

# Radical copolymerization of *N*-(1,1-dimethyl-3-oxobutyl)-acrylamide in different solvents

S. Franco and A. Leoni

Research Laboratories, 3M Italia SpA, 17016 Ferrania (Savona), Italy  
(Received 12 July 1972; revised 30 August 1972)

The influence of different solvents on the copolymerization behaviour of *N*-(1,1-dimethyl-3-oxobutyl)-acrylamide (diacetone acrylamide, DAAM) with styrene and methyl methacrylate has been investigated. The calculated relative reactivities of DAAM towards the polystyryl and poly(methyl methacryl) radicals ( $1/r_2$ ) are practically unaffected by the reaction medium; on the contrary, the relative reactivities of both styrene and methyl methacrylate monomers towards the poly(diacetone acrylamide) radical ( $1/r_1$ ) are influenced by the reaction solvents. This effect, however, is less significant than that found previously for *N*-methyl acrylamide copolymerization.

## INTRODUCTION

Previous papers have shown that in the free radical copolymerization of acrylamide, methacrylamide, and *N*-methyl acrylamide<sup>1-3</sup>, the reactivity ratios are strongly influenced by the reaction medium; on the contrary, in the case of *N,N*-dimethyl acrylamide<sup>4</sup> no significant influence of the solvent on the copolymer composition was shown. Several factors were considered in order to tentatively explain such peculiar solvent effects.

In the present paper the results obtained in the copolymerization of *N*-(1,1-dimethyl-3-oxobutyl)-acrylamide (diacetone acrylamide) with styrene and methyl methacrylate in different solvents are reported; this monomer is a *N*-monosubstituted acrylamide. The copolymerization of diacetone acrylamide has already been investigated by other authors<sup>5</sup>; this paper, however, does not consider the effect of solvents on copolymerization parameters.

## EXPERIMENTAL

Diacetone acrylamide (DAAM), styrene and methyl methacrylate (MMA) were commercial products and were purified before polymerization according to the usual techniques. Dioxane, ethanol and ethyl acetate were commercial products; they were dried and distilled before use. The initiator,  $\alpha,\alpha'$ -azodiisobutyronitrile, was crystallized twice from ethyl ether. All experiments were performed in glass tubes sealed in a nitrogen atmosphere and heated to 70°C. The total concentration of monomers was kept constant at 0.8 mol/l of solvent; the initiator was used at the rate of 0.4 g/l of solvent. The conversions to polymers were in each case lower than 10%. The detailed experimental procedures for copolymer separation, purification, analyses and infra-red (i.r.) spectra are reported in a previous paper<sup>3</sup>.

## RESULTS AND DISCUSSION

The experimental points and the calculated copolymerization curves are plotted in Figures 1 and 2 where monomer  $f_1$  and copolymer  $F_1$  compositions are expressed as molar ratios with respect to DAAM.

The data were plotted according to the method of Fineman and Ross<sup>6</sup>. The best values of  $r_1$  and  $r_2$  were obtained by the method of least squares and the associated standard deviations by regression analysis.

The calculated  $r_1$  and  $r_2$  values are reported in Table 1.

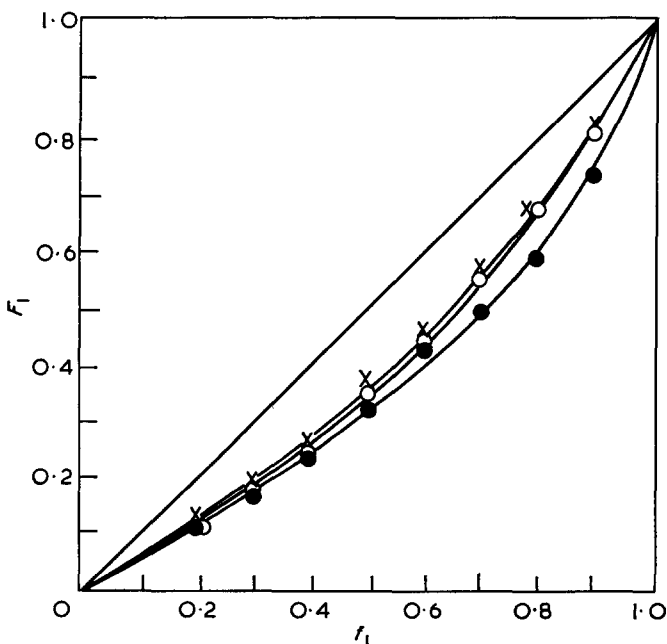


Figure 1 Copolymerization diagram for the system diacetone acrylamide ( $M_1$ )/styrene at 70°C.  $\circ$ , dioxane (line calculated for  $r_1=0.47$ ,  $r_2=1.85$ );  $\bullet$ , ethanol (line calculated for  $r_1=0.30$ ,  $r_2=1.80$ );  $\times$ , ethyl acetate (line calculated for  $r_1=0.49$ ,  $r_2=1.70$ )

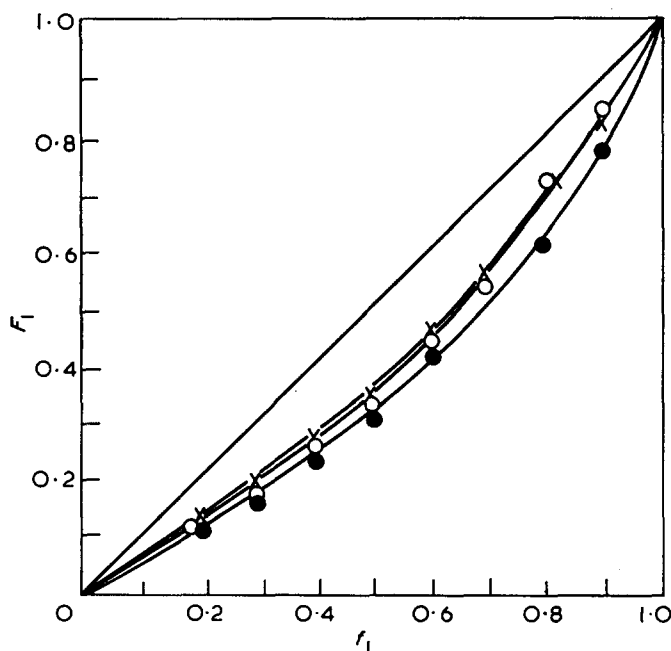
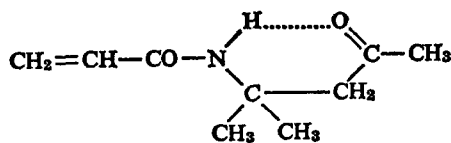


Figure 2 Copolymerization diagram for the system diacetone acrylamide ( $M_1$ )/methyl methacrylate at 70°C. ○, dioxane (line calculated for  $r_1=0.50$ ,  $r_2=1.80$ ); ●, ethanol (line calculated for  $r_1=0.31$ ,  $r_2=2.00$ ); ×, ethyl acetate (line calculated for  $r_1=0.46$ ,  $r_2=1.70$ )

Table 2 shows the corresponding  $Q$  and  $e$  values.

The experimental data show an evident influence of the solvents on these copolymerizations. It can be seen particularly that in each copolymerization system the copolymers obtained in dioxane and in ethyl acetate are always richer in DAAM than the copolymers obtained in ethanol. These differences can be seen by examining the i.r. spectra of copolymers obtained from 0.5 DAAM molar ratio of feeding. The intensity of absorption bands respectively of amide, styrene and methacrylic ester are in agreement with the found nitrogen contents.

It seems worth mentioning that the solvent effect is in the present case less significant compared to the effect found in the *N*-methyl acrylamide<sup>3</sup> copolymerization. In fact the mobility of the amido hydrogen giving the enolic form might be lowered by the presence of the substituent group on the amido nitrogen. In addition there is the possibility of intramolecular hydrogen bond formation according to:



although such effect should be rather reduced at polymerization temperature. The intramolecular hydrogen bonding should decrease the tendency of DAAM to give solute-solute associations<sup>7</sup> in low polarity solvents such as dioxane and ethyl acetate compared to *N*-methyl acrylamide. These considerations should be valid both for the monomers and the growing chain end radicals. All these facts could contribute to lowering the solvent influence on the copolymerization parameters.

In Tables 1 and 2 beside the  $r_1$ ,  $r_2$  and  $Q$ ,  $e$  values obtained in the present work in dioxane, ethyl acetate and in ethanol, the values obtained by Coleman *et al.*<sup>5</sup> in the

Table 1 Reactivity ratios for DAAM copolymerizations

Solvent	DAAM/styrene		DAAM/MMA	
	$r_1$	$r_2$	$r_1$	$r_2$
Dioxane <sup>a</sup>	$0.47 \pm 0.05$	$1.85 \pm 0.15$	$0.50 \pm 0.05$	$1.80 \pm 0.30$
Ethanol <sup>a</sup>	$0.30 \pm 0.03$	$1.80 \pm 0.10$	$0.31 \pm 0.02$	$2.00 \pm 0.10$
Ethyl acetate <sup>a</sup>	$0.49 \pm 0.04$	$1.70 \pm 0.10$	$0.46 \pm 0.03$	$1.70 \pm 0.10$
Benzene <sup>b</sup>	$0.49 \pm 0.06$	$1.77 \pm 0.08$	$0.57 \pm 0.03$	$1.68 \pm 0.06$

<sup>a</sup> Present work; <sup>b</sup> ref. 5

Table 2  $Q$  and  $e$  values for DAAM copolymerizations

Solvent	DAAM/styrene		DAAM/MMA	
	$Q$	$e$	$Q$	$e$
Dioxane <sup>a</sup>	0.43	-0.43	0.35	-0.04
Ethanol <sup>a</sup>	0.30	-0.03	0.28	-0.29
Ethyl acetate <sup>a</sup>	0.42	-0.37	0.36	-0.10
Benzene <sup>b</sup>	0.42	-0.42	0.41	-0.02

<sup>a</sup> Present work; <sup>b</sup> ref. 5

Reference values:  $Q=1.00$ ,  $e=-0.80$  for styrene;  $Q=0.74$ ,  $e=0.40$  for MMA

Table 3 Relative reactivities of DAAM monomer towards polystyryl and poly(methyl methacryl) radicals

Solvent	$1/r_2$	
	Polystyryl radical	Poly(methyl methacryl) radical
Dioxane <sup>a</sup>	0.54	0.55
Ethanol <sup>a</sup>	0.55	0.50
Ethyl acetate <sup>a</sup>	0.59	0.59
Benzene <sup>b</sup>	0.56	0.60

<sup>a</sup> Present work; <sup>b</sup> ref. 5

Table 4 Relative reactivities towards the poly(DAAM) radical of styrene and methyl methacrylate monomers

Solvent	$1/r_1$	
	Styrene monomer	Methyl methacrylate monomer
Dioxane <sup>a</sup>	2.12	2.00
Ethanol <sup>a</sup>	3.33	3.22
Ethyl acetate <sup>a</sup>	2.04	2.17
Benzene <sup>b</sup>	2.04	1.75

<sup>a</sup> Present work; <sup>b</sup> ref. 5

copolymerization of DAAM with styrene and methyl methacrylate in benzene are also reported. These values show that benzene behaves like dioxane and ethyl acetate. This could be attributed to the low dielectric constant of these solvents compared to that of ethanol.

The relative reactivities of DAAM monomer ( $1/r_2$ ) towards both the polystyryl and poly(methyl methacryl) radicals, listed in Table 3 are practically unaffected by the reaction solvents. On the contrary, the relative reactivities of both styrene and methyl methacrylate monomers ( $1/r_1$ ) towards the poly(DAAM) radical (Table 4) are remarkably affected by the reaction solvents: they are higher in the more polar solvent (ethanol) than in the other ones.



Similar results were previously found, and to a greater extent, for *N*-methyl acrylamide<sup>3</sup> and unsubstituted acrylamide<sup>1</sup>. Also these results could be explained by the above discussed association phenomena.

#### ACKNOWLEDGEMENTS

The authors express their thanks to Professor Guido Saini, Istituto Chimica Analitica dell'Università di Torino, for many helpful suggestions and stimulating discussions.

#### REFERENCES

- 1 Saini, G., Leoni, A. and Franco, S. *Makromol. Chem.* 1971, **144**, 235
- 2 Saini, G., Leoni, A. and Franco, S. *Makromol. Chem.* 1971, **147**, 213
- 3 Leoni, A., Franco, S. and Saini, G. *Makromol. Chem.* in press
- 4 Saini, G., Leoni, A. and Franco, S. *Makromol. Chem.* 1971, **146**, 165
- 5 Coleman, L. E., Bork, J. F., Wyman, D. P. and Hoke, D. I. *J. Polym. Sci. (A)* 1965, **3**, 1601
- 6 Fineman, M. and Ross, S. D. *J. Polym. Sci.* 1950, **5**, 259
- 7 Curtat, M., Jozefonvics, J. and Neel, G. *Eur. Polym. J.* 1969, **5**, 53

# Poly(ethyl acrylate) in dilute solution

K. S. V. Srinivasan and M. Santappa

Department of Physical Chemistry, University of Madras, Madras 25, India  
(Received 24 July 1972; revised 25 September 1972)

Poly(ethyl acrylate) (PEA), solution polymerized in methyl ethyl ketone by free radical initiation, was fractionated and the fractions were characterized by light scattering, viscometry and osmometry. Fractions obtained were in the molecular weight range of  $0.3 \times 10^6$  to  $1.6 \times 10^6$  with a polydispersity of 1.40. The following Mark-Houwink relations were established:

$$\begin{aligned} [\eta]_{\text{acetone}}^{35^\circ\text{C}} &= 4.15 \times 10^{-2} \bar{M}_w^{0.61} \\ [\eta]_{\text{MEK}}^{35^\circ\text{C}} &= 2.03 \times 10^{-2} \bar{M}_w^{0.66} \\ [\eta]_{\text{n-propanol}}^{39.5^\circ\text{C}} &= 7.89 \times 10^{-2} \bar{M}_w^{0.50} \end{aligned}$$

It was found that n-propanol at  $39.5^\circ\text{C}$  was a theta solvent for poly(ethyl acrylate) and that acetone was a poor solvent compared to methyl ethyl ketone. A relation between the molecular dimension and the molecular weight was established. It was observed that the chain dimensions of poly(ethyl acrylate) and poly(butyl acrylate) were considerably larger than poly(ethyl methacrylate) and poly(butyl methacrylate) respectively. The validity of various extrapolation procedures that have been proposed for calculating the unperturbed dimensions have been examined. The steric factor for PEA was 2.16 compared to 2.10 for poly(ethyl methacrylate). Root mean square end-to-end distances were calculated from the Debye-Bueche and Kirkwood-Riseman methods and compared with the experimental values.

## INTRODUCTION

A number of conformational and thermodynamic studies on polystyrene, poly(methyl methacrylate) (PMMA) and poly(ethyl methacrylate) have been made but little attention appears to have been paid to poly(methyl acrylate) (PMA), poly(ethyl acrylate) (PEA) or poly(butyl acrylate) (PBA). It was observed by Kotera *et al.*<sup>1</sup>, Matsuda and Inagaki<sup>2</sup> and Karunakaran and Santappa<sup>3</sup> that the chain dimension of PMA was considerably larger than that for PMMA. It was felt interesting to study the dilute solution properties of poly(ethyl acrylate) and poly(butyl acrylate) and to compare the chain dimensions of polyacrylates with the corresponding polymethacrylates. This communication deals with the fractionation of poly(ethyl acrylate) and the characterization of these fractions by light scattering and viscometry. Viscosity and molecular weight data obtained in different solvents have been used to establish the viscosity/molecular weight relations and unperturbed dimensions of PEA chains. Also the interaction of polymer in solution has been interpreted in terms of the current theories of polymer solutions.

## EXPERIMENTAL

### Materials

Methyl ethyl ketone (lab. reagent grade, BDH), acetone (analytical reagent grade, BDH), n-propanol,

methanol (lab. reagent grade, BDH), etc. were purified according to the standard procedure<sup>4</sup>. Ethyl acrylate (Chem. pure, India) was washed three times with sodium hydroxide (5%) followed by distilled water, dried over anhydrous  $\text{Na}_2\text{SO}_4$  and distilled in an atmosphere of dry nitrogen.

### Polymerization

Polymerization of ethyl acrylate in methyl ethyl ketone was carried out with benzoyl peroxide as initiator in an atmosphere of nitrogen at  $60^\circ\text{C}$ . The conversion was restricted to  $\sim 15\%$ . The polymer was precipitated with methanol-water (6:1 v/v). It was purified by dissolving in methyl ethyl ketone and reprecipitating with methanol-water (6:1 v/v) and dried in vacuum at  $60^\circ\text{C}$ . Fractionation and refractionation were carried out by fractional precipitation technique using methyl ethyl ketone and methanol-water (6:1 v/v) as the solvent/non-solvent pair at  $30^\circ\text{C}$  and fifteen fractions each weighing about 0.20–0.50 g were obtained.

### Characterization

*Viscosity.* Viscosity measurements were carried out with filtered solvent and polymer solutions (six concentrations in the range  $2 \times 10^{-3}$  to  $5 \times 10^{-4}$  g/ml) in a suspended level dilution viscometer (PCL, Colchester Instruments Ltd, UK) at  $35^\circ\text{C} \pm 0.01^\circ\text{C}$  in a constant temperature viscometer bath. The kinetic energy

correction was negligible. The limiting viscosity number  $[\eta]$  was obtained as a mean of three  $[\eta]$  values from the equations:

$$\begin{aligned} \eta_{sp}/c &= [\eta] + k_1[\eta]^2c \\ (\ln \eta_{rel})/c &= [\eta] - k_2[\eta]^2c \\ \eta_{sp}/c &= [\eta] + k_3[\eta]\eta_{sp} \end{aligned}$$

where  $k_1$ ,  $k_2$  and  $k_3$  are the Huggins constant, Kraemer's constant and the Schulz-Blaschke constant respectively.

**Osmotic pressure.** An osmometer (Pinner-Stabin, Colchester Instruments Ltd, UK) with preconditioned gel cellulose (PECEL 600) membranes was employed to measure the osmotic pressure of PEA<sub>D</sub> and PEA<sub>F</sub> samples in acetone at 30 ± 0.01°C. The number-average molecular weight ( $\bar{M}_n = 5.69 \times 10^5$ ,  $9.10 \times 10^5$  for PEA<sub>D</sub> and PEA<sub>F</sub> respectively) was obtained from a plot of  $(\pi/c)^{1/2}$  vs.  $c$ . The polydispersity of the fraction was calculated from the ratio of the molecular weights by light scattering and osmometry and was found to be 1.42 and 1.38 for PEA<sub>D</sub> and PEA<sub>F</sub> respectively.

**Light scattering.** Light scattering measurements of PEA in methyl ethyl ketone and acetone were carried out at 35 ± 0.5°C in a Brice-Phoenix universal light scattering photometer (Series 1999-12; Phoenix Precision Instruments Company, Philadelphia)<sup>5</sup> with the use of unpolarized light ( $\lambda = 4356 \text{ \AA}$ ) at various angles. The refractive index increment ( $dn/dc$ ) of PEA in acetone (0.106 ± 0.003) and methyl ethyl ketone (0.097 ± 0.002) were measured in a differential refractometer (Brice-Phoenix No. 1974; Phoenix Precision Instruments Company, Philadelphia)<sup>5a</sup>. The light-scattering data were treated according to the method of Zimm<sup>6</sup>. The weight-average molecular weight  $\bar{M}_w$ , the  $z$ -average mean square radius of gyration  $(\bar{S}^2)_z$  and the second virial coefficient were calculated from the plots of  $KC/R_\theta$  versus  $\sin^2 \theta/2 + 100c$ .  $(\bar{S}^2)_z$  was then converted to  $(\bar{r}^2)_w$  by the equation<sup>7, 21, 22</sup>:

$$(\bar{r}^2)_w = (\bar{S}^2)_z(3 + \beta)(2 + \beta)(h + 1)/(h + 2 + \beta)$$

where  $h = [(M_w/M_n) - 1]^{-1}$  in the Schulz-Zimm distribution function and  $\beta$  is obtained from  $(\bar{r}^2) = AM^{(1+\beta)}$

Table 1 Parameters obtained from light scattering and viscosity  
Polymer=poly(ethyl acrylate); solvent=acetone; temperature=35°C;  $\lambda = 4356 \text{ \AA}$ ;  $dn/dc = 0.106 \pm 0.002$ ;  $h = 2.5$ ;  $a = 0.60$ ;  $\beta = 0.07$

Fraction	$\bar{M}_w \times 10^{-6}$	$[\eta]$ (ml/g)	$k_1$	$(\bar{r}^2)_w^{1/2}$ (Å)	$(\bar{r}^2)_0^{1/2}$ (Å)	$A_2 \times 10^4$ (cm <sup>3</sup> mol g <sup>-2</sup> )	$\Phi \times 10^{-23}$
PEAA	0.490	121.5	0.25	945	463	2.20	0.68
PEAB	0.560	131.0	0.26	1001	495	—	0.71
PEAC	0.775	170.0	0.24	1177	589	2.00	0.78
PEAD	0.811	167.0	0.28	1180	597	1.80	0.80
PEAE	1.065	189.4	0.36	1380	681	2.44	0.74
PEAF	1.234	207.1	0.33	1520	733	1.76	0.71
PEAG	1.663	263.5	0.32	1758	854	1.53	0.83

Table 2 Parameters obtained from light scattering and viscosity  
Polymer=poly(ethyl acrylate); solvent=methyl ethyl ketone; temperature=35°C;  $\lambda = 4356 \text{ \AA}$ ;  $dn/dc = 0.097 \pm 0.002$ ;  $a = 0.66$ ;  $h = 2.5$ ;  $\beta = 0.085$

Fraction	$\bar{M}_w \times 10^{-6}$	$[\eta]$ (ml/g)	$(\bar{r}^2)_w^{1/2}$ (Å)	$(\bar{r}^2)_0^{1/2}$ (Å)	$A_2 \times 10^4$ (cm <sup>3</sup> mol g <sup>-2</sup> )	$\Phi \times 10^{-23}$
PEA <sub>1</sub>	0.412	102.0	800	348	1.8	0.80
PEA <sub>2</sub>	0.485	112.1	839	369	2.0	0.74
PEA <sub>3</sub>	0.811	165.5	1137	496	1.5	0.91
PEA <sub>4</sub>	0.868	167.0	1158	498	1.5	0.93
PEA <sub>5</sub>	1.079	232.0	1411	617	1.2	0.89
PEA <sub>6</sub>	1.676	263.5	1708	747	1.5	0.86

or  $\beta = (2a - 1)/3$  where  $A$  is the second virial coefficient,  $M$  is the molecular weight and  $a$  is the exponent in the Mark-Houwink equation (Tables 1 and 2).

## RESULTS AND DISCUSSION

The solution properties of fractionated poly(ethyl acrylate) in methyl ethyl ketone (six fractions designated as PEA<sub>1</sub> to PEA<sub>6</sub>) and in acetone (seven fractions designated PEA<sub>A</sub> to PEA<sub>F</sub>) were investigated by light scattering and viscosity measurements at 35°C.

### Mark-Houwink-Sakurada relation

The least square fit of the double log plots (Figure 1 and Tables 1, 2 and 3) of  $[\eta]$  and  $\bar{M}_w$  for PEA systems yielded the following Mark-Houwink-Sakurada relations for PEA:

$$\begin{aligned} [\eta]_{\text{MEK}}^{35^\circ\text{C}} &= 2.03 \times 10^{-2} \bar{M}_w^{0.66} \\ [\eta]_{\text{Acetone}}^{35^\circ\text{C}} &= 4.15 \times 10^{-2} \bar{M}_w^{0.61} \\ [\eta]_{\text{n-propanol}}^{39.5^\circ\text{C}} &= 7.89 \times 10^{-2} \bar{M}_w^{0.50} \end{aligned}$$

The low value of  $a$  (0.61) for PEA/acetone compared to that for PEA/methyl ethyl ketone indicated that acetone is a 'poor' (thermodynamically more ideal) solvent for PEA compared to methyl ethyl ketone. The  $a$  value of 0.50 in n-propanol at 39.5°C suggests that n-propanol at 39.5°C is a  $\theta$ -solvent.

### Relation between $(\bar{r}^2)_w^{1/2}$ and $\bar{M}_w$

Kuhn relations for these systems at 35°C were established by least square fits of the log-log plots (Figure 1 and Tables 1 and 2):

$$\begin{aligned} (\bar{r}^2)_w^{1/2} &= 0.89 \bar{M}_w^{0.51} \text{ for acetone} \\ (\bar{r}^2)_w^{1/2} &= 0.98 \bar{M}_w^{0.52} \text{ for methyl ethyl ketone} \end{aligned}$$

### $A_2$ - $\bar{M}_w$ relation

The second virial coefficient,  $A_2$  decreased as the size of the molecule increased for PEA/acetone and PEA/

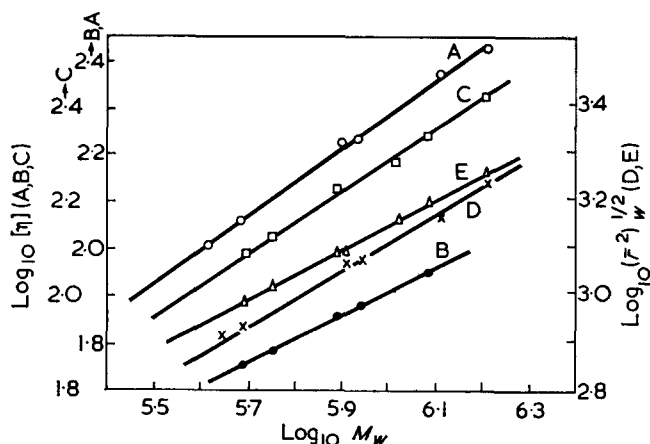


Figure 1 Plots of  $\log_{10}[\eta]$  versus  $\log_{10}\bar{M}_w$  in (A) methyl ethyl ketone, (B) n-propanol and (C) acetone; plots of  $\log_{10}(\bar{r}_0^2)^{1/2}$  versus  $\log_{10}\bar{M}_w$  in (D) methyl ethyl ketone and (E) acetone

Table 3 Evaluation of molecular parameters

Polymer=poly(ethyl acrylate); solvent=n-propanol; temperature=39.5°C;  $a=0.50$

Polymer sample	$\bar{M}_w \times 10^{-6}$	$[\eta]_{\theta}$	$k_1$
PEA <sub>A</sub>	0.490	54.2	0.42
PEA <sub>B</sub>	0.561	59.0	0.49
PEA <sub>C</sub>	0.775	69.5	0.60
PEA <sub>D</sub>	0.882	73.5	0.47
PEA <sub>F</sub>	1.234	85.9	0.40

methyl ethyl ketone but the points were too scattered to get any qualitative relation (Tables 1 and 2).

#### Evaluation of unperturbed dimensions

A number of graphical procedures are available for the determination of unperturbed dimensions of polymer molecules from intrinsic viscosity and molecular weight measurements in non-ideal solvents. In general all these methods involve determination of the constant  $K_{\theta}$  for the expression  $[\eta]_{\theta} = K_{\theta} M^{1/2}$  where  $K_{\theta} = \Phi_0 (\bar{r}_0^2/M)^{3/2}$  with  $\Phi_0 = 2.86 \times 10^{23}$ , the asymptotic value of the Flory constant and  $(\bar{r}_0^2)$ , unperturbed mean square end-to-end distance. Determining  $\bar{M}_w$  by light scattering in acetone and methyl ethyl ketone for poly(ethyl acrylate) and relating this  $\bar{M}_w$  to  $[\eta]$  in n-propanol at 39.5°C, the Mark-Houwink relation  $[\eta]_{\theta} = K_{\theta} M^{1/2}$  was established. From  $K_{\theta}(7.89 \times 10^{-2})$ , the value for  $(\bar{r}_0^2/M)^{1/2} = 673 \times 10^{11}$  cm was obtained taking into account the correction for heterogeneity as given by Kurata *et al.*<sup>8</sup> viz.

$$[\eta]_{\theta} = \frac{\Phi_0 \left( \frac{\bar{r}_0^2}{M_w} \right)^{3/2} M_w^{1/2}}{q_w}$$

where  $q_w = \Gamma(h+1.5)/(h+1)^{1/2} \Gamma(h+1)$ . The evaluation of the Flory constant  $K_{\theta}$  was also done by plotting  $[\eta]$  and  $\bar{M}_w$  data by three different methods based on the Flory-Fox-Schaeffgen<sup>9</sup> (FFS), the Stockmayer-Fixman<sup>10</sup> (SF) and the Ptitsyn-Inagaki<sup>11</sup> (PI) expressions. The  $K_{\theta}$  values obtained by these three methods respectively were:  $7.89 \times 10^{-2}$ ,  $7.74 \times 10^{-2}$ ,  $10.63 \times 10^{-2}$  in n-propanol;  $7.89 \times 10^{-2}$ ,  $11.09 \times 10^{-2}$ ,  $11.20 \times 10^{-2}$  in methyl ethyl ketone; and  $13.87 \times 10^{-2}$ ,  $14.30 \times 10^{-2}$ ,  $13.49 \times 10^{-2}$  in acetone. In theta solvents FFS and the SF methods gave almost identical values which are in good agreement with those obtained from the relation  $[\eta]_{\theta} = K_{\theta} M^{1/2}$ . The PI method gave a higher value in

theta solvents. This method is applicable only in good solvents<sup>12</sup>. In good solvents (methyl ethyl ketone) the FFS theory was found to give the same  $K_{\theta}$  value as that obtained in theta solvents. The SF and the PI methods gave a higher value of  $K_{\theta}$ . Cowie<sup>13</sup> has shown that the SF method gives reliable  $K_{\theta}$  values only when the molecular weight of the fractions are less than  $1 \times 10^6$  and the Mark-Houwink exponent is less than 0.7. Since the molecular weights of the fractions of PEA studied were not less than  $10^6$  it is evident that the SF method is not applicable for the present system. The  $K_{\theta}$  value for PEMA ( $5.64 \times 10^{-2}$ ) is far smaller than that of PEA ( $7.89 \times 10^{-2}$ ), showing that the unperturbed dimension of PEA is greater than that of PEMA which is in good agreement with the observations made on PMA and PMMA<sup>2</sup>.

#### Steric factor or conformational factor, $\sigma$

The unperturbed mean square end-to-end distance for the free rotation model of a polymer chain is given by:

$$\bar{r}_{0f}^2 = nl^2(1 - \cos\theta)/(1 + \cos\theta),$$

where  $n$  is the number of carbon atoms in the chain,  $l$  is the bond length and  $\theta$  is the valence angle;  $\bar{r}_{0f}^2$  is calculated taking  $l=1.54 \text{ \AA}$ ,  $\theta=109.5^\circ$ . The ratio  $(\bar{r}_0^2/\bar{r}_{0f}^2)^{1/2} = \sigma$  was found to be equal to 2.15.

#### Flory's universal parameter

The universal parameter,  $\Phi$  for PEA/acetone and PEA/methyl ethyl ketone was found to be less than  $1 \times 10^{23}$  (Tables 1 and 2) which was less than the normal value  $2.86 \times 10^{23}$ . Such low values have been obtained from the data reported in the literature for poly(methyl acrylate)<sup>1-3</sup> and poly(butyl acrylate)<sup>14</sup>. The possible factors that affect the magnitude of  $\Phi$  are: (a) non-Gaussian distribution of chain segments; (b) molecular weight heterogeneity; and (c) branching. It was observed that in the case of poly(methyl acrylate)<sup>16</sup> and other vinyl polymers, the non-Gaussian distribution of chain segments was small<sup>15, 17</sup>. Since  $\Phi$  values were very low, the effect of branching could be ruled out. Even after applying the correction for molecular weight heterogeneity and excluded volume effect, the values were low. Hence the reasons for the low values of  $\Phi$  obtained for poly(methyl acrylate), poly(ethyl acrylate) and poly(butyl acrylate) are not quite clear at present.

#### Calculation of root mean square end-to-end distance

Values of the end-to-end distance were calculated from Debye-Bueche theory<sup>18</sup> and Kirkwood-Riseman

Table 4 Comparison of root mean square end-to-end distance from hydrodynamic theory and experiment

Solvent=acetone;  $a=0.60$ ;  $\Phi(\sigma)=1.850$ ;  $X'(X')=0.970$

Fraction	$\bar{M}_w \times 10^{-6}$	$(\bar{r}_0^2)^{1/2} (\text{\AA})$		
		D-B	K-R	Expt.
PEA <sub>A</sub>	0.490	494	550	957
PEA <sub>B</sub>	0.561	530	590	1011
PEA <sub>C</sub>	0.775	644	717	1190
PEA <sub>D</sub>	0.811	650	723	1192
PEA <sub>E</sub>	1.065	741	825	1395
PEA <sub>F</sub>	1.234	802	894	1536
PEA <sub>G</sub>	1.663	979	1090	1778

D-B=Debye-Bueche

K-R=Kirkwood-Riseman

theory<sup>19</sup> (revised values<sup>20</sup>) to attempt to visualize the shape of the molecular chain in solution. It was observed that  $(\overline{r_z})_{\theta}^{1/2}$  measured by light scattering was 1.7 to 2.0 times higher than that calculated from the theories (Table 4).

#### REFERENCES

- 1 Kotera, A., Saito, Y., Watanabe, Y. and Ohama, M. *Makromol. Chem.* 1965, **87**, 195
- 2 Matsuda, H. and Inagaki, H. *Bull. Inst. Chem. Res. Kyoto Univ.* 1968, **46**, 2, 48
- 3 Karunakaran, K. and Santappa, M. *J. Polym. Sci. (A-2)* 1968, **6**, 713
- 4 Weissberger, A. and Proskauer, S. 'Techniques in Organic Chemistry', Interscience, New York, 1955
- 5 Brice, B. A., Halwar, M. and Speiser, R. *J. Opt. Soc. Am.* 1950, **40**, 768
- 5a Brice, B. A. and Speiser, R. *J. Opt. Soc. Am.* 1946, **36**, 363
- 6 Zimm, B. H. *J. Chem. Phys.* 1948, **16**, 1093, 1099
- 7 Cleland, R. L. *J. Polym. Sci.* 1958, **27**, 349
- 8 Kurata, M. and Stockmayer, W. H. *Fortschr. Hochpolym. Forsch.* 1963, **3**, 196
- 9 Flory, P. J. and Fox, T. G. *J. Am. Chem. Soc.* 1951, **73**, 1904
- 10 Stockmayer, W. H. and Fixman, M. *J. Polym. Sci.* 1963, **C1**, 137
- 11 Inagaki, H., Suzuki, H. and Kurata, M. in 'U.S.-Japan Seminar in Polymer Physics' (*J. Polym. Sci. (C)* 15), Interscience, New York, 1966, p 409
- 12 Patel, C. K. and Patel, R. D. *Makromol. Chem.* 1969, **128**, 157
- 13 Cowie, J. M. G. *Polymer* 1966, **7**, 487
- 14 Srinivasan, K. S. V., Karunakaran, K. and Santappa, M. *Curr. Sci.* 1971, **40**, 232
- 15 Benoit, H. and Doty, P. *J. Phys. Chem.* 1953, **57**, 958
- 16 Karunakaran, K. *PhD Thesis* University of Madras, 1967
- 17 Krigbaum, W. R. *J. Polym. Sci.* 1958, **28**, 213
- 18 Debye, P. and Bueche, A. M. *J. Chem. Phys.* 1948, **16**, 573
- 19 Kirkwood, J. G. and Riseman, J. *J. Chem. Phys.* 1948, **16**, 565
- 20 Kurata, M. and Yamakawa, H. *J. Chem. Phys.* 1958, **29**, 311
- 21 Peterlin, A. *J. Chem. Phys.* 1955, **23**, 2464
- 22 Matsumoto, M. and Ohayanagi, J. *J. Polym. Sci.* 1960, **46**, 441

# Characterization of the crystalline, intermediate and amorphous phase in poly(ethylene terephthalate) fibres by X-ray diffraction

W. L. Lindner

*Deutsches Wollforschungsinstitut an der RWTH-Aachen,  
Veltmanplatz 8, 51 Aachen, West Germany  
(Received 21 March 1972; revised 14 September 1972)*

An X-ray method is discussed for the formal characterization of three phases of fibres: the crystalline, intermediate and amorphous phase. Its application to the study of physically treated poly(ethylene terephthalate) (PET) fibres has been investigated. The crystalline phase index is correlated with the macroscopic density of fibres, whose non-crystalline densities were approximately equal. The least squares regression line is given by the following equation:  $\rho(\text{g/cm}^3) = 1.358 + 0.09k_{\text{cr}}$ , the correlation coefficient being 0.88. The deviations from the regression line are discussed by using specially drawn non-crystalline templates with different densities. The unit intercept of the regression line is at density  $1.448\text{g/cm}^3$ . This value is very close to the value of  $1.455\text{g/cm}^3$ , which is the density of the perfect crystal.

The results show that wide angle and density measurements alone are not sufficient to prove whether two different non-crystalline states with boundaries between both exist simultaneously in a semicrystalline drawn PET fibre or not. As long as no other suitable method is available, the two-phase model has to be regarded as an adequate approximation for PET fibres with respect to density.

## INTRODUCTION

The determination of the degree of crystallinity of fibres has been attempted over the last twenty years. A survey of the principles so far obtained has been given by Hermans<sup>1</sup>, Miller<sup>2</sup> and Ruscher<sup>3</sup>. The methods described have always involved some assumptions and simplifications. One of these is the two-phase model consisting of crystalline and amorphous substance with no transitions between the two.

It is the purpose of this paper to describe an internal X-ray method which allows an estimate to be made of the amount of the intermediate phase in poly(ethylene terephthalate) (PET) fibres subjected to different stretching and physical treatments. In 1956 Sandemann and Keller<sup>4</sup> proved the existence of an intermediate state of order between amorphous and crystalline in the case of nylon-6. Later Hyndman and Origlio<sup>5</sup> confirmed its existence from their nuclear magnetic resonance (n.m.r.) studies of polyethylene and polypropylene fibres. Sobue and Tabata<sup>6</sup> described polymorphic structures with differing physical phases on isotactic polypropylene filaments. Further experimental evidence for an intermediate state of order in polymers was given by Stern<sup>7</sup> in the case of nylon. Iwayanayi and Sakurai<sup>8</sup> proved the existence of a third n.m.r. component in addition to narrow and broadline components in polytetrafluoroethylene. It was assumed to be intermediate between the amorphous and

the crystalline phase. Jellinek *et al.*<sup>9</sup> measured an anisotropy of the diffuse scattering of the non-crystalline fraction on PET fibres subjected to thermal treatment at different temperatures and stresses, which could formally be subdivided into a diffuse isotropic halo and a diffuse arc on the equator.

Since the general methods used to measure crystallinity assume the division of the polymer sample into regions which are wholly crystalline or amorphous, Stern<sup>7</sup> inferred that the existence of an intermediate (mesomorphic) order renders its measurement invalid. This conclusion may be valid for nylon, since Stern proposed a paracrystalline structure for it, but this is not so in the case of polypropylene as Ruland<sup>10</sup> has shown.

These and other studies indicate that the two-phase model as defined earlier does not hold true for some polymers. The question that arises is: can we accept the two-phase model as an adequate approximation for PET fibres, or how far from this hypothesis and in which direction must we go to be consistent with the data? There are several methods available for determining crystallinity, each of which finds the spectrum order that may be present in the polymer sample differently. For this reason, agreement among results obtained by different techniques could be shown only in some cases. Farrow and Bagley<sup>11</sup> found an excellent correlation between change in density and X-ray crystallinity in undrawn

yarns, heat treated at different temperatures in the relaxed state. In drawn yarns this correlation was not present. Their conclusion was that the density of the non-crystalline material can no longer be assumed constant and therefore the measurement of crystallinity in drawn fibres by density measurements is unreliable. It is evident that the existence of an intermediate state of order and the capability of the experimental technique to respond to it becomes important in the discussion as to the correct interpretation of density measurements and whether the two-phase model is practical or not. The justification for the present study, which adds a new X-ray technique, is that it gives three X-ray phase criteria.

## EXPERIMENTAL

### Samples

The material used in this study was normal commercial production PET yarn with draw ratios of 3.0 and 3.3 which was subsequently physically treated.

### Density method

The apparent density was determined by the density-gradient column described by Kolb and Izard<sup>12</sup>. Based on studies by Kashmiri and Sheldon<sup>13</sup>, a carbon tetrachloride/heptane system was chosen as immersion liquid. Because of the time dependency of the apparent density measurement as shown by Juilfs<sup>14</sup> and Preston and Nimkar<sup>15</sup> the optimum shape of the sample and immersion time were previously selected. In the case of physically treated samples, the amount of retained liquid was determined. The measured density was corrected using the equation given by Moore and Sheldon<sup>16</sup>.

### X-ray method

The X-ray source was a microfocus X-ray unit (RDF50/1), 1200 W. A bundle of fibres 1 mm thick was given an exposure to nickel-filtered CuK $\alpha$  X-rays for 30 min. The X-ray diffraction lines were recorded on film (OSRAY DW: produced by Agfa-Gevaert) with a Debye-Scherrer camera (evacuated to eliminate air scattering).

After processing and drying, the diffractograms were scanned by a microdensitometer (Joyce double beam microdensitometer). The intensity data obtained from microdensitometer traces were used without correction for Lorentz-, polarization- and absorption-factors because the intensities compared were all measured at the same diffraction angle of  $2\theta$ .

### Principles of phase indices (PI)—scheme of measurement in the reciprocal space

All procedures developed so far to determine the 'degree of crystallinity' have a common first step: the division of the X-ray pattern into peaks and background. The relative method is based on the assumption that every crystalline or non-crystalline intensity measured either at one defined diffraction angle or about a limited angular range is proportional to the amount of crystalline or amorphous phase present in the partly crystalline polymer. If the unknown proportion factors can be eliminated then the problem is solved<sup>17-20</sup>. The absolute method includes the measurement of the intensity contributed by the crystalline as well as by the non-crystalline

phase. The basic principle is as follows: the total diffraction intensity of a substance, obtained by integrating in the three-dimensional reciprocal space, is independent of its state of order. Thus, if the total crystalline scattering in an X-ray pattern is  $J_{cr}$  and the total amorphous one is  $J_{am}$ , then the crystalline fraction is given by:

$$x = J_{cr} / (J_{cr} + J_{am}) \quad (1)$$

Naturally this principle is only valid if the total intensity has been measured by integrating either over the whole reciprocal space or over an angular range, which has been specially detected previously<sup>10</sup>. The errors arising from not observing this condition and by measuring over a limited range only (normally  $2\theta = 6^\circ$  to  $38^\circ$  in the case of PET<sup>11</sup>) shows very clearly that these 'crystallinities' are not absolute but only indices of crystallinity.

Another method measures the proportion of both intensities at one angle only. This is the simplest procedure both in the relative as well as in the absolute procedure. Table 1 gives a survey of the methods used so far but it is not claimed to be complete.

In the case of the oriented specimens all methods applied to date have made some provision for the elimination of the orientation in the sample. The reason is that any radial scan of an oriented pattern will give improper intensity data<sup>20, 21</sup>, since the different segments which give rise to the crystalline and non-crystalline halo do not have equal orientation. This has been accomplished by the spreading of the arcs into circles by either: (i) randomization of the sample<sup>21, 22</sup>; or (ii) rotation of the oriented specimen during the X-ray exposure<sup>9, 20, 23</sup>. However, Ruland<sup>23, 24</sup> and Jellinek *et al.*<sup>9</sup> in their studies of the diffuse disorder scattering of nylon-6,6 and PET fibres respectively, measured the diffraction pattern without this randomization procedure. The argument put forward was that, in the case of axial symmetry, these procedures produce systematic errors owing to the neglect of the azimuthal distribution of the diffuse disorder scattering. Jellinek *et al.* discussed the volume integrals of the intensity in the reciprocal space calculated with some approximations and restricted to the (010) reflection. The intensity of the crystalline scattering has been calculated by multiplying the maximum intensity (measured above the background) with the radial and azimuthal half width. It was assumed

Table 1 Survey of X-ray procedures for determining crystallinity

	Crystalline and/or amorphous intensity have been measured		
	at one angle only	over a short angular range	over the range $2\theta = 0^\circ$ to $180^\circ$
Relative method	Goppel <sup>24</sup>	Hermans and Weidinger <sup>18</sup> (cellulose)	
	Goppel and Arlmann <sup>17</sup>	Hermans and Weidinger <sup>19</sup> (polyethylene)	Statton <sup>20</sup> (PET)
Absolute method	Ruscher <sup>3</sup>	Matthews <i>et al.</i> <sup>25</sup> Falkai and Bodor <sup>26</sup> (PET) Johnson <sup>27</sup> (PET) Kilian <i>et al.</i> <sup>25</sup> (PET) Farrow and Preston <sup>21</sup> (PET)	Ruland <sup>10</sup>

that the integrated intensity of the diffuse anisotropy scattering is sufficiently represented by the product of the intensity of the maximum with the azimuthal half width, whereas the amorphous scattering has been represented by the peak intensity alone. It is clear that the intensities evaluated with the method just mentioned are not sufficient either for comparisons or for the evaluation of any index of order. The alterations on the diffractogram can be characterized in such a manner, but each of the three fractions must be discussed separately. Bearing in mind the fact that the macroscopic behaviour of any fibre is not only dependent upon the amount but also upon the distribution, the quality, and the percentage of the different phases, then it is apparent that the results obtained with this technique cannot be correlated with them.

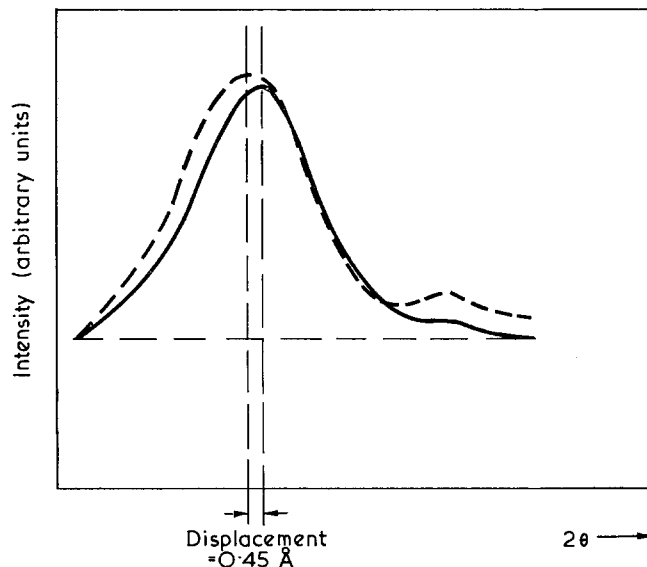
In the procedure discussed here, integration has not been carried out about any definite Bragg angle range. The measurements have been confined to the azimuthal distribution of the intensities to one Bragg angle (see *Figure 1*).

#### Equatorial scan

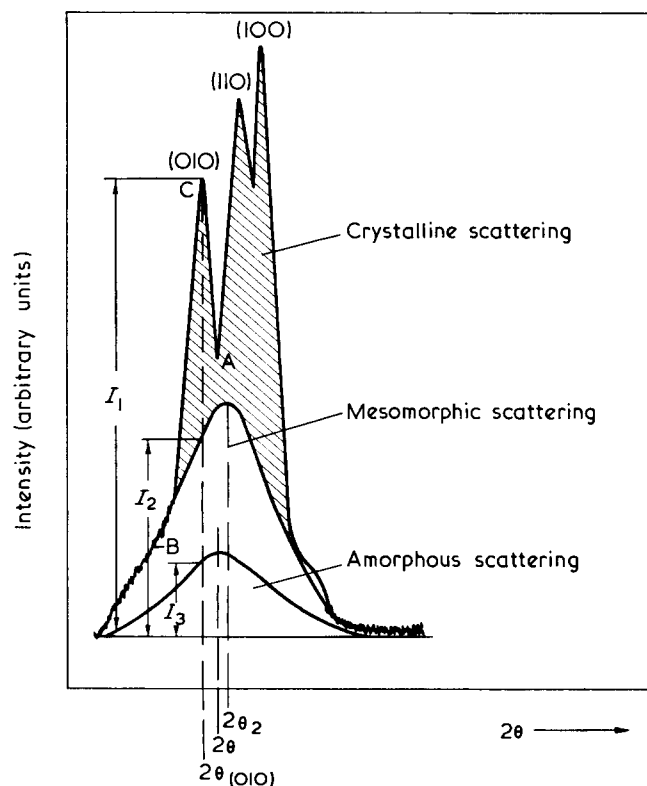
The shape of the background reflection curve in the equatorial scan can be reconstructed analogous to the method used by Kilian *et al.*<sup>25</sup>. They used relative heights  $h(2\theta) = I(2\theta)/I_{\max}(2\theta_2)$  [ $I(2\theta)$  being the intensity of the amorphous background;  $I_{\max}(2\theta_2)$  being the intensity at the Bragg angle  $2\theta_2$  of the maximum of the amorphous background] for reconstruction of the reflection contour of an amorphous template (*Figure 2*) in the diffractogram of a partly crystalline sample (*Figure 3*). The height A (*Figure 3*) is used as a reference position for fitting this curve to non-oriented samples, based on the assumption that the reflections (010) and (1 $\bar{1}$ 0) are not superimposed at this point.

Initially this technique was used; later, however, it appeared that, in many cases, the constructed background superimposed on the measured reflection curve in the region  $2\theta \leq 14^\circ$ . Thus, the minimum A has been rejected as a reference position. Assuming that there is no superposition of the non-crystalline spectrum by the crystalline scattering in this region<sup>25</sup>, the reconstructed background curve can be fitted. Since this discussion is restricted to the intensities arising at the Bragg angle of the maximum of the (010) reflection, a complete reconstruction of the background curve is not necessary.

The relative height  $h_B = I_{BT}/I(010)_T$  [ $I_{BT}$  being the intensity of the non-crystalline scattering of the template corresponding to the Bragg angle at point B (see *Figure 3*);



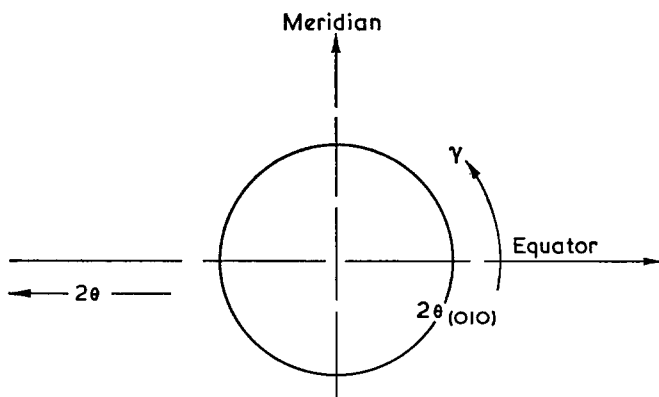
*Figure 2* Equatorial scans of non-crystalline isotropic PET (----) and an undrawn PET fibre (—)



*Figure 3* Radial scan along the equator of an oriented semi-crystalline PET sample. A, B, C, see text

$I(010)_T$  being the intensity of the template at the Bragg angle corresponding to the (010) reflection] is evaluated in the template (*Figure 2*). The background intensity of the  $i$ th partial crystalline sample corresponding to the (010) reflection is then given by the product of the relative height  $h_B$  with the intensity  $I_{Bi}$  [ $I_{Bi}$  being the intensity in the  $i$ th partly crystalline reflection curve at the Bragg angle corresponding to position B].

As can be seen in *Figure 3*, no attention has been paid to the intensity below the straight line fitting the reflection curve at  $2\theta = 6^\circ$  and  $2\theta = 36^\circ$ .



*Figure 1* Scheme of measurements in the reciprocal space



## Azimuthal scan

The construction of the azimuthal background reflection curve can be carried out analogously to the technique used for the crystalline orientation measurement by X-rays. The technique used by Hermans *et al.*<sup>26</sup> who scanned in their work dealing with the network formation in swollen hydrated cellulose the X-ray intensities with a microdensitometer at small increments of  $\alpha$  from the equator, has been adopted by Kast<sup>27</sup> and later by Farrow and Bagley<sup>11</sup>. The latter modified this procedure by using a polar table, which enabled them to reduce the determination to three scans only, two of which were along the azimuth of (100) and (010) reflections. This technique has been used here for the (010) reflection. The crystalline intensity can be separated on the azimuthal microdensitometer trace by the same relative height technique as discussed above. Reference points for the fitting of the non-crystalline template are given by the heights  $I_1$  and  $I_2$  in the equatorial trace (Figure 3). They can be reconstructed in the azimuthal scan (Figure 4) at  $\alpha=0$  degree (equator), starting from the fixed point C. Connecting the points on the trace where the intensity becomes independent of the azimuthal angular  $\alpha$ , by a straight line, we find the equatorial intensity  $I_3$  (Figure 4). Reconstructing  $I_3$  in the equatorial trace and doing so with each equatorial reflection, a curve analogous to that in Figure 3 can be reconstructed. Thus, the background due to diffuse disorder scattering can be formally subdivided into a diffuse isotropic and a diffuse anisotropic halo; the latter are called diffuse to correspond to the terminology used by Jellinek *et al.*

Regarding the template for the background reconstruction in the azimuthal scan, the assumption can be made that the shape of an oriented non-crystalline yarn is equal to that of the background radiation of an oriented semi-crystalline sample. Once the shape of the background is known from experience, it can be drawn in by eye without too great an error.

## Definition of the phase indices (PI)

From the azimuthal trace, which has been formally

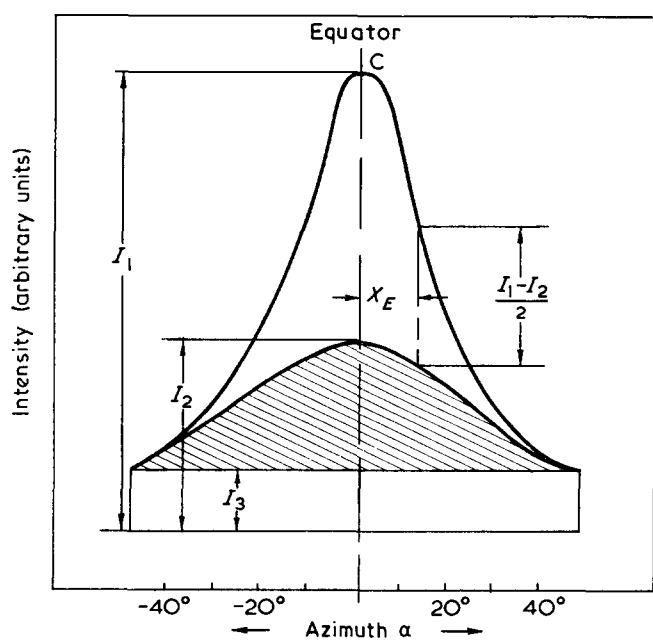


Figure 4 Azimuthal microdensitometer trace of sample reported in Figure 3 at a Bragg angle corresponding to the (010) plane

Table 2 Repetitive measurements of phase indices on PET fibres

Sample	Crystalline $PI_{k_{cr}}$	Intermediate $PI_{k_S}$	Amorphous $PI_{k_H}$
Exposure of sample 1	0.21	0.23	0.56
Exposure of a new sample 1	0.24	0.23	0.53
Exposure of sample 2	0.23	0.32	0.45
Exposure of a new sample 2	0.27	0.32	0.41
Exposure of sample 3	0.35	0.34	0.31
Exposure of a new sample 3	0.38	0.35	0.27

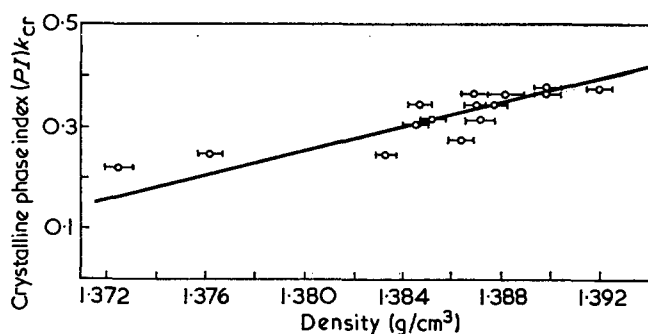


Figure 5 Crystalline phase index  $k_{cr}$  macroscopic density relationship for drawn PET filaments

subdivided as shown above, the  $PI$  are determined by measuring the integrated areas. The integration has to be performed over the whole range of the azimuthal reflection curve up to that angle where  $I(\alpha) = I_3$  (Figure 4). The indices are then given by:

$$k_{cr} = A_{cr} / \sum A_t \quad (\text{crystalline } PI) \quad (2a)$$

$$k_S = A_S / \sum A_t \quad (\text{intermediate } PI) \quad (2b)$$

$$k_H = A_H / \sum A_t \quad (\text{amorphous } PI) \quad (2c)$$

$$\sum A_t = A_{cr} + A_S + A_H$$

analogous to equation (1).  $A_{cr}$ ,  $A_S$  and  $A_H$  are the integrated areas of the crystalline, unisotropic and isotropic scattering curves.

## Precision

No special experiments have been done to work out a standard deviation for the measurement of X-ray phase indices, but an estimation has been obtained from several check tests on reproducibility. Two determinations were done on several fibres, i.e. two different samples were made and exposed to the X-ray beam. It has been established, that the precision is sufficient to detect differences in  $PI$  greater than 2%.

Values obtained for repetitive measurements of PET fibres are shown in Table 2.

## RESULTS AND DISCUSSION

In Figure 5 evaluated  $PI_{k_{cr}}$  values are correlated with the apparent densities. The measurements refer to PET yarns given different physical treatments but which have been previously drawn with the same draw ratio. The straight

line drawn in Figure 5 has been evaluated using the least squares regression and is given by the equation:

$$\bar{\rho} \text{ (g/cm}^3\text{)} = 1.359 + 0.0823k_{cr} \quad (3)$$

$$\text{range of availability: } 0.2 \leq k_{cr} \leq 0.4$$

The correlation coefficient  $r$  is 0.84. The density corresponding to the zero intercept ( $k_{cr}=0$ ) is 1.359 g/cm<sup>3</sup>, a value intermediate to the extrapolated non-crystalline densities obtained by Farrow and Ward<sup>28</sup> and Statton<sup>20</sup> (see Table 3).

The fact that a straight line relationship exists between the crystalline  $PI$   $k_{cr}$  and the apparent density asks the question as to whether it does coincide with the three-phase model. This relationship seems to be contrary to the possible existence of two different non-crystalline phases with boundaries between both (which has to be assumed in the case of a separate intermediate state) as can be seen by the following.

The macroscopic density is given by:

$$\rho = k_{cr}\rho_{cr} + k_S\rho_S + k_H\rho_H \quad (4)$$

where  $\rho_{cr}$ ,  $\rho_S$  and  $\rho_H$  are the densities of the crystalline, intermediate and amorphous phases. Taking into account the fact that the sum of the  $PI$ 's is equal to unity analogous to the equation:

$$k_{cr} + k_S + k_H = 1 \quad (5)$$

equation (4) can be transformed into equation (6):

$$\rho = k_{cr}(\rho_{cr} - \rho_H) + k_S(\rho_S - \rho_H) + \rho_H \quad (6)$$

If  $k_S \neq 0$ , equation (6) satisfies equation (3) only if the following condition is valid:

$$\rho_H = \rho_S \quad (7)$$

Any discussion regarding this discrepancy should start with the analysis of non-crystalline but drawn fibres, which can be made by drawing under special conditions<sup>29</sup>. This has the advantage that the discussion could be restricted to the non-crystalline phases.

Figure 6 shows the X-ray photographs of an undrawn PET fibre and a yarn drawn under necking at room temperature. In Table 4 the densities and intermediate  $PI$   $k_S$  of these uncrystallized fibres are listed together with the data of the bulk polymer and another sample with low draw ratio.

The increase in density with increasing intermediate  $PI$   $k_S$  as shown in Table 4 could be due to the existence of small crystallites. If this should be the case, the thickening of intensity on the equator as shown in Figure 6b is due to those crystallites small enough to produce only one diffuse reflection. Thus it has to be proved whether one or the other is valid. The fact that the X-ray pattern of

Table 3 Survey of amorphous and crystalline, theoretical and empirical densities for oriented and isotropic PET

	$\rho$ (g/cm <sup>3</sup> )	$\bar{v}$ (cm <sup>3</sup> /g)
Bulk polymer:		
100% amorphous	1.335–1.337 <sup>25</sup>	0.749–0.748
100% crystalline	1.455 <sup>32</sup> –1.498 <sup>25</sup>	0.687–0.668
Oriented polymer:		
100% amorphous	1.355 <sup>28</sup> –1.363 <sup>30</sup>	0.738–0.734
100% crystalline		

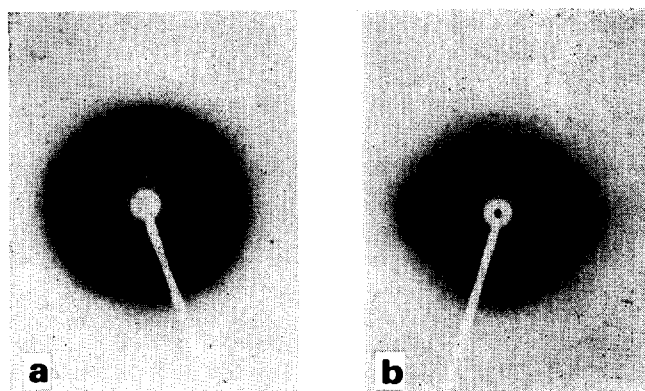


Figure 6 Diffraction photographs of PET fibres: (a) undrawn; (b) drawn under necking at room temperature

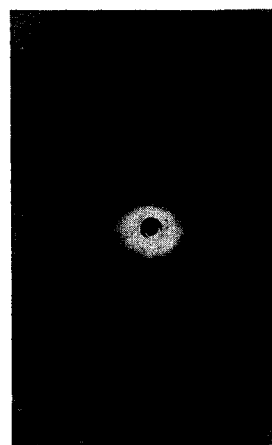


Figure 7 Small angle diffraction photograph of sample (b) reported in Figure 6 (see Table 4, sample D): the sharp Debye-Scherrer ring is due to MoS<sub>2</sub>, which has been used as reference; the sharp, weak reflections on the meridian correspond to 10.3 Å

Table 4 Density and intermediate  $PI$  ( $k_S$ ) for uncrystallized, drawn PET yarns

Sample	$\rho$ (g/cm <sup>3</sup> )	$k_S$
A	1.335	0.0
B	1.336	0.12
C	1.342	0.29
D	1.371	0.65

sample D (Figure 6b) has a weak meridional reflection (Figure 7), which cannot be found on the X-ray photograph of normal partly crystalline fibres, shows that this sample has a lattice which is intermediate to that of the amorphous and the crystalline. The spacing of this (001)\* plane is 10.3 Å, which is in good agreement with the  $c$  spacing of the triclinic lattice, being 10.75 Å<sup>30</sup>. The structure belonging to this X-ray photograph can be interpreted as being smectic arranged with a simultaneous formation of so-called *trans*-regions, as Bonart<sup>29</sup> has shown in his study on paracrystalline structure in poly(ethylene terephthalate). These *trans*-regions are characterized by the *trans* conformation of all monomer

\* The indication ( $hkl$ ) means that this plane is not identical with the corresponding plane of the crystal structure.

units of these zones. A partial separation in favour of a concentration of *trans* conformation has taken place.

The X-ray pattern of samples B and C in Table 4 show no (001)' reflection but only a concentration of intensity on the equator. The lack of the (001)' plane in these fibres leads to the conclusion that in contrary to sample D the existent *trans* conformations are not separated<sup>29</sup>, whereas the hexagonal rod packing is maintained. These domains of intermediate structures can be oriented by various means such as by extension<sup>22</sup>, as in the present case. Based on these interpretations it can be concluded in agreement with Bonart<sup>29</sup> and Vainshtein<sup>31</sup> that the 'amorphous' halo of the uncrystallized PET is compatible with a relatively high degree of order in the mutual disposition of the molecules. Thus the question which arose as to whether the increase in density of samples B, C and D in Table 4 is due to the existence of small crystallites or not, can be rejected.

The physical data of samples B, C and D are further evidence that non-crystalline polymers or regions do not have to be a system of chains irregularly interwoven. Crystallization of polymers, especially in drawn polymers, is not the only source of introduction of order.

In conclusion, we may assume that in the case of sample D, boundaries exist between the *trans*-zones and the amorphous phase. The macroscopic density of this sample is given by equation (6) with  $k_{cr}=0$ :

$$\rho = k_S(\rho_S - \rho_H) + \rho_H \quad (8)$$

The density of the smectic state can be evaluated if the density of the amorphous phase is known. Regarding its evaluation, sample D has to be treated more as a partly crystalline than as a non-crystalline sample insofar as its amorphous density does not have to be identical with that of the isotropic uncrystallized bulk polymer, as will be discussed later.

Thus, as a first approximation it seems reasonable to assume a continuous transition in densities from the nematic-hexagonal packing of samples B and C and the smectic structure of sample D. Figure 8 shows graphically the trend of change in density with the ratio of intermediate *PI* to amorphous *PI* ( $k_S/k_H$ ) of those non-crystalline samples. In Table 5 the samples from which the regression line in Figure 5 has been evaluated are listed in order of increasing intermediate *PI*  $k_S$  for the different crystalline *PI*  $k_{cr}$ . Using the corresponding ratios ( $k_S/k_H$ ) (column 3, Table 5), the non-crystalline density has been ascertained by means of the straight-line relationship shown in Figure 8. The corresponding non-crystalline densities are listed in column 5 of Table 5.

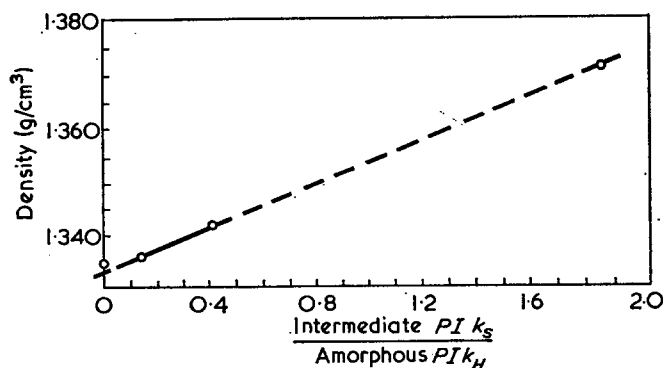


Figure 8 Correlation of macroscopic density with the coefficient (intermediate phase index/amorphous phase index) ( $k_S/k_H$ ) of non-crystalline PET fibres

Table 5 Phase indices and densities of oriented fibres

Sample number	$k_{cr}$	$k_S$	$k_S/k_H$	Macroscopic density $\rho$ (g/cm <sup>3</sup> )	Evaluated non-crystalline $\rho_S$ (g/cm <sup>3</sup> )
2	0.25	0.32	0.75	1.376	1.349
3	0.25	0.36	0.92	1.383	1.353
6	0.32	0.29	0.75	1.385	1.349
8	0.32	0.32	0.89	1.387	1.352
5	0.35	0.21	0.48	1.385	1.344
10	0.35	0.25	0.63	1.387	1.346
11	0.35	0.18	0.38	1.388	1.341
9	0.37	0.20	0.47	1.387	1.343
13	0.37	0.29	0.86	1.388	1.351
14	0.37	0.25	0.66	1.390	1.347
15	0.38	0.27	0.77	1.390	1.349
16	0.38	0.33	1.14	1.392	1.357

If we compare in Table 5 the macroscopic densities of samples with a constant crystalline *PI*  $k_{cr}$  but different intermediate *PI*  $k_S$  we can see that except for sample, numbers 11 and 14 the macroscopic density increases with increasing  $k_S$ . Although this correlation between the macroscopic and non-crystalline density gives a reasonable explanation for the fluctuations in the plot shown in Figure 5, it is clear from the difference between the mean non-crystalline density in Table 5, which is about 1.348 g/cm<sup>3</sup>, and the zero intercept of the regression line in Figure 5, which is about 1.359 g/cm<sup>3</sup>, that the evaluated densities listed in Table 5 are only rough estimates. As an explanation of this divergence it can be suggested that the non-crystalline density is not only influenced by drawing but also by heat treatment. This would also explain the non-agreement of sample numbers 11 and 14. The matter is complicated by the fact that: (i) Bonart (personal communication, 1970) and Konrad and Zachmann<sup>32</sup> have found that the non-crystalline density  $\rho_a$  of semi-crystalline unoriented PET is lower than the density of the fully amorphous polymer; (ii) Konrad and Zachmann<sup>32</sup> found for samples which have been crystallized at lower temperatures that  $\rho_{cr}$  was lower than 1.455 g/cm<sup>3</sup>. These findings resulted from small angle and density measurements. Thus none of the 3 densities in equation (4) can be assumed to be constant in any case.

The general picture which emerges from these facts is that as long as no further information is available regarding the crystalline and non-crystalline density, any decision, which is only based on density and wide-angle measurements, whether two different non-crystalline states with boundaries exist between both in partly crystalline oriented PET or not, is hypothetical in nature.

It can be concluded that the condition  $\rho_S = \rho_H$  holds true at least for the PET fibres listed in Table 5. In order to prove the range of availability of this finding, PET fibres heat treated under different tensions have been investigated. The details will be discussed elsewhere<sup>30</sup>. The regression line calculated using all measurements made on normal drawn and crystallized PET fibres to date is given by:

$$\rho \text{ (g/cm}^3\text{)} = 1.358 + 0.090k_{cr} \quad (9)$$

The correlation coefficient is 0.88. The number of samples tested was 27. As can be seen by comparing equations (3) and (9), there are only small differences between the corresponding constants.

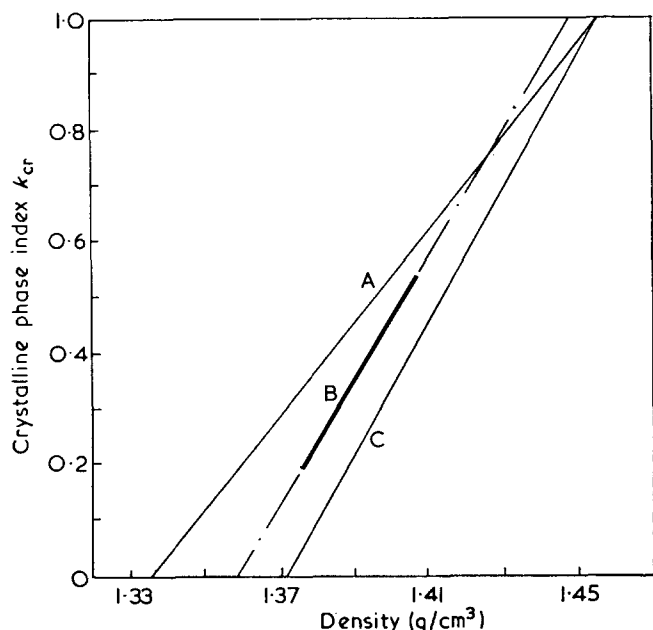


Figure 9 Crystalline phase index-macroscopic density map of PET. A, theoretical line drawn with the extreme values  $\rho_H = 1.335$  g/cm<sup>3</sup> and  $\rho_{cr} = 1.455$  g/cm<sup>3</sup>; B, regression line for the investigated oriented fibres; C, limiting line constructed with the density of the intermediate fibre  $\rho = 1.371$  g/cm<sup>3</sup> and the theoretical crystalline density

Using the theoretical crystalline density calculated by Bunn and Daubeny<sup>33</sup> of 1.455 g/cm<sup>3</sup>, the density of the fully amorphous polymer of 1.335 g/cm<sup>3</sup>, the constants of equation (9) and the density of sample D in Table 4, the diagram shown in Figure 9 can be constructed. The straight lines A and C limit the range of the crystalline  $PI$ -density relationship, assuming that the non-crystalline density does not decrease under those of the full amorphous polymer and does not increase above those of sample D in Table 4. The regression line B lies well within this range, at least within its range of availability. The density corresponding to the unity intercept ( $k_{cr} = 1$ ) of the regression line in Figure 9 is 1.448 g/cm<sup>3</sup>. This points to the fact that in fibres the crystalline density is lower than those of isotropic poly(ethylene terephthalate).

## CONCLUSIONS

An X-ray method could be devised which would be suitable for the characterization of the crystalline, intermediate and amorphous regions in drawn poly(ethylene terephthalate) fibres. From its application to the study of non-crystalline and partly crystalline PET fibres, the following conclusions can be drawn:

(1) The content of ordered segments can be ascertained successfully in the case of non-crystalline, but oriented fibres as well as in the case of partly crystalline drawn fibres, by applying the three-phases indices method.

(2) The two-phase model is, at least for PET fibres, a useful approximation regarding the density, provided the density of one of the two non-crystalline phases cannot be ascertained by the results of some other suitable method.

(3) The measurement of the amount of crystalline ordered regions by density alone is unreliable because of the high degree of variability of the density of the non-crystalline regions.

## ACKNOWLEDGEMENTS

The author wishes to express his thanks to the Landesamt für Forschung und Wissenschaft beim Ministerium für Bildung und Wissenschaft des Landes Nordrhein-Westfalen for its support of this work. Also thanks are due to Forschungskuratorium Gesamttextil and Verband der Chemischen Industrie for providing chemicals and the Chemiefonds for financial support. The author wishes to thank Glanzstoff A.-G., Wuppertal, Germany for making available the yarns. Helpful discussions with Prof. Dr-Ing. H. Zahn (Deutsches Wollforschungsinstitut, Aachen) and Prof. Dr-Ing. Bonart (TU Berlin) are gratefully acknowledged as is the technical assistance provided by Miss A. Augenadel.

The author is indebted to the Gemeinschaftslabor für Elektronenmikroskopie der RWTH Aachen for its support in supplying of a microdensitometer (Joyce, Loebel and Company Ltd).

## REFERENCES

- Hermans, P. H. *Experientia* 1963, **19**, 553
- Miller, R. L. 'Encyclopedia of Polymer Science and Technology', John Wiley, New York, Vol 4, 1966, p 449
- Ruscher, C. *Faserforsch. Textiltech.* 1964, **15**, 513
- Sandeman, I. and Keller, A. *J. Polym. Sci.* 1956, **19**, 401
- Hyndman, D. and Origlio, G. E. *J. Polym. Sci.* 1959, **39**, 556
- Sobue, Hiroshi and Tabata, Yoneho *J. Polym. Sci.* 1959, **39**, 427
- Stern, P. G. *Kolloid-Z. Z. Polym.* 1967, **215**, 140
- Iwayanai, Shigeo and Sakurai, Ikuko *J. Polym. Sci. (C)* 1966, **14**, 29
- Jellinek, G., Ringens, W. and Heidemann, G. *Ber. Bunsenges. Phys. Chem.* 1970, **20**, 564
- Ruland, W. *Acta Cryst.* 1961, **14**, 1180
- Farrow, G. and Bagley, J. *Text. Res. J.* 1962, **32**, 587
- Kolb, H. J. and Izard, E. F. *J. Appl. Phys.* 1949, **20**, 564
- Kashmiri, M. J. and Sheldon, R. P. *J. Polym. Sci. (B)* 1968, **6**, 45
- Juifls, J. *Forschungsber. Landes. Nordrhein-Westfalen No. 381* 1957
- Preston, J. M. and Nimkar, M. V. *J. Text. Inst.* 1950, **41**, 446
- Moore, W. R. and Sheldon, R. P. *Polymer* 1961, **2**, 315
- Goppel, J. M. and Arlman, J. *J. Appl. Sci. Res.* 1947, **A1**, 462; 1948, **A2**, 1
- Hermans, P. H. and Weidinger, A. *J. Polym. Sci.* 1949, **4**, 135
- Hermans, P. H. and Weidinger, A. *Makromol. Chem.* 1961, **24**, 44
- Statton, W. O. *J. Appl. Polym. Sci.* 1963, **7**, 803
- Farrow, G. and Preston, D. *Br. J. Appl. Phys.* 1960, **11**, 353
- Vainshtein, B. K. 'Diffraction of X-rays by Chain Molecules', Elsevier, Amsterdam and New York, 1966, p 359
- Ruland, W. *Norelco Reporter* 1967, **14**, 12
- Ruland, W. *Pure Appl. Chem.* 1969, **18**, 489
- Kilian, H. A., Halboth, H. and Jenckel, E. *Kolloid-Z.* 1960, **172**, 166
- Hermans, P. H., Kratky, O. and Platzek, P. *Kolloid-Z.* 1939, **86**, 245
- Kast, W. *Forschungsber. Wirtsch. Verkehrsminist. Nordrhein-Westfalen No. 35* 1953
- Farrow, G. and Ward, J. M. *Polymer* 1960, **1**, 330
- Bonart, R. *Kolloid-Z. Z. Polym.* 1966, **213**, 1
- Lindner, W. L. to be published
- Vainshtein, B. K. 'Diffraction of X-rays by Chain Molecules', Elsevier, Amsterdam and New York, 1966, p 107
- Konrad, G. and Zachmann, H. G. *Kolloid-Z. Z. Polym.* 1971, **247**, 851
- Bunn, C. W. and Daubeny, R. de P. *Trans. Faraday Soc.* 1954, **50**, 1173
- Goppel, J. M. *Appl. Sci. Res.* 1947, **A1**, 3
- Matthews, J. C. *et al. Acta Cryst.* 1949, **2**, 85
- Falkai, B. and Bodor, G. *Faserforsch. Textiltech.* 1957, **8**, 114
- Johnson, J. E. *J. Appl. Polym. Sci.* 1959, **2**, 205

# Flow induced crystallization of polyethylene melts

M. R. Mackley and A. Keller

*H. H. Wills Physics Laboratory, University of Bristol, Bristol BS8 1TL, UK  
(Received 31 July 1972; revised 30 August 1972)*

Longitudinal velocity gradients in a flowing system are known to extend molecules appreciably and have been found to be responsible for the fibrous crystallization of polyethylene from solution. In this paper the preliminary optical observations are given of the effect this type of velocity gradient has on flowing crystallizable polymer melts. By flowing molten polymer into two mutually opposed orifices a longitudinal velocity gradient is generated specifically along the symmetry axis of the system. It was found that fibrous crystallization of polyethylene melt appeared to occur preferentially along this axis, implying that longitudinal velocity gradients play an important part in the production of this fibrous crystallization. The structural implications of the resulting extrudates and filaments obtained are discussed. Additional observations of the effect a fine gauze has on the crystallization of polymer melts is also presented.

For crystalline polymers to approach their theoretical maximum stiffness two physical conditions must be satisfied. The molecular chains must crystallize in a manner such that they are highly aligned; and, equally important, the chains must possess appreciable continuity along the fibre direction<sup>1</sup>.

By cold drawing most crystalline polymers it is possible to obtain a high degree of molecular alignment; but the existence of chain discontinuities along the draw axis prevents a high modulus material being achieved.

Obviously the finite length of the molecules is one limiting factor on the degree of chain continuity that can be obtained; however, a very much larger contribution to chain discontinuities along the fibre axis can be expected to come from the existence of chain folding where the molecules fold back and forth a larger number of times. If a high modulus fibre is to be achieved an oriented extended chain type crystal structure relatively free from folds must be obtained<sup>1</sup>.

A possible way of producing oriented extended chain material is to align the molecules before crystallization by hydrodynamic means, and then allow the molecules to crystallize whilst in the extended configuration.

Previous experimental<sup>2,3</sup> and theoretical<sup>4,5</sup> studies have shown that in solution large polymer molecules can be readily stretched to their extended chain configuration in a longitudinal velocity gradient, whereas in the more common transverse velocity gradient the rotational nature of the flow severely restricts the extension of the molecules.

It was estimated that in solution<sup>3</sup> a longitudinal velocity gradient of magnitude about  $10^3 \text{sec}^{-1}$  was required to extend a significant proportion of the molecules. If it is assumed that in the melt longitudinal velocity gradients are also necessary to extend molecules, the magnitude necessary to obtain appreciable molecular

extension would be reduced somewhat because of the anticipated increase in relaxation times of molecules in the melt. However, a conventional fibre-spinning type apparatus can only supply a longitudinal velocity gradient at a maximum rate of about  $20 \text{sec}^{-1}$  which is a factor of 50 less than that estimated to be necessary in solution. Frank suggested a system of mutually opposed jets as a possible method of producing sufficiently high longitudinal velocity gradients<sup>2</sup>. A longitudinal velocity gradient would by symmetry be specifically generated along the symmetry plane and axis of the system. Regions away from these areas would not necessarily contain pure longitudinal velocity gradients and in all probability would be areas containing transverse velocity gradients.

Experiments carried out using a solution of polyethylene in xylene at low supercooling, where normally no crystallization would take place, resulted in a crystal deposit being obtained between the jets<sup>2</sup>. This deposit has a 'shish kebab' morphology of the type first studied by Pennings<sup>6,7</sup>. The 'shish kebab' consists essentially of a fibrous extended chain core onto which chain folded platelets are attached<sup>8,9</sup>.

The crystal deposit produced between the jets had little mechanical strength, presumably because of the weak compacting of the individual fibrils to form the crystal aggregate. In addition the fibre could not be produced as a continuous filament.

This paper reports the preliminary observations and their implications, made from similar experiments carried out in the melt.

In extending the work to the melt it was necessary to design a new apparatus capable of withstanding the larger pressures involved due to the increase in viscosity of the polymer melt. Details of the apparatus are given in the provisional patent specification for the system<sup>10</sup>. It is basically the suck jet experiment of ref. 2 except

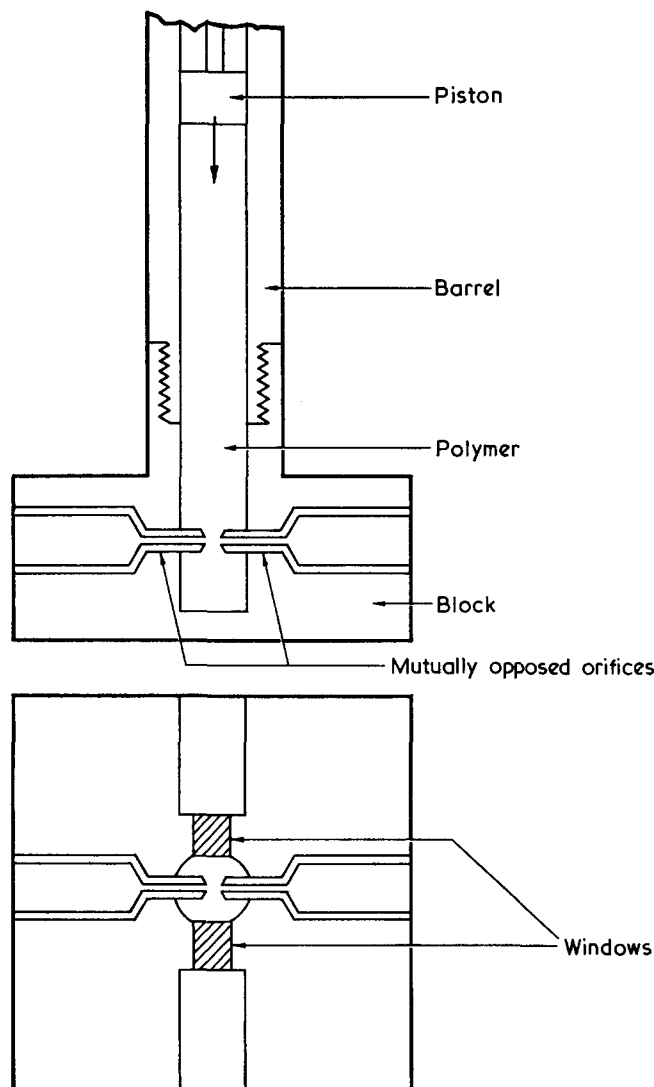


Figure 1 Apparatus used for flowing molten polymer into two mutually opposed orifices

that the polymer is forced through the jets not by suction applied to the jets but by pressure applied to the surrounding melt. The essential features of the apparatus shown in Figure 1 involve a barrel which is charged with polymer which is then melted. A piston forces the polymer down the barrel into a lower chamber where the melt is then forced out of two mutually opposed orifices. The barrel and chamber can be maintained at any chosen temperature. Optical windows are provided in the system to enable *in situ* observations of the crystallization to be made in the region of the jet orifices.

From the selected rate of advance of the piston and the known dimensions of both piston and jet orifices, the volumetric velocity,  $V$ , into the jets can be determined. It has been shown by tracer particle experiments<sup>3</sup> that the velocity at the centre of symmetry of the opposed orifice type of system, is essentially zero; thus the longitudinal velocity gradient  $\dot{\gamma}$  along the symmetry axis can be estimated to a first approximation simply by:

$$\dot{\gamma} = \frac{V}{d}$$

where  $d$  is the half distance between the jet orifices.

It is only possible to specify the longitudinal velocity gradient along the symmetry axis. Away from the symmetry axis predictions of the type and magnitude of the velocity gradients present cannot be specified in this precise manner.

The preliminary observed phenomena are best described with reference to Figure 2.

High density polyethylene Marlex 6002 was used as a sample polymer. All photographs were taken for a velocity gradient of  $50 \text{ sec}^{-1}$  using jets of internal diameter 1.0 mm.

At a temperature of  $150^\circ\text{C}$  the observed cross-polar and bright field flow patterns are shown in Figures 2a and 2b respectively. In Figure 2a with the polars crossed in the  $45^\circ$  position a highly symmetrical birefringence pattern is seen indicating molecular orientation in this region. Absolute determination of the magnitude of the birefringence would be difficult because the observed pattern is a result of varying optical paths through material where both the direction and magnitude of the birefringence are a function of position. A rough estimation of the overall birefringence can be made by dividing the observed retardation by a mean radius of the localized birefringence: an estimation of the maximum retardation being obtained by counting the number of interference fringes from outside the birefringent area to the symmetry axis, and knowing that each fringe corresponds to one wavelength retardation. In this manner an estimated birefringence of  $7.2 \times 10^{-3}$  is calculated. This is a factor of 8.0 below that calculated for the theoretical birefringence<sup>11</sup> expected for perfectly aligned polyethylene.

A point of immediate interest seen in Figure 2a is the beginning of cusping of the fringes as they approach the symmetry axis of the system. This strongly suggests that there is increased molecular orientation along the symmetry axis. The bright field photograph (Figure 2b) is included to contrast with later pictures; only the profile of the jets and slight contamination in the melt are visible in the photograph taken during flow.

Figures 2c and 2d show the cross-polar and bright field situation respectively for a temperature of  $140^\circ\text{C}$ . In addition to the features seen at  $150^\circ\text{C}$ , when either viewed between crossed polars or in bright field a discrete scattering line of about 0.1 mm diameter is seen along the symmetry axis of the jet geometry. This axial line was highly suggestive of a crystalline fibre being continuously produced along the symmetry axis with the ends of the fibre entering the jet nozzles along the jet axis. After flow the birefringence disappeared; however, the central line was seen to persist for up to 30 min after the cessation of flow.

Additional evidence to support the view that this discrete scattering line is a stable crystal form is shown in Figure 3. In this case the cross-polar photograph was taken when flow has terminated and the piston had been retracted slightly. In this way the pressure in the melt was returned to atmospheric pressure and some polymer 'sucked back' through the orifices. The picture shows clearly the discrete nature of the core. It also shows that the core extends into the orifices and that the core appears stable even at atmospheric pressure.

In Figure 2c the cusping of the interference bands is more enhanced than in Figure 2a indicating greater orientation along and near the symmetry axis. An estimation of the increase in birefringence along the

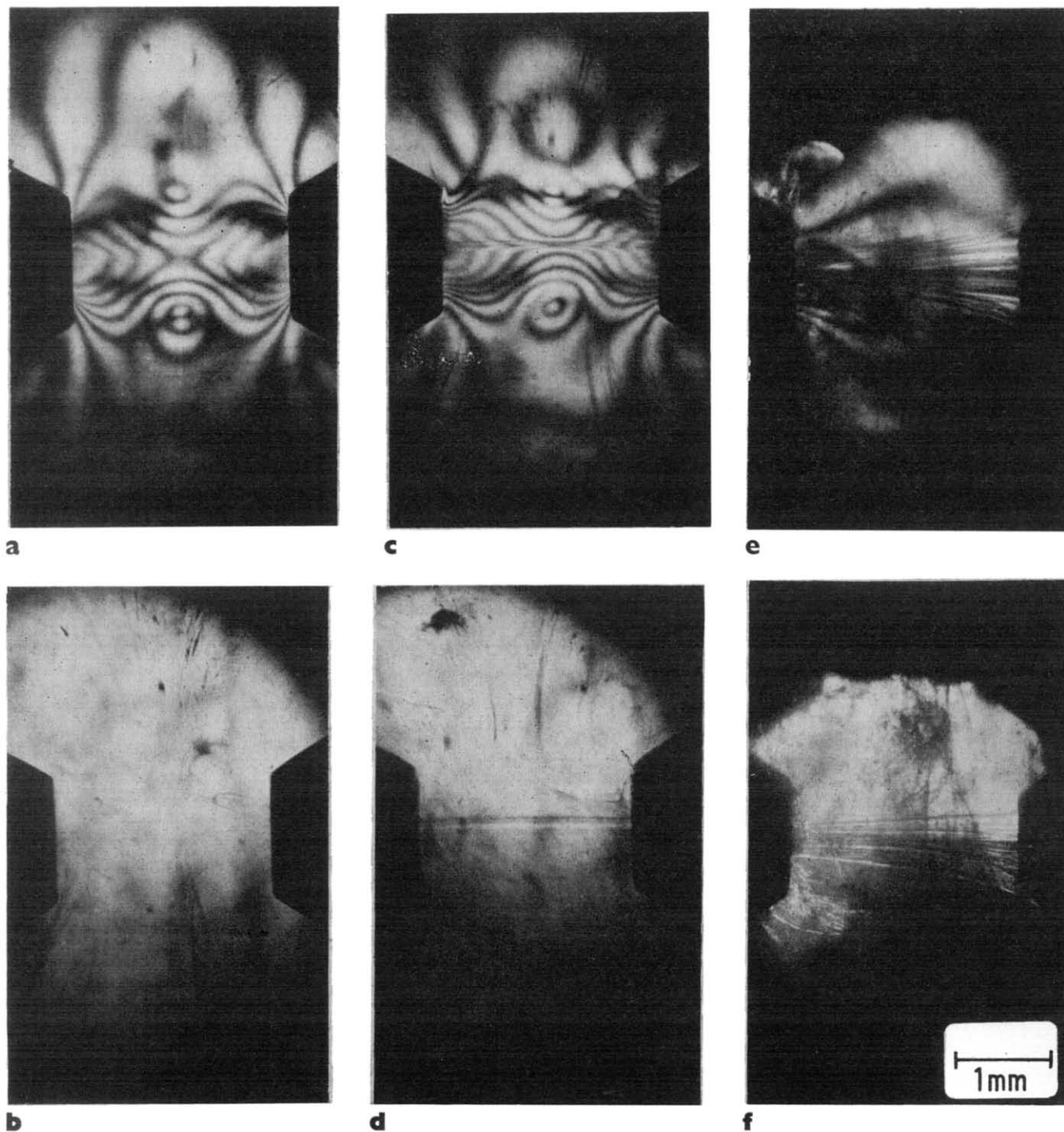


Figure 2 Photographs taken during flow of region between opposed orifices. (a) Polars crossed in 45° position,  $T=150^{\circ}\text{C}$ ; (b) bright field,  $T=150^{\circ}\text{C}$ ; (c) polars crossed in 45° position,  $T=140^{\circ}\text{C}$ ; (d) bright field,  $T=140^{\circ}\text{C}$ ; (e) polars crossed in 45° position,  $T=134^{\circ}\text{C}$ ; (f) bright field,  $T=134^{\circ}\text{C}$

symmetry axis can be made by dividing the increase in retardation seen near the symmetry axis by the thickness of the central thread. This gives a value of about  $1.7 \times 10^{-2}$  which is a factor of 2.4 greater than the estimated overall birefringence seen in Figure 2a. This makes the total birefringence along the central line only a factor of 2.5 below the theoretical value for fully aligned molecules.

Typical operating pressures for these experiments were 200 bar [ $1 \text{ bar} = 10^5 \text{ N/m}^2$ ]. For the above conditions, the polymer extruded through either of the jets could be removed as a plug or alternatively as a filament if slight tension was maintained on the extrudate as it left the exit side of the orifice. Both plug and filament showed a

similar form of X-ray pattern. Figure 4 shows an X-ray pattern from a filament. This consists of highly oriented equatorial arcs superimposed on arcs of much larger angular spread. The pattern obtained suggests molecular orientation of a two phase nature, one phase being more highly oriented than the other.

The likely interpretation of the phenomena described above is that the core fibre is produced within the melt by the crystallization of longitudinally aligned extended chain molecules. As the molecules are aligned in this highly oriented manner along the symmetry axis the polymer crystallizes as a fibre in an extended chain form and would be expected to have a higher melting point than the mass of surrounding material. This





Figure 3 Crossed polar photograph showing discrete nature of core, seen when piston had been retracted after flow

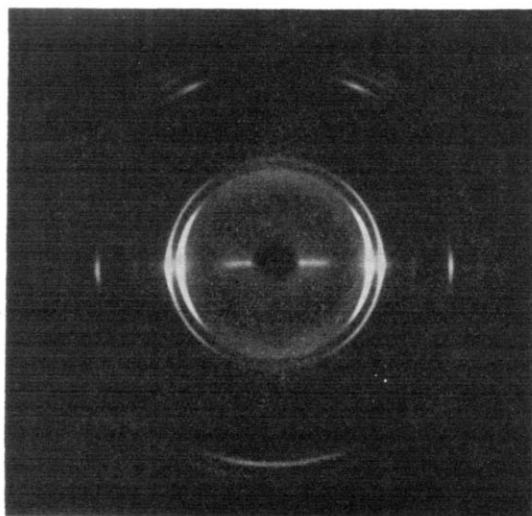


Figure 4 X-ray picture of filament, illustrating its two-phase nature

filament is continuously produced as the ends move outwardly along the high longitudinal velocity gradient centrally through the jet orifices. The polymer extruded around the core as it enters the orifices is obviously molten at this stage and acts as a 'lubricant' preventing the system from blocking. This molten material can be expected to crystallize onto the core at a later stage when the filament or plug leaves the heated region of the block, where the supercooling is sufficiently great to allow conventional chain-folded crystallization to take place.

This two-stage crystallization process offers an attractive explanation of the two-phase X-ray photograph obtained from the extrudate: the highly oriented phase corresponding to the crystalline core seen to form between the orifices and the less strongly oriented phase corresponding to the outer sheath of molten material which crystallizes onto the core in a conven-

tional manner when the extrudate has left the heated block.

Returning to the optical photographs, *Figures 2e* and *2f* show the cross-polar and bright field photographs respectively taken when flow had terminated after a run at a lower temperature of 134°C.

In this case further fibrils are seen to develop on or near the symmetry axis. As the amount of visible crystalline material was seen to increase the pressure within the melt rapidly increased until the maximum permissible pressure was reached where either one or both jets blocked. In this respect the experiment has similarities to observations of van der Vegt and Smit<sup>12</sup> and Porter and Southern<sup>13</sup> where they observe sudden increases in pressure resulting in total blockage when extruding polyethylene through tapered capillaries. They attributed this increase in pressure and blockage to the onset of crystallization. Using the apparatus described in this paper it is possible to confirm this type of phenomenon. The optical observations of the development of individual crystalline fibrils can be directly seen to be related to the increase in pressure of the system resulting in total blockage.

In an attempt to remove particle contamination from the melt a fine stainless-steel gauze supported on a rigid coarse gauze was placed in the polymer melt supply extending across the junction between the barrel and the bottom chamber. With the melt temperature in the barrel of 160°C the extrusion followed the same pattern described previously for this temperature. At a critical lower temperature of about 140°C where in the previous example a crystalline fibre was thought to be continuously produced; an additional part of the whole volume shown in *Figure 5* was filled with a number of fine crystalline fibrils each one appearing to originate from a single hole in the fine gauze. With the further development of the fibrils the system tended to block with a corresponding rise in pressure.

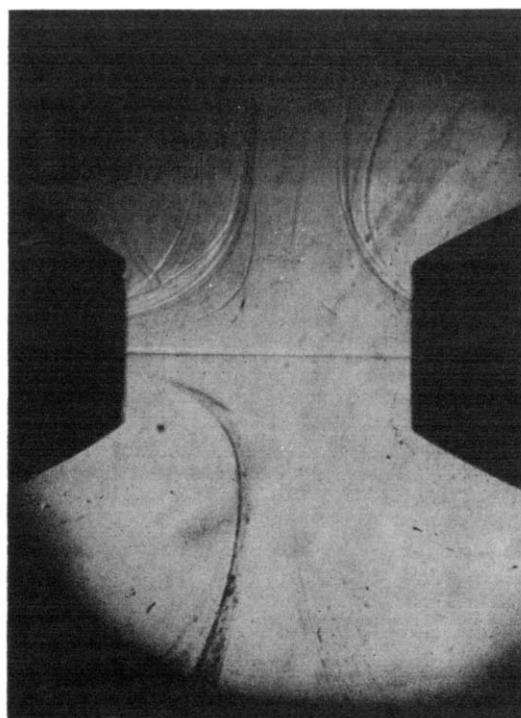


Figure 5 Photograph showing additional fibrous crystallization induced by putting gauze in polymer melt supply.  $T=140^{\circ}\text{C}$



It is apparent from the last example that fibrous crystallization can be induced through an array of fine holes in a gauze, presumably because of the longitudinal velocity gradient generated along the centre line of each hole. This observation may be relevant to the filtering of polymer melts in technical fibre spinning machines and to the origin of blockages which may occur.

In conclusion, it can be seen from the mutually opposed orifice experiment that longitudinal velocity gradients play a major part in inducing fibrous crystallization in the melt. Also there are sufficient indications from these preliminary observations to believe that continuous oriented filaments and/or fibril reinforced materials can be achieved effectively by careful design and control of hydrodynamic and thermodynamic parameters. Finally the experimental technique adopted in this paper of direct *in situ* optical observation of the flow and crystallization phenomena commends itself for studies of this kind.

#### ACKNOWLEDGEMENTS

One of us (M.R.M.) would like to acknowledge the

generous financial support of Courtauld's Educational Trust in support of this work. Also discussions with Professor F. C. Frank on this subject have been of great assistance to us both.

#### REFERENCES

- 1 Frank, F. C. *Proc. R. Soc.* 1970, **A319**, 127
- 2 Frank, F. C., Keller, A. and Mackley, M. R. *Polymer* 1971, **12**, 468
- 3 Mackley, M. R. *PhD Thesis* University of Bristol, 1972
- 4 Peterlin, A. *J. Polym. Sci. (B)* 1966, **4**, 287
- 5 Hlavacek, B. and Seyer, F. A. *Kolloid-Z. Z. Polym.* 1971, **243**, 32
- 6 Pennings, A. J. and Kiel, A. M. *Kolloid-Z. Z. Polym.* 1965, **205**, 160
- 7 Pennings, A. J. *J. Polym. Sci. (C)* 1967, **16**, 1799
- 8 Keller, A. and Willmouth, F. M. *J. Macromol. Sci. (Phys.)* 1972 **136**(3), 493
- 9 Pennings, A. J., van der Mark, J. M. A. A. and Kiel, A. M. *Kolloid-Z. Z. Polym.* 1970, **237**, 336
- 10 Frank, F. C., Keller, A. and Mackley, M. R. Br. Pat. 29840/72 (filed 26.6.72)
- 11 Bunn, W. W. R. and Daubeny, R. De P. *Trans. Faraday Soc.* 1954, **50**, 1173
- 12 van der Vegt, A. K. and Smit, P. P. A. *SCI Monogr.* 1967, **26**, 313
- 13 Porter, R. S. and Johnson, J. F. *Trans. Soc. Rheol.* 1967, **11**, 259

# Mechanical behaviour and permeability of ABS/glass bead composites

L. Nicolais\*, E. Drioli and R. F. Landel†

*Istituto di Principi di Ingegneria Chimica, University of Naples, 80125 Naples, Italy*  
(Received 8 May 1972; revised 4 July 1972)

The stress-strain behaviour of acrylonitrile-butadiene-styrene (ABS) containing up to 33.5 vol % of 10–40  $\mu\text{m}$  glass beads as filler was measured at one strain rate at room temperature. The beads eliminate the yielding and greatly enhance the ultimate elongation and work-to-break. The change in stress-strain response is associated with the dewetting and vacuole formation around the beads and with an increase in the amount of crazing. Initial experiments using water permeability to investigate the crazes are reported.

## INTRODUCTION

The straining of a polymeric glass results in a volume change that is the sum of an elastic recoverable change associated with the compressibility of the material and an irreversible non-linear change associated with microcavitation within the solid<sup>1</sup>. In many polymeric glasses, the microcavitation develops through the formation of crazes<sup>2, 3</sup>.

Crazes are very similar to cracks in appearance but quite different in other respects. The distinction was first made by Sauer *et al.*<sup>4, 5</sup>, who pointed out that polystyrene is capable of bearing considerable loads even after crazes have extended across the entire cross-section of the specimen. From X-ray diffraction evidence they concluded that crazes are composed of oriented polymer interspersed by voids<sup>9</sup>. According to Kambour<sup>3, 6</sup> and Spurr and Niegisch<sup>7</sup>, these crazes are structured regions analogous to that of a porous sponge in which the cell walls are highly drawn. In these zones, in fact, fibrils are drawn out of unoriented, amorphous coiled material and oriented in the direction of the tensile stress. These fibrils, then, contain oriented molecules.

The porous regions may be thought of as aggregates of microscopic cavities, which concentrate stress in a manner similar to a true crack.

In an unfilled polymeric glass, a unidirectional tensile load can cause crazes to nucleate and grow perpendicular to the direction of loading. While termination of the craze is related to the ability of the fibrils to form and to sustain a given load, the initiation of the crazes is considered to take place when a critical limit is reached in stress<sup>8–10</sup>, strain<sup>11</sup>, dilation<sup>12, 13</sup> or distortion strain energy<sup>14</sup> in the glassy polymer.

The presence of a particle in the polymeric matrix, however, causes stress concentrations around the particle which enhance the rate of craze formation<sup>8</sup>. The maximum stress concentration caused by a rigid inclusion, according to Goodier's<sup>15</sup> elastic analysis, is

about 1.5, whereas for a rubbery inclusion it is about 2<sup>12</sup> and for a hole, about 3<sup>8</sup>. Thus, in the case of rubber-modified polystyrene, such as acrylonitrile-butadiene-styrene (ABS), the presence of the low modulus particle provides a point of stress concentration which can act as a point of initiation of a craze. However, once the craze starts it does not continue to propagate through the sample because it comes up against another rubber particle and stops. This process has been illustrated by Bucknall and Smith<sup>9</sup>, who studied the deformation of high impact polystyrene in a thin film under the microscope. Recently a similar effect has been reported<sup>24</sup> in glassy polymers filled with rigid particles.

The dimensions of crazes are not yet well defined but seem to be a function of the specific polymer and of the stress level. Kambour found a value for polycarbonate of 20 to 200  $\text{\AA}$ <sup>6</sup> for the thickness of a craze\*. Naturally the stress level plays a role in the craze dimension in the sense that, after crazes are nucleated, the higher the values of stress, the larger the lateral dimension or length, though the thickness remains relatively fixed.

The density of this crazed material is very low, about 40–50% of the bulk material<sup>17</sup>. However, this value is not known with certainty and may well vary with the polymer and the condition under which the craze is developed. A clearer knowledge of this point would facilitate the understanding of the mechanism of craze propagation and the properties of the crazed material.

One way of investigating such porosity would be a direct measure of fluid transport (with or without the presence of an added solute) through a crazed specimen.

In the present work we report the effect of a hard filler on the mechanical properties of a material which does not craze as easily in their absence, and some preliminary results of the permeability of such materials. The emphasis, however, is almost solely on the mechanical properties, specifically the uniaxial stress-strain behaviour of ABS/glass bead composites at different filler levels.

\* Of the National Research Council, Italy.

† Fulbright Senior Research Scholar, Italy, 1971–72, on leave from the Jet Propulsion Laboratory, California Institute of Technology, USA.

\* Zhurkov *et al.*<sup>27</sup> report microcrack dimensions of about 90  $\text{\AA}$  for polycapromide, 320  $\text{\AA}$  for polypropylene and 400  $\text{\AA}$  for polyethylene. In this case, however, it is not clear whether such microcracks contain fibrils, as in the crazes discussed here.

## EXPERIMENTAL

The acrylonitrile-butadiene-styrene (ABS; Mazzucchelli Celluloide Sicoflex T 85 and Monsanto Co. Lustran I) having a glass transition temperature  $T_g=100^\circ\text{C}$  and a Poisson's ratio of 0.35, was used as received. The glass beads (Tradex Colori type 3000 CPO1 and Cataphote Corp. type 2740, both with a diameter range of 10–40  $\mu\text{m}$ ) were cleaned by refluxing with isopropyl alcohol for 24 h, after first removing the iron particles present with HCl (Tradex) or a large magnet (Cataphote). To prepare specimens the beads and polymer were mixed on a two-roll mill at  $180^\circ\text{C}$ .

For the mechanical tests, crude sheets were cut from the mill and then moulded to about 0.25 cm thick in a  $21 \times 7.5$  cm compression mould at  $185^\circ\text{C}$  under a pressure of  $55 \text{ kg/cm}^2$ . Specimens containing the following concentrations by volume of glass beads were prepared: 11.2, 20.5, 27.2 and 33.5%. In the present paper filler content is always expressed as volume concentration assuming that the density of the matrix is 1.05 and the density of glass beads  $2.5 \text{ g/cm}^3$ .

Tensile specimens were cut to the shape specified by ASTM D 638–64 T with a high speed roter and the filler content was determined by combustion of small pieces of broken samples. All samples were annealed at roughly  $10^\circ\text{C}$  below  $T_g$  for one day, to minimize moulding stresses and then conditioned at  $23^\circ\text{C}$  and 45–55% r.h. for 14 days before testing. Samples were tested in tension at a constant rate of strain and constant temperature with an Instron universal testing machine, using a strain gauge extensometer. Fracture surfaces were examined with a Cambridge electron scanning microscope.

For the permeability measurement the films were prepared in a similar manner, except that the film was created on the mill by adjusting the roller clearance<sup>18</sup>.

Permeability tests were conducted on two different types of equipment normally used in reverse osmosis laboratory tests. The first was an unstirred batch system (static cell) similar to the one described by Drioli<sup>19</sup>, working at a maximum pressure of 6.5 atm (1 atm  $\equiv$  101.33  $\text{kN/m}^2$ ). With the second apparatus<sup>20</sup> it was possible to make permeability measurements in laminar and turbulent flow with a maximum pressure of 50 atm.

## RESULTS AND DISCUSSION

Typical stress-strain curves for different concentrations of glass beads at  $24^\circ\text{C}$  and at a strain rate of  $0.131 \text{ min}^{-1}$  are shown in Figure 1. The modulus increases and the strength decreases as filler is added. In contrast to theoretical predictions for glassy polymers, the ultimate elongation of this system increases with the addition of the filler.

The curves for the filled materials exhibit an inflection and closer examination shows them to be bilinear with the discontinuity in slope occurring at about  $120 \text{ kg/cm}^2$ .

The stress at this point is practically independent of the filler concentration, as previously shown for styrene-acrylonitrile (SAN)/glass bead composites<sup>24</sup>, while the slope of the stress-strain curve above the discontinuity is strongly dependent on the bead content.

The change in slope is accompanied by stress whitening over the entire gauge length. A typical fracture surface

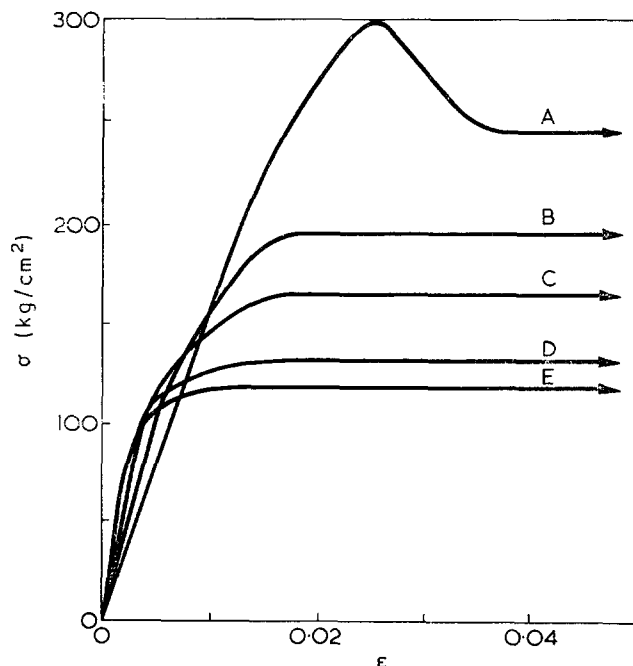


Figure 1 Stress-strain curve for ABS filled with glass beads to the volume percentage as shown. A,  $\phi=0\%$ ; B,  $\phi=11.6\%$ ; C,  $\phi=20.9\%$ ; D,  $\phi=28.2\%$ ; E,  $\phi=34.5\%$ .

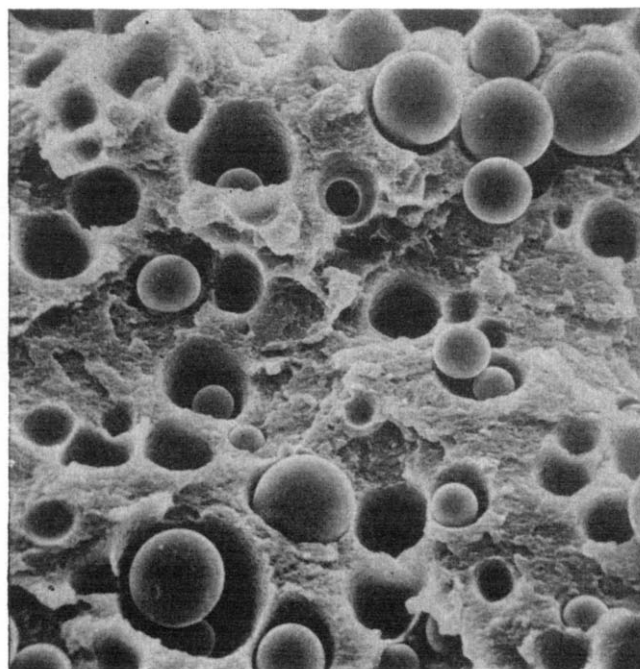


Figure 2 Electron scanning photomicrograph of the fracture surface of ABS/glass beads ( $440\times$ ) ( $\phi=0.20$ )

for a 20 vol% bead filled composite is shown in Figure 2. The denuded beads indicate that the adhesion of the ABS to the glass is poor, as would be expected with these materials.

At higher stresses the unfilled material shows a well-defined yielding, but the filled materials pass through a broad maximum with little change in the stress level. After this region of zero slope is attained, these samples continued to elongate with no further change in appearance and no necking.

The initial elastic modulus of the particulate composite  $E_c$  increases with filler content and can be expressed

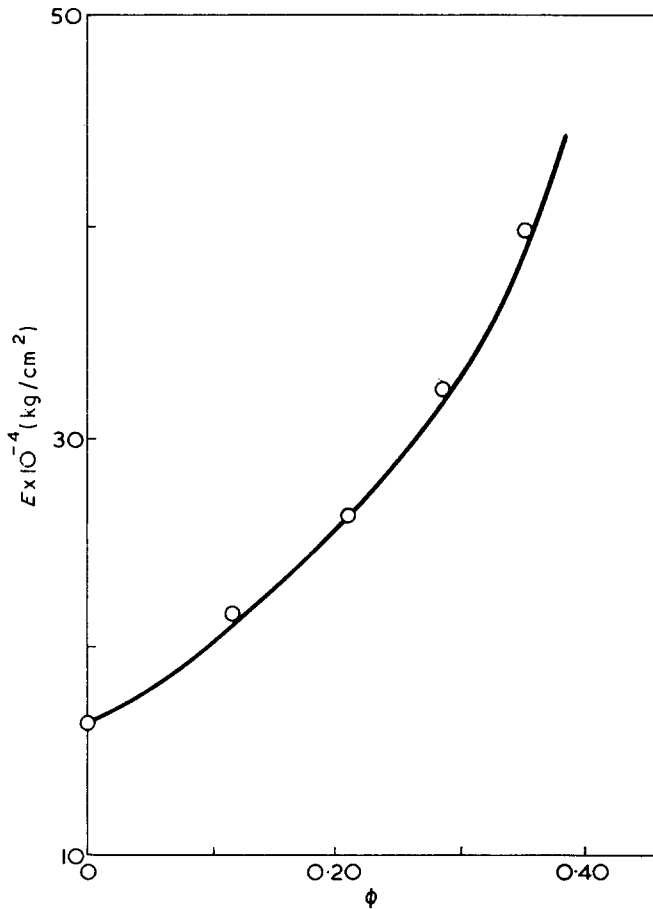


Figure 3 Initial modulus of ABS/glass bead composites versus  $\phi$  compared with equation (1)

as a function of its volume fraction,  $\phi$ , by the well known Kerner equation<sup>25</sup> as:

$$E_c = E_p \frac{1 + AC\phi}{1 - C\phi} \quad (1)$$

where

$$A = \frac{7 - 5\mu_p}{8 - 10\mu_p} = 1.17$$

and

$$C = \frac{E_f/E_p - 1}{E_f/E_p + A} = 0.97 \text{ for this polymer}$$

$\mu_p$  is the Poisson's ratio of ABS and  $E_f$ ,  $E_p$  are the Young's moduli of the filler and polymer respectively.

In Figure 3 the elastic moduli calculated from equation (1) are compared with the experimental values.

The strength of these composites decreases as the volume content of beads increases. This decrease is simply a reflection of the decreased cross-sectional area of the polymer bearing the load and can be expressed as a function of concentration by the following equation<sup>24</sup>:

$$\sigma_c = \sigma_p(1 - 1.21\phi^{2/3}) \quad (2)$$

where  $\sigma_c$  and  $\sigma_p$  are the strengths of the composite and the polymer respectively. In Figure 4 the experimental values of the strength are compared with those calculated.

Figure 5 shows the ultimate elongation of the ABS/glass bead composites as a function of filler content. It can

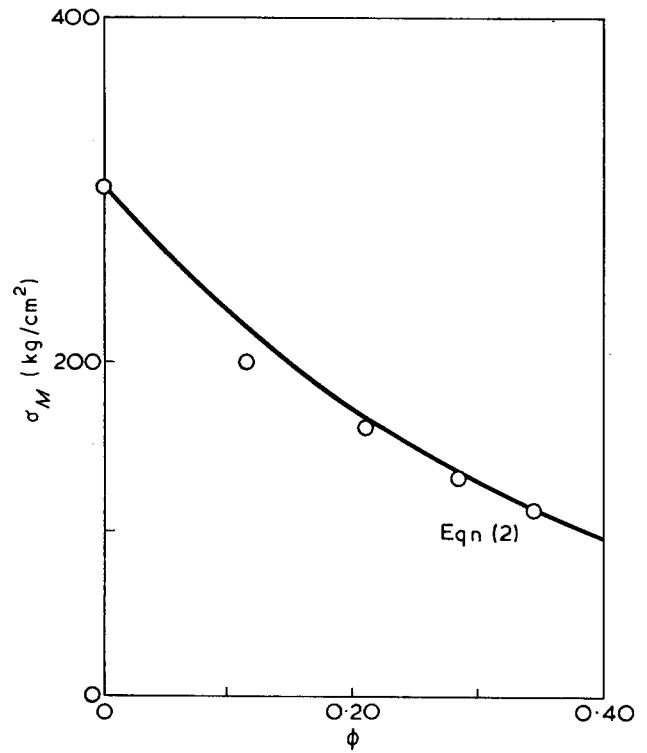


Figure 4 Strength of ABS/glass bead composites versus  $\phi$ , compared with equation (2)

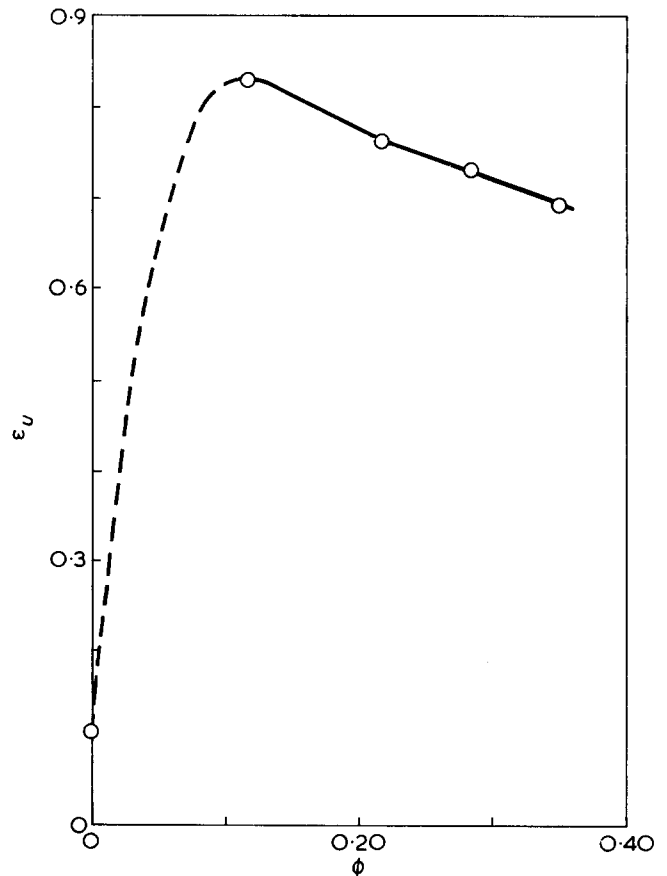


Figure 5 Ultimate elongation of ABS/glass bead composites as a function of filler content

be seen that, in contrast to theoretical predictions<sup>21, 22\*</sup> the ultimate elongation of these composites increases sharply when the filler is added, up to about 10 vol%,

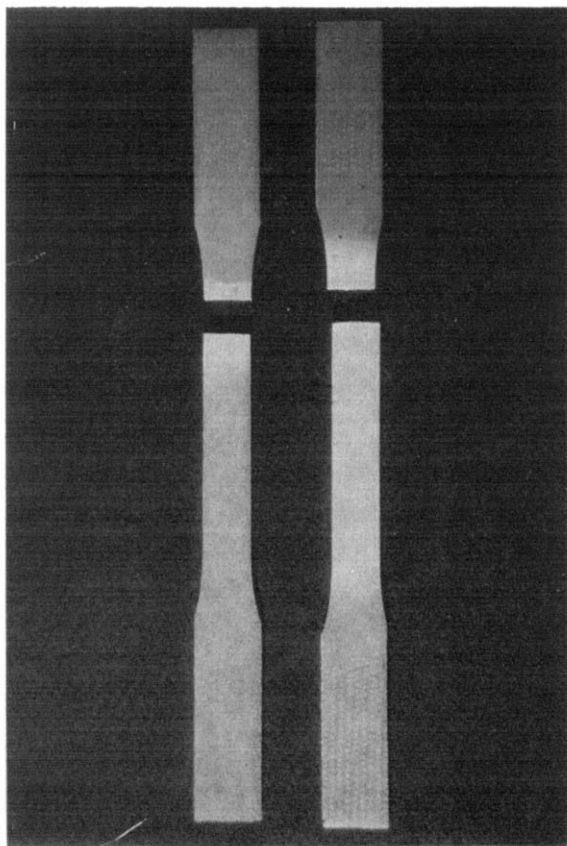
\* Smith<sup>23</sup> arrives at a similar prediction for a rubbery matrix.

and then decreases slowly. However, it should be recalled that the theories are only applicable to simple two-phase systems, not to those which are dilatant and can form a third phase.

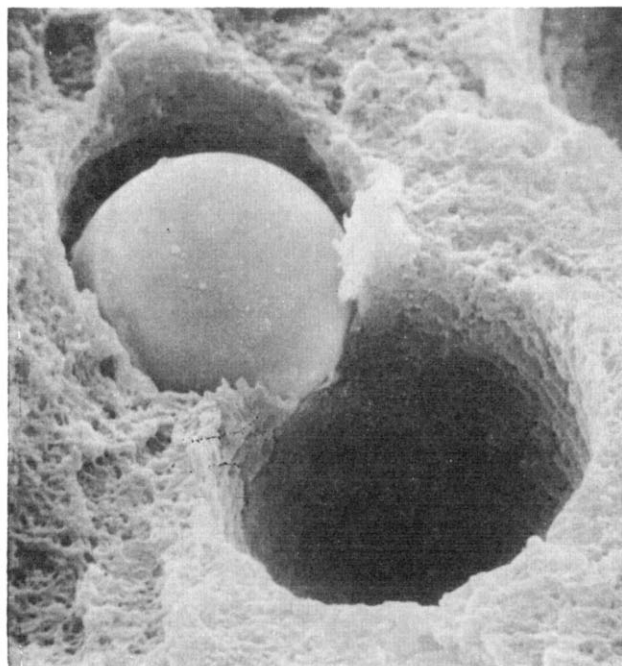
The local strain at the fractured surface in the unfilled ABS is quite high. While this is very revealing in terms of the mechanism of rupture, the fact remains that the ultimate elongation of the unfilled polymer is small for typical specimens by conventional standards.

This high elongation of the filled polymer can be explained if one can assume that the growth of crazes can be terminated by the glass beads or vacuoles around them. It is known<sup>13, 26</sup> that the rubber phase can act as a stress concentrator to initiate crazes and then assist in the terminating process. A similar process also occurs in glassy polymers filled with rigid particles. In fact if the propagating craze encounters a glass sphere to which the matrix is not strongly adherent, interfacial debonding can effectively blunt the tip of the craze and prevent further propagation. A similar but even more effective blunting occurs when a growing craze encounters a vacuole around a bead. In the case of ABS/glass bead composites these two processes act together to give a more extensive crazing which, when coupled with the added elongation associated with the vacuoles, permits the much greater specimen elongation.

Moreover, the effect of glass beads on the behaviour of the ABS is also that of equalizing the stress concentrations all along the specimen (throughout it, really) by causing crazes to initiate over the whole volume rather than just in a few localized regions. Thus *Figure 6* shows a picture of specimens with and without beads after fracture. It can be seen that the unfilled sample



*Figure 6* Appearance of two specimens after a tensile test, showing difference in stress-whitening. Unfilled, left, and filled with 20% glass beads, right



*Figure 7* Electron scanning photomicrograph of the fracture surface of ABS containing 20 vol% glass beads (3000 $\times$ )

shows a stress-whitening only in proximity to the fracture surface while the filled one is white over the whole gauge length.

However, it is not clear to what extent the stress-whitening in the filled material is due to void formation around the particles and how much is due to crazing *per se*. In the unfilled material, it must clearly be the latter. In the filled material, as indicated by *Figure 2*, and more clearly seen in *Figure 7*, there is a strong suggestion of the formation of elongated voids, such as are observed in filled elastomers<sup>1, 23, 28</sup>. Certainly it is evident that a strain of 80% must lead to elongated vacuoles if the beads dewet—the moot point is then whether the major part of the dewetting occurs first and causes crazing or subsequently, after the general initiation of crazing.

In any event, the picture emerges, to explain this high elongation, of the beads initiating crazes, either as rigid inclusions if they remain bonded until crazing starts or, if the dewetting occurs first, as sites for holes which are even more effective as stress raisers and hence initiators. Subsequently the beads or holes act as craze and crack stoppers, permitting other nuclei to grow and propagate. Eventually the resulting strain is large enough to dewet other beads in the matrix, with concurrent enhancement of further nucleation and further crack prevention capability.

The result of this combined dewetting and crazing leads to greatly improved toughness by the simple fact that a large volume of the specimen is involved in the deformation and hence increases the work-to-break.

Here we take toughness to mean simply the work-to-break in these uniaxial tensile tests. Notched impact or tensile tests, which localize the fracture plane, would be expected to show a lesser enhancement of toughness, thus measured, by the beads.

These results are very important practically in the fact that the addition of these rigid inclusions to the ABS leads to a new material with better mechanical properties.

The interesting point that only a small amount of glass beads increases the work to break very sharply is shown in Figure 8. The rapid fall-off at higher bead content indicates that the beads are more effective in stopping craze propagation than they are in initiating it. Even if the work is assumed to have been done only on the polymer and the results corrected for the decrease in polymer content, i.e.  $W_{pol} = W(1-\phi)^{-1}$  the work to break is still decreased by the higher bead contents (though it always remains greater than that for the unfilled polymer).

To investigate the resultant porosity in this material, sheet specimens were formed as previously indicated and are being tested for permeability to water. The unstrained material shows no permeability under a pressure of 36 atm for 24 h in a stirred cell, while a pre-strained sheet tested under the same dynamic conditions shows a flow rate as indicated in Figure 9. The initial high rate of 11 ml/min decreases with time towards an asymptotic value of roughly half this magnitude. This

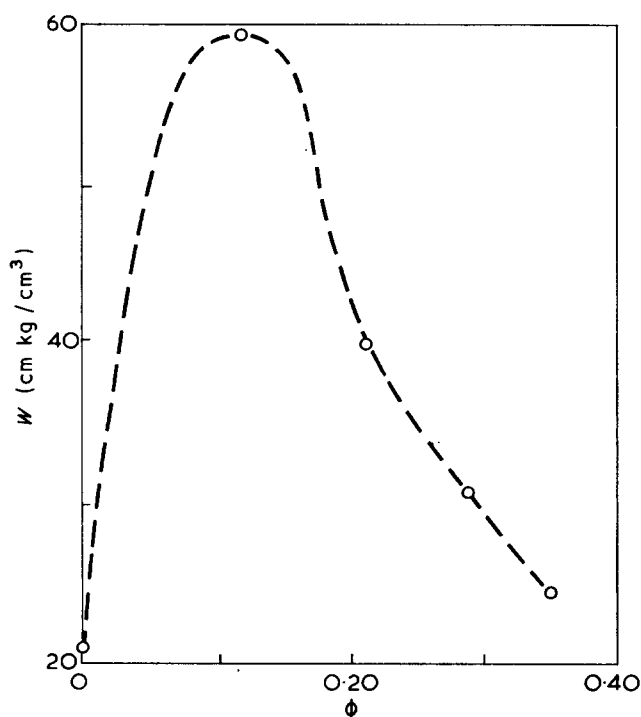


Figure 8 Work-to-break of ABS/glass bead composites as a function of bead content

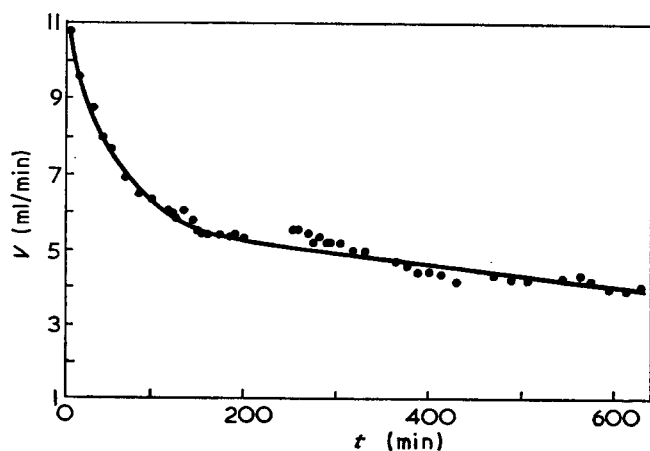


Figure 9 Flow rate  $V$  against time for an ABS/12% bead composite in a stirred cell under conditions as described in text

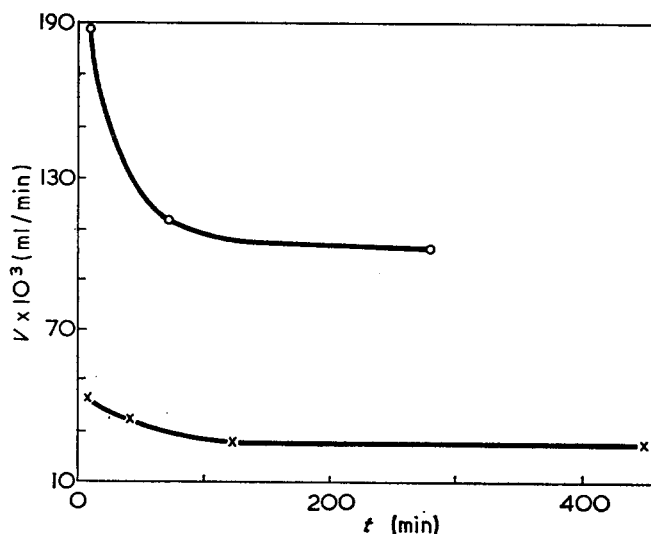


Figure 10 Flow rate against time for an ABS/16% bead composite during repetitive tests in a static cell under 6.5 atm pressure. O, Test immediately after mounting in cell; x, test after 576 hours of discontinuous operation for various periods of time

decrease, analogous to compaction in reverse osmosis membranes, is partly reversible. Figure 10 indicates the course of the permeability with time of another membrane in repeat experiments at 6.5 atm in an unstirred cell.

The strain in these sheets is unknown. To obtain a known value, the planar metal support plate in the static cell was replaced with a concave Teflon support plate. An unstrained sheet containing 12% beads was clamped in the cell and the applied pressure, 6.5 atm, was sufficient to stretch the sheet out against the plate. The hemispherical concavity in the plate was designed to give a maximum (biaxial) strain of 2.5%, i.e. above the strain at the discontinuity observed in the uniaxial stress-strain curve. The unstretched sheet showed a permeability of 0.11 ml/min, while the stretched sheet had an initial permeability of 0.17 ml/min. This permeability could result from any of three sources, pin-holes or other large defects, contiguous voids, or the crazes themselves. In the third case, the pore dimensions are such that a large polymer molecule would pass through with difficulty, if at all. Therefore 0.2% solutions of poly(oxypropylene glycol) (mol.wt  $\approx$  600 000) were used in both the static and dynamic test cells under the same conditions as used with the water. The effluent had a polymer concentration roughly half that of the original solution, which indicates that significant water permeation must have occurred through the crazes.

Further experiments to assess the utility of permeation as an investigative tool for such microporous materials are currently in progress.

## CONCLUSIONS

The addition of a hard filler to a glassy polymer enhances its toughness if the latter can craze, and the easier the craze formation the greatest the effect.

Thus glass beads have essentially no effect on polystyrene<sup>16</sup> but raise the elongation and work to break progressively in styrene-acrylonitrile, poly(phenylene oxide) (PPO) and acrylonitrile-butadiene-styrene. In the ABS the breaking strength depends on the available

polymer cross-section, according to equation (2), just as it does for SAN and PPO.

In this more readily crazed material, however, the elongation at break is very high. There is no adequate theory for this behaviour, though a reasonable explanation can be advanced based on craze initiation and propagation, coupled with the growth of voids around the beads.

The resulting porous materials are permeable to water with a pore size such that large flexible molecules seem to be excluded.

#### REFERENCES

- 1 Farris, R. J. *Trans. Soc. Rheol.* 1968, **12**, 2, 303
- 2 Kambour, R. P. *J. Polym. Sci. (A-2)* 1965, **3**, 1713; 1966, **4**, 17; 1966, **4**, 349
- 3 Kambour, R. P. *Polymer* 1964, **5**, 143
- 4 Sauer, J. A., Marin, J. and Hsiao, C. C. *J. Appl. Phys.* 1949, **20**, 507
- 5 Hsiao, C. C. and Sauer, J. A. *J. Appl. Phys.* 1950, **21**, 1071
- 6 Kambour, R. P. Conf. 'Yield, Deformation and Fracture of Polymers', 1970, Churchill College, Cambridge, Paper 4.1
- 7 Spurr, O. K., Jr and Niegisch, W. D. *J. Appl. Polym. Sci.* 1962, **6**, 585
- 8 Sternstein, S. S., Ongchin, L. and Silverman, A. *Appl. Polym. Symp.* 1968, **7**, 175
- 9 Bucknall, C. B. and Smith, R. R. *Polymer* 1965, **6**, 437
- 10 Nicolais, L. and Di Benedetto, A. T. *J. Appl. Polym. Sci.* 1971, **15**, 1585
- 11 Maxwell, B. and Rahm, L. F. *Ind. Eng. Chem.* 1948, **41**, 1988
- 12 Newman, S. and Strella, S. J. *J. Appl. Polym. Sci.* 1965, **9**, 2297
- 13 Strella, S. J. *J. Polym. Sci. (A-2)* 1966, **4**, 527
- 14 Matsuoka, S., Daane, J. H., Kwei, T. K. and Huseby, T. W. *Polym. Preprints*, 1969, **10**, 1198
- 15 Goodier, J. N. *Trans. ASME* 1933, **55**, A-39
- 16 Nicolais, L., Lavengood, R. E. and Narkis, M. *Ing. Chim. Ital.* 1972, **8**, 51
- 17 Kambour, R. P. *Nature* 1962, **195**, 1299
- 18 Drioli, E., Landel, R. F. and Nicolais, L. *Ital. Pat. Appl.* 48505 A/72 (22 Feb. 1972)
- 19 Drioli, E. *Ing. Chim. Ital.* 1969, **5**, 151
- 20 Drioli, E., Alfani, F. and Iorio, G. *Ing. Chim. Ital.* 1972, in press
- 21 Nielsen, L. E. *J. Appl. Polym. Sci.* 1966, **10**, 97
- 22 Kenyon, A. S. and Duffey, H. J. *Polym. Eng. Sci.* 1967, **7**, 1
- 23 Smith, T. L. *Trans. Soc. Rheol.* 1959, **3**, 113
- 24 Nicolais, L. and Narkis, M. *Polym. Eng. Sci.* 1971, **11**, 194
- 25 Kerner, E. H. *Proc. Phys. Soc. (B)* 1956, **69**, 808
- 26 Haward, R. N. in 'Advances in Polymer Blends and Reinforcement', Institution of the Rubber Industry, London, 1969
- 27 Zhurkov, S. N., Kuksenko, V. S. and Slutsker, A. I. Paper 46, *Proc. 2nd Int. Conf. Fracture, Brighton*, April 1969
- 28 Oberth, A. E. and Bruenner, R. S. *Trans. Soc. Rheol.* 1964, **9**, 165

# Rheological properties of emulsion viscoses:

## 1. Influence of alkali concentration, reaction time and order of addition of reactants

O. Y. Mansour, A. Nagaty and N. Shukry

Cellulose and Paper Laboratory, National Research Centre, Dokki, Cairo, Egypt  
(Received 3 May 1971; revised 20 March 1972)

Increased sodium hydroxide concentration resulted in a general decrease in structural and apparent viscosities of cellulose emulsion viscoses. For the same sodium hydroxide concentration, increased or decreased values of both types of viscosities accompanied increased reaction time and different orders of adding the reactants. With the viscose type of flow, the antithixotropic ones predominated among those viscoses produced in a short time by adding the carbon disulphide first, while the thixotropic ones predominated among those produced over a longer period of time either by adding the carbon disulphide or the sodium hydroxide first. The highest antithixotropy index was achieved with the lowest sodium hydroxide concentration. Opposite behaviour was shown for the thixotropic flow of the viscoses produced over a long period of time by adding the carbon disulphide first and then increasing the sodium hydroxide concentration. In general, the former viscoses showed higher thixotropic indices than the latter.

### INTRODUCTION

Polyelectrolyte solutions, even as dilute as 1–2%, exist in a state which is considered gel rather than fluid. When alkali is added, the gel-like mass tends to behave like an ordinary viscous fluid<sup>1</sup>. This fact indicates that the structure of aqueous solutions of polyelectrolytes is greatly modified by the presence of simple electrolytes. In general, the viscosity of a polyelectrolyte solution decreases markedly when a small amount of simple electrolyte is added<sup>2–5</sup>. According to Fuoss and Strauss<sup>6</sup>, the addition of such an electrolyte makes the polymer molecule smaller and smaller, thus approaching a limit of contraction.

If shear stresses,  $\tau$ , are plotted logarithmically against shear rates,  $D$ , straight lines are obtained, the slopes of which give the value of  $s$  in the equation:

$$\tau = bD^s \quad (1)$$

where  $s$  is designated as pseudoplasticity. Once  $s$  is obtained,  $b$ , which is taken as an indication of the viscosity, can be calculated as any experimental value of  $\tau$  divided by the corresponding  $D$  raised to the power  $s$ . For pseudoplastic flows, the value of  $s$  is less than 1, for dilatant ones  $s$  exceeds 1, while for Newtonian flows  $s=1$ <sup>7</sup>.

If the apparent viscosity,  $\eta$ , is plotted against the shear rate  $D$  on a log-log graph, approximate linear relations are obtained. The slopes of the resulting straight lines,  $-d \log \eta / d \log D$ , were utilized as a measure for the strength of solution structure<sup>1</sup>.

As regards the effect of cellulose properties on the structural viscosity of viscoses, Kiseleva *et al.*<sup>8</sup> showed

no interdependence between the average degree of aggregation of cellulose macromolecules in solution and the structural characteristics of viscoses prepared from various dissolving pulps. This structural property is mainly affected by the molecular polydispersity of the pulps.

An important factor contributing to polymer properties is the molecular weight or the length of the chain. The short chains of a low molecular weight polymer cause resistance to entangling when stress is applied. Hence the molecules can disentangle more readily under stress and produce a lower rupture point. As the average molecular weight increases, there is more entanglement of chains, resulting in an increase in strength properties<sup>9</sup>. On the other hand, Stein and Doty<sup>10</sup> stated that the greater the molecular weight the greater the coiling tendency becomes.

The dependence of viscosity on rate of shear of viscose was determined as a function of cellulose concentration, degree of polymerization, degree of maturation, sodium hydroxide content, sulphur content and temperature. The first two factors were of predominant importance; at very large rates of shear, the dependence of viscosity on concentration was linear while at low rates it was exponential. The structural viscosity was caused by uncoiling and orientation of chain molecules, rather than by their interaction<sup>11</sup>.

Thixotropy is similar to pseudoplasticity in that an increase in shearing stress produces a larger increase in rate of shear than expected but there is an important difference in that thixotropic changes are affected by time, whereas pseudoplastic changes are produced instantaneously. Thixotropy is believed to be due to



an internal structure which imparts rigidity to the system. This structure breaks down under shearing stress and when this happens the flow conforms to either the plastic or pseudoplastic type. Thus, if a plot is obtained of the rate of shear against shearing stress, a hysteresis loop is formed between the up and down curves. After the shearing stress is removed, the structure responsible for thixotropy reforms and the system returns to its original state but a significant time interval is required for this to take place<sup>12</sup>.

Thixotropy has also been defined as a reversible sol-gel transformation. It is difficult to measure and the usual criterion of measurement is the hysteresis loop, which is produced by non-linear up and down curves or consistency diagrams. The most useful measure of thixotropy is the coefficient of thixotropic breakdown with rate of shear, or the loss in shearing stress per unit area per unit increase in the rate of shear<sup>13</sup>.

Antithixotropy, on the other hand, is distinguished from thixotropy in that the rise in shearing stress causes a rise in viscosity and it is distinguished from structural viscosity in that recovery of the system is not instantaneous<sup>14</sup>.

Thixotropy has been found to increase with both concentration and temperature<sup>15</sup>. However, Fenson and Greenblatt<sup>16</sup> found that thixotropy decreased as the temperature increased, while it changed with concentration. Goodeve<sup>17</sup> showed that temperature has little effect on the coefficient of thixotropy over a fairly wide range but it normally has a large effect on the residual viscosity, i.e., the viscosity when the thixotropic effect is absent. The value of the coefficient of thixotropy increases as the square of the concentration.

In the present work, the aim was to investigate the influence of sodium hydroxide concentration, reaction time and order of addition of reactants on the flow properties of emulsion viscoses.

## EXPERIMENTAL

Wood pulp, shredded for 1 h at 50% moisture content and then dried at room temperature, was processed into viscoses in wide-mouthed glass bottles of 250 ml capacity, using 1 g cellulose and different sodium hydroxide concentrations, from 10 to 18%, at a liquor ratio of 30:1, carbon disulphide in the ratio of 1:1.8, for reaction periods of 3 and 6 h. Either the carbon disulphide or the sodium hydroxide was added first. The bottles were allowed to rotate at 9 rev/min in a water bath at  $20^{\circ} \pm 0.5^{\circ}\text{C}$ .

At the end of the reaction time, the viscose was centrifuged at 3000 rev/min for 5 min, and the dissolved amount of cellulose was estimated by oxidation using 1 N potassium dichromate solution and 68% (w/w) sulphuric acid, after destruction of the sulphur components with 5% sulphuric acid<sup>18</sup>.

The apparent viscosity of the viscose was then determined using a Rheo-viscometer after Höppler, thermostated at  $20^{\circ} \pm 0.05^{\circ}\text{C}$ . Thus, a known transferred volume of the viscose, defined by the mark of the suitable standard glass tube of the viscometer, was subjected to different shear stresses using weights allowing measurements within the range 10–200 g/cm<sup>2</sup>, and the corresponding times taken for a glass ball to pass through the viscose solution for a certain length recorded by a

dial are measured, from which the apparent viscosity was calculated from the following equation:

$$\eta = tK\tau$$

where  $t$  = measured time,  $K$  = constant for the standard tube, and  $\tau$  = shear stress.

## RESULTS AND DISCUSSION

### Structural viscosity

The ionized groups along a dissolved polymer chain repel one another, thus causing the chain to straighten out<sup>19</sup>. Such straightening might be accompanied by chain entanglement. Also, non-Newtonian behaviour would be due to the effect of shear on the number of links and the average life of a link<sup>20</sup>. Therefore, increasing the number of xanthate groups, i.e., increasing the  $\gamma$  number of the dissolved xanthated cellulose, would increase from the solution structure through increased entanglement as well as increased linking. As a result of their work, Fahmy and Fadl<sup>21</sup> showed that  $\gamma$  number for the dissolved xanthated cellulose increased as the sodium hydroxide concentration was increased. Accordingly, increasing the latter will, therefore, induce an increase in the structure of the viscose solution.

However, it is known that increased sodium hydroxide concentration results in increased degradation, i.e., increased shortening of the cellulose chains, and this will therefore lead to decreased entanglement; also, this will lead to a decreased number of xanthate groups per substituted cellulose chain molecule and hence induce a decrease in the solution structure.

Also, the introduction of a solvent electrolyte to a polyelectrolyte solution causes the repulsion between the neighbouring ionized groups along the polymer chain to become less, owing to the screening action of the electrolytes and, as a result, allows the polymer molecule to coil up into a more random configuration<sup>19</sup>. Such a coiling might be accompanied by chain disentanglement. According to Fuoss and Strauss<sup>6</sup> the polymer molecule becomes smaller and smaller, thus approaching a limit of contraction on addition of a simple electrolyte. Again, addition of alkali results in making the double layer around the polyion denser and hence the structure of the solution less tight, owing to the decrease in the electrostatic interaction between the polyions<sup>1</sup>. Therefore, increasing the sodium hydroxide concentration of the emulsion xanthation reaction, which is also accompanied by increased formation of the simple electrolytes reaction by-products (namely sodium thiocarbonate, sodium sulphide and some sodium carbonate<sup>21</sup>) induces increased loosening of the solution structure.

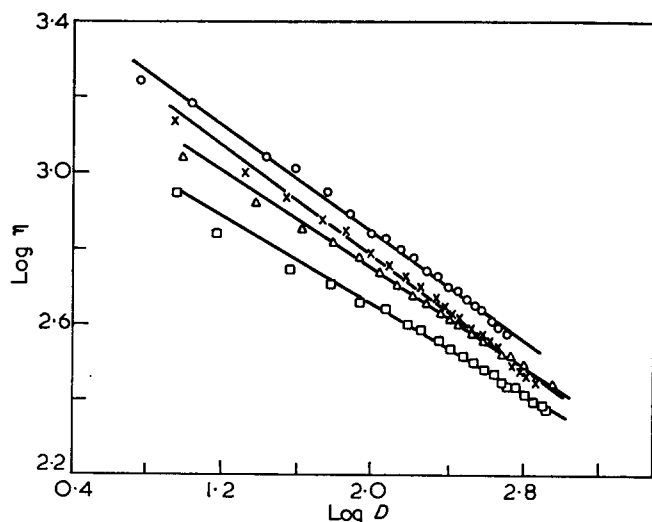
While increased sodium hydroxide concentration of the xanthation reaction tends, on the one hand, to make the structure of the solution more tight, it also tends to loosen it and the determined structural viscosity will thus be a product of both effects. The results achieved in this work, within the viscoses showing complete solubility and decreased structural viscosity with increased sodium hydroxide concentration (*Table 1* and *Figure 1*) therefore, reveal dominance of the factors affecting loosening of the structure over those affecting its tightness.

However, for viscoses showing incomplete solubility, other factors, such as concentration of the dissolved cellulose as well as molecular aggregates formation,

**Table 1** Influence of sodium hydroxide concentration, reaction time and order of addition of reactants on flow properties of emulsion viscoses\*

NaOH conc. (%)	Order of addition of reactants	Time (h)	Solubility (%)	Structural viscosity	Thixotropy/antithixotropy (A) index			
					$\eta_{50}$	$s$	$b$	$s$
10	CS <sub>2</sub> first	3	82	0.3481	912.10	1.8240(A)	0.6100	293.9
	CS <sub>2</sub> first	6	87	0.4350	965.95	1.2150	0.6200	313.8
	NaOH first	6	82	0.4553	935.15	2.4798	0.5400	243.0
12	CS <sub>2</sub> first	3	94	0.3603	704.65	0.1519	0.6392	271.9
	CS <sub>2</sub> first	6	100	0.4200	831.95	2.0514	0.5881	263.0
	NaOH first	6	100	0.3669	548.80	1.6716	0.6017	210.5
15	CS <sub>2</sub> first	3	100	0.3276	602.60	0.6837(A)	0.6451	252.2
	CS <sub>2</sub> first	6	100	0.3060	367.70	2.1273	0.7142	206.2
	NaOH first	6	100	0.3250	400.10	0.3609	0.6666	201.5
18	CS <sub>2</sub> first	3	100	0.2911	436.85	0.2279(A)	0.6875	223.1
	CS <sub>2</sub> first	6	100	0.2507	362.20	0.9300	0.7140	204.0
	NaOH first	6	90	0.2761	347.95	0.7597	0.7071	198.1

\* The viscoses were produced using 1 : 1.8 CS<sub>2</sub> ratio and 30 : 1 liquor ratio at 20°C



**Figure 1** Structural viscosity curves for viscoses produced in 3 h by adding CS<sub>2</sub> first. ○, 10% NaOH; ×, 12% NaOH; □, 15% NaOH; △, 18% NaOH

may interfere in influencing the solution structure. Thus, while decreased cellulose dissolution induces loosening of the structure, owing to a general decrease in the number of links within the entire structure, caused by a decreased linking strength through the resulting increased free spaces, the molecular aggregates induce increased solution structure. These molecular aggregates form by analogy to carboxymethyl cellulose solutions and to the presence of crystalline poorly soluble material which, serving as gel centres, entrap a relatively large amount of soluble material in a network held together by electrostatic and van der Waal forces<sup>22</sup>.

Therefore, for viscoses showing incomplete solubility, the structural viscosity will be a product of all the various effects related to the previously mentioned factors. This may explain the slightly increased and decreased structural viscosities of the viscose solutions produced with 12% sodium hydroxide by adding carbon disulphide first, for 3 and 6 h, respectively, compared with the corresponding ones similarly produced with 10% sodium hydroxide (Table 1).

For the same sodium hydroxide concentration, the structural viscosity has been found to undergo an increase or decrease in its value as the reaction time was increased from 3 to 6 hours (Table 1). Again, for

the same sodium hydroxide concentration and the same reaction time, the structural viscosity may show an increase or decrease following the differences in the order of addition of reactants, whether the sodium hydroxide or carbon disulphide is added first.

This may relate for the viscoses showing complete solubility to differences in the relative rates, which some or all the factors affecting the structural viscosity, namely  $\gamma$  number, amount of by-product formation and degree of degradation, may undergo as the reaction proceeds or the order of addition of reactants varies and which may differ with different sodium hydroxide concentrations, and to the formation of molecular aggregates and concentration of the dissolved cellulose, for viscoses showing incomplete solubility.

In this connection, it is worth mentioning that the rate of xanthation [degree of substitution ( $\gamma$  number) and cellulose dissolution], as well as the by-product formation (sulphides and trithiocarbonates), are higher on adding carbon disulphide rather than sodium hydroxide first, as can be seen from Table 2.

#### Pseudoplasticity

The slope of the straight lines resulting from plotting  $\log \tau$  vs.  $\log D$  and designated by the symbol  $s$  in equation (1) and which is less than 1 (Table 1 and Figure 2) is taken as an indication of the pseudoplasticity of the viscose solution. The increase in the  $s$  value means a decrease in the pseudoplasticity and hence the solution approaches Newtonian flow and *vice versa*. The results in the Table show, in general, that pseudoplasticity changes in accordance with the structural viscosity and both changes are in the same direction. However, the changes may not be of the same magnitude and even some few opposite changes may occur.

#### Apparent viscosity

From Figures 3, 4 and 5, it is clear that increased sodium hydroxide concentration resulted in decreased apparent viscosity. For the same sodium hydroxide concentration, increased or decreased values accompanied increased reaction time, or different orders of adding the reactants.

The different results achieved relate to the different factors affecting the apparent viscosity, namely, solution structure, concentration of the dissolved cellulose and length of the dissolved xanthated chains, i.e., extent of

Table 2 Influence of order of addition of reactants on rates of xanthation and by-product formation

	Time (min)				
	30	60	120	180	360
<b>CS<sub>2</sub> added first:</b>					
Dissolved cellulose (g%)	74.4	100	100	100	100
γ number <sup>24</sup>	32.0	42.4	63.6	85.6	106.7
<b>By-products<sup>25</sup></b>					
Sulphide (g)	0.21	0.35	0.42	0.53	0.66
Trithiocarbonate (g)	1.67	1.80	2.17	2.36	2.55
<b>NaOH added first:</b>					
Dissolved cellulose (g%)	—	34.6	46.5	84.2	90.0
γ number <sup>24</sup>	—	15.7	40.8	68.5	105.0
<b>By-products<sup>25</sup></b>					
Sulphide (g)	0.15	0.28	0.35	0.46	0.53
Trithiocarbonate (g)	1.45	1.75	1.98	2.01	2.18

The viscoses were prepared using 18% NaOH, 1 : 1.8 CS<sub>2</sub>: cellulose ratio, 30 : 1 liquor to cellulose ratio, at 20°C

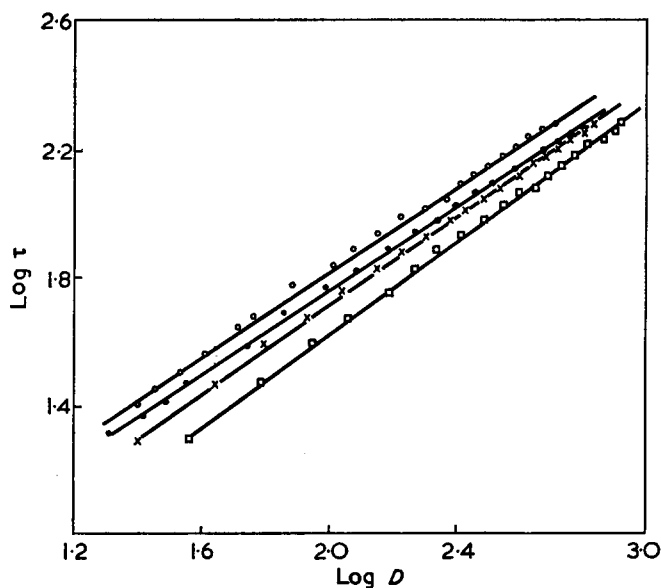


Figure 2 Pseudoplasticity curves for viscoses produced in 3 h by adding CS<sub>2</sub> first. ○, 10% NaOH; ●, 12% NaOH; ×, 15% NaOH; □, 18% NaOH

degradation, whose values may differ with the different sodium hydroxide concentrations, reaction times and orders of adding the reactants and of which the apparent viscosity is a product.

Thus, at the same cellulose solubility, sodium hydroxide concentration, and reaction time, where the last two are expected to lead to the same degree of degradation, the change in structural viscosity was accompanied by an analogous change in the apparent one. For example, both increased structural and apparent viscosities were achieved for the viscose produced with 12% sodium hydroxide, for 6 h, by adding carbon disulphide first, over the corresponding ones of that of the same solubility, similarly produced by adding sodium hydroxide first (Table 1 and Figures 4 and 5). Also the same, though the reverse, was achieved for the viscoses of the same cellulose solubility, produced for

6 h, with 15% sodium hydroxide, where the one produced by adding the carbon disulphide first, showed both decreased structural and apparent viscosities, below the corresponding ones of that produced by adding the sodium hydroxide first (Table 1 and Figures 4 and 5).

However, the decrease in the apparent viscosity, following that of the structural one, appears to take place up to a certain value beyond which any further decrease in the latter may be accompanied by little or no decrease in the former. This may reveal on comparing the viscoses produced with 15 and 18% sodium hydroxide, for 6 h, by adding the carbon disulphide first, where practically no change in the apparent viscosity was achieved, in spite of the distinct difference in their structural viscosities (Table 1 and Figure 4).

For different viscose solubilities or different degrees of degradation, or both, the apparent viscosity may behave differently from the structural one. Thus, although viscoses produced by adding the sodium hydroxide first for 6 h, with 10 and 18% sodium hydroxide concentrations, showed increased structural viscosities over the corresponding ones of those of the same cellulose chain lengths, similarly produced by adding the carbon disulphide first, yet they showed decreased apparent viscosities, owing to decreased solubilities (Table 1 and Figures 4 and 5).

Also, owing to a higher degree of degradation, accompanying the viscose solutions produced after 6 h, with 10 and 15% sodium hydroxide concentrations, by

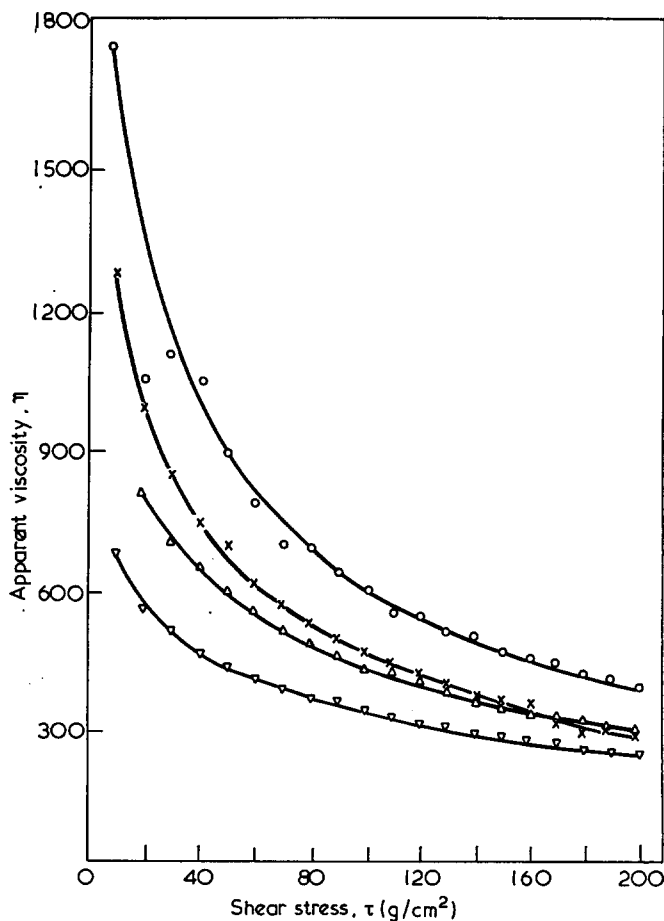


Figure 3 Viscosity curves for viscoses produced in 3 hours by adding CS<sub>2</sub> first. ○, 10% NaOH; ×, 12% NaOH; △, 15% NaOH; ▽, 18% NaOH

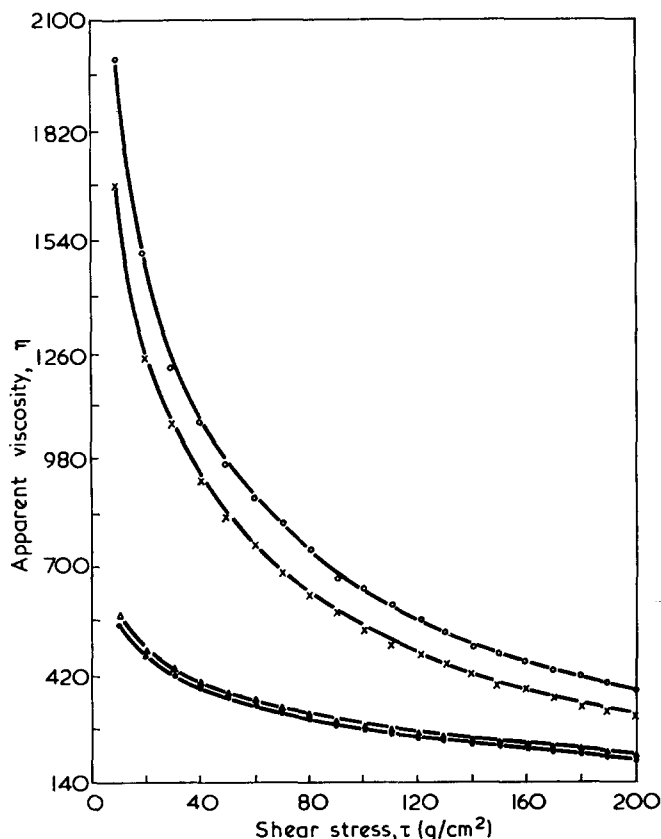


Figure 4 Viscosity curves for viscoses produced in 6 h by adding  $\text{CS}_2$  first. ○, 10% NaOH; ×, 12% NaOH; △, 15% NaOH; ●, 18% NaOH

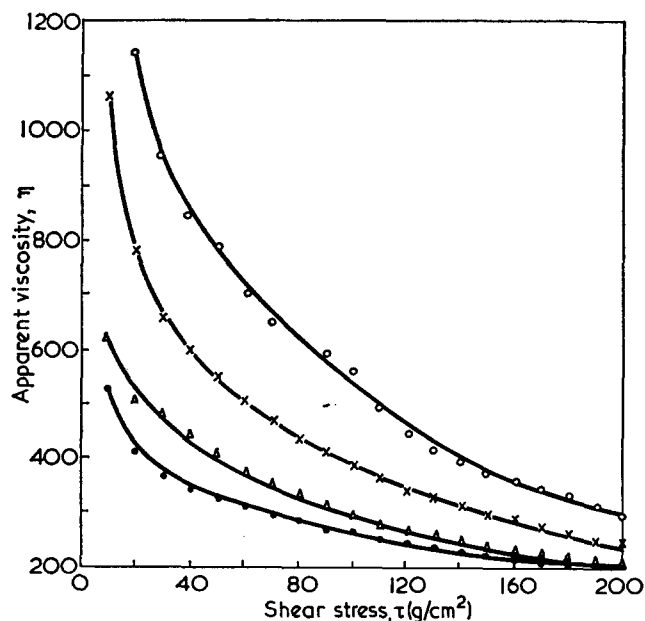


Figure 5 Viscosity curves for viscoses produced in 6 h by adding NaOH first. ○, 10% NaOH; ×, 12% NaOH; △, 15% NaOH; ●, 18% NaOH

adding the alkali first (it is known that the degree of degradation increases with time and sodium hydroxide concentration) they showed lower apparent viscosities than the corresponding ones of the same cellulose solubilities produced by adding the carbon disulphide

first, for 3 h, in spite of the higher structural viscosity achieved for the viscose produced after 6 h rather than 3 h with 10% sodium hydroxide concentration, and the practically equal ones for those produced for both times with 15% sodium hydroxide concentration (Table 1 and Figures 3 and 5). However, the decrease in apparent viscosity was distinct for the viscoses of 15% sodium hydroxide concentration, owing to the practically equal structural viscosities and only slight for those of 10% sodium hydroxide concentration, owing to the accompanying increase in structural viscosity.

By applying equation (1), the  $b$  value corresponding to a shear stress of  $50 \text{ g/cm}^2$  was calculated and it has been found that it does not approach the value of the apparent viscosity at the same shear stress,  $\eta_{50}$  (Table 1). However, the change of  $b$  value goes more or less parallel to that of the apparent viscosity at the same shear stress; only a few exceptions have been achieved.

#### Thixotropy and antithixotropy

The hysteresis loop produced by non-linear up and down curves on plotting shear stress against shear rate, has been taken as a measurement of the thixotropy and antithixotropy indices

$$= \text{area of the hysteresis loop} \times \text{shear stress} \times \text{shear rate}$$

$$= \text{cm}^2 \times (\text{g/cm}^2) \times \text{sec}^{-1} = \text{g sec}^{-1}.$$

According to Ree and Eyring<sup>23</sup>, two kinds of molecules—extended entangled and coiled disentangled—exist in a flow system of thixotropic substances; the former are non-Newtonian in their flow and the latter Newtonian. The relative amounts of the two kinds of molecules are determined by the equilibrium constant for entangled molecule  $\rightleftharpoons$  disentangled molecule. The equilibrium is shifted at high stresses and the entangled molecule is stretched and disentanglement is promoted and the network structure is thus destroyed.

Also, thixotropy and antithixotropy relate to differences in the rates of bond breaking and reformation, where for the former, the rate of reformation is slower than breaking, while the reverse takes place for the latter i.e., rate of reformation is higher than breaking<sup>20</sup>.

In dealing with the results achieved in this work, it is evident from Table 1 that while the antithixotropic flow dominates among viscoses produced by adding the carbon disulphide first, for 3 h, the thixotropic one prevails among those produced by adding either the carbon disulphide or the sodium hydroxide first, for 6 h; examples of the thixotropic and antithixotropic types of flow are shown in Figures 6 and 7, respectively.

Again, from Table 1, it is clear that the highest antithixotropy index was achieved with the lowest sodium hydroxide concentration i.e. 10%. Within the viscoses produced by adding the carbon disulphide first, for 6 h, the thixotropy index showed an increase with the increase of the sodium hydroxide concentration from 10 to 12%, remained practically constant as the concentration was increased to 15%, and finally decreased on further increasing the concentration to 18%; while, within those similarly produced by first adding the sodium hydroxide, it showed a decrease with the increase of sodium hydroxide concentration from 10 to 12 to 15%, and then an increase on further increasing the concentration to 18%.

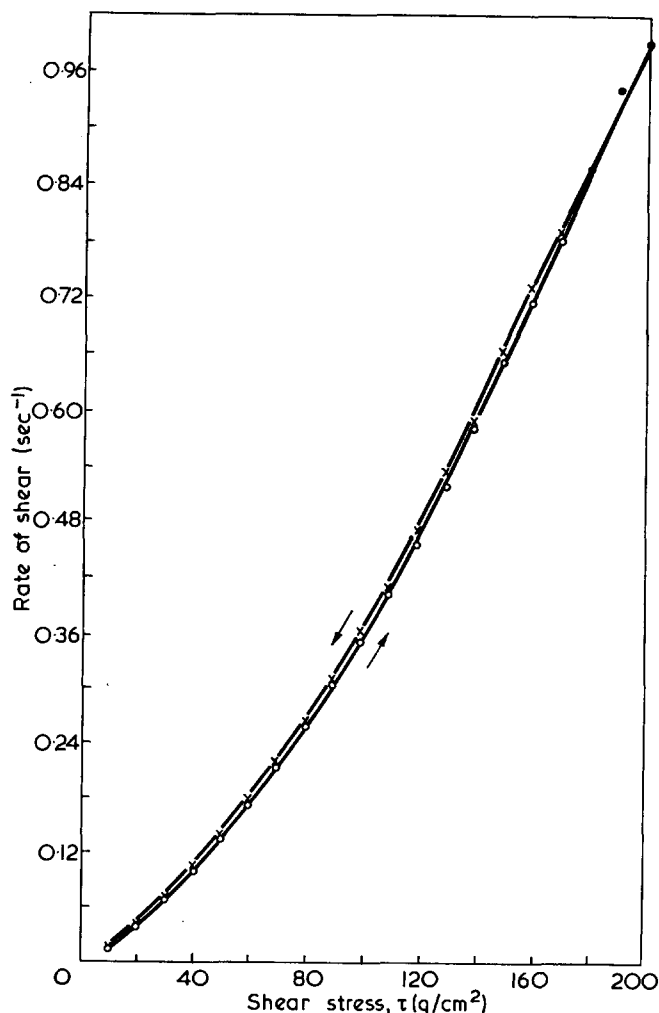


Figure 6 Consistency diagram of thixotropic flow for viscose produced with 15% NaOH in 6 h by adding CS<sub>2</sub> first. O, up; x, down

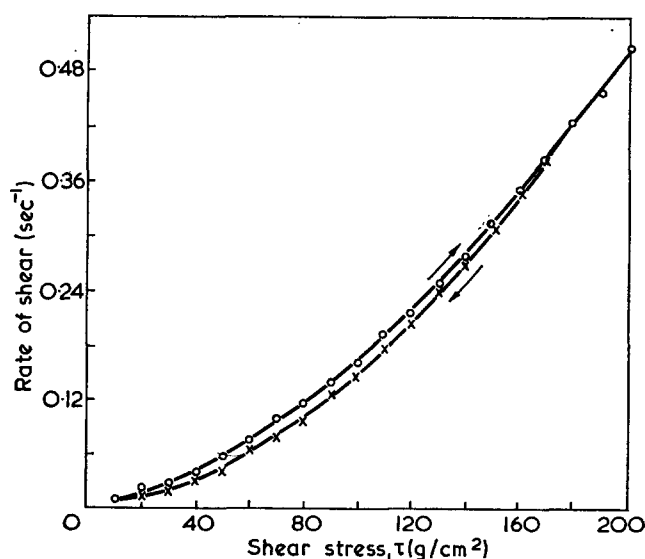


Figure 7 Consistency diagram of antithixotropic flow for viscose produced with 10% NaOH in 3 h by adding CS<sub>2</sub> first. O, up; x, down

The Table also reveals increased thixotropy indices for the viscoses produced, by adding the carbon disulphide first, for 6 h, than the corresponding ones of those similarly produced, by adding the sodium

hydroxide first; with 10% sodium hydroxide concentration, the reverse took place.

The different results achieved above relate primarily to the relative differences in the rates of xanthation and by-product formation, while the flow measurements were being carried out. These may differ with the sodium hydroxide concentration, reaction time and order of adding reactants. Thus, during the flow measurements, and due to by-product formation, promotion into coiled disentanglement and bond breaking induces increased thixotropy, while owing to the formation of new xanthate groups, promotion into extended entanglement and bond formation induces, on the contrary, decreased thixotropy and if the latter type of promotion dominates that of the former, the opposite type of flow (anti-thixotropy) is achieved.

In addition, incomplete cellulose solubility may induce increased or decreased thixotropy and antithixotropy indices or even transformation of one type of flow into the other, through the counteracting effects of the molecular aggregates formation, to which Ott<sup>22</sup> ascribed the thixotropic flows of carboxymethyl cellulose solutions and the increased free spaces which may allow proper extensions for the transformed molecules, respectively, increased entanglement and linking, while the flow measurements are being carried out. The latter influence may be observed when the viscose of incomplete cellulose solubility produced with 10% sodium hydroxide, for 3 h, showed a distinctly higher antithixotropy index (Table 1).

## CONCLUSIONS

(1) The solution structure of an emulsion viscose, being considered as a polyelectrolyte, is a product of several factors affecting the configuration of its xanthated cellulose chain molecules, as well as the bonding between the neighbouring chains. These factors are: sodium hydroxide concentration, degree of substitution, amounts of by-product formations, degree of degradation, percentage cellulose solubility and molecular aggregates formation.

(2) The apparent viscosity is affected by the solution structure, percentage cellulose solubility and degree of degradation, of which it is a product.

(3) The change of pseudoplasticity is in most cases in accordance with that of structural viscosity, while the *b* value agrees with that of the apparent one.

(4) The viscose type of flow is primarily affected by the relative rates of xanthation and by-product formation while the flow measurements are being carried out. Molecular aggregates formations and the increased free spaces between the molecules, which both accompany incomplete solubility of cellulose, may interfere.

## REFERENCES

- 1 Inagaki, H. *J. Colloid Sci.* 1956, **11**, 226
- 2 Pals, D. T. F. and Hermans, J. J. *J. Polym. Sci.* 1948, **3**, 897
- 3 Kruyt, H. R. and Edelman, H. J. *Kolloidchem. Beih.* 1932, **36**, 350
- 4 Mrakovitz, H. and Kimball, G. E. *J. Colloid Sci.* 1950, **5**, 115
- 5 Fuoss, R. M. and Strauss, U. P. *J. Polym. Sci.* 1948, **3**, 602
- 6 *Idem.* *Ann. N.Y. Acad. Sci.* 1949, **51**, 836
- 7 Merrill, E. W. *J. Colloid Sci.* 1956, **11**, 1
- 8 Kiseleva, V. P. and Kipershlak, E. Z. *Khim. Volokna* 1965, **5**, 29; *Chem. Abstr.* 1966, **64**, 3825b
- 9 'Rheology of Polymers', (Ed. E. T. Severs) Reinhold, New York; Chapman and Hall, London, 1962, pp 49-50

- 10 Stein, R. S. and Doty, P. *J. Am. Chem. Soc.* 1946, **68**, 159
- 11 Herrent, P., Lude, A. and Mouraux, F. *Bull. Soc. Chim. Belg.* 1951, **60**, 164; *Chem. Abstr.* 1952, **46**, 1253d
- 12 'Pulp and Paper', (Ed. J. P. Casey) Interscience, New York, 1960, p 1658
- 13 Ott, E. 'Cellulose and Cellulose Derivatives', Interscience, New York, 1954, Vol V, p 1210
- 14 Umstätter, H., *et al.* *Chem. Abstr.* 1949, **43**, 4541d
- 15 Glikman, S. A., Vladykina, N. Ya. and Perepelova, T. M. *Dokl. Akad. Nauk SSSR* 1949, **67**, 483; *Chem. Abstr.* 1949, **43**, 8235g
- 16 Fensom, D. and Greenblatt, J. H. *Can. J. Res.* 1948, **26B**, 215; *Chem. Abstr.* 1948, **42**, 4818a
- 17 Arnold, J. E. and Goodeve, C. F. *J. Phys. Chem.* 1940, **44**, 652
- 18 Fock, W. *Papier, Darmstadt* 1959, **13**, 92
- 19 Ott, E. 'Cellulose and Cellulose Derivatives', Interscience, New York, 1954, Vol V, p 1124
- 20 Kauzmann, W. and Eyring, H. *J. Am. Chem. Soc.* 1940, **62**, 3113
- 21 Fahmy, Y. A. and Fadl, M. H. *Sven. Papperstidn.* 1964, **67**, 105, 279, 576
- 22 Ott, E. and Elliott, J. H. *Makromol. Chem.* 1948, (18/19), 352
- 23 Hahn, S. J., Ree, T. and Eyring, H. *Ind. Eng. Chem.* 1959, **51**, 856
- 24 Whistler, R. L. 'Methods in Carbohydrate Chemistry', Academic Press, New York, 1963, Vol III, pp 247-251
- 25 de Wyss, G. *Ind. Eng. Chem.* 1925, **17**, 1044

# Rheological properties of emulsion viscoses :

## 2. Influence of cellulose origin, carbon disulphide ratio and temperature

O. Y. Mansour, A. Nagaty and N. Shukry

*Cellulose and Paper Laboratory, National Research Centre, Dokki, Cairo, Egypt*  
(Received 25 June 1971 ; revised 20 March 1972)

Celluloses of different origins or carbon disulphide of different ratios may affect different structural and apparent viscosities, thixotropy and antithixotropy indices for the produced viscoses. Change of temperature for the viscose flow measurements alone, or together with that for the viscose reaction may also have a similar effect or even convert one type of flow to the other, i.e., thixotropy into antithixotropy or *vice versa*. Apparent viscosity is affected by a change in structural viscosity, free space, cellulose solubility, degree of degradation and amounts of carbon disulphide included.

### INTRODUCTION

In Part 1 of this work<sup>1</sup>, investigations on the sodium hydroxide concentration, reaction time and order of addition of reactants have been carried out regarding their influence towards the structural and apparent viscosities and thixotropy and antithixotropy indices of the produced viscoses. The results achieved showed considerable variation, which has been attributed, for each property, to several factors whose effects may vary with the sodium hydroxide concentration, reaction time and order of addition of reactants and of which the state of the property is a product.

Thus the structural viscosity of a viscose solution is a product of the factors affecting the configuration of the constituent chain molecules as well as the bonding between the neighbouring chains. These factors are: sodium hydroxide concentration, degree of substitution amounts of by-product formation, degree of degradation, percentage cellulose solubility and molecular aggregates formation. The apparent viscosity is a product of the solution structure, percentage cellulose solubility and degree of degradation.

The thixotropic and antithixotropic flows are primarily affected by the differences in the relative rates of xanthation and by-product formation while the flow measurements are being carried out, as long as complete solubility is maintained; otherwise, other factors such as molecular aggregates formations and free spaces, owing to incomplete solubility, may interfere.

From the same work, it has also been shown that the pseudoplasticity changes in most cases in accordance with the structural viscosity while the *b* value changes with the apparent viscosity.

In the present work, the investigation has been further extended to include the influence of the cellulose origin from which the viscose was derived, carbon disulphide

ratio and the temperature used for its production together with the temperature at which the flow measurements have been carried out on the viscose flow properties.

### EXPERIMENTAL AND RESULTS

#### *Influence of cellulose origin*

Cotton sliver and viscose wood pulp of almost the same degree of polymerization, were processed into emulsion viscoses, using 18% sodium hydroxide solution, 1.8 : 1 carbon disulphide to cellulose ratio, 30 : 1 liquor to cellulose ratio at 20°C for 6 h. Either the carbon disulphide or the sodium hydroxide was added first.

From *Table 1*, it is clear that cotton sliver viscoses, produced by either adding the carbon disulphide first or the sodium hydroxide, showed distinct increases in structural viscosity over that of wood pulp viscose produced by the former type of addition and only a slight or indistinct one over that produced by the latter type. This may relate to differences in the relative rates of xanthation and by-product formation, following the differences in the cellulose origins from which the viscoses were derived—higher for the viscose of cotton sliver than for that of wood pulp. However, for viscoses showing incomplete solubility, interference of the molecular aggregates formation may take place so that the structural viscosity of wood pulp viscose produced by adding the sodium hydroxide first, approached those of cotton sliver viscoses produced by either type of addition of reactants.

Regarding the pseudoplasticity, the results of *Table 1* show that its change is different from the structural viscosity; higher structural viscosities of cotton sliver viscoses were accompanied by either almost constant or higher *s* values, than those of wood pulp.

Table 1 Influence of cellulose origin on flow properties of viscoses

Order of addition of reactants	Solubility (%)	Structural viscosity	$\eta_{50}$	Thixotropy index	s	b
Wood pulp viscose:						
CS <sub>2</sub> first	100	0.2507	362.20	0.9300	0.7140	204.0
NaOH first	90	0.2761	347.95	0.7597	0.7071	198.1
Cotton sliver viscose:						
CS <sub>2</sub> first	100	0.2894	727.70	0.3806	0.7222	343.1
NaOH first	90	0.2857	482.95	1.2501	0.7402	268.5

The viscoses were prepared using: 18% NaOH, 1 : 1.8 CS<sub>2</sub> and 30 : 1 liquor ratio, at 20°C, for 6 h

As far as the apparent viscosity is considered, its value at a shear stress of 50 g/cm<sup>2</sup> ( $\eta_{50}$ ), will be taken as representative, and from Table 1 it is clear that cotton sliver viscoses showed higher apparent viscosities than those of wood pulp. This may relate for the former viscoses either to a higher structural viscosity or lower degree of degradation which may accompany the cellulose cotton sliver.

The change in *b* value, has been found to follow that of apparent viscosity at the same shear stress ( $\eta_{50}$ ) (Table 1).

Again, from Table 1, the cotton sliver viscose produced by adding the carbon disulphide first, showed lower thixotropy indices than those of wood pulp viscoses produced by either type of addition of reactants, while that produced by adding the sodium hydroxide first showed a higher one. This may relate to a higher rate of xanthation than by-product formation, accompanying the flow measurements of the cotton sliver viscose produced by the former type of addition, as it is completely soluble; and to a higher percentage of gel centres and, molecular aggregates formation, accompanying the production of that produced by the latter type of addition, as it is incompletely soluble, owing to the higher lateral order and fibril packing of the cotton sliver cellulose.

#### Influence of carbon disulphide ratio

For such an investigation, two carbon disulphide ratios, namely, 1 : 1.8 and 1 : 3.6, were used for the production of wood pulp viscoses, with 18% sodium hydroxide, 30:1 liquor to cellulose ratio at 20°C for different reaction times, namely, 3 and 6 h, and order of addition of reactants, i.e., either the carbon disulphide or the sodium hydroxide added first.

From Table 2, it is clear that increasing the carbon disulphide ratio from 1:1.8 to 1:3.6 resulted in an

indistinct increase of structural viscosity and a distinct one, for viscoses produced by adding the carbon disulphide first, for 3 and 6 h, respectively, while, for those produced by adding the sodium hydroxide first, for 6 h, decreased viscosity was achieved. This may relate to a relatively higher rate of xanthation than by-product formation, accompanying the production of viscoses produced with the higher carbon disulphide ratio and by the former type of addition, as they are of complete cellulose solubility and which appear to be increased as the reaction time increased from 3 to 6 h, while to the dominance of the effect of the molecular aggregates formation, for the one produced with the lower carbon disulphide ratio, by the latter type of addition, as it is of incomplete cellulose solubility.

The results of pseudoplasticity show that its change, owing to the carbon disulphide ratio change mainly follows that of the structural viscosity (Table 2).

Regarding the apparent viscosity, it is clear from Table 2 that its value showed a slight decrease, increase, and again, increase, for the viscoses produced with the higher carbon disulphide ratio, by adding the carbon disulphide first, for the short and long reaction periods, and, by adding the sodium hydroxide first, for the long reaction period, respectively, over the corresponding ones similarly produced with the lower carbon disulphide ratio. This relates to the differences that may be affected in the cellulose solubility and structural viscosity, which may accompany the use of different carbon disulphide ratios; otherwise, it may relate to a higher percentage of carbon disulphide included within the viscose produced with the higher carbon disulphide ratio, which may thus lead to a decreased viscosity.

For the *b* value, its change again often follows that of  $\eta_{50}$  (Table 2).

As far as the flow behaviour is concerned, viscoses of the higher carbon disulphide ratio, showed increased antithixotropy and decreased thixotropy, for those

Table 2 Influence of carbon disulphide ratio on flow properties of viscoses

Order of addition of reactants	Time (h)	Solubility (%)	Structural viscosity	$\eta_{50}$	Thixotropy/antithixotropy (A) index	s	b
CS <sub>2</sub> ratio 1 : 1.8							
CS <sub>2</sub> first	3	100	0.2911	436.85	0.2279(A)	0.6875	223.1
CS <sub>2</sub> first	6	100	0.2507	362.20	0.9300	0.7140	204.0
NaOH first	6	90	0.2761	347.95	0.7597	0.7071	198.1
CS <sub>2</sub> ratio 1 : 3.6							
CS <sub>2</sub> first	3	100	0.2970	407.20	0.3039(A)	0.7302	231.2
CS <sub>2</sub> first	6	100	0.2910	447.30	0.3039	0.6608	212.4
NaOH first	6	100	0.2567	392.40	0	0.7430	229.6

The viscoses were prepared using: 18% NaOH and 30 : 1 liquor ratio, at 20°C



Table 3 Influence of temperature of flow measurements on flow properties of wood pulp viscoses

Temperature (°C)	20	30
Structural viscosity	0.3603	0.3472
$\eta_{50}$	704.65	388.00
Thixotropy index	0.1519	2.0514
$s$	0.6392	0.6625
$b$	271.90	193.10

The viscose solution was produced by adding the carbon disulphide first with 12% NaOH, 1 : 1.8 CS<sub>2</sub> and 30 : 1 liquor ratio, at 20°C, for 3 h

produced by adding the carbon disulphide first, for 3 and 6 h, respectively, and absence of thixotropy, for those produced by adding the sodium hydroxide first, for 6 h, as compared with the corresponding ones produced with the lower carbon disulphide ratio (Table 2). This may relate to a relatively higher rate of xanthation than by-product formation accompanying the flow measurements of the viscoses produced with the higher carbon disulphide ratio.

#### Influence of temperature

The temperature influence on the flow properties of emulsion viscoses has been investigated by varying either the temperature of the flow measurements only or together with that of the viscose reaction.

For the former purpose, the flow measurements of the viscose of wood pulp, produced by adding the carbon disulphide first, with 12% sodium hydroxide, 1:1.8 carbon disulphide ratio, and 30:1 liquor to cellulose ratio, at 20°C, for 3 h, were carried out once at 20°C, and again at 30°C (Table 3). The results showed decreased structural and apparent viscosities as well as decreased  $b$  values, while, the thixotropy index and the  $s$  value showed increases, for the measurements at the higher temperature.

According to Ree and Eyring<sup>2</sup>, raising the solution temperature results in an increase in the free spaces between the molecules and hence a decrease in the apparent viscosity. The latter, represented by  $\eta_{50}$ , is in turn accompanied by a decrease in the  $b$  value.

The decrease in structural viscosity may also be attributed to the increase in the free spaces which may then lead to decreased linking strength, or to an increase in the energy of the molecules, with which the bonds become more energetic and hence easily broken; non-Newtonian behaviour would be due to the effect of shear on the number of links and the average life of a link<sup>3</sup>. The decreased structural viscosity was as usual followed by decreased pseudoplasticity, i.e., increased  $s$  value.

The decreased rate of xanthation and that of increased by-product formation, which accompany increased temperature<sup>4</sup>, may contribute to the increased thixotropy, as they take place while the flow measurements are being carried out. However, the increased energy of the molecules, following the increased temperature, may lead to a change in the relative rates of bond breaking and reformation and hence interfere with the achieved result.

Regarding the effect of change of both the reaction and flow measurements temperature on the flow properties of viscose solutions, the investigations have been carried out on viscoses of wood pulp produced with 15 and 18% sodium hydroxide solutions using 1:1.8

carbon disulphide ratio and 30:1 liquor to cellulose ratio, by adding the carbon disulphide first, for 3 and 6 h, and, by adding the sodium hydroxide first, for 6 h, at 20, 30 and 50°C (Table 4) as well as on cotton sliver viscoses similarly produced with 18% sodium hydroxide, by adding first either the carbon disulphide or the sodium hydroxide, for 6 h (Table 5).

It is clear from Table 4 that increased temperature showed for the viscoses of wood pulp produced with 15% sodium hydroxide, different changes: increase and decrease, of structural viscosity, thixotropy and anti-thixotropy, and replacement of one type of flow by the other. Only for the viscoses produced by adding the carbon disulphide first, the increase of the temperature from 30 to 50°C resulted in almost no change in the structural viscosity; those produced with 18% sodium hydroxide showed increased structural viscosity and thixotropy and disappearance of the antithixotropic behaviour and its replacement by the thixotropic one. For the viscoses produced by adding the sodium hydroxide first, the increase of temperature from 20 to 30°C resulted in decreased structural viscosity and disappearance of the thixotropic behaviour. However, for cotton sliver viscoses, similarly produced to those of wood pulp with 18% sodium hydroxide, both decreased structural viscosities and thixotropy indices accompanied the rise of temperature from 20 to 30 to 50°C; only increased structural viscosity and thixotropy index were achieved, when the temperature was increased from 20 to 30°C, for the viscoses produced by adding the carbon disulphide first.

The above discrepancies were observed for the change of flow properties of the viscoses produced from the same cellulose origin, but with different sodium hydroxide concentrations or with the same sodium hydroxide concentration but from different cellulose origins, owing to temperature change, relate to different changes, the increase of temperature brings about the factors affecting the flow properties, which may vary with the sodium hydroxide concentration and the cellulose material from which viscoses were derived, and upon which the extent of the change of the flow properties depend.

Thus, besides these factors, which may affect the viscose flow properties owing to the change of the flow measurements temperature, and among which the decreased rate of xanthation and that of increased by-product formation may also result in the replacement of the antithixotropic type of flow by the thixotropic one, the following which are consequent of the change of the reaction temperature may be considered: (1) decreased cellulose solubility. This may affect: increased or decreased structural viscosity, thixotropy and anti-thixotropy or even conversion of one type of flow into the other, depending on the amount of gel centres produced; molecular aggregates formation, which increases structural viscosity and thixotropy, decreases antithixotropy and the antithixotropic-thixotropic conversion; and the resulting free spaces between the molecules, which increases the reverse effect; (2) decreased  $\gamma$ -number and increased by-product formation and this results in decreased structural viscosity.

As far as the apparent viscosity is considered, the results of both Tables 4 and 5, show decreased values for  $\eta_{50}$ , with the temperature increase, owing to the accompanying progressive decrease of cellulose solubility.

Table 4 Influence of temperature of reaction and flow measurements on flow properties of wood pulp viscoses

NaOH conc. (%)	Temp. (°C)	Order of addition of reactants	Time (h)	Solubility (%)	Structural viscosity	$\eta_{50}$	Thixotropy/antithixotropy (A) index	s	b
15	20	CS <sub>2</sub> first	3	100	0.3276	602.60	0.6837(A)	0.6451	252.2
		CS <sub>2</sub> first	6	100	0.3060	367.70	2.1273	0.7142	206.2
		NaOH first	6	100	0.3250	400.10	0.3609	0.6666	201.5
	30	CS <sub>2</sub> first	3	92.0	0.2970	245.85	0.7246	0.6923	150.0
		CS <sub>2</sub> first	6	96.5	0.3454	342.45	0.7246	0.6568	178.0
		NaOH first	6	92.0	0.2649	154.75	0.5442	0.7500	116.6
	50	CS <sub>2</sub> first	3	75.0	0.3010	161.35	1.3767(A)	0.6818	110.9
		CS <sub>2</sub> first	6	80.0	0.3130	199.75	9.4198(A)	0.6539	123.0
	18	20	CS <sub>2</sub> first	3	100	0.2911	436.85	0.2279(A)	0.6875
CS <sub>2</sub> first			6	100	0.2507	362.20	0.9300	0.7140	204.0
NaOH first			6	90.0	0.2761	347.95	0.7597	0.7071	198.1
30		CS <sub>2</sub> first	3	85.0	0.3039	239.30	0.9058	0.7222	154.3
		CS <sub>2</sub> first	6	90.0	0.3125	277.15	0.9420	0.7071	168.7
		NaOH first	6	87.0	0.2131	76.85	0	0.7549	69.0
50		CS <sub>2</sub> first	3	72.0	0.3627	133.90	4.3476	0.6363	93.9
		CS <sub>2</sub> first	6	75.0	0.3333	184.40	9.0575	0.6320	113.7

The viscoses were prepared using 1 : 1.8 CS<sub>2</sub> ratio and 30 : 1 liquor ratio

Table 5 Influence of temperature of reaction and flow measurements on flow properties of cotton sliver viscoses

Temp. (°C)	Order of addition of reactants	Solubility (%)	Structural viscosity	$\eta_{50}$	Thixotropy index	s	b
20	CS <sub>2</sub> first	100	0.2894	727.70	0.3806	0.7222	343.1
	NaOH first	90.0	0.2857	482.95	1.2501	0.7402	268.5
30	CS <sub>2</sub> first	90.0	0.3163	497.20	2.6085	0.6875	244.1
	NaOH first	87.0	0.2778	431.35	0.9238	0.7142	225.6
50	CS <sub>2</sub> first	75.0	0.1889	52.14	0	0.8190	51.6
	NaOH first	72.0	0.1329	28.54	0	0.8823	30.6

The viscoses were produced using 18% NaOH, 1 : 1.8 CS<sub>2</sub> and 30 : 1 liquor ratio, for 6h

The *b* value changes with  $\eta_{50}$ , and the *s* value changes in accordance with the structural viscosity, with the exception of very few cases.

## CONCLUSION

Change of viscose flow properties, following that of cellulose origin, carbon disulphide ratio or temperature of the flow measurements alone or, together with that of the viscose reaction, relates to the accompanying changes, which may occur in the relative rates of xanthation and by-product formations, amount of gel centres

produced, degree of degradation, free spaces between the molecules, cellulose solubility, amounts of included carbon disulphide within the produced viscose and energy of the molecules.

## REFERENCES

- Mansour, O. Y., Nagaty, A. and Shukry, N. *Polymer* 1973, **14**, 27
- 'Rheology of Polymers' (Ed. E. T. Severs), Reinhold, New York; London, Chapman and Hall, 1962, pp 18-21
- Kauzmann, W. and Eyring, H. *J. Am. Chem. Soc.* 1940, **62**, 3113
- Fahmy, Y. A. and Fadl, M. H. *Sven. Papperstidn.* 1964, **67**, 105, 279, 576

# Metal carbonyls as photoinitiators for the polymerizations of tetrafluoroethylene and vinyl monomers containing tetrafluoroethylene

C. H. Bamford and S. U. Mullik

*Department of Inorganic, Physical and Industrial Chemistry, Donnan Laboratories, University of Liverpool, Liverpool L69 3BX, UK  
(Received 22 August 1972)*

It is well-known that manganese and rhenium carbonyls in the presence of a suitable chlorine or bromine derivative  $RX$  (e.g.  $CCl_4$ ,  $BrCH_2COOH$ ) are efficient initiators of free-radical polymerization<sup>1</sup>. With  $Mn_2(CO)_{10}$  the process involves scission of a halogen atom with formation of initiating radicals  $R\cdot$  and a manganese pentacarbonyl halide  $Mn(CO)_5X$  which may subsequently enter into other reactions such as ligand exchange and polymerization<sup>2</sup>. In the absence of halides  $Mn_2(CO)_{10}$  is ineffective with common vinyl monomers, but  $Re_2(CO)_{10}$  gives rise to relatively slow photoinitiation which has been attributed to hydrogen abstraction<sup>3</sup>. We now report that both carbonyls are active photoinitiators of the free-radical polymerizations of liquid tetrafluoroethylene and other vinyl monomers containing low concentrations of tetrafluoroethylene. No halogen compound other than  $C_2F_4$  was present in any of the systems we consider in this communication, and radical generation follows a route quite different from those outlined above.

The optical system in the present experiments comprised a 250 W high-pressure mercury arc (AEI, type E/D) with a quartz lens (focal length 10 cm) to produce an approximately parallel beam. Wavelengths employed were 435.8 and 365 nm for  $Mn_2(CO)_{10}$  and  $Re_2(CO)_{10}$ , respectively; these were isolated by a pair of Wratten filters 2E+98 ( $\lambda=435.8$  nm) and a Chance OVI filter ( $\lambda=365$  nm). Reactants were thoroughly degassed by the conventional freeze-thaw technique and irradiated in a Pyrex tube of 1 cm internal diameter.

Tetrafluoroethylene, kindly supplied by ICI Ltd, London Division, was submitted to various treatments to ensure absence of impurities. Stabilizer was removed by passage of the gas through a glass spiral cooled to  $135^\circ C$ . About 6 g of the monomer were condensed in an evacuated Pyrex tube containing 1 mg  $Mn_2(CO)_{10}$ , then maintained at  $-93^\circ C$  with occasional shaking until the carbonyl had dissolved in the liquid tetrafluoroethylene. On irradiation at  $-93^\circ C$  rapid polymerization occurred, approximately 1 g of polymer being precipitated in 15 min. Similar results were obtained when the gaseous monomer was passed through concentrated sulphuric acid and over solid sodium hydroxide, or liquid  $C_2F_4$  was allowed to stand over sodium hydroxide, before reaction. In one series of experiments the monomer was distilled off after partial polymerization as described, and submitted to further irradiation after addition of  $Mn_2(CO)_{10}$ . When the

ensuing polymerization had proceeded for 15 min the process was repeated. In all, eight cycles were carried out, with essentially similar results at each stage. We believe these results demonstrate that the photopolymerization does not depend on the presence of low concentrations of adventitious impurities. Rhenium carbonyl, although not very soluble in liquid  $C_2F_4$  at  $-93^\circ C$ , also gave rise to rapid photopolymerization. In neither system was there any observable polymerization in the dark.

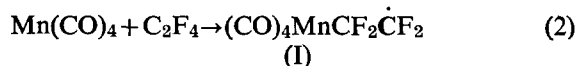
The free-radical polymerizations of styrene, methyl methacrylate and acrylonitrile photoinitiated by  $Mn_2(CO)_{10}/C_2F_4$  and  $Re_2(CO)_{10}/C_2F_4$  were studied at  $25^\circ C$ . In a typical experiment with methyl methacrylate with  $[C_2F_4]=0.2$  and  $[Mn_2(CO)_{10}]=8.5 \times 10^{-4} \text{ mol l}^{-1}$  a mean rate of polymerization of  $5.1 \times 10^{-4} \text{ mol l}^{-1} \text{ s}^{-1}$  was obtained. No polymerization was observed when  $C_2F_4$  was replaced by perfluorocyclohexane.

The manganese contents of polytetrafluoroethylene and poly(methyl methacrylate) prepared as described were determined by activation analysis after removal of uncombined manganese derivatives. Before analysis polytetrafluoroethylene was allowed to stand in contact with large volumes of benzene or methanol for 11 days, the liquids being changed eight times. The polymer was then washed five times and dried in vacuum at  $60^\circ C$  for one day. Poly(methyl methacrylate) was precipitated from benzene solution into methanol three times. The manganese content of the reprecipitated poly(methyl methacrylate) corresponded to 1.25 Mn atoms per polymer molecule. This is close to the value calculated (1.20) on the assumption that each growing polymer radical is initiated by, and remains attached to, a manganese atom (taking  $k_{tc}/k_{td}$  for methyl methacrylate at  $25^\circ C$  to be 0.52)<sup>4</sup>. The polytetrafluoroethylene contained 349 ppm by weight of manganese, implying, on the above basis, that the mean kinetic chain length in the polymerization was 1570.

Since  $Mn_2(CO)_{10}$  does not photosensitize the polymerization of methyl methacrylate in the absence of additives, initiation in the above experiments must involve participation of  $C_2F_4$ , so that the fluorine content of the polymer was of interest. Tetrafluoroethylene may be incorporated in the polymer in the initiation process, and also by copolymerization. The contribution of the latter was assessed by determining the fluorine content of polymers prepared by azodiisobutyronitrile initiation under similar conditions. It turns out that the mean

value of the ratio of fluorine to manganese atoms incorporated by initiation is 3.96, suggesting strongly that one  $C_2F_4$  molecule is incorporated with each Mn atom during initiation.

We therefore propose that initiation involves the following reactions:



Evidence for the photolytic step (1) has already been presented<sup>5</sup>. The radical-generating reaction (2) is favoured by the relatively high strength of the Mn-CF<sub>2</sub> bond. It is also possible that electron transfer from Mn(CO)<sub>4</sub> or photoexcited Mn<sub>2</sub>(CO)<sub>10</sub> to C<sub>2</sub>F<sub>4</sub> leads to a complex subsequently generating a propagating radical. Clearly this is much more probable with C<sub>2</sub>F<sub>4</sub> than with monomers (e.g. methyl methacrylate) which do not possess such powerfully electron-attracting groups. The vacant coordination position in (I) may be filled by CO or monomer. Subsequent propagation is represented by step (3) in which M represents C<sub>2</sub>F<sub>4</sub> or other polymerizable vinyl monomer. A similar mechanism is likely to hold for Re<sub>2</sub>(CO)<sub>10</sub>.

These experiments do not establish whether chain growth in liquid C<sub>2</sub>F<sub>4</sub> is stopped by bimolecular termination or radical occlusion<sup>6</sup>. No significant after-effects are observable on interrupting illumination, so that occlusion, if operative, must be extreme.

The polymerization of C<sub>2</sub>F<sub>4</sub> at -93°C photoinitiated by Mn<sub>2</sub>(CO)<sub>10</sub> is strongly retarded by low concentrations of styrene, methyl methacrylate or acrylonitrile; polymerization is almost completely suppressed by a concentration of methyl methacrylate of  $2 \times 10^{-2} \text{ mol l}^{-1}$

([Mn<sub>2</sub>(CO)<sub>10</sub>] =  $3.9 \times 10^{-3} \text{ mol l}^{-1}$ ). It appears that propagation between radicals with terminal methyl methacrylate units and C<sub>2</sub>F<sub>4</sub> is extremely slow at -93°C, although the experiments described earlier show that it occurs at 25°C.

We conclude with a brief reference to observations on osmium and ruthenium carbonyls. Os<sub>3</sub>(CO)<sub>12</sub> is sparingly soluble in liquid C<sub>2</sub>F<sub>4</sub> at -93°C and photoinitiated polymerization ( $\lambda = 365 \text{ nm}$ ) very slowly. Ru<sub>3</sub>(CO)<sub>12</sub>, although more soluble, behaves similarly. However, both carbonyls photoinitiate the polymerization of methyl methacrylate containing C<sub>2</sub>F<sub>4</sub> at 25°C.

We hope to publish shortly a full account of polymerizations photoinitiated by metal carbonyl/C<sub>2</sub>F<sub>4</sub> combinations.

#### ACKNOWLEDGEMENT

One of us (S.U.M.) gratefully acknowledges the award of an Academic Staff Fellowship by the Association of Commonwealth Universities.

#### REFERENCES

- 1 Bamford, C. H. *Eur. Polym. J. Suppl.* 1969, p 1 and references quoted
- 2 Bamford, C. H., Burley, J. W. and Coldbeck, M. *J. Chem. Soc., Dalton Trans.*, 1972, p1846
- 3 Bamford, C. H. and Mahmud, M. U. *Chem. Commun.* 1972, p 762
- 4 Bamford, C. H., Dyson, R. W. and Eastmond, G. C. *Polymer* 1969, **10**, 885
- 5 Bamford, C. H. and Paprotny, J. *Polymer* 1972, **13**, 208 and references quoted
- 6 Bamford, C. H., Barb, W. G., Jenkins, A. D. and Onyon, P. F. 'The Kinetics of Vinyl Polymerization by Radical Mechanisms', Butterworths, London, 1958, Ch 4

# Book Reviews

## Polymer characterization

Edited by Clara D. Craver

Plenum Press, New York, 1971, 279 pp. \$16.24

The book is a report of the proceedings of a symposium on 'Interdisciplinary Approaches to the Characterization of Polymers' sponsored by the American Chemical Society. It contains eighteen papers, and covers a wide range of techniques. Since the symposium additional data and background information have been added to some of the papers so as to make them more useful reference material.

The first four papers deal with the application of Raman spectroscopy to polymers. The introduction of laser sources has generated new interest in the technique and the book gives a good guide to the way the field is developing. Representative results are reported by F. J. Boerio and J. L. Koenig for a number of polymers, together with a comparative study of graphite and carbon black. The application of Raman spectroscopy to the study of biological polymers is dealt with in a paper by W. L. Peticolas, E. W. Small and B. Fanconi.

The other contributions which I feel should be noted are as follows. There is an interesting study by R. E. Baier and G. I. Loeb of the factors affecting the behaviour of interfacial films of poly(methyl glutamate). W. Wrasidlo reports extensive data on transitions and relaxation behaviour for a series of polyquinoxalines and other aromatic polymers. Finally, there is a paper by R. B. Fox and T. R. Price dealing with the scope and experimental problems associated with the application of luminescence spectroscopy in polymer science.

Taken as a whole the book provides a useful report of current achievements in a number of branches of the field and it can be recommended to research workers who wish to be kept informed of general developments.

C. Price

## Properties of polymers: correlations with chemical structures

D. W. van Krevelen

Elsevier, Amsterdam, 1972, 427 pp. \$27.25

This book is concerned with the relationships between polymer properties and structure. Thermophysical, optical, electrical, melting and flow and diffusion phenomena and all other important properties of polymers are dealt with.

The range of subject is great and necessarily the treatment of the theoretical background is frequently superficial and some topics are dealt with, briefly, where there are little or no data available. In this sense the author may have attempted too much for a single volume, but this criticism, if such it is, does not detract from the main purpose, and both the data and the correlations will be of the greatest value to the polymer scientist.

In a short review it is not possible to do more than refer to a few points on presentation and content. The arrangement of each chapter follows a more or less uniform pattern. The definitions and relationships, with their units clearly stated, are given first followed by tabular presentation of experimental data and calculated group contributions. The relationships are discussed critically and comparisons are made between different approaches. Where appropriate graphical correlations are given.

Numerical examples are provided which may appear hardly necessary for the professional scientist and more suited to the student, but to be fair the author makes modest claims both in regard to the composition of the book and the readership to which it is directed.

The text appears to be up to date, with 1969 and 1970 references, and no obvious errors or misprints were found. The book will clearly be of more than ephemeral value and the provision of space here and there for the insertion of newly published data would have been useful. The paper and printing are of good quality and the binding attractive.

Its cost (\$27.25) considering the problems of preparing a book of this type, is not excessive.

W. Cooper

## Film-forming compositions: Vol I, Part III

Edited by R. R. Myers and J. S. Long

Marcel Dekker, New York, 1972, 578 pp. \$48.75

This book is part of a five volume work aimed primarily at the surface coatings technologist. It purports to be an up-to-date and comprehensive work of reference on film-forming compositions. As a 'treatise' I expect such a book to present a systematic, comprehensive and detailed account of modern coatings technology. In fact it falls short of this on all three counts, even when considered in relation to the preceding two parts of the volume. The compilation of this type of work as a collection of authoritative reviews by experts in the field is undoubtedly a difficult task for the editors, and one in which they have been only partly successful. The method of compilation leads to variations in treatment, in depth and in material content which are difficult to reconcile in order to produce a cohesive book. The individual chapters are clearly written and well illustrated but their titles are misleading in some cases. Thus, unsaturated polyester resins are mentioned only in passing in the chapter on 'reactive polyesters'. A little more information is found on these important materials in the chapter on 'Dimer acids', otherwise one has to go to Volume I, Part I, for a slightly more detailed account. Similarly, fragmentation occurs with topics such as emulsion technology, polymerization, etc, emulsion polymerization being treated in an elementary fashion in the chapter on 'Surface-active agents'. The chapter on 'Emulsion technology' is of least value to the UK technologist since it deals only superficially with emulsion processes and equipment and is concerned with bodied linseed oil emulsions which are virtually unused in Europe. (Two whole pages of this chapter are devoted quite unnecessarily to the full canonical structures of common surface-active agents!)

Since this is the third and final part of Volume I of the treatise one may have hoped it to rectify omissions in the previous parts. However, important modern developments such as in the field of non-aqueous dispersion polymerization and powder coatings have been overlooked.

The chapters are generally well documented and the index for the book is adequate. It seems a pity that the editors did not include an index to the complete volume in this third and final part. As a work of reference it will be useful to the technologist as an introductory source of information on a wide range of film-forming materials, but it will not satisfy those who are seeking information in depth.

At \$48.75 I believe the book to be poor value for money.

R. Lambourne

## Plastics Technologist

The newly established Department of Materials Science and Engineering at Pahlavi University, Shiraz, Iran, is in need of a qualified faculty member in the field of plastics technology. Minimum requirements are:

- (i) Ph.D. degree in a related field;
- (ii) Industrial and/or teaching experience.

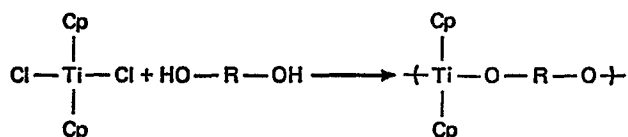
The post will be available in January 1973 and anyone interested should contact this department as soon as possible: Department of Materials Science and Engineering (Chairman: A. Ahmadi), School of Engineering, Pahlavi University, Shiraz, IRAN.

# Synthesis of titanium polyethers by the interfacial and aqueous solution techniques

C. E. Carraher Jr. and S. T. Bajah\*

Department of Chemistry, University of South Dakota,  
Vermillion, South Dakota 57069, USA  
(Received 14 August 1972)

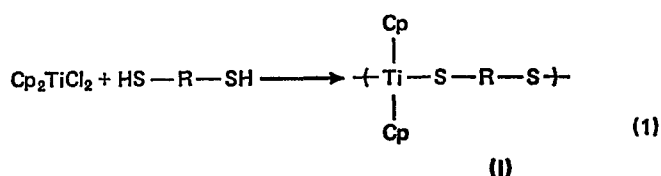
Titanium polyethers were formed via the interfacial and aqueous solution techniques as illustrated below. Synthesis was effected employing both aromatic and aliphatic diols



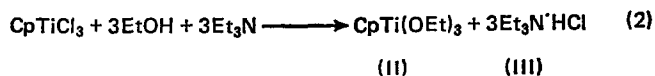
for the interfacial system but was effected only for aromatic diols when employing the aqueous solution technique. Some products exhibit Ti-OH and/or R-OH endgroups.

## INTRODUCTION

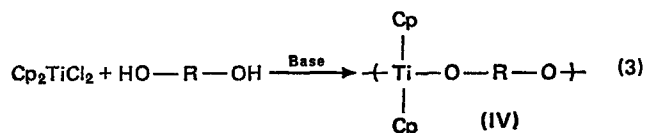
Relatively little work has been reported on the synthesis of organometallic polymers largely due to lack of suitable preparative methods. We are interested in the synthesis of polymers containing heavy metals in their backbone<sup>1-4</sup>. Recently we reported the synthesis of polyamines, polyesters and polythioethers as illustrated below for the synthesis of polythioethers via the interfacial and aqueous solution routes<sup>5-7</sup>.



The above work is based largely on the simple Lewis acid (the metal halide)—Lewis base (dithiols, etc.) concept. There is ample evidence that the formation of analogous Ti-O-R containing polymers should be effected under the proper conditions. For instance, metathetical reactions have been carried out with cyclopentadienyltitanium trichloride and ethanol in the presence of triethylamine as the acid scavenger<sup>8</sup>:



We now report the synthesis of polyethers as illustrated below using both the aqueous solution and interfacial techniques.



\* Portions of this paper are taken from the thesis of S.T.B. (1972).

The only previous report of the synthesis of titanium polyethers was by Schramm and Frijhauf<sup>9</sup> via a redox reaction involving the refluxing of Cp<sub>2</sub>TiCl<sub>2</sub> with dicarboxylate salts in the presence of heavy metals. The products were poorly characterized but reportedly exhibited good thermal stabilities. Additionally Giddings<sup>10</sup> reported the formation of organometallic products from refluxing R<sub>2</sub>TiX<sub>2</sub> products with various diols in toluene. No structure was given for the products.

There are several reasons for choosing Cp<sub>2</sub>TiCl<sub>2</sub> as the titanium-containing organometallic. It is commercially available and stable in air. Previously it has been shown to possess catalytic properties in certain reactions such as the synthesis of stereoregular polymers via the Ziegler catalyst route. A product containing the Cp<sub>2</sub>Ti moiety may possess similar properties. Cp<sub>2</sub>TiCl<sub>2</sub> ionizes in water to form Cp<sub>2</sub>Ti<sup>2+</sup> which is stable for longer than 1 h in neutral and acidic aqueous solutions. Lastly, Cp<sub>2</sub>TiCl<sub>2</sub> possess two readily identifiable colour sites, the yellow Cp-Ti colour site and the red Ti-Cl colour site, making rapid tentative identification of compounds containing these sites possible.

## EXPERIMENTAL

The following chemicals were used as received without further purification: dicyclopentadienyltitanium dichloride (from Alfa Inorganics, Inc., Beverly, Mass.); ethylene glycol (from Baker Chemical Co., Phillipsburg, N.J.); 1,4-benzenedimethanol, 1,3-dihydroxyacetone, 4,4'-isopropylidene diphenol, hydroquinone, chlorohydroquinone, tetrachlorohydroquinone, methylhydroquinone, t-butylhydroquinone, 2,5-di-t-butylhydroquinone, and dicyanohydroquinone (from Aldrich Chem Co., Milwaukee, Wis.).

Polymerization procedures are similar to those described in detail elsewhere<sup>7</sup>. Briefly, solutions of

$\text{Cp}_2\text{TiCl}_2$  are added to stirred aqueous solutions containing diol and any added base. For interfacial systems  $\text{Cp}_2\text{TiCl}_2$  is contained in a water-immiscible solvent whereas for aqueous solution systems  $\text{Cp}_2\text{TiCl}_2$  is contained in water. The reaction apparatus is similar to that described previously<sup>11</sup>. Essentially reaction occurs under rapidly stirred conditions in a 1 US pint (1 US gal  $\equiv$  3.785 dm<sup>3</sup>) Kimax Emulsifying Mill jar placed on a Waring Blendor with a recorded rotor speed of 23 500 rev/min (no load). Solutions are added through a large mouthed funnel placed in a hole in the jar lid. Addition is rapid such that 100 ml of solution can be added in less than 3 sec. A second hole in the jar lid acts as a vent. Timing for each reaction is begun after the second phase has been introduced into the stirring jar. Syntheses employing hydroquinone or substituted hydroquinones were accomplished under a nitrogen atmosphere using equipment described before<sup>11</sup>.

Polymer precipitates rapidly from the reaction jar as a tacky to 'powdery' solid. It is recovered using suction filtration, washed repeatedly with portions of water, and then transferred to a preweighed Petri dish for drying. After drying the Petri dish is weighed to determine product yield. The products vary in coloration from yellow to dark orange. Some dry to give glasses from which strong, flexible films are formed when they are scraped from the Petri dish while others dry to give salt-like solids. All can be ground to give powders which are electrostatic.

Solubility tests were conducted utilizing 0.001 g quantities of the polymer added to 2 ml of liquid. A wide range of solvents were used. The products were insoluble in all solvents tried. They undergo degradation in acid solutions, such as HCl and HNO<sub>3</sub>.

As with many organometallic polymers, elemental analysis by classical techniques is not possible. Titanium determinations were made using a technique given in ref. 12. Representative results follow: product from the condensation product of  $\text{Cp}_2\text{TiCl}_2$  with hydroquinone gave 15.3% Ti, calculated 16.8% Ti; with dicyanohydroquinone gave 14.4%, calculated 14.3% Ti.

Infra-red spectra were obtained using KBr pellets with a Beckman IR-10 and 12 and Perkin-Elmer 237-B spectrophotometers. Band sites for some of the products are contained in Table 1. Spectra of products agree with a product of form (IV). Some bands of particular interest are as follows. All of the products exhibit bands in the region of 815 cm<sup>-1</sup>, 1015 cm<sup>-1</sup> and 1440 cm<sup>-1</sup> characteristic of the  $\pi$ -Cp group. Products containing aliphatic groups contain bands in the 3000-2800 cm<sup>-1</sup>

region characteristic of C-H stretching. The product from 2,3-dicyanohydroquinone contains a sharp, strong band at 2240 cm<sup>-1</sup> characteristic of the nitrile group. The product from dihydroxyacetone exhibits a broad intense band in the region of 1620 cm<sup>-1</sup>, characteristic of the carbonyl group.

## RESULTS AND DISCUSSION

Yield results as a function of diol appear in Table 2. Polymerization is general for interfacial syntheses but has been effected with only aromatic diols utilizing aqueous solution systems. The reason(s) for the lack of polymer formation in aqueous solution systems for aliphatic diols is presently a matter of study. A possibility concerns the difference in acidity between aromatic and aliphatic diols. For instance hydroquinone is 99% mono-ionized at pH values >12 and over 99% di-ionized at pH values >13.8 (for hydroquinone  $\text{p}K_{\text{a}1} = 10^{13}$  and  $\text{p}K_{\text{a}2} = 12^{13}$ ). Aliphatic diols remain largely un-ionized even at a pH of 14 (for instance, ethylene glycol has a  $\text{p}K_{\text{a}1}$  of 15.1<sup>14</sup> and 1,3-dihydroxyacetone has a  $\text{p}K_{\text{a}1}$  of 13.5<sup>15</sup>). It is possible that polycondensation is only effected in aqueous solution with deprotonated diols whereas other criteria are critical for interfacial synthesis.

Reaction is rapid for both interfacial and aqueous solution syntheses (Table 3). Reaction is completed within 10 seconds for aqueous solution systems, but is slower for interfacial systems with yield reaching a plateau around 40 sec.

There exists at least three possible endgroups. These are R-OH, Ti-Cl and Ti-OH, the latter resulting from the hydrolysis of Ti-Cl. The presence of R-OH and Ti-OH endgroups has been confirmed for at least some products. Because of the overlapping of some of the R-OH bands (in the region of 3600 to 2500 cm<sup>-1</sup>) with bands due to the O-H stretching in Ti-OH (a broad, strong band in the 3500 to 3100 cm<sup>-1</sup> region) identification is not always possible. The Ti-Cl stretching band vibration has been assigned as 310 cm<sup>-1</sup>. This is in agreement with assignments made by others<sup>18, 19</sup>. None of the products exhibited a band in this region indicating a lack of detectable Ti-Cl endgroups. This may be due to the hydrolysis of Ti-Cl endgroups after polymerization was completed.

The only noticeable difference in the spectra of products synthesized using either the aqueous solution or interfacial techniques concerns bands associated with Ti-OH endgroups. These are often more intense for

Table 1 Infra-red bands of products of  $\text{Cp}_2\text{TiCl}_2$  condensed with various diols for the range 4000-700 cm<sup>-1</sup> (all band locations are given in cm<sup>-1</sup>)

### Diol: bands\*

2,5-di-t-butylhydroquinone: 3410 S; 2960 SSp; 2910 MSp; 2880 MSp; 1645 MSp; 1625 MSp; 1600 WSp; 1525 WSp; 1515 WSp; 1465 M; 1435 MSp; 1420 MSp; 1405 SSp; 1390 SSp; 1360 MSp; 1270 MSp; 1205 M; 1170 SSp; 1120 SSp; 1075 WSp; 1020 MSp; 920 M; 875 MSp; 855 MSp; 795 SSp.

Chlorohydroquinone: 3650-2500 SB; 1630-1600 MB; 1485 SSp; 1440 MSp; 1330 W; 1310 W; 1265 SSp; 1200 SSp; 1130 WSp; 1040 MSp; 1025 MSp; 810 SB (broad intense band in region 950-700).

4,4'-isopropylidenediphenol: 3500-3000 MB; 2990 MSp; 2925 MSp; 1605 MSp; 1500 SSp; 1480 WSp; 1445 M; 1390 W; 1365 MSp; 1350 WSp; 1250 S; 1180 SSp; 1120 WSp; 1105 WSp; 1090 WSp; 1020 MSp; 900-700 SB.

2,3-dicyanohydroquinone: 3520 SSp; 3250 W; 3100 W; 260-2450 WB; 2350 W; 2240 SSp; 1695 MSp; 1680 MSp; 1605 MSp; 1595 MSp; 1500 SSp; 1450 SSp; 1420 MSp; 1390 MSp; 1340 MSp; 1305 SSp; 1270 WSp; 1255 SSp; 1170 MSp; 1150 W; 1080 W; 1065 W; 1035 MSp; 1020 MSp; 985 M; 955 MSp; 945 W; 830 SSp; 800 M; 765 WSp.

\* S=strong; M=medium; W=weak; B=broad; Sp=sharp. If the band is between being broad and sharp no designation will be given

Table 2 Yield of polyether as a function of diol

Diol	Yield <sup>a</sup> (%) (aqueous solution)	Yield <sup>b</sup> (%) (interfacial)
1,3-Dihydroxyacetone	0	18
1,4-Benzenedimethanol	0	23
Ethylene glycol	0	24
4,4'-Isopropylidenediphenol	30	36
Hydroquinone	1	46
Chlorohydroquinone	41	61
2,3-Dicyanohydroquinone	70	72
2,5-Di-t-butylhydroquinone	74	41

a Reaction conditions: the aqueous phase consisting of  $Cp_2TiCl_2$  (0.001 mol) contained in 50 ml of water is added to stirred aqueous solutions containing the diol (0.001 mol) in 50 ml of water with added sodium hydroxide (0.002 mol) at 25°C for 1 min stirring time at a stirring rate of 23 500 rev/min (no load)

b *Ibid.* except the  $Cp_2TiCl_2$  is contained in 50 ml of  $CHCl_3$

Table 3 Yield as a function of stirring time

Stirring time (sec)	2,3-Dicyanohydroquinone		Hydro- quinone <sup>b,c</sup> yield (%)	Methyl- hydro- quinone <sup>b</sup> yield (%)
	Aqueous <sup>a</sup> yield (%)	Interfacial <sup>b</sup> yield (%)		
10	15	14	31	8
20	70	52	35	28
30	67	59	36	31
40	66	72		
60	70	72	70	60
80	66			
90	66	73	68	60
120	69	73	67	60
180			67	60

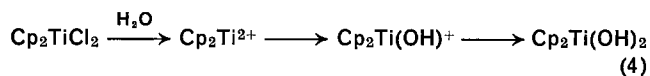
a Reaction conditions are the same as given in Table 2a

b Reaction conditions are the same as given in Table 2b

c Yield for aqueous systems is approximately constant after 10 sec stirring time

products synthesized using the aqueous solution technique in comparison with analogous products produced using the interfacial method.

While  $Cp_2TiCl_2$  ionizes in water to form  $Cp_2Ti^{2+}$  it does undergo subsequent mono- and di-hydroxylation:



$Cp_2Ti^{2+}$  is stable in neutral solutions for several hours, but hydroxylation is greatly accelerated in basic solutions<sup>16, 17</sup>. Such base-catalysed hydroxylations are presumably responsible for the presence of Ti-OH end-groups. To eliminate the importance of such hydroxylations, solutions containing the titanium moiety are made up just prior to reaction and the product is separated from the reaction solution just after (normally within 3 min) completion of reaction. None of the products studied exhibited Ti-OH bands greater than 5%, determined by comparison of the Ti-OH band to the Ti-Cp, 1440  $cm^{-1}$  band.

REFERENCES

- 1 Carraher, C. *Macromolecules* 1971, 4, 263
- 2 Carraher, C. and Dammeier, R. *Makromol. Chem.* 1971, 141, 245; 1971, 141, 251
- 3 Carraher, C. and Winter, D. *Makromol. Chem.* 1971, 141, 259; 1971, 141, 237
- 4 Carraher, C. and Scherubel, G. *J. Polym. Sci. (A-1)* 1971, 9, 983
- 5 Carraher, C. and Lessek, P. *Eur. Polym. J.* in press
- 6 Carraher, C. and Nordin, R. *J. Polym. Sci. (A-1)* 1972, 10, 521
- 7 Carraher, C. *Organic Coatings and Plastics* 1971, 31, 330, 338
- 8 Alexandrov, G., Gusev, A. and Struchkov, Yu. *Zh. Strukt. Khim.* 1968, 9, 333
- 9 Schramm, C. and Frijhauf, E. Fr. Pat. 1 397 533 (1965)
- 10 Giddings, S. U.S. Pat. 3 226 363 (1966)
- 11 Carraher, C. *J. Chem. Educ.* 1969, 46, 314
- 12 'Treatise on Analytical Chemistry' (Eds I. Kolthoff and P. Elving), Interscience, New York, 1961, Vol 5, Part II
- 13 Abichandianin, C. and Jatkar, S. *J. Indian Inst. Sci.* 1938, 21A, 417
- 14 Long, F. and Ballinger, P. *J. Am. Chem. Soc.* 1960, 82, 795
- 15 Carraher, C. *Diss. Abstr.* 1968, p 1488
- 16 Israeli, Y. *Bull. Soc. Chim. France* 1966, 3, 837
- 17 Carraher, C. unpublished work
- 18 Druce, P., Kingston, B., Lappert, M., Srivastava, R., Frazer, M. and Newton, W. *J. Chem. Soc. (A)* 1969, p 2814
- 19 Clark, R., Maresca, L. and Puddephatt, R. *Inorg. Chem.* 1968, 7, 1603



# Nuclear magnetic relaxation in poly(*N*-amyl maleimide) and poly(*N*-dodecyl) maleimide

J. Bailey, H. Block, D. R. Cowden and S. M. Walker

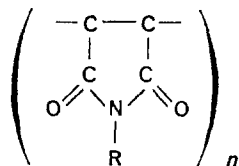
Department of Inorganic, Physical and Industrial Chemistry, University of Liverpool,  
PO Box 147, Liverpool L69 3BX, UK

(Received 3 August 1972; revised 12 October 1972)

Longitudinal relaxation times in the laboratory ( $T_1$ ) and rotating ( $T_{1\rho}$ ) frames have been measured for poly(*N*-amyl maleimide) and poly(*N*-dodecyl maleimide). The results are compared with information previously published using dielectric relaxation techniques. A total of three relaxation processes have been detected corresponding to methyl rotation, motion within the substituent alkyl chain and out-of-plane deformation of the maleimide ring. An attempt to fit the  $T_1$  data in the dodecyl derivative to theoretical equations is described.

## INTRODUCTION

The techniques of dielectric<sup>1</sup> and nuclear magnetic relaxation<sup>2-4</sup> are widely used for studying molecular motion in solid polymers. Both of these methods yield information on the molecular correlation times for various relaxation processes and on the apparent activation energy for the molecular motion involved. An extensive study using dielectric relaxation and broadline nuclear magnetic resonance (n.m.r.) measurements on a series of poly(*N*-substituted maleimides) (I) has recently been carried out<sup>5, 6</sup>.



These polymers, having in general very high glass transition temperatures and substantial backbone rigidity, are potentially important thermally stable materials. In this paper we report the results of a subsequent investigation into the longitudinal nuclear magnetic relaxation times of two of these polymers, poly(*N*-amyl maleimide) (R = C<sub>5</sub>H<sub>11</sub>) and poly(*N*-dodecyl maleimide) (R = C<sub>12</sub>H<sub>25</sub>), using pulsed rather than continuous wave techniques.

The behaviour of  $T_1$  as a function of temperature is given by the expression<sup>7</sup>:

$$\frac{1}{T_1} = \frac{2}{3} \left( \frac{1}{T_2''} \right)^2 \left[ \frac{\tau_C}{1 + \omega_R^2 \tau_C^2} + \frac{4\tau_C}{1 + 4\omega_R^2 \tau_C^2} \right] \quad (1)$$

where  $\omega_R$  is the resonance frequency and  $T_2''$  is the value of  $T_2$  for the rigid lattice, i.e. as  $T \rightarrow 0\text{K}$ .  $\tau_C$  is the molecular correlation frequency for the process which is occurring and is related to the activation energy  $E^*$  by the expression:

$$\tau_C = A \exp(E^*/RT) \quad (2)$$

where  $T$  is the temperature.

Equations (1) and (2) show that a plot of  $T_1$  versus temperature passes through a minimum when  $\omega_R \tau_C \approx 0.6$ . Furthermore at temperatures which are very much less or very much greater than the minimum temperature, a plot of  $\ln T_1$  versus  $1/T$  has a slope of  $\pm E^*$ , and hence the activation energy for molecular motion may be determined.

When applied to data on polymeric systems, however, the simple theory given above always gives rise to activation energies which are very low when compared with the corresponding quantity obtained by observing the same molecular motion by dielectric relaxation techniques<sup>8, 9</sup>. This non-correspondence is believed to arise from the neglect, in equation (1), of the distribution of relaxation times, which is always found for molecular motions in polymers. Connor<sup>9</sup> has shown how equation (1) may be modified to allow for a Fuoss-Kirkwood<sup>10</sup> relaxation time distribution. The result is:

$$\frac{1}{T_1} = \frac{2}{3} \left( \frac{1}{T_2''} \right)^2 \frac{\beta}{\omega_R} \left[ \frac{\omega_R \tau_C^\beta}{1 + (\omega_R \tau_C)^{2\beta}} + \frac{2(2\omega_R \tau_C)^\beta}{1 + (2\omega_R \tau_C)^{2\beta}} \right] \quad (3)$$

where  $\beta$  is the Fuoss-Kirkwood distribution parameter and is readily obtained from dielectric relaxation data.

Equations (3) and (2) show that the position of the  $T_1$  minimum is little affected by the value of  $\beta$ , and the main effect of the distribution of relaxation times is to 'broaden' the whole temperature range over which  $T_1$  varies<sup>9</sup>. Quantitatively, the slope of a graph of  $\ln T$  versus  $1/T$  now gives  $\pm \beta E^*$  at temperatures well above or below the  $T_1$  minimum. Since  $0 < \beta < 1$  it would be expected that the n.m.r. activation energies would initially be low.

The behaviour of  $T_{1\rho}$  in the temperature region of a molecular relaxation is rather more complex than that of  $T_1$ , although the results are qualitatively similar. The detailed theory<sup>11-13</sup> shows that  $T_{1\rho}$  goes through a minimum when  $\omega_L \tau_C \approx 0.5$ , but  $\omega_L$  is now the Larmor precessional frequency as given by equation (4). However, in contrast to the behaviour of  $T_1$ , the slopes of the lines on either side of the  $T_{1\rho}$  minimum bear no relation to the activation energy for the molecular process. Indeed these

two slopes are generally different<sup>14</sup> because different theories are applicable in the two temperature regions.

It is generally concluded, however, that the position of the  $T_{1\rho}$  minimum is not affected to any great extent by the presence of a distribution of molecular relaxation times.

It is, therefore, usual to proceed in one of two ways when deriving activation energies for molecular motion in polymers from nuclear spin relaxation data. If the molecular process can be seen to give rise to corresponding minima in  $T_1$  and  $T_{1\rho}$  then there are two values of the correlation time at two temperatures, which are not subject to distribution effects. Similarly, the behaviour of  $T_2$  as a function of temperature may also give a third value of the correlation time, but it is often found that molecular motion which affects the longitudinal relaxation time ( $T_1$  and  $T_{1\rho}$ ) has no effect on the transverse relaxation time<sup>15</sup> ( $T_2$ ). Alternatively the single accurate value of  $\tau_C$  at the  $T_1$  minimum may be seen to lie on the Arrhenius line for one of the dielectric processes in the material. If this is found to be so, then it is only necessary to multiply the apparent n.m.r. activation energy by  $1/\beta$ ,  $\beta$  being found from the dielectric measurements<sup>16</sup>. This latter procedure has certain disadvantages, because an apparent frequency correlation of this type may occasionally arise fortuitously even when the n.m.r. and dielectric relaxation methods are not observing the same process. Such a situation has been shown to exist for the line width measurements on poly(*N*-dodecyl maleimide)<sup>6</sup>. Furthermore, the relevant distribution parameters for a given molecular process may not be the same for the nuclear magnetic and dielectric relaxation methods.

We have attempted a further method of estimating  $\beta$  by a curve-fitting procedure on the  $T_1$  data using equations (2) and (3).

## EXPERIMENTAL

Nuclear magnetic relaxation experiments were carried out to determine the longitudinal relaxation times  $T_1$  and  $T_{1\rho}$  i.e. in the laboratory and rotating frames respectively. A Polaron pulsed n.m.r. spectrometer operating at a resonance frequency of 21 MHz was used for all the measurements. This corresponds to a stationary magnetic field ( $B_0$ ) of 0.5 T provided by a Newport Instruments 4 in. electromagnet.  $T_1$  was determined by a saturation recovery method using  $90^\circ$ - $\tau$ - $90^\circ$  pulse sequences<sup>4</sup>. The  $90^\circ$  pulse length was about 6  $\mu$ s and the receiver recovery time 8  $\mu$ s. Experiments in the rotating frame were carried out using a  $90^\circ$  pulse followed by a long (several ms) pulse, phase shifted by  $90^\circ$  relative to the first pulse<sup>14</sup>. This second pulse has the effect of 'locking' the spin system in the rotating frame, and  $T_{1\rho}$  is then obtained by observing the height of the (Bloch) decay following the long pulse as a function of the pulse length. The effective frequency of the  $T_{1\rho}$  measurements was calculated using the prescription<sup>14</sup>:

$$\omega_L = \gamma B_1 \quad (4)$$

where  $\gamma$  is the magnetogyric ratio and  $B_1$  is the radio-frequency field applied at right angles to  $B_0$ .  $\omega_L$  was found to be  $5 \times 10^4$  Hz in these experiments.

Some mention is also made in this paper of the transverse relaxation time  $T_2$ , although most of the  $T_2$  measurements were derived from the line width of the nuclear resonance signal. These measurements have been reported in detail in another paper<sup>6</sup>. Occasional checks were made on the earlier measurements of  $T_2$  in these polymers by

observing the time constant of the Bloch decay following a  $90^\circ$  pulse<sup>17</sup>. In all cases the values obtained in this way were found to be in satisfactory agreement with the earlier results.

The preparation of the polymers has been described elsewhere<sup>5</sup>. The samples consisted of a compressed pellet, 0.5 cm<sup>3</sup> volume and 0.7 cm long, this approximating to the ideal of 70% of the length of the transmitter coil. Samples were contained in a glass tube which was evacuated to  $10^{-2}$  mmHg for several hours before sealing. These particular polymers were found to be especially suitable for the nuclear magnetic relaxation experiments because their transverse relaxation times are reasonably long compared to the receiver recovery time. Therefore, very little of the Bloch decay is obscured and this provides a comparatively large signal amplitude with which to work.

Low temperatures were achieved by passing the vapour of boiling liquid nitrogen through a heater controlled by a thermistor bridge, the thermistor being situated adjacent to the sample tube. At high temperatures the nitrogen carrier gas was replaced by compressed air. Temperatures were measured using a chromel/alumel thermocouple.

## RESULTS AND DISCUSSION

### Poly(*N*-amyl maleimide)

Figure 1 shows the results of  $T_1$  and  $T_{1\rho}$  measurements for poly(*N*-amyl maleimide). The  $T_1$  data show two minima at 130 and 210K, but these were not well resolved.  $T_{1\rho}$  showed two rather more distinct minima, one at 150K, the other apparently situated below the temperature of boiling liquid nitrogen (77K). There was also a flattening of the  $T_{1\rho}$  curve between 200 and 290K, although no corresponding behaviour was seen for  $T_1$ . Above 310K both  $T_1$  and  $T_{1\rho}$  increased exponentially as a function of temperature.

Over some temperature ranges, the decay curve following the long pulse in the  $T_{1\rho}$  experiments was resolvable

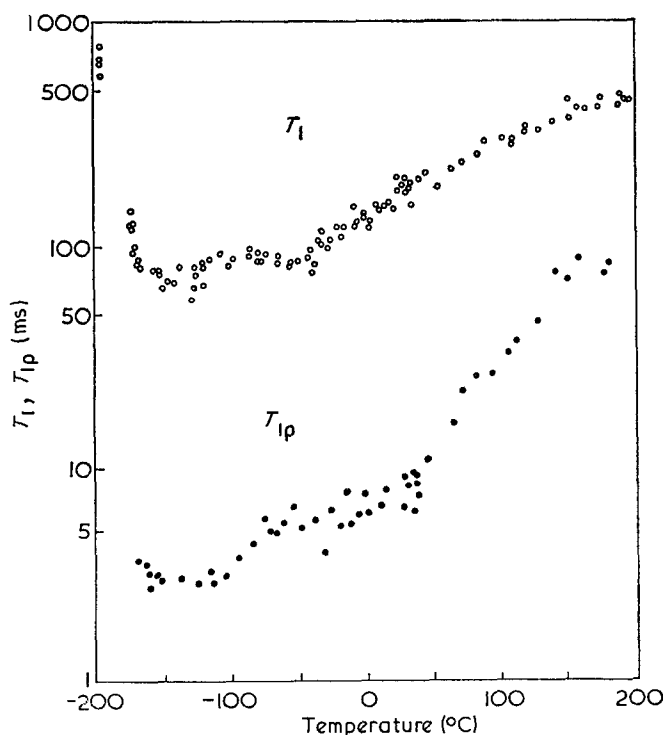


Figure 1  $T_1$  and  $T_{1\rho}$  measurements for poly(*N*-amyl maleimide)

into two exponential portions, indicating the presence of two simultaneous relaxation processes in the material. This behaviour is frequently observed in polymers, and is believed often to be due to different rates of molecular motion in the amorphous and crystalline regions of the sample<sup>2</sup>. For these materials, the fast decay region was, for the most part, too short for accurate assessment and the data in *Figure 1* refer exclusively to the 'long time constant' part of the decay curve.

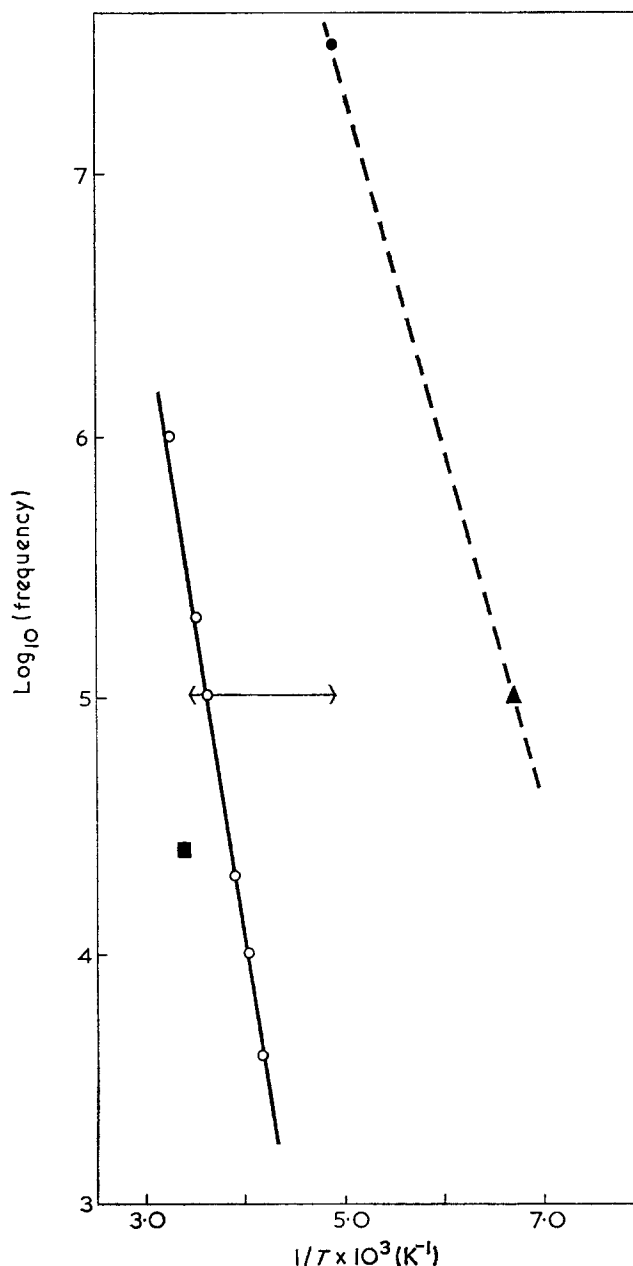
$T_{1\rho}$  minima in the region of 70–80K are frequently observed<sup>18–20</sup> for polymers which contain a terminal methyl group and these minima are generally associated with rotation of the methyl group about its three-fold axis. In this particular case, an approximate calculation of the activation energy for methyl group rotation can be obtained by assuming the  $T_{1\rho}$  minimum to be at 70K ( $\omega_L\tau_C=0.50$ ,  $\tau_C=1.0\times 10^{-5}$  s), and taking the  $T_1$  minimum at 130K ( $\omega_{RT}C=0.62$ ,  $\tau_C=2.95\times 10^{-8}$  s). The value obtained in this way is 7.2 kJ/mol. This compares very favourably with the 7.1 kJ/mol found experimentally in poly(propylene oxide)<sup>20</sup> but, in common with other experimental values, is lower than theoretical estimates<sup>21</sup> of this quantity.

The higher temperature relaxation found from  $T_1$  and  $T_{1\rho}$  in this polymer has an activation energy of 24 kJ/mol. On an Arrhenius diagram showing some of the other relaxation processes for poly(*N*-amyl maleimide) (*Figure 2*), this  $\delta$  relaxation mechanism is seen to occur at a far higher frequency than either the dielectric  $\gamma$  process or the process detected in the  $T_2$  measurements. Furthermore its activation energy is much lower than the prediction of Schatzki<sup>22</sup> and Boyer<sup>23</sup> for crankshaft motion in the pendant alkyl chain (55 kJ/mol). The  $T_2$  relaxation mechanism has previously been assigned to this latter process<sup>6</sup>. One cannot rule out the possibility of molecular motion involving the rotation of a dipole, since the region of this  $\delta$  process is above the frequency range of the earlier dielectric experiments. However, a similar process has been detected at a rather lower frequency in the dodecyl derivative and it seems more likely that some fast rotation about the carbon-carbon bonds of the alkyl chain is involved. This point will receive some further discussion in the next section.

The frequency/temperature position of the broad  $T_{1\rho}$  'minimum' (200–290K) is also shown in *Figure 2*. There is, of course, considerable uncertainty in the exact position of this minimum but *Figure 2* shows the range of possibilities. It seems very probable from this diagram that the minimum corresponds to the same mechanism as the dielectric  $\gamma$  process. This process in the maleimide polymers has been assigned to an out-of-plane deformation of the maleimide ring involving nitrogen inversion. Unfortunately it is not possible to calculate an activation energy from the n.m.r. measurements, because no parallel minimum in  $T_1$  is observed. On the basis of the dielectric activation energy (53 kJ/mol) a minimum in  $T_1$  would be expected around 310K, but no trace of such a minimum can be detected (cf. *Figure 1*). It is possible that this type of motional behaviour makes only a small contribution to the correlation time at the frequency of  $T_1$  measurement and is essentially not detected. This point is particularly well exemplified by the behaviour of the dodecyl derivative.

#### Poly (*N*-dodecyl maleimide)

Measurement of  $T_1$  in poly(*N*-dodecyl maleimide)



*Figure 2* Correlation frequency as a function of temperature for poly(*N*-amyl maleimide).  $\circ$ , Points for the dielectric  $\gamma$  process<sup>5</sup>;  $\bullet$ ,  $T_1$  minimum at 210K;  $\blacktriangle$ ,  $T_{1\rho}$  minimum at 150K;  $\blacksquare$ ,  $T_2$  measurement<sup>6</sup>.  $\leftrightarrow$  Flat portion of the  $T_{1\rho}$  data

showed the existence of a rather broad minimum extending over the temperature range 200–290K and centred on 253K. There was also a small 'shoulder' in the temperature dependence of  $T_1$  at 300K and a change in slope of the graph on the low temperature side of the minimum at 260K. Neither of these latter two phenomena could be described as true minima. The data are shown in *Figure 3*. This diagram also indicates the temperature dependence of  $T_{1\rho}$  for this polymer, and here two distinct and well resolved minima were observed at 150 and 240K.

The  $T_{1\rho}$  minimum at 150K and the  $T_1$  minimum at 250K are associated with the same molecular process, which has an activation energy of 17.2 kJ/mol. Both from the similarity of the activation energies, and from the similarity in the positions of the  $T_{1\rho}$  minima, it is suggested that this process is the same as the process detected in the amyl derivative. However, the activation energy is somewhat lower and this would seem to be in accord with the proposed mechanism; since a longer alkyl chain will

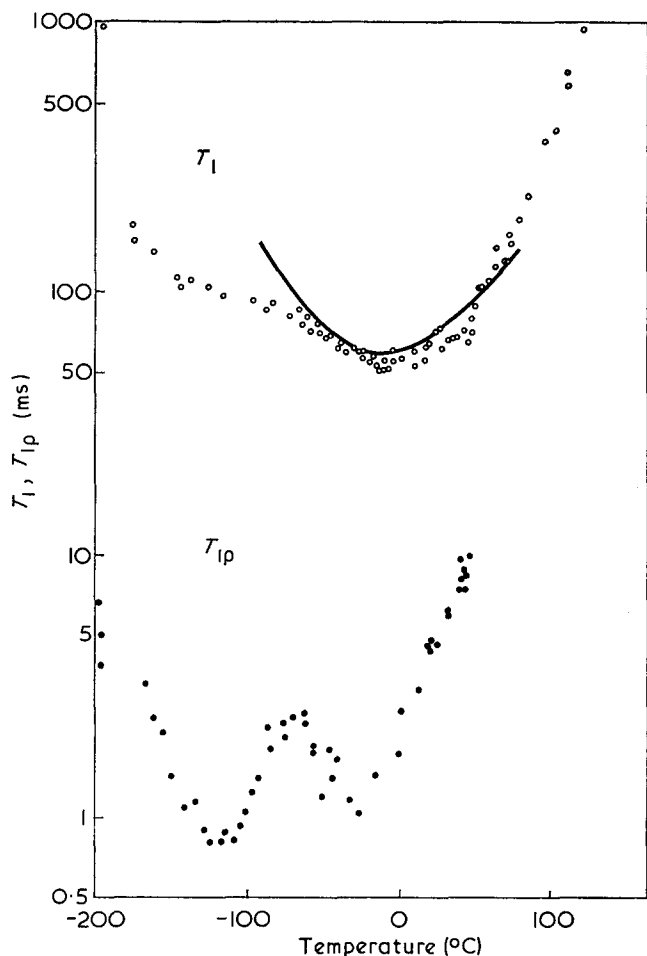


Figure 3  $T_1$  and  $T_{1\rho}$  measurements for poly(*N*-dodecyl maleimide). The curve superimposed on the  $T_1$  data is obtained from the curve-fitting procedure

create for itself a larger free volume in which it can move.

If one associates the 240 K  $T_{1\rho}$  minimum with the shoulder in  $T_1$  at 300K, then an activation energy of 55 kJ/mol is obtained for this second relaxation process. Figure 4 shows the frequencies and temperatures for both this process, the dielectric  $\gamma$  process and the broadline  $T_2$  process as obtained in earlier work. It is seen that the n.m.r.  $T_1$  process is only one or two decades faster in frequency than the dielectric  $\gamma$  process at the same temperature. Moreover, the activation energy found here is not very different from the 73 kJ/mol found for the  $\gamma$  relaxation. The comparatively small discrepancies in frequency correlation and in activation energy could be accounted for by the experimental uncertainties in the interpretation of the n.m.r. spectra, particularly in the location of the diffuse  $T_1$  minimum.

At this point it is worth pointing out that the  $\gamma$  process in these polymers markedly affects the longitudinal relaxation times ( $T_1$  and  $T_{1\rho}$ ) but no correlation could be established between this process and the transverse relaxation time  $T_2$ .

No evidence was found for a minimum in  $T_{1\rho}$  in the region of 70K in the dodecyl polymer. This is slightly surprising in view of the fact that this polymer contains  $\alpha$ -methyl groups which should give rise to a relaxation minimum in this temperature range [cf. poly(*N*-amyl maleimide)]. The only possible manifestation of methyl group rotation is the change in slope of the  $T_1$  graph observed at 200K. Hence it would appear that with long alkyl chains, the cooperation between methyl group

rotation and whole chain motion is so great that it is meaningless to speak of these as separate molecular processes. The expected effect of such cooperation would be to produce a very wide distribution of relaxation times in the single observed minimum. This in fact appears to be the case because the Fuoss-Kirkwood distribution parameter is reflected in the width of the  $T_1$  minimum<sup>9</sup>. Indeed even the dielectric  $\gamma$  process [the shoulder of  $T_1$  at 300K in poly(*N*-dodecyl maleimide)] is barely resolved from the general behaviour of  $T_1$  so that it would appear that this too is involved in a more cooperative motion than a simple statement of the mechanism would suggest.

An attempt was made to fit the minimum at 250K to equation (4) in order to extract the Fuoss-Kirkwood  $\beta$  value. Such a procedure could be useful when, for example, the true activation energy was required and no corresponding  $T_{1\rho}$  minimum was observed. Alternatively an independent value of  $\beta$  could be used as a point of comparison, when pulsed n.m.r. and dielectric techniques are observing the same molecular process, although this is not relevant in the present case.

The fitting procedure was based on a combination of equations (2) and (3) which gives:

$$\frac{1}{T_1} = \frac{2}{3} \left( \frac{1}{T_2} \right)^2 \frac{\beta}{\omega} \left[ \frac{(A\omega)^\beta \exp(\beta E^*/RT)}{1 + (A\omega)^{2\beta} \exp(2\beta E^*/RT)} + \frac{2(2A\omega)^\beta \exp(\beta E^*/RT)}{1 + (2A\omega)^{2\beta} \exp(\beta E^*/RT)} \right] \quad (5)$$

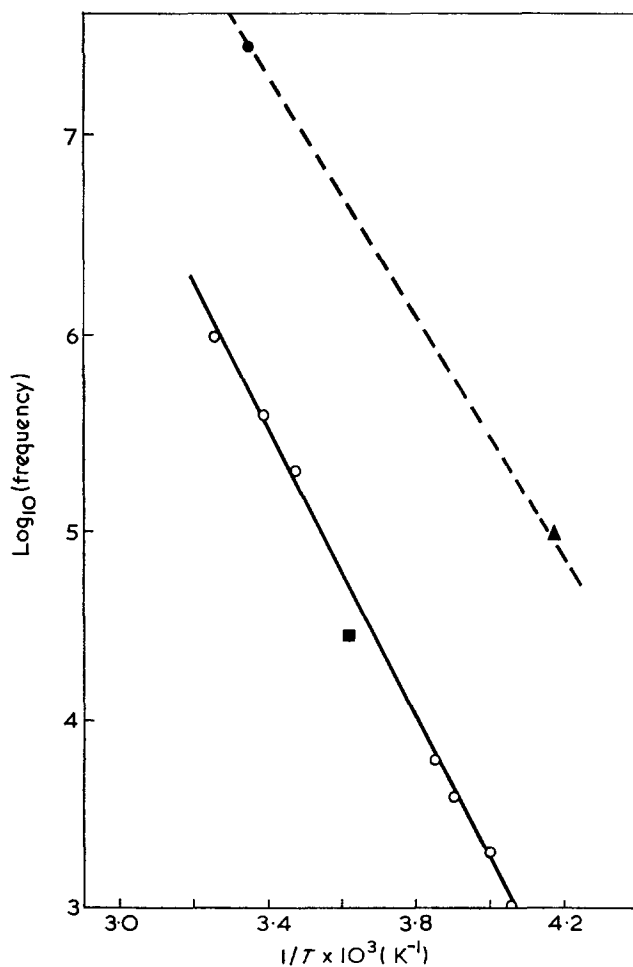


Figure 4 Correlation frequency as a function of temperature for poly(*N*-dodecyl maleimide).  $\circ$ , Points for the dielectric  $\gamma$  process<sup>5</sup>;  $\bullet$ ,  $T_1$  shoulder at 300K;  $\blacktriangle$ ,  $T_{1\rho}$  minimum at 240K;  $\blacksquare$ ,  $T_2$  measurement<sup>6</sup>

Taking  $\beta E^* = 12.0$  kJ/mol and  $T_2'' = 7.9 \times 10^{-6}$  s, a computer program was written to fit the experimental data to equation (5) using  $A$  and  $\beta$  as variables. The derived values were  $10^3$  s and 0.24 respectively, and Figure 3 shows that these values provide an excellent fit to the results. The derived  $E^*$  is apparently 50 kJ/mol, as opposed to 17.2 kJ/mol found by the more conventional method using the  $T_1$  and  $T_{1\rho}$  minima. The derived  $\beta$  value is obviously too low, and in fact the true  $\beta$  value must be around  $12.0/17.2 = 0.7$ . This is slightly surprising, since inspection indicates that the minimum is broader than would be suggested by a  $\beta$  of 0.7.

Since the  $T_{1\rho}$  information indicates the  $T_1$  minimum to comprise two relaxations, the closeness of the fitting procedure to the experimental data must imply that one of the relaxations is making only a very minor contribution to the  $T_1$  curve. The major influence of this process is to render quantitative evaluation of the energy and distribution parameters meaningless. It is clear that, in the absence of rotating frame data or information deduced from other relaxation techniques, curve-fitting to  $T_1$  data alone may yield misleading information even with an apparently good fit.

#### ACKNOWLEDGEMENTS

We would like to thank the SRC for providing funds for the purchase of the pulsed equipment and the Uni-

versity of Liverpool for a maintenance award to one of us (D.R.C.).

#### REFERENCES

- 1 McCrum, N. G., Read, B. E. and Williams, G. 'Dielectric and Anelastic Effects in Polymeric Solids', Wiley, London, 1967
- 2 McCall, D. W. and Douglas, D. C. *Appl. Phys. Lett.* 1965, **7**, 12
- 3 McCall, D. W. and Douglas, D. C. *Discuss. Faraday Soc.* 1969, **48**, 205
- 4 Farrar, T. C. and Becker, E. D. 'Pulse and Fourier Transform NMR', Academic Press, New York, 1971
- 5 Block, H., Groves, R. and Walker, S. M. *Polymer* 1972, **13**, 527
- 6 Bailey, J. and Walker, S. M. *Polymer* 1972, **13**, 561
- 7 Kubo, R. and Tomita, K. *J. Phys. Soc. Japan* 1954, **9**, 888
- 8 Powles, J. G. *IUPAC Symp. Rep., Weisbaden* 1959
- 9 Connor, T. M. *Trans. Faraday Soc.* 1964, **60**, 1574
- 10 Fuoss, R. M. and Kirkwood, J. G. *J. Am. Chem. Soc.* 1941, **63**, 385
- 11 Bloembergen, N., Purcell, E. M. and Pound, R. V. *Phys. Rev.* 1948, **73**, 679
- 12 Slichter, C. P. and Aillion, D. *Phys. Rev.* 1964, **135A**, 1099
- 13 Slichter, C. P. and Aillion, D. *Phys. Rev.* 1965, **137A**, 235
- 14 Connor, T. M. *Br. Polym. J.* 1969, **1**, 116
- 15 McCall, D. W. *Acc. Chem. Res.* 1971, **4**, 223
- 16 Connor, T. M. *J. Polym. Sci. (A-2)* 1970, **8**, 191
- 17 Bloch, F. *Phys. Rev.* 1946, **70**, 460
- 18 Stohrer, M., Noack, F. and Schütz, J. V. *Kolloid-Z. Z. Polym.* 1970, **241**, 937
- 19 Connor, T. M. and Hartland, A. *Phys. Lett.* 1966, **23**, 662
- 20 Connor, T. M. and Blears, D. J. *Polymer* 1965, **6**, 385
- 21 Stejskal, E. O. and Gutowsky, H. S. *J. Chem. Phys.* 1958, **28**, 388
- 22 Schatzki, J. F. *J. Polym. Sci.* 1962, **57**, 496
- 23 Boyer, R. F. *Rubber Rev.* 1963, **3**, 1303

# Studies on the formation of poly(ethylene terephthalate): 1. Propagation and degradation reactions in the polycondensation of bis(2-hydroxyethyl) terephthalate

Kosuke Tomita

Research and Development Center, Unitika Co. Ltd, Uji, Kyoto, Japan  
(Received 11 July 1972)

The polycondensation of bis(2-hydroxyethyl) terephthalate (BHET) was kinetically investigated in the presence of zinc acetate as a catalyst at 283°C. The reaction was followed by molecular weight measurements on the polymers formed. These molecular weights were found to have maximum values at a certain reaction time. To explain these observations an irreversible degradation reaction was assumed to occur simultaneously with the polycondensation reaction. If  $p$  and  $d$  are rate parameters associated with the rate constants of propagation and degradation reactions, respectively, and  $t$  is the reaction time, the following relation was finally obtained for the degree of polymerization ( $DP$ ):  $1/DP (=n) = dt + 1/(1+pt)$ . This simple equation was found to be in good agreement with the experimental results. Using this equation the effects of temperature and stirring could be studied for both reactions.

## INTRODUCTION

The preparation of poly(ethylene terephthalate) (PET) is usually carried out by polycondensation of bis(2-hydroxyethyl) terephthalate (BHET) or its oligomers at elevated temperature and under reduced pressure. In spite of the high industrial production of PET, there is little detailed knowledge about the chemical reactions by which PET is industrially synthesized.

Thus, only a few reports about the polycondensation process have been published<sup>1-6</sup>. The reaction conditions in previous work involve a sealed system or a limitation to the initial stage of the reaction. More specifically, no kinetic treatment of an industrial polycondensation process, over a wide range of conversions, has been given. In the latter case side reactions, such as thermal degradation, must be taken into account. This makes a kinetic treatment of the process more complicated.

In the present study, however, two main reactions are assumed to occur simultaneously: one reaction which increases the molecular weight (propagation reaction) and one reaction which decreases the molecular weight (degradation reaction). A kinetic treatment based on this assumption is shown to agree with experimental results. Furthermore, it is consistent with other information concerning the BHET polycondensation process.

## EXPERIMENTAL

### Reagents

The catalyst used was zinc acetate. A commercial product (guaranteed reagent grade) was used without further purification.

BHET was synthesized from dimethyl terephthalate (DMT) and ethylene glycol (EG). Starting with a molar ratio (EG/DMT) of five, the transesterification was carried out with sodium acetate ( $1 \times 10^{-2}$  mol/mol DMT) as a catalyst at 200°C. By repeated recrystallization of the product from water, pure BHET (m.p. 109°C) was obtained.

### Polycondensation

To a three-necked 300 ml glass vessel equipped with a stirrer and a take-off column, 0.3 mol BHET and  $3 \times 10^{-5}$  mol zinc acetate were introduced. The reaction was carried out in an open system with stirring (120 rev/min) under reduced pressure (0.02–0.05 mmHg). EG was continuously removed by distillation. The reaction temperature was maintained at 283°C with a dimethyl phthalate vapour bath. At suitable intervals nitrogen was introduced into the reactor, and the reaction mixture was sampled. A separate experiment was made in order to study the effect of this sampling operation on the polycondensation process. It was found to be negligible.

Other reaction temperatures were obtained by using vapour baths with  $\beta$ -naphthyl methyl ether (272°C) or diethyl phthalate (293°C) instead of dimethyl phthalate.

The reaction was also carried out with a reduced stirring rate (60 rev/min) in order to investigate the effect of stirring.

### Determination of molecular weight

The molecular weight of a formed polymer was determined viscometrically. The intrinsic viscosity  $[\eta]$  was measured, using a phenol-tetrachloroethane (1 : 1 w/w)

mixture as solvent at 20°C. This was converted to molecular weight by means of the following relation<sup>7</sup>:

$$[\eta] = 7.55 \times 10^{-4} \bar{M}_n^{0.685}$$

## RESULTS AND DISCUSSION

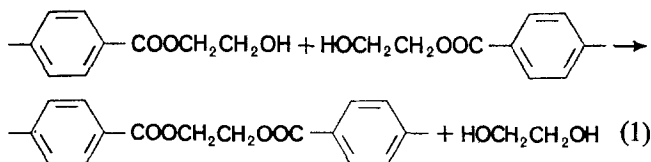
### Rate equation

Rigorous kinetic treatments of the polycondensation of BHET have been given by Challa<sup>1</sup> and Sumoto and Inoue<sup>2</sup> only for the equilibrium reaction in a sealed system. In open systems (with continuous removal of EG) the initial stage of the reaction has been studied by Griehl and Schnock<sup>3</sup>, Reinish *et al.*<sup>4</sup> and Stevenson and Nettleton<sup>5</sup>. In the work of Čefelín and Málek<sup>6</sup> the kinetic treatment is extended to a higher molecular weight ( $M_n = 30\,000$ ), but in this case the reaction was carried out in a solvent and at a lower temperature (260°C).

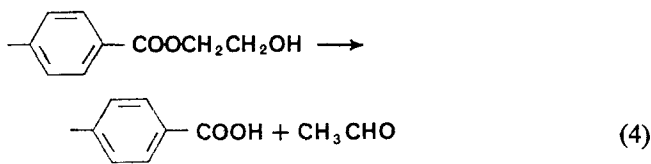
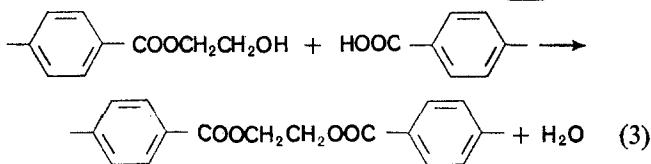
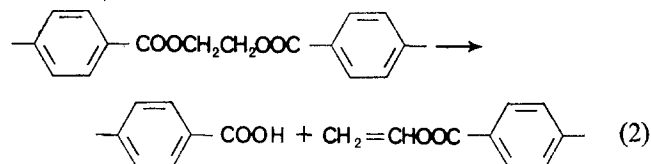
In commercial polycondensation of BHET the reaction would normally be carried out in a melt at about 280°C, under reduced pressure and in an open system. Under these conditions the molecular weight of the formed polymer has a maximum at a certain reaction time, as illustrated in Figure 1. This phenomenon indicates that the propagation reaction (which increases the molecular weight), corresponds to the polycondensation reaction, and the degradation reaction (which decreases the molecular weight) occur simultaneously.

In a rigorous kinetic approach to such a complex reaction, a treatment in terms of a competitive and consecutive reaction system is demanded. However, this would be rather complicated in a multistep reaction such as the polycondensation one\*. Accordingly the author attempted to approximate this reaction system as a parallel reaction system of two kinds of reaction: propagation and degradation reactions, as mentioned below.

The main reaction which leads to formation of PET can be represented as



From available information<sup>10</sup>, the following side reactions seem to occur in parallel with the above main reaction†.



\* In a limited-step reaction this demand can be occasionally met<sup>8</sup>.  
† Details on the side reactions will be reported separately.

Reaction (3) occurs as a result of reactions (2) and (4). The product from reaction (2), a terminal vinyl group, causes further complex reactions, but these reactions are omitted from the present discussion because of little connection with the purpose of this study.

Reactions (1) and (3) both contribute to the propagation process. However, the latter is of little importance, except when the number of terminal carboxyl groups approaches the number of terminal hydroxyethyl groups.

On the other hand, reactions (2) and (4) contribute to the degradation process. However, the latter is important only in the very first stage of the reaction.

Based on the above considerations, it may be considered reasonable to pay attention only to reactions (1) and (2). Both reactions are regarded as ones which change the mole number (the reciprocal of the degree of polymerization) of the polymer. Assuming that reaction (1) obeys second-order kinetics for the mole number and reaction (2) obeys first-order kinetics for the number of ester bonds, the rate of polycondensation may be represented by the equation

$$-\frac{dn}{dt} = k_1 n^2 - k_2 (n-1) \quad (5)$$

where  $n$  is a mole number of a polymer,  $k_1$  is a rate constant for reaction (1) and  $k_2$  is a rate constant for reaction (2).

Equation (5) can not explain the above-mentioned phenomenon that the molecular weight of the polymer has a maximum value at a certain reaction time. Because, if all the degradation products again contribute to the propagation reaction, nothing but the equilibrium state will be established. In order to account for the maximum, the terminal groups formed by reaction (2) are assumed to be inactive. Taking reaction (3) into account, this assumption is not strictly correct, but from the earlier considerations, it may be considered to be approximately valid over a wide conversion range in the polycondensation process.

Accordingly, equation (5) can be rewritten as:

$$-\frac{dn}{dt} = k_1 (n - \frac{1}{2} n_d)^2 - k_2 (n-1) \quad (6)$$

where  $n_d$  is a mole number of a degraded polymer, which is assumed to increase linearly with time as follows:

$$n_d = k_2 t \quad (7)$$

By substitution of equation (7) into equation (6), an equation which is not easy to solve analytically is obtained. Therefore, a Taylor series expansion was attempted.

Assuming that the solution of the above differential equation can be represented with a Taylor series, and that the higher-order terms in  $k_2$  can be neglected and putting,  $n_{t=0} = 1$ ,  $n$  can be obtained as a sum of series, which can be simplified by the binomial theorem as follows:

$$\begin{aligned} n &= \sum_{m=0}^{\infty} (-1)^{m-1} (k_1 t)^{m-1} + k_2 t \left\{ 1 - \sum_{m=0}^{\infty} (-1)^m (k_1 t)^m - \frac{1}{3} k_2 t^2 \sum_{m=0}^{\infty} (-1)^m (m+1) (k_1 t)^m \right\} \\ &= \frac{1}{1+k_1 t} + k_2 t \left\{ 1 - \frac{1}{1+k_1 t} - \frac{(k_1 t)^2}{3(1+k_1 t)^2} \right\} \quad (8) \end{aligned}$$

For large values of  $t$ , equation (8) becomes:

$$n = \frac{1}{1+k_1 t} + \frac{2}{3} k_2 t \quad (9)$$

By fitting equation (9) to experimental values of  $n$ ,  $k_1$  and  $k_2$  can be calculated. As it stands, equation (9) does not permit a simple fitting procedure. The existence of a maximum in the time-course of molecular weight, however, makes it easy to estimate  $k_1$  and  $k_2$ ; by setting  $dn/dt=0$ , it is found that:

$$\frac{1}{2}n_{\min} = \frac{1}{1+k_1t} = \frac{2}{3}k_2t \quad (10)$$

Using equation (10),  $k_1$  and  $k_2$  can be estimated.

Taking into account the approximations in the kinetic treatment, it may be preferable not to regard  $k_1$  and  $k_2$  as rate constants, but as two parameters associated with the propagation degradation reactions, respectively. Therefore, we will use  $p$  and  $d$  in place of  $k_1$  and  $k_2$ , in the following discussion.

According to the above consideration, equation (9) is rewritten as:

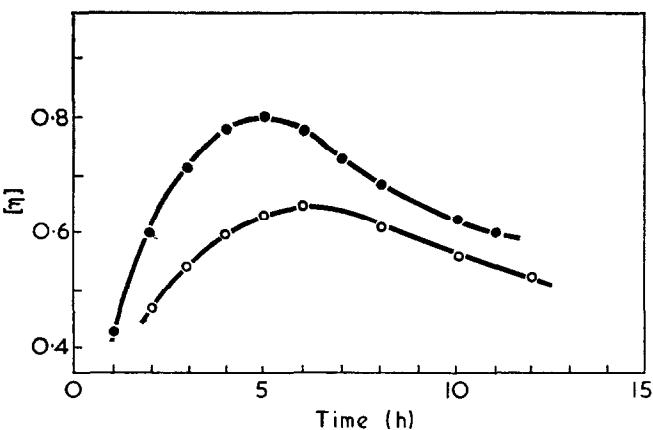


Figure 1 Effect of stirring on polycondensation of BHET. ●, 120 rev/min; ○, 60 rev/min

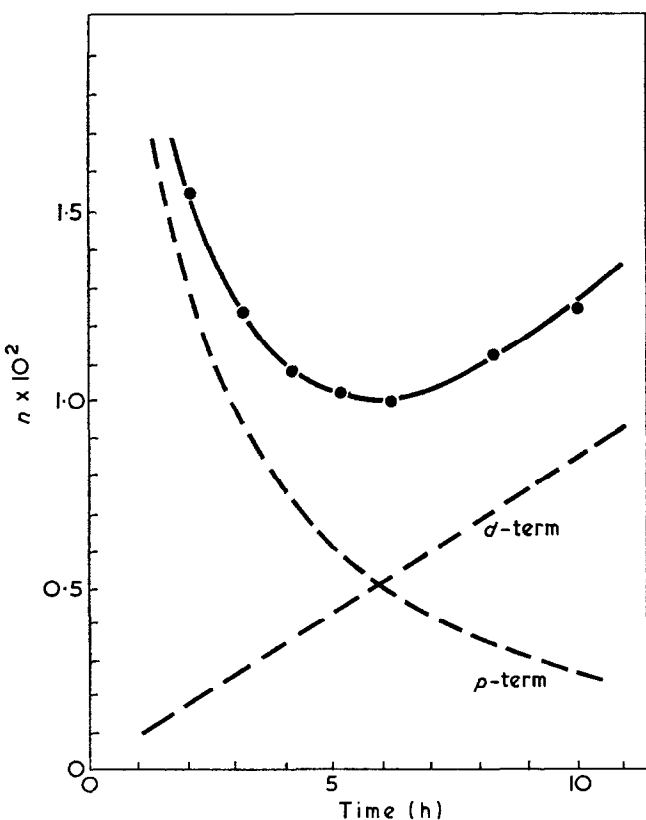


Figure 2 A  $p$ - $d$  analysis for polycondensation of BHET with 60 rev/min stirring

$$n = \frac{1}{1+pt} + dt \quad (11)$$

where  $p$  is a rate parameter for the propagation reaction and  $d$  is a rate parameter for the degradation reaction. We will call this kinetic expression a  $p$ - $d$  analysis.

The meaning of equation (11) is illustrated in Figures 2 and 3 or Figures 5 and 6. By means of equation (11) the time dependence of  $n$  can be separated into two components: one each for the propagation and degradation reactions.

As stated above,  $n$  at  $t=0$  was fixed at 1, and in the following calculation the molecular weight at  $t=0$  is fixed at one structural unit of PET. Accordingly  $n$  at arbitrary  $t$  may be calculated from equation (12):

$$n = \frac{192}{\text{molecular weight of formed polymer}}$$

#### Applications of a $p$ - $d$ analysis to the study of conditions of polycondensation of BHET

*Effect of stirring.* The time dependence of the polymer's intrinsic viscosity, using two different stirring rates, is shown in Figure 1. This Figure suggests that stirring is an important parameter, but does not give further information.

The applicability of equation (11) to the experimental values in Figure 1 is shown in Figures 2 and 3. In these two Figures each point represents an experimental value and the full lines represent equation (11) after fitting the parameters  $p$  and  $d$ . The contributions from the  $p$  and  $d$  terms in equation (11) are drawn separately with broken lines. From these Figures it is evident that equation (11) is

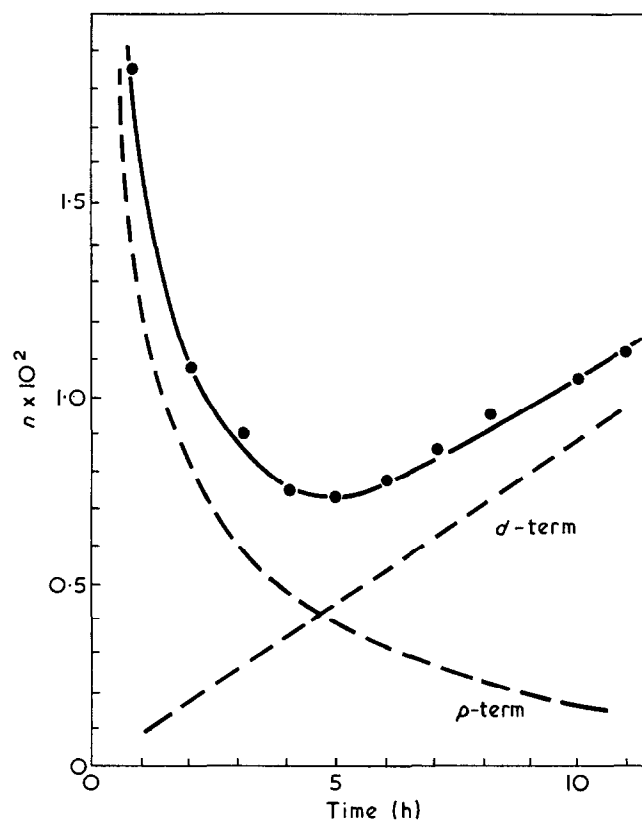


Figure 3 A  $p$ - $d$  analysis for polycondensation of BHET with 120 rev/min stirring



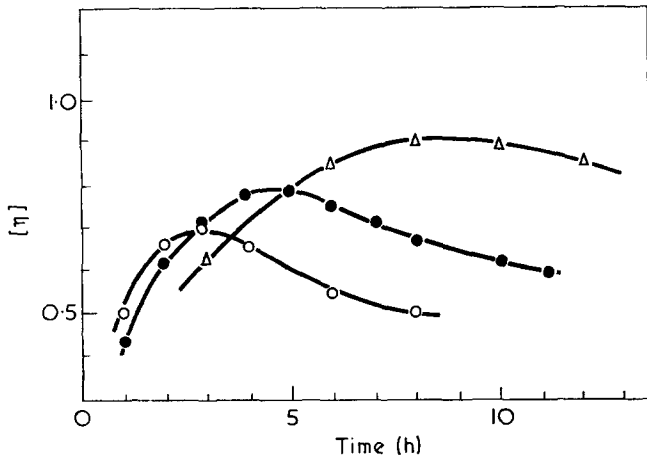


Figure 4 Effect of temperature on polycondensation of BHET.  $\Delta$ , 272°C;  $\bullet$ , 283°C;  $\circ$ , 293°C

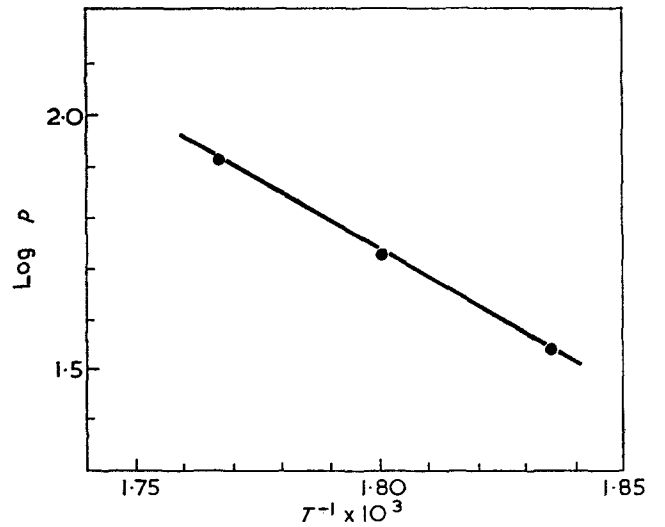


Figure 7 Arrhenius plot of the  $p$  values

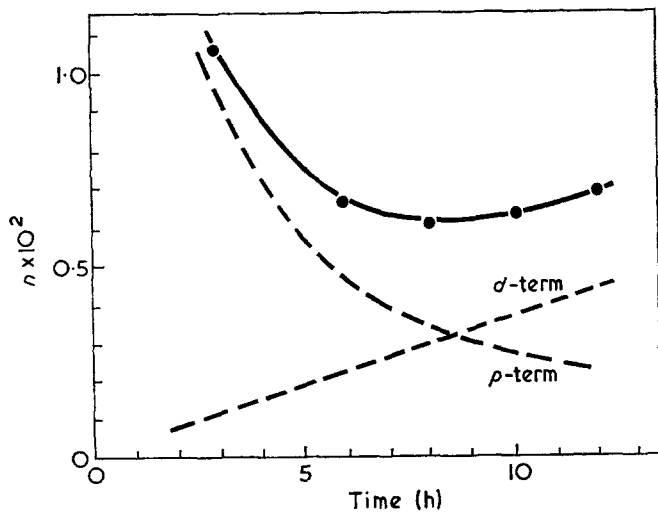


Figure 5 A  $p$ - $d$  analysis for polycondensation of BHET at 272°C

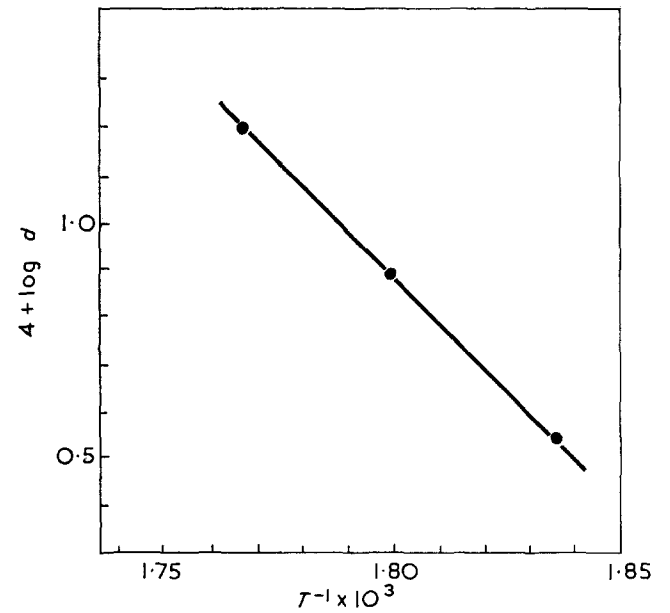


Figure 8 Arrhenius plot of the  $d$  values

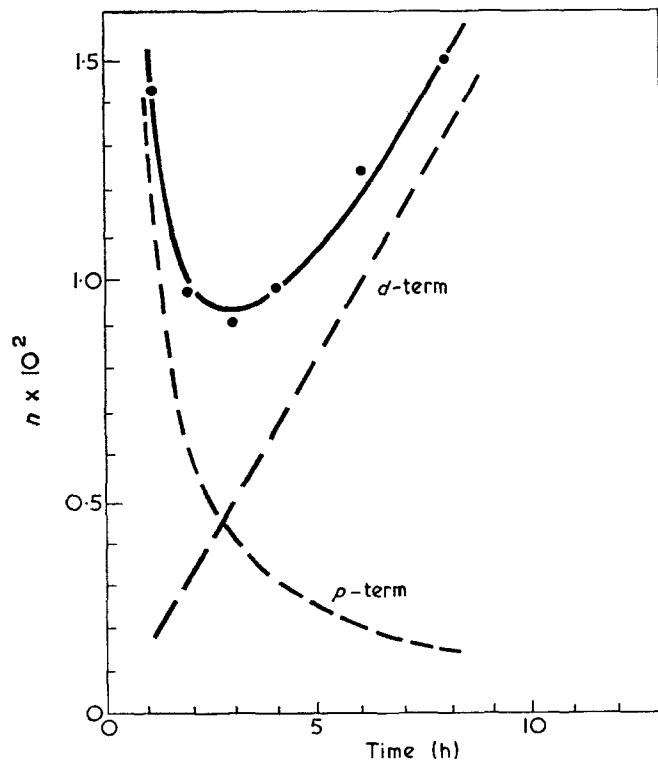


Figure 6 A  $p$ - $d$  analysis for polycondensation of BHET at 292°C

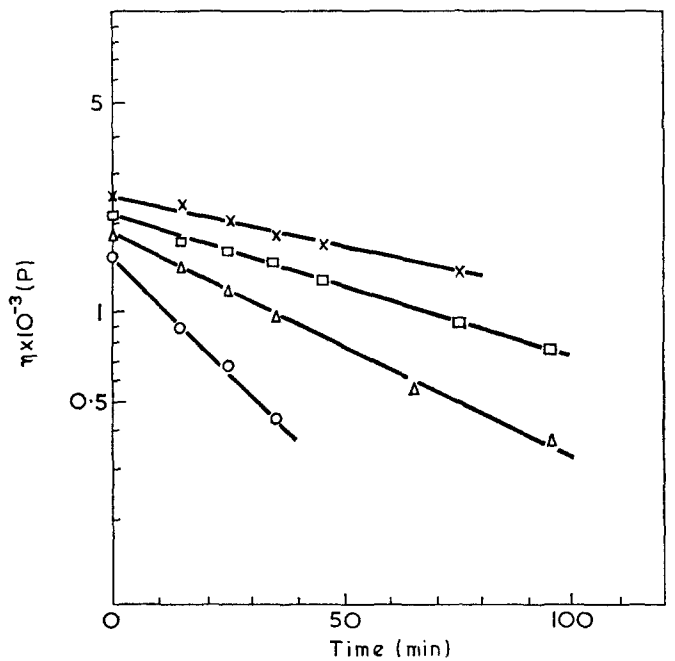


Figure 9 Effect of temperature on time dependence of the melt viscosity of PET obtained with zinc acetate as a catalyst.  $\times$ , 270°C;  $\square$ , 280°C;  $\triangle$ , 290°C;  $\circ$ , 300°C

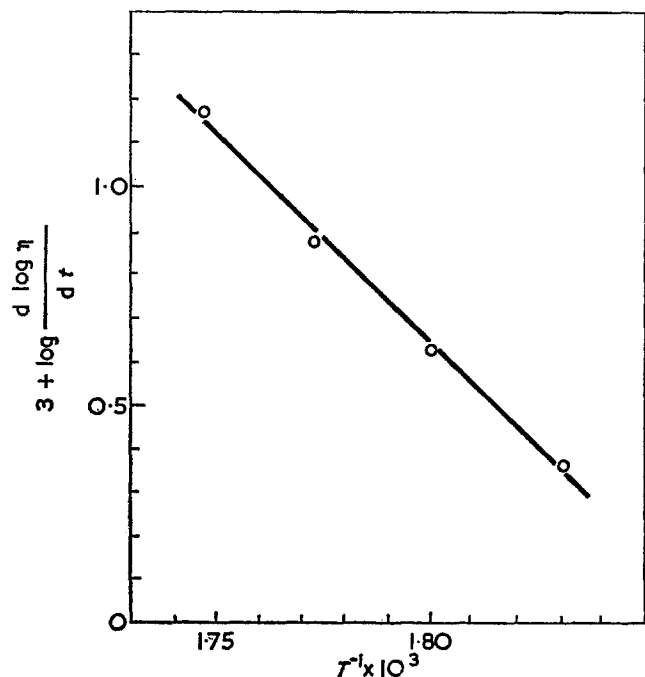


Figure 10 Arrhenius plot for the data in Figure 9

in good agreement with the experimental results. The  $p$ - $d$  analysis seems to disclose the features of the BHET polycondensation adequately.

The parameters of the fitted curves are:  $p = 34.0 \text{ mol}^{-1} \text{ h}^{-1}$ ,  $d = 9.0 \times 10^{-4} \text{ mol h}^{-1}$  with low stirring speed;  $p = 55.0 \text{ mol}^{-1} \text{ h}^{-1}$ ,  $d = 8.3 \times 10^{-4} \text{ mol h}^{-1}$  with high stirring speed. Thus stirring has a large influence on the propagation reaction and little influence on the degradation reaction. This behaviour is just as expected: the propagation reaction requires encounters between polymeric molecules and it is promoted by removal of EG, while the degradation reaction is unimolecular and not affected by the distillation of a product.

Thus, the effect of stirring on the polycondensation process can be clarified by the calculation of  $p$  and  $d$  values.

The above result illustrates the importance of having a reactor with efficient stirring for BHET polycondensations.

**Effect of temperature.** The polycondensation of BHET was carried out at 272, 283 and 293°C. The results are plotted in Figure 4. This Figure suggests that with rise of temperature the optimum reaction time and the maximum molecular weight are both reduced.

The application of  $p$ - $d$  analysis to these data is shown in Figures 3, 5 and 6. In all cases the fitted curves are in good agreement with the experimental values.

The  $p$  and  $d$  values of the fitted curves are the following:

$$272^\circ\text{C}: p = 36.3 \text{ mol}^{-1} \text{ h}^{-1}, d = 3.7 \times 10^{-4} \text{ mol h}^{-1}$$

$$283^\circ\text{C}: p = 55.0 \text{ mol}^{-1} \text{ h}^{-1}, d = 8.3 \times 10^{-4} \text{ mol h}^{-1}$$

$$292^\circ\text{C}: p = 78.6 \text{ mol}^{-1} \text{ h}^{-1}, d = 16.8 \times 10^{-4} \text{ mol h}^{-1}$$

Plots of  $\log p$  and  $\log d$  vs.  $1/T$  are given in Figures 7 and 8. From these Figures it is found that satisfactory linear relations exist. As apparent activation energies the following values were calculated:

$$E_p = 23.7 \text{ kcal/mol}; E_d = 46.6 \text{ kcal/mol}$$

In other words, the degradation reaction is much more influenced by a temperature change than the propagation reaction.

Consequently, the use of a lower temperature permits a higher molecular weight to be obtained.

According to Tuckett<sup>9</sup>, in a random degradation reaction a plot of  $\log \eta$  ( $\eta$  is the melt viscosity) vs. time gives a straight line, and its slope is related to the rate constant for the degradation reaction. For the purpose of comparison, the time dependence of the melt viscosity of the polymer obtained in one of the experiments above (the polycondensation at 283°C) was followed with a rheometer at 270, 280, 290, and 300°C (Figure 9). From an Arrhenius plot an activation energy was calculated:  $E_d = 44.0 \text{ kcal/mol}$  (Figure 10).

This value is comparable with  $E_d$ , which lends support to the  $p$ - $d$  analysis procedure.

#### ACKNOWLEDGEMENT

The author wishes to thank Professor Seizo Okamura (Kyoto University) for his interest in this work and his helpful criticism of the manuscript.

#### REFERENCES

- 1 Challa, G. *Makromol. Chem.* 1960, **38**, 105, 123, 138
- 2 Sumoto, M. and Inoue, R. *Kobunshi Kagaku (Chem. High Polym.)* 1960, **17**, 285
- 3 Griehl, W. and Schnock, G. *Faserforsch. Textiltech.* 1957, **8**, 408; *J. Polym. Sci.* 1958, **30**, 413
- 4 Reinisch, G., Zimmermann, H. and Rafler, G. *Faserforsch. Textiltech.* 1969, **20**, 225
- 5 Stevenson, R. W. and Nettleton, H. R. *J. Polym. Sci. (A-1)* 1968, **6**, 889
- 6 Čefelín, P. and Málek, J. *Colln Czech. Chem. Commun.* 1969, **34**, 419
- 7 Koepp, H. M. and Werner, H. *Makromol. Chem.* 1959, **32**, 79
- 8 Frost, A. and Pearson, R. G. 'Kinetics and Mechanism', 2nd edn, Wiley, New York, 1969, p 177
- 9 Tuckett, R. F. *Trans. Faraday Soc.* 1945, **41**, 351
- 10 Buxbaum, L. H. *Angew. Chem. (Int. Edn)* 1968, **7**, 182; Tomita, K., Yamaguchi, R., Asakawa, H. and Osaki, K. *Abstr. 18th A. Meet. Soc. Polym. Sci. Japan, Kyoto*, 1969, p 449

# Studies on the formation of poly(ethylene terephthalate): 2. Rate of transesterification of dimethyl terephthalate with ethylene glycol

Kosuke Tomita and Hiroaki Ida

Research and Development Center, Unitika Co. Ltd, Uji, Kyoto, Japan  
(Received 11 July 1972)

The transesterification of dimethyl terephthalate (DMT) with ethylene glycol (EG) was kinetically investigated in the presence of various catalysts at 197°C. The reaction was followed by the measurement of the quantity of methanol which distilled from the reaction vessel. This distillation made corrections of reactant and catalyst concentrations necessary. The transesterification was assumed to obey first-order kinetics with respect to DMT and EG, and a rate equation was derived. The reaction was found to be first order in catalyst concentration as well and when this finding was incorporated in the rate equation, excellent agreement between the observed and calculated values was recognized throughout the reaction. The first-order dependence on the catalyst concentration is valid below a critical concentration which was found to be dependent on the catalyst type. Above this concentration a lower reaction order was observed.

## INTRODUCTION

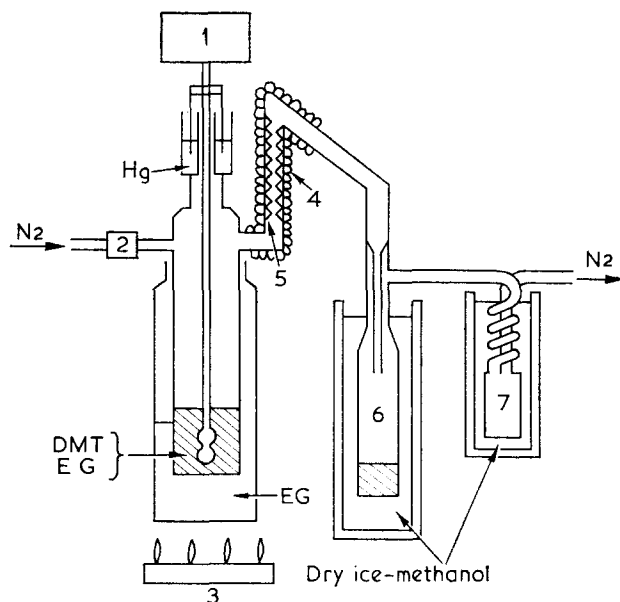
The preparation of poly(ethylene terephthalate) (PET) is usually carried out by polycondensation of bis(2-hydroxyethyl) terephthalate (BHET) or its oligomers. These can be formed by the transesterification of dimethyl terephthalate (DMT) with ethylene glycol (EG) or by the esterification of terephthalic acid (TPA) with EG. The transesterification process is generally preferred.

Knowledge of the kinetics of the transesterification reaction of DMT with EG is important for industry. A few reports on such investigations have been published previously<sup>1-5</sup>, but they do not account completely for the experimental observations. In the present study improvements have been made, and good agreement between experimental data and an appropriate rate expression is obtained over a wide conversion range.

## EXPERIMENTAL

### Apparatus

The apparatus used in this work is shown in *Figure 1*. For a kinetic study on the transesterification reaction, it is important to prevent methanol formed in this reaction from being retained, and to make it distil smoothly. Therefore, we have paid special attention to the following points: (i) nitrogen was made to flow through the reaction vessel at a steady rate of  $42 \pm 2$  ml/min; (ii) the tube connecting the reactor to a condenser was electrically heated at the inlet to prevent condensation of methanol; (iii) the length of the tube was reduced as far as possible in order to shorten the response time of the acceptor (a graduated cylinder); (iv) a Vigreux distillation column was incorporated in the tube in order to prevent distillation of reactants; (v) the whole acceptor



*Figure 1* Apparatus used in this work: 1, motor; 2, flow meter; 3, gas burner; 4, mantle heater; 5, distillation column; 6, acceptor (graduated cylinder); 7, trap

was cooled with a dry ice-methanol mixture in order to trap effluent methanol efficiently.

### Reagents

DMT was a commercial 'fiber grade' product and was used without further purification. EG was also a commercial 'fiber grade' product and was purified by distillation prior to use.

All catalysts were metal acetates. Commercial products (guaranteed reagent grade) were used without further

purification. However, antimony (III) acetate was synthesized according to the method of Nerdel and Kleinwächter<sup>6</sup> and then distilled under reduced pressure (b.p. 167–168°C at 5 mmHg; m.p. 120–124°C).

### Transesterification

To the reaction vessel 0.5 mol DMT, 1.0 mol EG and an adequate amount of catalyst were introduced. The reaction was carried out with stirring under a nitrogen atmosphere.

The temperature of the reaction mixture heated with the EG bath was measured with a thermocouple detector and was confirmed to be 197°C. The temperature of the distillation column was maintained at ~100°C.

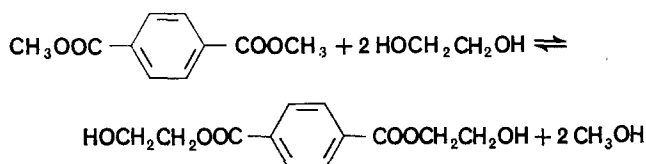
The reaction was considered to have started at the time when the methanol first condensed in the acceptor.

After that, the progress of the reaction was followed by measuring the quantity of methanol collected in the acceptor.

## RESULTS AND DISCUSSION

### Kinetic treatment

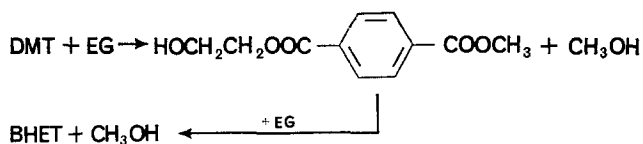
The mode of transesterification of DMT with EG is shown below in a simplified form, where methanol and bis(2-hydroxyethyl) terephthalate (BHET) are formed:



If less than 2 mol of EG are used, polycondensates, with a degree of condensation of 2 to 4, are formed as well as BHET. However, under the conditions of this work BHET and methanol are almost the only reaction products.

The transesterification is a reversible reaction as indicated in the equation above. Consequently, efficient removal of formed methanol is necessary in order to get a high yield of BHET. In this work, particular attention was paid to the removal of methanol, as mentioned above.

An important problem in the kinetic treatment is whether there is a difference between the rate constant of the first-step reaction, related to the reactivity of methyl ester groups in DMT, and that of the second-step reaction, related to the reactivity of methyl ester groups in *p*-methoxycarbonyl-2-hydroxyethyl benzoate, since DMT and EG form BHET in the following two steps.



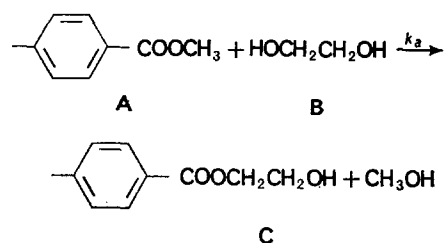
On this problem, Challa<sup>1</sup> reported that there is no difference. On the other hand, the presence of a difference was maintained by Peebles and Wagner<sup>2</sup>. From experiments with model compounds, we have concluded that such a difference is negligible, i.e. it may safely be assumed that the rate constant of the first-step reaction and that of the second-step reaction are much the same.

Consequently, the formation of BHET may be regarded as being merely the reaction between a methyl ester group and a hydroxyl group in EG.

In the paper by Challa<sup>1</sup>, the kinetics of the transesterification reaction in a closed system was studied. A similar study was made by Sumoto<sup>3</sup>. These papers are relevant for the reaction in non-distilling systems. In practice, however, the transesterification of DMT with EG should be made to proceed with removal of methanol. Very much simplified treatments of this case have been given by Griehl and Schnock<sup>4</sup> and Yoda *et al.*<sup>5</sup>. A more rigorous attempt was made by Peebles and Wagner<sup>2</sup> but it is possible to improve on their treatment. For example, in correcting concentrations of reactants—removal of formed methanol is accompanied by a decrease in volume—they did not apply such a correction to the catalyst concentration. Quantities of catalysts are usually kept constant in weight during the reaction, but their concentrations increase with a decrease in volume of the reaction mixture.

In the present study, according to the above considerations, transesterification of DMT with EG was kinetically treated as follows.

Schematically the reaction can be represented as:



Based on a material balance, the rate equations are

$$-\frac{dC_A}{dt} = k_a C_A C_B \quad (1)$$

$$-\frac{dC_B}{dt} = k_a C_A C_B \quad (2)$$

$$\frac{dC_C}{dt} = k_a C_A C_B \quad (3)$$

Volume corrections were made as follows:

$$C_A = \frac{\rho A}{224 + 32B}, \quad C_B = \frac{\rho B}{224 + 32B}, \quad C_C = \frac{\rho C}{224 + 32B} \quad (4)$$

where A, B and C are the quantities of reactants expressed in mol,  $\rho$  is the density of the reaction mixture and  $C_X$  is the concentration of X (X is A, B or C).

By substitution of equation (4) into equations (1)–(3),  $k_a$  may be obtained. This solution is imperfect since  $k_a$  is an apparent rate constant which may depend on the catalyst concentration. Therefore,  $k_a$  must be also corrected for a decrease in volume of the reaction mixture\*.

Provided that the reaction order with respect to the catalyst concentration is one, the correction factor is:

$$256/(224 + 32B) \quad (5)$$

Furthermore, it must be noticed that  $\rho$  varies with the extent of reaction.

In order to simplify the above equations, the degree of conversion,  $y$  (%), is introduced.

\* If the reaction considerably proceeds without catalysts, this volume correction may be of limited significance. However, under the usual conditions, the transesterification of DMT with EG does not proceed without catalysts. The reaction order with respect to the catalyst concentration will be discussed later.

Using this variables, equation (4) can be rewritten as:

$$C_A = \frac{A}{V_0 - \frac{V_0 - V_{100}}{100} y} = \frac{A_0 - \frac{A_0}{100} y}{V_0 - \frac{V_0 - V_{100}}{100} y} \quad (6)$$

where  $V$  is a volume of the reaction mixture and the suffixes 0 and 100 are used to denote the extent of conversion, 0% and 100%, respectively.

Similarly, the correction factor for the catalyst concentration will be:

$$\frac{V_0}{V_0 - \frac{V_0 - V_{100}}{100} y} \quad (7)$$

Under the present experimental conditions  $C_A = C_B$ . Consequently the rate of reaction is represented by:

$$-\frac{dC_A}{dt} = k_a \frac{V_0}{V_0 - \frac{V_0 - V_{100}}{100} y} \left\{ \frac{A_0 - \frac{A_0}{100} y}{V_0 - \frac{V_0 - V_{100}}{100} y} \right\}^2 \quad (8)$$

Equation (8) is simplified by assuming  $A_0 = 1$ , as follows:

$$-k_a dt = \frac{V_{100}}{V_0 \{1 - (V_0 - V_{100}) C_A\} C_A^2} dC_A \quad (9)$$

If the reaction starts from the direction:  $A_0 = 1$ ,  $y = 0$ , integration yields:

$$k_a t = \frac{V_{100}}{V_0} \left\{ \frac{V_{100} y}{100 - y} + (V_0 - V_{100}) \log \frac{100}{100 - y} \right\} = Y \quad (10)$$

If the decrease in volume of the reaction mixture can be neglected, equation (10) can be simplified to yield a normal second-order equation:

$$k_a t = \frac{V y}{100 - y} \quad (11)$$

#### Application of the rate equation

Figure 2 shows how the reaction proceeds with zinc acetate as a catalyst ( $1 \times 10^{-4}$  mol/mol DMT). By application of equation (10) to these data, and plotting the  $Y$  values thus obtained against time, the points in Figure 3 are obtained:  $Y$  represents the right hand side of equation (10). In accordance with equation (10), a plot of  $Y$  against  $t$  is found to be linear over a wide conversion range.

In Figure 4 the results obtained with a less careful treatment is compared with equation (10). In one case volume corrections are completely neglected [equation (11) is applied], and in another case the change in catalyst concentration is ignored [equation (13), derived in the Appendix, is applied]. It is easily seen that only equation (10) gives a straight line in the entire conversion range. Others give  $k_a$  values which increase with the reaction time. The above-mentioned difference, maintained by Peebles and Wagner<sup>2</sup> between the rate constants of the two reaction steps may relate with the above result brought by equation (13).

#### Catalyst concentration dependence

Formerly, little was known concerning the dependence of the rate on the catalyst concentration. Griehl and Schnock<sup>4</sup> suggested a first-order dependence, but their data were too poor to discuss such a problem.

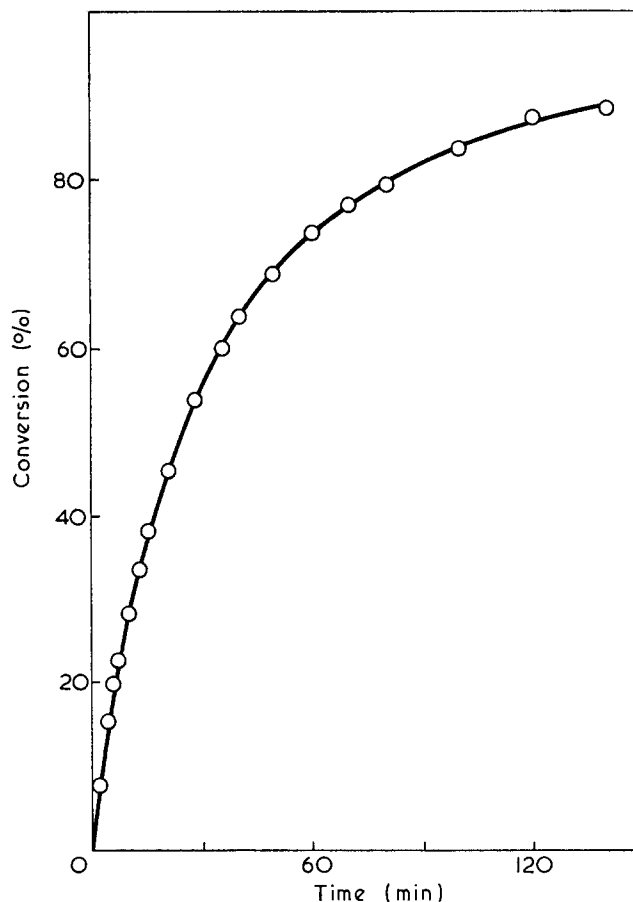


Figure 2 Time-conversion curve of the transesterification of DMT by EG with zinc acetate as a catalyst

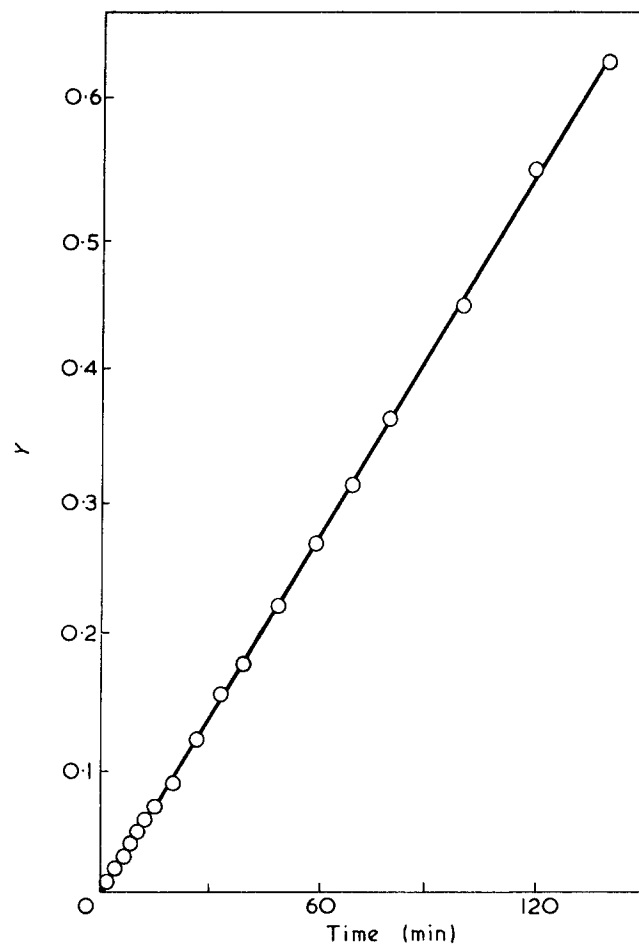


Figure 3 Application of equation (10) to data in Figure 2

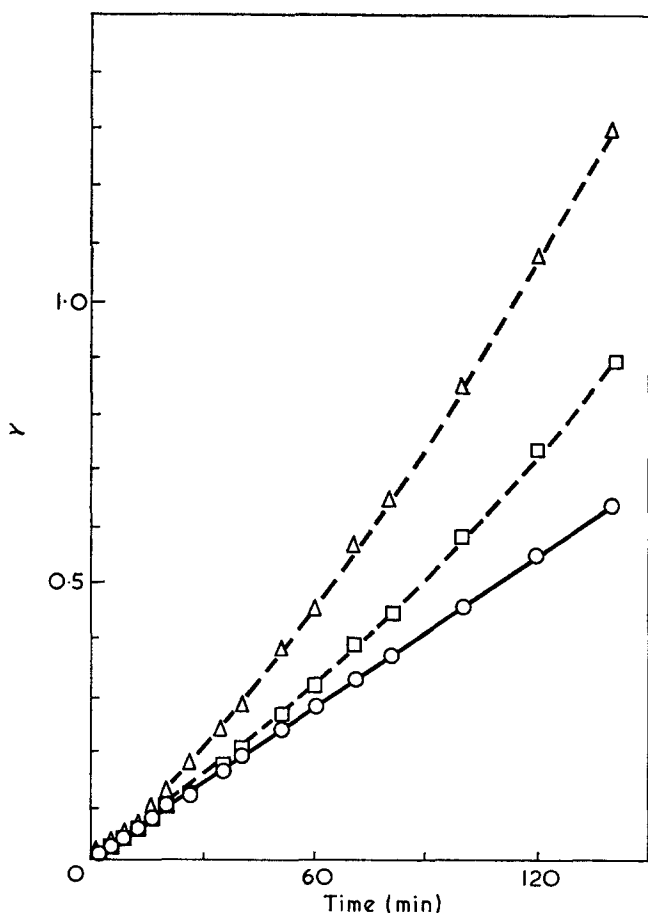


Figure 4 Comparison of three kinds of kinetic treatment for data in Figure 2: ○, the authors' treatment, equation (10) is applied; □, a change in catalyst concentration is ignored, equation (13) is applied; △, volume corrections are completely neglected, equation (11) is applied

For a satisfactory kinetic treatment it is necessary to clarify this problem, as mentioned in the above section. Therefore, the dependence of  $k_a$  on the catalyst concentration was investigated.

Some examples of the time-course of the collected methanol formed with various amounts of catalyst are shown in Figures 5 and 6. The corresponding plots according to equation (10) are shown in Figures 7 and 8.

Apparent rate constants,  $k_a$ , were calculated from the results shown in Figures 7 and 8. The relation between  $k_a$  and the catalyst concentration is illustrated as the double-logarithmic plot in Figure 9. It is seen in Figure 9 for all the different catalysts that a straight-line relation exists at not-too-high catalyst concentrations. The slope of this linear part, and therefore the reaction order is found to be 1.0 in all cases. This is consistent with the assumption made in the derivation of equation (10).

An interesting phenomenon can be observed in Figure 9: the linear relation with a slope of 1.0 is only valid within a limited range. When the catalyst concentration is increased beyond a certain value,  $\log k_a$  increases more slowly.

In order to explain this phenomenon, it was first considered that a diffusion control effect might occur. However, in this case the saturation phenomenon in  $k_a$  would appear at a constant value of  $k_a$  regardless of the catalyst type. Figure 9 shows that when magnesium acetate or manganese acetate is used as a catalyst this phenomenon appears at higher values of  $k_a$  than when

zinc acetate or stannous acetate is used. Thus the phenomenon depends on the kind of catalyst used, which suggests that it cannot be attributed to a simple diffusion control effect.

Instead, these results may shed some light on the mechanism of catalysis.\* A few remarks related to the phenomenon of catalyst saturation will be made.

The strength in Lewis acidity of the metal ion catalysts used in this work is considered to increase in the order of  $Mg^{2+} < Mn^{2+} < Zn^{2+}$ <sup>7</sup>, the same order as the limiting catalyst concentration. A possible explanation may be that there exists an association phenomenon with these metal compounds, which is related to the Lewis-acid strength of the metal ion species; during the experiments it was observed that an increase in the amount of zinc acetate makes the formation of a deposit, in which some catalyst may leave the reaction mixture, to appear earlier. Such a deposit formation may clearly counteract an increase in the catalyst concentration.

In the case of still stronger Lewis acids such as antimony (III) acetate, however, coordination bonding to the substrate (DMT) may occur preferentially. Therefore, the above-mentioned phenomenon may appear later.

In evaluation of the catalytic action above, certain facts must be kept in mind. If catalytic action is evaluated beyond above the critical point of  $k_a$ , the erroneous conclusion will be drawn and from a practical point of view, it will lead to a waste if the catalyst is used in a large excess quantity.

\* A more detailed discussion of this question will be published separately<sup>7</sup>.

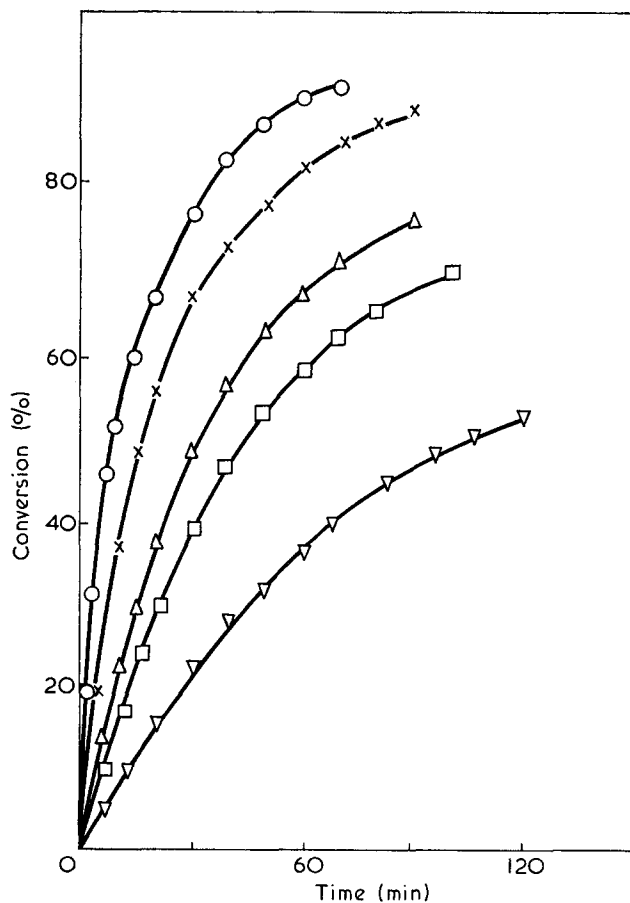


Figure 5 Time-conversion curves of the transesterification of DMT by EG with zinc acetate as a catalyst. Effect of catalyst concentration: ○,  $1 \times 10^{-3}$ ; ×,  $3 \times 10^{-4}$ ; △,  $7 \times 10^{-5}$ ; □,  $5 \times 10^{-5}$ ; ▽,  $3 \times 10^{-5}$  mol/mol DMT

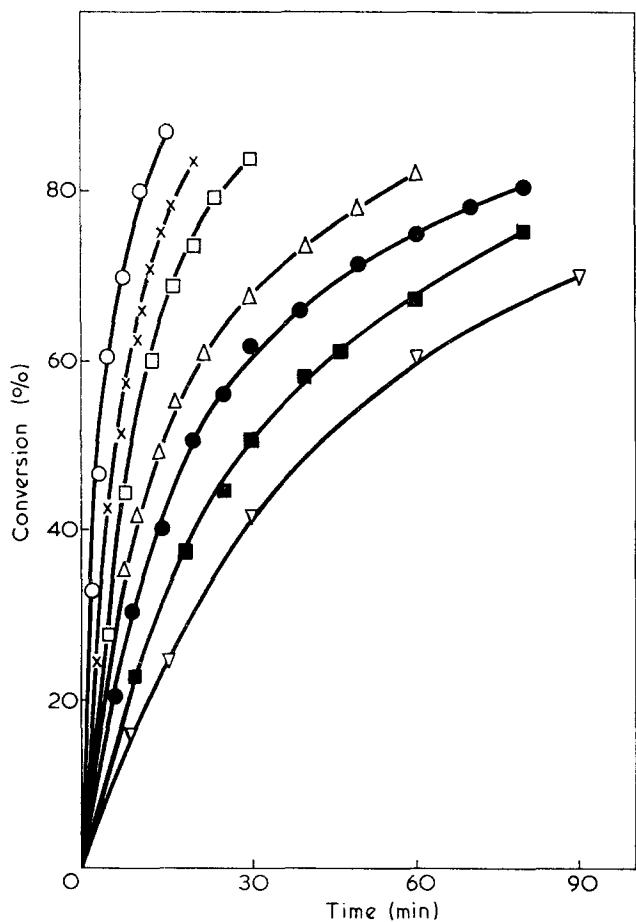


Figure 6 Time-conversion curves of the transesterification of DMT by EG with manganese acetate as a catalyst. Effect of catalyst concentration:  $\circ$ ,  $5 \times 10^{-3}$ ;  $\times$ ,  $1 \times 10^{-3}$ ;  $\square$ ,  $5 \times 10^{-4}$ ;  $\triangle$ ,  $2 \times 10^{-4}$ ;  $\bullet$ ,  $1.5 \times 10^{-4}$ ;  $\blacksquare$ ,  $1 \times 10^{-4}$ ;  $\nabla$ ,  $8 \times 10^{-5}$  mol/mol DMT

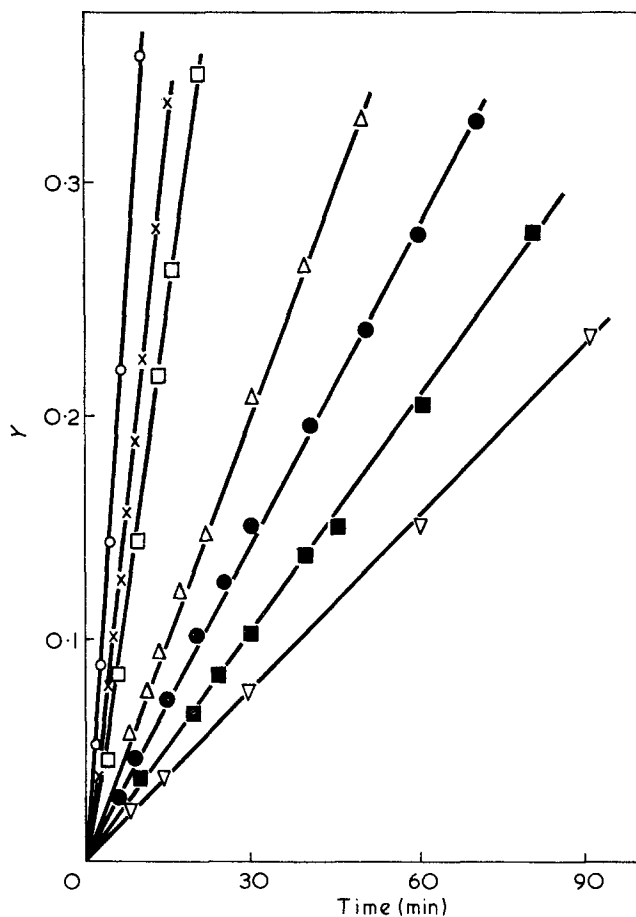


Figure 8 Application of equation (10) to data in Figure 6:  $\circ$ ,  $5 \times 10^{-3}$ ;  $\times$ ,  $1 \times 10^{-3}$ ;  $\square$ ,  $5 \times 10^{-4}$ ;  $\triangle$ ,  $2 \times 10^{-4}$ ;  $\bullet$ ,  $1.5 \times 10^{-4}$ ;  $\blacksquare$ ,  $1 \times 10^{-4}$ ;  $\nabla$ ,  $8 \times 10^{-5}$  mol/mol DMT

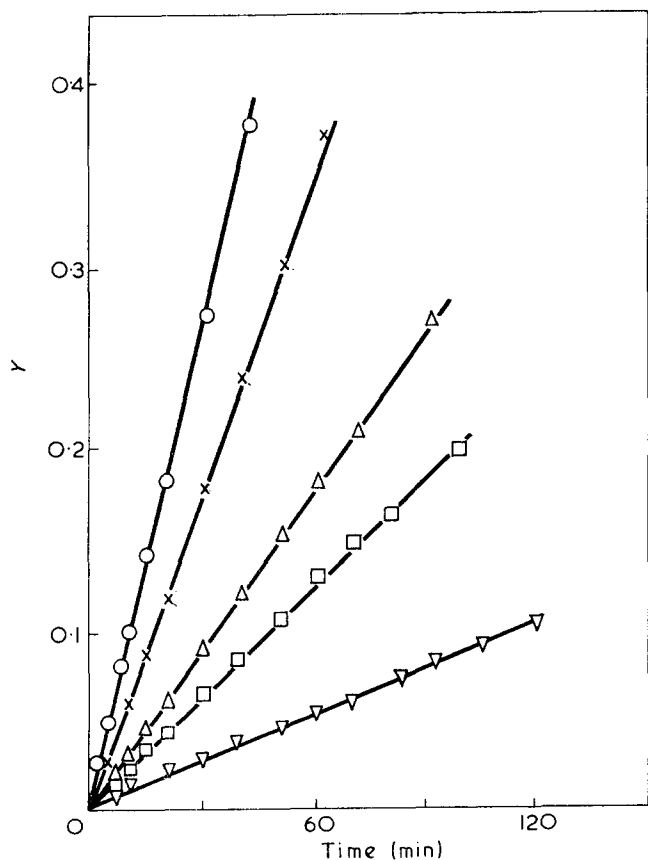


Figure 7 Application of equation (10) to data in Figure 5:  $\circ$ ,  $1 \times 10^{-3}$ ;  $\times$ ,  $3 \times 10^{-4}$ ;  $\triangle$ ,  $7 \times 10^{-5}$ ;  $\square$ ,  $5 \times 10^{-5}$ ;  $\nabla$ ,  $3 \times 10^{-5}$  mol/mol DMT

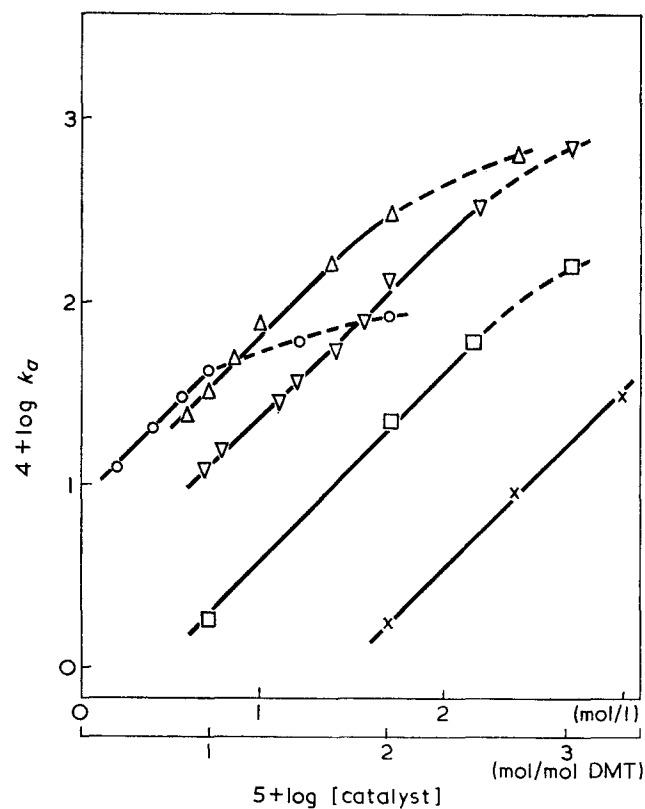


Figure 9 Rate dependence on the catalyst concentration. Metal acetate:  $\circ$ , Zn;  $\triangle$ , Mn;  $\nabla$ , Mg;  $\square$ , Sn;  $\times$ , Sb

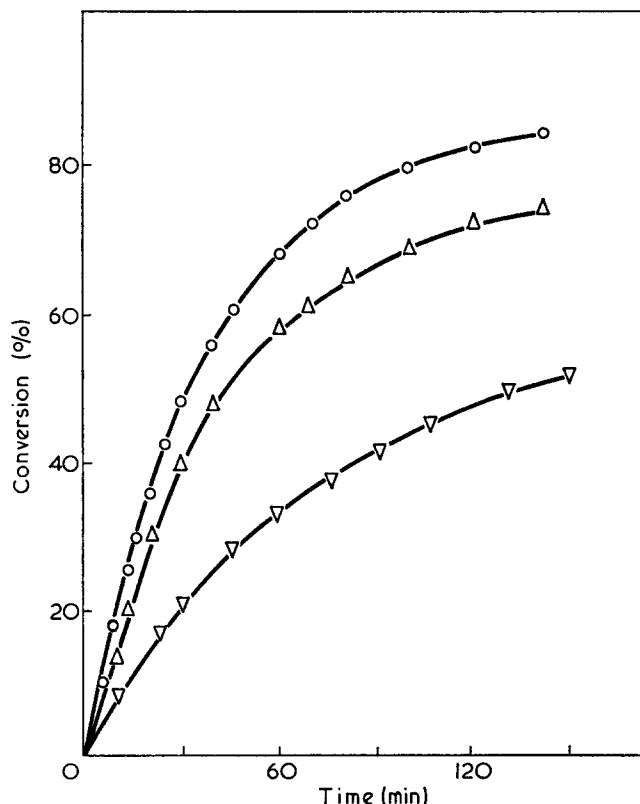


Figure 10 Time-conversion curves of the transesterification of DMT by EG with zinc acetate as a catalyst.  $\nabla$ , 160°C;  $\Delta$ , 170°C;  $\circ$ , 180°C

Temperature dependence

In Figure 10 methanol effusion curves from experiments at lower temperatures, zinc acetate ( $1 \times 10^{-4}$  mol/mol DMT) as a catalyst, are shown. By application of equation (10) the corresponding  $k_a$  values were computed. The activation energy was calculated from a plot of  $\log k_a$  vs.  $1/T$  (Figure 11) as  $E_a = 9.4$  kcal/mol.

This value is a little lower than that of alkaline hydrolysis of usual ester compounds.<sup>8</sup>

ACKNOWLEDGEMENT

The authors wish to thank Professor Seizo Okamuro (Kyoto University) for his interest in this work and his helpful criticism of the manuscript.

REFERENCES

- 1 Challa, G. *Rec. Trav. Chim.* 1960, **79**, 90
- 2 Peebles, Jr, L. H. and Wagner, W. S. *J. Phys. Chem.* 1959, **63**, 1206

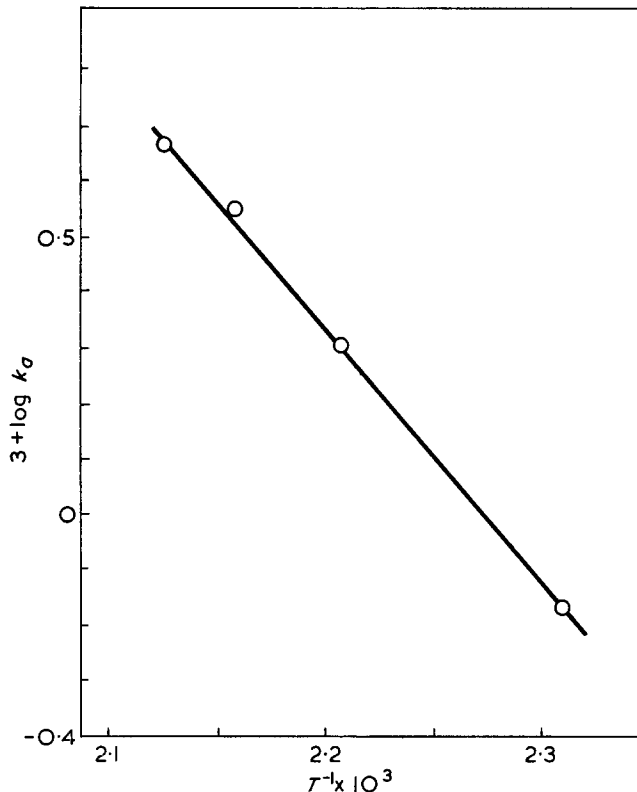


Figure 11 Arrhenius plot for data in Figure 10

- 3 Sumoto, M. *Kogyo Kagaku Zasshi (J. Chem. Soc. Japan, Ind. Chem. Sect.)* 1963, **66**, 1867
- 4 Griehl, W. and Schnock, G. *Faserforsch. Textiltech.* 1957, **8**, 408; *J. Polym. Sci.* 1958, **30**, 413
- 5 Yoda, K., Kimoto, K. and Toda, T. *Kogyo Kagaku Zasshi (J. Chem. Soc. Japan, Ind. Chem. Sect.)* 1964, **67**, 909
- 6 Nerdel, F. and Kleinwächter, J. *Chem. Ber.* 1957, **90**, 600
- 7 Tomita, K. and Ida, H. in preparation
- 8 Bender, M. L. *J. Am. Chem. Soc.* 1951, **73**, 1626

APPENDIX

When the change in catalyst concentration is ignored, equation (8) becomes:

$$-\frac{dC_A}{dt} = k_a \left\{ \frac{A_0 - \frac{A_0}{100}y}{V_0 - \frac{V_0}{100}y} \right\}^2 \quad (12)$$

If the reaction starts from the initial value:  $A_0 = 1, y = 0$ , integration yields:

$$k_{at} = \frac{V_{100}y}{100 - y} \quad (13)$$



# The structure of $\alpha$ -keratin

R. D. B. Fraser and T. P. MacRae

*Division of Protein Chemistry, CSIRO, Parkville, Melbourne, Victoria 3052, Australia*  
(Received 18 September 1972)

High-resolution low-angle meridional and near-meridional X-ray diffraction data have been collected from specimens of  $\alpha$ -keratin and various heavy-atom derivatives of  $\alpha$ -keratin. The observed reciprocal spacings of the layer lines satisfy the selection rule

$$Z = m/h + n/P + s/P_d$$

where  $h=67.1\text{\AA}$ ,  $P=220\text{\AA}$ ,  $P_d=235\text{\AA}$  and  $m$ ,  $n$  and  $s$  are integers. Taken in conjunction with observations on the lateral distribution of intensity this evidence suggests that the microfibrils in  $\alpha$ -keratin have a helical structure with pitch= $220\text{\AA}$  and unit height= $67.1\text{\AA}$  which is subject to a regular axial distortion of period  $235\text{\AA}$ . Possible relationships between this helix and the coiled-coil  $\alpha$ -helix rope segments of the constituent molecules are discussed.

## INTRODUCTION

Three distinct groups of proteins have been isolated from mammalian hard keratins<sup>1</sup>; a low-sulphur group, a high-sulphur group, and a high glycine-tyrosine group. The low-sulphur proteins possess regular secondary structure and are organized into filaments termed microfibrils whilst the proteins of the other two groups form a matrix of variable composition. Recent X-ray diffraction and electron microscope studies<sup>2-4</sup> have focused attention on the problem of determining the manner in which the low-sulphur proteins aggregate to form the microfibril and in the present paper new X-ray data are presented which permit the geometrical form of the aggregate to be deduced.

## INDEXING OF PATTERN

The series of low-angle meridional and near-meridional reflections observed in the X-ray diffraction pattern of  $\alpha$ -keratin (*Figure 1*) have generally been indexed<sup>5-8</sup> on an axial repeat of structure around  $200\text{\AA}$  but recently<sup>3</sup> it was found that the reciprocal spacings of many of the meridional reflections were significantly displaced from those calculated for any period in the vicinity of  $200\text{\AA}$ . It was shown, however, that the meridional reflections could be satisfactorily indexed on a repeat of about  $470\text{\AA}$ . In the present study the same specimens and procedures were used but the observations were extended to include both meridional and near-meridional reflections. It is difficult to calibrate fibre patterns with sufficient precision to combine results obtained from different specimens and the device was again adopted of selecting a well-resolved meridional reflection as an internal standard for comparative purposes.

Owing to the combined effects of lattice imperfections and disorientation the sharpness of the layer lines decreases rapidly with distance from the meridian

(*Figure 1*) and it is difficult to measure the layer line translation ( $Z$ ) for non-meridional reflections, particularly at high angles of diffraction. Attention was therefore concentrated on the low-angle pattern and the measured values of the layer-line translations for both meridional and near-meridional reflections are collected together in *Table 1*. A composite diagram illustrating the approximate lateral extents of the intensity distributions is given in *Figure 2*.

All the meridional reflections recorded in the present series of measurements can be indexed on a periodicity of  $470\text{\AA}$ , thus confirming the conclusion reached in an earlier study<sup>3</sup>. In this earlier study the layer-line translation of only one near-meridional reflection was determined and was found to be close to the value calculated for the 17th layer line of a  $470\text{\AA}$  periodicity. On this basis it was suggested that it might be possible to index the entire pattern on an axial repeat of structure of  $470\text{\AA}$ . The more complete data obtained in the present study (*Table 1*) indicate, however, that the true axial repeat is very much greater than  $470\text{\AA}$ . In particular, well-developed off-meridional reflections are observed with layer-line translations of  $Z=1/220\text{\AA}^{-1}$  in the chromium derivative (*Figure 1b*) and  $Z=3/220\text{\AA}^{-1}$  in wet quill (*Figure 1c*). Neither of these layer lines can be indexed in terms of a  $470\text{\AA}$  repeat of structure and it is apparent, from a consideration of the data recorded in *Table 1*, that the true axial repeat ( $c$ ) is too great to provide a suitable means for discussing the pattern, due to the correspondingly large values required for the indexing parameter  $l$ , where  $Z=l/c$ . Instead, it is more convenient and informative to relate prominent features of the diffraction pattern by means of a series of subsidiary parameters which may, if required, be related to  $l$ .

In the earlier study of the meridional reflections<sup>3</sup> it was noted that the pattern resembled that expected for a structure subject to periodic axial distortion. The

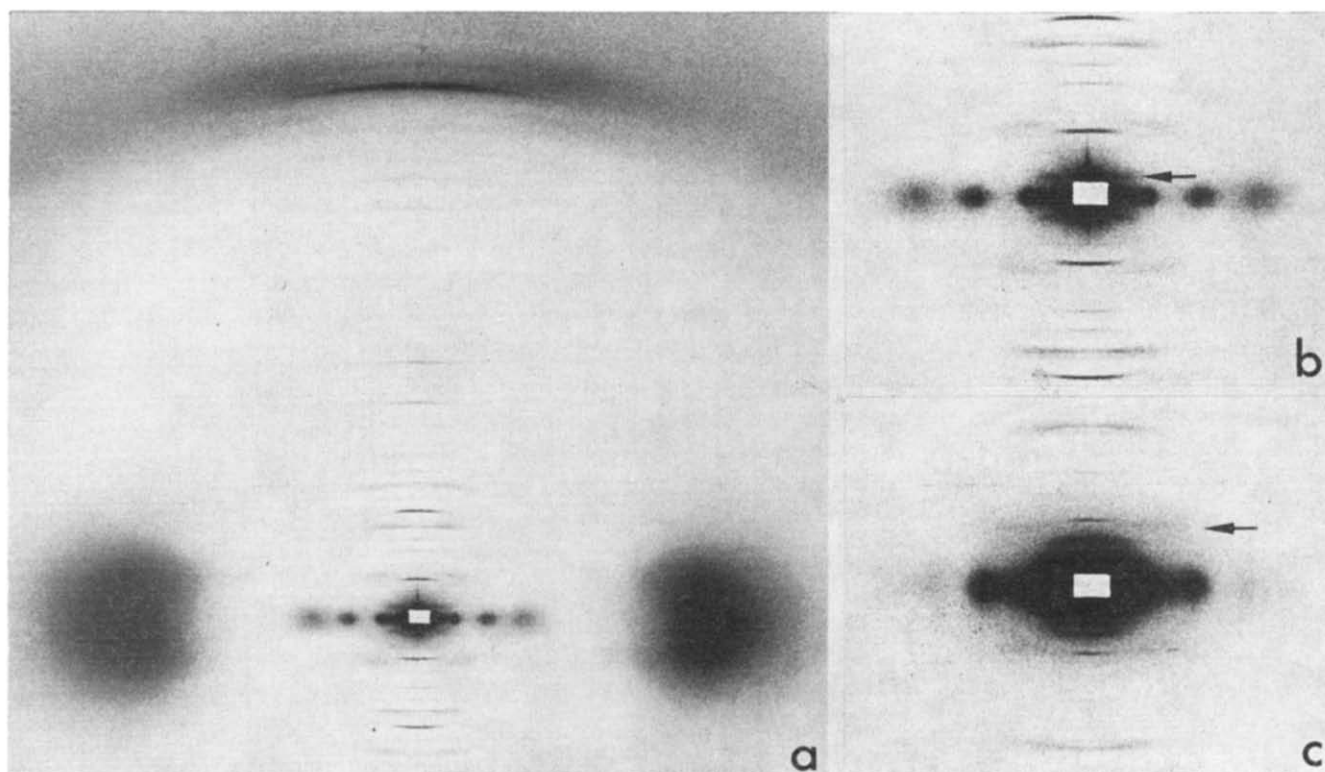


Figure 1 (a) X-ray diffraction pattern obtained from a chromium derivative of porcupine quill showing relationship between the high-angle and low-angle patterns. (b) Enlargement of central portion of (a) showing a layer line of spacing 220 Å (arrowed). (c) Low-angle pattern from wet quill showing a layer line of spacing 220/3 Å (arrowed)

Table 1 Layer line translations of the meridional and near-meridional reflections in the X-ray diffraction patterns obtained from porcupine quill and from certain heavy-atom derivatives

Selection rule parameters*			Z-value of layer line† (10 <sup>-3</sup> Å <sup>-1</sup> )	Observed Z-values (10 <sup>-3</sup> Å <sup>-1</sup> )‡				
				Untreated		Silver derivative	Chromium derivative	Mercury derivative
m	n	s	Dry	Wet				
0	0	1	4.3					4.2
0	1	0	4.6				4.6	
0	0	3	12.8		12.8			
0	3	0	13.6	13.4	13.5			
1	0	-2	6.4					6.3
1	0	-1	10.6		10.8	10.7	10.7	10.8
1	0	0	14.9	14.8	14.9	15.0	14.9	
1	1	0	19.4			19.4		19.5
2	-3	0	16.2				16.2	
2	0	-3	17.0				17.1	
2	0	-2	21.3			21.3		
2	0	-1	25.5	25.4	25.5		25.6	25.6
2	0	0	29.8			29.9	29.7	
2	1	0	34.3		34.3		34.3	34.5
3	0	-3	31.9				31.9	
3	0	-2	36.2				36.0	36.4
3	0	-1	40.4	40.4	40.4	40.4	40.4	40.4
3	0	0	44.7				44.9	
3	1	0	49.2				49.5	
4	0	-2	51.1				50.9	
4	0	-1	55.3	55.3	55.1		55.1	

\* See equation (2)

† Calculated from the relation  $Z = (7m + 2s)/470 + n/220$

‡ Relative values based on  $Z(m=3, n=0, s=-1) = 19/470 \text{ Å}^{-1}$

limited data collected in this earlier study favoured the identification of the meridional reflection with  $Z=0.0404 \text{ Å}^{-1}$  as the first order of the undistorted periodicity but the more complete data obtained in the present study suggests that the prominent meridional reflection with  $Z=0.0149 \text{ Å}^{-1}$  is a more likely choice. Originally

this possibility was rejected since the higher orders are weak but if the distortion of the periodicity is appreciable the satellite or 'ghost' reflections soon become as strong as or stronger than the orders of the undistorted periodicity<sup>9</sup>. The reciprocal spacings of the layer lines corresponding to the undistorted periodicity are given

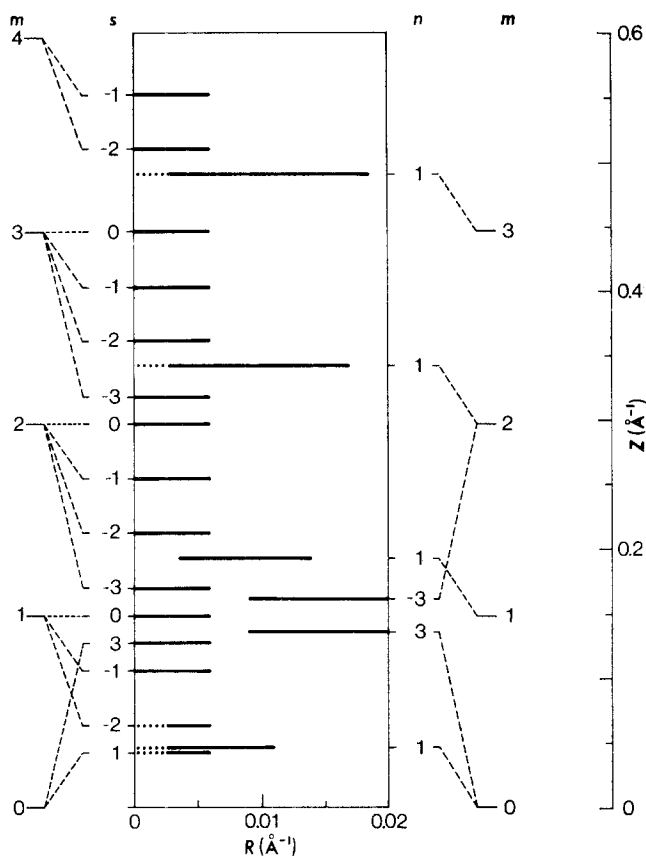


Figure 2. Composite diagram showing the translations and approximate lateral intensity distributions of layer lines observed in low-angle X-ray diffraction patterns of porcupine quill and of certain heavy-atom derivatives. The indexing scheme in terms of the integers  $m$ ,  $n$  and  $s$ , as discussed in the text, is indicated

by  $Z = 7m/470$ , where  $m$  is an integer and it was found that the meridional reflections could be indexed according to the selection rule:

$$Z = (7m + 2s)/470 \quad (1)$$

where  $s$  is an integer such that  $|s| \leq 3$  (Figure 2). The observation, mentioned earlier, that near-meridional reflections occur at low angles on layer lines related to a  $220 \text{ \AA}$  periodicity suggested that a term  $n/220$ , where  $n$  is an integer, be incorporated in equation (1) giving:

$$Z = m/67.1 + n/220 + s/235 \quad (2)$$

It will be seen from Table 1 that all the observed layer-line translations can, in fact, be fitted to such a scheme of indexing. It should be recalled that the numerical values in equation (2) are relative values and, as discussed elsewhere<sup>3</sup>, the precise values vary slightly with degree of hydration.

#### INTERPRETATION OF THE PATTERN

In biological structures formed by the self-assembly of identical structural units the units are generally equivalently or quasi-equivalently related<sup>10-14</sup>. In the first instance the continued operation of a translation and a rotation leads to a helical structure<sup>10</sup> and interpretation of the diffraction pattern is based on the fact that the layer line distribution is governed by the expression<sup>15, 16</sup>:

$$Z = m/h + n/P \quad (3)$$

where  $Z$  is the reciprocal space coordinate parallel to the meridian,  $h$  is the unit height,  $P$  is the pitch of the helix and  $m$  and  $n$  are integers. The parameter  $n$  determines the orders of Bessel functions which contribute to the intensity transform. Meridional reflections can occur when  $n=0$  and near-meridional reflections when  $n$  is small.

In the case of quasi-equivalently related units the situation is made more complex by the departures from equivalence but these will generally be periodic in nature and the effects on the diffraction pattern have been discussed in some detail by James<sup>9</sup>, Johnson<sup>17</sup> and by Caspar and Holmes<sup>18</sup>. The period of the distortion is often much greater than the undistorted period and this leads to the appearance of satellite layer lines around each layer line of the undistorted structure. In a helix subject to periodic axial distortion of amplitude  $z_a$  each meridional reflection is flanked by a series of satellite reflections and the intensity transform contains the factor  $J_s(2\pi Z z_a)$  where  $s$  is the 'order' of the satellite and  $J_s$  is a Bessel function of the first kind of order  $s$ . The  $Z$  coordinates of the meridional reflections in the distorted structure satisfy the relation:

$$Z = m/h + s/P_a \quad (4)$$

where  $P_a$  is the distortion period and  $m$  and  $s$  are integers. The set of meridional reflections obtained by setting  $s=0$  corresponds to the reflections given by the undistorted helix.

Combining equations (3) and (4) the expression for the layer-line translations of a helical structure subject to a periodic axial distortion becomes:

$$Z = m/h + n/P + s/P_a \quad (5)$$

and when this is compared with equation (2) it will be seen that the layer-line distribution in  $\alpha$ -keratin is explicable in terms of a helix with pitch  $220 \text{ \AA}$  and unit height  $67.1 \text{ \AA}$  which is subject to a regular axial distortion of period  $235 \text{ \AA}$ . In addition to axial distortion there will, in general, also be radial and azimuthal distortion. In this event the non-meridional reflections will also be flanked by satellite reflections and it is possible that these occur in the diffraction pattern of  $\alpha$ -keratin although they have not been identified with certainty in the present study.

Some ambiguity exists in the prediction of helical symmetry from the  $Z$  distribution of the meridional and near-meridional reflections due to the possibility that an  $N$ -fold parallel rotation axis of symmetry is present. If this is so  $n$  in equation (3) is limited<sup>16</sup> to multiples of  $N$  and the near-meridional reflections depend on factors in the expression for the intensity transform of the type  $J_{kN}^2(2\pi Rr)$  rather than  $J_k^2(2\pi Rr)$  where  $R$  is the radial coordinate in reciprocal space,  $r$  is the radial coordinate in real space and  $k$  is an integer. The first maximum of  $J_k^2(x)$  occurs at increasingly large values of  $x$  with increasing  $k$  and in the present case the observed lateral positions of the near-meridional reflections correspond to values of  $r \sim 35-45 \text{ \AA}$  for  $N=1$  and to very much larger values of  $r$  for  $N>1$ . Since the microfibril is believed<sup>2</sup> to have a radius of about  $36 \text{ \AA}$  it is unlikely that an  $N$ -fold rotation axis could be present in the  $\alpha$ -keratin microfibril.

Although the lateral positions of the maxima of the near-meridional reflections only give a very crude estimate of the radius of the diffracting object the

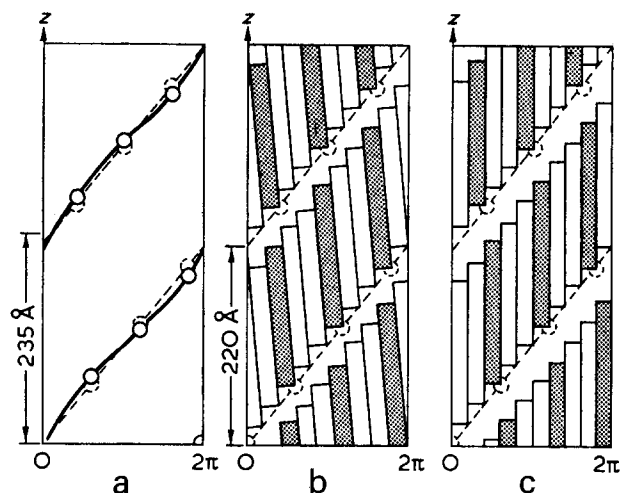


Figure 3 (a) Radial projection of the distribution of structural units at the surface of the microfibril as derived from the low-angle X-ray diffraction data. This arrangement is derived from a helix with a unit height of  $67.1 \text{ \AA}$  and a pitch of  $220 \text{ \AA}$  (broken line) by the superposition of an axial distortion of period  $235 \text{ \AA}$ . The resultant distorted helix is shown by a full line. (b) and (c) Examples of distributions of  $160 \text{ \AA}$  long coiled-coil rope segments that satisfy the symmetry requirements in (a). For simplicity the undistorted helices are shown. The molecular boundaries and the actual tilt of the segments are unknown

value obtained in the present study suggests that the low-angle pattern in  $\alpha$ -keratin is largely determined by projections from the surface of the microfibril. An estimate of the amplitude  $z_a$  of the axial distortion may be obtained<sup>9</sup> by comparing the way in which the range of satellite orders increases with increasing  $Z$  and a consideration of the observed intensity data suggests that the distortion amplitude  $z_a \sim 10 \text{ \AA}$ . Since the pattern of meridional and near-meridional reflections appears to originate primarily from the surface of the microfibril the value derived for the distortion amplitude also refers to this region.

The quasi-helical symmetry of the surface of the microfibril, derived from a consideration of the low-angle X-ray diffraction pattern, is illustrated in Figure 3a and it seems likely that this is a consequence of a similar or related symmetry in the internal structure of the microfibril. The  $5.15 \text{ \AA}$  meridional reflection, which is believed to originate from the coiled-coil  $\alpha$ -helix rope segments within the microfibril<sup>1, 2</sup>, consists of finely-spaced layer lines (Figure 1) but these are difficult to resolve owing to the effects of disorientation. In appropriately tilted specimens it is found that the strongest component has a  $Z$  coordinate which corresponds, within experimental error, to values of  $m=13$ ,  $n=s=0$  in equation (2), and a component is also present with  $m=13$ ,  $n=0$ ,  $s=1$ . Thus although the presently available data are very limited it supports the belief that the internal symmetry of the microfibril is basically that of a helix with a pitch of  $220 \text{ \AA}$  and an axial translation of  $67.1 \text{ \AA}$  between consecutive structural units. In the following sections the extent to which existing knowledge of the molecular structure can be reconciled with such a helical symmetry in the microfibril is examined.

#### NATURE OF THE STRUCTURAL UNIT

The *S*-carboxymethyl derivatives of the low-sulphur proteins from wool can be separated into two major

fractions, termed components 7 and 8, which have molecular weights respectively of about 53 000 and 45 000 and are present in a molar ratio of approximately 2 : 1<sup>19-21</sup>. The helix contents of these derivatives, as judged by measurements of the optical rotatory dispersion parameter  $b_0$ , are respectively 56 and 62% and it has been demonstrated that discrete helical and non-helical regions are present in the molecule<sup>22-24</sup>. The helix contents of the low-sulphur proteins in their native, solid state are unlikely to be the same as in the charged derivatives in solution and the estimates so obtained cannot be interpreted too literally. Various lines of evidence suggest that a specific aggregate may be formed between two molecules of component 7 and one of component 8<sup>23-35</sup> but this has not so far been demonstrated directly, for example by hydrodynamic measurements. A helix-rich fragment has been isolated from unfractionated preparations of the *S*-carboxymethyl derivatives of the low-sulphur proteins after partial hydrolysis with enzymes<sup>22</sup> and evidence from hydrodynamic<sup>23</sup>, electron microscope<sup>26</sup>, and X-ray diffraction<sup>27</sup> studies indicates that the fragment is rod-like and has a length of about  $160 \text{ \AA}$ . In summary the chemical studies of the low-sulphur protein derivatives suggest the possibility that there is a chemical unit of structure with a molecular weight of 151 000 and that about one-half of the polypeptide chain has an  $\alpha$ -helical conformation.

If there is, in fact, a chemical unit of molecular weight around 151 000 in the native structure it would occupy a volume

$$v_c = 1.66 \times 151\,000 / 1.3 = 1.93 \times 10^5 \text{ \AA}^3$$

assuming a density of  $1.3 \text{ g cm}^{-3}$ . The X-ray data discussed earlier suggest that the microfibril contains quasi-equivalently related structural units spaced at intervals of  $67 \text{ \AA}$  along the length of the microfibril and the low-sulphur proteins associated with this structural unit will occupy a volume  $v_s = 67\pi r^2$ , where  $r$  is the radius of a cylinder with the same volume per unit length as the microfibrillar proteins. The radius calculated for one chemical unit per structural unit ( $v_s = v_c$ ) is  $30 \text{ \AA}$  and for two ( $v_s = 2v_c$ ) is  $43 \text{ \AA}$ . Estimates of the effective radius of the microfibril based on stain exclusion or electron density distribution<sup>1</sup> are intermediate between these two values, but the radius so estimated is not necessarily identical with that defined above. It does not seem possible, therefore, on the basis of the existing evidence, to establish a definite correspondence between the chemical and structural units.

#### STRUCTURE OF THE MICROFIBRIL

##### Coiled-coil model

Crick<sup>28</sup> and Pauling and Corey<sup>29</sup> suggested independently that the  $\alpha$ -helices in  $\alpha$ -keratin were distorted into coiled coils and the high-angle X-ray diffraction pattern has been examined in some detail<sup>2, 8, 30-33</sup> for evidence of the characteristic features predicted for coiled-coil ropes. The problem of testing these and other suggestions is complicated by the presence of an overlying interference function associated with the substructure of the microfibril and by the limited length of the helical sections of chain and the likelihood of various types of disorder<sup>2</sup>. Initially it was thought that the best agreement with the observed data was obtained with a three-strand

rope model<sup>28, 31, 32</sup> and this model has also been favoured by Crewther and coworkers as providing the best explanation of their chemical and physico-chemical studies<sup>23, 24</sup>. Subsequent calculation of the intensity transform of a coiled-coil rope, in which the effects of background material were taken into consideration<sup>33</sup>, showed however that the differences between the transforms predicted for two-strand and three-strand ropes were not as great as originally supposed and the existing data did not enable a clear choice to be made between these two alternatives. Comparative studies of dried specimens of tropomyosin, myosin, paramyosin and  $\alpha$ -keratin showed that the scattering in the equatorial and near-equatorial region was very similar and since the first three proteins have two-strand rope structures it was concluded that on balance the data obtained favoured a two-strand rope structure for the helical fraction of  $\alpha$ -keratin<sup>33</sup>.

#### Arrangement of coiled-coil rope segments

Evidence concerning the arrangement of the coiled-coil rope segments in the microfibril has been obtained from both electron microscope and high-angle X-ray diffraction studies and in the present section this is discussed in relation to the quasi-helical symmetry derived from the low-angle X-ray study.

Filshie and Rogers<sup>34</sup> obtained electron micrographs of cross-sections of reduced wool that had been stained with osmium tetroxide and lead hydroxide and found that there was a ring about 20 Å in width and 60 Å in diameter in which the uptake of stain was small. In many cases a central unstained core about 20 Å in diameter was also observed. The unstained ring appeared to be broken up into subunits and it was suggested that the microfibril contained fine filaments about 20 Å in diameter arranged in the 9+2 pattern found in cilia and in certain flagella. The interpretation of these data in terms of a protofibrillar substructure has been the subject of some controversy<sup>35, 36</sup> but the ring-core feature has been confirmed both by direct imaging<sup>37</sup> and by a number of independent methods including image averaging<sup>38</sup> and direct Fourier synthesis from the equatorial low-angle electron diffraction pattern obtained from similarly stained specimens<sup>2</sup>. That the ring-core feature is not an artefact of staining has been shown by X-ray diffraction studies of untreated specimens<sup>2, 33, 39, 40</sup> (Figure 4a). It seems probable that the unstained ring and core visible in electron micrographs of cross-sections contain the coiled-coil portions of the low-sulphur protein molecules and that the densely stained annulus between them is occupied by the non-helical portions<sup>2</sup>.

The observed density of  $\alpha$ -keratin is close to  $1.3 \text{ g cm}^{-3}$  in the dry state<sup>41</sup> and thus the structure must be close-packed. It is not possible to build up a three-dimensionally regular assembly of coiled-coils which would achieve anything approaching this density but Rudall<sup>42</sup> has shown that a reasonable close packing can be obtained in a two-dimensional array of two-strand ropes if neighbouring ropes are rotated by  $\pi/2$  about the rope axis or displaced by  $P_c/4$  parallel to the axis, where  $P_c$  is the pitch of the coiled-coil (Figure 5a). This suggests the possibility that the ring in the microfibril contains a helical array of close-packed segments of coiled-coil ropes. In the case of a ring of  $M$  identical segments of rope (Figure 5b) it may be shown that close packing

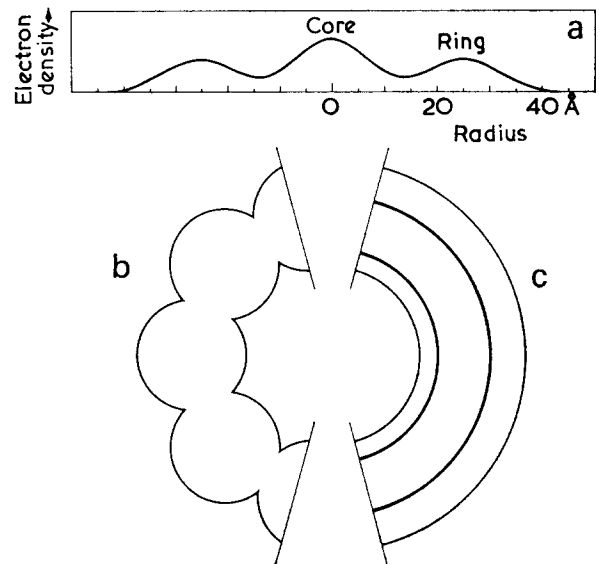


Figure 4 (a) Fourier synthesis of the cylindrically averaged electron density distribution in porcupine quill obtained from the low-angle equatorial X-ray diffraction pattern<sup>2</sup>. (b) Section through the model illustrated in Figure 3b for the ring portion of the microfibril. Only part of the section is shown; in the complete section two of the nine sites would be vacant. The core shown in (a) is believed to consist of  $\alpha$ -helical material<sup>1, 2</sup> but the present experiments do not give any information about its precise form. (c) In projection the ring would appear continuous since there is no reason *a priori* why the segments should be aligned exactly parallel to the axis of the microfibril

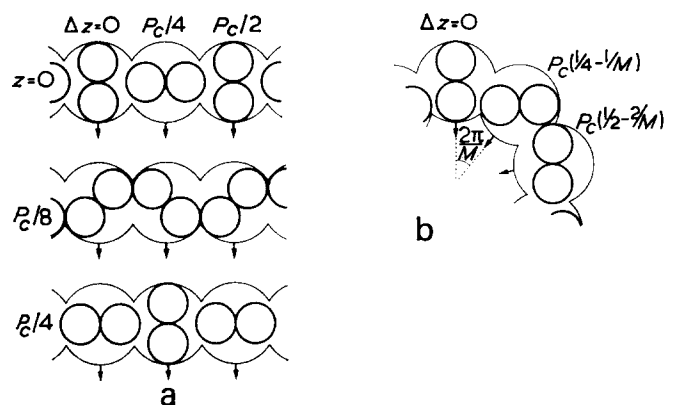


Figure 5 (a) Close-packing scheme for two-strand ropes suggested by Rudall<sup>42</sup>. Cross-sections illustrating the relative orientations of the strands in adjacent ropes are shown for three different values of  $z$ . The relative stagger ( $\Delta z$ ) of the ropes in the sheet is indicated. (b) Extension to helical array

occurs if there is an axial stagger between neighbouring segments of

$$\Delta z = P_c/4 - P_c/M + kP_c/2 \quad (6)$$

for two-strand ropes or

$$\Delta z = -P_c/M + kP_c/3 \quad (7)$$

for three-strand ropes where  $k=0, \pm 1, \pm 2 \dots$

Equations (6) and (7) represent necessary rather than sufficient conditions for close-packing. For example if  $M$  is odd an array of two-strand ropes can only be formed if the segment length is less than  $(M-1)P_c/M$ .

The number of structural units per turn in the quasi-helical arrangement illustrated in Figure 3a is

$$220/67.1 = 3.28$$

and if the internal arrangement of the microfibril has

the same symmetry there should be an integral number of rope segments associated with each structural unit. From a consideration of the physical dimensions of the ring the appropriate choice would appear to be 3, giving a value of  $M$  close to 10. When combined with the evidence, discussed earlier, that the helical segments are about 160 Å in length the general type of model shown in Figure 3c is arrived at. The symmetry does not require that the three rope segments be equivalent and so the axial stagger may be different for the three segments; however, equations (6) and (7) would still be applicable to the mean stagger. There is no *a priori* reason why the rope axes should be aligned exactly with the microfibril axis and Figure 3b illustrates how the azimuthal spacing in section can be varied from  $2\pi/10$  to  $2\pi/9$  by the introduction of a small tilt of the rope axis. The appearance of a section through the arrangement in Figure 3b is depicted diagrammatically in Figure 4b, and Figure 4c shows the corresponding projection. The latter is in good accord with the experimentally determined distribution of electron density shown in Figure 4a.

## DISCUSSION

The data obtained in the present study indicate that the microfibril in  $\alpha$ -keratin consists of a quasi-helical arrangement of structural units, and when combined with evidence obtained from studies of the extracted proteins and from high-angle X-ray and electron microscope studies, lead to a general type of model in which 160 Å lengths of coiled-coil rope are arranged in a helical band to form the ring portion of the microfibril. The present data do not permit any deduction to be made about the molecular boundaries and the relation between the structural unit and the postulated chemical unit is not immediately apparent. However, there is a numerological coincidence between the number of coiled-coil rope segments per structural unit in the ring portion of the microfibril (three) and the number of protein molecules in the postulated chemical unit (three). This suggests the possibility that there is one chemical unit per 67 Å in the ring portion of the microfibril.

There have been a number of earlier suggestions as to the organization of the polypeptide chain in the microfibril<sup>4, 39, 43-50</sup>. These suggestions have generally been designed to account for particular features of the physical properties or the diffraction pattern and have not been sufficiently comprehensive or stated in sufficiently precise terms to be tested experimentally by X-ray diffraction methods. In many cases the suggestions could probably be adapted to conform with a quasi-helical distribution of scattering matter. Spei *et al.*<sup>50-53</sup> have noted the presence of a layer line of spacing around 200 Å in chemically modified wool and mohair but it is not immediately clear as to how this should be indexed on the present scheme.

The data obtained in the present study relate essentially to the geometry of the arrangement of the structural units in the microfibril and in order to determine the molecular boundaries or to derive or test a detailed model it will be necessary to collect intensity data and to extend considerably the range of the observations. Many authors have noted that particular reflections in the X-ray diffraction pattern of  $\alpha$ -keratin are intensified

following chemical treatments where specific types of residue are modified. In view of the complexity of the diffraction pattern and its dependence on distortion amplitudes the interpretation of such intensifications directly in terms of periodic distributions of amino acids clearly requires some caution.

## ACKNOWLEDGEMENTS

The authors are indebted to Dr F. R. Hartley and Mr A. Kirkpatrick for the preparation of heavy-atom derivatives.

## REFERENCES

- 1 Fraser, R. D. B., MacRae, T. P. and Rogers, G. E. 'Keratins', C. C. Thomas, Springfield, Illinois, 1972
- 2 Fraser, R. D. B., MacRae, T. P., Millward, G. R., Parry, D. A. D., Suzuki, E. and Tulloch, P. A. *Appl. Polym. Symp.* 1971, **18**, 65
- 3 Fraser, R. D. B. and MacRae, T. P. *Nature* 1971, **233**, 138
- 4 Wilson, G. A. *Polymer* 1972, **13**, 63
- 5 MacArthur, I. *Nature* 1943, **152**, 38
- 6 Bear, R. S. *J. Am. Chem. Soc.* 1944, **66**, 2043
- 7 Bear, R. S. and Rugo, H. J. *Ann. N.Y. Acad. Sci.* 1951, **53**, 627
- 8 Lang, A. R. *Acta Cryst.* 1956, **9**, 446
- 9 James, R. W. 'The Optical Principles of the Diffraction of X-rays', Bell and Sons, London, 1948
- 10 Crane, H. R. *Sci. Mon.* 1950, **70**, 376
- 11 Pauling, L. *Discuss. Faraday Soc.* 1953, **13**, 170
- 12 Caspar, D. L. D. and Klug, A. *Cold Spring Harbor Symp. Quant. Biol.* 1962, **27**, 1
- 13 Caspar, D. L. D. 'Molecular Architecture in Cell Physiology', (T. Hayashi and A. G. Szent-Györgyi, Eds.), Prentice-Hall, Englewood Cliffs, 1966, p 191
- 14 Klug, A. 'Symmetry and Function of Biological Systems at the Macromolecular Level', (A. Engström and B. Strandberg, Eds.), Wiley, New York, 1969, p 425
- 15 Cochran, W., Crick, F. H. C. and Vand, V. *Acta Cryst.* 1952, **5**, 581
- 16 Klug, A., Crick, F. H. C. and Wyckoff, H. W. *Acta Cryst.* 1958, **11**, 199
- 17 Johnson, C. K. *PhD Thesis*, Massachusetts Institute of Technology, 1959
- 18 Caspar, D. L. D. and Holmes, K. C. *J. Mol. Biol.* 1969, **46**, 99
- 19 Thompson, E. O. P. and O'Donnell, I. J. *Aust. J. Biol. Sci.* 1965, **18**, 1207
- 20 Jeffrey, P. D. *Biochemistry* 1969, **8**, 5217
- 21 Jeffrey, P. D. *Aust. J. Biol. Sci.* 1970, **23**, 809
- 22 Crewther, W. G. and Harrap, B. S. *J. Biol. Chem.* 1967, **242**, 4310
- 23 Crewther, W. G., Dobb, M. G., Dowling, L. M. and Harrap, B. S. 'Symposium on Fibrous Proteins Australia 1967' (W. G. Crewther, Ed.), Butterworths (Australia), Sydney, 1968, p 329
- 24 Crewther, W. G. and Dowling, L. M. *Appl. Polym. Symp.* 1971, **18**, 1
- 25 Bhatnagar, G. M. and Crewther, W. G. *Aust. J. Biol. Sci.* 1967, **20**, 827
- 26 Crewther, W. G., Dobb, M. G. and Millward, G. R. *J. Text. Inst.* 1972, in press
- 27 Suzuki, E., Crewther, W. G., Fraser, R. D. B., MacRae, T. P. and McKern, N. M. *J. Mol. Biol.* 1972, in press
- 28 Crick, F. H. C. *Acta Cryst.* 1953, **6**, 689
- 29 Pauling, L. and Corey, R. B. *Nature* 1953, **171**, 59
- 30 Fraser, R. D. B. and MacRae, T. P. *Nature* 1961, **189**, 572
- 31 Fraser, R. D. B. and MacRae, T. P. *J. Mol. Biol.* 1961, **3**, 640
- 32 Fraser, R. D. B., MacRae, T. P. and Miller, A. *J. Mol. Biol.* 1964, **10**, 147
- 33 Fraser, R. D. B., MacRae, T. P. and Miller, A. *J. Mol. Biol.* 1965, **14**, 432
- 34 Filshie, B. K. and Rogers, G. E. *J. Mol. Biol.* 1961, **3**, 784
- 35 Dobb, M. G. and Sikorski, J. *J. Text. Inst.* 1969, **60**, 497
- 36 Fraser, R. D. B., MacRae, T. P. and Millward, G. R. *J. Text. Inst.* 1969, **60**, 498

- 37 Millward, G. R. *J. Ultrastruct. Res.* 1970, **31**, 349
- 38 Fraser, R. D. B., *et al.* *J. Text. Inst.* 1969, **60**, 343
- 39 Bailey, C. J., Tyson, C. N. and Woods, H. J. *3rd Int. Congr. Rech. Text. Lainiere*, Inst. Textile, France, 1965, Vol 1, p 21
- 40 Fraser, R. D. B., MacRae, T. P. and Parry, D. A. D. 'Symposium on Fibrous Proteins Australia 1967' (W. G. Crewther, Ed.), Butterworths (Australia), Sydney, 1968, p 279
- 41 King, A. T. *J. Text. Inst.* 1926, **17**, T53
- 42 Rudall, K. M. 'Lectures on the Scientific Basis of Medicine', British Postgraduate Medical Foundation, University of London, 1956, Vol 5, p 217
- 43 Fraser, R. D. B., MacRae, T. P. and Rogers, G. E. *Nature* 1962, **193**, 1052
- 44 Lundgren, H. P. and Ward, W. H. *Arch. Biochem. Biophys.* 1962, Suppl. 1, 78
- 45 Skertchly, A. R. B. *Nature* 1964, **202**, 161
- 46 Feughelman, M. *Appl. Polym. Symp.* 1971, **18**, 751
- 47 Hearle, J. W. S., Chapman, B. M. and Senior, G. S. *Appl. Polym. Symp.* 1971, **18**, 775
- 48 Menefee, E. *Appl. Polym. Symp.* 1971, **18**, 809
- 49 Crewther, W. G. *Text. Res. J.* 1972, **42**, 77
- 50 Spei, M. *Kolloid-Z. Z. Polym.* 1972, **250**, 207
- 51 Spei, M. *Kolloid-Z. Z. Polym.* 1972, **250**, 214
- 52 Spei, M., Heidemann, G. and Zahn, H. *Naturwiss.* 1968, **55**, 346
- 53 Spei, M. *Appl. Polym. Symp.* 1971, **18**, 659

# Molecular motion in a copolymer of styrene and maleic anhydride

H. Block, M. E. Collinson and S. M. Walker

*Department of Inorganic, Physical and Industrial Chemistry,  
University of Liverpool, PO Box 147, Liverpool L69 3BX, UK  
(Received 18 September 1972; revised 12 October 1972)*

Dielectric and mechanical relaxation techniques have been applied to the study of the molecular motions exhibited by an alternating copolymer of styrene and maleic anhydride. Three major relaxations were detected by these techniques and shown to correspond to motions already defined in homopolymers of substituted maleimides. A fourth relaxation was detected but insufficient evidence for assignment was obtained. The  $\alpha$  relaxation is attributed to gross main chain motion ( $T_g \sim 475\text{K}$ ), the  $\beta$  relaxation (activation energy 103 kJ) to local motion about the backbone and the  $\delta$  relaxation (activation energy 51 kJ) to deformation of the substituted succinic anhydride ring.

## INTRODUCTION

In our studies of the physical properties of thermally stable polymers, dielectric relaxation experiments have been carried out on a number of poly(*N*-substituted maleimides)<sup>1</sup> and copolymers of styrene with maleimides<sup>2</sup>. We report here the results of a similar investigation into a styrene-maleic anhydride copolymer, which includes mechanical as well as dielectric relaxation experiments.

Molecular motion in polymers may be detected by electrical measurements, providing the type of movement involves the realignment of dipoles. Such a process is manifest by changes in the complex permittivity ( $\epsilon^* = \epsilon' - i\epsilon''$ ) with variation of either the frequency, or temperature of measurement. The torsion pendulum used in these experiments to characterize the mechanical behaviour of the copolymer responds to changes in the complex shear modulus ( $G^* = G' + iG''$ ).

The several relaxations detected in this investigation are labelled, according to established practice, as  $\alpha$ ,  $\beta$ ,  $\gamma$  etc., in the sequence in which they occur from the highest to the lowest temperature at constant frequency (temperature plane) or from the lowest to the highest frequency at constant temperature (frequency plane).

## EXPERIMENTAL

### *Materials*

Styrene was purified by fractional distillation (b.p. 419K at 760 mmHg after removal of inhibitor. Maleic anhydride was recrystallized from chloroform.

The copolymer was prepared by the free-radical initiation of a 1 : 1 molar mixture of the monomers dissolved in acetone<sup>3</sup> (30 cm<sup>3</sup> per 7 g of maleic anhydride). Initiation was achieved with azobisisobutyronitrile at 323K (0.05 g per 7 g of anhydride) for 4.5 h.

The polymer was precipitated by running the reaction mixture into a ten-fold excess of petroleum ether (b.p. 333–353K), isolated by filtration, washed and vacuum dried (yield  $\sim 80\%$ ). Elemental analysis found: C,

70.62%; H, 5.02%. An alternating copolymer composition requires: C, 71.41%; H, 4.96%. The polymer was stored and handled in a dry atmosphere because of its relatively easy hydrolysis to the free acid. Infra-red (i.r.) spectral checks on the purity were performed before all the experiments.

The molecular weight was estimated viscometrically using dry tetrahydrofuran solvent and the previously established Mark-Howink parameters<sup>4</sup>. A value for  $\bar{M}_n$  of  $5.3 \times 10^5$  was obtained. Differential scanning calorimetry (Perkin Elmer DSC 1B, scan rate 16°C/min) showed an endothermic second order transition at 476K. Assignment of this to the glass-rubber transition is supported by the subsequent relaxation information.

### *Dielectric measurements*

The copolymer was compression moulded into 5.08 cm diameter, 0.1 cm (nominal) thick discs as previously described<sup>1</sup>. Sample behaviour was investigated in two frequency regions using the transient step response technique ( $10^{-5}$  to  $10^{-1}$  Hz) and transformer ratio-arm bridges ( $10^2$  to  $10^6$  Hz) over a temperature range of  $-190\text{K}$  to  $+475\text{K} \pm 1\text{K}$ . Full details of the equipment and experimentation have been given elsewhere<sup>1</sup>, as has the method of Fourier transformation involved in the data analysis obtained from the transient technique<sup>5</sup>.

### *Mechanical measurements*

Sample bars (8 cm long  $\times$  0.9 cm wide  $\times$  0.3 cm) were moulded at 500K in a stainless-steel die and tested on a Nonius torsion pendulum capable of oscillating at three frequencies between 0.5 and 4.5 Hz. Temperature variation over the range  $-140\text{K}$  to  $+475\text{K} \pm 1\text{K}$  was achieved by a gas flow system using nitrogen as thermostating medium.

## RESULTS AND DISCUSSION

Transient step-response dielectric experiments revealed the existence of two distinct relaxations in the temperature



range 300K to 475K (Figure 1). The high temperature peak (labelled  $\alpha$ ) is clearly the larger of the two and at several frequencies showed evidence of being composed of more than one relaxation. Cole-Cole plots (Figure 2) also suggest this possibility but since the data are insufficient to warrant further analysis we are unable to confirm the existence of multiple relaxations. A plot of  $\log_{10} f_{\max}$  against  $1/T$  is shown in Figure 3. The almost vertical slope of the apparent straight line obtained with the  $\alpha$  relaxation indicates a very high activation energy. Analysis of this line on an expanded scale reveals a degree of curvature, but the mean slope is 515 kJ. Extrapolation of this curve leads asymptotically to a value for  $1/T$  corresponding to a temperature of 470K. The close similarity of this temperature to that obtained for the transition on the differential scanning calorimeter implies that both techniques are detecting manifestations of the same molecular reorientation, namely the gross Brownian motion of backbone chains. The low frequency investigation necessary to detect this process reflects the high rigidity of the copolymer backbone structure. This has been a common feature of all the polymers recently studied<sup>1,2</sup> containing a five-membered ring unit in the backbone.

The  $\beta$  relaxation also derived from the transient measurements is shown as a function of frequency in Figure 4. This diagram shows distinct evidence for the existence of aliasing, in that the high frequency portion of the relaxation is emphasized at the expense of low

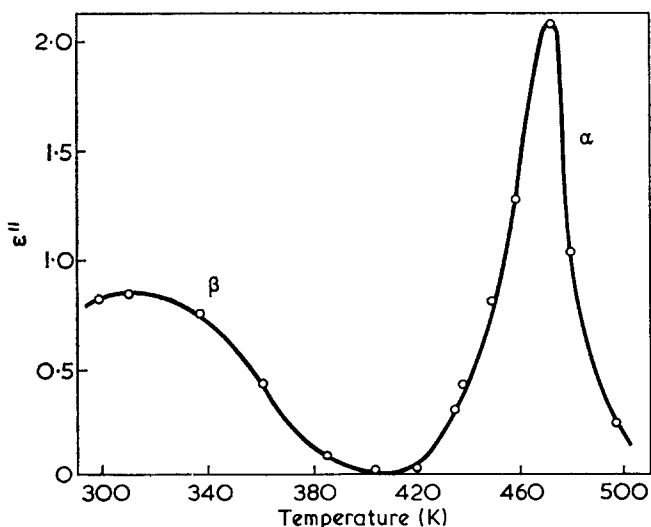


Figure 1 Dielectric loss as a function of temperature. The data points are derived from the transient step-response technique transformed to a frequency of  $2 \times 10^{-3}$  Hz

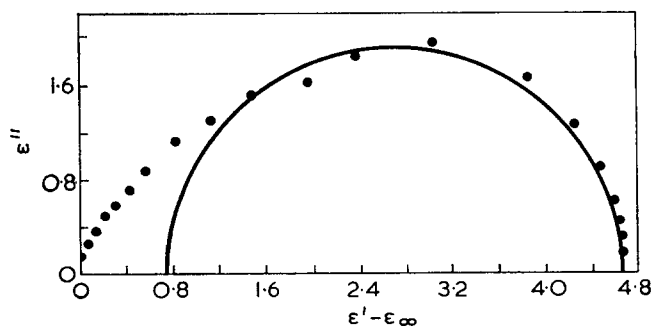


Figure 2 Cole-Cole plot at 458K showing asymmetry in the  $\alpha$  peak at high frequencies

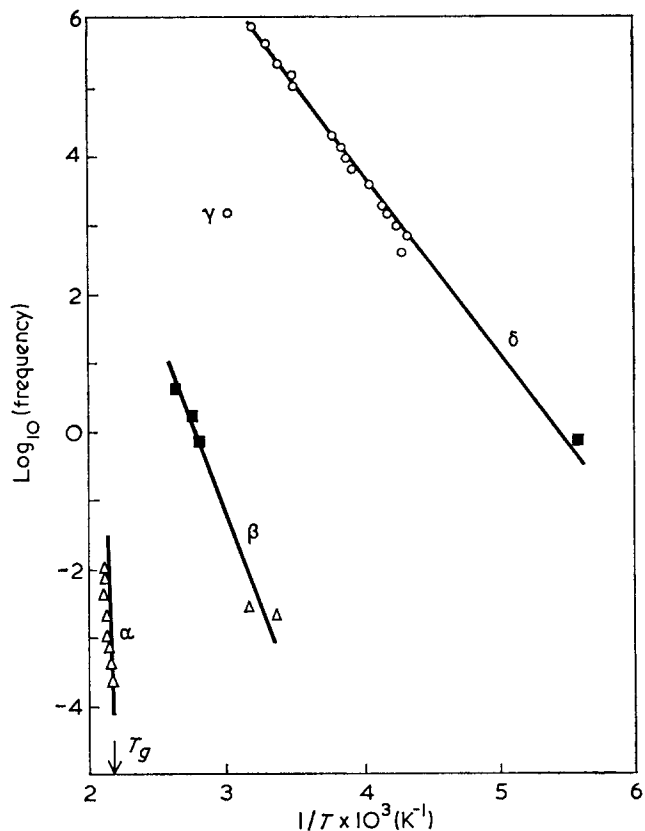


Figure 3 Activation energy plot of  $\log_{10} f_{\max}$  against  $T^{-1}$ .  $\Delta$ , Transient step response dielectric results;  $\blacksquare$ , torsion pendulum results;  $\circ$ , high frequency dielectric results

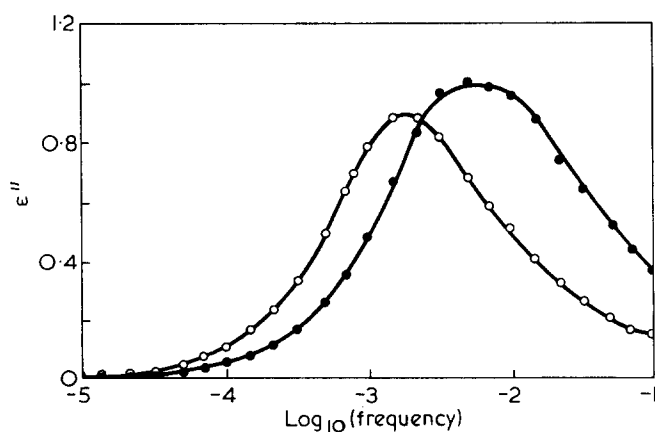


Figure 4 Dielectric loss as a function of frequency using data transformed from the step-response technique. The existence of 'aliasing' is revealed in the  $\beta$  peak at two temperatures:  $\circ$ , 298K  $\bullet$ , 313K

frequency contributions. Relaxations at higher frequencies ( $f > 10^{-1}$  Hz) are being 'folded back' on to the lower frequency region as a result of the numerical method of data treatment<sup>5</sup>, resulting in an apparently asymmetric loss peak. This effect is absent in the temperature plane (Figure 1) thereby proving that the observed asymmetry is not a true property of the relaxation. Unfortunately there is no known numerical technique for subtracting aliased information. However, the data are still included since the inaccuracies so introduced are negligible below about 0.05 Hz and the position and magnitude of the loss peaks are not affected. The  $\beta$  peak is well characterized at room temperature but the rapidly increasing influence of the glass-rubber relaxation masks the

position of this relaxation at higher temperatures. Consequently the activation energy diagram (Figure 3) shows only a few points covering a very limited temperature and frequency range. Fortunately this particular relaxation is well suited to study by the torsion pendulum and further discussion will be delayed until the data from this technique are assessed.

High frequency dielectric experiments reveal the existence of two further relaxations (Figure 5)—a substantial peak ( $\delta$ ) occurring at about 240K and a very much smaller one ( $\gamma$ ) at about 330K both at 1000 Hz. The latter peak occurs as a shoulder on the larger peak and we were unable to determine the activation energy of the process. These two relaxations are very similar in magnitude and position to relaxations occurring in many polymaleimides<sup>1,2</sup>. We have assigned these previously to a twisting of the maleimide ring sited in either the amorphous ( $\delta$ ) or crystalline ( $\gamma$ ) regions of the polymer. The structural similarity of styrene-maleic anhydride copolymer to maleimide homo- and copolymers inclines us to choose the same relaxation mechanism in this polymer. However, we were unable to detect crystallinity in this material by X-ray powder photography. Furthermore quenching of the polymer, which in the previous experiments proved of great importance in assignment, failed to provide useful information in this case. The dielectric behaviour after quenching was essentially unaltered although the activation energy of the  $\delta$  peak increased slightly (60 kJ/mol compared with 51 kJ/mol). The  $\delta$  peak corresponds in activation energy, position and magnitude with the amorphous phase ring twist in the polymaleimides. There is insufficient evidence to be more precise about the origin of the  $\gamma$  relaxation.

The torsion pendulum results provide excellent complementary data. Figure 6 shows that three mechanically active relaxations are present. At temperatures approaching the glass transition temperature the logarithmic decrement increases very rapidly and at about 375K the

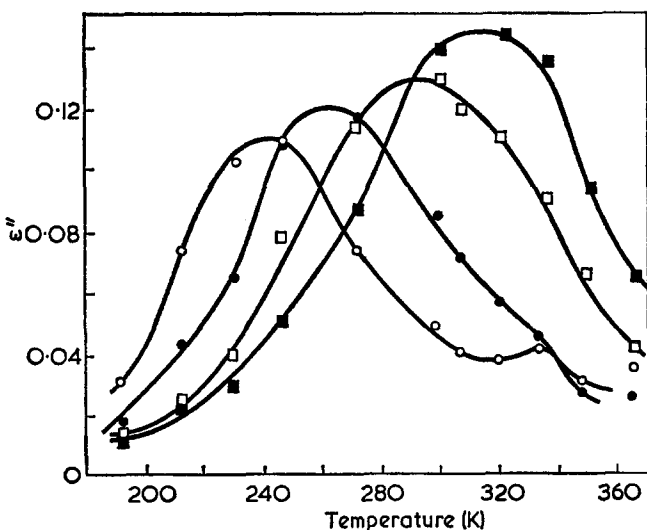


Figure 5 Dielectric loss as a function of temperature showing the  $\gamma$  and  $\delta$  peaks detected using the high-frequency bridge apparatus.  $\circ$ , 1.5 kHz;  $\bullet$ , 15 kHz;  $\square$ , 150 kHz;  $\blacksquare$ , 700 kHz

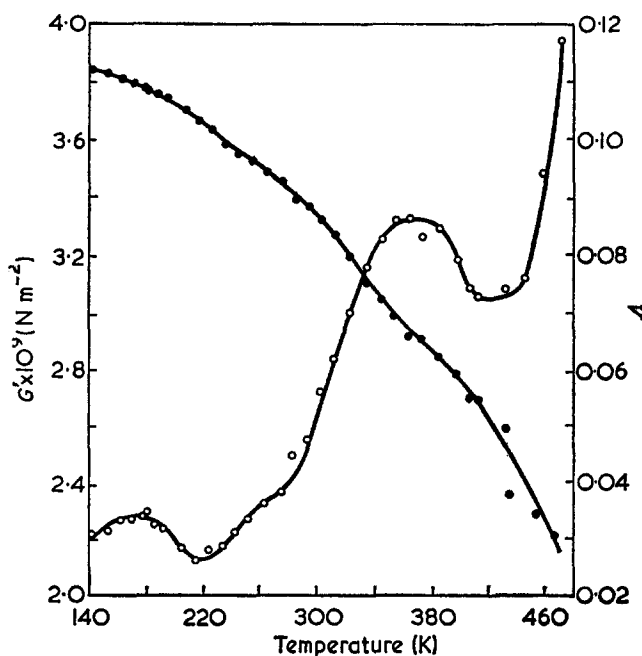


Figure 6 The logarithmic decrement as a function of temperature using the torsion pendulum at 1 Hz ( $\circ$ ).  $G'$  under the same conditions ( $\bullet$ )

$\beta$  relaxation becomes very prominent. The shear loss data derived from these experiments are plotted in Figure 3 where they can be seen to supplement the dielectric results. The activation energy resulting from the combined data of the two techniques is 103 kJ. In magnitude, this value together with its close relationship to the glass-rubber transition suggests a local mode process about the backbone chain as being responsible for the  $\beta$  process.

The mechanical loss peak at 170K correlates well with the dielectric  $\delta$  relaxation (Figure 3). The relatively small size of the mechanical loss peak *vis-à-vis* its electrical counterpart is not surprising in view of the proposed origin of the relaxation. Twisting of the five-membered ring would involve a proportionately small change in the mechanical characteristics of the material compared with the dielectric polarization change following inversion of the five membered ring.

The dielectric  $\gamma$  relaxation, which would be detected at about 260K, is not observed mechanically, possibly due to its very small magnitude.

#### ACKNOWLEDGEMENT

We wish to thank the SRC for an equipment grant.

#### REFERENCES

- Block, H., Groves, R. and Walker, S. M. *Polymer* 1972, **13**, 527
- Block, H., Lord, P. W. and Walker, S. M. in preparation
- Cubbon, R. C. P. *J. Polym. Sci. (C)* 1967, **16**, 387
- Endo, R., Hinokuma, T. and Takeda, M. *J. Polym. Sci. (A-2)* 1968, **6**, 665
- Block, H., Groves, R., Lord, P. W. and Walker, S. M. *JCS Faraday Trans. (II)* 1972, **68**, 1890
- McCrum, N. G., Read, B. E. and Williams, G. 'Anelastic and Dielectric effects in polymeric solids'. Wiley, London, 1967

# Deformation of *trans*-1,4-polyisoprene spherulite: small angle X-ray diffraction, thermal differential analysis and density studies

E. Martuscelli and C. Mancarella

Laboratorio di Ricerche su Tecnologia dei Polimeri e Reologia,  
CNR, Via Toiano 2, 80072 Arco Felice, Napoli, Italy  
(Received 19 June 1972; revised 11 September 1972)

The deformation behaviour of melt crystallized spherulitic samples of *trans*-1,4-polyisoprene was investigated by small-angle and wide-angle X-ray measurements and by density and differential thermal analysis. The X-ray diffraction experiments were carried out both on the fibres under strain with the two ends clamped and on the fibres after relaxation at room temperature. A substantially different trend is obtained in the plots of the long-spacing versus the degree of elongation for the clamped and free fibres. A limiting axial long-spacing  $L_T$  is found only in the case of the fibres with both ends fixed. The way in which isotropic *trans*-1,4-polyisoprene deforms seems to be dependent on the stretching conditions, on the thermal history, the pre-stretching conditioning and on the relative amount of polymorphic modification in the samples. A comparison with the deformation behaviour of polyethylene and polypropylene is made. The overall density and the mass crystallinity increase with the degree of elongation though a lowering in the melting point is observed. Linear relationships are obtained between the reciprocal of the long-spacing and the fusion temperature of the plastically deformed fibres.

## INTRODUCTION

Depending on crystallization conditions and thermo-mechanical treatment, *trans*-1,4-polyisoprene has two different structures probably brought about by different conformations of the polymer chains in the crystal<sup>1</sup>. The polymorphism of *trans*-1,4-polyisoprene is monotropic, no solid-solid transition having ever been observed<sup>2</sup>. The lower melting form (LM) is permanently metastable at room temperature, but may be converted to the higher melting modification (HM) by conditioning at elevated temperatures. The conversion can proceed only upon complete melting of the LM crystals<sup>3</sup>.

By quenching from the melt, polymer in the pure LM form can be easily obtained. On stretching, these samples assume a fibre-like morphology with a well-oriented pattern in the wide-angle X-ray region. Crystallization at high temperatures close to melting leads to samples of *trans*-1,4-polyisoprene with a high percentage of the higher-melting modification.

The stretching of these samples produces the orientation of the two modifications. The HM crystals always appear in association with the LM since all stretched samples, regardless of previous heat treatment show a high proportion of LM material<sup>4</sup>.

The morphology, the annealing behaviour and determination of some important thermodynamic parameters such as equilibrium melting point  $T_m^0$  and the end surface energy  $\sigma_e$  of solution grown and melt-crystallized

crystals of the LM and HM form of *trans*-1,4-polyisoprene have been the subjects of previous papers<sup>5</sup>.

In the literature there is little work describing the features of stretched *trans*-1,4-polyisoprene and the influence of external stress on the morphology and texture of this polymer. In the present paper, wide and small-angle X-ray diffraction, differential thermal analysis and density techniques have been applied to the study of the deformation of spherulitic synthetic guttapercha. The main objective was to elucidate the transition and transformation mechanism of isotropic microspherulitic melt crystallized polymer to the anisotropic fibre texture. In addition, we were concerned with correlating quantities such as degree of deformation, crystal size, melting points, density and crystallinity with the influence which the relative amounts of the two crystalline modifications in the starting samples has on them.

## EXPERIMENTAL

Synthetic *trans*-1,4-polyisoprene containing ~2% of 3,4-polyisoprene, as assessed by n.m.r. analysis, was kindly supplied by the Polymer Corporation Limited (Sarnia, Ontario, Canada). The registered trade mark of the polymer is 'transPIP' (lot 2026); number-average molecular weight ( $\bar{M}_n$ ) is 37 000.

Pellets of synthetic *trans*-1,4-polyisoprene were compression-moulded into 1 mm sheets by heating to ~80°C

and slowly cooling to room temperature. The film was cut into strips of the usual dumbbell shape. These strips were kept for about 30 min in boiling water to destroy any traces of crystallinity and were then isothermally crystallized. Straining was performed with an apparatus similar to that reported by Ishikawa *et al.*<sup>6</sup>. Both ends of the crystallized sample were clamped on the straining bars with nuts.

The samples were strained by rotation of the driving nuts by hand. The degree of elongation, defined by:

$$\epsilon = \frac{l - l_0}{l_0}$$

where  $l_0$  and  $l$  are the starting and the final sample length respectively, was determined by measuring the separation, before and after extension, of small India-ink fiducial marks placed a few millimetres apart along the longitudinal axis of the sample.

The samples were stretched isothermally in a thermostated water bath following a time conditioning of 30 min. After drawing, the sample was kept at the stretching temperature for 30 min, then removed from the thermostat and allowed to cool in air at room temperature. The degree of elongation  $\epsilon$  was measured as reported above on the sample under strain with both ends clamped.

Four sets of samples differing in thermal treatment, crystallization and stretching temperature were used for the experiments reported here.

Data on the preparation and characterization of the samples are summarized in *Table 1*.

#### X-ray measurements

Both wide (WAXS) and low (SAXS) angle reflections were recorded. The measurements were made at room temperature with a point-collimation Rigaku-Denki small-angle camera and a flat-plate camera.

CuK $\alpha$  radiation with a Ni filter was used. The photographs were taken with the beam perpendicular to the draw direction. The long periods were calculated according to Bragg's equation. Fibres were first examined by X-ray diffraction while still clamped and under strain. The fibres were then removed from the stretching frame and allowed to shrink at room temperature. A second diffraction was obtained on these free fibres. The long spacings of the fibre under strain and of the free fibre are referred to as  $L$  and  $L_1$  respectively. Correspondingly, the extension ratios are  $\epsilon$  and  $\epsilon_1$  (because of shrinkage

of the fibre  $\epsilon > \epsilon_1$ ). Thus, every deformed sample is characterized by two values of the extension ratio ( $\epsilon$ ,  $\epsilon_1$ ) whose two long spacing values correspond ( $L$ ,  $L_1$ ).

Wide angle measurements were mainly carried out to assess in the sample the presence of the two crystalline modifications and qualitatively, the degree of orientation induced by the applied strain.

#### Thermal and density measurements

A Perkin-Elmer differential scanning calorimeter DSC-1 was used to obtain melting points  $T_m$ , apparent heats of fusion  $\Delta H^*$  and crystallinities  $x_c$  of the strained polymer samples. The weight of polymer heated in each measurement was always less than 6 mg.

A heating rate of 16°C/min was used. The calorimeter was calibrated in the temperature scale, at the scanning speed to be used, using substances with standard melting points. The peak maximum temperatures were assumed to correspond to the melting temperature of the samples. They could be measured with a precision of  $\pm 0.5^\circ\text{C}$ . The apparent enthalpy of fusion  $\Delta H^*$  was computed by comparing the area under the fusion curve of the polymer samples with that obtained from a known weight of indium heated under the same conditions.

Finally, the overall mass crystallinity was obtained as the ratio between  $\Delta H^*$  and the true enthalpy of fusion  $\Delta H$  whose values for the LM and HM modification of *trans*-1,4-isoprene are 2302 and 3070 cal/mol respectively<sup>2</sup>.

Overall densities  $\rho$  were measured at 23°C by using a gradient column with isopropyl alcohol and ethylene glycol as miscible liquids. Results are accurate to  $\pm 0.001 \text{ g/cm}^3$ .

The crystallinity of the fibre was also determined by density measurement using the relation:

$$x_c = \frac{\frac{1}{\rho_a} - \frac{1}{\rho}}{\frac{1}{\rho_a} - \frac{1}{\rho_c}} \quad (1)$$

where  $\rho_c$  is the crystallographic density, and  $\rho_a$  the density of the completely amorphous polymer, was assumed to be equal to that of the amorphous rubber ( $0.91 \text{ g/cm}^3$ )<sup>7</sup>. The value of  $\rho_c$  ( $1.11 \text{ g/cm}^3$ ) was calculated from the crystallographic data of the LM modification<sup>1</sup>.

*Table 1* Crystallization, thermal stretching conditions and some physical properties of the samples of *trans*-1,4-polyisoprene used for the deformation studies

Sample	Crystallization conditions of the unstrained samples	Percentage of the two solid modifications in the melt crystallized sample*	Thermal treatment before the stretching	Temperature of stretching (°C)	Melting temperature of the unstrained samples (°C)	Long spacing of the unstrained samples (Å)
A	Crystallized from 100°C at 0°C	~100% LM ~0% HM	None	28.6	42	164
B	Crystallized from 100°C at 0°C	~100% LM ~0% HM	None	35	44	178
C	Crystallized from 100°C at 0°C	~100% LM ~0% HM	Annealed for 24 h in the unstrained state at 40°C	28.6	46	183
D	Crystallized from 100°C by slowly cooling to room temperature	~61% LM ~39% HM	None	35	LM 41 HM 49	173

\* By d.t.a. measurements.

## RESULTS

Following the crystallization and the thermal treatments indicated in *Table 1*, samples A, B and C of *trans*-1,4-polyisoprene crystallize in the pure LM modification while sample D proves to be a mixture of the LM and HM crystals.

The relative amounts of the two crystalline modifications were assessed qualitatively by WAXS and quantitatively by d.t.a. by measuring and comparing the areas of the endotherm peaks of the two forms whose melting temperatures differ by several degrees.

*X-ray scattering*

When a sample of *trans*-1,4-polyisoprene is deformed, the original homogeneous ring of the SAXS is transformed into a diagram with two distinct maxima on the meridian. Correspondingly, a fibre-like oriented pattern is obtained in the WAXS (see *Figures 1* and *2*). The degree of orientation increases with  $\epsilon$ , as expected. After relaxation, the fibres are still well oriented, as can be deduced by comparing the shape of the WAXS reflection of the clamped and free fibres (see *Figure 2*).

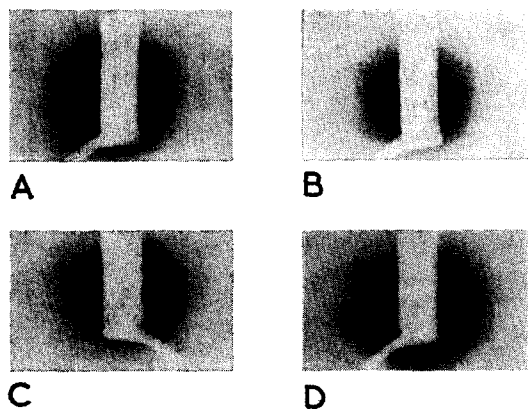
These observations lead to the conclusion that when *trans*-1,4-polyisoprene is stretched under the experimental conditions reported above, and allowed to shrink at room temperature, plastically deformed samples are obtained.

The long period ( $L$  for the clamped fibres and  $L_1$  for the free fibres) in the draw direction was derived from the position of the SAXS meridional maxima.

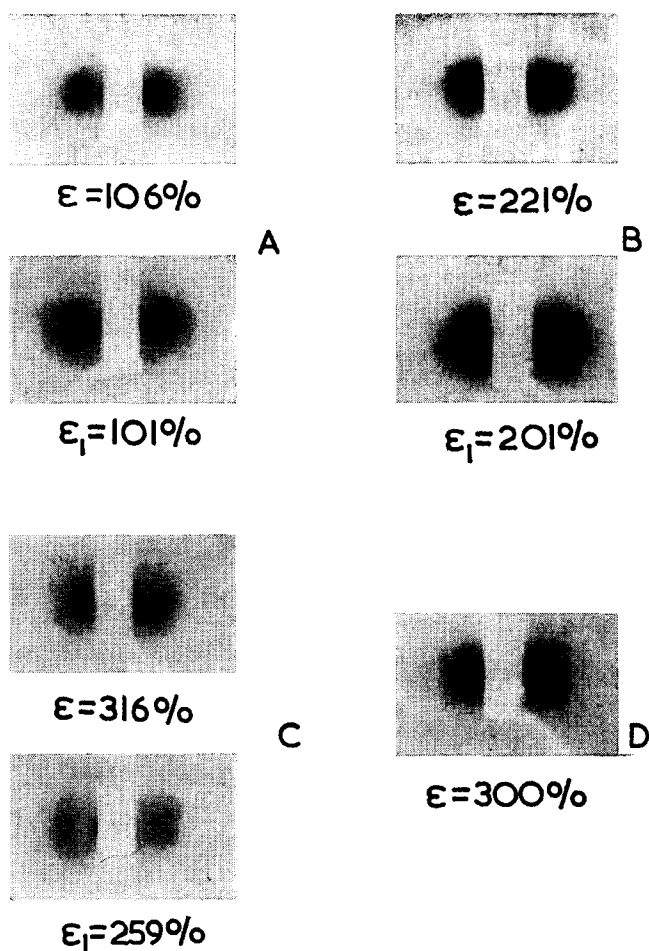
These quantities are plotted in *Figures 3* to *5* as functions of the degree of elongation  $\epsilon$  and  $\epsilon_1$  for samples A, B, C and D. Upon drawing in the case of samples B and C, the small-angle long spacing  $L$  drops from initial value  $L_0$  (178 for B and 183 for C) of the melt crystallized sample to an almost identical constant value of  $L$  ( $\approx 162$  Å). This final value is attained at an extension ratio of  $\sim 100\%$  and  $\sim 150\%$  for B and C respectively.

A levelling off of  $L$  with the draw ratio was observed by Samuels<sup>8</sup> and Peterlin<sup>9</sup> in the case of plastically deformed samples of polypropylene and polyethylene.

Samples A and D behave differently. In the same range of deformation, no levelling off is observed in the plot of  $L$  versus  $\epsilon$ . In fact, one obtains a gradual and continuous lowering of  $L$  versus  $\epsilon$  with an almost



*Figure 1a* Small angle X-ray diffraction pattern from undeformed melt crystallized samples A, B, C and D of *trans*-1,4-polyisoprene



*Figure 1b* Small angle X-ray diffraction patterns from deformed samples of *trans*-1,4-polyisoprene. The degree of elongation before ( $\epsilon$ ) and after ( $\epsilon_1$ ) relaxation of the fibres is indicated

linear trend. The rate of lowering seems to be higher for sample A.

The values of  $L_1$  are always lower than the corresponding values of  $L$  (see *Figures 3* to *5*). This indicates a contraction in the long-spacing in the draw direction when the fibres are allowed to relax and shrink at room temperature.

This process appears to be reversible, if the shrunken fibres are re-stretched at room temperature to a new  $\epsilon$  value, and the long-period measured on the clamped fibre, a point is obtained that falls on the curve of  $L$  versus  $\epsilon$ . This is illustrated for sample C in *Figure 5*. The numbers 1, 2 and 3 respectively refer to the clamped, relaxed and re-stretched fibre.

All the samples examined show a linear decrease of  $L_1$  with  $\epsilon_1$  even in the region of deformation where the corresponding meridional long-period  $L$  of the unrelaxed, clamped fibre, remains constant with  $\epsilon$  (compare the plots of  $L$  and  $L_1$  in the case of sample B and C in *Figures 4* and *5*).

*Density measurement results*

The macroscopic density  $\rho$  and the mass crystallinity  $x_c$  of the drawn samples A and B of *trans*-1,4-polyisoprene are reported in *Table 2* together with  $\epsilon_1$ ,  $L_1$  and the melting temperatures  $T_m$ . The fibres were allowed to shrink at room temperature before measurement. Both quantities  $\rho$  and  $x_c$  show a qualitatively similar

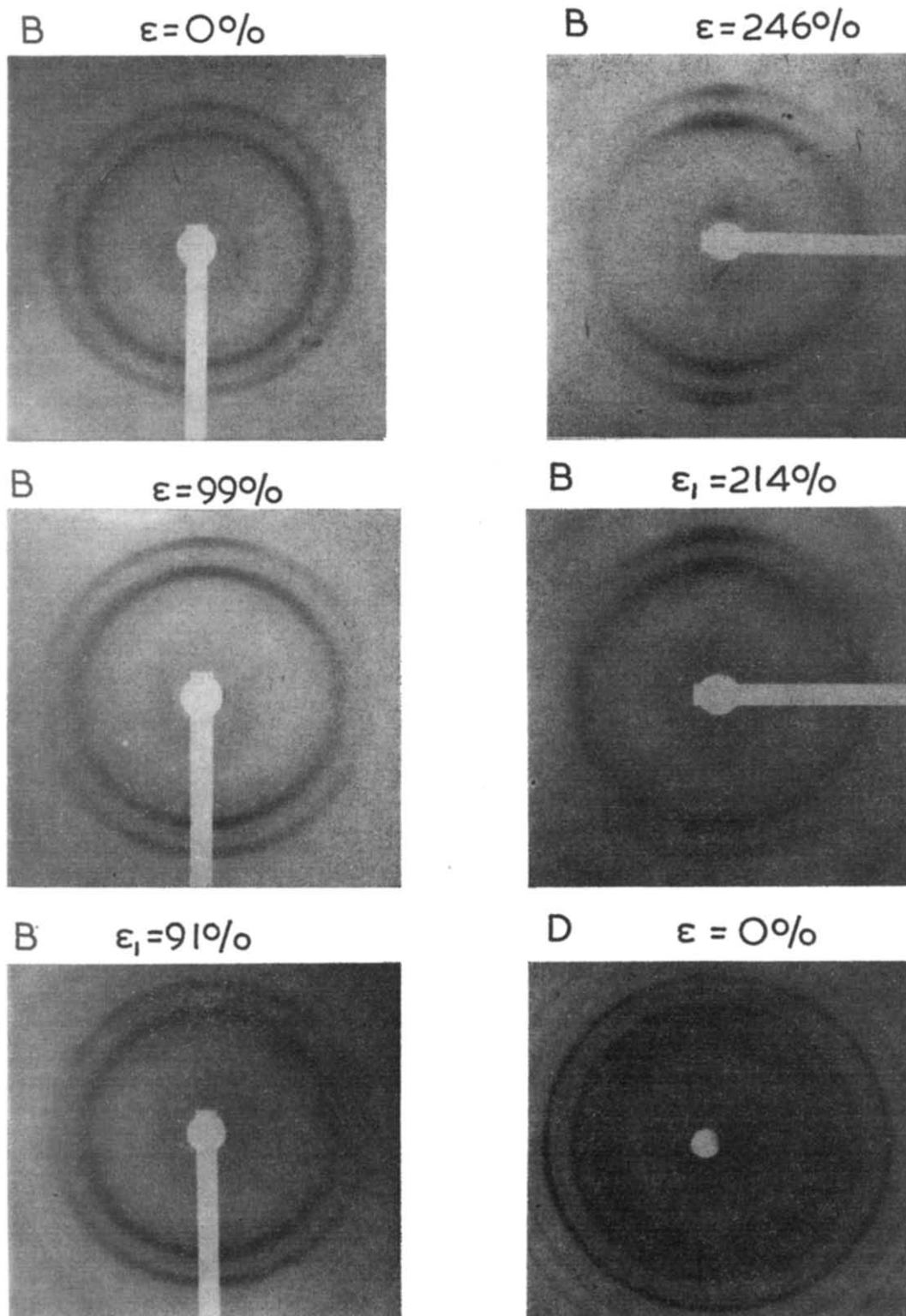


Figure 2 Wide angle X-ray diffraction patterns from undeformed and deformed samples of *trans*-1,4-polyisoprene (samples B and D). The degree of elongation is reported. Sample B ( $\epsilon=0$ ) is in a pure LM form; sample D ( $\epsilon=0$ ) is a mixture of the two crystalline modifications

dependence on  $\epsilon_1$ . In fact, a sudden change is observed from the values of the unstrained melt-crystallized material (0.9621 and 0.9625 g/cm<sup>3</sup> for the density and  $\sim 0.30$  for the crystallinity of B and A respectively) to new higher values. At a higher degree of deformation ( $\epsilon_1 \simeq 300\%$ ) density and crystallinity increase to 0.9713 g/cm<sup>3</sup> and  $\sim 0.35$  for sample B and to 0.9716 g/cm<sup>3</sup> and 0.35 for sample A.

The crystallinity has been calculated according to equation (1) assuming that the density of the crystalline

and amorphous regions is independent of the draw ratio.

#### Thermal data

Melting points  $T_m$  of the fibres of samples A, B and C after relaxation, as determined by the d.t.a. endotherm peaks, are reported in Table 2 and plotted versus the reciprocal of the long-spacing  $1/L_1$  in Figure 6.

All the samples show a gradual decrease in the melting point with  $\epsilon_1$ . All the experimental points reported in

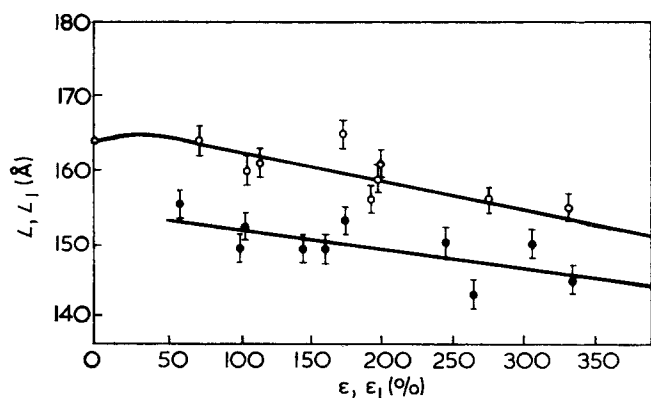


Figure 3 Long spacing (Å) of fibres of sample A of *trans*-1,4-polyisoprene as a function of the degree of elongation. ○, long spacings,  $L$ , and degree of elongation,  $\epsilon$ , measured on fibres with both ends fixed; ●, long spacings,  $L_1$ , and degree of orientation,  $\epsilon_1$ , measured on fibres with both ends free after relaxation at room temperature

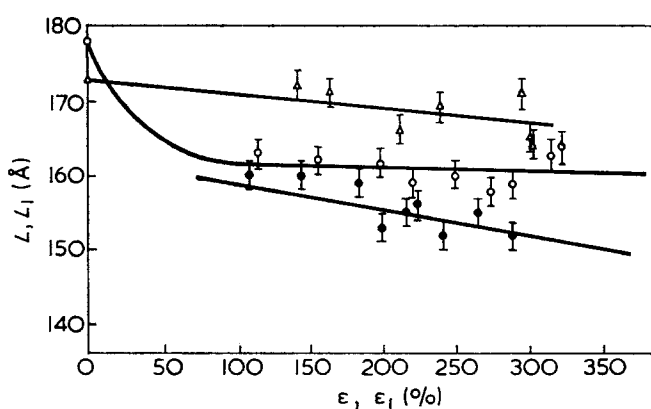


Figure 4 Long spacing of fibres of *trans*-1,4-polyisoprene as a function of the degree of elongation. ○, long spacing,  $L$ , and degree of elongation,  $\epsilon$ , measured on fibres of sample B with both ends fixed; ●, long spacing,  $L_1$ , and degree of elongation,  $\epsilon_1$ , measured on fibres of sample B with both ends free after relaxation at room temperature; △, long spacing,  $L$ , and degree of elongation measured on fibres of sample D with both ends fixed

Figure 6 (including that of the undeformed samples) can be fitted by the same straight line whose equation is:

$$T_m = 345 - 4688 \frac{1}{L_1} \quad (2)$$

The values of the coefficient of equation (2) does not change drastically if the points of the undrawn samples are not taken into consideration.

Assuming a two phase model for the fibre of *trans*-1,4-polyisoprene with crystalline and amorphous layers arranged periodically in the draw direction, the thickness of crystallites  $L_c$  can be calculated by using the equation:

$$L_c = \frac{x_c \cdot L_1}{\frac{\rho_c}{\rho_a} [1 - x_c] + x_c} \quad (3)$$

where  $L_1$  is the long-period in the fibre axis direction as derived from SAXS,  $x_c$  the mass crystallinity and  $\rho_c$  and  $\rho_a$  the density of the crystalline and amorphous regions respectively. In Table 2 the values of  $L_c$  and  $L_a$  ( $L_a = L_1 - L_c$ , is the thickness of the amorphous layer) are reported for samples A and B. The values of the

crystallinity used in the calculation of  $L_c$  and  $L_a$  were obtained by means of equation (1).

It is interesting to point out that the amorphous regions of the fibres are  $\sim 2.3$  times thicker than the crystalline ordered phase.

## DISCUSSION

First, it is interesting to consider the results of previous work which point to the explanation of the processes involved in the deformation of polymeric materials. Meinel *et al.*<sup>9</sup>, while plastically deforming polyethylene, found that the SAXS homogeneous ring of the melt crystallized material is first transformed into a pattern with four maxima whose angular and radial positions are dependent upon the value of the draw ratio and then, at high values of  $\epsilon$  ( $> 300\%$ ), a meridional two-point pattern arises whose spacing is independent of the draw ratio and of the long-period of the starting melt crystallized material.

A similar limiting axial long-period ( $L_T$ ) has also been observed in the case of polypropylene by Samuels<sup>8</sup>, by Balta-Calleja and Peterlin<sup>11</sup> and by Zubov<sup>12</sup> on fibres, films, and monofilaments respectively.

The values of  $L_T$  are shown to be dependent on the thermal stretching conditions only, increasing with the drawing temperature<sup>11</sup>. According to Samuels' results<sup>8</sup>,  $L_T$  seems related to the degree of orientation of

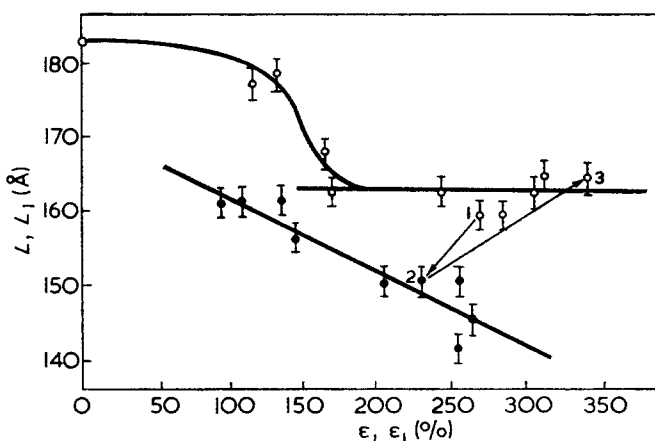


Figure 5 Long spacing (Å) of fibres of sample C of *trans*-1,4-polyisoprene as a function of the degree of elongation. ○, long spacing,  $L$ , and degree of elongation,  $\epsilon$ , measured on fibres with both ends fixed; ●, long spacing,  $L_1$ , and degree of orientation,  $\epsilon_1$ , measured on fibres with both ends free after relaxation at room temperature

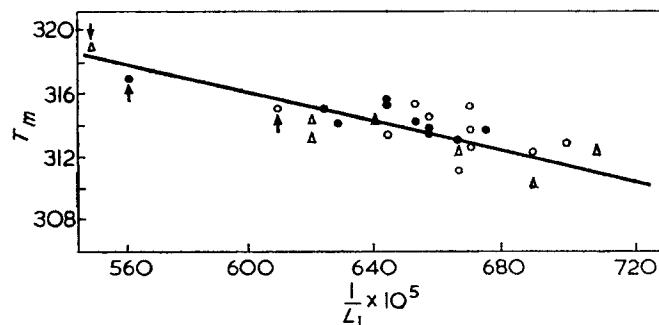


Figure 6 Melting temperatures (K) of fibres of *trans*-1,4-polyisoprene as function of the reciprocal of the long spacing  $L_1$  ( $\text{\AA}^{-1}$ ). ○, Sample A; ●, sample B; △, sample C. The arrows refer to the melt crystallized undeformed sample ( $\epsilon = 0$ )

Table 2 Long-spacing ( $L_1$ ), overall density ( $\rho$ ), mass crystallinity ( $x_c$ ), melting temperatures ( $T_m$ ), thickness of the crystallites ( $L_c$ ) and of the amorphous regions ( $L_a$ ) for plastically deformed fibres of samples A, B and C of *trans*-1,4-polyisoprene. The degree of elongation ( $\epsilon_1$ ) is also reported

Sample	$\epsilon_1$ (%)	$L_1$ (Å)	$\rho$ (g/cm <sup>3</sup> )	$x_c^*$ (%)	$T_m$ (K)	$L_c^\dagger$ (Å)	$L_1 - L_c = L_a$ (Å)
A	0	164	0.9625	30	315	—	—
A	105	152	0.9690	34	314	45	107
A	145	149	0.9692	34	315	44	105
A	175	153	0.9702	34	315	46	107
A	245	150	0.9705	35	313	46	104
A	265	143	0.9712	35	312	44	99
A	306	150	0.9719	35	311	45	105
A	335	145	0.9716	35	312	45	100
B	0	178	0.9621	30	317	—	—
B	109	160	0.9679	33	315	46	114
B	183	159	0.9685	33	314	46	113
B	217	155	0.9699	34	315	45	110
B	243	152	0.9693	34	314	45	107
B	266	155	0.9685	34	315	46	109
B	289	148	0.9696	34	313	40	108
B	289	152	0.9713	35	313	47	105
C	0	183	—	—	319	—	—
C	109	161	—	—	313	—	—
C	137	161	—	—	314	—	—
C	144	156	—	—	314	—	—
C	208	150	—	—	312	—	—
C	258	141	—	—	312	—	—
C	259	150	—	—	309	—	—
C	268	145	—	—	310	—	—

\*  $x_c$  from density measurements according to equation (1)

†  $L_c$  is calculated according to equation (3)

the  $\vec{c}$  axis of the crystals along the draw direction. In fact, in the case of isotactic polypropylene film it is attained only when the lamellae are almost fully oriented with their  $\vec{c}$  axis parallel to the deformation direction.

The WAXS patterns of plastically deformed polyethylene first show a split of the (200) and (020) reflection, but by increasing  $\epsilon$ , the angle of the split decreases until the reflections coalesce on the equatorial line.

At this point, the normal fibre-like WAXS pattern is attained. At high extension a line lattice is obtained and fibrillation occurs. Further deformation of the samples is obtained by *cleavage of crystallites* which is the predominating process.

During this latter process, the long-spacing is constant while the extension of the sample can still be increased. Furthermore, a decrease in the intensity of the meridional SAXS at high draw ratio seems to indicate that the disordered phase orients throughout the draw region since this intensity is proportional to the square of the difference in the electron density between the crystalline and non-crystalline regions<sup>8</sup>.

In conclusion, the discontinuity in the transformation of isotropic spherulitic microstructure into the fibre-like morphology, as revealed by low-angle, wide-angle and other techniques at higher degrees of elongation, is explained by the above mentioned authors assuming that the starting lamellae are broken into small blocks of folded chains and incorporated in microfibrils.

The work of deformation produces a heating of the sample up to a temperature that is characteristic of the drawing temperature. This process of heating allows the blocks to rearrange themselves in a new fibre morphology with well-defined long-spacing. In the case of deformation of samples of *trans*-1,4-polyisoprene, neither four-point patterns in the SAXS nor split in the equatorial

WAXS reflections is observed even at the lowest degree of elongation ( $\approx 50\%$ ).

Noteworthy is the difference in the trend of the plots of the long spacing *versus* the degree of elongation for the clamped and free fibres.

A clearly defined, limiting axial long-spacing  $L_T$  is obtained only in the case of samples B and C of *trans*-1,4-polyisoprene when the diffraction experiments are performed on the fibres with both ends fixed.

It is interesting to note that the values of  $L_T$  obtained are almost the same ( $\sim 162$  Å) although the thermal history and stretching temperature of the two samples are different (see Table 1). On the other hand, fibres of samples A and C, whose stretching temperatures are equal, show a totally different trend in the plots of  $L$  and  $L_1$  *versus*  $\epsilon$  and  $\epsilon_1$  respectively (see Figures 3 and 5). A substantial difference is also observed when the behaviour of fibres of pure LM *trans*-1,4-polyisoprene (sample B) is compared with that of samples containing both phases (sample D) when both are deformed at 35°C (see Figure 4).

As far as the permanently deformed fibres are concerned, the plots of  $L_1$  against  $\epsilon_1$  never show levelling off. Thus, no limiting values of  $L_1$  arise, but a continuous lowering is observed for all the samples examined.

According to our SAXS and WAXS results we conclude that the way in which isotropic *trans*-1,4-polyisoprene deforms is dependent not only on the stretching conditions, but also seems to be dependent in a rather complicated way on the thermal history, the pre-stretching conditioning and on the relative amount of polymorphic modification in the samples.

These conclusions are in contrast with the above mentioned findings on polyethylene and polypropylene.



Much work must still be done before we can describe and forecast the behaviour of a deformed polymer. We believe that, together with the straining conditions and thermal history of the samples, the mechanism of transition from isotropic spherulitic structure to anisotropic fibre is also very much dependent on the physical, chemical, morphological and thermomechanical properties of the polymeric material.

#### ACKNOWLEDGEMENTS

We thank Mr E. Scafora and Miss C. Carelli who actively contributed to this work.

#### REFERENCES

- 1 Bunn, C. W. *Proc. R. Soc.* 1942, **A180**, 40; Fisher, D. *Proc. Phys. Soc. (B)* 1953, **46**, 7
- 2 Mandelkern, L., Quinn, F. A. Jr. and Roberts, D. E. *J. Am. Chem. Soc.* 1956, **78**, 926
- 3 Leeper, H. M. and Schlesinger, W. *J. Polym. Sci.* 1953, **4**, 307; Lowering, E. G. and Wooden, D. C. *J. Polym. Sci. (A-2)* 1969, **7**, 1639
- 4 Hardin, J., Luch, D. and Yeh, G. S. Y. *J. Polym. Sci. (B)* 1971, **9**, 771
- 5 Keller, A. and Martuscelli, E. *Makromol. Chem.* 1972, **151**, 189; Martuscelli, E. *Makromol. Chem.* 1972, **151**, 159
- 6 Ishikawa, K., Miyasaka, K., Maeda, M. and Yamada, M. *J. Polym. Sci. (A-2)* 1969, **7**, 1259
- 7 'Polymer Handbook'. (Eds J. Brandrup and E. H. Immergut), Interscience, New York, 1967, VI-58
- 8 Samuels, R. J. *J. Polym. Sci. (A-2)* 1968, **6**, 1101
- 9 Meinel, G., Morosoff, N. and Peterlin, A. *J. Polym. Sci. (A-2)* 1970, **8**, 1723
- 10 Hoffman, J. D. *SPE Trans.* 1964, **4**, 315
- 11 Balta-Calleja, F. J. and Peterlin, A. *J. Polym. Sci. (A-2)* 1969, **7**, 1275
- 12 Zubov, A., Tsvankin, D. A., Markova, G. L. and Kargin, V. A. *Vysokomol. Soedin.* 1964, **6**, 406

## Crazing in a crystalline polymer (isotactic polypropylene) and the role of N<sub>2</sub>, O<sub>2</sub>, and CO<sub>2</sub> as crazing agents

H. G. Olf and A. Peterlin

Camille Dreyfus Laboratory, Research Triangle Institute, PO Box 12194,  
Research Triangle Park, North Carolina 27709, USA  
(Received 6 November 1972)

In a recent paper Lyakhovich *et al.*<sup>1</sup> described the temperature dependence of deformability of crystalline polymers and called attention to a significant increase in deformability of polypropylene and polyisobutylene with decreasing temperature around liquid nitrogen temperatures. As these authors state, such behaviour is in contrast to the usually observed decrease in deformability with lower temperature and particularly differs from the behaviour of polyethylene at liquid nitrogen temperatures. In an attempt to check this effect we investigated films of crystalline isotactic polypropylene in the temperature range from solid nitrogen to room temperature. The occurrence of large plastic deformation around liquid nitrogen temperatures was confirmed and found to be due to extensive crazing; it was further found to be an environmental effect similar to that observed by Parrish and Brown in amorphous polymers<sup>2</sup>. Polypropylene in contact with solid, liquid, or gaseous nitrogen shows both crazing and large plastic deformation between  $-210^{\circ}\text{C}$  and  $-140^{\circ}\text{C}$ . In a helium atmosphere or in vacuum neither is observed.

Crazing is commonly associated with glassy, amorphous polymers as recently reviewed by Rabinowitz and Beardmore<sup>3</sup> and by Kambour and Robertson<sup>4</sup>. A few reports in the literature indicate, however, that crazing can occur in crystalline polymers as well<sup>5-9</sup>. In particular, crystalline polypropylene was shown by van den Boogaart<sup>7</sup> to craze at room temperature and above. The present communication is concerned with crazing in crystalline, isotactic polypropylene at low temperatures, in the range from  $-210^{\circ}\text{C}$  to  $0^{\circ}\text{C}$ , and with the role played by gaseous environments in the crazing process.

The experiments here described were made with a polypropylene film of 0.125 mm thickness. This was an extruded and subsequently quenched film made of isotactic polypropylene by the Rexall Chemical Co. The X-ray diagram indicated that the crystallites are in the so-called smectic form and that they are randomly distributed, i.e., that the film is isotropic. Since residual orientation might affect the present results, many experiments were performed with the mechanical stress, applied to induce crazing, parallel as well as perpendicular to the extrusion direction. Since the results were identical in every respect, it was concluded that the film is indeed isotropic.

This polypropylene film was found to develop a myriad of crazes when stressed in liquid nitrogen, giving the sample the silvery appearance in reflected light so characteristic of crazing. That we are dealing with crazes rather than cracks is evident by the practically

unimpaired strength of the sample at both liquid nitrogen temperatures and room temperature. Optical microscopy and scanning electron microscopy revealed some of the well-known features of the craze: the typical 'lip', the fibrillar bridges across the craze, and the nearly perfect perpendicularity of the crazes to the stress direction.

A load *versus* strain curve obtained in liquid nitrogen is shown in *Figure 1a*. This is somewhat atypical in that it depicts the greatest strain to break we have so far observed in liquid nitrogen, more than 60%. The average of 20 samples in strain to break is 32%.

Crazes first appear when the load begins to level out. The load then remains remarkably constant while more crazes form and those already present grow to maturity. Finally, fracture occurs under gradual propagation of a crack which mostly starts at the edge of the sample.

Crazing also proceeds in nitrogen gas, provided the temperature is close to liquid nitrogen temperature,  $-196^{\circ}\text{C}$ . It also occurs in solid nitrogen, at  $-210^{\circ}\text{C}$ , a condition reached by reducing the pressure above the initially liquid nitrogen with a pump. The load *versus* strain curves obtained in solid and in liquid nitrogen are practically identical, as are those obtained in gaseous nitrogen at temperatures very close to  $-196^{\circ}\text{C}$ . The curves at higher temperatures, however, are quite different, the more so, the higher the temperature is above  $-196^{\circ}\text{C}$  (*Figures 1a* and *1b*). The yield and ductile stress and the stress to break increase, the strain to break decreases, and the crack propagation becomes faster with increasing temperature up to about  $-140^{\circ}\text{C}$  (*Figure 1a*); the tough ductile material becomes ductile brittle. Examination of the fractured specimens in the optical microscope showed that crazes had formed at all temperatures including  $-140^{\circ}\text{C}$ , although they became fewer in number and also finer and more difficult to detect as the temperature approached  $-140^{\circ}\text{C}$ .

At temperatures above  $-140^{\circ}\text{C}$  the stress to break decreases steadily (*Figure 1b*). Up to  $-100^{\circ}\text{C}$  crazes were practically absent. The sample drawn at  $-56^{\circ}\text{C}$  showed crazes again, but these were obviously different from those obtained around  $-196^{\circ}\text{C}$  in that they were very coarse and easily visible even with the naked eye. Above  $-56^{\circ}\text{C}$  more and more of this type of craze occurred on drawing. At  $-28^{\circ}\text{C}$  a definite, macroscopic neck appeared, encompassing the entire cross-section area of the sample. Whereas the crazes at lower temperatures were rather long, traversing the width of the sample, those at  $-28^{\circ}\text{C}$  were much shorter.

In summary, there are two temperature ranges in which crazing occurs in a nitrogen environment: one region around liquid nitrogen temperatures,  $-196^{\circ}\text{C}$  and another around  $-30^{\circ}\text{C}$ , in the neighbourhood of

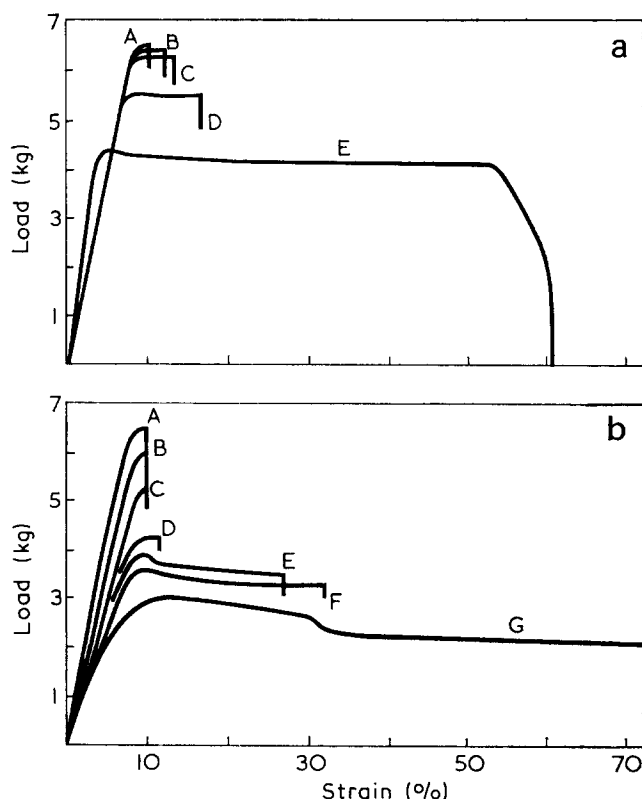


Figure 1 Load versus strain curves obtained with the extruded polypropylene film at different temperatures and in different environments: (a) between  $-196^{\circ}\text{C}$  and  $-140^{\circ}\text{C}$  (A,  $-140^{\circ}\text{C}$ ; B,  $-155^{\circ}\text{C}$ ; C,  $-170^{\circ}\text{C}$ ; D,  $-183^{\circ}\text{C}$ ; E,  $-196^{\circ}\text{C}$ ) and (b) between  $-140^{\circ}\text{C}$  and  $-28^{\circ}\text{C}$  (A,  $-140^{\circ}\text{C}$ ; B,  $-115^{\circ}\text{C}$ ; C,  $-101^{\circ}\text{C}$ ; D,  $-56^{\circ}\text{C}$ ; E,  $-36^{\circ}\text{C}$ ; F,  $-33^{\circ}\text{C}$ ; G,  $-28^{\circ}\text{C}$ ). Cross-section area of the samples at  $20^{\circ}\text{C}$ :  $0.0125 \times 0.5 \text{ cm}^2 = 0.00625 \text{ cm}^2$ ; gauge length: 1 cm. The data were obtained with an Instron (TM-M) apparatus at an extension rate of  $0.05 \text{ cm/min}$

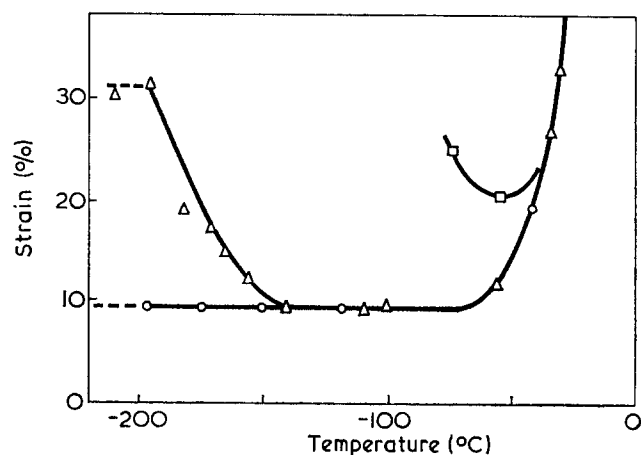


Figure 2 The average strain to break as a function of temperature;  $\Delta$ , in  $\text{N}_2$ ;  $\circ$ , in He and vacuum;  $\square$ , in  $\text{CO}_2$

the glass transition temperature of polypropylene. This behaviour is well represented in Figure 2 where the strain to break (average of several samples) appears plotted versus the test temperature. At temperatures where extensive crazing occurs the strain to break is comparatively high.

Similar experiments were performed in other environments: helium, oxygen, carbon dioxide, and vacuum. The results can be summarized as follows.

Oxygen, having a boiling point ( $-183^{\circ}\text{C}$ ) very close

to that of nitrogen, gave results very similar to those for nitrogen. In helium, which has a boiling point of  $-269^{\circ}\text{C}$ , crazing occurred only at temperatures around  $-30^{\circ}\text{C}$ , but not around  $-196^{\circ}\text{C}$ ; as a consequence the strain to break remains small at  $-196^{\circ}\text{C}$  in He (Figure 2). The load at break in He at  $-196^{\circ}\text{C}$  is about  $7.4 \text{ kg}$  which is 80% greater than the  $4.1 \text{ kg}$  in  $\text{N}_2$  at  $-196^{\circ}\text{C}$ . The results obtained in vacuum are very similar to those in He.

These results certainly suggest that a gas may promote crazing at temperatures near its condensation point. This is further supported by experiments in  $\text{CO}_2$  which has a sublimation point of  $-78^{\circ}\text{C}$ . Extensive crazing was observed in  $\text{CO}_2$  at  $-75^{\circ}\text{C}$ , resulting in a strain to break of 25% (Figure 2).

The crazing at temperatures around  $-30^{\circ}\text{C}$ , that is just below the glass transition temperature of polypropylene, is quite analogous to the well-known crazing of amorphous polymers below their glass transition temperatures<sup>3,4</sup> and requires little comment. It is the crazing at lower temperatures, promoted by gases near their condensation points, which demands an explanation. Parrish and Brown<sup>2</sup> have reported the effect for some amorphous polymers and argued that it is due to the gas or liquid becoming adsorbed on the polymer surface and causing a significant reduction in surface energy.

An alternative explanation is that these gases are absorbed in the polymer and act as plasticizers, thus making possible the plastic flow necessary in craze initiation and propagation. Gent has shown that poor swelling agents will become locally highly absorbed at the tip of a flaw or growing craze because of stress concentration at that point<sup>10</sup>. We submit that this mechanism may increase the absorption of the gas at a flaw or craze tip to the extent that the polymer becomes plasticized and capable of plastic flow and cavitation in the stress field.

A more detailed report will be published soon.

#### ACKNOWLEDGEMENTS

This work was supported by the Camille and Henry Dreyfus Foundation. The authors wish to thank Dr G. N. B. Burch of the Hercules Inc., Research Laboratories, Research Triangle Park, North Carolina for supplying the extruded polypropylene film, and Mr Harry Sugg of this laboratory for his expert help with the stress-strain experiments.

#### REFERENCES

- 1 Lyakhovich, I. S., Musayelyan, I. N. and Chirkov, N. M. *Vysokomol. Soedin.* 1968, **A10**, 715
- 2 Parrish, M. and Brown, N. *Nature (Phys. Sci.)* 1972, **237**, 122
- 3 Rabinowitz, S. and Beardmore, P. *CRC Crit. Rev. Macromol. Sci.* 1972, **1**, 1
- 4 Kambour, R. P. and Robertson, R. E. in 'Polymer Science', (Ed. A. D. Jenkins), North-Holland Publishing Co., Amsterdam, 1972, p 803
- 5 Farrow, B. and Ford, J. E. *Nature* 1964, **201**, 183
- 6 Prevorsek, D. and Lyons, W. J. *J. Appl. Phys.* 1964, **35**, 3152
- 7 van den Boogaart, A. in 'Physical Basis of Yield and Fracture', Inst. of Phys. and Phys. Soc. (Conference Series No. 1), Oxford, 1966, p 167
- 8 Harris, J. S. and Ward, I. M. *J. Mater. Sci.* 1970, **5**, 573
- 9 Daniels, R. K. *J. Appl. Polym. Sci.* 1971, **15**, 3109
- 10 Gent, A. N. *J. Mater. Sci.* 1970, **5**, 925

# Book Reviews

## **Keratins: their composition, structure and biosynthesis**

R. D. B. Fraser, T. P. MacRae and G. E. Rogers  
C. C. Thomas, Springfield, Ill., 1972, 304 pp. \$16.75

Although one of its manifestations is considered man's 'crowning glory' and another is the basis of one of the oldest industries, keratin has always been the least glamorous of the proteins. This dead, relatively inert substance, evolved as a protective layer between the higher vertebrates and their environment, could never compete on molecular biological terms with the structure-function relationships of other fibrous proteins such as myosin. The enzyme proteins appeared to outclass it completely.

However, the multi-detective story unveiled under the leadership of ace researchers Fraser, MacRae and Rogers changes this picture. The many-faceted keratin, hard, soft,  $\alpha$ ,  $\beta$ , matrix, amorphous, mammalian, avian, reptilian is exposed in a dance of a hundred veils which, despite attack from chemical, spectroscopic, microscopic, diffraction and any other method so far possible, still has another fifty to go.

This is a fascinating book, clear and detailed. Smoothly folded into 250 pages of text are no fewer than 599 assessed, criticized and evaluated references to original work on keratin. All this is done with tact and understanding, not only of the scientific problems involved, but also of the difficulties confronting researchers limited to the techniques and knowledge current at the time of the research. The vast experience of the authors in the field is continuously balanced by that of other researchers and the whole is a most gracious review of scientific investigation and investigators. The production is impeccable and the many photo- and electron-micrographs are superbly presented. The diagrams are precise and clear and these, as well as the illustrations and tables, are positioned meticulously so as to require a negligible amount of 'page-thumbing'.

Despite the ease of reading, the book is dense with facts and is destined to become the definitive work on keratin for many years. It will be an indispensable work of reference for those involved in fundamental research on keratin chemistry and structure and also, especially so because of the large chapter on biogenesis, be of great value to medical research.

No scientific criticism is warranted or necessary. Figure 5.16, the electron density map of  $\beta$ -keratin, may raise a few eyebrows as it did when the original paper was published in *Polymer* (1969, Vol 10, p 822). However, all X-ray diffraction work on keratin

has had to involve an eye of faith, from the very beginning of Astbury's investigations in the early thirties. It is perhaps hard for the 'older hands' in the game to find the  $\alpha$ - $\beta$  transformation relegated to one-half page, although this is mollified by appropriate reference.

Speculative comments are kept to a minimum throughout the book and fields where further investigation is necessary before worthwhile comment can be made are clearly indicated.

This book will be invaluable for all those concerned with fibrous protein systems and related biopolymer systems.

E. Beighton

## **Reviews in macromolecular chemistry**

Edited by G. B. Butler, K. F. O'Driscoll and M. Shen  
Marcel Dekker, New York, 1972, Vol 7, 305 pp. \$19.50;  
Vol 8, 337 pp. \$19.50

Although there are a growing number of review journals in the field of polymer science, the rapid proliferation of journals for the publication of original work creates a demand for periodic reviews of the tremendous variety of topics.

The present review volumes are hardbound versions of previously published journal editions and, whilst this provides a convenient opportunity to purchase individual volumes in a durable form, the duplication of publications can hardly be commended.

Volume 7 comprises reviews of Linear polyquinoxalines, Nylons—known and unknown, Recent advances in polymer fractionation, Rheology of adhesion, Solvation of synthetic and natural poly-electrolytes, and Hydrogen transfer (isomerization) polymerization with anionic catalysts.

Volume 8 comprises reviews of Polymerization of carbenoids, Carbenes and nitrenes, Collagen and gelation in the solid state, Ring opening polymerization of cyclo-olefins, Thermodynamics of (cationic) polymerization, Polymerization of *N*-vinyl carbazole initiated by metal salts, Vibration spectroscopy of polymers, and Polymer compatibility.

In both volumes the presentation is very good and there are useful author and subject indexes. Although the chapters are not uniform in either topicality or critical comment, all serve to provide a convenient reference point to progress in the various areas covered and afford this opportunity to those who do not subscribe to the journal edition.

A. Ledwith

## Reprinted Volumes of

# **POLYMER**

1960-1969 (Vols 1-10)

**Missing volume of POLYMER in your library?**

The first 10 volumes of POLYMER, covering the years 1960 to 1969, have now been reprinted in separate volumes (one per year) and are available at £15.00 (\$39.00) per volume.

All orders should be sent direct to:

Wm Dawson and Sons Ltd,  
Cannon House,  
Folkestone,  
Kent, UK

## Conference Announcement

### **Order in Polymer Solutions**

Midland, Michigan, 20-24 August 1973

The Midland Macromolecular Institute will sponsor a Symposium on 'Order in Polymer Solutions' to be held from August 20 to 24, 1973 in Midland, Michigan. The Symposium will consist of both invited and contributed papers. The invited papers will offer critical reviews on order in isolated biological and synthetic macromolecules, preferential solvation, association and morphological transitions in dilute and concentrated solutions. Contributed papers are solicited. For further information write to: Organizing Committee, Midland Macromolecular Institute, 1910 W. St Andrews Drive, Midland, Michigan 48640, USA.

# Synthesis and solution behaviour of polystyrene-g-polyisoprene copolymers

C. Price and D. Woods

Department of Chemistry, University of Manchester, Manchester M13 9PL, UK  
(Received 25 October 1972)

A graft copolymer was prepared by adding poly(isoprenyl lithium) to chloromethylated polystyrene. Four samples, isolated from the product by a liquid-liquid separation scheme, were characterized with respect to molecular weight and chemical composition. The intrinsic viscosities of the samples in methyl cyclohexane and n-decane were studied over a range of temperatures. On cooling in both solvents the results suggested that before the temperatures of liquid-liquid separation were reached segregation and partial collapse of the polystyrene main chains occurred.

## INTRODUCTION

Earlier studies have shown how the solution properties of graft copolymers are very dependent on the selectiveness of the solvent<sup>1-6</sup>. Numerous experiments have been carried out on graft copolymers in solvent mixtures. Systems investigated include polystyrene-g-poly(methyl methacrylate)<sup>1</sup>, poly(*p*-bromostyrene)-g-polystyrene<sup>7</sup>, poly(diphenyl propene)-g-polystyrene<sup>7</sup>, polystyrene-g-poly(2-vinyl pyridine)<sup>8</sup> and poly(2-vinyl pyridine)-g-polystyrene<sup>8</sup>. If a non-solvent for the main-chain of a graft copolymer is added to a solution of the latter in a good solvent there is observed a large decrease in the intrinsic viscosity<sup>7</sup>. At low concentrations it is believed that monomolecular micelles are formed in which unsolvated main chains are kept in solution by protective layers of the grafted blocks. However, as the concentration is increased there is some evidence that aggregation occurs. Similar trends have been observed by varying the temperature of solutions of graft copolymers in good solvents<sup>9</sup>. However, such studies have not been of a detailed nature, and the temperature ranges covered have been fairly narrow.

In the present investigation we have synthesized polystyrene-g-polyisoprene copolymers by adding poly(isoprenyl lithium) to chloromethylated polystyrene. The various stages of the synthesis were carefully monitored and the product was fractionated and characterized by light scattering, gel permeation chromatography (g.p.c.) and membrane osmometry. Intrinsic viscosities of fractions containing different numbers of grafts have been studied over a range of temperatures in decane and methyl cyclohexane.

## EXPERIMENTAL

### *Preparation of chloromethylated polystyrene*

The chloromethylation of polystyrene by chloromethyl methyl ether\* in the presence of Lewis acids such as

\* This material is carcinogenic and should be used with extreme caution.

ZnCl<sub>2</sub><sup>10</sup>, SnCl<sub>2</sub><sup>11</sup> and SnCl<sub>4</sub><sup>12</sup> is well known. However, there appears to be considerable confusion in the literature concerning reaction efficiency as a function of reagent concentration, temperature and polystyrene chain length. Consequently it was necessary to carry out a series of exploratory reactions to find the most suitable experimental procedure. The conditions eventually chosen were as follows: polystyrene,  $M_w/M_n \leq 1.06$  (supplied by Pressure Chemical Co.), was made up as a 5% solution in pure carbon tetrachloride. Chloromethyl methyl ether was added and the subsequent mixture was cooled to 0°C. SnCl<sub>4</sub> was injected via a serum cap and the mixture was shaken vigorously. The reaction was terminated by the addition of wet dioxane and the mixture was shaken with an aqueous solution of HCl. The organic layer was shaken twice more with the acid after which it was run into a large excess of methanol. The precipitated chloromethylated polystyrene was dried and freeze-dried to constant weight. A spectroscopic analysis of the product was carried out, and a reaction time of approximately 30 min was found to give a substitution level of one chloromethylated unit per 40 polystyrene repeat units. This material was used in the subsequent polymerization programme.

### *Materials*

All purification processes were carried out in a vacuum system.

*Isoprene.* BDH laboratory reagent grade isoprene was twice distilled from powdered calcium hydride and stored over lithium aluminium hydride for 24 h prior to use. Absence of adventitious impurities was ensured by distilling the reagent on to a sodium mirror. The required volume of isoprene was distilled directly from the polymerizing mixture into an ampoule which was then sealed from the vacuum line.

*Solvents.* All solvents were first distilled from crushed calcium hydride and stored over lithium aluminium hydride in the vacuum system. Remaining traces of impurity were removed by distillation of the solvent from a solution of poly(styryl lithium).

**Tetramethyl ethylene diamine (TMEDA).** BDH laboratory reagent grade TMEDA was distilled on to a sodium mirror from which the required volume was distilled into a detachable ampoule.

**Chloromethylated polystyrene.** This coupling agent was degassed and made up as a solution in tetrahydrofuran using the apparatus illustrated in Figure 1. Solvent from a solution of poly(styryl lithium) (A) was distilled on to the chloromethylated polystyrene contained in ampoule B which could be detached from the vacuum line at constriction C.

**n-Butyl lithium.** This was obtained as a 15% solution in n-hexane from the Koch-Light Chemical Co. and in this form it was used without further purification.

#### Polymerization procedure

All reactions were carried out using the vacuum apparatus illustrated in Figure 2. A benzene solution of poly(styryl lithium) was prepared in flask B. The apparatus was washed internally with this solution to ensure absence of all adventitious impurities, care being taken to avoid contact with the serum caps. The solution was returned to flask B, after which flask D and its surrounds were rinsed thoroughly using successive quantities of condensed solvent. Next a given quantity of benzene was distilled into flask D and the constriction C was sealed. The requisite quantity of n-butyl lithium, as required by the equation  $M_n = \text{weight of monomer}/\text{weight of initiator}$ , was injected into flask D via serum cap E. Constriction F was sealed and the breakseal of ampoule G was broken using the magnetic breaker L. A seeding technique<sup>13</sup> was employed to ensure low dispersity in the polyisoprenyl living ends. The polymerization was allowed to proceed with vigorous stirring for 24 h. Whereupon a sample was

removed in the detachable ampoule O. The sample was characterized using the standard techniques to be described.

Preliminary experiments revealed that addition of the coupling agent to poly(isoprenyl lithium) in benzene produces some metal-halogen interchange resulting in crosslinking of the coupling agent. Comb and star-shaped polystyrene prepared by similar techniques have involved the use of the poly(styryl lithium) in mixtures of benzene and tetrahydrofuran of varying composition<sup>12, 14, 15</sup>. Unfortunately poly(isoprenyl lithium) reacts readily with tetrahydrofuran and therefore this technique could not be used. The problem was circumvented by the addition of 1.2 equivalents of TMEDA from ampoule I, per equivalent of n-butyl lithium used. The original pale yellow poly(isoprenyl lithium) was observed to change rapidly to a deep yellow colour as a consequence of the solvating action of the amine.

The coupling agent, contained in ampoule J, was added dropwise from position M over a period of 2 h with vigorous stirring and with the poly(isoprenyl lithium) in large excess at all times. No visible crosslinking was observed and, as expected, the solution became slightly paler and noticeably more viscous. The reaction was allowed to proceed for 10 h, before it was finally terminated by adding degassed methanol from ampoule N.

#### Fractionation

After the coupling reaction the remaining mixture consisting of graft copolymer, polyisoprene and any trace of crosslinked material was fractionated at 25°C using the method of successive liquid-liquid separation. Successive quantities of methanol were added to a 1% solution of the polymer in a 1 : 1 (v/v) mixture of toluene and heptane. The two liquid phases obtained after each addition were equilibrated using the usual heating and cooling cycles and then separated by syphoning off the dilute phase. Fractions were isolated by freeze drying. They were then carefully characterized using the dilute solution and spectroscopic techniques to be described.

#### Characterization of fractions

**Gel permeation chromatography.** Gel permeation chromatograms were obtained for polymer samples in tetrahydrofuran (0.2–0.5 wt% concentrations) using a commercial instrument manufactured by Water Associates operated at 25°C. The injection time and flow rate were 120 sec and 1 ml/min respectively. The technique was employed primarily to investigate the homogeneity of fractions rather than to assess molecular weight.

**Intrinsic viscosities.** Solution flow times were measured in a modified Desreux-Bischoff viscometer. Efflux times were measured for at least three concentrations and plots of  $\eta_{sp}/c$  versus  $c$  and  $\ln \eta_r/c$  were extrapolated to zero concentration to obtain  $[\eta]$ . An investigation of the effect of temperature on  $[\eta]$  was made in methyl cyclohexane and n-decane. The thermostat bath was controlled to  $\pm 0.1^\circ\text{C}$ .

**Number-average molecular weights ( $M_n$ ).** The number-average molecular weights of the graft copolymer fractions and the chloromethylated polystyrene were determined using a Melabs (CSM2) recording membrane osmometer. Measurements on the terminated polyisoprene homopolymer were made using a Mechrolab vapour-phase osmometer. Toluene was used as the solvent in both instruments.

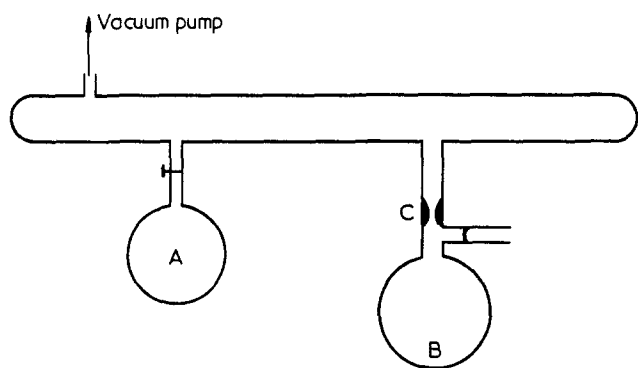


Figure 1 Apparatus used in making up a carefully purified solution of the chloromethylated polystyrene in tetrahydrofuran

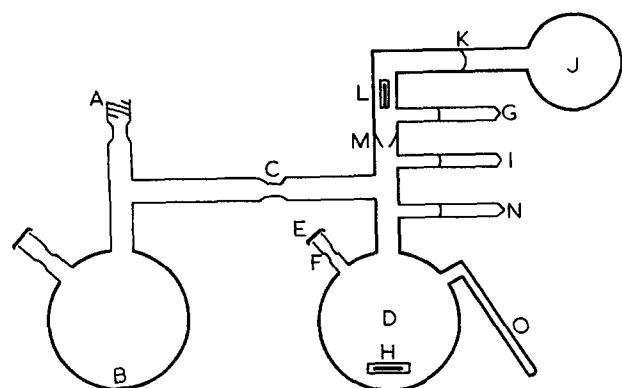


Figure 2 Apparatus used for carrying out the coupling reaction

**Light scattering.** Weight-average molecular weights were estimated from measurements made at  $30^\circ \pm 0.5^\circ\text{C}$  using a Sofica light scattering photometer. Polymer solutions and solvents were clarified by means of filtration. Light scattering was performed with light of wavelength 546 nm at ten angles between  $30^\circ$  and  $150^\circ$  for each of four dilutions with each solvent. The instrument was calibrated using benzene as standard. Results were plotted using the double extrapolation method of Zimm.

Bushuk and Benoit have extended the classical light scattering theory for polymer solutions to solutions of copolymers which are polydisperse in chain composition as well as molecular weight<sup>16</sup>. They showed that fluctuations in chain composition can lead to estimates of the molecular weight which are too high, and the observed value

$$M_{\text{app}} = M_w + 2P[(\nu_A - \nu_B)/\nu_0] + Q[(\nu_A - \nu_B)/\nu_0]^2$$

where  $M_w$  is the real weight-average molecular weight of the polymer mixture and  $\nu_A$ ,  $\nu_B$  and  $\nu_0$  are the refractive index increments ( $dn/dc$ ) in a particular solvent of the polymers forming the two types of block and of the copolymer mixture respectively. The two parameters  $P$  and  $Q$  are related to the heterogeneity in composition of the sample, and are given by:

$$2P = (1 - x_0)(M_w - M_B) - x_0(M_w - M_A)$$

and

$$Q = x_0(1 - x_0)(M_A + M_B - M_w)$$

where  $M_A$  and  $M_B$  are the weight-average molecular weights of the parts of the copolymer formed of monomer A and B respectively and  $x_0$  is the overall average weight fraction of component A. If values of  $M_{\text{app}}$ , determined in a variety of solvents, are plotted against  $(\nu_A - \nu_B)/\nu_0$  a parabola should be obtained from which the values of  $M_w$ ,  $P$  and  $Q$  can be estimated. It has been shown that the values of  $P$  and  $Q$  will vary between the following limits:

$$-x_0M_w \leq P \leq (1 - x_0)M_w$$

$$0 \leq Q \leq M_w[1 - x_0(1 - x_0)]$$

The parameter  $Q/M_w$ , whose maximum possible value is  $x_0(1 - x_0)$ , has been shown to provide a useful quantitative measure of the polydispersity in chain composition<sup>16</sup>.

In the study a Brice-Phoenix differential refractometer, which had been calibrated using aqueous sucrose solutions, was used to determine refractive index increments of the copolymers and polyisoprene in the appropriate solvents.

**U.v. spectroscopy.** U.v. analyses of chloroform solutions were used to estimate the polystyrene contents of the individual fractions. The procedure adopted was that described by Meehan<sup>17</sup>. Measurements were made using a Unicam SP800 spectrometer operating at a slit width of 0.5 mm with a path length of 1 cm.

## RESULTS AND DISCUSSION

### Fractionation and gel permeation chromatography

The fractions isolated by liquid-liquid separation are shown in Table 1. Fractions 2 and 3 were designated samples 1G2 and 1G3 respectively, and fractions 4 and 5 were combined together and designated sample 1G4. On examination the first fraction was found to contain a small quantity of microgel. It was therefore redissolved in

Table 1 Copolymer fractions obtained by liquid-liquid separation

Fraction No.	Weight %	Vol. methane		G.p.c. suggests
		Vol. 1 : 1 mixture		
1	17.8	0.240		—
2	13.3	0.243		Graft
3	16.5	0.246		Graft
4	9.4	0.252		Graft
5	5.3	0.256		Graft
6	8.0	0.264		Graft and polyisoprene
Residue	—	—		Graft and polyisoprene

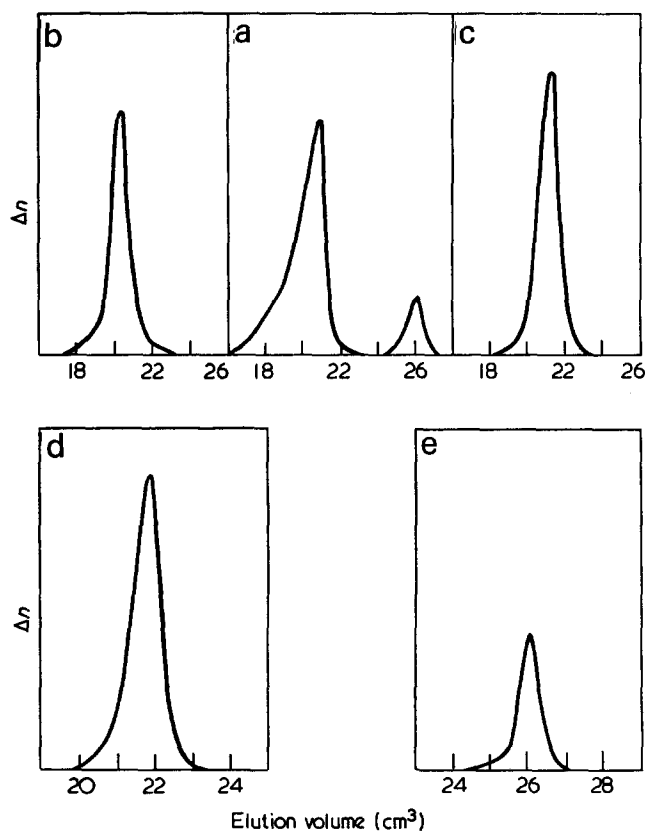


Figure 3 Gel permeation chromatograms of the unfractionated product (a), the chloromethylated polystyrene precursor (d), the terminated polyisoprene homopolymer (e) and the graft copolymer samples 1G1 and 1G4 (b and c)

benzene and separated into two fractions 1a and 1b by liquid-liquid separation using petroleum ether as non-solvent. Fraction 1a, which amounted to 30% by weight of the original fraction 1, contained microgel and was discarded. Fraction 1b was isolated and designated sample 1G1. Samples 1G1 → 1G4 were each characterized by the technique described in the last section.

The effectiveness of the fractionation process is demonstrated by the gel permeation chromatograms shown in Figure 3; traces are recorded for the unfractionated product, the chloromethylated polystyrene precursor, the terminated polyisoprene homopolymer and for two of the samples 1G1 and 1G4. On the basis of a conventional calibration plot established using polystyrene standards, all the fractions show a fairly low polydispersity  $M_w/M_n < 1.25$ .

### Molecular weight and composition

Number-average molecular weights determined by osmometry and percentage polystyrene contents determined by ultra-violet spectroscopy are given in Table 2.

Table 2 Number-average molecular weights and composition

Sample	$M_n \times 10^{-5}$	Weight % polystyrene	No. of side chains per main chain	
			A	B
1G1	5.5	29.2	29	34
1G2	4.9	34.9	24	27
1G3	4.2	38.1	18	22
1G4	3.9	40.6	16	19
Chloromethylated polystyrene	1.9	—	—	—
Polyisoprene	0.125	—	—	—

A. Estimated from number-average molecular weights of copolymer and homopolymers

B. Estimated from weight % polystyrene and number-average molecular weights of homopolymers

Table 3 Apparent weight-average molecular weights

Sample	Solvent	$M_{ap} \times 10^{-5}$	$M_{ap}/M_n$
1G2	Chloroform	5.7	1.16
1G2	Cyclohexane	5.6	1.14
1G2	Tetrahydrofuran	5.4	1.10
1G2	1-Chloropropane	5.5	1.12
1G1	Tetrahydrofuran	6.5	1.18
1G3	Tetrahydrofuran	5.1	1.21
1G4	Tetrahydrofuran	4.8	1.23

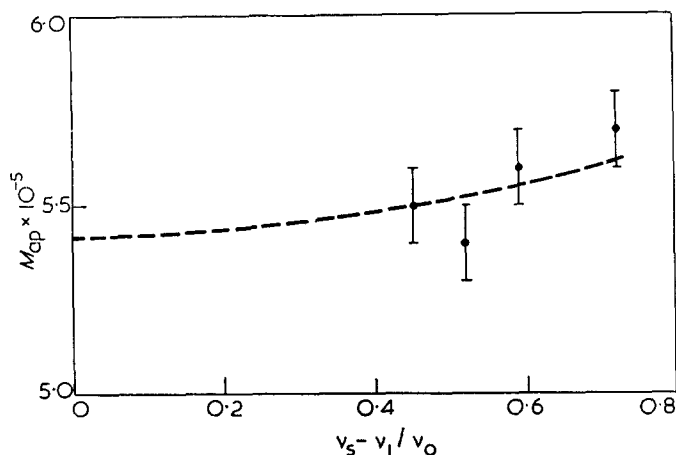


Figure 4 A plot of apparent molecular weights of sample 1G2 versus  $v_s - v_1 / v_0$

From these results we can obtain for each copolymer two separate estimates of the number of polyisoprene side-chains per polystyrene main chain. The two sets of values, which are given in columns 4 and 5 of Table 2 are seen to be in fair agreement. As might be expected it is seen that on passing from sample 1G1 to 1G4 the degree of grafting progressively decreases.

Apparent weight-average molecular weights have been determined for sample 1G2 in four different solvents (see Table 3). In accord with the usual procedure in Figure 4 we have plotted  $M_{ap}$  against  $v_s - v_1 / v_0$ . Unfortunately we have not covered a sufficiently wide range of refractive index increments to thoroughly investigate the heterogeneity of composition. However, the results available suggest that the heterogeneity parabola is very shallow and hence that  $Q/Q_{max}$  is small. For the other fractions measurements have only been carried out in one solvent. The values of  $M_{ap}$  (which again are likely to be close to  $M_w$ ) are given in Table 3.

### Solution properties

Intrinsic viscosities as a function of temperature are plotted in Figure 5 for the samples 1G1–1G4 in methyl cyclohexane. For samples 1G1 and 1G3 the measurements cover the range  $-20$  to  $60^\circ\text{C}$ . For both cases the curves contain two steep regions X and Z separated by a short shallow extension Y. On lowering the temperature the solutions used for viscometry became somewhat turbid on going below  $5^\circ\text{C}$ . However, the dispersions remained quite stable until much lower temperatures; for a 1% by weight solution liquid–liquid separation occurred for 1G1 at  $-65^\circ\text{C}$  and for 1G3 at  $-60^\circ\text{C}$ . Over the range  $0$  to  $60^\circ\text{C}$  we have collected data on all four samples 1G1–1G4, and it is interesting to compare behaviour within this domain. It can be seen that the effect of increasing the number of grafted polyisoprene blocks per polystyrene main chain is to shift the curves in a systematic manner down the temperature axis.

At the present time interpretation of the results in Figure 5 can only be somewhat speculative. At  $0^\circ\text{C}$ , methyl cyclohexane is a very poor solvent for polystyrene ( $\theta = 74^\circ\text{C}$ ), but is still a relatively good solvent for polyisoprene. We feel that the sharp, well defined decrease in  $[\eta]$  over the region designated Z is associated with an intramolecular phase separation on cooling leading to a species having a compact, but swollen, polystyrene core surrounded by a polyisoprene fringe. It should be possible to observe the transition using other experimental techniques which give more direct molecular information and this possibility is currently under investigation in our laboratory.

The more gradual change in  $[\eta]$  which is observed in the region above Z can be associated with the usual tempera-

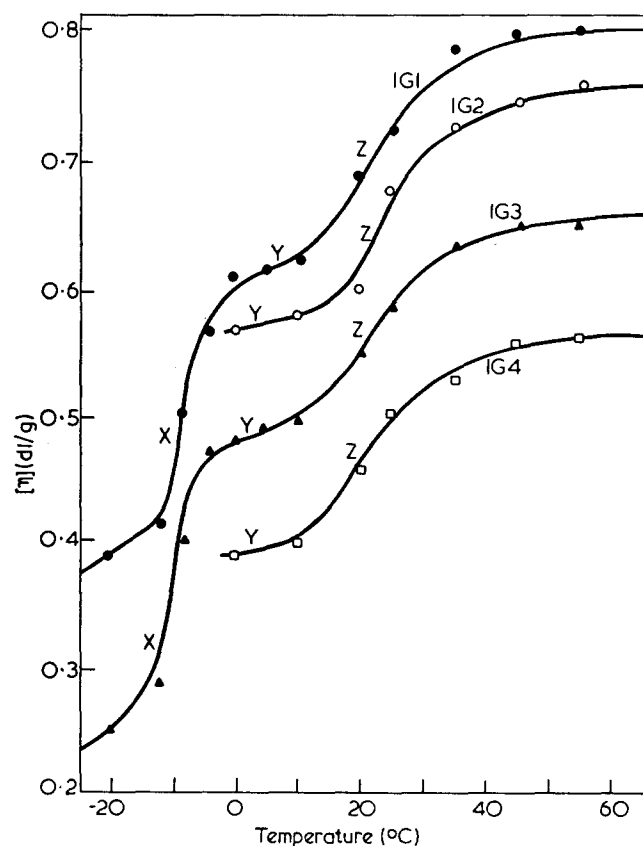


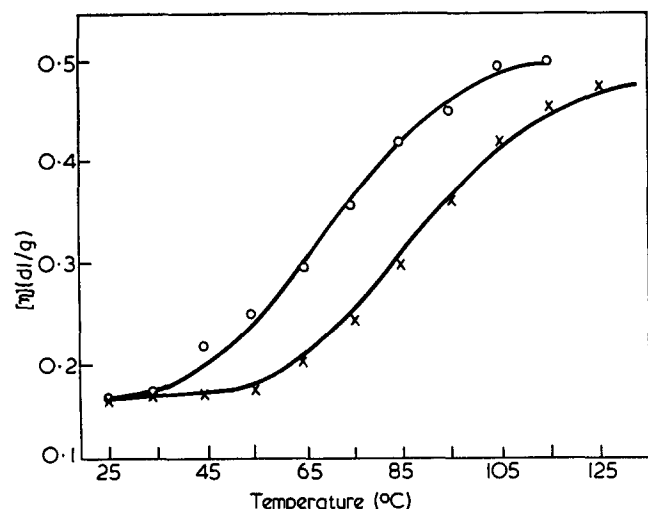
Figure 5 Plots of  $[\eta]$  versus temperature for the graft copolymer samples 1G1–1G4 in methyl cyclohexane



ture dependence of coil dimensions. As a measure of the coil expansion which may occur in solvents which are good for both components we list in *Table 4* the intrinsic viscosities of the four samples in toluene and tetrahydrofuran at 25°C; the intrinsic viscosity of the chloromethylated polystyrene is also given for comparison.

In the temperature range marked X, over which we have studied just two samples, a further sharp decrease in  $[\eta]$  is observed on cooling. We associate this lower transition with the formation of intermolecular aggregates. After heating and cooling cycles the results plotted in *Figure 5* were found to be completely reproducible.

n-Decane is a much poorer solvent for polystyrene than methyl cyclohexane. We would expect therefore that the sort of behaviour shown in *Figure 5* would be observed at higher temperatures for the graft copolymer in n-decane. Intrinsic viscosities in decane for the temperature range 20–120°C are plotted in *Figure 6* for samples 1G1 and 1G3. On cooling a 1% by weight solution 1G1 became turbid at approximately 70°C, and for 1G3 at 105°C; liquid-liquid separation occurred at –20°C for 1G1 and at –10°C for B. Both samples show a marked change in  $[\eta]$  over the range covered. However, this change is gradual and the curves do not have the same characteristic shape as those observed in methyl cyclohexane. However, whilst no abrupt decrease in  $[\eta]$  occurs on cooling the very low values of  $[\eta]$  are indicative of micelle formation. It is just possible that a further significant increase in  $[\eta]$  (corresponding to regions Z in *Figure 5*)



*Figure 6* Plots of  $[\eta]$  versus temperature for the graft copolymer samples 1G1 (○) and 1G3 (×) in n-decane

*Table 4* Intrinsic viscosities in toluene and tetrahydrofuran

Sample	$[\eta]$ in toluene (dl/g)	$[\eta]$ in THF (dl/g)
1G1	1.09	1.16
1G2	0.99	1.03
1G3	0.91	0.94
1G4	0.82	0.84
Chloromethylated polystyrene	0.77	0.78

occurs above 120°C; unfortunately we were not able to work at these higher temperatures because of the instability of the polyisoprene chains under these conditions.

#### ACKNOWLEDGEMENTS

The authors thank the Science Research Council for the award of a CAPS Studentship for D.W., and Esso Chemicals Research Centre, Abingdon, for their co-operation on the project. We thank Dr R. C. Price and Mr R. C. Watkins for the interest they have shown in the work. We acknowledge the technical assistance of Mr D. J. Roy and Mr D. Rowlinson with the g.p.c. studies.

#### REFERENCES

- Gallot, Y., Franta, E., Rempp, P. and Benoit, H. *J. Polym. Sci. (C)* 1964, **4**, 473
- Gramain, P., Leray, J. and Benoit, H. *J. Polym. Sci. (C)* 1967, **16**, 3983
- Dondos, A., Rempp, P. and Benoit, H. *J. Chim. Phys.* 1965, **62**, 821
- Dondos, A., Froelich, D., Rempp, P. and Benoit, H. *J. Chim. Phys.* 1967, **64**, 1012
- Dondos, A., Rempp, P. and Benoit, H. *Eur. Polym. J.* 1967, **3**, 657
- Dondos, A. *Eur. Polym. J.* 1969, **5**, 767
- Dondos, A., Rempp, P. and Benoit, H. *J. Polym. Sci. (B)* 1966, **4**, 293
- Gosnell, A. B., Woods, D. K., Gervasi, J. A., Williams, J. L. and Stannett, V. *Polymer* 1968, **9**, 561
- Danon, J. and Jozefonvicz, J. *J. Polym. Sci. (C)* 1970, **30**, 57
- Jones, G. D. *Ind. Eng. Chem.* 1952, **44**, 2686
- Blanchette, J. A. and Cottman, J. D. Jr. *J. Org. Chem.* 1958, **23**, 117
- Altare, T. Jr., Wyman, D. P., Allen, V. R. and Meyerson, K. *J. Polym. Sci. (A)* 1965, **3**, 4131
- Morton, M., Bostick, E. E. and Clarke, R. G. *J. Polym. Sci. (A)* 1963, **1**, 475
- Candau, F. and Franta, E. *Makromol. Chem.* 1971, **149**, 41
- Meunier, J.-C. and Van Leemput, R. *Makromol. Chem.* 1971, **142**, 1
- Bushuk, W. and Benoit, H. *Can. J. Chem.* 1958, **36**, 1616
- Meehan, E. J. *J. Polym. Sci.* 1946, **1**, 175

# Reaction of thiol to diene polymer in the presence of various catalysts

Koichi Yamaguchi, Nobuo Yamada and Yuji Minoura

Department of Applied Chemistry, Faculty of Engineering, Osaka City University,  
Sugimoto-cho, Sumiyoshi-ku, Osaka, Japan

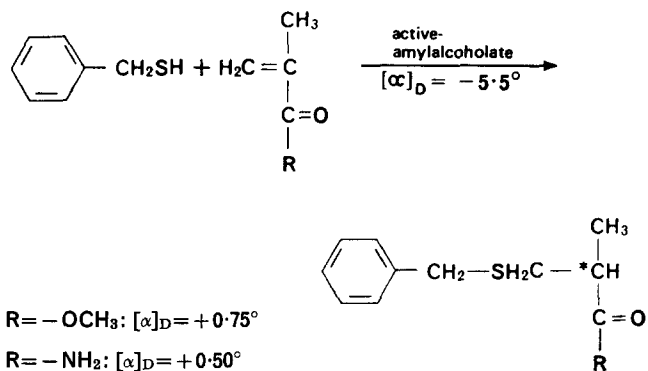
(Received 26 September 1972; revised 14 November 1972)

The addition reaction of benzylmercaptan to diene polymer (natural rubber, and *cis*-1,4-polyisoprene) by various optically active catalysts such as D-camphorsulphonic acid, D-percamphoric acid, and active-amylalcoholate (sodium and barium) were carried out in benzene or anisole at room temperature to 100°C. The optically active adduct polymer was only obtained from the reaction of benzylmercaptan to natural rubber and *cis*-1,4-polyisoprene by active-amylalcoholate (barium), but was not obtained by the other catalysts. The  $[\alpha]^{25}$  value of optically active adduct polymer was  $-0.1^{\circ}\text{C} \sim -0.6^{\circ}\text{C}$  (in benzene), and the optical rotatory dispersion curves were found to fit the simple Drude equation. The reaction of benzylmercaptan to *cis*-1,4-polybutadiene, various styrene-butadiene copolymers, and alternating butadiene-acrylonitrile copolymer were carried out, but the optically active adduct polymers were not obtained by these catalysts.

## INTRODUCTION

The addition reaction of thiol to olefin is well known; e.g. the reaction of thiol with acrylonitrile (or acrylic ester, methacrylic ester) by basic catalyst such as sodium ethoxide<sup>1</sup>, the reaction of propylene with thioacetic acid (AcSH) by sulphuric acid or phosphoric acid<sup>2</sup>, the reaction of maleic anhydride with AcSH by peroxide catalyst<sup>3</sup>, the reaction of maleic anhydride with benzylmercaptan (BzSH) by 35% aqueous solution of benzyltrimethylammonium hydroxide<sup>4</sup>, etc. have been reported. Further, many studies of the reaction of thiol to a carbon-carbon double bond in polymer, i.e. the reaction<sup>5</sup> of AcSH to natural rubber (NR) by peroxide, and irradiation of X-ray or ultra-violet radiation, have also been made. In connection with this reaction, one of the authors has reported that the polyaddition of *N,N'*-methylenebisacrylamide or diallydene pentaerythritol with ethylene dimercaptoacetate or ethylene dimercaptopropionate<sup>6</sup> by radical catalyst (benzyl peroxide), ultra-violet radiation, basic catalyst (sodium *t*-butoxide) and acidic catalyst (*p*-toluenesulphonic acid) can be carried out to obtain the polymer.

The asymmetric addition reaction of thiol to olefin was first presented by Tsuruta and co-workers<sup>7,8</sup>. They studied the asymmetric addition reaction of laurylmercaptan to methyl methacrylate with optically active amine catalyst. We also studied the asymmetric addition reaction of benzylmercaptan to methyl methacrylate and methacrylamide with active-amylalcoholate (barium)<sup>9</sup>, and obtained the optically active product as follows:



In this paper, the addition reaction of benzylmercaptan (BzSH) to diene polymers by optically active acidic catalyst (D-camphorsulphonic acid), radical catalyst (D-percamphoric acid) and basic catalysts [active-amylalcoholate (sodium and barium)] was carried out. The optically active adduct polymer was only produced in the addition reaction of thiol to NR and *cis*-1,4-polyisoprene by active-amylalcoholate (barium), but was not obtained by other catalysts or from other diene polymers (*cis*-1,4-polyisoprene, various styrene-butadiene copolymer and alternating butadiene-acrylonitrile copolymer).

## EXPERIMENTAL

### Reagents

The diene polymers used were NR, *cis*-1,4-polyisoprene, *cis*-1,4-polybutadiene, alternating butadiene-acrylonitrile

copolymer<sup>10</sup> (mole ratio of butadiene/acrylonitrile = 50.9/49.1,  $[\eta]^{30} = 1.55$  in dimethylformamide) and various SBR. The used SBR were Tafuden 1000R (styrene content 18 wt %,  $[\eta]^{30} = 1.60$  in THF) Nipol 1502 (styrene content 23.5 wt %)  $[\eta]^{30} = 1.03$  in THF), Solprene 1205F (styrene content 25 wt %,  $[\eta]^{30} = 1.06$  in THF), Buna Huls 190 (styrene content 40 wt %,  $[\eta]^{30} = 1.54$  in THF) and Hycar 2007J (styrene content 85 wt %,  $[\eta]^{30} = 0.54$  in THF). These diene polymers were reprecipitated from benzene or tetrahydrofuran (THF).

BzSH<sup>11</sup> was prepared from benzyl chloride with sodium hydrosulphide and was distilled at the boiling point (74.0–74.5°C at 10 mmHg).

The used catalysts were active-amylalcoholate (sodium and barium), D-percamphoric acid, and D-camphor-sulphonic acid.

Active-amylalcoholate (barium or sodium) was prepared from active-amylalcohol ( $[\alpha]_D^{25} - 5.5^\circ$ ) and barium or sodium metal. D-Percamphoric acid<sup>13</sup> ( $[\alpha]_D^{25} 60.0^\circ$ ) was prepared from D-camphoric acid with sodium peroxide and was recrystallized from diethyl ether. D-Camphor-sulphonic acid ( $[\alpha]_D^{25} 40.5^\circ$ ) was used as the commercial reagent and was recrystallized from ethanol.

Solvents (benzene, anisole, etc.) were purified by distillation.

#### Reaction of diene polymer with thiol

Diene polymer, BzSH, catalyst and benzene as solvent were placed in a glass tube connected to a vacuum line, the tube was thoroughly degassed and sealed and the reaction proceeded from room temperature to 90°C for 10–90 h (exposed to ultra-violet radiation in the reaction by D-percamphoric acid). After a suitable time, the reaction mixture was poured into a large excess of methanol. The product precipitated was filtered, washed with methanol and dried in a vacuum to constant weight.

After all reaction products were purified by reprecipitation, sulphur analysis, elemental analysis, optical rotation and infra-red spectra were measured. The addition percentage of thiol was calculated from the sulphur content of the reaction product.

#### Measurements

The infra-red spectra of reaction adduct polymers were measured with film and liquid state on an Infrared Spectrometer (Jasco IR-E, Japan Spectroscopic Co. Ltd).

The molecular weight of the reaction product was determined with a Knauer vapour pressure osmometer, acetone being used as solvent.

The sulphur quantitative analysis was determined by Schoniger's method<sup>14</sup> which used the combustion flask.

The D-line optical rotation of the reaction adduct polymer reprecipitated from benzene was measured by a Shimadzu Liebig type polarimeter with filtered sodium light. Optical rotatory dispersion data were obtained with a Shimadzu model QV-50 polarimeter equipped with a xenon source.

## RESULTS AND DISCUSSION

#### Reaction by acidic catalyst

The addition reaction of BzSH to NR by D-camphor-sulphonic acid as optically active catalyst was carried out in benzene at 100°C. The addition percentage of thiol increased with increasing concentration of catalyst, but

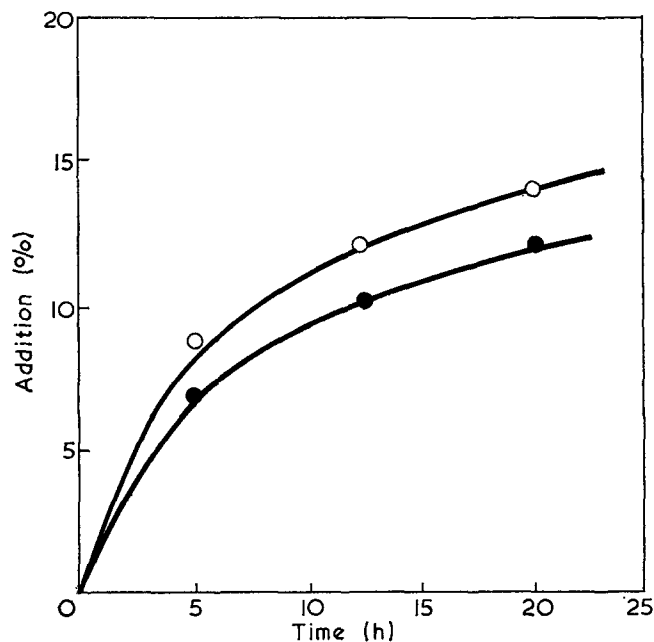
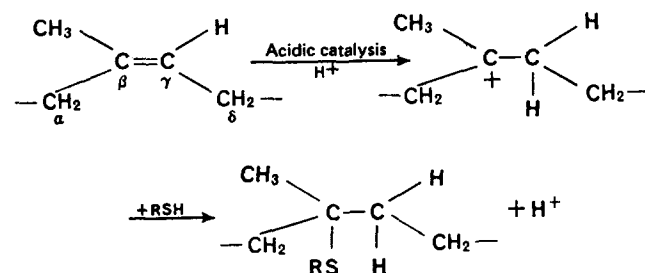


Figure 1 Relation between the percentage addition and the reaction time in the reaction of BzSH to NR with D-camphor-sulphonic acid. [NR] : [BzSH] : [catalyst] = 1 : 1 : 1 (○); = 1 : 1 : 0.5 (●)

the addition percentage was shown to be saturated at about 10–15% as shown in Figure 1. The adduct polymer did not show optical activity. Consequently, the optically active polymer was not obtained by this addition reaction but according to the reaction mechanism that follows:



Moreover, from the reaction of styrene with BzSH by D-camphorsulphonic acid in benzene,  $\alpha$ -phenylethyl benzylsulphide<sup>15</sup> (b.p. 134–135°C at 1.5 mmHg) was obtained, but did not have the same optical activity as above.

#### Reaction by radical catalyst

The reaction of AcSH or BzSH to NR by an optically active radical catalyst such as D-percamphoric acid was carried out in benzene at 90°C or room temperature by exposure to u.v. radiation. The results are shown in Table 1. It was found that the addition percentage was 20–30% in this condition, but the optically active adduct polymer was not obtained in accordance with the anti-Markownikov rule.

#### Reaction by basic catalyst

**Polyisoprene.** The addition reaction of BzSH to diene polymers (NR and *cis*-1,4-polyisoprene) by active-amylalcoholate (barium and sodium) as optically active basic catalyst was carried out in anisole at 90°C for 48 h. The results are shown in Table 2.

The adduct polymer by active-amylalcoholate (barium)

**Table 1** Reaction of thiolacetic acid or benzylmercaptan to natural rubber by D-percamphoric acid as radical catalyst in benzene [NR]=[RSH]=[per acid]=0.6 mol/l

RSH <sup>a</sup>	Temp.	Time (h)	Sulphur content of product (%)	Addition (%)	[ $\alpha$ ] <sub>D</sub> <sup>b</sup>
AcSH	Room temp.†	72	10.85	32.0	0
AcSH	70°C	72	9.98	29.4	0
BzSH	Room temp.†	72	9.35	20.6	0
BzSH	70°C	72	8.60	19.0	0

<sup>a</sup> AcSH: thiolacetic acid; BzSH: benzylmercaptan

<sup>b</sup> In benzene at 25°C

† U.v. irradiation

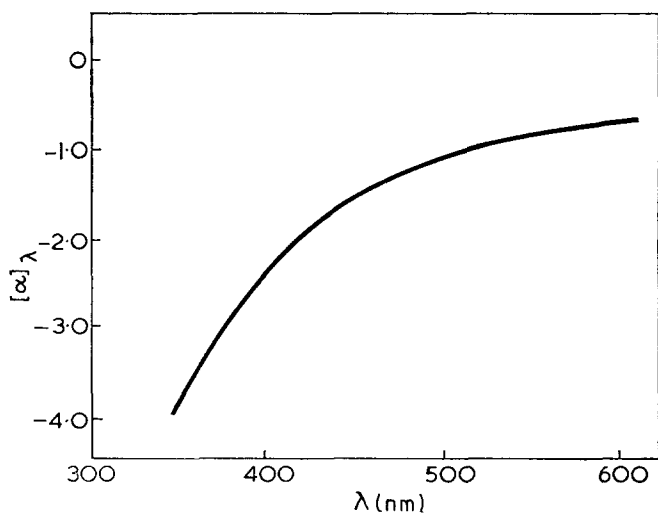
**Table 2** Reaction of benzylmercaptan to natural rubber and *cis*-1,4-polyisoprene by active-amylalcoholate (sodium, barium) in anisole at 90°C for 48 h

[Polymer] : [BzSH] : [alcoholate]=1 : 1 : 1

[Polymer]=0.44 mol/l

Polymer	Alcoholate	Analysis of product		Addition (%)	[ $\alpha$ ] <sub>D</sub> <sup>25*</sup>
		C (%)	H (%)		
Natural rubber	Na	84.06	11.23	14.0	0
Natural rubber	Ba	85.70	11.47	7.7	-0.6°
Polyisoprene	Na	85.01	11.33	10.2	0
Polyisoprene	Ba	85.76	11.51	7.5	-0.1°

\* In benzene at 25°C



**Figure 2** Optical rotatory dispersion of adduct polymer obtained from reaction of BzSH to NR with active-amylalcoholate (barium)

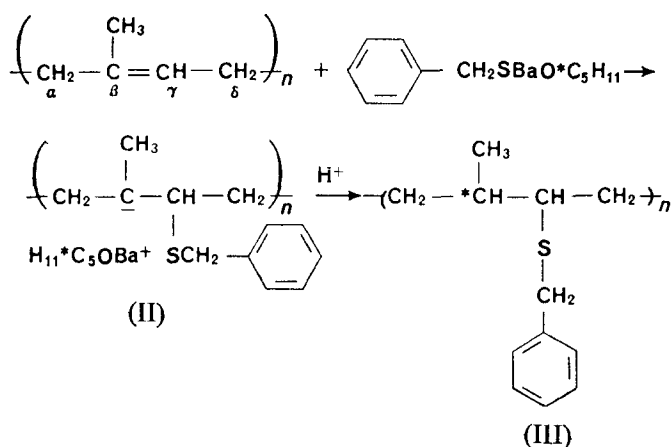
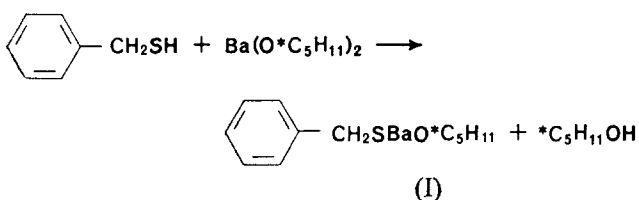
showed optical activity, but the adduct polymer by active-amylalcoholate (sodium) did not. The specific rotation was -0.6° for NR and -0.1° for *cis*-1,4-polyisoprene.

The optical rotatory dispersion of adduct polymer having [ $\alpha$ ]<sub>D</sub> = -0.6° is shown in *Figure 2*. This optical rotatory dispersion curve was satisfied by the simple Drude equation; the calculated  $\lambda_c$  value was 287 nm. This  $\lambda_c$  value is also based on absorption due to the thioether linkage.

**Other diene polymers.** The addition reaction of BzSH to other diene polymers (*cis*-1,4-polybutadiene, various SBR, alternating butadiene-acrylonitrile copolymer) by active-amylalcoholate (barium and sodium) was carried out at 90°C for 72–90 h in benzene. In all cases, the

optically active polymer was not obtained. The results are shown in *Table 3*.

**Mechanism.** From the above results, the mechanism of producing optically active adduct polymer was thought to be as follows:



In this addition reaction of thiol with polyisoprene by active-amylalcoholate (barium), at first, the product (I) is formed by the substitution reaction between the alkoxy group of alcoholate and the mercapto group, and the intermediate (II) is produced by the reaction of product (I) to the carbon-carbon double bond according to the anti-Markownikov rule. The product (III) is produced from the intermediate (II) by acid treatment. The  $\beta$ -carbon of the isoprene unit in the intermediate (II) becomes optically active by the addition reaction of (I); therefore, the optically active polymer, i.e. the product

**Table 3** Reaction of benzylmercaptan to diene polymer by active-amylalcoholate (sodium, barium) in benzene at 90°C for 72 h [Double bond of polymer] : [BzSH] : [alcoholate]=1 : 1 : 1 [Polymer]=0.44 mol/l

Diene polymer	Alcoholate	Analysis of product		Addition* (%)	[ $\alpha$ ] <sub>D</sub> <sup>25†</sup>
		C (%)	H (%)		
Polybutadiene	Na	83.10	9.86	16.1	0
	Ba	84.88	10.18	10.3	0
Tafuden 1000R	Na	85.05	9.70	31.5	0
	Ba	87.53	10.10	12.1	0
Nipol 1502	Na	86.84	9.84	19.5	0
	Ba	87.37	9.93	15.4	0
Solprene 1205F	Na	87.20	9.78	17.4	0
	Ba	88.05	9.96	11.3	0
Buna Huls 190	Na	88.88	9.52	10.8	0
	Ba	89.07	9.56	9.1	0
Hycar 2007J	Na	91.43	8.18	11.3	0
	Ba	91.58	8.19	7.2	0
Alternating butadiene-acrylonitrile copolymer	Na	75.84	8.21	20.1	0
	Ba	76.06	8.65	18.1	0

\* Addition percentage of BzSH for double bond of butadiene unit  
† In benzene at 25°C

(III) is obtained after acid treatment. On the other hand, in the addition of thiol to *cis*-1,4-polybutadiene, SBR, and alternating butadiene-acrylonitrile copolymer, all these adduct polymers did not show optical activity because of the pseudo-asymmetric carbon atom.

#### ACKNOWLEDGEMENT

The authors would like to express their grateful acknowledgement to Dr Junji Furukawa (Kyoto University) for providing the alternating butadiene-acrylonitrile copolymer.

#### REFERENCES

1 Hurd, C. D. and Gershhein, L. L. *J. Am. Chem. Soc.* 1947, **69**, 2328

- 2 Ipatieft, V. N. *J. Am. Chem. Soc.* 1938, **60**, 2731
- 3 Brown, R., Jones, W. E. and Pinder, A. R. *J. Chem. Soc.* 1951, p 2123
- 4 Szado, J. L. and Stiller, E. T. *J. Am. Chem. Soc.* 1948, **70**, 3667
- 5 Cunneen, J. I. *J. Chem. Soc.* 1947, p 134
- 6 Minoura, Y. and Zako, K. *Kogyo Kagaku Zasshi* 1966, **69**, 340
- 7 Tsuruta, T. and Inoue, S. *21st Meet. Chem. Soc. Japan, Preprints* 1968, p 2716
- 8 Inoue, S. and Ohashi, S. *19th Symp. High Polym. Japan, Preprints* 1970, p 431
- 9 Yamaguchi, K. and Minoura, Y. *Chem. Commun.* 1973, in press
- 10 Furukawa, J., Iseda, Y., Haga, K. and Kataoka, N. *J. Polym. Sci. (B)* 1969, **7**, 47
- 11 Bllingboe, E. K. *Org. Synth.* 1963, **4**, 928
- 12 Fromm, E. and Achert, O. *Chem. Ber.* 1903, **36**, 546
- 13 Miles, N. A. and McAlevy, A. *J. Am. Chem. Soc.* 1933, **55**, 349
- 14 Schoniger, W. *Mikrochim. Acta* 1956, p 860
- 15 Overberger, C. G. and Hogt, J. M. *J. Am. Chem. Soc.* 1951, **73**, 3305

# Kinetics of epoxy cure: 3. The systems bisphenol-A epoxides/dicy

E. Sacher

IBM Systems Development Division, PO Box 6, Endicott, NY 13760, USA  
(Received 27 October 1972)

Differential scanning calorimetry was used to study the cure of several bisphenol-A epoxide/dicy (dicyandiamide, cyanoguanidine) systems in the temperature range 170–220°C. It was found that, simultaneously with curing, the dicy decomposed into melamine, which was capable of further decomposition. With a higher molecular weight epoxide, reaction subsequent to cure resulted in a more rigid epoxy than expected. The addition of surfactant caused reaction to occur at lower temperatures, although the rate decreased and a change in mechanism appeared to have occurred.

## INTRODUCTION

Previous studies in this series<sup>1,2</sup> were concerned with epoxide/hardener systems which were mutually soluble and could thus be intimately mixed, on a molecular level, prior to reaction. The present hardener, dicy (dicyandiamide, cyanoguanidine), is one of a unique group of hardeners whose use depends on the fact that it is insoluble in the epoxide.

The insoluble dicy may be dispersed in the epoxide at the manufacturing site because reaction occurs only at the epoxide-dicy interface. This one-part epoxy system is stable enough to be shipped and stored for extended periods prior to use. The cure reaction begins when the temperature is raised to where the dicy dissolves.

Although the commercial use of the epoxide/dicy systems has definite economic advantages, there are several variables which have not yet been addressed in the literature. Among them are the effects of hardener particle size, epoxide molecular weight and added solubilizers. Further, the activation energy for the overall reaction would be expected to include, in addition to that for the reaction of the epoxide and the hardener, the energies necessary for dissolution and mixing. The present study was undertaken to resolve these points.

## EXPERIMENTAL

### Materials

Bisphenol-A epoxides have the general structure given in formula (I).

The two epoxides used in the present study were Dow DER 332, the diglycidyl ether of bisphenol-A, in which the value of  $x$  in formula (I) is zero, and Shell EPON 1001, a higher molecular weight mixture of bisphenol-A epoxides where  $x=2.0$ – $2.7$ . They, along with the dicy

(Aldrich) and surfactant (Atlas Tween 80), were used without further purification.

The epoxies were made immediately prior to use by dispersal in a cooled laboratory blender. All contained a 10% excess (eq/eq) of epoxide, and dicy whose particle size range was obtained on a set of nesting sieves. The blender speed was set low enough to minimize further breaking of the dicy particles. Where necessary, the epoxies were stored at  $-20^{\circ}\text{C}$ .

### Instrumental procedures

The infra-red (i.r.) absorption and d.c. conductivity methods used in the previous studies<sup>1,2</sup> were not presently used due to the heterogeneous nature of the epoxy system. Kinetic data were obtained using the previously described<sup>1</sup> differential scanning calorimetry (d.s.c.) technique. The temperature range was confined to 170–220°C, within which kinetic data were easily obtainable on a reasonable time scale. Isothermal d.s.c. traces had a slight, but discernible shoulder during the rise of the exotherm.

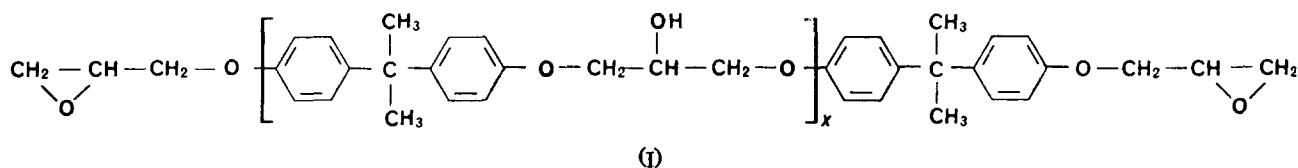
Transition temperatures were determined on a DuPont model 941 Thermomechanical Analyzer and i.r. spectra were obtained on a Perkin-Elmer model 521 Spectrophotometer.

### Treatment of data

The d.s.c. data were fitted to the equation<sup>3</sup>:

$$\frac{d\alpha}{dt} = k(1-\alpha)^n \quad (1)$$

where  $\alpha$  is the fraction reacted at time  $t$ ,  $k$  is the overall rate constant and  $n$  is the overall reaction order. All the data gave good Arrhenius plots, from which the activation energies were obtained.



## RESULTS

The course of the reaction was found to depend on the molecular weight of the epoxide, the dicy particle size and the presence and amount of surfactant. For the DER 332 epoxide and a dicy particle size of  $<125 \mu\text{m}$  (subsequently referred to as fine dicy),

$$k (\text{sec}^{-1}) = 3.85 \times 10^9 \exp(-24.1 \text{ kcal mol}^{-1}/RT)^* \quad (2)$$

where  $R$  is the gas constant and  $T$  is the absolute temperature;  $n$  values ranged from 0.7 to 1.4. For a dicy particle size of  $250\text{--}500 \mu\text{m}$  (subsequently referred to as coarse dicy),

$$k (\text{sec}^{-1}) = 2.45 \times 10^3 \exp(-12.1 \text{ kcal mol}^{-1}/RT) \quad (3)$$

while  $n$  values ranged from 1.0 to 2.1. For the EPON 1001 epoxide and the fine dicy particles,

$$k (\text{sec}^{-1}) = 2.20 \times 10^5 \exp(-16.6 \text{ kcal mol}^{-1}/RT) \quad (4)$$

with  $n$  values ranging from 1.0 to 1.2.

Using the DER 332/fine dicy system, the addition of 1.2% (w/w) surfactant gave:

$$k (\text{sec}^{-1}) = 1.46 \times 10^7 \exp(-19.3 \text{ kcal mol}^{-1}/RT) \quad (5)$$

for a range of  $n$  from 1.0 to 1.5. The addition of 6% (w/w) surfactant gave:

$$k (\text{sec}^{-1}) = 2.56 \times 10^6 \exp(-18.2 \text{ kcal mol}^{-1}/RT) \quad (6)$$

with  $n$  ranging from 1.1 to 1.9.

Table 1 Transition temperatures of cured epoxy systems

System	$T_1$ (°C)	$T_2$ (°C)	$T_3$ (°C)
DER 332/fine dicy	$73.7 \pm 4.3$	$124.9 \pm 3.9$	$145.6 \pm 1.0$
DER 332/fine dicy/1.2% surfactant	$48.9 \pm 4.5$	$121.5 \pm 2.9$	$140.6 \pm 2.2$
DER 332/fine dicy/6% surfactant	$41.6 \pm 1.1$	$118.7 \pm 4.1$	a
DER 332/coarse dicy	$57.7 \pm 6.7$	$106.6 \pm 7.3$	$134.8 \pm 1.7$
EPON 1001/fine dicy	$95.5 \pm 2.8$	a	a

No transition observed

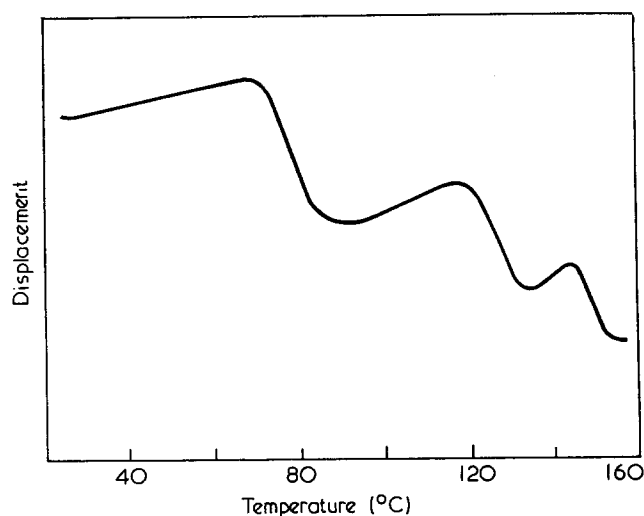


Figure 1 A thermomechanical analysis plot of the transitions in cured DER 332/fine dicy epoxy. The complete sample, containing both transparent upper layer and opaque lower layer, was used, after having been cured at  $200^\circ\text{C}$  for 4 h. The plot was made using a 20 g load on an expansion probe at a heating rate of  $5^\circ\text{C}/\text{min}$

\*  $1 \text{ kcal mol}^{-1} = 4.1868 \text{ kJ mol}^{-1}$

With the exception of the EPON 1001/fine dicy epoxy, whose cured d.s.c. samples were transparent, the cured samples of all the other epoxy systems had a transparent upper layer and an opaque, white lower layer. There was evidence of condensate in the d.s.c. cell and all the samples were full of microscopic bubbles.

While the EPON 1001/fine dicy epoxy had one transition temperature, the other epoxies had several, as seen in Table 1. By grinding off one of the layers, it was found that the transition occurring near  $120^\circ\text{C}$  ( $T_2$ ) was associated with the opaque layer, while  $T_1$  and  $T_3$  were associated with the transparent layer. All three transitions are seen in Figure 1.

## DISCUSSION

## Course of the reaction

The reaction of the dicy with phenyl glycidyl ether has previously been investigated<sup>4</sup> from the point of view of the structure obtained. The present results amplify what was previously found and show that the reaction is far more complicated than previously suspected.

On heating the epoxide/dicy mixture in open d.s.c. sample holders, the first observable phenomenon was the clarification of the opaque mixture: that is, the dicy dissolved. This was immediately followed by bubble formation, indicating the thermal decomposition of dicy into melamine<sup>5</sup> (2,4,6-triamino-s-triazine, cyanurotriamide), a process of commercial significance<sup>6</sup>. Since the reaction ultimately resulted in a glassy solid, decomposition occurred simultaneously with curing.

During bubble formation, and while the epoxy was curing, a white precipitate formed and settled to the bottom of the DER 332 epoxies, but not the EPON 1001 epoxy. The presence of such a layer has previously been noted<sup>7</sup> as being due to excess, insoluble dicy. There are three reasons why this is not so. First, the dicy was initially totally soluble. Second, thermal analysis gave no sign of a melting point near  $209^\circ\text{C}$  (dicy), but rather of a decomposition above  $358^\circ\text{C}$  (melamine). Finally, an i.r. of the opaque layer did not resemble that of dicy, but was quite similar to that of melamine, as in Figure 2. In the EPON 1001 system, melamine did not precipitate out, indicating the increased solubility of melamine in higher molecular weight bisphenol-A epoxides.

The two transitions in the clear layers of the DER 332 epoxies,  $T_1$  and  $T_3$ , are not unusual: multiple transitions have been found in other cured epoxies<sup>2</sup>. The transition associated with the melamine layer,  $T_2$ , is unusual, in that no data were found in the literature to indicate the existence of such a transition. However, thermal analysis of pure melamine (Figure 3) indicates that it undergoes decomposition at  $127^\circ\text{C}$ , as indicated by frothing. The i.r. spectrum of the decomposition product no longer resembles that of the starting melamine and has few characteristics of the opaque layer of the cured DER 332 epoxy, as seen in Figure 2. It was not further identified.

Reheating the melamine decomposition product showed no further  $T_2$  transition, although the cured DER 332 epoxies exhibited such a transition after several cycles. This indicates that the decomposition is reversible when its products are trapped in the cured epoxy matrix.

The EPON 1001 epoxy did not exhibit a  $T_2$  transition since, evidently, the soluble melamine reacted with the

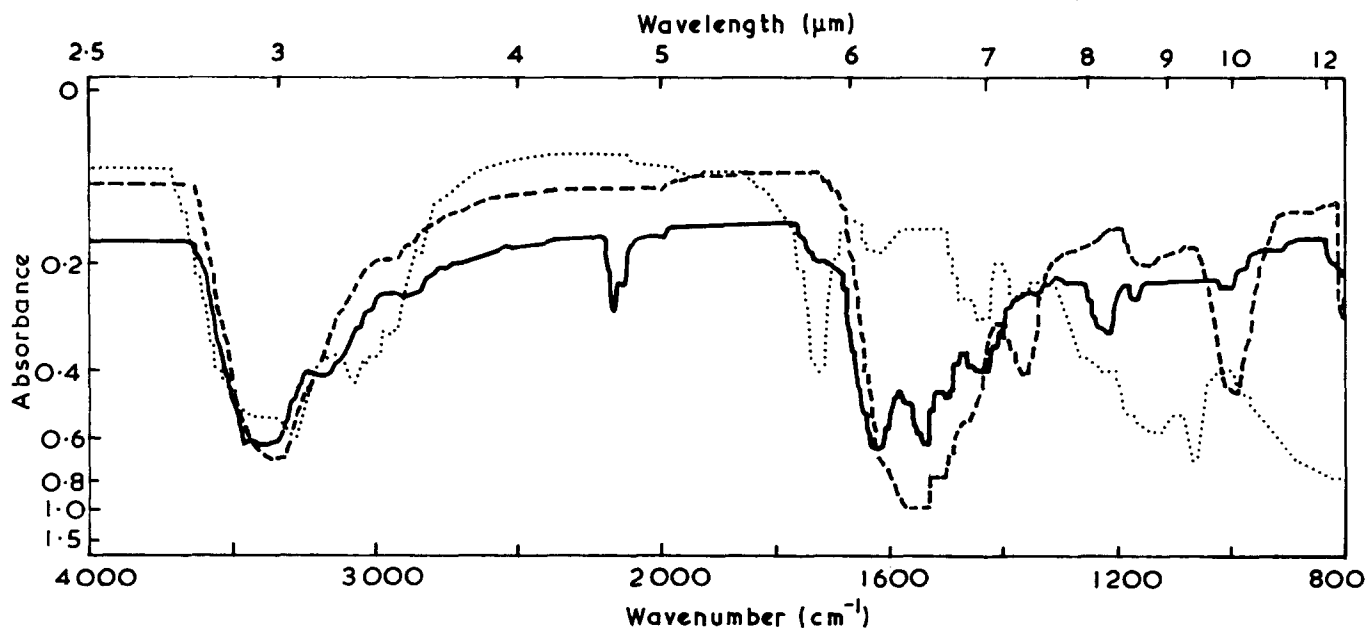


Figure 2 Infra-red spectra of the opaque lower layer of cured DER 332/fine dicy epoxy (—), of melamine (---) and of the melamine decomposition product (. . .). The presence of the nitrile peak ( $2200\text{ cm}^{-1}$ ) in the spectrum of the opaque layer is due to the presence of the epoxy matrix, which contains nitrile groups, in which the precipitate was formed

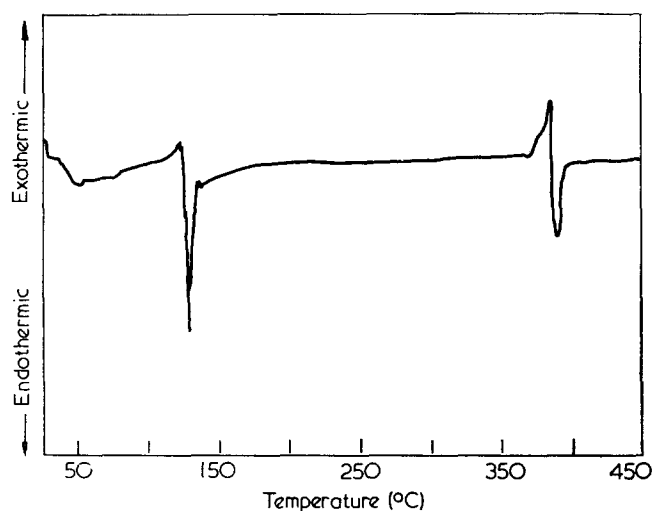


Figure 3 A differential thermal analysis plot of the decomposition of melamine at  $127^\circ\text{C}$ , followed by a premelt phenomenon beginning at  $375^\circ\text{C}$  and a melt at  $390^\circ\text{C}$ . When carried to completion, the final product was a black char, indicating decomposition during melting. The plot was made at a heating rate of  $5^\circ\text{C}/\text{min}$

epoxide or continued to decompose into the unidentified, soluble decomposition product, which reacted. The absence of a  $T_3$  transition suggests that this material differs structurally from the DER 332 epoxy. In a previous study<sup>4</sup>, it was found that a cured epoxy using phenyl glycidyl ether was capable of further reaction, through the addition of the hydroxyl group across the nitrile. An i.r. spectrum of the cured EPON 1001 epoxy (Figure 4) shows the presence of peaks at  $3400\text{ cm}^{-1}$  and at  $2200\text{ cm}^{-1}$ . Although the former may be due to the presence of, among others, hydroxyl groups, the latter is definitely due to nitrile groups. Thus, any addition of hydroxyl groups across the nitrile is incomplete. This will be further considered in a later section.

In summary, the reaction of dicy with epoxides is more complex than previously suspected. It is outlined schematically in Figure 5. What is clear is that the activation energies in equations (2) to (6) have contributions from the decomposition reactions, as well as from the cure reaction. Thus, the measured activation energy,  $\Delta E$ , is really some combination of  $\Delta E_{\text{reaction}}$  and  $\Delta E_{\text{catchall}}$ , where  $\Delta E_{\text{reaction}}$ , that for the cure proper, is expected to

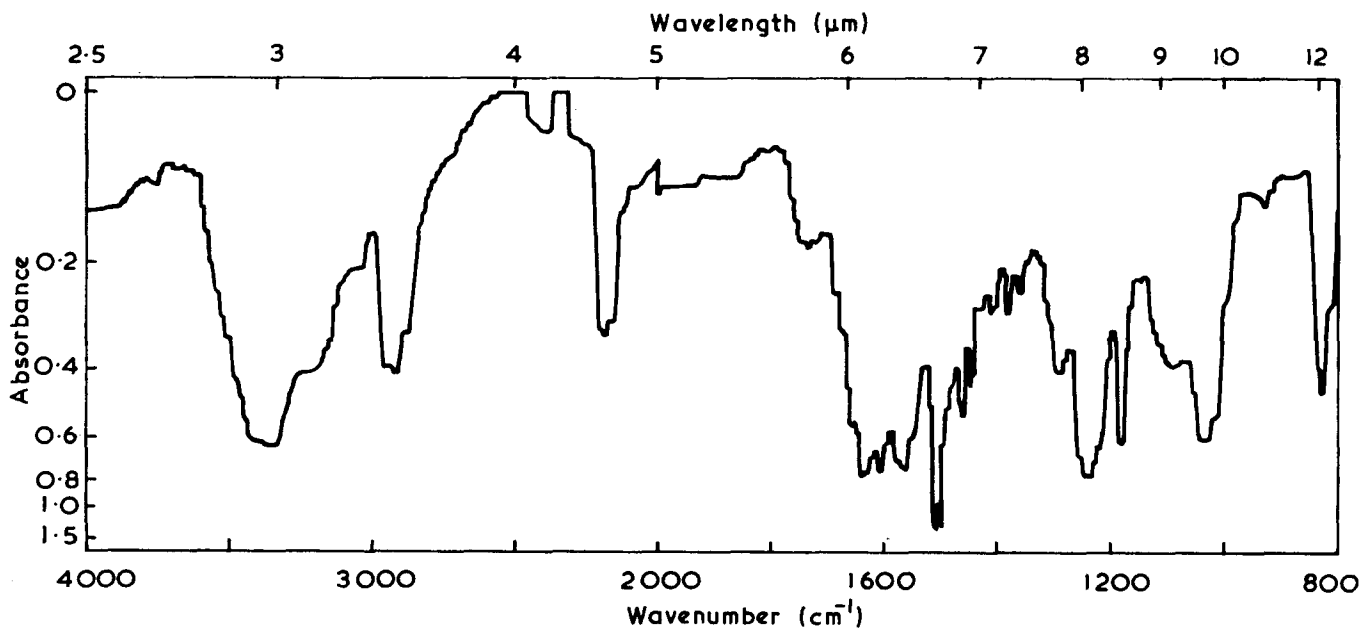


Figure 4 An infra-red spectrum of the cured EPON 1001/dicy epoxy



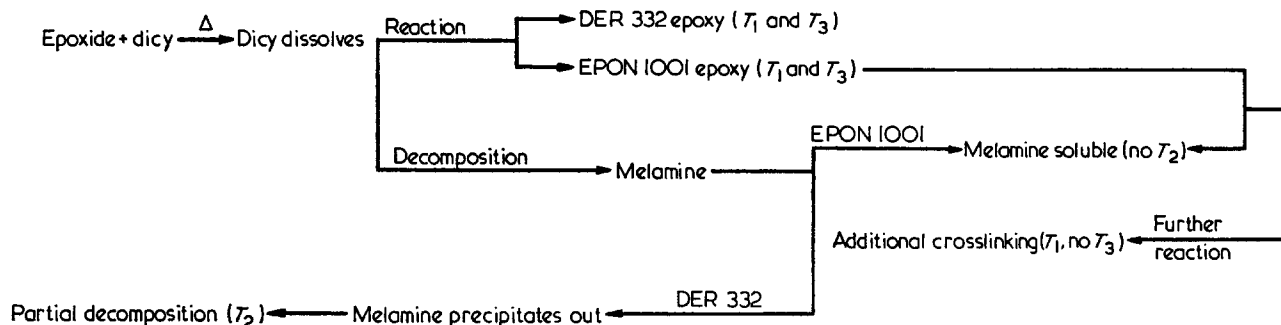


Figure 5 The cure/decomposition reaction scheme for the general bisphenol-A epoxide/dicy system

have a value<sup>1,2</sup> around  $13 \text{ kcal mol}^{-1}$  and  $\Delta E_{\text{catchall}}$  has an unknown value varying with the magnitudes of the appropriate dissolution, mixing, decomposition and precipitation contributions. Doubtless, these same contributions influence the pre-exponentials, as well. For these reasons, a comparison of rate equations may not be justified except in very similar cases and, even then, only qualitatively.

#### Effect of particle size

A comparison of equations (2) and (3) indicates that, for the DER 332 epoxies, the change from fine to coarse dicy reduced the pre-exponential by  $10^6 \text{ sec}^{-1}$  and the activation energy by half\*. The transition temperatures in Table 1 indicate a decrease in both  $T_1$  and  $T_3$  with increased particle size.

Dynamic d.s.c., at  $20^\circ\text{C}/\text{min}$ , indicated a small melting transition at  $209^\circ\text{C}$  for the DER 332/coarse dicy, after isothermal reaction at  $170^\circ\text{C}$ . This dicy m.p. is evidence of incomplete reaction. A similar transition was not found for the DER 332/fine dicy. That is, partial reaction occurred in the case of the coarse dicy, caused by the inability of the larger particles to react completely. This leads to a situation where regions of more completely reacted epoxide exist in a matrix of less completely reacted epoxide. This situation is believed to be the cause of the lowering of the transition temperatures in Table 1.

Equations (2) and (3) indicate that the magnitudes of the pre-exponentials and activation energies might be used to estimate dicy particle size. The activation energy for the fine dicy,  $\sim 24 \text{ kcal mol}^{-1}$ , is similar to that found for commercial bisphenol-A diglycidyl ether/dicy systems of unspecified particle size<sup>7</sup>, indicating that finer sized particles were used. However, the reason for using them does not appear to be because finer material gives a more complete cure reaction at a faster rate, but because it gives a more stable system at room temperature. This increased room temperature stability is mentioned in various monographs on epoxies<sup>8</sup>.

An example of this stability is seen in the following: in the present study, DER 332/fine dicy was found to be stable after a week at room temperature, while DER 332/coarse dicy was noticeably pasty after 48 hours. What appears to have occurred is reaction at the epoxide/dicy interface (i.e., the particle surface). Since reaction at relatively few sites is sufficient to immobilize a large particle, the material takes on a pasty consistency. On the other hand, the larger surface area available with the fine dicy leads to more interfacial reaction without a pasty consistency.

\* Since  $\Delta E \approx \Delta E_{\text{reaction}}$  in the coarse dicy case, the various contributions of  $\Delta E_{\text{catchall}}$  seem to have cancelled each other.

One might be tempted to use equation (1) to estimate room temperature stability. For example, letting  $n=1$  and assuming a gel point when  $\alpha=0.6$ , substitution of equations (2) and (3) indicates that, at  $23^\circ\text{C}$ , the time to gelation for the fine dicy is  $4 \times 10^4$  hours (4.6 years) and that for the coarse dicy is 90 hours. Such an extrapolation is, however, invalid since dicy is insoluble at  $23^\circ\text{C}$ .

#### Effect of surfactant

A surfactant lowers surface tensions. It was reasoned in the present study that the addition of surfactant would, by lowering the epoxide-dicy interfacial tension, increase the dicy solubility at a lower temperature. The minimum amount of surfactant to be added was determined in the following way: dynamic d.s.c. traces of the uncured DER 332/fine dicy were run at  $20^\circ\text{C}/\text{min}$  with increasing amounts of Tween 80 added, until the dicy m.p. at  $209^\circ\text{C}$  was no longer present. This minimum amount was 1.2% (w/w) and caused a diminution in both pre-exponential and  $\Delta E$ , as seen in equation (5). What is surprising is that, as a comparison of equations (5) and (6) shows, a five-fold increase in surfactant concentration caused no change in the rate, within experimental error<sup>1</sup>. That is, beyond a certain minimum amount, additional surfactant had little effect on the kinetics. Further, in spite of the increased dicy solubility, the system without added surfactant still had a higher overall rate. This may be due to surfactant at the epoxide-dicy interface acting as a barrier to the cure reaction.

Table 1 indicates that the addition of surfactant caused a reduction in the transition temperatures, particularly in  $T_1$ . This does not appear to be due to plasticization by the surfactant since it is not linear in surfactant concentration. The absence of  $T_3$  in the case of the 6% surfactant and the non-linearity of the  $T_1$  change suggest a change in reaction mechanism caused by the addition of the Tween 80, which according to company literature, is polyoxyethylene (20) sorbitan monooleate. This view, that a change in mechanism has caused a change in structure, is consistent with the experimental data, although a comparison of i.r. spectra was inconclusive on this point. The similarity of equations (5) and (6) suggests that the rate-determining step occurred early in the reaction; the mechanistic deviation suggested by the data in Table 1 must, then, have occurred later in the course of the reaction.

#### Effect of epoxide molecular weight

The epoxide molecular weight does not affect  $\Delta E_{\text{reaction}}$  since it is well known<sup>1,2</sup> that this term is essentially constant for a large variety of epoxides. Rather, it affects the dicy decomposition, in that the solubility of the melamine formed increased with increasing epoxide

molecular weight. In spite of this increased melamine solubility, dynamic d.s.c. did not indicate a similarly increased dicy solubility.

A comparison of equations (2) and (4) indicates that both the pre-exponential and  $\Delta E$  decreased with increasing molecular weight of the epoxide. Since  $\Delta E_{\text{reaction}}$  is expected to be the same regardless of epoxide molecular weight<sup>1,2</sup>, and the same particle size of dicy was used in both cases, it seems reasonable to suggest that the decrease in  $\Delta E$  is due entirely to a decrease in  $\Delta E_{\text{catalyst}}$  and is related to the absence of a heterogeneous layer in the EPON 1001 system.

It has been found<sup>2</sup> that an increase in chain flexibility is reflected in decreased transition temperatures and increased pre-exponentials. Table 1 indicates, however, that not only is  $T_1$  increased on going to EPON 1001,  $T_3$  is absent. In addition, the pre-exponential has decreased. Taken together, these indicate that the EPON 1001 epoxy differs structurally from the DER 332 epoxy.

One may speculate on the structural difference. As indicated in the discussion on the course of the reaction, the presence of i.r. peaks at  $2200\text{ cm}^{-1}$  and  $3400\text{ cm}^{-1}$  precludes any large-scale addition of hydroxyl across the nitrile. However, a comparison of the i.r. spectra of the

DER 332 and EPON 1001 epoxies, in Figure 6, shows the presence of many more absorption peaks, in the  $1500\text{--}1650\text{ cm}^{-1}$  range, for the EPON 1001 epoxy than for the DER 332 epoxy. Such absorptions are characteristic of amides. Amides have previously been found<sup>4</sup> to result from rearrangement of the hydroxyl-nitrile addition product during epoxy cure. It is unlikely that such an addition may have occurred across the nitriles, sufficient to stiffen the resulting epoxy, since, although hydroxyl groups sterically favourable for reaction are produced in both epoxy systems through the opening of the oxirane rings, few amide peaks are present in the DER 332 epoxy.

It is probable that, since the melamine remains soluble only in the EPON 1001 case, it or its decomposition product may be involved in reactions which produce amides and stiffen the resulting network. Thus, crosslinking in the regions responsible for  $T_3$  has suppressed this transition and stiffened the network, raising  $T_1$ . A similar situation has been shown<sup>2</sup> to occur with polyamide hardener, where the product of an early stage of the reaction was a reactant in a later stage.

## CONCLUSIONS

The cure of the systems bisphenol-A epoxides/dicy occurs with a simultaneous decomposition of the dicy into melamine. The melamine is soluble in higher molecular weight epoxides and is capable of further decomposition into an unidentified material. The melamine is insoluble in lower molecular weight epoxides and precipitates out, retarding its further degradation. The higher molecular weight epoxides are capable of further reaction and the resulting epoxy is more rigid than that obtained with bisphenol-A diglycidyl ether.

The addition of surfactant causes an increased dicy solubility at lower temperatures. In spite of this, the rates are lower than for the system without surfactant. Further, the presence of surfactant appears to cause a change in reaction mechanism.

## ACKNOWLEDGEMENTS

The author wishes to thank R. B. Prime for helpful discussions and D. G. Sedor for obtaining most of the experimental data.

## REFERENCES

- 1 Acitelli, M. A., Prime, R. B. and Sacher, E. *Polymer* 1971, **12**, 335
- 2 Prime, R. B. and Sacher, E. *Polymer* 1972, **13**, 455
- 3 Piloyan, G. O., Ryabchikov, I. D. and Novikova, O. S. *Nature* 1966, **212**, 1229
- 4 Saunders, T. F., Levy, M. F. and Serino, J. F. *J. Polym. Sci. (A-1)* 1967, **5**, 1609
- 5 Davis, T. L. and Underwood, H. W., Jr. *J. Am. Chem. Soc.* 1922, **44**, 2595
- 6 American Cyanamid Co., U.S. Pat. 2 737 513 (1956)
- 7 Eyerer, P. *J. Appl. Polym. Sci.* 1971, **15**, 3067
- 8 'Handbook of Epoxy Resins' (Eds H. Lee and K. Neville), McGraw-Hill, New York, 1967, Ch 10, p 16

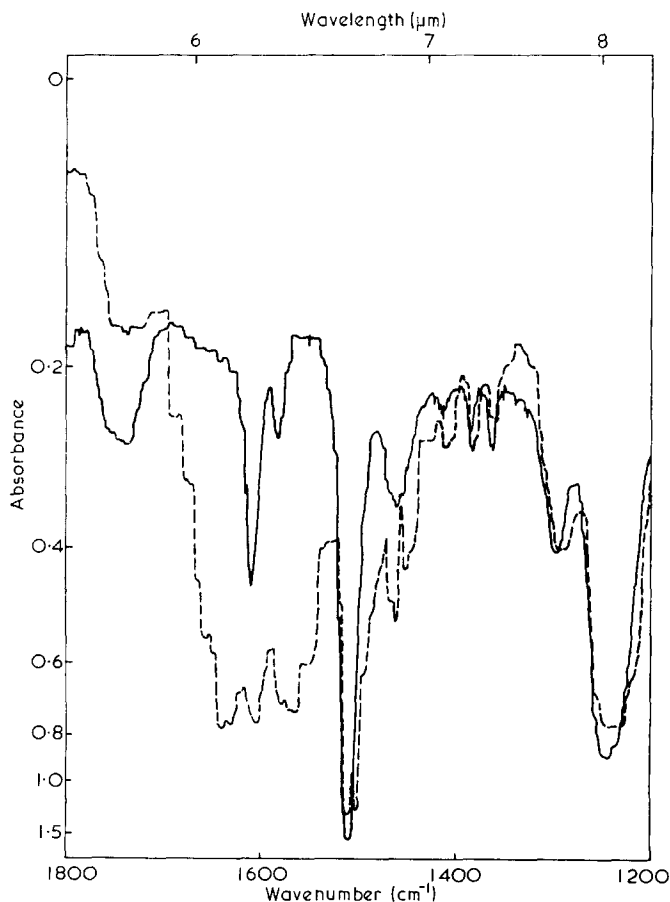


Figure 6 Infra-red spectra of the clear DER 332/dicy epoxy upper layer (—) and of the EPON 1001/dicy epoxy (---)

# Electron microscopy studies of fracture processes in amorphous thermoplastics\*

P. Beahan, M. Bevis and D. Hull

*Department of Metallurgy and Materials Science, University of Liverpool,  
PO Box 147, Liverpool L69 3BX, UK  
(Received 23 October 1972)*

The electron microscopy techniques which can be used to provide definite information about fracture processes in amorphous thermoplastics are summarized. A comparison is made of the micromorphology of crazes formed in thin films of polystyrene and the micromorphology of the fracture surfaces of bulk specimens. This shows that the fracture behaviour of thin films simulates closely the fracture behaviour of the bulk in craze controlled fracture and that the former procedure may therefore be used for high resolution studies of fracture processes. A brief description is also given of the precautions that have to be taken in the study of electron beam sensitive materials and of the developments in electron optical instruments which should result in an improvement in the facilities available for electron microscopy studies of polymers.

## INTRODUCTION

The main aim of this paper is to review the electron microscopy techniques which can be used to study fracture processes in amorphous thermoplastics, and to identify the procedures which are most likely to provide definite information about the fracture process in these materials. A more detailed discussion of the craze controlled fracture process in polystyrene which is used as the main example in this paper will be given elsewhere<sup>1</sup>.

The techniques fall into two main categories: first, those associated with the examination of fracture surfaces of bulk specimens using scanning electron microscopy and also replication combined with conventional transmission electron microscopy, and secondly, those associated with the transmission electron microscopy of thin polymer films or sections which provide information about the microstructure of the specimen and of the changes in internal structure which occur during the fracture process. Any changes in microstructure which occur during the fracture process are likely to be reflected in fracture surface morphology and as such the two approaches referred to complement one another. The resolution attainable with the conventional transmission electron microscope is considerably in excess of that attainable with the conventional scanning electron microscope so that the former should provide more definite microstructural information. On the other hand, the scanning electron microscope procedures provide direct information about bulk specimens which is easily and rapidly obtained. Working at the best resolutions currently attainable they provide sufficient detail to allow a comparison to be made between the microstructure associated

with the fracture process in thin films and the microstructure observed on the fracture surfaces of bulk specimens using optical microscopy techniques. In this paper the equivalence of structures observed is demonstrated for the case of craze controlled fracture. The experimental procedures which can be used to study the fracture process in amorphous thermoplastics are described. An outline is given of the potential of high resolution scanning electron microscopy based on instruments fitted with field-emission electron guns and of *in situ* experiments in high voltage transmission electron microscopes and conventional scanning electron microscopes.

There are inherent difficulties associated with electron beam damage in the electron microscopy of amorphous polymers just as in the case of crystalline polymers. These difficulties can be overcome to a limited extent by operating the microscope at low intensities and by keeping the specimen cold during examination. In order to establish the extent to which thin film experiments represent the behaviour of the bulk it is desirable to carry out experiments with materials which are relatively insensitive to the electron beam. The models of the microstructure, deformation and fracture processes which are developed for these materials can subsequently be modified for the case of the more beam sensitive polymers. This procedure has been adopted by the authors and the initial investigations were made with a general purpose grade of polystyrene. Most of the examples in this paper are taken from the results of our investigations with polystyrene, but some examples from electron microscopy studies of the more beam sensitive poly(methyl methacrylate) and polycarbonate are also included.

The examination by optical and scanning electron microscopy of fracture surfaces of bulk specimens of polystyrene<sup>2,3</sup> has resulted in the formulation of the model for the fracture process summarized in *Figures 1a* and *1b*. *Figure 1a* is an optical micrograph showing a

\* Text of a paper presented by M. Bevis at the symposium 'Application of electron microscopy to the study of polymers' on 12 September 1972 as part of the 5th European Congress on Electron Microscopy (EMCON 72) held at the University of Manchester.

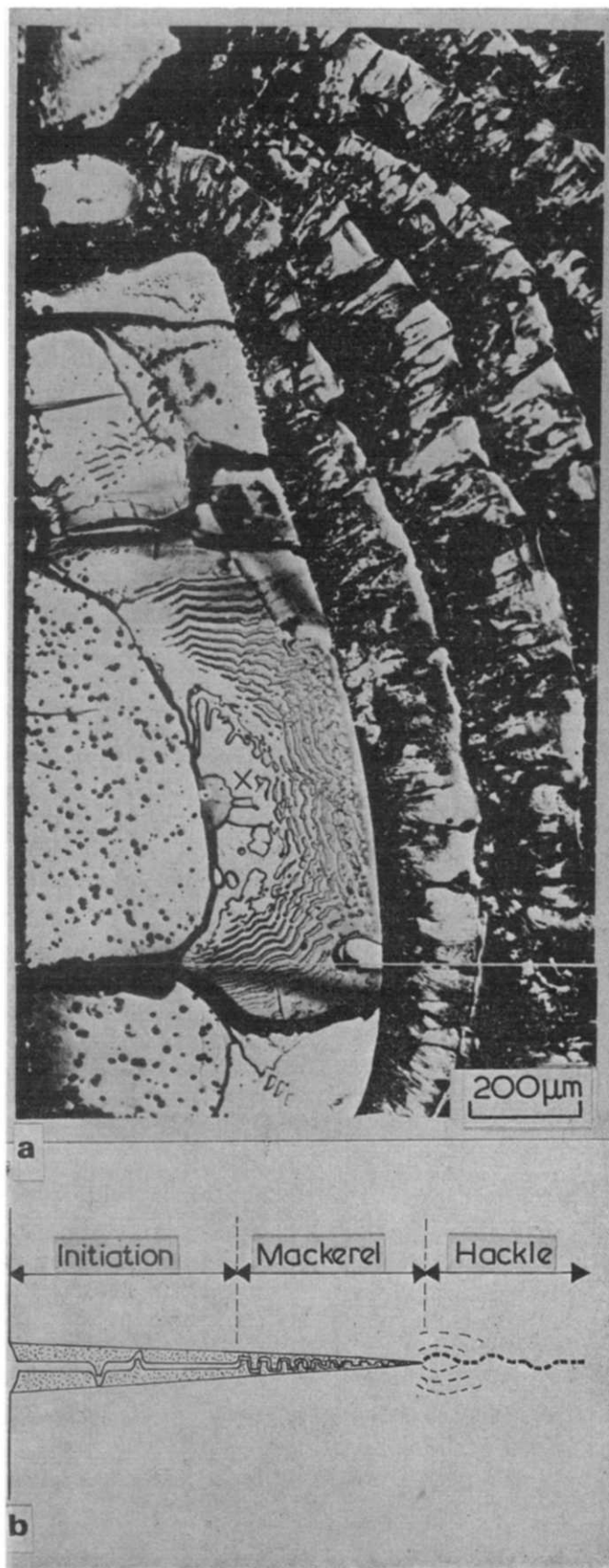


Figure 1 (a) Optical micrograph showing a plan view of the fracture surface of a bulk polystyrene specimen. Three distinct regions of the fracture surface are illustrated. The way in which these different areas arise in relation to craze controlled failure is illustrated in (b). The crazed region is shown shaded in this end elevation diagram and the direction of crack propagation is from left to right

typical fracture surface, and Figure 1b is a schematic diagram of the fracture process which is initially craze controlled in that the crack nucleates and grows within the craze. The hackle region of the fracture surface is associated with crack propagation through small crazes which form ahead of the advancing crack. This particular mode of fracture is quite common in amorphous thermoplastics and results from straining at low temperatures or high strain rates, the exact conditions of test and the resultant fracture surface morphology varying with the polymer or compounding formulation used. Discussion will be restricted to this type of fracture process.

#### TRANSMISSION ELECTRON MICROSCOPY OF THIN POLYMER FILMS

In a craze controlled fracture process it is to be expected that the microstructure of the polymer will influence the micromorphological characteristics of the craze, and hence the exact conditions for the nucleation and growth of the crack. There should also be some evidence of the craze microstructure on the fracture surfaces of bulk specimens. In order to understand the fracture process fully it is therefore necessary to be able to establish the effect of processing conditions, compounding, etc. on the morphology of crazes. The most effective way of doing this is to investigate the microstructure of crazes by transmission electron microscopy. However, it is essential that the results obtained be representative of the bulk and the best way of establishing this is to examine the remnants of crazes retained on the fracture surfaces of the bulk. It is also desirable to compare the morphology of fractures crazes which arise in *in situ* tensile testing in an electron microscope with that formed in the bulk.

The microstructure of crazes may be examined by transmission electron microscopy using the following procedures.

(a) Preparation of thin sections by the ultramicrotomy of precrazed bulk specimens<sup>4-6</sup>. Included in this category is the procedure used by Kambour and co-workers<sup>5,6</sup> which consists basically of impregnating crazes with a reinforcing agent to reduce damage of the craze during microtomy. The procedures of preparing thin sections of precrazed material directly or by the use of reinforcing agents are difficult and there is also the possibility that artefacts may be introduced as a result of their use.

(b) Preparation of thin sections by the ultramicrotomy of bulk specimens. Crazes can subsequently be formed<sup>4</sup> by straining the thin sections in a microstraining device.

(c) Preparation of solvent-cast thin films<sup>7</sup> by solvent evaporation. The polymer film is prepared by evaporation of the solvent from a clean glass slide or casting onto mercury<sup>8</sup>. Crazes can subsequently be formed by straining the thin films in a microstraining device whilst supported on an electron microscope grid. Thin films of a uniform thickness may be prepared in this way and it is also possible to carry out quantitative work on the effects of strain rate, total strain, etc.

(d) Preparation of a solvent cast thin film encapsulating an electron microscope grid<sup>7</sup>. The specimen can be made simply by placing the grid in a drop of the polymer solution and allowing the solvent to evaporate. The plastic encapsulated grid may then be strained using a microstraining device or even with pairs of tweezers. A complex and changing stress system occurs within the film in this type of experiment and it is therefore of limited value for

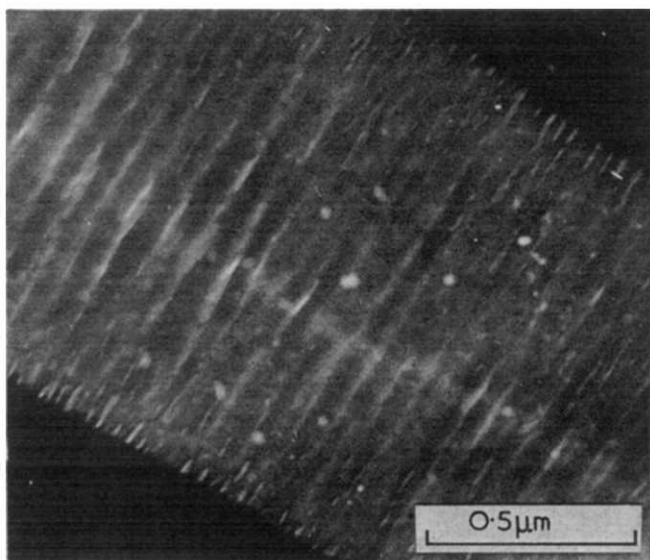
quantitative work. However, an indication of the type of craze microstructure which can occur is given rapidly and easily by the technique<sup>7</sup>.

(e) The preparation of large solvent-cast thin films<sup>7, 9, 10</sup> of dimensions of, for example, 30 × 5 mm. These films were prepared in a similar way to that described in (c) and subsequently strained on a Mylar substrate under well controlled conditions of testing with a tensile testing machine. Small sections identified by optical microscopy can be cut from the large film after removal of the film from the substrate by immersion in distilled water. The small sections supported by an electron microscope grid can then be examined in the electron microscope.

(f) Preparation of 'thick' thin films of up to several microns in thickness by solvent casting. These films may then be strained using a microstraining device with a supporting grid or in the case of very thick films without the use of a supporting grid. This type of specimen is particularly suited for high voltage electron microscopy and *in situ* experiments in the electron microscope, including testing *in situ* in active environments.

The microstructure of crazes formed in the bulk and studies using procedure (a) is similar to the microstructure of crazes formed by straining thin microtomed sections of bulk material using procedure (b)<sup>4, 7</sup>. Procedure (b) therefore provides a very effective way of studying the microstructure of crazes in amorphous plastics. An example of the microstructure of a craze produced by straining a microtomed section of bulk general purpose polystyrene is shown in *Figure 2*. The crazes formed in a plane normal to the major principal stress axis (the tensile axis) and exhibited the characteristic craze microstructure described previously<sup>7</sup>; that is, a planar interface between the matrix and the craze and fibrils of 250–500 Å in diameter parallel to the major principal stress axis and joined together by minor fibrils. Also present are bands of large voids at the centre (midrib) of the craze and at the craze–matrix interfaces.

The viability of technique (b) is dependent on being able to produce microtomed thin sections of the polymer. This can be a serious difficulty in the case of, for example, polycarbonate, where it is necessary to produce solvent cast thin films or alternatively to thin the bulk material



*Figure 2* Transmission electron micrograph of a craze formed by straining a microtomed thin section of polystyrene

using jet or ion bombardment thinning techniques<sup>14</sup>. It is possible in both of these situations that the deformation behaviour of the thin films will be modified by the procedure used for producing the films, particularly in the former case where the desirable effects of compounding in the bulk can be lost in the solvent casting. The importance of method (b) is that the properties of the material which are modified by compounding are not lost. Nevertheless, if it can be demonstrated that solvent cast films are representative of the bulk polymer, particularly in the case of simple formulations in compounding, then the uniformity of the films, their large dimensions, and large range of controllable thicknesses can be used to great advantage. Methods (d) and (e) have been described in detail previously<sup>7, 10</sup>, the latter in particular being useful in controlled strain rate and total strain experiments with ultra-thin films. In the case of general purpose polystyrene the microstructure of crazes formed in thin microtomed and solvent cast thin films have been shown to be very similar<sup>7</sup>. The microstructure and failure of crazes formed in 'thick' thin films are expected to be even more representative of the bulk. An example of a craze formed by straining a thick thin film is shown in *Figure 3*. The microstructure of the craze in this example is consistent with the model for the microstructure of a craze previously described by the authors<sup>7</sup>. The coarse fibres within the craze break down into fine fibres with increasing thickness of the craze resulting in bands of coarse voids at the centre of the craze and at the craze–matrix interfaces.

The next stages of development in 'thick' thin film experiments are *in situ* tensile experiments in the transmission electron microscope. Experiments of this type have been made<sup>11</sup> and in principle it is possible to follow the nucleation, growth and failure of crazes directly in the electron microscope. However, as is well known in this type of experiment a long time can be taken in detecting and following through a single 'event'. This type of experiment is, however, very important as it provides direct evidence about the fracture process by allowing the validity of the proposed mechanisms of failure to be established more definitely. This point is illustrated by *Figure 4* which is a transmission electron micrograph showing the region of a craze directly ahead of a crack in a 'thick' thin film. This micrograph was not recorded during an *in situ* experiment but during an examination of a prestrained film. The micrograph shows the existence of a mackerel type failure of the craze which is very similar to the mackerel pattern observed on bulk fracture surfaces and illustrated in *Figure 1*. The mackerel pattern in 'thick' thin films is formed by dilatation and subsequent failure of fibres at the craze–matrix interface alternating between the two surfaces of the craze.

The equivalence of the morphology of the mackerel pattern in this example and the mackerel pattern shown in *Figure 1* indicate that the fracture process in 'thick' thin films does simulate the fracture process in the bulk. The equivalence of these processes can be further demonstrated by the examination of the fracture surfaces using high resolution electron optical techniques.

#### HIGH RESOLUTION ELECTRON FRACTOGRAPHY OF BULK SPECIMENS

The best resolution that can be obtained in fractography of bulk specimens results from the examination of surface replicas with a transmission electron microscopy.

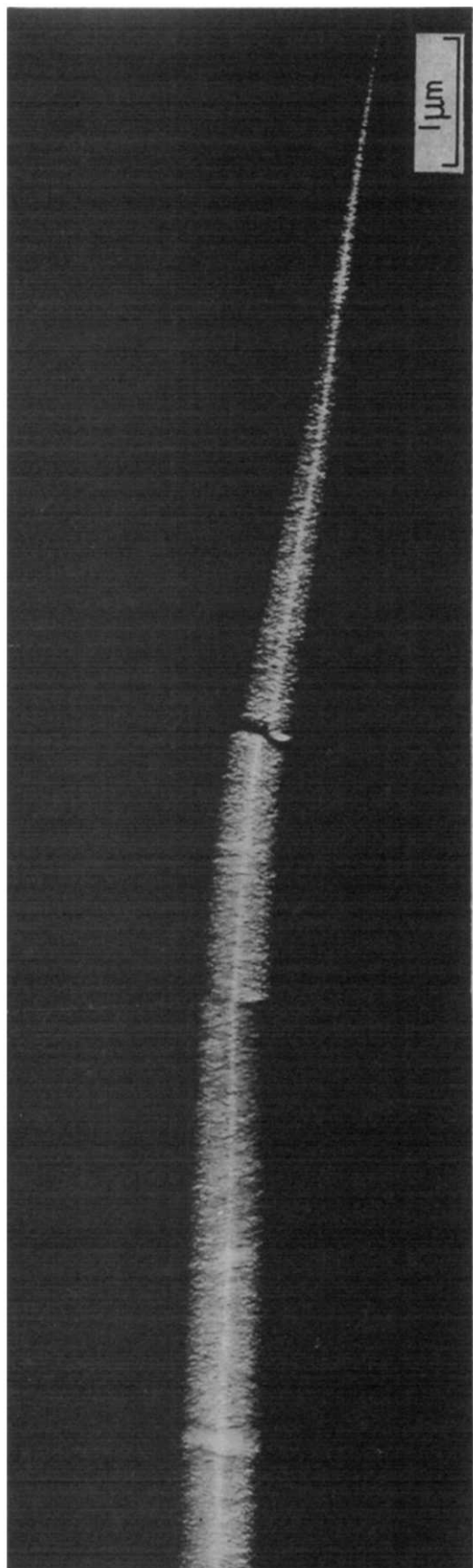


Figure 3 A composite electron micrograph of a craze formed in a 'thick' thin film of polystyrene. The existence of a band of voids at the centre (midrib) and at the craze-matrix interface is illustrated and so is the drawing down of the coarse fibrillar structure into a fine fibrillar structure in the wider regions of the craze

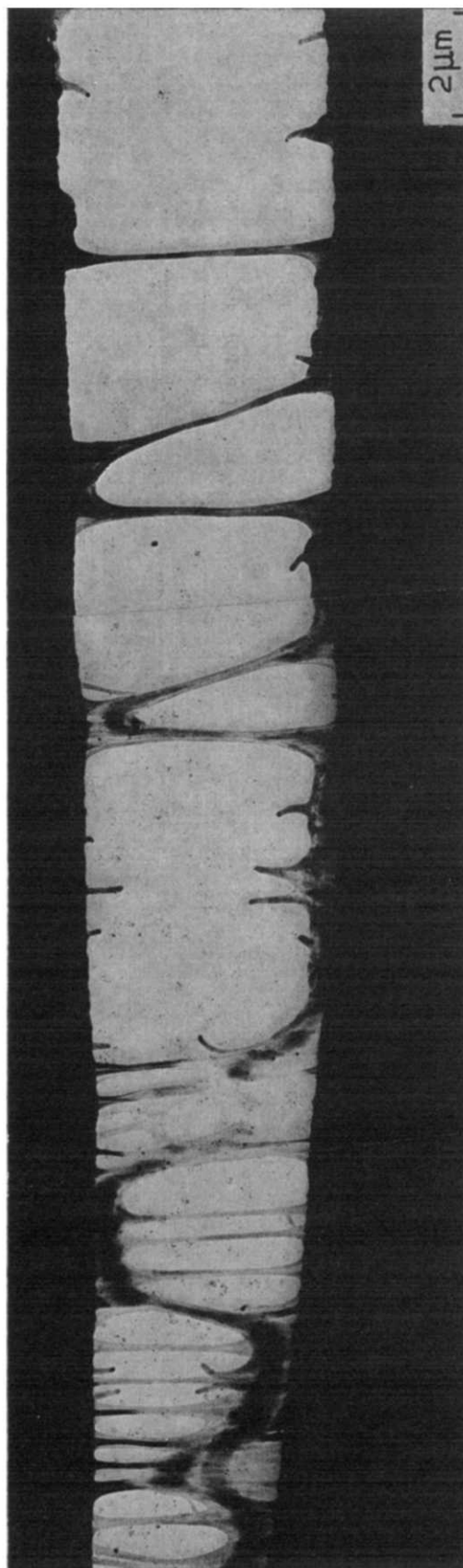


Figure 4 Composite transmission electron micrograph showing a 'mackerel' type failure of a craze in a 'thick' thin film of polystyrene



Figure 5 is a transmission electron micrograph of a two-stage carbon/platinum replica obtained from a polystyrene fracture surface using gelatin as the replicating material. The gelatin was softened by immersion in cold water before being placed on the fracture surface and allowed to dry. The replica was coated at an angle of  $60^\circ$  and the final C/Pt replicas were floated off in warm distilled water. The fibres observed on the replica are comparable in dimensions to the fibres observed within crazes formed in thin films. The detail that can be observed using replicas is, however, very dependent on the replication procedure used. The technique has been used extensively in the past<sup>12, 13</sup> for example, but has now in some areas of investigation tended to be superseded by high resolution scanning electron microscopy.

It is now possible with conventional scanning electron microscopes to achieve on a regular basis resolutions of approximately  $100 \text{ \AA}$ . In high-resolution reflection studies of polymers it is necessary to use high accelerating voltages and this may lead to specimen charging. Charging effects can be minimized without decreasing the resolution significantly by coating the specimen with a conductive film.

It is widely realised that the optimum conditions for scanning electron microscopy, including for example, cleanliness of the system, alignment of filament and apertures etc. are essential requirements for high resolution microscopy.

The micrographs described below were obtained under these conditions of operation and from polystyrene fracture surfaces which had been coated on a planetary stage using gold/palladium. Figure 6 is a scanning electron

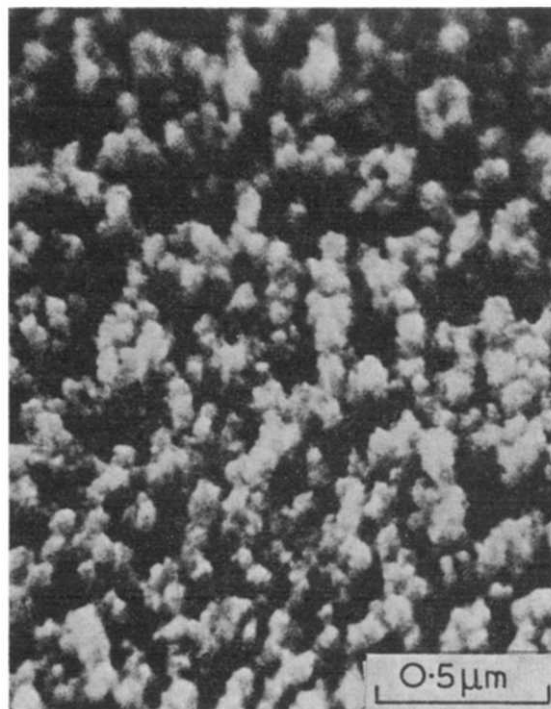


Figure 6 High-resolution scanning electron micrograph from the mirror region of a polystyrene fracture surface showing the existence of fractured fibrils of dimensions comparable with that observed in thin film experiments and replicas. The specimen was coated with gold/palladium and examined at 30 kV accelerating voltage with an aperture of  $100 \mu\text{m}$  diameter and optimum operating conditions

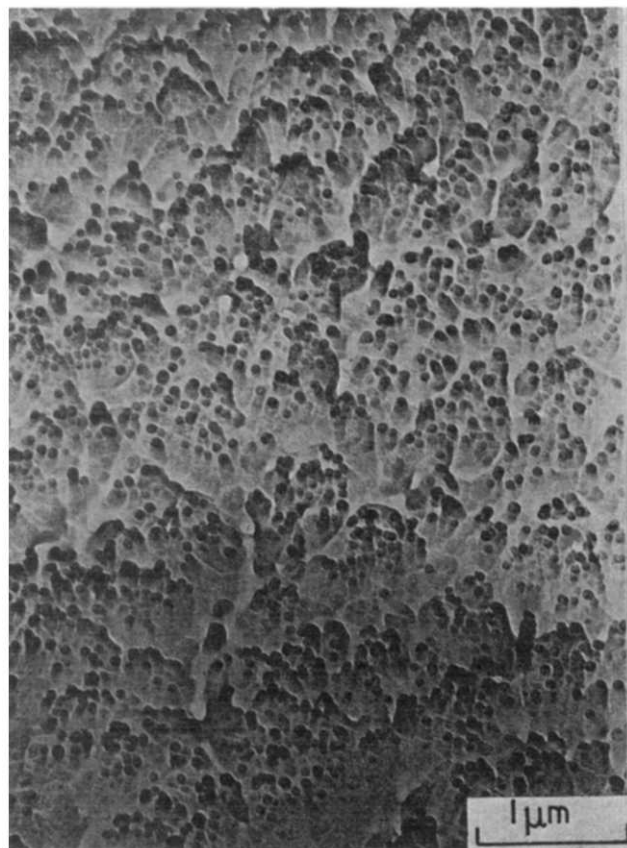


Figure 5 A transmission electron micrograph of a two-stage carbon-platinum replica showing the existence of a fibrillar structure in the mirror region of a polystyrene fracture surface

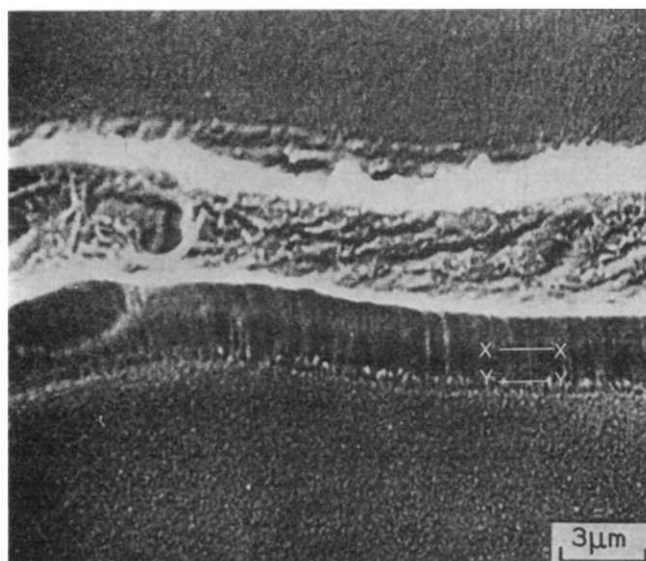


Figure 7 Scanning electron micrograph of the side of a 'mackerel' band showing details of the micromorphology of the craze which correlate well with the micromorphology observed in thin film studies. In particular the existence of a 'midrib' (X-X) and a coarse fibrillar structure (Y-Y) at the craze-matrix interface should be noted

micrograph from a polystyrene fracture surface and was obtained from an area similar to that indicated by X in Figure 1. The fibres illustrated in the micrograph are consistent with the dimensions of fibres observed in crazes formed in thin films. An examination of the sides of the mackerel bands on the fracture surface by scanning electron microscopy shows conclusively the existence of a change in morphology through the thickness of the craze.

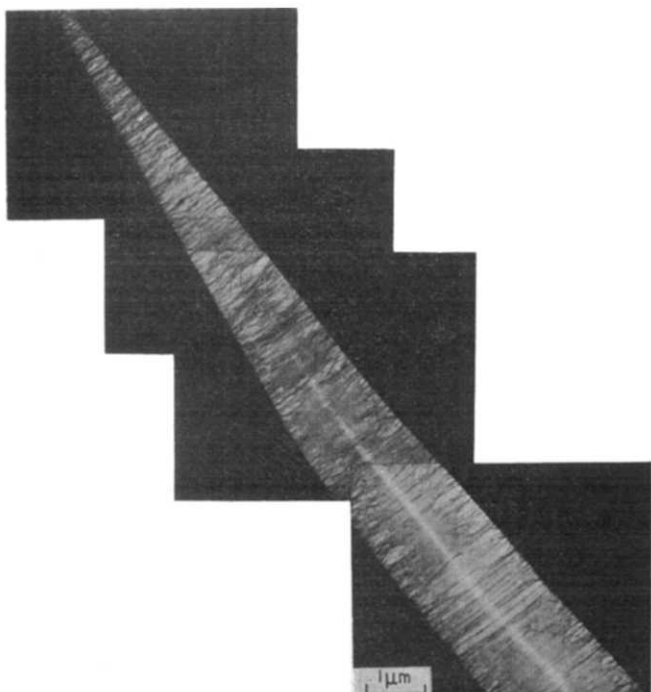
This is illustrated by *Figure 7* which shows the central row of voids at the centre of the craze and rows of voids at the craze-matrix interfaces.

#### APPLICATIONS OF THIN FILM ELECTRON MICROSCOPY

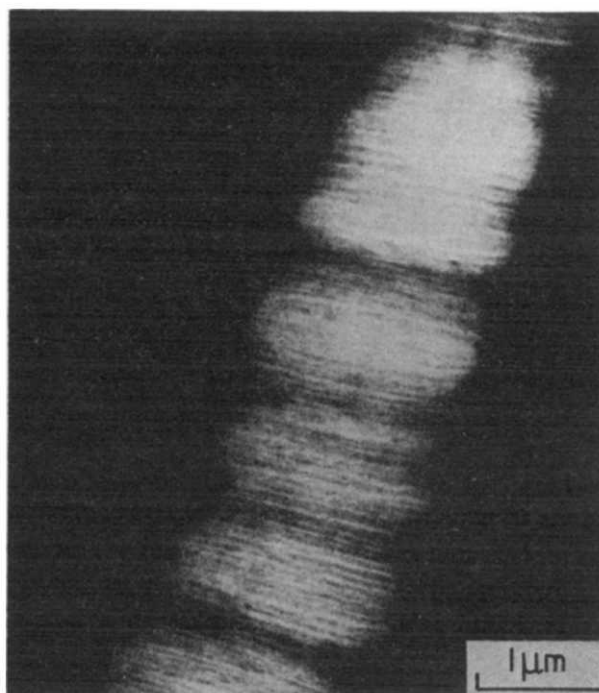
A comparison of the transmission electron micrographs of crazes formed in thin films and the scanning electron micrographs from polystyrene fracture surfaces shows that the micromorphology of crazes and the fracture processes associated with crazes in the two cases are very similar. It is therefore possible in principle to study the effect of the following variables on the micromorphology of crazes and the associated fracture processes by the transmission electron microscopy of ultra-microtomed thin sections of bulk specimens or solvent cast thin films: (i) heat treatments; (ii) strain rate; (iii) total strain; (iv) temperature; (v) environment; (vi) degree of crosslinking; (vii) compounding formulation; (viii) molecular orientation.

The thin film procedures are being used by Bevis, Hull *et al.* at Liverpool University to study the effect of the variables listed on the deformation and fracture processes in a wide range of amorphous thermoplastics. The techniques have quite general applicability and if great care is taken with experimental technique they also apply to beam sensitive materials. The time taken for marked degradation of amorphous polymers to occur in the electron microscope can be increased by maintaining the specimen at low temperatures during examination, and by operating at low beam intensities.

*Figure 8* is a transmission electron micrograph of a craze formed in a solvent cast film of poly(methyl methacrylate). It is quite clear from that micrograph,



*Figure 8* Composite transmission electron micrograph showing the variation in micromorphology with craze width in a craze formed in a solvent cast thin film of poly(methyl methacrylate). The micromorphology in this case is very similar to that observed in polystyrene under certain conditions



*Figure 9* Transmission electron micrograph showing the fibrillar structure observed within a craze formed in polycarbonate by straining in air after annealing at 110°C for three days (Low, A. and Bevis, M. work in progress)

which was recorded for a specimen maintained at 77K that the micromorphology of the craze in this case is similar to that of the polystyrene craze shown in *Figure 2*.

*Figure 9* is a transmission electron micrograph showing the 100 Å fibril microstructure of a craze formed in a thin film of polycarbonate which had been annealed at 110°C for three days prior to straining. A comparable extent of crazing in films which had not undergone heat treatment could only be developed by deforming in an active environment such as ethanol.

The techniques described above can also apply equally well to two phase materials. This is particularly so in the case of ABS systems<sup>11</sup> where the rubber phase can be comparable in dimensions to the thickness of 'thick' thin films.

#### CONCLUDING REMARKS

The main theme of this paper has been to demonstrate the ways in which electron microscopy can contribute in a definite way to the understanding of fracture and related processes in amorphous thermoplastics. The continued development of electron optical equipment should, however, lead to significant advances in the techniques available for the study of fracture problems in polymers.

High voltage transmission electron microscopes allow much thicker films to be examined. The use of very thick films allows *in situ* testing to be carried out in a controlled way without need for the Mylar substrate technique. More important, however, is that the space available in the specimen area in the high voltage electron microscopes is sufficient to allow *in situ* straining experiments to be carried out in active environments.

The development of scanning systems for conventional scanning electron microscopes operating at TV scanning rates and of versatile straining stages is also significant.



High resolution studies of *in situ* fracture experiments with bulk specimens are possible in principle, but generally difficult because of specimen charging effects. The technique is, however, a practical proposition with thick films and has considerable potential. It is possible to observe without significant charging effects when operating in reflection or transmission modes the existence of voids within crazes in thick films. Figure 10 is a scanning electron micrograph of a craze formed in a thick thin film and shows enhanced contrast at the midrib of the craze and at voids. *In situ* scanning electron microscope experiments and the use of TV scanning rates would therefore allow the nucleation and growth of cracks within crazes to be studied. This provides in some respects a more straightforward alternative to high voltage transmission electron

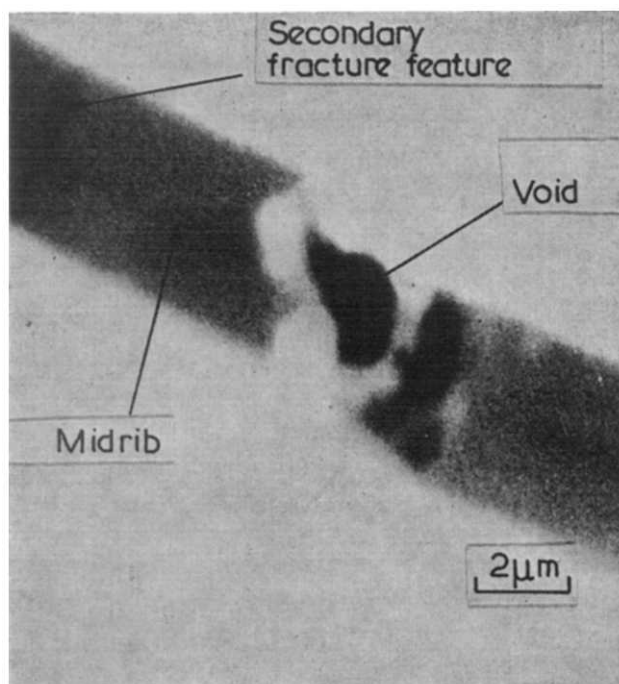


Figure 10 Reflection scanning electron micrograph showing a craze formed by straining a 'thick' thin film. The existence of secondary fracture features, the 'midrib' and voids can be distinguished. The specimens were not coated and this result indicates that *in situ* straining experiments for studying craze-controlled fracture processes are practicable with scanning electron microscopes equipped with TV scanning and *in situ* straining facilities. Experiments of this type are of value only in cases where the specimen material is not sensitive to electron beam damage, as for example, in the case of polystyrene

microscopy, although the resolution attainable and the ease of deforming in active environments do not compare favourably with the latter.

Probably the most important contribution that could be made to the development of the fractography of plastics would be an improvement in the resolution capability of scanning electron microscopes operating in the reflection mode. Fibre diameters within crazes described in this paper range from 30 Å to 500 Å illustrating the importance of attaining resolutions better than 100 Å. Resolutions of better than 100 Å would also be of great value in the study of crystalline polymers in relation to fractography studies and also to the identification of, for example, microstructural detail associated with processing which can be observed on etched sections of bulk specimens. The development of the high brightness field-emission electron guns for use in reflection scanning electron optical equipment should result in some improvement in resolution. More sophisticated instruments of this type also have great potential for transmission studies of polymers, and would allow thicker films to be examined for a given accelerating voltage and in some cases would give improved contrast and possibly improved degradation characteristics. These qualities are also of considerable importance in the study of crystalline polymers.

#### ACKNOWLEDGEMENTS

The authors gratefully acknowledge the support of the Science Research Council and the University of Liverpool in this research.

#### REFERENCES

- 1 Beahan, P., Bevis, M. and Hull, D. in preparation
- 2 Murray, J. and Hull, D. *J. Polym. Sci. (A-2)* 1970, **8**, 583
- 3 Hull, D. *J. Mater. Sci.* 1970, **5**, 357
- 4 Beahan, P., Bevis, M. and Hull, D. *Phil. Mag.* 1971, **24**, 1267
- 5 Kambour, R. P. and Holik, A. S. *J. Polym. Sci. (A-2)* 1969, **7**, 1393
- 6 Kambour, R. P. and Russell, D. R. *Polymer* 1971, **12**, 237
- 7 Beahan, P., Bevis, M. and Hull, D. *J. Mater. Sci.* in press
- 8 Bray, J. C. and Hopfenberg, H. B. *J. Polym. Sci. (B)* 1969, **7**, 679
- 9 Klement, J. J. and Geil, P. H. *J. Macromol. Sci.* 1972, **B6** (1), 31
- 10 Brady, T. E. and Yeh, G. S. Y. *J. Appl. Phys.* 1971, **42**, 4622
- 11 Bevis, M. *et al.* work in progress
- 12 Haward, R. N. and Brough, I. *Polymer* 1969, **10**, 724
- 13 Bird, R. J., Rooney, G. and Mann, J. *Polymer* 1971, **12**, 742
- 14 Lewis, P. R. paper presented at EMCON 72, University of Manchester, September 1972

# Some observations on the fracture of poly(ethylene terephthalate) film

R. J. Ferguson and J. G. Williams

Polymer Engineering Group, Department of Mechanical Engineering, Imperial College of Science and Technology, Exhibition Road, London SW7 2BX, UK  
(Received 12 September 1972)

Recent work on the applications of linear elastic fracture mechanics to the problem of ductile tearing and fracture of poly(ethylene terephthalate) film is reviewed. It is shown that, even for a brittle plastic, there can be no direct correlation between the amount of slow crack growth and stress intensity factor. The Dugdale model, combined with a constant crack opening displacement criterion, is then used to correlate both initiation and final fracture results for poly(ethylene terephthalate) film extended in the extrusion direction. Also, the model is able to justify the use of linear elastic fracture mechanics for a limited range of crack initiation results.

## INTRODUCTION

In a recent paper<sup>1\*</sup> Vincent described some experiments in which he had studied the slow growth of cracks in poly(ethylene terephthalate) film (PET). He had chosen PET as a representative ductile thermoplastic to investigate the usefulness of linear elastic fracture mechanics in describing the failure of this class of material.

In essence, Vincent's conclusion was that linear fracture mechanics could not correlate his test results and therefore cannot be applied to ductile plastics in general. In the main, this is certainly true, and indeed, Vincent shows clearly that a single value of stress intensity factor ( $K_c$ ) does not characterize the onset of slow growth in PET film; there is a clear dependence on crack length.

Although ductile fracture strictly exceeds the explanatory capacity of simple linear fracture mechanics theory, several useful comments on this topic can still be made. In the present paper the authors attempt to do this, and to show that some of the PET results can be correlated by using the Dugdale model to account for the effects of plasticity at the crack tip.

## EXPERIMENTAL TECHNIQUE AND RESULTS

Vincent's experiments<sup>1</sup> involved the loading of single edge notch 25  $\mu\text{m}$  thick film specimens of various crack lengths at 5 mm/min until a prescribed load, different for each specimen, was reached. The specimens were then unloaded, and the amount of slow crack growth was measured. This technique was probably adopted to remove the difficulty involved in directly measuring tiny amounts of crack growth as a function of load. Although this is acceptable for Vincent's tests, it would not be a good general method because further slow growth, or even catastrophic failure, could occur if

unloading were to begin when instability was imminent.

The results of Vincent's measurements are shown in Figures 1 and 2 where the amount of slow growth ( $\Delta a$ ) is plotted against the net section stress ( $\sigma_N$ ), and the stress intensity factor ( $K_c$ ) respectively.

From these Figures, it is clear that slow cracking does not initiate at a particular  $K_c$ , but there seems to be a threshold value of  $\sigma_N$  below which cracking will not occur. It must be pointed out, however, that if the data of Figure 1 are examined critically, then it becomes obvious that extrapolation to 40 MN/m<sup>2</sup> cannot be defended without additional evidence.

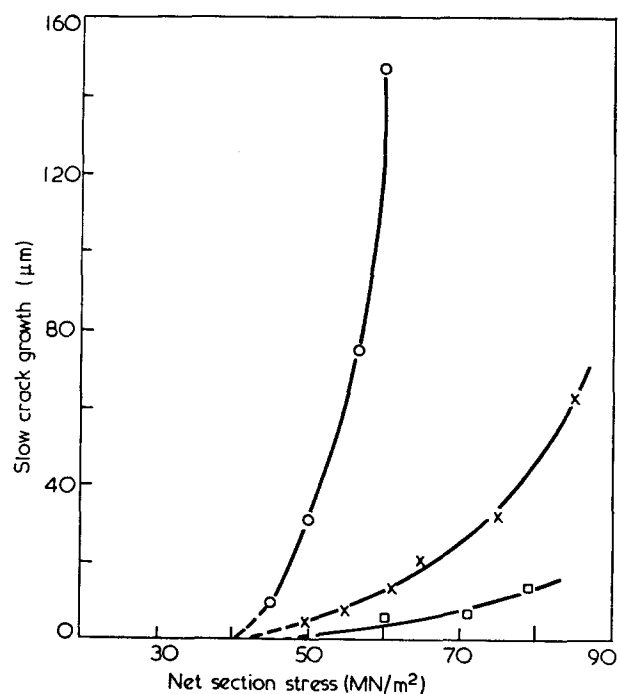


Figure 1 Slow crack growth in poly(ethylene terephthalate) film as a function of net section stress for various initial notch depths<sup>2</sup>:  $\circ$ , 4.34-4.63 mm;  $\times$ , 1.38-1.87 mm;  $\square$ , 0.36-0.39 mm

\* This work was an extension and, in part, a summary of two more extensive reports<sup>2, 3</sup>.

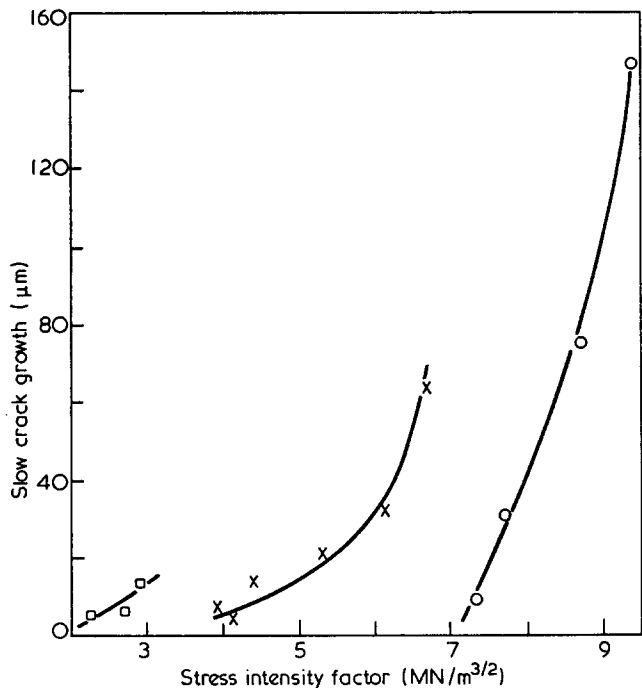


Figure 2 Slow crack growth in poly(ethylene terephthalate) film as a function of stress intensity factor<sup>1</sup>. For legend see Figure 1

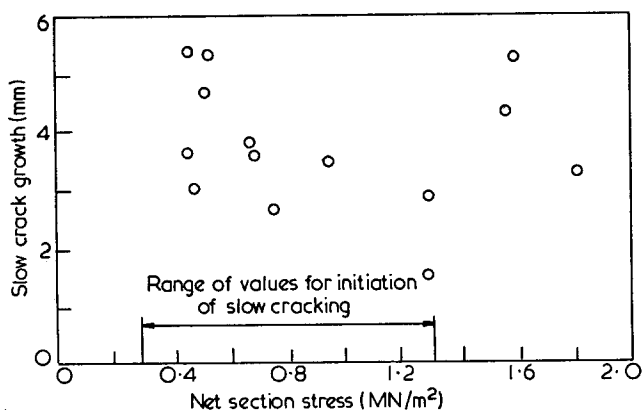


Figure 3 Slow crack growth in PMMA as a function of net section stress. (Data supplied by Marshall<sup>5</sup>.)

Since Vincent treats these measurements as a test of fracture mechanics, it is appropriate to review what would happen if similar experiments were done using poly(methyl methacrylate) (PMMA), the archetypal brittle plastic.

The initiation of slow cracking in PMMA occurs at a constant  $K_c$  for each strain rate<sup>4</sup>. For a tension test of a single edge notch specimen of brittle plastic, it can be shown that the amount of slow growth obtained depends on both the initial and final values of  $K_c$ , and on the initial crack length. In these circumstances there can be no simple relation between  $K_c$  and  $\Delta a$  which is independent of  $a$  itself.

A similar argument applies to the  $\Delta a$  versus  $\sigma_N$  plot. Since cracking initiates at a constant  $K_c$ , it cannot do so at a constant  $\sigma_N$  and again no simple relation exists. To illustrate these points, some data supplied by Marshall<sup>5</sup> are shown plotted in Figure 3. The data are from tension tests of single edge notch specimens of PMMA pulled at an extension rate of 0.5 mm/min. The same degree of scatter is obtained if the  $\Delta a$  versus  $K_c$  correlation is investigated.

Since crack growth measurements for a brittle plastic such as PMMA cannot be successfully correlated using either  $K_c$  or  $\sigma_N$ , it seems unlikely that it could be done for a ductile plastic such as PET.

The only way in which the  $K_c$  value and the behaviour of the moving crack could be related is by plotting the results as  $K_c$  versus crack speed. It has been shown that this is entirely valid for brittle plastics such as PMMA<sup>4</sup> and polystyrene<sup>6</sup>. The approach is not, however, a worthy possibility for PET since there is an experimentally proved dependence of  $K_c$  for crack initiation on crack length<sup>1</sup>. Accordingly, a different  $K_c$  versus  $\dot{a}$  curve would be generated for each  $a/W$  ratio tested. The curves themselves would have little significance since they would owe their existence and shape to the act of multiplying two monotonically increasing quantities, namely,  $a^{1/2}$  and the applied stress.

### THE DUGDALE MODEL

The Dugdale model<sup>7</sup> provides the first stage of refinement to linear fracture mechanics and can often be used for problems of semi-ductile fracture. Here it will serve to show that the  $K_c$ -crack length dependence is an inevitable result of ductility and that when it is combined with a constant crack opening displacement (COD) criterion, the model can correlate crack initiation and final fracture data for PET.

The simple Dugdale model envisages the growth of a line plastic zone from the tip of a crack in which the stress is equal to the yield stress of the material. The length of this zone can be calculated as can the COD<sup>8</sup> which must necessarily take place at the crack tip. Closed-form solutions for both these parameters exist for the case of a centre crack in an infinite plate, but more realistic geometries require the numerical solutions which are available in a recent paper by Hayes and Williams<sup>9</sup>. Their result for the single edge notch specimen forms Figure 4. The abscissa of the graph is COD ( $\delta$ ) non-dimensionalized by the factor:

$$\frac{\pi E}{4\sigma_y W} \text{ (for plane stress only)}$$

where  $E$  = Young's modulus,  $\sigma_y$  = yield stress, and  $W$  = plate width.

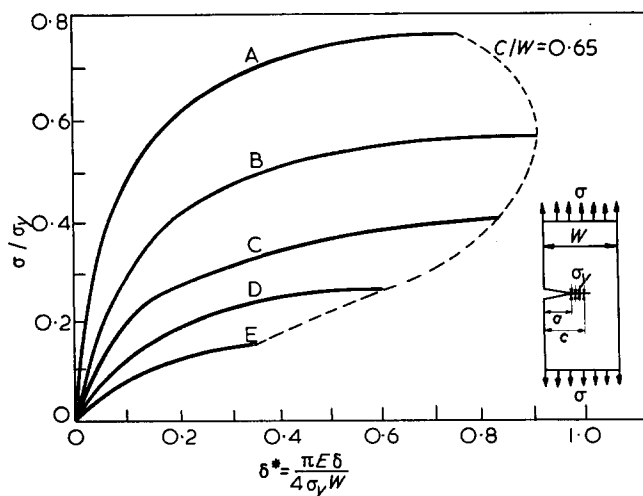


Figure 4 Crack opening displacement in the Dugdale model for the single edge notch specimen. (After Hayes et al.<sup>9</sup>) A,  $a/W=0.1$ ; B,  $a/W=0.2$ ; C,  $a/W=0.3$ ; D,  $a/W=0.4$ ; E,  $a/W=0.5$

If it is assumed that slow cracking begins at a constant  $COD$ , irrespective of crack length—a reasonable and a common assumption—then it is possible to calculate  $K_c$  for a material having  $\sigma_y = 100 \text{ MN/m}^2$  (approximately that for PET) for a range of  $\delta^*$  values. The results are displayed in Figure 5 and show that there is a significant dependence of  $K_c$  on crack length. This dependence becomes more pronounced as  $\delta^*$  increases since this implies increased ductility. For low values of  $\delta^*$  the dependence is reduced so that for PMMA ( $\delta^* \approx 0.003$ ) the constant  $COD$  and  $K_c$  criteria are satisfied simultaneously. The falling off of the curves at high values of  $a/W$  is attributable to interaction between the single edge notch finite plate correction factor<sup>10</sup>, and that inherent in the finite element results of Hayes and Williams (Figure 4).

#### CONSTANT $COD$ AS A FRACTURE CRITERION FOR PET

The postulate that  $\delta$  is a constant for crack initiation cannot be tested for the data of Vincent's paper<sup>1</sup> because not enough information is given. Figure 5 in the first of his two earlier reports<sup>2</sup> does, however, provide data for PET film which can be used for this purpose. In using these results it must be noted that the specimens were extended in the extrusion direction while those described in the most recent work<sup>1</sup> were extended in the transverse direction.

The fit obtained by assuming a  $\delta^*$  of 0.03 is shown in Figure 6 along with the relationship between stress and crack length which would be predicted by a constant  $K_c$  criterion. [The constant  $K_c$  is calculated from the values:  $a = 10 \text{ mm}$  and  $\sigma = 28 \text{ MN/m}^2$ .] The two criteria agree reasonably well down to an  $a/W$  ratio of 0.05. Below this the plasticity effects are of paramount importance since the plastic zone size becomes so large compared to the crack length, that linear elastic fracture mechanics can no longer apply and therefore the two results must diverge. For example, with  $\delta^* = 0.03$ , Hayes's finite plate version of the Dugdale model<sup>9</sup> predicts that the plastic zone length is approximately

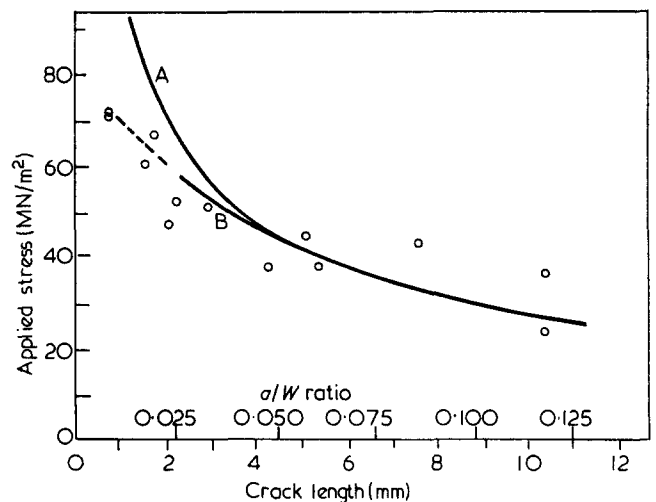


Figure 6 Comparison of theoretical curves and experimental results for crack initiation: A,  $K_c = \text{constant}$ ; B,  $\delta^* = 0.03$

equal to  $a/5$  when  $a/W = 0.125$ , but that it rises to over  $6a/5$  when  $a/W = 0.025$ .

There are two advantages to viewing crack initiation in PET in this way. First, the range of  $a/W$  ratios for which fracture data can be correlated is increased since the Dugdale model specifically accounts for the relatively large amount of crack tip plasticity which occurs for short cracks. Second, the model provides a theoretical justification for using a constant  $K_c$  criterion over a limited  $a/W$  range. This second advantage may be the principle one because  $K_c$  can be determined more easily than  $\delta$  since it is unnecessary to know the value of either  $E$  or  $\sigma_y$ . For initiation, for example,  $\delta^* = 0.03$  corresponds to  $\delta = 57 \mu\text{m}$  if  $\sigma_y = 100 \text{ MN/m}^2$  and  $E = 6000 \text{ MN/m}^2$ .

Since Vincent found that  $K_c$  was even less able to deal with final fracture data<sup>2</sup> than initiation data, it is interesting to attempt the correlation using the Dugdale model. As can be seen from Figure 7, it is possible to fit a curve to a significant portion of the data—the  $a/W$  range covered is twice that in Figure 6—using a  $\delta^*$  of 0.7 which corresponds to  $\delta = 189 \mu\text{m}$ . Also shown on the graph is the curve obtained when  $K_c$  is constant (calculated from the values  $a = 6 \text{ mm}$  and  $\sigma = 20 \text{ MN/m}^2$ ). Once again constant  $\delta^*$  and constant  $K_c$  give the same result until plasticity effects cause the two theoretical curves to diverge. Unfortunately the two criteria are united only in their inability to correlate the data beyond  $a/W \approx 0.25$ . The difference between theory and experiment is opposite to the one which might be due to work hardening effects. It may, however, be attributable to the discrepancy between the boundary conditions of the analysis, and the actual boundary conditions—one which will grow with increasing  $a/W$ . In particular, the analysis allows the specimen ends to rotate, but in the experiments the ends were clamped.

Finally, it will be noted that the results of Figure 7 have been plotted using the initial crack length and the maximum tensile stress attained in the test. In reality this combination does not exist because of the large amount of slow growth which takes place<sup>2</sup>. If the actual crack length is used, however, it is found that the Dugdale model can no longer correlate the results if the stress in the plastic zone is presumed equal to the yield stress of the material. This is a difficulty experienced with

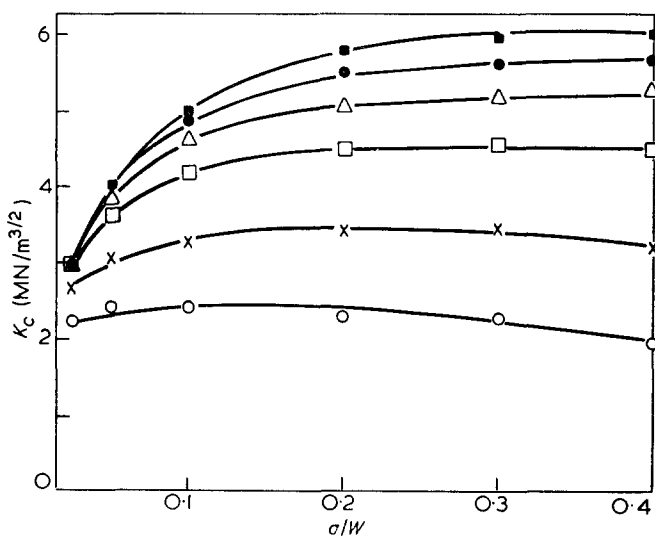


Figure 5 Dependence of  $K_c$  on  $a/W$  for a Dugdale material with  $\sigma_y = 100 \text{ MN/m}^2$ .  $\delta^*$ :  $\circ$ , 0.05;  $\times$ , 0.10;  $\square$ , 0.20;  $\triangle$ , 0.30;  $\bullet$ , 0.40;  $\blacksquare$ , 0.50

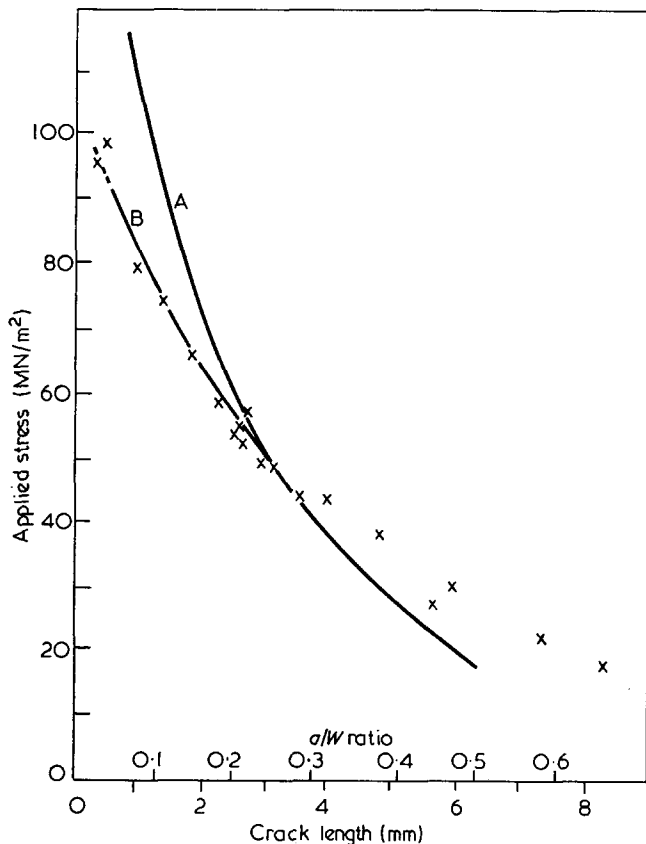


Figure 7 Comparison of theoretical curves and experimental results for final fracture: A,  $K_c = \text{constant}$ ; B,  $\delta^* = 0.7$

other tough plastics<sup>11</sup>, and can only be removed by measuring the actual zone length and then by using the Dugdale model twice: first to calculate the stress in the plastic zone, and then again to determine the *COD*.

When this process is complete, a more realistic model of the physical situation is available. Use of initial crack lengths can still be defended, however, since a reasonable estimate of *COD* can be made and because the failure stress of a cracked sheet can be predicted to a good degree of accuracy<sup>11</sup>.

## CONCLUSIONS

- (1) Linear elastic fracture mechanics does not suggest that attempts to correlate the amount of slow crack growth with either  $\sigma_N$  or  $K_c$  will be successful for even a brittle plastic such as PMMA.
- (2) By using the Dugdale model, it can be shown that a dependence exists between  $K_c$  and crack length for moderate to large values of non-dimensional *COD*.
- (3) The constant *COD* criterion can correlate both initiation and final fracture data for PET film extended in the extrusion direction. Also, for crack initiation, it can be shown that  $K_c$  is an appropriate criterion for a restricted range of crack length to width ratios.

## ACKNOWLEDGEMENTS

The authors thank Mr D. N. Fenner for providing additional data on the Dugdale model to supplement those of Hayes and Williams<sup>9</sup>, and Dr G. P. Marshall for his suggestions and discussion. Mr P. I. Vincent was kind enough to answer questions about his experimental work, and he also made several useful comments.

## REFERENCES

- 1 Vincent, P. I. *Polymer* 1971, **12**, 534
- 2 Vincent, P. I., Picknell, S. and Harding, G. F. *Tech. Rep. 73*, 1967, Division of Polymer Science, Case Western Reserve University, Cleveland, Ohio
- 3 Vincent, P. I. *Tech. Rep. 97*, 1968, Division of Polymer Science, Case Western Reserve University, Cleveland, Ohio
- 4 Marshall, G. P., Culver, L. E. and Williams, J. G. *Plastics and Polymers* 1969, **37**, 75
- 5 Marshall, G. P. personal communication
- 6 Marshall, G. P., Culver, L. E. and Williams, J. G. *Int. J. Fract. Mech.* 1972, in press
- 7 Dugdale, D. S. *J. Mech. Phys. Solids* 1960, **8**, 100
- 8 Burdekin, F. E. and Stone, D. E. W. *J. Strain Anal.* 1966, **1**, 143
- 9 Hayes, D. J. and Williams, J. G. *Int. J. Fract. Mech.* 1972, **8**, 239
- 10 Brown, W. F. and Srawley, J. E. 'Plane strain crack toughness testing of high strength metallic materials', *ASTM STP 410* 1966, p 12
- 11 Ferguson, R. J., Marshall, G. P. and Williams, J. G. *3rd Int. Conf. Fract., Munich* 1973, to be published

# Effects of poor solvents on radical-radical termination of polymerization

G. G. Cameron and J. Cameron

Department of Chemistry, University of Aberdeen, Aberdeen AB9 2UE, UK  
(Received 28 September 1972)

It is shown that in poor solvents for the polymer the rate coefficient for radical-radical termination in the polymerization of styrene and methyl methacrylate is diminished compared with that in bulk monomer. It is suggested that this effect is due to the formation of tightly coiled macroradicals which hinder the radical-radical reaction process.

## INTRODUCTION

The rate of radical-radical termination in polymerization of several monomers is sensitive to diluting liquids dissolved in the polymerizing monomer. The nature of this influence is dependent to a large extent upon how effective the diluent is as a solvent for the polymer. At one extreme, diluents which are thermodynamically good solvents for the polymer exert their influence on termination through their effect on the viscosity of the reaction medium. This has been known for some time for acrylate esters and has been found more recently to apply also to styrene<sup>1, 2</sup>. The termination of polymerization of these monomers is a diffusion-controlled process and the rate coefficient for termination,  $k_t$ , is inversely proportional to the viscosity of the medium; hence, very viscous diluents retard termination because they slow down the viscosity-dependent segmental rearrangement which brings the radical chain ends into a position where they can react. At the other extreme, diluents, regardless of their viscosity, which are very poor solvents and which bring about immediate precipitation of the polymer as it forms create a heterogeneous reaction system in which at least some of the active polymeric radicals are co-precipitated with inactive polymer<sup>3</sup>. These occluded radicals continue to propagate but termination in the solid or gelatinous precipitate is severely hindered. When this occurs the reaction rate and molecular weight of the polymer are abnormally high.

These two extreme situations are reasonably well understood but very little is known about the effects on radical-radical termination of reaction media with solvent powers in an intermediate range, i.e. poor solvents, but not sufficiently poor to bring about precipitation. Under such conditions the polymer molecules and active radicals remain in solution but adopt a tightly coiled configuration as opposed to the expanded coil configuration in good solvents. Therefore, the purpose of the present investigation was to ascertain if the macroradical configuration has a significant effect on  $k_t$ , or if the proportionality between  $k_t$  and medium fluidity is retained even in poorly solvating media.

For this purpose the thermal (at 60°C) and photo-

chemical (at 25°C) polymerizations of styrene and methyl methacrylate (MMA) were studied using methanol and various hydrocarbons to alter the solvent powers of the bulk monomers. At 60°C only the ratio  $k_p^2/k_t$  was derived but at 25°C the ratio  $k_p/k_t$  was also obtained using the rotating sector technique, and hence individual values of  $k_p$  and  $k_t$ ;  $k_p$  is the rate coefficient for propagation.

## EXPERIMENTAL

### Polymerization

Solvents, monomers and initiators were purified by standard techniques as described in earlier papers<sup>2, 4</sup>.

Polymerization rates were measured in vacuum-sealed dilatometers, the percentage conversion being calculated from the relation<sup>5</sup>:

$\% \text{ conversion} = \% \text{ contraction} \times V_{\text{sp, m}} / (V_{\text{sp, m}} - V_{\text{sp, p}})$   
where  $V_{\text{sp, m}}$  and  $V_{\text{sp, p}}$  are the specific volumes of monomer and polymer respectively under the particular conditions of polymerization.  $V_{\text{sp, p}}$  for poly(methyl methacrylate) (PMMA) in various media was determined as described below.

The rate of polymerization was varied by changing the initiator concentration, or incident light intensity in photo-initiated polymerizations. Azobisisobutyronitrile (AZBN) was used for thermal initiation of MMA and photo-initiation of styrene, and azobiscyclohexane carbonitrile (AZCN) for photo-initiation of MMA. None of the solvents absorbed the photo-initiating light (3650 Å) significantly and within experimental error the rates of polymerization,  $R_p$ , were always proportional to the square root of the initiator concentration or incident light intensity.

For molecular weight measurements the conversion was restricted to 2–4%. Polymer samples were isolated and purified by precipitation in methanol cooled with solid CO<sub>2</sub>.

### Polymer specific volumes

The value of  $V_{\text{sp, p}}$  of PMMA in monomer and of  $V_{\text{sp, m}}$  of MMA were available in the literature<sup>5</sup>.  $V_{\text{sp, p}}$  for PMMA in the other reaction media were calculated

Table 1 Monomer and polymer specific volumes in various media

Polymer or monomer	Reaction medium (parts by vol.)	Temperature (°C)	$V_{sp}$ (ml/g)	Reference
MMA	Bulk monomer	25	1.0695	5
MMA	Bulk monomer	60	1.115	5
Styrene	Bulk monomer	25	1.111	6
PMMA	Bulk monomer	25	0.8228	5
PMMA	MMA : toluene (50 : 50)	25	0.809 ± 0.002	This work
		60	0.820 ± 0.002	This work
PMMA	MMA : toluene : MeOH (50 : 15 : 35)	25	0.804 ± 0.003	This work
		60	0.809 ± 0.001	This work
PMMA	MMA : MeOH (50 : 50)	25	0.791 ± 0.003	This work
		60	0.808 ± 0.003	This work
PMMA	MMA : n-octane : n-nonane (75 : 5 : 20)	25	0.796 ± 0.030	This work
Polystyrene	Bulk monomer	25	0.9302	7

from pycnometer measurements of the densities of solutions of known weight composition. The values are shown in Table 1. The variations of  $V_{sp, p}$  in different media are small and no appreciable error in polymerization rates would have resulted if these had been neglected.

For the single experiment with styrene the literature values<sup>6,7</sup> of  $V_{sp, m}$  and  $V_{sp, p}$  were used uncorrected for changes in media, since the variation is in this case even less than with PMMA.

#### Determination of polymer molecular weights, $k_p^2/k_t$ and $k_p/k_t$

In all cases limiting viscosities were derived from measurements in toluene at 30°C using a suspended-level dilution viscometer. For styrene polymerization at 25°C in which termination is exclusively by combination of macroradicals, and when transfer reactions are negligible, it has been shown previously<sup>2</sup> that the relation between  $[\eta]$  and  $R_p$  is:

$$[\eta]^{-1/\alpha} = \frac{k_t R_p}{2M_0 k_p^2 [M]^2} \cdot \left[ \frac{2^{1+\alpha}}{K\Gamma(3+\alpha)} \right]^{1/\alpha} \quad (1)$$

in which  $M_0$  is the monomer molecular weight,  $K$  and  $\alpha$  the Mark-Houwink constants and  $\Gamma(\quad)$  the gamma function. In this work  $K$  and  $\alpha$  were  $11.0 \times 10^{-5}$  and 0.725 respectively<sup>8</sup> and the ratio  $k_p^2/k_t$  was obtained from the slope of the linear plot of  $[\eta]^{-1/\alpha}$  vs.  $R_p/[M]^2$ . This line passed within experimental error through the origin confirming the absence of significant transfer.

For MMA polymerization termination by both combination and disproportionation occurs, and in methanol and the octane/nonane mixture there is evidence of transfer to solvent. Under these conditions the number average degree of polymerization  $\bar{r}$  is given by:

$$\bar{r}-1 = \frac{k_f [S]}{k_p [M]} + \frac{k_t}{k_p^2} \cdot \frac{R_p}{[M]^2} \cdot \frac{2+y}{2(1+y)} \quad (2)$$

where  $k_f$  is the rate coefficient for transfer to solvent and  $y$  the ratio  $k_{tc}/k_{td}$ .  $k_{tc}$  and  $k_{td}$  are the rate coefficients for termination by combination and disproportionation respectively, and  $k_t = k_{tc} + k_{td}$ . The rate of termination here is defined as  $k_t[P\cdot]^2$ , where  $[P\cdot]$  is the macroradical concentration. In the experiments on MMA equation (2) was employed;  $\bar{r}$  was plotted against  $R_p/[M]^2$  and the slope yielded  $k_p^2/k_t$ ,  $y$  being taken as 0.47 and 0.174 at 25° and 60°C respectively<sup>9</sup>. Some typical plots are shown in Figure 1.  $\bar{r}$  was calculated from  $[\eta]$  using the relation:

$$[\eta] = K(M_0 \bar{r})^\alpha \left[ \frac{y(1+\alpha/2)+1+Z}{y+1+Z} \right]^\alpha \times \left[ \frac{y+2+2Z}{2(y+1+Z)} \right]^\alpha \Gamma(2+\alpha) \quad (3)$$

$K$  and  $\alpha$  were  $7.0 \times 10^{-5}$  and 0.71 respectively<sup>10</sup>.  $Z$  is given by:

$$Z = \left( \frac{k_t}{R_t} \right)^{1/2} k_f \frac{[S]}{k_{td}} \quad (4)$$

where  $R_t$  is the rate of initiation. In systems where transfer to solvent was evident  $\bar{r}$  was calculated as follows. First an approximate set of values of  $\bar{r}$  was obtained by assuming  $Z=0$ . Applying equation (2), these values were then used to calculate the unknown parameters in the right hand side of equation (4) to give an approximate value of  $Z$ . With this value of  $Z$  a fresh set of values of  $\bar{r}$  was then derived and this process was repeated until constant values of  $\bar{r}$  and  $Z$  were obtained. In practice, the corrected values of  $\bar{r}$  were always only marginally different from those obtained assuming  $Z=0$ . In other words, in all these polymerizations transfer reactions had a very small effect on the molecular weight distribution of the polymer.

The ratio  $k_p/k_t$  at 25°C was obtained by employing the rotating sector technique. For the MMA polymerizations AZCN was the photo-initiator so that no dark rate correction was necessary. For the styrene

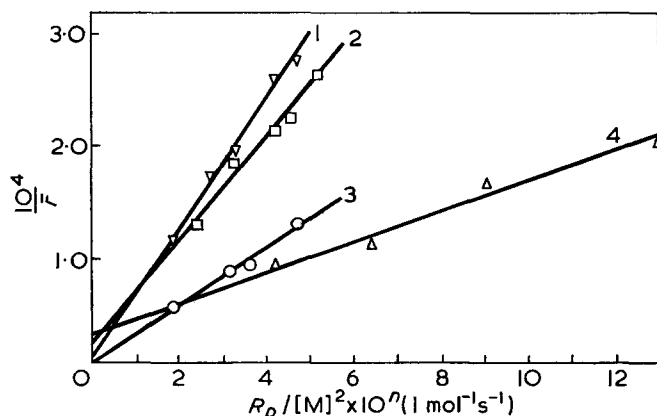


Figure 1 Reciprocal of degree of polymerization  $\bar{r}$  versus  $R_p/[M]^2$ . 1 and 2, thermal initiation at 60°C,  $n$  on abscissa scale 6; 3 and 4, photo-initiation at 25°C,  $n$  on abscissa scale, 7.  $\nabla$ , MMA : toluene (50 : 50);  $\square$ , MMA : toluene : MeOH (50 : 15 : 35);  $\circ$ , bulk monomer;  $\triangle$ , MMA : MeOH (50 : 50)

Table 2 Rate coefficients for the radical polymerization of styrene and MMA in various media

Reaction medium (parts by vol.)	Temperature (°C)	$k_p^2/k_t \times 10^3$ (l mol <sup>-1</sup> s <sup>-1</sup> )	$k_p/k_t \times 10^6$	$k_p \times 10^{-2}$ (l mol <sup>-1</sup> s <sup>-1</sup> )	$k_t \times 10^{-7}$ (l mol <sup>-1</sup> s <sup>-1</sup> )	$(\bar{S}^2)^{1/2} \times 10^5$ (mm)
MMA-toluene (50 : 50)	60	15.3	—	—	—	4.1
MMA-toluene-MeOH (50 : 15 : 35)	60	20.7	—	—	—	3.9
Bulk MMA	25	3.50	9.08	3.9 ± 0.4	4.2 ± 0.4	4.1
MMA-MeOH (50 : 50)	25	5.92	14.35	4.1 ± 0.4	2.9 ± 0.3	3.6
MMA/n-octane/n-nonane (75 : 5 : 20)	25	6.29	15.50	4.1 ± 0.4	2.6 ± 0.3	3.3
Bulk styrene <sup>a</sup>	25	6.6 × 10 <sup>-2</sup>	1.88	0.35 ± 0.07	1.9 ± 0.4	3.66
Styrene-dodecane (60 : 40)	25	6.6 × 10 <sup>-2</sup>	2.69	0.25 ± 0.03	0.9 ± 0.15	3.16

<sup>a</sup> From ref. 2.

polymerizations AZBN was employed and a dark rate correction, as described by Matheson *et al.*<sup>7</sup>, was applied. Radical lifetimes at four or five different flash times were found and the mean value used to calculate  $k_p/k_t$ .

## RESULTS AND DISCUSSION

The results of these kinetic measurements are summarized in Table 2. It should be noted that for each set of experiments with MMA the reaction media have been chosen to give contrasting solvent powers for the polymer but almost identical bulk viscosities. Thus,  $\eta_{\text{MMA-Tol}} : \eta_{\text{MMA-Tol-MeOH}}$  is 1.070 at 60°C, and  $\eta_{\text{MMA}} : \eta_{\text{MMA-MeOH}} : \eta_{\text{MMA-octane-nonane}}$  is

$$1.000 : 0.963 : 0.972$$

at 25°C. Therefore, comparisons can be made within these sets of data without having to consider the effects of different medium viscosities. For the styrene polymerizations the medium viscosities are more divergent— $\eta_{\text{styrene}} : \eta_{\text{styrene-dodecane}}$  is 0.902 at 25°C, and comparison of the rate coefficients is a little more complicated. An estimate of the solvent powers of the various media is given by the root-mean-square end-to-end separations  $(\bar{S}^2)^{1/2}$  in the last column of Table 2. These were calculated from the relation:

$$[\eta] \cdot \bar{M} = \Phi(\bar{S}^2)^{3/2}$$

$[\eta]$  was measured at 30°C in each solvent system, and for the samples of PMMA and polystyrene  $\bar{M}$  was  $3.75 \times 10^5$  and  $1.26 \times 10^5$  respectively. The universal Flory constant  $\Phi$  was  $2.1 \times 10^{21}$ . As methanol or aliphatic hydrocarbons are added to the polymerizing medium the solvent power diminishes as evidenced by the decrease in  $(\bar{S}^2)^{1/2}$ .

For the thermally initiated polymerization of MMA at 60°C a decrease in solvent power is accompanied by an increase in the ratio  $k_p^2/k_t$ . This increase could be caused by a decrease in  $k_t$ , an increase in  $k_p$ , or both. However, if we assume that the only solvent effect is that of viscosity on diffusion-controlled termination, then  $k_t$  can be calculated as previously<sup>4</sup> from its known value in bulk monomer, and hence  $k_p$ . The values of  $k_p$  obtained in this manner are  $6.18 \times 10^2$  and  $7.42 \times 10^2$  l mol<sup>-1</sup> s<sup>-1</sup> in toluene and toluene/methanol respectively. On the basis of previous results<sup>4</sup> this variation seems improbably large, and suggests that a contribution to the

increase in  $k_p^2/k_t$  in the poorer solvent must come from a decrease in  $k_t$ .

The sector experiments with MMA at 25°C support this view. As the solvating power of the medium decreases there is a marked increase in  $k_p/k_t$  and again in  $k_p^2/k_t$ . The resulting values of  $k_t$  show a decrease, well outside experimental error, as the solvating power of the medium is decreased. Furthermore, this decrease runs counter to the change that would be anticipated if only the viscosity affected  $k_t$  since the bulk viscosity of the bulk monomer is marginally higher than that of the other two media. It is also noteworthy that this change in solvent power from MMA to the MMA/n-octane/n-nonane mixture is close to the maximum achievable because the latter is very near to a theta system for the polymer. In all three media  $k_p$  appears unaffected within experimental error.

The results from the styrene polymerization again show a decrease in  $k_t$  as the solvent power of the medium is decreased. However, in this case the poor solvent is somewhat more viscous than pure monomer. It has been shown<sup>2</sup> that for styrene  $k_t \propto 1/\eta_{\text{mix}}$ , and on this basis alone  $k_t$  for the styrene-dodecane mixture would be expected to be  $1.7 \times 10^7$  l mol<sup>-1</sup> s<sup>-1</sup>. The observed value is still below this figure. Rather surprisingly,  $k_p$  also appears to decrease in the dodecane mixture.

The results quoted in Table 2 show clearly that the medium viscosity is not the only controlling agent on the rate of termination in free radical polymerization. The configuration of the polymer chain is also an important factor, and when the chain is tightly coiled, due to low macroradical-solvent interaction, termination is hindered. A parallel effect has been noted in some polycondensation reactions. Thus, the rate coefficient and the activation energy for polycondensation of 2,2-di(*p*-hydroxyphenyl) propane and its bis-chloroformate in solution were found to be strongly dependent upon the effectiveness of the solvent used and hence on the degree of macromolecule coiling<sup>11</sup>. These effects were explained on the basis that the diffusion constant of the reactive end of the macromolecule inside the coil is a function of the segment density in the coil. Although the rate coefficient in the polycondensation reaction is several orders of magnitude less than  $k_t$  the solvent effects and likely causes are essentially the same in each system.

The effects of chain coiling on polymer reactions are not restricted to reactions of end-groups. Schnabel and



Görlich<sup>12</sup> have recently found that the bimolecular rate coefficient  $k_R$  for side-group macroradicals generated in aqueous solution is dependent upon the coil dimensions. These dimensions in polymers, such as poly(vinyl alcohol), were altered by incorporating varying amounts of ionizable units, such as acrylic acid, in the polymer. In this case intramolecular coulombic repulsion causes coil expansion with a concomitant increase in  $k_R$  for  $R\cdot + R\cdot$ .

These investigations indicate that in the interpretation of kinetic studies of polymer-polymer reactions the solvent power of the reaction medium must be taken into account.

#### ACKNOWLEDGEMENT

J.C. thanks the Science Research Council for the award of a scholarship.

#### REFERENCES

- 1 see for example: North, A. M. and Reed, G. A. *Trans. Faraday Soc.* 1961, **57**, 859; North, A. M. *Makromol. Chem.* 1965, **83**, 15
- 2 Burnett, G. M., Cameron, G. G. and Joiner, S. N., *JCS Faraday Trans. I* 1973 **69**, 322
- 3 Bamford, C. H., Barb, W. G., Jenkins, A. D. and Onyon, P. F. 'The Kinetics of Vinyl Polymerization by Radical Mechanisms', Butterworths, London, 1958, pp 125-128
- 4 Burnett, G. M., Cameron, G. G. and Zafar, M. M. *Eur. Polym. J.* 1970, **6**, 823
- 5 Schulz, G. V. and Harborth, G. *Angew. Chem.* 1947, **A59**, 90
- 6 Patnode, W. and Sheiber, W. J. *J. Am. Chem. Soc.* 1939, **61**, 3449
- 7 Matheson, M. S., Auer, E. E., Bevilacqua, E. B. and Hart, E. J. *J. Am. Chem. Soc.* 1951, **73**, 1700
- 8 Danusso, F. and Moraglio, G. *J. Polym. Sci.* 1957, **24**, 161
- 9 Bevington, J. C., Melville, H. W. and Taylor, R. P. *J. Polym. Sci.* 1954, **12**, 449; *ibid.* 1954, **14**, 463
- 10 Cohn-Ginsberg, E., Fox, T. G. and Mason, H. F. *Polymer* 1962, **3**, 97
- 11 Turska, E. *J. Prakt. Chem.* 1971, **313**, 387
- 12 Schnabel, W. and Görlich, W. *Makromol. Chem.* in press; personal communication

# An investigation of molecular orientation in oriented poly(ethylene terephthalate) films

M. Kashiwagi\*, A. Cunningham, A. J. Manuel and I. M. Ward

Department of Physics, University of Leeds, Leeds LS2 9JT, UK  
(Received 2 October 1972)

Attempts to obtain a quantitative description of molecular orientation in one-way drawn poly(ethylene terephthalate) films are described using a combination of nuclear magnetic resonance (n.m.r.), optical and X-ray diffraction measurements. Complete theoretical developments are presented for the anisotropy of the n.m.r. second moment and for the optical anisotropy. The n.m.r. method shows severe limitations, primarily due to its inability to deal with the preferred orientation situation and to a lesser extent to the complications due to the presence of *gauche* conformations of the glycol residue. It has been shown, however, that the optical anisotropy is consistent with a simple scheme for the development of orientation during drawing. In this scheme a molecular chain axis undergoes the directional change of a line in the macroscopic body lying in the same direction, and preferred orientation is introduced by a simple mathematical approximation, which appears to hold well at high draw ratios.

## INTRODUCTION

In two recent publications, broad-line nuclear magnetic resonance (n.m.r.) studies of two very dissimilar polymers, low density polyethylene<sup>1</sup> and poly(methyl methacrylate)<sup>2</sup>, are described. In both cases the anisotropy of the n.m.r. second moment was used to obtain orientation distribution functions, based on the assumption that the partially oriented polymer can be regarded as an aggregate of anisotropic units of structure. The n.m.r. orientation functions were first shown to correlate well with the observed optical anisotropy, and then used to predict the mechanical anisotropy on the aggregate model, with very satisfactory results.

The present paper describes a similar investigation on one-way drawn poly(ethylene terephthalate) (PET) sheets. There are a number of reasons why this is of particular interest. In the first instance, these PET sheets are of comparatively low crystallinity, and it is known that the non-crystalline regions can achieve considerable orientation in this polymer<sup>3</sup>. The n.m.r. anisotropy will therefore arise from the orientation of both the crystalline and the non-crystalline regions, and we cannot neglect the orientation of the latter as was found adequate in low density polyethylene<sup>1</sup>. Secondly, these one-way drawn sheets are known to possess orthorhombic symmetry. This has been shown by X-ray diffraction measurements in our own previous work<sup>4</sup>, and even more extensively by other workers<sup>5, 6</sup>. There is considerable interest in extending the n.m.r. techniques developed for specimens of transverse isotropy to specimens of orthorhombic symmetry, and we will see that this exposes the limitations of the n.m.r. method.

Finally, these sheets have been extensively studied with regard to their yield behaviour and the formation of

deformation bands<sup>4, 7-9</sup>. In the latter work, the optical anisotropy of the initial sheets and of the material in the deformation band was found to relate directly to the deformation which had occurred from the original isotropic extruded state. Moreover, the refractive indices could be predicted in terms of the deformation using a simple deformation scheme<sup>9</sup>. In this deformation scheme the polymer is again regarded as an aggregate of anisotropic units of structure, where preferred axes rotate with deformation as would lines marked on the body of the material. We have called this the pseudo-affine deformation scheme and in this paper its relevance to the measured n.m.r. anisotropy, the optical anisotropy and the X-ray diffraction data will be examined in detail.

There are a number of previous publications on broad line n.m.r. in PET. The earliest of these were primarily concerned with the temperature dependence of the n.m.r. spectrum in isotropic polymer<sup>10, 11</sup>. There have, however, also been some studies of oriented PET<sup>12, 13</sup>, and Slonim<sup>14, 15</sup> has made a preliminary analysis of the n.m.r. anisotropy in terms of the molecular orientation which leaves the situation largely unresolved.

In addition to these experimental investigations, Roe<sup>16</sup> has recently reported an extension of our previous treatment for transversely isotropic specimens to the case where both the distribution and the structural unit possess orthorhombic symmetry. We will show that although Roe's treatment is very elegant, and is useful to the present studies in some respects, it has severe limitations in its practical application.

## THEORY OF THE ANISOTROPY OF THE SECOND MOMENT OF THE N.M.R. ABSORPTION CURVE

### General theory

We wish to develop a general theory for the n.m.r. second moment anisotropy which is not restricted to

\* On leave from Toray Industries, Inc., Basic Research Laboratories, Tebiro, Kamakura, 248 Japan.

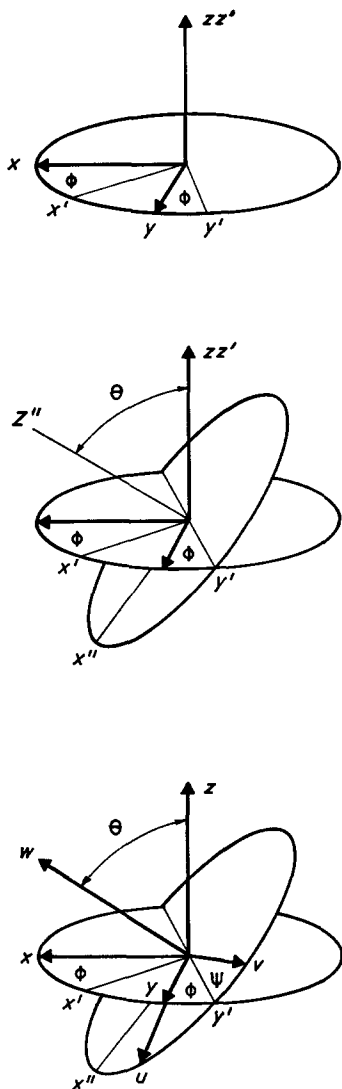


Figure 1 The specification of the orientation of the axes of a structural unit  $\{uvw\}$  with respect to the reference frame  $\{xyz\}$ . The Euler angles  $(\phi, \theta, \psi)$  represent successive rotations about the  $z$  axis, the  $y'$  axis and  $z''$  ( $w$ ) axis

systems showing transverse isotropy. Following the procedure of the previous papers we will take as our starting point the assumption that the partially oriented polymer can be regarded as an aggregate of anisotropic units of structure. At this stage we do not wish to be precise in structural terms regarding the composition of the units of structure. We will, in fact, propose and examine models where the unit of structure is taken to be of different composition.

We set up a system of orthogonal reference axes  $\{xyz\}$  fixed in the PET sheet with the  $xz$  plane in the plane of the sheet and the  $z$  axis parallel to the draw direction. We also set up a system of orthogonal reference axes  $\{uvw\}$  fixed within the structural unit. The orientation  $\{uvw\}$  of the structural unit with respect to the reference frame  $\{xyz\}$  is then specified by means of the Eulerian angles  $\phi, \theta, \psi$  (Figure 1). The angles  $\phi$  and  $\theta$  define the orientation of the unique direction  $w$  in the structural unit and  $\psi$  specifies the rotation of the unit around this unique direction.

The orientation distribution function of all the structural units in the sample is represented by  $\rho(\theta, \phi, \psi)$ , where:

$$\int_0^{2\pi} \int_0^{2\pi} \int_0^{\pi} \rho(\theta, \phi, \psi) \sin \theta d\theta d\phi d\psi = 1 \quad (1)$$

The Van Vleck formula<sup>17</sup> for the second-moment of the n.m.r. resonance absorption of a single magnetic species may be written:

$$\langle \Delta H^2 \rangle = \frac{G}{N} \sum_{j>k} r_{jk}^{-6} (3 \cos^2 \beta_{jk} - 1)^2 \quad (2)$$

where  $G = 3/2[I(I+1)g^2\mu_n^2]$ ,  $I$  is the nuclear spin number,  $g$  the nuclear  $g$  factor,  $\mu_n$  the nuclear magneton,  $N$  the number of magnetic nuclei over which the sum is taken,  $r_{jk}$  the length of the vector joining nuclei  $j$  and  $k$ , and  $\beta_{jk}$  the angle between the vector  $r_{jk}$  and the direction of the externally applied magnetic field  $H$ . This formula may be expressed in terms of the second order Legendre polynomial:

$$\langle \Delta H^2 \rangle = 4 \frac{G}{N} \sum_{j>k} r_{jk}^{-6} [P_2(\cos \beta_{jk})]^2 \quad (3)$$

and  $[P_2(\cos \beta_{jk})]^2$  can be written as a linear sum of Legendre polynomials as follows:

$$[P_2(\cos \beta_{jk})]^2 = \sum_{l=0,2,4} a_l P_l(\cos \beta_{jk}) \quad (4)$$

where  $a_0 = 1/5$ ,  $a_2 = 2/7$ , and  $a_4 = 18/35$ . We let the polar and azimuthal angles of  $H$  and  $r_{jk}$  be  $(\delta, \phi_\delta)$  and  $(\theta_{jk}, \phi_{jk})$  respectively, with reference to the axes  $\{uvw\}$  fixed in the structural unit. Application of the Legendre addition theorem<sup>18</sup> leads to:

$$P_l(\cos \beta_{jk}) = \sum_{m=-l}^{+l} Y_{lm}^*(\theta_{jk}, \phi_{jk}) Y_{lm}(\delta, \phi_\delta) \frac{4\pi}{2l+1} \quad (5)$$

To avoid complexity of the equations, and in order to allow the theory to be developed more clearly, the complex form of spherical harmonics is used. The application of real functions used in calculations is treated in the Appendixes.

To calculate the dependence of the second-moment on the direction of the magnetic field  $H$  in the sample, we define  $\gamma$  and  $\phi_\gamma$  as the polar and azimuthal angles respectively of the field  $H$  with respect to the main reference system  $\{xyz\}$  set up in the sample.  $Y_{lm}(\delta, \phi_\delta)$  and  $Y_{lm}(\gamma, \phi_\gamma)$  are related through a transformation matrix involving  $\phi, \theta, \psi$ <sup>18</sup>:

$$Y_{lm}(\delta, \phi_\delta) = \sum_{m'=-l}^l D_{m'm}^l(\phi, \theta, \psi) Y_{lm'}(\gamma, \phi_\gamma) \quad (6)$$

By substitution of equations (4), (5) and (6) into equation (3) we obtain:

$$\begin{aligned} \langle \Delta H^2 \rangle &= 4 \frac{G}{N} \sum_{l=0,2,4} \left( \frac{4\pi a_l}{2l+1} \right) \sum_{m=-l}^l \sum_{m'=-l}^l \left\{ r_{jk}^{-6} \times \right. \\ &\quad \left. Y_{lm}^*(\theta_{jk}, \phi_{jk}) D_{m'm}^l(\phi, \theta, \psi) Y_{lm'}(\gamma, \phi_\gamma) \right\} \\ &= 4G \sum_{l=0,2,4} \left( \frac{4\pi a_l}{2l+1} \right) \sum_{m=-l}^l \sum_{m'=-l}^l S_{lm} D_{m'm}^l(\phi, \theta, \psi) Y_{lm'}(\gamma, \phi_\gamma) \end{aligned} \quad (7)$$

where

$$S_{lm} = \frac{1}{N} \sum_{j>k} r_{jk}^{-6} Y_{lm}^*(\theta_{jk}, \phi_{jk}) \quad (8)$$

The lattice sum  $S_{lm}$  is a more generalized lattice sum than in the case of transverse isotropy<sup>1</sup>, and there are now in general 15 independent lattice sums instead of only 3. However, when the structural unit has symmetry properties, not all of them are mutually independent. For example, a structural unit of orthorhombic symmetry (which we shall consider later) has  $S_{lm} = S_{l\bar{m}}$  when  $m$  is even and  $S_{lm} = 0$  when  $m$  is odd, leaving only 6 independent lattice sums. Multiplying both sides of equation (7) by  $\rho(\theta, \phi, \psi)$  and integrating over the whole solid angle range of  $\theta, \phi, \psi$ , we obtain for the second-moment measurable in the experiment:

$$\langle \Delta H^2 \rangle_{av} = 4G \sum_{l=0,2,4} \left( \frac{4\pi a_l}{2l+1} \right) \times \sum_{m=-l}^l \sum_{m'=-l}^l S_{lm} \langle D_{m'm}^l(\phi, \theta, \psi) \rangle Y_{lm'}(\gamma, \phi_\gamma) \quad (9)$$

where

$$\langle D_{m'm}^l(\phi, \theta, \psi) \rangle = \int_0^{2\pi} \int_0^{2\pi} \int_0^\pi \rho(\theta, \phi, \psi) D_{m'm}^l(\phi, \theta, \psi) \sin\theta \, d\theta \, d\phi \, d\psi \quad (10)$$

Equation (9) expresses the measurable second-moment of the bulk specimen as a linear combination of 15 independent spherical harmonics  $Y_{lm}(\gamma, \phi_\gamma)$ .

$$\langle \Delta H^2 \rangle_{av} = \sum_l \sum_{m=-l}^l B_{lm} Y_{lm}(\gamma, \phi_\gamma) \quad (11)$$

From experimental measurements of  $\langle \Delta H^2 \rangle_{av}$  as a function of  $\gamma$  and  $\phi_\gamma$ , the coefficients  $B_{lm}$  can be determined. It is shown later that not all of the spherical harmonics are necessary when the distribution function and the structural unit have symmetry properties. It can be seen from equations (9) and (11) that the  $B_{lm}$  are related to  $S_{lm}$ ,  $\langle D_{m'm}^l(\phi, \theta, \psi) \rangle$  and  $\rho(\theta, \phi, \psi)$  through the following expression:

$$B_{lm} = 4G \left( \frac{4\pi a_l}{2l+1} \right) \sum_{m'=-l}^l S_{lm'} \langle D_{m'm}^l(\phi, \theta, \psi) \rangle \quad (12)$$

where  $\langle D_{m'm}^l(\phi, \theta, \psi) \rangle$  is defined in equation (10).

We now relate the experimentally determined  $B_{lm}$  to the distribution function  $\rho(\theta, \phi, \psi)$ . For this purpose we expand  $\rho(\theta, \phi, \psi)$  linearly in a series of basis functions. For this we use generalized spherical harmonics  $D_{m'm}^l(\phi, \theta, \psi)$ <sup>18</sup>.

$$\rho(\theta, \phi, \psi) = \sum_{L=0}^{\infty} \sum_{M=-L}^L \sum_{N=-L}^L \rho_{LMN} D_{MN}^{L*}(\phi, \theta, \psi) \quad (13)$$

where  $D_{MN}^{L*}$  is the complex conjugate of  $D_{MN}^L$  and  $\rho_{LMN}$  is a coefficient of the expansion. Substituting equation (13) into equation (12) and using the orthogonality relations of  $D$ , we obtain the following:

$$B_{lm} = 4G \left( \frac{4\pi a_l}{2l+1} \right) \sum_{L=0}^{\infty} \sum_{M=-L}^L \sum_{N=-L}^L \sum_{m'=-l}^l \rho_{LMN} \times \left( \frac{8\pi^2}{2L+1} \right) \delta_{Ll} \delta_{Mm} \delta_{Nm'} S_{lm'} \\ = 4G \left( \frac{4\pi a_l}{2l+1} \right) \left( \frac{8\pi^2}{2l+1} \right) \sum_{m'=-l}^l S_{lm'} \rho_{lmm'} \quad (14)$$

These relations are equivalent to those derived previously by Roe<sup>16, 19</sup>. Equation (14) represents the complete n.m.r. analysis of the distribution function  $\rho(\theta, \phi, \psi)$ . The macroscopic symmetry of the distribution function puts a constraint on the possible values of  $m$ , whereas the structural unit symmetry constrains  $m'$ . For example, in the case of the orthorhombic symmetry of both  $\rho(\theta, \phi, \psi)$  and the lattice sums we have:

$$\rho_{lmm'} = 0 \text{ for } m \text{ odd}; \quad S_{lm'} = 0 \text{ for } m' \text{ odd} \\ \rho_{l\bar{m}m'} = \rho_{lmm'} \neq 0 \text{ for } m \text{ even}; \quad S_{l\bar{m}m'} = S_{lm'm'} \neq 0 \text{ for } m' \text{ even}$$

In all cases  $l$  is positive and even<sup>17</sup>. Also for fixed values of  $l$  and  $m$  there are, in general  $(2l+1)$  unknowns  $\rho_{lmm'}$ . In principle, therefore, we cannot determine the distribution function  $\rho(\theta, \phi, \psi)$  up to  $l=4$  completely, using the n.m.r. method, unless we make some simplifying assumptions with regard to the distribution in  $\theta, \phi$ , or  $\psi$  (e.g. random distribution in  $\psi$ ). The physical meaning is that since we measure the second-moments through only two parameters, say  $\theta$  and  $\phi$ , we cannot get any information about the distribution in  $\psi$ . In this respect our conclusions differ from those of Roe<sup>16</sup>.

#### Application of the theory to systems of particular symmetry

Let us now consider three special cases relevant to this particular investigation.

*Case (i). Transverse isotropy ( $m=0$ )—Transversely isotropic structural unit ( $m'=0$ ).* To express this case we make both  $\phi$  and  $\psi$  random, and equations (13), (14) and (11) become:

$$\rho(\theta) = \sum_{l=0}^{\infty} \rho_{l00} Y_{l0}(\theta) \left( \frac{4\pi}{2l+1} \right)^{1/2} \quad (15)$$

$$B_{l0} = 4G \left( \frac{4\pi a_l}{2l+1} \right) \left( \frac{8\pi^2}{2l+1} \right) S_{l0} \rho_{l00} \quad (16)$$

$$\langle \Delta H^2 \rangle_{av} = \sum_l B_{l0} Y_{l0}(\gamma) \quad (17)$$

The distribution function coefficients can now be uniquely determined up to  $l=4$  by using equations (16) and (17). This is achieved by decomposing the measured second-moment variation with respect to the angle in accordance with equation (17), thus determining the expansion coefficients  $B_{l0}$ .

*Case (ii). Orthorhombic symmetry ( $m$  only positive and even)—(ii)a. Transversely isotropic structural unit ( $m'=0$ ).* In this case we obtain:

$$\rho(\theta, \phi) = \sum_{l=0}^{\infty} \sum_{m=-l}^l \left( \frac{4\pi}{2l+1} \right)^{1/2} \rho_{lm0} Y_{lm}(\theta, \phi) \quad (18)$$

$$B_{lm} = 4G \left( \frac{4\pi a_l}{2l+1} \right) \left( \frac{8\pi^2}{2l+1} \right) S_{l0} \rho_{lm0} \quad (19)$$

$$\langle \Delta H^2 \rangle_{av} = \sum_l \sum_m B_{lm} Y_{lm}(\gamma, \phi_\gamma) \quad (20)$$

The coefficients  $\rho_{lm0}$  can also be uniquely determined up to  $l=4$  by using equations (19) and (20).

*(ii)b. Orthorhombic structural unit ( $m'$  positive and even).* Earlier it was pointed out that the n.m.r. method could not be applied to determine directly the dependence of the

orientation distribution on the angle  $\psi$ . However, we wish to present an examination of the effect of making the simplifying assumption that  $\psi=0$ . Expressed mathematically:

$$\rho'(\theta, \phi) = \delta(\psi - 0)\rho(\theta, \phi, \psi)$$

where  $\rho'(\theta, \phi)$  is now independent of  $\psi$ . We feel that this assumption has particular relevance to the situation in highly drawn PET films and will be discussed fully later.

In Appendix A an expression (equation A12) for the second-moment  $\langle \Delta H^2 \rangle$  corresponding to equation (7) is derived in terms of real functions. By developing the theory using equation (A12) and carrying out the averaging as in equations (9) and (10) the following expression for  $\langle \Delta H^2 \rangle_{av}$  corresponding to equation (11) is obtained:

$$\begin{aligned} \langle \Delta H^2 \rangle_{av} = & B_{00} Y_{00} + B_{20} Y_{20}(\gamma, \phi_\gamma) + B_{22}^e Y_{22}^e(\gamma, \phi_\gamma) + \\ & B_{40} Y_{40}(\gamma, \phi_\gamma) + B_{42}^e Y_{42}^e(\gamma, \phi_\gamma) + \\ & B_{44}^e Y_{44}^e(\gamma, \phi_\gamma) \end{aligned} \quad (21)$$

where:

$$\begin{aligned} B_{00} = & (4Ga_0)(4\pi)^{3/2} S_{00} \rho'_{00} \\ B_{20} = & (4Ga_2) \left( \frac{4\pi}{5} \right)^{3/2} \left[ \left( \frac{5}{3} \right)^{1/2} S_{22}^e \rho'_{00} + \left( S_{20} - \frac{1}{3^{1/2}} S_{22}^e \right) \rho'_{20} \right] \\ B_{22}^e = & (4Ga_2) \left( \frac{4\pi}{5} \right)^{3/2} \left[ S_{20} \rho'_{22} + \left( \frac{5}{4\pi} \right)^{1/2} S_{22}^e \langle \cos \phi \rangle - \right. \\ & \left. \frac{1}{3^{1/2}} S_{22}^e \rho'_{22} \right] \\ B_{40} = & (4Ga_4) \left( \frac{4\pi}{9} \right)^{3/2} \left[ \left( \frac{1}{5^{1/2}} S_{42}^e + \frac{7}{35^{1/2}} S_{44}^e \right) \rho'_{00} + \right. \\ & \left. \left( S_{42}^e - \frac{2}{7^{1/2}} S_{44}^e \right) \rho'_{20} + \left( S_{40} - \frac{2}{5^{1/2}} S_{42}^e + \frac{1}{35^{1/2}} S_{44}^e \right) \rho'_{40} \right] \\ B_{42}^e = & (4Ga_4) \left( \frac{4\pi}{9} \right)^{3/2} \left[ \left( \frac{9}{4\pi} \right)^{1/2} S_{42}^e \langle \cos 2\phi \rangle - \left( \frac{24}{5} \right)^{1/2} S_{42}^e \rho'_{22} + \right. \\ & \left. \left( S_{40} - \left( \frac{8}{5} \right)^{1/2} S_{42}^e + \left\{ \left( \frac{2}{35} \right)^{1/2} + \frac{54}{7^{1/2}} \left( \frac{24}{5} \right)^{1/2} \right\} S_{44}^e \right) \rho'_{42} \right] \\ B_{44}^e = & (4Ga_4) \left( \frac{4\pi}{9} \right)^{3/2} \left[ \left( \frac{9}{4\pi} \right)^{1/2} S_{44}^e \langle \cos 4\phi \rangle + \right. \\ & \left. \left( \frac{9}{4\pi} \right)^{1/2} \left( \frac{7^{1/2}}{2} S_{42}^e - S_{44}^e \right) \langle \sin^2 \theta \cos 4\phi \rangle + \right. \\ & \left. \left( S_{40} - \left( \frac{8}{5} \right)^{1/2} S_{42}^e + \left( \frac{2}{35} \right)^{1/2} S_{44}^e \right) \rho'_{44} \right] \end{aligned} \quad (22)$$

Appendix B illustrates the derivation of  $B_{22}^e$ .

Equations (22) represent case (ii)b with  $\psi=0$  approximation. Six independent lattice sums ( $S_{00}$ ,  $S_{20}$ ,  $S_{22}^e$ ,  $S_{40}$ ,  $S_{42}^e$ ,  $S_{44}^e$ ) now characterize the orthorhombic structural unit. It is not possible, however, to solve equations (22) for all of the distribution function coefficients  $\rho'_{im}$ . Only limited information on the axial distribution of the structural units, in the form of  $\rho'_{20}$  and  $\rho'_{40}$ , can be obtained

uniquely. It can be shown that if  $\rho'(\theta, \phi)$  is represented by the first 6 terms in its linear expansion only, then equation (22) can be solved uniquely for all the 6 independent coefficients  $B_{lm}$ . The validity of this assumption rests on whether the molecular distribution can be approximately described by the truncated series. Theoretical work has shown that this is only true in the low draw ratio region and therefore cannot be applied to highly drawn PET films. We must therefore look to other methods to provide us with information regarding the  $\psi$  variable distribution.

By reducing the structural unit to transverse isotropy ( $S_{22}^e = S_{42}^e = S_{44}^e = 0$ ) equations (22) correspond to the real counterpart of equation (19) of case (ii)a [ $\rho'(\theta, \phi) = \rho(\theta, \phi)$ ]. Similarly by reducing the overall sample symmetry to transverse isotropy ( $\rho_{22}^e = \rho_{42}^e = \rho_{44}^e = 0$ ) we obtain the real counterpart of equation (16) of case (i) [ $\rho'(\theta, \phi) = \rho(\theta)$ ].

#### Identification of structural units for different model calculations

In our calculations above we have proposed three different models, with two types of structural unit: (i) transversely isotropic unit, (ii) orthorhombic unit. The transversely isotropic unit will be considered to be a small aggregate of crystalline and amorphous regions. Within the structural unit we set up a reference frame  $\{u, v, w\}$  and all the molecular chains in both the crystalline and amorphous regions are assumed to be fully extended with their chain axes (the crystallographic  $c$ -axis for those in the crystalline regions) parallel to  $w$ , but with no preferred orientation about  $w$ .

In the high draw ratio region of one-way drawn PET films X-ray diffraction data (Figure 2) show that the 100 crystalline planes have a preferred orientation tendency to lie in the plane of the film<sup>5</sup>. We propose to approximately describe this tendency by the introduction of an orthorhombic unit and the  $\psi=0$  approximation of case (ii)b as follows.

Let the orthorhombic unit of structure consist of fully extended molecular chains in the amorphous regions parallel to  $w$  but with no preferred orientation about  $w$ , together with crystalline regions whose  $c$  axes are, as before, parallel to  $w$  but now with all the 100 planes lying parallel to the  $\{uw\}$  plane. Such an arrangement produces a unit of orthorhombic symmetry. In the high draw ratio region, where both  $\theta$  and  $\phi$  describing the orientation of the unit  $w$  axis tend to be small, the  $\{uw\}$  plane, by definition of the Euler angles, already lies in or nearly in the plane of the film. This prescribes a degree of 100 plane preferred orientation without the need to introduce a  $\psi$  variation.

The two phase crystalline/amorphous nature of the units is represented quantitatively by assuming a mass fraction  $f$  of crystalline material. The overall lattice sums  $S_{im}^e$  are then given by:

$$S_{im}^e = f^c S_{im}^e + (1-f)^a S_{im}^e \quad (23)$$

where  $^c S_{im}^e$  are the lattice sums of the crystalline regions calculated on the basis of the crystal unit cell<sup>20</sup> and  $^a S_{im}^e$  are the lattice sums of the amorphous regions calculated on the assumption that these are equal to the intramolecular lattice sums of the crystalline regions, all intermolecular interactions being assumed to be isotropic. This latter assumption is identical to that adopted in

calculating the lattice sums for poly(methyl methacrylate) which is wholly amorphous.

#### THEORY OF OPTICAL ANISOTROPY FOR POLY(ETHYLENE TEREPHTHALATE) FILMS

We wish to apply our ideas regarding the molecular distributions within one-way drawn PET film to the prediction of the resultant optical anisotropy. For this we require the following intermediate theory which relates certain distribution function coefficients to the principal refractive indices of the sample. Let us consider the orientation of a structural unit, so defined by its coordinate frame ( $u, v, w$ ) with respect to the main reference system ( $x, y, z$ ). This orientation can be described by the three Euler angles and the transformation of the rotated frame ( $u, v, w$ ) is:

$$\begin{pmatrix} \cos\theta \cos\phi \cos\psi & -\cos\theta \cos\phi \sin\psi & \sin\theta \cos\phi \\ -\sin\phi \sin\psi & -\sin\phi \cos\psi & \\ \cos\theta \sin\phi \cos\psi & -\cos\theta \sin\phi \sin\psi & \sin\theta \sin\phi \\ +\cos\phi \sin\psi & +\cos\phi \cos\psi & \\ -\sin\theta \cos\phi & \sin\theta \sin\phi & \cos\theta \end{pmatrix} = \begin{pmatrix} a_{11} & a_{12} & a_{13} \\ a_{21} & a_{22} & a_{23} \\ a_{31} & a_{32} & a_{33} \end{pmatrix} \quad (24)$$

If we now define the principal polarizabilities of the unit along  $u, v, w$  as  $P_u, P_v, P_w$  and the resultant polarizabilities as seen along  $x, y, z$  as  $P_x, P_y, P_z$  then it can be shown that:

$$\begin{aligned} P_x &= a_{11}^2 P_u + a_{12}^2 P_v + a_{13}^2 P_w \\ P_y &= a_{21}^2 P_u + a_{22}^2 P_v + a_{23}^2 P_w \\ P_z &= a_{31}^2 P_u + a_{32}^2 P_v + a_{33}^2 P_w \end{aligned} \quad (25)$$

For an orthorhombic unit of principal polarizabilities  $P_u, P_v, P_w$  we make the approximation that  $\psi = 0$  [case (ii)b], then equations (25) reduce to:

$$\begin{aligned} P_x &= \cos^2\theta \cos^2\phi P_u + \sin^2\phi P_v + \sin^2\theta \cos^2\phi P_w \\ P_y &= \cos^2\theta \sin^2\phi P_u + \cos^2\phi P_v + \sin^2\theta \sin^2\phi P_w \\ P_z &= \sin^2\theta P_u + \cos^2\theta P_w \end{aligned} \quad (26)$$

If the unit is to possess only transverse isotropy we must randomize the  $\psi$  variable of equation (25). This gives:

$$\begin{aligned} P_x &= (\sin^2\phi + \cos^2\theta \cos^2\phi) \left( \frac{P_u + P_v}{2} \right) + \sin^2\theta \cos^2\phi P_w \\ P_y &= (\cos^2\phi + \cos^2\theta \sin^2\phi) \left( \frac{P_u + P_v}{2} \right) + \sin^2\theta \sin^2\phi P_w \\ P_z &= \sin^2\theta \left( \frac{P_u + P_v}{2} \right) + \cos^2\theta P_w \end{aligned} \quad (27)$$

where  $(P_u + P_v)/2$  is the effective transverse polarizability  $P_T$ . For a sample of overall transverse isotropy we average over  $\phi$  as well as  $\psi$  and obtain:

$$\begin{aligned} P_x &= \left( \frac{1}{2} + \frac{1}{2} \cos^2\theta \right) P_T + \sin^2\theta \frac{P_w}{2} \\ P_y &= \left( \frac{1}{2} + \frac{1}{2} \cos^2\theta \right) P_T + \sin^2\theta \frac{P_w}{2} \\ P_z &= \sin^2\theta P_T + \cos^2\theta P_w \end{aligned} \quad (28)$$

#### Polarizability values

We assume that  $P_u, P_v, P_w$  are given by:

$$P_{u,v,w} = f {}^c P_{u,v,w} + (1-f) {}^a P_{u,v,w} \quad (29)$$

where  $f$  is the mass fraction of the crystalline regions,  ${}^c P_{u,v,w}$  are the polarizabilities along the  $u, v, w$  axes due to the crystalline regions and  ${}^a P_{u,v,w}$  the corresponding values in the amorphous regions. The intrinsic polarizability of a PET monomer is defined in terms of  $P_1, P_2$  and  $P_3$ ; where  $P_3$  is the polarizability along the chain axis,  $P_2$  the polarizability at right angles to  $P_3$  but in the plane of the terephthalate residue and  $P_1$  the polarizability at right angles to both  $P_2$  and  $P_3$ . It is possible from known optical data on isotropic and drawn fibres of PET (measured at 551 nm) where molecular orientation was assumed to be that predicted from birefringence measurements, to obtain consistent values for  $P_3$  and  $(P_1 + P_2)/2$ , the chain axis and average transverse polarizability of the PET monomer respectively. We assume that the intrinsic polarizability of the monomer is dominated by the nature of the intramolecular interactions and so we can say, in terms of the previous nomenclature that:

$$\begin{aligned} P_3 &= {}^c P_w = {}^a P_w = 2.30 \times 10^{-23} \text{ cm}^3 \\ \left( \frac{P_1 + P_2}{2} \right) &= P_T = P_u = P_v = 1.70 \times 10^{-23} \text{ cm}^3 \end{aligned}$$

Independent experimental determination of  $P_1$  and  $P_2$  was not possible but predictions based on the summation of known bond polarizabilities<sup>21</sup> yield the following values:  $P_1 = 1.18 \times 10^{-23} \text{ cm}^3$ ;  $P_2 = 2.18 \times 10^{-23} \text{ cm}^3$ ;  $P_3 = 2.20 \times 10^{-23} \text{ cm}^3$  (determined for sodium D line). These values have a 2-3% overall error due to inaccuracies not only in the individual bond polarizabilities used but also in the structure representation. We therefore adjust  $P_3$  to be consistent with the experimentally determined value of  $2.30 \times 10^{-23} \text{ cm}^3$  but make no alteration in  $P_1$  and  $P_2$ . We will show later that the importance of these values lies not in their precision numerically, but in their characterization of the qualitative shape of the intrinsic polarizability anisotropy of the PET monomer.

Since the plane of the terephthalate residue makes about  $20^\circ$  to the 100 plane,  ${}^c P_{u,v}$  are calculated as follows:

$$\begin{aligned} {}^c P_u &= P_2 \cos^2 20^\circ + P_1 \sin^2 20^\circ = 2.06 \times 10^{-23} \text{ cm}^3 \\ {}^c P_v &= P_2 \sin^2 20^\circ + P_1 \cos^2 20^\circ = 1.30 \times 10^{-23} \text{ cm}^3 \end{aligned}$$

Assuming that the polarizabilities of each unit make an independent contribution to the polarizability of the aggregate, then the mean polarizabilities per unit volume, of the PET sample, will be given by:

$$\begin{aligned}\langle P_x \rangle &= \frac{\rho N}{M} \{ \langle \sin^2 \theta \cos^2 \phi \rangle (P_w - P_u) + \\ &\quad \langle \cos^2 \phi \rangle (P_u - P_v) + P_v \} \\ \langle P_y \rangle &= \frac{\rho N}{M} \{ \langle \sin^2 \theta \sin^2 \phi \rangle (P_w - P_u) + \\ &\quad \langle \cos^2 \phi \rangle (P_v - P_u) + P_u \} \\ \langle P_z \rangle &= \frac{\rho N}{M} \{ \langle \cos^2 \theta \rangle (P_w - P_u) = P_u \} \quad (30)\end{aligned}$$

where  $\rho$  is the density of the material,  $N$  is Avogadro's number,  $M$  is the molecular weight of one monomer unit of PET and  $\langle \cos^2 \theta \rangle$ , for example is expressed as follows in terms of the case (ii)b approximation:

$$\begin{aligned}\langle \cos^2 \theta \rangle &= \int_0^{2\pi} \int_0^{2\pi} \int_0^\pi \rho(\theta, \phi, \psi) \cos^2 \theta \sin \theta \, d\theta \, d\phi \, d\psi \\ &= \int_0^{2\pi} \int_0^\pi \rho'(\theta, \phi) \left( \frac{2}{3} \left( \frac{4\pi}{5} \right)^{1/2} Y_{20}(\theta) + \frac{1}{3} \right) \sin \theta \, d\theta \, d\phi \\ &= \frac{2}{3} \left( \frac{4\pi}{5} \right)^{1/2} \rho'_{20} + \frac{1}{3}\end{aligned}$$

Similarly:

$$\langle \sin^2 \theta \cos^2 \phi \rangle = \frac{2}{3} \left( \frac{3\pi}{5} \right)^{1/2} \rho'_{22} - \frac{1}{3} \left( \frac{4\pi}{5} \right)^{1/2} \rho'_{20} + \frac{1}{3}$$

$\langle \cos^2 \phi \rangle$  cannot be determined by the n.m.r. method. The procedure is identical for case (ii)a with  $\rho(\theta, \phi)$  replacing  $\rho'(\theta, \phi)$ . However, this case is independent of  $\langle \cos^2 \phi \rangle$  because  $P_u = P_v$  for the structural unit. The principal refractive indices are then related to the mean polarizabilities (to a good approximation) by the Lorentz-Lorenz equation:

$$n_x^2 = \frac{(8/3)\pi \langle P_x \rangle + 1}{1 - (4/3)\pi \langle P_x \rangle} \quad (31)$$

When  $n_x$  is the principal refractive index of the specimen in the  $x$  direction.

## EXPERIMENTAL

### Sample preparation

The oriented PET films were similar to those used in previous investigations of their deformation band behaviour<sup>7-9</sup> and were also supplied by Imperial Chemical Industries Limited, Plastics Division. The films were prepared by drawing at constant width to a series of nominal draw ratios. Measurements were also made on a transversely isotropic sample produced by cold drawing a rod of square cross-section to its natural draw ratio which was measured and found to be 3.25 : 1. Details of the films are given in *Table 1*.

### N.m.r. apparatus and second-moment determination

A low level marginal oscillator, based on the Robinson circuit<sup>22, 23</sup> was used throughout these experiments. To

*Table 1* PET sheets used in n.m.r. measurements

Draw ratio (sheets)	Density	Mean thickness (cm)
2 : 1	1.349	0.047
2.5 : 1	1.354	0.042
5 : 1	1.372	0.026

*Table 2* Coefficients of the second-moment expansion  $B_{lm}/a_l$

$B_{lm}/a_l$	Sample			
	2 : 1 Film	2.5 : 1 Film	5 : 1 Film	Transversely isotropic rod
$B_{00}/a_0$	+182.3	+182.8	+181.2	+196.46
$B_{20}/a_2$	-3.57	-4.76	-7.65	-8.48
$B_{22}^{e22}/a_2$	-0.85	-2.08	-4.31	0.00
$B_{40}/a_4$	+1.55	+2.81	+6.61	+4.29
$B_{42}^{e42}/a_4$	+0.19	+0.09	+2.21	0.00
$B_{44}^{e44}/a_4$	-0.04	+0.10	+1.15	0.00

ensure a rigid lattice the sample was cooled to  $-196^\circ\text{C}$ . The oscillator frequency was 25 MHz for proton resonance and the modulation frequency 20 Hz.

To obtain a good signal/noise ratio, necessary in the accurate determination of the second-moment, a large modulation amplitude ( $\pm 3.2$  G peak to peak) was used together with a Time Averaging Computer. After applying the Andrew correction<sup>24</sup> the estimated accuracy of the second-moment determination was  $\pm 0.3$  G<sup>2</sup>.

### Measurement of the second-moment anisotropy

We define the orientation of the film with respect to the main coordinate frame  $\{x, y, z\}$  as in the theoretical section. For a given sample, specimens were cut such that measurements could be made in the  $\{x, z\}$ ,  $\{x, y\}$ , and  $\{y, z\}$  planes. Orientation with respect to the magnetic field was achieved by means of a large goniometer placed directly above the probe containing the specimens. The second moment was measured with the applied magnetic field making angles between  $-20^\circ$  and  $+110^\circ$  with a particular coordinate  $x, y, z$  axis, at  $10^\circ$  intervals, for each specimen. This enabled the orthorhombic symmetry property of the second-moment variations to be used, to fix the  $0^\circ$  and  $90^\circ$  orientations to within  $\pm 1^\circ$ . Preliminary experiments showed that signal saturation occurred at comparatively low radiofrequency levels. Since it was not known how signal saturation was affected by draw ratio or orientation in the magnetic field, saturation curves were plotted for each sample at orientations of approximately  $0^\circ$ ,  $45^\circ$  and  $90^\circ$  before second-moment measurements were carried out. The signal levels used in obtaining second-moments were then chosen to be well below saturation levels. The coefficients of the least squares fit to the experimental second-moment data are listed in *Table 2*.

### Refractive index measurements

Refractive index measurements were made using immersion liquids and an image splitting interference microscope. The samples used were those on which the n.m.r. measurements had been made as well as a further 4 : 1 drawn sample. It was found that there existed a spread in the principal refractive indices for a given draw ratio. By measuring several specimens the errors in the mean values were reduced to less than  $\pm 0.005$ . All measurements were made at 551 nm.

*X-ray diffraction measurements*

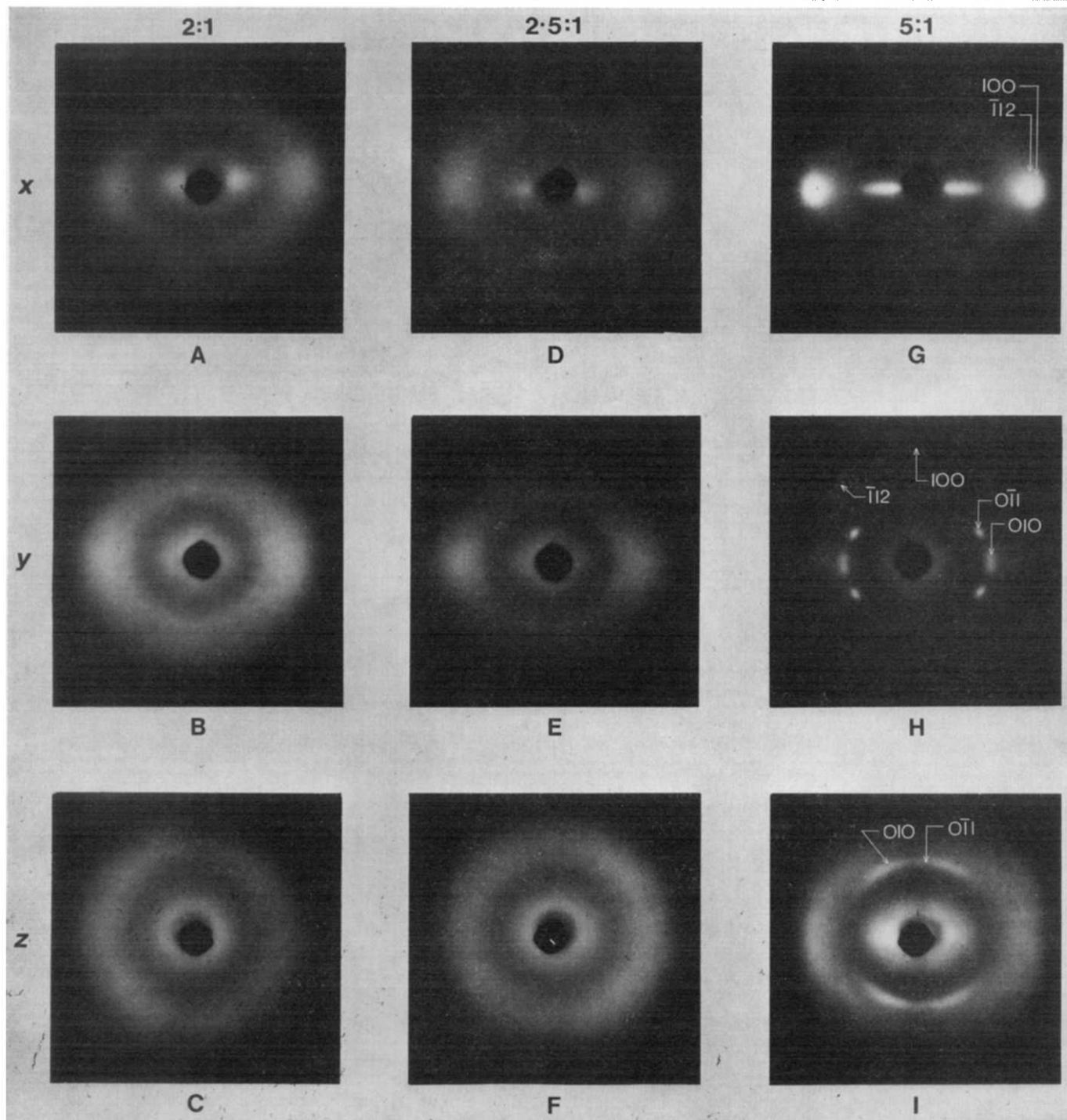
Wide-angle X-ray diffraction patterns were obtained from the actual n.m.r. samples of the three orthorhombic films. Photographs taken for the X-ray beam along three symmetry axes of the film are shown in *Figure 2*. For the film with a draw ratio of 5 : 1 the distinct differences in the patterns for the two X-ray beam directions ( $x, y$ ) normal to the draw direction ( $z$ ) indicate the presence of a preferred orientation as earlier reported for similar films by Heffelfinger and Burton<sup>5</sup>. The presence of a strong equatorial reflection by the 100 plane for the X-ray beam in the plane of the film ( $x$  direction) but its absence for the beam perpendicular to the film ( $y$  direction) indicates that

many more crystalline units are oriented with their 100 planes close to the plane of the film than normal to it. This view is reinforced by the well defined pattern due to reflections from the 010 and  $0\bar{1}1$  planes when the X-ray beam is normal to the film.

## RESULTS AND DISCUSSION

*Discussion of n.m.r. and optical results*

The second-moment data for the films of draw ratio 2.5 : 1 and 5 : 1 are shown in *Figures 3* and *4* respectively. Data for the 2 : 1 film are not shown, but orthorhombic symmetry was observed in all 3 cases.



*Figure 2* Wide angle X-ray diffraction patterns for one-way drawn PET films. The draw ratios are marked at the top of each column and the axes along which the X-ray beam was directed at the side of each row. The  $x, y$  and  $z$  axes are as in *Figures 3* and *4*. For the X-ray beam in the  $x$  and  $y$  directions the  $z$  axis was vertical; for the X-ray beam along the  $z$  direction the  $x$  axis was vertical



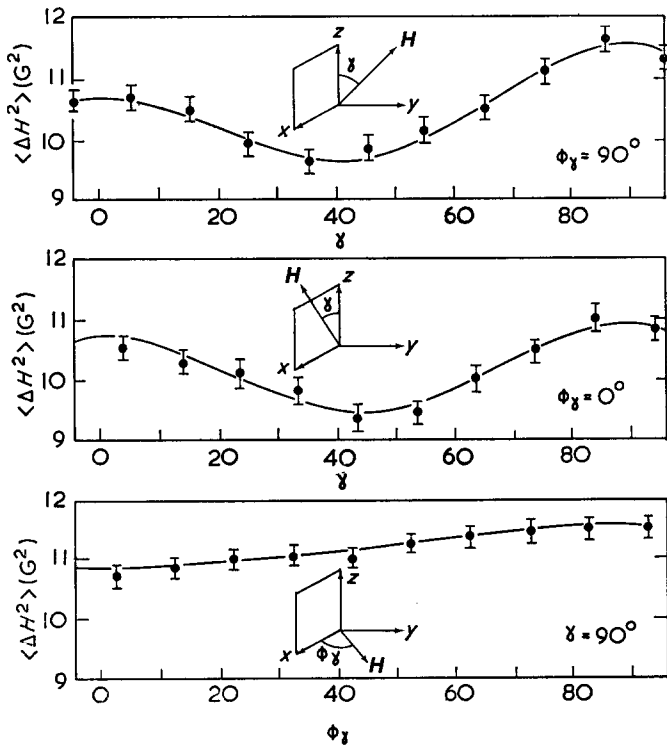


Figure 3 N.m.r. absorption second moment,  $\langle \Delta H^2 \rangle_{av}$ , PET film: draw ratio 2.5:1.  $\bullet$ , Experimental points; —, least squares fit of experimental points to equation (20) for  $l=0, 2, 4$ ;  $m=0, 2, 4$ . Total r.m.s. deviation  $0.11 G^2$

Table 3 Lattice sums—*trans* conformation based on ref. 20

	Intra	Inter	Total
$S_{00}$	+0.003027	+0.001211	+0.004238
$S_{20}$	-0.002057	-0.002210	-0.002267
$S_{22}^e$	-0.003141	-0.000464	-0.003605
$S_{40}$	+0.003151	-0.000393	+0.002758
$S_{42}^e$	+0.003100	-0.000815	+0.002285
$S_{44}^e$	+0.003676	-0.00022	+0.003654

To take into account the assumption that the intermolecular interactions in the amorphous phase are isotropic, the isotropic lattice sum  $S_{00}$  was adjusted, as in ref. 2, to a value consistent with the measured isotropic second moment of  $10.3 G^2$ . This required changes of only a few % in  $S_{00}$

*Application of case (ii)a.* This case allows a complete analysis of the second-moment data and determination of the refractive index anisotropy. Mathematically it represents the concept of only chain-axis orientation occurring under deformation, the structural unit being of intrinsic transverse isotropy. The three lattice sum values,  $S_{00}$ ,  $S_{20}$ ,  $S_{40}$ , needed to define the unit n.m.r. response are listed in Table 3. They were based on the crystal structure determination of Daubeny *et al.*<sup>20</sup>, the proton positions being calculated on the basis of known bond angles and lengths. The predicted refractive indices for the 2:1 and 2.5:1 drawn films are shown in Figure 5, together with the overall experimental optical anisotropy. Results for the 5:1 drawn sample are not shown since some of the angular functions derived from application of the theory to that sample produced physically unrealistic values. Although this does not happen for the low draw ratio samples, deviation between theory and experiment is still large. This was an unexpected result for the following reasons.

(1). The low draw ratio samples show a low degree of crystallinity ( $f=0.13$  at 2:1 draw ratio). Any complica-

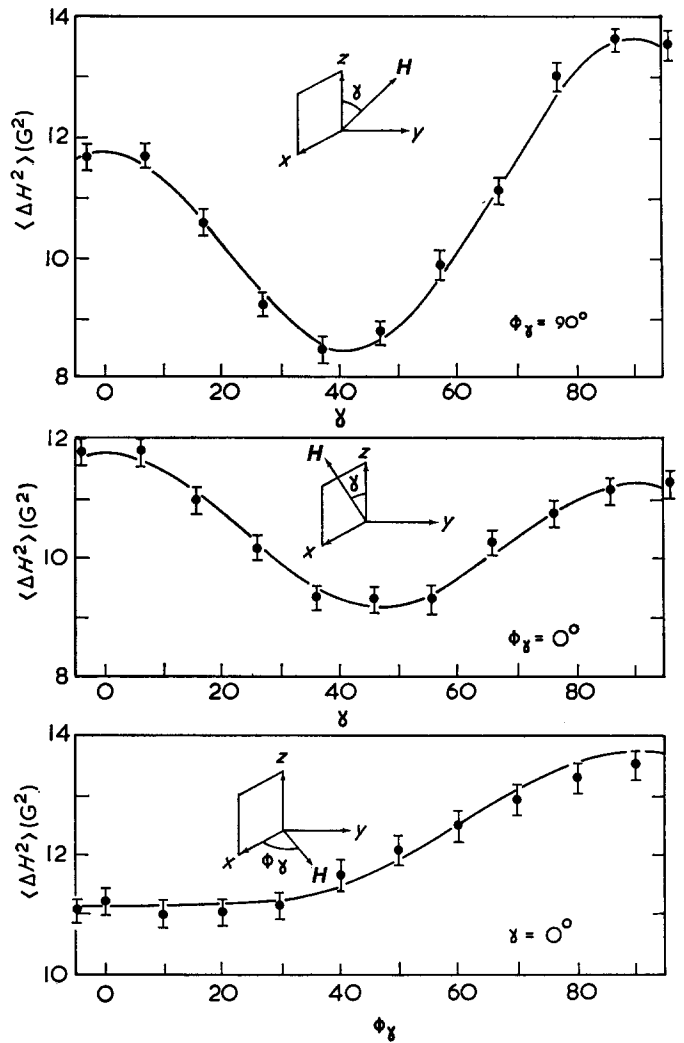


Figure 4 N.m.r. absorption second-moment,  $\langle \Delta H^2 \rangle_{av}$ , PET film: draw ratio 5:1.  $\bullet$ , Experimental points; —, least squares fit to equation (20) for  $l=0, 2, 4$ ;  $m=0, 2, 4$ . Total r.m.s. deviation  $0.15 G^2$

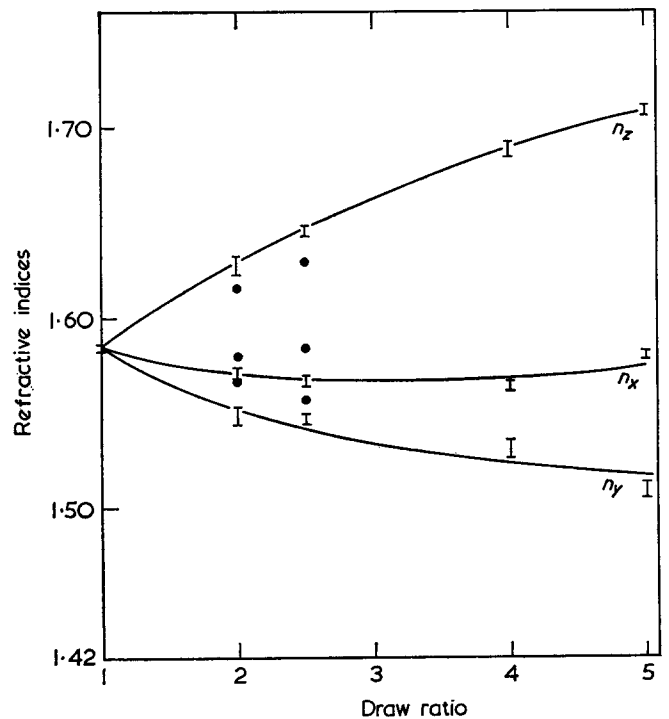


Figure 5 Comparison of the measured refractive indices for PET film with values calculated from the orientation functions determined from n.m.r. assuming transversely isotropic structural units. I, Experimental points;  $\bullet$ , predicted values

tions due to preferred orientation of the crystalline regions must therefore make a small contribution to the refractive index calculations. In fact, the X-ray diffraction photographs of the 2 : 1 and 2.5 : 1 draw ratio sheets show negligible preferred orientation of the 100 plane.

(2). Preferred orientation of the amorphous regions is also highly unlikely in this range of draw ratios. As can be seen from Figure 3, the n.m.r. anisotropy is close to showing transversely isotropic symmetry at low draw ratios ( $\{x-y\}$  anisotropy for the 2 : 1 draw ratio sample is 0.5 G<sup>2</sup>). We would therefore expect the resultant anisotropy to be predominantly due to main-chain orientation, and the assumption of a transversely isotropic structural unit to be valid in this range.

(3). The basic assumptions used at low draw ratios have been found to be adequate in predicting the refractive indices for the low draw ratio sheets in previous investigations, where the deformation band behaviour was used to predict effective deformation ratios<sup>9</sup>.

It was suspected at this stage that the reason for the discrepancies might lie in the incorrect estimates of the lattice sums. There are two reasons for suspecting this. First, the lattice sums are based on the crystal structure proposed on the basis of X-ray diffraction data, which cannot be very precise concerning the positions of the protons, and secondly, it has been assumed that the conformation of the molecule in the amorphous regions is identical to its conformation in the crystalline regions. The infra-red spectrum of amorphous PET is, however, consistent with the view that the glycol residue can also take up the *gauche* conformation rather than the *trans* which is the preferred conformation in the crystalline regions<sup>25-27</sup>. Although little work has been done determining the *gauche* fraction in oriented PET films, the results of Schmidt and Gay<sup>28</sup> indicate a value of approximately 0.25 for one-way drawn film of density 1.35 g cm<sup>-3</sup>.

It would be expected that lattice sums calculated on the basis of a *gauche* conformation would differ significantly in all but the isotropic lattice sums  $S_0$ , since such a conformation alters the methylene group orientation with respect to the chain axis, which is the dominant factor in determining the value of the anisotropic lattice sums  $S_{20}$ ,  $S_{40}$ .

In order to check our calculated values of the lattice sums, measurements were undertaken on an oriented sample produced by cold drawing a rod of square cross-section. This sample was transversely isotropic, and had two advantages. First, the theory for transversely isotropic specimens is very much simpler, and has been applied successfully to other polymers. Secondly, previous work suggests that in the cold drawing of PET the molecular orientation closely follows the pseudo-affine deformation scheme<sup>29</sup>. This means that there should be consistency, first, between the measured birefringence and the measured natural draw ratio, and secondly between the observed n.m.r. anisotropy and that predicted on the basis of the theory and the measured natural draw ratio. Direct refractive index measurements were therefore undertaken to determine the birefringence  $\Delta n$  of the specimen and it was found that  $\Delta n = 0.136$ . Using the relation:

$$\Delta n = \Delta n_{\max}(1 - 3/2\langle \sin^2\theta \rangle)$$

with  $\Delta n_{\max} = 0.23$ , it follows that  $\langle \sin^2\theta \rangle = 0.27$ . This value of  $\langle \sin^2\theta \rangle$  is consistent with the pseudo-affine deformation model for a draw ratio of 3, compared with the measured natural draw ratio of 3.25 for this sample. We can, how-

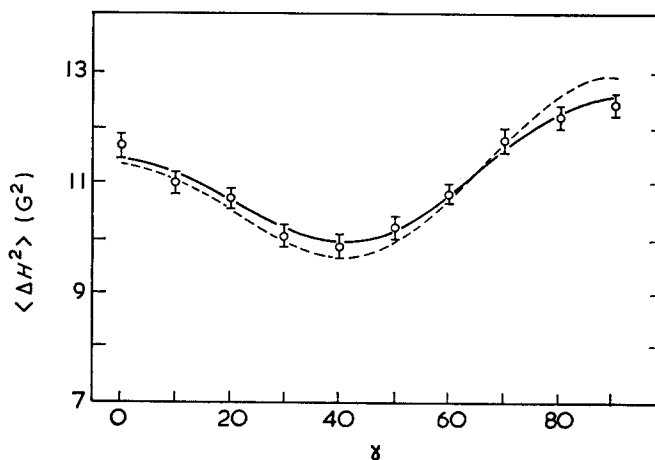


Figure 6 N.m.r. absorption second-moment, ( $\langle \Delta H^2 \rangle_{av}$ ), variation in transversely isotropic drawn PET rod; draw ratio 3.25:1.  $\circ$ , Experimental points; —, least squares fit to equation (20) for  $l=0, 2, 4; m=0$ . ---, predicted variation from lattice sums and pseudo-affine deformation for draw ratio 3:1

ever, assume that the distribution of molecular orientations is given by the pseudo-affine deformation scheme with this draw ratio of 3, and calculate  $\langle \sin^4\theta \rangle$ , which is found to be 0.16. Using these two values for  $\langle \sin^2\theta \rangle$  and  $\langle \sin^4\theta \rangle$ , we can proceed to calculate the n.m.r. anisotropy, assuming the values of the lattice sums obtained from the crystal unit cell. Figure 6 shows the measured second-moment anisotropy and that predicted on the basis of a pseudo-affine deformation. The failure to predict the measured second-moment variation clearly indicates that the lattice sum values used were incorrect. Consistency could be reached by adjusting the lattice sums  $S_{20}$ ,  $S_{40}$  to the following values:  $S_{20} = -0.00159$  and  $S_{40} = +0.00265$ . It will be shown in a further publication that these values for the lattice sums are consistent with a small fraction ( $\sim 20\%$ ) of the glycol residue being in the *gauche* conformation. We are at present attempting to quantify the situation by making spectroscopic determinations of the *gauche* content in this sample.

At this stage let us assume that the empirically adjusted lattice sums are an improvement on the original values in that they contain within them the majority of the alterations required due to the inaccuracies in the crystal structure determination and the *gauche* conformation contributions in the drawn state. Using these adjusted lattice sums, which characterize chain-axis orientation only, we predict a new set of refractive indices for the 2 : 1 drawn sheet.<sup>1</sup>

	Experimental	N.m.r. (initial lattice sums)	N.m.r. (adjusted lattice sums)
$n_x$	1.627	1.617	1.626
$n_y$	1.571	1.580	1.577
$n_z$	1.549	1.568	1.561

Although exact agreement is not obtained there is a marked improvement in all three predicted refractive indices. Failure to improve the situation by the above approach in the 5 : 1 drawn film strongly suggested that the chain axis orientation mechanism of case (ii)a was in itself inadequate in attempting to predict the optical anisotropy in the high draw ratio region.

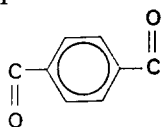
Application of case (ii)b. For reference, Table 3 lists the numerical values of the 6 lattice sums needed to characterize the orthorhombic structural unit. These are based on the unit construction of the earlier section and crystal unit cell data<sup>20</sup>. However, even with the approximate equations (22) we can still only obtain values for  $\langle \cos^2\theta \rangle$  and  $\langle \cos^4\theta \rangle$  (i.e. solving for  $\rho'_{20}$  and  $\rho'_{40}$ ). We must, therefore, look to a less restrictive technique in our study of the effects of the known preferred orientation tendency of the crystalline regions in highly drawn PET film. Such a technique is presented in the following section.

#### Planar orientation and the pseudo-affine deformation model

Although it has been possible to obtain tentative empirical estimates of the lattice sums  $S_{00}$ ,  $S_{20}$ ,  $S_{40}$ , the n.m.r. technique, as presented earlier, is considerably restricted in the investigation of PET primarily owing to the following three reasons: (1) the existence of the *gauche* conformation. This conformation exists only in the amorphous regions which makes it impossible, at the present time, to accurately determine its structure experimentally; (2) a dependence of the *trans/gauche* ratio on sample extension<sup>28</sup>. This ratio must therefore be independently determined for a given sample; (3) the intrinsic difficulty of the method to determine the molecular distribution function of systems possessing a degree of preferred molecular orientation.

An intermediate step which will now be shown to be extremely informative is to attempt a theoretical analysis, first using the pseudo-affine deformation scheme for chain-axis orientation only, with no preferred orientation otherwise, and secondly, using this scheme for chain-axis orientation and adding a constraint of preferred orientation of the 100 planes in the crystalline regions. We will now show that these two schemes throw considerable light on the orientation processes occurring during drawing. We would expect these analyses to be of value concerning the question of preferred orientation at high draw ratios for the following reasons:

(1). The molecules are now characterized intrinsically by their polarizabilities and not by their lattice sums. The magnitude and anisotropy of the molecular polarizabilities are dominated to a large extent by the



part of the molecule, which remains the same in both the *trans* and *gauche* conformations. Also, the difficulties met in the lattice sum calculations (the need to rely solely on the proton positions) is largely eliminated because the C-H bond polarizability is very nearly isotropic. The polarizability values for this bond along the axis and in the transverse plane are as follows<sup>21</sup>:

$$P(\text{bond axis}) = 8.2 \times 10^{-25} \text{ cm}^3$$

$$P(\text{transverse}) = 6.0 \times 10^{-25} \text{ cm}^3$$

The molecular polarizabilities are, therefore, more reliable, at present, to represent the state of molecular orientation than the lattice sums.

(2). Although quantitatively the angular averages predicted from a pseudo-affine deformation scheme might well differ considerably from the actual averages, the qualitative variation of these averages are realistic. This should be enough, when coupled to a particular molecular

model, to reproduce the general features of the optical anisotropy.

(3). It is reasonable to assume that planar orientation considerably affects the shape of the refractive index variation with draw ratio, particular the  $n_x$  variation. We would, therefore, expect that it would be possible to distinguish between a deformation which produced an optical anisotropy dominated by chain axis orientation and one which was dominated by planar orientation, by comparing the general features of the refractive index variations predicted on the basis of (1) and (2) with that found experimentally. The angular average variations with draw ratio<sup>9</sup> are shown in Figure 7. As can be seen, their trend is realistic, with both  $\langle \sin^2\theta \cos^2\phi \rangle_{ps}$  and  $\langle \sin^2\theta \sin^2\phi \rangle_{ps}$  tending to zero at high draw ratios. For a mechanism of chain axis orientation only, we use a transversely isotropic orienting unit defined by principal polarizabilities  $P_w$  and  $P_T$  as above. In this case the refractive index predictions based on equation (30) are independent of  $\langle \cos^2\phi \rangle$  and are shown in Figure 8. Here, we see that in the low draw ratio region the trend follows that found experimentally. However, at high draw ratios,  $n_x$  does not pass through a minimum, and  $n_y$  and  $n_z$  start to converge with the overall trend tending to transverse isotropy ( $n_x = n_y$ ). This confirms our earlier tentative conclusions from the n.m.r. results.

We now introduce the concept of preferred planar orientation. This is more difficult to describe using the pseudo-affine deformation scheme since such a deformation only prescribes the orientation of a chain axis, and does not prescribe the orientation about that axis. However, let us make the approximation [as assumed before in case (ii)b] that at high draw ratios, when a considerable number of the chain axes are lying nearly in the plane of the sheet, there is a tendency for the preferred orientation plane of the molecules to lie in the plane of the sheet. In this case, if we arrange our orienting unit such that a rotation of this plane about the chain axis is defined by the  $\psi$  rotation, then the preferred orientation constraint can be made by setting  $\psi = 0$ . In this case then:

$$\langle \cos^2\phi \rangle_{\text{unit}} = \langle \cos^2\phi \rangle_{\text{chain axis}} = \langle \cos^2\phi \rangle_{ps}$$

where:

$$\langle \cos^2\phi \rangle_{ps} = 1 - \frac{\lambda_x^2}{(\lambda_x^2 - \lambda_y^2)} \left( 1 - \frac{\lambda_y}{\lambda_x} \right)$$

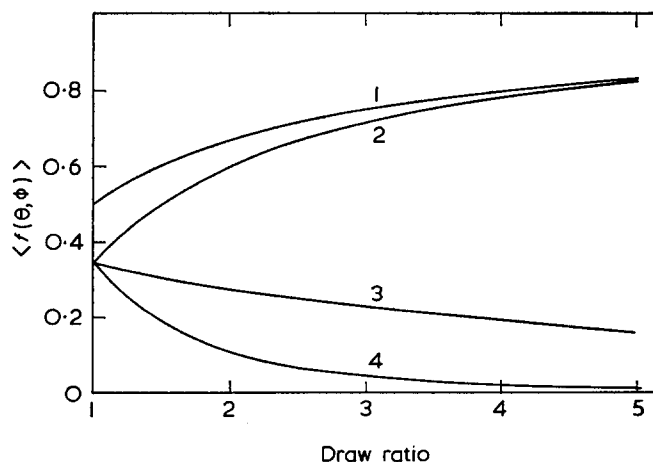


Figure 7 Calculated 'angular average' variations from a pseudo-affine deformation of one-way drawn film. (1),  $f(\theta, \phi) = \langle \cos^2\phi \rangle_{ps}$ ; (2),  $f(\theta, \phi) = \langle \cos^2\theta \rangle_{ps}$ ; (3),  $f(\theta, \phi) = \langle \sin^2\theta \cos^2\phi \rangle_{ps}$  (4),  $f(\theta, \phi) = \langle \sin^2\theta \sin^2\phi \rangle_{ps}$

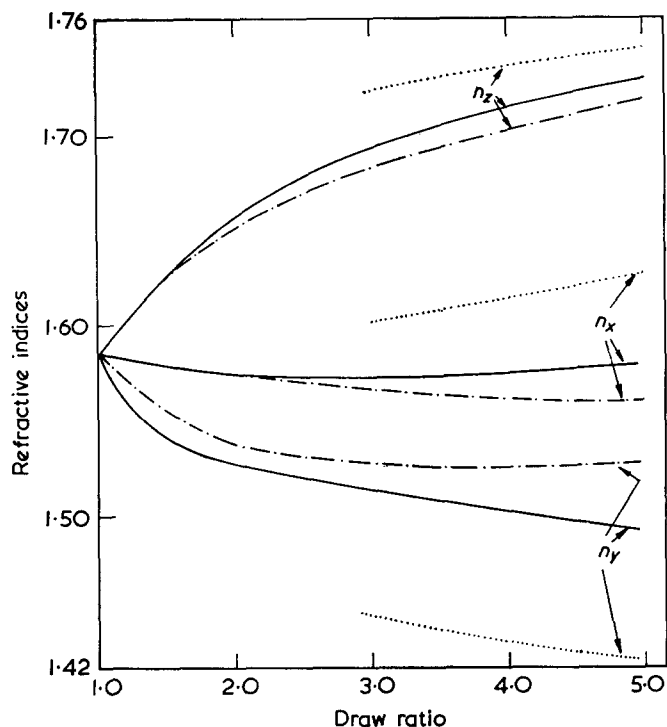


Figure 8 Theoretical refractive index variations with draw ratio using pseudo-affine deformation calculations. —, Based on a transversely isotropic structural unit with principal polarizabilities:  $P_w = 2.30 \times 10^{-23} \text{ cm}^3$ ;  $P_T = 1.70 \times 10^{-23} \text{ cm}^3$ . . . . ., Based on orthorhombic structural unit with preferred orientation:  $P_w = 2.30 \times 10^{-23} \text{ cm}^3$ ;  $P_U = 2.06 \times 10^{-23} \text{ cm}^3$ ;  $P_V = 1.30 \times 10^{-23} \text{ cm}^3$ . —, Restricting the preferred orientation to a mass fraction ( $f$ ) of each sample, equal to the approximate crystalline content from density measurements, the remainder of the structural units being assumed transversely isotropic: 2:1 draw ratio,  $f = 0.13$ ; 2.5:1 draw ratio,  $f = 0.17$ ; 5:1 draw ratio,  $f = 0.33$

$\lambda_x$ ,  $\lambda_y$ ,  $\lambda_z$  are the principal draw ratios in the  $x$ ,  $y$ ,  $z$  film directions respectively.

This approximation, therefore, enables us to predict the refractive index anisotropy with a preferred orientation constraint.

For the orthorhombic unit we take the n.m.r. description of the theoretical section and define the principal polarizabilities as described above. The predicted refractive index variations of the high draw ratio region based on an extreme model in which all the molecules in both the crystalline and amorphous regions have a preferred orientation constraint put upon them in the manner described above, is shown in Figure 8.

The overall shape of the Figure is not sensitive to whether we make the 100 plane or the benzene ring the preferred orientation plane. We now have  $n_y$  and  $n_x$  diverging at high draw ratios, which is what is observed experimentally. Comparing the experimental variations of Figure 5 with Figure 8 it can be seen that the assumption of a certain degree of preferred orientation at high draw ratios is sufficient to describe the general features of the experimental variations.

This is indeed what happens if we constrain a mass fraction of each sample approximately equal to its crystalline content. This is also shown in Figure 8 where the actual sample crystalline mass fractions have been used. (Compare with experimental variation of Figure 5.)

## CONCLUSION

To summarize the results of this investigation we can say that the optical anisotropy of one-way drawn PET films is

governed essentially by two types of molecular response. In the low draw ratio region the orthorhombic distribution of chain axes alone is sufficient to characterize the optical anisotropy, whereas in the high draw ratio region preferred planar orientation must be taken into account.

Work is at present in progress to test these conclusions using laser-Raman spectroscopy. This technique will enable us not only to make a direct measure of the *trans/gauche* ratio, but also to determine independent orientation functions for the *trans* and *gauche* conformations. With such information, it will then be possible to re-examine the n.m.r. results for these materials.

## ACKNOWLEDGEMENTS

We wish to thank Mr B. C. Goswami, Mr J. S. Foot and Mr N. H. Ladizesky for assistance with measurements of refractive index and X-ray diffraction. We are also indebted to Dr R. A. Duckett for discussions regarding calculation of the planar orientation. One of us (A.C.) is indebted to the Science Research Council for the award of a maintenance grant.

## REFERENCES

- 1 McBrierty, V. J. and Ward, I. M. *Br. J. Appl. Phys.* 1968, **1**, 1529
- 2 Kashiwagi, M., Folkes, M. J. and Ward, I. M. *Polymer* 1971, **12**, 697
- 3 Patterson, D. and Ward, I. M. *Trans. Faraday Soc.* 1957, **55**, 1516
- 4 Brown, N., Duckett, R. A. and Ward, I. M. *Phil. Mag.* 1968, **18**, 483
- 5 Heffelfinger, C. J. and Burton, R. C. *J. Polym. Sci.* 1960, **47**, 289
- 6 Dulmage, W. J. and Geddes, A. L. *J. Polym. Sci.* 1958, **31**, 499
- 7 Brown, N. and Ward, I. M. *Phil. Mag.* 1968, **17**, 961
- 8 Brown, N., Duckett, R. A. and Ward, I. M. *J. Phys. (D-Ser. 2)* 1968, **1**, 1369
- 9 Richardson, I. D., Duckett, R. A. and Ward, I. M. *J. Phys. (D: Appl. Phys.)* 1970, **3**, 649
- 10 Land, R., Richards, R. E. and Ward, I. M. *Trans. Faraday Soc.* 1959, **55**, 225
- 11 Ward, I. M. *Trans. Faraday Soc.* 1960, **56**, 648
- 12 Boyle, C. A. and Goodlett, V. W. *J. Appl. Phys.* 1963, **34**, 59
- 13 Farrow, G. and Ward, I. M. *Br. J. Appl. Phys.* 1960, **11**, 543
- 14 Slonim, I. Ya. and Urman, Ya. G. *Zh. Strukt. Khim.* 1963, **4**, (2), 216
- 15 Slonim, I. Ya. and Lyubimov, A. W. 'The NMR of Polymers', Plenum Press, New York, 1970, p 172
- 16 Roe, R. J. *J. Polym. Sci. (A-2)* 1970, **8**, 1187
- 17 Van Vleck, J. H. *Phys. Rev.* 1948, **74**, 1168
- 18 Rose, M. E. 'Elementary Theory of Angular Momentum', John Wiley, New York, 1957, Ch 4
- 19 Roe, R. J. *J. Appl. Phys.* 1963, **36**, 2024
- 20 Daubeny, R. de P., Bunn, C. W. and Brown, C. J. *Proc. R. Soc. (A)* 1954, **226**, 531
- 21 Pinnock, P. R. and Ward, I. M. *Br. J. Appl. Phys.* 1964, **15**, 1559
- 22 Robinson, F. N. H. *J. Sci. Instrum.* 1959, **36**, 481
- 23 Edmonds, D. T. and Robinson, F. N. H. *J. Sci. Instrum.* 1967, **44**, 475
- 24 Andrew, E. R. *Phys. Rev.* 1953, **91**, 425
- 25 Ward, I. M. *Chem. Ind.* 1956, p 905
- 26 Grime, D. and Ward, I. M. *Trans. Faraday Soc.* 1958, **54**, 959
- 27 Krimm, S. *Fortschr. Hochpolym-Forsch.* 1960, **2**, S-51-172
- 28 Schmidt, P. G. and Gay, F. P. *Angew. Chem.* 1962, **74**, (16), 638
- 29 Allison, S. W. and Ward, I. M. *Br. J. Appl. Phys.* 1967, **18**, 1151

## APPENDIX A

*N.m.r. second-moment as a function of the direction of the magnetic field, expressed in real spherical harmonic functions and real lattice sums*

We define the following real quantities:

$$Y_{10}(\theta, \phi) = \left( \frac{2l+1}{4\pi} \right)^{1/2} P_l(\cos\theta) \quad (\text{A1})$$

$$Y_{lm}^e(\theta, \phi) = \left(\frac{2l+1}{2\pi}\right)^{1/2} \left[\frac{(l-|m|)!}{(l+|m|)!}\right]^{1/2} P_l^m(\cos\theta) \cos m\phi \quad m > 0 \quad (A2)$$

$$Y_{lm}^o(\theta, \phi) = \left(\frac{2l+1}{2\pi}\right)^{1/2} \left[\frac{(l-|m|)!}{(l+|m|)!}\right]^{1/2} P_l^m(\cos\theta) \sin m\phi \quad m > 0 \quad (A3)$$

Equation (5) then becomes:

$$P_l(\cos\beta_{jk}) = \left(\frac{4\pi}{2l+1}\right) \left\{ Y_{l0}(\theta_{jk}, \phi_{jk}) Y_{l0}(\delta, \phi_\delta) + \sum_{m=1}^l Y_{lm}^e(\theta_{jk}, \phi_{jk}) Y_{lm}^e(\delta, \phi_\delta) + \sum_{m=1}^l Y_{lm}^o(\theta_{jk}, \phi_{jk}) Y_{lm}^o(\delta, \phi_\delta) \right\} \quad (A4)$$

From equation (6) and relations (A1), (A2) and (A3)  $Y_{l0}(\delta, \phi_\delta)$  is expressed as:

$$Y_{l0}(\delta, \phi_\delta) = C_{00}^l[n, n] Y_{l0}(\gamma, \phi_\gamma) + \sum_{m'=1}^l C_{0m'}^l[n, e] Y_{lm'}^e(\gamma, \phi_\gamma) + \sum_{m'=1}^l C_{0m'}^l[n, o] Y_{lm'}^o(\gamma, \phi_\gamma) \quad (A5)$$

where:

$$\begin{aligned} C_{00}^l[n, n] &= D_{00}^l(\phi, \theta, \psi) \\ C_{0m'}^l[n, e] &= \frac{1}{2^{1/2}} [D_{m'0}^l + D_{m'0}^l] \\ C_{0m'}^l[n, o] &= \frac{i}{2^{1/2}} [D_{m'0}^l - D_{m'0}^l] \end{aligned} \quad (A6)$$

Similarly,  $Y_{lm}^e(\delta, \phi_\delta)$  and  $Y_{lm}^o(\delta, \phi_\delta)$  are expressed as:

$$Y_{lm}^e(\delta, \phi_\delta) = C_{m0}^l[e, n] Y_{l0}(\gamma, \phi_\gamma) + \sum_{m'=1}^l C_{mm'}^l[e, e] Y_{lm'}^e(\gamma, \phi_\gamma) + \sum_{m'=1}^l C_{mm'}^l[e, o] Y_{lm'}^o(\gamma, \phi_\gamma) \quad (A7)$$

$$Y_{lm}^o(\delta, \phi_\delta) = C_{m0}^l[o, n] Y_{l0}(\gamma, \phi_\gamma) + \sum_{m'=1}^l C_{mm'}^l[o, e] Y_{lm'}^e(\gamma, \phi_\gamma) + \sum_{m'=1}^l C_{mm'}^l[o, o] Y_{lm'}^o(\gamma, \phi_\gamma) \quad (A8)$$

where

$$\begin{aligned} C_{m0}^l[e, n] &= \frac{1}{2^{1/2}} (D_{0m}^l + D_{0m}^l) \\ C_{mm'}^l[e, e] &= \frac{1}{2} (D_{m'm}^l + D_{m'm}^l + D_{m'm}^l + D_{m'm}^l) \\ C_{mm'}^l[e, o] &= \frac{i}{2} (D_{m'm}^l + D_{m'm}^l - D_{m'm}^l - D_{m'm}^l) \end{aligned} \quad (A9)$$

and

$$C_{m0}^l[o, n] = \frac{1}{(2)^{1/2}} (D_{0m}^l - D_{0m}^l)$$

$$\begin{aligned} C_{mm'}^l[o, e] &= \frac{1}{2^i} (D_{m'm}^l - D_{m'm}^l + D_{m'm}^l - D_{m'm}^l) \\ C_{mm'}^l[o, o] &= \frac{1}{2} (D_{m'm}^l - D_{m'm}^l - D_{m'm}^l + D_{m'm}^l) \end{aligned} \quad (A10)$$

The significance of the notation in the brackets of the coefficients  $C_{mm'}^l [i, j]$  is as follows:

$i = n$  when the spherical harmonic under expansion is of neutral parity or

= e for even parity

= o for odd parity

Similarly

$j = n$  when the spherical harmonic of which  $C_{mm'}^l [i, j]$  is the respective coefficient is of neutral parity or

= e for even parity

= o for odd parity

By substitution of equations (A5), (A7) and (A8) into equation (A4), we obtain:

$$\begin{aligned} P_l(\cos\beta_{jk}) &= \left(\frac{4\pi}{2l+1}\right) \left\{ \left[ C_{00}^l[n, n] Y_{l0}(\theta_{jk}, \phi_{jk}) + \sum_{m=1}^l C_{m0}^l[e, n] Y_{lm}^e(\theta_{jk}, \phi_{jk}) + \sum_{m=1}^l C_{m0}^l[o, n] Y_{lm}^o(\theta_{jk}, \phi_{jk}) \right] Y_{l0}(\gamma, \phi_\gamma) + \sum_{m'=1}^l \left\{ C_{0m'}^l[n, e] Y_{lm'}^e(\theta_{jk}, \phi_{jk}) + \sum_{m=1}^l C_{mm'}^l[e, e] Y_{lm}^e(\theta_{jk}, \phi_{jk}) + \sum_{m=1}^l C_{mm'}^l[o, e] Y_{lm}^o(\theta_{jk}, \phi_{jk}) \right\} Y_{lm'}^e(\gamma, \phi_\gamma) + \sum_{m'=1}^l \left\{ C_{0m'}^l[n, o] Y_{lm'}^o(\theta_{jk}, \phi_{jk}) + \sum_{m=1}^l C_{mm'}^l[e, o] Y_{lm}^e(\theta_{jk}, \phi_{jk}) + \sum_{m=1}^l C_{mm'}^l[o, o] Y_{lm}^o(\theta_{jk}, \phi_{jk}) \right\} Y_{lm'}^o(\gamma, \phi_\gamma) \right\} \quad (A11) \end{aligned}$$

By substitution of equations (A11) and (4) into equation (3), we obtain:

$$\begin{aligned} \langle \Delta H^2 \rangle &= 4G \sum_{l=0,2,4} \frac{4\pi a_l}{2l+1} \left\{ \left[ C_{00}^l[n, n] S_{l0} + \sum_{m=1}^l C_{m0}^l[e, n] S_{lm}^e + \sum_{m=1}^l C_{m0}^l[o, n] S_{lm}^o \right] Y_{l0}(\gamma, \phi_\gamma) + \sum_{m'=1}^l \left\{ C_{0m'}^l[n, e] S_{l0} + \sum_{m=1}^l C_{mm'}^l[e, e] S_{lm}^e + \sum_{m=1}^l C_{mm'}^l[o, e] S_{lm}^o \right\} Y_{lm'}^e(\gamma, \phi_\gamma) + \sum_{m'=1}^l \left\{ C_{0m'}^l[n, o] S_{l0} + \sum_{m=1}^l C_{mm'}^l[e, o] S_{lm}^e + \sum_{m=1}^l C_{mm'}^l[o, o] S_{lm}^o \right\} Y_{lm'}^o(\gamma, \phi_\gamma) \right\} \end{aligned}$$

$$\sum_{m=1}^l C_{mm'}^l [o, e] S_{im}^o Y_{im}^e(\gamma, \phi_\gamma) + \sum_{m'=1}^l \left\{ C_{0m'}^l [n, o] S_{i0} + \sum_{m=1}^l C_{mm'}^l [e, o] S_{im}^e + \sum_{m=1}^l C_{mm'}^l [o, o] S_{im}^o \right\} Y_{im}^o(\gamma, \phi_\gamma) \quad (A12)$$

where:

$$\begin{aligned} S_{i0} &= \frac{1}{N} \sum_{j>k} r_{jk}^{-6} Y_{i0}(\theta_{jk}, \phi_{jk}) \\ S_{im}^e &= \frac{1}{N} \sum_{j>k} r_{jk}^{-6} Y_{im}^e(\theta_{jk}, \phi_{jk}) \\ S_{im}^o &= \frac{1}{N} \sum_{j>k} r_{jk}^{-6} Y_{im}^o(\theta_{jk}, \phi_{jk}) \end{aligned} \quad (A13)$$

These are the lattice sums expressed by real quantities. Equation (A12) corresponds to equation (7).

APPENDIX B

Procedure for the calculation of the coefficients  $B_{lm}$  using  $B_{22}^e$  as an example

We define the following quantities:

$$D_{mn}^l(\phi, \theta, \psi) = e^{-im\phi} d_{mn}^l(\theta) e^{-in\psi} \quad (B1)$$

$$d_{mn}^l(\theta) = \left[ \frac{(l-n)!(l+m)!}{(l+n)!(l-m)!} \right]^{1/2} \frac{(\cos\theta/2)^{2l+n-m} (-\sin\theta/2)^{m-n}}{(m-n)!} \times {}_2F_1(m-l, -n-l, m-n+1; -\tan^2\theta/2) \quad (B2)$$

where  ${}_2F_1$  is a hypergeometric function<sup>18</sup>. For  $1 \leq l < 1$  and  $c$  not zero or a negative integer then

$${}_2F_1(a, b, c; z) = 1 + \frac{ab}{c}z + \frac{1}{2!} \frac{a(a+1)b(b+1)}{c(c+1)}z^2 + \dots \quad (B3)$$

We have expressed equation (7) in terms of real quantities in equation (A12). It is now possible by the use of equations (9) and (10) to derive the equivalent real expression for equation (12). Considering only the  $B_{22}^e$  coefficient we have:

$$B_{22}^e = (4Ga_2) \left( \frac{4\pi}{5} \right) \int_0^{2\pi} \int_0^{2\pi} \int_0^\pi \{ C_{02}^2 [n, e] S_{20} + C_{22}^2 [e, e] S_{22}^e \} \times \delta(\psi - 0) \rho(\theta, \phi, \psi) \sin\theta \, d\theta \, d\phi \, d\psi \quad (B4)$$

Referring to equation (A6) we can carry out the calculation for the first term in the integrand,  $I_1$ :

$$I_1 = \int_0^{2\pi} \int_0^{2\pi} \int_0^\pi C_{02}^2 [n, e] \delta(\psi - 0) \rho(\theta, \phi, \psi) \sin\theta \, d\theta \, d\phi \, d\psi$$

$$\begin{aligned} &= \int_0^{2\pi} \int_0^\pi \left[ \frac{1}{2^{1/2}} \{ D_{20}^2(\phi, \theta, 0) + D_{20}^2(\phi, \theta, 0) \} \rho'(\theta, \phi) \right] \times \sin\theta \, d\theta \, d\phi \\ &= \left( \frac{4\pi}{5} \right)^{1/2} \frac{1}{2^{1/2}} \int_0^{2\pi} \int_0^\pi \{ Y_{22}^*(\theta, \phi) + Y_{22}^*(\theta, \phi) \} \rho'(\theta, \phi) \times \sin\theta \, d\theta \, d\phi \\ &= \left( \frac{4\pi}{5} \right)^{1/2} \int_0^{2\pi} \int_0^\pi Y_{22}^e(\theta, \phi) \rho'(\theta, \phi) \sin\theta \, d\theta \, d\phi \\ &= \left( \frac{4\pi}{5} \right)^{1/2} \rho'_{22} \end{aligned} \quad (B5)$$

Using equation (A9) we calculate the contribution of the second term in the integrand,  $I_2$ :

$$\begin{aligned} I_2 &= \int_0^{2\pi} \int_0^{2\pi} \int_0^\pi C_{22}^2 [e, e] \delta(\psi - 0) \rho(\theta, \phi, \psi) \sin\theta \, d\theta \, d\phi \, d\psi \\ &= \int_0^{2\pi} \int_0^\pi \frac{1}{2} \{ [ D_{22}^2(\phi, \theta, 0) + D_{22}^2(\phi, \theta, 0) + D_{22}^2(\phi, \theta, 0) + D_{22}^2(\phi, \theta, 0) \} \rho'(\theta, \phi) \sin\theta \, d\theta \, d\phi \\ &= \int_0^{2\pi} \int_0^\pi \frac{1}{2} \{ [ D_{22}^2(\phi, \theta, 0) + D_{22}^2(\phi, \theta, 0) ] + [ D_{22}^2(\phi, \theta, 0) + D_{22}^2(\phi, \theta, 0) ] \} \rho'(\theta, \phi) \sin\theta \, d\theta \, d\phi \\ &= \int_0^{2\pi} \int_0^\pi \{ \text{Re}[D_{22}^2(\phi, \theta, 0)] + \text{Re}[D_{22}^2(\phi, \theta, 0)] \} \times \rho'(\theta, \phi) \sin\theta \, d\theta \, d\phi \end{aligned}$$

From relations (B1), (B2) and (B3)

$$\begin{aligned} \text{Re}[D_{22}^2(\phi, \theta, 0)] &= \cos 2\phi (\cos\theta/2)^4 \\ \text{Re}[D_{22}^2(\phi, \theta, 0)] &= \cos 2\phi (\sin\theta/2)^4 \end{aligned}$$

$$\therefore \text{Re}[D_{22}^2] + \text{Re}[D_{22}^2] = \cos 2\phi - \frac{1}{6} \left( \frac{2\pi \cdot 4!}{5} \right)^{1/2} Y_{22}^e(\theta, \phi)$$

(Re = real part)

Hence:

$$\begin{aligned} I_2 &= \int_0^{2\pi} \int_0^\pi \left\{ \cos 2\phi - \frac{1}{6} \left( \frac{2\pi \cdot 4!}{5} \right)^{1/2} Y_{22}^e(\theta, \phi) \right\} \times \rho'(\theta, \phi) \sin\theta \, d\theta \, d\phi \\ &= \langle \cos 2\phi \rangle - \frac{1}{6} \left( \frac{2\pi \cdot 4!}{5} \right)^{1/2} \rho'_{22} \end{aligned} \quad (B6)$$

Substituting equations (B5) and (B6) into (B4) we arrive at the expression for  $B_{22}^e$

$$B_{22}^e = (4Ga_2) \left( \frac{4\pi}{5} \right)^{3/2} \left[ \rho'_{22} S_{20} + \left( \frac{5}{4\pi} \right)^{1/2} \langle \cos 2\phi \rangle S_{22}^e - \frac{1}{3^{1/2}} \rho'_{22} S_{22}^e \right] \quad (B7)$$

# Note to the Editor

## Synthesis and polymerizability of *N*-ethyl-2-vinylcarbazole

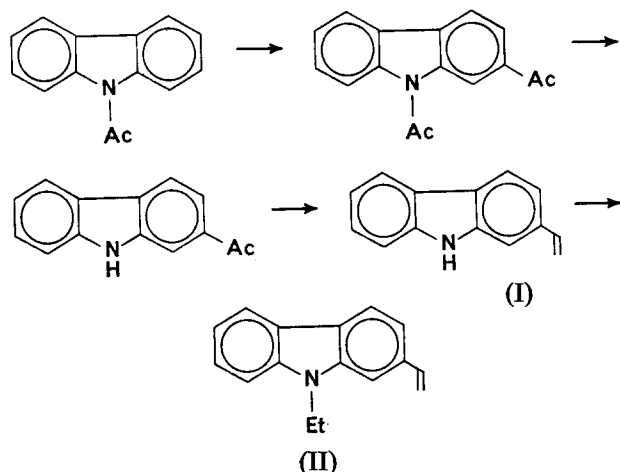
P. Hyde, L. J. Kricka and A. Ledwith

Department of Inorganic, Physical and Industrial Chemistry, University of Liverpool, Liverpool L69 3BX, UK  
(Received 27 November 1972)

### INTRODUCTION

Interest in vinylated carbazole derivatives centres around *N*-vinylcarbazole (NVC) and the commercial exploitation of poly(*N*-vinylcarbazole) in photocopying processes<sup>1, 2</sup>. Ring-substituted vinylcarbazoles are also known; Lopatinski and Sirotkina<sup>3</sup> have described the synthesis and polymerization of several *N*-alkyl-3-vinyl- and *N*-alkyl-3,6-divinyl-carbazoles.

We wish to report the synthesis and polymerizability of a new vinylated carbazole monomer, *N*-ethyl-2-vinylcarbazole (II).



Friedel-Crafts acetylation of *N*-acetylcarbazole using aluminium trichloride as catalyst, affords 2,9-diacetylcarbazole, the product of substitution *meta* to the nitrogen atom<sup>4</sup>. Subsequent acid-catalysed hydrolysis affords 2-acetylcarbazole, which upon reduction, using aluminium isopropoxide in xylene, gave 2-vinylcarbazole (I) in moderate yield. The alkylation of this base-sensitive monomer was achieved using thallium(I) ethoxide<sup>5</sup>. Treatment of a solution of 2-vinylcarbazole in DMF/ether with thallium(I) ethoxide and reaction of the thallium salt *in situ* with an excess of iodoethane afforded *N*-ethyl-2-vinylcarbazole (II).

### EXPERIMENTAL

<sup>1</sup>H n.m.r. spectra were measured at 60 MHz for solutions in deuteriochloroform with tetramethylsilane as internal standard. I.r. spectra were recorded for Nujol mulls. Mass spectra were measured by the Physico-Chemical Measurements Unit, Harwell.

Benzene and methanol were analytical grade reagents, and were used without further purification. Tetrahydrofuran and dichloromethane were purified by distillation

from calcium hydride. *n*-Butyl-lithium was a 15% solution in *n*-hexane (ex. Koch-Light). Tris-(*p*-bromophenyl)-aminium and tropylium hexachloroantimonate were prepared as outlined in the literature<sup>6, 7</sup>.

Friedel-Crafts acylation of 9-acetylcarbazole, m.p. 68–69°C (lit.<sup>8</sup>, 68–69°C) afforded 2,9-diacetylcarbazole, m.p. 105–106°C (lit.<sup>4</sup>, 106–107°C) which upon hydrolysis gave 2-acetylcarbazole, m.p. 229–230°C (lit.<sup>4</sup>, 230–231°C).

**2-Vinylcarbazole.** A mixture of 2-acetylcarbazole (24 g) and aluminium isopropoxide (40 g) in xylene (75 ml) was refluxed for 3 h, during which time the acetone formed was distilled from the reaction mixture. After cooling, the reaction mixture was filtered free of aluminium isopropoxide and poured into water. The xylene layer was separated and the aqueous layer was extracted with ether. The combined extracts were washed with water and dried (MgSO<sub>4</sub>/NaOH). Evaporation afforded 2-vinylcarbazole (12.0 g, 53%) as pale yellow crystals, m.p. 253–254°C from toluene. Found: C, 86.7%; H, 5.8%; N, 7.2%. C<sub>14</sub>H<sub>11</sub>N requires: C, 87.0%; H, 5.7%; N, 7.3%.  $\nu_{\max}$  3400 (N-H), 1625 (CH=CH<sub>2</sub>), 1610, 1340, 1240, 1080, 995, 875, 830, 750, and 730 cm<sup>-1</sup>.  $\tau$ [(CD<sub>3</sub>)<sub>2</sub>CO] 0.1 br. (NH), 1.9–3.1 (8H, m, ArH and an olefinic proton), 4.10 and 4.38 (1H, two d, *J*<sub>gem</sub> 2 Hz, *trans*, *gem* olefinic proton) and 4.75 and 4.93 (1H, two d, *cis*, *gem* olefinic proton). *m/e* 193(*M*<sup>+</sup>, 100%), 194(*M*+1, 21), 192(37), 191(26), 167(28), and 91(19).

**9-Ethyl-2-vinylcarbazole** (61%) as needles, m.p. 89–90°C was prepared by alkylation of 2-vinylcarbazole using thallium(I) ethoxide/ethyl iodide, as described previously<sup>5</sup>.

### RESULTS AND DISCUSSION

#### Free radical polymerization

Using AIBN as initiator at 50°C and solvents, benzene, tetrahydrofuran and methanol, polymer yields were less than 1% under conditions where *N*-vinylcarbazole (NVC) would give polymer yields of the order of 70%<sup>9–11</sup>. In contrast to NVC therefore, *N*-ethyl-2-vinylcarbazole shows remarkably little reactivity in free radical homopolymerization.

#### Copolymerization with maleic anhydride

AIBN initiated copolymerization of maleic anhydride with *N*-ethyl-2-vinylcarbazole in tetrahydrofuran at 50°C proceeded readily to give almost quantitative yields of 1 : 1 alternating copolymer (found: C, 74.4%; H, 5.3%; calculated for 1 : 1 copolymer: C, 75.2%,

H, 5.4%). Under identical conditions, NVC and maleic anhydride gave a 12% yield of a polymer which by i.r. analysis was largely homopolymer of NVC. This latter result is in agreement with observations of other workers<sup>12</sup> and again highlights the differences in reactivity between NVC and *N*-ethyl-2-vinylcarbazole.

#### Cationic polymerization

Following the procedures described for cationic polymerization of NVC, both tropylium hexachloroantimonate<sup>6</sup> and tris-(*p*-bromophenyl) aminium hexachloroantimonate<sup>7</sup> readily catalysed high conversion of *N*-ethyl-2-vinylcarbazole to polymer in methylene chloride. Values of  $\bar{M}_n$  for polymerizations at room temperature were in the region of 6000 and it is clear that cationic polymerizability of *N*-ethyl-2-vinylcarbazole is comparable to that of NVC.

#### Anionic polymerization

Preliminary investigation of the reactions between *n*-butyl-lithium and *N*-ethyl-2-vinylcarbazole in tetrahydrofuran at room temperature showed immediate formation of a deep red coloured anion, stable in the absence of air, and present continuously during polymerizations. High conversions to polymer ( $\bar{M}_n > 30\,000$ ) were readily achieved and experiments with initiation by living polystyryl anions confirmed the feasibility of block copolymer synthesis. In its anionic polymerizability therefore, *N*-ethyl-2-vinylcarbazole differs completely from NVC.

#### Ziegler-Natta polymerization

Attempts to polymerize *N*-ethyl-2-vinylcarbazole using  $\text{TiCl}_3/\text{AlEt}_3$  in heptane/benzene at room temperature failed. That the catalyst is deactivated or destroyed by the monomer is evidenced by the immediate colour change, purple  $\rightarrow$  brown, which occurs on addition of monomer. Under similar conditions addition of NVC does not affect the colour of the catalyst and 30–40% yields of polymer are obtained<sup>13</sup>.

#### Thermal stability and melting behaviour of poly(*N*-ethyl-2-vinylcarbazole) [PEVC]

For simplicity, anionically prepared poly(*N*-ethyl-2-vinylcarbazole) ( $\bar{M}_n \sim 30\,000$ ) was compared with free

radically prepared PNVC ( $\bar{M}_n \sim 40\,000$ ) using conventional melting point procedures (open tubes). Both polymers began softening around 200°C and melting was complete for PEVC at 225°C and for PNVC at 235°C. However, whereas PNVC became dark coloured and gelled when heated at 250°C for approximately 10 min, PEVC remained a pale straw coloured mobile liquid. Preliminary indications are, therefore, that PEVC has improved thermal or oxidative stability over PNVC.

#### CONCLUSIONS

Synthesis of a vinylated carbazole derivative in which the nitrogen atom is not directly conjugated with the vinyl group permits formation of a new homopolymer, and copolymers, having many of the desirable properties of PNVC including thermal stability, electron donor character and light absorption characteristics. The anionic reactivity is especially important because of current interest in block copolymers having rigid block components and this aspect of the polymerizability of *N*-ethyl-2-vinylcarbazole is being actively pursued.

#### ACKNOWLEDGEMENT

The authors are indebted to the SRC for Research Assistantships to P.H. and L.J.K.

#### REFERENCES

- Morimoto, K. *Jap. Electronic Eng.* 1969 (May), p 16
- Regensburger, P. J. *Photochem. Photobiol.* 1968, **8**, 429; Schaffert, R. M. *IBM J. Res. Dev.* 1971, **15**, 75
- Lopatinskii, V. P. and Sirotkina, E. E. *Metody Poluch. Khim., Reakt. Prep.* 1964, **11**, 40; *Chem. Abstr.* 1966, **65**, 2203
- Manske, R. H. F. and Kulka, M. *Can. J. Res.* 1950, **28B**, 443
- Kricka, L. J. and Ledwith, A. *JCS Perkin Trans. I* 1972, p 2292
- Bowyer, P. M., Ledwith, A. and Sherrington, D. C. *Polymer* 1971, **12**, 509
- Ledwith, A. *Acc. Chem. Res.* 1972, **5**, 133
- Berlin, A. A. *J. Gen. Chem. (USSR)* 1944, **14**, 438
- Ellinger, L. P. *J. Appl. Polym. Sci.* 1965, **9**, 3939
- Hughes, J. and North, A. M. *Trans. Faraday Soc.* 1966, **62**, 1866
- Jones, R. G., Catterall, E., Bilson, R. T. and Booth, R. G. *Chem. Commun.* 1972, p 22
- Ellinger, L. P. *Polymer* 1964, **5**, 559
- Heller J., Tieszen, D. O. and Parkinson, D. B. *J. Polym. Sci. (A)* 1963, **1**, 125



# Book Reviews

## Carbon fibres in composites

R. M. Gill

Iliffe Books, London, 1972, 207 pp. £5.00

It is six years since the newly hatched carbon fibre industry was revealed to public view accompanied by widespread acclaim and an excess of superlatives. Unfortunately the fledgling has since failed to reproduce in flight the confident performance predicted at the time, and its major attempt to leave the nest appeared to fall short of the target. There are signs, however, that growth towards maturity is now inexorably underway and this is therefore a propitious time for the publication of Dr Gill's monograph.

This book is not aimed at a specific group of people; it could be read with advantage by all who have interests in the materials field and can see that carbon fibre composites may interact with their work or businesses. Drawing on his experience with Morganite Modmor Ltd, the author has produced a comprehensive guide to present production techniques and the chemistry of the conversion processes for the major rayon-based and PAN-based fibres. Valuable data on fibre and composite properties and testing techniques have been compiled, together with information on a variety of matrix materials and hints for composite test-piece manufacture. These chapters form the core of the book and are authoritatively written with references to the principal papers and international patent literature. It has clearly been Dr Gill's intention to create in the reader the feeling that he has sufficient background information to evaluate these materials for himself. For this reason the fact that the description of composite and prepreg manufacturing methods does not represent the best present industrial practice is understandable. Simple methods are more likely to be successful with small quantities of fibre than complex techniques which may lead to punitive scrap costs in the event of an error. The author has also surveyed present carbon fibre reinforced plastics applications and future potential, acknowledging that these aspects are likely to change rapidly and be contentious in character. It will be interesting to evaluate actual performance in a few years time against these tentative predictions.

There are some incongruities in the book. For example, the chemical complexities of the pyrolysis process render the simple definitions of terminology, which appear a few pages before, insignificant by comparison. Imperial units are used throughout when the universal movement is towards metrication. In the useful chapter on resin matrix materials some of the proportions of constituents seem unfortunately to have been omitted.

These and a few other small objections do not detract from Dr Gill's main achievement which has been to produce an excellent primer on carbon fibre technology at a critical time in the growth of the field.

The book is generally easy to read, clearly laid out and very nicely produced but at £5 for 200 pages seems slightly on the expensive side.

J. W. Johnson

## Plasticisers, stabilisers and fillers

Edited by P. D. Ritchie

Iliffe Books, London, 1972, 333 pp. £8.00

It is unfortunate that the title of this book tends to be a misleading one, in that fourteen of its twenty chapters nominally deal with plasticizers, with three of the remainder on stabilizers and three on fillers. As mentioned in the preface this rather unbalanced treatment has been partially remedied by a separate monograph, 'Fillers for Plastics', edited by W. C. Wake. Another feature which is not indicated by the title is the considerable emphasis on additives for poly(vinyl chloride). Although this is justified, in the case of plasticizers for example, by the very much larger consumption of plasticizers for PVC, further information concerning other polymers would have been useful, particularly in the case of stabilizers and fillers.

Two short introductory chapters are followed by a chapter in which polymer types and additives are discussed. Useful information concerning requirements of additives, and types of additives used for different polymers are included in this chapter. The next

two chapters review the literature on theories of plasticizer action and compatibility, efficiency and permanence of plasticizers, but in the former case no work published later than 1961 is cited. Chapters on viscoelastic, mechanical, and electrical properties of polymers and polymer processing include much material which is available from other sources. In addition the large number of contributors has led to a certain amount of repetition, so that electrical properties, for example, are defined in two separate chapters. Much more relevant material is that on the manufacture, properties and analysis of plasticizers, while a chapter on formulation for specific applications is a useful one for reference purposes.

Useful chapters on stabilizers and additives for particular applications are also included in the last two sections of the monograph. Much information on the effect of different types of filler on properties is quoted.

Thus although parts of this monograph contain valuable reference material for the plastics technologist, other information presented is less relevant for a publication of this type, and the price of £8.00 is high for the amount of new material presented.

M. Gilbert

## Reviews in polymer technology, Vol I

Edited by Irving Skeist

Marcel Dekker, New York, 1972, 252 pp. \$19.50

This book is intended as the first volume of a series which will deal with current technology in the polymer-based industries and the six reviews included are illustrative of the range expected.

The style and nature of the contents varies considerably. *Plastics and other polymers in building* is a short marketing oriented article with statistical data for the use of polymers drawn from Germany and the UK as well as the USA. The technology is sparse. The longest and most technological is *Fire retardance in polymeric materials*. This is an extremely thorough review which seems to be written in three parts. It starts with theoretical matters, then follows a section on the use of additives with emphasis on glass fibre reinforced plastics, empirical test results and smoke development and it concludes by a return to some theory applied to actual data. This method of treatment involves some repetition even to the extent of Fig. 25 virtually repeating Fig. 4. There is also in this otherwise valuable article a failure to consider the level of knowledge to be expected of the reader. Many of the simple chemical equations are mere padding and Figs 9 and 10 occupying whole pages are too elementary. The mechanism discussion leans heavily on radical mechanisms to the exclusion of physical factors such as heat conductance, heats of combustion and vapour diffusion. The empirical and unsatisfactory state of fire retardance comes out clearly as the direct result of the complexity of the processes which occur. In fact one is surprised at the amount of order the authors have managed to impose.

The first review concerns *Coupling agents as adhesion promoters*. This also is extremely thorough in that it concludes with 346 references adding for good measure a page of general bibliography. As this suggests, it accepts all and in doing so fails to give the reader fresh to the subject a critical picture. Amino-silanes are not suitable coupling agents to use with polyesters but one doubts the ascription of release properties to the treated glass surface. In general, coupling agents will lower the surface energy of a metal or even a glass substrate but in so doing they discourage the preferential adsorption of water which would otherwise occur. Where direct chemical reaction between coupling agent and resin occurs it is true that simple displacement of resin by water is not possible but it is untrue to state that the primary bond is not susceptible to hydrolysis for most of the coupling agents used can hydrolyse although there is little loss in this since the polyester will itself hydrolyse given sufficient exposure to water.

*Processing powdered polyethylene* is a competent state-of-the-art review of this technology. To the present writer the most modern of these reviews is *Recent advances in photo-crosslinkable polymers*. This concerns the use of polymers in photo-resist systems used in a number of ways but principally in the manufacture of integrated circuits. The review considers new polymers and their synthesis including materials such as poly(vinyl cinnamate) and its derivatives, poly(vinyl-2-furyl-acrylate), aryl azido condensation polymers,

styryl ketones, methoxy stilbenes and acetylenic polyethers. Data are given for a range of photosensitizers and the whole is most interesting.

The last review, *Organic colorants for polymers*, classifies these materials and concludes with a list of colorant chemical types conveniently arranged within the primary colours. This should be valuable.

The printing and book binding are of the usual USA high standard, though the writing of some of the authors is less than elegant. For some unaccountable reason the review copy was printed on two different coloured papers; pp 1-111 being white and pp 113-252 having a distinct and very noticeable green tinge. This ought not to occur.

W. C. Wake

## Polymer science and materials

Edited by A. V. Tobolsky and H. F. Mark

Wiley, New York and London, 1972, 432 pp. £10.05

This book, which is the first of two volumes, is intended, in the words of the editors, 'for the beginning student of polymer science or engineering, whether undergraduate, graduate, or employed in the polymer industry', and it attempts 'to present the fundamental ideas of polymer science in as simple a manner as possible'. Furthermore, it is also stated that 'an attempt has been made to retain a certain uniformity in the mode of presentation'.

It must regrettably be admitted that these stated objectives have been only partly accomplished. Not only is the level of difficulty among the various contributors widely different, but the order of the chapters does not appear to be based on any obvious logical principle. Some of the earlier chapters in particular are overlaid with mathematical formulations before the fundamental qualitative concepts underlying these formulations have been sufficiently clearly explained. Thus in Chapter 3 (Conformations of polymer molecules) the reader is confronted with advanced chain statistics in which references are made to the 'random-walk necklace model', the 'wormlike chain model', the 'elastic dumbbell model', etc., with practically no preparation. In the treatment of rubber elasticity (Chapter 9) insufficient care is given to clarity of presentation. The Gaussian network formulae are given in a form which contains the volume, and although it is stated that the volume is essentially constant, this obscures the essential simplicity of the results. The force-length relation for a non-Gaussian chain is derived (p 197) without defining the angle  $\theta$ . No graphs are included to illustrate either the Gaussian or the non-Gaussian force-extension relations. The beginner would have great difficulty in understanding the relation between the mean-

square length of network chains and that of free chains, or the significance of the 'affine deformation' assumption. He would probably decide that rubber elasticity was not for him. This is a great pity, for the subject is one in which engineers in particular can find much of interest.

The chapters which are concerned more with actual properties are much clearer. Chapter 10 (Viscoelastic properties of polymers) could well have preceded Chapter 6 (Phase transitions and vitrification). The chapters on crystallinity, on strength and on diffusion are well done. Later chapters, rather curiously entitled Science of rubbers, Science of plastics, and Science of fibres, which in fact are more concerned with industrial and technological aspects, are also very readable. The final chapter (Equilibrium polymerization) appears to have been added as an afterthought.

There is much in this book that will be read with interest by those who are already familiar with polymer science. It definitely is not suitable for a first reading in the subject.

L. R. G. Treloar

## Glycoproteins

Edited by A. Gottschalk

Elsevier, Amsterdam, 1972, Parts A and B, 1378 pp. Dfl. 400 (approx. £50)

Since the first edition of this work appeared in 1966, the interest in glycoproteins has escalated dramatically and their relevance to a widening circle of biological interests has become apparent. It is a notable example of a subject, which just a few years ago was a somewhat despised poor cousin, now proverbially become the rich uncle. It is timely, therefore, that an authoritative survey such as this should be brought up-to-date in line with current results and ideas. The book, which now is published in two volumes, Parts A and B, is partly successful in achieving this aim. It gives a broad coverage of the whole area being concerned principally on the one hand with general aspects of glycoproteins (analytical techniques, structural analysis, applications of enzymes for study of chemical constitution etc.) and on the other with detailed considerations of well-defined classes of glycoproteins or individual members of this category. The closing chapters deal with some aspects of biosynthesis and functions of glycoproteins. Most of the authors who contributed to the first edition, happily, reappear in the second. In some cases, it is evident that their contributions have been extensively rewritten so as to embody much new information, while other chapters are republished virtually unchanged in substance or views. In one chapter, for example, only eight references to works post-1966 are quoted, while another section has only four references which post-date the first edition. The contribution on the physico-chemical methods for determination of purity, molecular size and shape is a lengthy but readable survey providing a useful introduction to the various commoner techniques available. Many readers will appreciate especially the succinct and informative review of gas-liquid chromatographic techniques pertinent to glycoproteins. Elsewhere, inclusion of a brief chapter effectively on glycosaminoglycans of connective tissue is of interest, if only for comparative purposes. In general, the chapters on individual glycoproteins are well-written and authors have made judicious selections of examples for discussion. The book is well printed, the figures are adequately presented in most cases but the binding scarcely does justice to the volumes as a whole.

Though one does not minimize the importance nor usefulness of the subject, it is difficult to avoid the conclusion that at \$125 the work is substantially overpriced. Few individuals will feel able to invest at such a price and some doubt will exist, even in the minds of some librarians, whether the proportion of new information which this new edition contains makes it worth the outlay. It can only be described as regrettable that a single subject index (though commendably thorough) to both Parts appears only at the end of Part B. Even if Part A is available separately, its use is seriously diminished without Part B. There is no author index to either Part.

Nevertheless, this work stands as an outstanding source volume which will be of great service to research workers in many fields, and will be undoubtedly an added stimulus to further investigations.

P. W. Kent

## Reprinted Volumes of POLYMER

1960-1969 (Vols 1-10)

Missing volume of **POLYMER** in your library?

The first 10 volumes of **POLYMER**, covering the years 1960 to 1969, have now been reprinted in separate volumes (one per year) and are available at £15.00 (\$39.00) per volume.

All orders should be sent direct to:

Wm Dawson and Sons Ltd,  
Cannon House,  
Folkestone,  
Kent, UK

# Book Reviews

## Carbon fibres in composites

R. M. Gill

Iliffe Books, London, 1972, 207 pp. £5.00

It is six years since the newly hatched carbon fibre industry was revealed to public view accompanied by widespread acclaim and an excess of superlatives. Unfortunately the fledgling has since failed to reproduce in flight the confident performance predicted at the time, and its major attempt to leave the nest appeared to fall short of the target. There are signs, however, that growth towards maturity is now inexorably underway and this is therefore a propitious time for the publication of Dr Gill's monograph.

This book is not aimed at a specific group of people; it could be read with advantage by all who have interests in the materials field and can see that carbon fibre composites may interact with their work or businesses. Drawing on his experience with Morganite Modmor Ltd, the author has produced a comprehensive guide to present production techniques and the chemistry of the conversion processes for the major rayon-based and PAN-based fibres. Valuable data on fibre and composite properties and testing techniques have been compiled, together with information on a variety of matrix materials and hints for composite test-piece manufacture. These chapters form the core of the book and are authoritatively written with references to the principal papers and international patent literature. It has clearly been Dr Gill's intention to create in the reader the feeling that he has sufficient background information to evaluate these materials for himself. For this reason the fact that the description of composite and prepreg manufacturing methods does not represent the best present industrial practice is understandable. Simple methods are more likely to be successful with small quantities of fibre than complex techniques which may lead to punitive scrap costs in the event of an error. The author has also surveyed present carbon fibre reinforced plastics applications and future potential, acknowledging that these aspects are likely to change rapidly and be contentious in character. It will be interesting to evaluate actual performance in a few years time against these tentative predictions.

There are some incongruities in the book. For example, the chemical complexities of the pyrolysis process render the simple definitions of terminology, which appear a few pages before, insignificant by comparison. Imperial units are used throughout when the universal movement is towards metrication. In the useful chapter on resin matrix materials some of the proportions of constituents seem unfortunately to have been omitted.

These and a few other small objections do not detract from Dr Gill's main achievement which has been to produce an excellent primer on carbon fibre technology at a critical time in the growth of the field.

The book is generally easy to read, clearly laid out and very nicely produced but at £5 for 200 pages seems slightly on the expensive side.

J. W. Johnson

## Plasticisers, stabilisers and fillers

Edited by P. D. Ritchie

Iliffe Books, London, 1972, 333 pp. £8.00

It is unfortunate that the title of this book tends to be a misleading one, in that fourteen of its twenty chapters nominally deal with plasticizers, with three of the remainder on stabilizers and three on fillers. As mentioned in the preface this rather unbalanced treatment has been partially remedied by a separate monograph, 'Fillers for Plastics', edited by W. C. Wake. Another feature which is not indicated by the title is the considerable emphasis on additives for poly(vinyl chloride). Although this is justified, in the case of plasticizers for example, by the very much larger consumption of plasticizers for PVC, further information concerning other polymers would have been useful, particularly in the case of stabilizers and fillers.

Two short introductory chapters are followed by a chapter in which polymer types and additives are discussed. Useful information concerning requirements of additives, and types of additives used for different polymers are included in this chapter. The next

two chapters review the literature on theories of plasticizer action and compatibility, efficiency and permanence of plasticizers, but in the former case no work published later than 1961 is cited. Chapters on viscoelastic, mechanical, and electrical properties of polymers and polymer processing include much material which is available from other sources. In addition the large number of contributors has led to a certain amount of repetition, so that electrical properties, for example, are defined in two separate chapters. Much more relevant material is that on the manufacture, properties and analysis of plasticizers, while a chapter on formulation for specific applications is a useful one for reference purposes.

Useful chapters on stabilizers and additives for particular applications are also included in the last two sections of the monograph. Much information on the effect of different types of filler on properties is quoted.

Thus although parts of this monograph contain valuable reference material for the plastics technologist, other information presented is less relevant for a publication of this type, and the price of £8.00 is high for the amount of new material presented.

M. Gilbert

## Reviews in polymer technology, Vol I

Edited by Irving Skeist

Marcel Dekker, New York, 1972, 252 pp. \$19.50

This book is intended as the first volume of a series which will deal with current technology in the polymer-based industries and the six reviews included are illustrative of the range expected.

The style and nature of the contents varies considerably. *Plastics and other polymers in building* is a short marketing oriented article with statistical data for the use of polymers drawn from Germany and the UK as well as the USA. The technology is sparse. The longest and most technological is *Fire retardance in polymeric materials*. This is an extremely thorough review which seems to be written in three parts. It starts with theoretical matters, then follows a section on the use of additives with emphasis on glass fibre reinforced plastics, empirical test results and smoke development and it concludes by a return to some theory applied to actual data. This method of treatment involves some repetition even to the extent of Fig. 25 virtually repeating Fig. 4. There is also in this otherwise valuable article a failure to consider the level of knowledge to be expected of the reader. Many of the simple chemical equations are mere padding and Figs 9 and 10 occupying whole pages are too elementary. The mechanism discussion leans heavily on radical mechanisms to the exclusion of physical factors such as heat conductance, heats of combustion and vapour diffusion. The empirical and unsatisfactory state of fire retardance comes out clearly as the direct result of the complexity of the processes which occur. In fact one is surprised at the amount of order the authors have managed to impose.

The first review concerns *Coupling agents as adhesion promoters*. This also is extremely thorough in that it concludes with 346 references adding for good measure a page of general bibliography. As this suggests, it accepts all and in doing so fails to give the reader fresh to the subject a critical picture. Amino-silanes are not suitable coupling agents to use with polyesters but one doubts the ascription of release properties to the treated glass surface. In general, coupling agents will lower the surface energy of a metal or even a glass substrate but in so doing they discourage the preferential adsorption of water which would otherwise occur. Where direct chemical reaction between coupling agent and resin occurs it is true that simple displacement of resin by water is not possible but it is untrue to state that the primary bond is not susceptible to hydrolysis for most of the coupling agents used can hydrolyse although there is little loss in this since the polyester will itself hydrolyse given sufficient exposure to water.

*Processing powdered polyethylene* is a competent state-of-the-art review of this technology. To the present writer the most modern of these reviews is *Recent advances in photo-crosslinkable polymers*. This concerns the use of polymers in photo-resist systems used in a number of ways but principally in the manufacture of integrated circuits. The review considers new polymers and their synthesis including materials such as poly(vinyl cinnamate) and its derivatives, poly(vinyl-2-furyl-acrylate), aryl azido condensation polymers,

styryl ketones, methoxy stilbenes and acetylenic polyethers. Data are given for a range of photosensitizers and the whole is most interesting.

The last review, *Organic colorants for polymers*, classifies these materials and concludes with a list of colorant chemical types conveniently arranged within the primary colours. This should be valuable.

The printing and book binding are of the usual USA high standard, though the writing of some of the authors is less than elegant. For some unaccountable reason the review copy was printed on two different coloured papers; pp 1-111 being white and pp 113-252 having a distinct and very noticeable green tinge. This ought not to occur.

W. C. Wake

## Polymer science and materials

Edited by A. V. Tobolsky and H. F. Mark

Wiley, New York and London, 1972, 432 pp. £10.05

This book, which is the first of two volumes, is intended, in the words of the editors, 'for the beginning student of polymer science or engineering, whether undergraduate, graduate, or employed in the polymer industry', and it attempts 'to present the fundamental ideas of polymer science in as simple a manner as possible'. Furthermore, it is also stated that 'an attempt has been made to retain a certain uniformity in the mode of presentation'.

It must regrettably be admitted that these stated objectives have been only partly accomplished. Not only is the level of difficulty among the various contributors widely different, but the order of the chapters does not appear to be based on any obvious logical principle. Some of the earlier chapters in particular are overlaid with mathematical formulations before the fundamental qualitative concepts underlying these formulations have been sufficiently clearly explained. Thus in Chapter 3 (Conformations of polymer molecules) the reader is confronted with advanced chain statistics in which references are made to the 'random-walk necklace model', the 'wormlike chain model', the 'elastic dumbbell model', etc., with practically no preparation. In the treatment of rubber elasticity (Chapter 9) insufficient care is given to clarity of presentation. The Gaussian network formulae are given in a form which contains the volume, and although it is stated that the volume is essentially constant, this obscures the essential simplicity of the results. The force-length relation for a non-Gaussian chain is derived (p 197) without defining the angle  $\theta$ . No graphs are included to illustrate either the Gaussian or the non-Gaussian force-extension relations. The beginner would have great difficulty in understanding the relation between the mean-

square length of network chains and that of free chains, or the significance of the 'affine deformation' assumption. He would probably decide that rubber elasticity was not for him. This is a great pity, for the subject is one in which engineers in particular can find much of interest.

The chapters which are concerned more with actual properties are much clearer. Chapter 10 (Viscoelastic properties of polymers) could well have preceded Chapter 6 (Phase transitions and vitrification). The chapters on crystallinity, on strength and on diffusion are well done. Later chapters, rather curiously entitled Science of rubbers, Science of plastics, and Science of fibres, which in fact are more concerned with industrial and technological aspects, are also very readable. The final chapter (Equilibrium polymerization) appears to have been added as an afterthought.

There is much in this book that will be read with interest by those who are already familiar with polymer science. It definitely is not suitable for a first reading in the subject.

L. R. G. Treloar

## Glycoproteins

Edited by A. Gottschalk

Elsevier, Amsterdam, 1972, Parts A and B, 1378 pp. Dfl. 400 (approx. £50)

Since the first edition of this work appeared in 1966, the interest in glycoproteins has escalated dramatically and their relevance to a widening circle of biological interests has become apparent. It is a notable example of a subject, which just a few years ago was a somewhat despised poor cousin, now proverbially become the rich uncle. It is timely, therefore, that an authoritative survey such as this should be brought up-to-date in line with current results and ideas. The book, which now is published in two volumes, Parts A and B, is partly successful in achieving this aim. It gives a broad coverage of the whole area being concerned principally on the one hand with general aspects of glycoproteins (analytical techniques, structural analysis, applications of enzymes for study of chemical constitution etc.) and on the other with detailed considerations of well-defined classes of glycoproteins or individual members of this category. The closing chapters deal with some aspects of biosynthesis and functions of glycoproteins. Most of the authors who contributed to the first edition, happily, reappear in the second. In some cases, it is evident that their contributions have been extensively rewritten so as to embody much new information, while other chapters are republished virtually unchanged in substance or views. In one chapter, for example, only eight references to works post-1966 are quoted, while another section has only four references which post-date the first edition. The contribution on the physico-chemical methods for determination of purity, molecular size and shape is a lengthy but readable survey providing a useful introduction to the various commoner techniques available. Many readers will appreciate especially the succinct and informative review of gas-liquid chromatographic techniques pertinent to glycoproteins. Elsewhere, inclusion of a brief chapter effectively on glycosaminoglycans of connective tissue is of interest, if only for comparative purposes. In general, the chapters on individual glycoproteins are well-written and authors have made judicious selections of examples for discussion. The book is well printed, the figures are adequately presented in most cases but the binding scarcely does justice to the volumes as a whole.

Though one does not minimize the importance nor usefulness of the subject, it is difficult to avoid the conclusion that at \$125 the work is substantially overpriced. Few individuals will feel able to invest at such a price and some doubt will exist, even in the minds of some librarians, whether the proportion of new information which this new edition contains makes it worth the outlay. It can only be described as regrettable that a single subject index (though commendably thorough) to both Parts appears only at the end of Part B. Even if Part A is available separately, its use is seriously diminished without Part B. There is no author index to either Part.

Nevertheless, this work stands as an outstanding source volume which will be of great service to research workers in many fields, and will be undoubtedly an added stimulus to further investigations.

P. W. Kent

## Reprinted Volumes of POLYMER

1960-1969 (Vols 1-10)

Missing volume of POLYMER in your library?

The first 10 volumes of POLYMER, covering the years 1960 to 1969, have now been reprinted in separate volumes (one per year) and are available at £15.00 (\$39.00) per volume.

All orders should be sent direct to:

Wm Dawson and Sons Ltd,  
Cannon House,  
Folkestone,  
Kent, UK

**Vinyl and applied polymers**  
**Vol 2: Vinyl chloride and vinyl acetate polymers**

G. A. R. Matthews

Iliffe Books, London, 1972, 401 pp. £8.50

Vinyl chloride is now a chemical of considerable commercial importance, polymers based on this monomer providing a wide range of products extending from rigid mouldings to flexible sheet, according to the composition and fabrication process adopted, and one welcomes the appearance of an authoritative textbook directed specifically to this field.

The Plastics Institute in association with the publishers were instrumental in producing the first of this series on vinyl polymers (*Polyolefins*, edited by P. D. Ritchie, Butterworths, 1968) and the present volume by George Matthews of the Polytechnic of the South Bank forms a worthy successor. The subject is very competently treated, both from the polymer science and the technological angles, the author having usefully drawn on his wide experience in industry and technical education to provide a useful and readable account.

After a brief introductory chapter, concerned largely with the history of PVC development, three chapters (55 pp) relate to the production of vinyl chloride and related monomers and the manufacture and general properties of derived polymers and copolymers, attention being given to the relevant scientific background on addition polymerization and the production processes involved, particularly with regard to suspension and emulsion methods.

Four chapters (94 pp) discuss degradation and stabilization, plasticizers and formulation, these being followed by comprehensive reviews (130 pp) of processing and fabrication (compounding, extrusion, calendering, moulding, use of pastes, etc.) in which not only polymer compositions but processing equipment and operating factors are fully considered; properties and applications of PVC are then discussed generally.

Experimental and test procedures form the subject of a lengthy chapter which will be of particular interest to those engaged in characterization, evaluation and control, since it details a wide series of tests and lists the relevant British Standard specifications and ISO methods. The inclusion of a section on molecular weight characteristics is especially useful in drawing attention to and clarifying the somewhat confused picture on  $K$  values and viscosity numbers as related to  $M_n$  and  $M_w$ .

The final chapter of the book is essentially a self-contained article by Llewellyn and Williams of BP Co. Ltd, and deals briefly with the manufacture and use of vinyl acetate and its polymers and copolymers.

The book brings together a great deal of information from diverse sources in the scientific, technical and patent literature and the logical presentation of the theoretical and practical content will be appreciated. Practical issues over a wide field are well displayed; indeed the only omission appears to be that of vinyl chloride in synthetic fibres.

Each chapter carries a comprehensive list of references while the whole book is provided with clear diagrams and a good index. Printing and binding are excellent and the book can be well recommended to all concerned with the development, manufacture and use of PVC and with related polymers. Students of polymer science and technology will also find it of value in that it displays important factors relating polymer theory to practice and properties and processes to applications.

R. J. W. Reynolds

**Proceedings of the Third Tihany Symposium on Radiation Chemistry**

*Edited by János Dobó and Péter Hedvig*

Akadémiai Kiadó, Budapest, 1972, Vols I and II, 1458 pp. £16.20

Part 2 of Vol I of these proceedings contains about 600 pages that deal with the radiation chemistry of polymers. Among the papers presented are the following: Radiation and photo-induced ionic polymerization; Solid state polymerization of methyl methacrylate; Calorimetric study of the post-polymerization of the acrylonitrile-urea channel complex; N.m.r. study of the solid state polymerization of  $\gamma$ -irradiated vinyl monomers; Radiation polymerization of crystalline *N*-vinylcarbazole; Large-scale radiation polymerization of maleimides in the  $\gamma$ -ray installation 'PXYHD-20 000'; Radiation chemical process of modification of wood by polymers; Electron beam polymerization of wood-plastic combinations; Irradiated concrete-polymer materials: influence of different polymers on strength properties; Heavy ion effects in polymers; Decay of free radicals in irradiated PMMA at high pressures; Radiation graft polymerization of *N*-vinylpyridine to capron and polypropylene fibres; Structural study of polyethylene-styrene graft copolymers; Syntheses and study of the properties of vinyl fluoride based statistic and graft copolymers; Radiothermoluminescence for investigating the thermal and radiation induced crosslinking of rubber mixtures; Radiation induced graft polymerization of vinyl monomers onto cellulose.

C. J. R.

*Conference Announcement*

**Order in Polymer Solutions**

Midland, Michigan, 20-24 August 1973

The Midland Macromolecular Institute will sponsor a Symposium on 'Order in Polymer Solutions' to be held from August 20 to 24, 1973 in Midland, Michigan. The Symposium will consist of both invited and contributed papers. The invited papers will offer critical reviews on order in isolated biological and synthetic macromolecules, preferential solvation, association and morphological transitions in dilute and concentrated solutions. Contributed papers are solicited. For further information write to: Organizing Committee, Midland Macromolecular Institute, 1910 W. St Andrews Drive, Midland, Michigan 48640, USA.

*Conference Announcement*

**Seventeenth Canadian High Polymer Forum**

St Jean, Quebec, 15-17 August 1973

The Seventeenth Canadian High Polymer Forum will be held at the Collège Militaire Royal, Quebec, Canada from August 15 to 17, 1973. Sponsored by the Macromolecular Sciences Division of the Chemical Institute of Canada and the National Research Council, the Forum concerns itself with all aspects of polymer science. Those wishing to contribute papers are invited to send titles, author's names and 200-300 word abstracts to the Program Chairman, Dr D. J. Worsfold, Chemistry Division, National Research Council, Ottawa K1A 0R9, Canada by April 30, 1973. Further details about registration etc. will be available from E. G. Lovering, Pharmaceutical Chemistry Division, Health Protection Branch, Tunney's Pasture, Ottawa K1A 0L2, Canada.

# Scanning electron microscopical study of fibre reinforced polymeric cage materials for rolling bearings\*

D. Scott and G. H. Mills

National Engineering Laboratory, East Kilbride, Glasgow G75 0QU, UK  
(Received 20 November 1972)

Under conditions of heavily loaded, unlubricated rolling contact, the use of cages in composite materials reduced the wear of the rolling elements and thus effected *in situ* lubrication with little wear of the cage material. Owing to the spreading of polytetrafluoroethylene (PTFE) on the bearing surface, PTFE material reinforced with carbon or glass fibres and MoS<sub>2</sub> was the most effective of the materials tested in reducing wear under all the arduous test conditions. Scanning electron microscopical investigations showed that, generally, cage failure by fracture occurred by cracks initiating at voids formed during the bearing test. These were usually in areas of fibre depletion in the polymeric material.

## INTRODUCTION

*In situ* lubrication from a special cage material offers an attractive solution to the lubrication problem of rolling bearings under arduous service conditions. Using an accelerated service-simulation test<sup>1</sup> an exploratory investigation of composite material cages for the *in situ* lubrication of rolling bearings has been carried out<sup>2</sup>. Cages machined from sheets of various types of fibre and lamellar solid reinforced polymeric materials and cages moulded from the same materials were investigated under lubricated, unlubricated, and elevated temperature conditions of rolling contact all of which had led to failure by wear of the rolling elements<sup>3, 4</sup>. The use of composite cages reduced wear of the rolling elements and thus effected *in situ* lubrication with little wear of the cage material. The polytetrafluoroethylene (PTFE)-based material was the most effective of the polymer materials used, because of transfer of a PTFE film to the bearing surface. PTFE containing carbon or glass fibres and molybdenum disulphide (MoS<sub>2</sub>) was found to be the most effective of the cage materials.

## EXAMINATION OF CAGE MATERIALS

Investigations of selected tested cages were carried out by scanning electron microscopy to obtain fine-scale information of interest in the elucidation of the mechanism of *in situ* lubrication. Failed and fractured cages were also examined to study the mechanism of failure and the controlling factors.

The surfaces of spacers which had been in rubbing contact appeared different in different materials. With materials containing the larger amounts of PTFE, the

rubbed surfaces appeared to be predominantly PTFE as if the PTFE had spread along the rubbing surfaces. MoS<sub>2</sub> content appeared to promote a smoother rubbed surface (*Figure 1a*). The rubbed surface of carbon fibre and MoS<sub>2</sub> reinforced PTFE (*Figure 1b*) showed good fibre/matrix bonding and a smeared surface layer of PTFE and MoS<sub>2</sub>; very few loose or broken carbon fibres were observed on the surface. PTFE reinforced with glass fibre and MoS<sub>2</sub> showed a similar rubbed surface appearance. In the absence of MoS<sub>2</sub>, although the general appearance of the fibre/matrix bond was good, more broken fibres were found on the rubbed surface. After test at elevated temperature, the rubbed surfaces of PTFE-based materials were very smooth owing to a thick layer of PTFE. The low wear rate of bearings using these cage materials at elevated temperature was attributed to the formation of this layer by softening of the PTFE, allowing easier smearing and transfer to the surfaces of the mating metal rolling elements.

*Figure 1c* shows a laminate interface of the rubbed surface of a five-ply laminate of carbon fibre reinforced epoxy resin; numerous surface cracks and broken fibres are evident. Large areas of fibres parallel to the rubbing direction appeared devoid of matrix material, indicative of poor fibre/matrix bond strength. *Figure 1d* shows the rough appearance of carbon fibre-reinforced polyformaldehyde with loose broken fibres.

The typical appearance of the fracture surface of a failed carbon fibre and MoS<sub>2</sub> reinforced spacer is shown in *Figure 2a*. The texture of the material has a close knit appearance with smeared PTFE and MoS<sub>2</sub> on the surface. On the other hand, the appearance of the fracture surface of the five-ply laminate of carbon fibre-reinforced epoxy resin (*Figure 2b*) shows relatively clean carbon fibres and the lack of a good fibre/matrix bond. Evidence of voids, areas of fibre depletion and

\* Presented at the symposium 'Application of electron microscopy to the study of polymers' on 12 September 1972 as part of the 5th European Congress on Electron Microscopy (EMCON 72) held at the University of Manchester.



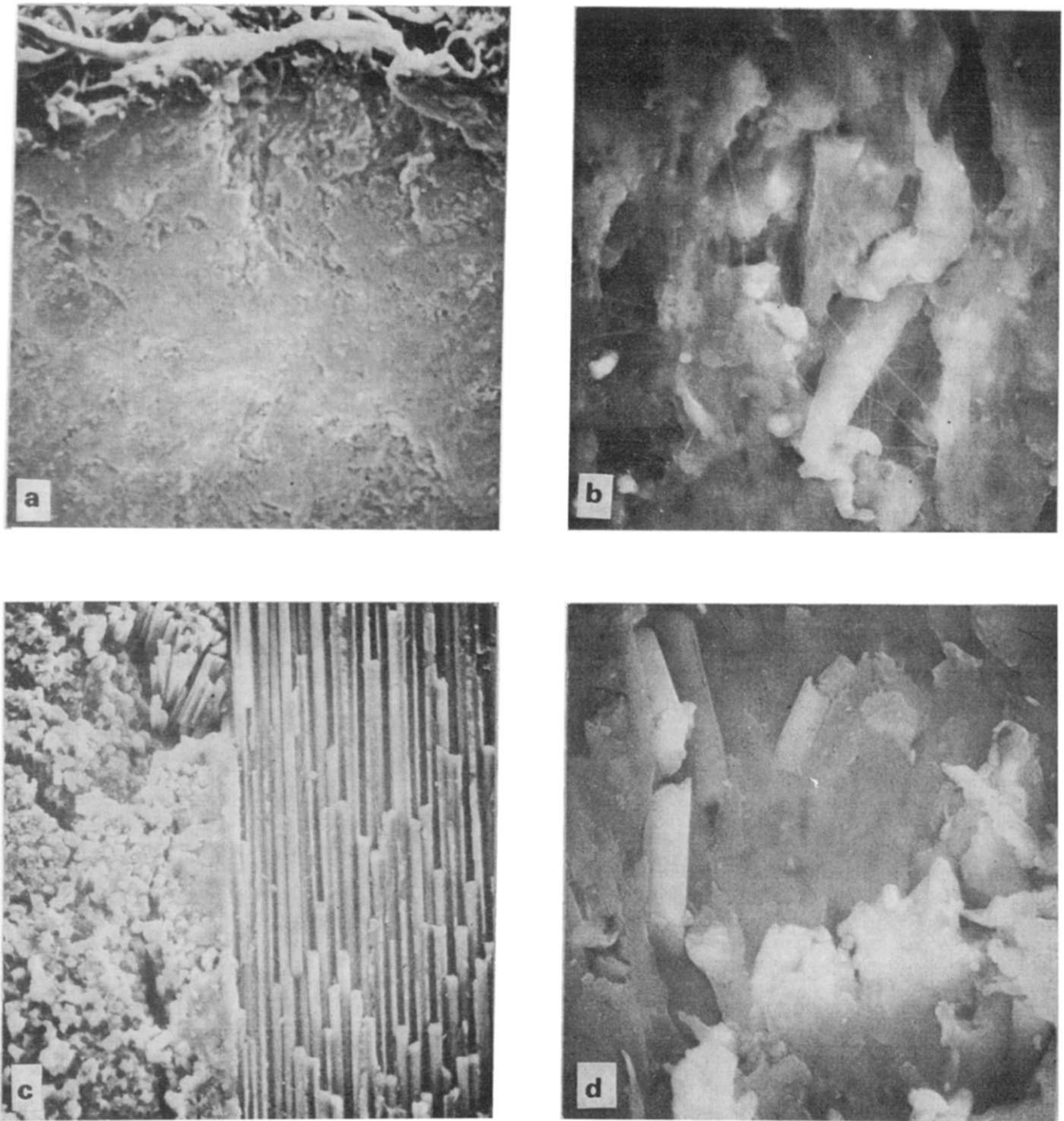


Figure 1 Scanning electron micrographs of the rubbed surface of cages. (a) Carbon fibre and  $\text{MoS}_2$  reinforced PTFE showing smooth surface ( $\times 150$ ); (b) carbon fibre and  $\text{MoS}_2$  reinforced PTFE showing smeared PTFE and  $\text{MoS}_2$  and a broken fibre ( $\times 1400$ ); (c) carbon fibre-reinforced epoxy resin laminate ( $\times 280$ ); (d) carbon fibre-reinforced polyformaldehyde showing rough surface and broken fibres ( $\times 1400$ )

fibre segregation was found in the fracture surface of carbon fibre-reinforced polyformaldehyde (Figure 2c). Voids, indicated at X (Figure 2d), were found in the fracture surface of the carbon fibre-reinforced PTFE; smearing of PTFE on the surface is also evident. No voids were found in the virgin material.

#### CONCLUSIONS

Electron microscopical examination revealed that, gener-

ally, failure of the cage materials by fracture occurred by cracks initiating at voids formed during bearing operation, usually in areas of fibre depletion. The better performance of PTFE-based materials appears to be due to the stronger fibre/matrix bond and the smearing of PTFE on the rubbing surface.  $\text{MoS}_2$  appears to aid the production of a smooth low-friction rubbing surface and is thus beneficial. Uniform distribution of the fibres and good bonding aids satisfactory performance.

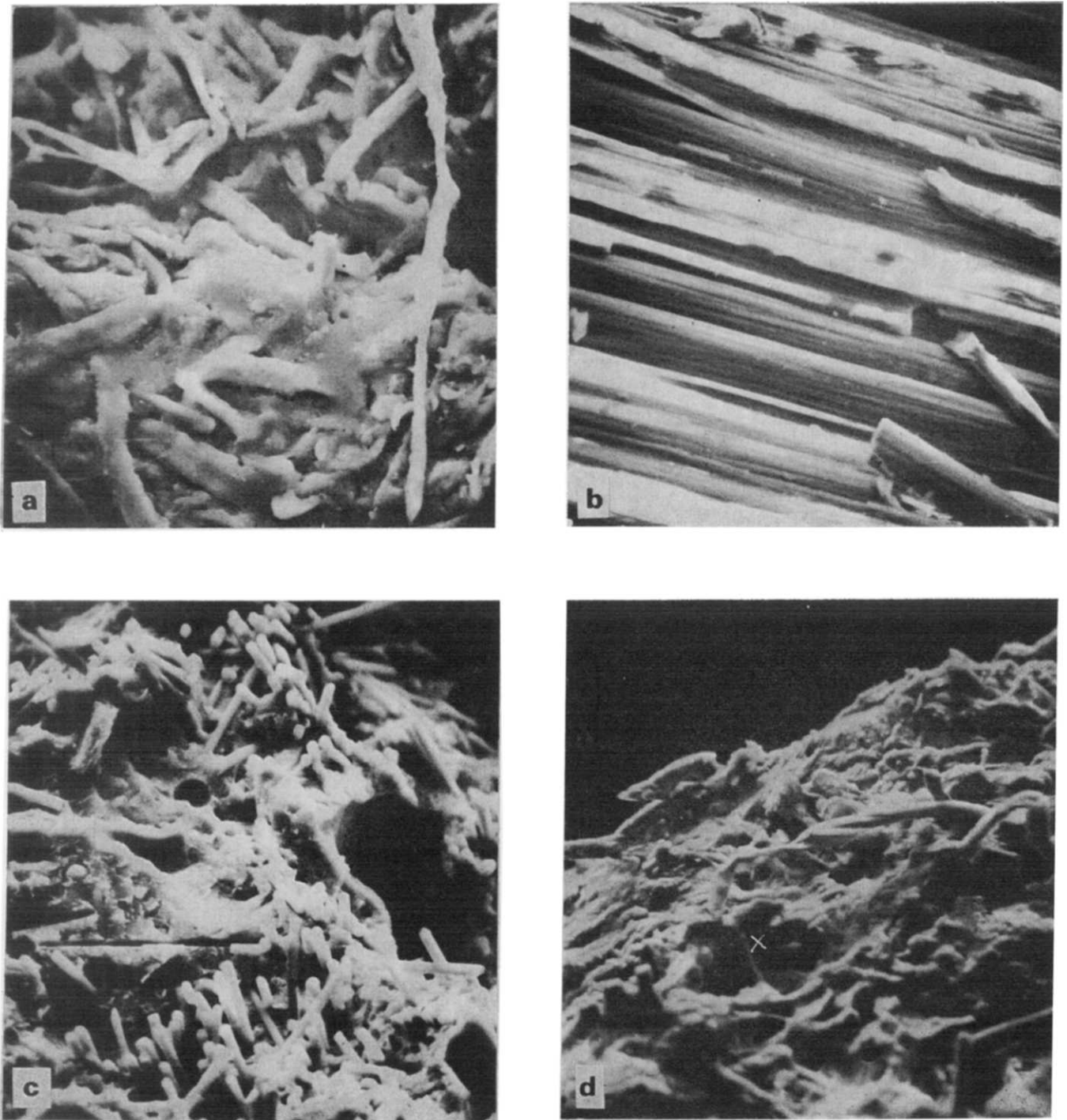


Figure 2 Scanning electron micrographs of fracture surfaces of failed cages. (a) Carbon fibre and  $\text{MoS}_2$  reinforced PTFE showing surface texture and smearing of PTFE and  $\text{MoS}_2$  ( $\times 360$ ); (b) carbon fibre-reinforced epoxy resin laminate showing clean fibres and poor bonding ( $\times 1300$ ); (c) carbon fibre-reinforced polyformaldehyde showing voids and areas of fibre depletion ( $\times 320$ ); (d) carbon fibre and  $\text{MoS}_2$  reinforced PTFE showing voids and smeared PTFE and  $\text{MoS}_2$  ( $\times 360$ )

#### ACKNOWLEDGEMENTS

This paper is published by permission of the Director, National Engineering Laboratory, Department of Trade and Industry. It is Crown copyright and is reproduced with the permission of the Controller, HMSO.

#### REFERENCES

- 1 Scott, D. and Blackwell, J. *Proc. 1st Lubr. Wear Conv. Inst. Mech. Eng.*, London, 1964, pp 292-298
- 2 Scott, D. *et al. Wear* 1970, **15**, 257
- 3 Scott, D. *Proc. Inst. Mech. Eng.* 1969, **183**, 9
- 4 Scott, D. and Blackwell, J. *Proc. Inst. Mech. Eng.* 1967, **181**, 70



# Variation of refractive index increment with molecular weight

D. Margerison, D. R. Bain and B. Kiely

*Department of Inorganic, Physical and Industrial Chemistry, University of Liverpool,  
PO Box 147, Liverpool L69 3BX, UK  
(Received 3 December 1972; revised 12 January 1973)*

The variation of the refractive index increment with molecular weight has been studied using solutions of monodisperse polystyrenes in toluene. The results show an asymptotic approach of the refractive index increment towards a limiting value characteristic of the infinite molecular weight polymer. It is shown that this limiting value is reached within experimental error in the molecular weight range between 50 000 and 100 000. A simple theory which postulates additivity of the specific refractions of the end groups and repeat units is used to account quantitatively for the results.

## INTRODUCTION

The rate of change of refractive index,  $\mu$ , with mass concentration,  $c$ , is an important experimental parameter in the treatment of data obtained from light scattering and gel permeation chromatography. Especially is this so in the study of solutions of high molecular weight polymers. In general, for these solutions, it is found that the refractive index increment,  $\partial\mu/\partial c$ , is a function of both concentration and molecular weight, i.e.  $\nu_c = \nu_c(c, M)$  where  $\nu_c$  stands for  $\partial\mu/\partial c$  and  $M$  stands for the molecular weight of the polymer. At low concentrations of polymer (say,  $c < 50$  g/l), the dependence of  $\nu_c$  on concentration may be neglected and so  $\nu_c \approx \nu_c(M)$ ;  $c < 50$  g/l. It has been normal practice to assume that the molecular weight dependence may also be neglected provided that the polymer does not contain a substantial mass fraction of species with molecular weights below about 10 000. However, recent work by Barrall *et al.*<sup>1</sup> has suggested that this assumption is not justified; using solutions of polystyrene in toluene and in methyl ethyl ketone, they claimed to detect a significant variation of refractive index increment with molecular weight extending up to molecular weights around 300 000.

Other studies of the variation of the refractive index increment with molecular weight have certainly not revealed anything like this far-reaching effect. Thus, Reed and Urwin<sup>2</sup> found no significant difference in refractive index increment for four synthetic polyisoprenes ranging in molecular weight from 28 000 to 220 000 using four different solvents. What changes have been found are confined to the low end of the molecular weight range. For example, Ziegler and co-workers<sup>3</sup> working with a series of methyl-substituted *p*-oligophenylenes found that the asymptotic value of the refractive index increment was effectively reached after something like 10 rings had been joined together—a molecular weight below 1000. Rempp<sup>4</sup> likewise found that the limiting value of the increment was reached for poly(ethylene glycol) in water at a molecular weight around 10 000.

In view of the importance of the refractive index increment in the characterization of polymers, it was decided to repeat the work of Barrall *et al.* with rather more emphasis placed on the assessment of the random errors of measurement. It seemed to us that their result might be an artefact originating in their failure to quantify the precision with which their reported refractive index differences could be measured and their consequent inability to separate a random fluctuation from a systematic variation.

## EXPERIMENTAL

A Brice-Phoenix Differential Refractometer, Model BP-2000-V, was used to measure the refractive index difference between solution and solvent. In this instrument, the deviation of the refracted beam is measured as a lateral displacement of a slit image in the focal plane of a microscope objective which is fitted with a filar micrometer eyepiece for this purpose. To convert the observed lateral shifts to refractive index differences, a series of calibration experiments with solutions of known refractive index is carried out. In both the calibration experiments and the experiments with the polymer solutions, five separate determinations of each lateral shift were made at each of the two positions of the optical cell, as recommended by the manufacturers of the instrument.

All determinations were made at 25°C using the mercury green line,  $\lambda = 546$  nm, as the monochromatic source of light.

### *Calibration experiments*

*Materials.* Solutions of KCl in water were employed. The KCl (AR grade) was dried in a vacuum oven at 130°C for about 72 hours before use. De-ionized water was purified by simple fractional distillation from alkaline  $\text{KMnO}_4$ .

*Solutions.* Solutions were made by weight covering the KCl mass fraction range 0.0025 to 0.05; this range

of concentration was chosen so as to give lateral shifts similar in size to those observed with the polymer solutions under investigation. Initially, a series of six KCl solutions was used to give a master calibration curve; thereafter, spot checks on the constancy of calibration were made at regular intervals using solutions whose concentrations were chosen at random within the master calibration range.

*Experiments with the polymer solutions*

**Materials.** Solutions of polystyrene in toluene were employed. The polystyrene samples used were sharp molecular weight fractions prepared by butyl lithium initiation; they were supplied by Waters Associates and ranged in molecular weight from 575 to 773 000. They were used directly without further purification. Toluene (Analar) was purified by fractionation on a 15-plate Fenske helice column; it was then deoxygenated by bubbling dry N<sub>2</sub> through it.

**Solutions.** For each molecular weight, solutions of varying concentration were made by weight in the polymer mass fraction range 0.004 to 0.03. The order of measurement of the lateral shift for any one molecular weight fraction was random so as to avoid any correlation of undetected systematic instrumental error with concentration. Likewise the runs with the various polymer fractions were not ordered with either increasing or decreasing molecular weight so as to ensure that any systematic instrumental change over the time scale of the whole experiment appeared as a random element in the molecular weight variation sequence.

**RESULTS AND TREATMENT OF DATA**

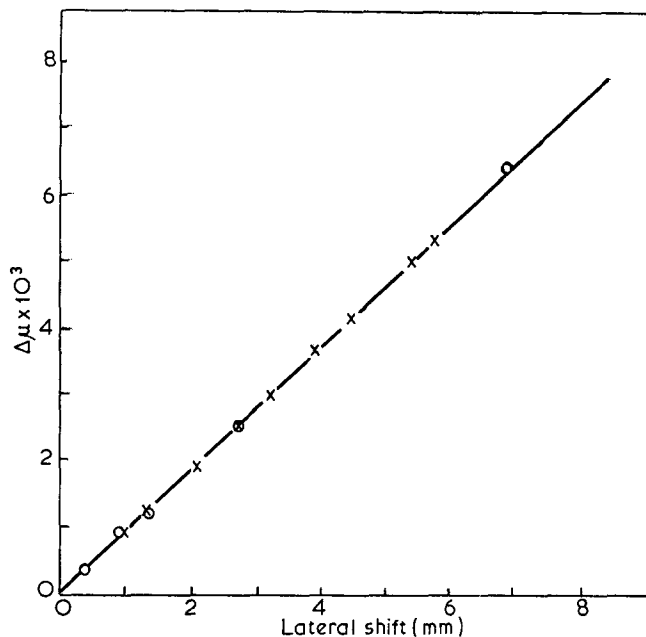
*Calibration of the instrument*

The purpose of the calibration experiment was to discover the relationship between the observed lateral shift and the refractive index difference between solution and solvent which produced that shift.

The refractive index differences for the aqueous KCl solutions employed were obtained by interpolation from the data of Kruis<sup>5</sup>. These data were linearized by plotting the listed refractive index differences against the mole fractions, *x*, of KCl used by Kruis. The slope of the best straight line through these points and the origin was computed by the method of least squares with equal weights allocated to all the experimental points. We write the result in the form

$$\Delta\mu_{\text{KCl}} = b_s x_{\text{KCl}}$$

where the subscript *s* signifies that the slope *b* was calculated from the *standard* literature data. We find  $b_s = 0.5400 \pm 0.0019$  (*DF* = 10) where the quoted error is the estimated standard deviation based on 10 degrees of freedom (*DF*). From this relation, the refractive index differences between water and the aqueous KCl solutions used in the calibration experiment were calculated; the variance estimates of the calculated refractive index differences were also computed so that the values of  $\Delta\mu$  could be weighted in subsequent calculations in accordance with the varying errors of interpolation. *Figure 1* shows that the calibration line of refractive index difference against lateral shift remained un-



*Figure 1* Refractive index difference between water and the aqueous KCl solutions employed in the calibration experiments plotted against lateral shift. The solid line represents the weighted least squares fit. O, Master calibration, x, monitor experiments

changed over the time scale of the experiment (about 8 weeks). This line is adequately represented by:

$$\Delta\mu = k_c l \tag{1}$$

*l* being the lateral shift and *k<sub>c</sub>* the instrumental constant obtained from the complete set of *calibration* data. *k<sub>c</sub>* was calculated as the slope of the regression line of  $\Delta\mu$  on *l* using the principle of least squares and weighting each value of  $\Delta\mu$  by the reciprocal of its variance estimate. In this way, some account is taken of the increasing uncertainty in the fitted value of  $\Delta\mu$  as the concentration of KCl goes to higher values. It is unnecessary to take into account the experimental errors in *l* since equation (1) is to be used purely for further interpolation using the lateral shift data obtained with the experiments on polystyrene. The point is that the lateral shifts measured with the polystyrene solutions were obtained under precisely the same conditions and in the same range as those obtained in the calibration experiments. Putting it another way, the value of *k<sub>c</sub>* obtained, viz.

$$k_c = (9.335 \pm 0.042) \times 10^{-4} \text{ mm}^{-1} \text{ (DF=13)}$$

is not necessarily the best estimate of the error-free value but is the best estimate for the purposes of prediction.

*Variation of refractive index difference with polymer concentration*

From the observed lateral shift and the calibration constant, *k<sub>c</sub>*, the difference in refractive index between the solution and the solvent was obtained at each of the concentrations of polymer employed; also obtained was an estimate of the variance of this quantity from the estimated variance of *k<sub>c</sub>*. In *Figure 2*, the resulting data are shown plotted against the mass fraction, *w*, of polymer in solution for a typical polystyrene of the set. It is clear that, in the range of polymer concentration employed, the refractive index difference may be written

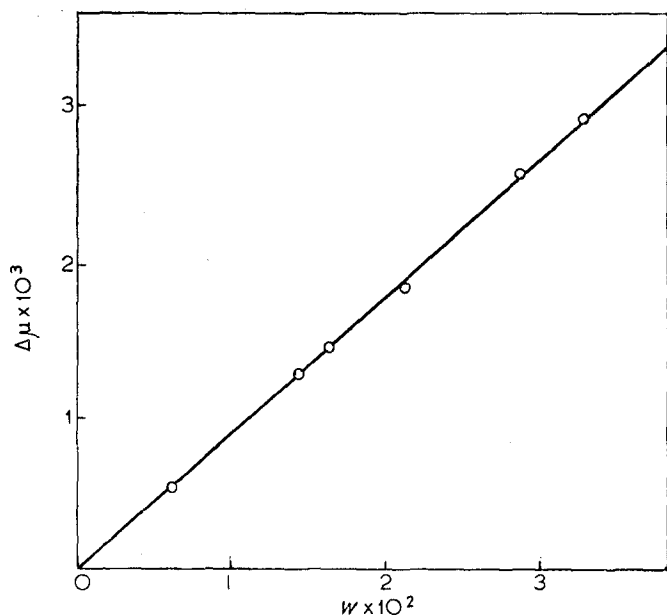


Figure 2 Refractive index difference between toluene and polymer solution plotted against mass fraction of polymer for a typical polymer of the set. The solid line represents the weighted least squares fit

Table 1 Values of  $\nu_m$  for the various polymers studied

Experiment No.	Polymer No.	Polymer molecular weight	$\nu_m \times 10^2$	$s(\nu_m) \times 10^2$	DF
7	1	773 000	9.165	0.038	5
4	2	404 000	9.192	0.013	5
1	3	193 000	9.239	0.027	4
8	4	96 200	9.258	0.027	4
2	5	49 000	8.965	0.059	5
3	6	9 700	9.001	0.030	5
5	7	4 600	8.675	0.045	5
6	8	1 950	8.487	0.053	5
9	9	575	6.766	0.023	5

as a linear function of the concentration,  $w$ , viz.

$$\Delta\mu = \nu_m w$$

where  $\nu_m$  is the refractive index increment corresponding to the polymer concentrations being expressed in terms of mass fraction of polymer. The best value of  $\nu_m$  was obtained for each polystyrene sample using the principle of least squares and weighting each value of  $\Delta\mu$  by the reciprocal of its estimated variance.

#### Variation of $\nu_m$ with molecular weight

Table 1 shows the values of  $\nu_m$  obtained for the different polystyrene samples. By inspection, it is clear that in the low molecular weight region these values show an unmistakable upward trend with increasing molecular weight. At the higher molecular weights, the values of  $\nu_m$  appear to go through a maximum value in the  $10^5$  molecular weight region. However, closer examination of the values and their estimated standard deviations,  $s(\nu_m)$ , shows that this conclusion may not be justified. For example, the  $\nu_m$  of the first four polymers lie within  $2s(\nu_m)$  of their common mean so that it is possible that this latter value represents the limit. In order to test the hypothesis that a limiting value of  $\nu_m$  is indeed reached, families of straight lines generating various sets of  $\nu_m$  were examined for homogeneity of

slope following a general procedure described by Guest<sup>6</sup>. In this procedure, the scatter of the individual set slopes about the weighted mean slope of the set is compared with the total scatter of the experimental points about the fitted lines. The question as to whether all the lines included in the set have or have not the same slope is then decided by assessing whether the test ratio of mean squares is or is not a likely value drawn from the appropriate population of the statistic,  $F$ . For our purpose, we repeated the test eight times with an increasing number of the polymer samples being included in the set; the first test included only the two highest molecular weights, the second test included the three highest molecular weights, and so on. Our data show that the test ratio exceeds the 5% critical value of  $F$  when the polymer sample of molecular weight 49 000 is included in the set. This means that the value of  $\nu_m$  obtained for this polymer is significantly different at the 5% level from the values of  $\nu_m$  obtained for the higher molecular weights. The change in the test ratio when polymer number 5 is included is sufficiently abrupt that other realistic choices of significance level do not alter this conclusion.

#### DISCUSSION

It is apparent from our results that, as the polymer molecular weight increases,  $\nu_m$  increases towards a limiting value characteristic of the infinite molecular weight polymer. This is illustrated in Figure 3. The point at which the systematic variation of  $\nu_m$  with molecular weight is rendered undetectable by the presence of random errors of measurement depends on the magnitude of these errors. In our work, these errors have been reduced to quite low levels as is shown by the values of the estimated standard deviations of  $\nu_m$  given in Table 1. Nevertheless, the estimated standard deviations are commensurate with some of the differences between successive values of  $\nu_m$ . It is this fact that makes it difficult to select a value of the polymer

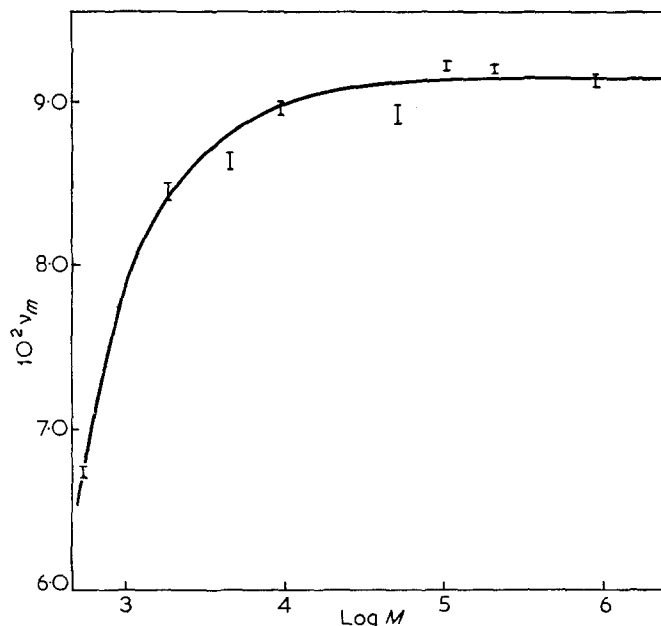


Figure 3 Refractive index increment  $\nu_m$  plotted against molecular weight. The error bars shown are of length  $2s(\nu_m)$ . The solid line shows the dependence of  $\nu_m$  on molecular weight calculated from the simple end-group theory

molecular weight above which  $\nu_m$  is effectively constant. Indeed without quantifying the random errors and using a statistical procedure which pools the data from several experiments (thus avoiding distortion of the random error component by one relatively poor experiment) it is not possible to make a statement about the effective constancy of  $\nu_m$ . However, with our technique of data analysis, we conclude that  $\nu_m$  effectively reaches its limiting value at a molecular weight somewhere between 50 000 and 100 000, the value being  $0.09210 \pm 0.00014$  ( $DF=18$ ).

We thus disagree with the conclusion of Barrall and co-workers who claim that the refractive index increment does not become sensibly constant until a molecular weight of 300 000 is reached. The origins of the disagreement are two-fold. First, Barrall *et al.* relied on a single determination of the refractive index difference between the solvent and a solution of known fixed concentration for each molecular weight studied; consequently, they did not have as many data as us with which to quantify their errors of measurement. Secondly, in the crucial region of molecular weight, namely 50 000 to 300 000, they only had available one polymer sample whose molecular weight was 97 200; had they decided that the refractive index increment found for this polymer was not significantly different from the values which they found for the higher molecular weight polymers, their conclusion would have been the same as ours.

Finally, we comment on the variation of refractive index increment ( $\nu_m$  or  $\nu_c$ ) with molecular weight. For this purpose, it is necessary to discuss the dependence of the refractive index,  $\mu$ , of a solution, on its composition. It is known<sup>7</sup> that the specific refraction,  $r$ , of a solution of density  $\rho$ , where

$$r = \frac{\mu^2 - 1}{\mu^2 + 2} \cdot \frac{1}{\rho}$$

is related to the specific refractions of its components,  $r_i$  (defined analogously) by:

$$r = \sum_i w_i r_i \quad (2)$$

where the  $w_i$  are the mass fractions of the various species. It may be shown that, if the Lorentz-Lorenz expressions for the specific refractions are replaced by the slightly less accurate but more tractable Gladstone and Dale versions, equation (2) reduces to:

$$\frac{1}{\rho} \Delta\mu = \sum_{i>1} \frac{w_i}{\rho_i} (\mu_i - \mu_1) \quad (3)$$

with the assumption of volume additivity. In this expression, the subscript 1 denotes the solvent and  $\Delta\mu$ , as before, represents the difference in refractive index between solution and solvent. Huglin<sup>8</sup> has given the binary solution equivalents of equations (2) and (3).

Within the limitations of the additivity principle embodied in equation (2), it is permissible to regard the specific refraction of a polymer solution as being the weighted sum of the specific refractions of the solvent, repeat units, and end groups. Hence, we may apply equation (3) to obtain an expression for  $\Delta\mu$  in terms of the refractive indices and densities of these species. In our case where the end groups are  $C_4H_9$  and H, it is unnecessary to include a term for the contribution of the hydrogen end groups since the weight fraction of

these species is always negligible. With his simplification, we obtain:

$$\frac{1}{\rho} \Delta\mu = \left[ \frac{\phi}{1+\phi} \left( \frac{\mu_r - \mu_1}{\rho_r} \right) + \frac{1}{1+\phi} \left( \frac{\mu_e - \mu_1}{\rho_e} \right) \right] w \quad (4)$$

Here,  $\mu_r$  and  $\mu_e$  are the refractive indices of the repeat units and butyl end groups, and  $\rho_r$  and  $\rho_e$  are their densities; the symbol  $w$ , as before, signifies the mass fraction of polymer and  $\phi$  is a molecular weight-dependent quantity, viz.  $nM_r/M_e$  where  $n$  is the number-average degree of polymerization and  $M_r$  and  $M_e$  are the molecular weights of the repeat unit and end group. Equation (4) shows that:

$$\nu_c = \frac{\phi}{1+\phi} \left( \frac{\mu_r - \mu_1}{\rho_r} \right) + \frac{1}{1+\phi} \left( \frac{\mu_e - \mu_1}{\rho_e} \right) \quad (5)$$

and

$$\nu_m = \nu_c \rho \quad (6)$$

Bodmann<sup>9</sup>, and Lorimer and Jones<sup>10</sup> have used similar arguments.

It follows from equation (6) that  $\nu_m$  varies with  $c$ ; however, at low concentrations of polymer the solution density is more or less that of the pure solvent. In our work, this approximation may be made without introducing any serious error and so  $\nu_m$  is independent of concentration as observed experimentally. This approximation enables us to convert our limiting value of  $\nu_m$  into a limiting value for  $\nu_c$ . We obtain a value of  $0.107 \text{ cm}^3/\text{g}$  in good agreement with the literature values<sup>11</sup>.

Finally, we see that the influence of molecular weight on  $\nu_m$  and  $\nu_c$  is entirely an end group effect. As the proportion of repeat units to end groups increases, so the refractive index increment approaches its limiting value. The parameter  $\phi$  in equations (4) and (5) quantifies the effect. At very high values of  $\phi$  corresponding to very high molecular weights, the limiting value of  $\nu_c$  is clearly  $(\mu_r - \mu_1)/\rho_r$ ; our data thus provide a numerical value for this quantity. Similarly our data on the lowest molecular weight polymer enable the other factor  $(\mu_e - \mu_1)/\rho_e$  to be computed. Hence it is possible on this simple theory to construct the whole curve showing the dependence of  $\nu_m$  on  $\bar{M}_n$ . This theoretical curve is shown in Figure 3 as a solid line. The good fit of the experimental points on the theoretical curve gives strong support to the end-group theory as discussed above and disposes of the speculations of Barrall and co-workers of the possibility of non-styrene moieties being incorporated into the polymers during synthesis.

## REFERENCES

- Barrall, II, E. M., Cantow, M. J. R. and Johnson, J. F. *J. Appl. Polym. Sci.* 1968, **12**, 1373
- Reed, P. J. and Urwin, J. R. *Aust. J. Chem.* 1970, **23**, 1743
- Ziegler, I., Freund, L., Benoit, H. and Kern, W. *Makromol. Chem.* 1960, **37**, 217
- Rempp, P. *J. Chim. Phys.* 1957, **54**, 421
- Kruis, A. *Z. Phys. Chem. (B)* 1936, **34**, 13
- Guest, P. J. 'Numerical Methods of Curve Fitting', Cambridge Univ. Press, Cambridge, 1961
- Glasstone, S. 'Textbook of Physical Chemistry', Macmillan, London, 1948
- Huglin, M. B. *J. Appl. Polym. Sci.* 1965, **9**, 4003
- Bodmann, O. *Makromol. Chem.* 1969, **122**, 210
- Lorimer, J. W. and Jones, D. E. G. *Polymer* 1972, **13**, 52
- Huglin, M. B. *J. Appl. Polym. Sci.* 1965, **9**, 3963

# Anionic polymerization of methyl acrylate

W. K. Busfield and J. M. Methven

Chemistry Department, University of Dundee, Dundee DD1 4HN, UK  
(Received 17 November 1972; revised 18 December 1972)

The homogeneous polymerization of methyl acrylate in tetrahydrofuran using a variety of sodium aryl catalysts has been investigated at  $-75^{\circ}\text{C}$  and  $-30^{\circ}\text{C}$ . The mode of action of each catalyst is discussed and its efficiency in producing high polymer has been calculated from the yields and polymer characteristics. Sodium trityl is the most effective catalyst at both temperatures. Dilatometry has shown that with sodium naphthalene at  $-70^{\circ}\text{C}$ , rapid initial polymerization to about 10% conversion in 4 min is followed by a very low rate period which proceeds at low temperature for at least 24 h when conversions up to 50% have been observed. Throughout this period a species is present which absorbs at 320 nm and which is immediately lost on addition of a proton donor. There is evidence suggesting that this dormant form of the poly(methyl acrylate) anion is an oxyanion. It is postulated that carbanions are formed initially and are responsible for the rapid polymerization rate. They also isomerize in an equilibrium reaction to form the unreactive oxyanions. The rate of further propagation is thus controlled by the value of the equilibrium constant which in this system is strongly in favour of the oxyanions. On the basis of this mechanism some rate constants have been calculated.

## INTRODUCTION

Although in the field of anionic polymerization of acrylates and methacrylates, methyl methacrylate has been studied more than any other monomer, certain important aspects of the polymerization are still not fully understood. Details of the methyl methacrylate system are fully described in previous reviews and papers<sup>1-4</sup>. In 1960 Goode *et al.*<sup>5</sup> reported that in certain respects methyl methacrylate, methyl acrylate (MA), isopropyl acrylate and ethyl acrylate behaved similarly in anionic polymerizations, and ever since many authors have tended to assume that the anionic polymerization of all acrylates and methacrylates can be described by a single mechanism. Although there is insufficient evidence to prove or disprove this philosophy, there is one factor arising from the results of Goode *et al.* and those of later workers which indicates a significant difference between the mechanisms of the polymerization of methyl methacrylate and MA. Methyl methacrylate is invariably polymerized by anionic catalysts to high conversion in short reaction times at temperatures from  $-78^{\circ}\text{C}$  to above room temperature. Many of these systems have been shown to be capable of initiating the polymerization of further increments of certain monomers, and hence to be truly live. On the other hand, in all reports of the anionic polymerization of methyl acrylate, only low yields (<10%) of polymer have been obtained above about  $-30^{\circ}\text{C}$ , and only intermediate yields (usually <30% except for one isolated report<sup>6</sup> of MA polymerizing to 63% conversion at  $-78^{\circ}\text{C}$  in 24 h) at temperatures below  $-30^{\circ}\text{C}$  even after many hours reaction time<sup>5,6</sup>. However, there has been no serious mechanistic investigation of the polymerization of MA since that by Goode *et al.*

Since that time most work has been directed towards an investigation of the stereochemistry of the propagation step by means of polymer stereoregularity studies<sup>6,7</sup>. Although this is an important aspect of a mechanistic investigation, it can by no means provide a complete answer to the problems on its own.

Two other acrylates which have attracted more attention than MA are isopropyl acrylate, because it produces crystalline polymers, and allyl acrylate, because of its potential bifunctional characteristics. Both behave more like methyl methacrylate than MA in that they polymerize to complete conversion (isopropyl)<sup>5</sup> or to high conversion (allyl)<sup>8,9</sup>. Ethyl and other saturated straight chain acrylates have not been studied in any detail, but apparently behave like MA in anionic polymerizations in that only low yields of polymer are produced.

Thus a mechanistic investigation of the anionic polymerization of MA may produce more detailed information on the differences from the corresponding methyl methacrylate systems, and may help to elucidate some of the unsolved problems of both. In this paper we describe the results of some preliminary but extensive experiments on the polymerization of MA in tetrahydrofuran using a range of anionic initiators. A more detailed investigation of selected aspects of this work will be undertaken and reported in the near future.

## EXPERIMENTAL

Conventional high vacuum technique was used throughout this work. Break tip seals and/or fragile bulbs were used in all reaction systems, thus eliminating the need for greased joints or taps.

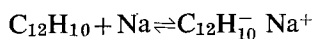
*Materials*

*Tetrahydrofuran (THF).* After prior rough drying THF was degassed, distilled on to a fresh sodium mirror and stored in a blackened vessel in the presence of sodium benzophenone.

*Methyl acrylate (MA).* After certain purification procedures MA, which was at least 99.9% pure by gas-liquid chromatography (g.l.c.) analysis, was found to 'popcorn' during storage *in vacuo*<sup>10</sup>. Thus, in addition to the g.l.c. standard of purity, we have used the criterion of non-'popcorn' formation after storage *in vacuo* at room temperature, as our standard of satisfaction. MA purified to this standard gave reproducible results in the anionic polymerization experiments. The purification method adopted was as follows. MA (Koch Light) including inhibitor, was degassed and distilled on to powdered CaH<sub>2</sub>, where it was stirred continuously for three days at room temperature. It was then vacuum distilled a further three times, each time discarding a generous first and last portion. Finally, known volumes were distilled into break-seal ampoules which were sealed off and stored at -20°C. It is worth noting that the often recommended procedure for removing inhibitor from MA<sup>11</sup> of washing with dilute NaOH solution causes some hydrolysis of MA.

*Catalyst solutions (sodium naphthalene, fluorene, benzophenone, biphenyl and trityl).* In each case the starting material after purification (fluorene, benzophenone and biphenyl were recrystallized from ethanol; cryoscopy grade naphthalene (BDH) was used as received; triphenyl methyl chloride was vacuum sublimed) was transferred to the appropriate volume of THF over a sodium mirror in a vacuum system. After stirring the mixture for at least 3 h (48 h for sodium trityl), the catalyst solution was filtered into an attached vessel from where it was dispensed into previously calibrated break-seal ampoules or fragile bulbs. These were sealed off with their contents at ambient temperature, and stored at -20°C until required for use, in most cases within one month of preparation.

In the case of biphenyl, allowance was not made for the fact that it does not react completely with excess sodium at room temperature. The true concentration of sodium biphenyl in the prepared solution was calculated from the observed absorption at 400 nm and the published extinction coefficient<sup>12</sup>. This gave 0.41 for the equilibrium constant for the reaction:



at ambient temperature in agreement with the published value of 0.36 at 20°C<sup>11</sup>.

Also there is some uncertainty about the degree of conversion of (C<sub>6</sub>H<sub>5</sub>)<sub>3</sub>CCl into sodium trityl using this method. For the purposes of calculations on the polymerization system, we have assumed it to be 100%.

*Sodium anthracene.* After twice recrystallizing from petroleum ether (b.p. 60-80°C), anthracene was converted to disodium anthracene in the manner described for sodium naphthalene. After filtration and before dispensing the catalyst solution, a second sample of an equal quantity of anthracene was added from an evacuated break-seal in order to convert the disodium salt to the monosodium salt. After dissolution the

catalyst solution was dispensed into ampoules and stored as described for sodium naphthalene.

*Sodium 1,1-diphenyl ethylene.* 1,1-Diphenyl ethylene (Koch Light) was fractionated under reduced pressure, and stored in a nitrogen glove box from where it was dispensed by syringe from a serum capped bottle into break-seal ampoules. Its u.v. spectrum was identical with that recorded in the literature<sup>13</sup>. The catalyst solution was prepared by adding 1,1-diphenyl ethylene in 1% excess to the main polymerization reactor immediately after adding an ampoule of sodium naphthalene solution to the main polymerization solvent. The reactants were stirred for 3 h prior to the commencement of the polymerization.

*Terminators.* Glacial acetic acid or methanol were, without further purification, degassed and distilled into break-seal ampoules.

*Purity of the catalyst solutions.* In keeping with common practice, catalyst ampoules were sealed off with the contents at ambient temperature. This practice inevitably causes pyrolysis of solvent vapour to CO<sub>2</sub> and H<sub>2</sub>O and consequently some loss of catalyst. At the concentrations used this was thought to result in less than 2% decomposition<sup>14</sup>. The u.v. spectra of the catalyst solutions exhibited the same characteristic features as those previously described<sup>15</sup>. That for sodium trityl has not previously been recorded.

*Polymerization*

*Polymer yield and polymer characteristics.* The reaction flask (250 ml) together with pendant monomer, catalyst and terminator ampoules was attached to the vacuum line where it was pumped and flamed to a pressure of 10<sup>-5</sup> mmHg. THF was distilled in and the whole was sealed off. After adding catalyst solution the mixture was stirred and cooled to the appropriate reaction temperature by immersion in an acetone/solid CO<sub>2</sub> slurry. The polymerization was then started by adding MA rapidly from its ampoule. For most experiments termination was effected by adding acetic acid after 2 h reaction time, but some were allowed to react for 24 h. The colourless terminated solutions were warmed to room temperature before the reactor was opened. A small quantity of the terminated reaction mixture was retained for g.l.c. analysis on a Pye 104 chromatograph using Porapak and silicone oil columns.

The remainder of the contents were added dropwise to a well-stirred 3-fold excess of methanol at -60°C. When the precipitated polymer had coagulated into a large mass, as the mixture warmed to -30°C it was filtered through a previously cooled sintered disc. The polymer was dried to constant weight in a vacuum oven at room temperature. In every case the mother liquor was slightly colloidal and filtration through the finest sinter did not produce a clear filtrate. The amount of involatile material remaining in the filtrate was measured by pumping off the solvent and other volatiles and weighing the residue. This is labelled 'precipitant soluble polymer' although it contains catalyst residue, colloidal polymer and products of side reactions.

The precipitated polymers were characterized by number-average molecular weight (Hitachi Perkin-Elmer

model 115), gel permeation chromatography (g.p.c.) (Waters model 200) and infra-red spectroscopy (Perkin-Elmer model 521). Polymer films for infra-red analysis were cast on NaCl plates from chloroform solutions, and dried in a vacuum oven at 80°C. Some tests were omitted due to insufficient polymer.

*U.v. spectral analysis of polymerizing solutions.* The apparatus (Figure 1a) was evacuated and was filled with the appropriate volume of THF by distillation before it was sealed off from the vacuum line. After adding the catalyst solution from C to the THF at room temperature, the whole solution was transferred to the quartz u.v. cell, Q. Vessel V was rinsed by solvent distillation, and then was sealed off at X. The u.v. cell was placed in a specially made cell holder which also acted as a thermostat jacket through which alcohol could be circulated from a Townson-Mercer -70 thermostat bath. The spectrum of the catalyst solution was recorded first at room temperature and then at -60°C. Magnetic manipulation of the spacer, S, a rectangular quartz block with four polished surfaces, enabled path lengths of either 1, 0.1 or 0.01 mm whichever was appropriate to be used. MA was next added from M and was stirred into the catalyst solution by agitation with the spacer. The spectrum of the polymerizing solution was recorded at -60°C usually within 4 to 6 min of monomer addition. In some experiments the reaction mixture was allowed to warm to room temperature, and a spectrum again recorded before termination. In all experiments the spectrum of the reaction mixture after termination with acetic acid was recorded. Finally the reactor was cut open and the polymer recovered in the manner described above. Spectra were recorded on a Unicam SP800 spectrophotometer.

*Reaction rates by dilatometry (sodium naphthalene reactions only).* Because of the rapid initial rates occurring in these reactions, the fragile bulb method of introducing catalyst to the monomer solution was employed. The

dilatometer (Figure 1b) was evacuated and was filled with solvent and MA by distillation, whilst attached to the vacuum line. After sealing off and allowing to come to thermal equilibrium in a thermostat bath at -70°C, the reaction was started by activating the electromagnet, E, thus crushing the catalyst bulb, F. It was followed with time using a cathetometer before termination was effected at the appropriate time by addition of acetic acid. The polymer was isolated and weighed as described previously. The dilatometer calibration factor was calculated from the degree of conversion at termination and the weight of polymer. In one experiment two fragile bulbs of catalyst solution were used (as illustrated in Figure 1b) so that the effect of adding a second sample of catalyst at an intermediate stage in the polymerization could be investigated.

## RESULTS

The results of the polymerization of MA using a range of homogeneous anionic catalysts in THF at -75°C and at -30°C are presented in Tables 1 and 2 respectively. The reaction time before termination was 2 h for all the experiments described in the main Tables. Polymer yields from two reactions allowed to run for 24 h at -75°C before termination are given in the footnote to Table 1. In all experiments the colour of the polymerizing solution was instantaneously discharged after mixing with terminating agent. The products detected by g.l.c. analysis of the terminated reaction mixtures included THF and MA as the major components and methanol as a minor component in all reactions at -75°C. In addition anthracene, naphthalene and biphenyl were detected in the sodium anthracene, sodium naphthalene and sodium biphenyl systems respectively. The products of reactions at -30°C and the 1,1-diphenyl ethylene system at -75°C were not tested.

Differential u.v. spectra of the polymerizing solutions were calculated by subtracting the absorbance spectrum of the terminated reaction mixture, taken at room temperature, from that of the polymerizing solution, taken at -60°C after about 4 min reaction time. They all showed a single absorption band having a maximum with the wavelength and absorbance (path length 1.0 cm) shown in Table 1. In specific tests on the sodium naphthalene system the absorbance of the 320 nm peak was found to be unchanged after 2 h standing at -60°C. After warming to room temperature, a procedure which took about 15 min, the absorbance dropped by about 20%.

Polymer g.p.c.'s are illustrated in Figure 2. While no specific data are available to convert the elution volumes directly to molecular size for poly(methyl acrylate), the elution profile itself can be taken as a qualitative measure of the molecular weight distributions.

The infra-red spectra of the polymers produced with all the catalysts were very similar. Of particular interest is the fact that they all have small absorption bands in the 3500 cm<sup>-1</sup> region, even after pumping for 24 h at 80°C in a vacuum oven. Such absorptions are almost absent from the spectrum of free radically prepared poly(methyl acrylate) and hence are presumably due to the presence of OH end groups. There are small differences in the spectra of some polymers in the

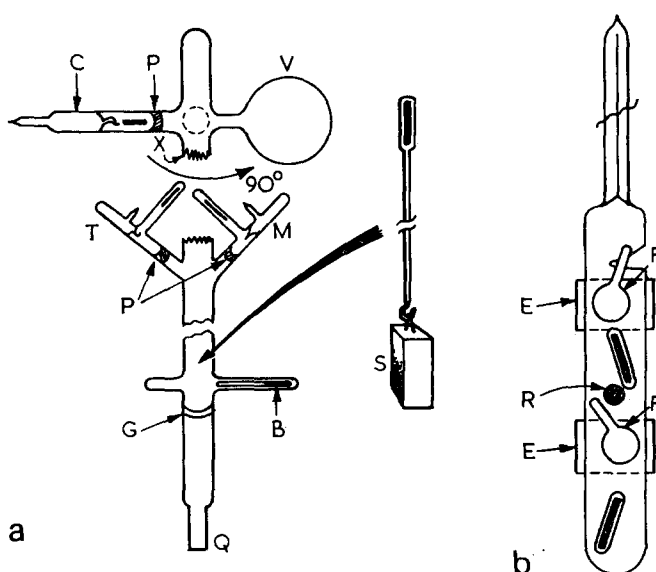


Figure 1 Polymerization reactors for (a) u.v. spectral analysis of catalysts and polymerizing solutions and (b) dilatometry. P, coarse sinter discs; T, terminator solution; B, spacer stop; G, graded seal; R, crushing rod; other symbols, see text

Table 1 Solution polymerization of MA at  $-75^{\circ}\text{C}$  in THF, reaction time 2 h

Catalyst (sodium salt)	Concentration		Conversion to polymer (%)	Precipitant <sup>c</sup> soluble polymer (%)	Solution colour	Polymer $DP_n$	$\lambda_{\text{max}}^g$ (nm)	Absorbance <sup>g</sup>
	Catalyst ( $\text{M} \times 10^3$ )	Monomer (M)						
Anthracene	9.4	1.58	26.5	3.1	yellow	89	320	1.17
Naphthalene	8.9	1.47	25.4	3.2	yellow	85	320	1.62
Trityl	8.3 <sup>a</sup>	1.89	24.4 <sup>e</sup>	3.0	yellow	62	320	0.77
1,1-Diphenyl ethylene	8.7	1.68	19.2 <sup>f</sup>	d	blue	d	d	d
Biphenyl	2.6 <sup>b</sup>	1.64	8.2	3.3	pale yellow	102	320	0.18
Fluorene	8.7	1.73	2.0	2.5	pale yellow	88	320	0.45
Benzophenone	9.8	1.67	1.6	3.9	blue	d	395	0.68

a May be high value (see experimental)

b Reason for low value, see experimental

c Expressed as mol% with respect to initial monomer

d Not measured

e Yield after 24 h with similar reaction conditions: 50%

f Yield after 24 h with similar reaction conditions: 35%

g Taken from differential u.v. spectra at  $-60^{\circ}\text{C}$  of polymerizing solutions with similar monomer and catalyst concentrations  
Path length 1.0 cm

Table 2 Solution polymerization of MA at  $-30^{\circ}\text{C}$  in THF, reaction time 2 h

Catalyst (sodium salt)	Concentration		Conversion to polymer (%)	Precipitant <sup>c</sup> soluble polymer (%)	Solution colour	Polymer $DP_n$
	Catalyst ( $\text{M} \times 10^3$ )	Monomer (M)				
Trityl	8.3 <sup>a</sup>	1.89	22.4	4.8	yellow	160
Anthracene	8.8	1.83	6.1	4.6	pale yellow	203
Fluorene	9.1	1.75	4.5	3.9	pale yellow	171
Naphthalene	8.7	1.76	2.5	4.9	pale yellow	216
Biphenyl	1.6 <sup>b</sup>	1.66	1.4	5.3	pale yellow	d
Benzophenone	8.5	1.77	0.4	5.5	green- yellow	d

a, b, c, d See footnotes to Table 1

$1500\text{cm}^{-1}$  region where aromatic C-H bending vibrations occur. In particular the polymers produced by sodium fluorene and sodium trityl catalysis had these absorptions.

The polymerization catalysed by sodium naphthalene was taken as a representative system for a study of the polymerization rate. A typical rate profile is shown in Figure 3. In one experiment a second ampoule of catalyst was added during the period of low rate following the first addition. The conversion time profile for the second period was almost identical with the first (see inset Figure 3).

## DISCUSSION

### Colour changes and yields

In respect of the colour changes occurring on adding MA to the catalyst solution and the u.v. spectra of the reactant solution, two systems were exceptional. With sodium benzophenone the characteristic blue colour of the catalyst anion was unchanged upon addition of MA and correspondingly little polymer was formed. Under similar reaction conditions we found that the benzophenone anion produced absolutely no polymer from methyl methacrylate in agreement with the findings

of Tsuruta *et al.*<sup>16</sup>. The benzophenone anion is apparently too weak to react significantly with either MA or methyl methacrylate. With sodium 1,1-diphenyl ethylene the characteristic red colour of the catalyst was immediately transformed to the characteristic blue colour of the sodium benzophenone anion upon addition of MA. In this case, however, a reasonable polymer yield was obtained in 2 h (relative to the other systems) and thus the benzophenone originates either as an impurity in the 1,1-diphenyl ethylene (it is known to be difficult to remove<sup>17</sup>) or from a side reaction of the anions with MA (benzophenone has been identified as a side product in the polymerization of acrylates with Grignard reagents<sup>5</sup>). In the following discussion the sodium benzophenone system has been omitted and it has been assumed that the presence of benzophenone has negligible effect (apart from colour and slightly on yield) on the sodium 1,1-diphenyl ethylene polymerization.

The visually observed colour changes in the reactions with the other catalysts show that: (i) catalyst anion reacts almost instantaneously with MA and at least some of the product species are yellow; (ii) the yellow colour is due to an anionic or pseudo-anionic species which reacts almost instantaneously with a proton donor such as acetic acid or methanol; (iii) the yellow



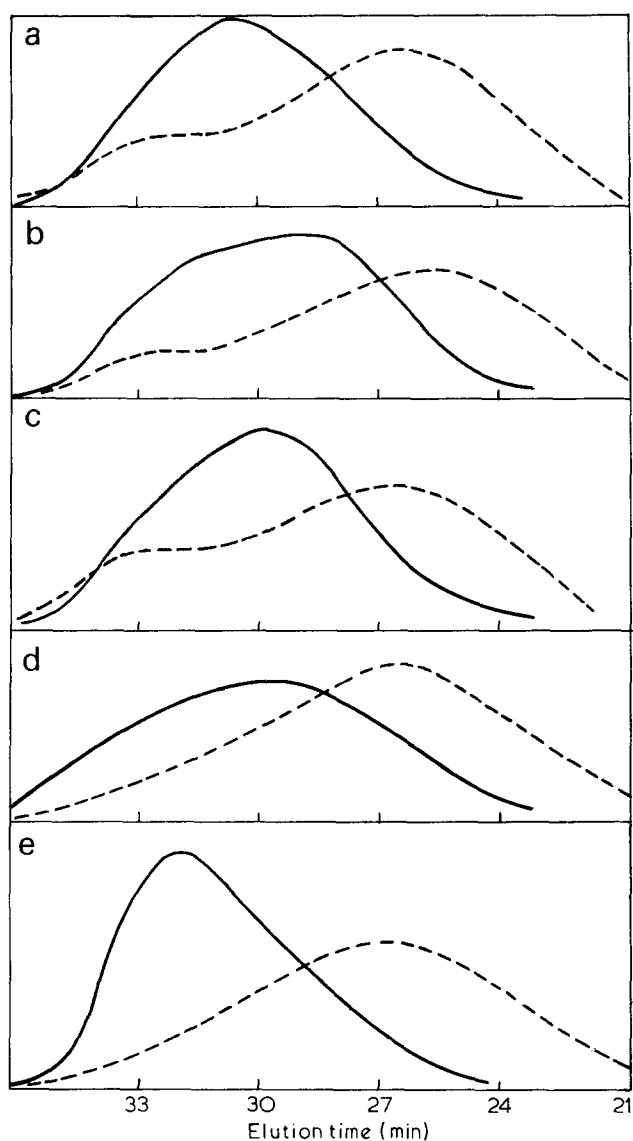


Figure 2 Gel permeation chromatograms of poly(methyl acrylate) made at  $-70^{\circ}\text{C}$  (—) and at  $-30^{\circ}\text{C}$  (---). (a) Sodium anthracene; (b) sodium biphenyl; (c) sodium naphthalene; (d) sodium trityl; (e) sodium fluorene. G.p.c. details: flow rate, 5 ml/min; solvent, THF; polymer concentrations, 0.3%

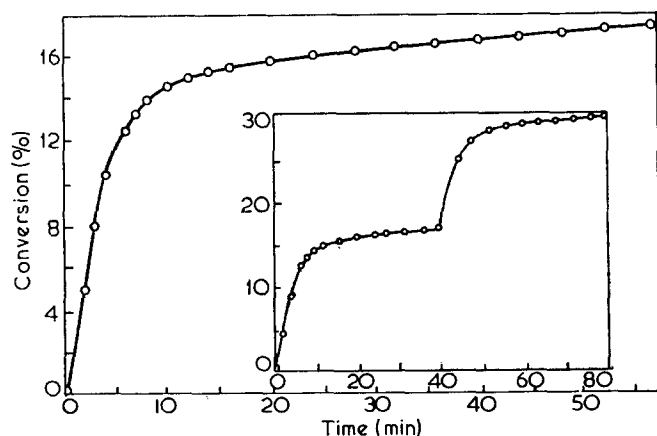


Figure 3 Rate of polymerization of MA catalysed by sodium naphthalene. Concentrations: MA, 1.50M, catalyst,  $8.6 \times 10^{-3}\text{M}$ . Inset: Effect of adding a second ampoule of catalyst at 40 min. Total catalyst concentration after second addition,  $17.2 \times 10^{-3}\text{M}$

species is stable indefinitely at  $-75^{\circ}\text{C}$  (our longest experiment was for 24h) and at temperatures up to ambient although slight fading was observed to occur over 2h at room temperature. This contrasts with the behaviour of allyl acrylate<sup>8</sup>; in the polymerization with BuLi the colour of the polymerizing solution was visibly observed to fade even at  $-70^{\circ}\text{C}$ . The u.v. spectra in the MA systems confirmed the visual observations and showed that the yellow colour originates from a single chromophore which absorbs at 320nm. Although the monomer concentrations were similar in each system there seems to be no relation between the size of the absorption peak and the polymer yield at  $-70^{\circ}\text{C}$  as would be expected if the absorption was related in some way to the propagating species. Thus the system is undoubtedly more complex than the u.v. spectrum indicates. There is a contrast with the observations on systems containing poly(methyl methacrylate) anions by Allen *et al.*<sup>4</sup>. They observed three peaks at about 290, 330 and about 440nm at low temperature, two of which (290 and 440nm) disappeared on warming the solutions. One might speculate that their 330nm peak and the 320nm peak observed in the MA system are due to corresponding anionic species and that one or both of the species absorbing at 290 and 440nm is the truly active species in the methyl methacrylate system. The corresponding species in the MA system have absorptions which are either hidden or are too weak to be observed under our conditions. The only information we can reasonably extract from the u.v. spectra is that the 320nm absorption is due to a dormant or partly dormant form of a poly(methyl acrylate) anion.

After a very fast reaction of catalyst anion with MA to form poly(methyl acrylate) anions and with similar reaction conditions one might expect similar polymer yields after the same reaction time even with different catalysts. In the series of experiments at  $-75^{\circ}\text{C}$  the sodium anthracene, sodium naphthalene and sodium trityl systems fit well into this category and hence can possibly be classed as clean systems. Sodium biphenyl cannot be categorized on this evidence since its concentration was very much lower (see above). Sodium 1,1-diphenyl ethylene either takes part in some side reactions or contains some impurity as already discussed, thus explaining the lower yield. The sodium fluorene system is obviously very different. Although there is a small concentration of poly(methyl acrylate) anions as evidenced by the u.v. spectrum and the colour, the polymer yield is very low. Sodium fluorenyl is known<sup>18</sup> to exist mainly as solvent separated ion pairs at  $-75^{\circ}\text{C}$ . Possibly these species are more reactive towards the carbonyl function of MA, thus causing many more side reactions to occur and consequently loss of the main polymer propagation species.

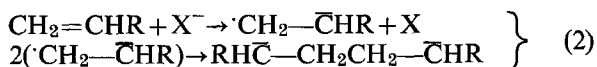
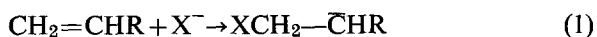
In the series of experiments at  $-30^{\circ}\text{C}$ , apart from the sodium trityl system, the yields were low despite the fact that the colour of the solution indicated the presence of poly(methyl acrylate) anions. Only with sodium fluorene was the yield greater at  $-30^{\circ}\text{C}$  than at  $-75^{\circ}\text{C}$ . This is consistent with the explanation of low yield at  $-75^{\circ}\text{C}$ , since it is known that as the temperature is increased, the concentration of contact ion pairs significantly increases in the sodium fluorene-THF system<sup>18</sup>. Thus at  $-30^{\circ}\text{C}$  either most of the catalyst is lost in side reactions or propagation is very much slower for some other reason.

In two experiments terminated after 24 h at  $-75^{\circ}\text{C}$  the polymer yield had increased to 50% with sodium trityl and 35% with sodium 1,1-diphenyl ethylene. Although these yields are significantly greater than yields after 2 h the rate of reaction is obviously much lower in the later stages. This is made clear by the results of the dilatometric experiments with the sodium naphthalene system at  $-70^{\circ}\text{C}$  which show conclusively that the high initial rate of about  $7.3 \times 10^{-4} \text{M sec}^{-1}$  steadily reduced to a rate of about  $1.0 \times 10^{-5} \text{M sec}^{-1}$  after about 25 min, and thereafter stayed reasonably constant at least for the 2 h period of our dilatometric experiments. Moreover, the fact that addition of a second ampoule of catalyst solution produced a second fast reaction period which again reduced to a low steady rate in an exactly analogous manner to the initial behaviour, shows that it is not loss of MA but loss of active species which is responsible for the deceleration. This conclusion is in agreement with the large amounts of MA observed by g.l.c. in the solutions remaining after termination.

The yellow colour of the polymerizing solutions did not vary visually from immediately after adding MA until termination in any experiment either at  $-75^{\circ}\text{C}$  or  $-30^{\circ}\text{C}$ . Also the u.v. spectrum of the polymerizing solutions at  $-70^{\circ}\text{C}$  did not vary between about 4 min after addition of MA until termination. Thus the species containing the chromophore which absorbs at 320 nm is not that which partakes in the fast propagation reaction. Unfortunately it was not experimentally convenient to obtain a u.v. spectrum during the fast reaction period, that is between zero and 4 min reaction time.

#### Initiation mechanisms and catalyst efficiency

Initiation in anionic systems is normally by either reaction (1) or by reaction (2). Recent work has shown that in some systems initiation can be by both reactions occurring simultaneously<sup>19, 20</sup>.



Some observations which may be used to distinguish between the two are: (a) the fate of the catalyst residue; (b) the shape of the resultant polymer molecular weight distribution (reaction 2 produces a bimodal distribution in the presence of some termination); (c) the relation between the resultant polymer  $DP_n$  and the initial monomer to catalyst ratio. The variable yields obtained with the MA systems make method (c) of doubtful validity.

Naphthalene, biphenyl and anthracene were identified, by g.l.c. analysis, in the solutions left after the polymerizations catalysed by sodium naphthalene, sodium biphenyl and sodium anthracene at  $-75^{\circ}\text{C}$  respectively. Thus, these three catalysts initiate, at least partly, by mechanism (2). The g.p.c.'s of polymers produced at  $-75^{\circ}\text{C}$  were not easy to categorize into single or bimodal distributions. Those of polymers produced at  $-30^{\circ}\text{C}$ , however, were distinctly bimodal for the same three catalysts whilst broad single peaks were obtained for polymers produced by sodium trityl and sodium fluorene catalysis. There is therefore agreement between the two methods. Neither data were available for the sodium

1,1-diphenyl ethylene system, but this is known to form dianions after reaction with sodium naphthalene.

The sodium anthracene system is the only surprising case since with methyl methacrylate there is evidence that initiation is predominantly<sup>19, 20</sup> by reaction (1).

$DP_n$  values (Tables 1 and 2) at each temperature are of similar magnitude showing that once the poly(methyl acrylate) anion is formed it grows at a rate dependent more on the temperature than on the initiating species. On this basis the polymers initiated by reaction (2) should grow to twice the  $DP_n$  of those initiated by reaction (1). Polymers formed by sodium trityl catalysis, which can only initiate by reaction (1), do have lower  $DP_n$  values than those formed by the electron transfer catalysts, but not by a factor of 2. Ignoring many possible complicating factors and using the sodium trityl system as a base, the fraction of each catalyst which initiates by reaction (1),  $x$ , can be evaluated by comparison of  $DP_n$  values. This of course only takes account of catalyst effective in producing high polymer. Values of  $x$  and  $(1-x)$ , the fraction of effective catalyst initiating by reaction (2), are given in Table 3. Only sodium fluorene acting at  $-75^{\circ}\text{C}$  gives an unexpected result. On the evidence presented earlier, it initiates mainly by reaction (1).

Taking the ideal mechanism as one in which each catalyst molecule leads, after propagation, to either one polymer molecule for initiation by reaction (1) or half a polymer molecule by reaction (2), then the catalyst efficiency in producing high polymer,  $f$ , is given by:

$$f = [\text{M}] \cdot Y \cdot 2 / DP_n \cdot [\text{C}] \cdot (1+x)$$

where  $[\text{M}]$  and  $[\text{C}]$  are the monomer and catalyst concentrations, and  $Y$  is the yield of high polymer. Although values of  $x$  are of doubtful validity, their precision is not critical in the evaluation of  $f$  (see Table 3). With all catalysts at  $-30^{\circ}\text{C}$  except sodium trityl and with sodium fluorene at  $-75^{\circ}\text{C}$  there is considerable loss of catalyst in side reactions, and only a small fraction is effective in producing high polymer. Since once formed the poly(methyl acrylate) anions are stable both at  $-75^{\circ}\text{C}$  and  $-30^{\circ}\text{C}$ , the catalyst loss must be due to non-polymer producing side reactions involving the catalyst ion. There are many possible products which could result from anionic attack at the carbonyl function of acrylates.

Table 3 Efficiency and mode of action of catalysts in producing high polymer

Catalyst (sodium salt)	Temperature ( $^{\circ}\text{C}$ )	$x$	$(1-x)$	Catalyst efficiency, $f$
anthracene	-75	0.55	0.45	0.64
	-30	0.72	0.28	0.07
biphenyl	-75	0.34	0.66	0.75
	-30	—	—	0.10 <sup>a</sup>
naphthalene	-75	0.62	0.38	0.61
	-30	0.65	0.35	0.03
fluorene	-75	0.57	0.43	0.06
	-30	0.93	0.07	0.05
trityl	-75	1.0	0	0.90 <sup>b</sup>
	-30	1.0	0	0.32 <sup>b</sup>

$x$  = fraction of effective catalyst which initiates by reaction (1)

$(1-x)$  = fraction of effective catalyst which initiates by reaction (2)

$f$  = fraction of catalyst effective in producing high polymer

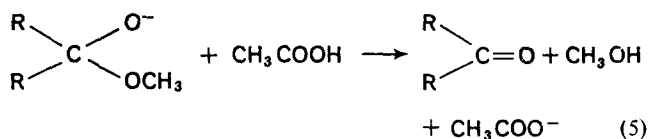
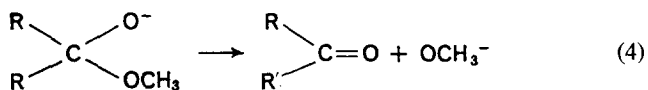
<sup>a</sup> Calculated using a guessed value for the polymer  $DP_n$  (209) and the  $x$  value found for the reaction at  $-75^{\circ}\text{C}$  (0.34)

<sup>b</sup> May be low values since true catalyst concentration not known (see experimental)

Lists of typical low molecular weight products are given by Goode *et al.*<sup>5</sup> and by Kawabata and Tsuruta<sup>21</sup> from the results of analysing the low molecular weight fraction obtained in similar systems. No attempt was made to analyse the precipitant soluble fraction obtained in this work. The amounts were reasonably consistent with the fraction of catalyst lost in side reactions.

Assuming that catalyst loss is all due to attack at the carbonyl group and that attack at the carbon carbon double bond leads to high polymer, then the ratio of the rate of attack at C=C to that at C=O in MA in THF by catalyst anion is in the order: (a) at  $-30^{\circ}\text{C}$ : trityl > biphenyl > anthracene > fluorene > naphthalene; (b) at  $-75^{\circ}\text{C}$ : trityl > biphenyl > anthracene  $\approx$  naphthalene > fluorene.

Side reactions involving loss of catalyst might be expected to lead to the formation of  $\text{CH}_3\text{O}^-$  which would end up as methanol after termination.  $\text{CH}_3\text{O}^-$  is known to be ineffective in initiating the polymerization of methyl methacrylate<sup>22</sup> and presumably therefore it is ineffective for MA. Small amounts of methanol were found by g.l.c. analysis of the acetic acid terminated reaction solutions after all experiments. Absolute amounts were not measured but in general about three times as much was produced from experiments at  $-30^{\circ}\text{C}$  as from experiments at  $-75^{\circ}\text{C}$  in general agreement with the relative magnitude of the catalyst efficiencies. Unfortunately the production of methanol gives little information about the mechanism because it could be produced during initiation by, for example, reaction (3), during propagation (reaction 4) or during termination by added proton donor (reaction 5).

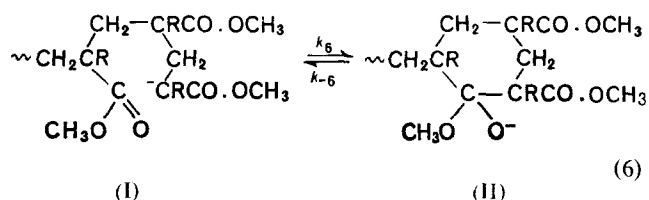


Kawabata and Tsuruta<sup>21</sup> estimated from the results of experiments at  $-70^{\circ}\text{C}$  in THF using 10% BuLi as catalyst and acetone as the reference substrate, that initiation by reaction (1) is over 5 times faster for MA than for methyl methacrylate. They also estimated that, under polymerization conditions, 60% of catalyst was effective in polymer formation for MA compared with only 25% for methyl methacrylate. Thus there is agreement with our observation of catalyst efficiencies for MA polymerization which are in general significantly greater than those observed by other workers for methyl methacrylate.

#### Reaction mechanism

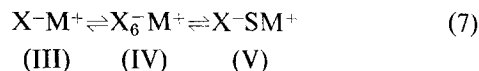
In the systems of high catalytic efficiency the drop in polymerization rate shows that the poly(methyl acrylate) anions almost lose their ability to add MA since the other reactant, MA, is still present in abundance at the end of the reaction. The most likely explanation is that an equilibrium is established between the very

active species, presumably the carbanion, which is present initially, and at least one other species which is either incapable or only capable of slow propagation. Such a stop-go polymerizing system would adequately explain the broad molecular weight distributions observed. This type of mechanism has been postulated previously for the corresponding methyl methacrylate system. Different authors have, however, suggested completely different reaction possibilities for the equilibrium. On the basis of the structure of side products identified from the reaction of acrylates and methacrylates with Grignard reagents at high concentration, Goode *et al.*<sup>5</sup> postulated that the dormant species was the anion of a cyclic hemi-ketal and was formed by a back-biting reaction of the initially formed carbanion:



They had evidence to show that the fairly extensive premature termination which occurred in their system was due to expulsion of  $\text{CH}_3\text{O}^-$  from (II) leaving a cyclic ketone as polymer end group.

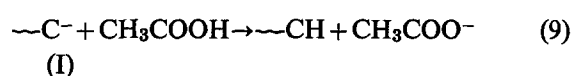
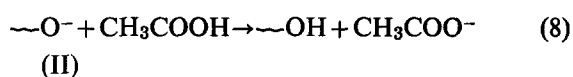
More recent authors<sup>4</sup> have accepted the cyclization postulate in order to explain the low molecular weight products in the methyl methacrylate system but prefer to postulate the existence of an equilibrium involving ion pairs in various stages of solvation (reaction 7) to explain the kinetic and molecular weight distribution effects observed in the main polymerization reaction. Species (III), (IV) and (V) are a contact ion pair, a peripherally solvated ion pair and a solvent separated ion pair respectively.



In the MA system an equilibrium similar to type (7) will exist and will be important in determining the stereochemistry of monomer addition but it cannot possibly explain the kinetic effects observed. The conversion time curve for the sodium naphthalene catalysed polymerization shows that the half-life for the establishment of equilibrium conditions is of the order of 2.5 min. Equilibria of the type described by reaction (7) will be established within a few  $\mu\text{sec}$ . The postulation of a slow relaxation phenomenon by Allen *et al.*<sup>4</sup> for such reactions is untenable. On the other hand equilibrium in the cyclization reaction (6) will take much longer to become established especially if cyclization is favoured only after a particular sequence of stereoregular monomer addition. By reference to molecular models Goode *et al.*<sup>5</sup> showed that ring closure in the methyl methacrylate system is very unlikely with an isotactic chain but quite probable with non-isotactic sequences in the last three units. The presence of an oxyanion in the system is further substantiated by the observation of some OH end groups by infra-red analysis of the terminated polymers. OH end groups have never been reported for methyl methacrylate polymers. Perhaps the expulsion of  $\text{CH}_3\text{O}^-$  from (II) is much more favourable when the two neighbouring C atoms have  $\text{CH}_3$  groups rather

than H atoms attached. Certainly there is much more premature termination in methyl methacrylate systems as evidenced by the large yields of low polymer which have been observed with several catalyst/solvent systems<sup>3</sup>.

We consider therefore that in the anionic polymerization of MA, initiation by reaction (1) or (2), depending upon the catalyst, results in the formation of a carbanion or dicarbanion of type (I). A certain proportion of catalyst is lost by attack at the carbonyl function of the monomer and leads to a variety of non-polymeric products. The extent of catalyst wastage depends upon the catalyst, its degree of solvation and is normally more extensive at higher temperatures. Species (I) can either add MA in a fast propagation reaction or isomerize to (II) by reaction (6). Apart from these two reactions species (I) and (II) are stable in the system at low temperatures but slow decomposition occurs at room temperature. Finally, addition of a proton donor produces instantaneous termination by reaction (5), (8) or (9).



Assuming that effective initiation is instantaneous and initially only produces species (I) and that only (I) can propagate, then  $k_p$ , the rate constant of propagation in THF at 203K can be calculated from the initial rate of the dilatometric experiment and the catalyst efficiency,  $f$ , given in Table 3,  $k_p(203\text{K}) = 0.09 \text{ M}^{-1} \text{ sec}^{-1}$ . Thus MA propagates much more slowly than methyl methacrylate under similar reaction conditions. The lower limit for  $k_p(203\text{K})$  for methyl methacrylate polymerization in high THF concentration and with sodium gegenion has been measured by Allen *et al.*<sup>4</sup> to be  $24 \text{ M}^{-1} \text{ sec}^{-1}$ .

Taking the half-life for the establishment of equilibrium in the dilatometric experiment as 2.5 min, the average lifetime of an initially formed carbanion is  $2.5/\ln 2 = 3.6$  min. From the conversion to polymer after 3.6 min (Figure 3), the initial catalyst and MA concentrations and the corresponding values of  $f$  and  $x$  (Table 3), the polymer  $DP_n$  after 3.6 min comes to be 35. Thus on average 35 monomer units add to a carbanion in its lifetime showing that the rate of propagation is 35 times greater than the rate of reaction (6).

$$k_6(203\text{K}) = k_p[M]/35 = 0.004 \text{ sec}^{-1}$$

By making the added assumption that the monomer concentration is constant during the dilatometric experi-

ment (it actually dropped from 1.49 M to about 1.2 M) the ratio of the concentrations of species (II) to species (I) is related to the initial rate,  $R_0$ , and the equilibrium rate,  $R_e$ , by the equation:

$$[\text{II}]/[\text{I}] = (R_0/R_e) - 1 = k_6/k_{-6}$$

From the observed values of  $R_0$  and  $R_e$  in three dilatometric experiments, the ratio of oxyanions to carbanions at equilibrium ( $[\text{II}]/[\text{I}]$ ) is 70 at 203K. Thus

$$k_{-6}(203\text{K}) = k_6/70 = 6 \times 10^{-4} \text{ sec}^{-1}$$

#### ACKNOWLEDGEMENTS

The authors would like to thank Dr G. G. Cameron, University of Aberdeen, for allowing them the use of g.p.c. equipment, Miss R. Black for technical assistance and ICI Plastics Division for a maintenance grant (J. M.).

#### REFERENCES

- 1 Szwarc, M. 'Carbanions, Living Polymers, and Electron Transfer Processes', Wiley, New York, 1968
- 2 Tsuruta, T. and O'Driscoll, K. F. 'Structure and Mechanism in Vinyl Polymerisation', Marcel Dekker, New York, 1969, pp 426-429
- 3 *Idem, ibid.*, pp 233-249
- 4 Allen, P. E. M., Chaplin, R. P. and Jordan, D. O. *Eur. Polym. J.* 1972, **8**, 271
- 5 Goode, W. E., Owens, F. H. and Myers, W. L. *J. Polym. Sci.* 1960, **47**, 75
- 6 Matsuzaki, K., Uryu, T., Ishida, A., Ohki, T. and Takenshi, M. *J. Polym. Sci. (A-1)* 1967, **5**, 2167
- 7 Yoshino, T., Komiyama, J. and Shinomiya, M. *J. Am. Chem. Soc.* 1964, **86**, 4482
- 8 Bywater, S., Black, P. E. and Wiles, D. M. *Can. J. Chem.* 1966, **44**, 695
- 9 D'Alelio, G. F. and Hoffend, T. R. *J. Polym. Sci. (A-1)* 1967, **5**, 323
- 10 Methven, J. M. *PhD Thesis* University of Dundee, 1971, p 139
- 11 'Vinyl and Diene Monomers', (Ed. E. C. Leonard), Part 1, Wiley-Interscience, New York, 1970, p 183
- 12 Ref 1, p 174
- 13 Curtin, D. Y. and Hendrikson, Y. G. *J. Org. Chem.* 1956, **21**, 1260
- 14 Spach, G., Montiero, H., Levy, M. and Szwarc, M. *Trans. Faraday Soc.* 1962, **58**, 1809
- 15 Ref 1, pp 172-175; Hogan Esch, T. F. and Smid, J. *J. Am. Chem. Soc.* 1966, **88**, 307; Hirota, N. and Weissman, S. I. *J. Am. Chem. Soc.* 1964, **86**, 2538
- 16 Tsuruta, T., Makimoto, T. and Nakayama, Y. *Makromol. Chem.* 1966, **90**, 12
- 17 Ref 1, p 154
- 18 Ref 2, p 373
- 19 Tobolsky, A. V. and Hartley, D. B. *J. Am. Chem. Soc.* 1962, **84**, 1391
- 20 Panayotov, I. M., Rashkov, I. B. and Berlinova, I. V. *Makromol. Chem.* 1972, **155**, 179
- 21 Kawabata, N. and Tsuruta, T. *Makromol. Chem.* 1965, **86**, 231
- 22 Wiles, D. M. and Bywater, S. *J. Phys. Chem.* 1964, **68**, 1983

# The cubic structure of a SIS three block copolymer

E. Pedemonte, A. Turturro, U. Bianchi and P. Devetta

*Istituto di Chimica Industriale, Università Genova, 16132 Genova, Italy*  
(Received 24 November 1972)

A commercial thermoelastic three block copolymer (styrene-isoprene-styrene) has been characterized with regard to its molecular weight, block length and original morphology. The morphology was also followed as a function of mechanical (extrusion) and thermal (annealing at 150°C) treatment. After thermal treatment the structure consists of a body-centred cubic arrangement of spherical polystyrene domains; large groups of polystyrene domains are differently oriented to the axis of observation. The appearance of these differently oriented 'grains' was shown to be consistent with a structural model, observed from a variety of directions.

## INTRODUCTION

Three block copolymers of the ABA type have been studied for many years<sup>1-4</sup> since in these materials the physical and mechanical properties of two different homopolymers are matched; generally the resulting characteristics are peculiar and different from those of a mixture of the two components.

This has to be correlated with the phase separation that occurs in the solid state owing to the thermodynamic incompatibility of A and B blocks<sup>5-13</sup>. Homogeneous elements of several macromolecules join together in separated domains and the morphology of the material depends primarily on the relative amounts of A and B. When A : B  $\approx$  1 a lamellar structure appears and each macromolecule has its own end blocks in two different lamellae; they are therefore connected by the central portions B of the chains. When the percentage of one component is noticeably higher than the other, the former forms a continuous matrix in which the domains of the latter are uniformly distributed; these domains have usually a spherical shape. When A : B  $\ll$  1 there are spherical domains of A plunged in the B matrix and joined by the central blocks of the macromolecules, so that a three-dimensional network is apparent.

The technique employed in the preparation of the specimens can modify the structure. The solvent has an influence on the morphology of the films cast from dilute solutions<sup>14-18</sup>, whereas mechanical and thermal treatments can influence specimens prepared directly from the bulk<sup>19-25</sup>. As a consequence the proportion of polystyrene is the main, but not the only factor responsible for the structure and therefore the properties; the copolymer composition is, of course, a primary characteristic of the material since specific morphologies can be induced by several treatments and hence peculiar properties can be obtained.

In the present paper the results concerning the molecular characterization and the morphology of a SIS (S = polystyrene; I = polyisoprene) three block copolymer

are reported, following the influence of extrusion and annealing treatments on the structure.

## EXPERIMENTAL

### *Materials and molecular characterization*

The SIS three block copolymer used was a commercial product supplied by Shell Company under the trade name of Kraton 1107. In *Table 1* some molecular and physical characteristics of this material are shown.

The techniques employed to obtain the reported data have been extensively described in a previous paper<sup>26</sup>. The number-average molecular weight was obtained by osmometry, while infra-red spectroscopy was used to measure the amount of polystyrene and the configurational composition of the elastic fraction. The glass transition temperature and the two values of the cubic expansion coefficients in the glassy and in the rubbery state were obtained by the dilatometric technique; the density was measured by flotation and the length of the elastic chains by swelling.

The data clearly show that this copolymer has a rather high molecular weight and a low content of polystyrene so that in the macromolecule a long central

*Table 1* Molecular and physical characteristics of the Kraton 1107 copolymer

Molecular weight, $\bar{M}_n$	$1.5 \times 10^5$
Polystyrene (%)	10
Molecular weight of each polystyrene terminal block	$7.5 \times 10^3$
Molecular weight of the central elastic block	$1.35 \times 10^5$
Configurational composition of the elastic block:	
<i>cis</i> -1,4-polyisoprene (%)	90
3,4-polyisoprene (%)	10
$T_g$ (°C)	60-63
$\alpha_g$ (°C) <sup>-1</sup>	$5.50 \times 10^{-4}$
$\alpha_r$ (°C) <sup>-1</sup>	$6.30 \times 10^{-4}$
$\rho$ (g cm <sup>-3</sup> )	0.89
$M_c$	$30 \times 10^3$

block of isoprene units, mainly in the *cis*-1,4 configuration, is joined to two very short end blocks.

The glass transition temperature is particularly far from the value of the bulk polystyrene; this result indicates that the polystyrene domains in the rubbery matrix have to be quite small in size<sup>10</sup>.

#### Morphology

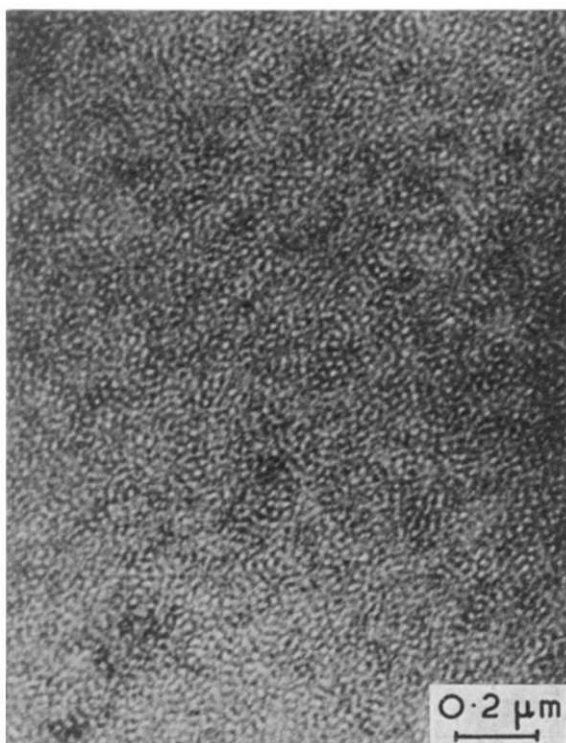
For the morphological analysis with the electron microscope, ultra-thin sections of the bulk material were prepared. For cutting elastic specimens, a low temperature ultra-microtome has to be used, the sample being cooled with liquid nitrogen to approximately  $-150^{\circ}\text{C}$ ; the technique employed with this SIS copolymer is described elsewhere<sup>27</sup>. The rubbery phase of the specimen was contrasted by exposing the sections to the vapour of an aqueous  $\text{OsO}_4$  solution at room temperature for several hours; consequently in the electron micrographs the isoprene phase will appear dark and the styrene phase bright.

The Kraton 1107 (K1107) copolymer was studied as supplied by the manufacturer and the evidence from mechanical and thermal treatments was used to study the effects on morphology. By extrusion at high temperature (about  $150^{\circ}\text{C}$ ; extrusion rate  $1.5\text{--}6\text{ mm}^3/\text{sec}$ ), cylindrical plugs with a diameter of 2 mm were obtained. The original material and the cylinders were annealed at  $150^{\circ}\text{C}$  under vacuum for a week; a longer annealing time (up to three months) was tested on the extruded plugs.

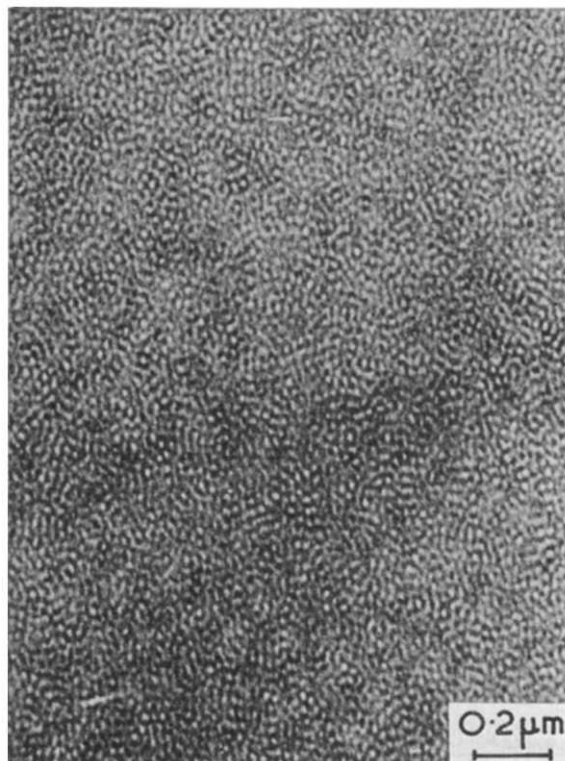
## RESULTS

#### Morphology of the original sample

In *Figure 1* the morphology of the original material is shown. The phase separation is quite visible and is characterized by circular domains of polystyrene em-



*Figure 1* Electron micrograph of an ultra-thin section of the K1107 original copolymer



*Figure 2* Electron micrograph of an ultra-thin section of an extruded plug of the K1107 copolymer, cut perpendicular to the extrusion axis

bedded in the rubbery matrix. In several areas the spots have the shape of perfect, isolated circles; in other areas the circles are degenerated into elongated spots, oriented along different directions in the different areas of the field.

We have to take into account that the sections viewed in the electron microscope are about  $500\text{ \AA}$  thick and that the osmium tetroxide stains the whole thickness of the section. Therefore we look at the projection on the observation plane of the three-dimensional structure of the copolymer. Circular domains of polystyrene may come out from spheres or from the exact cross-sectional view of cylinders with an orientation perpendicular to the cutting section; on the other hand, streaks and striated structures could be due either to local variations in the cylinder orientation within the field of view or to the projection of spherical domains lying down on the same row but at different depths in the section. As a consequence the micrograph of *Figure 1* does not allow us to draw any conclusion on the true morphology of the original copolymer; however, owing to the copolymer composition, it seems reasonable to assume that spherical domains of polystyrene are present.

We will not discuss this point any further and we will merely assume the morphology of the original material as the starting point to study the effect of mechanical and thermal treatments on the structure of the copolymer.

#### Morphology of the extruded plugs

The structure of the K1107 copolymer is not modified by the extrusion. In *Figure 2* a section cut perpendicular to the plug axis is shown and the morphology is clearly



similar to that of the original sample; in particular no orientation along the extrusion direction can be seen and the polystyrene domains are still randomly distributed in the rubbery matrix. As a consequence no birefringence is observed and the small-angle X-ray diffraction with the beam parallel to the plug axis gives a symmetrical ring (Figure 3).

These results seem to be peculiar to copolymers having a low proportion of polystyrene because it was found that the extrusion process leads to orientation of the domains when the weight percentage of polystyrene is in the range between 26<sup>20, 21</sup> and 33<sup>28</sup>.

*Morphology of extruded and annealed plugs*

In Figure 4 a section perpendicular to the extrusion axis of a specimen annealed for one week is shown.

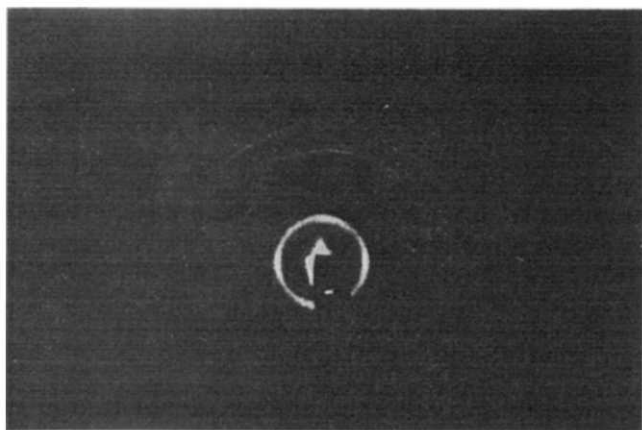


Figure 3 Small-angle X-ray diffraction pattern of an extruded plug with the beam parallel to the cylinder axis. The beam and the beam stop were not exactly centred and therefore some extraneous diffractions appear in the centre of the ring

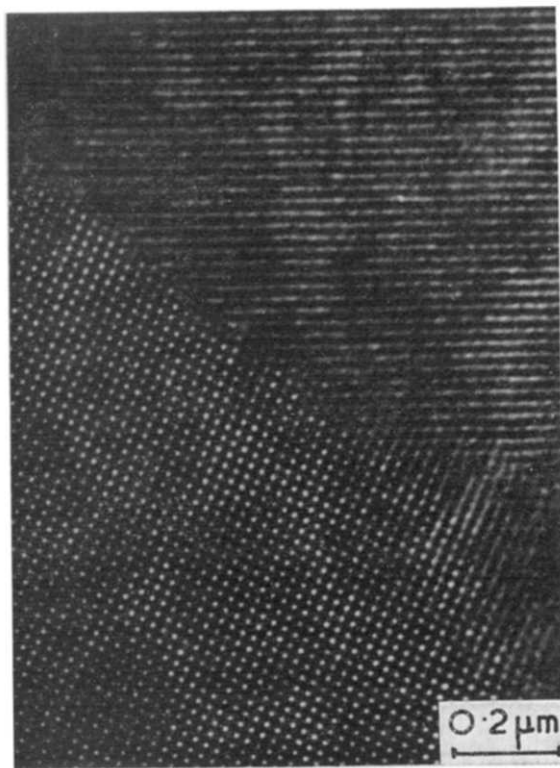


Figure 4 Electron micrograph of an ultra-thin section of an extruded and annealed plug of the K1107 copolymer; section cut perpendicular to the extrusion axis

The phase separation is clearly better than in the original copolymer and a striking re-organization of the polystyrene domains is observed.

The electron micrographs of extruded and annealed plugs show a long range order which extend over well defined areas appearing as 'grains of crystallinity'. In

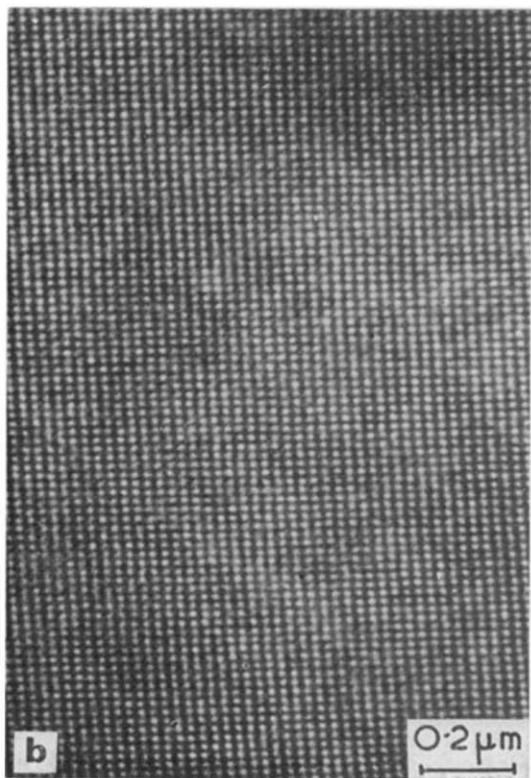


Figure 5 (a) Hexagonal and (b) rectangular arrangement of circular domains of polystyrene embedded in the rubbery matrix. Specimen annealed for 60 days at 150°C. Section cut perpendicular to the extrusion direction

each area the organization of the polystyrene domains in the rubbery matrix reveals a surprising uniformity and the boundaries are well defined. The size of each ordered region is rather small ( $< 2 \mu\text{m}$ ) when the annealing time is one week but increases progressively with annealing time and reaches exceptionally large values by extending the treatment up to three months. On the other hand, the dimensions of the polystyrene domains apparently do not change.

Different morphologies are present. Those more frequently observed are characterized by: hexagonal (Figure 5a), rectangular (Figure 5b) and square (Figure 4) arrangement of circular domains of polystyrene embedded in the rubbery matrix; striated structures, in which the thickness of the polystyrene striations is always constant but the spacing may have two different values (Figure 6).

As noted previously, the grains boundaries are well defined and in each region the morphology is very regular. The same observations can be made on sections but along the extrusion direction and on the original material when annealed for a long period of time.

The extruded specimens are still isotropic; the small-angle X-ray diffraction with the beam along the extrusion directions gives a symmetrical ring<sup>29</sup>.

## DISCUSSION

Sections of both the original material and of the extruded plugs show, after annealing, many different morphologies in ordered regions, whose dimensions increase with annealing time. We call these regions 'grains of crystallinity' because the structure of the copolymer looks like that of a crystalline low molecular weight substance.

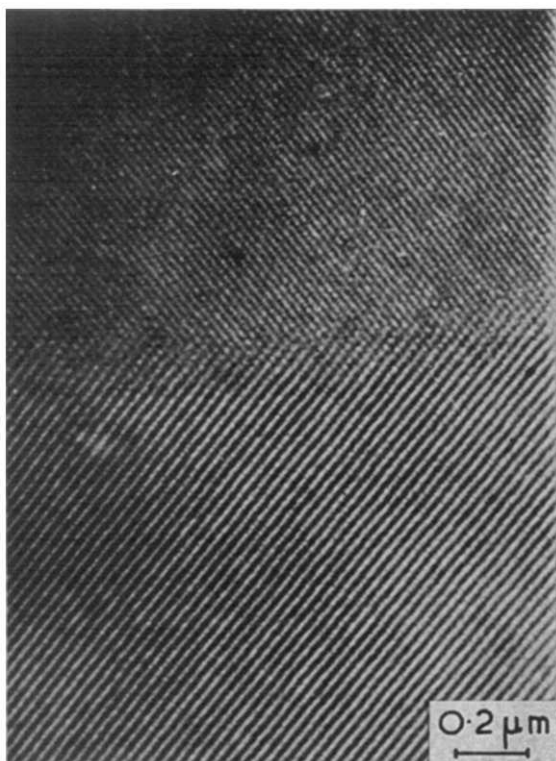


Figure 6 Striated structures. Specimen annealed for 60 days at  $150^{\circ}\text{C}$ . Section cut perpendicular to the extrusion direction

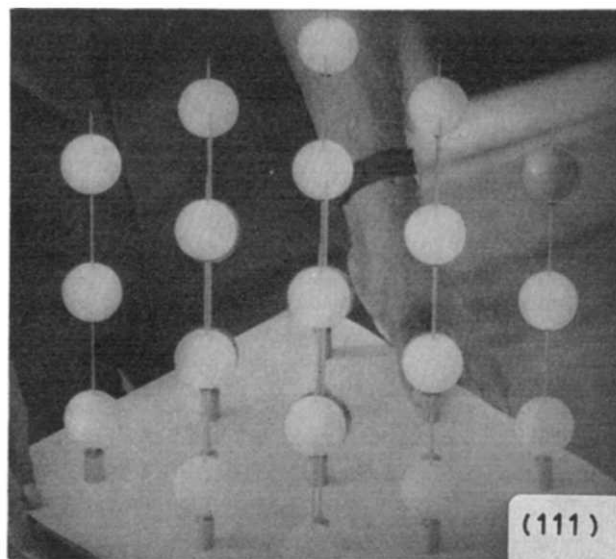


Figure 7 Body-centred cubic model viewed from the 111 plane

Keller and Odell<sup>29, 30</sup> assume the possibility of the coexistence of spherical and cylindrical domains of polystyrene to explain some results obtained with small-angle X-ray diffraction on the same K1107 copolymer. Also Hoffmann and coworkers<sup>13, 31-32</sup>, in their comprehensive work on the butadiene-styrene two-block copolymer, assume that cylinders and spheres can both be present; more recently<sup>33</sup>, for a copolymer having a content of styrene of about 17% by weight, the possibility of having cubic and hexagonal close packing of spheres is considered because the difference in energy between these two lattices is claimed to be extremely small.

We believe that the lattice of the polystyrene domains in K1107 is unique for the whole structure. Assuming that the polystyrene domains are spherical and arranged on a body-centred cubic lattice, we can explain our experimental observation if we take into account that each grain of crystallinity can have a different orientation.

This hypothesis is supported by the analysis of a structural model, made up with 'ping-pong balls' according to the ratio  $d/\phi$  between the domain to domain distance,  $d$ , and the domain diameter,  $\phi$ , experimentally observed in the hexagonal arrangement of circles of polystyrene (as in Figure 5a). The average value of many observations was considered and only spots perfectly circular were taken into account. This view would correspond to the (111) face of the lattice (Figure 7). Looking to the body-centred cubic lattice from the (100) and from the (110) planes respectively we have morphologies characterized by square and rectangular arrangement of spots (Figures 8a and b). By simply rotating the lattice around a definite crystallographic axis we go from one morphology to another; in the meantime a great number of transition structures are put into evidence and we draw attention to the high spacing and the low spacing striations, shown in Figures 9a and b. The striated structures shown in Figure 6 would therefore be the consequence of a particular three-dimensional distribution of spherical domains of polystyrene set on different crystallographic planes.

The agreement between the experimental results and the body-centred cubic lattice model is satisfactory not only qualitatively, as discussed so far, but also from



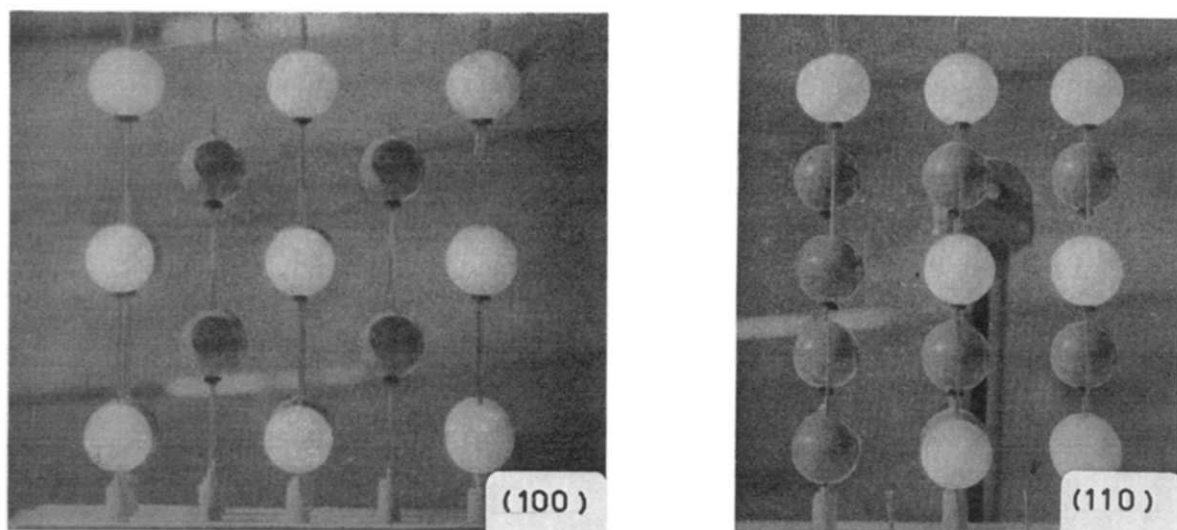


Figure 8 Body-centred cubic model viewed from the (100) and the (110) plane

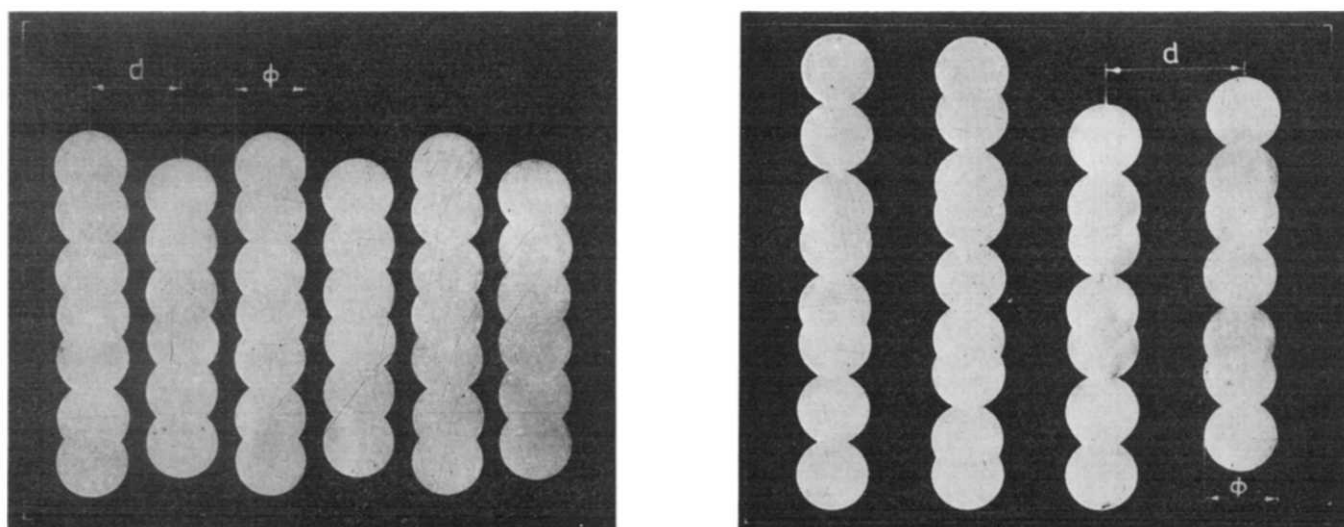


Figure 9 Diagram of the striated structures obtained by rotation of the body-centred cubic model

Table 2 Comparison between calculated and experimental values for body-centred cubic structure

$d$  = distance between the centres of two nearest polystyrene elements;  $\phi$  = dimension (thickness or diameter) of a polystyrene element

Morphology	$d/\phi$ (calc.)	$d/\phi$ (exp.)
Hexagonal (111)	—	2.0
Square (100)	1.85	1.7
Rectangular (110)	1.35/1.85	1.3/1.8
High density striation	1.35	1.4
Low density striation	1.85	1.9

a quantitative point of view. In Table 2 the values experimentally observed for the  $d/\phi$  ratios are compared with those calculated from the model.

We are aware of the errors that result from trying to measure the dimensions of elements of structures stained with osmium tetroxide. For this reason we do not discuss the possible variation of the polystyrene domains sizes with the annealing time. On average, the spheres show a diameter of about 130 Å.

## CONCLUSIONS

The comparison between the morphologies reported indicate the influence of mechanical and thermal treatments on the structure of the K1107 copolymer. Extrusion has no effect on the morphology; by annealing at high temperature both the original material and the extruded plugs, a re-organization of the spherical polystyrene domains takes place and a body-centred cubic lattice is produced. The specimens have the characteristics of a polycrystalline material so that the orientation of the grains of crystallinity is randomly distributed.

These results are completely different from those obtained with K1102<sup>20-22</sup> and can be correlated with the low amount of polystyrene present in the copolymer studied.

## ACKNOWLEDGEMENT

The authors thank Mr G. Dondero for technical assistance with the electron microscope.

REFERENCES

- 1 'Block copolymers', *J. Polym. Sci. (C)* 1969, **26**
- 2 'Block Polymers', (Ed. S. L. Aggarwal), Plenum Press, New York, 1970
- 3 Estes, G. M., Cooper, S. L. and Tobolsky, A. V. *J. Macromol. Sci.* 1970, **C4**, 313
- 4 Folkes, M. J. and Keller, A. in 'Physics of Glassy Polymers', (Ed. R. N. Haward). Elsevier, Amsterdam, 1973, in press
- 5 Fedors, R. F. *J. Polym. Sci. (C)* 1969, **26**, 189
- 6 Meier, D. J. *J. Polym. Sci. (C)* 1969, **26**, 81
- 7 Krause, S. *Macromolecules* 1970, **3**, 84
- 8 Krause, S. *J. Polym. Sci. (A-2)* 1969, **7**, 249
- 9 Bianchi, U., Pedemonte, E. and Turturro, A. *J. Polym. Sci. (B)* 1969, **7**, 785
- 10 Bianchi, U., Pedemonte, E. and Turturro, A. *Polymer* 1970, **11**, 268
- 11 Inoue, T. et al. in 'Block Polymers', (Ed. S. L. Aggarwal), Plenum Press, New York, 1970, p 53
- 12 Leary, D. F. and Williams, M. C. *J. Polym. Sci. (B)* 1970, **8**, 335
- 13 Kromer, H., Hoffmann, M. and Kamp, G. *Ber. Bunsenges, Phys. Chem.* 1970, **74**, 859
- 14 Matsuo, M. *Japan Plastic*, July 1968
- 15 Matsuo, M., Sagal, S. and Asai, H. *Polymer* 1969, **10**, 79
- 16 Fischer, E. *J. Macromol. Sci.* 1968, **A2**, 1285
- 17 Lewis, P. R. and Price, C. *Nature* 1969, **223**, 494; *Polymer* 1971, **12**, 258
- 18 Inoue, T., Moritani, H., Hashimoto, T. and Kawai, K. *Macromolecules* 1971, **4**, 500
- 19 Matsuo, M., Ueno, T., Horino, H., Chuyio, S. and Asai, H. *Polymer* 1968, **9**, 425
- 20 Keller, A., Pedemonte, E. and Willmouth, F. M. *Nature* 1970, **225**, 538
- 21 Keller, A., Pedemonte, E. and Willmouth, F. M. *Kolloid-Z. Z. Polym.* 1970, **238**, 385
- 22 Dlugosz, J., Keller, A. and Pedemonte, E. *Kolloid-Z. Z. Polym.* 1970, **242**, 1125
- 23 Arridge, R. G. C. and Folkes, M. J. *J. Phys. (D): Appl. Phys.* 1972, **4**, 344
- 24 Pedemonte, E., Turturro, A., Bianchi, U. and Devetta, P. *Chim. Ind. (Milan)* 1972, **54**, 689
- 25 Turturro, A. et al. *Chim. Ind. (Milan)* 1972, **54**, 782
- 26 Bianchi, U. et al. *Chim. Ind. (Milan)* 1972, **54**, 603
- 27 Dondero, G., Olivero, L., Devetta, P., Cartasegna, S. and Pedemonte, E. *La Nuova Chimica* 1972, (48), 1
- 28 Pedemonte, E., Cartasegna, S., Devetta, P., Turturro, A. and Bianchi, U. *Chim. Ind. (Milan)* to be published
- 29 Odell, J. A. *MSc Thesis* University of Bristol, 1971
- 30 Keller, A. and Odell, J. A. 1972, to be published
- 31 Kampf, G., Hoffmann, M. and Kromer, H. *Ber. Bunsenges. Phys. Chem.* 1970, **74**, 851
- 32 Hoffmann, M., Kampf, G., Kromer, H. and Pampus, G. *Adv. Chem. Ser.* 1971, **99**, 351
- 33 Kampf, G. and Kromer, H. *J. Macromol. Sci. (B)* 1972, **6**, 167

# Polymer translational diffusion: 1. Dilute theta solutions, polystyrene in cyclohexane

T. A. King, A. Knox, W. I. Lee and J. D. G. McAdam

Physics Department, Schuster Laboratory, University of Manchester,  
Manchester M13 9PL, UK

(Received 22 December 1972; revised 2 February 1973)

The translational diffusion coefficient for polystyrene in cyclohexane under theta conditions has been found to be concentration dependent, describable by an equation of the form:  $D(c) = D_0(1 + k_D c + \dots)$ , in which  $k_D$  is related to the weight-average molecular weight as  $k_D = (4.1 \pm 0.3) \times 10^{-4} \bar{M}_w^d$  dl/g with  $d = 0.48 \pm 0.04$ . The result is intermediate between the theoretical descriptions of: Yamakawa; Imai; and Pyun and Fixman. Diffusion coefficient measurements have been made with variation of molecular weight and concentration by detecting the linewidth of the Rayleigh light-scattered component in a laser light-scattering apparatus.

## INTRODUCTION

The purpose of this paper is to present our recent measurements on the concentration dependence of the diffusion coefficient of polymer molecules in dilute solution under theta conditions and to compare these results with the current theoretical situation. When a polymer solution is at thermal equilibrium in which a concentration gradient exists the diffusion process occurs. The concentration gradient can arise from chemical potential fluctuations of the solution and this origin of diffusion is applicable to the experimental technique described later.

The diffusion of the polymer molecule in solution can be described in terms of a matter flux  $\vec{J}$ , a diffusion coefficient  $D$ , the phenomenological coefficient  $L = c/f$  and the gradient in polymer chemical potential  $\vec{\nabla}_{\mu_1}$  as:

$$\vec{J} = -D \vec{\nabla} c = -\frac{c}{f} \vec{\nabla}_{\mu_1} \quad (1)$$

Here  $c$  is the solution concentration and  $f$  is the friction coefficient of the polymer.

From the Gibbs–Duhem relation and the virial expansion for the osmotic pressure of the solution the diffusion coefficient can be expressed<sup>1</sup> as:

$$D = \frac{kT}{f} \left( 1 - \frac{NV_1 c}{M} \right) (1 + 2A_2 M c + 3A_3 M c^2 + \dots) \quad (2)$$

in which  $M$  and  $V_1$  are the polymer molecular weight and volume,  $A_2$  and  $A_3$  are the second and third virial coefficients,  $k$  is Boltzmann's constant,  $N$  is Avogadro's number and  $T$  is the absolute temperature. In general the friction coefficient  $f$  may also be taken to depend on concentration<sup>1</sup> and may be expanded in  $c$  as:

$$f = f_0(1 + k_f c + k'_f c^2 + \dots) \quad (3)$$

with  $f_0$  denoting the friction coefficient at infinite dilution and  $k_f, k'_f \dots$  denoting molecular weight dependent

constants. The concentration dependence of the diffusion coefficient for dilute solutions can then be written as:

$$D(c) = D_0(1 + k_D c + k'_D c^2 + \dots) \quad (4)$$

In equation (4)  $D_0$  is given by the Einstein relation as  $D_0 = kT/f_0$ , being the diffusion coefficient at infinite dilution, and the thermodynamic and hydrodynamic dependence of  $k_D$  being given as:

$$k_D = 2A_2 M - k_f - \frac{NV_1}{M} \quad (5)$$

where the inclusion of the term  $NV_1/M$  in equation (5) has been recently discussed<sup>1</sup>.

When a polymer solution is at the theta temperature the term containing  $A_1$  may be taken as zero and equation (5) becomes:

$$k_D^{\theta} = - \left( k_f + \frac{NV_1}{M} \right) \quad (6)$$

and the corresponding expression for the diffusion coefficient to first order in  $c$ ,

$$D^{\theta}(c) = D_0^{\theta}(1 + k_D^{\theta} c + \dots) \quad (7)$$

Independent theoretical descriptions of the form of  $k_f$  have been given by Yamakawa<sup>2</sup>, Imai<sup>3</sup> and Pyun and Fixman<sup>4</sup> and these will be briefly described and compared with the results of this work later in this paper. Investigations related to  $k_f$  in equation (3) from diffusion and sedimentation measurements have not achieved a definite conclusion. In particular it has been predicted to have both zero and non-zero values. For polystyrene in cyclohexane, Cantow<sup>5</sup> found that  $k_f = 0$  and any concentration dependence he attributed to the next higher term ( $k'_f c^2$ ) or ( $-k'_f c^2$ ) and Klenine *et al.*<sup>6</sup> and Haug and Meyerhoff<sup>7</sup> found that the concentration dependence was negligible. Also for polystyrene in cyclohexane near the theta point Cowie and Cussler<sup>8</sup> found a noticeable decrease in  $D$  with increase in concentration although their data were not analysed fully

in terms of equation (7). Other measurements<sup>9-13</sup> mainly of polymer sedimentation have provided evidence for various non-zero values of  $k_f$ .

### DIFFUSION COEFFICIENT MEASUREMENTS

#### Experimental techniques

The polymer translational diffusion coefficients were obtained from laser light-scattering by Rayleigh linewidth measurements<sup>14</sup>. The molecular centre-of-mass motion introduces a range of quasi-elastic frequency shifts in the scattered light whose linewidth is characteristic of the ensemble average motion of the molecule. A description of the optical light-beating spectrometer will be published in more detail separately. The spectrometer resolves the optical linewidth of the scattered light by homodyne (intensity fluctuation spectroscopy) light-beating and the photomultiplier photocurrent from the detected scattered light is analysed with an autocorrelation function computer. In the present study a 60 mW Spectra-Physics model 125 He-Ne 6328 Å laser and a Hewlett-Packard model 3721A correlator used in autocorrelation mode have been used, with data being transferred on to paper tape for subsequent computer analysis.

This study is based on the observation of the dynamics of polystyrene random coils in cyclohexane maintained very close to the theta temperature; also included for comparison are  $D$  values in butan-2-one at 25°C. A set of polystyrene samples (from the Pressure Chemical Company) of varying molecular weight and with a polydispersity equal to or better than 1.3 was used. Some details of the samples are given in Table 1. The polymer characterization data are largely as given by the suppliers except for the sample with weight-average molecular weight  $\bar{M}_w = 2.7 \times 10^6$ . For this sample the molecular weight information has been obtained from viscosity and gel permeation chromatography (g.p.c.) analysis. Cyclohexane solutions of chosen concentration were prepared in an oven at 40°C and particular care was taken with sample cleaning before performing the light-scattering experiments. All solutions were prepared free of particulate matter by centrifugation for up to 2 hours at 40°C, with rotor speeds up to 20 000 rev/min giving  $35\,000 \times g$  acceleration, and then transferred directly into pre-cleaned sample cells. The measurement cells were contained in a high thermal mass temperature-controlled chamber maintained at  $35 \pm 0.1^\circ\text{C}$  for the theta point measurements.

An example of the form of the correlator output for the time autocorrelation function for measurements on the  $\bar{M}_w = 2.7 \times 10^6$  sample is shown in Figure 1.

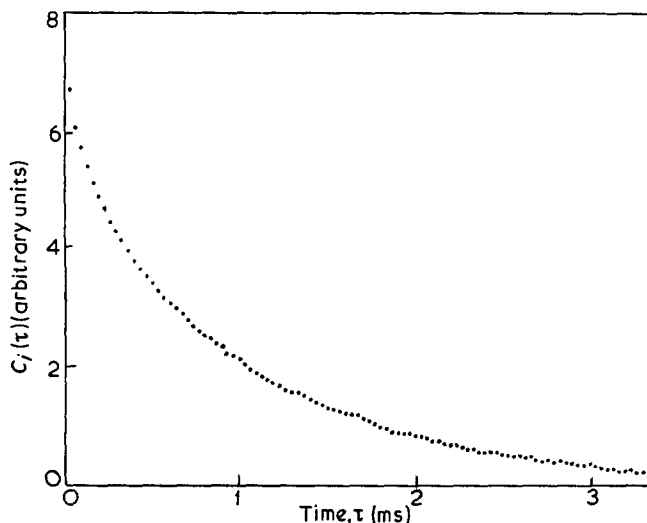


Figure 1 Photomultiplier photocurrent time autocorrelation function  $C_i(\tau)$  for a polystyrene polymer of  $\bar{M}_w = 2.7 \times 10^6$  in cyclohexane at 35°C at a concentration of 0.05 g/dl with  $K^2 = 6.28 \times 10^9 \text{ cm}^{-2}$

For molecules small compared to the wavelength of light the autocorrelation function is exponential with a time constant  $\tau_c$  given by<sup>14, 15</sup>:

$$\tau_c = [2K^2 D(c)]^{-1} \quad (8)$$

with  $K^2 = [16\pi^2 n^2 \sin^2(\theta_s)/2]/\lambda_0^2$  in which  $K$  is the scattering wave-vector in a medium of refractive index  $n$  for an incident light wave of wavelength  $\lambda_0$  in vacuum and scattered angle  $\theta_s$ . Thus the diffusion coefficient is obtained directly from the time constant of the exponential autocorrelation function.

Preliminary calculations indicate that the appropriate molecular weight average to use in this diffusion type of experiment lies between the weight and  $z$  averages and so, for consistency,  $\bar{M}_w$  has been used. Also the diffusion coefficient measured is sensitive to sample polydispersity and narrow distribution samples have been used. This dependence has been the subject of study<sup>16</sup> and preliminary calculation and measurement shows that for the small polydispersity of the samples used here the correction to  $D$  would be within the experimental uncertainty of the measurement itself.

The precision of the experiment is a function of the solution scattering power. Typically for a solution of  $\bar{M}_w = 2 \times 10^5$  at a concentration of 0.5 g/dl the measured diffusion coefficient is estimated to have an accuracy of  $\pm 2\%$ . The diffusion coefficients at zero concentration,  $D_0$ , which are obtained from an extrapolation of the concentration dependence of the diffusion coefficient

Table 1 Description of polystyrene samples and values of the diffusion coefficient at  $c=0$ ,  $D_0$ , for cyclohexane (at 35°C) and butan-2-one (at 25°C) The diffusion coefficient concentration dependence parameter  $k_D^0$  and the ratio  $(k_D^0 + 9.4 \times 10^{-3})\bar{M}_w^{-1/2}$  are given for theta conditions

Sample	$\bar{M}_w$	$\frac{\bar{M}_w}{\bar{M}_n}$	$D_0 \times 10^7 \text{ (cm}^2/\text{s}^{-1}\text{)}$		$k_D^0$ (dl/g)	$(k_D^0 + 9.4 \times 10^{-3})\bar{M}_w^{-1/2}$ ( $\times 10^4$ )
			Cyclohexane at 35°C	Butan-2-one at 25°C		
PC-14b	$2.7 \times 10^6$	1.3	0.84	1.37	-0.56	-3.36
PC-13a	$6.7 \times 10^5$	<1.15	1.66	2.95	-0.34	-4.03
PC-1c	$2 \times 10^5$	<1.06	3.05	5.96	-0.16	-3.36
PC-4b	$1.1 \times 10^5$	<1.06	4.20	7.90	-0.18	-5.12
PC-2b	$2.1 \times 10^4$	<1.06	8.97	22.5	-0.09	-5.52

random coil polymer at the theta point

$$\Phi^{1/3}/P = 2.65 \times 10^6,$$

we obtain:

$$\frac{NV_h}{M} = 0.20[\eta]_\theta \quad (10)$$

where  $[\eta]_\theta$  is the value of the intrinsic viscosity at the theta temperature. Literature values of the Mandelkern invariant differ from the mean value of  $2.65 \times 10^6$  by up to  $\pm 6\%$  and the limiting values have the effect of making the coefficient in equation (10) range from 0.18 to 0.24. For the purposes of this paper the mean value of the invariant is adequate.

For the polystyrene-cyclohexane system the intrinsic viscosity variation with  $\bar{M}_w$  is<sup>19</sup>:

$$[\eta]_\theta = 8.4 \times 10^{-4} \bar{M}_w^{0.5} \text{ (dl/g)} \quad (11)$$

and

$$\frac{NV_h}{M} = 1.7 \times 10^{-4} \bar{M}_w^{0.5} \text{ (dl/g)} \quad (12)$$

The limiting concentration  $c_m$  is then given as:

$$c_m = 6.0 \times 10^2 \bar{M}_w^{-0.5} \text{ (g/dl)} \quad (13)$$

Consequently  $c_m$  is, for example, calculated as 1.3 g/dl for  $\bar{M}_w = 2 \times 10^5$  and 0.36 g/dl for  $\bar{M}_w = 2.7 \times 10^6$  the largest polymer for which measurements are reported in this study. This type of calculation provides a useful guide to the concentration range to be used in investigating equation (7).

### Results

From measurements of the typical form of Figure 1 the diffusion coefficient,  $D(c)$ , and its concentration dependence is obtained for various molecular weights; data on five molecular weights are reported here. Two examples of the concentration dependence are shown in Figure 2 for  $\bar{M}_w = 2 \times 10^5$  and  $\bar{M}_w = 2.7 \times 10^6$ . For each of the five samples a value of the diffusion coefficient at  $c=0$ ,  $D_0$ , has been derived and a value of the concentration dependence parameter  $k_D^0$ , within the concentration limits discussed in the previous section. The low concentration regions of the  $D(c)$  curves either for cyclohexane or butan-2-one solutions do not provide any evidence, within the limit of the experimental sensitivity, for a concentration-independent region of the type given by Cantow<sup>5</sup>.

The molecular weight dependence of  $D_0$  is shown in Figure 3. This dependence can be well represented by the relation:

$$D_0^0 = k_T \bar{M}_w^{-b} \quad (14)$$

in which in this study the sample temperature is held constant to enable the temperature-dependent value to be obtained for  $k_T = (1.3 \pm 0.2) \times 10^{-4} \text{ cm}^2/\text{s}$  and  $b = 0.497 \pm 0.006$ . The molecular weight dependence of  $D_0^0$  is in agreement with theoretical and other experimental investigations<sup>1, 5</sup>.

The sign of  $k_D^0$  over the investigated molecular weight range has been found to be always negative for cyclohexane solutions. This contrasts with the butan-2-one data in which a sign change is found as is illustrated by the butan-2-one data in Figure 2. The values of  $k_D^0$  for the cyclohexane solutions are given in Table 1 and plotted

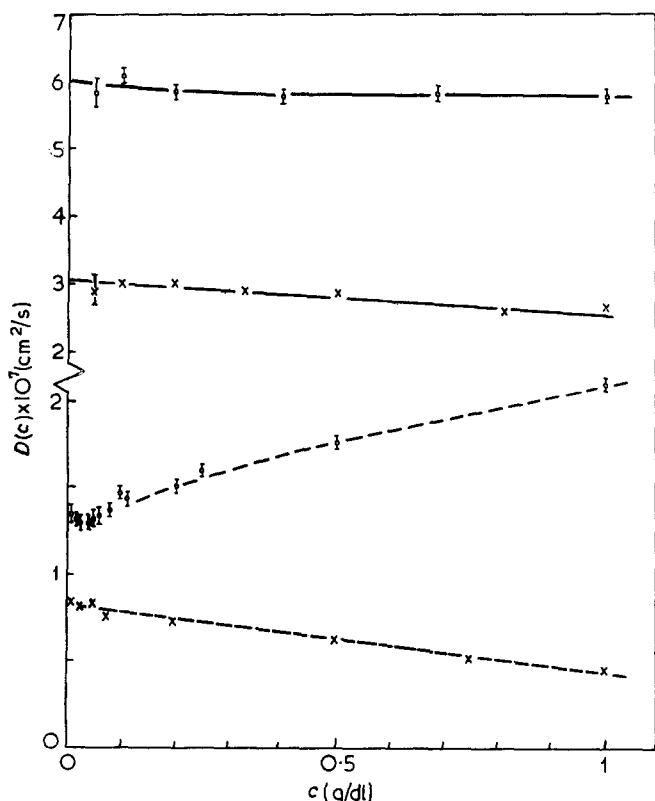


Figure 2 Concentration dependence of  $D(c)$  for polystyrene samples in cyclohexane at 35°C (x) and butan-2-one at 25°C (O). —,  $\bar{M}_w = 2 \times 10^5$ ; - - - -,  $\bar{M}_w = 2.7 \times 10^6$

cient data, are estimated to have an accuracy of  $\pm 5\%$  for  $\bar{M}_w \sim 10^5$  and  $\pm 3\%$  for  $\bar{M}_w = 2.7 \times 10^6$ . Two such dependences for  $\bar{M}_w = 2 \times 10^5$  and  $\bar{M}_w = 2.7 \times 10^6$  are shown in Figure 2. The cyclohexane results are there compared with butan-2-one measurements. The non-theta point butan-2-one results can be seen to be of a different nature and those measurements form part of a larger study of the diffusion coefficient of polystyrene under non-theta conditions. The results of this study are to be reported in a subsequent separate publication.

### Limitation of dilute solution range

In order to satisfy the condition for dilute solution behaviour and still determine  $k_D$ , consideration needs to be given to the concentration range over which measurements are made. The criterion adopted here is that the distance between the neighbouring centres of mass of two chain molecules should be at least twice the linear effective diameter of the polymer. Or alternatively, the total volume occupied by the polymer molecules should not be greater than about 10% of the volume of the solution. If the maximum useful concentration is  $c_m$  and  $V_h$  is the solute hydrodynamic volume, the condition becomes:

$$\frac{Nc_m V_h}{M} \leq 0.1 \quad (9)$$

From the empirical equations of Flory and Fox<sup>17</sup> connecting the intrinsic viscosity  $[\eta]$  and molecule radius of gyration  $R_G$ ,

$$[\eta] = 6^{3/2} \Phi \frac{R_G^3}{M}$$

and an average value of the Mandelkern invariant for a

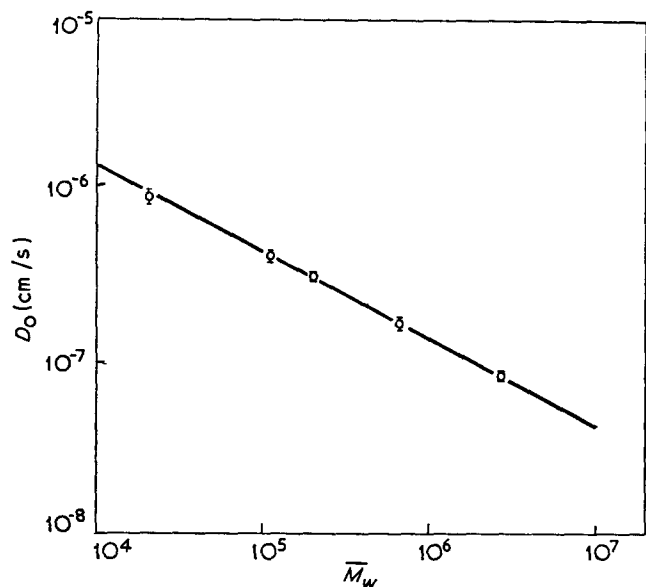


Figure 3 Dependence of  $D_0$  the diffusion coefficient at  $c=0$ , on molecular weight  $\bar{M}_w$  for polystyrene in cyclohexane at 35°C

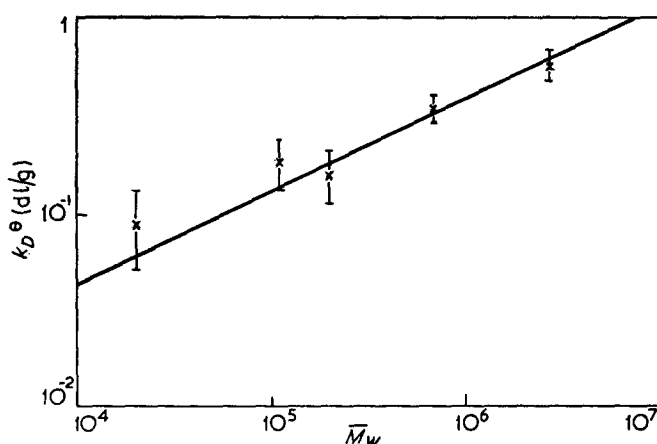


Figure 4 Variation of  $k_D^0$  with  $\bar{M}_w$  for polystyrene in cyclohexane at 35°C

in Figure 4 and a concentration dependence is found for  $D^0$  over the experimental range reported here of  $\bar{M}_w$  ranging from  $2 \times 10^4$  to  $2.7 \times 10^6$ . At this point we are now concerned with how this result compares with the theories of the diffusion or sedimentation coefficients.

### DISCUSSION

The nature of the  $D^0(c)$  concentration dependence from these results indicates that equation (7) can describe the low concentration behaviour of the polystyrene-cyclohexane system under theta conditions. Also the linear concentration dependence applies down to very low concentrations, e.g. for  $\bar{M}_w = 2.7 \times 10^6$  down to  $c = 10^{-3}$  g/dl and no real evidence for a concentration independent region as reported by Cantow<sup>5</sup> has been found which is outside the experimental uncertainty. Qualitative evidence for the higher order terms in  $D(c)$  is found for both theta (cyclohexane) and non-theta (butan-2-one) solvents.

The quantity  $k_D^0$  contains the polymer volume term and the coefficient  $k_f$  from the frictional dependence. The available theories for  $k_f$  may be divided into two

theoretical approaches. Yamakawa<sup>2</sup> and Imai<sup>3</sup> have used similar models based on the random coil polymer and the Kirkwood-Riseman theory to show:

$$k_f = 1.2A_2M + \frac{NV_h}{M} \quad (Y) \quad (15)$$

where  $V_h$  is the hydrodynamic volume of the polymer molecule, and

$$k_f = c_0M^{1/2}(\alpha_\eta - \alpha_\eta^{-1}) + \frac{NV_h}{M} \quad (I) \quad (16)$$

Here  $\alpha_\eta$  is the viscosity-radius expansion factor and  $c_0 = 2/(3^{3/2})N\Phi(X)[(nb_0^2/M)]^{3/2}$  is a constant with  $X$  = the effective volume of a polymer segment,  $n$  = the number of segments in the polymer and  $b_0$  = bond length. The term  $NV_h/M$  did not appear in the original publications<sup>2,3</sup> and occurs merely as a result of a coordinate transformation from the molecular frame to the laboratory frame in order to eliminate the surface effect<sup>1</sup> and conserve solution volume.

An alternative approach by Pyun and Fixman<sup>4</sup> used a spherical polymer model and considered the potential interaction as well as the hydrodynamic interaction. This gave for a soft interpenetrating sphere-like polymer:

$$k_f = [7.16 - K(A)] \frac{NV_h}{M} \quad (PF) \quad (17)$$

for the calculation when the concentration is in units of g/dl. In equation (17),  $K(A)$  is a monotonically decreasing function of  $A$  which is related to the second virial coefficient for segment-segment interaction.

At the theta temperature  $A \rightarrow 0$  and it is found<sup>4</sup> that  $K(A) = 4.93$ . Also under theta conditions  $\alpha_\eta = 1$  and then equations (15), (16) and (17) reduce to:

$$k_f = \frac{NV_h}{M} \quad (Y, I) \quad (18)$$

$$k_f = 2.23 \frac{NV_h}{M} \quad (PF) \quad (19)$$

We can use equations (18) and (19) to develop equation (6) further as:

$$k_D^0 = -\frac{N}{M}(V_1 + V_h) \quad (Y, I) \quad (20)$$

or

$$k_D^0 = -\frac{N}{M}(V_1 + 2.23V_h) \quad (PF) \quad (21)$$

The polymer molecular volume can be related to the polymer density  $\rho$  as

$$V_1 = \frac{M}{N\rho} \quad (22)$$

A measure of the polymer hydrodynamic volume can be obtained from the values of  $D_0^0$  found in this work. From equations (4) and (14) we can write:

$$D_0^0 = \frac{kT}{f_0} = \frac{kT}{6\pi\eta R_h} = k_T \bar{M}_w^{-b} \quad (23)$$

Here  $R_h$  is the hydrodynamic radius of the polymer such that the hydrodynamic volume  $V_h$  is given as:

$$V_h = \frac{4}{3}\pi R_h^3 = \frac{4}{3}\pi \left( \frac{kT}{6\pi\eta k_T} \right)^3 \bar{M}_w^{3/2} \quad (24)$$

Using the values of  $k_T = 1.3 \times 10^{-4} \text{ cm}^2/\text{s}$ ,  $\rho = 106 \text{ g/dl}$  and cyclohexane viscosity at  $35^\circ\text{C}$ ,  $\eta = 0.75 \text{ cP}$ , equations (20) and (21) reduce to:

$$k_D^\theta = -2.8 \times 10^{-4} \bar{M}_w^{1/2} - 9.4 \times 10^{-3} \quad (Y, I) \quad (25)$$

and

$$k_D^\theta = -6.2 \times 10^{-4} \bar{M}_w^{1/2} - 9.4 \times 10^{-3} \quad (PF) \quad (26)$$

The quantity  $(k_D^\theta + 9.4 \times 10^{-3}) \bar{M}_w^{-0.5}$  has a value of  $-2.8 \times 10^{-4}$  on the Yamakawa<sup>2</sup> and Imai<sup>3</sup> theories and a value of  $-6.2 \times 10^{-4}$  from the theory of Pyun and Fixman<sup>4</sup>. The results of this present study, as presented in Table 1, show that the experimental values of that quantity fall between the theoretical values for all the results from the five molecular weights reported. For small molecular sizes the experimental results move towards the Pyun and Fixman value. As indicated in Figure 4 the uncertainty in  $k_D^\theta$  ranges from  $< 5\%$  for  $\bar{M}_w = 2.7 \times 10^6$  to near  $50\%$  for  $\bar{M}_w = 2 \times 10^4$ . It may be expected that the low molecular weight polymers may not fit into the theoretical descriptions. If a weighting proportional to their experimental uncertainty is given to each of the five points in Figure 4 the form of the  $k_D^\theta$  data can be represented as:

$$k_D^\theta = (4.1 \pm 0.3) \times 10^{-4} \bar{M}_w^{0.48 \pm 0.04} \text{ dl/g} \quad (27)$$

The development of the description of  $D(c)$  as given briefly in the first section shows that the theories predict a concentration dependence for  $k_f$  and  $k_D^\theta$ . As found by other workers the concentration dependence is weaker in a poor solvent than a good solvent. If the polymer does not change its size much with concentration at the theta point we might expect the soft sphere model of Pyun and Fixman to be reasonable. Here the agreement is found to become better for  $\bar{M}_w \sim 10^5$ . The hydrodynamic contribution to  $k_f$  may possibly have other terms in addition to  $\langle (R_{ls})^{-1} \rangle_{av}$  which Yamakawa and Imai considered as the only source of concentration dependence. Also Imai indicates that a further dependence on concentration may be extracted from his theory if certain approximations are removed.

In comparing the diffusion coefficient obtained by the techniques of this study—a free diffusion method—and by sedimentation velocity or equilibrium measurements consideration needs to be given to the change of polymer conformation due to the applied force field which alters the frictional drag. There are reports<sup>8, 20</sup>

of sedimentation measurements giving values of  $k_f$  in a range which is higher than the value derived from the work of Pyun and Fixman and much higher than the value from Yamakawa and Imai. Also Kotaka *et al.*<sup>21</sup> found that  $k_f$  depended on the centrifugation speed. In the method of this paper, where the polymer moves under a diffusion process due to spontaneous concentration fluctuations in the solution and minimum perturbation of the polymer molecule is introduced, the assumptions of Yamakawa and Imai may be adequate.

#### ACKNOWLEDGEMENTS

The authors gratefully thank Professor G. Allen and Professor S. F. Edwards for discussions on the motion of polymer molecules and Dr C. Booth for providing viscosity and g.p.c. polystyrene characterization. They acknowledge with thanks financial support from the Science Research Council.

#### REFERENCES

- 1 Yamakawa, H. 'Modern Theory of Polymer Solutions', Harper and Row, New York, 1971, Ch 6
- 2 Yamakawa, H. *J. Chem. Phys.* 1962, **36**, 2995
- 3 Imai, S. *J. Chem. Phys.* 1969, **50**, 2116
- 4 Pyun, C. W. and Fixman, M. *J. Chem. Phys.* 1964, **41**, 937
- 5 Cantow, H. *J. Makromol. Chem.* 1959, **30**, 169
- 6 Klenine, S., Benoit, H. and Daune, M. *C.R. Acad. Sci.* 1960, **250**, 3174
- 7 Haug, A. and Meyerhoff, G. *Makromol. Chem.* 1962, **53**, 91
- 8 Cowie, J. M. G. and Cussler, E. L. *J. Chem. Phys.* 1967, **46**, 4886
- 9 Billick, I. H. *J. Phys. Chem.* 1962, **66**, 1941
- 10 Homma, T., Kawahara, K., Fujita, H. and Ueda, M. *Makromol. Chem.* 1963, **67**, 132
- 11 McIntyre, D., Wims, A., Williams, L. C. and Mandelkern, L. *J. Phys. Chem.* 1962, **66**, 1932
- 12 Noda, I., Saito, S., Fujimoto, T. and Nagasawa, M. *J. Phys. Chem.* 1967, **71**, 4048
- 13 Wales, M. and Rehfeld, S. *J. Polym. Sci.* 1962, **62**, 179
- 14 Cummins, H. Z. and Swinney, H. L. *Progr. Optics* 1970, **8**, 133
- 15 Pecora, R. *J. Chem. Phys.* 1968, **49**, 1032
- 16 Pecora, R. and Tagami, Y. *J. Chem. Phys.* 1969, **51**, 3298
- 17 Flory, P. J. and Fox, T. G. *J. Am. Chem. Soc.* 1951, **73**, 1904
- 18 Mandelkern, L. and Flory, P. J. *J. Chem. Phys.* 1952, **20**, 212
- 19 Berry, G. C. *J. Chem. Phys.* 1967, **46**, 1338
- 20 Petrus, V., Danihel, I. and Bohdanecky, M. *Eur. Polym. J.* 1971, **7**, 143
- 21 Kotaka, T. and Donkai, N. *J. Polym. Sci. (A-2)* 1968, **6**, 1457

# Kinetics of crosslinking of linear polyethylene with t-butyl peroxide

T. R. Manley and M. M. Qayyum

Department of Materials Science, Newcastle upon Tyne Polytechnic,  
Newcastle upon Tyne NE1 8ST, UK

(Received 28 September 1972; revised 27 November 1972)

The kinetics of the curing of polyethylene with di-t-butyl peroxide have been studied using a Wallace-Shawbury curometer and a Monsanto rheometer. Results obtained for the activation energy of the crosslinking reaction are of comparative value only, because the temperature of the specimen is not known with sufficient accuracy; this applies especially to the rheometer. It was not possible to crosslink polyethylene premixed with carbon black; the addition of carbon black to the mixture of polyethylene and peroxide greatly reduced the degree of crosslinking obtained.

## INTRODUCTION

The effect of peroxide concentration on the physical and mechanical properties of crosslinked polyethylene<sup>1</sup> and its behaviour at elevated temperatures<sup>2</sup> have been investigated.

Raley *et al.*<sup>3</sup> found that di-t-butyl peroxide decomposes by a first order dissociation reaction with an activation energy of 39 kcal/mol. The t-butoxy radicals formed tend to lose methyl radicals at higher temperatures rather than to abstract hydrogen<sup>4</sup>. Rado and Simunkova<sup>5</sup> using dicumyl peroxide found that temperature was the controlling factor for the rate, but had no effect on the efficiency of crosslinking. Moore and Watson found that t-butyl peroxide crosslinked natural rubber without causing degradation<sup>6</sup>.

In this paper an account is given of a study of the kinetics of the crosslinking of linear polyethylene with di-t-butyl peroxide at different temperatures using two commercial instruments, the Shawbury curometer and the Monsanto rheometer, that are widely used to study the curing of elastomers. The effect of carbon black on the kinetics of the crosslinking reaction was also investigated.

## EXPERIMENTAL

The linear polyethylene used (British Petroleum Rigidex 476) had a molecular weight ( $M_v$ ) of  $2.716 \times 10^5$  and an intrinsic viscosity in decalin of 2.96 at 135°C. The peroxide used was di-t-butyl peroxide (Trigonox B) in a hydrocarbon solvent (special boiling point spirit No. 4, Shell-Mex and BP) with Midland Silicones Ltd MS 550 as a dispersant in the ratio 10 : 10 : 4 parts as in previous work<sup>1</sup>.

The polyethylene was mixed with different amounts of peroxide in an Engel<sup>7</sup> pressure chamber at 130°C. The design pressure of the chamber was  $1.034 \times 10^9$  N/m<sup>2</sup> (150 000 lbf/in<sup>2</sup>). All the polyethylene samples containing peroxide were stored at -20°C.

The rate of cure was ascertained from a Wallace-Shawbury curometer MK III<sup>8</sup> (H. Wallace, Croydon) and a Monsanto rheometer (Model 100). The latter was used at a rotor speed of 100 cycles/min with an arc of oscillation of  $\pm 5^\circ$  and a standard die. Both apparatuses measure the change in modulus of the crosslinkable polyethylene against time at constant temperature. Seval Carbon Black (MT) of particle size 400  $\mu$ m and pH 8.4 was pre-mixed with the polyethylene in a Banbury mixer or added with the peroxide in a ball mill.

### Wallace-Shawbury curometer

A small fixed volume of powdered polymer containing peroxide is subjected to sinusoidal strain at a chosen temperature and any change in stiffness is recorded. The width of the trace is adjusted to compensate for the softness of the molten sample.

A curometer trace at 200°C with 3.6% peroxide is shown in Figure 1. The initial part of the trace indicates the flow in the sample when it is placed in the heated platen. The second portion of the trace shows the onset of crosslinking and it continues until a minimum distance between two curves is obtained.

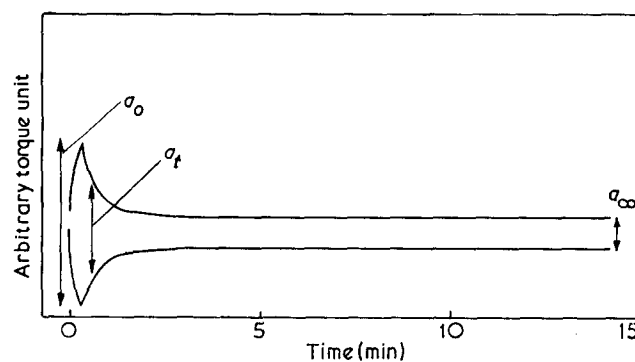


Figure 1 Curometer trace of crosslinked polyethylene at 200°C containing 3.6% peroxide



The shear modulus is given<sup>9</sup> by:

$$G = K \left( \frac{b}{a} - 1 \right)$$

where  $K$  and  $b$  are constants characteristic of the machine and stroke setting respectively and  $a$  is the width of stroke.

The modulus is taken to be proportional to the number of crosslinks<sup>10</sup> and the rate of crosslinking is taken to be first order. The number of crosslinks,  $Z$ , still to be formed after time  $t$  relative to the total number that can be formed is:

$$Z = \frac{(1/a_\infty) - (1/a_t)}{(1/a_\infty) - (1/a_0)}$$

where  $a_0$  = the greatest width of the trace at the start,

$a_t$  = width at time  $t$ ,

$a_\infty$  = width of the trace at infinite time.

The width of the trace when the lines are parallel gives the value for  $a_\infty$ , as degradation occurs if the experiment is prolonged.

Thus this equation is expressed in arbitrary torque (or shear modulus) units since the width of the trace varies with the shear modulus of the sample. The plot of the logarithm of this equation against time should be linear, i.e. first order, although initially during the warming up period this is not so. It is shown in *Figure 2* at 175°, 200°, and 220°C with 1.36% peroxide.

The cure time is taken as the time for 90% of the crosslinks to be formed, i.e. when  $-\log Z = 1.0$ . The values obtained and the activation energies are given in *Table 1*.

#### Monsanto rheometer

The specimen is subjected to a shear strain by means of an oscillating biconical disc. The torque required to oscillate the disc gives a measure of the shear modulus of the polymer. *Figure 3* shows an initial increase in torque (polymer viscosity) followed by a fall due to increasing temperature. When crosslinking occurs the torque rises. The cure shows a decrease in torque with time if chain scission takes place or a continual increase if a slow crosslinking reaction occurs.

A kinetic interpretation has already been given by Coran<sup>11</sup>.

Assuming that crosslinking is a first order reaction after an induction period  $t_i$ , we get:

$$\log_{10} (R_{\max} - R_t) = \log_{10} R_{\max} + \frac{k(t - t_i)}{2.303}$$

The torque at a time  $t$  ( $R_t$ ) and the maximum torque ( $R_{\max}$ ) are taken from the rheometer trace. *Table 2* gives the overall rate constant  $k$  obtained by plotting the log of  $(R_{\max} - R_t)$  against time, and the time for 90% of the crosslinks to be formed ( $t_{90}$ ). This is the number of minutes taken to reach a torque  $R_{90}$  given by:

$$R_{90} = 0.9 (R_{\max} - R_{\min}) + R_{\min}$$

## RESULTS

#### Shawbury curometer

The cure times for polyethylene containing different amounts of peroxide are shown in *Table 1*. As expected,

extra peroxide reduces the time for curing (90%) to occur. This is seen at 150°C but at higher temperatures the curing times are too short for any noticeable effect to be visible.

The minimum amount of peroxide required is 0.24%<sup>1</sup>. This figure is low because the process uses high molecular weight and high density polyethylene and disperses the peroxide efficiently.

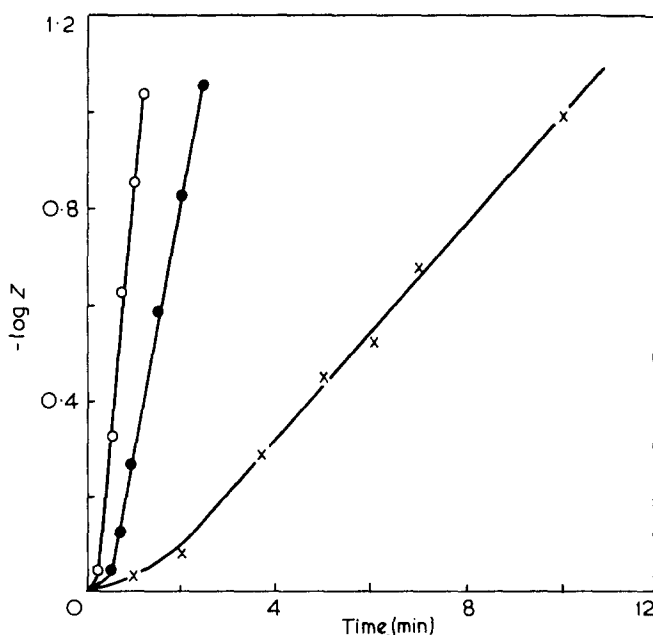
The slope of the cure curves, shown in *Figure 2*, is used as a measure of the rate of cure ( $k$ ) and the values obtained along with the activation energies calculated for the reaction over this range of temperature are given in *Table 1*. The gel content (mesitylene, 24 h heating) of crosslinked polyethylene samples containing 6.87% peroxide was found to be 87% giving good correlation with the theoretical values (90%). An exception occurs at 220°C when the value falls to 81% showing that the polymer is degrading at this temperature. 200°C is thus the preferred working temperature.

#### Monsanto rheometer

The time required for 90% crosslinking ( $t_{90}$ ) at 175°, 190° and 200°C is shown in *Table 2*. At 150°C the peroxide is being activated very slowly as is shown by the long scorch time and slow rise in viscosity; it was not possible to obtain reliable results. No noticeable differences are shown between the samples.

At 200°C the rheograph (*Figure 3*) is similar to that obtained with rubbers. It shows a rapid fall in viscosity to a minimum followed by a short dwell time before crosslinking starts to take place. Crosslinking continues as shown by the increase in torque until the maximum is reached. At 175°C the rate of crosslinking is considerably reduced while at 190°C the rate is faster than at 175°C, as would be expected.

The times for 90% crosslinking show an increase with increase of peroxide. This could be due to the presence of some scission reactions owing to shear strain.



*Figure 2* Rate of formation of crosslinks in linear polyethylene (1.36% peroxide) using Wallace-Shawbury curometer. x, 175°C; ●, 200°C; ○, 220°C

Table 1 Activation energy for the crosslinking of polyethylene using Wallace-Shawbury curometer

Number	Peroxide (%)	Temperature (°C)	Cure time* for 90% crosslinking (min)	Overall rate constant, $k$	$E$ (kcal/mol)
1	0.24	150	92.30	0.008	7.6
		175	21.00	0.075	
		200	2.56	0.469	
		220	1.04	1.12	
2	0.78	150	85.15	0.012	7.4
		175	11.21	0.087	
		200	2.22	0.52	
		220	1.12	1.10	
3	1.36	150	65.45	0.015	6.9
		175	10.33	0.108	
		200	2.11	0.53	
		220	1.07	1.06	
4	2.55	150	60.30	0.017	7.2
		175	9.54	0.105	
		200	2.04	0.69	
		220	1.12	1.16	
5	3.60	150	61.36	0.013	7.6
		175	11.26	0.093	
		200	2.31	0.65	
		220	1.18	1.10	
6	6.87	150	61.48	0.014	6.8
		175	12.46	0.086	
		200	2.36	0.45	
		220	1.13	1.03	

\* Mean of three results

Table 2 Activation energy for the crosslinking of polyethylene using Monsanto rheometer

Number	Peroxide (%)	Temperature (°C)	$t_{90}$ (min)	Overall rate constant, $k$	$E$ (kcal/mol)
1	0.24	175	29.0	0.044	9.2
		190	9.54	0.175	
		200	5.19	0.544	
2	0.78	175	30.30	0.042	10.8
		190	8.06	0.250	
		200	5.08	0.628	
3	1.36	175	32.0	0.036	10.1
		190	9.06	0.210	
		200	5.32	0.572	
4	2.55	175	32.50	0.038	10.2
		190	8.36	0.253	
		200	5.43	0.555	
5	3.60	175	33.0	0.041	10.2
		190	9.36	0.210	
		200	6.00	0.594	
6	6.87	175	34.0	0.032	10.6
		190	9.48	0.220	
		200	6.00	0.618	

The overall first order rate constant  $k$  obtained from the slope of reaction curve and the activation energy calculated for this reaction is shown in Table 2. The amount of peroxide, in excess of 0.24%, has no effect on  $E$ . The values are fairly constant over this range of temperature.

#### Effect of carbon black

Carbon black (MT) was mixed with polyethylene in a Banbury mill at 150°C for 10 min and then further milled on a two-roll mill for 5 min at 130°C. The material was ground into powder and then different amounts of peroxide were mixed with it in the Engel process at

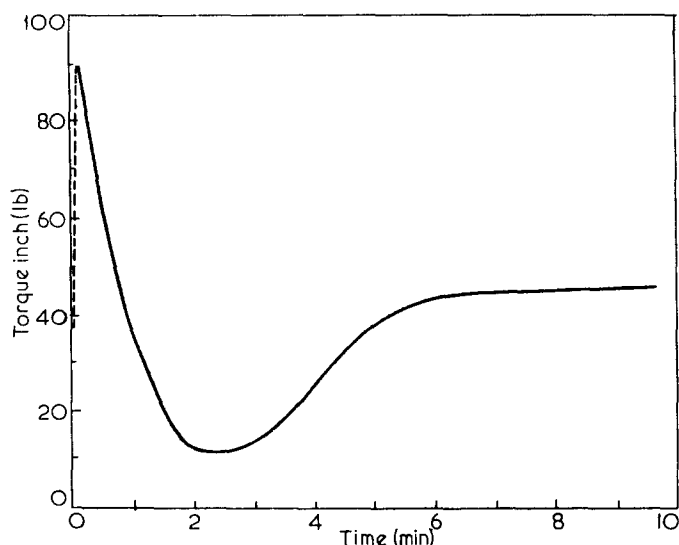


Figure 3 A rheograph of crosslinked polyethylene at 200°C containing 2.55% peroxide

130°C. The effect of 10, 25 and 40% carbon black on the curing of polyethylene was investigated using both the curometer and the Monsanto rheometer. In neither instrument was it possible to crosslink this carbon black filled polyethylene.

In the second trial polyethylene samples containing different amounts of peroxide, which were used in the main experiments, were ball milled with 10, 25 and 40% MT carbon black for 24 h at room temperature. The samples were subjected to the same investigation. The crosslinking reaction was considerably reduced. The curing test was repeated after a week, no measurable crosslinking was recorded.

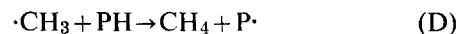
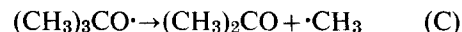
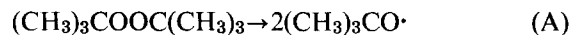
## DISCUSSION

The most important factor to be considered in comparing the instruments is the temperature of the specimen. In neither instrument is the temperature of the specimen directly measured. The sample in the curometer is very small while the rheometer requires a large specimen. Polyethylene has a very low thermal conductivity and the time required to raise the temperature of the inside of a thick specimen is relatively long. (It is for this reason that small specimens give better results in thermoanalytical studies where temperature measurement is crucial.) The results from a machine that requires large specimens should be viewed with caution. Downing and Stuckey<sup>12</sup> found that specimens used in the Monsanto rheometer had a considerable time lag between the temperature in the centre of a thick piece and that on the outside. This factor tends to cause variations in the state of cure within the specimen. On the other hand, there is a 2°C drop in temperature initially in the curometer which, owing to its fast heating rate, takes a few seconds to recover to original temperature.

The different type of strain used in both instruments makes it difficult to compare their results because the strain rate plays an important role. It was difficult to crosslink polyethylene in the rheometer with an arc of oscillation of  $\pm 3^\circ$ . All the specimens crosslinked with an arc of  $\pm 5^\circ$ . This could be due to the small arc of oscillation which is not sufficient to overcome the resistance of the material. It is also possible that a

large amplitude or a high frequency results in a substantial rise in the interior temperature of the material and helps to crosslink it faster than at low frequency.

Moore and Watson<sup>6</sup> made a detailed analysis of the *t*-butyl peroxide vulcanization of natural rubber. They proposed that the reaction scheme was:

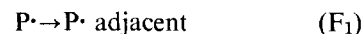


where PH denotes a polymer molecule and P $\cdot$  the polymer radical resulting from hydrogen abstraction. They confirmed it by product analysis which showed that the decomposed peroxide was recovered fully as *t*-butanol and acetone while the methane and ethane together were equivalent to the acetone formed. Reaction by this scheme gives the number of crosslinks as equivalent to the amount of *t*-butanol and methane. This basic work of Moore and Watson relied on the absence of any scission during vulcanization.

Interpretations of the results from the Monsanto rheometer are based on the assumption that the increase in torque during crosslinking is proportional to the crosslinking density. If crosslinking is the only reaction then one would expect a linear dependence of crosslinking on peroxide concentration.

In practice a slight levelling off of the curve is found because some peroxide is wasted (e.g. reaction E, formation of ethane). From Table 3 it is seen that the torque (maximum modulus) increases with the increase in peroxide (up to 2.55%) and then decreases. This decrease is due to the scission reaction already discussed.

It is known<sup>13</sup> that under the high pressure used in this work the mobility of polymer chain segments decreases resulting in a corresponding decrease in free radical decay. The formation and decay of radicals is too fast to be measured by these instruments. It is the slowest reaction which is being recorded. It appears that reaction (F) occurs in two stages. The first is the movement of radicals along the chains to positions adjacent to those of radicals in other chains. The second is the formation of crosslinks by intermolecular migration of the radicals:



Both instruments measure reaction F<sub>2</sub>, i.e. the rate of formation of crosslinks. This rate is accelerated by higher

Table 3 Maximum modulus [in (lb)] of crossed polyethylene from Monsanto rheometer at various temperatures

Number	Peroxide (%)	Temperature (°C)		
		175	190	200
1	0.24	41	39	39
2	0.78	87	103	84
3	1.36	72	63	72
4	2.55	105	87	91
5	3.60	75	71	65
6	6.87	56	52	52

temperatures but the amount of crosslinking is not affected. The curing time and activation energy found by the curometer is lower than that for the rheometer at all temperatures. The activation energy found by the curometer (7.2 kcal/mol) is preferred to that of the rheometer (10.2 kcal/mol) although the latter is closer to the 10 kcal/mol found in irradiation studies<sup>14</sup>. The activation energy given by the curometer is preferred to the result from the rheometer because the small platens of the curometer are heated very rapidly to the curing temperatures and a small sample is used. In the rheometer the temperature of the initial stages of cure is less accurately known.

The presence of carbon black has a considerable effect on the crosslinking of polyethylene. In the first case when peroxide is injected, it is being absorbed by the carbon black so no crosslinking reactions can occur.

In the second case when carbon black is mixed with polyethylene containing peroxide from 0.14 to 6.87%, the crosslinking reaction is reduced. This is attributed to the reaction of radicals present on the carbon black with the radicals produced by the peroxide.

#### CONCLUSIONS

The Wallace-Shawbury curometer is a simple and convenient method for studying the kinetics of crosslinking reactions. The Monsanto rheometer enables one to differentiate between the crosslinking and scission reactions and the rheograph is easily interpreted. The rheometer is not recommended for kinetic studies.

The rate of crosslinking increases with rise in temperature but the amount of crosslinking is unchanged. The amount of peroxide required may be varied from 0.24% to 2.5% without affecting the efficiency of the crosslinking; above 2.5% degradation occurs. Carbon black inhibits the crosslinking reaction.

#### ACKNOWLEDGEMENTS

We thank Mr C. W. Evans for his continued interest and encouragement and Dunlop Ltd for permission to publish.

#### REFERENCES

- 1 Manley, T. R. and Qayyum, M. M. *Polymer* 1971, **12**, 176
- 2 Manley, T. R. and Qayyum, M. M. *Polymer* 1972, **13**, 587
- 3 Raley, J. H., Rust F. R. and Vaughan, W. E. *J. Am. Chem. Soc.* 1948, **70**, 88
- 4 Raley, J. H., Rust, F. R. and Vaughan, W. E. *J. Am. Chem. Soc.* 1948, **70**, 1336
- 5 Rado, R. and Simunkova, D. *Chem. Průmysl* 1961, **11**, 657
- 6 Moore, C. G. and Watson, W. F. *J. Polym. Sci.* 1956, **19**, 327
- 7 Engel, T. *Plastics and Polymers* 1970, **38**, 174
- 8 RAPRA Report No. 135, Class No. 35725, November 1964
- 9 Pinfold, R. N. F. *Trans. Inst. Rubber Ind.* 1961, **37**, 206
- 10 Payne, A. R. *Plast. Rubber Wkly* 1963, No. 144, p 293
- 11 Coran, A. T. *Rubber Chem. Technol.* 1964, **37**, 689; 1965, **38**, 1
- 12 Downing, M. S. and Stuckey, J. E. *Rubber J.* 1969 (November), p 2
- 13 Szocs, F., Placok, J. and Borsig, E. *J. Polym. Sci. (B)* 1971, **9**, 753
- 14 Dole, M., Killing, C. D. and Rose, D. G. *J. Am. Chem. Soc.* 1954, **76**, 4304

# Transition magnitudes and impact improvement in rubber-modified plastics

R. E. Wetton

*Department of Chemistry, University of Technology, Loughborough, Leics LE11 3TU, UK*

and J. D. Moore and P. Ingram

*International Synthetic Rubber Company Limited, Southampton SO9 3AT, UK  
(Received 15 September 1972; revised 8 December 1972)*

Impact strength at room temperature and dynamic mechanical properties over a temperature range have been studied for a number of rubber reinforced glassy state plastics. The rubber phases in every case were butadiene copolymers of known composition and particle size and selected for their good dispersion after blending into the various matrices. This dispersion was checked by electron microscopy and the *in situ* particle size evaluated. The matrices were based on homo- and co-polymers of styrene, methyl methacrylate and acrylonitrile. A vibrating reed apparatus was employed to measure the storage component of Young's modulus ( $E'$ ) and loss factor ( $\tan \delta$ ) at essentially constant frequency ( $\sim 300$ Hz) through the rubber relaxation region. The Izod impact strength was measured in accordance with the standard method ASTM D-256. A gross parallel was found between impact strength and transition magnitude as measured by the change in modulus between  $-100^\circ\text{C}$  and  $20^\circ\text{C}$  ( $\Delta E'$ ) or the  $\tan \delta$  peak area with, for example, increasing volume fraction of rubber phase. However, when the same rubber was dispersed in different matrices a more subtle effect was an inverse proportionality of  $\tan \delta$  area with  $E'$  measured at the peak temperature. Conversely  $\Delta E'$  after correction for matrix modulus change was shown both theoretically and experimentally to be directly proportional to  $E'$  of the matrix at room temperature. The impact strength actually increases with  $\Delta E'$  and not with  $\tan \delta$  area in these cases. However, a more important requirement for good impact is compatibility between the rubber and matrix, but neither  $\Delta E'$  nor  $\tan \delta$  reflect this. After correction of  $\tan \delta$  areas to constant matrix modulus there remains an increase of area with particle size. Impact strength also increases strongly with particle size for compatible systems. The applicability of Hashin's central equation and Mackenzie's equation in describing the systems is discussed.

## INTRODUCTION

A number of authors have pointed out that there is often a correspondence of low temperature transition magnitude in small strain dynamic mechanical behaviour with impact strength at room temperature. This has been proposed<sup>1</sup> both for glassy state homopolymers in which the low temperature relaxation is a secondary ( $\beta_a$ ) process and for rubber modified glassy thermoplastics<sup>2</sup> in which it is due largely to the dispersed rubber phase main relaxation process ( $\alpha_a$ ). Nielsen<sup>3</sup>, however, concluded that correlations of transition magnitudes with impact behaviour, although they existed, were imperfect, while more recently Heijboer<sup>4</sup> has suggested a rationalization of the homopolymer case by limiting impact correlations to those  $\beta_a$  processes arising from in-chain modes of motion.

The situation in rubber-modified plastics is very much more complex than in the homopolymer case. The nature and morphology of the rubber phase together with properties of the interface now become important. Furthermore, in all the important cases of impact

improved plastics stress-whitening occurs at the fracture surface. It is generally accepted that crazing is the origin of the stress-whitening and that, as proposed by Bucknall and Smith<sup>5</sup>, this is the essential energy absorbing process conferring toughness. The correlation of small strain dynamic data, no matter how imperfect, with the large strain yielding process occurring on impact is thus somewhat surprising.

The present paper is concerned with investigating the factors influencing transition magnitude and impact strength. In the long term, understanding is sought of the physical basis of meaningful correlations between the two properties. It is virtually impossible to vary the morphology (e.g. particle size) of the dispersed rubber without altering the properties of the rubber at the same time. The approach chosen in the present work was thus to disperse a number of different commercial and experimental latex grafted rubbers in a series of different matrices. The morphology of a given rubber can be checked, by electron microscopy, to be constant over the range of different matrices.

## EXPERIMENTAL

The rubber phase was provided by commercially available emulsion graft copolymers, either of styrene and methyl methacrylate on to styrene-butadiene rubber (MBS), or of styrene and acrylonitrile (ACN) on to polybutadiene rubber (ABS). Details of their compositions are given in *Table 1*. A comparison was made with ungrafted styrene-butadiene rubber (Intol SBR 1006), together with this and a polybutadiene latex grafted in our laboratories.

The compositions were determined using the method of Hilton<sup>15</sup> for bound styrene and Kjeldahl for nitrogen content to give the bound acrylonitrile. Where applicable the methyl methacrylate content was determined by an infra-red method using the peak at 5.8  $\mu\text{m}$ .

A commercially available polystyrene (Sterling ST 90) and a styrene-acrylonitrile copolymer containing 25% acrylonitrile by weight (Monsanto Lustran) provided two of the matrices. The remaining thermoplastic matrices were prepared by bulk polymerization. The first series was one of styrene-methyl methacrylate copolymers containing between 50% and 100% by weight of methyl methacrylate. These were prepared using small amounts of tertiary dodecyl mercaptan (TDM) as molecular weight regulator and 0.3 parts by weight of tertiary butyl peroxoate (TBPO) as initiator with polymerization for 36 h at 65°C. After cooling the blocks were sawn and granulated.

The second series was of styrene and acrylonitrile copolymers containing 0, 5, 10, 15, 20 and 25% by weight of acrylonitrile. These were prepared using 0.1, 0.15, 0.2, 0.25, 0.3 and 0.35 parts by weight of TDM and 0.2, 0.2, 0.15, 0.15, 0.1, 0.1 parts of TBPO as initiator. The temperature cycle was 24 h at 60°C and 4 h at 120°C. The materials were granulated in a similar manner to the styrene-methyl methacrylate copolymers.

The rubber reinforced thermoplastics were prepared by blending the powdered graft copolymers and granulated thermoplastic matrices in a Brabender Plastograph at 180°C, and mixing for 7 min. The formulation contained 0.5% by weight of an antioxidant, Plastanox 425<sup>®</sup> (Cyanamid Company).

The commercial MBS and the ABS materials 'A' and 'B' were blended with the styrene-methyl methacrylate copolymers and poly(methyl methacrylate) (PMMA) to give 20%, 15% and 10% content of *parent rubber* [butadiene (BD) or SBR] by weight. The percentages of *total graft rubber* are higher than these figures and can be evaluated from *Table 1*. The commercial ABS 'A' was blended with polystyrene and the range of styrene-acrylonitrile copolymers at a rubber level of

15% by weight of the parent rubber (butadiene) while all three commercial ABS materials were blended with SAN containing 25% acrylonitrile to give a parent rubber (butadiene) content of 15% by weight. SBR 1006, its MBS graft and the experimental MB rubber were blended into a range of styrene-methyl methacrylate copolymer matrices to give a 12.5% content of parent rubber.

The Izod impact strength of the blends prepared were determined on compression moulded test pieces of  $2\frac{1}{2}$  in  $\times$   $\frac{1}{2}$  in  $\times$   $\frac{1}{8}$  in, cut with a notch of radius 0.01 in, using a pendulum type machine in accordance with ASTM D-256.

The microstructure and the particle size of each blend prepared were examined by electron microscopy of thin sections, using the staining and hardening technique of Kato<sup>6</sup>, employing a solution of osmium tetroxide. In the case of the commercial graft copolymers it was found that the dispersion and therefore discrete particle size did not vary with the composition of the matrix.

The dynamic mechanical behaviour at very small strains was determined over a temperature range -120°C to +20°C using a previously described vibrating reed apparatus<sup>7</sup>. Bar specimens were cut from the same sheet as the impact specimens and each was clamped at one end against a piezoelectric ceramic transducer, while the other end was vibrated electromechanically. Measurements were performed around the resonant frequency ( $\sim 300$  Hz) which decreases slightly [as  $(E')^{1/2}$ ] with increasing  $T$ . The storage component of Young's modulus is determined from the resonant frequency ( $f_0$ ), as discussed previously<sup>7</sup>, while  $\tan \delta = \Delta f/f_0$ , where  $\Delta f$  is the half power width of the amplitude resonance curve. The loss component of Young's modulus follows immediately as  $E'' = E' \tan \delta$ . Corresponding data were also obtained for the matrix materials alone.

## RESULTS AND DISCUSSION

Dynamic mechanical data, similar to those shown in *Figure 1* for the commercial ABS 'A' rubber in a PMMA matrix, were obtained for each sample. In each case a damping peak at  $\sim -71^\circ\text{C}$  is observed for the polybutadiene based rubber grafts while the peak for the SBR based grafts was  $\sim -43^\circ\text{C}$ . The skirts of the peaks varied slightly in shape from series to series, but this aspect will not be discussed further here. The damping associated with the rubber phase only, is estimated by drawing in a background to give an area  $A_R$ , when plotted against reciprocal temperature. The background is of course due to damping processes

*Table 1* Analysis of grafted rubber phase

Graft copolymer	Rubber main chain	Composition of grafted rubber (% by wt.)				Rubber phase particle diameter in blends ( $\mu\text{m}$ )	Weight average diameter ( $\mu\text{m}$ )
		BD	Styrene	ACN	MMA		
Commercial MBS	SBR	53.6	32.2 (total) 18.8 (grafted)	—	14.2	0.05-0.1	0.06
Commercial ABS 'A'	PBD	63	27.7	9.3	—	0.2-0.5	0.4
Commercial ABS 'B'	PBD	48.7	39.0	12.3	—	0.1-0.2	0.15
Commercial ABS 'C'	PBD	49.7	37.8	12.5	—	0.2-0.7	0.4
Intol 1006	SBR	76	24	—	—	Uneven particles	$\sim 0.6$
1006 graft MBS	SBR	52	15 (grafted)	—	15	0.2	0.2
Experimental MB	PBD	60	—	—	40	—	0.42

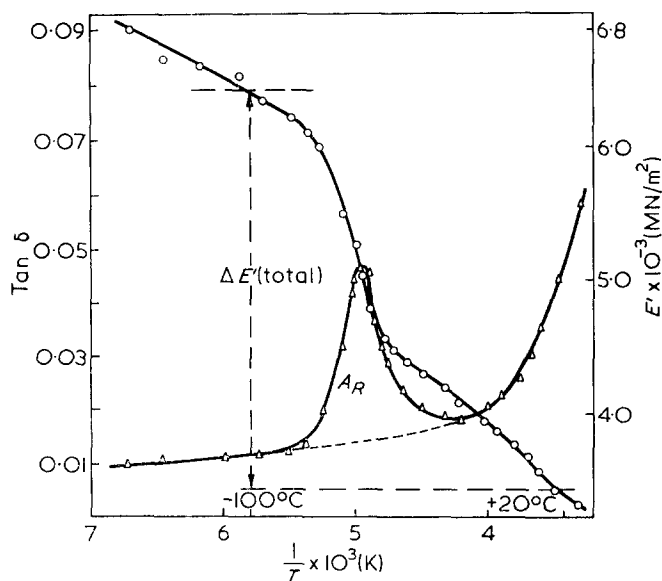


Figure 1 Storage modulus  $E'$  and  $\tan \delta$  measured at  $\sim 300$  Hz plotted against  $1/T$  for PMMA containing 24% of ABS 'A' rubber graft.  $A_R$  defines the loss peak area due to the  $\alpha$  relaxation process of the rubber phase

operating in the matrix material. The total relaxation magnitude of both rubber and matrix may be measured via the change in modulus from some very low temperature. It was found that the rubber phase relaxation commenced well above  $-100^\circ\text{C}$  and  $\Delta E'$  (total) was thus taken from  $-100^\circ\text{C}$  to  $+20^\circ\text{C}$ .

It is worth pointing out the significance of these damping peak locations. As will be discussed later, the fact that the rubber is embedded in a matrix distorts the rubber damping peak very little, one or two degrees being typical. The position of the peaks are certainly within  $10^\circ\text{C}$  of the damping peak expected from the parent (ungrafted) rubber, e.g. polybutadiene  $\sim -80^\circ\text{C}$ . Typically the rubber grafted systems contain 30–50% polystyrene or similar graft. If this were dispersed molecularly it would certainly elevate the rubber glass transition by tens of degrees (as in SBR itself) rather than by a few. Thus although the rubber grafts appear free of inclusions by electron microscopy, the dynamic mechanical evidence indicates phase separation of the polystyrene or other graft component. This is further evidenced by the high modulus of the experimental butadiene latex graft (MB) which was amenable to direct measurement. This exhibited a damping peak at  $-77^\circ\text{C}$  and a rubbery modulus of  $\sim 500 \text{ MN/m}^2$ , yet showed no inclusions by electron microscopic techniques which would be expected to reveal  $100 \text{ \AA}$  inclusions. The poly(methyl methacrylate) phase size in the rubber graft is thus less than this figure and we expect this

condition to hold in all the rubber grafts employed in this work.

The grafted rubbers used in this work retained their original particle size distribution after mechanical blending into the different matrices. This is probably due in part to a degree of crosslinking in the rubber and in part to the presence of the phase separated polystyrene segments. Mechanical blending of non-grafted rubbers gave poorly reproducible morphology which was highly dependent on the blending conditions. By using grafted rubbers in different matrices and ensuring good dispersion, constant morphology is achieved for any of the rubber grafts. Different rubber grafts have different morphology of course. Changes in impact strength and transition magnitude in any single series can thus be related to other parameters than morphological changes and this is a greatly simplifying factor.

In Table 2 are shown the pertinent parameters for different styrene-methyl methacrylate (SMMA) copolymer matrices containing the same ABS 'A' rubber. This illustrates two main points which are generally found to hold with constant morphology. The first is that the transition temperatures are constant within experimental error and the second that both transition magnitudes  $A_R$  or  $\Delta E'$  and impact strengths increase with volume fraction of the rubber. This is the gross correlation between impact strength and transition magnitude. However, it is clear from the same data that there is a more subtle variation in the parameters with changing matrix. The trends in these data are representative of all the systems studied.  $\Delta E'$  changes in sympathy with impact strength whereas the  $\tan \delta$  area ( $A_R$ ) does not. In fact  $A_R$  decreases as the modulus of the matrix increases. Any relationship between loss peak area and matrix modulus will involve the modulus in the same region as that in which the loss occurs. In Figure 2 therefore the  $E'$  value at  $-70^\circ\text{C}$  is plotted against styrene/acrylonitrile matrix composition together with  $A_R$  and impact strength for ABS 'A' at a level of 24%.  $\Delta E'$ , although not shown here, again increases with impact strength and  $E'$  while  $A_R$  is reciprocally related. These trends are found consistently in all the systems studied in this work as will be shown in combined plots later (Figures 3 and 6). It must be emphasized that the base matrices have very similar impact strengths at  $0.15 \pm 0.01 \text{ J per cm of notch}$ .

It is found that  $\Delta E'$  (total) increases with  $E'$  for all systems. The reason for this and a theoretical formulation of a quantitative relationship may be seen by examining Mackenzie's equation for a voided system<sup>8</sup>, i.e. the present situation if  $E'(\text{rubber}) \ll E'(\text{matrix})$ . Under these conditions:

$$E'_c = E'_1 \left[ 1 - \frac{15(1 - \nu_1)}{7 - 5\nu_1} \phi \right]$$

Table 2 Dynamic mechanical data for commercial ABS 'A' blends

Matrix	Rubber (%)	Impact strength ( $\text{J cm}^{-1}$ )	Loss peak temp. ( $^\circ\text{C}$ )	Tan $\delta$ , $A_R$	$\Delta E'_{173-293}$ ( $\text{GN m}^{-2}$ )	$E'_{293}$ ( $\text{GN m}^{-2}$ )
SMMA 50:50	15	0.69	-71	18.5	2.44	2.58
SMMA 25:75	15	1.1	-70.5	18	2.38	2.74
PMMA	15	1.2	-71.5	14	2.96	3.39
SMMA 50:50	10	0.26	-69.5	12.5	1.95	2.82
SMMA 25:75	10	0.53	-71.5	9.0	2.31	3.13
PMMA	10	0.58	-73	8.0	2.52	3.75

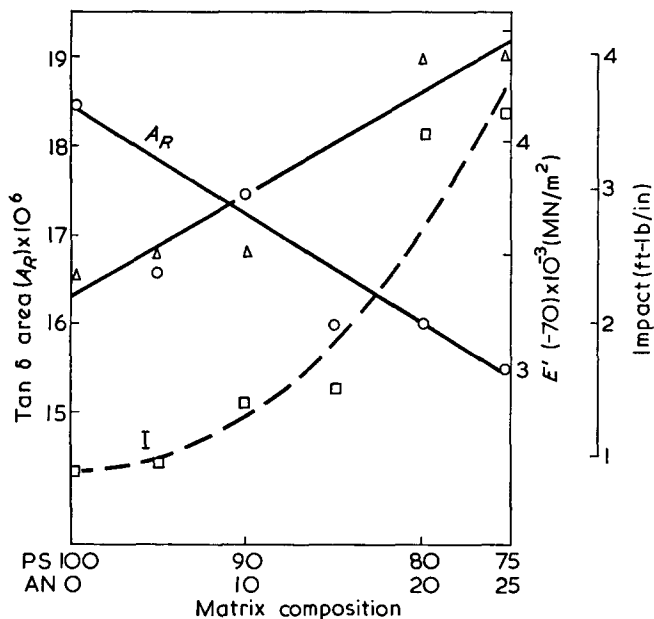


Figure 2 Tan  $\delta$  area ( $A_R$ ), impact strength and matrix modulus at the peak loss temperature ( $-70^\circ\text{C}$ ) plotted as a function of matrix composition for ABS 'A' (24% rubber graft) in styrene-acrylonitrile copolymer matrices. (1 ft-lb/in = 0.53 J/cm)

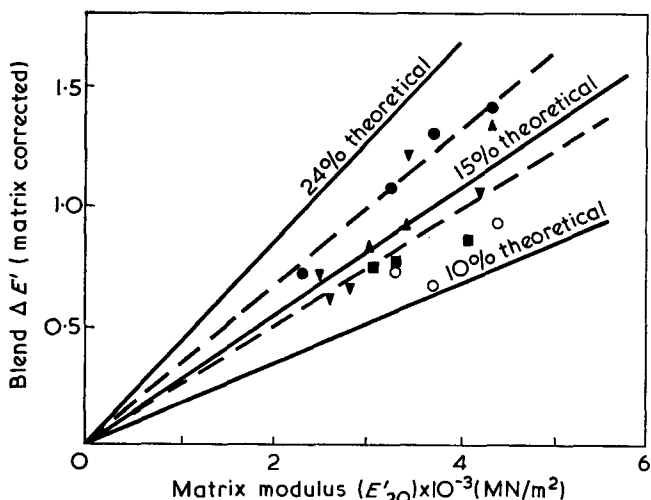


Figure 3 Transition strength ( $\Delta E'$ ) after subtraction of matrix change in region versus matrix modulus (300Hz) at  $20^\circ\text{C}$ . Theoretical lines according to equation (1).  $\bullet$ , 24% ABS 'A' in S/MMA matrices;  $\blacktriangledown$ , 24% ABS 'A' in S/AN matrices;  $\blacktriangle$ , 30% ABS 'C' in S/AN, and S/MMA matrices;  $\blacksquare$ , 31% ABS 'B' in S/MMA matrices (all filled points 15% parent polybutadiene);  $\circ$ , 16% ABS 'A' in S/MMA matrices (10% parent polybutadiene)

which may be rearranged to give

$$E'_1 - E'_c = E'_1 \left[ \frac{15(1 - \nu_1)}{7 - 5\nu_1} \phi \right]$$

where  $E_1$  and  $E_c$  are the Young's moduli of the matrix and composite respectively measured at  $20^\circ\text{C}$  in the present context,  $\phi$  the volume fraction of disperse phase and  $\nu_1$  Poisson's ratio for the matrix. Now if  $\Delta E'$  (total) is corrected by subtraction of the relaxation occurring in the matrix modulus between  $-100^\circ\text{C}$  and  $20^\circ\text{C}$ , then

$$\Delta E'(\text{matrix corrected}) \approx E'_1 - E'_c = E'_1 \left[ \frac{15(1 - \nu_1)}{7 - 5\nu_1} \phi \right] \quad (1)$$

The approximation involved is that at  $-100^\circ\text{C}$  the composite modulus is not significantly different from that of the matrix. The above equation (1) is tested with the present data in Figure 3. Remembering the rather large experimental errors which accrue in measuring absolute moduli and their differences, each set of data can be approximated by a straight line through the origin.

The line predicted from equation (1) on the basis of 15% or 10% very soft phase ( $E_2 \ll E_1$ ) actually represents these data fairly well. Each rubber particle, however, contains glassy inclusions by virtue of the grafting reactions, so that the total graft rubber phase varies from 15.9% to 30.8% for the data shown. These heavily included phases have moduli which are not trivial compared to  $E_1$ . The experimental MB graft has  $E_2 = 520 \text{ MN/m}^2$  at  $20^\circ\text{C}$ . If this value is typical of the other grafts  $E_2/E_1 \sim 0.14$ . The situation should now be described more accurately by the central equation of Hashin<sup>9</sup>:

$$E_c = E_1 \left[ 1 - \frac{15(1 - \nu_1)(1 - E_2/E_1)\phi}{(7 - 5\nu_1) + (8 - 10\nu_1)[E_2/E_1 + (1 - E_2/E_1)\phi]} \right] \quad (2)$$

which reduces to Mackenzie's equation (1) if  $E_1 \gg E_2$  (rubber modulus) and  $\phi$  small. (The relation in this form will only hold if both Poisson's ratios,  $\nu_1$  and  $\nu_2$ , are less than  $\sim 0.4$ .) Using  $E_2/E_1 = 0.14$  and  $\phi = 0.24$  for total graft rubber ABS 'A' in the glassy matrices, gives  $\Delta E'$  (equation 2) = 0.66  $\Delta E'$  (equation 1). The experimental data are then equally well described by equation (2), treating the total graft rubber phase as a significant modulus filler. This treatment is undoubtedly more correct, but the simpler form of equation (1) is appealing and it clearly demonstrates that  $\Delta E'$  depends most significantly on  $E_1$  and  $\phi$  for these systems.

It was thought useful to investigate the more general applicability of equation (2) over the whole temperature range. The purpose is primarily to seek a theoretical relationship for the variation of loss peak areas with matrix modulus. For the experimental MB graft good data have been obtained for all the required moduli against temperature at the same measuring frequency ( $\sim 300 \text{ Hz}$ ). For illustration the case of 21% of this graft dispersed in a 50:50 styrene-methyl methacrylate copolymer matrix is taken. The storage components  $E'_1$  and  $E'_2$  are combined via equation (2) on a point to point basis at each temperature,  $\nu_1 = 0.33$  was assumed throughout. The calculated value of  $E_c$  is compared with the experimentally observed data in Figure 4. The out-of-plane components  $E''_1$  and  $E''_2$  are similarly combined via the same relation to give  $E''_c$ . Tan  $\delta_c$  was then evaluated as  $E''_c/E'_c$  from the two calculations. The results of the theoretical calculations and the experimental data for the composite are shown in Figure 5 together with tan  $\delta$  for each phase separately. We note the predicted tan  $\delta_c$  in the loss peak region is significantly lower than the experimental value but agrees with it outside this region. The application of the same coupling equation to elastic and viscous components was shown to be sound by Goodier<sup>10</sup> and the results used by both Smallwood<sup>11</sup> and Guth<sup>12</sup>. The cause of the discrepancy probably lies in the fact that  $E''_2$  exceeds the matrix value  $E''_1$  in the loss region and that the stress coupling has changed. In the loss



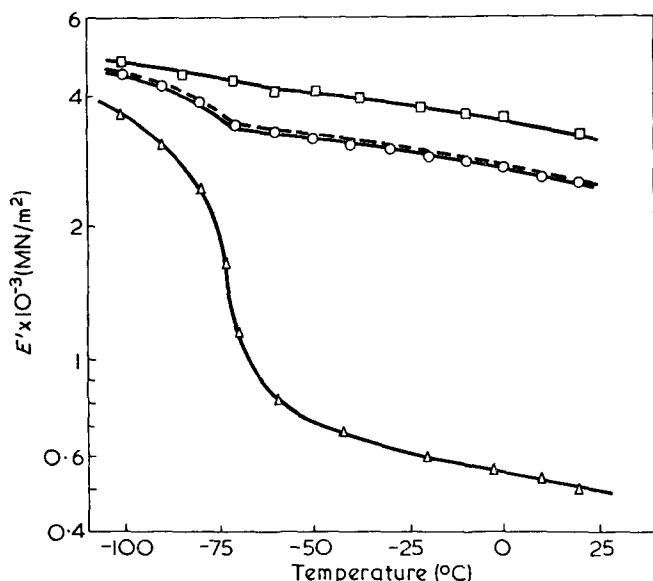


Figure 4 Experimental Young's moduli for experimental MB rubber graft ( $\Delta$ ), 50:50 S/MMA copolymer matrix ( $\square$ ) and a 21% blend of the rubber in the matrix ( $\circ$ ). ---, theoretical prediction of Hashin's central relation, equation (2).  $\bar{D}_w = 4.210 \text{ \AA}$

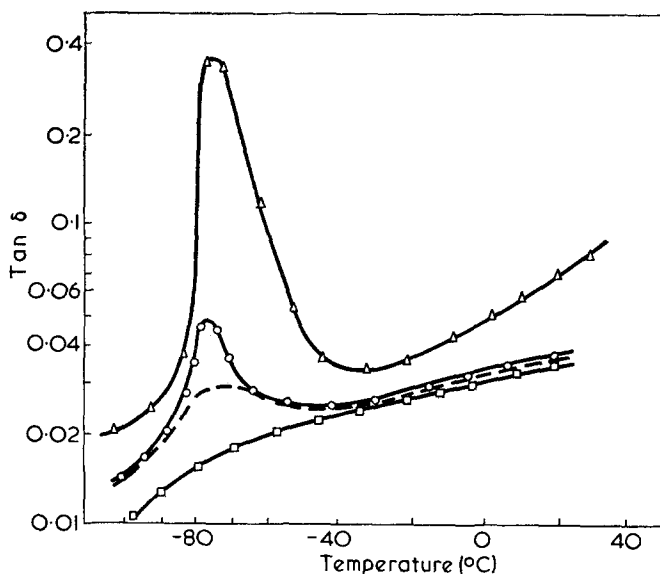


Figure 5 As with Figure 4 but comparing experimental and predicted loss factors. Note the discrepancy in the transition region

region the system has moved towards the equal strain situation approaching Hashin's upper bound values. The coupling situation will of course be changing continuously so that no one equation yet proposed will describe the situation through the whole region. It is also worthy of note that the loss peak position on the theoretical curve has shifted to  $-72^\circ\text{C}$  whereas experimentally it is practically unchanged at  $-76^\circ\text{C}$ . This erroneous peak prediction by the extremes of Hashin's bounds is clearly evident in the calculations of Bucknall and Hall<sup>13</sup>.

From equation (2) can be derived without approximation:

$$\tan \delta_c = \tan \delta_1 \left[ 1 + \phi \left( \frac{1 - E'_2/E'_1}{1 + E'_2/E'_1} - \frac{1 - E''_2/E''_1}{1 + E''_2/E''_1} \right) \right]$$

Without further approximation, this is not particularly useful in predicting the dependence of the loss area

$A_R$  on matrix modulus and as the equation fails to predict the correct loss peak size for the composite, this argument is not pursued further. Instead we note empirically for all the systems containing ABS 'A' graft at the 24% level that

$$A_R = K/E'_1(\text{peak } T) \quad (3)$$

where  $K = 7 \times 10^4 \text{ N m}^{-2} (\text{K})^{-1}$ . In looking for the reason for this relationship we note the expression relating total loss area (on a  $1/T$  plot) to the modulus change through the transition for a single relaxation time<sup>14</sup>,

$$\int_{-\infty}^0 \tan \delta \cdot d(1/T) = \frac{(E'_\infty - E'_0)\pi R}{(E'_\infty E'_0)^{1/2} 2Q}$$

where the limiting low  $E'_\infty$  and high  $E'_0$  temperature moduli could be replaced in the present work by  $E'_{-100}$  and  $E'_{20}$  respectively for the composite.  $Q$  in this relation is the activation enthalpy. This indicates that if the product  $(E'_{-100} \times E'_{20})$  increased faster than  $\Delta E'$  (total) on changing to a higher modulus matrix then the total loss area will decrease. This might be the reason why  $A_R$ , the rubber loss peak area, shows a reciprocal relation with the modulus of the matrix at the loss peak temperature but application of approximations such as equation (1) then erroneously predict  $A_R$  independent of the modulus. Qualitatively the present authors believe that the rubber phase can be considered as becoming more mechanically isolated the higher the modulus of the matrix in which it is dispersed and that it is the conditions of stress coupling changing with modulus that produce the observed area changes.

The empirical equation (3) is expected to apply to each type of rubber but with its own slightly different  $K$  value. Instead of evaluating this rather meaningless  $K$  value for each system the  $K$  value of  $7 \times 10^4 \text{ N m}^{-2} (\text{K})^{-1}$  has been taken as a standard and all  $A_R$  values for other systems corrected to a constant matrix modulus of  $4.9 \text{ GN/m}^2$  by using the same value of  $K$ . Differences in  $A_R$  values from system to system will then be largely dependent on morphology and factors other than matrix modulus. In Figure 6 corrected (circled points) and uncorrected  $A_R$  values are plotted against weight average particle diameter, which is believed to be the important morphological difference between the present systems. All data are for composites with 15% parent rubber dispersed as spherical particles. Correction to a constant matrix modulus strengthens the evidence that  $A_R$  increases with particle size and tends to a lower limit as the particle size decreases to zero. It is not known whether the cause of this increasing trend with particle size is chemical or physical. A shell of grafted glassy state material on the outside of the rubber particles could decrease the rubber effective in generating  $A_R$ , the larger the particle the less the volume fraction of effective rubber would be modified. This argument requires that  $A_R \rightarrow 0$  as diameter  $\rightarrow 0$ , which in the present limited size range is not observed. Against this trend in chemical composition is the fact that the largest particle size shown was for ungrafted rubber and yet the relationship with size is still maintained. Thus the weight of evidence at the moment is in favour of a physical origin through changes in stress coupling patterns in the transition region. It seems that the loss modulus of the rubber is more parallel coupled to the

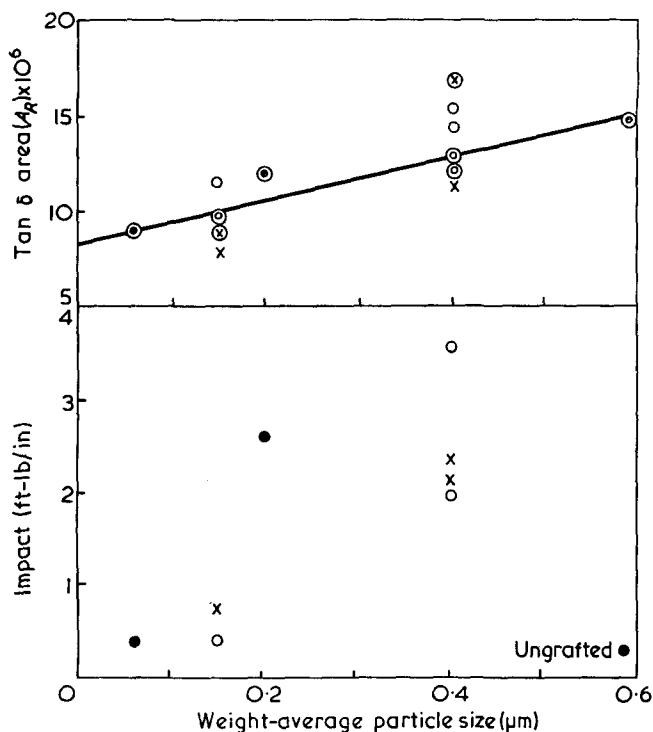


Figure 6 Tan  $\delta$  area ( $A_R$ ) and impact strength (1ft-lb/in=0.53 J/cm) versus particle size in the indicated matrices. The encircled  $A_R$  values are 'corrected' to a common matrix modulus of 4.9 GN/m<sup>2</sup> via equation (3). All data are for composites containing 15% parent rubber. x, MMA matrix; O, S/AN matrix; ●, S/MMA (50:50)

matrix (tending towards the equal strain bound) the larger the particle size.

The impact strength shown in Figure 6 also increases with particle size, this time very strongly. This is true only if the rubbers are compatible with the matrix. The ungrafted SBR of large particle size does not show any significant improvement. The grafted rubbers are of markedly higher modulus than the ungrafted parent material and this may be a contributing cause in the impact enhancement. Other work which will be reported shortly<sup>16</sup>, however, clearly demonstrates that good compatibility is a major requirement for good impact strength. It is interesting to conjecture that the increased parallel coupling proposed to explain the tan  $\delta$  area increase may also be at least partly responsible for the improved impact strength with particle size, provided that the rubber/matrix interface shows good adhesion under large strain conditions. The effect of particle size on impact strength will be discussed further in a later publication<sup>17</sup>.

## CONCLUSIONS

Much of the subtle change in transition magnitudes observed in systems of constant morphology can be

explained purely by reference to the modulus of the matrix. The increase in the total change in modulus through the rubber transition,  $\Delta E'$ (total) with matrix modulus,  $E'$ , at room temperature can be neatly explained by Mackenzie's equation for voided systems or Hashin's central equation with  $E_1 > E_2$ . The opposite trend in the tan  $\delta$  loss areas due to the rubber phase is proposed to be the result of changing patterns of stress coupling with different levels of matrix moduli. Certainly Hashin's central equation fails to predict the correct loss peak magnitude in the transition region even though it applies well to all data outside this region.

After due allowance is made for the modulus of the matrix, tan  $\delta$  areas and impact strength show the same increasing trend with particle size, although in the impact case it is more dramatic. This suggests that a change towards parallel coupling between phases as the particle size increases might be responsible for both effects. Impact strength, however, is always dependent on good compatibility between the rubber and the matrix. Without this the impact strength, being a large strain property, is disastrously low, whereas the transition magnitudes reflect little or nothing of the nature of the interphase boundary.

## ACKNOWLEDGEMENTS

The authors wish to thank Professor E. W. Duck of the I.S.R. laboratories without whose help and encouragement this work would not have been possible. The assistance of Dr I. J. W. Bowman with electron microscopy is gratefully acknowledged.

## REFERENCES

- Wada, Y. and Kasahara, T. *J. Appl. Polym. Sci.* 1967, **11**, 1661
- Turley, S. G. *J. Polym. Sci. (C)* 1963, **1**, 101; *Appl. Polym. Symp.* 1968, **7**, 273
- Nielsen, L. E. 'Mechanical Properties of Polymers', Reinhold, New York, 1962, p 173
- Heijboer, J. J. *J. Polym. Sci. (C)* 1968, **16**, 3755
- Bucknall, C. B. and Smith, R. R. *Polymer* 1965, **6**, 437
- Kato, K. *Polym. Eng. Sci.* 1967, **7**, 38
- Wetton, R. E. and Fielding-Russell, G. S. *Plastics and Polymers*, 1970, **38**, 179
- Mackenzie, J. K. *Proc. Phys. Soc. (B)* 1950, **63**, 2
- Hashin, Z. *J. Appl. Mech.* 1962, **29**, 143
- Goddier, J. N. *Phil. Mag.* 1936, **22**, 678
- Smallwood, H. M. *J. Appl. Phys.* 1944, **15**, 758
- Guth, E. J. *J. Appl. Phys.* 1944, **15**, 768
- Bucknall, C. B. and Hall, M. M. *J. Mater. Sci.* 1971, **6**, 95
- Read, B. E. and Williams, G. *Trans. Faraday Soc.* 1961, **57**, 1979
- Hilton, C. L. *Rubber Age* 1959 (August), p 783
- Ingram, P. and Wetton, R. E. *Plastics and Polymers* to be submitted
- Moore, J. D. and Wetton, R. E. *Plastics and Polymers* to be submitted

# Influence of cooling rate on the heat capacity and thermal transitions of amorphous polyhexene-1

J. Bourdariat, A. Berton, J. Chaussy, R. Isnard and J. Odin

*Centre de Recherches sur Les Très Basses Températures et Laboratoire d'Electrotechnique, CNRS, BP 166, 38042 Grenoble, France*  
(Received 21 November 1972)

Heat capacity measurements have been made on an amorphous polyhexene-1 sample between 20 and 300K, with an adiabatic calorimeter giving a low dispersion on the  $C_p$  curve (0.2–0.4%). The measured sample was prepared by a new method increasing its thermal diffusivity. The heat capacities were measured for different cooling rates (250K/h and 0.15K/h) through the glass transition. This large difference of the cooling rates did not change  $T_g$  very much (215.5 to 213.5K), but a peak was added to the usual  $\Delta C_p$  at  $T_g$ . An anomalous behaviour was observed at 80K, which is consistent with an experiment described elsewhere. Around 80K dielectric and mechanical relaxations were found in other experiments. In conclusion, the importance of the glass transition is pointed out, its effect being visible down to the lowest temperatures.

## INTRODUCTION

In the study of the physical properties of solid polymers, heat capacity measurements play a very important role. Differential calorimetry and differential thermal analysis (d.t.a.) may be used to determine glass and melting transitions easily and quickly in glass-forming systems or in semi-crystalline polymers. However, the absolute and precise specific heat curve, as measured in an adiabatic calorimeter, can give much more information about the vibrational states of the sample, and about possible sub-glass transitions, which will be very small compared to the heat capacity. The apparatus we have used is capable of very precise measurements. As a first stage of the study of amorphous polyhexene-1, we have measured two samples cooled through the glass transition at different cooling rates. Indeed, it is now well established that the way of decreasing the temperature through  $T_g$  is of fundamental importance for all the low-temperature physical properties (for instance see ref. 1). Recently some authors<sup>2</sup> tried to explain the anomalous thermal properties of glass below 1 K by a theory based on the possibility of molecular unit of a glass being frozen at  $T < T_g$  in two equilibrium positions, defined by the cooling through  $T_g$ . The possible existence of two equilibrium positions shows the interest of knowing the relaxational properties of vitreous polymers. Thus in this study, we will refer to two sets of measurements made on polyhexene: mechanical and dielectric loss tangent, both of which have been measured over a wide temperature range below the glass-transition temperature.

## EXPERIMENTAL

### *Apparatus*

The calorimeter used allows the adiabatic determination of absolute specific heat to be made over a wide temperature range (20–300 K)<sup>3</sup>. The sample is thermally isolated from the environment: conduction through the nylon suspension wires and through the constantan wires of the heating resistors and the thermometers is negligible; convection and conduction through the helium atmosphere is negligible, since the pressure in the calorimeter is less than  $10^{-6}$  mmHg; no thermal exchange by radiation can occur. A system of three gold-plated shields with low emissivity is electronically temperature regulated, so that the maximum temperature difference between the sample and the nearest shield is less than 0.01 K. Thus the thermal exchange between the sample and its environment is less than  $10^{-3}$  mW.

The temperature is measured by a platinum resistor [ $R(273.15 \text{ K}) = 200 \Omega$ ] using a  $100 \mu\text{A}$  measuring current. The voltage is measured by a Tinsley potentiometer which has a maximum accuracy of 10 nV. The out of balance reading of the potentiometer is amplified by a galvanometer amplifier, multiplying the input by  $10^4$ , then read on a Fluke numeric voltmeter. The accuracy in the measurement of the  $\Delta T$  temperature rise after the heating of the sample is  $10^{-4}$  K. The heat capacity is given by:

$$C_p = \frac{V_H \cdot I_H \cdot t}{\Delta T}$$

$\Delta T$  varies from 0.5 K at 20 K to 2.5 K at 300 K.  $V_H$ ,  $I_H$ ,  $t$  are respectively the voltage, current and duration of heating.  $t$  was equal to 6 min for nearly the whole temperature range. After heating, 15 or 20 min were needed for the temperature to attain a constant value. The heat capacity of the sample was computed directly by subtracting the heat capacity of the sample vessel and addenda from the measured heat capacity using a small Hewlett-Packard computer. Between 20 and 300 K, a great number (from 150 to 180) of measurements were made. We estimate that the specific heat curves below  $T_g$  have a maximum dispersion of 0.2–0.4%.

#### Sample preparation

Polyhexene-1 at room temperature has the appearance of an amorphous polymer in a rubber state. Some X-ray diffraction experiments made at various temperatures (from 88 to 300 K) do not show any diffraction peak on the pattern, which confirms that polyhexene-1 is a completely amorphous polymer at all temperatures<sup>5,6</sup>. The average molecular weight  $M_n$  is 350 000 and the polydispersion index is equal to 3. The density is 0.8540 g/cm<sup>3</sup><sup>7</sup>.

The main problem in the thermal study of polymers is their low thermal diffusivity. Some authors<sup>8</sup> did their experiments with a powdered sample, placing it in a sealed container with helium exchange gas. The exchange gas aided the heat distribution and increased the thermal diffusivity of the sample. A new method we have used for polyhexene was very satisfactory. We made sandwiches of very thin gold foils (0.002 mm) and the polymer. Then we piled up 4 of them, and rolled and pressed them to form a cylindrical sample 15 mm diameter and 30 mm long.

## RESULTS AND DISCUSSION

The heat capacity curves, shown in Figures 1 and 2, were determined for two different cooling rates. The sample (A) (Figure 1), quickly cooled, was cooled at a rate of 250 K/h, and the sample (B) (Figure 2), slowly cooled, at a rate of 0.15 K/h. The latter was cooled for two weeks from 225 to 165 K through the glass transition temperature. It is possible to obtain an analogous effect by annealing at a temperature inferior but close to  $T_g$ <sup>9,11</sup>.

**Sample (A) (Figure 1).** The curve has the classical shape for amorphous compounds. The glass transition temperature starts at about 205 K and ends at around 230 K.

**Sample (B) (Figure 2).** We can see two anomalies if we compare this curve with that for sample (A). First, during the glass transition, a sharp peak is added to the usual  $\Delta C_p$  at  $T_g$ . Secondly, a much smaller anomaly may be seen around 80 K, which is, however, outside the experimental error.

If we compare the two experiments, the absolute values of the heat capacity do not present any important differences outside of the transition temperature ranges. The experimental values are listed in Table 1.

#### Glass transition (interval)

If we calculate the enthalpy  $H$ , we can plot it as a function of temperature, and thus determine  $T_g$  (Figure 3). Above  $T_g$ ,  $H(T)$  is approximately linear and below  $T_g$ ,  $H(T)$  varies approximately as  $T^2$ .  $T_g$  is the tem-

perature at which these two curves intersect. We obtain: sample (A),  $T_g = 215.5 \pm 1$  K; sample (B),  $T_g = 213.5 \pm 1$  K.

The Gibbs and DiMarzio model<sup>10</sup> predicts a temperature  $T_2$  where a second order transition occurs in

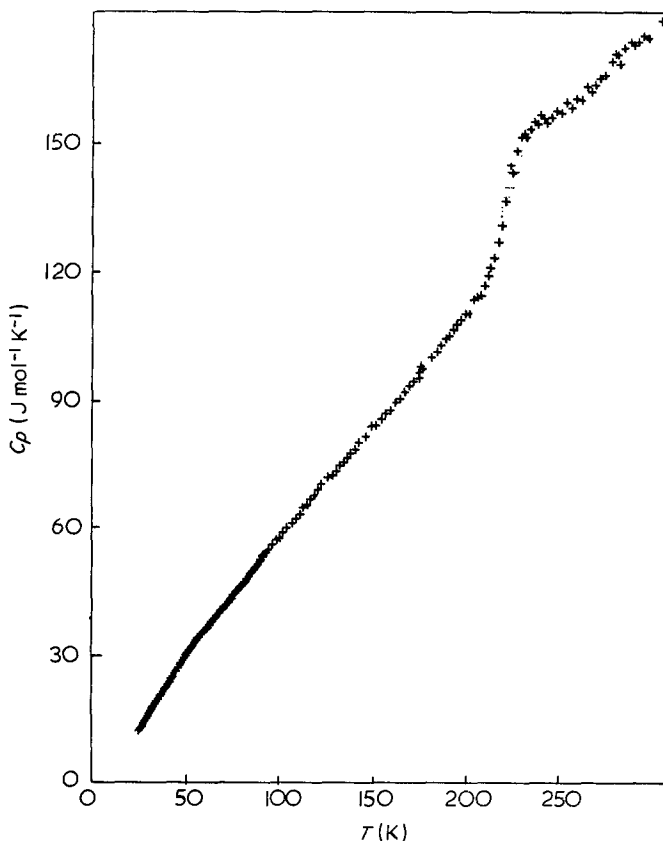


Figure 1 Heat capacity of sample (A), cooled at a rate of 250 K/h

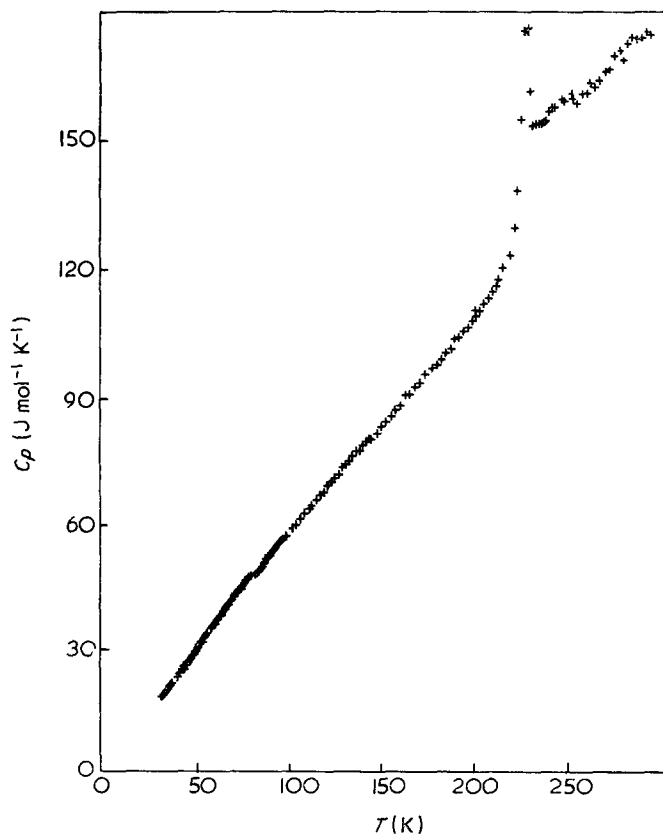


Figure 2 Heat capacity of sample (B), cooled at a rate of 0.15 K/h

Table 1 Comparison of the experimental values of polyhexene  $C_p$  for quickly and slowly cooled samples

T (K)	A		B		$C_p(B)$ $C_p(A)$ (%)
	$C_p$ (J mol <sup>-1</sup> K <sup>-1</sup> )	$\Delta T$ (K)	$C_p$ (J mol <sup>-1</sup> K <sup>-1</sup> )	$\Delta T$ (K)	
20	9.091	0.733			
25	12.35	0.519			
30	16.42	0.590			
35	20.24	0.456	20.37	0.728	+0.6
40	24.00	0.604	23.94	0.86	-0.25
45	26.98	0.932	27.23	0.807	+0.9
50	30.16	0.711	30.60	0.702	+1.5
55	33.65	0.633	33.78	0.631	+0.4
60	36.71	0.569	37.02	0.571	+0.8
65	39.86	0.874	40.22	0.518	+0.9
70	42.67	0.808	43.32	0.803	+1.5
75	45.32	0.760	46.19	0.727	+1.9
80	48.33	0.712	48.66	0.706	+0.7
85	50.99	1.05	50.14	0.676	-1.7
90	53.74	0.735	53.46	0.998	-0.5
95	56.65	1.38	56.55	0.958	-0.2
100	59.08	1.89	59.80	1.53	+1.2
105	61.71	2.26	61.90	2.27	+0.3
110	64.30	2.19	64.35	2.16	+0.1
115	66.39	2.08	66.90	2.09	+0.8
120	69.61	2.04	69.68	2.04	+0.1
125	72.38	2.01	72.10	1.97	-0.4
130	74.68	1.91	74.73	1.92	+0.1
135	77.27	1.86	77.32	1.86	+0.1
140	79.88	2.82	79.77	1.80	-0.1
145	82.21	2.78	81.81	2.77	-0.5
150	84.96	2.69	84.22	2.70	-0.9
155	87.61	2.44	86.67	2.64	-1.1
160	89.69	2.57	89.31	2.67	-0.4
165	92.46	2.52	91.98	2.50	-0.5
170	95.11	2.46	94.52	2.36	-0.6
175	98.17	1.97	97.07	2.09	-1.1
180	100.9	2.33	98.93	2.38	-2.0
185	104.7	2.25	101.6	2.34	-3.0
190	106.4	2.24	104.6	2.28	-1.7
195	109.4	2.22	107.2	2.25	-2.0
200	111.4	2.18	110.1	2.20	-1.2
205	115.0	2.13	113.0	2.16	-1.7
210	118.8	2.08	116.5	2.12	-1.9
215	125.6	1.99	121.4	1.95	-3.3
220	137.3	1.82	128.5	1.97	-6.4
225	148.3	1.76	166.1	1.61	+12.0
227.31	152.1	1.71	176.6	1.58	+16.1
230	152.2	1.72	156.7	1.67	+3.0
235	155.6	1.69	154.7	1.46	-0.6
240	156.3	1.41	158.0	1.67	+1.1
245	158.2	2.65	160.0	1.62	+1.1
250	159.6	2.64	161.3	1.65	+1.1
255	160.5	2.63			
260	162.4	2.59			
265	163.5	2.59			
270	166.5	2.55			
275	170.7	2.50			
280	172.4	2.28			
285	174.5	2.45			
290	175.1	2.42			
295	175.8	2.40			
301.08	179.30	2.38			

supercooled liquids, which are cooled at an infinitely slow rate. In this model, it seems justified that decreasing the cooling rate makes  $T_g$  decrease. However, the large difference ( $> 10^3$ ) between our two cooling rates decreases  $T_g$  only by 2 K. This is consistent with the experiment of Chang and Bestul<sup>11</sup>, achieved on *o*-terphenyl, for which a diminution of the cooling rate implied a small decrease (2 K) of  $T_g$ . As has been pointed out by certain authors<sup>12</sup>, the kinetics of glass-transition, which were not considered in the Gibbs and Dimarzio

model, are of fundamental importance, so that the temperature  $T_2$  remains quite theoretical.

The peak at  $T_g$  has already been found in some other molecular glasses, such as diethylphthalate<sup>9</sup> and in polystyrene<sup>13</sup> annealed below  $T_g$ , but its origin is

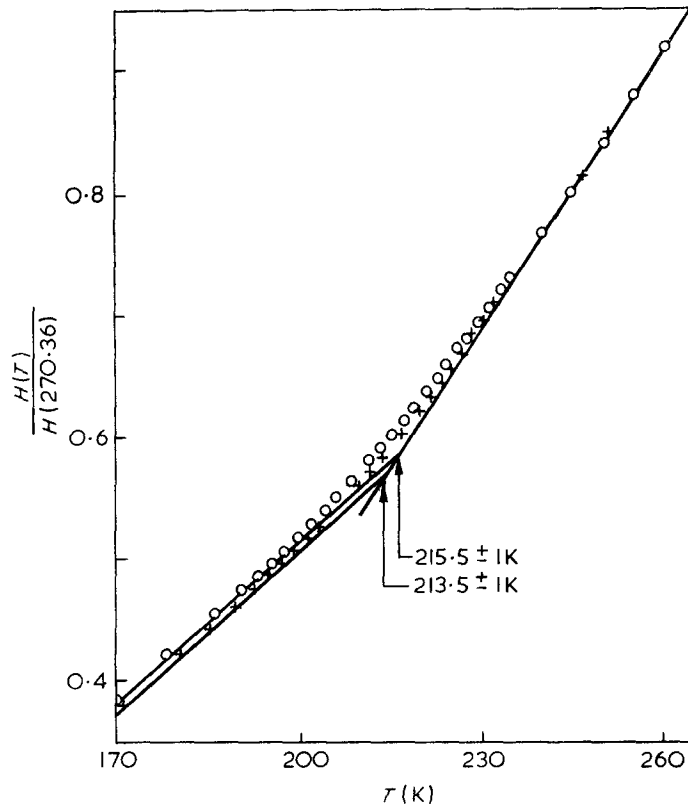


Figure 3 Enthalpy of samples (A) and (B) in the glass transition temperature range. The curves are that of  $H(T)/H(270.36)$  versus  $T$ . O, 250 K/h; +, 0.15 K/h

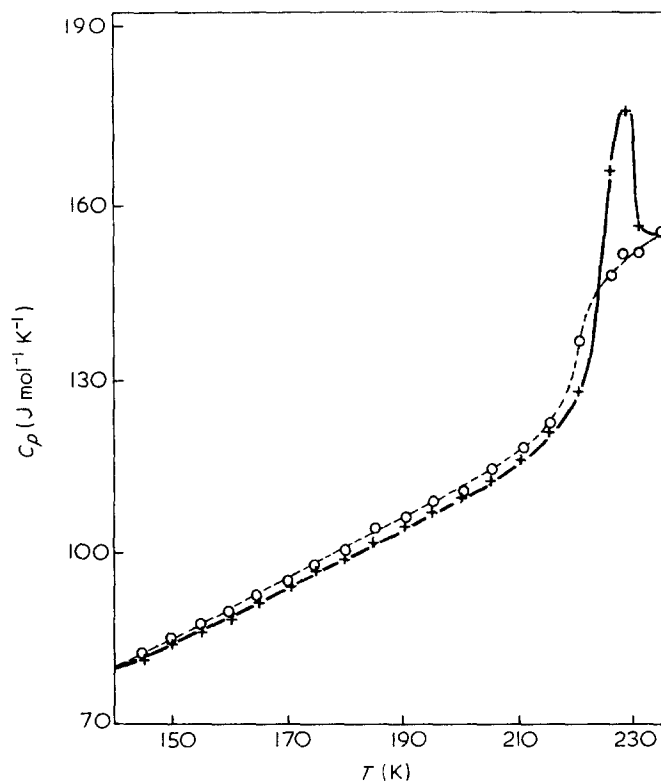


Figure 4 Comparison of both heat capacities in the glass transition temperature range. O, A; +, B

not yet understood. Below  $T_g$ , the heat capacity of sample (B) becomes smaller than sample (A) by 1 to 3%, but below 150 K, the maximum difference between both heat capacities becomes less than 0.5%. Both curves are plotted in Figure 4 in the glass transition temperature range.

#### Subglass anomaly

A different sample of polyhexene showed a low temperature anomaly of the same type during an experiment with an unknown cooling rate. This anomalous behaviour of  $C_p$  occurred at a temperature close to 60 K<sup>14</sup>. An experiment giving the dielectric loss tangent performed at the same time showed the presence of a shoulder on the loss tangent *versus* temperature curve between 60 and 80 K.

In the experiment we are describing now, where cooling rates are clearly defined, we notice a discontinuity on the sample (B) heat capacity curve (Figure 5). At lower temperatures the heat capacity of sample (B) is greater by 0.5 to 1% than sample (A). (This difference is outside the experimental error.) This deviation increases to 3% at 79 K, after which the maximum heat capacity difference becomes less than 0.5%. The shape of this anomalous behaviour would indicate that a transition takes place. The existence of mechanical<sup>15</sup> and dielectric relaxations at the same temperature is the proof that a movement occurs. Some authors have noted that a very low temperature relaxation cannot be explained by a classical activation process. The possibility of a quantum mechanical tunnelling was then pointed out<sup>16</sup>.

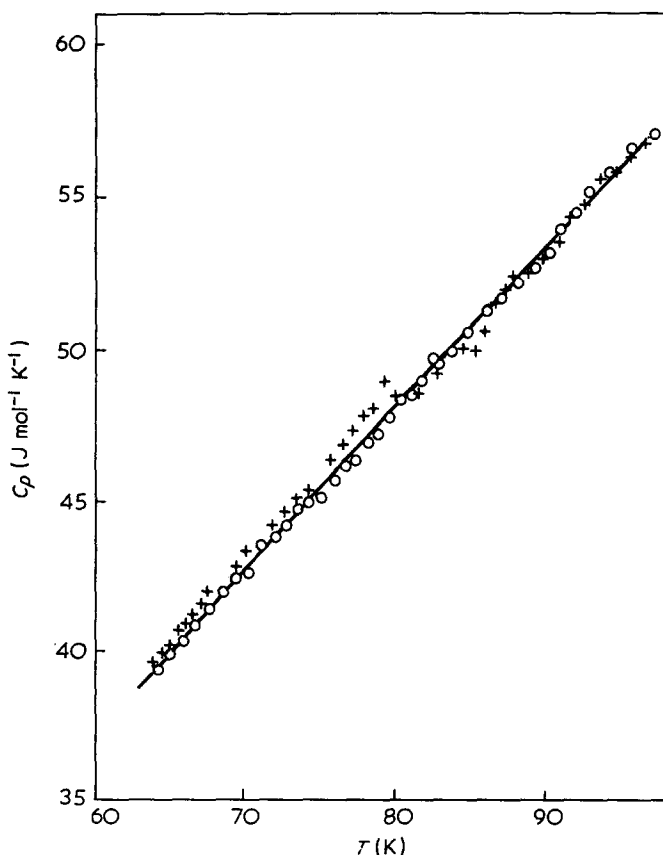


Figure 5 Comparison of both heat capacities in the neighbourhood of sub-glass anomaly. O, A; +, B

However, such a relaxation would be observed in a calorimetric experiment only if a coupling exists between the groups which relax. More work is necessary before looking for any explanation of this phenomenon.

#### CONCLUSION

The amorphous character of polyhexene makes it the most interesting material if we compare it with other polyolefins. The study of its thermal and vibrational properties<sup>17</sup>, and the measurement of its heat capacity at lower temperatures will complete our knowledge of this polymer. Even if the  $10^3$  factor between the two cooling rates does not make  $T_g$  vary very much, it changes some aspects of the  $C_p$  *versus* temperature curve. The anomalous behaviour at 80 K shows that the cooling rate has a very important influence on the physical properties of glasses at low temperature. Thus, the freezing of molecular groups in two different equilibrium positions, which occurs at  $T_g$ , is an important phenomenon, even at temperatures much lower than  $T_g$ . We are continuing the study of polyhexene-1 in an attempt to increase our understanding of molecular glass behaviour at very low temperatures.

#### ACKNOWLEDGEMENTS

We are grateful to Dr Guillot from Institut de la Catalyse and Drs May, Grandaud and Berticat from Chimie Macromoléculaire, Faculté des Sciences de Lyon, for their part in polymerizing and characterizing the polyhexene sample.

We are indebted to Mr Martoña, without whom this work could not be achieved.

#### REFERENCES

- 1 Shen, M. C. and Eisenberg, A. 'Progress in Solid State Chemistry', Pergamon Press, London, 1967, Vol 3
- 2 Anderson, P. W., Halperin, B. I. and Varma, C. M. *Phil. Mag.* 1972, **25**, 1
- 3 Berton, A. and Chaussy, J. to be published
- 4 O'Reilly, J. M. and Karasz, F. E. *J. Polym. Sci. (C)* 1966, **14**, 49
- 5 Kurath, S. F., Passaglia, E. and Parisier, P. *J. Appl. Phys.* 1957, **28**, 499
- 6 Grandaud, J. L., May, J. F., Berticat, P. and Vallet, G. *C.R. Acad. Sci.* 1971, **273 C**, 500
- 7 Grandaud, J. L. personal communication
- 8 Dainton, F. S. *et al. Polymer* 1962, **3**, 286; Sterett, K. F. *et al. J. Res. Nat. Bur. Stand.* 1965, **69 C** (1), 19; Karasz, F. E. *et al. Polymer* 1968, **8**, 547
- 9 Chang, S. S., Horman, J. A. and Bestul, A. B. *J. Res. Nat. Bur. Stand. (Phys. Chem.)* 1967, **71 A** (4), 293
- 10 Gibbs, J. H. and DiMarzio, E. A. *J. Chem. Phys.* 1958, **28**, 373
- 11 Chang, S. S. and Bestul, A. B. *J. Chem. Phys.* 1972, **56**, 503
- 12 Adam, G. and Gibbs, J. H. *J. Chem. Phys.* 1965, **43**, 139
- 13 Karasz, F. E., Bair, H. E. and O'Reilly, J. M. *J. Phys. Chem.* 1965, **69**, 2657
- 14 Bourdariat, J., Chaussy, J., Berton, A., Odin, J. and Pineri, M. *C.R. Acad. Sci.* 1972, **274B**, 190
- 15 Pineri, M. to be published
- 16 Philipps, W. A. *Proc. R. Soc.* 1970, **A319**, 565; Eisenberg, A. and Reich, S. *J. Chem. Phys.* 1969, **51**, 5706; 1970, **53**, 2847
- 17 Bourdariat, J., Isnard, R. and Odin, J. *J. Polym. Sci.* to be published

## Notes to the Editor

### Characterization of stereoblock polymers of poly(methyl methacrylate) by thin-layer chromatography

R. Buter, Y. Y. Tan and G. Challa

Laboratory of Polymer Chemistry, State University Groningen, The Netherlands  
(Received 28 December 1972)

Inagaki *et al.*<sup>1,2</sup> reported the application of thin-layer chromatography (t.l.c.) to separate mixtures of isotactic and syndiotactic poly(methyl methacrylate) (i-PMMA, s-PMMA) into their components. During the development i-PMMA remained on the starting line ( $R_f=0$ ), while s-PMMA moved to the neighbourhood of the solvent front ( $R_f=0.9$ ).

We have applied this t.l.c. method on an analytical as well as on a preparative scale to characterize polymers formed during so-called replica polymerizations of methyl methacrylate (MMA)<sup>3,4</sup>. Silica gel type G, activated at 110°C, was used as stationary phase and ethyl acetate as developing solvent. The position of the polymer was marked by spraying a 1% methanol solution of iodine on the layer. The adsorbed species were recovered by extraction with hot acetone.

The polymer products were obtained by use of the following polymerization procedures: (i) polymerization of MMA by a radical initiator at 25°C in dimethylformamide (DMF) in the presence of preformed i-PMMA as a matrix<sup>3</sup>; and (ii) bulk polymerization of MMA initiated at 90°C by dissolved preformed i-PMMA<sup>4</sup>. The total polymer products were separated by extraction with boiling acetone into soluble and insoluble fractions and each fraction was characterized by 60 MHz nuclear magnetic resonance spectroscopy (n.m.r.) and by t.l.c.

The acetone-insoluble fractions appeared to be composed of *i,s*-stereocomplexes<sup>3</sup>, which are partly crystalline as shown by X-ray diffraction and could be decomposed into their components by dissolution in a 'non-complexing' solvent such as chloroform<sup>5,6</sup>. The chromatogram in Figure 1, in which conventional (c-)PMMA (1), i-PMMA (2), and s-PMMA (3) were developed simultaneously for comparison, shows that such 'decomposed' stereocomplex could be separated into i-PMMA and s-PMMA (4).

The high persistence ratio<sup>7</sup> ( $\rho=2IS/h$  where *I* and *S* are isotactic and syndiotactic diads, respectively) of the acetone-soluble fractions indicated the occurrence of *i,s*-stereoblock polymers. Considering their solubility in acetone it was unlikely that these fractions consisted of mixtures of i-PMMA and s-PMMA. The stereoblock polymers were also submitted to t.l.c. and their chromatograms show, in contrast to mixtures of i-PMMA and s-PMMA, only one spot with an intermediate  $R_f$  value.

From Table 1, and Figure 2, in which the  $R_f$  values are plotted against the *i*-triad contents of the polymers, it is seen that  $R_f$  values decrease continuously from

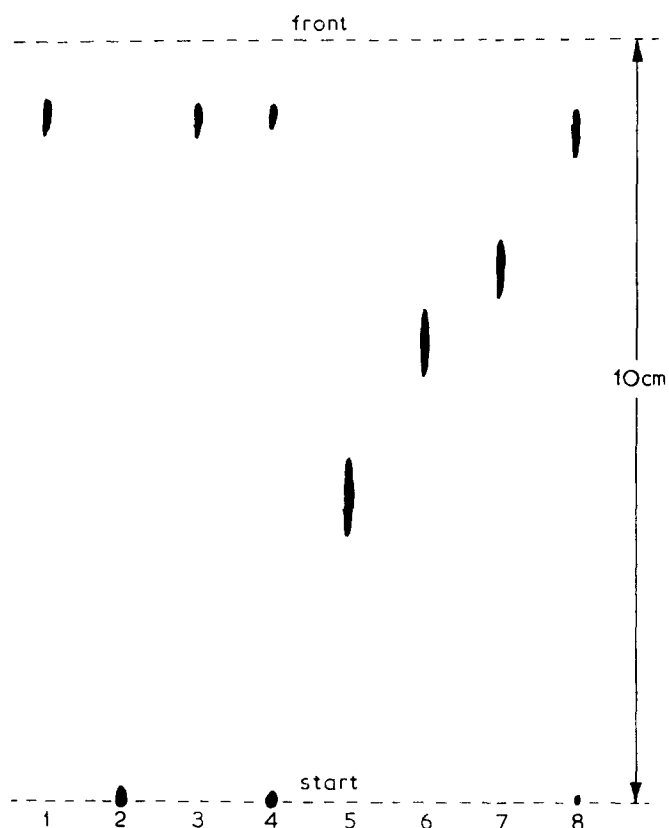


Figure 1 T.l.c. chromatogram obtained from (1) c-PMMA, (2) i-PMMA, (3) s-PMMA, (4) 1:1 *i,s*-stereocomplex, (5)–(8) stereoblock polymers

Table 1  $R_f$  values and tacticities

PMMA	<i>i</i>	<i>h</i>	<i>s</i>	$R_f$
c-PMMA	0.08	0.27	0.65	0.90
i-PMMA	0.90	0.07	0.03	0
s-PMMA	0.02	0.07	0.91	0.90
block	0.11	0.37	0.52	0.80
block	0.17	0.20	0.63	0.70
block	0.23	0.16	0.61	0.60
block	0.24	0.16	0.60	0.60
block	0.31	0.12	0.57	0.50
block	0.33	0.21	0.46	0.50
block	0.35	0.05	0.60	0.45
block	0.39	0.12	0.49	0.40
block	0.55	0.05	0.40	0.30
block	0.61	0.08	0.31	0.25

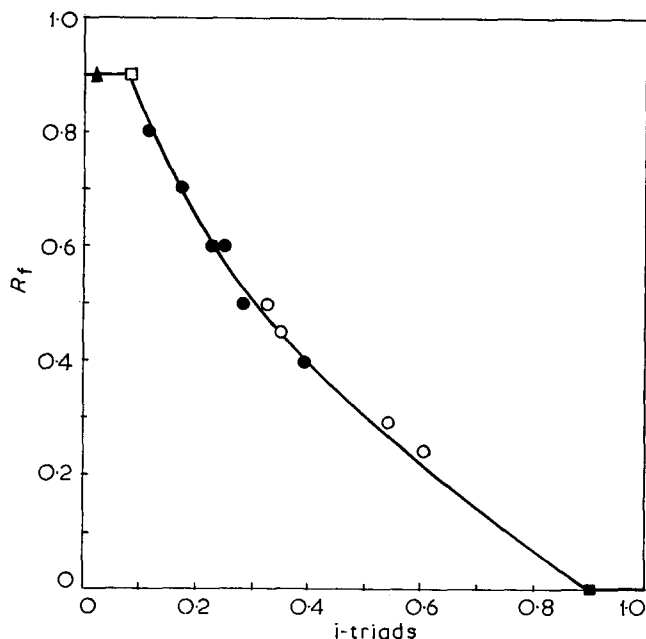


Figure 2  $R_f$  values versus i-triad contents of s-PMMA (▲), c-PMMA (□), i-PMMA (■), stereoblock polymers from replica polymerizations in DMF (●), and stereoblock polymers from bulk polymerizations (○)

0.9 to 0 with increasing isotactic triad contents. Syndiotactic polymers with about 0–10% isotactic triads all have  $R_f=0.9$  and isotactic polymers with about 90–100% isotactic triads all have  $R_f=0$ .

In addition it was found that at low conversion of the polymerization the percentage of isotactic triads of the acetone-soluble fractions was too high in relation with the  $R_f$  value. However, in these cases an additional lower spot with  $R_f=0$  was observed, due to excess non-complexed preformed isotactic polymer matrix [Figure 1 (8)].

The results show that t.l.c. is a feasible method to distinguish mixtures of i-PMMA and s-PMMA from i,s-stereoblock polymers and also to estimate tacticities from  $R_f$  values.

#### REFERENCES

- 1 Inagaki, H., Miyamoto, T. and Kamiyama, F. *J. Polym. Sci. (B)* 1969, 7, 329
- 2 Miyamoto, T. and Inagaki, H. *Macromolecules* 1969, 2, 554
- 3 Buter, R., Tan, Y. Y. and Challa, G. *J. Polym. Sci. (A-1)* 1972, 10, 1031
- 4 Buter, R., Tan, Y. Y. and Challa, G. *J. Polym. Sci. (A-1)* to be published
- 5 Liu, H. Z. and Liu, K. *J. Macromolecules* 1968, 1, 157
- 6 Borchard, W., Pyrlík, M. and Rehage, G. *Makromol. Chem.* 1971, 145, 169
- 7 Coleman, F. D. and Fox, T. G. *J. Chem. Phys.* 1963, 38, 1065

## Anionic polymerization of $\beta$ -nitrostyrene

R. W. H. Berry and R. J. Mazza

Department of Science, Medway and Maidstone College of Technology, Chatham, Kent, UK  
(Received 30 October 1972; revised 11 January 1973)

Apart from the polymerization of styrene by potassium amide in liquid ammonia<sup>1,2</sup>, the only quantitative work, which has been carried out on anionic polymerization, has involved either bulk polymerization or the use of inert solvents<sup>3</sup>. The present work is a spectrophotometric study on the kinetics of the anionic polymerization of  $\beta$ -nitrostyrene by sodium methoxide in methanol.

Sodium methoxide ( $\sim 10^{-4}$  M) reacts with  $\beta$ -nitrostyrene ( $\sim 10^{-1}$  M) in methanol solution at 22°C producing, almost immediately, a white suspension. The dry product melts at about 285°C (m.p. of  $\beta$ -nitrostyrene = 58°C<sup>4</sup>) and its infra-red spectrum when compared with the spectrum of  $\beta$ -nitrostyrene does not have a band at 1630  $\text{cm}^{-1}$ , which is attributed to the carbon-carbon double bond.

The ultra-violet spectrum of the monomer shows a  $K$  band ( $\pi \rightarrow \pi^*$ ) at 309 nm,  $\Sigma(\text{max})=16700$ , which is due to an electron migration along the conjugated system. However, after addition of a methanolic solution of sodium methoxide, this  $K$  band decreases in intensity whilst a band at about 210 nm increases in intensity. Furthermore, as the peak at 309 nm decreases in intensity another band, which has been previously masked, becomes apparent at 260 nm. The decrease in the intensity of the  $K$  band ( $\pi \rightarrow \pi^*$ ) at 309 nm is due to the disappearance of the monomer. Since a decrease in the

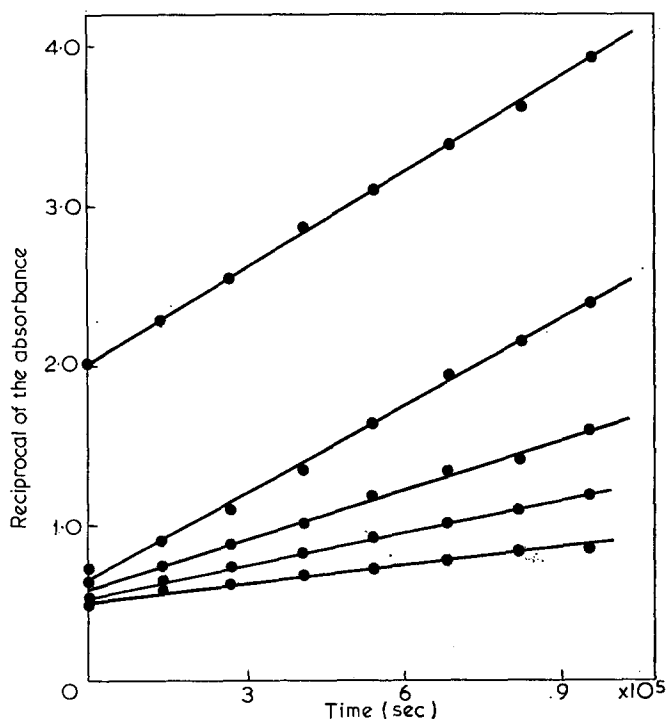


Figure 1 Plots of the reciprocal of the absorbance against time for kinetic runs with a constant concentration of initiator



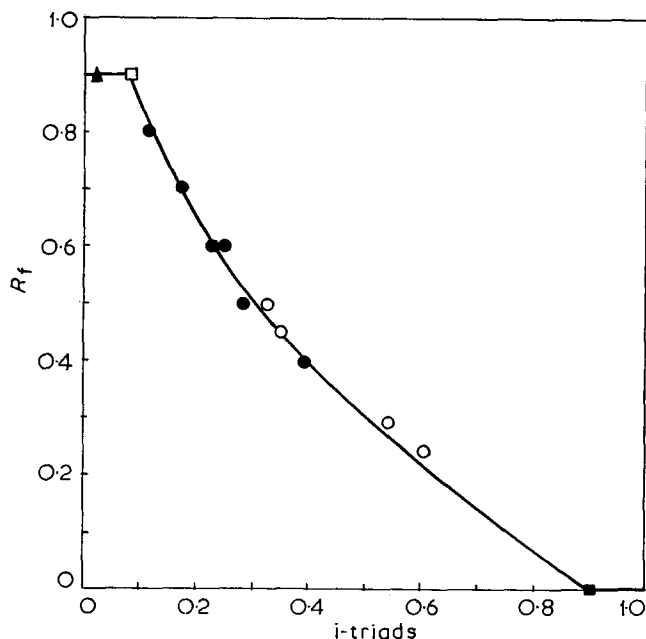


Figure 2  $R_f$  values versus i-triad contents of s-PMMA (▲), c-PMMA (□), i-PMMA (■), stereoblock polymers from replica polymerizations in DMF (●), and stereoblock polymers from bulk polymerizations (○)

0.9 to 0 with increasing isotactic triad contents. Syndiotactic polymers with about 0–10% isotactic triads all have  $R_f=0.9$  and isotactic polymers with about 90–100% isotactic triads all have  $R_f=0$ .

In addition it was found that at low conversion of the polymerization the percentage of isotactic triads of the acetone-soluble fractions was too high in relation with the  $R_f$  value. However, in these cases an additional lower spot with  $R_f=0$  was observed, due to excess non-complexed preformed isotactic polymer matrix [Figure 1 (8)].

The results show that t.l.c. is a feasible method to distinguish mixtures of i-PMMA and s-PMMA from i,s-stereoblock polymers and also to estimate tacticities from  $R_f$  values.

#### REFERENCES

- 1 Inagaki, H., Miyamoto, T. and Kamiyama, F. *J. Polym. Sci. (B)* 1969, 7, 329
- 2 Miyamoto, T. and Inagaki, H. *Macromolecules* 1969, 2, 554
- 3 Buter, R., Tan, Y. Y. and Challa, G. *J. Polym. Sci. (A-1)* 1972, 10, 1031
- 4 Buter, R., Tan, Y. Y. and Challa, G. *J. Polym. Sci. (A-1)* to be published
- 5 Liu, H. Z. and Liu, K. *J. Macromolecules* 1968, 1, 157
- 6 Borchard, W., Pyrlík, M. and Rehage, G. *Makromol. Chem.* 1971, 145, 169
- 7 Coleman, F. D. and Fox, T. G. *J. Chem. Phys.* 1963, 38, 1065

## Anionic polymerization of $\beta$ -nitrostyrene

R. W. H. Berry and R. J. Mazza

Department of Science, Medway and Maidstone College of Technology, Chatham, Kent, UK  
(Received 30 October 1972; revised 11 January 1973)

Apart from the polymerization of styrene by potassium amide in liquid ammonia<sup>1,2</sup>, the only quantitative work, which has been carried out on anionic polymerization, has involved either bulk polymerization or the use of inert solvents<sup>3</sup>. The present work is a spectrophotometric study on the kinetics of the anionic polymerization of  $\beta$ -nitrostyrene by sodium methoxide in methanol.

Sodium methoxide ( $\sim 10^{-4}$  M) reacts with  $\beta$ -nitrostyrene ( $\sim 10^{-1}$  M) in methanol solution at 22°C producing, almost immediately, a white suspension. The dry product melts at about 285°C (m.p. of  $\beta$ -nitrostyrene = 58°C<sup>4</sup>) and its infra-red spectrum when compared with the spectrum of  $\beta$ -nitrostyrene does not have a band at 1630  $\text{cm}^{-1}$ , which is attributed to the carbon-carbon double bond.

The ultra-violet spectrum of the monomer shows a  $K$  band ( $\pi \rightarrow \pi^*$ ) at 309 nm,  $\Sigma(\text{max})=16700$ , which is due to an electron migration along the conjugated system. However, after addition of a methanolic solution of sodium methoxide, this  $K$  band decreases in intensity whilst a band at about 210 nm increases in intensity. Furthermore, as the peak at 309 nm decreases in intensity another band, which has been previously masked, becomes apparent at 260 nm. The decrease in the intensity of the  $K$  band ( $\pi \rightarrow \pi^*$ ) at 309 nm is due to the disappearance of the monomer. Since a decrease in the

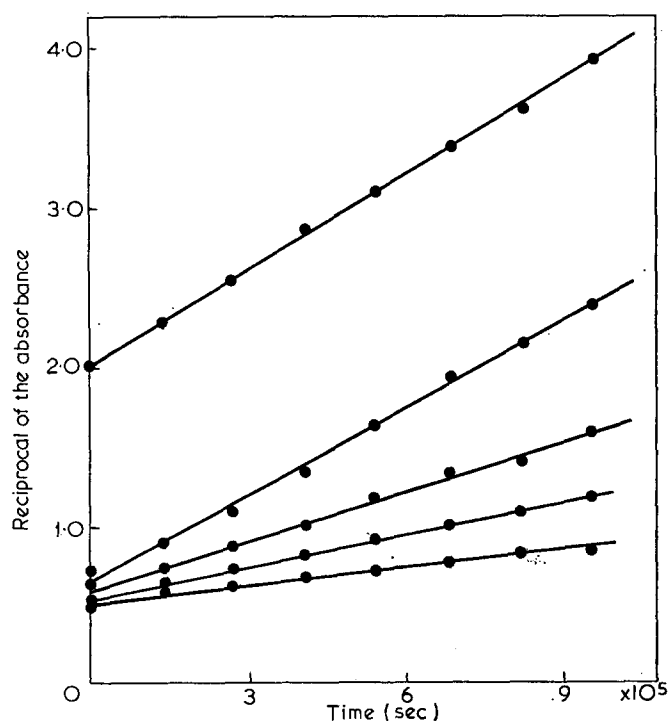
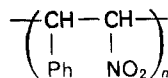


Figure 1 Plots of the reciprocal of the absorbance against time for kinetic runs with a constant concentration of initiator

length of the conjugated system occurs during the polymerization process, the polymer absorbs at shorter wavelengths than the monomer. The resulting spectrum resembles quite closely that of ethyl benzene in ethanol which has a peak at 208 nm assigned to the *K* band ( $\pi \rightarrow \pi^*$ ) and a band at 260 nm attributed to the *B* band ( $\pi \rightarrow \pi^*$ )<sup>5</sup>.

The spectral evidence is consistent with the formation of a substance of the general formula:



Moreover, the disappearance, with time, of the band at 309 nm is suitable for following the kinetics of the reaction. This was carried out first, by varying the monomer concentration and keeping the initiator concentration constant, and secondly, by keeping the monomer concentration constant and varying the initiator concentration.

The rate of consumption of  $\beta$ -nitrostyrene was found to be second order with respect to  $\beta$ -nitrostyrene concentration as plots of the reciprocal of the absorbance against time were linear (Figure 1) for kinetic runs with a constant concentration of initiator. A plot of the slopes of the graphs in Figure 2 against the concentration

of initiator (Figure 3), when the initial concentration of monomer was kept constant, also yields a straight line indicating that the reaction is first order with respect to initiator concentration, [I]. Thus, a plausible mechanism for the reaction is as follows:

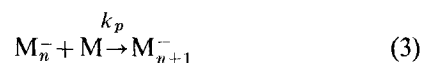
Initiation:



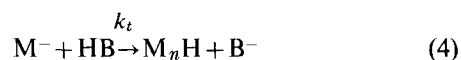
Propagation:



Or, in general:



Termination (by chain transfer to solvent):



where M is monomer, B<sup>-</sup> is  $\text{O}^-\text{CH}_3$  and HB is  $\text{CH}_3\text{OH}$ . (N.B. The species B<sup>-</sup>, produced in step (4), is then capable of re-initiation.)

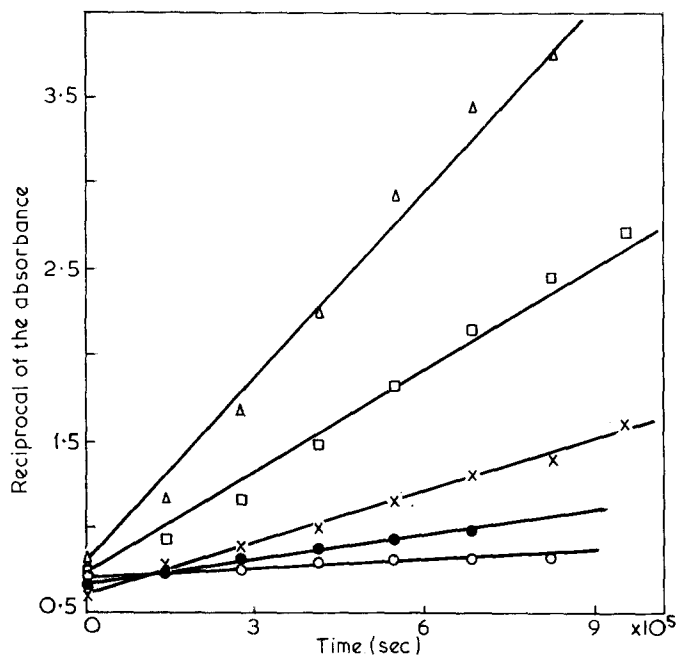


Figure 2 Plots of the reciprocal of the absorbance against time for kinetic runs with a constant initial concentration of monomer

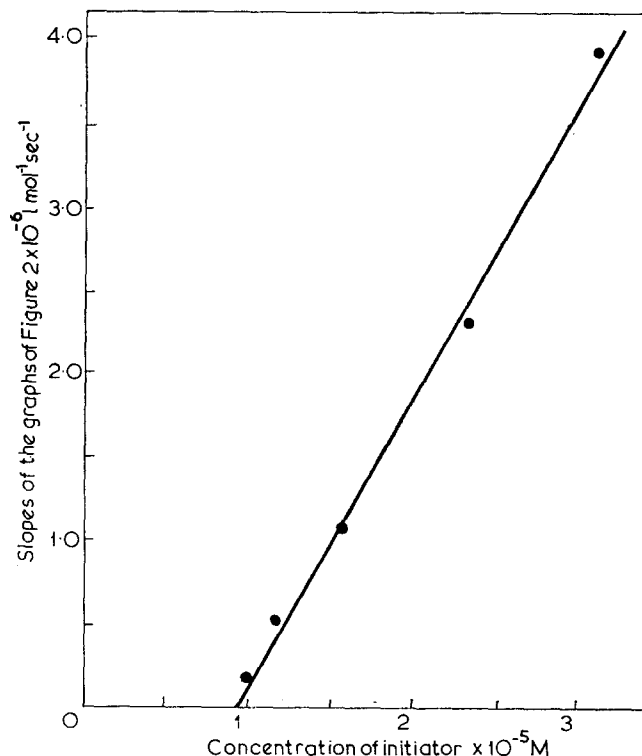


Figure 3 Plot of the slopes of the graphs in Figure 2 against the concentration of initiator

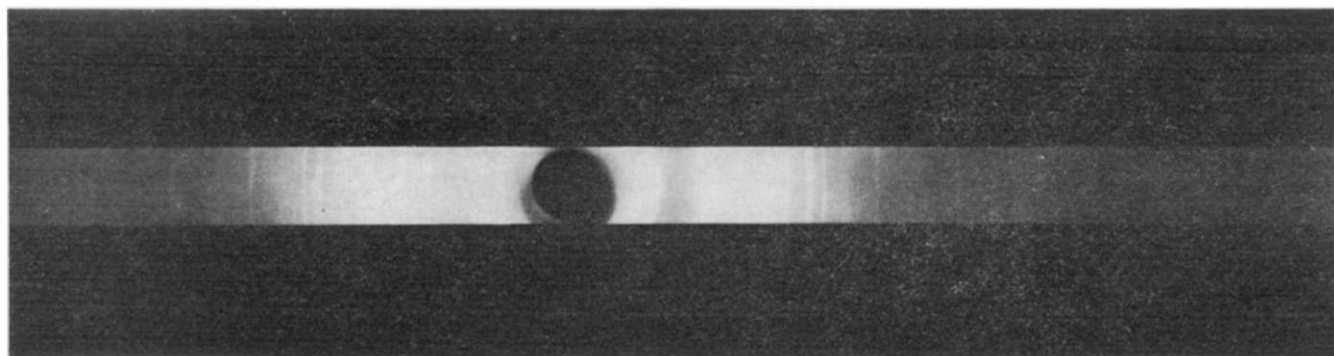


Figure 4 Diffraction powder photograph of the polymer

If  $k_p$  and  $k_t$  are assumed to be independent of the chain length of the growing polymer molecule, application of the stationary-state hypothesis to the appropriate rate equations leads to the following overall kinetic expression for the reaction:

$$-\frac{d}{dt} [M] = \frac{k_t k_p [M]^2 [I]}{k_t [\text{CH}_3\text{OH}]} \quad (5)$$

Thus, the results are consistent with a mechanism involving chain transfer to the solvent.

The high melting point of the product and its insolubility in numerous solvents seems to indicate that it is stereoregular. This is supported by an X-ray diffraction powder photograph (Figure 4) which clearly shows that the polymer is crystalline.

A preliminary radiochemical study suggests a molecular weight of approximately 26 000. Although this value may be high due to self-absorption of the sample during suspension counting in a liquid scintillation counter, the presence of recurring units in the mass spectrum demonstrates the polymeric nature of the substance.

Currently, this system is being investigated further in an attempt to measure the molecular weight of the polymer precisely.

#### ACKNOWLEDGEMENTS

The authors thank Messrs P. Smith and M. J. Turner for some technical assistance.

#### REFERENCES

- 1 Evans, M. G., Higginson, W. C. E. and Wooding, N. S. *Rec. Trav. Chim.* 1949, **68**, 1069
- 2 Higginson, W. C. E. and Wooding, N. S. *J. Chem. Soc.* 1952, p 760
- 3 Lenz, W. R. 'Organic Chemistry of Synthetic High Polymers', Interscience, New York, 1967; Billmeyer, F. W. 'Textbook of Polymer Science', Interscience, New York, 1962
- 4 'Handbook of Chemistry and Physics', 46th edn, The Chemical Rubber Company, Cleveland, Ohio, 1967
- 5 Braude, E. A. *J. Chem. Soc.* 1949, p 1902

# ENERGY POLICY

A NEW QUARTERLY JOURNAL

## *The economics and planning of energy*

*ENERGY POLICY* will deal with the economics and planning of the production, conversion and use of energy. It will publish articles, reports and book reviews that deal with the availability of fuels and with the efficiency, applicability and acceptability of different forms of energy production and conversion.

*ENERGY POLICY* will be

*International:* covering the resources and capabilities of particular countries and regions and the increasing interdependence of their needs:

*Integrative:* including coal, oil, gas, nuclear, hydro and alternative energy sources:

*Interdisciplinary:* drawing together studies by technologists with those of economists, geographers, environmentalists and political scientists.

*ENERGY POLICY'S* aim will be to help the manager and planner concerned with the fuel and energy industries develop a coherent overall picture of this complex and fast-changing subject.

*ENERGY POLICY* will be guided by a distinguished international editorial board. Each issue will contain in depth articles and these will be complemented by reports and reviews of publications.

Published quarterly in March, June, September, December, commencing with the June 1973 issue.

One-year subscription (four issues) £14.00 (\$36.40)

\*Special pre-publication offer £10.00 (\$26.00) if ordered before 31st May 1973.

For full details apply to  
IPC Science and Technology Press Limited, (Dept AD.EP.2F)  
IPC House, 32 High Street, Guildford, Surrey, England.  
Telephone: Guildford (0483) 71661

# Book Reviews

## Reverse osmosis membrane research

Edited by H. K. Lonsdale and H. E. Podall

Plenum Press, New York, 1972, 503 pp. \$32.00

This book is primarily a collection of papers presented in a symposium on Polymers for Desalination held at the 162nd National Meeting of the American Chemical Society in Washington, D.C. in September 1971. Several additional papers have been especially contributed to the monograph so as to improve the coverage of membrane research and development.

The introduction, written by the editors, is designed to serve two purposes; it gives a general description of the principles and problems of practical reverse osmosis and it surveys and summarizes the following papers by organizing them into five groups.

The book is likely to interest most intently readers personally connected with research on membrane separation processes. For them the general description is scarcely necessary but the survey and summaries of the papers are extremely valuable and relieve the reviewer of one of his more difficult tasks. The potential purchaser should certainly read this editors' survey. It gives a strong impression of the creative activity and ingenuity which now characterizes attempts to improve the commercial viability of membrane processes. The practical research papers are all of USA origin although the two papers on Fundamentals: on the membrane process (by O. Kedem) and on the membrane/solution interfacial process (by W. Pusch), are from elsewhere. This restriction of origin is more apparent than real because by far the greatest amount of truly innovative membrane research at the present time is being carried out in the USA.

Although no book of this size could give a truly complete account of the field nor could it be truly up-to-date even at the date of publication, the collection of papers presented here give a balanced and stimulating picture of the mainstreams of research towards improving reverse osmosis. The book closes with a chapter by W. S. Gillan setting out trends and hopes for the future. There is a short and rather inadequate index.

P. Meares

## Comportement thermique des polymères synthétiques

F. Rocaboy

Masson et Cie, Paris, 1972, Vol 1, 301 pp. 140F

This is the first volume of what promises to be a rather curious book, in which the entire range of synthetic polymers is described from the aspect of their thermal properties. An attempt is made to classify the principal properties in relation to behaviour upon heating, mainly by division into reversible and irreversible changes. In particular, an attempt is made to identify the structural and chemical factors which favour resistance to degradation at high temperatures, with a special interest in polymers accepted as 'thermally stable' or 'thermally resistant'. In practice, this means that most of the text published so far consists of a catalogue of every conceivable vinyl and carbocyclic polymer, with tables of fusion temperatures and, where possible, differential thermal analysis curves tacked on the end of each section. Many of these sections are so brief that they are misleading without the addition of further critical comment. As a quick reference, the thermal data provided are useful; the supporting references quoted are, at times, somewhat unexpectedly chosen. To precede this section, there are four introductory chapters, which discuss the configuration of macromolecular chains, crystal structure and polymer morphology, the rheology of polymers (which is clearly stated but barely relevant in this context), and the general principles of thermal behaviour. At the end of the book, an appendix lists, by type of polymer, the commercial names of synthetic fibres based on carbon chains. The list is long, includes many obscure and probably obsolete brand-names, and seems quite pointless.

In sum, this is a polemical work, of some value to workers concerned with the thermal properties of polymers, but the approach is too eccentric for it to be used in isolation. It is well printed, with many figures, but is rather expensive for its likely value to most readers.

C. A. Finch

## Light scattering from polymer solutions

Edited by M. B. Huglin

Academic Press, London, 1972, 885 pp. £14.50

Light scattering from polymer solutions has become a routine characterization technique in many laboratories. The experimental work involved, however, is exceptionally demanding and a great deal of care and considerable experience is required to obtain reliable results. Research workers from a variety of disciplines, who use light scattering as a tool, will find the wealth of technical information and experimental know-how recorded in this work extremely useful. Undoubtedly it is a book which will find its place on or near the laboratory bench. In all it contains eighteen chapters and there are twenty contributors.

The first sections deal with experimental procedures, theoretical background, and treatment of results. Especially noteworthy here is the extensive tabulation of useful data (e.g. specific refractive index increments and physical properties of solvents). The rest of the work deals with the effect of external parameters and applications to particular types of systems. Included are chapters on the Influence of pressure and temperature (G. V. Schulz and M. Lechner), Electric field light scattering (B. R. Jennings), the Study of association and aggregation via light scattering (H.-G. Elias), the Application of light scattering to copolymers (H. Benoit and D. Froelich), Light scattering from polyelectrolytes (M. Nagasawa and A. Takahashi), Selected topics in biopolymeric systems (W. Burchard and J. M. G. Cowie). My main criticism of the book is the omission of Rayleigh light scattering spectroscopy which in recent years has become an important tool for studying the dynamic properties of polymers in dilute solution. There are at least two chapters which I feel could have been left out to make room for the treatment of this rapidly developing topic.

The book is well presented and the contents show a logical development. It can be recommended to those concerned with day-to-day problems of polymer characterization. Beginners to this field should find certain sections particularly helpful.

C. Price

## Plastic foams

Edited by K. C. Frisch and J. H. Saunders

Marcel Dekker, New York, 1972, Part 1, 450 pp. \$36.50

This is Part 1 of a two-part monograph concerning cellular plastics and rubber flexible foams; semi-rigid and rigid foams are to be covered in Part 2 still awaiting publication. Reviews of current practice in major areas of the cellular polymer field have been written by a team of authors each a known specialist in the appropriate polymer class. Most of the material presented is already published elsewhere and little new information revealed the prime purpose served by the editors being to collect this scattered data in a reasonably concise format. Consequently, some detail essential to these materials and their processes has been eliminated.

Chapters are devoted to foams from the following polymer classes: polyurethanes, solid and latex rubber, polyolefins, poly(vinyl chloride), and silicones, each including the basic chemistry of blowing but with pronounced emphasis on primary processing, mixing and dispensing equipment illustrated by selected application examples of cellular products. Formulations are quoted throughout to illustrate each blowing technique. This has resulted in a balanced blend of chemistry and related technology which is most readable.

Special chapters have been included on the mechanism of foam formation and testing procedures for cellular materials which are based entirely on ASTM methods, there being no cross references to equivalent BSI or ISO specifications. A useful marketing trend and historical chapter is included.

USA trade names are used throughout, supplemented by chemical names in most instances so that identification with equivalent types should not be too difficult for potential users.

Individual chapter authors have, in most instances, given adequate literature references so that the book has become a minor bibliography of current cellular foam technology with American literature receiving dominant representation. It is possible to dip into the various sections at will adding to general usefulness.

No cumulative index has been included in Part 1 and it is to be hoped that Part 2 will contain such an index without which the usefulness of these monographs as reference sources will be severely limited. It is the only book to the reviewer's knowledge which attempts to cover both plastic and rubber materials jointly in this industrially important field reflecting growing rationalization in the cellular polymeric materials field. To this extent it must be regarded as unique which possibly would justify the high price of £15.25. It is still unusual to find rubber polymers in a book with plastics as its only key word title, the two materials possessing quite different properties and such misrepresentation of contents could well affect readership.

C. Hepburn

### Dielectric properties of polymers

Edited by Frank E. Karasz

Plenum Press, New York, 1972, 374 pp. \$26.00

This book comprises a collection of 15 papers originally presented at a Symposium on the Dielectric Properties of Polymers at the American Chemical Society meeting in Los Angeles, March 1971. The authors include many leading authorities in the field and the papers encompass a wide range of topics within the dielectrics area.

With regard to polymer solutions, a particularly encouraging aspect of the book concerns the inclusion of dielectric theories based on more detailed models of polymer chains than the well established Rouse-Zimm bead-spring model. Such developments are, for example, necessary for understanding the various types of relaxation behaviour possible for chains with local dipole components perpendicular to the chain axis. Clark and Zimm describe in detail a theory for chains containing 'perpendicular' dipoles which incorporates a measure of the extent to which the motions of chain dipoles are correlated, and yields insight into the observation that average relaxation times are usually independent of molecular weight. A first attempt to apply the detailed rotational isomeric state model to the dielectric relaxation of short chain polymers is also made by Jernigan. There is clearly a need for more extensive and systematic dielectric studies on dilute polymer solutions to support these theoretical developments, and only one experimental paper, on *para*-substituted polystyrenes (Baysal, Lowry, Yu and Stockmayer), is concerned with solution work.

Regarding the dielectric behaviour of bulk amorphous polymers, Williams and Watts have contributed a clear and concise review

of their extensive work on the combined effects of frequency, temperature and pressure. They emphasize the relationships observed between the mechanisms of the multiple loss peaks, and suggest that environmental rather than intrachain cooperation is of major concern in the motional processes exhibited by solid polymers. Matsuoka, Roe and Cole provide evidence for a similar view from a study of chlorinated polyethylenes and Wetton concludes that long range intermolecular interactions provide the major restriction to methoxy group motions in *para*-substituted polystyrenes. The effects of pressure on the dielectric relaxation in crystalline methyl stearate are interpreted by Broadhurst in terms of bulk thermodynamic properties.

Several papers are devoted specifically to solid copolymers. Smith, Corrado and Work discuss equilibrium dipole moments in terms of correlations both in the type and orientation of chain repeat units and MacKnight and Emerson have quantitatively correlated the dispersions observed in ethylene-acrylic and ethylene-methacrylic acid copolymers with the orientation of dissociated carboxylic acid groups. Current interest in the properties of multi-phase segmented or block copolymers is reflected in the papers by Pochan and Crystal and by Dev, North and Reid. The latter authors give more than usual attention to the low frequency effects associated with ionic conduction and interfacial polarization, and the practically important ionic processes are also considered in detail by Reed from the point of view of impurity effects in an amorphous poly(phenylene oxide). Creswell, Perlman and Kabayama have investigated the charge storage stability of a wide range of polymers (electrets) and a useful account of experimental methods, suitable for both solid and liquid polymers, is presented by Porter and Boyd.

As stated in the Preface to the book, it is obviously useful to have related material of this kind published in a single volume. However, in view of the high standards and clarity of the individual contributions, it seems a pity that a collective and critical discussion is not included, since this would tend to minimize the lack of coherence inevitable in a book of this kind.

The book is produced by the photocopying of typed manuscripts, a procedure which often yields an unsightly product and which has been rightly criticized in past reviews. In the present case, the typescript is uniform throughout, reasonably attractive and appears to contain few errors. The book should prove a useful acquisition for specialists in dielectrics and related polymer fields, providing that they can afford the inflated price of \$26. If not, they can find a summary of most of the papers in the *ACS Polymer Preprints* (1971, Vol 12, No 1).

B. E. Read

#### Conference Announcement

### Composites - standards, testing and design

National Physical Laboratory, Teddington  
8-9 April 1974

This conference will highlight and discuss problems inhibiting the effective use of composites as engineering materials, and will identify the needs for standards and tests necessary to set criteria for the safe, efficient and economic use of composites. The areas it will cover include the aircraft, marine, transport, building, chemical and civil engineering industries. Invited speakers will give keynote papers which will be supplemented by shorter contributions. Fuller details will be circulated in due course but intending participants are invited to notify Mr R. P. Miller, Division of Inorganic and Metallic Structure, NPL, Teddington, Middlesex TW11 0LW, UK.

#### Summer Program Announcement

### Institute in Science and Technology

Mohonk Lake, New York,  
4 June to 13 July 1973

The State University of New York is organizing the following summer Institutes in Science and Technology:

- 4-8 June Scanning electron microscopy
- 11-15 June New techniques and methods of polymerization
- 18-22 June Fundamentals and technology of plastic foams
- 25-29 June Disposal and utilization of plastic wastes

9-13 July Photoconductivity in polymers  
The fee for each is \$275. Further details may be obtained from Professor A. V. Patsis, Department of Chemistry, State University of New York, New Paltz, New York, USA.

# Book Reviews

## Reverse osmosis membrane research

Edited by H. K. Lonsdale and H. E. Podall

Plenum Press, New York, 1972, 503 pp. \$32.00

This book is primarily a collection of papers presented in a symposium on Polymers for Desalination held at the 162nd National Meeting of the American Chemical Society in Washington, D.C. in September 1971. Several additional papers have been especially contributed to the monograph so as to improve the coverage of membrane research and development.

The introduction, written by the editors, is designed to serve two purposes; it gives a general description of the principles and problems of practical reverse osmosis and it surveys and summarizes the following papers by organizing them into five groups.

The book is likely to interest most intently readers personally connected with research on membrane separation processes. For them the general description is scarcely necessary but the survey and summaries of the papers are extremely valuable and relieve the reviewer of one of his more difficult tasks. The potential purchaser should certainly read this editors' survey. It gives a strong impression of the creative activity and ingenuity which now characterizes attempts to improve the commercial viability of membrane processes. The practical research papers are all of USA origin although the two papers on Fundamentals: on the membrane process (by O. Kedem) and on the membrane/solution interfacial process (by W. Pusch), are from elsewhere. This restriction of origin is more apparent than real because by far the greatest amount of truly innovative membrane research at the present time is being carried out in the USA.

Although no book of this size could give a truly complete account of the field nor could it be truly up-to-date even at the date of publication, the collection of papers presented here give a balanced and stimulating picture of the mainstreams of research towards improving reverse osmosis. The book closes with a chapter by W. S. Gillan setting out trends and hopes for the future. There is a short and rather inadequate index.

P. Meares

## Comportement thermique des polymères synthétiques

F. Rocaboy

Masson et Cie, Paris, 1972, Vol 1, 301 pp. 140F

This is the first volume of what promises to be a rather curious book, in which the entire range of synthetic polymers is described from the aspect of their thermal properties. An attempt is made to classify the principal properties in relation to behaviour upon heating, mainly by division into reversible and irreversible changes. In particular, an attempt is made to identify the structural and chemical factors which favour resistance to degradation at high temperatures, with a special interest in polymers accepted as 'thermally stable' or 'thermally resistant'. In practice, this means that most of the text published so far consists of a catalogue of every conceivable vinyl and carbocyclic polymer, with tables of fusion temperatures and, where possible, differential thermal analysis curves tacked on the end of each section. Many of these sections are so brief that they are misleading without the addition of further critical comment. As a quick reference, the thermal data provided are useful; the supporting references quoted are, at times, somewhat unexpectedly chosen. To precede this section, there are four introductory chapters, which discuss the configuration of macromolecular chains, crystal structure and polymer morphology, the rheology of polymers (which is clearly stated but barely relevant in this context), and the general principles of thermal behaviour. At the end of the book, an appendix lists, by type of polymer, the commercial names of synthetic fibres based on carbon chains. The list is long, includes many obscure and probably obsolete brand-names, and seems quite pointless.

In sum, this is a polemical work, of some value to workers concerned with the thermal properties of polymers, but the approach is too eccentric for it to be used in isolation. It is well printed, with many figures, but is rather expensive for its likely value to most readers.

C. A. Finch

## Light scattering from polymer solutions

Edited by M. B. Huglin

Academic Press, London, 1972, 885 pp. £14.50

Light scattering from polymer solutions has become a routine characterization technique in many laboratories. The experimental work involved, however, is exceptionally demanding and a great deal of care and considerable experience is required to obtain reliable results. Research workers from a variety of disciplines, who use light scattering as a tool, will find the wealth of technical information and experimental know-how recorded in this work extremely useful. Undoubtedly it is a book which will find its place on or near the laboratory bench. In all it contains eighteen chapters and there are twenty contributors.

The first sections deal with experimental procedures, theoretical background, and treatment of results. Especially noteworthy here is the extensive tabulation of useful data (e.g. specific refractive index increments and physical properties of solvents). The rest of the work deals with the effect of external parameters and applications to particular types of systems. Included are chapters on the Influence of pressure and temperature (G. V. Schulz and M. Lechner), Electric field light scattering (B. R. Jennings), the Study of association and aggregation via light scattering (H.-G. Elias), the Application of light scattering to copolymers (H. Benoit and D. Froelich), Light scattering from polyelectrolytes (M. Nagasawa and A. Takahashi), Selected topics in biopolymeric systems (W. Burchard and J. M. G. Cowie). My main criticism of the book is the omission of Rayleigh light scattering spectroscopy which in recent years has become an important tool for studying the dynamic properties of polymers in dilute solution. There are at least two chapters which I feel could have been left out to make room for the treatment of this rapidly developing topic.

The book is well presented and the contents show a logical development. It can be recommended to those concerned with day-to-day problems of polymer characterization. Beginners to this field should find certain sections particularly helpful.

C. Price

## Plastic foams

Edited by K. C. Frisch and J. H. Saunders

Marcel Dekker, New York, 1972, Part 1, 450 pp. \$36.50

This is Part 1 of a two-part monograph concerning cellular plastics and rubber flexible foams; semi-rigid and rigid foams are to be covered in Part 2 still awaiting publication. Reviews of current practice in major areas of the cellular polymer field have been written by a team of authors each a known specialist in the appropriate polymer class. Most of the material presented is already published elsewhere and little new information revealed the prime purpose served by the editors being to collect this scattered data in a reasonably concise format. Consequently, some detail essential to these materials and their processes has been eliminated.

Chapters are devoted to foams from the following polymer classes: polyurethanes, solid and latex rubber, polyolefins, poly(vinyl chloride), and silicones, each including the basic chemistry of blowing but with pronounced emphasis on primary processing, mixing and dispensing equipment illustrated by selected application examples of cellular products. Formulations are quoted throughout to illustrate each blowing technique. This has resulted in a balanced blend of chemistry and related technology which is most readable.

Special chapters have been included on the mechanism of foam formation and testing procedures for cellular materials which are based entirely on ASTM methods, there being no cross references to equivalent BSI or ISO specifications. A useful marketing trend and historical chapter is included.

USA trade names are used throughout, supplemented by chemical names in most instances so that identification with equivalent types should not be too difficult for potential users.

Individual chapter authors have, in most instances, given adequate literature references so that the book has become a minor bibliography of current cellular foam technology with American literature receiving dominant representation. It is possible to dip into the various sections at will adding to general usefulness.

No cumulative index has been included in Part 1 and it is to be hoped that Part 2 will contain such an index without which the usefulness of these monographs as reference sources will be severely limited. It is the only book to the reviewer's knowledge which attempts to cover both plastic and rubber materials jointly in this industrially important field reflecting growing rationalization in the cellular polymeric materials field. To this extent it must be regarded as unique which possibly would justify the high price of £15.25. It is still unusual to find rubber polymers in a book with plastics as its only key word title, the two materials possessing quite different properties and such misrepresentation of contents could well affect readership.

C. Hepburn

### Dielectric properties of polymers

Edited by Frank E. Karasz

Plenum Press, New York, 1972, 374 pp. \$26.00

This book comprises a collection of 15 papers originally presented at a Symposium on the Dielectric Properties of Polymers at the American Chemical Society meeting in Los Angeles, March 1971. The authors include many leading authorities in the field and the papers encompass a wide range of topics within the dielectrics area.

With regard to polymer solutions, a particularly encouraging aspect of the book concerns the inclusion of dielectric theories based on more detailed models of polymer chains than the well established Rouse-Zimm bead-spring model. Such developments are, for example, necessary for understanding the various types of relaxation behaviour possible for chains with local dipole components perpendicular to the chain axis. Clark and Zimm describe in detail a theory for chains containing 'perpendicular' dipoles which incorporates a measure of the extent to which the motions of chain dipoles are correlated, and yields insight into the observation that average relaxation times are usually independent of molecular weight. A first attempt to apply the detailed rotational isomeric state model to the dielectric relaxation of short chain polymers is also made by Jernigan. There is clearly a need for more extensive and systematic dielectric studies on dilute polymer solutions to support these theoretical developments, and only one experimental paper, on *para*-substituted polystyrenes (Baysal, Lowry, Yu and Stockmayer), is concerned with solution work.

Regarding the dielectric behaviour of bulk amorphous polymers, Williams and Watts have contributed a clear and concise review

of their extensive work on the combined effects of frequency, temperature and pressure. They emphasize the relationships observed between the mechanisms of the multiple loss peaks, and suggest that environmental rather than intrachain cooperation is of major concern in the motional processes exhibited by solid polymers. Matsuoka, Roe and Cole provide evidence for a similar view from a study of chlorinated polyethylenes and Wetton concludes that long range intermolecular interactions provide the major restriction to methoxy group motions in *para*-substituted polystyrenes. The effects of pressure on the dielectric relaxation in crystalline methyl stearate are interpreted by Broadhurst in terms of bulk thermodynamic properties.

Several papers are devoted specifically to solid copolymers. Smith, Corrado and Work discuss equilibrium dipole moments in terms of correlations both in the type and orientation of chain repeat units and MacKnight and Emerson have quantitatively correlated the dispersions observed in ethylene-acrylic and ethylene-methacrylic acid copolymers with the orientation of dissociated carboxylic acid groups. Current interest in the properties of multi-phase segmented or block copolymers is reflected in the papers by Pochan and Crystal and by Dev, North and Reid. The latter authors give more than usual attention to the low frequency effects associated with ionic conduction and interfacial polarization, and the practically important ionic processes are also considered in detail by Reed from the point of view of impurity effects in an amorphous poly(phenylene oxide). Creswell, Perlman and Kabayama have investigated the charge storage stability of a wide range of polymers (electrets) and a useful account of experimental methods, suitable for both solid and liquid polymers, is presented by Porter and Boyd.

As stated in the Preface to the book, it is obviously useful to have related material of this kind published in a single volume. However, in view of the high standards and clarity of the individual contributions, it seems a pity that a collective and critical discussion is not included, since this would tend to minimize the lack of coherence inevitable in a book of this kind.

The book is produced by the photocopying of typed manuscripts, a procedure which often yields an unsightly product and which has been rightly criticized in past reviews. In the present case, the typescript is uniform throughout, reasonably attractive and appears to contain few errors. The book should prove a useful acquisition for specialists in dielectrics and related polymer fields, providing that they can afford the inflated price of \$26. If not, they can find a summary of most of the papers in the *ACS Polymer Preprints* (1971, Vol 12, No 1).

B. E. Read

#### Conference Announcement

### Composites - standards, testing and design

National Physical Laboratory, Teddington  
8-9 April 1974

This conference will highlight and discuss problems inhibiting the effective use of composites as engineering materials, and will identify the needs for standards and tests necessary to set criteria for the safe, efficient and economic use of composites. The areas it will cover include the aircraft, marine, transport, building, chemical and civil engineering industries. Invited speakers will give keynote papers which will be supplemented by shorter contributions. Fuller details will be circulated in due course but intending participants are invited to notify Mr R. P. Miller, Division of Inorganic and Metallic Structure, NPL, Teddington, Middlesex TW11 0LW, UK.

#### Summer Program Announcement

### Institute in Science and Technology

Mohonk Lake, New York,  
4 June to 13 July 1973

The State University of New York is organizing the following summer Institutes in Science and Technology:

- 4-8 June Scanning electron microscopy
  - 11-15 June New techniques and methods of polymerization
  - 18-22 June Fundamentals and technology of plastic foams
  - 25-29 June Disposal and utilization of plastic wastes
  - 9-13 July Photoconductivity in polymers
- The fee for each is \$275. Further details may be obtained from Professor A. V. Patsis, Department of Chemistry, State University of New York, New Paltz, New York, USA.

# Flow birefringence of polyelectrolytes: a poly(amide carboxylic acid) from pyromellitic anhydride and benzidine—influence of triethylamine on the molecular dimensions

J. W. M. Noordermeer and H. Janeschitz-Kriegl

Laboratory of Physical Chemistry, Delft University of Technology, Delft 8, The Netherlands

and A. Horvath

Polymer-Institut der Universität Karlsruhe, 75 Karlsruhe, West Germany

(Received 27 November 1972)

The flow birefringence of a number of solutions of a poly(amide carboxylic acid) from pyromellitic anhydride and benzidine was measured at 30°C. *N,N*-dimethyl acetamide was used as a solvent. Addition of the organic base triethylamine to this polyacid (0 to 15 g-equiv. with respect to the number of —COOH— groups) results in a strong increase of the stress-optical coefficient. This increase can successfully be interpreted in terms of an expansion of the molecular coils. An increase of the stress-optical coefficient is also obtained, when the concentration of the poly(amide carboxylic acid) is decreased. This is in agreement with the observed increase of the reduced viscosity,  $\eta_{sp}/c$ . A relation is deduced, which describes the dependence of the stress-optical coefficient on concentration with reasonable accuracy. Making use of this relation the degree of expansion of this polyelectrolyte can be determined for infinite dilution.

From the behaviour of the extinction angle the conclusion is drawn that the hydrodynamic behaviour of the investigated polyelectrolyte molecules does not undergo a fundamental change with expansion: after a correction for polydispersity the results seem to indicate that the expanded molecules still approximately behave like Gaussian chains.

## INTRODUCTION

It is well known that, in many respects, the behaviour of polyelectrolyte molecules strongly differs from that of uncharged macromolecules. The coil dimensions of polyelectrolytes in solution are influenced by the electrostatic repulsion of charges, which are introduced on the macromolecular chain by ionization. A large number of charges on the chain causes a strong expansion of the coil.

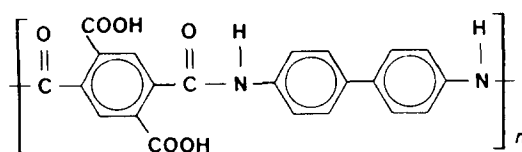
Counter-ions are known to shield the electrostatic charges on the chain so that the degree of expansion is influenced also by the presence of these ions. The local concentration of counter-ions can be increased by addition of a low-molecular electrolyte or by an increase of the concentration of the polyelectrolyte itself. In this way, an increase of the polyelectrolyte concentration causes a decrease of the mean dimensions of the molecules.

Coil expansion can, for example, be observed with the aid of the angular dependence of light-scattering (radius of gyration) and derived from a strong increase of the viscosity of the polyelectrolyte solution. In this respect, many examples are already known.

On the contrary, only a few investigations of the flow birefringence of polyelectrolyte solutions have been published until now. The investigations of Fuoss and

Signer<sup>1</sup> and of Jordan and co-workers<sup>2,3</sup> on poly(4-vinyl-*N*-butyl pyridinium bromide) and poly(4-vinyl pyridinium chloride) have shown that extinction angle and birefringence considerably change with an increasing degree of ionization of the macromolecules. The investigations of Kuhn *et al.*<sup>4</sup> and of Tsvetkov and co-workers<sup>5</sup> on poly(acrylic acid) and poly(methacrylic acid) in aqueous solutions give similar results. The interpretation of these results, however, is complicated by a considerable contribution of the form birefringence. This birefringence becomes considerable if too large a difference exists between the refractive indices of polymer and solvent. In such a case the coil-molecule as a whole contrasts too much with the solvent.

Vollmert and Horvath<sup>6-8</sup> recently performed viscosity and light-scattering measurements on a poly(amide carboxylic acid) (PACA) from pyromellitic anhydride and benzidine:





As a solvent *N,N*-dimethyl acetamide (DMA) was used. On ionization of this polyacid with the organic base triethylamine (TEA) the viscosity of the solution sharply increases. For the ionized PACA the dependence of  $\eta_{sp}/c$  on  $c$  is characterized by the typical increase which is always observed with polyelectrolytes when concentration is lowered. On the other hand, for the un-ionized PACA the dependence of  $\eta_{sp}/c$  on  $c$  corresponds to that for uncharged macromolecules.

The degree of ionization and with it the coil expansion of the PACA are determined by the equilibrium constant of the acid-base reaction, the concentration of the dissolved PACA and the concentration of TEA. As an excess of unreacted TEA remains non-ionic, it does not contribute to the ionic strength of the solution.

This work describes the flow birefringence of this polyelectrolyte system. Because of the stiffness of the PACA chain and the great number of aromatic rings this polyelectrolyte has a very high intrinsic anisotropy even in the uncharged state. As will be shown later, the stress-optical coefficient of this uncharged PACA is about ten times as large as that of polystyrene, for example. Therefore the influence of the form birefringence will be relatively small, in spite of the rather high refractive index increment ( $dn/dc=0.375$  ml/g<sup>6</sup>). In such a case also the ionic atmosphere of the protonated TEA molecules around the charged PACA molecules will have only a minor influence on the anisotropy of the macromolecule. Another advantage of the high optical anisotropy of the PACA molecules is that the flow birefringence of its solutions can be measured at very low concentrations of the PACA, where the polyelectrolyte effects are most pronounced.

It may be concluded that the described system must be extremely suitable for the investigation and interpretation of changes of optical properties as caused by ionization.

## THEORY

Flow birefringence is characterized by two quantities, which are measured separately, viz. the extinction angle and the birefringence, both as functions of shear rate. In addition, the viscosity of the solution must be known for the interpretation of the measurements.

From the theory for Gaussian chain molecules a stress-optical relation can be derived<sup>9-11</sup>. According to this relation proportionality should exist between the deviatoric components of the stress-tensor and the polarizability-tensor. The proportionality constant, which is also called the stress-optical coefficient, should only depend on the optical properties of the macromolecule, but not on its molecular weight or the concentration of the solution. The following equation holds under these conditions:

$$C = \frac{\Delta n \sin 2\chi}{2q(\eta - \eta_0)} = \frac{2\pi(n^2 + 2)^2}{27n} \frac{\gamma_1 - \gamma_2}{kT} \quad (1)$$

where

- $C$  = stress-optical coefficient,
- $q$  = shear rate,
- $\Delta n$  = birefringence at shear rate  $q$ ,
- $\chi$  = extinction angle, i.e. the smallest angle between one of the extinction directions and the direction of flow, at shear rate  $q$ ,
- $\eta$  = viscosity of the solution at shear rate  $q$ ,
- $\eta_0$  = viscosity of the solvent,
- $n$  = refractive index of the solution,

$k$  = Boltzmann constant,

$T$  = absolute temperature,

$\gamma_1 - \gamma_2$  = average difference of polarizabilities with respect to directions parallel and perpendicular to the end-to-end distance of the molecule in a stationary solution. As was pointed out by Kuhn and Gr $\ddot{u}$ n<sup>12</sup>, this parameter is independent of the length of the Gaussian chain.

Equation (1) is only valid if the refractive index of the solvent is very similar to that of the polymer ('matching solvent'). Otherwise the birefringence, caused by the shape of the macromolecular coil (form birefringence), gives a complicated contribution to the stress-optical coefficient.

The stress-optical coefficient actually appears to be a constant for many polymers, independent of shear rate and, in the absence of the form birefringence effect, also independent of molecular weight<sup>5</sup> and concentration<sup>10</sup>. However, solutions of relatively stiff or too short chain molecules may show a deviation from this rule; a decrease of the measured value of the stress-optical coefficient is found with increasing shear rate. It seems that deviation from Gaussian behaviour is more apparent in a flowing solution. As a consequence, equation (1) seems to remain valid for many molecules in the limiting case of zero shear rate<sup>13</sup>.

The ionization of a polyelectrolyte causes an expansion of the molecular coil, which can be described by an increase of the mean square end-to-end distance of the coil with regard to the un-ionized state<sup>4,14</sup>. For the expanded state Gaussian statistics may still be applied, if the expansion is not too large.

The charges on the molecular chain lead to a 'long-range' repulsion, as well as to a 'short-range' repulsion, which particularly influences the local chain-stiffness. Both effects together lead to an increase of the coil dimensions. For a moderate expansion, we may apply a well-known relation, derived originally by Kuhn and Gr $\ddot{u}$ n<sup>12</sup> for uncharged molecules:

$$\gamma_1 - \gamma_2 \sim \frac{\langle r^2 \rangle}{\langle r_0^2 \rangle} \quad (2)$$

where  $\langle r_0^2 \rangle$  is the mean-square end-to-end distance in the undisturbed, i.e. uncharged, state and  $r$  is an arbitrarily chosen end-to-end distance. If an external couple of forces is applied to the end-points, an averaging over the square of this end-to-end distance seems reasonable. In this way the action of the electrostatic repulsion forces is rudely taken into account. Admittedly, this procedure is equivalent to the introduction of an effective statistical random link which increases in length with the degree of ionization.

From equations (1) and (2) it can be concluded that an expansion of the coil must result in an increase of the stress-optical coefficient  $C$ . The more the coil expands, the more  $C$  increases.

On the other hand, the anisotropy  $\gamma_1 - \gamma_2$  of the macromolecule will also be influenced by a change of the chemical structure of the macromolecule, as caused by the ionization of the chain. This means that, in principle, the changes in the stress-optical coefficient must be ascribed to several effects.

A relation for the extinction angle  $\chi$  can be derived

from the theory of the 'bead-spring' model<sup>11, 15</sup>:

$$\cot 2\chi = J_{eR}\beta \quad (3)$$

The constant  $J_{eR}$  is known as the reduced steady-state compliance<sup>16</sup>. The reduced shear rate<sup>17</sup>  $\beta$  is defined by:

$$\beta = \frac{Mq(\eta - \eta_0)}{cRT} \quad (4)$$

where  $M$  = molecular weight of the polymer,  
 $c$  = the concentration (g/ml),  
 $R$  = the gas constant,  
 $\eta$  = here the zero shear viscosity of the solution.

For equation (3) it is again assumed that no form birefringence effect occurs.

When the parameter  $\beta$  is used, as given by equation (4), one aims at a reduction of experimental data with respect to temperature, molecular weight and concentration. However, the suggested reduction with respect to the concentration is often found to be less accurate<sup>11</sup>. For the value of  $J_{eR}$  one obtains 0.4 in the 'free-draining' case and 0.205 in the 'non-draining' case<sup>15</sup>. The value of  $J_{eR}$  depends only slightly on the excluded volume<sup>11</sup>. On the other hand, the extinction angle is very much affected by the polydispersity of the polymer.

It can be deduced<sup>11, 17</sup> that equation (3) reads for a polydisperse system:

$$\cot 2\chi = J_{eR} \frac{\langle \beta^2 \rangle_n}{\langle \beta \rangle_n} \quad (3a)$$

where  $\langle \rangle_n$  means the number average. With the introduction of a polydispersity factor  $p$ , where

$$p = \frac{\langle \beta^2 \rangle_n}{\langle \beta \rangle_n^2} \quad (5)$$

equation (3a) reads:

$$\cot 2\chi = p J_{eR} \langle \beta \rangle_n \quad (3b)$$

The quantity  $\langle \beta \rangle_n$  can directly be obtained from equation (4), if the number-average molecular weight is inserted. According to Peterlin<sup>17, 18</sup> the polydispersity factor  $p$  can be calculated, if the molecular weight distribution and the exponent  $\alpha$  in the Mark-Houwink relation are known for the polymer. As is well known, this relation reads  $[\eta] = KM^\alpha$ , where  $[\eta]$  is the intrinsic viscosity and  $0.5 \leq \alpha \leq 1.0$ .

Using the latter relation one obtains:

$$p = \frac{\langle M^{2\alpha+2} \rangle_n}{\langle M^{\alpha+1} \rangle_n^2} \quad (6)$$

These complicated molecular weight averages can be calculated with the aid of the molecular weight distribution. For an example, Peterlin and Munk<sup>18</sup> give a relation for  $p$ , if the molecular weight distribution is of the Schulz-Zimm type. For this type of distribution one obtains:

$$\frac{\langle M \rangle_w}{\langle M \rangle_n} = \frac{z+2}{z+1} \quad (7)$$

where  $\langle M \rangle_n$  and  $\langle M \rangle_w$  are the number- and weight-average molecular weights, respectively, and  $z$  is an adjustable parameter. The corresponding relation for  $p$  reads:

$$p = \frac{z!(z+2+2\alpha)!}{(z+1+\alpha)!^2} \quad (8)$$

Peterlin and Munk<sup>18</sup> gave  $p$ -values for a series of chosen values of  $\langle M \rangle_w / \langle M \rangle_n$  and  $\alpha$ .

## EXPERIMENTAL

For the present investigation a sample of PACA was used, previously described by Horvath and Vollmert<sup>6-8</sup>. Its weight-average molecular weight  $\langle M \rangle_w$  was 125 000, and its polydispersity index  $\langle M \rangle_w / \langle M \rangle_n$  was 2.4.

The solvent *N,N*-dimethyl acetamide (Fluke A.G.) was dried over KOH and P<sub>2</sub>O<sub>5</sub>, and distilled in vacuum. The triethylamine (Fluka A.G.) was distilled from KOH in a nitrogen atmosphere.

The concentrations of PACA varied from  $0.1 \times 10^{-3}$  to  $2.0 \times 10^{-3}$  g/ml. The amount of TEA added varied from 0 to 15 g-equiv. (with respect to the number of —COOH— groups). The solutions were prepared by addition of about half the required amount of DMA to a weighed amount of a 5% solution of PACA in DMA. To this solution an amount of a solution of TEA in DMA was added. This amount depended on the required number of g-equiv. Finally, DMA was added until the right volume was attained.

At high concentrations of PACA ( $2 \times 10^{-3}$  g/ml) and large amounts of TEA (5 g-equiv. and more) a precipitation occurred.

The refractive index increment of the PACA in DMA is 0.375 ml/g<sup>6</sup>. Normally such a high refractive index increment results in a rather great influence of the form birefringence. This latter effect can be calculated as a contribution  $C_f$  to the stress-optical coefficient  $C$  [equation (5.3) of Janeschitz-Kriegl<sup>11</sup>]. For the un-ionized PACA one obtains:

$$C_f/C = 1.67 \times 10^{-2} \quad (9)$$

when the value of  $C$  is taken from the measurements to be described. This contribution is small enough to lie completely within the limits of accuracy of this technique. Therefore, it can be disregarded throughout the present investigation.

The pure DMA does not show any measurable flow birefringence. This means that all the equations can be used without a correction for the solvent contribution to the flow birefringence.

The flow birefringence measurements were carried out in the equipment previously described<sup>11, 19</sup>. The viscosity measurements were done with the aid of ordinary Ubbelohde viscometers. To remove dust all solutions were filtered through glass filters. All measurements were carried out at 30°C.

## RESULTS OF FLOW BIREFRINGENCE MEASUREMENTS

Figure 1 gives an example for the type of extinction angle curves found. In this Figure the number of g-equiv. TEA per carboxyl group serves as a parameter. The concentration of the chosen solution is  $0.3 \times 10^{-3}$  g PACA per ml. The corresponding measurements of the birefringence  $\Delta n$  are given in Figure 2.

It is observed that, with increasing amounts of TEA, the deviation of the extinction angle from 45° rapidly increases, while also the birefringence appreciably increases. For the un-ionized PACA (0 g-equiv. of TEA), however, the deviation of the extinction angle

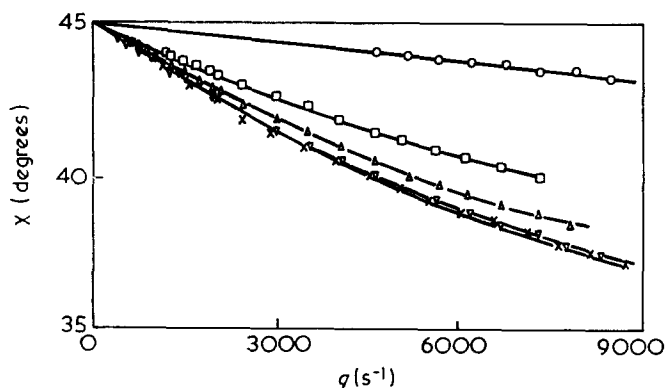


Figure 1 Extinction angle against shear rate of a series of solutions of PACA in DMA with varying amounts of TEA added. Concentration of PACA:  $0.3 \times 10^{-3}$  g/ml. Amounts of TEA added, expressed in g-equiv. per  $-\text{COOH}-$  group:  $\circ$ , 0;  $\square$ , 1;  $\triangle$ , 2;  $\nabla$ , 5;  $\times$ , 15

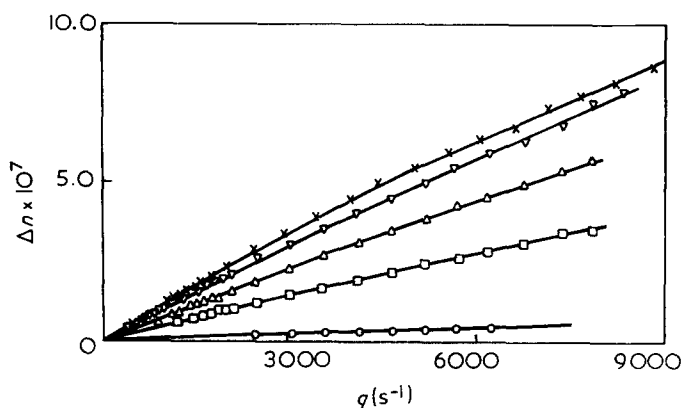


Figure 2 Flow birefringence against shear rate for the solutions specified in the caption to Figure 1

from  $45^\circ$  and the birefringence at low shear rates are so small, that reliable measurements are possible only at rather high shear rates.

In both Figures a tendency to saturation can be observed with regard to the influence of large quantities of TEA. If only a small quantity of TEA is added, the relation between the measured birefringence and the shear rate is linear. If larger quantities of TEA are added, a downward curvature is noticed at high shear rates. This points to a deviation from the stress-optical relation (equation 1).

In Figure 3 an example is given of the usefulness of the reduced shear rate  $\langle \beta \rangle_n$ . The points correspond to measurements at a variety of concentrations of PACA. About 5 g-equiv. of TEA per COOH group are added to each solution. All points fall on the same line within the accuracy of these measurements; for the rather low concentrations of PACA, used in this investigation, the reduction with respect to these concentrations seems successful.

At the highest  $\langle \beta \rangle_n$  values a slight deviation can be observed from the proportionality between  $\cot 2\chi$  and  $\langle \beta \rangle_n$ . This points, like the deviation from linearity in Figure 2, to a deviation from the Gaussian behaviour of the chains. At lower  $\langle \beta \rangle_n$  values, where the relation between  $\cot 2\chi$  and  $\langle \beta \rangle_n$  is still linear,  $pJ_{eR}$  can be determined. The obtained values of  $pJ_{eR}$  are given in Figure 4. This Figure surveys the results of the entire investigation, as far as the extinction angle is concerned. Both the concentration and the added amount

of TEA, seem to have no significant influence on  $pJ_{eR}$ . The averaged value of  $pJ_{eR}$  amounts to 1.60.

The larger scatter, which is obtained when less TEA is added, is caused by the inaccuracy in measuring small deviations of the extinction angle from  $45^\circ$  (compare Figure 1). Moreover, with these measurements also the birefringence is very small, making an accurate determination still more difficult.

With the aid of equation (1) stress-optical coefficients can be calculated from the measurements. The obtained values are given in Figure 5 as functions of the number of g-equiv. TEA per COOH group and with the concentrations of PACA as parameters. Since several solutions show deviations from the proportionality between birefringence and shear rate, all values are taken after extrapolation to zero shear rate.

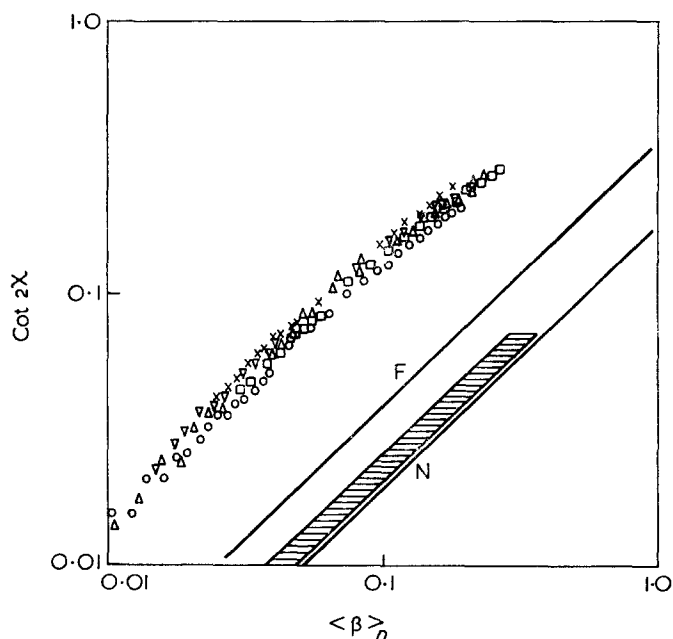


Figure 3 Example of a reduction of the extinction angle  $\chi$  with respect to concentration. Concentrations in g PACA per ml solution are:  $\times$ ,  $0.1 \times 10^{-3}$ ;  $\nabla$ ,  $0.2 \times 10^{-3}$ ;  $\triangle$ ,  $0.3 \times 10^{-3}$ ;  $\square$ ,  $0.5 \times 10^{-3}$ ;  $\circ$ ,  $1.0 \times 10^{-3}$ . To all solutions 5 g-equiv. of TEA per COOH group are added. F=free-draining approximation; N=non-draining approximation. Shaded area: location of the measured points after a correction for polydispersity

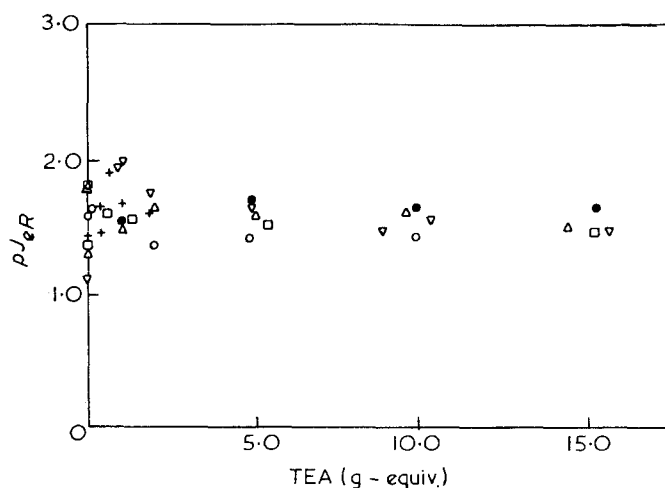


Figure 4 Values of  $pJ_{eR}$  for all investigated solutions, as calculated from their extinction angle curves. The values are plotted against number of g-equiv. TEA per COOH group added. Concentrations in g PACA per ml are:  $\bullet$ ,  $0.1 \times 10^{-3}$ ;  $\nabla$ ,  $0.2 \times 10^{-3}$ ;  $\triangle$ ,  $0.3 \times 10^{-3}$ ;  $\square$ ,  $0.5 \times 10^{-3}$ ;  $\circ$ ,  $1.0 \times 10^{-3}$ ;  $+$ ,  $2.0 \times 10^{-3}$

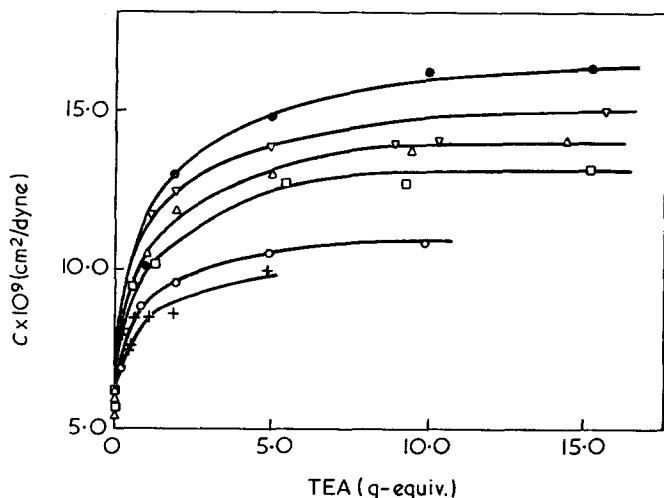


Figure 5 Stress-optical coefficient  $C$ , calculated for all solutions, against number of g-equiv. TEA per COOH— group added. Concentrations of PACA: symbols as in Figure 4

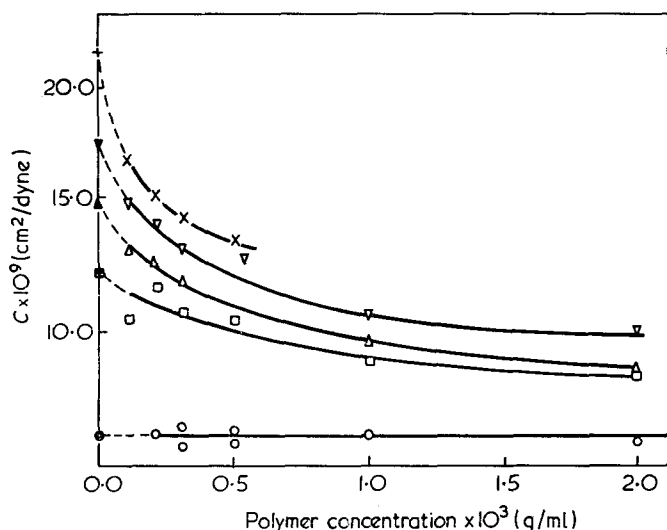


Figure 6 Stress-optical coefficient  $C$  against concentration of PACA. Number of g-equiv. TEA per COOH— group added: symbols as in Figure 1. Closed points and +: values of  $C$  extrapolated to zero concentration, according to equation (11)

From an inspection of Figure 5 the following facts can be deduced: on addition of TEA the stress-optical coefficient first shows a considerable increase. On the other hand, a clear saturation of the stress-optical coefficient is noticed at larger amounts of TEA added. An increase of the concentration of PACA suppresses the expansion effects.

Figure 6 gives the same results, now as functions of the concentration of PACA and with the numbers of g-equiv. of TEA per COOH group as parameters. One clearly observes that a decrease of the concentration of PACA results in an increase of the stress-optical coefficient.

The curves in both Figures show a clear resemblance to the  $\eta_{sp}/c$  vs.  $c$  curves of this PACA<sup>6,8</sup>. A detailed discussion of this fact will be given later.

Finally, it should be noticed that the stress-optical coefficient of the un-ionized PACA (0 g-equiv. TEA) is independent of concentration. This is normally found for uncharged polymers of molecular weight high enough for the formation of Gaussian coils.

## DISCUSSION

It is quite obvious that the increase of the stress-optical coefficient of the PACA must be ascribed to an expansion of the macromolecules. Especially the resemblance of Figure 6 to the  $\eta_{sp}/c$  vs.  $c$  curves characteristic for polyelectrolytes seems to prove this. Also the equilibrium character of the acid–base reaction is clearly manifested by the saturation effect in Figure 5.

On the other hand, the un-ionized PACA shows no changes in the stress-optical coefficient, when the concentration of PACA is changed. From this fact the conclusion may be drawn that PACA in DMA is incapable of spontaneous ionization. Admittedly, such an ionization will be detectable only at low concentrations. The question remains, whether at these concentrations changes in the stress-optical coefficient can be observed with sufficient accuracy.

As is well known, quantitative conclusions about the coil expansion of polyelectrolytes cannot be drawn from viscosity measurements, as the results of these measurements cannot safely be extrapolated to zero concentration. As a matter of fact the same is true for the stress-optical coefficient. Only when isoionic dilution, according to Pals and Hermans<sup>20</sup> is applied to viscosity measurements on polyelectrolytes, normal results are obtained, which can be extrapolated to zero concentration.

However, Fuoss and Strauss<sup>21</sup> found an empirical relation which seems to describe the dependence of  $\eta_{sp}/c$  on  $c$  at low polyelectrolyte concentrations with reasonable accuracy. This Fuoss–Strauss relation reads:

$$\eta_{sp}/c = \frac{A}{1 + B \times (c)^{1/2}} \quad (10)$$

where  $A$  and  $B$  are adjustable parameters. This equation has been extremely useful for many polyelectrolytes. In fact, Horvath and Vollmert<sup>6,8</sup> have shown that it can also be applied to the changes of the viscosity of the PACA solutions.

Because of the resemblance of the curves in Figure 6 to the  $\eta_{sp}/c$  vs.  $c$  curves of this PACA we tried a similar relation for the dependence of the stress-optical coefficient on the concentration of our PACA:

$$C = \frac{A'}{1 + B' \times (c)^{1/2}} \quad (11)$$

When  $1/C$  is plotted as a function of the square root of PACA concentration, a straight line should be obtained. This is demonstrated in Figure 7 for several

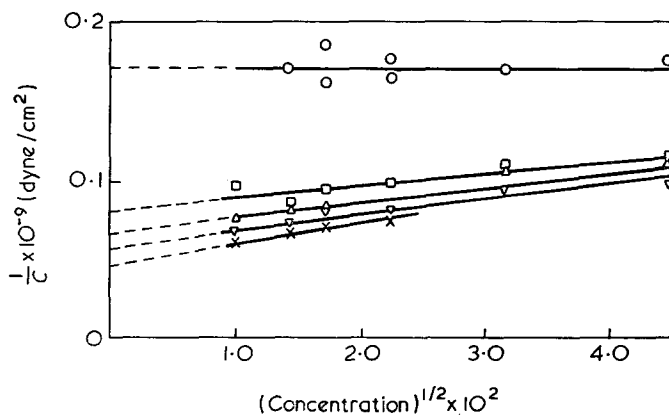


Figure 7 Extrapolation of the stress-optical coefficient to zero concentration, according to equation (11). Number of g-equiv. TEA per COOH— group added: symbols as in Figure 1

quantities of TEA added. Within the limits of accuracy a reasonable extrapolation to zero concentration can be carried out with the aid of equation (11). The values of the stress-optical coefficient, extrapolated in this way, are given in Table 1 (column 2). They are also shown in Figure 6 as closed points at the ordinate axis.

At infinite dilution no mutual shielding of charges on separate macromolecules takes place. The coil expansion is then determined only by the charges on the same molecular chain.

The —COOH— groups on our PACA molecule are located opposite to each other on the aromatic rings in the chain. The charges, introduced by ionization, are uniformly distributed along the molecular chain. Therefore, it seems probable that the anisotropy per unit length of the PACA chain (in 'stretched' conformation) will hardly be changed by the ionization. This supports the assumption that the increase of the stress-optical coefficient is mainly caused by the expansion of the macromolecular coil.

In this case the degree of expansion, expressed as an increase of the mean square end-to-end distance, can be calculated with the aid of equations (1) and (2). The results of this calculation are given in Table 1 (column 3).

Another way of interpretation is found in Figure 8, in which the stress-optical coefficient, as extrapolated to zero concentration, is plotted on a double logarithmic scale against the intrinsic viscosity, measured at corresponding degrees of ionization. If the above made assumption with respect to the usefulness of the stress-optical coefficient as a measure of coil expansion is correct, one should obtain a curve of slope 2/3, since

Table 1 Stress optical coefficient and coil-expansion for several amounts of TEA added

TEA (g-equiv.)	$\lim_{\substack{c \rightarrow 0 \\ \alpha \rightarrow 0}} C \times 10^9$ (cm <sup>2</sup> /dyne)	$\frac{\langle r^2 \rangle}{\langle r_0^2 \rangle}$
0	5.9	1
1	12.2	2.1
2	14.9	2.5
5	17.4	2.9
10	19.6	3.3
15	21.2	3.6

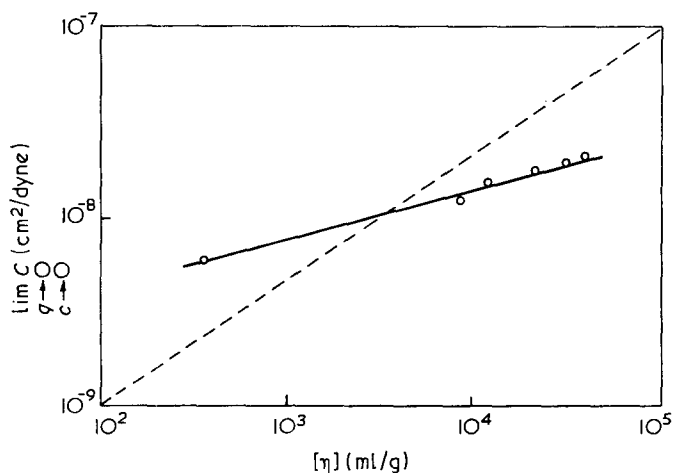


Figure 8 Stress-optical coefficient  $C$ , extrapolated to zero concentration, against intrinsic viscosity  $[\eta]$ , at various degrees of ionization. ---, slope 2/3

the viscosity is proportional to the 3/2 power of the mean square end-to-end distance of the coiled molecule.

In Figure 8 a broken line of slope 2/3 is drawn for comparison. From this Figure it becomes clear, however, that the growth of the stress-optical coefficient with increasing degree of ionization is considerably slower than would be expected from the corresponding growth of the intrinsic viscosity. More detail should probably not be deduced from Figure 8 because of the limited reliability of the extrapolation method. The interpretation of this fact may probably be that the difference of main polarizabilities  $\gamma_1 - \gamma_2$  of the chain is more sensitive to the local stiffening of the chain than to the expansion by long range interaction forces, whereas the intrinsic viscosity is influenced by both effects more equally. This interpretation should, nevertheless, be considered with some extra reserve as we do not know the influence of the growing number of charges on the polarizabilities.

As a next point of discussion we now choose the behaviour of the extinction angle. For this purpose Figure 3 is considered. Except for the highest  $\langle \beta \rangle_n$  values, where a slight downward tendency can be observed, the linear relation between  $\cot 2\chi$  and  $\langle \beta \rangle_n$  as postulated by equation (3b), is obeyed by this polymer. This means that the macromolecules behave hydrodynamically as flexible molecules.

For a comparison of these measurements with the results of Zimm's treatment of the 'bead-spring' model<sup>15</sup>, two theoretical lines are also given in Figure 3. The upper line, denoted by F, stands for the free-draining approximation, the lower one, designated by N, for the non-draining case. However, all experimental points lie far outside the theoretically expected area between the F and N line. From the experience with other polymers one may expect that this deviation is mainly caused by the polydispersity of the polymer sample. In order to confirm this assumption, Peterlin's method, which is explained in the theoretical part of this paper, is applied to the experimental results.

As is well known, a polycondensation reaction, like the one which takes place during the synthesis of this PACA, actually gives rise to a molecular weight distribution of the Schultz-Zimm type. A polydispersity index of 2.4 as found for this PACA corresponds to a value of  $-0.286$  for the adjustable parameter  $z$  in equation (7).

Unfortunately, Horvath and Vollmert<sup>6,7</sup> only give the Mark-Houwink equation at 25°C for the un-ionized PACA in DMA containing LiBr:

$$[\eta] = 3.40 \times 10^{-2} \times \langle M \rangle_w^{0.78} \quad (12)$$

A few measurements in pure DMA give higher values for the intrinsic viscosity of the PACA as a function of  $\langle M \rangle_w$ . The exponent in the Mark-Houwink equation, however, does not seem to be changed. The difference of 5°C between the temperatures at which the measurements of Horvath and Vollmert and the present measurements were carried out, seems of minor importance to us. Thus, a value of 0.78 is used for the constant  $\alpha$  which occurs in equation (8). In this way one obtains for the polydispersity factor  $p$  a value:  $p = 6.25$ . Using the average value for  $pJ_{eR} = 1.60$ , as derived from Figure 4, one finally obtains for  $J_{eR}$  the value.  $J_{eR} = 0.25$ . This value actually lies between the 'free-draining' and the 'non-draining' limits of Zimm<sup>15</sup>, as was found

earlier for many uncharged molecules<sup>11</sup>. In *Figure 3* the locations of the measurements, corrected for polydispersity, are indicated by a shaded area.

From this two conclusions can be drawn: (a) the dynamic behaviour of the expanded chain does not deviate considerably from that of the uncharged polymer (*Figure 4*); (b) also the expanded chains behave like molecular coils in which the solvent is non-draining. This conclusion agrees well with the opinion expressed by Vollmert and Horvath<sup>7</sup> that the PACA molecule must be highly solvated in DMA.

Finally, it may be concluded that the value of the stress-optical coefficient is a sensitive measure for the coil expansion of this polyelectrolyte. Owing to the high anisotropy of this PACA, even semi-quantitative conclusions as to the degree of expansion can be drawn. Unfortunately, this will be impossible for most of the more conventional polyelectrolytes in aqueous solution, because of the rather low optical anisotropy of these polymers.

#### ACKNOWLEDGEMENTS

The authors are indebted to Professor B. Vollmert for his aid in establishing the cooperation between the two laboratories and for his interest in this work.

#### REFERENCES

- 1 Fuoss, R. M. and Signer, R. *J. Am. Chem. Soc.* 1951, **73**, 5872
- 2 Jordan, D. O., Mathieson, A. R. and Porter, M. R. *J. Polym. Sci.* 1956, **21**, 463
- 3 Jordan, D. O. and Kurucsev, T. *Polymer* 1960, **1**, 202
- 4 Kuhn, W., Künzle, O. and Katchalski, A. *Helv. Chim. Acta* 1948, **31**, 1994
- 5 Tsvetkov, V. N. in 'Newer Methods of Polymer Characterisation' (B. Ke, Ed.), Interscience, New York, 1964
- 6 Horvath, A. *Thesis* 1970, University of Karlsruhe
- 7 Vollmert, B. and Horvath, A. *Angew. Makromol. Chem.* 1972, **23**, 117
- 8 Horvath, A. and Vollmert, B. *Angew. Makromol. Chem.* 1972, **23**, 141
- 9 Hermans, J. J. *Physica* 1943, **10**, 777
- 10 Janeschitz-Kriegl, H. *Makromol. Chem.* 1960, **40**, 140
- 11 Janeschitz-Kriegl, H. *Fortschr. Hochpolym.-Forsch.* 1969, **6**, 170
- 12 Kuhn, W. and Grün, F. *Kolloid-Z.* 1942, **101**, 248
- 13 Janeschitz-Kriegl, H. and Burchard, W. *J. Polym. Sci. (A-2)* 1968, **6**, 1953
- 14 Morawetz, H. in 'High Polymers', Vol XXI, Interscience, New York, 1965, Ch VII
- 15 Zimm, B. H. *J. Chem. Phys.* 1956, **24**, 269
- 16 Tschoegl, N. W. *J. Chem. Phys.* 1966, **44**, 4615
- 17 Peterlin, A. *J. Chem. Phys.* 1963, **39**, 224
- 18 Peterlin, A. and Munk, P. in 'Physical Methods of Chemistry', Vol I, Part IIIc (A. Weissberger and B. Rossiter, Eds.), John Wiley, New York, 1972
- 19 Janeschitz-Kriegl, H. and Nauta, R. *J. Sci. Instrum.* 1965, **42**, 880
- 20 Pals, D. T. F. and Hermans, J. J. *J. Polym. Sci.* 1950, **5**, 733
- 21 Fuoss, R. M. and Strauss, U. P. *J. Polym. Sci.* 1948, **3**, 602

# Equilibrium ring concentrations and the statistical conformations of polymer chains: Part 11. Cyclics in poly(ethylene terephthalate)

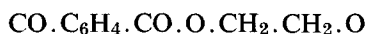
D. R. Cooper\* and J. A. Semlyen

*Department of Chemistry, University of York, Heslington, York YO1 5DD, UK  
(Received 20 December 1972)*

Methods have been developed for extracting cyclic oligomers from poly(ethylene terephthalate) samples and for analysing the extracts by gel permeation chromatography. These methods have been used to measure the molar cyclization equilibrium constants  $K_x$  for cyclics  $(\text{CO} \cdot \text{C}_6\text{H}_4 \cdot \text{CO} \cdot \text{O} \cdot \text{CH}_2 \cdot \text{CH}_2 \cdot \text{O})_x$  with  $x=3-9$  in the undiluted polymer at 543K and in solution in 1-methyl naphthalene at 523K. The close agreement between the measured  $K_x$  values over the range  $x=3-9$  shows that oligomeric ethylene terephthalate chains adopt similar conformations in the two environments (which contain 95% w/w and 6% w/w linear polymer respectively).  $K_x$  values were calculated by the Jacobson and Stockmayer theory by assuming that the corresponding open chain molecules obey Gaussian statistics and describing their statistical conformations by Williams and Flory's rotational isomeric state model. These theoretical values were found to be lower than the experimental values by factors of at least two over the whole range of cyclics  $x=3-9$ . Poor agreement between experiment and theory was also obtained when  $K_3$  and  $K_4$  values were calculated by computing the end-to-end distances of acyclic trimeric and tetrameric ethylene terephthalate chains in all discrete conformations defined by the Williams and Flory model. It is suggested that these discrepancies might result, at least in part, from substantial correlations between the positions and directions of the termini of oligomeric ethylene terephthalate chains. Observed decreases in the concentrations of cyclics in commercial poly(ethylene terephthalate) samples resulting from heating the samples in the solid state are discussed briefly.

## INTRODUCTION

Poly(ethylene terephthalate) (PET) consists of linear chains containing the repeat unit



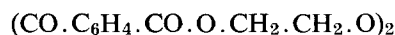
In common with a wide range of polymers prepared by condensation polymerizations or ring-to-chain equilibration reactions, PET contains cyclic as well as linear molecules. This paper describes the results of experimental and theoretical investigations of the concentrations of cyclic oligomers in PET equilibrates, carried out as part of a general study of the relationship between the concentrations of cyclics in polymers undergoing ring-chain equilibration reactions and the statistical conformations of the corresponding open chain molecules.

A basis for the investigations to be described here has been provided by the experimental work of several groups of chemists, who have reported the extraction of cyclics from commercial samples of PET film, fibre and chip, as well as the preparation and characterization of individual cyclic oligomers. The first report of a cyclic

oligomer of PET was by Ross and his coworkers<sup>1</sup>, who obtained about 1% w/w cyclic trimer



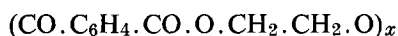
by extracting commercial PET film with trichloroethylene. This finding was confirmed later by Giuffria<sup>2</sup>. In the detailed investigations of Goodman and Nesbitt<sup>3</sup>, PET fibre and chip were extracted with mixed xylenes and with 1,4-dioxane to yield 1.3-1.7% w/w material, consisting mainly of cyclic trimer, but also containing cyclic tetramer and pentamer. Goodman and Nesbitt found none of the cyclic dimer



in their extracts, but they did isolate small amounts of a cyclic containing one ethylene glycol linkage,  $\text{O} \cdot \text{CH}_2 \cdot \text{CH}_2 \cdot \text{O}$ , and one diethylene glycol linkage,  $\text{O} \cdot \text{CH}_2 \cdot \text{CH}_2 \cdot \text{O} \cdot \text{CH}_2 \cdot \text{CH}_2 \cdot \text{O}$ . The unexpected appearance of this latter compound was connected with the observation that diethylene glycol residues had been incorporated into the polymer as a result of side-reactions during the melt polymerization reaction<sup>4,5</sup>. Zahn and Kusch<sup>6</sup> were the first to use gel permeation chromatography to analyse oligomeric extracts from PET. They were able to obtain samples of the individual cyclics

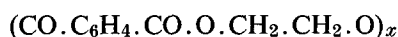
\* Present address: Department of Chemistry, University of Manchester, Manchester M13 9PL, UK.

$(\text{CO} \cdot \text{C}_6\text{H}_4 \cdot \text{CO} \cdot \text{O} \cdot \text{CH}_2 \cdot \text{CH}_2 \cdot \text{O})_x$  from the trimer ( $x=3$ ) to the hexamer ( $x=6$ ). In a recent study, Peebles *et al.*<sup>7</sup> used paper and column adsorption chromatography to resolve the mixtures obtained by extracting PET fibre and finely powdered chip with xylenes and 1,4-dioxane at temperatures close to the boiling points of the solvents. These authors found cyclics with three to five monomeric units in their extracts, together with a cyclic pentamer containing one diethylene glycol residue and several other compounds that were incompletely characterized. Individual cyclic oligomers of PET have also been obtained by direct synthesis, and high dilution techniques have been developed for the preparation of all the cyclic oligomers



from the dimer ( $x=2$ ) to the heptamer ( $x=7$ )<sup>8-12</sup>. These cyclic oligomers have been characterized and studied by a range of physico-chemical techniques<sup>11-20</sup>.

In this paper, experimental molar cyclization equilibrium constants for cyclics



(with  $x=3-9$ ) in melt and solution equilibrates of PET are presented and compared with theoretical predictions of the Jacobson-Stockmayer cyclization theory<sup>21, 22</sup>, applied in conjunction with the Williams and Flory<sup>23</sup> rotational isomeric state model of PET.

## EXPERIMENTAL

### Equilibration reactions

The starting material for the ring-chain equilibration reactions was PET chip of high molecular weight ( $\bar{M}_w = \sim 5 \times 10^4$ ) and low cyclic content ( $\sim 0.7\%$  w/w cyclics containing three to nine monomeric units).

The melt equilibration reactions were carried out by heating 50g samples of the polymer chip with 0.5% w/w antimony trioxide in evacuated glass ampoules at 543K for periods of up to 36h. The reactions were quenched by cooling to room temperature. The ampoules were then opened to air and the polymer was broken up. Oligomers were extracted from portions of the polymer as described below. The density of a PET melt equilibrate at 543K was assumed to be the literature value<sup>24</sup> of 1.22g/ml.

The solution equilibration reactions were carried out by mixing 5g samples of the polymer chip with 1-methyl naphthalene to give polymer concentrations of 10% w/w and adding zinc acetate as catalyst at concentrations of 0.5% w/w. The mixtures were sealed in glass ampoules under vacuum and heated at 523K for periods of up to 96h. The reactions were quenched by cooling the ampoules to room temperature. The density of a solution equilibrate at 523K was found to be  $0.86 \pm 0.03$  g/ml.

### Extraction of oligomers

Cyclic oligomers were obtained from undiluted PET equilibrates and commercial PET chip using the following extraction procedure. A 15-20g sample of the solid polymer was dissolved in 100ml of freshly distilled 1-methyl naphthalene by heating the mixture with vigorous stirring at 473-483K in a stream of dry nitrogen. The polymer dispersed within a period of 10min. The solution was then cooled so that the polymer reprecipi-

tated. The mixture of swollen polymer and 1-methyl naphthalene was washed into a beaker with chloroform and filtered. The polymer was then repeatedly extracted with chloroform until no more oligomeric material was obtained. The filtrates were combined and the chloroform was removed using a rotary evaporator. 1-Methyl naphthalene was then distilled off at a temperature below 323K using a short-path molecular still and solid oligomeric extract was obtained as a residue in the still.

The solution equilibrates were treated differently from the solid polymers. When the ampoules were cooled to room temperature, PET precipitated. The product was filtered and the solid residue was extracted several times with chloroform. The filtrate and the chloroform extracts were then combined and the solvents were removed to yield the solid oligomeric extract.

### Preparation of reference materials

Several samples of cyclic and linear oligomers of PET were prepared for identification purposes and for calibration of the gel permeation chromatograph.

A sample of cyclic trimer



was prepared by the pyrolytic depolymerization method of Carothers<sup>25, 26</sup> as follows. 10g PET containing 1% w/w antimony trioxide were heated in a small molecular still at 570-580K at a pressure of 0.05mmHg. Approximately 1g of the trimer sublimed from the polymer over a period of 36h. It was freed from contamination by terephthalic acid by taking advantage of the insolubility of the latter in chloroform. It was purified further by reprecipitation.

A mixture of low molecular weight oligomers terminated with ethylene glycol groups was produced by the transesterification of dimethyl terephthalate by ethylene glycol using calcium acetate as catalyst<sup>27</sup>.

### Gel permeation chromatography (g.p.c.)

Cyclic extracts were analysed using a gel permeation chromatograph fitted with a Waters Model R4 differential refractometer detector. The instrument was fitted with four sample columns (each 4ft long  $\times$  0.3in. i.d.) packed with SX-1 Bio-beads (lightly crosslinked polystyrene beads supplied by Biorad Laboratories, St Albans). Samples were analysed at room temperature using chloroform as the solvent. Cyclics above the trimer were not completely resolved and a least squares analysis was developed in order to apportion the area of the tracing between the different components<sup>28</sup>.

The molecular weights of high molecular weight PET samples were determined using a g.p.c. instrument manufactured by Waters Associates Ltd. This was fitted with columns packed with Styragel and used hot *m*-cresol as the solvent.

### Spectroscopic methods

Proton nuclear magnetic resonance spectra were obtained in deuteriochloroform or trifluoroacetic acid using a Perkin-Elmer 60MHz Model R10 spectrometer.

Infra-red spectra were obtained from hexachlorobutadiene mulls and potassium bromide discs, using Unicam SP200 and SP200G instruments.



### Viscosity measurements

The molecular weights of polymeric products were determined by intrinsic viscosity measurements in *o*-chlorophenol at 298K using the relationship established by Ravens and Ward<sup>29</sup>:

$$[\eta] = 3.0 \times 10^{-4} \bar{M}_n^{0.77}$$

## RESULTS AND DISCUSSION

### Extraction of oligomers from PET samples

Oligomeric extracts from PET samples were analysed by g.p.c. Figure 1 shows a typical chromatogram of a mixture of cyclics  $(\text{CO} \cdot \text{C}_6\text{H}_4 \cdot \text{CO} \cdot \text{O} \cdot \text{CH}_2 \cdot \text{CH}_2 \cdot \text{O})_x$  from trimer to nonamer obtained by a single extraction of a commercial PET sample using the procedure described in the experimental section. This procedure was found to be effective for removing the cyclic oligomers from PET samples without significant degradation or redistribution reactions. After the first extraction, the polymer residues were thoroughly dried and then re-extracted. The second extracts were always much smaller than the first and they contained mainly the larger cyclic oligomers. In a typical case, the first extract comprised 2.2% w/w of the polymer and the second only 0.35% w/w.

The conventional procedures for extracting oligomers from PET samples using low boiling solvents<sup>1-3, 6, 7</sup> were also investigated. Such procedures resulted in the extraction of most of the cyclic trimer but little of the higher cyclic oligomers. Figure 2a shows a g.p.c. tracing of a sample obtained from commercial PET fibre using the extraction procedure employing 1,4-dioxane described by Goodman and Nesbitt<sup>3</sup>. Figure 2b shows a g.p.c. tracing of another sample obtained by drying the extracted fibre and then re-extracting with 1-methyl naphthalene. The g.p.c. tracings of these samples showed that oligomeric chains were formed when the fibre was extracted over a period of many hours by refluxing 1,4-dioxane, but not when it was re-extracted by the 1-methyl naphthalene method.

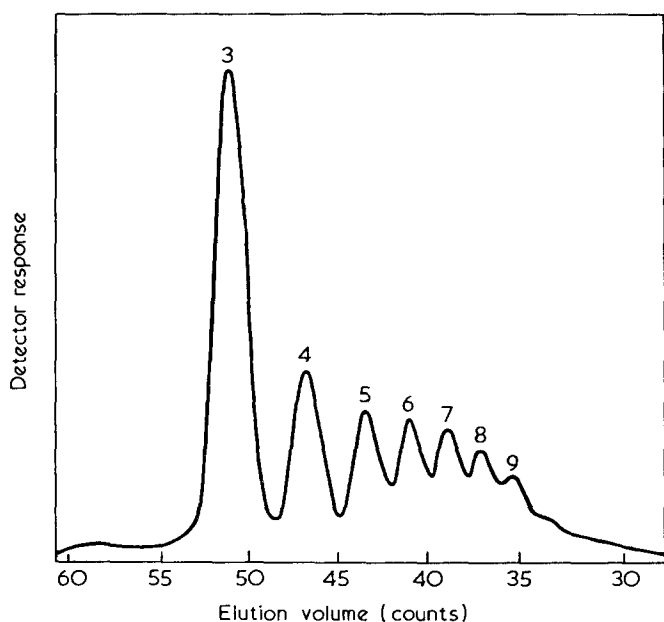


Figure 1 G.p.c. of cyclics  $(\text{CO} \cdot \text{C}_6\text{H}_4 \cdot \text{CO} \cdot \text{O} \cdot \text{CH}_2 \cdot \text{CH}_2 \cdot \text{O})_x$  with  $x=3-9$  obtained by extracting melt polymerized samples of PET with 1-methyl naphthalene

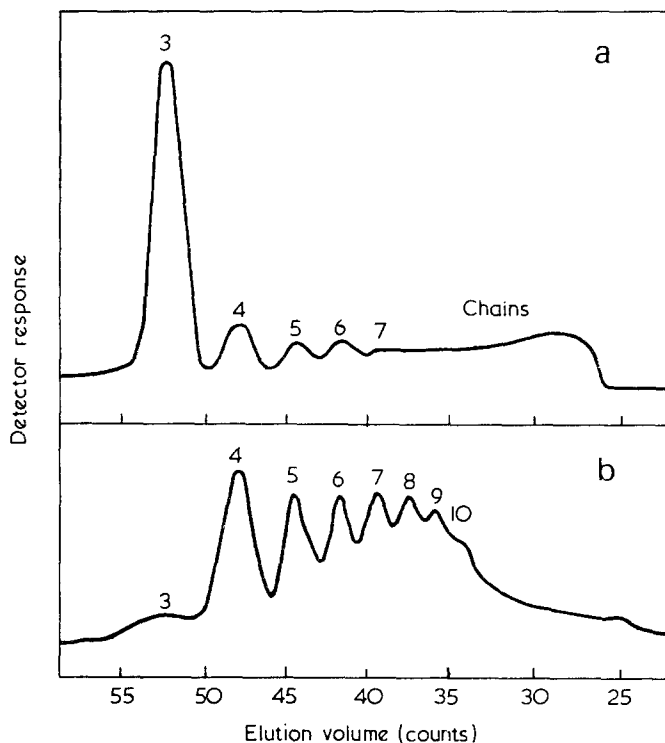
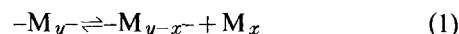


Figure 2 G.p.c. of two extracts from a melt polymerized sample of PET showing the cyclics  $(\text{CO} \cdot \text{C}_6\text{H}_4 \cdot \text{CO} \cdot \text{O} \cdot \text{CH}_2 \cdot \text{CH}_2 \cdot \text{O})_x$  with  $x=3-10$ . (a) Extract A was obtained by extracting the sample once with 1,4-dioxane by the method of Goodman and Nesbitt<sup>3</sup>. (b) Extract B was obtained by extracting the same polymer again with 1-methyl naphthalene

### Experimental molar cyclization equilibrium constants for cyclics in melt and solution equilibrates

The equilibrium between ring and chain molecules in molten PET or in a 1-methyl naphthalene solution of PET may be represented as:



where M symbolizes a monomeric unit



Shaw<sup>24</sup> has used g.p.c. to show that there is a most probable distribution of chain lengths in melt equilibrates of PET, and molar cyclization equilibrium constants  $K_x$  for cyclics  $M_x$  in undiluted and solution equilibrates of PET were calculated using the relation<sup>21, 22</sup>:

$$K_x = [M_x]/p^x \quad (2)$$

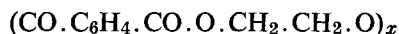
where  $p$  represents the extent of reaction of functional groups in the chain polymer. This latter quantity was found for each polymer by measuring the number-average molecular weight of the polymer residue remaining after extraction of the cyclic oligomers and applying Flory's<sup>30</sup> relation:

$$\bar{M}_n = M_0/(1-p) \quad (3)$$

where  $M_0$  is the molecular weight of a monomeric unit.

Ring-chain equilibration reactions were carried out on molten PET samples containing 0.5% w/w antimony trioxide at 543K, and on 10% w/w solutions of PET in 1-methyl naphthalene containing 0.5% w/w zinc acetate at 523K. Antimony trioxide was replaced by zinc acetate for the reactions in 1-methyl naphthalene solution because it was found to be a more stable catalyst under the conditions used. All the samples were quenched by

cooling after fixed periods of time and the oligomers were obtained by the extraction method using 1-methyl naphthalene described above. The g.p.c. tracings, infra-red and nuclear magnetic resonance spectra of all the oligomeric extracts corresponded to those expected for mixtures of cyclics<sup>6, 11, 18</sup>



although the g.p.c. tracings and infra-red spectra of some of them indicated that small amounts of linear oligomers were also present. The concentrations of individual cyclics in the oligomeric extracts were obtained from g.p.c. tracings. Due allowance was made for the presence of small amounts of linear oligomers, as well as for the somewhat greater response of the differential refractometer detector to the cyclic trimer as compared to the larger cyclic oligomers.

The concentrations of cyclics in PET samples prepared by heating the molten polymer plus catalyst for periods of 1, 12 and 36 h are plotted as the logarithms of their molar concentrations divided by  $p^x$  in Figure 3. It is believed that equilibrium between ring and chain molecules was effectively attained in the melt after 12 h at 543K. Further heating resulted in partial thermal degradation of the polymer, with darkening of the melt

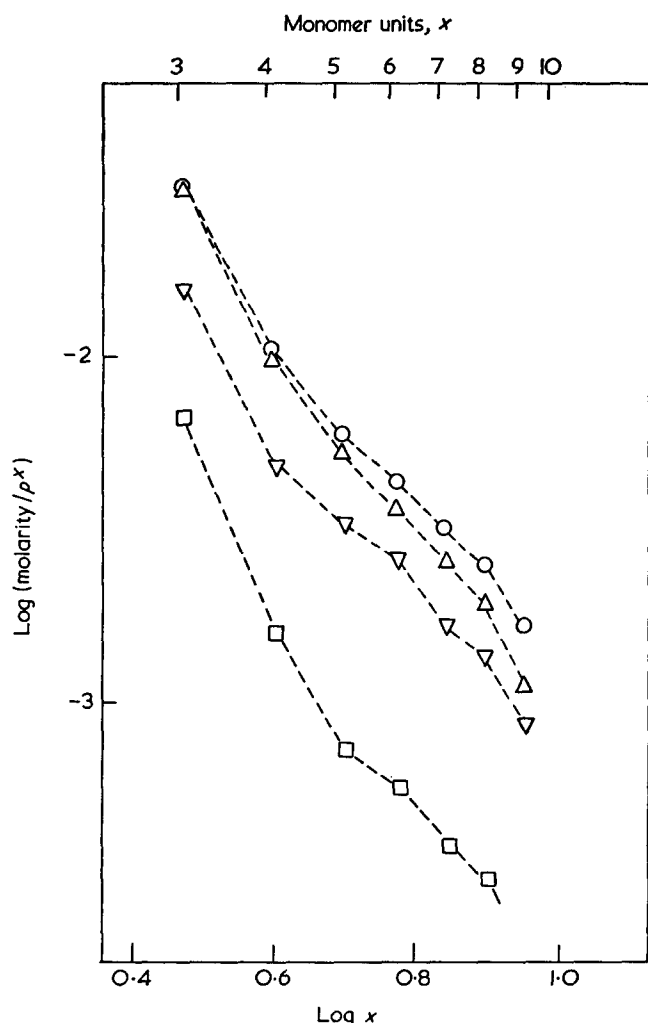


Figure 3 Plot of  $\log(\text{molarity}/p^x)$  against  $\log x$  for cyclics  $(\text{CO} \cdot \text{C}_6\text{H}_4 \cdot \text{CO} \cdot \text{O} \cdot \text{CH}_2 \cdot \text{CH}_2 \cdot \text{O})_x$  in samples of PET containing 0.5%w/w antimony trioxide, which were heated in the melt at 543K for 1 h ( $\nabla$ ), 12 h ( $\Delta$ ) and 36 h ( $\circ$ ). Concentrations of cyclics in the starting polymer are denoted  $\square$

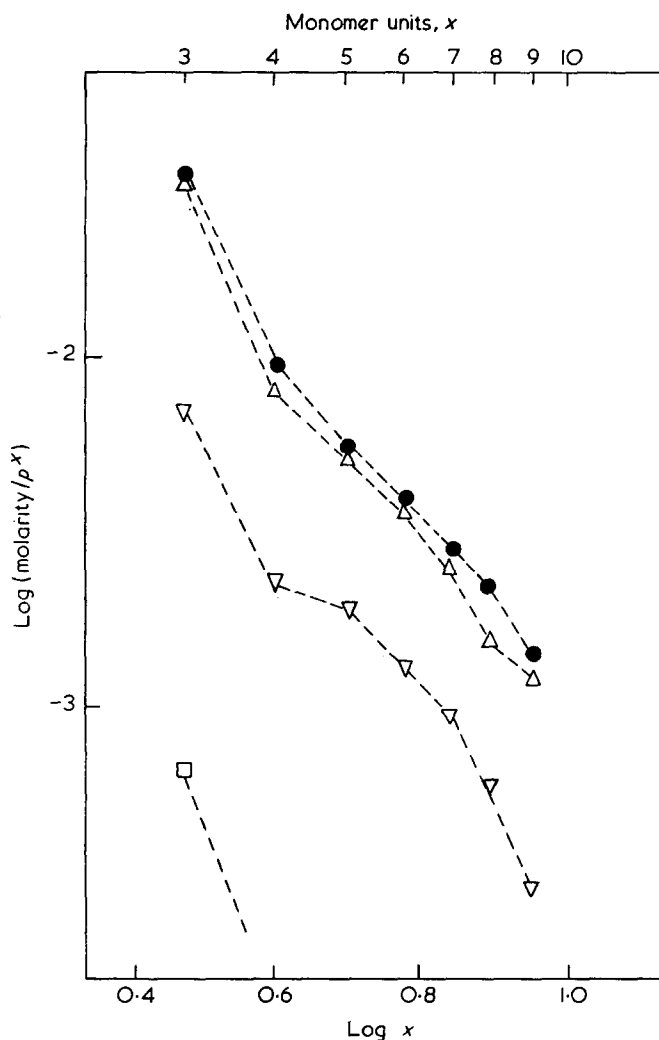


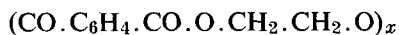
Figure 4 Plot of  $\log(\text{molarity}/p^x)$  against  $\log x$  for cyclics  $(\text{CO} \cdot \text{C}_6\text{H}_4 \cdot \text{CO} \cdot \text{O} \cdot \text{CH}_2 \cdot \text{CH}_2 \cdot \text{O})_x$  in samples of PET containing 0.5%w/w zinc acetate heated in 1-methyl naphthalene solution at concentrations of 10%w/w for 7 h ( $\nabla$ ) and 96 h ( $\Delta$ ). Concentrations of cyclics in the starting solution are denoted  $\square$ . Concentrations of cyclics in a melt equilibrate at 543K are denoted  $\bullet$

and the formation of small amounts of acyclic oligomers. The experimental molar cyclization equilibrium constants  $K_x$  for cyclics in melt equilibrates of PET at 543K were assumed to be the averages of the values plotted in Figure 3 for the sample heated for 12 h and for the sample heated for 36 h. These  $K_x$  values were close to those estimated for another PET sample, which was heated in the melt at 543K for 24 h. Following an assessment of sources of uncertainty in the experimental measurements, the following limits of accuracy were placed on the  $K_x$  values obtained:  $\pm 15\%$  for  $K_3, K_4$ ;  $\pm 25\%$  for  $K_5, K_6, K_7$ ; and  $\pm 40\%$  for  $K_8, K_9$ .

The concentrations of cyclics in solutions of PET in 1-methyl naphthalene after 7 h and 96 h at 523K are plotted as the logarithms of their molar concentrations divided by  $p^x$  in Figure 4, where they are compared with the  $K_x$  values for cyclics in the melt equilibrate at 543K. After 96 h, 37%w/w of the PET was in the form of cyclics with three to nine monomeric units compared with only 0.7%w/w in the starting polymer.

From these results it is concluded that thermodynamic equilibria between ring and chain molecules can be established in PET melts after  $\sim 12$  h and in solutions of PET in 1-methyl naphthalene at 523K after a some-

what longer period of time. Furthermore, since the concentrations of unstrained cyclics in polymeric equilibrates are related directly to the probabilities of intramolecular cyclization of the corresponding open chain molecules<sup>21, 22</sup>, the close agreement between the molar concentrations of cyclics



with  $x=3-9$  in the melt equilibrate containing 95% w/w linear polymer and in the solution equilibrate containing only 6% w/w linear polymer (see Figure 4) provides convincing evidence that PET chains adopt similar average conformations in the two environments.

*Comparison of experimental cyclization equilibrium constants with theoretical predictions made using Williams and Flory's rotational isomeric state model of PET*

The Jacobson and Stockmayer equilibrium theory of macrocyclization relates the molar cyclization equilibrium constants  $K_x$  for large, unstrained cyclics  $(\text{CO} \cdot \text{C}_6\text{H}_4 \cdot \text{CO} \cdot \text{O} \cdot \text{CH}_2 \cdot \text{CH}_2 \cdot \text{O})_x$  formed by the forward step of equation (1) to the densities  $W_x(\mathbf{r})$  of end-to-end vectors  $\mathbf{r}$  of the corresponding  $x$ -meric chains in the region  $\mathbf{r}=\mathbf{0}$  as follows<sup>21, 22</sup>:

$$K_x = W_x(\mathbf{0})/2N_A x \quad (4)$$

where  $K_x$  is in units of mol/l,  $W_x(\mathbf{0})$  is in units of molecules/l and  $N_A$  is the Avogadro constant. This expression neglects possible correlations between the directions and positions of terminal groups in the intramolecular cyclization process<sup>22</sup>. Neglect of such correlations would be expected to be valid for long chain molecules in random-coil conformations. Furthermore, provided such chains are of sufficient length and flexibility, the densities  $W_x(\mathbf{r})$  of end-to-end vectors  $\mathbf{r}$  should be spherically symmetrical in the region  $\mathbf{r}=\mathbf{0}$  and given by the Gaussian expression:

$$W_x(\mathbf{0}) = (3/2\pi \langle r_x^2 \rangle)^{3/2} \quad (5)$$

where  $\langle r_x^2 \rangle$  represents the mean-square distance between the ends of the  $x$ -meric chains. Hence, the  $K_x$  values for macrocyclics in PET equilibrates should be given by the relation:

$$K_x = (3/2\pi \langle r_x^2 \rangle)^{3/2} (1/2N_A x) \quad (6)$$

As in previous studies of cyclic concentrations in polymeric equilibrates<sup>31</sup>, experimental  $K_x$  values for the cyclics  $(\text{CO} \cdot \text{C}_6\text{H}_4 \cdot \text{CO} \cdot \text{O} \cdot \text{CH}_2 \cdot \text{CH}_2 \cdot \text{O})_x$  will be compared with theoretical values calculated by equations (5) and (6) using a rotational isomeric state model to describe the statistical conformations of the corresponding open chain molecules. The Williams and Flory<sup>23</sup> model of PET was used for this purpose. It was set up following a detailed analysis of the molecular structure of the linear polymer and it reproduces the experimental unperturbed dimensions of PET, viz.:

$$\langle r_x^2 \rangle_0 / x M_0 \cong 1.0 \text{ \AA}^2 (\text{g mol wt})^{-1}$$

in the limit  $x \rightarrow \infty$ . These dimensions were deduced by Krigbaum<sup>32</sup>, by Williams and Flory<sup>23</sup> and by Wallach<sup>33</sup> from the results of osmometric, light scattering and intrinsic viscosity measurements of dilute solutions of linear PET chains in good solvents<sup>33-35</sup>, using the methods of Krigbaum<sup>36</sup>, Orofino and Flory<sup>37</sup>, Stockmayer and Fixman<sup>38</sup> and Kurata and Stockmayer<sup>39</sup> to

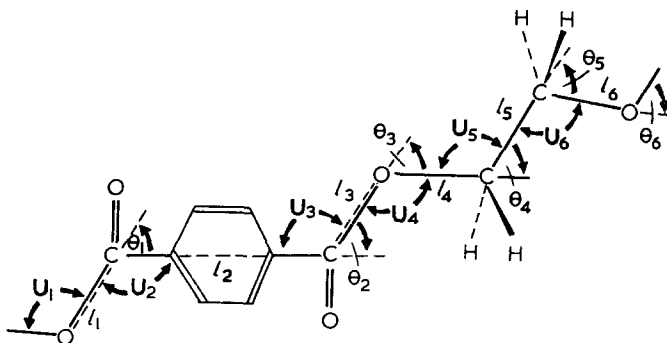


Figure 5 Section of the PET chain in the all-trans conformation. Structural parameters were assigned to the chain by Williams and Flory<sup>23</sup> as follows:  $l_1=l_3=1.34 \text{ \AA}$ ,  $l_2=5.74 \text{ \AA}$ ,  $l_4=l_6=1.44 \text{ \AA}$ ,  $l_5=1.53 \text{ \AA}$ ,  $\theta_1=\theta_2=66^\circ$ ,  $\theta_3=\theta_6=67^\circ$ ,  $\theta_4=\theta_5=70^\circ$ . The statistical weight matrices  $U_1-U_6$  take account of the mutual interdependence of rotational states about the pairs of bonds shown

estimate the magnitude of chain expansion resulting from long-range intramolecular interactions.

The Williams and Flory rotational isomeric state model can be described with reference to Figure 5, which shows a section of the PET chain in the all-trans conformation. Structural parameters were assigned to the chain by Williams and Flory and they are listed in the legend to this Figure. In the Williams and Flory model, each terephthaloyl group is assigned to either a *cis* or *trans* conformational position with equal probability and each O-CH<sub>2</sub>, CH<sub>2</sub>-CH<sub>2</sub> and CH<sub>2</sub>-O bond to rotational isomeric states in *trans* ( $\phi=0^\circ$ ) or *gauche* ( $\phi=\pm 120^\circ$ ) positions. The interdependences of rotations about adjacent pairs of skeletal bonds are taken into account by means of six statistical weight matrices  $U_i$  ( $i=1-6$ ). The elements of these matrices are indexed on the rows and columns by the rotational states of pairs of skeletal bonds  $i-1$  and  $i$  as shown in Figure 5, and they are defined by Boltzmann factors as:

$$u_{\zeta\eta; i} = \exp(-E_{\zeta\eta; i}/RT) \quad (7)$$

where  $R$  is the gas constant,  $T$  is the temperature and  $E_{\zeta\eta; i}$  represents the difference between the conformational energy of a section of the chain when skeletal bonds  $i-1$  and  $i$  are in rotational states  $\zeta$  and  $\eta$  (and all other bonds are *trans*), and the corresponding conformational energy after bond  $i$  is rotated into its *trans* state. In the temperature range of 523-543K used for the ring-chain equilibration reactions, the elements of the statistical weight matrices  $U_1-U_6$  are given by the Williams and Flory model as follows

$$U_1 = 1 \quad (8)$$

$$U_2 = \begin{bmatrix} 1 & 1 \end{bmatrix} \quad (9)$$

$$U_3 = \begin{bmatrix} 1 \\ 1 \end{bmatrix} \quad (10)$$

$$U_4 = \begin{bmatrix} 1 & 0.7 & 0.7 \end{bmatrix} \quad (11)$$

$$U_5 = \begin{bmatrix} 1 & 1.2 & 1.2 \\ 1 & 1.2 & 0.4 \\ 1 & 0.4 & 1.2 \end{bmatrix} \quad (12)$$

$$U_6 = \begin{bmatrix} 1 & 0.7 & 0.7 \\ 1 & 0.7 & 0.2 \\ 1 & 0.2 & 0.7 \end{bmatrix} \quad (13)$$

The mean-square end-to-end distances  $\langle r_x^2 \rangle$  of  $x$ -meric chains  $\text{-(CO.C}_6\text{H}_4\text{.CO.O.CH}_2\text{.CH}_2\text{.O)-}_x$  (with  $x=2-9$ ) were identified with their unperturbed values  $\langle r_x^2 \rangle_0$  and calculated by the mathematical methods of Flory and Williams<sup>40,41</sup> using the statistical weight matrices given in equations (8)–(13) and the structural parameters of PET listed in the legend to Figure 5. Theoretical molar cyclization equilibrium constants  $K_x$  were obtained by substituting the  $\langle r_x^2 \rangle_0$  values into equation (6) and they are compared with the corresponding experimental values in Figure 6.

There are substantial differences between the experimental  $K_x$  values and those calculated assuming the  $x$ -meric chains obey Gaussian statistics over the range of cyclic ethylene terephthalate oligomers containing 18 to 54 skeletal bonds.\* The experimental  $K_x$  values are larger than the calculated values by factors of at least two, and in the case of  $K_3$  and  $K_8$  by factors close to three. These results contrast with those found for cyclics in all the other systems that have been studied up to the present time, including polysiloxanes<sup>22, 42, 44,</sup>

\* For present purposes CO.C<sub>6</sub>H<sub>4</sub>.CO groups are counted as single skeletal bonds.

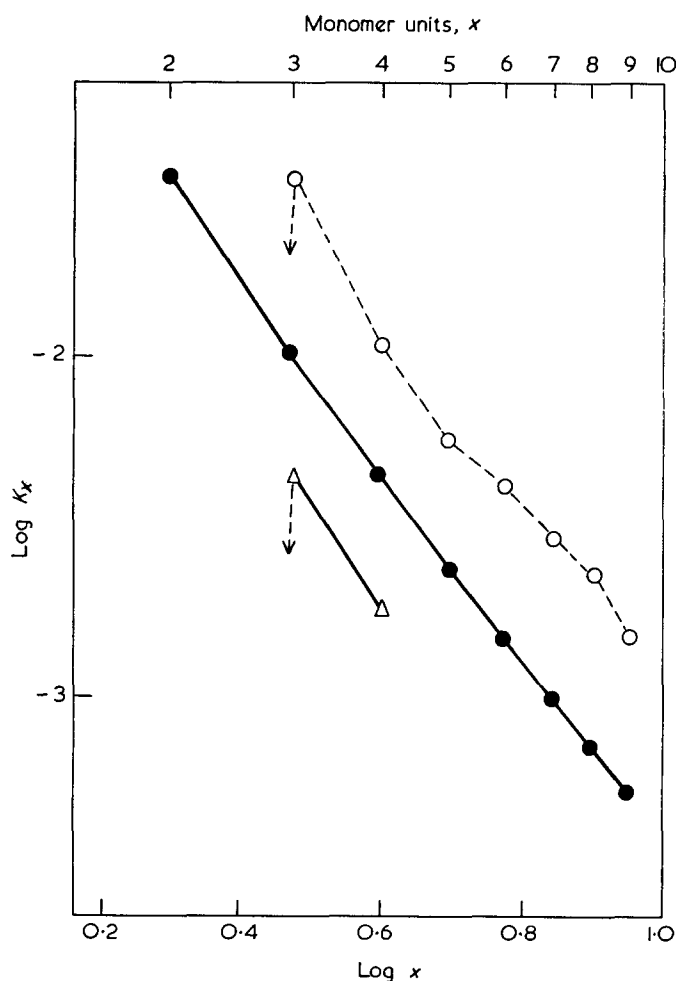


Figure 6 Experimental molar cyclization equilibrium constants  $K_x$  (in mol/l) for cyclics  $\text{(CO.C}_6\text{H}_4\text{.CO.O.CH}_2\text{.CH}_2\text{.O)}_x$  with  $x=2-9$  in the melt at 543K (denoted  $\circ$ ) are plotted as  $\log K_x$  against  $\log x$ . They are compared with theoretical values calculated by equation (6) which assumes that the corresponding open chain molecules obey Gaussian statistics (these values are denoted  $\bullet$ ). Theoretical  $K_3$  and  $K_4$  values calculated by equation (4) using the direct computational method (see Table 1) are denoted  $\triangle$

nylon-6<sup>45, 46</sup>, poly(1,3-dioxolane)<sup>47</sup> and poly(2,2,7,7-tetramethyl-1-oxa-2,7-disilacycloheptane)<sup>48</sup>. The experimental  $K_x$  values for cyclics  $[\text{R}(\text{CH}_3)\text{SiO}]_x$ ,  $[\text{NH}(\text{CH}_2)_5\text{CO}]_x$ ,  $\text{(CH}_2\text{.O.CH}_2\text{.CH}_2\text{.O)}_x$  and  $[(\text{CH}_3)_2\text{Si}-(\text{CH}_2)_4-(\text{CH}_3)_2\text{Si-O}]_x$  with more than  $\sim 15$  skeletal bonds are either smaller than the values calculated by assuming that the corresponding open chain molecules obey Gaussian statistics or are in good agreement with them. The striking discrepancies between the experimental  $K_x$  values for the larger cyclic oligomers in PET equilibrates and those calculated by equation (6) could arise from a failure of the corresponding open chain molecules to obey the Gaussian formula for the probability of intramolecular cyclization; but it may also result from correlations between the positions and directions of the chain termini in their highly-coiled conformations resulting in asymmetric distributions of end-to-end vectors and non-random relative orientations of terminal bonds.

The molar cyclization equilibrium constants  $K_3$  and  $K_4$  for the cyclic trimer and cyclic tetramer were also calculated using the Williams and Flory model by a direct computational method that has been applied to calculate equilibrium cyclic concentrations in several polymeric systems<sup>49-52</sup>. In this method, the  $x$ -meric chains are not assumed to obey Gaussian statistics but the densities  $W_x(\mathbf{r})$  end-to-end vectors  $\mathbf{r}$  of  $x$ -meric chains in the region  $\mathbf{r} \cong \mathbf{0}$  are calculated by computing the statistically weighted fraction of the total number of discrete conformations defined by the model that have the centres of their terminal atoms within the range  $0-r \text{ \AA}$  and dividing this fraction by the volume  $(4/3)\pi r^3$  (see Table 1). The values of  $K_3$  and  $K_4$  that were calculated by equation (4) for small but finite values of  $r$  were found to be approximately independent of  $r$  when  $2 < r < 5 \text{ \AA}$  (see ref. 24), and the values plotted in Figure 6 were obtained by taking  $r=3 \text{ \AA}$ . They are lower than

Table 1 Calculation of  $K_x$  values by the direct computational method using the Williams and Flory model\*

Value of $r$ ( $\text{\AA}$ )	Number of conformations of the chain molecule $\text{-(CO.C}_6\text{H}_4\text{.CO.O.CH}_2\text{.CH}_2\text{.O)-}_x$ that have the centres of terminal carbon and oxygen atoms within the range $0-r \text{ \AA}$	Molar cyclization equilibrium constant $K_x$ (in mol/l) calculated by equation (4)
Cyclic trimer ( $x=3$ )†:		
2	38	0.00469
3	120	0.00405
4	258	0.00353
5	538	0.00646
Cyclic tetramer ( $x=4$ ):		
2	942	0.00156
3	3 190	0.00167
4	6 902	0.00167
5	13 570	0.00210

\* As noted in ref. 24, the distances between the centres of the terminal carbon and oxygen atoms of the acyclic dimer  $\text{-(CO.C}_6\text{H}_4\text{.CO.O.CH}_2\text{.CH}_2\text{.O)-}_2$  are greater than  $7 \text{ \AA}$  in all the 486 conformations defined by the Williams and Flory model. Hence, the value of  $K_2$  calculated by equation (4) is zero, and this is in agreement with the fact that cyclic dimer cannot be detected in melt equilibrates of PET

† These values are identical with those quoted in ref. 24

the corresponding values calculated by equation (6) by factors of two or more, and lower than the corresponding experimental values by factors of seven and six respectively. The substantial discrepancies between the experimental  $K_3$  and  $K_4$  values and those calculated by equation (4) using the direct computational method may result in part from an inability of the Williams and Flory model to provide reliable values for  $W_3(0)$  and  $W_4(0)$  and in part from the assumption [implicit in equation (4)] that the termini of such chains are randomly oriented in their highly coiled conformations.

#### Changes in the cyclic oligomer content of PET samples resulting from heating the samples in the solid state

When samples of either PET or nylon-6 (which have been prepared by melt polymerization reactions) are heated in the solid state below their melting points, the molecular weights of the polymers increase<sup>53,54</sup> and, in the case of nylon-6, the concentrations of cyclic monomer decrease<sup>55</sup>.

In connection with our studies of cyclic oligomer concentrations in PET equilibrates, we have carried out some preliminary studies of changes in the amounts of cyclic oligomers in PET samples resulting from heating the samples below their melting points. Four samples of PET chip were prepared by catalysed melt polymerization reactions. The cyclic oligomer concentrations in two of the samples (I) and (II) were measured directly. The remaining samples (III) and (IV) were each heated in the solid state at 508K for periods of 18h, then cooled and their cyclic concentrations were measured. In Table 2, the percentages by weight of cyclics with  $x=3-9$  in the four samples are compared with values found for two melt equilibrates (see above). The large decreases in the cyclic oligomer concentrations resulting from heating the samples at 508K show that chemical ring-to-chain interconversion reactions readily take place in the solid polymer. Following Wichterle<sup>55</sup>, these changes can be interpreted in terms of the formation of crystalline regions free of cyclic oligomers, together with residual amorphous regions containing cyclics in concentrations close to their equilibrium values in the molten polymer.

Table 2 Cyclic content of PET samples\*

Value of $x$ in cyclic	%w/w cyclics in samples (I)-(VI)					
	(I)	(II)	(III)	(IV)	(V)	(VI)
3	1.15	1.25	0.32	0.33	1.39	1.32
4	0.29	0.19	0.10	0.12	0.57	0.56
5	0.24	0.27	0.06	0.07	0.34	0.38
6	0.19	0.18	0.05	0.06	0.29	0.32
7	0.14	0.16	0.04	0.04	0.22	0.26
8	0.10	0.11	0.04	0.04	0.19	0.22
9	0.06	0.07	0.02	0.02	0.11	0.16

Samples (I) and (II): PET chip prepared by melt polymerization reactions

Samples (III) and (IV): PET chip prepared by melt polymerization reactions, then heated in the solid state at 508K for 18h. The molecular weights of these samples were approximately twice those of samples (I) and (II). Further heating in the solid state resulted in appreciable thermal degradation of the samples

Samples (V) and (VI): PET prepared by ring-chain equilibration reactions in the melt at 543K (see Figure 3)

\* Samples (I)-(IV) were prepared by staff at ICI Fibres Ltd, Harrogate and samples (V)-(VI) were prepared at the University of York

Similar decreases in the concentrations of cyclic oligomers have been found to result when melt equilibrated samples of nylon-6 are heated in the solid state<sup>46</sup>, and these will be reported at a later date.

#### ACKNOWLEDGEMENTS

This work was carried out during the tenure of a SRC(CAPS) Research Studentship by D.R.C. We are indebted to Mr J. E. McIntyre, Dr J. Mather and Mr A. J. Thompson of ICI Fibres Ltd, Harrogate, Yorkshire for their interest and practical help over the past three years. We thank the staff of ICI Fibres Ltd for g.p.c. analyses, viscometric determinations and for gifts of many commercial PET samples.

We thank Mr D. Symphon of our Departmental Workshops for designing and constructing a g.p.c. instrument, column packing equipment and an oven heater, as well as for helpful technical advice and assistance.

We gratefully acknowledge extensive computational facilities at the University of York.

#### REFERENCES

- Ross, S. D., Coburn, E. R., Leach, W. A. and Robinson, W. B. *J. Polym. Sci.* 1954, **13**, 406
- Giuffria, R. *J. Polym. Sci.* 1961, **49**, 427
- Goodman, I. and Nesbitt, B. F. *Polymer* 1960, **1**, 384
- Kirby, J. R., Baldwin, A. J. and Heidner, R. H. *Analyt. Chem.* 1965, **37**, 1306
- Hovenkamp, S. G. and Munting, J. P. *J. Polym. Sci. (A-1)* 1970, **8**, 679
- Zahn, H. and Kusch, P. *Z. Gesamte Text.-Ind.* 1967, **69**, 880
- Peebles, L. H., Huffman, M. W. and Ablett, C. T. *J. Polym. Sci. (A-1)* 1969, **7**, 479
- Meraskentis, E. and Zahn, H. *J. Polym. Sci. (A-1)* 1966, **4**, 1890
- Hamb, L. and Trent, L. C. *J. Polym. Sci. (B)* 1967, **5**, 1057
- Meraskentis, E. and Zahn, H. *Chem. Ber.* 1970, **103**, 3034
- Zahn, H. and Repin, J. F. *Chem. Ber.* 1970, **103**, 3041
- Repin, J. H. and Papanikolaou, E. *J. Polym. Sci. (A-1)* 1969, **7**, 3126
- Seidel, B. Z. *Elektrochem.* 1958, **62**, 214
- Grime, D. and Ward, I. M. *Trans. Faraday Soc.* 1958, **54**, 959
- Ward, I. M. *Chem. Ind.* 1956, p 905; *Chem. Ind.* 1957, p 1102
- Binns, G. L., Frost, J. S., Smith, F. S. and Yeadon, E. C. *Polymer* 1966, **7**, 583
- Ito, E. and Okajima, S. *J. Polym. Sci. (B)* 1969, **7**, 483
- Ito, E. and Okajima, S. *Polymer* 1971, **12**, 650
- Hashimoto, S. and Sakai, J. *Kobunshi Kagaku* 1966, **23**, 422
- Hashimoto, S. and Jinnai, S. *Kobunshi Kagaku* 1967, **24**, 36
- Jacobson, H. and Stockmayer, W. H. *J. Chem. Phys.* 1950, **18**, 1600
- Flory, P. J. and Semlyen, J. A. *J. Am. Chem. Soc.* 1966, **88**, 3209
- Williams, A. D. and Flory, P. J. *J. Polym. Sci. (A-2)* 1967, **5**, 417
- Walker, G. R. and Semlyen, J. A. *Polymer* 1970, **11**, 472
- Hill, J. W. and Carothers, W. H. *J. Am. Chem. Soc.* 1933, **55**, 5031; 1935, **57**, 925
- Spanagel, E. W. and Carothers, W. H. *J. Am. Chem. Soc.* 1935, **57**, 929; 1936, **58**, 654
- Cramer, F. B. in 'Macromolecular Syntheses' (Ed. C. G. Overberger), Wiley, New York, 1963, Vol 1, p 17
- Cooper, D. R. *J. Chromatog.* in press
- Ravens, D. A. S. and Ward, I. M. *Trans. Faraday Soc.* 1961, **57**, 150
- Flory, P. J. 'Principles of Polymer Chemistry', Cornell University Press, Ithaca, NY, 1953
- Parts 1-10 of this series published in *Polymer* (1969-1972): Semlyen, J. A. and Wright, P. V. *Polymer* 1969, **10**, 543; Semlyen, J. A. and Walker, G. R. *Polymer* 1969, **10**, 597; Wright, P. V. and Semlyen, J. A. *Polymer* 1970, **11**, 462; Walker, G. R. and Semlyen, J. A. *Polymer* 1970, **11**, 472;

- Beevers, M. S. and Semlyen, J. A. *Polymer* 1971, **12**, 373;  
Semlyen, J. A. *Polymer* 1971, **12**, 383;  
Andrews, J. M. and Semlyen, J. A. *Polymer* 1972, **13**, 142;  
Beevers, M. S. and Semlyen, J. A. *Polymer* 1972, **13**, 385;  
Cooper, D. R. and Semlyen, J. A. *Polymer* 1972, **13**, 414;  
Beevers, M. S. and Semlyen, J. A. *Polymer* 1972, **13**, 523
- 32 Krigbaum, W. R. *J. Polym. Sci.* 1958, **28**, 213  
33 Wallach, M. L. *Makromol. Chem.* 1967, **103**, 19  
34 Lanka, W. A., unpublished results quoted in ref. 32  
35 Conix, A. *Makromol. Chem.* 1958, **26**, 226  
36 Krigbaum, W. R. *J. Polym. Sci.* 1955, **18**, 315  
37 Orofino, T. A. and Flory, P. J. *J. Chem. Phys.* 1957, **26**, 1067  
38 Stockmayer, W. H. and Fixman, M. *J. Polym. Sci. (C)* 1963, **1**, 137  
39 Kurata, M. and Stockmayer, W. H. *Fortschr. Hochpolym. Forsch.* 1963, **3**, 196  
40 Flory, P. J. and Williams, A. D. *J. Polym. Sci. (A-2)* 1967, **5**, 399
- 41 Flory, P. J. 'Statistical Mechanics of Chain Molecules', Interscience, New York, 1969  
42 Semlyen J. A. and Wright, P. V. *Polymer* 1969, **10**, 543  
43 Wright, P. V. and Semlyen, J. A. *Polymer* 1970, **11**, 462  
44 Wright, P. V. *J. Polym. Sci.* in press  
45 Semlyen, J. A. and Walker, G. R. *Polymer* 1969, **10**, 597  
46 Andrews, J. M. *DPhil. Thesis* University of York, 1972  
47 Andrews, J. M. and Semlyen, J. A. *Polymer* 1972, **13**, 142  
48 Beevers, M. S. and Semlyen, J. A. *Polymer* 1972, **13**, 523  
49 Semlyen, J. A. *Trans. Faraday Soc.* 1967, **63**, 2342  
50 Semlyen, J. A. *Polymer* 1971, **12**, 383  
51 Beevers, M. S. and Semlyen, J. A. *Polymer* 1972, **13**, 385  
52 Cooper, D. R. and Semlyen, J. A. *Polymer* 1972, **13**, 414  
53 Zimmerman, J. J. *J. Polym. Sci. (B)* 1964, **2**, 959  
54 Wunderlich, B. *Adv. Polym. Sci.* 1968, **5**, 568  
55 Wichterle, O. *Makromol. Chem.* 1960, **35**, 174

# Determination of frozen-in stresses in thermoplastic injection mouldings\*

M. Jensen† and R. R. Whisson

*Rubber and Plastics Research Association, Shawbury, Shrewsbury SY4 4NR, UK  
(Received 15 December 1972)*

A method and apparatus for providing an overall numerical value of the frozen-in stresses in injection mouldings was developed and compared with existing methods. The developed technique was more rapid and could be employed on either opaque or transparent samples and was more suitable for production quality control purposes. Frozen-in stress values of a number of different thermoplastics moulded under varying conditions of melt temperature and pressure were determined. Some results on the influence of melt flow pattern are also included.

## INTRODUCTION

The most dominant and influential factor affecting the service performance of thermoplastic injection mouldings is the degree and distribution of the stress forces which have been locked into the product during its manufacture. The occurrence of these stresses is an inherent characteristic of the injection moulding process in which the plastics material is rapidly heated to an elevated temperature and subjected to high shearing forces and pressures to cause plastification and flow into a mould followed by rapid cooling.

The greater the frozen-in stress developed the greater the differential shrinkage arising with resultant warpage of the moulding. Mechanical properties are substantially dependent on the directional stress differences occurring in the moulding. Its resistance to heat distortion and environmental stress cracking can be significantly weakened by higher built-in stresses. When the properties quoted by the raw material manufacturer are not duplicated in production, as a result of the processing treatment, misunderstanding often arises between custom moulder and customer. There are several types of stress occurring in injection mouldings denoted by the term 'frozen-in' or 'built-in' stress but by far the largest component is derived from alignment of polymer chains or orientation during processing. As the polymer melt flows into the channels leading to the mould it develops a flow front. A melt flow velocity gradient occurs between the hotter, faster flowing, inner core and the colder, moving, outer layers. The polymer chains tend to become stretched from their randomly coiled state because of the shearing effect occurring between the different layers of polymer. The greater the differences in the velocity of the layers the greater the shear rate developed and the higher will be the ensuing orientation. The lower the melt temperature, the greater will be the melt viscosity with the occurrence of chain disentanglement under a higher stress

level and a consequent increase in orientation. As the polymer melt enters the mould cavity the hot central core flows outwards and solidifies rapidly against the colder mould walls. This initial thin skin of material is relatively free of orientation since it has solidified from a higher melt temperature and is not subject to further shearing forces. The layers of melt which form the immediate sub-surface cool at an increasingly slower rate towards the centre. Melt viscosity increases and melt flow persists under the injection pressure resulting in a region of considerably higher orientation near the surface skin of the moulding. The oriented melt in the central region, being hotter than the outer layers undergoes more relaxation or unstretching until this is prevented by the rapid increase in viscosity when the cavity is full and the polymer cools. An orientation gradient is also formed in the length direction as well as the thickness direction of the moulding. The gradient will be at a minimum at the flow front and rise to a maximum at a point near to the gate. Orientation will also increase to a maximum at the gate if additional melt is packed on to cooling melt already there.

Differential orientation is not the only source of gradient effects. Density gradients occur in crystallizable polymers arising from varying degrees of crystallization. This may result from unbalanced cooling in the mould, inadequate cooling times or pressure losses in the melt.

It was apparent that for the investigation of reproducibility of the injection moulding process<sup>1, 2</sup> it was necessary to obtain a realistic value of the frozen-in stresses of mouldings produced under monitored conditions. The interrelationships between stress, other properties affecting product quality and the respective processing conditions employed could then be established. After reviewing the existing methods for determining stress<sup>3</sup> it was obvious that all of them were inadequate to varying degrees for utilization of what amounted to a production inspection test during the course of the moulding trials being conducted. Birefringence methods are only applicable to small areas of transparent plastics. Hot wire and stress corrosion techniques are primarily a means of detection of surface orientation. Although bulk stresses

\*RAPRA Research Report No. 197

† Present address: Centro Chileno-Danes, Casilla 91-Maipu, 16 Santiago, Chile.

can be revealed by the heat reversion test<sup>4</sup> the reproducibility is doubtful. Except for birefringence the results obtained from the aforementioned methods are difficult to quantify. Although some tests for change in mechanical properties are useful they involve the careful preparation of test specimens with the attendant problem of stress relaxation or crack propagation being induced during subsequent machining.

From this survey a set of requirements emerged to which a single method would have to comply. The method should be applicable to opaque and transparent polymers. It should give a numerical value of the bulk or overall stress forces in a sample taken from a moulding—if not the whole moulding. Furthermore, the test procedure should be quick, sufficiently accurate, reproducible and involve simple equipment and calculation. In this report the experience and results obtained from a method developed at RAPRA<sup>5</sup> are described and compared with other existing methods.

### PREPARATION OF SAMPLES

The samples examined were obtained from an injection mould which produced two 76.2 mm (3 in) square plaques, 2.0 mm thick from a central runner whose sides formed a film gate along one edge of each plaque of 0.6 mm depth (Figure 1). Most of the development work was performed on a g.p. polystyrene with additional data obtained by a more confined examination and comparison of g.p. polypropylene copolymer, nylon-6, polysulphone and an impact grade of acrylonitrile-butadiene-styrene (ABS).

Mouldings were produced on a 5.0 oz (141.75 g) reciprocating screw injection machine with hydraulic clamping action (Bone Craven's Johns Model 75-IX-5). For each material the mouldability range of injection pressure was determined (i.e. between short and flashed mouldings). The injection pressure was varied in 400 lbf/in<sup>2</sup> (1 lbf/in<sup>2</sup> ≡ 6894.76 N/m<sup>2</sup>) steps over the injection pressure range for polystyrene and—for the other materials—the two extreme conditions and an intermediate

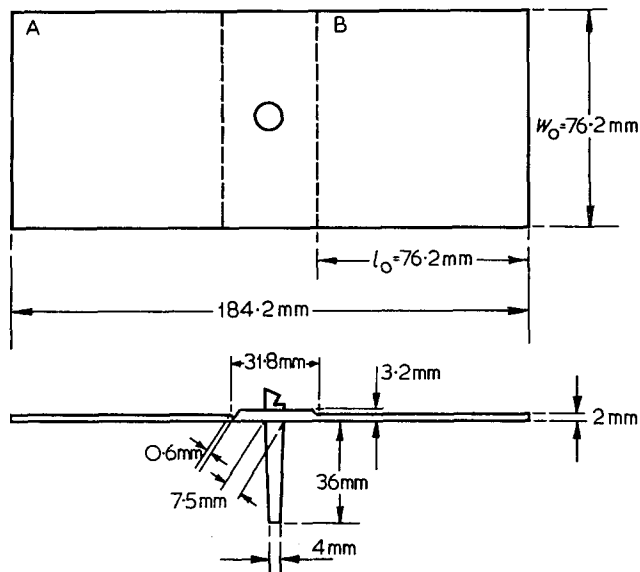


Figure 1 Test specimen for stress relaxation analysis

setting were taken. Except for pressure changes other process settings were unaltered and maintained at the values shown in Table 1.

In the project on injection moulding reproducibility it has been determined that steady moulding conditions as evidenced by analysis of shot weight distribution were developed after the first 30 mouldings. Samples for stress determination were therefore taken at each of the pressure settings after this point. Approximately 80 mouldings were taken at each setting.

### RAPRA STRESS RELAXATION METHOD

The method was developed from original work conducted by Hathaway<sup>6</sup> and subsequently used by Pokigo and Flodman<sup>7</sup> on plastics film. Here a strip of film was clamped between the jaws of a tensile load tester and rapidly heated by radiant heaters until the load-time curve indicated a peak reading. This peak was recorded

Table 1 Injection moulding process settings

	Polystyrene	Polypropylene	Nylon-6	Polysulphone	ABS
<b>Temperature (°C):</b>					
Barrel zone 1	220	220	280	355	250
Barrel zone 2	190	190	230	350	190
Nozzle	220	220	280	360	250
Mould water set	60	60	95	98	60
<b>Pressure (lbf/in<sup>2</sup>):</b>					
Injection run 1	5800	6000	7000	15 000	18 000
Injection run 2	6200	7000	6000	—	10 000
Injection run 3	6600	5000	5000	—	9 000
Injection run 4	7000	—	—	13 500	—
Injection run 5	7400	—	—	16 500	—
Injection run 6	7800	—	—	—	—
Preplasticizing	1000	1000	1000	1 000	1 000
Clamping	3000	3000	3000	3 000	3 000
<b>Time (sec):</b>					
Hold on	20	20	20	15	20 <sup>a</sup>
Mould open	3.4	3.4	3.4	3.4	3.4
Complete cycle	38	38	38	38	38
<b>Other:</b>					
Predrying				overnight 120°C	

<sup>a</sup> 15 sec for 9000 lbf/in<sup>2</sup> injection pressure



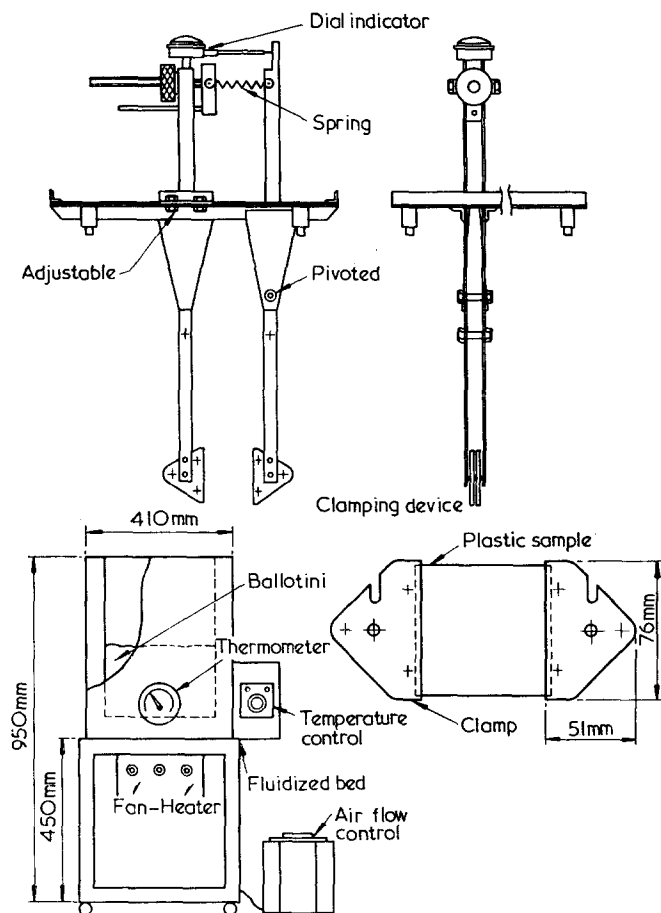


Figure 2 RAPRA Stress Relaxometer for thermoplastics

as the orientation stress value. Orientation stress was defined as the force released when the material shrinks on heating to above its glass transition temperature,  $T_g$ .

The equipment developed at RAPRA for testing mouldings was based upon the lever arm principle and consisted of two long arms each ending in a pair of jaws (Figure 2). The specimen was held edgewise between the jaws. Both arms of the apparatus were fixed at right angles to a supporting framework: one rigidly, the other pivoted. A spring of known load extension characteristics was fixed between the short-end of the pivoted arm and the rigidly held arm. When the specimen shrank between the grips the spring was extended and the deflection was registered on a micrometer dial gauge adjacent to the spring. A cubical bed of ballotini was utilized as the heating source. It was preferred for ease of fluidizing that the particles of the fluidizing medium were substantially spherical and, therefore, ballotini which consisted of very small glass spheres was particularly suitable. The depth of the fluidized bed was 200 mm. Air at a low pressure was blown through a sintered glass tile forming the base of the bed. The bed was heated by a 1 kW heater situated over the porous base of the container. The framework of the specimen clamping and measuring device rested conveniently across the open end of the fluidization chamber with the clamped specimen immersed in the preheated ballotini. Springs of differing load extension characteristics were calibrated from applied static load measurements.

To determine the temperature at which maximum stress relaxation occurred a series of deflection-time curves were plotted for each material examined for a

series of test temperatures increasing in  $10^\circ\text{C}$  steps. The temperature used to derive the curve with the highest most pronounced peak was taken as the test temperature for the fluidized bed and the peak deflection recorded on that curve was taken as the stress relaxation value for that sample.

#### Results with polystyrene

The resultant curves for polystyrene samples moulded at 5800 lbf/in<sup>2</sup> and 7800 lbf/in<sup>2</sup> injection pressure and tested at temperatures from  $80^\circ\text{C}$  to  $140^\circ\text{C}$  are shown in Figures 3 to 8. Tests were carried out with samples measuring 3 in  $\times$  3 in, 3 in  $\times$  2 in and 3 in  $\times$   $\frac{1}{2}$  in. All tests were performed with the samples clamped in the melt flow direction, the latter two sizes being cut parallel to the flow direction from the central section of the plaque. Balanced flow and filling time of each cavity in a multi-cavity mould seldom, if ever, occurs in practice. One or more cavities may differ in shot weight, dimensions or other properties. This difference occurred in the mould tool employed, one plaque having a higher stress value than the other. All testing was therefore performed on mouldings produced in this cavity (plaque A).

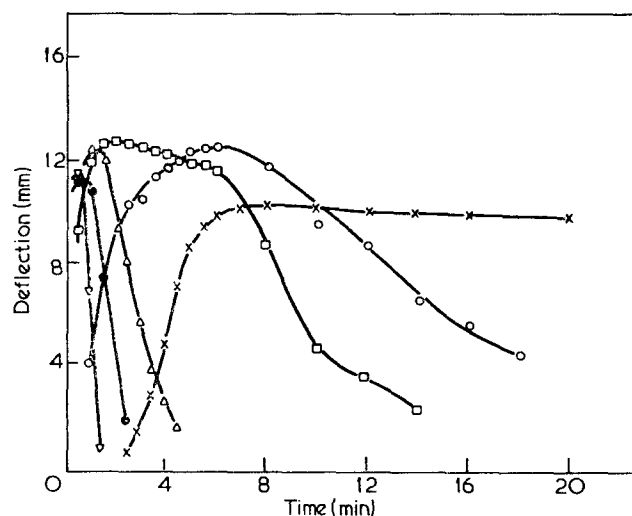


Figure 3 Deflection curve for 3 in polystyrene plaque, moulded at 5800 lbf/in<sup>2</sup>. Initial tests between  $90^\circ\text{C}$  and  $140^\circ\text{C}$ .  $\times$ ,  $90^\circ\text{C}$ ;  $\circ$ ,  $100^\circ\text{C}$ ;  $\square$ ,  $110^\circ\text{C}$ ;  $\triangle$ ,  $120^\circ\text{C}$ ;  $\bullet$ ,  $130^\circ\text{C}$ ;  $\nabla$ ,  $140^\circ\text{C}$

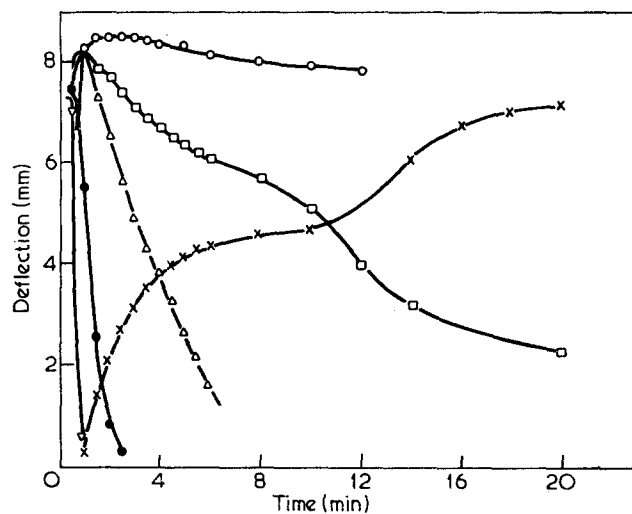


Figure 4 Deflection curve for 2 in polystyrene plaque moulded at 5800 lbf/in<sup>2</sup>. Initial tests between  $90^\circ\text{C}$  and  $140^\circ\text{C}$ .  $\times$ ,  $90^\circ\text{C}$ ;  $\circ$ ,  $100^\circ\text{C}$ ;  $\square$ ,  $110^\circ\text{C}$ ;  $\triangle$ ,  $120^\circ\text{C}$ ;  $\bullet$ ,  $130^\circ\text{C}$ ;  $\nabla$ ,  $140^\circ\text{C}$

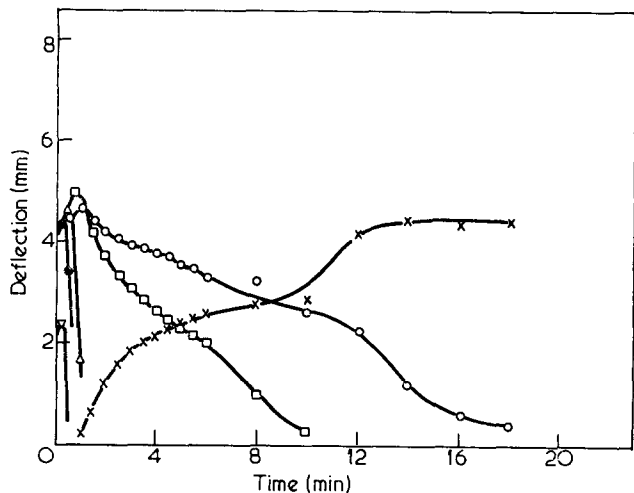


Figure 5 Deflection curve for 1 in polystyrene sample moulded at 5800 lbf/in<sup>2</sup>. Initial tests between 90°C and 140°C. x, 90°C; o, 100°C; □, 110°C; △, 120°C; ●, 130°C; ▽, 140°C

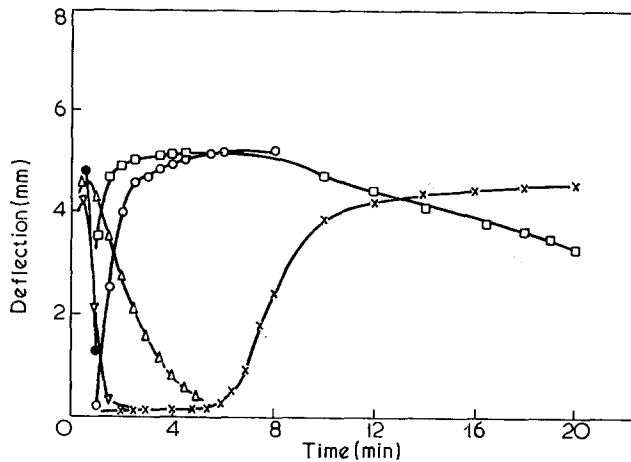


Figure 7 Deflection curve for 1 in polystyrene sample moulded at 7800 lbf/in<sup>2</sup>. Initial tests between 90°C and 140°C. x, 90°C; o, 100°C; □, 110°C; △, 120°C; ●, 130°C; ▽, 140°C

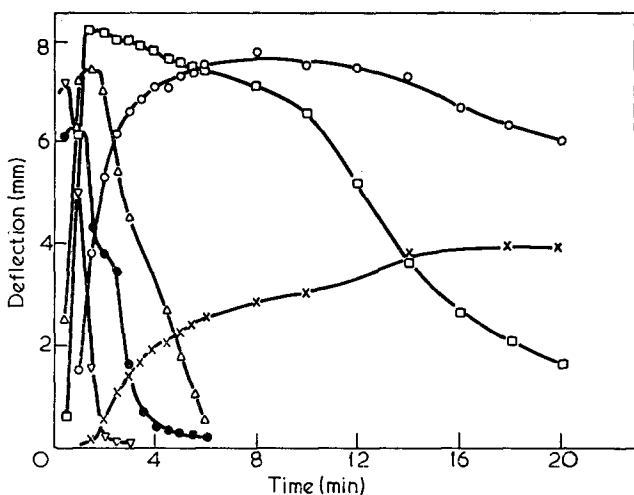


Figure 6 Deflection curve for 3 in polystyrene sample moulded at 7800 lbf/in<sup>2</sup>. Initial tests between 90°C and 140°C. x, 90°C; o, 100°C; □, 110°C; △, 120°C; ●, 130°C; ▽, 140°C

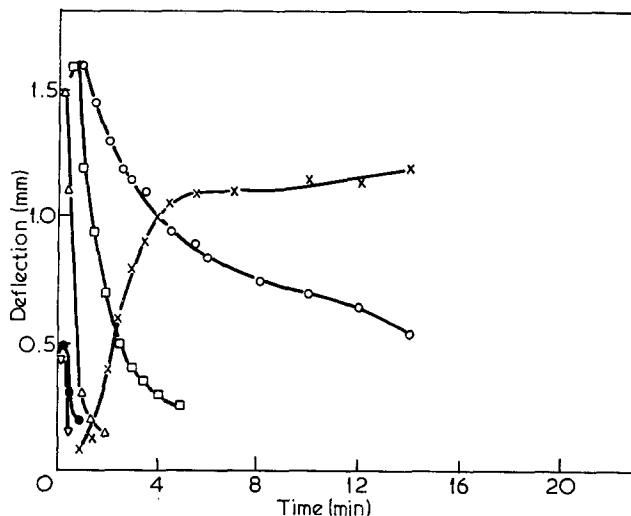


Figure 8 Deflection curve for 2 in polystyrene sample moulded at 7800 lbf/in<sup>2</sup>. Initial tests between 90°C and 140°C. x, 90°C; o, 100°C; □, 110°C; △, 120°C; ●, 130°C; ▽, 140°C

From this examination it was found that non-reproducible results were obtained at 80°C. Poorly defined peak values occurred at temperatures below 120°C but as the temperature was increased the peak value decreased. This is assumed to be due to uneven heat transfer through the specimen. If the edges of the specimen are heated too rapidly they will lose their stress before the main body of the sample is adequately heated. In the case of the polystyrene mouldings a test temperature of 120°C was chosen.

The curves also show that the peak stress value at 120°C is reached at different times, when the sample size is reduced as follows:

Sample size 3 in × 3 in peak value reached after 1.0 min

Sample size 3 in × 2 in peak value reached after 0.75 min

Sample size 3 in × 1 in peak value reached after 0.5 min

The relaxation force and frozen-in stress at the peak value at 120°C for samples of different size are shown in Table 2. The figures quoted are the mean of the three middle values of five samples.

It can be seen that specimens moulded at 7800 lbf/in<sup>2</sup> have a stress level from 31.8% to 33.2% lower than specimens moulded at 5800 lbf/in<sup>2</sup> when the sample is cut from the centre of the plaque. The corresponding figures for samples cut from the side of the plaque are 37.2% for the 3 in × 1 in specimen but only 11.0% for the 3 in ×

Table 2 Relaxation force parallel to flow and orientation stress for samples from different positions of the plaque

Injection pressure (lbf/in <sup>2</sup> )	Relaxation force (N)			Frozen-in stress (kN/m <sup>2</sup> )	
	Centre of plaque			Side of plaque	
	3 × 3 in	3 × 2 in	3 × 1 in	3 × 1 in	3 × ½ in
5800	62 785 (380)	47 775 (428)	33 060 (593)	24 625 (440)	17 365 (622)
7800	42 770 (248)	31 785 (284)	22 565 (440)	15 450 (277)	15 450 (553)

$\frac{1}{2}$  in specimen. The stress measured in samples from the centre of the plaque 2 in and 1 in wide moulded at 5800 lbf/in<sup>2</sup> is 14.1% and 58.1% higher than in a sample 3 in wide. The corresponding figures for samples moulded at 7800 lbf/in<sup>2</sup> are 11.9% and 58.5%. The stress measured in samples from the side of the plaque  $\frac{1}{2}$  in wide moulded at 5800 lbf/in<sup>2</sup> is 41.3% higher than in a sample 1 in wide. The corresponding figures for samples moulded at 7800 lbf/in<sup>2</sup> are 100%. The consistency of the results gives a picture of almost similar stress distribution for samples moulded at the two different injection pressures. One anomaly is the unexpected high value for the  $\frac{1}{2}$  in sample moulded at 7800 lbf/in<sup>2</sup>. A second test confirmed this result with a stress level of 550 kN/m<sup>2</sup>.

Orientation stress will also occur in the direction transverse to melt flow and, as expected from other published work, its level will be considerably lower than in the melt flow direction.

Table 3 shows the orientation stress for samples cut transverse to flow from the middle of the plaque. A sample length of 2 in was the smallest to be tested. The results for a 3 in  $\times$  3 in sample are given in parentheses.

The difference in stress between samples moulded at 7800 lbf/in<sup>2</sup> and 5800 lbf/in<sup>2</sup> was found to be 20.7% which was lower than the value for the sample in the parallel to flow direction.

When compared with the 3 in  $\times$  3 in sample the stress was found to be 48.2% lower for samples moulded at 5800 lbf/in<sup>2</sup> and 39.6% lower for samples moulded at 7800 lbf/in<sup>2</sup>. As the area of the plaque is reduced by one-third only, this could indicate a very high stress in the two  $\frac{1}{2}$  in strips cut from the plaque, presumably concentrated in the  $\frac{1}{2}$  in near the gate. As can be seen in Table 2 the relaxation force measured in a 1 in sample from the centre of the plaque is higher than in a 1 in sample from the side. Also the  $\frac{1}{2}$  in sample cut from the side has a proportionately higher stress than the 1 in sample.

It will be shown later that stress corrosion tests indicated a surface stress distribution with least orientation in the centre. This pattern, however, was not found with birefringence, which shows the bulk orientation.

One possible distribution of the orientation across the plaque is proposed in Figure 9. The hatched parts in this Figure indicate areas where the main orientation is supposed to be found in a cross-section of the plaque at right angles to the direction of flow. The size of these areas is in agreement with the relaxation force measured. This pattern is, of course, influenced by the position of the cooling channels, shown in Figure 10, around which the isotherms are believed to follow concentric circles.

The influence from heat transfer through the sample on the deflection measured can be analysed when relaxation forces for samples of reduced area are added as shown in Table 4.

Table 4 shows results for different parts of the plaque tested separately. In this case the total force is higher than when the whole plaque is tested. A satisfactory agreement exists, irrespective of how the samples are

Table 3 Orientation stress transverse to flow for samples 2 in  $\times$  3 in

Injection pressure (lbf/in <sup>2</sup> )	Orientation stress (kN/m <sup>2</sup> ) at 120°C	
	2 $\times$ 3 in	3 $\times$ 3 in
5800	194	(380)
7800	154	(248)

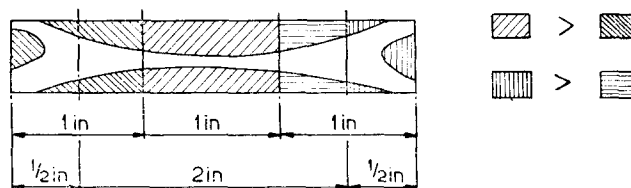


Figure 9 Orientation distribution across the plaque (not to scale)

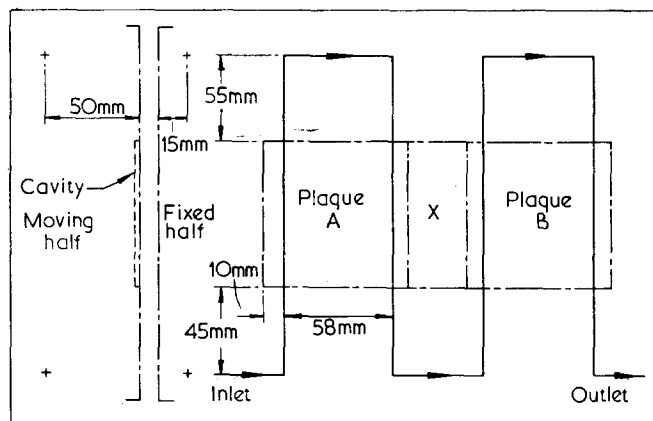


Figure 10 Outline of mould cooling system

Table 4 Relaxation forces in specimens of varying surface area

Injection pressure (lbf/in <sup>2</sup> )	Force (N) for specimens		
	$\frac{1}{2}$ in S $\times$ 2 + 2 in C	1 in S $\times$ 2 + 1 in C	3 in
5800	82.505	82.310	62.785
7800	62.685	53.465	42.770

Table 5 Orientation stress transverse to flow for 1 in  $\times$  3 in samples

Injection pressure (lbf/in <sup>2</sup> )	Orientation stress (kN/m <sup>2</sup> )	
	Adjacent gate 1 $\times$ 3 in	Opposite gate 1 $\times$ 3 in
5800	30	30
7800	31	31

cut, for specimens moulded at 5800 lbf/in<sup>2</sup> injection pressure, but a somewhat poorer agreement for specimens moulded at 7800 lbf/in<sup>2</sup>. This is probably due to the unexpectedly higher value for the  $\frac{1}{2}$  in sample which is probably due to greater orientation at the sides.

The stress in transverse to flow for specimens moulded at 5800 lbf/in<sup>2</sup> and 7800 lbf/in<sup>2</sup> was determined for 1 in  $\times$  3 in samples cut transverse to flow from the side adjacent to and opposite to the gate. Table 5 shows that no variation was found between samples cut transverse to flow from different parts of the plaque for mouldings made at the same injection pressure.

The result obtained, however, should be interpreted with care due to the low values, where the influence from thermal expansion of the samples and the non-linear characteristic of the spring is more distinct. Frozen-in stress was finally determined for specimens moulded at pressures between 5800 and 7800 lbf/in<sup>2</sup> in 400 lbf/in<sup>2</sup> steps. The samples were tested parallel and transverse to flow and the result is given in Figure 11.

Figure 11 shows that the frozen-in stress parallel to flow decreased as the injection pressure increased. In

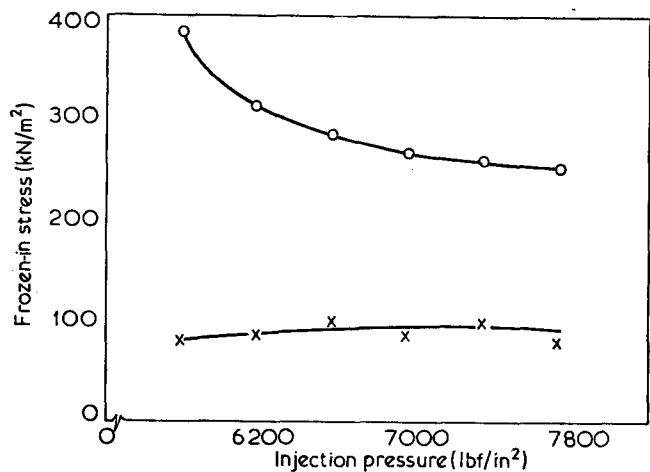


Figure 11 Effect of injection pressure on frozen-in stress in polystyrene. ○, parallel to flow; ×, transverse to flow

Table 6 Effect of injection pressure on frozen-in stress parallel to flow in a 3 in × 3 in plaque

Material	Injection pressure (lbf/in <sup>2</sup> )	Test temperature (°C)	Orientation stress (kN/m <sup>2</sup> )
Polystyrene	5 800	120	380
	7 800		248
Polypropylene	5 000	170	234
	6 000		221
	7 000		207
Polysulphone	13 500	215	111
	15 000		106
	16 500		085
ABS	8 000	140	280
	9 000		253
	10 000		238

contrast the stress in the transverse to flow direction increased only slightly as the injection pressure increased.

#### Results obtained with other materials

Table 6 shows the materials tested and the results obtained. Nylon-6 did not give any indication of orientation, even when tested over a wide temperature range, although a distinct discoloration due to oxidation took place. For comparison, results with polystyrene are given.

For 1 in samples cut parallel to flow from the centre and the side of the plaque the results given in Table 7 were obtained.

Table 6 showed that the orientation stress in the materials tested decreased as the injection pressure increased. As can be seen in Table 7 this tendency was

not followed when a 1 in sample was cut from the side of the plaque and only in the case of polypropylene when the sample is cut from the centre. In the samples tested the highest stress was found in specimens moulded at the injection pressure in the middle of the range.

The figures also seem to indicate a change in stress distribution across the sample with increasing injection pressure. A similar observation was made with tensile strength but this will be discussed later.

As can be seen from Table 8 a very poor agreement was found when the relaxation force for a 3 in. sample was compared with the relaxation force for three 1 in samples, two from the sides and one from the centre.

It is to be expected that the deflection recorded should be proportional to the sample size so that the added force would correspond to the force for a whole plaque. This is not the case, so the extra surfaces introduced with the smaller samples must lead to a more spontaneous relaxation because of the quicker heating. This disagreement makes a comparison with absolute values doubtful.

It has been assumed that the instrument did not apply any external force on the sample. However, a larger variation in the results was found with the smaller samples. This could be due to play in the bearings and the more unstable characteristic of the spring for a low load.

The thermal expansion of the sample and equipment and friction in the equipment should in fact be added to the force measured because these are working against the relaxation force. However, the thermal expansion of the clamps and friction in the equipment is considered to be negligible.

Figure 12 shows a 2 in sample after testing. Since there is an uneven stress intensity across the sample and the sample is held rigidly thus preventing unrestrained distortion as in a heat reversion test, differential displacement of material takes place and the part nearest to the gate becomes thicker.

## EVALUATION OF OTHER METHODS

### Birefringence methods

Measurement of birefringence, or the difference in refractive index, along and across the direction of an oriented sample provides a convenient method for determining the degree of molecular orientation in transparent polymers. When examined under plane-polarized white light an injection moulded specimen exhibits a repeating series of coloured fringes, each colour indicating a fixed amount of molecular orientation.

Table 7 Effect of injection pressure on orientation stress parallel to flow in samples 3 in × 1 in

Material	Injection pressure (lbf/in <sup>2</sup> )	Test temperature (°C)	Orientation stress (kN/m <sup>2</sup> )	
			Centre of plaque 3 × 1 in	Side of plaque 3 × 1 in
Polystyrene	5 800	120	593	440
	7 800		404	277
Polypropylene	5 000	170	591	513
	6 000		560	588
	7 000		419	432
Polysulphone	13 500	215	278	178
	15 000		286	246
	16 500		214	218
ABS	8 000	140	550	560
	9 000		575	580
	10 000		575	565

Table 8 Relaxation force for a 3 in sample compared with three 1 in. samples

Material	Injection pressure (lbf/in <sup>2</sup> )	Relaxation force (N)		
		3 in	1 in × 3	%*
Polypropylene	5 000	35·705	86·650	41
	6 000	34·825	91·235	38
	7 000	33·354	69·160	48
Polysulphone	13 500	18·640	35·705	52
	15 000	18·395	46·600	39
	16 500	18·150	44·635	41
ABS	8 000	45·371	90·745	50
	9 000	42·430	96·875	44
	10 000	41·200	96·630	43

$$*\% = \frac{3 \text{ in}}{1 \text{ in} \times 3} \times 100$$

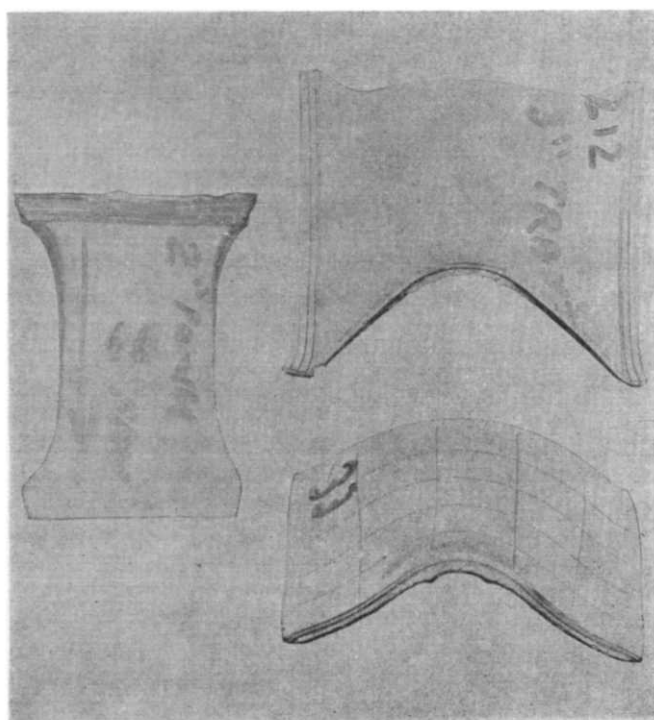


Figure 12 Distorted polystyrene samples

Polariscope determinations show the overall orientation pattern whereas exact point to point measurements by means of a Babinet's Compensator can be used to determine variation in orientation over the sample. Both techniques were examined.

*Determination with polariscope.* Specimen birefringence was measured with a polariscope using the technique described by Ballman and Toor<sup>8</sup>. Birefringence was calculated from the formula:

$$\eta = \frac{R}{t}$$

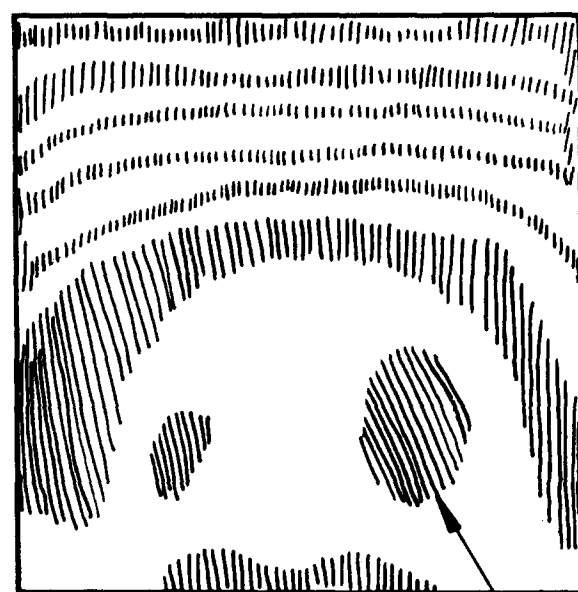
where the wavelength of the polariscope white light source  $\eta$  was estimated to be about 5500 Å. The retardation  $R$  was determined by counting the number of orders, each order consisting of the sequence of colours yellow-red-green, and assigning the various colours the following fractional order values:

- yellow 0·3
- red 0·7
- green 1·0

so that, for example, a twelfth order yellow would have a retardation of 11·3, a sixth order green would be 6·0, etc.;  $t$  is the thickness of the specimen. A typical birefringence pattern is shown in Figure 13.

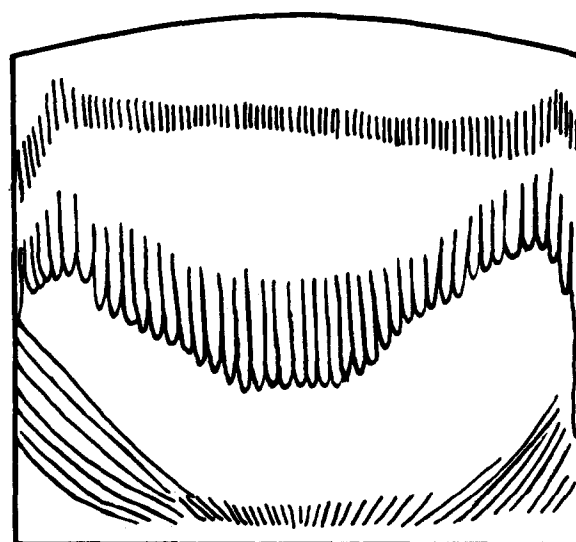
The maximum orientation is reached near the gate and the sequence of colours then reverses indicating a negative orientation gradient over the remainder of the specimen. In order to be able to express the orientation present in the specimen by a single number the birefringence maximum was arbitrarily chosen (see Figure 13). The values shown in Table 9 are total birefringence values which in effect integrate the varying degrees of orientation present through the cross-section of the sample. Several specimens from each experimental run were tested, the result quoted being the sample with the most typical value.

Some point regarding the interpretation of the birefringence should be made. First, it is assumed that birefringence is primarily a function of molecular alignment,



a

Max



b

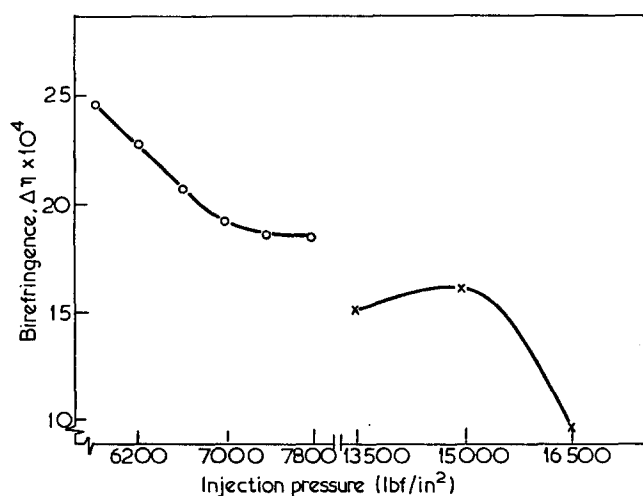
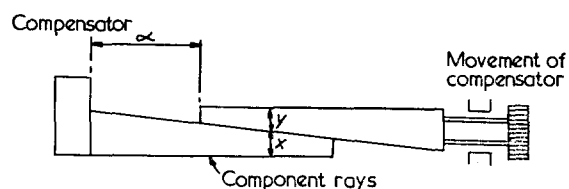
Figure 13 Typical birefringence pattern for polystyrene. (a) Full shot; (b) short shot

**Table 9** Effect of injection pressure on total birefringence in polystyrene (A) and polysulphone (B)

	Injection pressure (lb/in <sup>2</sup> )	No. of bands			$R_{\max}$ (orders)	Average thickness (mm)	$\eta \times 10^4$
		Yellow	Red	Green			
A.	5 800	9	10	9	10 red	2.085	25.55
	6 200	9	9	8	9 red	2.100	22.80
	6 600	8	8	8	8 green	2.130	20.65
	7 000	6	8	7	8 red	2.200	19.25
	7 400	7	7	7	7 green	2.185	17.60
	7 800	6	7	7	7 green	2.195	17.55
B.	13 500	5	6	6	6 green	2.180	15.1
	15 000	6	7	6	7 red	2.280	16.2
	16 500	5	5	4	5 red	2.710	9.5

rather than of valence bond distortion or of density variation. Secondly, it must be remembered that the birefringence observed in a moulding is a composite of two competing effects: orientation induced by shearing forces during flow and subsequent molecular relaxation caused by Brownian motion when the shear forces are removed. Superimposed on both of these effects is the point temperature history of the moulding. These factors result in a rather complex series of interrelated events, the order and nature of which must be deduced from the evidence offered by the moulding.

Birefringence as a function of injection pressure is shown in *Figure 14*. This Figure shows that for polystyrene the total birefringence decreased as the injection pressure was increased. For polysulphone the birefringence first increased and then rapidly decreased as the injection pressure increased. The dark band in *Figure 13* is the accumulation of points at which the relative retardation is an integral number of wavelengths of white light. The relative retardation in a plastics material depends uniquely on the degree of orientation of the molecules; thus the increase in band order throughout the plaque gives a convenient measure of the orientation. *Figure 13* also demonstrates the increase in orientation in moving from the edge of the plaque remote from the gate towards the centre. With polystyrene, the birefringence pattern for a short shot showed a distinct difference from the full shot pattern, as is illustrated (see section on melt flow and stress distribution).


**Figure 14** Effect of injection pressure on birefringence. ○, Polystyrene; ×, polysulphone

**Figure 15** Babinet Compensator

Polysulphone samples produced a somewhat similar pattern of birefringence to polystyrene, but lower overall values were obtained as shown in *Table 9*. Also the third of the plaque remote from the gate did not show orientation at all. The phenomenon of a frame of unoriented material, approximately 2 mm wide, was found on polysulphone samples only. This effect was most pronounced with samples moulded at the highest injection pressure.

*Determination with Babinet's Compensator.* The magnitude of birefringence, that is the difference between the two refractive indices, is most conveniently measured by means of the Babinet Compensator<sup>9</sup>.

This instrument consists of two wedge-shaped prisms of quartz cut at a very small angle as shown in *Figure 15*.

The optical axes are parallel and perpendicular respectively to the two refracting edges. When plane polarized light is incident normally on the compensator with the plane of vibration at some arbitrary angle  $\theta$  to the optical axes, it will be broken up into two components. These two components travel at different speeds through the prisms, at the boundary between the two prisms the components are interchanged owing to the optical axis of the second being perpendicular to that of the first prism; The result is that one prism tends to cancel out the effect of the other. Along the centre, where both prisms have equal thickness, both paths are equal and the cancellation is therefore complete. A dark line forms along the centre flanked on both sides by coloured bands corresponding to the path difference between the components.

The compensator and a polaroid plate set is mounted on a microscope, and a sample is introduced between the polaroid plate and the compensator. With an oriented sample there will be a shift of the dark line, owing to the path difference introduced by the sample between the components of the polarized light. The experimental procedure is then to slide the one prism with respect to the other until the dark fringe is in the centre of the eye piece again. This distance can be measured very accurately by a micrometer screw. The exact path difference can be calculated from the geometry of the system. At the

black line the path difference introduced by the sample is cancelled out by the compensator, that is:

$$t(\eta_1 - \eta_2) + (x - y)(\gamma_1 - \gamma_2) = 0 \quad (1)$$

where

$\eta_1 - \eta_2$  = difference between refractive indices in the sample

$\gamma_1 - \gamma_2$  = difference between refractive indices in the compensator

$x - y$  = difference between thickness of wedges for  $\alpha = \alpha_i$

$t$  = thickness of sample.

With no sample we have:

$$\eta_1 = \eta_2$$

$$x - y = 0$$

$$\alpha = \alpha_0$$

where

$\alpha$  = micrometer reading

Now since  $x - y$  varies linearly with  $\alpha$  and is 0 for  $\alpha = \alpha_0$  we have:

$$(y - x) \propto (\alpha - \alpha_0)$$

and

$$t(\eta_1 - \eta_2) = k(\alpha - \alpha_0)$$

where

$$k = \text{'wedge constant'} = \frac{\gamma_1 - \gamma_2}{\tan \beta}$$

( $1.763 \times 10^{-4}$  for instrument used)

then

$$\Delta\eta = \eta_1 - \eta_2 = \frac{K}{t}(\alpha - \alpha_0)$$

As both  $\eta_1 - \eta_2$  and  $\gamma_1 - \gamma_2$  (therefore also  $k$ ) depend on the colour, accurate measurements must be made with monochromatic light (e.g. a sodium flame, or mercury lamp); in practice, however, sufficient accuracy is usually obtainable by the use of white light.

It was found with polystyrene that samples cut from different parts of the plaque produced a dark pattern off scale. The compensator used had a total movement of  $\pm 13$  mm, hence the birefringence in the 2 mm thick sample tested must be above  $11.5 \times 10^{-4}$ , as can be seen from equation (1). A 'double-sample' technique in order to offset the scale did not prove successful either.

With polysulphone, only samples moulded with the highest injection pressure were tested. With these samples it was not possible to determine birefringence closer to the gate than 47 mm, because of the high degree of orientation in the comparatively thick sample. The result is given in Table 10.

Table 10 shows the difference in results with the two methods. The values obtained with the polariscope are one band order lower than that obtained with the compensator.

The compensator also clearly showed the 2 mm un-oriented frame on the polysulphone sample.

#### Heat reversion test

The reversion test was carried out by heating specimens floating on talc powder in a hot-air oven for 20 min at the following temperatures:

Polystyrene	120°C
Polypropylene	170/175/180°C
Nylon-6	220/225°C
Polysulphone	220°C
ABS	130°C

After reversion the transparent specimens were examined between crossed polaroids. The residual birefringence in the sample was negligible.

Three specimens from each experimental run were tested. Polystyrene samples from the two extreme moulding conditions were allowed to cool down to room temperature for 4 h, to see if the cooling rate after heating had any significant influence on the final distortion. This was found not to be the case. Prior to heating the specimens were scribed with a grid of lines in order to facilitate measurement of the distorted specimen. Figure 12 shows a distorted specimen, and indicates how the shrinkage at any position on the plaque can be estimated from the resulting changes in the initial 15 mm square grid pattern. The overall flow pattern is clearly seen, but owing to the curvature of the reverted moulding caused by non-uniform flow accurate measurements are tedious and difficult. Length and width values after reversion were calculated as an average of  $2 \times 30$  dimensional measurements on each plaque.

The final result was calculated as an average of three specimens from each run with the following formulae:

$$\text{Width reversion: } 1 - \frac{w_0}{w}$$

$$\text{Length reversion: } \frac{l_0}{l_t} - 1$$

where

$l_0$  and  $w_0$  = length and width before reversion

$l_t$  and  $w_t$  = average length and width after reversion.

Nylon-6 was tested at 220 and 225°C but although the samples were nearly floating, and showed a very pronounced colour change due to oxidation, no distortion occurred.

Table 10 Birefringence in polysulphone as measured with Babinets Compensator and polariscope

Position on plaque		Babinets Compensator			Polariscope	
(mm) from		Thickness Reading			$R_{max}$	
Gate	Edge	(mm)	(mm)	$\eta \times 10^4$	(orders)	$\eta \times 10^{-4}$
47	20	2.65	12.95	8.6	3 red	5.6
47	125	2.65	12.56	8.4		
57	125	2.63	9.19	6.2	2 green	4.2

Table 11 Shrinkage after reversion testing as a function of injection pressure

Materials	Injection pressure (lbf/in <sup>2</sup> )	Heating temperature (°C)	Reversion	
			Length	Width
Polystyrene	5 800	120	1.20	0.14
	6 200		0.96	0.15
	6 600		0.86	0.14
	7 000		0.70	0.13
	7 400		0.70	0.14
	7 800		0.63	0.11
Polypropylene	5 000	175	0.77	0.17
	6 000		0.64	0.15
	7 000		0.93	0.19
Polysulphone	13 500	220	0.29	0.19
	15 000		0.34	0.14
	16 500		0.29	0.14
ABS	8 000	130	0.59	0.09
	8 000		0.51	0.09
	10 000		0.51	0.09

Polypropylene was tested at 170°C, 175°C and 180°C. Testing at 170°C gave very inconsistent results. Using a test temperature of 180°C a very large reversion took place. The grid pattern was still clearly seen, but with large variations in thickness, measurements were of little value. The results of these experiments are shown in Table 11.

#### Hot wire test

The use of a hot wire to reveal surface orientation has been proposed by Atkinson *et al.*<sup>11</sup> and evaluated by Smith and Stevens<sup>12</sup>. The test essentially consists of applying a red hot wire across a set of scribed lines on the surface of the sample. Melting of the surface and sub-surface takes place and the heated portions of the scribed lines will form a series of peaks pointing in the direction of melt flow. The amount by which the lines have shifted from the original scribed lines is a measure of the degree of orientation in that area. From the line shift distribution the nature of the overall stress pattern can be deduced. The phenomenon produced is associated with relaxation of polymer chains which have become stretched by the melt flow during moulding and have been frozen with their chain 'head' pointing slightly downwards into the centre of the moulding. On the application of localized heat the polymer chains in that region will have their 'tails' unfrozen first and will relax towards their frozen 'heads'.

The method consisted of stretching a single nichrome wire about 1 mm thick across the surface of the sample and at right angles to the scribed lines. The height of the wire above the surface of the sample can be adjusted. The wire itself was kept taut by means of a weight. The clamps holding the wire were connected to a 12 V battery and the wire was brought to red heat for several seconds. It was found with the polystyrene samples tested, that lines did not shift further after heating for more than 30 sec. However, a shorter period of heating, say 20 sec, gave better results and caused less distortion of the surface. For other materials the optimum heating time varied. Care should be taken when results are compared quantitatively, because the wire tended to become hotter over a period of time.

Polystyrene samples from the six different experimental settings were tested. Lines were drawn with 5 mm spacing parallel to the gate across the samples. The hot wire was applied perpendicular to the lines and heated

for 20 sec. The wire was applied 5 times to each half of the plaque assuming the two halves were identical.

A typical pattern obtained with polystyrene with lineshifts varying between 0.1 and 4.0 mm is shown in Figure 16. The height of each individual peak was measured and the values for all peaks on one-half of a plaque were added with the intention of obtaining an overall value for the surface orientation of the plaque. This value did not vary significantly from sample to sample, but there seemed to be a tendency towards a higher value for specimens moulded at a higher injection pressure. The difference between the lowest and highest figure was found to be approximately 7%. Both surfaces of the plaque were tested. The lineshifts shown between full-drawn lines on the right side of the plaque were obtained on the side of the sample moulded adjacent to the moving mould-half. In most cases a somewhat higher lineshift was found on this surface. As can be seen from Figure 16 the peaks tend to converge towards the sprue. Tests with the hot wire at different angles to the gate in a direction towards the sprue did not show an essentially higher peak value, compared to the value found at the same position tested with the wire perpendicular to the gate. Specimens annealed at 120°C for 20 min, and specimens tested with the hot wire parallel to the gate did not show lineshifts at all. The hot wire technique was also applied on the other four materials, of these, nylon-6 did not show any indication of orientation at all. With polysulphone orientation was only indicated in the two-thirds of the plaque nearest the gate with little variation of peak height across the plaque. With polypropylene and ABS an overall pattern similar to polystyrene was obtained.

#### Stress crazing techniques

Solvent stress crazing or environmental stress crazing has been defined<sup>13</sup> as the superficial crazing undergone by materials subjected to internal or external stresses and simultaneously exposed to certain vapours or liquids. According to Ziegler<sup>15</sup> the rather wide acceptance of n-heptane as a general purpose stress crazing solvent

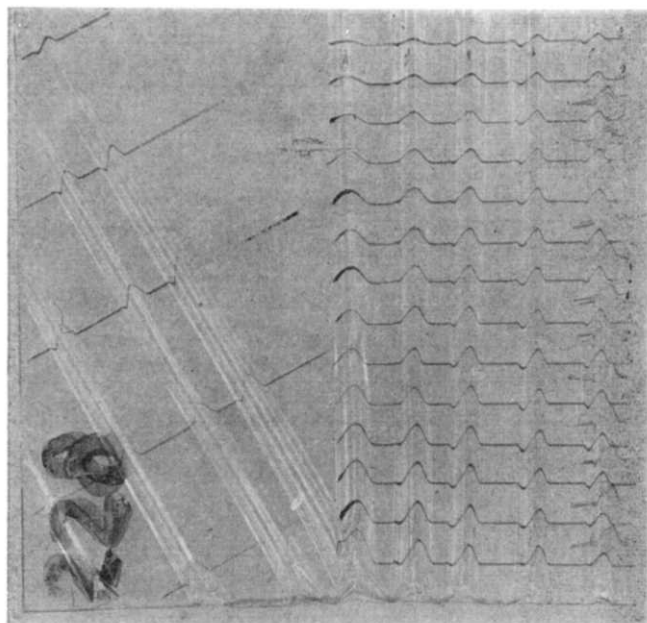


Figure 16 Polystyrene sample tested with hot-wire



for polystyrene mouldings should be interpreted with care, and it should only be employed after the operational details and significance of the test are thoroughly understood and preferably only after correlation with actual end use has been established. 'Crazing' is the fine cracks on or under the surface of a plastic. These cracks may range from those of relatively large size, individually visible to the unaided eye, down to those of almost microscopic size visible *en masse* as 'water-bloom'. Stress-crazing, as the name implies, is associated with stresses contained in or exerted on the plastic moulding, and indicates that crazing strength and orientation are directly associated.

The purpose of the tests performed was primarily to obtain an indication of the orientation intensity over the surface of the plaque, and secondly to visualize the effect of injection pressure on stress-corrosion.

n-Heptane was chosen for experiments on polystyrene because the asymptotic value of craze depth is reached very rapidly in heptane. n-Heptane is so effective in lowering the critical elongation of polystyrene that stresses above 50 lbf/in<sup>2</sup> (345 kN/m<sup>2</sup>) will cause crazing at 90°F (32.2°C).

Specimens from each experimental setting were immersed in n-heptane for periods from a few hours up to seven days. All specimens were regularly inspected during the test period, and it was found that a characteristic cloudiness or whitening took place after a few hours immersion, depending on room temperature.

A typical example of this is shown in Figure 17. This Figure shows that two patterns of whitening can be observed—a 'bowl' pattern superimposed on the usual pattern for 'plug' filling of the mould. The former was observed to be mainly associated with the surface of the plaque, whereas the latter seemed to be mainly in the subsurface.

A somewhat similar observation was made with birefringence studies of short-shots, where it appeared that under certain conditions the birefringence pattern changed from the 'bowl' type to the 'plug' type when the moulding approached the size of a full shot. A further discussion of this phenomena will be made later.

The whitening apparently stopped towards the end of the seven day test period, at which time the sample had become completely opaque.

A specimen annealed at 120°C for 20 min did not show any tendency to whitening, even after immersion for more than seven days, so it seems reasonable to suggest a relationship between whitening and surface orientation.

Scanning of the sample in a stereo-binocular microscope showed some evidence of a series of microcracks on the surface but it is most reasonable to relate the whitening to crazing as defined by Hsiao and Sauer<sup>14</sup>. In their fundamental work Hsiao and Sauer refer to 'crazing' occurring in the form of a blush or haze on a previously transparent material and they consider 'crazing cracks' to be the visible cracks produced only after crazing, in the form of real but submicroscopic discontinuities. In other words, crazing is not actually cracking but may be some sort of infinitesimal openings, which are either still within the field of molecular attraction or are physically prevented by neighbouring molecules from developing into cracks.

It was observed that visible cracks, which must be distinguished from the above mentioned crazing,

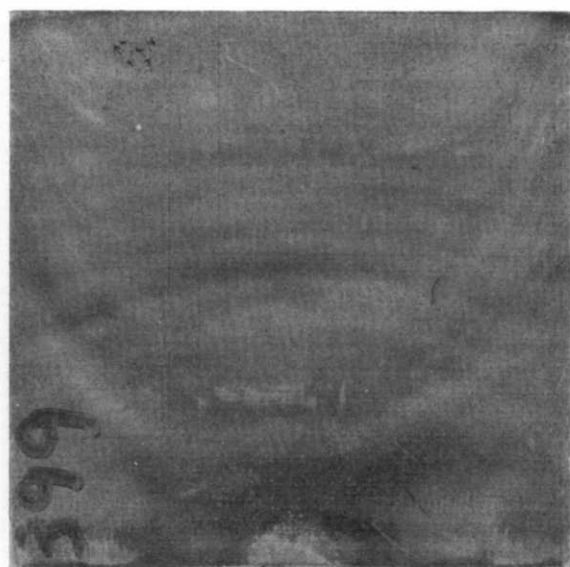
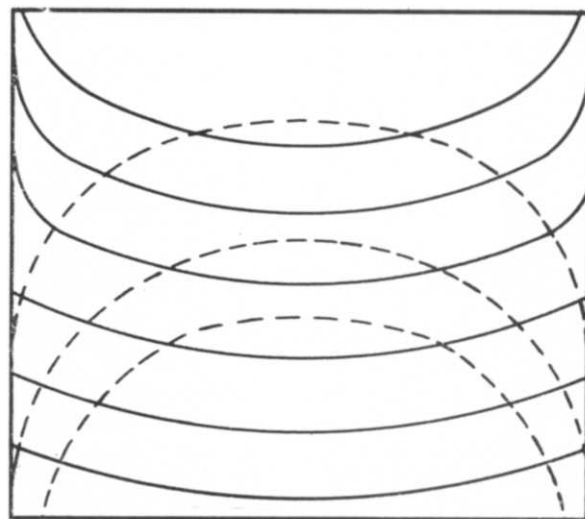


Figure 17 'Crazing' of polystyrene with outline sketch above

appeared first on specimens moulded with the highest injection pressure. These cracks appeared after 2 days and their length increased very slightly during the remaining test period. Cracks appeared in a direction roughly towards the sprue, except near to the edges perpendicular to the runner, where the lines of cracks were deflected perpendicular to the edge. Most of the cracks were found on the third of the plaque next to the runner and near the edges perpendicular to the runner, leading to the assumption that these areas have the highest surface orientation. There was a distinct difference between the two surfaces of the plaque, the surface moulded by the moving half of the mould having considerably more cracks than the opposite surface. This could be caused by a higher degree of shear when the material is forced from the runner over the edges of the gate into the cavity or more probably by a difference in the surface temperature of the mould halves. After seven days immersion, the thickness of the specimen had increased by approximately 0.02 mm.

*Nylon-6.* Carbon tetrachloride has been found to cause cracks on samples of nylon-6<sup>16</sup>. However, no effect was found on samples moulded at the three different injection pressures after immersion in carbon tetrachloride for more than 2 days.

Tests on polysulphone. The critical stress levels for polysulphone in selected solvents<sup>17</sup> at 20°C are:

Solvent	Approximate critical stress	
	(lbf/in <sup>2</sup> )	(kN/m <sup>2</sup> )
Acetone	200	1.38
1,1,1-Trichloroethane	500-600	3450-4140
Ethylene glycol monobutyl ether	1400	9690
Carbon tetrachloride	2400-2600	16 600-17 950

Samples were immersed in acetone for 2 or 5 min. Cracks appeared very quickly, after only wetting the surface. No effect was found on samples which had been stress relieved by heat. There was a distinct difference between the two surfaces of the sample with only a few cracks on the surface moulded by the fixed half of the mould. Nearly all cracks were perpendicular to the runner, and not, as was expected, more or less towards the sprue. Cracks had not propagated into the stress-free areas as measured by birefringence studies. A pronounced delamination took place after approximately 2 min immersion. It was found that most cracks appeared on the samples moulded at 15 000 lbf/in<sup>2</sup> and least cracks on the samples moulded at 16 500 lbf/in<sup>2</sup>.

The order of orientation stress determined was similar to that exhibited by birefringence experiments. Neither carbon tetrachloride or ethylene glycol monobutyl ether had any noticeable effect on polysulphone mouldings after 6 days immersion and a tendency to dissolve the plastic occurred with trichloroethane after 1 day.

#### Measurement of tensile strength

A useful adjunct to an investigation of changes in frozen-in stress in injection mouldings and a practical outcome is to relate these to a mechanical property. The mechanical test itself must be sufficiently sensitive to the stress variation and give reproducible results. Tensile strength measurements when plotted against birefringence measurements have been shown to change significantly for small changes in orientation<sup>18</sup> and for this reason they were chosen in this study. Tensile strength was tested at different parts of the plaque for samples moulded at the two extreme injection pressures. As a reference non-oriented samples were prepared from polystyrene by compression moulding of plaques 6 in × 6 in × 2.5 mm.

The results of the test are shown in Table 12, the figures quoted being the median of five results. The dumbbell was milled to shape after being cut from the plaque with a band-saw. The Table shows clearly that the tensile properties of polystyrene transverse to flow are lower than those parallel to flow. The results also show that the tensile strength for polystyrene specimens moulded at 7800 lbf/in<sup>2</sup> was higher than those moulded at 5800 lbf/in<sup>2</sup> when the sample was cut from the side of the plaque, and *vice versa* for the sample cut from the middle of the plaque. The same tendency was shown by samples cut transverse to flow, where specimens moulded at the highest pressure showed a proportionately greater difference to samples cut near to and opposite the gate. This could indicate a different stress distribution in the two types of samples and could lead to the conclusion that samples moulded at 7800 lbf/in<sup>2</sup> have a high degree

Table 12 Variation in tensile strength with injection pressure and orientation

Test specimen: type C dumbbell; pulling speed: 5.5 mm/sec

Material	Injection pressure (lbf/in <sup>2</sup> )	Tensile strength at yield point (MN/m <sup>2</sup> )	
		Specimen position parallel to flow	
		Centre of plaque	Side of plaque
Polystyrene	5 800	44.9	40.4
	7 800	20.9	44.4
Polypropylene	5 000	26.2	24.5
	7 000	24.2	26.7
Nylon-6	5 000	53.8	54.7
	7 000	51.4	53.3
Polysulphone	13 500	65.8	65.9
	16 500	69.0	69.1
ABS	8 000	46.1	44.9
	10 000	43.3	43.8
Transverse to flow			
		Near gate	Opposite gate
Polystyrene	5 800	14.2	14.9
	7 800	23.6	18.8
Unoriented polystyrene		Random 32.0	

of orientation in the corners, since this part is filled first. As a reference the tensile strength of the unoriented sample is quoted. The value is approximately 25% lower than most commercial figures quoted; these, however, can often be considered to represent ideal values. A similar pattern of results at a lower order of tensile strength was exhibited by the polypropylene samples. With nylon-6 and ABS the samples taken from the side of the plaques moulded at the lowest injection pressure had the greatest strength, the figures for nylon being higher than those obtained from the centre of the plaque. In contrast polysulphone samples exhibited the highest tensile strength at the higher injection pressure in both areas and only a marginal indication of greater strength at the side of the plaque.

#### COMPARISON OF METHODS EXAMINED

From the investigation conducted only birefringence methods, heat reversion, the RAPRA stress relaxation method and tensile strength measurements are directly comparable. The first three methods provide a numerical value of the bulk stress in an injection moulded sample whilst the latter gives an indirect measure of stress variation. Both the hot wire and solvent crazing tests detect surface orientation and are therefore not included in this comparison.

The RAPRA Stress Relaxometer showed with all materials tested except nylon-6 that the frozen-in stress decreases as the injection pressure increases. This is in agreement with an observation by Spencer and Gilmore<sup>19</sup>. They found that sealing of the mould by 'freezing' of polymer in the gate was characterized by a critical rate of flow for a given gate, polymer softening point, and mould wall temperature. This led to an approximately linear relationship between the temperature and pressure in the mould at the sealing point. Clearly the speed with which the gate can seal decreases as the velocity of the fluid passing through the gate

increases. In any case when the plastic wave front encounters the end of the cavity, the velocity of the melt at the gate drops to nearly zero and its rate of skin growth accelerates enormously, rapidly seals the gate and closes off the cavity from further pressure transfer. Shearing forces in the cavity then disappear, thus allowing more relaxation to take place. In the mould in question the position of the cooling channels favoured a rapid sealing of the cavity.

The stress was found to decrease more than proportionately with injection pressure. This is to be expected since the rate of flow increases much more than proportionately with increasing driving force. As the injection pressure increases the temperature of the melt in the nozzle and sprue will increase owing to a higher degree of shear, and a higher melt temperature will generally allow more relaxation to take place.

The lack of measured stress in nylon-6 was also apparent with other techniques used except for the tensile strength test, which showed a slight variation across the specimen. This property was not unexpected since the grade used had a homogeneous and finely crystalline structure, ensuring a largely isotropic behaviour of the specimen. The pronounced tendency to crystallize is combined with quick solidification. The material retained its tough-and-hard character up to just below its melting point (217–221°C) without any appreciable softening. Less than 3% variation was found for the relaxation force for polysulphone. This observation is in agreement with its low degree of shear sensitivity which produces a high melt viscosity during processing, and results in specimens with uniform physical properties that vary little with direction of flow.

#### Birefringence versus frozen-in stress

The correlation between birefringence and frozen-in stress for polystyrene and polysulphone is shown in Figure 18. This Figure shows fairly good agreement for polystyrene in those samples having the greatest stress.

With polysulphone a somewhat poorer agreement was found at a moulding pressure of 15 000 lbf/in<sup>2</sup>. These samples were found by birefringence, stress-corrosion and length reversion to have a higher degree of orientation than those moulded at a higher or a lower injection pressure.

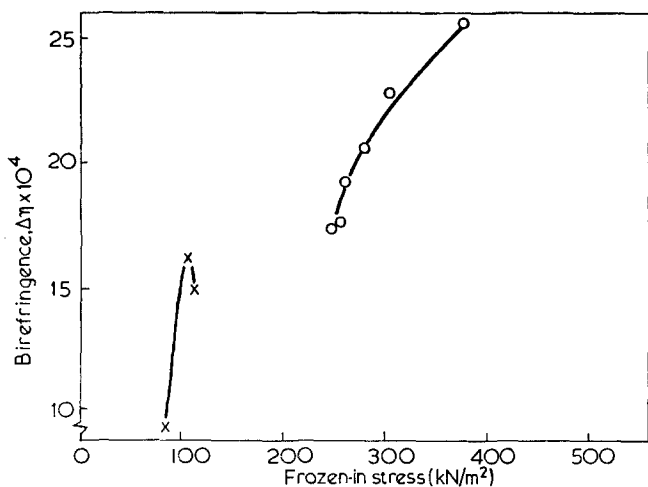


Figure 18 Birefringence versus frozen-in stress. O, Polystyrene; x, polysulphone

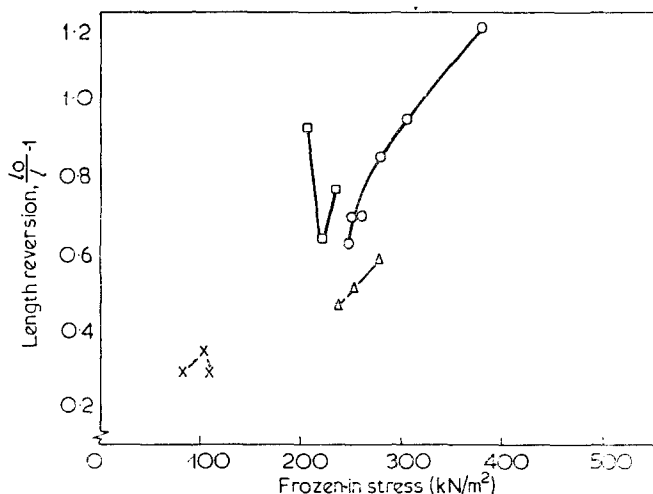


Figure 19 Length reversion versus frozen-in stress. O, Polystyrene; □, polypropylene; x, polysulphone; △, ABS

#### Reversion on heating versus frozen-in stress

The correlation between length reversion on heating and frozen-in stress is shown in Figure 19. As with birefringence, polystyrene shows a good agreement for the highly oriented samples.

ABS shows very good agreement but no correlation seems to exist with polypropylene and polysulphone. Polypropylene, which caused some difficulties in the reversion test, had its lowest value for reversion at the middle injection pressure, where polysulphone had its highest value. One would assume that reversion would either decrease or increase linearly with injection pressure.

#### Tensile strength versus frozen-in stress

Tensile strength parallel to flow was found to decrease with increasing injection pressure for all materials except polysulphone. This is in good agreement with the other test measurements. Tensile strength was tested in the melt flow direction for 1 in samples cut from the centre and the side of the plaque. Specimens from two different injection pressures were tested. With both methods it was found that a low injection pressure led to high stress in the centre and conversely a high injection pressure led to low stress.

The agreement in evidence of this hypothesis given by the two test methods is shown in Table 13. Agreement is enhanced because the tensile strength showed little variation with sample position in the plaque mouldings

Table 13 Agreement with tensile strength (TS) and frozen-in stress (FS) in valuation of stress distribution

		Poly-styrene	Poly-propylene	Nylon-6	Poly-sulphone	ABS
Low injection pressure	TS	X	X	O	(X)	X
High orientation in centre	FS	X	X	—	X	O
High injection pressure	TS	X	X	X	X	X
Low orientation in centre	FS	O	X	—	X	X

X, Agreement with hypothesis; O, incongruity with hypothesis; —, no results

and that the reproducibility of results with 1 in wide sample was less than with the 3 in sample.

MELT FLOW AND STRESS DISTRIBUTION

One of the problems in a comparative study of techniques for measurement of orientation stress is that the stress intensity and the stress distribution over the plaque is unknown.

It has been proposed that the orientation stress gradient across the specimen can be divided into three parts: (a) a very thin essentially unoriented layer near or at the surface; (b) a highly oriented layer at the subsurface; (c) the bulk of the specimen with a varying degree of orientation. However, this is a general picture only, and the profile will vary considerably with processing conditions. Orientation is generally considered to be a function of locality; in the case of simple symmetric moulds for example, it is a function of the distance from the gate. Even this is a simplification and as the following study has shown flow into the mould is more complex than revealed in most published work.

The filling of the mould and the melt flow pattern can be studied by a short-shot technique, by increasing the feed setting (i.e. the screw stroke) on the machine and by the use of mixed feeds, i.e. by admixing a few granules of polypropylene with polystyrene, in the hopper. There are, according to Smith and Stevens<sup>8</sup>, deficiencies in such procedures. For example, measurement of heat history is difficult; this is important in assessing internal relaxation and the extent of crystallization, for those materials which crySTALLIZE. Both techniques were used, the results from the short-shot technique are shown in Figure 20 and the flow pattern with mixed feeds is shown in Figure 21.

Figure 20 shows that with polystyrene the two cavities of the mould are not filled at the same rate, the A cavity being filled slightly faster than the B cavity. The difference in length is approximately 3-4% for nearly full shot. This is in contrast to what is expected since the A cavity is the one which is cooled first.

The following mechanism for mould filling is proposed on the basis of these filling patterns. The pressure difference between the screw tip and the cavity causes hot melt to be forced from the sprue via the runner and gate into the cavity. The pressure gradient is at a maximum in the nozzle and decreases to zero at the wavefront. The shearing stress causing orientation at any point is directly proportional to this gradient. However, it must be remembered that orientation in a moulding is a composite of two competing effects; orientation induced by shearing forces during flow and subsequent molecular relaxation caused by Brownian motion when the shear forces are decreased. Superimposed on both these effects is the point temperature history of the moulding. These factors result in a rather complex series of inter-related events, the order and nature of which must be deduced from the evidence offered by the moulding.

Figure 20 shows that the melt fills the sprue, sprue puller and runner evenly. As the number designating the flow front increases it signifies an increased feed setting. The melt then contacts the centre of the gate, where, mainly owing to the position of the cooling channels (see Figure 10) it freezes instantaneously restricting flow through that part of the gate (see Figure 20). As the gate is restricted the material then fills the runner com-

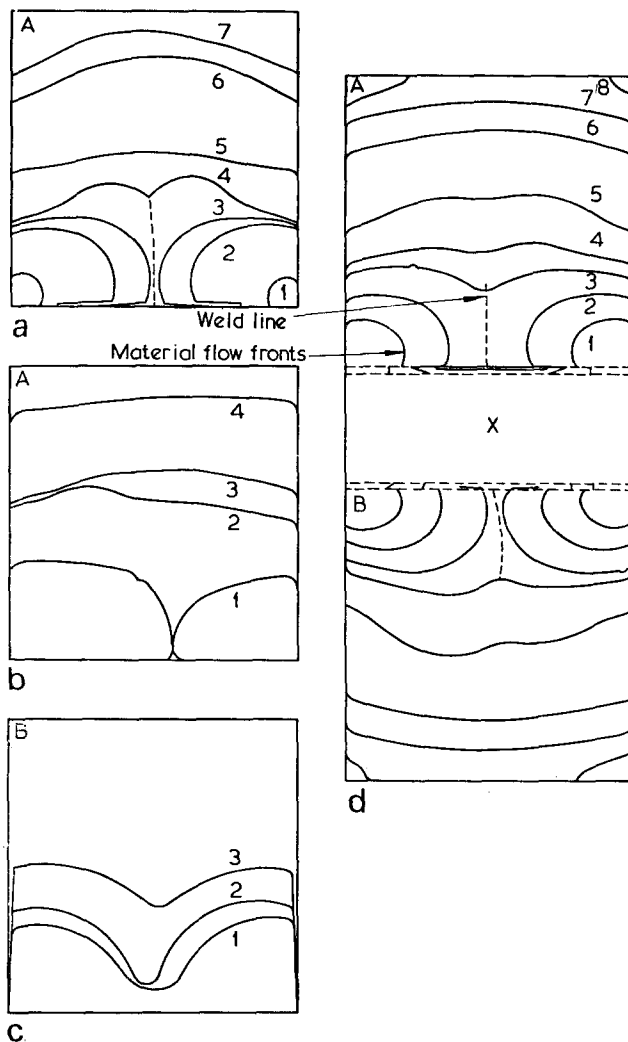


Figure 20 Cavity fill-out patterns. (a) ABS; (b) polysulphone; (c) polypropylene; (d) polystyrene (whole plaque)

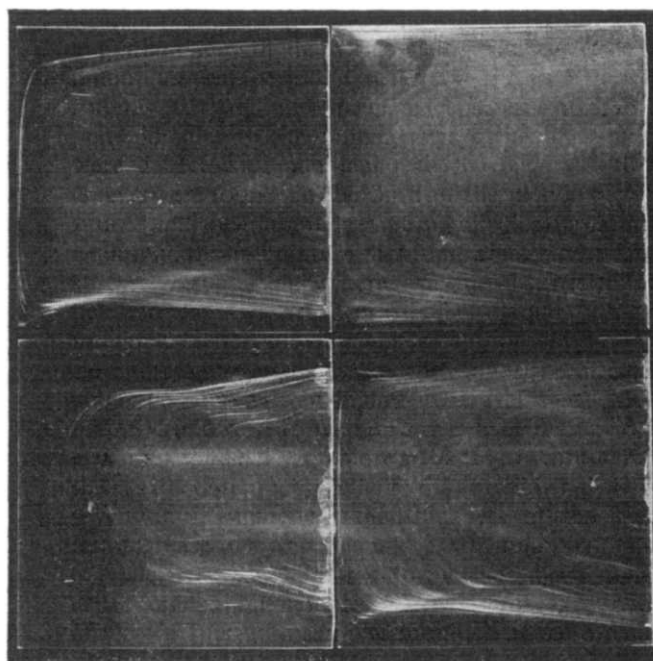


Figure 21 Flow studies with mixed feeds

pletely. The cavity then starts to fill from the corners of the gate which, despite its remote distance from the sprue, gives less resistance to the flow because in this part of the gate the material has had less time for cooling. The flow fronts widen out from the corners of each cavity as more material is forced into the mould until after a short distance they merge and weld together in the centre. The central portion of the gate is not used at this stage and more than half of the cavity is filled before the whole length of the gate is used. Welding of the two flow fronts leads probably to a thawing of the middle third of the gate.

As stage 6 shows, a circular flow front develops which probably means that an equilibrium temperature has been reached. From this stage filling takes place in the expected way with a normal plug-type flow.

Birefringence at this stage produces a 'bowl-type' pattern (Figure 13) similar to the stress-corrosion pattern for a full shot (Figure 17). With increasing shot-weight the birefringence pattern changes to the 'plug-type' pattern. This observation could indicate that the surface freezes very quickly and that the bulk orientation as shown by birefringence is built-up at a later stage.

The birefringence pattern gave some evidence of departure from parallel flow near the gate. This may introduce a degree of biaxial orientation with an increase in strength in the transverse to flow direction in the gate region. In fact only samples moulded at the highest injection pressure had a greater tensile strength across the plaque near the gate.

The above mentioned mechanism for filling only applies to the polystyrene tests. With polysulphone for example, solvent stress crazing and birefringence gave evidence that an almost parallel flow pattern developed from the gate. Nearly all the cracks developed in the stress crazing test in a direction at right angles to the gate. Little variation in relaxation force was found with polysulphone, probably because the material is not sensitive to shear.

It was observed from the solvent stress crazing test and in part from hot-wire tests that increasing injection pressure gave increasing surface orientation. There also seemed to be a difference in cracking between the two surfaces of the sample, the surface towards the injection side having the least number of cracks. This surface should be cooled more since it is closer to the cooling channels. In addition less shear probably occurs in this part of the mould as the gate is restricted on the opposite side. Orientation will become more marked when there is a diminution of selection.

By comparing tensile strength and orientation stress for 1 in samples cut from the side and the centre of the plaque it was found that a low injection pressure led to highest orientation in the centre and the reverse occurred with a high injection pressure (see Table 13). This is thought to be due to a variation in viscosity during filling. With a higher injection pressure, flow rate and shear rate will increase. If the increase in shear rate is higher than the decrease in viscosity, then the orientation will increase with increasing shear rate. With increasing injection pressure the viscosity in the centre will decrease more than the shear rate increment and give less orientation. At the edges the shear rate increases faster than the rate of decrease in viscosity because the melt is already cooled. This will give higher orientation. The pattern obtained with mixed feeds did not support any of the

above mentioned observations, although it is believed that areas with only a small distance between subsequent lines represents those parts of the moulding with high orientation. It was found that the pattern appears in the bulk of the specimen only and indicated a very symmetrical 'plug-type' filling.

The relaxation force per unit square area has been used as a means of comparison in the study. By doing this the influence of a variation in thickness is eliminated. An increase in thickness, however, can increase relaxation and if there is such an effect it will appear more pronounced when the force is divided by the thickness of the sample. Polysulphone showed this clearly. Less than 3% variation was found in relaxation force but this was indicative of more than 23% in stress owing to the abnormal thickness of samples moulded at the highest pressure. This effect was less noticeable with the other materials examined.

## CONCLUSIONS

A test apparatus and technique was developed for the rapid determination of moulded-in stresses in flat injection moulded samples in either opaque or transparent thermoplastics. The method was more applicable to production quality control purposes than the other methods examined for the reasons discussed. It provided an overall numerical value of the frozen-in stresses in injection mouldings without preferentially determining certain components of frozen-in stress. For example, stress crazing and hot wire tests determined the stresses, essentially orientation, in the skin and immediate sub-surface of mouldings. A measure of the bulk stresses may be more realistic since it is only partly understood what the contribution and interaction of external and internal effects is towards dimensional and environmental stability. In support of this it was found that a considerably more complex stress pattern existed in the relatively simple plaque mould than was expected. This was clearly demonstrated by the mould filling experiments and the evidence revealed by the different methods which preferentially measured either internal or external stresses. Bulk stress, as measured by the RAPRA technique, decreased with increasing injection pressure or melt temperature<sup>20</sup> in the sample. On the other hand, surface orientation as measured by hot wire tests increased with increasing injection pressure and the surface of the plaque produced by the moving half of the tool was more oriented than the injection side.

The distribution of the stress pattern drew attention to the importance of the arrangement of cooling channels in the tool so as to provide for uniform cooling of the melt in the cavity, the effects of uneven and differential mould surface temperature and the influence of gate dimensions on the sealing point of the mould cavity.

Good correlation was obtained between frozen-in stress measured by the RAPRA method and tensile strength measurements.

## REFERENCES

- 1 Scott, K. A., Humpidge, R. T., Whisson, R. R. and Harbert, F. C. *RAPRA Res. Rep.* 170 1968 (May)
- 2 Whisson, R. R. and Scott, K. A. *Plastics and Polymers* 1970, 38, 251
- 3 Jensen, M. and Whisson, R. R. *RAPRA Tech. Rev.* (unpublished)

*Frozen-in stresses in thermoplastic injection mouldings: M. Jensen and R. R. Whisson*

- 4 BS 3126: 1959, Appendix F, British Standards Institution, London
- 5 Whisson, R. R. *RAPRA Bull.* 22 1968, p 82
- 6 Hathaway, C. T. *SPE Journal* 1961, **17**, 567
- 7 Pokigo, F. J. and Flodman, R. E. *SPE Journal* 1963, **19**, 289
- 8 Ballman, R. L. and Toor, H. L. *SPE Antec.* 1950, **5**, Paper 51, p 1
- 9 Treloar, L. R. G. *Trans. Faraday Soc.* 1941, **37**, 84
- 10 van Leeuwen, J. 'Control of plastics processing' in *Conf. Processing Plastics to Polymers, Amsterdam* 1966 (October)
- 11 Atkinson, E. B., Brooks, P. B., Lewis, T. D., Smith, R. R. and White, K. A. *Trans. J. Plast. Inst.* 1967, **35**, 549
- 12 Smith, R. R. and Stevens, M. J. 'Limitations of plastics moulding process: non-uniformity in injection mouldings', in *Proc. Polym. Symp. Salford Univ.* Institution of Chemical Engineers, London, 1970
- 13 Stuart, H. A., Markowski, G. and Jeschke, D. *Kunststoffe* 1964, **54**, 618
- 14 Hsiao, C. C. and Sauer, J. A. *J. Appl. Phys.* 1950, **21**, 1071
- 15 Ziegler, E. E. *SPE Journal* 1954, **10**, 12
- 16 Reid, D. R. and Horsley, R. A. *Br. Plast.* 1959, **33**, 156
- 17 Plastics Materials Guide (supplement to *Br. Plast.*) 1970, p 112
- 18 Jackson, G. B. and Ballman, R. L. *SPE Journal* 1960, **16**, 1150
- 19 Spencer, R. S. and Gilmore, G. D. *J. Colloid Sci.* 1951, **6**, 118
- 20 Whisson, R. R. *RAPRA Res. Rep.* 188 1971 (January)

# Stability of wedge and channel flow of highly viscous and elastic liquids

J. R. A. Pearson\* and T. J. F. Pickup†

Department of Chemical Engineering, University of Cambridge, Pembroke Street,  
Cambridge CB2 3RA, UK  
(Received 23 November 1972)

Experiments are reported on the flow of a highly elasticoviscous polymer solution into a slit, in which instability was observed. This instability was manifest as an irregularity in the output along the slit and as an unsteadiness in the extentional flow into the slit. The onset of irregular flow was well-defined, and its intensity increased with flow rate. Similar results were noted for axial flow into a tube. Simplified linearized stability analyses bearing on the observed flow are given briefly in Appendixes 2 and 3. It is concluded that existing theories are inadequate to explain the observed phenomena.

## OBSERVATIONS

An experiment was described in an earlier report<sup>1</sup> in which the flow of a highly elasticoviscous polymer solution (Separan AP30 in 50:50 glycerol-water mixture) into a slit was observed. The flow geometry is shown diagrammatically in *Figures 1* and *2*. The channel width  $h_0$  was fixed; the slit width  $h_s$  and the wedge entry angle  $\alpha$  could be varied. The channel breadth (in the  $z$  direction) was  $10h_0$  and it was assumed that along the central ( $x, y$ ) plane, a two-dimensional ( $u_x, u_y$ ) flow would arise. The channel length (upstream of the slit) was taken to be infinite and so a fully developed viscometric channel flow was established. The slit length  $l_s$  was not varied. The object of the experiment was primarily to investigate the kinematics and dynamics of the slit-entry flow, and this is described in detail by Pickup<sup>1,2</sup>. We are concerned here with the instability of this flow.

The results were briefly:

(1) At very slow flow rates, all fluid within the channel flowed steadily out of the slit; there were no closed streamlines.

(2) At slightly higher flow rates, two steady recirculating vortices, an upper ( $4^U$ ) and a lower ( $4^L$ ), became established. The oncoming viscometric (simple shear) flow in region 1 went through a surprisingly short transition region 2, short compared with  $h_0$  (i.e. only a few mm long), level with the vortex attachment lines  $V^U$  and  $V^L$ , and entered a region 3 of essentially pure shear. In this last region the downstream velocity could conveniently be regarded as a function of  $x$  only,  $u(x)$ , and was reasonably well approximated by the functional form:

$$u = u_0 \exp(\beta x) \quad (1)$$

\* Present address: Department of Chemical Engineering, Imperial College of Science and Technology, London SW7, UK.

† Present address: Central Research Laboratories, Dupont of Canada, Kingston, Ontario, Canada.

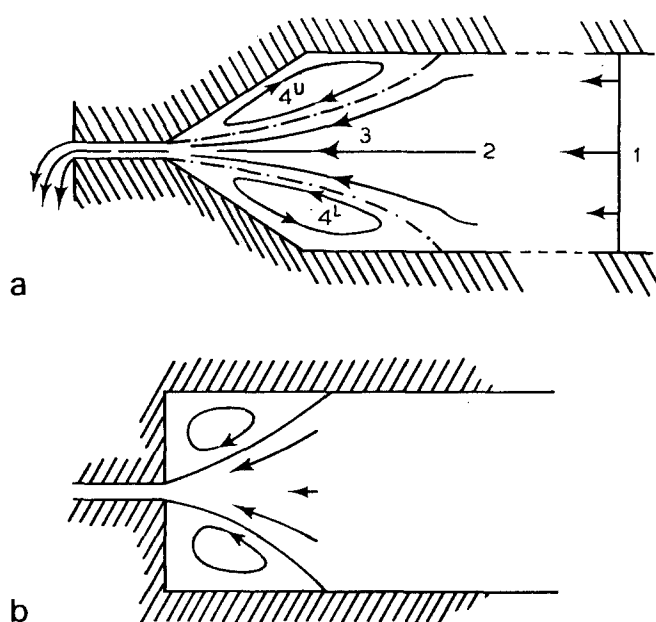


Figure 1 Flow geometry diagram for a highly elasticoviscous polymer solution (Separan AP30 in 50:50 glycerol-water mixture) flowing into a slit. (a) Wedge entry; (b) flat entry

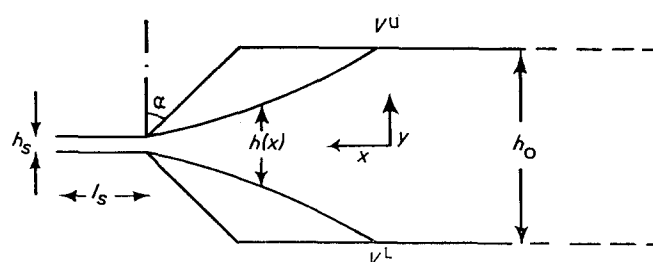


Figure 2 Coordinate system and dimensions for the flow of a highly elasticoviscous polymer solution (Separan AP30 in 50:50 glycerol-water mixture) into a slit

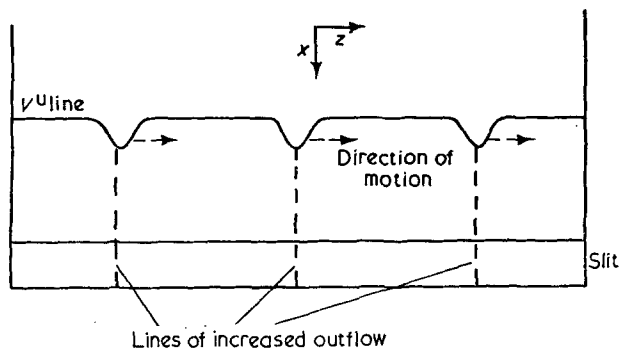


Figure 3 Non-uniformity of two-dimensional flow of a highly elasticoviscous polymer solution (Separan AP30 in 50:50 glycerol-water mixture) into a slit at high flow rate

where clearly

$$uh = u_0 h_0 = u_s h_s \quad (2)$$

Hence:

$$h = h_0 \exp(-\beta x) \quad (3)$$

The origin for  $x$  is located near the transition zone and

$$h_s = h_0 \exp(-\beta x_s) \quad (4)$$

$\beta$  was found to be a function of  $\alpha$ ,  $u_0$  and  $h_s$ , as well as of polymer concentration. The length of the vortices increased with flow rate.

(3) At still higher flow rates, the flow became asymmetric and unsteady. This was manifest in two ways. Viewed in the  $(x, y)$  plane, either the upper or the lower vortices grew in size and the central elongational zone 3 consequently moved down or up; if the flow rate was further increased, this asymmetry fluctuated vigorously, the upper and lower vortices alternately growing and decaying, with the elongational zone flapping up and down and the attachment lines  $V^U$  and  $V^L$  moving back and forth. Viewed from above in the  $(x, z)$  plane, this apparently two-dimensional flow pattern was seen to be non-uniform. Figure 3 shows diagrammatically how, at fairly regular but well spaced intervals, the upper attachment line curved sharply and approached the slit. These stations corresponded with a local increase in flow rate through the slit; these irregularities moved slowly sideways (in the  $z$ -direction) across the channel.

These flow irregularities set in at a well defined value of flow rate, for any given fluid and any given geometry, and increased in intensity with increase in flow rate. Below the critical flow rate, untoward disturbances were damped out; above the critical flow rate, steady flow was essentially unattainable except for an initial period of up to a minute or so.

Similar and evidently related effects were noted for entry flow from a wide circular-cylindrical tube into a much smaller diameter coaxial tube, using various entry cone angles. At very low flow rates, a steady efflux without recirculation was obtained. As the flow rate was increased, a toroidal vortex formed; however, this was scarcely ever axisymmetric or stable, the upstream attachment line showing one section significantly closer to the exit tube. This helical irregularity processed slowly around the tube, and intensified with increase in flow-rate.

## DISCUSSION

The steady two-dimensional flow with recirculating regions has been carefully discussed and analysed by

Pickup<sup>1,2</sup>. The irregular and unsteady flow reported above was only investigated qualitatively<sup>2</sup>. One of the reasons for this was the very complex flow pattern involved; another was the considerable difficulty encountered in trying to describe at all fully the rheological properties of the fluids used. These properties are relevant when complex patterns of flow arise. The phenomenon itself was dependent on fluid properties, on flow rate and on channel geometry, i.e. on 2 geometrical, one operating and an indefinite number of physical parameters. Some values of these parameters are given in Appendix 1.

We do not believe that a simple criterion for the onset of disturbances to the steady flow is likely to exist and we seek here to discuss some of the factors and mechanisms that appeared to be relevant.

First, we note that the Reynolds number of the flow was low, and that rheological (elasticoviscous) forces dominated. Next, we note that the polymer solution was sufficiently concentrated for interactions between polymer molecules to be expected. This interpretation is consistent with the strongly shear-dependent viscosity, and the high first and second normal-stress differences observed in simple shear flow; also with the very high elongational viscosity measured in pure shear.

The tensile stresses developed in the elongational zone 3 dominate the dynamics of the entry flow to such an extent that the vortex flow can to first order be taken as inviscid. This yields a basically free-boundary model for the rapidly elongating zone, with the vortices acting rather as lubricating layers, particularly when  $\alpha$  is relatively large and the vortices are thin. A stability and sensitivity analysis for a completely free extending sheet of Newtonian liquid is given by Pickup<sup>2</sup> and more exhaustively by Yeow<sup>3</sup>; an outline is given in Appendix 2. These results cannot be applied directly, because the material in question here is demonstrably not Newtonian. However, the stability and sensitivity results obtained suggest strongly that rapidly extending sheets of fluid are prone to gross amplification of minor entry disturbances and, when extension rates and inlet or outlet boundary conditions are so conducive, total breakdown of the symmetric flow on an infinitesimal disturbance theory may be expected; in practice the latter situation would lead to a vigorous secondary flow, whether steady or unsteady.

The situation encountered in these experiments differs from the Pickup-Yeow model in various respects.

(1) The material in the vortices is essentially incompressible and so the consequent constraint on vortex volume must introduce an additional factor in the stability mechanism. In particular, it can lead to a change of position of the attachment lines  $V^U$  or  $V^L$  and so to a variation in the input plane (taken to be  $x=0$  in the steady flow); also, if there is a fluctuation in  $h$  at the output slit,  $x=x_s$ , continuity would require excess fluid arriving in zone 3 to displace the vortices, or alternatively fluid from the vortices 4 to flow into the slit. Both of these effects were observed.

(2) The material in the vortices is in a different structural state to the fluid reaching the slit in zone 3, i.e. its instantaneous rheological behaviour is different, because it has suffered a different deformation (or stress) history. This in turn means that a minor change in flow pattern at the slit entry could lead to a large change in stress distribution and hence trigger off a



major change in flow and stress patterns in the whole of the entry flow. This is particularly true if the material displays a significant elastic response to sudden imposition of tensile stress, followed by a rapid increase in tensile viscosity, as appears to be the case with this and many other polymeric fluids.

(3) The flow in the transition zone and in the slit do not provide fixed boundary conditions, in that they cannot be specified independently of the entry flow.

Another point is that, although the stresses in the vortices are relatively small compared to those in region 3, they are nevertheless anything but isotropic. At the shear rates involved<sup>2</sup> difference-of-normal-stresses are so large that the flat vortex flow might itself be unstable to small disturbances, according to the predictions of Giesekus<sup>4</sup> and Bhatnagar and Giesekus<sup>5</sup>. Thus the source of observed fluctuations both in the  $(x, y)$  and in the  $(x, z)$  planes might be within the vortices  $4^U$  and  $4^L$ .

Lastly, there is the question of what happens to inlet flow fluctuations as they pass through the slit along its length  $l_s$ . Will they amplify, decay or propagate without change of form? Certainly non-uniformities in output as a function of the coordinate  $z$ , measured across the mean flow direction, were observed at the output of the whole apparatus. Several earlier authors have sought a cause for instability within the slit itself; they have so far restricted themselves to fully developed flow and not to any interaction with the inlet flow. First there are the results of Bhatnagar and Giesekus<sup>5</sup> mentioned earlier which have considered disturbances of the form  $\exp(i\nu z)$ ; also those of Pearson and Petrie<sup>6,7</sup> and Porteous and Denn<sup>8</sup> which considered disturbances of the form  $\exp(i\lambda x)$ ; they are not mutually exclusive. All authors are agreed that, in certain circumstances, instabilities caused by elasticoviscous forces alone could lead to a breakdown of uniform two-dimensional flow.

In Appendix 3, we consider a very simple model to try to analyse the stability of flow in the slit of two distinct fluids. These have been chosen to represent very crudely a central layer of fluid entering from the elongation zone and two boundary layers of fluid entering from the vortex zones; for simplicity they are taken to have constant Newtonian viscosity and not to mix across a separating interface. It will be seen that the approximation relates to a short fast flow in the slit, in that relaxation effects are neglected. Two-dimensional linearized perturbations in the  $(x, y)$  plane only were considered. The results are that simple sinusoidal disturbances, whether varicose or sinuous, propagate downstream without change of form; the phase velocity is a function of frequency and so a general disturbance could be expected to change shape. All such sinusoidal disturbances are essentially neutrally stable. They are therefore expected neither to cause nor to suppress inlet flow instabilities. We have not studied in detail either the effect of  $z$ -direction variations or of more subtle viscoelastic properties.

## CONCLUSIONS

(A) Isothermal flows of highly elastic polymer solutions can exhibit instabilities of the type long known as elastic turbulence, or melt flow instability.

(B) These instabilities are clearly fluid mechanical and

viscous. Although catastrophic internal material failure may be a cause of some observed 'melt fracture', although shear waves involving large acceleration forces<sup>9</sup> may sometimes be relevant and although heat generation or heat transfer effects can lead to instability, a wide range of non-linear effects, including unsteadiness and non-uniformity, must undoubtedly be due to fluid rheology alone.

(C) Existing theories are insufficient to explain the observed phenomena in rational quantitative mechanical terms.

## REFERENCES

- Pickup, T. J. F. *Can. J. Chem. Eng.* 1973, submitted
- Pickup, T. J. F. *PhD Thesis* University of Cambridge, 1970
- Yeow, Y. L. *PhD Thesis* University of Cambridge, 1972
- Giesekus, H. *Prog. Heat Mass Transfer* 1972, 5, 187
- Bhatnagar, R. K. and Giesekus, H. *Rheol. Acta* 1970, 9, 53, 412
- Pearson, J. R. A. and Petrie, C. J. S. *Proc. 4th Int. Congr. Rheol.* 1965, Interscience, New York, Vol 3, p 265
- Pearson, J. R. A. and Petrie, C. J. S. 'Deformation and Flow in High Polymer Systems' (Eds R. E. Wetton and R. W. Whorlow), 1967, Macmillan, London, p 163
- Porteous, K. C. and Denn, M. M. *Trans. Soc. Rheol.* 1972, 16, 295, 309
- Coleman, B. D. and Gurtin, M. E. *J. Fluid Mech.* 1968, 33, 165

## APPENDIX 1

### Equipment geometry

Channel breadth, 254 mm
Channel width, $h_0$ , 25.4 mm
Slit width, $h_s$ , 1.34–2.57 mm
Slit length, $l_s$ , 25.4 mm
Die entry angle, $\alpha$ , 0°, 30°

### Fluid properties

A solution of 0.2, 0.3 or 0.4% Separan AP30 in a mixture of glycerol and water. Specific gravity=1.27. Typical rheogoniometric data, viscometric flow, 0.3% solution.

Shear rate (sec <sup>-1</sup> )	Shear stress (N/m <sup>2</sup> )	1st normal stress difference (N/m <sup>2</sup> )	2nd normal stress difference (N/m <sup>2</sup> )
1	0.9	—	—
10	5	-8	~10
100	10	-90	—

Estimated relaxation time, 0.1 sec at 10 sec<sup>-1</sup>

Typical elongational data, pure strain, 0.3% solution:

Elongation rate, 30 sec<sup>-1</sup>

Elongation stress, 200 N/m<sup>2</sup>

For further details, see Pickup<sup>2</sup>.

### Kinematic data

Fluid conc. (%)	Slit width, $h_s$ (mm)	$\alpha$ (rad)	$\beta$ (m <sup>-1</sup> )	$u_s h_s$ (mm <sup>2</sup> /sec)	Elongational rates (sec <sup>-1</sup> )	
					$x=0$	$x=x_s$
0.2	1.34	0	170	240	1.4	29.4
0.2	1.45	0	150	320	1.6	28.2
0.2	2.57	0	250	680	6.0	60.0
0.3	1.45	0	135	520	2.7	51.0
0.3	1.45	$\pi/6$	160	440	2.9	52.0
0.4	1.34	0	140	275	1.7	31.0
0.4	1.45	0	140	500	2.9	46.0
0.4	2.57	0	250	1000	10.3	82.0

Conditions just before flow became unstable for various cases observed

Typical Reynolds number in flow field based on a volume flux of 500 mm<sup>2</sup>/sec, a viscosity of 1 N sec/m<sup>2</sup> and a density of 1.27 × 10<sup>3</sup> N sec/m<sup>4</sup> is 0.63.

APPENDIX 2

Stability analysis for extending sheet

Consider the flow in region 3. Take obvious length and velocity scales (with associated variables) so that the undisturbed flow pattern is given by:

$$U^{(0)} = (U, V, W)^{(0)} = (e^{\gamma\xi}, -\gamma\gamma e^{\gamma\xi}, 0)$$

$$H^{(0)} = e^{-\gamma\xi}$$

A neutrally stable linearized disturbance, varying sinusoidally in the z (or ζ) direction, can be written:

$$U^{(1)} = [\bar{U}(\xi), \bar{V}(\xi)\eta, i\bar{W}(\xi)]e^{\gamma\xi}\exp(i\Gamma\zeta)$$

$$H^{(1)} = \bar{H}(\xi)e^{-\gamma\xi}\exp(i\Gamma\zeta)$$

where real parts are implied. Continuity requires that:

$$\bar{V} = -\gamma\bar{U} + \bar{U}' + \Gamma\bar{W}$$

We now suppose that the interface between regions 4 and 3 is a material surface, and that the fluid in the vortices exerts merely a constant uniform normal pressure on the material in the extending sheet. We suppose also that γ is small. A mass balance on the slightly disturbed sheet requires that:

$$\frac{\partial}{\partial\xi}(HU) + \frac{\partial}{\partial\xi}(HW) = 0$$

i.e. that

$$\bar{H}' + \bar{U}' - \Gamma\bar{W} = 0$$

A force balance can then be applied to the sheet in the directions ξ and ζ to give:

$$\frac{\partial}{\partial\xi}(HP_{\xi\xi}) + \frac{\partial}{\partial\xi}(HP_{\xi\xi}) = 0$$

and

$$\frac{\partial}{\partial\xi}(HP_{\xi\zeta}) + \frac{\partial}{\partial\xi}(HP_{\xi\zeta}) = 0$$

Here P<sub>ξξ</sub> is the normal stress (above that existing at the interface) and P<sub>ξζ</sub> the shear stress (in the ζ direction) across planes ξ = constant. Similarly for P<sub>ζξ</sub>. If we take μ<sub>A</sub> to be the apparent Newtonian viscosity of the fluid then

$$P_{\xi\xi} = 2\mu_A(\partial U/\partial\xi - \partial V/\partial\eta); P_{\xi\zeta} = \mu_A(\partial U/\partial\zeta + \partial W/\partial\xi);$$

$$P_{\zeta\xi} = 2\mu_A(\partial W/\partial\xi - \partial V/\partial\eta)$$

Thus we obtain, using the relation given above for V̄:

$$4\gamma\bar{H}' + 4\bar{U}'' + 4\gamma\bar{U}' - \Gamma^2\bar{U} - 3\Gamma\bar{W}' - \Gamma\gamma\bar{W} = 0$$

and

$$2\Gamma\gamma\bar{H} + 3\Gamma\bar{U}' + \bar{W}'' + \gamma\bar{W}' + 2\Gamma(\gamma - 2\Gamma)\bar{W} = 0$$

We write q = γ/Γ and change to a new variable X = Γξ. The set of equations obtained have 'constant' coefficients (dependent only on the parameter q). Thus the general solution will be of the form:

$$(\bar{U}, \bar{W}, \bar{H}) = \sum_{i=1}^5 (A_i, B_i, C_i)\exp(p_i X)$$

where the (A<sub>i</sub>, B<sub>i</sub>, C<sub>i</sub>) are arbitrary and the p<sub>i</sub>(q) are solutions of the equation:

$$4p^5 + 4qp^4 - 8p^3 - 2qp^2 + 4p - 2q = 0$$

i.e. p<sub>1</sub> = 1, p<sub>2</sub> = -1 and p<sub>3</sub>, p<sub>4</sub> and p<sub>5</sub> given by the roots of:

$$2p^3 + 2qp^2 - 2p + q = 0$$

(Minor complications arise if any two of the roots are equal. Complex roots can be accommodated by treating all variables as complex.)

The (A<sub>i</sub>, B<sub>i</sub>, C<sub>i</sub>) are determined by the boundary conditions, to be imposed at 0 and X<sub>s</sub>, of which there must be five. Thus, for example, one of Ū(0), W̄(0), H̄(0), Ū(X<sub>s</sub>), W̄(X<sub>s</sub>), H̄(X<sub>s</sub>) is predicted by the solution given above if the other 5 are prescribed. The parameter defining the undisturbed flow may be taken as qX<sub>s</sub> = ln(h<sub>0</sub>/h<sub>s</sub>); the parameter defining the wavelength of the disturbance is X<sub>s</sub>.

Two types of solution may be sought. A true stability analysis treats the problem as an eigen value problem, with X<sub>s</sub> (or qX<sub>s</sub>) as the eigen value, and homogeneous boundary conditions applied at ξ = 0 and X<sub>s</sub>. This corresponds to a situation where no disturbance is imposed from outside, yet an arbitrarily large finite disturbance Ū, W̄, H̄, can exist within the flow field. Yeow<sup>3</sup> has concentrated on this aspect of the solution,

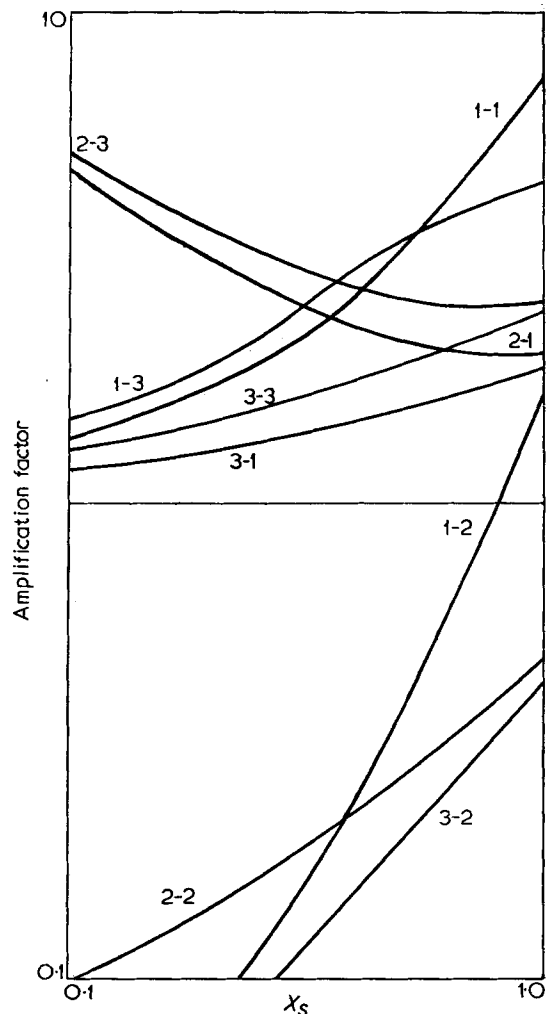


Figure 4 Sensitivity analysis for elongating sheet. Curves are labelled i-j where i refers to initial disturbance and j to consequent disturbance at slit. 1, Ū; 2, W̄; 3, H̄; qX<sub>s</sub> = 2.9

for the case where  $\bar{U}(0) = \bar{W}(0) = \bar{H}(0) = \bar{W}(X_s) = 0$ , and either  $\bar{U}(X_s) = 0$  or the total tension at  $X_s$  is fixed. The main result is that solutions exist only for values of  $qX_s > 3.0$  and that the first to appear is for the rather special case of  $\Gamma = 0$ . We have not investigated the situation fully for other boundary conditions, such as  $\bar{H}(X_s) = 0$ , which would have relevance in this case.

A sensitivity analysis may also be carried out, whereby one of  $\bar{U}(0)$ ,  $\bar{W}(0)$  or  $\bar{H}(0)$  is put equal to unity and one of  $\bar{U}(X_s)$ ,  $\bar{W}(X_s)$  or  $\bar{H}(X_s)$  is not constrained; the rest are put equal to zero. The value of the unconstrained quantity is called the amplification factor. Figure 4 shows predictions for the amplification factor, for a choice of  $qX_s = 2.9$  corresponding to one of the flows most carefully observed for instability, and values of  $X_s$  lying in the range observed. It will be noted that amplification ( $> 1$ ) is predicted; however, it was clear that the most sensitive disturbances arose for values of  $X_s > 2$ , and so there was no direct correspondence between this rather crude theory and observation, as might be expected, because no account has been taken of the interaction between the elongating flow and any of the other flow zones.

APPENDIX 3

Stability analysis for channel flow of two Newtonian fluids

Figure 5 shows the geometry for the undisturbed flow, with the interfaces shown as full lines. This is described by:

$$\left. \begin{aligned} U_{0+} &= \frac{G}{2\mu N}(y^2 - 1) & y_0 \leq |y| \leq 1 \\ U_{0-} &= \frac{G}{2\mu}(y^2 - y_0^2) + \frac{G}{2\mu N}(y_0^2 - 1) & |y| \leq y_0 \end{aligned} \right\} \quad (A1)$$

where  $\mu$  is the viscosity of the fluid in the central layer  $|y| < y_0$  and  $\mu N$  the viscosity in the outer layer  $y_0 \leq |y| \leq 1$ ;  $G$  is the pressure gradient.

A small perturbation for the region  $y > 0$  is introduced as:

$$\left. \begin{aligned} U &= U_0 - \epsilon \text{Re}\{if''(y)\exp[i\lambda(x - ct)]\} \\ V &= \epsilon \text{Re}\{\lambda f(y)\exp[i\lambda(x - ct)]\} \\ \eta &= y_0 + \epsilon \text{Re}\{i\exp[i\lambda(x - ct)]\} \end{aligned} \right\} \quad (A2)$$

where  $\epsilon \ll 1$  and  $\lambda$ ,  $c$  and  $f(y)$  may be complex. The disturbance has been chosen to satisfy continuity, and involves a wavenumber  $\lambda$  and wave speed  $c$ .  $\eta$  is the position of the interface and is shown by broken lines in Figure 5, for two forms of disturbance, sinuous and varicose.

Taking the Reynolds number to be low and therefore neglecting inertia forces, the equations of motion become:

$$\frac{\partial P}{\partial x} = \mu N_{\pm} \left( \frac{\partial^2 U}{\partial x^2} + \frac{\partial^2 U}{\partial y^2} \right); \quad \frac{\partial P}{\partial y} = \mu N_{\pm} \left( \frac{\partial^2 V}{\partial x^2} + \frac{\partial^2 V}{\partial y^2} \right)$$

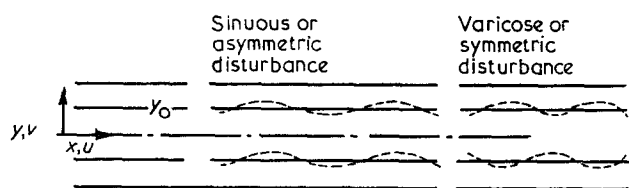


Figure 5 Geometry and coordinate system for two-fluid channel flow—schematic form of sinuous and varicose disturbances

where  $N_+ = N$  for  $y > \eta$  and  $N_- = 1$  for  $y < \eta$ . On eliminating  $P$ , the equation for  $f$  becomes:

$$f'''' - 2\lambda^2 f'' + \lambda^4 f = 0 \quad (A3)$$

This has a general solution:

$$f_{\pm}(y) = A_{\pm} \sinh \lambda y + B_{\pm} \cosh \lambda y + C_{\pm} y \sinh \lambda y + D_{\pm} y \cosh \lambda y \quad (A4)$$

where the subscripts + and - refer to regions  $y > \eta$  and  $y < \eta$  respectively.

The boundary conditions are:

(i) from no slip at  $y = 1$ ,

$$f_+(1) = f'_+(1) = 0 \quad (A5i)$$

(ii) for sinuous disturbance at  $y = 0$ ,

$$f'_-(0) = f''_-(0) = 0 \quad (A5iis)$$

or for varicose disturbance at  $y = 0$ ,

$$f_-(0) = f''_-(0) = 0 \quad (A5iiv)$$

(iii) from continuity of velocity at the interface  $y = \eta$ , i.e.  $V_+(\eta) = V_-(\eta)$ ,  $U_+(\eta) = U_-(\eta)$ , and expanding the upper and lower solutions about  $y = y_0$  by Taylor series,

$$f_+(y_0) = f_-(y_0)$$

$$U'_{0+}(y_0) - f'_+(y_0) = U'_{0-}(y_0) - f'_-(y_0) \quad (A5iii)$$

(iv) from continuity of stress at the interface  $y = \eta$ , i.e. of

$$\mu N_{\pm} [(\partial U_{\pm} / \partial y) + (\partial V_{\pm} / \partial x)]$$

and of

$$\mu N_{\pm} [(\partial^2 U_{\pm} / \partial y^2) + (\partial^2 U_{\pm} / \partial x^2)]$$

using Taylor expansions about  $y = y_0$ ,

$$N \{f''_+(y_0) - \lambda^2 f_+(y_0)\} = f''_-(y_0) - \lambda^2 f_-(y_0) \quad (A5iv)$$

$$N \{\lambda^2 f'_+(y_0) - f''_+(y_0)\} = \lambda^2 f'_-(y_0) - f''_-(y_0)$$

Finally, because the interface is a streamline:

$$V = \frac{D\eta}{Dt} = U \frac{\partial \eta}{\partial x} + \frac{\partial \eta}{\partial t}$$

or

$$f_{\pm}(y_0) = U(y_0) - c \quad (A6)$$

Table 1 Values for wave velocity for varicose ( $c_v$ ) and sinuous ( $c_s$ ) disturbances when  $G/\mu = 1$  for various values of  $\lambda$ ,  $N$  and  $y$

$\lambda$	$N$	$y_0$	$c_v$	$c_s$
0.01	0.1	0.2	$-1.1 \times 10^5$	$-4.0 \times 10$
0.02	0.1	0.2	$-1.4 \times 10^4$	$-2.0 \times 10$
0.05	0.1	0.2	$-8.8 \times 10^3$	$-7.8$
0.1	0.1	0.2	$-1.1 \times 10^2$	$-3.6$
0.5	0.1	0.2	1.2	1.3
1.0	0.1	0.2	4.3	3.8
10	0.1	0.2	$4.7 \times 10$	$4.7 \times 10$
0.5	0.1	0.5	$-1.8 \times 10$	$-5.0$
0.5	0.1	0.8	$-1.5 \times 10^2$	$-3.0 \times 10$
0.5	0.5	0.2	$3.5 \times 10^{-1}$	$3.6 \times 10^{-1}$
0.5	0.5	0.5	-1.7	$-2.1 \times 10^{-1}$
0.5	0.5	0.8	$-1.2 \times 10$	-1.5
0.5	2.0	0.2	$1.8 \times 10^{-1}$	$1.6 \times 10^{-1}$
0.5	2.0	0.5	$9.7 \times 10^{-1}$	$2.4 \times 10^{-1}$
0.5	2.0	0.8	3.1	$3.4 \times 10^{-1}$
0.5	10	0.2	$1.3 \times 10^{-1}$	$5.9 \times 10^{-2}$
0.5	10	0.5	$8.7 \times 10^{-1}$	$9.5 \times 10^{-2}$
0.5	10	0.8	1.5	$1.3 \times 10^{-1}$

The undisturbed solution (A1) specified  $y_0$  and  $N$ . The small perturbation in (A2) involves  $\lambda$  and  $c$ ; of these  $\lambda$  may be chosen arbitrarily. The general solution (A4) of equation (A3) has eight parameters  $A_{\pm}$ ,  $B_{\pm}$ ,  $C_{\pm}$ ,  $D_{\pm}$  to be determined along with  $c$  as functions of  $y_0$ ,  $N$  and  $\lambda$  by use of the nine boundary conditions (A5) and (A6). Results were obtained by numerical computation.

For  $\gamma$  real,  $c$  will clearly be real. *Table 1* shows some typical values obtained; these correspond to neutrally stable disturbances in a very long channel. It will be seen that  $c$  is proportional to  $U(y_0)$  and, for fixed

$(N, y_0)$ , is a function of  $\lambda$ . Waves may move upstream or downstream.

Detailed results for  $\lambda$  complex ( $=\lambda_R+i\lambda_I$ ) are given by Pickup<sup>2</sup>. The  $\exp(-\lambda_I x)$  factor corresponds, at fixed time, to a spatially decaying or growing component, and so would be relevant only in a tube of finite length. The related factor  $\exp\{(\lambda_I c_R + \lambda_R c_I)t\}$  corresponds, at fixed  $x$ , to a disturbance growing or decaying in time. Careful analysis of the results obtained showed that they could all be related, physically, to the more easily described results for  $\lambda$  real.

# Polymerization studies using modified Ziegler–Natta catalysts: 1. Polymerization of vinyl chloride

R. N. Haszeldine, T. G. Hyde\* and P. J. T. Tait

Department of Chemistry, University of Manchester Institute of Science and Technology, Manchester M60 1QD, UK

(Received 27 November 1972; revised 22 January 1973)

The polymerization of vinyl chloride by a number of modified Ziegler–Natta catalysts has been investigated. The most effective catalyst system is the soluble system prepared from vanadium oxytrichloride, tri-isobutylaluminium, and tetrahydrofuran. All three components are necessary for the formation of an active catalyst. The kinetics of the polymerization of vinyl chloride by this catalyst system has been examined at 30°C, and the dependence of the overall rate of polymerization on the transition halide concentration, aluminium alkyl concentration, monomer concentration and temperature established. Kinetic and copolymerization studies indicate that the polymerization process is not free radical in nature but is similar to that encountered in more conventional Ziegler–Natta systems.

## INTRODUCTION

It is now well established that although Ziegler–Natta catalysts are particularly effective for the polymerization of electron rich monomers, such as  $\alpha$ -olefins and diolefins they are often ineffective when used as catalysts for the polymerization of monomers containing hetero atoms. In particular, there are but few examples of halogen-containing monomers being successfully polymerized by conventional Ziegler–Natta systems. When attempts are made to polymerize monomers such as vinyl chloride<sup>1</sup> and allyl chloride<sup>2</sup>, using the catalyst systems  $\text{TiCl}_4/\text{AlEt}_3$  and  $\text{TiCl}_3/\text{AlEt}_2\text{Cl}$  respectively, evolution of hydrogen chloride takes place, and little polymer can be isolated. Halogenated olefins can, however, be polymerized by means of modified Ziegler–Natta catalysts, and a considerable number of these modified systems have been reported in the literature.

Suitable modification of a Ziegler–Natta catalyst may be achieved by substitution of the transition metal halide by a transition metal alkoxide and replacement of the aluminium alkyl by an aluminium chloro alkyl, alkoxide or chloro alkoxide. Thus, suitable catalysts which can polymerize vinyl chloride have been prepared from  $\text{Et}_2\text{AlOEt}$  and  $\text{VO}(\text{OEt})_3$ ,  $\text{EtAl}(\text{OEt})\text{Cl}$  and  $\text{VO}(\text{C}_5\text{H}_7\text{O}_2)_2$ <sup>3</sup>;  $\text{EtAl}(\text{OEt})\text{Cl}$  and  $\text{BuOTiCl}_3$ <sup>4</sup>;  $\text{EtAlCl}_2$ ,  $\text{Et}_2\text{AlCl}$  or  $\text{AlEt}_3$  and  $\text{Ti}(\text{OBu})_3$ <sup>5</sup>; and  $\text{Al}(\text{iBu})_2\text{Cl}$  and  $\text{Ti}(\text{OBu})_4$ <sup>6</sup>. The catalyst system  $(\text{iBu})\text{Al}(\text{OiBu})\text{Cl}/\text{VO}(\text{C}_5\text{H}_7\text{O}_2)_2$  has been used for the polymerization and copolymerization of vinyl fluoride<sup>7</sup>. The polymerization process, however, in many of these systems has been shown<sup>3, 6, 7</sup> to proceed by a free radical rather than by a co-ordination mechanism.

Ziegler–Natta catalyst systems may also be suitably

modified by the addition of complexing agents such as ethers, esters, ketones, tertiary amines and nitro-aromatics, and these have been used to polymerize vinyl chloride<sup>8–11</sup>.

The aim of the present study is to investigate the possibilities of using Ziegler–Natta type catalysts for the polymerization of vinyl chloride, and to make a detailed study of the overall polymerization process. To achieve this a large number of catalyst systems have been prepared from transition metal compounds, and used in conjunction with alkyls of aluminium and zinc to polymerize vinyl chloride.

## EXPERIMENTAL

### Reagents

*Vinyl chloride.* This monomer was kindly supplied by ICI Ltd, Petrochemical and Polymer Laboratories, Runcorn. The monomer was dried over phosphorous pentoxide, purified by means of trap-to-trap distillation into traps cooled with solid carbon dioxide in ethanol ( $-72^\circ\text{C}$ ), and finally distilled into a trap cooled in liquid nitrogen. The vinyl chloride fraction, collected at  $-72^\circ\text{C}$ , and shown to be pure by infra-red spectroscopy, was used in the polymerization experiments.

*Methyl methacrylate and vinyl acetate.* These monomers were fractionally distilled and dried over anhydrous sodium sulphate.

*Benzene.* The Analar solvent was dried by refluxing over sodium wire for 1 h. The middle fraction was then stored over sodium wire in a dry box.

*Tetrahydrofuran.* The Analar solvent was dried by refluxing over sodium wire for 2 h and was then fractionated. The purified tetrahydrofuran was re-dried and re-fractionated every five days.

\* Present address: Development Department, Industrial Chemicals Division, Ciba-Geigy, Trafford Park, Manchester, UK.

**Vanadium oxytrichloride.** This compound was kindly supplied by Magnesium Elektron Ltd, Clifton Junction, Manchester, and was purified by fractionation under an atmosphere of nitrogen.

**Tri-isobutylaluminium and diethylaluminium chloride.** These alkyls were kindly supplied by Shell Chemical Co. Ltd, Carrington. Analyses for both compounds, before delivery, were given as: Al(iBu)<sub>3</sub>, 89.2%; Al(iBu)<sub>2</sub>H, 7.8%; Al(nBu)<sub>3</sub>, 0.8%; Al(OBu)<sub>3</sub>, 2.2%; and AlEt<sub>2</sub>Cl, 95.2%.

**Di-isopropylzinc.** This alkyl was prepared according to the method of Krug and Tang<sup>12</sup>, and was fractionated before use.

**Polymerization procedure**

All experiments were carried out in either glass vessels or dilatometers<sup>13</sup>. Both the vessels and the dilatometers contained glass enclosed iron stirrers which could be operated magnetically. The catalyst components were introduced into the reaction vessel in a dry box containing a dried atmosphere of nitrogen. Solutions of the catalyst components were prepared in benzene using a dry box. Benzene was added to the dilatometer by means of a syringe, then the solutions of the catalyst components were added in the following order: vanadium oxytrichloride, tetrahydrofuran, tri-isobutylaluminium. The dilatometer was removed from the dry box, attached to the high vacuum line, the contents were frozen down in liquid nitrogen and then degassed, when a known amount of monomer was distilled into the dilatometer. The amount of monomer was determined by allowing the gaseous monomer to expand into a 5 l bulb whose volume was accurately known. After all the monomer had been distilled into the dilatometer, and whilst the contents were still solid, the dilatometer neck was sealed. The dilatometer was then attached to the stirrer and placed in the thermostat bath. The contents of the dilatometer melted and expanded up the capillary tube, the excess flowing into the side arm. A cathetometer reading to ±0.01 mm and fitted with a 3 in objective was used to follow the fall in the meniscus during polymerization.

**Isolation of polymer**

The polymer mixture was sucked out of the dilatometer and poured into methanol containing hydrochloric acid, which had been cooled previously by the addition of solid carbon dioxide. The dilatometer was then washed out with a little benzene which was then added to the methanol solution. In this way the polymer was freed from any inorganic materials, and also from any excess monomer. The polymer was again digested with methanolic hydrochloric acid, washed with methanol, and dried under high vacuum.

**COMPARISON OF VARIOUS CATALYTIC SYSTEMS**

Initially an attempt was made to polymerize vinyl chloride using di-isopropylzinc and either vanadium trichloride or vanadium oxytrichloride. Zinc alkyls were chosen because, unlike aluminium alkyls, they do not react with primary or secondary alkyl halides<sup>14, 15</sup>. These polymerizations were, however, unsuccessful; no solid polymer was produced and only an oil was isolated.

A similar situation was found to be the case when a wide variety of other catalyst systems were used.

The addition of tetrahydrofuran, however, produced an effective catalyst system for the polymerization of vinyl chloride at 30°C (Table 1). No significant signs of chlorine stripping by this catalyst system was detected, as is shown in Table 2. Similar results were found at 60°C.

All three components in the catalytic systems, VCl<sub>3</sub>/Al(iBu)<sub>3</sub>/THF and VOCl<sub>3</sub>/Al(iBu)<sub>3</sub>/THF were found to be necessary. No polymerization could be effected unless all three components were present.

The catalyst systems VOCl<sub>3</sub>/Al(iBu)<sub>3</sub>/A where A was (C<sub>2</sub>H<sub>5</sub>)<sub>3</sub>N, (C<sub>2</sub>H<sub>5</sub>)<sub>2</sub>O, CH<sub>3</sub>CO<sub>2</sub>C<sub>2</sub>H<sub>5</sub> or C<sub>4</sub>H<sub>4</sub>S were investigated in order to examine the effect on catalytic activity of substituting other electron donor compounds for tetrahydrofuran. All these systems, however, gave yields of less than 0.5% when polymerizations were carried out for 48 h at 30°C.

The effect on catalytic activity of using other inorganic chlorides instead of vanadium oxytrichloride was also examined. The catalyst systems MX/Al(iBu)<sub>3</sub>/THF, where MX was PCl<sub>3</sub>, CoCl<sub>2</sub> or SnCl<sub>4</sub> were found to be ineffective, all giving yields of less than 0.1% at 30°C. A yield of 65% was, however, obtained using the catalyst system FeCl<sub>3</sub>/Al(iBu)<sub>3</sub>/THF.

It was concluded from these experiments that the most effective catalyst system for the polymerization of vinyl chloride was that prepared from vanadium oxytrichloride, tri-isobutylaluminium, and tetrahydrofuran.

**KINETICS OF POLYMERIZATION**

The solution of vanadium oxytrichloride and tetrahydrofuran in benzene is opaque and coloured black. Addition, however, of tri-isobutylaluminium to this solution (Al : V = 2.5 : 1) yields a transparent brown coloured

Table 1 Attempted polymerization of vinyl chloride by Ziegler-Natta catalysts

[Vinyl chloride] = 2.10 mol/l; [transition metal halide] = 0.033 mol/l; [metal alkyl] : [transition metal halide] = 1 : 1; [THF] : [transition metal halide] = 2 : 1; polymerization time = 48 h; temperature = 30°C

Catalyst	Result
VCl <sub>3</sub> /Zn(iPr) <sub>2</sub> /THF	30% Conversion
VCl <sub>3</sub> /Zn(iPr) <sub>2</sub>	An oil. No polymer
VOCl <sub>3</sub> /Zn(iPr) <sub>2</sub> /THF	35% Conversion
VOCl <sub>3</sub> /Zn(iPr) <sub>2</sub>	An oil. No polymer
VCl <sub>3</sub> /Al(iBu) <sub>3</sub> /THF	40% Conversion
VCl <sub>3</sub> /Al(iBu) <sub>3</sub>	An oil. No polymer
VOCl <sub>3</sub> /Al(iBu) <sub>3</sub> /THF	60% Conversion
VOCl <sub>3</sub> /Al(iBu) <sub>3</sub>	An oil. No polymer
VOCl <sub>3</sub> /AlEt <sub>2</sub> Cl/THF	10% Conversion

Table 2 Analysis of polymers and oils  
Experimental details as in Table 1

Catalyst	Polymer/oil	Analysis (%)					
		Experimental			Calculated*		
		C	H	Cl	C	H	Cl
VOCl <sub>3</sub> /Al(iBu) <sub>3</sub> /THF	Polymer	37.4	4.6	55.0	38.4	4.8	56.8
VOCl <sub>3</sub> /Al(iBu) <sub>3</sub>	Oil	82.0	17.6	1.1			

\* For poly(vinyl chloride)

solution. The catalyst prepared in this way is completely soluble, and no precipitation occurs even when the solution is left standing for several hours, or when centrifuged at 2000 rev/min for 30 min.

Figure 1 shows a typical plot of percentage conversion against time. It can be seen that there is an immediate and rapid fall off in rate, and that there is no induction period. This decreasing overall rate of polymerization as a function of time is characteristic of many Ziegler-Natta catalyst systems when these have been prepared from higher valence state transition metal halides in the liquid form<sup>16, 17</sup>, or when metal alkyl halides have been used<sup>18</sup>. Most soluble Ziegler-Natta catalyst systems also show similar behaviour<sup>7, 19</sup>.

The dependence of the initial overall rate of polymerization on the concentrations of the components of the catalyst system was investigated systematically.

#### Dependence of rate on monomer concentration

The effect of increasing the monomer concentration on the rate of polymerization was investigated at 30°C. A series of polymerizations in dilatometers were carried out in which the concentration of monomer was varied from 0.90 to 2.30 mol/l whilst the catalyst concentration remained constant. Experimental details of these experiments are given in Table 3. It can be seen that the initial rate of polymerization is first order with respect to the monomer concentration.

The determination of the order with respect to the monomer concentration within a given polymerization

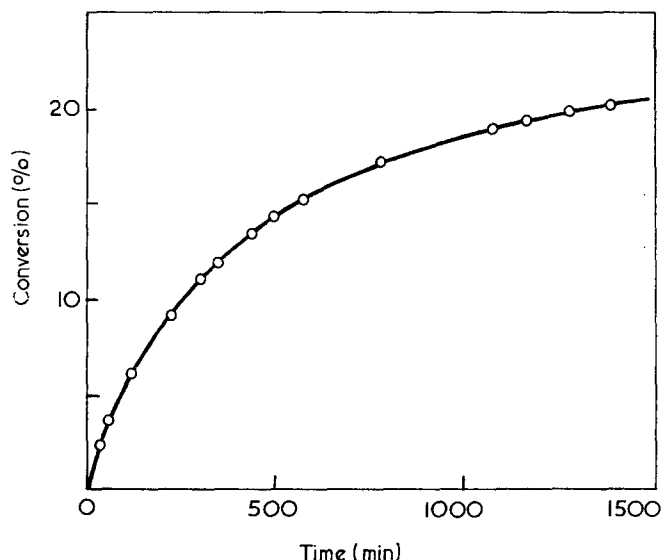


Figure 1 Plot of % conversion versus time at 30°C. [Vinyl chloride]=1.96 mol/l; [VOCl<sub>3</sub>]=0.0104 mol/l; [Al(iBu)<sub>3</sub>] : [VOCl<sub>3</sub>]=5.3 : 1; [THF] : [VOCl<sub>3</sub>]=10 : 1; solvent=benzene

Table 3 Variation of initial rate of polymerization with monomer concentration

[VOCl<sub>3</sub>]=0.0105 mol/l; [Al(iBu)<sub>3</sub>] : [VOCl<sub>3</sub>]=2.5 : 1; [THF] : [VOCl<sub>3</sub>]=7.7 : 1; temperature=30°C

Concentration of vinyl chloride (mol/l)	Initial rate $\times 10^4$ ( $R_p$ ) (mol/l min)	$\frac{R_p \times 10^4}{[\text{vinyl chloride}]}$
0.90	3.6	4.0
1.25	5.8	4.6
1.56	6.6	4.2
1.94	8.0	4.1
2.30	8.7	3.8

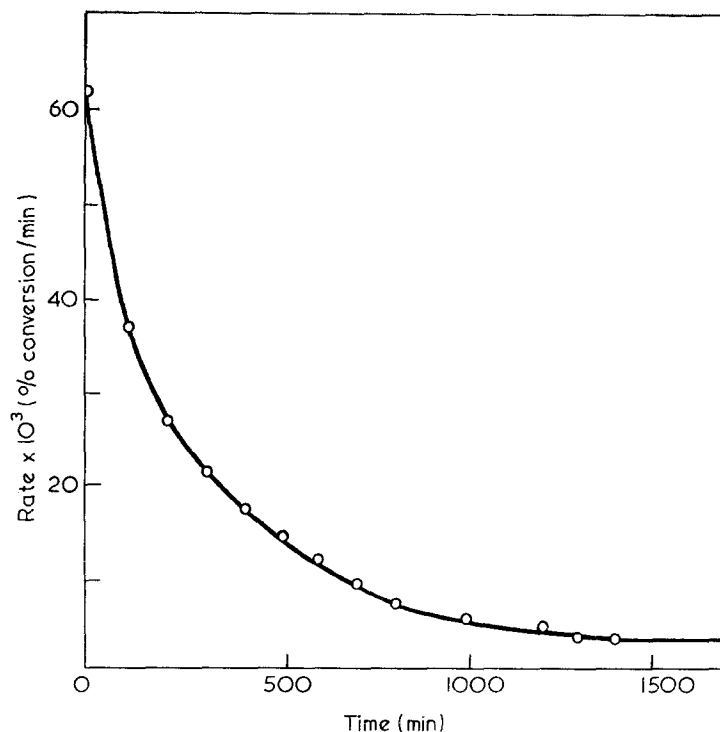


Figure 2 Plot of rate of polymerization versus time at 30°C. Experimental details as for Figure 1

was not found to be so simple. The polymerization process was characterized by an initial maximum rate which quickly decreased with time, and with depletion in monomer concentration. This effect is shown in Figure 2. Since the polymerization process has been shown to be first order with respect to the monomer concentration, a plot of time against  $\log(100 - \% \text{ conversion})$  should be linear provided that the catalyst concentration remains constant. That this is not so can be established from Figure 3, and indicates that the concentration of active centres does not remain constant throughout the duration of these polymerizations<sup>20</sup>. Evidently these systems, unlike conventional Ziegler-Natta systems, are not very stable.

#### Dependence of rate on [VOCl<sub>3</sub>]

In this series of polymerizations the tri-isobutylaluminium to vanadium oxytrichloride ratio and the tetrahydrofuran to vanadium oxytrichloride ratio were kept constant, whilst the vanadium oxytrichloride concentration was varied from  $1.06 \times 10^{-3}$  to  $1.06 \times 10^{-1}$  mol/l. The initial overall rate of polymerization was found to be directly proportional to the concentration of vanadium oxytrichloride, as is evident from the results shown in Figure 4. A similar dependency of the rate on the transition metal halide concentration has been observed in most Ziegler-Natta systems<sup>18, 21-23</sup>.

#### Dependence of rate on [Al(iBu)<sub>3</sub>]

The results of experiments in which the concentrations of monomer and vanadium oxytrichloride remained constant, whilst the tri-isobutylaluminium to vanadium oxytrichloride ratio was varied from 0.38 : 1 to 6.3 : 1 are shown in Figure 5. Sufficient tetrahydrofuran was added to each experiment to ensure that the tetrahydrofuran to tri-isobutylaluminium ratio remained constant.

It can be seen that the initial rate rapidly increases as the ratio of tri-isobutylaluminium to vanadium oxytri-

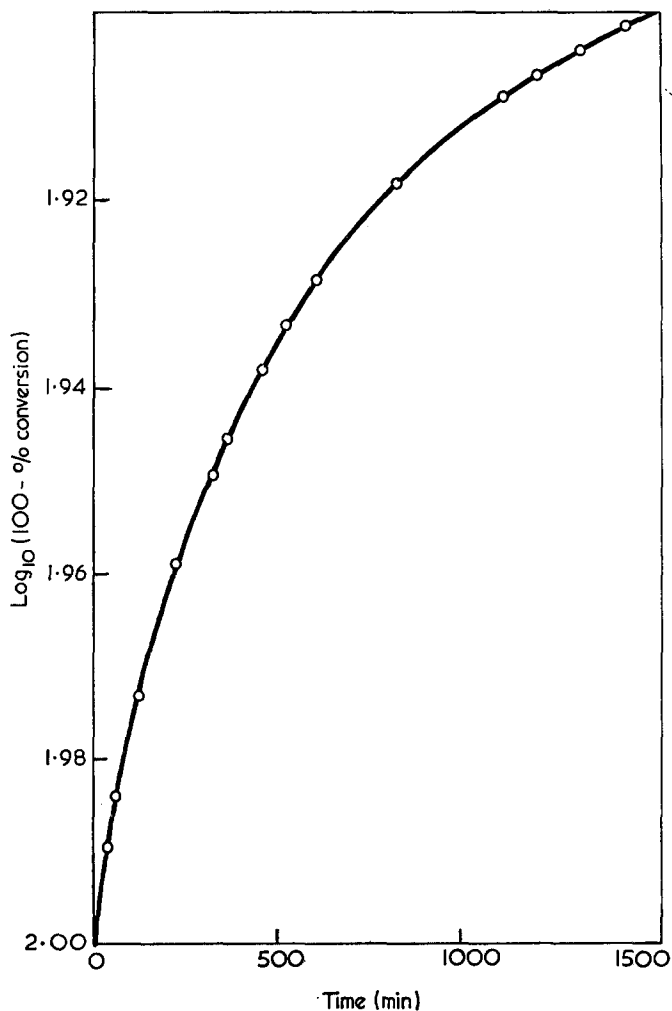


Figure 3 Plot of  $\log_{10}(100-\% \text{ conversion})$  versus time at  $30^\circ\text{C}$ . Experimental details as for Figure 1

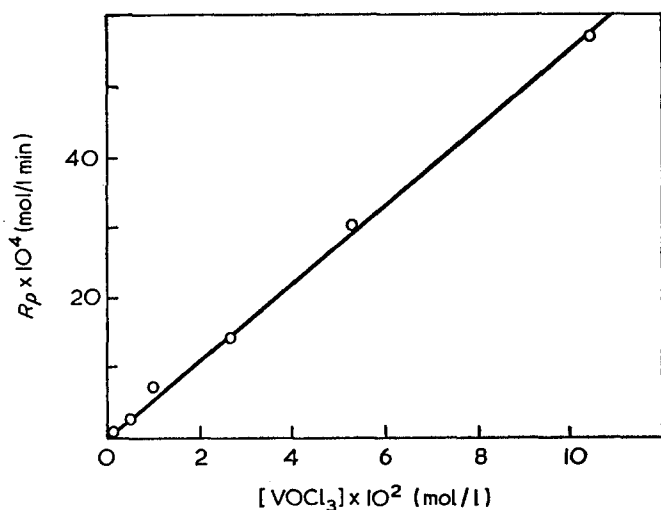


Figure 4 Variation in rate of polymerization with vanadium oxytrichloride concentration at  $30^\circ\text{C}$ . [Vinyl chloride]= $1.89 \text{ mol/l}$ ;  $[\text{Al}(\text{iBu})_3]=2.5:1$ ;  $[\text{THF}]:[\text{VOCl}_3]=10:1$ ; solvent=benzene

chloride is increased, and then flattens out somewhat as the limiting ratio is reached. This complex behaviour of rate on the aluminium to vanadium ratio is common to many Ziegler-Natta systems, and will be more fully discussed in a later publication<sup>24</sup>.

#### Dependence of rate on [THF]

In the next series of polymerizations the concentrations of vanadium oxytrichloride and tri-isobutylaluminium remained constant, whilst the tetrahydrofuran to vanadium oxytrichloride ratio was varied from 0.5 : 1 to 487 : 1. The results are shown in Table 4. The overall rate of polymerization increases as the tetrahydrofuran to vanadium oxytrichloride ratio is increased up to a ratio of 6 : 1. Above this ratio the rate remains fairly constant even to very high ratios.

#### Dependence of rate on temperature

It was not, unfortunately, possible to investigate a very wide temperature range, owing to the thermal decomposition of aluminium alkyls at temperatures greater than  $100^\circ\text{C}$ . The range covered was  $30^\circ\text{C}$  to  $60^\circ\text{C}$ , and all experiments were carried out using the same concentrations of reactants. The activation energy was found to be  $16.1 \pm 0.5 \text{ kcal/mol}$  ( $67.4 \pm 2.1 \text{ kJ/mol}$ ) which is comparable to that found in many Ziegler-Natta catalyst systems<sup>22, 23</sup>.

#### Copolymerization studies

It was found possible to copolymerize vinyl chloride with both methyl methacrylate and vinyl acetate. The polymers produced appeared to be true copolymers since

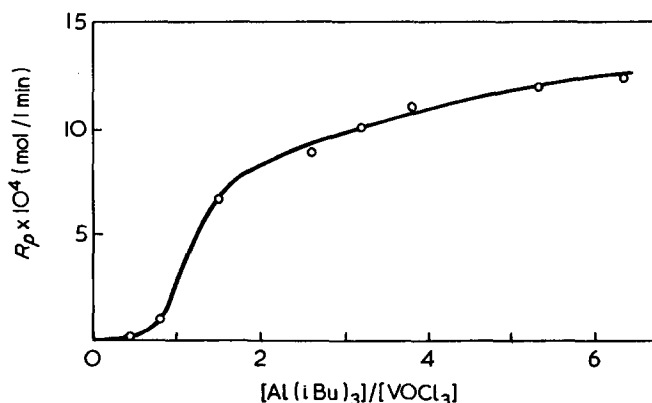


Figure 5 Plot of rate of polymerization versus  $[\text{Al}(\text{iBu})_3]/[\text{VOCl}_3]$  at  $30^\circ\text{C}$ . [Vinyl chloride]= $1.96 \text{ mol/l}$ ;  $[\text{VOCl}_3]=0.0104 \text{ mol/l}$ ; [THF] :  $[\text{Al}(\text{iBu})_3]=10:1$ ; solvent=benzene

Table 4 Dependence of rate on tetrahydrofuran concentration [Vinyl chloride]= $1.96 \text{ mol/l}$ ;  $[\text{VOCl}_3]=0.0104 \text{ mol/l}$   $[\text{Al}(\text{iBu})_3]:[\text{VOCl}_3]=2.5:1$ ; temperature= $30^\circ\text{C}$

Concentration of tetrahydrofuran $\times 10^2$ (mol/l)	$\frac{[\text{THF}]}{[\text{VOCl}_3]}$	Initial rate $\times 10^4$ (mol/l min)
0.5	0.5	—
2.0	1.9	0.7
4.2	4.0	5.7
6.5	6.2	7.3
8.0	7.7	7.8
9.2	8.8	8.2
12.1	11.6	8.6
15.2	14.6	8.2
39.0	37.5	8.0
65.5	63.0	9.0
116	112	8.6
350	337	8.0
506	487	8.2
Tetrahydrofuran	as solvent	8.8



it was not found possible to separate any homopolymer by means of solvent extraction. The determination of the reactivity ratios affords a method for checking on the nature of the polymerization process<sup>3, 7, 9, 25</sup>, since reactivity ratios for free radical propagation are known<sup>26, 27</sup>. The amount of copolymer produced was never allowed to exceed 5% conversion. The copolymers were carefully isolated, dried and analysed for chloride using the Volhard method.

The copolymer reactivity ratios were calculated by means of Fineman-Ross plots<sup>28</sup>. The best straight line was drawn through the points using the methods of least squares (Figures 6 and 7). The reactivity ratios calculated from the Fineman-Ross graph, together with the reactivity ratios quoted for free radical copolymerization<sup>26, 27</sup> are listed in Table 5. The difference between these sets of reactivity ratios is considerable.

These results show that the mechanism for the polymerization of vinyl chloride by the catalyst system  $\text{VOCl}_3/\text{THF}/\text{Al}(\text{iBu})_3$  cannot be a conventional free radical type. Moreover, additional evidence for this conclusion comes from recent studies<sup>29</sup> on active centre concentrations in these systems using tritiated methanol<sup>30, 31</sup>. These studies conclusively prove that the

growing polymer chain involves a metal-carbon bond since the observed rates of polymerization can be related to the numbers of active centres determined in this way.

Using the evidence obtained from similar copolymerization studies Ashikari<sup>9</sup> has concluded that the polymerization of vinyl chloride by the catalyst system  $\text{VCl}_3/\text{BuOH}/\text{AlEt}_3$  is non-radical in nature.

## PROPERTIES OF POLYMERS

Some interesting differences in the properties of the poly(vinyl chloride) prepared by the catalyst system  $\text{VOCl}_3/\text{THF}/\text{Al}(\text{iBu})_3$  from control samples, prepared by conventional free radical initiators, were observed.

The polymers melted over the temperature range 150–180°C, and differential thermal analysis (d.t.a.) indicated a decomposition temperature of 275–335°C; the corresponding temperature range for free radical initiated polymer is 250–295°C.

The infra-red spectra of these polymers also showed differences (Figure 8). In order to make a detailed assignment of the bands in the infra-red spectrum Krimm<sup>32, 33</sup> has studied the deuterated analogues of poly(vinyl chloride), and has reached the following conclusions concerning the origins of the non-crystalline bands. The 615  $\text{cm}^{-1}$  arises from syndiotactic pairs only, while the 638  $\text{cm}^{-1}$  band is due to isotactic pairs only; the band at  $\sim 690 \text{ cm}^{-1}$  contains contributions from both isotactic and syndiotactic placements, comprising the most stable form of the former and the less stable form of the latter.

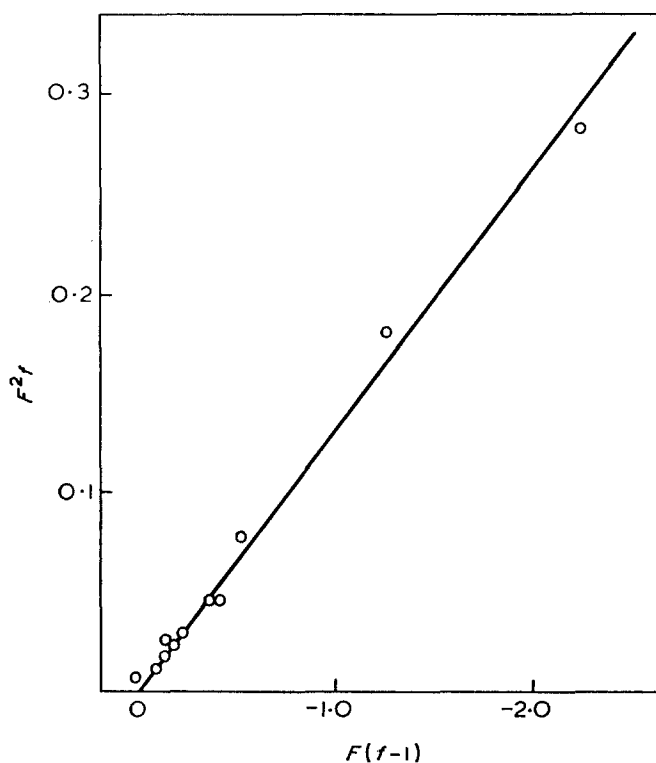


Figure 6 Fineman-Ross plot for the copolymerization of vinyl chloride and methyl methacrylate at 45°C.  $[\text{Monomer}]_{\text{total}} = 2.00 \text{ mol/l}$ ;  $[\text{VOCl}_3] = 0.115 \text{ mol/l}$ ;  $[\text{Al}(\text{iBu})_3] : [\text{VOCl}_3] = 1.1 : 1$ ;  $[\text{THF}] : [\text{VOCl}_3] = 3.5 : 1$ ; solvent = benzene

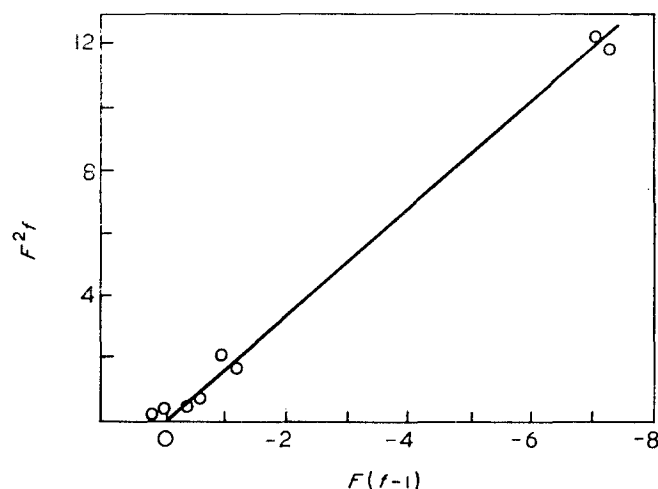


Figure 7 Fineman-Ross plot for the copolymerization of vinyl chloride and vinyl acetate at 40°C.  $[\text{Monomer}]_{\text{total}} = 2.00 \text{ mol/l}$ ;  $[\text{VOCl}_3] = 0.0103 \text{ mol/l}$ ;  $[\text{Al}(\text{iBu})_3] : [\text{VOCl}_3] = 2.6 : 1$ ;  $[\text{THF}] : [\text{VOCl}_3] = 11 : 1$ ; solvent = benzene

Table 5 Comparison of reactivity ratios in copolymerization with typical reactivity ratios for free radical initiation

Monomer pair	Catalyst	$r_1$	$r_2$	$r_1 r_2$
Vinyl chloride (1)-methyl methacrylate (2)	$\text{VOCl}_3/\text{Al}(\text{iBu})_3/\text{THF}^a$	$0.008 \pm 0.004$	$7.3 \pm 1.2$	0.058
Vinyl chloride (1)-methyl methacrylate (2)	Free radical <sup>a</sup>	0.020	15	0.30
Vinyl chloride (1)-vinyl acetate (2)	$\text{VOCl}_3/\text{Al}(\text{iBu})_3/\text{THF}^b$	$0.58 \pm 0.10$	$0.020 \pm 0.007$	0.012
Vinyl chloride (1)-vinyl acetate (2)	Free radical <sup>b</sup>	$1.35 \pm 0.05$	$0.65 \pm 0.04$	0.88

<sup>a</sup> Temperature = 45°C;  $[\text{VOCl}_3] = 0.115 \text{ mol/l}$ ;  $[\text{Al}(\text{iBu})_3] : [\text{VOCl}_3] = 1.1 : 1$ ;  $[\text{THF}] : [\text{VOCl}_3] = 3.5 : 1$ ;  $[\text{Monomer}]_{\text{total}} = 2.00 \text{ mol/l}$

<sup>b</sup> Temperature = 40°C;  $[\text{VOCl}_3] = 0.0103 \text{ mol/l}$ ;  $[\text{Al}(\text{iBu})_3] : [\text{VOCl}_3] = 2.6 : 1$ ;  $[\text{THF}] : [\text{VOCl}_3] = 11 : 1$ ;  $[\text{Monomer}]_{\text{total}} = 2.00 \text{ mol/l}$

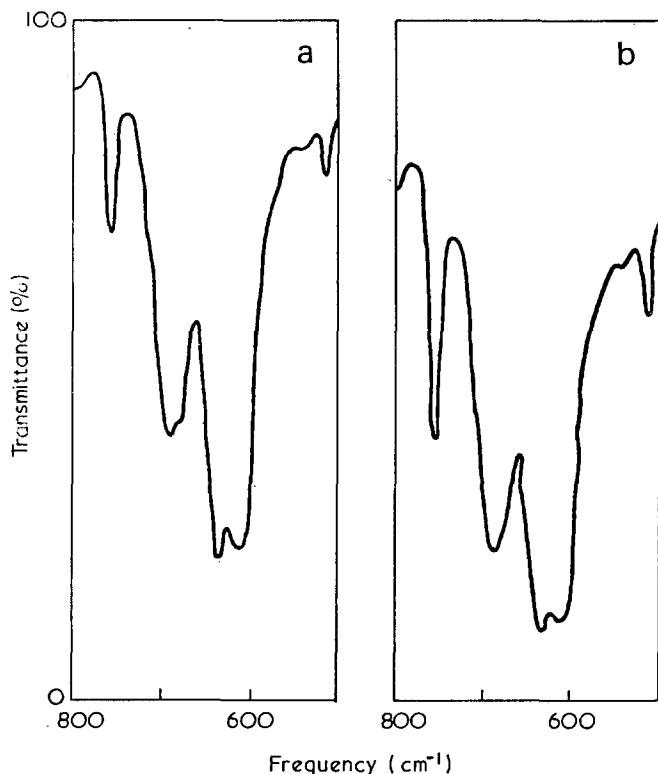


Figure 8 Infra-red spectra of poly(vinyl chloride). (a) Prepared using  $\text{VOCl}_3/\text{Al}(\text{iBu})_3/\text{THF}$ ; (b) prepared using a free radical initiator

Bands were found at  $\sim 690$ ,  $638$  and  $615 \text{ cm}^{-1}$  indicating that both isotactic and syndiotactic placements are present in the chains. The ratios of the integrated areas associated with the bands at  $638$  and  $690 \text{ cm}^{-1}$  are not the same in these samples (Figure 8). More details will be given in a later publication<sup>34</sup>.

## CONCLUSIONS

(1) The most satisfactory modified Ziegler-Natta catalyst for the polymerization of vinyl chloride is that obtained when vanadium oxytrichloride and tri-isobutylaluminium react together in the presence of excess tetrahydrofuran in an inert diluent. All three components are required for the formation of an active catalyst system which is homogeneous.

(2) The overall kinetics of polymerization follow the general pattern observed in many Ziegler-Natta systems. In particular, the initial overall rate of polymerization is proportional to the monomer and vanadium oxytrichloride concentrations, and increases as the concentration of tetrahydrofuran is increased up to a tetrahydrofuran to tri-isobutylaluminium ratio of 6 : 1. The variation of the initial overall rate of polymerization with respect to the tri-isobutylaluminium concentration is complex; increase in aluminium alkyl concentration

initially causes an increase in initial rate, whilst further increase in concentration gives rise to a limiting value.

(3) The activation energy of the overall polymerization process is  $16.1 \text{ kcal/mol}$  ( $67.4 \text{ kJ/mol}$ ), and is similar to that found for other Ziegler-Natta polymerization systems.

(4) Copolymerization studies with vinyl acetate and methyl methacrylate show marked differences from the behaviour observed in free radical polymerization.

(5) D.t.a. and infra-red analyses demonstrate structural differences between poly(vinyl chloride) prepared by the catalytic system  $\text{VOCl}_3/\text{THF}/\text{Al}(\text{iBu})_3$  and control samples prepared by free radical initiation.

## REFERENCES

- 1 Solvay and Cie, Belg. Pat. 545, 968 (1956)
- 2 Murahashi, S., Nozakura, S. and Hatada, K. *Bull. Chem. Soc. Japan* 1961, **34**, 631
- 3 Giannini, U. and Cesca, S. *Chim. Ind. (Milan)* 1962, **44**, 371
- 4 Natta, G., Mazzanti, G., Giannini, U. and Cesca, S. Belg. Pat. 611, 654
- 5 Yamazaki, N., Sasaki, K. and Kambara, S. *J. Polym. Sci. (B)* 1964, **2**, 487
- 6 Budanova, G. P. and Mazurek, U. V. *Vysokomol. Soedin.* 1967, **A9**, 1393
- 7 Caporiccio, G. and Sianesi, D. *Chim. Ind. (Milan)* 1970, **52**, 139
- 8 Hercules Powder Co., Br. Pat. 834, 937 (1961)
- 9 Ashikari, N. *Rev. Elect. Commun. Lab.* 1964, **12**, 570
- 10 Ashikari, N. *Chem. High Polymers (Japan)* 1962, **19**, 718
- 11 Hyde, T. G. *PhD Thesis* University of Manchester, 1965
- 12 Krug, R. C. and Tang, P. J. C. *J. Am. Chem. Soc.* 1954, **76**, 2262
- 13 Anderson, I. H., Burnett, G. M. and Tait, P. J. T. *J. Polym. Sci.* 1962, **56**, 391
- 14 Coates, G. E. 'Organometallic Compounds', Methuen, London, 1956, p 40
- 15 Zeiss, H. 'Organometallic Chemistry', Reinhold, New York, 1960, p 198
- 16 Natta, G., Pino, P., Mazzanti, G. and Longi, P. *Gazz. Chim. Ital.* 1957, **87**, 549
- 17 Smith, W. E. and Zelmer, R. G. *J. Polym. Sci. (A)* 1963, **1**, 2587
- 18 Burnett, G. M. and Tait, P. J. T. *Polymer* 1960, **1**, 151
- 19 Henrici-Olivé, G. and Olivé, S. *Angew. Chem. (Int. Edn)* 1967, **6**, 791
- 20 Haszeldine, R. N., Hyde, T. G. and Tait, P. J. T. *Polymer* 1973, **14**, 224
- 21 Natta, G. *J. Polym. Sci.* 1959, **34**, 21
- 22 Medalia, A. I., Orzenchowski, A., Trinckera, J. A. and Morley, J. P. *J. Polym. Sci.* 1959, **41**, 241
- 23 McKenzie, I. D., Tait, P. J. T. and Burfield, D. R. *Polymer* 1972, **13**, 307
- 24 Chesworth, A. E., Haszeldine, R. N. and Tait, P. J. T. to be published
- 25 Furukawa, J. and Tsuruta, T. *Bull. Inst. Chem. Res. (Kyoto Univ.)* 1960, **38**, 319
- 26 Tkanchenko, G. V., Stupen, L. V., Kaufman, L. A. and Karacheva, L. A. *Zh. Fiz. Khim.* 1958, **32**, 2492
- 27 Kimura, T. and Yoshida, K. *Kagaku Kogyo* 1958, **29**, 43
- 28 Fineman, M. and Ross, S. D. *J. Polym. Sci.* 1950, **5**, 259
- 29 Shore, G. S. and Tait, P. J. T. to be published
- 30 Feldman, C. F. and Perry, E. *J. Polym. Sci.* 1960, **46**, 217
- 31 Burfield, D. R. and Tait, P. J. T. *Polymer* 1972, **13**, 315
- 32 Krimm, S. *J. Polym. Sci. (A)* 1963, **1**, 2647
- 33 Krimm, S. *J. Polym. Sci. (C)* 1964, **7**, 3
- 34 Tait, P. J. T. to be published

# Polymerization studies using modified Ziegler-Natta catalysts: 2. Polymerization of vinyl fluoride

R. N. Haszeldine, T. G. Hyde\* and P. J. T. Tait

Department of Chemistry, University of Manchester Institute of Science and Technology, Manchester M60 1QD, UK

(Received 27 November 1972; revised 22 January 1973)

Vinyl fluoride has been polymerized by modified Ziegler-Natta catalysts. As in the case of vinyl chloride the most effective catalyst system at 30°C is the soluble system prepared from vanadium oxytrichloride, tri-isobutylaluminium and tetrahydrofuran. All three components are necessary for the formation of an active catalyst. The overall kinetics of polymerization follow the general pattern observed in many Ziegler-Natta systems and that observed in the polymerization of vinyl chloride by the same catalyst system.

## INTRODUCTION

There are but few literature references to the polymerization of fluorinated olefins by Ziegler-Natta catalysts. The polymerization of tetrafluoroethylene and hexafluoropropylene has been reported<sup>1, 2</sup>. Overberger and Davidson<sup>3</sup> have polymerized 4,4,4-trifluorobutene-1, 5,5,5-trifluoropentene-1, 3-trifluoromethylbutene-1, and 4-trifluoromethylpentene-1 using the catalyst system  $\text{VCl}_3/\text{Al}(\text{iBu})_3$ . Polymerization of trifluorochloroethylene, vinyl fluoride, and fluorinated butadienes by  $\text{AlEt}_2\text{Br}$  and  $\text{TiCl}_4$  in the presence of  $\text{CCl}_4$  has been effected<sup>4, 5</sup>. Catalytic combinations of titanium tetra-alkoxides or vanadyl acetylacetonate, and di or monoalkylaluminium derivatives have been reported<sup>6</sup> to polymerize 3,3,3-trifluoropropylene. More recently the polymerization and copolymerization of vinyl fluoride has been described by Caporiccio and Sianesi<sup>7</sup> using catalyst systems based on vanadyl acetylacetonate and  $\text{AlR}(\text{OR})\text{Cl}$ .

The polymerization of vinyl chloride by modified Ziegler-Natta catalysts has been reported in the previous paper<sup>8</sup>, and this publication describes the use of some of these catalysts for the polymerization of vinyl fluoride.

## EXPERIMENTAL

Details of materials, other than vinyl fluoride, and experimental procedure have already been described<sup>8</sup>.

*Vinyl fluoride.* This monomer was supplied by Du Pont Ltd. The monomer was purified by trap-to-trap distillation through slush baths of diethyl ether (-120°C) and isopentane (-160°C), and collected in a trap cooled in liquid nitrogen. The purity of the vinyl fluoride was checked by infra-red spectroscopy.

Owing to the high vapour pressure of vinyl fluoride (3092 kN/m<sup>2</sup> at 30°C) most of these experiments using vinyl fluoride were carried out in thick-walled glass

reaction vessels.

The catalyst solution was added to the reaction vessels in a dry box. The reaction vessels were then taken out of the dry box, attached to the high vacuum line, and the catalyst solution was degassed. A known amount of vinyl fluoride was distilled into the reaction vessels, which were then sealed, removed from the vacuum line, and placed in a stirrer tank at 30°C. The polymerizations were terminated by the addition of methanol, and the polymer was isolated<sup>8</sup>.

## COMPARISON OF VARIOUS CATALYTIC SYSTEMS

Table 1 shows that the addition of tetrahydrofuran produces an active catalyst for the polymerization of vinyl fluoride, although the conversion to polymer is much lower than that obtained in the case of vinyl chloride<sup>8</sup>. As before polymerization proceeds without halogen stripping (Table 2).

The catalytic activity of the systems  $\text{VOCl}_3/\text{Al}(\text{iBu})_3/\text{A}$  where A was  $(\text{C}_2\text{H}_5)_3\text{N}$ ,  $(\text{C}_2\text{H}_5)_2\text{O}$ ,  $\text{CH}_3\text{CO}_2\text{C}_2\text{H}_5$  or  $\text{C}_4\text{H}_4\text{S}$  was investigated in order to examine the effect

Table 1 Attempted polymerization of vinyl fluoride by Ziegler-Natta catalysts  
[Vinyl fluoride]=2.92 mol/l; [transition metal halide]=0.033 mol/l; [metal alkyl]:[transition metal halide]=1:1; [THF]:[transition metal halide]=2:1; polymerization time=48 h; temperature=30°C

Catalyst	Result
$\text{VCl}_3/\text{Zn}(\text{iPr})_2/\text{THF}$	0.05% Conversion
$\text{VCl}_3/\text{Zn}(\text{iPr})_2$	An oil. No polymer
$\text{VOCl}_3/\text{Zn}(\text{iPr})_2/\text{THF}$	An oil. No polymer
$\text{VOCl}_3/\text{Zn}(\text{iPr})_2$	An oil. No polymer
$\text{VCl}_3/\text{Al}(\text{iBu})_3/\text{THF}$	0.05% Conversion
$\text{VCl}_3/\text{Al}(\text{iBu})_3$	An oil. No polymer
$\text{VOCl}_3/\text{Al}(\text{iBu})_3/\text{THF}$	5% Conversion
$\text{VOCl}_3/\text{Al}(\text{iBu})_3$	An oil. No polymer
$\text{VOCl}_3/\text{AlEt}_2\text{Cl}/\text{THF}$	0.5% Conversion

\* Present address: Development Department, Industrial Chemicals Division, Ciba-Geigy, Trafford Park, Manchester, UK.

of substituting other electron donor compounds for tetrahydrofuran. Only the catalyst system containing  $(C_2H_5)_2O$  produced polymer (0.5% conversion in 48 h at 30°C).

Substitution of  $PCl_3$ ,  $SnCl_4$ ,  $CoCl_2$  or  $FeCl_3$  for  $VOCl_3$  produced inactive catalyst systems.

It was concluded from these polymerization experiments that, as in the case of vinyl chloride, the most effective catalyst system was that prepared from vanadium oxytrichloride, tri-isobutylaluminium and THF.

KINETIC FEATURES OF THE POLYMERIZATION

This study was undertaken in order to gain some information on the nature of the polymerization process, and to afford a comparison of the polymerization of vinyl fluoride and vinyl chloride. Additional difficulties were encountered in these polymerizations. Vinyl fluoride is much less reactive than vinyl chloride. This is probably due to increased deactivation of the double bond owing to the higher electronegativity of the fluorine atom. Also it was not possible, except at very low monomer concentrations, to use dilatometry to follow the rates of polymerization.

Overall polymerization process

A series of experiments was performed in order to obtain information concerning the nature of the polymerization process, and to determine the optimum catalyst concentrations. Experimental details and results are given in Table 3.

It is evident that much higher catalyst concentrations ( $\times 20$ ) are required for these polymerizations than for the polymerization of vinyl chloride<sup>8</sup>.

The characteristics of the polymerization process were investigated at low monomer concentration by means of dilatometry. At these low monomer concentrations it was not possible to isolate any solid polymer, since only oils were obtained, and for this reason only plots of percentage decrease in volume against time were obtained. From Figure 1 it can be seen that the same polymerization characteristics are exhibited as were encountered in the polymerization of vinyl chloride. In particular, the overall rate of polymerization rapidly

Table 2 Analysis of polymers and oils  
Experimental details as in Table 1

Catalyst	Polymer/ oil	Analysis (%)					
		Experimental			Calculated*		
		C	H	F	C	H	F
$VOCl_3/Al(iBu)_3/THF$	Polymer	50.2	6.1	39.7	52.2	6.5	41.3
$VOCl_3/Al(iBu)_3$	Oil	83.1	14.0	1.1			

\* Calculated for poly(vinyl fluoride)

Table 3 Polymerization of vinyl fluoride at 30°C

$[VOCl_3]$ (mol/l)	$[Al(iBu)_3]$ $[VOCl_3]$	[Vinyl fluoride] (mol/l)	$[THF]$ $[VOCl_3]$	Conversion (%)
0.021	1.5	2.00	3.0	No polymer
0.035	3.8	2.00	12.0	3.2
0.070	3.8	2.93	12.0	5.7
0.105	3.8	2.93	12.0	6.2
0.175	2.3	2.93	7.7	9.2

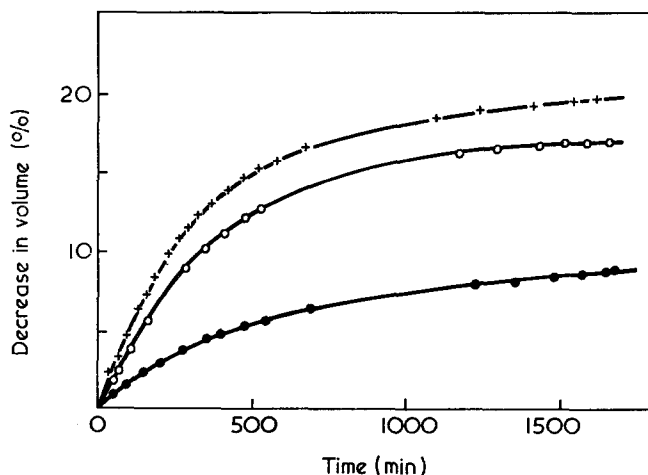


Figure 1 Plots of % conversion versus time at 30°C. [Vinyl fluoride]=1.01 mol/l;  $[Al(iBu)_3]:[VOCl_3]=1:1$ ;  $[THF]:[VOCl_3]=3:1$ .  $[VOCl_3]$ : +, 0.84; O, 0.70; ●, 0.31 mol/l

Table 4 Effect of monomer concentration on percentage conversion

$[VOCl_3]=0.314$  mol/l;  $[Al(iBu)_3]:[VOCl_3]=1:1$ ;  $[THF]:[VOCl_3]=3:1$ ; polymerization time=25 h; temp. = 30°C

[Vinyl fluoride] (mol/l)	Conversion (%)
0.49	No polymer
1.95	19.3
2.24	18.1
2.92	18.8
3.41	20.0
3.90	25.0
4.87	27.0

decreases with time. This is probably due to a depletion in the concentration of active centres.

Dependence of polymer yield on [vinyl fluoride]

The concentrations of vanadium oxytrichloride, tri-isobutylaluminium and tetrahydrofuran were kept constant whilst the monomer concentration was varied from 0.49 mol/l to 4.87 mol/l. The polymerizations were carried out in sealed tubes, and the polymer was isolated after 25 h. The results are shown in Table 4. At very low concentrations of monomer only an oil was isolated. Between monomer concentrations of 1.95 mol/l and 3.41 mol/l the overall rate appears to be first order with respect to monomer concentration. Above a vinyl fluoride concentration of 3.90 mol/l the percentage conversion of monomer to polymer increases somewhat. It will be realized, however, that the procedure used here is not an accurate one for the determination of reaction order.

Dependence of rate on  $[VOCl_3]$

The effect of increasing the vanadium oxytrichloride concentration at constant monomer, constant tetrahydrofuran to vanadium oxytrichloride ratio and constant tri-isobutylaluminium to vanadium oxytrichloride ratio was studied. Dilatometers were used for these experiments, and because of this a low concentration of vinyl fluoride was used. The initial rate of polymerization, under these conditions, was found to be proportional to the vanadium oxytrichloride concentration as is shown in Figure 2.

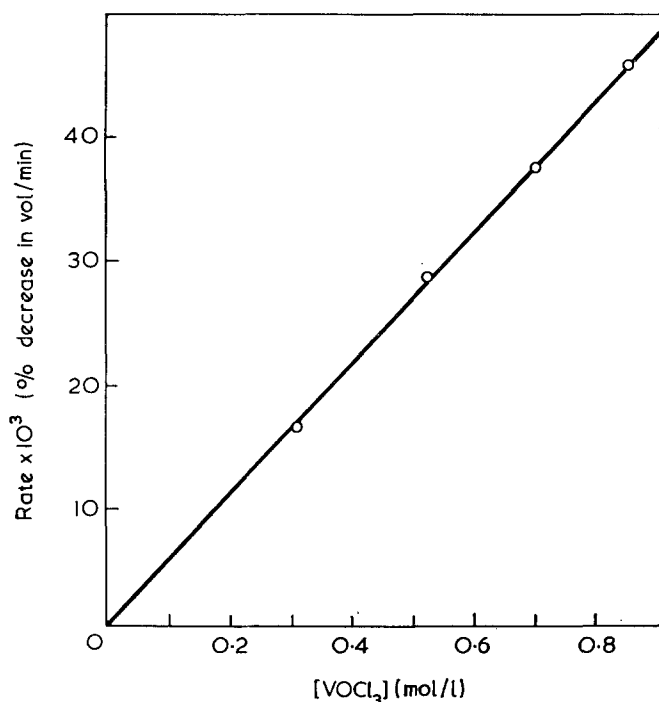


Figure 2 Plot of rate of polymerization versus concentration of vanadium oxytrichloride at 30°C. [Vinyl fluoride]=1.01 mol/l; [Al(iBu)<sub>3</sub>]:[VOCl<sub>3</sub>]=1:1; [THF]:[VOCl<sub>3</sub>]=3:1

#### Dependence of rate on [Al(iBu)<sub>3</sub>]

The concentrations of vanadium oxytrichloride and vinyl fluoride were kept constant and the concentration of tetrahydrofuran was adjusted to maintain a tetrahydrofuran to tri-isobutylaluminium ratio of 4:1, whilst the tri-isobutylaluminium concentration was increased from 0.09 mol/l to 1.87 mol/l. The polymerizations were carried out in sealed tubes, and the polymer was isolated after 24 h. The results are given in Table 5. The maximum conversion was obtained at a tri-isobutylaluminium to vanadium oxytrichloride ratio of 1.6:1. Above this ratio the percentage conversion decreased as the tri-isobutylaluminium concentration was increased. This behaviour is typical of a wide range of Ziegler–Natta polymerization catalysts when used under similar conditions<sup>9</sup>.

#### Dependence of rate on [THF]

The concentrations of vanadium oxytrichloride, tri-isobutylaluminium and vinyl fluoride were kept constant whilst only the concentration of tetrahydrofuran was varied. The polymerizations were carried out in sealed

Table 5 Effect of [Al(iBu)<sub>3</sub>] on yield  
[VOCl<sub>3</sub>]=0.246 mol/l; [vinyl fluoride]=2.92 mol/l;  
[THF]:[Al(iBu)<sub>3</sub>]=4:1; polymerization time=24 h;  
temperature=30°C

[Al(iBu) <sub>3</sub> ] (mol/l)	[Al(iBu) <sub>3</sub> ] [VOCl <sub>3</sub> ]	Conversion (%)
0.09	0.38	2.0
0.13	0.52	3.1
0.19	0.76	16.1
0.39	1.60	22.0
0.57	2.30	19.2
0.69	2.80	16.2
0.94	3.80	10.0
1.18	4.80	8.0
1.40	5.70	7.1
1.87	7.60	5.0

Table 6 Effect of [THF] on yield  
[VOCl<sub>3</sub>]=0.175 mol/l; [vinyl fluoride]=2.92 mol/l;  
[Al(iBu)<sub>3</sub>]:[VOCl<sub>3</sub>]=2.27:1; polymerization time  
=48 h; temperature=30°C

[THF] (mol/l)	[THF] [VOCl <sub>3</sub> ]	Conversion (%)
0.12	0.7	No polymer
0.25	1.4	No polymer
0.40	2.3	9.8
1.02	5.8	8.9
1.52	8.7	9.4
2.05	11.7	12.4
3.06	17.5	10.3
4.48	25.6	11.6
10.21	58.3	11.0

tubes, and the polymer was isolated after 25 h. Experimental details and results are given in Table 6.

Below a tetrahydrofuran to vanadium oxytrichloride of 2.3:1 no polymer was produced. Between the ratios of 2.3:1 and 58:1, however, the percentage conversion remained more or less constant. From these results it is concluded that within this region the rate of polymerization is substantially independent of the tetrahydrofuran concentration. This suggests that tetrahydrofuran itself does not take part in the polymerization process, but acts as a complexing agent for the tri-isobutylaluminium and the vanadium oxytrichloride.

#### CONCLUSIONS

(1) As in the case of the polymerization of vinyl chloride the most satisfactory modified Ziegler–Natta catalyst for the polymerization of vinyl fluoride is that obtained when vanadium oxytrichloride and tri-isobutylaluminium react together in the presence of excess tetrahydrofuran in an inert diluent. All three components are necessary for the formation of an active catalyst. Vinyl fluoride, however, shows a much reduced activity in this polymerization system.

(2) The overall kinetics of polymerization follow the general pattern observed in many Ziegler–Natta systems and that observed in the polymerization of vinyl chloride by the same catalyst system. The overall rate is proportional to the monomer and vanadium oxytrichloride concentrations. The variation of the yield of polymer with tri-isobutylaluminium concentration is complex but, nevertheless, similar to that in many Ziegler–Natta systems. The yield of polymer is independent of the tetrahydrofuran concentration above a tetrahydrofuran to vanadium oxytrichloride ratio of 2.3:1.

#### REFERENCES

- Montecatini, Belg. Pat. 618 320 (1962)
- Sianesi, D. and Caporiccio, G. *Makromol. Chem.* 1963, **60**, 213
- Overberger, C. G. and Davidson, E. B. *J. Polym. Sci.* 1962, **62**, 23
- U.S. Pat. 3 084 144 (1963)
- U.S. Pat. 3 089 866 (1963)
- Sianesi, D. and Caporiccio, G. *Makromol. Chem.* 1964, **81**, 264
- Caporiccio, G. and Sianesi, D. *Chim. Ind. (Milan)* 1970, **52**, 139
- Haszeldine, R. N., Hyde, T. G. and Tait, P. J. T. *Polymer* 1973, **14**, 215
- Burfield, D. R., McKenzie, I. D. and Tait, P. J. T. *Polymer* 1972, **13**, 302

# Polymerization studies using modified Ziegler-Natta catalysts: 3. The catalyst system

R. N. Haszeldine, T. G. Hyde\* and P. J. T. Tait

Department of Chemistry, University of Manchester Institute of Science and Technology, Manchester M60 1QD, UK

(Received 27 November 1972; revised 22 January 1973)

The catalyst system  $\text{VOCl}_3/\text{Al}(\text{iBu})_3/\text{THF}$  has been examined and the role of the individual catalyst components investigated. Tetrahydrofuran is believed to undergo complex formation with the other catalyst components thus restricting reduction of the vanadium to V(IV). The complex  $\text{VOCl}_2 \cdot 2\text{THF}$  has been isolated and, when used with tri-isobutyl-aluminium in the presence of excess tetrahydrofuran, shown to produce polymerization systems of comparable activity to the  $\text{VOCl}_3/\text{Al}(\text{iBu})_3/\text{THF}$  systems. The kinetic behaviour of the  $\text{VOCl}_3/\text{Al}(\text{iBu})_3/\text{THF}$  system has been investigated and shown to be consistent with a simple Ziegler-Natta kinetic scheme involving a rapid bimolecular decomposition of either a transition metal alkyl compound, or of a complex formed on interaction of a transition metal alkyl with an aluminium alkyl.

## INTRODUCTION

Earlier publications<sup>1,2</sup> describe the polymerization of vinyl chloride and vinyl fluoride by the modified Ziegler-Natta catalyst system  $\text{VOCl}_3/\text{Al}(\text{iBu})_3/\text{THF}$ . The aim of the present study is to determine the role played by the individual components of the catalyst system.

## EXPERIMENTAL

Details of materials, other than vanadium oxydichloride and vanadium oxydichloride tetrahydrofuranate, have been described previously<sup>1,2</sup>.

### Vanadium oxydichloride

Vanadium oxydichloride was prepared from vanadium oxytrichloride by reduction with sulphur. Vanadium oxytrichloride (45.7g) was refluxed (under nitrogen) for 3 h with sulphur (5.0g). The excess vanadium oxytrichloride was removed by vacuum distillation at 90°C, leaving the solid green vanadium oxydichloride. Analysis: (IV), 36.4% (calc. 37.0%); Cl, 50.6% (calc. 51.5%).

### Vanadium oxydichloride tetrahydrofuranate

Vanadium oxydichloride (10.0g) was dissolved in tetrahydrofuran (250 cm<sup>3</sup>) when a dark blue solution was produced. This solution was filtered and concentrated to 50 cm<sup>3</sup>. Dry hexane (25 cm<sup>3</sup>) was added, and the solution allowed to stand overnight. After 24 h light green needle-like crystals (10.5 g) were produced. These operations were performed in a dry box in an atmosphere of dried nitrogen.

Analysis: V(IV), 18.0% (calc. 18.2%); Cl, 25.0% (calc. 25.2%); C, 34.4% (calc. 34.1%); H, 6.0% (calc. 5.7%).

\* Present address: Development Department, Industrial Chemicals Division, Ciba-Geigy, Trafford Park, Manchester, UK.

## RESULTS AND DISCUSSION

### Role of tetrahydrofuran

In order to determine the role of the tetrahydrofuran in the polymerization process, experiments using vinyl fluoride and vinyl chloride were performed in which the solvent (benzene) together with the tetrahydrofuran were distilled off, and analysed after polymerization had taken place. The concentration of tetrahydrofuran was determined from measurement of the refractive index of the benzene/tetrahydrofuran distillate. Experimental details are listed in *Table 1*.

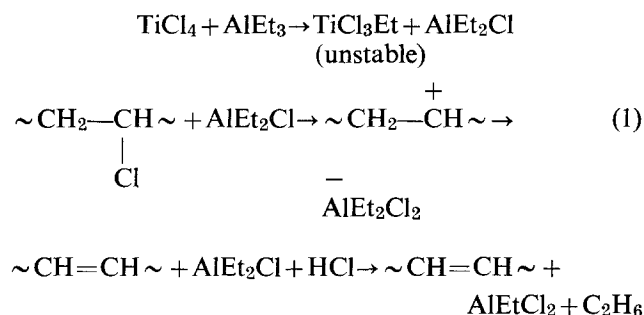
These results show that tetrahydrofuran is not being destroyed or removed to any appreciable extent either during the polymerization process or by interaction with the other components of the catalyst system, and they are consistent with earlier kinetic results<sup>1,2</sup> which indicated that the tetrahydrofuran probably acted only as a complexing agent. The possibility that small amounts of tetrahydrofuran are being used to produce active centres is not, however, excluded by this analysis, since it is known that the concentrations of active centres in these systems is very low<sup>3</sup>.

Only a small yield of polymer is obtained from the polymerization of vinyl chloride by the catalyst system  $\text{TiCl}_4/\text{AlEt}_3$  in the absence of additives such as

*Table 1* Recovery of tetrahydrofuran  
[Vinyl halide]=2.54 mol/l; solvent=benzene; polymerization time=48h; temperature=30°C

Monomer	Concentration of tri-isobutyl-aluminium (mol/l)	[THF]		Recovery of tetrahydrofuran (%)
		[ $\text{VOCl}_3$ ]	[ $\text{Al}(\text{iBu})_3$ ]	
Vinyl fluoride	0.527	1:1	4.6:1	96
Vinyl chloride	0.0105	2.5:1	6:1	95

tetrahydrofuran<sup>4</sup>. On interaction of the catalyst components evolution of hydrogen chloride has been reported<sup>4</sup>. By analogy with the findings of Bacskai<sup>5</sup> it is possible that in these systems the following reactions take place leading to the elimination of hydrogen chloride, and the formation of polymer with a low chlorine content:



Aluminium alkyls are known<sup>6</sup> to form complexes with tetrahydrofuran. Such complex formation would considerably reduce the reactivity of the aluminium alkyl, and hence prevent the formation of the carbonium ion. It is now well established that when aluminium chloroalkyls react with poly(vinyl chloride) carbonium ion formation results<sup>7</sup>. The suppression of this carbonium ion formation is one of the fundamental conditions for obtaining a successful Ziegler-Natta type catalyst for the polymerization of vinyl chloride.

The vanadium compound in the catalyst system would also be expected to be complexed by the tetrahydrofuran; both the complexes  $\text{VOCl}_3 \cdot \text{THF}$  and  $\text{VOCl}_2 \cdot 2\text{THF}$  have been reported in the literature<sup>8</sup>.

#### Oxidation state of vanadium

A potentiometric method<sup>9</sup> was used to determine the oxidation state of the vanadium in the catalyst. Experimental details together with results are given in Table 2.

Immediate reduction of V(V) to V(IV) occurs on mixing the catalyst components. Thereafter only slow reduction of V(IV) to V(III) occurs. Even after 3 days there is still 79% V(IV) present in the system.

Petrov and Korotkov<sup>10</sup> have studied the catalyst system  $\text{VOCl}_3/\text{AlEt}_3$  in benzene solution. They found that the oxidation state of the vanadium decreased with increase in triethylaluminium to vanadium oxytrichloride ratio; above a ratio of 2:1 the vanadium was present as V(II). Our results, however, show that using a tri-isobutylaluminium to vanadium oxytrichloride ratio of 2.5:1, the tetrahydrofuran restricts reduction below V(IV). Further reduction takes place only very slowly.

It is considered that there is a connection between the reduction of vanadium beyond V(IV) and the

Table 2 Oxidation state of vanadium in catalyst used for the polymerization of vinyl chloride  
[ $\text{VOCl}_3$ ] = 0.0105 mol/l; [Al(iBu)<sub>3</sub>]:[ $\text{VOCl}_3$ ] = 2.5:1  
[THF]:[ $\text{VOCl}_3$ ] = 7.7:1; temperature = 30°C

Ageing time (min)	V(V) (%)	V(IV) (%)	V(III) (%)	V(II) (%)
5	0	100	0	0
30	0	100	0	0
1440	0	92	8	0
4320	0	79	21	0

Table 3 Analysis of precipitate from cooling catalyst system to -193°C and raising to +5°C

[ $\text{VOCl}_3$ ] = 0.527 mol/l; [Al(iBu)<sub>3</sub>]:[ $\text{VOCl}_3$ ] = 1:1; [THF]:[ $\text{VOCl}_3$ ] = 4:1

Compound	Percentage in precipitate (wt %)
THF	55-65
Al	2.5-3
V	9-11

Table 4 Oxidation state of vanadium in precipitate and supernatant from catalyst system

[ $\text{VOCl}_3$ ] = 0.527 mol/l; [Al(iBu)<sub>3</sub>]:[ $\text{VOCl}_3$ ] = 1:1; [THF]:[ $\text{VOCl}_3$ ] = 4:1; temperature = 30°C

Ageing time (h)	Oxidation state of vanadium in precipitate				Oxidation state of vanadium in supernate			
	V(V) (%)	V(IV) (%)	V(III) (%)	V(II) (%)	V(V) (%)	V(IV) (%)	V(III) (%)	V(II) (%)
1/2	0	96	4	0	0	77	23	0
24	0	92	8	0	0	65	35	0
48					0	52	48	0
120					0	30	70	0

decrease in the rate of polymerization with time which was observed in earlier polymerizations<sup>1,2</sup>. Although the time scales of the two processes appear very different the percentage of V atoms active in polymerization is low<sup>3</sup>.

#### Isolation of $\text{VOCl}_2 \cdot 2\text{THF}$

When the polymerization system:



was cooled to low temperatures a light green precipitate was produced. Several of these precipitates were isolated by cooling the catalyst mixtures to -193°C, and then allowing the temperature to rise to 5°C. The precipitates were separated from the catalyst solutions by centrifugation for 30 min at 2000 rev/min at 5°C. Experimental details are listed in Table 3.

These results are somewhat inconclusive. The precipitates, isolated in this way, all contain small percentages of aluminium, which could arise through complex formation, adsorption, or even by freezing out of the aluminium alkyl.

Moreover, both the precipitate and the supernate polymerized vinyl fluoride to give about 10% conversion after 48 h.

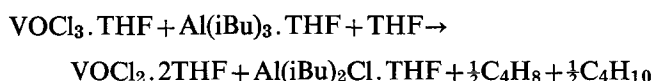
The oxidation state of the vanadium in the precipitate and the supernate was studied, and the results are listed in Table 4.

Vanadium is present in the precipitate as 96% V(IV), and therefore the vanadium compound present is most probably vanadium oxydichloride. Furthermore, since vanadium oxydichloride forms the complex  $\text{VOCl}_2 \cdot 2\text{THF}$  it is possible that the precipitate is largely  $\text{VOCl}_2 \cdot 2\text{THF}$  (see below).

#### Identification of gas produced on mixing catalyst components

When tri-isobutylaluminium is added to a solution of vanadium oxytrichloride and tetrahydrofuran a vigorous exothermic reaction takes place and a gas is

evolved. A solution of tri-isobutylaluminium in benzene was slowly added to a solution of vanadium oxytrichloride and tetrahydrofuran in benzene. The apparatus was connected to a nitrogen supply, and a slow stream of dried nitrogen was passed through the system. The gas liberated was collected in a trap. When all the alkyl had been added, the catalyst was stirred for 30 min. The trap was then removed from the apparatus, connected to a high vacuum system, and the gas was introduced into the distillation train. The gas was then purified by trap-to-trap distillation to remove any benzene which had been carried over by the nitrogen stream. This purification was effected by trap-to-trap distillation through traps cooled in slush baths of solid carbon dioxide in ethanol ( $-72^{\circ}\text{C}$ ), diethyl ether ( $-120^{\circ}\text{C}$ ) and liquid nitrogen ( $-196^{\circ}\text{C}$ ). The molecular weight of the gas liberated was found to be 58. Mass spectrographic analysis of the gas identified this as isobutane. The reaction between vanadium oxytrichloride and tri-isobutylaluminium in the presence of tetrahydrofuran may, therefore, be formulated as:



The formation, in these Ziegler-Natta systems, of an alkane through some hydrogen abstraction process has been well established. In both the reaction between trimethylaluminium and titanium tetrachloride<sup>11</sup> and trimethylaluminium and titanium trichloride<sup>12</sup> methane is evolved. The reaction between triethylaluminium and titanium tetrachloride has been studied<sup>13</sup> in the presence of carbon tetrachloride. No ethyl chloride was found. de Vries<sup>14</sup> and van Heerden<sup>15</sup> have shown that alkyl titanium compounds decompose by a bimolecular process yielding an olefin and an alkane, viz.:



This bimolecular process only occurs to a substantial degree when there is a hydrogen atom on the  $\beta$ -carbon atom of the titanium alkyl halide. No isobutene was identified in the gas liberated in the present experiments, but it is possible, however, that any isobutene produced could have been converted into solid polymer.

*Polymerization of vinyl chloride using tetravalent vanadium compounds*

Attempts were made to polymerize vinyl chloride using the following catalyst combinations:  $\text{VOCl}_2$ ;  $\text{VOCl}_2/\text{Al}(\text{iBu})_3$ ;  $\text{VOCl}_2/\text{Al}(\text{iBu})_3/\text{THF}$ . All these combinations produced heterogeneous systems. The results are shown in Table 5. Use of vanadium oxydichloride alone produces no polymer. In the other two catalyst systems the yield of polymer is low when compared to that obtained from the system  $\text{VOCl}_3/\text{Al}(\text{iBu})_3/\text{THF}$ . Evidently the active catalyst system



is not simply derived from vanadium oxydichloride.

The following catalyst combinations were then investigated:



The catalysts were prepared by addition of vanadium

oxydichloride tetrahydrofuranate to benzene followed by tetrahydrofuran and tri-isobutylaluminium when required. All these catalyst combinations produced homogeneous systems. Addition of tri-isobutylaluminium to a solution of vanadium oxydichloride tetrahydrofuranate in tetrahydrofuran changed the colour from pale blue to brownish green.

As can be seen from Table 6 use of vanadium oxydichloride tetrahydrofuranate alone does not produce an active catalyst. The most active catalyst is that produced when sufficient tetrahydrofuran is added to complex all the tri-isobutylaluminium. Figure 1 shows that the course of the polymerization is similar to that observed for polymerization using the catalyst system  $\text{VOCl}_3/\text{Al}(\text{iBu})_3/\text{THF}$ . As can be seen from Table 7 there is no appreciable increase in the initial rate of polymerization when the tetrahydrofuran to tri-isobutylaluminium ratio is increased from 1:1 to 40:1. This differs somewhat from the behaviour established for

Table 5 Polymerization of vinyl chloride using catalysts prepared from vanadium oxydichloride

[Vinyl chloride]=2.54 mol/l;  $[\text{VOCl}_2]=0.0104$  mol/l; polymerization time=24 h; temperature= $30^{\circ}\text{C}$

Catalyst	$\frac{[\text{Al}(\text{iBu})_3]}{[\text{VOCl}_2]}$	$\frac{[\text{THF}]}{[\text{VOCl}_2]}$	Conversion (%)
$\text{VOCl}_2$	—	—	No polymer
$\text{VOCl}_2/\text{Al}(\text{iBu})_3$	2:1	—	Traces
$\text{VOCl}_2/\text{Al}(\text{iBu})_3/\text{THF}$	2:1	7.7:1	3.3*

\* Corresponding value for catalyst system  $\text{VOCl}_3/\text{Al}(\text{iBu})_3/\text{THF}$  is 25%.

Table 6 Polymerization of vinyl chloride using catalysts prepared from vanadium oxydichloride tetrahydrofuranate

[Vinyl chloride]=2.54 mol/l;  $[\text{VOCl}_2 \cdot 2\text{THF}]=0.0104$  mol/l; polymerization time=24 h; temperature= $30^{\circ}\text{C}$

Catalyst	$\frac{[\text{Al}(\text{iBu})_3]}{[\text{VOCl}_2 \cdot 2\text{THF}]}$	$\frac{[\text{THF}]}{[\text{VOCl}_2 \cdot 2\text{THF}]}$	Conversion (%)
$\text{VOCl}_2 \cdot 2\text{THF}$	—	—	No polymer
$\text{VOCl}_2 \cdot 2\text{THF}/\text{Al}(\text{iBu})_3$	1:1	—	8
$\text{VOCl}_2 \cdot 2\text{THF}/\text{Al}(\text{iBu})_3/\text{THF}$	1:1	1:1	13

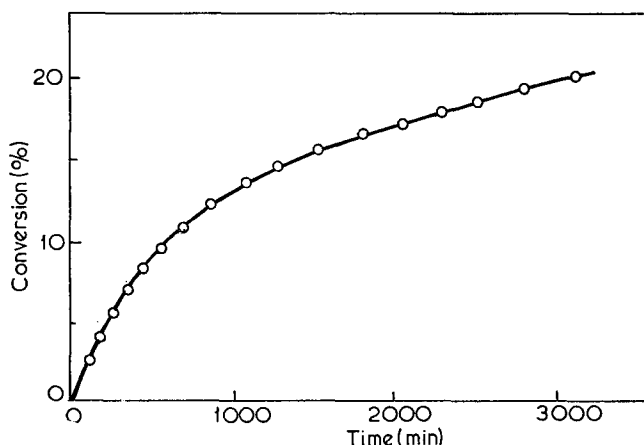


Figure 1 Plot of % conversion versus time for the polymerization of vinyl chloride with a catalyst prepared from vanadium oxydichloride. [Vinyl chloride]=2.54 mol/l;  $[\text{VOCl}_2 \cdot 2\text{THF}]=0.0104$  mol/l;  $[\text{Al}(\text{iBu})_3]:[\text{VOCl}_2 \cdot 2\text{THF}]=2:1$ ;  $[\text{THF}]:[\text{Al}(\text{iBu})_3]=3:1$ ; solvent=benzene; temperature= $30^{\circ}\text{C}$



**Table 7** Effect of tetrahydrofuran concentration on the initial rate of polymerization

[Vinyl chloride]=2.54 mol/l; [VOCl<sub>2</sub>.2THF]=0.0104 mol/l; [Al(iBu)<sub>3</sub>]:[VOCl<sub>2</sub>.2THF]=2:1; temperature=30°C

Concentration of tetrahydrofuran (mol/l)	$\frac{[\text{THF}]}{[\text{Al}(\text{iBu})_3]}$	Initial rate $\times 10^4$ (mol/l min)
—	—	5.1
0.021	1:1	10.2
0.063	3:1	10.2
0.84	40:1	10.9

**Table 8** Comparison of values of initial rates using VOCl<sub>3</sub> with those using VOCl<sub>2</sub> in the catalyst system

[Vinyl chloride]=2.54 mol/l; [vanadium compound]=0.0104 mol/l; [Al(iBu)<sub>3</sub>]:[vanadium compound]=2:1; [THF]:[Al(iBu)<sub>3</sub>]=3:1; temperature=30°C

Catalyst system	Initial rate $\times 10^4$ (mol/l min)
VOCl <sub>3</sub> /Al(iBu) <sub>3</sub> /THF	7.2
VOCl <sub>2</sub> .2THF/Al(iBu) <sub>3</sub> /THF	10.2

the more complex VOCl<sub>3</sub>/Al(iBu)<sub>3</sub>/THF system in which the critical ratio was found to be 6:1. However, as was observed for polymerizations using the catalyst system VOCl<sub>3</sub>/Al(iBu)<sub>3</sub>/THF the initial rate of polymerization is first order with respect to monomer and vanadium compound concentrations. Moreover, *Table 8* shows that the initial rates of polymerization by these two systems are very similar indeed.

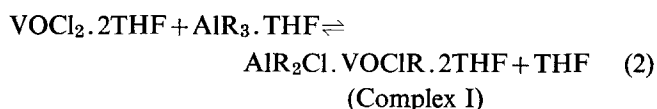
## DISCUSSION

The results presented in this paper demonstrate that the active centres in the catalyst system

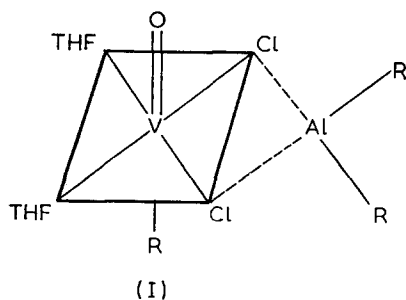


are formed by the interaction of vanadium oxydichloride tetrahydrofuranate and tri-isobutylaluminium in the presence of tetrahydrofuran. The first stage of this reaction is believed to be rapid complex formation as is indicated by the instantaneous colour change observed on adding the tri-isobutylaluminium.

In general the initial stage of the reaction may be formulated as<sup>16</sup>:



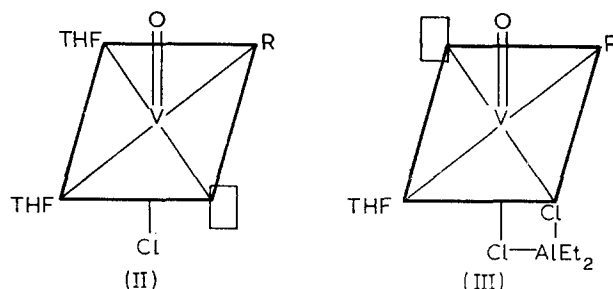
Complex I probably has the structure<sup>17</sup>:



In addition, the following equilibria may be established in the catalyst system:



Complex II has not been isolated, but would be expected to have the structure:

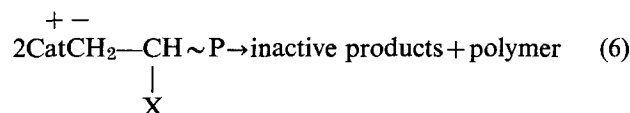


Such a complex is octahedral, possesses a vacant coordination position, and by analogy with the Cossee-Arlman theory<sup>18</sup> of heterogeneous Ziegler-Natta polymerization, could be considered a potential active site. Furthermore it would be present only in small concentrations since the equilibrium in reaction (3) would lie to the far left<sup>19</sup>. However, the active site could be a bimolecular complex of the type suggested by Henrici-Olivé and Olivé<sup>17</sup> (complex III) but this is considered somewhat less likely since the tetrahydrofuran would be expected to dominate the scene by its superior complexing power not only to vanadium (complex II) but it would encourage reactions (3) and (4) by complexing with AlR<sub>2</sub>Cl and Al<sub>2</sub>R<sub>5</sub>Cl. This would also explain why nearly maximum initial rate is attained at [THF]/[VOCl<sub>3</sub>] just over 4 (see *Table 4* of Part 1<sup>1</sup>).

The most striking feature of the kinetic results presented earlier<sup>1, 2</sup> was the rapid decrease in the overall rate of polymerization as a function of time. Evidently, the active centres are formed immediately the catalyst components are mixed. These centres are unstable and decompose. Many transition metal alkyl derivatives are known to decompose by means of a bimolecular process<sup>14, 15, 17</sup>, and if this were the case in the present system, then the rate of decrease of active centre concentration (C) would be given by the equation:

$$-\frac{dC}{dt} = k_d C^2 \quad (5)$$

where  $k_d$  is the rate constant for the bimolecular decomposition process:



Equation (5) assumes that no further active centres are generated in the system after the catalyst components are mixed.

Integration of equation (5) between  $t=0$  and  $t=t$  gives:

$$C_t = \frac{1}{k_d t + 1/C_0} \quad (7)$$

where  $C_0$  and  $C_t$  are the active centre concentrations at  $t=0$  and  $t=t$  respectively.

Under conditions where the concentration of monomer is constant, or nearly so:

$$\frac{C_t}{C_0} = \frac{R_t}{R_0} \quad (8)$$

where  $R_0$  and  $R_t$  are the overall rates of polymerization at  $t=0$  and  $t=t$  respectively.

Thus equation (7) becomes:

$$\frac{R_0}{R_t} = C_0 k_a t + 1 \quad (9)$$

A plot of  $(R_0/R_t) - 1$  against  $t$  should therefore be a straight line of slope  $k_a C_0$ .

At low conversions such a plot is indeed linear, and a typical plot is shown in Figure 2. Above about 5% conversion deviation from linearity occurs.

Earlier kinetic results have shown that the initial rate of polymerization is proportional to the monomer (M) and catalyst concentrations. If chain propagation is assumed to proceed by means of the insertion mechanism, believed to operate in Ziegler-Natta systems, the rate of polymerization ( $R_p$ ) will be given by:

$$R_p = \frac{-dM}{dt} = k_p C_t [M] \quad (10)$$

where  $k_p$  is the rate constant for propagation.

Substitution for  $C_t$  from equation (7) yields:

$$\frac{-dM}{[M]} = \frac{k_p dt}{k_a t + 1/C_0} \quad (11)$$

Integration between the limits  $t=0$  and  $t=t$  gives:

$$\ln \frac{[M]_0}{[M]_t} = \frac{k_p}{k_a} \ln(k_a C_0 t + 1) \quad (12)$$

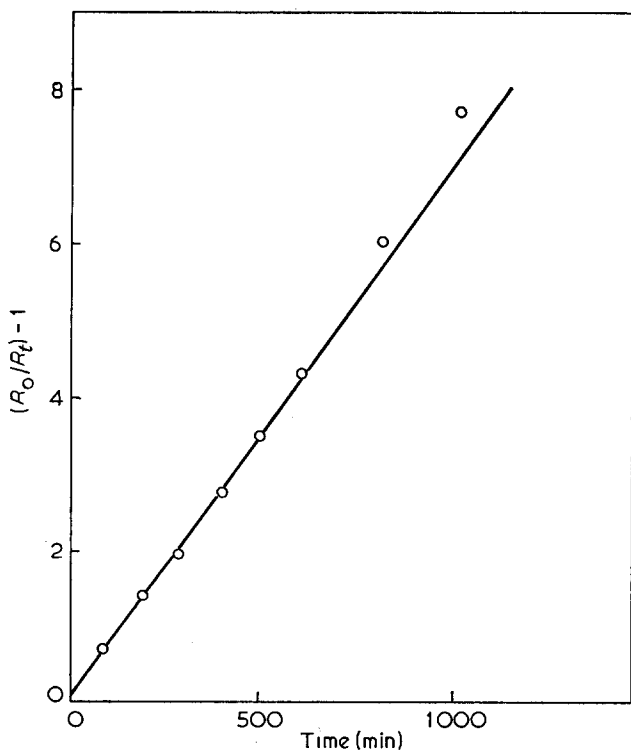


Figure 2 Plot of  $(R_0/R_t) - 1$  versus time at 30°C. [Vinyl chloride]=1.96 mol/l;  $[VOCl_3]=0.0104$  mol/l;  $[Al(iBu)_3]:[VOCl_3]=5.3:1$ ;  $[THF]:[VOCl_3]=10:1$

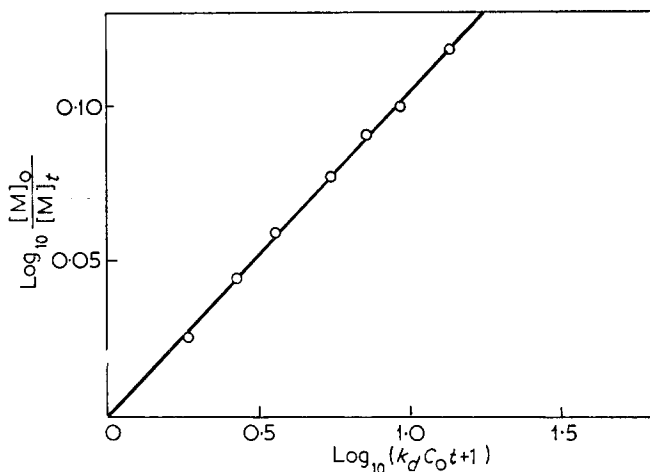


Figure 3 Plot of  $\log_{10}[M]_0/[M]_t$  versus  $\log_{10}(k_d C_0 t + 1)$ . Experimental details as for Figure 2

Table 9 Variation of  $k_d C_0$ ,  $k_p/k_d$  and  $k_p C_0$  with tetrahydrofuran concentration

[Vinyl chloride]=1.96 mol/l;  $[VOCl_3]=0.0104$  mol/l;  $[Al(iBu)_3]:[VOCl_3]=2.5:1$ ; temperature=30°C

$[THF] \times 10^2$ (mol/l)	$\frac{[THF]}{[VOCl_3]}$	$k_d C_0 \times 10^3$ (min <sup>-1</sup> )	$\frac{k_p}{k_d}$	$k_p C_0 \times 10^3$ (min <sup>-1</sup> )
4.2	4.0	3.57	0.09	0.33
6.5	6.2	1.75	0.28	0.49
39.0	37.5	1.75	0.28	0.49
116	112	1.75	0.28	0.49
350	337	1.75	0.28	0.49
506	481	1.75	0.28	0.49

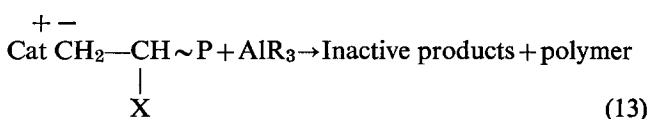
where  $[M]_0$  and  $[M]_t$  are the monomer concentrations at  $t=0$  and  $t=t$  respectively.

A plot of  $\ln[M]_0/[M]_t$  against  $\ln(k_a C_0 t + 1)$  should therefore be linear and of slope  $k_p/k_a$ . Such a plot is shown in Figure 3 and is considered to be excellent confirmation of the proposed theory.

The effect of variation of the ratio of tetrahydrofuran to vanadium oxytrichloride on the values of  $k_a C_0$ ,  $k_p C_0$  and  $k_p/k_a$  was investigated, and the results are shown in Table 9. Above a ratio of tetrahydrofuran to vanadium oxytrichloride of 6.5:1  $k_a C_0$  is strictly constant, indicating a constant number of active centres in the polymerization system. The reason for the higher value of  $k_a$  at a ratio of tetrahydrofuran to vanadium oxytrichloride of 4.0:1 is probably because insufficient tetrahydrofuran is present to complex all the vanadium and tri-isobutylaluminium; a ratio of 4.5:1 is required for this.

The effect of variation of the tri-isobutylaluminium concentration on the values of  $k_a C_0$ ,  $k_p C_0$  and  $k_p/k_a$  is shown in Table 10. It is evident that in this case there is a gradual increase in the number of active centres and also an increase in  $k_a$  with increase in tri-isobutylaluminium concentration. Evidently the postulated kinetic scheme has been too simplified.

An increase in  $C_0$  with increase in the tri-isobutylaluminium concentration could arise from either reaction (4) or (2), whilst the apparent increase in  $k_a$  may be due to reactions such as:



which have not been allowed for in the reaction scheme.

Table 10 Variation of  $k_d C_0$ ,  $k_p/k_d$  and  $k_p C_0$  with tri-isobutyl-aluminium concentration

[Vinyl chloride]=1.96 mol/l; [VOCl<sub>3</sub>]=0.0104 mol/l; [THF]:  
[Al(iBu)<sub>3</sub>]=10:1; temperature=30°C

[Al(iBu) <sub>3</sub> ] × 10 <sup>2</sup> (mol/l)	[Al(iBu) <sub>3</sub> ] [VOCl <sub>3</sub> ]	$k_d C_0 \times 10^3$ (min <sup>-1</sup> )	$\frac{k_p}{k_d}$	$k_p C_0 \times 10^3$ (min <sup>-1</sup> )
1.56	1.5	0.80	0.41	0.33
2.70	2.6	1.75	0.28	0.49
3.32	3.2	2.06	0.23	0.48
3.95	3.8	2.40	0.26	0.62
4.90	4.8	4.6	0.16	0.73
5.51	5.3	7.3	0.106	0.78
6.55	6.3	9.8	0.104	1.02

In conclusion the kinetic behaviour of this somewhat novel catalyst system is consistent with the mechanism believed to operate in many Ziegler-Natta systems, and can be accounted for by means of a simple kinetic scheme, which involves a rapid bimolecular decomposition of a transition metal alkyl compound, or of a complex formed on interaction of a transition metal alkyl with an aluminium alkyl.

## REFERENCES

- 1 Haszeldine, R. N., Hyde, T. G. and Tait, P. J. T. *Polymer* 1973, **14**, 215
- 2 Haszeldine, R. N., Hyde, T. G. and Tait, P. J. T. *Polymer* 1973, **14**, 221
- 3 Shore, G. S. and Tait, P. J. T. to be published
- 4 Solvay and Cie, Belg. Pat. 545 968 (1956)
- 5 Bacskai, R. *J. Polym. Sci. (A)* 1965, **3**, 2491
- 6 Bonitz, E. *Chem. Ber.* 1955, **88**, 742
- 7 Thame, N. G., Lunberg, R. D. and Kennedy, J. P. *J. Polym. Sci. (A-1)* 1972, **10**, 2507
- 8 Kern, R. *J. Inorg. Nucl. Chem.* 1962, **24**, 1105
- 9 Carrick, W. L., Reichle, W. T., Pennella, F. and Smith, J. J. *J. Am. Chem. Soc.* 1960, **82**, 3888
- 10 Petrov, G. N. and Korotkov, A. *Dokl. Akad. Nauk. SSSR* 1961, **141**, 632
- 11 Ziegler, K., Martin, H. and Stedefeder, J. *Tetrahedron Lett.* 1959, **20**, 12
- 12 Rodriguez, L. and Gabant, J. *J. Polym. Sci.* 1962, **57**, 881
- 13 Eden, C. and Feilchenfeld, H. *Tetrahedron* 1962, **18**, 233
- 14 de Vries, H. *Rec. Trav. Chim. Pays-Bas* 1961, **80**, 866
- 15 van Heerden, C. *J. Polym. Sci.* 1959, **34**, 47
- 16 Gilman, H. and Jones, R. G. *J. Org. Chem.* 1945, **10**, 505
- 17 Henrici-Olivé, G. and Olivé, S. *Angew. Chem. (Int. Edn)* 1963, **67**, 2477
- 18 Arlman, E. J. *J. Catalysis* 1964, **3**, 89
- 19 Rodriguez, L. A. M., van Looy, H. M. and Gabant, J. A. *J. Polym. Sci. (A-1)* 1966, **4**, 1905

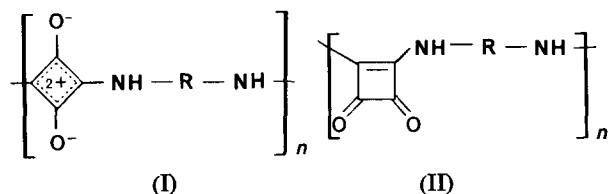
# Note to the Editor

## Polyamides derived from squaric acid

Brian R. Green and Eberhard W. Neuse

Department of Chemistry including Biochemistry, University of the Witwatersrand, Johannesburg, South Africa  
(Received 2 January 1973)

In a recent study<sup>1,2</sup>, Gauger and Manecke obtained polyamides from squaric acid (1,2-dihydroxycyclobuten-3,4-dione) and difunctional amines, such as *p*-phenylenediamine or hexamethylenediamine, by solution polymerization and other techniques. Structures I (R = 1,4-phenylene, 4,4'-biphenylene, polymethylene) were ascribed to representative polymers on the strength of i.r. spectral data and by comparison with analogous non-polymeric amidation reactions of squaric acid<sup>3-6</sup>. The same workers prepared polyamides assigned the isomer structure II from diethyl squarate (1,2-diethoxycyclobuten-3,4-dione) and difunctional amines by similar solution polymerization techniques.



More recent work in our laboratory on non-polymeric amidation reactions of squaric acid<sup>7</sup> suggested, however, that the experimental conditions of Gauger and Manecke should be conducive to 1,3- as well as 1,2-orientation (albeit the former predominant) of the substituents on the four-membered ring system and so should furnish polycondensation products not precisely of the type I, but rather possessing a 'copolymer' structure that comprises the units of both I and II in its backbone.

A synthetic programme involving the polycondensation of squaric acid with *p*-phenylenediamine by solution polymerization techniques, including those employed previously<sup>1,2</sup>, has indeed confirmed these expectations. Duplicating the condensations of Gauger and Manecke<sup>2</sup>, we condensed equimolar quantities of squaric acid and *p*-phenylenediamine in refluxing glycerol. The dark brown polymer separated and purified as described<sup>2</sup> gave an i.r. spectrum that exhibited the strong cyclobutenediylidyl diolate absorption<sup>2,5,9</sup> near 1600 cm<sup>-1</sup> (superimposed on a phenylene ring-vibrational mode at this position) and additionally gave in moderate intensity the characteristic pair of (*asym* and *sym*) carbonyl stretching bands<sup>2,5,8</sup> of the cyclobutenedione system near 1786 and 1675 cm<sup>-1</sup>, the latter appearing as a shoulder on the diolate absorption band. A similar absorption pattern was observed with polymers obtained from the same starting materials on solution polymerization in *N*-methylpyrrolidone (containing 5% LiCl) or polyphosphoric acid (83% P<sub>2</sub>O<sub>5</sub> content) under the conditions summarized in Table 1.

In a 1,3-diamide structure, as represented by I, the cyclobutenedione absorption in the 1680–1840 cm<sup>-1</sup> region should be strictly absent<sup>5</sup>, and any bands appearing at this position should then be entirely due to (monosubstituted) squaryl end groups. In this case, however, in view of the relatively low concentrations of such end groups in the polymers synthesized (especially those possessing higher viscosities), one would expect lower band intensities than observed. Furthermore, the intensities of the two bands should increase with de-creas-

Table 1 Solution polymerization of squaric acid and *p*-phenylenediamine<sup>a</sup>

Exp. No.	Heating conditions	Solvent <sup>b</sup>	Squaric acid conc. (mol/l)	Polymer yield (%)	$\eta_{inh}^c$ (ml/g)	Remarks	Ref.
1	10 min at reflux temp. <sup>d</sup>	glycerol	0.25	91.5	15.8	product precipitates from soln during heating period	1,2
2	4 h at reflux temp.	NMP	0.09	61.3 <sup>e</sup>	9.7 <sup>f</sup>	product precipitates partly from soln during reaction; second portion precipitated by excess water	this work
3	20 h at 160°C 2.5 h at 220°C	PPA	0.17	92.5	17.1	product remains in soln throughout, is precipitated by excess water	this work
4	15 h at 165°C	PPA	0.67	96.8	29.1	as in 3	this work

<sup>a</sup> Equimolar quantities of reactants. All solvents degassed; experiments conducted under N<sub>2</sub>. Crude products reprecipitated from 98% H<sub>2</sub>SO<sub>4</sub>. Acceptable elemental analyses obtained on all polymers

<sup>b</sup> NMP = *N*-methylpyrrolidone; PPA = polyphosphoric acid

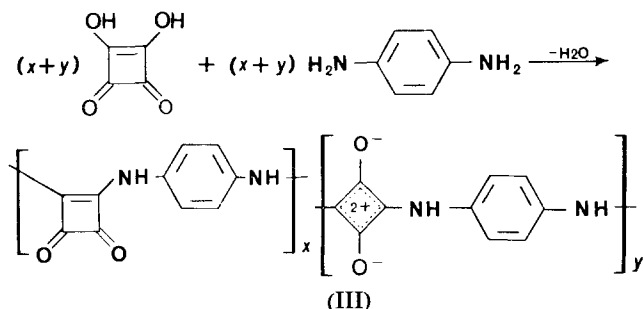
<sup>c</sup> 0.5% (w/v) at 30°C in 98% H<sub>2</sub>SO<sub>4</sub>

<sup>d</sup> Additional 40 min at reflux, as solvent is partly distilled off

<sup>e</sup> Yield of portion precipitating during reaction (additional 38% of product precipitated by water)

<sup>f</sup> Determined on portion precipitating during reaction (7.3 on product precipitated by water)

ing molecular weight, a trend that we were, at least qualitatively, unable to observe on fractionated material. Finally, squaryl end groups and hence carbonyl band intensities should undergo a drastic decrease upon further reaction of the polymers with excess *p*-phenylenediamine. Such an experiment was performed with polymer No. 1 (3 h at 150°C in polyphosphoric acid), but no change in intensities of the two bands could be noticed. We are thus led to conclude that the polyamides here described must be represented by the copolymer structure III, with both unit types likely to be randomly distributed along the chain. As far as the relative occurrence of the two units is concerned, we can only qualitatively assess at this stage that  $y > x$ . This question is being examined in more quantitative terms.



The viscosity data listed in *Table 1* point to the advantage in using polyphosphoric acid as the reaction medium,

this advantage deriving from superior efficacy of polyphosphoric acid as a condensing agent and, more importantly, from retained product solubility throughout the reaction, allowing for homogeneous chain-growth conditions.

Efforts to study the electronic absorption characteristics of the described polyamides and related polymers derived from squaryl esters and squaryl dichloride are in progress.

## REFERENCES

- 1 Gauger, J. and Manecke, G. *Angew. Chem.* 1969, **81**, 917; *Angew. Chem. (Int. Edn)* 1969, **8**, 898
- 2 Manecke G. and Gauger, J. *Makromol. Chem.*, 1969, **125**, 231; Gauger, J. and Manecke, G. *Kinet. Mech. Polyreactions, Int. Symp. Macromol. Chem. Prepr.* 1969, **1**, 31; *Chem Abstr.* 1971, **75**, 64331
- 3 Manecke, G. and Gauger, J. *Tetrahedron Lett.*, 1967, p 3509; 1968, p 1339
- 4 Sprenger, H.-E. and Ziegenbein, W. *Angew. Chem.* 1968, **80**, 541; *Angew. Chem. (Int. Edn)* 1968, **7**, 530
- 5 Gauger, J. and Manecke, G. *Chem. Ber.* 1970, **103**, 2696, 3553
- 6 Sprenger, H.-E., DBP.-Anm. C 41650 IVb/120 (1967); Offenleg. 1618211 (1971)
- 7 Neuse, E. and Green, B. *Liebigs Ann. Chem.* in press
- 8 Baglin, F. G. and Rose, C. B., *Spectrochim. Acta* 1970, **26A**, 2293
- 9 Treibs, A. and Jacob, K. *Liebigs Ann. Chem.* 1966, **699**, 153

# ENERGY POLICY

A NEW QUARTERLY JOURNAL

## *The economics and planning of energy*

**ENERGY POLICY** will deal with the economics and planning of the production, conversion and use of energy. It will publish articles, reports and book reviews that deal with the availability of fuels and with the efficiency, applicability and acceptability of different forms of energy production and conversion.

**ENERGY POLICY** will be

**International:** covering the resources and capabilities of particular countries and regions and the increasing interdependence of their needs:

**Integrative:** including coal, oil, gas, nuclear, hydro and alternative energy sources:

**Interdisciplinary:** drawing together studies by technologists with those of economists, geographers, environmentalists and political scientists.

**ENERGY POLICY'S** aim will be to help the manager and planner concerned with the fuel and energy industries develop a coherent overall picture of this complex and fast-changing subject.

**ENERGY POLICY** will be guided by a distinguished international editorial board. Each issue will contain in depth articles and these will be complemented by reports and reviews of publications.

Published quarterly in March, June, September, December, commencing with the June 1973 issue.

One-year subscription (four issues) £14.00 (\$36.40)  
\*Special pre-publication offer £10.00 (\$26.00) if ordered before 31st May 1973.

For full details apply to  
IPC Science and Technology Press Limited, (Dept AD.EP.2F)  
IPC House, 32 High Street, Guildford, Surrey, England.  
Telephone: Guildford (0483) 71661

Conference Announcement

10 — 14 September 1973

The Chemical Society

## IUPAC International Symposium on Macromolecules

### University of Aberdeen

The 1973 IUPAC International Macromolecular Symposium will take place in the King's College area of Old Aberdeen, which is the main centre of the University, from 10 to 14 September. The scientific programme will include the following Invited Lectures:

- Crystal structure and morphology of polymers from solid state reactions  
*W. W. Fischer and G. Wagner (University of Mainz)*
- The Phillips polyethylene process  
*J. P. Hogan (Phillips Petroleum Company)*
- Compatibility of polydisperse polymers  
*R. Koningsveld (Dutch State Mines)*
- New thermally stable adhesive resins  
*C. S. Marvel (University of Arizona)*
- Polymerization and cyclopolymerization of 2-oxazoline  
*T. Saegusa (Kyoto University)*
- Fundamental problems concerning interrelation of polymer structures and their rheological properties in the fluid state  
*G. V. Vinogradov (USSR Academy of Sciences)*
- Neutron scattering studies of self-diffusion in rubbers and polymeric melts  
*G. Allen (University of Manchester)*
- Liquid systems for rubber products including tyres  
*G. Alliger (Firestone Tyre and Rubber Company)*
- Elastic properties of crosslinked polymers  
*G. Rehage (Technical University, Clausthal)*
- Morphology and mechanical properties in semi-crystalline polymers  
*E. H. Andrews (Queen Mary College, London)*
- Block copolymers—structure and properties  
*H. C. Benoit (CNRS, Strasbourg)*
- Towards a molecular interpretation of material transport in polymers  
*P. Meares (University of Aberdeen)*
- Synthesis and properties of asymmetric polymers  
*C. G. Overberger (University of Michigan)*
- Viscoelastic behaviour and yielding processes of glassy and composite polymers in multiaxial stress states  
*S. S. Sternstein (Rensselaer Polytechnic Institute)*
- Development and application of *trans*-1,5-poly-pentamer (TPR)  
*D. Theisen (Farbenfabriken Bayer AG)*
- Problems in crosslinking  
*G. M. Burnett (University of Aberdeen)*
- Chain orientation and crystallization  
*A. Keller (University of Bristol)*
- Some relaxation studies of environmental effects in solid polymers  
*A. M. North (University of Strathclyde)*
- Influence of morphology on the transport of liquids, vapours and gases in crystalline polymers  
*A. Peterlin (Research Triangle Institute, North Carolina)*
- Chemical reactions in polymeric systems  
*G. Smets (University of Louvain)*
- Fracture mechanics of craze growth in polymers  
*J. G. Williams (Imperial College, London)*

In addition there will be 24 Symposium Lectures as well as numerous contributed papers. Full details of these, together with abstracts and accommodation details will be given in the final programme to be sent out in August.

The second circular and application forms are now available from Dr John F. Gibson, Chemical Society, Burlington House, London W1V 0BN, England and to whom completed registration forms should be sent by 16 July 1973. Intending participants are advised, however, to finalize their travel and hotel accommodation arrangements before this date, although accommodation will be available in halls of residence at the University.

Further details about the ladies programme and social events, including the afternoon/evening excursions on Wednesday, 12 September when no scientific sessions/formal functions are scheduled, are given in Circular 2.

# Stereoregular polymerization of vinyl chloride with the redox system ferrous sulphate/hydrogen peroxide/oxalic acid: 1. Influence of some synthesis conditions on the stereoregularity of PVC

K. Dimov and L. Slavtcheva

*Higher Institute of Chemical Technology, Sofia 56, Bulgaria  
(Received 14 November 1972; revised 6 February 1973)*

The emulsion polymerization of vinyl chloride with the redox catalyst system ferrous sulphate/hydrogen peroxide/oxalic acid has been studied in the temperature range  $-30^{\circ}\text{C}$  to  $+20^{\circ}\text{C}$ . The effects of the catalyst components' ratio and polymerization temperature on the stereoregular structure, thermostability and molecular weight of the obtained poly(vinyl chloride) were investigated.

## INTRODUCTION

Obtaining poly(vinyl chloride) (PVC) of stereoregular structure and minimum content of chain branches with higher thermostability characteristics is of interest in the production of fibres and foil.

Until recently low temperature polymerization<sup>1</sup> has predominantly applied as a method for obtaining a polymer of stereoregular structure and higher thermostability but now investigations are being carried out also at temperatures above  $0^{\circ}\text{C}$ <sup>2</sup>.

The stereoregularity of poly(vinyl chloride) is increased by applying emulsion, suspension or bulk polymerization of vinyl chloride with redox-type catalysts. These can be water-soluble (inorganic salts of Fe, Cu, Ni, Co, Mn inorganic peroxides, for instance the system ferrous sulphate/hydrogen peroxide/oxalic acid<sup>3</sup>) or soluble in the monomer (carboxylic acid salts/organic peroxides, for instance ferrous caproate/lauryl peroxide<sup>4</sup>.) The use of chloroacetyl peroxides<sup>5</sup> for initiation of low temperature polymerization of vinyl chloride is well known.

However, a number of problems pertaining to the realization of stereoregular polymerization of vinyl chloride including the use of the redox system ferrous sulphate/hydrogen peroxide/oxalic acid, are not yet explained, irrespective of the above mentioned investigations. The effect of polymerization temperature ( $T_p$ ) on stereoregularity and the yield of PVC remains an undecided problem. Also, no complete investigation has been made about the dependence of structure and softening temperature on the molar ratio of components in the redox system.

The present investigations are intended to follow the effect of  $T_p$  and the ratio of components in the redox system ferrous sulphate/hydrogen peroxide/oxalic acid on the thermostability and stereoregularity of the poly(vinyl chloride) obtained.

## EXPERIMENTAL

### *Materials*

*Monomer.* Commercial vinyl chloride was purified by distillation in which its vapour bubbled through concentrated aqueous NaOH solution to eliminate inhibitors (hydroquinone and t-butyl catechol) and all traces of hydrochloric acid. Then the gas (b.p.  $-13.9^{\circ}\text{C}$ ) was dried over granulated KOH and collected in a cooled glass vessel. The monomer purity was determined by gas chromatographic analysis<sup>6</sup> in a Perkin-Elmer F11 gas chromatograph. It was 99.8% vinyl chloride, 1,1'-dichloroethane appearing as an impurity.

*Catalyst.* The catalyst system components were commercial products: ferrous sulphate (analytical reagent grade), containing 99% active substance, was purified by recrystallization from water; hydrogen peroxide (perhydrol) was analytical reagent grade (non-stabilized) containing 30%  $\text{H}_2\text{O}_2$ ; oxalic acid was purified by recrystallization from an aqueous solution, m.p.  $101.5^{\circ}\text{C}$ .

*Emulsifier E30.* This was a commercial product representing the sodium salt of mepasin\* sulphonic acid ( $\text{C}_n\text{H}_{n+1}\text{SO}_3\text{Na}$ ,  $n=12-18$ ). The emulsifier content of mepasin sulphonate was over 92%. In the polymerization process E30 was used in the form of a 25% aqueous solution.

*Solvent for the polymer.* Cyclohexanone, was an imported product of VEB Laborchemie Apolda (GDR), of purum level purity:  $n_D^{20}=1.4507$ ; m.p.  $155^{\circ}\text{C}$ .

### *Methods*

Polymerization of vinyl chloride was carried out in a stainless-steel autoclave fitted with a magnetic stirrer and a coil for heat circulation. Reaction temperature

\* Mersenburg Paraffinen Syntese: fraction of synthetic petrol obtained by the Fischer-Tropsch synthesis, which was purified from unsaturated and oxy-compounds by hydration.

conditions were maintained by means of an ultrathermostat and were controlled by a thermometer incorporated in a special case welded to the cap of the autoclave.

The initial charge was 0.450 l of aqueous methanol solution (2:1 water:methanol), ferrous sulphate (from 0.0315 to 0.538% by weight against VC) 0.250 g of oxalic acid and emulsifier (0.975% by weight against the aqueous methanol phase). The autoclave was purged with pure nitrogen (oxygen content <0.1%) and was then evacuated three times for 15 min each time at 20°C to a resulting pressure of 10 mmHg. In the intervals between the evacuations it was purged with nitrogen. The autoclave was then cooled to -30°C and charged with 186 g of vinyl chloride and hydrogen peroxide (from 0.247 to 0.860% by weight against VC). Exact doses of monomer were determined by volume. The process was carried out in nitrogen with continuous stirring.

When the reaction was completed, the suspension was filtered and the filtrate was precipitated with a 5% aqueous solution of potassium aluminium sulphate. The additionally coagulated polymer was filtered, washed and dried in vacuum at 60°C.

The poly(vinyl chloride) obtained was characterized by determining its relative viscosity (0.5% solution in cyclohexanone at 25°C) and Fikentsher  $K$  value. According to Krimm and Liang<sup>7</sup> fluctuations of the conformation are shown by i.r. absorptions between 600 and 700  $\text{cm}^{-1}$  and so the syndiotactic index  $D_{635/692}$  was obtained by infra-red spectroscopy using a Carl Zeiss (GDR) IR-20 apparatus. The softening temperature ( $T_g$ ) was obtained by differential thermal analysis carried out in a derivatograph (Paulik-Paulik-Erdey system, Orion type).

## RESULTS AND DISCUSSION

Polymerization was carried out by an emulsion method in water-methanol.

The redox system used is related to the water-soluble systems. Its decomposition in the water-methanol solution of vinyl chloride (VC) is slowed down by increasing the content of methanol in the VC. Increased concentration of methanol in the system leads to increased solubility of VC in the aqueous phase and to partial sedimentation from this phase of the polymer obtained, i.e. a heterogeneous process occurs. The amount of the so called 'pearl' polymer (precipitated polymer) thus obtained is variable and depends on the polymerization temperature and agitation of the reaction medium. Best yields are obtained at a polymerization temperature of -30°C (58% to 70% of the total amount of the obtained polymer). Its content at temperatures higher than -15°C is below 1% of the total polymer. It should be noted that quality indices of the 'pearl' poly(vinyl chloride) are different from those of the polymer separated by coagulation with potassium aluminium sulphate. In carrying out vinyl chloride polymerization at low temperatures best results are obtained at a 50% content of methanol in the aqueous phase.

Participation of oxalic acid is intended to reduce  $\text{Fe}^{3+}$  to  $\text{Fe}^{2+}$  which gives an opportunity for more complete use of the redox components and of the reducing agent in particular. It helps in addition to establish a pH of 3 in the medium for the process to proceed.

In emulsion polymerization the present redox system

reacts in both acidic and alkaline media but heterogeneous polymerization of vinyl chloride in methanol occurs only in an acidic medium<sup>8</sup>. Preferably organic acids which do not decrease thermostability of the polymer are used for this.

Figure 1 and Figure 2 give the results obtained in the investigation of the effect of molar ratio of the redox system components on the yield and properties of the poly(vinyl chloride) obtained at a polymerization temperature of -20°C. As can be seen from data in these Figures, a polymer of highest yield and molecular weight, of highest content of the crystalline phase and highest glass-transition temperature ( $T_g$ ) is obtained at a ratio of the molar concentration of the reducing to the oxidizing agent  $C_1/C_2=0.093$ , where  $C_1$  is molar concentration of ferrous sulphate and  $C_2$  is the molar concentration of hydrogen peroxide.

Figure 3 and Figure 4 illustrate the results from the investigation of the effect of  $T_p$  on the yield and properties of the polymer. Figure 3 shows that as expected the molecular weight of the polymer increases as  $T_p$  is decreased. This increase is very rapid below -20°C while the change of temperature from -20°C to +20°C

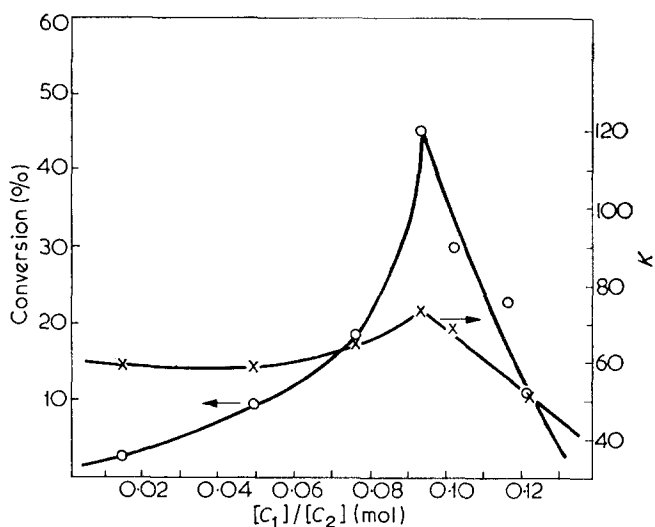


Figure 1 Dependence on the rate of polymerization of vinyl chloride (O) and the molecular weight of the polymer (x) on the molar ratio in the redox system. Polymerization temperature, -20°C; duration of process, 7 h

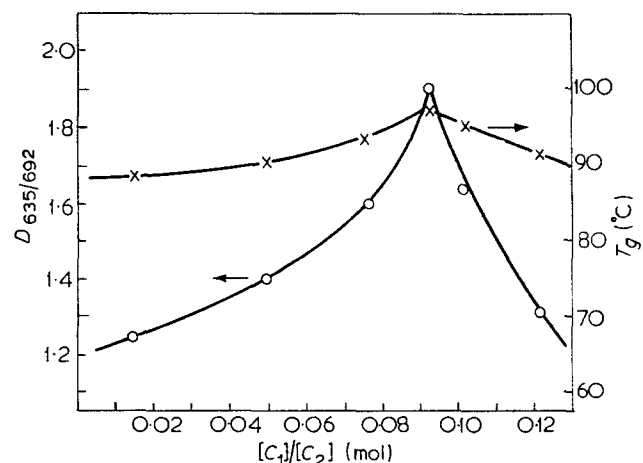


Figure 2 Dependence of syndiotactic level (O) and  $T_g$  (x) of poly(vinyl chloride) on the molar ratio in the redox system. Polymerization temperature, -20°C; duration of process, 7 h



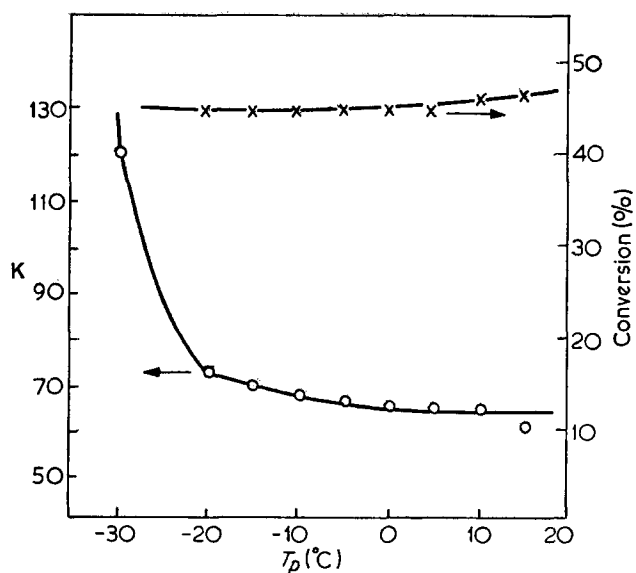


Figure 3 Dependence of the molecular weight (O) and the yield (x) of poly(vinyl chloride) on polymerization temperature. Molar ratio of ferrous sulphate to hydrogen peroxide, 0.093; duration of process, 7 h

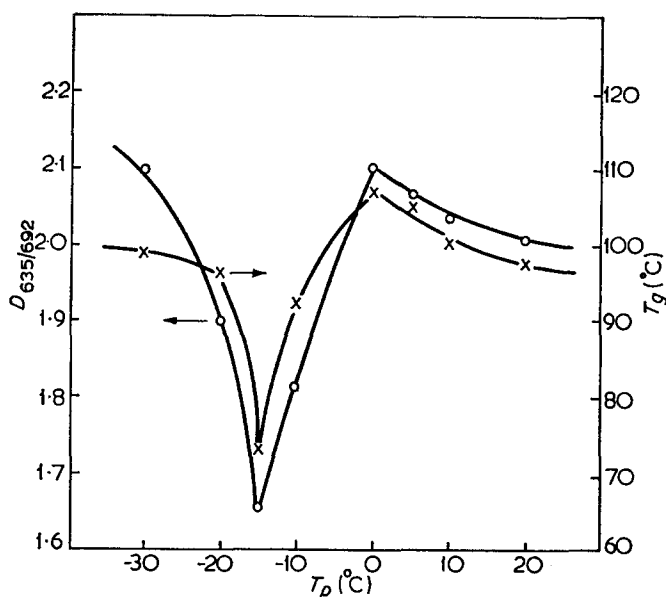


Figure 4 Dependence of syndiotactic level (O) and  $T_g$  (x) of poly(vinyl chloride) on polymerization temperature. Molar ratio of reducing to oxidizing agent 0.093; duration of process, 7 h

gives only a slight effect. Polymerization temperature has a negligible effect on the yield of PVC.

Figure 4 gives the dependence of the stereoregular structure of PVC and of  $T_g$  on  $T_p$ . In contrast to expectations for a predominant quantity of atactic PVC at reaction temperatures above  $-13.9^\circ\text{C}$ , the present

investigations have shown that when the redox system ferrous sulphate/hydrogen peroxide/oxalic acid is used at temperatures above  $0^\circ\text{C}$  a polymer of a characteristic stereoregular structure is obtained. The syndiotactic index is quite high (2.02) even at a temperature close to room temperature ( $15^\circ\text{C}$ ). The  $T_g$  of PVC also increases when it is obtained at reaction temperatures above the VC b.p. In the investigated temperature range of polymerization, maximum  $T_g$  and syndiotactic ratio are both obtained at  $0^\circ\text{C}$ .

The maximum and minimum points on the curves reflecting the change of  $D_{635/692}$  and  $T_g$  are seen in Figure 4, at the f.p. of water and the b.p. of VC. To explain this we proceed from the generally accepted assumption that a suitable preliminary orientation of the monomer molecules involved in polymerization is favourable for obtaining polymers of higher stereoregular structure. In conforming with these conditions, the stereoregularity of the PVC obtained and simultaneously its  $T_g$  should increase with decreasing polymerization temperature. In our investigations this dependence is valid for reaction temperatures below the b.p. of VC. The range of temperatures above  $-13.9^\circ\text{C}$  is of interest. Here a continuous growth of  $D_{635/692}$  and  $T_g$  to  $0^\circ\text{C}$  is observed, after which these magnitudes change slightly with a trend to reduction.

#### CONCLUSION

Polymerization of vinyl chloride with the redox system ferrous sulphate/hydrogen peroxide/oxalic acid was studied.

The molar ratio of components in the catalyst system and polymerization temperature exert a marked effect on the yield,  $T_g$  and syndiotactic level of PVC.

PVC of the highest yield,  $T_g$  and syndiotactic level in the conditions under investigation is obtained at  $0^\circ\text{C}$  and a ratio of 0.093 of ferrous sulphate to hydrogen peroxide.

PVC of good  $T_g$  and syndiotactic level may also be obtained with the use of the investigated redox system at a polymerization temperature of  $15^\circ\text{C}$ .

#### REFERENCES

- 1 Sharetskyi, A. M., Svetozarskyi, S. V., Kotliar, I. B. and Zilberman, E. N. *Plast. Massy* 1968, 3, 6
- 2 Sharetskyi, A. M., Svetozarskyi, S. V., Kotliar, I. B. and Zilberman, E. N. *Vysokomol. Soedin.* 1970, 12B, 476
- 3 Jap. Pat. 18 588 (23/12/60)
- 4 Konishi, A. and Nambu, K. *J. Polym. Sci.* 1962, 56, 225
- 5 Jap. Pat. 4011 (26/4/61)
- 6 Slavtcheva, L. H. and Lutsкая, B. E. *A. Rep. Res. Inst. Chem. Ind. Sofia* 1971, 11, 60
- 7 Krimm, S. and Liang, C. G. *J. Polym. Sci.* 1969, 22, 95
- 8 Zavalov, A. N. and Krupstov, B. K. *Plast. Massy* 1969, 1, 3

# Estimation of heat of dilution of polymer solution: a trial on a correction of the heat of stirring ascribed to the viscosity difference before and after dilution

Katsutoshi Tamura, Sachio Murakami and Ryoichi Fujishiro

*Department of Chemistry, Osaka City University, Sumiyoshi-ku, Osaka, Japan  
(Received 15 January 1973)*

The heat of dilution for the polystyrene and methyl ethyl ketone system was measured using an isothermal calorimeter, and the heat correction due to the change of stirring before and after dilution was estimated from the observed change in heat of dilution. The net heat of dilution of the polystyrene and methyl ethyl ketone system obtained was very small and the system was considered to be almost athermal. The heat correction due to the change of stirring was unexpectedly large, and often exceeded the net heat of dilution. The interaction parameters obtained for the polystyrene and methyl ethyl ketone system were +0.035, +0.012, -0.022, and -0.062 for molecular weights of 2100, 22 000, 57 500, and 212 000, respectively, at 298.15 K.

## INTRODUCTION

Many authors<sup>1-3</sup> have measured the osmotic pressure of the polystyrene and methyl ethyl ketone system and have indirectly estimated the heat of dilution to be slightly exothermic for polystyrene of molecular weight greater than  $10^5$ . On the other hand, we have directly estimated the heat of dilution to be slightly endothermic for polystyrene of degree of polymerization = 244 using a twin-type conductive calorimeter<sup>4</sup>. To solve this inconsistency, we have again tried to measure the heat of dilution for the polystyrene and methyl ethyl ketone system using a newly constructed isothermal calorimeter. Results obtained show that stirring the solution has a considerable effect on the heat of dilution which is very small in absolute magnitude. In this paper, we discuss the effect of stirring on the heat of dilution and report net heats of dilution which are endothermic for polystyrene of low molecular weight and exothermic for polystyrene of high molecular weight.

## EXPERIMENTAL

### Materials

Polystyrene of molecular weight = 2100 was supplied by Pressure Chemical Co.; that of molecular weight = 22 000 by Asahi Dow Chem. Co.; and those of molecular weights = 57 500 and 212 000, by Dr Hamada (Kyoto University).

Methyl ethyl ketone (special grade) was purified by the standard method<sup>5</sup>.

### Apparatus

The mixing cell (total volume ~ 90 cm<sup>3</sup>) is shown in *Figure 1*. The calorimeter is a modified one of the Van

Ness type of isothermal displacement calorimeter described in a previous paper<sup>6</sup>.

The mixing cell is a Dewar vessel with a polished glass bottom. About 40 cm<sup>3</sup> of polymer solution (or solvent) is introduced into the mixing cell and then the solvent (or polymer solution) is added from the piston burette through a Teflon tube, the inner diameter of which is 3 mm. The solution in the mixing cell is stirred by a Teflon-coated magnetic spin bar with two glass paddles, activated by an external magnet rotating at 300 rev/min by means of a constant-speed motor. The temperature change of the solution in the mixing cell is detected by the thermistor (which is ~ 37 k $\Omega$  at the temperature of the experiment, 298.15 K), Wheatstone bridge, micro-voltmeter, and recorder. The manganin wire heater, with a resistance of about 50  $\Omega$ , is used for thermal compensation. The heater power is calculated by measuring the voltage across the heater and a 1  $\Omega$  standard resistance by means of a digital voltmeter. In order to maintain the isothermal state of the calorimeter, the Peltier cooling effect of a thermomodule is used and the electric current through it is supplied by a stabilized d.c. power supply, the drift of current being monitored on a recorder.

### Procedure

The measurement procedure for exothermic and endothermic processes is schematically illustrated in *Figure 2*. The upper part of *Figure 2* corresponds to an exothermic process and the lower one to an endothermic one. Time axes for them are in the horizontal direction from left to right. Each process is divided into three steps.

*First step (before mixing).* The stirrer is rotated and a given amount of current is supplied to the heater (*I*

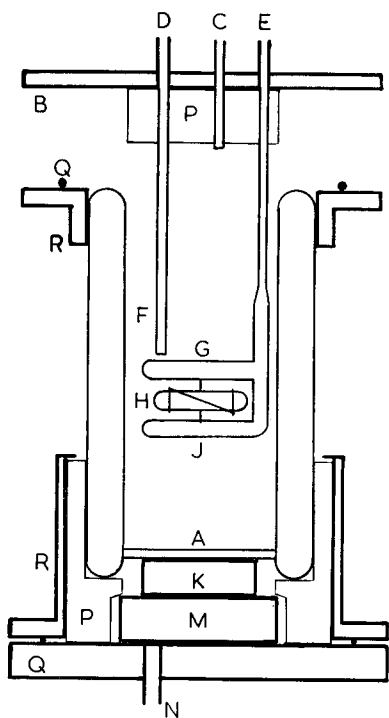


Figure 1 Mixing cell of the isothermal calorimeter. A, Dewar vessel with a polished glass bottom; B, lid; C, inlet of second solution from piston burette; D, outlet of lead wires of thermistor; E, outlet of lead wires of heater; F, thermistor and glass sheath; G, heater and glass sheath; H, Teflon-coated magnetic spin bar with two glass paddles; J, support for spin bar; K, copper block for thermal conduction; M, thermomodule for cooling the cell; N, outlet of lead wires of thermomodule; P, Teflon covers; Q, Viton O-rings; R, brass covers for supporting the cell

and  $V$  are measured by a digital voltmeter) from a stabilized d.c. supply through a potential adjustment assembly. Then the current supplied to the thermomodule (cooling device) is adjusted so that the work of the thermomodule ( $W_{th}$ ) is balanced by the sum of the heat produced by the heater ( $W_b$ ) and the stirrer ( $W_{st}$ ). The above operations give a linear base line on the recorder (through the thermistor, Wheatstone bridge, and amplifier) since the heat produced in the cell ( $W_b + W_{st}$ ) and the heat absorbed by the thermomodule ( $W_{th}$ ) balance each other. The temperature in the cell is adjusted to that of the thermostated bath to make the thermal exchange between the cell and the bath as small as possible.

*Second step (mixing period).* On dilution, in order to balance the heat produced, the heater current is changed to  $W_t$  and the cell temperature is held in the neighbourhood of the initial set value. In actual operation, the heater current is decreased (increased for an endothermic case) by a definite amount, and the flow rate of solvent from the piston burette is adjusted step by step if the cell temperature deviates from the base line. This step interval is counted by the digital clock.

*Third step (after mixing).* As soon as dilution is over, the heater current is adjusted to an amount ( $W_a$ ) so that the heating and stirring heats are balanced by the cooling of the thermomodule which is always constant. Thus, the base line after mixing returns to the original one.

## RESULTS AND DISCUSSION

Each experimental run gives the following information: work of heating ( $W_b$ ,  $W_t$ , and  $W_a$ ), time interval  $t$ , initial and final volume fractions of polymer  $\phi_2$  and  $\phi_2'$ , and volume change  $\Delta V$  and, if necessary, volume fraction of polymer in piston burette,  $\phi_{20}$ .

The difference of  $W_b$  and  $W_a$  corresponds to the change of stirring work  $\Delta W_{st}$  before and after dilution. The plots of integrated amount of  $\Delta W_{st}$  against the change of volume fraction of polymer due to the dilution are given in Figures 3 and 4. In these Figures  $\Delta W_{st}$  is positive when the stirring work decreases, since a decrease of the stirring work corresponds to an endothermic process in the experiment. Figure 3 shows the decrease

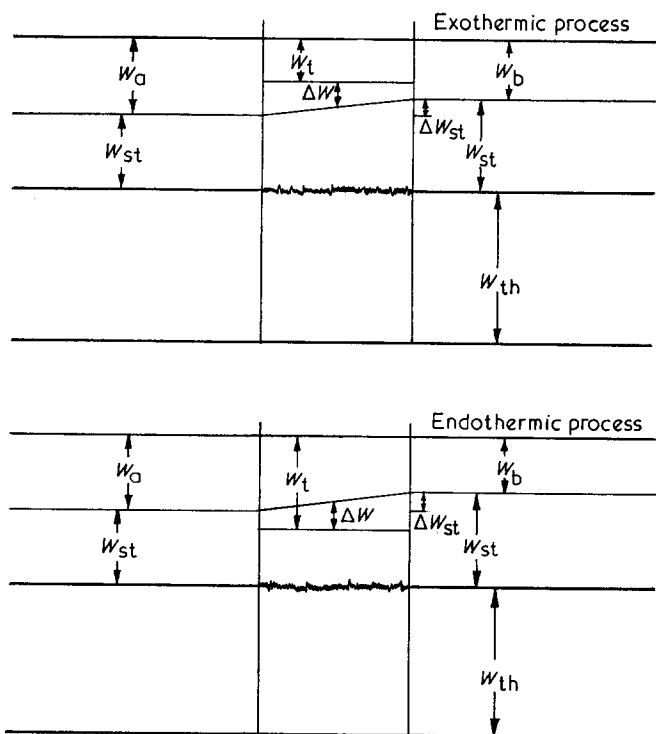


Figure 2 Schemes of dilution processes

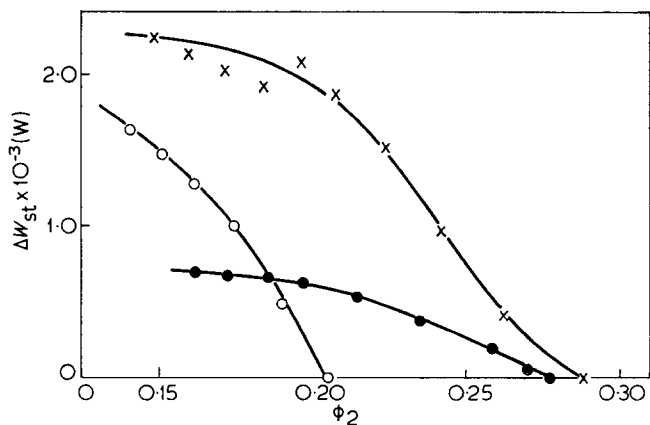


Figure 3 Plot of the integrated amount of stirring work (case of decrease of stirring work). Molecular weights: ●, 2100; ×, 22 000; ○, 57 500

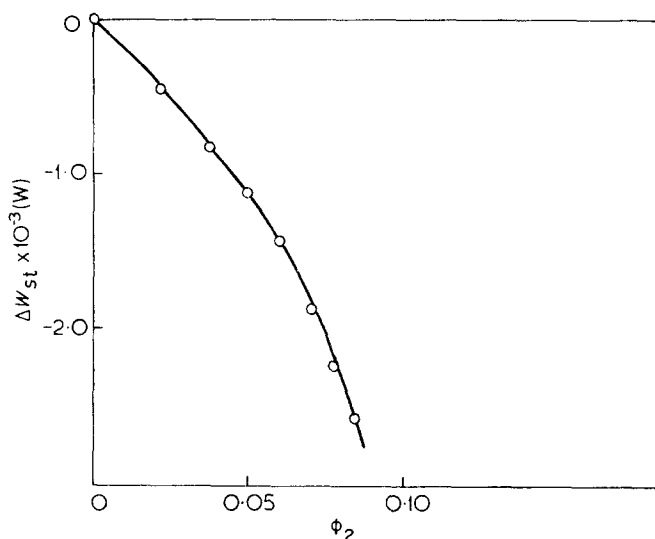


Figure 4 Plot of the integrated amount of stirring work (case of increase of stirring work). Molecular weight=212 000

of stirring work with the decrease of volume fraction of polymer. Figure 4 represents the increase of stirring work with the increase of volume fraction of polymer. The slopes of these curves seem to change reasonably with molecular weight and concentration of polymer. Naturally, these values may depend also on the shape of the stirrer, the power of stirring and the volume of solution in the cell. The effect of  $\Delta W_{st}$  on the error of the heat of dilution is discussed below.

The heat of dilution can be estimated from  $W_b$ ,  $W_t$ ,

$W_a$ , and  $t$ , by using the following equation, assuming that the work of stirring on dilution changes linearly with time:

$$Q = [W_t - (W_b + W_a)/2]t \quad (1)$$

$\Delta W$  in Figure 2 is equal to  $[W_t - (W_b + W_a)/2]$ .

In the actual run, however, the flow rate of titre is not constant and the change of the volume fraction is not linear with time. This deviation from linearity with time brings an error ( $\delta Q$ ) in  $Q$  in equation (1). Since the maximum value of the error is  $\delta Q_{max} = \Delta W_{st} \cdot t/2$ , the error may be in the following range;  $0 < |\delta Q| < |\delta Q_{max}|$ . Usually the deviation from linearity is not expected to be so large; hence it may not be unreasonable to put tentatively:

$$|\delta Q| = |\delta Q_{max}|/2 = \Delta W_{st} \cdot t/4 \quad (2)$$

The heat of dilution  $Q$  is related to the interaction parameter  $\kappa$  and the initial and final volume fractions  $\phi_2$  and  $\phi_2'$  by the following modified Van Laar equation:

$$Q = (RT/V_1)\kappa(\Delta V)(\phi_2 - \phi_{20})(\phi_2' - \phi_{20}) \quad (3)$$

where  $V_1$  is the molar volume of solvent,  $R$  the gas constant,  $T$  the absolute temperature, and  $\phi_{20}$  the volume fraction of polymer of the titre.

The heats of dilution,  $Q$ , obtained when the polymer solution is diluted from  $\phi_2$  to  $\phi_2'$  are given in Table 1, together with the  $\kappa$  parameters calculated from equations (2), (3) and (4):  $\Delta W_{st}$ ,  $\Delta W_{st} \cdot t/Q$ ,  $\Delta \kappa_{st}$ , and  $\kappa'$ . Since  $\Delta W_{st} \cdot t/Q$  represents the ratio of the heat of stirring to the net heat of dilution and sometimes amounts to considerable values, as seen in Table 1, the stirring

Table 1 Heats of dilution of the polystyrene and methyl ethyl ketone system at 298.15K and related values

$\phi_2$	$\phi_2'$	$\Delta V$ (cm <sup>3</sup> )	$Q$ (J/mol)	$\kappa$	$\Delta W_{st}$ $\times 10^{-3}$ (W)	$\Delta W_{st} \cdot t/Q$	$\Delta \kappa_{st}$	$\kappa'$
Molecular weight of polystyrene=2100								
0.2779	0.2704	1.31	+0.0321	+0.009	+0.0485	+1.04	+0.009	+0.018
0.2704	0.2588	2.17	+0.0910	+0.017	+0.1482	+1.43	+0.024	+0.041
0.2588	0.2355	4.99	+0.3344	+0.032	+0.1842	+0.41	+0.012	+0.044
0.2355	0.2145	5.44	+0.2434	+0.026	+0.1501	+0.52	+0.013	+0.039
0.2111	0.1972	4.39	+0.1117	+0.018	+0.0811	+0.14	+0.003	+0.021
0.1972	0.1856	4.10	+0.2419	+0.047	+0.0496	+0.10	+0.005	+0.052
0.1856	0.1729	5.18	+0.4116	+0.072	0	0	0	+0.072
0.1729	0.1618	5.19	+0.3041	+0.061	+0.0331	+0.65	+0.040	+0.101
Molecular weight of polystyrene=22 000								
0.2889	0.2630	4.18	-0.1714	-0.016	+0.4304	-0.41	+0.007	-0.009
0.2630	0.2419	4.06	+0.1715	+0.019	+0.5424	+2.21	+0.042	+0.061
0.2419	0.2242	3.99	+0.2387	+0.032	+0.5404	+0.61	+0.019	+0.051
0.2242	0.2077	4.33	+0.2177	+0.031	+0.3600	+0.43	+0.013	+0.044
0.2077	0.1965	3.37	+0.1442	+0.030	+0.1943	+0.09	+0.003	+0.033
0.1965	0.1838	4.29	-0.0516	-0.010	-0.1486	+1.38	+0.014	+0.004
0.1838	0.1707	5.11	+0.0322	+0.006	+0.0907	+1.02	+0.006	+0.012
0.1707	0.1593	5.11	-0.0009	-0.000	+0.1184	-23.78	+0.005	+0.005
0.1593	0.1489	5.36	+0.0011	+0.000	+0.1124	+10.91	+0.003	+0.003
Molecular weight of polystyrene=57 500								
0.2049	0.1898	3.48	-0.1043	-0.022	+0.490	-2.0	+0.044	+0.022
0.1898	0.1748	4.06	-0.0576	-0.012	+0.517	-2.0	+0.024	+0.012
0.1748	0.1621	4.06	-0.1077	-0.027	+0.2837	-0.43	+0.012	-0.015
0.1621	0.1508	4.13	-0.1023	-0.029	+0.1961	-0.21	+0.006	-0.023
0.1508	0.1406	4.35	-0.1056	-0.033	+0.1418	-0.13	+0.004	-0.029
Molecular weight of polystyrene=212 000; $\phi_{20}=0.1678$								
0	0.0202	4.95	-0.2244	-0.053	-0.4507	+0.24	-0.013	-0.066
0.0202	0.0366	5.10	-0.1937	-0.057	-0.3801	+0.28	-0.016	-0.073
0.0366	0.0495	5.06	-0.1501	-0.056	-0.2950	+0.29	-0.016	-0.072
0.0495	0.0601	5.01	-0.0971	-0.044	-0.2974	+0.87	-0.038	-0.082
0.0601	0.0690	5.03	-0.1265	-0.068	-0.4551	+0.38	-0.027	-0.095
0.0690	0.0765	5.02	-0.1156	-0.074	-0.3877	+0.49	-0.036	-0.110
0.0765	0.0835	5.50	-0.1157	-0.079	-0.3181	+0.75	-0.059	-0.138

during dilution has a significant effect on the heat of dilution. The  $\kappa$  values (expressed by  $\kappa'$  in Table 1) obtained in the experiments, from which the effect of stirring is not separated, are larger than our  $\kappa$  values by amounts  $\Delta\kappa_{st}$ , which are the contribution of stirring to  $\kappa$ , calculated from:

$$\Delta\kappa_{st} = \kappa(\Delta W_{st} \cdot t/Q) \quad (4)$$

As shown in Table 1, the contribution of  $\Delta\kappa_{st}$  to  $\kappa'$  varies and in some exothermic cases  $\kappa'$  shows a different sign from that of  $\kappa$ . Thus stirring plays an important role in the experimental determination of the interaction parameter  $\kappa$  for such polymer solutions as polystyrene in methyl ethyl ketone for which the absolute value of  $\kappa$  is very small.

Further inspection of Table 1 reveals that  $\kappa$  parameters change with molecular weight of polymer from positive values to negative ones.

In Figure 5 the plot of average  $\kappa$  values against the logarithm of molecular weight of polystyrene is shown. From this Figure it may be seen that the  $\kappa$  parameters are very small and change their sign at a molecular weight of about  $2-3 \times 10^4$ .

These  $\kappa$  values are compared with the values obtained by other authors<sup>1-4</sup> in Table 2. According to a personal communication from Dr Hamada, the  $\kappa$  parameter of this system obtained by high pressure osmometry is slightly exothermic at 298.15 K for a polymer of molecular weight 107 000. Flory and Hocker<sup>7</sup> report that the  $\kappa$  parameters of this system (in which the molecular

Table 2  $\kappa$  parameters of the polystyrene and methyl ethyl ketone system at 298.15 K

Molecular weight $\times 10^3$	$\kappa$	Method	Reference
2.1	+0.02	Calorimetry	This work
22	+0.01	Calorimetry	This work
( $DP^*=244$ )	+0.08	Calorimetry	Ref. 4
57.5	-0.02	Calorimetry	This work
160	-0.03	Osmotic pressure	Ref. 3
212	-0.06	Calorimetry	This work
237	-0.00	Osmotic pressure	Ref. 2
316	-0.02	Osmotic pressure	Ref. 3
520	-0.02	Osmotic pressure	Ref. 1

\*  $DP$  is degree of polymerization

weights of the polymer are 51 000 and 97 200, respectively) are slightly endothermic at 298.15 K in the experimental region of the volume fraction ( $0.1 < \phi_2 < 0.4$ ) and may change their sign at a volume fraction of less than 0.1.

Our results are in good agreement with the values obtained by osmotic pressure measurements. The value in our previous paper<sup>4</sup> is slightly larger and opposite in sign: most of this discrepancy may be due to disregarding the heat of stirring.

Until now, in the measurement of the heat of dilution of polymer solutions, the effect of stirring has been neglected or underestimated. However, as shown here, the stirring effect ascribed to the viscosity difference before and after dilution, cannot be neglected and correction for this effect must be made even if a twin-type calorimeter is used. The authors are going to construct a calorimeter in which this effect is removed.

## REFERENCES

- Schick, M. J., Doty, P. and Zimm, B. *J. Am. Chem. Soc.* 1950, **72**, 530
- Schulz, G. V. and Hellfritz, H. *Z. Elektrochem.* 1953, **57**, 835
- Bawn, C. E. H. and Wajid, M. A. *J. Polym. Sci.* 1954, **12**, 109
- Kagemoto, A., Murakami, S. and Fujishiro, R. *Bull. Chem. Soc. Japan* 1966, **39**, 15
- 'Organic Solvents', (Ed. Weissberger, A.) Wiley-Interscience, New York, 3rd edn, 1970
- Tanaka, R., Murakami, S. and Fujishiro, R. *Bull. Chem. Soc. Japan* 1972, **45**, 2107
- Flory, P. J. and Hocker, H. *Trans. Faraday Soc.* 1971, **67**, 2258

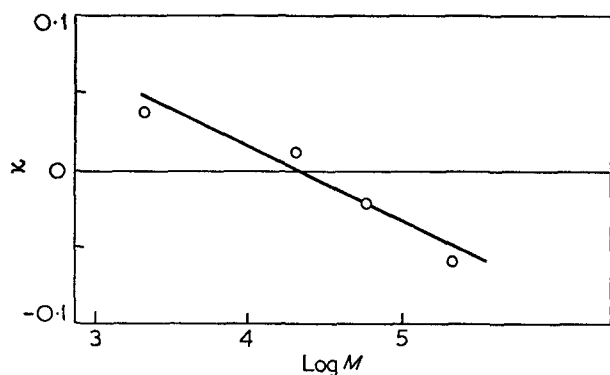


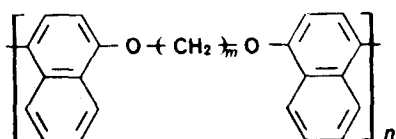
Figure 5 Plot of the mean values of  $\kappa$  parameters of the polystyrene and methyl ethyl ketone system against the logarithm of molecular weight of polymer

# Preparation of poly(dinaphthyl alkylene ethers) by oxidative polyarylation and their crystallization behaviour

R. G. Feasey, A. Turner-Jones, P. C. Daffurn and J. L. Freeman

Imperial Chemical Industries Limited, Plastics Division, Welwyn Garden City, Herts, UK  
(Received 30 November 1972; revised 25 January 1973)

Di-1-naphthoxy alkanes are found to polycondense in a surprisingly clean oxidative polyarylation reaction, effected by iron(III) chloride in nitrobenzene solution at room temperature. By this reaction, polymers with the structure

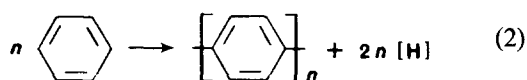


in which  $m=2-7$  were prepared as high molecular weight, crystallizable, apparently linear thermoplastics. Glass transition temperatures,  $T_g$ , have been measured and show considerable variation with reduced solution viscosity and with previous thermal history; the polymer in which  $m=4$  has the highest melting point,  $324^\circ\text{C}$ . From the melt and from the amorphous state at room temperature, the rates of crystallization of the  $m$ -even polymers decrease with increasing  $m$ , but the  $m$ -odd polymers do not crystallize by thermal treatment. The  $m=3$  polymer crystallizes in contact with boiling xylene and the  $m=5$  polymer crystallizes from chloroform/*N*-methyl pyrrolidone.

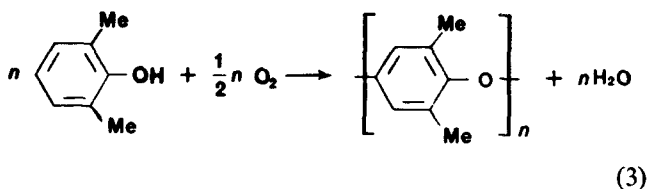
## PART I: PREPARATION AND ANALYSIS OF POLY(DINAPHTHYL ALKYLENE ETHERS)

### INTRODUCTION

Oxidative polyarylation is the direct formation of an aromatic polymer involving the coupling of aromatic nuclei by an oxidative process. Equation (1) shows the general form of an oxidative polyarylation and equation (2) a specific example, the oxidative coupling of benzene to form poly(*p*-phenylene).

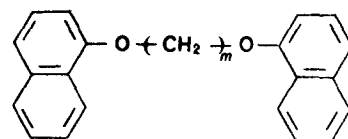


Equation (3), by comparison, shows a well known<sup>1</sup> example of the preparation of an aromatic polymer by an oxidative polymerization process which is not an oxidative polyarylation. Substituent O-aromatic C coupling rather than aromatic C-aromatic C coupling is involved in this reaction and so it is classified as an oxidative polyetherification.

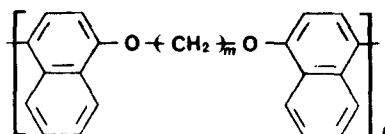


Although the literature contains several reports of oxidative polyarylation reactions, notably by Kovacic *et al.*<sup>2</sup>, none have previously reported the preparation of a high molecular weight, linear polymer by this process. A typical example of the oxidative polyarylations reported by Kovacic<sup>3</sup> is the reaction of benzene with the  $\text{AlCl}_3\text{-CuCl}_2$  reagent system to yield an infusible product of indeterminate composition, which could not be regarded as a high molecular weight thermoplastic. Although Bilow and Miller<sup>4</sup> have extended Kovacic's work to prepare high molecular weight, fusible polyphenylenes, this was achieved only at the expense of destroying the linearity of the resin structure.

In this paper we describe the polycondensation of di-1-naphthoxy alkanes (I) to form linear, high molecular weight poly(dinaphthyl alkylene ethers) (II).



(I)



(II)

## EXPERIMENTAL

## Preparation of model compounds

*1-Ethoxy naphthalene.* 1-Naphthol (235 g; 1.63 M) was slowly added to a stirred mixture, under nitrogen and initially at room temperature, of an aqueous solution of potassium hydroxide (187 g; 1.64 M) and dimethyl sulphoxide. The temperature of the solution rose to 53°C, and iodoethane (254 g; 1.63 M) was added over 15 min. The mixture was stirred for a further 1.5 h without external cooling, then diluted with water and extracted with dichloromethane. The dichloromethane solution was washed with potassium hydroxide solution (0.1 N), washed with water and then dichloromethane was removed by distillation. The residue was distilled at 106–108°C and 5 mmHg to yield a colourless liquid (280 g; 71%) which had b.p. 106–108°C at 5 mmHg (Clowes<sup>6</sup> reports b.p. 136–138°C at 15 mmHg).

*4,4'-Diethoxy-1,1'-dinaphthyl.* To a stirred solution of 8.11 g (0.05 mol) FeCl<sub>3</sub> and 25 cm<sup>3</sup> nitrobenzene, contained in a flask equipped with a nitrogen inlet and dropping funnel, at 25°C was slowly added 8.61 g (0.05 mol) of 1-ethoxy naphthalene. The liberated HCl was passed into water and titrated against N sodium hydroxide solution to a steady value (after 2 h). The whole reaction mixture was poured into 150 cm<sup>3</sup> of methanol, a brown solid was filtered off and washed with cold methanol until the filtrate was colourless. The residue (8.7 g; ~100%) was recrystallized from a 50:50 vol./vol. mixture of benzene/acetone to yield colourless plates (4.8 g; 56%) m.p. 214–216°C (lit.<sup>5</sup> m.p. 212–213°C).

## Monomer preparation

Di-1-naphthoxy alkanes (I) were prepared by the procedure illustrated by the following typical example: 1-naphthol (288.3 g; 2.00 M) was added slowly to a stirred mixture under nitrogen and initially, at room temperature, of an aqueous solution of potassium hydroxide (229.4 g; 2.00 M) and dimethyl sulphoxide (500 cm<sup>3</sup>). To the resulting green solution at 45°C was added slowly a solution of 1,5-dibromopentane (230.0 g; 1.00 M) in dimethyl sulphoxide (300 cm<sup>3</sup>). The temperature of the reaction mixture rose to 75°C during this addition. The resulting mixture was stirred for 2 h, diluted with water (1 dm<sup>3</sup>) and extracted into chloroform. The combined chloroform extracts were washed three times each with aqueous sodium hydroxide solution (~10% wt./vol.) and then water, were dried over anhydrous sodium sulphate and then evaporated to dryness. The residue was crystallized from ethanol-acetone solution (90:10% vol./vol.) to yield 1,5-di-1-naphthoxy pentane (264.6 g; 75%).

All monomers thus prepared gave satisfactory elemental analyses, and infra-red, nuclear magnetic resonance (n.m.r.) and mass spectra consistent with their expected structure. Melting points were recorded for the monomers as follows: 1,2-di-1-naphthoxyethane, m.p. 132.5–134°C (Clowes<sup>6</sup> reports m.p. 129–131°C); 1,3-di-1-naphthoxypropane, m.p. 101–102.5°C; 1,4-di-1-naphthoxybutane, m.p. 123–124°C; 1,5-di-1-naphthoxypentane, m.p. 79.5–80.5°C (Ashley *et al.*<sup>7</sup> reports m.p. 79–81°C); 1,6-di-1-naphthoxyhexane, m.p. 111–112.5°C; 1,7-di-1-naphthoxyheptane, m.p. 98–99°C.

Di-1-naphthyl ether was prepared according to the method described by Rodionow and Manzow<sup>8</sup> for the

preparation of di-2-naphthyl ether and had m.p. 105–106°C (lit. m.p. 110°C).

## Polymerizations

Polymerizations were carried out by the procedure illustrated by the following typical example: 1,5-di-1-naphthoxypentane (7.13 g; 0.020 M) and anhydrous iron(III) [ferric] chloride (7.00 g; 0.043 M) were charged to a 250 cm<sup>3</sup> three-necked round-bottom flask fitted with a stirrer, nitrogen inlet (<10 ppm water), and a nitrogen outlet leading into a flask containing stirred water to dissolve the hydrogen chloride evolved. Sufficient time was allowed for air in the flask to be displaced by nitrogen, the stirrer was started and nitrobenzene (50 cm<sup>3</sup>) was introduced. The reaction mixture became intensely coloured, its temperature increased and hydrogen chloride evolution commenced. The reaction was allowed to proceed for 4 h and then the reaction mixture in the form of a viscous slurry, was poured into stirred methanol (500 cm<sup>3</sup>). A buff solid precipitated, which was collected, extracted with boiling methanol and then dried at 80°C *in vacuo* (7.0 g; 99%) and had reduced viscosity 1.28, measured as a 1% wt./vol. solution in 1-chloronaphthalene at 25°C.

Titration of the aqueous solution of evolved hydrogen chloride with aqueous sodium hydroxide solution (1.00 N; phenolphthalein indicator) showed it to contain 0.0380 M hydrogen chloride. Titration of aliquots of the combined methanol liquors from the work-up of the polymer with aqueous cerium(IV) sulphate solution (0.95 M; *o*-phenanthroline-iron(II) sulphate indicator) showed them to contain 0.0398 M of Fe<sup>2+</sup> ion. Mass spectral analysis of the liquors did not indicate the presence of any compound which might have been a product of the reduction of nitrobenzene.

## Elemental and spectral analysis

Satisfactory elemental analysis and mass, infra-red and n.m.r. spectra were obtained for all monomeric compounds prepared. Data relating to the poly(1-naphthoxy alkanes) (II), prepared by oxidative polyarylation, are shown in Table 1.

Nuclear magnetic resonance spectra were recorded in CDCl<sub>3</sub> solution on a Varian HD100 spectrometer and the infra-red data on a Perkin Elmer 457 Grating Spectrometer.

The elemental analyses (Table 1) and infra-red spectra of the polymers are consistent with the structure (II) proposed for them, as are the n.m.r. spectra of the soluble polymers. The infra-red spectra of all members of the polymer series are virtually identical and are very

Table 1 Data relating to polymers of formula II (*m*=2 to 7) prepared by oxidative polyarylation

Polymer	Elemental analysis				RV*
	Found		Calculated		
	C (%)	H (%)	C (%)	H (%)	
II, <i>m</i> =2	84.8	5.1	84.6	5.1	NS
<i>m</i> =3	84.7	5.5	84.7	5.5	1.28
<i>m</i> =4	86.9	6.0	84.7	5.9	NS
<i>m</i> =5	84.6	6.3	84.7	6.2	1.30
<i>m</i> =6	84.8	6.7	84.7	6.5	NS
<i>m</i> =7	85.8	6.8	84.8	6.9	0.90

\* Reduced viscosity of a 1% wt./vol. solution in 1-chloronaphthalene at 25°C

NS=not soluble



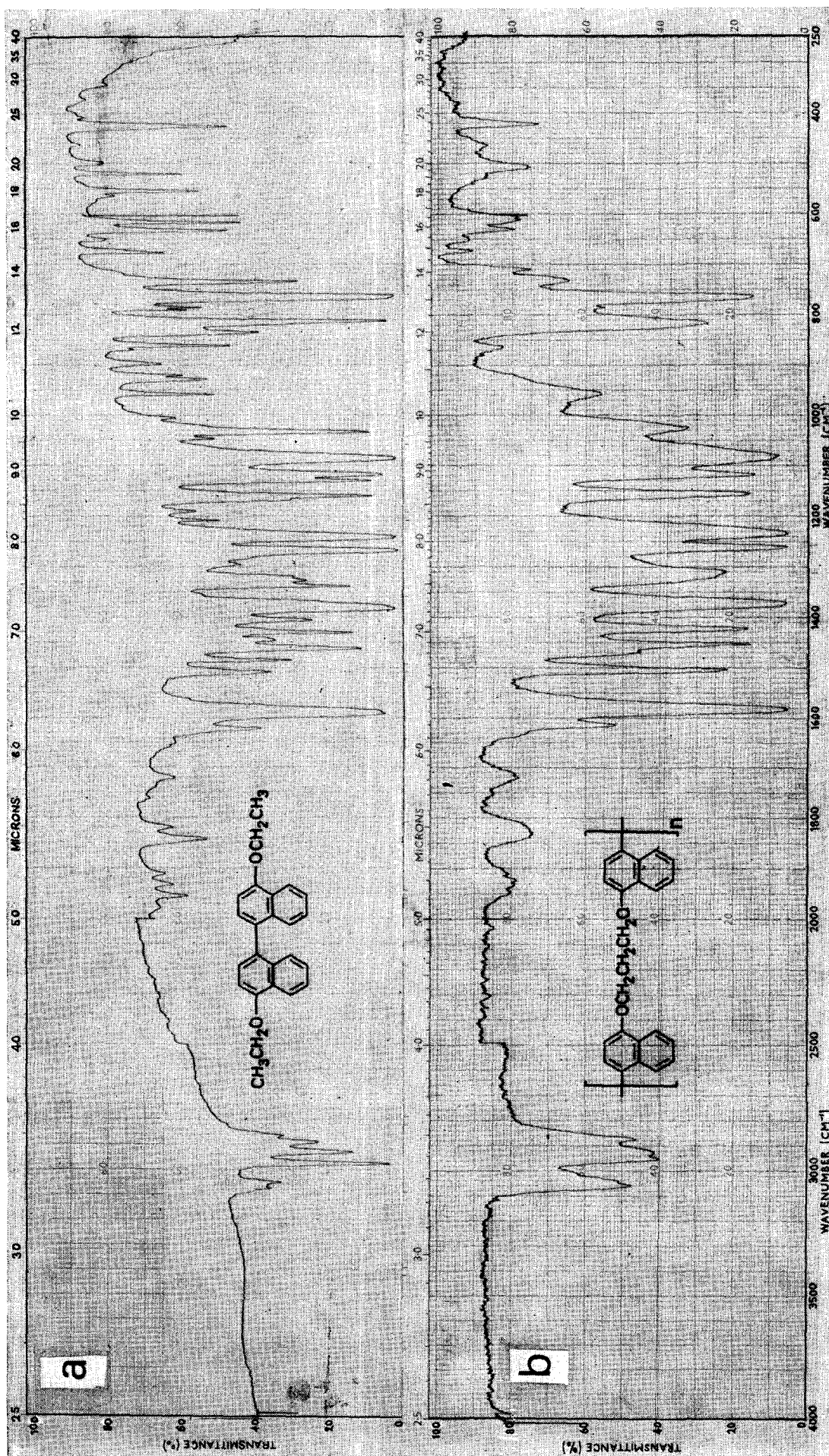


Figure 1 Infrared spectra of (a) the model compound 4,4'-diethoxy-1,1'-dinaphthyl and (b) poly(dinaphthyl propylene ether)



similar to the spectrum of the model compound 4,4'-diethoxy-1,1'-dinaphthyl. Figure 1 shows the infra-red spectrum of a typical member of the polymer series with the formula II,  $m=3$ , together with the spectrum of the model compound. Typical of the n.m.r. spectra of the soluble polymers is that of the polymer of formula II,  $m=3$ . This spectrum is shown in Figure 2 in comparison with that of the model compound 4,4'-diethoxy-1,1'-dinaphthyl. In the spectrum of the polymer, resonances assigned to 4,4'-disubstituted-1,1'-dinaphthyl protons occur between 6, 8 ppm and 8.5 ppm. Resonances at 4.45 ppm and 2.6 ppm are assigned to methylene protons and integration of band areas is consistent with both the assignments made and the structure proposed for the polymer.

## RESULTS AND DISCUSSION

### Model reaction

Our approach to the problem of preparing a high molecular weight, linear thermoplastic by oxidative polyarylation started with a model reaction. This reaction, equation (4), was the Scholl reaction<sup>5</sup> of 1-ethoxy naphthalene (III) in the presence of  $\text{AlCl}_3$  and in nitrobenzene solution to form 4,4'-diethoxy-1,1'-dinaphthyl (IV) in 70% yield.

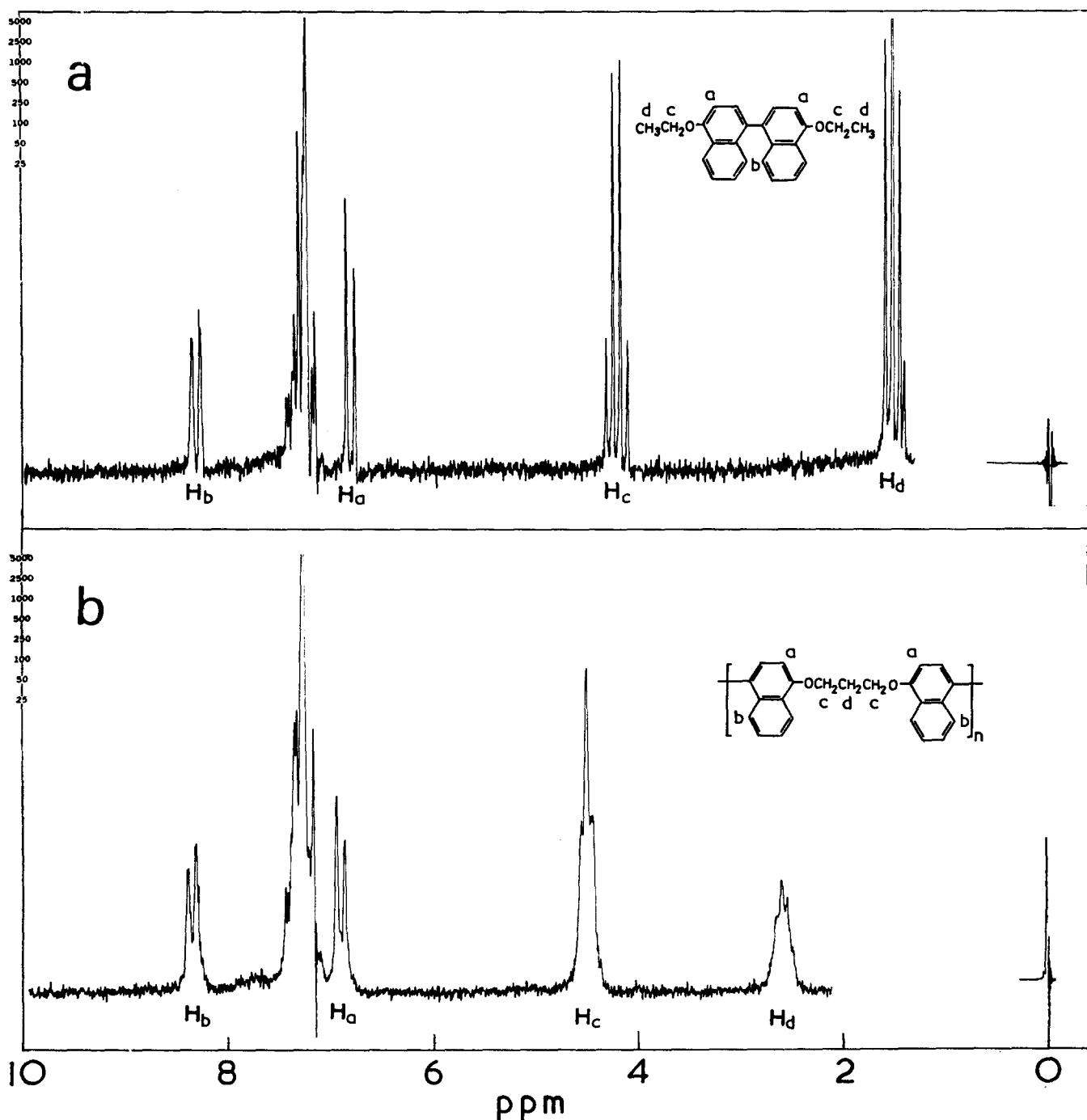
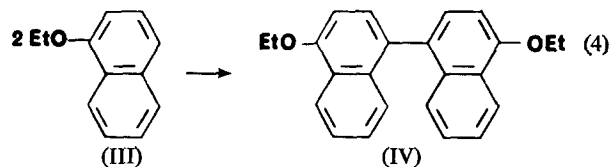
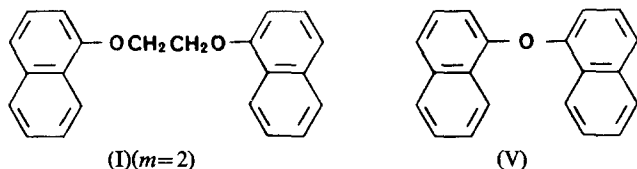


Figure 2 Nuclear magnetic resonance spectra of (a) the model compound 4,4'-diethoxy-1,1'-dinaphthyl and (b) poly(dinaphthyl propylene ether)

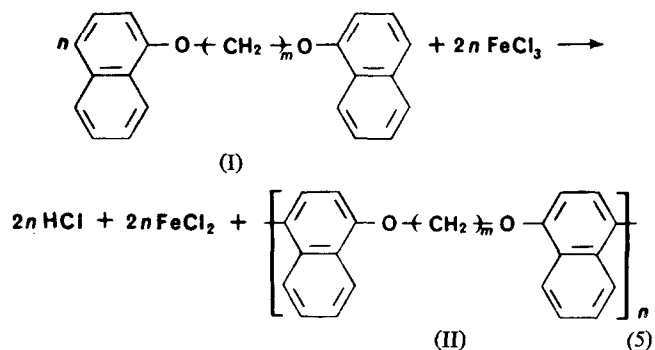
Clowes<sup>6</sup> attempted to apply this reaction to the preparation of polymers by reacting 1,2-di(1-naphthoxy) ethane, I ( $m=2$ ) and di-1-naphthyl ether (V) with  $\text{AlCl}_3$  in nitrobenzene solution but obtained only low molecular weight materials of indeterminate composition.



We have found that the model reaction (4) proceeds with improved yield (up to 86% of isolated product) in the presence of  $\text{FeCl}_3$  in nitrobenzene solution and that this reaction may be successfully adapted to the preparation of high molecular weight, linear thermoplastic polymers.

#### Polymerization of di-1-naphthoxy alkanes

It is found that compounds of the general formula (I) react with ferric chloride in nitrobenzene solution at room temperature to form polymers of the general formula (II), according to:



In practice polymers of highest molecular weight are obtained when the polymerization is carried out in the

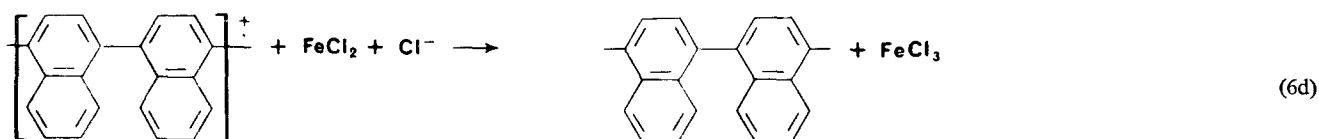
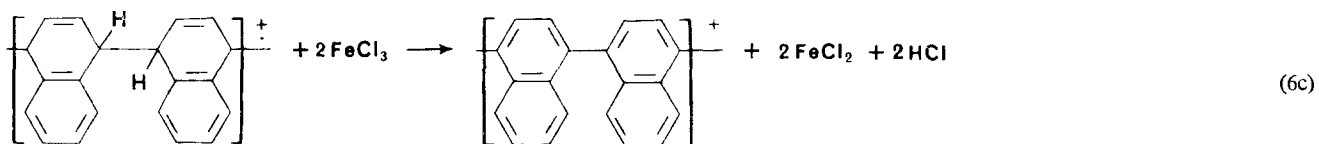
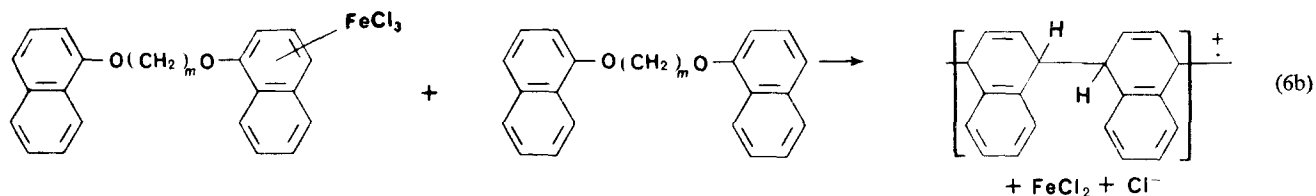
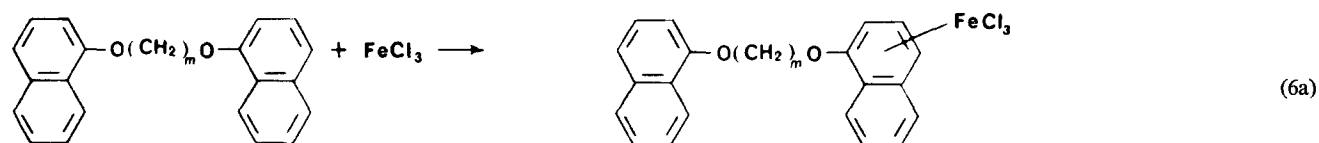
presence of a small (2 to 10 mol%) excess of ferric chloride which, presumably, compensates for loss of ferric chloride by hydrolysis either by atmospheric moisture or by water contained in the nitrobenzene solvent. The polymerization is also best carried out in the absence of oxygen and water, and under conditions, e.g. of vigorous agitation, which assist removal of hydrogen chloride from the reaction mixture. The polymerization, which is exothermic and accompanied by an intense red coloration, is generally complete within 6 h to give reaction mixtures in the form of dark viscous slurries.

All the polymers are crystallizable but after being quenched to the amorphous state they are soluble in certain solvents.

The films obtained by compression moulding polymers of formula II,  $m=3, 5$  and  $7$ , were amorphous, transparent, amber in colour and tough in that they could be creased without fracture. However, films similarly obtained of polymers of formula II,  $m=2, 4$  and  $6$ , were similar in appearance but fractured when creased, owing to the presence of crystallinity as discussed in Part II. The polymers were also thermoplastic in that they could be repeatedly melt fabricated without 'setting-up'. Both the above and the analysis of the polymers suggests that they all have substantially linear structures.

#### Mechanism

We tentatively propose a mechanism (6a-6d) for the oxidative polyarylation of di-1-naphthoxy alkanes (I) involving the initial formation of a ferric chloride-substrate charge transfer species which, effectively, carries out an electrophilic attack on the substrate to form an unstable coupled dihydro radical cation which is rapidly dehydrogenated to a relatively stable aromatic radical cation which finally accepts an electron from an iron(II) species:



## PART II: CRYSTALLINITY AND MELTING POINTS OF FORMULA II POLYMERS

## EXPERIMENTAL AND RESULTS

The crystallinity in the polymers was judged visually by X-ray diffraction photographs. Melting points and crystallization from the melt and from the amorphous state were investigated by differential scanning calorimetry (d.s.c.) with a Perkin Elmer DSC-1B instrument using 10mg samples and heating and cooling rates of 16°C/min. Temperature calibration for heating runs in the melting region was carried out by observing the onset of melting of standard metal samples (tin and cadmium). As the backgrounds of the scans obtained with the DSC-1B are curved and the slopes tend to differ the d.s.c. heating and cooling scans shown in *Figure 3* have been normalized to a horizontal background in order to facilitate comparison between them. The scans are all on the same vertical ( $C_p$ ) scale but no attempt has been made to quantify the data only to compare the crystallization behaviour of the copolymers. Quantitative data are in any case difficult to obtain and may be misleading because as is now well known melting and crystallization can be occurring even where there is no clear change in  $C_p$ .

*Melting points*

The melting points of the polymers as originally prepared are shown in *Table 2*. On heating to just below their melting points and slow cooling at 6°C/h to room temperature both the crystallinity and some melting points increased. After this thermal treatment some polymers showed double melt endotherms which must arise from recrystallization during this treatment; only the higher melting peaks are quoted. The melting points given may still not be maximal for each polymer, since

*Table 2* Melting points  
10mg samples; heating rate 16°C/min

<i>m</i>	X-ray crystallinity as made	D.s.c. $T_p$ (°C)	Slow cooled 6°C/h from	X-ray crystallinity	D.s.c. $T_p$ (°C)
2	Moderate	276	270	High	291
	Mod. good	274			
3	Mod. good	277	270	High	278
4	Mod. good	325	320	High	324
5	Amorphous	—	175*	Moderate	196*
6	Moderate	271	270	High	280
7	Moderate	219	214	Mod. good	~239

$T_p$ =peak of melt endotherm after appropriate instrumental calibration

\* Crystallized from chloroform/*N*-methyl pyrrolidone and then cooled 6°C/h from 175°C

melting point depends upon prior thermal treatment, and a full investigation has not been made. The very high melting point of the  $m=4$  polymer seems out of line and is discussed later. Only one crystal form has been identified so far for each of the polymers except  $m=2$  (see next section).

*Crystallization from the melt*

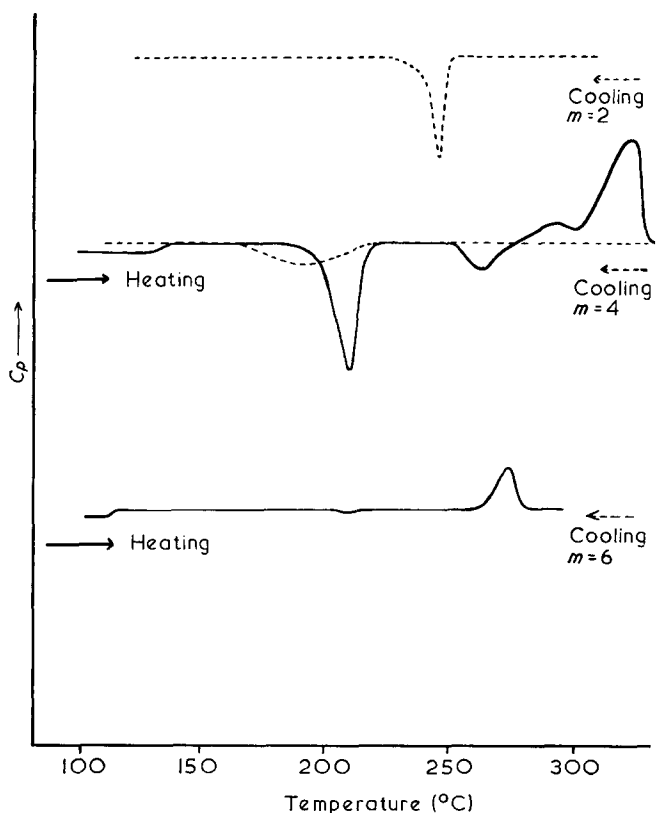
The samples were cooled at 16°C/min after holding for 1 min at 20–30°C above their original melting peaks. The crystallization exotherm of the  $m=2$  and  $m=4$  polymers are shown as broken lines in *Figure 3*. The sharp peak shown by the  $m=2$  polymer indicates faster crystallization occurring at a higher temperature than in the  $m=4$  polymer where a shallow broad exotherm is observed. No exotherm was observed on cooling the  $m=6$  polymer, but poor crystallinity had developed at room temperature. This underlines the point made above that thermal processes may be occurring which are not detectable in a single d.s.c. scan. Good crystallinity was regained in the  $m=6$  polymer on heating to 250°C. The  $m=2$  polymer developed a slightly different X-ray pattern (B) from that present originally (A) which, unless the change can be ascribed to degradation products, indicates two crystal forms. Polymers with  $m$ -odd gave amorphous products under these cooling conditions.

Whether crystallization could be induced by much slower cooling from the melt was examined by cooling polymers with  $m=2, 3, 5, 6, 7$  at 6°C/h from 300°C. Those with  $m$ -odd remained amorphous. The  $m=6$  polymer developed moderate crystallinity. The  $m=2$  polymer developed the second (B) X-ray pattern but no melting endotherm was observed on reheating probably owing to severe degradation as suggested by a low proportion of polymer crystallinity and the colour of the specimen.

Attempts to recrystallize the  $m=3$  polymer by thermal treatment from the amorphous state failed but treatment with boiling xylene induced good crystallization into the crystal form first observed. The  $m=5$  polymer crystallized from chloroform/*N*-methyl-2-pyrrolidone solution.

*Crystallization from the amorphous state and  $T_g$  measurements*

All the crystalline polymers were heated to some 20°C above their original melting points,  $T_p$ , and either



*Figure 3* D.s.c. heating and cooling thermograms for polymers with  $m=2, 4$  and  $6$

cooled in the d.s.c. as fast as possible or quenched into liquid nitrogen. All except the  $m=2$  polymer were obtained amorphous. The  $m=2$  polymer remained crystalline after quenching into liquid nitrogen from 310°C and 320°C when form (B) developed.

All the amorphous samples were reheated in the d.s.c. at 16°C/min and the  $T_g$  values observed are given in Table 3. As shown in the next section for the  $m=3$  polymer, the  $T_g$  can vary considerably with change in reduced viscosity ( $RV$ ). It will also be seen in Table 3 that the  $T_g$  values of the  $m$ -odd polymers can be raised by slow cooling from the melt. It is therefore difficult to comment on the variations in  $T_g$  observed in relation to structure.

During the reheating process, the polymers with  $m=4$  and  $m=6$  crystallized. Their cold crystallization exotherms and final melting points are shown in Figure 3 (solid lines). The polymers with  $m$  odd did not crystallize at this heating rate. The  $m=4$  polymer crystallized much faster than the  $m=6$  polymer and developed much more crystallinity as evidenced by the much larger final endotherm. The reason for the double crystallization exotherms and double melting peaks shown by the  $m=4$  polymer have yet to be investigated.

#### Variation of $T_g$ with $RV$

A series of samples of the  $m=3$  polymer with  $RV$  varying between 0.27 and 1.28 were investigated. Some were amorphous as received and others showed some crystallinity. The latter were made amorphous by rapid cooling from the melt in the d.s.c. The  $T_g$  values measured as before are given in Table 4 and show a rapid increase from 119°C to ~170°C at  $RV=0.5$  but levelled off to ~180–190°C at higher reduced viscosity.

## DISCUSSION

#### Crystallinity and melting points in relation to structure

On structural grounds it would be expected that the  $m$ -even and  $m$ -odd polymers would behave differently. Single chains of the  $m=2, 4$  and other  $m$ -even polymers, in the fully extended chain conformation, form a related structural series in which the oxygen atoms are on alternate sides of the aliphatic planar zig-zag (see Figures 4a and b). A different series is formed by the  $m$ -odd polymers with the oxygens of each aliphatic portion on the same side of the planar zig-zag (Figure 4c).

This is borne out in practice both in their crystallization behaviour, where the  $m$ -even polymers are all more

Table 3 Glass-rubber transitions  
10 mg samples; heating rate 16°C/min

$m$	D.s.c.	
	$T_g$ (°C) <sup>a</sup>	$T_g$ (°C) <sup>b</sup>
2	*	
3	119–187 <sup>c</sup>	191
4	130	
5	143	159
6	109	
7	118	141

\* Not obtained amorphous

<sup>a</sup> After quenching to amorphous stage

<sup>b</sup> After cooling 6°C/h from melt

<sup>c</sup> See Table 4

$T_g$  measured at start of process after appropriate instrumental correction

Table 4  $T_g$  vs.  $RV$  for  
polymers with  $m=3$

$RV$	D.s.c. $T_g$ (°C)
0.23	119
0.34	148
0.44	182–187
0.54	171
0.64	187
0.66	182
0.72	184
1.28	184

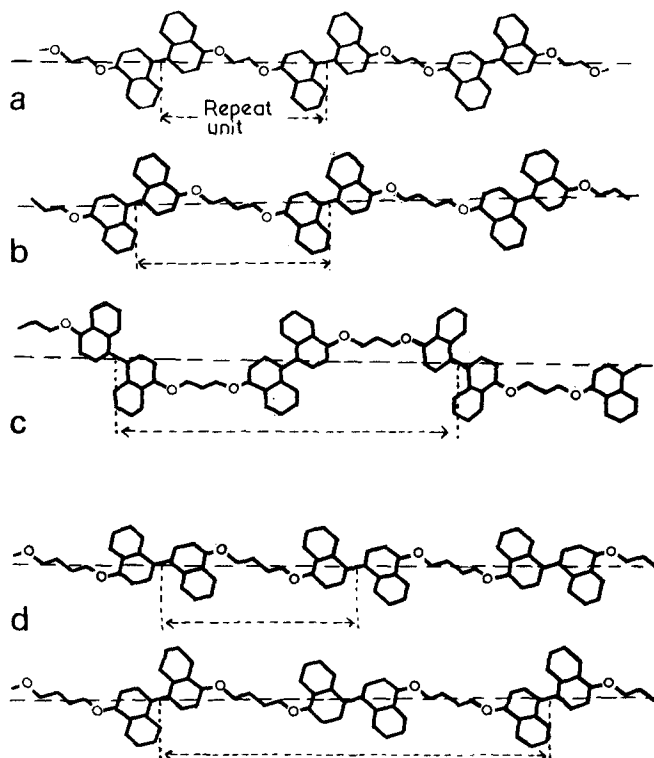


Figure 4 Diagrammatic representation of possible chain conformations for poly(dinaphthyl alkylene ethers) with  $m$  odd or even. (a)  $m=2$ ; (b)  $m=4$ ; (c)  $m=3$ ; (d)  $m=4$ ; (e)  $m=5$

readily crystallizable than the  $m$ -odd series and in their crystal structures. The X-ray patterns of the  $m=2, 4, 6$  polymers are similar to each other with principal diffraction lines at the same spacings and of similar intensities, indicating basically similar structures. These reflections are at  $d$ -spacings of 6.4 Å ( $m$ ), 5.4 Å ( $ms-s$ ), 4.8 Å ( $mw$ ), 3.85 Å ( $vs$ ), 3.2 Å ( $w$ ). These reflections were all shown to be equatorial reflections from a crystalline oriented fibre obtained from the  $m=6$  polymer and hence indicate a similar side-by-side packing of the chains. Other reflections are also present, the number that can be clearly distinguished varying with the degree of crystallinity attained, and also a strong reflection of high spacing which increases as  $m$  increases and is clearly associated with the chain repeat.

The X-ray pattern of the  $m=3$  polymer has lines at similar spacings, 6.2 Å ( $w$ ), 5.7 Å ( $s$ ), 4.7 Å ( $m$ ), 3.65 Å ( $ms$ ), 3.45 Å ( $w$ ) but with different relative intensities. When  $m=5, 7$  the pattern is becoming more like those of the even series for reasons which are discussed later.

#### Melting points

A point which requires explanation is the high melting point of the  $m=4$  polymer. In a series such as this various

factors can affect the melting point, sometimes operating in opposite directions. As far as a single chain is concerned, the large aromatic groups will produce a high melting point which will decrease as their frequency along the chain drops and as the length of the flexible methylene portion of the chain increases, i.e. with increase in  $m$ . The oxygen atoms produce points of increased flexibility in the chains and will therefore contribute to a slight increase in melting point with increasing  $m$ , because their frequency decreases, but this will be offset because the polarity of the oxygen atoms tends to increase melting point. If the chains are considered in isolation, on balance we should expect a continuously decreasing melting point with increasing  $m$ . Even allowing for the fact that the maximum melting point of all the polymers has not yet been achieved, it appears that the melting point of the  $m=4$  polymer is too high to fall in the expected series on this basis alone.

Another very important factor which affects melting point is the packing of the chains. Where a good packing can be achieved with no 'holes' left in the crystal structure so that atoms of adjacent chains can get as close as is permissible, then the cohesion between the chains will be maximal and the melting point as high as possible. The negatively charged oxygen atoms in adjacent chains also need to get as far as possible from each other and as near as possible to any positively charged atoms.

It is therefore probable that we have to look to the packing of the chains to explain the high melting point of the  $m=4$  polymer. As we have only obtained oriented crystalline fibres from one polymer ( $m=6$ ), we have little crystallographic data to go on and it is only possible to speculate in a preliminary way on the type of packing that is likely to occur.

Figure 5a gives a purely diagrammatic representation of the kind of packing that might be envisaged for the  $m=4$  polymer, with the molecules arranged in planar sheets. It will be seen that the aromatic groups of one chain fit conveniently into the spaces between the aromatic groups of adjacent chains with no very bad contact distances and no 'holes'. On the other hand, if a similar packing is considered for  $m=2$  polymer (Figure 5b) and naphthalene group A is placed in the same relation to group B, then a bad contact develops between C and D. The chains must move further apart and the packing will be less close than for the  $m=4$  polymer. A similar packing for the  $m=6$  polymer produces a gap in the structure as marked by the broken ring in Figure 5c, so that here again close packing is less readily achieved. (In this case the aromatic groups of the second chain have had to be rotated slightly with respect to the first to keep the chain directions parallel.)

The length of the aliphatic portion of the  $m=4$  chain therefore seems optimal for close packing and this could explain its high melting point. The above reasoning can also explain why the  $m=6$  polymer does not take up a fully extended form in its crystal structure. Shortening of the aliphatic portion of the chain can take place by rotation around chain bonds, so that the aromatic groups can pack more closely.

A similar shortening of the aliphatic portion of the  $m=7$  polymer chain is likely and rotations around chain bonds may occur which allow the aromatic groups to twist round and pack side by side in a manner similar to that in the  $m=4$  and  $m=6$  polymers. This would explain the resemblance between the  $m=7$  X-ray pattern

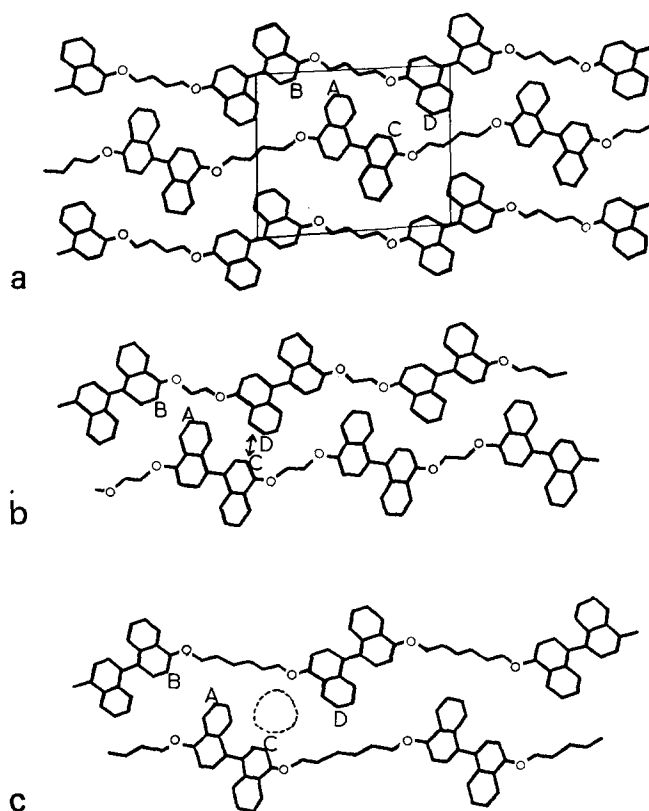


Figure 5 Diagrammatic representation of chain packings for polymers with (a)  $m=4$ , (b)  $m=2$  and (c)  $m=6$

and those of the  $m$ -even polymers. In other words, the precise conformation of the aliphatic portion and the positions of the oxygen atoms are now not of great importance, because they are shielded by the large aromatic groups which determine the packing. In the  $m=3$  polymer, the aliphatic portion is too short for this to occur and a quite different packing results because of the basically different chain structure. The low melting point of the  $m=5$  polymer may result from difficulty in achieving close packing or because so far only a relatively low degree of crystallinity has been achieved. It is not for one moment suggested that the packing of the chains is as shown in Figures 5a, b and c. There are some crystallographic indications that it cannot be quite like this. Such a sheet-like packing is not very likely in any case, but serves to illustrate the principle involved. The aromatic groups may well rotate out of the plane of the sheet around the bond joining the naphthalene groups to relieve poor interchain contact distances. Moreover, there are other basic chain conformations to be considered such as those shown for the  $m=4$  polymer in Figures 4d and 4e.

#### Rates of crystallization

Somewhat similar considerations apply to rates of crystallization, although now close packing is not necessarily an important factor. Poly(4-methylpentene) crystallizes with a very open packing of low density and yet crystallizes very fast. More important is the ease with which the chains can take up the conformation which occurs in the crystal. This is dependent upon various factors such as the packing itself, the ease of rotation around chain bonds and the length of the fibre repeat.

The molecular movements required to pack molecules correctly in a structure with a long repeat unit are greater than those for a polymer with a very short repeat unit. This is one of the reasons for the very fast crystallization of polyethylene. Hence the greater flexibility of the chain as  $m$  increases would tend to lead to faster crystallization, but this can be offset by the longer repeat unit and the more complicated rotations around chain bonds required to get the aromatic groups into the correct position. The last factor is tied up with the much larger number of chain conformations possible in the melt. It is also possible that the low flexibility of the  $m=2$  polymer with its high proportion of aromatic groups, means that order (i.e. basic chain conformation) is retained in the melt which will act as nuclei for crystallization.

#### ACKNOWLEDGEMENTS

The authors wish to thank Messrs M. E. A. Cudby, A. Bunn and J. M. Chalmers for n.m.r. and infra-red data and its expert interpretation.

#### REFERENCES

- 1 Hay, A. S. *et al. J. Am. Chem. Soc.* 1959, **81**, 6335
- 2 Ramsey, J. S. and Kovacic, P. *J. Polym. Sci. (A-1)* 1969, **7**, 127 and references cited therein
- 3 Kovacic, P. and Kyriakis, A. *Tetrahedron Lett.* 1962, **11**, 467
- 4 Bilow, N. and Miller, L. *J. J. Macromol. Sci.* 1957, **A1** (1), 183
- 5 Scholl, R. and Seer, C. *Ber. Dt. Chem. Ges.* 1922, **55**, 330
- 6 Clowes, C. A. *J. Chem. Soc. (C)* 1968, p 2519
- 7 Ashley, J. N. *et al. J. Chem. Soc.* 1948, p 263
- 8 Rodionow, W. M. and Manzow, S. *J. J. Soc. Chem. Ind.* 1923, **42**, 509
- 9 'Handbook of Chemistry and Physics', 31st edn, Chemical Rubber Publishing Co., Cleveland, Ohio, p 964

# Rôle of semi-pinacol radicals in the benzophenone-photoinitiated polymerization of methyl methacrylate

J. Hutchison, M. C. Lambert and A. Ledwith

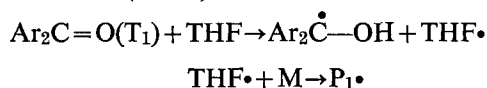
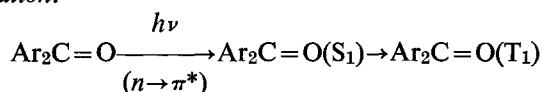
Department of Inorganic, Physical and Industrial Chemistry, University of Liverpool,  
PO Box 147, Liverpool L69 3BX, UK  
(Received 3 December 1972)

Semi-pinacol radicals ( $\text{Ph}_2\dot{\text{C}}\text{-OH}$ ), generated by photolysis of benzophenone in the presence of benzhydrol, are shown to act as terminating species in free radical polymerization of methyl methacrylate (MMA) at 30° and 70°C; initiation by  $\text{Ph}_2\dot{\text{C}}\text{-OH}$  radicals is significant only at the higher temperature. Polymerizations of MMA photoinitiated by substituted benzophenones ( $\text{Ar}_2\text{C=O}$ ) in hydrogen donor solvents are affected by these reactions and, contrary to previous assumption, the present results demonstrate that combination of  $\text{Ar}_2\dot{\text{C}}\text{-OH}$  with solvent derived radicals is a process which competes with initiation. Results from the photochemical experiments are discussed in relation to those of other workers, obtained by thermal generation of semi-pinacol radicals.

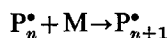
## INTRODUCTION

The results of a detailed study of the efficiencies of benzophenone, 3,3',4,4'-benzophenone tetracarboxylic dianhydride (BTDA) and 3,3',4,4'-tetramethoxycarbonyl benzophenone (TMCB) as photoinitiators for the polymerization (at 30°C) of methyl methacrylate (MMA) have been reported previously<sup>1</sup>. Photoinitiation was found to be most effective when the reactions were carried out in solvents, such as tetrahydrofuran (THF), having readily abstractable hydrogen atoms. Most of the experimental observations were consistent with the reaction scheme shown below.

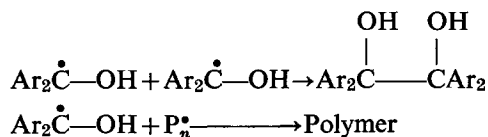
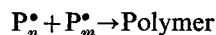
### Initiation:



### Propagation:



### Termination:



Termination of a significant proportion of the polymer chains by semi-pinacol radicals ( $\text{Ar}_2\dot{\text{C}}\text{-OH}$ ) was proposed in order to account for the observed relationship

between rates of polymerization and molecular weights of the polymers produced; gradients of plots of reciprocal viscosity-average molecular weight ( $1/\bar{M}_v$ ) versus rate of polymerization ( $R_p$ ) were considerably greater for MMA polymerizations photoinitiated by the benzophenones, than for those initiated (thermally and photochemically) by azobisisobutyronitrile (AIBN). The effect was most pronounced for benzophenone itself (Ar = phenyl) although addition of benzophenone (and also benzhydrol, and benzopinacol) to MMA polymerizations initiated thermally by AIBN (at 50°C, in THF solution) had no appreciable effect on  $R_p$  or  $\bar{M}_v$ . These observations seemed to exclude the possibility that additional chain transfer reactions, occurring in the presence of benzophenone, were responsible for the relatively low molecular weight polymers obtained in the benzophenone-photoinitiated polymerizations. However, for other photoinitiators, enhanced transfer activity under irradiation conditions over that observed in thermal systems has been reported<sup>2-4</sup>, and it has been suggested that photo-excited initiator molecules (and monomer molecules<sup>4</sup>) may take part more readily in transfer reactions than molecules in the ground state. Conceivably then, benzophenone, although not exhibiting transfer activity in thermal systems, may do so under photolysis conditions. If so, this would be an alternative explanation for the  $1/\bar{M}_v$  against  $R_p$  relationship observed for the benzophenone-photoinitiated polymerizations. Moreover, the work of Braun *et al.*<sup>5,6</sup> has shown that semi-pinacol radicals, rather than acting as terminating species, can in fact initiate the polymerization of MMA (above 40°C).

In this paper, the results of a further investigation into the rôle of semi-pinacol radicals in the benzophenone-photoinitiated polymerization of MMA are

reported and evidence has been obtained which supports the proposition that semi-pinacol radicals do act as terminating species. In addition, spectrophotometric studies are described which indicate that a combination reaction between semi-pinacol radicals and solvent-derived radicals takes place. Ways in which this reaction may influence the overall polymerization kinetics are suggested.

## EXPERIMENTAL

### Materials

Methyl methacrylate (Hopkin and Williams stabilized monomer) was washed five times with 10% v/v portions of 5M aqueous sodium hydroxide to remove the inhibitor, then with de-ionized water to constant pH. The monomer was dried over calcium chloride and fractionated under reduced pressure, with a nitrogen bleed, through an 80cm heated column packed with Fenske helices. The middle fraction, boiling at 43°C, 90mm, was collected at a reflux ratio of 2:1.

Benzene (May and Baker 'pure, crystallizable') was washed five times with 10% v/v portions of concentrated sulphuric acid, twice with 25% v/v portions of de-ionized water, twice with 10% v/v portions of 5M sodium hydroxide, and finally twice more with 25% v/v portions of water. After standing for several days over calcium hydride, the benzene was distilled at atmospheric pressure on the Fenske helices column and the middle fraction (b.p. 80°C) was collected.

The purified methyl methacrylate and benzene were each degassed several times on the high-vacuum line ( $\sim 10^{-4}$  mmHg) and then distilled into their respective storage vessels.

Benzophenone (Hopkin and Williams) was recrystallized from absolute ethanol to yield large, transparent crystals, m.p. 48°C (lit.<sup>1</sup> 48°C).

Benzhydrol (Hopkin and Williams) was also recrystallized from absolute ethanol to yield fine white needles, m.p. 65–67°C (lit.<sup>1</sup> 68°C).

Benzopinacol was prepared by ultra-violet irradiation of a 4% w/v solution of benzophenone in isopropanol. After 12h, the benzopinacol was filtered off and recrystallized from absolute ethanol, to yield white crystals, m.p. 174°C (lit.<sup>1</sup> 170–180°C).

Azobisisobutyronitrile (Eastman Kodak) was recrystallized from methanol. The resulting white crystals, m.p. 102–103°C (lit.<sup>1</sup> 103°C), were stored under vacuum at 0°C in the dark.

Tetrahydrofuran (BDH laboratory reagent, stabilized with 0.1% hydroquinone) was refluxed for 48h over calcium hydride, then distilled through a Vigreux column at a reflux ratio of 4:1. The fraction boiling between 66.0 and 66.5°C was collected, and stored in the dark over sodium wire.

### Polymerization procedure

Initiators and additives were weighed into individual reaction ampoules (8mm diam. Pyrex tubes) which were then glass-blown on to the high vacuum line, and evacuated prior to the introduction of monomer and solvent. After filling and sealing, the reaction ampoules were warmed to near room temperature and the contents ( $\sim 5\text{cm}^3$ ) were mixed by shaking. For thermally initiated reactions, the ampoules were wrapped in

aluminium foil and placed in the constant temperature bath for an appropriate time. In the case of the photo-initiated reactions, irradiation was by means of a 250W medium-pressure mercury discharge lamp operated from a stabilized d.c. power supply. Light from the lamp was collimated and directed on to a soda-glass window ( $\sim 6.5\text{cm}$  in diameter), in the side of the constant temperature bath, which effectively filtered out short-wavelength u.v. light ( $\lambda < 310\text{nm}$ ). The reaction ampoules were placed about 1cm behind the window and for each run, two ampoules were positioned side-by-side so that the intensity of light incident on each would be the same. Thus the temperature and irradiation conditions could be considered identical for each member of a particular pair of ampoules. Since conditions may have varied slightly among different pairs of photo-sensitized runs (owing for example to temperature fluctuation, ageing of the lamp, or in the positioning of the lamp and ampoules) comparisons of polymerization rates observed for unpaired ampoules were considered to be less reliable than the comparisons made between paired ampoules.

On removal from the bath, the ampoules were opened, and the contents were precipitated in 300cm<sup>3</sup> of methanol. After filtration, the polymer samples were dried to constant weight at 50°C in a vacuum oven. Molecular weights of some of the polymer samples were determined by gel permeation chromatography (Waters model 200), and the more reliable weight-averages taken.

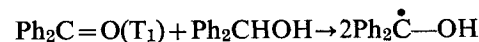
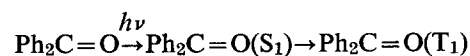
### Spectrophotometric studies

Solutions of benzophenone in THF, or THF/MMA mixtures, were made up in 1cm spectrophotometer cells, flushed with oxygen-free nitrogen for about 20min and irradiated with light from a 250W medium pressure mercury discharge lamp through a water filled heat filter and a 366nm interference filter. Ultra-violet spectra of the solutions were recorded after various times of irradiation (in the region 0–40min) by means of a Unicam SP1800 spectrophotometer.

## RESULTS

### Polymerization experiments

*Effects of benzhydrol on the benzophenone-photo-initiated polymerization of MMA in benzene.* The results of a series of 'paired' photolysis experiments are summarized in Table 1. It can be seen that for each paired run, one of the  $\sim 30\%$  v/v MMA/benzene mixtures contained both benzophenone ( $\sim 5 \times 10^{-3}\text{M}$ ) and benzhydrol ( $\sim 0.14\text{M}$ ), and the other benzophenone alone. The aim was to encourage increased semi-pinacol radical formation in the former mixtures, since it was anticipated that triplet-excited benzophenone would abstract a hydrogen atom from benzhydrol (rather than from benzene or MMA) giving rise to semi-pinacol radicals from both precursors, i.e.



The experiments were carried out at 30°C and 70°C. At 30°C, it is evident that the presence of benzhydrol



Table 1 Benzophenone-photoinitiated polymerizations in the presence and absence of benzhydrol (30°C and 70°C)

Temperature (°C)	Vol.% MMA in benzene (20°C)	[Ph <sub>2</sub> C=O] 10 <sup>3</sup> M	[Ph <sub>2</sub> CHOH] (M)	Polymerization rate (mol l <sup>-1</sup> h <sup>-1</sup> )	$\bar{M}_w \times 10^{-3}$ (by g.p.c.)
30	29.5	5.1	0.144	$5.7 \times 10^{-3}$	62 ± 4
	29.6	5.2	none	$10.3 \times 10^{-3}$	336 ± 22
	30.0	5.6	0.141	$7.1 \times 10^{-3}$	—
	30.6	5.6	none	$14.3 \times 10^{-3}$	—
70	29.6	4.8	0.142	$4.3 \times 10^{-2}$	257 ± 18
	29.8	4.6	none	$3.5 \times 10^{-2}$	649 ± 54
	30.0	6.3	0.154	$5.7 \times 10^{-2}$	—
	29.7	6.1	none	$5.2 \times 10^{-2}$	—

has had a considerable retarding effect on the polymerization rate. This retardation is not apparent at 70°C; at this temperature the presence of benzhydrol has, if anything, tended to increase the overall rate of polymerization. At both temperatures, the (weight-) average molecular weight of the polymer formed is significantly reduced when the reactions are carried out in the presence of benzhydrol.

*Effect of benzhydrol on the AIBN-photoinitiated polymerization of MMA.* In order to ascertain whether the retarding effect of benzhydrol in the 30°C experiments described above was due to interaction of the benzhydrol molecule itself with the growing polymer radicals, AIBN-photoinitiated polymerization rates in the presence and absence of benzhydrol were compared. (Photo-excited AIBN dissociates to form nitrogen and cyano-isopropyl radicals, which initiate polymerization.) No retardation by benzhydrol could be detected and the molecular weight of the polymer produced was not affected by the presence of benzhydrol. Thus, at the concentrations employed, and under the photolysis conditions, it may be assumed that benzhydrol itself acts neither as a terminating species, nor as a transfer agent, in the free-radical polymerization of MMA.

*Comparison of photopolymerization rates in the presence and absence of benzophenone.* Under the photolysis conditions, higher polymerization rates (at 30°C) were observed for MMA/benzene mixtures containing benzophenone ( $5.5 \times 10^{-3}$  M) than for 'paired' mixtures containing no benzophenone (Figure 1). This confirmed that photoinitiation by benzophenone does take place, even when benzene is used as solvent. The effect was more marked than observed previously<sup>1</sup>, when lower benzophenone concentrations were employed ( $8 \times 10^{-4}$  M). In the absence of benzophenone, a reaction order of 1.5 with respect to MMA concentration is indicated. This would be consistent with initiating radicals being produced by direct photo-excitation of MMA. The lower monomer exponent obtained in the presence of benzophenone is to be expected on the basis that, in this case, most of the initiating radicals result from excitation of the benzophenone.

*Thermal initiation using benzopinacol.* The presence of benzopinacol ( $\sim 3 \times 10^{-2}$  M) in  $\sim 30\%$  v/v MMA/benzene mixtures, heated in the dark at 70°C, gave rise to an approximately twenty-fold increase in the polymerization rate over that observed for blank mixtures, containing no benzopinacol. Initiation is presumably brought

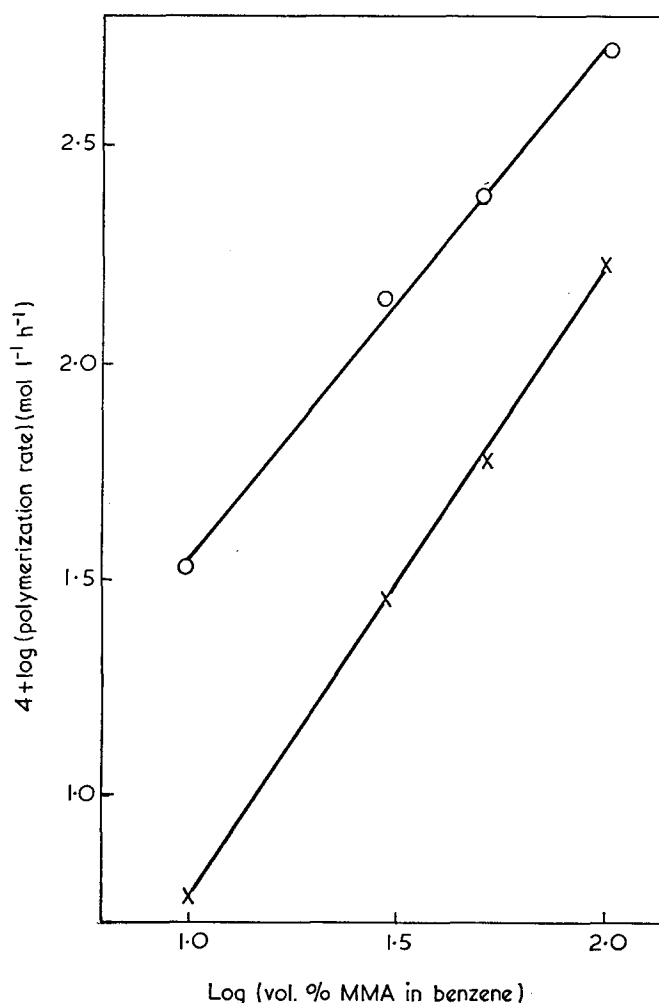


Figure 1 Photopolymerization of MMA at 30°C. O, Containing  $5.5 \times 10^{-3}$  M benzophenone, gradient 1.2; X, absence of benzophenone, gradient 1.5

about by semi-pinacol radicals formed by the thermal dissociation of benzopinacol<sup>5,6</sup>.

#### Spectrophotometric studies

On irradiating a solution of benzophenone ( $5.5 \times 10^{-3}$  M) in THF with light of wavelength 366 nm, a reaction occurred which was monitored by recording the absorption spectrum of the solution between 300 and 370 nm (Figure 2, solid lines). By analogy with studies of the photoreduction of benzophenone in isopropanol<sup>7,8</sup>, the increase in absorption may be ascribed to the formation of an adduct arising from the combination of the two radicals formed as a result of hydrogen abstraction from THF by triplet-excited benzophenone.

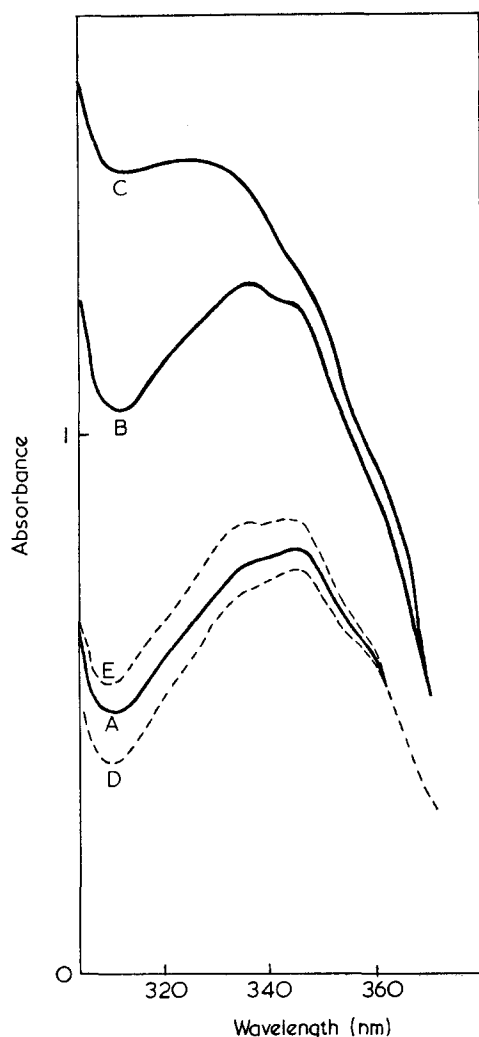


Figure 2 U.v. absorption spectra of benzophenone solutions in THF (—) after (A), 0, (B) 10 and (C) 40 min irradiation times and 50% v/v THF/MMA (---) after (D) 0 and (E) 40 min irradiation times

The spectra recorded before and after irradiation (for 40 min) of a solution of benzophenone in 50% v/v THF/MMA (Figure 2, broken lines) show a considerably reduced rate of adduct formation. Figures 3 (a)–(d) confirm that the rate of adduct formation decreases with increasing MMA concentration over the 0–50% v/v range investigated.

## DISCUSSION

Since, in the AIBN-photoinitiated polymerizations benzhydrol affected neither the polymerization rate, nor the average molecular weight of the polymer produced, then it is reasonable to assume that the effects of benzhydrol on the benzophenone-photoinitiated polymerizations were due to more semi-pinacol radicals being formed in the presence of benzhydrol than in its absence. If this is accepted, then the fact that in the 30°C photolysis experiments benzhydrol caused a marked reduction in both the polymerization rate and the molecular weight of the polymer, demonstrates conclusively that semi-pinacol radicals act as terminating species in the polymerization of MMA at this temperature.

The possibility that semi-pinacol radicals also initiate polymerization to some extent at 30°C cannot be alto-

gether excluded. That initiation is brought about by semi-pinacol radicals at higher temperatures is shown by the thermal reactions carried out at 70°C using benzopinacol. Braun *et al.*<sup>5,6</sup> have previously reported that vinyl monomers can be polymerized by semi-pinacol radicals (again produced from aromatic pinacols) above 40°C. In the photolysis experiments carried out at 70°C, the presence of benzhydrol resulted in a marginal increase in the rate of polymerization, but a considerable reduction in the molecular weight of the polymer formed. Thus it can be concluded that although semi-pinacol radicals undoubtedly initiate at this temperature, termination is still an important effect.

This conclusion is of relevance to the point raised earlier, namely, that for some photoinitiators, chain transfer constants measured in the irradiated systems have been found to be appreciably higher than those determined in thermally initiated (non-irradiated) polymerizations. For example Minoura and Toshima<sup>2</sup> reported this to be so for a series of chlorosilane compounds,  $(\text{CH}_3)_n\text{SiCl}_{4-n}$ , and assumed that when activated with u.v. light these compounds take part more readily in the chain transfer reaction than chlorosilanes in the ground state. However, an alternative explanation could be that, as in the case of benzophenone, one of the radical species formed in the photochemical reaction terminates a significant proportion of the polymer chains.

If the following assumptions can be considered valid: (i) the terminating radical species does not also initiate polymerization, being consumed otherwise only by interaction with itself, e.g. by self-combination; (ii) the other sensitizer-derived radical is *not* consumed by self-interaction, i.e. it is a highly efficient initiator of polymer chains, then kinetic analysis of the system is relatively straightforward<sup>1</sup>, and predicts that the polymerization will be half-order with respect to photoinitiator<sup>4</sup> concentration and first-order in monomer (as was found for the chlorosilanes<sup>2</sup>).

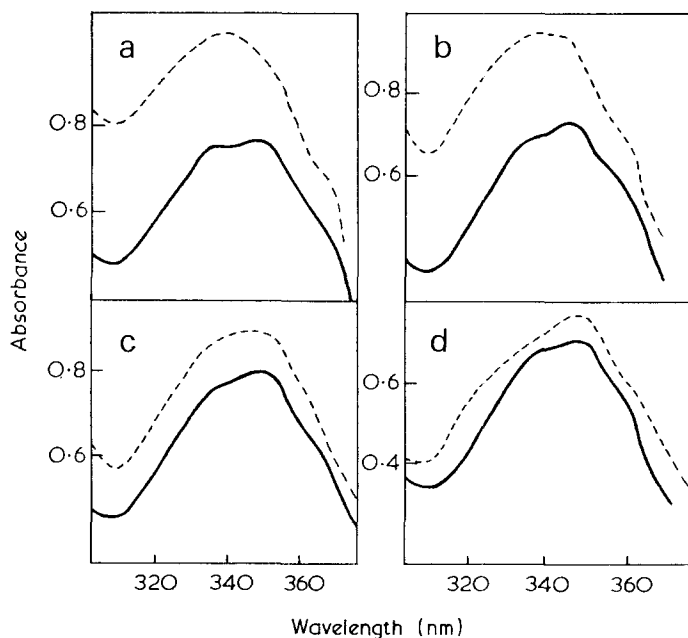


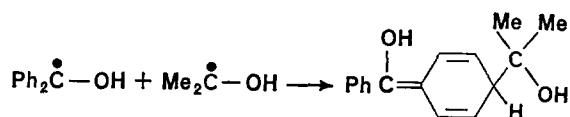
Figure 3 U.v. absorption spectra of benzophenone solutions in MMA/THF mixtures before irradiation (—) and after 5 min irradiation (---). (a) Bulk THF; (b) 5 vol.% MMA; (c) 20 vol.% MMA; (d) 50 vol.% MMA

A more complex kinetic situation arises when a radical species derived from a sensitizer, or from a thermal initiator, both initiates and terminates polymer chains<sup>9</sup>. Such behaviour affects the dependence of the polymerization rate on both initiator and monomer concentrations; the order with respect to initiator tending to be reduced (i.e. <0.5), and that in monomer increased (i.e. >1.0). MMA polymerizations initiated thermally by benzopinacol would be expected to exhibit these tendencies, since it has been shown that semi-pinacol radicals, as well as initiating the polymerization of MMA, also act as terminating species. For this system, Braun *et al.*<sup>6</sup> did in fact find the order in MMA to be significantly greater than 1.0, the results being more consistent with an order of 1.5; but in the case of this monomer, they do not provide data for the order with respect to benzopinacol. For the benzopinacol-initiated polymerization of styrene, their results were again consistent with a monomer order of 1.5, but a linear relationship was obtained between polymerization rate and the square root of benzopinacol concentration. (Braun *et al.* interpreted their results in terms of a reaction scheme which did not include termination of polystyryl chains by semi-pinacol radicals.)

The spectrophotometric studies relate to the efficiency of initiation by solvent-derived radicals in the benzophenone-photoinitiated polymerization of MMA in THF<sup>1</sup>. From the changes observed in the u.v. absorption spectra on irradiation of solutions of benzophenone in THF and THF/MMA mixtures, it may be inferred that a combination reaction takes place between THF radicals and semi-pinacol radicals:



As mentioned previously, this is analogous to reactions observed in photolysis of benzophenone in isopropanol. For the latter system, Filipescu and Minn<sup>7</sup> have proposed the following structure for the adduct giving rise to increased u.v. absorption between 300 and 370 nm:



It was observed that in the benzophenone/THF/MMA system, the rate of adduct formation decreases with increasing MMA concentration. Two possible mechanistic interpretations of this are as follows.

(1) The quantum yield for production of THF• and Ar<sub>2</sub>C•-OH radicals remains constant (unity?) over the MMA concentration range investigated, but the proportion of THF• radicals which react with MMA (initiating polymerization) increases with increasing MMA concentration, thus decreasing the number of THF• radicals available for combination with semi-pinacol radicals, i.e. reducing the rate of adduct formation.

(2) The proportion of THF• and Ar<sub>2</sub>C•-OH radicals which combine to give adduct remains constant (cage

recombination?), but the rate of formation of THF• and Ar<sub>2</sub>C•-OH radicals decreases with increasing MMA concentration, owing to quenching of triplet-excited benzophenone by MMA. The quenching reaction may or may not give rise to species which themselves initiate polymerization.

Both of these interpretations would require that the efficiency, *f*, of the initiation process changes with MMA concentration (*f* may be defined as the fraction of triplet-excited benzophenone molecules which, by some intermediate process, lead to the initiation of polymer chains). Interpretation (1) would involve *f* increasing with increasing MMA concentration. This would tend to increase the order of the polymerization reaction with respect to MMA concentration. Interpretation (2) would involve *f* decreasing with increasing MMA concentration assuming that the species formed as the result of quenching of triplet-excited benzophenone by MMA initiated polymerization less efficiently than the solvent-derived radicals (i.e. THF•). This would tend to decrease the order of the polymerization reaction with respect to MMA concentration. The reaction scheme proposed by Block *et al.*<sup>1</sup> (which did not include the combination of THF• with Ar<sub>2</sub>C•-OH radicals) predicted that the polymerization would be first-order with respect to MMA concentration. However, their analysis of the data obtained for the polymerization of MMA in THF photoinitiated by benzophenone itself gave a value of 0.84 for the monomer exponent, and it could be argued that this result favours interpretation (2).

An important observation in the earlier study of photo-initiation of MMA polymerization by benzophenones<sup>1</sup> was the relative rate sequence



This was ascribed mostly to increasing efficiency of termination by the respective semi-pinacol radicals (Ar<sub>2</sub>C•-OH). It was further assumed that there would be a common quantum efficiency for radical production for the three ketones and that there would be no adducts formed between Ar<sub>2</sub>C•-OH and solvent derived radicals. The latter assumption is now clearly untenable and relative efficiencies of initiation by radicals derived from photoexcited aromatic carbonyl compounds will undoubtedly be affected by relative efficiencies of adduct formation.

## REFERENCES

- 1 Block, H., Ledwith, A. and Taylor, A. R. *Polymer* 1971, **12**, 271
- 2 Minoura, Y. and Toshima, H. *J. Polym. Sci. (A-1)* 1969, **7**, 2837
- 3 Tsuda, K., Kobayashi, S. and Otsu, T. *Bull. Chem. Soc. Japan* 1965, **38**, 1517
- 4 Baysal, B. and Tobolsky, A. V. *J. Polym. Sci.* 1951, **8**, 529
- 5 Braun, D. and Becker, K. H. *Angew. Makromol. Chem.* 1969, **6**, 186
- 6 Braun, D. and Becker, K. H. *Makromol. Chem.* 1971, **147**, 91
- 7 Filipescu, N. and Minn, F. L. *J. Am. Chem. Soc.* 1968, **90**, 1544
- 8 Weiner, S. A. *J. Am. Chem. Soc.* 1971, **93**, 425
- 9 North, A. M. 'The Kinetics of Free Radical Polymerisation'. Pergamon Press, Oxford, 1966, p 79

# Effect of segment size and polydispersity on the properties of polyurethane block polymers

H. N. Ng, A. E. Allegrezza, R. W. Seymour and S. L. Cooper

*Department of Chemical Engineering, University of Wisconsin, Madison, Wisconsin 53706, USA  
(Received 22 December 1972; revised 19 February 1973)*

The dynamic-mechanical and thermal scanning behaviour of a series of specially synthesized linear segmented polyurethanes is presented. These materials possess a well defined segment molecular weight and molecular weight distribution and no possibility of intermolecular hydrogen bonding. The dynamic-mechanical transitions observed are assigned to specific molecular motions and the effect of segment size and molecular weight distribution is described. The results are explained in terms of hard segment domain perfection. Differential scanning calorimetry (d.s.c.) curves of annealed samples indicate that domain morphology may be affected by thermal treatment. A comparison of dynamic mechanical and d.s.c. results to hydrogen-bonded polyurethanes is made.

## INTRODUCTION

The development of thermoplastic elastomers in recent years has led to extensive studies of the morphology and viscoelastic properties of these materials. Thermoplastic elastomers are block copolymers produced by joining alternating blocks of two dissimilar polymer chains. At service temperatures, one of the polymer chains is a viscous or rubbery component (soft segment), the other, a glassy or highly crystalline thermoplastic (hard segment). In the thermoplastic elastomers, the soft segments are the major component, and each polymer chain contains at least two hard segments.

It is now widely accepted that many of the unusual properties of these polymeric systems can be attributed to microphase separation of the hard segments into domains dispersed in a matrix of soft segments<sup>1</sup>. The rigid domains reinforce the elastomeric matrix by functioning both as tie-down points and as filler particles. Such elastomeric block polymers exhibit properties characteristic of crosslinked elastomers at moderate temperatures but flow as thermoplastics at temperatures above the softening point of the higher modulus component.

An important class of thermoplastic elastomers are the linear segmented polyurethanes<sup>2-6</sup>. These polymers have the general structure  $(A-B)_n$  where B (the soft segment) is usually formed from a polyester or poly(ether macroglycol) of molecular weight less than 2000. The hard segment is formed by extending an aromatic diisocyanate with a low molecular weight diol such as 1,4-butanediol. The soft and the hard segments are relatively short blocks which alternate  $n$  times to give a polymer of high molecular weight. Electron microscopic<sup>7</sup> and X-ray<sup>8-10</sup> studies have demonstrated the existence of separate domains of hard and soft segments.

The synthesis of a typical macroglycol as well as its subsequent reaction with diisocyanate and low molecular

weight diol is done by stepwise polymerization reactions. This results in a broad molecular weight distribution in both of the segments and in the final polymer.

It is known that the molecular weight distribution ( $MWD$ ) affects the mechanical properties of homopolymers as well as the more extensively studied ABA triblock polymers<sup>11</sup>. It was therefore of interest to study the effect of varying  $MWD$  on the properties of segmented polyurethanes.

Materials chosen for this study were prepared from poly(tetramethylene oxide glycol) (PTMEG), piperazine and 1,4-butanediol bischloroformate. They were synthesized in a carefully designed manner in order to control the molecular weight and molecular weight distribution of the hard segments. While the effect of other molecular parameters on the properties of polyurethanes have been studied extensively, a study of the effects of  $MWD$  has received little attention. With the polymers used in this study, it is now possible to begin this work.

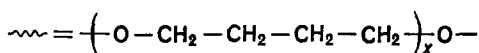
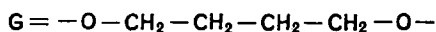
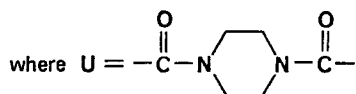
Another important feature of this system is that in contrast to the polyurethanes commonly investigated these materials have no potential for intermolecular hydrogen bonding. Although hydrogen bonding is important in determining some properties of polyurethane elastomers, it imposes considerable complexity on structure-property relations and renders interpretations difficult. Fortunately, with piperazine-based hard segments, the possibility of hydrogen bonding is excluded. Thus, the structure of the hard domains, the nature of the intermolecular association due to crystallization of the soft and hard segments and other morphological features can be studied in a simplified manner. Furthermore, the thermal behaviour of these non-hydrogen-bonded polyurethanes (as studied by differential scanning calorimetry) may be compared to analogous systems of the more common polyurethanes.

EXPERIMENTAL

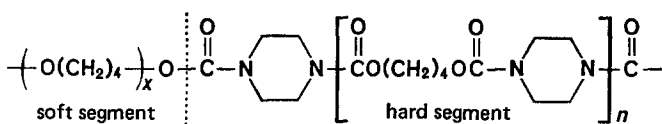
Materials

The materials used in this study were obtained through the courtesy of Dr L. L. Harrell, Jr, of E. I. Du Pont de Nemours & Company and are described below.

Overall structure:



Segmented structure:



The soft segment  $-(O-CH_2-CH_2-CH_2-CH_2)_x$  is poly(tetramethylene oxide) whose length is specified by  $x$ , the degree of polymerization. In this series of materials,  $x$  took on an average value of either 13.7 or 24, yielding a molecular weight of 1003 or 1744 for the soft segment. The hard segments  $-(UG)_n$  were prepared by reacting 1,4-butanediol bischloroformate with piperazine. The resulting urethane linkage formed between the bischloroformate and piperazine was designated as U, while G represents the chain extender, 1,4-butanediol. The value of  $n$  varied from 1 to 4. For convenience, the molecular weight of the hard segment has been expressed as a weight percentage. A summary of the structural parameters for the polymers investigated in this work is presented in Table 1.

A detailed synthetic procedure for the preparation of these polymers has been published by Harrell<sup>12</sup>. Mono-disperse hard segments were produced by a sequence of reactions that allowed the addition of one hard unit at a time to give hard segments with  $n=1, 2, 3$  or 4. Polydisperse hard segments were easily prepared via the stepwise reaction between 1,4-butanediol bischloroformate and piperazine, to give average values of  $n=1, 2, 3$ , and 4. The polyurethanes were formed by the stepwise reaction of the preformed hard segments and the polyether segments.

Table 1 Structural parameters of segmented polyurethanes

Designation	Soft segment mol. wt.	Hard segment (wt.%)	$x$	$n$	Segment size distribution <sup>a</sup>	
					Soft	Hard
BB1-2	1003	37.2	13.7	2	B	B
BB1-4	1003	51.4	13.7	4	B	B
BN1-2	1003	37.2	13.7	2	B	N
BN1-4	1003	51.4	13.7	4	B	N
NN2-3	1744	32.0	24.0	3	N	N
BB2-3	1744	32.0	24.0	3	B	B

<sup>a</sup> B=broad; N=narrow

The molecular weight distribution of the soft segment follows that of the starting PTMEG. Hence, soft segments with a broad distribution were readily obtained from commercial, unfractionated PTMEG, whereas those with a narrow distribution were prepared from a fractionated sample of the same PTMEG.

The segmented polyurethanes used in this study are designated in the following manner. The molecular weight distribution in the soft and the hard segments are designated as B (broad) or N (narrow), the description for the hard segments being preceded by that for the soft segments. This is followed by a number indicating the molecular weight of the soft segments rounded to the nearest thousand. The last number indicates the number of repeat units ( $n$ ) in the hard segments. Hence, a polymer with a code such as BN1-2 has a broad molecular weight distribution in the soft segments and a narrow one in the hard segments, with the soft segments having a molecular weight of 1000 and the hard segments having two repeat units ( $n=2$ ).

Sample preparation

All samples used in dynamic mechanical testing and differential scanning calorimetry (d.s.c.) were prepared as films. The polymer was dissolved in methylene chloride, cast onto a clean glass surface and the solvent was allowed to evaporate slowly at room temperature. Removal of the film without distortion was accomplished by applying a small amount of water at the polymer/glass interface. The films were then vacuum-dried at ambient temperature for 4 hours.

Dynamic mechanical measurements

A direct reading dynamic viscoelastometer, Vibron model DDV-II (Toyo Measuring Instruments Company) was employed to make dynamic mechanical measurements at three frequencies (110, 11, and 3.5 Hz) for temperatures from about  $-140^\circ\text{C}$  to  $+180^\circ\text{C}$ . The rate of temperature change was maintained at about  $1^\circ\text{C}/\text{min}$ . The film dimensions were  $0.1 \times 5 \times 20$  mm. Apparent activation energies for various relaxation processes were determined from a plot of frequency versus the reciprocal of the absolute temperature at the loss peak maximum ( $T_{\text{max}}$ ) using the following equation:

$$\Delta H^* = 2.303R \times \frac{d(\log f_{\text{max}})}{d(1/T_{\text{max}})} \quad (1)$$

where  $\Delta H^*$  is the apparent activation energy,  $f_{\text{max}}$  the frequency at the loss peak maximum, and  $R$  the gas constant.

Differential scanning calorimetry

D.s.c. measurements were made using a Du Pont model 900 Thermal Analyzer with the d.s.c. module at a programmed heating rate of  $14^\circ\text{C}/\text{min}$ . Annealed samples were held at the specified temperatures for a period of 4 h and allowed to cool slowly to room temperature at a rate of  $1^\circ$  to  $2^\circ\text{C}/\text{min}$ . The sample size was 10–20 mg.

RESULTS AND DISCUSSION

Dynamic mechanical testing

The modulus temperature curves for the polyurethanes studied are shown in Figures 1–5. Loss peaks are observed for all polymers at about  $-100^\circ\text{C}$ ,  $-50^\circ\text{C}$ ,  $40^\circ\text{C}$ , and

Table 2 Transition temperatures (°C)

	Dynamic mechanical					D.s.c. (control)		
	$\gamma$	$\alpha_s$	$\alpha_h$	$\delta$	$\alpha_c$	$\alpha_s$	$\alpha_c$	$\delta$
BB1-2	-100	-50	25	110*	~10	-74	—	120*
BB1-4	-100	-45	25	135*	—	-72	—	150*
BN1-2	-100	-50	35	100*	—	-74	—	105
BN1-4	-100	-45	35	140*	~10	-74	—	160
NN2-3	-105	-55	35	105*	—	-76	—	105
BB2-3	-105	-50	35	170*	10	-77	8	175*

\* Estimated values—peaks are not well-defined

Table 3 Apparent activation energies ( $\Delta H^*$ )

Material	$\Delta H^*$ (kcal/mol)	
	$\gamma$	$\alpha_s$
BB1-2	10	47
BN1-2	13.5	65
BB1-4	9.5	65
BN1-4	7	51
BB2-3	15	48

above 100°C. These are designated  $\gamma$ ,  $\alpha_s$ ,  $\alpha_h$  and  $\delta$  respectively and are summarized in Table 2. In addition, a small peak appears as a shoulder at about 10°C ( $\alpha_c$ ) for polymers BB2-3, BB1-2, and BN1-4. Table 3 contains activation energy data for the  $\gamma$  and  $\alpha_s$  relaxations of the five materials studied.

**Soft segment relaxations.** The primary relaxation observed near -50°C in the dynamic mechanical behaviour at 110 Hz of all the samples is designated as the  $\alpha_s$  relaxation and assigned to the glass transition ( $T_g$ ) of the soft segments. The storage modulus drops by about two orders of magnitude in this relaxation region and the calculated activation energies for all the samples range from 47 to 65 kcal/mol, typical values for primary glass transitions. The  $T_g$  of the poly(tetramethylene oxide) (PTMO) homopolymer has been reported to be -65°C at 100 Hz<sup>13</sup>. In addition, a  $T_g$  for all 5 materials is observed in d.s.c. testing at about -70°C (Figure 6).

The secondary relaxation at about -100°C at 110 Hz is labelled the  $\gamma$  relaxation. The activation energy calculated from equation (1) ranges from 7 to 15 kcal/mol (Table 3). Willbourn<sup>14</sup> observed a secondary relaxation in PTMO at -100°C at a frequency of about 100 Hz, and ascribed it to motion of the methylene sequence. The actual mechanism of the  $\gamma$  relaxation remains controversial and it is not clear whether the relaxation occurs in both the crystalline and amorphous phases of the polymer. Although both the soft and hard segments contain the methylene sequence, the major contribution to the  $\gamma$  relaxation presumably comes from the soft segments because of its relatively high content in the polymer.

In addition to these relaxations, BB2-3, BB1-2, and BN1-4 possess a small shoulder (around 10°C) between the  $\alpha_s$  and  $\alpha_h$  relaxations, denoted  $\alpha_c$ . A deep endotherm was found at a similar temperature in the d.s.c. curve for polymer BB2-3 (Figure 6). The  $\alpha_c$  relaxation is attributed to the melting of the crystalline phase of the PTMO comprising the soft segments. The melting point of the PTMO homopolymer is 35°C<sup>13</sup>. The lower melting temperature of the soft segments of BB2-3 than that of

the homopolymer is probably due to the fact that the molecular weight of the PTMO segments in the block polymer is considerably less than in the homopolymer.

**Hard segment relaxations.** Dispersions above the melting point of the soft segments are attributed to relaxations within the hard segments. A small loss peak appears as a shoulder around 40°C, considered to be due to micro-Brownian motion of the amorphous phase in the hard segments. The corresponding glass transition (about 40°C) is rather ill-defined in the d.s.c. curves (Figure 6) because of the low hard segment content.

The high temperature loss process observed in the temperature range from 100°C to 190°C is designated at the  $\delta$  relaxation and is assigned to the melting of hard segment micro-crystallites. This assignment is confirmed by the d.s.c. endotherm (peak II in Figure 6) located at about the same temperature as the  $\delta$  relaxation.

**Comparison to hydrogen-bonded polyurethanes.** It is interesting to compare the dynamic mechanical properties of the present system, which has no hydrogen bonding, with the polyurethanes studied by Huh and Cooper<sup>6</sup>. In the latter study, the soft segments were either poly(tetramethylene adipate) or poly(tetramethylene oxide) and the hard segment, *p,p'*-dimethylmethane diisocyanate extended with 1,4-butanediol. These polymers are extensively hydrogen-bonded. The relaxation spectra for the two systems are remarkably similar, the primary difference being the location of the  $\alpha_s$  peak which occurs about 40° higher in the hydrogen-bonded polymers. This may be due to the influence of hydrogen bond interactions on the soft segment mobility. Infra-red studies have established that there is a significant amount of hydrogen bonding between the soft and hard segments<sup>4</sup>, which might serve to restrict local motion. Since this bonding persists above the soft segment  $T_g$ <sup>4,15</sup> it is evident that the  $\alpha_s$  transition is not accompanied by total disruption of these bonds.

#### Effect of segment size and polydispersity on the relaxation spectra

In the present system the  $\gamma$  transition is not affected by changes in *MWD* of the segments, but becomes broader at higher hard segment content. This is consistent with the belief that the  $\gamma$  transition is due to a local motion of methylene sequences in the soft segments.

The  $\alpha_s$ , or glass transition of the soft segments, appears to be influenced by the hard segment content, but not by the hard segment molecular weight or *MWD*. For example, in Figures 1 and 2 it can be seen that the  $\alpha_s$  transitions of BB1-2 and BB1-4 are equal to those of the analogous polymers which have narrow hard segment *MWD* (BN1-2 and BN1-4 respectively). Thus the hard segment *MWD* does not affect  $\alpha_s$ .

However, the  $\alpha_s$  transition of BN1-4 occurs at a higher temperature than that of BN1-2 (Figure 3) as does that of BB1-4 over BB1-2. The 5° or so increase in  $\alpha_s$  of the *n*=4 polymers is ascribed to the higher hard segment content and not to higher hard segment molecular weight. This is borne out by the fact that the  $\alpha_s$  transition temperature of BB2-3 is equivalent to the other polymers having the approximately same composition (BN1-2 and BB1-2) despite the higher hard segment molecular weight of BB2-3. The hard segments act as filler particles which

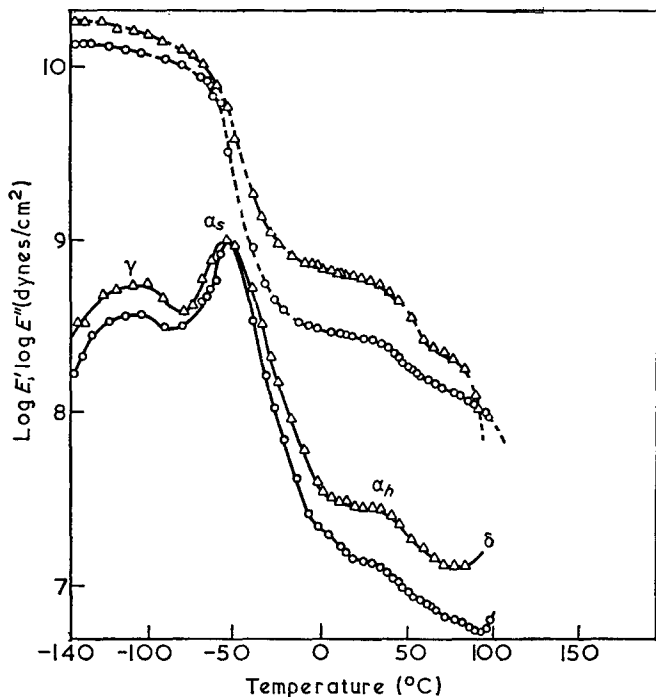


Figure 1 Dynamic mechanical properties of BB1-2 (O) and BN1-2 (Δ) at 110Hz. ---,  $E'$ ; —,  $E''$

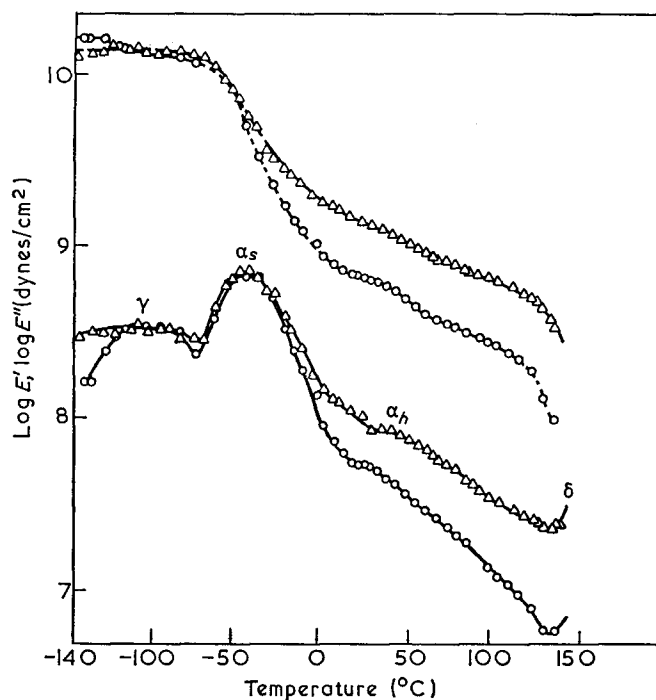


Figure 2 Dynamic mechanical properties of BB1-4 (O) and BN1-4 (Δ) at 110Hz. ---,  $E'$ ; —,  $E''$

interact with the matrix to raise its  $T_g$ , the effect being dependent upon filler content.

The hard segments influence the  $\alpha_s$  transition in another way. It can be seen that the slope of this transition ( $dE'/dT$ ) is less for BB1-4 and BN1-4 (53% hard segments), than for the other polymers, including BB2-3. According to Tobolsky and Narkis<sup>16</sup> this may be interpreted as indicating that the hard segment domains are more diffuse, that is, diluted with interpenetrating soft segments. The overall effect of such a diffuse morphology would be to hinder the total motion of the soft segment broadening their distribution of relaxation times.

The  $\alpha_h$  transition, or  $T_g$  of the hard segments, occurs at a higher temperature as the  $MWD$  narrows when polymers of similar composition are compared. For example, the  $\alpha_h$  transitions of BN1-2 and BN1-4 occur at a higher temperature than BB1-2 and BB1-4 respectively (Table 2). It would appear that here,  $MWD$  is at least as important a molecular parameter as hard segment content or molecular weight. This is shown by the fact that the  $\alpha_h$  value for NN2-3 is comparable to those of polymers having higher hard segment content and molecular weight (e.g. BN1-4).

The increase in  $\alpha_h$  with narrowing  $MWD$  of the hard segments may be due to improved microphase separation and crystallization. The absence of high and especially low molecular weight hard segments should result in higher degree of order within the domains and a concomitant increase in  $\alpha_h$ .

The important effects of hard segment  $MWD$  on  $E'$  can be explained in terms of domain perfection and crystallization. A comparison of the modulus-temperature curves in the plateau region between  $\alpha_s$  and  $\alpha_h$  shows the effect of polymer structure very well. Figure 1, a comparison of the modulus-temperature curves of BB1-2 and BN1-2 and, Figure 2, which compares the curves for BB1-4 and BN1-4, show that the modulus in the plateau region has a higher value for the polymers of narrower hard segment  $MWD$ , other molecular parameters being equal. The higher degree of hard segment order in BN1-2 and BN1-4 is also demonstrated in the d.s.c. traces of Figure 6 by the sharpness of the melting endotherm.

The same effect can also be seen in polymers of lower hard segment content. Figure 3 compares the modulus-temperature curves of NN2-3 and BB2-3. In this case, the curve for NN2-3 decreases more sharply at  $\alpha_s$  yet crosses that of BB2-3 to give a higher modulus in the plateau region. This may also be explained in terms of a more perfect hard segment domain. Further evidence of this is found in the sharp hard segment melting endo-

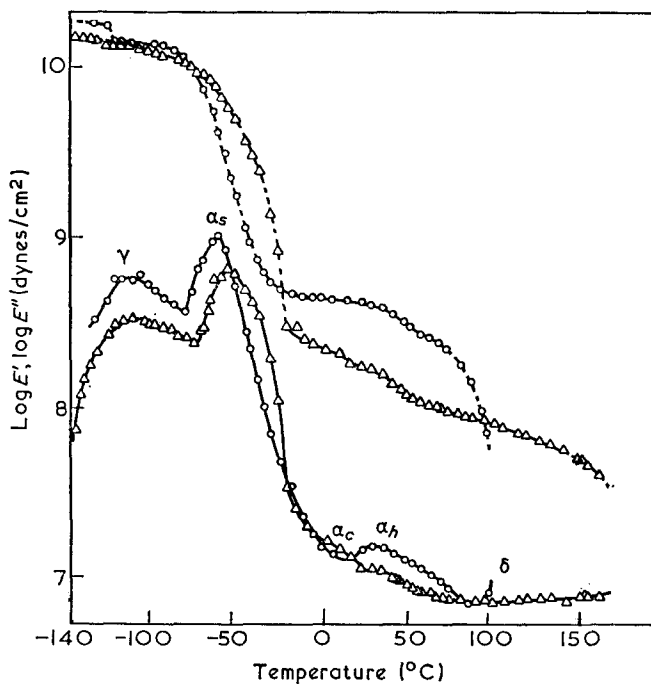


Figure 3 Dynamic mechanical properties of BB2-3 (Δ) and NN2-3 (O) at 110Hz. ---,  $E'$ ; —,  $E''$

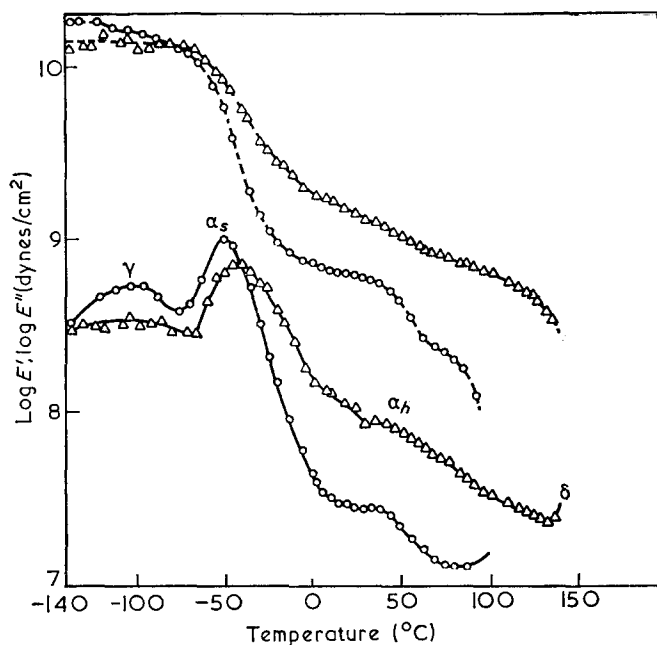


Figure 4 Dynamic mechanical properties of BN1-2 (O) and BN1-4 ( $\Delta$ ) at 110Hz. ---,  $E'$ ; —,  $E''$

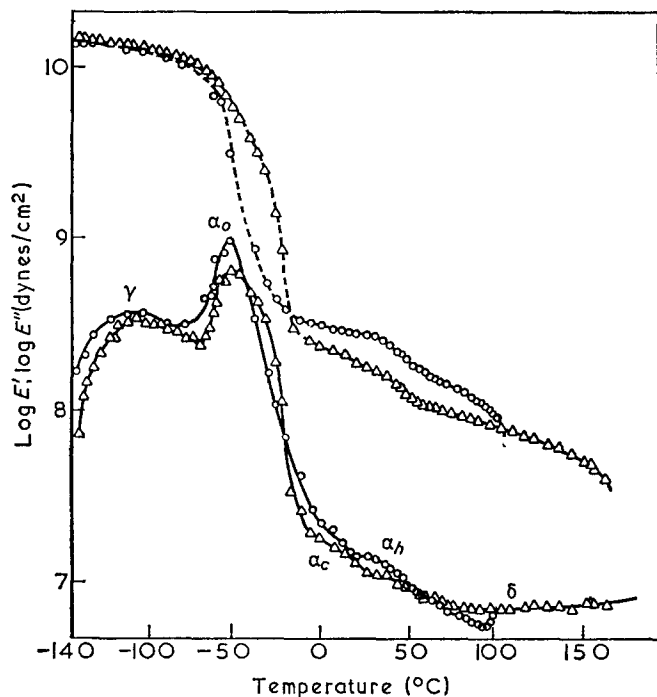


Figure 5 Dynamic mechanical properties of BB1-2 (O) and BB2-3 ( $\Delta$ ) at 110Hz. ---,  $E'$ ; —,  $E''$

therm of NN2-3 as compared to a very broad and indistinct melting transition for BB2-3 (Figure 6).

Figure 4 shows that for the higher hard segment content, the modulus in the plateau region has a higher value. This is the expected result, since an increased hard segment content is essentially the same as increasing the reinforcing filler content.

Figure 5 is a comparison of the modulus-temperature curves of BB1-2 and BB2-3. At the  $\alpha_s$  transition, the  $E'$  versus temperature curve for BB1-2 decreases more sharply than does that for BB2-3 and then crosses so that the modulus of BB1-2 is higher in the plateau region. This latter effect is to be expected owing to the slightly higher hard segment content of BB1-2 while the sharper

decrease of the modulus at  $\alpha_s$  for BB1-2 is felt to be due to the presence of relatively more perfect domains.

These results may be explained by considering the relative degree of phase separation and perfection in the various polymers. In considering the results shown in Figures 1 and 2, it is felt that the polymers with narrow *MWD* hard segments have a higher modulus in the plateau region because the domains formed are more perfect than those of comparable polymers of broad hard segment *MWD*. Studies done by Morton<sup>11</sup> have indicated that the modulus of the hard blocks in ABA

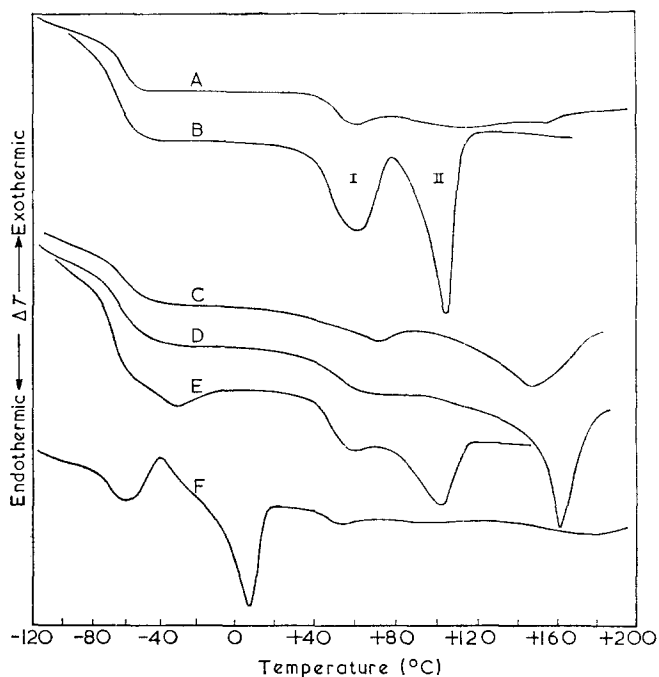


Figure 6 D.s.c. curves of polyurethane control samples. A, BB1-2; B, BN1-2; C, BB1-4; D, BN1-4; E, NN2-3; F, BB2-3

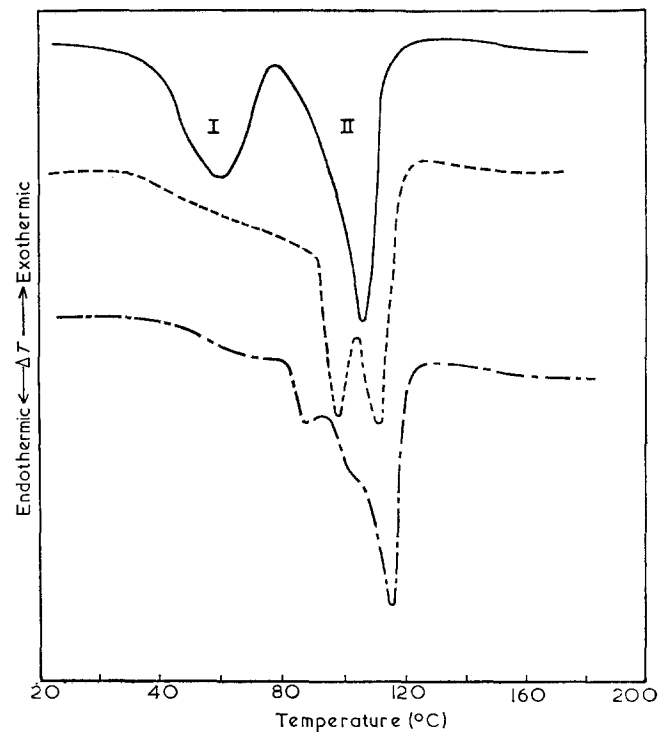


Figure 7 Effect of annealing on the thermal behaviour of BN1-2. —, Control; ---, annealed at 90°C for 4h; - - - -, annealed at 110°C for 4h



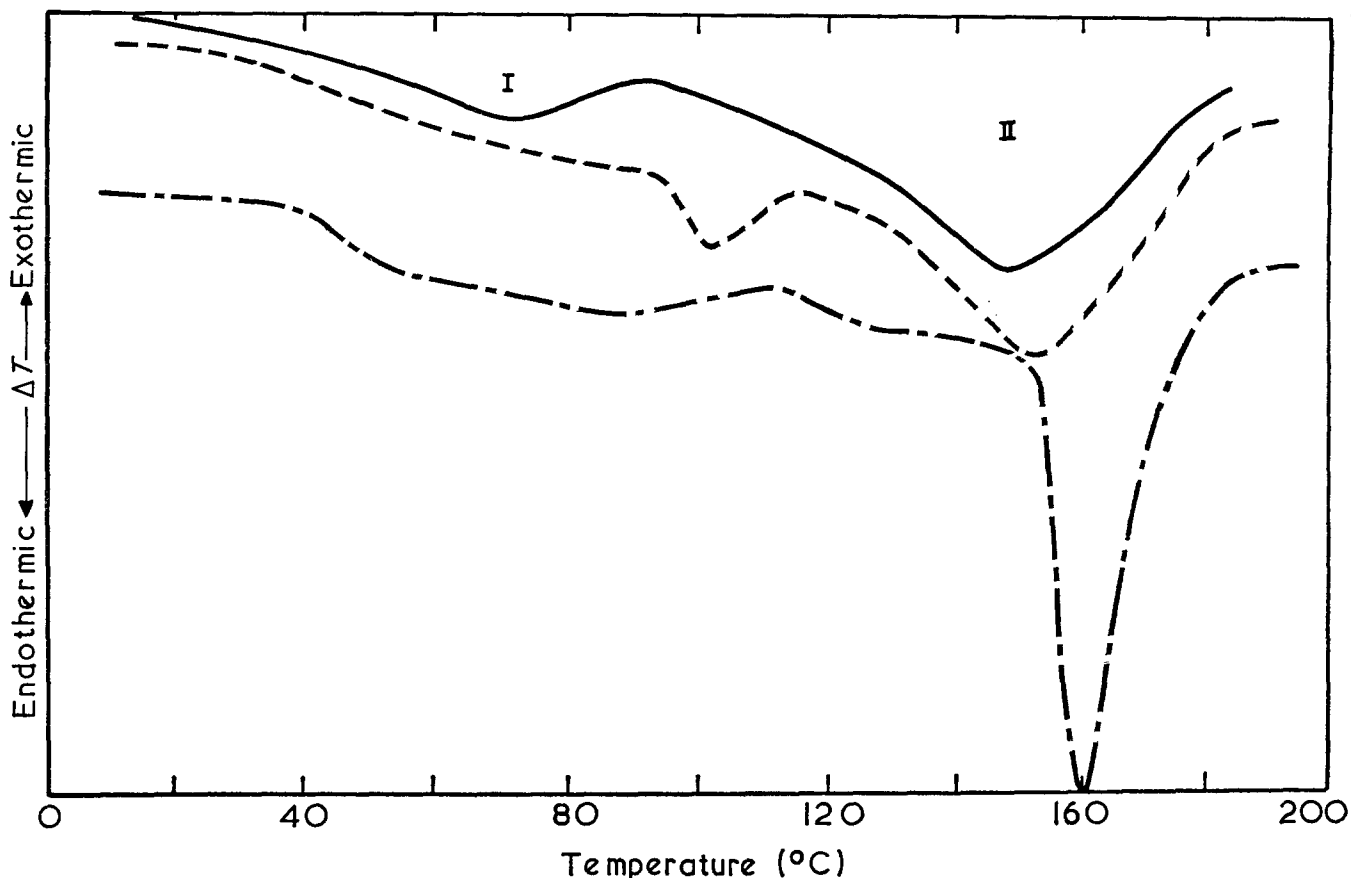


Figure 8 Effect of annealing on the thermal behaviour of BB1-4. —, Control; ----, annealed at 90°C for 4h; - · - · -, annealed at 150°C for 4h

triblock copolymers influences the modulus and tensile properties of the overall polymer. While a direct comparison between the present system and the ABA copolymers is not possible, a qualitative comparison of the filler effect of the domains in both is reasonable. Therefore, it is felt that the less perfect, or more diffuse domains, would cause a lower overall modulus.

In the case of the results shown in Figure 5, the data indicate that the polymer containing the higher molecular weight segments (BB2-3) formed less perfect domains than a polymer of slightly higher hard segment content. This result may be attributed to the kinetics of the film-making process, that is, during the drying time of the film-casting process, the diffusion of the hard segments into domains of BB2-3 is hindered by their higher molecular weight and by the more viscous matrix of the higher molecular weight soft segments.

#### D.s.c. results

D.s.c. curves for unannealed control samples are shown in Figure 6. D.s.c. estimates of the  $\alpha_s$ ,  $\alpha_c$  and  $\delta$  transition temperatures are summarized in Table 2. The soft segment glass transition occurs at about  $-70^\circ\text{C}$  in all samples. In BB2-3 it is followed by an *in situ* crystallization exotherm at  $-40^\circ\text{C}$  and a melting endotherm at  $10^\circ\text{C}$ .

A high temperature melting endotherm (II in Figure 6) is well defined for samples with narrow hard segment molecular weight distributions. This may be identified with the melting of the microcrystalline regions of the hard segment domains. This is defined as the  $\delta$  relaxation in the dynamic mechanical test.

The final feature of the d.s.c. curves in Figure 6 is an endotherm around  $60^\circ\text{C}$ , labelled I. Figures 7 and 8 show that annealing shifts the position of this peak upscale until it merges with the II peak. This effect is observed for all samples and is analogous to that reported by Seymour and Cooper<sup>15,17</sup> for hydrogen-bonded polyurethanes. These investigators concluded that the I peak thus represents disordering of more poorly ordered hard segments. The morphology responsible for the I peak may be improved by annealing until the microcrystalline morphology of peak II is reached. Further annealing intensifies and shifts the combined I-II peak to a slightly higher temperature. However, the low temperature endotherms and transitions pertaining to the soft segments are not affected by annealing.

#### ACKNOWLEDGEMENTS

The authors wish to thank Dr L. L. Harrell, Jr, of E. I. Du Pont de Nemours Co. for supplying us with the polymers described in this work. We are also grateful to the National Science Foundation for support of this research through Grant GH-31747.

#### REFERENCES

- 1 Estes, G. M., Cooper, S. L. and Tobolsky, A. V. *J. Macromol. Sci.* 1970, **C4** (1), 167
- 2 Cooper, S. L. and Tobolsky, A. V. *Text. Res. J.* 1966, **36**, 800
- 3 Cooper, S. L. and Tobolsky, A. V. *J. Appl. Polym. Sci.* 1966, **10**, 1837
- 4 Seymour, R. W., Estes, G. M. and Cooper, S. L. *Macromolecules* 1970, **3**, 579

- 5 Estes, G. M., Seymour, R. W. and Cooper, S. L. *Macromolecules* 1971, **4**, 452
- 6 Huh, D. S. and Cooper, S. L. *Polym. Eng. Sci.* 1971, **11**, 369
- 7 Koutsky, J. A., Hien, N. V. and Cooper, S. L. *J. Polym. Sci. (B)* 1970, **8**, 353
- 8 Clough, S. B., Schneider, N. S. and King, A. O. *J. Macromol. Sci.* 1968, **B2**, 641
- 9 Bonart, R., Morbitzer, L. and Hentze, G. *J. Macromol. Sci.* 1969, **B3**, 337
- 10 Bonart, R. *J. Macromol. Sci.* 1968, **B2**, 115
- 11 Morton, M. *Adv. Chem. Ser.* 1971, **99**, 490
- 12 Harrell, L. L. Jr, *Macromolecules* 1969, **2**, 607
- 13 McCrum, N. G., Read, B. E. and Williams, G. 'Anelastic and Dielectric Effects in Polymeric Solids', John Wiley, New York, 1967
- 14 Willbourn, A. H. *Trans. Faraday Soc.* 1958, **61**, 2132; *J. Polym. Sci.* 1959, **34**, 569
- 15 Seymour, R. W. and Cooper, S. L. *Macromolecules* 1973, **6**, 48
- 16 Tobolsky, A. V. and Narkis, M. *J. Macromol. Sci.* 1970, **B4** (4), 877
- 17 Seymour, R. W. and Cooper, S. L. *J. Polym. Sci. (B)* 1971, **9**, 689

# A theoretical treatment of die swell in a Newtonian liquid

F. Horsfall

Rubber and Plastics Research Association of Great Britain, Shawbury,  
Shrewsbury SY4 4NR, UK  
(Received 4 January 1973)

A finite-difference technique is used to calculate the die swell of a Newtonian liquid emerging from a capillary at zero Reynolds number. There is semi-quantitative agreement with experimental results. The experimental die swell is 13.5%; this theory predicts a die swell of 6.3%.

## INTRODUCTION

When a polymer melt emerges from the die in an extruder there is an increase in cross-sectional area, a phenomenon known as the 'Barus effect', 'post extrusion swelling' or simply 'die swell'. This effect is of practical importance since allowance must be made for it in the design of dies.

A theory relating die swell to fundamental flow properties such as normal stress or elastic recovery would be useful in die design. Such a theory would also provide a means of assessing the various equations of state that have been proposed for polymer melts. Several attempts have been made to explain die swell; probably the most popular theory was due to Metzner *et al.*<sup>1</sup> and was based on momentum balance. The theory, although successful for polymer solutions, was unsuccessful for polymer melts<sup>2,3</sup>. More recently theories have been developed that assume the flow of liquid can be approximated by steady shear flow suddenly followed by elastic recovery<sup>3-5</sup>. These theories appear to be successful but the assumed flow history is a considerable simplification and the theories do not explain the die swell of a Newtonian liquid. An alternative and more satisfactory procedure would be to solve the coupled equations of state and motion over a region extending both upstream and downstream from the die exit.

At low shear rates the die swell of a polymer melt tends towards the Newtonian value of about 13.5%<sup>3,6</sup>. Furthermore, the viscosity of a polymer melt becomes independent of shear rate at low shear rates. It seems reasonable therefore to develop a theory for the die swell of a Newtonian liquid before attempting the more complex polymer melt. In this report a numerical technique is described for determining the shape of an extrudate of Newtonian liquid emerging from a capillary at zero Reynolds number. The effects of gravity and surface tension have been neglected.

One of the main difficulties with the calculation lies in specifying the boundary conditions on the free surface, since the position of the surface is unknown. Duda and Vrentas<sup>7</sup> overcame this difficulty by re-arranging the Navier-Stokes equations and the boundary conditions so that the stream function was an independent variable and the distance from the axis a dependent variable.

However, they only solved the equations for large Reynolds numbers when the equations became parabolic. In our procedure an arbitrary boundary shape is chosen and the stress tangential to the surface is made zero. The stress distribution normal to the surface is calculated and a boundary shape is chosen to give a minimum normal stress distribution. The equations used are less complicated than those obtained by Duda and Vrentas.

## THE PROBLEM

Consider a system of cylindrical polar coordinates in which the origin is the centre of the exit of the capillary and the  $z$  axis points downstream. If we assume that the angular velocity component is negligible and the liquid is incompressible, the movement of the liquid at zero Reynolds number is described by the equation:

$$\frac{\partial^4 \psi}{\partial z^4} + 2 \frac{\partial^4 \psi}{\partial z^2 \partial r^2} + \frac{\partial^4 \psi}{\partial r^4} - \frac{2}{r} \frac{\partial^3 \psi}{\partial z^2 \partial r} - \frac{2}{r} \frac{\partial^3 \psi}{\partial r^3} + \frac{3}{r^2} \frac{\partial^2 \psi}{\partial r^2} - \frac{3}{r^3} \frac{\partial \psi}{\partial r} = 0 \quad (1)$$

Stokes' stream function  $\psi$  is defined in terms of the velocity components by:

$$V_z = \frac{1}{r} \frac{\partial \psi}{\partial r}; \quad V_r = -\frac{1}{r} \frac{\partial \psi}{\partial z}$$

Equation (1) can be obtained from the Navier-Stokes equations (Aris<sup>8</sup>, p 182) by eliminating the isotropic pressure.

Die swell decreases with increasing length of die to a limiting value when the die is several die diameters long. Consequently we can assume that the upstream boundary condition is:

$$\psi = \frac{Q}{2\pi} \left[ 2 \left( \frac{r}{R_0} \right)^2 - \left( \frac{r}{R_0} \right)^4 \right] \quad (z = -\infty) \quad (2)$$

where  $R_0$  is the radius of the capillary and  $Q$  is the volume rate of flow. This implies that the velocity distribution is parabolic. Die swell increases with distance from the die exit to a limiting value several die diameters downstream. Consequently we can assume that the velocity profile across the extrudate is flat at the downstream boundary, i.e.

$$\psi = \frac{Q}{2\pi} \left( \frac{r}{R_\infty} \right)^2 \quad (z = +\infty) \quad (3)$$

where  $R_\infty$  is the final radius of the extrudate. Inside the capillary, at the wall, the boundary condition is

$$\frac{\partial \psi}{\partial r} = 0 \quad \text{and} \quad \psi = \frac{Q}{2\pi} \quad (z < 0, r = R_0) \quad (4)$$

This implies that the liquid does not slip on the wall of the capillary. On the free surface of the extrudate the stress tangential to the surface  $p_T$  is taken to be zero, i.e.

$$p_T = 0; \quad \psi = \frac{Q}{2\pi} \quad (z > 0, r = R_z) \quad (5)$$

where  $R_z$  is the radius of the extrudate. The stress tangential to the free surface is given by:

$$p_T = \frac{\eta}{R_z(1+\beta^2)} \left[ (1-\beta^2) \left( \frac{\partial^2 \psi}{\partial r^2} - \frac{\partial^2 \psi}{\partial z^2} \right) - (1+\beta^2) \frac{1}{r} \frac{\partial \psi}{\partial r} - 4\beta \frac{\partial^2 \psi}{\partial z \partial r} \right]_{r=R_z} \quad (6)$$

where  $\beta$ , the gradient the free surface makes with the  $z$  axis, is given by:

$$\beta = - \left( \frac{\partial \psi}{\partial z} / \frac{\partial \psi}{\partial r} \right)_{r=R_z}$$

and  $\eta$  is the viscosity. Equation (6) can be obtained by resolving components of the stresses parallel to the surface (Aris<sup>8</sup>, p 181). Similarly, an expression for the stress normal to the free surface can be obtained:

$$p_N = -p + \frac{2\eta}{R_z(1+\beta^2)} \left[ (-1+\beta^2) \frac{\partial^2 \psi}{\partial z \partial r} + \beta \left( \frac{\partial^2 \psi}{\partial z^2} - \frac{\partial^2 \psi}{\partial r^2} \right) \right]_{r=R_z} \quad (7)$$

where  $p$  is the isotropic pressure which can be obtained from the Navier-Stokes equations:

$$\frac{\partial p}{\partial z} = \eta \left[ \frac{1}{r} \frac{\partial^3 \psi}{\partial r^3} - \frac{1}{r^2} \frac{\partial^2 \psi}{\partial r^2} + \frac{1}{r^3} \frac{\partial \psi}{\partial r} + \frac{1}{r} \frac{\partial^3 \psi}{\partial z^2 \partial r} \right] \quad (8)$$

$$\frac{\partial p}{\partial r} = \eta \left[ -\frac{1}{r} \frac{\partial^3 \psi}{\partial z^3} - \frac{1}{r} \frac{\partial^3 \psi}{\partial z \partial r^2} + \frac{1}{r^2} \frac{\partial^2 \psi}{\partial z \partial r} \right]$$

The problem then is to choose the extrudate profile  $R_z$  so that the normal stress distribution  $p_N$  is zero.

FINITE DIFFERENCE FORM OF THE EQUATIONS

The flow field was covered by a square mesh of grid points with spacing  $h$ . The usual finite difference representation of the first three terms of equation (1) was used with an error of order  $O(h^2)$  (Abramowitz and Stegun<sup>9</sup>, p 883). The remaining terms had errors of higher order since all five points in the  $r$  direction were used. This makes the finite-difference equation compatible with equation (2) upstream, removing any unnecessary anomalies.

Using the local notation illustrated in Figure 1, at the point (0, 0) equation (1) becomes:

$$\psi_{2,0} + (2-t)\psi_{1,1} - 8\psi_{1,0} + (2+t)\psi_{1,-1} + (1-t - \frac{1}{4}t^2 + \frac{1}{4}t^3)\psi_{0,2} + (-8 + 4t + 4t^2 - 2t^3)\psi_{0,1} + (20 - 7\frac{1}{2}t^2)\psi_{0,0} + (-8 - 4t + 4t^2 + 2t^3)\psi_{0,-1} + (1+t - \frac{1}{4}t^2 - \frac{1}{4}t^3)\psi_{0,-2} + (2-t)\psi_{-1,1} - 8\psi_{-1,0} + (2+t)\psi_{-1,-1} + \psi_{-2,0} = 0 \quad (9)$$

where  $t = h/r$  and  $r$  is the radial coordinate at (0, 0). The boundary condition upstream was represented by

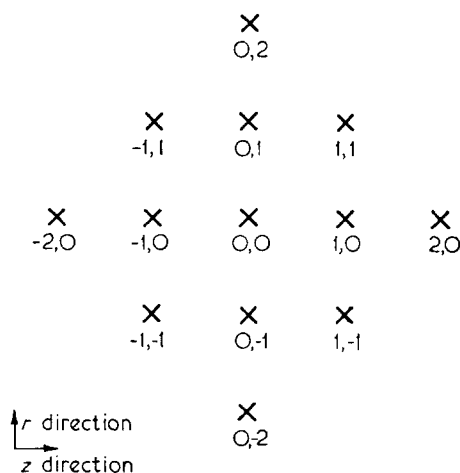


Figure 1 Mesh points used for equation (9)

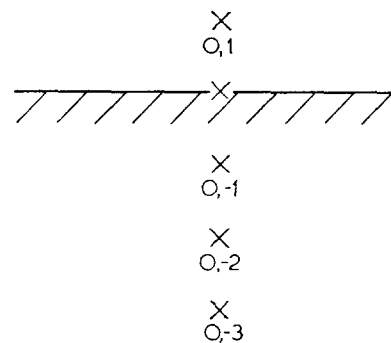


Figure 2 Mesh points near wall of capillary

two adjacent columns of stream values given by equation (2) at the positions  $z = -N_u h$  and  $-(N_u + 1)h$ . Similarly at positions  $z = N_d h$  and  $(N_d + 1)h$  equation (3) was used to represent the downstream boundary condition. Because of the symmetry the axis is effectively a boundary so the mesh points on the axis were given the value zero and the rows on either side of the axis were taken to be identical. On the wall of the capillary equation (4) was represented (Figure 2) by:

$$-0.1\psi_{0,-3} + 0.6\psi_{0,-2} - 1.8\psi_{0,-1} + 0.3\psi_{0,1} + \frac{Q}{2\pi} = 0 \quad (10)$$

The use of five grid points in the  $r$  direction makes the equations compatible with the upstream boundary condition.

The boundary conditions on the free surface were arranged to be of order  $O(h^2)$  on the lines  $r = R_0$  and  $r = R_0 + h$ . We therefore assumed that the boundary lies in this region; this was found to be justified. The finite difference form of equations (5) at the point (0,  $\alpha$ ) in Figure 3 were:

$$\begin{aligned} & [\alpha(1-\beta^2) + (1+2\alpha)\beta]\psi_{1,1} + [(1-\alpha)(1-\beta^2) - 4\alpha\beta]\psi_{1,0} + \\ & [- (1-2\alpha)\beta]\psi_{1,-1} + \\ & [- (1+3\alpha)(1-\beta^2) + (\frac{1}{2} + \alpha)(1+\beta^2)t]\psi_{0,1} + \\ & [5\alpha(1-\beta^2) - 2\alpha(1+\beta^2)t]\psi_{0,0} + \\ & [- (1+3\alpha)(1-\beta^2) - (\frac{1}{2} - \alpha)(1+\beta^2)t]\psi_{0,-1} + \\ & [\alpha(1-\beta^2) - (1+2\alpha)\beta]\psi_{-1,1} + \\ & [(1-\alpha)(1-\beta^2) + 4\alpha\beta]\psi_{-1,0} + [(1-2\alpha)\beta]\psi_{-1,-1} + \\ & [\alpha(1-\beta^2)]\psi_{0,-2} = 0 \end{aligned} \quad (11)$$

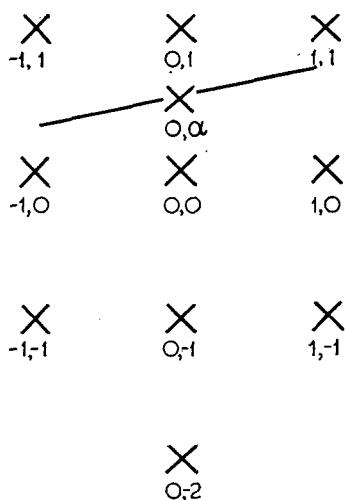


Figure 3 Mesh points near free surface

and

$$\alpha(1 + \alpha)\psi_{0,1} + 2(1 - \alpha^2)\psi_{0,0} - \alpha(1 - \alpha)\psi_{0,-1} - \frac{Q}{\pi} = 0 \quad (12)$$

where  $t = h/R_z$  and  $\alpha = (R_z - R_0)/h$ . Equations (9)–(12), (2) and (3) produced  $(N_u + N_d - 1)(N_r + 1)$  simultaneous equations. These were solved to give the stream function at all grid points, which enabled the normal stress distribution to be calculated. By using equation (6) with  $p_T = 0$  equation (7) can be simplified to:

$$p_N = -p - \frac{z\eta}{R_z(1 + \beta^2)} \left[ (1 + \beta^2) \frac{\partial^2 \psi}{\partial z \partial r} + \beta \frac{1}{r} \frac{\partial \psi}{\partial r} \right]_{r=R_z} \quad (13)$$

using the notation of Figure 3 the finite difference form of equation (13) is:

$$p_N = -p + \frac{\eta}{h^2 R_z (1 - \beta^2)} \times \left[ \begin{aligned} &[-(\frac{1}{2} + \alpha)(1 + \beta^2)]\psi_{1,1} + [2\alpha(1 + \beta^2)]\psi_{1,0} + \\ &[(\frac{1}{2} - \alpha)(1 + \beta^2)]\psi_{1,-1} + [-(1 + 2\alpha)\beta t]\psi_{0,1} + \\ &[4\alpha\beta t]\psi_{0,0} + [(1 - 2\alpha)\beta t]\psi_{0,-1} + \\ &[(\frac{1}{2} + \alpha)(1 + \beta^2)]\psi_{-1,1} + [-2\alpha(1 + \beta^2)]\psi_{-1,0} + \\ &[-(\frac{1}{2} - \alpha)(1 + \beta^2)]\psi_{-1,-1} \end{aligned} \right]$$

The isotropic pressure  $p$  was found by integrating equation (8) along the three lines  $r = R_0 - h$ ,  $r = R_0$  and  $r = R_0 + h$  using Simpson's rule. The integrations were performed twice starting at the points  $z = N_d h$ , and  $z = (N_d + 1)h$  with  $p = 0$  to give the pressure at each grid point. Using the notation of Figure 4 the finite difference form of equation (8) at the point (0, 0) is:

$$\frac{\partial p}{\partial z} = \frac{\eta}{2R_z h^3} \times \left[ \begin{aligned} &3\psi_{1,0} - 4\psi_{1,-1} + \psi_{1,-2} + \\ &[-1 - 4t + 3t^2]\psi_{0,0} + [-10 + 10t - 4t^2]\psi_{0,-1} + \\ &[22 - 8t + t^2]\psi_{0,-2} + [-14 + 2t]\psi_{0,-3} + 3\psi_{0,-4} + \\ &3\psi_{-1,0} - 4\psi_{-1,-1} + \psi_{-1,-2} \end{aligned} \right]$$

To obtain  $p$  on the free surface the following interpolation equation was used:

$$p = \frac{1}{2}\alpha(1 + \alpha)p_{R_0+h} + (1 - \alpha^2)p_{R_0} + \frac{1}{2}\alpha(-1 + \alpha)p_{R_0-h}$$

## RESULTS AND DISCUSSION

A computer programme was written in Fortran for calculating the normal stress distribution from the equations developed in the previous section. The programme was supplied with the boundary shape and the number of mesh spaces upstream ( $N_u$ ), downstream ( $N_d$ ), and between the axis and the capillary wall ( $N_r$ ). The programme was run on the University of London Atlas computer. In the numerical method the upstream and downstream boundaries are a finite distance from the exit. Hence we require the boundary profile that gives a minimum normal stress distribution with  $N_u$ ,  $N_d$  and  $N_r$  large enough for the normal stress to be independent of  $N_u$ ,  $N_d$  and  $N_r$ . The normal stress at the downstream boundary was taken to be zero.

In the first calculations we assumed that the extrudate profile was flat, i.e. the die swell was zero. The dimensionless normal stress distribution obtained,  $p_N D^3 / \eta Q$ , where  $D = 2R_0$  is illustrated in Figure 5 (curve 1). The number

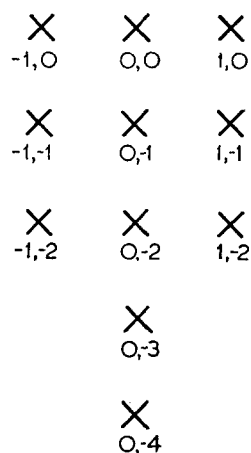


Figure 4 Mesh points used for calculating isotropic pressure

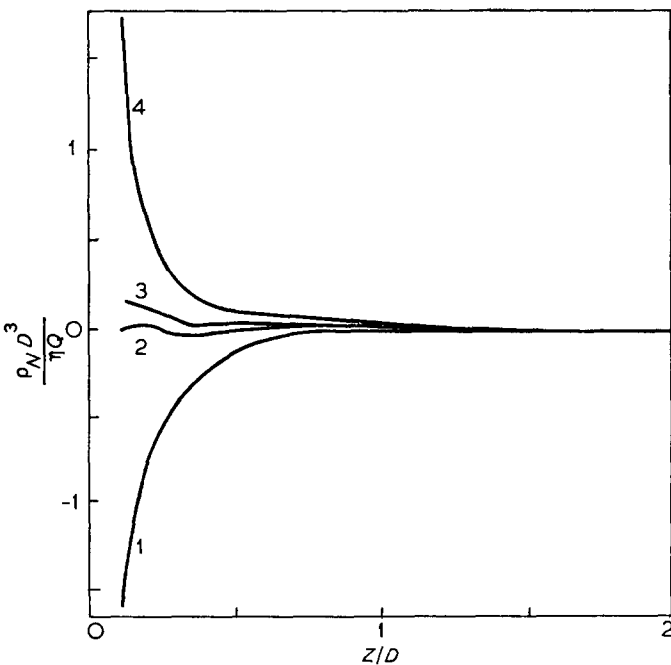


Figure 5 Stress normal to free surface for different extrudate profiles. 1,  $A=0$ ; 2,  $A=6.26$ ,  $B=5.22$ ; 3,  $A=7.6$ ,  $B=4.40$ ; 4,  $A=13.5$ ,  $B=4.12$

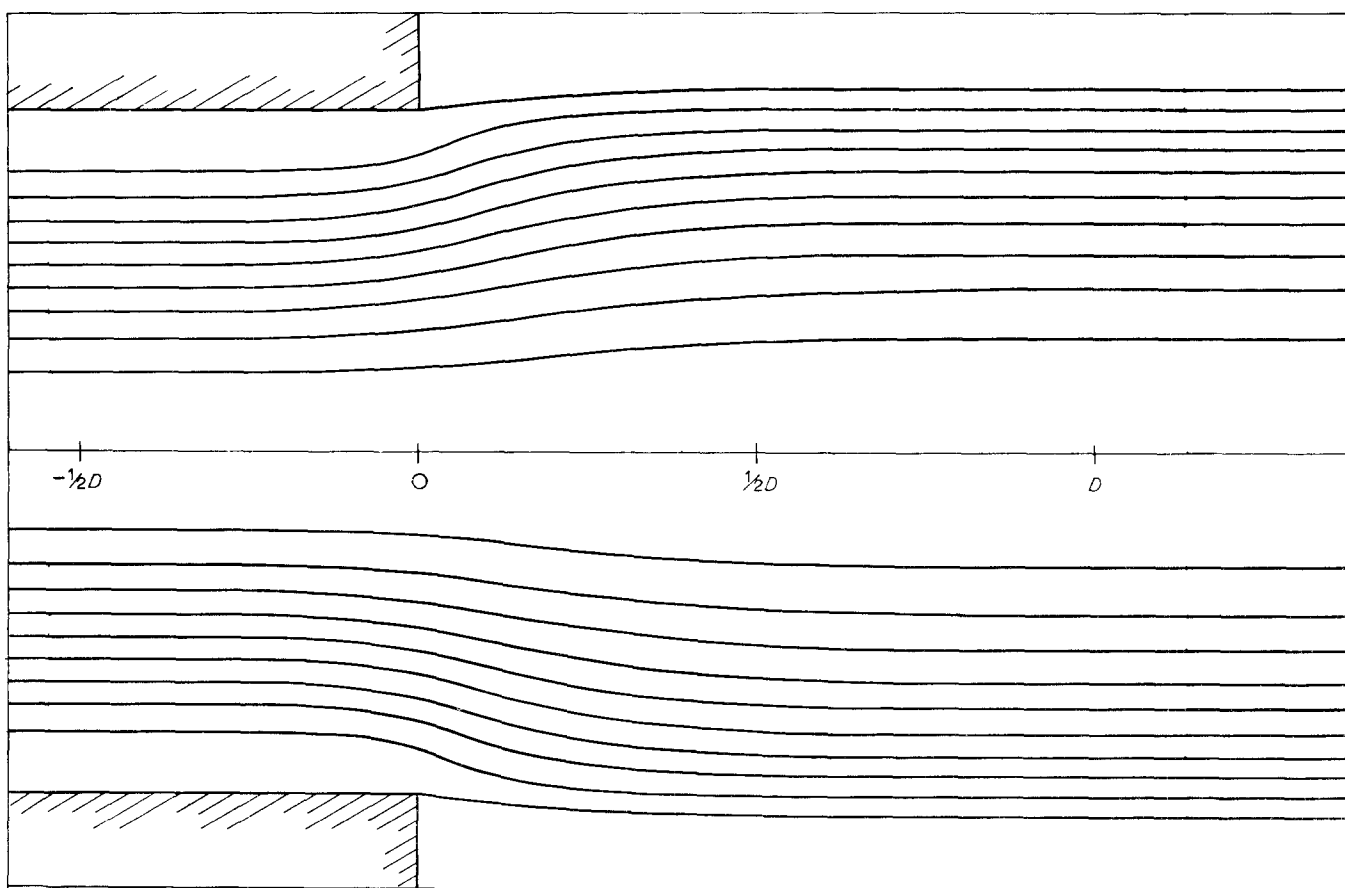


Figure 6 Streamlines for calculated die swell

of grid spaces  $N_u$  was varied from 16 to 24,  $N_d$  from 23 to 40, and  $N_r$  from 9 to 12. The change in normal stress was about 1% of the minimum obtained. Hence the stress distribution is negative. This implies that the liquid is pushing outwards and that in the absence of constraining forces the boundary would move outwards and give rise to die swell. A similar stress distribution was obtained by Richardson<sup>10</sup> by an analytical technique for a Newtonian liquid emerging from an infinitely wide slit.

Batchelor *et al.*<sup>6</sup> found that the shape of the free boundary of the Newtonian liquid was adequately described by an exponential of the form:

$$y = A \left[ 1 - \exp\left(-B \frac{z}{D}\right) \right]$$

where  $y$  is the percentage increase in diameter at a distance  $z$  from the capillary exit. The theoretical boundary was therefore assumed to have this shape. The two adjustable parameters  $A$  and  $B$  were chosen to make the sum of squares of the normal stresses a minimum. For  $N_u=16$ ,  $N_d=40$  and  $N_r=9$  this minimum was obtained when  $A=6.26$  and  $B=5.22$ . These results may be compared with experimental values of  $A=13.5$  and  $B=4.12$ . The stress distribution corresponding to the theoretical values is illustrated in Figure 5 (curve 2); the streamlines are shown in Figure 6 and the axial velocity distributions at various cross-sections in Figure 7. In this Figure it is interesting to compare the velocity distribution at the exit ( $z/D=0$ ) with the parabolic distribution upstream ( $z/D=-\frac{1}{2}$ ). The momentum balance approach assumes that the parabolic velocity

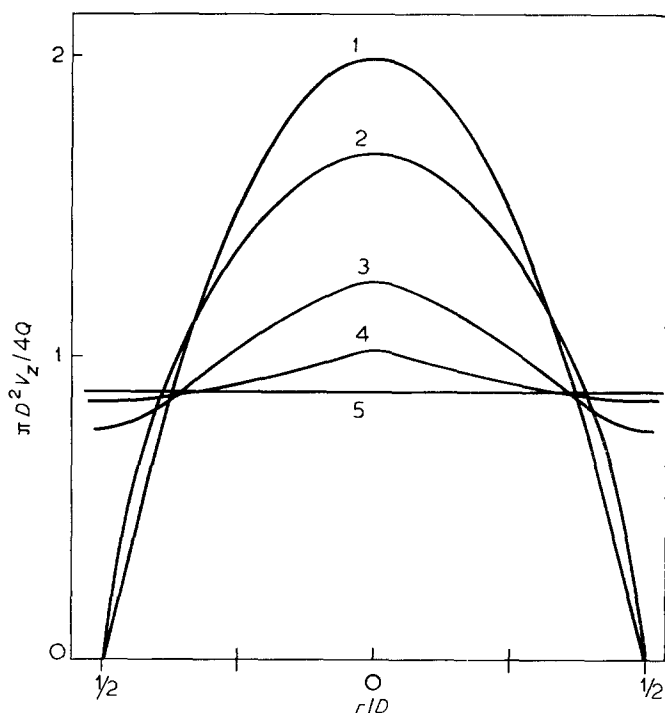


Figure 7 Axial velocity distributions at various distances from the exit. 1,  $-\frac{1}{2}D$ ; 2, 0; 3,  $\frac{1}{4}D$ ; 4,  $\frac{1}{2}D$ ; 5,  $2D$

distribution persists up to the exit for the Newtonian liquid.

The estimates of  $A$  and  $B$  are probably not very accurate since  $p_N$  is not very sensitive to changes in  $A$

and  $B$ . In Figure 5 curve 3 gives the pressure distribution corresponding to  $A=7.6$  and  $B=4.40$ . Changes in the number of grid spaces of approximately 50% gave a minimum for the sum of squares in roughly the same region but because of the costs involved a detailed examination was not possible. The pressure distribution was independent of the position of the upstream and downstream boundary positions provided they were at a distance greater than 1 and 2 die diameters from the die exit respectively. The stress distribution corresponding to the experimentally obtained boundary shape  $A=13.5$  and  $B=4.12$  is shown in Figure 5 (curve 4).

The treatment given here may not be rigorous in specifying the boundary conditions at the capillary wall in the exit plane. Within the capillary we assume that there is no slip at the wall and hence the tangential stress is finite. On the free surface of the extrudate the tangential stress is taken to be zero. The finite difference equations used here may not represent this discontinuity accurately. There is clearly a need for an analysis of the behaviour at this point similar to that given by Michael<sup>11</sup> for the two dimensional flow of a viscous liquid past the edge of a solid boundary. Such a local solution could be incorporated into the more general finite difference solution given here.

#### CONCLUSIONS

The theoretical analysis described in this report provides

a semi-quantitative explanation for the experimental observation that a Newtonian liquid exhibits a die swell of 13½%. The suggested equations of state for polymer melts are much more complicated than that for a Newtonian liquid and the resultant equations equivalent to those used in this analysis would be correspondingly more complicated. At present therefore the cost of a solution based on the above approach but for a non-Newtonian liquid does not appear to be justified.

#### REFERENCES

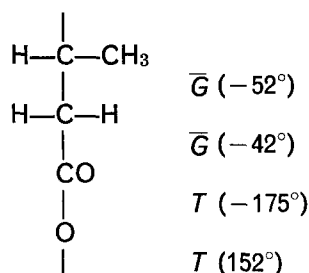
- 1 Metzner, A. B., Houghton, W. T., Sailor, R. A. and White, J. L. *Trans. Soc. Rheol.* 1961, **5**, 133
- 2 Berry, J. P. and Batchelor, J. *RAPRA Res. Rep.* 184 1970
- 3 Graessley, W. W., Glasscock, S. D. and Crawley, R. L. *Trans. Soc. Rheol.* 1970, **14**, 519
- 4 Mendelson, R. A., Finger, F. L. and Bagley, E. B. *J. Polym. Sci.* 1971, **C35**, 177
- 5 Tanner, R. I. *J. Polym. Sci. (A-2)* 1970, **8**, 2067
- 6 Batchelor, J., Berry, J. P. and Horsfall, F. *Polymer* 1973, **14**, in press
- 7 Duda, J. N. and Vrentas, J. S. *Chem. Eng. Sci.* 1967, **22**, 855
- 8 Aris, A. 'Vectors, Tensors, and the Basic Equations of Fluid Mechanics', Prentice Hall, Englewood Cliffs, NJ, 1962
- 9 Abramowitz, M. and Stegun, I. A. 'Handbook of Mathematical Functions', Dover, New York, 1965
- 10 Richardson, S. *Rheol. Acta* 1970, **9**, 193
- 11 Michael, D. H. *Mathematika* 1958, **5**, 82

# Structural studies of polyesters: 5. Molecular and crystal structures of optically active and racemic poly( $\beta$ -hydroxybutyrate)

M. Yokouchi, Y. Chatani, H. Tadokoro, K. Teranishi and H. Tani

Department of Polymer Science, Osaka University, Toyonaka, Osaka, 560 Japan  
(Received 26 January 1973)

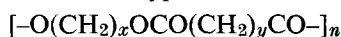
The molecular and crystal structure of naturally occurring optically active poly( $\beta$ -hydroxybutyrate) was analysed by X-ray diffraction. The unit cell is orthorhombic,  $P2_12_12_1-D_2^4$ , with  $a=5.76 \text{ \AA}$ ,  $b=13.20 \text{ \AA}$ , and  $c(\text{fibre period})=5.96 \text{ \AA}$  and two molecules pass through the unit cell. The molecule has a conformation shown by the Fischer projection for the case of a rectus polymer, giving a left-handed (2/1) helix.



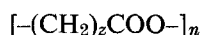
The crystalline synthesized racemic polymer gave the same X-ray diffraction pattern as the naturally occurring optically active polymer. This result indicates that the racemic polymer has an isotactic configuration and consists of two kinds of crystallites, each composed only of the left-handed helices of rectus polymer chains, or only of the right-handed helices of sinister polymer chains.

## INTRODUCTION

Several polyesters of the types



and



have been studied systematically by the authors using X-ray diffraction, infra-red, and Raman spectroscopic methods ( $x=2$  and  $y=0$ ,  $x=2$  and  $y=2^1$ ,  $x=2$  and  $y=4^2$ ,  $z=1^3$ ,  $z=2^4$ , and  $z=5^{5,6}$ ). As an extension of these studies, analyses of polyesters with side chains have been undertaken. In the present paper, the structures of optically active and racemic poly( $\beta$ -hydroxybutyrate)  $[-\text{CH}(\text{CH}_3)\text{CH}_2\text{COO}-]_n$  are reported. The naturally occurring optically active polymer plays an important role in bacteria as a storage material and is isolated from various bacteria.

There have been several papers on the crystal structures of polyesters with side chains: polypivalolactone  $[-\text{CH}_2\text{C}(\text{CH}_3)_2\text{COO}-]_n^{7,8}$ , and optically active poly( $\beta$ -hydroxybutyrate)<sup>9</sup>. The conformation of the modification (II) of poly( $\beta$ -propiolactone)  $[-(\text{CH}_2)_2\text{COO}-]_n$  is planar zigzag<sup>4</sup>, while the conformation of polypivalolactone is a two-fold helical structure of the type  $(G_2T_2)_2$ . It would be interesting to compare the molecular conformations of poly( $\beta$ -propiolactone), polypivalolactone, and poly( $\beta$ -hydroxybutyrate); these three polymers have the same main chain structure.

In 1967, Okamura and Marchessault proposed a crystal structure of optically active poly( $\beta$ -hydroxybutyrate) based upon the qualitatively observed X-ray intensity data<sup>9</sup>. In the present paper, the crystal structures of optically active and racemic poly( $\beta$ -hydroxybutyrate) are reported in detail. After completion of the present study, the authors were informed through Okamura's review<sup>10</sup> and a personal communication from Marchessault that these authors had independently found the same crystal structure of the optically active polymer as us.

STRUCTURE DETERMINATION

### Samples

Naturally occurring optically active poly( $\beta$ -hydroxybutyrate) was obtained by extracting *Pseudomonas solanasearum* with chloroform and was purified by reprecipitation with diethyl ether (m.p. 174–177°C; measured under a polarizing microscope). The racemic polymer was prepared by polymerizing DL- $\beta$ -methyl- $\beta$ -propiolactone with  $[\text{Et}_2\text{AlOCPPhNPh}]_2$  catalyst (m.p. 167–169°C)<sup>11</sup>. The samples for X-ray measurements

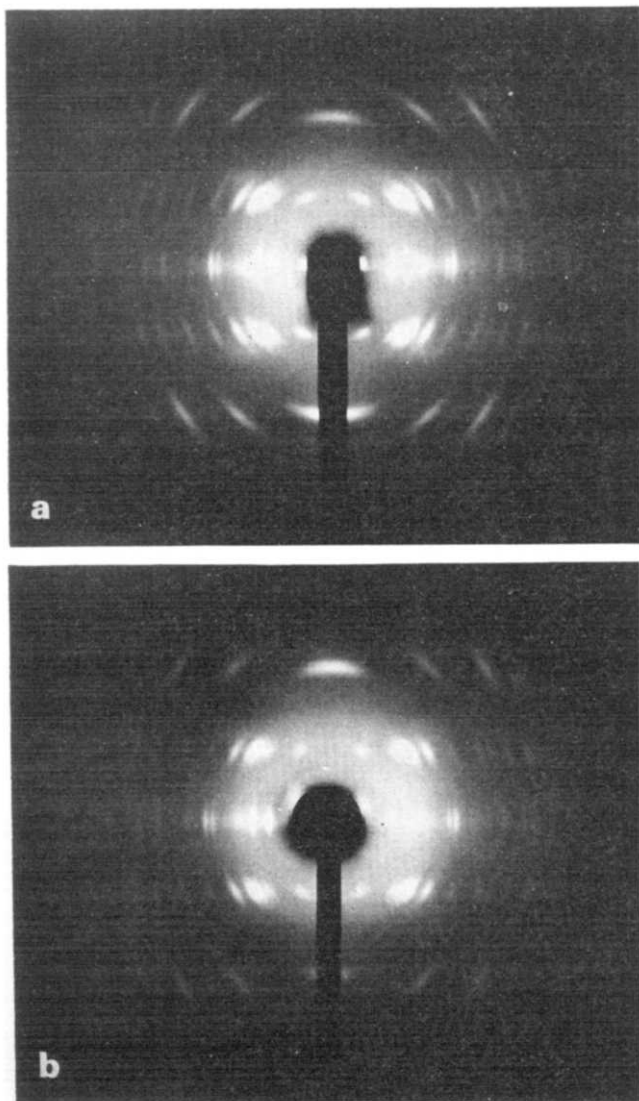


were made by heating to just below the melting point and then drawing quickly.

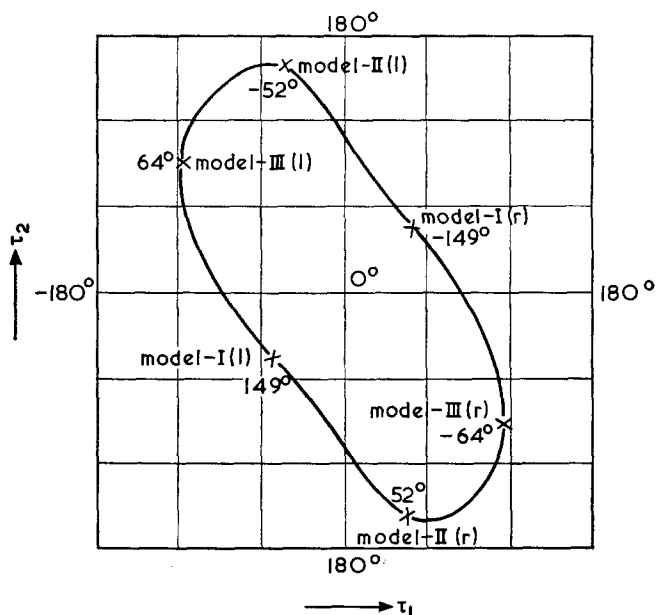
*X-ray measurements*

Ni-filtered Cu-K $\alpha$  radiation was used throughout the present X-ray studies. The X-ray photographs of the optically active polymer and the racemic polymer are shown in *Figures 1a* and *b*, respectively. The X-ray diffraction pattern of the racemic polymer is essentially the same as that of the optically active polymer. It was expected that the naturally occurring optically active polymer has a higher regularity than the synthesized racemic polymer. Therefore, for a detailed structure analysis, the photographs of the naturally occurring polymer were used. The meridional reflection data were taken from the photograph using a Weissenberg camera where the sample was oscillated about an axis normal to the fibre axis.

Forty-two independent reflections were observed. The reflection intensities of the fibre diagram obtained by the multiple film method were measured by visual comparison with a standard intensity scale. The corrections for Lorentz polarization factors and the obliquity effect in the fibre diagram were made.



*Figure 1* X-ray fibre photographs of poly( $\beta$ -hydroxybutyrate). (a) Naturally occurring optically active polymer; (b) synthesized racemic polymer



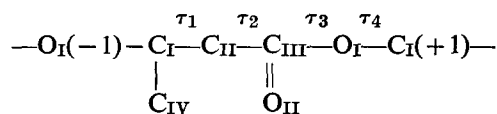
*Figure 2* Three-dimensional closed curve showing the relationship between  $\tau_1$ ,  $\tau_2$ , and  $\tau_4$  for possible conformation of the main chain of poly( $\beta$ -hydroxybutyrate)

*Unit cell and space group*

The reflections observed on the photograph could be indexed by an orthorhombic cell;  $a = 5.76 \text{ \AA}$ ,  $b = 13.20 \text{ \AA}$ , and  $c$  (fibre period) =  $5.96 \text{ \AA}$ . These values were calibrated by using the spacings of the reflections of aluminium powder and they agreed with those reported by Okamura and Marchessault<sup>9</sup>. It was assumed that there are four monomeric units in a unit cell, by comparing the calculated density of  $1.26 \text{ g/ml}$  with the observed density of  $1.23\text{--}1.25 \text{ g/ml}$  measured by the flotation method<sup>12</sup>. The following systematic absences were found;  $h00$  when  $h$  is odd,  $0k0$  when  $k$  is odd, and  $00l$  when  $l$  is odd. Therefore the possible space group is  $P2_12_12_1-D_2^4$ . This space group is a suitable one for an optically active material. It was assumed from these experimental data that this polymer molecule has a two-fold screw axis relating two monomeric units, and two molecules pass through the unit cell.

*Molecular models*

Here the rectus polymer model was assumed, since the naturally occurring optically active poly( $\beta$ -hydroxybutyrate) is considered to be rectus because hydrolysis and autolysis of this polymer give D(-)- $\beta$ -hydroxybutyric acid<sup>13</sup>. At first, the molecular models with two-fold screw axis were constructed by assuming the following bond lengths and bond angles:  $C_I-C_{II} = C_I-C_{IV} = 1.54 \text{ \AA}$ ,  $C_{II}-C_{III} = 1.52 \text{ \AA}$ ,  $C_{III}-O_I = 1.36 \text{ \AA}$ ,  $C_{III}-O_{II} = 1.23 \text{ \AA}$ ,  $O_I-C_I(+1) = 1.43 \text{ \AA}$ ,  $\angle O_I(-1)C_I C_{II} = \angle O_I(-1)C_I C_{IV} = \angle C_{IV}C_I C_{II} = \angle C_I C_{II} C_{III} = 109.5^\circ$ ,  $\angle C_{II}C_{III}O_I = 115.0^\circ$ ,  $\angle C_{II}C_{III}O_{II} = \angle O_{II}C_{III}O_I = 122.5^\circ$ , and  $\angle C_{III}O_I C_I(+1) = 112.0^\circ$ . The numbering of the atoms and the internal rotation angles are as follows;



By assuming the two-fold screw symmetry, the number of independent internal rotation angles is three. From the results of the structure analyses of polyesters of the types

$[-O(CH_2)_xOCO(CH_2)_yCO-]_n$  and  $[-(CH_2)_zCOO-]_n$ , it is reasonable to fix  $\tau_3$  at  $180.0^\circ$ . By fixing  $\tau_3$  at  $180.0^\circ$  and varying  $\tau_1$  and  $\tau_2$  from  $-180^\circ$  to  $180.0^\circ$ , the values of  $\tau_4$  for all possible molecular models were obtained which satisfy the identity period of  $5.96 \text{ \AA}$ . A set of the internal rotation angles was on one closed curve in a cube defined by the three-dimensional Cartesian coordinates,  $\tau_1$ ,  $\tau_2$ , and  $\tau_4$ , each covering from  $-180.0^\circ$  to  $180.0^\circ$ . In Figure 2, the projection to the  $\tau_1\tau_2$  plane is shown and  $\tau_4$  values of several points are given on the closed curve. From this Figure, six models with plausible internal rotation angles (nearly *trans* (*T*), skew (*S*), and

*gauche* (*G*)) could be obtained: three left-handed helices and three right-handed helices. The internal rotation angles of the left-handed helices are given as follows and the right-handed helical models [model I(r), model II(r), and model III(r)] can be given by changing the sign of all the internal rotation angles of the left-handed helical models;

Model	$\tau_1(^{\circ})$	$\tau_2(^{\circ})$	$\tau_3(^{\circ})$	$\tau_4(^{\circ})$
I(l)	-50	-45	180	149
II(l)	-45	159	180	-52
III(l)	-115	92	180	64

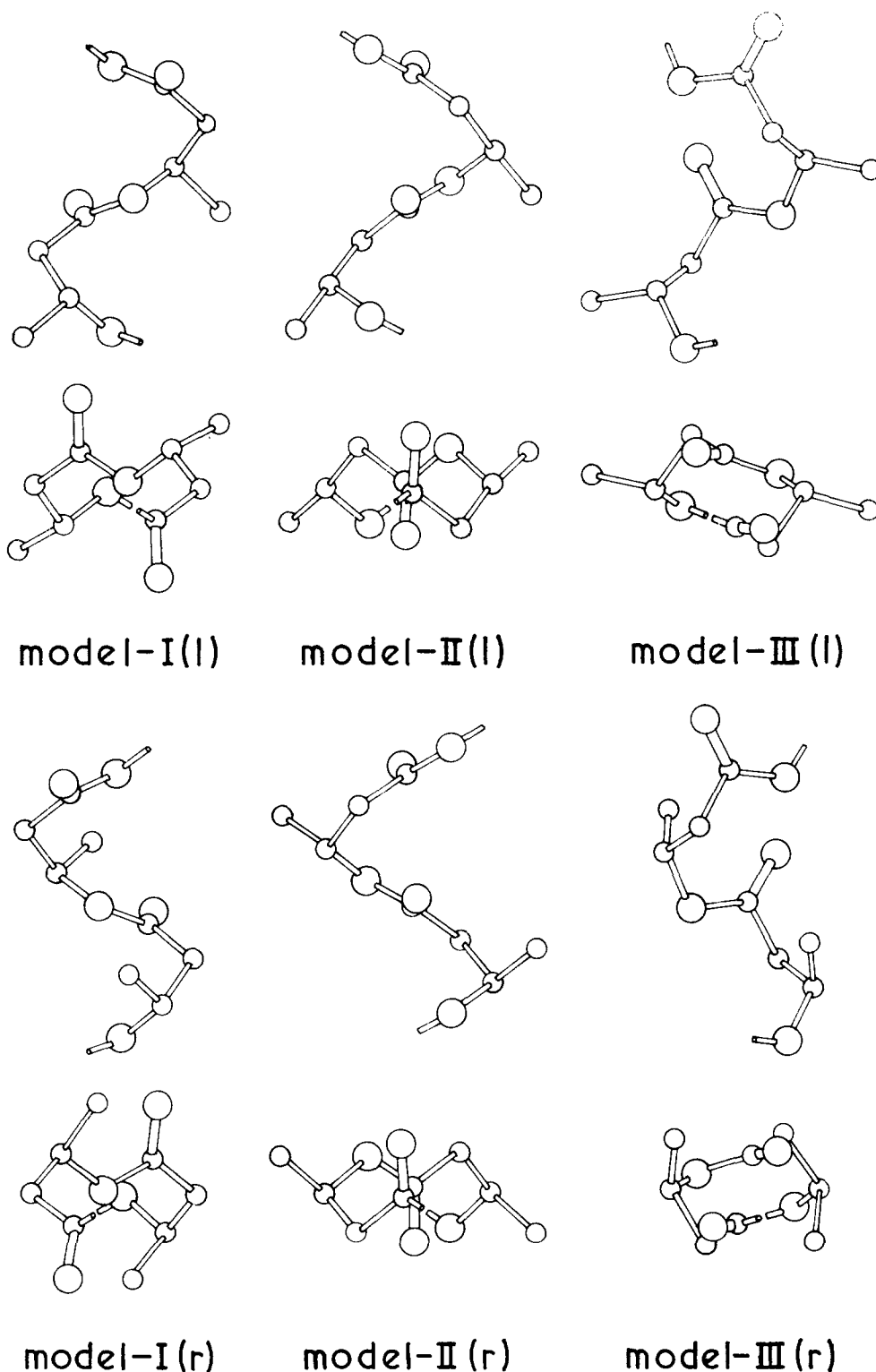


Figure 3 Six models with probable internal rotation angles

These six rectus polymer models are shown in Figure 3.

Structure factor calculations

At first, the structure factors of the equatorial reflections for the six models were calculated. Good agreement between observed and calculated structure factors could be obtained only for the structure in which model I(I) was located so that the direction connecting two methylene groups on the *ab* projection is nearly parallel to the *b* axis. The model I(I) is considered the most probable molecular conformation. But, there remains another parameter, the translation along the *c* axis (parallel to the fibre axis). Referring to the observed intensities of the meridional reflections, the model I(I) was placed as the *z*-coordinate of the carbonyl carbon atom to be nearly zero. At this stage, the contribution of the hydrogen atoms was included in the structure factor calculations, by assuming the C-H bond length to be 1.09 Å and the ∠CCH and ∠HCH bond angles to be 109.5°. As a result, the calculated structure factors for the all

Table 1 Atomic coordinates and thermal coefficients

	<i>x</i>	<i>y</i>	<i>z</i>	<i>B</i> (Å <sup>2</sup> )
C <sub>I</sub>	0.437	-0.068	0.217	4.7
C <sub>II</sub>	0.318	-0.139	0.389	3.3
C <sub>III</sub>	0.143	-0.077	0.513	5.1
C <sub>IV</sub>	0.587	-0.140	0.052	7.1
O <sub>I</sub>	0.232	0.017	0.585	5.1
O <sub>II</sub>	-0.057	-0.105	0.558	5.7
Assumed values for hydrogen atoms				
H(I)	0.557	-0.020	0.294	10.0
H(II-1)	0.447	-0.171	0.499	10.0
H(II-2)	0.226	-0.200	0.301	10.0
H(IV-1)	0.667	-0.092	-0.076	12.0
H(IV-2)	0.464	-0.192	-0.036	12.0
H(IV-3)	0.710	-0.182	0.143	12.0

Table 2 Comparison of obs. and calc. structure factors for naturally occurring optically active poly(β-hydroxybutyrate)

<i>h</i>	<i>k</i>	<i>l</i>	( <i>I</i> <sub>o</sub> ) <sup>1/2a</sup>	( <i>I</i> <sub>c</sub> ) <sup>1/2b</sup>
0	2	0	86.3	70.0
1	1	0	85.5	86.3
1	2	0	(5.1) <sup>c</sup>	17.3
1	3	0	38.6	43.3
0	4	0	50.9	49.6
2	0	0		
1	4	0	28.3	25.6
2	1	0		
2	2	0	21.8	18.2
2	3	0	38.3	28.2
1	5	0		
0	6	0	34.7	42.3
2	4	0		
1	6	0	21.6	12.1
2	5	0	(8.4)	2.0
3	1	0	29.1	35.6
3	2	0	(8.7)	14.6
1	7	0	(8.8)	9.8
3	3	0		
2	6	0	39.0	36.5
3	4	0		
0	8	0	26.1	18.2
1	8	0		
2	7	0	27.3	28.6
3	5	0	(9.9)	5.0
3	6	0		
4	0	0		
2	8	0		
4	1	0	25.6	23.1
1	9	0		
4	2	0		

Table 2 (continued)

<i>h</i>	<i>k</i>	<i>l</i>	( <i>I</i> <sub>o</sub> ) <sup>1/2a</sup>	( <i>I</i> <sub>c</sub> ) <sup>1/2b</sup>
4	3	0	(10.8)	14.0
3	7	0		
0	10	0	29.4	28.9
0	1	1	24.3	23.3
0	2	1	43.3	36.8
1	0	1	54.7	53.9
1	1	1	62.9	79.1
0	3	1		
1	2	1	55.6	59.8
1	3	1	38.8	33.3
0	4	1	10.5	9.3
2	0	1		
1	4	1	38.8	36.7
2	1	1		
0	5	1		
2	2	1	31.5	24.9
2	3	1		
1	5	1	47.3	42.4
0	6	1		
2	4	1	46.3	41.0
1	6	1	26.0	26.0
2	5	1		
3	0	1	22.2	18.1
3	1	1		
0	7	1	30.8	28.9
3	2	1	(4.6)	4.4
1	7	1	(4.7)	8.8
3	3	1		
2	6	1	23.9	25.4
3	4	1		
0	8	1	23.8	13.8
1	8	1	(5.2)	4.3
2	7	1	(5.2)	3.1
3	5	1	(5.3)	10.6
0	9	1		
3	6	1		
4	0	1		
4	1	1		
1	9	1		
0	3	2		
1	2	2	47.6	57.3
1	3	2	27.7	26.2
0	4	2	28.7	22.5
2	0	2		
1	4	2		
2	1	2	63.9	66.7
0	5	2		
2	2	2	25.4	23.9
2	3	2		
1	5	2	49.7	44.1
0	6	2		
2	4	2	28.7	26.9
1	6	2	(8.5)	6.7
2	5	2		
3	0	2	41.6	46.8
3	1	2		
0	7	2	(9.0)	1.8
3	2	2	(9.2)	15.2
1	7	2	(9.3)	13.3
3	3	2		
2	6	2	19.7	11.1
3	4	2		
0	8	2	(9.9)	13.3
1	8	2		
2	7	2	32.8	22.2
3	5	2		

a The observed structure factors (*I*<sub>o</sub>)<sup>1/2</sup> were put on the same scale as the (*I*<sub>c</sub>)<sup>1/2</sup> [= (*mF*<sub>o</sub><sup>2</sup>)<sup>1/2</sup>] values by setting Σ*k*(*I*<sub>o</sub>)<sup>1/2</sup> = Σ(*mF*<sub>o</sub><sup>2</sup>)<sup>1/2</sup> where *k* is the scale factor and *m* is the multiplicity

b (*I*<sub>c</sub>)<sup>1/2</sup> values of the reflections which overlap on the X-ray fibre photograph are (Σ*mF*<sub>o</sub><sup>2</sup>)<sup>1/2</sup>

c For non-observed reflections, (*I*<sub>o</sub>)<sup>1/2</sup> values were assumed to be half of the most weakly observed intensity

reflections satisfactorily agreed with the observed structure factors. The discrepancy factor  $R$

$$= \frac{\sum |(I_o)^{1/2} - (I_c)^{1/2}|}{\sum (I_o)^{1/2}}$$

was 15.6% (only for forty-two observed reflections). Then, the atomic coordinates and thermal coefficients were refined by the diagonal least-squares method. The discrepancy factor  $R$  was reduced to 13.5%. Table 1 lists the atomic coordinates and thermal coefficients. The observed and calculated structure factors are given in Table 2.

For all computations in the present study, the NEAC-2200 electronic computer in this university was used.

## RESULTS AND DISCUSSION

### Optically active poly( $\beta$ -hydroxybutyrate)

The molecular conformation of naturally occurring optically active poly( $\beta$ -hydroxybutyrate) was found to be approximately  $(G_2T_2)_2$ . In Figure 4 the molecular dimensions of this polymer are shown. The values of the bond lengths and bond angles are reasonable. The crystal structure of this optically active polymer is shown in Figure 5. In the case of polypivalolactone, right- and left-handed molecules coexist in the crystal lattice. On the other hand, the crystal lattice of the optically active poly( $\beta$ -hydroxybutyrate) contains two left-handed helical molecules in antiparallel orientation. The oxygen atoms of the carbonyl groups are located nearly at the same level,  $z=0$  and  $1/2$ . No abnormal atomic distances were found and the packing of the molecules was reasonable.

### Racemic poly( $\beta$ -hydroxybutyrate)

It has already been mentioned that the X-ray photograph of the synthesized crystalline racemic poly( $\beta$ -

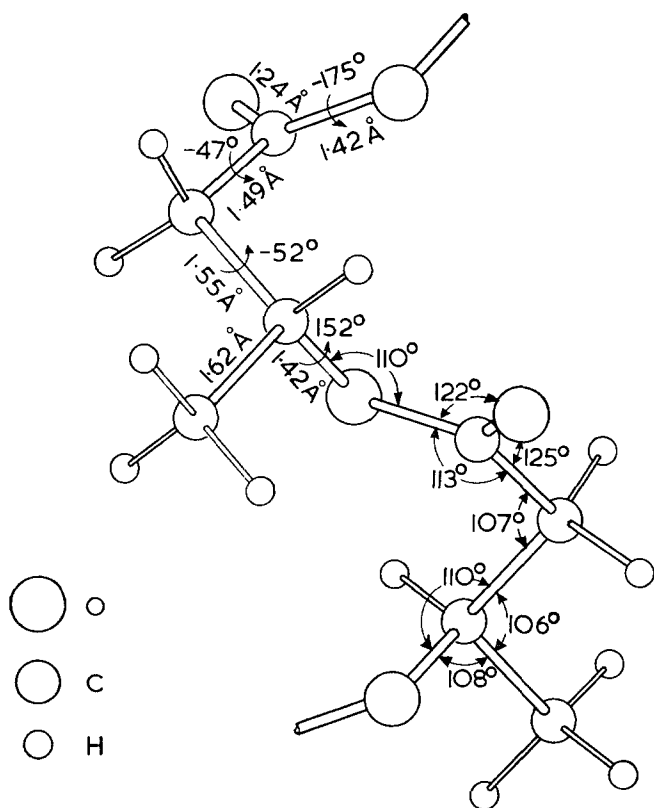


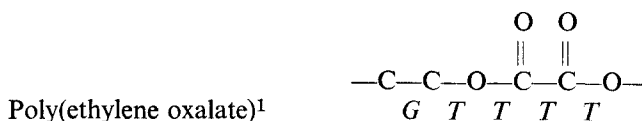
Figure 4 Final molecular model of naturally occurring optically active poly( $\beta$ -hydroxybutyrate)

hydroxybutyrate) was essentially the same as the naturally occurring optically active polymer (Figures 1a and b). Accordingly, it may be concluded that the crystalline polymer prepared from the racemic monomer is isotactic. Naturally occurring optically active polymer was found to be a left-handed helix because the configuration of the  $\beta$ -carbon atom is rectus, and the sinister polymer should be right-handed. From these results based on the X-ray analysis, it is conceivable that the bulk sample of this racemic polymer consists of two kinds of crystallites, each composed only of the rectus polymer chains, or only of the sinister polymer chains. Such a type of polymer has already been reported by the authors in the case of poly(propylene sulphide)<sup>14</sup>.

### Molecular conformations of polyesters

The skeletal conformations of some polyesters analysed so far are summarized below:

	O				
	-C-C-O-C-C-				
Poly( $\beta$ -propiolactone) <sup>4</sup>		T	T	T	T
Poly( $\epsilon$ -caprolactone) <sup>5</sup>		T	T	T	T
Poly(ethylene adipate) <sup>15</sup>		T	S	T	T
Poly(ethylene sebacate) <sup>15</sup>		T	S	T	T
Poly(ethylene succinate) <sup>1</sup>		G	T	T	G
Poly(tetramethylene succinate) <sup>2</sup>		G	T	T	T
Polypivalolactone <sup>7,8</sup>		G	T	T	G
Poly( $\beta$ -hydroxybutyrate)		G	T	T	G



The C(O)-O bond of all these polyesters has *trans* conformation. In the cases of the polyesters of the types  $[-O(CH_2)_xOCO(CH_2)_yCO-]_n$  and  $[-(CH_2)_zCOO-]_n$ , the C-C(O) bond is stable in the *trans* form and also O-C bond preferably takes the *trans* form. In the cases of polypivalolactone and poly( $\beta$ -hydroxybutyrate), which have side chains, the C-C(O) bond is in the *gauche* form. But the C(O)-O and O-C bonds are in the *trans* form just as in the cases of the polyesters with no side chains. This suggests that the conformation of C-C(O) bond in a polyester is liable to be affected by introduction of substituent groups. Poly( $\beta$ -hydroxybutyrate) and polypivalolactone take  $(G_2T_2)_2$  conformation. Such a  $(G_2T_2)_2$  type conformation was also found in the cases of the modification (III) of polyoxacyclobutane<sup>16</sup> and syndiotactic polypropylene<sup>17</sup>.

### Disordered modification

When a sample of poly( $\beta$ -hydroxybutyrate) was stretched even further after necking, there appeared another modification with a fibre period of 4.70 Å. Figure 6 is a fibre photograph of a sample containing this modification, which shows a sharp reflection on the equator and streaks on the layer lines. This feature may suggest this modification is in a kind of paracrystalline structure in which the molecular chains are arranged regularly in the lateral direction, but irregularly along the fibre axis. From the observed fibre identity period (4.70 Å) it is considered that this modification has a twisted planar zigzag conformation. A detailed structure analysis is now being made.

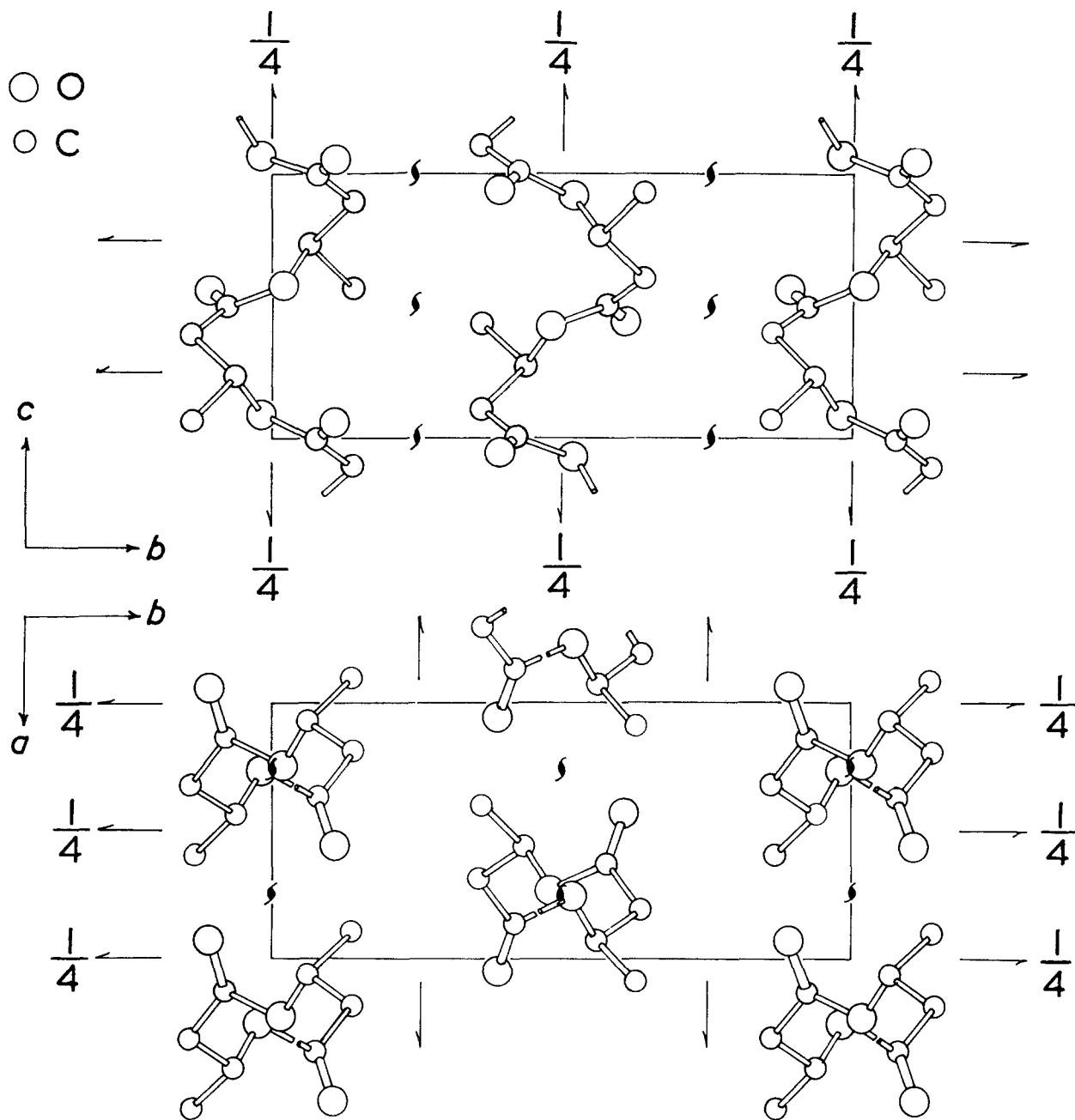


Figure 5 Crystal structure of naturally occurring optically active poly( $\beta$ -hydroxybutyrate).  $a=5.76 \text{ \AA}$ ;  $b=13.20 \text{ \AA}$ ;  $c=5.96 \text{ \AA}$  (fibre axis)

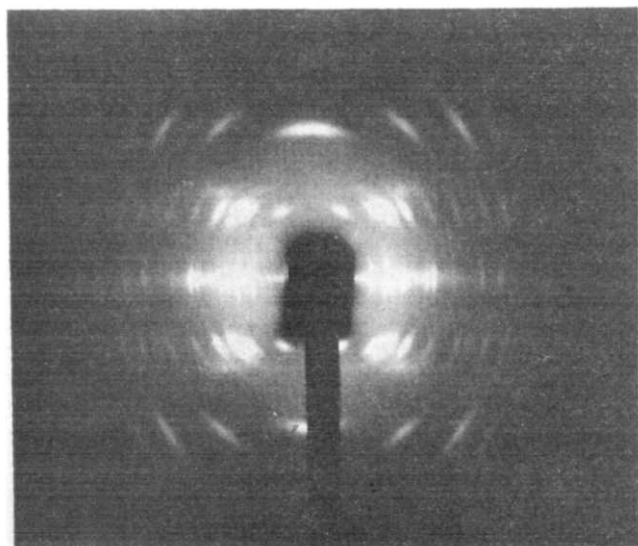


Figure 6 X-ray fibre photograph of naturally occurring optically active poly( $\beta$ -hydroxybutyrate) containing another modification

#### REFERENCES

- 1 Ueda, A. S., Chatani, Y. and Tadokoro, H. *Polymer J.* 1971, **2**, 387
- 2 Hasegawa, R. K., Chatani, Y. and Tadokoro, H. *A. Meet. Soc. Polym. Sci. (Japan)* 1971 (May), Tokyo
- 3 Chatani, Y. et al. *Makro-mol. Chem.* 1968, **113**, 215
- 4 Suehiro, K., Chatani, Y., Tadokoro, H., Kato, R. and Tanaka, A. *A. Meet. Soc. Polym. Sci. (Japan)* 1966 (May), Nagoya
- 5 Chatani, Y. et al. *Polymer J.* 1970, **1**, 555
- 6 Tadokoro, H. et al. *J. Chem. Phys.* 1968, **49**, 3359
- 7 Carazzolo, G. *Chim. Ind. (Milan)* 1964, **46**, 525
- 8 Perego, G. et al. *Makromol. Chem.* 1972, **157**, 269
- 9 Okamura, K. and Marchessault, R. H. 'Conformation of Biopolymers', (Ed. G. N. Ramachandran), Vol. 2, Academic Press, New York, 1967, pp 709-720
- 10 Okamura, K. *Kobunshi* 1972, **21**, 525
- 11 Tani, H., Yamashita, S. and Teranishi, K. *Polymer J.* 1972, **3**, 417
- 12 Williamson, D. H. and Wilkinson, J. F. *J. Gen. Microbiol.* 1958, **19**, 198
- 13 Leomoigne, M. *Ann. Inst. Pasteur* 1925, **39**, 144
- 14 Sakakihara, H. et al. *Macromolecules* 1969, **2**, 515
- 15 Turner-Jones, A. and Bunn, C. W. *Acta Cryst.* 1962, **15**, 105
- 16 Tadokoro, H. et al. *Makromol. Chem.* 1967, **109**, 96
- 17 Natta, G., Pasquon, I., Corradini, P., Peraldo, M., Pegoraro M., and Zambelli, A. *Atti Accad. Naz. Lincei Rend., Cl. Sci. Fis. Mat. Nat. Sez. II* (8) 1960, **28**, 539

# Electron microscope studies of textile fibres and materials\*

J. W. S. Hearle

Department of Textile Technology, University of Manchester  
Institute of Science and Technology, Manchester M60 1QD, UK

and S. C. Simmens

Shirley Institute, Didsbury, Manchester, UK  
(Received 1 December 1972)

## INTRODUCTION

Historically, the examination of fibres occurred early in the use of electron microscopes. Two of the first seven commercial RCA electron microscopes to come to this country under lend-lease in 1942, went to the Shirley Institute (then the British Cotton Industry Research Association) and the Textile Physics Laboratory of the University of Leeds. In the 1950s, Chapman *et al.*<sup>1,2</sup>, as part of a study of fibre friction, developed the use of the reflection mode of a direct electron microscope† to study fibre surfaces—a technique now superseded by scanning electron microscopy. Later, the first scanning electron microscope to be used in an applications laboratory was made at Cambridge University and sent to the Pulp and Paper Research Institute of Canada; and two of the first three commercial instruments went to textile fibre laboratories. However, despite this priority, it remains true that the electron microscopy of individual textile fibres is really just a special case of the electron microscopy of polymer materials, providing also, in natural fibres, a link to biological studies, though without the severe problems associated with the collapse of cells on drying.

Some special features do arise from the size and shape of fibres, which, are by definition, long fine units of matter. The lateral dimensions of fibres (around 10  $\mu\text{m}$ ) are only a little greater than the wavelength of light, and consequently even comparatively gross features of fibre structure, below about a tenth of a fibre diameter, cannot be examined effectively by optical microscopy. In practice, the restricted depth of focus is as severe a difficulty as the limited resolution. For example, the general morphology of fibre fracture surfaces could not be clarified until the use of scanning electron microscopy (s.e.m.).

In electron microscopy, the fineness and cylindrical shape of fibres cause some difficulties in replication, because it is necessary either to prevent the replicating

material wholly or partly encasing the fibre or to find some means of breaking open a replicating skin around a fibre. Sectioning also has its special difficulties with fine fibres.

At lower magnifications, the study of fibre assemblies, textile yarns and fabrics, is a use of scanning electron microscopy which has many special problems and applications. Direct electron microscopy has no application to the study of fibre assemblies.

In this review, we shall first outline the general range of techniques and applications for electron microscopy in textile and fibre laboratories, describing in more detail some recent techniques; and, second, comment on two topics of continuing interest—the nature of the fine structure, where direct electron microscopy gives information, and fibre fractography, where scanning electron microscopy is important.

## USE OF ELECTRON MICROSCOPES IN TEXTILE LABORATORIES

A direct electron microscope is a necessary tool in any laboratory concerned with experimental studies of fibre structure or fibre surfaces, and is found in the research laboratories of the major fibre producers and in cooperative and academic laboratories. The scanning electron microscope, and indeed the optical microscope, is a complementary instrument for fibre studies, and has also greatly increased the range of textile problems which can be studied by electron microscopy (e.m.): the applications to textile fibres have been pioneered by Billica's group in du Pont (Kinston, North Carolina), Sikorski's group at Leeds, and the group at UMIST.

However, the heavy utilization of an electron microscope of either type in a textile laboratory is partly made up of other applications: the study of additives, such as starches, pigments, and resins; the study of metal, plastic, or ceramic machine parts; and service work in completely different fields.

### *Direct electron microscopy*

Table 1 lists those techniques which would be regarded as being in the standard repertoire of a fibre electron microscope laboratory and indicates the nature of the applications. In this section we briefly consider the

\* Presented at the symposium 'Application of electron microscopy to the study of polymers' on 12 September 1972 as part of the 5th European Congress on Electron Microscopy (EMCON 72) held at the University of Manchester.

† The term *direct electron microscope* is used to denote an electron microscope of the earlier type, often, misleadingly, called a *transmission, conventional, or traditional* electron microscope.

**Table 1** Common techniques and applications of direct electron microscopy to fibres

Techniques	Applications
<b>Basic specimen:</b>	
Replica of fibre surface*	Surface structure (e.g. scales on wool), roughness, and modification. Surface defects or damage. Observation of soiling or foreign objects
Thin transverse section (low magnification)*	Observation of fibre cross-sectional shape, and gross structural features
Whole fibre silhouette*	Fibre axial shape
Replica of cut surface†	
Replica of peeled surface†	
Replica of fractured surface†	
Mechanical disintegration (blendor)*†	Contribution to elucidation of fine structure of fibres
Ultrasonic disintegration*†	
Chemical disintegration*†	
Thin transverse or longitudinal section (high magnification)	
<b>Other features:</b>	
Enhancement of contrast by shadowing* or staining	
Dark-field viewing*	
Selected area diffraction*	Crystal structure or identification

\* In common current use at Shirley Institute

† At high magnification; use s.e.m. for lower magnification

application of some general laboratory techniques or day-to-day applications of direct e.m. for which experience shows that there is a continuing use. As those who work in the field are all too aware, textile fibres are too big in their entirety for fine structure to be shown up in transmission electron microscopy, yet they offer practical difficulties in handling because of their small diameter and chemical nature. However, for a number of purposes there is in fibres a level of detail not yet accessible by other means.

Of the various approaches that can be used to obtain information many have a very long history of development and refinement; but, even so, relative newcomers to the field, like ourselves, find difficulty in translating published techniques into reliable routine methods, and we propose here only to discuss those general techniques that work for us.

Considering first the surface detail of fibres, replication is necessary in order to examine this; and the major problem involved is that, owing to their small diameter, fibres are liable to be encapsulated by the replication. Dlugosz<sup>3</sup> and Ramanathan *et al.*<sup>4</sup> realized this many years ago, and applied the principle of first semi-embedding the fibre in some medium such as gelatine or resin for up to half its depth or thickness; the exposed upper portion of the fibre was then replicated by a silver/carbon or similar technique. This method, though having several steps, works well when one has fibres that are in a shape or form that can be semi-embedded and it gives a final resolution as good as any that can be obtained. In the intervening years since this approach was introduced other semi-embedding media have been used. Fibres that can tolerate a temperature around 150°C can be laid on a thin disc of freshly pressed polystyrene which is then heated; the fibres sink into the polystyrene with, fortunately, a contact angle of about 90°, the depth of embedding being controlled by time and temperature. Thin discs of polystyrene can be used

in another way; a piece of fabric can be shadowed and carbon-coated and pressed lightly or even laid on the heated polystyrene. When cool the fabric can be stripped, mechanically or chemically, and the replica fragments recovered by dissolving the polystyrene.

In *Figure 1*, the surface detail on a nylon filament can be seen at relatively high magnification. This is a replica made in the way described. The feature of interest is the numerous needle shaped crystals of about 200 × 6 nm size. This fibre was in a fabric that did not bond well to a foam laminate; it was found that the use of acid dyestuffs followed by a synthetic tanning agent produced poor bonding and this was associated with the presence of the crystal detail seen on the fibre surface. This technique is not unlike that of Scott<sup>5</sup>, who used chromium instead of carbon, then placing the filament into a viscous solution of poly(acrylic acid) and subsequently stripping chemically or mechanically to leave the chromium behind in the poly(acrylic acid) from which it was recovered by dissolution of the poly(acrylic acid) in hot water.

In *Figure 2*, we see this method applied to the surface of a polyester filament—the titanium pigment can be seen to be exposed at the fibre surface and suggests how guides and knitting needles come to be cut by an easily deformable polymer substance.

*Figure 3* shows a fibre surface after etching in a glow discharge with argon<sup>6</sup>; this was done to examine the effect of such treatment on the soiling properties of polyester fabric and is a further example of the technique of Scott.

Although the literature contains numerous papers wherein a plastic has been used for replication, our experience is that plastic replicas at best give low or poor resolution and at worst misleading artifacts; nowadays better and more reliable pictures can be obtained by s.e.m. We do, however, find Chippendale's technique<sup>7</sup> useful at times (he used Formvar softened

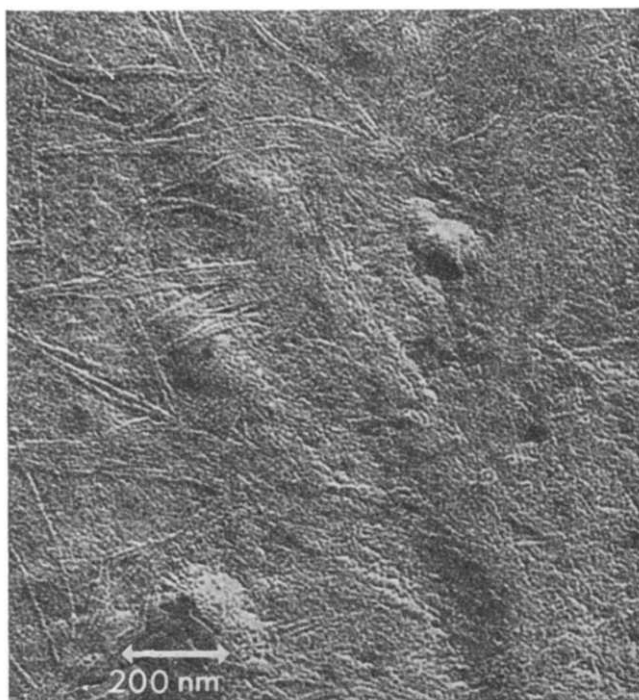
**Figure 1** Pre-shadowed carbon replica of nylon filament surface showing numerous fine dyestuff crystals (S.C.S.)





Figure 2 Chromium replica of a polyester filament surface showing exposed titanium pigment (S.C.S.)

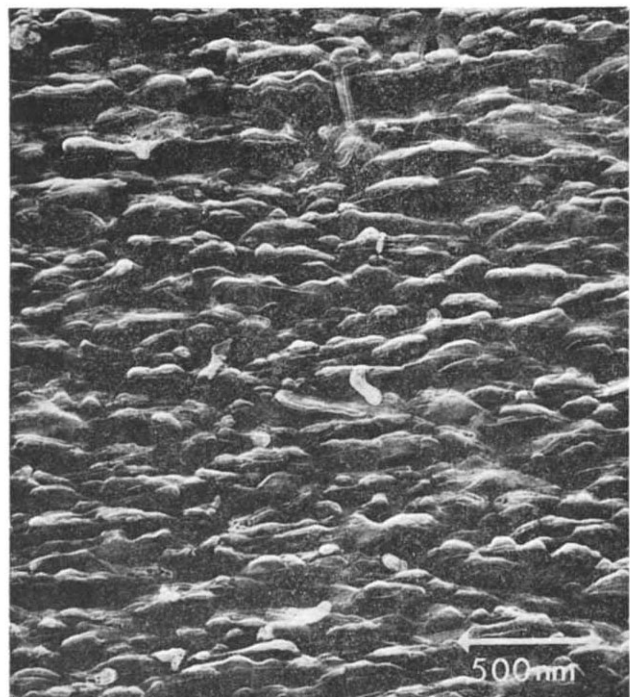


Figure 3 Chromium replica of polyester filament surface after a glow discharge treatment (S.C.S.)

with acetone as the primary replicating medium) on account of the fact that it will often strip a deposit from a fibre; the deposit finishes up in a carbon replica, and thus becomes accessible to electron diffraction (ED).

In Figure 4 we have the final carbon replica, from Chippendale's method, of a cotton fabric containing a deposit. At higher magnifications we can see that the

deposit contains much plate-like material and the ED pattern from this is compatible with a clay deposit.

From Table 1, it can be seen that various techniques are available for the examination of internal detail in fibres; the apparently most direct is that of sectioning and over the years much effort has been expended in this direction. From the results published it is clear that useful information about the internal structure of wool, in particular, and also cotton can be and still is being obtained; but that with man-made fibres this is not a profitable line of approach. Mainly this arises from the difficulties associated with the sectioning of polymers, and so far there appears to be little information that cannot be obtained more easily by other means. Consider, for example, the titanium pigment present in most polyamide and polyester fibres and about which there is a continuing need for information as pigment can vary in size, shape and degree of aggregation. Sectioning may seem a direct approach but let us look at a different one.

Figure 5 shows a polyester filament etched in a glow-discharge with argon. It provides an excellent view of the distribution of the pigment in the fibre, as here the discharge has been allowed to etch well into the fibre allowing the pigment particles to stand out. Incidentally they are now accessible to extraction techniques, if we want to look at them closely or use ED. This appears to us a worthwhile approach to the study of pigment distribution in fibres. It can be further supplemented by direct examination of the particles (Figure 6); here the yarn was dissolved, the pigment separated out, washed and sprayed on to a carbon coated grid.

A further means of opening up the internal structure of fibres is by mechanical or physical disintegration. Beating in a blender device and ultrasonics have been used, and, as discussed later, we have recently applied freeze-pressing as a method to break down fibres. The



Figure 4 Carbon replica (Chippendale technique) illustrating the removal of a deposit from cotton fibres (S.C.S.)



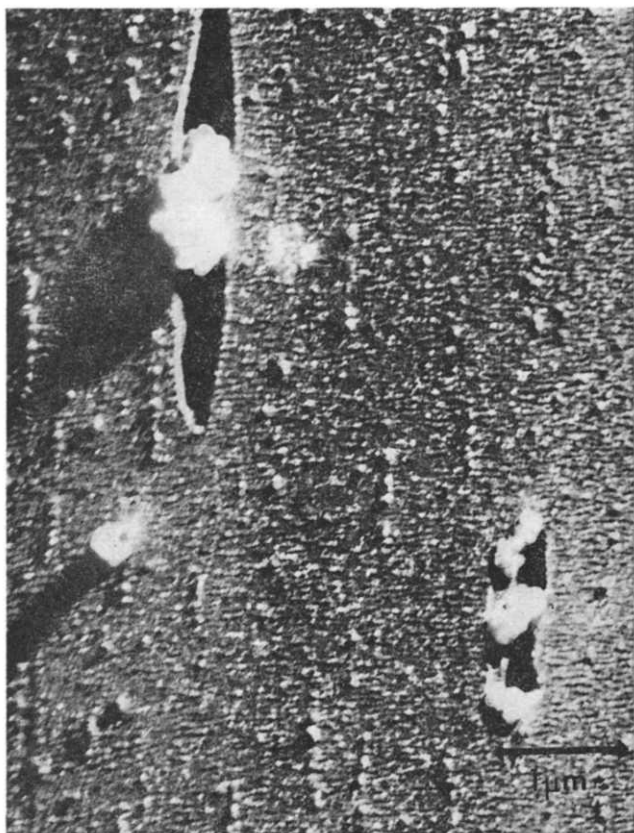


Figure 5 Polyester filament strongly etched in a glow discharge to show the distribution of the titanium pigment (S.C.S.)

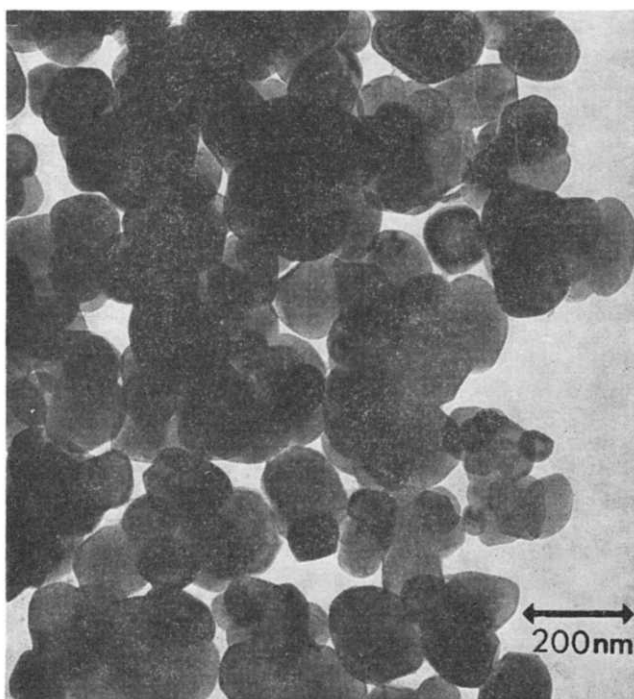


Figure 6 Titanium pigment extracted from polyester filament (S.C.S.)

preparation from some fibres made by this method are excellent for *ED* work; in some respects this form of disintegration is superior to using a blender. It does not, for example, produce so much of the extremely finely degraded material (flour-like in the micrographs) as the blender does.

Mechanical disintegration of fibres in a blender,

however, is still much used in a routine way. The choice of liquid in which the beating is done is of importance: cotton in white spirit cannot be fibrillated, but cotton in water readily fibrillates into microfils having a size around 100 Å, some of which split at the ends into finer strands (Figure 7). With prolonged beating, much ultra-fine fibrillar material, 50 Å and less, is obtained. Cotton beaten in caustic soda passes quickly from microfibrils of 100 Å, or less, to an extremely finely divided material.

Internal detail can also be examined by the splitting and peeling techniques, described by Scott<sup>5</sup>, in which a nick is cut in the fibre surface and then peeled back to display an internal surface for replication.

#### Scanning electron microscopy

The usual repertoire for scanning electron microscopy is given in Table 2, with a list of typical applications. As in all scanning electron microscopy, the ease of preparation, the apparent directness (despite the instrumental indirectness) of observation, and the ease of manipulation of specimens is a great advantage. The standard procedure at UMIST would be to take a textile specimen as provided, stick it to Twinstick previously mounted on the stub and coated with a thin layer of gold or silver\*, then coat the specimen with gold or silver, and examine it in the s.e.m. at 5 kV. Where fibre ends have to be examined, the fibre would usually be held between Sellotape, with 1 mm projecting, and then clamped in a split stub and coated with gold or silver. There are circumstances where metal coating is undesirable. An antistatic agent such as Duron can be used as an alternative; at UMIST we commonly soak the material and

\* Silver is suitable for immediate use; but gold is used for specimens which need to be kept for some time.

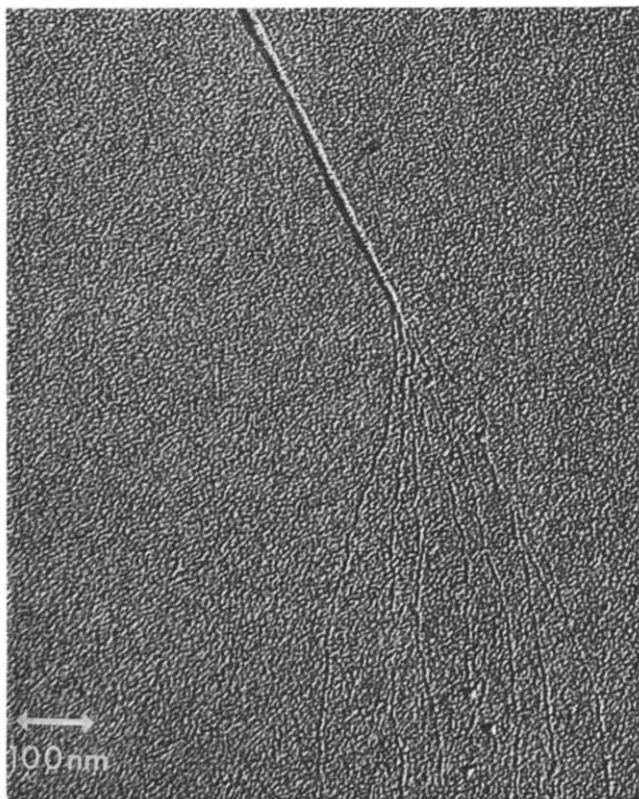


Figure 7 Cotton microfibril showing splitting into finer units (S.C.S.)

Table 2 Common techniques and applications of scanning electron microscopy to fibres, yarns and fabrics

Techniques	Applications
Basic specimen:	Low magnification
Direct observation of sample*	Assembly structure—arrangement of fibres in yarns or non-woven fabrics, and yarns in woven or knitted fabrics as produced or modified
Cut end (plate method)*	
Section, moderately thick ( $>1 \mu\text{m}$ )*	Presence of soil or foreign objects
Disintegration of fibres	Identification of fibres in structure (blend distribution, faulty fibres)
Peeling of fibres	Observation of damage in textile products
Thin section	
Examination of original, cut or ruptured surfaces*	Medium magnification:
Other features:	Fibre shape and form
Reduction of charging by metal-coating, or soaking or spraying with antistat*	Fibre surface structure, roughness, defects or damage
	Particles on fibre surface
	Fracture morphology
	Gross internal features (cell structure in wool, voids, macrofibrils, etc)
	Distribution of resins or finishes (external or internal) location of variations in composition
Choice of viewing angle conditions and magnification*	
Analysis of X-ray emission	High magnification:
Imaging in X-ray mode	Fracture detail
	Contribution to elucidation of fibre fine structure

\* In frequent use at UMIST

then allow it to dry before examination. The Duron may be sprayed on, but this has the disadvantage of giving droplets on the specimen.

It should also be noted that it is often possible to examine specimens as received without any antistatic treatment, if the viewing conditions are carefully chosen.

In general, the choice of viewing conditions involves a compromise and, in any except the easy specimens, effort spent in securing the best compromise in relation to the type of specimen and the needs of the investigation will do much to improve the results. The parameters available for variation are accelerating voltage, beam current, lens currents, aperture sizes, viewing distance, astigmatism correction, and exposure time: these interact together to influence resolution, contrast, depth of focus, penetration and spread in specimen, charging troubles, specimen damage, and specimen movement or vibration error. These problems and, in particular, the advantage of using relatively low voltages for fibre examination are discussed by Hearle *et al.*<sup>8</sup>.

The plate method is an easy method for examining fibre cross-sections. The individual fibres, or the yarn, are surrounded with a bundle of packing yarn, and then pulled through a hole in the stub with a wire or strong yarn. The surface is then cut flush and coated. It is necessary to ensure that the yarns are tightly packed before cutting.

Comments on disintegration, peeling and sectioning of fibres have already been made in connection with direct electron microscopy.

Some examples selected from our studies at UMIST using these methods are shown in Figure 8.

The X-ray emission mode is being used for identification of location of finishes, soil particles etc. Cathodo-

luminescence can also be used, though care is needed in interpretation of results on complicated surfaces, because the contrast arises both from differential light emission and direction (topographical contrast).

## SOME SPECIAL TECHNIQUES

### Swelling and staining

The central problem in the use of electron microscopy to help in understanding fibre structure is to find a means of showing up structural elements which may be present.

It has been common practice to stain fibre sections to enhance contrast, e.g. heavy-metal containing substances such as osmium tetroxide are taken up differentially by wool fibres depending on variations in protein composition. However, the range of techniques is steadily being expanded. For example, Swift<sup>9</sup> has developed specific stains for particular amino acid residues in hair fibres. Stains can also be used to show up differences in accessibility, and for this purpose a mild swelling treatment may first be given. Ingram<sup>10,11</sup> treats cellulose fibres, such as Ramie, with caustic soda and then phosphotungstic acid in order to show up a fibrillar structure.

A further development has been reported by Billica *et al.*<sup>12</sup>. A synthetic fibre is swollen in the vapour of boiling methyl methacrylate (or some other vinyl monomer) for about 3 h; polymerization of the monomer then occurs over a few days and, finally, the reactive polymer, which now impregnates the fibre, is stained with osmium tetroxide. In addition to opening up the material slightly in order to clarify the structure, the impregnation also helps to support the fibre and preserve structure during sectioning.

Another swelling and staining technique is described by Sotton *et al.*<sup>13-15</sup>. Fibres are first exposed to hydrogen sulphide under pressure and then reacted with silver nitrate. Some examples are shown in Figure 9.

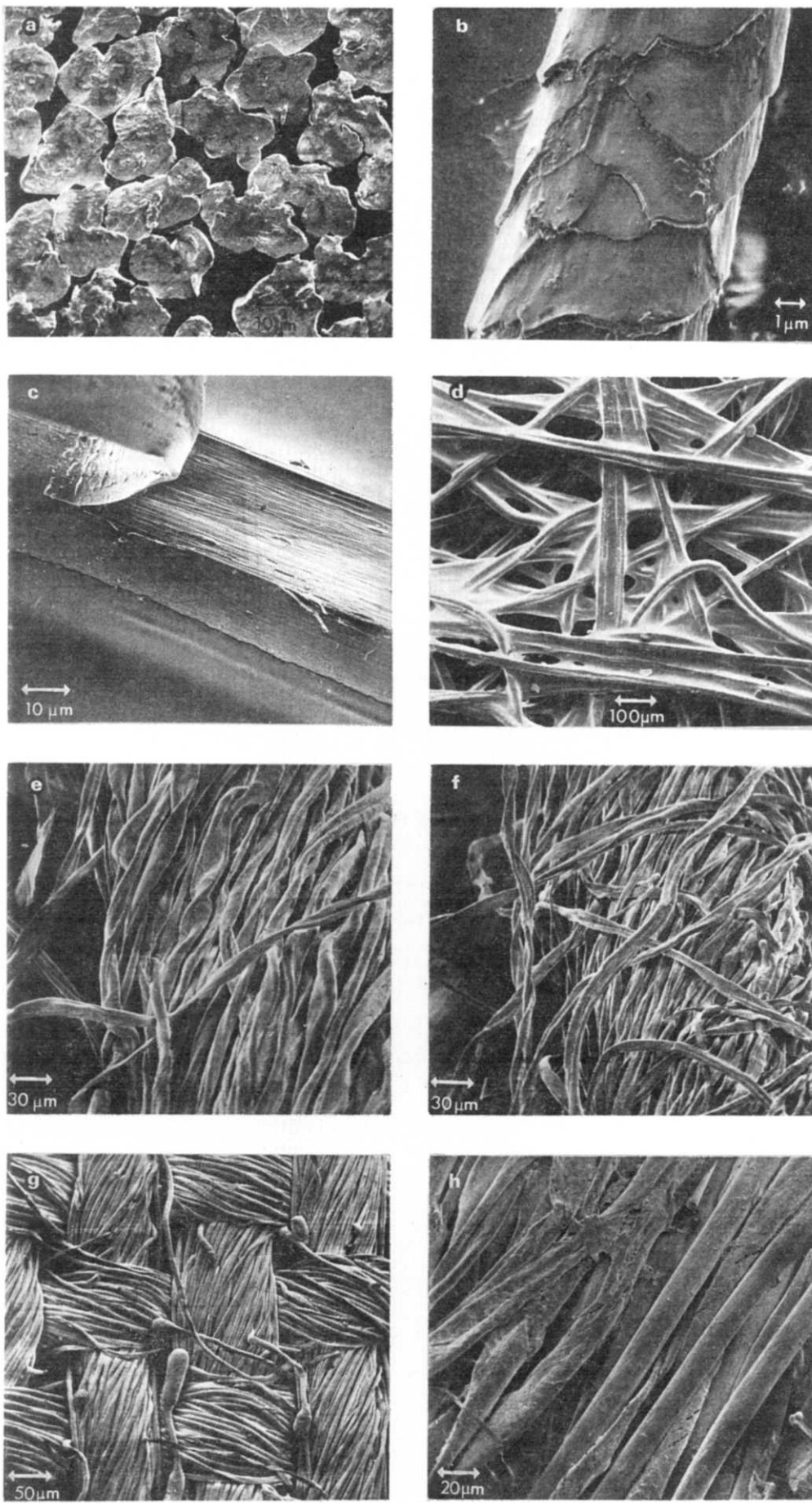
### Dark-field (diffraction contrast)

Where a specimen contains crystalline regions, contrast can be generated by dark-field viewing. By selecting one part of the diffraction pattern, and using it to form the image, crystallites with a particular orientation show up as bright patches. Ingram<sup>10,11</sup> has used this method to show up continuity of orientation over lengths of about 40 nm in fibrils in cellulose fibres; but he points out that it is difficult to get good results because cellulose is very susceptible to electron damage, and so it is necessary to use a low beam intensity, which with weak diffraction gives a very weak signal.

Earlier, Peterlin *et al.*<sup>16</sup> applied the technique more successfully on laboratory-prepared specimens of polyethylene, but it is a technique which might be explored more in studying synthetic fibre structure.

### Disintegration

Another way of studying fine structure is to break up the fibre. The classical methods are well-known and have already been mentioned. A comparatively new method, utilizing the X-press equipment of Biotec, involves forcing a frozen mixture of water and fibres through an orifice under high pressure. The principles were described by Edebo<sup>17</sup>. At  $-25^\circ\text{C}$  and  $2 \times 10^5 \text{ kg/mm}^2$ , ice undergoes a crystal lattice transition. At the



**Figure 8** Examples of scanning electron microscope studies of textiles. (a) Cross-sectional shape of cellulose acetate fibres by the plate method; (b) wool fibre; (c) internal surface of nylon-6 filament revealed by peeling; (d) bonded-fibre fabric; (e) conventional (ring-frame) cotton yarns; (f) comparative study of break-spun yarn; (g) cotton-polyester blend fabric, showing general structure and singed fibre ends; (h) used cotton-nylon sheets showing fibre damage. [From work of B. Lomas, B. H. Bhutta and K. L. Ghandi (UMIST)]

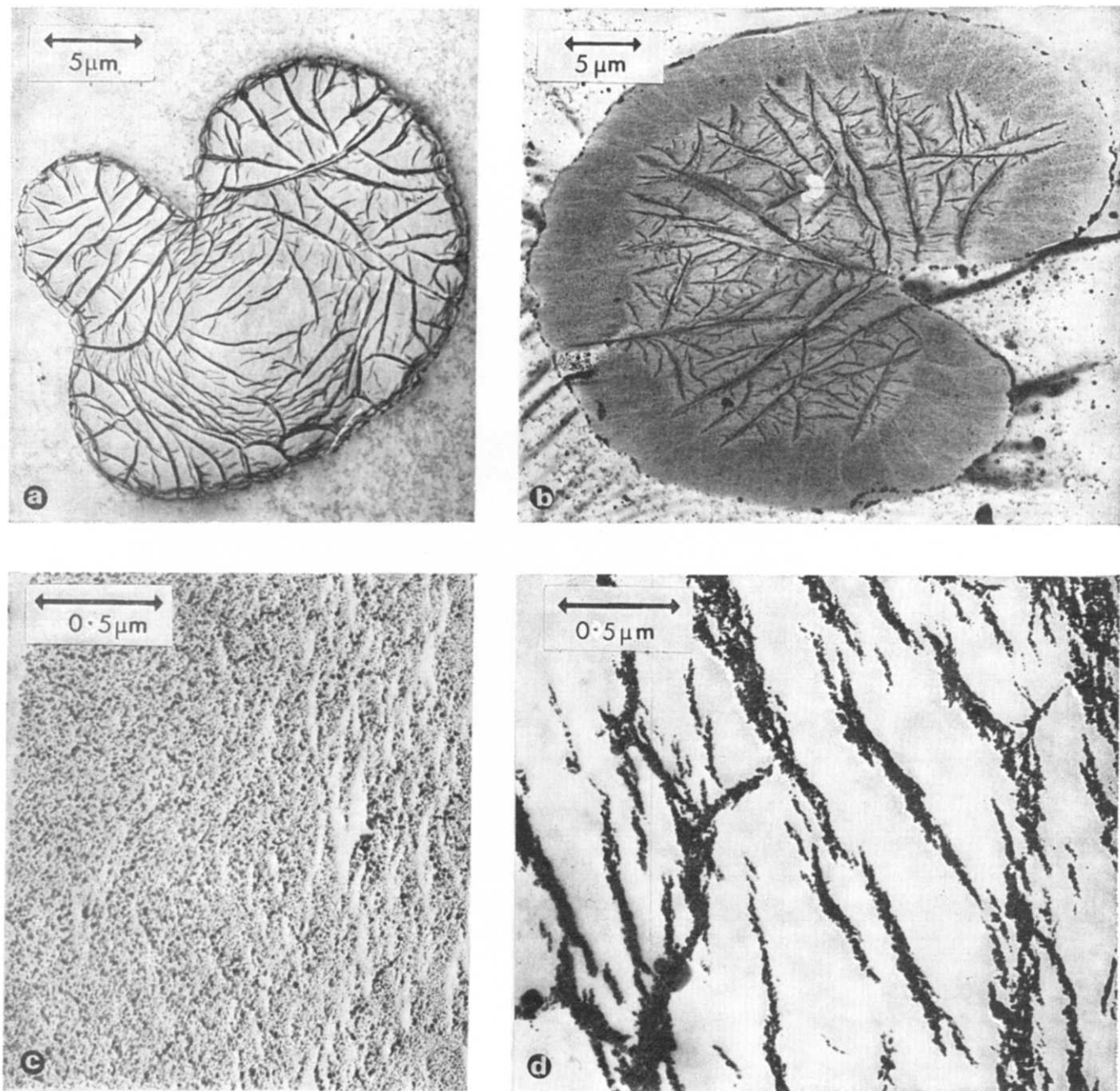


Figure 9 Use of staining methods by Sotton<sup>13-15</sup>—treatment with  $H_2S$  followed by  $AgNO_3$  to show structural differences. (a), (b) stained acrylic fibres; (c), (d) surface region of polyester fibres. (Pictures by courtesy of M. Sotton, Institut Textile de France)

moment of the transition there is a degree of mobility which allows some material to pass through a small orifice. The high pressures serve to disintegrate the fibres. Some examples are shown in Figure 10.

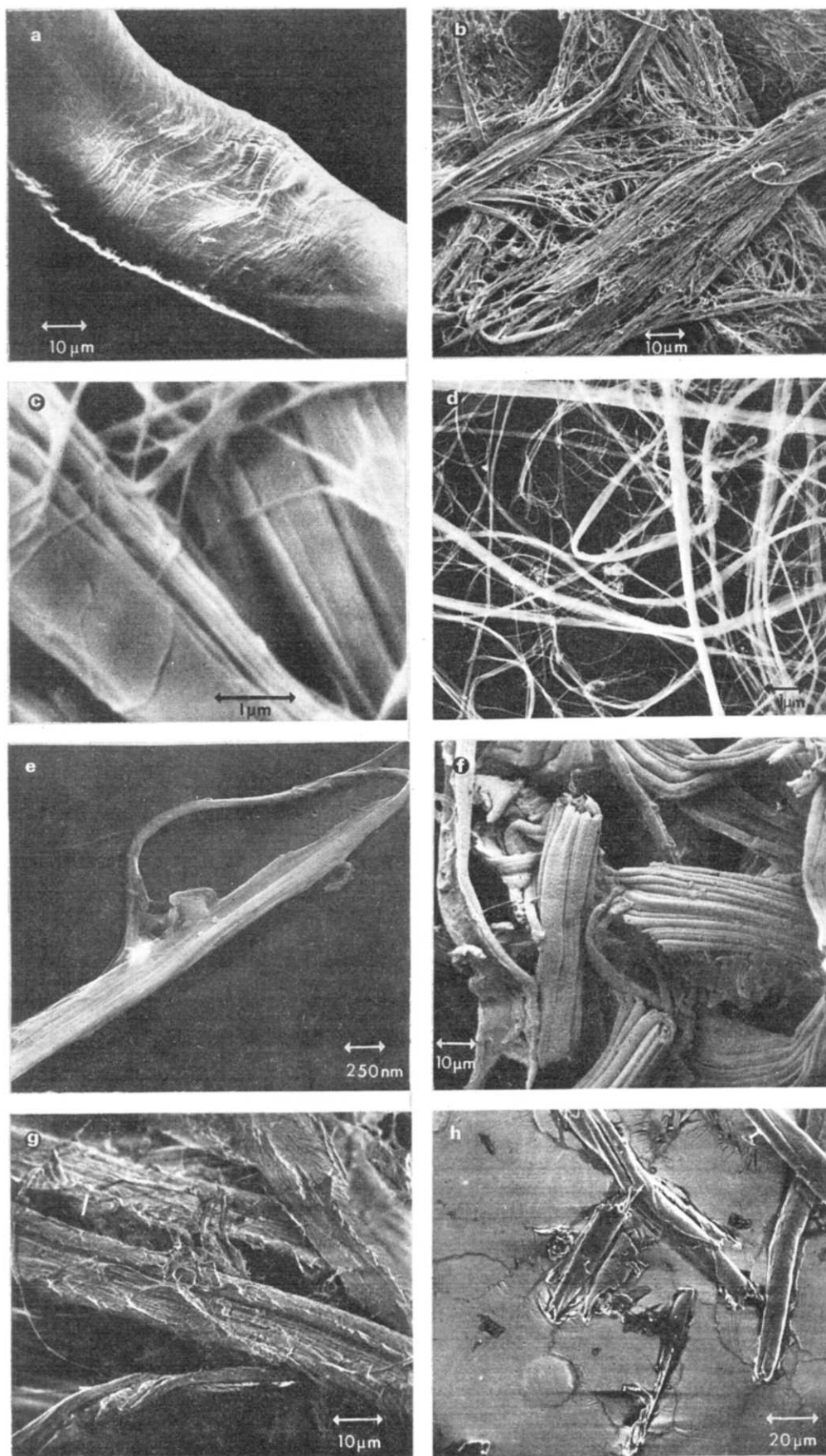
There are interesting differences between fibres. Nylon is barely affected by 10 passes, but du Pont's fibre B splits readily into fibrils. The illustrations demonstrate how, in this application, the s.e.m. runs out of useful magnification between  $2000\times$  and  $20\,000\times$ , but the direct electron microscope can go on to higher magnifications. There are also differences in appearance in the two microscopes. Viscose rayon splits into short pieces. Untreated cotton fibrillates, with some difficulty, but resin crosslinked cotton breaks into short pieces. Acrylic fibres (not illustrated) vary in their ease of fibrillation.

#### High-voltage electron microscopy

If the fibre will survive examination, high-voltage electron microscopy can be used on complete fibres. Sharp and Burnay<sup>18</sup> have used the method to examine carbon, metal and ceramic fibres. Figure 11 shows two views of the same fractured carbon fibres, seen in a s.e.m. and at 1 MV in the high-voltage transmission microscope. The internal void shown in the high voltage picture can be related to external features visible with the s.e.m.

Only thin specimens of the comparatively low-melting polymers used for textile fibres can be examined in the high-voltage microscope. Thick specimens, such as whole fibres, melt quickly owing to the energy absorption. It is possible that scanning high-voltage microscopy might solve this problem.





**Figure 10** Use of X-press method on fibres. (a) Nylon, after 10 passes, showing little change apart from distortion due to buckling (s.e.m.); (b) fibre B, after 10 passes (s.e.m.); (c) fibre B, after 10 passes (s.e.m. higher magnification); (d) fibre B, after 10 passes (direct electron microscope); (e) fibre B, after 10 passes (direct electron microscope, higher magnification); (f) viscose rayon, after 10 passes; (g) cotton, after 2 passes; (h) resin crosslinked cotton after 2 passes. [Pictures by B. Lomas and J. T. Sparrow (UMIST) and S.C.S.]

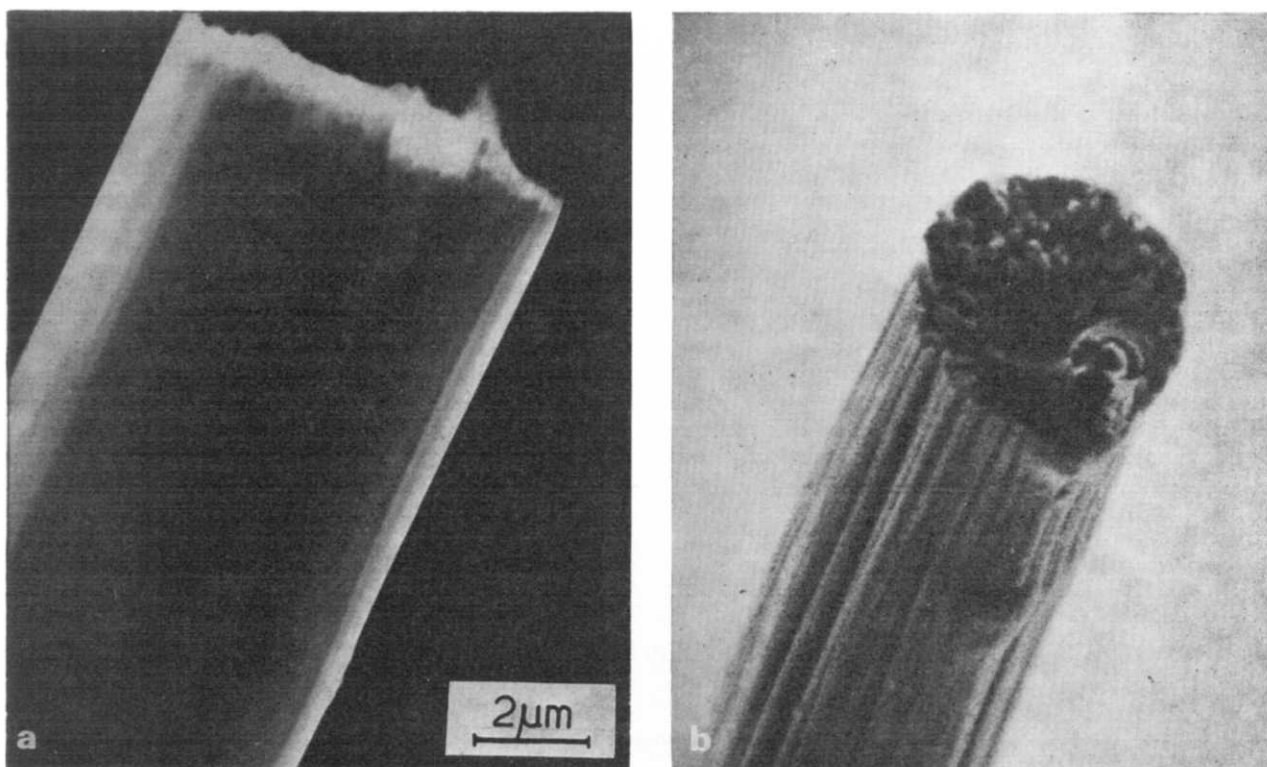


Figure 11 (a) High-voltage transmission electron microscope view of a fractured carbon fibre; (b) s.e.m. view of fibre. (Pictures by courtesy of J. V. Sharp, AERE, Harwell)

#### *S.e.m. filming*

The use of TV-scanning to show up dynamic experiments on fibres and textiles is a very useful technique. At UMIST Hearle *et al.*<sup>10</sup> have preferred to use lapsed-time cinephotography in order to show up the sequence of events in, for example, the extension and failure of bonded-fibre fabrics, the deformation of yarns and knitted fabrics, and the fracture mechanisms of cotton fibres.

#### *Reliability of information*

There are many applications of electron microscopy to fibres where there is little difficulty in interpreting the results, but there are also many interesting problems where the method may be pushed to a limit and where doubts arise. A due degree of scepticism is a virtue.

The errors due to specimen damage during preparation or viewing, to charging, and to similar causes are fairly well appreciated, if not always understood. But, near the limit of resolution, it is important to consider the nature of image formation. Lipson and Lipson<sup>20</sup> have recently pointed out the difficulties which arise from the strong interaction of electrons with matter, and which may upset the usual theory of image formation as a simple pair of Fourier transforms. They state that the limit of resolution will be about  $4(\lambda t)^{1/2}$ , where  $\lambda$  is the electron wavelength and  $t$  is the specimen thickness. For specimens of thickness 1000 Å, this indicates a resolution of about 30 Å. Images, such as those of lattice planes in carbon fibres, with apparently well-resolved smaller spacings are really Young's fringes, and not actual images of the object. This is pointed out in work at Leeds University<sup>21</sup>.

In order to overcome the possibilities of misinterpretation in difficult cases, more use might be made of careful searching for invariance under transformation. Those

features which are invariant in a variety of ways of examining or preparing the specimen are more likely to be real and not artifacts. There are many possible variations on this theme: through-focusing as shown in the Leeds exhibit<sup>21</sup>, change of viewing conditions, use of different knives in sectioning, use of different stains or swelling agents, the combination of studies with quite different modes of preparation and examination etc.

## TWO CURRENT TOPICS

### *Fine structure of fibres*

In both natural and synthetic fibres there remain interesting problems of fine structure concerning which electron microscopy has already provided some clues, and should yield more, but which remain unsolved. Rather curiously, the structural situation is qualitatively, if not quantitatively, clearer for the regenerated cellulose fibres. The two important groups of natural fibres—cotton and other plant fibres, wool and other hair fibres—have very different structure but in both the wealth of gross structural features are well-established and there is clearly a fibrillar fine structure at a level of the order of 10 nm; what is uncertain is whether there are appreciably finer fibrillar units. In the melt-spun synthetics (acrylic fibres are rather different) the structure is generally more uniform over the whole fibre, except possibly for a skin; what is uncertain is whether the fine structure is a comparatively uniform system of intermediate order (paracrystalline, a highly defective crystal, or amorphous with correlation) or whether it contains recognizable crystallites and, if so, whether these are fibrillar, micellar or even lamellar. The varying views of synthetic fibre structure are not necessarily exclusive: the structure may differ according to the history of fibre formation and subsequent treatment. In the family of rayon fibres, we

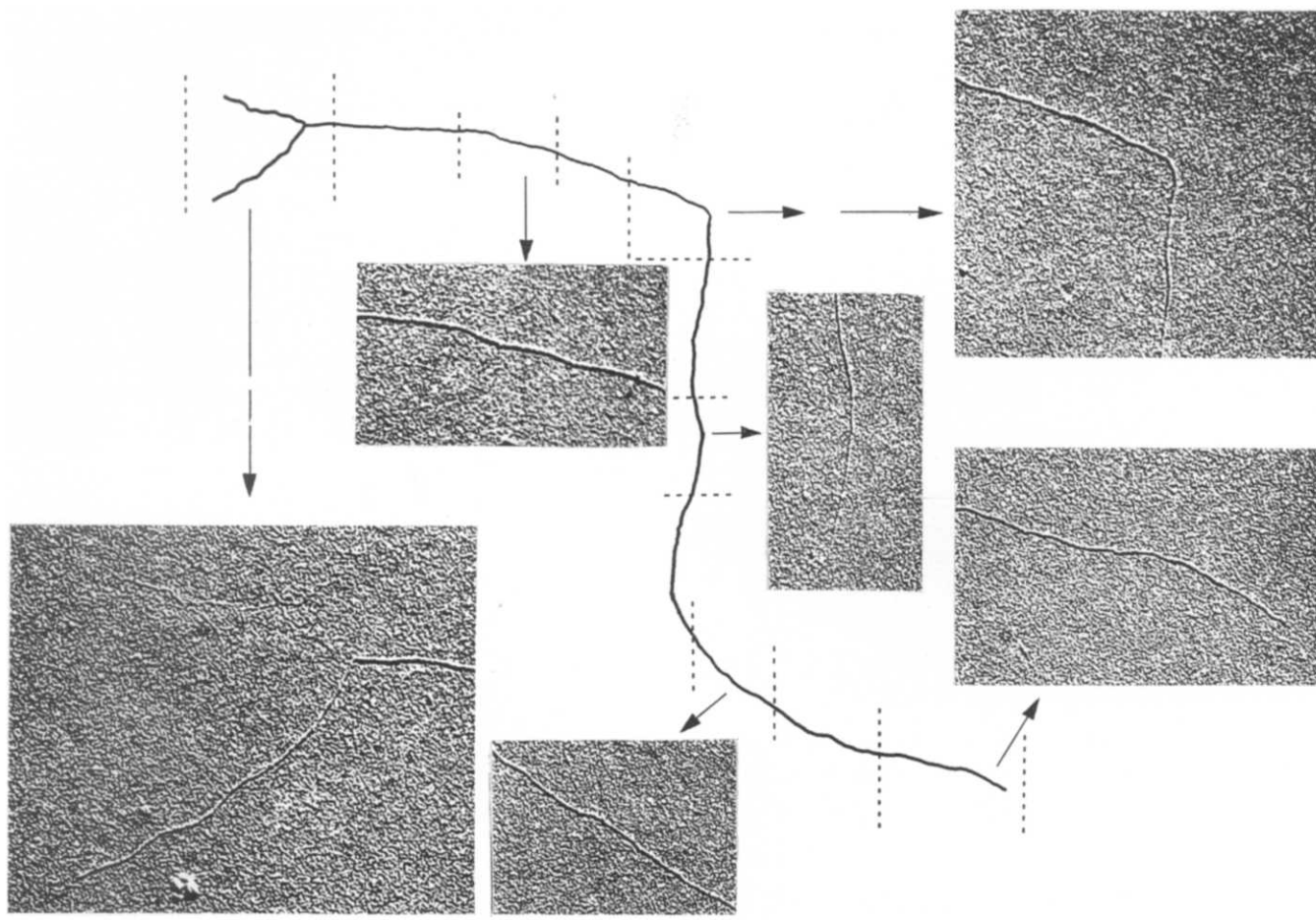


Figure 12 Fibril of cotton (65 000 $\times$ ) (S.C.S.). Short sections, located on the line diagram, are shown to allow adequate magnification in the print

can interpret the difference between fibres which are formed by direct crystallization (precipitation) from solution, followed by stretching, and those which are formed by crystallization in the oriented solid state as being a difference between a micellar and a fibrillar texture.

In natural cellulose fibres, there is clearly a coarse fibrillar structure, and this breaks down into separate fibrils. The problem of the identity of the ultimate microfibril is well illustrated by Figures 7 and 12, which show cotton mechanically disintegrated in a blender. In Figure 12, there is an enormous length of a fibril, about 7  $\mu\text{m}$ , with lateral dimensions of about 120  $\text{\AA}$ ; but at the end, it splits into finer fibrils. The question is whether these represent a smaller basic unit (a protofibril), or whether they are merely the result of cleavage between the molecules in the coarser fibrillar crystallite. Examination of the residue left on evaporation of the liquor shows globular particles which may well be single molecules resulting from the ultimate splitting of the crystals. Thus there is doubt about evidence from disintegration studies, even if one can accept the measurements of the size of the protofibrils, near the limit of resolution. Fibrils can be shown up in thin sections, or disintegrated lamellar fragments, by developing contrast by the staining methods mentioned earlier, as shown in Figure 13. Ingram<sup>10,11</sup> states that this suggests that the secondary walls in cotton are lamellae consisting of partly coalesced fibrils of about 50  $\text{\AA}$  in lateral width. Manley<sup>22</sup> has proposed very specific crystallographic modes of fibre formation, and finds support in his electron microscope studies. However, the detailed interpretation of the

electron microscope pictures is not easy or unambiguous, and Preston<sup>23</sup> argues strongly that the basic fibrillar units are thicker. Evidence from other sources (X-ray diffraction, chemistry, biosynthesis) is inconclusive or conflicting.

In wool, fibrillar disintegration does not easily occur, but the staining of sections shows microfibrils about 70  $\text{\AA}$  in diameter spaced 100  $\text{\AA}$  apart in a matrix (Figure 14). A wealth of circumstantial evidence identifies the microfibrils with helical crystalline material made of low-sulphur protein and the matrix with amorphous material of high-sulphur (cystine crosslinked) protein. There is believed to be a continuity between the helical segments of chains in the microfibril and their tails in the matrix. In the stained cross-sections, the eye of faith, looking with some reason for double or triple helices, can see indications of a protofibrillar internal structure of the microfibrils; but interpretation of the electron micrographs at this level is difficult, though Fraser *et al.*<sup>24</sup> have shown that it can be helped by optical filtering.

More convincing evidence came with the apparent isolation of protofibrils by disintegration of wool. However, Millward<sup>25</sup> and Fraser *et al.*<sup>26</sup> have shown that the 'protofibrils' can arise from contamination of the specimen with cellulose—providing, incidentally, in their studies of disintegrated Kleenex tissue some of the best pictures of finer cellulose fibrils. Dobb and Sikorski<sup>27, 28</sup> do not accept that the observed protofibrils always arise in this way. They show by selected area electron diffraction that fragments from a disintegrated Merino wool fibre were indeed keratin; however, these were relatively large sheets not isolated protofibrils and, as in other

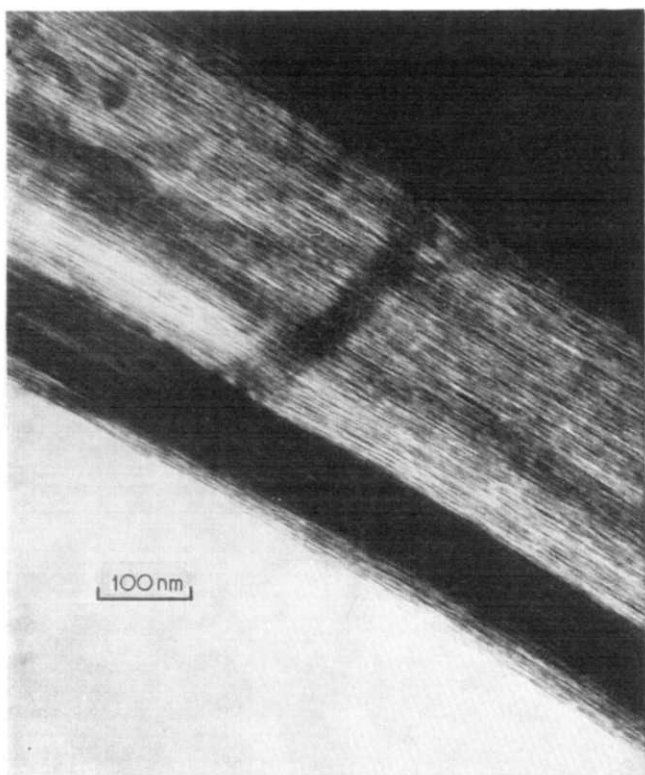


Figure 13 Stained section of ramie (122 500 $\times$ ). (Picture by courtesy of P. Ingram, Research Triangle Institute, North Carolina)

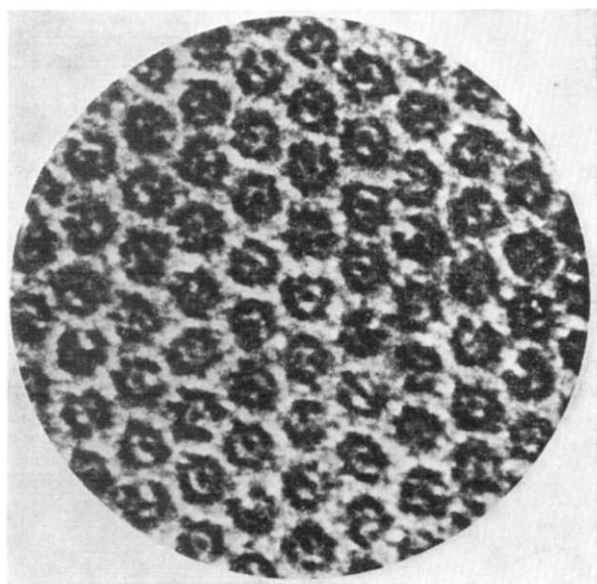


Figure 14 Stained section of wool. [Reproduced from *J. Textile Inst.* (1969, 60, 498) by permission of the Textile Institute]

such specimens, the evidence that they were composed of 2 nm filaments does not seem conclusive. At the moment, it is difficult to avoid taking the view that while protofibrils may exist in wool, there is no convincing evidence for their existence.

The main evidence against a fibrillar fine structure in polyamide and polyester fibres is the difficulty of producing fibrils by fibre disintegration or fracture—in comparison, for example, with the ease with which fibrillation occurs in cotton or wet-spun acrylic fibres. This would suggest that the structure is a partially ordered network of shorter elements or a micellar

structure. Rather coarse fibrils are seen in some peeled fibres, but this may reflect the influence of fluctuations within the coagulating stream during fibre formation or in the fibre during drawing, or it may be an artifact of peeling mechanics. The staining methods of Van Veld *et al.*<sup>29</sup> do apparently show a fine fibrillar texture, not very clearly resolved, with nodes along the fibre. Hearle and Greer<sup>30</sup> have suggested that this may be the result of the aggregation of micelles in pseudo-fibrils.

More comprehensive studies, using many techniques including electron microscopy, on a set of well-characterized samples are needed to establish the nature of the fine structure of these fibres. It is likely that if the same effort was put into the electron microscope study of synthetic fibres as has been put into cotton and wool, useful results would ensue. For the ignorance about synthetic fibres is related to structure at the level of 10 to 20 nm, in contrast to the finer level where the uncertainties now rest with the natural fibres.

At first sight, the disintegration of fibre B shown in Figure 10, might seem to be convincing evidence of a fibrillar fine structure. But there does not appear to be any limiting preferred size for the fibrillar units, and it is more likely that what is observed is merely a splitting between molecules in a very well-oriented fibre. The splitting would continue on down to a molecular level, just as a crystal of mica goes on splitting, and so would only be evidence that the material is a highly ordered linear polymer.

In order to check whether an observed fibrillar structure is evidence for a real fibrillar unit in the fibre before disintegration (or other specimen preparation), it is necessary to check, either by casual observation or more explicitly, whether there is a statistical predominance of fibrils of a particular size. If there is a sharply peaked distribution then this is evidence for a basic fibrillar unit; if there is a continuous broad distribution of sizes it is evidence against.

#### Fibre fractography

The advent of scanning electron microscopy has opened up the subject of fibre fractography, and has been the most important aspect of our s.e.m. work at UMIST. Because it shows the whole specimen in focus (as compared with the very limited depth of focus in an optical microscope) the general features of fibre fracture are clearly visible in s.e.m. views and, in addition, much fine detail can be examined at higher magnification.

The work is important for several reasons: (a) for its general scientific interest; (b) for the insight into mechanisms of failure in fibres, and thus as a guide to the possibility of improvement of fibre properties by the fibre producer; (c) for the insight into the causes of failure in use and processing and thus as a guide to improvement in processing methods or into construction of yarns, fabrics and garments; (d) as a means of diagnosis of causes by failure.

The results can be briefly summarized by a classification of the forms of fracture which have been observed. There are, however, many variants and combinations of the basic forms, and a full account of the work is, or will be, contained in other papers, including a continuing Atlas of pictures<sup>31</sup>.

The fibre fractures, so far observed, can be divided into the following classes.



*Elastic crack growth fractures.* Glass fibres show the classical brittle fracture from a Griffith's crack; similar fractures, though with large deformation, may occur in the tensile failure of elastomeric fibres. In these instances, the crack becomes less stable as it grows.

*Ductile crack growth fractures.* In nylon and other synthetics, as described by Hearle and Cross<sup>32</sup>, the crack growth is accompanied by drawing of the remainder of the cross-section and so the crack opens as a V-notch before the final catastrophic failure occurs (Figure 15). In this case, the crack requires a greater load for propagation the deeper it gets; this is a situation in which more detailed analysis of fracture mechanics is required. On rare occasions fracture of this type is initiated at an interior flaw.

*Fractures with axial splitting.* In the tensile fracture of cotton, described by Hearle and Sparrow<sup>33</sup>, and in the torsional fracture of some acrylic fibres, the dominant feature is a splitting of the structure along its length as shown in Figure 16. This is associated with the marked fibrillar nature of these fibres.

*Axial splitting due to fatigue.* Hearle and Bunsell<sup>34</sup> have shown that tensile fatigue can cause cracks to run along the fibre parallel to the tensile stress axis, giving breaks with long tails as shown in Figure 17. In order to promote this fatigue failure in nylon it is necessary that the load should fall to zero in each cycle. With a peak load much less than the normal breaking load, failure occurs in  $10^5$  to  $10^6$  cycles, owing to an initial surface crack turning and running along the fibre, getting gradually deeper. In polyester and acrylic fibres long internal cracks develop.

*Fracture perpendicular to the fibre axis.* Rayon, acrylic fibres, wool, and crosslinked cotton show breaks which run across the fibre with no clear crack morphology and moderate roughness. An example is shown in Figure 18. Sometimes, there is a marked discontinuity along the

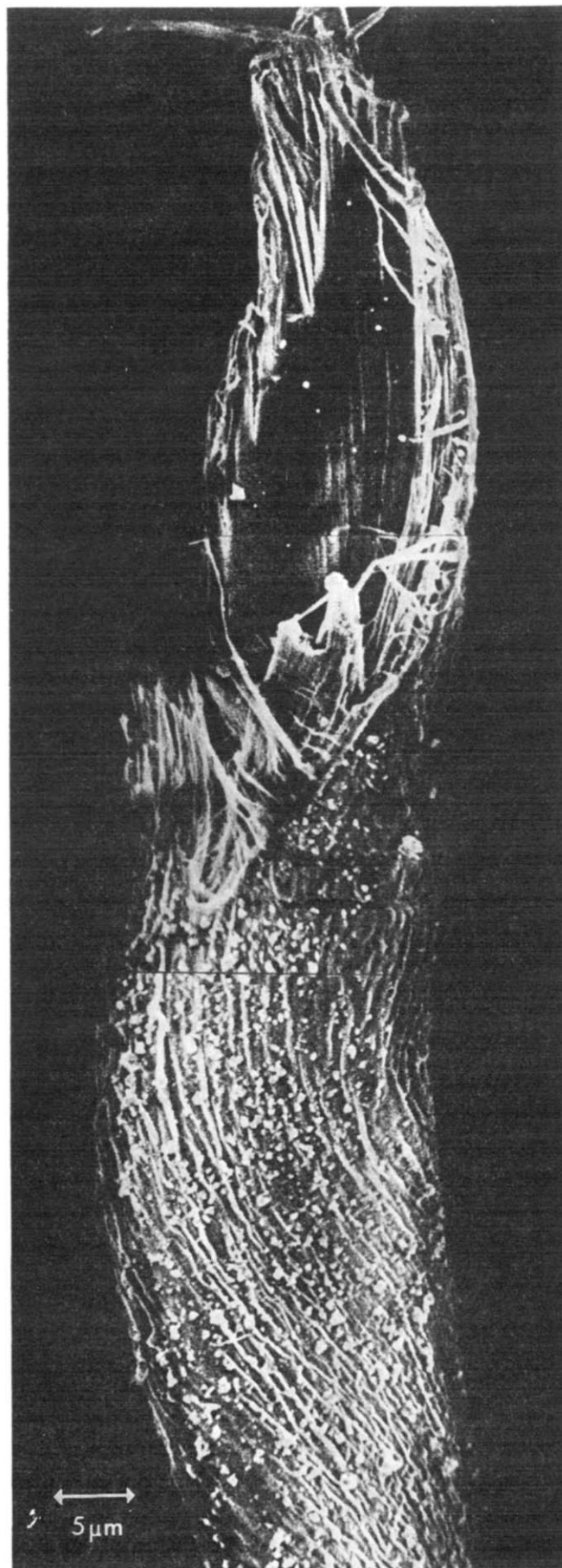


Figure 16 Cotton tensile fracture. [Picture by J. T. Sparrow (UMIST)]

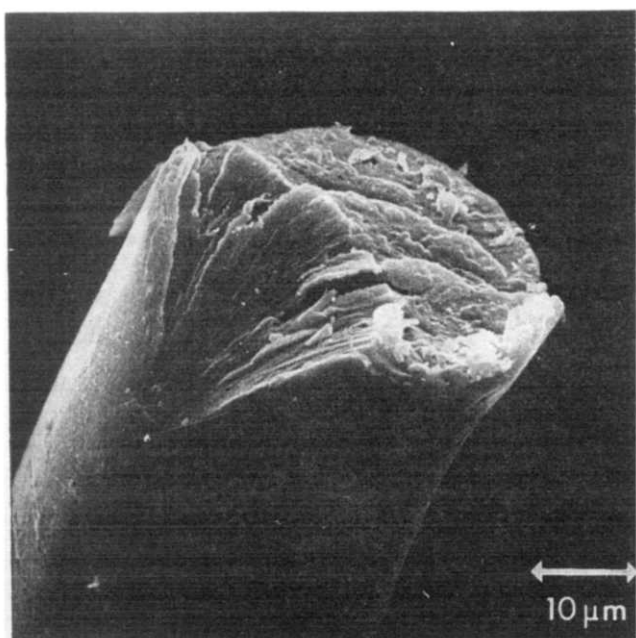


Figure 15 Nylon tensile fracture. [Picture by B. Lomas (UMIST)]

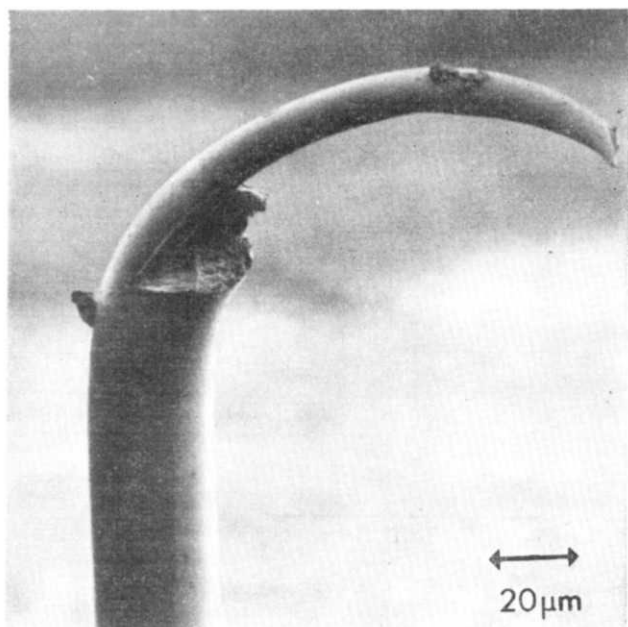


Figure 17 Fatigue failure of nylon. [Picture by A. R. Bunsell and L. Konopasek (UMIST)]

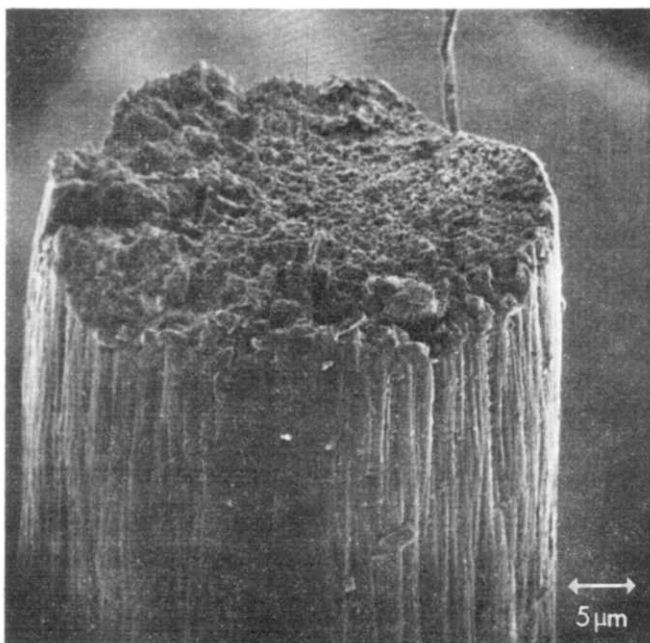


Figure 18 Acrylic fibre tensile fracture. [Picture by B. Lomas (UMIST)]

fibre axis to give breaks in two or more steps. This type of failure resembles, at many orders of magnitude smaller in scale, the fracture of fibre-reinforced composites and is probably due to the separate rupture of fibrils within the fibre.

*Failure from kink-bands.* Fibres in compression, for example on the inside of a bend, develop oblique bands visible in polarized light. Under repeated flexing, failure occurs along these bands. This is an area of current study.

*Other breaks or fibre ends.* This is a miscellaneous group not separately classified. It includes fibres which are cut,

or have their ends melted or chemically attacked. It also includes fibres broken to make staple fibres and fibres which have failed in use.

As the work proceeds, other forms will, no doubt, be recognized.

#### REFERENCES

- 1 Chapman, J. A. and Menter, J. W. *Proc. R. Soc. (A)* 1954, **226**, 400
- 2 Chapman, J. A., Pascoe, M. W. and Tabor, D. *J. Text. Inst.* 1955, **46**, 3
- 3 Dlugosz, J. *Proc. 1st Eur. Reg. Conf. Electron Microsc., Stockholm* 1956, p 283
- 4 Ramanathan, N., Sikorski, J. and Woods, H. J. *Proc. Int. Conf. Electron Microsc., London* 1954, p. 482
- 5 Scott, R. G. *ASTM Spec. Tech. Publ. No. 257* 1959, p 121
- 6 Byrne, G. A. and Brown, K. C. *J. Soc. Dyers Colour.* 1972, **88**, 113
- 7 Chippendale, P. J. *J. Text. Inst.* 1960, **5** (11), T392
- 8 Hearle, J. W. S., Lomas, B. and Sparrow, J. T. *J. Microsc.* 1970, **92**, 205
- 9 Swift, J. A. *J. Text. Inst.* 1972, **63**, 64, 129
- 10 Ingram, P. *Papers of SIRTEC, Institute Textile de France*, 1969, p 519
- 11 Peterlin, A. and Ingram, P. *Text. Res. J.* 1970, **40**, 345
- 12 Billica, H. R., van Veld, R. D. and Davis, H. A. *7th Int. Electron Microsc. Congr. Grenoble* 1970, p 335
- 13 Sotton, M. *C.R. Acad. Sci. Paris* 1970, **270**, 1261
- 14 Sotton, M. and Vialard, A-M. *C.R. Acad. Sci. Paris* 1971, **272**, 1381
- 15 Sotton, M. and Vialard, A-M. *Text. Res. J.* 1971, **41**, 834
- 16 Peterlin, A., Ingram, P. and Kiho, H. *Makromol. Chem.* 1965, **86**, 294
- 17 Edebo, L., *J. Biochem. Microbiol. Technol. Eng.* 1960, **2**, 453
- 18 Sharp, J. V. and Burnay, S. G. *Proc. 25th Anniv. Meet. EMAG Inst. Physics, London*, 1971, p 28
- 19 Hearle, J. W. S., Clarke, D. J., Lomas, B., Reeves, D. A. and Sparrow, J. T. *Proc. 25th Anniv. Meet. EMAG Inst. Physics, London*, 1961, p 210
- 20 Lipson, H. and Lipson, S. G. *J. Appl. Cryst.* 1972, **5**, 239
- 21 University of Leeds, Textile Industries Department, exhibit at EMCON 1972
- 22 Manley, R. St. J. *J. Polym. Sci. (A-2)* 1971, **9**, 1025
- 23 Preston, R. D. *J. Microsc.* 1971, **93**, 7
- 24 Fraser, R. D. B., MacRae, T. P. and Millward, G. R. *J. Text. Inst.* 1969, **60**, 343
- 25 Millward, G. R. *J. Cell Biol.* 1969, **42**, 317
- 26 Fraser, R. D. B., MacRae, T. P. and Millward, G. R. *J. Text. Inst.* 1969, **60**, 498
- 27 Dobb, M. G. and Sikorski, J. *J. Text. Inst.* 1969, **60**, 497
- 28 Dobb, M. G. and Sikorski, J. *Appl. Polym. Symp.* 1971, **18**, 743
- 29 van Veld, R. D., Morris, G. and Billica, H. R. *J. Appl. Polym. Sci.* 1968, **12**, 2709
- 30 Hearle, J. W. S. and Greer, R. *J. Text. Inst.* 1970, **61**, 243
- 31 'An Atlas of Fibre Fracture', (continuing series) *Text. Manuf.* 1972 (January), No. 1
- 32 Hearle, J. W. S. and Cross, P. M. *J. Mater. Sci.* 1970, **5**, 507
- 33 Hearle, J. W. S. and Sparrow, J. T. *Text. Res. J.* 1971, **41**, 736
- 34 Bunsell, A. R. and Hearle, J. W. S. *J. Mater. Sci.* 1971, **6**, 1303

#### General references

- J. A. Chapman in 'Physical Methods of Investigating Textiles', (Eds J. W. S. Hearle and R. Meredith), Interscience, New York, 1959, Ch 3
- 'Fibre Structure', (Eds J. W. S. Hearle and R. H. Peters), Butterworths, London, 1963
- J. W. S. Hearle and R. Greer, *Text. Progr.* 1970, **2**, (4)
- 'The Use of the Scanning Electron Microscope', (Eds J. W. S. Hearle, J. T. Sparrow, and P. M. Cross), Pergamon Press, Oxford, 1972

# Note to the Editor

## Electrical properties of polymers containing isoxazoline and isoxazole heterocycles

Suck-Ju Hong

Department of Chemical Engineering, Kon-kuk University, Seoul, Korea  
(Received 12 February 1973)

### INTRODUCTION

The interest in semiconducting polymers has been constantly increasing. Investigations concerned with semiconducting polymers with heterocyclic rings in the polymer main chain, such as polybenzimidazole<sup>1</sup>, and polypyrrole<sup>2</sup> had attracted our attention. Recently, electrical conductivities of partially conjugated polymers, such as polyrhodanine<sup>3</sup>, polythiohydantoin<sup>4</sup>, and polyoxazole<sup>5</sup>, have been reported. However, these had shown relatively high values of resistivity,  $10^{12}$ – $10^{14}$   $\Omega$  cm.

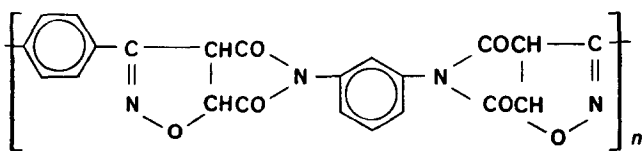
Previously the author reported the synthesis of polyisoxazoline and polyisoxazole<sup>6</sup>, and the physical properties of polyisoxazole concerned with its e.s.r. and crystallinity<sup>7</sup>. In conjunction with these investigations, the author wishes to present some further interesting results on the electrical properties of polyisoxazolines and polyisoxazole.

### EXPERIMENTAL

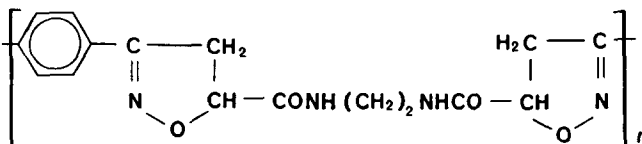
#### Polymer sample

Polyisoxazolines (I) and (II) and polyisoxazole (III) were synthesized from the reactions of terephthalohydroxamoyl chloride with corresponding dipolarophiles in refluxing toluene and were purified by extracting in hot methanol<sup>6</sup>.

Polyisoxazoline [poly(phenylene- $\Delta^2$ -isoxazoline)]:

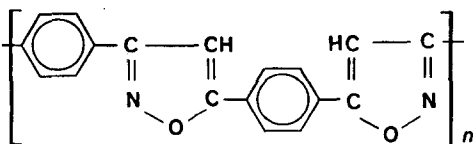


(I):  $\eta_{sp}/c = 0.11$  in 0.2 g/dl of DMF at 30°C



(II):  $\eta_{sp}/c = 0.25$  in 0.1 % g/dl of dichloroacetic acid at 30°C

Polyisoxazole (polyphenyleneisoxazole):



(III):  $\eta_{sp}/c = 0.24$  in 0.5 g/dl of sulphuric acid at 30°C

### Resistivity

Temperature-resistivity profiles were obtained for compressed discs as follows<sup>5</sup>. Finely powdered sample was compressed to form a disc under a pressure of about 200 kg/cm<sup>2</sup> applying suction to remove air and moisture. Then the disc mounted in a cylinder was placed between stainless-steel electrodes. A pressure of 40 kg/cm<sup>2</sup> was applied to the disc of the sample throughout the measurement. The compressed disc of the sample was kept for 30 min under a given temperature and electrical voltage, and the measurement of conductivity was carried out by using a Takeda-Riken model TR-84 electrometer. Applied voltages from batteries for polyisoxazolines and polyisoxazole were 3.05 and 15.8 V respectively. The thickness of the disc was measured with the micrometer after measurement of the conductivity.

### RESULTS AND DISCUSSION

The electrical resistivities of (I), (II) and (III) were measured at various temperatures under a pressure of 40 kg/cm<sup>2</sup>. The results are summarized in Table 1.

The resistivity data of Table 1 appear to obey the usual exponential equation for semiconductive behaviour,  $\rho = \rho_0 \exp E_g/2kT$ , where  $\rho$  = resistivity ( $\Omega$  cm);  $E_g$  = the energy gap for the conduction (eV);  $k$  is Boltzmann's constant and  $T$  is the absolute temperature. The values of the energy gaps for (I), (II) and (III) calculated from the linear relationship between  $\log \rho$  and  $1/T$  by the exponential equation are shown in Table 2.

As indicated in Table 1, resistivities of (I) and (II) are decreased with increasing temperature. Resistivities of (I) and (II) are in the range  $10^6$ – $10^9$   $\Omega$  cm. Polyisoxazoline(II) having  $-\text{NHCO}-$  bond and higher crystallinity<sup>6</sup>, even though containing an aliphatic unit in the main

Table 1 Electrical resistivities of polyisoxazolines and polyisoxazole\*

(I) at 3.05 V†		(II) at 3.05 V		(III) at 15.8 V	
Temp. (°C)	$\rho$ ( $\Omega$ cm)	Temp. (°C)	$\rho$ ( $\Omega$ cm)	Temp. (°C)	$\rho$ ( $\Omega$ cm)
28	$3.80 \times 10^9$	29	$3.05 \times 10^8$	28	$1.15 \times 10^{11}$
46	$2.19 \times 10^9$	49	$8.66 \times 10^7$	48	$2.66 \times 10^{11}$
57	$1.63 \times 10^9$	72	$2.12 \times 10^7$	93	$4.93 \times 10^{11}$
78	$9.92 \times 10^8$	96	$4.23 \times 10^6$	113	$9.86 \times 10^{11}$
140	$2.94 \times 10^8$	125	$1.81 \times 10^6$	130	$1.64 \times 10^{12}$

\* Surface area of sample, 1.3067 cm<sup>2</sup>; thickness of sample, (I)=0.543 mm; (II)=0.523 mm; (III)=0.598 mm

† Applied voltage; different voltages were applied because a battery was used instead of a regulated voltage supply

Table 2 Values of energy gaps for (I), (II), and (III)

Sample	Temp. range (°C)	$E_g$ (eV)
(I)	28–140	0.486
(II)	29–125	1.107
(III)	28–130	-0.510

chain of the polymer, exhibits considerably lower resistivity than (I). This might result from the development of crystallinity caused by the interaction of amide bonds between the polymer molecules.

However, the resistivity of polyisoxazole(III) with the highest crystallinity among the polymers<sup>6, 7</sup> is comparatively high and is increased with increasing temperature. Eventually the resistivity of polyisoxazole(III) has a positive dependence on temperature. The value of the energy gap is negative as shown in Table 2. This clearly demonstrates the nature of positive thermistor<sup>8</sup>. These results are in significant contrast with cases of polyisoxazolines.

The electrical energy losses of (I), (II), and (III) were very small. Further investigation is in progress.

These new findings may initiate further interest in studying the semiconductive behaviour of polymers with heterocyclic rings.

#### ACKNOWLEDGEMENTS

The author is grateful to Professors J. S. Shim, J. H. Lee, K. Uno, and Dr R. Hirohashi for their valuable discussions.

#### REFERENCES

- 1 Pohl, H. A. *J. Polym. Sci. (A-2)* 1964, **2**, 2787
- 2 Botto, H. A. and Weiss, D. W. *Aust. J. Chem.* 1963, **16**, 1076
- 3 Hirohashi, R. *Kogyo-Kagaku Zasshi* 1968, **71**, 1744; 1970, **73**, 1450
- 4 Hirohashi, R. *Kogyo-Kagaku Zasshi* 1969, **72**, 1394
- 5 Hirohashi, R. *Polymer* 1970, **11**, 297
- 6 Iwakura, Y., Uno, K. and Hong, S. J. *Polymer J.* 1971, **2**, 36
- 7 Hong, S. J., Iwakura, Y. and Uno, K. *Polymer* 1971, **12**, 526
- 8 Futaki, H. 'Thermistor and its Application', 1969, Nichi-Kan Kogyo Press Co, Tokyo, Ch 1

## Book Reviews

### Polymer science: a materials science handbook

Edited by A. D. Jenkins

North-Holland, Amsterdam/London, 1972, Vols 1 and 2, 1822 pp. £49.00

Those concerned with polymers, no matter whether their interests be related to synthesis, characterization, properties, or even to something more specific, like polyelectrolytes or composites, often have occasion to seek information on wider issues connected with the subject, and are then faced with the problem of a search for the appropriate textbooks, review articles and papers, some of which may not be readily to hand. An encyclopaedia presentation of polymer science and technology is, of course, available but there is usually first the wish to go to a convenient bookshelf rather than to a main library.

Consideration of the contents of these two volumes and a discerning look at the index indicates the breadth of polymer topics dealt with. Excellently printed and bound, they comprise 27 authoritative chapters contributed by specialists from the USA and the UK. One of my colleagues has described the work as a 'mini-encyclopaedia'; perhaps it could be better termed as a series of monographs assembled to provide a 'jumbo-sized' handbook.

Chapters in the first volume (932 pp) deal with chemistry, structure, crystallinity, molecular behaviour, viscoelastic and optical properties, and then cover plasticization, fracture, and the mechanical properties of plastics and fibres (but with less reference to elastomers). In the second volume (888 pp) the subjects are of a wider—and perhaps less integrated—nature, dealing with such aspects as adhesion, friction and wear, solutions, polyelectrolytes, electric and dielectric properties, far infra-red, n.m.r. and neutron spectroscopy, degradation (thermal, photo- and oxidative), radiation effects, identification and analysis, polymers for use at high temperatures, and composites. There is thus cover wide enough to satisfy many readers but it will be found that some items such as vulcanization or even chemical treatments in general, elastomers and fillers, get less attention.

The editor, Professor A. D. Jenkins of the University of Sussex, has done well in bringing the chapters together in a reasonably standard form despite the large number of contributors and inevitable differences in style and treatment. Some chapters are more detailed and comprehensive than others, some are more superficial or general in approach, but taken in all they form a very acceptable up-to-date collection and are made all the more useful by inclusion of the many references at the end of each.

The comprehensive nature and excellent presentation, however, bring in another feature, that of price. At £49, the work represents a costly acquisition, pagewise much more so than a fuller encyclopaedia; however, a good distillate is rarely cheap. There are many who will find these volumes useful and wish to have them available, perhaps not as a personal possession but in a departmental or works library where information is sought on a variety of areas in polymer science and technology.

R. J. W. Reynolds

### The use of the scanning electron microscope

Edited by J. W. S. Hearle, J. T. Sparrow and P. M. Cross

Pergamon Press, Oxford, 1972, £8.80

The number of scanning electron microscopes in general use has grown enormously over the last few years and workers in a variety of fields have gained access to instruments. There is therefore a need for a book which gives a simple and straightforward account of scanning electron microscopy, whilst at the same time covering the types of practical and interpretive problems encountered by the average user. The editors and contributors to this book are to be congratulated on successfully meeting this need.

The book contains thirteen chapters and there are eight contributors. However, the treatment is uniform and the ground is covered in a systematic manner. Basic principles, background knowledge, and instrument design and use are dealt with in Chapters 1 to 4. Specimen preparation and modes of operation are discussed in Chapters 4 and 5. Chapters 6 to 9 are given over to specialist applications in the fields of metals, electronic devices, fibres and polymers, and biological materials respectively. Faults and dimensional measurements are dealt with in Chapters 10 and 11. For those fortunate enough to possess an instrument, some tips on instrument management are given in Chapter 12, while Chapter 13 considers possible future developments in the field. The book contains comprehensive author and subject indexes and there is a useful list of manufacturers and suppliers. The quality of the paper, printing and numerous micrographs is good.

The book can be recommended to workers who wish to make best use of the scanning electron microscope technique. It will also be of value to those who would like to become generally acquainted with the potentialities and limitations of this branch of microscopy. By present day standards the book is reasonably priced.

C. Price

Table 2 Values of energy gaps for (I), (II), and (III)

Sample	Temp. range (°C)	$E_g$ (eV)
(I)	28-140	0.486
(II)	29-125	1.107
(III)	28-130	-0.510

chain of the polymer, exhibits considerably lower resistivity than (I). This might result from the development of crystallinity caused by the interaction of amide bonds between the polymer molecules.

However, the resistivity of polyisoxazole(III) with the highest crystallinity among the polymers<sup>6, 7</sup> is comparatively high and is increased with increasing temperature. Eventually the resistivity of polyisoxazole(III) has a positive dependence on temperature. The value of the energy gap is negative as shown in Table 2. This clearly demonstrates the nature of positive thermistor<sup>8</sup>. These results are in significant contrast with cases of polyisoxazolines.

The electrical energy losses of (I), (II), and (III) were very small. Further investigation is in progress.

These new findings may initiate further interest in studying the semiconductive behaviour of polymers with heterocyclic rings.

#### ACKNOWLEDGEMENTS

The author is grateful to Professors J. S. Shim, J. H. Lee, K. Uno, and Dr R. Hirohashi for their valuable discussions.

#### REFERENCES

- 1 Pohl, H. A. *J. Polym. Sci. (A-2)* 1964, **2**, 2787
- 2 Botto, H. A. and Weiss, D. W. *Aust. J. Chem.* 1963, **16**, 1076
- 3 Hirohashi, R. *Kogyo-Kagaku Zasshi* 1968, **71**, 1744; 1970, **73**, 1450
- 4 Hirohashi, R. *Kogyo-Kagaku Zasshi* 1969, **72**, 1394
- 5 Hirohashi, R. *Polymer* 1970, **11**, 297
- 6 Iwakura, Y., Uno, K. and Hong, S. J. *Polymer J.* 1971, **2**, 36
- 7 Hong, S. J., Iwakura, Y. and Uno, K. *Polymer* 1971, **12**, 526
- 8 Futaki, H. 'Thermistor and its Application', 1969, Nichi-Kan Kogyo Press Co, Tokyo, Ch 1

## Book Reviews

### Polymer science: a materials science handbook

Edited by A. D. Jenkins

North-Holland, Amsterdam/London, 1972, Vols 1 and 2, 1822 pp. £49.00

Those concerned with polymers, no matter whether their interests be related to synthesis, characterization, properties, or even to something more specific, like polyelectrolytes or composites, often have occasion to seek information on wider issues connected with the subject, and are then faced with the problem of a search for the appropriate textbooks, review articles and papers, some of which may not be readily to hand. An encyclopaedia presentation of polymer science and technology is, of course, available but there is usually first the wish to go to a convenient bookshelf rather than to a main library.

Consideration of the contents of these two volumes and a discerning look at the index indicates the breadth of polymer topics dealt with. Excellently printed and bound, they comprise 27 authoritative chapters contributed by specialists from the USA and the UK. One of my colleagues has described the work as a 'mini-encyclopaedia'; perhaps it could be better termed as a series of monographs assembled to provide a 'jumbo-sized' handbook.

Chapters in the first volume (932 pp) deal with chemistry, structure, crystallinity, molecular behaviour, viscoelastic and optical properties, and then cover plasticization, fracture, and the mechanical properties of plastics and fibres (but with less reference to elastomers). In the second volume (888 pp) the subjects are of a wider—and perhaps less integrated—nature, dealing with such aspects as adhesion, friction and wear, solutions, polyelectrolytes, electric and dielectric properties, far infra-red, n.m.r. and neutron spectroscopy, degradation (thermal, photo- and oxidative), radiation effects, identification and analysis, polymers for use at high temperatures, and composites. There is thus cover wide enough to satisfy many readers but it will be found that some items such as vulcanization or even chemical treatments in general, elastomers and fillers, get less attention.

The editor, Professor A. D. Jenkins of the University of Sussex, has done well in bringing the chapters together in a reasonably standard form despite the large number of contributors and inevitable differences in style and treatment. Some chapters are more detailed and comprehensive than others, some are more superficial or general in approach, but taken in all they form a very acceptable up-to-date collection and are made all the more useful by inclusion of the many references at the end of each.

The comprehensive nature and excellent presentation, however, bring in another feature, that of price. At £49, the work represents a costly acquisition, pagewise much more so than a fuller encyclopaedia; however, a good distillate is rarely cheap. There are many who will find these volumes useful and wish to have them available, perhaps not as a personal possession but in a departmental or works library where information is sought on a variety of areas in polymer science and technology.

R. J. W. Reynolds

### The use of the scanning electron microscope

Edited by J. W. S. Hearle, J. T. Sparrow and P. M. Cross

Pergamon Press, Oxford, 1972, £8.80

The number of scanning electron microscopes in general use has grown enormously over the last few years and workers in a variety of fields have gained access to instruments. There is therefore a need for a book which gives a simple and straightforward account of scanning electron microscopy, whilst at the same time covering the types of practical and interpretive problems encountered by the average user. The editors and contributors to this book are to be congratulated on successfully meeting this need.

The book contains thirteen chapters and there are eight contributors. However, the treatment is uniform and the ground is covered in a systematic manner. Basic principles, background knowledge, and instrument design and use are dealt with in Chapters 1 to 4. Specimen preparation and modes of operation are discussed in Chapters 4 and 5. Chapters 6 to 9 are given over to specialist applications in the fields of metals, electronic devices, fibres and polymers, and biological materials respectively. Faults and dimensional measurements are dealt with in Chapters 10 and 11. For those fortunate enough to possess an instrument, some tips on instrument management are given in Chapter 12, while Chapter 13 considers possible future developments in the field. The book contains comprehensive author and subject indexes and there is a useful list of manufacturers and suppliers. The quality of the paper, printing and numerous micrographs is good.

The book can be recommended to workers who wish to make best use of the scanning electron microscope technique. It will also be of value to those who would like to become generally acquainted with the potentialities and limitations of this branch of microscopy. By present day standards the book is reasonably priced.

C. Price

Table 2 Values of energy gaps for (I), (II), and (III)

Sample	Temp. range (°C)	$E_g$ (eV)
(I)	28-140	0.486
(II)	29-125	1.107
(III)	28-130	-0.510

chain of the polymer, exhibits considerably lower resistivity than (I). This might result from the development of crystallinity caused by the interaction of amide bonds between the polymer molecules.

However, the resistivity of polyisoxazole(III) with the highest crystallinity among the polymers<sup>6, 7</sup> is comparatively high and is increased with increasing temperature. Eventually the resistivity of polyisoxazole(III) has a positive dependence on temperature. The value of the energy gap is negative as shown in Table 2. This clearly demonstrates the nature of positive thermistor<sup>8</sup>. These results are in significant contrast with cases of polyisoxazolines.

The electrical energy losses of (I), (II), and (III) were very small. Further investigation is in progress.

These new findings may initiate further interest in studying the semiconductive behaviour of polymers with heterocyclic rings.

#### ACKNOWLEDGEMENTS

The author is grateful to Professors J. S. Shim, J. H. Lee, K. Uno, and Dr R. Hirohashi for their valuable discussions.

#### REFERENCES

- 1 Pohl, H. A. *J. Polym. Sci. (A-2)* 1964, **2**, 2787
- 2 Botto, H. A. and Weiss, D. W. *Aust. J. Chem.* 1963, **16**, 1076
- 3 Hirohashi, R. *Kogyo-Kagaku Zasshi* 1968, **71**, 1744; 1970, **73**, 1450
- 4 Hirohashi, R. *Kogyo-Kagaku Zasshi* 1969, **72**, 1394
- 5 Hirohashi, R. *Polymer* 1970, **11**, 297
- 6 Iwakura, Y., Uno, K. and Hong, S. J. *Polymer J.* 1971, **2**, 36
- 7 Hong, S. J., Iwakura, Y. and Uno, K. *Polymer* 1971, **12**, 526
- 8 Futaki, H. 'Thermistor and its Application', 1969, Nichi-Kan Kogyo Press Co, Tokyo, Ch 1

## Book Reviews

### Polymer science: a materials science handbook

Edited by A. D. Jenkins

North-Holland, Amsterdam/London, 1972, Vols 1 and 2, 1822 pp. £49.00

Those concerned with polymers, no matter whether their interests be related to synthesis, characterization, properties, or even to something more specific, like polyelectrolytes or composites, often have occasion to seek information on wider issues connected with the subject, and are then faced with the problem of a search for the appropriate textbooks, review articles and papers, some of which may not be readily to hand. An encyclopaedia presentation of polymer science and technology is, of course, available but there is usually first the wish to go to a convenient bookshelf rather than to a main library.

Consideration of the contents of these two volumes and a discerning look at the index indicates the breadth of polymer topics dealt with. Excellently printed and bound, they comprise 27 authoritative chapters contributed by specialists from the USA and the UK. One of my colleagues has described the work as a 'mini-encyclopaedia'; perhaps it could be better termed as a series of monographs assembled to provide a 'jumbo-sized' handbook.

Chapters in the first volume (932 pp) deal with chemistry, structure, crystallinity, molecular behaviour, viscoelastic and optical properties, and then cover plasticization, fracture, and the mechanical properties of plastics and fibres (but with less reference to elastomers). In the second volume (888 pp) the subjects are of a wider—and perhaps less integrated—nature, dealing with such aspects as adhesion, friction and wear, solutions, polyelectrolytes, electric and dielectric properties, far infra-red, n.m.r. and neutron spectroscopy, degradation (thermal, photo- and oxidative), radiation effects, identification and analysis, polymers for use at high temperatures, and composites. There is thus cover wide enough to satisfy many readers but it will be found that some items such as vulcanization or even chemical treatments in general, elastomers and fillers, get less attention.

The editor, Professor A. D. Jenkins of the University of Sussex, has done well in bringing the chapters together in a reasonably standard form despite the large number of contributors and inevitable differences in style and treatment. Some chapters are more detailed and comprehensive than others, some are more superficial or general in approach, but taken in all they form a very acceptable up-to-date collection and are made all the more useful by inclusion of the many references at the end of each.

The comprehensive nature and excellent presentation, however, bring in another feature, that of price. At £49, the work represents a costly acquisition, pagewise much more so than a fuller encyclopaedia; however, a good distillate is rarely cheap. There are many who will find these volumes useful and wish to have them available, perhaps not as a personal possession but in a departmental or works library where information is sought on a variety of areas in polymer science and technology.

R. J. W. Reynolds

### The use of the scanning electron microscope

Edited by J. W. S. Hearle, J. T. Sparrow and P. M. Cross

Pergamon Press, Oxford, 1972, £8.80

The number of scanning electron microscopes in general use has grown enormously over the last few years and workers in a variety of fields have gained access to instruments. There is therefore a need for a book which gives a simple and straightforward account of scanning electron microscopy, whilst at the same time covering the types of practical and interpretive problems encountered by the average user. The editors and contributors to this book are to be congratulated on successfully meeting this need.

The book contains thirteen chapters and there are eight contributors. However, the treatment is uniform and the ground is covered in a systematic manner. Basic principles, background knowledge, and instrument design and use are dealt with in Chapters 1 to 4. Specimen preparation and modes of operation are discussed in Chapters 4 and 5. Chapters 6 to 9 are given over to specialist applications in the fields of metals, electronic devices, fibres and polymers, and biological materials respectively. Faults and dimensional measurements are dealt with in Chapters 10 and 11. For those fortunate enough to possess an instrument, some tips on instrument management are given in Chapter 12, while Chapter 13 considers possible future developments in the field. The book contains comprehensive author and subject indexes and there is a useful list of manufacturers and suppliers. The quality of the paper, printing and numerous micrographs is good.

The book can be recommended to workers who wish to make best use of the scanning electron microscope technique. It will also be of value to those who would like to become generally acquainted with the potentialities and limitations of this branch of microscopy. By present day standards the book is reasonably priced.

C. Price



# Study of thermoelastic properties of ethylene–vinyl acetate copolymer

V. Pollák, A. Romanov and K. Marcinčin

*Polymer Institute of Slovak Academy of Sciences, Bratislava, Czechoslovakia  
(Received 15 January 1973)*

The thermoelastic properties of the random ethylene–vinyl acetate copolymer crosslinked with dicumyl peroxide were investigated. It was found that the relationships between equilibrium stress and temperature showed a discontinuity in the temperature range 38–42°C which was due to the crystalline character of the samples. The value of energetic contribution  $f_U$  is negative at elongations ranging from 1.1 to 2.1 while it assumes a relatively high value at greater elongations. The values of relative energetic contribution  $f_U/f$  change with elongation and are in agreement with the values of  $f_U/f$  calculated from shear modulus for the region of medium elongations in the investigated range. The character of the relationship between  $f_U$  or  $f_U/f$  and elongation indicates that a change in the intra- and inter-molecular interaction energies occurs in the case of uniaxial strain of the investigated copolymer.

## INTRODUCTION

The elasticity of real elastomers does not show a pure entropy character since a change in the intrinsic energy of the strained sample also occurs<sup>1,2</sup>. The energetic term of elastic strain calculated from the relationship between equilibrium stress and temperature at low deformations corresponds to the change in the conformational energy of the chains<sup>3</sup> and is related to the thermal coefficient of unperturbed dimensions of these chains<sup>4,5</sup>. Besides the changes in intramolecular interaction energies, the change in the intermolecular interaction energies is not negligible, especially at large elongations<sup>6,7</sup>. The intramolecular interaction energy does not depend on elongation until the contour length of chains is attained while the intermolecular energy changes with strain.

This paper is devoted to the study of the thermoelastic properties of ethylene–vinyl acetate copolymer.

## EXPERIMENTAL

### Materials

A commercial copolymer of ethylene with vinyl acetate (Levapren 450) containing 75 mol% of ethylene and  $M_n = 4.73 \times 10^4$  was used in this study. Dicumyl peroxide (DCP), precipitated three times from ethanol, was used as a crosslinking agent.

### Methods

The vulcanizing mixtures were prepared in a laboratory masticator at 300 rev/min. The mixtures of ethylene–vinyl acetate copolymer (EVA) contained 2.5 parts by weight of DCP to 100 parts by weight of EVA. The samples were crosslinked in the form of sheets (50 × 10 × 1 mm) at 160°C for 45 min.

The values of equilibrium stress at varying temperatures were measured with a Cambridge Textile Extensometer

which was adapted for the thermostating of samples. The temperature was controlled to  $\pm 0.1^\circ\text{C}$ . The constant values of stress were obtained after 4–5 h relaxation at 80°C. The rate of temperature decrease and increase was 1.5°C/min. A period of 20 min was necessary to achieve the equalization of temperatures of sample and its surroundings. A correction with respect to thermal expansion was carried out by using a cathetometer (KM-6). The thermal coefficient of linear expansion was equal to  $2.5 \times 10^{-4} \text{ deg}^{-1}$  in the temperature range from 50 to 80°C.

The values of the thermodynamic quantities were obtained from the relations:

$$f = (\partial U / \partial L)_{T,V} - T(\partial S / \partial L)_{T,V} = f_U + f_S \quad (1)$$

$$-(\partial S / \partial L)_{T,V} = (\partial f / \partial T)_{V,L} \quad (2)$$

where  $f$ ,  $U$ ,  $S$ ,  $L$ ,  $V$  and  $T$  denote equilibrium stress, intrinsic energy, entropy, length of sample, volume of sample, and absolute temperature. The coefficient  $(\partial f / \partial T)_{p,\alpha}$  found experimentally was corrected for thermal linear expansion of the sample as recommended by Flory *et al.*<sup>8</sup>:

$$(\partial f / \partial T)_{p,\alpha} = (\partial f / \partial T)_{V,L} + f\lambda \quad (3)$$

where  $\lambda = L^{-1}(\partial L / \partial T)_p$  and  $\alpha = L/L_0$ , i.e. relative elongation. The term  $f_U/f$  was calculated from the following relation<sup>8</sup>:

$$f_U/f = 1 - \left( \frac{\partial \ln f}{\partial \ln T} \right)_{p,\alpha} + T\lambda = T \frac{d \ln \bar{r}_0^2}{dT} \quad (4)$$

Differential thermal analysis was carried out by use of a Perkin-Elmer differential scanning calorimeter (d.s.c.).

## RESULTS AND DISCUSSION

Figure 1 shows the dependence of equilibrium stress on temperature for ethylene–vinyl acetate copolymer. In the temperature range 38° to 42°C a discontinuity appears

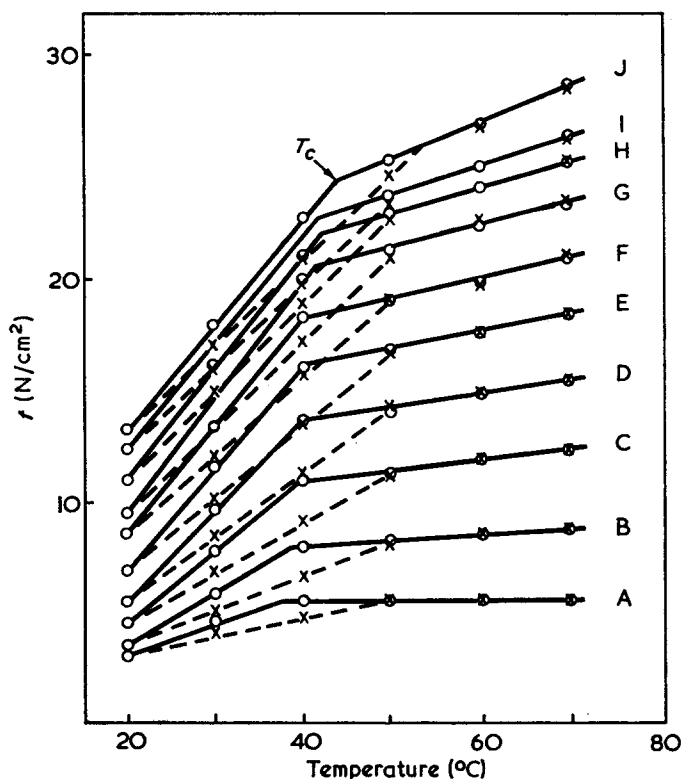


Figure 1 Variation of equilibrium stress with temperature for crosslinked ethylene-vinyl acetate copolymer.  $T_c$  = crystallization temperature of sample. Elongations: A = 1.106; B = 1.112; C = 1.324; D = 1.432; E = 1.540; F = 1.646; G = 1.751; H = 1.858; I = 1.964; J = 2.072.  $\circ$ , Decreasing temperature;  $\times$ , increasing temperature

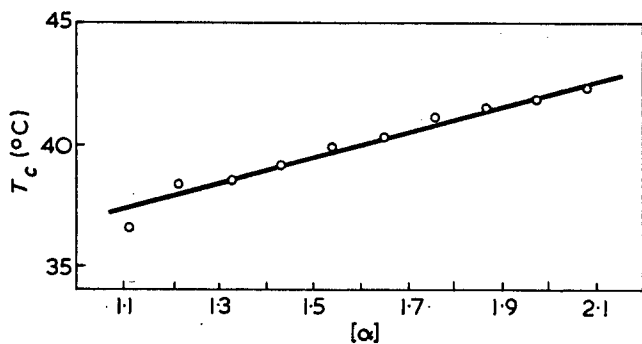


Figure 2 Crystallization temperature of ethylene-vinyl acetate copolymer ( $T_c$ ) as a function of elongation

on the plots which is due to the crystallization of the sample<sup>9,10</sup>. A similar phenomenon was observed with an ethylene-propylene copolymer containing a higher percentage of ethylene<sup>10,11</sup>. If the temperature rises, the discontinuity appears at about 50°C. The shift of the discontinuity with temperature is due to the hysteresis of the crystallization process.

It is clear from Figure 2 which shows the dependence of  $T_c$  on elongation, that  $T_c$  rises with increasing elongation (effect of strain on the formation of crystallites). At the given content of ethylene in copolymer (75 mol%), it is also possible that some nuclei of crystallites of polyethylene segments are present which may enhance the formation of crystallites.

The d.s.c. curve (Figure 3) shows that the melting of crystallites in unstrained sample sets in at 46°C. The positions of  $T_c$  (Figure 1) and  $T_m$  (Figure 3) may be affected by the different methods of determination as well as the different history of the thermal treatment of sample during measurement.

The equilibrium stress at temperatures above 50°C has the same value independent of whether equilibrium is approached by increase or decrease in temperature and this demonstrates the reversibility of the process. The values of  $f_U$  and  $f_S$  were calculated for the temperature of 60°C at which the sample is amorphous. Figure 4 presents the variation of  $f_U$ ,  $f_S$ , and  $f$  with  $\alpha$ . The term  $f_U$  is the most important for the study of the properties of polymer network and it is evident from Figure 4 that the value of  $f_U$  is negative over the total range of elongations. It assumes relatively high values at greater elongations and this may be caused by the interactions between the chains which align as the result of uniaxial strain<sup>7</sup>. It is also possible that some contribution arises from intra- and inter-molecular interactions of the polar group of vinyl acetate.

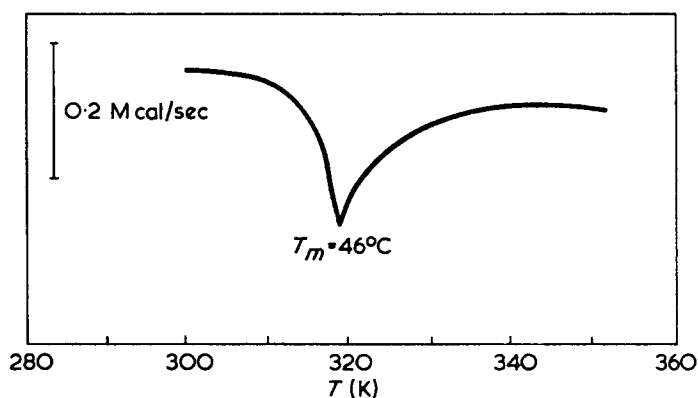


Figure 3 D.s.c. curve for ethylene-vinyl acetate copolymer.  $T_m$  = melting point of crystallites

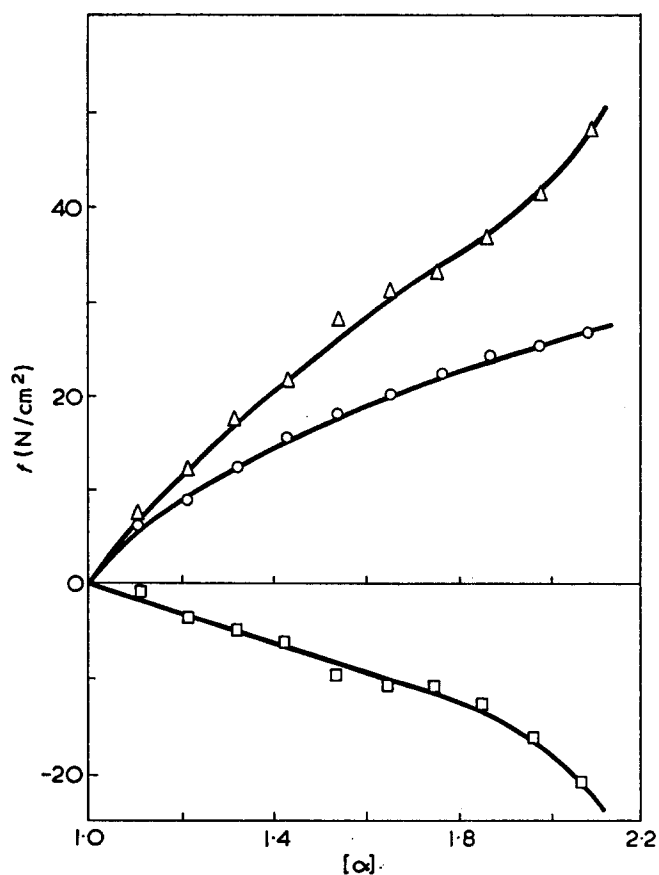


Figure 4 Variation of equilibrium stress ( $f$ ) and entropy ( $f_S$ ) and intrinsic energy ( $f_U$ ) contribution to equilibrium stress with elongation for crosslinked ethylene-vinyl acetate copolymer at 60°C.  $\circ$ ,  $f$ ;  $\Delta$ ,  $f_S$ ;  $\square$ ,  $f_U$



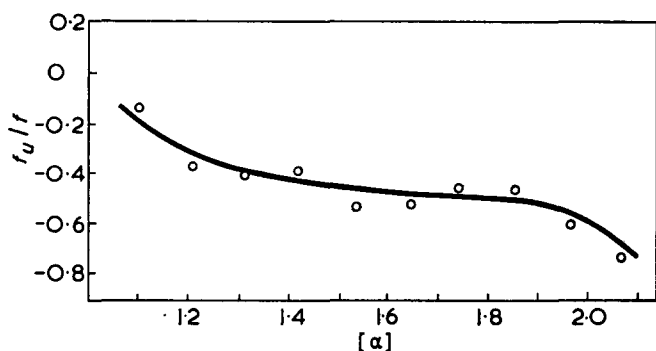


Figure 5 Variation of relative energetic contribution  $f_U/f$  with elongation for crosslinked ethylene-vinyl acetate copolymer at 60°C

The value of  $f_U/f$  calculated from equation (4) (Figure 5) varies with  $\alpha$  which is not in agreement with the random theory of rubber elasticity and does not assume any interaction between the chains of polymer network. The character of the plots of  $f_U/f$  versus  $\alpha$  (Figure 5) indicates a change in the interactions between the chains of ethylene-vinyl acetate copolymer during strain. At small elongations, the accuracy in the determination of  $\alpha^{12}$  may also account for the curvature of the plot of  $f_U/f$  versus  $\alpha$ . The value of  $f_U/f$  calculated from shear modulus according to Shen and Blatz<sup>13</sup> equals  $-0.428$ . This agrees approximately with the values of  $f_U/f$  determined from thermoelastic curves in the region of elongation  $\alpha = 1.3-1.6$  (Figure 5). The value of the thermal coefficient of the unperturbed dimensions of chains calculated according to Shen and Blatz<sup>13</sup> is equal

to  $-1.29 \times 10^{-3} \text{ deg}^{-1}$ . A comparison with the values determined for homopolymers (polyethylene:  $-1.1 \times 10^{-3} \text{ deg}^{-1}$ <sup>14</sup>; poly(vinyl acetate):  $-2.1 \times 10^{-3} \text{ deg}^{-1}$ <sup>15</sup>) shows that the value found for ethylene-vinyl acetate copolymer has the same sign and is close to the value of the ethylene component.

#### REFERENCES

- 1 Flory, P. J. 'Principles of Polymer Chemistry', Cornell University Press, Ithaca, 1953
- 2 Treloar, L. R. G., 'The Physics of Rubber Elasticity', Oxford University Press, London, 1958
- 3 Volkenstein, M. V. 'Configurational Statistics of Polymeric Chains', Interscience, New York, 1963
- 4 Flory, P. J., Hovee, C. A. J. and Ciferri, A. *J. Polym. Sci.* 1959, **34**, 337
- 5 Tobolsky, A. V., Carlson, D. W. and Indictor, N. *J. Polym. Sci.* 1961, **54**, 175
- 6 Natta, G., Crespi, G. and Flisi, U. *J. Polym. Sci. (A)* 1963, **1**, 3569
- 7 Van der Hoff B.M.E., *J. Macromol. Sci. (A)* 1971, **5**, 661
- 8 Flory, P. J., Ciferri, A. and Hovee, C. A. J. *J. Polym. Sci.* 1960, **45**, 235
- 9 Flisi U., Crespi, G. and Valvassori, A. *Rubber Chem. Technol.* 1970, **43**, 778
- 10 Flisi, U., Valvassori, A. and Novaira, G. *Rubber Chem. Technol.* 1971, **44**, 1093
- 11 Flisi, U., Crespi, G. and Valvassori, A. *Kautsch. Gummi Kunstst.* 1969, **22**, 154
- 12 Shen, M. *Macromolecules* 1969, **2**, 358
- 13 Shen, M. and Blatz, P. J. *J. Appl. Phys.* 1968, **39**, 4937
- 14 Abe, A., Jernigan, R. L. and Flory, P. J. *J. Am. Chem. Soc.* 1966, **88**, 631
- 15 Patrone, E. and Bianchi, U. *Ric. Sci.* 1966, **36**, 17

# Polymer translational diffusion: 2. Non-theta solutions, polystyrene in butan-2-one

T. A. King, A. Knox and J. D. G. McAdam

Physics Department, Schuster Laboratory, University of Manchester, Manchester M13 9PL, UK

(Received 14 February 1973)

The diffusion of linear polystyrene under non-theta conditions in butan-2-one has been studied by Rayleigh light scattered linewidth measurements for the molecular weight range of  $2.08 \times 10^4$  to  $8.7 \times 10^6$  and as a function of concentration. By extrapolation of diffusion coefficient values to zero concentration we find that  $D_0 = 5.5 \times 10^{-4} \bar{M}_w^{-0.561} \text{cm}^2 \text{s}^{-1}$ . The first order concentration dependence  $k_{DC}$  changes sign as the molecular weight increases,  $k_D$  being fairly small and negative at low molecular weights and increasingly positive above  $\bar{M}_w \approx 230\,000$ .

## INTRODUCTION

In this paper we describe how intensity fluctuation spectroscopy has been applied to the study of translational diffusion in dilute polymer solutions under non-theta conditions, as exemplified by the polystyrene/butan-2-one system. A similar study has recently been carried out on the polystyrene/cyclohexane theta-point system<sup>1</sup> (I). The homodyne light-beating technique employed here for observing concentration fluctuations has been used since 1965 and is amply reviewed elsewhere<sup>2</sup>. Interpretation of data is based on Pecora's theory<sup>3</sup> which predicts for the usual case of dominant centre-of-mass motion a Lorentzian lineshape with half-width at half-height:

$$\Delta w_{1/2} = 2K^2 D \quad (1)$$

where  $D$  is the translational diffusion coefficient and  $K = (4\pi/\lambda) n \sin(\theta/2)$  is the wave-vector change in the quasi-elastic scattering,  $\lambda$  being the wavelength of the incident laser light,  $n$  the solution refractive index and  $\theta$  the scattering angle. Measurements of  $D$  by this method can be rapid, accurate, and are performed on a solution at equilibrium thus giving valuable information on polymer conformations and solution hydrodynamics.

## EXPERIMENTAL

A 60 mW helium-neon laser (Spectra-Physics model 125) was used as the monochromatic light source and scattered radiation was detected with a red-sensitive photomultiplier tube (Amperex 56 TVP) with some electronic focusing to reduce noise. The photocurrent signal was analysed by a hybrid correlator (Hewlett-Packard 3721 A), the computed autocorrelation function being in effect the Fourier transform of the power spectrum. Least-squares computer fitting of the resulting exponential function yields the translational diffusion coefficient with a typical accuracy of a few percentage units from a single run. Other details of the apparatus and spectrometer design are described more fully elsewhere<sup>4</sup>.

A range of narrow molecular weight distribution polystyrene samples were supplied by the Pressure Chemical Company and solutions were made up with spectroscopic grade butan-2-one solvent. The removal of particulate matter from the solutions is essential to avoid distortion of the autocorrelation function and the most effective cleaning procedure was found to be centrifugation of samples for 2 h at over  $30\,000 \times g$ . Measurements of the autocorrelation function were made at room temperature and results corrected by at most 4% to 25°C for variations in temperature and viscosity.

Deviations from a single exponential due to internal motions in the polymer coils were observed at large scattering angles for the very high molecular weight samples and are discussed elsewhere<sup>5</sup>.

## RESULTS

The data for solution concentrations below  $0.02 \text{ gml}^{-1}$  are shown in Figures 1 and 2, each point being the average value of  $D(c)$  calculated from many runs at several different angles. The curves drawn through these points for the various molecular weights are summarized in Table 1 where  $k_D$ , as defined by equation (3) below, is the value of the initial slope of the concentration dependence in the dilute solution range. The extent of this range is estimated via the procedure outlined in I. The  $D_0$  values quoted are the results of smooth extrapolations to zero concentration. Preliminary studies, using samples cleaned by filtering, showed a pronounced decrease in  $D$  with decrease in concentration at low concentration. This effect disappeared with more careful cleaning using ultra-centrifugation; the effect is attributed to dirt contamination which is likely to be more troublesome in this region. Tsvetkov and Klenin<sup>6</sup> have derived a concentration dependence for polystyrene having  $M = 3.5 \times 10^6$  in butan-2-one which is in good agreement with that predicted from the form of sample PC-14b of this work. Calculations indicate that the appropriate molecular weight average to use in this type of experiment lies

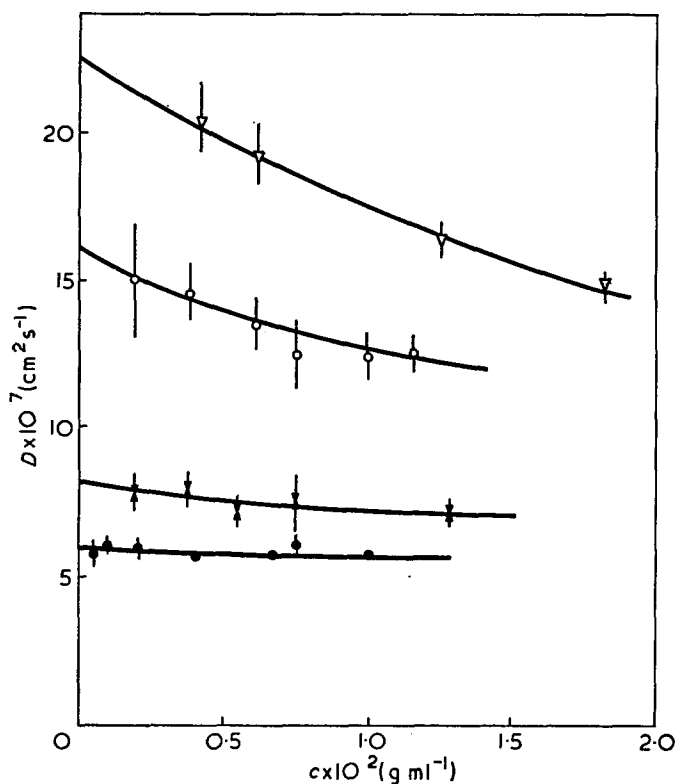


Figure 1 Diffusion coefficient concentration dependence,  $\bar{M}_w=2.08 \times 10^3$  to  $\bar{M}_w=2 \times 10^5$  polystyrene in butan-2-one. ●, PC-1c; ×, PC-4b; ○, PC-7b; ▽, PC-2b

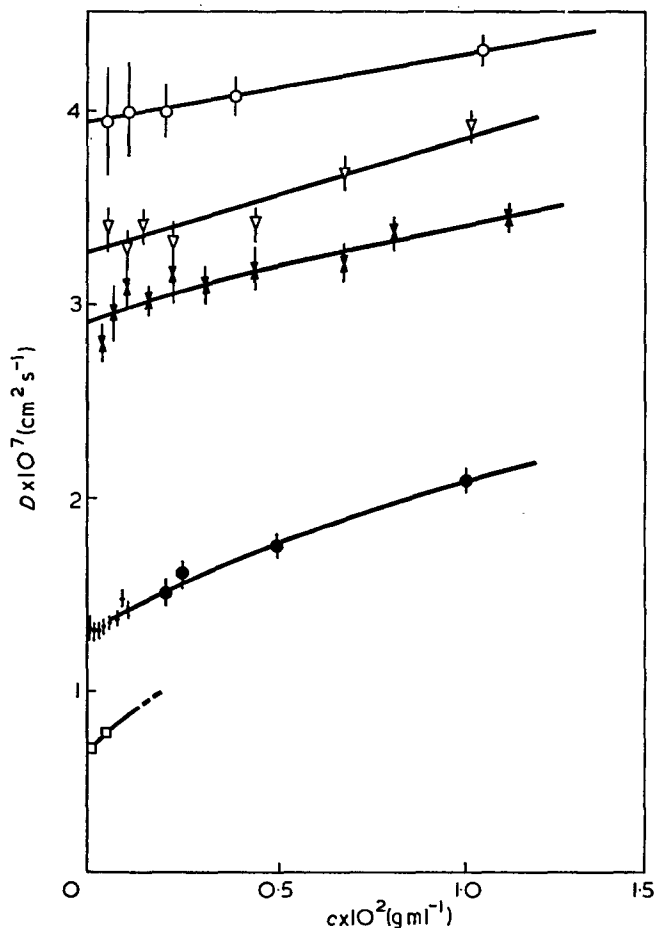


Figure 2 Diffusion coefficient concentration dependence,  $\bar{M}_w=3.92 \times 10^5$  to  $\bar{M}_w=8.7 \times 10^6$  polystyrene in butan-2-one. □, JCH-7M; ●, PC-14c; ×, PC-13a; ▽, PC-5a; ○, PC-3b

Table 1 A summary of the molecular weight and polydispersity of polystyrene samples with experimentally determined values of the diffusion coefficient concentration dependence parameter  $k_D$  and values of  $D_0$ , the diffusion coefficient from extrapolation to  $c=0$ .

Sample	$\bar{M}_w$	$\bar{M}_w/\bar{M}_n$	$D_0 \times 10^7$ (cm <sup>2</sup> s <sup>-1</sup> )	$k_D$ (ml g <sup>-1</sup> )
PC-2b	20 800	1.06	22.5 ± 1.0	-25 ± 5
PC-7b	33 000	1.06	16.0 ± 0.6	-26 ± 5
PC-4b	111 000	1.06	8.1 ± 0.3	-11 ± 4
PC-1c	200 000	1.06	5.95 ± 0.1	-2 ± 3
PC-3b	392 000	1.1	3.95 ± 0.15	9 ± 4
PC-5a	507 000	1.2	3.30 ± 0.10	19 ± 4
PC-13a	670 000	1.1	2.9 ± 0.1	27 ± 4
PC-14b	2.7 × 10 <sup>6</sup> a	1.3	1.30 ± 0.03	72 ± 5
JVC-7M	8.7 × 10 <sup>6</sup> b	1.3	0.70 ± 0.03	—

a  $\bar{M}$  from viscosity measurements

b Sample generously supplied by Dr J. V. Champion, City of London Polytechnic

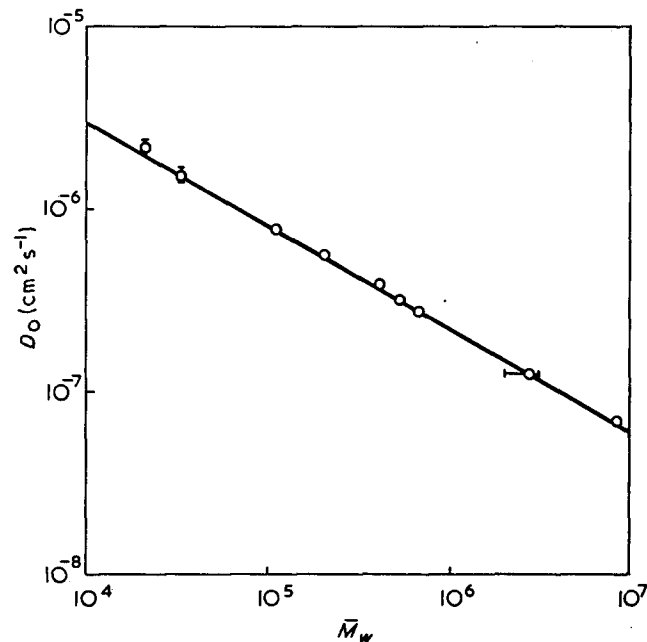


Figure 3 Molecular weight dependence of  $D_0$ , the diffusion coefficient by extrapolation to  $c=0$

between the weight and  $z$ -averages<sup>4</sup>, consequently  $\bar{M}_w$  has been used in some subsequent analysis. For sample PC-14b the molecular weight distribution was checked by viscometry and by gel permeation chromatography (g.p.c.) because of anomalies in the manufacturer's data supplied with the sample. In this case the viscosity-average molecular weight is preferred as this was found to lie between  $\bar{M}_w$  and  $\bar{M}_z$  from g.p.c. analysis and is in agreement with  $\bar{M}_w$  from fractionation data.

A plot of  $\log D_0$  vs.  $\log \bar{M}_w$  (in Figure 3) in analogy to the Mark-Houwink relationship for intrinsic viscosities shows that the results closely obey the expression:

$$D_0 = k \bar{M}_w^{-b} = (5.5 \pm 0.2) \times 10^{-4} \bar{M}_w^{-(0.561 \pm 0.005)} \text{ cm}^2 \text{ s}^{-1} \quad (2)$$

The values of  $k$  and  $b$  differ from the values of Ford *et al.*<sup>7</sup> for an investigation covering a similar molecular weight range.

### DISCUSSION

If the relation between the exponent  $b$  in equation (2) and the exponent  $a$  in the viscosity Mark-Houwink equation,

$[\eta] = k'M^a$ , is taken as<sup>8</sup>:  $b = (a+1)/3$ , values of  $b$  calculated from literature viscosity data, for which  $a$  ranges from 0.58 to 0.635 for polystyrene in butan-2-one, cover the range  $b = 0.527$  to  $b = 0.545$ . This range is lower than the value measured in this work and the diffusion-viscosity exponent relationship may be worthy of further investigation.

From equation (4) of I we see that the diffusion coefficient can be expanded to first order in concentration as

$$D = D_0(1 + k_D c + \dots) \quad (3)$$

in which thermodynamic and hydrodynamic factors can be combined in  $k_D$  as

$$k_D = 2A_2M - k_f - \bar{v} \quad (4)$$

where  $A_2$  is the second virial coefficient,  $k_f$  (or equivalently  $k_s$  in sedimentation coefficient terminology) is the first order friction coefficient concentration dependence and  $\bar{v}$  is the specific volume of the polymer.

Although second virial coefficients for polystyrene/butan-2-one solutions are relatively small at around  $10^{-4} \text{ ml g}^{-2}$ , significant differences from the theta-solvent behaviour reported in I are observed. The most noticeable feature of the variation of  $k_D$  with molecular weight in Figure 4 is the change from negative values at low  $\bar{M}_w$  to positive and increasing values above the cross-over point at  $\bar{M}_w \approx 230\,000$ . As  $\bar{v}$  remains essentially constant at about  $0.9 \text{ ml g}^{-1}$  this must be due to the increasing importance of the first thermodynamic term in equation (4) relative to  $k_f$ .

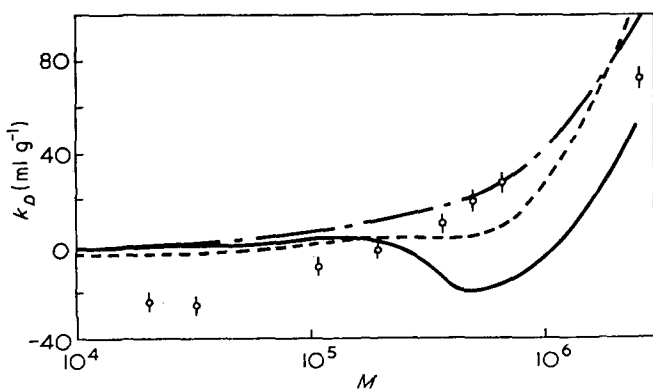


Figure 4 Molecular weight dependence of the first order concentration dependence coefficient  $k_D$ .  $\odot$ , experimental points; theoretical curves: - - - -, Yamakawa<sup>11</sup>; - · - ·, Pyun and Fixman<sup>13</sup>; —, Imai<sup>12</sup>

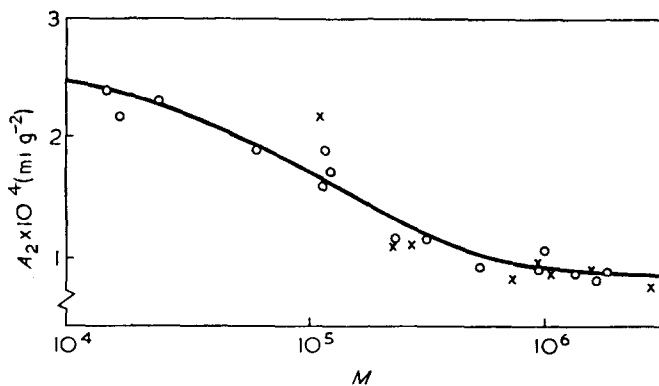


Figure 5 Values of the second virial coefficient  $A_2$  from Outer et al.<sup>9</sup> ( $\circ$ ) and from Oth and Desreux<sup>10</sup> ( $\times$ )

The second virial coefficient has been the subject of several determinations and from two of the most extensive studies on this system<sup>9,10</sup> it can be seen from Figure 5 that  $A_2$  has only a small dependence on molecular weight, going roughly as  $M^{-0.2}$ . It is noticeable that the values show considerable variations, however, and equation (4) could provide the basis for more accurate measurements of this parameter. The molecular weight dependence of  $k_f$  has been briefly discussed in I in conjunction with the theoretical expressions derived by Yamakawa<sup>11</sup>, Imai<sup>12</sup> and by Pyun and Fixman<sup>13</sup>. These can be summarized as:

$$k_f = \lambda(x) A_2 M + \frac{NV_h}{M} \quad (Y) \quad (5a)$$

$$k_f = C_0 M^{1/2} \left( \alpha_\eta - \frac{1}{\alpha_\eta} \right) + \frac{NV_h}{M} \quad (I) \quad (5b)$$

$$k_f = k_f^\phi \frac{NV_h}{M} \quad (PF) \quad (5c)$$

where  $N$  is Avogadro's number,  $\alpha_\eta$  is the viscosity expansion factor, and  $V_h$  is the hydrodynamic volume of the polymer molecule. This can be deduced from equation (2) by means of the Stokes-Einstein relationship as:

$$V_h = \frac{4\pi}{3} \left( \frac{kT}{6\pi\eta D_0} \right)^3 \quad (6)$$

and hence taking the viscosity to be 0.40 cP:

$$\frac{NV_h}{M} \approx 2.47 \times 10^{-3} \bar{M}_w^{0.683} \text{ ml g}^{-1} \quad (7)$$

In Yamakawa's extension of the Kirkwood-Riseman formalism for the friction coefficient, the function  $\lambda(x)$  can be taken as 1.2 in the non-draining limit. Imai's constant  $C_0$  which depends upon the parameters of the unperturbed polymer chain is best found by fitting his expression to the available data for  $k_s$ <sup>6,14,15</sup>, though this virtually means that  $k_s$  values are interpolated from those already measured. Pyun and Fixman's model of an equivalent soft sphere for a macromolecule leads to a value of  $k_f^\phi = 2.23$  for theta conditions increasing monotonically to the hard sphere limit of 7.16. We have therefore chosen the intermediate value of  $k_f^\phi = 5$  which is unlikely to be in error by more than 50% for this parameter. Thus by combining equations (4), (5) and (7) these theoretical models can be compared with the data for  $k_D$ , and are plotted in Figure 4.

It is clear that agreement between theory and experiment is poor, though in all cases this can be improved at the higher molecular weights because of the flexibility of the parameters involved. Also, calculated  $k_D$  values are strongly dependent on  $A_2$  and values taken from the continuous curve in Figure 5 could well be in error by at least 10%.

We are able to conclude, however, that none of the theories in their present form predict the relatively large negative  $k_D$  values at low molecular weight. This is equivalent to saying that  $k_f$  (or  $k_s$ ) remains finite and positive as  $M$  becomes small. Further work is therefore necessary, perhaps involving higher order terms and draining effects, before these theories describe experimental behaviour over a wide molecular weight range.

ACKNOWLEDGEMENTS

We should like to thank Professor G. Allen of the Chemistry Department for interest, encouragement and discussions through the course of this work. The participation of Dr W. I. Lee during his stay in Manchester and the polymer characterization provided by Dr C. Booth are gratefully acknowledged. Funding for this project has been given by the Science Research Council.

REFERENCES

- 1 King, T. A., Knox, A., Lee, W. I. and McAdam, J. D. G. *Polymer* 1973, **14**, 151
- 2 Cummins, H. Z. and Swinney, H. L. *Prog. Optics* 1970, **8**, 134
- 3 Pecora, R. J. *Chem. Phys.* 1964, **40**, 1604
- 4 Knox, A. *PhD Thesis* University of Manchester, 1972
- 5 King, T. A., Knox, A. and McAdam, J. D. G. *Chem. Phys. Lett.* 1973, **19**, 351
- 6 Tsvetkov, V. N. and Klenin, S. I. *J. Polym. Sci.* 1958, **30**, 187
- 7 Ford, N. C., Karasz, F. E. and Owen, J. E. M. *Discuss. Faraday Soc.* 1970, **49**, 228
- 8 Flory, P. J. 'Principles of Polymer Chemistry', Cornell Univ. Press, Ithaca, 1953, Ch 14
- 9 Outer, P., Carr, C. I. and Zimm, B. H. *J. Chem. Phys.* 1950, **18**, 830
- 10 Oth, J. and Desreux, V. *Bull. Soc. Chim. Belg.* 1954, **63**, 285
- 11 Yamakawa, Y. *J. Chem. Phys.* 1962, **36**, 2995
- 12 Imai, S. *J. Chem. Phys.* 1969, **50**, 2116
- 13 Pyun, C. W. and Fixman, M. *J. Chem. Phys.* 1964, **41**, 937
- 14 Newman, S. and Eirich, F. J. *Colloid Sci.* 1950, **5**, 541
- 15 Schick, A. F. and Singer, S. J. *J. Phys. Chem.* 1950, **54**, 1028

# Die swell in elastic and viscous fluids

J. Batchelor\*, J. P. Berry and F. Horsfall

Rubber and Plastics Research Association of Great Britain,  
Shawbury, Shrewsbury SY4 4NR, UK

(Received 22 December 1972; revised 5 March 1973)

Measurements of die swell have been made on an elastic liquid and a Newtonian liquid of similar viscosity ( $\sim 10^4 \text{ N s m}^{-2}$ ). The Reynolds number was about  $10^{-8}$ . The Newtonian liquid has a die swell of 13.5% which was independent of shear rate. The die swell of the elastic liquid increased with shear rate and seemed to be asymptotic to the Newtonian die swell at low shear rates.

## INTRODUCTION

The phenomenon of die swell is well known in polymer melt extrusion and it must be taken into account when dies are designed. In practice this is achieved by 'rule of thumb' methods even for dies of simple shape because there are no means of predicting die swell from the fundamental flow properties of the melt<sup>1</sup>. Die swell is known to be associated with elasticity and normal stresses<sup>2</sup>, and Newtonian liquids also exhibit die swell<sup>3</sup>. However, very few measurements have been made at the low Reynolds numbers relevant to polymer processing, i.e.  $\ll 1$ .

In this paper we describe the results of die swell measurements on the capillary flow of an elastic liquid and a Newtonian liquid with viscosities similar to polymer melts. The measurements were made at shear rates below  $1 \text{ sec}^{-1}$  so that they could be compared with shear flow measurements made on a Weissenberg rheogoniometer. The Reynolds number in the die swell measurements was about  $10^{-8}$ .

## EXPERIMENTAL

### Apparatus

The measurements were carried out on a capillary viscometer similar to the one described by Atkinson and Nancarrow<sup>4</sup>. The apparatus was designed for use with a Hounsfield tensometer which was mounted vertically to facilitate the measurements of die swell. The barrel wall was hollow so the sample temperature could be controlled by circulating a thermostatically controlled liquid.

The capillaries were made of stainless-steel tubing embedded in a brass sleeve to give rigidity; this was jacketed so that the temperature controlled liquid could be circulated. A constant speed motor drove the piston at speeds from about  $4.2 \times 10^{-4}$  to  $1.3 \times 10^{-2} \text{ mm/s}$  via a system of pulleys.

The piston movement was measured by a displacement transducer. A proof ring transducer measured the load on the piston. The outputs from the two transducers were displayed on an ultra-violet recorder and the piston speed was calculated from the displacement time trace.

\* Present address: British Rail Research Department, Railway Technical Centre, Derby, UK.

### Procedure

The two materials studied were a depolymerized natural rubber (Lorival R25) and a modified alkyd resin (Paralac 385). Lorival displays large normal stresses whereas Paralac does not; it is a Newtonian fluid. The experimental conditions were chosen so that the materials had similar viscosities ( $\sim 10^4 \text{ N s m}^{-2}$ ). The steady shear flow characteristics obtained on the rheogoniometer are shown in Figure 1.

A small quantity of pigment ( $\sim \frac{1}{4}\%$ ) was incorporated into the Paralac to make the extrudate visible. This had no measurable effect on the flow properties. To eliminate the effect of gravity the materials were extruded into an optical cell containing an inert liquid of the same density.

Capillaries 1, 3 and 4 (Table I) were used for the Lorival and 2, 3 and 4 for the Paralac experiments. Data on Paralac using capillary 1 could not be obtained because

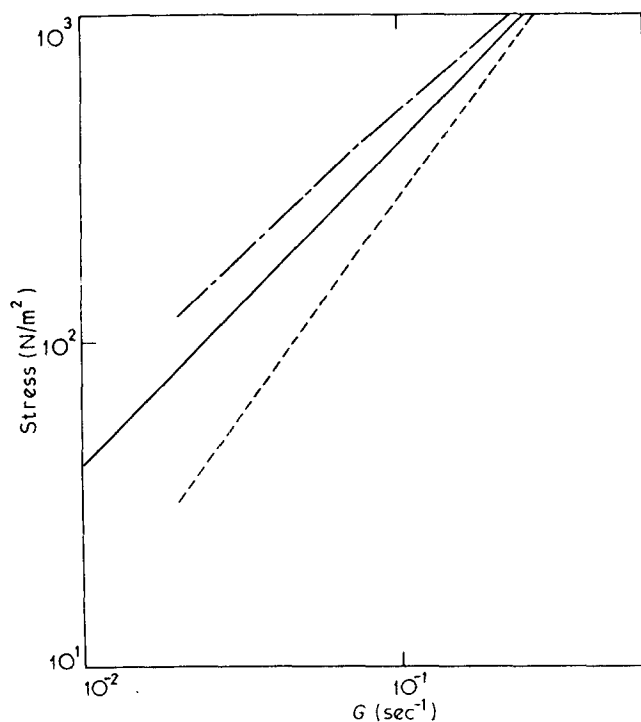


Figure 1 Steady shear flow data obtained on rheogoniometer. —,  $p_{21}$ , Paralac, 65°C; - - -,  $p_{21}$ , Lorival, 23.5°C; - · - ·, ( $p_{11} - p_{22}$ ), Lorival, 23.5°C

Table 1 Capillary dimensions

Capillary	D (mm)	L/D
1	2.51 ± 0.02	77.4
2	2.51 ± 0.02	58.1
3	1.95 ± 0.02	76.1
4	1.33 ± 0.04	75.8

of the poor temperature control with a long die at elevated temperatures.

When the load and piston speed reached steady values the diameter of the extrudate was measured with a travelling microscope. For Lorival we measured the diameter at 2 mm intervals from the capillary exit up to a distance of 16 mm. The extrudate diameter was constant over this range and the final die swell was therefore calculated from the average value. Measurements were carried out much closer to the capillary exit with Paralac so that we could obtain the complete shape of the extrudate.

The effect of viscosity was studied with Paralac by carrying out experiments at 60°C and 65°C, which altered the viscosity by a factor of three. The temperature control in the Paralac experiments was ± 1.5°C; for Lorival the temperature was 23.5 ± 0.25°C.

## RESULTS AND DISCUSSION

The load and piston speed were recorded in a series of experiments with Lorival so that the viscosity could be calculated and compared with measurements made on the rheogoniometer. Some of the pressure drop along the capillary occurs in the regions at the ends where convergent and divergent flow occurs. However, these effects will be negligible with the long capillaries used<sup>5</sup>. Hence we calculated the shear stress at the wall of the capillary  $p_{21}(R)$  using the formula<sup>2</sup>:

$$p_{21}(R) = \Delta p D / 4L \quad (1)$$

where  $\Delta p$  is the pressure drop along the capillary of length  $L$  and diameter  $D$ . The shear rate at the wall  $G(R)$  was evaluated using the formula due to Rabinowitsch:

$$G(R) = \left( \frac{3}{4} + \frac{n}{4} \right) \left( \frac{32Q}{\pi D^3} \right)$$

where

$$n = \frac{d \ln(32Q/\pi D^3)}{d \ln[p_{21}(R)]} \quad (2)$$

and  $Q$  is the volume rate of flow. The results are shown in Figure 2 compared with data obtained on the rheogoniometer using a cone and plate system. The agreement between the two instruments is good.

Die swell depends on the  $L/D$  ratio and on the geometry of the die entry<sup>6</sup>. But with the large  $L/D$  ratio ( $\geq 58$ ) in the present experiments the die swell becomes independent of  $L/D$ . This was checked using Lorival with capillaries 1 and 2.

Some typical Paralac die swell results are shown in Figure 3 and we see that a Newtonian liquid exhibits a significant amount of die swell. The points are a random selection of results obtained at various piston speeds, die diameters and viscosities. The curve in Figure 3 is an exponential of the form

$$y = A [1 - \exp(-Bx/D)] \quad (3)$$

where  $y$  is the percentage increase in diameter at a distance  $x$  from the capillary exit.  $A$  and  $B$  are constants which were obtained by least squares.  $A$  is the final die swell and  $B$  is a shape factor. Using the results of all 16 runs we found that  $A = 13.5$  and  $B = 4.12$ . We see from Figure 3 that equation (3) is an adequate fit to the experimental data. The die swell for each run was calculated by the least squares technique and the results are shown in Figure 4 with the Lorival data. The die swell for the Newtonian liquid was independent of capillary diameter, viscosity and volume rate of flow. For the elastic fluid die swell increased with shear rate but did not depend on capillary diameter. At low shear rates the die swell for the elastic fluid appears to be asymptotic to the Newtonian value.

Graessley *et al.*<sup>7</sup> have measured the die swell of molten polystyrene at low Reynolds numbers ( $10^{-5}$ – $10^{-9}$ ). At low shear rates the viscosity of the materials with narrow molecular weight distributions became independent of

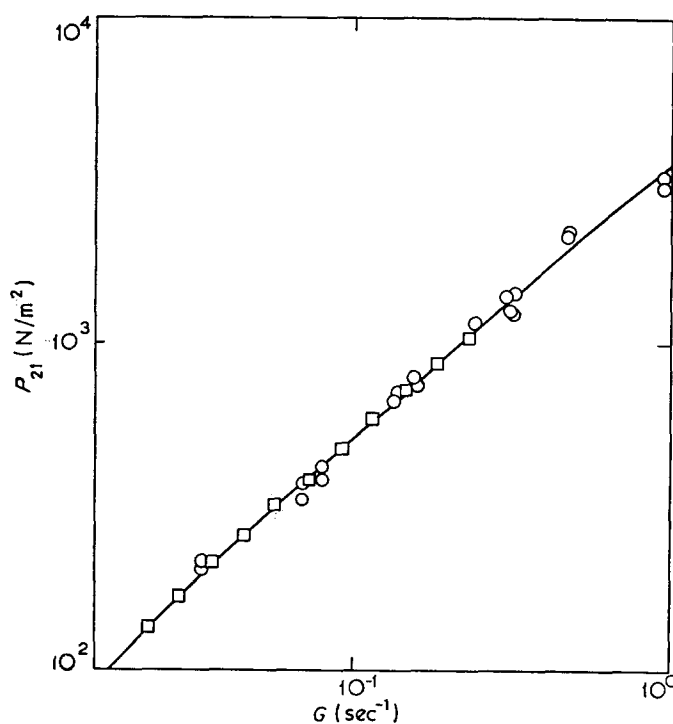


Figure 2 Comparison of cone-plate and capillary rheometers for Lorival at 23.5°C. □, Cone-plate (rheogoniometer); ○, capillary

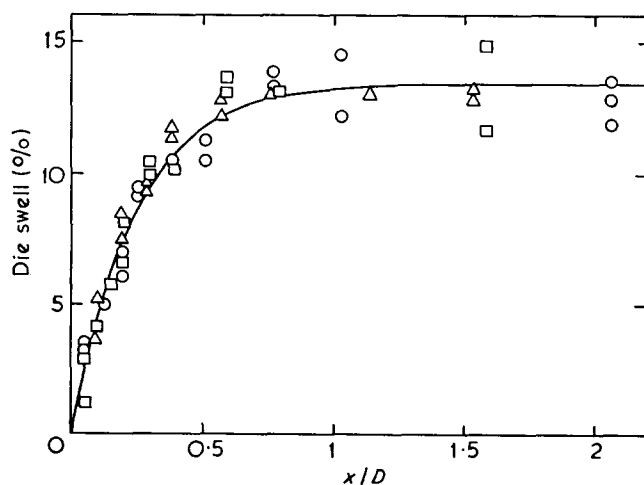


Figure 3 Shape of extrudate of Paralac

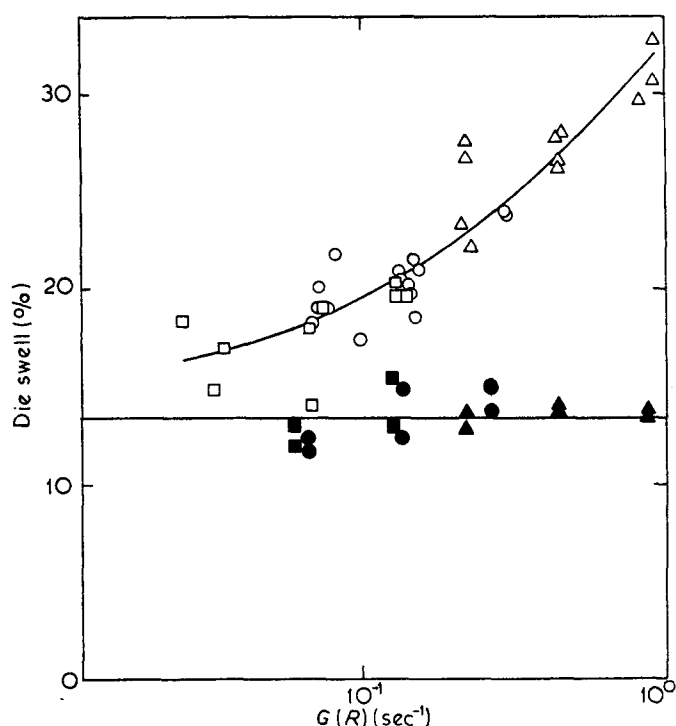


Figure 4 Die swell as a function of shear rate

$D$ (mm)	Lorival	Paralac
2.51	□	■
1.95	○	●
1.33	△	▲

shear rate and the die swell reached a constant value of 10%. Measurements were, however, made on the hardened extrudate. The die swell of Newtonian liquids

over a wide range of Reynolds number down to a Reynolds number of about 4 is given by Goren and Wronski<sup>8</sup>. A figure of 13.5 at very low Reynolds numbers appears to be a better extrapolation of their curve than 10%.

The normal stress difference ( $p_{11} - p_{22}$ ) was calculated from the die swell data of Lorival by the momentum balance approach<sup>9</sup>. The calculated values were 7 orders of magnitude lower than the values shown in Figure 1. Clearly, the momentum balance theory of die swell is not appropriate to polymer melts.

#### CONCLUSIONS

We have confirmed that Newtonian fluids exhibit a significant amount of die swell at low Reynolds numbers. Thus there are two contributions to the die swell of polymer melts. The first is associated with a viscous effect and superimposed on this is an effect due to the elastic nature of polymer melts. Initially it will be necessary to study theoretically the flow of a Newtonian fluid out of a capillary before we can hope to understand the phenomenon of die swell in polymer melts.

#### REFERENCES

- 1 Batchelor, J. *PhD Thesis*, CNA A, 1970
- 2 Lodge, A. S. 'Elastic Liquids', Academic Press, London, 1964
- 3 Middleman, S. and Gavis, J. *Phys. Fluids* 1961, **4**, 355
- 4 Atkinson, E. B. and Nancarrow, H. A. 'Proc. Int. Congr. on Rheology', North-Holland, Amsterdam, 1949, Part 2, p 103
- 5 Metzner, A. B., Carley, E. L. and Park, I. K. *Mod. Plast.* 1960, **37**, (11), 133
- 6 Bagley, E. B., Storey, S. H. and West, D. C. *J. Appl. Polym. Sci.* 1963, **1**, 1661
- 7 Graessley, W. W., Glasscock, S. D. and Crawley, R. L. *Trans. Soc. Rheol.* 1970, **14**, 519
- 8 Goren, S. L. and Wronski, S. *J. Fluid Mech.* 1966, **25**, 185
- 9 Metzner, A. B., Houghton, W. T., Sailor, R. A. and White, J. L. *Trans. Soc. Rheol.* 1961, **5**, 133



# Melting of low molecular weight poly(ethylene oxide) with acetoxy- and trimethylsiloxy-end-groups

P. C. Ashman and C. Booth

*Department of Chemistry, University of Manchester, Manchester M13 9PL, UK  
(Received 9 February 1973)*

Melting points and lamellar spacings are reported for samples of low molecular weight poly(ethylene oxide) with acetoxy- and trimethylsiloxy-end-groups. The results, together with others reported earlier for hydroxy-, phenoxy- and chloro-ended polymers, show that the melting point can be much affected by the end-group. The main causes of the effects are ascribed to differences in end-end and end-chain interactions and to end-group dimensions.

## INTRODUCTION

Recently<sup>1,2</sup> we have reported measurements of the melting points of hydroxy-, phenoxy- and chloro-ended samples of low molecular weight poly(ethylene oxide). It was found<sup>1</sup> that the melting temperature was substantially affected when hydroxy-ends were replaced by less polar ends. Here we present further measurements of melting points, supplemented by low-angle X-ray scattering measurements, for acetoxy- and trimethylsiloxy-ended poly(ethylene oxide) samples.

## EXPERIMENTAL

### *Preparation of samples*

Acetoxy- and trimethylsiloxy-ended samples of poly(ethylene oxide) were prepared by reacting hydroxy-ended polymers in solution in pyridine with either acetic anhydride or NO-bis(trimethylsilyl) acetamide. Pyridine was dried over and distilled from calcium hydride. The other reagents were used as received (BDH Chemicals Ltd). Hydroxy-ended poly(ethylene oxide) samples were of nominal molecular weights 1500 (Shell Chemical Co. Ltd) and 2000 (Hoechst Chemicals Ltd). Low molecular weight fractions were removed by precipitating the samples from dilute solutions in benzene at 0°C by adding iso-octane. The precipitates were freeze-dried from benzene before use. Benzene and iso-octane, used in recovery of the polymer were dried over and distilled from calcium hydride.

*Acetoxy-ended polymer.* Poly(ethylene oxide) (5 g, mol. wt. 1500, hydroxy-ended) was dissolved in dry pyridine (40 ml). Excess acetic anhydride (20 ml) was added (by syringe via a serum cap) and the mixture was refluxed, under calcium chloride guard tube, for 45 min. Volatiles were removed by rotary evaporation. The residue was dissolved in dry benzene and the cloudy solution was clarified by centrifugation (15 000 × *g* for 1 h). The polymer was recovered and purified by repeated precipitation at 0°C (by adding excess iso-octane). A similar

procedure was used for poly(ethylene oxide) of mol. wt. 2000.

*Trimethylsiloxy-ended polymer.* Poly(ethylene oxide) (5 g, mol. wt. 1500, hydroxy-ended) was dissolved in dry pyridine (40 ml). NO-bis(trimethylsilyl) acetamide (3 ml) was added (by syringe via a serum cap) and the mixture was refluxed, under calcium chloride guard tube, for 45 min. The polymer was recovered as described above for the acetoxy-ended materials. A similar procedure was successful for poly(ethylene oxide) of mol. wt. 2000, but reaction with poly(ethylene oxide) of mol. wt. 4000 was incomplete (< 30% replacement of hydroxy-groups).

### *Characterization of samples*

Infra-red spectra of hydroxy-ended poly(ethylene oxide) samples showed strong adsorption at 3100–3700 cm<sup>-1</sup> due to hydroxy stretching, which was absent in the acetoxy- and trimethylsiloxy-ended polymers. The infra-red spectra of the acetoxy-ended samples showed strong adsorption at 1740 cm<sup>-1</sup> due to ester carbonyl stretching. <sup>1</sup>H n.m.r. spectra of trimethylsiloxy-ended samples (in carbon tetrachloride) showed resonances at 6.5τ (–OCH<sub>2</sub>–) and 10τ (SiCH<sub>3</sub>) with relative intensities consistent with about 95% replacement of hydroxy- by trimethylsiloxy-groups.

Gel permeation chromatography (Water Associates Inc., tetrahydrofuran at 45°C, 1 ml/min flow rate, 2 ml injection of 0.25% solution, 4 Styragel columns of nominal pore size in the range 5 to 150 nm) showed no differences in shape of molecular weight distribution between the samples before and after end-group reaction. The molecular weight ratio  $M_w/M_n$  for all samples was near to 1.05 (results corrected for adventitious dispersions<sup>3</sup>). Vapour pressure osmometry (Mechrolab Inc., tetrahydrofuran at 25°C) likewise showed no changes in number-average molecular weight which could be attributed to degradation of the samples during their preparation. Number-average chain lengths ( $x_n$ ) were close to those calculated from the nominal molecular weights of the samples.

### Melting points

Small samples of polymer (<200 mg) were placed in glass dilatometers, outgassed and confined with mercury. The dilatometers were immersed in boiling water for 15 min, and then their contents were allowed to crystallize at the required temperature ( $T_c \pm 0.01^\circ\text{C}$ ). Melting was effected by placing the dilatometer in an oil bath held a degree or so below the melting point and then raising the temperature by 6 deg/h. Expansion was followed by means of a cathetometer. The melting point was taken to be that point at which detectable crystallinity (judged by volume) disappeared.

### Lamellar spacings

Thin films of polymer (thickness 0.05 cm), supported on Melinex polyester film, were melted at  $100^\circ\text{C}$  and were then transferred to a hot plate held at the required crystallization temperature ( $T_c \pm 0.01^\circ\text{C}$ ). Films were exposed to copper  $K\alpha$  radiation in a Rigaku-Denki slit collimated low angle camera. The diffraction pattern was recorded photographically. Lamellar spacings were calculated, directly from the photographs, by use of Bragg's law.

## RESULTS AND DISCUSSION

Lamellar spacings are reported in Table 1. The extended chain lengths of poly(ethylene oxide) 1500 and 2000 are 10 and 13 nm respectively, so that the crystals are identified as extended-chain type irrespective of their end-group. This was assumed in the earlier paper<sup>1</sup>.

Melting points, listed in Table 2, are practically independent of crystallization temperature. These melting points, and those for similar low molecular weight poly(ethylene oxide) samples with other end-groups<sup>1,2</sup>, are given in Table 3.

Values of the end interfacial free energy of lamellar crystals ( $\sigma_e$ ) have been calculated by comparison of the

Table 1 Lamellar spacings of poly(ethylene oxide) samples

Sample		$T_c$ ( $^\circ\text{C}$ )	Lamellar spacing (nm)
Mol. wt.	End-group		
1500	-OH	35	11
	-OCOMe	29	10
	-OSiMe <sub>3</sub>	28	10
2000	-OH	36	13
	-OCOMe	36	14
	-OSiMe <sub>3</sub>	36	14

Table 2 Melting points of poly(ethylene oxide) samples

Sample		$T_c$ ( $^\circ\text{C}$ )	$T_m$ ( $^\circ\text{C}$ )
Mol. wt.	End-group		
1500	-OCOMe	28.7	45.0
		31.5	45.1
		33.2	45.2
	-OSiMe <sub>3</sub>	27.0	41.4
		28.8	41.4
		30.4	41.3
2000	-OCOMe	33.8	41.6
		41.0	51.9
	-OSiMe <sub>3</sub>	28.8	48.5
		33.2	48.9
		36.1	49.1

Table 3 Melting points ( $T_m$ ) and end interfacial free energies ( $\sigma_e$ ) of poly(ethylene oxide)

Sample		$T_m$ (K)	$\sigma_e$ (kJ/mol)
End-group	Mol. wt.		
-OH	1000	312.3	7.2
	1500	322.2	7.9
	2000	327.0	8.9
-OCOMe	1500	318.3	9.7
	2000	325.1	10.0
-OPh	1000	303.9	9.6
	1500	316.2	10.6
-Cl	1000	303.2	9.8
	1500	316.8	10.3
-OSiMe <sub>3</sub>	1500	314.7	11.2
	2000	322.0	11.7

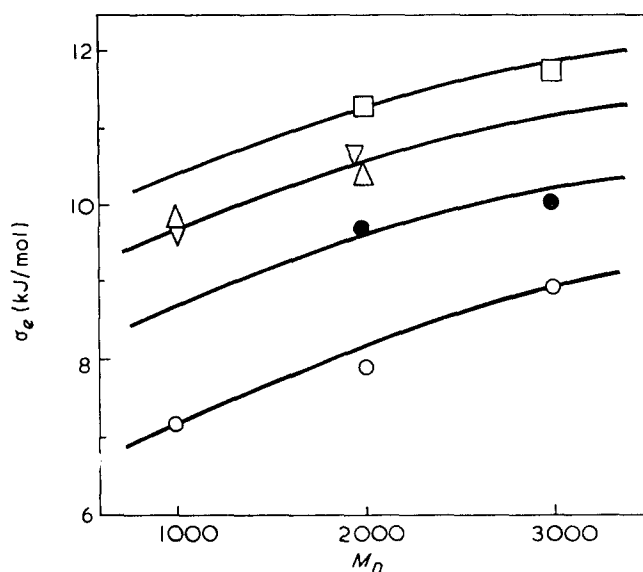


Figure 1 End interfacial free energy ( $\sigma_e$ ) versus molecular weight for poly(ethylene oxide) with hydroxy- (○), acetoxo- (●), phenoxy- (▽), chloro- (△) and trimethylsiloxy- (□) end-groups

measured melting points (Table 3) with calculated values. The melting point of a low molecular weight polymer is given by:

$$T_m = \frac{T_m^0 \left(1 - \frac{2\sigma_e}{\Delta h \zeta}\right)}{\left(1 + \frac{RT_m^0 Q}{\Delta h}\right)} \quad (1)$$

where  $T_m^0$  is the thermodynamic melting point ( $349\text{K}^{4,5}$ ),  $\Delta h$  is the heat of fusion ( $\sim 8\text{ kJ/mol}$  of chain units<sup>6</sup>),  $\zeta$  is the lamellar thickness ( $\sim x_n$  chain units) and  $Q$  is a function of  $\zeta$ ,  $x_n$  and the chain length distribution and varies according to the model adopted for the crystalline polymer. Certain possible forms of  $Q$  have been explored earlier<sup>2</sup> and we note that the form adopted does not significantly change relative values of  $\sigma_e$  obtained via equation (1) provided samples have similar molecular weight distributions. In Table 3 we quote values of  $\sigma_e$  calculated by use of the Flory-Vrij<sup>7</sup> model for lamellar crystals of a polydisperse (Schulz-Zimm<sup>8</sup> distribution) polymer crystallized (via chain folding if necessary<sup>2</sup>) to its maximum extent. Figure 1 is a plot of  $\sigma_e$  against molecular weight for the variously ended poly(ethylene oxide) samples.

The end interfacial free energy of a predominantly extended-chain crystal is largely the free energy of

transfer of chain ends from the melt to the interlamellar layer. Low molecular weight poly(ethylene oxide) samples are of high crystallinity, so the amount of interlamellar material is low (probably less than 10%). Consequently the process of formation of end interface is accompanied by an almost complete interchange of end-chain interactions for end-end interactions. For chloro-ended poly(ethylene oxide) the end-chain and end-end interactions will be similar and the interchange free energy will be negligible (provided steric effects are unimportant—see later). Accordingly a convenient parameter with which to characterize the interchange process is  $\Delta\sigma_e$ , the end interfacial free energy difference from that of the chloro-ended polymer of the same molecular weight. Approximate values of  $\Delta\sigma_e$ , read off *Figure 1*, are listed in *Table 4*. These values indicate that, relative to chloro-ends, hydroxy- and acetoxy-ends stabilize the interface whereas trimethylsiloxy-ends make the interface less stable.

We have already shown<sup>1</sup> that the stabilization of the interface by hydroxy-ends is consistent (semi-quantitatively) with almost complete interchange of hydroxy-ether hydrogen bonds in the melt for hydroxy-hydroxy hydrogen bonds in the interlamellar layer. The stabilization due to acetoxy-ends likewise probably derives from extensive dipolar interaction of the ester groups in the interlamellar layer. (We note that esters are treated by some authors<sup>9</sup> as associated liquids.)

The decreased stability of the end interface with trimethylsiloxy-ends is not so readily explained. For non-polar liquids an interchange free energy can be estimated from solubility parameter theory<sup>10</sup>. For separation of mixtures with poly(ethylene oxide) chain units (solubility parameter<sup>11</sup> ( $J^{1/2}/cm^{3/2}$ )  $\delta=17.6$ ) we estimate values of the interchange free energy (kJ/mol)

Table 4 End interfacial free energy differences ( $\Delta\sigma_e$ )

End-group	$\Delta\sigma_e$ (kJ/mol)
—OH	—2.4
—OCOMe	—1.0
—OPh	0.0
—OSiMe <sub>3</sub>	+0.7

of 0.0 for chloroethane ( $\delta=17.8$ ), —0.1 for phenetole ( $\delta=18.9$ ) and —2.2 for trimethylethoxysilane ( $\delta=12.9$ ). By obvious analogy the value of  $\Delta\sigma_e$  predicted for trimethylsiloxy-ends is opposite in sign to that found here (*Table 4*). We suggest that the low stability of the interface containing trimethylsiloxy-ends is due to their large size. We calculate, from unit cell dimensions<sup>12</sup>, an area of 0.26 nm<sup>2</sup> per chain emerging from the end interface of a poly(ethylene oxide) crystal. The areas of cross-section (nm<sup>2</sup>) of the various non-polar end-groups, estimated from van der Waals radii, are 0.16 (chloro-), 0.36 (phenoxy-, rotating) and 0.54 (trimethylsiloxy-). Presumably with the large trimethylsiloxy-end the negative entropic and positive energetic contributions to the interchange free energy (due to configurational restrictions and packing effects) outweigh the negative contribution to the interchange free energy of the intermolecular interactions.

#### ACKNOWLEDGEMENTS

We thank Messrs D. J. Roy, D. Rowlinson and A. Friday for assistance with the characterization and preparation of polymers. P. C. A. acknowledges receipt of a Science Research Council Studentship.

#### REFERENCES

- Booth, C., Bruce, J. M. and Buggy, M. *Polymer* 1972, **13**, 475
- Ashman, P. C. and Booth, C. *Polymer* 1972, **13**, 459
- Aldhouse, S. T. E. and Stanford, D. M. *5th Int. Gel Permeation Chromatog. Seminar, London* 1968
- Beech, D. R. and Booth, C. *J. Polym. Sci. (B)* 1970, **8**, 731
- Affi-Effat, A. M. and Hay, J. N. *JCS Faraday Trans. II* 1972, **68**, 656
- Beaumont, R. H., Clegg, B., Gee, G., Herbert, J. B. M., Marks, D., Roberts, R. C. and Sims, D. *Polymer* 1966, **7**, 401; Booth, C., Devoy, C. J. and Gee, G. *Polymer* 1971, **12**, 327
- Flory, P. J. and Vrij, A. *J. Am. Chem. Soc.*, 1963, **85**, 3548
- Schulz, G. V. *Z. Phys. Chem.* 1939, **B43**, 25; Zimm, B. H. *J. Chem. Phys.* 1948, **16**, 1093
- Burrell, H. *Interchem. Rev.* 1955, **14**, 31
- Hildebrand, J. H., Prausnitz, J. M. and Scott, R. L. 'Regular and Related Solutions', Van Nostrand-Reinhold, New York, 1970
- Small, P. A. *J. Appl. Chem., Lond.* 1953, **3**, 71
- 'Polymer Handbook', Interscience, New York, 1966

# N.m.r. studies of the helix-coil transition of polypeptides in non-protonating solvent mixtures

E. M. Bradbury and C. Crane-Robinson

*Biophysics Laboratories, Physics Department, Portsmouth Polytechnic, Portsmouth PO1 2QG, UK*

and L. Paolillo and P. Temussi

*Laboratorio per la Chimica e Fisica di Molecole di Interesse Biologico del CNR, Arco Felice, Naples, Italy*  
(Received 16 February 1973)

High resolution nuclear magnetic resonance (n.m.r.) spectra have been obtained for poly( $\beta$ -benzyl aspartate), poly( $\gamma$ -benzyl glutamate) and several of their copolymers in the solvent system dimethylsulphoxide/chloroform, in which no amide protonation can occur. 'Double-peak'  $\alpha$ CH and peptide NH resonances are observed in the helix-coil transition region of the same form as seen in trifluoroacetic acid/chloroform solutions. It is concluded that protonation of peptide groups is not essential, either for inducing the helix to coil transition itself or for observation of different and characteristic helix and coil  $\alpha$ CH and NH shifts.

## INTRODUCTION

Strong organic acids, in particular trifluoroacetic (TFA) and dichloroacetic (DCA) acids are the normally used agents for inducing transition to the coil of helical polypeptides in organic solvents such as chloroform ( $\text{CHCl}_3$ ), methylene chloride or ethylene dichloride. Sulphuric and perchloric acids have also been used. The usual explanation for the breakdown of the helix is that the acid molecules form stronger hydrogen bonds with the amide groups in the coil than occur intramolecularly in the helix. An alternative explanation, originally proposed by Hanlon and Klotz and coworkers<sup>1,2</sup> is that the acid molecules protonate the amide groups and the juxtaposition of positive charges causes breakdown of the helix. The degree of protonation is thought to increase with TFA content and the helix-coil transition to occur when only a proportion of the amide groups are in the charged form. Hanlon<sup>3</sup> later proposed that not all polypeptides are protonated to the same extent in the same solvent mixture; poly(L-alanine) (PLA), for example, being largely protonated in as little as 6% DCA. Poly( $\gamma$ -benzyl-L-glutamate) (PBLG) was thought to show two stages of protonation and the helix to be capable of accommodating up to 50% of charged amide groups. The random coil form was taken to be highly protonated and also hydrogen bonded to the acid. Viscometry studies of PBLG have been interpreted as indicating that the polymer behaves as a polyelectrolyte in DCA and is therefore protonated under these conditions<sup>4</sup>. There has been a great deal of opposition to the thesis of amide protonation in polypeptides, although there is agreement

that model compounds such as *N*-methyl acetamide can be protonated at high acid contents. Detailed studies of model amides in TFA and DCA, both by nuclear magnetic resonance (n.m.r.)<sup>5</sup> spectroscopy and by circular dichroism (c.d.)<sup>6</sup> have led to the result that little protonation takes place and it was concluded that random coil polypeptides are likewise not protonated but only solvated by haloacetic acids. Quadrifoglio and Urry<sup>7</sup> found that addition of TFA to a chloroform solution of PBLG produced no change in the 222 nm negative c.d. band up to the point of the helix-coil transition, suggesting no marked protonation of helical PBLG. Infra-red spectra of poly(L-alanine) in acid-containing solvent mixtures were found to show little change in the amide II vibrations at  $1550\text{ cm}^{-1}$  as compared to helical PLA in a cast film<sup>8</sup>. Since the amide II vibration is a C-N stretching and N-H bending coupled mode, either N- or O- protonation would cause a marked change in the amide II band and it can be concluded that the coil form of PLA is not strongly protonated under these conditions. At low acid contents the presence of a new band at  $1616\text{ cm}^{-1}$  in the spectra was interpreted as due to a strong interaction between the helical form of PLA and the acid molecules.

The high resolution n.m.r. spectra of polypeptides undergoing the helix-coil transition in chloroform ( $\text{CDCl}_3$ )/TFA solutions show double  $\alpha$ CH and amide NH resonances in the transition region for low molecular weight samples. In the case of the  $\alpha$ CH resonance the upfield peak may be assigned to the helix and the lowfield peak to the coil, while the reverse is true of the NH

resonance. Although this assignment has been questioned<sup>9-11</sup>, the constancy of the total  $\alpha\text{CH}$  area relative to an internal standard<sup>12</sup> and the good correlation of the areas of the separate peaks with the optical rotatory dispersion (o.r.d.) parameter  $b_0$ <sup>13</sup>, provide strong support for the assignment. The observation of separate helix and coil peaks is general, though not universal; it has been argued elsewhere<sup>14a, 14b</sup> that this is not a consequence of slow helix-coil exchange processes, but due rather to conformational heterogeneity in the transition region as a result of molecular weight polydispersity. This has been fully confirmed by recent studies on fractionated PBLG samples<sup>15</sup>. None of the n.m.r. results obtained to date have provided proof of why the  $\alpha\text{CH}$  coil peak is always found to lowfield of the helix peak. The chemical shift difference between the conformations could be intrinsic to the polypeptide chain or be a result of differing solvation in the helix and coil. Clearly a combination of the two effects is also possible. Theoretical predictions of the intrinsic shift-difference between the conformations vary widely<sup>16-18</sup>, due largely to uncertainties in the amide group anisotropy. Experimentally it has been observed that in water the shift difference is very much smaller ( $\sim 0.1$  ppm) than in TFA/DCA/ $\text{CDCl}_3$  solvent systems ( $\sim 0.5$  ppm). The relative importance of the intrinsic and solvation effects is thus unclear. J. H. Bradbury *et al.*<sup>10</sup> have argued that the shift difference is due entirely to protonation of the amide group such that the lowfield peak can be assigned to protonated helix and coil. Since the helix in solution is unlikely to support a large degree of protonation, the lowfield peak must be very largely protonated coil and the good correlation of peak areas with  $b_0$  indicates that the upfield peak must therefore be due very largely to unprotonated helix. This explanation thus implies virtually complete protonation of the coil form. Tam and Klotz<sup>11</sup> have also favoured protonation as the cause of the helix-coil shift difference in PLA.

In this work we have studied the helix-coil transition of a number of polypeptides in dimethylsulphoxide ( $\text{DMSO-d}_6$ )/ $\text{CDCl}_3$  solvent systems. For certain polypeptides and copolypeptides, particularly those containing a considerable proportion of  $\beta$ -benzyl aspartate,  $\text{DMSO}$  favours the random coil conformation. Addition of  $\text{CDCl}_3$  to these systems thus induces a coil to helix transition. For these polymers  $\text{DMSO}$  can be regarded as a direct substitute for TFA, i.e. an alternative denaturant of the secondary structure that contains no acidic protons. In fact in the presence of acid,  $\text{DMSO}$  is somewhat basic and in this respect in strong contrast to TFA. Data from the  $\text{DMSO-d}_6$ / $\text{CDCl}_3$  solvent system are directly compared therefore with those from TFA/ $\text{CDCl}_3$ . For PBLG it has been found that low molecular weights are partly random coil in  $\text{DMSO}$ , whilst samples with  $DP=100$  are fully helical; this has provided the first n.m.r. study of a polypeptide in two conformations in a single solvent. It was hoped that by using the  $\text{DMSO}$  solvent system one could obtain greater understanding of the importance of solvation, whether protonation or not, in the helix-coil transition and its n.m.r. manifestation. A brief report of some of this work has already appeared<sup>19</sup>.

#### METHOD

N.m.r. spectra were obtained at 100 MHz on a Varian HA 100-15 spectrometer using 5 mm tubes and internal

tetramethylsilane (TMS) as reference.  $b_0$  values were obtained on a Bendix Polarmatic 62 spectropolarimeter over the wavelength range 345 to 278 nm using Moffitt's equation with a  $\lambda_0$  value of 212 nm. These  $b_0$  values have been included directly in the Figures for comparison with the n.m.r. results.

#### RESULTS

Figure 1 shows the 100 MHz spectrum of a sample of high molecular weight poly( $\beta$ -benzyl-L-aspartate) (PBLA) in pure  $\text{DMSO-d}_6$ . It can be seen that the  $\alpha\text{CH}$  and amide  $\text{NH}$  peaks are relatively sharp, whilst the two  $\beta\text{CH}_2$  protons are almost equivalent. These observations indicate a random coil conformation for PBLA in  $\text{DMSO}$ . This is supported by a  $b_0$  measurement of  $-130^\circ$ , a value similar to that observed for random coil L-aspartates in TFA-containing solvents. The shift values of the  $\alpha\text{CH}$  and  $\text{NH}$  peaks are 4.64 and 8.15 ppm, and differ from the corresponding values in TFA/ $\text{CDCl}_3$  of 4.80 and 7.90 ppm respectively. Addition of chloroform to this  $\text{DMSO-d}_6$  solution induces transition to the left-handed (LH) helical form, the mid-point of the transition lying at about 59%  $\text{CDCl}_3$  by volume. The changes in the  $\alpha\text{CH}$  spectrum are shown in Figure 2 and a characteristic double-peak phenomenon is seen with the helix peak at 4.30 ppm, as expected for the LH helix of PBLA<sup>19</sup>. The shift difference  $\Delta_{\text{H/C}}(\alpha\text{CH})$  between the helix and coil is thus 0.34 ppm in this solvent mixture as compared to 0.50 ppm in  $\text{CDCl}_3$ /TFA. Since the LH helical  $\text{NH}$  peak is observed at 8.75 ppm, the corresponding value of  $\Delta_{\text{H/C}}(\text{NH})$  is 0.60 ppm, as compared to 0.85 ppm in  $\text{CDCl}_3$ /TFA. This reduction in both the shift differences  $\Delta_{\text{H/C}}$  between the LH helix and coil is due to changes in the coil shifts resulting from replacing TFA by  $\text{DMSO-d}_6$  and shows that the conformationally dependent peak displacements are at least in part a consequence of solvation differences. More important is the finding that the normal double-peak phenomenon is obtained when the helical form of PBLA is broken down to the coil by a non-protonating solvent. It follows that neither the helix-coil transition itself nor its n.m.r. manifestation as the appearance of separate helix and coil peaks of characteristic shift, is dependent on protonation of the amide groups.

In contrast to PBLA, a sample of PBLG (S416, see ref. 14b) having average  $DP=100$ , when dissolved in  $\text{DMSO-d}_6$  gave a  $b_0$  of  $-578^\circ$  and relatively broad  $\alpha\text{CH}$  and  $\text{NH}$

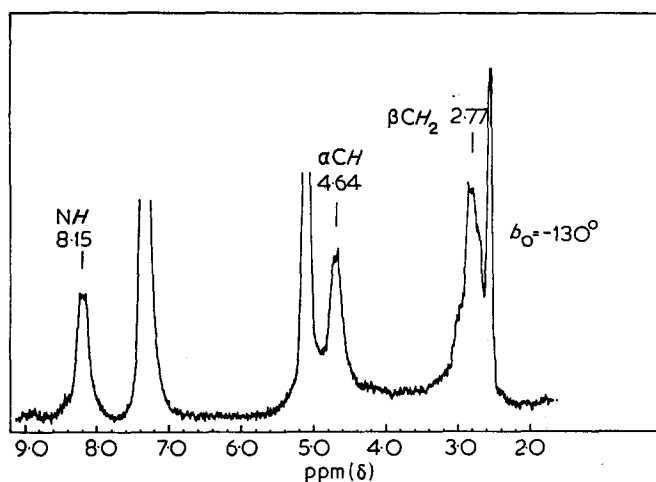


Figure 1 Poly(benzyl-L-aspartate) sample 426 in pure  $\text{DMSO-d}_6$

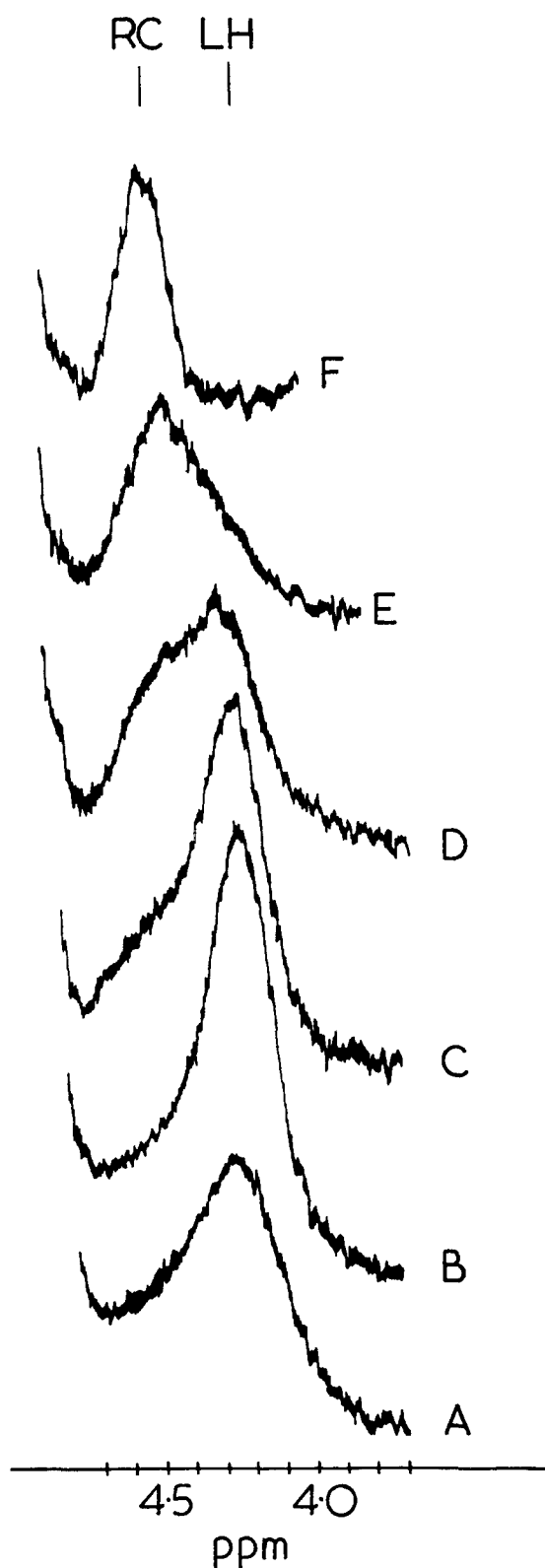


Figure 2 Poly(benzyl-L-aspartate) sample 426 in  $\text{CDCl}_3/\text{DMSO-d}_6$ . A, neat  $\text{CDCl}_3$  ( $b_0 = +600^\circ$ ); B, 23%; C, 33%; D, 41%; E, 47%; F, 56% v/v  $\text{DMSO-d}_6$  ( $b_0 = -130^\circ$ )

peaks centred at 3.94 ppm and 8.25 ppm respectively. This indicates a helical conformation for PBLG in  $\text{DMSO-d}_6$  and it is noteworthy that the shifts of the main-chain protons are very close to those of PBLG in chloroform. It is then of interest to measure the chemical shift of random coil benzyl-L-glutamate residues in  $\text{DMSO-d}_6$  in order to establish whether the conformational shift difference  $\Delta_{\text{H/C}}(\alpha\text{CH})$  is the same as for

aspartates. This is found to be so in  $\text{CDCl}_3/\text{TFA}$  despite the fact that the absolute magnitudes of the shifts in aspartates are about 0.3 ppm to lowfield of glutamates. This was achieved firstly by the use of very low molecular weight polymers. Although  $\text{CDCl}_3$  induces the helical conformation in all but a few terminal residues of a PBLG molecule, the same is not found to be so for  $\text{DMSO}$ , in which a higher molecular weight is necessary for the fully helical conformation.  $\text{DMSO}$  may thus be regarded as a 'weaker' helix-supporter for PBLG than is  $\text{CDCl}_3$ . The two samples of PBLG used were those characterized previously<sup>13</sup> as a 21-mer and a 7-mer and Figure 3 shows their  $\alpha\text{CH}$  spectra in pure  $\text{DMSO-d}_6$ . It is clear that the broad upfield peak at 3.95 ppm can be

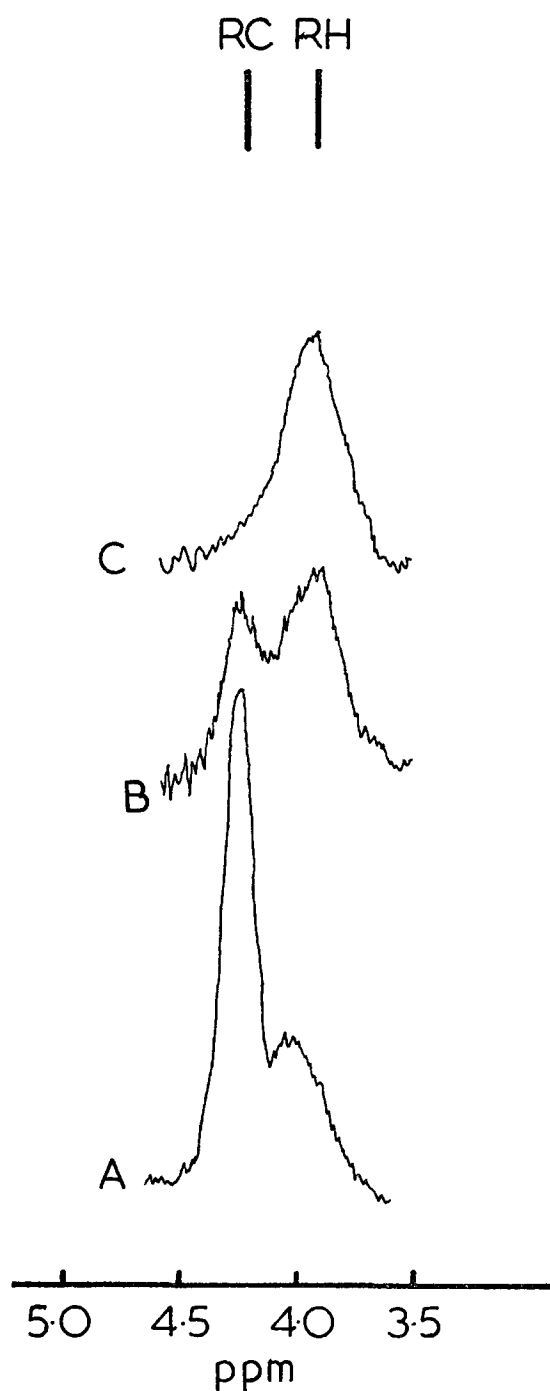


Figure 3 Poly(benzyl-L-glutamate) in  $\text{DMSO-d}_6$  at  $30^\circ\text{C}$ . Samples with different molecular weights: A,  $\text{DP}=7$  ( $b_0 = -313^\circ$ ); B,  $\text{DP}=21$  ( $b_0 = -489^\circ$ ); C,  $\text{DP}=100$  ( $b_0 = -578^\circ$ )

assigned to helix and the sharp lowfield peak at 4.26 ppm to coil. The second method used to observe random coil benzyl-L-glutamate residues was incorporation in PBLA as a random copolymer. Figure 4 shows the  $\alpha$ CH spectra of two such copolymers, both largely random coil in

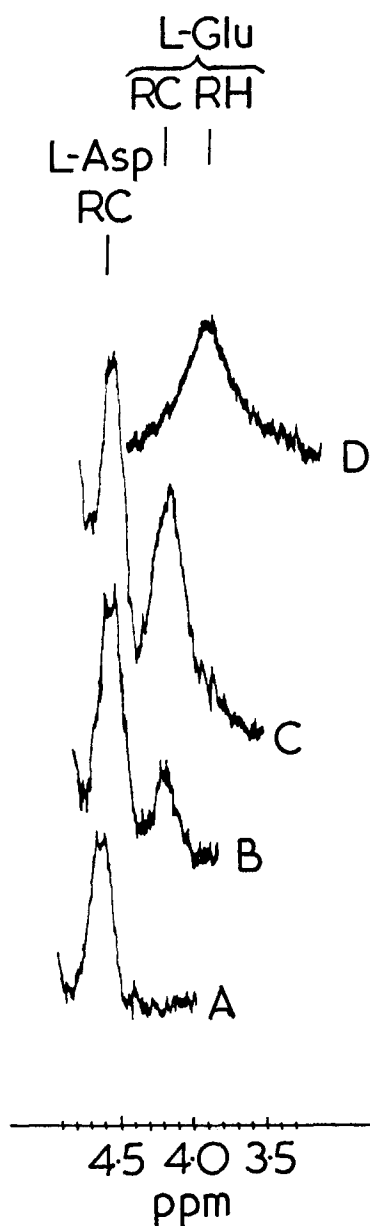


Figure 4 Several homo- and co-polymer spectra in DMSO-d<sub>6</sub>. A, poly(benzyl-L-aspartate) ( $b_0 = -130^\circ$ ); B, copoly[(benzyl-L-aspartate)<sub>75</sub>(benzyl-L-glutamate)<sub>25</sub>] ( $b_0 = -175^\circ$ ); C, copoly[(benzyl-L-aspartate)<sub>50</sub>(benzyl-L-glutamate)<sub>50</sub>] ( $b_0 = -270^\circ$ ); D, poly(benzyl-L-glutamate) in 90 : 10 DMSO-d<sub>6</sub>/CDCl<sub>3</sub> ( $b_0 = -571^\circ$ )

DMSO-d<sub>6</sub>, together with random coil PBLA and helical PBLG. The benzyl-L-glutamate residues give an  $\alpha$ CH peak at 4.20 ppm in the copolymers, confirming the above random coil assignment. It follows that for PBLG in DMSO-d<sub>6</sub>,  $\Delta_{H/C}(\alpha CH)$  is approximately 0.3 ppm and close to the value found for PBLA in DMSO-d<sub>6</sub>/CDCl<sub>3</sub>. The amide NH peak of coil PBLG in DMSO-d<sub>6</sub> is observed at approximately 7.95 ppm, close to the position in CDCl<sub>3</sub>/TFA and the value of  $\Delta_{H/C}(NH) \approx 0.3$  ppm is thus similar to that in CDCl<sub>3</sub>/TFA. Table 1 summarizes values of the conformational shift differences  $\Delta_{H/C}$  (and the observed shifts) in such a way as to allow comparison between the solvent systems CDCl<sub>3</sub>/TFA and CDCl<sub>3</sub>/DMSO-d<sub>6</sub>. All differences between the solvent systems are due to changes in the coil shifts since the helical shifts are not to a first approximation dependent on the amount of TFA or DMSO-d<sub>6</sub> present. In particular the  $\alpha$ CH shift of helical PBLG is the same in DMSO-d<sub>6</sub> as in CDCl<sub>3</sub> (3.95 ppm; see Figure 3). Large quantities of TFA do, however, produce small downfield shifts of almost all peaks in the spectrum and this must be taken into account in obtaining precise  $\Delta_{H/C}$  values. The data in the Table are accurate to  $\pm 0.05$  ppm.

In order to confirm the above data and to measure the shifts of both aspartate helix senses, several other copolymers were studied in the DMSO-d<sub>6</sub> solvent systems. Figure 5 shows the  $\alpha$ CH spectra of a series (441) of random copoly(benzyl-D-glutamate, benzyl-L-aspartate) samples in DMSO-d<sub>6</sub>. When the L-aspartate is in excess [sample numbers 441(4) and 441(5)] the polymers are random coil and the peaks are at the same shift as those of the copolymers of Figure 4, viz. 4.60 ppm, aspartate and 4.26 ppm, glutamate. As the amount of D-glutamate residues increases, the helicity of the polymer rises as seen from the  $b_0$  values and the peaks move to the positions characteristic of the helical conformation, viz. 4.30 ppm, LH L-aspartate and 3.95 ppm, LH D-glutamate. It is apparent from the spectra, particularly that of 441(7) in which the helicity is about 50%, that the helical regions formed include both types of residue and not only those which naturally assume the helical conformation in DMSO-d<sub>6</sub>, the D-glutamates. This supports our previous finding<sup>19</sup> from titration against TFA in CDCl<sub>3</sub>, that series 441 behaves as truly random copolymers. The polymer containing 90% D-glutamate is largely helical in DMSO-d<sub>6</sub> and there is no apparent resonance at the position of random coil aspartate. The LH helical benzyl-L-aspartate residues in this polymer resonate at 4.2–4.3 ppm, (the shift is 4.30 ppm in CDCl<sub>3</sub>) showing that LH helical L-aspartate in pure DMSO-d<sub>6</sub> (just as RH helical L-glutamate) shows an  $\alpha$ CH shift very close to that in pure CDCl<sub>3</sub>.

Table 1 Absolute shifts in ppm from TMS and shift differences for the main chain  $\alpha$ CH and peptide NH protons

	$\Delta_{H/C}(\alpha CH)$		$\Delta_{H/C}(NH)$	
	CDCl <sub>3</sub> /DMSO-d <sub>6</sub> (or pure DMSO-d <sub>6</sub> )	CDCl <sub>3</sub> /TFA	CDCl <sub>3</sub> /DMSO-d <sub>6</sub> (or pure DMSO-d <sub>6</sub> )	CDCl <sub>3</sub> /TFA
L-Glutamate	0.31 3.95(H)-4.26(C)	0.50 3.95(H)-4.45(C)	0.30 8.25(H)-7.95(C)	0.30 8.25(H)-7.95(C)
L-Aspartate	0.34 4.30(H)-4.64(C)	0.50 4.30(H)-4.80(C)	0.60 8.75(H)-8.15(C)	0.85 8.75(H)-7.90(C)
	0.24 4.40(H)-4.64(C)	0.40 4.40(H)-4.80(C)	0.1 8.3(H)-8.15(C)	0.4 8.3(H)-7.90(C)

H=helix; C=coil

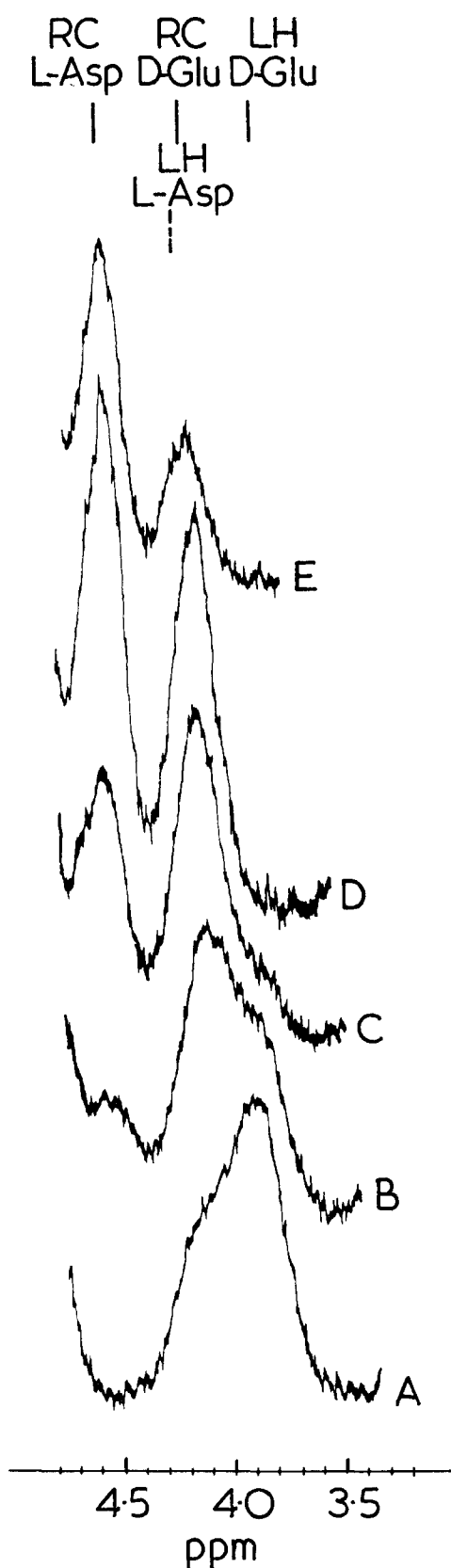


Figure 5 Random copoly[(benzyl-D-glutamate)<sub>m</sub>(benzyl-L-aspartate)<sub>n</sub>] in DMSO-d<sub>6</sub>. A: sample 441(8);  $m=90$ ;  $n=10$ ;  $b_0=+474^\circ$ . B: sample 441(7);  $m=75$ ;  $n=25$ ;  $b_0=+337^\circ$ . C: sample 441(6);  $m=60$ ;  $n=40$ ;  $b_0=+111^\circ$ . D: sample 441(5);  $m=45$ ;  $n=55$ ;  $b_0=-56^\circ$ . E: sample 441(4);  $m=30$ ;  $n=70$ ;  $b_0=-90^\circ$

Figure 6 shows the conversion of the partly helical (~50%) copolymer 441(7) (25% L-aspartate, 75% D-glutamate) in DMSO-d<sub>6</sub> into the fully helical state by the addition of 33% CDCl<sub>3</sub>. As expected from the above and the data of ref. 21, both types of residue assume the

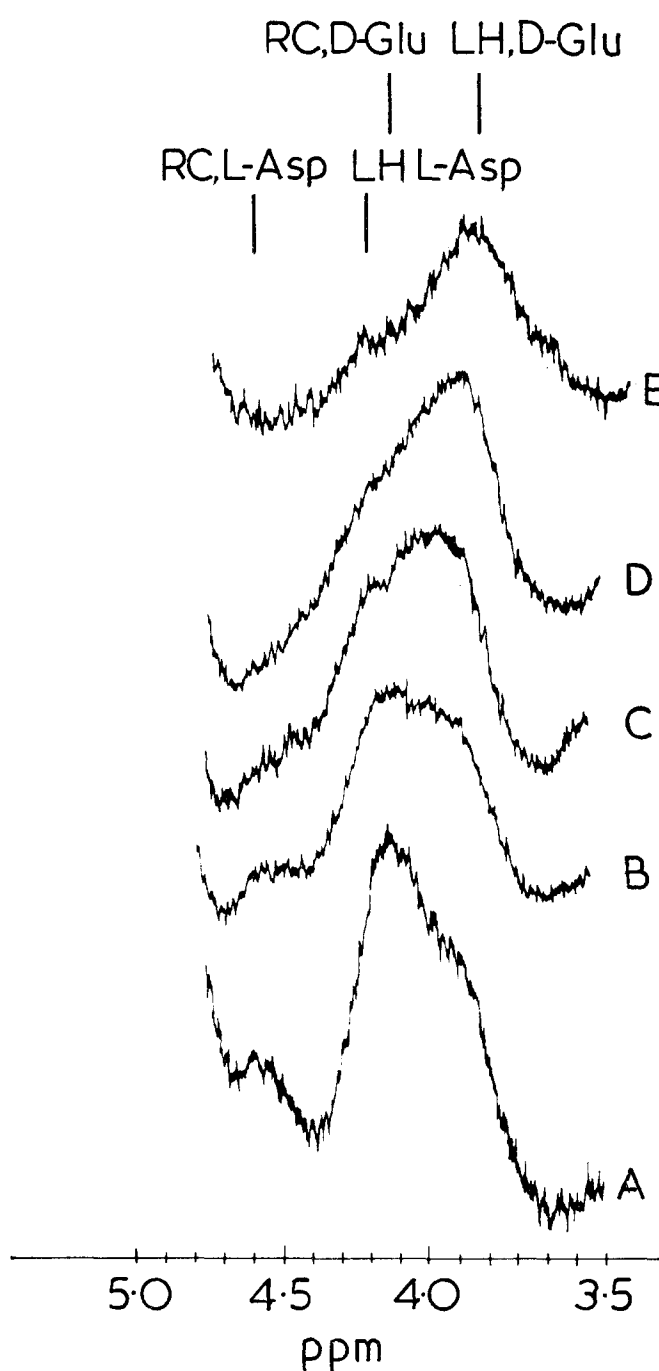


Figure 6 Random copoly[(benzyl-L-aspartate)<sub>25</sub>(benzyl-D-glutamate)<sub>75</sub>] sample 441(7) in CDCl<sub>3</sub>/DMSO-d<sub>6</sub> mixtures. A, neat DMSO-d<sub>6</sub> ( $b_0=+337^\circ$ ); B, 5% v/v CDCl<sub>3</sub>; C, 9% v/v CDCl<sub>3</sub> ( $b_0=+430^\circ$ ); D, 20% v/v CDCl<sub>3</sub>; E, 33% v/v CDCl<sub>3</sub> ( $b_0=+585^\circ$ )

helical conformation together and the final peak positions are close to those in pure CDCl<sub>3</sub>. In order to observe the shifts of benzyl-L-aspartate residues in the RH helix form (i.e., the unnatural sense for this as a homopolymer) spectra were obtained of random copoly(75% benzyl-L-aspartate, 25% benzyl-L-glutamate) series 432(3)<sup>21</sup> which is random coil in pure DMSO-d<sub>6</sub>. Increasing amounts of CDCl<sub>3</sub> were added (to induce the coil to helix transition) and spectra run at 50°C owing to limited solubility of the polymer when helical. The  $\alpha$ CH resonances are shown in Figure 7 and the final RH helical L-aspartate shift of 4.43 ppm is close to that found in pure CDCl<sub>3</sub> (4.40 ppm). On the basis of the data given above, there seems little reason to doubt that this would also be the shift if RH helical L-aspartate could be observed in pure DMSO-d<sub>6</sub>.



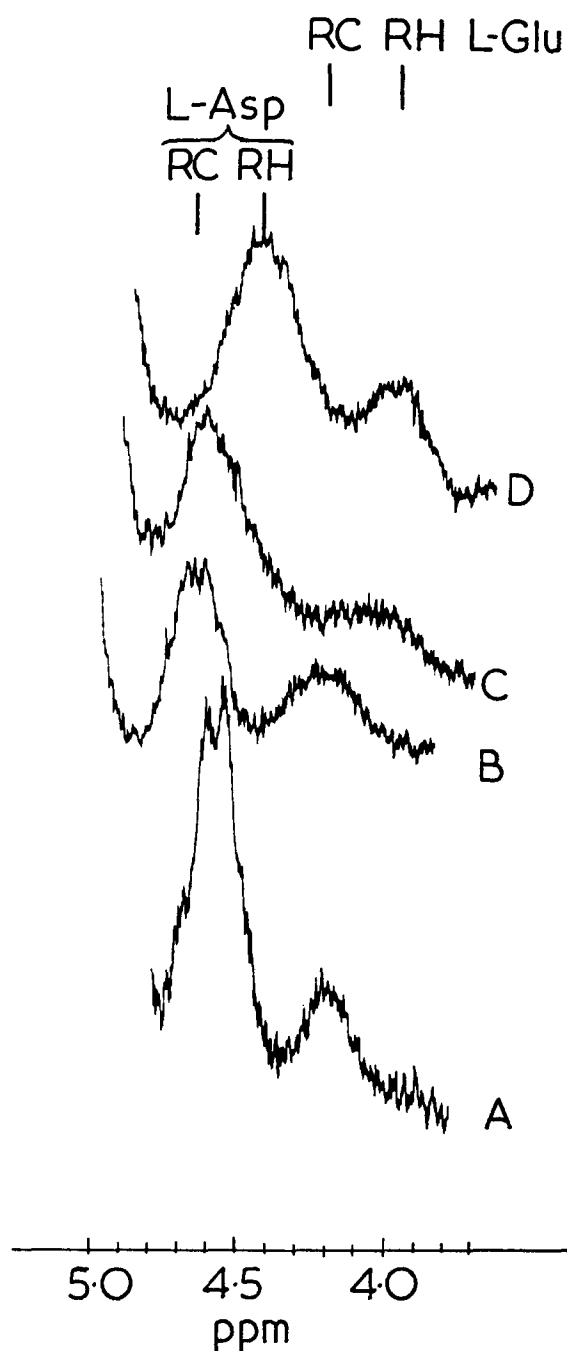


Figure 7 Random copoly[(benzyl-L-aspartate)<sub>75</sub>(benzyl-L-glutamate)<sub>25</sub>] sample 432(3) in DMSO-d<sub>6</sub>/CDCl<sub>3</sub> mixtures at 50°C. A, neat DMSO-d<sub>6</sub> ( $b_0 = -175^\circ$ ); B, 30% v/v CDCl<sub>3</sub>; C, 38% v/v CDCl<sub>3</sub> ( $b_0 = -380^\circ$ ); D, 60% v/v CDCl<sub>3</sub> ( $b_0 = -590^\circ$ )

From the spectra of partly helical copolymer in 30% to 38% CDCl<sub>3</sub> it can be seen that the L-glutamate residues undergo transition to the helix at significantly lower CDCl<sub>3</sub> contents than do the L-aspartate residues. Such an effect is also observed in TFA/CDCl<sub>3</sub>, indicating some non-randomness in the copolymerization of series 432<sup>21</sup>.

#### DISCUSSION

For a number of polymers DMSO-d<sub>6</sub> can replace TFA as the random coil promoting solvent in mixtures of various composition with CDCl<sub>3</sub>. Both benzyl glutamate and benzyl aspartate residues are found to show  $\alpha$ CH and NH random coil shifts in DMSO-d<sub>6</sub> different from those in CDCl<sub>3</sub>/TFA. For RH helical PBLG and LH helical

PBLA, however, the shifts in pure DMSO-d<sub>6</sub> are the same as in pure CDCl<sub>3</sub>/TFA. The chemical shift differences  $\Delta_{H/C}$  between the conformations are thus dependent on solvent and cannot be completely intrinsic to the secondary structure. In every way other than the precise shift values, the transitions in DMSO-d<sub>6</sub>/CDCl<sub>3</sub> are similar to those in TFA/CDCl<sub>3</sub> and in particular the 'double-peak' phenomenon is observed for the  $\alpha$ CH and NH resonances in the region of the helix-coil transition of low molecular weight polymers. Since DMSO-d<sub>6</sub> contains no acidic (or even exchangeable) protons, it follows that protonation of amide groups is not essential either for inducing the helix to coil transition or for observation of different and characteristic helix and coil shifts for the main chain protons in the n.m.r. spectra of polypeptides.

#### ACKNOWLEDGEMENTS

We are grateful to Mrs J. Brnjac-Kraljevic for assistance with o.r.d. measurements. Two of us (E.M.B. and C.C.-R.) are grateful to the Consiglio Nazionale delle Ricerche of Italy for fellowships, during the tenure of which the work was carried out and to the SRC of Great Britain for research support.

#### REFERENCES

- Hanlon, S., Russo, S. F. and Klotz, I. M. *J. Am. Chem. Soc.* 1963, **85**, 2024
- Klotz, I. M., Russo, S. F., Hanlon, S. and Stake, M. A. *J. Am. Chem. Soc.* 1964, **86**, 4774
- Hanlon, S. *Biochemistry* 1966, **5**, 2049
- Bradbury, J. H. and Fenn, M. D. *J. Mol. Biol.* 1968, **36**, 231
- Steigman, J., Silvio, A., Montagner, C. and Strasorier, L. *J. Am. Chem. Soc.* 1969, **91**, 1829
- Bovey, F. A. *Rev. Pure Appl. Chem.* 1968, **16**, 417
- Quadrifoglio, F. and Urry, D. W. *J. Phys. Chem.* 1967, **71**, 2364
- Bradbury, E. M. and Rattle, H. W. E. *Polymer* 1968, **9**, 201
- Joubert, F. J., Lotan, N. and Scheraga, H. A. *Biochemistry* 1970, **9**, 2197
- Bradbury, J. H., Fenn, M. D. and Moritz, A. G. *Aust. J. Chem.* 1969, **22**, 2443
- Tam, J. W. O. and Klotz, I. M. *J. Am. Chem. Soc.* 1971, **93**, 1313
- Bradbury, E. M., Cary, P., Crane-Robinson, C., Paolillo, L., Tancredi, T. and Temussi, P. A. *J. Am. Chem. Soc.* 1971, **93**, 5916
- Bradbury, E. M., Crane-Robinson, C., Goldman, H. and Rattle, H. W. E. *Nature* 1968, **217**, 812
- Ullman, R. *Biopolymers* 1970, **9**, 471
- Bradbury, E. M., Crane-Robinson, C. and Rattle, H. W. E. *Polymer* 1970, **11**, 277
- Nagayama, K., Nakanishi, M., Tsuboi, M., Wada, A. and Saton, S. *Biopolymers* in press
- Sternlicht, H. and Wilson, D. *Biochemistry* 1967, **6**, 2881
- Conti, F. 'Magnetic Resonance in Biological Research', (Ed. C. Franconi), Gordon and Breach, New York, 1971
- Tigelaar, H. L. and Flygare, W. H. *J. Am. Chem. Soc.* 1972, **94**, 343
- Bradbury, E. M., Crane-Robinson, C., Paolillo, L. and Temussi, P. *J. Am. Chem. Soc.* 1973, **95**, 1683
- Bradbury, E. M., Carpenter, B. G., Crane-Robinson, C. and Goldman, H. *Macromolecules* 1971, **4**, 557
- Paolillo, L., Temussi, P. A., Bradbury, E. M. and Crane-Robinson, C. *Biopolymers* 1972, **11**, 2043

#### Note added in proof

It has been brought to our attention that Prof. H. N. Rydon *et al.* were the first to show that DMSO induced the helix-coil transition in PBLA (*Polym. Preprints* 1969, **10**, 25). We apologize for this omission.

# Polymer/particulate filler interaction—the bound rubber phenomena

C. M. Blow

*Institute of Polymer Technology, Loughborough University of Technology,  
Leics LE11 3TU, UK  
(Received 3 January 1973)*

In Part I, after an historical note on the subject of bound rubber, the experimental determination of bound rubber and the many factors affecting the value, in the case of the organic rubber/carbon black and silicone rubber/silica systems, are reviewed. Mention is made of the relation between swelling index and bound rubber and, in Part II, the accuracy and significance of bound rubber values are appraised.

Some experimental work on the natural rubber/fine particle black system is described in Part III; this assesses qualitatively the rigidity of swollen jellies of the (unvulcanized) mixtures and shows how it is not correlated with either bound rubber or solvent content. Other experiments lead to the conclusion that the uptake of solvents of different solubility parameters compares with that of a pure gum vulcanisate, indicating no significant or substantial change in the solubility parameter of the rubber on becoming insolubilized. Results are reported on bound rubber determinations in solutions of rubber and it is suggested that these provide a method of arriving at the true bound rubber value. The discussion which forms Part IV suggests how the two structures, postulated recently as present in polymer/filler systems, might be further analysed to explain the phenomena.

## PART I: A REVIEW

### INTRODUCTION

The study of the reinforcement of rubbers by particulate fillers has resulted in a vast literature over the past 40–50 years and there is evidence to day of some rationalization of the many theories that have been put forward. The greatest attention has been paid to vulcanisates prepared in the conventional manner by mixing the filler and other ingredients into the polymer on a two-roll mill or in an internal mixer and heating under pressure to vulcanize; strength and strength changes, modulus and modulus changes over a wide variety of strains under dynamic as well as static conditions, hysteresis and stress-softening have all been exhaustively investigated in relation to such factors as chemical surface characteristics of the particle, its size and structure and the degree of dispersion achieved; the influence of polymer type and the part played by promoters have also received attention.

The very interesting phenomena displayed by the unvulcanized mixtures of rubber and filler have also been the subject of study, and discussion has ranged over the possible bases for the polymer–filler interaction displayed, in particular, by unsaturated rubbery polymers and carbon blacks.

The insolubilization of the rubber in such mixtures is the subject of this paper, this part of which is primarily a critical review of the literature from a rather narrow viewpoint.

### HISTORICAL NOTE

It is as well to remind ourselves of the earliest recorded observations of Twiss<sup>1</sup>. In a note on the 'theory of vulcanization', Twiss<sup>1</sup> pointed out that 'the presence of carbon black greatly reduces the ease of solubility of raw rubber in the customary solvents in much the same way as does vulcanization'. The rubber–black mixture in the solvent retains its shape, although swollen, and the supernatant solvent remains clear but it is found to contain dissolved rubber. During the following five years other workers reported similar aspects of the phenomenon<sup>2–7</sup>.

Stamberger<sup>8</sup> discussed the phenomena and the behaviour not only of the active channel or gas black but many other fillers in (natural) rubber and observed how the amount of filler carried by the rubber, as it is allowed to diffuse into solvent, is an indication of the activity or the interaction of rubber and filler. The values are given in *Table 1*. These draw attention to the fact that carbon black is not unique in 'reacting' with natural rubber. Furthermore Stamberger<sup>3,9</sup> recorded how a well-masticated rubber—killed rubber, he termed it—of no strength, after a certain time of standing with 20% of carbon black added, gains such strength that it cannot easily be torn by hand. Furthermore whereas the freshly made mixture dissolves readily in a solvent such as benzene, the stiff material after standing a few days only swells. It is interesting to note that McBain<sup>10</sup> explained

**Table 1** Amount of filler diffusing  
[Reproduced from Stamberger, P. 'Colloid Chemistry of Rubber', 1929, by permission of Oxford University Press]

Filler	Amount diffused (%)
Gas black	100
Zinc oxide	98
Magnesium carbonate	87.5
Magnesia	44
Lead oxide	44
Clay	2
Barytes	0.37

the changes as resulting from an orientation of the rubber molecules taking place on standing. A few years later, Cotton<sup>11</sup> referred to the idea of rubber molecules being orientated between particles of reinforcing filler although he made no mention of the insolubilization phenomenon. He cited Blow<sup>12</sup> as showing that the viscosity of solutions of mixes of rubber with low proportions of gas black increased as the time of resting between mixing and dissolving was lengthened. Boiry<sup>7</sup> reported that the time of milling, the time of resting between milling and immersion in solvent and the type and amount of filler alter the extent of insolubilization.

Fielding<sup>13</sup> is usually credited with the first use of the term 'bound rubber' and Wiegand<sup>14</sup>, in recognizing the importance and significance of the phenomenon, also used this term at about the same time.

After this early interest, the subject seems to have aroused less study; it is noteworthy that there is no mention in the index of the IRI Annual Reports on the Progress of Rubber Technology from the first issue in 1937 until 1951 of 'bound rubber' or 'carbon gel'. After White *et al.*<sup>15</sup> had noted that bound rubber developed in GR-S (SBR), which was by then in wide usage under wartime conditions, some quite important work was carried out by workers at Columbian Carbon among others; this is discussed below.

Goldfinger<sup>16, 17</sup>, by removing GR-S from GR-S/black mixtures and by other experiments, established that it is not justifiable to assume that the rubber between pigment particles is equivalent in properties to the original gum stock without pigment, because the addition of pigment induces fractionation of the rubber in such a manner as to concentrate preferentially one molecular configuration around pigment particles and hence leave the rubber richer in some other configurations in the spaces between particles.

Around this time the physical *versus* chemical attachment theories began to be discussed. For example, Dannenberg<sup>18</sup> from swelling measurements on unvulcanized rubber/carbon black (various) mixtures concluded that no chemical bonding of rubber to filler exists, it being a simple physical mixture only, the two components associated through adsorptive forces of the van der Waals type.

Sweitzer *et al.*<sup>19</sup>, of Columbian Carbon, centred their interest, first, on the presence of polymer gel and the effect of high mixing temperatures on the stiffness of vulcanisates. Gel, they defined, as the benzene-insoluble fraction of polymer determined by standard solubility methods<sup>20</sup>. They noted that bound rubber, in rubber/black mixtures, develops at temperatures far below those required for

polymer gel to form in the absence of black. They reported on adsorption experiments which suggest that lower molecular weight fractions of rubber are adsorbed by carbon in dilute solution whereas in concentrated non-solvent mixtures the carbon adsorbs the higher molecular weight fractions.

As a result, they proposed 'carbon gel' or 'carbon gel complex' as preferable to 'bound rubber'. They proceeded to consider the effect of mixing temperature on carbon gel development, including experiments on solutions of mixes made immediately after mixing. They found differences between carbons of equal pH, particle size and structure indicating a chemical effect. Oxygen in small amounts promotes gelation but in large amounts scission is favoured. By implication it is suggested that carbon gel is responsible for modulus increases and differences of modulus increase associated with different black types. This aspect is, however, outside the scope of this discussion, as also is a consideration of the practical effects of bound rubber on processing behaviour.

It may be remarked that it is rare to find workers who have, of recent years, adapted the Einstein and Guth-Gold viscosity/concentration equations to the modulus relationships in rubber/filler systems, accepting the possibility of the  $E_0$  (the Young's modulus of the rubber matrix) not being the same in the mixture as in the pure gum.

From electron microscope studies of carbon gel, Ladd and Ladd<sup>21</sup> of the same laboratories arrived at a picture of highly pigmented carbon gel units separated by polymer gel and areas of low carbon concentration. In later papers, Sweitzer<sup>22, 23</sup> showed that carbon gel increased as the particle size of the black was reduced, although not all blacks showed good correlation. Higher mixing temperatures and higher molecular weight polymers led to higher gel values<sup>24</sup>.

The inference of early workers that different mechanisms were involved in solution adsorption and in bound rubber formation because low molecular weight polymer was preferentially adsorbed, while high molecular weight polymer was preferentially bound was quite logical. The later demonstration<sup>25-27</sup> that both processes preferentially involve high molecular weight polymer removed this particular piece of evidence.

#### EXPERIMENTAL DETERMINATION OF BOUND RUBBER

The term 'bound rubber' rather than 'carbon gel' appears to be generally established.

In reading the literature it is apparent that methods of determining bound rubber have varied in details such as testpiece form—comminuted or not—solvent, ratio of solvent to rubber mix, extent of disturbance of the rubber as it swells in the solvent, method of separation of gel from sol, etc. It may well be that these differences are not significantly important insofar as the effects reported in each investigation are comparable and absolute bound rubber values are not necessary to the overall argument. The usual temperature of test has been 20–25°C but Sircar and Voet<sup>28</sup> worked with boiling solvents (see below).

On the other hand, some workers have been interested not only in the amount of rubber occurring in the solvent—the sol rubber—from which they arrive at the bound rubber, but also in the solvent/rubber ratio in the swollen

jelly. In the latter case particularly the conditions such as degree of testpiece comminution, agitation and method of separation may well affect the result.

Another point that should be made is that, in particular, both Gessler<sup>29</sup> and W. F. Watson<sup>30,31</sup> made measurements only when the cubical dimensions of the testpieces, regardless of the extent of the swell, were fully maintained during the immersion period. In some determinations corrections had to be made because some black diffused with the sol rubber into the solvent.

It is to be regretted that so many authors appear to have ignored the well known effect of time of resting between mixing and immersion on the value; often an arbitrary 24 or 48 hours is set. The back-pressure effect (the presence of rubber dissolved in the solvent reduces the equilibrium solvent/rubber ratio in the jelly) reported by Blow and Stamberger<sup>32</sup> was considered theoretically by Boyer<sup>33</sup> but has not been taken note of, in practical bound rubber determinations, by anyone until Southwart and Hunt<sup>34</sup> in their work on the silicone rubber/silica system. The other point worthy of mention is that of equilibrium being reached in both the bound rubber and swelling values. The Cabot workers generally allow 3 days for extraction, whereas others have assumed that 6–7 days is adequate but this may be far from the truth<sup>34,35</sup>. It is to be noted that two methods are commonly employed for expressing 'bound rubber': the ratio of rubber insolubilized as gel (a) to the total rubber originally present or (b) to the amount of filler present.

Adsorption, as opposed to bound rubber, determinations<sup>16,17,25–27,36</sup> are carried out by methods of which the following is typical: 5 g of polymer are dissolved in 1000 cm<sup>3</sup> of cyclohexane; 4 g of black are stirred into 100 cm<sup>3</sup> of this solution for 30 h; the black is allowed to settle for 1 h and the amount of polymer in the clear solution is determined<sup>29</sup>.

#### RELATION OF BOUND RUBBER TO VULCANISATE PROPERTIES

As already mentioned, considerable attention has been directed to and use made of bound rubber values in the study of the effect of carbon black and other fillers on the physical properties of vulcanisates. There are many contradictions to be resolved but this subject is outside the scope and purpose of this paper<sup>37</sup>. Bound rubber may well be related to some vulcanisate properties, e.g. high extension modulus<sup>38</sup>, but whether or not it remains identifiable in the vulcanisate is open to question.

#### FACTORS AFFECTING THE BOUND RUBBER VALUE (Organic rubber/carbon black systems)

##### Solvent type

Gessler<sup>39</sup> determined the bound rubber value of mixes using a wide range of solvents and concluded that it was virtually independent of solvent type.

##### Extraction temperature

Sircar and Voet<sup>28</sup> determined the amount of unextractable polymer from unvulcanized polymer/filler mixtures at the boil using a number of solvents, boiling in the range 69–196°C; SBR, IIR and polyisobutylene were the polymers examined, compounded with HAF-HS, Graphon and other blacks. The values of unextractables fell sharply from 20% as the temperature was raised. They

concluded that the immobilized unextractable elastomer existing at the carbon black surface points to the existence of chemisorption, defined as higher energy bonding. The gradual decline of the immobilized amount with increasing extraction temperature indicates a spectrum of bonding energies.

##### Time of resting between mixing or milling and extraction

The earlier workers recognized this effect. For example, Dannenberg and Collyer<sup>40</sup> showed the increase in bound rubber formation with resting time before extraction and the behaviour of a fine furnace black is different from that of a channel black; the latter shows a greater increase in bound rubber with ageing. Bound rubber is low in freshly prepared material (if it can be determined) and continues to increase up to 50 days<sup>39,41</sup> (Table 2). In the case of SBR loaded with 50 parts per hundred of rubber (pphr) of HAF black, there is little difference in the storage effect whether in air or *in vacuo*<sup>41</sup>.

Table 2 Effect of storage after milling on bound rubber

[Reproduced from *J. Appl. Polym. Sci.* 1961, 3, 213 by permission of John Wiley, New York]

Hours storage	BRC	BRF	CD
0	0.405	0.212	1.5
8	1.008	0.526	11.1
24	1.040	0.546	12.2

BRC = weight of rubber per g of black in the gel  
BRF = fraction of total rubber rendered insoluble by association with filler  
CD = chain density, number of moles of effective network ( $\times 10^6$ ) associated with 1 g of filler

It is surprising that Parkinson<sup>42</sup> does not refer to this time dependence, because undoubtedly this phenomenon does hinder or reduce the usefulness of bound rubber as an analytical tool. Brennan *et al.*<sup>43</sup> gave data showing how the amount of bound rubber increased during mixing with no mention of the storage time effect; indeed, Boonstra<sup>44</sup> has stated recently that bound rubber is formed immediately during mixing and increases only slightly during storage. Perhaps the effect is modified not only by the amount and type of black but also by the temperature of mixing.

##### Carbon black characteristics

*Type and proportion of black.* Gilliland and Guttoff<sup>45</sup> reported that channel blacks bind more butyl rubber after Banbury mixing than does HAF and the reverse is the case for adsorption from solution. Others have reported this same type of difference. Generally bound rubber, however, shows a good correlation with the specific surface of the black and, if calculated as weight per unit of filler, decreases or remains nearly constant with loading, depending on the black<sup>42</sup>. Brennan *et al.*<sup>43</sup> give the values shown in Table 3 for bound rubber in polybutadiene rubber at 50 pphr.

Gessler<sup>46,47</sup> studied low and high structure HAF black in NR, EPR, CIIR and BR. With low structure black, the extent of bound rubber formation varies with the activity of the polymer functionality. With high structure black, the primary carbon-polymer bonding effects are overshadowed by the formation *in situ* of a facile new radical source which it is proposed results from the

**Table 3** Bound rubber values at 50 pphr black in polybutadiene rubber [Reproduced from *J. Appl. Polym. Sci.* 1964, 8, 2687 by permission of John Wiley, New York]

Black type	Bound rubber
HAF-HS	41.7
HAF	30.3
GPF	12
SRF	11
MT	0

mechanical breakage of the aggregated carbon black structure during mixing.

**Pretreatment of black.** J. W. Watson<sup>35</sup> investigated surface chemical treatments of blacks for their effect on reinforcement of vulcanisates in terms of abrasion and tear. Some data were included indicating that bound rubber values were not changed. Graphitized black gives very low bound rubber values (5 to 7%<sup>36, 43</sup>). Gessler<sup>48</sup> showed that attrited carbon blacks gave bound rubber figures 2 to 3 times higher than the standard blacks. Dannenberg and Donnet<sup>49</sup> have studied how modifying the surface of the black alters the bound rubber value.

#### Milling treatment

Reference must now be made to the classic work of W. F. Watson and the apparent revival of interest and work in this field by him, Gessler, Berry and Cayre, and others. Prior to the publications by W. F. Watson<sup>30, 31</sup>, Kolthoff and Gutmacher<sup>27</sup> reported that substantial amounts of bound rubber are formed when equal weights of black and rubber are mixed by adding the black to the rubber swollen in solvent (chloroform) and drying *in vacuo* at 80°F (26.7°C). Bound rubber, according to these authors, can be formed without milling or high temperature treatment.

Watson's contribution has been summarized by Gessler<sup>46</sup>. Bound rubber gel is quickly formed when a solution-made master batch is passed through the mill, the percentage gel increasing at first and then decreasing. [Values reported by Berry and Cayre<sup>41</sup> do not show the subsequent decrease (*Table 4*)]. The interaction between rubber and black on the mill is characterized by a negative temperature coefficient; the extent of gel formation is greater in nitrogen than in air; the development of bound rubber gel on milling is reduced or prevented when free radical acceptors are added in the system to compete with carbon black for polymer free radicals.

With regard to the effect of molecular weight of the polymer, W. F. Watson<sup>31</sup> found that milling deproteinized crepe in air to different viscosities before preparing the dispersions of black led to lower gel contents.

**Table 4** Effect of milling on bound rubber [Reproduced from *J. Appl. Polym. Sci.* 1961, 3, 213 by permission of John Wiley, New York]

No. of passes through mill	BRC	BRF	CD
0	0.204	0.118	0.54
1	0.326	0.189	1.4
5	0.531	0.307	3.0
100	1.013	0.586	17.2

BRC, BRF, CD—see *Table 2*

In the conventional mixing of black and rubber, there is ample evidence that bound rubber increases with mixing time, although much of the data lacks recognition of the resting effect. On the other hand, milling of rested or heated mixtures reduces bound rubber content<sup>19, 31, 39</sup>.

J. W. Watson<sup>35</sup> and Glander<sup>50</sup> have concluded that the free radical interacting between carbon black and rubber, which contributes to reinforcement, occurs mainly during vulcanization and not during milling.

#### Heating

In a study of the effect of resting, milling and heating the mixtures on bound rubber values Gessler<sup>39, 47</sup> showed how the resting effect can be accelerated by heating for 45 min at 307°F (154°C) and indeed that longer periods of heating lead to higher values. Similar results have been given recently by Brennan and Lambert<sup>51</sup>. The increase of bound rubber value with heating increases as the unsaturation of the polymer increases. No increase occurs with polyisobutylene; it is doubled with SBR<sup>29</sup>.

#### Polymer type

Many authors have drawn attention to the fact that 'unsaturation' in the polymer is necessary for bound rubber development. For reasons of stability, and lack of gel formation, even in the presence of sulphur, Gessler<sup>39</sup>, however, chose butyl rubber with a low unsaturation for much of his exhaustive and careful study of the phenomena.

W. F. Watson<sup>31</sup>, who used deproteinized crepe wholly soluble in benzene at room temperature in 48 hours, showed that ribbed smoked sheets and extracted pale crepe, lightly milled in air to solubilize macrogel and to reduce viscosity to that of the deproteinized crepe, gave similar results; but unextracted pale crepe gave much reduced gel content.

#### Sulphur addition

There are suggestions to be found in many papers over the last 30 years that vulcanization in the presence of fine particle carbon black is in some way different from vulcanization in its absence<sup>52</sup> and sulphur addition in the absence of any crosslinking due to polymer-sulphur interaction has been shown to affect bound rubber contents. Rehner<sup>53</sup> states that sulphur is the common bonding agent in both polymer crosslinks and polymer/filler attachments.

Gessler<sup>29, 46</sup> carried out considerable work on this subject and showed that the inclusion of 2% sulphur leads to high bound rubber values only if heated and if both black and sulphur are present in the polymer. He concludes that there is a close relationship between vulcanization and reinforcement. Of all the polymers examined, the most marked effect was in the case of butyl, with the bound rubber value (at 70 pphr of black) increasing from 30 to 60 on sulphur addition; SBR and EPDM also showed a considerable increase.

#### Additives

W. F. Watson had shown earlier that radical acceptors reduce bound rubber and later Berry and Cayre<sup>41</sup> found that bound rubber and chain density (see later) values were all reduced by adding thiophenol prior to heat treatment. This additive also eliminates the increase of the values on resting before solvent immersion. The anti-

oxidant normally present in SBR (removed in the above experiments by extraction) acts similarly to thiophenol.

There are promoters of the interaction. Harris *et al.*<sup>54</sup> reported an increase in bound rubber when *N*,4-dinitroso-*N*-methylaniline (0.2 pphr) was present in NR, IIR and SBR mixtures with ISAF black over the range 20–70 pphr. The results were in line with reduction of hysteresis.

#### FACTORS AFFECTING THE BOUND RUBBER VALUE (Silicone rubber/silica system)

In this review so far attention has been directed almost exclusively to the organic rubber/carbon black system. Not only for the sake of completeness would it be undesirable to omit the technologically important silicone rubber/silica system but some of the recent observations of this system are very relevant and will be the subject of further discussion and analysis in later sections of this paper<sup>55</sup>.

Warrick and Lauterbur<sup>56</sup> showed that bound rubber is measurable in solution mixtures of silicone rubber and fine particle silica and the amount is increased by heating or milling.

More recently, Southwart and Hunt<sup>57</sup> have published the results of a detailed study of this system. Measurements were made of several properties of the unvulcanized mixtures including Young's modulus, mill breakdown time, bound rubber and swelling in solvents; in particular, they draw attention to the effects of storage, heating, milling, humidity and pH on the properties.

These workers demonstrated first, the much more intense reaction of silica with silicone rubber, compared with that of carbon black with organic rubbers, leading to bound rubber values as high as 90%, i.e. 90% of the rubber initially present in the mix is apparently rendered insoluble in solvents. Secondly, apart from the large increase in bound rubber as the percentage of silica in the rubber is increased, there is a marked and substantial increase of bound rubber (a) on storage at room temperature, (b) on heating at temperatures in the range 100–250°C, and (c) on changing from an acid to an alkaline filler. Their data are summarized in *Table 5* and generally relate to a 24 hour immersion period for the bound rubber determination.

In the third paper of the series, Southwart and Hunt<sup>57</sup>

*Table 5* Bound rubber values for silicone rubber/silica systems (data from Southwart and Hunt)

Storage (days at room temp.)	Silica loading				
	20	30	40		
2	37	44	43		
7	51	64	72		
20	78	76	84		
30	78	81	85		
<hr/>					
Silica loading:	20	32			
Heated: at 150°C	Control	10	at 250°C	Control	55
	10'	61	240'	87	
	30'	66			
<hr/>					
Silica loading 35					
	Acid treated	Alkali treated	Control		
Storage: 5 days	72	91	89		

report a more detailed study of the swelling behaviour of the system and establish that, in some instances, equilibrium is not reached in a 24 h immersion; very much longer times—weeks rather than days—may be required, although they do appreciate that other changes may be occurring to give the effect of non-equilibrium conditions. In mixtures with low proportions of silica the uptake of solvent with time passes through a maximum, which is reached much more rapidly than in the case of the more highly filled mixtures; these, in fact, give a lower uptake, showing no maximum.

The back pressure or osmotic pressure effect mentioned earlier has been investigated in a preliminary way<sup>34</sup> and further reference to this work is made later.

In concluding this section of the review, reference may be made to fine particle silica incorporation in organic rubbers. W. F. Watson<sup>30</sup> included silica in his study of bound rubber development and prevention by milling in the absence and presence of radical acceptors. Wagner and Sellers<sup>58</sup> refer to silica in IIR and SBR but do not report bound rubber values. Contrary to Watson's findings, Endter and Westlinning<sup>59</sup> observed the development of bound rubber with silica in natural rubber not during milling but during storage.

#### RELATION BETWEEN SWELLING INDEX AND BOUND RUBBER

Whereas a number of workers determined and recorded the amount of solvent held by the gel fraction, not many have attempted to draw conclusions from the values.

J. W. Watson<sup>35</sup> plotted swelling index [weight of solvent (benzene) per unit weight of insoluble rubber in the jelly] against bound rubber (insoluble rubber per unit weight of black) and found a good correlation for a range of blacks including Graphon at 50 pphr loading in pale crepe. The higher the bound rubber the lower the swelling index, i.e. on the supposition that crosslinking occurs between rubber and black, the greater the amount of the rubber attached to it, the more it is crosslinked and the lower the swelling. Southwart<sup>60</sup> has published a plot of bound rubber (insoluble rubber per 100 of original rubber by weight) vs. swelling index showing a linear relationship with little scatter of points representing different immersion times, storage times and filler contents (see *Figure 8* below).

From the swollen and dry weights of gel, Gessler<sup>29</sup> calculated the crosslink density using the equation of Flory<sup>61</sup> and the interaction coefficients of Kraus<sup>62</sup>. Berry and Cayre<sup>41</sup> determined sol fraction and swollen weight of jelly and from the Flory-Rehner theory calculated chain density, i.e. the number of moles of effective network chains associated with 1 g of filler.

In a study of the effect of solvent type, Gessler<sup>39</sup> found that the volume of swollen jelly/g of polymer increased fourfold in going from benzene to carbon tetrachloride.

#### DISCUSSION

From the foregoing it is apparent that there are many gaps in our understanding of the phenomena of bound rubber and its significance. The latter is the subject of the next part of this paper because it seems desirable to consider certain fundamental aspects in some detail. The third part of the paper reports some experimental work along hitherto little studied lines, and in the fourth part, current theories are discussed and some comments and suggestions made to advance our understanding.

## PART II: CRITICAL APPRAISAL OF THE ACCURACY AND SIGNIFICANCE OF 'BOUND RUBBER' VALUES

### INTRODUCTION

There is, in the literature, very little analysis of the observations and processes occurring during a bound rubber determination. Rather, it seems, have workers tended to adopt a standard method as mentioned earlier, and not analysed how far the value obtained depends on the particular conditions chosen in relation to the particular structure of which they are determining the bound rubber content.

### LIMITED AND UNLIMITED SWELLING; GEL AND SOL FRACTIONS

The classical distinction used to be made between substances—colloidal, high molecular weight substances—which showed limited swelling and those that showed unlimited swelling in liquids with which they are compatible. A substance showing limited swelling maintains its original shape and form; i.e. a sheet sample remains as a sheet with clearly defined faces and edges, after absorbing the liquid in quite considerable quantities. A substance showing unlimited swelling soon loses its shape and form and the boundary between solid and liquid becomes diffuse and eventually a solution of high viscosity is obtained.

Polymers dissolve in solvents of similar cohesive energy densities or solubility parameters. Swelling, as opposed to solution, occurs when the mobility of the polymer molecules is restricted (a) by attachments to one another—chemical crosslinks as in vulcanized rubbers, (b) by entanglements, (c) by 'association' with a second phase, in particular, a fine particle filler.

In the first case, except in the instance where the number of chemical crosslinks is very small, the polymer swells on immersion in solvents or liquids (in which in the uncrosslinked state it would dissolve) and no polymer is found to diffuse into the solvent.

In the second case, frequently observed in raw natural rubber, dried natural rubber latex films, and high molecular weight raw synthetic rubbers, in which it is now known some crosslinked structures are present, the polymer will absorb solvent, swell and retain its shape sufficiently for a separation to be made into a supernatant solvent phase which contains polymer—sol rubber—and a gel fraction. There is considerable literature on the subject of the insoluble fraction of rubbers.

In the third case, that of filled polymers, the behaviour bears some resemblance to that of the second case.

For the original testpiece shape to be retained, i.e. the swelling to be limited, it seems essential for there to be a three-dimensional structure. Chemical crosslinking provides this. Polymer molecules 'attached' to a second phase—a fine particle filler, be it carbon black or silica—and bridging the spaces between particles also provide such a three-dimensional network. Unattached molecules can diffuse out of such a structure if they are small enough and mobile enough in relation to the network; provided also that the thermodynamic situations permit, e.g. the solvent outside the jelly contains a lower concentration of polymer than that in the jelly. Whereas the gel content of polymers can be determined if swelling is unlimited, a bound rubber value cannot so readily be obtained; in

practice, most workers do not attempt it (see above), because of the filler entering the solvent.

### BOUND RUBBER DETERMINATIONS

#### *Storage changes*

Presumably the changes which take place on storage can continue during the determination of bound rubber and this is the first complication. Conceivably, if the active sites or groups on filler and rubber take time to find one another, then the expansion of the system by solvent may, on the one hand, increase the mobility of the molecules and the chance of 'reaction', but, on the other hand, may remove the active sites further apart. There is thus considerable uncertainty as to what time dependent processes take place during a bound rubber determination.

#### *Processes occurring during the determination*

There are three processes proceeding at once when an (aged) rubber/carbon black mix is immersed in solvent: (i) the carbon black particle/polymer molecule/carbon black particle (B-P-B) three-dimensional network is absorbing the solvent to the limit of the extensibility of the polymer molecules; (ii) the polymer molecules attached to only one particle are extending into the solvent and taking with them the black particle if such particle is not attached to another particle by a polymer molecule; (iii) unattached polymer molecules are dispersing in the solvent and diffusing, as much as physically possible, into the solvent outside the jelly.

#### *Diffusion—a major factor?*

The entry of rubber into the solvent is a diffusion controlled process and the rate at which this soluble unattached, unreacted rubber leaves the jelly and enters the solvent phase depends on its molecular weight and the size of the interstices, i.e. on the compactness or degree of expansion of the rubber/filler gel structure by the solvent. Southwart<sup>60</sup> has pointed out that, at low silica contents, a silicone rubber/filler mixture shows a high rate of swell and a high final swell value which, in fact, passes through a maximum with time of immersion. Much of the bound rubber data does not give a detailed complete picture because, in the determination, procedures such as degree of agitation, separation technique, etc. will affect the proportion of rubber taken as gel and influence the degree to which the jelly remains intact, e.g. how many B-P-B links are broken.

#### *'Back' or osmotic pressure effect*

There is a third factor complicating or modifying the value of bound rubber and that is the 'back' pressure effect, already referred to previously and originally reported by Blow and Stamberger<sup>32</sup> as occurring in swelling tests on dried latex rubber films which show limited swelling with a proportion of soluble rubber diffusing into the solvent. As the amount of free solvent is varied in relation to a fixed weight of rubber, the concentration of sol rubber in the solvent will vary and affect the swelling because of a back pressure or osmotic pressure effect. In bound rubber determinations a similar



effect is present and the amount of solvent to rubber will affect the degree of swelling and the value of bound rubber obtained. It is questionable whether the term 'osmotic pressure' should be used.

#### Equilibrium states

There are a number of equilibrium states that can be considered: (a) by repeated change of solvent until no more extraction/diffusion of rubber occurs from the jelly and the solvent surrounding the jelly contains no dissolved rubber, it is possible to obtain an apparent true bound rubber value; but there may still be associated with the bound rubber some sol rubber that is of such high molecular weight that it does not diffuse out of the jelly; (b) an equilibrium can be established between jelly and solution by leaving rubber in contact with solvent; this apparent bound rubber value will contain a proportion of soluble rubber, the back pressure effect will have restricted the swelling and, therefore, reduced the amount of soluble rubber diffusing out of the jelly; (c) in the case of both (a) and (b) no account is taken of the polymer/filler interaction possibly not having reached equilibrium either at the beginning or during the bound rubber determination. The amount of soluble polymer may increase by chain breakdown or decrease by attachment to filler particles, and these changes may be influenced by the presence of solvent.

It is erroneous to suppose that, because bound rubber values change on changing the solvent during the determination, equilibrium is not achieved; there can be equilibrium as stated [(b) above] subject to changes as mentioned in (c).

#### APPLICABILITY OF SWELLING THEORY

Swelling theory is based on the assumption that the crosslinks are uniformly distributed, which may well be the case and is usually so when chemical. In a system consisting of a filler particle of 200 to 400 Å diameter, to the surface of which several polymer molecule ends or active sites are attached, the situation is very different in that a number of polymer molecules are associated or aggregated; the cohesion of the polymer around the filler particles may be increased. It is often stated that the swelling of the polymer molecules attached to the particle is nil or less than normal. Molecules do not swell; they separate in a solvent because their cohesion is similar to that of the solvent; if they do not dissolve it is because they are not free and separate entities—they are cross-linked, entangled, entrapped, physically adsorbed or chemically bound on a second phase<sup>63</sup>.

If it is accepted that the 'crosslinks' are non-uniformly distributed in such rubber/filler systems, swelling theory cannot be applied.

#### SWELLING INDEX VERSUS BOUND RUBBER

Swelling index, i.e. the amount of solvent associated with one part of insoluble rubber in the jelly (either on a volume or weight basis), on samples as storage proceeded was reported by Southwart<sup>60</sup> to give a linear plot against bound rubber, with only small scatter on varying silica proportion in silicone rubber/silica mixtures. Furthermore, on extrapolation the line passed through the point 100% bound rubber, nil swelling (approximately). As

Southwart remarks, swelling and bound rubber may be manifestations of the same reaction and as such correlate well. Alternatively, the three-dimensional structure due to rubber/filler interaction restricts the swelling and because the expansion of the structure is limited in this way, the amount of soluble rubber diffusing out is proportional to the amount of swelling. A further point to be made is that there may be a balance between sol rubber concentration in the solvent phase, liquid uptake by the insoluble rubber, and the soluble rubber concentration in the solvent present in the jelly.

Southwart's plot, however, draws attention to the fact that, in practice, the bound rubber values of different samples are determined at different degrees of swelling.

#### Partition of sol between solvent inside and outside the jelly

In all bound rubber values so far reported in the literature it is probably correct to say that the soluble rubber present in the solvent phase of the jelly is included in the value. Because the activity of the solvent in the jelly is lowered by the presence of insoluble rubber bound by the filler, it is to be expected that the sol rubber/solvent ratio inside the jelly will differ from that in the liquid phase with which it is in equilibrium. This partition coefficient would be expected to vary as the amount of filler to rubber is varied.

Southwart and Hunt<sup>34</sup> have described experiments in which bound rubber determinations of silicone rubber/silica mixtures were carried out in solutions of the silicone rubber in solvent.

Initially the silicone rubber/silica mixture consists of  $S_g$  parts of soluble polymer,  $B$  of insoluble, bound polymer and  $F$  of active filler, and is immersed in  $T_1$  parts of solvent containing  $S_s$  parts of dissolved polymer.

This becomes, at equilibrium, a jelly consisting of  $S'_g$  parts of soluble polymer,  $B$  of insoluble,  $F$  of filler and  $T_2$  of solvent (assuming no diffusion of filler from the jelly); immersed in a solution phase consisting of  $T_3$  of solvent and  $S'_s$  of dissolved polymer. The following equivalences will hold:

$$T_1 = T_2 + T_3 \quad (1)$$

$$S_g + S_s = S'_g + S'_s \quad (2)$$

and  $G$ , the bound rubber value as reported,  $= S'_g + B$  (3.) Assume  $B$  is a constant for any filler/polymer ratio and is independent of the method of extracting the soluble rubber, and  $P$ , a partition coefficient for soluble polymer between jelly and solution  $= S'_g T_3 / S'_s T_2$  (4). Then, from equations (3) and (4),  $G = (P S'_s T_2 / T_3) + B$ , and a plot of  $G$  against  $S'_s T_2 / T_3$  should yield a straight line, from which  $P$  and  $B$  can be obtained as constants for any particular mixture. Plotting the data of Southwart and Hunt for three silicone rubber/silica mixtures immersed in a range of solutions with equilibrium approached from the dry mix and swollen jelly, one does indeed obtain linear plots and values of  $B$  and  $P$  as given in Table 6 and Figure 1.

As the silica content decreases the true insolubilized content decreases and the partition coefficient increases to approach one for zero bound rubber (Figure 2).

#### True bound rubber values

This suggests a method of arriving at the true bound rubber from two determinations of the apparent bound rubber of the mixture immersed in solutions of different concentrations. One final point should perhaps be made



Table 6 Bound rubber values and partition coefficients (Derived from immersion tests in range of solutions; Southwart and Hunt)

Silica loading per 100 silicone rubber	'True' bound rubber	Partition coefficient
8	23	0.56
26	58	0.27
44	76	0.13

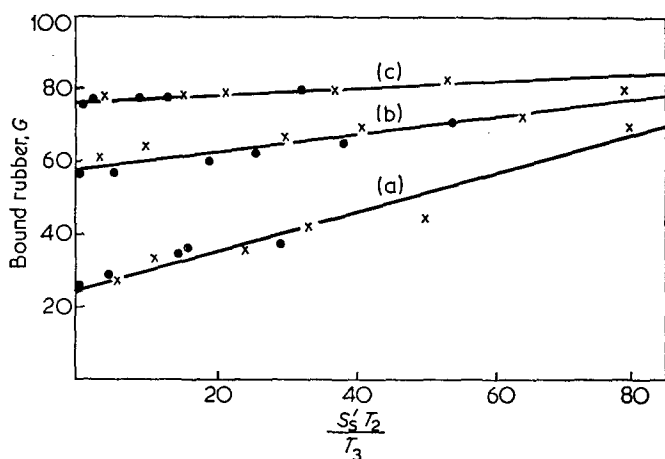


Figure 1 Bound rubber (G) vs.  $S_2^2 T_2 / T_3$  for silicone rubber/silica mixtures. (a), 8; (b), 26; (c), 44 pphr silica. x, Dry testpieces; ●, preswollen testpieces. [Data from Southwart and Hunt, *J. Inst. Rubber Ind.* 1968, 2, 142, Tables VI and VII]

to justify bound rubber determinations. If the attachments, in whatever structure finally results from the interaction of filler and polymer, are essentially physical it is likely that the solvent, according to type, will disturb these attachments and a true bound rubber would be unlikely to be obtainable. If the attachments are essentially chemical, there should be a true bound rubber value.

### PART III: A STUDY OF NATURAL RUBBER-FINE PARTICLE BLACK SYSTEMS

#### INTRODUCTION

The object in the experiments described here was (a) to study the swelling behaviour of natural rubber/carbon black mixtures, in particular the rigidity of swollen jellies, after various times and conditions of storage between mixing and immersion in solvent, (b) to investigate the behaviour of the mixtures in different solvents, and (c) to suggest the use of the back pressure effect to arrive at a true bound rubber value.

#### MATERIALS

Ribbed smoked sheets (RSS) and constant viscosity standard Malaysian rubber (SMR-CV) were used without extraction but in both cases were given extensive mastication before addition of black.

MPC (C—channel), HAF-HS (H—high structure) and HAF-LS (L—low structure) blacks were used as the fillers.

The solvent for swelling tests was toluene.

#### GEL RIGIDITY

##### Preliminary investigation

A 400 g batch of RSS was masticated for 1 h on a 12 in x 6 in (1 in ≡ 25.4 mm) mill at friction speed with

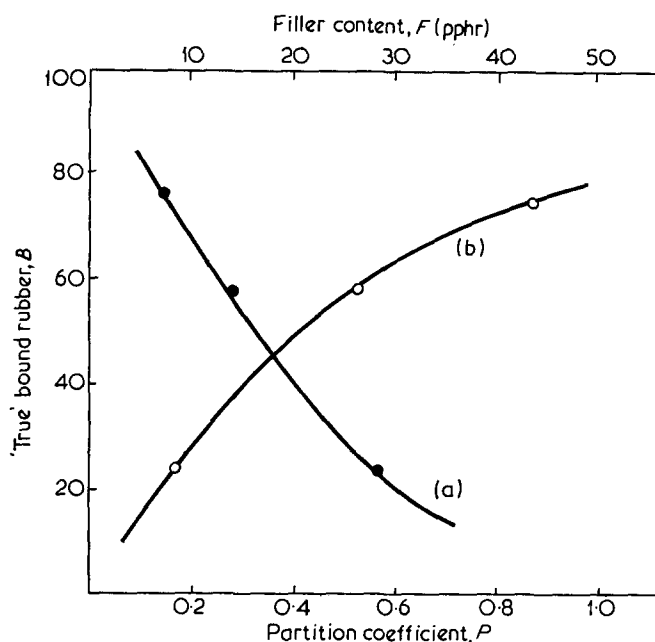


Figure 2 'True' bound rubber (B) vs. (a) partition coefficient (P) and (b) filler content (F) in pphr by weight. (From Figure 1)

Because the solvent type has little effect on the bound rubber value<sup>39</sup> and true bound rubber values are apparently obtainable (see later section), the evidence mounts for chemical attachments. The two problems are then (a) to decide when the interaction is complete; is the frequently reported increase of determined bound rubber on heating a different reaction or only an acceleration to the same final value as is reached on prolonged storage at room temperature? and (b) to make an accurate determination of the true bound rubber value in as short a time as possible before other changes take place.

cold water cooling; 200 g were removed and the remaining 200 g were masticated for a further hour and a half. A 200 g batch of SMR-CV was masticated for 2 h at which time it appeared to be similar to the second batch of RSS in softness. All three batches were too soft to obtain Mooney values at 100°C.

50 g portions of each batch were mixed with 10 g of the three fillers on a mill with 3 in roll width; nip settings and mixing and grinding times being kept constant as far as possible. Within 10 min of being taken off the mill, 1 g portions of each were immersed in toluene; further samples were immersed in toluene after resting at room temperature for 2, 11 and 36 days. The mixtures were not disturbed except for examination at intervals.

The behaviour of the rubber mix was recorded from visual observation and assessment of the rigidity of the jelly, the colour of the free toluene, etc. In addition to complete solution, it proved easy to rate the gel rigidity into six categories; with increasing time of immersion beyond 3 or 4 days the rating changed very little and in no case affected the general conclusion from these observations, as recorded in Figure 3. RSS developed much more rigid jellies more rapidly than the CV rubber; HAF-HS black behaved similarly to MPC but HAF-LS gave significantly softer jellies particularly in the RSS.

Approximately 10 months after mixing, the CV/C and

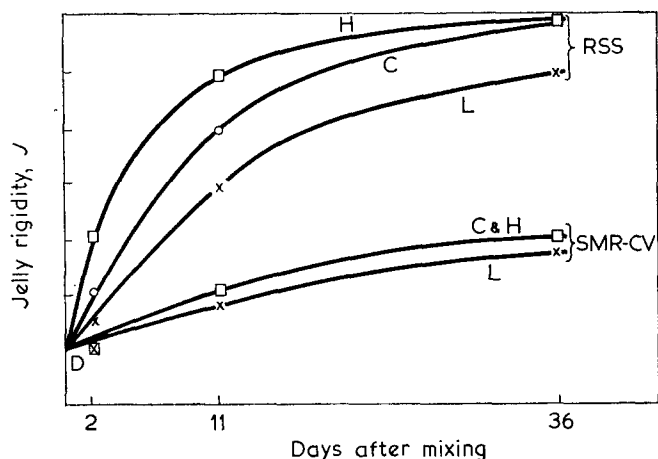


Figure 3 Jelly rigidity (*J*) vs. time of resting between mixing and immersion in solvent; RSS and SMR-CV with 20 pphr of MPC (C), high (H) and low (L) structure HAF blacks

Table 7 *S<sub>r</sub>* values determined 19 months after mixing

	Black MPC	Black HAF-LS	Black HAF-HS
RSS-A	6.95	7.1	5.75
SMR-CV	5.65	4.6	—
Milled 19 months after mixing			
RSS-A			
0 days rested	Dissolved	Dissolved	
17 days rested	Dissolved	9.1	

*S<sub>r</sub>* = weight of solvent in jelly per unit weight of rubber in original mix, assuming no loss to solvent

CV/L mixes were passed approximately 10 times through the nip of a mill and were found to be immediately soluble in toluene. Nineteen months after the original mixing date portions of some batches, not remilled, were immersed in toluene and were all found to give rigid jellies with a perfectly clear black-free solvent. The jellies were separated from the free solvent and weighed to calculate the weight of solvent per unit weight of rubber in the jelly, taking no account of loss of rubber to the solvent (Table 7). At the same time, the least masticated RSS/C and /L batches were passed through the nip and on immersing in toluene immediately were found to be soluble. Seventeen days later the mix containing the low structure black gave a jelly.

Fuller investigation

It was decided to carry out a fuller investigation with greater emphasis on: (a) comparative viscosity and plasticity values of the masticated rubbers; (b) working at two or more levels of plasticity; (c) more precise recording of jelly strength, etc.; (d) estimation of bound rubber; and (e) estimation of weight of solvent in jelly related to original mix, gel rubber, black content.

The investigation is incomplete but already some facts have come to light.

Mastication and mixing. RSS and SMR-CV were masticated and four batches of each were selected and designated RSS1 to RSS4 and CV1 to CV4, 1 being the least masticated and 4 being the most masticated. In fact, only batches 1 and 4 have been used to date, and only MPC and HAF-HS blacks, again at 10 parts by weight per 50 of rubber.

Viscosity and plasticity determinations. Mooney viscosity tests were possible on masticated rubbers 1 and 2, (ML 100°C 1+4) values being as follows: RSS1, 23; RSS2, 14; CV1, 24; CV2, 12.

Parallel-plate plastimeter tests were carried out on all batches of masticated rubber and black mixes; the recorded values in Table 8 are the amounts of compression, occurring under the load after 60 and 120 sec, as a percentage of the original testpiece thickness, and are the means of duplicates. It is to be noted that the plasticities of the corresponding masticated batches were very close in the case of 1, 2 and 4. Of the mixed batches, the CV were softer than the RSS and the HAF-HS softer than the MPC (Table 8). [Plasticity values of some of the batches of the preliminary investigation were also obtained at this time, 19 months after mixing. It is to be noted that the remilled material has not recovered its hardness even after 9 months' storage (Table 9).]

Storage conditions. Within 24 h of mixing portions of each mix were placed in storage under the following conditions: over silica gel; over water; *in vacuo*; in a refrigerator at -1°C 48 h later.

Immersion conditions. At intervals 0.4 g testpieces, approximately 2.5 mm thick, were placed in 10 cm<sup>3</sup> of toluene at room temperature and allowed to swell for 24 hours. Separation was then made and the weight of the swollen jelly was determined; jelly and free solvent solution were then dried and the sol and gel contents were

Table 8 Parallel plate plasticity tests (% compression of testpiece under 250 g load at room temperature)

Batch	RSS		CV	
	After 60 sec	After 120 sec	After 60 sec	After 120 sec
1	15.5	19.3	17.2	21.0
2	20.9	25.1	20.2	25.1
3	27.8	34.0	34.0	41.2
4	35.3	44.2	36.6	44.2
Black mixes (20 pphr) 24 h after mixing				
	MPC		HAF-HS	
	After 60 sec	After 120 sec	After 60 sec	After 120 sec
RSS1	19.0	23.0	20.8	26.6
CV1	19.4	24.6	24.4	29.0
RSS4	26.7	32.8	30.0	35.3
CV4	29.7	35.7	35.0	42.7

Table 9 Parallel plate plasticity tests (Mixes used in preliminary experiment)

	MPC		HAF-HS	
	After 60 sec	After 120 sec	After 60 sec	After 120 sec
A: RSS-A	7.5	8.1	9.5	10.5
CV	5.0	5.2	3.5	3.6
B: CV	35.0	38.8	34.8	38.6

A. 19 months after mixing (500 g load)  
 B. Remilled 10 months after mixing; tested 9 months later (250 g load)

determined. At the same time, a note was made of the jelly strength and the colour of the solvent.

*Assessments.* Five gradings of solvent colour, (1 clear to 5 blackest) and seven of jelly strength were possible; the latter grading being relatively easy, the higher the value the greater the rigidity: (1) an extremely mobile jelly, original shape and form lost, disperses with slight agitation—separation impossible; (2) a less mobile jelly—separation not possible; (3) a jelly that could be just separated from the free solvent, but flowed and broke up; (4) a more rigid jelly, separable without much difficulty, but tended to cling to the sides of the flask and break up into small lumps; (5) more rigid still with only very slight tendency to cling to the vessel and break up; (6) a form-steady jelly, easily separable, but edges and corners rounded; (7) in this case the edges and corners of the separated jelly were well-defined.

The photographs of the dried jellies (*Figure 4*) are representative of the gradings 2 to 7 inclusive. The high rigidity jelly (7) did not spread and on drying shrank to a small area. The low rigidity jelly (2), not completely separable from the solvent phase, flowed to a very much larger area and dried with relatively little area contraction. The area covered by the swollen jelly is just discernible (not to be confused with the labels on the underside of the Petri dishes).

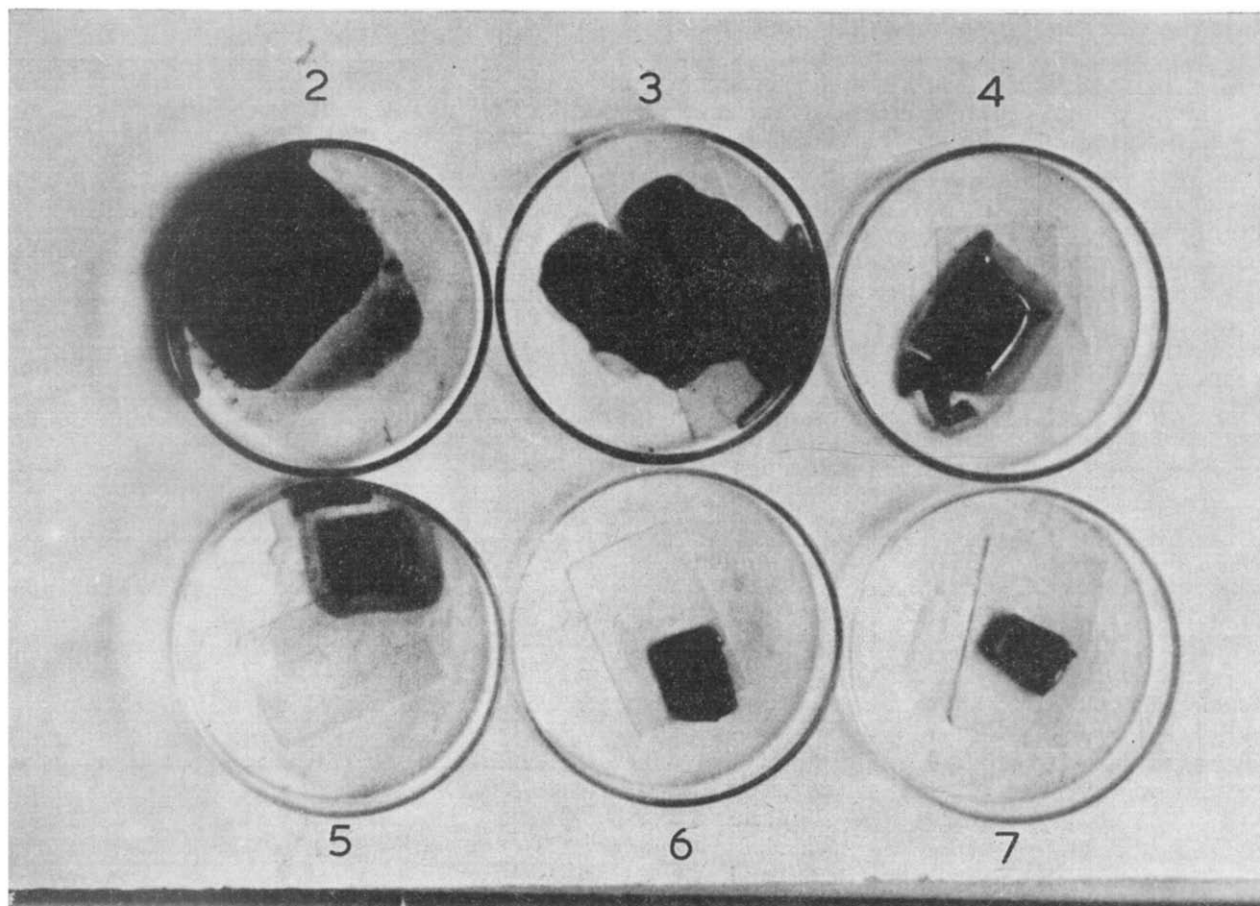
*Analysis of results and discussion.* The qualitative and quantitative results are recorded in *Tables 10* and *11*.

The qualitative results show that: (a) the CV rubber, as in the preliminary investigation, gave much weaker jellies

under all conditions and times of storage than the corresponding RSS mixes. More black diffused into the solvent in the case of the CV rubber mixes; (b) refrigeration of the sample delayed the strengthening of the jelly, and the development of black-free solvent; (c) dry storage tended to accelerate the development of rigidity; e.g. the only case of a CV mix, from the softer masticated rubber giving a clear sol was after dry storage; (d) more often than not the HAF-HS black gave a weaker jelly than MPC; (e) on average the more masticated rubber (batch 4) gave weaker jellies than the less masticated (batch 1).

In the early part of the investigation, the sol rubber was not determined so only values of  $S_r$ , the weight of solvent in the jelly per unit weight of original rubber, are given. In the latter part, the weight of solvent in the jelly per unit weight of insoluble or unextracted rubber and the amount of rubber retained in the jelly were determined. From these results:  $W_{rb}$  = bound rubber/black ratio in the jelly, by weight;  $W_{rs}$  = bound rubber/solvent ratio in the jelly, by weight; and  $W_{bs} = W_{rs}/W_{rb}$  = black/solvent ratio in the jelly, by weight.

It is appreciated that swelling and bound rubber were not always carried to equilibrium but this was because the interest lay in the jelly strength and amount of black diffusing out with the rubber. The  $S_r$  and  $W_{rs}$  values, representing the composition of the jelly, show poor correlation with  $J$ , the jelly rigidity. A plot, however, of  $W_{rb}$  vs.  $W_{rs}$  (*Figure 5*) for the testpieces that had rested for from 49 to 59 days before immersion shows a hint of a relationship insofar as several points, representing a particular jelly rigidity, lie on lines more or less parallel to



*Figure 4* Photographs of dried jellies, illustrating the different rigidities graded 2-7 inclusive

Table 10 Colour of solvent  
1=clear; 5=black

Time of resting (days)	Batch 1					Batch 4				
	R.T.	Ref.	Dry	Wet	Vacuo	R.T.	Ref.	Dry	Wet	Vacuo
MPC in RSS:										
7	4	—	—	—	—	4	—	—	—	—
21-23	—	4	1	1	1	—	5	1	1	1
42	1	—	—	—	—	1	—	—	—	—
57-59	—	3	1	1	—	—	4	1	1	—
MPC in CV:										
7	4	—	—	—	—	4	—	—	—	—
21-23	—	5	4	4	4	—	5	4	5	5
42	2	—	—	—	—	3	—	—	—	—
57-59	—	5	3	2	—	—	5	3	5	—
HAF-HS in RSS:										
7	4	—	—	—	—	4	—	—	—	—
28-30	—	—	1	1	1	—	5	1	1	1
49-51	—	3	1	1	1	—	4	1	2	1
HAF-HS in CV:										
7	—	—	—	—	—	5	—	—	—	—
28-30	—	4	1	1	1	—	5	1	4	4
49-51	—	5	1	2	2	—	5	2	4	3

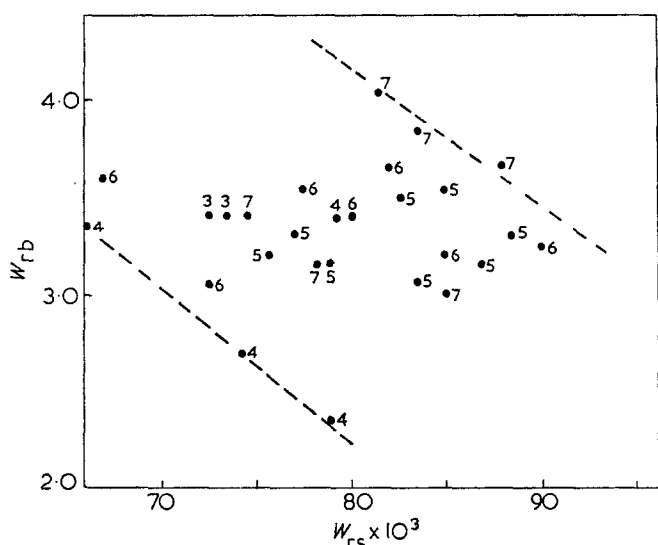


Figure 5 Bound rubber: black ratio in jelly ( $W_{rb}$ ) vs. bound rubber: solvent ratio in jelly ( $W_{rs}$ ); numerals indicate jelly rigidity ( $J$ )

each other. Because the cold-stored testpieces and the CV based mixes are included, a range of rigidities is present. The most rigid jellies have the highest  $W_{rb}$  and/or the highest  $W_{rs}$  values and *vice versa*, as is to be expected. There are, nevertheless, instances of jellies of nearly the same  $W_{rs}$  values (rubber to solvent ratio) with different rigidities; e.g.

RSS4/MPC/Refrigerated and Dry:

$$W_{rs} = 0.0725 \text{ and } 0.0745; J = 3 \text{ and } 7$$

CV4/MPC/Refrigerated and Wet:

$$W_{rs} = 0.085 \text{ and } 0.087; J = 2 \text{ and } 5$$

The difference in rigidity of two jellies of equal composition can only be explained by assuming that the weaker one has fewer crosslinking molecules (interparticulate rubber); the adsorbed molecules attached at one end or

one point only to a black particle surface contribute only marginally to the rigidity. It is to be noted that low viscosity rubber was used so that any residue of sol rubber in the jelly will contribute little to its modulus; and incidentally provide little shearing action to generate free radicals during black addition.

#### BEHAVIOUR OF RUBBER/CARBON BLACK MIXTURES IN VARIOUS SOLVENTS

##### Introduction

In the literature, there is a frequently repeated suggestion that the shell or adsorbed rubber appearing as insoluble will not swell or only swell to a small extent. It is an attractive and reasonable suggestion that the cohesive energy density of the bound rubber is different from that of unbound rubber. Whereas, from some aspects, cohesive energy density (or its square root, the widely used solubility parameter) is a fundamental of a molecule of a liquid, Beerbower *et al.*<sup>64</sup> have pointed out, in the case of polymers and particularly copolymers, that there are several complicating and modifying factors. Furthermore, if polymer and filler react chemically, it is to be expected that the solubility parameter of the polymer might be changed. From this one could argue that the peak in the plot of the volume uptake (in a range of liquids) vs. their solubility parameters would be shifted compared with a chemically crosslinked system such as occurs in a pure gum vulcanisate.

##### Experimental

Portions of the mixture RSS1C, used for the investigation described in the previous section and stored for many months at room temperature and therefore assumed to have reached a stable state, were immersed in toluene to extract a substantial proportion of the soluble rubber present; the solvent was dried off to give samples of mix containing carbon black, insoluble rubber and some soluble rubber. These were then immersed in the four

Table 11 Jelly rigidity,  $S_r$ ,  $W_{rb}$ ,  $W_{rs}$  and  $W_{bs}$  values

Time of resting (days)		Batch 1					Batch 4				
		R.T.	Ref.	Dry	Wet	Vacuo	R.T.	Ref.	Dry	Wet	Vacuo
<b>MPC in RSS:</b>											
7	$J$	4	—	—	—	—	4	—	—	—	—
	$S_r$	11.1	—	—	—	—	11.5	—	—	—	—
21-23	$J$	—	4	6	6	6	—	3	6	6	6
	$S_r$	—	9.2	9.4	9.8	10.5	—	10.6	9.5	9.9	7.9
42	$J$	7	—	—	—	—	7	—	—	—	—
57-59	$J$	—	6	7	7	—	—	3	7	6	—
	$W_{rb}$	—	3.6	4.05	3.85	—	—	3.4	3.4	3.4	—
	$W_{rs}$	—	0.067	0.082	0.084	—	—	0.073	0.075	0.080	—
	$W_{bs}$	—	0.018	0.020	0.022	—	—	0.021	0.022	0.024	—
<b>MPC in CV:</b>											
7	$J$	4	—	—	—	—	2	—	—	—	—
	$S_r$	11.3	—	—	—	—	—	—	—	—	—
21-23	$J$	—	3	4	4	5	—	1	4	5	3
	$S_r$	—	10.9	10.5	10.8	11.0	—	—	9.9	9.1	8.2
42	$J$	5	—	—	—	—	5	—	—	—	—
57-59	$J$	—	4	6	6	—	—	2	4	5	—
	$W_{rb}$	—	3.35	3.05	3.55	—	—	3.55	3.4	3.15	—
	$W_{rs}$	—	0.066	0.073	0.078	—	—	0.085	0.079	0.087	—
	$W_{bs}$	—	0.020	0.024	0.022	—	—	0.024	0.023	0.026	—
<b>HAF-HS in RSS:</b>											
7	$J$	4	—	—	—	—	4	—	—	—	—
	$S_r$	9.1	—	—	—	—	7.8	—	—	—	—
28-30	$J$	—	4	7	5	5	—	3	7	5	6
	$S_r$	—	8.5	9.0	8.0	9.0	—	8.2	6.5	7.1	6.6
49-51	$J$	—	5	7	5	7	—	5	7	6	4
	$W_{rb}$	—	3.3	3.65	3.2	3.15	—	3.15	3.0	3.25	2.7
	$W_{rs}$	—	0.077	0.088	0.076	0.078	—	0.079	0.085	0.090	0.074
	$W_{bs}$	—	0.023	0.024	0.024	0.025	—	0.025	0.028	0.028	0.027
<b>HAF-HS in CV:</b>											
7	$J$	2	—	—	—	—	1	—	—	—	—
28-30	$J$	—	3	4	3	4	—	1	6	4	4
	$S_r$	—	9.2	8.8	9.8	8.8	—	—	7.3	7.2	5.9
49-51	$J$	—	3	6	5	5	—	1	6	5	4
	$W_{rb}$	—	3.4	3.65	3.5	3.3	—	—	3.2	3.05	2.35
	$W_{rs}$	—	0.074	0.082	0.083	0.089	—	—	0.085	0.084	0.079
	$W_{bs}$	—	0.022	0.022	0.024	0.027	—	—	0.027	0.027	0.034

$J$ =jelly rigidity; 1 the weakest, 7 the strongest

$S_r$ =weight of solvent in jelly per unit weight of rubber in original mix; assumes no loss of rubber into the solvent

$W_{rb}$ =ratio of bound rubber to carbon black in the jelly, by weight

$W_{rs}$ =ratio of bound rubber to solvent in the jelly, by weight

$W_{bs}$ =ratio of carbon black to solvent in the jelly, by weight

Batch 1 is least masticated; batch 4 most masticated

solvents, hexane, cyclohexane, toluene and methyl ethyl ketone with solubility parameters of 7.3, 8.2, 8.9 and 9.2. Two series were carried out; the first with a pre-immersion period of 3 days, and the second with a pre-immersion period of 10 days. Some further extraction of soluble rubber occurred in all cases, except for MEK, as is to be expected. The solvent uptake was calculated on the basis of the dried weight of the sample less its black content. In parallel, portions of a pure gum vulcanisate [containing (in parts by weight): natural rubber (RSS), 100; zinc oxide, 4; stearic acid, 2; sulphur, 3; mercaptobenzthiazole, 1; antioxidant, 1; vulcanized for 20 min at 150°C] were swollen to equilibrium in the same solvents and the solvent uptake was again calculated on the dried weight of the rubber. The swelling results are given in Table 12 and plotted against the solubility parameters in Figure 6. There seems no evidence that the solubility parameter (cohesive energy density) of the rubber has been significantly altered by being adsorbed or reacted with the carbon black.

Table 12 Immersion of RSS1C mix in toluene and after drying, in other solvents—as indicated

Solvent	S.P.	3 days immersion		10 days immersion		Swelling index of pure gum vulcanisate
		Bound rubber (57.8)*	Swelling index (14.7)	Bound rubber (34.5)	Swelling index (17.6)	
Hexane	7.3	28.3	11.4	24.4	11.2	1.55
Cyclohexane	8.2	31.0	15.0	24.2	19.6	3.28
Toluene	8.9	24.0	23.6	21.5	26.0	3.80
MEK	9.2	—	0.86	—	0.93	0.69

\* Figures in parentheses are values after initial immersion in toluene

BACK PRESSURE EFFECT AS A MEANS OF ARRIVING AT A TRUE BOUND RUBBER VALUE

Experimental

Samples of the same RSS1C mix were immersed in a series of solutions of the two masticated rubbers, RSS1

Table 13 Back pressure effects

Swelling behaviour of RSS1C mix in solutions of masticated rubbers RSS1 and RSS4 in toluene; final (equilibrium ?) conditions; data based on 100 parts of the rubber in the original RSS1C mix (by weight)

	RSS1 solutions				RSS4 solutions			
Jelly: Insol G	43.1	63.5	80.7	92.2	32.3	51.2	76.6	90.4
Solvent $T_2$	520	546	507	401	651	529	495	467
Solution: Sol $S_s$	155	225	374	481	67.7	255	420	526
Solvent $T_3$	2500	2220	2390	1940	3140	3110	2910	2660
$\frac{S_s T_2}{T_3}$	32.2	55.5	79.2	99.5	14.0	43.4	71.6	90.5

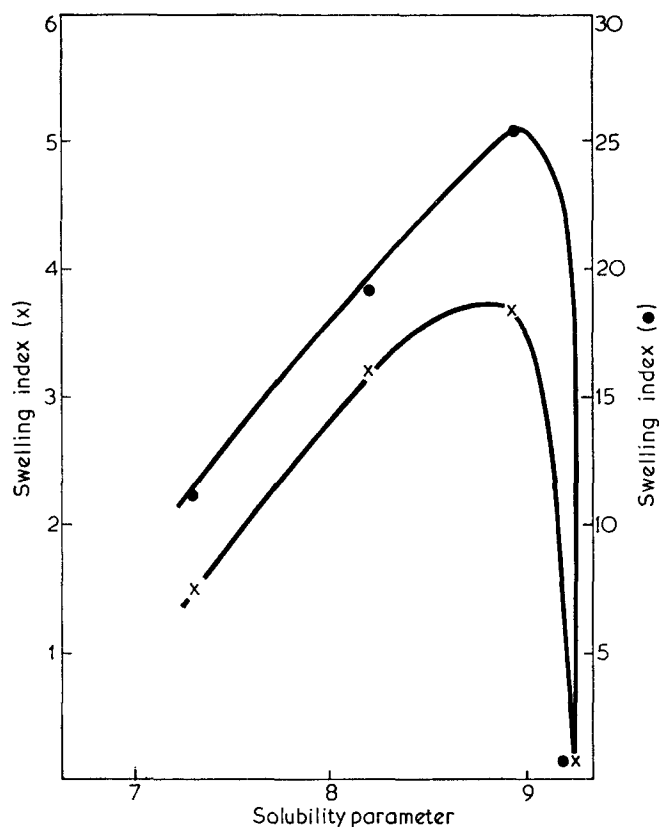


Figure 6 Swelling index vs. solubility parameter. ●, Mix RSS1C (unvulcanized); x, pure gum natural rubber vulcanisate

and RSS4, representing two levels of mastication and molecular weight; 7 days immersion was allowed to reach equilibrium and then separation of swollen carbon black rubber jelly from the solution was effected; the weights of jelly, solution, dried jelly and dried solution were measured

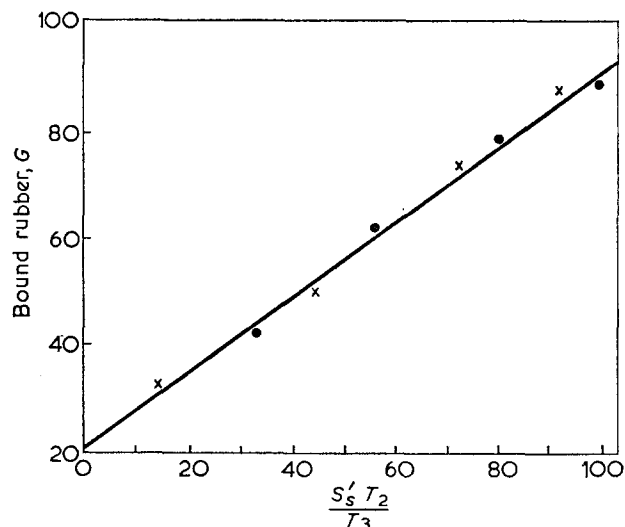


Figure 7 Bound rubber (G) vs.  $S_s T_2 / T_3$  for natural rubber/MPC (20 pphr) mix RSS1C, immersed in solutions of RSS1 (●) and RSS4 (x) masticated rubbers

and the data given in Table 13 were calculated, all quantities being based on 100 parts by weight of the original rubber/carbon black mixture.

#### Discussion

The plot of  $G$  vs.  $S_s T_2 / T_3$  in Figure 7 shows a linear relation and it is to be noted that the points from the RSS1 and RSS4 solutions are on the same line indicating no effect on the back pressure of a difference in molecular weight. From the line the true bound rubber is 21% and the partition coefficient is 0.75. The former value appears to agree well with the values obtained in the experiment described in the previous section.

### PART IV: DISCUSSION

#### PHENOMENA TO BE EXPLAINED

Any structure proposed for the insoluble rubber/active filler substance must take account of the facts that it takes time to develop, is truly elastic within small strains and shows limited swelling.

#### TWO-STRUCTURE THEORIES

Several workers during the past five years have postulated that the polymer molecules in such polymer/filler mixtures can exist in two or more 'structures'<sup>59, 60</sup>. One of the most recent suggestions<sup>60</sup> is that there are adsorbed polymer molecules and interparticular polymer molecules; the former are attached to one filler particle only at one or more points, and the latter form a three-dimensional

structure by reason of one molecule being bound to two or more filler particles.

The above mentioned postulate can explain qualitatively the changes observed on milling and on exposure to different humidities and pH conditions in the case of the silicone rubber/silica system, if degradation of the siloxane chain by hydrolysis, leading to scission, is accepted. Furthermore qualitative explanations of the Young's modulus changes with milling, heating, etc. are also possible; the lack of correlation between bound rubber values and Young's modulus, processability (Southwart and Hunt's breakdown time), etc. can also be understood if one accepts that both adsorbed and interparticular rubbers are included in the bound rubber value, but contribute in different ways to these properties.

Opinion is probably still divided as to the nature of the polymer/filler reaction and attachments<sup>65</sup>, which may well differ from one system to another, i.e. silicone/silica, NR/black, etc.

Stickney and Falb<sup>66</sup>, in their comprehensive review of 'bound rubber', come down firmly in favour of chemical attachments between rubber and black, arising probably and principally from free radical formation during milling/mixing processes. They suggest two phases, one highly crosslinked localized around filler particles and the other a matrix resembling, more or less, the gum vulcanisate.

From an n.m.r. study, Kaufman, Slichter and Davis<sup>67</sup> concluded that there is a region of immobilized rubber immediately surrounding the black and a region of intermediate mobility where the polymer segments are less immobilized but constrained in comparison with the pure rubber.

To consider the change that leads from solubility to insolubility and continued increase in the proportion insoluble on resting or heating, there appear to be two main points. Firstly, as suggested by several authors<sup>41</sup> free radicals persist in the mixture after mixing and milling and it takes time for them to find one another. This is difficult to understand when there is so much oxygen about\*. To explain the increase in bound rubber on heating, either free radicals are generated thermally or the alignment of the reactive positions on the polymer chain with the active groups on the particle surface takes time and is accelerated by increased mobility at the higher temperatures. Certainly milling is not essential to produce some bound rubber but there is a large difference between the amount of rubber insolubilized by black in dilute solution and in standard mill mixes. Heating the former increases insoluble rubber into the range of the latter<sup>23</sup>. Kraus and Dugone<sup>36</sup> suggest, from adsorption of elastomers from solution by carbon black, that the insolubilization takes place in two steps: a rapid physical adsorption followed by a slower reaction of the adsorbed polymer with the black.

Perhaps some of the phenomena have been overlooked by workers because they have studied mixes with 50 pphr of black—the amount in a tyre tread compound.

#### QUANTITATIVE DETERMINATION OF THE PROPORTION OF THE TWO STRUCTURES PRESENT

##### Bound rubber

Carbon black particles with adsorbed, that is, chemically or physically attached, polymer molecules on their surfaces will not cohere without interparticular polymer molecules, and pieces of rubber containing such filler particles will not swell and retain their shape in a solvent but disperse. Nevertheless, it is probable that many of the techniques for determining bound rubber or gel content will yield a value.

The difficulty over attempting to use bound rubber determinations to investigate these systems is the impossibility of distinguishing the adsorbed and interparticular rubbers. One has therefore to seek other methods.

##### Jelly rigidity

In Part III of this paper, evidence is presented of a lack of correlation of the rigidity and strength of the jelly with

\* When rubber is milled in nitrogen, the broken ends, in the absence of oxygen or radical acceptor, recombine immediately.

the swelling behaviour as measured by liquid uptake and bound rubber. In quantitative determinations of the rigidity of swollen jellies in conjunction with a mathematical model may lie a method of separating and arriving at values for the proportion of polymer in the two types of structure.

##### Swelling index vs. bound rubber relation

As an adjunct to this a more detailed study of the swelling/insoluble rubber relation already discussed by Southwart is worth considering. Whereas the results on a series of mixtures of silicone rubber/silica after various times of storage fall on a straight line, without an undue amount of scatter, and which, when extrapolated, passes through 100% bound rubber/nil swelling, other results reported by Southwart by no means follow this pattern. For example, the results on the above series of mixtures repeatedly remilled after different storage times give separate lines for each rubber/filler ratio and these lines, moreover, are both widely separated and of different slopes; none of them passes through the point 100% BR/nil swell. At any one bound rubber value, mixes of identical composition give different swell values depending on whether they have been remilled or not; the higher swell is given by the remilled samples. Figure 8 is typical and relates to a 20 pphr filler mix. Remilling breaks the interparticular rubber molecules and therefore increases the proportion of adsorbed polymer. It is the interparticular molecules that restrict the swelling of the mixture and the fewer there are the greater is the swelling.

To suggest that the adsorbed polymer swells little or not at all, apart from the logical criticism already discussed seems contrary to experimentally observed facts in

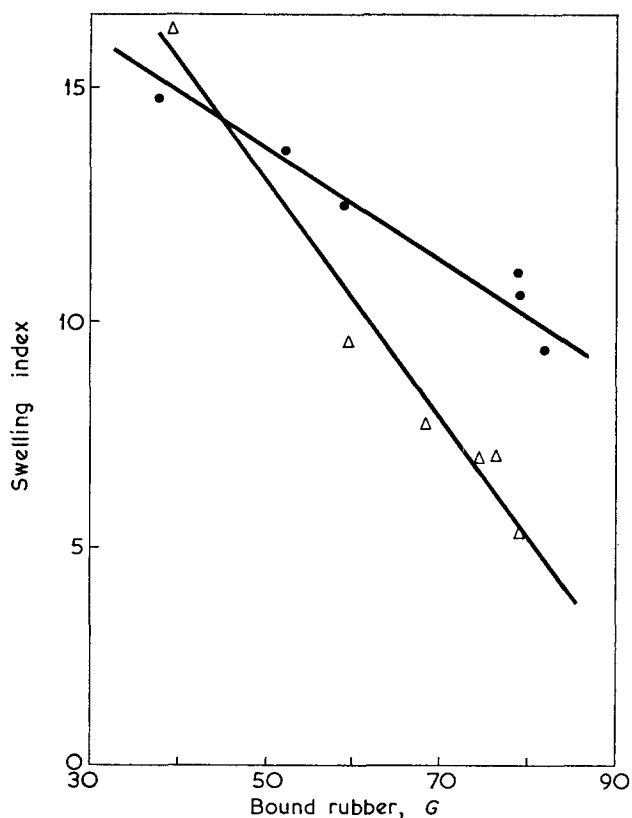


Figure 8 Swelling index vs. bound rubber (G) for silicone rubber/silica 20 pphr mix after different times of resting between mixing and immersion in solvent. Δ, Mix not remilled; ●, mix remilled at each stage. [Data from Southwart, University of Manchester MSc Thesis 1969, Tables 2 and 3]

the case of unvulcanized mixtures. Mixtures with a high proportion of the bound rubber as adsorbed rubber swell more than those with a low proportion. The fact is that for limited swelling there must be interparticulate rubber or intense entanglement of the adsorbed polymer of adjacent filler particles. Without these conditions, the mixture will show unlimited swelling and dissolve but the polymer adsorbed on filler will exist in solution as a gel phase with a solvent content less than that of the surrounding matrix rubber.

## CONCLUSIONS

It appears to the present author that a mathematical model is required to lead to an expression relating the rigidity modulus of the system (filler particle, polymer molecules linking particles and adsorbed 'shell' of polymer molecules in a matrix of rubber and solvent) to filler particle diameter, polymer/filler/solvent proportions, viscosity of polymer solution, etc. This coupled with quantitative values for jelly rigidity and data regarding swelling index and bound rubber may confirm or otherwise theories and ideas proposed to explain the several phenomena, associated with bound rubber.

## ACKNOWLEDGEMENTS

The author's thanks are due to Professor R. J. W. Reynolds for granting facilities for the experimental work to be carried out and for helpful comments. Many and lengthy conversations between the author and David Southwart have contributed greatly to the writing of this paper. Thanks are due to him also for permission to use original data to calculate the results given in *Table 6* and *Figure 1*.

## REFERENCES

- Twiss, D. F. *J. Soc. Chem. Ind.* 1925, **44**, 106T
- LeBlanc, M., Kroger, M. and Kloz, G. *Kolloidchem. Beih.* 1925, **20**, 356
- Stamberger, P. *Kolloid-Z.* 1928, **42**, 295
- Goodwin, N. and Park, C. R. *Ind. Eng. Chem.* 1928, **20**, 621
- Depew, H. A. *Ind. Eng. Chem.* 1929, **21**, 1027
- Fielding, J. H. *Ind. Eng. Chem.* 1929, **21**, 1027
- Boiry, F. *Rev. Gen. Caoutch.* 1931, **8**, 108
- Stamburger, P. 'The Colloid Chemistry of Rubber', Oxford University Press, 1929
- Stamberger, P. *Kautschuk* 1931, **7**, 182
- McBain, J. W. *J. Am. Chem. Soc.* 1927, **49**, 2230
- Cotton, F. H. *Trans. Inst. Rubber Ind.* 1930, **6**, 248
- Blow, C. M. *Trans. Inst. Rubber Ind.* 1929, **5**, 417
- Fielding, J. H. *Ind. Eng. Chem.* 1937, **29**, 880
- Wiegand, W. E. *Can. Chem. Metall.* 1937, **21**, 17
- White, L. M., Ebers, E. S., Shriver, G. E. and Birch, S. J. *Ind. Eng. Chem.* 1945, **37**, 770
- Goldfinger, G. *Rubber Chem. Technol.* 1945, **18**, 286
- Goldfinger, G. *J. Polym. Res.* 1946, **1**, 58; *Rubber Chem. Technol.* 1946, **19**, 614
- Dannenberg, E. M. *Ind. Eng. Chem.* 1948, **40**, 2199
- Sweitzer, C. W., Goodrich, W. C. and Burgess, K. A. *Rubber Age* 1949, **65**, 651
- Fuller, C. S. *Bell System Tech. J.* 1946, **25**, 351
- Ladd, W. A. and Ladd, M. *Ind. Eng. Chem.* 1951, **43**, 2564
- Sweitzer, C. W., Goodrich, W. C. and Burgess, K. A. *Rubber Age* 1952, **72**, 55
- Sweitzer, C. W. and Lyon, F. *Ind. Eng. Chem.* 1952, **44**, 125
- Braendle, H. A. *Rubber Age* 1952, **72**, 205
- Kolthoff, I. M. and Kahn, A. *J. Phys. Chem.* 1950, **54**, 251
- Kolthoff, I. M., Gutmacher, R. G. and Kahn, A. *J. Phys. Chem.* 1951, **55**, 1240; Duke, J., Taft, W. K. and Kolthoff, I. M. *Ind. Eng. Chem.* 1951, **43**, 2885; *Rubber Chem. Technol.* 1952, **25**, 500
- Kolthoff, I. M. and Gutmacher, R. G. *J. Phys. Chem.* 1952, **56**, 740
- Sircar, A. K. and Voet, A. *Rubber Chem. Technol.* 1970, **43**, 973
- Gessler, A. M. *Proc. Int. Rubber Technol. Conf., Brighton* 1967, p 249
- Watson, W. F. *Proc. Rubber Technol. Conf., London* 1954, p 553
- Watson, W. F. *Ind. Eng. Chem.* 1955, **47**, 1281
- Blow, C. M. and Stamberger, P. *Recl Trav. Chem.* 1929, **48**, 681
- Boyer, R. F. *J. Chem. Phys.* 1945, **13**, 363
- Southwart, D. W. and Hunt, T. J. *Inst. Rubber Ind.* 1968, **2**, 140
- Watson, J. W. *Trans. Inst. Rubber Ind.* 1956, **32**, 204
- Kraus, G. and Dugone, J. *Ind. Eng. Chem.* 1955, **47**, 1809; Kraus, G. *Rubber Chem. Technol.* 1965, **38**, 1070
- Garten, V. A. and Sutherland, G. K. *Proc. Rubber Technol. Conf. London* 1954, p 536
- Brennan, J. J. and Jermyn, T. E. *J. Appl. Polym. Sci.* 1965, **9**, 2749; *Rubber Chem. Technol.* 1967, **40**, 817
- Gessler, A. M. *Rubber Age* 1969, **101**, 12, 54
- Dannenberg, E. M. and Collyer, H. J. *Ind. Eng. Chem.* 1949, **41**, 1607
- Berry, J. P. and Cayre, P. J. *J. Appl. Polym. Sci.* 1961, **3**, 213
- Parkinson, D. 'Reinforcement of Rubbers', Institution of the Rubber Industry, London, 1957
- Brennan, J. J., Jermyn, T. E. and Boonstra, B. B. *J. Appl. Polym. Sci.* 1964, **8**, 2687
- Boonstra, B. B. *J. Appl. Polym. Sci.* 1967, **11**, 389
- Gilliland, E. R. and Gutoff, E. B. *J. Appl. Polym. Sci.* 1960, **3**, 26
- Gessler, A. M. *Rubber Chem. Technol.* 1969, **42**, 850, 858
- Gessler, A. M. *Rubber Chem. Technol.* 1969, **42**, 1494
- Gessler, A. M. *Rubber Age* 1961, **87**, 64
- Dannenberg, E. M. *Trans. Inst. Rubber Ind.* 1966, **42**, T26; Donnet, J. B. *Carbon* 1968, **6**, 161
- Glander, F. *Kautsch. Gummi* 1957, **10**, WT180
- Brennan, J. J. and Lambert, D. H. *Rubber Chem. Technol.* 1972, **45**, 94
- Boonstra, B. B. and Dannenberg, E. M. *Rubber Age* 1958, **82**, 838; *Rubber Chem. Technol.* 1959, **32**, 825
- Rehner, Jr., J. 'Reinforcement of Elastomers', (Ed. G. Kraus), Interscience, New York, 1965, p 153
- Harris, J. O., Kerwood, J. E. and Walker, L. A. *Proc. 4th Rubber Technol. Conf., London*, 1962, p 27
- Galanti, A. V. and Sperling, L. H. *J. Polym. Sci. (B)* 1970, **8**, 115; *Polym. Eng. Sci.* 1970, **10**, 3, 177
- Warrick, E. L. and Lauterbur, P. C. *Ind. Eng. Chem.* 1955, **47**, 486
- Southwart, D. W. and Hunt, T. J. *Inst. Rubber Ind.* 1968, **2**, 77, 79, 140; 1969, **3**, 249; 1970, **4**, 74, 77
- Wagner, M. P. and Sellers, J. W. *Ind. Eng. Chem.* 1959, **51**, 961
- Endter, F. and Westlinning, H. *Angew. Chem.* 1957, **69**, 219; *Rubber Chem. Technol.* 1957, **30**, 1103
- Southwart, D. W. *Inst. Rubber Ind. Conference, Loughborough* 1969
- Flory, P. J. *J. Phys. Chem.* 1950, **18**, 108
- Kraus, G. *Rubber World* 1956, **135**, 67, 254
- Porter, M. *Rubber Chem. Technol.* 1967, **40**, 868
- Beerbower, A., Pattison, D. A. and Staffin, G. D. *Am. Soc. Lubr. Eng. Trans.* 1963, **6**, 80; *Rubber Chem. Technol.* 1964, **37**, 246; Beerbower, A., Kaye, L. A. and Pattison, D. A. *Chem. Eng.* 1967, **74**, 26, 118; Beerbower, A. and Dickey, J. R. *Am. Soc. Lubr. Eng. Trans.* 1969, **12**, 1
- Deviney, M. L. *Adv. Colloid Interface Sci.* 1968, **2**, 237
- Stickney, P. B. and Falb, R. D. *Battelle Tech. Rev.* 1964, **13**(9), 8; *Rubber Chem. Technol.* 1964, **37**, 1299
- Kaufman, S., Slichter, W. P. and Davis, D. D. *J. Polym. Sci. (A-2)* 1971, **9**, 829



# Poly(methyl methacrylate-co-acrylonitrile)

Raymond B. Seymour, Don R. Owen and Glenn A. Stahl

Department of Chemistry, University of Houston, Houston, Tx 77004, USA  
(Received 1 January 1973)

Stable macroradicals of methyl methacrylate were prepared by the azobisisobutyronitrile-initiated polymerization of methyl methacrylate in hexane whose solubility parameter value ( $\delta$ ) differed from that of the macroradical by more than 1.8 hildebrand units and in 1-propanol at temperatures below its theta temperature (84.5°C). The rates of heterogeneous polymerization in hexane and 1-propanol were much faster than that of the homogeneous polymerization in benzene. Stable macroradicals were not obtained in benzene which was a good solvent nor at temperatures above the glass transition temperature ( $T_g$ ) of the macroradicals. Thus, stable macroradicals of butyl methacrylate ( $T_g$  20°C) and methyl acrylate ( $T_g$  3°C) were not obtained at a polymerization temperature of 50°C. Good yields of block copolymers of methyl methacrylate and acrylonitrile were obtained by the addition of acrylonitrile to the methyl methacrylate macroradical in methanol, ethanol, 1-propanol and hexane at 50°C. The rate of formation of the block copolymer decreased in these poor solvents as the differences between the solubility parameter of the solvent and macroradical increased.

The block copolymer samples prepared at temperatures of 50°C and above were dissolved in benzene which is a non-solvent for acrylonitrile homopolymer, but is a good solvent for poly(methyl methacrylate) and the block copolymer. The presence of acrylonitrile and methyl methacrylate in the benzene-soluble macromolecule was demonstrated by pyrolysis gas chromatography, infra-red spectroscopy and differential thermal analysis.

## INTRODUCTION

It has been shown previously that since some polymers are insoluble in their monomers, insoluble trapped free radicals are produced when vinyl chloride<sup>1</sup> or acrylonitrile<sup>2</sup> are polymerized in bulk. Macroradicals are also produced when styrene is polymerized in alcohols<sup>3</sup> and when other vinyl monomers are polymerized in poor solvents<sup>4</sup>. That the rate of polymerization of methyl methacrylate<sup>5</sup> and that of the copolymerization of styrene and maleic anhydride was faster in poor solvents than in good solvents has been observed previously<sup>6, 7</sup>.

It has also been shown that heterogeneous solution polymerization takes place when the hildebrand solubility parameter values<sup>8, 9</sup> of the solvent and polymer differ by at least 1.8 units<sup>10</sup>. The presence of macroradicals in precipitated polymers has been demonstrated by electron spin resonance (e.s.r.) techniques<sup>11</sup>.

Block copolymers have been obtained by the addition of styrene to acrylonitrile macroradicals, by the addition of styrene or methyl methacrylate to vinyl chloride macroradicals<sup>12</sup> and by the addition of various monomers to styrene-maleic anhydride macroradicals<sup>13</sup>. It has been shown previously that block copolymers are produced when a vinyl monomer is added to a suspension of a macroradical in a poor solvent providing the difference in the solubility parameter values of the monomer and macroradical are not greater than 3.1 units<sup>13</sup>.

This investigation was undertaken to determine the effect of variables on the stability of methyl methacrylate macroradicals and on the rate of formation of a block copolymer of acrylonitrile with this macroradical.

## EXPERIMENTAL

Freshly distilled methyl methacrylate was polymerized

in the absence of oxygen and in the presence of 1.5% recrystallized azobisisobutyronitrile as a 10% solution in the freshly distilled solvent at a specified temperature such as 50°C. The rate of polymerization was monitored by a precision dilatometer. The presence of macroradicals was demonstrated by measuring the decrease in free radicals when the macroradicals were added to DPPH (2,2-diphenyl-1-picrylhydrazyl).

The macroradical was separated by filtering and solvent washing in an oxygen-free atmosphere. Block copolymers were produced by the addition of freshly distilled acrylonitrile to a suspension of the macroradical in a poor solvent (usually at 50°C in the absence of azobisisobutyronitrile and in an inert atmosphere). The rate of copolymerization was monitored by observing aliquot yield data. The block copolymers were filtered, solvent washed and dried. These products were characterized by yield, solubility and pyrolysis g.c.

## RESULTS AND DISCUSSION

As shown in *Figure 1*, the rate of polymerization of methyl methacrylate was much slower in a good solvent such as benzene ( $\delta=9.0$ ) than in poor solvents such as 1-propanol ( $\delta=11.9$ ) or hexane ( $\delta=7.3$ ). The solubility parameter ( $\delta$ ) of poly(methyl methacrylate) which was 9.1 was within 1.8 hildebrand units of that of benzene and therefore conventional termination steps produced dead macromolecules in this homogeneous solution polymerization. In contrast the solubility parameter differences ( $\Delta\delta$ ) between the polymer and other solvents were 2.8 and 1.8 respectively. It is of interest to note that macroradicals were produced in poor solvents having solubility parameter values ( $\delta$ ) both above and below that of the macroradical whose  $\delta$  value is identical to that of the polymer.

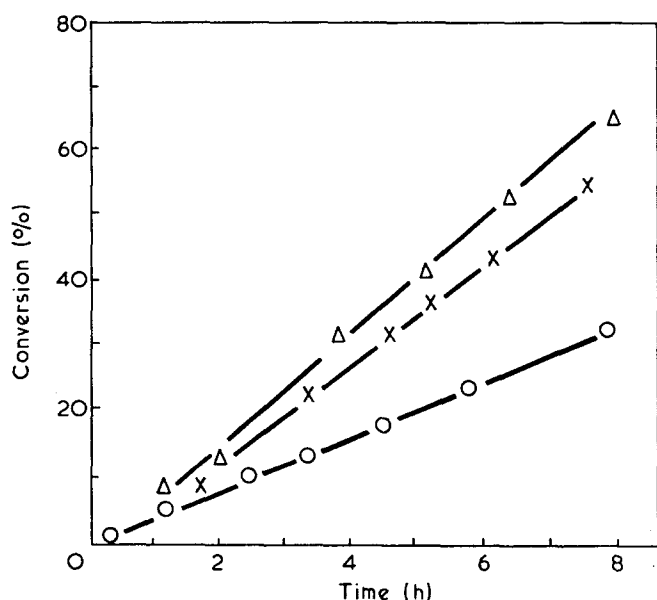


Figure 1 Rate of solution polymerization of methyl methacrylate'  $\Delta$ , Hexane;  $\times$ , 1-propanol;  $\circ$ , benzene

The theta temperature for the poly(methyl methacrylate)/1-propanol system is  $84.5^{\circ}\text{C}$ . By definition<sup>14,15</sup>, the polymer should exist as a statistical coil at its theta temperature. Thus, as shown in Figure 2, the yield of insoluble macroradicals obtained by the polymerization of methyl methacrylate for 48 h dropped dramatically as the polymerization temperature approached the theta temperature.

There is little chain motion of amorphous polymers or their macroradicals at temperatures below the glass transition temperature ( $T_g$ ). Hence, one would expect macroradicals to be stable in inert atmospheres at temperatures below  $T_g$ . The  $T_g$  value for poly(methyl methacrylate) is  $105^{\circ}\text{C}$ , and no decrease in activity was noted when its macroradicals were heated at temperatures as high as  $90^{\circ}\text{C}$ . Poly(ethyl methacrylate) ( $T_g$   $65^{\circ}\text{C}$ ) was also stable at  $50^{\circ}\text{C}$ . In contrast, macroradicals of butyl methacrylate ( $T_g$   $20^{\circ}\text{C}$ ) and methyl acrylate ( $T_g$   $3^{\circ}\text{C}$ ) were unstable at  $50^{\circ}\text{C}$ .

It has been shown previously that monomers will form block copolymers with macroradicals if the difference in solubility parameters ( $\Delta\delta$ ) between the monomers and macroradicals is less than 3.1 hildebrand units<sup>13</sup>. Thus, acrylonitrile ( $\delta=10.5$ ) readily produces a block copolymer with methyl methacrylate macroradicals ( $\delta=9$ ), since the  $\Delta\delta$  value is equal to 1.4 hildebrand units. This reaction was used to ascertain the degree of stability of macroradicals.

These macroradicals are unstable in the presence of oxygen, good solvents, at temperatures above  $T_g$  and above the theta temperature. Hence, it is essential to add the vinyl monomers to poor solvents in an inert atmosphere at temperatures below  $T_g$  and at temperatures below the theta temperature. Thus, as shown in Figure 3, the yield of acrylonitrile block copolymer decreased dramatically when the temperature of the macroradical/1-propanol system was increased above the theta temperature of  $84.5^{\circ}\text{C}$ . The macroradicals noted in Figure 3 were produced at the same temperature used for copolymerization and were stored for 24 h before the addition of acrylonitrile.

Since the formation of block copolymer from vinyl

monomers and solid macroradicals is diffusion controlled, the rate is most rapid when the macroradical is highly swollen by the solvent. Thus, Minoura<sup>12</sup> produced block copolymers in good yields by the addition of good solvents to a suspension of macroradical, vinyl monomer and poor solvent.

As shown in Figure 4, optimum yields of acrylonitrile block copolymer were obtained when a suspension of the methyl methacrylate macroradical in acrylonitrile and 1-propanol was heated at  $70^{\circ}\text{C}$  for 72 h. The original

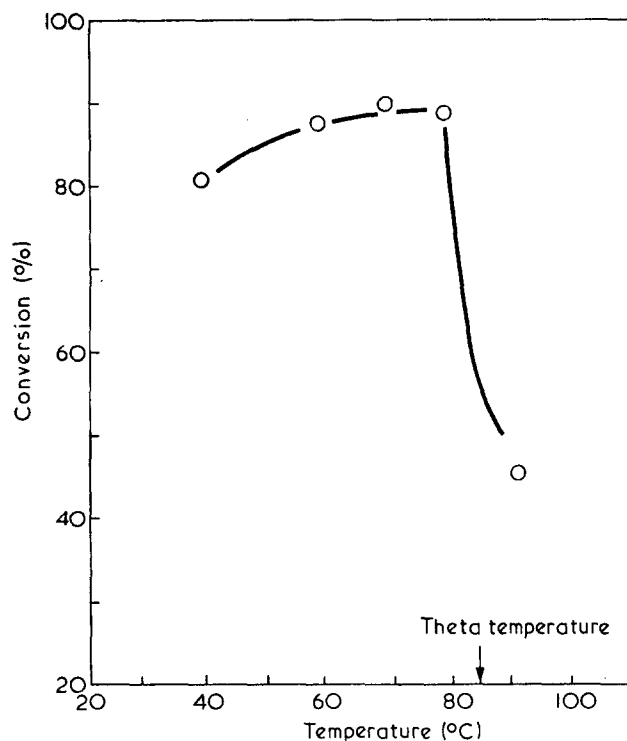


Figure 2 Effect of temperature on the yield of methyl methacrylate macroradicals in 1-propanol

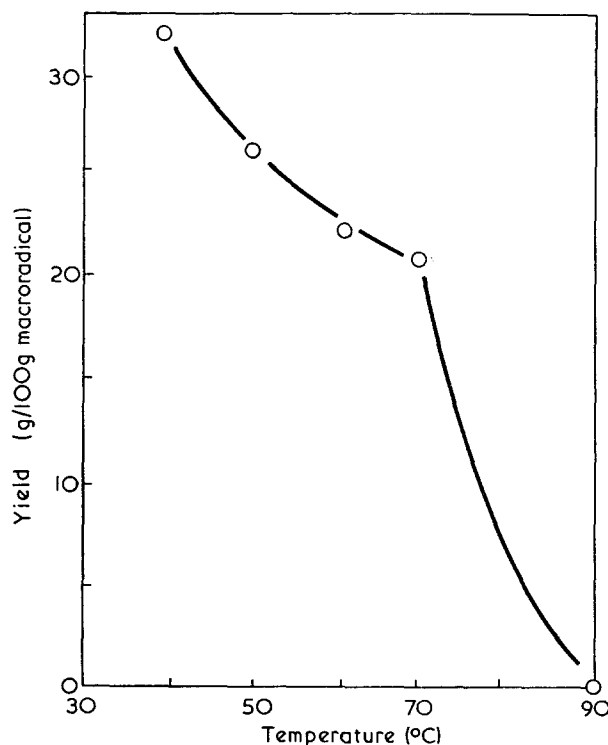


Figure 3 Formation of block copolymer from acrylonitrile and methyl methacrylate macroradicals in 1-propanol

macroradical was produced by the polymerization of methyl methacrylate at 50°C for 72 h. A weight of acrylonitrile equal to that of the macroradical was added and the mixture was heated for 72 h at the temperature shown in Figure 4.

Presumably, the rate of block copolymer formation is slower at temperatures below 70°C because of slower diffusion of acrylonitrile into the slightly swollen macroradicals. The yield at 70°C was essentially quantitative because of rapid diffusion of acrylonitrile into the swollen macroradicals. As the temperature approached the theta temperature (84.5°C), some of the macroradicals terminated by coupling before copolymerization took place. Since the block copolymer macroradicals were stable at this temperature, the optimum conditions for copolymer preparation would include formation of the initial block copolymer macroradicals at 70°C followed by further copolymerization at a higher temperature.

The rate of block copolymer formation is also dependent on the solubility parameter of the solvent and is most rapid in poor solvents having solubility parameters comparable to that of the macroradical. Thus, as shown in Figure 5, no block copolymer was produced when acrylonitrile was added to a polymer of methyl methacrylate in benzene and the mixture was heated at 50°C for 72 h. This is not unexpected since the difference in the solubility parameter values of the macroradical and the benzene solvent ( $\Delta\delta = 0.1$ ) was less than 1.8 hildebrand units.

However, as stated previously, the  $\Delta\delta$  value for the hexane system is 1.8 hildebrand units. Thus, the macroradicals in this heterogeneous polymerization system are highly swollen and acrylonitrile diffuses rapidly into these swollen particles to produce a block copolymer. Since the  $\Delta\delta$  value for the 1-propanol system is 2.8, the rate of copolymerization is slower than in hexane but sufficiently fast to increase the weight of the macroradicals by over 35% after 72 h at 50°C. Since the  $\Delta\delta$  values for ethanol

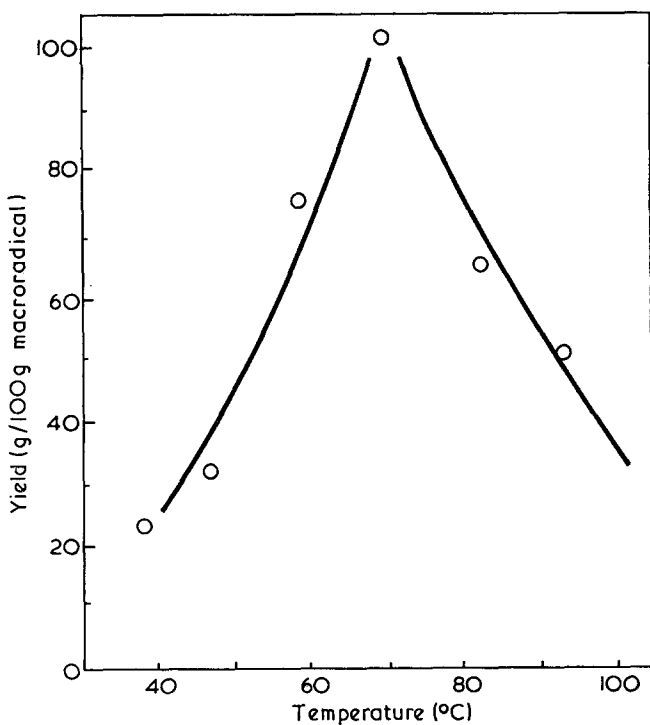


Figure 4 Formation of methyl methacrylate macroradicals in 1-propanol at 50°C and subsequent formation of block copolymers at temperatures shown

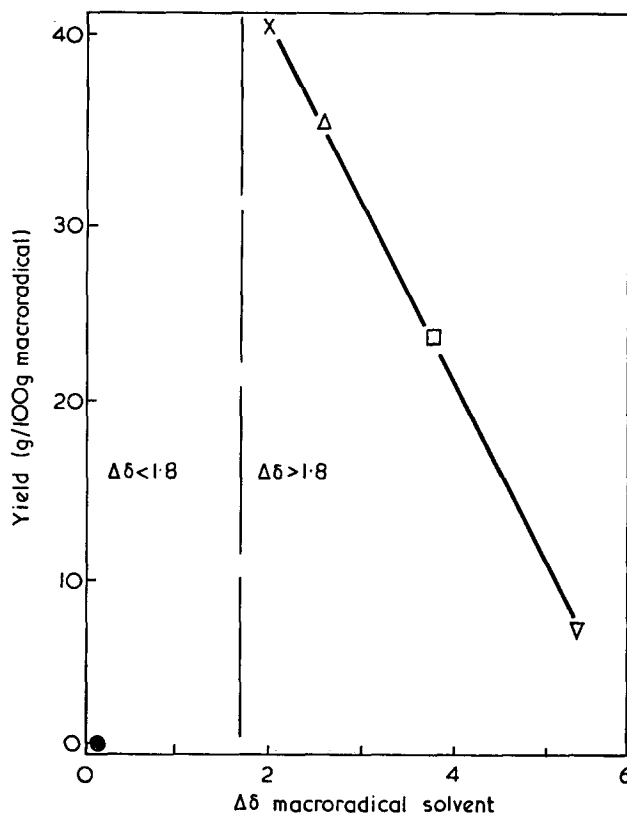


Figure 5 Effect of solubility parameter of solvent on the rate of formation of block copolymer of acrylonitrile and methyl methacrylate. ●, Benzene; ×, hexane; Δ, 1-propanol; □, ethanol; ▽, methanol

and methanol are 3.8 and 5.4 hildebrand units respectively the rate of copolymerization decreases in these systems.

Because of the presence of a small amount of residual azobisisobutyronitrile in the poor solvent systems used for the polymerization of methyl methacrylate at temperatures of 40°C and less, some benzene-insoluble homopolymer of acrylonitrile was noted in addition to the block copolymer. However, less than 1% of benzene-insoluble product was observed when acrylonitrile was added to methyl methacrylate macroradicals at temperatures of 50°C or above. The benzene-soluble portion was precipitated in isopropyl alcohol and the dried macromolecules were characterized. That block copolymers of methyl methacrylate and acrylonitrile were present in the benzene-soluble fractions was demonstrated by characteristic chromatograms, spectrograms and thermograms in pyrolysis g.c., i.r. spectroscopy and d.t.a.

#### REFERENCES

- ICI Ltd., Br. Pat. 366 897 (1929)
- Bamford, C. H. and Jenkins, A. D. *Proc. R. Soc.* 1953, **216**, 515
- Chapiro, A. *J. Chem. Phys.* 1950, **47**, 747
- Hiemeleers, J. and Smets, G. *Makromol. Chem.* 1961, **47**, 7
- Atkinson, B. and Cotten, G. R. *Trans. Faraday Soc.* 1958, **54**, 877
- Tsuchida, E. U., et al. *J. Chem. Soc. Japan* 1967, **70**, 573
- Seymour, R. B., et al. *Texas J. Sci.* 1969, **21** (1), 13
- Burrell, H. 'Polymer Handbook' (J. Brandrup and E. H. Immergut, Eds), Interscience, New York, 1965, Ch 4
- Seymour, R. B. *Mod. Plast.* 1971, **48** (10), 150
- Seymour, R. B., et al. *Adv. Chem. Ser.* 1971, **99**, 418
- Bamford, C. H. *J. Polym. Sci.* 1960, **48**, 37
- Minoura, Y. and Ogata, Y. *J. Polym. Sci. (A-1)* 1969, **7**, 2547
- Seymour, R. B., et al. *Polym. Prepr.* 1972, **13** (1), 522
- Flory, P. J. *J. Chem. Phys.* 1949, **17**, 303
- Elias, H.-G., Dietschy, H. J., Etter, O., et al. in ref. 8

# Some steric regulation on radical polymerization of perfluorobutadiene\*

Madeline S. Toy and J. C. DiBari

Stanford Research Institute, Menlo Park, Calif. 94025, USA  
(Received 16 January 1973; revised 10 April 1973)

Polymer initiation by irradiation alone exerts only a minor effect on the steric regulation of polyperfluorobutadiene. Under ultra-violet irradiation the extent of stereoregularity for 1,2-polymerization increases with increasing concentration of the free radical catalyst, while the solvent effect under ultra-violet initiation is not as significant in steric regulation nor in improving the yield of the homopolymer. This study demonstrated some stereoregularity of polyperfluorobutadiene through variation of the experimental conditions under ultra-violet irradiation.

## INTRODUCTION

Previously it was found that radical polymerizations of perfluorobutadiene under low pressure and ambient temperature formed 1,2- and 1,4-polyperfluorobutadiene<sup>1,2</sup>. With the presence of higher concentrations of radical initiator during bulk polymerization, the polymer was reported to consist of higher 1,2-moieties<sup>3</sup>. In the present investigation, experimental conditions are being sought that will demonstrate that radical polymerization of perfluorobutadiene can allow polymerization to favour one or both olefinic bonds of the monomer. In other words, the objective is to show that a high ratio of 1,2- or 1,4-polymer can be selectively obtained under some polymerization conditions.

The molecule perfluorobutadiene, unlike butadiene monomer, adopts a *cis*-bent conformation with the dihedral angle being  $42 \pm 15$  degrees or  $47.60 \pm 0.58$  degrees, in keeping with later electron diffraction data<sup>4,5</sup>. The non-planar conformation of perfluorobutadiene does not allow the *p* orbitals to overlap effectively, and thus extensive delocalization of this monomer is precluded. Because of the less conjugated nature of the two double bonds of the monomer and its comparatively slow rate of polymerization under low pressure and ambient temperature, radical polymerization of this monomer was undertaken to demonstrate some steric orientation effects of the polymer by varying the radiation dose rate, polarity of the aprotic solvent, and concentration of the free radical catalyst under gamma and electron irradiation<sup>6</sup>. This paper reports the continuing work on the solvent and catalyst effects under ultra-violet (u.v.) irradiation and the various results so far achieved.

## EXPERIMENTAL

### *Materials and polymerization techniques*

Perfluorobutadiene and  $\text{CF}_3\text{OOCF}_3$  (from Peninsular ChemResearch, PCR) were checked by methods described previously<sup>2,7</sup>. The solvents ( $n\text{-C}_4\text{F}_9$ )<sub>3</sub> (from 3M Co.),  $\text{CCl}_3\text{F}$  (from duPont de Nemours), and  $n\text{-C}_8\text{F}_{18}$  from PCR were checked by infra-red spectra only.

\* Paper presented at the Joint Pacific Conference on Chemistry and Spectroscopy, San Francisco, California, October 1972.

The polymerizations of perfluorobutadiene were carried out in bulk, in solution, and in the presence of  $\text{CF}_3\text{OOCF}_3$  catalyst in evacuated sealed quartz tubes under autogenous pressure of about 0.8 atm (1 atm  $\equiv$  101.33 kN/m<sup>2</sup>). They were then placed in the polymer tumbling apparatus under external ultra-violet irradiation at ambient temperature for a week.

At the end of the polymerization period, the sealed polymerization tubes were cooled to solid, opened, and the unconverted monomer was removed through the vacuum system. The polymer samples in the presence of solvents were centrifuged and the decanted liquids were combined with the  $\text{CCl}_3\text{F}$  extracts from the fractionations of the solid polymers. The combined liquids were evaporated to dryness and evacuated over anhydrous  $\text{MgSO}_4$  as  $\text{CCl}_3\text{F}$ -soluble fractions. The fractionations of various solid polymer samples were carried out by  $\text{CCl}_3\text{F}$  solvent extractions under identical conditions.

### *Polymerization apparatus and intensity of the u.v. source*

A Hanovia medium pressure mercury arc lamp was introduced at the centre of the previously described polymer tumbling apparatus<sup>8</sup> in a double-walled quartz cooling jacket and at  $4\frac{1}{2}$  in distance from the sealed quartz polymerization tubes. The light intensity for the u.v.-induced polymerization was determined by the liquid chemical actinometer using a potassium ferrioxalate system<sup>9-11</sup>. In experiments, the  $\text{K}_3\text{Fe}(\text{C}_2\text{O}_4)_3$  solution was placed in two quartz polymerization tubes at the same distance for polymerization and irradiated in the polymer tumbling apparatus. The unirradiated  $\text{K}_3\text{Fe}(\text{C}_2\text{O}_4)_3$  solution was used as a reference to set the zero reading. The measured optical densities from the Beckman DU spectrophotometer ( $\log_{10} I/I_0$ , 1.23 and 1.29) and the calculated light intensities ( $I_0^i$ , 6.005 and  $6.250 \times 10^{16}$  quanta/sec) give average  $I_0^i$  as  $6.127 \times 10^{16}$  quanta/sec.

## RESULTS AND DISCUSSION

Polymer initiation by irradiation alone seems to polymerize the unsaturated perfluorobutadiene monomer with only limited specific control of configuration. When irradiation is combined with another factor, however, such as the presence of free radical catalyst  $\text{CF}_3\text{OOCF}_3$  under ultra-violet irradiation or the presence of a non-

Steric regulation on polymerization of perfluorobutadiene: M. S. Toy and J. C. DiBari

Table 1 Solvent effect on polymerization of perfluorobutadiene in the presence of catalyst under u.v. irradiation (monomer, 4.43 g)

Solvent	Catalyst	Yield of product (g)	After CCl <sub>3</sub> F extraction		
			Fraction	Yield (g)	I.r. absorbance ratio 5.6/5.8
0	0	0.30	Soluble	0.19	1.1
			Insoluble	0.11	1.2
0	5% CF <sub>3</sub> OOCF <sub>3</sub>	0.89	Soluble*	0.65	2.7
			Insoluble*	0.24	1.6
(n-C <sub>4</sub> F <sub>9</sub> ) <sub>3</sub> N, 1 ml	5% CF <sub>3</sub> OOCF <sub>3</sub>	0.88	Soluble†	0.68	2.6
			Insoluble†	0.20	1.6
3 ml	0	0.23	Soluble	0.14	1.1
			Insoluble	0.09	1.0
3 ml	2% CF <sub>3</sub> OOCF <sub>3</sub>	0.47	Soluble	0.34	2.1
			Insoluble	0.13	1.8
3 ml	5% CF <sub>3</sub> OOCF <sub>3</sub>	0.75	Soluble‡	0.64	3.0
			Insoluble	0.11	1.9
6 ml	5% CF <sub>3</sub> OOCF <sub>3</sub>	0.63	Soluble	0.54	2.4
			Insoluble	0.09	1.7
n-C <sub>8</sub> F <sub>18</sub> , 1 ml	5% CF <sub>3</sub> OOCF <sub>3</sub>	0.64	Soluble	0.56	2.5
			Insoluble	0.08	1.9
3 ml	5% CF <sub>3</sub> OOCF <sub>3</sub>	0.58	Soluble	0.50	2.4
			Insoluble	0.08	2.2
6 ml	5% CF <sub>3</sub> OOCF <sub>3</sub>	0.58	Soluble	0.50	1.8
			Insoluble	0.08	1.8

\* Mol. wt. of CCl<sub>3</sub>F solution fraction=6200 and insoluble fraction=6300

† Mol. wt. of CCl<sub>3</sub>F solution fraction=6000 and insoluble fraction=6800

‡ Mol. wt. of CCl<sub>3</sub>F solution fraction=5730

polar aprotic solvent under gamma irradiation in the absence of catalyst<sup>6</sup>, the incoming monomer unit seems in some way to favour 1,2-polymerization for the former and 1,4-polymerization for the latter. Table 1 shows that under u.v. irradiation both the stereoregulation for 1,2-polymerization and the polymer yield increase with increasing concentration of the free radical catalyst. Table 1 also shows that bulk polymerization in the presence of CF<sub>3</sub>OOCF<sub>3</sub> catalyst under u.v. irradiation gave polyperfluorobutadiene (molecular weight around 6000) with higher 1,2-moieties and better yield than in the absence of catalyst. For solution polymerizations with the same amount of catalyst, the presence of more polar aprotic solvent, (n-C<sub>4</sub>F<sub>9</sub>)<sub>3</sub>N, is preferred over non-polar solvent (n-C<sub>8</sub>F<sub>18</sub>).

The pendant perfluorovinyl bonds (-CF=CF<sub>2</sub>) from 1,2-addition polymerization appear at 5.6 μm and the internal perfluorovinylene bonds (-CF=CF-) from 1,4-addition polymerization appear at 5.8 μm. Thus, in Tables 1 and 2, a large infra-red absorbance ratio (5.6/5.8) indicates more 1,2-polymerization.

Table 2 shows that the solvent effect under u.v. initiation is not a significant factor in steric regulation nor in improving the yield of the homopolymer. The converse is true for homopolymerization under gamma irradiation, where the extent of stereoregularity for 1,4-polymerization and the yield of the homopolymer increase with decreasing polarity of the aprotic solvents<sup>6</sup>.

In summary, under ultra-violet irradiation the predominance of 1,2-moieties is in the lower molecular weight fraction and is enhanced by increasing the concentration of the free radical catalyst. For the preparation of high 1,4-moieties, see ref. 6.

ACKNOWLEDGEMENTS

This work is sponsored in part by Stanford Research Institute and in part by National Aeronautics and Space Administration under Contract NAS3-15577.

Table 2 Solvent effect on polymerization of perfluorobutadiene under u.v. irradiation (monomer, 4.43 g)

Solvent	Yield of product (g)	After CCl <sub>3</sub> F extraction		
		Fraction	Yield (g)	I.r. absorbance ratio 5.6/5.8
0	0.30	Soluble*	0.19	1.1
		Insoluble*	0.11	1.2
(n-C <sub>4</sub> F <sub>9</sub> ) <sub>3</sub> N, 1 ml	0.31	Soluble	0.21	1.1
		Insoluble	0.10	1.0
3 ml	0.23	Soluble	0.14	1.1
		Insoluble	0.09	1.0
6 ml	0.20	Soluble	0.13	1.1
		Insoluble	0.07	1.0
n-C <sub>8</sub> F <sub>18</sub> , 1 ml	0.34	Soluble	0.19	1.1
		Insoluble	0.15	1.2
3 ml	0.28	Soluble	0.17	1.2
		Insoluble	0.11	1.3
6 ml	0.18	Soluble	0.14	1.3
		Insoluble	0.04	1.2

\* Mol. wt. of CCl<sub>3</sub>F solution fraction = 2700 and insoluble fraction = 9800

REFERENCES

- 1 Toy, M. S. 'Photochemistry of Macromolecules', (Ed. R. F. Reinisch), Plenum Press, New York, 1970, pp 135-144
- 2 Toy, M. S. and Lawson, D. D. *J. Polym. Sci. (B)* 1968, 6, 639
- 3 Toy, M. S. *Polym. Prepr.* 1971, 12(1), 385
- 4 Brundle, C. R. and Robin, M. B. *J. Am. Chem. Soc.* 1970, 92, 5550
- 5 Andreassen, A., Chang, C. H. and Bauer, S. H. Paper presented at 160th Am. Chem. Soc. Meeting, Chicago, Sept. 1970
- 6 Toy, M. S. and DiBari, J. C. *Ind. Eng. Chem. (Prod. Res. Develop.)* 1972, 11, 404
- 7 Toy, M. S. and Newman, J. M. *J. Polym. Sci. (A-1)* 1969, 7, 2333
- 8 Toy, M. S. and Newman, J. M. *Polym. Prepr.* 1970, 11(1), 121
- 9 Hatchard, C. G. and Parker, C. A. *Proc. R. Soc.* 1956, A235, 518
- 10 Calvert, J. G. and Pitts, J. N. 'Photochemistry', John Wiley, New York, 1967, pp 769-814
- 11 Skoog, D. and West, D. M. 'Fundamentals of Analytical Chemistry', Holt, Rinehart and Winston, New York, 1966

# Notes to the Editor

## Glass transition temperatures of oligosaccharides

Elisabeth Alfthan and Alf de Ruvo

Physics Department, Swedish Forest Products Research Laboratory, Box 5604, S-114 86 Stockholm, Sweden

and Wyn Brown

Department of Physical Chemistry, University of Uppsala, Uppsala, Sweden

(Received 1 March 1973)

### INTRODUCTION

This note reports the determination of the glass transition temperatures of different oligosaccharide series and the acetylated materials. The results are briefly discussed with regard to the influence of conformation and cohesive energies on the rigidity of the oligosaccharide backbone.

### EXPERIMENTAL

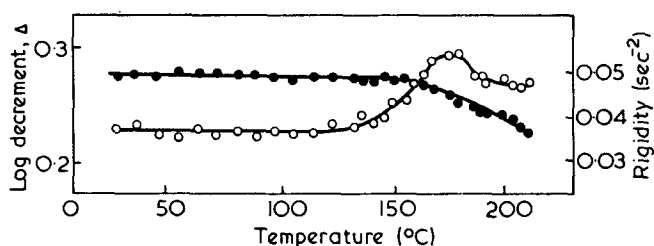
Xylo- and cello-dextrins with chain lengths of up to six units were produced as described in previous papers<sup>1, 2</sup>. The samples were acetylated in an equal mixture of pyridine and acetic anhydride according to the usual techniques<sup>3</sup>. Determination of the degree of acetylation yielded values between 2.9 and 2.7 for all samples.

The temperature of glass transition was measured by a torsional braid analyser (TBA, Chemical Instruments Corp.). The principle of this testing technique has been previously described in detail<sup>4</sup>. The samples were deposited onto the glass braid by evaporation of solvent from solution containing the sample at a concentration of 5–10% by weight. Owing to the small amount of available material (50–100 mg) it was not possible to load the braids with more than 10–20 mg of each oligosaccharide.

The damping number and rigidity were evaluated as a function of temperature for all samples in a nitrogen atmosphere (flow rate 20 ml/min) and at a temperature scanning rate of 1°C/min. The resonance frequency of the free oscillation was between 0.1 and 0.5 Hz. All damping curves were directly analysed by a computer by means of an analog-digital converter connected to the output of the TBA. Damping and rigidity were evaluated by a least-square technique and the results were automatically plotted as the mechanical parameters *versus* temperature<sup>5</sup>. A typical mechanical spectrum is illustrated in *Figure 1*.

### RESULTS

*Table 1* lists the glass transition values,  $T_g$ , found in this investigation. To check agreement with theory, a plot of  $1/T_g$  *versus*  $1/M$  according to Ueberreiter<sup>6</sup> is shown in *Figure 2*. The intercept on the  $y$ -axis should yield  $T_g$  corresponding to infinite molecular weight. These data should thus correspond with the  $T_g$  values of cellulose, xylan, cellulose acetate and xylan acetate. It should be noted that the degree of crystallinity may interfere with the determination of  $T_g$ <sup>7</sup>. No absolute means are available to determine the crystallinity of the samples on the braid. However, the heat of solution of the samples were measured



*Figure 1* Rigidity and logarithmic decrement *versus* temperature for cellohexaose as obtained with torsional braid analyser (TBA)

*Table 1* Molecular weight and  $T_g$  of oligosaccharides

Sample	DP	$1/T_g \times 10^3$ (K <sup>-1</sup> )	$1/M \times 10^3$	$T_g$ (°C)	$T_g$ extrapolated (°C)
Cellodextrin	2	2.58	2.92	114	217
	4	2.32	1.50	158	
	5	2.26	1.21	169	
	6	2.23	1.01	175	
	∞		0		
Acetylated cellodextrin	2	3.00	1.47	60	190 (190) <sup>a</sup>
	4	2.58	0.80	115	
	5	2.53	0.65	122	
	6	2.49	0.57	128	
	∞		0		
Xylodextrin	4	2.45	1.82	135	200
	5	2.39	1.46	145	
	6	2.35	1.23	152	
	∞		0		
	Acetylated xylodextrin	4	2.65	1.03	
5		2.54	0.84	120	
6		2.48	0.71	130	
∞			0		

<sup>a</sup> Measured on the braid

after being subjected to the same procedure used for deposition on the braid. In no cases could endothermic enthalpies be detected, thus indicating that the crystallinity of the samples is small.

The  $T_g$  for cellulose, given by the extrapolation, is in good agreement with that reported in the literature<sup>8</sup>. Similarly the  $T_g$  values for cellulose acetate and high molecular weight xylan obtained by extrapolation are in agreement both with data previously reported<sup>9</sup> and measured directly by torsion braid experiments.

The experimental points fit well with the expression given by Ueberreiter and also yield reasonable values for the softening temperatures of the polymer. A plot of  $T_g$  *versus*  $1/M$  as recommended by Flory<sup>10</sup> also gave linear plot and no significant changes of  $T_{g\infty}$ . Consequently it may be concluded that the use of oligomers for determining  $T_g$  may avoid the objection of

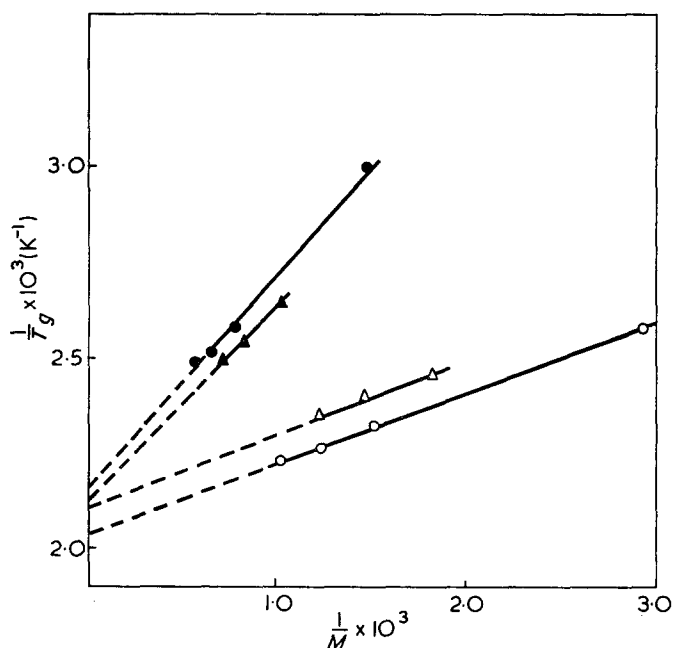


Figure 2 The glass transition temperatures ( $T_g$ ) of oligosaccharides versus molecular weight.  $\circ$ , Cellodextrins;  $\bullet$ , acetylated cellodextrins;  $\triangle$ , xylodextrins;  $\blacktriangle$ , acetylated xylodextrins

subjecting polymers to drastically high temperatures. In the case of polysaccharides pyrolytic degradation becomes severe at  $180^\circ\text{C}$ <sup>11</sup>.

#### CONCLUSIONS

The high  $T_g$  values of the oligosaccharides are due to the high cohesive energy between the chains (intermolecular

forces) and the limited rotational freedom between the monomer units in these molecules<sup>12</sup>. Since changes in the cohesive energy by acetylation are not found to alter  $T_g$  to any great extent, at least for the xylodextrins, it seems probable that the inherent chain stiffness is the primary reason for the high  $T_g$  values.

The structure of the monomer unit evidently influences the  $T_g$  values. In the absence of the primary hydroxyl group (xylodextrins) the  $T_g$  values are reduced by about  $20^\circ\text{C}$ . It seems reasonable to assume that this is due to intramolecular coupling by hydrogen bonding between adjacent rings that has been demonstrated between the hydroxyls at  $\text{C}_6$  and  $\text{C}_2$  in contiguous units<sup>13</sup>. This interpretation is in line with the results on the acetylated compounds. In this case hydrogen bonding is absent and similar  $T_g$  values are observed. Thus chain stiffness and cohesive energies should be about equal and equal  $T_g$  values would be expected.

#### REFERENCES

- 1 Brown, W. J. *Chromatogr.* 1970, **52**, 273
- 2 Brown, W. and Andersson, Ö. *J. Chromatogr.* 1971, **57**, 255
- 3 Marton, J. *et al. Adv. Chem. Ser.* 1966, **59**, 125
- 4 Lewis, A. F. and Gillham, J. K. *J. Appl. Polym. Sci.* 1962, **6**, 422
- 5 Karlsson, H. *Thesis* Royal Institute of Technology, Stockholm
- 6 Ueberreiter, K. and Kanig, G. *J. Colloid Sci.* 1952, **7**, 569
- 7 Read, B. E. *Polymer* 1962, **3**, 529
- 8 Back, E. L. and Didriksson, E. I. E. *Sven. Papperstidn.* 1969, **72**, 687
- 9 Goring, D. A. I. *Pulp Paper Mag. Can.* 1963, **64**, T-517
- 10 Fox, T. G. and Flory, P. J. *J. Appl. Phys.* 1950, **21**, 581
- 11 Arseneau, D. F. *Can. J. Chem.* 1971, **49**, 632
- 12 Boyer, R. F. *Rubber Chem. Technol.* 1963, **36**, 1303
- 13 Mann, J. and Marrison, H. I. *J. Polym. Sci.* 1956, **21**, 301

## Introduction of hydroxymethyl groups into polystyrene and styrene

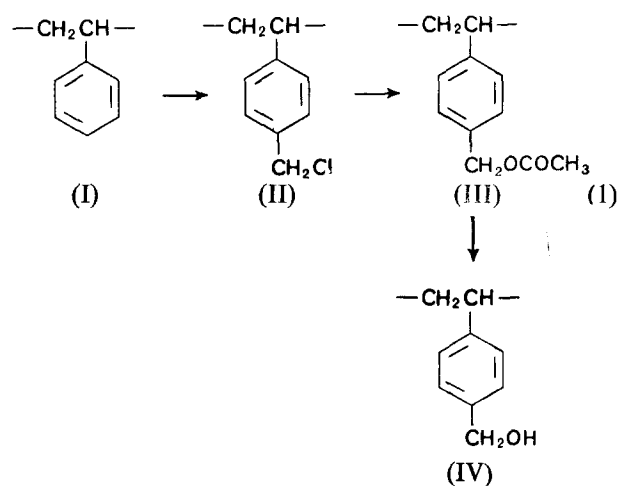
C. H. Bamford and H. Lindsay

Department of Inorganic, Physical and Industrial Chemistry, Donnan Laboratories, University of Liverpool, PO Box 147, Liverpool L69 3BX, UK  
(Received 15 March 1973)

The controlled inter- and intra-molecular crosslinking of polymers is of current interest in several contexts<sup>1,2</sup> and generally must be effected through functional groups attached to the polymer chains. Polystyrene has advantages in studies of this type since it may be prepared with narrow molecular weight distributions and its physical properties have been extensively investigated. Use of hydroxyl as the functional group is attractive; for example it may readily be converted to a halogenated ester capable of network formation<sup>1</sup>. The preparation of hydroxystyrenes<sup>3-5</sup> and their polymerization<sup>6,7</sup> have been studied extensively. There are, however, no reports in the literature of the synthesis of (hydroxymethyl)styrene polymers, and indeed some of the difficulties encountered are well documented<sup>8</sup>. The purposes of this communication are to point out that the introduction of hydroxymethyl groups into polystyrene may readily be carried out by known reactions, and that the direct preparation of *p*-vinylbenzyl alcohol from styrene monomer may also be effected in a similar way.

#### POLYSTYRENE CONTAINING *p*-CH<sub>2</sub>OH GROUPS

The synthesis follows the route shown in (1) below:



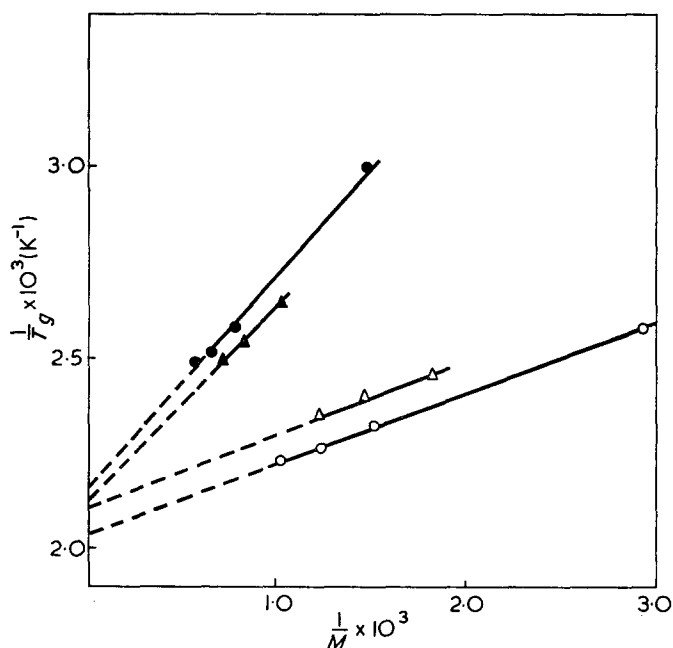


Figure 2 The glass transition temperatures ( $T_g$ ) of oligosaccharides versus molecular weight.  $\circ$ , Cellodextrins;  $\bullet$ , acetylated cellodextrins;  $\triangle$ , xylodextrins;  $\blacktriangle$ , acetylated xylodextrins

subjecting polymers to drastically high temperatures. In the case of polysaccharides pyrolytic degradation becomes severe at  $180^\circ\text{C}$ <sup>11</sup>.

#### CONCLUSIONS

The high  $T_g$  values of the oligosaccharides are due to the high cohesive energy between the chains (intermolecular

forces) and the limited rotational freedom between the monomer units in these molecules<sup>12</sup>. Since changes in the cohesive energy by acetylation are not found to alter  $T_g$  to any great extent, at least for the xylodextrins, it seems probable that the inherent chain stiffness is the primary reason for the high  $T_g$  values.

The structure of the monomer unit evidently influences the  $T_g$  values. In the absence of the primary hydroxyl group (xylodextrins) the  $T_g$  values are reduced by about  $20^\circ\text{C}$ . It seems reasonable to assume that this is due to intramolecular coupling by hydrogen bonding between adjacent rings that has been demonstrated between the hydroxyls at  $\text{C}_6$  and  $\text{C}_2$  in contiguous units<sup>13</sup>. This interpretation is in line with the results on the acetylated compounds. In this case hydrogen bonding is absent and similar  $T_g$  values are observed. Thus chain stiffness and cohesive energies should be about equal and equal  $T_g$  values would be expected.

#### REFERENCES

- 1 Brown, W. J. *Chromatogr.* 1970, **52**, 273
- 2 Brown, W. and Andersson, Ö. *J. Chromatogr.* 1971, **57**, 255
- 3 Marton, J. *et al. Adv. Chem. Ser.* 1966, **59**, 125
- 4 Lewis, A. F. and Gillham, J. K. *J. Appl. Polym. Sci.* 1962, **6**, 422
- 5 Karlsson, H. *Thesis* Royal Institute of Technology, Stockholm
- 6 Ueberreiter, K. and Kanig, G. *J. Colloid Sci.* 1952, **7**, 569
- 7 Read, B. E. *Polymer* 1962, **3**, 529
- 8 Back, E. L. and Didriksson, E. I. E. *Sven. Papperstidn.* 1969, **72**, 687
- 9 Goring, D. A. I. *Pulp Paper Mag. Can.* 1963, **64**, T-517
- 10 Fox, T. G. and Flory, P. J. *J. Appl. Phys.* 1950, **21**, 581
- 11 Arseneau, D. F. *Can. J. Chem.* 1971, **49**, 632
- 12 Boyer, R. F. *Rubber Chem. Technol.* 1963, **36**, 1303
- 13 Mann, J. and Marrison, H. I. *J. Polym. Sci.* 1956, **21**, 301

## Introduction of hydroxymethyl groups into polystyrene and styrene

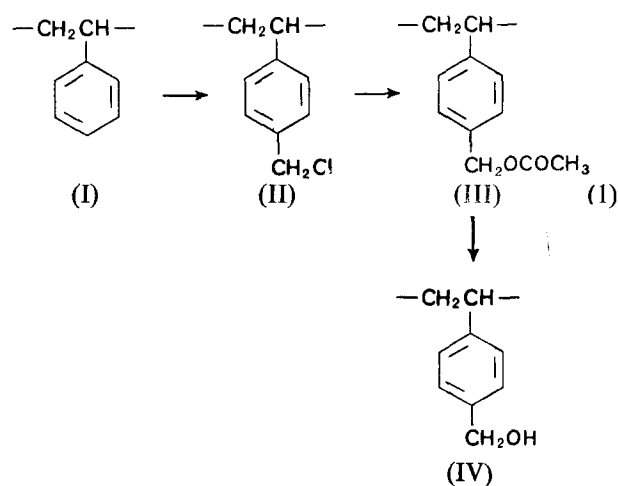
C. H. Bamford and H. Lindsay

Department of Inorganic, Physical and Industrial Chemistry, Donnan Laboratories, University of Liverpool, PO Box 147, Liverpool L69 3BX, UK  
(Received 15 March 1973)

The controlled inter- and intra-molecular crosslinking of polymers is of current interest in several contexts<sup>1,2</sup> and generally must be effected through functional groups attached to the polymer chains. Polystyrene has advantages in studies of this type since it may be prepared with narrow molecular weight distributions and its physical properties have been extensively investigated. Use of hydroxyl as the functional group is attractive; for example it may readily be converted to a halogenated ester capable of network formation<sup>1</sup>. The preparation of hydroxystyrenes<sup>3-5</sup> and their polymerization<sup>6,7</sup> have been studied extensively. There are, however, no reports in the literature of the synthesis of (hydroxymethyl)styrene polymers, and indeed some of the difficulties encountered are well documented<sup>8</sup>. The purposes of this communication are to point out that the introduction of hydroxymethyl groups into polystyrene may readily be carried out by known reactions, and that the direct preparation of *p*-vinylbenzyl alcohol from styrene monomer may also be effected in a similar way.

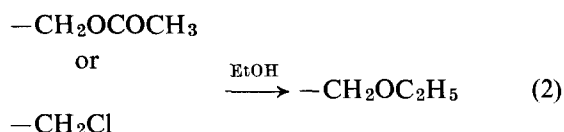
#### POLYSTYRENE CONTAINING *p*-CH<sub>2</sub>OH GROUPS

The synthesis follows the route shown in (1) below:





The almost quantitative conversion of polystyrene (I) into poly(*p*-vinylbenzyl chloride) (II) has been described by Schlögl and Fabitschowitz<sup>9</sup>, who used chlorodimethyl ether both as solvent and reagent for chloromethylation. Anhydrous zinc chloride is a suitable catalyst. Other reagents, such as stannic chloride<sup>10</sup>, have been suggested but the reaction is often too vigorous and leads to gel formation. In our preparations the polymer was dissolved in carbon disulphide or carbon tetrachloride and a proportion of the stoichiometric weight of chlorodimethyl ether was employed. Conversion of poly(*p*-vinylbenzyl chloride) (II) to poly(*p*-vinylbenzyl acetate) (III) was described by Ayres and Mann<sup>11</sup>. These authors carried out the reaction on a polystyrene gel, so that the isolation of the product in our case is different. Saponification of (III) to the required poly(*p*-vinylbenzyl alcohol) (IV) has not been described in the literature, although the corresponding reaction with non-polymeric analogues is recorded<sup>12,13</sup>. A variety of conditions was examined, and the results led to the following conclusions: (i) saponification is only successful in homogeneous solution; and (ii) ethanol must be absent from the reaction mixture, otherwise ether derivatives are formed. A similar reaction occurs if unconverted chloromethyl groups remain:



There are reports in the literature<sup>8</sup> that direct hydrolysis of poly(*p*-vinylbenzyl chloride) to poly(*p*-vinylbenzyl alcohol) cannot be accomplished, and our experience bears out this conclusion.

### Experimental

**Styrene/*p*-vinylbenzyl chloride copolymer.** Commercial grade polystyrene (5 g) was dissolved in carbon disulphide (50 ml) and chlorodimethyl ether (3.5 ml) was added together with anhydrous zinc chloride (1 g). The mixture was shaken for 1 h and a further 1 g of zinc chloride was added. Shaking was continued for 9 h at room temperature and the mixture was then filtered. The solution was poured into methanol (2 l) to precipitate the polymer which was filtered and washed successively with hot water (1 l) and methanol (2 l). Reprecipitation was carried out from tetrahydrofuran or chloroform solution (30 ml) into methanol, to give a white fibrous polymer which was dried *in vacuo* at 60°C for 4 h (yield 5.5 g).

The degree of substitution may be controlled through the reaction time. Observation of the intensity of the *p*-substitution band at 1220 cm<sup>-1</sup> provides a convenient method of monitoring the progress of reaction once the necessary calibration (based on elemental analysis) has been established. The conditions specified above would give 10% substitution, approximately.

**Styrene/*p*-vinylbenzyl acetate copolymer.** Chloromethylated polystyrene (5 g) and anhydrous potassium acetate (30 g) were suspended by stirring in dimethyl sulphoxide (300 ml) at 40°C for 48 h. The resulting slurry was poured into cold water (2 l) and the precipitate was filtered off

and washed with hot water (3 l). Reprecipitation was carried out from tetrahydrofuran (or chloroform) solution (30 ml) into methanol, to give a white fibrous polymer which was dried *in vacuo* at 40°C for 5 h (yield 5 g).

The infra-red spectrum showed strong C=O peaks at 1740 and 1230 cm<sup>-1</sup>.

The chloromethylated polymer used in this stage must be finely divided; it may be obtained in a suitable form by precipitation from dilute solution.

**Styrene/*p*-vinylbenzyl alcohol copolymer.** The styrene/*p*-vinylbenzyl acetate copolymer (5 g) was dissolved in dioxane (300 ml); water (about 10 ml) was added dropwise until the polymer just remained in solution, then solid sodium hydroxide (4 g). The mixture was stirred for 10 h at 40°C and then poured into water (2 l) acidified with hydrochloric acid (25 ml). The polymer was filtered off, redissolved in tetrahydrofuran (30 ml) and reprecipitated in water (2 l). The fibrous white polymer was washed in methanol (1 l) and after separation by filtration was dried *in vacuo* at 30°C for 5 h.

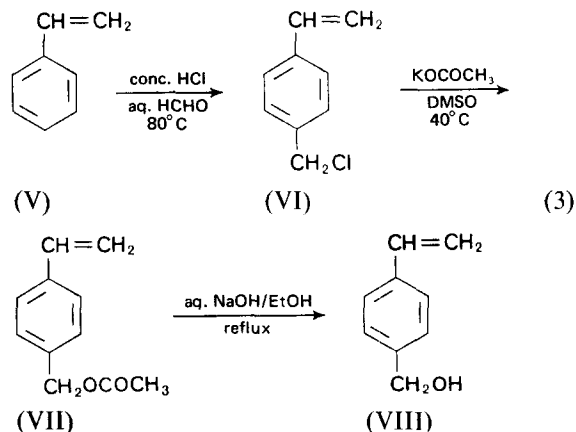
The infra-red spectrum showed the disappearance of the carbonyl peaks and the appearance of a broad hydroxyl peak at 3400–3500 cm<sup>-1</sup>.

### *p*-VINYL BENZYL ALCOHOL FROM STYRENE

Two types of procedure for the synthesis of *p*-vinylbenzyl alcohol have been described. Yakubovich *et al.*<sup>14</sup> employed the Grignard reagent from *p*-chlorostyrene and reacted this with gaseous formaldehyde. However, *p*-chlorostyrene requires a lengthy preparation and is expensive.

The second procedure involves chloromethylation of  $\beta$ -chloroethyl benzene<sup>13</sup> or ethyl benzene<sup>12</sup>, followed by conversion of the chloromethyl to an acetoxymethyl group by reaction with potassium or sodium acetate and acetic acid. Simultaneous saponification and dehydrochlorination then led to the desired product in the former case, while in the latter, conversion of the ethyl substituent into  $\alpha$ -acetoxyethyl is a necessary preliminary. There is also considerable contamination from the *o*-isomers of the intermediate products.

Both of these routes involve a large number of steps. Direct synthesis from styrene is more convenient, and may be effected by the route shown in (3):



Styrene monomer (V) was chloromethylated using concentrated hydrochloric acid and aqueous formaldehyde solution<sup>15</sup>. Potassium acetate in dimethylsulphoxide was used to replace the chlorine in (VI) by an acetate

group (a method adapted from that of Ayres and Mann<sup>11</sup>) and the resulting ester (VII) was saponified to *p*-vinylbenzyl alcohol (VIII).

Attempts to hydrolyse the chloromethyl group in (VI) directly with ethanolic or aqueous sodium hydroxide produced ethyl(*p*-vinylbenzyl) ether in the absence of water and failed completely in aqueous solution. Blanchette and Cotman<sup>8</sup> similarly found that halogen in chloromethylated polystyrene could not be directly replaced by hydroxyl groups.

#### Experimental

***p*-Chloromethylstyrene.** A mixture of styrene (172 ml), conc. hydrochloric acid (750 ml), sulphur as inhibitor (10 g) and formaldehyde solution (aq. 30%; 150 ml) was stirred at 80°C for 8 h. An equal volume of water was added, the mixture was filtered and the oily layer separated. The aqueous layer was extracted twice with 50 ml portions of chloroform and the organic layers were combined. After drying (Na<sub>2</sub>SO<sub>4</sub>), *p*-chloromethylstyrene was obtained on fractionation as a colourless oil (108 g) b.p. 89–92°C (4 mmHg) [lit.<sup>15</sup> b.p. 114–115°C (13 mmHg)]; i.r. (liquid) 1654 and 970 cm<sup>-1</sup> (vinyl group); n.m.r. centred at δ 3.95 (2H, chloromethyl CH<sub>2</sub>), δ 6.25 (2H, vinyl CH<sub>2</sub>) and δ 7.25 (5H, ring protons and vinyl CH).

***p*-Vinylbenzyl acetate.** A mixture of *p*-chloromethylstyrene (108 g), potassium acetate (80 g) and dimethylsulphoxide (DMSO) (250 ml) was stirred at 40°C for 48 h. The mixture was filtered, water (1.5 l) was added, and the oil which separated was extracted with four 100 ml portions of chloroform. The extracts were dried (Na<sub>2</sub>SO<sub>4</sub>) and distilled under reduced pressure to give a colourless oil, b.p. 96–100°C (10 mmHg). This product was then washed twice with 50 ml portions of water to remove any residual DMSO. After drying (Na<sub>2</sub>SO<sub>4</sub>) the organic layer was distilled to give *p*-vinylbenzyl acetate (109 g) as a colourless oil b.p. 97–99°C (4 mmHg) [lit.<sup>12</sup> 136–139°C (15 mmHg)]; i.r. (liquid) 1735 and 1240 (ester C=O) and 975 cm<sup>-1</sup> (vinyl group); n.m.r. centred at δ 1.85 (3H, ester CH<sub>3</sub>), δ 4.60 (2H benzyl CH<sub>2</sub>), δ 6.35 (2H, vinyl CH<sub>2</sub>) and δ 7.25 (5H, ring protons and vinyl).

***p*-Vinylbenzyl alcohol.** A mixture of *p*-vinylbenzyl acetate (109 g), sodium hydroxide (50 g) in water (50 ml) and ethanol (300 ml) was refluxed for 1.5 h. The mixture was diluted with water (1.5 l) and extracted with four 100 ml portions of chloroform. The extracts were dried (Na<sub>2</sub>SO<sub>4</sub>) and distilled under reduced pressure to give *p*-vinylbenzyl alcohol (73.5 g), a pale yellow oil, b.p. 100–101°C (4 mmHg) [lit.<sup>12</sup> 132–137°C (15 mmHg)], which solidified on cooling to feathery crystals m.p. 23–24°C (lit.<sup>8</sup> 24°C). The phenyl urethane melted at 93–94°C (lit.<sup>13</sup> 95–96°C); i.r. (liquid) 975 and 1640 (vinyl group) and 3320 (OH) cm<sup>-1</sup> (complete absence of any carbonyl bands); n.m.r. centred at δ 4.05 (2H, benzyl CH<sub>2</sub>), δ 4.92 (1H, hydroxyl), δ 6.20 (2H, vinyl CH<sub>2</sub>) and δ 7.10 (5H, ring protons and vinyl CH).

#### REFERENCES

- Bamford, C. H., Ashworth, J. and Smith, E. G. *IUPAC Conf. Chem. Transformations of Polymers, Bratislava, 1971* Butterworths, London, 1972, p 25
- Walsh, D. J. *Thesis*, University of Manchester, 1972
- Flood, S. A. and Nieuwland, J. A. *J. Am. Chem. Soc.* 1928, **50**, 2566
- Dale, W. J. and Hennis, H. E. *J. Am. Chem. Soc.* 1958, **80**, 3645
- Corson, B. B., Heintzelman, W. J., Schwartzman, L. H. *et al. J. Org. Chem.* 1958, **23**, 544
- Stern, R., English, (Jr) J. E. and Cassidy, H. G. *J. Am. Chem. Soc.* 1957, **79**, 5792
- Kato, M. *J. Polym. Sci. (A-1)* 1969, **7** 2175
- Blanchette, J. A. and Cotman, J. D. *J. Org. Chem.* 1958, **23**, 1117
- Schlögl, K. and Fabitschowitz, H. *Monatsh. Chem.* 1954, **85**, 1223
- Jones, G. D. *Ind. Eng. Chem.* 1952, **44**, 2686
- Ayres, J. T. and Mann, C. K. *J. Polym. Sci. (B)* 1965, **3**, 503
- Emerson, W. S., Heyd, J. W., Lucas, V. E., Lyness, W. I., Owens, G. R. and Shortridge, R. W. *J. Am. Chem. Soc.* 1947, **69**, 1905
- Abrams, J. G. and Chapin, E. C. *J. Org. Chem.* 1961, **26**, 2671
- Yakovovich, A. Ya., Ginsburg, V. A., Spiridova, T. G. and Popakova, G. I. USSR Pat. 172 293 (1965); *Chem. Abstr.* 1965, **63**, 16260g
- Wichterle, O. and Černý, J. Czech. Pat. 83 721 (1955); *Chem. Abstr.* 1956, **50**, 5738h

## On the importance of 2:1 water-DMSO complex in the n.m.r. spectra of 2'-deoxyadenosine in DMSO-water mixtures

G. Venkoba Rao\*, M. Balakrishnan and N. Venkatasubramanian

Department of Chemistry, Vivekananda College, Madras 600004, India  
(Received 5 March 1973)

In their study of n.m.r. and u.v. spectra of 2'-deoxyadenosine (dA) in DMSO-water mixtures, Jang *et al.*<sup>1</sup> noticed two types of upfield shifts of C<sub>2</sub> and C<sub>8</sub> protons of the base moiety. One type of upfield shift decreasing with decreasing water concentration upto 40% water in DMSO-water mixtures was found to be concentration dependent. The other type of upfield shift increases in the region 60%–100% DMSO and is concentration independent. While the first type was due to stacking

interactions, the second type was interpreted by these authors in terms of hydration.

We wish to point out in this communication that Jang *et al.* have completely overlooked one of the most important features of the DMSO-water system *viz.* the formation of a complex between DMSO and water. The novel results of Jang *et al.* can be explained only on the basis of this complex formation. Further, the possibility of hydration of the substrate at water concentrations less than 40% in DMSO-water mixtures is negligible and the upfield shift of C<sub>2</sub> and C<sub>8</sub> protons is due to a novel type

\* Present address: Harihar Polyfibers, Harihar, Mysore, India.

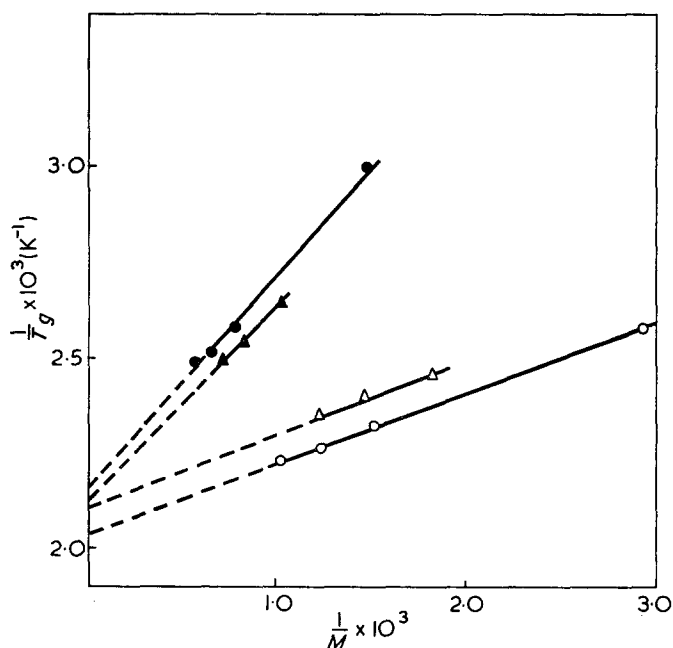


Figure 2 The glass transition temperatures ( $T_g$ ) of oligosaccharides versus molecular weight.  $\circ$ , Cellodextrins;  $\bullet$ , acetylated cellodextrins;  $\triangle$ , xylodextrins;  $\blacktriangle$ , acetylated xylodextrins

subjecting polymers to drastically high temperatures. In the case of polysaccharides pyrolytic degradation becomes severe at  $180^\circ\text{C}$ <sup>11</sup>.

#### CONCLUSIONS

The high  $T_g$  values of the oligosaccharides are due to the high cohesive energy between the chains (intermolecular

forces) and the limited rotational freedom between the monomer units in these molecules<sup>12</sup>. Since changes in the cohesive energy by acetylation are not found to alter  $T_g$  to any great extent, at least for the xylodextrins, it seems probable that the inherent chain stiffness is the primary reason for the high  $T_g$  values.

The structure of the monomer unit evidently influences the  $T_g$  values. In the absence of the primary hydroxyl group (xylodextrins) the  $T_g$  values are reduced by about  $20^\circ\text{C}$ . It seems reasonable to assume that this is due to intramolecular coupling by hydrogen bonding between adjacent rings that has been demonstrated between the hydroxyls at  $\text{C}_6$  and  $\text{C}_2$  in contiguous units<sup>13</sup>. This interpretation is in line with the results on the acetylated compounds. In this case hydrogen bonding is absent and similar  $T_g$  values are observed. Thus chain stiffness and cohesive energies should be about equal and equal  $T_g$  values would be expected.

#### REFERENCES

- 1 Brown, W. J. *Chromatogr.* 1970, **52**, 273
- 2 Brown, W. and Andersson, Ö. *J. Chromatogr.* 1971, **57**, 255
- 3 Marton, J. *et al. Adv. Chem. Ser.* 1966, **59**, 125
- 4 Lewis, A. F. and Gillham, J. K. *J. Appl. Polym. Sci.* 1962, **6**, 422
- 5 Karlsson, H. *Thesis* Royal Institute of Technology, Stockholm
- 6 Ueberreiter, K. and Kanig, G. *J. Colloid Sci.* 1952, **7**, 569
- 7 Read, B. E. *Polymer* 1962, **3**, 529
- 8 Back, E. L. and Didriksson, E. I. E. *Sven. Papperstidn.* 1969, **72**, 687
- 9 Goring, D. A. I. *Pulp Paper Mag. Can.* 1963, **64**, T-517
- 10 Fox, T. G. and Flory, P. J. *J. Appl. Phys.* 1950, **21**, 581
- 11 Arseneau, D. F. *Can. J. Chem.* 1971, **49**, 632
- 12 Boyer, R. F. *Rubber Chem. Technol.* 1963, **36**, 1303
- 13 Mann, J. and Marrison, H. I. *J. Polym. Sci.* 1956, **21**, 301

## Introduction of hydroxymethyl groups into polystyrene and styrene

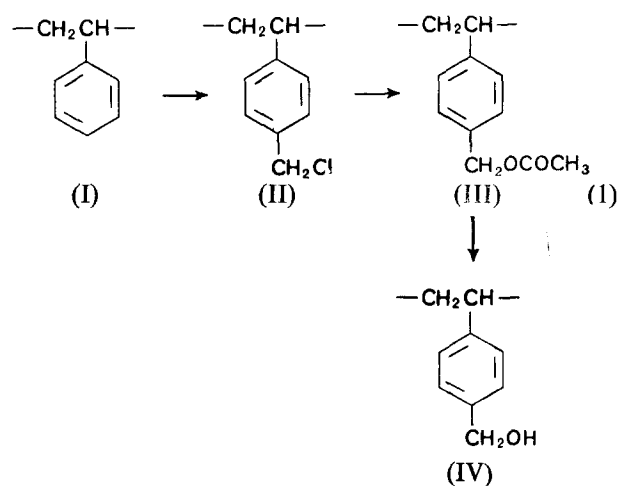
C. H. Bamford and H. Lindsay

Department of Inorganic, Physical and Industrial Chemistry, Donnan Laboratories, University of Liverpool, PO Box 147, Liverpool L69 3BX, UK  
(Received 15 March 1973)

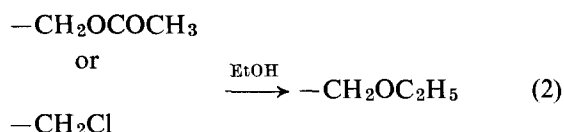
The controlled inter- and intra-molecular crosslinking of polymers is of current interest in several contexts<sup>1,2</sup> and generally must be effected through functional groups attached to the polymer chains. Polystyrene has advantages in studies of this type since it may be prepared with narrow molecular weight distributions and its physical properties have been extensively investigated. Use of hydroxyl as the functional group is attractive; for example it may readily be converted to a halogenated ester capable of network formation<sup>1</sup>. The preparation of hydroxystyrenes<sup>3-5</sup> and their polymerization<sup>6,7</sup> have been studied extensively. There are, however, no reports in the literature of the synthesis of (hydroxymethyl)styrene polymers, and indeed some of the difficulties encountered are well documented<sup>8</sup>. The purposes of this communication are to point out that the introduction of hydroxymethyl groups into polystyrene may readily be carried out by known reactions, and that the direct preparation of *p*-vinylbenzyl alcohol from styrene monomer may also be effected in a similar way.

#### POLYSTYRENE CONTAINING *p*-CH<sub>2</sub>OH GROUPS

The synthesis follows the route shown in (1) below:



The almost quantitative conversion of polystyrene (I) into poly(*p*-vinylbenzyl chloride) (II) has been described by Schlögl and Fabitschowitz<sup>9</sup>, who used chlorodimethyl ether both as solvent and reagent for chloromethylation. Anhydrous zinc chloride is a suitable catalyst. Other reagents, such as stannic chloride<sup>10</sup>, have been suggested but the reaction is often too vigorous and leads to gel formation. In our preparations the polymer was dissolved in carbon disulphide or carbon tetrachloride and a proportion of the stoichiometric weight of chlorodimethyl ether was employed. Conversion of poly(*p*-vinylbenzyl chloride) (II) to poly(*p*-vinylbenzyl acetate) (III) was described by Ayres and Mann<sup>11</sup>. These authors carried out the reaction on a polystyrene gel, so that the isolation of the product in our case is different. Saponification of (III) to the required poly(*p*-vinylbenzyl alcohol) (IV) has not been described in the literature, although the corresponding reaction with non-polymeric analogues is recorded<sup>12,13</sup>. A variety of conditions was examined, and the results led to the following conclusions: (i) saponification is only successful in homogeneous solution; and (ii) ethanol must be absent from the reaction mixture, otherwise ether derivatives are formed. A similar reaction occurs if unconverted chloromethyl groups remain:



There are reports in the literature<sup>8</sup> that direct hydrolysis of poly(*p*-vinylbenzyl chloride) to poly(*p*-vinylbenzyl alcohol) cannot be accomplished, and our experience bears out this conclusion.

### Experimental

**Styrene/*p*-vinylbenzyl chloride copolymer.** Commercial grade polystyrene (5 g) was dissolved in carbon disulphide (50 ml) and chlorodimethyl ether (3.5 ml) was added together with anhydrous zinc chloride (1 g). The mixture was shaken for 1 h and a further 1 g of zinc chloride was added. Shaking was continued for 9 h at room temperature and the mixture was then filtered. The solution was poured into methanol (2 l) to precipitate the polymer which was filtered and washed successively with hot water (1 l) and methanol (2 l). Reprecipitation was carried out from tetrahydrofuran or chloroform solution (30 ml) into methanol, to give a white fibrous polymer which was dried *in vacuo* at 60°C for 4 h (yield 5.5 g).

The degree of substitution may be controlled through the reaction time. Observation of the intensity of the *p*-substitution band at 1220 cm<sup>-1</sup> provides a convenient method of monitoring the progress of reaction once the necessary calibration (based on elemental analysis) has been established. The conditions specified above would give 10% substitution, approximately.

**Styrene/*p*-vinylbenzyl acetate copolymer.** Chloromethylated polystyrene (5 g) and anhydrous potassium acetate (30 g) were suspended by stirring in dimethyl sulphoxide (300 ml) at 40°C for 48 h. The resulting slurry was poured into cold water (2 l) and the precipitate was filtered off

and washed with hot water (3 l). Reprecipitation was carried out from tetrahydrofuran (or chloroform) solution (30 ml) into methanol, to give a white fibrous polymer which was dried *in vacuo* at 40°C for 5 h (yield 5 g).

The infra-red spectrum showed strong C=O peaks at 1740 and 1230 cm<sup>-1</sup>.

The chloromethylated polymer used in this stage must be finely divided; it may be obtained in a suitable form by precipitation from dilute solution.

**Styrene/*p*-vinylbenzyl alcohol copolymer.** The styrene/*p*-vinylbenzyl acetate copolymer (5 g) was dissolved in dioxane (300 ml); water (about 10 ml) was added dropwise until the polymer just remained in solution, then solid sodium hydroxide (4 g). The mixture was stirred for 10 h at 40°C and then poured into water (2 l) acidified with hydrochloric acid (25 ml). The polymer was filtered off, redissolved in tetrahydrofuran (30 ml) and reprecipitated in water (2 l). The fibrous white polymer was washed in methanol (1 l) and after separation by filtration was dried *in vacuo* at 30°C for 5 h.

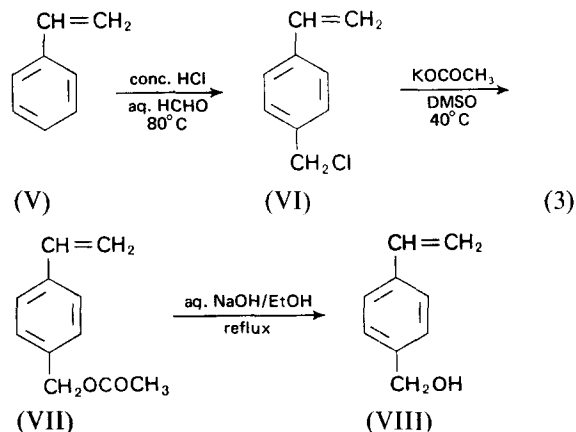
The infra-red spectrum showed the disappearance of the carbonyl peaks and the appearance of a broad hydroxyl peak at 3400–3500 cm<sup>-1</sup>.

### *p*-VINYL BENZYL ALCOHOL FROM STYRENE

Two types of procedure for the synthesis of *p*-vinylbenzyl alcohol have been described. Yakubovich *et al.*<sup>14</sup> employed the Grignard reagent from *p*-chlorostyrene and reacted this with gaseous formaldehyde. However, *p*-chlorostyrene requires a lengthy preparation and is expensive.

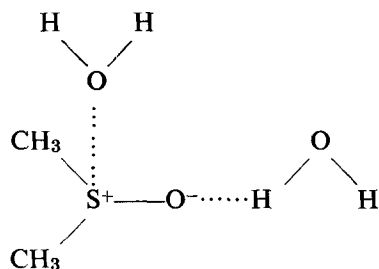
The second procedure involves chloromethylation of  $\beta$ -chloroethyl benzene<sup>13</sup> or ethyl benzene<sup>12</sup>, followed by conversion of the chloromethyl to an acetoxymethyl group by reaction with potassium or sodium acetate and acetic acid. Simultaneous saponification and dehydrochlorination then led to the desired product in the former case, while in the latter, conversion of the ethyl substituent into  $\alpha$ -acetoxyethyl is a necessary preliminary. There is also considerable contamination from the *o*-isomers of the intermediate products.

Both of these routes involve a large number of steps. Direct synthesis from styrene is more convenient, and may be effected by the route shown in (3):



Styrene monomer (V) was chloromethylated using concentrated hydrochloric acid and aqueous formaldehyde solution<sup>15</sup>. Potassium acetate in dimethylsulphoxide was used to replace the chlorine in (VI) by an acetate

of interaction between dA and DMSO. The fact that DMSO forms 1 : 2 complex with water is well established<sup>2</sup>.



There is spectral evidence to show that there is hydrogen bonding between the two liquids<sup>3</sup>. The maxima in viscosity isotherms at mole fractions of DMSO equal to 0.3 and the large heat of evolution on mixing DMSO with water also show that there is strong association between these two liquids<sup>4</sup>. Thus at the mole fraction of DMSO = 0.28 corresponding to 60% DMSO in DMSO-water mixtures the formation of complex is complete and very little 'free water' is available in the system for hydration purposes above 60% DMSO. There have been evidences for this from our kinetic studies as well<sup>5</sup>.

The first type of upfield shift of C<sub>2</sub> and C<sub>8</sub> protons in 2'-deoxyadenosine has been attributed to solute-solute or stacking interactions<sup>1</sup>. These solute-solute interactions have been previously reported in the literature and in aqueous solutions such increased upfield shift of signals of base protons with increasing concentration of the solute have been noticed<sup>6, 7</sup>. This concentration dependent upfield shift of C<sub>2</sub> and C<sub>8</sub> protons of the base moiety in dA is found to decrease with decreasing water concentrations and vanishes at 40% water. This is because at this concentration of water corresponding to 60% DMSO, almost all the water is bound to DMSO in the form of a complex and at this percentage of water (40% water-60% DMSO) no concentration dependent upfield shift is noticed. We attribute the non-availability of 'free water' as the major cause of this. This non-dependence of the upfield shift on concentration at 40% water has not been explained by Jang *et al.*

When the concentration of water is still further decreased below 40%, the signals of C<sub>2</sub> and C<sub>8</sub> protons shift to higher field, the upfield shift increasing with decreasing water concentrations. The upfield shift being concentration independent cannot be due to stacking

interactions. Jang *et al.* attribute this to hydration, a solvent-solute interaction. We feel that the results are better explained by invoking a different type of solvent-solute interaction, *viz.* the interaction between DMSO and the solute rather than water and solute (hydration) as these authors have proposed. This looks more plausible because: (1) the concentration of 'free water' available for hydration is negligible when the percentage of DMSO exceeds 60% in DMSO-water mixtures; and (2) in 100% DMSO also a concentration independent upfield shift is noticed. In 100% DMSO no water is available for hydration purposes and hence 'hydration' is not responsible for these upfield shifts.

We attribute the increased upfield shifts in concentrations of DMSO exceeding 60% to a possible interaction between the positive end of the sulphoxide dipole in DMSO and the lone pair of electrons on the ring nitrogen atoms. This type of interaction will affect the 'ring current' and will then be the reason for the upfield shift of C<sub>2</sub> and C<sub>8</sub> protons. What we envisage here is an ion-pair formation between the positive end of the DMSO dipole and the lone pair on ring nitrogen atoms or alternatively a situation similar to 'collision complexes' postulated between benzene and *N,N*-dimethyl formamide<sup>8</sup>. This hypothesis is further confirmed by the fact that the upfield shift increases with decreasing dielectric constant of the medium (increasing DMSO concentration in aqueous DMSO) and it is well known that ion-pair formation will increase with decreasing dielectric constant.

We wish to point out here that interaction between DMSO and  $\pi$  electrons of the ring is not significant as evidenced by the superimposability of the n.m.r. spectra of ethyleneglycol dibenzoate in DMSO and CDCl<sub>3</sub><sup>9</sup>.

## REFERENCES

- 1 Jang, C. G., Bartl, P. and Williams, T. *Polymer* 1972, **13**, 520
- 2 Parker, A. J. *Chem. Rev.* 1969, **69**, 1
- 3 Tamres, U. and Searless, S. J. *Am. Chem. Soc.* 1959, **81**, 2100
- 4 Tommila, E. and Murto, M. L. *Acta Chem. Scand.* 1963, **17**, 1947
- 5 Venkoba Rao, G. and Venkatasubramanian, N. *Ind. J. Chem.* 1972, **10**, 178
- 6 Broom, A. D., Schweizer, M. P. and Ts'o, P. O. P. *J. Am. Chem. Soc.* 1967, **89**, 3612
- 7 Jardetzky, O. *Biopolymers* 1964, Symp. 1, 501
- 8 Hatton, J. V. and Richards, R. E. *Mol. Phys.* 1962, **5**, 139
- 9 Venkoba Rao, G., Balakrishnan, M. and Venkatasubramanian, N. unpublished results

## Molecular-sieve catalysed polymerization of isobutylene\*†

R. A. Rhein and Jeanne S. Clarke

Jet Propulsion Laboratory, California Institute of Technology, Pasadena, Calif. 91103, USA  
(Received 16 February 1973)

### INTRODUCTION

There are only two other reports of molecular-sieve catalysed polymerization of isobutylene. Norton<sup>1</sup> stated that isobutylene polymerized more readily than did

\* This paper presents the results of one phase of research carried out at the Jet Propulsion Laboratory, California Institute of Technology, under Contract No. NAS7-100, sponsored by the National Aeronautics and Space Administration.

† Part of this paper is based upon a presentation to the 97th Meeting of the Division of Rubber Chemistry, ACS, Washington DC, May 1970 (paper 10).

propylene or ethylene, and that the order of molecular sieve reactivities towards propylene polymerization for sieves of different designations was: type 10X < 13X < 5A < 4A < 3A = 0, but there was no discussion of the isobutylene polymerization products. Gensheimer and Brown<sup>2</sup> reported that a molecular sieve of type 5A (and also 4A, 10X and 13X) could polymerize isobutylene to di(isobutylene) and higher polymers. However, if the sieve was preheated in an inert oxygen-free gas, it would polymerize isobutylene to di(isobutylene) to the extent of 1-3%.

In this work, a variety of molecular sieves and conditions of temperature and reaction time were employed for isobutylene polymerization catalysis. The products were primarily low-boiling telomers, but polymers were formed in nearly every case.

#### EXPERIMENTAL AND RESULTS

Molecular sieves selected as catalysts included the types A, X, Y<sup>3,4</sup>, and L<sup>5,6</sup>. The types and pore diameters of the most common commercially available molecular sieves used in this work are: type 3A, 3 Å; type 4A, 4.2 Å; type 5A, 5 Å; type 10X, 8 Å; and type 13X, 10 Å.

Other molecular sieves used as catalysts (Linde Division of Union Carbide Corp.) were: SK45 (a potassium-exchanged type L<sup>5</sup>); SK100 (decaionized type Y with 0.5% Pd<sup>7</sup>); SK110 (partly decaionized type Y with 5.2% MnO and 0.5% Pd<sup>7</sup>); SK200 (calcium-exchanged type Y with 0.5% Pt<sup>7</sup>); SK310 (calcium-exchanged type Y with 0.5% Pd<sup>7</sup>); SK400 (sodium-exchanged type Y with 1.0% Ni<sup>7</sup>); SK410 (sodium-exchanged type Y with 1.0% Cu<sup>7</sup>); and SK500 (type Y with 35% cations, 15% Na<sub>2</sub>O and 50% mixed rare earth oxides<sup>8</sup>).

Although a variety of experimental methods and approaches were employed (a more detailed discussion of experimental procedure is presented in ref. 9), there were features common to all of the experiments. In most cases,  $7.5 \times 10^{-5} \text{ m}^3$  (75 ml) of isobutylene were added to 0.025 kg of molecular sieve (pretreated by heating to 373–473 K and evacuating to 0.133 N/m<sup>2</sup> for 1 day)

in a  $2.5 \times 10^{-4} \text{ m}^3$  (250 ml) bulb. The reaction temperature was ambient (about 298 K) in most cases, although the reaction was studied also at 193 K, 273 K and 373 K.

After the reaction period, the reaction bulb was then opened to a cooled graduated tube, in which non-reacted isobutylene was collected and its volume measured. The products in the reaction bulb were washed with several portions of n-pentane. Then the mixture of pentane and reaction products, in a  $5 \times 10^{-4} \text{ m}^3$  (500 ml) beaker or flask, was opened to the atmosphere for a period of 1–4 days to permit the pentane to evaporate.

The resulting liquid product was then heated to approximately 423 K and evacuated to approximately 6.7 N/m<sup>2</sup> for a period of 1–3 days; to remove the volatile telomers, consisting of mixtures of di-, tri- and tetra-isobutylene.

The refractive index and infra-red spectrum were determined for each polymer. The number-average and weight-average molecular weights were obtained from gel-permeation chromatograms.

Nearly every polyisobutylene sample was characterized by a bimodal molecular weight distribution. The peak molecular weights were approximately 250 for the low-molecular weight peak and 3000–5000 for the high-molecular weight peak. This bimodal distribution accounts for polydispersity values ranging from 4 to 6.

The unsaturation was estimated by the mercuric acetate method<sup>10</sup>, and by a method using the increase in weight of a polymer sample, smeared on ground-glass disc (0.06 m diam.), after immersion in bromine vapour

Table 1 Experimental conditions and results

Molecular sieve type and size	Reaction time (days)	Stirring	Unreacted isobutylene	Yield of polymer (%)	Number-average molecular weight $M_n$	Weight-average molecular weight $M_w$
3A, 1/16 pellets	7	No	100	0		
4A, 100/120 mesh	7	No	100	0		
5A, 1/16 pellets	10	No	0	22.7	555	1325
5A, 40/50 mesh	4	Yes	0	54.3	350	b
5A, 40/50 mesh	4	Yes	0	52.6	322	1032
5A, 40/50 mesh	10	No	0	18.9	515	1264
5A, 80/90 mesh	10	No	0	43.6	469	1397
5A, 120/130 mesh	4	Yes	0	56.3	526	1641
5A, 160/170 mesh	10	No	0	48.7	663	1963
5A, 160/170 mesh	1	Yes	0	9.6	1241	3669
5A, 160/170 mesh <sup>a</sup>	1	Yes	0	8.0	1229	3438
5A powder, 1–4 μm	10	No	0	0		
10X, 100/120 mesh	7	No	0	4.5	300	480
10X, 100/120 mesh	9	Yes	0	3.9	575	1390
13X, 100/110 mesh	7	No	50	7.8	2569	5989
13X, 100/110 mesh	9	Yes	13.3	10.9	1140	4896
SK45 powder, 1–4 μm	5	Yes	b	b	839	2566
SK45 powder, 1–4 μm	9	Yes	76.0	0.2	1417	3292
SK100, 1/16 pellets	5	Yes	b	b	315	365
SK100, 1/16 pellets	9	Yes	0	5.6	639	1830
SK110, 1/16 pellets	3	Yes	b	b	982	2164
SK110, 1/16 pellets	9	Yes	0	4.4	832	1950
SK200, 1/16 pellets	3	Yes	b	b	781	1232
SK200, 1/16 pellets	9	Yes	0	0.5	564	1124
SK310, 1/16 pellets	3	Yes	0	1.2	457	761
SK400, 1/16 pellets	3	Yes	60	2.2	448	2114
SK400, 1/16 pellets	9	Yes	66.6	2.5	1233	3807
SK410, 1/16 pellets	3	Yes	80	0		
SK500, 1/16 pellets	3	Yes	0	2.0	610	1608

<sup>a</sup> Polymerized at 0°C. All others polymerized at room temperature

<sup>b</sup> Not determined

Table 2 Processing conditions and experimental results for the polymerization of isobutylene by molecular sieve 13X

Exp. No.	Reaction time (days)	Temp. (K)	Ratio of catalyst to monomer $\text{kg/m}^3 \times 10^3$ (gm/ml)	Stirring	Unreacted isobutylene (%)	Yield of polymer (%)	Number-average molecular weight, $M_n$	Weight-average molecular weight, $M_w$
1	0.333	298	0.333	Yes	66.6	2.6	911	3275
2	1	298	0.333	Yes	57.8	7.1	1565	4935
3	2	298	0.333	Yes	26.7	4	1293	4405
4	4	298	0.333	Yes	22.6	24.4	802	4279
5	6	298	0.333	Yes	0	14.7	863	4933
6	12	298	0.333	Yes	5.3	11.1	889	3971
7	15	298	0.333	Yes	6.7	16.7	770	4229
8	20	298	0.333	Yes	6.7	16	839	4049
9	9	298	0.5	Yes	19	43.4	865	4688
10	9	298	0.25	Yes	4	11.3	807	4135
11	9	298	0.5	Yes	2	30.3	586	3081
12	9	298	1	Yes	0	12.2	1264	3500
13	9	298	2.5	Yes	0	8.3	717	1405
14	1	193	0.333	No	97.6	0.1	1715	5267
15	4	193	0.333	No	31.4	12.2	780	3257
16	7	193	0.333	No	72	4.7	1107	5210
17	1	273	0.333	No	31.4	9.1	1137	5399
18	4	273	0.333	No	25	21.3	712	3369
19	7	273	0.333	No	0	30	820	3363
20	1	298	0.333	No	54.7	9.6	489	2507
21	4	298	0.333	No	20	22.9	613	3095
22	1	373	0.333	No	0.7	11	971	5710
23	4	373	0.333	No	6.7	16	393	1454
24	7	373	0.333	No	9.3	33.1	370	1678

Table 3 Parameters influencing the characteristics of the reaction products from the molecular-sieve-catalysed polymerization of isobutylene

Independent variable	Dependent variable		
	Polymer yield (%)	Polymer molecular wt., $M_n$	Isobutylene reacted (%)
Pore diameter	No yield $\leq 4.2 \times 10^{-10}$ m (4.2 Å) maximum at $5 \times 10^{-10}$ m (5 Å)	Increasing with increasing pore diameter	None $\leq 4.2 \times 10^{-10}$ m (4.2 Å); maximum (5–8) $\times 10^{-10}$ m (5–8 Å)
Exchanged cation	Generally cations > cations + MnO > Na <sub>2</sub> O > (Na <sub>2</sub> O + cations + rare earth oxides) > CaO	Generally (cations + MnO) ~ Na <sub>2</sub> O > CaO > (cations + Na <sub>2</sub> O + rare earth oxides) > cations	Generally (cations) ~ (cations + NaO) ~ CaO ~ (Na <sub>2</sub> O + cations + rare earth oxides) > Na <sub>2</sub> O
Type of sieve	A > X > Y > L	L > Y, L > A, otherwise indeterminate	A $\geq$ Y $\geq$ X > L
Catalyst on sieve	Pd > Pt, Ni > Cu	Pt > Pd	Pt = Pd, Ni > Cu
Particle size	Increasing yield for increased size	Increasing $M_n$ for decreasing particle size	Indeterminate
Temperature	Increased	Decreased	Increased
Time of reaction	Increasing	Generally decreased	Generally increasing
Ratio catalyst/monomer	Decreased	Decreased	Decreased
Effect of stirring	Decreased	Increased	Increased

for 60 sec.\* Unsaturation functionality substantially higher than unity was not observed for any of the polymers.

The data for the polymers are presented in Tables 1 and 2; these data include the weight percentage polymer yield (based upon the initial monomer weight), the percentage monomer that reacted, and the number-average and weight-average molecular weights.

From the experimental conditions, the character of the molecular sieves and the nature of the reaction products (Tables 1 and 2) comparative relationships

between the experimental variables and the reaction products were obtained. The dependent variables considered were the weight percentage polymer yield, the number-average molecular weight of the polymer, and the percentage monomer that reacted.

The following were regarded as independent variables: pore diameter (of the molecular sieve), the exchanged cation, the type of molecular sieve, the polymerization temperature, the reaction time, and the effect of stirring the reactants. Table 3 presents the qualitative relationships between each of the dependent variables to each of the independent variables in this work.

## DISCUSSION AND CONCLUSION

Since isobutylene polymerizes by a cationic mechanism<sup>11</sup>, it appears that the polymerization of isobutylene by molecular sieves occurs at cationic sites within the molecular sieve cavity. This is supported by the fact that

\* The method and apparatus is described in a brochure, 'Instructions for use of Heidbrinck Weight Glass, Cat. M30640', from Metro Scientific Inc., Farmingdale, NY. This method was found to be accurate for unsaturation determination of 1-octadecene and tetraisobutylene, and registered essentially no unsaturation (as expected) for Nujol mineral oil and for 2,6,10,14-tetramethylpentadecane.

polymerization only occurs when the cavity pores are  $\geq 5 \times 10^{-10}$  m ( $\geq 5 \text{ \AA}$ ) [i.e. the isobutylene cannot enter through pores  $< 5 \times 10^{-10}$  m ( $< 5 \text{ \AA}$ )] that polymer yield and fraction of isobutylene reacted were greatest for molecular sieves with cationic exchanged sites, and that the polymer was essentially monofunctional in unsaturation.

The polymerization reaction is rather slow, since both polymer yield and fraction of reacted isobutylene increased over a period of days. In addition, the polymer molecular weight decreased with increasing temperature, as generally observed in isobutylene polymerization.

In conclusion, types A, X, Y and L molecular sieves have served as catalysts for the polymerization of isobutylene. In all cases, the polymerization reaction was relatively slow. The polymerization evidently occurs within the cavities of the molecular sieve structure, since polymerization does not take place if the pore size is less than  $5 \times 10^{-10}$  m ( $5 \text{ \AA}$ ).

The polymerization products included viscous, non-volatile polymers, along with volatile telomers of isobutylene. The polymers in most cases were characterized by bimodal molecular weight distributions. Unsaturation

determination by means of mercuric acetate addition and bromine addition indicated about one unsaturated group per mole.

#### REFERENCES

- 1 Norton, C. J. *Ind. Eng. Chem. (Process Design and Develop.)* 1964, 3, (3) 230
- 2 Gensheimer, D. E. and Brown, E. C. U.S. Pat. 3 061 654 (20 Oct. 1962)
- 3 'Linde Molecular Sieves', *Tech. Bull. F-1979B* Union Carbide Corp., Linde Div., New York
- 4 Breck, D. W. *J. Chem. Educ.* 1964, 48, 678
- 5 Breck, D. W. and Flanigen, E. M. 'Molecular Sieves', London, Society of Chemical Industry, 1967
- 6 Barrer, R. M. and Villiger, H. Z. *Kristallog.* 1969, 128, 352
- 7 'A Report on Molecular Sieve Catalysis', *Bull. F-1578*, Union Carbide Corp., Linde Div., New York, 1967
- 8 *Bull. F-2808*, Union Carbide Corp., Linde Div., New York, 1967
- 9 Rhein, R. A. 97th Meet. Div. of Rubber Chem., ACS Washington D.C., May 1970, Paper No. 10
- 10 Fritz, J. S. and Hammond, G. S. 'Quantitative Organic Analysis', John Wiley, New York, 1957, p 72
- 11 Schildknecht, C. E. 'Vinyl and Related Polymers', John Wiley, New York, 1952, Ch 10

## Book Reviews

### Physical methods in macromolecular chemistry

Edited by Benjamin Carroll

Marcel Dekker, New York, 1972, Vol. 2, 369 pp. \$23.50

This book is volume two of a series which aims, according to the preface, to provide the scientist with the understanding needed to select the most useful method for his research problem. By focusing attention on the interpretation of experimental data, the editor assures us, the contributors point out important features and principal limitations of the methods they describe. Judged by these intentions, this particular book is a failure. In fact, the majority of the book is an uncritical catalogue of the various research papers which have been published. Of course, the book is quite useful as a source of references.

The nearest the book comes to fulfilling its objectives is in the fourth chapter by E. P. Manche and B. Carroll which is devoted to the applications of thermal methods to polymers. The article by D. J. R. Laurence on the Interactions of polymers with small ions and molecules, on the other hand, illustrates precisely my complaint; it will be unlikely to tell the expert anything new while for the beginner it fails to concentrate attention on the key papers but merely lumps them in with the morass—in some 70 pages of text, 386 references are given! The other two articles lie somewhere between in usefulness. The article on gel permeation chromatography by D. D. Bly is rather pedestrian but adequately summarizes the technique. The remaining article on the electrical properties of proteins by E. O. Forster and A. P. Minton is rather better but is restricted in scope to this particular type of polymer.

I also find the printing unattractive with its non-aligned right hand columns and small type face. The uninspired quality of the contributions, the unattractive printing, and the high price make me advise unequivocally private individuals or libraries not to purchase this book.

D. Margerison

### Differential thermal analysis

Edited by R. C. Mackenzie

Academic Press, London and New York, 1972, Vol 2, 607 pp. £12.50

The book opens with four excellent short chapters in a section entitled 'Physical chemistry'. The chapter on kinetics provides a useful corrective to some optimistic views in later pages. A chapter on Low temperature studies would logically have appeared in Vol 1 under instrumentation. The final section 'Applications in industry' has chapters on ceramics, building materials, cements, glass, minerals, soils, catalysts, atomic energy, explosives, plastics and rubbers, textiles, pharmaceuticals, oils, fats, soaps and waxes, foods, forest products and dusts.

Although this volume, unlike Vol 1, does not regard organic compounds chiefly as impurities in soils we still find plastics and rubbers treated as one chapter with the result that the coverage of the former relies unduly on the technical literature of instrument manufacturers. The author's criticism of published d.t.a. curves of polymers (p 411) is illuminating but this chapter on the whole is disappointing, probably because it is approximately six years old. The chapter on textiles contains much useful information in a mass of verbiage. The other chapters contain little of interest to polymer scientists. From the standing of the authors, one would expect good reviews of the topics and this they appear to provide. There is, however, a good deal of repetition amongst the various chapters as well as much extraneous material. One presumes that the book is intended to be available in a library rather than in a personal bookcase; the price of £25.00 for both volumes supports this view. D.t.a. is used by workers in many disciplines throughout the world, and the editor has endeavoured to reflect this in his choice of authors and subjects. This Herculean task has not been completely successful but the two volumes together provide the best general reference on d.t.a. known to me.

T. R. Manley



polymerization only occurs when the cavity pores are  $\geq 5 \times 10^{-10}$  m ( $\geq 5 \text{ \AA}$ ) [i.e. the isobutylene cannot enter through pores  $< 5 \times 10^{-10}$  m ( $< 5 \text{ \AA}$ )] that polymer yield and fraction of isobutylene reacted were greatest for molecular sieves with cationic exchanged sites, and that the polymer was essentially monofunctional in unsaturation.

The polymerization reaction is rather slow, since both polymer yield and fraction of reacted isobutylene increased over a period of days. In addition, the polymer molecular weight decreased with increasing temperature, as generally observed in isobutylene polymerization.

In conclusion, types A, X, Y and L molecular sieves have served as catalysts for the polymerization of isobutylene. In all cases, the polymerization reaction was relatively slow. The polymerization evidently occurs within the cavities of the molecular sieve structure, since polymerization does not take place if the pore size is less than  $5 \times 10^{-10}$  m (5 Å).

The polymerization products included viscous, non-volatile polymers, along with volatile telomers of isobutylene. The polymers in most cases were characterized by bimodal molecular weight distributions. Unsaturation

determination by means of mercuric acetate addition and bromine addition indicated about one unsaturated group per mole.

#### REFERENCES

- 1 Norton, C. J. *Ind. Eng. Chem. (Process Design and Develop.)* 1964, 3, (3) 230
- 2 Gensheimer, D. E. and Brown, E. C. U.S. Pat. 3 061 654 (20 Oct. 1962)
- 3 'Linde Molecular Sieves', *Tech. Bull. F-1979B* Union Carbide Corp., Linde Div., New York
- 4 Breck, D. W. *J. Chem. Educ.* 1964, 48, 678
- 5 Breck, D. W. and Flanigen, E. M. 'Molecular Sieves', London, Society of Chemical Industry, 1967
- 6 Barrer, R. M. and Villiger, H. Z. *Kristallog.* 1969, 128, 352
- 7 'A Report on Molecular Sieve Catalysis', *Bull. F-1578*, Union Carbide Corp., Linde Div., New York, 1967
- 8 *Bull. F-2808*, Union Carbide Corp., Linde Div., New York, 1967
- 9 Rhein, R. A. 97th Meet. Div. of Rubber Chem., ACS Washington D.C., May 1970, Paper No. 10
- 10 Fritz, J. S. and Hammond, G. S. 'Quantitative Organic Analysis', John Wiley, New York, 1957, p 72
- 11 Schildknecht, C. E. 'Vinyl and Related Polymers', John Wiley, New York, 1952, Ch 10

## Book Reviews

### Physical methods in macromolecular chemistry

Edited by Benjamin Carroll

Marcel Dekker, New York, 1972, Vol. 2, 369 pp. \$23.50

This book is volume two of a series which aims, according to the preface, to provide the scientist with the understanding needed to select the most useful method for his research problem. By focusing attention on the interpretation of experimental data, the editor assures us, the contributors point out important features and principal limitations of the methods they describe. Judged by these intentions, this particular book is a failure. In fact, the majority of the book is an uncritical catalogue of the various research papers which have been published. Of course, the book is quite useful as a source of references.

The nearest the book comes to fulfilling its objectives is in the fourth chapter by E. P. Manche and B. Carroll which is devoted to the applications of thermal methods to polymers. The article by D. J. R. Laurence on the Interactions of polymers with small ions and molecules, on the other hand, illustrates precisely my complaint; it will be unlikely to tell the expert anything new while for the beginner it fails to concentrate attention on the key papers but merely lumps them in with the morass—in some 70 pages of text, 386 references are given! The other two articles lie somewhere between in usefulness. The article on gel permeation chromatography by D. D. Bly is rather pedestrian but adequately summarizes the technique. The remaining article on the electrical properties of proteins by E. O. Forster and A. P. Minton is rather better but is restricted in scope to this particular type of polymer.

I also find the printing unattractive with its non-aligned right hand columns and small type face. The uninspired quality of the contributions, the unattractive printing, and the high price make me advise unequivocally private individuals or libraries not to purchase this book.

D. Margerison

### Differential thermal analysis

Edited by R. C. Mackenzie

Academic Press, London and New York, 1972, Vol 2, 607 pp. £12.50

The book opens with four excellent short chapters in a section entitled 'Physical chemistry'. The chapter on kinetics provides a useful corrective to some optimistic views in later pages. A chapter on Low temperature studies would logically have appeared in Vol 1 under instrumentation. The final section 'Applications in industry' has chapters on ceramics, building materials, cements, glass, minerals, soils, catalysts, atomic energy, explosives, plastics and rubbers, textiles, pharmaceuticals, oils, fats, soaps and waxes, foods, forest products and dusts.

Although this volume, unlike Vol 1, does not regard organic compounds chiefly as impurities in soils we still find plastics and rubbers treated as one chapter with the result that the coverage of the former relies unduly on the technical literature of instrument manufacturers. The author's criticism of published d.t.a. curves of polymers (p 411) is illuminating but this chapter on the whole is disappointing, probably because it is approximately six years old. The chapter on textiles contains much useful information in a mass of verbiage. The other chapters contain little of interest to polymer scientists. From the standing of the authors, one would expect good reviews of the topics and this they appear to provide. There is, however, a good deal of repetition amongst the various chapters as well as much extraneous material. One presumes that the book is intended to be available in a library rather than in a personal bookcase; the price of £25.00 for both volumes supports this view. D.t.a. is used by workers in many disciplines throughout the world, and the editor has endeavoured to reflect this in his choice of authors and subjects. This Herculean task has not been completely successful but the two volumes together provide the best general reference on d.t.a. known to me.

T. R. Manley

# Thermoelastic and thermomechanical studies on natural rubber vulcanized in the swollen state

C. Price, K. A. Evans and F. de Candia\*

Department of Chemistry, University of Manchester, Manchester M13 9PL, UK  
(Received 1 March 1973)

Three samples of natural rubber were crosslinked in n-decane solution. After the solvent had been removed, a thermodynamic investigation was made of the elastic behaviour of the samples in simple extension. Thermoelastic measurements at constant pressure and length were carried out on the first two samples. The third sample was subjected to a thermomechanical heat of extension study using a Calvet microcalorimeter. The experiments enabled the temperature coefficient of the mean-square unperturbed dimensions,  $\langle r_0^2 \rangle$ , to be derived. From the thermoelastic measurements average values for  $d \ln \langle r_0^2 \rangle / dT$  of  $(0.44 \pm 0.08) \times 10^{-3} \text{ deg}^{-1}$  and  $(0.38 \pm 0.07) \times 10^{-3} \text{ deg}^{-1}$  were obtained, whilst the thermomechanical measurements gave a value of  $(0.54 \pm 0.04) \times 10^{-3} \text{ deg}^{-1}$ .

## INTRODUCTION

When applied to the case of uniaxial extension and compression the statistical<sup>1, 2</sup> theory of rubber elasticity gives:

$$f = \nu kT (\langle r_i^2 \rangle / \langle r_0^2 \rangle) (\alpha - \alpha^{-2}) \quad (1)$$

where  $f$  is the equilibrium force per unit cross-sectional area of the undeformed sample,  $\nu$  is the number of active chains per unit volume of the sample,  $k$  is the Boltzmann constant,  $\langle r_i^2 \rangle$  and  $\langle r_0^2 \rangle$  are the mean-square end-to-end dimensions for chains constrained by the network and for free chains in the bulk state respectively, and  $\alpha$  is the extension ratio.

For rubbers crosslinked in the dry state the force-extension behaviour is found to deviate significantly from the  $\alpha$ -dependence predicted by equation (1). Over a restricted range of  $\alpha$  above 1.1 the behaviour has been shown to be adequately described by the empirical relationship<sup>3-5</sup>:

$$f = C_1(\alpha - \alpha^{-2}) + C_2(1 - \alpha^{-3}) \quad (2)$$

Differentiation of equation (1)<sup>2</sup> with respect to temperature whilst holding the pressure  $P$  and length  $L$  constant yields:

$$(\partial \ln (f/T) / \partial T)_{L, P} = -d \ln \langle r_0^2 \rangle / dT - \beta_{L, P} / (\alpha^3 - 1) \quad (3)$$

where  $\beta_{L, P} = (\partial \ln V / \partial T)_{L, P}$  is the coefficient of cubical expansion of a sample maintained at constant length, while if the volume  $V$  rather than the pressure is held constant

$$(\partial \ln (f/T) / \partial T)_{L, V} = -d \ln \langle r_0^2 \rangle / dT \quad (4)$$

In spite of the observed deficiencies of equation (1),

\* Permanent address: Laboratorio di Ricerche su Tecnologia dei Polimeri e Reologia, CNR, Arco Felice, Napoli, Italy.

thermoelastic measurements have provided the most extensively used method of obtaining  $d \ln \langle r_0^2 \rangle / dT$ .

The force-extension behaviour of solution-vulcanized natural rubber<sup>7</sup> and *cis*-polybutadiene<sup>8,9</sup> in the dry state have been found to be in closer agreement with the  $\alpha$ -dependence predicted by equation (1) than vulcanisates prepared in the dry state. In the case of natural rubber<sup>7</sup> the magnitude of  $C_2/C_1$  was shown to be quite small (or zero) for values of  $\phi_r$  from 0.15 up to 0.40, where  $\phi_r$  is the volume fraction of rubber present during crosslinking. For *cis*-polybutadiene low values of  $C_2/C_1$  were obtained up to  $\phi_r = 0.30$ <sup>8</sup>. For solution vulcanized rubbers it would seem that there is rather more justification for the use of equations (3) and (4) to obtain  $d \ln \langle r_0^2 \rangle / dT$  than for the case of conventional vulcanisates. In the present study we have determined  $d \ln \langle r_0^2 \rangle / dT$  for natural rubber from (a) thermoelastic measurements and (b) thermomechanical measurements, carried out on solution vulcanized materials at constant pressure in the dry state.

## EXPERIMENTAL

### Crosslinking procedure

A weighed amount of natural rubber (light masticated crepe) was packed in small pieces into a 14 mm wide Pyrex tube sealed at one end. Recrystallized dicumyl peroxide was dissolved in an inert high boiling solvent (n-decane) and the requisite volume of the solution was added to the rubber in the tube; three parts of dicumyl peroxide per 100 parts by weight of rubber were used. The rubber solution was well stirred and left for a period of several weeks to equilibrate. (Any tubes in which bubbles did not disappear after a reasonable length of time were rejected.) The space above the solution was flushed with nitrogen and the tube was

sealed. The system was then crosslinked either by heating to 135°C for 2 h (sample NR3) or to 140°C for 2 h (samples NR1-2); under the chosen conditions no syneresis was observed. Afterwards the system was slowly cooled to room temperature and the tube was opened at the top. To ensure that the gel came away cleanly from the tube without fracture or surface damage a small quantity of methanol was added in order to de-swell it. After the gel had been removed from the tube, the solvent, catalyst residues and any uncrosslinked rubber were removed by continuous extraction with benzene. The sample was dried on a vacuum line to constant weight; this took a period of several weeks. Finally, the ends of the specimen were trimmed perpendicular to the principal axis of the cylinder, and stainless-steel pieces were bonded onto the end using Eastman 910 adhesive.

#### Force-extension measurements

The force-extension characteristics of the samples were studied using a Hounsfield Model E tensile tester fitted with an environmental chamber. Measurements were made for both increasing and decreasing loads. Between increments the sample was stretched at a rate of 1 cm/min. On reaching the required extension the sample was allowed to reach equilibrium each time. The extension was obtained by measuring the distance apart of two marks on the sample with a cathetometer to an accuracy of  $\pm 0.005$  cm. The equilibrium force was obtained using calibrated 0-5 lb or 0-50 lb (1 lb = 0.4536 kg) load cells.

#### Force-temperature measurements

Values of  $(\partial f/\partial T)_{L,P}$  at a range of extension between  $\alpha = 1.1$  and 2.0 were determined in the manner described previously<sup>12</sup> from linear plots of equilibrium force versus temperature over the range 35-65°C. The extended rubber was left thermostating at 70°C before each determination. The equilibrium forces required to maintain the length constant were measured at  $\sim 35$  minute intervals for progressively decreasing temperatures. Some measurements were also taken at progressively increasing temperatures to check the reversibility of the values. Using this schedule the linear plots of force versus temperature were found to be reversible and repeated determinations gave slopes which were constant to within  $\pm 2\%$ . The plots were similar to those shown previously<sup>8</sup> and in each determination measurements were taken at eight temperatures.

#### Thermomechanical studies

The change in enthalpy  $\Delta H$ , of a rubber sample on extending it from length  $l_1$  to length  $l_2$  at constant pressure is given by  $q + w$ , where  $q$  is the heat absorbed during the deformation process and

$$w = \int_{l_1}^{l_2} f dl$$

is the mechanical work done on the system. The quantity  $q$  was measured by stretching the rubber sample in a Calvet microcalorimeter using the procedure to be described later. Ideally, the quantity  $w$  should have been determined during the same deformation process. Indeed, in a preliminary investigation an apparatus was constructed which permitted this to be done. However, the

system was cumbersome and difficult to operate. In the investigation therefore it was decided to determine  $w$  from force-extension measurements carried out under identical strain rates in a subsidiary experiment.

**Calorimetry.** The Calvet microcalorimeter (Setram, Lyon) was the standard commercial model, capable of operating from ambient temperature to 200°C. A detailed description of the theory, construction, and calibration of the instrument may be found elsewhere<sup>10</sup>. Briefly, the instrument consisted of an aluminium heat sink containing two cavities into which fitted twin cylindrical cells (stainless steel: 1.7 cm dia.  $\times$  8.5 cm long). In each cavity a thermopile (496 copper/constantan thermocouples) was interposed between cell and metallic block. The metallic block was thermostated to  $\pm 0.001^\circ\text{C}$  by use of a Sefram R.T.64 temperature regulator. The thermopiles were connected in opposition, and the net output from them was fed to a galvanometer. The galvanometer assembly consisted of a Sefram Verispot galvanometer in conjunction with a projection lantern and Photodyne spot-follower. The twin cells, which were seated in silver sockets coated with a thin layer of mica, could easily be removed for charging. The deformation process under investigation was carried out in the 'laboratory' cell and the other was set up as the 'reference' cell. Either a quarter or three-quarters of the thermocouples in the pile surrounding the 'laboratory' cell could be used to generate a compensating Peltier effect. Because the thermal fluxes developed in our experiments were always relatively small, this facility was not employed and the microcalorimeter was operated on the highest sensitivity range throughout.

**Tian equation.** In using this equation we assume that the internal boundary which contacts the pile is at a uniform temperature. If  $W$  is the thermal power developed in the 'laboratory' cell at time  $t$ , and  $\theta$  is the difference between the temperature of the internal boundary  $\theta_i$  and that of the external boundary  $\theta_e$ , then we can write

$$W = p\theta + \mu \frac{d\theta}{dt} \quad (5)$$

where  $p$  is a constant, and  $\mu$  is the thermal capacity of the cell contents. Since the mechanical inertia of the galvanometer and the self induction of the calorimeter are negligible, the e.m.f. generated by the heat flux produces a recorder deviation  $\Delta = g\theta$  where  $g$  is a constant. Thus we can write  $W = (p/g)\Delta + (\mu/g)d\Delta/dt$ . The quantity of heat emitted by the cell contents between times  $t_1$  and  $t_2$  is given by:

$$q_{t_1}^{t_2} = \int_{t_1}^{t_2} W dt \\ = (p/g) \int_{t_1}^{t_2} \Delta dt + (\mu/g) \int_{\Delta_1}^{\Delta_2} d\Delta \quad (6)$$

The first term on the right-hand side of equation (6) can be determined from the area  $A$  under the recorded curve and a knowledge of the calibration constant, whilst the second term is zero in our experiment since experiments were started and ended on the same baseline (i.e.  $\Delta_1 = \Delta_2 = 0$ ). Hence equation (6) becomes  $q_{t_1}^{t_2} = (p/g)A$ .

**Cell assembly.** The experimental assembly within the 'laboratory' cell G is shown schematically in Figure 1. One of the metal end-pieces attached to the rubber sample, A, was screwed into cap B in the base of the cell, whilst the other end-piece was connected to steel rod D via a Teflon spacer C. The Teflon plug, E, formed the roof of the cell. The length of the sample could be varied by winding the rod D up or down at a constant rate; the position of the rod, and hence the length of the sample, could be determined by means of the micrometer screw gauge, F. The assembly within the 'reference' cell was similar to that in the 'laboratory' cell except for the omission of a sample.

The microcalorimeter was calibrated electrically in the recommended manner using Joule heating.

**Experimental procedure.** When a stable base line had been established the sample was extended at a fixed rate from  $\alpha=1.0$  to the chosen extension. The rate of strain was arranged to be as near as possible equal to that used in the subsidiary force-extension measurements. However, a number of test runs carried out at deliberately erroneous rates (as much as 25% too high, and too low) showed that over the range of interest the results were not very sensitive to quite moderate variations in this parameter. When the recorder trace had returned to the base line, the applied stress was removed and the sample was allowed to relax back to  $\alpha=1.0$ . The described procedure was repeated for a series of  $\alpha$  values.

RESULTS

Force-extension studies

These were carried out on three solution vulcanized natural rubber samples NR1-NR3 in the dry state. The ranges covered by the measurements were  $1.1 < \alpha < 2.0$  for samples NR1 and NR2 and  $1.1 < \alpha < 4.0$  for sample NR3. Plots of  $f/(\alpha - \alpha^{-2})$  against  $\alpha^{-1}$  are shown in Figure 2. Given in Table 1 are values of  $C_1$  and  $C_2$  obtained on fitting the experimental data over the range  $1.1 < \alpha < 2.0$  to equation (2) by the method of least squares. The results confirm that over the range of interest solution crosslinked rubbers show smaller departures from the  $\alpha$ -dependence predicted by equation (1) than do conventional vulcanisates. However, even if the measurements taken up to  $\alpha=4.0$  are included in the fit for sample NR3 the values obtained

$$(C_1 = 1.64 \times 10^5 \text{ N m}^{-2}, C_2 = 0.36 \times 10^5 \text{ N m}^{-2})$$

remain fairly close to those given in Table 1.

Thermoelastic studies

Force-temperature measurements at constant pressure and length were carried out on two solution crosslinked rubbers NR1 and NR2 in the dry state. The results are collected together in Table 2, together with values of  $d \ln \langle r_0^2 \rangle / dT$  calculated using equation (3); also given is the fraction of the total force which is energetic in origin  $f_e/f$  obtained from:

$$f_e/f \equiv (\partial U / \partial l)_{T, V} / f = T d \ln \langle r_0^2 \rangle / dT \quad (7)$$

Equation (7) like equation (3) is based on the statistical theory of rubber elasticity.

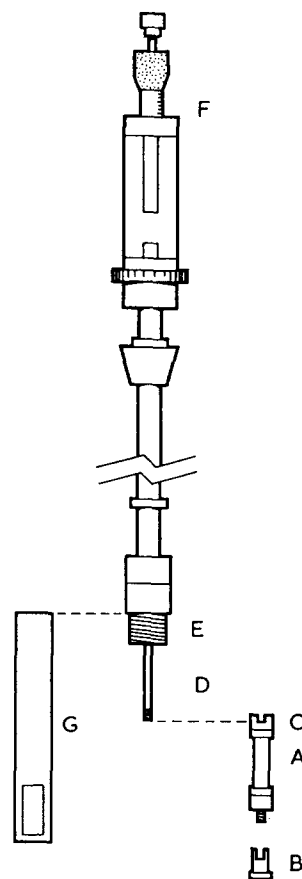


Figure 1 Experimental assembly within the 'laboratory' cell of the Calvet microcalorimeter

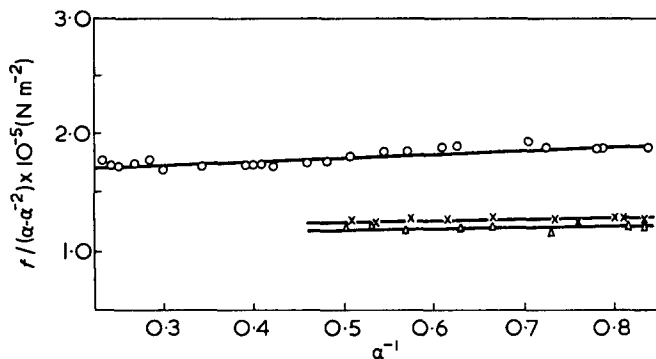


Figure 2 Mooney-Rivlin plots for dry samples of natural rubber crosslinked in the presence of n-decane.  $\Delta$ , NR1;  $\times$ , NR2;  $\circ$ , NR3

Table 1 Values of  $C_1$  and  $C_2$  for dry samples of natural rubber crosslinked in the presence of n-decane

Sample	$\phi_r$	$C_1 \times 10^{-5}$ ( $\text{N m}^{-2}$ )	$C_2 \times 10^{-5}$ ( $\text{N m}^{-2}$ )	$T$ ( $^\circ\text{C}$ )
NR1	0.20	1.15	0.11	30
NR2	0.28	1.22	0.11	30
NR3	0.34	1.81	0.15	25

Thermomechanical studies

Calorimetric measurements were made on sample 3 in the dry state for extensions up to  $\alpha \approx 1.8$ . All the measurements were made at  $25^\circ\text{C}$ . The mechanical work done on the system during the deformation process was obtained by integration of the force-extension curves established at the same strain rate. The results

Table 2 Results from thermoelastic studies

Sample	$\alpha$	$f(50^\circ\text{C}) \times 10^{-5}$ ( $\text{N m}^{-2}$ )	$(\partial f/\partial T)_L, P \times 10^{-2}$ ( $\text{N m}^{-2} \text{ deg}^{-1}$ )	$d \ln \langle r_0^2 \rangle / dT \times 10^3$ ( $\text{deg}^{-1}$ )	$f_e / f$
NR1	1.192	0.628	1.00	0.55	0.178
	1.312	0.915	1.93	0.46	0.148
	1.401	1.143	2.64	0.41	0.132
	1.533	1.477	3.62	0.39	0.126
	1.641	1.628	4.05	0.41	0.134
	1.707	1.780	4.66	0.31	0.101
	1.843	2.011	5.09	0.44	0.142
	1.926	2.079	5.11	0.53	0.171
	NR2	1.212	0.736	1.30	0.48
1.304		0.979	2.21	0.30	0.096
1.431		1.313	3.19	0.32	0.104
1.515		1.486	3.71	0.33	0.107
1.620		1.616	3.94	0.45	0.147
1.716		1.890	4.97	0.30	0.098
1.796		1.981	5.03	0.42	0.135
1.901		2.211	5.64	0.43	0.139
2.038		2.402	6.31	0.38	0.123

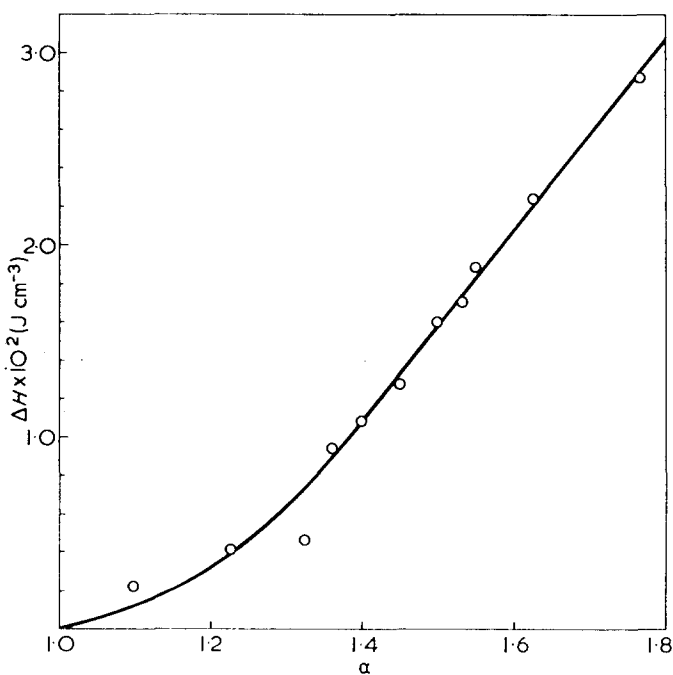

 Figure 3 Enthalpy changes on stretching sample NR3 from the unstrained state to  $\alpha$ 

Table 3 Results from thermomechanical studies on sample NR3 at 25°C

$\alpha$	$-q \times 10^2$ ( $\text{J cm}^{-3}$ )	$w \times 10^2$ ( $\text{J cm}^{-3}$ )	$\Delta H \times 10^2$ ( $\text{J cm}^{-3}$ )	$f_e \times 10^2$ ( $\text{J cm}^{-4}$ )	$d \ln \langle r_0^2 \rangle \times 10^3$ $dT$ ( $\text{deg}^{-1}$ )	$f_e / f$
1.098	0.05	0.27	0.22			
1.227	1.01	1.42	0.41			
1.323	2.36	2.82	0.46			
1.360	2.40	3.34	0.94			
1.398	2.92	4.00	1.08	3.02	0.58	0.174
1.448	3.68	4.95	1.27	3.18	0.57	0.169
1.498	4.41	6.01	1.60	3.31	0.55	0.164
1.531	5.05	6.75	1.70	3.38	0.54	0.161
1.548	5.29	7.17	1.88	3.42	0.53	0.159
1.623	6.82	9.05	2.23	3.57	0.51	0.152
1.765	10.16	13.03	2.87	3.81	0.47	0.141

are recorded in Table 3. As shown in Figure 3 a plot of  $\Delta H$  versus  $\alpha$  was found to be virtually linear for values of  $\alpha$  above  $\sim 1.36$ . From the slope of the plot

in this region  $(\partial H/\partial L)_{P,T}$  was obtained ( $=4.98 \times 10^{-2} \text{ J cm}^{-4}$ ) and values of  $f_e$  were calculated using:

$$f_e = \left( \frac{\partial H}{\partial L} \right)_{P,T} \frac{f \beta_L P T}{\alpha^3 - 1}$$

which like equation (3) is derived from the statistical theory of rubber elasticity. The quantity  $d \ln \langle r_0^2 \rangle / dT$  was then calculated from equation (4). Values of  $f_e$ ,  $d \ln \langle r_0^2 \rangle / dT$  and  $f_e / f$  are listed in Table 3.

#### DISCUSSION

Thermoelastic studies made on samples NR1 and NR2 gave average values for  $d \ln \langle r_0^2 \rangle / dT$  of  $(0.44 \pm 0.08) \times 10^{-3} \text{ deg}^{-1}$  and  $(0.38 \pm 0.07) \times 10^{-3} \text{ deg}^{-1}$  respectively, whilst the thermomechanical study made on sample NR3 gave a value of  $(0.54 \pm 0.04) \times 10^{-3} \text{ deg}^{-1}$ . The results obtained from the thermomechanical studies correspond to a temperature of 25°C and those from the thermoelastic studies to a mean temperature of 50°C. This difference would not be expected to lead to any significant change in the observed value of  $d \ln \langle r_0^2 \rangle / dT$ . It is therefore gratifying that the two different approaches we have used give results which are in fair agreement. It provides satisfactory evidence that under chosen conditions the mechanical deformation of solution-vulcanized rubbers can be treated as thermodynamically reversible.

Previous studies of  $d \ln \langle r_0^2 \rangle / dT$  made on conventional natural rubber vulcanisates give in nearly all cases values which fall within the range  $0.32 \times 10^{-3}$  to  $0.64 \times 10^{-3} \text{ deg}^{-1}$ . The majority of studies involved the measurement of force-temperature coefficients at constant pressure on samples in simple extension followed by application of an equation such as (3). From thermoelastic measurements in torsion Boyce and Treloar<sup>11</sup> obtained a value for  $d \ln \langle r_0^2 \rangle / dT$  of

$$0.43 \pm 0.05 \times 10^{-3} \text{ deg}^{-1}.$$

In a very extensive investigation Allen *et al.* determined values of  $d \ln \langle r_0^2 \rangle / dT$  from thermoelastic measurements made in simple extension at both constant volume and constant pressure and obtained  $0.38 \pm 0.06 \times 10^{-3}$  and  $0.57 \pm 0.09 \times 10^{-3} \text{ deg}^{-1}$  respectively<sup>12</sup>; average values of  $C_1$  and  $C_2$  for the samples used in the latter study were  $2.2 \times 10^5 \text{ N m}^{-2}$  and  $1.0 \times 10^5 \text{ N m}^{-2}$  respect-

ively. The agreement of the present results with those obtained previously for conventionally crosslinked samples indicates that values derived from equation (3) are not significantly influenced by deviations from the Gaussian theory represented in terms of the Mooney equation. Indirectly this implies that the empirical constants  $C_1$  and  $C_2$  are both mainly governed by the intramolecular behaviour of network chains.

#### REFERENCES

- 1 Flory, P. J., Hovee, C. A. J. and Ciferri, A. *J. Polym. Sci.* 1959 **34**, 337
- 2 Flory, P. J. *Trans. Faraday Soc.* 1961, **57**, 829
- 3 Mooney, M. J. *Appl. Phys.* 1940, **11**, 582
- 4 Gumbrell, S., Mullins, L. and Rivlin, R. S. *Trans. Faraday Soc.* 1953, **49**, 1945
- 5 Blokland, R. 'Elasticity and Structure of Polyurethane Networks', Rotterdam University Press, 1968
- 6 Mark, J. E. *Rubber Chem. Technol.* 1973, **46**, in the press
- 7 Price, C., Allen, G., de Candia, F., Kirkham, M. C. and Subramaniam, A. *Polymer* 1970, **11**, 486
- 8 de Candia, F., Amelino, L. and Price, C. *J. Polym. Sci. (A-2)* 1972, **10**, 975
- 9 Mark, J. E. *J. Am. Chem. Soc.* 1970, **92**, 7252
- 10 Calvet, E. and Prat, H. 'Recent Progress in Microcalorimetry' (Edited and translated by H. A. Skinner), Pergamon Press, Oxford and New York, 1963
- 11 Boyce, P. H. and Treloar, L. R. G. *Polymer* 1970, **11**, 21
- 12 Allen, G., Kirkham, M. C., Padget, J. and Price, C. *Trans. Faraday Soc.* 1971, **67**, 1278

# Heat of dilution and density data for poly( $\beta$ -propiolactone) and poly( $\epsilon$ -caprolactone) in dioxane

Giorgio Manzini and Vittorio Crescenzi

Laboratorio di Chimica delle Macromolecole, Istituto di Chimica,  
Università di Trieste, Trieste, Italy

(Received 12 January 1973; revised 23 February 1973)

Solution properties of two polyesters, poly( $\beta$ -propiolactone) and poly( $\epsilon$ -caprolactone) in dioxane have been studied. Data reported are: polymer densities, thermal expansion coefficients, thermal pressure coefficients, solution densities (volume changes on mixing:  $\Delta V_M$ ) and heats of dilution ( $\Delta H_1$ ). It is found that the solution properties of the two polyesters in dioxane differ; e.g. poly( $\beta$ -propiolactone):  $\Delta V_M < 0$ ;  $\Delta H_1 > 0$ ; poly( $\epsilon$ -caprolactone):  $\Delta V_M > 0$ ;  $\Delta H_1 < 0$ . Flory's theory is used to interpret these results. The theory contains one adjustable parameter ( $X_{12}$ ) which is fixed by fitting the theory to the heat of dilution data. Sign and order of magnitude of the volume changes on mixing are then correctly predicted.

## INTRODUCTION

Previous studies from this laboratory have dealt with the configurational statistics of polylactone chains in the amorphous or unperturbed state<sup>1</sup> and with the thermodynamics of melting of crystalline poly( $\beta$ -propiolactone) (P $\beta$ L) and poly( $\epsilon$ -caprolactone) (P $\epsilon$ L).<sup>2</sup>

We wish to report here additional data concerning certain properties of the above-mentioned polylactones in solution, namely heat of dilution and density data for P $\beta$ L and P $\epsilon$ L mixtures with dioxane, at 25°C.

We find that in the case of P $\beta$ L the enthalpy of dilution is endothermic but the excess volume of mixing is negative while for P $\epsilon$ L the opposite holds true. The observed effects are, however, quite small. Nevertheless no explanation can be found for them on the basis of 'conventional' theories of polymer solutions. On the contrary, adoption of the theory of Flory and co-workers<sup>3a</sup> permits at least a qualitative description of our data. This theory has, among other valuable features, the advantage of assuming a simple analytical form for the equation of state of pure liquid components and of their mixtures. In our case, to fulfill the requirements of the theory of initial accurate information on the properties of pure P $\beta$ L and P $\epsilon$ L, the thermal pressure coefficient values reported in a previous paper<sup>2</sup> have been retained while more accurate thermal expansion coefficient and density data have been redetermined for both polymers.

## EXPERIMENTAL

### Samples

Poly( $\epsilon$ -caprolactone) was a Union Carbide sample (PCL 300-R-1014) of molecular weight  $M_w = 1.7 \times 10^4$ , purified by dissolution in benzene and precipitated with petroleum ether, then desiccated under vacuum. Poly( $\beta$ -propiolactone) was obtained by bulk polymerization

at about 0°C with pyridine as catalyst<sup>4</sup>. The sample was dissolved in chloroform and precipitated with diethyl ether, then desiccated under vacuum. The molecular weight was determined by viscometry using the relation reported by Kagiya *et al.*<sup>4</sup>, resulting in  $M_v = 1.5 \times 10^4$ . Dioxane (Carlo Erba, RP reagent), was desiccated over sodium wire, distilled and stored over sodium wire.

### Dilatometric measurements

For each polymer a 'weighing dilatometer' of the type described by Flory *et al.*<sup>5</sup> was used, employing about 3 g of sample. The dilatometer bulbs had a volume of about 7 cm<sup>3</sup> and, after introduction of the sample and sealing off, they were filled with pure mercury under vacuum.

The densities of polymer samples were determined just before the dilatometric measurements, both using a pycnometer for solids and determining the density of zinc chloride aqueous solution of the same density as the sample. The results were consistent within 0.1%:  $\rho = 1.150 \pm 0.001$  g/cm<sup>3</sup> for P $\epsilon$ L and  $\rho = 1.354 \pm 0.001$  g/cm<sup>3</sup> for P $\beta$ L.

Being partly crystalline at 25°C, the densities of the amorphous polymers at this temperature were determined by extrapolation of the dilatometric curves from data above the melting temperatures,  $T_m$  (about 60°C for P $\epsilon$ L and about 80°C for P $\beta$ L). Accounting for the uncertainty in the extrapolation, accuracies in the amorphous polymer densities were evaluated to be about 0.2%:  $\rho_a = 1.095 \pm 0.002$  g/cm<sup>3</sup> for P $\epsilon$ L and  $\rho_a = 1.306 \pm 0.002$  g/cm<sup>3</sup> for P $\beta$ L.

After the usual corrections for Pyrex glass and mercury dilatation, the expansion coefficients  $\alpha = 1/V \cdot (dV/dT)$  of the amorphous polymers were determined; they resulted in being nearly constant between  $T_m$  and 100°C, and these values were assumed also at 25°C:

$$\alpha = 0.72 \times 10^{-3} \text{ } ^\circ\text{C}^{-1}$$

for PεL and  $\alpha=0.76 \times 10^{-3} \text{ }^\circ\text{C}^{-1}$  for PβL with an accuracy within  $\pm 2\%$ .

For dioxane the values deduced from Timmermans<sup>6</sup> were adopted:  $\rho=1.0280 \text{ g/cm}^3$  at  $25^\circ\text{C}$ ,  $\alpha=1.10 \times 10^{-3} \text{ }^\circ\text{C}^{-1}$  at  $25^\circ\text{C}$ ;  $\rho_{25^\circ\text{C}}$  was confirmed by pycnometry within  $0.01\%$ .

*Thermal pressure coefficients*

For the thermal pressure coefficient  $\gamma$  of the polymers, the values obtained from measurements described in a previous paper<sup>2</sup> were adopted. Correction from the temperature of the measurement to  $25^\circ\text{C}$  was made with the aid of the relation given by Flory<sup>5</sup>:

$$\frac{d \ln \gamma}{dT} = -\frac{(1+2\alpha T)}{T}$$

Such a procedure inevitably implies an uncertainty in the  $\gamma$  values<sup>5, 7, 8</sup> which, in our case, we estimate to be of the order of  $10\%$ .

The  $\gamma$  values are: (1) for PεL,  $\gamma_{70^\circ\text{C}}=0.28 \pm 0.005$  and  $\gamma_{25^\circ\text{C}}=0.34 \pm 0.03 \text{ cal/cm}^3$ ; (2) for PβL,  $\gamma_{90^\circ\text{C}}=0.52 \pm 0.01$  and  $\gamma_{25^\circ\text{C}}=0.70 \pm 0.07 \text{ cal/cm}^3$ .

For dioxane the value  $\gamma_{25^\circ\text{C}}=0.395 \text{ cal/cm}^3$ , derived from the value at  $20^\circ\text{C}$  ( $\gamma_{20^\circ\text{C}}=0.407 \text{ cal/cm}^3$ ) reported by Allen *et al.*<sup>9</sup>, was adopted.

*Excess volumes*

Density measurements were performed using a pycnometer for liquids consisting of a bulb of approximately  $7 \text{ cm}^3$  with a capillary tube of  $0.95 \text{ mm}^2$  cross-section. The exact volume of the pycnometer was determined using mercury, and confirmed by determining the density of triply distilled water; reproducibility was about  $\pm 0.3 \text{ mm}^3$ , i.e.  $\sim 0.004\%$ .

All measurements were made in a thermostat at  $25 \pm 0.02^\circ\text{C}$  by preparing the solutions by weight, injecting them in the pycnometer with the aid of a syringe and finally weighing the pycnometer. All weighings were corrected for buoyancy. The accuracy of the final density data should be about  $0.01\%$ . The theoretical specific volumes of the polymer-dioxane mixtures corresponding to perfect additivity of volumes on mixing,  $v_{sp}^0$ , were calculated using the specific volumes of the pure components listed in Table 1.

Knowing the experimental specific volumes,  $v_p$ , the relative excess volumes  $v_E$  were finally computed from:  $v_E = (v_{sp} - v_{sp}^0)/v_{sp}^0$ .

*Enthalpy of dilution*

Heat of dilution data were collected using a LKB 10700-2 batch-type microcalorimeter. In a typical

experiment  $4 \text{ cm}^3$  of polymer solutions were mixed with  $\sim 1 \text{ cm}^3$  of solvent. The reproducibility was rather limited, but sufficient in our opinion, particularly in view of the small heat exchanges measured (from  $0.2$  to  $2 \text{ mcal}$ ). The correction for possible thermal effects arising from the variation in solvent vapour pressure during the mixing<sup>10</sup> was not applied, for, considering the approximate relation of Flory<sup>11</sup>:

$$P_1 = P_1^0 \phi_1 \exp(\phi_2 + \chi \phi_2^2)$$

(where  $\phi_1$  and  $\phi_2$  are the volume fractions of solvent and polymer), such correction would result, for reasonable values of the polymer-solvent interaction parameter  $\chi$ , in smaller values than the scattering of the experimental points.

Both excess volume and enthalpy of dilution measurements were necessarily limited to low polymer concentrations, for PεL by the high viscosity of the solutions above  $\sim \phi_2=0.25$  and for PβL by the onset of slight turbidity beyond  $\phi_2 \sim 0.07$ , at  $25^\circ\text{C}$ .

RESULTS

*Data for the pure compounds*

Information on the properties of pure amorphous PβL and PεL and of dioxane, i.e. specific volume,  $v_{sp}$ , thermal expansion coefficient,  $\alpha$ , and thermal pressure coefficient,  $\gamma$ , data together with the values of the characteristic parameters,  $p^*$ ,  $v^*$  and  $T^*$  are listed in Table 1.

The latter parameters were calculated on the basis of the equation of state<sup>3</sup> (at  $p \rightarrow 0$ ):

$$\tilde{T} = (\tilde{v}^{1/3} - 1)/\tilde{v}^{4/3} \tag{1}$$

and the relationships:

$$\tilde{v}^{1/3} = 1 + \alpha T/3(1 + \alpha T) \tag{2}$$

$$\tilde{p} = p/\gamma T \tilde{v}^2 \tag{3}$$

In fact, knowing  $\alpha$ , equation (2) yields  $\tilde{v}$  and thus  $V^*$  (the hard-core volume per mole); equation (1) then gives  $T^*$ . The characteristic pressure  $p^*$  follows from  $\gamma$  according to equation (3). In the following, subscripts 1 and 2 will specify parameters for dioxane and PβL or PεL respectively.

It is interesting to note that the characteristic pressure of PβL is quite high indeed. The estimated accuracies of the data reported in Table 1 are separately specified in the experimental section.

*Data for the mixtures*

*PβL-dioxane.* The experimental data on the heat of dilution are reported in Figure 1a as a plot of:

$$\chi_H = \frac{\Delta Q}{\Delta n_1} \cdot \frac{1}{RT \phi_2 \cdot \phi_2'}$$

against  $(\phi_2 \cdot \phi_2')^{1/2}$ .

$\Delta Q$  is the heat exchange measured (at  $25^\circ\text{C}$ ) when the number of moles of solvent in the solution was increased by  $\Delta n_1$  thereby reducing the polymer volume fraction from  $\phi_2$  to  $\phi_2'$ . The experimental points are quite scattered; in our opinion, however, the attainment of a higher precision (with apparatuses available) would be very difficult in view of very small heat effects to be measured.

Table 1 Properties of pure components

	Dioxane	PεL	PβL
$v_{sp}$ ( $\text{cm}^3/\text{g}$ )	0.9727	0.913	0.765
$\alpha \times 10^3$ ( $^\circ\text{C}^{-1}$ )	1.10	0.72	0.76
$\gamma$ ( $\text{cal}/\text{cm}^3 \cdot ^\circ\text{C}$ )	0.395	0.34	0.70
$\tilde{v}$	1.2678	1.1873	1.1963
$T^*$ ( $^\circ\text{C}$ )	4970	6363	6149
$p^*$ ( $\text{cal}/\text{cm}^3$ )	190	143	298
$v_{sp}^0$ ( $\text{cm}^3/\text{g}$ )	0.7673	0.769	0.640

$\tilde{v} = V/V^*$ ; likewise,  $\tilde{p} = p/p^*$  and  $T = T/T^*$  by definition (see text)



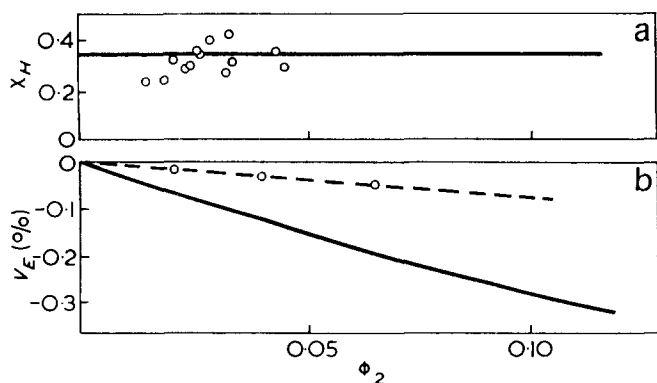


Figure 1 (a) Reduced partial molar enthalpy of dilution  $\chi_H$ , for P $\beta$ L-dioxane mixture:  $\circ$ , experimental measurements; —, theoretical curve. (b) Relative excess volume on mixing P $\beta$ L and dioxane:  $\circ$  (and - - - -), experimental; —, theoretical

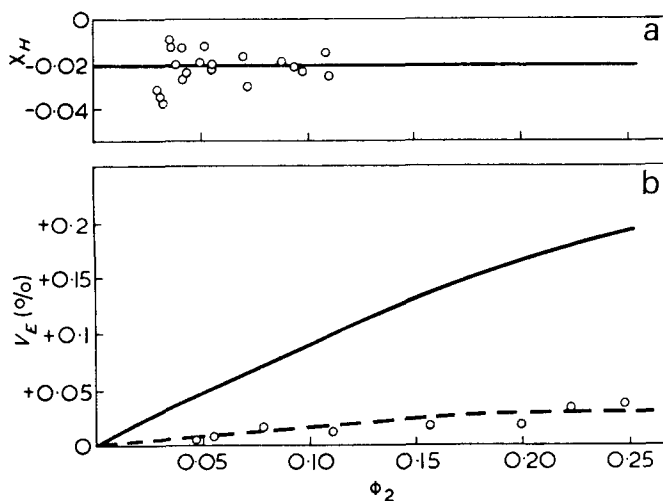


Figure 2 (a) Reduced partial molar enthalpy of dilution  $\chi_H$ , for P $\epsilon$ L-dioxane mixture:  $\circ$ , experimental measurements; —, theoretical curve. (b) Relative excess volume on mixing P $\epsilon$ L and dioxane:  $\circ$  (and - - - -), experimental; —, theoretical

A positive value of  $\chi_H$  in the range 0.3–0.4 results from the data of Figure 1a, in the range of  $\phi_2$  considered.

The excess volumes of P $\beta$ L-dioxane mixtures, obtained from density data as explained in the experimental section, are plotted in Figure 1b against polymer volume fraction,  $\phi_2$ . The  $v_E$  values are quite small indeed, and should be affected by an error of about  $\pm 2 \times 10^{-3} \phi_2$  mainly as a consequence of the uncertainty in the value of the specific volume of pure amorphous P $\beta$ L estimated to be around 0.2%. In any case  $v_E$ , though small in absolute value, is seen to be negative for the P $\beta$ L-dioxane system at 25°C.

**P $\epsilon$ L-dioxane.** For this system the  $\chi_H$  and  $v_E$  values are reported in Figures 2a and 2b respectively. Both entities are seen to be small, in the limited range of  $\phi_2$  values practically explorable. In any case we are led to conclude that, beyond experimental errors,  $v_E$  is positive but  $\chi_H$  is negative for P $\epsilon$ L-dioxane mixtures at 25°C.

## DISCUSSION

On the basis of the theory of Flory *et al.*<sup>3a</sup> of the thermodynamic properties of binary mixtures the expression for  $\chi_H$ , i.e. the reduced partial molar enthalpy of the

solvent is:

$$\chi_H = \frac{\bar{H}_1^R}{RT\phi_2^2} = \frac{P_1^* \cdot V_1^*}{RT\phi_2^2} \left[ \left( \frac{1}{\bar{v}_1} - \frac{1}{\bar{v}} \right) + \frac{\alpha T}{\bar{v}} \left( \frac{\bar{T}_1}{\bar{T}} - 1 \right) \right] + \frac{V_1^* (1 + \alpha T) X_{12} \theta_2^2}{\bar{v} RT \phi_2^2} \quad (4)$$

In the limit for  $\phi_2 \rightarrow 0$ , we have:

$$\chi_{H,1} = \frac{P_1^* V_1^*}{\bar{v}_1 RT} [Y_{12}(1 + \alpha_1 T) - \frac{2}{3} A^2 \alpha_1^2 T^2 (1 + \alpha_1 T)] \quad (5)$$

where:

$$\theta_2 = \frac{\phi_2 (S_2/S_1)}{\phi_1 + \phi_2 (S_2/S_1)} \quad (6)$$

$$Y_{12} = \frac{X_{12} (S_2/S_1)^2}{P_1^*}; \quad A = \left( 1 - \frac{T_1^*}{T_2^*} \right) \cdot \frac{P_2^*}{P_1^*} - \frac{X_{12} (S_2/S_1)}{P_1^*} \quad (7)$$

In these equations the parameter  $X_{12}^\dagger$ , accounts for the difference in energy density between like and unlike types of molecular contacts. ( $S_2/S_1$ ) is the ratio of number of polymer-solvent contact sites per 'hard-core' volume.

In equation (4), reduced quantities without subscript refer to the mixture and can be evaluated according to equations (8) and (9), respectively, once of course appropriate values of  $X_{12}$  and of  $S_2/S_1$  have been chosen:

$$P^* = \phi_1 P_1^* + \phi_2 P_2^* - \phi_1 \theta_2 X_{12} \quad (8)$$

$$T^* = \frac{P^*}{(\phi_1 P_1^*/T_1^* + \phi_2 P_2^*/T_2^*)} \quad (9)$$

Furthermore, on the basis of equation (1) for the mixture and of equation (9) the value of  $\bar{v}$  and hence of the excess volume  $\bar{v}_E$  may be determined for each  $\phi_2$  value:

$$\bar{v}_E = \bar{v} - \bar{v}_0 = \bar{v} - (\phi_1 \bar{v}_1 + \phi_2 \bar{v}_2) \quad (10)$$

which may be directly compared with experimental density data since:

$$\frac{\bar{v}_E}{\bar{v}_0} = v_E = \frac{v_{sp} - v_{sp}^0}{v_{sp}^0} \quad (11)$$

where

$$v_{sp}^0 = (w_1 v_{sp,1} + w_2 v_{sp,2}) / (w_1 + w_2) \quad (12)$$

in which  $w_1$  and  $w_2$  are the amounts (in g) of solvent and polymer, respectively.

In the case of P $\beta$ L, the  $S_2/S_1$  ratio has been estimated assuming a dioxane molecule to be a disc of volume  $V_1^*/N$  and of height equal to 3/2 of the radius, and the polymer repeating unit to be a cylinder of volume  $V_1^*/N$ , 4.80 Å high<sup>3b, 12†</sup>.

In this way the value of  $S_2/S_1$  results as 0.75. (If the dioxane molecules were assimilated to spheres of volume  $V_1^*/N$ ,  $S_2/S_1$  would rise to 0.90: an uncertainty of the order of 10–20% in  $S_2/S_1$  does not, however, sensitively influence the results of the following calculations.)

Thus, imposing  $S_2/S_1 = 0.75$ , the value of  $S_{12}$  which through equations (8), (9) and (10) yields the best agreement between calculated and experimental  $\chi_H$

† To be derived from experimental data from the mixtures.

‡  $V_u^* = v_{sp,2}^* \cdot M_u$ , where  $M_u$  is the molecular weight per repeating unit (72.06 for P $\beta$ L and 114.15 for P $\epsilon$ L), and  $V_1^* = v_{sp,1}^* \cdot M_1$  for dioxane. Of course, equations (4)–(9) are consistent with the choice of equal hard-core volumes *per segment*.

data was found. The result is:  $X_{12} = +7 \text{ cal/cm}^3$ , which also yields (see equation 5):  $\chi_{H,1} = +0.35$ . The calculated  $\chi_H$  against  $\phi_2$  curve is drawn in Figure 1a. Next, using the values given above of  $X_{12}$  and  $S_2/S_1$  and with the aid of equations (8), (9) and (10) the theoretical  $v_E - \phi_2$  relationship has been calculated (see Figure 1b).

In the case of P $\epsilon$ L calculations similar to those indicated above for P $\beta$ L have yielded the following set of results for  $S_2/S_1 = 0.70$ , i.e. assimilating the polymer repeating units to cylinders of volume  $V_u^*/N$ , 8.50 Å in height ( $S_2/S_1 = 0.85$  if dioxane molecules are taken as spheres):  $X_{12} = 0.4 \text{ cal/cm}^3$ ,  $\chi_{H,1} = -0.02$ . The theoretical  $\chi_H$  vs.  $\phi_2$  and  $v_E$  vs.  $\phi_2$  curves are drawn in Figures 2a and 2b.

Comparison of theory and experiment indicates that for both systems considered sign and order of magnitude of  $v_E$  are consistently predicted using  $X_{12}$  values derived from microcalorimetric data and equation (5).

The disparity between experimental and calculated  $v_E$ , might be reduced for P $\epsilon$ L in dioxane only at the expense of taking a negative  $X_{12}$  value, i.e. of assuming particular attractive interactions between polymer segments and solvent molecules<sup>13</sup>.

On the contrary for the P $\beta$ L-dioxane system a much higher  $X_{12}$  had to be assumed to obtain a calculated  $v_E$  vs.  $\phi_2$  curve superimposable on to the experimental points.

For both polymers such changes in the  $X_{12}$  parameter might be accommodated in the fitting of the calorimetric data only by proper, combined changes of the equation of state parameters.

On the other hand, this would imply changing the values of the primary variables,  $\alpha$ ,  $\rho$  and  $\gamma$ , beyond experimental errors. The  $\gamma$  values are incidently the

more uncertain ones: however, even allowing for the maximum estimated experimental errors a relevant uncertainty in  $X_{12}$  but only minor changes in the calculated  $v_E$  values would result.

Investigations are in progress in our laboratory on other polyesters and polylactone solutions to try to contribute a better understanding of the possible correlation between  $X_{12}$  values and polymer chain chemical constitution.

#### ACKNOWLEDGEMENT

This work has been sponsored by the Consiglio Nazionale delle Ricerche, Rome.

#### REFERENCES

- 1 Brückner, S., Crescenzi, V. and Zotteri, L. *Eur. Polym. J.* 1971, **7**, 1473
- 2 Crescenzi, V., Manzini, G., Calzolari, G. and Borri, C. *Eur. Polym. J.* 1972, **8**, 449
- 3 (a) Flory, P. J. *J. Am. Chem. Soc.* 1965, **57**, 1833; (b) Eichinger, B. E. and Flory, P. J. *Trans. Faraday Soc.* 1968, **64**, 2035
- 4 Kagiya, T., Sano, T. and Fukui, K. *Kogyo-Kagaku Zasshi* 1964, **67**, 951
- 5 Höcker, H., Blake, G. J. and Flory, P. J. *Trans. Faraday Soc.* 1971, **67**, 2251
- 6 Timmermans, I. 'Physico-Chemical Constants of Pure Organic Compounds', Elsevier, New York, 1950, p 502
- 7 Orwoll, R. A. and Flory, P. J. *J. Am. Chem. Soc.* 1967, **69**, 6814
- 8 Eichinger, B. E. and Flory, P. J. *Macromolecules* 1968, **1**, 285
- 9 Allen, G., Gee, G. and Wilson, G. J. *Polymer* 1960, **1**, 456
- 10 Lewis, G. and Johnson, A. F. *J. Chem. Soc. (A)* 1969, p 1816
- 11 Flory, P. J. 'Principles of Polymer Chemistry', Cornell University Press, Ithaca, New York, 1953, p 514
- 12 Flory P. J. and Höcker, H. *Trans. Faraday Soc.* 1971, **67**, 2258
- 13 Booth, C. and Devoy, C. J. *Polymer* 1971, **12**, 309

# Investigation of the compatibility of butadiene–acrylonitrile copolymers with poly(vinyl chloride)

G. A. Zakrzewski

Film Department, E. I. du Pont de Nemours & Co. (Inc.), Experimental Station, Wilmington, Delaware 19898, USA

(Received 11 March 1973)

Various methods were used to study the compatibility of butadiene–acrylonitrile copolymers with poly(vinyl chloride). These blends were investigated by phase contrast microscopy, differential scanning calorimetry and torsion pendulum analysis. We conclude that the copolymers are compatible with poly(vinyl chloride) in all PVC compositions within the range 23–45% acrylonitrile. These blends exhibit a single  $T_g$  in the torsion pendulum studies and differential scanning calorimetry studies and follow a Fox expression in the variation of  $T_g$  with composition. Experimental densities are also higher than those calculated assuming volume additivity, implying better packing and a negative heat of mixing leading to molecular compatibility.

## INTRODUCTION

Many authors have studied the compatibility of poly(vinyl chloride) with butadiene–acrylonitrile copolymers. In these studies authors have given conflicting opinions as to the compatibility of the polymers<sup>1–3</sup> and this work was done to get new information on this subject.

## EXPERIMENTAL

### Polymers

Opalon 630 poly(vinyl chloride) (PVC) was obtained from the Monsanto Chemical Company and stabilized with 2 pph (parts per hundred) Thermolite 831 obtained from the M & T Chemical Company. The butadiene–acrylonitrile (BD–AN) copolymers were FR–N–500, FR–N–504, and FR–N–510 obtained from the Firestone Synthetic Rubber and Latex Company. Compositional characteristics are shown in *Table 1*.

### Blend preparations

PVC and BD–AN were blended on a rubber mill at 175°C using conventional milling techniques. The blend was then removed from the rolls and pressed into 6 in × 6 in films between ferrotype plates at 190°C and at 25 000 lbf (1 lbf ≡ 4.448 N) and quenched in ice water. A list of the blends and their properties is shown in *Table 2*.

*Table 1* Composition of butadiene–acrylonitrile copolymers

	BD–AN (wt.%)	Mooney viscosity (ML4 at 212°F)
FR–N–500	77:23	45
FR–N–504	55:45	50
FR–N–510	68:32	75

### Density

Density measurements were made with a heptane–CCl<sub>4</sub>, ethyl alcohol–CaNO<sub>3</sub> or CaNO<sub>3</sub>·H<sub>2</sub>O density gradient tube following ASTM procedure D150S.

### Phase contrast microscopy

Phase contrast photomicrographs (320×) were taken using the Zernike phase contrast condenser on a Leitz microscope at 25°C. This films [0.5–1.0 mil (1 mil ≡ 0.0245 mm)] specimens were employed.

### Torsion pendulum experiments

Film samples (10–20 mil × ¼ in × 1.00 in) were examined with a torsion pendulum described in an earlier publication<sup>4</sup>. Free oscillations of ~1 Hz were employed. The details of the procedures and computation can be obtained from the literature.

### Differential scanning calorimetry (d.s.c.)

The Du Pont Differential Thermal Analyzer with the d.s.c. cell was used in these experiments. The sampling and procedures were described earlier<sup>4</sup>. Thermograms were obtained using 20°C/min testing rate and the relative glass transition temperatures ( $T_g$ ) were obtained by graphical methods previously described<sup>5</sup>.

### X-ray measurements

X-ray goniometer traces were obtained at 25°C with a General Electric XRD-5 X-ray diffractometer using MoK $\alpha$  radiation.

## RESULTS AND DISCUSSION

Phase contrast microscopy and optical clarity were used as a first determination of compatibility of the blends. The refractive indices of PVC and the BD–AN

Table 2 Properties of PVC/BD-AN blends

Number	BD-AN		$T_g$ (torsion pendulum) (°C)	Density (g/cm <sup>3</sup> )	Crystallinity index (%)	Symbol
	Type	Wt. %				
100	—	0	+74	1.376	5	■
101	FR-N-500	30	+42	1.260	5	△
102	FR-N-504	30	+42	1.299	5	▲
103	FR-N-510	10	+62	1.330	5	□
104	FR-N-510	30	+36	1.301	5	▽
105	FR-N-510	50	+15	1.178	5	○
FR-N-500	FR-N-500	100	-14	0.951		×
FR-N-504	FR-N-504	100	-12	1.005		▼
FR-N-510	FR-N-510	100	-26	0.980		●

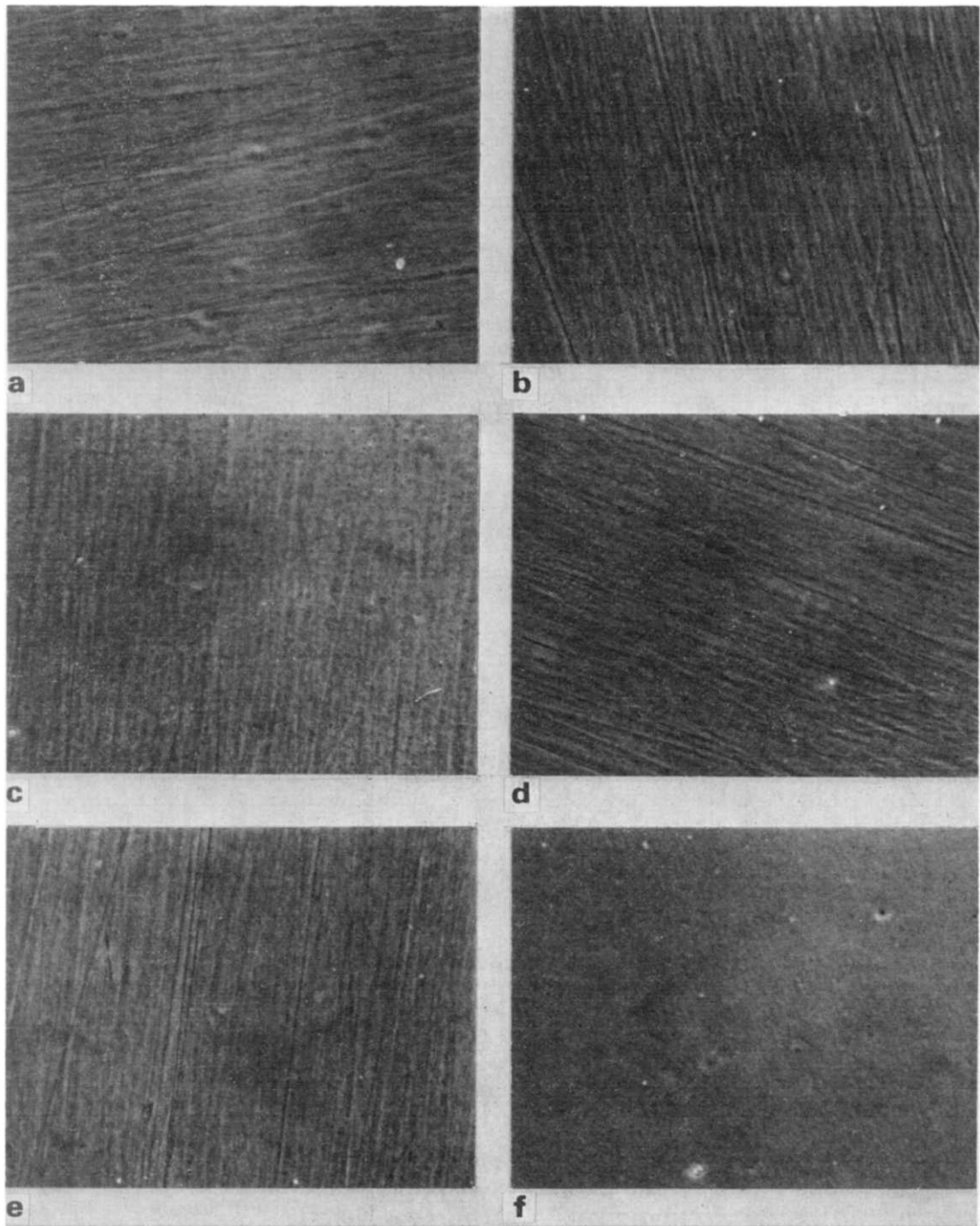


Figure 1 Phase contrast photomicrographs: (a) PVC; (b) Blend 101; (c) Blend 102; (d) Blend 103; (e) Blend 104; (f) Blend 105

copolymers (1.54=PVC, 1.51=FR-N-500, 1.51=FR-N-504, and 1.51=FR-N-520) should be sufficiently different to yield microscopic evidence if the phase domains are larger than  $0.1\ \mu\text{m}$ . No obvious phase separation is observed in Figure 1 and the phase photomicrographs of all blends, 101, 102, 103, 104 and 105 are identical with those of PVC (100) itself.

The microscopy and optical clarity has indicated the absence of large phase domains. Ikeda *et al.*<sup>4</sup>, however, have shown that domains of smaller dimension can exist and the phase separation remains undeterminable by optical phase contrast microscopy. These can, however, be seen easily by using torsion pendulum analysis of the samples.

Torsion pendulum analysis of homogeneous polymers, truly random copolymers and polymer-polymer solutions, will yield one  $T_g$ . In a compatible polymer-polymer solution the  $T_g$  should vary with composition as shown in an expression by Fox<sup>6</sup>:

$$\frac{1}{\bar{T}_g} = \frac{W_1}{T_{g_1}} + \frac{W_2}{T_{g_2}} \quad (1)$$

Table 3 Glass transition temperatures of PVC/BD-AN blends and blend components

	$T_g$ (calculated) (°C)	$T_g$ (measured) using torsion pendulum (°C)	$T_g$ (measured d.s.c.) (°C)
PVC		+74	+74
FR-N-500		-14	-13
FR-N-504		-12	-12
FR-N-510		-26	-25
101	+42	+42	+40
102	+43	+42	+45
103	+61	+62	+58
104	+36	+36	+35
105	+15	+10	-5

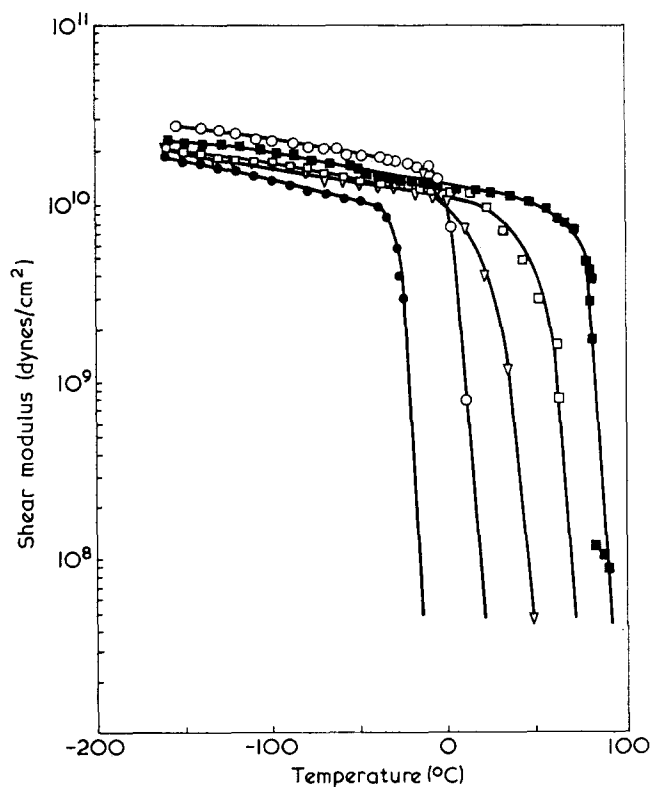


Figure 2 Temperature variation of modulus for PVC/FR-N-510 blends. Samples and symbols identified in Table 2

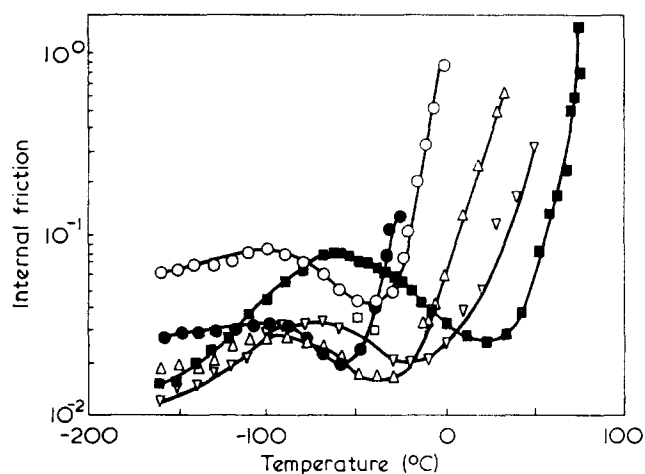


Figure 3 Internal friction versus temperature for PVC/FR-N-510 blends. Samples and symbols identified in Table 2

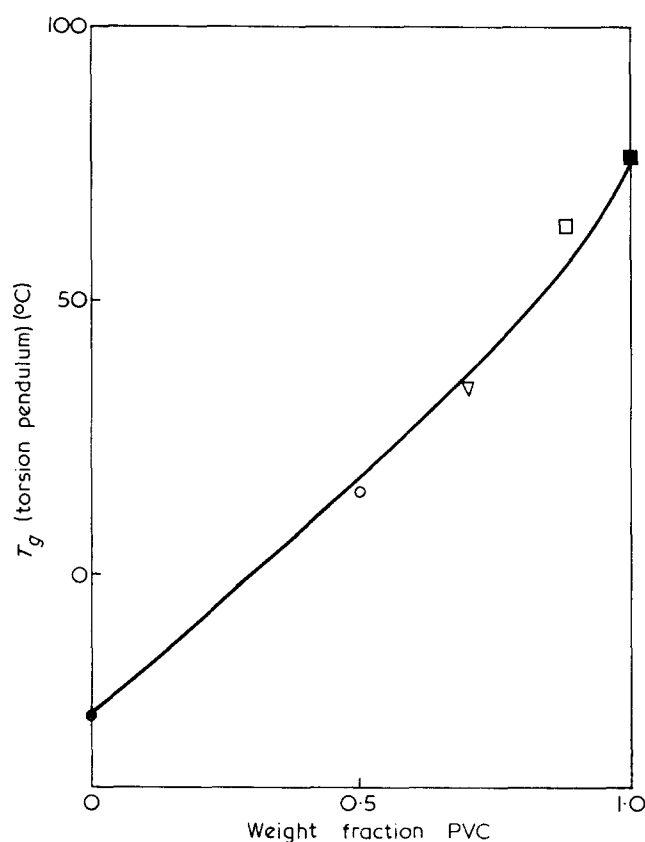


Figure 4  $T_g$  (measured by torsion pendulum) versus composition for PVC/FR-N-510 blends. Samples and symbols identified in Table 2

where  $T_g$  is the glass transition temperature of the mixture,  $T_{g_1}$  and  $T_{g_2}$  are the glass transition temperatures of the respective homogeneous components and  $W_1$  and  $W_2$  are their respective weight fractions. Table 3 and Figure 4 give a comparison of the blend  $T_g$  values as calculated using the Fox equation with the  $T_g$  values measured from the torsion pendulum curves. We can see the agreement of these calculated and experimental quantities. Figure 2 shows shear modulus versus temperature for the blends and blend components. Figure 3 shows internal friction versus temperature for the blends and blend components. We can see in these curves the large (2-3 decade) fairly sharp decrease in the modulus at the  $T_g$  and the decrease in the  $T_g$  as the BD-AN

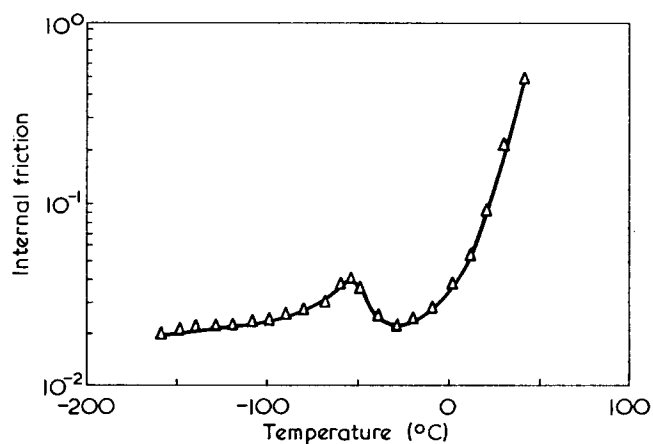


Figure 5 Internal friction versus temperature for 70:30wt.% PVC/FR-N-500 blend

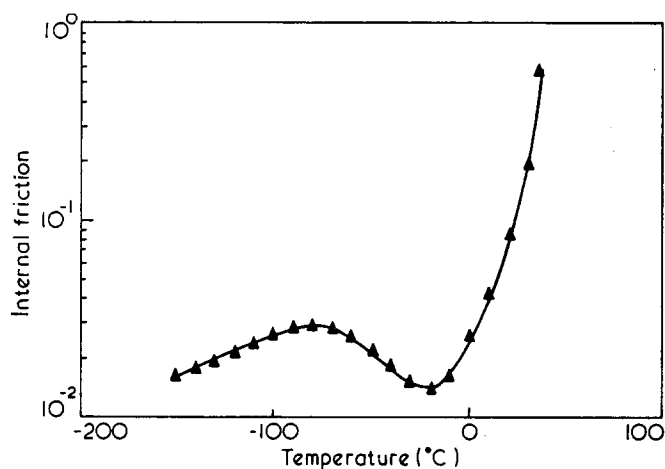


Figure 6 Internal friction versus temperature for 70:30wt.% PVC/FR-N-504 blend

copolymer concentration is increased (Figure 3). Figures 5 and 6 show the single  $T_g$  peaks for PVC/FR-N-500 and PVC/FR-N-504 blends.

In a multicomponent system we would expect to see a  $T_g$  for each component in the mixture. In the shear modulus and internal friction curves of blends 101, 102 and 103, we can find no such peaks for PVC at +74°C or to FR-N-510 at -26°C. This is very strong evidence indicating the true compatibility of the system. The secondary relaxations are very broad, and it is not possible to interpret any intensity variation or peak shifts corresponding to compatibility on a molecular level as evidenced in PVC/E-VA-SO<sub>2</sub> blends by Ikeda and Hickman<sup>7</sup>.

D.s.c. studies of these blends confirm torsion pendulum analysis. The  $T_g$  values graphically determined from the d.s.c. curves are very close to those obtained from torsion pendulum analysis (Table 3). These thermograms (Figure 7) show a single relatively sharp  $T_g$  for the PVC/BD-AN blends. If the blends are incompatible we should be able to find a  $T_g$  peak for PVC at +74°C and another for BD-AN at -26°C. Torsion pendulum studies are difficult above the  $T_g$  of the blends and the PVC probably could not be seen. The BD-AN peaks, however, are absent.

An interesting observation can be made from the densities of the compatible blends. If the interaction between blend components is small, then we may expect

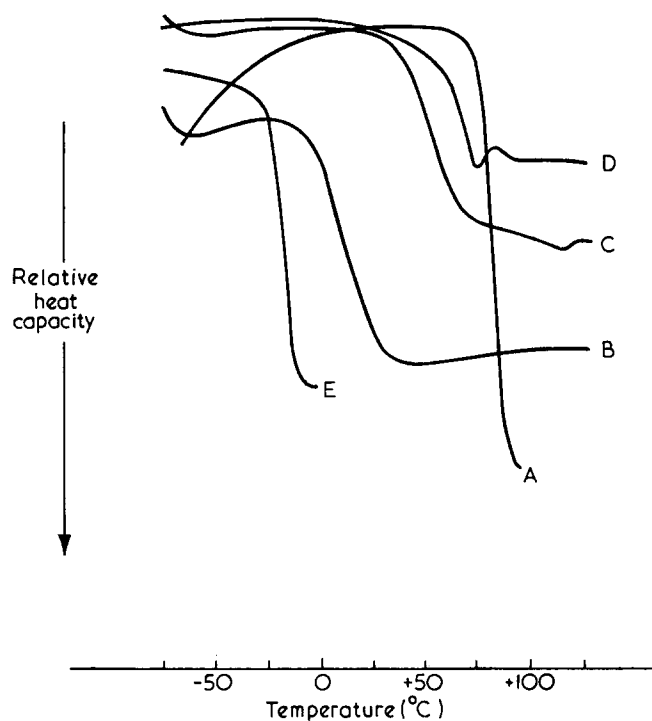


Figure 7 D.s.c. thermograms of PVC/FR-N-510 blends. A, PVC; B, 50:50 PVC/BD-AN; C, 70:30 PVC/BD-AN; D, 90:10 PVC/BD-AN; E, BD-AN

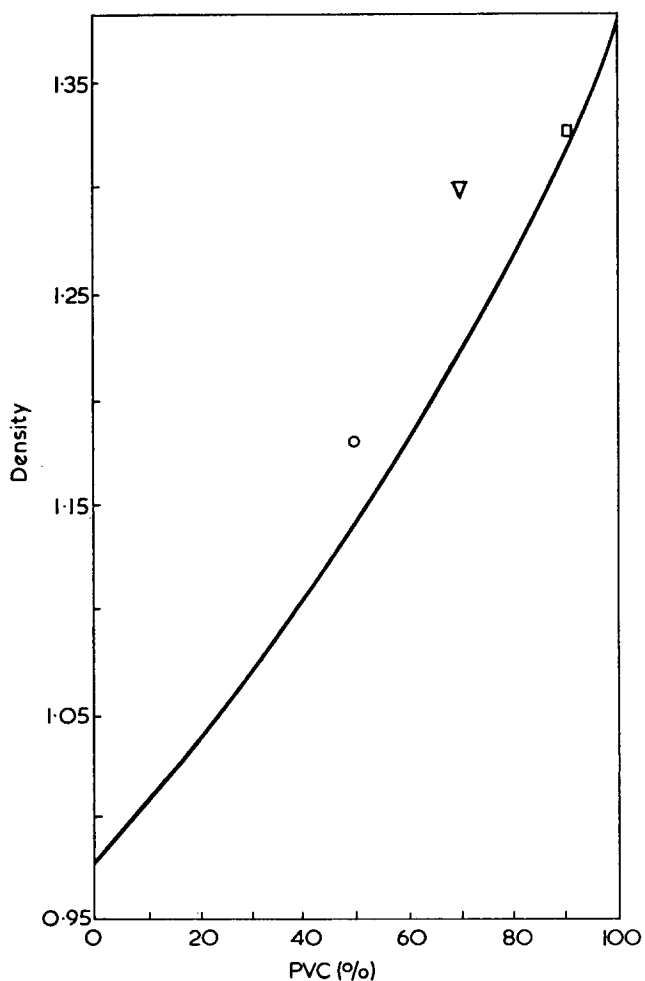


Figure 8 Density versus composition curve for PVC/FR-N-510 blends. Symbols and samples identified in Table 2. Continuous curve calculated from equation (2)

to calculate the density of a polymer-polymer solution using the expression:

$$\frac{1}{\rho} = \frac{W_1}{\rho_1} + \frac{W_2}{\rho_2} \quad (2)$$

where  $\rho$ ,  $\rho_1$  and  $\rho_2$  are the respective densities of the blend, component 1 and component 2 and  $W_1$  and  $W_2$  are the weight fractions of the same respective material. By calculating these quantities we observe that all our measured densities for PVC/BD-AN blends are significantly greater (*Figure 8*) than these calculated quantities.

To investigate the possibility of crystallinity accounting for the difference in densities we have run X-ray goniometer traces on the same film at 25°C. Data in *Table 1* show that all blends are substantially amorphous, with crystallinity <10%. These crystallinity differences do not account for the differences in the calculated and measured densities.

We believe that these differences are due to strong molecular interaction leading to better chain packing and high densities. Such a big positive interaction would

also yield a negative heat of mixing which would explain the solubility of BD-AN copolymer in PVC.

Our data show that PVC is compatible with these copolymers of BD-AN over the range 23-45% AN. We believe that decreasing numbers of polar AN groups providing strong interaction with PVC will limit compatibility below this range. There is probably also an upper limit to the AN concentration in the copolymers which will be reached when the intermolecular interaction is greater than the intramolecular interaction.

#### REFERENCES

- 1 Feldman, D. and Rosu, M. *Eur. Polym. J.* 1970, **6**, 627
- 2 Rezhikou, R. *et al. Kolloid Zh.* 1953, **15**, 108
- 3 Chandler, L. and Collins, E. *J. Appl. Polym. Sci.* 1969, **13**, 1385
- 4 Angelo, R. J., Ikeda, R. M. and Wallach, M. L. *Polymer* 1965, **6**, 141
- 5 Ikeda, R. M., Wallach, M. L. and Angelo, R. J. 'Block Polymers', Plenum Press, New York, 1970, p 43
- 6 Fox, T. G. *Am. Phys. Soc.* 1956, **1**, 123
- 7 Hickman, J. J. and Ikeda, R. M. to be published

# Cationic polymerization of acenaphthylene and methyl acenaphthylenes

S. Cohen, P. Belliard and E. Marechal

*Institut National Supérieur de Chimie Industrielle de Rouen (Institut Emile Blondel),  
76130 Mont-Saint-Aignan, France*

*(Received 26 February 1973; revised 2 April 1973)*

Cationic polymerization of acenaphthylene was studied both by experimental methods and theoretical calculations. Very pure acenaphthylene was obtained by double sublimation and its polymerization kinetics were studied with  $\text{SnCl}_4$  as initiator. Reactivity ratios were determined for methyl-1, methyl-3 and methyl-5 acenaphthylenes, while values of stabilization energies,  $(\Delta E)_s^\ddagger$ , have been calculated. There is good agreement between the trends of the two sets of values. In the case of acenaphthylene, the comparison of results obtained by Hückel's and by Pople's methods has shown the contribution of ring strain to the reactivity of acenaphthylenic monomers.

## INTRODUCTION

We have recently published a review on electronic and steric effects of substituents on the reactivity of aromatic monomers in cationic polymerization<sup>1</sup>. The comparison of experimental and theoretical results provided much information on the mechanisms of cationic polymerization. Our results have been, up to now, mainly concerned with monomers derived from indene and styrene<sup>2-10</sup>. Acenaphthylene and related compounds are particularly interesting because the strain of the pentagonal ring has a determining influence on their reactivity towards cations (as will be shown later) and also because numerous quantum chemistry calculations have been published about these compounds<sup>11-13</sup>.

## EXPERIMENTAL AND RESULTS

Acenaphthylene and its derivatives were prepared and purified as reported previously<sup>14</sup>. There is generally very little information on the purity of the acenaphthylene used for the polymerizations described in the literature. Particularly important is the acenaphthene content of acenaphthylene; very small quantities of this saturated compound have been shown to have a drastic influence on the results of the polymerization. Polymerizations were carried out under dry nitrogen. Polymer was precipitated from the polymerization solution by addition of methanol and isolated by filtration; the quantity of unprecipitated oligomers was very small. The rates have been followed by determination of the conversion at various times.

### *Polymerization of acenaphthylene by stannic chloride*

Numerous studies have been published about cationic polymerization of acenaphthylene. The only aim of this short preliminary paper is to compare our monomer and one of our initiators with those of previous studies.

We have studied the  $\text{SnCl}_4$  initiated polymerization

in detail. When the temperature is  $+15$  or  $-20^\circ\text{C}$ , the internal order of overall rate of polymerization is 2 and the overall rate  $V$  is given by the following relation:

$$V_2 = K_2[M]^2$$

with  $K_2 = 5.46 \times 10^{-3} \text{ l mol}^{-1} \text{ sec}^{-1}$  when the temperature is  $+15^\circ\text{C}$ , and  $K_2 = 1.37 \times 10^{-3} \text{ l mol}^{-1} \text{ sec}^{-1}$  when the temperature is  $-20^\circ\text{C}$ .

Guisti and Andruzzi<sup>15</sup> have obtained the same relationship and order of magnitude for  $K$  with the system acenaphthylene- $\text{BF}_3$ -dichloroethane when the temperature is  $30^\circ\text{C}$ .

The initial order of polymerization with respect to monomer, in the temperature range between  $+15^\circ\text{C}$  and  $-40^\circ\text{C}$ , is 1. Polton<sup>16</sup> obtained the same value for the  $\text{SnCl}_4$  initiated polymerization of indene.

### *Homopolymerization of monomethylacenaphthylenes*

The synthesis of these monomers is described elsewhere<sup>14</sup>. Some of them were obtained in very small amount, hence the restricted number of determinations.

The results obtained with various initiators are reported in *Table 1* where  $R$  (%) is the yield of precipitated polymer,  $[\eta]$  the intrinsic viscosity (100 ml/g). For all polymerizations  $\theta = -72^\circ\text{C}$  and the initiator concentration  $[A]$  and the monomer concentration  $[M]$  have optimum values for each polymerization.

### *Determination and study of reactivity ratios*

The reactivity ratios have been determined by differential and integral methods. The results are reported in *Table 2*. Indices 1 and 2 are respectively assigned to acenaphthylene and to styrene. All these reactivity ratios have been obtained with  $[\text{TiCl}_4] = 0.01$ ,  $[M] = 0.304$ , solvent  $\text{CH}_2\text{Cl}_2$ , polymerization temperature  $0^\circ\text{C}$ . The average degree of polymerization is about 30. The conversion ranges from 40 to 50% when  $r_1$  and  $r_2$  are



Table 1 Yields and intrinsic viscosities for the homopolymerization of monomethylacenaphthylenes

Initiator	R(%)				
	Acenaphthylene	Me-1	Me-3	Me-5	
TiCl <sub>4</sub>	90	90	0	48	95
SnCl <sub>4</sub>	0	0	2	92	92
BF <sub>3</sub> , OEt <sub>2</sub>	0	0	0	33	57
BF <sub>3</sub>	95	94	0	100	100
AlCl <sub>3</sub>	—	0	—	—	—
SbCl <sub>5</sub>	46	48	—	—	—

	[ $\eta$ ]				
	Acenaphthylene	Me-1	Me-3	Me-5	
TiCl <sub>4</sub>	0.10	0.10	—	0.10	0.29
SnCl <sub>4</sub>	0	0	Trimer*	0.36	0.19
BF <sub>3</sub> , OEt <sub>2</sub>	0	0	—	0.10	0.55
BF <sub>3</sub>	0.11	0.14	—	0.30	0.17
AlCl <sub>3</sub>	—	0	—	—	—
SbCl <sub>5</sub>	0.06	0.12	—	—	—

\* It has been possible to show by n.m.r. that the poly(methyl-1 acenaphthylene) obtained in SnCl<sub>4</sub> initiated polymerization is a trimer ended by a methyl-1 acenaphthylene unit

Solvent=CH<sub>2</sub>Cl<sub>2</sub> except for first column=C<sub>2</sub>H<sub>5</sub>Cl

Table 2 Reactivity ratios and stabilization energies for various monomers

Monomer	$r_1$	$r_2$	$1/r_2$	$(\Delta E)_s$
Methyl-1 acenaphthylene	0.4±0.05	0.11±0.05	9.1	0.949
Methyl-3 acenaphthylene	9.3±0.5	0.23±0.05	4.3	0.869
Methyl-5 acenaphthylene	11.7±1	0.15±0.05	6.7	0.877
Acenaphthylene	17.5±1.5	0.25±0.05	4	0.847

determined by the Mayo and Lewis method and below 8% when determined by the intersection method.

Moreover, we have studied the influence of several parameters on reactivity ratios of acenaphthylene and styrene.

The influence of the polymerization temperature is described in Figure 1 where variations of  $\log r_1$  and  $\log r_2$  versus  $10^3/T$  are reported. The initiator concentration is 0.01, the monomer concentration 0.13 and the solvent CH<sub>2</sub>Cl<sub>2</sub>.

The influence of initiator and monomer concentrations have been carefully studied but are very small and the variations of  $r_1$  and  $r_2$  with [A] and [M] are always smaller than the experimental uncertainty.

There are only small changes in the values of reactivity ratios when the nature of the solvent and of the initiator are changed.

Thus, when the solvent is CH<sub>2</sub>Cl<sub>2</sub>, the temperature  $\theta = -78^\circ\text{C}$  and the initiator and the monomer concentrations are respectively  $10^{-2}$  and 0.125, the following values were obtained:

TiCl<sub>4</sub> as initiator:  $r_1 = 11.3$ ;  $r_2 = 0.17$

SnCl<sub>4</sub> as initiator:  $r_1 = 14.2$ ;  $r_2 = 0.5$

On the other hand, with [TiCl<sub>4</sub>]=0.01, [M]=0.125 and  $\theta = -20^\circ\text{C}$  the following values have been obtained with various solvents:

toluene ( $\epsilon = 2$ ):  $r_1 = 14.1$ ;  $r_2 = 0.13$

CH<sub>2</sub>Cl<sub>2</sub> ( $\epsilon = 10$ ):  $r_1 = 16.8$ ;  $r_2 = 0.14$

CH<sub>3</sub>NO<sub>2</sub> ( $\epsilon = 35$ ):  $r_1 = 11.5$ ;  $r_2 = 0.15$

## DISCUSSION AND CONCLUSIONS

Examination of Table 1 shows that the polymerization of methyl-1 acenaphthylene is hindered by the methyl group on carbon 1. It is possible to obtain a trimer with a very low yield when the initiator is SnCl<sub>4</sub>. However, methyl-1 acenaphthylene is able to copolymerize and has a high reactivity due to the inductive effect of the methyl group. The behaviour of methyl-1 acenaphthylene is very similar to the behaviour of methyl-3 indene; however, it has not been possible to show a penultimate effect<sup>17</sup>.

Using Hückel's method and Yonezawa's relations we calculated the stabilization energies  $(\Delta E)_s^*$  involved in the attack of styryl cation by the various acenaphthylenes studied. The unit for stabilization energies is  $(\Delta\beta)/\beta$  where  $\Delta\beta$  is the resonance integral of the bond between the atom  $r$  of the cation and the atom  $s$  of the monomer. The values obtained are reported in Table 2.

The classification of monomers obtained from these values and those obtained from  $1/r_2$  values are quite consistent.

However, the stabilization energy for styrene is 0.912, i.e. greater than the value obtained for acenaphthylene. This result is inconsistent with the comparison of the value of  $1/r_2$ . Styrene and acenaphthylene are both conjugated with  $\pi$  bonds so it is rather strange to observe a failure of Hückel's method with this compound. However, as early as 1951 Pullman<sup>13</sup> observed that there is a discrepancy between the theoretical and the experimental results when Hückel's method is applied to acenaphthylene. This author thinks that the failure of Hückel's method to give correct values is due to the strain of the pentagonal ring. We tried to confirm this assumption in the case of polymerization with the help of Pople's method (C.N.D.O. II). Indeed this

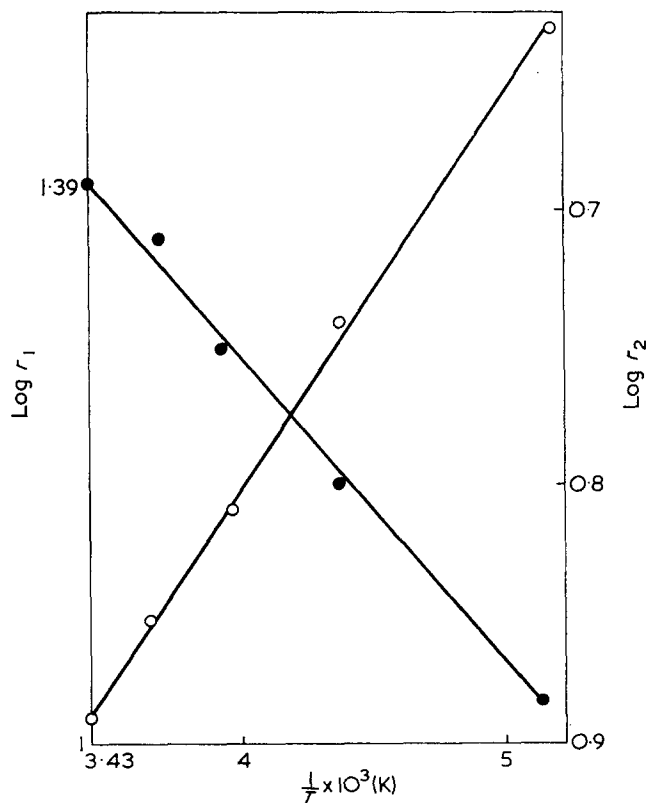


Figure 1 Variations of  $\log r_1$  (●) and  $\log r_2$  (○) versus  $10^3/T$  (K) for acenaphthylene: [M]=0.13; [TiCl<sub>4</sub>]=0.01; solvent: CH<sub>2</sub>Cl<sub>2</sub>

method is not only more accurate than Hückel's but moreover takes into account the geometry of the molecule.

The stabilization energies calculated by this method (with the same unit) are 6756 for styrene and 6993 for acenaphthylene when the cation is styryl. So, with Pople's method which takes into account the geometry of the molecule, the discrepancy between theoretical and experimental results disappears. This fact is a proof of the contribution of ring strain to the reactivity of acenaphthylene in cationic polymerization.

The results obtained through the study of the influence of experimental parameters on the values of reactivity ratios for acenaphthylene and styrene are worth more careful analysis.

The nature of the initiator and the solvent have only a slight influence on the values of  $r_1$  and  $r_2$ , but the influence of temperature is much more interesting. The results are reported in *Figure 1*.

Imoto<sup>18</sup> determined the variations of  $r_1$  and  $r_2$  with respect to temperature for n-butyl vinyl ether (M2) and acenaphthylene (M1) with  $\text{BF}_3 \cdot \text{OEt}_2$  as initiator in benzene. He found that, whatever the cation, the reactivity of M2 was greater than that of M1. However, the direction of variation for  $r_1$  and  $r_2$  was opposite to ours. From the relation:

$$r_1 = k_{11}/k_{12} = \left\{ \exp \left( \frac{\Delta S_{11} - \Delta S_{12}}{R} \right) \right\} \cdot \left\{ \exp - \left( \frac{E_{11} - E_{12}}{RT} \right) \right\}$$

he obtained  $E_{11} - E_{12} = -(E_{22} - E_{21}) = 2.6 \text{ kcal/mol}$  and  $(\Delta S_{11} - \Delta S_{12}) = -(\Delta S_{22} - \Delta S_{21}) = 6.5 \text{ cal mol}^{-1} \text{ deg}^{-1}$ .

From *Figure 1*, we obtained  $E_{11} - E_{12} = 1.57 \text{ kcal/mol}$  and  $E_{22} - E_{21} = -0.57 \text{ kcal/mol}$ ;  $\Delta S_{11} - \Delta S_{12} = 6.76 \text{ cal mol}^{-1} \text{ deg}^{-1}$  and  $\Delta S_{22} - \Delta S_{21} = -4.25 \text{ cal mol}^{-1} \text{ deg}^{-1}$ .

Contrary to Imoto, we do not have the same value for  $\Delta S_{11} - \Delta S_{12}$  and  $\Delta S_{22} - \Delta S_{21}$  since in our case the product  $r_1 r_2$  is not equal to 1.

The fact that  $r_1$  increases with  $T$  although it is greater than 1 may appear inconsistent with the relation  $d \log r_1 / d(1/T) = T \log r_1$ <sup>19</sup>.

However, this relation has been obtained because  $\Delta S_{11} - \Delta S_{12} = X$  has been ignored; when  $X$  is taken into account the result is:

$$\frac{d \log r_1}{d \left( \frac{1}{T} \right)} = T \left( \log r_1 - \frac{X}{R} \right)$$

which is, for all the values we have obtained, negative and consequently consistent with the direction of variation.

#### REFERENCES

- 1 Marechal, E. *J. Macromol. Sci. (A)*, 1973, 7, 433
- 2 Marechal, E. *C.R. Acad. Sci.* 1969, 269, 752
- 3 Marechal, E. *C.R. Acad. Sci.* 1969, 268C, 1121
- 4 Marechal, E. *Bull. Soc. Chim. Fr.* 1969, p 1459
- 5 Zaffran, C. and Marechal, E. *Bull. Soc. Chim. Fr.* 1970, p 3521
- 6 Tortai, J. P. and Marechal, E. *Bull. Soc. Chim. Fr.* 1971, p 2673
- 7 Anton, A. and Marechal, E. *Bull. Soc. Chim. Fr.* 1971, p 3753
- 8 Zweggers, J. and Marechal, E. *Bull. Soc. Chim. Fr.* 1972, p 1157
- 9 Quere, J. P. and Marechal, E. *Bull. Soc. Chim. Fr.* 1969, p 4087
- 10 Marechal, E. *J. Macromol. Sci. (A)* 1973, 7, in the press
- 11 Sandorfy, C., Trinble, W. Q., Laforgue, A. and Daudel, R. *J. Chim. Phys.* 1949, 46, 655
- 12 Crawford, W. A. and Coulson, C. A. *J. Chem. Soc.* 1948, p 1990
- 13 Pullman, B., Bergman, E. D., Berthier, G., Fisher, E., Highberg, Y. and Pontis, J. *J. Chim. Phys.* 1951, 48, 359
- 14 Belliard, P. and Marechal, E. *Bull. Soc. Chim. Fr.* 1972, p 4255
- 15 Giusti, P. and Andruzzi, F. *Gaz. Chim. Ital.* 1966, p 1563
- 16 Polton, A. *Thesis*, University of Paris, 1968
- 17 Sigwalt, P. and Marechal, E. *Eur. Polym. J.*, 1966, 2, 5
- 18 Imoto, M. and Takemoto, K. *J. Polym. Sci.* 1958, 31, 210
- 19 O'Driscoll, K., *J. Macromol. Sci. (A)* 1969, 3, 307

# Equilibrium bulk polymerization of 1,3-dioxolan

R. Binet and J. Leonard

Department of Chemistry, Université Laval, Quebec 10, Canada  
(Received 9 March 1973)

Cationic bulk polymerization of 1,3-dioxolan has been carried out in sealed ampoules using a high vacuum technique. The polymerization is initiated with triethyl oxonium hexafluorophosphate and the equilibrium between monomer and active polymer is attained within a few hours. Specific volumes of pure monomer and polymer in solution of its own monomer have been measured. Equilibrium measurements have been performed in the 40° to 141.4°C temperature range and the ceiling temperature is estimated to be 144° ± 2°C. The effect of short polymer chains on the equilibrium is discussed briefly. Values of  $\Delta G_{lc}$ , the free energy of polymerization of one mole of pure liquid monomer to one base-mole of amorphous polymer, are computed making allowance for the non-ideal mixing. Respective values of  $-17.5 \pm 0.8$  kJ/mol and  $-47.9 \pm 2.2$  J K<sup>-1</sup> mol<sup>-1</sup> are deduced for the corresponding  $\Delta H_{lc}$  and  $\Delta S_{lc}$ .  $\Delta G_{lc}$  is also computed from published data on equilibrium polymerization of 1,3-dioxolan in various solvents and the combined results for both types of polymerization yield  $\Delta H_{lc} = -16.7 \pm 0.5$  kJ/mol and  $\Delta S_{lc} = -45.8 \pm 1.5$  J K<sup>-1</sup> mol<sup>-1</sup> for the 20° to 140°C range.

## INTRODUCTION

It is well known that cationic polymerization of 1,3-dioxolan may lead to a state of equilibrium between monomer and active polymer chains and equilibrium polymerizations of that monomer in solution have been reported by several groups of workers<sup>1-7</sup>.

In the present paper, we wish to report results obtained for the cationic bulk polymerization of 1,3-dioxolan under equilibrium conditions. Polymerizations were carried out in the 40° to 141.4°C temperature range. Our results are compared with published data on the equilibrium polymerization of 1,3-dioxolan in solution.

## EXPERIMENTAL

### Materials

1,3-Dioxolan (Eastman) was degassed over calcium hydride for several days, and then distilled *in vacuo* onto a sodium mirror. A small amount of naphthalene was added and the green colour of the sodium naphthalene complex was used as an indicator for the purity of dioxolan. Upon the fading out of the green colour, the monomer was distilled onto a fresh sodium mirror.

Triethyl oxonium hexafluorophosphate was used as initiator and its purification has been described elsewhere<sup>8</sup>.

### Polymerization

Polymerizations were carried out in sealed ampoules using high vacuum techniques. The general procedure is similar to the one used for the polymerization of tetrahydrofuran<sup>8</sup>. 1,3-Dioxolan reacts readily with the initiator at room temperature and initial heating of the monomer is unnecessary. This behaviour is in contrast to that observed for the polymerization of these two monomers initiated with triethyl oxonium tetrafluoro-

borate where an induction period for the polymerization of 1,3-dioxolan is reported<sup>9</sup>. In all cases equilibrium was attained within 24 hours.

Reversibility of the polymerization was checked by following the variation of the meniscus height in the capillary of a dilatometer. The procedure is illustrated in *Figure 1* where the meniscus height is plotted against time for two ranges of temperature. In section (a), the bath is set at a given temperature and the meniscus height is observed until it remains constant (equilibrium). Then the temperature is changed and the procedure is repeated (section b). After equilibrium has been reached, the bath is re-set at its original temperature (section c). In the case of a reversible polymerization, the final meniscus height should coincide with its initial equilibrium height. In experiment A, the temperature was allowed to vary from 30° to 50°C and in experiment B from 120° to 130°C.

After equilibrium had been reached, the polymerization was terminated by adding a mixture of benzene and a primary alcohol to the reacting mixture at equilibrium temperature. In order to avoid loss of monomer, for polymerizations above 60°C, the alcohol was kept in a side ampoule equipped with a break-seal so that the reaction could be terminated in a closed system. After termination, the polymer-monomer mixture was removed quantitatively from the ampoule and transferred into a preweighted flask. The monomer was removed and the polymer was dried *in vacuo* to constant weight. The initial amount of monomer and equilibrium amount of polymer being known, the amount of monomer present under equilibrium conditions is deduced.

### Molecular weights

Average molecular weights of dead polymer samples were determined through intrinsic viscosity at 25°C in

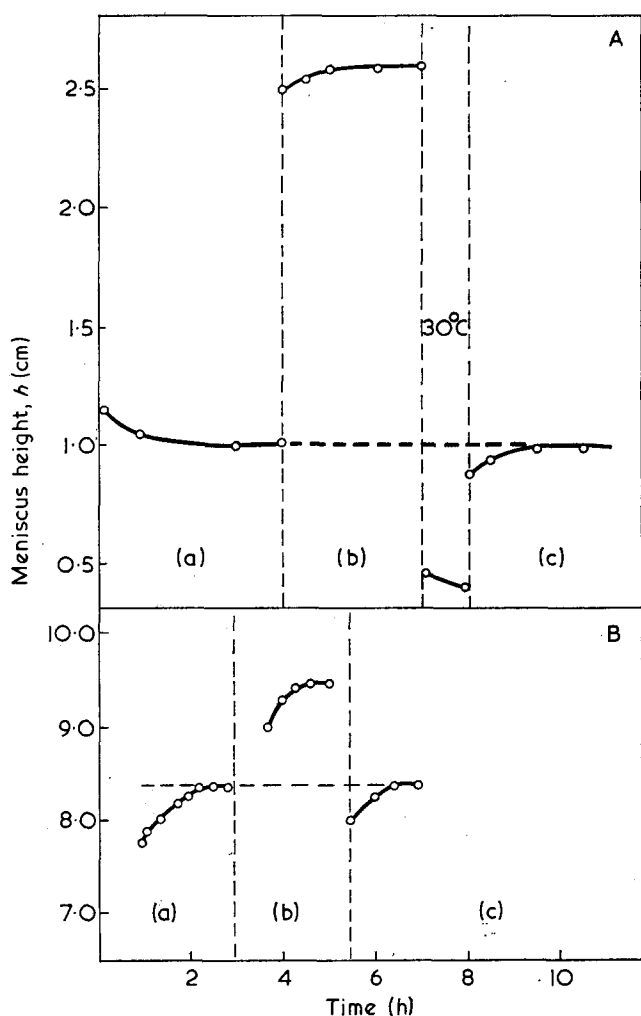


Figure 1 Reversibility of the bulk polymerization of 1,3-dioxolan. Variation of  $h$ , the meniscus height, with time for two series of dilatometric measurements. Experiment A: (a) 35°C; (b) 50°C; (c) 35°C. Experiment B: (a) 120°C; (b) 130°C; (c) 120°C

chlorobenzene, using a Ubbelohde viscometer. Molecular weights were computed through the relation<sup>10</sup>:

$$[\eta] = 2 \times 10^{-3} \bar{M}_v^{0.5} \quad (1)$$

where  $[\eta]$  is the intrinsic viscosity and  $\bar{M}_v$ , the viscosity-average molecular weight. The intrinsic viscosity was determined by a one-point method<sup>11</sup>. Results obtained from the one-point method were in excellent agreement with those obtained from the extrapolation of  $\eta_{sp}/c$ .

## RESULTS AND DISCUSSION

### Specific volumes of monomer and polymer

Specific volumes of pure 1,3-dioxolan using both dilatometry and picnometry have been measured in the 10° to 70°C temperature range. The variation of  $\bar{v}_m$ , the specific volume, with  $t$ , the temperature (in °C) is expressed by:

$$\bar{v}_m = 0.9198 (1 + 1.116 \times 10^{-3} t + 1.56 \times 10^{-6} t^2) \pm 0.002 \text{ ml} \quad (2)$$

Apparent specific volumes of polymer,  $\bar{v}_p$ , in solution of its own monomer were also measured. Dilatometric measurements of a solution 18.34 % (w/w) in polymer ( $\bar{M}_v = 71\,400$ ) were performed in the 25° to 75°C temperature range.  $\bar{v}_p$  was computed from:

$$\bar{v}_p = (V - w_m \bar{v}_m) / w_p$$

where  $V$  is the total volume (in ml),  $w_m$  and  $w_p$  are the weights (in g) of monomer and polymer respectively. The variation of  $\bar{v}_p$  with temperature is given by:

$$\bar{v}_p = 0.812 (1 + 7.0 \times 10^{-4} t) \pm 0.002 \text{ ml} \quad (3)$$

### Equilibrium bulk polymerization

Table 1 shows results obtained for the bulk polymerization of 1,3-dioxolan in the 40° to 141.4°C temperature range. The initial concentration of initiator measured at 25°C,  $[I]_{25}^0$ , varies from 2.0 to  $4.0 \times 10^{-3}$  mol/l except for the highest temperatures where the concentration is  $0.6 \times 10^{-3}$  mol/l.  $n$  is the average degree of polymerization computed from  $\bar{M}_v$ . The weight fraction of polymer,  $m_p$ , present at equilibrium, or the degree of conversion, is given in column 2. The volume fraction of polymer,  $\phi_p$ , is computed from:

$$\phi_p = m_p / [m_p + (\bar{v}_m / \bar{v}_p)(1 - m_p)] \quad (4)$$

values of  $\bar{v}_m$  and  $\bar{v}_p$  being obtained through equations (2) and (3) for each temperature.

Variation of  $\phi_p$  with temperature is shown in Figure 2. The extrapolation of  $\phi_p$  to  $\phi_p = 0$  yields a ceiling temperature of  $144 \pm 2^\circ\text{C}$  for the polymerization of pure monomer. The extrapolation of  $m_p$  gives an identical result. This value is in good agreement with the estimated value of 150°C obtained from the equilibrium polymerization of 1,3-dioxolan in benzene<sup>7</sup>. However, our result differs appreciably from the reported values of 155°C<sup>1</sup>, 160°C<sup>2</sup> and 165°C<sup>3</sup>. These values were deduced from the extrapolation of  $\ln[M]_e$  computed under various conditions of polymerization without taking into account the variation of the monomer molar volume with temperature. When treated in this fashion, our own results yield a ceiling temperature of 155°C, which is obviously too high.

### Free energies of polymerization

The present set of values can be used to compute free energies of polymerization, making allowance for the non-ideality of the polymerization system. Assuming formation of polymer of infinite molecular weight,  $\Delta G_{1c}$ , the free energy change upon the conversion of one mole of pure liquid monomer to one base-mole of amorphous polymer, is computed from<sup>12</sup>:

$$\Delta G_{1c} = RT [\ln \phi_m + 1 + \chi_{mp} (\phi_p - \phi_m)] \quad (5)$$

where  $\phi_m (= 1 - \phi_p)$  is the equilibrium monomer volume

Table 1 Equilibrium bulk polymerization of 1,3-dioxolan

$t$ (°C)	Conversion (%)	$[I]_{25}^0 \times 10^3$ (mol/l)	$n \times 10^{-2}$
40.0	91.8	2.6	9.6
50.0	88.3	2.5	13.0
60.0	87.6	2.6	7.3
70.0	81.8	2.7	20.0
80.0	76.2	3.2	9.9
	75.2	2.6	4.6
95.0	64.5	2.1	5.8
109.2	53.5	3.9	13.0
	52.3	4.0	26.0
120.0	37.5	3.7	0.9
129.8	27.6	2.0	13.0
140.8	6.9	0.6	2.5
141.4	5.3	0.6	0.6

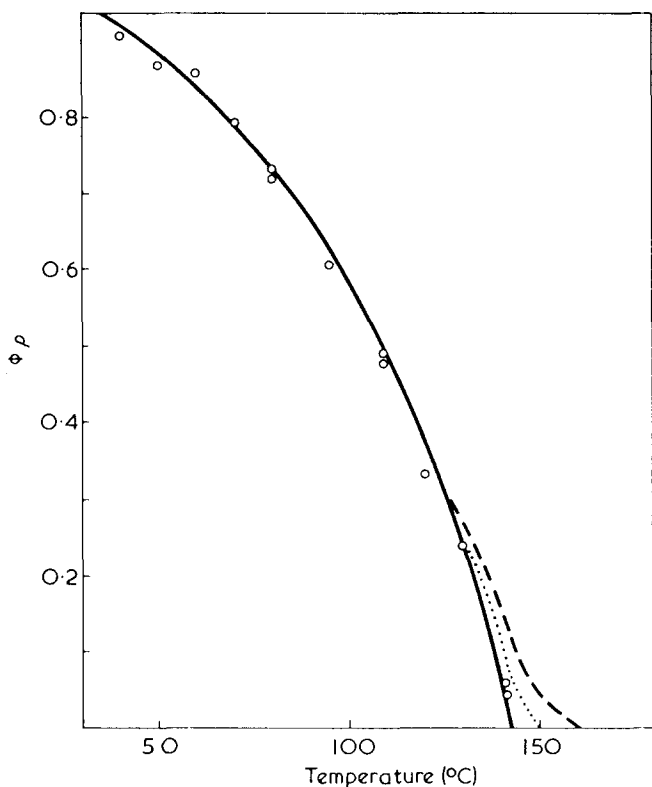


Figure 2 Variation of the polymer volume fraction,  $\phi_p$ , with temperature. ---, Computed curve with  $n=20$ ; ·····, with  $n=50$

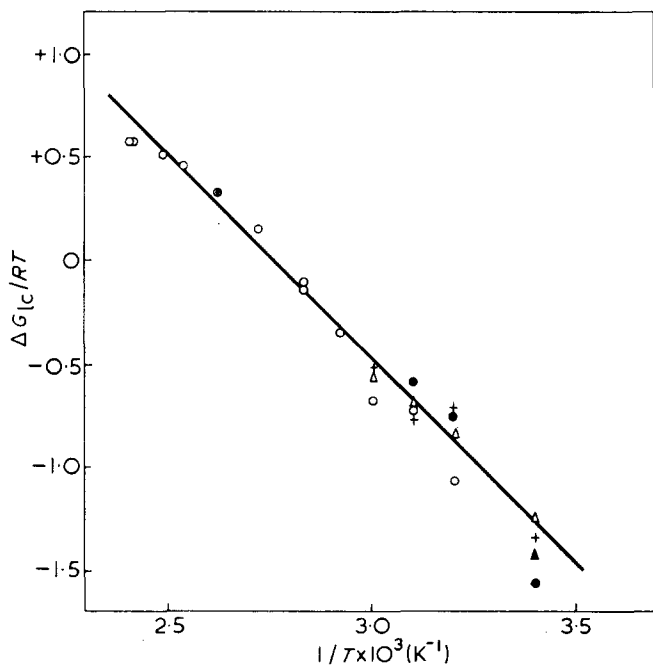


Figure 3 Computation of  $\Delta G_{1c}/RT$ : ○, bulk polymerization; ●, in *p*-dioxane; +, in benzene; △, in methylene chloride; ▲, in ethyl chloride

fraction and  $\chi_{mp}$  is the monomer-polymer interaction parameter.  $\Delta G_{1c}/RT$  is computed assuming a constant value of 0.4 for  $\chi_{mp}$  and its variation with  $1/T$  is shown in Figure 3. The value of 0.4 represents an average value since  $\chi_{mp}$  is bound to change over the considerable range of 40° to 140°C. A value of 0.3 above 120°C and 0.5 below 70°C would yield a better straight line. As can be seen from equation (5), the value of  $\chi_{mp}$  has little effect on  $\Delta G_{1c}/RT$  for  $\phi_p$  around 0.5.

Equation (5) is valid when  $n$  is large and the polymer volume fraction, not too small. From Table 1, it can be seen that in some cases,  $n$  is rather small. The effect of short chains on the equilibrium position can be checked through the original equation<sup>12</sup>:

$$\Delta G_{1c} = RT [\ln \phi_m + \chi_{mp} (\phi_p - \phi_m) + 1 - (\ln \phi_p)/n - (1/n)] \quad (6)$$

Just as in the case of equilibrium polymerization in solution<sup>13</sup>,  $\Delta G_{1c}/RT$  is assumed to be independent of chain length and  $\phi_p$  is computed from equation (6) for different values of  $n$  at various temperatures. Figure 2 shows computed curves for  $n$  equal to 20 and 50 with  $\chi_{mp}=0.3$ . The value of 0.3 was selected since the best agreement between extrapolated and experimental values of  $\Delta G_{1c}/RT$  is observed for this value of  $\chi_{mp}$  in the considered temperature range. As can be seen, the presence of short chains may lead to an overestimate of the ceiling temperature. The present results do not seem to be influenced by short-chain effect although Table 1 shows that, in a few cases,  $n$  is lower than expected. The presence of short chains may be explained through chain scission during and after polymerization<sup>1, 3, 14</sup>.

$\Delta G_{1c}/RT$  being essentially independent of the polymerization system, the values obtained here may be compared with those obtained from the equilibrium polymerization of 1,3-dioxolan in solution. Recently, it has been shown that for the anionic polymerization of  $\alpha$ -methylstyrene<sup>15, 16</sup> and for the cationic polymerization of tetrahydrofuran<sup>8</sup> in solution, at a given temperature,  $\phi_m$  varies linearly with  $\phi_p$  according to:

$$\phi_m = \phi_m^0 + b\phi_p \quad (7)$$

$\Delta G_{1c}/RT$  is computed through comparison of equation (7) with<sup>13, 15</sup>:

$$\phi_m = \frac{-(\Delta G_{1c}/RT) + \ln a + \beta}{\beta + \chi_{mp} - 1/a} + \frac{\chi_{mp} - \beta}{\beta + \chi_{mp} - 1/a} \phi_p \quad (8)$$

where  $\beta$  is a term including a solvent-monomer and a solvent-polymer interaction parameter and  $\alpha$  is identical to  $\phi_m^0$ . Equilibrium polymerization of 1,3-dioxolan using various initial monomer concentrations have been reported<sup>1, 5</sup> so that equations (7) and (8) are applicable. Values of  $\phi_m$  and  $\phi_p$  are obtained from the plot of

Table 2 Thermodynamic parameters computed from equilibrium polymerization of 1,3-dioxolan in solution

$t$ (°C)	Solvent	$a$	$-b$	$-\beta$	$\Delta G_{1c}/RT$ (with $\chi_{mp}=0.4$ )	Refs
60	CH <sub>2</sub> Cl <sub>2</sub>	0.27	0.17	0.21	-0.56	5
	Benzene	0.25	0.13	0.07	-0.54	5
50	CH <sub>2</sub> Cl <sub>2</sub>	0.23	0.14	0.16	-0.70	5
	Benzene	0.20	0.11	0.08	-0.74	5
	Dioxane	0.21	0.08	0.06	-0.58	5
40	CH <sub>2</sub> Cl <sub>2</sub>	0.19	0.10	0.11	-0.83	5
	Benzene	0.16	0.04	-0.20	-0.71	5
	Dioxane	0.18	0.07	-0.04	-0.74	5
20	CH <sub>2</sub> Cl <sub>2</sub>	0.11	0.04	-0.03	-1.23	5
	Benzene	0.12	0.07	0.15	-1.34	5
	Dioxane	0.14	0.14	0.62	-1.55	5
	C <sub>2</sub> H <sub>5</sub> Cl	0.07	0.009	-0.27	-1.42	1

$[M]_e$ , the equilibrium monomer concentration, against  $[M]_0$ , the initial monomer concentration, for the polymerization in methylene chloride<sup>5</sup>; from the plot of  $\ln \phi_m$  against  $\phi_p$  for the polymerization in benzene and in *p*-dioxane<sup>5</sup>; and from the plot of  $([M]_0 - [M]_e)$  against  $[M]_0$  for the polymerization in ethyl chloride<sup>1</sup>. In all cases  $\phi_m$  varies linearly with  $\phi_p$  in accordance with equation (7) and values of the thermodynamic parameters computed from equation (8) are given in Table 2. Variation of  $\Delta G_{1c}/RT$  with  $1/T$  are shown in Figure 3 together with the results obtained for bulk polymerization. Values of  $-17.5 \pm 0.8$  kJ/mol and  $-47.9 \pm 2.2$  JK<sup>-1</sup>mol<sup>-1</sup> are deduced for  $\Delta H_{1c}$  and  $\Delta S_{1c}$  respectively for the bulk polymerization. The combined results of bulk and solution polymerization yield

$$\Delta H_{1c} = -16.7 \pm 0.5 \text{ kJ/mol}$$

and  $\Delta S_{1c} = -45.8 \pm 1.5$  JK<sup>-1</sup>mol<sup>-1</sup>. These latter values should be retained if the 293° to 413°K range is considered. Data for the *p*-dioxane system were not used in the computation of  $\Delta H_{1c}$  as copolymerization of *p*-dioxane with 1,3-dioxolan cannot be ruled out completely: copolymerization of *p*-dioxane with monomers such as 3,3-bis(chloromethyl) oxacyclobutane<sup>17</sup> and epichlorohydrin<sup>18</sup> has been reported. Our results are comparable with the values of  $-14.6$  kJ/mol and  $-36.7 \pm 3.0$  JK<sup>-1</sup>mol<sup>-1</sup> for  $\Delta H_{1c}$  and  $\Delta S_{1c}$  respectively, obtained from the equilibrium between gaseous monomer and amorphous polymer<sup>19</sup>. However, they differ to a considerable extent from  $\Delta S_{1c} = -66 \pm 6$  JK<sup>-1</sup>mol<sup>-1</sup> computed from the heat capacities of monomer and polymer<sup>20</sup>.

#### ACKNOWLEDGEMENTS

The authors gratefully acknowledge financial support

from the Defence Research Board of Canada, Grant No. DRB-9530-85 (UG). R. B. wishes to thank the National Research Council of Canada for the award of a fellowship.

#### REFERENCES

- 1 Berman, Ye. L., Lyudvig, Ye. B., Ponomarenko, V. A. and Medvedev, S. S. *Vysokomol. Soedin.* 1969, **11**, 200
- 2 Chil'-Gevorgyan, G. M., Bonetskaya, A. K., Skuratov, S. M. and Yenikolopyan, N. S. *Vysokomol. Soedin.* 1967, **9**, 1363
- 3 Kharitonova, L. A., Rakova, G. V., Shaginyan, A. A. and Yenikolopyan, N. S. *Vysokomol. Soedin.* 1967, **9**, 2586
- 4 Kučera, M. and Pichler, J. *Vysokomol. Soedin.* 1965, **7**, 10
- 5 Kuzub, L. I., Markevich, M. A., Berlin, A. A. and Yenikolopyan, N. S. *Vysokomol. Soedin.* 1968, **10**, 2007
- 6 Plesch, P. H. and Westermann, P. H. *J. Polym. Sci. (C)* 1968, **16**, 3837
- 7 Yamashita, Y., Okada, M., Suyama, K. and Kasahara, H. *Makromol. Chem.* 1968, **114**, 146
- 8 Leonard, J. and Maheux, D. *Polym. Preprints* 1972, **13**, 78
- 9 Yamashita, Y., Kozawa, S., Chiba, K. and Okada, M. *Makromol. Chem.* 1970, **135**, 75
- 10 Pravikova, N. A., Berman, Y. B., Lyudvig, Y. B. and Davtyan, A. G. *Vysokomol. Soedin.* 1970, **12**, 580
- 11 Berlin, A. A. *Vysokomol. Soedin.* 1966, **8**, 1336
- 12 Ivin, K. J. and Leonard, J. *Polymer* 1965, **6**, 621
- 13 Leonard, J. *Macromolecules*, 1969, **2**, 661
- 14 Gorin, S. and Monnerie, L. *Bull. Soc. Chim. Fr.* 1966, p 2047
- 15 Ivin, K. J. and Leonard, J. *Eur. Polym. J.* 1970, **6**, 331
- 16 Leonard, J. and Malhotra, S. L. *J. Polym. Sci. (A-1)* 1971, **9**, 1983
- 17 Tsuda, T., Nomura, T. and Yamashita, Y. *Makromol. Chem.* 1965, **86**, 301
- 18 Stirna, U., Pernikis, R. and Surna, J. *Apsite B. Latv. PSR Zivat. Akad. Vestis, Kim. Ser.* 1969, p 113
- 19 Busfield, W. K., Lee, R. M. and Merigold, D. *Makromol. Chem.* 1972, **156**, 183
- 20 Clegg, G. A. and Melia, T. P. *Polymer* 1969, **10**, 912

# Light scattering Rayleigh linewidth measurements on some globular protein solutions

D. B. Sellen

*Astbury Department of Biophysics, University of Leeds, Leeds LS2 9JT, UK  
(Received 1 February 1973; revised 11 March 1973)*

An apparatus previously described for investigating the Rayleigh linewidth of light scattered from macromolecular solutions by means of the optical homodyne technique has been modified so as to obtain the autocorrelation function of the fluctuations in scattered intensity. Its operation is described and some results presented for three commercially obtainable globular proteins: chymotrypsinogen, bovine plasma albumin and urease. Measurements were made in unbuffered 0.2M NaCl aqueous solutions and the diffusion constants,  $D_{20w}$ , found to be  $7.4 \pm 0.3 \times 10^{-7} \text{ cm}^2 \text{ s}^{-1}$ ,  $5.8 \pm 0.1 \times 10^{-7} \text{ cm}^2 \text{ s}^{-1}$  and  $3.4 \pm 0.1 \times 10^{-7} \text{ cm}^2 \text{ s}^{-1}$  respectively. There was no detectable concentration dependence. In each case the results agreed well with theoretical predictions both as regards angular variation and shape of the autocorrelation function. The effects of polydispersity are discussed.

## INTRODUCTION

During the past decade it has become possible, largely owing to the advent of the laser, to investigate the spectra of light scattered from macromolecular solutions<sup>1-8</sup>. The most convenient method of making these measurements is by means of the optical homodyne technique in which the power spectrum of a photoelectric signal is investigated. In recent years it has been found advantageous to do this by obtaining the autocorrelation function<sup>3,4</sup>. An apparatus previously described<sup>8</sup> has been modified to use an autocorrelation function computer and the present paper describes its operation and presents some results for three commercially obtainable globular proteins.

### *Theory of the spectral broadening of light scattered from macromolecular solutions*

The theory of the spectral broadening of light scattered from macromolecular solutions is set out in a series of publications by Pecora<sup>6</sup>. The quantity first calculated is the phase correlation function:

$$F(\tau) = \frac{1}{T} \int_0^T A_t A_{t+\tau} dt \quad (1)$$

where  $T \gg \tau$ ,  $A_t$  is the scattered amplitude at time  $t$  and  $A_{t+\tau}$  that component which is in the same phase at time  $t + \tau$ . For a monodisperse system in which broadening arises only from changes in the phase of scattered light due to translational diffusion this becomes for positive values of  $\tau$ :

$$F(\tau) = I \exp(-K^2 D \tau) \quad (2)$$

where  $F(\tau)$  is symmetrical about  $\tau = 0$ .  $D$  is the translational diffusion constant,  $I$  the scattered intensity and

$$K = \frac{4\pi}{\lambda} \sin \theta / 2 \quad (3)$$

where  $\theta$  is the angle of scatter relative to the incident direction and  $\lambda$  the wavelength *in the solution*. The spectral intensity distribution function of the shift  $\omega$  relative to the frequency of the incident beam is then given by the Fourier transform of  $F(\tau)$ . This is a Lorentzian  $I_\omega$ :

$$I_\omega = \frac{IK^2 D}{\pi(\omega^2 + K^4 D^2)} \quad (4)^*$$

Spectral broadening will also arise from any other cause which results in fluctuations of the scattered amplitude or phase and in general  $F(\tau)$  is a sum of exponentials and  $I_\omega$  the corresponding sum of Lorentzians. For non-interacting systems there are two possible additional sources of broadening, rotational or configurational changes in the particle scattering factor  $P(\theta)$ , and rotational variation of polarizability. For a solution of globular proteins  $P(\theta)$  is unity at all angles and cannot fluctuate with time. For the case of optically anisotropic molecules with an axis of symmetry Pecora<sup>6</sup> gives the relations:

$$F_V(\tau) = I_V \left[ \left( 1 - \frac{4}{3} \rho_V \right) \exp(-K^2 D \tau) + \frac{4}{3} \rho_V \exp(-(K^2 D + 6\Theta)\tau) \right] \quad (5)$$

$$F_H(\tau) = I_H \exp[-(K^2 D + 6\Theta)\tau] \quad (6)$$

where the incident light is vertically polarized and the two equations refer to the vertically and horizontally polarized components of the scattered light.  $\Theta$  is the

\* In an earlier publication by the author<sup>8</sup> a derivation of equation (4) was given in which the scattered light was regarded as a random succession of damped oscillations whose amplitude varied with time as  $\exp(-K^2 D t)$ .  $I_\omega$  is then given by the *square* of the modulus of the Fourier transform of a function which varies as  $\exp(-K^2 D t)$  for positive times and is *zero* for negative times.

rotational diffusion constant and  $\rho_V$  the depolarization factor. For globular proteins  $6\Theta$  is of the order of  $10^7 \text{ s}^{-1}$ ,  $K^2 D$   $10^4 \text{ s}^{-1}$  or less and  $\rho_V$  about 0.01. The above equations may therefore be simplified, spectral broadening of the vertically and horizontally polarized components being attributed entirely to translational and rotational diffusion respectively. If no attempt is made to separate the two components the low value of  $\rho_V$  will render the observed spectrum dependent upon translational diffusion alone. Also frequency shifts associated with rotational diffusion are of the order of MHz and beyond the frequency range of the present apparatus. The results presented in this paper may therefore be interpreted entirely in terms of translational diffusion. It is worth noting, however, that in principle rotational diffusion constants can be determined from the spectral distribution of depolarized light. This would also afford a useful method of finding  $\rho_V$  as the spectral width of any horizontally polarized light of a spurious nature would be several orders of magnitude smaller than that of the true depolarized light.

For a polydisperse system where only translational diffusion is considered, the phase correlation function becomes a sum of exponentials associated with each component, viz:

$$F(\tau) = \sum_n I_n \exp(-K^2 D_n \tau) \quad (7)$$

where  $I_n$  is the scattered intensity from that component having diffusion constant  $D_n$ . The spectral distribution is then the corresponding sum of Lorentzians.

#### The optical homodyne

The simplest method of investigating the spectra of scattered light where the frequency shifts are small (of the order of 1 kHz) as is the case here, is by employing the optical homodyne technique. Provided that the coherence length of the source is long compared with the various differences in optical path length involved, and this is easily achieved with a laser, the different frequency components of the scattered light will beat with each other and result in fluctuations in scattered intensity. The spectrum of these intensity fluctuations can be investigated photoelectrically and if the signal is scanned with a wave analyser of bandwidth  $\Delta B$  the signal at angular frequency  $B$  will be given by  $s_B$  where<sup>8</sup>:

$$\overline{s_B^2} = 2c^2 \gamma^2 \Delta B \int_0^\infty I_{\frac{1}{2}B-\Omega} I_{\frac{1}{2}B+\Omega} d\Omega \quad (8)$$

$I$  is the spectral intensity distribution function,  $c$  the overall photosensitivity of the detecting system and  $\gamma$  a coherence factor which depends upon the geometry of the scattered light receiver system.  $\gamma$  has a maximum value of unity and increases as the smallest illuminated volume resolvable by the receiver system (in an image forming sense), approaches the volume of solution from which scattered light is actually received. A focused beam together with small stops in the receiver system are therefore needed otherwise complete phase cancellation of the beats occurs. Substitution of equation (4) in equation (8) yields:

$$\overline{s_B^2} = \frac{c^2 \gamma^2 \Delta B}{2} \frac{I^2 K^2 D}{\pi \left( \frac{B^2}{4} + K^4 D^2 \right)} \quad (9)$$

i.e. a Lorentzian of twice the spectral width. For a

polydisperse system this becomes:

$$\overline{s_B^2} = \frac{c^2 \gamma^2 \Delta B}{\pi} \sum_m \sum_n \frac{I_m I_n K^2 (D_m + D_n)}{B^2 + K^4 (D_m + D_n)^2} \quad (10)$$

Investigation of the intensity fluctuations by scanning with a wave analyser has three major disadvantages: (i) the beat spectrum has to be scanned making measurements at one frequency at a time using a time constant which is long compared with  $1/\Delta B$ <sup>8</sup>. In order to preserve resolution at low frequencies  $\Delta B$  has to be about six cycles so that each point on the spectrum takes about five minutes to obtain; (ii) provision has to be made for subtracting photoelectric shot noise<sup>8</sup>; and (iii) equation (10) shows that  $\overline{s_B^2}$  is very difficult to interpret if the solution is polydisperse. These disadvantages may be largely overcome by obtaining the autocorrelation function of the photoelectric signal using a suitable computer. This is defined by  $\phi(\tau)$  where:

$$\phi(\tau) = \frac{1}{T} \int_0^T s_t s_{t+\tau} dt \quad (11)$$

with  $T \gg \tau$  and is the Fourier transform of  $\overline{s_B^2}$ . It is also proportional to the square of  $F(\tau)$ , viz:

$$\phi(\tau) = \frac{c^2 \gamma^2}{2} [F(\tau)]^2 \quad (12)$$

For the case of a monodisperse system where spectral broadening is due to translational diffusion alone this becomes:

$$\phi(\tau) = \frac{c^2 \gamma^2 I^2}{2} \exp(-2K^2 D \tau) \quad (13)$$

and for a polydisperse system:

$$\phi(\tau) = \frac{c^2 \gamma^2}{2} \left[ \sum_n I_n \exp(-K^2 D_n \tau) \right]^2 \quad (14)$$

Thus  $\phi(\tau)$  is much easier to interpret than  $\overline{s_B^2}$ . Provided that the integration time  $T$  is long enough photoelectric shot noise is averaged out and contributes to  $\phi(\tau)$  only for very small values of  $\tau$  if the electronic system has a large bandwidth.  $T$  also has to be long enough for  $\phi(\tau)$  to be properly defined, i.e.  $T \gg \tau$ , and the time taken to obtain  $\phi(\tau)$  for a particular value of  $\tau$  will be of the same order of magnitude as that required to obtain a point on the  $\overline{s_B^2}$  spectrum. However, computers are available which enable  $\phi(\tau)$  to be obtained for one hundred different values of  $\tau$  simultaneously thus considerably reducing the total time required.

#### APPARATUS

The apparatus used has been described previously. It was modified by the addition of an autocorrelation function computer (Princeton Applied Research Corporation Model 100A) and by replacing the He-Ne laser with one having a higher output (50 mW uniphase nominal). The latter has enabled smaller stops to be used in the receiver system so raising  $\gamma$  from 0.01 to 0.10 independent of angle of scatter.  $\gamma$  may be found experimentally from the value of  $\phi(\tau)$  at  $\tau=0$  [equations (13) and (14)].

The computer obtains  $\phi(\tau)$  for one hundred different values of  $\tau$  simultaneously and is of the analogue type, i.e. the input is analysed as a continuous signal and the remarks which follow apply only to analysis of this type.



They will not in general be applicable to photon counting systems<sup>3</sup>. The operation of the apparatus is best illustrated by Figure 1 which shows the computer output for light scattered from a 2% solution of chymotrypsinogen at  $\theta=30^\circ$ . This is displayed on an oscilloscope and then transferred to an X-Y recorder for analysis. The integration time is 20s and achieved by means of RC filters so that in principle complete curves can be obtained in about 2min. The autocorrelation function of the photoelectric shot noise is obtained by analysing a beam direct from the laser attenuated to the same intensity as the scattered light in the manner described previously<sup>8</sup>. After the initial decay this remains equal to zero indicating the absence of any significant modulation on the laser output or spurious pick-up in the electronics. The initial decay is the Fourier transform of the Lorentzian response curve of the electronic system and therefore exponential, the decay time being determined by the bandwidth which can be varied by means of a low pass filter placed before the computer. Reduction of bandwidth is desirable so that the photoelectric signal due to the scattered light may be made as large as possible without overloading the computer with shot noise. However, the resulting autocorrelation function (shown as 'beats plus photoelectric shot noise' in Figure 1) can be analysed only for those delay times above which the autocorrelation function of the shot noise is negligible and the value of  $\phi(\tau)$  for  $\tau=0$  must be found by extrapolation. The choice of bandwidth is therefore a compromise. The computer operates, however, by scanning through the delay times with a recycling time equal to one-hundredth of the maximum delay on the selected range, so that for this reason also it is advisable to remove high frequencies and ignore data corresponding to the first 10% of the delay times. The bandwidth is accordingly adjusted so that the autocorrelation function of the shot noise occupies the first 10% of the time scale. When the scattered intensity is very low it nevertheless becomes necessary to make measurements near to the computer baseline, especially when the solution under investigation necessitates using the very short delay ranges so that a wide electronic bandwidth must be employed. For the very short delay ranges (50  $\mu$ s maximum to 200  $\mu$ s maximum) the baseline

consists of spurious oscillations associated with the computation process. These are systematic, however, and their effect may be minimized by subtracting the two curves.

Measurements are made more difficult by the presence of dust in the solutions. Dust particles cause transient signals as they move in and out of the beam, the effect of which is to cause the autocorrelation function to execute spasmodic vertical movements sometimes causing the computer to be overloaded. To some extent this effect may be reduced by removing low frequencies from the signal and an adjustable high pass filter is placed before the computer for this purpose. The cleanliness of the solution, however, ultimately determines the time required to make a measurement as it is necessary to wait for a 2min period during which no dust particles move in or out of the beam.

As both high and low pass filters are placed in the electronic system it is necessary to calculate the extent to which these distort the autocorrelation function. If the normalized function is given by  $\exp(-2K^2D\tau)$  then the effect of simple RC filters is to change this to:

$$\exp(-2K^2D\tau) - \frac{2K^2D}{\Omega} \exp(-\Omega\tau) \quad (15)$$

for the case of a low pass filter and:

$$\exp(-2K^2D\tau) - \frac{b}{2K^2D} \exp(-b\tau) \quad (16)$$

for the case of a high pass filter where  $\Omega$  and  $b$  are the angular frequencies of the 3db points and  $\Omega \gg 2K^2D \gg b$ . No correction for the presence of the low pass filter is therefore necessary as the data are ignored in the region where the second term is effective. The second term in equation (16) may be calculated using an approximate value of  $K^2D$  obtained by plotting  $\log\phi(\tau)$  against  $\tau$ . For the data shown in Figure 1 where the lower 3db point is at 30 Hz this correction changes the calculated value of  $D$  by about 4%.

The apparatus employs a semi-cylindrical cell of the type supplied by the Aminco (American Instrument Co. Inc., Silver Spring, Maryland, USA) apparatus in which conventional light scattering measurements can be made on the same solutions. Thus both kinds of measurements can be made over a wide range of angles. When conventional light scattering measurements are made on macromolecular solutions which have a dissymmetry of scatter, a correction has to be made for light scattered from the beam reflected at the glass/air interface where the incident beam leaves the cell. This is done by subtracting from the intensity scattered at any given angle 4% of the intensity scattered at the supplementary angle. At first sight it might appear that a similar correction should be applied to the spectral distribution of scattered light as this will be different for supplementary angles of scatter. This, however, is not so as ordinary light scattering cells are not made with sufficient precision for the light scattered from the reflected beam to enter the receiver system from the same coherence volume, i.e. there will be no heterodyne effect between the light scattered from the two beams. The output from the computer will simply be the sum of the autocorrelation functions resulting from the two spectral distributions and as these are proportional to the square

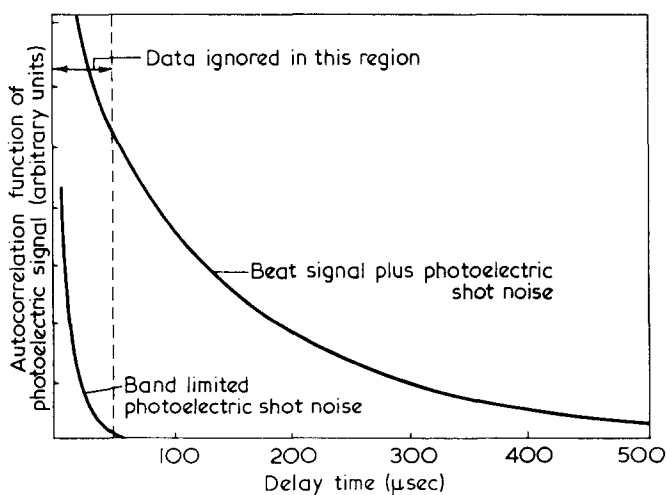


Figure 1 Autocorrelation function computer output for a 2% solution of chymotrypsinogen: angle of scatter  $30^\circ$ . The 3db points of the electronics are 30 Hz and 14 kHz

of the scattered intensity the contribution from the reflected beam will be negligible.

RESULTS AND DISCUSSION

In an earlier publication<sup>8</sup> measurements on a 0.5% solution of Ludox (Du Pont Ltd) were reported which were made by scanning the photoelectric signal with a wave analyser. As a check on its performance these measurements were repeated with the present apparatus and the equivalent hydrodynamic diameter of 17 nm confirmed.

Three globular proteins chosen so as to represent a wide range of molecular weights: chymotrypsinogen, bovine plasma albumin and urease were investigated. These were commercially available samples and their sources are listed in Table 1. The solvent in each case was a 0.2 M aqueous solution of NaCl with no buffers added, the pH being about 5 in the case of chymotrypsinogen and bovine plasma albumin, and about 6 in the case of urease. All measurements were made on the same day as the solutions were made up. Solutions were clarified by centrifuging for 2 h at 30 000 × g and passing through a Millipore filter of pore size 1.2 μm directly into the cell. Conventional light scattering measurements were made in the Aminco apparatus. In no case was any dissymmetry of scatter observed after the solutions had been properly clarified and the molecular weights were found to be 29 000 for chymotrypsinogen, 68 000 for bovine plasma albumin and 60 000 for urease. The last result is in serious disagreement with the accepted value (about 500 000) and arises because the sample contains a high proportion of very low molecular weight material such as ammonia and free amino acids which is not detected at all by light scattering.

Normalized autocorrelation functions plotted against  $\tau \sin^2\theta/2$  for chymotrypsinogen, bovine plasma albumin and urease are shown in Figures 2, 3 and 4 respectively. The points are taken from the read-out on the X-Y recorder and as predicted by theory all the data lie on the same curve. The solid line in each case represents the best fit of an exponential curve to the data. Values of  $D_{20w}$  were calculated assuming the validity of the Stokes-Einstein equation and these are shown as a function of concentration for each protein in Figure 5. Measurements were actually made at room temperature but this was never outside the range 18°C to 22°C. The concentrations shown for urease are those estimated

Table 1 Sources of globular proteins and summary of results

Globular protein	Description and source	$M_w$	$D_{20w} \times 10^7$ ( $\text{cm}^2 \text{s}^{-1}$ )
Chymotrypsinogen	From bovine pancreas 6 × crystallized (Sigma cat. C4879)	29 000	$7.4 \pm 0.3$
Bovine plasma albumin	Fraction V from bovine plasma (Armour Pharmaceutical Co.)	68 000	$5.8 \pm 0.1$
Urease	From jack bean meal 2 × crystallized (Calbiochem B grade cat. 66613)	60 000*	$3.4 \pm 0.1$

\* See text

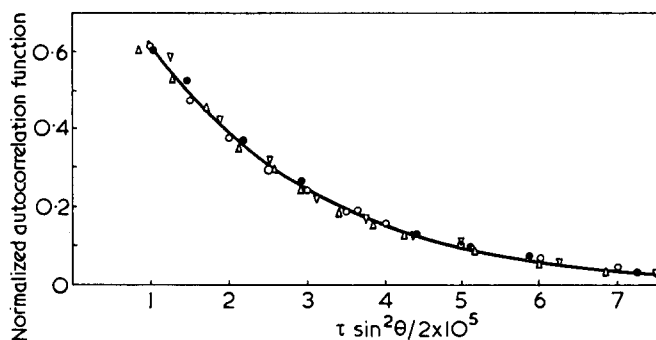


Figure 2 Normalized autocorrelation function of intensity fluctuations of light scattered from a 2% solution of chymotrypsinogen in 0.2 M NaCl.  $\Delta$ , 30°;  $\nabla$ , 45°;  $\bullet$ , 60°;  $\circ$ , 90°

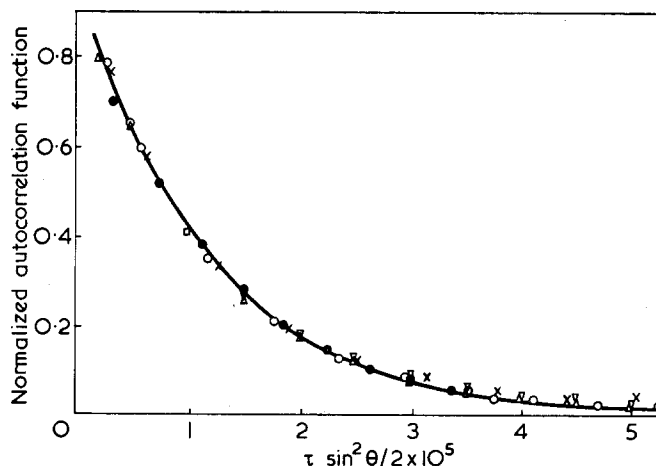


Figure 3 Normalized autocorrelation function of intensity fluctuations of light scattered from a 2% solution of bovine plasma albumin in 0.2 M NaCl.  $\times$ , 29°;  $\circ$ , 40°;  $\Delta$ , 60°;  $\nabla$ , 90°;  $\bullet$ , 120°

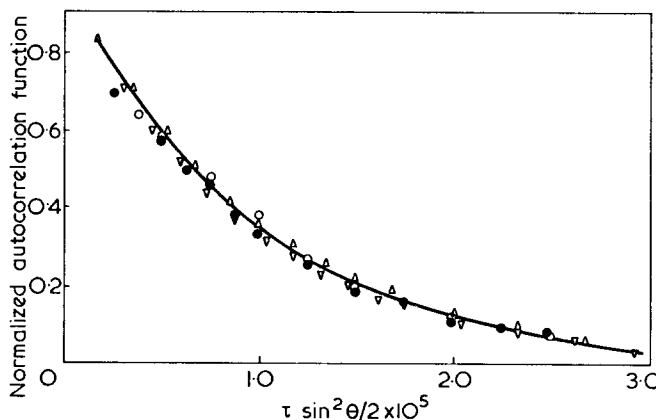


Figure 4 Normalized autocorrelation function of intensity fluctuations of light scattered from a 0.2% solution of urease in 0.2 M NaCl.  $\Delta$ , 135°;  $\circ$ , 90°;  $\nabla$ , 60°;  $\bullet$ , 45°

for the true globular protein on the basis of the measured molecular weight for the whole sample. It can be seen that in no case is there a detectable variation with concentration and the mean values are shown in Table 1.

During the experiments it was found that in all cases where there was any significant dissymmetry of scatter due to aggregation with time, or insufficient clarification, the  $\sin^2\theta/2$  law no longer applied, the decay time on a  $\tau \sin^2\theta/2$  scale increasing with decreasing angle although no deviation from the exponential shape was observed. This does not arise from fluctuations in  $P(\theta)$  due to rotation of the aggregates as these would be virtually

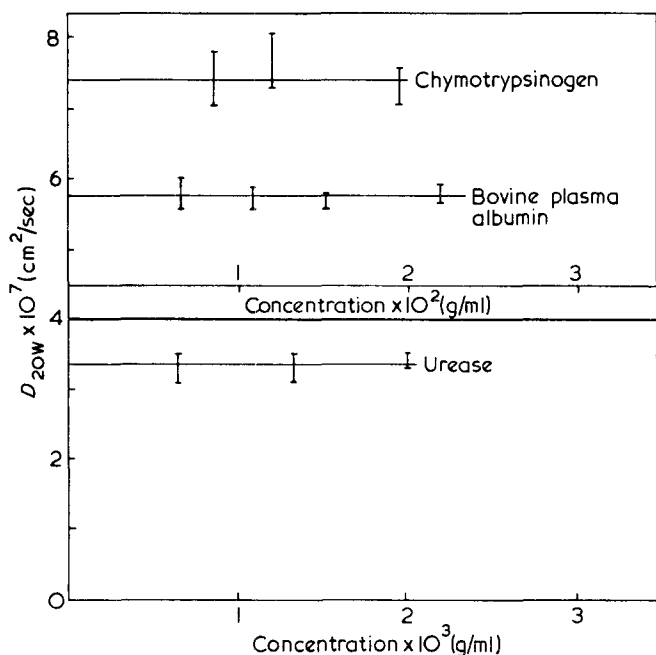


Figure 5 Diffusion constant as a function of concentration for three globular proteins. Measurements were made in 0.2M NaCl

undetectable in a globular system. It is due to the fact that the relative contribution of the aggregates to the scattered intensity increases with decreasing angle. In passing it should be emphasized that the systematic deviation from the  $\sin^2\theta/2$  law is in the same direction both for polydispersity and rotational or configurational variation of  $P(\theta)$  so that systems under investigation must be very carefully characterized before any interpretation in terms of the latter is made.

Where there is no dissymmetry of scatter the  $\sin^2\theta/2$  law should apply rigorously whatever the polydispersity if rotational variation of polarizability is negligible<sup>8</sup> although the autocorrelation function may not be quite exponential. The exponential shapes obtained for the three globular proteins, however, do not necessarily indicate that they are monodisperse and it is necessary to discuss the effects of polydispersity before comparing the results with those of other authors. For a polydisperse system the autocorrelation function is given by equation (14) and if  $\ln\phi(\tau)$  is plotted against  $\tau$  the slope of the graph is:

$$\frac{1}{\phi(\tau)} \frac{d\phi(\tau)}{d\tau} = \frac{2 \sum_n -K^2 D_n I_n \exp(-K^2 D_n \tau)}{\sum_n I_n \exp(-K^2 D_n \tau)} \quad (17)$$

which for  $\tau=0$  becomes:

$$-2K^2 \frac{\sum_n D_n I_n}{\sum_n I_n} \quad (18)$$

Unless the degree of polydispersity is very high there will be a tendency for the exponential terms to cancel out even though they are under the summation signs. In this case the autocorrelation function will be exponential and the slope of a plot of  $\ln\phi(\tau)$  against  $\tau$  given by equation (18). It is not possible to determine the type of average of  $D$  so calculated without postulating how  $D$  varies with molecular weight  $M$ . If it is postulated that  $M_n \propto 1/D_n^3$ , i.e. the system is globular and all components have the same shape and that  $I_n \propto N_n M_n^2$

where  $N_n$  is the number of molecules with molecular weight  $M_n$  then equation (18) becomes:

$$\frac{-2K^2}{(1/D)_{z+3}} \quad (19)$$

where

$$(1/D)_{z+3} = \frac{\sum_n N_n / D_n^5}{\sum_n N_n / D_n^6} \quad (20)$$

The molecular weight of that component which has this value of  $1/D$  is given by  $M_D$  where:

$$M_D = \left[ \frac{\sum_n N_n M_n^2}{\sum_n N_n M_n^{5/3}} \right]^3 \quad (21)^*$$

This usually lies somewhere between the weight and  $z$ -average depending upon the type of distribution. In general for polydisperse solutions the value of  $D$  calculated from the autocorrelation function will correspond to a somewhat larger molecular weight than that found from conventional light scattering measurements.

The result for chymotrypsinogen is somewhat lower than that determined using conventional techniques by Schwert<sup>9</sup> ( $9.5 \times 10^{-7} \text{ cm}^2 \text{ s}^{-1}$ ) who found a negative concentration dependence at very low concentrations. His value of molecular weight calculated from subsequent ultracentrifuge measurements was 23 000 compared with the presently accepted value of 26 000 suggesting that his value for the diffusion constant may be about 10% too high. The solvent used by Schwert was an aqueous solution consisting of 0.18 M NaCl plus 0.02 M NaCOOH. This solvent was accordingly tried in the present work and yielded a value of  $8.4 \times 10^{-7} \text{ cm}^2 \text{ s}^{-1}$  at a concentration of about 2% which decreased with decreasing concentration to yield approximately the same extrapolated value at infinite dilution as for the unbuffered solution. Measurements were not possible, however, at concentrations below  $7 \times 10^{-3} \text{ g/ml}$ . Although the sample exhibited a single peak by gel-filtration chromatography this does not necessarily indicate monodispersity and in fact the measured weight average molecular weight is about 10% higher than the accepted value. This would not itself affect the diffusion constant appreciably but, as has been shown above, the measured constant corresponds to a molecule somewhat larger than this. A low value is therefore to be expected. Thus a combination of the foregoing considerations is enough to account for the discrepancy with the earlier work and determination of the true diffusion constant must await Rayleigh linewidth measurements on a sample of high purity.

Physical measurements on bovine plasma albumin from the same source as that cited here have been made by many authors and the value of the diffusion constant agrees well both with authors using this technique<sup>3</sup> and conventional techniques<sup>10</sup>. Some denaturation on storing the sample in the dry state was observed however, the value of  $D$  falling to  $5.5 \times 10^{-7} \text{ cm}^2 \text{ s}^{-1}$  after six months although there was no dissymmetry of scatter or change

\* Average values of macromolecular parameters are sometimes defined using the molecular weight as the weighting function rather than the parameter itself. In this case equation (18) shows that  $D_z$  is obtained irrespective of the relationship between  $D$  and  $M$ .  $M_D$  is still given by equation (21) which applies only for a globular system.

of molecular weight. Measurements on bovine plasma albumin in distilled water yielded identical results to those in salt solution as did measurements in 0.2 M NaCl plus 0.02 M phosphate buffer (pH = 7).

In spite of the low purity of the sample the results for urease agree well with the early work of Sumner *et al.*<sup>11</sup>. This would be expected if the impurities made little contribution to the scattered intensity and the true globular protein possibly represents the largest particle present. Data obtained for a low purity sample, however, must always be suspect and the results presented here serve mainly to illustrate measurements on a molecule of this size.

The measurements presented in this paper have been made mainly on unbuffered solutions in the presence of NaCl and consequently the values of pH were not strictly controlled. A fuller investigation would have to include variation of the diffusion constant with pH together with a thorough investigation of any concentration dependence involved and its variation with the molarity of both salt and buffer.

### CONCLUSIONS

Light scattering Rayleigh linewidth measurements made upon solutions of three globular proteins representing a wide range of molecular weights by investigating the autocorrelation function of the fluctuations in scattered intensity, indicate the viability of the technique. Results agree well with theoretical predictions both as regards angular variation and shape of the autocorrelation function.

There is little concentration dependence of the diffusion

constants of these proteins: chymotrypsinogen, bovine plasma albumin and urease, when measured in unbuffered salt solutions, and the values are  $7.4 \pm 0.3 \times 10^{-7} \text{ cm}^2 \text{ s}^{-1}$ ,  $5.8 \pm 0.1 \times 10^{-7} \text{ cm}^2 \text{ s}^{-1}$  and  $3.4 \pm 0.1 \times 10^{-7} \text{ cm}^2 \text{ s}^{-1}$  respectively. Comparison with the work of other authors is complicated by the unknown polydispersities of the samples. Only for extreme polydispersity would the exponential shape of the autocorrelation function be altered and the results correspond to a molecule with molecular weight somewhat higher than the weight average. The results for bovine plasma albumin, however, agree well with those of other authors, who obtained their material from the same source.

### REFERENCES

- 1 Cummins, H. Z., Knable, N. and Yeh, Y. *Phys. Rev. Lett.* 1964, **12**, 150
- 2 Dubin, S. B., Lunacek, J. H. and Benedek, G. B. *Proc. Nat. Acad. Sci. US* 1967, **67**, 1164
- 3 Foord, R., Jakeman, E., Oliver, C. J. *et al. Nature* 1970, **227**, 242
- 4 Ford, N. C., Karasz, F. E. and Owen, J. E. M. *Discuss. Faraday Soc.* 1970, **49**, 228
- 5 French, M. J., Angus, J. C. and Walton, A. G. *Science* 1969, **163**, 345
- 6 Pecora, R. *Discuss. Faraday Soc.* 1970, **49**, 222 and references cited therein
- 7 Rimai, L., Hickmott, J. T., Cole, T. and Carew, E. B. *Biophys. J.* 1970, **10**, 20
- 8 Sellen, D. B. *Polymer* 1970, **11**, 374
- 9 Schwert, G. W. *J. Biol. Chem.* 1951, **190**, 799
- 10 Wagner, M. L. and Scheraga, H. A. *J. Phys. Chem.* 1956, **60**, 1066
- 11 Sumner, J. B., Gralen, N. and Eriksson-Quensel, I-B. *J. Biol. Chem.* 1938, **125**, 37

# Highly active catalysts for ethylene polymerization by the reduction of $\text{TiCl}_4$ with organomagnesium compounds

R. N. Haward\*, A. N. Roper and K. L. Fletcher

Carrington Plastics Laboratory, Shell Research Ltd, Urmston, Manchester M31 4AJ, UK  
(Received 19 March 1973)

The effect of introducing metal halides other than  $\text{AlCl}_3$  into a  $\text{TiCl}_3$  catalyst, by the reduction of  $\text{TiCl}_4$  with various metal alkyls is examined. Magnesium halides are shown to be most effective in increasing catalyst activity for the polymerization of ethylene. The influence of the type of organomagnesium compound on catalyst activity is studied, together with the effect of reaction conditions in the reduction step. The composition and structure of the catalysts is discussed. The results show conclusively that the activity of a  $\text{TiCl}_3$  catalyst in the Ziegler polymerization of ethylene is strongly affected by the presence of other metal compounds.

## INTRODUCTION

The factors which control the activity of catalysts in the heterogeneous Ziegler polymerization of ethylene are of great scientific and technical interest both on their own account and as part of the more general problem of heterogeneous catalysis. Much is known about the performance of Ziegler catalysts, but among the very extensive literature there is more information available concerning the factors affecting the performance of particular transition compound preparations than is available concerning the factors responsible for the activity of different types of catalyst. Further, in the case of ethylene, which is the monomer studied here, there is also a problem of gas/liquid mass transfer which makes it extremely difficult to determine the true activity of the most active catalysts. From the technical and commercial viewpoint, the development of more active catalysts makes it possible to prepare polymers having a high purity, without the use of additional purification processes. For this purpose a yield of 20 000 g polymer/g  $\text{TiCl}_3$  is desirable and this value is not easily reached with the conventional type of Ziegler catalyst in which  $\text{TiCl}_4$  is reduced with aluminium alkyls or alkyl halides<sup>1</sup>.

Recently a number of publications have indicated some of the factors which influence the activity of the preferred type of Ziegler catalyst for ethylene polymerization, i.e. a catalyst in which a solid particle containing or consisting of  $\text{TiCl}_3$  is activated by an aluminium alkyl.

In the first place it is clear that the catalysts prepared in this manner are not pure, and that the  $\text{TiCl}_3$  crystals actually have a composition better represented as

$\text{Ti}[\text{Cl}]_3 \cdot n[\text{AlCl}_3]$  where  $n \sim 0.3^1$ . However, the  $\text{AlCl}_3$  appears to be incorporated in a single crystalline phase together with  $\alpha$ ,  $\beta$ ,  $\gamma$  or  $\delta$   $\text{TiCl}_3$  and cannot be detected by X-ray diffraction or easily removed by sublimation<sup>2</sup>. There is no doubt that the activity of these catalysts is enhanced by the presence of the  $\text{AlCl}_3$ <sup>3,4</sup>. Claims have been made in the patent literature that activity, the stereospecificity for poly( $\alpha$ -olefins), and polymer molecular weight can all be controlled by using mixed crystals of  $\text{TiCl}_3$  and other metal halides<sup>5</sup>. The influence of different metal halides can also be made plausible qualitatively according to molecular-orbital theory, as a result of the fact that the active titanium surface ions are conditioned by their near-neighbour chloride ions and that a very subtle balance is necessary to make this titanium suitable for the different steps in one incorporation step of the olefin. One can visualize, therefore, that the conditioning by the surrounding chloride ions can be modified by replacing the next nearest neighbour titanium ions by aluminium ions<sup>6</sup>. Most commercial catalysts have, however, for some time been formulated to provide a near optimum composition in these respects.

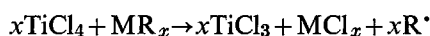
However, it has also been clear that catalyst activity has by no means reached a fundamental limit, since it has also been found that conventional  $\text{TiCl}_3$  catalysts can show a very high activity over short periods when employed with aluminium triethyl as a co-catalyst<sup>7</sup>, although these high rates soon decay to a much lower value (Figure 1). This decay has been ascribed to the further reduction of  $\text{TiCl}_3$  to  $\text{TiCl}_2$  by the aluminium alkyl<sup>8</sup>. Another possible explanation is that the co-crystallized  $\text{AlCl}_3$  is converted into  $\text{Al}(\text{C}_2\text{H}_5)\text{Cl}_2$  which is reported to inhibit polymerization<sup>9</sup>. Whatever the chemical reasons for the decay, the existence of these

\* Present address: Department of Chemistry, University of Birmingham, PO Box 363, Edgbaston, Birmingham B15 2TT, UK.

high activities shows that there is no fundamental physical limitation that forbids greater activity.

More recently a further discovery has shown that the activity of  $\text{TiCl}_3$  can be greatly increased by supporting it on a metal halide or oxyhalide support<sup>10</sup>. The preferred compound here is  $\text{Mg}(\text{OH})\text{Cl}$  and in this way the titanium atoms become highly activated. These developments also pointed to the possible significance of magnesium compounds in Ziegler catalysis.

One method of introducing a second metal halide would be to ball-mill the halide with pure  $\alpha\text{-TiCl}_3$ . In this work we preferred the alternative method of reducing  $\text{TiCl}_4$  with the appropriate different metal alkyl although it is more restricted in its scope. The equation



expresses the overall reaction taking place in this process.

## EXPERIMENTAL

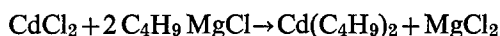
Stringent precautions were taken at all stages to reduce the amounts of oxygen and water to less than 2 ppm in all reagents used. Glass equipment was oven dried at 120°C and then assembled hot with pure dry nitrogen as purge gas. Gases (ethylene, hydrogen and nitrogen) were passed through columns of Linde 4A molecular sieves and  $\text{MnO}$ . Solvents were distilled under pure dry nitrogen from high surface sodium (deposited on  $\text{Na}_2\text{CO}_3$ ).

Reference will be made frequently to the use of SBPA as solvent. This is a commercial solvent containing mainly aliphatic hydrocarbons, of which we used a fraction with the boiling range 105–117°C.

### Metal alkyls

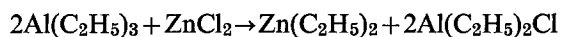
$\text{Li}(\text{n-C}_4\text{H}_9)$  was made by reacting  $\text{n-BuCl}$  with lithium 'sand' in SBPA suspension. Reaction was incomplete, but the unreacted butyl chloride was not removed before the alkyl solution was used.

$\text{Cd}(\text{n-C}_4\text{H}_9)_2$  was made by reacting anhydrous  $\text{CdCl}_2$  with  $\text{n-C}_4\text{H}_9\text{MgCl}$  in tetrahydrofuran (THF)<sup>11</sup>:



The THF was distilled off and replaced by benzene as the reaction proceeded to give finally a solution of the Cd alkyl in the latter solvent. The  $\text{MgCl}_2$  was removed by filtration.

$\text{Zn}(\text{C}_2\text{H}_5)_2$  was made by reacting aluminium triethyl and anhydrous zinc chloride:



The zinc and aluminium alkyls were separated by fractional distillation.

Methods used to obtain hydrocarbon solutions of magnesium alkyls were essentially those described by Bryce-Smith and Cox<sup>12</sup>. A small quantity of the neat alkyl halide was heated with predried Mg powder under nitrogen to initiate reaction. The remaining alkyl halide, in total 90% of theoretical, was then added either neat or as a solution in toluene, SBPA or isooctane. The latter method was preferred, refluxing of the solvent being used to control the temperature. If initiation was difficult the initial addition of 5% M (on total alkyl halide) isopropanol was usually effective.

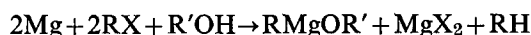
The products obtained were typically viscous grey slurries containing unreacted magnesium, magnesium halide and magnesium alkyl, the latter mainly present as a solid. Repeated hot extraction with fresh solvent followed by decantation or filtration was employed to recover the active material in solution. This was a difficult process owing to the generally low solubility of the magnesium alkyl and the high viscosity of the solution and slurry.

By solvating a magnesium alkyl with a suitable ether or amine, its solubility in hydrocarbons is increased very markedly. The ether or amine was added, at a 1:1 or 2:1 molar ratio on alkyl halide, to the solution of the latter before reaction with the magnesium. The product was a low viscosity solution from which magnesium halide and unreacted Mg could easily be filtered.

Alkyl magnesium alkoxides are also quite soluble in hydrocarbons. These were prepared either by reacting the appropriate alcohol with an alkyl magnesium halide slurry in hydrocarbon, made as above, or by direct reaction of alcohol and alkyl halide with magnesium<sup>13–15</sup>:



or



Alkyl solutions were analysed for active (C–Mg) content by hydrolysis with excess standard HCl and back titration with NaOH. The (Mg–X) content was determined by Volhard's method for halogens. The non-solvated alkyls usually had high (C–Mg)/(Mg–X) ratios, i.e. disproportionation to dialkyl was appreciable. Their structure is therefore uncertain, but for convenience they will be referred to as the appropriate 'alkyl magnesium halide'.

$\text{Al}(\text{C}_2\text{H}_5)_2\text{Cl}$  and  $\text{Al}(\text{C}_2\text{H}_5)_3$  were obtained from Shell Chemicals (UK) Limited.  $\text{Al}(\text{C}_{11}\text{H}_{23})_3$  was made by reacting the olefin with  $\text{Al}(\text{C}_2\text{H}_5)_3$ .  $\text{Al}(\text{C}_8\text{H}_{17})_3$  was obtained from Schering AG (West Germany).

### Reduction of $\text{TiCl}_4$

A standardized procedure was adopted, the reduction being done in a 250 ml cylindrical flat-bottomed vessel, fitted with a stainless-steel turbine and vertical baffles. 100 cm<sup>3</sup> of a solution containing 30 mmol (C–Mg) were placed in the reactor which was then immersed in a bath at the desired temperature. The  $\text{TiCl}_4$ , as a molar solution, was added to the vigorously agitated alkyl over 20–30 min from a dropping funnel. The whole system was blanketed with pure dry nitrogen. After completion of the reduction the catalyst slurry was analysed for di- and tri-valent Ti content. The method used employs oxidation of the Ti to  $\text{Ti}^{4+}$  with  $\text{H}_2\text{SO}_4$  and a ferric salt under controlled conditions, followed by determination of the liberated  $\text{Fe}^{2+}$  with ceric sulphate<sup>16</sup>.

### Determination of catalyst activity

The activity of the catalysts was determined by using a standard ethylene polymerization procedure which gave a reasonable measure of relative activity although it was not fully quantitative (see below). Polymerization was carried out at atmospheric pressure under the following conditions. Volume of solvent (SBPA or

iso-octane), 3 litres; concentration of  $\text{TiCl}_3$ , 0.10 mmol/l; concentration of alkyl cocatalyst, 1.0 mmol/l; temperature, 80°C; ethylene input rate, 100 l/h; hydrogen (chain transfer agent) input rate, 100 l/h; polymerization time, 3 h.

The equipment used was a 5 litre flask fitted with a gas inlet dip leg, agitator, reflux condenser and thermometer pocket. The flask was immersed in a thermostated water bath. Gas inlet rates were measured using calibrated rotameters and the total outlet gas with a wet gas meter. The solvent was saturated with the ethylene/hydrogen mixture at reaction temperature before adding first the cocatalyst and then the catalyst. After 3 h, polymerization was stopped by addition of a small amount of water. The solvent was removed by steam distillation and the polymer was dried in an oven and weighed.

The average specific polymerization rate (*ASPR*) was calculated as the g polymer per g  $\text{TiCl}_3$  per hour per bar ethylene pressure.

The intrinsic viscosity (decalin 120°C) was either determined directly or derived from the melt index using a relationship previously found experimentally<sup>17</sup>. The melt index was determined using ISO R 292 (Method A).

## RESULTS AND DISCUSSION

### Comparison of metal halides as promoters of the catalytic activity of $\text{TiCl}_3$

$\text{TiCl}_4$  was reduced to  $\text{TiCl}_3$  using the following metal alkyls or alkyl halides:  $\text{Al}(\text{C}_2\text{H}_5)_2\text{Cl}$ ;  $\text{LiC}_4\text{H}_9$ ;  $\text{Cd}(\text{C}_4\text{H}_9)_2$ ;  $\text{Zn}(\text{C}_2\text{H}_5)_2$ ;  $\text{MgC}_4\text{H}_9\text{Br}$  (exact composition uncertain). In all cases a purely hydrocarbon system was employed; the Al, Li and Zn alkyls were used in SBPA solution, the Cd alkyl in benzene solution and the Mg alkyl as a slurry in SBPA. The  $\text{TiCl}_4$  was dissolved in SBPA in each case. A 1:1 molar ratio of alkyl to  $\text{TiCl}_4$  was employed and the reductions were carried out at low temperatures: 0°C in the case of the Mg alkyl, -30°C with  $\text{Al}(\text{C}_2\text{H}_5)_2\text{Cl}$  and -60°C with the other alkyls. The dark brown precipitates obtained were in each case washed several times with SBPA before use. The  $\text{Al}(\text{C}_2\text{H}_5)_2\text{Cl}$  reduced catalyst was also heated at 160°C for 2 hours to convert it into the  $\gamma$ -form, but the others were not given this heat treatment.

Using the standard polymerization conditions described in the experimental section, the activity of each catalyst for ethylene polymerization was determined. The results obtained are compared in Table 1.

Longer chain aluminium trialkyls, i.e.  $\text{Al}(\text{C}_8\text{H}_{17})_3$  and  $\text{Al}(\text{C}_{11}\text{H}_{23})_3$  were used as co-catalysts in some of these tests and gave higher average activities than did either  $\text{Al}(\text{C}_2\text{H}_5)_3$  or  $\text{Al}(\text{C}_2\text{H}_5)_2\text{Cl}$ . The influence of co-catalyst chain length is shown in Figure 1 for a series of polymerizations using an  $\text{Al}(\text{C}_2\text{H}_5)_2\text{Cl}$  reduced catalyst. The ethylene absorption rate is lower initially but decays less rapidly as chain length is increased. Above  $\text{C}_{11}$ , however, the maximum rate obtained begins to decrease; thus the highest average rates are obtained with  $\text{Al}(\text{iC}_4\text{H}_9)_3$ ,  $\text{Al}(\text{C}_8\text{H}_{17})_3$  and  $\text{Al}(\text{C}_{11}\text{H}_{23})_3$ .

The catalysts made by reduction with Al, Li or Cd alkyls all have very similar activities. The  $\text{Zn}(\text{C}_2\text{H}_5)_2$  reduced catalyst is less active. The  $\text{Mg}(\text{C}_4\text{H}_9)\text{Br}$  reduced catalyst is, however, at least three times more active

Table 1 Comparison of metal alkyls as reducing agents for  $\text{TiCl}_4$

Alkyl used to reduce $\text{TiCl}_4$	Activity test		$[\eta]_{\text{decalin}}^{120^\circ\text{C}}$ (dl/g)
	Alkyl co-catalyst	<i>ASPR</i> *	
$\text{Al}(\text{C}_2\text{H}_5)_2\text{Cl}$	$\text{Al}(\text{C}_2\text{H}_5)_2\text{Cl}$	330	2.24
	$\text{Al}(\text{C}_2\text{H}_5)_3$	376	1.86
	$\text{Al}(\text{C}_8\text{H}_{17})_3$	580	2.28
	$\text{Al}(\text{C}_{11}\text{H}_{23})_3$	730	2.44
$\text{LiC}_4\text{H}_9$	$\text{Al}(\text{C}_2\text{H}_5)_2\text{Cl}$	250	3.89
	$\text{Al}(\text{C}_{11}\text{H}_{17})_3$	760	2.15
$\text{Cd}(\text{C}_4\text{H}_9)_2$	$\text{Al}(\text{C}_8\text{H}_{17})_3$	700	2.55
	$\text{Al}(\text{C}_2\text{H}_5)_3$	negligible	—
$\text{Zn}(\text{C}_2\text{H}_5)_2$	$\text{Al}(\text{C}_{11}\text{H}_{23})_3$	460	1.90
	$\text{Al}(\text{C}_2\text{H}_5)_2\text{Cl}$	870	n.d.
	$\text{Al}(\text{C}_2\text{H}_5)_3$	750	2.12
	$\text{Al}(\text{C}_8\text{H}_{17})_3$	2040	2.72
$\text{Mg}(\text{C}_4\text{H}_9)\text{Br}$	$\text{Al}(\text{C}_{11}\text{H}_{23})_3$	2200	4.50

\* *ASPR* = average specific polymerization rate [g polymer g<sup>-1</sup>  $\text{TiCl}_3$  h<sup>-1</sup> bar<sup>-1</sup> (C<sub>2</sub>H<sub>4</sub>)]

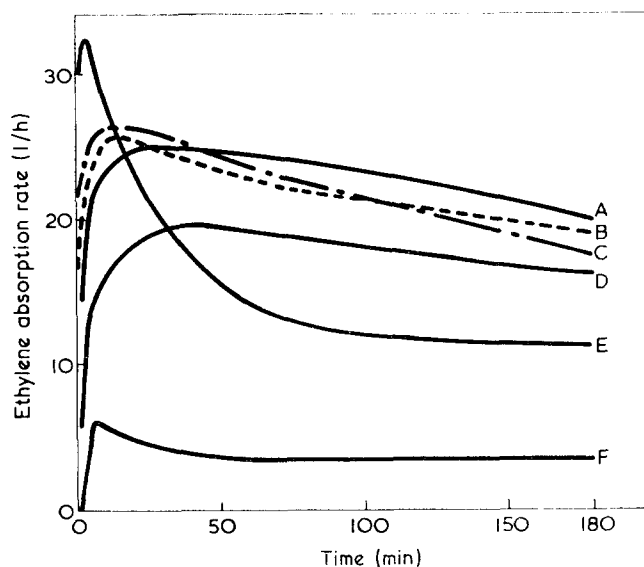


Figure 1 Effect of trialkyl co-catalyst on polymerization of ethylene. Catalyst:  $\text{TiCl}_3$  made by reduction of  $\text{TiCl}_4$  with  $\text{Al}(\text{C}_2\text{H}_5)_2\text{Cl}$ . A,  $\text{Al}(\text{C}_{11}\text{H}_{23})_3$ ; B,  $\text{Al}(\text{iBu})_3$ ; C,  $\text{Al}(\text{nOctyl})_3$ ; D,  $\text{Al}(\text{C}_{14}\text{H}_{29})_3$ ; E,  $\text{Al}(\text{C}_2\text{H}_5)_3$ ; F,  $\text{Al}(\text{C}_{18}\text{H}_{37})_3$

than that made using the Al alkyl. In view of the marked increase found with the Mg alkyl, further work was concentrated in this area.

### Reduction of $\text{TiCl}_4$ with organomagnesium compounds

Mg alkyl or aryl halides (Grignard reagents) are usually made in an ether, in which they are, as a rule, completely soluble. Reduction of  $\text{TiCl}_4$  by butyl magnesium chloride in diethyl ether solution does not, however, give an active catalyst. Hence the use of a purely hydrocarbon system, in which the alkyl magnesium halide is not very soluble, for the experiments already described. The hydrocarbon slurries are, however, very difficult to handle and contain variable quantities of magnesium halide and unreacted Mg and efforts were devoted to obtaining alkyl solutions free from these impurities.

*Non-solvated Mg alkyl or aryl halides*<sup>18</sup>. Short chain Mg alkyl halides are only slightly soluble in aliphatic hydrocarbons and the chlorides are less soluble than the bromides. Longer chain alkyls have, however,

Table 2 Catalysts made with non-solvated magnesium alkyl/aryl halides

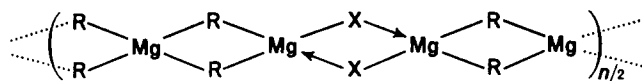
Catalyst preparation				Activity test		$[\eta]_{\text{decalin}}^{120^\circ\text{C}}$ (dl/g)	
Reduction temp. ( $^\circ\text{C}$ )	Reducing alkyl*	Solvent medium	Form used	Alkyl co-catalyst	ASPR		
0	$\text{MgC}_{12}\text{H}_{25}\text{Br}$	SBPA	Slurry	$\text{Al}(\text{C}_{11}\text{H}_{23})_3$	3040	3.46	
-60			Solution	$\text{Al}(\text{C}_8\text{H}_{17})_3$	2340	1.39	
		Toluene		$\text{Al}(\text{C}_{11}\text{H}_{23})_3$	2940	1.40	
				$\text{Al}(\text{C}_8\text{H}_{17})_3$	3710	1.31	
			$\text{Al}(\text{C}_{11}\text{H}_{23})_3$	3770	1.82		
0	$\text{MgC}_4\text{H}_9\text{Br}$	SBPA	Slurry	$\text{Al}(\text{C}_8\text{H}_{17})_3$	2040	2.72	
-60			Solution		2400	1.56	
	$\text{MgC}_4\text{H}_9\text{Cl}$	Toluene			2030	1.63	
-60		SBPA	Slurry	$\text{Al}(\text{C}_8\text{H}_{17})_3$	900	2.59	
	$\text{MgC}_4\text{H}_9\text{I}$	Toluene			2240	1.54	
-30		SBPA	Solution	$\text{Al}(\text{C}_8\text{H}_{17})_3$	2330	2.48	
	$\text{MgC}_6\text{H}_5\text{Cl}$	C <sub>6</sub> H <sub>5</sub> Cl	Toluene		2060	2.61	
-60			C <sub>6</sub> H <sub>5</sub> Br	Slurry	$\text{Al}(\text{C}_8\text{H}_{17})_3$	2470	1.65
				Solution		2230	1.33
					2480	1.27	

\* Ratio of [C-Mg]:TiCl<sub>4</sub> used=2:1

higher solubility and using dodecyl bromide, solutions containing 500–600 mmol/l of active material were obtained in toluene, SBPA or iso-octane. The composition of the alkyl was found to be nearer to that of Mg didodecyl than that of Mg dodecyl bromide, i.e. the Schlenk equilibrium:



had been shifted very much to the dialkyl in the absence of an ether. The ratio of C-Mg to Mg-Br found was 7–10:1. Bryce-Smith and Cox<sup>12</sup> have suggested linearly associated bridge bonded structures of the type:



for these compounds of intermediate composition, association being the reason for the observed high viscosity of the solutions.

In Table 2 the activity of catalysts made using slurries and solutions of ' $\text{MgC}_{12}\text{H}_{25}\text{Br}$ ' and ' $\text{MgC}_4\text{H}_9\text{Br}$ ' are compared. (These simple formulae, although not expressing the true compositions will be used for convenience.) Activities are all high but polymers obtained using catalysts made with alkyl solutions have a lower intrinsic viscosity (molecular weight). Thus less hydrogen will be required with these catalysts to obtain a given molecular weight polymer.

The bromides and iodides are more soluble than the chlorides, but the catalyst activities obtained with the different Mg butyl halides are generally very similar (Table 2).

Phenyl magnesium chloride and bromide can be made using a large excess of the phenyl halide as solvent, although their solubility is low. Reduction of TiCl<sub>4</sub> with these compounds produced catalysts of similar high activity to that obtained with the Mg alkyl halides (Table 2). The excess phenyl halide was removed from the TiCl<sub>3</sub> slurries by repeated washing with SBPA before use in polymerization.

*Solvated Mg alkyl halides*<sup>19</sup>. The hydrocarbon solubility of Mg alkyl halides can be greatly increased by solvation with an ether or a tertiary amine. Mg butyl

Table 3 Catalysts made with solvated magnesium butyl chloride

Catalyst preparation <sup>a b</sup>		Activity test <sup>c</sup> ASPR	$[\eta]_{\text{decalin}}^{120^\circ\text{C}}$ (dl/g)
Solvating agent	Post-reduction treatment		
Diethyl ether	None	2450	1.98
	Washed	2070	1.90
Di-n-butyl ether	None	2500	1.69
	Washed	2400	1.66
Tetrahydrofuran	None	3090	1.94
	Washed	2690	1.75
Triethylamine	None	580	2.43
	Washed	1260	2.15
Tri n-butylamine	Washed	1640	2.01
Pyridine	None	2020	1.66
	Washed	1450	1.82

a Ratio  $\text{MgC}_4\text{H}_9\text{Cl}:\text{TiCl}_4=2:1$ 

b Solvent SBPA

c Alkyl co-catalyst  $\text{Al}(\text{C}_8\text{H}_{17})_3$ All catalysts made at  $-60^\circ\text{C}$ 

chloride was obtained as a molar solution in SBPA by carrying out the preparation in the presence of n-butyl ether at a 1:1 molar ratio on the butyl chloride. No disproportionation occurred and the [C-Mg]:[Mg-Cl] ratio in the product was 1:1. Similar results were obtained with other ethers and tertiary amines and the activities of the catalysts made using these solutions are compared in Table 3. Generally speaking, the ether-solvated alkyls gave catalysts of equal activity to those derived from unsolvated alkyls; slightly lower activities were obtained when tertiary amines were used. Washing the catalyst before use to remove any free ether or amine tended to reduce the activity rather than increase it. In fact, higher concentrations of ethers could be tolerated without significant loss in activity, as is shown by the results in Table 4. Activity did not begin to fall until more than a 3:1 ratio of ether: $\text{C}_4\text{H}_9\text{Cl}$  had been used in making the alkyl solution.

*Alkyl magnesium alkoxides*<sup>20</sup>. Butyl and dodecyl magnesium isopropoxides were made as described in the experimental section and found to be quite soluble in SBPA or toluene. These compounds reduced TiCl<sub>4</sub> to highly active catalysts similar in performance to those



given by the Mg alkyl halides. Results are given in Table 5.

*Influence of reduction conditions.* Most of the catalysts described were made at  $-60^{\circ}\text{C}$ ; where temperatures of  $-30^{\circ}$  and  $0^{\circ}\text{C}$  were used, this was because high viscosity or solidification of the alkyl solution prevented the use of the lower temperature. In fact, temperature of reduction was not found to have a great influence on catalyst activity between  $-60^{\circ}$  and  $0^{\circ}\text{C}$ .

A 2:1 molar ratio of alkyl to  $\text{TiCl}_4$  or more precisely of  $[\text{C-Mg}]$  to  $\text{TiCl}_4$  was used as standard, although theoretically a 1:1 ratio should suffice. The reason was that incomplete reduction occurred sometimes in the initial work with slurries when a 1:1 ratio was used. This may well have been due to inaccuracies in the determination of the

$[\text{C-Mg}]$  concentration in the slurries. More precise work showed in fact that higher activities could be obtained at a 1:1 ratio. This is illustrated by the results in Table 6, obtained with solvated and unsolvated alkyls. In the latter case no definite effect was shown under the standard polymerization conditions using  $0.1 \text{ mmol TiCl}_3/\text{l}$ . When, however, the  $\text{TiCl}_3$  catalyst concentration was reduced to  $0.02 \text{ mmol/l}$  not only was there a marked decrease above a ratio of 1.5:1 but much higher average specific polymerization rates (ASPR) were obtained. This effect of catalyst concentration, which is related to the limited rate of mass transfer of ethylene between gas and liquid phases, will be discussed in more detail below.

As the ratio of reducing alkyl to  $\text{TiCl}_4$  was increased there was, not surprisingly, an increase in the divalent Ti content of the catalysts obtained, but even with a  $\text{Ti}^{2+}$  content of 40% the catalyst was highly active. The intrinsic viscosity, which is a measure of the molecular weight, was affected by the increasing alkyl to  $\text{TiCl}_4$  ratio but in directly opposing fashion for the two types; it increased with the solvated alkyl and decreased with the unsolvated alkyl. Ethers have been observed in earlier unpublished work to increase molecular weight when added to a  $\gamma\text{-TiCl}_3$  catalyst system.

*Catalyst composition and structure.* A number of catalysts were analysed to determine their composition. From the amounts of Ti, Mg, Cl and Br found the following empirical formulae were calculated, assuming that Mg was divalent in every case.

(a) Two catalysts made by reduction of  $\text{TiCl}_4$  with  $\text{MgC}_{12}\text{H}_{25}\text{Br}$  (toluene solution;  $[\text{C-Mg}]:[\text{Mg-Br}]=5.0:1$ )

Table 4 Effect of ether:alkyl halide ratio on catalyst activity

Catalyst preparation <sup>a</sup>			
Molar ratio ether:alkyl halide	Post-reduction treatment	Activity test <sup>b</sup> ASPR	$[\eta]_{\text{decalin}}^{120^{\circ}\text{C}}$ (dl/g)
1.1	None	2500	1.69
	Washed	2400	1.66
2.1	None	2350	1.98
	Washed	2550	1.77
3.1	None	3060	2.13
	Washed	2940	1.71
6.1	None	200	n.d.
	Washed	980	3.04

<sup>a</sup> Ether:  $n\text{-(C}_4\text{H}_9)_2\text{O}$ ; alkyl halide:  $\text{MgC}_4\text{H}_9\text{Cl}$ ; solvent: SBPA; molar ratio  $\text{MgC}_4\text{H}_9\text{Cl}:\text{TiCl}_4=2:1$ ; reduction temperature:  $-60^{\circ}\text{C}$

<sup>b</sup> Alkyl co-catalyst  $\text{Al(C}_8\text{H}_{17})_3$

Table 5 Catalysts made with alkyl magnesium alkoxides

Catalyst preparation			Activity test		
Reduction temp. ( $^{\circ}\text{C}$ )	Reducing alkyl*	Solvent	Alkyl co-catalyst	ASPR	$[\eta]_{\text{decalin}}^{120^{\circ}\text{C}}$ (dl/g)
$-60$	$\text{C}_4\text{H}_9\text{MgOC}_3\text{H}_7$	SBPA	$\text{Al(C}_8\text{H}_{17})_3$	2930	1.66
			$\text{Al(C}_{11}\text{H}_{23})_3$	3040	1.74
			$\text{Al(C}_8\text{H}_{17})_3$	1460	1.74
$-30$	$\text{C}_{12}\text{H}_{25}\text{MgOC}_3\text{H}_7$	Toluene	$\text{Al(C}_{11}\text{H}_{23})_3$	3040	1.48
		SBPA	$\text{Al(C}_{11}\text{H}_{23})_3$	3040	1.48

\* Ratio  $[\text{C-Mg}]:\text{TiCl}_4=2:1$

Table 6 Effect of  $[\text{C-Mg}]:\text{TiCl}_4$  ratio on catalyst performance

Catalyst preparation				Activity test <sup>c</sup>			
Reducing alkyl <sup>a</sup>	$[\text{C-Mg}]/[\text{TiCl}_4]$	Solvent	$\text{Ti}^{2+}$ content of catalyst (wt.%)	$[\text{TiCl}_3]=0.10 \text{ mmol/l}$		$[\text{TiCl}_3]=0.02 \text{ mmol/l}$	
				ASPR	$[\eta]_{\text{decalin}}^{120^{\circ}\text{C}}$ (dl/g)	ASPR	$[\eta]_{\text{decalin}}^{120^{\circ}\text{C}}$ (dl/g)
$\text{MgC}_4\text{H}_9\text{Cl} \cdot (\text{C}_4\text{H}_9)_2\text{O}$	1.00	SBPA	2.0	3260	1.44	b	b
	1.50		10.0	2950	1.50	b	b
	2.00		18.0	2240	1.63	b	b
	3.00		25.0	1100	1.87	b	b
	3.00		25.0	1100	1.87	b	b
' $\text{MgC}_{12}\text{H}_{25}\text{Br}$ ' $[\text{C-Mg}]/[\text{Mg-Br}]=7.8$	1.00	Iso-octane	1.0	3070	2.13	5720	2.78
	1.25		16.0	2860	1.91	6240	2.40
	1.50		20.0	2560	1.69	6040	2.03
	1.75		28.0	3280	1.34	4500	2.08
	2.00		41.0	2950	1.62	3720	2.02

<sup>a</sup> Temperature of reduction  $-60^{\circ}\text{C}$

<sup>b</sup> Not tested under these conditions

<sup>c</sup> Alkyl co-catalyst  $\text{Al(C}_8\text{H}_{17})_3$

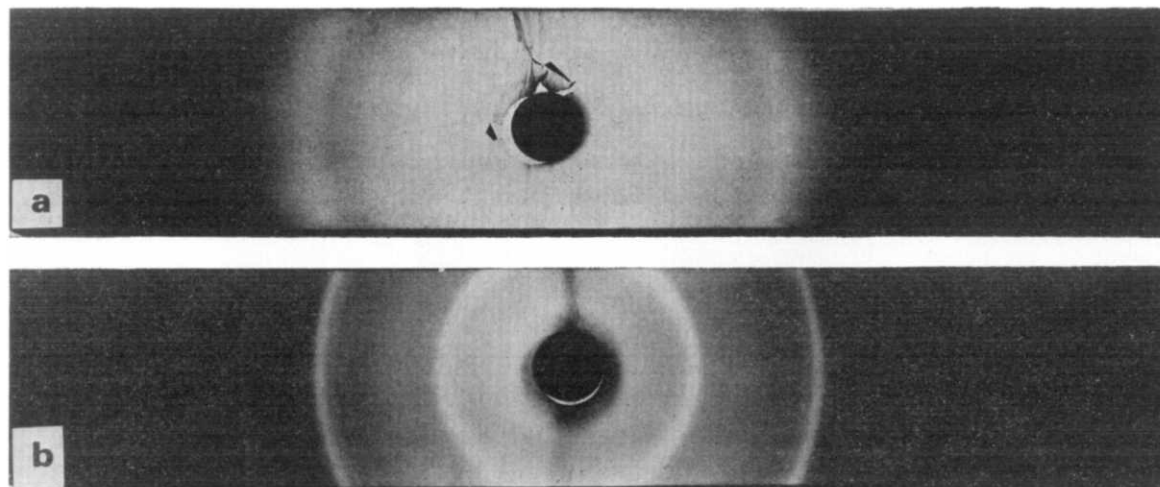
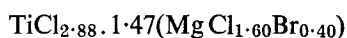
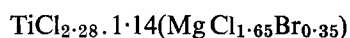


Figure 2 (a)  $\text{TiCl}_3$  made by reduction of  $\text{TiCl}_4$  with 'MgC<sub>12</sub>H<sub>25</sub>Br'; (b)  $\beta\text{-TiCl}_3$  made by reduction of  $\text{TiCl}_4$  with  $\text{Al}(\text{C}_2\text{H}_5)_2\text{Cl}$

at a 2:1 ratio of [C-Mg]:[TiCl<sub>4</sub>] had the following compositions:



If the alkyl composition is taken to be equivalent to  $2\text{Mg}(\text{C}_{12}\text{H}_{25})_2 + \text{MgC}_{12}\text{H}_{25}\text{Br}$  and only 75% of it is assumed to have reacted, the theoretical composition of the catalyst should be:



The actual amount of magnesium halide present is thus in each case considerably more than might be expected.

(b) A catalyst made by reduction of  $\text{TiCl}_4$  with  $\text{MgC}_4\text{H}_9\text{Cl} \cdot (\text{C}_4\text{H}_9)_2\text{O}$  at a 2:1 ratio of [C-Mg]:[TiCl<sub>4</sub>] had the composition:



In this case the composition is as expected if only 75% of the alkyl has reacted.

The actual amount of magnesium halide present in all three catalysts exceeds that of titanium halide. This is quite different from the case of aluminium alkyl reduced catalysts where less than 0.5:1 of  $\text{AlCl}_3:\text{TiCl}_x$  is found.

Many of the catalysts made were examined by X-ray diffraction. Figure 2 shows a typical example of the diffuse pattern obtained in comparison with the well defined  $\beta\text{-TiCl}_3$  structure of a catalyst made by reduction with  $\text{Al}(\text{C}_2\text{H}_5)_2\text{Cl}$  under similar conditions. (The activity of the latter catalyst for ethylene polymerization is essentially unchanged on conversion to  $\gamma\text{-TiCl}_3$  by heating to 160°C.) There are no identifiable lines which can be assigned either to  $\text{TiCl}_3$  or to  $\text{MgCl}_2$  in the picture given by the Mg alkyl reduced catalyst. The crystallite size must therefore be very small.

Transmission electron micrographs (Pt shadowed C replicas) were obtained of a number of catalysts. Figure 3 shows the very fine nodular structure revealed. The primary particle size is apparently less than 50 nm.

'Absolute' activity of the catalysts. The rate of ethylene polymerization during a standard polymerization test run of 3 h duration falls from an initial peak, decreasing at a rate which depends to some extent on the co-catalyst being used (see Figure 1). The decline is much faster

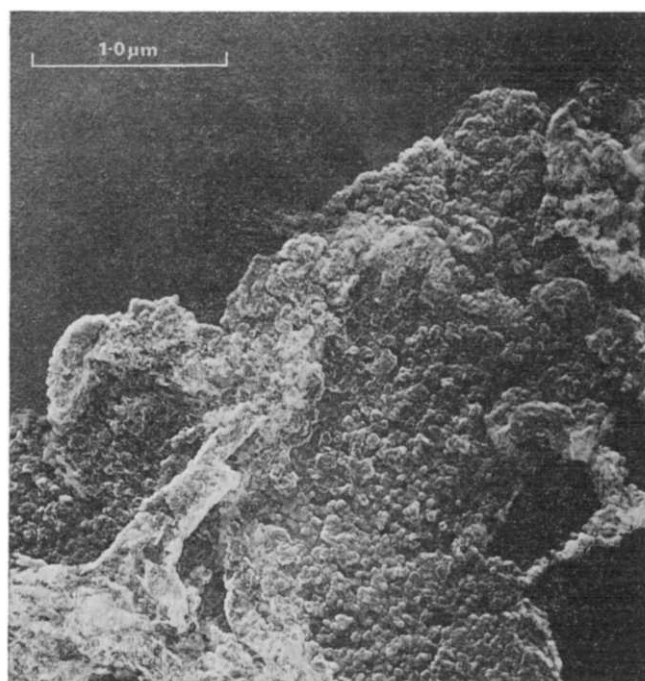


Figure 3 Electron micrograph of  $\text{TiCl}_3$  catalyst made by reduction of  $\text{TiCl}_4$  with 'MgC<sub>12</sub>H<sub>25</sub>Br' ( $\times 25\,000$ )

with  $\text{Al}(\text{C}_2\text{H}_5)_3$  than with  $\text{Al}(\text{C}_8\text{H}_{17})_3$  and in the former case the rate may fall to zero within 3 h. In addition to kinetic factors the rate of polymerization is also controlled by the purely physical process of mass transfer of ethylene from the gaseous to liquid phases<sup>21</sup>. At all practical catalyst concentrations the mass transfer effect is very significant and thus any calculated catalyst activity may be only an indication of the true activity if access to monomer were unrestricted. This mass transfer effect is shown quite clearly by the results already quoted above where a reduction in catalyst concentration from 0.10 to 0.02 mmol/l doubled the calculated specific activity.

To obtain some indication of the 'absolute' activity of these catalysts a series of polymerizations were carried out at progressively lower catalyst concentrations down to 0.005 mmol/l. All other conditions were held constant. By plotting the reciprocal of  $\text{C}_2\text{H}_4$  absorption rate against time for each experiment and extrapolating

back to zero time, figures for the rates in the absence of catalyst decay were obtained. An earlier theoretical consideration of the processes involved in polymerization under similar conditions led to the derivation of a linear correlation between the reciprocal rate of polymerization (equated to rate of absorption) and the reciprocal catalyst concentration<sup>21</sup>. This relationship had then been shown to be obeyed by a  $\gamma$ -TiCl<sub>3</sub> catalyst. In the present case too a linear relationship was found when the rates at zero time were used (Figure 4). The slope of the line gives the true kinetic rate of polymerization and the intercept the maximum rate of transfer of ethylene from gas to liquid under the experimental conditions employed. The values derived are: maximum transfer rate = 100 l/h; true maximum kinetic rate of polymerization = 36 200 g g<sup>-1</sup> TiCl<sub>3</sub> h<sup>-1</sup> bar<sup>-1</sup> (C<sub>2</sub>H<sub>4</sub>).

This rate is much higher than the average specific rate previously reported for two reasons: (1) maximum initial rates are of course higher than the average rate during a 3 hour polymerization; (2) the gas/liquid mass transfer effect.

These factors may be illustrated by noting that the average specific rates for a 3 hour polymerization are 6250 and 2510 g g<sup>-1</sup> h<sup>-1</sup> bar<sup>-1</sup> respectively with 0.02 and 0.10 mmol/l TiCl<sub>3</sub> concentrations. This indicates the influence of mass transfer. On the other hand, the maximum initial rate at 0.02 mmol/l is 21 900 g g<sup>-1</sup> h<sup>-1</sup> bar<sup>-1</sup> showing the difference due to the type of measurement. The fall in rate with time is somewhat greater than with the aluminium reduced catalyst shown in Figure 1.

In the light of these results it will be clear that the measurement of very high catalyst activities in ethylene polymerization is not at all easy. When working at concentrations of 0.01 mmol/l of TiCl<sub>3</sub> purity requirements clearly become more difficult to meet.\* On the other hand, straightforward polymerization experiments of the type described will give low activities for very active catalysts. It can, however, be confidently asserted that the activities reported here can readily be achieved and that more precise methods of evaluation will lead to higher results. From this practical point of view, however, the evaluation of catalyst activity over a period of time (e.g. 3 h) is desirable, since the achievement of momentary high rates is of little value.

**Catalyst structure and activity.** Two possible mechanisms whereby these very high catalyst activities are obtained may be considered. Either the intrinsic site activity is enhanced by the incorporation of magnesium halide into the crystal lattice or the number of active and potentially active sites is greatly increased. Both mechanisms could conceivably operate together.

The ionic radius of magnesium, 0.65 Å, is very close to that of titanium, 0.68 Å, in comparison with the 0.50 Å of aluminium. Magnesium halides also have a layer-lattice structure, although half the octahedral holes are occupied compared to one-third with  $\alpha/\gamma$ -TiCl<sub>3</sub> or AlCl<sub>3</sub>. Thus substitution of magnesium for titanium in the crystal lattice should readily occur. It should be noted, however, that under the experimental conditions used in this work, the TiCl<sub>3</sub> will be formed as the  $\beta$

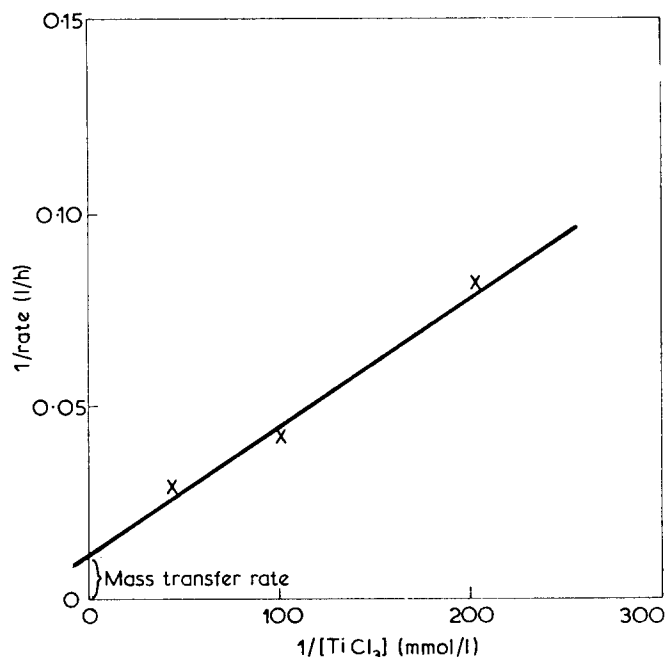


Figure 4 Determination of 'absolute' activity. Polymerization at 80°C; 50% hydrogen; iso-octane; C<sub>2</sub>H<sub>4</sub> partial pressure 0.224 bar; Al(C<sub>6</sub>H<sub>17</sub>)<sub>3</sub> co-catalyst. Catalyst made by reduction of TiCl<sub>4</sub> with MgC<sub>12</sub>H<sub>25</sub>Br; derived maximum transfer rate of C<sub>2</sub>H<sub>4</sub> from gas-liquid = 100 l/h

modification, which does not have a layer-lattice structure, and no heat treatment is given to convert it into the latter. Cocrystallization of magnesium halide and TiCl<sub>3</sub> might therefore be expected to lead to a very disordered structure more like a glass than a crystal, as is indicated by X-ray diffraction (Figure 2). Observations on large TiCl<sub>3</sub> crystals by a number of workers have shown that active sites occur on edges and at crystal defects (e.g. Rodriguez and van Looy<sup>22</sup>). As crystal size decreases the number of such sites will increase and activity has been shown to increase correspondingly<sup>23</sup>. Thus the very disordered structure of the present catalysts would be expected to lead to a high concentration of active sites and so to high catalyst activity.

On the other hand, effects due to magnesium atoms acting as promoters through the chlorine atoms as described by Cossee (personal communication) for the action of Al in AlCl<sub>3</sub>-promoted catalysts cannot be excluded. Actual measurements of the active site concentration would be required to clarify the situation. Simultaneous determinations of active site concentration and polymer yield could be used to resolve the question of a specific promoter effect on site activity due to the magnesium.

**Polymerization to high yield on catalyst.** So far only results obtained by polymerization at atmospheric pressure have been quoted, and the yields of polymer on catalyst in these experiments were relatively low. In order to obtain the higher yields which would be required commercially a number of polymerizations were carried out at a pressure of 7.9 bar (absolute) and the polymers examined in some detail. Results obtained are given in Table 7.

By adjustment of the amount of hydrogen used as modifier a full commercial range of molecular weights (melt indices between 0.02 and 10.0 dg/min) has been covered and the polymers are all non-corrosive and of

\* Comparison with more conventional types of Ziegler catalyst may be made with reference to Reich, L. and Schindler, A. 'Polymerisation by Organometallic Compounds', John Wiley, New York, 1966, Ch II. Experiments quoted are mainly in the range of 1-100 mmol Ti/l, i.e. 10-1000 times those employed here.

Table 7 Properties of polyethylenes made at high yield  
 Polymerization conditions: pressure, 7.9 bar (abs); temperature, 80°C; solvent, SBPA; co-catalyst,  $\text{Al}(\text{C}_8\text{H}_{17})_3$

Hydrogen used (%)	25 <sup>a</sup>	35 <sup>b</sup>	40 <sup>b</sup>	50 <sup>b</sup>	60 <sup>b</sup>
Polymer yield (g/g $\text{TiCl}_3$ )	75 000	40 000	32 000	27 000	17 000
Melt index (dg/min)	0.02	0.14	2.0	3.5	10.2
Intrinsic viscosity (decalin, 120°C) (dl/g)	4.50	3.00	1.71	1.52	1.22
Density (g/cm <sup>3</sup> )	n.d.	0.953	0.959	0.961	0.967
1% Secant modulus (MN/m <sup>2</sup> )	n.d.	$1.12 \times 10^3$	$1.15 \times 10^3$	$1.24 \times 10^3$	$1.33 \times 10^3$
Titanium content (calc.) (ppm)	4	7.5	10	12	18
Colour	n.d.	96	93	95	94
Corrosivity <sup>d</sup>	n.d.	6	3	n.d.	2

<sup>a</sup> Residence time 3 h

<sup>b</sup> Residence time 4 h

<sup>c</sup> Comparison with standard white surface rated 100

<sup>d</sup> Mild steel plates. Ratings below 7 classed as non-corrosive

excellent colour. This shows that the quantities of catalyst residues in the polymers are too low to have any harmful effect. Further the observation of a yield of 75 000 g/g  $\text{TiCl}_3$  shows that the catalyst can continue to be active even when it is associated with very high proportions of polymer, without prohibitive physical blocking of the polymerization sites.

## CONCLUSIONS

Highly active Ziegler-Natta catalysts can be made by reducing  $\text{TiCl}_4$  with organomagnesium compounds<sup>18</sup>. They contain appreciable amounts of magnesium halide and are much more active in the polymerization of ethylene than the well known forms of  $\text{TiCl}_3$  made by reduction of  $\text{TiCl}_4$  with aluminium alkyls and which contain  $\text{AlCl}_3$ . The primary crystal size is apparently very small in these new catalysts. The high activity may, therefore, be due to the increased number of active sites available as a result, rather than to any chemical activation of the site.

By the use of these catalysts it is possible to obtain polyethylene at yields which are high enough to eliminate any necessity for removal of catalyst residues.

## ACKNOWLEDGEMENTS

Thanks are due to R. J. Bird (Thornton Research Centre) for the electron microscopy and to G. T. Chamberlain for chemical analyses and X-ray diffraction work. The detailed experimental work was carried out by G. A. Brown, Mrs M. J. Hamilton, T. E. Moss, A. J. Nummelin, M. R. M. Swingle and E. A. Wilson, whose efforts are gratefully acknowledged. The authors are

indebted to Shell Research Limited, for permission to publish.

## REFERENCES

- Natta, G., Corradini, P. and Allegra, G. *J. Polym. Sci.* 1961, **51**, 399
- Tornquist, E. G. M., Richardson, J. T., Wilchinsky, Z. W. and Looney, R. W. *J. Catal.* 1967, **8**, 189
- Chem. Eng. News* 1967 (29 May) p 42
- Tornquist, E. G. M. *Ann. N.Y. Acad. Sci.* 1969, **155** (2), 447
- Br. Pat. 872 142
- Cossee, P. (personal communication)
- Berger, M. N., Boocock, G. and Haward, R. N. *Adv. Catalysis* 1969, **19**, 211
- Ambroz, J., Osecky, P., Mejzlik, J. and Hamrick, O. *J. Polym. Sci. (C)* 1967, **6**, 423
- Caunt, A. D. *J. Polym. Sci. (C)* 1963, **4**, 49
- Solvay et Cie, Fr. Pat. 1 375 127
- Cason, J. and Prout, F. S. *J. Am. Chem. Soc.* 1944, **66**, 46
- Bryce-Smith, D. and Cox, G. F. *J. Chem. Soc.* 1961, p 1175
- Bryce-Smith, D. and Blues, E. T. *Chem. Ind.* 1960, p 1533
- Bryce-Smith, D. and Wakefield, B. J. *Proc. Chem. Soc.* 1963, p 376
- Bryce-Smith, D. and Graham, I. F. *Chem. Commun.* 1966, p 559
- Martin, H. and Stedefeder, J. *Ann. Chem.* 1958, **618**, 17
- Williamson, G. R., Wright, B. and Haward, R. N. *J. Appl. Chem.* 1964, **14**, 13
- Shell Int. Res. Mij., OLS 2 003 075 (German Pat.); Br. Pat. 1 299 862
- Shell Int. Res. Mij., OLS 2 116 045 (German Pat.)
- Shell Int. Res. Mij., OLS 2 024 558 (German Pat.)
- Haward, R. N. and Boocock, G. 'The Chemistry of Polymerisation Processes', SCI Monograph No. 20, Society of Chemical Industry, 1966, p 3
- Rodriguez, L. A. M. and van Looy, H. M. *J. Polym. Sci. (A-1)* 1966, **4**, 1971
- Schnecko, H., Dost, W. and Kern, W. *Makromol. Chem.* 1969, **121**, 159

# Morphology and structure of poly(ethylene-co-carbon monoxide) single crystals

G. C. Alfonso, L. Fiorina, E. Martuscelli\*, E. Pedemonte and S. Russo

*Istituto di Chimica Industriale, Università Genova, 16132 Genova, Italy*  
(Received 26 February 1973)

Random copolymers from ethylene and carbon monoxide, containing different numbers of carbonyl groups in the main chain, have been crystallized from dilute solutions. The self-seeding technique has been applied. Monolayer single crystals are obtained and some results concerning their morphology and the unit cell dimensions as functions of the carbonyl content are reported. The annealing treatment supports a structural transition previously noted for other polymers.

## INTRODUCTION

In recent years, random copolymers from ethylene and carbon monoxide have received considerable attention, mostly for fundamental studies on the mechanisms of polymer photodegradation<sup>1-4</sup>. The kinetics<sup>5-8</sup> and the mechanism<sup>9</sup> of the copolymerization reaction have already been published in detail. The resultant copolymers show a polyketonic structure of the type:  $-(CH_2CH_2)_n-(CO)-$ , with  $n$  changing as a function of the monomer feed composition<sup>6</sup>.

The present paper is a preliminary report of a thorough study on the morphology and the structure of solution-grown single crystals of these polyketones, as functions of the carbonyl content.

## EXPERIMENTAL

### *Materials and their characterization data*

Poly(ethylene-co-carbon monoxide) samples were obtained by free radical polymerization of ethylene and carbon monoxide, both from the gaseous phase (PCO-1) at room temperature, using  $\gamma$ -rays<sup>10</sup>, and from benzene solution (PCO-2, PCO-3) using chemical initiators at 70°C<sup>11</sup>. As reference materials, polyethylene samples were obtained by  $\gamma$ -ray polymerization of ethylene at room temperature from the gaseous phase<sup>10</sup>. In all cases conversion was kept very low (<0.2%) in order to reduce any branching formation<sup>8,12</sup> and to ensure chemical homogeneity in the copolymers<sup>8</sup>. No fractionations have been performed on the specimens. Carbonyl content, molecular weights, apparent heats of fusion, and other characterization data of the original materials are summarized in *Table 1*.

The solvents used for the preparation of the single crystals—xylene (a mixture of three isomers), *o*-dichlorobenzene (DCB) and dimethylformamide (DMF), were commercial products, undistilled.

### *Techniques of crystallization*

The preparation of the single crystals was carried out following the self-seeding technique introduced by

Keller and coworkers some years ago<sup>13-15</sup>. The copolymer is wholly dissolved in the solvent at high temperature  $T_{sol}$ , and completely crystallized at a suitable temperature  $T_{cc}$ ; this suspension is thereupon heated up from  $T_{cc}$  to the 'seeding temperature'  $T_s$  at a controlled heating rate of about 10°C/h. The seeding temperature is some degrees above the optical clearing temperature of the suspension. After a short storage time at  $T_s$  (about 1 h), the solution is crystallized at  $T_c$ ;  $T_s$  and  $T_c$  must be carefully controlled ( $\pm 0.05^\circ\text{C}$ ) and accurately chosen if single crystals uniform in size and with a simple morphology are to be prepared successfully.

It is well known<sup>14,15</sup> that the technique so far summarized involves the preservation both of the primary nuclei and of many fragments of the crystalline lamellae above the optical clearing temperature of the suspension; they act as seeds in the final crystallization. Their folding period would eventually be correlated with the seeding temperature,  $T_s$ .

No special precaution to avoid the degradation of the copolymers during preparation of the single crystals has been applied. However, brown test tubes have been used to keep out the u.v. radiation from the CO groups<sup>16</sup> and the solutions have been removed as soon as possible from the high temperatures necessary for the dissolution of the polymer or for the seeding process.

*Table 1* Characterization data of the original materials

Sample	Carbonyl content (%) <sup>a</sup>	$M_n$ <sup>b</sup>	$\Delta H^*$ (cal/g) <sup>c</sup>	$T_m$ (°C)
PE	—	—	34.7	—
PCO-1	9	—	29.7	104
PCO-2	32	4700	15.9	104
PCO-3	37	8300	12.5	113

<sup>a</sup> Number of CO groups/(number of CO groups+number of ethylene units)  $\times 100$ . These data have been obtained with a Carlo Erba Mod. 3102 CHNO elemental analyser

<sup>b</sup> Measured by vapour pressure osmometry, using DCB as the solvent at 110°C

<sup>c</sup> Apparent melting enthalpies of the original materials have been measured by a Perkin-Elmer Differential Scanning Calorimeter. The calibration was performed with indium

\* Laboratorio di Tecnologia dei Polimeri e Reologia, CNR, 80072 Arco Felice, Napoli, Italy.

*Morphological observations*

The external shape of the single crystals has been examined by using a Philips E.M. 300 electron microscope, following the usual technique<sup>17</sup>.

Electron diffraction patterns were obtained using the same electron microscope with the beam normal to the main surface of the crystals. The crystals were shadowed with gold, which was used as the internal calibration standard to calculate the spacings from the polymer reflections.

The thickness of the crystals was obtained by means of low-angle X-ray diffraction on oriented single crystal mats. A pinhole-collimated Rigaku-Denki camera was used. The long-spacing, calculated according to the Bragg relation, was assumed to correspond to the thickness of the lamellae.

*Annealing and thermal measurements*

Fragments of the single crystal mats, wrapped in aluminium foil, were annealed in glass tubes, which were sealed under nitrogen and immersed in thermostat baths. The annealing was performed in the dark for a constant time of 24 h.

The same sample was used both for X-ray diffraction and thermal measurements. A DSC-1 Perkin-Elmer differential scanning calorimeter was used to obtain apparent heats of fusion  $\Delta H^*$ . All samples (2 or 3 mg) were scanned at 16°C/min. The area under the differential scanning calorimetry melting curve was expressed in cal/g using a typical calibration factor determined from melting a known weight of indium.

The small angle X-ray scattering spectra were performed at room temperature.

*Wide angle X-ray diffraction measurements*

Wide angle X-ray diffraction patterns were obtained either photographically with a flat camera or by means of an X-ray spectrometer (North America Philips Co. Inc.). Ni-filtered  $\text{CuK}\alpha$  radiation was used throughout. The mass crystallinity of bulk materials was calculated from X-ray diffraction traces according to the method proposed by Hermans and Weidinger<sup>18, 19</sup> for powder samples.

RESULTS AND DISCUSSION

*Crystallinity and heat of fusion of original materials*

Wide angle X-ray diffraction traces of polymers with different carbonyl intrachain content are reported in Figure 1. The crystallinity and the Bragg angles of the most relevant reflections are also indicated.

The crystallinity decreases notably with increasing numbers of carbonyl groups in the chain; however, the reported figures could be a result of the preparation technique for the copolymers. From the values of the apparent heat of fusion noted in Table 1 it appears that the melting enthalpy of the copolymers is remarkably lower than that of the pure polyethylene (68.5 cal/g):  $\Delta H^*/x_c$  is 49.5 and 45.8 cal/g for PCO-1 and PCO-3 respectively. It seems that this parameter does not change greatly with the composition of the copolymers.

*Preparation and morphology of the single crystals*

The polyethylene (PE), prepared as reference material by  $\gamma$ -irradiation, can be submitted to the self-seeding

process without any particular precaution. The seeding temperatures which yield single crystals are 80–90°C in xylene and 85–95°C in DCB respectively; in these temperature ranges the number of seeds decreases with increasing  $T_s$  and simultaneously the morphology of the crystals becomes more and more complicated.

The crystals shown in Figure 2 indeed look very similar to the diamond-shaped single crystals that can be obtained from the commercial high density polyethylene<sup>14, 15, 20</sup> or from sharp fractions of it<sup>21, 22</sup>, but generally show less regular edges and more growth. Since the low density polyethylene produced by high pressure polymerization has been reported to form oval-shaped crystals<sup>23, 24</sup>, we can therefore assume that only

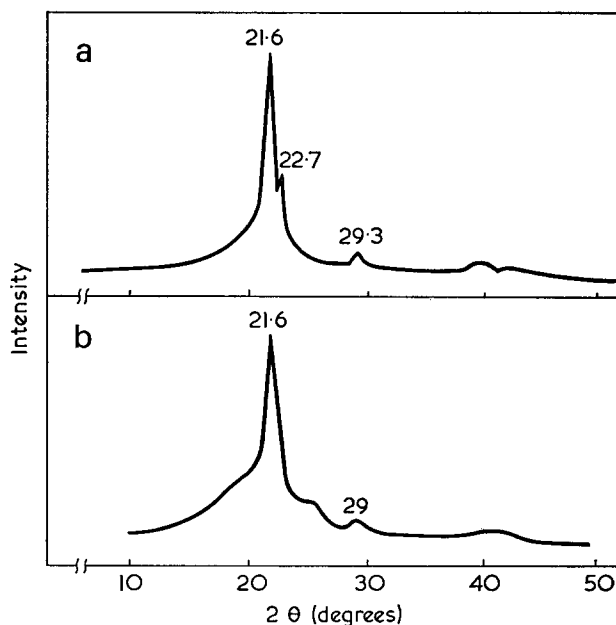


Figure 1 Powder spectrum of bulk (a) PCO-1 and (b) PCO-3. The spectra were registered with a proportional counter ( $\text{CuK}\alpha$ ). Mass crystallinity  $x_c$ : (a) 0.60; (b) 0.27

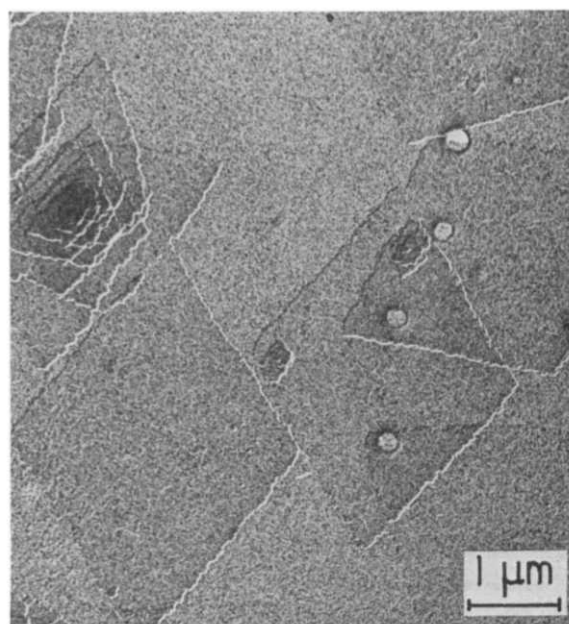


Figure 2 Seeded single crystals of polyethylene (PE) (prepared by  $\gamma$ -irradiation) from xylene.  $c=1.0 \times 10^{-3}\%$ ;  $T_{sol}=120^\circ\text{C}$ ;  $T_{cc}=T_c=50^\circ\text{C}$ ;  $T_s=83.0^\circ\text{C}$



few and very short branches, if any, are present in the main chain of the polymer; also since the copolymers would be less branched than the polymer itself<sup>8</sup>, they can be confidentially submitted to the self-seeding process.

PCO-1 single crystals can be obtained in the same solvents used for pure polyethylene, say xylene and DCB.

In Figure 3 the unseeded crystals, as obtained from the first crystallization of the solution in the experimental conditions indicated in the caption, are shown. The crystals from very dilute solutions of both solvents used, but particularly from DCB, have indeed a rather simple morphology because their sizes are not too large; the lozenge shape of pure polyethylene single crystals is observed, with some growths on the main diagonal. It is noteworthy that the morphology does not change greatly over a large range of the crystallization temperatures and, rather surprising, it becomes less complicated if  $T_{cc}$  is reduced to room temperature.

In Figure 4a the seeded crystals obtained from a very dilute solution in DCB ( $c=1.0 \times 10^{-3}\%$ ) with  $T_s=88^\circ\text{C}$  and  $T_c=53.2^\circ\text{C}$  are shown. They are usually monolayers with an almost circular shape; their sizes are very small but uniform, according to the self-seeding treatment. The primary nuclei are well visible as protrusions in the central area of the lamellae and this is again a consequence of the self-seeding treatment, i.e. the stabilization of the seeds at  $T_s$ , involving a folding period for the nuclei higher than that for the whole crystal.

On the outline of the crystals a step or a variation in the thickness of the lamellae is clearly visible. This involves a change in the crystallization temperature. If we raise  $T_c$  up to  $60^\circ\text{C}$  (Figure 4b) a larger amount of polymer does not crystallize in these conditions and therefore the step appears in the inner part of the lamellae. These observations can be explained either assuming that the crystallization of the copolymer in dilute solutions occurs so slowly that even after many days it is not yet finished or assuming that some material with a very low molecular weight may not be crystallized

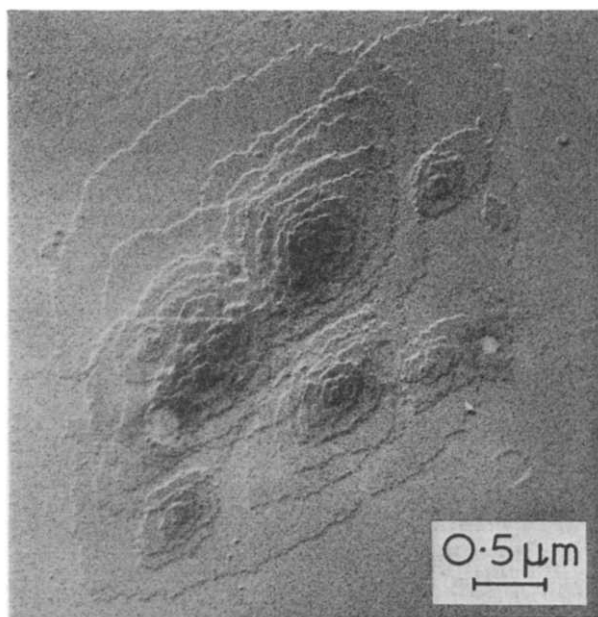


Figure 3 Unseeded crystals of PCO-1 from DCB.  $c=5.0 \times 10^{-4}\%$ ;  $T_{sol}=120^\circ\text{C}$ ;  $T_{cc}=25^\circ\text{C}$

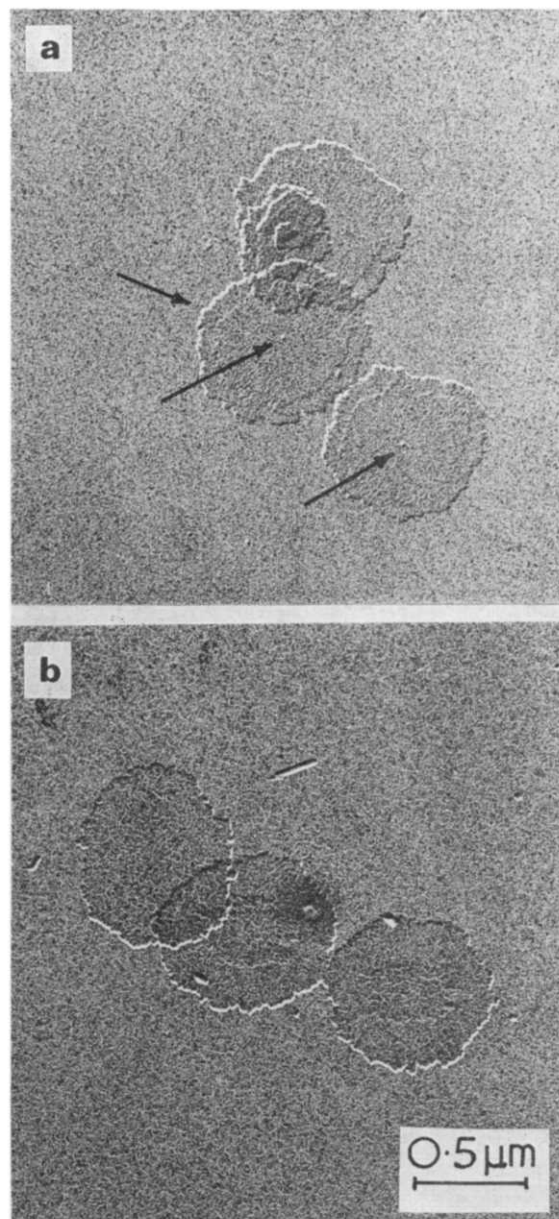


Figure 4 Seeded single crystals of PCO-1 from DCB.  $c=1.0 \times 10^{-3}\%$ ;  $T_{sol}=112^\circ\text{C}$ ;  $T_{cc}=60^\circ\text{C}$ ;  $T_s=88.0^\circ\text{C}$ . (a)  $T_c=53.2^\circ\text{C}$ ; (b)  $T_c=60.0^\circ\text{C}$ . The arrows indicate the primary nuclei and the steps on the outline of the crystals

at such temperatures. It seems that the latter hypothesis would be more realistic, as the copolymer is not fractionated.

This conclusion would also explain the unusual observation that the dimensions of the seeded crystals apparently do not change greatly with the seeding temperature; raising  $T_s$  from  $85^\circ\text{C}$  to  $89.1^\circ\text{C}$  only the growth becomes more and more complicated. Actually, the amount of the uncrystallized polymer available for each seed increases with  $T_s$  and more complicated multilayer crystals come out.

Figure 4b also shows that by increasing the crystallization temperature the morphology of the seeded crystals becomes more elongated. This means that the basic shape of the PCO-1 copolymer single crystals is still the lozenge characteristic of the pure polyethylene; we have here a very high value of the truncation ratio<sup>20</sup>.

Owing to the low number of carbonyl groups in the main chain of the PCO-1 copolymer, xylene is a solvent thermodynamically better than DCB and therefore, with the same values of the seeding temperatures, single crystals with larger sizes and more growths are obtained from the former (Figure 5a). In both cases the polymer concentration of the initial suspension influences the results. Decreasing the concentration from  $1.0 \times 10^{-3}$  to  $5.0 \times 10^{-4}$  in xylene (Figure 5b) we obtain smaller crystals; we will not discuss this point any further because a similar phenomenon has been recently obtained for pure polyethylene<sup>22</sup>.

With copolymers having a larger number of carbonyl groups in the main chain (PCO-2 and PCO-3) it is more difficult to find the experimental conditions leading to monolayer single crystals with a simple morphology because the results obtained with the self-seeding technique are less reproducible. We do not have any explanation for this; nevertheless we think it reasonable to assume that the copolymers themselves, unfractionated,

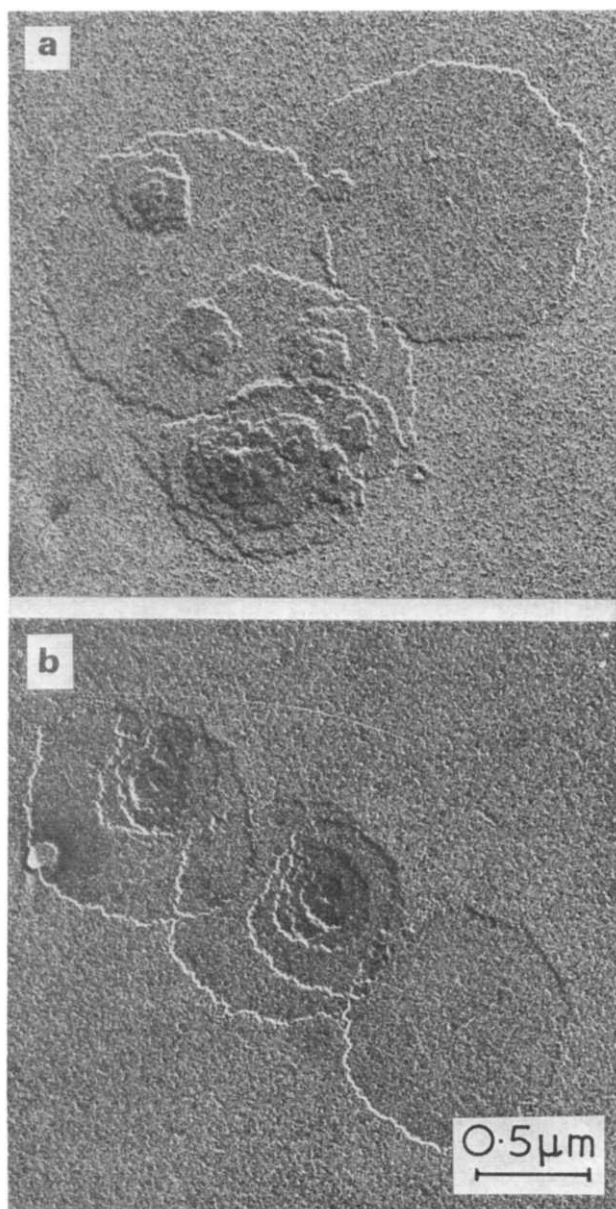


Figure 5 Seeded single crystals of PCO-1 from xylene.  $T_{sol}=112^{\circ}\text{C}$ ;  $T_{cc}=T_c=60^{\circ}\text{C}$ ;  $T_s=87.1^{\circ}\text{C}$ . (a)  $c=1.0 \times 10^{-3}\%$ ; (b)  $c=5.0 \times 10^{-4}\%$



Figure 6 Seeded single crystals of PCO-3 from DMF;  $c=2.0 \times 10^{-2}\%$ ;  $T_{sol}=99^{\circ}\text{C}$ ;  $T_{cc}=21^{\circ}\text{C}$ ;  $T_s=84.5^{\circ}\text{C}$ ;  $T_c=42^{\circ}\text{C}$

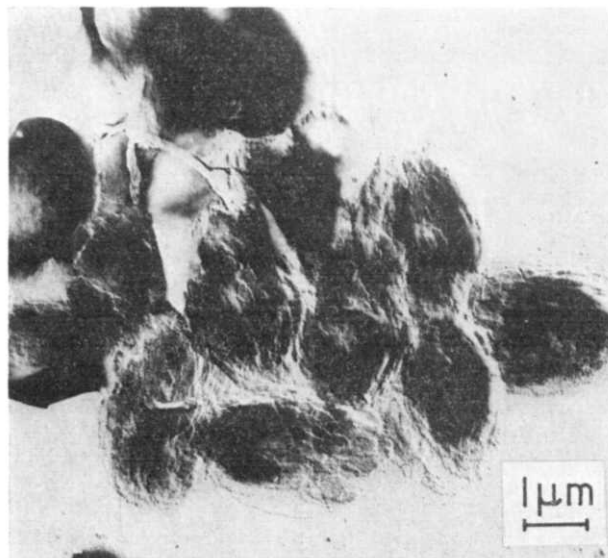


Figure 7 Seeded single crystals of PCO-3 from xylene;  $c=1.0 \times 10^{-3}\%$ ;  $T_{sol}=112^{\circ}\text{C}$ ;  $T_{cc}=T_c=50^{\circ}\text{C}$ ;  $T_s=86.0^{\circ}\text{C}$

could not be homogeneous as far as both the distribution of the carbonyl groups in the main chain and the amount of CO in each single chain are concerned.

The solvents used were again xylene and DCB; some experiments have been carried on in DMF. Owing to the larger number of carbonyl groups in the main chain DCB and DMF are now better solvents than the xylene.

In Figures 6-8 some results obtained in the experimental conditions indicated in the captions are shown. Normally multilayer crystals come out.

The best results have been obtained in DCB; generally we have many growths and no effect of the seeding temperature on the sizes of the crystals but nevertheless the self-seeding technique does work (in Figure 8 the arrow indicates the nucleus of a monolayer crystal) and decreasing the concentration of the suspension the results



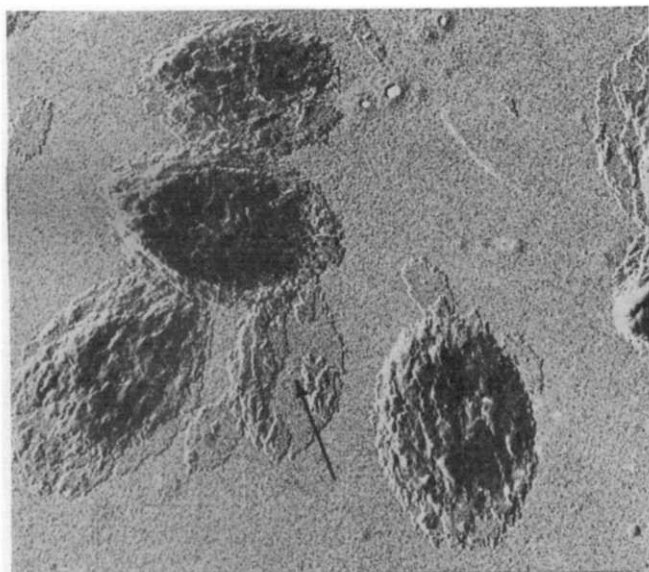


Figure 8 Seeded single crystals of PCO-3 from DCB.  $c=1.0 \times 10^{-1}\%$ ;  $T_{sol}=120^\circ\text{C}$ ;  $T_s=80.8^\circ\text{C}$ ;  $T_{cc}=50^\circ\text{C}$ ;  $T_c=60^\circ\text{C}$

Table 2 Indices and spacings of PCO-3 single crystal reflections from electron diffraction patterns. The spacings of the corresponding planes for linear polyethylene (PE) are also reported for comparison

Diffraction planes	PCO-3 spacings (Å)	PE spacings (Å)
110	4.19	4.10
200	4.01	3.70
210	3.10	2.92
020	2.43	2.46
220	2.07	2.03

remarkably improve and monolayer lamellae with very small dimensions can be obtained.

#### Electron diffraction results

A typical electron diffraction pattern from solution-grown single crystals of a sample of PCO-3 and the electron micrograph of the corresponding crystal in their reciprocal orientation are shown in Figure 9. The orientation of the unit cell parameters  $a^*$  and  $b^*$  is indicated with reference to the crystal. The molecular axis is perpendicular to the platelet; therefore, by the familiar argument, the molecules must fold back on themselves many times on the surface of the crystal.

The interplanar spacings, listed in Table 2 with their crystallographic indices, were determined by internal calibration with gold. Comparing the spacings of the corresponding planes of linear polyethylene an expansion of the unit cell in the case of the copolymers is observed. The expansion is more pronounced in the  $a$  axis direction. This result clearly indicates that some C=O groups become part of the lattice as defects. These results are in good agreement with those previously reported by Chatany *et al.*<sup>25</sup>.

The reciprocal angle  $\gamma^*$ , determined from the electron diffraction pattern, is  $90^\circ$ .

#### Annealing results

In Figure 10 the long-spacing (Å) and the apparent enthalpy of fusion  $\Delta H^*$  (cal/g) of oriented single crystal

mats of PCO-1 polymer (9% of CO) are plotted *versus* the annealing temperature. The crystals were grown at  $50^\circ\text{C}$  from DCB using a seeding temperature of  $86^\circ\text{C}$  and a polymer concentration of 0.01% (w/w).

A discontinuity in the trend of the long-spacing is observed at an annealing temperature of  $\sim 80^\circ\text{C}$ . Correspondingly, in the range of annealing temperatures from  $70$  to  $80^\circ\text{C}$ , the apparent melting enthalpy of the single crystal aggregates starts to decrease dramatically.

The same kind of correlation between long-spacing and apparent heat of fusion has already been observed in polymers such as polydodecener<sup>26</sup>, polyoctener<sup>27</sup> and branched polyethylenes<sup>28</sup>.

The critical value  $T_a^*$  of the annealing temperature at which the increase in the long-spacing and the falling off of the crystallinity starts, has been related to a morphological transition of the type schematically illustrated in Figure 11<sup>26</sup>. Following the scheme of

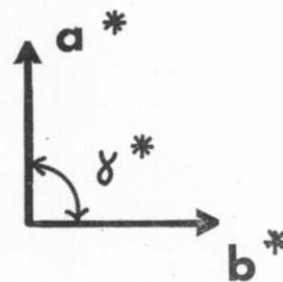
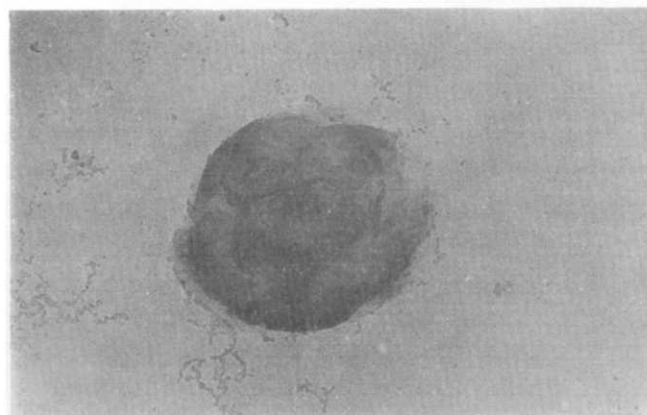


Figure 9 Electron diffraction pattern and electron micrograph of a PCO-3 single crystal. The orientation of the unit cell parameters  $a^*$  and  $b^*$  is indicated with reference to the crystal

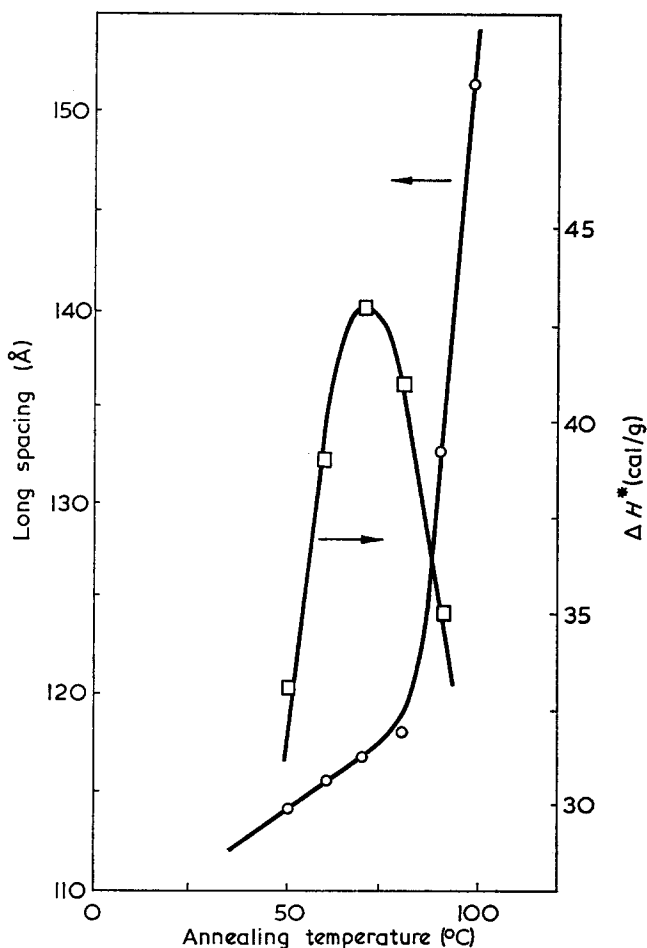


Figure 10 Long spacing (○) and apparent enthalpy of fusion (□) of oriented crystal aggregates of PCO-1 as function of the annealing temperature

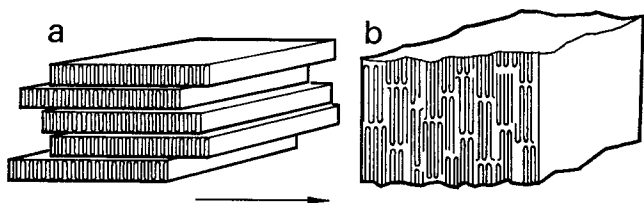


Figure 11 Change in the overall morphology of the crystal aggregate system at the annealing temperature  $T_a^*$ . (a) Below  $T_a^*$  the system shows the morphology of oriented single crystal aggregate; (b) above  $T_a^*$  a complicated morphology is attained and the lamellae lose their individuality

transition of Figure 11, at the critical annealing temperature the characteristic morphology of single crystal aggregates is lost and the system assumes a more complicated morphology very close to that of a melt crystallized material, although the orientation of the chain is retained.

#### REFERENCES

- 1 Guillet, J. E., Dhanray, J., Golemba, F. J. and Hartley, G. H. *Adv. Chem. Ser.* 1968, **85**, 272
- 2 Heskins, M. and Guillet, J. E. *Macromolecules* 1968, **1**, 97
- 3 Hartley, G. H. and Guillet, J. E. *Macromolecules* 1968, **1**, 165
- 4 Heskins, M. and Guillet, J. E. *Macromolecules* 1970, **3**, 224
- 5 Munari, S., Russo, S. and Rossi, C. *Proc. 2nd Tihany Symp. Radiat. Chem.* 1967, p 501
- 6 Russo, S. and Munari, S. *J. Polym. Sci. (B)* 1967, **5**, 827
- 7 Russo, S. and Munari, S. *Atti Conv. Chim. Radiaz. Radioelem., Roma* 1967, p 46
- 8 Munari, S., Russo, S. and Vigo, F. *J. Polym. Sci. (B)* 1968, **6**, 23
- 9 Russo, S., Munari, S. and Biagini, E. *J. Phys. Chem.* 1969, **73**, 378
- 10 Caffarelli, E. *Thesis* University of Genoa, 1973
- 11 Sorrentino, V. *Thesis* University of Genoa, 1972
- 12 Munari, S. and Russo, S. *J. Polym. Sci. (B)* 1966, **4**, 733
- 13 Blundell, D. J., Keller, A. and Kovacs, A. J. *J. Polym. Sci. (B)* 1966, **4**, 481
- 14 Blundell, D. J. and Keller, A. *J. Macromol. Sci. (B)* 1968, **2**, 301
- 15 Blundell, D. J. and Keller, A. *J. Macromol. Sci. (B)* 1968, **2**, 337
- 16 Trozzolo, A. M. and Winslow, H. J. *Macromolecules* 1968, **1**, 98
- 17 Kay, D. 'Technique for electron microscopy', Blackwell, Oxford, 1965
- 18 Hermans, P. H. and Weidinger, A. *Makromol. Chem.* 1961, **44-46**, 24
- 19 Hermans, P. H. and Weidinger, A. *Makromol. Chem.* 1961, **50**, 98
- 20 Valenti, B. and Pedemonte, E. *Chim. Ind. (Milan)* 1972, **54**, 112
- 21 Keller, A. and Pedemonte, E. *J. Cryst. Growth* 1973, **18**, 111
- 22 Alfonso, G., Valenti, B. and Pedemonte, E. to be published
- 23 Eppe, R., Fischer, E. W. and Stuart, H. A. *J. Polym. Sci.* 1959, **34**, 721
- 24 Geil, P. H. *J. Polym. Sci.* 1961, **51**, 510
- 25 Chatani, Y., Takizawa, T. and Murahashi, S. *J. Polym. Sci.* 1972, **62**, S27
- 26 Martuscelli, E. and Vittoria, V. *Polymer* 1972, **13**, 360
- 27 Facioni, E. and Martuscelli, E. *J. Polymer. Sci. (B)* 1972, **10**, 423
- 28 Martuscelli, E. and Pracella, M. to be published

# Application of small angle X-ray scattering to semi-crystalline polymers: 1. Experimental considerations and analysis of data

D. S. Brown, K. U. Fulcher\* and R. E. Wetton

Department of Chemistry, University of Technology, Loughborough LE11 3TU, UK  
(Received 14 December 1972; revised 20 March 1973)

Experimental problems in studying small angle X-ray scattering from semi-crystalline bulk polymers are discussed and data obtained from slit optics compared, after desmearing, with pin-hole data. Theoretical correlation functions are derived for a model based on alternating layers of crystalline and amorphous phases. Different types of distribution functions for layer thicknesses were employed and compared with experimental correlation functions from polyethylene, poly(trimethylene oxide) and poly(tetramethylene oxide). For the latter polymer with crystallinity ~40%, Gaussian distributions for the thicknesses of both phases gave good agreement, whereas log normal distributions did not. For high crystallinity polymers choice of distribution is not critical. The fraction crystallinity obtained from different X-ray techniques is discussed.

## INTRODUCTION

Small angle X-ray scattering (SAXS) has been widely used for the estimation of lamellar thickness in semi-crystalline polymers<sup>1-3</sup>, assuming a two phase model. It has been shown that for correct determination of this parameter considerable care must be taken in the interpretation of results<sup>4-6</sup>. Direct application of Bragg's law will result in erroneous  $d$  spacings from the broad diffraction maxima normally obtained from bulk semi-crystalline polymers. A more correct average periodicity perpendicular to the layers is obtained by multiplying the desmeared intensity function by  $\theta^2$  and only subsequently applying Bragg's law to the peak position<sup>7</sup>. Calculation of average periodicities gives no insight into the thickness distributions of amorphous and crystalline layers. The experimental correlation function defined by Debye *et al.*<sup>5, 8, 9</sup> contains this information and from a detailed comparison with model correlation functions it is possible to obtain such parameters as the sizes and relative distribution of the crystalline and amorphous regions, the volume fraction crystallinity, and the surface area per unit volume between phases. Further information can be obtained if the integrated scattered intensity is converted to an absolute scale by the use, for example, of a standard calibration sample<sup>10-12</sup>.

This paper demonstrates, by comparison with pin-hole data, how reliable information can be obtained fairly rapidly by correct desmearing of data obtained with slit optics. Consideration is given to the various experimental and theoretical factors which must be taken into account to obtain meaningful results. In particular different model correlation functions are evaluated by comparison with experimental correlation functions obtained for poly-

ethylene, poly(trimethylene oxide) and poly(tetramethylene oxide). Detailed results on the crystallization of the latter polymer will be reported subsequently.

## EXPERIMENTAL

All measurements were made with a Rigaku-Denki goniometer (catalogue no. 2202), in conjunction with a Philips PW 1010 generator. Slit and pin-hole optics were taken from the point focus of a fine focus tube. Samples were in the form of discs approximately 1 mm thick. The path between sample and detector (film or Geiger counter) was evacuated and monochromatization of the copper radiation was achieved by using balanced Ni and Co filters<sup>13</sup>. In order to correct for dead-time errors in the Geiger counter, a paralysis circuit of known dead-time (400  $\mu$ sec), and greater than that of the Geiger tube, was introduced. In the cases where high resolution and accurate documentation of the scattering curve were required, counting methods of detection were employed, combined with very slow angular scanning or step scanning. Film detection was employed for pin-hole optics with intensities measured with a microdensitometer.

Tables 1 and 2 summarize the settings we have used for slit and pin-hole optics respectively. These represent a good balance between intensity and resolution.

Table 1 Optimum slit arrangement

Target to	Slit number			Sample	Slit number		Detector
	1	2	3		4	5	
(distance in mm)	80	430	514	530	872	912	915
Slit widths (mm)	0.2	0.1	0.22		0.30	0.10	

\* Present address: Koninklijke/Shell Laboratory, Amsterdam, The Netherlands

Table 2 Optimum pin-hole arrangement

Focal spot to	Pinhole number		Sample	Detector
	1	2		
(distance in mm)	80	430	530	835
Pin-hole diameters (mm)	0.3	0.2		

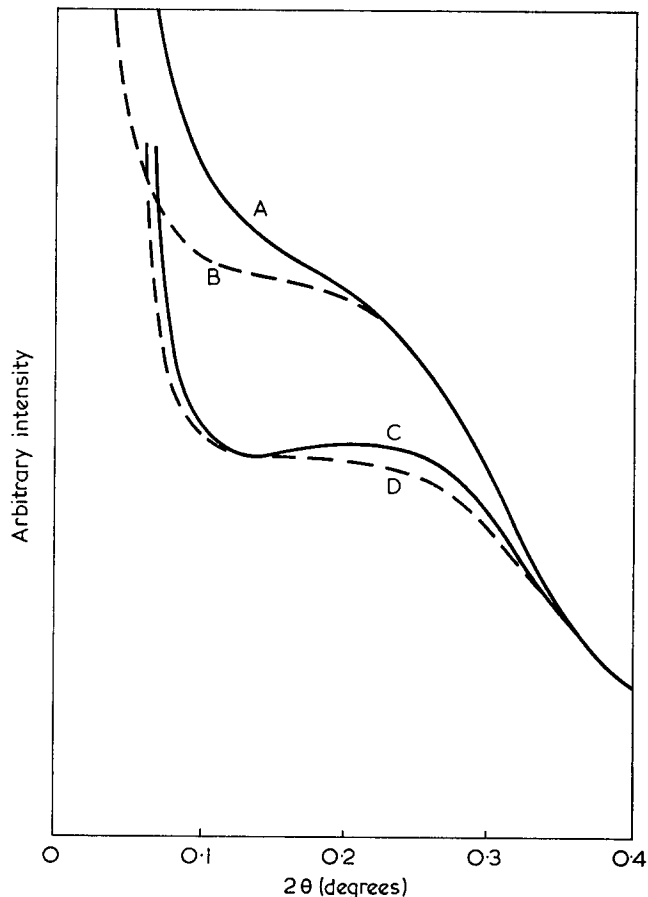


Figure 1 Effect of third slit width on the SAXS pattern of polyethylene. Slit width is progressively reduced in the sequence (A) to (D). The third slit at setting D has impinged on the primary beam, thus making C the choice for optimum resolution

The positioning and width of the third slit, the purpose of which is to cut out parasitic scattering from the second slit, were found to be extremely critical. Although the settings of the third slit may be calculated on a theoretical basis, in practice they are best found by trial and error. Figure 1 illustrates the effect of different settings of the third slit on the SAXS pattern of polyethylene. For curve D, the third slit has impinged on the primary beam and hence effectively behaves as the second slit. For high resolution the parasitic scattering is measured separately with the sample in an absorbing position between the fifth slit and the Geiger counter.

RESULTS AND DISCUSSION

The settings discussed above allow an effective angular resolution of 0.07° for slit collimation. Collimation corrections for slit smeared curves were applied using the method of Dijkstra et al.<sup>4</sup>

Figure 2 shows the SAXS pattern from polyethylene (sample 1b, ref. 6) before and after applying the desmearing programme. The peak is not only sharpened but also

shifted to a higher scattering angle upon desmearing. This is compared with the undistorted scattering curve from the same sample obtained using pin-hole optics. The two curves are in good agreement showing the validity of the desmearing process. The second-order peak is clearly discernible and occurs at half the Bragg spacing upon desmearing. The data are also in agreement with those obtained by Vonk<sup>6</sup> for the same sample using a Kratky camera with slit collimation and subsequent desmearing.

The SAXS diagrams obtained from samples of poly(tetramethylene oxide) ( $\bar{M}_n=435\,000$ ) crystallized at 23.5°C for 2.5 months, and poly(trimethylene oxide) ( $\bar{M}_n=327\,000$ ) crystallized at -10°C for 2.5 months, are shown in Figures 3 and 4. Figures 5 and 6 show the one- and three-dimensional correlation functions obtained from the desmeared experimental scattering curves of the two polymers. The first maximum in the one-dimensional

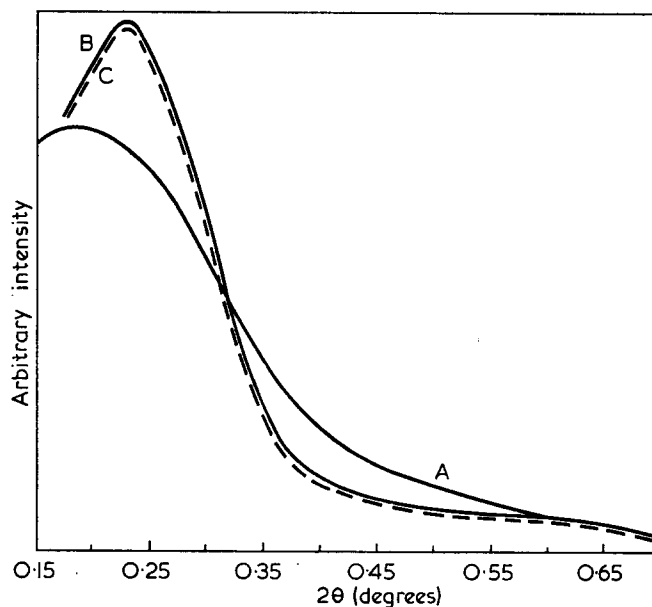


Figure 2 Effect of desmearing on the SAXS pattern of polyethylene. Curve A represents the experimental data with slit optics (CuK $\alpha$  radiation, data obtained using balanced Co and Ni filters<sup>10</sup>). Curve B shows these data mathematically desmeared and curve C the experimental pattern obtained using pin-hole optics

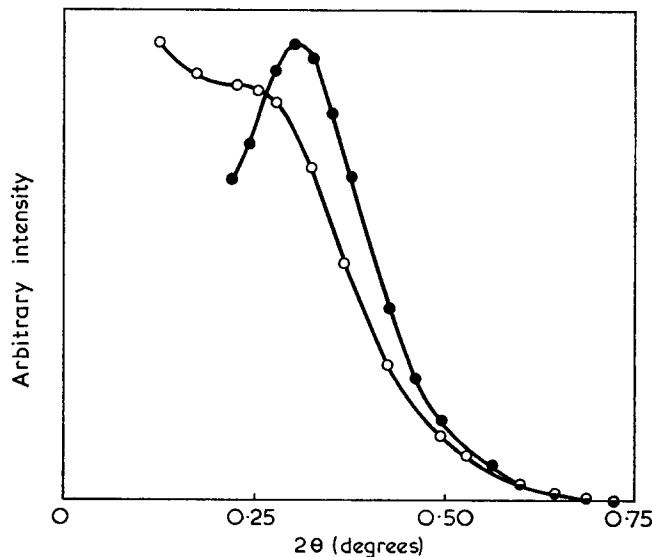


Figure 3 SAXS diagrams for poly(tetramethylene oxide) ( $\bar{M}_n=435\,000$ ) crystallized at 23.5°C for 2.5 months. O, Slit smeared; ●, desmeared

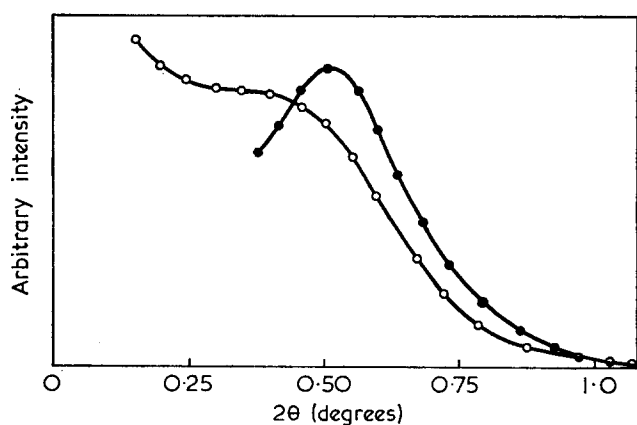


Figure 4 SAXS diagrams for poly(trimethylene oxide) ( $\bar{M}_n = 327\,000$ ) crystallized at  $-10^\circ\text{C}$  for 2.5 months. ○, Slit smeared; ●, desmeared

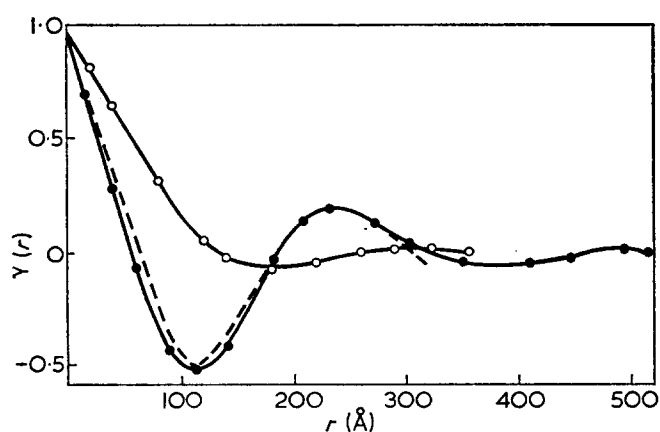


Figure 5 One-dimensional (●) and three-dimensional (○) experimental correlation functions derived from the SAXS curves for poly(tetramethylene oxide) shown in Figure 3. ----, theoretical best match with parameters  $\phi = 0.4$ ,  $\beta_c = 0.1$  and  $\beta_a = 0.7$

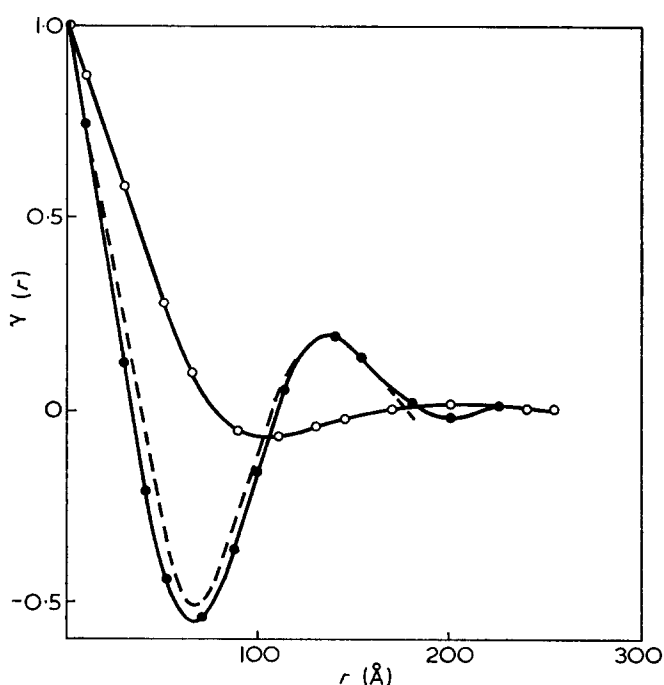


Figure 6 One-dimensional (●) and three-dimensional (○) experimental correlation functions derived from the SAXS curves for poly(trimethylene oxide) shown in Figure 4. ----, theoretical best match with parameters  $\phi = 0.45$ ,  $\beta_c = 0.1$  and  $\beta_a = 0.8$

correlation function occurs at a smaller spacing than the three-dimensional case. It is the maximum in the one-dimensional correlation function which gives the average repeat distance perpendicular to the lamellae and represents the sum of amorphous and crystalline thicknesses.

In order to obtain satisfactory matches of the experimental with the theoretical correlation functions, a distribution of layer thicknesses must be assumed. Kortleve and Vonk<sup>6</sup> have shown that the log normal function

$$P(x) = [\exp(\beta^2/2)/\phi\beta\pi^{1/2}] \exp - \{ [3\beta^2/4 + \ln(x/\phi)]^2 / \beta^2 \}$$

with the same distribution width parameter,  $\beta$ , for crystalline and amorphous thickness can be used to obtain a reasonably good fit between the experimental and theoretical functions for polyethylene. However, for the two polyethers which have much lower crystallinities ( $\phi < 0.5$ ), separate distribution width parameters are required for the crystalline ( $\beta_c$ ) and amorphous ( $\beta_a$ ) layers to obtain even moderate agreement. The broken lines in Figures 5 and 6 show the closest fitting theoretical correlation functions using log normal distributions and treating  $\phi$  as a variable as well as the width parameter. In both polyethers a considerable amount of secondary crystallization has occurred. In such samples, where the distributions are relatively sharp, the choice of distribution function type is not critical. However, in less well crystallized samples the shapes of the theoretical correlation functions differ considerably for different types of distribution function. Figure 7 shows the experimental one-dimensional correlation function for poly(tetramethylene oxide) crystallized at  $20^\circ\text{C}$  for 112 days, normalized such that the maximum occurs at a correlation distance  $x = 1.0$ . This is compared with theoretical functions which have the types of distribution and distribution parameters shown in Table 3.

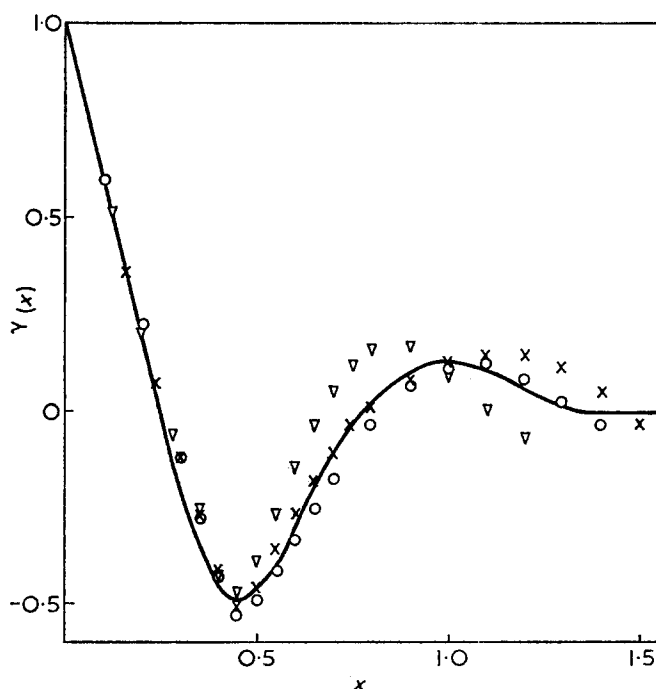


Figure 7 Experimental one-dimensional correlation function [ $\gamma(x)$ ] for poly(tetramethylene oxide) ( $\bar{M}_n = 227\,000$ ), but normalized to give the first maximum at  $x = 1.0$ . The points are the closest fits computed from a lamellar model with crystalline and amorphous distributions respectively: ○, Gaussian/Gaussian; ▽, log normal/log normal; ×, Gaussian/square. Breadth parameters are given in Table 3

Table 3 Distribution functions, crystallinity and width parameters for theoretical curves

	Crystalline distribution function	Amorphous distribution function	$\phi$	$\beta_c$	$\beta_a$
A	Gaussian	Gaussian	0.45	0.02	0.33
B	Log normal	Log normal	0.45	0.05	0.90
C	Gaussian	Square	0.45	0.02	0.45

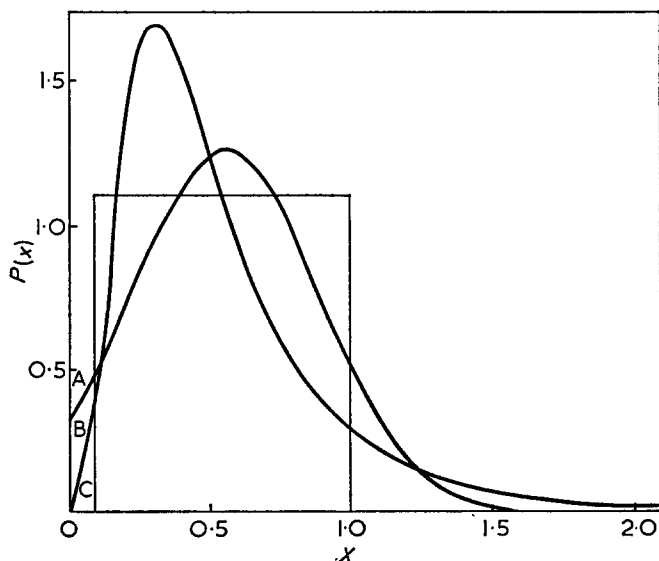


Figure 8 Plots of amorphous thickness distribution functions A, B and C of Table 3, used in calculating the theoretical correlation functions in Figure 7. The crystalline thickness distribution functions are very sharp in comparison

The log normal function has been defined earlier. The Gaussian function is defined by:

$$P(x) = \{1/\beta(2\pi)^{1/2}\} \exp - [(x - \phi)^2/2\beta^2]$$

For physical reasons, negative values of  $x$  were not permitted and in order to compensate for any cut-off at  $x=0$ , the whole function was multiplied by a normalizing constant to make the positive area 1. The square function is defined by:

$$P(x) = 1/2\beta \text{ between } \phi - \beta \text{ and } \phi + \beta$$

otherwise  $P(x) = 0$ . The three different types of size distribution functions chosen for the amorphous layers are plotted in Figure 8. It will be appreciated that the width parameters  $\beta$  have different mathematical significances for the different functions. The position of the first maximum in the correlation function is sensitive to the type of distribution used and it will be seen that the proposed theoretical correlation functions do not have their first maximum occurring at precisely  $x = 1.0$ . In order to attempt an exact fit of the data, the experimental function must be normalized such that the position of the first maximum coincides with that in the theoretical function. When this is done, it is found that only the case with two Gaussian distributions gives satisfactory agreement with the experimental data. Figure 9 shows the exactness of the fit so obtained.

Thus, crystallizations of poly(tetramethylene oxide) and poly(trimethylene oxide) under the conditions cited yield crystalline regions of fairly constant size separated by amorphous regions which vary much more in thickness. Although the model assumes a lamellar structure of

approximately parallel layers, the finite probability of having zero amorphous thickness (indicated by the cut-off at  $x=0$  in the Gaussian function) could be accounted for by branching or impingement of the crystallites.

The determination of the volume fraction crystallinity  $\phi$  by using it as a variable parameter in the theoretical correlation function has an estimated error of  $\pm 0.05$ .  $\phi$  may also be determined from the experimental correlation function, from the total integrated intensity on an absolute scale and from wide angle scattering measurements. In each case a slightly different physical quantity is measured. Table 4 shows crystallinities estimated by various methods for poly(tetramethylene oxide) crystallized for 112 days at 20°C.

The value obtained from wide angle scattering was calculated making no allowance for lattice defects or disorder. These together with chain folds contribute to the amorphous scattering so that wide angle scattering would be expected to yield lower crystallinities than those obtained from small angle scattering. The first abscissa intercept [ $\phi(1-\phi)$ ] on the one-dimensional experimental correlation function leads to an estimate of  $\phi$ . This method is only approximate since curvature of the correlation function necessitates a rather inaccurate extrapolation of the first linear part of the correlation function. Further, the product  $\phi(1-\phi)$  changes very little when  $\phi$  is

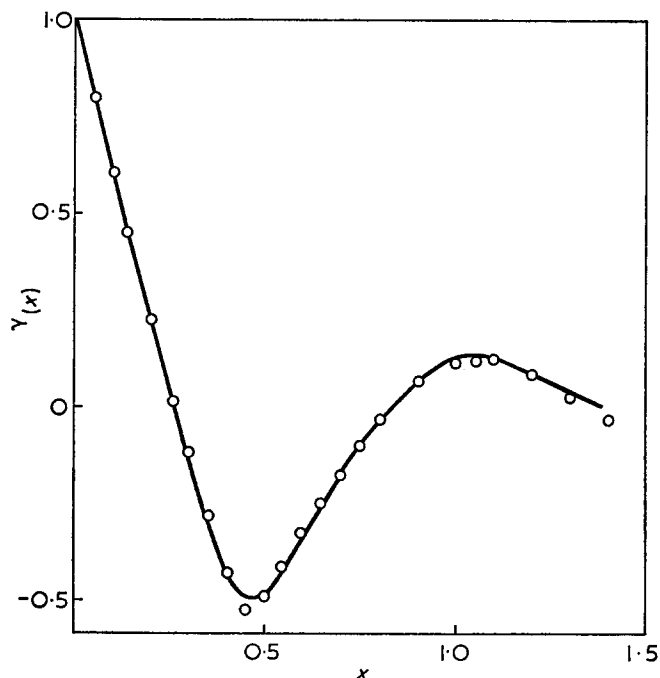

 Figure 9 Normalized experimental (—) one-dimensional correlation function for the poly(tetramethylene oxide) as in Figure 7, compared with the theoretical correlation function A of Table 3 (○) showing the best fit by adjusting the position of the theoretical function maximum on the  $x$  axis

Table 4 Comparison of crystallinities from different X-ray methods

Method	$\phi$
Matching theoretical and experimental correlation functions	0.45
From first abscissa intercept of experimental correlation function	0.45
Wide angle scattering	0.37
Total integral assuming $\Delta\rho = 138 \text{ kg m}^{-3}$	0.34
Total integral assuming $\Delta\rho = 132 \text{ kg m}^{-3}$	0.42

in the range 0.4 to 0.6. In practice, therefore, it is only useful at high crystallinities.

The total integral of the scattered intensity is proportional to  $\phi(1-\phi)\Delta\rho^2$ , where  $\Delta\rho$  is the density difference between the phases. Assuming a density difference of  $138\text{ kg m}^{-3}$ , the total integral crystallinity calculates less than that obtained from wide angle scattering. It would appear that the assumed value of  $\Delta\rho$  is too high and a more reasonable value is obtained with  $\Delta\rho=132\text{ kg m}^{-3}$ . This agrees, within experimental error, with the value obtained from the absolute densities of crystalline and amorphous phases<sup>14</sup>.

We thus conclude that although the choice of distribution function is less critical for well-crystallized polymers of high crystallinity ( $\phi>0.5$ ), the choice becomes more critical the lower the crystallinity and the broader the distribution widths. A knowledge of the correct distributions of layer thicknesses is of prime importance in understanding the morphology of the semi-crystalline polymer. The reasonable agreement between theory and experiment indicates the validity of the two-phase lamellar model when applied to polymers of low crystallinity (<50%) as well as to polyethylene.

#### ACKNOWLEDGEMENTS

We would like to thank Dr C. G. Vonk and Ir G. Kortleve of the Dutch State Mines for the donation of computer

programs and for very helpful discussions. Thanks are also due to Mr E. J. Miller for technical assistance with the setting-up of the SAXS system and to Professor O. Kratky for supplying a standard calibration Lupolen sample.

We thank the SRC for financial support and the award of a studentship to K.U.F.

#### REFERENCES

- 1 Geil, P. H. 'Polymer Single Crystals', Interscience, New York, 1963
- 2 Mandelkern, L. 'Crystallization of Polymers', McGraw-Hill, New York, 1964
- 3 Keller, A. *Rep. Progr. Phys.* 1968, **31**, 623
- 4 Dijkstra, A., Kortleve, G. and Vonk, C. G. *Kolloid-Z. Z. Polym.* 1966, **210**, 121
- 5 Vonk, C. G. and Kortleve, G. *Kolloid-Z. Z. Polym.* 1967, **220**, 19
- 6 Kortleve, G. and Vonk, C. G. *Kolloid-Z. Z. Polym.* 1968, **225**, 124
- 7 Guinier, A., Fournet, G., Walker, C. B. and Yudowitch, K. L. 'Small Angle X-ray Scattering of X-rays', Wiley, New York, 1955, p 181
- 8 Debye, P. and Bueche, A. M. *J. Appl. Phys.*, 1949, **20**, 518
- 9 Porod, G. *Kolloid Z.* 1951, **124**, 83; 1952, **125**, 51, 109
- 10 Kratky, O., Pilz, I. and Schmidt, P. J. *J. Colloid Interface Sci.* 1966, **21**, 24
- 11 Pilz, I. and Kratky, O. *J. Colloid Interface Sci.* 1967, **24**, 211
- 12 Pilz, I. *J. Colloid Interface Sci.* 1969, **30**, 140
- 13 Ross, P. D. *Phys. Rev.* 1926, **28**, 425
- 14 Bowman, I. J. W., Brown, D. S. and Wetton, R. E. *Polymer* 1969, **10**, 716

# Steady flow and dynamic viscoelastic properties of branched polyethylene

J. J. Labaig and Ph. Monge

*Thermodynamics Laboratory, University of Pau, 64016 Pau, France*

and J. Bednarick

*S.N.P.A.-ATO Plastics, Research Centre of Lacq, 64170 Lacq, France*

*(Received 19 February 1973)*

The presentation of viscoelastic properties of molten high polymers in a complex plane makes three characteristic rheologic parameters appear. These are examined for a series of commercial samples of low density polyethylene. For instance, it enables products to be recognized which are very similar as far as the melt index is concerned but have different molecular weight distribution, different long chain branching index and consequently different processing properties.

## INTRODUCTION

Recent studies have shown that molten high polymers have a mechanical relaxation<sup>1</sup> in the frequency range between  $10^{-3}$  and 20 Hz. The curves representing the variations of real and imaginary parts of the complex viscosity:

$$\eta^*(\nu) = \eta'(\nu) - j\eta''(\nu)$$

are actually very typical of this phenomenon.

$\eta''(\nu)$  is maximum for a value  $\nu_c$  of the frequency and  $\eta'(\nu)$  goes through an inflexion point.  $\eta'$  and  $\eta''$  are not independent values; they depend on each other through the very general Kramers-Kronig relationship<sup>2</sup>.

It is interesting to note the results in the complex plane. Experimental points are located for each product on a circular arc.

Thus, we can define three experimental parameters:

$\eta_0$  = zero shear rate viscosity,

$\tau_0$  = characteristic relaxation time such as  $\tau_0 = 1/2\pi\nu_c$ ,

$h$  = coefficient such as  $h\pi/2 = \theta$ , angle between diameter going through the origin and the real axis.

Variations of  $\eta_0$  and  $\tau_0$  with temperature follow the Arrhenius law with similar activation energies for the two parameters.  $h$  does not depend upon temperature.

We propose to use the Cole-Cole analytical expression<sup>3</sup> in order to represent the complex viscosity of polymers:

$$\eta^* = \frac{\eta_0}{1 + (j\omega\tau_0)^{1-h}}$$

This study shows the interest of such a representation.

## EXPERIMENTAL

A rheologic study was conducted under steady flow (Instron capillary rheometer) and dynamic oscillatory experiments (Contraves-Kepes Balance-Rheometer) of

ten samples of commercial branched polyethylene. They were separated into two groups. Group I samples (A, B, C, D, E, F) have roughly the same melt index. Group II samples (F, G, H, I, J) cover a large range of melt indices.

Structural parameters of studied products are shown in Table 1.  $d$  represents the density,  $MI$  the melt index,  $[\eta]$  the intrinsic viscosity measured in trichlorobenzene at 135°C,  $M_w^*$  the weight average apparent molecular weight,  $P^*$  the apparent polydispersity and  $\langle g'_\eta \rangle$  the long chain branching index. The definition of the last three parameters and the method of measurement have been given by Prechner *et al.*<sup>4</sup>.

We can observe that structural parameters of group I samples are clearly different although their melt indices are very close.

## Procedure

Measurements with Instron capillary rheometer have been achieved in the same conditions for all samples,

Table 1 Structural parameters of the samples studied

Ref.	$d$	$MI$	$[\eta]$ (dl/g)	$M_w^*$	$P^*$	$\langle g'_\eta \rangle$
Group I:						
A	0.919	1.9	0.982	256 000	28.9	0.357
B	0.9248	1.85	0.807	78 400	6.4	0.650
C	0.9225	2.15	0.858	124 200	6.7	0.495
D	0.9216	2	1.04	117 200	8.4	0.694
E	0.9245	2.15	0.810	85 700	5.4	0.609
F	0.926	2.10	0.837	64 000	6.1	0.832
Group II:						
G	0.9227	0.4	1.093	114 000	7.45	0.758
H	0.922	0.62	0.984	125 000	8.0	0.617
F	0.926	2.10	0.837	64 000	6.1	0.832
I	0.920	5.40	0.835	126 000	10.6	0.506
J	0.918	15.2	0.775	111 000	11.9	0.535



i.e. at a temperature of 190°C with a capillary whose ratio of length to diameter is 16. Since we are interested in comparing the samples we did not apply either the Bagley or the Rabinovitch corrections. The apparent viscosity of products was measured according to shear rates varying between 3.1 s<sup>-1</sup> and 1555 s<sup>-1</sup>. The accuracy of the measurements was about 2%.

Dynamic measurements have been achieved with a Contraves-Kepes Balance-Rheometer. The torque momentum was recorded using a stress gauge. Complex viscosity was measured at 190°C with frequency varying between 10<sup>-3</sup> Hz and 20 Hz. The accuracy on  $\eta'$  and  $\eta''$  was about 4%.

## RESULTS

Table 2 shows the values of the apparent viscosity measured for a shear rate value of 3.1 s<sup>-1</sup> (called  $\eta_{3.1}$ ) and the ratio  $\eta_{3.1}/\eta_{31}$ .

In Figure 1, flow curves are presented for a large range of shear rates. We can see that the flow curves relating to the group I samples are practically the same.

The Balance-Rheometer results have been given as Cole-Cole plots for group I products (Figure 2) and group II products (Figure 3).

In Table 2, we have shown the values of the parameters  $\eta_0$ ,  $\tau_0$  and  $h$  previously defined and the parameter  $G_0 = \eta_0/\tau_0$  which is an elasticity coefficient.

Considering the experimental uncertainties, since  $\eta_0$  is given by extrapolation of the curves and the maximum of the curve  $\eta''(\nu)$  is rather smooth,  $\eta_0$  is known to a certainty of 5%,  $\tau_0$  to a certainty of 10%; therefore the certainty relative to  $G_0$  is 15%. Nevertheless, there are significant differences for this parameter.

Table 2 Viscoelastic properties of sample studies

Ref.	MI	$\eta_{3.1}(P)$	$\frac{\eta_{3.1}}{\eta_{31}}$	$\eta_0(P)$	$h$	$\tau_0$ (sec)	$G_0$ (dyne/cm <sup>2</sup> )
Group I:							
A	1.9	36 400	2.44	110 000	0.50	4.80	23 000
B	1.85	36 400	2.21	51 500	0.49	0.40	12 900
C	2.15	33 000	2.13	66 000	0.51	1.17	56 600
D	2	31 600	2.19	68 000	0.52	1.27	53 500
E	2.15	33 000	2.19	40 000	0.49	0.26	51 500
F	2.10	36 400	2.74	73 400	0.47	1.0	73 400
Group II:							
G	0.4	86 600	3.36	605 000	0.55	19.1	31 700
H	0.62	68 700	3.03	365 000	0.52	11.4	32 000
F	2.10	36 400	2.74	73 400	0.47	1.0	73 400
I	5.40	17 900	2.24	28 000	0.49	0.55	51 000
J	15.2	8 600	1.91	10 200	0.51	0.21	48 600

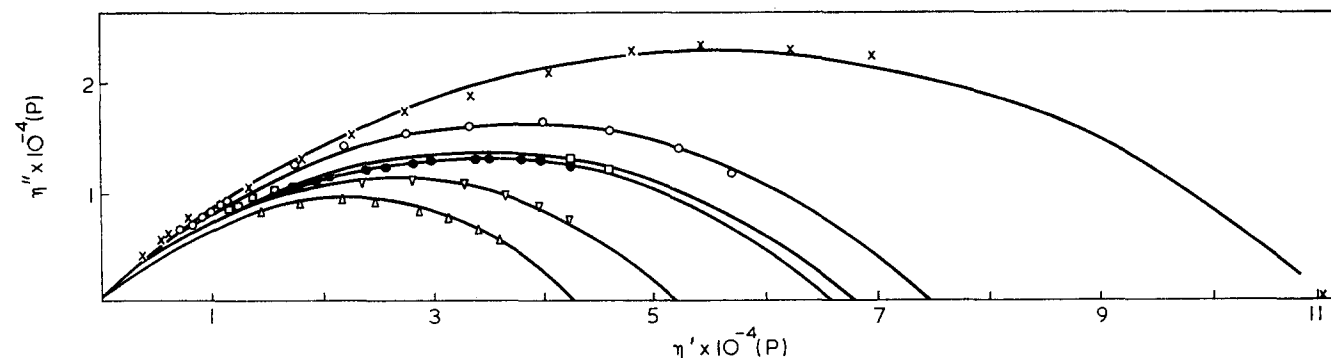


Figure 2 Cole-Cole's representation: imaginary part of the complex viscosity plotted against real part for group I products.  $\times$ , A;  $\nabla$ , B;  $\bullet$ , C;  $\square$ , D;  $\triangle$ , E;  $\circ$ , F

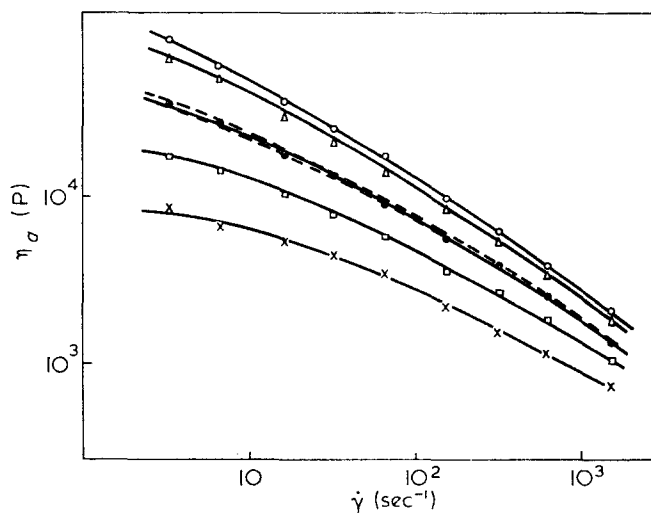


Figure 1 Flow curves of non-Newtonian viscosity against shear rate for group II products.  $\bullet$ , F;  $\circ$ , G;  $\triangle$ , H;  $\square$ , I;  $\times$ , J

Figures 4 and 5 show the distribution function of the logarithms of the relaxation times  $N(\tau) = \tau H(\tau)$ , computed using the Cole-Cole expression,  $H(\tau)$  being the distribution function currently used in rheology<sup>5, 6</sup>.

## DISCUSSION

Group I samples with the same grade have a very similar steady flow behaviour, briefly described by  $\eta_{3.1}$  and  $\eta_{3.1}/\eta_{31}$ .

On the other hand their processing properties (e.g. die swell, melt fracture and retractability) are very different. The differences between these products are also shown in their dynamic behaviour<sup>7</sup> and may be described by the two parameters  $\eta_0$  and  $\tau_0$ .

However, there is no significant difference between dynamic parameters for samples C and D although their long chain branching indices are clearly different. This shows a limit to the present state of our investigations.

Parameter  $h$  is constant for all the products. We can get a general approach of the behaviour of the products through their assimilation to a simple Maxwell model with a single relaxation time  $\tau_0$  and an elasticity  $G_0$ .

Using  $\eta_0$  and  $\tau_0$  we can draw for group II samples a master curve relative to the steady flow curves. As a matter of fact, if we plot the ratio  $\eta_a/\eta_0$  where  $\eta_a$  is the apparent viscosity versus  $\dot{\gamma}\tau_0$ , all experimental points (groups I and II) are located on the same master curve (Figure 6).

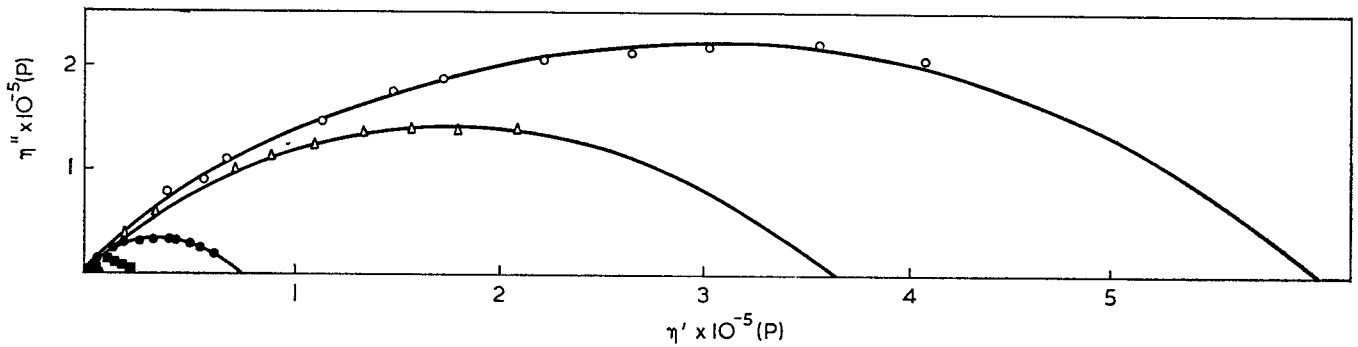


Figure 3 Cole-Cole's representation: imaginary part of the complex viscosity plotted against real part for group II products. ●, F; ○, G; △, H; ■, I; ×, J

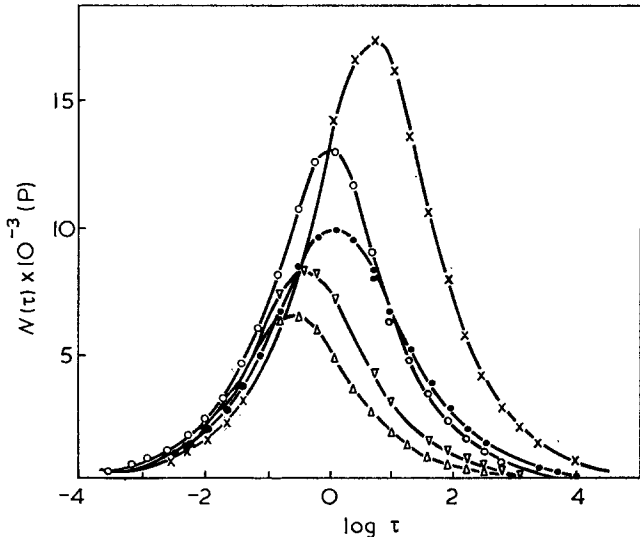


Figure 4 Distribution function of the logarithm of the relaxation times against the logarithm of the relaxation times for group I products. ×, A; ▽, B; ●, C; △, E; ○, F

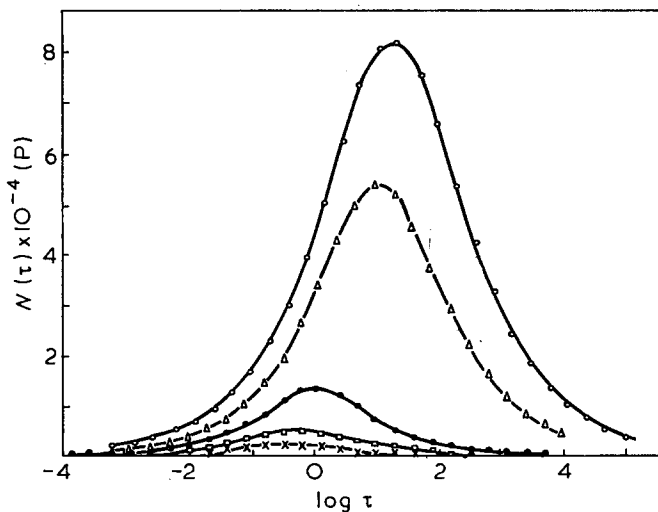


Figure 5 Distribution function of the logarithm of the relaxation times against the logarithm of the relaxation times for group II products. ●, F; ○, G; △, H; □, I; ×, J

This last result is in agreement with previous studies<sup>8,9</sup> and shows that the characteristic relaxation time  $\tau_0$  we defined has to be related to the maximum relaxation time which was introduced in some high polymer molecular theories<sup>10-12</sup>.

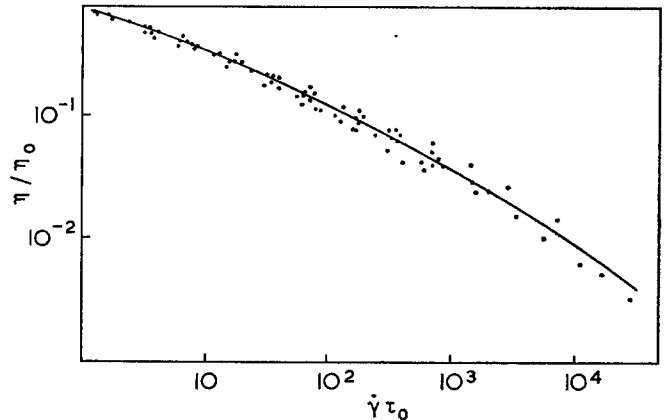


Figure 6 Master curve of  $\log \eta/\eta_0$  against  $\log \dot{\gamma}\tau_0$  for group II products

## CONCLUSIONS

Plotting the dynamical parameters of branched polyethylene in the Cole-Cole plane has been an efficient method for comparing these products.

Differences in molecular weight distribution and long chain branching index induce large variations in the two parameters: zero shear rate viscosity  $\eta_0$  and a characteristic relaxation time  $\tau_0$ .

These two parameters appear to be useful for a better understanding of the processing properties of branched polyethylene.

## REFERENCES

- 1 Monge, Ph. and Labaig, J. J. *Proc. 6th Int. Congr. Rheol., Lyon 1972*, in press
- 2 Landau, L. and Lifchitz, E. 'Electrodynamique des milieux continus', (Ed. Mir) Moscow, 1969, p 336
- 3 Cole, K. S. and Cole, R. H. *J. Chem. Phys.* 1941, **9**, 341
- 4 Prechner, R., Panaris, R. and Benoit, H. *Makromol. Chem.* 1972, **156**, 39, 54
- 5 Gross, B. 'Mathematical Structures of the Theories of viscoelasticity', Hermann et Cie, Paris, 1953
- 6 Williams, M. L. and Ferry, J. D. *J. Polym. Sci.* 1953, **11**, 169
- 7 Chartoff, R. P. and Maxwell, B. *J. Polym. Sci. (A-2)* 1970, **9**, 455
- 8 Blyer, L. L. *Trans. Soc. Rheol.* 1969, **13**, 39
- 9 Shida, M. and Cancio, L. U. *Polym. Eng. Sci.* 1971, **11**, 2
- 10 Rouse, P. F. *J. Chem. Phys.* 1953, **21**, 1272
- 11 Bueche, F. and Harding, S. W. *J. Polym. Sci.* 1958, **32**, 177
- 12 Graessley, W. W. *J. Chem. Phys.* 1967, **47**, 6

# Lamellar thickening and chain-extended growth of polyethylene

D. C. Bassett and D. R. Carder

*J. J. Thomson Laboratory, University of Reading, Reading RG6 2AF, UK  
(Received 9 March 1973; revised 10 April 1973)*

The lamellar thickness of chain-extended polyethylene produced by annealing at high pressure increases logarithmically with time. The rate of increase is faster than for the same material annealed at 1 bar ( $\equiv 10^5$  N/m<sup>2</sup>), but the large crystal thickness owes more to the initial increase than to enhanced thickening. The similarity of high and low pressure behaviour on annealing supports the hypothesis that chain-folded and chain-extended growth of polyethylene are models, one of the other.

## INTRODUCTION

The discovery that crystallization of polyethylene from the melt at pressures of the order of 5 kbar (1 bar  $\equiv 10^5$  N/m<sup>2</sup>) produced very thick lamellae in comparison to those familiar from work at 1 bar<sup>1</sup> posed several questions, among them (a) do the layers consist of molecules in fully extended conformation, (b) how does the large thickness develop and (c) what is the relationship of crystal growth at high pressures to normal chain-folded crystallization? The first of these has already been answered in the negative. Molecules are usually folded in pressure-crystallized polyethylene. The average layer thickness increases with the time and temperature of crystallization, the same trends observed for crystallization at atmospheric pressure<sup>2</sup>. This paper is concerned with the other two issues and supplements recent work which has shown that chain-extended crystallization is distinct from chain-folded<sup>3</sup> and is associated with the appearance at high pressures of a new phase of polyethylene<sup>4</sup>. It concludes that although long-term lamellar thickening contributes substantially to the final thickness of chain-extended layers, it is not the primary cause of the large molecular extension. In addition it provides further experimental support for the hypothesis that chain-folded and chain-extended crystallization are models, one of the other.

## EXPERIMENTAL AND RESULTS

The specimens used were of Rigidex 2 (BP Chemicals Ltd) polyethylene about 0.2 mm thick which had been oriented by cold drawing to a natural draw ratio of eight. They were punched out in the form of tensile test-pieces 50 mm long parallel to the draw direction and 1.5 mm central width. For high pressure treatment these were suspended, lightly clamped at one end, in silicone oil inside a piston-cylinder apparatus. The precise details of the apparatus and relevant techniques identical to those used in this work have been described for an associated investigation<sup>5</sup>. A pressure of  $5.34 \pm 0.03$  kbar was imposed at room temperature before heating over about 2 h to the controlled temperature of

$245 \pm 0.5^\circ\text{C}$  which was approached at  $\sim 0.3^\circ\text{C}/\text{min}$  and then maintained for varying times up to 24 h. Subsequently the apparatus was cooled to ambient temperature, the pressure was released, and excess silicone oil was removed from the samples by washing in cold xylene.

*Figure 1* records the density and number-average lamellar thickness of polyethylene treated in this way as a function of annealing time. The first measurement was obtained at  $23.0 \pm 0.1^\circ\text{C}$  with a density gradient column containing carbon tetrachloride and toluene. The second came from replicas of fracture surfaces photographed in the electron microscope, sampled by our usual technique<sup>2, 5</sup> and calibrated against a standard grating.

In *Figure 2* are data obtained on identical material annealed at 1 bar and  $130 \pm 0.2^\circ\text{C}$  by immersion in silicone oil at this temperature and then quenched in more silicone oil. These length measurements were given by converting the position of a single diffraction maximum seen in small angle X-ray scattering, using Bragg's law.

*Figure 3* shows the two sets of thicknesses plotted against the logarithm of time. A linear relationship holds for both. The slope at 5 kbar is  $185 \text{ \AA}/\text{decade}$  of minutes and at 1 bar  $78 \text{ \AA}/\text{decade}$ , while the lengths extrapolated back to 1 minute are 1140 and 220  $\text{\AA}$  respectively.

## DISCUSSION

Impetus was given to the investigation of the role of time dependence in high pressure crystallization phenomena by the discovery that chain-folded lamellae could be transformed through a continuous spectrum of molecular extensions to chain-extended dimensions<sup>6, 7</sup>, a result which is now amply confirmed<sup>5</sup>, notwithstanding earlier criticisms<sup>8, 9</sup>. This was relevant to the issue of whether the large thicknesses of chain-extended crystals developed by pressure-enhanced thickening of chain-folded lamellae, e.g. as formulated by Peterlin<sup>10</sup> or formed directly in crystal growth. While at first sight this discovery seemed to support the former hypothesis

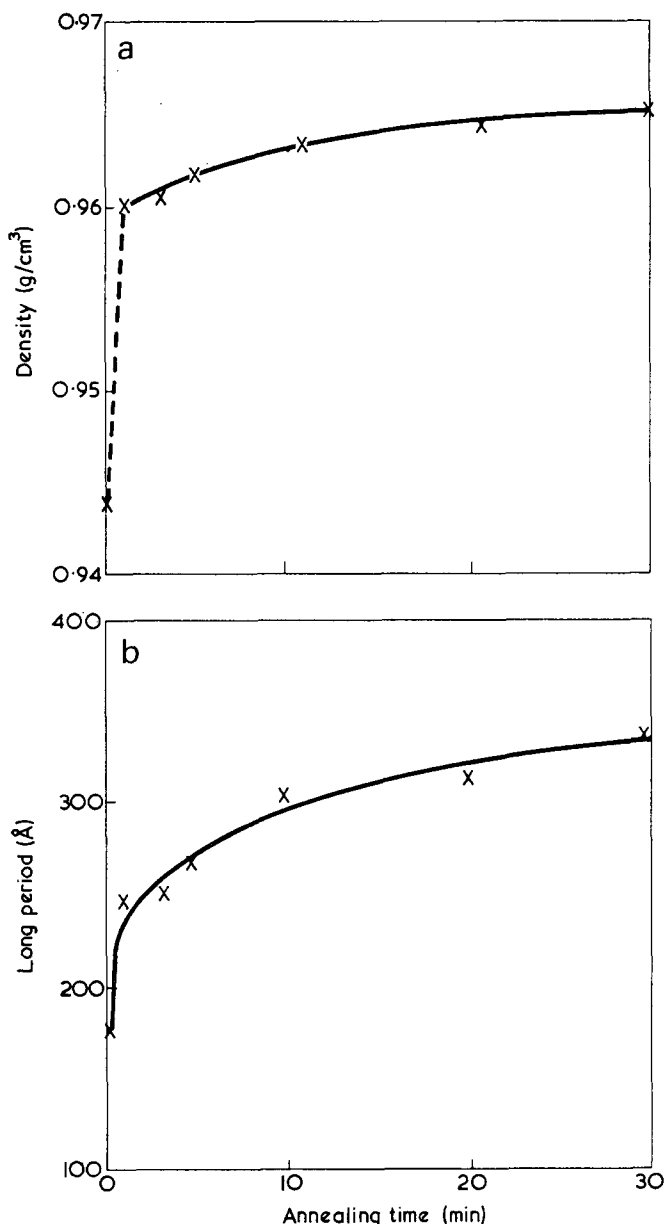


Figure 1 Variation of (a) density and (b) long period with time for drawn polyethylene annealed at 130°C and 1 bar

it was also evident that to consider the matter adequately much more needed to be known about the basic details of crystal growth of polyethylene at high pressures. Accordingly a programme of research was undertaken which looked first at crystallization from the melt at 5 kbar using good fractions. This showed that, contrary to what had been generally supposed, the average thickness of chain-extended crystals was not constant, and did increase with time, but also that the situation was more akin to chain-folded crystallization at 1 bar in that lamellar thickness increased with both the time and temperature of crystallization<sup>2</sup>. Preliminary comparison has shown that there is a similar proportional dependence of fold length on supercooling at 5 kbar and under vacuum<sup>11</sup>. Now, the similarity between high and low pressure behaviour is reinforced by the data reported here of the time dependence of lamellar thickening on annealing.

It is well known that whole polymer annealed at 1 bar increases its fold length logarithmically with time<sup>12</sup>. Figure 3 shows that this is also the case at 5 kbar and

that the long-term thickening is faster at the higher pressure. Nevertheless, although the figure of 185 Å/decade recorded at 5 kbar is more than twice that measure at 1 bar\*, and is also higher than atmospheric values of others<sup>12</sup>, it is clear from Figure 3 that the large thickness of chain-extended crystals produced by high pressure annealing has more to do with the initial increase (from 180 Å to over 1300 Å in 15 min) than with 400 Å of subsequent thickening in 24 h. This is a conclusion we should also expect to apply to high pressure crystallization, because we have argued elsewhere<sup>5</sup> that annealing of polyethylene can now be regarded without difficulty as due to a combination of melting and recrystallization.

This evidence is in accord with other, later work in this laboratory, which has shown that chain-extended crystallization of polyethylene is distinct from chain-folded and does not result from conversion of preformed chain-folded lamellae<sup>3</sup>. Indeed at the same pressure and temperature chain-extended crystals form before chain-folded. The occurrence of chain-extended growth has also been correlated with the appearance of a new, high pressure phase of polyethylene<sup>4</sup>. It thus becomes especially pertinent to enquire whether, as a first hypothesis, chain-extended growth is simply chain-folded crystallization operating between different phases than usual. What little data are available is not inconsistent with this suggestion<sup>4</sup>. Moreover, the finding that for first temperature<sup>11</sup> and now time dependence there are formal similarities between chain-folded and chain-extended behaviour supports the idea that each is a model for the other. If this is true, then the crystallization of polyethylene at high pressures takes on a wider relevance. Its great crystal size and associated comparative ease of examination might also make it a more

\* This comparison may be exaggerated because annealing was carried out closer to the final melting point of chain-extended material at high pressure. According to our measurements this parameter is 254°C at 5.3 kbar<sup>5</sup>. Conversely if allowance is made for the two different techniques of measuring length, using the empirical correction derived elsewhere<sup>5</sup>, the difference is accentuated.

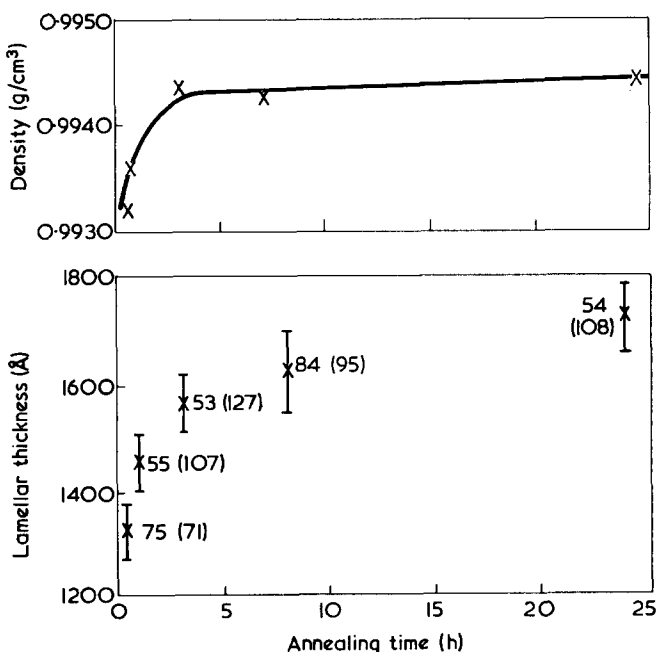


Figure 2 Variation of (a) density and (b) lamellar thickness for drawn polyethylene annealed at 245°C and 5.3 kbar

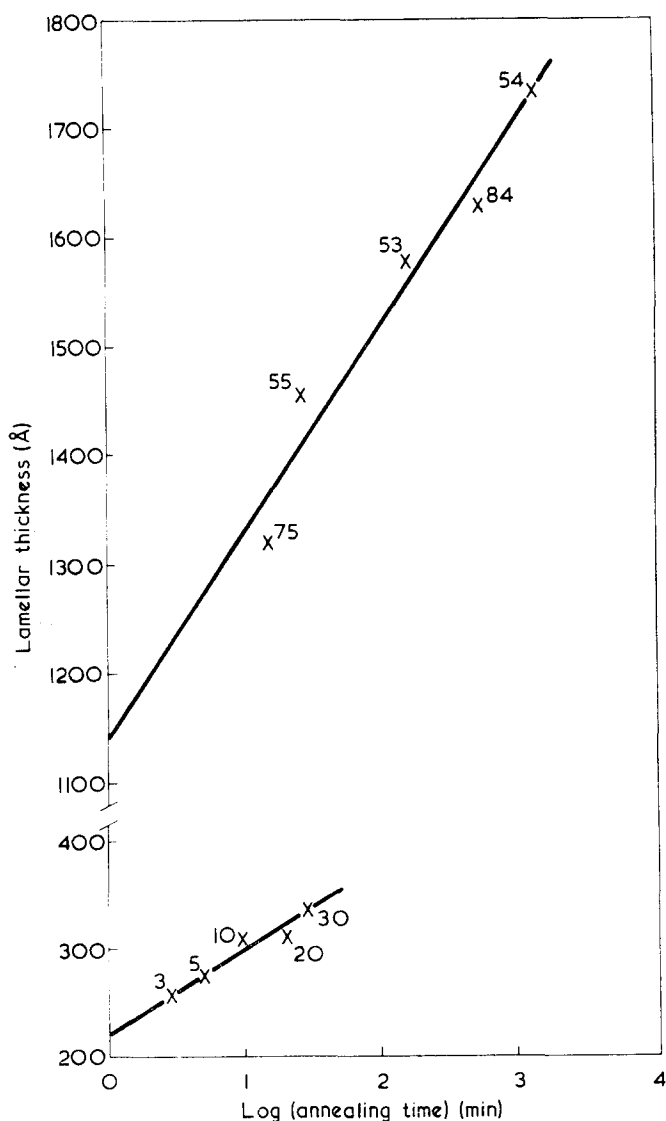


Figure 3 The crystal thickness data of Figures 1 (lower data; slope=78 Å/decade) and 2 (upper data; slope=185 Å/decade) replotted as functions of log annealing time.

valuable system than chain-folded crystallization on which to investigate fundamentals of growth from the melt. In particular observations on chain-extended growth which have been interpreted in terms of final crystal thickness being determined by a process more complicated than the simple deposition of a chain-folded molecular strip on a substrate, would be of more general application<sup>11, 13</sup>.

Lastly, we note, comparing the thicknesses of chain-extended and chain-folded crystals, that whereas the relative changes produced by crystallization temperature are in proportion to lamellar thicknesses, those given by time dependent thickening are more nearly equal. This suggests that isothermal thickening does not directly involve units of the full layer thickness as it would, for example, in secondary crystallization or fold length doubling, but rather is restricted to something like the adjustment of fold surface roughness where the proportionate effect of lamellar thickness is subdued.

#### ACKNOWLEDGEMENT

This work was carried out with the support of the Procurement Executive, Ministry of Defence.

#### REFERENCES

- 1 Geil, P. H., Anderson, F. R., Wunderlich, B. and Arakawa, *J. Polym. Sci. (A)* 1964, **2**, 3707
- 2 Rees, D. V. and Bassett, D. C. *J. Polym. Sci. (A-2)* 1971, **9**, 385
- 3 Bassett, D. C., Khalifa, B. A. and Turner, B. *Nature (Phys. Sci.)* 1972, **239**, 106
- 4 Bassett, D. C. and Turner, B. *Nature (Phys. Sci.)* 1972, **240**, 146
- 5 Bassett, D. C. and Carder, D. R. *Phil. Mag.* (in press)
- 6 Rees, D. V. and Bassett, D. C. *Nature* 1968, **219**, 368
- 7 Rees, D. V. and Bassett, D. C. *J. Polym. Sci. (B)* 1969, **7**, 273
- 8 Fischer, E. W. and Puderbach, H. *Kolloid-Z.* 1969, **235**, 1260
- 9 Gruner, C. L., Wunderlich, B. and Bopp, R. C. *J. Polym. Sci. (A-2)* 1969, **7**, 2099
- 10 Peterlin, A. *Polymer* 1965, **6**, 25
- 11 Bassett, D. C. and Phillips, J. M. *Polymer* 1971, **12**, 730
- 12 Fischer, E. W. and Schmidt, G. F. *Angew. Chem.* 1962, **74**, 551
- 13 Bassett, D. C. and Khalifa, B. A. *Polymer* 1973, **14**, 390

# Chain-extended crystallization of polyethylene: effect of sample thickness

D. C. Bassett and B. A. Khalifa

*J. J. Thomson Laboratory, University of Reading, Reading RG6 2AF, UK  
(Received 9 March 1973)*

Films of polyethylene varying in thickness from 100 Å to 1 mm have been melted and recrystallized at 5 kbar ( $1 \text{ bar} \equiv 10^5 \text{ N/m}^2$ ). All produced the spherulitic texture characteristic of chain-extended growth, but the average lamellar thickness increased with that of the specimen by a factor of about ten from hundreds to thousands of Å. The effect is discussed in terms of processes involved in the establishment of layer thickness. It also offers a means of removing the major difficulty in regarding lamellar thickening of polyethylene on annealing as a combination of melting and recrystallization.

## INTRODUCTION

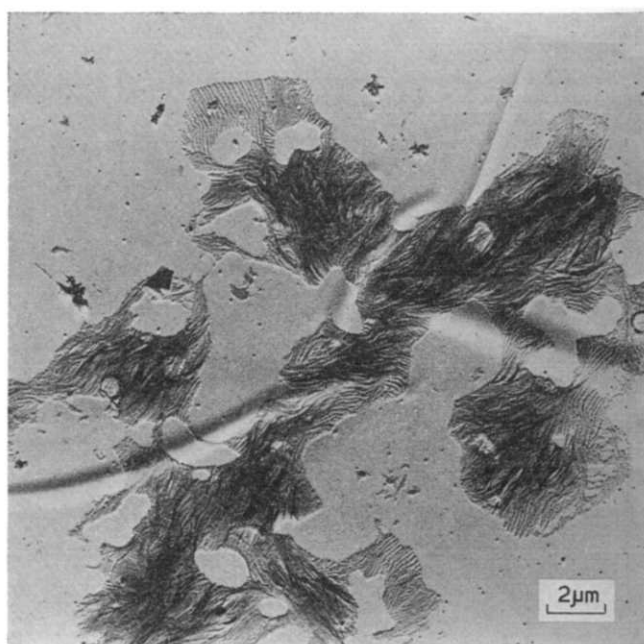
This work was originally undertaken as part of a wider investigation into the morphology of chain-extended polyethylene which sought to prepare thin films of this material and to examine them by transmission electron microscopy. In this way it was hoped to observe whole crystals rather than having to rely on those cross-sections preferentially revealed in fracture surfaces. From the first, however, it was evident that crystallization of polyethylene in very thin films at high pressures did not produce thick crystals. Instead the lamellae formed were very similar to those crystallized at 1 bar ( $\equiv 10^5 \text{ N/m}^2$ ), being only a few hundred Å thick. This observation led to the present work which is singled out from the wider investigation (to be reported elsewhere) because it reveals a new effect in polymeric crystallization which moreover, offers a solution to the main difficulty in regarding lamellar thickening of polyethylene on annealing as being due to a combination of melting and recrystallization.

## EXPERIMENTAL RESULTS

The first experiments used polyethylene crystals grown from dilute solution in xylene which were then sedimented on cleaved mica substrates. After recrystallization from the melt at 4.95 kbar they appeared as in *Figure 1*. The surprising formation of thin crystals when thick, chain-extended layers were produced in bulk polymer prompted three actions. First, specimens were scrutinized for molecular degradation. For microscopic samples this was restricted to subsequent melting and recrystallization behaviour but for larger amounts, carbonyl absorption was looked for at  $1720 \text{ cm}^{-1}$  in the infra-red. None of these tests proved positive. Second, experiments were conducted to see whether nucleation by partly extended molecules, as e.g. in 'shish-kebabs' would alter the situation. It did not, reflecting the common experience in polymer crystallization that primary nucleation is not important for lamellar

thicknesses. Third, the effect of specimen dimensions on layer thickness was examined.

The appearance of thin layers after recrystallization at 5 kbar remains for films thousands of Å thick, prepared either by melting multilayer crystals grown from concentrated solution in xylene, or by solvent casting. As *Figure 2* shows, even microtomed films  $3 \mu\text{m}$  thick, when recrystallized reveal surface steps of a few hundred Å and have a similar textural appearance to the thinnest films. Yet such samples have melting points of  $\sim 140^\circ\text{C}$ , are brittle at room temperature, revealing fracture surfaces as in *Figure 3a* and would be regarded as chain-extended even on the old arbitrary criteria of melting point and crystal size. Moreover, it is clear both from replication of fracture surfaces and from transmission



*Figure 1* Appearance of solution-grown crystals of polyethylene which were melted then recrystallized at 4.95 kbar

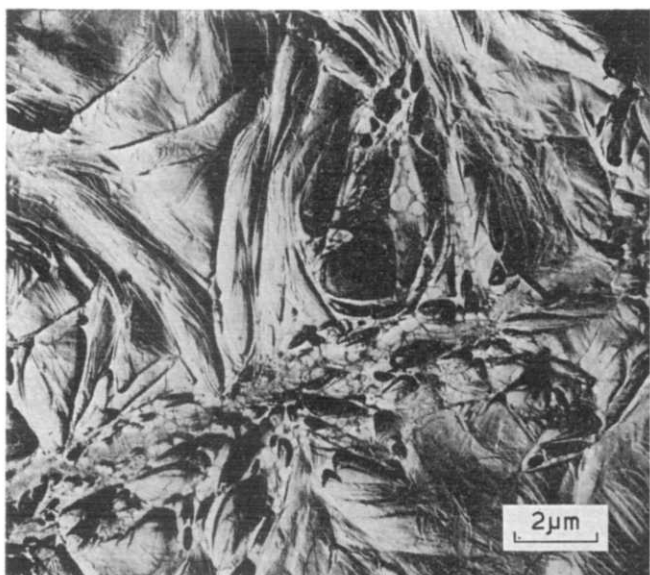


Figure 2 Replica of the free surface of a microtomed section of polyethylene, initially  $3\mu\text{m}$  thick, after recrystallization at  $4.95\text{kbar}$

microscopy with 1 MeV electrons that there is no special surface texture, but that the steps seen there represent fractional differences of the full layer thicknesses. The continuity in spherulitic texture from the thinnest to the thickest samples reflects the common formation by the distinct high-pressure growth process which for historical reasons has had to be denoted 'chain-extended'<sup>1</sup>, although this nomenclature is now unfortunately seen to have to embrace lamellae only hundreds of Å thick. Qualitatively, however, these experiments show clearly that the thicknesses of chain-extended lamellae are depressed in thin films.

More quantitative measurements have been made for several runs involving films microns or more thick because these can be fractured to allow measurements on clearly identifiable lamellar thicknesses, rather than using step heights seen on top surfaces. All the data show the same trend of behaviour, but the precise figures do not repeat exactly from run to run, suggesting that with a variable as crude as film thickness certain more vital, microscopic, factors are not under control. Here we quote measurements for one particular experiment only, as an illustration, in which four samples of nominal thicknesses 3, 10 and  $50\mu\text{m}$  were crystallized side by side with a pellet ( $\sim 1\text{mm}$  cube) of the same polymer, Rigidex 9 (BP Chemicals Ltd).

The two thinnest specimens were cut to their nominal size with a microtome, while the  $50\mu\text{m}$  one was part of a drawn film whose thickness was calculated by weighing a measured area. All the films were sandwiched between cleaved mica surfaces, one of which was coated with carbon to facilitate subsequent treatment. The four samples were then individually loosely wrapped in platinum foil and encapsulated in water inside the high pressure apparatus. Pressure was raised to  $2.8\text{kbar}$  and controlled while samples were heated to  $229.5^\circ\text{C}$ . Then a pressure of  $4.95\text{kbar}$  was imposed which caused a rise of some degrees for a few minutes until the temperature was again controlled at  $229.5^\circ\text{C}$  for 1 h. After this the press was cooled to room temperature and pressure was finally released. From subsequent experience it is likely that crystallization occurred during

the temperature transient, i.e. a degree or two above  $229.5^\circ\text{C}$ . This does not affect the comparison of the three films, nor does the fact that each became non-uniform in thickness, with an overall thickening, during the treatment. The separation of the two edges of specimens fractured in planes approximately parallel to the film normal was as much as twice the nominal film thickness. This includes multiplication by the secant of the angle between the fracture face and film normal but it is unlikely to account for all the apparent increase in thickness.

Detail of fracture surface replicas of the four specimens is shown in Figures 3a-3d. The two thinnest seem to contain thinner lamellae than the third, which in turn shows a smaller molecular extension than the bulk sample. This is confirmed by measurements, using our standard technique of random sampling<sup>2</sup>, which are summarized in the normalized histograms of Figure 4. 200 lamellae were sampled for each of the three thinnest films and 197 for the bulk polymer. The number-average mean figures for molecular extension, i.e. crystal thickness along  $c$  and their standard errors are respectively  $1418 \pm 63 \text{ \AA}$ ,  $1616 \pm 63 \text{ \AA}$ ,  $2048 \pm 90 \text{ \AA}$  and  $3071 \pm 121 \text{ \AA}$ . It is to be noted that the breadth of the distribution also increases with the mean.

## DISCUSSION

That physical constraints might restrict crystal growth is intuitively a plausible idea, one which insofar as it is contained within the term 'entanglement' goes back to the early development of polymer science. Since the recognition of the lamellar nature of crystalline polymers, the role of crystallization temperature via the associated supercooling has been recognized to be the dominant factor controlling layer thickness. What this work shows, however, is that specimen size has an influence at least as great as, and probably greater than, any other variable. For polyethylene crystallized from solution, a two-fold variation is possible from crystallization temperature in contrast to variables such as solvent, molecular weight and concentration which have much less effect<sup>3</sup>. In melt growth, crystallization time becomes important, but its influence is small in comparison with the range from, say, 200 to over  $1000 \text{ \AA}$  produced by varying the temperature<sup>4</sup>. For melt growth at  $5\text{kbar}$ , crystallization for moderate times over a comparatively wide temperature range on a fractionated polyethylene ( $\bar{M}_w = 57\,200$ ,  $\bar{M}_n = 50\,100$ ) produced a variation of nearly two, from  $1900$  to  $3400 \text{ \AA}$ , in number-average lamellar thickness<sup>2,5</sup>. In contrast a factor of two is produced by specimen size, according to the data of Figure 4, but this represents only the upper end of a continuous morphological spectrum down, according to Figure 1, to sizes of a few hundred Å, so that an overall factor of about ten would seem more realistic.

Kinetic theories of polymeric crystallization relate lamellar thickness to secondary nucleation at the growing crystal edge, which specimen size might affect through constraining molecular configurations in the melt, or in altered diffusion conditions. Theory has so far considered the deposition of a molecular strip in its final configuration which appears to give a satisfactory explanation of data for solution growth provided that the effective surface free energy,  $\sigma_{\text{eff}}$ , for growth is as much as 50% higher than that measured during melting<sup>6</sup>.

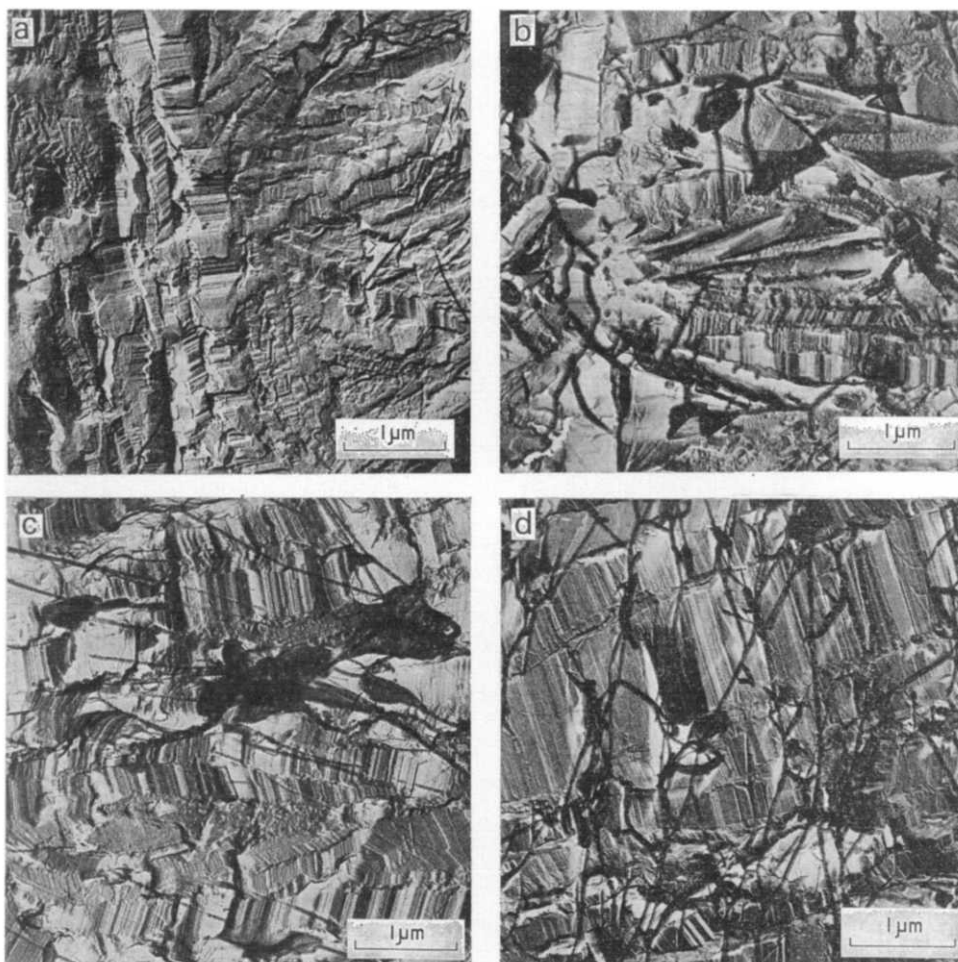


Figure 3 Replicas of fracture surfaces of polyethylene films after recrystallization at 4.95 kbar. Initial thicknesses nominally (a) 3  $\mu\text{m}$ , (b) 10  $\mu\text{m}$ , (c) 50  $\mu\text{m}$  and (d) 1 mm (bulk)

When one turns to melt growth, the situation is not so satisfactory. A typical crystal thickness would be, say, 400 Å in contrast to about 150 Å for solution growth at a comparable supercooling. Because the surface free energy measured from variation of melting point with fold length shows little difference between the two cases, the increased thickness implies that  $\sigma_{\text{eff}}$  would need to be much increased for melt growth. This is a parameter associated with surface roughness and while one might anticipate a small increase in changing from solution to melt conditions, that actually required is hard to explain. Moreover, observations on melt growth at high pressures, which appears to be a model system for atmospheric crystallization (related to the intervention of a new high pressure phase<sup>7</sup>), suggest that the process actually involved in establishing crystal thickness is more complicated than just depositing a single strip on a substrate.

Wunderlich has drawn attention to the increasing thickness of chain-extended lamellae with radial distance in spherulites<sup>8</sup>, while Rees and Bassett considered their morphological observations best interpreted in terms of lamellae propagating with a tapering edge<sup>2</sup>, a conclusion which is supported by our own, as yet unpublished, work on thin films. Direct evidence of increasing lamellar thickness with time has been found for both crystallization<sup>2</sup> and annealing<sup>9</sup> of polyethylene at high pressure. Indeed recent work has strengthened the analogy of chain-extended and chain-folded systems by

showing a logarithmic time dependence for annealing in both cases<sup>10</sup>. It has also shown, however, that time dependence is not a sufficient explanation of the large thicknesses produced at high pressure although it does contribute significantly to the final layer thickness. It may even be that there is a partial separation of the time dependent and initial contributions to thickness in the data of this paper, where there is still a significant reduction in lamellar thickness for samples nominally 50  $\mu\text{m}$  thick, a dimension within the range of spherulitic diameters. This is supported by Figure 4 which shows that it is the thickest layers which are suppressed in the thinnest films. One way in which this might arise is that lamellae growing outwards in a spherulite may be deflected and concentrated by the outer specimen surfaces and then be unable to thicken to their normal extent. Certainly on the conventional explanation of layer thickness it is hard to account for its marked response to specimen dimensions large compared with molecular lengths.

If specimen size also restricts fold lengths in chain-folded growth, then the effect is relevant to the interpretation of lamellar thickening of polyethylene on annealing. Such is the similarity to crystallization behaviour, not just at 1 bar but also at 5 kbar<sup>9</sup>, that it is easy to see why lamellar thickening on annealing has often been supposed to be equivalent to melting part of the sample (i.e. the thinnest lamellae) and then recrystallizing it at a higher, more stable thickness on



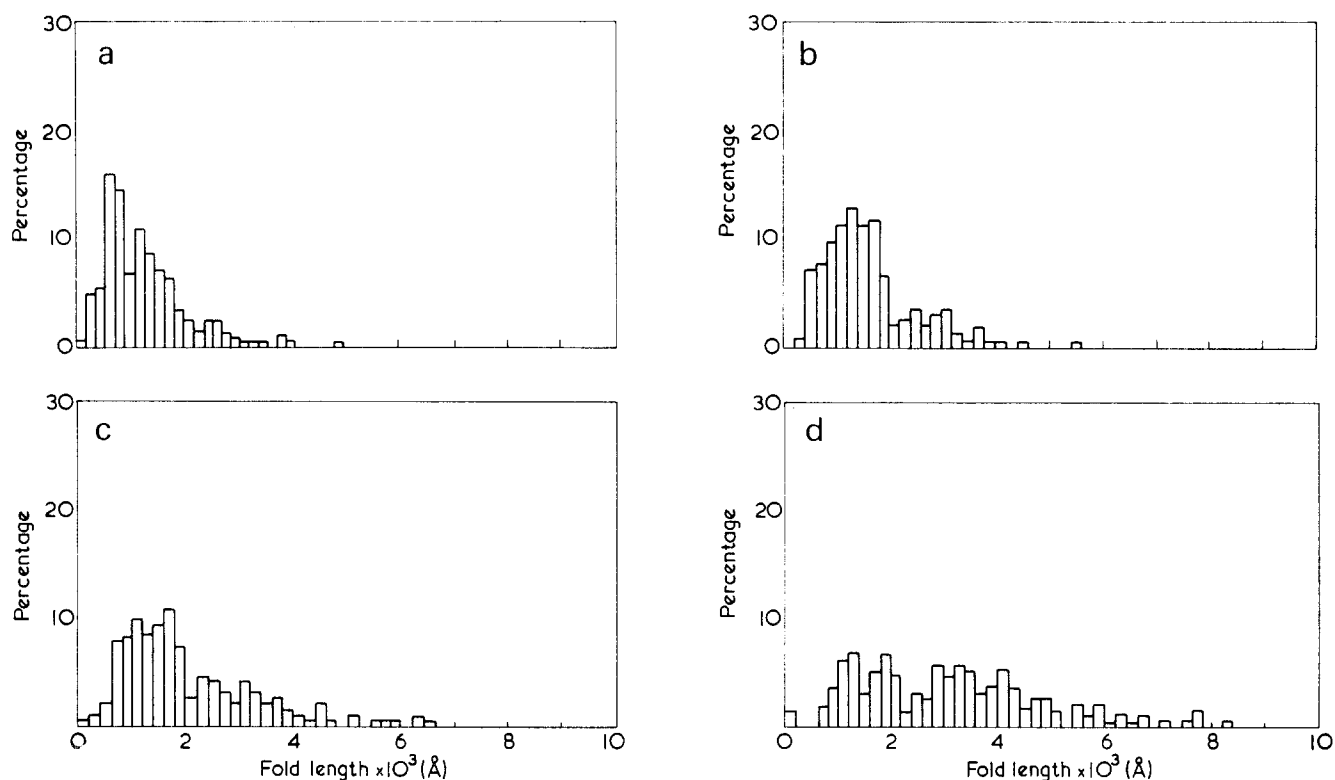


Figure 4 Normalized histograms of the frequency distribution of lamellar thicknesses parallel to  $c$  measured on the samples of Figure 3. (a)  $N=200$ ;  $L_n=1418$  Å;  $SD=63$  Å. (b)  $N=200$ ;  $L_n=1616$  Å;  $SD=63$  Å. (c)  $N=200$ ;  $L_n=2048$  Å;  $SD=90$  Å. (d)  $N=197$ ;  $L_n=3071$  Å;  $SD=122$  Å

the remainder. This could account for the maintenance of orientation during annealing, which is the main distinction between an annealed and a recrystallized sample, and also for the general experience with several polymers of spacings achieved by annealing being close to, but always below, those formed by recrystallization at the same temperature<sup>11</sup>. A more serious difficulty, however, has always seemed to us to be the effect of sample prehistory.

Baltá Calleja *et al.*<sup>12</sup> showed that if two polyethylene samples of different fold lengths were annealed side by side then that with lower initial fold length eventually attained higher crystal thicknesses than the other sample. Rees and Bassett confirmed the effect with fractionated polymer, showing that the earlier work was not due to differences in molecular weight<sup>2</sup>. If constraining the volume of recrystallizing material can restrict lamellar thickness, then we now have a possible solution to this difficulty.

In the experiment just described, the sample of lower average fold length will contain more lamellae of lower thickness so that at a particular annealing temperature more of this sample will melt than the other. On average therefore, polymer would recrystallize from larger local volumes in this sample and produce correspondingly higher fold lengths. If there were no such effect, then the fold length plots against temperature for the two samples would merge, but not cross. By 'local volume' is meant the effective volume contributing to the recrystallization of a particular lamella. At low annealing temperatures, especially those below the onset of macroscopic flow, this is likely to be restricted to a few molecular

segments immediately adjacent to the crystal edge, in which case the local volumes for the two samples would be the same and they would therefore retain their respective ranking of fold lengths. With higher temperatures, local volume should rise gradually to that appropriate to initial lamellar thicknesses thereby enabling the fold length of one sample to overtake that of its partner. Local volume will rise with temperature so that with its increase one might anticipate the eventual disappearance of the effect of initial fold length. There is no evidence on this last point, so far as we are aware. But for the rest, the qualitative picture outlined matches the known behaviour of polyethylene on annealing.

#### REFERENCES

- 1 Bassett, D. C., Khalifa, B. A. and Turner, B. *Nature (Phys. Sci.)* 1972, **239**, 106
- 2 Rees, D. V. and Bassett, D. C. *J. Polym. Sci. (A-2)* 1971, **9**, 385
- 3 Bassett, D. C. and Keller, A. *Phil. Mag.* 1962, **7**, 1553
- 4 Geil, P. H. 'Polymer Single Crystals', Interscience, New York, 1963
- 5 Rees, D. V. *PhD Thesis* University of Reading, 1970
- 6 Lauritzen, J. I. and Passaglia, E. *J. Res. Nat. Bur. Stand.* 1967, **71A**, 261
- 7 Bassett, D. C. and Turner, B. *Nature (Phys. Sci.)* 1972, **240**, 146
- 8 Wunderlich, B. and Melillo, L. *Makromol. Chem.* 1968, **118**, 250
- 9 Bassett, D. C. and Carder, D. R. *Phil. Mag.* in press
- 10 Bassett, D. C. and Carder, D. R. *Polymer* 1973, **14**, 387
- 11 Blais, J. J. B. P. and Manley, R. St. J. *J. Macromol. Sci. (B)* 1967, **1**, 525
- 12 Balta Calleja, F. J., Bassett, D. C. and Keller, A. *Polymer* 1963, **4**, 269

# Notes to the Editor

## Ionic end-groups in polymaleimide

C. H. Bamford and J. W. Burley

Department of Inorganic, Physical and Industrial Chemistry, University of Liverpool, Liverpool L69 3BX, UK  
(Received 10 April 1973)

Several workers<sup>1,2</sup> have reported the development of a red coloration during the polymerization of maleimide in dimethylformamide (DMF) solution and also the isolation of red polymers. The suggestion has been made<sup>1</sup> that unsaturated end-groups in the polymer might be responsible for the colour, but the exact origin of the latter was not elucidated.

We have observed similar coloration in solutions of polymaleimide in DMF and have studied these solutions spectrophotometrically. Polymaleimide was prepared by free radical polymerization of the monomer in methanol or acetone/water (90:10 v/v); generally initiation by azobisisobutyronitrile was used, but photoinitiation<sup>3</sup> ( $\lambda=435.8\text{ nm}$ ) by  $\text{Mn}_2(\text{CO})_{10}/\text{CCl}_4$  yielded polymers with identical properties for purposes of the present work. A 1:1 copolymer of maleimide and styrene was prepared similarly. Molecular weights of polymaleimide were determined viscometrically in DMF at 30°C with the aid of the relation<sup>3</sup>  $[\eta]=2.61 \times 10^{-4} \bar{M}_n^{0.701}$ . Commercially available DMF was used, also DMF which had been subjected to rigorous purification by allowing the liquid to stand for several 24 h periods over  $\text{P}_2\text{O}_5$  and distilling twice in vacuum. Pure DMF was stored in vacuum.

The visible absorption spectrum of a solution of polymaleimide ( $\bar{M}_n=3.1 \times 10^4$ ) in unpurified DMF (1 g/l) is shown in Figure 1 (curve A) and exhibits a peak at 496 nm. The solution is initially red but on standing in air the colour gradually changes to purple; this transformation is accompanied by a marked change in the visible absorption spectrum, which after 45 h shows two new maxima at 456 and 558 nm [Figure 1 (curve D)]. These and intermediate spectra such as those in Figure 1 (curves B and C) pass through isosbestic points at 470 and 517 nm indicating the occurrence of a relatively simple chemical change. Solutions of poly-

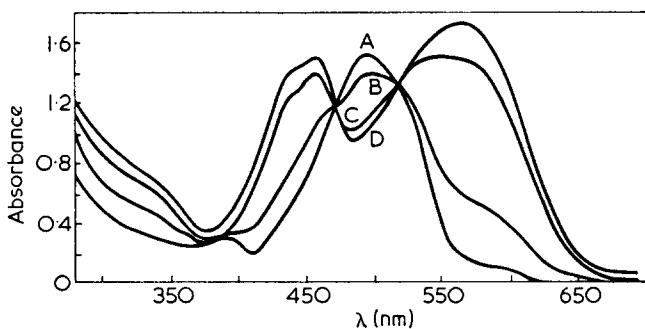


Figure 1 Absorption spectra of solutions of polymaleimide ( $\bar{M}_n=3.1 \times 10^4$ , 1 g/l) in unpurified DMF after standing for various times (h) in contact with air: A, 0.5; B, 3.0; C, 19.5; D, 45

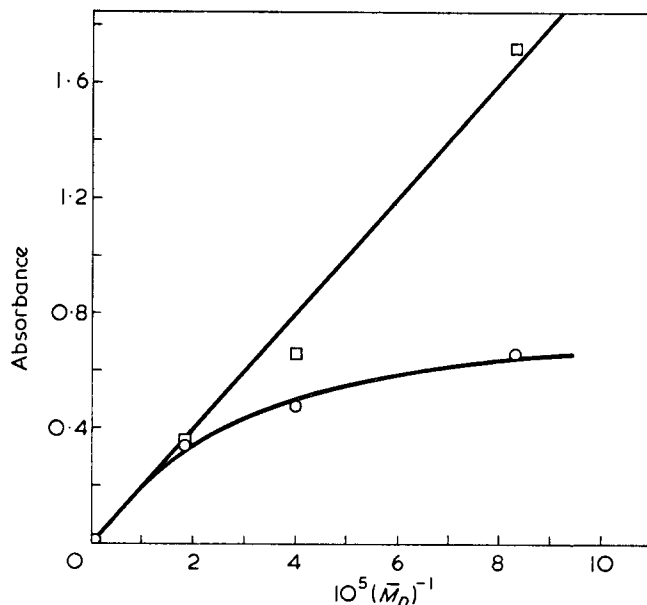
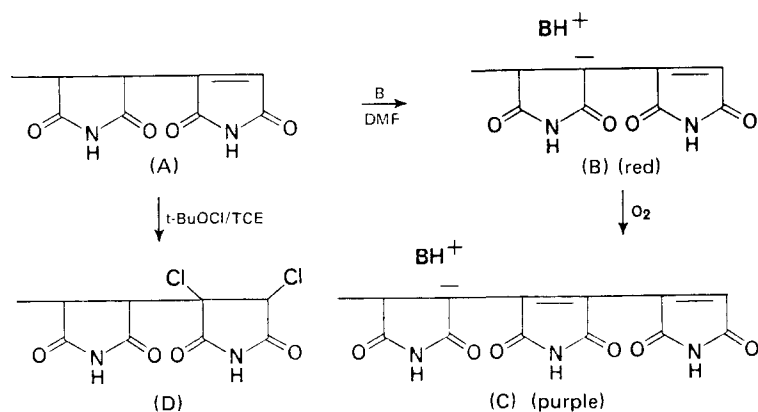


Figure 2 Absorbance of solutions of polymaleimide in DMF as a function of molecular weight. Spectra recorded after 100h:  $\square$ , purple band (560nm);  $\circ$ , red band (496nm)

maleimide in pure DMF were almost transparent in the visible region; however, addition of pyridine (Py) to the solutions resulted in the appearance of the red colour. Thus it seems likely that the origin of the coloration in commercial DMF lies in the presence of basic impurities. Both the red and purple colorations were dispersed by the addition of nitric acid, probably indicating protonation of anionic species.

When a solution of polymaleimide in DMF was prepared in vacuum the typical red colour developed but spectroscopic observations confirmed that no further change took place within 96 h. On exposing the liquid to the atmosphere or bubbling oxygen through the solution the red-purple transformation again occurred.

The intensities of the absorption bands were found to be directly related to the molecular weights of the polymaleimide. Figure 2 shows the relationship between the observed optical density and the reciprocal of the molecular weight for both the red and purple bands. A good straight line is obtained for the purple species (spectra recorded after 100h, approximately) but the plot for the initial product shows distinct curvature; the latter must reflect the slowness of the initial reaction responsible for the production of the red coloration (values of the optical density recorded at later times would not be helpful since the rate of the secondary process appears to be comparable to that of the primary



reaction leading to the red product). These observations suggest that the chromophores responsible for the absorption bands are terminal groups in the polymaleimide molecules.

Bamford *et al.*<sup>3</sup> showed that the termination process in the free radical polymerization of maleimide proceeds exclusively through a disproportionation reaction resulting in half the dead polymer chains having unsaturated end-groups (A); we believe that all the experimental observations can be explained in terms of the reactions of this type of end-group as follows. The initial reaction of polymaleimide in DMF is proton abstraction by pyridine or other base from the  $\alpha$  position to the double bond to give (B), in which there will be extensive delocalization of the negative charge, especially if tautomerism in the terminal ring is involved. Oxidation then results in the development of further unsaturation in the polymer backbone and hence in the formation of a more highly conjugated species (C). Evidently continuation of this oxidation process may occur and is probably responsible for the green coloration we have observed in aged solutions ( $\sim 8$  weeks). These showed substantial absorption above 600 nm but no distinct maxima were observed. We are not able to propose a mechanism for the oxidation process at present since no kinetic data are available.

Further evidence for the origin of the coloured solutions was obtained from chlorination of polymaleimide samples with *t*-butyl hypochlorite in *sym*-tetrachloro-

ethane (TCE). Reaction in this medium typically gives rise to *N*-chlorinated products<sup>4</sup> but samples isolated at short reaction times (1 h) (when no *N*-chlorination could be detected by infra-red spectroscopy) yielded transparent solutions of polymaleimide in DMF. These solutions remained colourless when pyridine was added. We therefore propose that chlorination of the reactive end-groups gives rise to saturated end-groups (D). A solution of the copolymer of styrene and maleimide in DMF was also transparent in the visible region; this would be expected since termination in the homopolymerization of styrene occurs solely by combination and cross-termination reactions would reduce the concentration of (A) groups in the polymer.

The linear relationship between optical density and  $\bar{M}_n^{-1}$  (for the purple band) presents the intriguing possibility that molecular weights of polymaleimide samples may simply be obtained from spectroscopic studies of their solutions in DMF. The extinction coefficients of the 496 and 558 nm bands were calculated to be 0.88 and  $1.06 \times 10^4$  respectively.

#### REFERENCES

- 1 Tawney, P. O. *et al. J. Org. Chem.* 1961, **26**, 15
- 2 Block, H. personal communication
- 3 Bamford, C. H., Bingham, J. F. and Block, H. *Trans. Faraday Soc.* 1970, **66**, 2612
- 4 Zimmer, H. and Audrieth, L. F. *J. Am. Chem. Soc.* 1954, **76**, 3856

## Dienolysis of lignin: cleavage of $\beta$ -aryl ethers by Diels-Alder synthesis

Wolfgang G. Glasser

Department of Forestry and Forest Products, Virginia Polytechnic Institute and State University, Blacksburg, Virginia 24061, USA

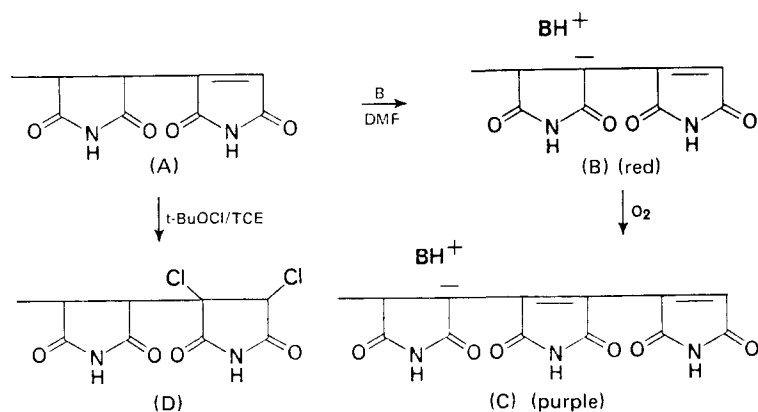
(Received 30 March 1973)

#### INTRODUCTION

In a recent paper by Glasser and Sandermann<sup>1</sup>, lignin model compounds with ethylenic double bonds in conjugation with aromatic rings were tested with respect to their reactivities in Diels-Alder reactions. Maleic anhydride, chloromaleic anhydride and tetracyanoethylene had served as dienophiles in this previous investigation. It was demonstrated that lignin-like  $\beta$ -substituted styrene derivatives can indeed serve as

dienes in the diene synthesis, and the isolation of a number of tetralin and dihydronaphthalene derivatives was reported<sup>1</sup>.

Styrene configurations, however, are reportedly rare in lignin as the content of unsaturated sidechains is estimated to be only 0.09 per  $C_9$ -unit<sup>2</sup>. In order to increase the concentration of diene configurations in lignin, elimination of water from benzyl alcohols had been considered. Thus, adduct (III) had been syn-



reaction leading to the red product). These observations suggest that the chromophores responsible for the absorption bands are terminal groups in the polymaleimide molecules.

Bamford *et al.*<sup>3</sup> showed that the termination process in the free radical polymerization of maleimide proceeds exclusively through a disproportionation reaction resulting in half the dead polymer chains having unsaturated end-groups (A); we believe that all the experimental observations can be explained in terms of the reactions of this type of end-group as follows. The initial reaction of polymaleimide in DMF is proton abstraction by pyridine or other base from the  $\alpha$  position to the double bond to give (B), in which there will be extensive delocalization of the negative charge, especially if tautomerism in the terminal ring is involved. Oxidation then results in the development of further unsaturation in the polymer backbone and hence in the formation of a more highly conjugated species (C). Evidently continuation of this oxidation process may occur and is probably responsible for the green coloration we have observed in aged solutions ( $\sim 8$  weeks). These showed substantial absorption above 600 nm but no distinct maxima were observed. We are not able to propose a mechanism for the oxidation process at present since no kinetic data are available.

Further evidence for the origin of the coloured solutions was obtained from chlorination of polymaleimide samples with *t*-butyl hypochlorite in *sym*-tetrachloro-

ethane (TCE). Reaction in this medium typically gives rise to *N*-chlorinated products<sup>4</sup> but samples isolated at short reaction times (1 h) (when no *N*-chlorination could be detected by infra-red spectroscopy) yielded transparent solutions of polymaleimide in DMF. These solutions remained colourless when pyridine was added. We therefore propose that chlorination of the reactive end-groups gives rise to saturated end-groups (D). A solution of the copolymer of styrene and maleimide in DMF was also transparent in the visible region; this would be expected since termination in the homopolymerization of styrene occurs solely by combination and cross-termination reactions would reduce the concentration of (A) groups in the polymer.

The linear relationship between optical density and  $\bar{M}_n^{-1}$  (for the purple band) presents the intriguing possibility that molecular weights of polymaleimide samples may simply be obtained from spectroscopic studies of their solutions in DMF. The extinction coefficients of the 496 and 558 nm bands were calculated to be 0.88 and  $1.06 \times 10^4$  respectively.

#### REFERENCES

- 1 Tawney, P. O. *et al. J. Org. Chem.* 1961, **26**, 15
- 2 Block, H. personal communication
- 3 Bamford, C. H., Bingham, J. F. and Block, H. *Trans. Faraday Soc.* 1970, **66**, 2612
- 4 Zimmer, H. and Audrieth, L. F. *J. Am. Chem. Soc.* 1954, **76**, 3856

## Dienolysis of lignin: cleavage of $\beta$ -aryl ethers by Diels-Alder synthesis

Wolfgang G. Glasser

Department of Forestry and Forest Products, Virginia Polytechnic Institute and State University, Blacksburg, Virginia 24061, USA

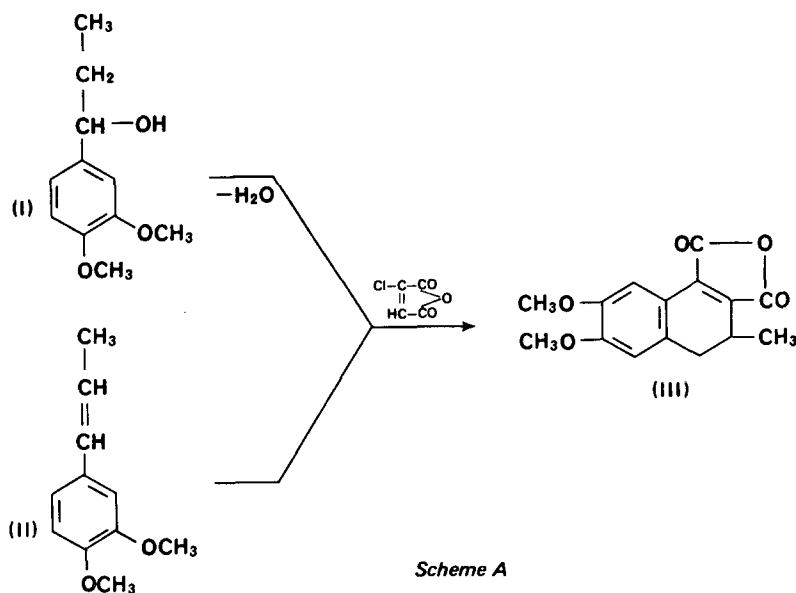
(Received 30 March 1973)

#### INTRODUCTION

In a recent paper by Glasser and Sandermann<sup>1</sup>, lignin model compounds with ethylenic double bonds in conjugation with aromatic rings were tested with respect to their reactivities in Diels-Alder reactions. Maleic anhydride, chloromaleic anhydride and tetracyanoethylene had served as dienophiles in this previous investigation. It was demonstrated that lignin-like  $\beta$ -substituted styrene derivatives can indeed serve as

dienes in the diene synthesis, and the isolation of a number of tetralin and dihydronaphthalene derivatives was reported<sup>1</sup>.

Styrene configurations, however, are reportedly rare in lignin as the content of unsaturated sidechains is estimated to be only 0.09 per  $C_9$ -unit<sup>2</sup>. In order to increase the concentration of diene configurations in lignin, elimination of water from benzyl alcohols had been considered. Thus, adduct (III) had been syn-



thesized from 1-(3,4-dimethoxyphenyl)-propanol-1 (I) and chloromaleic anhydride, and it was found to be identical with (III) formed by isoeugenol methyl ether (II) under the same reaction conditions (see *Scheme A*). Dehydration was probably promoted by hydrogen chloride eliminated from chloromaleic anhydride during the course of this reaction.

The objective of this study is to demonstrate the possibility of reacting  $\alpha$ -hydroxylated phenylpropanes, substances representative of lignin, as dienes with tetracyanoethylene as dienophile in Diels-Alder reactions.

## EXPERIMENTAL

### Procedure

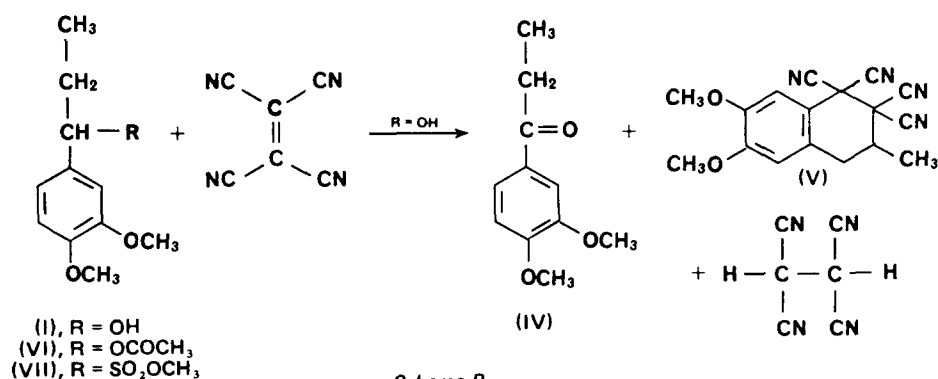
Reactions of lignin model compounds and tetracyanoethylene were carried out by refluxing for 2–4 h in any one of the three solvents dichloroethane, toluene or xylene. Subsequent to the synthesis the reactants were evaporated to dryness at reduced pressure, and a sample of the crude mixture was dissolved in a deuterated solvent (chloroform, acetone or pyridine) suitable for analysis by n.m.r. spectroscopy. Whenever possible, thin-layer chromatography was performed and compounds were identified by comparison with pure substances.

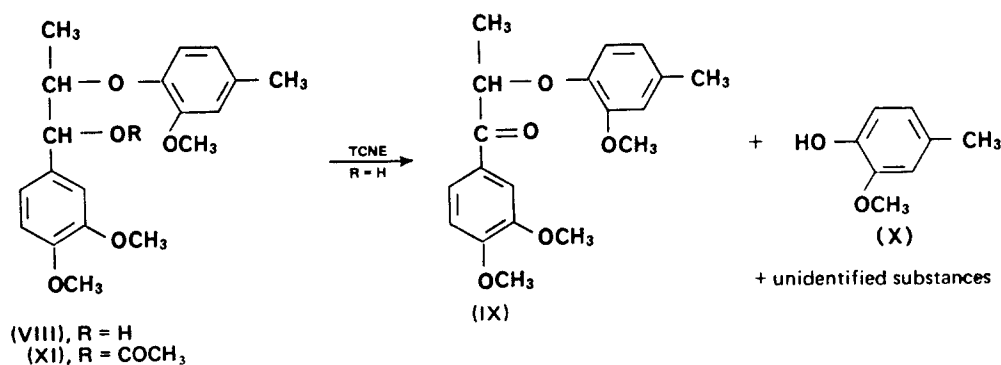
### Compounds

Lignin model compounds were prepared in accordance with known procedures reported in the literature.

## RESULTS AND DISCUSSION

The reaction of veratryl carbinol (I) with tetracyanoethylene (TCNE) in boiling xylene resulted in the formation of a mixture of veratryl ketone (IV), adduct (V) and presumably tetracyanoethane, as shown in *Scheme B*. Thin-layer chromatography and n.m.r. spectroscopy of the mixture indicated that the reaction was complete after 30 min, and the ratio of (IV):(V) was 60:40, respectively. No other products were detected. The formation of ketone (IV) in the reaction mixture can be explained with dehydrogenation of carbinol (I) and simultaneous reduction of TCNE to tetracyanoethane. This type of hydrogen abstraction by TCNE had previously been reported to occur with thiols, among others<sup>3</sup>. Adduct (V) was found to be identical with the reaction product of isoeugenol methyl ether (II) and TCNE. Its formation from carbinol (I) can be interpreted with dehydration of the benzyl alcohol resulting in the formation of a double bond as intermediate step. In this reaction TCNE seems to function as a Lewis acid attacking the aliphatic hydroxyl group. The potential strength of TCNE as a Lewis acid has been pointed out by Merrifield and Phillips on theoretical





Scheme C

grounds<sup>4</sup>. These authors determined the  $\pi$ -acid strengths of five compounds and found that TCNE possesses a greater electron affinity than any of the other known Lewis acids, which included chloranil, maleic anhydride, 1,2-dicyano-1,2-dicarbethoxyethylene and *p*-quinone. The reactivity of TCNE with such nucleophilic groups as alkoxy or hydroxy has been demonstrated in another paper<sup>5</sup>.

Acetate (VI) which was prepared through acetylation of carbinol (I) with pyridine/acetic anhydride, yielded adduct (V) as the sole reaction product when treated with TCNE in boiling xylene or dichloroethane for 3 h. The crystalline reaction product was identical with (V) obtained with (II) (n.m.r., chromatography, melting point). Hydrolysis, initiated by the strong dienophilic Lewis acid TCNE, must be held responsible for the reaction. There are substituents other than hydroxyl and acetoxy groups in  $\alpha$ -position of lignin model compounds that might also conceivably be eliminated by TCNE. A sulphonate group, however, proved to be resistant when the sulphonic acid methyl ester (VII) was subjected to boiling xylene and TCNE for 4 h.

Most  $\alpha$ -hydroxyphenylpropanes in lignin are present in the form of phenylglyceryl- $\beta$ -aryl ethers. The hydrolysis of such ethers by acid, sulphonation, hydrogenation, or other methods has been the subject of many research endeavours reported in the literature (for review, see ref. 2). In order to test the reactivity of lignin-like carbinols containing aroxy substituents in the  $\beta$ -position, ether (VIII) (Scheme C) was synthesized following pathways described by Adler *et al.*<sup>6</sup> Its erythro-form was obtained in crystalline form (m.p. 45–47°C) following column chromatography; n.m.r. spectroscopic data of this substance have been reported elsewhere<sup>7</sup>.

When the erythro-form of  $\beta$ -ether (VIII) was treated with TCNE in boiling xylene for 2 h, the resulting mixture contained keto- $\beta$ -ether (IX) and creosol (X) as identifiable reaction products. The yield of ketone (IX) corresponded to 60% of the starting carbinol; column chromatography rendered (IX) in crystalline state (m.p. 94–95°C). The yield of phenol (X) matched

40% ether cleavage. Other compounds were present in the reaction mixture as indicated by thin-layer chromatography, but have not yet been isolated. Acetate (XI) was found to be unreactive; it withstood treatment with TCNE in boiling dichloroethane, toluene, or xylene for up to 24 h. Only unreacted  $\beta$ -ether acetate (XI) could be recovered. Its stability might be based on steric factors.

Cleavage of  $\beta$ -aryl ether groups by Lewis acids has been accomplished before as in the case of acetic anhydride<sup>8</sup> or thioacetic acid and borotrifluoride<sup>9</sup>, or resorcinol and hydrogen chloride<sup>10</sup>. It has never been demonstrated, however, that this predominant ether linkage in lignin can also be cleaved by such dienophiles as tetracyanoethylene under the conditions of a diene synthesis. It is proposed, therefore, to name this type of ether cleavage 'Dienolysis', in analogy to other  $\beta$ -ether cleaving solvolysis reactions, such as acidolysis, alcoholysis, sulphitolysis, hydrogenolysis, and others.

Presently, experiments are underway aiming at the isolation of dienolysis products of  $\beta$ -ethers and at reaction products with milled wood lignins.

## REFERENCES

- 1 Glasser, W. G. and Sandermann, W. *Sven. Papperstidn.* 1970, **73**, 246
- 2 Lai, Y. Z. and Sarkanen, K. V. in 'Lignins—Occurrence, Formation, Structure and Reactions', (Eds K. V. Sarkanen and C. H. Ludwig), Wiley-Interscience, New York, 1971, p 195
- 3 Middleton, W. J., Heckert, R. E., Little E. L. and Krespan, C. G. *J. Am. Chem. Soc.* 1958, **80**, 2783
- 4 Merrifield, R. E. and Phillips, W. D. *J. Am. Chem. Soc.* 1958, **80**, 2778
- 5 Cairns, T. L., Carboni, R. A., Coffman, D. D., Engelhardt, V. A. *et al. J. Am. Chem. Soc.* 1958, **80**, 2775
- 6 Adler, E., Delin, S. and Miksche, G. E. *Acta Chem. Scand.* 1966, **20**, 1035
- 7 Glasser, W. G., Gratzl, J. S., Collins, J. J., Forss, K. and McCarthy, J. L. *Macromolecules* 1973, **6**, 114
- 8 Nimz, H. *Liebigs Ann. Chem.* 1966, **691**, 126
- 9 Nimz, H. *Chem. Ber.* 1969, **102**, 3803
- 10 Nimz, H. *Holzforschung* 1969, **23**, 84

# Letter

## Molecular orientation in PET studied by polarized Raman scattering

We describe here the first quantitative experimental determination, as far as is known, of molecular orientation in a polymer by polarized Raman spectroscopy. For simplicity we have restricted ourselves to a transversely isotropic system by choosing uniaxially oriented specimens of poly(ethylene terephthalate) (PET), although the theory has been established for more general systems in a previous publication<sup>1</sup>.

### Theory

In the Raman experiment the intensity of the scattered radiation,  $I_s$ , is given by:

$$I_s = I_0 \sum_{ij} (l'_i l_j \alpha_{ij})^2 \quad (1)$$

In this equation,  $I_0$  is a constant depending on the incident light intensity and instrumental factors, the direction cosines  $(l_1, l_2, l_3)$ ,  $(l'_1, l'_2, l'_3)$  define, respectively, the polarization directions of the incident light and the analyser (with respect to a set of axes  $0-x_1x_2x_3$  fixed in the sample) and  $\alpha_{ij}$  is the  $ij$ th component of the Raman tensor for the vibration under examination. The scattered light intensity can therefore be regarded as depending on the experimentally chosen direction cosines  $l'_i$  and  $l_j$ , together with quantities  $\Sigma \alpha_{ij} \alpha_{pq}$ , which depend on the distribution of molecular orientations and the principal components  $\alpha_1, \alpha_2, \alpha_3$  of the Raman tensor. For the case of uniaxial symmetry, the Raman scattering depends on the distribution of orientations only through  $\cos^2\theta$  and  $\cos^4\theta$ . The angle  $\theta$  is the angle between the molecular chain axis and the draw direction and the averages are taken over the distribution of orientations in the polymer.

We shall assume that, in addition to the overall uniaxial statistical symmetry of the samples, the individual molecular chains have no preferred orientation around the chain axis. We shall further assume that for the particular Raman line on which measurements have been made the Raman tensor has cylindrical symmetry ( $\alpha_1 = \alpha_2 \neq \alpha_3$ ) and that its unique axis makes an angle  $\gamma$  with the chain axis. If  $0x_3$  is chosen parallel to the unique axis of the sample then we can write the quantity  $\Sigma \alpha_{ij} \alpha_{pq}$  as:

$$\Sigma \alpha_{ij} \alpha_{pq} = 16\pi^4 N_0 \sum_{l=0,2,4} [2/(2l+1)]^{1/2} M_{100} D_{100} A_{100}^{ijpq} \quad (2)$$

[see equations (15) and (19) of ref. 1], where the summation on the left is over all  $N_0$  chain segments and  $ijpq$  is of the form  $ijjj$  or  $ijij$ .

In this expansion, the terms  $M_{100}$  are coefficients in the expansion of the molecular orientation distribution

in a series of Legendre polynomials  $P_l(\cos\theta)$ , the  $D_{100}$  are equal to  $P_l(\cos\gamma)$  (and take fixed values for a particular line) and the  $A_{100}^{ijpq}$  are linear sums of quadratic terms in the principal components of the Raman tensor, i.e. terms such as  $\alpha_1^2, \alpha_1\alpha_2$  etc. (see Table I of ref. 1). For an isotropic sample it follows from equation (2) that:

$$(\Sigma \alpha_{ij}^2)/(\Sigma \alpha_{ii}^2) = (1 - 2r + r^2)/(8r^2 + 4r + 3) \quad (3)$$

where  $r = \alpha_1/\alpha_3$ . Thus by determining the scattered intensity from an oriented sample for at least three suitably chosen combinations of polarization vectors and combining this with the result for isotropic samples, we can find  $M_{200}$  and  $M_{400}$ , and hence  $\overline{\cos^2\theta}$  and  $\overline{\cos^4\theta}$ , together with the value of  $\alpha_1/\alpha_3$ .

### Experimental

The PET samples were produced, by melt spinning, in the form of thin tapes with cross-section approximately  $1.5 \times 10^{-3}$  m by  $1.0 \times 10^{-4}$  m. The number-average molecular weight was estimated from intrinsic viscosity measurements to be  $2.3 \times 10^4$ . The samples were subsequently oriented by drawing around a smooth stationary 'pin', heated to  $80^\circ\text{C}$ , located between rollers rotating at different rates. An additional specimen was produced by cutting a sample from an injection moulded plaque so that its cross-section was 3 mm square and cold drawing it to a draw ratio of 3.25. X-ray photographs showed the crystallinity of the samples to be low, and measurements both of dimensions and refractive indices (at 551 nm) showed that, to a very good approximation, they were uniaxially oriented. Data from two randomly oriented samples were used. One was produced by annealing an as-spun tape at  $90^\circ\text{C}$  in an air oven until no birefringence was observable and one was produced from an injection moulded plaque.

The Raman intensity measurements were made using a Coderg PHO spectrometer and a CRL 52A argon ion laser tuned to 488 nm. The tape samples were mounted parallel to the spectrometer slit. The partially focused laser beam was incident normally on them and the scattered light was collected in directions making approximately  $180^\circ$  with the incident light direction. The incident and scattered light polarization vectors could be chosen parallel or perpendicular to the length of the tapes so that intensities proportional to  $\Sigma \alpha_{33}^2, \Sigma \alpha_{11}^2, \Sigma \alpha_{23}^2$  and  $\Sigma \alpha_{31}^2$  could be determined. The polarization of the incident beam was checked after it had passed through the specimen and the depolarization was found to be less than 1%. It was therefore assumed that the depolarization of both the incident and Raman-scattered light by its passage through the surface and the thickness of the specimen could be neglected.

The Raman line chosen for this work was that at  $1616\text{cm}^{-1}$ , which is due<sup>2,3</sup>, to the benzene ring mode 8a (in Wilson's notation) the form of which is shown in Figure 1. The Raman tensor has one of its principal

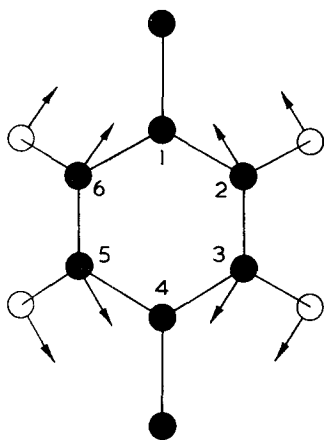


Figure 1 Form of vibration 8a in *p*-disubstituted benzenes

axes parallel to  $C_1-C_4$  (corresponding to  $\alpha_3$ ) and one perpendicular to the plane of the ring, corresponding to  $\alpha_1$  or  $\alpha_2$ .

The assumption that  $\alpha_1 = \alpha_2$  is not easy to justify except by the results obtained, but inspection of the forms of the  $A_{lmn}^{ijpq}$  shows that provided these two components are of the same sign and not very different in magnitude equation (2) with  $\alpha_1 = \alpha_2$  is a very good approximation, particularly if  $\gamma$  is small. The angle  $\gamma$  is the angle between the  $C_1-C_4$  direction in the benzene ring and the chain axis direction and has been assumed to be the same as in the crystal phase. It is calculated from the data of Daubeny *et al.*<sup>4</sup> to be  $19^\circ 12'$ .

The chosen line does not appear to overlap any other Raman line and the peak height above the baseline was taken as a measure of the intensity. The directly measured intensities were corrected for the differential polarization sensitivity of the spectrometer and the inequality of the intensities of the exciting line for the two polarization directions. The intensities proportional to  $\Sigma\alpha_{13}^2$  and  $\Sigma\alpha_{31}^2$  were then found to be equal within experimental error.

The bulk samples were illuminated using the more conventional right-angle viewing technique, care being taken that the incident and scattered beams passed either through a large thickness of material, so that polarization scrambling was complete, or through such a small thickness that essentially no scrambling took place. From these samples it was possible to obtain intensities proportional to  $\Sigma\alpha_{22}^2$ ,  $\Sigma\alpha_{33}^2$ ,  $\Sigma\alpha_{12}^2$ ,  $\Sigma\alpha_{13}^2$  and  $\Sigma\alpha_{32}^2$ .

### Results

The values of  $r$  determined from the data on the random samples were  $-0.19_2$ ,  $-0.17_6$ . The mean value was used, together with the intensity data for the tapes, to calculate values of  $\overline{\cos^2\theta}$  and  $\overline{\cos^4\theta}$  from equation (2). A good straight line is obtained when  $\overline{\cos^2\theta}$  is plotted against birefringence (Figure 2), as predicted theoretically<sup>5, 6</sup>, and the indicated maximum birefringence is 0.24, in good agreement with the value 0.23 given by Kashiwagi *et al.*<sup>7</sup> Figure 3 shows the relationship between  $\overline{\cos^2\theta}$  and  $\overline{\cos^4\theta}$  compared with theoretical curves for the affine rubber elasticity model<sup>8</sup> and for the pseudo-affine deformation scheme<sup>9</sup>. This comparison is only given here to show that the values of  $\overline{\cos^4\theta}$  are also reasonable; detailed discussion of deformation

mechanisms will be deferred until more extensive studies have been completed.

Figures 2 and 3 also show points for the oriented bulk sample calculated from intensities proportional to  $\Sigma\alpha_{33}^2$ ,  $\Sigma\alpha_{12}^2$  and  $\Sigma\alpha_{23}^2$  by assuming  $r = -0.184$ . The predicted value for the intensity proportional to  $\Sigma\alpha_{22}^2$  was  $21.1$  and the experimental value was  $20 \pm 3$ . This suggests that the assumption that  $r$  is independent of the distribution of orientations is reasonable. (The largest intensity, that proportional to  $\Sigma\alpha_{33}^2$ , was  $89 \pm 3$  units.)

### Conclusion

The results reported here confirm that polarized Raman spectroscopy can give quantitative information about molecular orientation in polymers. More detailed studies are to be undertaken on PET and results will shortly be published of a detailed study of oriented poly(methyl methacrylate).

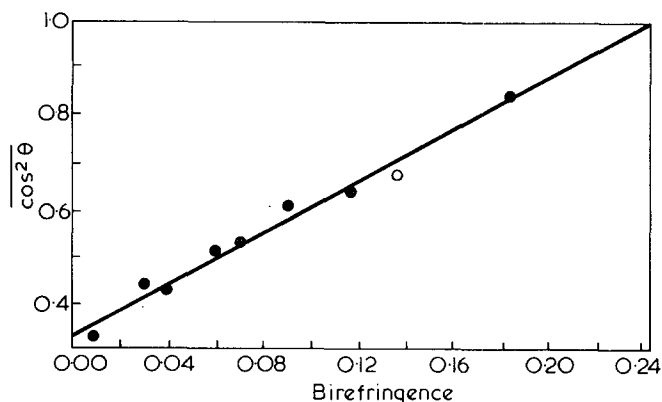


Figure 2 Variation of  $\overline{\cos^2\theta}$  obtained from polarized Raman scattering with birefringence. ●, Tape specimens; ○, bulk specimen

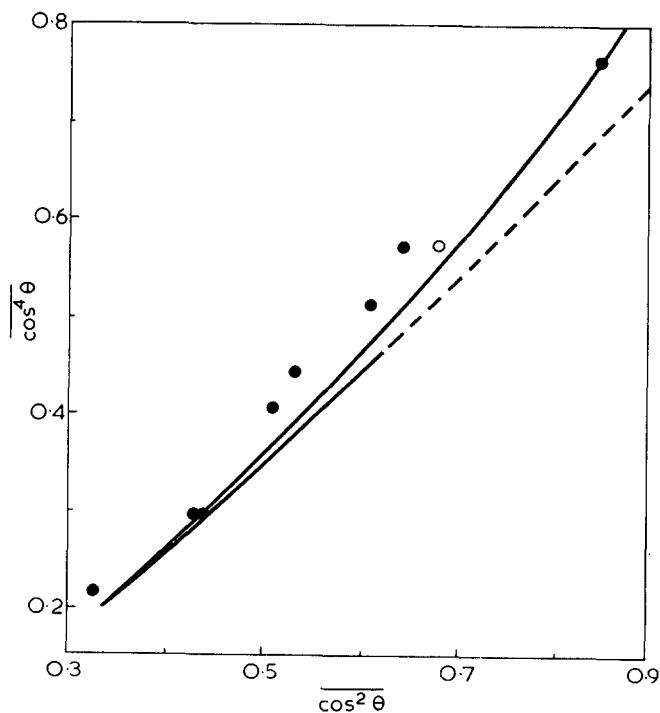


Figure 3 Comparison of  $\overline{\cos^4\theta}$  and  $\overline{\cos^2\theta}$  obtained from polarized Raman scattering. ●, Tape specimens; ○, bulk specimen. Lower curve shows relationship between  $\overline{\cos^4\theta}$  and  $\overline{\cos^2\theta}$  according to affine rubber elasticity model and upper curve shows relationship according to the pseudo-affine deformation scheme



### Acknowledgements

We have had useful discussions with several colleagues. In addition, we wish to thank Mr J. Nobbs and Mr A. Cunningham for preparing the oriented specimens and ICI Fibres Division, Harrogate for providing melt-spinning facilities. One of us (J.P.) is indebted to the Science Research Council for the award of a maintenance grant.

J. Purvis, D. I. Bower and I. M. Ward

Department of Physics,  
University of Leeds,  
Leeds LS2 9JT, UK

(Received 9 May 1973;  
revised 24 May 1973)

### References

- 1 Bower, D. I. *J. Polym. Sci. (Polym. Phys.)* 1972, **10**, 2135
- 2 Varsanyi, G. 'Vibrational Spectra of Benzene Derivatives', Academic Press, New York, 1969, p 152
- 3 Julien-Laferriere, S. and Lebas, J-M. *Spectrochim. Acta* 1971, **27A**, 1337
- 4 Daubeny, R. de P., Bunn, C. W. and Brown, C. J. *Proc. R. Soc.* 1954, **226A**, 531
- 5 Hermans, P. H. 'Physics and Chemistry of Cellulose Fibres', Elsevier, New York, 1949, Part 2, Ch 4
- 6 Pinnock, P. R. and Ward, I. M. *Br. J. Appl. Phys.* 1964, **15**, 1559
- 7 Kashiwagi, M., Cunningham, A., Manuel, A. J. and Ward, I. M. *Polymer* 1973, **14**, 111
- 8 Roe, R. J. and Krigbaum, W. R. *J. Appl. Phys.* 1964, **35**, 2215
- 9 Ward, I. M. 'Mechanical Properties of Solid Polymers', Wiley, London, 1971, p 258

## Book Review

### IUPAC International Conference on Chemical Transformations of Polymers

Edited by R. Rado

Butterworths, London, 1972, 300 pp. £8.50

It is a sobering reflection on progress in chemical transformations in polymers that if Charles Goodyear were miraculously resurrected for the Conference whose Plenary and 18 Main Lectures make up this book, he would have found the vulcanization of rubber by sulphur still a subject for discussion, and could probably have contributed a few sensible remarks on the practical aspects of a process which he discovered in 1839. Wohler, who transmuted ammonium cyanate to urea only 11 years earlier, would hardly fare so well at a modern conference on the metamorphosis of small molecules. Insofar as 'chemical transformation' implies purposeful improvement, polymer chemists are scarcely off the starting-line in comparison with their small-molecule confreres, partly of course because of the late recognition of large molecules, but also because until relatively recently most of the effort expended on polymeric transformations was designed to avoid them; the more appropriate term 'degradation' was not coined by a man who was pleased with what he saw.

This preventive aspect of polymer transformation underlies 7 of the main lectures, with predominant emphasis on photochemical processes which, combined with ketone carbonyl groups produced by atmospheric oxidation, are the main cause of deleterious 'weathering'. The general background of energy transfer from excited states in small molecules is discussed by Fox, who goes on to examine emission spectra (fluorescent/phosphorescent) in polymers, where the photophysical process may be influenced by the orbital overlap of a succession of chromophores allowing energy migration along a chain to a weak link 'energy-trap'. Guillet examines practical aspects of u.v. stabilization with screening and absorbing agents, and mentions briefly the formation of chromophores in polyolefins by oxidative processes. (The testing and performance of antioxidants are reviewed by Scott, and that of specific u.v. absorbers by Heller and Blattman.) Photochemical aspects of degradation are rounded off by Golub on polydienes, a specialized but important area which is starting to make progress again after twenty years' neglect following Bateman's pioneering work in 1945.

There is a satisfying chapter by Grassie on the thermal degradation of acrylates (which fragment) and methacrylates (which unzip)—satisfying because the careful and detailed experiments described lead to an integrated mechanism which resolves the question of why such closely allied polymers break down in different ways. Finally, a relative newcomer to the degradation scheme is the break down of polymers caused by Ziegler-Natta catalyst residues, on which Vesely and coworkers make a start by analysing similar reactions of small molecules to isolate individual steps in the overall process.

Turning to purposeful transformations, the formation of block, graft and network copolymers (a distant descendant of Goodyear's vulcanization) is most commonly done with carbanionic systems, here reviewed by Rempp and Franta, but there is an interesting account by Ashworth, Bamford and Smith of network formation in a free-radical system using molybdenum carbonyl catalysts, where polymer chains containing Cl atoms yield free radicals (which subsequently act as growth sites) in a redox process. The vulcanization of rubbers using peroxides instead of sulphur, giving a simpler system which is also chemically related to electron irradiation curing has a chapter by Loan, and the preparation of semi-permeable membranes is discussed by Pegoraro. The general behaviour of free radicals in polymeric systems covers three chapters: Braun on stable polyradicals (in German), Butiagin on the decay of radicals, and a brief account by Jenkins of the application of the Patterns system to polyradicals.

The starting-point for most polymer modification is the introduction of functional groups along the polymer chain, and since most of our knowledge of the reactivity of such groups is derived from their behaviour in small molecules, it is important to know if and how this reactivity is affected in polymeric surroundings. These 'polymeric effects' are discussed in detail by R. C. Schulz for three specific instances (optical racemization, electron donor-acceptor complex formation, and the reactivity of chlorine in *N*-chlorinated nylon-6,6). Chemically attached groups scattered along the polymer chain may also have a profound direct effect on the physical properties of the polymer, acting as built-in plasticizers or modifying crystallization behaviour. This complex field is reviewed by Platé, with a final hint of things to come in the effects of such 'micromodification' on the catalytic activity of synthetic proteolytic enzymes. The remaining two lectures scarcely fit in the general context of the book—Chapiro on controlled propagation in associated monomer aggregates and Okamura on solid-state polymerization—and though both competent reviews on their own ground add little to the main theme.

Finally, the Plenary Lecture by Smets on the photochromic behaviour of polymeric systems is perhaps over-detailed on too narrow a front, considering the scope of the book as a whole. Reversible colour formation on exposure to light is a feature of certain small-molecule organic structures, and the author is chiefly concerned with the 'polymeric effect' on the photochromism of spirobenzopyrans, which is most marked in the solid state and depends strongly on the glass transition temperature of the polymer. One of the more interesting practical applications of such systems is the possibility of using photochromes to detect local motions in a polymer chain and to pinpoint secondary glass transition temperatures.

Overall, the lectures are a rather diverse collection gathered somewhat uneasily under one roof. No single reader is likely to find more than two or three chapters of direct interest, and at £8.50 it is a book for the library rather than the private shelf.

R. O. Colclough

### Acknowledgements

We have had useful discussions with several colleagues. In addition, we wish to thank Mr J. Nobbs and Mr A. Cunningham for preparing the oriented specimens and ICI Fibres Division, Harrogate for providing melt-spinning facilities. One of us (J.P.) is indebted to the Science Research Council for the award of a maintenance grant.

J. Purvis, D. I. Bower and I. M. Ward

Department of Physics,  
University of Leeds,  
Leeds LS2 9JT, UK

(Received 9 May 1973;  
revised 24 May 1973)

### References

- 1 Bower, D. I. *J. Polym. Sci. (Polym. Phys.)* 1972, **10**, 2135
- 2 Varsanyi, G. 'Vibrational Spectra of Benzene Derivatives', Academic Press, New York, 1969, p 152
- 3 Julien-Laferriere, S. and Lebas, J-M. *Spectrochim. Acta* 1971, **27A**, 1337
- 4 Daubeny, R. de P., Bunn, C. W. and Brown, C. J. *Proc. R. Soc.* 1954, **226A**, 531
- 5 Hermans, P. H. 'Physics and Chemistry of Cellulose Fibres', Elsevier, New York, 1949, Part 2, Ch 4
- 6 Pinnock, P. R. and Ward, I. M. *Br. J. Appl. Phys.* 1964, **15**, 1559
- 7 Kashiwagi, M., Cunningham, A., Manuel, A. J. and Ward, I. M. *Polymer* 1973, **14**, 111
- 8 Roe, R. J. and Krigbaum, W. R. *J. Appl. Phys.* 1964, **35**, 2215
- 9 Ward, I. M. 'Mechanical Properties of Solid Polymers', Wiley, London, 1971, p 258

## Book Review

### IUPAC International Conference on Chemical Transformations of Polymers

Edited by R. Rado

Butterworths, London, 1972, 300 pp. £8.50

It is a sobering reflection on progress in chemical transformations in polymers that if Charles Goodyear were miraculously resurrected for the Conference whose Plenary and 18 Main Lectures make up this book, he would have found the vulcanization of rubber by sulphur still a subject for discussion, and could probably have contributed a few sensible remarks on the practical aspects of a process which he discovered in 1839. Wohler, who transmuted ammonium cyanate to urea only 11 years earlier, would hardly fare so well at a modern conference on the metamorphosis of small molecules. Insofar as 'chemical transformation' implies purposeful improvement, polymer chemists are scarcely off the starting-line in comparison with their small-molecule confreres, partly of course because of the late recognition of large molecules, but also because until relatively recently most of the effort expended on polymeric transformations was designed to avoid them; the more appropriate term 'degradation' was not coined by a man who was pleased with what he saw.

This preventive aspect of polymer transformation underlies 7 of the main lectures, with predominant emphasis on photochemical processes which, combined with ketone carbonyl groups produced by atmospheric oxidation, are the main cause of deleterious 'weathering'. The general background of energy transfer from excited states in small molecules is discussed by Fox, who goes on to examine emission spectra (fluorescent/phosphorescent) in polymers, where the photophysical process may be influenced by the orbital overlap of a succession of chromophores allowing energy migration along a chain to a weak link 'energy-trap'. Guillet examines practical aspects of u.v. stabilization with screening and absorbing agents, and mentions briefly the formation of chromophores in polyolefins by oxidative processes. (The testing and performance of antioxidants are reviewed by Scott, and that of specific u.v. absorbers by Heller and Blattman.) Photochemical aspects of degradation are rounded off by Golub on polydienes, a specialized but important area which is starting to make progress again after twenty years' neglect following Bateman's pioneering work in 1945.

There is a satisfying chapter by Grassie on the thermal degradation of acrylates (which fragment) and methacrylates (which unzip)—satisfying because the careful and detailed experiments described lead to an integrated mechanism which resolves the question of why such closely allied polymers break down in different ways. Finally, a relative newcomer to the degradation scheme is the break down of polymers caused by Ziegler-Natta catalyst residues, on which Vesely and coworkers make a start by analysing similar reactions of small molecules to isolate individual steps in the overall process.

Turning to purposeful transformations, the formation of block, graft and network copolymers (a distant descendant of Goodyear's vulcanization) is most commonly done with carbanionic systems, here reviewed by Rempp and Franta, but there is an interesting account by Ashworth, Bamford and Smith of network formation in a free-radical system using molybdenum carbonyl catalysts, where polymer chains containing Cl atoms yield free radicals (which subsequently act as growth sites) in a redox process. The vulcanization of rubbers using peroxides instead of sulphur, giving a simpler system which is also chemically related to electron irradiation curing has a chapter by Loan, and the preparation of semi-permeable membranes is discussed by Pegoraro. The general behaviour of free radicals in polymeric systems covers three chapters: Braun on stable polyradicals (in German), Butiagin on the decay of radicals, and a brief account by Jenkins of the application of the Patterns system to polyradicals.

The starting-point for most polymer modification is the introduction of functional groups along the polymer chain, and since most of our knowledge of the reactivity of such groups is derived from their behaviour in small molecules, it is important to know if and how this reactivity is affected in polymeric surroundings. These 'polymeric effects' are discussed in detail by R. C. Schulz for three specific instances (optical racemization, electron donor-acceptor complex formation, and the reactivity of chlorine in *N*-chlorinated nylon-6,6). Chemically attached groups scattered along the polymer chain may also have a profound direct effect on the physical properties of the polymer, acting as built-in plasticizers or modifying crystallization behaviour. This complex field is reviewed by Platé, with a final hint of things to come in the effects of such 'micromodification' on the catalytic activity of synthetic proteolytic enzymes. The remaining two lectures scarcely fit in the general context of the book—Chapiro on controlled propagation in associated monomer aggregates and Okamura on solid-state polymerization—and though both competent reviews on their own ground add little to the main theme.

Finally, the Plenary Lecture by Smets on the photochromic behaviour of polymeric systems is perhaps over-detailed on too narrow a front, considering the scope of the book as a whole. Reversible colour formation on exposure to light is a feature of certain small-molecule organic structures, and the author is chiefly concerned with the 'polymeric effect' on the photochromism of spirobenzopyrans, which is most marked in the solid state and depends strongly on the glass transition temperature of the polymer. One of the more interesting practical applications of such systems is the possibility of using photochromes to detect local motions in a polymer chain and to pinpoint secondary glass transition temperatures.

Overall, the lectures are a rather diverse collection gathered somewhat uneasily under one roof. No single reader is likely to find more than two or three chapters of direct interest, and at £8.50 it is a book for the library rather than the private shelf.

R. O. Colclough

# A variance analysis of the line broadening of X-ray profiles from Fortisan

A. K. Kulshreshtha, R. E. Hunter and N. E. Dweltz

Ahmedabad Textile Industry's Research Association, Ahmedabad-380015, India  
(Received 20 February 1973; revised 1 May 1973)

A variance range analysis has been performed on the meridional 020 and 040 profiles from saponified stretched acetates (Fortisan) having a cellulose II lattice. Variance range functions for 020 and 040 profiles are found to be practically identical to each other in all cases, indicating structural perfection of Fortisan crystallites. A slope analysis of the variance range function of the 020 profiles indicates that the average crystallite length in Fortisan seems to be a function of the stretch applied to the cellulose acetate precursor before saponification. The differences in the stress-strain curves of various Fortisan samples have been explained as due to the difference in their crystallite length distribution.

## INTRODUCTION

The fine structure of dry spun cellulose acetate yarn can be conveniently modified by steam-stretching the yarn under pressure. Sprague<sup>1</sup> has extensively studied the rate of diffusion of disperse dyes for stretched acetates as a function of their fine structure. A study on the fine structure and various mechanical properties of stretched acetate yarns (stretch varying from 50% to 2000%) and of the saponification products derived therefrom by the Fortisan process has also been published<sup>2</sup>. The present paper deals with the line broadening analysis<sup>3-5</sup> of various saponified stretched acetates (Fortisan) which have a cellulose II lattice. The analysis has been performed on the profiles of 020 and 040 meridional reflections from various regenerated cellulose samples. Such an analysis reveals the values of average crystallite length and lattice distortions (if any), which characterize the polydispersity of the specimens under investigation.

## EXPERIMENTAL

### Materials

The Fortisan samples used in the present study were obtained by the saponification of their cellulose acetate precursors, stretched under pressure in steam to extents varying from 50% to 1000%. Thus Fortisan-200% would mean a cellulose sample regenerated by the Fortisan process from cellulose acetate yarns and stretched to 200% (before saponification).

### X-ray measurements

Intensity measurements were made at 25°C with a Philips Diffractometer (PW 1050) using  $\text{CuK}\alpha$  radiation at 35 kV and 20 mA. A combination of  $\text{K}\alpha_1$  and  $\text{K}\alpha_2$  was thus employed. The diffractometer was used in the transmission mode in conjunction with a curved crystal focalizer (PW 1075) which minimizes instrumental broadening and gives rise to intense, sharp X-ray

diffraction profiles. A scintillation counter (PW 1964) and a pulse height discriminator (PW 1365) were employed in order to get a monochromatized diffracted beam. The meridional line profiles were recorded using step scan gears (PW 1063) at a scanning speed of 0.02°/min and a chart speed of 200 mm/h. The line profiles due solely to instrumental aberrations were recorded using a thin film of crystalline powdered sodium chlorate. Details about sample preparation, line profile measurements and subsequent data processing have been published<sup>6,7</sup> earlier.

### Processing of data

The intervals used for sampling of line profile data were 0.035 (°2 $\theta$ ) for various Fortisan samples and 0.01 (°2 $\theta$ ) for the  $\text{NaClO}_3$  standard. The correction of line profile data for background, absorption and Lorentz polarization factors were made according to the standard procedure<sup>5,6</sup>. The background was found to be linear in the range of the profile considered for all samples. The variance range functions for 020 and 040 profiles (which have centroids near 17.33° and 34.85° 2 $\theta$  respectively) and their corresponding instrumental profiles were obtained using the computer programme<sup>6</sup> published earlier for an IBM 1620 computer.

### Interpretation of line broadening

*Background.* The line profiles usually recorded on a powder diffractometer are characterized by long, Cauchy-like tails. The second central moment, or variance<sup>8,9</sup> of such a profile will have a very large value, approaching infinity in the case of a Cauchy profile. Thus, in practice, after eliminating the background, the line profile is truncated<sup>10</sup> (so as to get rid of the tails) between limits of 2 $\theta$  or  $2\sin\theta/\lambda$  which are nearly symmetrical about the centroid of the truncated portion and the variance of the truncated portion of the profile is evaluated<sup>11</sup>. The range of truncation is increased continuously to include more of the tails each time and the variance is

computed for each range<sup>6,12</sup>. The variance range function thus obtained has contributions from instrumental broadening and from various imperfections in the specimen such as small size of crystallites, lattice distortions, faulting, etc. The observed variance range function can be corrected<sup>5</sup> for instrumental broadening by a simple subtraction procedure to obtain the intrinsic variance range curves. Theoretical formulations<sup>5,8,9</sup> have been developed to express the intrinsic variance range curve in terms of specimen imperfections and methods have been standardized<sup>13,14</sup> for the separation of broadening contributions due to finite crystal size and lattice distortions. The variance range method has found wide application in the determination of crystallite size<sup>15-17</sup>, analysis of faulting in refractory alloys<sup>18</sup>, analysis of lattice distortions in metals<sup>19</sup>, metallic filings<sup>20</sup> and fibrous polymers<sup>13</sup>.

*Theory.* The variance range function can be expressed as<sup>5</sup>:

$$W_{PD}(S) = K_{0s}\sigma(S) - W_{0s}$$

where the slope

$$K_{0s} = \frac{g^2 k^2}{b} + \frac{1}{2\pi^2 \bar{M}_1} = \frac{(W_{0s})^{1/2}}{\pi} \quad (1)$$

In equation (1),  $b$  denotes the lattice spacing between reflecting (*oko*) planes,  $k$  the order of reflection,  $\bar{M}_1$  the number-average crystallite size<sup>21</sup>, and  $g$  the degree of 'paracrystalline' lattice distortions<sup>22</sup>. The variance range function is expressed as a function of the reciprocal space variable  $S = 1/\lambda \cdot (2\sin\theta - 2\sin\theta_0)$ ,  $2\theta_0$  being the centroid of the line profile and  $\lambda$  the wavelength of X-rays.  $\sigma(S)$  denotes the range (in  $2\sin\theta/\lambda$  units) of truncation used to evaluate variance. If the slope of the variance range function  $K_{0s}$  is independent of the order or reflection  $k$  then the line broadening is solely due to small crystallite size and for this particular case:

$$K_{0s} = \frac{1}{2\pi^2 \bar{M}_1} \quad (2)$$

## RESULTS

When the variance range functions were computed, it was found that the 020 and 040 profiles gave rise to practically overlapping variance range functions for each Fortisan sample. This is conclusive evidence that line broadening for these samples is due only to small crystallite size and no lattice distortions are present. *Figure 1* depicts the 020 profiles and their variance range functions for various Fortisan samples together with

Table 1 Results of X-ray line profile analysis

No.	Sample	Slope of variance range function* $K_{0s} \times 10^{-3} (\text{\AA}^{-1})$	Average crystallite length $\bar{M}_1$ calculated from eqn (2) ( $\text{\AA}$ )
1.	Fortisan—50%	0.917	55
2.	Fortisan—100%	0.622	82
3.	Fortisan—150%	0.564	90
4.	Fortisan—200%	0.522	97
5.	Fortisan—300%	0.460	110
6.	Fortisan—500%	0.413	123
7.	Fortisan—1000%	0.413	123

\* Slope,  $K_{0i}$ , of variance range function of instrument profile has the magnitude  $0.142 \times 10^{-3} \text{\AA}^{-1}$

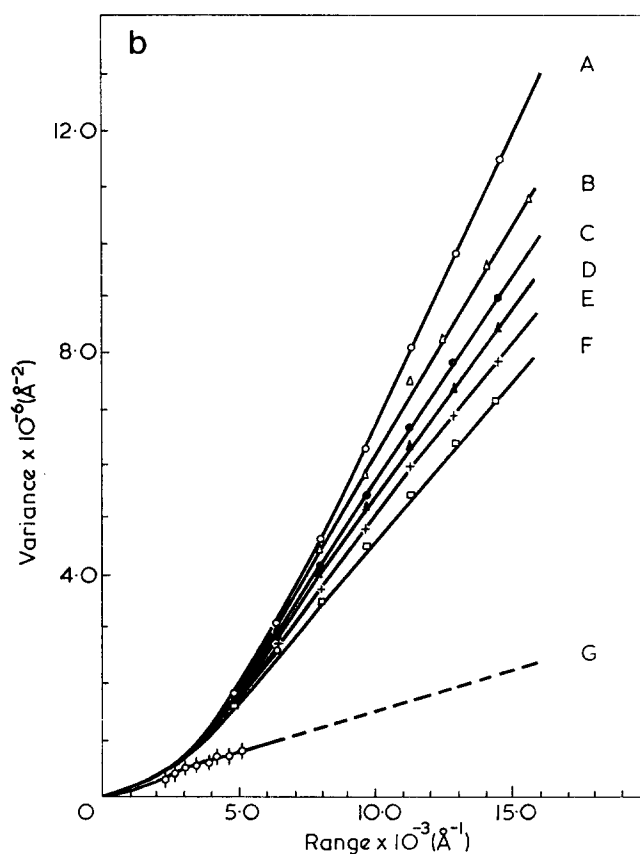
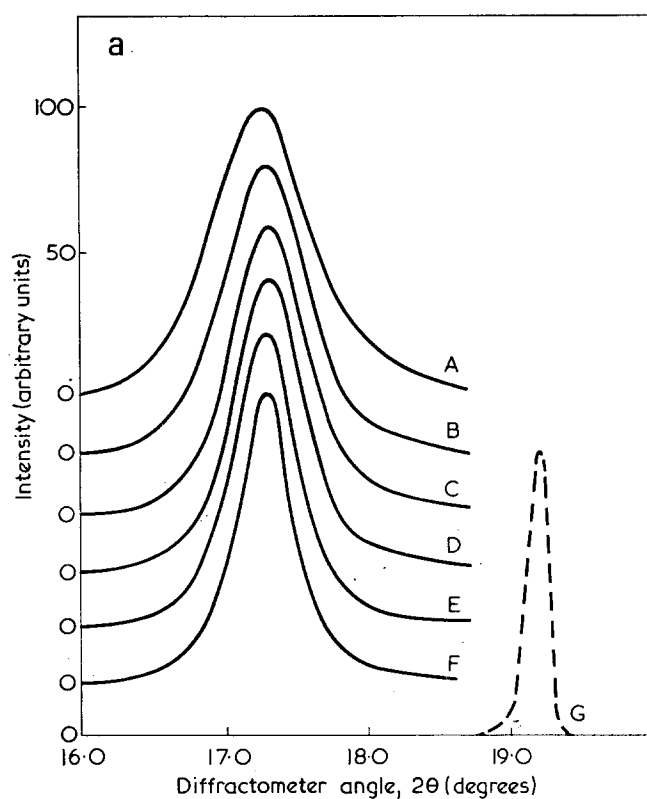


Figure 1 (a) 020 profiles and (b) their observed variance range curves for: A, Fortisan—50%; B, Fortisan—100%; C, Fortisan—150%; D, Fortisan—200%; E, Fortisan—300%; F, Fortisan—500%; and for the 110 profile of sodium chlorate, the instrumental standard (G)

those of the corresponding instrument profile. The slopes of these curves after correction for instrumental effects are listed in *Table 1* for various samples.

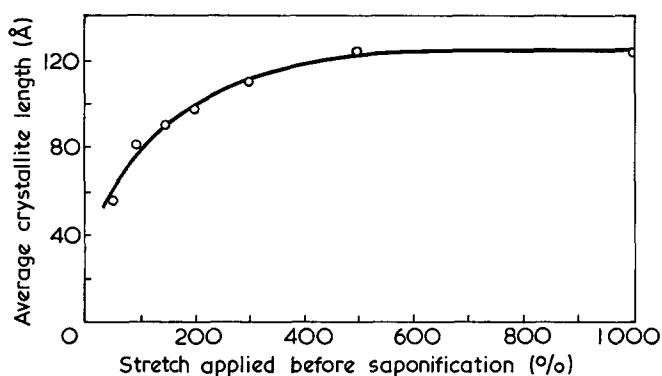


Figure 2 Average crystallite length attained in various Fortisan samples as a function of stretch applied before saponification to their cellulose acetate precursors

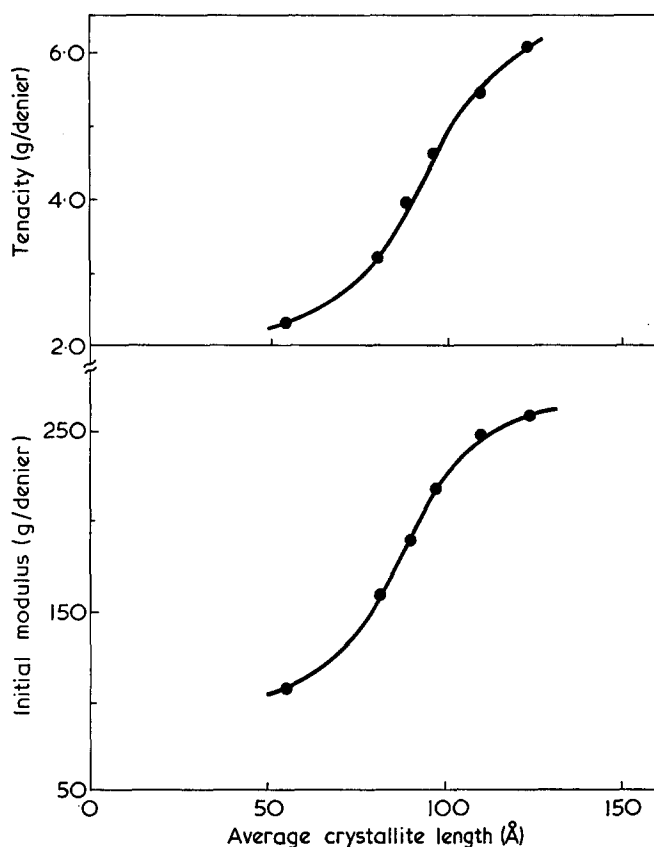


Figure 3 Initial modulus and tenacity for various Fortisan samples plotted as a function of average crystallite length

Figure 2 shows a plot of the average crystallite length  $\bar{M}_1$  of Fortisan against the stretch applied before saponification to the corresponding cellulose acetate precursor yarn. Figure 3 illustrates the relationship between the mechanical properties, such as initial modulus and tenacity, and the average crystallite length  $\bar{M}_1$ , the data on mechanical properties having been taken from Table II of ref. 2.

#### DISCUSSION

The order independent nature of the variance range functions for various Fortisan samples suggests that the crystallites in these materials, though having a small finite size, are perfect and free from any significant distortion in the axial direction. This is to be expected since the cellulose acetate precursors of the Fortisan samples, although non-crystalline, are highly oriented and the

conditions of crystallization into a very stable cellulose II lattice are ideal.

As pointed out by Sprague and Noether<sup>2</sup>, there is a close dependence of structural order and mechanical properties of saponified stretched acetates (Fortisan) upon the corresponding parameters of their cellulose acetate precursors. The relationship between stretch applied to cellulose acetate yarns before saponification and the average crystallite length attained after saponification (Figure 2) further substantiates this view.

The correspondence between mechanical properties of a fibrous polymer on the one hand and its fine structure parameters on the other, is of great practical interest. Figure 3 demonstrates the relationship between average crystallite length and some parameters derived from the stress-strain curves of the various Fortisan samples. The increase in tenacity or initial modulus with increasing length of the crystallite is in accordance with theoretical expectations. The use of crystallite length for comparison with the characteristics of the stress-strain curves is pertinent since the latter are modified as a result of the lengthwise rearrangement of fibre structure.

#### ACKNOWLEDGEMENTS

The authors wish to thank Dr B. S. Sprague and Dr H. D. Noether of the Celanese Corporation of America for very kindly providing the Fortisan samples used in the present study. They also wish to thank the Director, ATIRA for his permission to publish this work.

#### REFERENCES

- 1 Sprague, B. S. *J. Polym. Sci. (C)* 1967, **20**, 159
- 2 Sprague, B. S. and Noether, H. D. *Textile Res. J.* 1961, **31**, 858
- 3 Wilson, A. J. C. 'X-Ray Optics', Methuen, London, 1962
- 4 Grimes, N. W., Pearson, J. M., Fane, R. W. and Neal, W. E. *J. Phil. Mag.* 1970, **21**, 177
- 5 Kulshreshtha, A. K., Dweltz, N. E. and Radhakrishnan, T. *J. Appl. Crystallogr.* 1971, **4**, 116
- 6 Kulshreshtha, A. K., Kothari, N. R. and Dweltz, N. E. *J. Appl. Crystallogr.* 1971, **4**, 125
- 7 Kulshreshtha, A. K., Dweltz, N. E. and Radhakrishnan, T. *Proc. 12th Joint Technol. Conf. ATIRA, BTRA and SITRA, Coimbatore* 1969
- 8 Wilson, A. J. C. *Proc. Phys. Soc.* 1962, **80**, 286
- 9 Wilson, A. J. C. *Proc. Phys. Soc.* 1963, **81**, 41
- 10 Wilson, A. J. C. *Proc. Phys. Soc.* 1965, **85**, 807
- 11 Langford, J. I. and Wilson, A. J. C. in 'Crystallography and Crystal Perfection', (Ed. G. N. Ramachandran), Academic Press, London, 1963, pp 207-222
- 12 Hilleard, R. J. and Webster, J. A. *J. Appl. Crystallogr.* 1969, **2**, 193
- 13 Kulshreshtha, A. K., Dweltz, N. E. and Radhakrishnan, T. *Ind. J. Pure Appl. Phys.* 1971, **9**, 986
- 14 Aqua, E. N. *Acta Crystallogr.* 1966, **20**, 560
- 15 Longford, J. I. *J. Appl. Crystallogr.* 1968, **1**, 131
- 16 Louer, P. D., Weigel, D. and Langford, J. I. *J. Appl. Crystallogr.* 1972, **5**, 353
- 17 Lewis, D. and Northwood, D. O. *Br. J. Appl. Phys.* 1969, **2**, 21
- 18 Aqua, E. N. and Wagner, C. N. *J. AEC Access. No. 9649*, Report No. AD-608738, CFSTI, 1964, 34 pp
- 19 Vishnyakov, Ya. D., Ivanov, A. N. and Peregudov, M. N. *Kristallografia* 1968, **13**, 1093
- 20 Halder, N. C. and Wagner, C. N. *J. Adv. X-Ray Anal.* 1966, **9**, 91
- 21 Guinier, A. 'X-Ray Diffraction in Crystals, Imperfect Crystals and Amorphous Bodies', Freeman, San Francisco & London 1963, Ch 5
- 22 Hosemann, R. *Polymer* 1962, **3**, 349

# Mechanisms and relative efficiencies in radical polymerization photoinitiated by benzoin, benzoin methyl ether and benzil

J. Hutchison and A. Ledwith

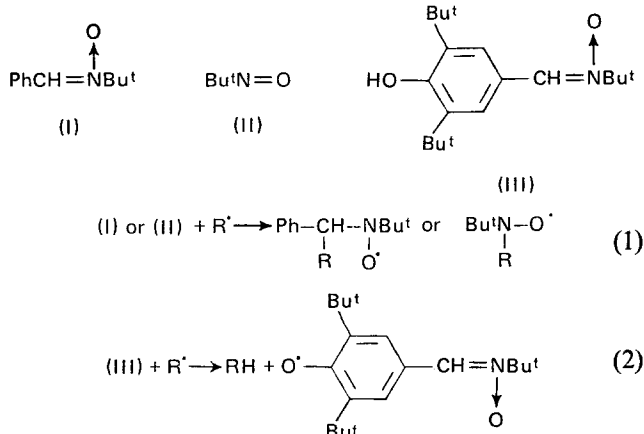
Department of Inorganic, Physical and Industrial Chemistry, University of Liverpool,  
PO Box 147, Liverpool L69 3BX, UK  
(Received 13 April 1973; revised 25 April 1973)

Contrary to widely held views, detailed studies of light absorption characteristics, reaction rates, and molecular weights in radical polymerization of methyl methacrylate photoinitiated by benzoin and benzoin methyl ether indicate that the two photoinitiators have comparable efficiencies; benzil is much less efficient. Mechanisms for initiation, and possible termination processes, for systems involving all three photoinitiators are discussed in the light of results from studies of radical characterization by the spin trapping technique.

## INTRODUCTION

Benzoin,  $\text{PhCO}\cdot\text{CH}(\text{OH})\text{Ph}$  (BN), its methyl ether  $\text{PhCOCH}(\text{OMe})\text{Ph}$  (BME), and benzil,  $\text{PhCOCOPh}$ , (BL), are well known and extensively used photoinitiators of free radical polymerization<sup>1</sup>. Benzoin derivatives in particular have found appreciable use as photoactivators for a wide range of image recording processes based on vinyl polymerization<sup>2</sup>, and for activation of light induced curing of surface films<sup>3</sup>. Although most reports of the use of these materials as photoactivators are to be found in the patent literature, a common inference<sup>3</sup> is that benzoin alkyl ethers are more efficient than benzoin, and that benzil is less efficient than the benzoin derivatives<sup>4</sup>.

Recently we have reported on the use of the diamagnetic radical scavengers (I)–(III) as spin traps for radicals produced on photolysis of benzoin, benzoin methyl ether and benzil, under a variety of reaction conditions<sup>5</sup>. For scavengers (I) and (II), radicals are trapped and characterized by direct addition to the N–O function (equation 1); the scavenger (III) traps radicals in a similar manner but may also scavenge by hydrogen transfer from the reactive phenolic group (equation 2).



An important conclusion<sup>5</sup>, from the spin trapping experiments, is that whilst both BN and BME undergo fragmentation ( $\alpha$ -cleavage) to give  $\text{Ph}\dot{\text{C}}\text{O}$  and  $\text{Ph}\dot{\text{C}}\text{HOR}$  radicals on photolysis, BL does *not* give rise to radicals by corresponding  $\alpha$ -cleavage. Radicals produced by photo-excitation of BL arise, apparently, only from hydrogen abstraction processes, thus offering a possible explanation for the lower efficiency of BL in photoinitiating radical polymerization. The spin trapping experiments also demonstrate a hydrogen abstraction capability (i.e. from III) for photo-excited BN and BME suggesting that the respective excited states have significant lifetimes and are not completely dissociative, as is commonly assumed.

Radical formation from BN and BME, as evidenced by the spin trapping experiments, appears to be much more efficient in the case of the latter sensitizer, in accord with observations from polymerization studies noted earlier. However, it is quite possible that this apparent relative efficiency for radical production results entirely from the different light absorption characteristics of the two sensitizers and, in order to clarify the position, we have studied light absorption characteristics, reaction rates, and molecular weights in polymerization of methyl methacrylate photoinitiated by BN, BME, and BL.

## EXPERIMENTAL

Benzoin and benzil were recrystallized twice from methanol, m.p. 138° and 96°C respectively. Benzoin methyl ether was recrystallized twice from petroleum ether (b.p. 80–100°C), m.p. 49–50°C.

The purification of methyl methacrylate (MMA), tetrahydrofuran (THF) and azobisisobutyronitrile (AIBN) have been fully described in an earlier paper<sup>6</sup>, as have the high-vacuum techniques employed for the polymerization experiments<sup>7</sup>. Reaction tubes for the latter were constructed out of 7 mm i.d. Pyrex

tubing and contained 2 cm<sup>3</sup> of solutions of the photoinitiators usually in bulk MMA. These were placed in a 30°C constant temperature bath behind a soda-glass window and irradiated by a 250 W mercury discharge lamp (Mazda type ME/D). The soda-glass window filtered out short-wavelength u.v. light ( $\lambda < 310$  nm). Polymerization rates were determined gravimetrically, the polymer being precipitated in 300 cm<sup>3</sup> methanol, filtered, and dried to constant weight at 50°C in a vacuum oven. The number-average molecular weights of the polymers were measured using a Hewlett-Packard 502 high speed membrane osmometer.

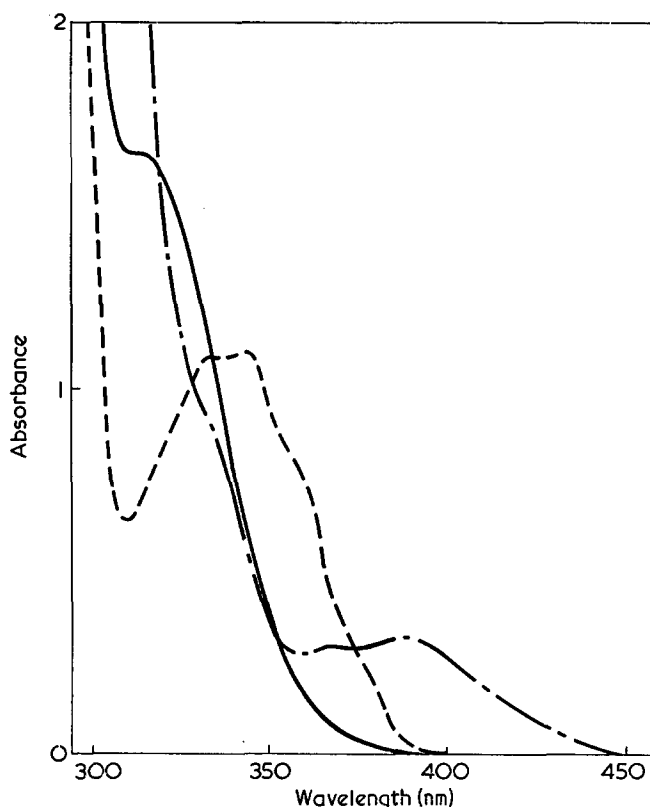
A potassium ferrioxalate actinometer<sup>8</sup> was used to determine the relative amounts of light absorbed by the photoinitiators in MMA solution over the concentration range investigated in the polymerization experiments. The photoinitiator solution was placed in a spectrophotometer cell of path length 5 mm, which was considered to be a close approximation to the effective path length of the 7 mm diam. tubes used for the polymerizations. Another cell containing the acetate-buffered potassium ferrioxalate/1,10-phenanthroline solution was positioned immediately behind the photolysis cell. A piece of soda-glass similar to the window of the constant temperature bath was placed in front of the u.v. lamp and the light transmitted by the photoinitiator solution was monitored by measuring the rate of formation of the ferrous 1,10-phenanthroline complex in the actinometer. The latter rate was subtracted from that observed when MMA containing no photoinitiator was present in the 5 mm cell. The method assumed that the quantum yield for complex formation in the actinometer was constant over the wavelength range absorbed by the photoinitiators.

The u.v. absorption spectra of solutions of the photoinitiators in MMA and in methanol were recorded using a Unicam SP1800 spectrophotometer.

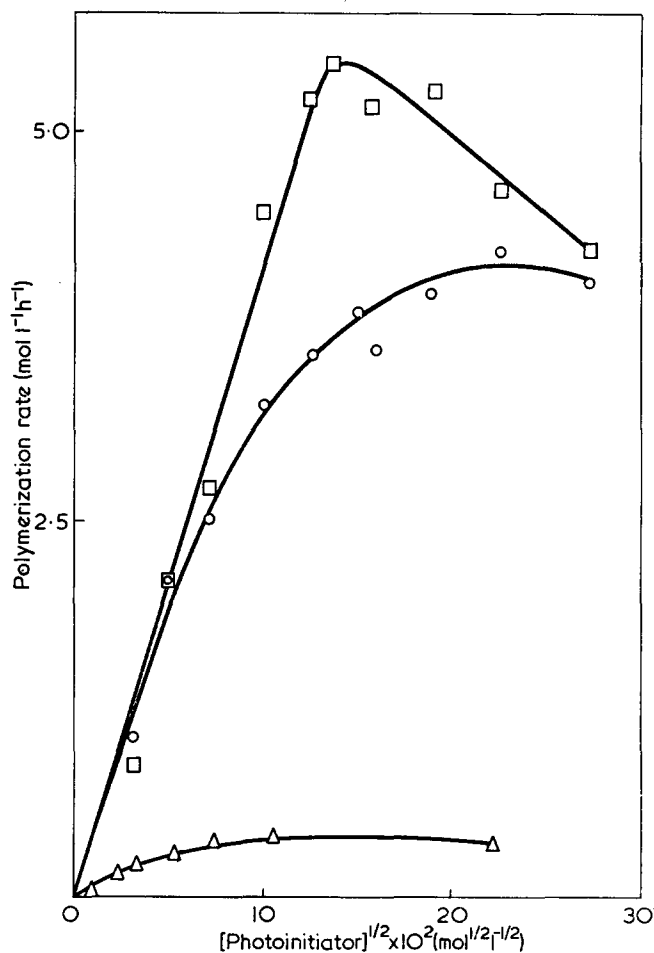
## RESULTS AND DISCUSSION

The u.v. absorption spectra of MMA solutions of BN, BME and BL are shown in *Figure 1*. A striking feature is the dissimilarity between the BN and BME spectra. This is ascribed largely to the presence of strong intramolecular hydrogen bonding in the BN molecule, this not being possible in the case of BME. In methanol solution, the BN and BME spectra were found to resemble each other much more closely (BN:  $\lambda_{\max}$  318 nm,  $\log \epsilon = 2.44$ ; BME:  $\lambda_{\max}$  326 nm,  $\log \epsilon = 2.42$ ) hydrogen bonding between methanol and the carbonyl group of BME having produced the characteristic blue shift of the  $n-\pi^*$  transition. The small red shift observed in the case of BN ( $\lambda_{\max}$  313 nm in MMA, 318 nm in MeOH) is an interesting effect, and may be a result of intermolecular hydrogen bonding disrupting the intramolecular hydrogen-bonded structure. Acetoin has been reported to exhibit similar behaviour<sup>9</sup>.

Rates of polymerization observed on irradiation of solutions containing various concentrations of the three photoinitiators in bulk MMA are shown in *Figure 2*. These results, when considered in relation to those obtained from the actinometry experiments (*Figure 3*) show that BL is much less efficient as a photoinitiator of bulk MMA polymerization than BN or BME. Moreover, the quantum efficiencies for initiation by BN and BME clearly do not differ to any significant extent,



*Figure 1* U.v. absorption spectra of benzoin (—), benzoin methyl ether (---) and benzil (-·-·-) in MMA ( $1.0 \times 10^{-2}$  M, 5 mm path length)



*Figure 2* Polymerization rates (30°C) observed on irradiation of solutions of benzoin (○) benzoin methyl ether (□) and benzil (△) in bulk MMA

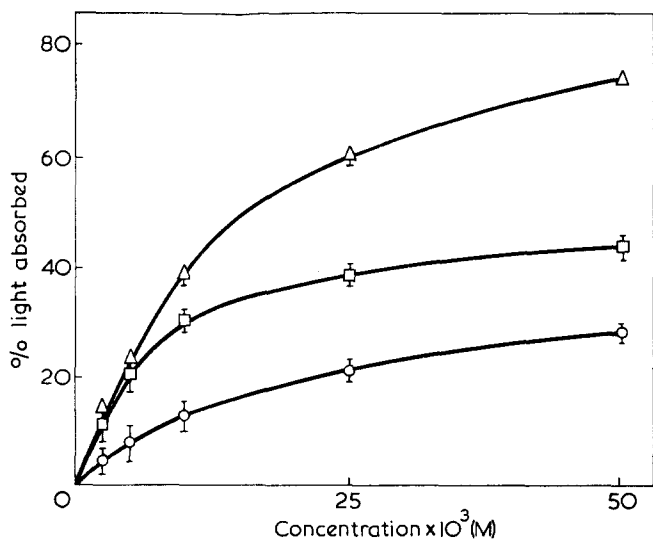


Figure 3 Concentration dependence of light absorbed by benzoin (O), benzoin methyl ether (□) and benzil (Δ) in bulk MMA, 5mm path length

the generally higher rates of polymerization obtained with BME being more than adequately accounted for by the greater amount of light absorbed under the photolysis conditions employed. The fact that all three plots in Figure 2 exhibit marked curvature is not surprising in view of the non-linear relationships between light absorption and concentration of the photoinitiators over the range investigated. The actual decrease in polymerization rate observed for BME concentrations above  $2 \times 10^{-2}$  M, and less obviously for the highest concentrations of BN and BL used, requires further explanation. Since in all cases the total amount of light absorbed continues to increase with concentration over the whole range, then the total number of initiating radicals produced per unit time would also be expected to increase. However, the *distribution* of initiating radicals will become less uniform at higher concentrations, more and more being formed in a relatively narrow region nearest to the light source. Because of the half-order dependence of free-radical polymerization rates on the rate of initiation, non-uniformity of the latter in the system will tend to decrease the observed overall rate of polymerization. It is quite conceivable that a stage will be reached when this effect more than compensates for the increase in total light absorption.

Values obtained for the number-average molecular weights of the polymers produced in the photoinitiated reactions are expressed in the form of reciprocal degree of polymerization vs. rate of polymerization plots in Figure 4. (Points corresponding to photoinitiator concentrations in excess of those giving the maximum observed polymerization rates exhibit divergence from the general trends, as would be expected from the argument given in the previous paragraph.) From the gradients of these plots, apparent values for  $k_p/k_t^{1/2}$  were calculated using the equation:

$$\frac{k_p}{k_t^{1/2}} = \frac{1}{[\text{MMA}] \times \text{gradient}^{1/2}}$$

( $k_p$  and  $k_t$  being the rate constants for propagation and termination). This equation assumes that transfer to initiator does not take place, and that termination occurs exclusively by disproportionation of the polymer radicals. The error involved in ignoring the combination

mode of termination<sup>10</sup> at this temperature is estimated<sup>11</sup> to be less than 10%. The  $k_p/k_t^{1/2}$  values calculated from the BN- and BME-photoinitiated polymerizations were  $0.063 \pm 0.003$  and  $0.059 \pm 0.002 \text{ mol}^{-1/2} \text{ l}^{1/2} \text{ s}^{-1/2}$  respectively, and are not considered to differ significantly from the value of  $0.066 \text{ mol}^{-1/2} \text{ l}^{1/2} \text{ s}^{-1/2}$  obtained previously<sup>7</sup> for MMA polymerizations initiated by AIBN and carried out in THF solution at 30°C. From the polymerizations initiated using BL,  $k_p/k_t^{1/2}$  was calculated to be  $0.038 \pm 0.004 \text{ mol}^{-1/2} \text{ l}^{1/2} \text{ s}^{-1/2}$ , somewhat lower than the values obtained using BN and BME. However, there are reservations in attaching significance to this since the polymerization rates obtained with BL were so low and covered a comparatively narrow range not fully investigated with BN and BME. That BL itself, in the ground state, does not act as a retarder or transfer agent was demonstrated by investigating its effect on bulk MMA polymerizations initiated thermally by AIBN ( $5 \times 10^{-2}$  M, 30°C). No reduction in either the rate of polymerization or the number-average molecular weight of the polymer was observed for BL concentrations up to 0.1 M. However, it should be noted that other workers<sup>1g, 1h</sup> have reported significant incorporation of BME and BN in photoinitiated polymerizations of MMA and styrene, to an extent indicative of copolymerization of photoexcited initiators.

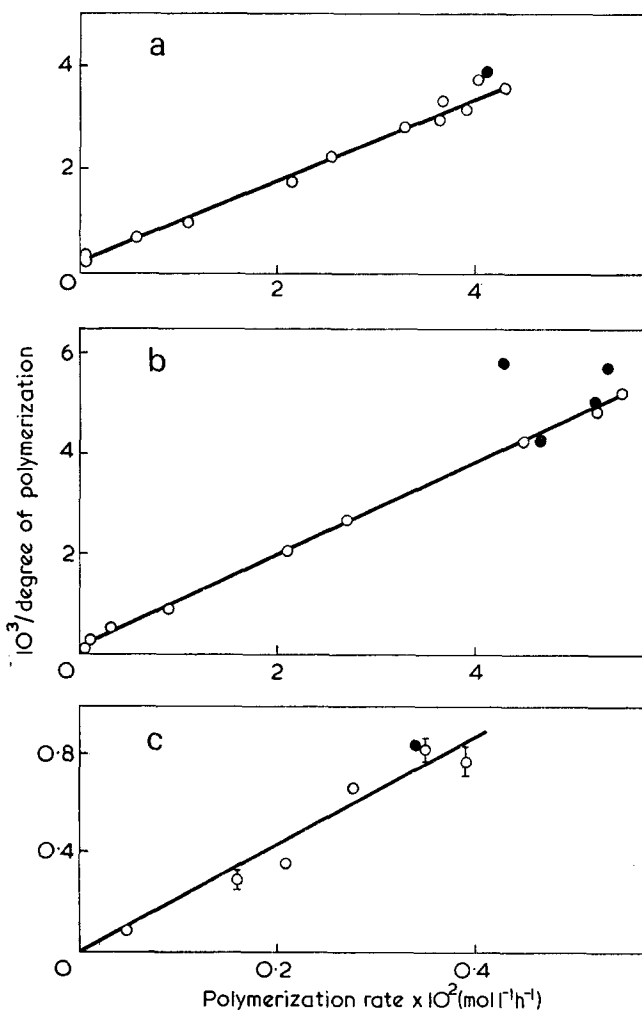
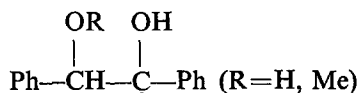


Figure 4 Reciprocal degree of polymerization versus rate of polymerization of bulk MMA photoinitiated by (a) benzoin, (b) benzoin methyl ether and (c) benzil. ●, correspond to photoinitiator concentrations in excess of those giving the maximum observed polymerization rates

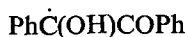


Previous studies<sup>3, 5, 12, 13</sup> of the photochemistry of BN and BME are consistent with the radical-forming process being Norrish type I cleavage of the photo-excited states of these molecules to produce  $\text{Ph}\dot{\text{C}}=\text{O}$  and  $\text{Ph}\dot{\text{C}}\text{HOH}$  or  $\text{Ph}\dot{\text{C}}\text{HOME}$  radicals. The results presented here show that, taking into account the light absorption characteristics of these two compounds, their efficiencies as photoinitiators for the polymerization of bulk MMA are comparable. The simplest interpretation of this is that the quantum yields for dissociation of BN and BME are similar and that there is no marked difference in the ability of the resulting pairs of radicals to initiate the polymerization of MMA. Any alternative explanation of the results would involve a counterbalancing of these properties. If the former situation holds, it follows that in bulk MMA the reactivities of the  $\text{Ph}\dot{\text{C}}\text{HOH}$  and  $\text{Ph}\dot{\text{C}}\text{HOME}$  radicals are approximately the same. This is interesting in view of the recent suggestion by Heine *et al.*<sup>3</sup> that  $\text{Ph}\dot{\text{C}}\text{HOH}$ , but not  $\text{Ph}\dot{\text{C}}\text{HOME}$ , may initiate polymerization by a fragmentation mechanism analogous to that proposed by Braun<sup>14</sup> for semibenzopinacol radicals, i.e. transfer to monomer of the hydroxyl hydrogen atom. Heine *et al.*<sup>3</sup> (who have studied the reactivities of a number of benzoin derivatives in the light-induced curing of unsaturated polyester resins) imply that the chain thus started may cause premature termination of the one initiated by  $\text{Ph}\dot{\text{C}}=\text{O}$  in the immediate vicinity, thereby reducing the effectiveness of the photoinitiator. The  $k_p/k_t^{1/2}$  values calculated for the BN- and BME-initiated MMA polymerizations are not unusually low, and from this it is concluded that 'premature' termination of polymer chains, including termination by the primary radicals themselves, does not occur to any significant extent in either case. Nevertheless the efficiency of benzoin in promoting hardening of illuminated surface coatings is clearly much less than that of benzoin methyl ether and, in addition to the differing light absorption characteristics, it is also possible that, in less mobile environments, initiation by both benzoin and its methyl ether may involve hydrogen abstraction from the environment, as well as fragmentation. Evidence for hydrogen abstraction by photo-excited benzoin and its methyl ether has been provided by the spin trapping experiments referred to in the introduction. Hydrogen abstraction from the environment would yield radicals of the type



and there is clear evidence<sup>6, 7</sup> for differing tendencies to terminate radical chains by semi-pinacol radicals of similar types. Thus it may be that the benzoin derived radical is more efficient in terminating radical chains than its methyl homologue, and that this contributes to the apparent lower efficiency of BN in photo-induced crosslinking processes.

The photochemical behaviour of BL has been shown by Bunbury *et al.*<sup>15</sup> to be related to the hydrogen-donating power of the solvent. These authors conclude that photo-excited BL can abstract hydrogen atoms from good hydrogen-donor solvents forming



and solvent-derived radicals. The comparatively low initiating efficiency of BL in bulk MMA may be due

to the participation of such a mode of reaction producing radicals which are poor initiating species. The apparently low  $k_p/k_t^{1/2}$  value calculated from the BL-initiated polymerizations could result from termination of polymer radicals by  $\text{Ph}\dot{\text{C}}(\text{OH})\text{COPh}$ , since this has been shown to occur for analogous radicals derived from benzophenone<sup>6</sup>. The latter is also a relatively poor photoinitiator for the polymerization of bulk MMA, but shows considerably increased efficiency when a good hydrogen-donor solvent, such as THF, is present<sup>7</sup> (the solvent-derived radical being held chiefly responsible for initiation). The effect of THF on the BL/MMA system was therefore tested. Irradiation of a  $10^{-2}$  M solution of BL in 10% v/v THF/MMA gave rise to an approximately three-fold increase in polymerization rate (30°C) over that observed for the same concentration of BL in bulk MMA (THF had no appreciable effect on BN- and BME-photoinitiated polymerizations). This supports the view that radical production from photo-excited BL proceeds by a hydrogen-abstraction mechanism rather than by direct dissociation. The latter would give rise exclusively to benzoyl radicals and it may be argued that this is unfavourable since there is evidence<sup>16</sup> that the unpaired electron of the benzoyl radical is not delocalized into the aromatic ring. In contrast, the dissociation of BN and BME will be facilitated by simultaneous formation of relatively stable substituted benzyl radicals.

## REFERENCES

- (a) Cooper, W., Vaughan, G., Miller, S. and Fielden, M. *J. Polym. Sci.* 1959, **34**, 651; (b) Chen, C. T. and Huang, W. D. *J. Chin. Chem. Soc. (Taipei)* 1969, **16**, 46; (c) Rafikov, S. R. and Gladyshev, G. P. *Vysokomol. Soedin.* 1962, **4**, 1345 (*Chem. Abstr.* 1962, **58**, 14097f); (d) Heine, H. G., Fuhr, K., Rudolph, H. and Schnell, H. S.Afr. Pat. 6904, 724 (*Chem. Abstr.* 1970, **73**, 46220); (e) Okamura, S. and Motoyama, T. *Kobunshi Kagaku* 1958, **15**, 847 (*Chem. Abstr.* 1960, **54**, 11552a); (f) Sun Chemical Corp. Br. Pat. 1 198 259 (*Chem. Abstr.* 1970, **73**, 57311); (g) Mochel, W. E., Crandall, J. L. and Peterson, J. H. *J. Am. Chem. Soc.* 1955, **77**, 494; (h) Bevington, J. C. 'Radical Polymerisation', Academic Press, London, 1961, p 77
- Kosar, J. 'Light-sensitive Systems', Wiley, New York, 1965, Ch 5
- Heine, H. G., Rosenkranz, H.-J., and Rudolph, H. *Angew. Chem. (Int. Edn)* 1972, **11**, 974; Heine, H. G. *Tetrahedron Lett.* 1972, p 4755
- Whyte, R. B. and Melville, H. W. *J. Soc. Dyers Colour.* 1949, p 703; Chinmayanandam, R. B. and Melville, H. W. *Trans. Faraday Soc.* 1954, **50**, 73
- Ledwith, A., Russell, P. J. and Sutcliffe, L. H. *JCS Perkin Trans. II* 1972, p 1925
- Hutchison, J., Lambert, M. C. and Ledwith, A. *Polymer* 1973, **14**, 250
- Block, H., Ledwith, A. and Taylor, A. R. *Polymer* 1971, **12**, 271
- Kurien, K. C. *J. Chem. Soc. (B)* 1971, p 208
- Baum, E. J., Hess, L. D., Wyatt, J. R. and Pitts, Jr. J. N. *J. Am. Chem. Soc.* 1969, **91**, 2461
- Bevington, J. C., Melville, H. W. and Taylor, R. P. *J. Polym. Sci.* 1954, **12**, 449; 1954, **14**, 463
- Bamford, C. H. and Brumby, S. *Makromol. Chem.* 1967, **105**, 122
- Kornis, G. and DeMayo, P. *Can. J. Chem.* 1964, **42**, 2822
- Closs, G. L. and Paulson, D. R. *J. Am. Chem. Soc.* 1970, **92**, 7229
- Braun, D. and Becker, K. H. *Angew. Makromol. Chem.* 1969, **6**, 186; *Makromol. Chem.* 1971, **147**, 91
- Bunbury, D. L. and Wang, C. T. *Can. J. Chem.* 1968, **46**, 1473; Bunbury, D. L. and Chuang, T. T. *Can. J. Chem.* 1969, **47**, 2045
- Solly, R. K. and Benson, S. W. *J. Am. Chem. Soc.* 1971, **93**, 1592

# Copolymers of methyl methacrylate with cinnamic acid

J. C. Bevington, F. R. Colley\* and J. R. Ebdon

Department of Chemistry, University of Lancaster, Lancaster, UK  
(Received 25 April 1973)

Methyl methacrylate (MMA) and cinnamic acid (CA) have been copolymerized radically at 60°C; the amounts of CA incorporated in copolymers are surprisingly low. The CA units sensitize the MMA units towards alkaline hydrolysis. The copolymers are less soluble than the homopolymer of MMA in toluene; their thermal stabilities are significantly higher and their glass transition temperatures are slightly lower.

## INTRODUCTION

The methyl methacrylate (MMA) units in polymers made by radical polymerization are sensitized towards alkaline hydrolysis by the presence of certain comonomer units<sup>1-4</sup>. For copolymers of MMA with methyl acrylate or methacrylic acid, the sensitization has been attributed to a neighbouring group effect involving anions derived from the comonomer units<sup>1,4</sup>. Copolymers of MMA with cinnamic acid (CA) have now been examined to see if this comonomer produces similar effects.

## EXPERIMENTAL

Monomeric MMA was purified and <sup>14</sup>C-MMA was prepared and purified by methods described already<sup>5</sup>; the specific activity of the labelled monomer was ~0.18 μCi/g. *trans*-CA was recrystallized from water; CA labelled at the 3-position and having a specific activity of ~0.40 μCi/g was prepared using benzaldehyde labelled with <sup>14</sup>C in the carbonyl group (supplied by Dr P. Hodge of these laboratories). *N,N*-dimethylformamide (DMF) and benzoyl peroxide (BP) were purified by standard procedures.

Copolymers were prepared at 60°C using mixtures of MMA and CA at a total concentration of 3.8 mol/l in DMF with BP at 1 g/l. Polymerizations were stopped at about 5% conversion. Copolymers were recovered by precipitation in methanol and then purified by two such precipitations from benzene; they were finally freeze-dried from benzene solution. Compositions of copolymers were determined by a tracer method using <sup>14</sup>C-CA in some cases and <sup>14</sup>C-MMA in others. Labelled materials were assayed by scintillation counting of benzene solutions using equipment supplied by Isotope Developments Ltd and phosphor solution NE 211 (Nuclear Enterprises Ltd). Observed counting rates were corrected for background; allowance was made for quenching by finding the counting rates for samples of various weights and extrapolating to give counts s<sup>-1</sup>mg<sup>-1</sup> at zero weight of sample.

Solutions of copolymers (50 mg) in benzene (25 cm<sup>3</sup>) were treated with solutions of sodium hydroxide (1 g)

in methanol (7 cm<sup>3</sup>) at 80°C for various periods. The copolymers were recovered by precipitation in methanol or in petroleum ether acidified with HCl; they were purified by reprecipitation in acidified petroleum ether from dioxane solutions and dried in a vacuum oven. Proton magnetic resonance spectra of copolymers were recorded on a Varian A60A 60 MHz spectrometer using solutions in pyridine; degrees of hydrolysis were found by comparison of the spectra of the original and modified copolymers.

Glass transition temperatures were found using a Perkin-Elmer DSC-1B differential scanning calorimeter. Weight losses during pyrolysis under nitrogen between 250 and 500°C were measured on a Perkin-Elmer TGS-1 thermobalance.

## RESULTS AND DISCUSSION

The mole fraction (*x*) of CA in a copolymer with MMA is given by:

$$\frac{25C_p}{37C_A - 12C_p} \quad \text{for } ^{14}\text{C-CA with unlabelled MMA}$$

or

$$\frac{25(C_M - C_p)}{25C_M + 12C_p} \quad \text{for unlabelled CA with } ^{14}\text{C-MMA}$$

where *C<sub>A</sub>*, *C<sub>M</sub>* and *C<sub>p</sub>* are the counting rates (counts s<sup>-1</sup>mg<sup>-1</sup>) for CA, MMA and copolymer respectively. Results are summarized in *Table 1* which includes values of the number-average molecular weight and the average numbers of CA units per copolymer molecule (calculated from the analyses and the values of  $\bar{M}_n$ ). There are only quite small amounts of CA in the copolymers and there is no detectable homopolymerization of CA under the conditions used in these experiments; *r*<sub>2</sub> (taking CA as monomer-2) is therefore very close to zero.

From *Figure 1*, it is evident that the usual copolymer composition equation is not strictly obeyed but *r*<sub>1</sub> must have a very high value, say 300 (see *Figure 2*). For the copolymerization of styrene (monomer-1) with CA<sup>6</sup>, *r*<sub>1</sub> is 1.85; from published *Q* and *e* values<sup>7</sup>, a value of

\* Present address: Plastanol Ltd, Belvedere, Kent, UK.

about 4 might be expected for  $r_1$  in the system MMA/CA. The discrepancies may be attributed to a marked steric effect between a radical with a terminal MMA unit and an approaching molecule of CA. Table 1 shows that both rate of polymerization and  $\bar{M}_n$  of the resulting polymer are depressed by increasing the proportion of CA in the feed. These effects are consistent with rather a slow reaction between monomeric MMA and a polymer radical with a terminal CA unit.

The fraction ( $h$ ) of MMA units hydrolysed was calculated from n.m.r. spectra of copolymers using the expression:

$$h = 1 - \frac{A'_M/A'_T}{A_M/A_T}$$

where

$A_M$  and  $A'_M$  = peak area from the methoxy protons before and after hydrolysis, respectively

$A_T$  and  $A'_T$  = the corresponding total proton peak areas

For copolymers containing mole fractions of CA of 0.013, 0.009 and 0.005, the percentages of MMA units

Table 1 Copolymers of methyl methacrylate (MMA) and cinnamic acid (CA)

Mole fraction CA in feed	Mole fraction CA in copolymer	Time (h) for ~5% conversion	No. average mol. wt of copolymer $\times 10^{-4}$	Average no. of CA units per copolymer molecule
0.40	0.0038	2.5	16	6
0.47	0.0047	3.0	—	—
0.55	0.0060	3.5	10	6
0.65	0.0082	4.75	9	8
0.70†	0.0094	5.25	7	7
0.75	0.0114	6.25	—	—
0.80†	0.0131	10.5	—	—
0.85	0.0160	15.0	—	—
0.90†	0.0229	25.0	5	12

† Experiments with  $^{14}\text{C}$ -MMA; others with  $^{14}\text{C}$ -CA

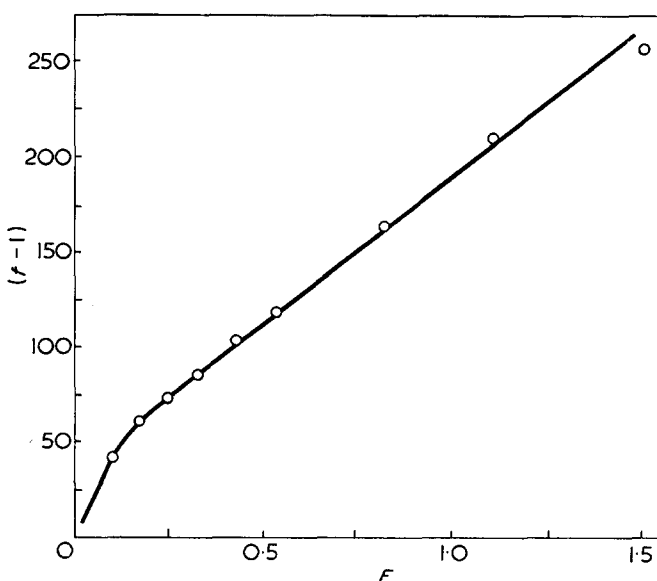


Figure 1 Plot of  $(f-1)$  against  $F$  for copolymerization of MMA with CA.  $f$  and  $F$  = molar ratio MMA:CA in copolymer and feed respectively. The Fineman-Ross equation can be written as  $f-1=r_1F$  when  $r_2$  is very close to zero

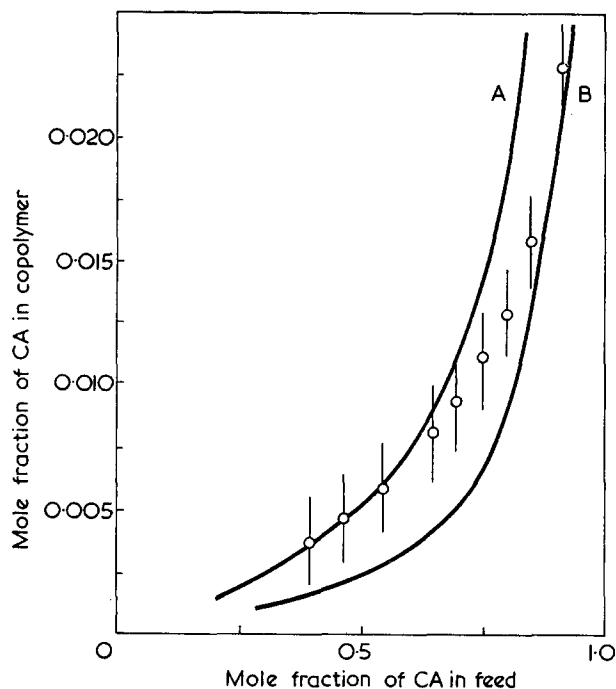


Figure 2 Copolymer composition plotted against feed composition. Points correspond to experimental results; line A is drawn for  $r_1=200$  and line B for  $r_1=400$

hydrolysed after treatment for 52 h were 12, 5 and 4 respectively; the corresponding percentages for 96 h treatment were 16, 14 and 7. The results for the copolymer containing least CA are close to those for the homopolymer of MMA<sup>1</sup>. The extent of hydrolysis increased with the CA content of the copolymers; in this respect, CA resembles other comonomers.

The introduction of a few CA units into a MMA chain produces changes in certain properties of the polymer. From the measurements of osmotic pressures of toluene solutions, it is apparent that the second virial coefficient is lower for the copolymers than for the homopolymer; this result indicates that toluene is better as a solvent for the homopolymer than for the copolymers. The glass transition temperature was reduced slightly by the presence of CA units in the MMA chain. The copolymers were significantly more thermally stable than the homopolymer.

ACKNOWLEDGEMENT

The work reported here was supported by a grant from the Science Research Council.

REFERENCES

- Baines, F. C. and Bevington, J. C. *J. Polym. Sci. (A)* 1968, 6, 2433
- Bevington, J. C., Brinson, R. and Hunt, B. J. *Makromol. Chem.* 1970, 134, 327
- Bevington, J. C. and Ebdon, J. R. *Makromol. Chem.* 1972, 153, 165
- Smets, G. and de Loecker, W. *J. Polym. Sci.* 1959, 41, 374
- Blackley, D. E. and Melville, H. W. *Makromol. Chem.* 1955, 18, 16
- Barson, C. A. *J. Polym. Sci.* 1962, 62, S128
- Young, L. J. 'Polymer Handbook' (Eds J. Brandup and E. H. Immergut), Interscience, New York, 1966, pp II-341

# Electron microscopic studies on the useful life of liquid permeated membranes

S. K. Ghosh\* and M. G. Krishna

*Indian Institute of Petroleum, Dehradun, India*

and V. D. Vankar

*Department of Physics, Banaras Hindu University, Varanasi-221005, India*

*(Received 3 January 1973; revised 18 April 1973)*

Morphological changes occurring on the surface of a polyethylene membrane used in liquid permeation of hydrocarbons have been studied by electron microscopy. The upstream surface of the membrane in contact with liquid feed has been shown to be eroded considerably whereas the downstream surface remained sensibly unaffected. Thus, the useful life of a particular membrane is limited depending on temperature and nature and quantity of the feed used.

## INTRODUCTION

Membrane separation processes such as reverse osmosis, ultra-filtration, membrane permeation (gas or liquid) etc. have become popular in recent years. In the field of low molecular weight separation of hydrocarbons and other organic liquid mixtures by physical methods, liquid permeation shows much promise and has been studied in detail by various authors<sup>1-7</sup>.

In liquid permeation the liquid feed mixture remains in contact with the upstream side of a thin membrane (25 to 100  $\mu\text{m}$  thick) and the permeant, in the form of vapour, is withdrawn from the downstream side which is maintained at a reduced pressure. The membrane is a film of synthetic polymer (polyethylene, cellulose acetate etc.) containing no discrete holes or pores thus prohibiting any hydrodynamic flow through it.

Sanders and Choo<sup>6</sup> studied the useful life of a membrane (of undisclosed nature) for the system isopropanol-water and found that the membrane withstood about 5000 h without failure, although the rate increased slightly and the selectivity of separation decreased. The instability of the membrane may be due to (1) physico-chemical changes and/or (2) mechanical changes brought about within the polymer by contact with the permeant molecules for a long time.

Baddour *et al.*<sup>7</sup> and Müller *et al.*<sup>8</sup> found that crystallinity of the membrane increased up to a limiting value after liquid permeation which amounts to an increase in membrane strength. Consequently, attention was paid to the second reason.

The following discussion will be restricted to low density polyethylene (crystallinity about 44% by volume and hydrocarbon permeants, used in the present studies.

Below about 70°C, the amorphous content of polyethylene does not change appreciably with temperature<sup>9</sup> and also the solubility of polyethylene in hydrocarbon is negligible<sup>10</sup> though not nil. So, a micro amount of polymeric material (amorphous part only, leaving the crystalline part intact, as has been observed by Mackie

and Rudin<sup>11</sup>) at the upstream side of the membrane goes into solution during permeation runs. The non-uniformity developed this way impairs the mechanical stability of the membrane. Here, an electron microscopic study carried out on the solvent action of hydrocarbons on the membrane surface has been discussed. The entire procedure was divided into two steps: sample preparation, and electron microscopy.

## EXPERIMENTAL

### *Sample preparation*

Samples were prepared by prolonged permeation runs for each system. *Figure 1* shows a self-explanatory schematic diagram of the apparatus.

The membrane was mounted and the assembly was made leak-proof. Both temperature and downstream pressure were maintained at the desired level. The feed liquid (~500 ml), preheated to the run temperature, was poured into the feed chamber carefully and the stirrer was started. The fraction cutter and other traps were filled with dry ice. The permeated sample was taken out regularly, weighed and fed back to the feed chamber every 30 min. This feed back, the quantity being very small, did not show temperature variation of more than 0.5°C in the feed chamber. At the end of about 5 h (attainment of steady state required about 3 h as indicated by the constancy in weight of product samples) about 450 ml of feed was syphoned out while the run was continuing; another instalment of 450 ml of preheated feed was added and the run continued. In a similar way about 5 to 6 litres of feed have been run covering a period of 60 to 90 h, although in one case run has been continued up to 450 h until the membrane yielded.

At the end of the run, the whole of the feed liquid was syphoned out, the permeation cell was removed from the bath and opened up to take out the membrane. These membranes were vacuum-dried, labelled and preserved.

The loss in weight of the membrane at saturation with

\* Present address: Engineers India Ltd, New Delhi-1, India.

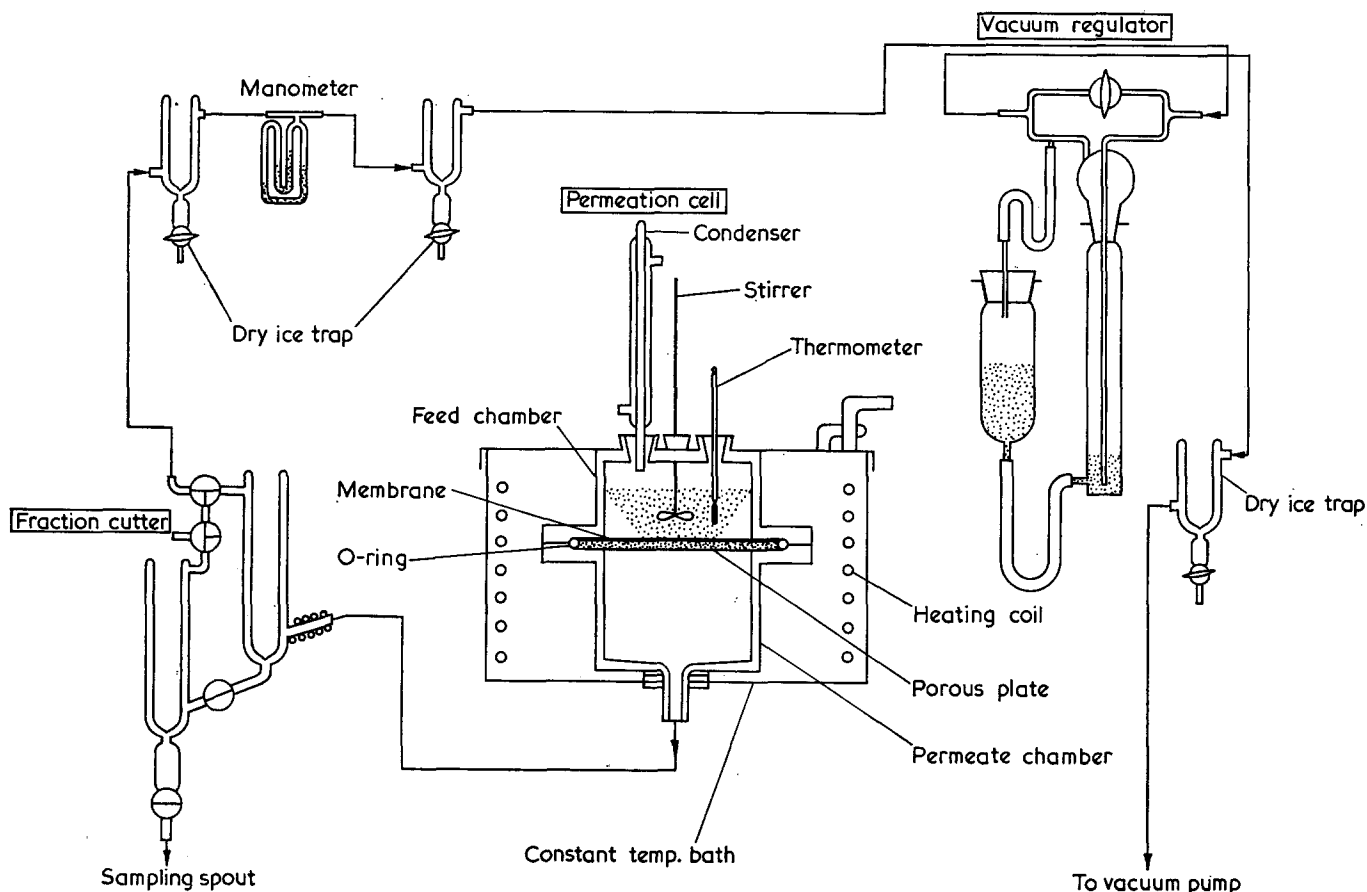


Figure 1 Schematic diagram of liquid permeation assembly

Table 1 Experimental conditions and loss in weight of membranes due to dissolution in hydrocarbons

Surface	Feed	Temp. (°C)	Down-stream pressure (mmHg)	Dura-tion (h)	Loss in weight (%)	Figure
Fresh	—	—	—	—	—	2
Down-stream	Methyl-cyclo-hexane	40	35	60	1.06	3
Upstream	Methyl-cyclo-hexane	40	35	60	1.06	4
Upstream	Methyl-cyclo-hexane	30	35	60	0.75	5
Upstream	Benzene	40	30	450	0.96	6
Upstream	Benzene	40	30	450	0.96	7
Upstream	Toluene/2,2,4-trimethyl-pentane (50:50)	40	25	90	1.09	8

various hydrocarbons has been determined in an electro balance. Table 1 describes the details of the samples, the experimental conditions and the percentage weight loss of membranes due to dissolution in hydrocarbons.

Electron microscopy

The surface was cleaned with acetone and flooded over by a special replicating solution meant for synthetic polymer surfaces in particular (supplied by Ladd Research Inc., USA). A small piece (2 cm x 2 cm) of

replicating tape was cut and immediately pressed onto the wet surface and the bubbles were removed. After about 30 min the tape was taken off the surface. This, being the first tape, was discarded and the same process was repeated. After rejecting two or three, the next tape with the impression side upwards was mounted on a glass slide by adhesive tape. This was shadow-cast with gold (about 10 Å thickness) at an angle of ~14° and then a film of carbon (~100 Å) was deposited on it. A small portion (3 mm x 3 mm) of this tape was cut and dissolved in acetone solution (containing 30% water by volume) taking care that the replica always floated on the surface. After about 1 h the floating replica was picked up on a grid and washed with pure acetone and examined in the electron microscope after drying.

RESULTS AND DISCUSSION

All the micrographs presented (for descriptions see Table 1) here are positive prints so that the dark areas represent hollow regions in the membrane; white areas the unetched regions; and the grey areas the etched regions with severity varying according to shades of grey.

It may be noted that the regular shaped (mostly round or elliptical) dark spots (as in Figures 2, 3, 6 and 7) are defects which occurred during the processing and are not to be taken as characteristic features. These did not appear in other specimens investigated.

Figure 2 shows the general features of a fresh film at a magnification of 3400. The ordered patterns shown here are probably due to uneven surfaces of the rollers used during manufacture of the film from melt. Figure 3

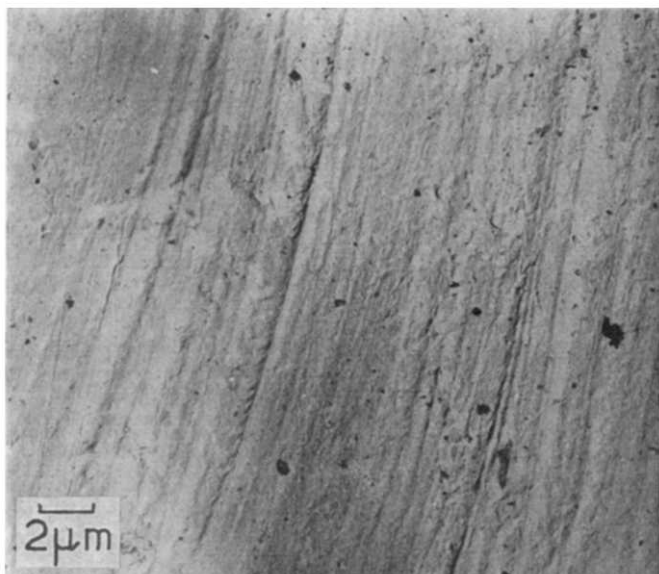


Figure 2 General features of a fresh membrane showing ordered patterns

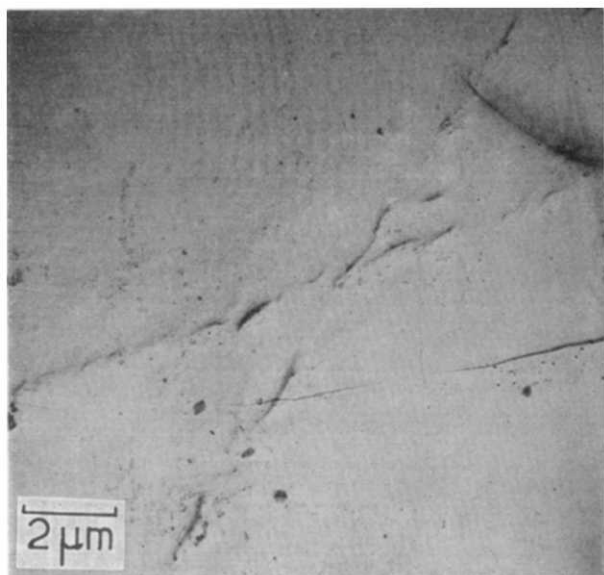


Figure 3 Downstream surface of the membrane showing characteristic features the same as in the fresh one with its unevenness smoothed out. Treated with methylcyclohexane at 40°C for 60h

shows the downstream surface of the membrane (used in permeation run) at a magnification of 6100. The characteristic features appear to be the same as in the fresh film with its unevenness smoothed out probably by continuous long exposure (60h) to hydrocarbon vapour at 40°C. The absence of any significant change in the downstream surface of the membrane could be expected to occur, the permeant being in the form of vapour.

Comparison of Figure 4 ( $\times 4000$ ) and Figure 5 ( $\times 4600$ ) reveals the severity of hydrocarbon attack with respect to temperature. In both cases 5 litres of methylcyclohexane have been used as feed. Although the magnifications are slightly different, it may be readily concluded that the attack is much stronger at elevated temperature. This indicates that with the present systems, permeation runs are not possible at much higher temperatures and the upper limit has been demonstrated<sup>5</sup> to be about 55–60°C.

Figure 5 shows that at 30°C, the surface is practically unetched. On the other hand, Figure 4 reveals clearly the surface roughness due to erosion of amorphous portion of the polymer leaving the crystalline part unaffected<sup>12</sup>. The dark lines are deeply eroded portions which would have developed to microcracks had the permeation runs been continued further.

Both Figure 6 ( $\times 4600$ ) and 7 ( $\times 2300$ ) are for two different locations on the upstream surfaces of the same membrane used in permeation of benzene at 40°C and continued until leakage developed. Figure 6 clearly shows the linear micro-cracks and pores which developed around the etched region having widths of between 0.1 and 0.2 μm. Referring to Figures 6 and 7 it can be seen that the degree of solvent attack is not uniform over the entire membrane surface, indicating possible imperfections in the polymer where hydrocarbons can act more readily.

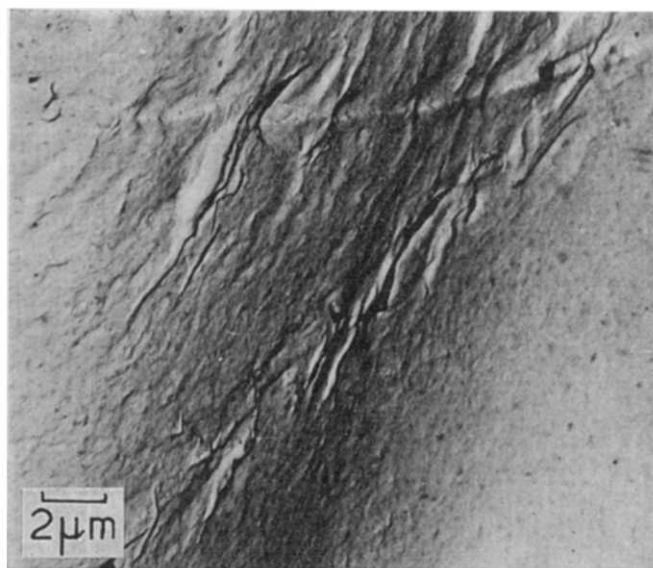


Figure 4 Upstream surface of the membrane showing severity of hydrocarbon attack with respect to temperature. Treated with methylcyclohexane at 40°C for 60h

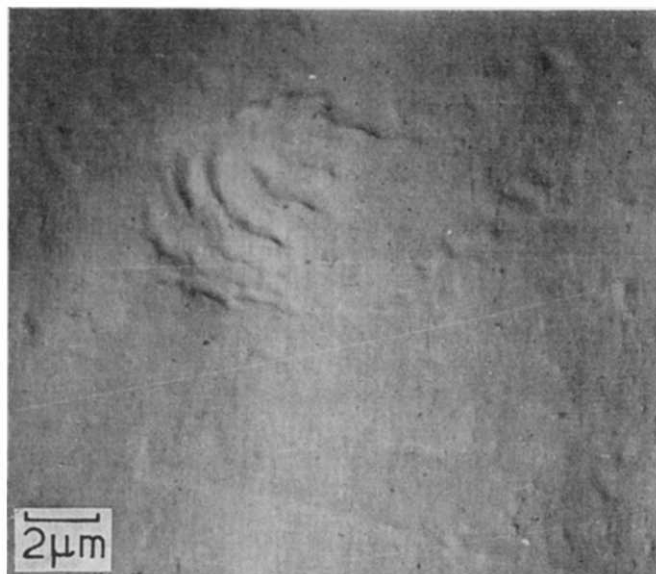


Figure 5 Upstream surface of the membrane showing severity of hydrocarbon attack with respect to temperature. Treated with methylcyclohexane at 30°C for 60h



Figure 8 ( $\times 7600$ ) represents the mode of solvent attack at  $40^{\circ}\text{C}$  when a binary mixture is used. Here the solvent attack is less severe than that with methylcyclohexane (Figure 4) and benzene (Figure 6) at the same temperature (although the run duration was higher than that of methylcyclohexane by 50%), but more than methylcyclohexane at  $30^{\circ}\text{C}$  (Figure 5). It is quite likely that 2,2,4-trimethylpentane (having lower solubility) masks the etching power of toluene (having higher solubility). In this specimen, the etching pattern has not followed any apparent regularity as is evident in the others. From the limited number of micrographs available it is difficult to ascertain if this is a result of permeation of a binary liquid mixture instead of a pure compound.

#### CONCLUSION

These micrographs have thus provided visual evidence that during liquid permeation there is dissolution of polymer into the feed liquid. Although the solubility

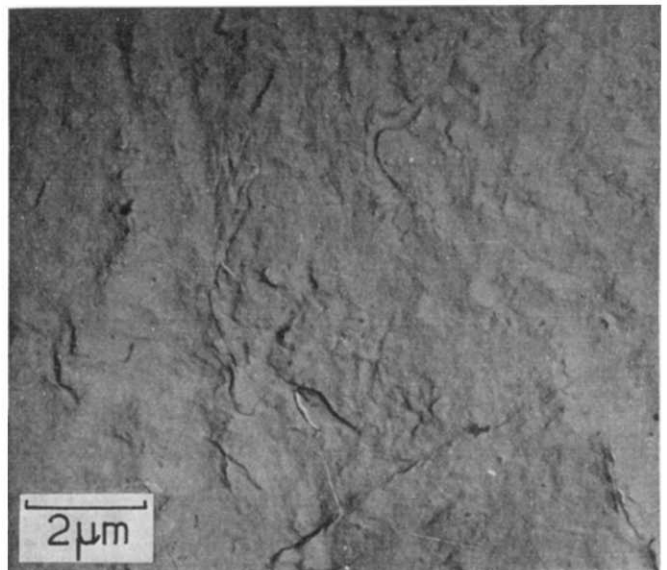


Figure 8 Upstream surface of the membrane showing mode of solvent attack at  $40^{\circ}\text{C}$  when a binary mixture (toluene/2,2,4-trimethylpentane) is used

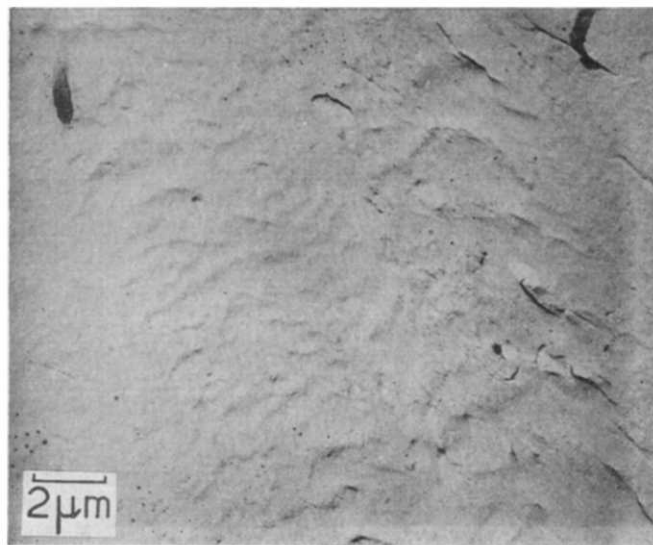


Figure 6 Upstream surface of the membrane used in permeation of benzene at  $40^{\circ}\text{C}$  and continued until leak developed

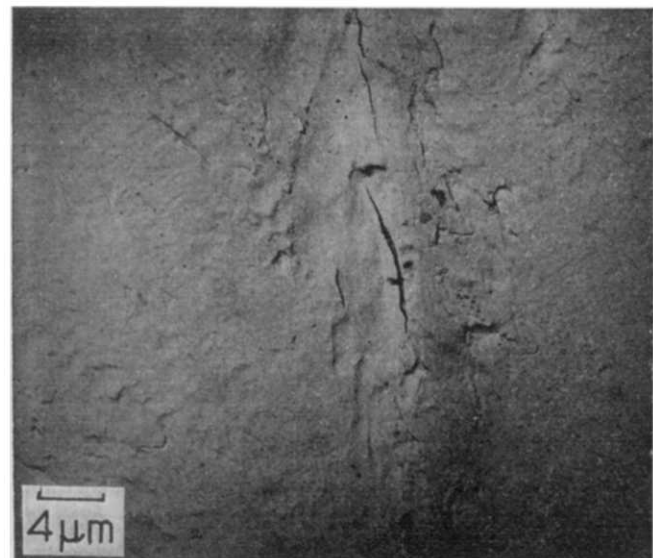


Figure 7 Upstream surface of the membrane used in permeation of benzene at  $40^{\circ}\text{C}$  and continued until leak developed

is very small, it is still sufficient to impart mechanical instability to the membrane. The extent of such damage depends upon the nature of the hydrocarbon, its quantity and temperature. The attack is restricted to the upstream side only, whereas the downstream side is practically unaffected. Thus, it is evident that the useful membrane life is limited owing to loss of mechanical strength with use, consequent to removal of amorphous polymer material from the membrane surface by dissolution. As a result, the working life of a membrane is limited depending upon the temperature and nature of the feed and its replacement is essential after a certain quantity of feed is handled. These observations on a low density polyethylene membrane could reasonably be extrapolated to cover the range of all non-polar polymeric membranes, e.g. high density polyethylene, polypropylene, polyisobutylene etc.

#### ACKNOWLEDGEMENTS

Thanks are due to Mr B. S. Rawat for his help in preparation of the etched membrane samples and to Mr P. K. Gargya for help in electron microscopic preparations. Thanks are also due to Dr D. L. Bhattacharya for discussions and encouragement.

#### REFERENCES

- 1 Binning, R. C., Lee, R. J., Jennings, J. F. and Martin, E. C. *Ind. Eng. Chem.* 1961, **53**, 45
- 2 Choo, C. Y. 'Advances in Petroleum Chemistry and Refining', Interscience, New York, Vol VI, 1962, p. 112
- 3 Eisenmann, J. L. and Berger, C. 141st Am. Chem. Soc. Meeting, 1962
- 4 Long, R. B., *Ind. Eng. Chem. (Fundamentals)* 1965, **4**, 445
- 5 Ghosh, S. K. *Doctorate Thesis* Calcutta University, 1971
- 6 Sanders, B. H. and Choo, C. Y. *Petrol. Refiner* 1960, **39** (6), 133
- 7 Baddour, R. F., Michaels, A. S., Bixler, H. J., DeFillipi, P. and Barrie, J. A. *J. Appl. Polym. Sci.* 1964, **8**, 897
- 8 Müller, F. H. and Hellmuth, E. *Kolloid Z.* 1961, **177**, 1
- 9 Richards, R. B. *Trans. Faraday Soc.* 1946, **42**, 10
- 10 Myers, C. S. *J. Polym. Sci.* 1954, **13**, 549
- 11 Mackie, J. S. and Rudin, A. *J. Polym. Sci.* 1961, **49**, 407
- 12 Fischer, E. W. and Goddar, H. *J. Polym. Sci. (C)* 1969, **16**, 4405

# Cloud-point curves of the polystyrene–cyclohexane system near the critical point

N. Kuwahara, M. Nakata and M. Kaneko

Department of Polymer Science, Hokkaido University, Sapporo, Japan  
(Received 3 April 1973)

Cloud-point curves for solutions of five polystyrene samples, including three well-fractionated polystyrenes, in cyclohexane have been examined near their critical points. Even for a solution of polystyrene characterized by  $M_w/M_n < 1.03$ , the critical point determined by the phase-volume method is generally situated on the right hand branch of the cloud-point curve. The precipitation threshold concentration is appreciably lower than the critical concentration, while the threshold temperature slightly deviates from the critical temperature. The agreement of the precipitation threshold point with the critical point has been found for a solution of polystyrene characterized by  $M_w = 20 \times 10^4$  and  $M_w/M_n < 1.02$  in cyclohexane. The  $\chi(\phi)$  function derived from critical miscibility data is expressed by  $\chi(\phi) = 0.2798 + 67.50/T + 0.3070\phi + 0.2589\phi^2$ , which yields  $\theta$  of  $33.2^\circ\text{C}$  and  $\psi_1$  of  $0.22$ .

## INTRODUCTION

Schultz and Flory<sup>1</sup> measured cloud points as a function of the concentration in some polymer solutions and developed a method for the determination of the  $\theta$  temperature, which is identified as the critical miscibility temperature in the limit of infinite molecular weight. Since then, the cloud-point curves carried out on polymer fractions differing in molecular weight have been widely used as a relatively simple method for the determination of the  $\theta$  temperature<sup>2</sup>. The use of the temperature at the maximum of the cloud-point curve instead of the critical temperature is basically incorrect because of identification of the polymer solution with a binary mixture. However, if the fractions have the same distribution in the molecular weight heterogeneity, the same value of  $\theta$  can be expected<sup>3</sup>.

Stockmayer<sup>4</sup> theoretically examined the effect of the polydisperse character of polymer samples on the critical concentration. Tompa<sup>5</sup> examined the feature of the phase diagrams for mixtures of one solvent component and two polymer homologues differing in chain length. He clearly revealed the difference in the phase behaviour between ternary and binary systems. It has been found by recent studies on the cloud-point curves<sup>3, 6–9</sup> that the precipitation threshold point of the polymer–solvent system does not generally coincide with a true critical point because of the macromolecular constituents. Kuwahara *et al.*<sup>10</sup> and Borchard and Rehage<sup>11</sup> found that the angular dissymmetry of scattered light intensity has its maximum at a concentration much lower than the critical concentration. Koningsveld<sup>3, 7–9</sup> have revealed that the difference of the threshold point from the critical point is ascribed to the molecular weight distribution.

In this paper it is shown empirically that the critical point generally lies at a higher concentration and lower temperature than the precipitation threshold point depending on the molecular weight heterogeneity. It is also shown that the precipitation threshold point for a

solution of a very carefully fractionated polystyrene in cyclohexane can be identified with the critical mixing point. The critical miscibility data are utilized for determinations of the pair interaction parameters by the aid of the method developed by Koningsveld<sup>8</sup>.

## EXPERIMENTAL

Polystyrenes (Pressure Chemical Co. products 1c:  $M_w = 20 \times 10^4$ ;  $M_w/M_n < 1.06$ , and 13a:  $M_w = 67 \times 10^4$ ;  $M_w/M_n < 1.10$  with  $M_w$  and  $M_n$  being the weight- and number-average molecular weight) were fractionated into six fractions, respectively. Fractionation was sequentially carried out through the solution fractionation technique known as the coacervation method. The polystyrene–cyclohexane solution at a concentration less than  $0.04 \text{ g/ml}$  was kept for 2 days at a temperature a little below its precipitation temperature in a water thermostat controlled to  $\pm 0.002^\circ\text{C}$ . After a complete attainment of the phase equilibrium the dilute solution phase, in which lower molecular weight polystyrene is richer, was separated from the other concentrated solution phase. A fractionated polystyrene was obtained from the dilute phase and the concentrated phase was diluted by reagent grade cyclohexane for further fractionations.

Reagent grade cyclohexane, dried thoroughly over anhydrous calcium chloride, was purified by fractional distillation through a column of 100 cm length and 10 mm diameter packed with stainless-steel helices. Purified cyclohexane was dried over silica gel for 7 days and then further dried for 10 days over chromatographic neutral alumina (activity grade 1, M-Woelm-Eschwege), which had been heated at  $600^\circ\text{C}$  for 24 h. It was then distilled with a small distillation apparatus set in a dry box under an atmosphere of dry nitrogen. Particular caution was paid to avoid the moisture in air, because a slight trace of water in cyclohexane leads to the considerable rise of the precipitation temperature.



All solutions were prepared in the dry box under dry nitrogen and were thoroughly stirred at the temperature by about 5°C higher than the phase separation temperature for a few days. The volume fraction  $\phi$  of polystyrene was calculated from the density of cyclohexane and the specific volume of polystyrene in cyclohexane.

The cells used for determinations of the cloud point and the critical point were made of Pyrex tubing (6 mm i.d.) and were sealed with two closely machined Teflon plugs and a silicone rubber stopcock. The solution cells were immersed in the water bath controlled to  $\pm 0.001^\circ\text{C}$  and slowly cooled. In the vicinity of the cloud point the temperature of the bath was lowered in steps of  $0.001\text{--}0.002^\circ\text{C}$ . After each temperature change we allowed sufficient time for the solution to achieve equilibrium. The precipitation temperature  $T_p$  was detected with an accuracy of  $\pm 0.002^\circ\text{C}$  on a relative scale for measurements very near the critical temperature by observing the pattern of He-Ne laser beam transmitted through the solution cell<sup>12</sup>. Temperature was measured using a 6° Beckman thermometer which had been calibrated with a platinum resistance thermometer.

RESULTS AND DISCUSSION

Quantitative features of the cloud-point curves

The volumes of two coexisting phases in equilibrium at an overall concentration  $\phi$  were measured as a function of temperature. A temperature  $T$  at which the volume ratio of two coexisting phases is unity was determined for each  $\phi$  as shown in Figure 1. The cloud-point curves are shown in Figures 2 and 3, in which the sets of  $(\phi, T)$  representing the unit phase-volume ratio are also included. The critical point was determined by extrapolation of the curve of unit phase-volume ratio to the cloud-point curve. The precipitation threshold and critical points are listed in Table 1, where the subscripts  $t$  and  $c$  denote the threshold and critical points, respectively. As compared with the result by Koningsveld et al.<sup>8</sup> our values of  $T_c$  are lower by  $0.5^\circ\text{C}$  or more.

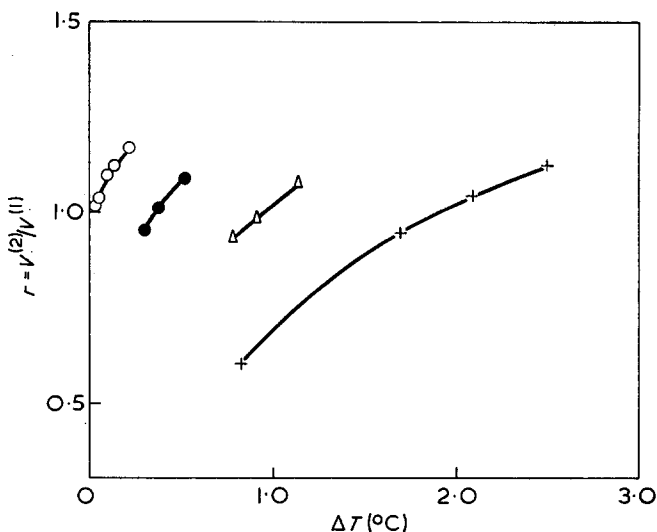


Figure 1 Phase-volume ratio  $r$  as a function of  $\Delta T = T_p - T$  for the sample 1c-5 in cyclohexane. The overall polymer concentration:  $\circ$ ,  $\phi = 0.785$ ;  $\bullet$ ,  $\phi = 0.0844$ ;  $\Delta$ ,  $\phi = 0.0937$ ;  $+$ ,  $0.1083$ . The superscripts (1) and (2) refer to the concentrated and dilute phases

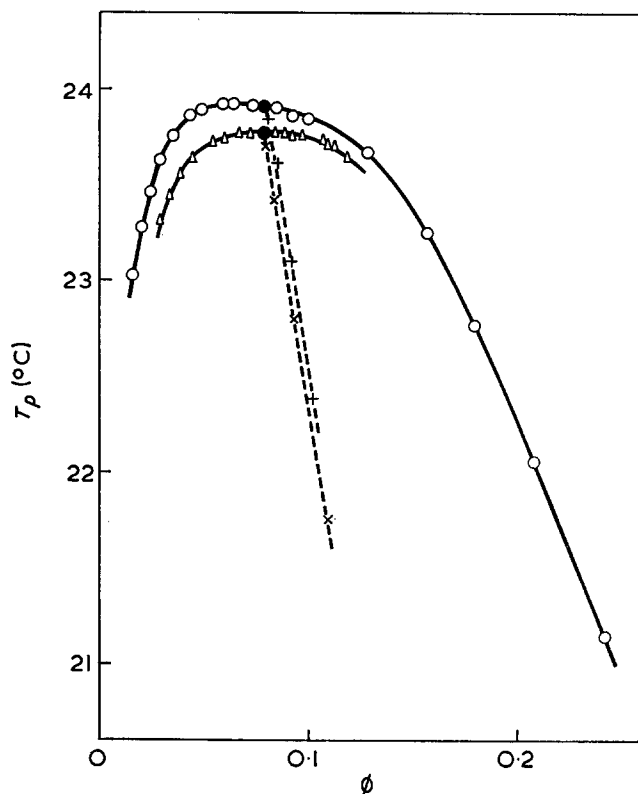


Figure 2 Phase diagrams for the polystyrene samples in cyclohexane:  $\circ$ , 1c-6;  $\Delta$ , 1c-5.  $\bullet$ , Critical point; ----, rectilinear diameter

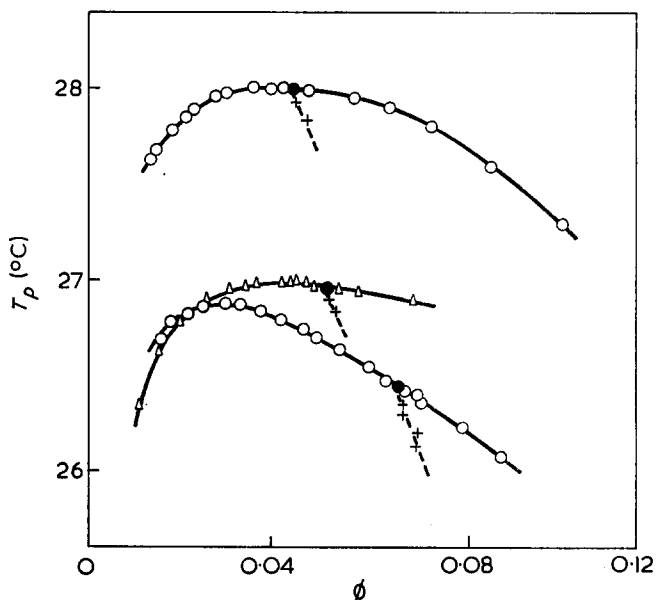


Figure 3 Phase diagrams for the polystyrene samples in cyclohexane:  $\circ$  (upper), 13a-5;  $\Delta$ , 3a;  $\circ$  (lower), mixture.  $\bullet$  and ---- are the same as in Figure 2

A comparison of the precipitation threshold and critical points for 13a-5 suggests that the difference between  $\phi_t$  and  $\phi_c$  is not small, even if  $T_t - T_c = 0.002^\circ\text{C}$ . On the other hand, the critical point for the well-fractionated sample 1c-5 lies at the maximum of its cloud-point curve. The cloud-point curve for 1c-5 may be identified with the coexistence curve and thus the well-fractionated polystyrene solution behaves as if it were a binary mixture. The critical indices which govern the shape and magnitude of the coexistence curve near

Table 1 Characteristics of the polystyrene samples and their critical and precipitation threshold points in cyclohexane

Sample	$M_w \times 10^5$	$M_w/M_n$	$h$	$T_c$ (°C)	$\phi_c$	$T_t$ (°C)	$\phi_t$	$T_t - T_c$ (°C)
1c-5	2.00	1.02 <	67	23.78 <sub>2</sub>	0.077 9	23.78 <sub>2</sub>	0.077 9	0.00 <sub>0</sub>
1c-6	2.06	1.03 <	50	23.92 <sub>3</sub>	0.078 1	23.94 <sub>3</sub>	0.068	0.02 <sub>0</sub>
3a	4.15	1.06 <	17	26.95 <sub>7</sub>	0.052 3	26.98 <sub>0</sub>	0.043	0.02 <sub>3</sub>
13a-5	6.80	1.02 <	67	28.02 <sub>5</sub>	0.044 6	28.02 <sub>7</sub>	0.041	0.00 <sub>2</sub>
Mixture*	4.50	1.44		26.44 <sub>5</sub>	0.067 7	26.89 <sub>5</sub>	0.031	0.45

\* Mixture 52 wt % 1c-5; 48 wt % 13a-5;  $M_z/M_w = 1.30$

the critical point were estimated<sup>13</sup> as  $\beta = 0.345 \pm 0.005$  and  $B_\phi = 0.51$  by fitting experimental points to the equation:

$$(\phi^{(1)} - \phi^{(2)})/2 = B_\phi(1 - T/T_c)^\beta$$

in which the superscripts (1) and (2) refer to the concentrated and dilute phases.

The solution of sample designated by mixture can be considered as a quasi-ternary system, which comprises the polystyrene samples of  $M_w = 20 \times 10^4$ ;  $M_w/M_n < 1.02$  and of  $M_w = 68 \times 10^4$ ;  $M_w/M_n < 1.02$  in cyclohexane. Any molecular weight distribution corresponding to the same  $M_w$  must have the same quasi-binary spinodal curve, which coincides with the binary spinodal of the monodisperse polymer of equal  $M_w$ <sup>8,9</sup>. The z-average molecular weight  $M_z$  must be taken into consideration for comparison at equal  $M_w$  of  $\phi_c$ . The critical point for the mixture of  $M_w = 45 \times 10^4$ ;  $M_z/M_w = 1.30$  lies at a much higher concentration and lower temperature in comparison with 3a of  $M_w = 41.5 \times 10^4$ ;  $M_z/M_w < 1.06$ , as is theoretically predicted<sup>5,8,9</sup>.

In the case of the solution of the sample 3a characterized by  $M_w/M_n < 1.06$ ,  $\phi_t$  is remarkably lower than  $\phi_c$ . However, the difference between  $T_t$  and  $T_c$  is only 0.02<sub>3</sub>°C. Since the small difference of  $T_t - T_c = 0.02_3$ °C is within the limits of error in the ordinary cloud-point measurements, the threshold temperature for samples with  $M_w/M_n < 1.06$  and  $M_z/M_w < 1.06$  can be used for the usual determinations of the  $\theta$  temperature.

#### Evaluations of the pair interaction parameter

In the original Flory-Huggins theory<sup>2,14</sup> the pair interaction parameter  $g$ , which is directly related to the commonly used  $\chi$  parameter, was assumed to be independent of concentration. However, it has been widely accepted that the interaction parameter  $g$  generally depends on the polymer concentration<sup>8,9,15-20</sup>. It seems to be preferable to assume a concentration dependence of  $g(\phi)$  by:

$$g = g_0 + g_1\phi + g_2\phi^2$$

If the well-known interaction parameter  $\chi$  is written by a polynomial in the concentration<sup>5</sup>:

$$\chi = \chi_1 + \chi_2\phi + \chi_3\phi^2$$

the  $g$  parameter is related to the  $\chi$  parameter by:

$$\chi_{k+1} = (k+1)(g_k - g_{k+1})$$

Koningsveld *et al.*<sup>8</sup> have recently applied the spinodal and critical conditions to the system obeying the Flory-Huggins expression with  $g$  dependent on  $\phi$  and derived the following equations expressed by:

$$2g_0 = (1 - \phi)^{-1} + (\phi x_w)^{-1} + 2g_1(1 - 3\phi) + 6g_2(1 - 2\phi)\phi \quad (1)$$

for the spinodal and:

$$g_1 - g_2 + 4g_2\phi_c = (1/6)[(1 - \phi_c)^{-2} - x_z/x_w^2\phi_c^2] = Y \quad (2)$$

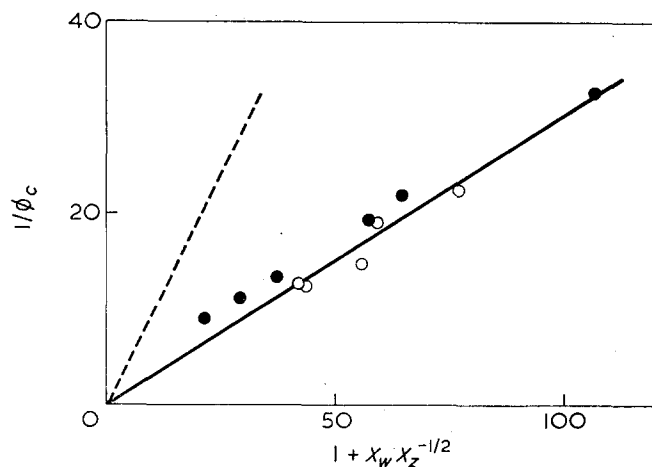


Figure 4 Plots of  $1/\phi_c$  against  $1 + x_w x_z^{-1/2}$ .  $\circ$  and  $\bullet$  are obtained from this work and reference 8, respectively. ---- represents the Stockmayer relation<sup>4</sup>

for the consolute state. In these formulae  $x_w$  and  $x_z$  are the weight- and z-average ratios of the molar volumes of the polymer and solvent. If  $g$  is taken independent of  $\phi$ , equations (1) and (2) reduce to the Stockmayer relations<sup>4</sup> written by:

$$2g = (1 - \phi)^{-1} + (\phi x_w)^{-1} \quad (3)$$

for the spinodal and

$$\phi_c = 1/(1 + x_w x_z^{-1/2}) \quad (4)$$

for the consolute state.

The  $1/\phi_c$  is plotted against  $1 + x_w x_z^{-1/2}$  in Figure 4, which also indicates that the critical concentrations are roughly three times as big as those predicted by equation (4). Our values of  $\phi_c$  are higher than those of Koningsveld<sup>8</sup> at equal  $M_w$  especially in the region of low molecular weight. The discrepancy between the two sets of data may be brought about by different molecular weight distributions. Exact estimation of  $M_z/M_w$  for the well-fractionated samples characterized by

$$M_w/M_n < 1.03$$

was out of the limit of ability of the gel permeation chromatography. Only existence of trace amounts of high molecular weight components which brought about a high value of  $M_z$  was examined through the gel permeation chromatography measurements. None of the trace amounts was observed. For estimation of  $M_z$  we assumed a Zimm-Schulz exponential distribution<sup>21,22</sup> given by:

$$g(M) = (y^{h+1}/h!) M^h \exp(-yM)$$

where:

$$y = h/M_n = (h+1)/M_w$$

As a result slightly smaller values of  $M_z/M_w$  as compared with  $M_w/M_n$  were estimated for all the present samples except for the mixture. Values of  $h$  assumed for the samples are given in Table 1. The value of  $M_z/M_w$  for the mixture was estimated from superposition of the molecular weight distributions for 1c-5 and 13a-5.

The ordinary plot of  $T_c^{-1}$  against  $1/x_w^{1/2} + 1/2x_w$  yields values of  $\theta = 33.2^\circ\text{C}$  and  $\psi_1 = 0.78$ , which is much higher than the value of  $\psi_1 = 0.23$  obtained by osmotic pressure and vapour pressure measurements<sup>15</sup>. The low value of  $\theta = 33.2^\circ\text{C}$ , compared with the values reported by several investigators<sup>1, 2</sup>, is mainly attributed to the high purification of cyclohexane, in which a trace amount of water is minimized by the use of the dry box during the present work. We frequently found that a trace amount of moisture in the air lead to a considerable rise of the precipitation temperature. The discrepancy of experiment from equation (4) for  $\phi_c$  and of the value of  $\psi_1$  from  $\psi_1 = 0.23$  may be attributed to the concentration dependence of  $g$ .

The critical state expressed by equation (2) can be employed to determine  $g_1$  and  $g_2$ . Having evaluated  $g_1$  and  $g_2$ , the spinodal equation (1) can be used to determine the temperature dependence of  $g_0$ . In the present treatment, a possible temperature dependence of  $g_1$  and  $g_2$  was ignored and  $g_0$  was supposed to be the usual linear function of  $1/T$  written by:

$$g_0 = g_{00} + g_{01}/T$$

The values of  $Y$  are plotted against  $\phi_c$  in Figure 5. The values of  $g_1 = 0.2398$  and  $g_2 = 0.0863$  were evaluated. The  $g_0$  function and its extrapolation to the  $\theta$  temperature, at which  $g_0 - g_1 = 0.5$ , is given in Figure 6. The plot of  $g_0$  against  $1/T$  yields the value of  $\theta = 33.2^\circ\text{C}$  in accordance with the extrapolation of the plot of  $1/T_c$  against  $1/x_w^{1/2} + 1/2x_w$ . The values of  $g_{00} = 0.5196$  and  $g_{01} = 67.50$  were evaluated by using the slope of the plot of  $g_0$  against  $1/T$ . Consequently  $g(\phi)$  function is expressed by:

$$g(\phi) = 0.5196 + 67.50/T + 0.2398\phi + 0.0863\phi^2$$

and  $\chi(\phi)$  function is written by:

$$\chi(\phi) = 0.2798 + 67.50/T + 0.3070\phi + 0.2589\phi^2$$

In the usual terminology we have:

$$g_0 - g_1 = 1/2 - \psi_1 + \psi_1\theta/T$$

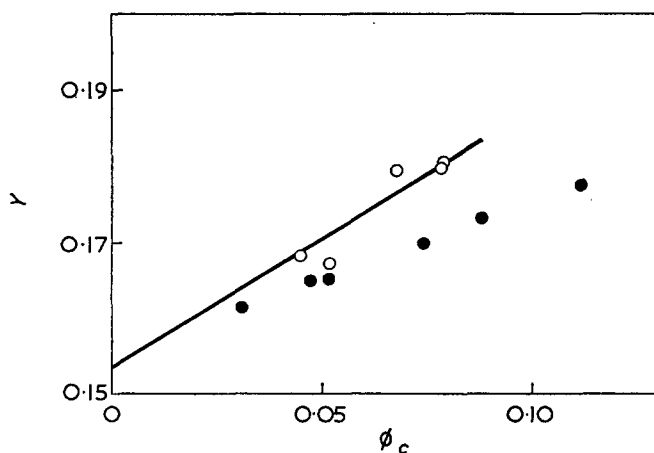


Figure 5 Plots of  $Y$  against  $\phi_c$ . The symbols are the same as in Figure 4

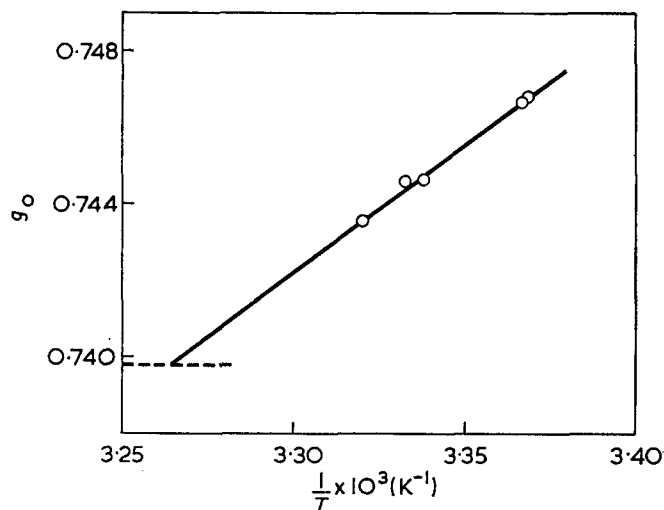


Figure 6 Plots of  $g_0$  against  $1/T$ . The horizontal broken line represents the value of  $g_0 - g_1$  of 0.5

Evaluation of  $\psi_1$  gives 0.22, which is in excellent quantitative agreement with the value of 0.23 obtained by Krigbaum and Geymer<sup>15</sup>.

The concentration dependence of the present  $\chi(\phi)$  agrees well with that found by Krigbaum and Geymer<sup>15</sup> as well as with that derived by Koningsveld *et al.*<sup>8, 9</sup> in the concentration range of  $\phi = 0-0.8$ . Further, the  $\chi(\phi)$  function is quantitatively consistent with those found from the data of sedimentation-diffusion equilibrium in the ultracentrifuge<sup>18, 19</sup> and light-scattering measurements<sup>20</sup>. Höcker *et al.*<sup>23</sup> have derived the concentration dependence of the  $\chi(\phi)$  for the polystyrene-cyclohexane system by the statistical thermodynamic theory, which also predicts a lower critical solution temperature in agreement with experiments<sup>24, 25</sup>. The value of  $\chi$  expressed by the segment fraction  $s$  instead of the volume fraction is in good agreement in the range of  $s = 0-0.8$ . A further check of the  $g(\phi)$  function is also possible by comparing the spinodals calculated by means of equation (1) with those deduced from measurements of intensity and linewidth studies<sup>10, 20, 26, 27</sup> of the scattered light at temperatures above the phase separation temperature. Experiments are under way for obtaining the spinodals from the light scattering measurements.

#### ACKNOWLEDGEMENT

The authors gratefully acknowledge the Ministry of Education in Japan for grant-in-aid.

#### REFERENCES

- Shultz, A. R. and Flory, P. J. *J. Am. Chem. Soc.* 1952, **74**, 4760
- Flory, P. J. 'Principles of Polymer Chemistry', Cornell University Press, Ithaca, 1953, p 541
- Koningsveld, R. and Staverman, A. J. *J. Polym. Sci. (A-2)* 1968, **6**, 349
- Stockmayer, W. H. *J. Chem. Phys.* 1949, **17**, 538
- Tompa, H. 'Polymer Solutions', Butterworths, London, 1956, p 174
- Rehage, G., Möller, D. and Ernst, O. *Makromol. Chem.* 1965, **88**, 232
- Koningsveld, R. and Staverman, A. J. *J. Polym. Sci. (A-2)* 1968, **6**, 305
- Koningsveld, R., Kleintjens, L. A. and Shultz, A. R. *J. Polym. Sci. (A-2)* 1970, **8**, 1261

- 9 Koningsveld, R. and Kleintjens, L. A. *Macromolecules* 1971, **4**, 637
- 10 Kuwahara, N. et al. *J. Chem. Phys.* 1971, **55**, 1140
- 11 Borchard, W. and Rehage, G. *Adv. Chem. Ser.* 1971, **99**, 42
- 12 Lee, S. P., Tschurnuter, W., Chu, B. and Kuawahara, N. *J. Chem. Phys.* 1972, **57**, 4240
- 13 Kuwahara, N., Kojima, J., Kaneko, M. and Chu, B. to be published
- 14 Huggins, M. L. *Ann. NY Acad. Sci.* 1942, **43**, 1
- 15 Krigbaum, W. R. and Geymer, D. O. *J. Am. Chem. Soc.* 1959, **81**, 1859
- 16 Rehage, G. *Kolloid Z.* 1964, **196**, 97
- 17 Kuwahara, N., Okazawa, T. and Kaneko, M. *J. Polym. Sci. (C)* 1968, **23**, 543
- 18 Scholte, Th. G. *J. Polym. Sci. (A-2)* 1970, **8**, 841
- 19 Rietveld, B. J., Scholte, Th. G. and Pijpers, J. P. L. *Br. Polym. J.* 1972, **4**, 109
- 20 Scholte, Th. G. *J. Polymer Sci. (A-2)* 1971, **9**, 1553
- 21 Schulz, G. V. *Z. Phys. Chem.* 1939, **B43**, 25
- 22 Zimm, B. H. *J. Chem. Phys.* 1948, **16**, 1099
- 23 Höcker, H., Shih, H. and Flory, P. J. *Trans. Faraday Soc.* 1971, **67**, 2275
- 24 Delmas, G. and Patterson, D. *Polymer* 1966, **7**, 513
- 25 Saeki, S., Kuwahara, N., Konno, S. and Kaneko, M. *Macromolecules* 1973, **6**, 246
- 26 Chu, B., Schoenes, F. J. and Fisher, M. E. *Phys. Rev.* 1969, **185**, 219
- 27 Scholte, Th. G. *J. Polym. Sci. (C)* 1972, **39**, 281

# Polymers from the hydrolysis of tetraethoxysilane\*

B. W. Peace and K. G. Mayhan

Graduate Center for Materials Research and Department of Chemical Engineering,  
University of Missouri-Rolla, Rolla, Mo 65401, USA

and J. F. Montle

Carboline Company, St. Louis, Missouri, USA  
(Received 26 March 1973)

The hydrolysis of tetraethoxysilane was studied under various solvent and temperature conditions. A method was developed by which reaction rates can be measured even in the presence of alcohols other than ethanol. The structures of the resulting polymers were dependent upon the reaction conditions employed, those formed at high temperature being highly condensed materials.

## INTRODUCTION

The acid-catalysed hydrolysis of tetrafunctional silicon compounds has been the subject of numerous investigations<sup>1, 2</sup>. The acid-catalysed exchange of polar groups at silicon is widely documented<sup>2, 3</sup>. Since a tetrafunctional molecule is involved, a wide variety of linear and cyclic structures is possible as products from these reactions<sup>3</sup>. A common practice is to hydrolyse tetraethoxysilane in alcoholic solvents to obtain condensed polysilicates<sup>4, 5</sup>. When an alcohol other than ethanol is employed as the reaction medium, the final polymer structure is further complicated by incorporation of some solvent through the exchange process.

Recently in our laboratories, it became necessary to know with some certainty the structures of condensed polysilicates obtained from the hydrolysis of tetraethoxysilane under several different solvent and temperature conditions. Furthermore, it was necessary to determine the rate of both the hydrolysis and the ester exchange reactions. Thus, it was advantageous to develop a method of investigating the hydrolysis and the resulting polysilicate.

## EXPERIMENTAL

A Victoreen 4000 Series gas chromatograph employing a 2 m × 3 mm Porapak Q column and a thermal conductivity cell was used for all gas chromatographic (g.c.) analyses. Nuclear magnetic resonance spectra (n.m.r.) were obtained using a Varian A-56/60 spectrometer. All n.m.r. spectra were obtained in 20% solutions of carbon tetrachloride using tetramethylsilane as an internal standard. Number-average molecular weights were determined in toluene using a Mechrolab Model 301 Osmometer. Waters Associates polystyrene standards with number-average molecular weights of 1220 and 2020 were used for calibration.

\* Contribution No. 177 from Graduate Center for Materials Research, University of Missouri-Rolla.

## G.c. calibration procedure

Mixtures of varying mole ratios of ethanol and solvent alcohol were prepared and 1.00 ml of methyl ethyl ketone was added to each as an internal standard. The mole ratios of alcohols chosen were expected to cover the range encountered during hydrolysis. G.c. analysis was performed on each mixture and a plot of relative peak areas (alcohol/ketone), versus mole of alcohol was constructed for both ethanol and the solvent alcohol in question. Methyl ethyl ketone was chosen as the internal standard since it did not react with the system, had no apparent effect upon the solubility of the silicate, and was sufficiently different in its retention time from the alcohols to allow accurate measurements.

## General hydrolysis procedure

All reactions at 25°C were performed in Pyrex flasks sealed with septum caps. Reactions at 110°C were carried out in heavy walled, sealed Pyrex tubes. A mixture of solvent alcohol (0.125 mol), tetraethoxysilane (0.050 mol), water (0.080 mol) and methyl ethyl ketone (1.00 ml) was blended to give a homogeneous solution. Hydrochloric acid (0.20 ml of 0.10 N) was added and the reaction vessel was sealed. During the low temperature runs, samples for g.c. analyses were periodically withdrawn through the septum cap. Relative peak areas (alcohol/ketone), were converted to moles of alcohol from the calibration curve. In this way, the course of the reactions was easily followed as a function of time.

## Isolation of condensed polysilicates

After hydrolysis, the reaction mixtures were frozen in liquid nitrogen and the flask was connected to a vacuum system. A vacuum of 0.01 mmHg was maintained while the solutions were slowly warmed to room temperature. G.c. analyses before and after this procedure showed identical compositions of the alcohols.

RESULTS AND DISCUSSION

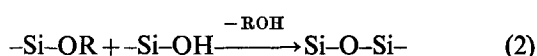
Hydrolysis and ester exchange

Theoretically, the acid-catalysed hydrolysis of tetraethoxysilane in two or more equivalents of water leads to the formation of silicon dioxide and ethanol as the only products. If, however, the reaction is carried out in an alcoholic solvent with limited amounts of water, partly hydrolysed condensed silicates are produced<sup>4</sup>. In theory, the condensed polysilicates can form either as linear chains or as ring systems.

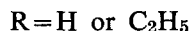
The formation of the condensed polysilicates is the result of a complex sequence of reactions. First, the silicate ester is hydrolysed as shown by:



The polysilicate is then formed through condensation of either silicate hydroxyl groups or hydroxyl and ester groups:



where



The alternating sequence of hydrolysis and condensation steps continues until the ultimate molecular weight is attained and all water is consumed. When an alcohol other than ethanol is employed as the solvent, a third reaction, that of ester exchange, must also be considered. The final structure of the condensed polysilicate must reflect all three reactions.

In general, the production of ethanol can be taken as a measure of the progress of the hydrolysis reaction. However, when an alcohol other than ethanol is employed as the reaction medium, ethanol is formed both by hydrolysis and by ester exchange and these processes must be separated. This was accomplished by simultaneously measuring the amount of ethanol liberated and the amount of solvent alcohol consumed. The amount of solvent alcohol consumed must be equal to the amount of ethanol liberated by the exchange process. Thus, the amount of ethanol generated by hydrolysis is obtained by subtracting that amount liberated by exchange from the total ethanol produced during the reaction. From these data the ratio Si:OC<sub>2</sub>H<sub>5</sub>:solvent in the final polymer structure can be calculated. Here, percentage exchange is based upon the final polymer composition.

The hydrolysis of tetraethoxysilane at 25°C was carried out in alcohols of differing structural types. As shown in Table 1, no trend was established with respect to the hydrolysis reaction. Since very small amounts of water cause large changes in the amount of apparent hydrolysis, the difference in the percentage hydrolysis may reflect residual water in the solvents. Table 1 does, however, show that the distribution of alkyl groups in the condensed polysilicate is highly dependent upon the structure of the solvent alcohol.

Table 1 Hydrolysis and ester exchange of tetraethoxysilane at 25°C

Solvent	Hydrolysis (%)	Exchange (%)
methanol	76	44.7
Cellosolve (ethylene glycol mono ethyl ether)	63	45.9
isopropanol	63	35.2
t-butanol	67	0

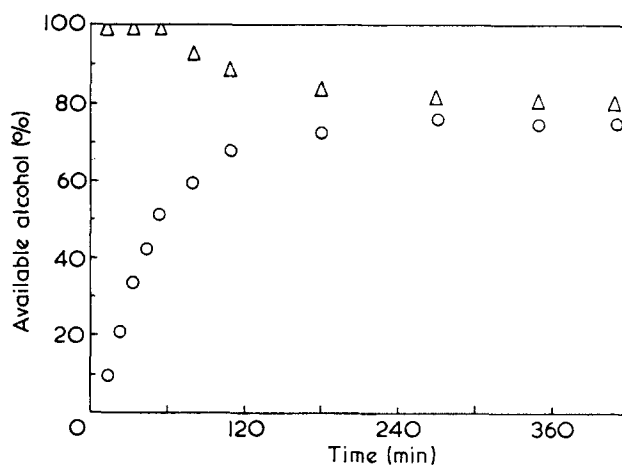


Figure 1 Rate of hydrolysis and ester exchange during the polymerization of tetraethoxysilane in isopropanol at 25°C. Δ, Isopropanol; ○, ethanol

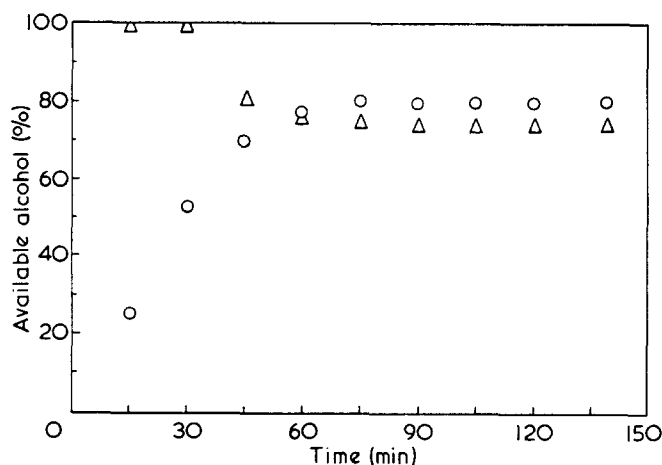


Figure 2 Rate of hydrolysis and ester exchange during the polymerization of tetraethoxysilane in Cellosolve at 25°C. Δ, Cellosolve; ○, ethanol

With respect to the exchange process primary alcohols are more reactive than secondary alcohols while the tertiary alcohol did not undergo exchange.

Reaction rate data for the production of ethanol at 25°C was obtained in the case of Cellosolve and isopropanol. Examination of Figures 1 and 2 reveals that the rate of hydrolysis (generation of ethanol) is more rapid in Cellosolve than in the secondary alcohol. The initial rate in Cellosolve was  $3.5 \times 10^{-2}$  mol/min as compared to  $2.5 \times 10^{-2}$  for isopropanol. It is interesting to note that the ester exchange reaction occurs only after hydrolysis is complete.

As shown in Table 2, increased reaction temperatures had little influence upon the extent of the ester exchange reaction, but did increase the apparent percentage hydrolysis. The term 'apparent hydrolysis' is used here since the 110°C reaction results in a more highly condensed polymer.

The ester exchange reaction was also examined using ethanol as the solvent. This was accomplished by performing the hydrolysis in β-deuterated ethanol. In this case, the exchange reaction resulted in an equal distribution of the ethanols between polymer and solvent. Thus, the exchange reaction is solely a function of the alcoholic medium employed as solvent.

The distribution of alkoxy groups in the final condensed polysilicate is highly dependent upon the mole fraction of solvent alcohol employed. Polymers with a

Table 2 Effect of temperature upon the tetraethoxysilane hydrolysis and ester exchange

Solvent	Temperature (°C)	Hydrolysis (%)	Exchange (%)
isopropanol	25	63	35.2
isopropanol	110	78	38.7
Cellosolve	25	63	45.9
Cellosolve	110	75.5	44.5

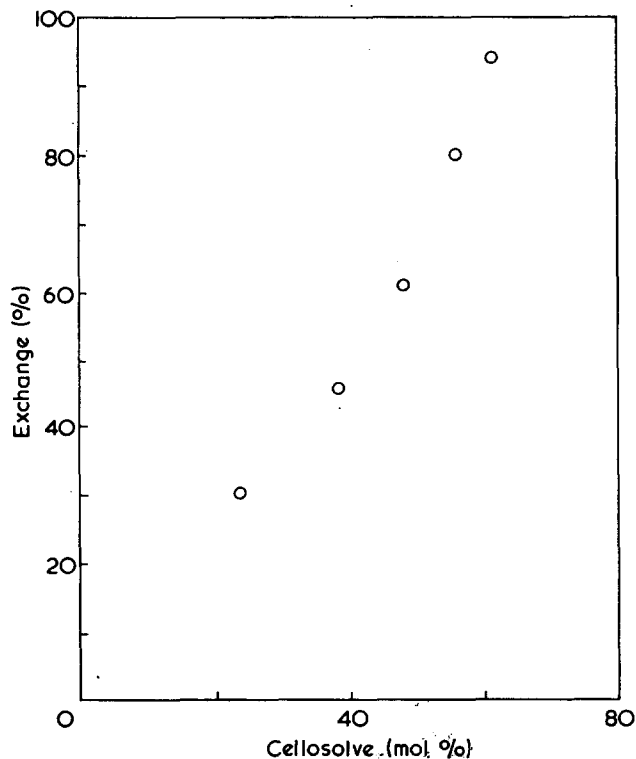


Figure 3 Extent of the exchange reaction as a function of the Cellosolve concentration

Cellosolve content from 0 to 100% can be obtained simply by adjusting the mole ratio of Cellosolve to tetraethoxysilane (Figure 3).

Polymer structure

The g.c. method described previously yields information regarding the relative ratios of silicon to alcohols. In order to have a complete description of the polysilicate, however, the silicon to hydroxy ratio must also be known since it will reflect the extent of condensation. This was done by removing the solvents and hydrochloric acid, and then measuring the n.m.r. spectra of the pure polymers. In all cases, the methyl groups appeared as overlapping multiplets centred at  $\tau=9.17$ . The methylene groups and the secondary proton of isopropanol appeared as overlapping multiplets centred at  $\tau=6.34$ . The hydroxy proton appeared as a broad peak at  $\tau=5.34$ . By comparing the area under the hydroxyl proton peaks to that under the alkyl peak, sufficient information was obtained to generate an empirical formula.

The condensed polysilicate obtained from the 25°C hydrolysis of tetraethoxysilane in isopropanol was found to have the empirical formula

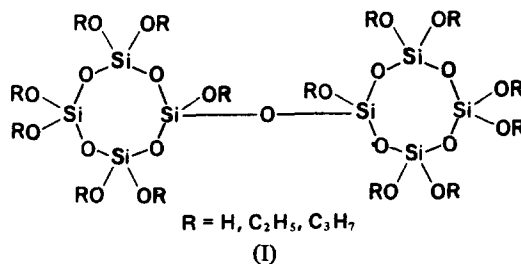


This formula is significant in that it requires a cyclic structure and not linear chains. A completely linear system would have the formula  $\text{Si}_n(\text{OR})_{2n+2}$ , where

OR represents the total of all hydroxy and alkoxy groups. It was not possible to draw a structure for the empirical formula as given. However,



can be drawn as two connected rings each containing four silicon atoms as shown in structure (I). The number-

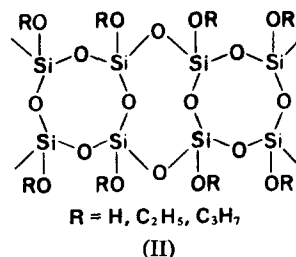


average molecular weight of the polymer was determined to be 1002 which is in good agreement with the calculated molecular weight of 996.

The structure of the hydrolysis product obtained at 110°C in isopropanol is much more complex. The products empirical formula was found to be



Here the silicon to OR ratio is almost 1:1 indicating a highly condensed material. Structure (II) is one possible way to represent such a structure.



The molecular weight of this material was determined to be 2212. However, it is much more than a 'dimer' of (I) since a much higher ratio of silicon to alkoxy is observed. The polysilicate (II) contains approximately 28 silicon atoms and can be derived by condensation of molecules of (I).

Structures identical to (I) and (II) were also obtained and identified from the Cellosolve reactions.

CONCLUSIONS

The combined use of g.c., n.m.r. and molecular weight measurements provides a technique for the determination of the exact structures of condensed polysilicates. Since the structures of the polymer obtained by hydrolysis of alkoxy silanes vary widely with reaction conditions, the method should be of assistance to other investigators working in this area. The method is also useful for obtaining hydrolysis and ester exchange rate data.

REFERENCES

- 1 Eaborn, C. 'Organosilicon Compounds', Butterworths, London, 1960
- 2 Noll, W. 'Chemistry and Technology of Silicones', Academic Press, New York, 1968, p 648
- 3 Moedritzer, K. 'Advances in Organometallic Chemistry', (F. G. A. Stone and R. West, Eds), Academic Press, New York, 1968, Vol 6, p 171
- 4 Iler, R. K. 'The Colloid Chemistry of Silica and Silicates', Cornell University Press, Ithaca, 1955, p 76
- 5 Aelion, R., Toebel, A. and Eirich, F. *Rec. Trav. Chim.* 1950, 69, 61

# Molecular motions in poly(dimethyl siloxane) oligomers and polymers

J. M. G. Cowie and I. J. McEwen

Department of Chemistry, University of Stirling, Stirling FK9 4LA, UK  
(Received 28 February 1973; revised 9 April 1973)

The glass transition temperatures of fifteen samples of poly(dimethyl siloxane) polymers and oligomers have been measured by differential scanning calorimetry. Polymers with  $M_n > 2400$  exhibit an asymptotic value of  $T_g(\infty) = 148\text{K}$ , but for shorter chains the  $T_g$  is lower. The thermomechanical behaviour has also been examined using a torsional braid analyser and this has served to confirm the chain length dependence of  $T_g$ . A sub-glass transition, located in the temperature range 80–120K for short chain samples, has been attributed to methyl group rotation.

## INTRODUCTION

Significant changes in the physical properties of a polymer are obtained when the transition from a glass into a rubber-like state is accomplished. It is important to determine the temperature,  $T_g$ , at which this transition takes place if the material is to be characterized effectively.

One of the factors which can affect the  $T_g$  is the chain length of the polymer. If the glass transition temperature of the monomer can be measured it is found to be much lower than that of the high molecular weight polymer, consequently some variation of  $T_g$  with increasing chain length ought to be observed. In general the glass transition temperatures of a homologous series of polymers increase asymptotically with increasing degree of polymerization. This behaviour has been reported for a number of polymers<sup>1-8</sup>.

The polymer studied here is poly(dimethyl siloxane) which has one of the lowest values of  $T_g$  recorded for high molecular weight polymers. Several measurements of  $T_g$  for both linear and crosslinked samples have been reported; Weir *et al.*<sup>9</sup> found  $T_g = 150\text{K}$  as did Polmanteer and Hunter<sup>10</sup>, while Barrie *et al.*<sup>11</sup> recently reported a value of  $T_g = 148\text{K}$ . Ke<sup>12</sup> measured the  $T_g$  of two cross-linked samples and found values of 153K and 161K, the latter being obtained for the more crystalline of the two polymers.

As all the data published refer to samples with relatively large molecular weights, a study of the behaviour of short chains was undertaken. Values of  $T_g$  for oligomers and polymers ranging from dimer to  $M_n = 1.36 \times 10^5$  are reported and the influence of chain length on  $T_g$  is discussed in relation to current theory.

## EXPERIMENTAL

Samples of a number of poly(dimethyl siloxane), PDMS, fluids were obtained from Hopkin and Williams, and were characterized. In all cases the polymer chains were terminated by methyl groups.

The limiting viscosity number  $[\eta]$  was measured for

each sample using a Cannon-Ubbelohde semi-micro dilution viscometer, which could be reproducibly positioned by means of a triple point suspension system in a thermostat bath. The solvents used were either toluene at 298K or 2-butanone at 293K. Number-average molecular weights ( $M_n$ ) were calculated from:

$$[\eta] = 2.0 \times 10^{-2} M_n^{0.66} \text{ (toluene)}$$

when molecular weights were in the range 3000 to 200 000<sup>13</sup> or

$$[\eta] = 8.1 \times 10^{-2} M_n^{0.5} \text{ (2-butanone)}$$

when molecular weights were lower than 3000<sup>14</sup>.

These relations are valid for  $[\eta]$  expressed in units of  $\text{cm}^3/\text{g}$ . The results are shown in Table 2. Four other oligomers, the dimer hexamethyl disiloxane ( $M_n = 162$ ), the trimer PDMS-1.0 ( $M_n = 236$ ), the tetramer PDMS-1.5 ( $M_n = 310$ ), and the pentamer PDMS-2.0 ( $M_n = 384$ ), were also used.

Calculation of  $M_n$  from the Mark-Houwink equations will, of course, be subject to some error if the molecular weight distributions of the samples differ from those of the original calibrating fractions. Accurate knowledge of  $M_n$  is only essential for the lower molecular weights, however, which show a deviation of  $T_g$  from the asymptotic value. The dimer to pentamer are readily characterized from their known boiling and melting points, while the  $M_n$  values for samples 3 and 10 were verified by vapour pressure osmometer measurements carried out by Dr W. K. Busfield of Dundee University. A spot check was carried out on two of the higher molecular weight samples using a membrane osmometer and  $M_n$  was found to be 8–10% lower than that calculated from viscosity measurements. Consequently any analysis, based on the  $M_n$  values quoted in Table 2 should be valid.

The glass transition temperature  $T_g$  for each sample was measured using a Du Pont 900 DSC module.  $T_g$  was taken to be the temperature at which the initial base line intersected with the extrapolated sloping portion of the curve, caused by the base line shift during the transition. Measurements were made in triplicate.



**Table 1** Effect of heating rate in d.s.c. cell on  $T_g$  for sample PDMS-1000

Heating rate (K/min)	$T_g$ (K)
40	153
30	151.5
20	150
10	149
2	148.5
Extrapolated value	148

Regular daily calibration of the instrument was carried out using mercury and gallium standards.

The effect of various heating rates on the value of  $T_g$  was determined and the results shown in *Table 1* indicate that  $T_g$  is raised by about 1 K for every 10 K/min rise in heating rate.

The values of  $T_g$  quoted in *Table 2* were obtained by using a heating rate of 10 K/min and applying a correction based on the assumption that the trend shown in *Table 1* was common to all.

#### Dynamic mechanical response

The thermomechanical behaviour of eight poly(dimethyl siloxane) samples and one poly(methyl phenyl siloxane) (PMPS) was measured over the temperature range 80–200 K, using a Torsional Braid Analyser<sup>15</sup> (TBA).

Glass sample braids were impregnated with the polymers, all of which were liquids at room temperature. The braid was then suspended in the sample chamber of the TBA, cooled to liquid nitrogen temperature and allowed to equilibrate for 30 min.

The system was then allowed to warm up slowly, during which time the dynamic mechanical response of the sample was measured at 2–4 K intervals. Values of the mechanical damping index ( $1/n$ ), which is a function of the loss modulus, were calculated from the number of oscillations ( $n$ ) measured between arbitrarily fixed boundary amplitudes of the decay pattern. The frequency of measurement was approximately 1 Hz.

## RESULTS AND DISCUSSION

#### Relation between $T_g$ and $M_n$

The values of  $T_g$  for fifteen samples of PDMS and one of PMPS, measured from d.s.c. scans, are listed in *Table 2*. These are in reasonable accord with  $T_g$  estimated from the TBA spectra. The asymptotic value  $T_g(\infty)$  for PDMS was 148 K, which corresponds with that reported by Barrie *et al.*<sup>11</sup> and this remains constant down to  $M_n$  of about 2400. Below this there is a monotonic decrease to  $T_g = 112$  K for the dimer.

This variation of  $T_g$  with molecular weight has not been reported previously, presumably because the effect is restricted to very short chain lengths.

It can be seen from *Figure 1*, that the dependence of  $T_g$  on  $M_n^{-1}$  is linear over the molecular weight range covering non-asymptotic behaviour. This can be contrasted with data reported for poly(methyl methacrylate)<sup>3</sup>, poly( $\alpha$ -methyl styrene)<sup>5</sup> and poly(vinyl chloride)<sup>7</sup> where distinct curvature was obtained in similar plots. For these systems linearity was observed over part of the molecular weight range, but never lower than  $M_n$  of 3000 to 5000.

A number of relations have been proposed to predict the dependence of  $T_g$  on chain length. Two of general interest are

$$T_g = T_g(\infty) - K/M_n \quad (1)$$

$$1/T_g = 1/T_g(\infty) + K^1/M_n \quad (2)$$

where  $T_g$  is measured in K,  $T_g(\infty)$  is the asymptotic value, and  $K$  and  $K^1$  are constants whose interpretation depends on the assumptions made concerning the nature of the factors governing the glass transition.

There are a number of primary assumptions from which interpretations of the glass transition phenomenon have been developed.

Ueberreiter and Kanig<sup>2</sup> favoured the form of equation (2) which was reinterpreted by Kanig<sup>6</sup> using a thermodynamic approach and presented as:

$$\frac{1}{T_g} = \frac{RM_0}{\phi_{f2}^* A_{MM}^*} \left( \frac{V_{f1}^*}{V_{fM}^*} \right) \cdot \frac{1}{M_n} - \frac{R(\ln \phi_{f1}^* + \phi_{f2}^*)}{(\phi_{f2}^*)^2 \cdot A_{MM}^*} \quad (3)$$

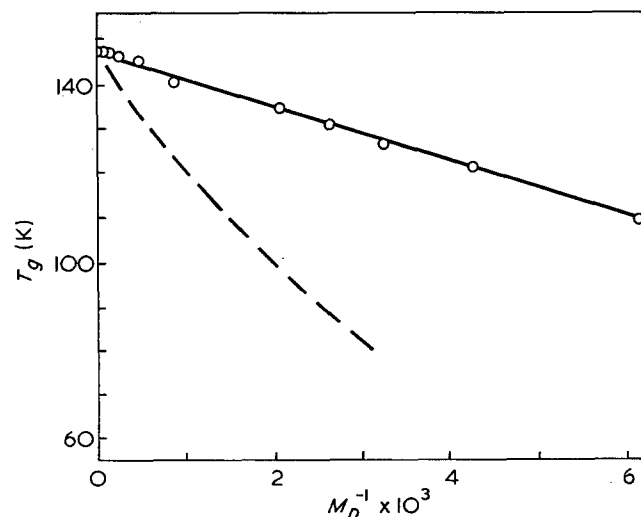
**Table 2** Limiting viscosity numbers, and glass transition temperatures for poly(methyl phenyl siloxane) and poly(dimethyl siloxanes) of varying chain length

Sample	$[\eta]^\dagger$ (cm <sup>3</sup> /g)	$M_n$	$x$	$T_g$ (K) <sup>‡</sup>	
				D.s.c.	TBA
Hexamethyl disiloxane	—	162	4	112	—
PDMS-1	—	236	6	123	126
PDMS-1.5	—	310	8	128	—
PDMS-2	—	384	10	133	130
PDMS-3	0.6*	540	14	136	133
PDMS-10	2.8*	1 200	32	141	138
PDMS-20	4.0*	2 400	64	146	138
PDMS-50	5.0	4 200	114	147	—
PDMS-100	7.3	7 700	208	148	—
PDMS-200	9.9	12 200	330	148	—
PDMS-350	11.7	15 500	418	148	153
PDMS-500	13.1	19 000	514	148	—
PDMS-1000	16.8	27 000	730	148	148
PDMS-12 500	27.6	57 000	1 540	148	148
PDMS-200 000	49.0	136 000	3 680	149	—
PMPS	—	6 300	—	190	191

\* Measured in 2-butanone at 293 K

† Measured in toluene at 298 K except for \*

‡ Estimated error in  $T_g$  is  $\pm 1$  K


**Figure 1** Dependence of  $T_g$  on  $M_n^{-1}$  for poly(dimethyl siloxanes). —, plotted as for equation (1) and has a slope  $K = 5.9 \times 10^{-3}$ . ---, derived from the Gibbs-DiMarzio equation

Here  $R$  is the gas constant and  $M_0$  the monomer molecular weight. The parameter  $A_{MM}^*$  is the energy required to form a mole of holes and can be identified with the cohesive forces in the solid,  $(V_{f1}^*/V_{fM}^*)$  is the ratio of the hole volume to the vibrational expansion volume,  $\phi_{f2}^* = (1 - \phi_{f1}^*)$  where  $\phi_{f1}^*$  has been treated as a universal constant of 0.6 but is actually the ratio  $(\alpha_L - \alpha_G/\alpha_L)$ . Here  $\alpha_L$  and  $\alpha_G$  are the slopes of the volume-temperature lines above and below the glass transition respectively. From data tabulated by Mandelkern<sup>16</sup>,  $\phi_{f1}^*$  can fall in the range 0.46–0.76. Using the values of  $\alpha_L = 9.5 \times 10^{-4}$  and  $\alpha_G = 4.5 \times 10^{-4}$  for poly(dimethyl siloxane)<sup>16</sup> one obtains  $\phi_{f1}^* = 0.57$ . This means that the asymptotic value of  $T_g$  can be expressed as:

$$T_g(\infty) = \frac{A_{MM}^*}{0.746R} \quad (4)$$

showing that the basic assumption here is that  $T_g$  is governed entirely by cohesive forces in the system. On this analysis  $A_{MM}^* = 916 \text{ J/mol}$  for PDMS, which can be compared with  $2042 \text{ J/mol}$  for polystyrene<sup>6</sup> and  $2607 \text{ J/mol}$ <sup>5</sup> for poly( $\alpha$ -methyl styrene).

Ellis<sup>17</sup> proposed that equation (2) could also be plotted as  $M_n/T_g$  against  $M_n$  and this results in linearity over the entire range of molecular weights, as shown in Figure 2.

A different interpretation was placed on equations (1) and (2) by Patterson and Somcynsky<sup>18</sup>, based on the Prigogine theorem of corresponding states. In this treatment samples of different molecular weight are assumed to be in corresponding states at their glass transition temperature, which leads to equation (2) in the form:

$$\frac{1}{T_g} = \frac{1}{T_g(\infty)} + \left( \frac{b}{a} \frac{M_0}{T_g(\infty)} \right) \frac{1}{M_n} \quad (5)$$

the ratio  $(b/a)$  is a quantity which is a measure of the chain flexibility. As the chain becomes more flexible,  $(b/a)$  decreases and for a flexible polymer with low frequency bending vibrations Patterson estimates  $(b/a) = 0.5$ . For PDMS chains  $(b/a)$ , calculated using equation (5), is found to be 0.54, which suggests they are highly flexible polymers. On this formulation  $(b/a)$  is directly proportional to  $(V_{f1}^*/V_{fM}^*)$  of the Kanig theory.

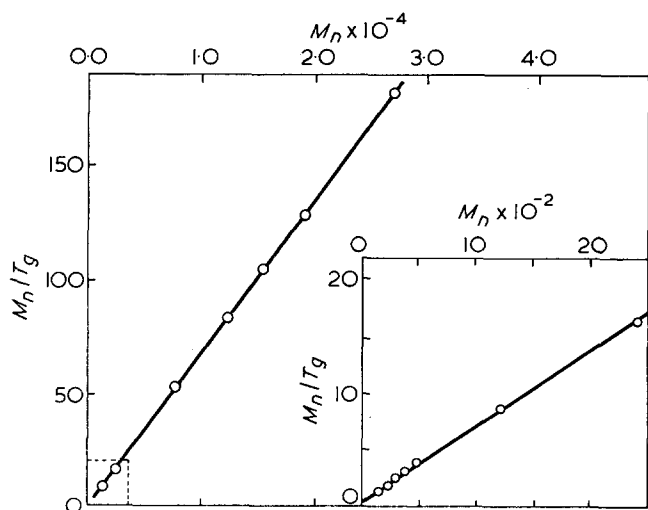


Figure 2  $M_n/T_g$  data plotted according to the method proposed by Ellis. Inset shows detail in the low molecular weight region

The simple free volume concept is based on the premise that the free volume contribution in a polymer is constant up to the glass transition but increases thereafter. The departure of  $T_g$  from the asymptotic value as  $M_n$  decreases is attributed to the additional contribution to the free volume of the system from an increasing number of chain ends.  $K$  in equation (1) is interpreted by Bueche<sup>19</sup> as  $[2\rho N_A \theta / (\alpha_L - \alpha_G)]$ . Here  $\rho$  is the polymer density,  $N_A$  is the Avogadro number, and  $\theta$  is the free volume contribution from each chain end. For a value of  $\rho = 1.105 \text{ g/cm}^3$  the free volume contribution  $\theta$  is  $2.2 \text{ \AA}^3$  ( $1 \text{ \AA} = 10^{-10} \text{ m}$ ). This is a very low value in comparison to  $\theta = 11 \text{ \AA}^3$  for propylene oxide<sup>7</sup> or  $85 \text{ \AA}^3$  for poly( $\alpha$ -methyl styrene)<sup>5</sup>. The concept presents some inconsistencies, however, as in poly(methyl methacrylate), where  $\theta = 26 \text{ \AA}^3$  for the isotactic form and  $80 \text{ \AA}^3$  for the syndiotactic form<sup>4</sup>. This implies that the same chain end makes a different contribution to the free volume. It is more reasonable to postulate that the chain packing in the sample is affected by the different microstructures which in turn alters the free volume. The low value of  $\theta$  for poly(dimethyl siloxane) presumably indicates that the free volume in the vicinity of  $T_g$  is virtually unaffected by chain ends, chain packing or any other factors.

In a number of systems<sup>3, 5, 7</sup> the Gibbs–DiMarzio treatment<sup>20</sup> of chain length and  $T_g$  has proved successful. These authors relate the sample  $T_g$  to the number of chain atoms  $x$ , in the macromolecule using the equation:

$$\frac{x}{x-3} \left\{ \ln V_0 + \frac{1+V_0}{1-V_0} \ln \left[ \frac{(x+1)(1-V_0)}{2xV_0} + 1 \right] + \frac{\ln 3(x+1)}{x} \right\} = \frac{2\beta \exp \beta}{(1+2\exp \beta)} - \ln(1+2\exp \beta) \quad (6)$$

where  $\beta = -\epsilon/kT_g$ ,  $k$  is the Boltzmann constant,  $\epsilon$  is the flex energy and  $V_0$  the free volume fraction at  $T_g$ . The curve shown in Figure 1 was derived from equation (6) using values of  $V_0 = 0.036$ <sup>21</sup> and  $\epsilon/k = 345.5 \text{ K}$  which correctly predict  $T_g(\infty)$  for the polymer, but the agreement is very poor below  $T_g(\infty)$ . This shows that the Gibbs–DiMarzio theory cannot predict the depression of  $T_g$  as the chain length decreases. No significant improvement is obtained if different values of  $V_0$  are assumed.

#### Thermomechanical spectra

Typical damping curves for poly(dimethyl siloxanes) and poly(methyl phenyl siloxane) are shown in Figure 3. In all cases the most prominent damping peak corresponded to the glass transition, whereas the melting transition, when observed, was seen as an increase in damping, typically that shown in Figure 3(c). For samples with  $M_n$  less than 1200, a smaller peak was detected at temperatures lower than  $T_g$ . This peak was quite broad and began close to the lower limits of the temperature range employed. Although the breadth of these damping peaks makes accurate location of the maxima difficult, there was an apparent shift to higher temperatures as the chain length increased (see Table 3).

For PDMS samples with molecular weights higher than 1200 there was little evidence of this sub-glass transition, although the shape of the damping curves was altered somewhat. When the minor peak was obvious the damping rose sharply to the glass transition temperature. For higher molecular weight samples the

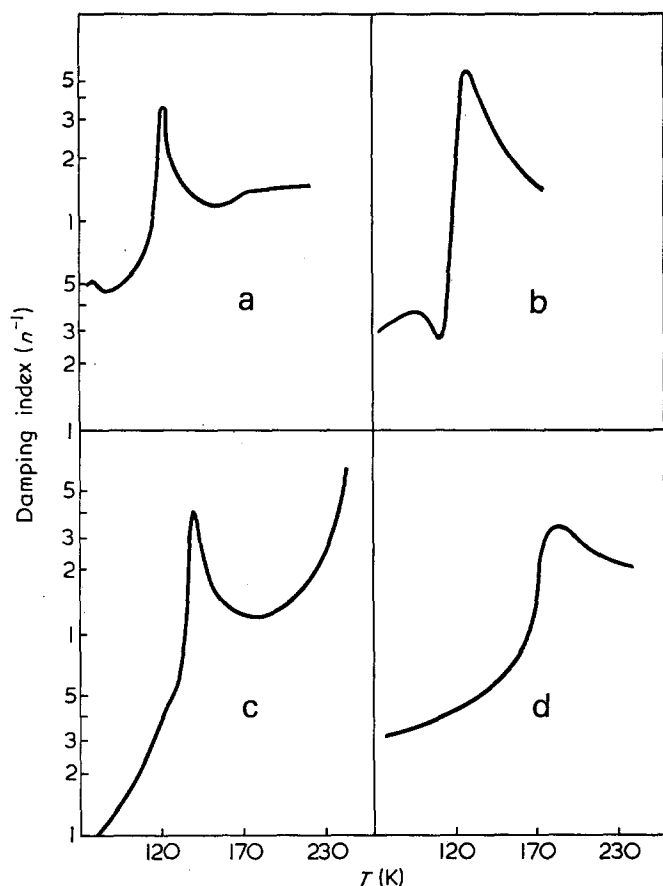


Figure 3 Thermomechanical damping spectra of (a) PDMS—1, (b) PDMS—3, (c) PDMS—12 500 and (d) a sample of poly(methyl phenyl siloxane) for comparison

Table 3 Approximate position of minor damping peak as a function of sample chain length

Sample	Minor damping peak temperature (K)
PDMS—1	86
PDMS—2	104
PDMS—3	105
PDMS—10	116
PDMS—20	119

rise in damping was more gradual and it may be that the minor peak is absorbed into the main glass transition peak.

Barrie *et al.*<sup>11</sup> observed a minimum in their spin-lattice relaxation measurements in the region of 100 K which they attributed to methyl group rotation and it is reasonable to interpret the sub-glass transition detected

here also as methyl group rotation. No damping peak which would correspond to methyl group rotation was observed in the PMPS sample and this suggests that the bulky phenyl groups restrict methyl rotation in the glass. The same restrictions to methyl rotation, but by other chains, could be postulated for higher molecular weight PDMS samples and it is interesting to note that the minor damping peak is only detected in samples whose  $T_g$  is lower than  $T_g(\infty)$ . It is impossible to say whether the ability of the methyl group to rotate is a contributing factor to the depression of  $T_g$  or simply a consequence of the greater freedom of movement in the glassy state for short chains which arises from other factors. The fact that the peak is apparently displaced towards higher temperatures as the chain length increases indicates that the energy required to move the methyl group is also increasing and that in longer chains the motion is largely restricted until the glass transition is reached.

Other systems are now being studied to determine chain length effects on the mechanical response.

#### REFERENCES

- 1 Fox, T. G. and Flory, P. J. *J. Appl. Phys.* 1950, **21**, 581
- 2 Ueberreiter, K. and Kanig, G. *J. Colloid Sci.* 1952, **7**, 569
- 3 Beevers, R. B. and White, E. F. T. *Trans. Faraday Soc.* 1960, **56**, 744
- 4 Thompson, E. V. *J. Polym. Sci. (A-2)* 1966, **4**, 199
- 5 Cowie, J. M. G. and Toporowski, P. M. *Eur. Polym. J.* 1968, **4**, 621
- 6 Kanig, G. *Kolloid Z.* 1963, **190**, 1
- 7 Pezzin, G., Zilio-Grandi, F. and Sanmartin, P. *Eur. Polym. J.* 1970, **6**, 1053
- 8 Onder, K., Peters, R. H. and Spark, L. C. *Polymer* 1972, **13**, 133
- 9 Weir, C. F., Leser, W. H. and Wood, L. A. *J. Res. Nat. Bur. Stand.* 1950, **44**, 367
- 10 Polmanteer, K. E. and Hunter, M. J. *J. Appl. Polym. Sci.* 1959, **1**, 3
- 11 Barrie, J. A., Fredrickson, M. J. and Sheppard, R. *Polymer* 1972, **13**, 431
- 12 Ke, B. *J. Polym. Sci. (B)* 1963, **1**, 167
- 13 Barry, A. J. *J. Appl. Phys.* 1946, **17**, 1020
- 14 Flory, P. J., Mandelkern, L., Kinsinger, J. B. and Schulz, W. B. *J. Am. Chem. Soc.* 1952, **74**, 3364
- 15 Gillham, J. K. and Lewis, A. F. *J. Appl. Polym. Sci.* 1963, **7**, 2293
- 16 Mandelkern, L., Sharma, S. C. and Stehling, F. C. *J. Polym. Sci. (B)* 1972, **10**, 345
- 17 Ellis, B. in 'Amorphous Materials', Wiley-Interscience, New York, 1972, p 375
- 18 Somcynsky, T. and Patterson, D. *J. Polym. Sci.* 1962, **62**, 151
- 19 Bueche, F. 'Physical Properties of Polymers', Interscience, New York, 1962
- 20 Gibbs, J. H. and DiMarzio, E. A. *J. Chem. Phys.* 1958, **28**, 373
- 21 Eisenberg, A. and Saito, S. *J. Chem. Phys.* 1966, **45**, 1673

# Asymmetric addition of thiol to diene polymer in the presence of optically active amines as catalyst

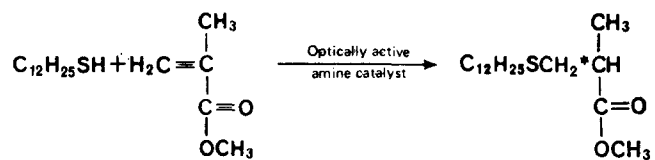
Koichi Yamaguchi, Nobuo Yamada and Yuji Minoura

Department of Applied Chemistry, Faculty of Engineering, Osaka City University, Sugimoto-cho, Sumiyoshi-ku, Osaka, Japan  
(Received 19 December 1972)

The asymmetric addition reaction of thiolacetic acid or benzylmercaptan to diene polymer (natural rubber, *cis*- and *trans*-1,4-polyisoprene, *cis*-1,4-polybutadiene, various styrene-butadiene copolymers and alternating acrylonitrile-butadiene copolymer) by optically active catalysts such as *D*-bornylamine ( $[\alpha]_D -45.2^\circ$ ), *L*-aspartic diethyl ester ( $-11.2^\circ$ ), *L*-aspartic dibutyl ester ( $-5.3^\circ$ ) were carried out in benzene at room temperature to  $90^\circ\text{C}$ . The optically active polymers were obtained from natural rubber and *cis*-1,4- and *trans*-1,4-polyisoprene, but were not obtained from *cis*-1,4-polybutadiene, styrene-butadiene copolymers, and butadiene-acrylonitrile copolymer. The  $[\alpha]_D^{25}$  value of optically active derivatives was  $-0.1^\circ \sim -1.0^\circ$  (in benzene), and the optical rotatory dispersion curves were found to fit the simple Drude equation.

## INTRODUCTION

The asymmetric addition reaction of thiol to olefin was first reported by Tsuruta and coworkers<sup>1,2</sup>. They studied the asymmetric addition reaction of methyl methacrylate with laurylmercaptan with optically active catalysts such as *S*-isobutyl ethyleneimine, poly(*S*-butyl ethyleneimine) and (–)  $\alpha$ -phenyl ethylamine, and obtained the optically active product as follows:



Further, they studied the poly-addition of ethylene dimethacrylate with tetramethylene dimercaptan by *S*-isobutyl ethyleneimine ( $[\alpha]_D -15.68^\circ$ ) or poly(*S*-isobutyl ethyleneimine) ( $[\alpha]_D +56.1^\circ$ ) as catalyst, and obtained the optically active polymer ( $[\alpha]_D +1.40^\circ$ ,  $+0.62^\circ$ ).

In this paper, the asymmetric syntheses by the addition reaction of thiol [thiolacetic acid (AcSH) and benzylmercaptan (BzSH)] to diene polymer [natural rubber (NR), *cis*-1,4-polyisoprene and *trans*-1,4-polyisoprene] by optically active basic catalysts such as *D*-bornylamine, *L*-aspartic diethyl ester, and *L*-aspartic dibutyl ester were carried out. The optically active adduct polymer was produced by the optically active amine catalyst used, but was not obtained by aniline and dimethylaniline. Further, the effects of reaction temperature and reaction time on the addition reaction were studied.

Moreover, the reactions of thiol to *cis*-1,4-polybutadiene, alternating butadiene-acrylonitrile copolymer, and various styrene-butadiene copolymers (SBR) were

carried out by optically active amine, but the optically active adduct polymer was not obtained.

## EXPERIMENTAL

### Reagents

The diene polymers used were natural rubber (NR), *cis*-1,4-polyisoprene, *trans*-1,4-polyisoprene, *cis*-1,4-polybutadiene, alternating butadiene-acrylonitrile copolymer<sup>3</sup> (mole ratio of butadiene/acrylonitrile = 50.9:49.1,  $[\eta]^{30} = 1.55$  in dimethylformamide) and various SBR. The used SBR were Tafuden 1000R (styrene content 18 wt %,  $[\eta]^{30} = 1.60$  in THF) Nipol 1502 (styrene content 23.5 wt %,  $[\eta]^{30} = 1.03$  in THF), Solprene 1205F (styrene content 25 wt %,  $[\eta]^{30} = 1.06$  in THF), Buna Huls 190 (styrene content 40 wt %,  $[\eta]^{30} = 1.54$  in THF) and Hycar 2007J (styrene content 85 wt %,  $[\eta]^{30} = 0.54$  in THF). These diene polymers were reprecipitated from benzene or tetrahydrofuran (THF).

AcSH<sup>4</sup> was prepared by the reaction of acetic anhydride with hydrogen sulphide and was distilled at the boiling point ( $86-87^\circ\text{C}$ ). BzSH<sup>5</sup> was prepared from benzyl chloride with sodium hydrosulphide and was distilled at the boiling point ( $74.0-74.5^\circ\text{C}$  at 10 mmHg).

The optically active basic catalysts used were *D*-bornylamine, *L*-aspartic diethyl ester, and *L*-aspartic dibutyl ester. *D*-Bornylamine was prepared as follows<sup>6</sup>: *D*-camphoroxime was prepared from *D*-camphor with hydroxylamine and was reduced to form *D*-bornylamine. It was recrystallized from diethyl ether [m.p.  $162.5-163^\circ\text{C}$ ,  $[\alpha]_D -45.2^\circ$  (in benzene)]. *L*-Aspartic diethyl ester<sup>7</sup> [b.p.  $121.6-122^\circ\text{C}$  at 11 mmHg,  $[\alpha]_D -11.2^\circ$  (in ethanol),  $-6.1^\circ$  (in benzene)] and *L*-aspartic dibutyl ester [b.p.  $150.0^\circ\text{C}$  at 5 mmHg,  $[\alpha]_D -5.3^\circ$  (in ethanol)] were supplied by Tanabe Pharmaceutical Co. Aniline and dimethylaniline were purified by distillation.

Solvents (benzene, anisole, etc.) were purified by distillation. Stilbene was also purified by recrystallization from ethanol.

*Reaction of diene polymer with thiol*

The addition reaction of thiol to diene polymer in the presence of basic catalyst was carried out as follows. Diene polymer, AcSH (or BzSH), catalyst and benzene as a solvent were placed in a glass tube connected to a vacuum line, and the tube was thoroughly degassed, sealed and the reaction proceeded from room temperature to 90°C for 10–90 h. The reaction mixture was poured into a large excess of methanol after a suitable time interval. The product precipitated was filtered, washed with methanol and dried in a vacuum to constant weight.

After all reaction products were purified by reprecipitation, sulphur analysis, elemental analysis, optical rotation, and infra-red spectra were measured. The percentage addition of thiol to polymer was calculated from the sulphur content of the reaction product.

*Reaction of stilbene with benzylmercaptan by L-aspartic diethyl ester*

In a 100 ml flask, a solution of 5.0 g (0.028 mol) of *trans*-stilbene, 3.28 ml (0.028 mol) of BzSH and 0.69 g (0.028 mol) of L-aspartic dibutyl ester as a catalyst in 40 ml of benzene were allowed to react at room temperature (20°C) under a stream of nitrogen for 20 days with stirring in the dark, and then a large amount of aqueous sodium hydroxide solution was added. The extraction of mixed solution was taken out by diethyl ether, and the extract was distilled to remove diethyl ether. After unreacted stilbene was removed by sublimation from the residue, the reaction product was recrystallized from acetone.

*Measurements*

The D-line optical rotation of the reaction adduct polymer reprecipitated from benzene was measured by a Shimadzu Liebig type polarimeter with filtered sodium light. Optical rotatory dispersion data were obtained with a Shimadzu model QV-50 polarimeter equipped with xenon source.

The infra-red spectra of reaction adduct polymer and products were measured with film on an Infra-red Spectrometer (Jasco IR-E, Japan Spectroscopic Co. Ltd).

The molecular weight of the reaction product was determined with a Knauer vapour pressure osmometer, acetone being used as solvent.

The sulphur quantitative analysis was carried out by Schoniger's method<sup>8</sup> which used the combustion flask.

**RESULTS AND DISCUSSION**

*Reaction of natural rubber*

The reaction of AcSH to NR by aniline and dimethyl aniline as basic catalysts in a sealed tube was carried out at 100°C in benzene. The relationship between the reaction time and the percentage addition of AcSH to NR are shown in Figure 1. As shown in Figure 1, the percentage addition of thiol to NR by both basic catalysts increased with increase in concentration of thiol and basic catalyst, and was saturated at about 20–30%.

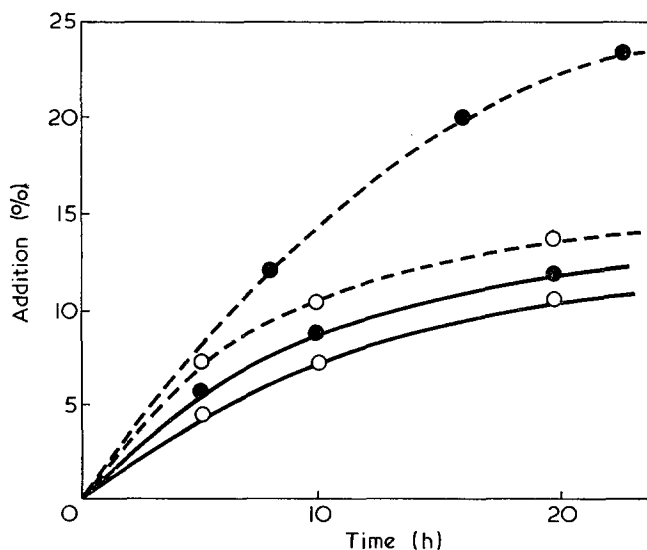


Figure 1 Relation between the percentage addition and reaction time in the reaction of natural rubber with thiolacetic acid by aniline (—) or dimethylaniline (---). [NR] : [AcSH] : [catalyst] = 1 : 1 : 0.5 (O); = 1 : 2 : 1 (●)

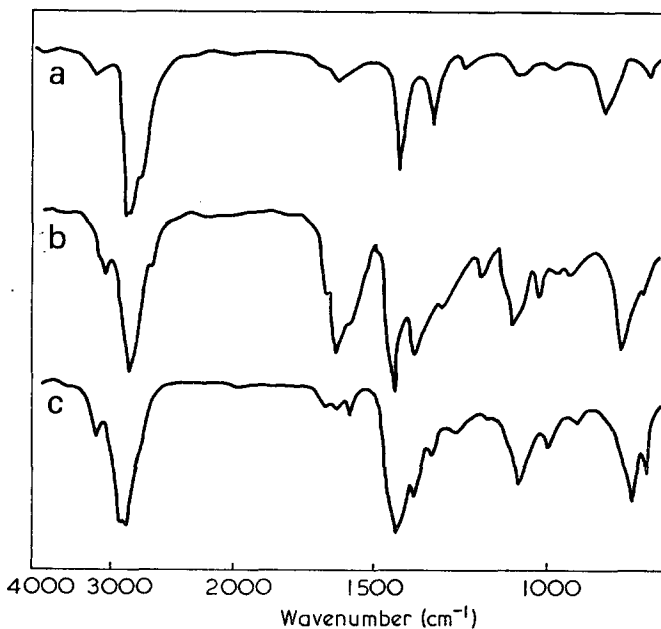


Figure 2 Infra-red spectra of (a) natural rubber, (b) the adduct polymer obtained from natural rubber with thiolacetic acid by D-bornylamine and (c) the adduct polymer obtained from natural rubber with benzylmercaptan by D-bornylamine

Similarly, the addition reaction of AcSH and BzSH to NR by D-bornylamine, L-aspartic diethyl ester, and L-aspartic dibutyl ester as optically active basic catalysts were carried out in benzene at 90°C. The results are shown in Figure 3.

The infra-red spectra of the product obtained from the reaction of NR with AcSH (b) and BzSH (c) by D-bornylamine are shown in Figure 2. The spectrum (b) had absorption bands at 1670 cm<sup>-1</sup> due to a carbonyl group and at 670 cm<sup>-1</sup> due to a thioether linkage and the spectrum (c) had absorption bands at 1600 and 700 cm<sup>-1</sup> due to a phenyl group and at 660 cm<sup>-1</sup> due to a thioether linkage. Both spectra showed decreased absorption of carbon-carbon double bond (950 cm<sup>-1</sup>) compared with the unreacted NR.

From these results, it was found that AcSH or BzSH

was added to NR and that the percentage addition of thiol was little changed after 10 h reaction time and was 10–20% (AcSH) and 15–25% (BzSH).

#### Optical properties

The addition reaction of thiol to NR by basic catalyst took place according to the anti-Markownikov rule, and the  $\beta$ - and  $\gamma$ -carbon atom of the isoprene unit which added  $\text{SH}^-$  and  $\text{H}^+$  induced the asymmetric carbon. If the optically active basic catalyst was used in this reaction, the optically active adduct polymer would be produced due to the asymmetric carbon. Actually, in the reaction with aniline and dimethylaniline, the optically active adduct polymer was not obtained. But, in the reaction with optically active amine catalyst, the optically active adduct polymer was obtained as shown in Figure 3, and specific rotation ( $[\alpha]_D^{25}$ ) was  $-0.1 \sim -0.2$  for the adduct polymer by the reaction of AcSH to NR and  $-0.4^\circ \sim -0.9^\circ$  for the adduct polymer by the reaction of BzSH to NR.

The relationship between the percentage addition of thiol and the specific rotation of adduct polymer is shown in Figure 3. The specific rotation was increased with increasing percentage addition. The asymmetric-inducing ability of these catalysts was L-aspartic dibutyl ester, L-aspartic diethyl ester and D-bornylamine, which increase in that order.

The optical rotatory dispersion were measured in benzene at 25°C and the curves of optical rotatory dispersion are shown in Figure 4 in which curve (A) is based on the adduct polymer of AcSH to NR by L-aspartic diethyl ester and curve (B) is based on the adduct polymer of BzSH to NR by L-aspartic dibutyl ester.

These optical rotatory dispersion curves are satisfied by the simple Drude equation, and the calculated  $\lambda_c$  value was 260–280 nm (in the reaction of NR with AcSH) and 280–290 nm (in the reaction of NR with BzSH). These  $\lambda_c$  values are based on absorption due to the thioether linkage.

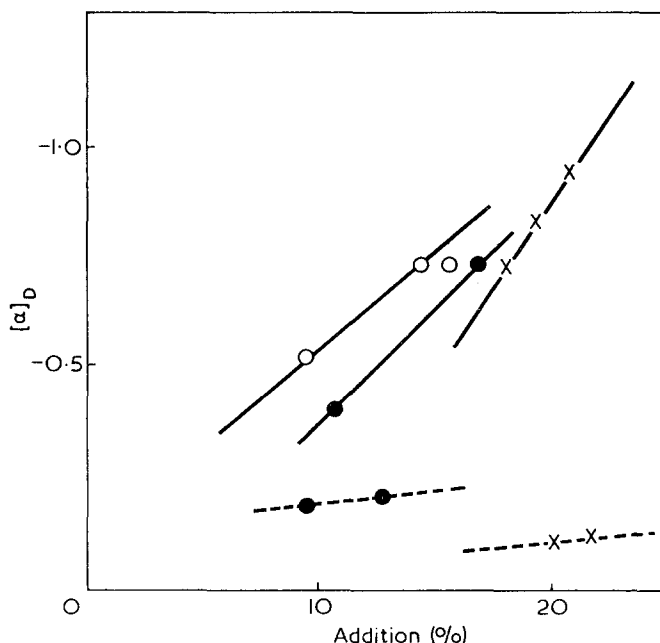


Figure 3 Relation between the specific rotation and percentage addition of adduct polymers obtained from natural rubber with benzylmercaptan (—) and thiolacetic acid (---) by L-aspartic dibutyl ester (○), L-aspartic diethyl ester (●) and D-bornylamine (×)

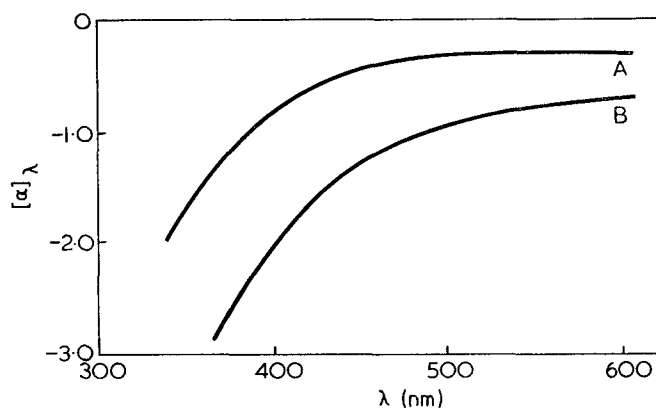


Figure 4 Optical rotatory dispersion of (A) the adduct polymer obtained from natural rubber with thiolacetic acid by L-aspartic diethyl ester and (B) the adduct polymer obtained from natural rubber with benzylmercaptan by L-aspartic dibutyl ester

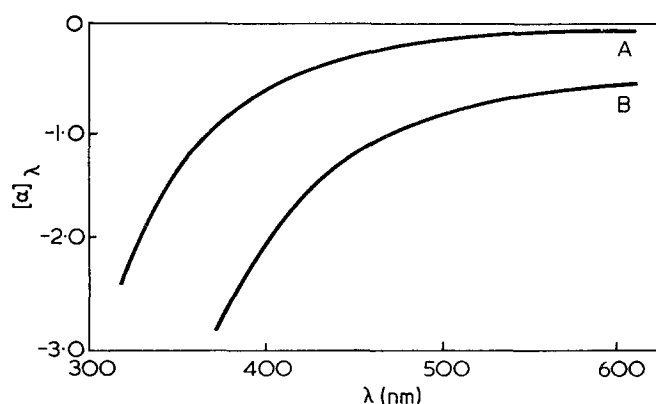


Figure 5 Optical rotatory dispersion of (A) the adduct polymer obtained from *cis*-1,4-polyisoprene with benzylmercaptan by L-aspartic dibutyl ester and (B) the adduct polymer obtained from *trans*-1,4-polyisoprene with benzylmercaptan by L-aspartic dibutyl ester

From these results, it was found that the addition reaction of thiol (AcSH and BzSH) to NR by an amine catalyst used has enabled the asymmetric synthesis, and the optical activity of reaction product was due to the asymmetric carbon atom of the adduct polymer.

#### Reaction of *cis*- and *trans*-1,4-polyisoprene

The addition reaction of AcSH and BzSH to *cis*-1,4-polyisoprene by L-aspartic diethyl ester and L-aspartic dibutyl ester was carried out in benzene at room temperature to 90°C. The results are shown in Tables 1 and 2.

From the sulphur analysis and the infra-red spectrum, it was confirmed that the reaction product was adduct polymer of thiol (AcSH or BzSH) to *cis*-1,4- and *trans*-1,4-polyisoprene as well as the reaction to NR.

In the reaction of *cis*-1,4-polyisoprene, the percentage addition was 15–30% (AcSH) and 10–14% (BzSH) and increased with increasing reaction time, and the specific rotation was  $-0.1^\circ \sim -0.2^\circ$  (AcSH) and  $-0.1^\circ \sim 1.0^\circ$  (BzSH) as shown in Table 1. In the reaction of *trans*-1,4-polyisoprene, the percentage addition was 16.1% (AcSH) and 10–18% (BzSH), and the specific rotation was  $-0.1^\circ$  (AcSH) and  $-0.1 \sim -0.6$  (BzSH) as shown in Table 2.

The optical rotatory dispersion curves of optically active adduct polymer are shown in Figure 5. These

Table 1 Reaction of thiolacetic acid or benzylmercaptan to *cis*-1,4-polyisoprene by L-aspartic diethyl ester or L-aspartic dibutyl ester as basic catalyst in benzene [Polyisoprene]=0.44 mol/l

RSH	Catalyst*	Mole ratio		Temp. (°C)	Time (h)	Sulphur content of product (%)		[ $\alpha$ ] <sub>D</sub> <sup>25</sup> †
		Polymer	RSH : Catalyst			of product	Addition	
AcSH	—	1	1 : 1 : 0	90	70	2.60	6.54	0
	AEE	1	1 : 1 : 1	90	70	6.60	16.6	-0.2
		1	2 : 1	90	70	5.90	15.0	-0.2
	ABE	1	1 : 1 : 1	90	70	9.40	25.7	-0.1
		1	2 : 1	90	70	10.5	29.6	-0.2
BzSH	—	1	1 : 1 : 0	90	70	2.71	6.79	0
	AEE	1	1 : 1 : 1	90	20	3.99	10.0	-0.7
		1	1 : 1 : 1	90	70	4.52	11.6	-0.7
		1	2 : 1	90	70	5.26	14.0	-0.8
	ABE	1	1 : 1 : 1	Room temp.	20	2.23	5.18	-0.1
		1	1 : 1 : 1	50	20	3.84	9.59	-0.6
		1	1 : 1 : 1	90	20	4.39	11.2	-0.8
		1	1 : 1 : 1	90	70	5.18	13.8	-1.0

\* AEE=L-aspartic diethyl ester; ABE=L-aspartic dibutyl ester

† In benzene at 25°C

Table 2 Reaction of thiolacetic acid or benzylmercaptan to *trans*-1,4-polyisoprene by L-aspartic diethyl ester or L-aspartic dibutyl ester as basic catalyst in benzene [Polyisoprene]=0.44 mol/l

RSH	Catalyst*	Mole ratio		Temp. (°C)	Time (h)	Sulphur content of product (%)		[ $\alpha$ ] <sub>D</sub> <sup>25</sup> †
		Polymer	RSH : Catalyst			of product	Addition	
AcSH	—	1	1 : 1 : 0	90	20	2.10	5.27	0
	AEE	1	1 : 1 : 1	90	20	6.42	16.1	-0.1
BzSH	—	1	1 : 1 : 0	90	20	2.54	7.10	0
	AEE	1	1 : 1 : 1	90	20	6.17	17.3	-0.1
		1	1 : 1 : 1	Room temp.	20	4.03	10.0	-0.1
	1	1 : 1 : 1	50	20	4.93	13.0	-0.5	
1	1 : 1 : 1	90	20	6.25	17.5	-0.6		

\* AEE=L-aspartic diethyl ester; ABE=L-aspartic dibutyl ester

† In benzene at 25°C

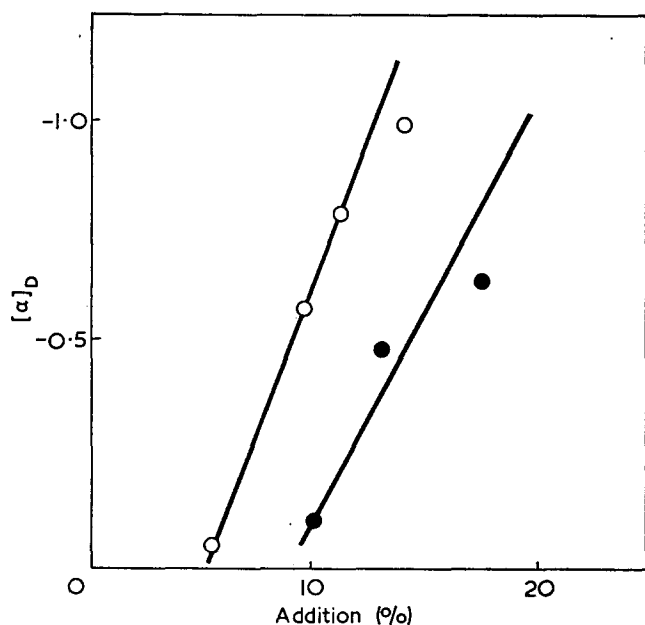


Figure 6 Relation between the specific rotation and the percentage addition of adduct polymers obtained from *cis*-1,4-polyisoprene (○) or *trans*-1,4-polyisoprene (●) with benzylmercaptan by L-aspartic dibutyl ester

optical rotatory dispersion curves (A: *cis*-1,4-polyisoprene; B: *trans*-1,4-polyisoprene) are satisfied by the simple Drude equation, and the calculated  $\lambda_c$  value was 270–290 nm. This  $\lambda_c$  value is also based on absorption due to the thioether linkage.

The relationship between the percentage addition and the specific rotation is shown in Figure 6. The specific rotation was increased with increasing percentage addition. The increasing tendency was almost identical with the reaction of these polyisoprenes (*cis*-1,4- and *trans*-1,4-). The specific rotation of adduct polymer from *cis*-1,4-polyisoprene was higher than that of adduct polymer from *trans*-1,4-polyisoprene. For example, when the percentage addition was 10%, the specific rotation from *cis*-1,4-polyisoprene was  $-0.6^\circ$  and that from *trans*-1,4-polyisoprene was  $-0.1^\circ$ . This reason was considered due to the difference of *cis*- or *trans*-conformation of surrounding an asymmetric carbon atom.

#### Reaction of other diene polymers

The reaction of BzSH to other diene polymers (*cis*-1,4-polybutadiene, various SBR, and alternating butadiene-acrylonitrile copolymer) by L-aspartic dibutyl ester as optically active basic catalyst were carried out at 90°C for 72 to 90 h in benzene. The results are shown

Table 3 Reaction of benzylmercaptan to diene polymer by L-aspartic dibutyl ester in benzene at 90°C for 72 h. [Double bond in polymer] : [BzSH] : [Catalyst]=1 : 1 : 1. [Polymer]=0.44 mol/l

Diene polymer	Analysis of product			Addition* (%)	[α] <sub>D</sub> <sup>25</sup> †
	C(%)	H(%)			
Polybutadiene	83.15	9.76	16.1	0	
Tafuden 1000 R	85.10	9.80	31.5	0	
Nipol 1502	86.84	9.73	17.3	0	
Solprene 1205F	86.61	9.64	19.1	0	
Buna Huls 190	89.68	9.55	6.1	0	
Hycar 2007J	92.92	8.30	2.0	0	
Alternating butadiene-acrylonitrile copolymer	76.11	8.26	15.7	0	

\* Percentage addition of B<sub>2</sub>SH for double bond of butadiene unit  
† In benzene at 25°C

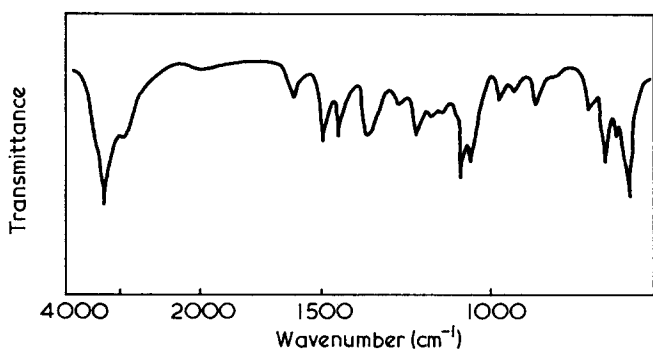
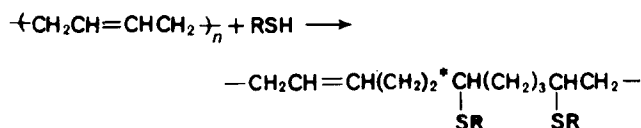


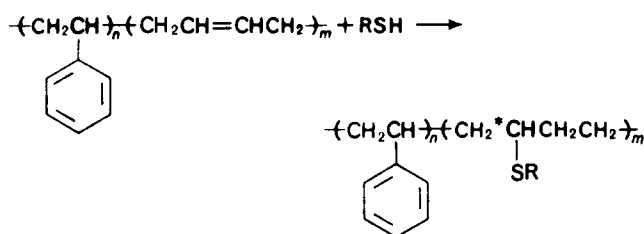
Figure 7 Infra-red spectrum of the product obtained from stilbene with benzylmercaptan by L-aspartic dibutyl ester

in Table 3. From the qualitative sulphur analysis and the infra-red spectrum, it was confirmed that the reaction product was adduct polymer of BzSH to these diene polymers. However, in some cases the optically active polymer was not obtained. The addition reaction of thiol to *cis*-1,4-polybutadiene, SBR and alternating butadiene-acrylonitrile copolymer was considered as follows.

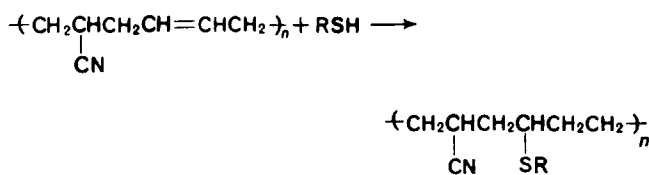
Polybutadiene:



SBR:



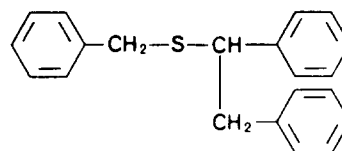
Alternating butadiene-acrylonitrile copolymer:



and the asymmetric carbon was induced at the β-carbon atom of the butadiene unit which added SR<sup>-</sup>. The

product of optically inactive adduct polymer, in comparison with the reaction of thiol to NR or polyisoprene, was due to the following reason. The asymmetric carbon atom which caused optical activity was H<sup>+</sup> added carbon atom rather than the SR<sup>-</sup> added carbon atom. In order to confirm this reason, the addition reaction of BzSH to *trans*-stilbene with L-aspartic dibutyl ester was carried out in mixed solvent of tetrahydrofuran and benzene at room temperature (20°C) in the dark. The reaction product having melting point 195°C was obtained. The infra-red spectrum is shown in Figure 7. This had absorption bands at 2900 and 2850 cm<sup>-1</sup> due to a methine group and 1600, 1080, and 720 cm<sup>-1</sup> due to phenyl groups, but did not have an absorption band at 950 cm<sup>-1</sup> due to the *trans*-carbon-carbon double bond of stilbene. The molecular weight was 260. Calculated for C<sub>21</sub>H<sub>20</sub>S: C, 82.89%; H, 6.57%; S, 10.54%. Found: C, 80.09%; H, 6.70%; S, 10.31%.

From the results of elemental analysis, molecular weight and infra-red spectrum, it was found that the reaction product was identical to benzyl dibenzyl sulphide which is a new compound:



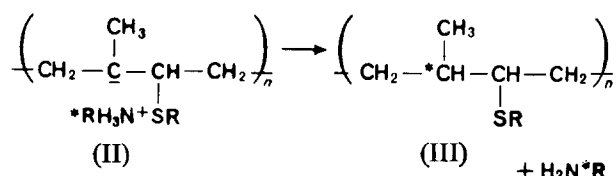
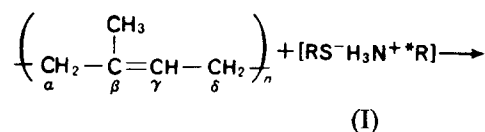
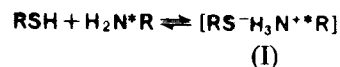
Molecular weight 260 (calculated 258)

However, benzyl dibenzyl sulphide did not show optical activity. The asymmetric carbon atom of the catalyst was independent of the addition of SR<sup>-</sup> to polymer.

Consequently, it was found that the asymmetric synthesis in the addition reaction of thiol to these diene polymers was quite impossible in spite of the position of added SR<sup>-</sup>.

#### Mechanism of asymmetric addition

From the above described results, the reaction mechanism of the asymmetric synthesis of NR and polyisoprene is now considered as follows:



In this reaction of thiol with polyisoprene by the optically active amine catalyst, first the complex (I) is formed by the reaction between thiol and catalyst, and the intermediate (II) is prepared by the addition reaction of the complex (I) to polyisoprene according to the anti-Markownikov rule. The product (III) is produced from the intermediate (II) by hydrogen addition from \*RH<sub>3</sub>N<sup>+</sup>.



Therefore, the  $\beta$ -carbon atom of the isoprene unit in polymer has optical activity.

Accordingly, in this asymmetric addition of polyisoprene by optically active amine catalysts, the optically active asymmetric carbon which caused optical activity was the  $H^+$  added carbon atom, rather than the  $SR^-$  added carbon atom, i.e. the addition of  $SR^-$  to the polymers does not produce the optically active asymmetric carbon. Therefore, it was found that the optically active adduct polymer was produced from NR, *cis*-1,4-polyisoprene and *trans*-1,4-polyisoprene having a  $\beta$ -carbon atom which changed into an asymmetric carbon by the  $H^+$  addition, but was not produced from polybutadiene, SBR and alternating butadiene-acrylonitrile copolymer whose  $\beta$ -carbon atom did change into an asymmetric carbon by the  $H^+$  addition.

#### ACKNOWLEDGEMENT

The authors would like to express their grateful acknowledgment to Dr Junji Furukawa (Kyoto University) for providing the alternating butadiene-acrylonitrile copolymer.

#### REFERENCES

- 1 Tsuruta, T. and Inoue, S. *21st Meet. Chem. Soc. Japan, Preprints* 1968, p 2716
- 2 Inoue, S. and Ohashi, S. *19th Symp. High Polym. Japan, Preprints*, 1970, p 431
- 3 Furukawa, J., Iseda, Y., Haga, K. and Kataoka, N. *J. Polym. Sci. (B)* 1969, 7, 47
- 4 Bllingboe, E. K. *Org. Synth.* 1963, 4, 928
- 5 Fromm, E. and Achert, O. *Chem. Ber.* 1903, 36, 546
- 6 Frankland, B. *J. Chem. Soc.* 1909, 95, 2024
- 7 Fischer, F. *Chem. Ber.* 1901, 34, 453
- 8 Schoniger, W. *Mikrochim. Acta* 1956, p 860

# Solid-state polymerization of derivatives of 2,4,6-octatriyne: 9. Topochemical reactions of monomers with conjugated triple bonds

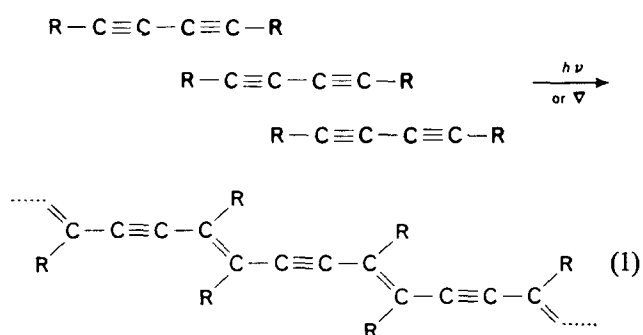
Jitsuo Kiji\*, J. Kaiser, G. Wegner† and R. C. Schulz‡

Sonderforschungsbereich 'Makromoleküle Mainz-Darmstadt' (SFB 41), West Germany  
(Received 29 March 1973)

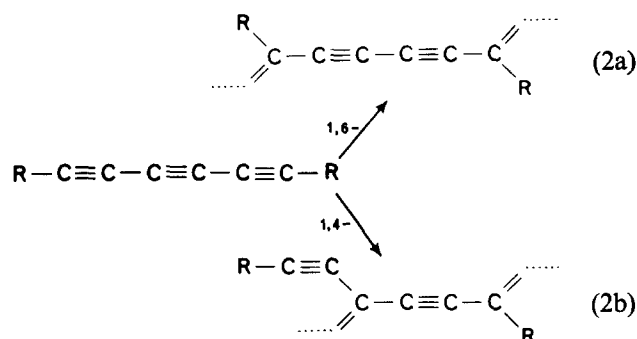
The solid-state polymerization of monomers with three conjugated triple bonds gives rise to polymer single crystals. The lattice parameters of the polymers from 2,4,6-octatriyne-1,8-diol and 2,4,6-octatriyne-1,8-diol-bis(phenyl urethane) were determined. Based on these data and considering the mechanical properties and dichroism of the polymer crystals, it is concluded that polymerization proceeds according to a 1,4-addition to the triple bond system of the monomers. Only two of the three triple bonds of the monomers are affected by polymerization to form the polymer backbone of regularly alternating double, single and triple bonds. The residual triple bond is regularly arranged in the all-*trans* position as part of the substituents. The kinetics of the thermal and photopolymerization of these monomers are quite similar to those of the corresponding diynes. The activation energy of thermal polymerization was found to be 23 kcal/mol as compared to 19 kcal/mol for comparable diynes. The long wavelength limit of photosensitivity was found to be at about 380 nm as compared to 330 nm for diynes.

## INTRODUCTION

Solid-state polymerization of monomers with two conjugated triple bonds is best described as a 1,4-addition polymerization, yielding a polymer with a backbone of conjugated unsaturated bonds<sup>1</sup>. The solid-state polymerization has been proposed to proceed according to:



This concept prompted us to investigate the solid-state polymerization of higher polyynes. Several different products are to be expected when monomers with three conjugated or even higher conjugated triple bonds are allowed to polymerize as shown by:



Therefore, it seemed to be of considerable interest to investigate the course of the polymerization of monomers with three conjugated triple bonds in the solid-state. Preparation and optical properties of conjugated polyynes have been studied extensively<sup>2,3</sup>. It is also well known that the thermal and photochemical stability decreases rapidly with increasing number of conjugated triple bonds per molecule. Until now, however, no effort was made to elucidate the structure of the polymers resulting from the photosensitive conjugated polyynes. This paper deals with the preparation and the structure of crystalline polymers obtained from the triynes. Additionally, some mechanistic studies are reported.

## EXPERIMENTAL

### X-ray diffraction and physical measurements

Throughout the present study the X-ray photographs (compare Figure 2) were taken by using Ni-filtered CuK $\alpha$  radiation and with both the rotating crystal and

\* Present address: Dept. of Synthetic Chemistry, Faculty of Engineering, Kyoto University, Kyoto, Japan

† To whom all correspondence should be addressed: Institut für Physikalische Chemie, Universität Mainz, D 65 Mainz, West Germany

‡ Institut für Makromolekulare Chemie, Technische Hochschule Darmstadt, West Germany

the Weissenberg technique. The conditions employed to obtain the data given in Table 2 were 20 mA, 30 kV with a Philips generator fitted with a normal focus X-ray tube. The crystals were mounted in their monomer form on the goniometer head. On exposure to the X-ray beam, the monomer crystals polymerized rapidly and quantitatively so that the reflections obtained are due to the polymer form of the crystals.

The spectra in the solid-state and the photoreactivity of the crystals on irradiating with monochromatic light were measured using a Leitz UV microscope photometer. All melting points are uncorrected.

#### Materials

Commercially available thionyl chloride, phenyl isocyanate and hexamethylene diisocyanate were used without further purification. *n*-Butyl isocyanate was purified by distillation. *p*-Toluene chlorosulphonate was purified by recrystallization. Paraformaldehyde was dried over phosphorus pentoxide. Commercially available gaseous ammonia was dried by passing through a cold trap ( $-30^{\circ}\text{C}$ ).

#### 2,4,6-Octatriyne-1,8-diol (I)

The procedure, given by Armitage *et al.*<sup>4</sup>, was employed. 2,4-Hexadiyne-1,6-dichloride<sup>5</sup> was reacted first with sodium amide in liquid ammonia and then with paraformaldehyde. 2,4-Hexadiyne-1,6-dichloride (10.9 g) was added to a suspension of sodium amide<sup>6</sup> (Na, 6.9 g; liquid ammonia, 150 ml;  $\text{Fe}(\text{NO}_3)_3 \cdot 6\text{H}_2\text{O}$ , 0.05 g) at  $-78^{\circ}\text{C}$  with vigorous stirring for 10 min. After an additional 5 min, paraformaldehyde (4.5 g) was added as a suspension in ether (150 ml). After the solution was stirred for 19 h, ammonium chloride (7.5 g) was added, and ammonia was allowed to evaporate while more ether was added. The residue was extracted three times with 100 ml of ether. The ethereal solution was percolated through a thin layer of alumina (5 g). Evaporation of ether under reduced pressure gave (I). Recrystallization from ethyl acetate/petroleum ether (b.p.  $50-70^{\circ}\text{C}$ ) gave thin plates of the diol (2.9 g) in 29% yield. According to Armitage<sup>4</sup> the diol melts at  $138-140^{\circ}\text{C}$ . However, on heating slowly, the diol polymerized and showed no melting point up to  $300^{\circ}\text{C}$ .

#### 2,4,6-Octatriyne-1,8-diol-bis(phenyl urethane) (II)

Diol (I) (0.5 g) was dissolved in 10 ml of tetrahydrofuran and 2.5 ml of phenyl isocyanate, 1 drop of triethylamine and a trace of di-*n*-butyltin diacetate were added to the solution at  $-10^{\circ}\text{C}$ . The mixture was stirred for 3 h, during which the temperature was raised gradually from  $-10^{\circ}\text{C}$  to room temperature. Then, the solution was poured into a large amount of petroleum ether with stirring. Crystals of (II) separated at once. They were filtered off and well washed with petroleum ether. The crystals were dissolved in dioxane/benzene (1:2) and percolated through a thin layer of alumina. The filtrate was again poured into a large amount of petroleum ether. Colourless fine needles were obtained (1 g). Recrystallization from hot benzene/petroleum ether (3:1), after percolation through a thin layer of alumina, by cooling very slowly in the dark gave long needles, which did not show a definite melting point upon to  $300^{\circ}\text{C}$ . Calculated for  $\text{C}_{22}\text{H}_{16}\text{O}_4\text{N}_2$ : C, 70.96%; H, 4.33%; N, 7.52%. Found: C, 70.67%; H, 4.36%; N, 7.60%.

#### 2,4,6-Octatriyne-1,8-diol-bis(*n*-butyl urethane) (III)

This monomer was prepared from the reaction of (I) with *n*-butyl isocyanate under the same conditions described above for the preparation of (II). Recrystallization from benzene/petroleum ether (1:1) gave colourless plates, which did not melt but decomposed around  $260^{\circ}\text{C}$ . Calculated for  $\text{C}_{18}\text{H}_{24}\text{O}_4\text{N}_2$ : C, 65.04%; H, 7.27%; N, 8.43%. Found: C, 65.05%; H, 7.40%; N, 8.35%.

#### 2,4,6-Octatriyne-1,8-diol-bis(benzoate) (IV)

The diol (I) (0.13 g) was dissolved in 3 ml of tetrahydrofuran and 0.35 g of benzoyl chloride was added at  $-10^{\circ}\text{C}$ . The temperature was raised gradually to room temperature and the solution was stirred overnight. A solution of potassium hydroxide (0.2 g KOH dissolved in 3 ml  $\text{H}_2\text{O}$ ) was added to the solution at  $0^{\circ}\text{C}$ . The solution was stirred for 30 min and then poured into a large amount of ice water. The crystals were filtered off. Recrystallization from benzene/cyclohexane gave colourless needles (m.p.  $120-121^{\circ}\text{C}$ ). Calculated for  $\text{C}_{22}\text{H}_{14}\text{O}_4$ : C, 77.18%; H, 4.12%. Found: C, 77.69%; H, 4.18%.

#### 2,4,6-Octatriyne-1,8-diol-bis(*p*-toluene sulphonate) (V)

This monomer was prepared in analogy to the method described by Wegner<sup>7</sup>. Recrystallization from 95% methanol gave light violet plates (m.p.  $116-118^{\circ}\text{C}$ ). Calculated for  $\text{C}_{22}\text{H}_{18}\text{S}_2\text{O}_6$ : C, 59.71%; H, 4.08%. Found: C, 59.69%; H, 4.05%.

#### Poly(2,4,6-octatriyne-1,8-diol-hexamethyl urethane) (VII)

This polymer was prepared from the reaction of (I) (0.2 g) with hexamethylene diisocyanate (0.24 g) under the same conditions as described for the preparation of (II) and (III). After the reaction had taken place the solution was poured into a large amount of petroleum ether. White powdery product (0.36 g) was reprecipitated from dioxane by adding petroleum ether.

#### Polymerization

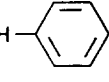

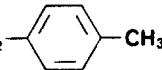
Photopolymerization was carried out in a beaker-like vessel, fitted with a cooling jacket, using a u.v. medium-pressure mercury lamp. The crystalline monomers were directly irradiated without using dispersion medium. The distance from the light source to the monomer was kept at 12 cm. Thermal polymerization was achieved by annealing the monomers in the dark. Conversion was determined by extracting unreacted monomer with hot acetone using a Soxhlet extractor.

## RESULTS AND DISCUSSION

#### Reactivity of triynes and the structure of the polymers

We have examined the polymerization of 2,4,6-octatriyne-1,8-diol (I) and its derivatives as model compounds. Most of these monomers are colourless when freshly prepared. They are highly photosensitive in the solid state. Especially on brief exposure of (I) and 2,4,6-octatriyne-1,8-diol-bis(phenyl urethane) (II) to light, extensive polymerization occurs on the surface of the crystals and they develop a deep colour. On the other hand, they are not so reactive in solution so that they could be stored without formation of polymers.

Table 1 Polymerization of triyne derivatives: R—C≡C—C≡C—C≡C—R

Triyne R	Photopolymerization <sup>a</sup>		Thermal polymerization		
	Polymer <sup>b</sup> yield	Colour <sup>c</sup>	Temp. (°C)	Time (h)	Polymer yield (%)
I —CH <sub>2</sub> OH	+++	red-purple	60 100	52 0.1	87 — <sup>d</sup>
II —CH <sub>2</sub> OCNH— 	+++	dark blue	60 70 100	50 70 22	6.7 14 71
III —CH <sub>2</sub> OCNHC <sub>4</sub> H <sub>9</sub>	++	blue	70	70	0
IV —CH <sub>2</sub> OC— 	+	brown	100	20	88
V —CH <sub>2</sub> OSO <sub>2</sub> —  —CH <sub>3</sub>	++	violet	70 83 100	70 40 1	0 — <sup>e</sup> — <sup>e</sup>

<sup>a</sup> By medium pressure mercury lamp at room temperature for 3 h

<sup>b</sup> —, no polymerization; +, low yield (<1%); ++, moderate yield (<10%); +++, high yield (>20%)

<sup>c</sup> Of the mixture of monomer and polymer as polymerized

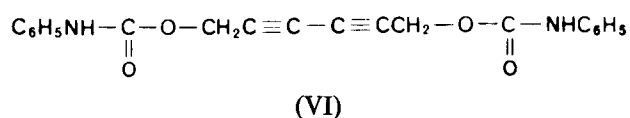
<sup>d</sup> Rapid carbonization occurred

<sup>e</sup> The infra-red spectrum of the polymer showed that elimination of sulphonate groups had occurred

Typical results of the thermal and photo-induced polymerization are summarized in *Table 1*.

Diol (I) is so reactive that it turned already light purple during recrystallization even when it was crystallized in the dark at low temperature. At 100°C rapid carbonization occurred. 2,4,6-Octatriyne-1,8-diol-bis(phenyl urethane) (II) was highly reactive either on u.v. or high energy irradiation or on heating. Annealing at temperatures above 100°C gave a crystalline polymer in high yield. Bis(*n*-butyl urethane) (III) and bis(benzoate) (IV) were not so photosensitive as (I) or (II). Bis(*p*-toluene sulphonate) (V) was also photosensitive, but no polymer was obtained on heating. At 80°C elimination of the sulphonate groups occurred and at temperatures below 70°C no appreciable change in the monomer was observed. From these observations phenyl urethane (II) seemed to be the best monomer to investigate the reactivity of triynes and the structure of the polymers. Most of our work employed (II).

As a complicating fact it is usually observed in solid-state polymerizations that different modifications of the same compound show different reactivity because of the close relationship between packing of the monomer molecules and chemical reactivity inside the crystal lattice. It was reported that 2,4-hexadiyne-1,6-diol-bis(phenyl urethane) (VI) appears in different modifications depending on recrystallization conditions. Single crystals of:



obtained from dioxane-water<sup>8,9</sup> are particularly reactive, while those prepared from anisole are far less reactive<sup>10,11</sup>. We have attempted recrystallization of (II) from various solvents, but petroleum ether/benzene gave the best results. Long needle shaped single crystals were obtained quite suitable for physical measurements.

The infra-red spectra of (II) and its polymer are shown in *Figure 1*. These spectra are very similar except that the peaks of the polymer are broadened. The spectra of the thermally and photochemically obtained polymers were quite similar and there was no significant difference between them. The elemental analysis of the polymer gave the same value as that of the monomer within the limits of experimental error, indicating that no decomposition had occurred during polymerization. The polymer was insoluble in common organic solvents. It consists of single crystals which show dichroism with the main axis of absorption parallel to the needle axis.

#### Crystallographic characterization of the polymers

The lattice parameters of the polymer crystals of the bis(phenyl urethane) (II) and the diol (I) were determined by rotation and Weissenberg photographs. From the knowledge of the lattice parameters in connection with the dichroic and cleavage behaviour of the crystals as obtained by solid-state polymerization definite conclusions can be drawn with regard to the chemical structure of the polymers. The chain direction is easily determined in the case of the solid-state polymerized acetylenes by looking to the dichroism<sup>1,9</sup> which is always parallel to the chain-axis and parallel to the direction of maximum mechanical strength of the polymer crystals. Rotation photographs around this axis yield the repeat distance in chain direction. A value of 4.8 to 5.2 Å has to be expected if polymerization of the monomer occurs according to a 1,4-addition to give a polymer with a planar structure as shown in equation (2b). The other possibility discussed in equation (2a) would afford a repeat distance of ~7.5 Å as can be calculated assuming normal bond angles and distances.

The lattice constants for the polymers of compounds (I) and (II) are compiled in *Table 2*. For comparison, lattice parameters of the related diacetylene derivatives 2,4-hexadiin-1,6-diol and the bis(phenyl urethane) (VI) of this diol (Mod. II<sup>10</sup>) are also given in *Table 2*. It is

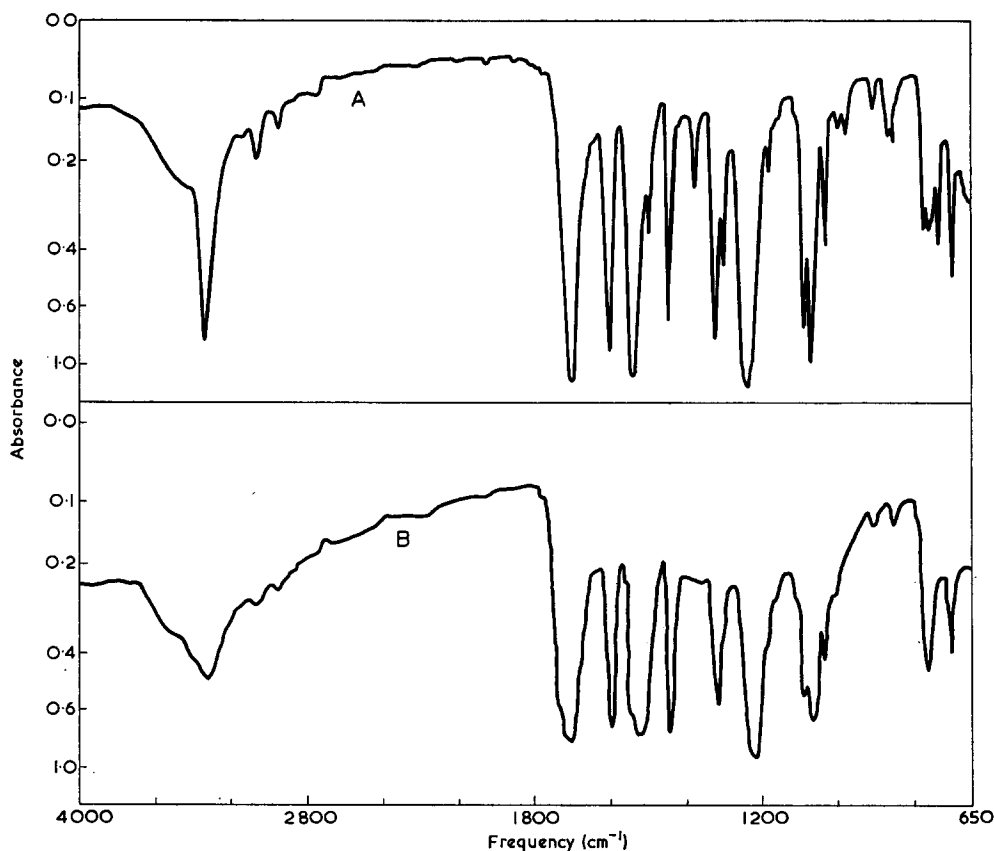
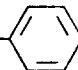


Figure 1 Infra-red spectra of 2,4,6-octatriyne-1,8-diol-bis(phenyl urethane) (A) and its polymer (B) in KBr disc

Table 2 Lattice parameters of polymer single crystals obtained from corresponding monomer single crystals of diynes and triynes by solid-state polymerization. General structure of monomer:  $R-(C\equiv C)_n-R$

Monomer structure:	R=CH <sub>2</sub> OH		$R = -CH_2OCNH-$ 	
	n=3 (I)	n=2	n=3 (II)	n=2 (VI)
Crystal system	monoclinic	monoclinic <sup>14</sup>	monoclinic	monoclinic <sup>10</sup>
Lattice constants:				
a (Å)	4.11	4.09	24.65	23.5
b (Å)	19.59	15.99	30.74	7.86
c (Å)	4.80	4.77	4.89	18.82
β (degrees)	109	106.6	92.2	94.5
Identity period (Å)	5.20	5.32	4.89	4.71
in chain direction	a/c-diagonal	a/c-diagonal	c-axis	1/4 c-axis
Space group	P 2 <sub>1</sub> /c	P 2 <sub>1</sub> /c	P 2 <sub>1</sub> /c	C 2/c
Molecules per unit cell	2	2	8	8
Density (g/cm <sup>3</sup> )	1.29	1.22	1.29	1.33

clearly evident from these data that the polymerization of the two triynes (I) and (II) gives polymers with repeat distances in chain direction compatible only with a 1,4-addition. This immediately tells that only two of the three acetylene groups take part in the polymerization and a regular arrangement of the residual triple bonds as the substituents is achieved in all-*trans* position according to equation (3). It is worth mentioning that the perfection of the polymer crystals obtained from single crystals of the triynes is quite high as can be judged from the many clear and sharp reflections of the Weissenberg photographs. As an example the Weissenberg photograph of the (*hko*) plane of a polymer single

crystal of the bis(phenyl urethane) (II) is shown in Figure 2. This is another indication that the lattice and packing properties of the molecules need not be affected in the solid-state polymerization of conjugated acetylenes. However, it should be mentioned that the diyne derivatives whose data are given in Table 2 do not polymerize completely because relaxation of the newly formed chains inside the monomer lattice occurs at 20–40% conversion due to a slight misfit between the packing properties of the monomer and polymer molecules<sup>10</sup>. The modification of the diyne (VI) which is crystallographically comparable to the corresponding triyne-bis-(phenyl urethane) (II) is not the most active

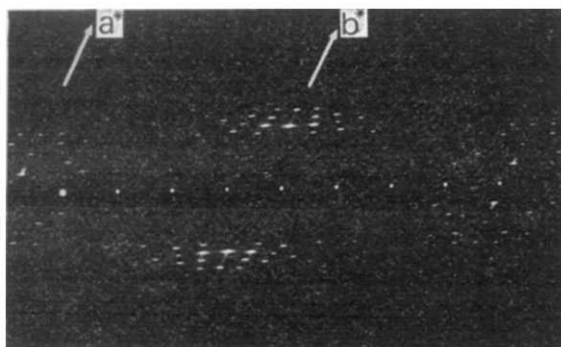


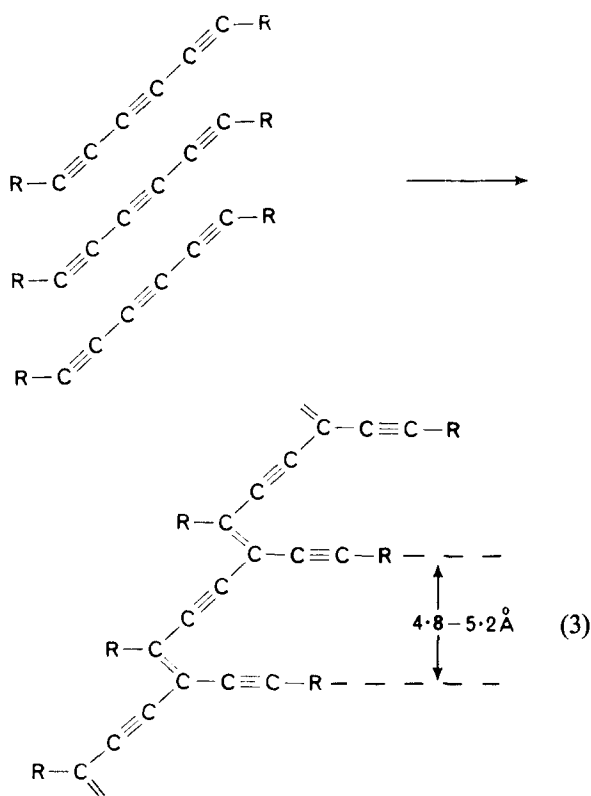
Figure 2 Weissenberg photograph of the  $(hko)$  plane of a polymer single crystal prepared by solid-state polymerization starting with a monomer single crystal of 2,4,6-octatriyne-1,8-diol-bis(phenyl urethane) (II)

Table 3 Longest wavelength bands of monomers in 95% methanol

Monomer	$\lambda_{\max}$ (nm)	$\epsilon$
I <sup>4</sup>	312	190
II	313	300*
V	315	400*

\* To eliminate insoluble parts, the solution was filtered before the measurement.

one<sup>10</sup>. From a more active modification of the same monomer perfect single crystals of the polymer were obtained and their structure was determined<sup>9</sup>.



#### Thermal polymerization

The thermal polymerization of (II) was carried out simply by annealing the monomer crystals at temperatures below 110°C. The shape of the crystals did not change during polymerization. After heating for a definite time the unreacted monomer was extracted

with hot acetone. At low conversion the colour of the polymerizing crystals was dark-blue and the pure polymer, after extracting the unreacted monomer, was dark-gold. At higher conversion, however, the colour of the polymerizing crystals and the pure polymer was dark-brown. Since the polymer was insoluble in all common solvents, molecular weight measurements were impossible. With the use of a u.v. microscope photometer the spectral change of polymerizing single crystals could be followed as a function of conversion. The spectrum of thermally polymerizing crystals shows no absorption maximum and the optical density increases monotonously from 650 to 400 nm, while the pure polymer, after extracting unreacted monomer, possesses a very broad adsorption maximum between 500 and 600 nm. It was confirmed by measuring the u.v. spectrum that the extract of the polymerizing crystals contained no species other than the monomer.

To gain insight into the polymerization of the phenyl urethane (II), time-conversion curves were measured at various temperatures between 60 and 110°C. Typical time-conversion curves are shown in Figure 3. At 70°C the polymerization proceeded very slowly, while at 110°C polymerization occurred quite fast and the polymer was rapidly obtained in quantitative yield. In all cases no induction period was observed and straight lines were obtained. The rate of reaction was independent of crystal size, i.e. small and large crystals polymerized with the same velocity indicating that the reaction is not governed by surface effects. The apparent activation energy of the polymerization was determined to be 23 kcal/mol. We derived this value from the Arrhenius plot of the slopes of the time-conversion curves (Figure 4), assuming that the rate of reaction can be expressed in terms of conversion/10 h. The activation energy is somewhat higher than that for thermal polymerization of the corresponding diyne derivative (VI)<sup>8</sup> (19 kcal/mol).

Heating (IV) at 100°C gave black polymer in 88% yield. The infra-red spectra of the monomer and polymer are not significantly different from each other. We have not studied the polymerization further.

We have extended the solid-state polymerization of triyne derivatives to solid-state crosslinking of polymers

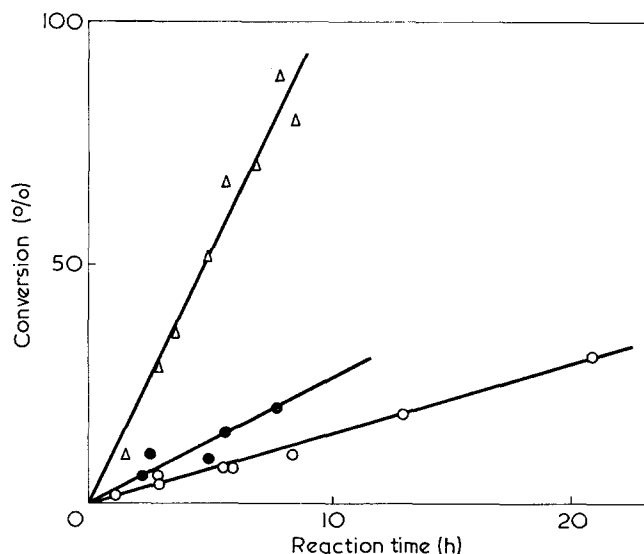


Figure 3 Time-conversion curves for the thermal polymerization of (II). ○, 90°C; ●, 100°C; △, 110°C

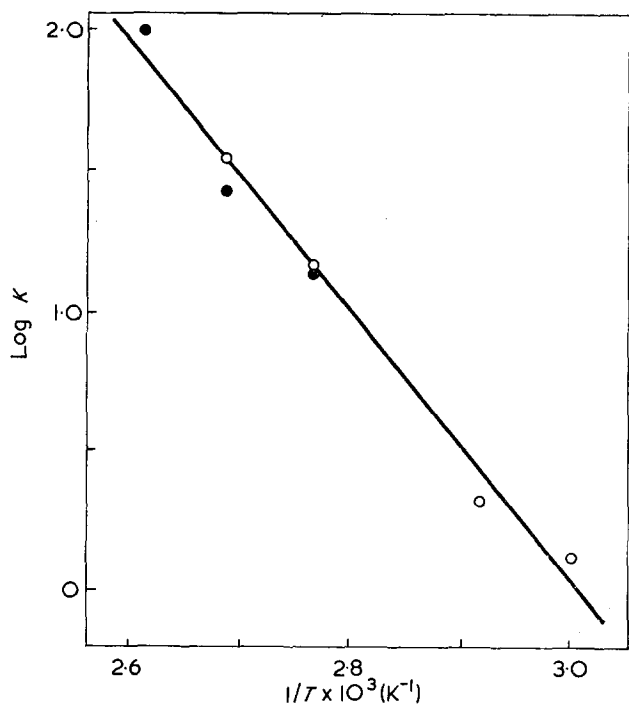
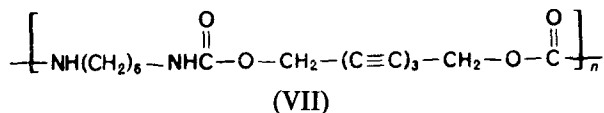


Figure 4 Arrhenius plots for the thermal polymerization of (II). O, Long needles; ●, fine needles

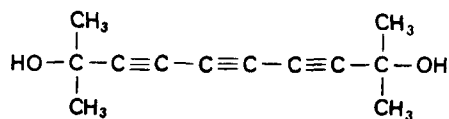
containing three conjugated triple bonds. Polyurethane (VII) from 2,4,6-octatriyne-1,8-diol (I) and hexamethylene diisocyanate was readily obtained. The polymer also showed solid-state reactivity. The polymer was crosslinked in solid-state on annealing at 70°C for 48 h or u.v. irradiation for 3 h. Extracting by hot dioxane



gave reddish-brown crosslinked polymer in 75% or 13% yield, respectively. Similar behaviour was observed for polymers containing two conjugated triple bonds as structural elements<sup>12, 13</sup>.

#### Photopolymerization

As already mentioned, many triyne derivatives are photosensitive and polymerize rather fast even on standing in diffuse daylight. The results in Table I are only qualitative. Contrary to thermal polymerization, the rate of conversion depends upon the size of crystals, since the photopolymerization occurs at first on the crystal surface and once the surface is covered by coloured polymer no appreciable polymerization occurs in the inside of the crystals. Generally speaking, reactivity of the triyne derivatives decreases in the following order: diol (I) > phenyl urethane (II) > tosylate (V) > n-butyl urethane (III) > benzoate (IV). Photopolymerization of 2,9-dimethyldeca-3,5,7-triyn-2,9-diol (VIII) was also attempted. However, no appreciable change of the monomer crystals was observed. We have studied the



photopolymerization by measuring the change in visible spectra of polymerizing single crystals using an u.v. microscope photometer. In this study suitable single crystals of the monomers (I) and (II) were placed on the microscope stage between quartz cover slides and were irradiated by monochromatic light in the wavelength range from 320 to 380 nm. In the case of the monomer (II) it was impossible to obtain sufficiently large single crystals of the pure monomer. For the preparation of suitable single crystals, hot saturated solutions of the monomer had to be cooled very slowly so that the crystallizing monomer had already started to polymerize thermally. Therefore, the long needles obtained by careful crystallization were already deep violet because of thermal polymerization. For this reason, we had to use aggregates of fine needles to measure the change in optical density during photopolymerization. Such fine colourless needles were easily obtained by rapid quenching of saturated solutions of the monomer. In any case, however, the monomer crystals were so reactive that we never succeeded in measuring the spectra of a completely colourless specimen. Since the extinction coefficient of the polymer and the intermediates seems to be quite high, deeply coloured crystals were obtained even on slight exposure, although no appreciable conversion takes place considering the very small amount of polymer which was obtained after extraction of the crystals with a solvent of the monomer.

Slightly coloured monomers (I) and (II) polymerized at a considerable rate when they were irradiated with light of wavelength 320–360 nm. Irradiation at longer wavelengths than 380 nm was almost ineffective. It is interesting to note that photopolymerization of the single crystals is achieved in a wavelength range where no appreciable absorption of the dissolved monomer molecules is observed, a fact which was already described in the case of photopolymerization of monomers with two conjugated triple bonds<sup>11</sup>. For comparison, the position and extinction coefficients of the longest wavelength bands of the monomers dissolved in 95% ethanol are compiled in Table 3.

Figure 5 shows typical absorption spectra obtained on irradiating the monomer (II) at 360 nm (monochromatic light) for various irradiation times. The spectra obtained of the photochemically polymerizing crystals of monomer (II) are quite similar to those

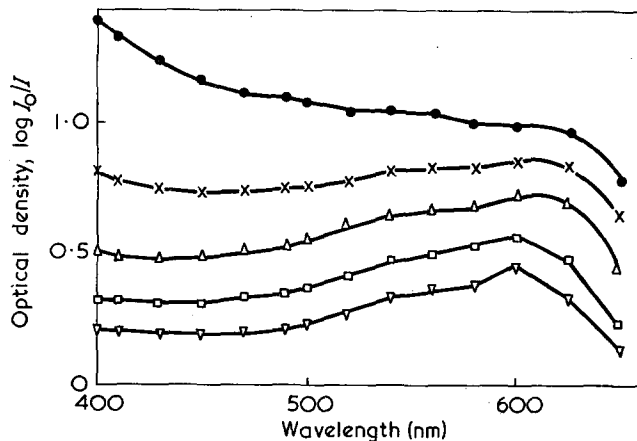


Figure 5 Spectra of polymerizing crystals of urethane (II) as depending on irradiation time. The crystals were irradiated with monochromatic light at 360 nm. ▽, 0; □, 1/4; △, 1; ×, 5; ●, 30 min

obtained from thermally polymerizing crystals. This indicates that the polymerization occurs through the same or similar intermediates. A quantitative analysis of the polymerization rate at wavelengths between 320 and 360 nm is quite complex, particularly because of the instability of the monomers. In each measurement we had to use fresh crystals. Consequently, thickness and size of the crystals were different from each other and so direct comparison of the effect of wavelength on the polymerization rate was impossible. A comparison of the photopolymerization of the urethane (II) and (VI) which differ only in the number of conjugated triple bonds is interesting, however. In the photopolymerization of (VI), at least two absorption maxima at 560 and 600 nm were obtained which have been attributed to two kinds of 'living' chain ends<sup>11</sup>. The relative intensity of these absorptions changed as a function of irradiation time and conversion. Generally speaking, these absorptions disappeared with increasing conversion and finally an absorption with broad maximum at 490 nm due to the 'dead' polymer was observed. During polymerization of the urethane (II) with three conjugated triple bonds per molecule no absorption maximum is observed in this region but optical density increases monotonously over the whole wavelength range starting from about 700 nm towards shorter wavelengths.

Contrary to the polymerization of (II), the change of absorption spectra of the monomer crystals of (I) (Figure 6) shows some similarities with the polymerization behaviour of diynes. The optical density in the range from 650 to 500 nm where the absorption due to the 'living' chain ends are to be expected, first increases very much at short irradiation times and then decreases with increasing conversion. It is, however, impossible to draw definite conclusions about the structure or behaviour of such intermediates as the above mentioned 'living' chain ends from the present study. But it seems to be a safe statement, based on the present results, to propose that both thermal and photochemical polymerization behaviour of triynes is not principally different from that reported for compounds with two conjugated triple bonds except that the range of photosensitivity is broader and that the upper limit for photopolymerization is shifted from 330 to 380 nm.

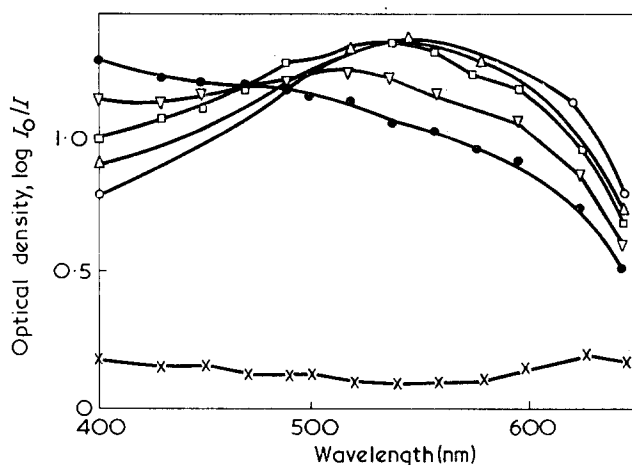


Figure 6 Spectra of polymerizing single crystal of diol (I) as depending on irradiation time. The crystals were irradiated with monochromatic light at 360 nm. x, 0; ○, 10; △, 15; □, 3; ▽, 10; ●, 25 min

#### ACKNOWLEDGEMENTS

We gratefully acknowledge the support of this work by the Alexander von Humboldt Foundation in the form of a fellowship grant to J. K. and the help of Dr K. Takeda in photochemical measurements.

#### REFERENCES

- 1 Wegner, G. *Makromol. Chem.* 1972, **154**, 35
- 2 Akiyama, S. and Nakagawa, M. *Bull. Chem. Soc. Japan* 1971, **44**, 2237, and refs cited therein
- 3 Bohlmann, F. *et al. Chem. Ber.* 1964, **97**, 794
- 4 Armitage, J. B. *et al. J. Chem. Soc.* 1952, p 2010
- 5 Cook, C. L. *et al. J. Chem. Soc.* 1952, p 2883
- 6 Vaugen, T. H., Vogt, V. R. and Newland, J. A. *J. Am. Chem. Soc.* 1934, **56**, 2120
- 7 Wegner, G. *Makromol. Chem.* 1971, **145**, 85
- 8 Wegner, G. *Z. Naturforsch.* 1969, **24b**, 824
- 9 Hädicke, E., Mez, E. C., Krauch, C. H., Wegner, G. and Kaiser, J. *Angew. Chem.* 1971, **83**, 253
- 10 Kaiser, J., Wegner, G. and Fischer, E. W. *Israel J. Chem.* 1972, **10**, 157
- 11 Takeda, K. and Wegner, G. *Makromol. Chem.* 1972, **160**, 349
- 12 Hay, A. S., Bolou, D. A., Leimer, K. R. and Clerk, R. F. *J. Polym. Sci. (B)* 1970, **8**, 97
- 13 Wegner, G. *Makromol. Chem.* 1970, **134**, 219
- 14 Hädicke, E., Penzien, K. and Schnell, W. *Angew. Chem.* 1971, **83**, 1024



# Aliphatic poly(amido acids) and polyimides with cyclobutane ring in the main chain

Fusae Nakanishi and Masaki Hasegawa

Research Institute for Polymers and Textiles, 4 Sawatari, Kanagawa-ku, Yokohama 221, Japan

and Hiroshi Takahashi

Fuji Photo Film Co. Ltd., Odawara, Japan

(Received 8 March 1973)

New aliphatic polyimides with cyclobutane ring in the main chain have been synthesized successfully from cyclobutane tetracarboxylic dianhydride and diamine. In order to establish the reaction path poly(amido acids), intermediates to polyimides, were isolated and characterized. All poly(amido acids) are hygroscopic and were found to be converted into polyimides through dicarboacetoxy intermediate by heating in dimethylformamide at 100°C in the presence of acetic anhydride. Thermal study by means of thermal gravimetric analysis and differential scanning calorimetry revealed that conversion of poly(amido acid) to polyimide also occurred by thermal cyclocondensation reaction at around 180°C. These reactions were confirmed by parallel reaction of the model compounds. Properties of polyimides thus obtained were characterized and are discussed in comparison with known polymers with polyimide or cyclobutane ring structures.

## INTRODUCTION

Only a few papers have reported work on polyimides derived from aliphatic tetracarboxylic dianhydride as a carboxylic anhydride component<sup>1-3</sup>, whereas polyimide resin prepared by the reaction of aromatic tetracarboxylic anhydride with diamines, is one of the best known heat stable polymers<sup>4</sup>. In literature studies on aliphatic polyimides, a well-defined structure of either the intermediate, poly(amido acid) or the resulting polyimide has never been demonstrated except in the case of polyimide from tricyclodecene tetracarboxylic dianhydride<sup>1</sup>. While in the last five years a number of polymers with cyclobutane ring in the main chain have been prepared through various preparative routes<sup>5-8</sup>, most of them involve a stepwise photocycloaddition reaction of bis-olefinic compounds and consequently result in a polymer with various types of steric configuration of cyclobutane ring in the main chain except in the case of crystalline state photopolymerization<sup>5</sup> where the polymer with a sole configuration of cyclobutane is obtained.

In the present work preparation and characterization of the intermediate [poly(amido acid)] to the polyimide, were undertaken in order to establish the reaction path during the preparation of polyimide and to reveal real features of aliphatic polyimides unambiguously. Then, the poly(amido acid) was converted into the corresponding polyimide by means of a convenient thermal cyclocondensation reaction. Since another purpose of the present work is to learn more about the properties of the polymer with cyclobutane ring in the main chain, tetracarboxylic dianhydrides of *cis*, *trans*, *cis*-cyclobutane

or citraconic acid dimer were employed as an acid anhydride component for the polyimide. These new polymers thus obtained were characterized and are discussed in terms of comparison to known poly(amido acids), polyimides or polymers with cyclobutane ring in the main chain.

## EXPERIMENTAL

### *Reaction of cis, trans, cis-cyclobutane-1,2,3,4-tetracarboxylic dianhydride (I) with diamines*

According to Schenk's method<sup>9</sup>, (I) was prepared by irradiating a solution of maleic anhydride in dioxane with a high pressure mercury lamp [m.p. 300°C (decomp.)]. 1.468 g (0.0075 mol) of (I), which was recrystallized twice from acetic anhydride, was dissolved into 20 ml of carefully dried dimethylformamide (DMF). To this solution, 0.870 g (0.0075 mol) of hexamethylene diamine in 20 ml of DMF was added dropwise with stirring. The reaction temperature was kept between 15 and 16°C. Then, the solution was stirred overnight at room temperature. The solution was poured into a large amount of ether and a colourless polymer (II) was precipitated {[ $\eta$ ] 0.37-0.49 (in DMF at 30°C)}. Almost the same method was employed for the reaction of (I) with other diamines, nonamethylene diamine or *p,p'*-diaminodiphenylmethane in order to obtain linear high poly(amido acids) (III and IV). Poly(amido acids) (II-IV) thus obtained are very hygroscopic, especially when they include the solvent, and are apt to be tar-like during the separation process in the atmosphere.

Moisture regain of these polymers was determined from the difference in weight when they are dried in a desiccator with phosphorus pentoxide at room temperature and when they are kept for a satisfactory period in 65% relative humidity. Then, to 0.50 g of poly(amido acid) (II) dissolved in 30 ml of DMF, 20 ml of acetic anhydride were added and stirred for 1 h at 100°C. A white product was partly precipitated during the reaction. The reaction mixture was poured into the large amount of ether in that condition and faintly yellow polyimide (II') was isolated.

According to a similar procedure, other polyimides (III' and IV') were obtained from the poly(amido acids) (III and IV), respectively. Among these polyimides (II'-IV'), only the polyimide (III') was soluble in trifluoroacetic acid  $\{[\eta]=0.57$  (trifluoroacetic acid, 30°C)}. Calcd. for polyimide (II',  $C_{14}H_{16}N_2O_4$ ), %: C, 60.86; H, 5.84; N, 10.14. Found, %: C, 56.52; H, 5.85; N, 8.52. Calcd. for polyimide (III',  $C_{17}H_{22}N_2O_4$ ), %: C, 64.14; H, 6.97; N, 8.80. Found, %: C, 60.70; H, 6.66; N, 8.86. Calcd. for polyimide (IV',  $C_{21}H_{14}N_2O_4$ ), %: C, 70.39; H, 3.94; N, 7.82. Found, %: C, 69.13; H, 3.99; N, 7.16.

#### Reaction of *cis*, *trans*, *cis*-1,3-dimethyl-cyclobutane-1,2,3,4-tetracarboxylic dianhydride (V) with diamines

According to Schenk's method<sup>9</sup>, (V) was prepared by irradiating a solution of citraconic anhydride in dioxane with a high pressure mercury lamp [m.p. 350°C (decomp.)]. Since (V) is insoluble in DMF, mixing of the two reactants was carried out in such two ways that to a suspension of (V) in DMF, a DMF solution of hexamethylene diamine was added, or a finely powdered crystal of (V) was added to a DMF solution of hexamethylene diamine. Higher molecular weight poly(amido acid) was obtained by the latter procedure. After mixing, the reaction mixture was kept at 15–16°C and stirred overnight. Dilute hydrochloric acid was used for reprecipitation of the polymer from the reaction mixture. For the measurement of moisture regain the same method was adopted as described before. For the conversion from polyamido acids to polyimides (VI, VII and VIII→VI', VII' and VIII'), almost the same experimental conditions were adopted as described before (II→II'). However, in the present case no precipitant was observed during the polymerization reaction. Polyimides were precipitated by adding a large amount of dilute hydrochloric acid to the reaction mixture.

#### Preparation of model compounds, *cis*, *trans*, *cis*-cyclobutanetetracarboxylic acid di-*n*-butyl amide (IX) and the same diimide (X)

To a solution of *n*-butyl amine, 0.804 g (0.011 mol) in 10 ml of DMF, 1.066 g (0.0054 mol) of finely powdered (I) was added. After standing for 1 h, DMF was distilled off under reduced pressure and the residue was recrystallized from ethanol. Colourless plate-like crystals (m.p. 263–265°C) were obtained, yield 1.312 g (77.0%).

Infra-red (i.r.) spectra show peaks at 3300 ( $\nu_{NH}$ ), 1690 (amide I), 1640 (amide II), and 1700 ( $\nu_{C=O}$  carboxyl)  $cm^{-1}$ . Calcd. for (IX) ( $C_{16}H_{26}N_2O_6$ ), %: C, 56.13; H, 7.07; N, 8.18. Found, %: C, 56.47; H, 7.94; N, 8.04. From the results the product is confirmed to be the expected diacid diamide (IX).

Furthermore, when 0.50 g of (IX) was heated in 20 ml of acetic anhydride at 100°C for 1 h and allowed to stand at room temperature, a small amount of transparent plate-like product was crystallized, m.p. 300°C (decomp.). From the i.r. spectrum of the product, the peaks at 1770 and 1700  $cm^{-1}$  which are assigned to the five-membered imide ring, are seen. Calcd. for (X) ( $C_{16}H_{22}N_2O_4$ ), %: C, 62.80; H, 7.24; N, 9.09. Found, %: C, 62.15; H, 7.27; N, 9.11. From the results the structure of the product is confirmed to be the imide compound (X) from (IX).

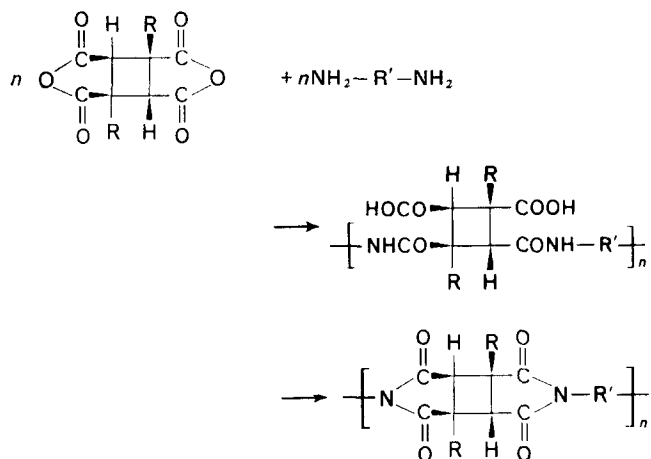
#### D.s.c. and t.g.a. measurement of amido acid and imide

Differential scanning calorimetry (d.s.c.) measurements were carried out with a Perkin-Elmer DSC 1B, at a heating rate of 32°C/min. Thermogravimetry curves were obtained by a duPont thermogravimetric analyser (t.g.a.) Type 950, at a heating rate of 10°C/min (nitrogen current speed, 250 ml/min).

## RESULTS AND DISCUSSION

### Preparation and properties of the polymers

The polymerization reaction is shown below:



where R represents H or  $CH_3$  and R' represents  $-(CH_2)_6-$ ,  $-(CH_2)_9-$  or 1,4- $C_6H_4-CH_2-1,4-C_6H_4$ , respectively. The structure of the intermediate, poly(amido acid), is shown tentatively. This will be the case hereafter. The *trans*-configuration of two five-membered carboxylic anhydride rings attached to the cyclobutane ring of (I) has been already established in the literature. On the other hand, the configuration of (V), which had been prepared by Schenk *et al.*<sup>9</sup>, was revised by Ziffer *et al.*<sup>10</sup>, to be a head-to-tail *trans*-configuration by identification of its derivative the structure of which was established by X-ray crystallographic analysis.

Accordingly, all the imides prepared in the present work ought to have only a *trans*-configuration attached to the cyclobutane ring. Similar polyimides had been prepared by means of a solution photopolymerization technique of bis-maleimide derivatives by de Schryver *et al.*<sup>6</sup>. These polyimides should be assumed to consist of various types of configuration attached to the cyclobutane ring. Furthermore, vinyl-type polymerization or intramolecular cyclization, which disturb the formation of a linear high polymer in good yield, cannot be suppressed satisfactorily in some instances.

In Figure 1 i.r. spectra of the polymers (II) and (II') and the corresponding model compounds (IX) and (X)

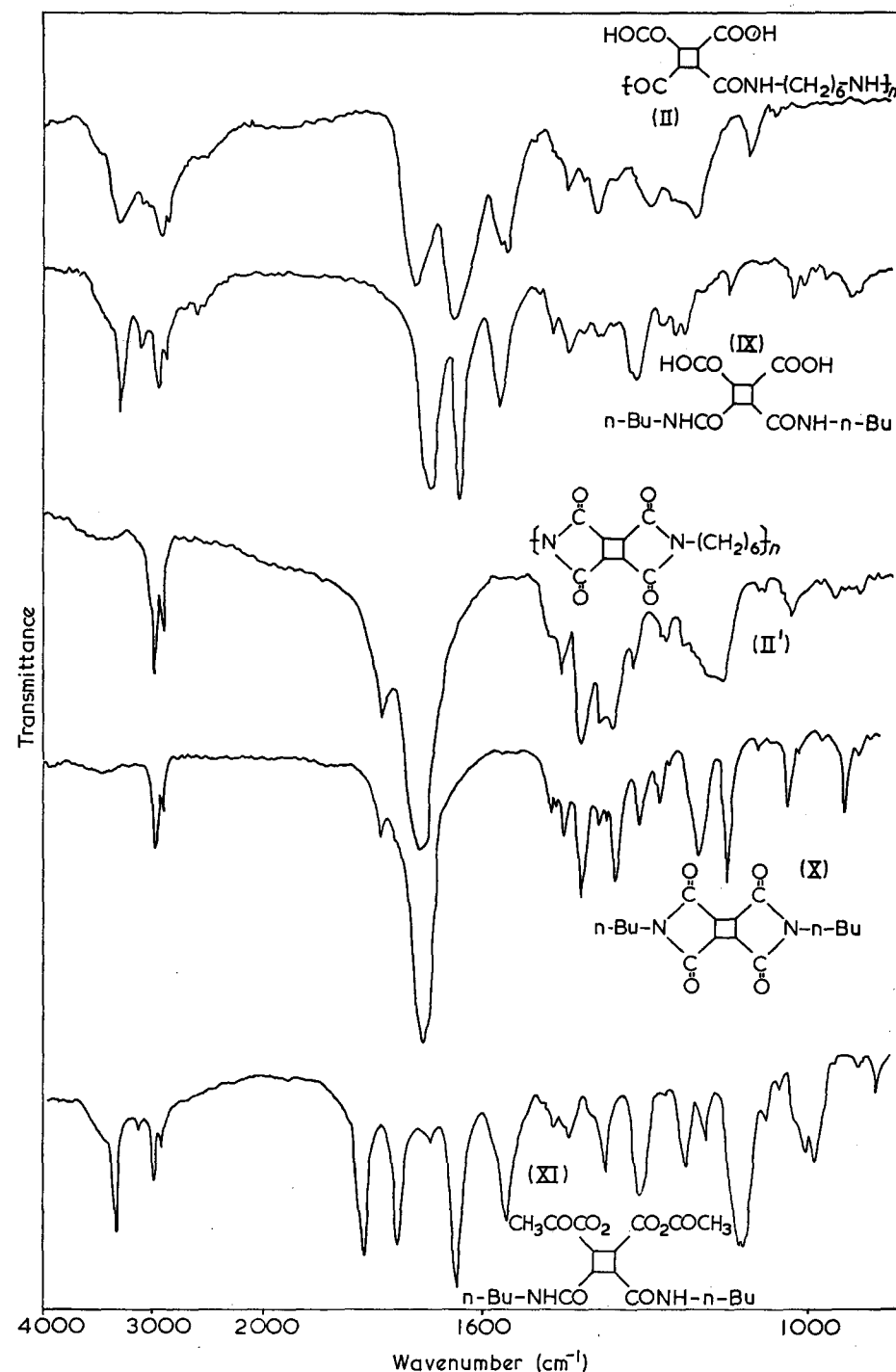


Figure 1 I.r. spectra of poly(amido acid), polyimide and the model compounds

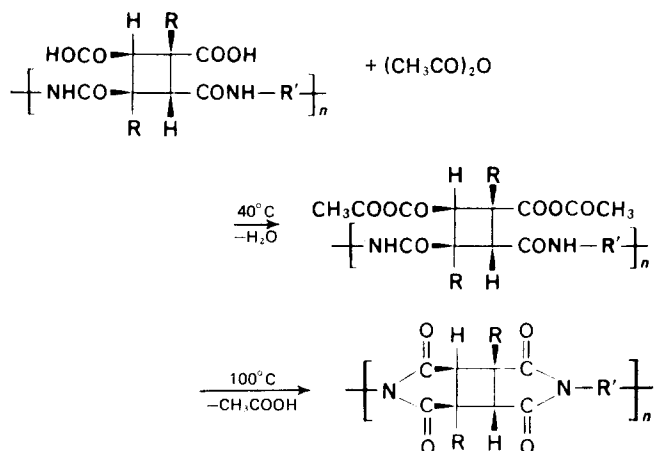
are shown. Another spectrum of the compound (XI), which was obtained by warming (IX) in acetic anhydride at 40°C for 40 min, is also shown in Figure 1. The spectra of poly(amido acid) (II) and polyimide (II') agree with those of the model compounds (IX) and (X) at all the main peaks, showing that the repeating units in the polymers have essentially the same structure as those of the corresponding model compounds.

For the compound (XI), the peaks due to residual amide group at 3300, 1640 and 1550  $\text{cm}^{-1}$  are seen with the peaks at 1815 and 1750  $\text{cm}^{-1}$ , not due to five-membered anhydride ring, but due to the ring-opened anhydride. In addition, the peak at 1700  $\text{cm}^{-1}$  due to the carboxyl group ( $\nu_{\text{C=O}}$ ) disappears.

Hence, compound (XI) can be considered to be

cyclobutane dicarboacetoxy di-n-butyl amide. Assumed structure is further supported by the fact that on heating in acetic anhydride at 100°C for 1 h, (XI) was converted into (X) in good yield. On the other hand, when (IX) was heated at 100°C in DMF solution for 1 h, cyclization to the imide ring did not proceed but only the starting material was recovered. When poly(amido acid) (II) was kept in DMF solution with some acetic anhydride at room temperature for a week, a soluble polymer the i.r. peaks of which correspond to the structure of the polymer with amide, imide and acetic anhydride was isolated. This polymer was also converted into the polyimide under the imide formation condition. From these results, the following reaction scheme is assumed to be the reaction path from amido acid to imide in the

presence of acetic anhydride:



i.e. the poly(amido acid) is not converted to the imide in DMF solution below  $100^\circ\text{C}$  in the absence of acetic anhydride. However, in the presence of acetic anhydride it is gradually converted to the imide through the acetylated intermediate even at  $40\text{--}100^\circ\text{C}$ . Results of elemental analysis of the poly(amido acids) do not show always good agreement with the calculated values. The facts are explained by assuming the imperfect repeating structure in poly(amido acid) that can be caused in the presence of a polar carboxylic group or to the partial formation of imide group by dehydrating cyclization during the desiccation.

Thus, compared with the elemental analysis of poly(amido acid), much better agreements are seen with

those of polyimides even from the deviated poly(amido acid) except in the case of polyimide (II').

The intrinsic viscosities and moisture regains of poly(amido acids) (II–IV, VI–VIII) are shown in Table 1. Poly(amido acids) are highly hygroscopic and soluble in ordinary polymer solvents such as *m*-cresol, DMF, dimethyl sulphoxide and trifluoroacetic acid.

A transparent strong film is obtained by casting a solution of poly(amido acid) and drying at  $40^\circ\text{C}$  *in vacuo*.

#### Thermal behaviour of poly(amido acid) and polyimide

D.s.c. curves of poly(amido acid) (II) and the model compound (IX) are shown in Figure 2. (IX) shows an endothermic peak at  $260^\circ\text{C}$  corresponding to the melting point that was followed by an exothermic peak. The exothermic peak is doubtlessly attributed to the imide ring formation with elimination of water. This was further confirmed from a thermal gravimetric analysis (t.g.a.) study which is described later. For the polymer (II) smaller endo- and exo-thermic peaks are observed nearly at the same temperature.

Above  $300^\circ\text{C}$  both curves of (II) and (IX) deviate to the endothermic side suggesting thermal degradation. Furthermore, these d.s.c. curves above the temperature of imide ring formation exactly agree with those of the imide compounds (II' and X). From the results of the d.s.c. study, the amido acid, independently of its molecular weight, seems to cyclize to the imide at around  $260^\circ\text{C}$  under the experimental conditions carried out.

A t.g.a. study was carried out in order to recognize the dehydrating ring formation of poly(amido acids)

Table 1 Intrinsic viscosities and moisture regains of poly(amido acids)

	Poly(amido acid)	Intrinsic viscosity	Moisture regain (%)
II		0.49	9.9
III		0.61	11.9
IV		0.40	12.4
VI		0.53	9.7
VII		0.21	9.9
VIII		0.42	10.6

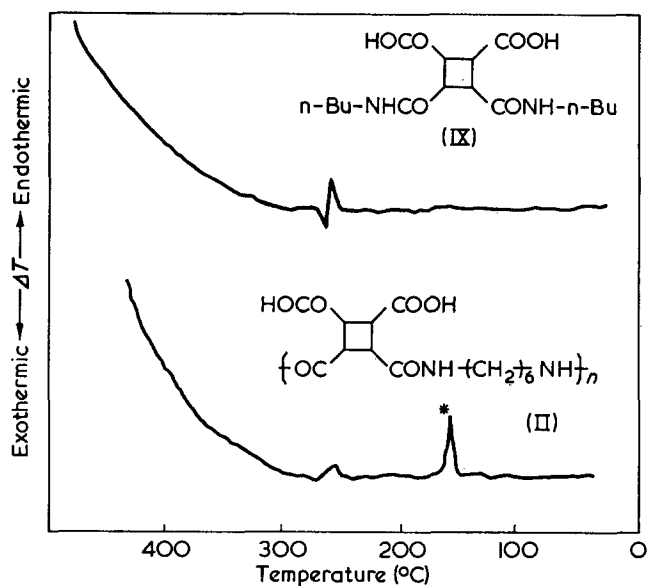


Figure 2 D.s.c. curves of poly(amido acid) and its model compound

\* This peak is due to the vaporization of DMF included in the polymer

Table 2 Thermal behaviour of poly(amido acids)

Poly(amido acid)	Ring formation temperature (°C)	Amount of eliminated water		Starting temperature of degradation accompanied by weight reduction (°C)
		Calcd. (%)	Found (%)	
II	160	11.5	12	440
IV	200	9.1	8.5	400
VI	175	10.6	9.5	410
VIII	200	8.5	8.5	400

(II, IV, VI and VIII) and thermal degradative behaviours of the resulting polyimides (II', IV', VI' and VIII'). The ring formation temperature, the amount of eliminated water, and the starting temperature of the degradation accompanied by weight reduction, are shown in Table 2.

Compared with the ring formation temperature obtained from d.s.c. curves, the weight reduction, which is attributed to the dehydrating ring formation reaction, is observed at considerably lower temperatures. This discrepancy can be understood in terms of difference of the heating rates at these two thermal measurements (10°C/min for t.g.a. and 32°C/min for d.s.c.). If this is the case, the temperature obtained from t.g.a. may be

the true value of the ring formation temperature. The observed amount of eliminated water shows good agreement with the calculated values for the conversion of the amido acid into the corresponding imide. With the known data on degradation temperature, it is concluded from the present thermal study that thermal cleavage of cyclobutane ring or crosslinking of the imide ring in the polymer chain are initiated above 300°C (based on d.s.c. data), and above nearly 400°C relatively low molecular weight fragments produced by degradation, begin to vaporize (based on t.g.a. data).

## CONCLUSIONS

Aliphatic polyimides with cyclobutane ring in the main chain were synthesized from *cis, trans, cis*-cyclobutane-1,2,3,4-tetracarboxylic dianhydride or *cis, trans, cis*-1,3-dimethylcyclobutane-1,2,3,4-tetracarboxylic dianhydride with hexamethylene diamine, nonamethylene diamine or *p, p'*-diaminodiphenylmethane. In order to establish the reaction path to polyimide, precursors, poly(amido acids), were isolated and characterized. They are hydroscopic and were converted into polyimides through dicarboacetoxy intermediate by heating in DMF at 100°C in the presence of acetic anhydride. Without acetic anhydride, the reaction did not proceed under the same conditions. Poly(amido acids) were also converted into polyimides by a thermal cyclocondensation reaction at around 180°C. The resulting polyimides begin to degrade above 300°C from the results of t.g.a. and d.s.c. studies.

## ACKNOWLEDGEMENTS

The authors express their thanks to Mr Yoshiro Okino and Mr Yoshimasa Suzuki for assistance in the performance of the experimental work.

## REFERENCES

- 1 Tabuse, I., Tanimura, N. and Oda, R. *Kogyo Kagaku Zasshi* 1964, **67**, 1084
- 2 Asakura, S. and Fukui, M. *ibid.* 1967, **70**, 2388
- 3 Asakura, S. and Fukui, M. *ibid.* 1968, **71**, 918
- 4 E. I. duPont, Br. Pat. 903 272 (1962)
- 5 Hasegawa, M., Suzuki, Y., Suzuki, F. and Nakanishi, H. *J. Polym. Sci. (A-1)* 1969, **7**, 743
- 6 de Schryver, F. C., Feast, W. J. and Smets, G. *J. Polym. Sci. (A-1)* 1970, **8**, 1939
- 7 Hall, H. K., Jr. *et al. J. Am. Chem. Soc.* 1971, **93**, 110
- 8 Takahashi, H., Sakuragi, M., Hasegawa, M. and Takahashi, H. *J. Polym. Sci. (A-1)* 1972, **10**, 1399
- 9 Schenk, G. O. *et al. Chem. Ber.* 1962, **95**, 1642
- 10 Ziffer, H. and Williams, J. R. *J. Org. Chem.* 1968, **33**, 920

# Electrical conductivity in poly(vinyl chloride)

Paolo Parrini

Montedison SpA, Centro Ricerche Ferrara, 44100 Ferrara, Italy  
(Received 19 March 1973)

An interpretation by mathematical theory of experimental data already published by the author is given, concerning the electrical conductivity measurement, in direct current, of PVC and plasticizer compositions. The electrical conduction in PVC is due to two mechanisms: one of polarization, which predominates at low temperature, below a transition temperature  $T_0$  and one of ionic conduction which predominates at high temperature above  $T_0$ . The mathematical expressions for polarization conductivity  $k_p$  and ionic conductivity  $k_0$ , agree very well with the experimental data and justify also the great difference in activation energy between the two mechanisms and the independence of activation energy of ionic conductivity from the system viscosity and type of ions.

## INTRODUCTION

The electrical properties of high polymers, as regards both the dependence of the dielectric constant and the loss factor on the temperature and frequency, and the electrical conductivity in direct current and its dependence on the temperature and other factors, have been the subject of a great number of papers. References 1 and 2 form a review of these subjects.

One of the materials most studied is plasticized poly(vinyl chloride), whose behaviour in direct current has been fully studied<sup>3-7</sup>. It has thus been established that in certain temperature and composition conditions the current through the PVC-plasticizer system takes a certain time, which is sometimes very long, to reach a constant value; this value also depends on the temperature and composition<sup>6, 7</sup>.

Both the current during the transition period and the steady-state current are proportional to the added field, at least in the case of moderately intense fields<sup>6</sup>; the ratio between the current density and the applied field which then has the significance of an electrical conductivity  $K$  is given by the sum of two terms:

$$K = k_0(T, C) + k_p(T, C, t)$$

where:  $k_0$  is the steady-state conductivity, a function of the temperature ( $T$ ) and of the percentage of plasticizer ( $C$ );

$k_p$  is the conductivity in the transition period (of polarization) which is found to be a decreasing function of the time  $t$ , tending to zero when the time tends to infinity, as well as of the temperature and of the percentage of plasticizer<sup>6</sup>.

The conductivity  $k_0$  does not depend on time and is essentially ionic in nature, as was demonstrated by indirect tests; it varies with the percentage of hydrochloric acid present in the PVC-plasticizer system<sup>6\*</sup> and

\* As is well known, during the thermal stresses accompanying the processing of PVC either pure or plasticized, a decomposition process occurs with formation of hydrochloric acid. The ions produced following partial dissociation of the latter into  $H^+$  and  $Cl^-$  are among those responsible for the steady-state conductivity.

with the type of stabilizer used<sup>7</sup>.

With regard to this, reference is made to the dependence of the logarithm of conductivity  $K$ , measured experimentally, versus the inverse of the absolute temperature  $1/T$ , in Figures 1 and 2<sup>6, 7</sup>. Figure 1 clearly shows that beyond a certain temperature the conductivity is not a function of the time of application of the voltage

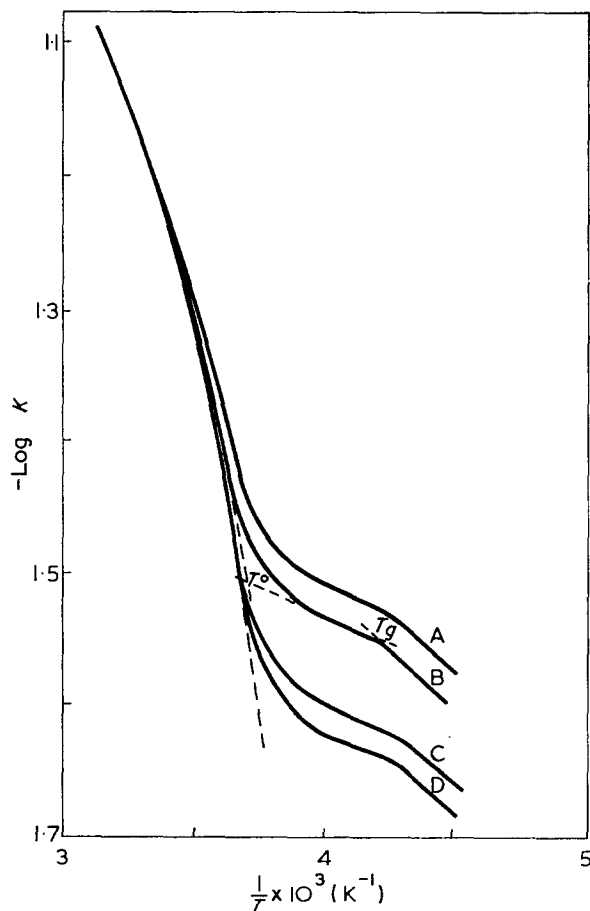


Figure 1 Logarithm of conductivity  $K$  versus inverse of the absolute temperature for several times of application of the voltage: A, 0.5 min; B, 1 min; C, 5 min; D, 10 min. PVC/DOP ratio=100:50

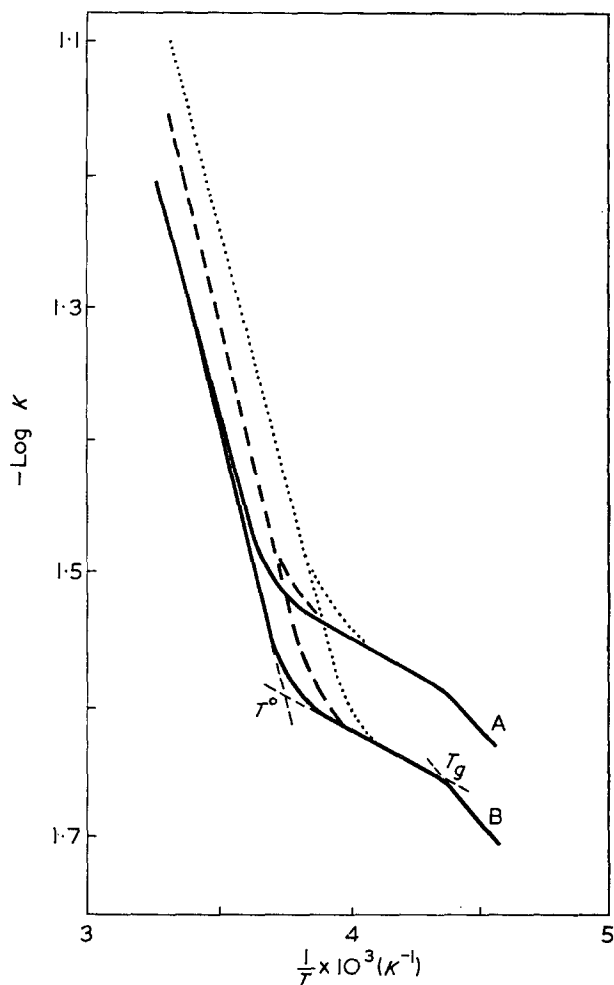


Figure 2 Logarithm of conductivity  $K$  versus the inverse of the absolute temperature for several concentrations of HCl in the sample and therefore of ions: —, 70mg HCl/100g; ---- 120mg HCl/100g; ·····, 180mg HCl/100g. A, 1min; B, 10min. PVC/DOP ratio=100:50

to the sample. Figure 2 illustrates quite clearly that there is a component of the conductivity which is not influenced by the presence of a larger number of ions but is, instead, a function of the time (as well as of the composition and temperature).

This component of conductivity has been called 'polarization conductivity',  $k_p$  and is independent of the type and number of the ions present<sup>6,7</sup> but is due instead, to the movement of the various dipoles forming in the system under the action of the electric field, from the initial isotropic distribution to the steady-state distribution<sup>6</sup>. In fact, it falls with increase of time and with increased viscosity of the system (i.e. when either the temperature or the percentage of plasticizer drops) and tends to zero when the dipolar orientation process ends.

The conductivity  $k_p$  may be obtained from the complex dielectric constant at various frequencies and temperatures<sup>8</sup> on the basis of the following equations where  $H(\ln\tau)$  represents the spectrum of the times of electrical relaxation:

$$k_p = \frac{1}{4} \int_{-\infty}^{+\infty} \frac{1}{\tau} H(\ln\tau) \exp(-t/\tau) d(\ln\tau)$$

$$\epsilon' = \epsilon_0 + \int_{-\infty}^{+\infty} \frac{H(\ln\tau) d(\ln\tau)}{1 + \omega^2 \tau^2}$$

$$\epsilon'' = \frac{4\pi k_0}{\omega} + \int_{-\infty}^{+\infty} \frac{H(\ln\tau) \omega \tau d(\ln\tau)}{1 + \omega^2 \tau^2}$$

where  $\omega$  is the angular frequency,  $\epsilon_0$  is the dielectric constant at infinite frequency,  $\tau$  the time of electrical relaxation and  $t$  the time of application of the voltage to the sample. On the basis of Maxwell's equations, we have demonstrated<sup>6</sup>, as further confirmation of the polar origin of part of the conductivity, that there is excellent agreement between the experimental values of  $k_p$  and those obtained from the above equations.

A comparison between conductivity in direct current and loss factor for plasticized PVC has been made also by Reddish<sup>9</sup> on the basis of previous work by Hamon<sup>10</sup>.

As for the dependence of the conductivity on the temperature, a detailed study<sup>6</sup> is reported regarding the PVC/2-ethylhexyl phthalate (DOP) (100:50) system, which is also shown in Figure 1. This shows three distinct regions characterized by different values of the apparent activation energy  $d \ln K / d(1/T)$  delimited by two singular temperatures  $T^\circ$  and  $T_g$ .

In the first zone, the contribution is essentially ionic ( $T > T^\circ$ ) and in the other two it is essentially dipolar ( $T < T^\circ$ ) but with different energies of activation according to whether we are above or below  $T_g$ . This latter temperature is simply the glass transition temperature of the system and has been checked also by dilatometric measurements<sup>6</sup>. The increase in the activation energy when the temperature falls below  $T_g$  is demonstrated by the data on systems with different plasticizer content, as is clearly shown by the curves of Figure 3<sup>7</sup>. The same Figure also shows that the apparent activation energy for ionic conductivity (for  $T > T^\circ$ ) does not depend in practice on the percentage of plasticizer or the presence of other ingredients<sup>7</sup>.

As for the dependence of the polarization conductivity on time, the data reported in refs. 6 and 8 show excellent

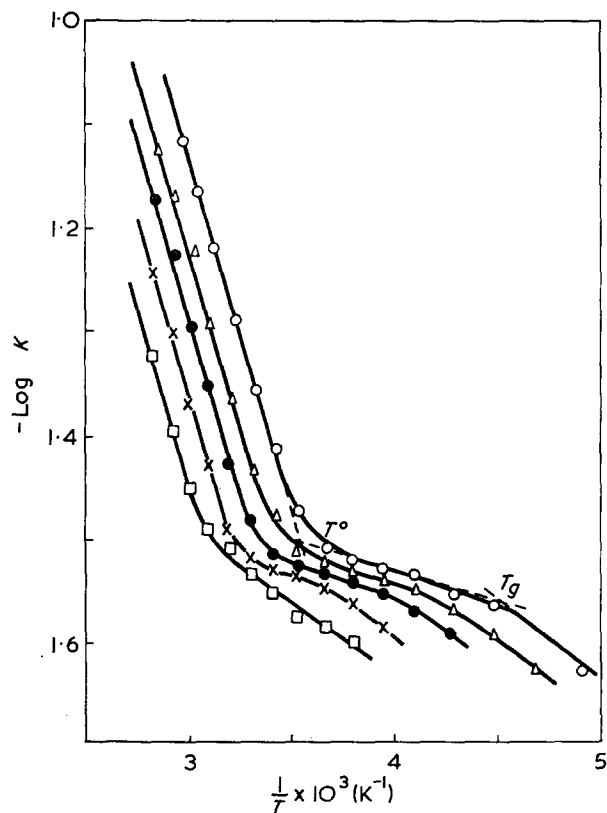


Figure 3 Logarithm of conductivity  $K$  versus the inverse of absolute temperature for several system compositions: ○, 100:60; △, 100:50; ●, 100:40; ×, 100:30; □, 100:20 PVC/DOP

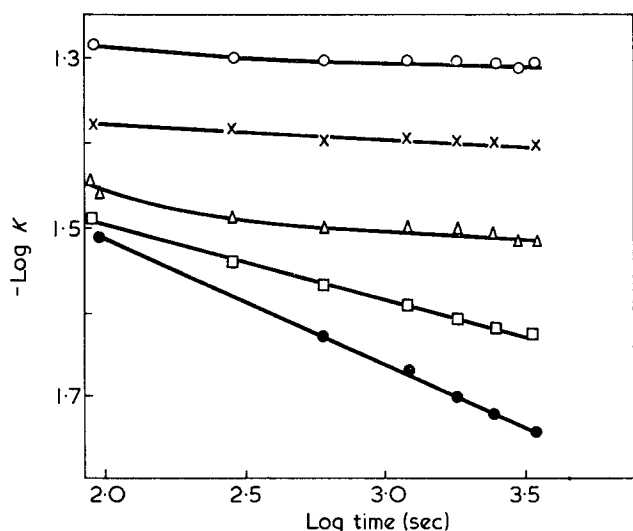


Figure 4 Logarithm of conductivity  $K$  versus logarithm of time for several temperatures<sup>6</sup>.  $\circ$ , 20°C;  $\times$ , 10°C;  $\triangle$ , 0°C;  $\square$ , -10°C;  $\bullet$ , -20°C

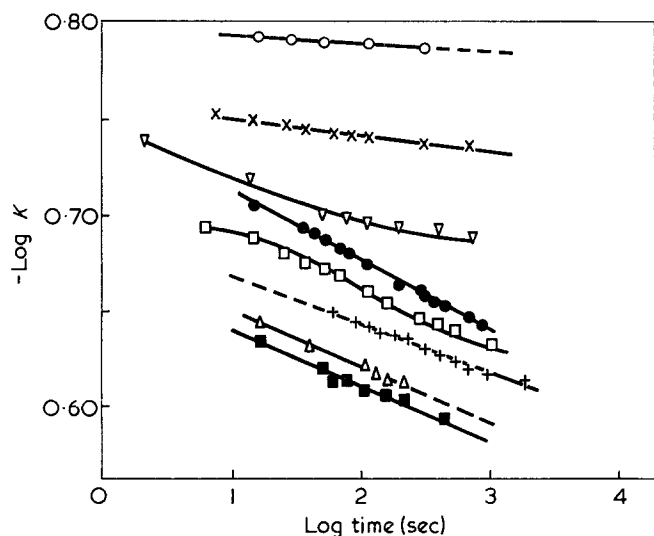


Figure 5 Logarithm of conductivity  $K$  versus logarithm of time for several temperatures<sup>9</sup>.  $\circ$ , 100°C;  $\times$ , 90°C;  $\nabla$ , 80°C;  $\bullet$ , 69°C;  $\square$ , 60°C;  $+$ , 51°C;  $\triangle$ , 30°C;  $\blacksquare$ , 20.8°C

approximation that it is proportional to  $t^{-n}$  (with  $n$  positive); Figure 4 gives the  $\log k_p$  against  $\log t$  plots for the PVC/DOP (100:50) system using the experimental data of ref. 6, while Figure 5 gives similar plots for the PVC/DOP (100:5) system taken from the experimental data reported in ref. 9.

This work has the purpose of demonstrating mathematically the lay-out given in the previous articles and obtaining expressions for ionic and polarization conductivity besides justifying on this basis both the great difference in their activation energies and the independence of the activation energy of the ionic component on the percentage of plasticizer and the type of ions present.

## EXPERIMENTAL AND RESULTS

For a complete description of the experimental method used, the reader is referred to the earlier papers<sup>6,7</sup>. We wish to mention here that the PVC consisted of a commercial polymer polymerized in suspension and of the type for electrical purposes: Montecatini-Edison's

Vipla KE. This polymer was transformed into calibrated cables with copper cores which were then used for electrical conductivity measurements with a Jhare Teraohmmeter, by the direct method. Mercury was used as the contact liquid for the outer surface of the cable. The measurement of temperature from  $-60^\circ\text{C}$  to  $+50^\circ\text{C}$  was accurate to  $\pm 1^\circ\text{C}$ . Measurement voltages ranged from 250 to 1000 V.

The percentage of plasticizer was determined analytically on the sample subjected to measurement. Both the plasticizer and the outer ingredients (stabilizers and fillers) were of analytical grade. To increase the percentage of hydrochloric acid present in the cable, the plasticizer DOP was saturated with gaseous HCl; the quantity of HCl present was determined analytically on the cable before performing the measurements.

### Polarization conductivity

As already stated, the movement of dipoles under the action of the electrical field applied to the system produces a current; we now propose to obtain an expression of this magnitude.

Let us first consider the case of a system consisting of  $n_0$  dipoles per unit volume of moment  $\mu$  all being equal. The number of dipoles per unit volume which at time  $t$  form with the direction of the effective field  $F_e^+$  an angle falling between  $\theta$  and  $\theta+d\theta$  are indicated by  $2\pi f(\theta, t)\sin\theta d\theta$ ; the function  $f(\theta, t)$  satisfies the following<sup>11</sup>:

$$\zeta \frac{\partial f}{\partial t} = \frac{1}{\sin\theta} \frac{\partial}{\partial \theta} \left[ \sin\theta \left( kT \frac{\partial f}{\partial \theta} + \mu F_e^+ \sin\theta \cdot f \right) \right] \quad (1)$$

where  $k$  is Boltzmann's constant,  $T$  the absolute temperature and  $\zeta$  a constant (with regard to  $\theta$  and  $t$ ) proportional to the viscosity and linked to the resistance which the dipoles encounter in their movement. In the hypothesis that  $\mu F_e^+ / kT \ll 1$ , as is the case here, a solution of equation (1) which satisfies the following three conditions:

$$f(\theta, 0) = n_0/4\pi \quad (2)$$

$$\lim_{t \rightarrow \infty} f(\theta, t) = (n_0/4\pi) [1 + (\mu F_e^+ / kT) \cos\theta] \quad (3)$$

$$2\pi \int_0^\pi f(\theta, t) \sin\theta d\theta = n_0 \quad (4)$$

is the following:

$$f(\theta, t) = (n_0/4\pi) [1 + (\mu F_e^+ / kT) \cos\theta (1 - \exp(-t/\tau))] \quad (5)$$

where  $\tau = \zeta/2kT$  (delay time). The physical significance of conditions (2), (3) and (4) is clear; (2) indicates that at the moment of application of the field the distribution of the dipoles is isotropic; (3) shows that once the steady-state distribution has been reached (i.e., after infinite time) the distribution function must be that envisaged by the Maxwell-Boltzmann theory in the case where  $\mu F_e^0 / kT \ll 1$ ; and (4) indicates that the number of dipoles per unit volume is independent of time.

Having fixed a general surface  $S$  normal to the field (Figure 6) we calculate the charge which crosses this surface in unit time.

If the length of the dipole of moment  $\mu$  is  $2l$  (so that charge  $e$  is equal to  $\mu/2l$ ) it is clear that the only dipoles

† The effective field  $F_e^+$  acting on the dipoles will be a function of the time tending to the limiting value  $F_e^0$ . We shall deal later with the relation between  $F_e^0$  and the macroscopic field  $E$ .



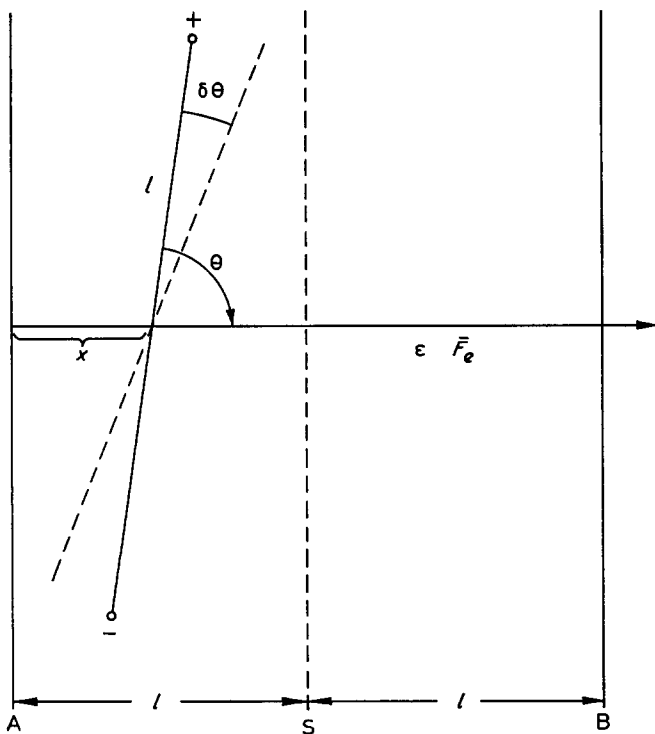


Figure 6 Scheme of movement of dipoles in an electrical field

which can cross section S are found in the volume bordered by planes A and B. Let us consider a dipole with its centre at a distance  $x$  from plane A; in time  $\delta t$  it will form an angle  $\delta\theta$  and will cross section S if the angle  $\theta$  which it forms at time  $t$  is linked to  $x$  by the relation  $l \cos\theta = l - x$ . Thus, presuming that the positive charge which crosses, left to right in time  $\delta t$ , unit surface of the section S, due to the dipoles present in the volume between A and S, is given by:

$$\begin{aligned} \delta q' &= \delta t \cdot \epsilon \int_0^l 2\pi f(\theta, t) \sin\theta \frac{\delta\theta}{\delta t} \cdot dx \\ &= \delta t \mu \pi \int_0^{\pi/2} f(\theta, t) \sin^2\theta \frac{\delta\theta}{\delta t} d\theta \end{aligned}$$

the contribution of the dipoles present in the volume between S and B is, as can be checked immediately:

$$\delta q'' = \delta t \mu \pi \int_{\pi/2}^{\pi} f(\theta, t) \sin^2\theta \frac{\delta\theta}{\delta t} d\theta$$

While bearing in mind the contribution due to the negative charge which crosses S from right to left, we shall have, finally for the charge crossing the unit surface S in time  $\delta t$  the expression:

$$\delta q = \delta t 2\mu \pi \int_0^{\pi} f(\theta, t) \sin^2\theta \frac{\delta\theta}{\delta t} d\theta \quad (6)$$

To calculate  $\delta\theta/\delta t$ , the relation:

$$f(\theta + \delta\theta, t + \delta t) = f(\theta, t)$$

must hold true, as the dipoles which at time  $t$  form an angle  $\theta$  with the direction of the field, at time  $t + \delta t$  form an angle  $\theta + \delta\theta$ . Thus:

$$\frac{\delta\theta}{\delta t} = - \frac{(\partial f/\partial t)_\theta}{(\partial f/\partial \theta)_t} = \frac{1}{\tan\theta} \frac{1}{\tau} \frac{\exp(-t/\tau)}{1 - \exp(-t/\tau)} \quad (7)$$

Introducing (7) into (6) and remembering that  $\delta q/\delta t = j_p$  (current density) we have:

$$j_p = \frac{n_0 \mu^2 \exp(-t/\tau)}{3kT} \cdot F_e^0 \quad (8)$$

In order to express (8) as a function of the macroscopic field  $E$  instead of the effective field  $F_e^0$ , the following procedure can be followed.

The polarizability (i.e. the average electrical moment of the unit volume<sup>11</sup>) can be calculated from (5) and from this the dielectric constant. It is easy to obtain:

$$\epsilon = \epsilon_0 + (4\pi n_0 \mu^2 / 3kT) (1 - \exp(-t/\tau)) F_e^0 / E \quad (9)$$

where  $\epsilon_0$  is the square of the refractive index (equal to the dielectric constant at time  $t=0$ , before movement of the dipoles starts).

The static dielectric constant is given by:

$$\epsilon^* = \epsilon_0 + (4\pi n_0 \mu^2 / 3kT) (F_e^0 / E) \quad (10)$$

If (10) is combined with Onsager's relation<sup>12</sup> (already used by Fuoss and Kirkwood<sup>13</sup> when considering the electrical properties of plasticized PVC):

$$(\epsilon^* - \epsilon_0)(2\epsilon^* + \epsilon_0) / \epsilon^*(\epsilon_0 + 2)^2 = 4\pi n_0 \mu^2 / kT$$

from which we obtain:

$$F_e^0 / E = (\epsilon_0 + 2)^2 \alpha / 3 \pm (1/4\alpha) \{ [\epsilon_0 + (\epsilon_0 + 2)^2 \alpha / 3]^2 + 8\epsilon_0^2 \}^{1/2} \quad (11)$$

where

$$\alpha = 4\pi n_0 \mu^2 / 3kT$$

It may be observed that  $F_e^0/E$  varies between  $(\epsilon_0 + 2)^2/9$  and  $(\epsilon_0 + 2)^2/6$  with variation of  $\alpha$  from zero to infinity. Therefore it is possible to have  $F_e^0/E = h(\epsilon_0 + 2)^2/9$  with  $h$  constant, ranging from 1 to 1.5, and independent of the number and moment of the dipoles and of the temperature. This approximation simplifies subsequent treatment relative to a system consisting of different dipoles.

Defining a polarization conductivity  $k_p = j_p/E$ , obtain from (8):

$$k_p = [h(\epsilon_0 + 2)^2 n_0 \mu^2 / 27kT\tau] \exp(-t/\tau) \quad (12)$$

In the case of a polymer, whether pure or plasticized, not merely one type of dipole should be considered, but it should be recalled that it is made up of dipoles with various relaxation times and dipole moments.  $n_{i,j}$  are used to indicate the number of dipoles per unit volume with lag time  $\tau_i$  and moment  $\mu_j$ . We shall therefore obtain for  $k_p$  the expression:

$$k_p = [h(\nu^2 + 2)^2 / 27kT] \sum_{i,j} (n_{i,j} \mu_j^2 / \tau_i) \exp(-t/\tau_i) \quad (13)$$

where  $\nu$  is the refractive index and  $h$  ranges from 1 to 1.5; for the dielectric constant:

$$\epsilon = \epsilon_0 + [4\pi h(\nu^2 + 2)^2 / 27kT] \sum_{i,j} n_{i,j} \mu_j^2 [1 - \exp(-t/\tau_{ij})] \quad (14)$$

from which it is immediately checked that:

$$k_p = \frac{1}{4\pi} \frac{d\epsilon}{dt}$$

This equation, already given in ref. 6, is also derived from the phenomenological treatment of the dependence of the conductivity on time, discussed in ref. 8. It can be seen from (13) that the polarization conductivity falls with increase in time, tending to zero when the time tends to infinity; this behaviour is that observed experimentally. The form of the equation  $k_p = k_p(t)$ , at constant temperature, depends on  $n_{i,j}$  and on their relation with  $\tau_i$ .

As for the dependence of the polarization conductivity on the temperature, it must be pointed out that the delay time according to Debye's theory<sup>11</sup> is proportional to the viscosity; admitting that the dependence on the temperature is *the same* for each  $\tau_i$ , in the sense that  $\log \tau_i/d(1/T)$  is independent of  $T_i$ , and that it is of the type:

$$\tau = \tau_{i0} \exp(W/RT) \quad (15)$$

with  $\tau_{i0}$  practically independent of the temperature<sup>†</sup>, we have, neglecting the dependence of  $(\nu^2 + 2)^{2/T}$  on the temperature:

$$d \ln k_p / d(1/T) = \frac{W}{R} \sum_{i,j} \frac{(n_{ij} h_{ij} \mu_{ij}^2 / T_i) (t/\tau_i - 1) \exp(-t/\tau_i)}{\sum (n_{ij} h_{ij} \mu_{ij}^2 / \tau_i) \exp(-t/\tau_i)} \quad (16)$$

Bearing in mind that

$$d \log k_p / d \log t = - \frac{\sum (n_{ij} h_{ij} \mu_{ij}^2 / \tau_i) (t/\tau_i) \exp(-t/\tau_i)}{\sum (n_{ij} h_{ij} \mu_{ij}^2 / \tau_i) \exp(-t/\tau_i)} \quad (17)$$

we immediately have

$$d \ln k_p / d(1/T) = - \frac{W}{R} [(d \log k_p / d \log t) + 1] \quad (18)$$

It may be seen from this equation that  $k_p$  can increase or decrease with temperature according to whether  $d \log k_p / d \log t$  (always negative) is, in absolute values, greater or less than 1.

The experimental data reported in Figures 4 and 5 show that  $d \log k_p / d \log t$  is  $< 1$ , in absolute values and, moreover, practically independent of the time and temperature in the intervals considered by us. Results show that  $R d \ln k_p / d(1/T)$  is constant but lower than the activation energy of the viscous flow, in spite of the fact that the viscosity is the parameter determining the movement of the dipoles.

Applying equation (18) to the experimental data of Figures 1 and 2, a value ranging from 50 to 60 kcal/mol is obtained for  $W$ . In spite of such a high value, the polarization conductivity varies little with the temperature as  $d \log t_p / d \log t$  differs little from unity.

### Ionic conductivity

If the charge of the ions of species  $i$  is indicated by  $q_i$ , their average speed in the direction of the field by  $v_i$  and their number per unit volume by  $n_i$ , then the current density  $j_0$ , due to the ions, will be given by:

$$j_0 = \sum_i q_i n_i v_i \quad (19)$$

The average speed  $v_i$  under steady-state conditions, will be linked to the field by the following approximate equation:

$$\lambda_i v_i = q_i F_0^0 \quad (20)$$

where  $\lambda_i$  is a quantity proportional to the viscosity  $\eta$  of the system in which the ions move ( $\lambda_i = \lambda_i / \eta$ ).

The ions taking part in the conduction process are

† The possibility of constructing, by superimposition, master curves for the various electrical properties confirms the validity of the hypothesis that  $d \log \tau_i / d(1/T)$  does not depend on  $T_i$ . Moreover, the experimental data given in Figures 1, 2 and 3 as well as in ref. 8, together with the discussion which follows, show how an equation of type (15) is justified.

of a different nature; they include those originating from the hydrochloric acid formed during thermal decomposition of the polymer. On indicating the number of moles of hydrochloric acid formed by  $\nu$ , the degree of dissociation by  $\alpha$  and the equilibrium constant for:



by  $k$ , with  $\nu_{\text{H}^+} = \nu_{\text{Cl}^-}$  the number of  $\text{H}^+$  and  $\text{Cl}^-$  ions formed, we have  $\nu_{\text{H}^+} = \nu_{\text{Cl}^-} = \alpha \nu$  where  $\alpha$  is given by:

$$\nu \alpha^2 / (1 - \alpha) = k$$

The dependence on the temperature is given by:

$$k = k_0 \exp(-U_0 / 2 \epsilon RT) \quad (21)$$

where  $U_0$  is the energy of dissociation of hydrochloric acid in vacuum and  $\epsilon$  is the macroscopic dielectric constant<sup>14</sup>.

Considering the various results, we get:

$$\nu_{\text{H}^+} = \nu_{\text{Cl}^-} = (\nu k_0)^{1/2} \exp(-U_0 / 2 \epsilon RT) \quad (22)$$

in the hypothesis that  $\alpha$  is small compared with 1 as is presumably the case. It is advisable to emphasize that the number of moles of hydrochloric acid figuring in the previous equations is that referring to the hydrochloric acid present and not to the hydrochloric acid formed. In fact, it should be remembered that part of the hydrochloric acid formed by thermal decomposition is eliminated as a result of the presence of stabilizers.

Moreover, ions originating from specific types of stabilizers (e.g., based on tin) or other impurities may be present; the number of these ions may or may not depend on the temperature.

Using equations (20) and (22) and what has been stated previously about the relation between  $F_0^0$  and  $E$ , the ionic conductivity  $K_0$ , defined by  $j_0 / E$ , is given by:

$$K_0 = [h(\epsilon_0 + 2) / 9\eta] \{ (1/\lambda_{\text{H}^+} + 1/\lambda_{\text{Cl}^-}) (\nu k_0)^{1/2} \times \exp(-U_0 / 2 \epsilon RT) + \sum (q_i^2 n_i / \lambda_i, 0) \} \quad (23)$$

where the first two terms take into account the  $\text{H}^+$  and  $\text{Cl}^-$  ions, and the sum of the contribution of the other types of ions.

As for the dependence of  $K_0$  on the temperature, it must be observed that it is due to the term  $1/\eta$  which will be of the form  $\exp(-H/RT)$  and to a term  $\exp(-U/2\epsilon RT)$  and other terms similar to the latter which take into account the dependence of the number of other types of ions on the temperature.  $U_0$  is equal to 102.7 kcal/mol<sup>15</sup> and, bearing in mind that  $\epsilon$  is about 13<sup>8</sup> we have that  $U_0/2\epsilon$  is equal to about 4; this value is certainly much smaller than the energy of activation,  $H$ .

Presumably, similar considerations may apply also to the possible dependence on the temperature of the number of other species of ions and therefore it may be assumed that the dependence of the ionic conductivity on the temperature is predominantly given by the term  $\exp(-H/RT)$ . The fact that  $d \log k_0 / d(1/T)$  is practically constant in a narrow temperature range therefore appears to be justified as also that this derivative is almost independent of the number and type of ions, as well as of the percentage of plasticizer, because it is quite plausible that the 'viscosity' may depend on the

temperature in the same way as the change in composition. Conversely, the value of  $k_0$  at constant temperature depends on the number of ions present and the viscosity; a drop in the conductivity under steady-state conditions due to an increase in the content of suitable stabilizers (which block the hydrochloric acid formed) is due to a fall in the number of ions,  $\nu$ .

The increased conductivity due to the presence of tin-based stabilizers is due to the presence of other types of ions ( $n_i$  of equation (23)), while the drop in conductivity due to the decreased plasticizer content is, instead, due to an increase in the viscosity.

#### ACKNOWLEDGEMENTS

Thanks are due to Dr A. Coen for his fundamental contribution to this work.

#### REFERENCES

- 1 'Engineering Design for Plastics' (Ed. E. Baer) Reinhold, New York, 1964, Ch 7, p 437
- 2 Miller, M. L. 'The Structure of Polymers' Reinhold, New York, 1966, Ch 13, p 657
- 3 Coen, A. and Parrini, P. *Mater. Plast.* 1955, **21**, 850
- 4 Coen, A. and Parrini, P. *Mater. Plast.* 1956, **22**, 357
- 5 Coen, A. and Parrini, P. *Mater. Plast.* 1957, **23**, 216
- 6 Coen, A. and Parrini, P. *Mater. Plast.* 1959, **25**, 931
- 7 Coen, A. and Parrini, P. *Mater. Plast.* 1961, **27**, 760
- 8 Coen, A. and Protospataro, F. *Mater. Plast.* 1964, **30**, 250
- 9 Reddish, W. 'The Physical Properties of Polymers', *SCI Monogr.* 5, Society of Chemical Industry, London, 1959, p 138
- 10 Hamon, B. W. *Proc. Inst. Electr. Eng.* 1952, **27**, 99
- 11 Debye, P. 'Polar Molecules', Dover, New York, 1929, p 77
- 12 Onsager, L. *J. Am. Chem. Soc.* 1936, **58**, 1886
- 13 Fuoss, R. W. and Kirkwood, F. G. *J. Am. Chem. Soc.* 1941, **63**, 385
- 14 Hearle, J. W. S. *J. Textile Inst.* 1953, **44**, T177
- 15 Pauling L. 'The nature of the chemical bond', Cornell University Press, Ithaca, 1948

# The fracture of rubber-modified polystyrene

R. J. Ferguson\*, G. P. Marshall and J. G. Williams

*Polymer Engineering Group, Department of Mechanical Engineering, Imperial College of Science and Technology, Exhibition Road, London SW7 2BX, UK  
(Received 20 March 1973)*

This paper reports a successful attempt to apply the theories of fracture mechanics to the failure of impact polystyrene in air. The results show that linear elastic fracture mechanics is limited to correlating crack initiation data but that both maximum load and initiation data can be correlated using a constant crack opening displacement criterion calculated from the Dugdale model. The results are supported by similar calculations made from experiments with two other commercially important plastics: PVC and polycarbonate. The toughness of these materials and that of PMMA, polystyrene, and poly(ethylene terephthalate) are compared in terms of Rice's contour integral,  $J$ .

## INTRODUCTION

Linear elastic fracture mechanics cannot be applied when the fracture event being studied occurs at a stress level which is above 70% of the applied stress<sup>1</sup>. This number may only be taken as a general guide, however, and the most practical approach is to perform a series of tests to determine whether the fracture toughness is a function of some geometrical factor to an extent which cannot be set aside for good theoretical reasons. The finite plate correction factors of Brown and Srawley<sup>2</sup>, for example, remove the dependence of fracture toughness on crack length to specimen width ratio for crack tip stress fields which are essentially elastic.

In the work described here, fracture tests of a commercial grade of impact polystyrene (IPS) were carried out over a wide range of Instron cross-head displacement rates to check the applicability of fracture theories. The linear theory, using a  $K_c$  criterion, proved capable of correlating crack initiation results, but was unable to cope with the maximum load data. Correlation was achieved using a constant crack opening displacement (COD) criterion calculated from the Dugdale model<sup>3</sup>. Since the model can only provide a one-dimensional representation of the overall effects of crack tip plasticity, it could not match the real experimental situation exactly. The use of this method can be justified, however, because failure stress predictions to within  $\pm 5\%$  were possible for two different specimen geometries.

Finally, a comparison is made between the results for IPS and those obtained by the authors for other tough plastics. These show that the analysis can be successfully applied to a range of materials and that the fracture toughness test has considerable potential for comparing one material with another.

## THEORY OF FRACTURE MECHANICS

### Linear theory

Griffith's energy balance argument<sup>4</sup>—that a sharp crack in an elastic brittle solid would extend when the

energy which would be released by an infinitesimal crack extension was greater or equal to the surface energy of the newly created surface—was extended by Irwin<sup>5</sup> and Orowan<sup>6</sup> to quasi-brittle materials. They pointed out that the work of plastic deformation involved in crack growth far exceeded the true surface energy even for materials as apparently brittle as glass. The elasticity solution for the energy release rate  $G$ , introduced by Irwin<sup>5, 8</sup> would still be valid, however, if the size of the yielded zone was small compared to the crack length. For an infinite plate in plane strain  $G$  is given by:

$$G = \frac{\sigma^2 \pi a}{E} (1 - \nu^2) \dagger$$

where  $\sigma$  = the applied stress,

$2a$  = the crack length,

$E$  = Young's modulus,

$\nu$  = Poisson's ratio.

Irwin<sup>5, 8</sup> also introduced the stress intensity factor ( $K$ ) concept by showing that the stresses in the crack tip region could be characterized by  $K$ , the value depending only upon the loading conditions and specimen geometry. He also showed that  $K$  and  $G$  are equivalent; in plane strain:

$$K^2 = \frac{EG}{1 - \nu^2} = \sigma^2 \pi a$$

If a fracture event can be shown by experiment to occur at the same *critical* value of stress intensity factor  $K_c$  despite changes in specimen geometry (assuming that plane strain conditions obtain), the validity of using the  $K_c$  approach is established and  $K_c$  can be considered to be a material property.  $K$  does, however, vary with temperature, crack speed, type of chemical environment, strain rate, and in plane stress, with specimen thickness.

Fracture test results which show that  $K_c$  depends on crack length (providing the appropriate geometrical correction factors have been employed<sup>2</sup>) violate the

\* Present address: Royal Military College, Kingston, Ont., Canada.

† In all of these equations for plane stress set  $(1 - \nu^2) = 1$ .

geometry independence requirement in the most basic way. In such cases, another analysis must be used which accounts for crack tip yielded zones which are of a size comparable to the crack length.

*Extensions to the linear theory*

If yielding takes place ahead of the crack tip, then it is clear that the faces of the crack must separate a certain amount. It has been argued<sup>9</sup> that this crack opening displacement (*COD*) characterizes the strain environment in the crack tip region and can function as a fracture criterion. If it can be validated by experiment, the *COD* criterion provides a conceptually simple fracture parameter.

The first model of crack tip yielding was proposed by Dugdale<sup>3</sup>. He envisaged the growth of an equilibrium line plastic zone at the tip of the crack in which the stress was equal to the yield stress. The details of the model are shown in *Figure 1*. For a centre crack in an infinite plate, values of *COD* and equilibrium plastic zone length can both be determined from closed form solutions<sup>3, 10</sup>. For practical geometries numerical results must be used<sup>11, 12</sup>. *Figure 2* gives non-dimensionalized *COD* results for the single edge notch (*SEN*) geometry in the form of a nomogram for the benefit of others who may wish to make trial calculations similar to those to be made here. Non-dimensional *COD* or  $\delta^*$  is

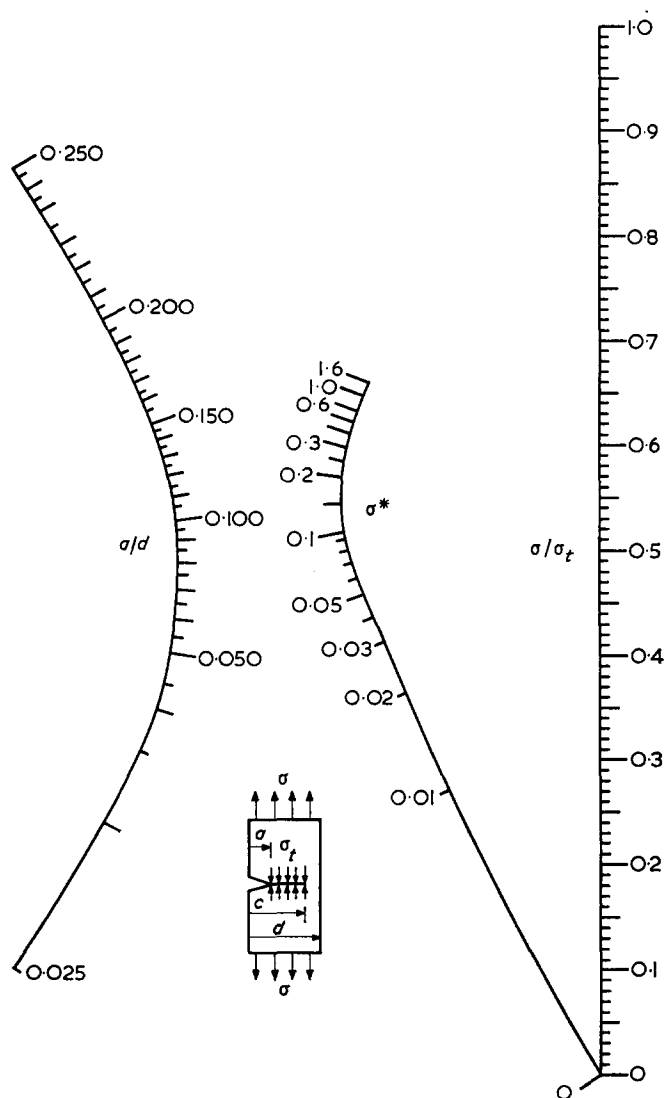
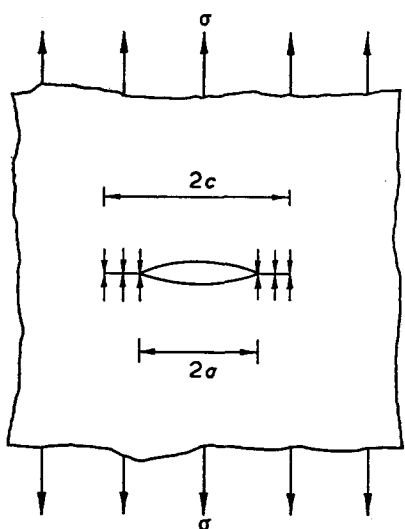


Figure 2 *COD* in the Dugdale model for the *SEN* specimen (uniaxial tension)

given by:

$$\delta^* = \frac{\pi E \delta}{4 \sigma_t d (1 - \nu^2)} \quad (\text{plane strain})$$

where  $\delta = \text{COD}$ ,

$d = \text{plate width}$ ,

$\sigma_t = \text{the stress in the plastic zone which is here defined as the yield stress } (\sigma_y)$ .

In the case of small scale yielding, i.e. when  $\sigma \ll \sigma_y$ , then the Dugdale model shows that *COD* and  $K_c$  are directly related and provide equivalent fracture criteria.

$$\delta = \frac{K_c^2}{E \sigma_y} (1 - \nu^2) \quad (\text{plane strain})$$

If the constant *COD* criterion is applied to the Dugdale model data of Hayes and Williams<sup>11</sup> for the *SEN* specimen, then the curves of *Figure 3* are produced. For low values of  $\delta^*$  the shape of the curve approaches that which would be predicted by an inverse square relationship between applied stress and crack length. Indeed, a plot of  $K_c$  versus  $a/d$  ratio for various values of  $\delta^*$  shows that a marked dependence of  $K_c$  on crack length does not begin to be important until  $\delta^* > 0.10$  except for very short cracks<sup>13</sup>.

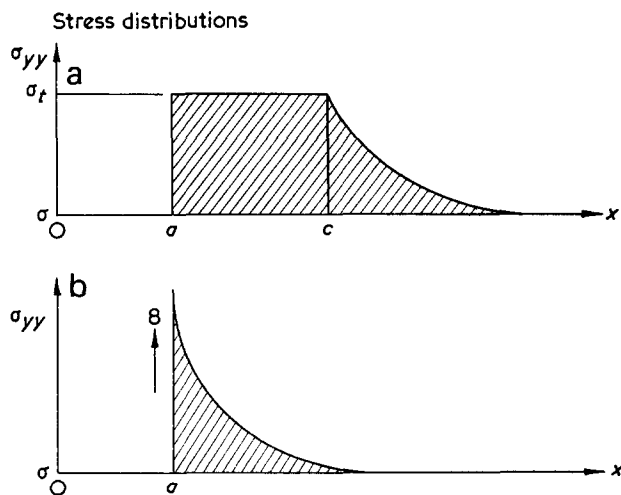


Figure 1 The Dugdale model. (a) Dugdale model; (b) elastic model

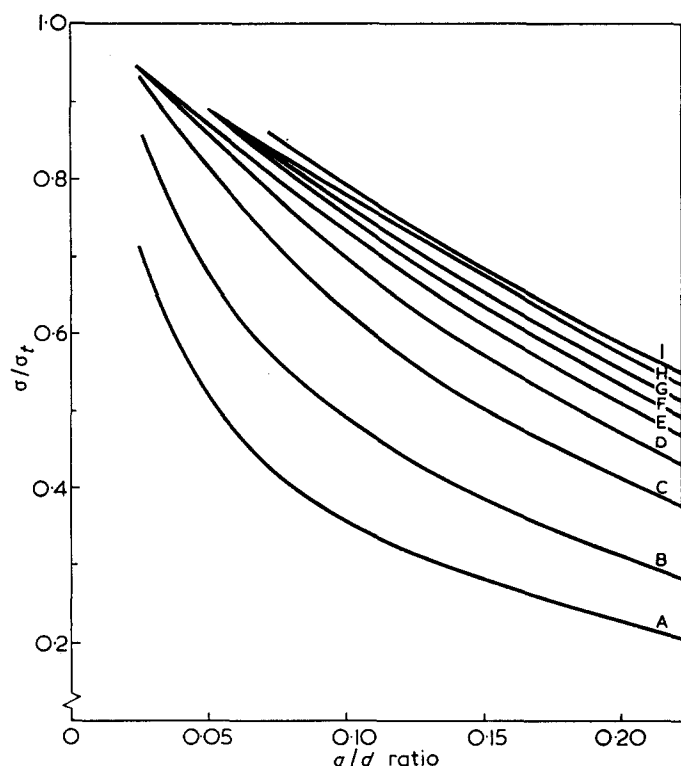


Figure 3  $\sigma/\sigma_y$  versus crack length for constant  $\delta^*$  SEN specimen Dugdale model.  $\delta^*$ : A, 0.05; B, 0.1; C, 0.2; D, 0.3; E, 0.4; F, 0.5; G, 0.6; H, 0.8; I, 1.0

#### The J concept

The application of energy methods to fracture problems began to have renewed practical importance following the work of Rice<sup>14</sup> who developed a relationship for the change in energy of a body due to the growth of a crack or void. The relationship is of particular value because it provides a general statement describing the strain field near the crack tip from which all of the fracture parameters of current interest can be calculated.

Rice's expression is given in terms of a path-independent integral  $J$  whose application is restricted only by the neglect of kinetic energy and heat transfer effects, and by the requirement that the strain energy density function:

$$W(\epsilon_{mn}) = \int_0^{\epsilon_{mn}} \sigma_{ij} d\epsilon_{ij}$$

be single valued.  $J$  is given by:

$$J = \int_{\Gamma} \left( W dy - T_i \frac{\partial u_i}{\partial x} ds \right)$$

where  $\Gamma$  is any closed contour around the crack tip,

$s$  is the arc length of the contour,

$T_i$  are the tractive components of stress acting at the contour,

$u_i$  are the displacements,

$i, j, m, n$  are the subscripts of tensor notation.

If the Dugdale model is analysed using this integral, then it can be shown that  $J$  is given by:

$$J = \sigma_y \delta \quad (1)$$

In plane strain and for  $\sigma \ll \sigma_y$ ,  $J$  and  $K$  are related

by:

$$J = \frac{K^2}{E} (1 - \nu^2) = G \quad (2)$$

so that  $J$  may be regarded as a measure of the work done at the crack tip.

#### TEST PROGRAMME

The bulk of the experimental effort was devoted to impact polystyrene (IPS) and the discussion of experimental technique will be largely restricted to that material. The samples of PVC and polycarbonate (PC) which were tested were treated in the same way as IPS except where noted. All testing was done in an air-conditioned laboratory (temperature,  $20 \pm 0.5^\circ\text{C}$ ; relative humidity,  $50 \pm 5\%$ ).

#### Materials

**IPS:** an unpigmented medium impact grade supplied by BP Chemicals Ltd, in compression moulded sheets of 1.5, 3.0 and 6.0 mm thickness.

**PC:** Bayer Makrolon, extruded sheet, 3 mm thick.

**PVC:** unplasticized ICI Darvic 110, compression moulded, 3.0 mm thick.

#### Notching

IPS is translucent and therefore it is difficult to see whether a good notch has been produced. This is a critical point because reproducibility of results depends on a consistent notch quality and because the lowest value of  $K_c$  can only be obtained for the sharpest notch. For polystyrene, for example,  $K_c$  can vary by a factor of five if the best and worst notching methods are compared<sup>15</sup>.

The technique finally adopted was to force a razor blade into the material slowly to a depth of about 0.5 mm. If the blade is pushed in too quickly or deeply a large craze bundle is formed and the fracture loads are considerably affected. The razor blade was mounted in a Vickers hardness tester so that penetration could be controlled carefully. It was important to use a fresh part of the blade for each specimen.

PC specimens were also prepared in this way but PVC had to be notched using the impact notching technique that has been previously described by Marshall *et al.*<sup>15</sup>.

#### Specimen geometries

Most of the tests were carried out using the SEN specimen. Crack lengths were varied from 2 to 12 mm and the possible existence of a thickness effect was investigated for IPS at one cross-head speed.

One series of four-point bending tests was performed to ensure that the results were truly geometry independent.

Figure 4 shows both specimen configurations.

#### IPS: FRACTURE TESTING

##### Procedure

After notching, the specimens were tested in batches of ten or twenty at cross-head rates from 0.05 to 50 cm/min. For the slow speeds it was possible to note the moment of crack initiation through a microscope

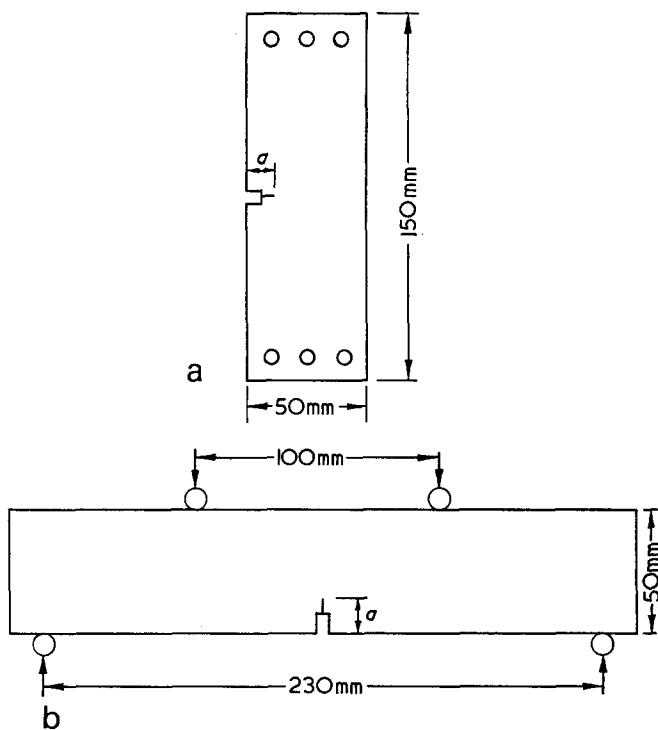


Figure 4 Specimen geometries. (a) Single edge notch; (b) four-point bend

and to make a measurement of COD at maximum load. For the medium speeds (1 and 2 cm/min), a Bolex ciné camera was used to record each test and at the higher speeds a Fastax camera was employed. These films were subsequently analysed and values of crack initiation load, COD at maximum load and, in one case, plastic zone length, were derived from them.

*Tensile failure of notched IPS specimens*

**General.** The grade of IPS tested did not fail in a brittle manner even at the highest cross-head speed available, 50 cm/min, and all of the failures were characterized by extensive slow growth. At the lower testing speeds, slow growth continued beyond the maximum load point and failure took place by ductile tearing as the load dropped towards zero. At the higher speeds, fast fractures were observed after an amount of unloading which decreased with increasing testing speed. Typical load-extension curves are shown in Figure 5. This behaviour is due, in part, to the normal effect of increasing straining rate on the ease with which a stiff machine can keep up with a sudden change in specimen elongation (cf. the comprehensive discussion of this for steels by Rogan<sup>16</sup>). It may also be due to a progressive decrease in the capacity of the material to form an energy absorbing crazed zone as crack speed rises with straining rate. It is certainly true that the extent of the crazed zone decreases with increasing crack speed.

**Development of the crazed zone.** The addition of styrene-butadiene or polybutadiene rubber to polystyrene has the effect of increasing the volume of craze matter produced and thus improves the energy absorbing capacity of the material. In a tensile test of a notched specimen, this behaviour manifests itself in the development of a large crazed zone at the crack tip. Figure 6 presents a series of drawings of the development

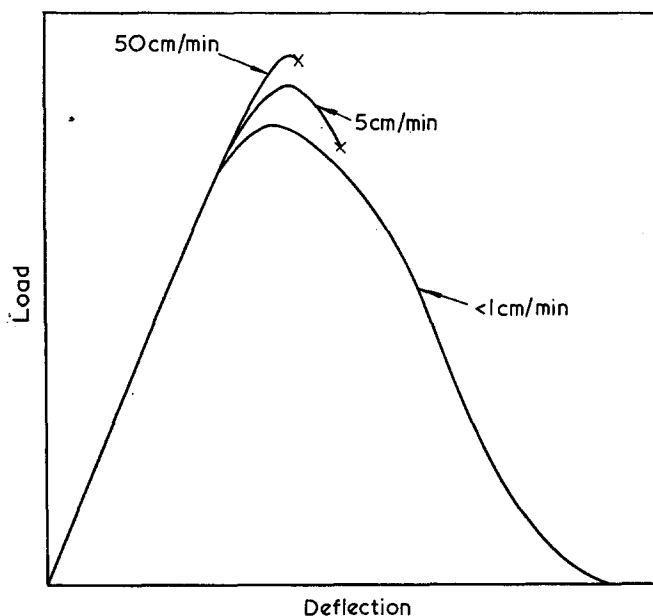


Figure 5 Typical load deflection curves for IPS

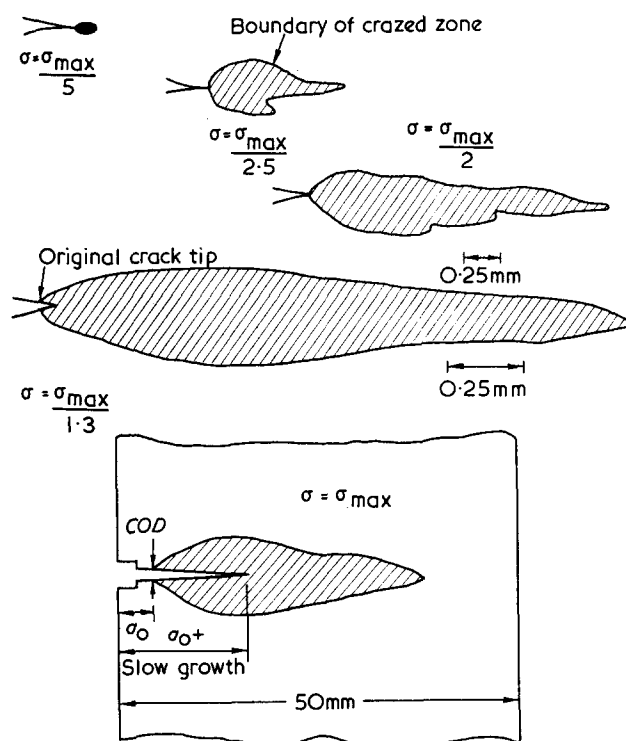


Figure 6 Development of the crazed zone in IPS

of the heavily stress-whitened core of the zone made from a ciné film record of craze growth in black-pigmented IPS. Photographs of unpigmented material taken using transmitted light show a haze of secondary crazes covering a much larger area (cf. Figure 17).

*Crack initiation data*

Crack initiation results usually show a considerable amount of scatter because the selection of the moment when slow cracking begins is necessarily influenced by human error. With this in mind, the typical data shown in Figure 7 are quite acceptable and demonstrate that the  $K_c$  criterion can apply at crack initiation for IPS. (In the Figure the ordinate is  $\sigma^2 Y^2$  where  $Y$  is the

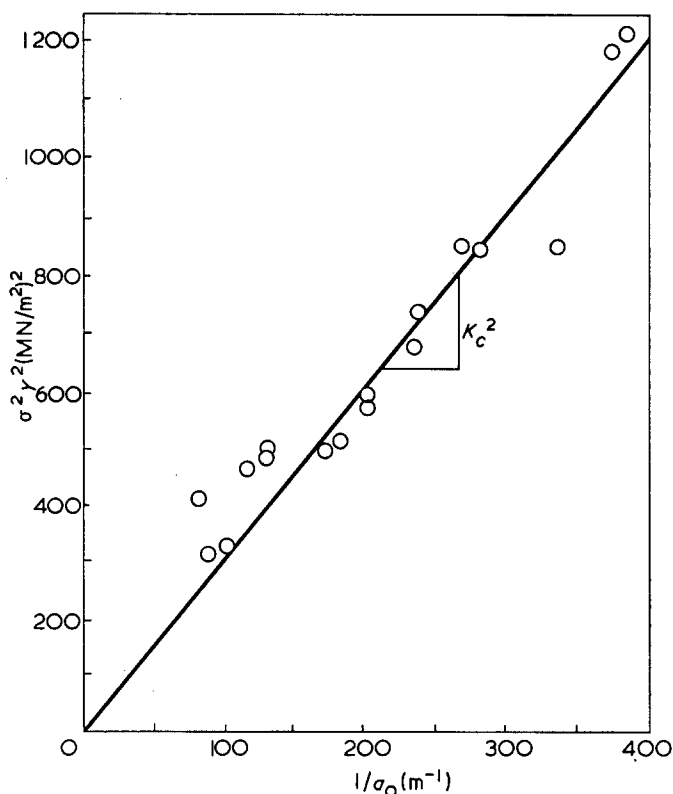


Figure 7 Typical crack initiation data for IPS in air. Cross-head speed, 0.5 cm/min;  $K_c = 1.75 \text{ MN/m}^{3/2}$

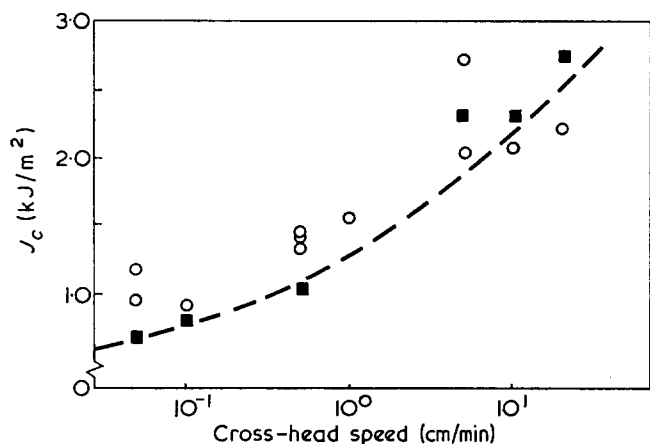


Figure 8  $J_c$  for crack initiation, IPS.  $\circ$ , from computed COD;  $\blacksquare$ , from measured COD; ---, polystyrene results<sup>15</sup>

Brown and Srawley<sup>2</sup> correction factor for the SEN specimen.)

If  $K_c$  is converted to  $J_c$  by equation (2) and the results are plotted against cross-head rate (Figure 8), it is seen that  $J_c$  for crack initiation is rate sensitive in common with PMMA and polystyrene<sup>15, 17</sup>.

Figure 8 also shows the agreement between  $J_c$  calculated from  $K_c$  (equation 2) and that calculated using equation (1) from values of COD obtained by measurement from filmed test records. The agreement is excellent. Also noteworthy is the good agreement between different batches of specimens tested on different days; each circle represents a batch of ten or more specimens of varying crack lengths.

The broken curve in Figure 8 represents the variation in  $J_c$  for final fracture in polystyrene when that material is razor notched in the same way as IPS. The coincidence

of these results is useful evidence of the toughening effect of the rubber particles in IPS. If it is assumed that razor notching produces a craze bundle of about the same size in both materials, then it seems reasonable to postulate that the energy input required to break through the bundle will be the same also. In polystyrene, final fracture follows immediately; however, in IPS the material can continue to extend the craze to an extent which would be disastrous in polystyrene and therefore the transition from slow cracking to instability is delayed.

Applicability of the Dugdale model to IPS

The Dugdale model is an equilibrium model and therefore its application to a situation in which load is increasing must be verified by experiment. From the outset it was clear that the shape of the crack tip from the moment of crack initiation until maximum load is reached did not match the ideal assumed here and shown in Figure 9. The crack tip does not become more blunt or remain stationary as load rises but moves slowly forward maintaining roughly the same tip radius (Figure 6). Despite this drawback the simple approach produces useful results and in other respects the model provides an adequate description of the overall effect of crack tip yielding.

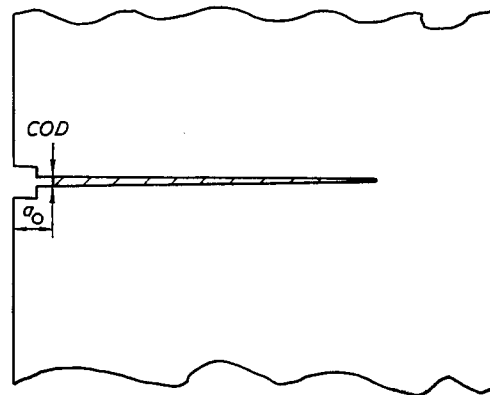


Figure 9 Idealized crack tip geometry at maximum load (cf. Figure 6)

To check on the validity of the Dugdale model for describing the fracture of IPS, the following tests were performed.

**Constant load tests.** A series of razor-notched IPS specimens was tested under constant load. Once the craze had grown to equilibrium length the craze stress was calculated using the Dugdale model results of Fenner<sup>12</sup> (here presented in the form of a nomogram, Figure 10). It was found that the value of craze stress predicted by the model was constant and did not depend on  $a/d$  ratio (Figure 11). The value of craze stress determined can be associated with the yield stress of the material for testing times of about 14 h which was a typical time taken for a craze to reach equilibrium length.

**Growing craze tests.** Another series of notched specimens, in this case pigmented with a black dye so that the developing craze could be seen more easily, was tested at 0.5 cm/min. A film was taken of the tests and measurements of craze length from it were matched to



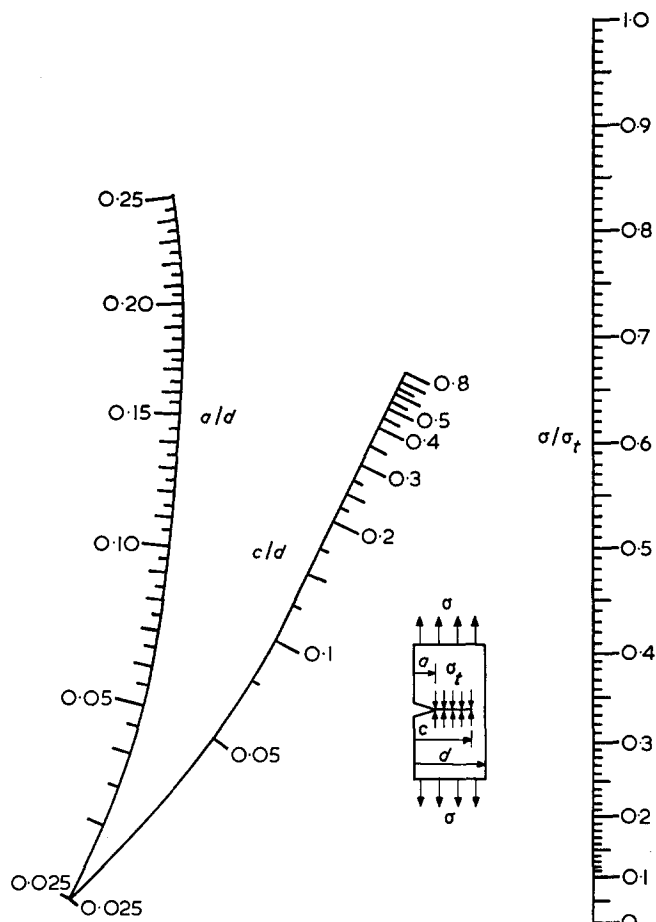


Figure 10 Plastic zone length in the Dugdale model for SEN specimen (uniaxial tension)

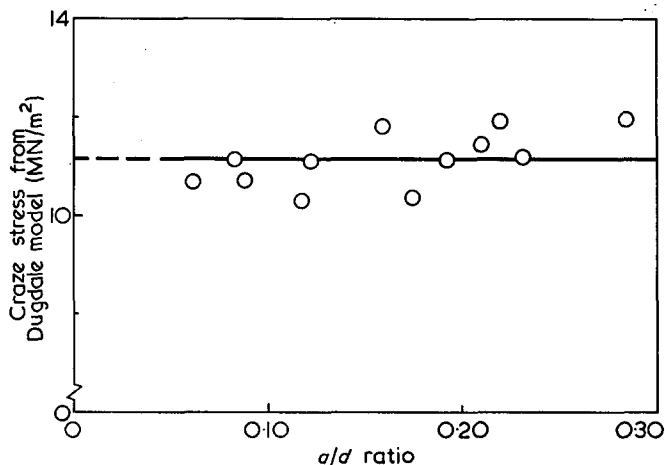


Figure 11 Craze stress calculations, constant load tests

the appropriate load and then a craze stress was calculated from Fenner's data<sup>12</sup>. A typical result is shown in Figure 12. In the early stages of craze growth the craze does not reach its equilibrium length and hence the predicted stress is much higher than the yield stress. As loading proceeds, however, the combination of slow crack and craze growth is such that the predicted stress is asymptotic to a constant which turns out to be the yield stress of the bulk material at the strain rate of the test.

#### Maximum load data

**SEN tests.** As would be expected from the large amount of crazing around the crack tip which is observed

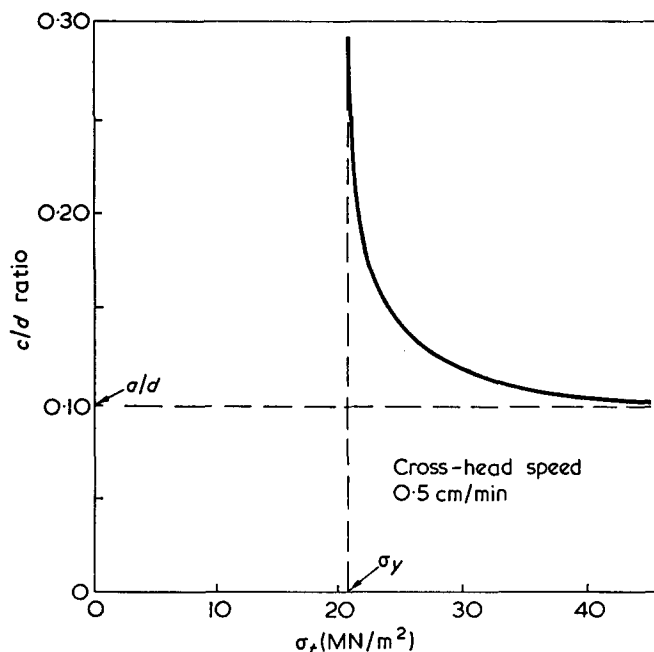


Figure 12 Craze stress calculation, constant straining rate test. Cross-head speed, 0.5 cm/min

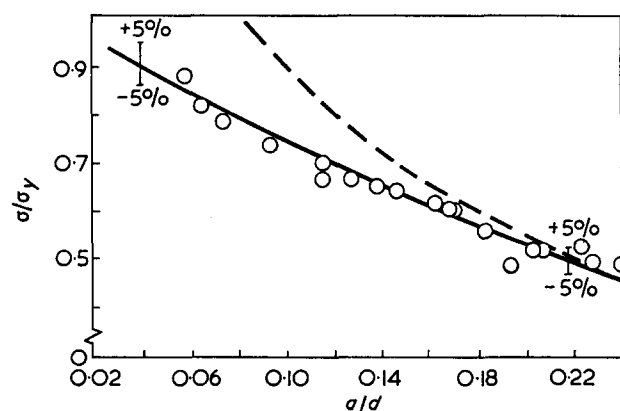


Figure 13 Typical maximum load data for IPS in air showing fit achieved with constant COD criterion. —,  $\delta = 0.25$  mm; ---,  $K_c = \text{constant}$ ; cross-head speed, 0.05 cm/min;  $\sigma_y$ , 17.51 MN/m<sup>2</sup>

at the moment the maximum load is reached (Figure 6), the  $K_c$  criterion cannot be expected to characterize the crack tip stress field and will therefore be unable to correlate the experimental results. The constant COD criterion, on the other hand, works rather well. The results from Fenner's<sup>12</sup> finite element analysis (Figure 2) were interpolated to determine the COD for each specimen using: the maximum stress achieved in the test, the initial crack length (in accordance with the identity represented in Figure 9), and the  $\sigma_y$  and Young's modulus appropriate to the testing speed. For IPS the crack speeds are low and hence bulk material values of  $\sigma_y$  and  $E$  are representative of those for the region ahead of the crack. The average COD for each batch of specimens was taken as the fracture criterion and a curve was fitted to the data. A typical result is shown in Figure 13. The fit is a good one and the superiority of the analysis over the constant  $K_c$  criterion, indicated by a broken line, is unquestionable. The results of all of the test series are given in Figure 14 in terms of  $J_c$  as a function of cross-head speed. This is done to reflect

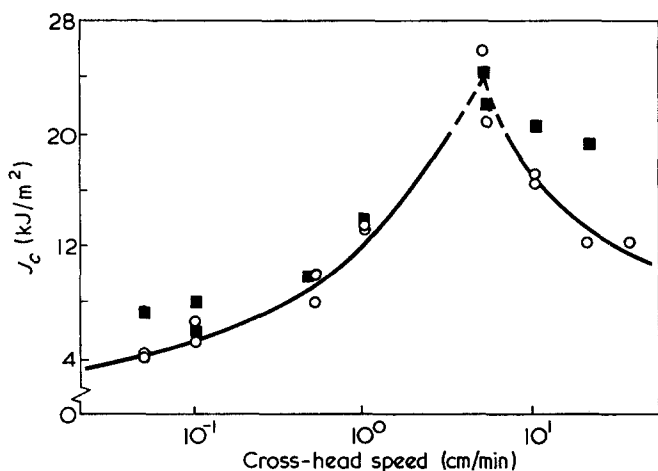


Figure 14  $J_c$  at maximum load, IPS. ○, from computed COD; ■, from measured COD

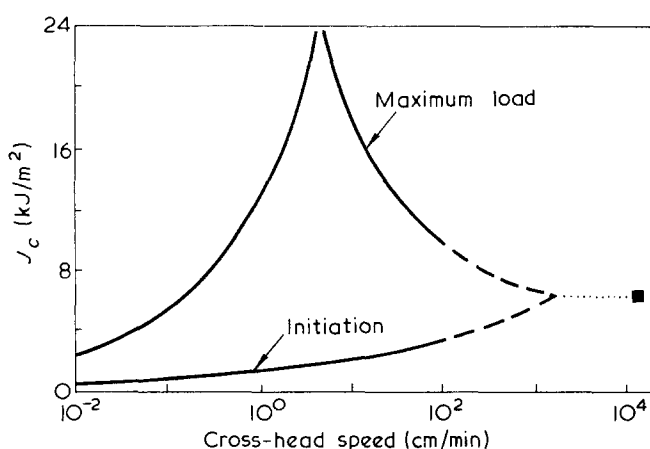


Figure 15 Correlation of fracture data, Instron to impact speeds. ■, Charpy test

the increases in both  $COD$  and  $\sigma_y$  with testing speed. As before, a comparison with  $J_c$  values obtained using  $COD$  measurements from the filmed test records is made, and the good agreement is clear up to a cross-head rate of 5 cm/min. Beyond this point accurate  $COD$  measurements become difficult because of the short duration of the test (less than 1 sec). The agreement between computed results from different batches of specimens is, however, excellent throughout the range.

The apparent peak in the curve at a cross-head speed of 5 cm/min coincides with the onset of instability in the tearing process. The trend to lower values of  $J_c$  as cross-head speed rises beyond this point seems reasonable because of the rate sensitivity of the crazing process. At low speeds crazing has ample time to proceed and can prevent rapid crack growth. The amount of crazing which does take place is reflected by the  $COD$ . As the speed rises both the yield stress and  $COD$  increase and hence  $J_c$  rises also. However, a point is reached where crazing no longer has time to take place and the  $COD$  will fall even though  $\sigma_y$  continues to rise.

Figure 15 shows the maximum load and initiation  $J_c$  versus cross-head speed curves plotted together. Extrapolation to higher speeds makes the curves cross at a value of approximately 6 kJ/m<sup>2</sup>. From this point onward fracture would be expected to occur without significant stress whitening. Charpy impact test results supplied

by Woodward (personal communication) support this argument. He obtained a  $J_c$  of 5.9 kJ/m<sup>2</sup> for a theoretical striker (cross-head) velocity of  $1.46 \times 10^4$  cm/min and no stress whitening was observed.

**Four-point bend tests.** Although no geometry effect due to thickness or change in crack length was observed in tensile fracture testing of IPS, either at crack initiation or at maximum load, it was decided that another specimen geometry should be tried. It was considered especially important to verify the appropriateness of the ideal of the crack tip profile which had been employed.

Accordingly, a series of four-point bend (4PB) test specimens cut from 12 mm thick sheets was tested at a cross-head speed of 0.5 cm/min. By a suitable choice of specimen dimensions, it was found that, in terms of strain rate,  $SEN$  and 4PB tests at 0.5 cm/min could be directly compared. The maximum moment which could be applied to the beam was determined by using the  $COD$  found in the  $SEN$  tests at 0.5 cm/min and the results of Hayes and Williams<sup>11</sup>. The moment which would cause crack initiation was found using  $K_c$  and the Brown and Srawley formula which includes a finite depth correction factor<sup>2</sup>.

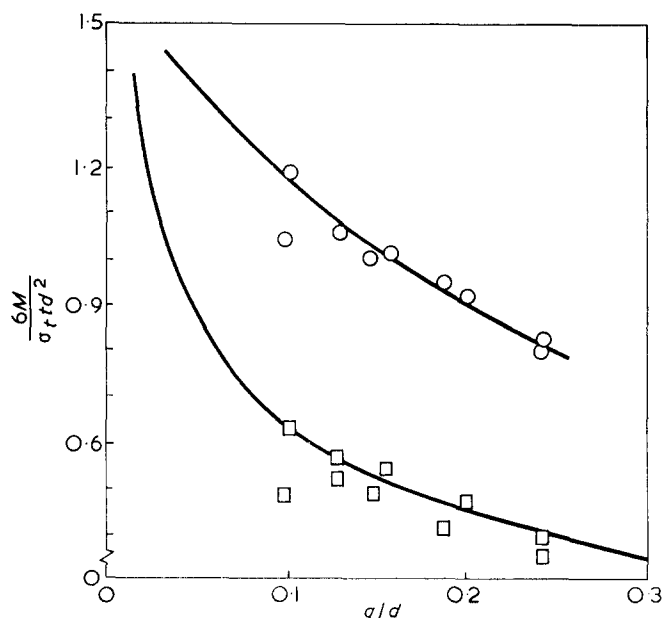


Figure 16 Four-point bend tests results, IPS tested at 0.5 cm/min compared with  $SEN$  predictions. ○,  $SEN$  data, constant  $COD=0.43$  mm criterion maximum load; □,  $SEN$  data, constant  $K_c$ , criterion initiation

Both the predictions and the corresponding experimental results are given in Figure 16. The ordinate is non-dimensionalized bending moment

$$\frac{6M}{\sigma_t t d^2}$$

where  $M$  = applied moment,  $t$  = thickness,  $d$  = depth of beam,  $\sigma_t = \sigma_y$  = yield stress. From Figure 16, it is clear that  $SEN$  results can be successfully used to predict both initiation and final fracture loads in four-point bending. This agreement is encouraging and lends confidence to the approach to ductile failure given here.

POLYCARBONATE AND PVC: FRACTURE TESTING

Polycarbonate

Polycarbonate can fracture in a brittle manner at high Instron testing speeds. At lower speeds failure

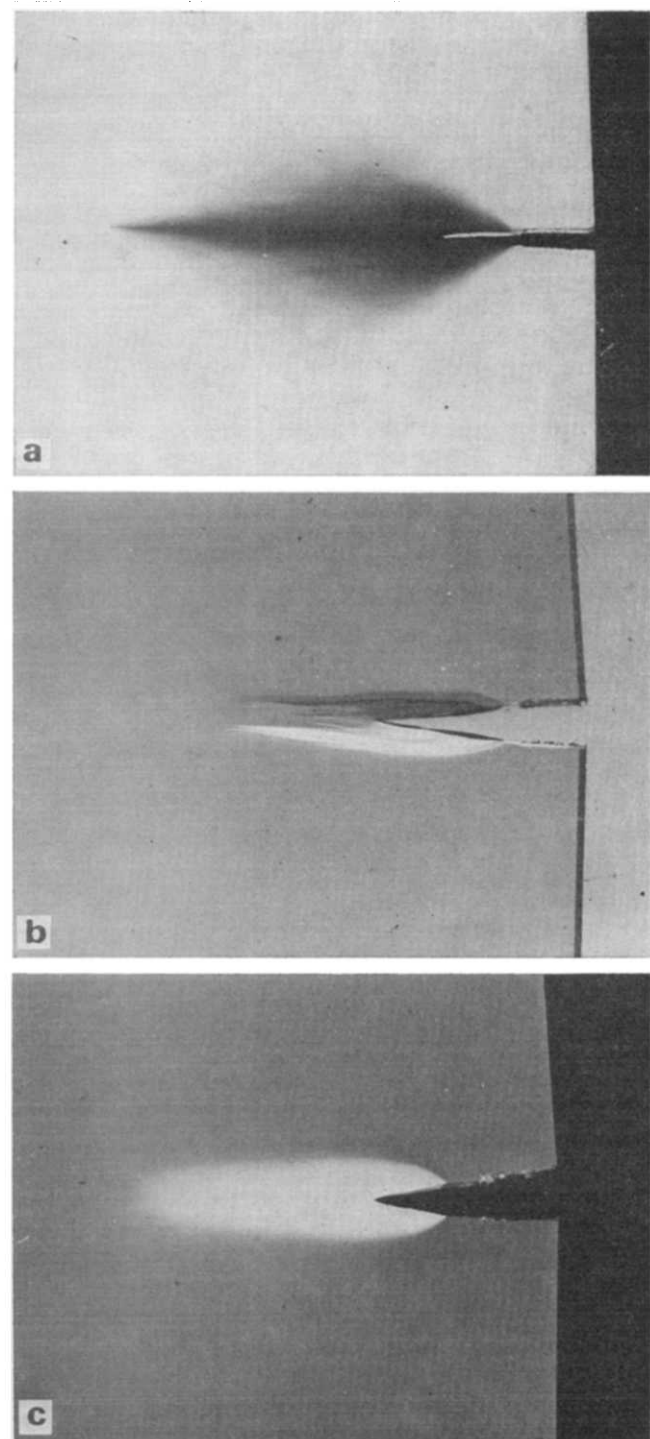


Figure 17 Comparison of crack tip plasticity at maximum load for (a) IPS, (b) PC and (c) PVC

takes place by ductile tearing under plane stress conditions (see Figure 17 where IPS, PC, and PVC are compared). The transition from ductile to brittle behaviour is a function of thickness—ductile failures are observed throughout the Instron speed range for 3mm thick sheet and brittle failures for 5mm thick sheet above 10 cm/min.

The ductile failures were analysed by the methods previously described for IPS;  $K_c$  was used to correlate initiation data and the constant  $COD$  criterion to correlate maximum load data (Figure 18).

If the  $J_c$  values for maximum load at different cross-head rates are compared (Table 1) it is seen that  $J_c$  drops with increasing testing speed. This is the correct trend because the fracture toughness must fall as the ductile-brittle transition is approached. It is unlikely, however, to be possible to extrapolate directly to the brittle fracture toughness value since the transition is a sudden one.

Because relatively few specimens were tested, it is not possible to comment confidently on the crack initiation results given in Table 1 for PC. The tests at 5 cm/min were particularly prone to error and confirmatory experiments are necessary. These will be included in a separate investigation into the nature of the ductile-brittle transition.

PVC

Unplasticized PVC also fails in plane stress and its fracture behaviour is similar to that of IPS and PC (see Figure 17), and can be analysed in the same way (see, e.g., Figure 19). A ductile-brittle transition is not observed at Instron testing speeds for 3mm sheet; however, the trend of the  $J_c$  results given in Table 1 indicates that one may exist at some higher speed.

As was true for PC, the PVC crack initiation results

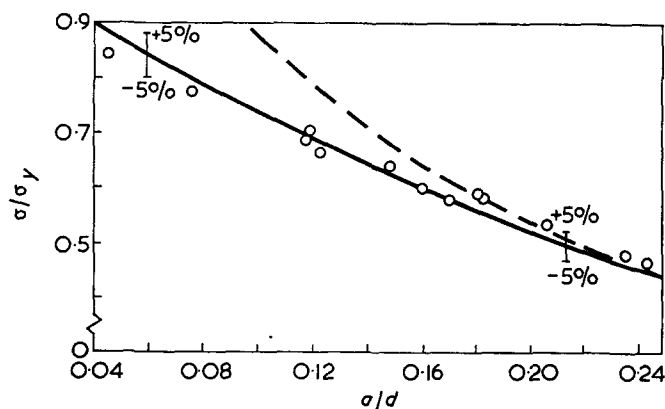


Figure 18 Typical maximum load data for PC in air showing fit achieved with constant  $COD$  criterion. Cross-head speed, 0.5 cm/min;  $\sigma_y = 56 \text{ MN/m}^2$ ; —,  $\delta = 0.75 \text{ mm}$ ; - - -,  $K_c = \text{constant}$

Table 1  $J_c$  values ( $\text{kJ/m}^2$ ) for initiation and maximum load at different cross-head speeds

Cross-head speed (cm/min)	PMMA		Polystyrene		IPS		PVC		PC		PET	
	Init.	Max.	Init.	Max.	Init.	Max.	Init.	Max.	Init.	Max.	Init.	Max.
0.05	0.27	0.91	0.23	0.39	0.85	4.2	—	74.9	—	49.1	—	—
0.50	0.32	0.91	0.25	0.36	1.40	9.0	1.69	66.2	3.00	41.8	5.7	18.9
5.00	—	0.91	—	—	2.08	24.2	1.34	61.5	2.55	41.3	—	—

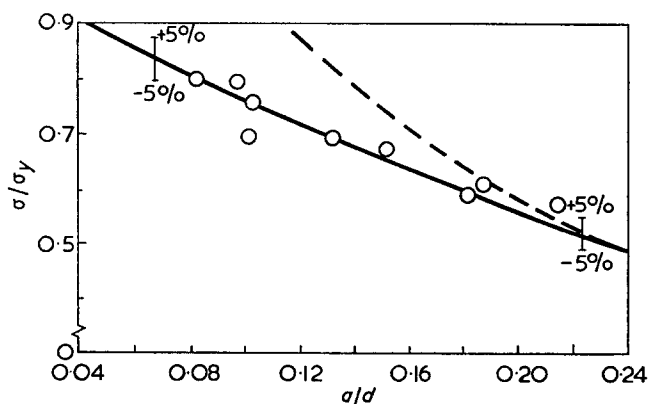


Figure 19 Typical maximum load data for PVC in air showing fit achieved with constant  $COD$  criterion. Cross-head speed, 0.5 cm/min;  $\sigma_y = 54 \text{ MN/m}^2$ ; —,  $\delta = 1.2 \text{ mm}$ ; - - - - ,  $K_c = \text{constant}$

are tentative and require confirmation. This will be part of a separate investigation.

### CONCLUSIONS

The primary aim of this work was to demonstrate the possibility of analysing the ductile fracture of IPS. This aim has been supported by similar experiments using PVC and PC. From all of these results it is clear that the  $K_c$  criterion cannot be applied to any aspect of the fracture behaviour of such ductile materials beyond the point of crack initiation. By using the  $J_c$  criterion it is possible to characterize the deformation in the crack tip region and valid comparison between materials can be made.

Table 1 contains the fracture toughness values for six thermoplastics at three representative cross-head speeds. The results for PMMA and polystyrene are from the work of Marshall *et al.*<sup>15, 17</sup> and those for poly(ethylene terephthalate) film from ref. 13. It is interesting to compare the ranking of the six materials in order of toughness by Izod impact strength, critical  $J$  at maximum load, and on the basis of the maximum stress which can be applied to a specimen containing an initial sharp notch of length  $0.1d$ . This is done in Table 2. Clearly  $J_c$  provides the most sensitive measure of toughness. The difference in order-of-merit for PVC and PC between Izod and fracture tests is not surprising given the difference in notching technique and strain rate that is involved. Polycarbonate is less sensitive to strain rate than PVC and it is entirely feasible that the

Table 2 Comparison of order of toughness by Izod impact strength, critical  $J$  at maximum load and failure stress

	The order of toughness at 0.5 cm/min	Relative toughness by		
		Impact*	$J_c$	Failure stress†
1 Polystyrene	0.36 kJ/m <sup>2</sup>	1	1	1
2 PMMA	0.91 kJ/m <sup>2</sup>	1.5	2.5	1.6
3 IPS	9.0 kJ/m <sup>2</sup>	4	25	2.3
4 PET	18.9 kJ/m <sup>2</sup>	?	52	11
5 PC	41.8 kJ/m <sup>2</sup>	70	116	11
6 PVC	66.2 kJ/m <sup>2</sup>	10	184	5.9

\* Approximate values Izod test (ASTM D256) from *Properties of Plastics* Shell Chemicals (UK) Limited, London

† Stress at maximum load for a *SEN* specimen where  $a/d = 0.1$ , cross-head rate = 0.5 cm/min

ranking order from a fracture test would be reversed for brittle fractures at high strain rates.

### ACKNOWLEDGEMENTS

The authors would like to thank the BP Plastics Department of BP Chemicals (International) Limited, who kindly supplied the impact polystyrene used in this study, and Miss E. Plati and Mr M. Parvin who assisted in obtaining the PVC and PC experimental data.

### REFERENCES

- Liu, H. W. 'Fracture toughness testing and its applications', *ASTM STP 381* 1965, p 23
- Brown, W. F. and Srawley, J. E. 'Plane strain crack toughness testing of high strength metallic materials', *ASTM STP 410* 1966, pp 12, 13
- Dugdale, D. S. *J. Mech. Phys. Solids* 1960, **8**, 100
- Griffith, A. A. *Phil. Trans. R. Soc. (A)* 1921, **221**, 163
- Irwin, G. R. 'Fracturing of metals', Am. Soc. Metals, Cleveland, 1948
- Orowan, E. *Rep. Prog. Phys.* 1949, **12**, 185
- Irwin, G. R. *J. Appl. Mech.* 1957, **24**, 361
- Irwin, G. R. *9th Int. Congr. Appl. Mech., Brussels* 1957
- Wells, A. A. *Br. Weld. Res. Assoc. Rep.* 1963, M13/1963
- Burdekin, F. E. and Stone, D. E. W. *J. Strain Anal.* 1966, **1**, 143
- Hayes, D. J. and Williams, J. G. *Int. J. Fract. Mech.* 1972, **6**, 239
- Fenner, D. N. *Int. J. Fract. Mech.* in press
- Ferguson, R. J. and Williams, J. G. *Polymer* 1973, **14**, 103
- Rice, J. R. *J. Appl. Mech.* 1968, **35**, 379
- Marshall, G. P., Culver, L. E. and Williams, J. G. *Int. J. Fract. Mech.* in press
- Rogan, J. *PhD Thesis* 1965, University of London
- Marshall, G. P., Culver, L. E. and Williams, J. G. *Plastics and Polymers* 1969, **37**, 75

# Note to the Editor

## Light scattering from terpolymer solutions

Hirotaro Kambe

*Institute of Space and Aeronautical Science, University of Tokyo, Komaba, Meguro-ku, Tokyo, Japan*

and Y. Kambe and C. Honda

*Showa College of Pharmaceutical Sciences, Tsurumaki, Setagaya, Tokyo, Japan*

(Received 24 April 1973)

The apparent molecular weight of terpolymer obtained from light scattering measurements is affected by the heterogeneity in composition as well as in molecular weight. In this note, we have extended the relationship between the apparent molecular weight and refractive index increment of a binary copolymer to the ternary system, and present some experimental results.

Terpolymer species  $i$  is characterized by the molecular weight  $M_i$  and the compositions  $w_{Ai}$ ,  $w_{Bi}$ , and  $w_{Ci}$ , i.e. weight fractions of the monomer units in a molecule of that species. Notations follow Yamakawa's system<sup>1</sup>. Apparent molecular weight obtained from Rayleigh ratio is expressed by:

$$M_{app} = \nu^{-2} \sum_i \nu_i^2 M_i w_i \quad (1)$$

where  $w_i = c_i/c$ , the ratio of the concentration of species  $i$  and the total concentration of terpolymer. The refractive index increments are written for species  $i$ :

$$\nu_i = w_{Ai} \nu_A + w_{Bi} \nu_B + w_{Ci} \nu_C$$

and for the terpolymer:

$$\nu = w_A \nu_A + w_B \nu_B + w_C \nu_C \quad (2)$$

where  $w_A$ ,  $w_B$ , and  $w_C$  are average compositions of the terpolymer, and  $\nu_A$ ,  $\nu_B$ , and  $\nu_C$  are the increments for respective homopolymers. The deviations of composition from the average value are expressed by

$\delta w_{Ai} = w_{Ai} - w_A$ ,  $\delta w_{Bi} = w_{Bi} - w_B$ , and  $\delta w_{Ci} = w_{Ci} - w_C$  where

$$\delta w_{Ai} + \delta w_{Bi} + \delta w_{Ci} = 0 \quad (3)$$

Substituting equations (2) and (3) into equation (1) and eliminating  $\delta w_{Ci}$ , we obtain the apparent molecular weight:

$$\begin{aligned} M_{app} &= \sum_i M_i w_i \left\{ 1 + \left( \frac{\nu_A - \nu_C}{\nu} \right) \delta w_{Ai} + \left( \frac{\nu_B - \nu_C}{\nu} \right) \delta w_{Bi} \right\}^2 \\ &= \langle M_w \rangle + 2P_A \left( \frac{\nu_A - \nu_C}{\nu} \right) + 2P_B \left( \frac{\nu_B - \nu_C}{\nu} \right) + \\ &\quad Q_A \left( \frac{\nu_A - \nu_C}{\nu} \right)^2 + Q_B \left( \frac{\nu_B - \nu_C}{\nu} \right)^2 + \\ &\quad 2R \left( \frac{\nu_A - \nu_C}{\nu} \right) \left( \frac{\nu_B - \nu_C}{\nu} \right) \end{aligned} \quad (4)$$

where

$$\begin{aligned} \langle M_w \rangle &= \sum_i M_i w_i, \\ P_A &= \sum_i M_i w_i (\delta w_{Ai}), \\ P_B &= \sum_i M_i w_i (\delta w_{Bi}), \\ Q_A &= \sum_i M_i w_i (\delta w_{Ai})^2, \\ Q_B &= \sum_i M_i w_i (\delta w_{Bi})^2, \end{aligned}$$

and

$$R = \sum_i M_i w_i (\delta w_{Ai})(\delta w_{Bi})$$

By putting  $C=B$ , equation (4) is reduced to the equation derived by Leng and Benoit<sup>2</sup> for the A-B binary copolymer. The weight-average molecular weight  $\langle M_w \rangle$  and the deviation parameters  $P_A$ ,  $P_B$ ,  $Q_A$ ,  $Q_B$  and  $R$  could be calculated from the measurements of the apparent molecular weight in at least six different solvents.

Terpolymer sample T74 was synthesized by radical polymerization corresponding to a 'partial azeotrope'<sup>3</sup> having a constant styrene/acrylonitrile ratio. Terpolymer T43 is far from 'partially' azeotropic and heterogeneous in composition. The compositions of terpolymers are shown in Table 1.

The composition of terpolymers at the beginning of terpolymerization and that at the given conversion are calculated by the Skeist method<sup>4</sup> with the Alfrey and Goldfinger's equation<sup>5</sup>, and are shown as the composition range in Table 1. The partially azeotropic terpolymer T74 has a negligibly small heterogeneity in composition and was fractionated due to the molecular weight<sup>6</sup>. The refractive index increment is calculated<sup>7</sup> with the terpolymer composition and refractive index increments of the parent homopolymers by equation (2). The results are consistent with the observed values. It means that equation (2) is confirmed in this system.

All measurements of light scattering from terpolymer solutions were carried out at 20°C with the Shimadzu Photometer PG-21 over the angular range 45° to 135°

Table 1 Composition of terpolymers

Sample	Monomer feed (mole fraction)			Conversion (wt %)	Composition range of terpolymer (wt fraction)			DMF $\nu_{calc.}$	DMF $\nu_{obs.}$
	S	AN	MMA		S	AN	MMA		
T74	0.55	0.15	0.30	6.1	0.6081~0.6075	0.0889~0.0886	0.3029~0.3039	0.1274~0.1272	0.1240
T43	0.147	0.693	0.160	8.5	0.4940~0.4725	0.2959~0.3052	0.2101~0.2223	0.1204~0.1182	0.1162

with a cylindrical cell and with a light source of 436 nm. Each solution was purified by centrifugation at  $20\,000 \times g$  for 1 h. The apparent molecular weight was determined from the Zimm plot. Refractive index increments were measured with light of 436 nm at  $20^\circ\text{C}$  with the Shimadzu Differential Refractometer DR-3. The apparent molecular weights, refractive index increments and the second virial coefficients in various solvents are shown in Table 2.

The refractive index increments for the homopolymer  $\nu_A$ ,  $\nu_B$  and  $\nu_C$  were calculated with the Gladstone-Dale equation, if all three homopolymers could not be dissolved in the solvent. The refractive index and density of a solvent are those referred to in data collected by Huglin<sup>8</sup>.

The typical Zimm plots in dioxane are shown in Figure 1. The second virial coefficient is apparently affected by the difference of composition in T74 and T43.

By solving six simultaneous equations corresponding to equation (4), we could obtain the parameters in equation (4). The data for six solvents are insufficient, however, to obtain the accurate values of deviation parameters, from which we could discuss the dispersion of composition in terpolymers. As shown in Table 2,

Table 2 Molecular weight,  $M_{app}$ , refractive index increment,  $\nu$  and second virial coefficient,  $A_2$  for terpolymers in various solvents

Solvent	T74			T43		
	$\nu$	$M_{app} \times 10^4$	$A_2 \times 10^{-4}$	$\nu$	$M_{app} \times 10^4$	$A_2 \times 10^{-4}$
Acetonitrile		insoluble		0.189	29.0	2.3
Methyl ethyl ketone	0.181	44.5	3.8	0.166	30.6	5.0
Tetrahydrofuran	0.159	47.6	7.8	0.147	29.1	7.3
Dimethylformamide	0.124	50.0	5.5	0.116	40.5	10.8
Dioxane	0.142	45.5	6.8	0.123	26.3	1.3
Chloroform	0.123	58.8	10.3	0.114	50.0	9.5
Toluene	0.065	52.6	3.6		insoluble	

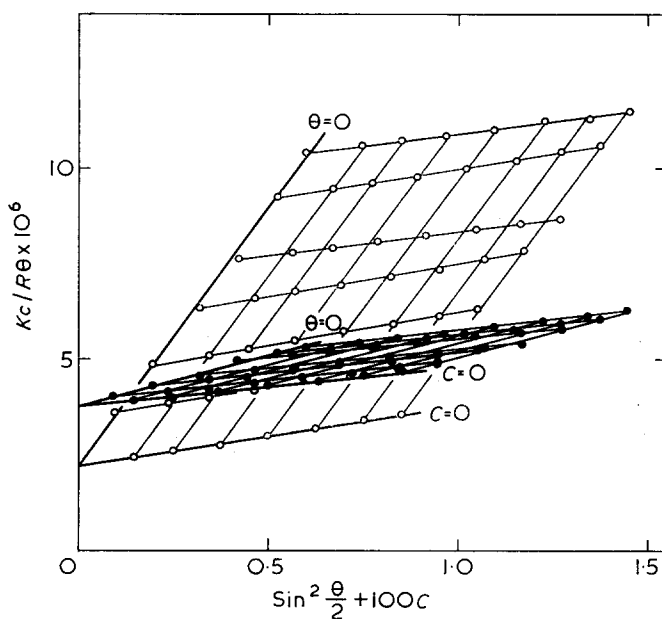


Figure 1 Zimm plots of T74 (○) and T43 (●) in dioxane at  $20^\circ\text{C}$  with 436nm light

the apparent molecular weights of T74 obtained with different solvents show a smaller dependence on solvent. On the other hand,  $M_{app}$  of T43 is varied significantly with solvent. This result corresponds to the width of composition range shown in Table 1.

REFERENCES

- 1 Yamakawa, H. 'Modern Theory of Polymer Solutions', Harper and Row, New York, 1971
- 2 Leng, M. and Benoit, H. *J. Chim. Phys.* 1961, **58**, 480
- 3 Ham, G. E. *J. Macromol. Chem.* 1966, **1**, 93
- 4 Skeist, I. *J. Am. Chem. Soc.* 1946, **68**, 1781
- 5 Alfrey, T. and Goldfinger, G. *J. Chem. Phys.* 1944, **12**, 322
- 6 Kambe, Y. *J. Macromol. Sci. (A)* 1973, **7**, 547
- 7 Kambe, Y. and Honda, C. *Angew. Makromol. Chem.* 1972, **25**, 163
- 8 Huglin, M. B. 'Light Scattering from Polymer Solutions', Academic Press, London, 1972

# Letters

## On the molecular weight distribution in condensation polymerization

### Introduction

The most probable molecular weight distribution in batch condensation polymerization was stated by Flory<sup>1</sup> to be

$$x_r = p^{(r-1)}(1-p) \quad (1)$$

where  $x_r$  is the number fraction of  $r$ -mers in a mixture formed by polymerization of a monomer with two functional groups. Here  $p$  is the fraction of the original number of such groups which have reacted in the formation of the mixture.

It is assumed that all groups are of the same reactivity, independent of the length of the chain to which they are attached.

Flory's argument was a statistical one, and is given in slightly different forms in other texts<sup>2,3</sup>. A kinetic derivation, based on an assumed order of reaction with a common value of the rate constant for condensation of molecules of all sizes, can also be carried through<sup>4</sup>.

In teaching this point students are not easily convinced by the statistical proof (the chance of a unit having reacted is indeed  $p$  but it may have reacted 'into' a molecule of any size, not only that under consideration). The kinetic treatment requires a particular model of the course of the reaction for the derivation to be given (though such a model is not unique). Watterson and Stafford<sup>5</sup> discuss the kinetic derivation of the molecular weight distribution, and take into account by-product concentrations and the fact that equilibrium (rather than complete reaction) may be attained. They also note that 'some of the steps in Flory's derivation are not conceptually easy to follow'.

The following derivation may be of interest. It relates directly to the way in which any one molecule is formed. The convolution integral involved is not a very deep concept, and the treatment is similar to that for the residence time distribution in a sequence of volumes or chemical plants.

### Derivation

For simplicity, let us consider the batch polymerization of HO-R-COOH (the copolymerization of di-alcohols with di-acids can be similarly dealt with). Let there be  $N_0$  molecules of HO-R-COOH initially in the batch, and let  $p'$  be the proportion of the original reactive end groups (henceforward called *groups*) which has reacted by the time  $t'$ . The symbols  $p'$  and  $t'$  will be used as running variables during the time period  $0 \rightarrow t$ , at the end of which the proportion of original groups remaining is  $(1-p)$ .

At any time  $t$  the number of unreacted monomer molecules will be  $N_0(1-p)^2$ , since for any one monomer to survive both its groups must remain unattacked, and this involves the square of the probability of either one of them remaining unattacked. The total number of groups, initially  $2N_0$ , is  $2N_0(1-p)$  at time  $t$ , so the total number of molecules is  $N_0(1-p)$ . Hence the

number fraction of monomer molecules is  $(1-p)$  at  $t$ , or  $(1-p')$  at  $t'$ .

Consider now the formation of dimer molecules in the time interval  $t'$  to  $t'+dt'$ . This is obtained by multiplying the number of groups on monomer molecules by the chance of any one group in the mixture reacting, and finally multiplying this product by the chance that such reaction as does occur is with another monomer molecule.

(A). Since the number of unreacted molecules at time  $t'$  is  $N_0(1-p')^2$ , the number of groups on monomer molecules is  $2N_0(1-p')$  at time  $t'$ .

(B). The rate of destruction of groups at time  $t'$  is  $2N_0(dp'/dt')$ . To express this as a fraction of groups existing at  $t'$  we must divide by  $2N_0(1-p')$ . Hence the chance of any one group reacting in the time interval  $t'$  to  $t'+dt'$  is  $(1-p')^{-1} \cdot (dp'/dt') \cdot dt'$ .

(C). The fraction of such reaction as is considered in (A) and (B) above being with another monomer molecule is  $(1-p')$ , since all molecules are assumed to have the same reactivity and the number fraction of monomer in the mixture surrounding a given group is  $(1-p')$ .

The product of (A), (B) and (C) is easily seen to be  $2N_0(1-p')^2 \cdot (dp'/dt') \cdot dt'$ . We must now divide by 2 since each monomer-monomer combination in the time interval  $dt'$  would otherwise be counted twice.

The number of dimer molecules formed in the time interval  $t'$  to  $t'+dt'$  is thus  $N_0(1-p')^2 \cdot (dp'/dt') \cdot dt'$ . We must now see how many of these will survive from time  $t'$  to  $t$ . The total number of groups at time  $t'$  is  $2N_0(1-p')$ , which number falls to  $2N_0(1-p)$  at time  $t$ . The fraction of groups at time  $t'$  which survive to time  $t$  is therefore  $(1-p)/(1-p')$ .

For a dimer molecule at time  $t'$  to survive to time  $t$  both its groups must remain unattacked, and its chance of survival is thus  $(1-p)^2/(1-p')^2$ . We therefore multiply the product of (A), (B) and (C) by

$$(1-p)^2/(1-p')^2$$

to find the number of dimer molecules formed between  $t'$  and  $t'+dt'$  and surviving until  $t$ . This result is:

$$N_0(1-p)^2 dp' \quad (2)$$

The total number of dimer molecules at time  $t$  is thus expression (2) integrated over all values of  $t'$  from 0 to  $t$ . This integral is:

$$N_0(1-p)^2 \int_0^p dp' = N_0 p (1-p)^2 \quad (3)$$

which gives the number fraction of dimers at time  $t$  as  $p(1-p)$ .

Consider now the formation of a trimer molecule. The previous derivation can be carried through until paragraph (C). We now wish to consider the reaction of a group on a monomer molecule with a *dimer*, and the number fraction of dimers in the mixture surrounding the given group is  $p'(1-p')$ . Also we do not divide by two, since our procedure for considering monomer-dimer reaction does not count each such event twice.

We could have considered dimer combining with monomer, with a similar resultant expression; but we must not consider this combination *as well as* the monomer combining with dimer.

The resultant expression equivalent to expression (2) is:

$$2N_0(1-p)^2 p' dp' \quad (4)$$

which, integrated over all values of  $t'$  from 0 to  $t$ , gives:

$$2N_0(1-p)^2 \int_0^p p' dp' = N_0 p^2 (1-p)^2 \quad (5)$$

which is to be compared with equation (3).

For the formation of tetramer we consider the combination of monomer+trimer (*or*, but not *as well as*, trimer+monomer), and dimer+dimer (which will require a factor of  $\frac{1}{2}$  to prevent double counting).

Paragraph (A) requires alteration for dimer-dimer combination, but this is straightforward, and following through the derivation gives:

$$N_0(1-p)^2 \int_0^p 3(p')^2 dp' = N_0 p^3 (1-p)^2 \quad (6)$$

Since the formation of  $r$ -mer from two blocks in all possible ways leads to:

$$N_0(1-p)^2 \int_0^p (r-1)(p')^{r-2} dp' = N_0 p^{r-1} (1-p)^2 \quad (7)$$

we have the general expression for number fraction as  $p^{r-1}(1-p)$ .

The consequences of this molecular weight distribution (and the derived number-averages, weight-averages, viscosity-averages, etc.) are well known. If the velocity constants for different sized molecules are not all equal the simple statistical arguments become invalid. The treatment given here could possibly be adapted, but such a situation focuses attention on the actual kinetics, and a kinetic derivation is thus to be preferred. Great care with the velocity constants between like and unlike molecules is required if incorrect factors of 2 are to be avoided.

The molecular weight distribution which will be obtained from a continuous polymerizing reactor will depend on the flow through and mixing in the reactor. This has been considered by, among others, Denbigh, and some of his results are to be found in Denbigh and Turner<sup>6</sup>. For the reason mentioned in the last paragraph there are some errors there, which I regret. These will be corrected, but the reader may care to find them for himself.

#### Acknowledgements

The purpose of this letter is to present an approach which was not previously known to me or my colleagues. I am grateful to a student, S. G. Trotter, whose persistence forced me to produce this treatment, to D. A. Blackadder for helpful comments, and to the referee, who required greater clarity in the presentation.

J. C. R. Turner

Department of Chemical Engineering,  
University of Cambridge,  
Cambridge CB2 3RA, UK

(Received 7 May 1973;  
revised 27 June 1973)

#### References

- 1 Flory, P. J. *J. Am. Chem. Soc.* 1936, **58**, 1877
- 2 Mark, H. and Tobolsky, A. V. 'Physical Chemistry of High Polymeric Systems', 2nd Edn, Interscience, New York, 1950, p 369
- 3 Tanford, C. 'Physical Chemistry of Macromolecules', John Wiley, New York, 1961, p 139
- 4 *Idem, ibid.* p 592
- 5 Watterson, J. G. and Stafford, J. W. *J. Macromol. Sci.* 1971, **A5**, 679
- 6 Denbigh, K. G. and Turner, J. C. R. 'Chemical Reactor Theory', 2nd Edn, Cambridge University Press, Cambridge, 1971, p 111

#### Crystallization of polyamides under elevated pressure: nylon-6 (polycapramide)

It is well known that elevated pressures, above 3 kbar, may strongly enhance the rate at which polymers such as polyethylene crystallize in extended chain conformation<sup>1, 2</sup>. Extended chain crystals may be grown either by pressure induced crystallization<sup>1</sup> or by annealing of folded chain crystals near the melting temperature as was reported for polyethylene by Rees and Bassett<sup>2</sup>.

This preliminary account describes the conditions that were found for extended chain crystallization of nylon-6 under elevated pressure. The polymer used throughout this study was synthesized by alkaline polymerization. The molecular weight was approximately  $90 \times 10^3$  as estimated from viscosity measurements. The crystallization experiments were carried out using a high pressure dilatometer, which consisted of two pistons and a thick-walled cylinder equipped with an appropriate heating device. The pressure was generated by a simple hydraulic press<sup>3</sup>.

Initially crystallization experiments were carried out by heating the nylon-6 samples to temperatures in the range 240 to 310°C and by applying pressures between 3 kbar and 8 kbar. These conditions did not lead to extended chain crystals but appear to favour severe decomposition of the polymer.

We succeeded in growing extended chain crystals after the caprolactam was removed and the nylon-6 was purified. This was accomplished by dissolving the polymer in formic acid. Subsequently the polymer was precipitated by pouring the solution into an excess of a 50% by weight mixture of acetone and water. Another essential step in the procedure was the removal of air from the sample by heating it up to 100°C and applying a pressure of 8 kbar for 15 h. After releasing the pressure the sample was heated to temperatures in the range of 240° to 310°C and crystallization was induced by applying pressures exceeding 3 kbar. The period of isothermal crystallization was 24 h after which the sample was cooled to room temperature at a speed of 10°C/h. That extended chain crystals were grown by this technique was inferred from the marked increase in melting temperature from 220°C for folded chain crystals to 240°C for pressure crystallized polymer. There is also a substantial difference between the fracture surfaces of the two types of crystals. The replicas of the folded chain crystals appear to be spherulitic in the electron microscope (*Figure 1*). An electron micrograph of the fracture surface of the extended chain crystals, shown in *Figure 2*, reveals that the surface is rather rough and that only little extended chain lamellae are



We could have considered dimer combining with monomer, with a similar resultant expression; but we must not consider this combination *as well as* the monomer combining with dimer.

The resultant expression equivalent to expression (2) is:

$$2N_0(1-p)^2 p' dp' \quad (4)$$

which, integrated over all values of  $t'$  from 0 to  $t$ , gives:

$$2N_0(1-p)^2 \int_0^p p' dp' = N_0 p^2 (1-p)^2 \quad (5)$$

which is to be compared with equation (3).

For the formation of tetramer we consider the combination of monomer+trimer (*or*, but not *as well as*, trimer+monomer), and dimer+dimer (which will require a factor of  $\frac{1}{2}$  to prevent double counting).

Paragraph (A) requires alteration for dimer-dimer combination, but this is straightforward, and following through the derivation gives:

$$N_0(1-p)^2 \int_0^p 3(p')^2 dp' = N_0 p^3 (1-p)^2 \quad (6)$$

Since the formation of  $r$ -mer from two blocks in all possible ways leads to:

$$N_0(1-p)^2 \int_0^p (r-1)(p')^{r-2} dp' = N_0 p^{r-1} (1-p)^2 \quad (7)$$

we have the general expression for number fraction as  $p^{r-1}(1-p)$ .

The consequences of this molecular weight distribution (and the derived number-averages, weight-averages, viscosity-averages, etc.) are well known. If the velocity constants for different sized molecules are not all equal the simple statistical arguments become invalid. The treatment given here could possibly be adapted, but such a situation focuses attention on the actual kinetics, and a kinetic derivation is thus to be preferred. Great care with the velocity constants between like and unlike molecules is required if incorrect factors of 2 are to be avoided.

The molecular weight distribution which will be obtained from a continuous polymerizing reactor will depend on the flow through and mixing in the reactor. This has been considered by, among others, Denbigh, and some of his results are to be found in Denbigh and Turner<sup>6</sup>. For the reason mentioned in the last paragraph there are some errors there, which I regret. These will be corrected, but the reader may care to find them for himself.

#### Acknowledgements

The purpose of this letter is to present an approach which was not previously known to me or my colleagues. I am grateful to a student, S. G. Trotter, whose persistence forced me to produce this treatment, to D. A. Blackadder for helpful comments, and to the referee, who required greater clarity in the presentation.

J. C. R. Turner

Department of Chemical Engineering,  
University of Cambridge,  
Cambridge CB2 3RA, UK

(Received 7 May 1973;  
revised 27 June 1973)

#### References

- 1 Flory, P. J. *J. Am. Chem. Soc.* 1936, **58**, 1877
- 2 Mark, H. and Tobolsky, A. V. 'Physical Chemistry of High Polymeric Systems', 2nd Edn, Interscience, New York, 1950, p 369
- 3 Tanford, C. 'Physical Chemistry of Macromolecules', John Wiley, New York, 1961, p 139
- 4 *Idem, ibid.* p 592
- 5 Watterson, J. G. and Stafford, J. W. *J. Macromol. Sci.* 1971, **A5**, 679
- 6 Denbigh, K. G. and Turner, J. C. R. 'Chemical Reactor Theory', 2nd Edn, Cambridge University Press, Cambridge, 1971, p 111

#### Crystallization of polyamides under elevated pressure: nylon-6 (polycapramide)

It is well known that elevated pressures, above 3 kbar, may strongly enhance the rate at which polymers such as polyethylene crystallize in extended chain conformation<sup>1, 2</sup>. Extended chain crystals may be grown either by pressure induced crystallization<sup>1</sup> or by annealing of folded chain crystals near the melting temperature as was reported for polyethylene by Rees and Bassett<sup>2</sup>.

This preliminary account describes the conditions that were found for extended chain crystallization of nylon-6 under elevated pressure. The polymer used throughout this study was synthesized by alkaline polymerization. The molecular weight was approximately  $90 \times 10^3$  as estimated from viscosity measurements. The crystallization experiments were carried out using a high pressure dilatometer, which consisted of two pistons and a thick-walled cylinder equipped with an appropriate heating device. The pressure was generated by a simple hydraulic press<sup>3</sup>.

Initially crystallization experiments were carried out by heating the nylon-6 samples to temperatures in the range 240 to 310°C and by applying pressures between 3 kbar and 8 kbar. These conditions did not lead to extended chain crystals but appear to favour severe decomposition of the polymer.

We succeeded in growing extended chain crystals after the caprolactam was removed and the nylon-6 was purified. This was accomplished by dissolving the polymer in formic acid. Subsequently the polymer was precipitated by pouring the solution into an excess of a 50% by weight mixture of acetone and water. Another essential step in the procedure was the removal of air from the sample by heating it up to 100°C and applying a pressure of 8 kbar for 15 h. After releasing the pressure the sample was heated to temperatures in the range of 240° to 310°C and crystallization was induced by applying pressures exceeding 3 kbar. The period of isothermal crystallization was 24 h after which the sample was cooled to room temperature at a speed of 10°C/h. That extended chain crystals were grown by this technique was inferred from the marked increase in melting temperature from 220°C for folded chain crystals to 240°C for pressure crystallized polymer. There is also a substantial difference between the fracture surfaces of the two types of crystals. The replicas of the folded chain crystals appear to be spherulitic in the electron microscope (*Figure 1*). An electron micrograph of the fracture surface of the extended chain crystals, shown in *Figure 2*, reveals that the surface is rather rough and that only little extended chain lamellae are

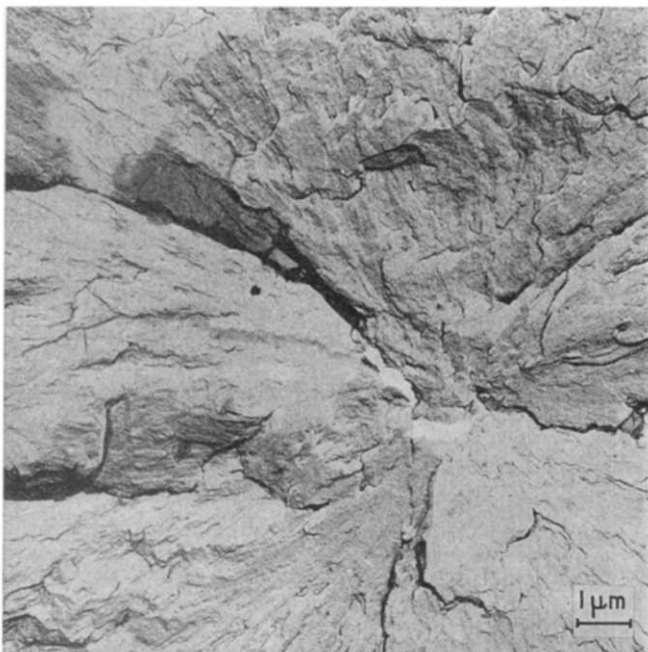


Figure 1 Electron micrograph of a replica of a fracture surface of nylon-6 crystallized at ambient pressure

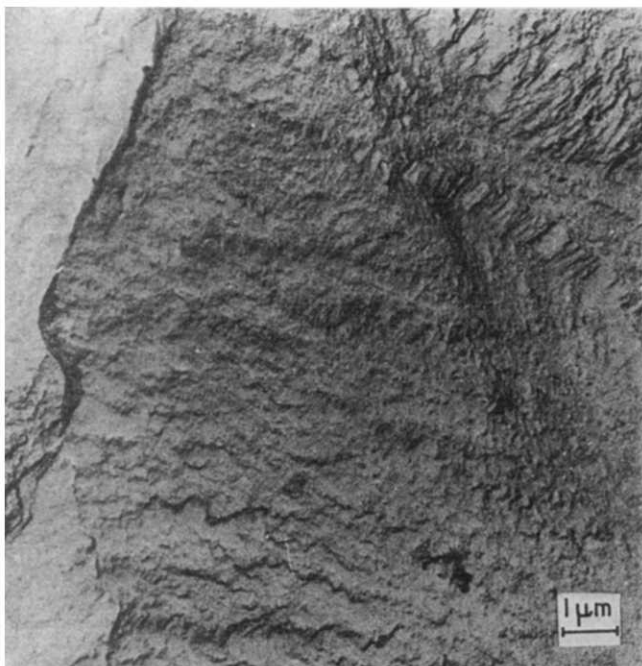


Figure 2 Electron micrograph of a fracture surface of purified nylon-6 crystallized at 260°C for 24 h under a pressure of 6 kbar

present of the type that was found abundantly in polyethylene samples. A similar surface structure was observed by Liberti and Wunderlich<sup>4</sup> for zone polymerized nylon-6. The rare occurrence of these striated extended chain lamellae in these fracture surfaces might be due to the fact that the surface free energy of 001 planes, containing the chain ends, is considerably lower than that of the lateral planes, some of which are bound by the strong hydrogen bonds, so that the high pressure crystallized samples fracture preferentially along the 001 planes. Evidence for this supposition is provided by infra-red reflection spectroscopy<sup>5-7</sup> on the fracture surfaces. Figure 3 shows that in the spectrum of the

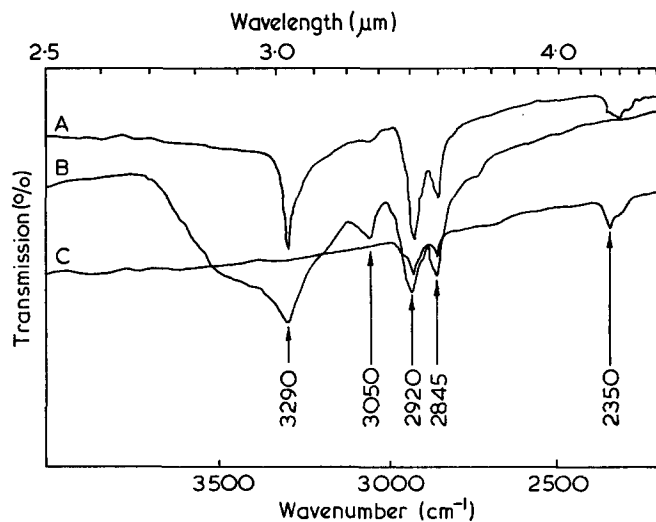


Figure 3 Infra-red spectra of nylon-6 surface of: A, internal reflection spectrometry technique applied to folded chain crystals; B, transmission spectrum of extended chain crystals; C, i.t.r. technique applied to surface of extended chain crystals

fractured surface of the extended chain nylon-6, as taken by the infra-red internal reflection spectrometry (i.r.s.), the strong absorption band at 3300  $\text{cm}^{-1}$  which is associated with stretching vibration of the NH bond connected by hydrogen bonding to the carbonyl group of neighbouring chain is totally absent. This hydrogen bond absorption peak does occur in the i.r.s. spectrum of folded chain crystals and in the transmission spectrum of the extended chain crystals. The i.r.s. spectrum of the fracture surface of the extended chain nylon-6 reveals a relatively strong absorption at 2350  $\text{cm}^{-1}$  which also occurs much less pronounced in the i.r.s. spectrum of the folded chain crystals. This peak originates from impurities which apparently were rejected quite effectively from crystal growth front in the high pressure crystallization experiment.

More details about the high pressure crystallization of polyamides and the application of the i.r.s. method to the study of fracture surfaces will be given in future publications.

S. Gogolewski

On leave from:

Technical University of Łódź,  
Institute of Artificial Fibres,  
Dept. of Physical Chemistry of Polymers,  
Łódź, Zwirki 36, Poland

and A. J. Pennings

Dept. of Polymer Chemistry,  
State University of Groningen,  
Groningen, The Netherlands

(Received 9 July 1973)

#### References

- 1 Wunderlich, B. and Arakawa, T. *J. Polym. Sci. (A)* 1964, 2, 3697
- 2 Rees, D. V. and Bassett, D. C. *Nature* 1968, 219, 368
- 3 Pennings, A. J. and Pijpers, M. F. J. to be published
- 4 Liberti, F. N. and Wunderlich, B. *J. Polym. Sci. (A-2)* 1968, 6, 833
- 5 Harrick, N. J. *Int. Conf. Mol. Spectros. Bologna* 1959
- 6 Harrick, N. J. *Phys. Rev. Lett.* 1960, 4, 224
- 7 Fahrenfort, J. *Spectrochim. Acta* 1961, 17, 698

# New polymer systems: chain extension by dianhydrides\*

R. A. Rhein and J. D. Ingham

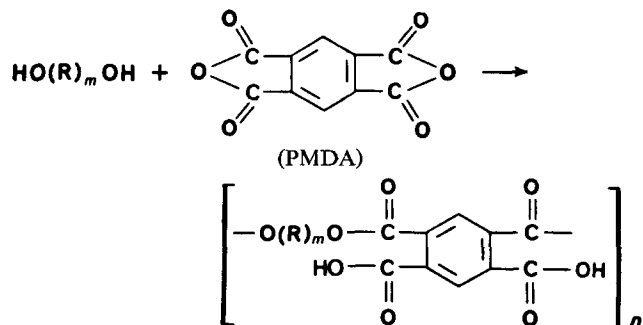
Jet Propulsion Laboratory, California Institute of Technology, Pasadena, Calif. 91103, USA  
(Received 13 December 1972)

New highly stable polymers are required for materials applications on future long-term planetary missions. The results of a systematic investigation on the use of anhydrides to prepare stable elastomeric materials using mild reaction conditions are presented. The three anhydrides investigated were found to provide effective chain extension of hydroxy-terminated poly(alkylene oxides) and polybutadienes. These were tetrahydrofuran tetracarboxylic dianhydride, pyromellitic dianhydride, and benzophenone tetracarboxylic dianhydride. The most effective catalyst investigated was ferric acetylacetonate, which resulted in chain extension at 333 K. A novel feature of these anhydride reactants is that they are difunctional as anhydrides, but tetrafunctional if conditions are selected that lead to reaction of all carboxyl groups. Therefore, chain extension can be effected and then followed by crosslinking via the residual carboxyl groups.

## INTRODUCTION

The objective of this work is the development of stable elastomeric systems for solid-propellant binders applicable to long-term planetary missions. Achieving this objective requires dimensional and mechanical stability as well as insensitivity to radiation. Such elastomers should evolve a minimum of volatile products. These new elastomers should be useful in other applications. Previous work has shown that anhydrides can be used to chain-extend hydroxy-terminated prepolymers (ref. 1 and related unpublished JPL work); however, chain extension was limited and reaction conditions were relatively severe. The work reported here was conducted to obtain higher molecular weights and determine the effects of different catalysts, diols, and dianhydrides.

Diols included poly(propylene oxide) (PPO), poly(ethylene oxide) (PEO), and polybutadienes. For a polymer of increased stability, saturated hydrocarbon prepolymers will be more extensively tested in future work. Anhydrides included tetrahydrofuran tetracarboxylic dianhydride (THFTDA), pyromellitic dianhydride (PMDA), and extension can be illustrated by:



\* This paper presents the results of one phase of research carried out at the Jet Propulsion Laboratory, Calif. Inst. of Technol., under Contract No. NAS7-100, sponsored by the National Aeronautics and Space Administration and was published in *JPL Q. Tech. Rev.* 1972, 1 (4), 97 and *Rubber Chem. Technol.* 1972, 45, 1554.

where R is a monomeric unit in the prepolymer; extension can be illustrated by where R is a monomeric unit in the prepolymer,  $m$  is the prepolymer degree of polymerization, and  $n$  is the degree of polymerization of the extended prepolymer.

## RESULTS AND DISCUSSION

For most of the experiments, poly(propylene oxide) of mol.wt. 2000 and hydroxyl of 1.0 equiv./kg (Union Carbide, Lot 439430) was used as the diol. Approximate intrinsic viscosities  $[\eta]$  were calculated from:

$$\eta_{sp}/C = [\eta] + 0.39[\eta]^2C$$

from measurements at one concentration  $C$  in benzene-dimethylformamide at 303 K. This relation is strictly valid only for PPO-toluene diisocyanate (TDI) polymers<sup>2</sup> but is used here for comparison of anhydride polymers with the values obtained for PPO-TDI, as an approximation of the degree of chain extension. For the extension of prepolymers, the dianhydride and low molecular weight polymer were stirred at 448–468 K to dissolve the anhydride; the catalyst (if any) was added, and the solution was cured in a vacuum oven at the desired temperature.

Since imidazole had been found to be a catalyst for the reaction of alcohols with PMDA for hydroxyl analytical methods<sup>3</sup>, it was tested as a catalyst for the reaction of PPO with PMDA. The desired catalytic effect was found to be negligible. At a mole ratio of PMDA to PPO (AN/OH) of 1.0 and a curing temperature of 373 K, the values of  $[\eta]$  were 1.6 and 1.5 m<sup>3</sup>/kg in the presence (21 h cure) and absence (24 h cure) of imidazole, respectively. The catalyst concentration was 0.2 mol per mol of PMDA. There are two functions of a catalyst in systems of this type. Not only should it increase the rate of the desired chain-extension reaction, but it is also desirable that it increases this ratio relative to side-reaction rates. Therefore, although imidazole was found

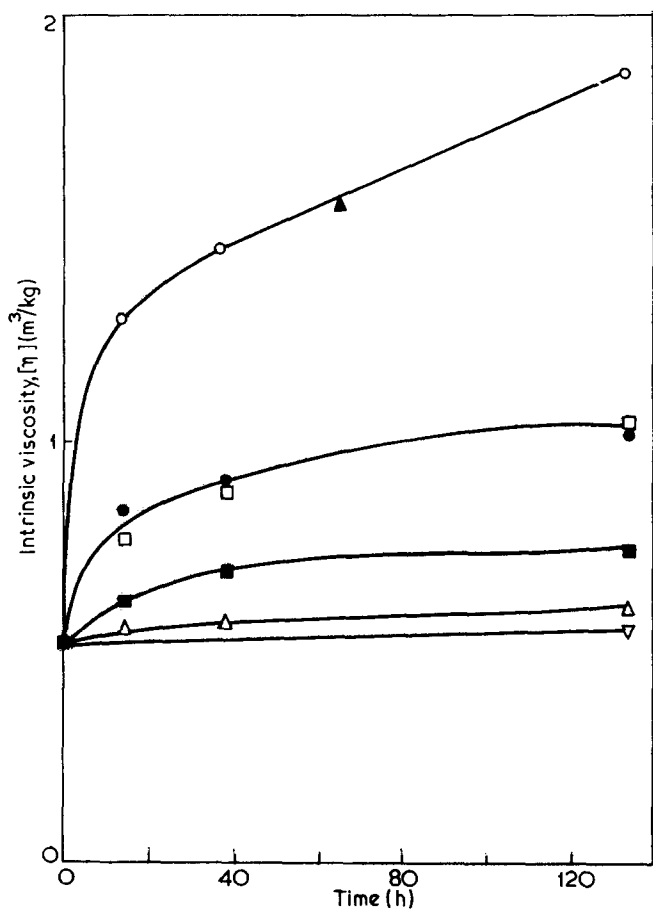
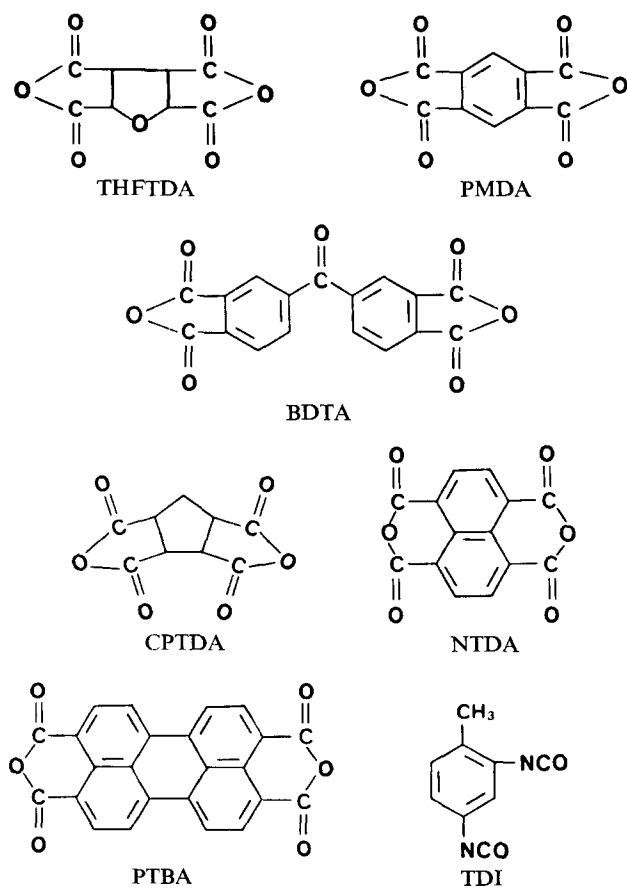


Figure 1 Solution viscosity of anhydride chain-extended poly(propylene oxide). Temperature=333 K; AN/OH=1.05. ○, THFTDA; ●, PMDA; □, BTDA; ■, CPTDA; △, NTDA; ▽, PTBA; ▲, TDI



to increase the chain-extension rate at times shorter than 24 h, the final molecular weight for longer cure times was no higher when it was present, indicating that side-reaction rates were also catalysed. When short reaction times are desired, as for analytical methods, imidazole is an effective catalyst for anhydride-hydroxyl reaction. Further work showed that imidazole, pyrrole, and pyridine did not give higher values of  $[\eta]$  than no catalyst for cure times from 14 to 134 h at 333 K with a mole ratio of PMDA to PPO of 1.05. The intrinsic viscosities were always  $1.1 (\pm 0.3) \text{ m}^3/\text{kg}$  under these conditions.

However, the presence of ferric acetylacetonate (FeAA) resulted in an intrinsic viscosity of  $\sim 2.4 \text{ m}^3/\text{kg}$  in 66 h at 333 K. The ratio of FeAA/anhydride was 0.2; thus, the catalyst concentration was higher and the effect less than for isocyanate-hydroxyl reactions. In an experiment in which the FeAA to anhydride or diisocyanate ratio was 0.002, the extended anhydride and isocyanate polymers had  $[\eta] = 1.8$  and  $8.8 \text{ m}^3/\text{kg}$ , respectively. However, the reactant ratio was probably more nearly optimum for the urethane polymer, accounting for part of the larger increase in molecular weight.

Figure 1 indicates the effect on  $[\eta]$  when PPO was chain-extended with several different anhydrides in the absence of catalyst at 333 K. THFTDA resulted in the highest molecular weights and was as effective as TDI under these conditions. Inspection of the results in Figure 1 indicates that the rate of chain extension may depend on the solubility parameters of anhydride and diol.

From Figure 2, it can be seen that the anhydride-hydroxyl mole ratio is in the vicinity of 1.05 for maximum chain extension. The value appears to be relatively

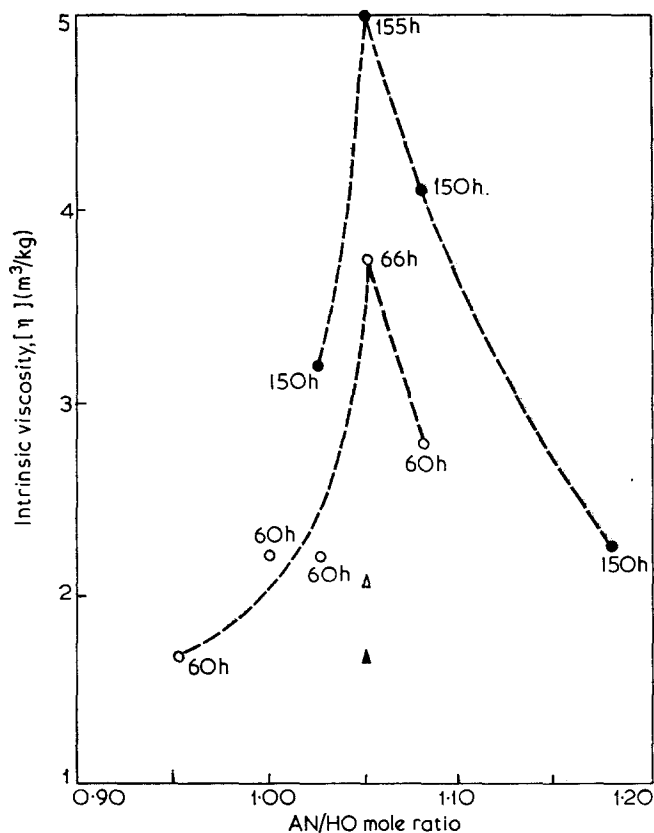


Figure 2 Solution viscosity of anhydride-poly(propylene oxide) versus anhydride to hydroxyl mole ratio. Temperature=345 K; ○, ●, FeAA/THFTDA mole ratio=0.2; △, CuAA (66 h); ▲, NiAA (66 h)

critical and somewhat less than the value of 1.10 generally used for NCO/OH ratios. Figure 2 also shows that FeAA is a much more effective catalyst for anhydride extension than CuAA or NiAA, which is also true for the isocyanate reaction.

Some experiments were also carried out at higher temperatures, for which gelation times were measured. Results are indicated in Figure 3. Because of esterification following anhydride ring opening, it appears that a crosslinked network can be formed and gelation may occur in 150 h at 373 K. The apparent upward curvature at lower temperatures is probably real but even if it is not, the relative rate of anhydride opening would be approximately six times faster than esterification at 333 K (60°C), indicating that negligible esterification would take place under normal low-temperature curing conditions for this system.

Table 1 shows some results obtained for chain extension and crosslinking of poly(ethylene oxide), polybutadienes and a reduced saturated polybutadiene. The higher temperature, 463 K, was used to dissolve the anhydride in the prepolymer. For these prepolymers, considerable chain extension and some crosslinking took place during the dissolution, as indicated by high initial intrinsic viscosities and gel formation within 10 min at 463 K in some cases.

Table 1 Prepolymer chain extension with THFTDA

Prepolymer	Time (min)	Temperature (K)	Mole ratio AN/OH	Initial $[\eta]^a$ (m <sup>3</sup> /kg)	Final $[\eta]^a$ (m <sup>3</sup> /kg)
Poly(ethylene oxide) <sup>b</sup>	3960 (66 h)	345	1.05 <sup>c</sup>	0.8	1.6
Telagen-Sd	10	463	1.05	0.8	2.3
Telagen-Sd	60	463	1.16 <sup>c</sup>	—	Gel
Telagen-Sd	1080 (18 h)	345	1.05	—	Gel
Hycar HTB <sup>e</sup>	10	463	1.00	0.6	6.4
Butarez HTS <sup>f</sup>	10	463	1.05	1.5	3.0
Butarez HTS <sup>f</sup>	18	345	1.05	—	Gel
Poly-BD, CN-15 <sup>g</sup>	10	463	1.05	—	Gel
Poly-BD, R-45M <sup>g</sup>	10	463	1.05	—	Gel
Poly-BD, R-15M <sup>g</sup>	10	463	1.05	—	Gel
Poly-BD, R-45HT <sup>g</sup>	10	463	1.05	—	Gel
Poly-BD, CS-15 <sup>g</sup>	10	463	1.05	—	Gel

<sup>a</sup> Viscosities obtained by single-point measurements using  $\eta_{sp}/C = [\eta] + 0.4[\eta]^2 C$

<sup>b</sup> A. G. Fluka, mol.wt. 2000

<sup>c</sup> Contained FeAA/anhydride mole ratio = 0.05

<sup>d</sup> Saturated polybutadiene  $\alpha, \omega$ -diol, GT and R, Lot 242 AM 148AH, hydroxyl 0.91 equiv./kg

<sup>e</sup> Polybutadiene  $\alpha, \omega$ -diol, B. F. Goodrich, Lot V-74, hydroxyl 0.38 equiv./kg

<sup>f</sup> Polybutadiene  $\alpha, \omega$ -diol, Phillips Petroleum, Lot 4760, hydroxyl 0.51 equiv./kg

<sup>g</sup> Hydroxy-terminated polybutadienes, ARCO Chemical (all hydroxyl values from suppliers data): CN-15, Lot 003061, hydroxyl 0.58 equiv./kg; R-45, Lot 008281, hydroxyl 0.70 equiv./kg; R-15M, Lot 710291, hydroxyl 0.65 equiv./kg; R-45HT, Lot 006041, hydroxyl 0.84 equiv./kg; CS-15, Lot 912211, hydroxyl 0.62 equiv./kg

## CONCLUSIONS AND RECOMMENDATIONS

It has been found that THFTDA readily chain-extends PPO to high molecular weights in the presence of FeAA catalyst at 343 K or lower. The reaction with hydrocarbon prepolymers appears to take place at higher rates, even in the absence of a catalyst.

Further work, particularly with saturated hydrocarbon prepolymers, should be conducted to define the minimum dissolution temperature and to determine which dianhydride will produce maximum chain extension and minimum esterification at moderate temperatures. Crosslinking of the carboxyl groups formed on ring opening should be investigated further, especially to form crosslinks at temperatures below 373 K. Trifunctional hydroxyl compounds, as well as metallic salts or oxide, should be tested. The former would be analogous to triols in urethane system, whereas the latter should provide salt crosslinks that would react with some of the free carboxyl groups and may tend to increase chemical stability.

## REFERENCES

- Ingham, J. D. in 'Supporting Research and Advanced Development', Space Programs Summary 37-52, Jet Propulsion Laboratory, Pasadena, Calif., 1968, Vol III, pp 97-98
- Moacanin, J. J. *Appl. Polym. Sci.* 1959, 1, 272
- Kingston, H. M., Garey, J. J. and Hellwig, W. B. *Analyt. Chem.* 1969, 41, 86

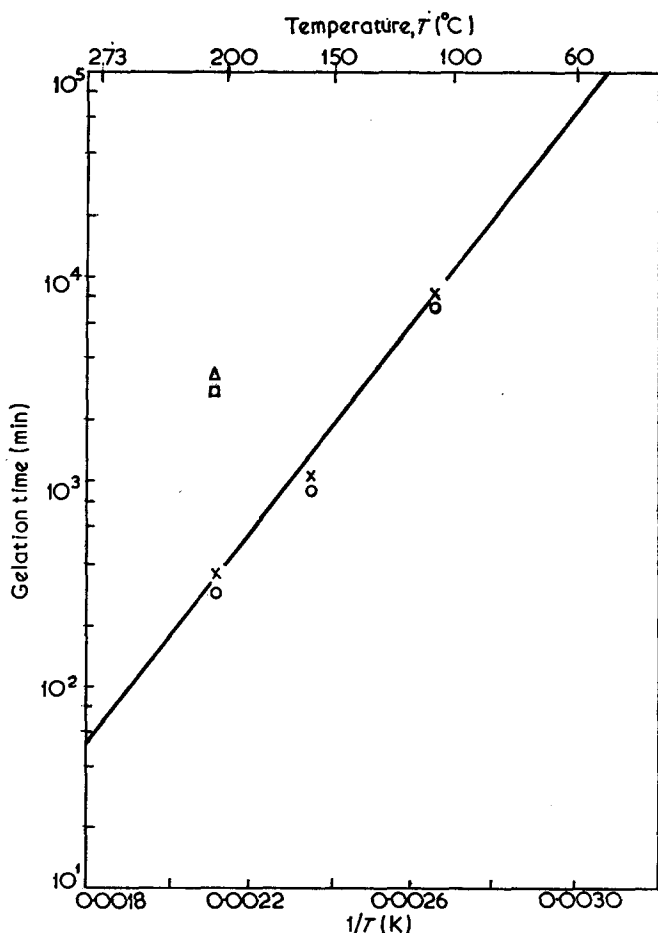


Figure 3 Gelation time versus temperature for anhydride-poly(propylene oxide) polymers. x, THFTDA; o, THFTDA + 0.05 FeAA<sub>3</sub>; Δ, PMDA; □, PMDA + 0.05 FeAA<sub>3</sub>

# Craze shape and fracture in poly(methyl methacrylate)

H. R. Brown\* and I. M. Ward

Department of Physics, University of Leeds, Leeds LS2 9JT, UK  
(Received 14 March 1973; revised 24 May 1973)

The shape of the primary craze at the tip of a crack has been studied by optical microscopy for two grades of poly(methyl methacrylate). The craze shapes are compared with the predictions of the Dugdale model for the plastic zone at a crack tip, and used to obtain a quantitative estimate of the craze stress and the effective stress intensity factor. The values of the stress intensity factor are then compared with those obtained directly from fracture toughness measurements.

## INTRODUCTION

It is now generally accepted that crazing is an essential part of the failure mechanism in brittle polymers such as poly(methyl methacrylate) (PMMA) and polystyrene<sup>1</sup>. Kambour<sup>2</sup>, following the pioneering research of Berry<sup>3</sup>, has shown that a slow crack propagates through a primary craze with the crack and craze tip growing together. Kambour<sup>4</sup> and Bessenov and Kuvshinskii<sup>5</sup> have studied the nature of the primary craze and shown that it can readily be observed in PMMA and polystyrene using optical microscopy.

The aim of the research now reported is to make quantitative measurements of the shape of this primary craze, under both loaded and relaxed conditions, and to compare these shapes with the predictions of the Dugdale model<sup>6</sup> for the plastic zone at a crack tip. In this way it is possible to make the link with fracture mechanics measurements for slow crack propagation under stable conditions, a situation which has been extensively studied in recent years<sup>7-9</sup>. The measurements of the craze shape will be used to obtain a quantitative estimate of the craze stress and the effective stress intensity factor, which can be compared with that obtained directly from fracture mechanics measurements. The results then provide valuable information concerning the nature of crazes and their modes of failure.

## EXPERIMENTAL

### Materials

Measurements were made on two types of PMMA: a commercial grade manufactured by ICI Ltd, Perspex cast sheet; and a cast sheet from an experimental sample of PMMA plasticized with 7% dibutyl phthalate. The latter sample has an appreciably lower modulus and yield stress.

### Measurements of craze shape

The measurements were made using the compact tension (CT) specimens shown in *Figure 1* (see also ref. 10). This method has the advantage that providing

the initial notch (the saw cut) is sufficiently long the crack travels in a straight line across the specimen without the latter being grooved. For the stress intensity measurements the specimen dimensions were 50 mm × 46.7 mm, the shape being in accordance with the requirements proposed by Brown and Srawley<sup>11</sup>. For determination of the craze dimensions, a similar specimen of smaller dimensions (~5 mm × 10 mm) was examined in an optical microscope, looking down vertically on to the crack tip in a direction normal to the crack plane (arrow in *Figure 1*). The craze and crack tip was observed in reflected light, as in the previous investigations of Kambour, and Bessenov and Kuvshinskii.

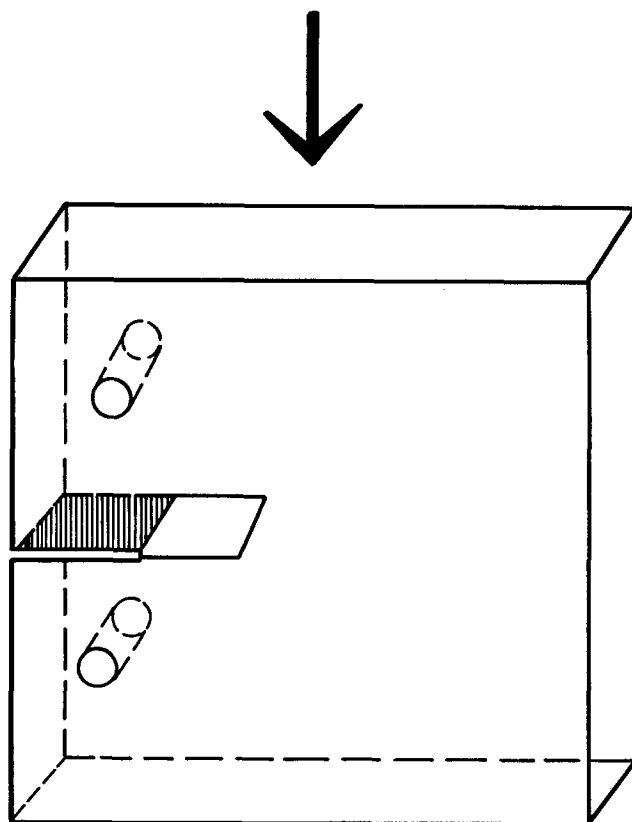


Figure 1 Compact tension specimen

\* Seconded from ICI Corporate Laboratory, Runcorn, Cheshire, UK.

The crack was initiated and propagated by pushing a razor blade slowly into the CT specimen. This method gave excellent control of the crack propagation which is important because of the small field of view in the microscope. Photographs were taken in both white and monochromatic light of the fringe patterns associated with moving cracks, stationary loaded cracks and unloaded cracks. The high level of illumination required to photograph the moving cracks was obtained with a mercury arc lamp. The photographic negatives were scanned with a microdensitometer to obtain accurate fringe positions.

#### Fracture toughness measurements

The measurements of fracture toughness were undertaken by the method described in a previous paper<sup>10</sup>. The initial crack formed by slowly pushing a razor blade into the base of the saw cut and the specimen pulled apart on an Instron testing machine at constant cross-head speed so that the crack travelled across the specimen at approximately constant speed. The stress intensity factors ( $K_1$ ) were calculated using the boundary collocation calculations of Brown and Srawley<sup>11</sup>, from the load  $P$  as the crack passed scratch lines marked along the crack path. The Young's modulus,  $E$ , of the polymer was also determined using the Irwin-Kies relation<sup>12</sup>:

$$\frac{K_1^2}{E^*} = \frac{P^2}{2B} \frac{dc}{da} \quad (1)$$

where  $c$  is the compliance of the specimen,  $B$  and  $a$  the width and length of the crack respectively, and  $E^*$  the reduced modulus. [ $E^* = E$ , in plane stress and  $E/(1 - \nu^2)$  in plane strain, where  $\nu$  is Poisson's ratio].

Brown and Srawley give:

$$K_1 = \frac{P}{B} Y(a) \quad (2)$$

where  $Y(a)$  is a function of crack length. Combining equations (1) and (2) we have:

$$c = \frac{1}{E^*} \int Y^2(a) da \quad (3)$$

$E^*$  can then be obtained from a plot of the calculated value of  $\int Y^2(a) da$  against the experimentally measured compliance.

## RESULTS

### The craze shape: general considerations

Examples of the fringe patterns observed are shown in Figures 2-7 and typical microdensitometer traces in Figures 8 and 9. If it is assumed that the refractive index within the craze is a constant, the shape of the crazes can be plotted from these results. These shapes are shown in Figures 10, 11 and 12, where the vertical scale contains the unknown refractive index of the craze. This is a function of the strain in the craze, which in turn depends on the conditions of the test. In the Perspex specimens the stationary loaded craze and the moving craze showed very similar dimensions. It can be seen by comparison of Figures 10 and 11, that the moving craze shows a slight decrease in maximum craze thickness, which is in agreement with previous observations by Kambour. This was not the case for the plasticized

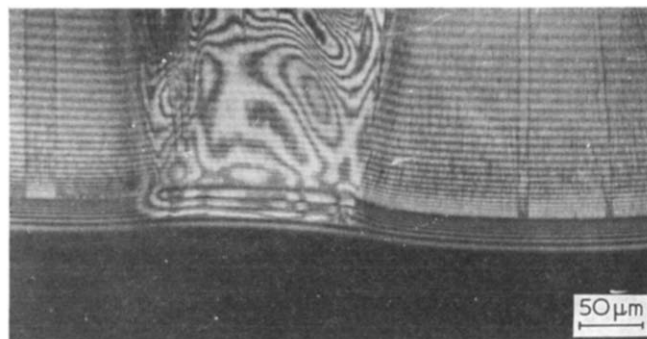


Figure 2 Overall view of crack and craze in Perspex

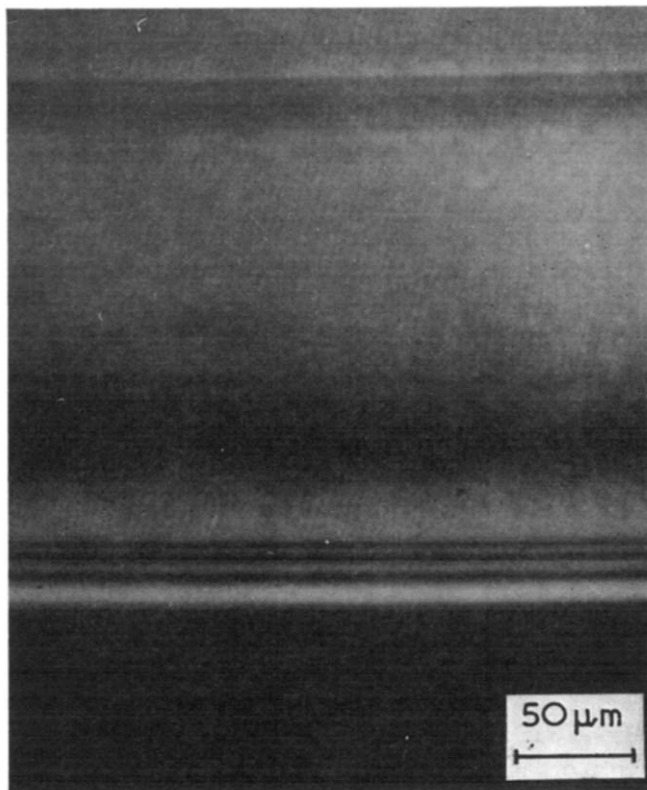


Figure 3 Unloaded crack and craze in Perspex

PMMA, where both the length and thickness of the craze were seen to be very velocity dependent, the moving craze always possessing smaller dimensions.

The fringe patterns observed as the crack was unloaded and reloaded showed that the craze is highly elastic, as previously reported by Kambour<sup>4</sup>. On unloading, about four of the fringes in the crack disappeared on a line at its tip and on reloading they reappeared. This showed that the crack tip is extremely blunt, and suggests a shape of the form shown in Figure 10.

### The craze shape: quantitative considerations

As has been mentioned, the vertical scale in Figures 10, 11 and 12 contains the unknown refractive index of the craze, which is a function of the strain in the craze, and in turn depends on the loading situation and the test conditions.

The observations reported in the previous section confirm the previous conclusions of Kambour that the material in the craze can be regarded as a spongy elastic



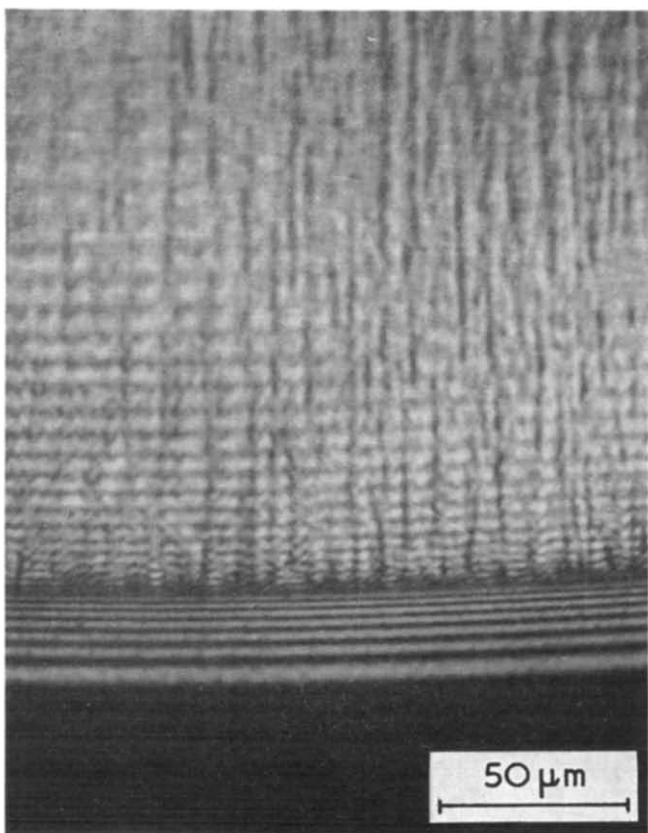


Figure 4 Loaded crack and craze in Perspex

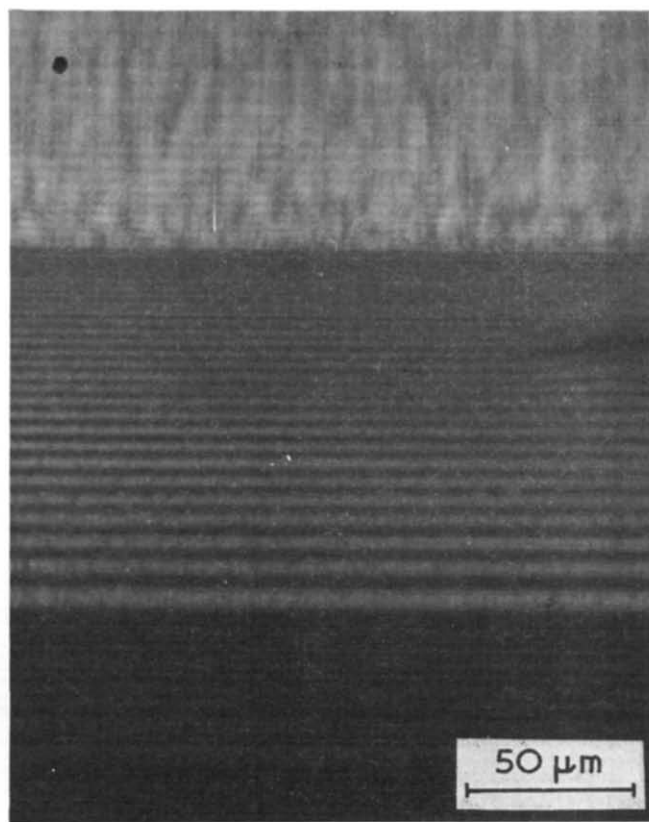


Figure 6 Loaded stationary crack and craze in plasticized PMMA

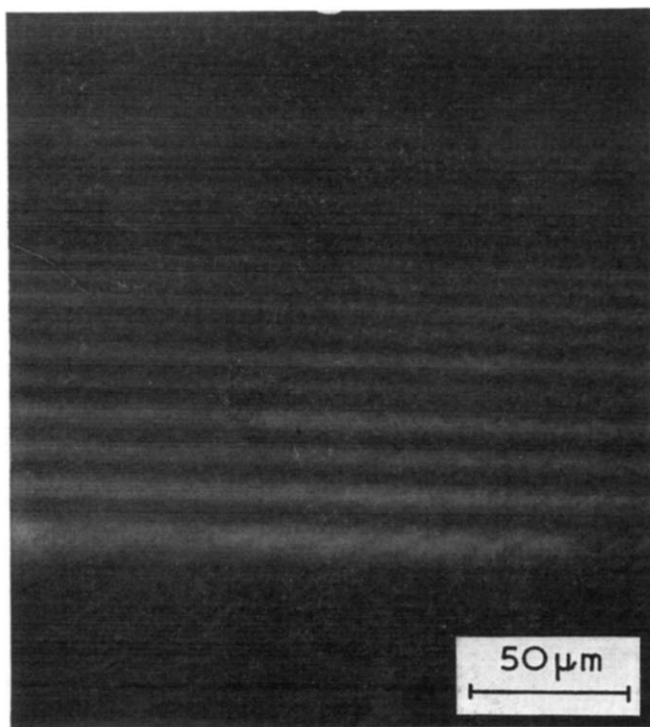


Figure 5 Unloaded crack and craze in plasticized PMMA

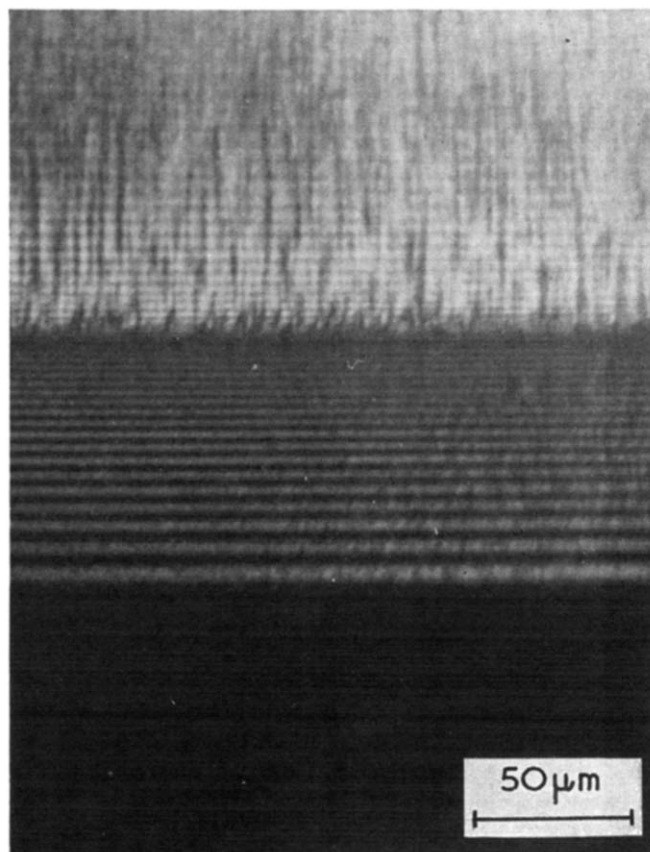


Figure 7 Loaded moving crack and craze in plasticized PMMA

solid<sup>4</sup>. His approach is followed to calculate the refractive index of the craze in terms of the strain in the craze, but as there is an apparent error in his calculation the result is derived from first principles.

The refractive index of the unstrained craze  $\mu_0$ , is related to the mean polarizability per unit volume  $\bar{p}$  by

the Lorentz-Lorenz equation:

$$\frac{\mu_0^2 - 1}{\mu_0^2 + 2} = \frac{4}{3} \pi \bar{p} \quad (4)$$



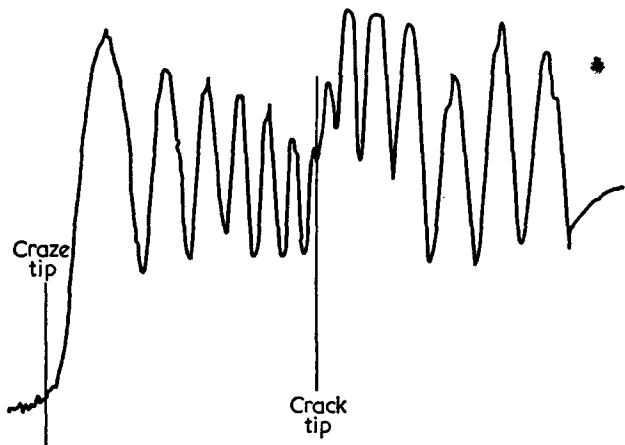


Figure 8 Microdensitometer trace of crack and craze in Perspex

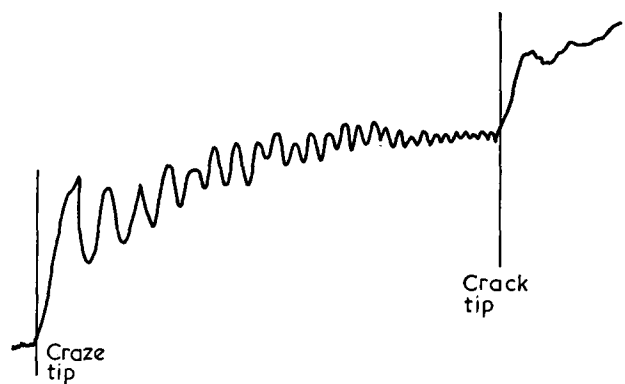


Figure 9 Microdensitometer trace of craze in plasticized PMMA

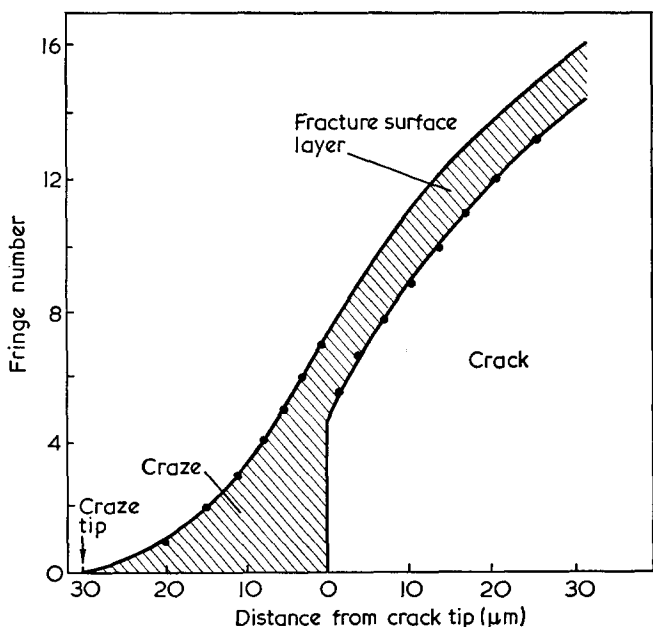


Figure 10 Configuration of crack tip and craze in Perspex under loaded stationary conditions, calculated from the interference patterns

If we assume that the craze extends with complete lateral constraint, the principal effect of strain will be a decrease in  $\bar{p}$  due to the decrease in density  $\rho$ , any orientational effects being very much smaller [cf. birefringence for extension ratio  $3=1 \times 10^{-3}$  (ref. 13)]. We have:

$$\bar{p} = \frac{\rho_0 \rho}{\rho_0} = \frac{\rho_0}{\lambda} \quad (5)$$

where  $\lambda$  is the extension ratio of the craze and the new refractive index  $\mu$  is given by:

$$\frac{\mu^2 - 1}{\mu^2 + 2} = \frac{4}{3} \pi \bar{p} = \frac{4}{3} \pi \frac{\rho_0}{\lambda} = \frac{\mu_0^2 - 1}{\mu_0^2 + 2} \cdot \frac{1}{\lambda} \quad (6)$$

Adopting the value for  $\mu_0$  of 1.32 proposed by Kambour<sup>14</sup>, we have:

$$\frac{\mu^2 - 1}{\mu^2 + 2} = \frac{0.2}{\lambda}$$

which gives  $\mu^2 = 1 + 0.6/(\lambda - 0.2)$ .

If  $n_b$  and  $n_0$  are the number of fringes in the craze at break and unloaded respectively, then

$$\frac{n_b}{n_0} = \frac{\mu_B \lambda}{\mu_0} = \left\{ 1 + \frac{0.6}{\lambda - 0.2} \right\}^{1/2} \frac{\lambda}{1.32}$$

$$= 1 + \frac{\lambda - 1}{1.32} \quad (\text{to a very good approximation})$$

or

$$\lambda - 1 = 1.32 \left\{ \frac{n_b}{n_0} - 1 \right\}$$

This formula differs from that previously obtained by Kambour<sup>4</sup>.

The experimental results showed values of  $n_b/n_0$  in the range 2-3 which gives  $\lambda$  in the range 2.3-3.6 and the refractive index of the craze at break  $\mu_B$  in the

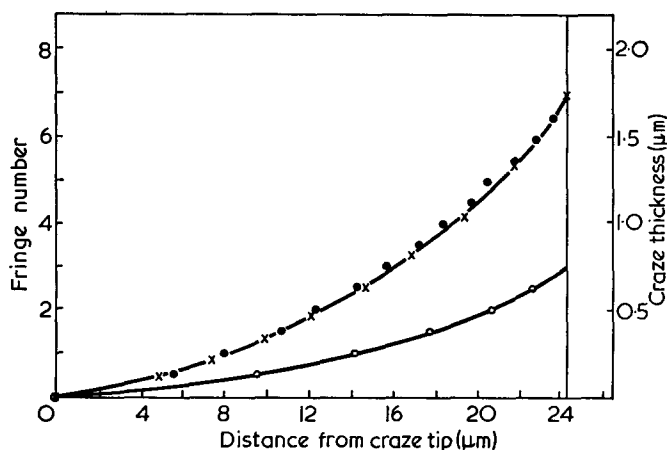


Figure 11 Shape of loaded moving (●) and unloaded (○) crazes in Perspex calculated from the interference patterns. ×, best fit to the Dugdale model

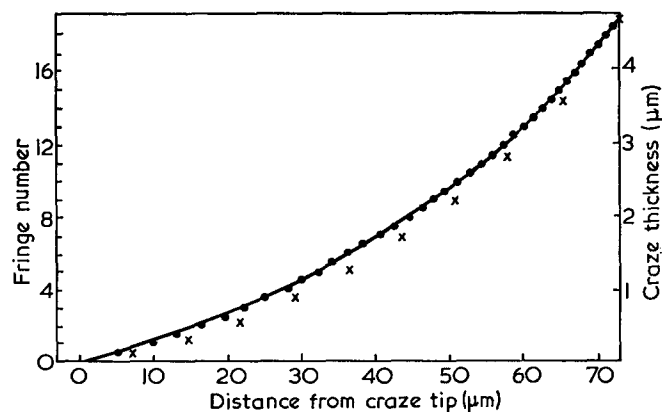


Figure 12 Shape of loaded moving craze in plasticized PMMA, calculated from the interference patterns. ×, best fit to the Dugdale model

range 1.15–1.09. Figure 11 shows that to a very good degree of approximation, the retardation pattern of the craze at break is exactly proportional to that at zero load. The simplest explanation of this result is that the refractive index of the craze is constant along the craze, so that the retardation pattern gives an exact representation of the shape of the craze. With this assumption the shape of the crazes can be plotted in terms of the absolute dimensions, and this has been done on the right hand side of Figures 11 and 12.

#### Fracture toughness measurements

The stress intensity factors for Perspex and the plasticized PMMA were found to be in the ranges 0.97–0.92 MN m<sup>-3/2</sup> and 0.91–0.87 MN m<sup>-3/2</sup> respectively, with the crack velocity varying from 9 to 5 mm/min. This value for Perspex agrees very well with that reported by Marshall *et al.*<sup>15</sup>. The values of  $E^*$  for the Perspex and plasticized PMMA obtained from Figure 13 were  $(2.90 \pm 0.05) \times 10^9$  N m<sup>-2</sup> and  $(2.38 \pm 0.03) \times 10^9$  N m<sup>-2</sup>, demonstrating the considerable plasticization of the latter material. The value of  $E^*$  for Perspex agrees very well with the low strain time independent value of the Young's modulus  $E$  quoted by Ogorkiewicz<sup>16</sup>. This agreement confirms that the majority of the elastic stored energy involves material at low strain, and moreover affords some support for the assumption of plane stress.

#### DISCUSSION

##### Comparison of craze dimensions with Dugdale plastic zone

We now wish to compare the shapes of these primary crazes with the shapes predicted by the Dugdale plastic zone model<sup>6</sup>. This model describes the situation in an infinite plate with a crack in the  $x_1$  direction for  $x_1 \leq 0$ , which is loaded by a uniform stress  $\sigma$  applied at infinity in the  $x_2$  direction (Figure 14). The stress field produced by the stress  $\sigma$  is given by expressions of the form:

$$\sigma_{ij} = \frac{K_1}{(2\pi r)^{1/2}} f_{ij}(\theta) \quad (7)$$

where  $\sigma_{ij} = \sigma_{11}, \sigma_{12}, \sigma_{22}$ ;  $r = [x_1^2 + x_2^2]^{1/2}$ ; and  $f_{ij}(\theta)$  are simple trigonometrical functions (see for example ref. 17, p 216). Yielding of the material at the crack tip is con-

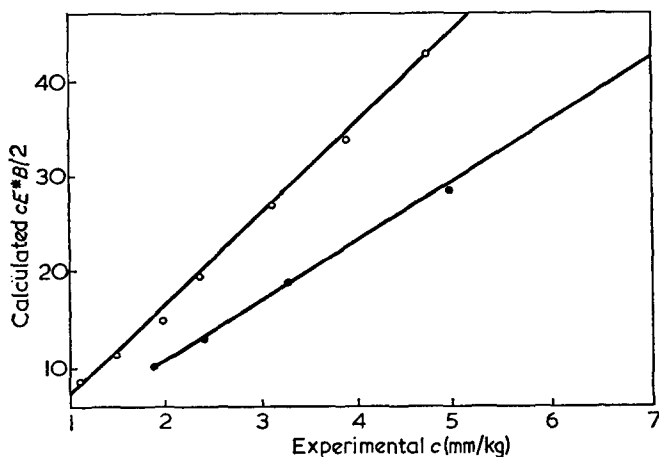


Figure 13 Calculated values of  $cE^*B/2$  against measured compliance  $c$  for Perspex (○) and plasticized PMMA (●). (For symbols see text).

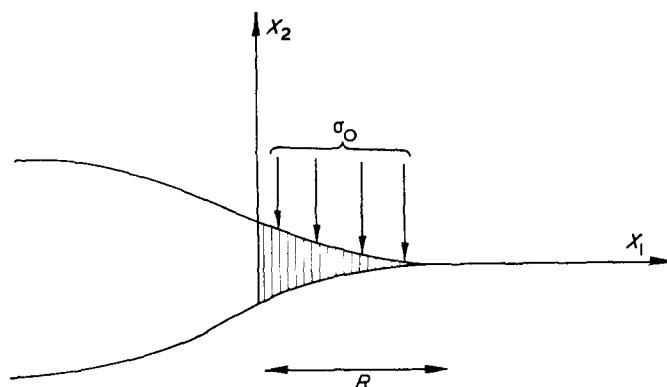


Figure 14 The Dugdale plastic zone

sidered as making the crack longer by the length  $R$  of the plastic zone and there is a series of internal tensile stresses of magnitude  $\sigma_0$  in the  $x_2$  direction acting on the extended crack surface over the region  $0 < x_1 < R$ . These internal stresses are chosen so that the stress singularities produced by the two stress fields just cancel, and no stresses exist in excess of the yield stress of the material.

The length of the plastic zone is then given by:

$$R = \frac{\pi}{8} \frac{K_1^2}{\sigma_0^2} \quad (8)$$

and the corresponding separation distance  $\delta$  in the plastic zone is:

$$\delta = \frac{8}{\pi E^*} \sigma_0 R \left[ \xi - \frac{x_1}{2R} \log \left( \frac{1+\xi}{1-\xi} \right) \right] \quad (9)$$

where  $\xi = \left( 1 - \frac{x_1}{R} \right)^{1/2}$

These expressions have been derived by Rice<sup>17</sup>.

The crack opening displacement  $\delta_t$  is the value of the separation distance  $\delta$  at the crack tip where  $x_1 = 0$ , and is therefore:

$$\delta_t = \frac{8\sigma_0 R}{\pi E^*} = \frac{K_1^2}{\sigma_0 E^*} \quad (10)$$

In the application of the Dugdale zone model to metals it is assumed that the plastic deformation is confined to the plane of the crack and  $\sigma_0$  is conventionally taken as the uniaxial tensile yield stress. It is now required to establish whether the model can also apply to the situation of a crack travelling through the primary craze in a polymer. In this case one could not expect a perfect fit because there is a finite volume of crazed material which means that the boundary on which the internal stresses (now assumed to be equal to the craze stress of the polymer) act is not a plane. However, the discrepancies can be expected to be small because the thickness of the craze is small compared with its length.

An important feature of this model is that it is not very dependent on the stress criteria for craze formation. The line of travel of the crack  $x_1 = 0$  is a line of zero shear stress within the plane but maximum triaxial stress. From our understanding of the stress criteria for crazing<sup>18</sup> we can argue that such a stress field will favour crazing and that since the craze length is determined by the requirement that the stress singularity at the crack tip is cancelled the stress at the crack tip will rise to meet the stress criteria for crazing.

Figure 11 shows the shape of a craze in front of a crack in the Perspex cast sheet travelling at  $3 \times 10^{-5}$  mm/sec, together with the best fit of these results to equation (9). The excellent fit suggests that the Dugdale model represents the situation very well. In this case the moving craze had a length of  $24.2 \mu\text{m}$  and a thickness corresponding to 7.0 fringes. The unloaded craze showed approximately 3 fringes. From these results the refractive index of the craze at break was calculated to be 1.10, giving a craze thickness at the crack tip of  $1.73 \mu\text{m}$ . This provides a value for the crack opening displacement  $\delta_t$  which can be used together with the experimental value of  $E^*$ , to calculate the stress intensity factor  $K_1$  and the craze stress  $\sigma_0$ , on the basis of equations (8) and (10). We find  $K_1 = 0.65 \text{ MN m}^{-3/2}$  and  $\sigma_0 = 8.1 \times 10^7 \text{ N m}^{-2}$ . This value for the stress intensity factor is appreciably lower than the value of  $0.95 \text{ MN m}^{-3/2}$  found for this material at the faster crack speeds  $\sim 7$  mm/min, but compares very well with the value of  $0.71 \text{ MN m}^{-3/2}$  found by Marshall *et al.*<sup>9</sup> at the lower crack speeds of these craze studies. The excellent agreement confirms the basic assumption involved in the model, in particular that the stress across the craze is constant along the length of the craze. The value for the craze stress would be expected to be similar to that for the tensile yield stress in Perspex at room temperature, as typically crazing and yield can be seen to occur simultaneously in a tensile test<sup>19</sup>. The shear stress at a strain rate of  $4 \times 10^{-4} \text{ sec}^{-1}$  was found to be  $5 \times 10^7 \text{ N m}^{-2}$ <sup>20</sup> (corresponding to a tensile yield stress of rather less than  $10 \times 10^7 \text{ N m}^{-2}$ ). Again, therefore, there is good quantitative agreement between the Dugdale zone model and other experimental data.

In the case of the plasticized PMMA, there is not such a good fit between the observed shape of the craze and that predicted by the Dugdale zone model. In Figure 12 the experimental results are compared with Dugdale plastic zones of first the same maximum width and second the same maximum length. It can be seen that the fit is not as good as in Perspex, possibly because the craze length is too long for all the elastic stresses except the singular one to be ignored in the calculations.

The similarity between the deviations from the Dugdale model for the loaded and unloaded crazes does suggest that again the stress across the craze is constant along the length of the craze. With some reservations in this case we can proceed to calculate the stress intensity factor  $K_1$  and the craze stress  $\sigma_0$ , from the length of the craze and the crack opening displacement determined from the craze thickness at the crack tip. For the moving crack we find  $K_1 = 0.83 \text{ MN m}^{-3/2}$  and  $\sigma_0 = 6.2 \times 10^7 \text{ N m}^{-2}$ . This value for the stress intensity factor is not very different from that measured at much faster rates in the direct experiments and suggests that the effects of crack speed in this material may be much less than in unplasticized PMMA. The value for the craze stress is very much lower than for the unplasticized PMMA, as is to be expected, and the comparatively similar value of the fracture toughness arises because there is a considerable relative increase in the crack opening displacement.

#### Variability in the craze patterns

The crack front in Perspex was very dependent on the manner of starting the crack, and the general view in Figure 2 shows that it was also rough in places across

a given crack front. From this Figure it can also be seen that the rough fracture mode was tougher than the smooth mode. We would therefore expect the direct bulk measurement of  $K_1$  to yield a greater value than that obtained from craze measurements of the smooth fracture areas. The memory which Perspex exhibits<sup>21</sup> in its fracture behaviour is probably due to the co-existence of these two stable crack propagation modes which are set up by the initial notching procedure.

The plasticized PMMA, on the other hand, showed no tendency to produce rough cracks. In this case it would therefore be expected, first that the value of  $K_1$  measured from craze dimensions would agree better with the direct bulk measurement value, and secondly that there would be no material memory effects.

These observations, which are subsidiary to the present study, offer scope for future investigations concerned with the relationships between macroscopic fracture toughness measurements and the nature of the crack and craze patterns.

## CONCLUSIONS

The results reported show that the Dugdale plastic zone model provides a good starting point for a study of the quantitative relationship between primary craze formation and fracture toughness measurements in polymers. This suggests a model for crack propagation in which the craze nucleates well in front of the crack and steadily enlarges as it approaches the crack tip. We have shown that the simplest interpretation of the craze interference patterns is that the material in the craze, no matter what its thickness, is extended to a fixed extension ratio  $\lambda$  (in the range 5–7 with respect to the uncrazed material) as the crack propagates. For the relaxed craze we have  $\lambda \sim 2$ . The success of the Dugdale model implies that the stress across this extended craze is just the stress necessary to craze more material (i.e. the critical craze stress, similar to the yield stress), and does not depend on the stress-strain properties of the craze itself. As in the application of the Dugdale model to metals we have replaced a complicated elastic-plastic problem by an equivalent problem in small strain elasticity, and made an assumption equivalent to perfect plasticity by assuming that the stress behaviour of the craze can be represented by a single parameter, the craze stress.

The other important parameter in these experiments is the crack opening displacement  $\delta_t$ . When the craze reaches this limiting thickness it breaks on a line down the middle, and the broken craze material contracts within a very short distance to the thickness expected for an unloaded craze of density  $\sim 60\%$  that of PMMA.

It is interesting to consider what factors may control the maximum craze thickness and why the craze should in general break down the middle. In this respect it is important to note that there is no evidence that the stress across the craze increases at the critical opening displacement. A possible explanation is that craze fracture is an activated process. The craze then breaks down the middle because this is the material which has been subjected to stress for the longest time. Moreover, the craze length and hence the craze thickness will be controlled by the stress-time dependence of fracture with no stress increase at the crack tip.

We then have to understand how the craze shows

considerable extensibility and fails at the comparatively low stress of  $\sim 10^7 \text{ N m}^{-2}$ . There are at least two proposals which one has to consider. One is the suggestion of Gent<sup>22</sup> that crazing is a process in which the dilation causes a drop in  $T_g$  to the experimental temperature so that the polymer is in the rubbery state. Studies of the fracture of rubbers<sup>23</sup> confirm that a stress of  $6\text{--}8 \times 10^7 \text{ N m}^{-2}$  is required to fracture a rubber at room temperature at a strain rate of  $1 \text{ sec}^{-1}$ , the breaking extension being  $\sim 5$ . The other view, supported by Kambour<sup>24</sup>, is that the craze is like an open-cell polymer foam. This accounts for the high elasticity of the craze and the measured values of craze modulus, but leaves craze fracture as a complex, time-dependent process involving large amounts of viscous energy. It should prove of particular value to extend the present studies by varying polymer composition and test conditions (e.g. presence of hostile environments) in order to throw light on these ideas.

#### REFERENCES

- 1 Rabinowitz, S. and Beardmore, P. Ford Motor Company, Publication Preprint 1971
- 2 Kambour, R. P. *J. Polym. Sci. (A)* 1965, **3**, 1713
- 3 Berry, J. P. in 'Fracture Processes in Polymeric Solids', (Ed. B. Rosen), Interscience, New York, 1964
- 4 Kambour, R. P. *J. Polym. Sci. (A-2)* 1966, **4**, 349
- 5 Bessenov, M. I. and Kuvshinshii, E. V. *Soviet Phys. (Solid State)* 1961, **3**, 1957
- 6 Dugdale, D. S. *J. Mech. Phys. Solids* 1960, **8**, 100
- 7 Benbow, J. J. and Roesler, F. C. *Proc. Phys. Soc.* 1957, **B70**, 201
- 8 Berry, J. P. *J. Polym. Sci.* 1961, **50**, 313
- 9 Marshall, G. R., Culver, L. E. and Williams, J. G. *Plastics and Polymers* 1968, **36**, 75
- 10 Brown, H. R. and Ward, I. M. *J. Mater. Sci.* in press
- 11 Brown, Jr, W. F. and Srawley, J. F. *ASTM STP* 1966, p 410
- 12 Irwin, G. R. and Kies, J. A. *Welding J. Res. Suppl.* 1954, **33**, 1935
- 13 Kashiwagi, M., Folkes, M. J. and Ward, I. M. *Polymer* 1971, **12**, 697
- 14 Kambour, R. P. *Polymer* 1964, **5**, 143
- 15 Marshall, G. P., Culver, L. E. and Williams, J. G. personal communication (1970)
- 16 'Engineering Properties of Thermoplastics' (Ed. R. M. Ogor-kiewicz) Wiley-Interscience, London, 1970
- 17 Rice, J. R. in 'Fracture—An Advanced Treatise' (Ed. H. Liebowitz) Academic Press, New York and London, 1968, Ch 3
- 18 Sternstein, S. S., Ongchin, L. and Silverman, A. *Appl. Polym. Symp.* 1968, **7**, 165
- 19 Beardmore, P. *Phil. Mag.* 1969, **19**, 389
- 20 Duckett, R. A., Rabinowitz, S. and Ward, I. M. *J. Mater. Sci.* 1970, **5**, 909
- 21 Williams, J. G. personal communication
- 22 Gent, A. N. *J. Mater. Sci.* 1970, **5**, 925
- 23 Smith, T. L. 'Rheology', Vol 5, Academic Press, New York, 1969, Ch 4
- 24 Kambour, R. P. General Electric Company Report No. 68-C-304, Schenectady, New York, 1968

# Morphology and fracture of compression moulded TPX

T. W. Owen and D. Hull

*Department of Metallurgy and Materials Science, University of Liverpool, PO Box 147, Liverpool L69 3BX, UK*  
(Received 30 April 1973)

The microstructure of compression moulded TPX, a semi-crystalline copolymer based on poly(4-methylpentene-1), has been examined using several techniques and has been shown to consist of small clusters of lamellar blocks about  $5\ \mu\text{m}$  in diameter. It is suggested that the clusters represent the early stage of spherulitic growth. The tensile properties of this material have been measured at temperatures between 77 and 420K. There is a sharp change in tensile ductility at about 290K which corresponds with a change in the micro-deformation processes. Optical studies have shown that between 285 and 330K ductility is associated with stress whitening and that above 330K large scale drawing occurs. Optical observations together with examination of thin sections in the electron microscope indicate that whitening is due to the formation of a large number of very fine irregular crazes. The microstructure of the crazes resemble those formed in polystyrene and other amorphous polymers.

## INTRODUCTION

The present work is concerned with understanding the fracture morphology of compression moulded TPX which is an ICI grade of semi-crystalline copolymer based on poly(4-methylpentene-1) (P4MP1). The polymer was first described in 1955 by Natta *et al.*<sup>1</sup> and possesses several unusual properties, one of which is transparency. The material has a low density ( $0.83\ \text{g/cm}^3$ ) and a high melting point (513K). In the crystalline state, the molecules take up a helical arrangement<sup>2</sup> and the conformation consists of seven monomer units for every two turns of the helix. Because of the space required for this arrangement, the density of the crystalline regions is slightly less than the density of the amorphous regions at room temperature<sup>3</sup>. Degrees of crystallinity have been reported by several people for compression moulded P4MP1. Both Crissman *et al.*<sup>4</sup> using density measurements, and Woodward *et al.*<sup>5</sup> using an n.m.r. technique obtained values of 50%. This is consistent with the value given for the commercial polymer by ICI.

## EXPERIMENTAL

The material was supplied by the Plastics Division of ICI in the form of pellets. Compression moulded sheets, 3 mm thick, were prepared by preheating the pellets to 548K for 10 min and compressing them for 5 min between chrome-plated glazing sheets in a picture frame mould at a pressure of  $5\ \text{MN/m}^2$ . The sheets were then cooled whilst under pressure.

For etching studies, sections were prepared by cutting with a jeweller's saw followed by hand grinding on emery papers and hand polishing on 'Gamma Alumina' paste. The most satisfactory etching was achieved with 6M chromic acid at 353K for 12 h. The solution was

agitated every 2 h. The etched sections were examined using a scanning electron microscope (Stereoscan).

Tensile specimens, which were cut from the sheets using a jeweller's saw, had a parallel gauge length of 30 mm and the edges were polished in a similar way to the etched sections. The tensile tests were carried out on an Instron tensile machine, using a crosshead speed of  $0.05\ \text{cm/min}$  for the majority of the tests. A Wessel apparatus<sup>6</sup> was used for the low temperature tests in a liquid nitrogen vapour. For the high temperature tests, a hot air oven was used. The fractured specimens were examined using optical microscopy and the Stereoscan. For scanning microscopy the specimens were coated with a gold-palladium alloy in a vacuum evaporation unit.

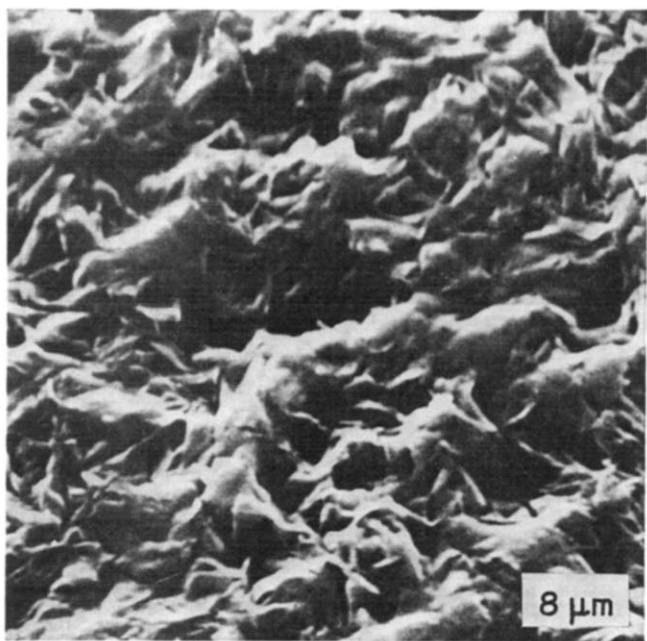
Thin slices, approximately  $750\ \text{\AA}$  thick, for examination by transmission electron microscopy were prepared at room temperature using an LKB ultramicrotome. The sections were collected on copper grids and were not stained or shadowed. Some sections were strained whilst on the grid using a separate tensile stage, and were then subsequently examined in the microscope.

## OBSERVATIONS

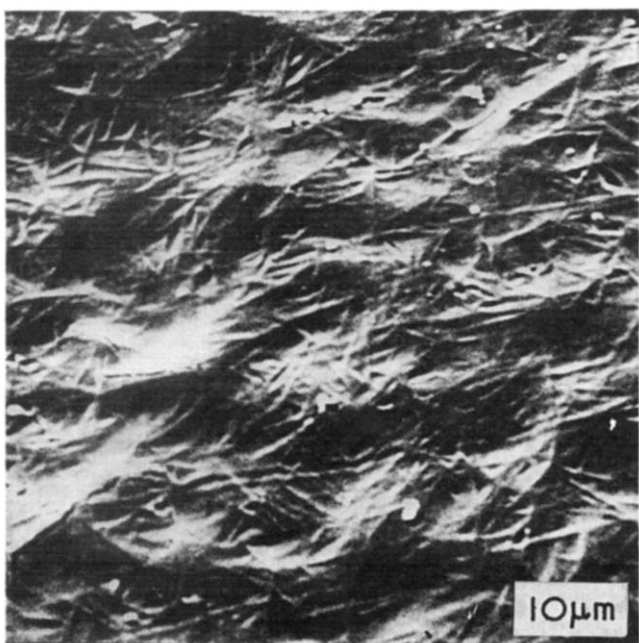
### *Structure*

The structure of this material was examined briefly. Thin sections were prepared parallel and normal to the sheet and examined using the wide angle X-ray diffraction method. The photographs showed no evidence of preferred orientation in either section. Smooth, sharp and continuous diffraction lines were obtained. The Bragg angles were consistent with a tetragonal unit cell as determined by Frank *et al.*<sup>2</sup>, with lattice parameters  $a$  and  $c$  of  $18.60\ \text{\AA}$  and  $13.53\ \text{\AA}$  respectively.

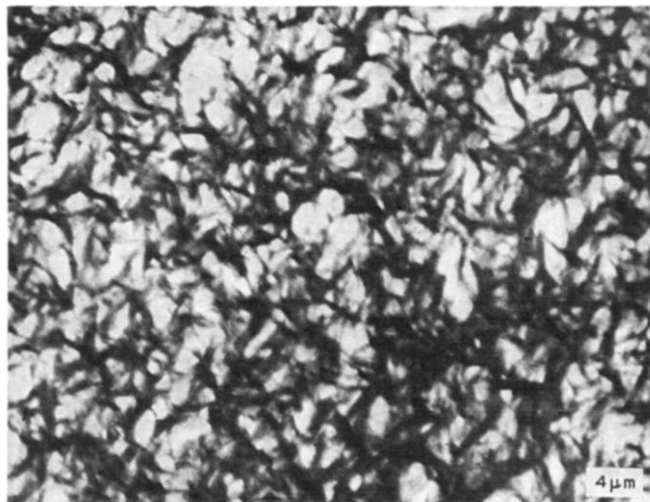
Sections were cut parallel and at right angles to the sheet, and were then polished and etched. The surface had a fine matt appearance and was uniformly attacked by the etchant, again indicating that there was no preferred orientation. The surface morphology was examined in the Stereoscan and the structure is shown in *Figure 1*. The dimension of the uniform hillock structure is approximately 3 to 5  $\mu\text{m}$ . Compression moulded surfaces and hand polished surfaces were studied directly in the Stereoscan. During observation, the originally smooth surface became rumpled as a result of beam heating and 'damage' (*Figure 2*). The rumpling is in the form of rounded undulations and is similar to that observed by Heavans *et al.*<sup>7</sup> in polyoxymethylene in similar circumstances. A needle-like structure is superimposed on the



*Figure 1* Stereoscan micrograph of an etched section of compression moulded TPX



*Figure 2* Micrograph of a TPX sheet surface illustrating the Stereoscan beam damage. Before observation the surface was perfectly smooth



*Figure 3* Electron micrograph of a microtomed section of compression moulded TPX

undulations suggesting a fibrillar structure. The average spacing of the undulations is again between 3 and 5  $\mu\text{m}$ . Microtomed sections were examined in the electron microscope and the same 5  $\mu\text{m}$  dimension could be detected as shown in *Figure 3*. The structure appears to consist of crude spherulites with a radial ill-defined dispersion of needles or fibrils.

It is concluded from these observations that the compression moulded material has a poorly developed structure corresponding to the initial stages of spherulite formation which is uniform throughout the material.

#### *Deformation and fracture at 293K*

The material was deformed by carrying out uniaxial tensile tests on parallel gauge length specimens. A typical stress-strain curve at 293K is illustrated in *Figure 4*. All specimens were ductile and showed a yield drop. The maximum stress was 20.7 MN/m<sup>2</sup> and occurred at 6% strain. The specimens remained transparent up to 90% of the maximum load at which point a slight milkiness appeared in a small region of the specimen. This region grew to fill the gauge length until the specimen became completely opaque. The stress whitening was homogeneous to the naked eye and was reversible in that a specimen recovered and became transparent when it was cycled to strains less than the yield strain (6%). Examination of the specimen surface after large strains showed that it contained a large number of crazes which formed perpendicular to the tensile axis. *Figure 5* is an optical micrograph of the surface of a stress whitened specimen which failed at about 20% strain. The crazes have a maximum width of 2  $\mu\text{m}$  at the surface and are very short and irregular.

Fracture occurs in a ductile manner by the formation of an edge cavity. This is illustrated in *Figure 6* which is a Stereoscan micrograph of the fracture surface of a compression moulded specimen. The opposite fracture surface was a mirror image of the one shown in *Figure 6*. Each surface shows a well defined line associated with a change in the fracture morphology which is probably due to a change in the speed of crack propagation. A high magnification micrograph of the region of slow crack speed (*Figure 7*) indicates that a large amount of drawing has taken place and that the resulting structure is extremely fibrous.

To investigate the stress whitening phenomenon

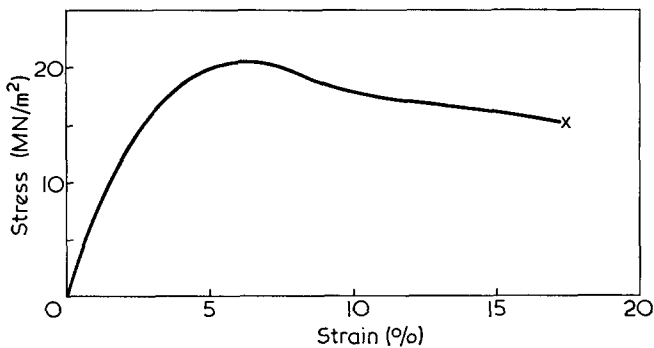


Figure 4 Typical stress-strain curve for a TPX specimen tensile tested at 293K and at a strain rate of  $2.8 \times 10^{-4} \text{ sec}^{-1}$

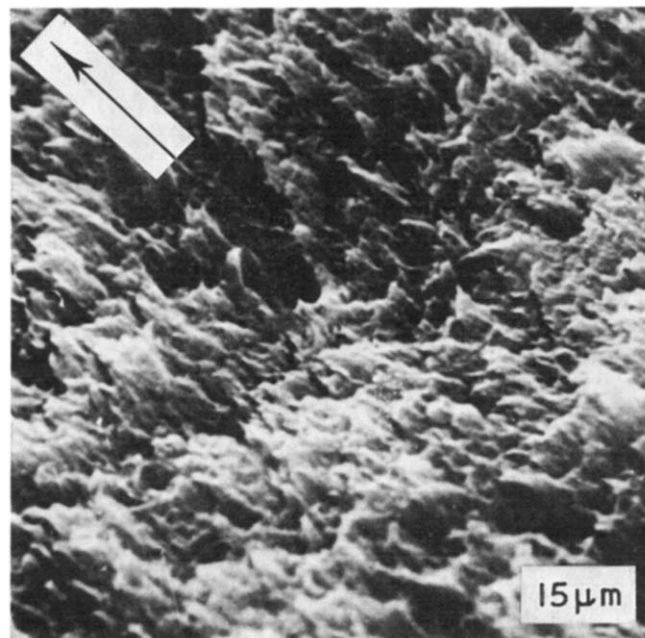


Figure 7 Stereoscan micrograph of the slow crack growth region. The arrow indicates the direction of crack growth

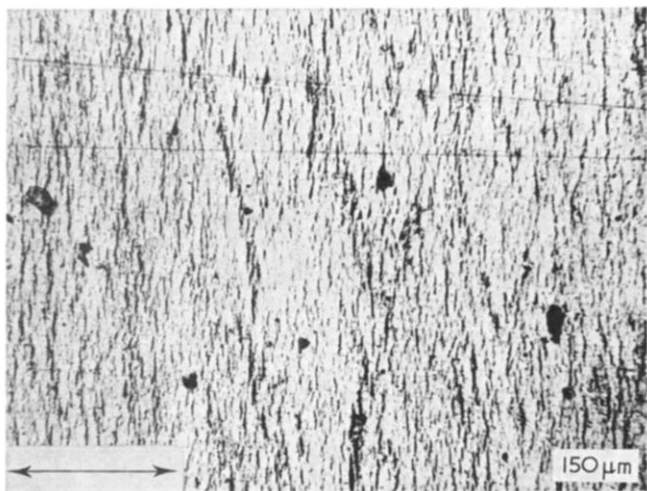


Figure 5 Optical micrograph of the surface of a stress whitened specimen showing short and irregular crazes

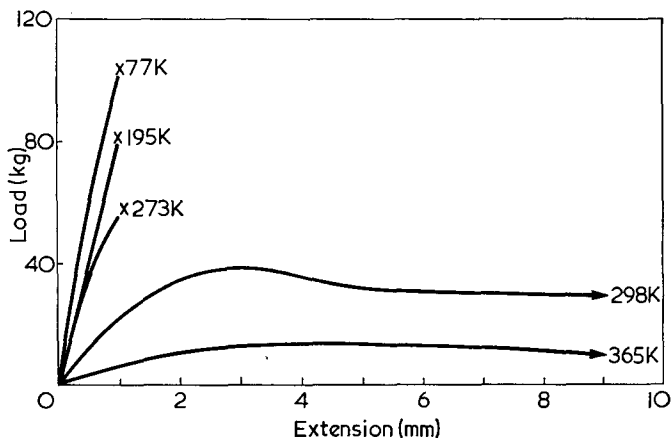


Figure 8 Load-extension curves for tensile specimens of compression moulded TPX plotted as a function of temperature

further, specimens of compression moulded TPX were deformed in a three point bending jig fitted to the optical microscope. The first signs of deformation appeared when there was a slight 'milky' in the specimen. At this stage, a small number of short surface crazes were observed. The crazes formed perpendicular to the tensile axis and were approximately  $7 \mu\text{m}$  in length. Several crazes initiated at scratches and impurity particles. With increasing strain the number of crazes grew and their average length increased to  $25 \mu\text{m}$ . At still larger strains, the crazes became much wider, and it could be clearly seen that they contained highly reflective material.

#### Effect of temperature

Tensile tests were carried out on curved gauge length specimens of compression moulded TPX at a range of temperatures and the results are shown in Figure 8. As the testing temperature was decreased the material became brittle. There was a sharp change in the tensile modulus between 270K and 290K (Figure 9) which is associated with the glass transition temperature,  $T_g$ ; dilatometry experiments gave a value of 280K for  $T_g$ .

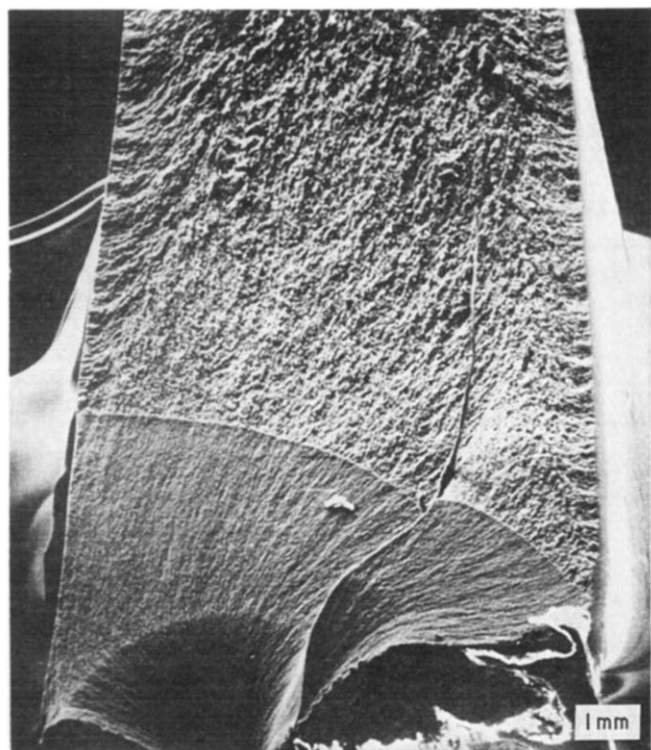


Figure 6 Stereoscan micrograph of the fracture surface of a stress whitened specimen. The boundary is caused by a change in crack speed



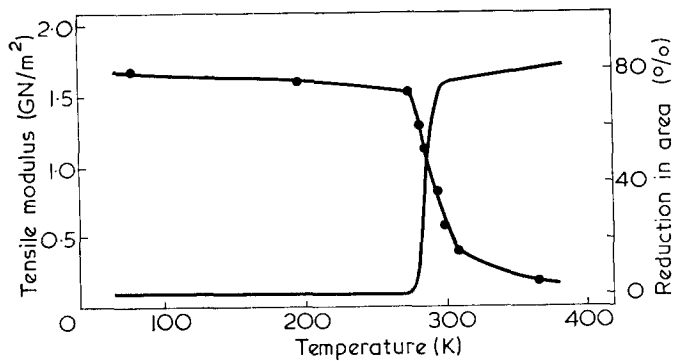


Figure 9 Effect of temperature on the tensile modulus (●) and reduction in area at fracture

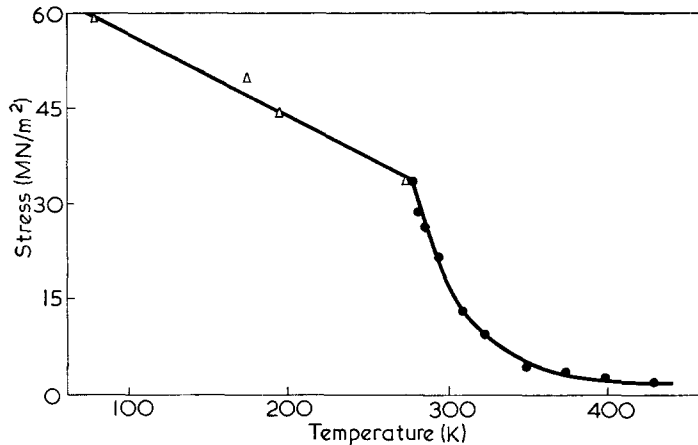


Figure 10 Effect of temperature on the fracture stress ( $\Delta$ ) and yield stress (●)

The fracture stresses and yield stresses are plotted against temperature in Figure 10. The change from ductile yielding to brittle fracture was accompanied by changes in the mode of fracture. Specimens tested between 285K and 330K deformed by a stress whitening mechanism. At the lower temperatures in this range failure occurred after only small elongations, whereas at temperatures approaching 330K stress whitening was accompanied by drawing. These changes are reflected in the change in reduction in area at fracture also shown in Figure 9. At temperatures above 330K, the specimens drew to their natural draw ratio, which increased with temperature; no stress whitening occurred. Specimens tested below 285K did not show stress whitening and failed in a completely brittle manner. However, a large amount of fine surface crazing was noted in specimens tested at 77K when immersed in liquid nitrogen.

No systematic studies were made of the fracture surfaces. However, the brittle fractures at low temperatures were of some interest. Figure 11 is an optical micrograph of the fracture surface of a specimen tested at 220K. There is a well defined initiation region which is approximately planar surrounded by rough irregular surfaces. Stereoscan observations indicated that fine cavitation was involved in the initiation process.

## DISCUSSION

Crystallinity in polymers has been recognized for some time but it is only recently, through detailed examination of single crystals and acceptance of chain folds, that the structure of bulk polymers has been understood.

When polymers are crystallized from the melt under stress-free conditions, the resulting structure is usually spherulitic. Keith and Padden<sup>8</sup> have pointed out in their theory of crystallization that spherulite-forming materials are multicomponent systems in which certain components are likely to be rejected preferentially by growing crystals. In polymers, one component will be the crystalline phase and the other phase will consist of molecules of low molecular weight and atactic material. This second phase will be accommodated between growing fibrils and at spherulitic boundaries. Factors that will influence the spherulitic structure include (a) those that alter the viscosity of the melt and the growth rate (temperature of crystallization), and (b) those that alter the nucleation density (impurity particles). The present system (TPX) contains a nucleating agent and this, coupled with the fact that the sheets are water-cooled after fabrication, will result in a very high density of nuclei. The crystallization process will occur very rapidly and it is unlikely that well defined spherulites will form.

At 298K stress whitening occurs when compression moulded TPX is deformed in uniaxial tension. Haward<sup>9</sup> was amongst the first to report whitening which he observed whilst stretching cellulose nitrate film. He suggested that it was due to the formation of holes in the material, 200 Å in diameter. Either the size of the holes or their distance apart are on such a scale as to scatter light. Other workers<sup>10, 11</sup> are of the opinion that the turbidity in PMMA is due to the formation of voids. Stress whitening has also been reported by Bucknall and Smith<sup>12</sup> in high-impact polystyrene and by Matsuo<sup>13</sup> in ABS polymer. They showed quite clearly by examination of thin sections that the whitening was due to an increased density of crazing. Whitening also occurs in certain grades of nylon (Bessell, T. personal communication) and appears after the maximum tensile load. In this case whitening is attributed to a large number of cracks forming in the specimen.

In contrast to the nylon, stress whitening in TPX occurs just before the yield point. The observations

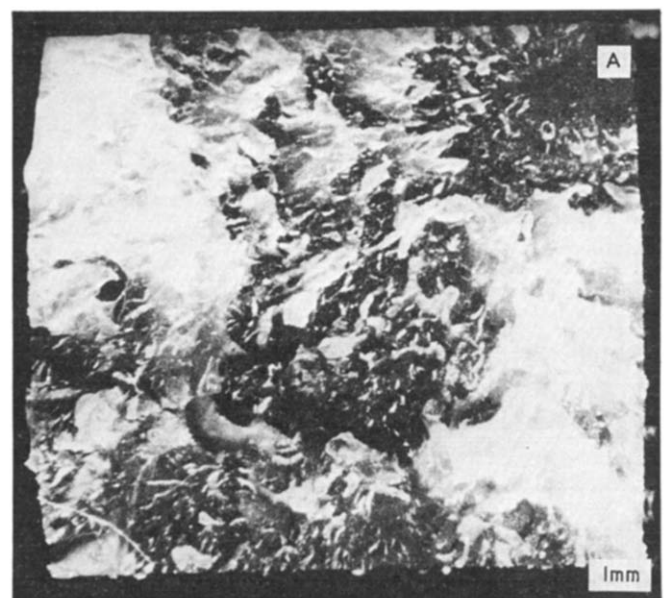


Figure 11 Optical micrograph of the fracture surface of a TPX specimen tested in tension at 220K. The surface is very irregular but a small initiation region can be seen at A





Figure 12 Transmission electron micrograph of a strained microtomed section of compression moulded TPX. The arrows indicate the stretching direction

reported here indicate that in compression moulded TPX the whitening is a form of crazing on a very fine scale. There is evidence from the deformation of injection moulded TPX<sup>14</sup> that two different types of crazing can occur in the same tensile specimen. At low magnifications one type has all the features of stress whitening and in the other type large thin crazes are formed. The two types of craze occur at different stress levels.

It was hoped to gain further information about the whitening by examining microtomed sections from stress whitened material. However, the sections were very similar in appearance to the unstrained material suggesting that they had relaxed during sectioning. To examine the deformation structure more directly, microtomed sections of the undeformed compression moulded TPX were mounted on copper grids which were then strained on a microstraining device. The sections were examined in the electron microscope and showed extensive evidence for non-uniform deformation (Figure 12). The microstructure is similar to the microstructure of crazes formed in polystyrene<sup>15</sup>. However, the craze boundaries are much more irregular than in polystyrene and the orientation of the fibrils within the crazes is not as pronounced. This is to be expected particularly for small crazes since they have grown through ill-defined bundles of lamellar blocks of crystalline material that have many different orientations with respect to the applied stress. The dimensions of the lamellar blocks are

comparable to those of the fibrils in the deformed structure.

It seems likely that the craze-like structure observed in the strained microtomed sections is responsible for the stress whitening observed in the bulk material, and one can conclude that stress whitening is due to the formation of a large number of fine, irregular crazes, and is similar to conventional crazing.

## CONCLUSIONS

It has been shown by various techniques that the microstructure of compression moulded TPX consists of small, poorly developed spherulites. Tensile tests on the material indicate that stress whitening is the initial mode of deformation between 285K and 330K. Below 285K the material fractures in a completely brittle manner whereas above 330K specimens draw to their natural draw ratio.

A detailed optical study of the specimens together with the examination of thin sections suggest that stress whitening is due to the formation of a large number of fine crazes.

## ACKNOWLEDGEMENTS

Thanks are due to ICI Plastics Division, for supplying the material and the Science Research Council for a studentship to support T. W. O.

## REFERENCES

- 1 Natta, G., Pino, P., Mazzanti, G., Corradini, P. and Giannini, V. *Atti Accad. Naz. Lincei, Rend. Classe Sci. Fis. Mat. Nat.* 1955, **19**, 397
- 2 Frank, F. C., Keller, A. and O'Connor, A. *Phil. Mag.* 1959, **4**, 200
- 3 Griffith, J. H. and Rånby, B. G. *J. Polym. Sci.* 1960, **44**, 369
- 4 Crissman, J. M., Sauer, J. A. and Woodward, A. E. *J. Polym. Sci. (A)* 1964, **2**, 5075
- 5 Woodward, A. E., Odayima, A. and Sauer, J. A. *J. Phys. Chem.* 1961, **65**, 1384
- 6 Ives, G. C. and Mead, J. A. *Mater. Res. Stand.* 1961, **1**, 194
- 7 Heavans, J. W., Keller, A., Pope, J. M. and Rowell, D. M. *J. Mater. Sci.* 1970, **5**, 53
- 8 Keith, H. D. and Padden, F. J. *J. Appl. Phys.* 1963, **34**, 2409
- 9 Haward, R. N. *Trans. Faraday Soc.* 1942, **38**, 394
- 10 Zhurkov, S. N., Marikhin, V. A. and Slutsker, A. I. *Sov. Phys. (Solid State)* 1960, **1**, 1060
- 11 Rosen, B. 'Fracture Processes in Polymeric Solids', (Ed. B. Rosen), Interscience, New York, 1964, p 293
- 12 Bucknall, C. B. and Smith, R. R. *Polymer* 1965, **6**, 437
- 13 Matsuo, M. *Polym. Eng. Sci.* 1969, **9**, 206
- 14 Owen, T. W. and Hull, D. to be published
- 15 Beahan, P. G., Bevis, M. J. and Hull, D. *Phil. Mag.* 1971, **24**, 1267

# Solid and liquid state relaxations in spin-labelled poly(ethylene glycol) at high temperatures ( $T > T_g$ )

P. Törmälä, H. Lattilä and J. J. Lindberg

Department of Wood and Polymer Chemistry, University of Helsinki, Helsinki, Finland  
(Received 21 March 1973; revised 11 June 1973)

Free and covalently bonded (esterified) nitroxyl radicals experienced in poly(ethylene glycols) (PEG;  $\bar{M}_n$  200–22 000) at temperatures  $T > T_g$  several different isotropic rotational relaxation regions. As a first approximation it was assumed, that in the polyglycols  $\bar{M}_n \geq 1000$  there are at least three rotational relaxation regions: the liquid state (I), the melting state (II) and the solid state (III). The existence of the fourth region, the frozen solid state (IV), was also concluded. The existence of the relaxation region (II) indicated the close interaction between radicals and the crystalline phase. The order of rotational activation energies ( $E_a$ ) was  $E_a^{II} > E_a^{III} > E_a^I > E_a^{IV}$  ( $\bar{M}_n \geq 1000$ ). In the polymer melts (I)  $E_a$  values of free and bonded radicals first diminished as a consequence of the decrease of the end group effect and they achieved constant high molecular weight values ( $\sim 15$  and  $25$  kJ respectively).  $E_a$  changed in the solid state as a function of  $\bar{M}_n$  principally in the same manner except of the higher numerical values ( $\sim 40$  kJ).

$E_a$  of free and covalently bonded radicals in the transition region (II) gained a maximum at  $\bar{M}_n$  1550 (125 and 170 kJ) and another at  $\bar{M}_n > 9500$  (130 and 165 kJ) expressing the high degree of order in these polymers in the solid state.

The results obtained correlated well with the proton magnetic resonance measurements but they did not correlate with the amorphous dielectric relaxation measurements.

It was concluded that the following factors may affect the rotational relaxations of nitroxyl radicals in PEG: the free volume of the polymer, the crystallinity, the chain packing and the end-group effect. The segmental character of the relaxation process was clearly indicated.

## INTRODUCTION

Various types of measurements indicate the existence of relaxation transitions in poly(ethylene glycols) (PEG) at temperatures above their glass transitions ( $T_g = 206\text{K}$ ). So, for example, crystalline PEG generally shows two dielectric absorptions caused by the disordered region<sup>1</sup>. It is considered that they are due to the diffusional segmental motions of main chains in the amorphous region ( $\alpha$ -abs.) and to the local twisting motion of main chains in both amorphous polymer and in defective regions of the crystals ( $\beta$ -abs.). Porter and Boyd<sup>2</sup> found that the  $\beta$ -relaxation in PEG goes continuously over into the melt state with respect to the location of the loss region and the width of the dispersion range. The strength of the relaxation is discontinuous on melting and roughly proportional to the amount of amorphous material present. The results were consistent with a model for the crystalline solid where the relaxations take place in discrete amorphous regions similar to the melt and the chain lengths involved in the motions are shorter than typical interlamellar chain lengths.

Allen *et al.*<sup>3</sup> measured the spin-lattice relaxation time  $T_1$  in a series of PEG as a function of temperature and molecular weight. Accordingly  $T_1$  was virtually independent of the molecular weight of PEG for  $M_w$  in

excess of  $5 \times 10^3$ . The inference was that the molecular motions associated with spin-lattice relaxation are segmental in nature and not properties of the whole chain at high  $M_w$  values. Hikichi and Furuichi<sup>4</sup> have also shown that a molecular motion such as rotation or oscillation is able to occur even in crystalline regions well below the melting point.

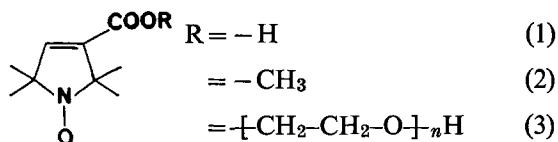
Read<sup>5</sup> studied the mechanical relaxations of PEG at a frequency of 1 Hz in the  $M_w$  range from about  $4 \times 10^3$  up to  $5 \times 10^6$ . The relaxations were attributed to the motions of chain segments in the disordered regions of the polymer. From the dynamic mechanical measurements of PEG at 0.1 Hz it was inferred that there is a slow decrease of modulus with temperature up to about  $60^\circ\text{C}$ , a rapid decrease of modulus from  $60^\circ\text{C}$  to the melting point and a relatively constant modulus above the melting point<sup>6</sup>.

There is an abrupt change of the internal pressure of PEG in the melting region<sup>7</sup>. It has been suggested that the major contribution to this phenomenon is the freezing-in of chain conformations in the solid PEG.

The rotational mobility of nitroxyl radicals in the rotational range  $10^{-7}$ – $10^{-11}$  sec affords a straightforward method to study the motions of polymer molecules. Spin-probe and spin-labelling techniques permit the

evaluation of relaxation times and energetic characteristics of motion of polymer segments<sup>8-12</sup>.

In this study we have therefore measured the rotational relaxation times ( $\tau$ ) of the spin-probe 3-methoxy carbonyl-2,2,5,5-tetramethylpyrroline-1-oxyl (2) and of the corresponding spin-label (3) [3-carbonyl-2,2,5,5-tetramethylpyrroline-1-oxyl radical (1) esterified with polymer] in poly(ethylene glycols) (PEG) of various molecular weights.



In a recent report<sup>12</sup> the authors expressed that four different relaxation regions exist in PEG of  $\bar{M}_n$  4000 at  $T > T_g$ . In this paper the nature of these relaxations is studied in the  $\bar{M}_n$  range 200–22 000. The molecular basis of these processes and their relationships to other relaxation phenomena are also discussed.

## EXPERIMENTAL

The PEG samples were of commercial origin (Fluka AG and E. Merck AG). They showed a quite narrow molecular weight distribution,  $M_w/M_n$  (see Table 1), and were therefore used as unfractionated. The organic reagents benzene, pyridine and thionyl chloride were purified by distillation and stored in desiccators.

### Preparation of radicals (1) and (2)

Radical (1) was prepared by the method of Rozantsev *et al.*<sup>13</sup>. From radical (1) its acid chloride derivative was prepared by the method of Krinitskaya *et al.*<sup>14</sup>. To its benzene/pyridine (1:1) solution was added an equivalent amount of dry methanol. The solution was left at room temperature overnight. The precipitated salts were filtered off, the solution was evaporated and the product, radical (2), was purified by column chromatography on Al<sub>2</sub>O<sub>3</sub> with chloroform as an eluant. The structure of the end product was confirmed by infra-red spectrometry (Perkin-Elmer 457 Grating Infra-red Spectrometer, KBr technique).

### Incorporation of radicals into PEG

The PEG samples containing the spin-probe radicals (2) (set A in Table 1) (radical concn 1:20 000 repeating

Table 1 Molecular characteristics of PEG samples and the melting points of the solid polymers. Sets A and B represent the samples containing free and bonded radicals respectively

$\bar{M}_n$	$\bar{M}_w/\bar{M}_n$	$T_m$ (°C)	
		Set A	Set B
200 ± 10	1.14	—	—
400 ± 20	1.20	—	—
600 ± 30	1.16	—	—
1 000 ± 50	1.24	36.5	33.5
1 550 ± 100	1.28	50.0	48.0
2 050 ± 150	1.28	56.0	48.5
3 000 ± 300	1.29	56.0	54.5
4 000 ± 500	1.28	58.5	55.5
6 700 ± 700	1.23	59.0	55.5
9 500 ± 500	1.10	59.5	57.5
15 000 ± 2 000	1.09	60.0	60.5
22 000	1.08	61.0	62.0

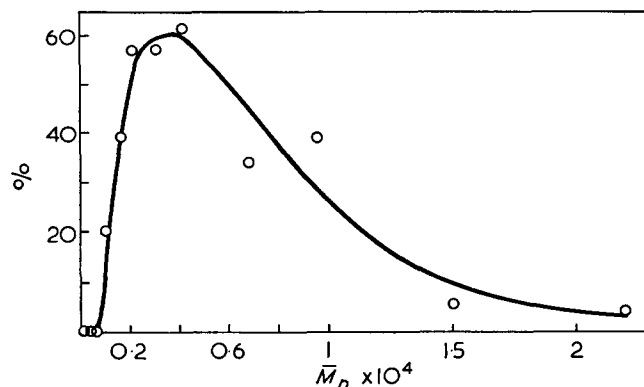


Figure 1 Degree of labelling of PEG as a function of  $\bar{M}_n$

units) were prepared by dissolving suitable amounts of dry PEG and radical (2) into chloroform and by evaporating the solvent.

Spin-labelled PEG (set B) was prepared by a Schotten-Baumann reaction in the following manner. To a solution of  $1 \times 10^{-4}$  mol of radical (1) in 0.3 ml of benzene/pyridine mixture (1:1) was added  $1.2 \times 10^{-4}$  mol of SOCl<sub>2</sub> and, after 15 min,  $0.5 \times 10^{-4}$  mol of vacuum-dried PEG in 4.5 ml of pyridine. The solution was shaken and left overnight. The unreacted label was removed by pouring the solution into a large excess of ether. The light yellow labelled polymer was sintered, dried in vacuum and dissolved in chloroform. The chloroform solution was precipitated with ether. The dissolving-precipitating procedure was repeated three times. The degree of labelling of the product was measured by comparing the intensities of the electron spin resonance (e.s.r.) spectra of spin-labelled PEG and radical (1) in dilute chloroform solutions. The degree of labelling as a function of  $\bar{M}_n$  as a percentage of the theoretical value is given in Figure 1. We suppose that the low degree of labelling at  $\bar{M}_n \leq 600$  values was caused by difficulties in removing the adsorbed water from PEG. The decreasing of labelling yield at high  $\bar{M}_n$  values is a plain high molecular weight effect.

To eliminate the intermolecular spin-spin exchange, which was not done in our first communication<sup>15</sup> it was necessary to dilute the radical concentrations in samples. It was experimentally found that the spin-spin exchange is totally absent when the ratio of radicals to the repeating units of polymer is  $\lesssim 1:20\ 000$ . Samples with this amount of radicals were prepared by dissolving into chloroform suitable amounts of spin-labelled and non-labelled PEG. The polymer was precipitated with ether, filtered and dried in vacuum (set B in Table 1).

The molecular weights ( $\bar{M}_n$ ) of polymers were measured using a vapour pressure osmometer (Perkin-Elmer Model 115) in chloroform at 32°C. The  $\bar{M}_n$  values of samples are given in Table 1. The molecular weight distributions were estimated by gel filtration at room temperature using Sephadex G-25 and G-75 gels and 0.1 M NaCl solution as an eluant. Calibration was done by plotting  $\log_{10} \bar{M}_n$  against the observed peak maxima. The molecular characteristics of the samples are given in Table 1. The molecular weight values of the commercial samples and of the samples containing minute amount of radicals were the same. This indicated that the radicals did not affect the molecular characteristics of the polymers.

The melting points ( $T_m$ ) of solid polymers were

measured by a differential scanning calorimeter (Perkin-Elmer DSC 1B)<sup>16</sup>. The  $T_m$  values are given in Table 1.

#### E.s.r. measurements

The polymer samples were evacuated in e.s.r. tubes in high vacuum ( $1 \times 10^{-3}$  mmHg) for 4 h and sealed under dynamic vacuum.

The e.s.r. spectra were obtained from evacuated samples on a Varian E-4 spectrometer operating at a microwave frequency of 9.5 GHz. The magnetic field was modulated with an amplitude less than one-sixth of the linewidth. The microwave power was 1 mW to avoid saturation effects. The measurements were made in the range 120–373 K using a Varian E-257 variable temperature accessory with an accuracy  $\pm 2$  K, calibrated with an iron/constantan thermocouple. The glass spectra at 100 K were measured by using liquid nitrogen containing Dewar thermostat.

The measurements were done, beginning from the low temperatures. The temperature was raised in steps of 4–10°C depending on the rate of change of the e.s.r. spectrum. The stabilization time was 6 min.

## RESULTS

It has been stated that under conditions where the intermolecular interactions between radicals are eliminated, the rotational frequencies of radicals of small molecules

are affected by the motions of the surrounding molecules<sup>8, 11</sup>.

In Figures 2a and b are given some examples of the e.s.r. spectra of free and bonded radicals in PEG 4000, respectively. The motion of radicals is in both cases isotropic but the rotation in the case of Figure 2b is plainly more hindered than in Figure 2a. Radicals behaved in other PEG samples in principle in the same manner, except the dependence of rotation rate on the  $\bar{M}_n$ . If the outermost peak-to-peak separations of the e.s.r. spectra are expressed as a function of temperature sigmoidal curves result as has been found earlier<sup>12, 17</sup>. In every PEG sample studied the sharp decrease of the peak-to-peak separation (=the inflection point of the sigmoidal curve) occurred at a temperature ( $T_i$ ) which was well above  $T_g$  but below  $T_m$  as can be seen from Figure 3 where  $T_i$  is given as a function of  $\bar{M}_n$  for free ( $\Delta$ ) and covalently bonded ( $\circ$ ) radicals. From Figure 3 it can be seen that  $T_i$  increases when  $\bar{M}_n$  increases from 200 to  $\bar{M}_n=1550$ . Thereafter  $T_i$  decreases although  $\bar{M}_n$  increases but at  $\bar{M}_n=4000$  it increases again and reaches its maximum value at  $\bar{M}_n=9500$ . It is well known that the peak-to-peak separation correlates inversely to the isotropic motional freedom of radicals<sup>18</sup>. Therefore in this case the motional freedom of radicals (2) and (3) in PEG gets a minimum at  $\bar{M}_n=1550$ . In samples  $\bar{M}_n=2050$  and 3000 the motional freedom is greater and it diminishes again when  $\bar{M}_n$  grows.

A more quantitative treatment of the results was done

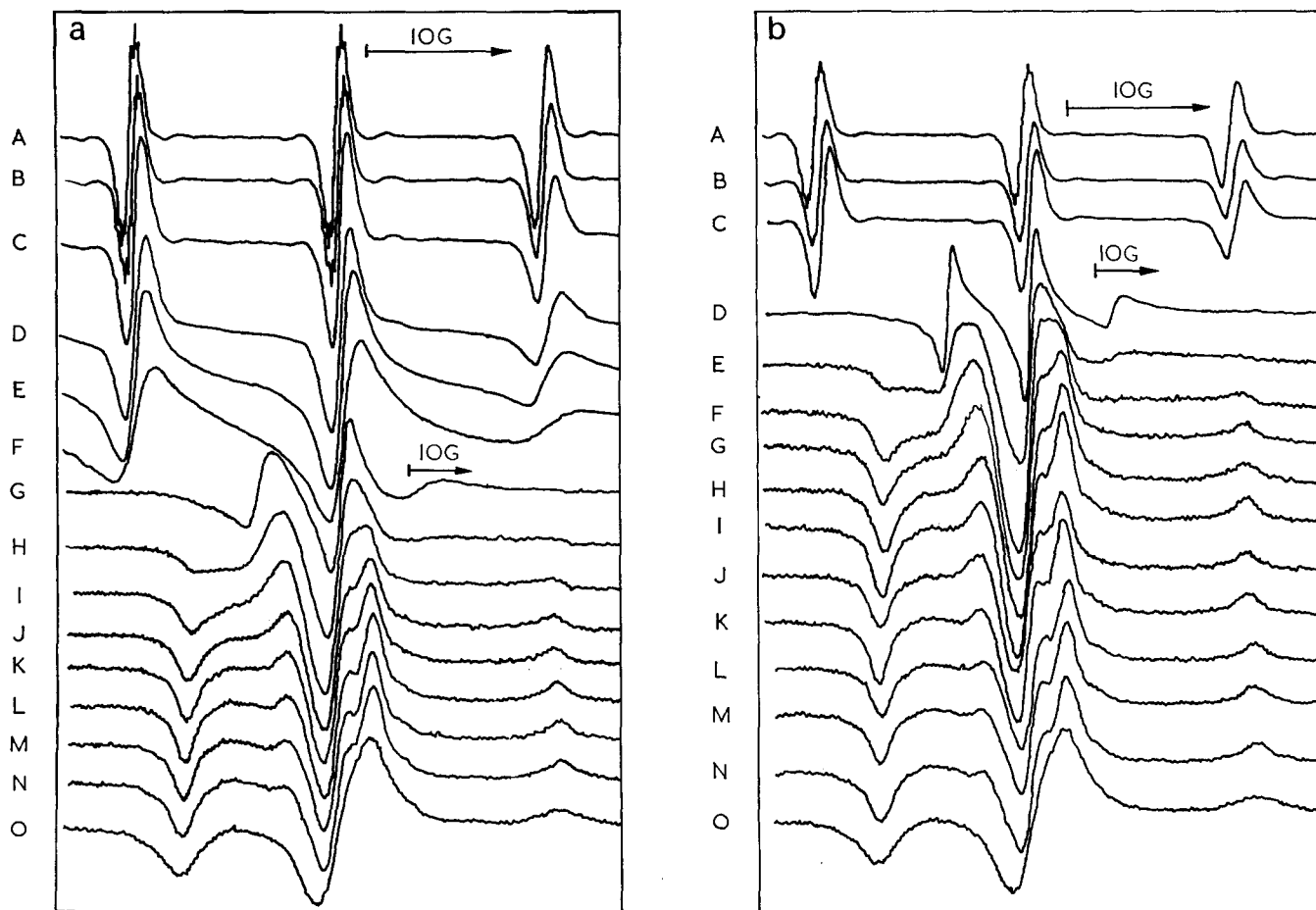


Figure 2 E.s.r. spectra of (a) free and (b) covalently bonded nitroxyl radicals in PEG of  $\bar{M}_n=4000$ . The measurement temperatures (K) were the following: A, (373); B, (348); C, (333); D, (323); E, (313); F, (303); G, (293); H, (283); I, (273); J, (263); K, (253); L, (233); M, (213); N, (173); O, (100)

by estimating the rotational correlation times ( $\tau$ ) of radicals from the e.s.r. spectra. In the region of rapid rotations ( $\tau \sim 5 \times 10^{-9} - 5 \times 10^{-11}$  sec) these could be calculated by equations (1) and (2) which are based on Kivelson's theory<sup>19, 20</sup>:

$$\tau_1 = 8.7 \times W_0 [(h_0/h_1)^{1/2} - (h_0/h_{-1})^{1/2}] \times 10^{-10} \text{ sec} \quad (1)$$

$$\tau_2 = 7.9 \times W_0 [(h_0/h_1)^{1/2} + (h_0/h_{-1})^{1/2} - 2] \times 10^{-10} \text{ sec} \quad (2)$$

where  $W_0$  is the line width (Gauss) of the centreline in e.s.r. spectrum and  $h_1$ ,  $h_0$  and  $h_{-1}$  are the intensities of the low, centre and high field components. The numerical

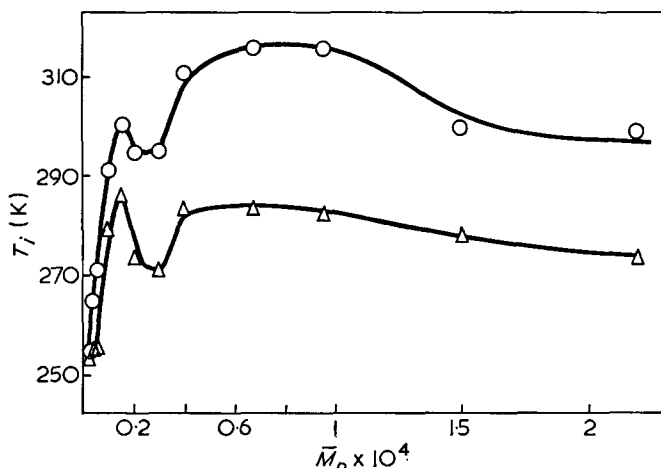


Figure 3  $T_i$  (=the temperature region at which the outermost separation of the e.s.r. spectrum changes most drastically) as a function of  $\bar{M}_n$ .  $\Delta$ , Free radicals;  $\circ$ , bonded radicals

parameters are dependent on the magnetic field and on the  $\bar{g}$  and  $\bar{T}$  tensors for which were used values given by Ohnishi *et al.*<sup>21</sup>. The differences between the two values of  $\tau$  were as a rule  $< 10\%$ . The mean values of  $\tau_1$  and  $\tau_2$  are used in this work. The calculation of  $\tau$  is reviewed more thoroughly elsewhere<sup>18, 22</sup>. By doing several measurements and by taking into account the measurement error of spectral components it was found that the error of  $-\ln \tau$  was  $\leq \pm 0.1$ . So the accuracy of measurements was quite good in the rotation region, where the spectral components do not overlap each other.

In the region of slow rotations ( $\tau \sim 10^{-7} - 5 \times 10^{-9}$  sec) the spectral components overlap and therefore Kivelson's theory is not valid. Kuznetsov *et al.*<sup>23</sup> and Shimshick *et al.*<sup>24, 25</sup> have done theoretical calculations to correlate the relative positions of derivative peaks to  $\tau$ . Accordingly we calculated the values of  $\tau$  in the region of slow rotations by using the treatment of Shimshick *et al.*<sup>24</sup>. The relative position of the high field peak was compared to the corresponding one measured at  $-180^\circ\text{C}$  (the difference =  $\Delta H$ ). It was assumed that at  $-180^\circ\text{C}$  the viscosity of sample was nearly infinite. The high field peak was used because the effects of polarity in this case are smallest<sup>25</sup>. A small capillary containing  $10^{-5}$  M aq. solution of radical (1) fixed on the outer surface of the thermostat was used as an external standard. The error of  $-\ln \tau$  calculated by this method was  $\leq \pm 0.5$  when  $-\ln \tau$  was between 19 and 16.5. When the frequency of rotations was  $\leq 10^7$  (1/s),  $\Delta H$  was so small that its relevant determination was not possible.

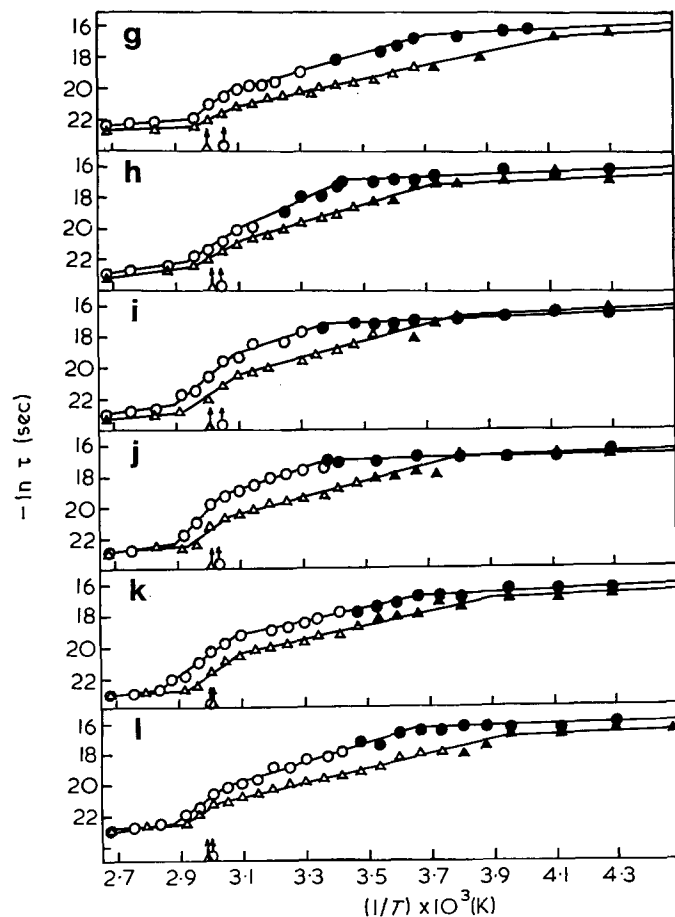
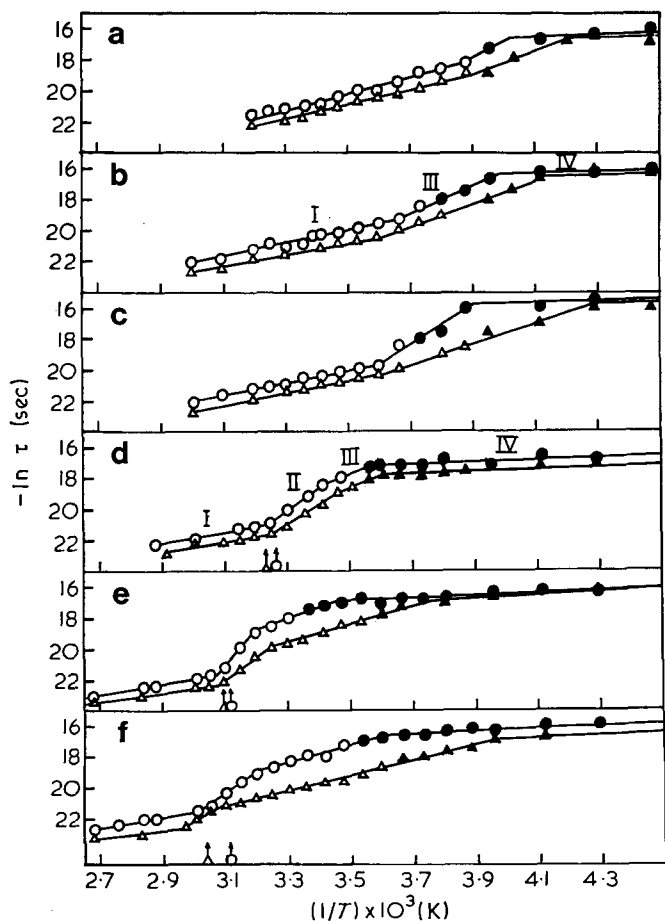


Figure 4  $1/T$  against  $-\ln \tau$  plots of PEG containing free ( $\Delta$ ) and covalently bonded ( $\circ$ ) radicals. The values of  $\tau$  calculated according to Shimshick *et al.*<sup>24</sup> are given by solid symbols. The melting points of the solid polymers (measured from the maximum of the endothermic peak height) are given by arrows. (a) 200; (b) 400; (c) 600; (d) 1000; (e) 1550; (f) 2050; (g) 3000; (h) 4000; (i) 6700; (j) 9500; (k) 15 000; (l) 22 000

The values of  $\tau$  which were calculated by the methods of Kivelson and Shimshick correlated as a rule quite well with each other (see Figure 4).

In Figure 4  $-\ln \tau$  is plotted as a function of  $1/T$  for PEG samples of  $\bar{M}_n=200-22\,000$ . The melting points of the solid polymers are also given.

The rotations of the radicals may be treated as a rate process in terms of the theory of absolute reaction rates<sup>8</sup>. It can be seen from Figure 4 that the temperature changes in the correlation times of radicals do not obey the Arrhenius law  $\tau=\tau_0\exp(E/RT)$  over the whole temperature range. Therefore, we conclude that the activation energy associated with rotational mobility is phase dependent. By assuming that the Arrhenius law is valid in each phase we suppose that when  $\bar{M}_n \geq 1000$  the following relaxation regions can be detected in Figure 4: the liquid state (I), the melting region (II), the solid state (III) and perhaps also the glassy state (IV). The measurements indicating the relaxation regions I-III are quite reliable because the rotations of radicals are so rapid that the spectral components do not overlap even in the solid state (except at the lowermost temperatures). The existence of the region IV is much more poorly documented because of the roughness of the measurements. The order of the rotational activation energies  $E_a^{II} > E_a^{III} > E_a^I > E_a^{IV}$  is, however, valid. In the samples of  $\bar{M}_n=200, 400$  and  $600$  there are at least two well documented relaxation regions, the liquid state (I) and the solid state (III). It is also probable that the glassy state (IV) exists. In these cases the relation  $E_a^{III} > E_a^I > E_a^{IV}$  is valid. However, the crystallization of PEG 200 containing bonded radicals occurred at so low a temperature that the region III could not be indicated in this case. The values of  $E_a$  were calculated from the slopes of lines by the least squares method. The change of the slope of the Arrhenius plot at certain

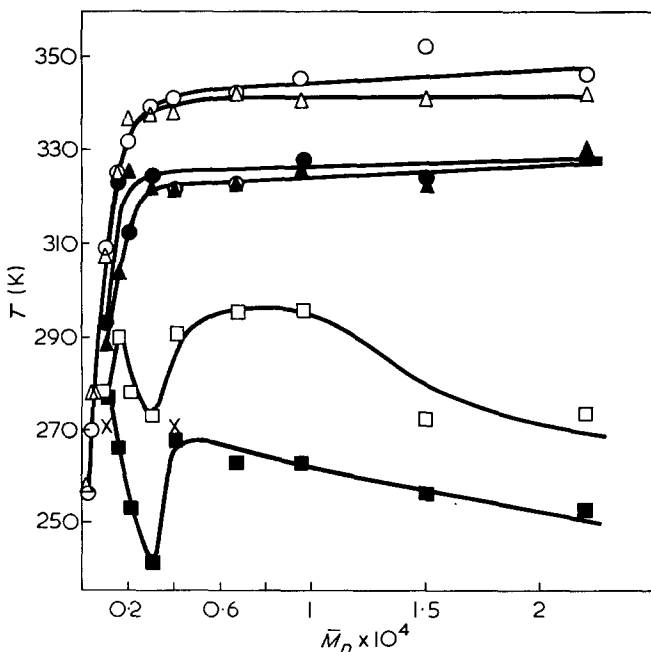


Figure 5 Temperatures, at which the slopes of Arrhenius plots change, as a function of molecular weight;  $\Delta$  and  $\circ$  give the transition temperature between relaxation regions I and II;  $\blacktriangle$  and  $\bullet$  between regions II and III;  $\blacksquare$  and  $\square$  between regions III and IV. The first symbol represents in each case the value of free radicals and the second symbol the value of bonded radicals. The results of n.m.r. measurements of Hikichi and Furuichi<sup>4</sup> are given by  $\times$

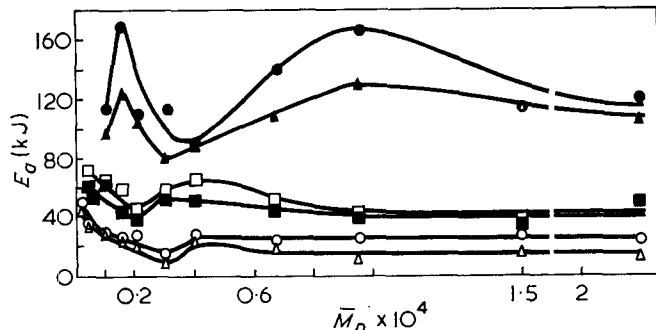


Figure 6  $E_a$  values of the used nitroxyl radicals in PEG as a function of  $\bar{M}_n$ .  $\Delta$  and  $\circ$  give the  $E_a$  values of free and bonded radicals in the relaxation region I ( $E_a^I$ );  $\blacktriangle$  and  $\bullet$  give  $E_a^{II}$ ;  $\blacksquare$  and  $\square$  give  $E_a^{III}$

Table 2 Differences of activation energies ( $\Delta E_a$ ) of bonded and free radicals in relaxation regions I-III

$\bar{M}_n$	$E_a^I$ (kJ)	$E_a^{II}$ (kJ)	$E_a^{III}$ (kJ)
200	7.0	—	—
400	3.0	—	10.5
600	0	—	6.0
1 000	2.0	17.0	0
1 550	2.5	45.0	15.5
2 050	8.5	5.5	6.0
3 000	7.0	32.5	5.5
4 000	3.5	32.5	15.0
6 700	4.5	14.0	8.0
9 500	14.0	36.5	4.0
15 000	11.0	0	0
22 000	11.0	34.0	8.0

temperatures shows that some kind of change has occurred in the relaxation process. In Figure 5 these temperatures are given as a function of  $\bar{M}_n$ .

In Figure 6 are given the values of  $E_a$  in the relaxation regions I-III as a function of  $\bar{M}_n$ . It is seen that the differences between the  $E_a$  values of free and bonded radicals ( $\Delta E_a$ ) are quite small in the relaxation regions I and III. In the transition region (II)  $E_a$  and  $\Delta E_a$  have two maxima (at  $\bar{M}_n=1550$  and  $9500$ ). In all these regions the rotations of bonded radicals are as a rule more restricted than those of free ones. In the region IV the accuracy of measurements was poor but it seems that  $E_a$  in these cases is nearly independent of  $\bar{M}_n$ . No clear differences between  $E_a$  values of free and bonded radicals can be seen ( $E_a^{IV} \sim 6$  kJ).

In Table 2 are given the differences of the activation energies of bonded and free radicals ( $\Delta E_a$ ) in relaxation regions I-III. Because the covalently bonded radicals follow more intimately the movements of host polymers than the free radicals the changes in  $\Delta E_a$  can be expressed partly as the changes of the molecular conformation. Table 2 shows that the greatest  $\Delta E_a$  values are found in the region II.

## DISCUSSION

### PEG in the liquid state

The relations of the PEG melt are the most simple ones because only the end groups,  $\bar{M}_n$  and temperature affect the dynamic state of the polymer.

Figure 4 shows that the  $E_a^I$  values of both free and bonded radicals behave principally in the same manner when  $\bar{M}_n$  increases. The decreasing of  $E_a^I$  when  $\bar{M}_n$  increases from 200-3000 is evidently caused by the

loosening of the intermolecular interaction. This effect is probably due to the diminution of the amount of hydrogen bonds. At higher  $\bar{M}_n$  values  $E_a^I$  remains almost constant, which clearly demonstrates the segmental character of the process.

The magnitudes of  $\Delta E_a^I$  values of *Table 2* indicate that the rotations of bonded radicals are hindered only by a small energy barrier in the melted PEG. It may be assumed that both free and bonded radicals are affected by the hydrogen bonds in their environments in the same manner. Therefore it may be concluded that  $\Delta E_a^I$  demonstrates the intramolecular polymer-radical interaction. In the region of  $\bar{M}_n$  200–6700 the order of magnitude of  $\Delta E_a^I$  is about one degree of rotational freedom ( $\sim 4$  kJ/mol). When  $\bar{M}_n$  is  $> 6700$   $\Delta E_a^I$  increases. This is evidently caused by the intramolecular high molecular weight effect of the PEG backbone to the end group radical (i.e. when  $\bar{M}_n$  grows the host polymer may gain conformations which restrict the rotations of the end group). The results suggest that the bonded radicals rotate quite freely at the ends of random coil PEG molecules. The host polymer must experience a rapid isotropic segmental diffusion because order parameter effects are practically absent<sup>22</sup>. The segmental character of the process is clearly demonstrated also in *Figure 4* which indicates that  $\tau$  of both free and bonded radicals remains almost constant when  $\bar{M}_n > 2000$  although the bulk viscosity of the melted polymer increases significantly<sup>26</sup>.

#### PEG in the transition region

It is evident that the specific volume of the polymer contributes to the  $\tau$  values of radicals. If the radicals were in a purely amorphous environment without influence of crystalline phases there should not be an  $E_a$  maximum in the transition region because the specific volume (and therefore even free volume) of amorphous polymers do not change abruptly in the melting region. So the existence of the transition region in the  $1/T$  against  $-\ln \tau$  plot indicates that the rotations of nitroxyl radicals are affected by the crystalline phase of the polymer. On the basis of these measurements, however, it is not possible to say what is the exact location of radicals in the polymer matrix. They could be situated in the amorphous phase between the crystalline lamellae, in the crystalline phase or in both phases. Studies on this question will be reported lately. The isotropy of e.s.r. spectra refers to the amorphous environment of radicals. It is also possible that bulky radicals, if situated in the crystalline phase, distort around themselves the ordered crystal lattice. However, the radicals must experience the ordered forces in their amorphous-like environment created by the crystal lattice. These results indicate that the mechanism of segmental relaxations found by nitroxyl radicals differs from the mechanism of amorphous dielectric relaxations. This is evident from the dielectric studies of amorphous loss peaks of PEG<sup>2</sup> and nylon-6,10<sup>27</sup>, which indicated that the loss peaks ( $\beta$  and  $\alpha$  processes respectively) go continuously into the melt with respect to location in the frequency-temperature domain and with respect to the shape of the peak.

*Figure 6* indicates that there are two marked maxima in the  $\bar{M}_n$  against  $E_a^{II}$  plot. It can also be seen from *Figure 6* that  $E_a^I$  changes only weakly (if compared to  $E_a^{II}$ ) when  $\bar{M}_n \geq 1000$ . Great  $E_a^{II}$  values at  $\bar{M}_n = 1550$

and 9500 indicate that during the melting process there occurs a strong diminution of the ordered state of the polymer molecules. It seems evident that these  $E_a$  maxima are not caused by the variations in the molecular weight distributions because the samples were effectively monodisperse although not single component systems, as can be seen from *Table 1*. Baltá Calleja and Keller<sup>28</sup> measured by X-ray diffraction the long spacings for the extended PEG molecules. The molecular weight above which the long spacing became independent of molecular length was 1500. So we suppose that the regularity of the structure of PEG 1550 reflected by the exceptional high  $E_a^{II}$  value is caused by the fact that in this case the molecule chains are staying straight in the lamellae. At  $\bar{M}_n = 2050$  the first folding has occurred and this has diminished the regularity of the structure<sup>29</sup>. Thus Beech *et al.*<sup>29</sup> found that the proportion of folded chain crystals increases as the crystallization temperature decreases, i.e. as the crystallization rate increases. Because our PEG samples were processed at room temperature the chain folding at  $\bar{M}_n = 2050$  seems to be certain. The free hydroxyl end groups may also affect considerably the  $E_a^{II}$  value because in the transition region the mobility of molecules increases which increases the possibility of hydrogen bond formation. The hydrogen bond formation diminishes the mobility of polymer end segments and may therefore diminish also the specific volume of polymer molecules. The varying degree of crystallinity of PEG samples does not explain the differences in  $E_a^{II}$  values at  $\bar{M}_n$  values  $\geq 1000$  because all the samples were highly crystalline ( $> 80\%$  crystallinity) and the differences of crystallinities in the  $\bar{M}_n$  range 1550–4000 were small<sup>16</sup>.

Although the  $T_m$  values obtained by d.s.c. of samples containing bonded radicals (set B) are lower than those of samples with free radicals (set A) (*Table 1*) the transition temperature between relaxation regions I and II (relaxational melting point) is in most cases higher in the case of bonded radicals (see *Figure 4*). This indicates that still several degrees above  $T_m$  some kind of entropy effect not observable by d.s.c. exists in the polymer radical system. Because it is more marked in the case of bonded radicals it may be concluded that the random-coil conformation is achieved only some degrees above the end point of the endothermic melting. The relaxation melting point changes as a function of  $\bar{M}_n$  in the same manner as the melting points obtained by other techniques<sup>16, 30, 31</sup> (see *Figure 5*) although the absolute values differ from each other because the histories and the molecular weight distributions of polymers differ from each other.

The  $E_a^{II}$  maximum at  $\bar{M}_n > 9500$  may be a crystallization effect because the amount of end groups is already negligible and the lamellae already contain many folded chains.

#### PEG in the solid state

*Figures 4* and *6* show that the rotation of radicals is more restricted in the relaxation region III than in the first-mentioned one. This indicates that the rotation frequency of radicals and the specific volume of polymer are in direct relation to each other. It also supports the hypothesis given above, that the radicals are in close interaction with the crystalline phase. The exactness of  $\Delta E_a^{II}$  values as a function of  $\bar{M}_n$  is quite poor (*Table 2*); however, they seem to be roughly about two degrees

of rotational freedom ( $\sim 8\text{kJ/mol}$ ). In the low  $\bar{M}_n$  region  $E_a^{\text{III}}$  of radicals decreases when  $\bar{M}_n$  increases. The high  $E_a^{\text{III}}$  values at low  $\bar{M}_n$  values may be explained by the great amount of end-group hydrogen bonds<sup>33</sup> and by the easiness of short chains to form extended chain lamellae<sup>28</sup>. In the high  $\bar{M}_n$  region  $E_a^{\text{III}}$  is practically constant which is in accordance with the short range nature of the relaxation.

The temperature plot of the transition point from relaxation region III to region IV describes the disordered structure of PEG 2050 and PEG 3000, because the segmental motions in these polymers increase strongly at lower temperatures than in other samples. The locking effect of the polymer backbone on the rotations of bonded radicals can be clearly observed because their transition temperatures (from region III to IV) are about  $20^\circ\text{C}$  higher than those of free radicals. These transition temperatures for free radicals correlate fairly well with the nuclear magnetic resonance (n.m.r.) measurements of Hikichi and Furuichi<sup>4</sup>. Their results for the beginning of rapid narrowing of the broad n.m.r. signal from crystalline regions of PEG 1000 and 4000 are also given in Figure 5. Hikichi and Furuichi supposed that the molecular motions which caused the narrowing of the broad n.m.r. signal were rotational or oscillational motions about the helical axis. Our results (that the segmental relaxations of PEG 1000 and 4000 contributing to rotations of free radicals increase notably at  $T \sim 270\text{K}$ ) evidently express the same phenomenon. This evidence further supports our hypothesis that the crystalline phase contributes to the rotations of radicals.

The low  $E_a$  value of relaxation region IV reflects the stable structure of PEG in this temperature region. It is probable that the motional freedom of polymer segments occurring at frequency  $\sim 10^7\text{Hz}$  is strongly inhibited and perhaps only oscillational motions take place. Of course, rotational movements with slower frequencies can occur, but they cannot be identified by e.s.r. techniques because these kinds of movements do not affect the linewidths of the e.s.r. spectra.

It has been stated that the  $\tau$  depends on the rate of molecular motions in the media containing the radicals<sup>8</sup>. On the basis of our work we conclude that  $E_a$  is not solely the activation energy of the motion of polymer segments but it depends strongly on the rate of changes in the total dynamic state of polymer as a function of temperature.

#### ACKNOWLEDGEMENTS

The authors wish to thank Jaakko Brotherus and Antti Savolainen, for valuable discussions during this work.

The authors are also indebted to the National Research Council for Sciences, to the Foundation of Neste Oy and to the University of Helsinki for financial aid.

#### REFERENCES

- 1 Ishida, Y. *J. Polym. Sci. (B)* 1965, **3**, 321
- 2 Porter, C. H. and Boyd, R. H. *Macromolecules* 1971, **4**, 589
- 3 Allen, G., Connor, T. M. and Pursey, H. *Trans. Faraday Soc.* 1963, **59**, 1525
- 4 Hikichi, K. and Furuichi, J. *J. Polym. Sci. (A)* 1965, **3**, 3003
- 5 Read, B. E. *Polymer* 1962, **3**, 529
- 6 Hartmann, B. *Polymer* 1972, **13**, 460
- 7 Allen, G. and Sims, D. *Polymer* 1963, **4**, 105
- 8 Wasserman, A. M., Buchachenko, A. L., Kovarskii, A. L. and Neiman, M. B. *Eur. Polym. J.* 1969, **5**, 473
- 9 Bullock, A. T., Butterworth, J. H. and Cameron, G. G. *Eur. Polym. J.* 1971, **7**, 445
- 10 Törmälä, P., Silvennoinen, K. and Lindberg, J. *Acta Chem. Scand.* 1971, **25**, 2659
- 11 Gross, S. C., *J. Polym. Sci. (A-1)* 1971, **9**, 3327
- 12 Törmälä, P., Lättilä, H. and Lindberg, J. J., in 'ESR Applications to Polymer Research', (Eds P. Kinell, B. Rånby and V. Runnström-Reio), Almqvist & Wiksell, Stockholm, 1973, p 267
- 13 Rozantsev, E. G. and Krinitskaya, L. A. *Tetrahedron* 1965, **21**, 491
- 14 Krinitskaya, L. A., Buchachenko, A. L. and Rozantsev, E. G. *Zh. Org. Khim.* 1966, **2**, 1301
- 15 Törmälä, P., Martinmaa, J., Silvennoinen, K. and Vaahtera, K. *Acta Chem. Scand.* 1970, **24**, 3066
- 16 Törmälä, P. and Savolainen, A. *Acta Chem. Scand.* in press
- 17 Rabold, G. P. *J. Polym. Sci. (A-1)* 1969, **7**, 1203
- 18 Griffith, O. H. and Waggoner, A. S. *Acc. Chem. Res.* 1969, **2**, 17
- 19 Kivelson, D. *J. Chem. Phys.* 1960, **33**, 1107
- 20 Waggoner, A. S., Griffith, O. H. and Christensen, C. R. *Proc. Nat. Acad. Sci. US* 1967, **57**, 1198
- 21 Ohnishi, S., Boeyens, J. C. A. and McConnell, H. M. *Proc. Nat. Acad. Sci. US* 1966, **56**, 809
- 22 Törmälä, P., Brotherus, J. and Lindberg, J. *J. Meddn Finska KemSamf.* 1972, **81**, 11
- 23 Kuznetsov, A. N., Wasserman, A. M., Volkov, A. U. and Korst, N. N. *Chem. Phys. Lett.* 1971, **12**, 103
- 24 Shimshick, E. J. and McConnell, H. M. *Biochem. Biophys. Res. Commun.* 1972, **46**, 321
- 25 McCalley, R. C., Shimshick, E. J. and McConnell, H. M., *Chem. Phys. Lett.* 1972, **13**, 115
- 26 Lindberg, J. J., Törmälä, P. and Lähtenmäki, M. *Acta Chem. Fenn. (B)* 1972, **45**, 295
- 27 Boyd, R. H. and Porter, C. H. *J. Polym. Sci. (A-2)* 1972, **10**, 647
- 28 Baltá Calleja, F. J. and Keller, A. *J. Polym. Sci. (A)* 1964, **2**, 2171
- 29 Beech, D. R., Booth, C., Dodgson, D. V., Sharpe, R. R. and Waring, J. R. S. *Polymer* 1972, **13**, 73
- 30 Afifi-Effat, A. M. and Hay, J. N. *JCS Faraday Trans. II* 1972, **68**, 656
- 31 Alfthan, E. and de Ruvo, A. personal communication
- 32 Booth, C., Bruce, J. M. and Buggy, M. *Polymer* 1972, **13**, 475



# Phosphonitrilic chloride: 21. Synthesis of chelating polymers with cyclophosphazene thiocarbamate and the properties of chelating polymers

M. Kajiwara, M. Hashimoto and H. Saito

*Department of Applied Chemistry, Faculty of Engineering, Nagoya University, Nagoya, Japan  
(Received 26 March 1973)*

Chelating polymers containing copper, nickel and cobalt have been formed from cyclophosphazene thiocarbamate trimer and copper, nickel or cobalt ions. These polymers obtained from the reaction are amorphous and the values of electron conductivity are  $2.7 \times 10^{11} \Omega\text{-cm}$ ,  $3.6 \times 10^{13} \Omega\text{-cm}$  and  $1.5 \times 10^{13} \Omega\text{-cm}$  for the Cu, Ni and Co polymers respectively. The Cu polymer is the most thermally stable on heating to  $500^\circ\text{C}$  in air.

## INTRODUCTION

Complexes of phosphazene derivatives have been reviewed by Allcock<sup>1</sup>. The first type of complex is by coordination of the metal to the skeletal phosphorus atom, for example  $(\text{NPCl}_2)_3\text{AlCl}_3$ . The second type is by coordination of the metal to a skeletal nitrogen atom, for example  $(\text{NPCl}_2)_3\text{AlBr}_3$ . The third type of complex of unknown structure is formed from various cyclophosphazene derivatives and metal salts, or ions.

In this work, cyclophosphazene dichloride trimer  $(\text{NPCl}_2)_3$ , potassium thiocyanate (KSCN), and dry ammonia gas ( $\text{NH}_3$ ) are reacted together, and the product obtained in this substitution reaction is then chelated with various metal ions. The properties of the chelate-polymer are investigated.

## EXPERIMENTAL

Cyclophosphazene dichloride trimer  $(\text{NPCl}_2)_3$  was prepared by the modified method of Saito and Kajiwara<sup>2</sup>. Pure trimer was obtained by repeated fractional crystallization from light petroleum ether. The trimer had a m.p. of  $112^\circ\text{C}$ . Cyclophosphazene thiocarbamate trimer  $[\text{NP}(\text{NHCSNH}_2)_2]_3$  (PTT) was formed from the cyclophosphazene dichloride trimer, potassium thiocyanate and dry ammonia gas by dissolving the isothiocyanophosphazene trimer  $[\text{NP}(\text{SCN})_2]_3$  formed by the method reported by Audrith<sup>3</sup> in dry ether. A white precipitate was obtained by passing dry ammonia into the ether solution. The product was separated by filtration and then the product is in fair agreement with the chemical composition  $[\text{NP}(\text{NHCSNH}_2)_2]_3$ . The product melted at  $190^\circ\text{C}$ , and dissolved in water, pyridine, and most organic solvents.

Chelated polymers were formed from PTT and copper, nickel or cobalt as follows.  $0.586 \text{ g}$  ( $0.001 \text{ M}$ ) PTT was dissolved in water, and  $5 \text{ ml}$  pyridine were

added to this aqueous solution.  $0.006 \text{ M}$  aqueous acetate salt solutions of the metal ions were used, and were added dropwise to warm PTT solution with vigorous

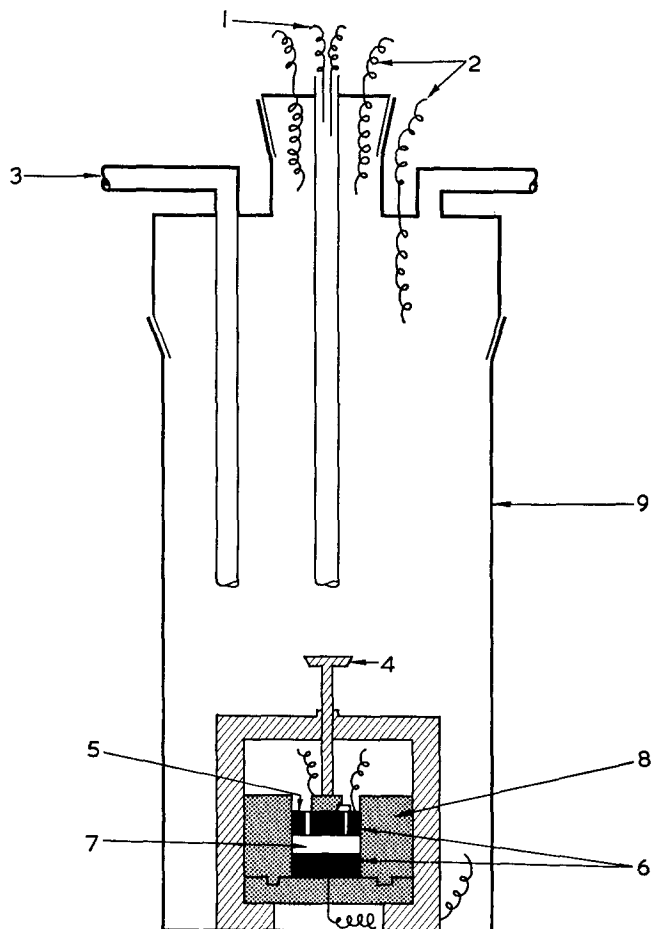


Figure 1 Electrical conductivity measurement apparatus. 1, Thermocouple; 2, Pt electrodes; 3, gas entry; 4, suppressed electrodes; 5, guard ring; 6, electrodes; 7, sample; 8, Teflon, 9, Pyrex tube

stirring. When the reaction was over, the mixture was warmed on a water bath for 15 min. The precipitate was filtered and washed with distilled water, ethanol, and ether, and then dried in an air oven for 24 h at 100°C. Infra-red (i.r.) spectra of the products were obtained using the pressed KBr disc technique. The variation of resistivity with temperature for the chelated polymers was measured with a Takeda TR-8651 type ammeter using Pt and guarded electrodes to eliminate the surface current. The apparatus is shown in Figure 1. The electrical conductivity of the polymers of PTT was measured by a d.c. method.

## RESULTS

The chemical analysis and i.r. spectra of the chelated polymers formed from PTT and each metal salt are summarized in Table 1 and Figures 2 and 3.

Further, the thermal stability of the polymers was investigated using a thermal balance and the results are shown in Figure 4.

The variation of resistivity with temperature is shown

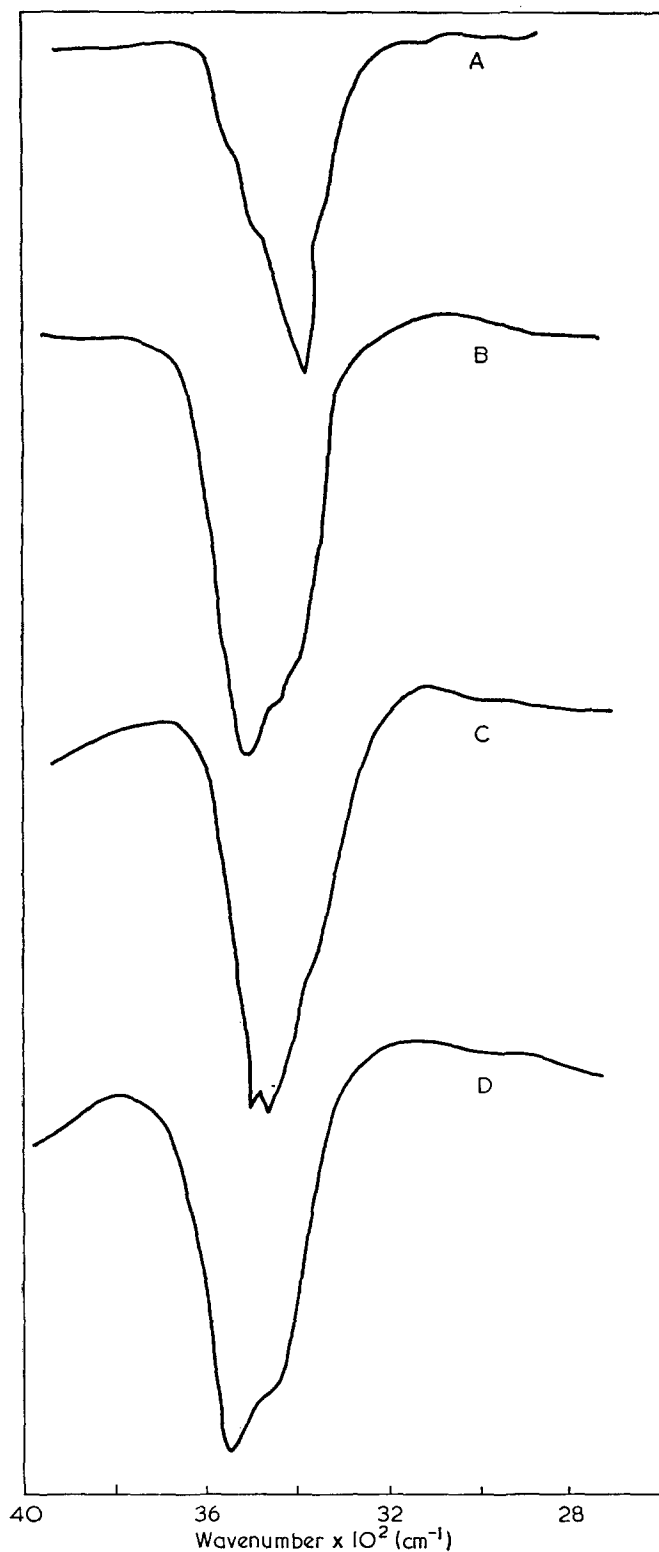


Figure 2 Infra-red absorption of chelating polymers in the region of 4000 to 2800  $\text{cm}^{-1}$ . (A), PTT; (B) PTT/Co/Py; (C) PTT/Ni/Py; (D) PTT/Cu/Py

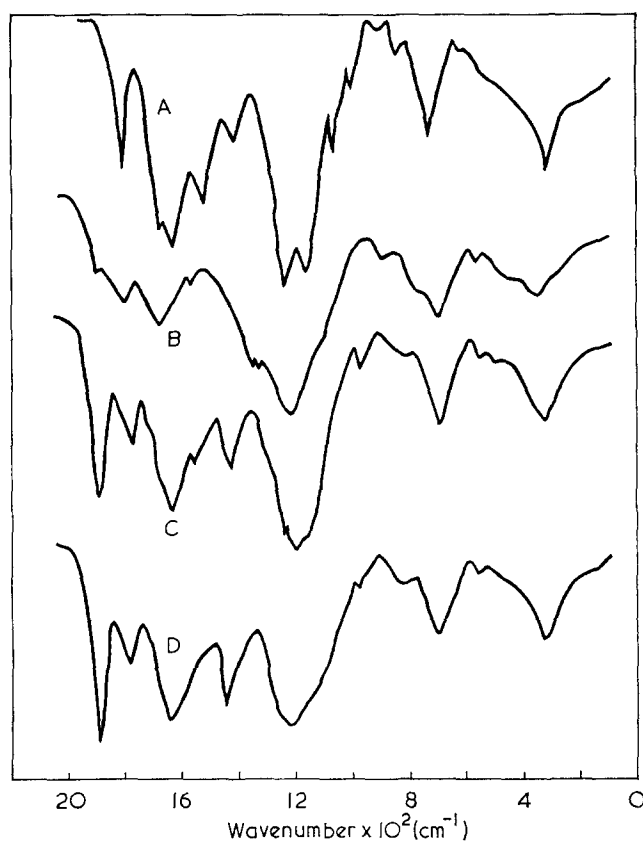


Figure 3 Infra-red absorption of chelating polymers in the region of 2000 to 200  $\text{cm}^{-1}$ . (A) PTT; (B) PTT/Cu/Py; (C) PTT/Ni/Py; (D) PTT/Co/Py

Table 1 Chemical analysis of the polymers formed from phosphazene thiocarbamate trimer and metal ions

Chemical compositions	Calcd. (%)			Found (%)			Nature of the polymers
	P	N	Metal	P	N	Metal	
(I) $[\text{N}_3\text{P}_3(\text{NCSNH})_6\text{Cu}_6\text{Py}_6]_x$	6.47	20.48	26.56	6.2	20.72	26.48	Green. Amorphous. Insoluble in most organic solvents
(II) $[\text{N}_3\text{P}_3(\text{NCSNH}_2)_6\text{Ni}_3\text{Py}_6]_y$	7.55	23.90	14.32	7.9	24.00	14.10	Grey. Amorphous. Insoluble in most organic solvents
(III) $[\text{N}_3\text{P}_3(\text{NCSNH}_2)_6\text{Co}_3\text{Py}_6]_z$	7.55	23.90	14.36	7.3	24.80	14.00	Orange. Amorphous. Insoluble in most organic solvents

Py=Pyridine

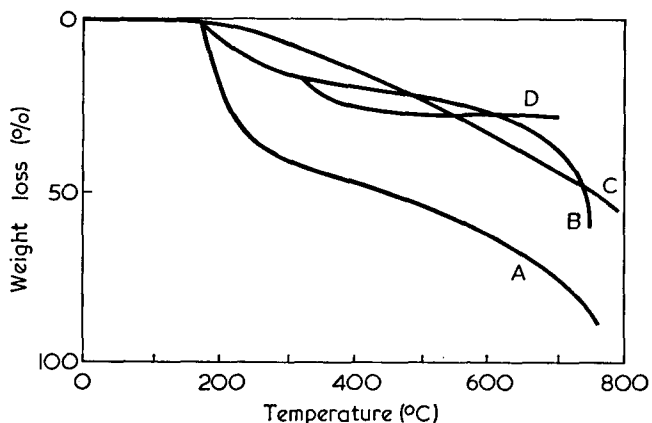
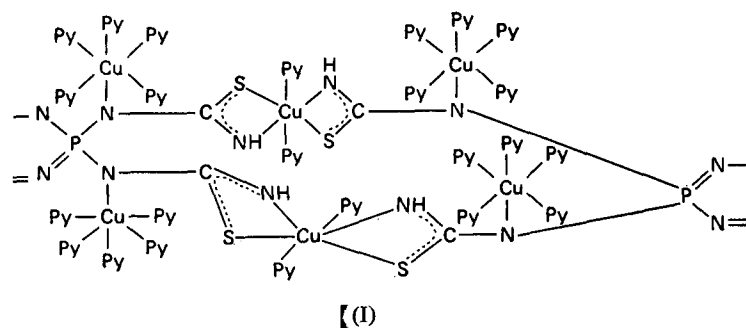


Figure 4 Thermal balance of chelating polymers formed from phosphazene thiocarbamate and metal salts in air at 5°C/min. (A) PTT; (B) PTT/Co/Py; (C) PTT/Cu/Py; (D) PTT/Ni/Py

Table 2 Energy gaps and the value of resistivity of chelated polymers and phosphazene thiocarbamate trimer

Polymers	$\rho_{25^\circ\text{C}}$ ( $\Omega\text{-cm}$ )	$\Delta E$ (eV)
(I) Cu	$2.7 \times 10^{11}$	1.24
(II) Ni	$3.6 \times 10^{13}$	1.65
(III) Co	$1.5 \times 10^{13}$	1.65
(IV) Phosphazene thiocarbamate trimer	$3.4 \times 10^9$	1.23



in Figure 5, and the energy gaps of the polymers calculated from the general relation for organic semiconductors  $\rho = \rho_0 \exp(\Delta E/2RT)$  are summarized in Table 2.

### DISCUSSION

The  $\text{-NH}_2$  frequency of the products (I), (II) and (III) in the region of  $3360\text{ cm}^{-1}$  remains as a shoulder. The absorption characteristic of the  $\text{-NH}$  frequency is in the region of  $3400\text{ cm}^{-1}$ .

The difference in the absorption of the  $\text{N-C=S}$  frequency is observed in the i.r. spectra. The  $\text{N-C=S}$  frequency of PTT is in the region of  $1485\text{ cm}^{-1}$ . However, it has changed to  $1350\text{ cm}^{-1}$  in (I) and  $1355\text{ cm}^{-1}$  in (II) and (III). This suggests that  $\text{N-C=S}$  bonding has become  $\text{N-C-S}$ .

From the chemical analysis and i.r. spectra of the products (I), (II) and (III), the structures are proposed as follows with a coordination number of six. However, the materials did not melt and were insoluble in most organic solvents or water. Consequently, their molecular weights were not determined.

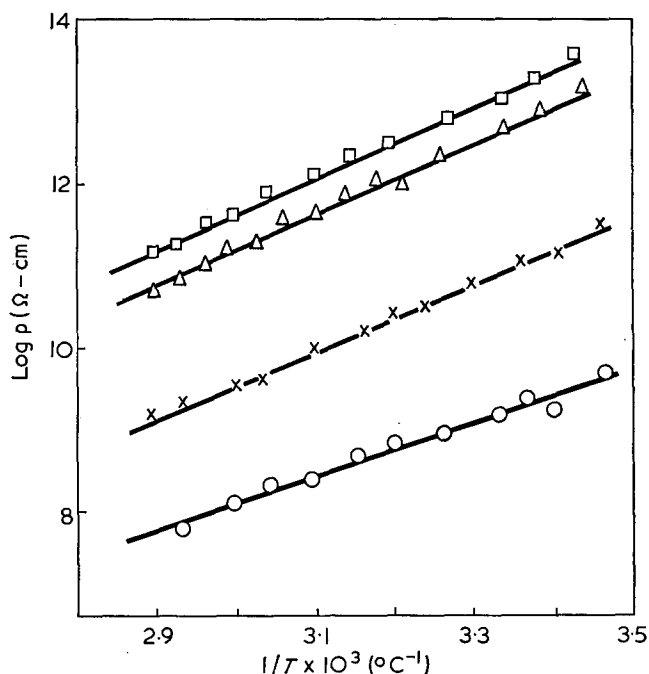
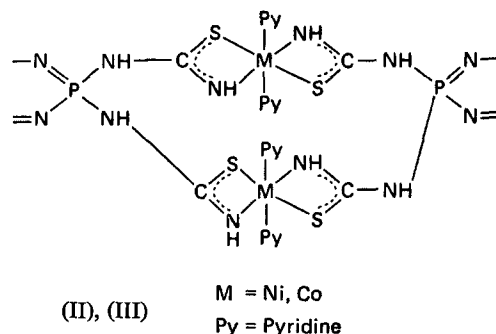


Figure 5 Electrical conductivity of chelating polymers formed from phosphazene thiocarbamate and metal salts. O, PTT; x, Cu;  $\Delta$ , Co;  $\square$ , Ni



The value of  $\rho$  and  $\Delta E$  of the products (I), (II) and (III) tended to decrease with a smaller ionic radius.

The intermolecular actions are inhibited because the products are amorphous, and there is no conjugation between  $\text{P}_3\text{N}_3$  and the chelating rings.

The thermal stability of the chelating polymers was investigated with the thermal balance. The thermal decomposition of PTT occurs at  $200^\circ\text{C}$ ; however, the three polymers chelated with metals are more stable. It is assumed that the chelating ring produced by the reaction leads to thermal stability. Under  $500^\circ\text{C}$  the order of thermal stability is as follows:  $\text{PTT/Cu/Py} > \text{PTT/Ni/Py} > \text{PTT/Co/Py}$ . This is similar to the electron conductivities, the most thermally stable polymer being  $\text{PTT/Cu/Py}$  from room temperature to  $500^\circ\text{C}$ .

### REFERENCES

- 1 Allcock, H. R. *Chem. Rev.* 1972, 72, 315
- 2 Saito, H. and Kajiwara, M. *J. Chem. Soc. Japan (Ind. Chem. Sect.)* 1963, 66, 618
- 3 Audrith, L. F. et al. *J. Am. Chem. Soc.* 1960, 82, 528

# Elastic modulus of linear polymer crystals

T. R. Manley and C. G. Martin

Department of Materials Science, Newcastle upon Tyne Polytechnic,  
Newcastle upon Tyne NE1 8ST, UK  
(Received 19 March 1973)

A method based on energy balance over the repeat unit is used for the calculation of the elastic modulus of linear polymer crystals. The result for polyethylene agrees with that of Treloar who used a statical analysis over the whole molecule. Both methods are much simpler than those of Shimanouchi and Miyazawa, the latter being based on the complete potential function for the polymer. Using force constants based on a Urey Bradley force field, the following values of modulus were found (all syndiotactic except PE) in GN/m<sup>2</sup>: PE, 299; PVC, 153; PVF, 212; PVA, 142; PAN, 236; PMMA, 63.

## INTRODUCTION

The method of Jaswon *et al.*<sup>1</sup> for the calculation of the elastic moduli of cellulose was modified and applied to the helical polymer crystals of poly(phosphonitrilic chloride)<sup>2</sup> and values for Young's modulus of 0.138 GN/m<sup>2</sup> and 1.66 GN/m<sup>2</sup> obtained for the uniform helix and *cis*-planar structures respectively. These results are similar to those calculated for other helical polymers, but as all experiments with (NPCl<sub>2</sub>)<sub>n</sub> used amorphous rubber, no direct comparison is possible.

The method is equally applicable to linear polymers and it was therefore decided to apply it to crystals of polyethylene and the syndiotactic forms of poly(vinyl chloride) (PVC), poly(vinyl fluoride) (PVF), poly(vinyl alcohol) (PVA), polyacrylonitrile (PAN) and poly(methyl methacrylate) (PMMA).

Different solutions have been proposed for both polyethylene<sup>3-5</sup> and PVC<sup>6</sup>. Treloar<sup>4</sup> performed a statical analysis using simple valence force constants. On the other hand, the Japanese workers<sup>3, 5, 6</sup> calculated the modulus directly from the complete potential function for the molecule.

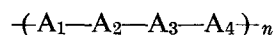
We assume that the polymer chain in the crystal is isolated and infinite; the repeat unit alone is characterized. The problem of a free or fixed end group does not arise. The bond lengths and bond angles of the repeating unit are taken as degrees of freedom which can be varied independently of one another. This simplifies the choice of force constants since we derive the extensions due to bond stretching separately from those due to angular deformation. The force constants are selected from a Urey Bradley force field (*UBFF*), in which only the 'pure' stretching or bending constants for the appropriate bond are taken. The mixed terms, i.e. bending-stretching interaction constants are meaningless in our method of modulus calculation. In obtaining these force constants we do, however, consider the effect of adjacent non-bonded atoms on the particular stretching or bending force constant in question. The number of force constants required for our analysis is a minimum and they are calculated from a knowledge of *K*, *H* and *F*, the stretching, bending and repulsive force constants for the

appropriate bonds or angles, which may be transferred from smaller molecules<sup>7</sup>.

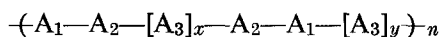
The methods of Shimanouchi *et al.*<sup>3, 6</sup> and Miyazawa<sup>5</sup> require the setting up of the complete Urey Bradley force field for the polymer repeat unit including both stretching-stretching and stretching-bending interaction terms.

The relationships between internal parameters and the helical parameters of the particular polymer structure are also required.

Some knowledge and expertise in spectroscopic techniques are required in order to set up the potential energy equation, remove the redundancies from it and derive the relationships between the helical and internal parameters. The calculation of the modulus requires the differentiation of all these equations and the solution of the resultant simultaneous equations. The present method, therefore, is much simpler. This advantage is particularly important with polymers more complex than polyethylene. The Japanese workers<sup>5, 6</sup> have treated polymers with up to four different chain units, e.g.



but excluding  $-(A_1-A_2-[A_3]_x)_n$ . On the other hand, the present method is readily applicable to polymers such as:



## POLYETHYLENE

The polyethylene molecule has an extended planar zig-zag structure in which the repeating unit is the  $-\text{CH}_2-$  group. This is characterized by the bond length *r* and bond angle  $\phi$  (see *Figure 1*). The translational repeat unit is defined as  $SS'$  and is made up from  $\frac{1}{2}r_1$ ,  $\phi$ ,  $r_2$ ,  $\phi$ ,  $\frac{1}{2}r_1$ , (*Figure 2*). It is more convenient, however, to base it on  $C_1C'_1$  bearing in mind that  $\phi$  occurs twice. Both definitions give the same equations but the latter is more convenient.

A set of rectangular Cartesian axes related to these quantities can be superimposed by choosing one of the carbon atoms as an origin and identifying one of the bonds as the direction of the *x* axis as shown in *Figure 2*. The *y* axis is then perpendicular to  $C_1C_2$  and is in the

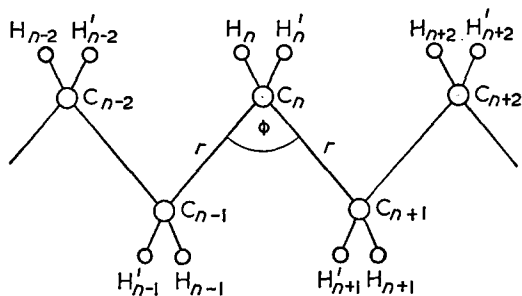


Figure 1 Structure of polyethylene molecule

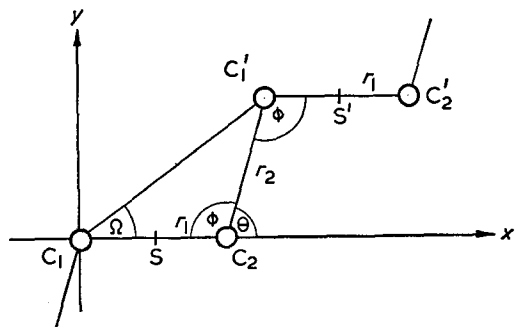


Figure 2 Translational repeat unit of PE

plane of the molecule. The  $z$  axis is out of the paper but is not required for this linear planar molecule.

The auxiliary angle  $\theta$  is the angle between bond  $C_2C'_1$  and the  $x$  axis and is related to  $\phi$  by:

$$\phi = \pi - \theta \quad (1)$$

Vector components can now be assigned to the bonds in the repeat unit:

$$C_1C_2 = (1, 0)r_1$$

$$C_2C'_1 = (\cos\theta, \sin\theta)r_2$$

The repeat unit vector is given as:

$$C_1C'_1 = \bar{n} \cdot L = (\cos\Omega, \sin\Omega)L \quad (2)$$

where  $\Omega$  is the angle between the fibre direction along  $C_1C'_1$  and the  $x$  axis and  $L$  is the repeat distance given by:

$$L = (r_1^2 + r_2^2 - 2r_1r_2 \cos\phi)^{1/2} \quad (3)$$

When the chain is deformed by a uniform strain along its axis the symmetry is still preserved and hence the three quantities  $r_1$ ,  $r_2$  and  $\phi$ , still describe the chain configuration. These can be considered as three degrees of freedom which can be varied independently of one another and will be designated as  $l_i$  using our previous notation<sup>2</sup>.

If we consider the repeating unit  $L$  to undergo a change in length  $dL$ , this change is made up of the sum of the small changes due to a small change in each degree of freedom, i.e.

$$dL = \sum dL_i; \quad i = 1, 3 \quad (4)$$

These small changes are given as follows:

$$dL_1 = \bar{n}(1, 0)dl_1 = \cos\Omega dl_1 \quad (5)$$

$$dL_2 = \bar{n}(\cos\theta, \sin\theta)dl_2 = (\cos\Omega, \cos\theta + \sin\Omega, \sin\theta)dl_2 \quad (6)$$

and

$$dL_3 = \bar{n}l_2 \frac{\partial}{\partial \phi} [\cos\theta, \sin\theta] d\phi = \bar{n}l_2 \left[ -\sin\theta \frac{d\theta}{d\phi}, \cos\theta \frac{d\theta}{d\phi} \right] d\phi$$

Now from equation (1)

$$\phi = \pi - \theta$$

$$\therefore d\phi = -d\theta$$

$$\text{i.e. } dL_3 = \bar{n}l_2 [\sin\theta, -\cos\theta] d\phi$$

$$\therefore dL_3 = (\cos\Omega \sin\theta - \sin\Omega \cos\theta) l_2 d\phi \quad (7)$$

Then utilizing the Jaswon *et al.* formula<sup>1</sup>:

$$C^{-1} = \sum \left( \frac{\partial L}{\partial l_i} \right)^2 / \frac{\partial^2 W}{\partial (dl_i)^2} \quad (8)$$

the overall force constant  $C$  for the repeat unit can be obtained from:

$$C^{-1} = \frac{(dL_1)^2}{K} + \frac{(dL_2)^2}{K} + \frac{(dL_3)^2}{2H} \quad (9)$$

where  $K$  and  $H$  are the bond stretching and bond angle deformation force constants for  $-\text{CH}_2-\text{CH}_2-$  and  $-\text{CH}_2-\text{CH}_2-\text{CH}_2-$  respectively. The factor  $2H$  arises since the degree of freedom  $\phi$  occurs twice in the repeat distance, (cf.  $SS'$  in Figure 2).

The overall force constant  $C$  is then related to the elastic constant  $c_{22}$  by the energy balance:

$$\frac{1}{2} c_{22} e_2^2 V = W = \frac{1}{2} C (dL)^2 = CL^2 e_2^2 \quad (10)$$

$$\therefore c_{22} = \frac{CL^2}{V} = \frac{CL}{A} \quad (11)$$

where  $A$  is the effective cross-sectional area of the repeating unit.

The force constants used were taken from a *UBFF*, the deviation of which is shown in the Appendix and are in the form:

$$K = K_2 = K_{CC} + 2s_2^2 F_{CC} + 4s_4^2 F_{HC} \quad (12)$$

and

$$H = b^2 H_2$$

where

$$H_2 = H_{CCC} + t_2^2 F_{CC} + 3\kappa / (8^{1/2} b^2) \quad (13)$$

Force constant data were taken from refs 3 and 8, since no complete set of *UBFF* constants was available for the polyethylene molecule.

The molecular parameters are given in Table 1 and the values used in the force constant calculations in Table 2.

The modulus ( $c_{22}$ ) for polyethylene is calculated as: 299 GN/m<sup>2</sup>.

### SYNDIOTACTIC PVC

Syndiotactic PVC has an extended planar zig-zag structure as shown in Figure 3 and the modulus may be calculated in the manner used for PE.

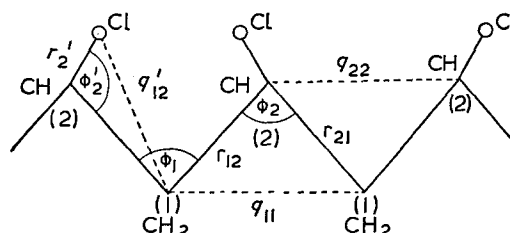


Figure 3 Structure of s-PVC

**Table 1** Molecular parameters used in modulus calculations  
Tetrahedral bond angles are used throughout ( $109^{\circ}28'$ )  
C-C bond distances are all 0.154 nm

Polymer (CH <sub>2</sub> CXY) <sub>n</sub>	Nature of		Bond distances		Cross-sectional area, * A (nm <sup>2</sup> )	Repeat distance L' (nm)
	X	Y	R(C-X) (nm)	R(C-Y) (nm)		
PE <sup>a</sup>	H	H	0.109	0.109	0.1824	0.2515
s-PVC <sup>b</sup>	Cl	H	0.177	0.109	0.2746	0.2515
s-PVFc	F	H	0.135	0.109	0.2121	0.2520
s-PVA <sup>c</sup>	OH	H	0.413	0.109	0.2152	0.2520
s-PAN <sup>c</sup>	CN	H	0.216	0.109	0.3111	0.2550
s-PMMA <sup>c</sup>	COOCH <sub>3</sub>	CH <sub>3</sub>	0.154	0.154	0.5565	0.2510

\* From unit cell measurements except for PMMA

<sup>a</sup> Ref. 12

<sup>b</sup> Ref. 6

<sup>c</sup> Alexander, L. E. 'X-ray diffractions in polymer science'. Wiley, N.Y. 1969, p. 473

**Table 2** Force constant data used in modulus calculations

Polymer (CH <sub>2</sub> CXY) <sub>n</sub>	Nature of		K <sub>C-C</sub> (N/m)	F <sub>CH<sub>2</sub>-CH<sub>2</sub></sub> (N/m)	F <sub>CXY-CXY</sub> (N/m)	F <sub>CX</sub> (N/m)	F <sub>CY</sub> (N/m)	H <sub>1</sub> (N/m)	H <sub>2</sub> (N/m)	κ (aNm)
	X	Y								
PE <sup>a,b</sup>	H	H	280	96	96	40	40	11	11	0.2
s-PVC <sup>c</sup>	Cl	H	340	33	96	60	40	11	20	0.23*
s-PVFc	F	H	340	33	150*	130	40	11	25*	0.25*
s-PVA <sup>d</sup>	OH	H	280	33	30	28 <sup>d</sup>	40	20*	11	0.17
s-PAN <sup>e</sup>	CN	H	200	38	44	44	54	34	27	κ <sub>1</sub> =0.01 κ <sub>2</sub> =0.11
s-PMMA <sup>f</sup>	COOCH <sub>3</sub>	CH <sub>3</sub>	340	96	33	33	40	11	20	0.1

\* Estimated value

<sup>a</sup> Ref. 3

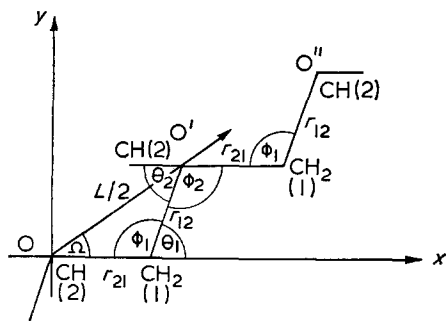
<sup>b</sup> Ref. 8

<sup>c</sup> Ref. 6

<sup>d</sup> From propyl alcohol

<sup>e</sup> Ref. 11

<sup>f</sup> From polyisobutylene and polypropylene<sup>6</sup>



**Figure 4** Translational repeat unit for s-PVC

The rectangular Cartesian axes are superimposed as for PE with a C atom as origin and a bond  $r_{21}$  as the  $x$  axis as shown in *Figure 4*.

Although there are four C atoms in the repeat unit we are only considering deformation of the carbon skeleton and since  $\phi_1 = \phi_2$  the alternate nature of the chlorine atoms along the chain will be mechanically indeterminate. Hence we need only consider half of the actual repeat unit with four degrees of freedom to be varied  $r_{21}$ ,  $r_{12}$ ,  $\phi_1$  and  $\phi_2$  and defining the auxiliary angles  $\theta_1$  and  $\theta_2$ .

The mechanical model is, therefore, almost exactly the same as for polyethylene and gives the following expressions for the small changes  $dL_i$ .

$$dL_1 = \bar{n}(1, 0)dl_1$$

where  $\bar{n}$  is the direction cosine of the repeat distance vector

$$00'' = (\cos\Omega, \sin\Omega)L = \bar{n} \cdot L$$

or in this case

$$00'' = (\cos\Omega, \sin\Omega)\frac{L}{2} = \bar{n}\frac{L}{2} = \bar{n}L'$$

$$\therefore dL_1 = \cos\Omega dl_1 \quad (14)$$

$$dL_2 = \bar{n}(\cos\theta_1, \sin\theta_1)dl_2 \\ = (\cos\Omega \cos\theta_1 + \sin\Omega \sin\theta_1)dl_2 \quad (15)$$

which are exactly the same as in polyethylene.

The angles  $\phi_1$ , i.e.  $\angle \text{CHCl}-\text{CH}_2-\text{CHCl}$  and  $\phi_2$ , i.e.  $\angle \text{CH}_2-\text{CHCl}-\text{CH}_2$  are not equivalent although some authors have used the same force constant for both angular deformations<sup>6</sup>:

$$dL_3 = \bar{n}\frac{r_{12}}{2} \frac{\partial}{\partial \phi_1} [\cos\theta_1, \sin\theta_1]d\phi_1 \\ = \bar{n}\frac{r_{12}}{2} [\sin\theta_1, -\cos\theta_1]d\phi_1$$

since  $d\theta_1 = -d\phi_1$

$$\therefore dL_3 = \frac{r_{12}}{2} (\cos\Omega \sin\theta_1 - \sin\Omega \cos\theta_1)d\phi_1 \quad (16)$$

and also

$$dL_4 = \bar{n}\frac{r_{12}}{2} \frac{\partial}{\partial \phi_2} [-\cos\theta_2, -\sin\theta_2]d\phi_2$$

$$dL_4 = \bar{n}\frac{r_{12}}{2} [-\sin\theta_2, \cos\theta_2]d\phi_2$$

since  $d\phi_2 = -d\theta_2$

$$\therefore dL_4 = \frac{r_{12}}{2} [-\cos\Omega \sin\theta_2 + \sin\Omega \cos\theta_2]d\phi_2 \quad (17)$$

The overall force constant  $C$  for the repeat unit can then be obtained from:

$$C^{-1} = \frac{(dL_1)^2}{K} + \frac{(dL_2)^2}{K} + \frac{(dL_3)^2}{H_1^\phi} + \frac{(dL_4)^2}{H_2^\phi} \quad (18)$$

where  $K$  and  $H_1^\phi$ ,  $H_2^\phi$  are the stretching and bending force constants for  $-\text{CHCl}-\text{CH}_2-$ ,  $-\text{CHCl}-\text{CH}_2-\text{CHCl}-$  and  $-\text{CH}_2-\text{CHCl}-\text{CH}_2-$  respectively.

#### DERIVATION OF THE FORCE CONSTANTS $K$ , $H_1^\phi$ , $H_2^\phi$

The Urey Bradley force field (UBFF) used for PVC is similar to that for polyethylene given in the Appendix but contains more terms due to the difference between  $\text{CH}_2$  and  $\text{CHCl}$ , i.e. the term in  $\Delta R_n$  in polyethylene ( $C_n - C_{n+1}$ ) becomes a term in  $\Delta r_{12}$  and  $\Delta r_{21}$ .

Similarly the term in  $\Delta \phi_n$  becomes a term in  $\Delta \phi_1$  and  $\Delta \phi_2$ .

Thus the required force constants are:

$$K = Kr_{11} = Kr_{21} = K_{CC} + s_{11}^2 F_{\text{CH}_2\text{CH}_2} + s_{22}^2 F_{\text{CHClCHCl}} + s_{12}^2 F_{\text{CCl}} + 3s_{21}^2 F_{\text{CH}} \quad (19)$$

and

$$H_1^\phi = \rho^2 H_1 + t_{22}^2 \rho^2 F_{\text{CHClCHCl}} + \rho^2 3\kappa / (8^{1/2} r_{21} r_{12}) \quad (20)$$

$$H_2^\phi = \rho^2 H_2 + t_{11}^2 \rho^2 F_{\text{CH}_2\text{CH}_2} + \rho^2 3\kappa / (8^{1/2} r_{12} r_{21}) \quad (21)$$

where

$$s_{11} = (r_{12} - r_{21} \cos \phi_2) / q_{11}$$

$$s_{22} = (r_{21} - r_{12} \cos \phi_1) / q_{22}$$

$$s_{12} = (r_{12} - r_2' \cos \phi_2') / q_{12}$$

$$s_{21} = (r_{21} - r_1' \cos \phi_1') / q_{21}$$

$$t_{11} = \rho \sin \phi_2 / q_{11}$$

$$t_{22} = \rho \sin \phi_1 / q_{22}$$

and

$$\rho = (r_{12} r_{21})^{1/2}$$

$$q_{11}^2 = r_{12}^2 + r_{21}^2 - 2r_{12}r_{21}\cos\phi_2$$

$$q_{22}^2 = r_{21}^2 + r_{12}^2 - 2r_{21}r_{12}\cos\phi_1$$

$$q_{12}^2 = r_{12}^2 + r_2'^2 - 2r_{12}r_2'\cos\phi_2'$$

$$q_{21}^2 = r_{21}^2 + r_1'^2 - 2r_{21}r_1'\cos\phi_1'$$

Using the values in Tables 1 and 2 the elastic constant  $c_{22}$  of s-PVC was calculated as  $c_{22} = 153 \text{ GN/m}^2$ .

The simplicity of this method for calculating the elastic moduli of planar zig-zag polymer chains of type  $(A_1-A_2-A_1-A_2)$  enabled us to calculate the moduli of other linear polymers, e.g. PVF, PVA and PAN, by substituting data into equations (14) to (21) as for the s-PVC calculation.

The parameters from Tables 1 and 2 gave the results shown in Table 3.

#### SYNDIOTACTIC POLY(METHYL METHACRYLATE)

In this case very little X-ray information about the unit cell is available so the cross-sectional area of the unit cell was calculated from the X-ray density-volume relation:

$$\text{density} = \frac{Z \times M}{V \times N} \quad (22)$$

Table 3 Calculated moduli of several polymer crystals

Polymer	Calculated results (GN/m <sup>2</sup> )		Experimental results <sup>9</sup> (GN/m <sup>2</sup> )
	p	q	
PE	299	340 <sup>a</sup>	235
	182	182 <sup>b</sup> 290 <sup>c</sup> 160 <sup>d</sup>	
s-PVC	153	160 <sup>d</sup>	251
s-PVF	212		
s-PVA	142		
s-PAN	236		
s-PMMA	63		

<sup>a</sup> Ref. 3

<sup>b</sup> Ref. 4

<sup>c</sup> Ref. 5

<sup>d</sup> Ref. 6

<sup>p</sup> This work

<sup>q</sup> Other authors

where  $Z$  is the number of monomer units per unit cell (in this case  $Z=4$ ),

$M$  = molecular weight of a monomer unit (100.11),

$V$  = volume of the unit cell,

$N$  = Avogadro's number =  $6.023 \times 10^{23} \text{ mol}^{-1}$ ,

and the chain length  $L = 5.02014 \times 10^{-8} \text{ cm}$ .

The only X-ray density available for s-PMMA was  $1.19 \text{ g/cm}^3$  obtained from the amorphous region. The crystalline density will be slightly higher but for the approximate nature of this calculation for cross-sectional area the value was thought to be adequate. The cross-sectional area of the 'unit cell' was thus calculated as  $111.291 \times 10^{-16} \text{ cm}^2$  giving an effective cross-sectional area of chain as  $55.645 \times 10^{-16} \text{ cm}^2$ . Substituting the above in equations (14) to (22) gave the modulus of s-PMMA as  $c_{22} = 63 \text{ GN/m}^2$ .

This low value of the modulus is attributed to the large cross-sectional area of the chain =  $55 \times 10^{-16} \text{ cm}^2$  compared with  $18.24 \times 10^{-16} \text{ cm}^2$  for polyethylene,  $27.46 \times 10^{-16} \text{ cm}^2$  for PVC, etc., which is caused by the bulky methyl and ester groups in the side chain.

#### EXTENSIBILITY

The values of modulus for polymers of type  $(A_1-A_2)_n$  in Table 3 were used to calculate the extensibility or  $f$  value. The extensibility is the force required to stretch a molecule by 1% in the direction of the molecular axis and may be calculated from the modulus and cross-sectional area of a single chain<sup>9</sup>.

The  $f$  value is mainly dependent on conformation and for planar zig-zag type polymers usually falls in the range 0.4–0.5 nN. The  $f$  values for each of the polymers are shown in Table 4.

#### DISCUSSION

The value for polyethylene obtained by the present method is identical to that of Treloar<sup>4</sup> if the same force constants are employed (Table 3). The improved values for the force constants in the present paper give a result lower than that of Shimanouchi<sup>3</sup> but close to that of Miyazawa<sup>5</sup>. A much better result is expected when force constant values from a single source are available. As

Table 4 Extensibilities ( $f$  values) of several polymer crystals

Polymer	Modulus (GN/m <sup>2</sup> )	Cross-sectional area (nm <sup>2</sup> )	$f$ value (nN)
PE	299	0.1824	0.545
s-PVC	153	0.2746	0.420
s-PVF	212	0.2121	0.449
s-PVA	143	0.2152	0.31
s-PAN	236	0.3111	0.73
s-PMMA	63	0.556	0.35

expected, the theoretical value of the elastic modulus in each case is higher than the experimental value obtained using X-ray methods<sup>9</sup>. The present method is preferred because it is simplest.

For s-PVC, this method gives a value close to that calculated by Asahina and Enomoto<sup>6</sup> (see Table 3). No X-ray data were available for PVC, but the  $f$  value obtained is within the expected range (see Table 4).

Similarly, no experimental or calculated data are available for s-PVF but the extensibility falls within the expected range (see Table 4).

Syndiotactic PVA gave a low result when compared to the experimental result (see Table 3). This could be due to lack of suitable force constants for substitution into the *UBFF*, but is more likely to be due to neglect of secondary bonding effects.

We consider an isolated polymer chain, i.e. neglecting intermolecular forces. These are normally very small when compared with the primary valence forces along the chain and hence the single chain approximation is quite reasonable. However, infra-red studies on PVA<sup>10</sup> show that strong intermolecular H-bonding occurs between adjacent chains, but no intramolecular H-bonding (in the chain direction) occurs. Sakurada<sup>9</sup> also noted that H-bonding affected only the modulus perpendicular to the chain.

As the PVA chain is extended it tends to contract laterally and when two adjacent chains are extended this will result in the H-bonds between them being stretched. Therefore the H-bond force constant also contributes to the elastic modulus in the chain direction and the single chain approximation becomes invalid. Jaswon *et al.*<sup>1</sup> gave a treatment for secondary bonding in cellulose and it is hoped to extend this to PVA in the near future.

The elastic modulus of s-polyacrylonitrile was calculated as 236 GN/m<sup>2</sup>. No experimental or calculated moduli were available for comparison, but the  $f$  value obtained was well outside the expected range for a planar zig-zag polymer (see Table 4). The force constants used were obtained from a recent detailed treatment of the alkylnitriles<sup>11</sup> and are regarded as reliable. The high extensibility value is due to the extremely polar nature of the polymer. Polyoxymethylene (POM) also exhibits strong intramolecular dipole-dipole interactions resulting in high modulus and extensibility values<sup>9</sup>. The calculated values for the modulus and  $f$  value of s-acrylonitrile, therefore appear to be quite reasonable.

The low modulus and  $f$  values obtained for s-PMMA are shown in Tables 3 and 4. The  $f$  value is only slightly lower than the expected range and is due to the uncertainty in the calculation for the cross-sectional area of the chain using X-ray density measurements rather than unit cell parameters.

## ACKNOWLEDGEMENT

We thank the Science Research Council for a scholarship to C.G.M.

## REFERENCES

- Jaswon, M. A., Gillis, P. P. and Mark, R. E. *Proc. R. Soc. (A)* 1968, **306**, 389
- Manley, T. R. and Martin, C. G. *Polymer* 1971, **12**, 775
- Shimanouchi, T., Asahina, M. and Enomoto, S. *J. Polym. Sci.* 1962, **59**, 93
- Treloar, L. R. G. *Polymer* 1960, **1**, 95
- Miyazawa, T. *Rep. Progr. Polym. Phys. Japan* 1965, **8**, 47
- Asahina, M. and Enomoto, S. *J. Polym. Sci.* 1962, **59**, 101
- Overend, J. and Scherer, J. R. *J. Chem. Phys.* 1960, **32**, 1289, 1296, 1720
- Shimanouchi, T. *J. Chem. Phys.* 1949, **17**, 245, 734, 848
- Sakurada, I. and Kaji, K. *J. Polym. Sci. (C)* 1970, **31**, 57
- Kuhn, L. P. *J. Am. Chem. Soc.* 1954, **76**, 4323
- Fujiyama, T. *Bull. Chem. Soc. Japan* 1971, **44**, (1), 89
- Bunn, C. W. *Trans. Faraday Soc.* 1939, **35**, 482

## APPENDIX

*Derivation of the force constants K and H*

Assuming a Urey-Bradley type field for polyethylene, the terms in the potential function involving the coordinates of the  $n$ th CH<sub>2</sub> group are given as<sup>6</sup>:

$$\begin{aligned}
 V_n = & K'_{\text{CH}a}(\Delta r_n + \Delta r'_n) + \frac{1}{2}K_{\text{CH}}[(\Delta r_n)^2 + (\Delta r'_n)^2] + \\
 & K'_{\text{C}cb}(\Delta R_n) + \frac{1}{2}K_{\text{CC}}(\Delta R_n)^2 + \\
 & H'_{\text{H}c}a^2(\Delta \theta_n) + \frac{1}{2}H_{\text{H}c}a^2(\Delta \theta_n)^2 + \\
 & H'_{\text{C}cb}b^2(\Delta \phi_n) + \frac{1}{2}H_{\text{C}cb}b^2(\Delta \phi_n)^2 + \\
 & H'_{\text{H}c}cab(\Delta \psi_n + \Delta \psi'_n + \Delta \psi''_n + \Delta \psi'''_n) + \\
 & \frac{1}{2}H_{\text{H}c}cab[(\Delta \psi_n)^2 + (\Delta \psi'_n)^2 + (\Delta \psi''_n)^2 + (\Delta \psi'''_n)^2] + \\
 & F'_{\text{H}H}(2a \sin \alpha) \Delta q_n + \frac{1}{2}F_{\text{H}H}(\Delta q_n)^2 + \\
 & F'_{\text{C}C}(2b \sin \alpha) \Delta Q_n + \frac{1}{2}F_{\text{C}C}(\Delta Q_n)^2 + \\
 & F'_{\text{H}H}[\Delta P_n + \Delta P'_n + \Delta P''_n + \Delta P'''_n] + \\
 & \frac{1}{2}F_{\text{CH}}[(\Delta P_n)^2 + (\Delta P'_n)^2 + (\Delta P''_n)^2 + (\Delta P'''_n)^2] \quad (\text{A1})
 \end{aligned}$$

where internal coordinates  $R_n$ ,  $r_n$  etc., denote the distances and angles respectively with equilibrium values as indicated in parenthesis:

$$\begin{aligned}
 R_n(C_n - C_{n+1} = b) \\
 r_n(C_n - H_n = a) \quad r'_n(C_n - H'_n = a) \\
 \phi_n(< C_{n+1} - C_n - C_{n-1} = 2\beta) \\
 \theta_n(< H_n - C_n - H'_n = 2\alpha) \\
 \psi_n(< H_n - C_n - C_{n+1} = 2\gamma) \\
 \psi'_n(< H'_n - C_n - C_{n+1} = 2\gamma) \\
 \psi''_n(< H_n - C_n - C_{n-1} = 2\gamma) \\
 \psi'''_n(< H'_n - C_n - C_{n-1} = 2\gamma) \\
 Q_n(C_{n-1} \dots C_{n+1} = 2b \sin \beta) \\
 q_n(H_n \dots H'_n = 2a \sin \alpha) \\
 P_n(H_n \dots C_{n+1} = \alpha) \\
 P'_n(H'_n \dots C_{n+1} = \alpha) \\
 P''_n(H_n \dots C_{n-1} = \alpha) \\
 P'''_n(H'_n \dots C_{n-1} = \alpha)
 \end{aligned}$$

where

$$\alpha^2 = a^2 + b^2 - 2ab \cos 2\gamma \quad \text{and} \quad \cos 2\gamma = -\cos \alpha \cos \beta$$

When the coordinates  $Q_n$ ,  $q_n$ ,  $P'_n$ ,  $P''_n$  and  $P'''_n$  for changes of distances between non-bonded atoms are expressed



in terms of the other coordinates<sup>6</sup> the potential energy becomes:

$$\begin{aligned}
 2V_n = & K_1[(\Delta r_n)^2 + (\Delta r'_n)^2] + K_2(\Delta R_n)^2 + \\
 & H_1(a\Delta\theta_n)^2 + H_2(b\Delta\phi_n)^2 + \\
 & H_3ab[(\Delta\psi_n)^2 + (\Delta\psi'_n)^2 + (\Delta\psi''_n)^2 + (\Delta\psi'''_n)^2] + \\
 & 2K_{11}(\Delta r_n)(\Delta r'_n) + 2K_{22}(\Delta R_n)(\Delta R_{n-1}) + \\
 & 2K_{12}[(\Delta r_n)(\Delta R_n) + (\Delta r'_n)(\Delta R_n) + (\Delta r_n)(\Delta R_{n-1}) + \\
 & \quad (\Delta r'_n)(\Delta R_{n-1})] + \\
 & 2F_{11}(a\Delta\theta_n)(\Delta r_n + \Delta r'_n) + 2F_{22}(b\Delta\phi_n)(\Delta R_n + \\
 & \quad \Delta R_{n-1}) + \\
 & 2F_{13}(ab)^{1/2}[(\Delta r_n)(\Delta\psi_n) + (\Delta r'_n)(\Delta\psi'_n) + \\
 & \quad (\Delta r_n)(\Delta\psi''_n) + (\Delta r'_n)(\Delta\psi'''_n)] + \\
 & 2F_{23}(ab)^{1/2}[(\Delta R_n)(\Delta\psi_n) + (\Delta R_n)(\Delta\psi'_n) + \\
 & \quad (\Delta R_{n-1})(\Delta\psi''_n) + (\Delta R_{n-1})(\Delta\psi'''_n)] + \\
 & 2H_{13}a(ab)^{1/2}[(\Delta\theta_n)(\Delta\psi_n) + (\Delta\theta_n)(\Delta\psi'_n) + \\
 & \quad (\Delta\theta_n)(\Delta\psi''_n) + (\Delta\theta_n)(\Delta\psi'''_n)] + \\
 & 2H_{23}b(ab)^{1/2}[(\Delta\phi_n)(\Delta\psi_n) + (\Delta\phi_n)(\Delta\psi'_n) + \\
 & \quad (\Delta\phi_n)(\Delta\psi''_n) + (\Delta\phi_n)(\Delta\psi'''_n)] + \\
 & 2H_{33}ab[(\Delta\psi_n)(\Delta\psi'_n) + (\Delta\psi_n)(\Delta\psi''_n) + \\
 & \quad (\Delta\psi'_n)(\Delta\psi'''_n) + (\Delta\psi''_n)(\Delta\psi'''_n)] \quad (A2)
 \end{aligned}$$

where

$$\begin{aligned}
 K_1 &= K_{CH} + t_1^2 F'_{HH} + s_1^2 F_{HH} + 2t_3^2 F'_{HC} + 2s_3^2 F_{HC} \\
 K_2 &= K_{CC} + 2t_2^2 F'_{CC} + 2s_2^2 F_{CC} + 4t_4^2 F'_{HC} + 4s_4^2 F_{HC} \\
 H_1 &= H_{HCH} - s_1^2 F'_{HH} + t_1^2 F_{HH} + (3\kappa/8^{1/2}a^2) \\
 H_2 &= H_{CCC} - s_2^2 F'_{CC} + t_2^2 F_{CC} + (3\kappa/8^{1/2}b^2) \\
 H_3 &= H_{HCC} - s_3s_4 F'_{HC} + t_3t_4 F_{HC} + (3\kappa/8^{1/2}ab)
 \end{aligned}$$

$$\begin{aligned}
 K_{11} &= -t_1^2 F'_{HH} + s_1^2 F_{HH} \\
 K_{22} &= -t_2^2 F'_{CC} + s_2^2 F_{CC} \\
 K_{12} &= -t_3t_4 F'_{HC} + s_3s_4 F_{HC} \\
 F_{11} &= t_1s_1(F'_{HH} + F_{HH}) \\
 F_{22} &= t_2s_2(F'_{CC} + F_{CC}) \\
 F_{13} &= (b/a)^{1/2}(t_3s_4 F'_{HC} + s_3t_4 F_{HC}) \\
 F_{23} &= (a/b)^{1/2}(t_4s_3 F'_{HC} + s_4t_3 F_{HC}) \\
 H_{13} &= \kappa/a(2ab)^{1/2} \\
 H_{23} &= \kappa/b(2ab)^{1/2} \\
 H_{33} &= \kappa/2^{1/2}ab
 \end{aligned}$$

and

$$\begin{aligned}
 s_1 &= \sin\alpha, s_2 = \sin\beta \\
 s_3 &= (a - b\cos 2\gamma)/\alpha \\
 s_4 &= (b - a\cos 2\gamma)/\alpha \\
 t_1 &= \cos\alpha \\
 t_2 &= \cos\beta \\
 t_3 &= b\sin 2\gamma/\alpha \\
 t_4 &= a\sin 2\gamma/\alpha
 \end{aligned}$$

Since in our modulus calculation we are considering the small changes in  $C_n - C_{n-1}$ , i.e.,  $R_n$  and in  $C_{n+1} - C_n - C_{n-1}$ , i.e.,  $\phi_n$  the required force constants are  $K_2$  and  $H_2$ .

$$\therefore K = K_2 = K_{CC} + 2s_2^2 F_{CC} + 4s_4^2 F_{HC} \quad (A3)$$

and

$$H_2 = H_{CCC} + t_2^2 F_{CC} + 3\kappa/8^{1/2}b^2 \quad (A4)$$

neglecting the first order terms since they have little effect on the value of the modulus.

# Elastic properties and structure of a composite elastomeric system

F. de Candia, A. Dontsov\*, G. Micera and A. Pusino

Laboratorio su Tecnologia dei Polimeri e Reologia, CNR, 80072 Arco Felice, Napoli, Italy  
(Received 1 March 1973)

In the present paper the structural and mechanical properties of an elastomeric system, obtained by vulcanizing a mixture of nitrile rubber and magnesium methacrylate, have been analysed. The structural properties have been studied using the small angle X-ray technique. The mechanical data have been treated with the Mooney–Rivlin phenomenological equation. Experimental data clearly indicate that the examined system is a composite one. Phase separation plays an important role in the mechanical behaviour which is directly related to the morphological and topological properties. The results are discussed at the molecular level and give some critical evidence on the Gaussian theory of rubber elasticity.

## INTRODUCTION

It is well known that the stress–strain isotherms of an elastomeric network, unidirectionally elongated, very closely follow the Mooney–Rivlin phenomenological equation:

$$\tau = 2C_1(\alpha - \alpha^{-2}) + 2C_2(\alpha - \alpha^{-2})^2 \quad (1)$$

where  $\tau$  is the stress on the unit of cross-sectional area,  $\alpha$  the strain ratio and  $C_1$  and  $C_2$  two phenomenological constants. A problem of great relevance is the investigation of the molecular significance of the two coefficients,  $C_1$  and  $C_2$ . While for highly swollen systems it seems possible to identify  $2C_1$  with the theoretical Gaussian modulus<sup>1–4</sup>, i.e. a molecular parameter<sup>5, 6</sup>, nothing is known about the molecular significance of the  $C_2$  term. However, recent experimental results<sup>3, 4, 7–9</sup> indicate that  $C_2$  could be related to intermolecular phenomena present in the amorphous material. In particular, some authors<sup>7–9</sup> suggest the presence of molecular aggregates (bundles) as the direct origin of experimental deviations from the Gaussian theory, of which  $C_2$  can be considered a measure. This interesting hypothesis is strongly supported by recent results<sup>10</sup>. With regard to this problem, it is useful to investigate the mechanical behaviour of elastomeric systems with known structural properties in order to obtain experimental data about the relationships between mechanical and structural parameters.

In a previous paper<sup>11</sup>, the elastic properties and the structure of a network obtained by vulcanizing *cis*-polybutadiene in admixture with magnesium methacrylate are analysed. Results indicate that in this system a phase separation takes place with magnesium methacrylate clustering. Moreover, mechanical properties analysed in terms of the Mooney–Rivlin equation, show that  $C_1$  and  $C_2$  values reflect the structural situation that, on the other hand, can be changed by using different swelling solvents.

\* Permanent address: M. V. Lomosov Moscow Institute of Fine Chemical Technology, Moscow, USSR.

In the present paper, the same kind of analysis has been carried out on networks obtained by vulcanizing nitrile rubber in admixture with different amounts of magnesium methacrylate. The purpose is to give further support to the conclusions previously reported<sup>11</sup>, and to test whether a different polymeric system can give a different experimental response.

## EXPERIMENTAL

In this work a butadiene–acrylonitrile copolymer (NBR, SNAM) containing 50% by weight of acrylonitrile was used. The magnesium salt and the vulcanization mixture were prepared as described previously<sup>11</sup>. The initiator was dicumyl peroxide and vulcanization was carried out at 155°C for 30 min. The stress–strain measurements were carried out at 30°C, stretching the sample step by step with 30 min intervals between each stress level. For swollen samples the stress was corrected by the term  $V_S^{1/3}$  where  $V_S$  is the volume fraction of the rubber.

X-ray analysis at low angles was carried out with a Kratky camera. The experimental conditions were: CuK $\alpha$  ( $\lambda = 1.54 \text{ \AA}$ ) radiation; 45 kV voltage; 20 mA intensity; distance sample-registration plane, 28.6 cm; Angular range 0–90' in steps of 0.6'. At every angle the counter gives the intensity diffused in 100 sec. Three samples with different amounts of salt were studied. These samples are indicated as GN0, GN10 and GN20 and correspond to a salt content of 0, 10 and 20% respectively.

## RESULTS

### Mechanical properties

Figure 1 shows in terms of the Mooney–Rivlin equation, the stress–strain isotherms obtained on sample GN0. Two different swelling solvents with different polarities were used: benzonitrile and *N,N*-dimethylformamide. As shown, the behaviour is similar to that with rubber-like materials. In fact,  $C_1$  is constant in

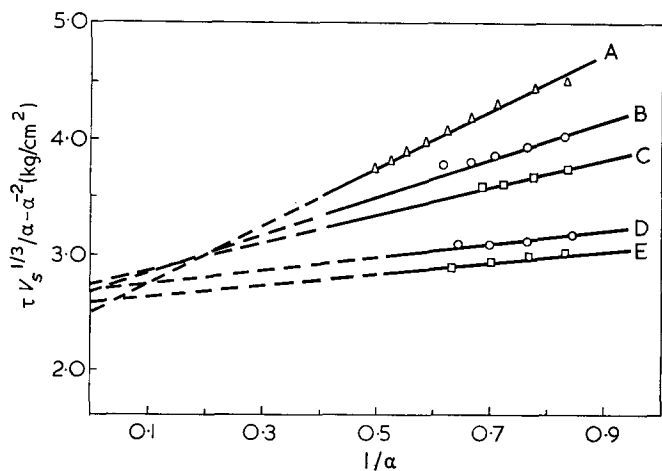


Figure 1 Mooney-Rivlin plots obtained on sample GN0.  $\Delta$ , Dry sample;  $\circ$ , *N,N*-dimethylformamide swollen samples;  $\square$ , benzonitrile swollen samples. A,  $V_s=1$ ; B,  $V_s=0.839$ ; C,  $V_s=0.748$ ; D,  $V_s=0.567$ ; E,  $V_s=0.462$

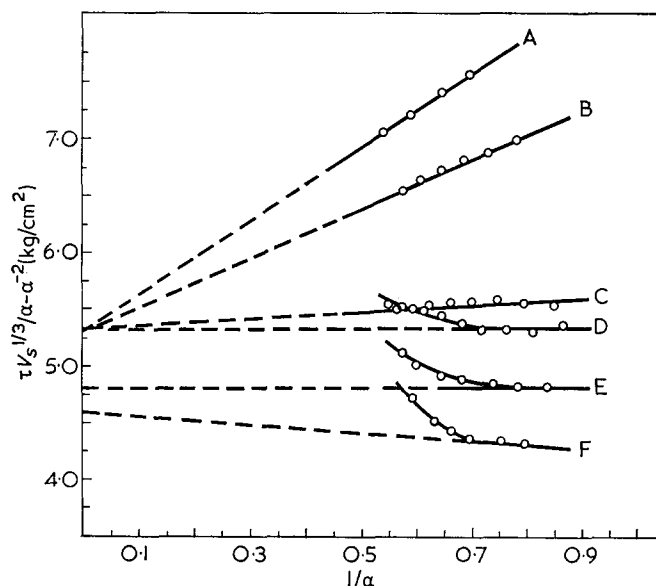


Figure 3 Mooney-Rivlin plots obtained on sample GN10 with benzonitrile as swelling solvent. A,  $V_s=1$ ; B,  $V_s=0.753$ ; C,  $V_s=0.628$ ; D,  $V_s=0.568$ ; E,  $V_s=0.532$ ; F,  $V_s=0.439$

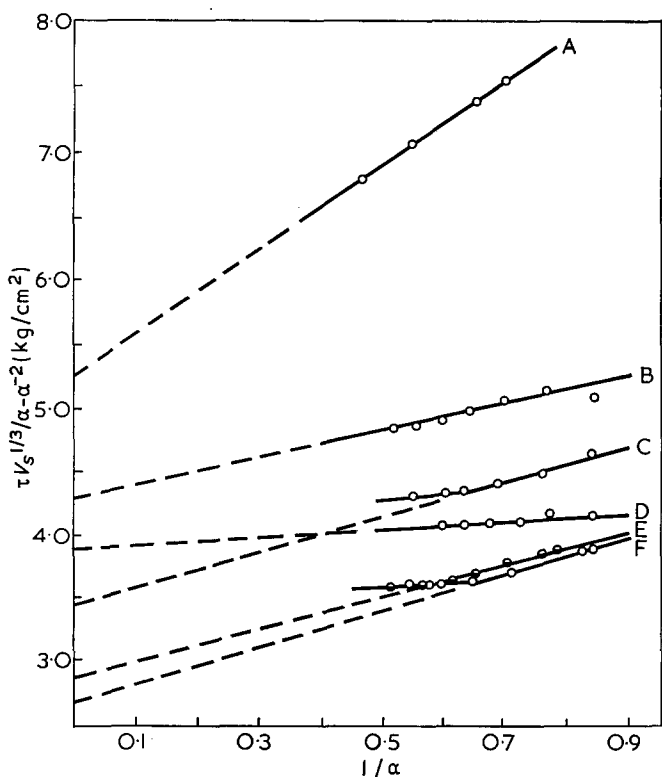


Figure 2 Mooney-Rivlin plots obtained on sample GN10 with *N,N*-dimethylformamide as swelling solvent. A,  $V_s=1$ ; B,  $V_s=0.876$ ; C,  $V_s=0.744$ ; D,  $V_s=0.665$ ; E,  $V_s=0.534$ ; F,  $V_s=0.509$

all swelling ranges investigated, while  $C_2$  decreases as the solvent amount increases. In Figures 2 and 3, the data obtained on sample GN10 are reported. Figure 2 refers to data obtained using *N,N*-dimethylformamide as swelling solvent, while in Figure 3 the swelling solvent was benzonitrile. It seems clear that the experimental behaviour is quite different from that of sample GN0.  $C_1$  decreases with swelling;  $C_2$  also decreases and in the benzonitrile swollen samples, at high degrees of swelling, gives rise to a sharp change in the sign.

The upturn in the Mooney-Rivlin plots, with  $C_2$  changing from positive to negative values, can be due to crystallization under stress or to non-Gaussian behaviour<sup>12</sup>. Excluding the first hypothesis in highly swollen systems, it seems possible to assign this behaviour to non-Gaussian phenomena. The observed trend is

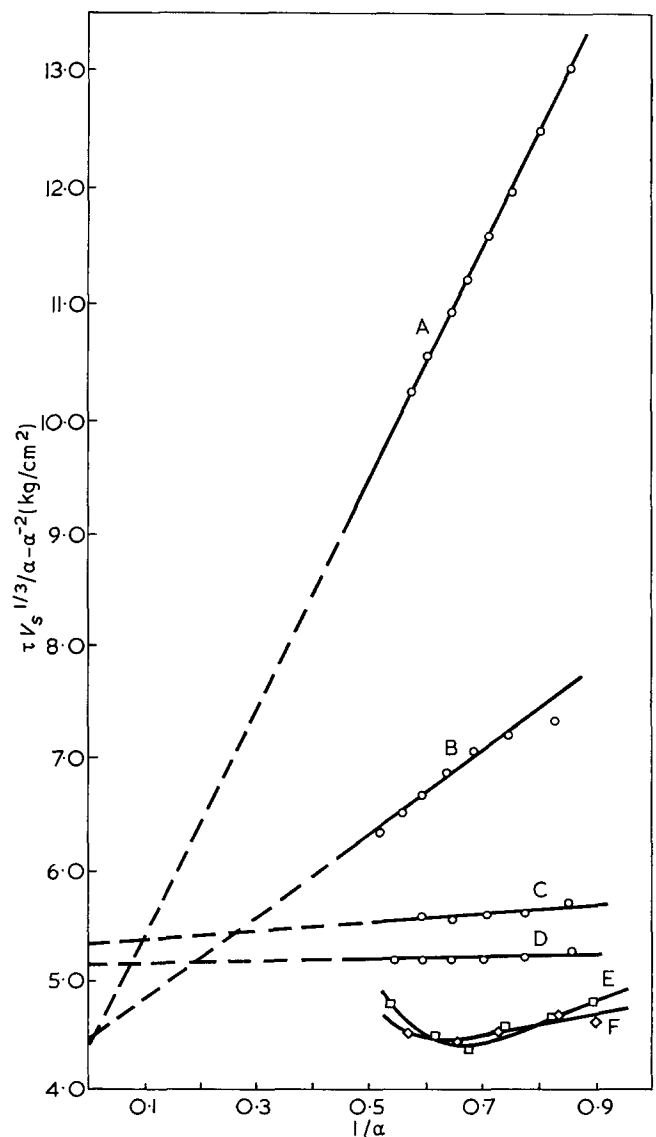


Figure 4 Mooney-Rivlin plots obtained on sample GN20 with *N,N*-dimethylformamide as swelling solvent. A,  $V_s=1$ ; B,  $V_s=0.933$ ; C,  $V_s=0.732$ ; D,  $V_s=0.696$ ; E,  $V_s=0.612$ ; F,  $V_s=0.661$

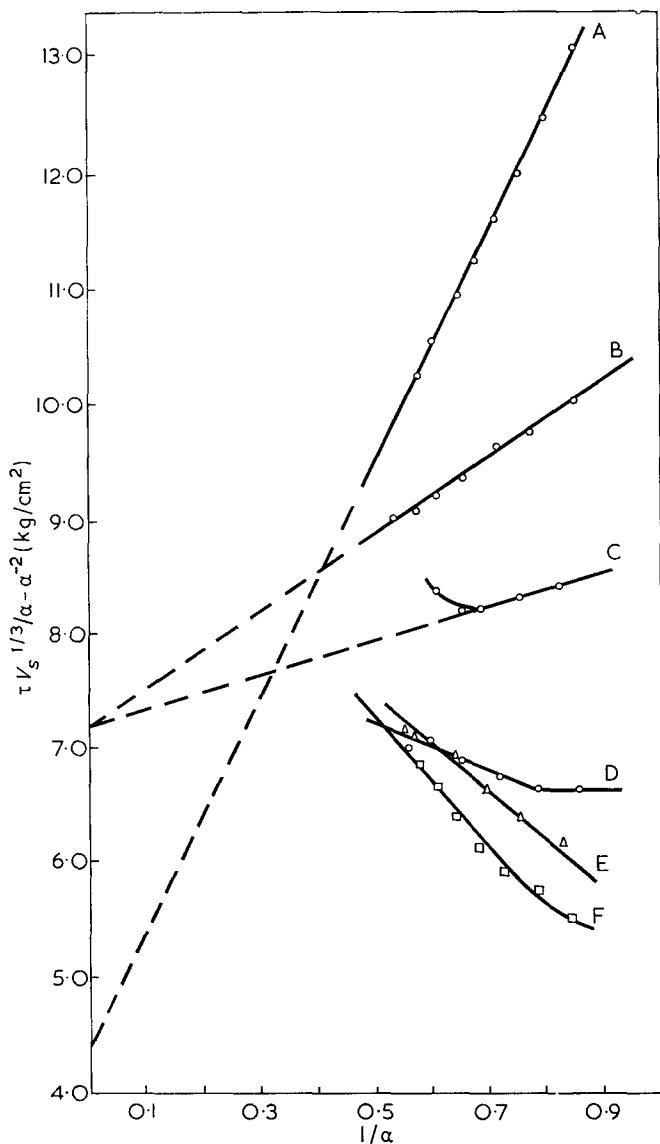


Figure 5 Mooney-Rivlin plots obtained on sample GN20, with benzonitrile as swelling solvent. A,  $V_s=1$ ; B,  $V_s=0.817$ ; C,  $V_s=0.678$ ; D,  $V_s=0.628$ ; E,  $V_s=0.506$ ; F,  $V_s=0.493$

more pronounced in Figures 4 and 5, where the data obtained on sample GN20 are reported. Figure 4 refers to *N,N*-dimethylformamide swollen samples while in Figure 5 the solvent was benzonitrile. In both cases, non-Gaussian behaviour is present but is more evident in Figure 5 where, at high degrees of swelling the upturn is not visible since  $C_2$  is also negative at low strain values. On the other hand, when it is possible to obtain a significant  $C_1$  value,  $C_1$  increases with the swelling, apparently at variance with the trend observed on sample GN10.

Samples GN10 and GN20 were taken after three days in swelling equilibrium with *N,N*-dimethylformamide and dichloroacetic acid (DCA), in the ratio of 0.95:0.05 respectively, and then dried. Such treated samples show a mechanical behaviour as reported in Figures 6 and 7. The swelling solvent was dimethylformamide. It seems evident that the observed trend is very similar to that reported in Figure 1 for sample GN0.

#### X-ray analysis

X-ray small angle analysis was carried out on the dry and swollen samples. Experimental data are reported

in Figures 8, 9 and 10 where the intensity is given as a function of the diffusion angle. The collective data obtained on dry samples GN0, GN10 and GN20 are shown in Figure 11. Diffused intensity indicates a non-homogeneous electronic density for all samples; in other words, it seems to indicate a phase separation, as is evident from Figure 11 where GN0, GN10 and GN20 give a spectrum with an appreciable difference from the background. In Figure 11 a dependence of the diffused intensity upon the amount of salt is also visible, because the former increases as the salt concentration is increased.

On the other hand, in Figures 8, 9 and 10 the effect of the solvent treatment is shown. The solvent reduces intensity and *N,N*-dimethylformamide in a more pronounced way. Moreover, on the samples treated with hydrolysing agent (*N,N*-dimethylformamide/DCA), the intensity strongly decreases moving very near the background. The data of Figures 9-11, when possible, were treated following the Guinier analysis<sup>13</sup>.

This analysis gives the approximate dimensions of particles producing X-ray diffraction. The numerical data indicate limiting values, but it is not possible to say anything about the relative population. Experi-

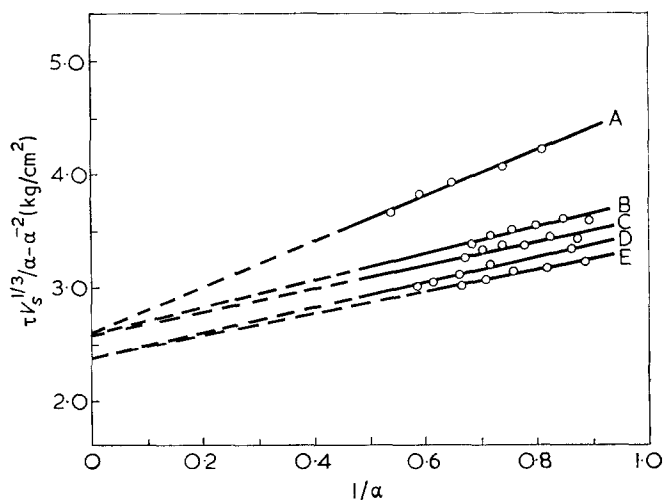


Figure 6 Mooney-Rivlin plots obtained on sample GN10 treated with *N,N*-dimethylformamide/DCA. Swelling solvent is *N,N*-dimethylformamide. A,  $V_s=0.937$ ; B,  $V_s=0.872$ ; C,  $V_s=0.833$ ; D,  $V_s=0.630$ ; E,  $V_s=0.522$

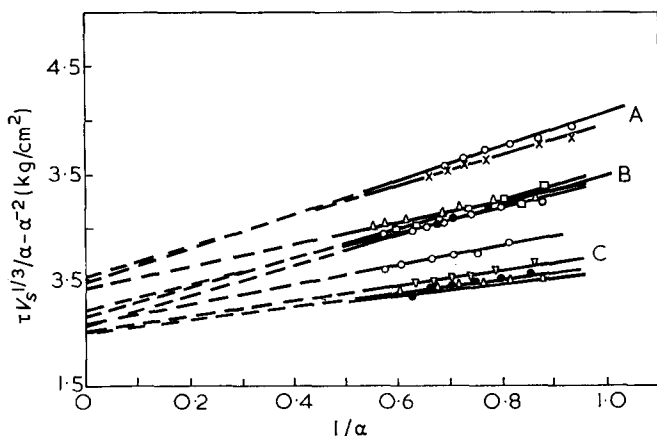


Figure 7 Mooney-Rivlin plots obtained on sample GN20 treated with *N,N*-dimethylformamide/DCA. Swelling solvent is *N,N*-dimethylformamide. A group:  $\circ$ ,  $V_s=0.942$ ;  $\times$ ,  $V_s=0.906$ . B group:  $\square$ ,  $V_s=0.985$ ;  $\triangle$ ,  $V_s=0.663$ ;  $\bullet$ ,  $V_s=0.811$ ;  $\circ$ ,  $V_s=0.935$ . C group:  $\triangle$ ,  $V_s=0.844$ ;  $\bullet$ ,  $V_s=0.774$ ;  $\nabla$ ,  $V_s=0.774$ ;  $\circ$ ,  $V_s=0.690$ . A, B and C groups refer to three different specimens

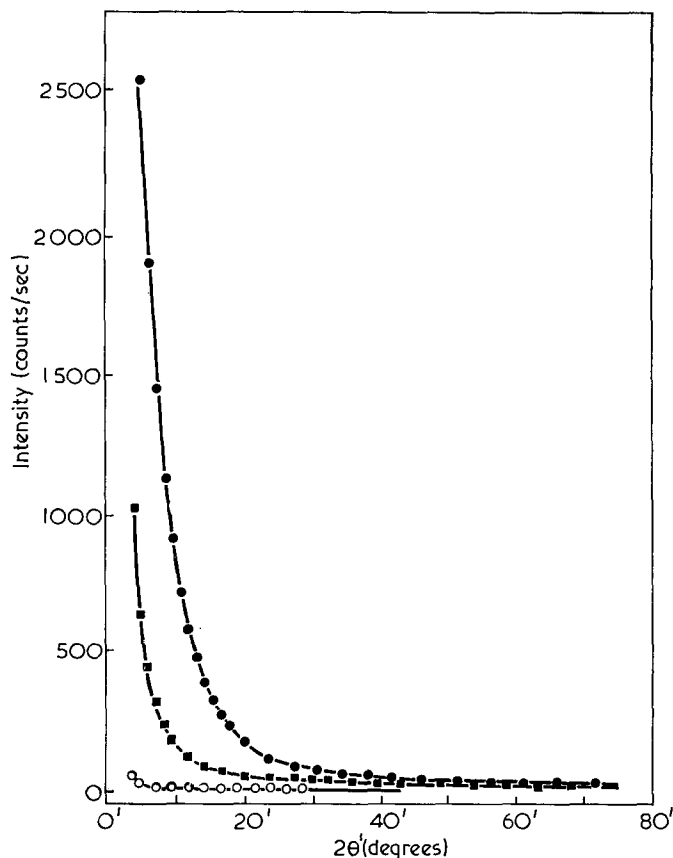


Figure 8 Small angle X-ray scattering plots of sample GN0. ●, Dry; ■, *N,N*-dimethylformamide swollen sample  $V_S \approx 0.5$ ; ○, background

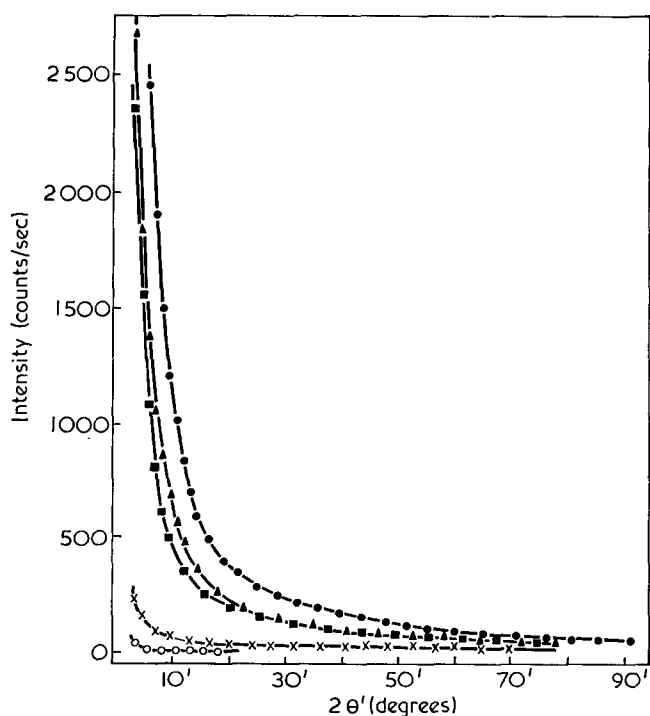


Figure 9 Small angle X-ray plots of sample GN10. ●, Dry; ▲, Benzotrile swollen  $V_S \approx 0.5$ ; ■, *N,N*-dimethylformamide swollen,  $V_S \approx 0.5$ ; ×, hydrolysed sample; ○, background

mental data are reported in Table 1. The data for GN0 are not given either because a linear range was not visible in the Guinier plot, or because an appreciable diffuse intensity is present only at very low angle values, where the experimental error is great.

DISCUSSION

The feature of salt vulcanizates is, as reported<sup>11,14</sup>, the presence in the network of two kinds of crosslinks. In the first group there are covalent carbon-carbon bonds due to peroxide action while in the second we have ionic bonds due to the presence of magnesium salt.

The experimental X-ray data indicate that a phase separation is present with distribution of particles in the amorphous material. It is believed that there is a high concentration of ionic bonds in these particles. In other words, the poly(magnesium methacrylate) formed during vulcanization<sup>14</sup> is distributed in the elastomeric network in the form of particles linked to the elastic chains by a grafting process which takes place in the radical vulcanization reaction. There is, therefore, a composite system whose chemical nature and structure are known and which can be modified by swelling treatment.

On this basis, critical examination of the experimental results can provide some important information regarding the problem of deviations from the rubber elasticity theory as related to topological and molecular parameters. The first point is the behaviour of the term  $C_2$

Table 1 Dimensions of the particles as given by the Guinier analysis

Sample	Dimension range (Å)
GN10 dry	70-220
GN10 benzotrile	70-228
GN10 <i>N,N</i> -dimethylformamide	87-304
GN20 dry	66-178
GN20 benzotrile	64-175
GN20 <i>N,N</i> -dimethylformamide	66-190

For the swollen samples  $V_S$  was about 0.5.

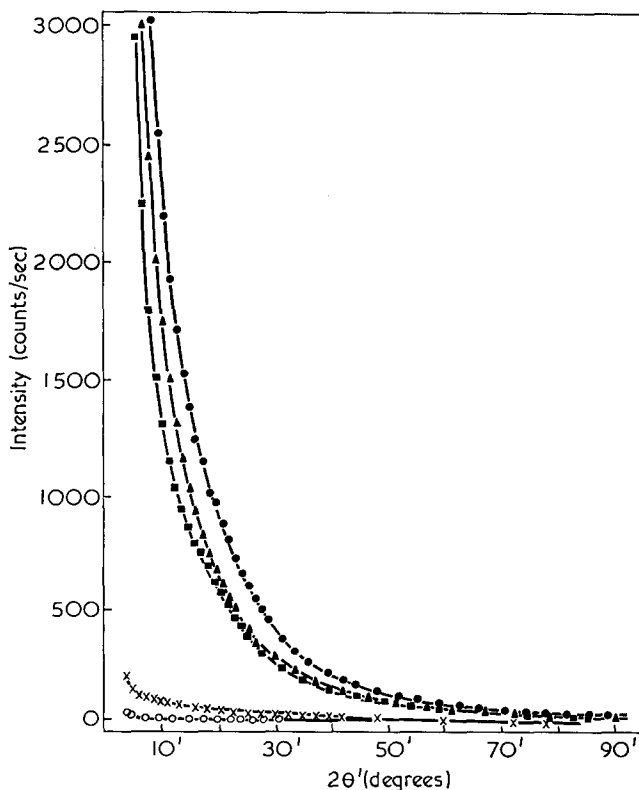


Figure 10 Small angle X-ray plots of sample GN20. ●, Dry; ▲, benzotrile swollen  $V_S \approx 0.5$ ; ■, *N,N*-dimethylformamide swollen  $V_S \approx 0.5$ ; ×, hydrolysed sample; ○, background

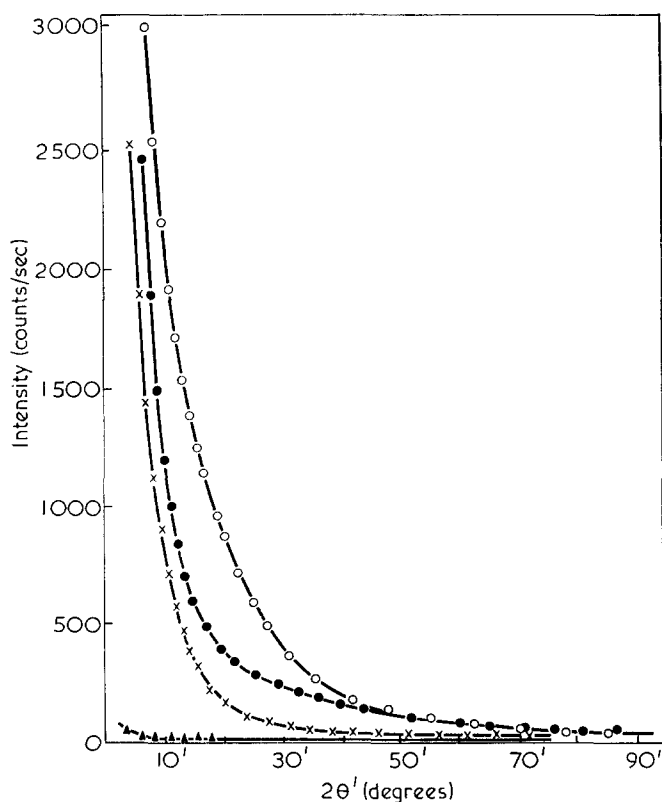


Figure 11 Small angle X-ray plots on dry samples. ○, GN20; ●, GN10; ×, GN0; ▲, background

as a function of the salt amount. We have for  $C_2$  the values 2.24, 3.36 and 10.22 kg/cm<sup>2</sup> for samples GN0, GN10 and GN20 respectively. There is, therefore, a relative increase of the  $C_2$  term with the clustering process. Considering the clusters as a particular phenomenon of interchain aggregation, this influence on the value of  $C_2$  is evident. A second effect shown by the experimental data is the non-Gaussian behaviour of swollen samples GN10 and GN20. This phenomenon is related to the selective action of the solvent that swells only the elastomeric fraction.

Swelling treatment increases the mean distances between particles and therefore stretches the chains linked to them to lengths in the non-Gaussian region. Essentially this is due to the freedom of the macromolecules which is greatly reduced by the presence of clusters, as was explained in a previous paper<sup>11</sup>.

This explanation is supported by the X-ray data. Benzonitrile and *N,N*-dimethylformamide neither change the structure, as shown in Figures 8–10, nor do they swell the clusters, as reported in Table 1. Slight swelling of the clusters is visible for *N,N*-dimethylformamide, and this explains the more pronounced non-Gaussian behaviour present in benzonitrile swollen samples.

On the other hand, treatment with dimethylformamide/DCA, hydrolysing the salt bonds, destroys the ionic crosslinks and the cluster structure disappears, as is clear in the X-ray data. The destruction of the clusters gives the materials the ability to follow the swelling behaviour of sample GN0 (see Figures 1, 6 and 7). The last point that deserves attention is the behaviour of the  $C_1$  coefficient.

The data of Figures 2–5 must be corrected taking into account the effect of the particles. We can use the Guth–Smallwood equation<sup>15</sup>:

$$2C_1(F) = 2C_1(1 + 2.5\phi_s + 14.1\phi_s^2) \quad (2)$$

where  $C_1(F)$  is the experimental value,  $C_1$  the corrected value and  $\phi_s$  the volume fraction of the particles. The use of equation (2) is approximate in this case, but can still give some indication about the trend.  $\phi_s$  has been calculated considering the selective swelling. Data so obtained indicate  $C_1$  to be constant for GN10 and  $C_1$  to increase with swelling for GN20. The increase of  $C_1$  in sample GN20 reflects the more pronounced non-Gaussian behaviour upon which the increase in the modulus depends. It is important, however, to note that  $C_1$  given by the dry samples does not give the Gaussian ideal modulus. In fact, as previously pointed out<sup>2–4</sup>,  $C_1$  gives the ideal modulus only in highly swollen systems or when the swelling behaviour indicates  $C_1$  to be constant with the degree of swelling. Finally one may consider the data of Figure 8 which also suggest phase separation for sample GN0. The rubber used was butadiene–acrylonitrile copolymer with a composition of 50:50.

With so high an acrylonitrile concentration we cannot exclude a block-like distribution with phase separation. However, the situation is quite different in respect to samples GN10 and GN20 where, as explained, the clustering is due to the presence of magnesium salts. In fact, in sample GN0 the *N,N*-dimethylformamide is sufficient to destroy the structure and give an absolutely usual mechanical behaviour (see Figure 1).

#### ACKNOWLEDGEMENTS

The authors wish to thank Dr A. Ferrero and Dr N. Roveri for their interest in this work and their help with X-ray measurements.

Thanks are also due to Mr V. Capodanno for his diligent preparation of the graphs.

#### REFERENCES

- Mullins, L. J. *Appl. Phys.* 1959, 2, 1
- de Candia, F. and Ciferri, A. *Makromol. Chem.* 1970, 134, 335
- de Candia, F. and Amelino, L. *J. Polym. Sci. (A-2)* 1972, 10, 715
- de Candia, F. *Macromolecules* 1972, 5, 102
- Flory, P. J. *J. Am. Chem. Soc.* 1956, 78, 5222
- Treolar, L. R. G. 'The Physics of Rubber Elasticity,' Oxford University Press, 1958
- Blokland, R. and Prins, W. *J. Polym. Sci. (A-2)* 1969, 7, 1595
- Dusek, K. and Prins, W. *Adv. Polym. Sci.* 1969, 6, 1
- Ilavsky, M. and Prins, W. *Macromolecules* 1970, 3, 415
- de Candia, F. and Vittoria, V., to be published
- Dontsov, A., de Candia, F. and Amelino, L. *J. Appl. Polym. Sci.* 1972, 16, 505
- Smith, K. J., Green, A. and Ciferri, A. *Kolloid-Z. Z. Polym.* 1964, 194, 49
- Alexander, L. E. 'X-Ray Diffraction Methods in Polymer Science,' Interscience, New York, 1969
- Dontsov, A. A., Soldatov, V. F. *et al. Colloid J. USSR* 1969, 31, 293

# Sedimentation equilibrium study on preferential interaction of protein with solvent components\*

Hideo Inoue

Shionogi Research Laboratory, Shionogi & Co. Ltd, Fukushima-ku, Osaka 553, Japan  
(Received 9 April 1973; revised 29 May 1973)

A sedimentation equilibrium equation was derived in weight-per-volume concentration units to evaluate the degree of preferential binding of one solvent component to a homogeneous neutral macromolecule in a mixture of two components. Using the equation, the preferential binding of chloroethanol to  $\beta$ -lactoglobulin A was calculated from sedimentation equilibrium data, and the result showed good agreement with values obtained by light scattering and refractive index increment experiments. It was also demonstrated that the preferential interaction can in principle be determined by density increment measurements under different conditions: at constant molality and at constant chemical potential of solvent.

## INTRODUCTION

Study of the optical properties of proteins has shown that a conformational change of protein frequently takes place when an additive such as alcohol or electrolyte is added to an aqueous solution of a protein<sup>1</sup>. Thermodynamic investigation has made it clear that the conformation of a protein in solution depends to a great extent on the interaction between the protein and the solvent component<sup>1, 2</sup>. We have previously investigated the preferential interaction of proteins with solvent components in mixed water-organic solvent systems by light scattering and refractive index increment measurements together with the proper application of multi-component theory<sup>3, 4</sup>.

In this communication we derive equations by which the degree of preferential binding of one of the solvent components to protein can be calculated from sedimentation equilibrium data and density increment measurements. Application of this method is demonstrated by sedimentation equilibrium experiments carried out on  $\beta$ -lactoglobulin A ( $\beta$ -Lg A) solutions at various concentrations of chloroethanol. The degree of preferential binding to  $\beta$ -Lg A calculated with use of the equations is in satisfactory to good agreement with the values obtained from the light scattering and refractive index increment experiments.

## THEORY

Fujita<sup>5</sup>, and Casassa and Eisenberg<sup>6</sup> have derived a sedimentation equilibrium equation for a solution of a homogeneous neutral macromolecular component in a medium which consists of two components of low molecular weight. We use here the Scatchard<sup>7</sup>-Stockmayer<sup>8</sup> notation for a three-component system: the principal solvent is component 1, the additional diffusible solvent

is component 3, and the macromolecule is component 2.

$$\left(\frac{d \ln w_2}{dr^2}\right)^{-1} L_2 = \frac{1}{M_2 \Lambda} + 2 \frac{A^{(w, R)}}{\Lambda} w_2 + O(w_2^2) \quad (1)$$

where

$$L_2 \equiv \frac{\omega^2}{2RT} (1 - \bar{v}_2 \rho) = \frac{V_m \omega^2}{2000RT} \left(\frac{\partial \rho}{\partial w_2}\right)_{P, w} \quad (1a)$$

$$\Lambda = 1 + \frac{\left(\frac{\partial \rho}{\partial w_3}\right)_{P, w} \left(\frac{\partial w_3}{\partial w_2}\right)_{P, \mu}}{\left(\frac{\partial \rho}{\partial w_2}\right)_{P, w}} \quad (1b)$$

$w_J$  is the concentration of component  $J$  in g/g of principal component,  $r$  is the distance from the centre of rotation in the ultracentrifuge,  $M$  is the molecular weight,  $A^{(w, R)}$  is the virial coefficient for light scattering on the  $w$  concentration scale (see ref. 6 for details),  $\bar{v}_J$  is the partial specific volume of component  $J$ ,  $\rho$  is the density of the solution,  $V_m$  is the volume of solution (in ml) containing 1000 g of principal solvent,  $\omega$  is the angular velocity,  $R$  is the gas constant,  $T$  is the temperature, the subscripts  $P$  and  $\mu$  are used to denote partial differentials subject to constant pressure and constant chemical potentials of diffusible components, and the subscripts  $P$  and  $w$  denote differentials subject to constant pressure and constant concentrations of all components except the one whose concentration is being varied. Throughout this work the temperature is constant and is therefore omitted from the partial differential subscripts. The degree of preferential interaction of the macromolecule with the third component is represented by  $(\partial w_3 / \partial w_2)_{P, \mu}$  the weight in g of component 3 which must be added to the solution per g of component 2 in order to maintain constancy of  $P$  and  $\mu$ .

For the sake of experimental convenience the concentration unit is changed from a weight-per-weight basis to a weight-per-volume basis:  $c_J$  in g/ml of solution.

\* This work was read in part before the 23rd Annual Meeting of the Chemical Society of Japan, Tokyo, Japan, April 1970.

Using the relations  $w_J = c_J V_m / 1000$  and  $V_m = 1000(\bar{v}_1 + w_2 \bar{v}_2 + w_3 \bar{v}_3)$ , equation (1) becomes:

$$\frac{\omega^2}{2RT} (1 - \bar{v}_2 \rho) (1 - \bar{v}_2 c_2) \left( \frac{d \ln c_2}{dr^2} \right)^{-1} = \frac{1}{M_2 \Lambda} + \frac{2V_m A^{(w, R)}}{1000 \Lambda} c_2 + O(c_2^2) \quad (2)$$

Assuming the constancy of  $\bar{v}_2$  with respect to the concentration of component 2, the term  $(1 - \bar{v}_2 \rho)$  may be approximated by:

$$(1 - \bar{v}_2 \rho) = (1 - \bar{v}_2 \rho^0) (1 - \bar{v}_2 c_2) \quad (3)$$

where  $\rho^0$  is the density of the mixed solvent. Then, substitution of equation (3) into equation (2) and rearrangement leads to the final sedimentation equilibrium equation for the three-component system in weight-per-volume concentration units:

$$\frac{\omega^2}{2RT} (1 - \bar{v}_2 \rho^0) \left( \frac{d \ln c_2}{dr^2} \right)^{-1} = \frac{1}{M_2 \Lambda} + \left( \frac{2\bar{v}_2}{M_2 \Lambda} + \frac{V_m A^{(w, R)}}{500 \Lambda} \right) c_2 + O(c_2^2) \quad (4)$$

Substitution of the relation  $(\partial \rho / \partial w_J)_{P, w} = (1000 / V_m) (1 - \bar{v}_J \rho)$  into equation (1b) gives:

$$\Lambda = 1 + \frac{(1 - \bar{v}_3 \rho) (\partial w_3)}{(1 - \bar{v}_2 \rho) (\partial w_2)_{P, \mu}} \quad (4a)$$

It is possible to estimate the degree of preferential binding,  $(\partial w_3 / \partial w_2)_{P, \mu}$ , through  $\Lambda$  by using equation (4) provided that the true molecular weight of component 2 and the partial specific volumes of components 2 and 3 are known. The situation is very like that we found to hold for light scattering<sup>3,6</sup>. The molecular weight of the macromolecular component is needed in the three-component system being considered in order to evaluate the preferential binding.

By expressing the density as a function of composition at constant pressure, we obtain:

$$\left( \frac{\partial \rho}{\partial w_2} \right)_{P, \mu} = \left( \frac{\partial \rho}{\partial w_2} \right)_{P, w} + \left( \frac{\partial \rho}{\partial w_3} \right)_{P, w} \left( \frac{\partial w_3}{\partial w_2} \right)_{P, \mu} \quad (5)$$

Comparison of this equation with equation (1b) yields:

$$\left( \frac{\partial \rho}{\partial w_2} \right)_{P, \mu} = \Lambda \left( \frac{\partial \rho}{\partial w_2} \right)_{P, w} \quad (6)$$

Introduction of equation (6) reduces the sedimentation equilibrium equation (1) to:

$$\frac{\omega^2 V_m}{2000 RT} \left( \frac{\partial \rho}{\partial w_2} \right)_{P, \mu} \left( \frac{d \ln w_2}{dr^2} \right)^{-1} = \frac{1}{M_2} + 2A^{(w, R)} w_2 + O(w_2^2) \quad (7)$$

In view of the facility of measuring  $c_2$  in the experiments, a conversion of  $w_2$  to  $c_2$  is desirable. The density increment with respect to  $w_2$  at constant pressure and chemical potential is transformed to that with respect to  $c_2$  by:

$$\left( \frac{\partial \rho}{\partial w_2} \right)_{P, \mu} = \left( \frac{\partial \rho}{\partial c_2} \right)_{P, \mu} \frac{1000}{V_m} (1 - \bar{v}_2^+ c_2) \quad (8)$$

where for convenience we introduce the symbol:

$$\bar{v}_2^+ \equiv \frac{1}{1000} \left( \frac{\partial V_m}{\partial w_2} \right)_{P, \mu} \quad (9)$$

Recall, for comparison, the definition of partial specific volume

$$\bar{v}_2 = \frac{1}{1000} \left( \frac{\partial V_m}{\partial w_2} \right)_{P, w} \quad (10)$$

Introduction of equation (8) into equation (7) and rearrangement results in:

$$\frac{\omega^2}{2RT} \left( \frac{\partial \rho}{\partial c_2} \right)_{P, \mu} \left( \frac{d \ln c_2}{dr^2} \right)^{-1} = \frac{1}{M_2} + \left( \frac{\bar{v}_2 + \bar{v}_2^+}{M_2} + \frac{V_m A^{(w, R)}}{500} \right) c_2 + O(c_2^2) \quad (11)$$

The density increment  $(\partial \rho / \partial c_2)_{P, \mu}$  differs only insensibly from the more readily accessible derivatives<sup>6,9</sup>,  $(\partial \rho / \partial c_2)_{\mu}$ , which can be measured for solutions that have been brought to a state of osmotic equilibrium with solvent. Therefore, the molecular weight of macromolecules is obtainable through equation (11) by the sedimentation equilibrium and density measurements on solutions equilibrated with the solvent.

Once  $M_2$  is obtained, we can evaluate the preferential interaction of the macromolecule with one of the solvent components by the sedimentation equilibrium and density measurements at constant molality of solvent components, using equations (4) and (4a).

We can develop another method to obtain the degree of preferential solvation from equation (5). Transformation of density increments with respect to  $w_J$  into those with respect to  $c_J$  in equation (5) leads to:

$$\left( \frac{\partial w_3}{\partial w_2} \right)_{P, \mu} = \frac{1}{1 - \bar{v}_3 \rho} \times \left[ (1 - \bar{v}_2^+ c_2) \left( \frac{\partial \rho}{\partial c_2} \right)_{P, \mu} - (1 - \bar{v}_2 c_2) \left( \frac{\partial \rho}{\partial c_2} \right)_{P, w} \right] \quad (12)$$

Infinite dilution of component 2 reduces the equation to:

$$\begin{aligned} \left( \frac{\partial w_3}{\partial w_2} \right)_{P, \mu}^0 &= \frac{1}{1 - \bar{v}_3 \rho^0} \left[ \left( \frac{\partial \rho}{\partial c_2} \right)_{P, \mu}^0 - \left( \frac{\partial \rho}{\partial c_2} \right)_{P, w}^0 \right] \\ &= \frac{1}{1 - \bar{v}_3 \rho^0} \left[ \left( \frac{\partial \rho}{\partial c_2} \right)_{P, \mu}^0 - (1 - \bar{v}_2^0 \rho^0) \right] \end{aligned} \quad (13)$$

where the superscript zero refers to vanishing concentration of component 2. For the reason given above, the density increment  $(\partial \rho / \partial c_2)_{P, \mu}^0$  can be replaced by  $(\partial \rho / \partial c_2)_{\mu}^0$ , which is determinable more easily by dialysis experiment. Equation (13) is identical with that derived by Reisler and Eisenberg<sup>10</sup>. Using equation (13), the preferential solvation of a macromolecule may be calculated by measurement of the density increments under two different conditions: (i) keeping the weight molality of component 3 constant, and (ii) keeping the chemical potentials of components 1 and 3 constant.

## EXPERIMENTAL

The data used here are from the previously reported<sup>4</sup> sedimentation equilibrium experiments on  $\beta$ -Lg A in water/2-chloroethanol mixtures.  $\beta$ -Lactoglobulin A was prepared from cow's milk by standard techniques<sup>11</sup> and recrystallized before use.

The sedimentation equilibrium experiments were carried out at 25°C in a Beckman model E analytical ultracentrifuge, equipped with Rayleigh interference optics. The rotor speed was set at around 39 000 rev/min. In all cases, the protein concentration was 0.5 mg/ml. The value of  $\bar{v}_2$  of  $\beta$ -Lg A was taken to be 0.751<sup>12</sup>.



## RESULTS AND DISCUSSION

From the interference patterns photographed on Kodak plates at sedimentation equilibrium, the fringe displacements were measured as a function of the radial distance. An example is shown in Figure 1, where the logarithm of the fringe displacement (in  $\mu\text{m}$ ) is plotted against the square of the radius for  $\beta$ -Lg A in 40% chloroethanol solution. The points in each plot for  $\beta$ -Lg A in different concentrations of chloroethanol lie almost in a straight line as shown in Figure 1. The plot for 80% chloroethanol does display an upward curvature at the bottom of the cell, which must reflect the aggregation observed in light scattering at protein concentrations above 2 mg/ml<sup>3</sup>, though, even in this case, a linear relationship is retained for the rest of the cell. From a least square slope of all points in each plot, the amount of the left-hand side of equation (4) was calculated. This was independent of the radial distance, i.e. of protein concentration, since the latter is a function of the former. The apparent molecular weight of the protein,  $\Lambda M_2$ , was obtained as a reciprocal of the amount thus calculated. Light scattering and refractive index increment measurements on  $\beta$ -Lg A at different concentrations of chloroethanol under the condition of constant chemical potential of solvent have shown that the molecular weight of the protein does not change in the range of chloroethanol concentration investigated<sup>3</sup>. Dividing the apparent molecular weight by the true molecular weight of the protein yielded  $\Lambda$ . Then, the preferential binding of chloroethanol to  $\beta$ -Lg A was evaluated by equation (4a). The results are given in Table 1, where in the last column the amounts  $(\partial w_3/\partial w_2)_\mu$  obtained from light-scattering experiments<sup>3</sup> are compared with those from sedimentation experiments. A fairly good agreement is observed between them.

Very recently, an application of equation (13) was reported for determination of preferential solvation by measuring the density increment. Kratochvil *et al.*<sup>13</sup> have measured the preferential binding of 2,2,3,3-tetrafluoropropanol (TFP) to poly(methyl methacrylate) in a

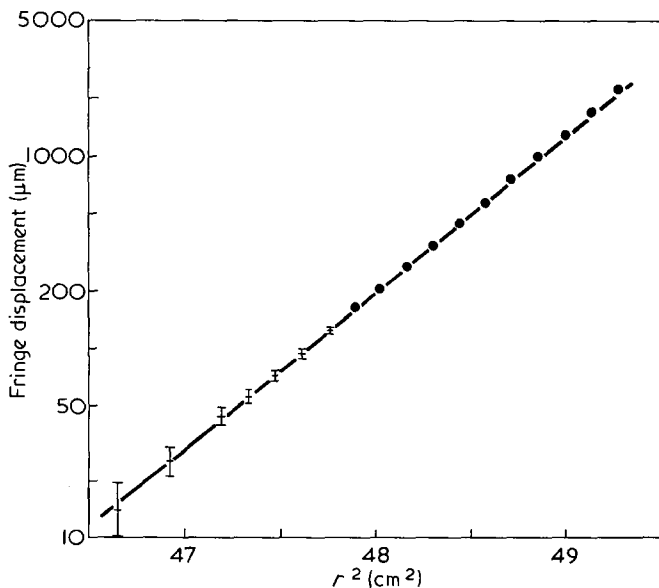


Figure 1 Plot of the logarithm of the fringe displacement (in  $\mu\text{m}$ ) against the square of the radial distance (in  $\text{cm}^2$ ) for the equilibrium sedimentation of  $\beta$ -lactoglobulin A with 4 mm solution column in 40% chloroethanol solution at 25°C. Rotor speed was 39 150 rev/min, and the initial protein concentration was 0.5 mg/ml. The error bars correspond to an estimated uncertainty of  $\pm 5 \mu\text{m}$  in the determination of the fringe displacement

Table 1 Preferential binding of chloroethanol to  $\beta$ -Lg A in water-chloroethanol mixtures, determined from the sedimentation equilibrium

Chloroethanol (vol. %)	$M_{\text{app}}$	$\rho^0$	$\bar{v}_3$	$(\frac{\partial w_3}{\partial w_2})_\mu$	
				Sedimentation equilibrium	Light scattering
0	18 800	0.9971			
5	18 100	1.0098	0.7934	-0.026	0.114
10	20 400	1.0226	0.7965	0.128	0.161
30	26 000	1.0708	0.8125	0.611	0.706
40	26 000	1.0915	0.8220	0.711	0.714
80	14 600	1.1652	0.8340	-0.933	-0.624

mixture of benzene and TFP, and shown that the results are in good agreement with the data obtained by the established refractive index increment method.

In the derivation of the equations for evaluation of preferential interaction, several assumptions were made: (i) the constancy of  $\bar{v}_2$  with respect to concentration  $c_2$ ; (ii) the negligible compressibility of the solution; (iii) the electroneutrality of the macromolecular component; and (iv) the negligible change in  $w_3$  with respect to the radial distance. The first assumption is a satisfactory approximation in many cases, provided that the concentration of component 2 is low enough throughout the ultracentrifuge cell. When the angular speed is low and the column height is short (the condition obtaining in sedimentation equilibrium experiments with a short column), the second assumption is also satisfied even though the third component is an organic solvent. Proteins are in general a kind of polyelectrolyte. So, to meet the third assumption all the solutions and the solvents contained 0.02 M NaCl<sup>3, 14</sup>. Any effect of NaCl on the three-component theory was considered to be negligibly small because of its very low concentration as compared to that of chloroethanol. If the concentration distribution of the solute or the solvent could be measured independently, it would not be necessary for the fourth assumption to hold. However, Rayleigh interference and Schlieren optics cannot distinguish between the two distributions; so to meet the last assumption the sedimentation equilibrium experiments should be carried out at a dilute concentration of component 2, and the blank concentration distribution of the solvent must be subtracted from the experimental curves.

## ACKNOWLEDGEMENTS

The author is grateful to Professor S. N. Timasheff for his stimulation to this work.

## REFERENCES

- 1 Tanford, C. *Adv. Protein Chem.* 1968, **23**, 121
- 2 Timasheff, S. N. *Acc. Chem. Res.* 1970, **3**, 62
- 3 Inoue, H. and Timasheff, S. N. *J. Am. Chem. Soc.* 1968, **90**, 1890
- 4 Timasheff, S. N. and Inoue, H. *Biochemistry* 1968, **7**, 2501
- 5 Fujita, H. 'Mathematical theory of sedimentation analysis', Academic Press, New York, 1962, p 255
- 6 Casassa, E. F. and Eisenberg, H. *Adv. Protein Chem.* 1964, **19**, 287
- 7 Scatchard, G. *J. Am. Chem. Soc.* 1946, **68**, 2315
- 8 Stockmayer, W. H. *J. Chem. Phys.* 1950, **18**, 58
- 9 Stigter, D. *J. Phys. Chem.* 1960, **64**, 842
- 10 Reisler, E. and Eisenberg, H. *Biochemistry* 1969, **8**, 4572
- 11 Aschaffenburg, R. and Drewry, J. *Biochem. J.* 1957, **65**, 273
- 12 Pedersen, K. O. *Biochem. J.* 1936, **30**, 961
- 13 Kratochvil, P., Pouchly, J. and Sedlacek, B. *J. Polym. Sci. (A-2)* 1972, **10**, 2057
- 14 Mijnlief, P. F. 'Ultracentrifugal analysis in theory and experiment' (Ed. J. W. Williams) Academic Press, New York, 1963, p 81

# Coupling of diffusion flux and chemical reaction in an asymmetric catalytically active membrane

M. Kubín and P. Špaček

*Institute of Macromolecular Chemistry, Czechoslovak Academy of Sciences,  
Prague, Czechoslovakia  
(Received 7 March 1973)*

The behaviour of a catalytically active membrane vectorized by a permanent transversal gradient of catalytic activity has been analysed mathematically. Under the simplifying assumption that the gradient of the catalytic activity profile across the membrane is linear, it is possible to express the steady state concentrations of the reaction components inside the membrane, governed by the diffusion-controlled chemical reaction, by means of tabulated Airy functions. For enzyme-catalysed reactions which follow Michaelis-Menten kinetics, two analytical solutions have been found for high and low substrate concentrations, respectively. If such an asymmetric membrane separates two compartments with the same (and constant) substrate concentrations, it behaves as an active barrier capable of pumping the product against its own concentration gradient. The effects of membrane thickness, slope of the activity profile and diffusion coefficient on the overall rate of product formation and on the pumping efficiency of the membrane are discussed.

## INTRODUCTION

In connection with the increasing importance of enzymes bound to macromolecular carriers in therapy, analytical chemistry and industrial processing, considerable attention has been paid recently to the theoretical analysis of diffusion-controlled, enzymatically catalysed reactions<sup>1-3</sup>. Several authors<sup>4-6</sup> have also proposed mathematical and/or real models of the so-called 'active transport' in which a compound diffuses against its concentration gradient on account of a concurrent chemical reaction. This 'up-hill' transport is very important in living organisms; however, in spite of the vast amount of experimental evidence collected in the past (e.g. ref. 7), very little is actually known about the true mechanism or mechanisms involved.

In this paper we present a mathematical analysis of a simple system based on an enzymatically active membrane having an uneven distribution of catalytic activity. It is shown that such a membrane, placed between two solutions with the same concentration of the substrate, behaves as an active barrier, capable of enriching one of the solutions by the product of the chemical reaction considered.

General conclusions from the results presented in this communication are valid in all similar systems where the diffusion-controlled chemical reaction is first order both with respect to the reactant and to the catalyst.

## STATEMENT OF PROBLEM

A membrane in which the diffusion flux is driven by a chemical reaction must be in some way vectorized, as the Curie Principle<sup>8</sup> forbids the coupling of phenomena of different tensorial order in an isotropic medium.

In this paper we analyse mathematically the behaviour of the probably simplest model of such a membrane, one in which there exists a stable linear gradient of catalytic activity obeying the equation:

$$E = \kappa x \quad (1)$$

where  $x$  ( $0 \leq x \leq l$ ) is the spatial coordinate perpendicular to the membrane surface,  $l$  is the membrane thickness and  $E$  is the concentration of an enzyme capable of catalysing a first-order chemical transformation of a substrate,  $S$ , to a product,  $P$ . The membrane separates two large reservoirs with solutions in which the substrate concentrations are the same and can be considered constant,  $S = S_0$ ; the situation is depicted schematically in Figure 1.

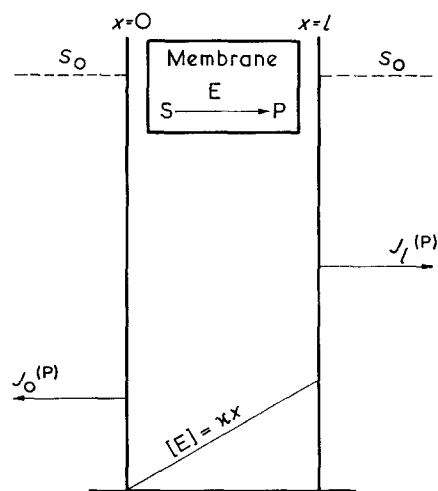


Figure 1 Schematic representation of the system under consideration

Designating by  $v_R$  the local reaction rate (rate of disappearance of the substrate, which in reactions of this type is equal to the rate of product formation) and limiting our considerations to the steady state, we have the following two differential equations for the concentration profiles of the substrate and product within the membrane, governed by the diffusion-controlled chemical reaction:

$$(\partial S/\partial t) = D_S(\partial^2 S/\partial x^2) - v_R = 0 \quad (2)$$

and

$$(\partial P/\partial t) = D_P(\partial^2 P/\partial x^2) + v_R = 0 \quad (3)$$

where  $S$  and  $P$  are the concentrations of substrate and product, respectively,  $D_S$  and  $D_P$  are the corresponding diffusion coefficients (assumed to be independent of concentration and constant throughout the membrane) and  $t$  is time.

Enzymatic reactions usually follow Michaelis–Menten kinetics:

$$v_R = k_2 ES/(K_m + S) \quad (4)$$

where  $k_2$  is the turnover number and  $K_m$  the Michaelis constant; the validity of equation (4) has been confirmed also for enzymes immobilized in membranes<sup>5</sup>.

The problem will be solved for the two limiting cases of high and low substrate concentration.

## SOLUTIONS

For low substrate concentration

If  $S \ll K_m$ , equation (4) reduces to:

$$v_R = k_2 ES/K_m \quad (5)$$

which in combination with equations (1) and (2) yields the differential equation:

$$(d^2 S/dx^2) - \lambda x S = 0 \quad (6)$$

with

$$\lambda = k_2 \kappa / K_m D_S \quad (7)$$

to be solved together with the boundary conditions:

$$S = S_0 \text{ at } x=0 \text{ and } x=l \quad (8a)$$

The steady-state concentration profile of the substrate inside the membrane is then given by:

$$S = S_0 [a \text{Ai}(\lambda^{1/3} x) + b \text{Bi}(\lambda^{1/3} x)] \quad (9)$$

the Airy functions  $\text{Ai}$  and  $\text{Bi}$  are two independent solutions<sup>9</sup> of the differential equation  $y'' - xy = 0$ . From the boundary conditions (8a) we then get for the two integration constants  $a$  and  $b$  the relations:

$$a = [\text{Bi}(\lambda^{1/3} l) - \text{Bi}(0)] / [\text{Ai}(0) \text{Bi}(\lambda^{1/3} l) - \text{Ai}(\lambda^{1/3} l) \text{Bi}(0)] \quad (10a)$$

$$b = [\text{Ai}(0) - \text{Ai}(\lambda^{1/3} l)] / [\text{Ai}(0) \text{Bi}(\lambda^{1/3} l) - \text{Ai}(\lambda^{1/3} l) \text{Bi}(0)] \quad (10b)$$

In order to find the concentration profile of the species  $P$  in the membrane, we make use of the fact that it is connected with the substrate concentration according to the relation:

$$-D_P(d^2 P/dx^2) = D_S(d^2 S/dx^2) \quad (11)$$

which follows from a comparison of equations (2) and (3). Integrating equation (11) twice we have:

$$-D_P P = D_S S + I_1 x + I_2$$

The integration constants  $I_1$  and  $I_2$  can be determined from the boundary conditions (8a) and (8b):

$$P = 0 \text{ for } x=0 \text{ and } x=l \quad (8b)$$

which are approximately valid if the volumes of the two compartments are large or if the experiment is performed in a through-flow arrangement.

Thus:

$$P = (D_S/D_P)(S_0 - S) \quad (12a)$$

or, after substitution from equation (9):

$$P = S_0 (D_S/D_P) [1 - a \text{Ai}(\lambda^{1/3} x) - b \text{Bi}(\lambda^{1/3} x)] \quad (12b)$$

On the basis of equation (12b) we may now calculate the diffusion fluxes of the product  $J_0^{(P)}$  and  $J_l^{(P)}$  at the two faces of the membrane (see Figure 1):

$$J_0^{(P)} = -D_P \left( \frac{dP}{dx} \right)_{x=0} = S_0 D_S \lambda^{1/3} [a \text{Ai}'(0) + b \text{Bi}'(0)] \quad (13a)$$

and

$$J_l^{(P)} = -D_P \left( \frac{dP}{dx} \right)_{x=l} = S_0 D_S \lambda^{1/3} [a \text{Ai}'(\lambda^{1/3} l) + b \text{Bi}'(\lambda^{1/3} l)] \quad (13b)$$

and therefrom also two important parameters, viz. the overall rate of product formation per unit area of the membrane,  $\text{div } P$ , defined as:

$$\text{div } P = |J_0^{(P)}| + |J_l^{(P)}| \quad (14)$$

and the ratio of the fluxes,

$$\gamma = |J_l^{(P)} / J_0^{(P)}| \quad (15)$$

which characterizes the pumping efficiency of the membrane.

The quantity  $(\text{div } P)/S_0$  calculated from equations (10), (13) and (14) on the basis of extensively tabulated<sup>9</sup> Airy functions and their derivatives is plotted in Figures 2 and 3 (solid lines) as a function of the parameter  $K = k_2 \kappa / K_m$  (proportional to the slope of the activity profile in the membrane) for two membranes of different

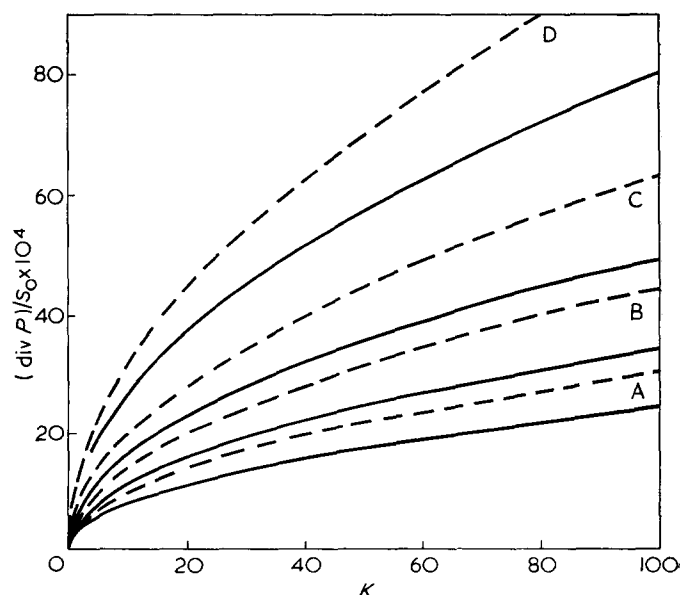


Figure 2 Dependence of the total rate of product formation on the parameter  $K = k_2 \kappa / K_m$  in a membrane 0.1 cm thick. — Vectorized membrane; - - - - -, membrane of uniform enzymatic activity  $\bar{E}$  corresponding to the given  $K$ ,  $\bar{E} = \kappa / 2$ .  $D_S$  (cm<sup>2</sup> s<sup>-1</sup>): A,  $5 \times 10^{-7}$ ; B,  $10 \times 10^{-7}$ ; C,  $20 \times 10^{-7}$ ; D,  $50 \times 10^{-7}$

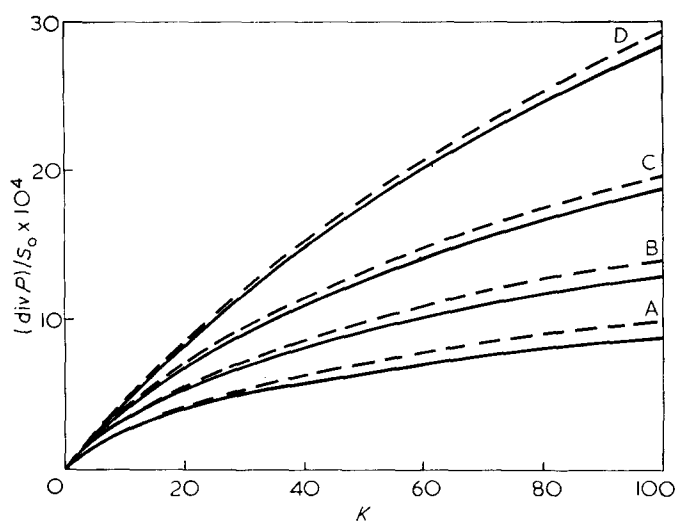


Figure 3 Dependence of the total rate of product formation on the parameter  $K$  in a membrane 0.01 cm thick. See caption to Figure 2 for full description

thickness ( $l=0.1$  and  $0.01$  cm, respectively) and for several values of the diffusion coefficient  $D_s$ . The rate of product formation increases with increasing  $K$  due to the higher mean catalyst concentration in (otherwise identical) membranes having a higher slope of catalytic activity,  $\kappa$ . For the same reason, the rate of product formation is higher in the thicker membrane (Figure 2), although this enhancement is not proportional by far to the increase in  $l$ , as the reaction will proceed much slower in the thicker membrane due to more pronounced diffusion control. The quantity  $(\text{div } P)/S_0$  also increases with the diffusion coefficient of the substrate,  $D_s$ , as expected in a diffusion-controlled process.

The ratio of the two diffusion fluxes, which can serve as a measure of the pumping efficiency of the membrane, is plotted as a function of the parameter  $K$  in Figure 4 for the same values of the relevant parameters  $l$  and  $D_s$  as before. For physical reasons, all the lines in Figure 4 must intersect at the ordinate  $\gamma=1$  in the limit of zero  $K$  (i.e., for zero activity gradient in the membrane); hence, the pumping efficiency strongly increases in the region of low  $K$ , so that even moderate values of the gradient of catalytic activity will bring about a considerable rise in the ratio of the diffusion fluxes. It is of interest to note that the ratio depends on the diffusion coefficient  $D_s$  of the substrate in the opposite way than the rate of product formation,  $\text{div } P$ . With increasing  $D_s$  the pumping efficiency of the asymmetric membrane decreases. This can be easily understood by taking into consideration the fact that the membrane must represent a barrier of relatively low permeability in order to maintain a sufficiently high ratio of the two diffusion fluxes in the steady state.

With every asymmetric membrane one might associate a membrane of uniform catalytic activity equal to the mean activity of the vectorized membrane:

$$\bar{E} = \kappa l / 2 \quad (16)$$

The broken lines in Figures 2 and 3 correspond to the rate of product formation  $(\text{div } P)/S_0$  by these associated membranes of constant catalytic activity; the kinetic behaviour of such membranes has been analysed in detail<sup>1-3</sup>. It is seen from the Figures that the total output of the vectorized membrane is always lower

than that of the corresponding uniform membrane having the same mean catalytic activity. This is in accord with the notion that, in the case of the asymmetric membrane, a part of the actual driving force which is the affinity of the proceeding chemical reaction is needed for maintaining a non-zero difference of the two diffusion fluxes of the product.

The effect of the membrane thickness  $l$  on its pumping efficiency as reflected in the ratio  $\gamma$  is illustrated by the results summarized in Table 1. The calculations were performed for two membranes of thickness 0.1 and 0.01 cm, respectively. However, it is not appropriate to compare directly two membranes of different thickness having the same gradient of catalytic activity  $\kappa$ , as the thinner of the two would be handicapped in that it then has a lower mean catalytic activity [see equation

Table 1 Comparison of the product flux ratio  $\gamma = |J^{(P)}_1/J^{(P)}_2|$  for two membranes of different thickness ( $l=0.01$  and  $0.1$  cm)

$K = k_2 \kappa / K_m^*$	$D_s \times 10^7 \text{ (cm}^2 \text{ s}^{-1}\text{)}$							
	50		20		10		5	
	$\gamma_{0.01}$	$\gamma_{0.1}$	$\gamma_{0.01}$	$\gamma_{0.1}$	$\gamma_{0.01}$	$\gamma_{0.1}$	$\gamma_{0.01}$	$\gamma_{0.1}$
20	2.1	3.7	2.2	4.3	2.3	4.8	2.5	5.4
50	2.2	4.3	2.3	5.0	2.6	5.6	2.9	6.3
100	2.3	4.8	2.6	5.6	2.9	6.3	3.2	7.1

\* Value corresponding to the membrane with  $l=0.01$  cm (see text)

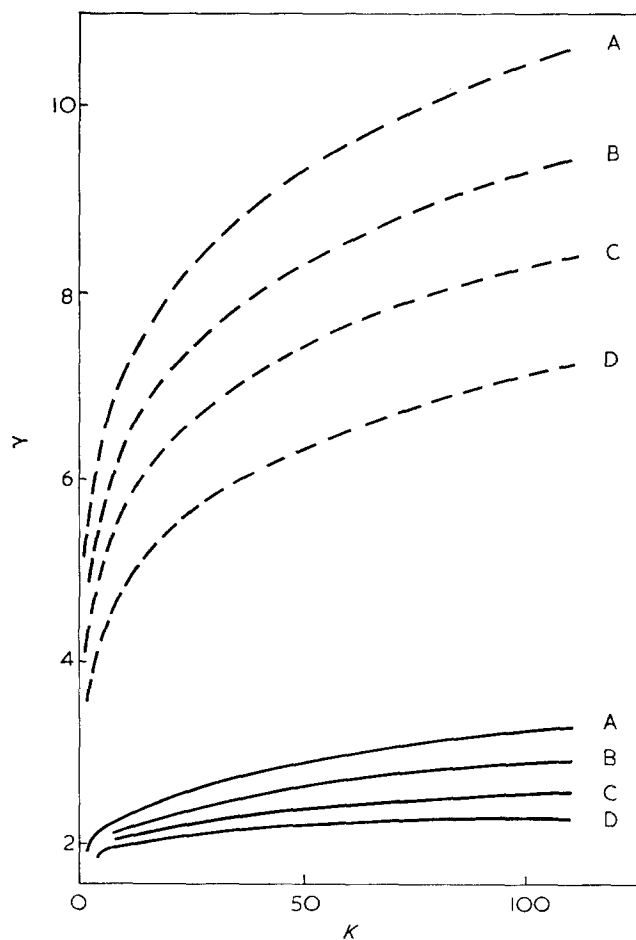


Figure 4 Dependence of the pumping efficiency of a vectorized membrane as expressed by the ratio of the two diffusion fluxes  $\gamma = |J^{(P)}_1/J^{(P)}_2|$  on the parameter  $K = k_2 \kappa / K_m$ . —,  $l=0.01$ ; - - -,  $l=0.1$ .  $D_s$  (cm<sup>2</sup> s<sup>-1</sup>): A,  $5 \times 10^{-7}$ ; B,  $10 \times 10^{-7}$ ; C,  $20 \times 10^{-7}$ ; D,  $50 \times 10^{-7}$

(16)]. Therefore, the comparison in the Table is made for two membranes with the same mean catalytic activity  $\bar{E}$ , i.e. with the same value of the maximum activity at one of their faces—the thicker membrane then must have a  $\kappa$  ten times lower (and therefore a  $K$  ten times lower) than the value shown in the first column of the Table.

The results in Table 1 show that even under these conditions the thicker membrane always has the higher ratio of the diffusion fluxes, which confirms the view already expressed about the importance of low membrane permeability for its pumping efficiency.

The solution of the problem contained in equations (1)–(4) can be further generalized:

(a) if the profile of the enzymatic activity in the membrane is of a more general linear form:

$$E = \kappa_1 + \kappa_2 x$$

we have to solve (again assuming  $K_m \gg S$ ) the differential equation:

$$D_S \frac{d^2 S}{dx^2} - \frac{k_2(\kappa_1 + \kappa_2 x)}{K_m} S = 0$$

Introducing a new variable

$$\xi = \kappa_1 + \kappa_2 x$$

we recover the original form of the differential equation:

$$\frac{d^2 S}{d\xi^2} - \sigma \xi S = 0$$

and the new parameter  $\sigma$  is defined by:

$$\sigma = k_2 / \kappa_2^2 D_S K_m$$

(b) analytical solutions (in terms of modified Bessel functions of fractional order<sup>10</sup>) exist also for the case when the catalytic activity inside the membrane is of the general parabolic form:

$$E = \kappa_3 x^m, \quad m > 1$$

For high substrate concentration

For  $K_m \ll S$  we have a rather trivial case of zero-order kinetics with respect to the substrate, as in this case equation (4) reduces to:

$$v_R = k_2 \kappa x \quad (17)$$

assuming again that the catalytic activity in the membrane follows equation (1). The resulting simple differential equation:

$$D_S (d^2 S / dx^2) - k_2 \kappa x = 0 \quad (18)$$

has a solution:

$$S = S_0 \left\{ 1 - \frac{k_2 \kappa l^3}{6 S_0 D_S} [(x/l) - (x/l)^3] \right\} \quad (19)$$

which satisfies the boundary conditions (8a).

For the species  $P$  it again holds:

$$P = (D_S / D_P)(S_0 - S) \quad (12a)$$

and the two diffusion fluxes of the product follow from equations (19) and (12a) as:

$$J_P^{(P)} = k_2 \kappa l^2 / 3 \quad (20a)$$

$$J_P^{(Q)} = -k_2 \kappa l^2 / 6 \quad (20b)$$

Hence, the total rate of product formation is now given by:

$$\text{div } P = k_2 \kappa l^2 / 2 \quad (21)$$

and depends neither on the substrate concentration in the outer solutions,  $S_0$ , nor on its diffusion coefficient,  $D_S$ .

As a consequence of the simplicity of assumptions underlying this derivation, it follows from equations (20a) and (20b) that in this case of high substrate concentration the diffusion fluxes of the product differ by a constant factor 2.

It must be said in conclusion that the simple model of active transport discussed (as well as the processes in the other models of active transport so far constructed) might be quite different from the processes involved in the up-hill transport in living cells. Nevertheless, these attempts can contribute to our better understanding of the principles underlying this complex phenomenon.

#### ACKNOWLEDGEMENT

The assistance of Mrs J. Hromádková in the numerical calculations is gratefully acknowledged.

#### REFERENCES

- 1 Goldman, R., Kedem, O. and Katchalski, E. *Biochemistry* 1968, 7, 4518
- 2 Meyer, J., Sauer, F. and Voermann, D. *Ber. Buns. Phys. Chem.* 1970, 74, 245
- 3 Blaedel, W. J. and Kissel, T. R. *Analyt. Chem.* 1972, 44, 2030
- 4 Blumenthal, R., Caplan, S. R. and Kedem, O. *Biophys. J.* 1967, 7, 735
- 5 Selegny, E., Brown, G. and Thomas, D. *C.R. Acad. Sci. (Paris)* 1970, 271D, 1423
- 6 Aris, R. and Keller, K. H. *Proc. Nat. Acad. Sci. USA* 1972, 69, 777
- 7 Kotyk, A. and Janáček, K. 'Cell Membrane Transport', Plenum Press, New York, 1970
- 8 de Groot, S. R. and Mazur, P. 'Non-Equilibrium Thermodynamics', North-Holland, Amsterdam, 1962, p 57
- 9 Antosiewicz, H. A. in 'Handbook of Mathematical Functions', (Abramowitz, M. and Stegun, I. A., Eds.), Dover, New York, 1965, p 446
- 10 Jahnke, E. and Emde, F. 'Tables of Higher Functions', B. G. Teubner, Leipzig, 1960, p 150

# An etch technique for morphological studies of multiphase polymers containing polycarbonates

G. C. Eastmond and E. G. Smith

Department of Inorganic, Physical and Industrial Chemistry, University of Liverpool,  
PO Box 147, Liverpool L69 3BX, UK  
(Received 22 March 1973; revised 4 June 1973)

An etch technique for studying the morphology of multiphase polymers containing a polycarbonate phase, based on the alkaline hydrolysis of polycarbonates, is described. The application of this technique to polycarbonate/polystyrene blends is illustrated. Difficulties which can occur in applying this technique to crosslinked materials under conditions such that only partial phase separation exists are discussed.

## INTRODUCTION

Morphological studies of multiphase amorphous polymers by electron microscopy are often hindered by lack of contrast between the phases. Most work in this field has concentrated on rubber-toughened plastics, such as high-impact polystyrene and acrylonitrile-butadiene-styrene copolymers, and on block copolymers containing chains of polyisoprene or polybutadiene. Two approaches have been adopted towards the morphological examination of such polymers. First, the unsaturated component is readily stained by osmium tetroxide<sup>1</sup>, which serves the dual purpose of hardening the rubber component to facilitate cutting and of rendering it visible under the electron microscope. The second approach is to selectively remove one phase by etching the polymer surface and subsequently examining its topography. Gas-discharge<sup>2</sup> and preferential-solvent<sup>3</sup> etching techniques have been reported for rubber-containing materials and Bucknall *et al.*<sup>4</sup> have recently described a chromic acid etching technique for the same polymers; chromic acid preferentially removes the rubber component. Bucknall *et al.* have listed advantages of etching methods which avoid distortion of the morphology during cutting of thin sections. The growing interest in multicomponent polymers requires the development of more techniques to distinguish phases, especially in non-rubber-containing polymers.

We are at present engaged in a study of the structure-property relations of multicomponent crosslinked polymers, in which a halogen-containing polymer is crosslinked by chains of a second polymer prepared by free-radical polymerization; methods of preparing the crosslinked structures are described elsewhere<sup>5</sup>. One class of materials of interest at present is polycarbonate [derived from 1,1,1-trichloro-bis-2-(*p*-hydroxyphenyl) ethane] crosslinked by chains of vinyl polymers. Prior to investigating the properties of these materials an attempt was made to devise a method for studying their morphologies. As a result of this work an etch technique, based on the alkaline hydrolysis of polycarbonate and suitable for examining the morphology of two-phase materials in which one phase is a polycarbonate, was developed and

is reported in this paper. Uncertainties in the interpretation of micrographs, obtained with this and other etch techniques, which can arise from materials in which only partial phase separation occurs are described. In these experiments polystyrene was used as the second component.

## EXPERIMENTAL

### Materials

The polycarbonate (mol. wt. = 7500) was prepared by condensation of phosgene and 1,1,1-trichloro-bis-2-(*p*-hydroxyphenyl) ethane. Polystyrene used in blends had a molecular weight of 120 000. Samples of polycarbonate crosslinked with polystyrene were prepared using manganese carbonyl, in conjunction with the polycarbonate, as the photo-initiating system<sup>5</sup>.

Polycarbonates are susceptible to hydrolysis by a variety of bases. Since, in general, the second polymeric component may dissolve or swell in organic bases, an aqueous solution of potassium hydroxide (~30% w/v) was chosen as etching agent.

### Sample preparation

Films of polycarbonate-polystyrene blends and of lightly crosslinked (soluble) materials were prepared by casting from solutions in ethyl acetate.

Thick films (~0.5 mm) of blends were cast (from ~15% w/v solution) in small polyethylene dishes. Under these conditions phase separation occurred in solution, forming droplets of a solution of one component; this method produced large domains of one polymer. Pieces of film were attached to Araldite blocks and the surfaces were etched by submerging the assembly in the etching solution. After washing and drying, the Araldite blocks were attached to specimen holders, and the surfaces were coated with gold/palladium to prevent charging. The etched surfaces were examined in a Cambridge Mk III Stereoscan microscope.

In an attempt to produce films containing smaller domains, thin films of blends (3–5 μm thick) were prepared by casting from dilute polymer solution (1.5% w/v)

onto glass slides. Small portions of the films were separated from the slide and floated upside down on the etching solution. After etching, the specimens were washed on a clean water surface, inverted to leave the etched surface uppermost, collected on glass cover-slips and dried. The glass cover-slips were glued to specimen holders and the samples were coated and examined as for thick films.

Films of lightly crosslinked materials were prepared for examination in a manner identical with that for thick films. More highly crosslinked samples which could not be cast as films were swollen in ethyl acetate and dried. The samples were attached to Araldite blocks, faced in an ultra-microtome and subsequently the smooth surfaces were etched and prepared for examination as for thick films of blends.

For transmission electron microscopy very thin films ( $\sim 600$  nm) of blends and lightly crosslinked materials were cast from dilute solution (0.3% w/v) and etched and washed as for thin films for scanning microscopy. The specimens were collected on microscope grids and either coated with carbon or shadowed with platinum and examined in a JEM 7 electron microscope.

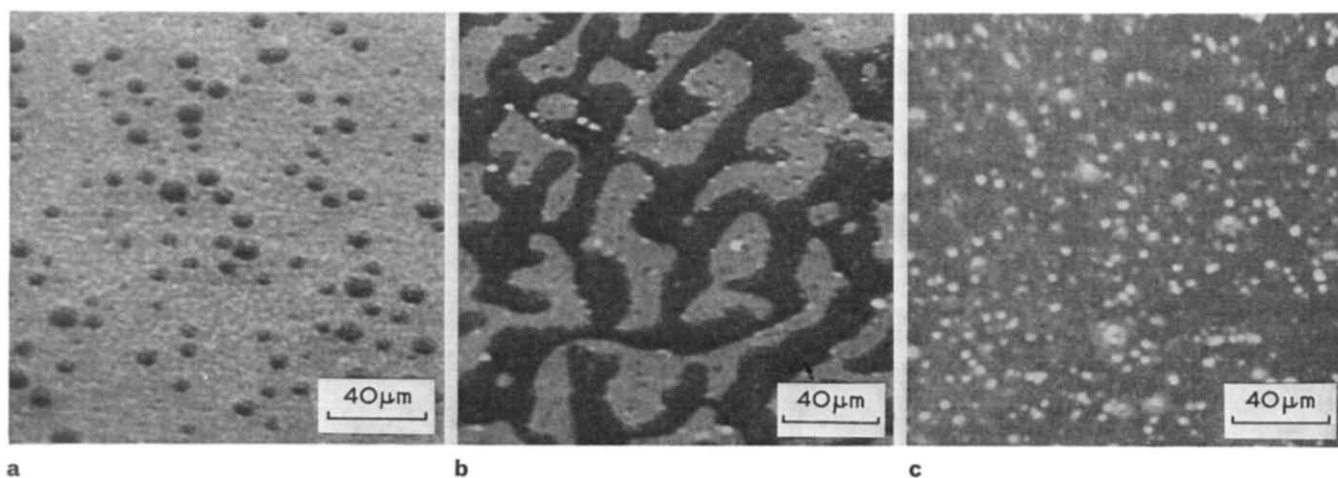
Prior to carrying out electron microscope studies on two-component systems it was confirmed that the particular polycarbonate used in these experiments was readily attacked by the potassium hydroxide etching solution; thin films of polycarbonate homopolymer were

completely destroyed in 24 h while comparable polystyrene films remained unaffected.

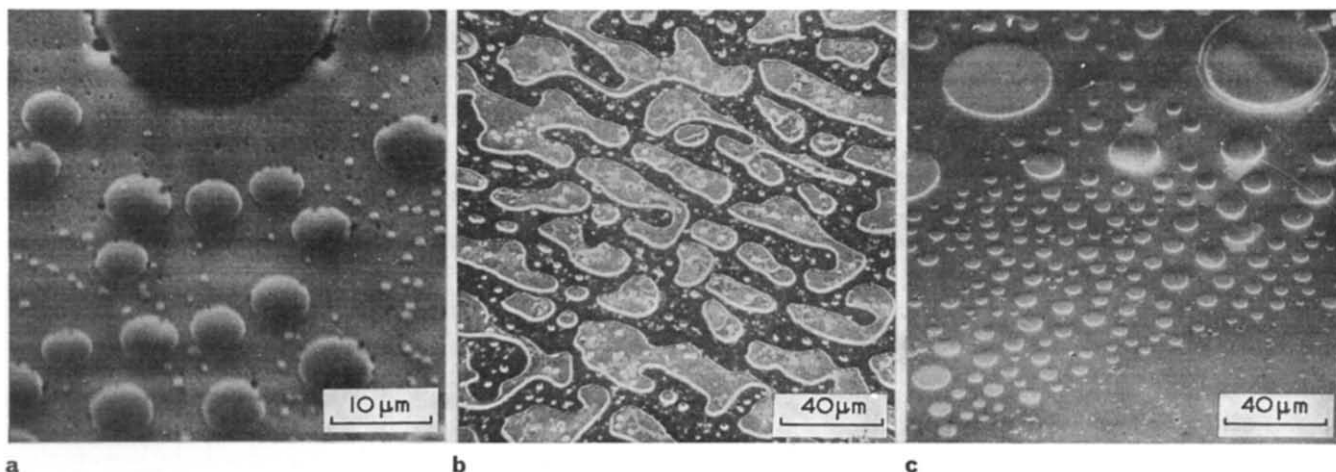
## RESULTS AND DISCUSSION

*Figure 1* shows scanning electron micrographs of unetched top surfaces of thin films of a series of polycarbonate-polystyrene blends, and confirms that normal variations of morphology with composition occur. In this particular system the phases can be distinguished without recourse to staining or etching; the polystyrene appears dark and the polycarbonate light. It cannot be expected that such contrast will be seen in all multicomponent materials containing a polycarbonate component and probably arises in this particular example from the presence of the trichloromethyl groups on the polycarbonate; here it is a confirmatory aid in the identification of the phases.

*Figure 2* is a corresponding set of scanning electron micrographs for blends after etching, and comparison with *Figure 1* illustrates how the morphology of the films is revealed by etching. *Figure 2a* shows the emergence of spherical polystyrene domains accompanying the degradation of the surrounding polycarbonate matrix. The wide distribution of domain sizes, frequently encountered in blends, can be seen in this photograph. Under conditions such that the degradable polymer is the matrix, as in *Figure 2a*, it cannot be expected that all the domains are in their original relative positions. As the matrix is



*Figure 1* Scanning electron micrographs of unetched thin films of polycarbonate-polystyrene blends containing (a) 9%, (b) 50% and (c) 91% polystyrene



*Figure 2* Scanning electron micrographs of thin films of polycarbonate-polystyrene blends after etching for times indicated. (a), 9% polystyrene (4 h); (b), 50% polystyrene (3 h); (c), 91% polystyrene (4 h)



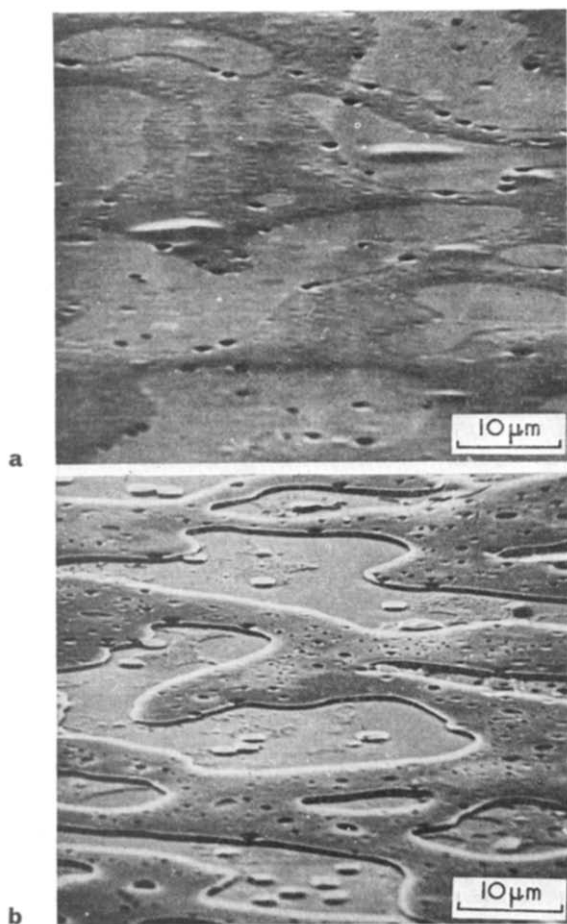


Figure 3 Scanning electron micrographs of a 1:1 polycarbonate-polystyrene blend (thin film). (a), Unetched, (b), etched for 3 h

destroyed the domains will be left essentially unsupported, and may, therefore, be lost when they are completely exposed by the destruction of the surrounding matrix, while some may adhere to the reacting surface as etching proceeds. Nevertheless, the etched film shows the sizes and shapes of the domains. Figure 2c demonstrates the formation of depressions in the surface of the film as surface domains of polycarbonate are etched away, the surrounding polystyrene matrix remaining unaffected. The intermediate situation, for a blend containing equal proportions of the constituent polymers, is seen in Figure 2b, and demonstrates how the detailed morphology is revealed by etching.

Figures 1b and 2b were obtained by viewing the sample at about 45° to the normal to the sample surface. The effects of etching can be seen in greater relief by viewing the samples at an angle of 80° to the normal (Figures 3a and 3b) when the depth of etching becomes more apparent. It can be seen in Figure 3 how depressions appear in the originally smooth surface of the polystyrene rich regions by removal of polycarbonate domains and, conversely, how the presence of polystyrene domains is revealed in the polycarbonate rich regions.

The morphology of thick films of blends was controlled by the phase separation which occurred when concentrated solutions of the polymers were mixed. On drying, this produced large domains of one polymer in a matrix of the other. Figure 4a shows the unetched top surface of such a film containing 67% polystyrene. The initial surface contained numerous depressions, the larger being concentrated in groups and the smaller distributed at random between those groups. Etching for a short time (Figure 4b) demonstrates that the depressions are within the surfaces of polystyrene domains which are revealed as large

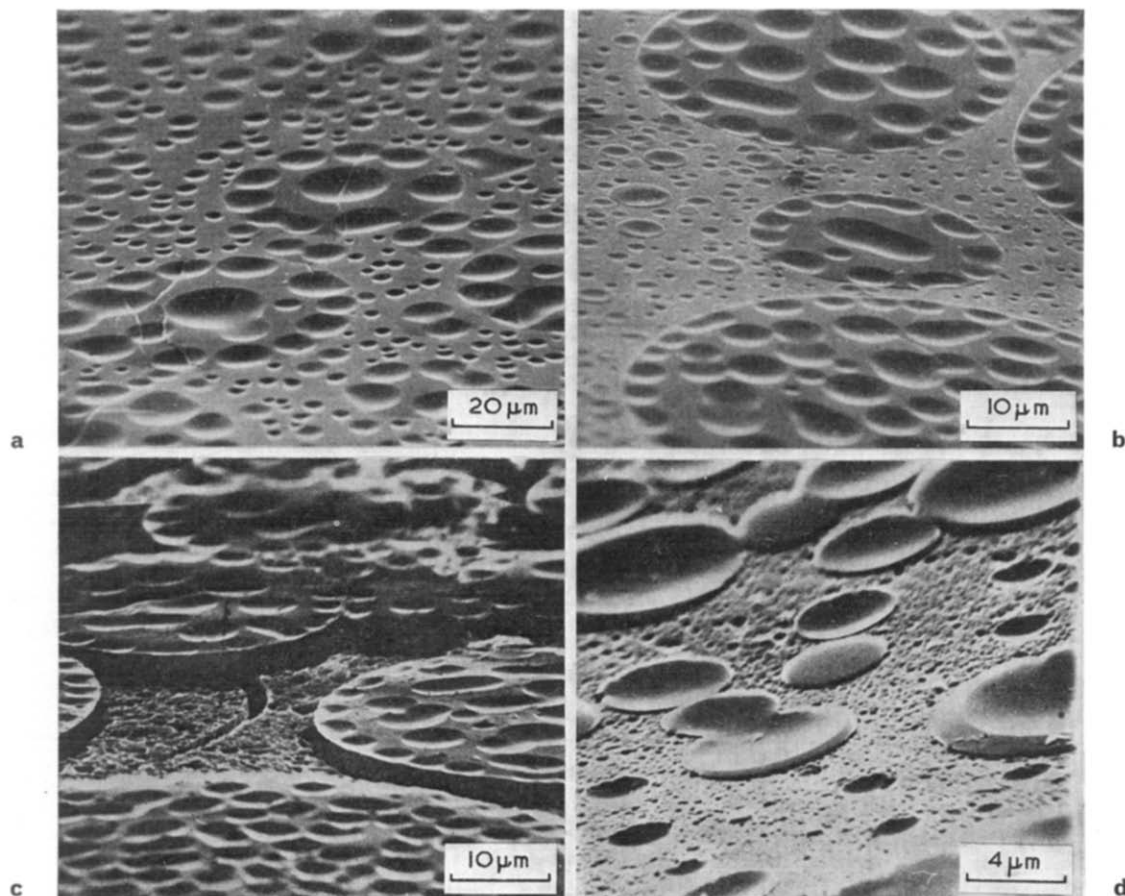


Figure 4 Micrographs of top surfaces of 1:2 polycarbonate-polystyrene blends (thick films) etched for (a) 0 h, (b) 4 h, (c) 3 days and (d) 4 h



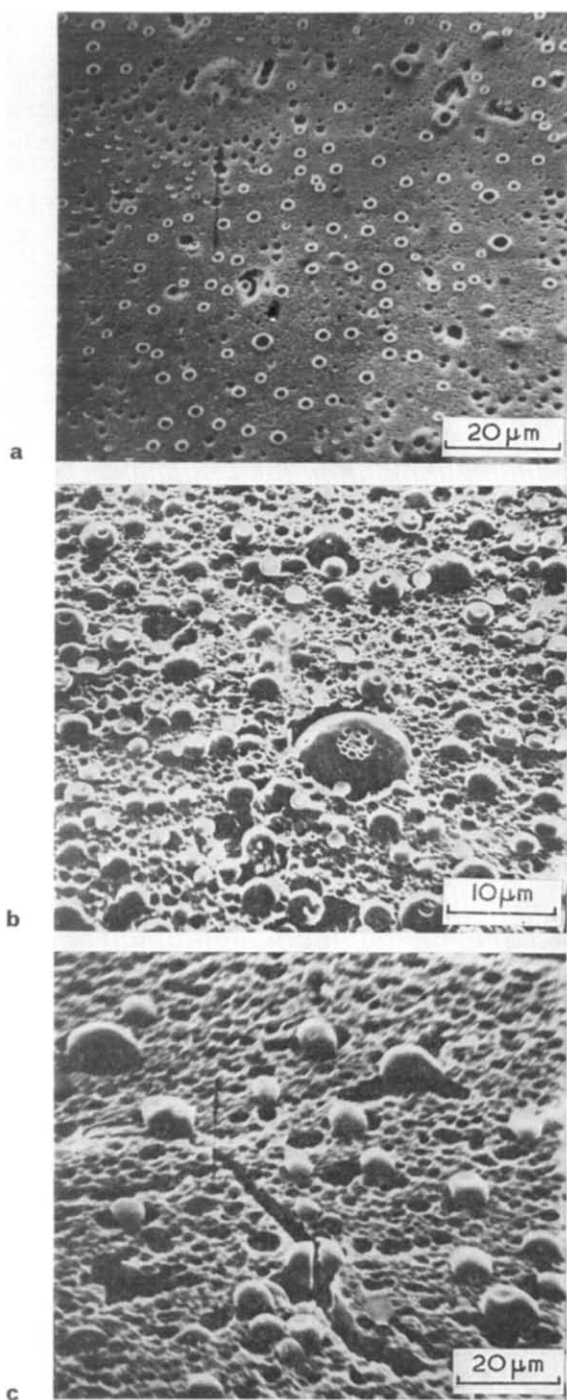


Figure 5 Micrographs of bottom surfaces of 1 : 1 polycarbonate-polystyrene blends (thick films) etched for (a) 12 h, (b) 3 days and (c) 3 days

pancake-like structures on the surface of the film. The larger domains are seen in greater relief in Figure 4c, taken at a different angle after a longer period of etching. The smaller depressions in the initial surface (Figure 4d) arise from smaller polystyrene domains, each responsible for an individual surface depression, distributed randomly between the larger domains.

Similar studies on the bottom surfaces of thick films, containing 50% polystyrene, revealed domains formed from droplets which had fallen to the bottom of the solution during film casting. Initially the bottom surfaces were smooth apart from a random distribution of holes about  $1\ \mu\text{m}$  in diameter. Surface etching caused the appearance of rings of polystyrene (Figure 5a). More

extensive etching revealed the presence of spherical polystyrene domains, many having a hole in the surface (Figure 5b). These holes appear to correspond to those present in the unetched surface and in the centres of at least some of the ring structures seen in Figure 5a; domains further removed from the initial surface appear approximately spherical and devoid of such features.

Figure 5c shows a fracture passing through a polystyrene domain and the matrix. It is reasonable to assume that the fracture was formed prior to etching, when we may conclude that: (i) the polystyrene domains are not artifacts produced during etching; (ii) the relative positions of the fragments and the matrix shows that distortion does not occur on etching; and (iii) sharp edges on the fragments demonstrate that the polystyrene remains unaffected.

When the surface of a pure polycarbonate film is etched, pits form in the surface due to uneven etching, as seen in Figure 6. The pits presumably arise from local variations in the structure of the polycarbonate and their diameters vary up to several hundred nanometres. It would not necessarily be correct to attribute such pits to holes formed by the loss of polystyrene domains. Smaller, but similar, structures have been observed by Frank *et al.*<sup>6</sup> using an ion-etching technique.

Examination of crosslinked materials produced difficulties which may be encountered with this and other techniques for studying polymer morphologies. Untreated thin films showed no evidence of domain formation. On etching, however, polystyrene domains ( $0.25\text{--}1\ \mu\text{m}$  diameter) appeared on the surfaces of the films, as seen in Figure 7. The domain diameters were greater than twice the extended chain length of the polystyrene chains (degree of polymerization 460), and it is inconceivable that the domains are pure polystyrene formed by phase separation during film preparation. It is probable that these observations are consequences of incomplete phase separation in the crosslinked polymers. For example, polystyrene may have been initially dispersed throughout the film and have aggregated during etching. Such an explanation would be consistent with greater resistance of these films to etching compared with blends. Evidence for such incomplete phase separation has been obtained for other crosslinked multicomponent polymers<sup>7</sup>, and also for polydimethylsiloxane-polycarbonate block copolymers<sup>8</sup>.

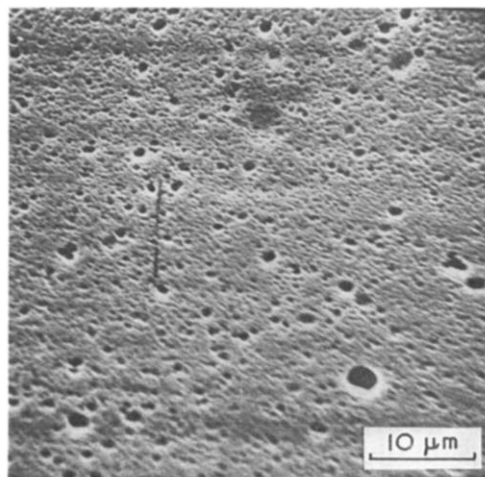


Figure 6 Scanning electron micrograph of polycarbonate surface etched for 12 h

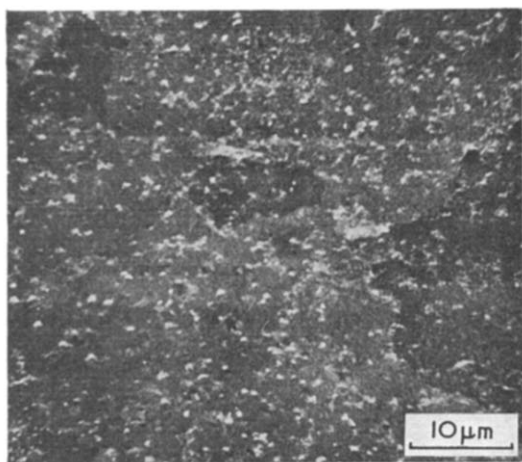


Figure 7 Scanning electron micrograph of a cross-linked polycarbonate-polystyrene polymer etched for 2 days

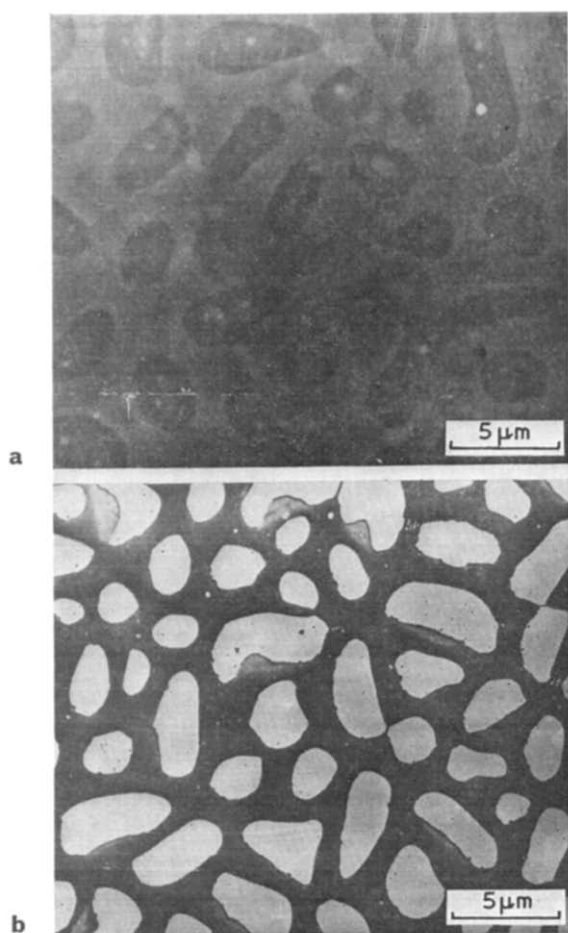


Figure 8 Transmission electron micrographs of a 1 : 1 polycarbonate-polystyrene blend. (a) Unetched; (b) etched

Restricted phase separation represents a general limitation on the use of electron microscopy in morphological studies. While electron micrographs may demonstrate the existence of separate phases, allow identification of the major component in a given phase and the determination of domain sizes, the micrographs do not provide information on the composition of the phases. To obtain more information on such materials, electron microscope studies must proceed in parallel with measurements which provide information on phase composition, such as glass-transition temperatures and coefficients of expansion<sup>7</sup>.

Where complete phase separation occurs in crosslinked materials it is probable that, if the components are of low molecular weight, domains with diameters of less than 50 nm may be present, which is on the limit of satisfactory operation of the scanning microscope. Under such conditions it would be necessary to use higher magnifications available on the transmission microscope. Figure 8a is a transmission electron micrograph of a 50 : 50 blend, corresponding to the scanning micrograph in Figure 1b. Transfer to transmission microscopy, of course, reverses the contrast, the polycarbonate now appearing dark. Confirmation of this assignment is obtained by etching, which produces holes corresponding to the removal of the domains, as seen in Figure 8b, the polystyrene matrix now appears dark relative to the holes.

Shadowing or replica techniques could be used, in conjunction with the transmission microscope to examine materials containing very small domains. If polycarbonate is the predominant phase care must be taken, in both cases, not to attribute incorrectly effects arising from pits in the pure polycarbonate, described earlier. Probably the best results would be obtained under conditions such that the non-degradable polymer forms the matrix, when the polycarbonate could be etched away completely.

In a partly etched film of a blend the depth of etching can be determined readily by normal shadowing techniques. This approach was applied to lightly crosslinked materials, the surfaces of which, after etching, were seen to contain numerous small domains, about 50 nm in diameter. It is just conceivable that these domains could have been present in the initial material but in view of the observations from scanning microscopy such a conclusion can only be adopted with reservations.

## CONCLUSIONS

The possibilities of using an etch technique, based on alkaline hydrolysis of polycarbonates, to study the morphologies of multicomponent materials containing a polycarbonate have been examined for both blends and crosslinked materials containing polycarbonate and polystyrene. In blends there are no restrictions on molecular re-organization and good phase separation can occur. Under these conditions the etch technique offers a simple method of determining the morphology, without causing distortion, either by scanning or by transmission electron microscopy. It is preferable to use the etch technique under conditions where the degradable polymer forms the domains and can be completely etched away without disturbing the second phase. If the degradable polymer forms the matrix, shapes and sizes of domains can still be determined.

With crosslinked materials molecular re-organization is more restricted and there is the possibility that such materials will form mixed phases containing both polymeric components. In these cases care must be exercised in interpreting micrographs, since the ultimate fate of the non-degradable component is uncertain. It is possible that, as the polycarbonate is destroyed, chains of the non-degradable component may aggregate to produce particles resembling domains which could have been present in the initial polymer. For such materials microscopy must be supported by additional data. This reservation applies to the application of any etch technique to such materials.

**ACKNOWLEDGEMENTS**

The authors wish to thank Unilever Research Port Sunlight Limited for financial assistance for one of us (E.G.S.) and the Department of Metallurgy and Materials Science for use of the electron microscope facilities.

**REFERENCES**

- 1 Kato, K. *J. Electron Microsc.* 1965, **14**, 220
- 2 Spit, B. *J. Polymer* 1963, **4**, 109

- 3 Keskkula, H. and Taylor, P. A. *J. Appl. Polym. Sci.* 1967, **11**, 2361
- 4 Bucknall, C. B., Drinkwater, I. C. and Keast, W. E. *Polymer* 1972, **13**, 115
- 5 Bamford, C. H., Dyson, R. W. and Eastmond, G. C. *J. Polym. Sci. (C)* 1967, **16**, 2425
- 6 Frank, W., Goddar, H. and Stuart, H. A. *J. Polym. Sci. (B)* 1967, **5**, 711
- 7 Bamford, C. H., Eastmond, G. C. and Whittle, D. *Polymer* 1971, **12**, 247
- 8 Le Grand, D. G. *J. Polym. Sci. (B)* 1969, **7**, 579; 1970, **8**, 195

# Reaction of poly(vinyl chloride) with ethylenediamine hydrotrisulphide and properties of the products

Kunio Mori and Yoshiro Nakamura

*Department of Applied Chemistry, Iwate University, Morioka, Iwate, Japan  
(Received 9 April 1973)*

The chemical structure and the properties of the products of the reaction of poly(vinyl chloride) (PVC) with ethylenediamine hydrotrisulphide were investigated. PVC derivatives containing a polysulphide crosslinkage and a hydropolysulphide pendant (PSC-PVC) were obtained by the reaction of PVC with ethylenediamine hydrotrisulphide in ethylenediamine (EN) as well as in EN-diglyme, and EN-benzene at 20–50°C for 0.5–5 h. The chemical structure of PSC-PVC was determined from crosslinking density before and after iodine oxidation and elemental analysis. Scission of polysulphide crosslinkage in PSC-PVC by some thiols was carried out in tetrahydrofuran-triethylamine solution at 30°C for 1–4 h as well as in a hot roller mill at 125–180°C for 2–8 min. The former product was photocrosslinked under ultra-violet irradiation in air and the latter showed the properties of a plastic, a leather, and a rubber with increasing weight of dioctyl phthalate.

## INTRODUCTION

Polymers containing a disulphide crosslinkage and a thiol group, such as wool, protein and modified nylon, have been reported<sup>1,2</sup>. However, the synthesis and properties of a poly(vinyl chloride) derivative containing the polysulphide crosslinkage and hydropolysulphide pendant (PSC-PVC) have not been described in detail.

In our previous paper<sup>3</sup>, a poly(vinyl chloride) derivative containing the polysulphide crosslinkage was reported to be prepared from poly(vinyl chloride) (PVC) and octamic sulphur or ethylenediamine hydrotrisulphide (EN.H<sub>2</sub>S<sub>3</sub>).

In this paper, the reaction conditions of PVC with EN.H<sub>2</sub>S<sub>3</sub>, and the chemical structure of the reaction products are investigated. Further, the properties of PSC-PVC are examined in regard to the scission of polysulphide crosslinkage by some thiols in tetrahydrofuran (THF) solution or in a hot roller mill, and the applications to photocrosslinking and reversible crosslinking polymer are also examined.

## EXPERIMENTAL

### *Reaction of PVC with EN.H<sub>2</sub>S<sub>3</sub> (synthesis of PSC-PVC)*

PVC powder (Geon 101 EP, p:1450, 100 mesh) was added to a solution of EN.H<sub>2</sub>S<sub>3</sub> in EN or to a mixed solvent such as EN-benzene (EN-BN) or EN-diglyme (EN-DG), and then the mixture was stirred for 0.5–5 h at 35°C under nitrogen. Crude PSC-PVC was separated from the solution by filtration, and EN.H<sub>2</sub>S<sub>3</sub>, EN, and free sulphur were removed by washing with methanol, water, and benzene.

### *Iodine oxidation of hydropolysulphide pendant to polysulphide crosslinkage*

0.5 g of PSC-PVC was added to 20 ml of 0.02 N benzene solution of iodine. After the mixture was allowed to stand at 25°C for 24 h, oxidized PSC-PVC (OPS-PVC) was separated from the mixture by filtration and extracted with benzene (BN) to remove iodine.

### *Scission of polysulphide crosslinkage by thiols*

*In THF solution.* PSC-PVC (0.5 g) was added to a solution of thiophenol (1.1 g) and triethylamine (TEA) (0.1–1.0 g) in 30 ml of THF, and the mixture was stirred under the conditions given in Table 3. The insoluble material in the mixture was rapidly separated with IG-3 glass-filter. The percentage of gel was found from the ratio of the weight of the dried gel and the weight of the original PSC-PVC. The degree of scission of polysulphide crosslinkage was indicated by the decrease in the percentage of gel.

*In a hot two-roller mill.* PSC-PVC, β-thionaphthol and dibutylbis(dodecylthio)tin, were blended in a two-roller mill with heating at 125–180°C for 2–8 min. The recipes are shown in Table 6 and Figure 7. The degree of scission of the polysulphide crosslinkage was indicated by the percentage of gel in the blended sheet (0.5 g) in THF (50 ml).

### *Synthesis and photocrosslinking of PSP-PVC*

The mixture of thiophenol (2 g) or nitrothiophenol (2.8 g), PSC-PVC (1 g), and triethylamine (2 g) in 30 ml of THF was stirred at 30°C for 24 h, and was then poured into ethanol to give a PVC derivative containing

phenyl or nitrophenylenepolysulphide and hypopoly-sulphide pendant [PSP-PVC (1)]. Alternatively, benzenesulphonyl chloride (4 g) or benzoyl chloride (3.5 g), and triethylamine (2 g) were added to the above mixture before pouring into ethanol. The reaction mixture was stirred at 10–20°C for 15–60 min, and poured into ethanol to give PVC derivatives containing phenylpolysulphide and benzenesulphonyl or benzoyl polysulphide pendant [PSP-PVC (2)]. The film of PSP-PVC (1) or PSP-PVC (2), about 0.04 mm thick was obtained after evaporation of the solvent from THF solution (20 ml) of each PSP-PVC (0.3 g). Ultra-violet irradiation of the film was carried out at 30 cm from a 400 W photochemical mercury lamp (Toshiba H-400 p, light intensity:  $1.15 \times 10^{-19}$  quanta/cm<sup>2</sup>h). The degree of photocrosslinking was estimated from the percentage of gel in the films after irradiation.

#### Analysis

Sulphur and chlorine were determined by the Schöniger method and nitrogen was determined by the Kjeldahl method. The crosslinking density of PSC-PVC or OPS-PVC was evaluated from the values of  $v_2$  in the following Flory–Rehner equation:

$$v = \frac{1}{V} \frac{2.30 \log(1-v_2) + v_2 + \mu v_2^2}{(v_2 \rho - v_2/2)} + \frac{2}{M} \quad (\text{mol/g})$$

where  $V$  = molecular volume of THF (81.2)

$\rho$  = specific gravity of PVC (1.36)

$\mu$  = interaction parameter of PVC–THF (0.14)

$M$  = molecular weight of used PVC (90 600)

$v_2$  was determined by the measurement of the volume ratio of polymer before and after swelling in a measuring cylinder as described in a previous paper<sup>4</sup>. Tensile strength and elongation at break, and yield strength were determined with a recording Autograph P-100 at a drawing rate of 5 mm/min at 25°C.

## RESULTS AND DISCUSSION

### Reaction of PVC with EN.H<sub>2</sub>S<sub>3</sub>

The reactions of PVC with EN.H<sub>2</sub>S<sub>3</sub> in EN or in the mixed solvents were carried out in a heterogeneous system. Here, EN.H<sub>2</sub>S<sub>3</sub> dissolves in EN or in the mixed solvent, but PVC disperses in a state of swelling. EN acts as an acid acceptor as well as an activator of the thiol group<sup>5</sup>. Therefore, the reaction seems to occur by the EN.H<sub>2</sub>S<sub>3</sub> and EN permeating into the PVC granule<sup>6</sup>.

The reaction variables were examined for effect on sulphur and chlorine content of PSC-PVC. As shown in Figures 1 and 2, the sulphur content of PSC-PVC was much influenced by such variables as reaction temperature, time, and the concentration of EN.H<sub>2</sub>S<sub>3</sub>, but little by the weight of PVC in the reaction mixture. At temperatures higher than 50°C, the resulting PSC-PVC was brown in colour, and the formation of a double bond as well as a small amount of nitrogen were detected by i.r. spectroscopy ( $\nu_{C=C}$ : 1650 cm<sup>-1</sup>) and elemental analysis. The sulphur content of PSC-PVC reached equilibrium at a reaction time of over 3 h. As observed in a previous reaction of PVC with sulphur in EN<sup>3</sup>, sulphur content was not found to decrease

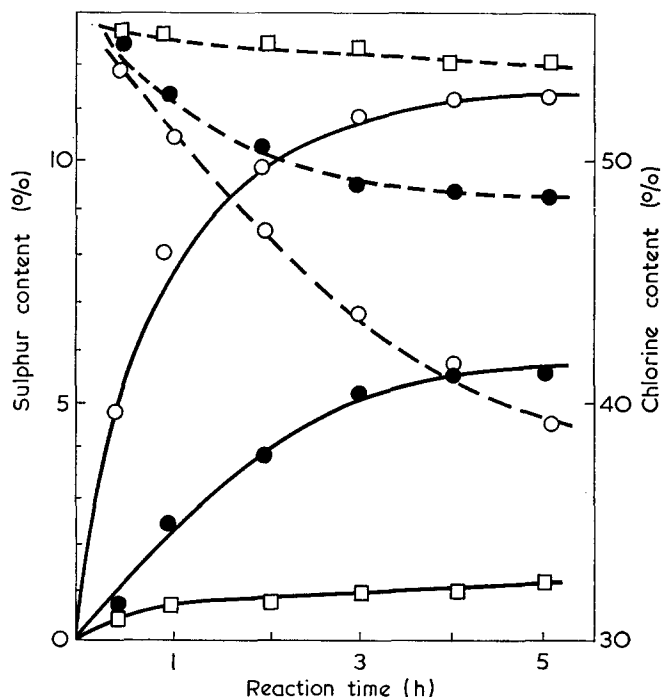


Figure 1 Effect of reaction temperature and time on sulphur (—) and chlorine (---) content. □, 20°C; ●, 35°C; ○, 50°C. Reactants: PVC, 10g; EN.H<sub>2</sub>S<sub>3</sub>, 3g. Solvent: EN, 30ml

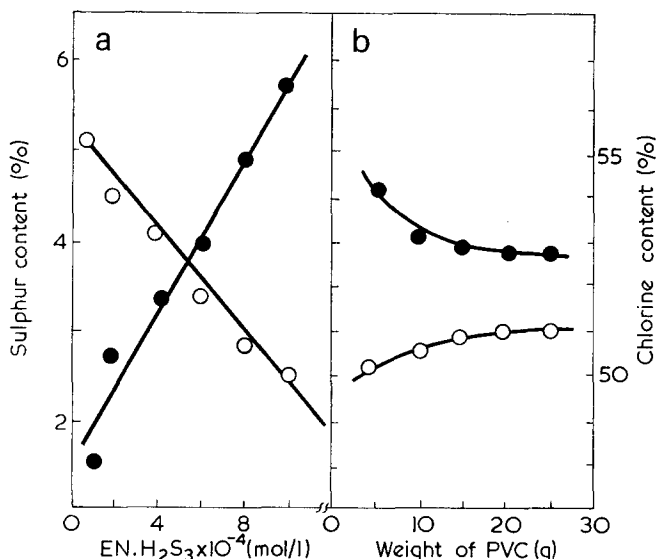


Figure 2 Effect of EN.H<sub>2</sub>S<sub>3</sub> concentration (a) and weight of PVC (b) on sulphur (●) and chlorine (○) content of PSC-PVC. Conditions: 30°C; 3h. Solvent: EN, 30ml

with an increase in reaction time. Therefore, the occurrence of desulphurization in the present reaction seems to be difficult.

The effect of the mixed solvent such as EN–DG or EN–BN was to facilitate the diffusion of EN and EN.H<sub>2</sub>S<sub>3</sub> into the PVC granule. As shown in Figures 3 and 4, the sulphur content of the resulting PSC-PVC in the mixed solvent (e.g. 10 ml of BN or BG and 40 ml of EN) was greater than that in EN. Further, the sulphur content of PSC-PVC, obtained from the mixed solvent of EN–DG which highly swells PVC, was larger than that in EN–BN (Figure 3). An increase in the volume of DG or BN against EN, however, decreased the sulphur content markedly (Figure 4). This is compensated on the basis of the following two factors: (i) the facilitated

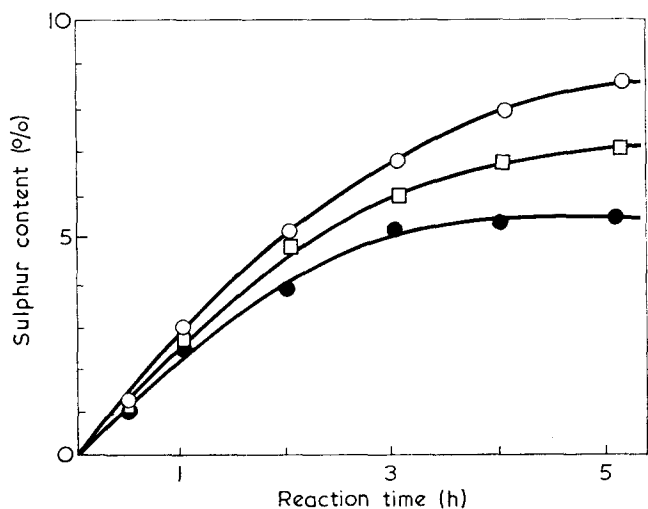
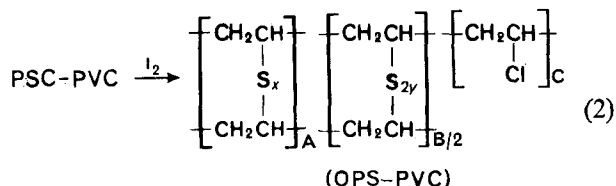
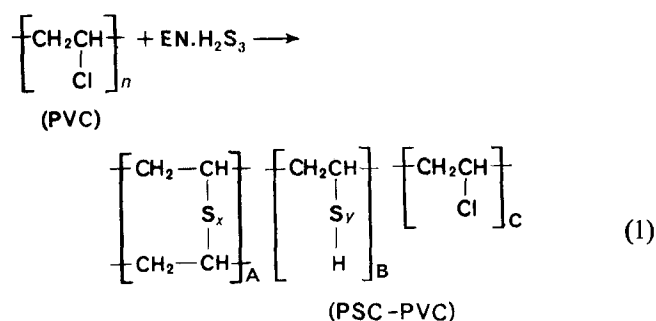


Figure 3 Effect of mixed solvents on sulphur content in the reaction of PVC and EN.H<sub>2</sub>S<sub>3</sub> at 35°C. ●, 50 ml EN; ○, 40:10 by vol. EN-DG; □, 40:10 by vol. EN-BN. Reactants: PVC, 10g; EN.H<sub>2</sub>S<sub>3</sub>, 3g

diffusion of EN.H<sub>2</sub>S<sub>3</sub> into granular PVC with increasing volume of BN or DG; (ii) the limited dissociation of EN.H<sub>2</sub>S<sub>3</sub> in the mixed solvent.

#### Structure of PSC-PVC

As described below, PSC-PVC obtained by the reaction of PVC with EN.H<sub>2</sub>S<sub>3</sub> in EN or in the mixed solvent, has been found to contain both the polysulphide crosslinkage and the hydropolysulphide pendant:



All hydropolysulphide pendants in PSC-PVC can form the polysulphide crosslinkage by iodine oxidation, as shown in scheme (2). The relations between crosslinking density ( $\nu$  or  $\nu'$ ) and the percentage of gel ( $G$  or  $G'$ ) of PSC-PVC or OPS-PVC are shown for the three solvent systems in Figure 5. Taking into account each crosslinking density, the percentage of gel in PSC-PVC or OPS-PVC seems to be much less than that estimated from the relation between percentage of sol and crosslinking density of crosslinking polymer<sup>7</sup>. This suggests that the crosslinking density of the outer layer of granular PVC differs from that of the inner layer remarkably. The difference of the gel fraction

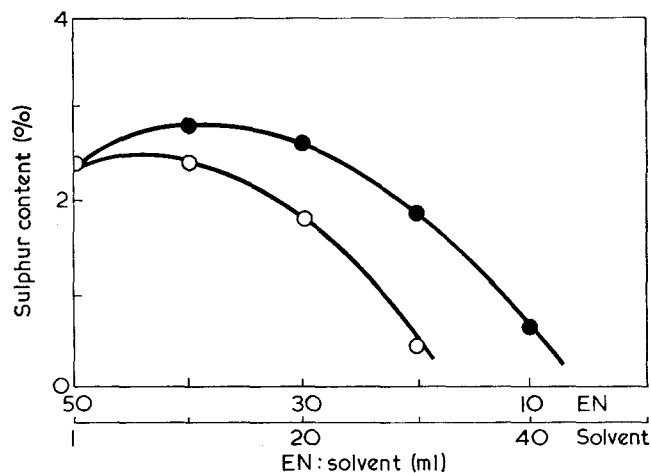


Figure 4 Effect of the proportion of mixed solvents on sulphur content in the reaction of PVC with EN.H<sub>2</sub>S<sub>3</sub>. ●, EN-DG; ○, EN-BN. Conditions: 35°C; 1h. Reactants: PVC, 10g; EN.H<sub>2</sub>S<sub>3</sub>, 3g

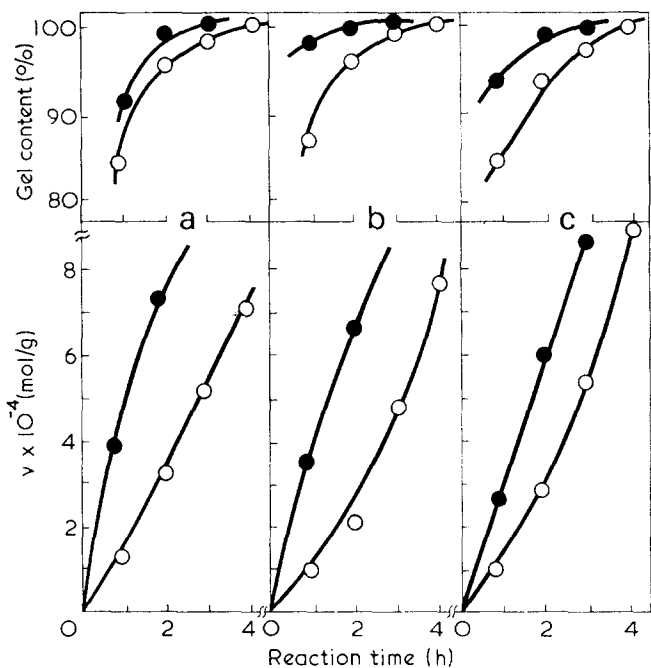


Figure 5 Relation between crosslinking density ( $\nu$ ) and gel content before (○) and after (●) iodine oxidation of PSC-PVC at 35°C. Reactants: PVC, 10g; EN.H<sub>2</sub>S<sub>3</sub>, 3g. Solvents: (a) 30 ml EN; (b) 40:10 by vol. EN-DG; (c) 40:10 by vol. EN-BN

or crosslinking density between PSC-PVC and OPS-PVC in the three solvent systems increases in the order EN < EN-BN < EN-DG. The difference means the presence of the hydropolysulphide pendant in PSC-PVC.

Now, the mole of the crosslinkage (A) and the pendant (B) in 1 g of PSC-PVC can be determined from  $\nu$  and  $\nu'$  as follows:  $A = \nu/2$ ;  $B = \nu - \nu'$ .

The crosslinking density in Figure 5 is expressed as  $\nu$  and in terms of A and B in Figure 6. Commonly, A increases with increase in reaction time, and B shows a maximum value. These results suggest that A increases progressively with the reaction between PVC and the hydropolysulphide pendant, and B decreases owing to the decrease of the diffusion velocity of EN.H<sub>2</sub>S<sub>3</sub> into the inner layer of granular PSC-PVC with the increase of crosslinking density. A in the maximum is larger in the EN-DG system which swells PVC more easily and

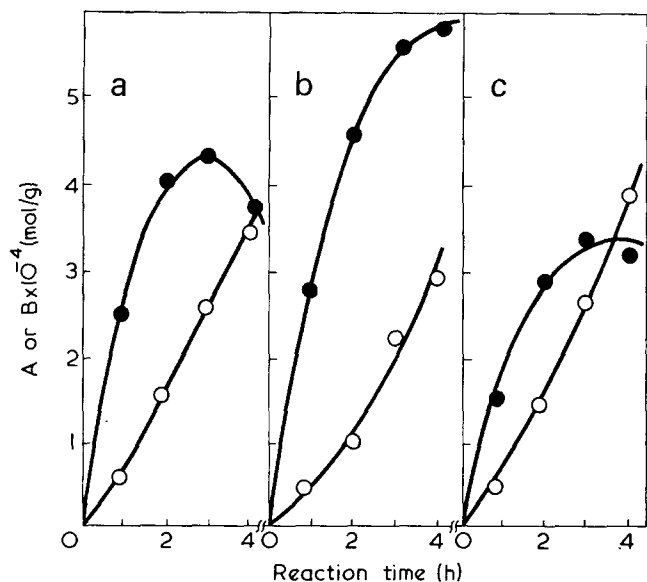


Figure 6 Relation between reaction time and polysulphide crosslinkage (A) or hydropolysulphide pendant (B) in PSC-PVC resulting in three solvent systems at 34°C. O, A; ●, B. Reactants: PVC, 10g; EN.H<sub>2</sub>S<sub>3</sub>, 3g. Solvents: (a) 30ml EN; (b) 40:10 by vol. EN-DG; (c) 40:10 by vol. EN-BN

solvates EN.H<sub>2</sub>S<sub>3</sub>. In the EN-BN system, EN.H<sub>2</sub>S<sub>3</sub> does not seem to be solvated although PVC swells and then B decreases with the elimination of H<sub>2</sub>S between hydropolysulphide pendants.

On the other hand, the number of sulphur chains ( $\bar{X}$  and  $\bar{Y}$ ) of the crosslinkage and pendant in PSC-PVC cannot be determined independently from analytical data and crosslinking density. The average number ( $\bar{X} + \bar{Y}$ ) of the sum of  $\bar{X}$  and  $\bar{Y}$ , however, can be calculated from:

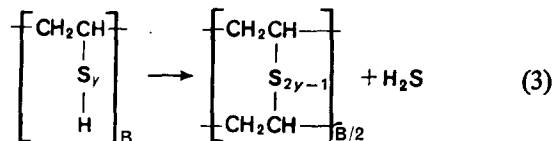
$$\bar{X} + \bar{Y} = \frac{aX + bY}{a + b} = \frac{\text{sulphur content}/32}{a + b}$$

( $\bar{X} + \bar{Y}$ ) is assumed to be 3 on the basis of the formation of dibutyltrisulphide from the reaction of butylchloride with EN.H<sub>2</sub>S<sub>3</sub> in dimethylformamide<sup>8</sup>. However, as shown in Table 1,  $\bar{X} + \bar{Y}$  of PSC-PVC obtained in EN, or EN-DG, is in the range of about 2 to 3. Although in the EN-BN system,  $\bar{X} + \bar{Y}$  is larger than 3 at the initial stage of reaction, this seems to be due to the elimination of H<sub>2</sub>S between hydropolysulphide pendants in PSC-PVC as shown in scheme (3):

Table 1 Effect of reaction conditions on sulphur chain number of PSC-PVC

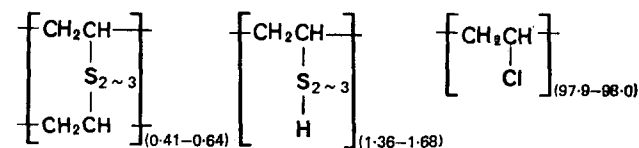
Reaction conditions				PSC-PVC <sup>a</sup>		
Reaction time (h)	Solvent (ml/ml)	Sulphur (%)	(A+B) × 10 <sup>-4</sup> (mol/g)	$\bar{X} + \bar{Y}$ (No. of sulphur atoms)		
1	EN 30	2.45	3.10	2.4		
2	4	5.55	7.51	2.3		
3	1	EN/DG 40/10	2.83	3.15	2.8	
4	4	8.00	9.45	2.6		
5	1	EN/BN 40/10	2.28	2.16	3.3	
6	4	6.85	7.68	2.8		

<sup>a</sup> Each sample was obtained by reacting PVC (10g) with EN.H<sub>2</sub>S<sub>3</sub> (3g) at 35°C for 1 or 4h, in EN or mixed solvents. EN: ethylenediamine; DG: dimethyl glycol; BN: benzene



Commonly,  $\bar{X} + \bar{Y}$  tends to decrease with increase in reaction time owing to easier desulphurization of polysulphide in the presence of EN<sup>8, 8</sup>. The desulphurization in the mixed solvent seems to be depressed because of higher ( $\bar{X} + \bar{Y}$ ) than that in EN. In the EN-DG system, the elimination of H<sub>2</sub>S and desulphurization seems to be the most difficult of the three solvent systems.

PSC-PVC containing residual hydromono- or polysulphide pendant reacts to produce post PSC-PVC with additional mono- or poly-sulphide crosslinkage by immersing PSC-PVC in EN at 35°C for 1h<sup>6</sup>. When a monosulphide crosslinkage occurs in the resulting post PSC-PVC, it cannot be dissolved in a THF solution of thiophenol and TEA as shown earlier. Post PSC-PVC, however, always dissolves perfectly in THF by the above described reduction. The above results suggest that PSC-PVC or post PSC-PVC contains neither hydromonosulphide pendant nor monosulphide crosslinkage, respectively. Therefore,  $\bar{X}$  and  $\bar{Y}$  in PSC-PVC are estimated to be more than 2. The chemical structure of typical PSC-PVC is generally shown as:



#### Properties of PSC-PVC

**Stability of PSC-PVC.** In general, polymers containing the thiol group are known to be unstable since they are easily oxidized in air. The stability of the hydropolysulphide pendant in PSC-PVC was examined at 30–60°C in air or in vacuum. As shown in Table 2, a higher temperature and a longer time decrease the sulphur content as well as B and increase A. These results cannot be accounted for on the basis of the formation of polysulphide crosslinkage by the oxidation of the thiol group, but by the elimination of H<sub>2</sub>S between hydropolysulphide pendants. This seems to be supported also by the similar results with PSC-PVC in vacuum.

#### Scission of polysulphide crosslinkage in THF solution of thiols

Linear PSP-PVC (I), containing both R-polysulphide and hydropolysulphide pendants as shown in scheme (4), was prepared when the mixture of PSC-PVC and

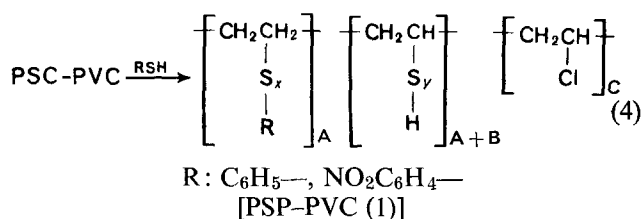
Table 2 Stability of hydropolysulphide group of PSC-PVC in air and vacuum

Condition <sup>a</sup>			PSC-PVC <sup>b</sup>		
Temp. (°C)	Time (days)		Sulphur (%)	A × 10 <sup>-4</sup> (mol/g)	B × 10 <sup>-4</sup> (mol/g)
—	—		2.31	0.56	2.56
20	7	air	2.39	0.60	2.50
40	7	air	2.29	0.66	2.45
60	6 (h)	air	2.28	0.61	2.55
60	7	air	2.09	0.98	2.08
30	7	vacuum	2.12	0.85	2.18

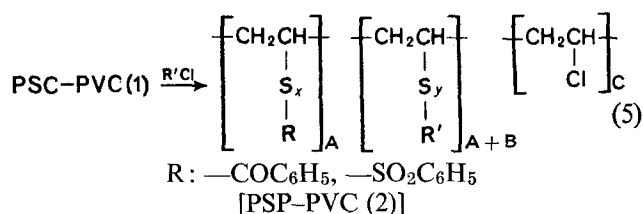
<sup>a</sup> Reaction conditions: 35°C, 1h

<sup>b</sup> Reactant system: PVC, 10g; EN.H<sub>2</sub>S<sub>3</sub>, 3g; EN, 30ml

THF solution of RSH (thiophenol or nitrothiophenol) and TEA was stirred at 30°C for 1–5 h as indicated in Table 3.



However, PSP-PVC (1) with a large sulphur content (over 2.66%) sets to gel on separation from the THF solution as shown in Table 4. This gelation seems to result from the desulphurization between hypopoly-sulphide pendants as shown in scheme (3) and the oxidation of the thiol group. The soluble PSP-PVC (2) with a large sulphur content can be obtained by pouring into alcohol after the addition of R'Cl (benzoyl chloride or benzenesulphonyl chloride) to the above mixture. It seems reasonable that PSP-PVC (2) containing replaced thiol group with the benzoyl or benzenesulphonyl group as shown in scheme (5) no longer sets to gel on isolation.



Schemes (4) and (5) are supported by the i.r. spectrum and elemental analysis as shown in Table 4.

#### Photocrosslinking of PSP-PVC (1) and (2)

On the photocrosslinking of PSP-PVC (1) or (2), an effective wave, percentage of gel (degree of photocrosslinking), and structure of photocrosslinkage was shown in Table 5. An effective wave for PSP-PVC (1) and (2) was in the range of 290 to 330 nm, and for PSP-PVC (2) was spread to a wave of 380 nm by the introduction of the internal sensitizing group such as the nitrophenylene and benzoyl group. PSP-PVC (1) was generally more sensitive than PSP-PVC (2) to ultra-violet light, and a mechanism of the photocrosslinking of PSP-PVC (1) and (2) seems to be different in the structure of crosslinkage as estimated through thiophenol reduction (Table 5). PSP-PVC (1) and (2) were not sensitized

Table 3 Scission of polysulphide crosslinkage of PSC-PVC in THF solution of thiophenol in the presence or absence of triethylamine

No.	PSC-PVC					Conditiona			Gel in THF mixture (%)
	Sulphur (%)	Gel (%)	A × 10 <sup>-4</sup> (mol/g)	B × 10 <sup>-4</sup> (mol/g)	$\bar{X} + \bar{Y}$ (No. of sulphur atoms)	Time (h)	TP (g)	TEA (g)	
1	2.39	85.5	0.58	2.58	2.8	1	1.0	0	15.6
2	2.39	85.5	0.58	2.58	2.8	1	1.1	1.0	0
3	6.07	99.5	1.65	5.32	2.6	1	1.1	0	83.2
4	6.07	99.5	1.65	5.32	2.6	1	1.1	0.1	54.0
5	6.07	99.5	1.65	5.32	2.6	1	1.1	1.0	34.6
6	6.07	99.5	1.65	5.32	2.6	5	1.1	1.0	0

a Conditions: temperature, 30°C; PSC-PVC, 0.5 g, under nitrogen; TP: thiophenol; TEA: triethylamine

Table 4 Preparation of PSP-PVC(1) and PSP-PVC(2)

No.	Reactants			Products							
	PSC-PVC sulphur (%)	Thiols (RSH) R—	Active organic chloride (R'Cl) R'—	PSP-PVC(1) <sup>c</sup>				PSP-PVC(2) <sup>d</sup>			
				Sulphur (%)	Gel (%)	I.r. (cm <sup>-1</sup> )		Sulphur (%)	Gel (%)	I.r. (cm <sup>-1</sup> )	
1	2.39 <sup>a</sup>	C <sub>6</sub> H <sub>5</sub> —	C <sub>6</sub> H <sub>5</sub> SO <sub>2</sub> —	2.66	0	C <sub>6</sub> H <sub>5</sub> —S— 760	2.75	0	O=S=OS 1340		
2	6.07 <sup>b</sup>	C <sub>6</sub> H <sub>5</sub> —	C <sub>6</sub> H <sub>5</sub> SO <sub>2</sub> —	6.43	46.3	C <sub>6</sub> H <sub>5</sub> —S— 760	6.55	0	O=S=OS 1340		
3	6.07 <sup>b</sup>	NO <sub>2</sub> C <sub>6</sub> H <sub>4</sub> —	C <sub>6</sub> H <sub>5</sub> CO—	6.25	45.5	NO <sub>2</sub> C <sub>6</sub> H <sub>4</sub> — 1340	5.86	0	C=OS 1730		

a, b PSC-PVC shown at No. 1 and No. 3 in Table 3 respectively

c PSP-PVC(1) was obtained by the reaction of PSC-PVC with RSH under the conditions in the experimental section

d PSP-PVC(2) was obtained by the reaction of PSC-PVC, RSH and R'Cl under the conditions in the experimental section

Table 5 Effect of R and R' in PSP-PVC on effective wave, percentage of gel and crosslinking structure in photocrosslinking

No.	PSP-PVC(1) or PSP-PVC(2) <sup>a</sup>			Photocrosslinked PSP-PVC(1) or PSP-PVC(2) <sup>b</sup>			
	R	R'	Sulphur (%)	Effective wave (nm)	Gel (%)	Insoluble fraction in THF solution of TP (%)	Structure of crosslinkage estimated
1	C <sub>6</sub> H <sub>5</sub> —	H	2.66	290–330	56.3	0	C—S <sub>x</sub> —C(x ≥ 2)
2	C <sub>6</sub> H <sub>5</sub> —	C <sub>6</sub> H <sub>5</sub> SO <sub>2</sub> —	2.75	290–330	28.5	0	C—S <sub>x</sub> —C(x ≥ 2)
3	C <sub>6</sub> H <sub>5</sub> —	C <sub>6</sub> H <sub>5</sub> SO <sub>2</sub> —	6.55	290–330	68.5	98.6	C—S—C
4	NO <sub>2</sub> C <sub>6</sub> H <sub>4</sub> —	C <sub>6</sub> H <sub>5</sub> CO—	5.86	290–380	58.5	60.5	C—S <sub>x</sub> —C(x ≥ 1)

a Samples 1–3 are shown in Table 4

b Irradiating for 30 min at 25°C in air; TP: thiophenol



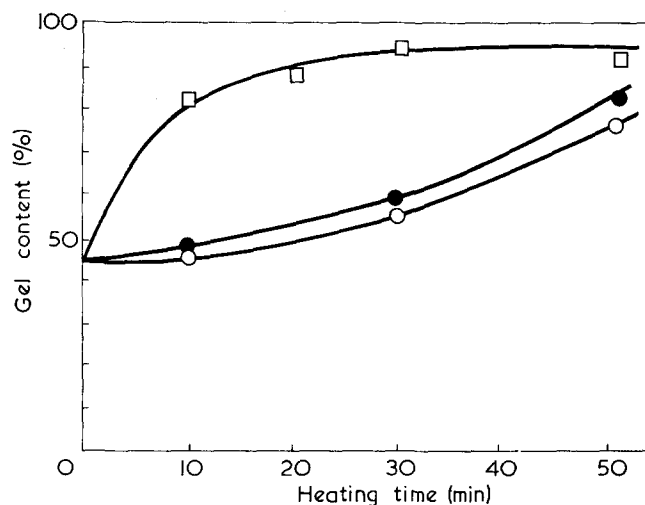
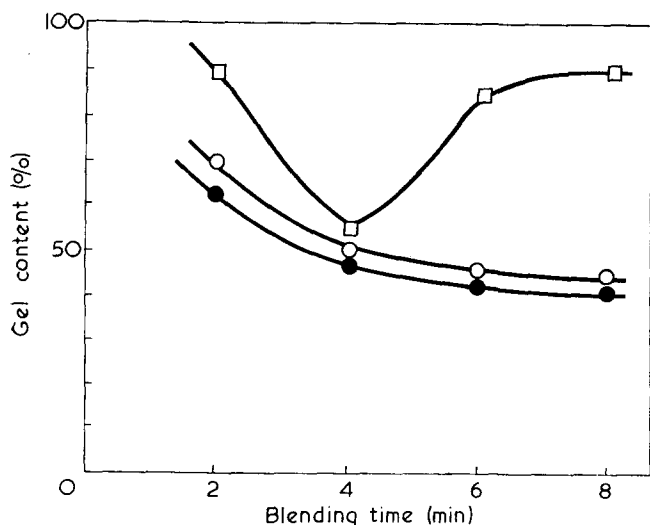


Figure 7 Effect of roller temperature and blending time on scission of polysulphide crosslinkage in PSC-PVC by  $\beta$ -thionaphthol.  $\circ$ , 125°C;  $\bullet$ , 150°C;  $\square$ , 180°C. Reactants: PSC-PVC, 10g;  $\beta$ -thionaphthol, 1g; ID-3, 0.2g

Figure 8 Effect of heating time between 125°C and 180°C on recrosslinking of PSC-PVC cleavage by thionaphthol.  $\circ$ , 125°C;  $\bullet$ , 160°C;  $\square$ , 180°C

Table 6 Mechanical properties of PSC-PVC reduced by  $\beta$ -thionaphthol

	I	II	III	IV	V
PSC-PVC <sup>a</sup> (phr)	100	100	100	100	100 <sup>e</sup>
DOP <sup>b</sup> (phr)	10	20	20	60	60
TN <sup>c</sup> (phr)	10	10	10	10	—
ID-3 <sup>d</sup> (phr)	2	2	2	2	2
$T_s$ at yield (kg/cm <sup>2</sup> )	497 (606)	115 (127)	—	—	—
$T_s$ at break (kg/cm <sup>2</sup> )	279 (—)	330 (309)	245 (230)	163 (127)	110
Elongation (%)	23 (9)	177 (177)	274 (252)	290 (279)	450
Modulus at 100% (kg/cm <sup>2</sup> )	—	266 (250)	110 (109)	66 (54)	33
Modulus at 200% (kg/cm <sup>2</sup> )	—	—	196 (195)	119 (103)	59
Gel content (%)	46 (59)	46 (63)	47 (72)	47 (75)	0

<sup>a</sup> S content: 2.15%; gel content: 86%;  $\nu=1.22 \times 10^{-4}$  mol/g. Gel content: 99%.  
 $\nu'=2.94 \times 10^{-4}$  mol/g after iodine oxidation of PSC-PVC

<sup>b</sup> Dioctyl phthalate. <sup>c</sup> Thionaphthol

<sup>d</sup> Dibutylbis(dodecylthio)tin as stabilizer (Nittokasei Co., Osaka, Japan)

<sup>e</sup> Original PVC

Figures in parentheses refer to heating at 160°C for 30 min

by such sensitizers as anthraquinone, benzophenone, acetylacetone or Michler's ketone. But, from the results in Table 5, a more sensitized PSP-PVC will be obtained by the selection of sensitive substituents in PSP-PVC (2). This will be presented in a subsequent paper.

#### Scission of polysulphide crosslinkage by $\beta$ -thionaphthol in a two roller mill

PSC-PVC powder did not wind round a roller mill with heating at 125–180°C, on blending without addition of  $\beta$ -thionaphthol. 100 parts of PSC-PVC powder with addition of 10 parts of  $\beta$ -thionaphthol, wound easily round on blending at 150°C for 1–2 min and a sheet of PSC-PVC was obtained by blending for an additional 4–6 min.

Polysulphide crosslinkage of the resulting sheet is estimated to be severely reduced by  $\beta$ -thionaphthol on the blending in a two roller mill, as the percentage of gel of the resulting sheet is less than that of the original PSC-PVC (Figure 7). On blending at 180°C, however, the percentage of gel in blends increases contrary to the increase of blending time over about 4 min, and the blending is no longer easy. The resulting blends seem to contain monosulphide or carbon-carbon crosslinkages as these are insoluble in THF solution of thiophenol and TEA. The formation of sheet is difficult

at 125°C although scission of polysulphide crosslinkage occurs on blending.

On the other hand, from the measurement of percentage of gel of the moulds (Figure 8), polysulphide pendants were found to recombine to form polysulphide crosslinkage on moulding at 160°C for 10–50 min under a pressure of 50 kg/cm<sup>2</sup>. The partly recrosslinked PSC-PVC sheet with excellent mechanical properties could be obtained with addition of  $\beta$ -thionaphthol and 10–60 parts of dioctylphthalate (DOP) as shown in Table 6. Sheets I, III, and IV in Table 6 show the properties of a plastic, a leather, and a rubber respectively with increasing weight of DOP.

#### REFERENCES

- 1 Weigmann, H. *et al. Textile Res. J.* 1966, **36**, 535
- 2 Astbury, W. *et al. Phil. Trans. R. Soc. (A)* 1933, **232**, 333
- 3 Mori, K. and Nakamura, Y. *J. Polym. Sci. (B)* 1970, **8**, 7
- 4 Mori, K. and Nakamura, Y. *Kobunshi Kagaku* 1973, **30**, 299
- 5 Mori, K. and Nakamura, Y. *Kobunshi Kagaku* 1971, **28**, 85
- 6 Mori, K. and Nakamura, Y. *J. Polym. Sci. (A-1)* 1971, **9**, 639
- 7 Charlesby, A. 'Atomic radiation and polymers', Asakura Press, Tokyo, 1962, p 132
- 8 Mori, K. and Nakamura, Y. *J. Org. Chem.* 1971, **36**, 3041

# Notes to the Editor

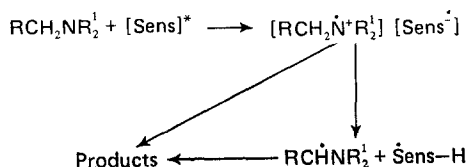
## Initiation of free-radical polymerization by photoinduced electron transfer processes

A. Ledwith and M. D. Purbrick

Department of Inorganic, Physical and Industrial Chemistry, University of Liverpool, PO Box 147, Liverpool L69 3BX, UK  
(Received 2 June 1973)

Previously<sup>1</sup> we have shown that photoinduced electron transfer reactions between *N*-vinylcarbazole and a wide range of sensitizers, leads to efficient, catalytic cyclodimerization of the olefin. Sensitizers employed range from aromatic ketones such as benzophenones and fluorenone, through pyrylium salts and rhodamine dyes, to long wavelength visible light absorbing dyes such as methylene blue and thionine. Whilst the sensitizers may act via lowest lying excited singlet or triplet states, according to type, the primary process in all cases involves electron transfer from olefin to photo-excited sensitizer, and it is now clear that this highly efficient photocyclodimerization is just a special case of the photo-oxidation of amines, especially tertiary amines, by aromatic carbonyl compounds<sup>2</sup> and certain dye molecules<sup>3</sup>.

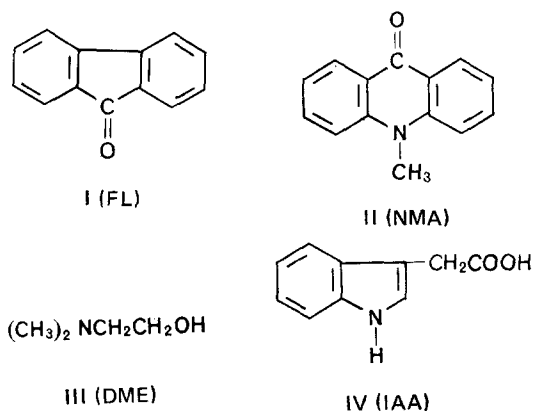
The reactions may be represented as indicated below, although products vary according to the nature of the amine substituents and the sensitizer:



As part of a continuing interest in initiation of free radical polymerization by photo-excited aromatic carbonyl compounds<sup>4,5</sup>, we have studied photo-redox processes between (mainly) aromatic carbonyl compounds and amines and present a summary of their value as initiating systems for the free radical polymerization of methyl methacrylate.

All the sensitizers, effective for photodimerization of *N*-vinylcarbazole<sup>1</sup>, were useful photoinitiators for free-radical polymerization of methyl methacrylate (MMA) when used in conjunction with other tertiary amines but we have found it particularly useful to employ 9-fluorenone (I) (FL), and *N*-methylacridone (II) (NMA). Most tertiary amines (e.g. triethylamine, *N,N*-dimethylaniline) were effective as co-initiators with these (and the other) sensitizers, but for experimental convenience we have preferred *N,N*-dimethyl ethanolamine (III) (DME). Davidson and coworkers<sup>6</sup> have demonstrated that photoreduction of certain aromatic ketones and dye molecules may be brought about by carboxylic acids having electron donor function, such as *N*-phenylglycine, and we find that these reagents are equally effective in co-initiating free-radical polymerization. However, again

for experimental convenience, we have preferred the readily available indol-3-yl-acetic acid (IV) (IAA), as reductant.



For both photoinitiators, and either of the two amines, a small induction period was observed during free radical polymerization of MMA carried out (bulk, or benzene solutions) in air-saturated systems. The induction periods were not observed when corresponding reactions were carried out in high vacuum degassed systems, and it seems clear that they represent scavenging of oxygen from the systems by highly efficient reactions<sup>3</sup> with products of the initial photoredox process, e.g.  $\text{RCH}_2\dot{\text{N}}\text{R}_2^1$ ,  $\dot{\text{Sens}}-\text{H}$ .

A full study of the kinetics and molecular weight dependencies of MMA (1–8 M) polymerization in benzene at 30°C, photoinitiated by FL ( $0.3\text{--}1.8 \times 10^{-4}$  M), activated by DME, gave rise to the expression:

$$-\frac{dM}{dt} = k[\text{FL}]^{0.5}[\text{I}_0]^{0.5}[\text{MMA}]$$

where  $\text{I}_0$  = light intensity. The effect of varying [DME] on rate of polymerization was more complex but very similar to the effects of varying amine concentration on photoreduction of fluorenone reported by other workers<sup>2</sup>; above a certain concentration ( $\sim 10^{-1}$  M) the rate of polymerization was essentially independent of [DME].

Determinations of  $\bar{M}_n$  values for polymer samples produced in the kinetic studies yielded a value for  $k_p/k_t^{1/2} = 0.054$ , in good agreement with data for MMA reported by other workers<sup>4,7</sup>, and indicating that transfer and termination processes in these systems are not particularly affected by the initiating components or their photoredox products.

Table 1 Spectroscopic data and quantum yields for initiation  $\phi$  of MMA polymerization in benzene at 30°C

Photo-initiator	$\lambda_{\max}$ (nm) ( $\epsilon_{\max}$ l/mol cm)	Amino compound	$\lambda$ (nm) for measurement of $\phi$	$\phi$
9-fluorenone	380 (321)	DME	370	0.2
9-fluorenone	380 (321)	IAA	370	0.2
<i>N</i> -methyl-acridone	406 (8470)	IAA	406	0.15

Very similar kinetic and molecular weight data have been determined for polymerization of MMA photo-initiated by the combinations FL/IAA and NMA/IAA; relative efficiencies may be compared by means of the quantum yield data shown in Table 1, and in all cases, the carbonyl compound was consumed during reaction. From Table 1 it can be seen that the relatively high absorption characteristics of *N*-methylacridone make it particularly useful as a photoinitiator.

Photoinitiation of MMA polymerization co-activated by amines, especially IAA, is not restricted to the aromatic carbonyl compounds. Semi-quantitative experiments have demonstrated that comparable efficiencies are shown by 2-*t*-butyl anthraquinone, benzil, 2,4,6-triphenylpyrylium tetrafluoroborate, acriflavine, rhodamine 6G, and methylene blue, although these observations are not corrected for the differing light absorption characteristics of the sensitizers. However, it is perhaps worth noting that the efficiency of methylene blue as a photo-activator for free radical polymerization of non-degassed solutions, appears to increase with solvent polarity and with the presence of added electrolytes. Both effects are known to favour equilibrium formation of dye aggregates<sup>8</sup>, and this particular aspect of the work is now being studied in detail. Methylene blue/IAA combinations are effective for degassed systems where the blue dye is completely bleached during reaction, and the colour restored on opening the vessel to air.

Solvent effects on photoinitiation by fluorenone parallel known effects of solvents on the facility for triplet state formation<sup>9</sup>. Generally speaking, increasing solvent dielectric (including increasing amine concentration) lowers the intersystem crossing efficiency and decreases effectiveness as photoinitiator. In contrast, for the IAA/FL system, comparable rates of polymerization of MMA were observed in benzene and acetonitrile and there is a close correlation between the efficiency of IAA as a quencher for fluorenone fluorescence, and photoinitiation, suggesting that, for this system, *singlet* excited fluorenone is involved.

Semi-pinacol-type radicals ( $\text{Ar}_2\dot{\text{C}}\text{-OH}$ ) produced by reduction of aromatic ketones<sup>4</sup> are not noticeably active in initiation of polymerization of MMA at 30°C and, taken with the bleaching-recolouration observations noted for photoinitiation by methylene blue, it is reasonable to conclude that the important initiation process involves reaction of amine derived radicals (e.g.  $\text{RCHNR}_2^{\cdot}$ ) with monomer; for IAA activated systems it is likely<sup>6</sup> that the initiating radical is derived by photo-decarboxylation.

In all cases a photoinduced electron transfer reaction is a primary requisite for production of initiating radicals. Other workers<sup>10</sup> have recently suggested a similar mechanism for polymerizations initiated by benzophenone/triethylamine combinations, and photoinduced electron transfer from reducing anions to dyes of the methylene blue type is a well established initiation process<sup>11</sup>. The range of sensitizer and amino compound combinations now shown to be active suggests that this should be regarded as a general and highly convenient technique for polymerization, and crosslinking, by radical processes and may provide a better mechanistic rationalization of other reports<sup>12</sup> of photoinitiated polymerizations involving certain dye molecules.

## EXPERIMENTAL

Techniques for purification of solvents and monomer, and for photopolymerization have been described previously<sup>4,5</sup>. Indol-3-yl-acetic acid (BDH) was purified by recrystallization, finally from ether (m.p. 169–170°C). *N,N*-dimethylethanolamine (BDH) was fractionated to give a middle fraction, b.p. 134°C. 9-Fluorenone (BDH) was recrystallized from ethanol, m.p. 82.5–83.5°C. Irradiation was by means of a 250 W medium pressure mercury lamp, with appropriate interference filters, for the carbonyl sensitizers, and by a 500 W tungsten filament lamp for photoinitiation by rhodamine 6G and methylene blue (the dyes were used as supplied by BDH). Quantum yields were estimated by ferrioxalate actinometry<sup>13</sup>.  $M_n$  values were determined by membrane osmometry.

## ACKNOWLEDGEMENT

The authors are indebted to the SRC for a research studentship to M.D.P.

## REFERENCES

- Ledwith, A. *Acc. Chem. Res.* 1972, **5**, 133
- Cohen, S. G., Parola, A. and Parsons, G. *Chem. Rev.* 1973, **73**, 141
- Bartholomew, R. F. and Davidson, R. S. *J. Chem. Soc. (C)* 1971, p 2347
- Block, H., Ledwith, A. and Taylor, A. R. *Polymer* 1971, **12**, 271; Hutchison, J., Lambert, M. C. and Ledwith, A. *Polymer* 1973, **14**, 250
- Ledwith, A., Russell, P. J. and Sutcliffe, L. H. *JCS Perkin Trans. II* 1972, p 1925; Hutchison, J. and Ledwith, A. *Polymer* 1973, **14**, 405
- Davidson, R. S., Harrison, K. and Steiner, P. R. *J. Chem. Soc. (C)* 1971, p 3480; Davidson, R. S. and Steiner, P. R. *ibid.* 1971, p 1682
- Bamford, C. H. and Brumby, S. *Makromol. Chem.* 1967, **105**, 122
- McKay, R. B. and Hillson, P. J. *Trans. Faraday Soc.* 1966, **62**, 1439; 1965, **61**, 1800; Schubert, M. and Levine, A. *J. Am. Chem. Soc.* 1955, **77**, 4197
- Caldwell, R. A. *Tetrahedron Lett.* 1969, p 2121; Guttenplan, J. B. and Cohen, S. G. *ibid.* 1969, p 2125
- Sandner, M. R., Osborn, C. L. and Trecker, D. J. *J. Polym. Sci. (A-1)* 1972, **10**, 3173
- Rust, J. B., Miller, L. J. and Margerum, J. D. *Phot. Sci. Eng.* 1968, **12**, 177
- Oster, G. and Yang, N. L. *Chem. Rev.* 1968, **68**, 125; Maiti, S., Saha, M. K. and Palit, S. R. *Makromol. Chem.* 1969, **127**, 224
- Kurien, K. C. *J. Chem. Soc. (B)* 1971, p 2081

# Proton magnetic resonance study of conformational transitions in heterogeneous oxidized-wool proteins

B. J. Dale and D.W. Jones

School of Chemistry, University of Bradford, Bradford, BD7 1DP, UK  
(Received 14 February 1973; revised 25 May 1973)

Of the changes in high-resolution proton magnetic resonance (p.m.r.) spectra which accompany a transition from random-coil to helical form in polypeptides or proteins<sup>1-7</sup>, the most marked are the 0.3–0.6 ppm upfield shift of the  $\alpha$ -CH resonance and the increase in linewidth attributed to non-averaging of dipolar interactions. Variations with temperature and with addition of urea in the p.m.r. spectra of aqueous solutions of several heterogeneous protein fractions from oxidized wool have been interpreted as indicating a predominance of the random-coil conformation<sup>5, 6</sup>. However, attempts to induce conformational transitions in trifluoroacetic acid (TFA)/chloroform- $d_1$  ( $CDCl_3$ ) and TFA/*m*-cresol solvent systems were unsuccessful<sup>6</sup>. In this communication, evidence is presented which suggests that, for two heterogeneous wool proteins in formic acid- $d_2$  (DCOOD)/ $CDCl_3$  mixtures, p.m.r. spectral changes arise from a transition to a helical structure.

100 MHz p.m.r. spectra were recorded at 302–339K on a JEOL MH-100 spectrometer for 4% w/w solutions in DCOOD/ $CDCl_3$  mixtures, internally referenced with tetramethylsilane (TMS), of  $\alpha$ -keratose, urea-soluble (U.S.)3, and  $\gamma$ -keratose. Optical rotatory dispersion (o.r.d.) spectra of 5% w/w solutions of  $\gamma$ -keratose and U.S.3 in DCOOD/ $CDCl_3$  ( $CDCl_3$  concentration, 0 to 50% w/w) were recorded at room temperature in 1 mm cells on a Thorn-Bendix Polarmatic 62 over the range 590–355 nm. The plain curves were analysed for the constants  $a_0$  and  $b_0$  (Table 1) of the Moffitt–Yang<sup>8</sup> equation, with a calculated<sup>9</sup> mean residue weight,  $M$ , of 112.9 for U.S.3 and with  $\lambda_0 = 212$  nm. Precipitation restricted  $CDCl_3$  concentrations to the range 0 to 50% w/w.  $\alpha$ -Keratose and U.S.3, with only 5.3 and 7.5 cysteic acid residues per 100, are so-called low-sulphur fractions; they contain small percentages of other amino acids, e.g. proline and serine, known not to favour a helical conformation<sup>10</sup>. In contrast,  $\gamma$ -keratose<sup>9</sup>, with 19.3 cysteic acid residues per 100, is a high-sulphur fraction and contains a higher percentage of amino acids unfavourable to helical conformation.

As the concentration of  $CDCl_3$  in a  $CDCl_3$ /DCOOD mixture is increased to 50% w/w, most resonances in the p.m.r. spectra of  $\alpha$ -keratose and U.S.3 at 302K broaden. Since chemical shift differences between TFA and DCOOD as solvents are expected to be small<sup>7</sup>, most of the assignments<sup>6</sup> made for TFA should be valid for DCOOD. For the composite leucyl/isoleucyl/valyl

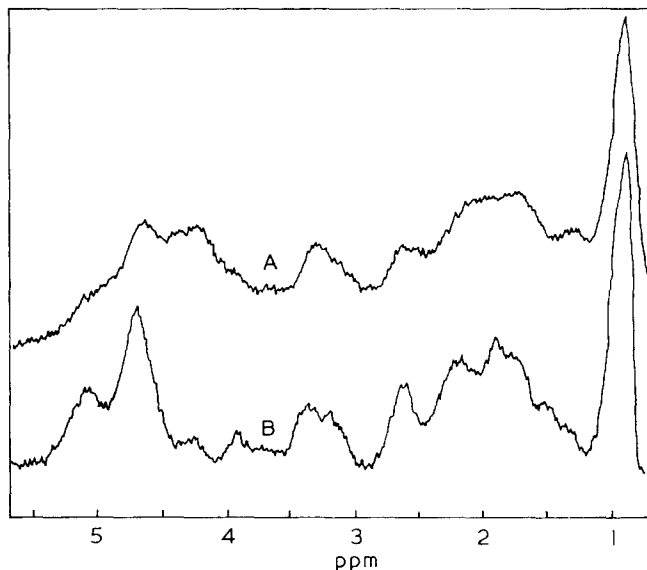


Figure 1 100 MHz p.m.r. spectra of low-sulphur wool fraction U.S.3. A, in 50% DCOOD/50%  $CDCl_3$  solution; B, in DCOOD solution

$CH_3$  peak at 0.9 ppm downfield from TMS, the half-height width,  $\Delta\nu_{1/2}$ , increases from 20 Hz to 25 Hz; other resonances are appreciably broadened; e.g., for a peak at 2.6 ppm,  $\Delta\nu_{1/2}$  increases from 25 Hz to about 40 Hz. The small (approximately 0.1 ppm) shifts in side-chain resonances probably result from changes in shielding with solvent composition. However, in the  $\alpha$ -CH region (4.0–5.2 ppm), some of the absorption shows a substantial (0.4–0.5 ppm) upfield shift (Figure 1); the intensity of these shifted regions, and presumably the number of protons affected, increases with increasing  $CDCl_3$  concentration.

The spread of these changes, suggestive of an increase in helicity, over a wide range of solvent compositions is presumably a consequence of the heterogeneity and polydispersity of each fraction<sup>11</sup>. The presence of appreciable helical structure in  $\alpha$ -keratose and U.S.3 is consistent with their amino acid compositions<sup>9</sup> and with o.r.d. measurements for the low-sulphur SCMKA<sup>12</sup> and U.S.3 protein fractions from wool. Moreover, p.m.r.<sup>5, 6</sup> and o.r.d. (ref. 13 and Table 1) studies on high-sulphur proteins suggest that  $\gamma$ -keratose remains in a random-coil conformation; addition of up to 50% w/w  $CDCl_3$  made no significant changes in linewidth or chemical shift to spectra recorded in DCOOD (Figure 2). P.m.r. estimation of the helix content of U.S.3 at 302K is rendered difficult by peak width and overlap in the  $\alpha$ -CH region; for example, at 5.0 ppm, residues which participate in the coil-to-helix transition overlap with those at 4.5 ppm remaining in a random-coil conformation. While the reduction in area of the 5.0 ppm peak and the emergence of the 4.2 ppm peak correspond to an increase in helix content by  $50 \pm 20\%$  in DCOOD/ $CDCl_3$  (50:50% w/w) relative to DCOOD, our o.r.d. results (Table 1) indicate

Table 1 Estimates of helicities of wool fractions from o.r.d.

Protein fractions	Solvent	$a_0$ (degrees)	$b_0$ (degrees)	Helix content (%)
U.S.3	DCOOD	248	-175	28
	DCOOD/ $CDCl_3$ (50 : 50% w/w)	108	-300	48
$\gamma$ -keratose	DCOOD	440	+2	0

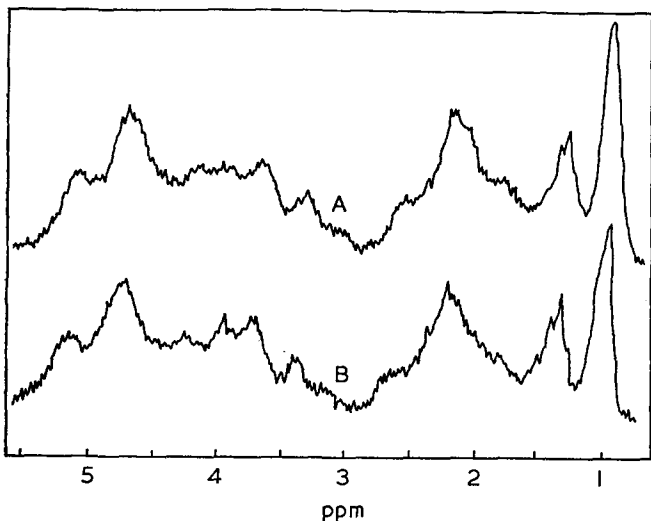


Figure 2 100 MHz p.m.r. spectra of high-sulphur wool fraction  $\gamma$ -keratose. A, in 50% DCOOD/50%  $\text{CDCl}_3$  solution; B, in DCOOD solution

a smaller but substantial increase. The implication that U.S.3 retains appreciable helicity in DCOOD is consistent with Harrap's observation<sup>12</sup> that  $b_0 = -100^\circ$ , corresponding to 15% helix content, for another low-sulphur protein, *S*-carboxymethylkeratine (SCMKA). Despite somewhat different  $b_0$  values, the p.m.r. linewidths for U.S.3 and  $\gamma$ -keratose in DCOOD are closely similar, suggesting that at lower helicities amino acid overlap may have more influence on the appearance of the spectrum than changes in rotational freedom. In all DCOOD/ $\text{CDCl}_3$  mixtures examined, the p.m.r. spectra of U.S.3 sharpened with increase of temperature to 339K, while some of the  $\alpha$ -CH resonances shifted downfield, corresponding to a reduction in helix content; when the sample was cooled to 302K, some of the lost helicity

appears to be recovered. These results are consistent with the view that the low-sulphur proteins are extracted from the helical wool fibrils, while the high-sulphur materials emanate from the amorphous matrix region<sup>14</sup>.

#### ACKNOWLEDGEMENTS

The samples of  $\alpha$ -keratose, U.S.3, and  $\gamma$ -keratose were kindly provided by Dr J. C. Fletcher; we are grateful to Dr D. N. Jones for facilitating o.r.d. measurements and to the Wool Industries Research Association for financial support to B.J.D.

#### REFERENCES

- 1 Rowe, J. J. M., Hinton, J. and Rowe, K. L. *Chem. Rev.* 1970, **70**, 1
- 2 Sheard, B. and Bradbury, E. M. *Prog. Biophys. Mol. Biol.* 1970, p 187
- 3 Roberts, G. C. K. and Jardetzky, O. *Adv. Protein Chem.* 1970, **25**, 447
- 4 Bovey, F. A. 'High resolution n.m.r. of macromolecules', Academic Press, New York, 1972
- 5 Bartle, K. D., Jones, D. W. and L'Amie, R. *Studia Biophys.* 1969, **13**, 53
- 6 Bartle, K. D., Jones, D. W. and L'Amie, R. *Appl. Polym. Symp.* 1971, **18**, 85
- 7 Bradbury, J. H. and King, N. L. R. *Aust. J. Chem.* 1969, **22**, 1083
- 8 Moffitt, W. and Yang, J. T. *Proc. Natl Acad. Sci. USA* 1956, **42**, 596
- 9 Corfield, M. C., Fletcher, J. C. and Robson, A. in 'Symposium on Fibrous Proteins, Australia, 1967', (Ed. W. G. Crewther). Butterworths, Sydney, 1968, p 299
- 10 Davies, D. R. *J. Mol. Biol.* 1964, **9**, 605
- 11 Bradbury, E. M., Crane-Robinson, C. and Rattle, H. W. E. *Polymer* 1970, **11**, 277
- 12 Harrap, B. S. *Aust. J. Biol. Sci.* 1963, **16**, 231
- 13 Gillespie, J. M. and Harrap, B. S. *Aust. J. Biol. Sci.* 1963, **16**, 252
- 14 Bendit, E. G. *Text. Res. J.* 1968, **38**, 15

## Effects of long branching on distribution of degree of polymerization: 2

P. A. Small

Department of Chemistry, University of Manchester, Manchester M13 9PL, UK  
(Received 18 June 1973)

The method of generating functions (*GF*) has been applied<sup>1</sup> to calculate the moments of the distribution for a model described by Mullikin and Mortimer<sup>2</sup> characterized by the assumption of two constant probabilities, one (*p*) for addition of a further monomer unit, and one (*b*) for branching at each potential site. There are  $\alpha$  equivalent sites per monomer unit in the polymer; termination by combination is assumed absent.

Mullikin and Mortimer have now<sup>3</sup> calculated the first and second moments, and the ratio of the weight-average degree of polymerization to the number average, for a more realistic model which should well represent a perfectly stirred continuous-flow reaction system. In this improved model the probability of branching  $b_\phi$  depends upon the time of residence in the reactor,  $\phi$ , through the relation<sup>3</sup>:

$$b_\phi = 1 - e^{-A\phi} \quad (1)$$

while the probability of residence has the usual negative exponential dependence on  $\phi$  with a rate constant  $\tau$ . The mean probability of branching per site,  $\bar{b}$ , is obtained by integrating  $b_\phi$  over the distribution of residence times and is:

$$\bar{b} = A/(A + \tau) \quad (2)$$

It is the purpose of this note to show how the *GF* method can be applied to Mullikin and Mortimer's improved model.

The derivation given in ref. 1 must be modified to take into account the dependence of branching probability on residence time. The expression (9) of that reference will represent the *GF* for all molecules derived from primary chains of *n* units and of age  $\phi$ , with the expression above for  $b_\phi$  substituted for *b*, that is:

$$u^n [e^{-A\phi} + zG(1 - e^{-A\phi})]^{zn} \quad (3)$$

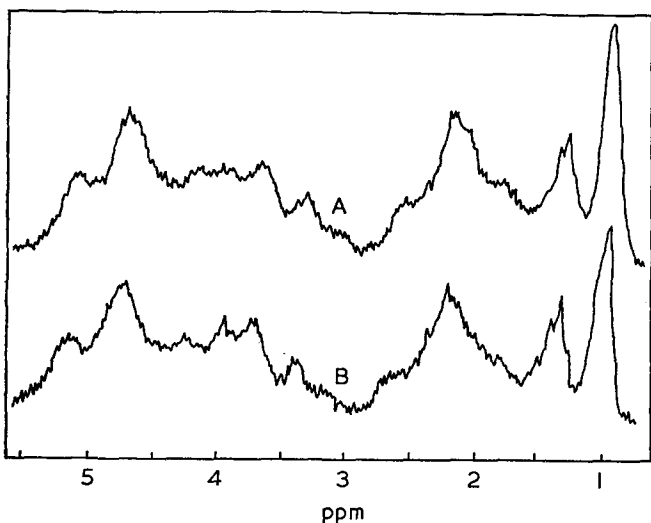


Figure 2 100 MHz p.m.r. spectra of high-sulphur wool fraction  $\gamma$ -keratose. A, in 50% DCOOD/50%  $\text{CDCl}_3$  solution; B, in DCOOD solution

a smaller but substantial increase. The implication that U.S.3 retains appreciable helicity in DCOOD is consistent with Harrap's observation<sup>12</sup> that  $b_0 = -100^\circ$ , corresponding to 15% helix content, for another low-sulphur protein, *S*-carboxymethylkeratine (SCMKA). Despite somewhat different  $b_0$  values, the p.m.r. linewidths for U.S.3 and  $\gamma$ -keratose in DCOOD are closely similar, suggesting that at lower helicities amino acid overlap may have more influence on the appearance of the spectrum than changes in rotational freedom. In all DCOOD/ $\text{CDCl}_3$  mixtures examined, the p.m.r. spectra of U.S.3 sharpened with increase of temperature to 339K, while some of the  $\alpha$ -CH resonances shifted downfield, corresponding to a reduction in helix content; when the sample was cooled to 302K, some of the lost helicity

appears to be recovered. These results are consistent with the view that the low-sulphur proteins are extracted from the helical wool fibrils, while the high-sulphur materials emanate from the amorphous matrix region<sup>14</sup>.

#### ACKNOWLEDGEMENTS

The samples of  $\alpha$ -keratose, U.S.3, and  $\gamma$ -keratose were kindly provided by Dr J. C. Fletcher; we are grateful to Dr D. N. Jones for facilitating o.r.d. measurements and to the Wool Industries Research Association for financial support to B.J.D.

#### REFERENCES

- 1 Rowe, J. J. M., Hinton, J. and Rowe, K. L. *Chem. Rev.* 1970, **70**, 1
- 2 Sheard, B. and Bradbury, E. M. *Prog. Biophys. Mol. Biol.* 1970, p 187
- 3 Roberts, G. C. K. and Jardetzky, O. *Adv. Protein Chem.* 1970, **25**, 447
- 4 Bovey, F. A. 'High resolution n.m.r. of macromolecules', Academic Press, New York, 1972
- 5 Bartle, K. D., Jones, D. W. and L'Amie, R. *Studia Biophys.* 1969, **13**, 53
- 6 Bartle, K. D., Jones, D. W. and L'Amie, R. *Appl. Polym. Symp.* 1971, **18**, 85
- 7 Bradbury, J. H. and King, N. L. R. *Aust. J. Chem.* 1969, **22**, 1083
- 8 Moffitt, W. and Yang, J. T. *Proc. Natl Acad. Sci. USA* 1956, **42**, 596
- 9 Corfield, M. C., Fletcher, J. C. and Robson, A. in 'Symposium on Fibrous Proteins, Australia, 1967', (Ed. W. G. Crewther). Butterworths, Sydney, 1968, p 299
- 10 Davies, D. R. *J. Mol. Biol.* 1964, **9**, 605
- 11 Bradbury, E. M., Crane-Robinson, C. and Rattle, H. W. E. *Polymer* 1970, **11**, 277
- 12 Harrap, B. S. *Aust. J. Biol. Sci.* 1963, **16**, 231
- 13 Gillespie, J. M. and Harrap, B. S. *Aust. J. Biol. Sci.* 1963, **16**, 252
- 14 Bendit, E. G. *Text. Res. J.* 1968, **38**, 15

## Effects of long branching on distribution of degree of polymerization: 2

P. A. Small

Department of Chemistry, University of Manchester, Manchester M13 9PL, UK  
(Received 18 June 1973)

The method of generating functions (*GF*) has been applied<sup>1</sup> to calculate the moments of the distribution for a model described by Mullikin and Mortimer<sup>2</sup> characterized by the assumption of two constant probabilities, one (*p*) for addition of a further monomer unit, and one (*b*) for branching at each potential site. There are  $\alpha$  equivalent sites per monomer unit in the polymer; termination by combination is assumed absent.

Mullikin and Mortimer have now<sup>3</sup> calculated the first and second moments, and the ratio of the weight-average degree of polymerization to the number average, for a more realistic model which should well represent a perfectly stirred continuous-flow reaction system. In this improved model the probability of branching  $b_\phi$  depends upon the time of residence in the reactor,  $\phi$ , through the relation<sup>3</sup>:

$$b_\phi = 1 - e^{-A\phi} \quad (1)$$

while the probability of residence has the usual negative exponential dependence on  $\phi$  with a rate constant  $\tau$ . The mean probability of branching per site,  $\bar{b}$ , is obtained by integrating  $b_\phi$  over the distribution of residence times and is:

$$\bar{b} = A/(A + \tau) \quad (2)$$

It is the purpose of this note to show how the *GF* method can be applied to Mullikin and Mortimer's improved model.

The derivation given in ref. 1 must be modified to take into account the dependence of branching probability on residence time. The expression (9) of that reference will represent the *GF* for all molecules derived from primary chains of *n* units and of age  $\phi$ , with the expression above for  $b_\phi$  substituted for *b*, that is:

$$u^n [e^{-A\phi} + zG(1 - e^{-A\phi})]^{zn} \quad (3)$$

and the  $GF$  for all molecules from such primary chains is obtained by integrating this expression over the distribution of residence times:

$$u^n \int_0^\infty \tau e^{-\tau \phi} [e^{-A\phi} + zG(1 - e^{-A\phi})]^{an} d\phi \quad (4)$$

or writing  $e^{-A\phi} = x$ ,  $\tau/A = r$ :

$$ru^n \int_0^1 x^{r-1} [x + zG(1-x)]^{an} dx \quad (5)$$

The  $GF$  for all molecules  $G$  is obtained by summing this expression, multiplied by the probability that the primary chain has  $n$  units, over  $n$ . That is:

$$G = r(1-p) \sum_{n=1}^{\infty} p^{n-1} u^n \int_0^1 x^{r-1} [x + zG(1-x)]^{an} dx \quad (6)$$

$r$  is related to  $\bar{b}$  by the expression:

$$r = (1/\bar{b}) - 1 \quad (7)$$

so that as  $\bar{b} < 1$ ,  $r > 0$ . It is possible to obtain expressions for the right-hand side of equation (6) in terms of Gaussian hypergeometric functions, but these are not very useful. The moments of the distribution are obtained<sup>1</sup> from the derivatives of  $G(u, z)$  with respect to  $u$  and  $z$  at  $u = z = 1$ ;  $G(1, 1) = 1$  of course. It is legitimate to differentiate equation (6) under the summation and integration signs, and set  $u = z = 1$  before carrying out the integration

and summation; the integrations then reduce to cases of standard result:

$$\int_0^1 x^{r-1} (1-x)^{s-1} dx = \Gamma(r)\Gamma(s)/\Gamma(r+s) \quad (8)$$

when  $r > 0$ ,  $s > 0$ .

This procedure gives for the first and second moments  $\langle m \rangle$  and  $\langle m^2 \rangle$ ,

$$\langle m \rangle = \partial G(1, 1)/\partial u = 1/(1-p-\alpha\bar{b}) \quad (9)$$

and

$$\langle m^2 \rangle = \partial^2 G(1, 1)/\partial u^2 + \partial G(1, 1)/\partial u \quad (10)$$

$$\begin{aligned} & \{(1+p)(1+\bar{b})(1-p-\bar{b})[1-p+(2\alpha-1)\bar{b}] \\ & + 2\bar{b}^2[\alpha^2(1+p)-\alpha(1-p)]\} \\ & = \frac{\quad}{(1-p-\alpha\bar{b})^3(1-p)(1+\bar{b})} \quad (11) \end{aligned}$$

In the case  $\alpha = 1$ , these expressions reduce to those given by Mullikin and Mortimer<sup>3</sup>. Expressions for the higher moments become complex, and will not be discussed here.

#### REFERENCES

- 1 Small, P. A. *Polymer* 1972, 13, 536
- 2 Mullikin, R. V. and Mortimer, G. A. *J. Macromol. Sci. (A)* 1970, 4, 1495
- 3 Mullikin, R. V. and Mortimer, G. A. *J. Macromol. Sci.* in press

## Electron spin resonance studies of spin-labelled polymers: Part 5. Synthesis and characterization of meta-labelled polystyrene

A. T. Bullock, G. G. Cameron and P. M. Smith

Department of Chemistry, University of Aberdeen, Old Aberdeen, AB9 2UE, UK  
(Received 17 May 1973)

Linewidth measurements on the electron spin resonance (e.s.r.) spectra of macromolecules carrying stable nitroxide radicals can yield information on the dynamics of the polymer chains. This spin-labelling technique has recently been used to study the motions of polystyrene both in dilute solution<sup>1,2</sup> and in the solid polymer<sup>3</sup>. The polystyrene samples used in these experiments were labelled with phenyl nitroxide<sup>1</sup> or *t*-butyl nitroxide<sup>2</sup> groups specifically at the *para*-position of the aromatic ring. The latter groups were attached by reaction of the *para*-lithiated polymer with 2-methyl-2-nitrosopropane<sup>4</sup>. However, for the complete and unambiguous interpretation of correlation times from spin-labelling studies it is desirable to compare correlation times when the polymer is labelled at different positions.

Lithiated polymers are convenient intermediates for the labelling reaction. It has been reported that direct metallation of polystyrene using butyl lithium complexed with *N,N,N',N'*-tetramethylethylenediamine (TMEDA) leads to *meta*-substitution in the aromatic ring<sup>5</sup>. This reaction therefore appeared to offer a convenient route to *meta*-labelled polystyrene, presenting at the same time a means of confirming the position of lithiation under these conditions.

In order to keep the degree of labelling small (to prevent spin-exchange effects) and to avoid undesirable side reactions the procedure developed by Chalk and

Hay<sup>6</sup>, to lithiate poly(phenylene ethers), was followed. 0.5 g polystyrene ( $\bar{M}_n = 126\,000$  with a broad molecular weight distribution) was dissolved in 50 ml dry benzene and added to a stirred mixture of 10 mmol *n*-BuLi and 10 mmol TMEDA in 20 ml dry hexane under nitrogen. The resulting orange coloured solution was stirred at room temperature for 30 min, then an excess (0.7 g) of 2-methyl-2-nitrosopropane in benzene was added. The product was precipitated from methanol, redissolved in toluene and shaken with silver oxide to ensure complete oxidation of the hydroxylamine to the nitroxide. The toluene solution was filtered and the labelled polymer was purified by repeated precipitations in methanol from toluene. During the work-up a small amount of gel appeared and was removed by filtration. The occurrence of some crosslinking was confirmed by gel permeation chromatography which showed an increased proportion of high molecular weight material in the labelled polymer.

The e.s.r. spectrum of the labelled polystyrene is shown in *Figure 1*. There is the usual marked dependence of linewidth on  $m_N$ , the <sup>14</sup>N magnetic quantum number, which permits evaluation of  $\tau_c$ , the rotational correlation time. The slight asymmetry in each of the three multiplets is caused by a weak linewidth dependence on  $m_H$ , the resultant proton magnetic quantum number. Each line of the nitrogen triplet shows a hyperfine proton structure of eight lines in the intensity ratio 1:1:3:3:3:3:1:1 as

and the  $GF$  for all molecules from such primary chains is obtained by integrating this expression over the distribution of residence times:

$$u^n \int_0^\infty \tau e^{-\tau \phi} [e^{-A\phi} + zG(1 - e^{-A\phi})]^{an} d\phi \quad (4)$$

or writing  $e^{-A\phi} = x$ ,  $\tau/A = r$ :

$$ru^n \int_0^1 x^{r-1} [x + zG(1-x)]^{an} dx \quad (5)$$

The  $GF$  for all molecules  $G$  is obtained by summing this expression, multiplied by the probability that the primary chain has  $n$  units, over  $n$ . That is:

$$G = r(1-p) \sum_{n=1}^{\infty} p^{n-1} u^n \int_0^1 x^{r-1} [x + zG(1-x)]^{an} dx \quad (6)$$

$r$  is related to  $\bar{b}$  by the expression:

$$r = (1/\bar{b}) - 1 \quad (7)$$

so that as  $\bar{b} < 1$ ,  $r > 0$ . It is possible to obtain expressions for the right-hand side of equation (6) in terms of Gaussian hypergeometric functions, but these are not very useful. The moments of the distribution are obtained<sup>1</sup> from the derivatives of  $G(u, z)$  with respect to  $u$  and  $z$  at  $u = z = 1$ ;  $G(1, 1) = 1$  of course. It is legitimate to differentiate equation (6) under the summation and integration signs, and set  $u = z = 1$  before carrying out the integration

and summation; the integrations then reduce to cases of standard result:

$$\int_0^1 x^{r-1} (1-x)^{s-1} dx = \Gamma(r)\Gamma(s)/\Gamma(r+s) \quad (8)$$

when  $r > 0$ ,  $s > 0$ .

This procedure gives for the first and second moments  $\langle m \rangle$  and  $\langle m^2 \rangle$ ,

$$\langle m \rangle = \partial G(1, 1)/\partial u = 1/(1-p-\alpha\bar{b}) \quad (9)$$

and

$$\langle m^2 \rangle = \partial^2 G(1, 1)/\partial u^2 + \partial G(1, 1)/\partial u \quad (10)$$

$$\begin{aligned} & \{(1+p)(1+\bar{b})(1-p-\bar{b})[1-p+(2\alpha-1)\bar{b}] \\ & + 2\bar{b}^2[\alpha^2(1+p)-\alpha(1-p)]\} \\ & = \frac{\quad}{(1-p-\alpha\bar{b})^3(1-p)(1+\bar{b})} \quad (11) \end{aligned}$$

In the case  $\alpha = 1$ , these expressions reduce to those given by Mullikin and Mortimer<sup>3</sup>. Expressions for the higher moments become complex, and will not be discussed here.

#### REFERENCES

- 1 Small, P. A. *Polymer* 1972, 13, 536
- 2 Mullikin, R. V. and Mortimer, G. A. *J. Macromol. Sci. (A)* 1970, 4, 1495
- 3 Mullikin, R. V. and Mortimer, G. A. *J. Macromol. Sci.* in press

## Electron spin resonance studies of spin-labelled polymers: Part 5. Synthesis and characterization of meta-labelled polystyrene

A. T. Bullock, G. G. Cameron and P. M. Smith

Department of Chemistry, University of Aberdeen, Old Aberdeen, AB9 2UE, UK  
(Received 17 May 1973)

Linewidth measurements on the electron spin resonance (e.s.r.) spectra of macromolecules carrying stable nitroxide radicals can yield information on the dynamics of the polymer chains. This spin-labelling technique has recently been used to study the motions of polystyrene both in dilute solution<sup>1,2</sup> and in the solid polymer<sup>3</sup>. The polystyrene samples used in these experiments were labelled with phenyl nitroxide<sup>1</sup> or *t*-butyl nitroxide<sup>2</sup> groups specifically at the *para*-position of the aromatic ring. The latter groups were attached by reaction of the *para*-lithiated polymer with 2-methyl-2-nitrosopropane<sup>4</sup>. However, for the complete and unambiguous interpretation of correlation times from spin-labelling studies it is desirable to compare correlation times when the polymer is labelled at different positions.

Lithiated polymers are convenient intermediates for the labelling reaction. It has been reported that direct metallation of polystyrene using butyl lithium complexed with *N,N,N',N'*-tetramethylethylenediamine (TMEDA) leads to *meta*-substitution in the aromatic ring<sup>5</sup>. This reaction therefore appeared to offer a convenient route to *meta*-labelled polystyrene, presenting at the same time a means of confirming the position of lithiation under these conditions.

In order to keep the degree of labelling small (to prevent spin-exchange effects) and to avoid undesirable side reactions the procedure developed by Chalk and

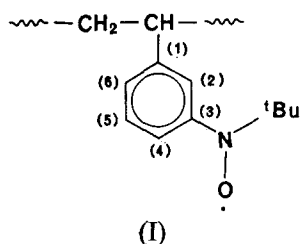
Hay<sup>6</sup>, to lithiate poly(phenylene ethers), was followed. 0.5 g polystyrene ( $\bar{M}_n = 126\,000$  with a broad molecular weight distribution) was dissolved in 50 ml dry benzene and added to a stirred mixture of 10 mmol *n*-BuLi and 10 mmol TMEDA in 20 ml dry hexane under nitrogen. The resulting orange coloured solution was stirred at room temperature for 30 min, then an excess (0.7 g) of 2-methyl-2-nitrosopropane in benzene was added. The product was precipitated from methanol, redissolved in toluene and shaken with silver oxide to ensure complete oxidation of the hydroxylamine to the nitroxide. The toluene solution was filtered and the labelled polymer was purified by repeated precipitations in methanol from toluene. During the work-up a small amount of gel appeared and was removed by filtration. The occurrence of some crosslinking was confirmed by gel permeation chromatography which showed an increased proportion of high molecular weight material in the labelled polymer.

The e.s.r. spectrum of the labelled polystyrene is shown in *Figure 1*. There is the usual marked dependence of linewidth on  $m_N$ , the <sup>14</sup>N magnetic quantum number, which permits evaluation of  $\tau_c$ , the rotational correlation time. The slight asymmetry in each of the three multiplets is caused by a weak linewidth dependence on  $m_H$ , the resultant proton magnetic quantum number. Each line of the nitrogen triplet shows a hyperfine proton structure of eight lines in the intensity ratio 1:1:3:3:3:3:1:1 as



would be expected from the radical<sup>4</sup>:

Figure 2a shows the central multiplet of Figure 1



expanded. Figure 2b shows a computer simulation of this multiplet, based on the radical I with three equivalent *ortho*- and *para*-protons having  $a_H = 5.0$  MHz and a single *meta*-proton having  $a_H = 2.5$  MHz. It is known that in small aryl nitroxides the coupling constants of protons in *ortho*- and *para*-positions to the nitroxide group are about twice those of *meta*-protons<sup>7</sup>.

The spectra in Figures 1 and 2 prove conclusively that the nitroxide groups occur at the *meta*-position of the aromatic ring. This supports the conclusion of Plate *et al.*<sup>5</sup>, based on infra-red evidence, that direct lithiation, being nucleophilic in nature, takes place at the *meta*-position in the aromatic nuclei in polystyrene.

Figure 1 yields a nitrogen coupling constant  $a_N = 35.6 \pm 0.3$  MHz, and an isotropic  $g$ -factor = 2.00589 (from centrepoint comparison with charred dextrose<sup>8</sup> for which  $g = 2.00259$ ). The  $g$ -factor and the nitrogen and proton coupling constants are very similar to those of the *para*-labelled polystyrene<sup>2</sup>. It can therefore be assumed that the anisotropic spin Hamiltonian parameters in the linewidth expression:  $T_2(m_N)^{-1} = A +$

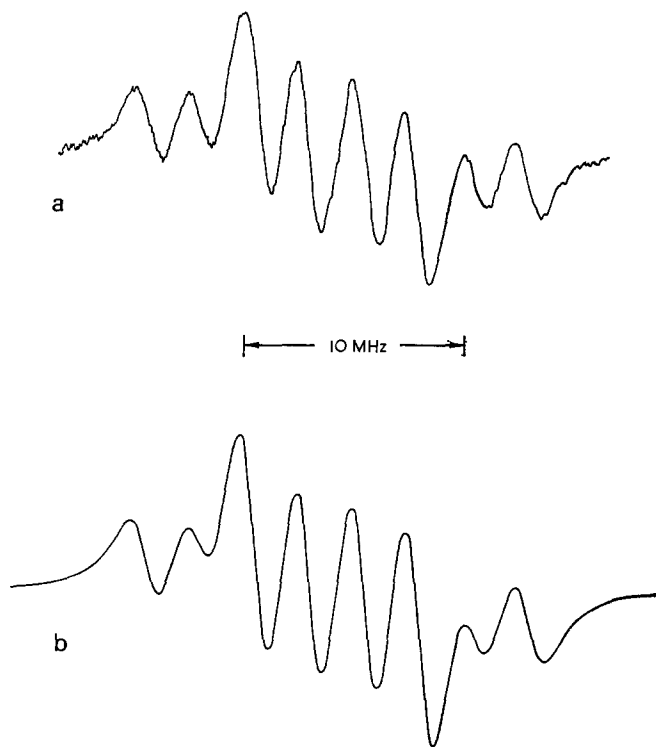


Figure 2 (a) Expanded central multiplet from Figure 1; (b) computer simulated multiplet

$Bm_N + Cm_N^2$  are similar. Consequently the parameters used for the line-width analysis of the *para*-labelled polymer<sup>2</sup> can be used to calculate a rotational correlation time for the *meta*-labelled polystyrene. This procedure yields  $\tau_c = (3.9 \pm 0.4) \times 10^{-10}$  sec at 52°C. The value for the corresponding *para*-labelled polymer is  $(3.2 \pm 0.3) \times 10^{-10}$  sec at 52°C. This concordance, within experimental error, lends further support to our earlier contention<sup>2</sup> that segmental re-orientation is the main factor controlling  $\tau_c$  in labelled polystyrenes of high molecular weight. Non-cooperative phenyl ring rotation or rotation about the C<sub>(3)</sub>-N bond do not significantly affect  $\tau_c$ .

#### ACKNOWLEDGEMENTS

P. M. S. gratefully acknowledges the award of a studentship from Imperial Chemical Industries Ltd. We are grateful to the Science Research Council for an equipment grant.

#### REFERENCES

- 1 Bullock, A. T., Butterworth, J. H. and Cameron, G. G. *Eur. Polym. J.* 1971, 7, 445
- 2 Bullock, A. T., Cameron, G. G. and Smith, P. M. *J. Phys. Chem.* 1973, 77, 1635
- 3 Bullock, A. T., Cameron, G. G. and Smith, P. M. *J. Polym. Sci. (A-2)* in press
- 4 Bullock, A. T., Cameron, G. G. and Smith, P. M. *Polymer* 1972, 13, 89
- 5 Plate, N. A., Jampolskaya, M. A., Davydova, S. L. and Kargin, V. A. *J. Polym. Sci. (C)* 1969, 22, 547
- 6 Chalk, A. J. and Hay, A. S. *J. Polym. Sci. (A-1)* 1969, 7, 691
- 7 Forrester, A. R., Hay, J. M. and Thomson, R. H. 'Organic Chemistry of Stable Free Radicals', Academic Press, London and New York, 1968, pp 202-203
- 8 Vana, N. J. and Unfried, E. *J. Magn. Resonance* 1972, 6, 655

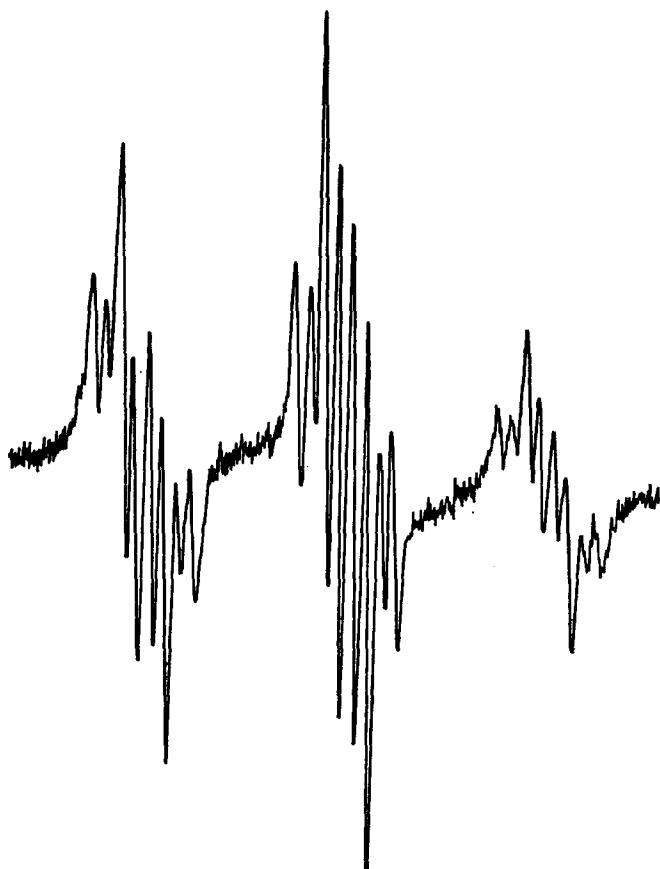
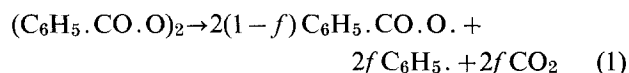


Figure 1 E.s.r. spectrum of spin-labelled polystyrene in toluene solution (5%) at 52°C

## Photo-dissociation of benzoyl peroxide

Studies of end-groups of polymer molecules have shown that there are some important differences between the natures of the radicals produced in thermal and photochemical dissociations of benzoyl peroxide in solution. It was shown<sup>1</sup> that thermally the peroxide molecules dissociate to pairs of benzoyloxy radicals some of which may dissociate further to phenyl radicals and carbon dioxide. It was deduced<sup>2</sup> that photochemical dissociation leads to the direct production of some phenyl radicals according to:



and that  $f$  is about 0.30 for a particular set of conditions.

These conclusions were reached by comparing the numbers of benzoyloxy and phenyl end-groups in polymers prepared using monomeric styrene at various concentrations in benzene. The ratio of these types of end-group varies with the concentration of monomer; extrapolation of the results to a system where the concentration of monomer is infinitely high showed that, if benzoyl peroxide were used as a thermal initiator, all the end-groups would be benzoyloxy groups because the primary radicals escaping cage recombination would be captured by monomer before they could possibly dissociate. In photochemical systems, however, the extrapolation indicated that polymers prepared at infinitely high concentration of monomer would contain an appreciable proportion of phenyl end-groups; it was argued that this result showed that some phenyl radicals are formed directly from the peroxide and not from benzoyloxy radicals.

The end-group analyses involved the use as initiator of benzoyl peroxide labelled in the rings with <sup>14</sup>C (R-peroxide). The sum of the number of benzoyloxy and phenyl end-groups was calculated directly from the specific activity of the purified polymer. The number of phenyl end-groups was found from the specific activity of the polymer after all the benzoyloxy end-groups had been detached by hydrolysis<sup>3</sup>.

If benzoyl peroxide could give rise to benzoyl end-groups, end-group analysis by the procedure just described would show them as phenyl end-groups because they would be unaffected by hydrolysis. It seems possible that the peroxide to some extent might dissociate photochemically according to:



If benzoyl peroxide labelled in the carboxyl groups with <sup>14</sup>C (C-peroxide) were used as a photoinitiator and if the resulting polystyrene contained some benzoyl end-groups, then hydrolysis of the polymer could not cause its specific activity to fall to zero as it does for

polystyrene prepared using C-peroxide as thermal initiator.

Experimental procedures were similar to those used previously<sup>2,3</sup>. The light source was a Hannoveria medium pressure Hg lamp and the light was filtered through Pyrex glass. Samples were assayed by scintillation counting in solution<sup>4</sup>.

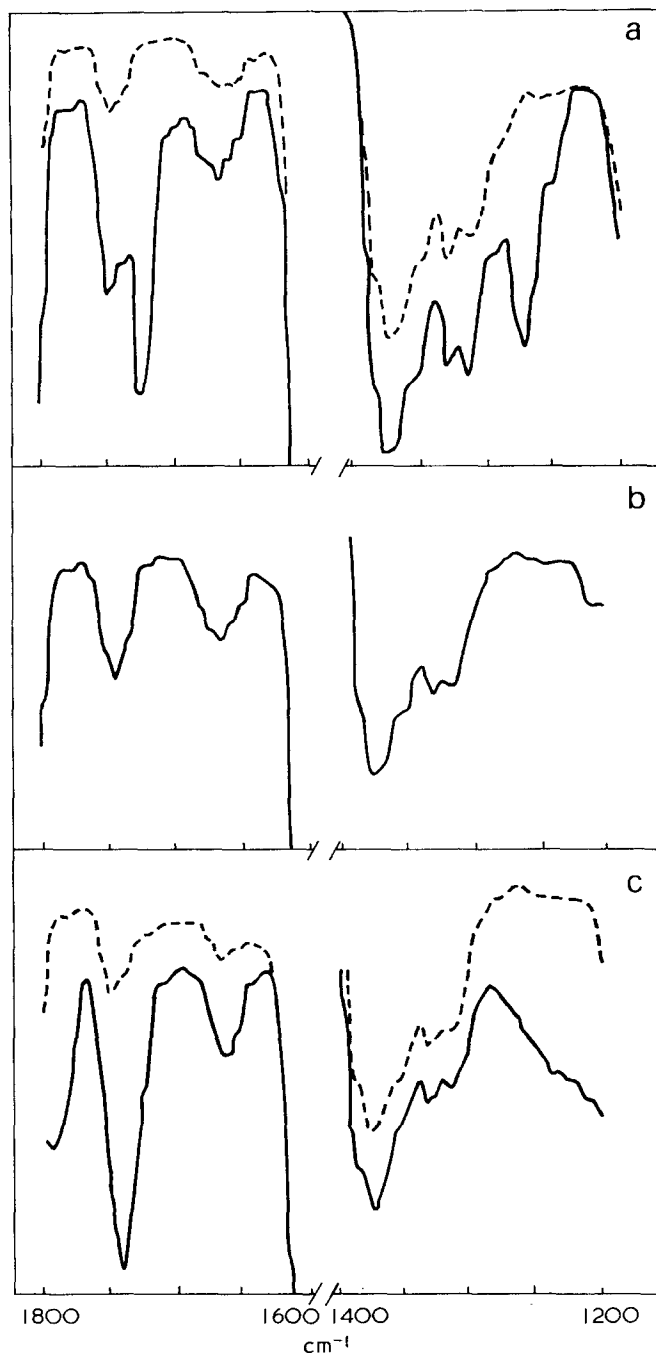


Figure 1 Infra-red spectra of polystyrene samples. (a) Using benzoyl peroxide as photoinitiator; (b) polymerized thermally without any initiator; (c) using benzoyl peroxide as thermal initiator (60°C), —, Before hydrolysis; ---, after hydrolysis

Previous results<sup>2</sup> were confirmed using R-peroxide as photoinitiator. Samples of polystyrene, prepared similarly with C-peroxide at 25°C with monomer at 8.37, 6.28, 4.19, 2.79 and 1.05 mol/l in benzene, retained 4.4, 3.1, 2.8, 4.3 and 4.5% respectively of their activity after hydrolysis. If these residual activities are attributed to benzoyl end-groups, it must be noted that these end-groups are much less numerous than benzoyloxy end-groups and that there are far too few to provide an alternative explanation of the results of Bevington and Lewis<sup>2</sup>.

Spectroscopic examination of samples of polystyrene, before and after hydrolysis, showed that absorption due to carbonyl groups was removed completely by the chemical treatment for polymers prepared using benzoyl peroxide either as a thermal- or as a photoinitiator (see Figure 1).

If benzoyl radicals were produced during the photolysis of benzoyl peroxide in pure benzene, appreciable further dissociation to phenyl radicals and carbon monoxide would be expected. Carbon monoxide could not be detected under these circumstances either by mass spectrometry or by tracer techniques (for C-peroxide).

It is concluded that there is no evidence for significant production of benzoyl radicals during photolysis of benzoyl peroxide in solution, at least for wavelengths exceeding about 3000 Å.

#### Acknowledgement

P. K. S. thanks the Royal Society for a Commonwealth Award.

P. K. SenGupta

On leave from:

Dept. of Applied Chemistry,  
University of Calcutta,  
Calcutta, India

and J. C. Bevington

Dept. of Chemistry,  
University of Lancaster,  
Lancaster, UK

(Received 11 August 1973)

#### References

- 1 Bevington, J. C. *Proc. R. Soc. (A)* 1957, **239**, 420
- 2 Bevington, J. C. and Lewis, T. D. *Trans. Faraday Soc.* 1958, **54**, 1340
- 3 Bevington, J. C. and Brooks, C. S. *J. Polym. Sci.* 1956, **22**, 257
- 4 Bevington, J. C. and Jemmett, J. A. L. *JCS Faraday Trans. I* 1973, **69**, 1866

## Book Review

### Identification and analysis of plastics

J. Haslam, H. A. Willis and D. C. M. Squirrel  
Iliffe Books, London, 1972, 748 pp. £18.00

This is a much enlarged and revised edition of the book first published in 1965. While all parts have been extended, the main changes are the inclusion of an introductory chapter on instrumental methods of analysis, and a number of n.m.r. reference spectra.

Throughout, very precise experimental details are given enabling it to be used as a laboratory handbook, often without referring to the original literature cited. Particularly useful details are comments on possible experimental errors, hazards involved, and in some cases addresses of suppliers for specialized chemicals and equipment.

The introductory chapter on instrumental methods, including u.v., visible, i.r. and atomic absorption spectrophotometry, X-ray fluorescence spectrometry, n.m.r. spectroscopy, and gas chromatography is followed by a chapter on the combined use of heating, burning and chemical tests and infra-red spectroscopy, in qualitative analysis, for which the use of n.m.r. is also exemplified. A useful table concerning polymer solubility is included.

Eight further chapters discuss in detail the analysis of particular types of polymers, and relevant additives. The arrangement of these chapters is slightly modified from that of the first edition, and increased reference is made to instrumental methods throughout. In their preface the authors explain that the areas covered are those in which they have practical experience, so that some are dealt with in greater depth than others. However, many specific methods given could be fairly readily adapted. Each chapter has an introduction detailing the particular types of analysis covered, followed by methods of chemical analysis, gas chromatography and special instrumental techniques, i.r. analysis, and finally n.m.r. analysis.

The final chapter discusses the analysis of plasticizers, fillers and solvents and some of the sophisticated methods necessary to separate complex mixtures of solvents are described.

As in the first edition the appendix contains an excellent collection of i.r. reference spectra. This collection has increased in size; an index to these spectra is a useful addition. Significant features in the spectra are described in the text, while a bibliography of other published i.r. spectra is also included.

Presentation of this edition is good although some typographical errors were found. In view of the size of the book a more detailed contents list would have been helpful, including some of the information given in the chapter introductions. However, after becoming familiar with the layout, most information could be found fairly readily. One anomaly is the treatment of information on polyurethanes, dealt with in three separate chapters.

This book is to be well recommended to any laboratories involved in the analysis of plastics. The authors make available their experience of many years, and the detailed methods and large collection of interpreted reference spectra are both invaluable. With the current availability of more sophisticated analytical methods, those already familiar with the first edition of this book are likely to find extra information, in this edition, to their advantage.

M. Gilbert

#### ERRATUM

'Some steric regulation on radical polymerization of perfluorobutadiene' by Madeline S. Toy and J. C. DiBari, *Polymer* 1973, **14**, 327-328.

Page 328, Table 2, caption:  
for monomer, 44.43 g read monomer, 4.43 g

We apologize for this error.

Previous results<sup>2</sup> were confirmed using R-peroxide as photoinitiator. Samples of polystyrene, prepared similarly with C-peroxide at 25°C with monomer at 8.37, 6.28, 4.19, 2.79 and 1.05 mol/l in benzene, retained 4.4, 3.1, 2.8, 4.3 and 4.5% respectively of their activity after hydrolysis. If these residual activities are attributed to benzoyl end-groups, it must be noted that these end-groups are much less numerous than benzoyloxy end-groups and that there are far too few to provide an alternative explanation of the results of Bevington and Lewis<sup>2</sup>.

Spectroscopic examination of samples of polystyrene, before and after hydrolysis, showed that absorption due to carbonyl groups was removed completely by the chemical treatment for polymers prepared using benzoyl peroxide either as a thermal- or as a photoinitiator (see Figure 1).

If benzoyl radicals were produced during the photolysis of benzoyl peroxide in pure benzene, appreciable further dissociation to phenyl radicals and carbon monoxide would be expected. Carbon monoxide could not be detected under these circumstances either by mass spectrometry or by tracer techniques (for C-peroxide).

It is concluded that there is no evidence for significant production of benzoyl radicals during photolysis of benzoyl peroxide in solution, at least for wavelengths exceeding about 3000 Å.

#### Acknowledgement

P. K. S. thanks the Royal Society for a Commonwealth Award.

P. K. SenGupta

On leave from:

Dept. of Applied Chemistry,  
University of Calcutta,  
Calcutta, India

and J. C. Bevington

Dept. of Chemistry,  
University of Lancaster,  
Lancaster, UK

(Received 11 August 1973)

#### References

- 1 Bevington, J. C. *Proc. R. Soc. (A)* 1957, **239**, 420
- 2 Bevington, J. C. and Lewis, T. D. *Trans. Faraday Soc.* 1958, **54**, 1340
- 3 Bevington, J. C. and Brooks, C. S. *J. Polym. Sci.* 1956, **22**, 257
- 4 Bevington, J. C. and Jemmett, J. A. L. *JCS Faraday Trans. I* 1973, **69**, 1866

## Book Review

### Identification and analysis of plastics

J. Haslam, H. A. Willis and D. C. M. Squirrel  
Iliffe Books, London, 1972, 748 pp. £18.00

This is a much enlarged and revised edition of the book first published in 1965. While all parts have been extended, the main changes are the inclusion of an introductory chapter on instrumental methods of analysis, and a number of n.m.r. reference spectra.

Throughout, very precise experimental details are given enabling it to be used as a laboratory handbook, often without referring to the original literature cited. Particularly useful details are comments on possible experimental errors, hazards involved, and in some cases addresses of suppliers for specialized chemicals and equipment.

The introductory chapter on instrumental methods, including u.v., visible, i.r. and atomic absorption spectrophotometry, X-ray fluorescence spectrometry, n.m.r. spectroscopy, and gas chromatography is followed by a chapter on the combined use of heating, burning and chemical tests and infra-red spectroscopy, in qualitative analysis, for which the use of n.m.r. is also exemplified. A useful table concerning polymer solubility is included.

Eight further chapters discuss in detail the analysis of particular types of polymers, and relevant additives. The arrangement of these chapters is slightly modified from that of the first edition, and increased reference is made to instrumental methods throughout. In their preface the authors explain that the areas covered are those in which they have practical experience, so that some are dealt with in greater depth than others. However, many specific methods given could be fairly readily adapted. Each chapter has an introduction detailing the particular types of analysis covered, followed by methods of chemical analysis, gas chromatography and special instrumental techniques, i.r. analysis, and finally n.m.r. analysis.

The final chapter discusses the analysis of plasticizers, fillers and solvents and some of the sophisticated methods necessary to separate complex mixtures of solvents are described.

As in the first edition the appendix contains an excellent collection of i.r. reference spectra. This collection has increased in size; an index to these spectra is a useful addition. Significant features in the spectra are described in the text, while a bibliography of other published i.r. spectra is also included.

Presentation of this edition is good although some typographical errors were found. In view of the size of the book a more detailed contents list would have been helpful, including some of the information given in the chapter introductions. However, after becoming familiar with the layout, most information could be found fairly readily. One anomaly is the treatment of information on polyurethanes, dealt with in three separate chapters.

This book is to be well recommended to any laboratories involved in the analysis of plastics. The authors make available their experience of many years, and the detailed methods and large collection of interpreted reference spectra are both invaluable. With the current availability of more sophisticated analytical methods, those already familiar with the first edition of this book are likely to find extra information, in this edition, to their advantage.

M. Gilbert

#### ERRATUM

'Some steric regulation on radical polymerization of perfluorobutadiene' by Madeline S. Toy and J. C. DiBari, *Polymer* 1973, **14**, 327-328.

Page 328, Table 2, caption:  
for monomer, 44.43 g read monomer, 4.43 g

We apologize for this error.

# The far infra-red spectrum (400–10 cm<sup>-1</sup>) of isotactic polypropylene

M. Goldstein and M. E. Seeley

*Department of Chemistry, The Polytechnic of North London, Holloway Road, London N7 8DB, UK*

and H. A. Willis and V. J. I. Zichy

*Imperial Chemical Industries Limited, Plastics Division, Welwyn Garden City, Herts, UK*  
(Received 4 May 1973)

Infra-red spectra of isotactic polypropylene samples having different crystallinity have been observed in the range 400 to 10cm<sup>-1</sup>. Eleven bands have been identified, whereas only eight internal modes are predicted for this region on the basis of line group symmetry. Experimental evidence, including dichroic behaviour of the bands, indicates that contrary to previous reports one of these additional features arises from a lattice mode and the others from the effect of crystal symmetry.

## INTRODUCTION

In the  $\alpha$ -crystalline form, the isotactic polypropylene (IPP) chain assumes a helical conformation (with three monomer units in one turn of the helix) having  $C_3$  line group symmetry<sup>1</sup>. The far infra-red spectrum of IPP has been recorded previously by several authors<sup>2-5</sup> and assigned in terms of normal coordinate analyses based on the  $C_3$  line group<sup>2-4,6-8</sup>. These results are summarized in *Table 1*. It may be noted that there is considerable disagreement amongst previous workers in the observation and assignment of the spectrum below  $\sim 260$  cm<sup>-1</sup>. There are two principal reasons for this. First, samples previously examined do not appear to have been sufficiently crystalline for all the features in the spectrum to be well defined. Secondly, no detailed account has been taken hitherto of the space group symmetry, i.e. of the possible effects of site symmetry, correlation splitting, or the occurrence of lattice modes. We consider the importance of these points in the discussion.

## EXPERIMENTAL

Highly isotactic (from n.m.r. measurements) polypropylene powder of medium molecular weight (melt-flow index=20) was pressed between stainless-steel plates, with aluminium release sheets, at a temperature of  $\sim 180^\circ\text{C}$  for 5 min at  $\sim 15\,000$  lbf/in<sup>2</sup> pressure ( $\sim 100$  MN/m<sup>2</sup>). The sample was then rapidly cooled to  $\sim 30^\circ\text{C}$  by passing water through the platens. These samples were 3.2 mm thick and between 58 and 66% crystalline.

The crystallinity of the sample was increased by annealing under oxygen-free nitrogen (to prevent oxidation), the general conditions for which have been described<sup>9</sup>. The actual sequence used in the present work was as follows: (i) heating to  $150^\circ\text{C}$  at a rate of  $20^\circ\text{C/h}$ ; (ii) heating from 150 to  $162^\circ\text{C}$  at a rate of  $1^\circ\text{C/h}$ ; (iii) maintaining the temperature at  $162^\circ\text{C}$  for  $\sim 20$  min; (iv) cooling to ambient temperature at a rate of  $6^\circ\text{C/h}$ . The crystallinity of the final product increases with the time for which the sample is held at  $162^\circ\text{C}$  [stage (iii)]. Samples of highest crystallinity which we examined

*Table 1* Summary of existing data (cm<sup>-1</sup>) on the far infra-red spectrum of isotactic polypropylene

Mode	Ref. 2		Ref. 3*		Ref. 4*		Ref. 5 $\nu(\text{obs.})$	Ref. 6* $\nu(\text{calc.})$	Ref. 7 $\nu(\text{calc.})$	Ref. 8 $\nu(\text{calc.})$
	$\nu(\text{calc.})$	$\nu(\text{obs.})$	$\nu(\text{calc.})$	$\nu(\text{obs.})$	$\nu(\text{calc.})$	$\nu(\text{obs.})$				
$\nu_{22}(A)$	381	398	371	398	375	396		391	392	392
$\nu_{23}(E)$	294	321	289	321	287	318	320	309	314	311
$\nu_{23}(A)$	266	251	245		249	248	248	260	272	267
$\nu_{24}(E)$	222	210					} 170		207	198
$\nu_{24}(A)$	216	200							203	195
$\nu_{25}(E)$	145	169	127		130	168	110†	138	162	147
$\nu_{25}(A)$	138	155	110		109		98†	118	157	140
$\nu_{26}(E)$	70	106					55		90	63

\* In these cases, simplified calculations were performed (ignoring torsional coordinates) so that fewer modes were calculated. We have re-numbered these according to the nearest equivalent vibrations used for the full model in refs. 2 and 8

† Resolved only at low temperatures ( $\sim 140$  K); broad band at  $103\text{cm}^{-1}$  at room temperature

had been treated at stage (iii) for 1 h and were 75% crystalline.

In order to obtain a sample of lower crystallinity, a thin ( $\sim 1$  mm) mould was used and the hot pressing rapidly quenched in a bath at  $-78^\circ\text{C}$ .

Crystallinities were determined by an X-ray diffraction method<sup>9</sup>, using a Philips PW 1010 diffractometer.

Preparation of a sufficiently well-oriented sample for the polarization measurements required the use of IPP powder of very high molecular weight (melt-flow index = 0.06)<sup>10</sup>. The optical quality and the draw ratio were improved by rolling the sample before drawing in a tensile testing machine. The crystallinity of the samples was subsequently increased by heat-setting under tension in an oven at  $150^\circ\text{C}$  for 10 min followed by slow cooling to ambient temperature. The sample obtained in this manner was 1.2 mm thick and had been extended 400%. It was shown to have a significant axial orientation from the parallel dichroism of the  $1044\text{cm}^{-1}$  doublet in the mid-infra-red spectral region. The occurrence of well-defined far infra-red bands indicated that the sample was also highly crystalline.

Spectra were recorded using RIIC FS-520 ( $400\text{--}60\text{cm}^{-1}$ ) and FS-720 ( $100\text{--}10\text{cm}^{-1}$ ) interferometers, the latter instrument at the PCMU, Harwell, UK. For the region  $100\text{--}10\text{cm}^{-1}$ , two or more pieces of sample, each 3.2 mm thick, were sandwiched together; dry liquid paraffin was placed between the pieces to eliminate interference fringes. For the polarized spectra, a polyethylene-backed grid polarizer was used. Loss of radiation by scattering from the oriented samples was severe, and in order to obtain polarized spectra with well defined bands, the following conditions were used: (i) the spectra were recorded with the samples cooled

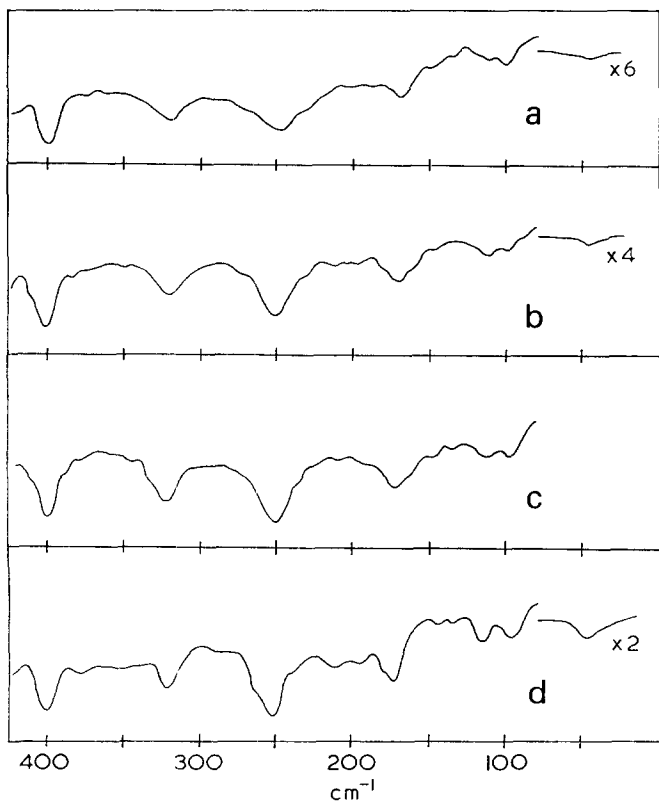


Figure 1 Far infra-red spectra of  $\alpha$ -IPP samples at room temperature. X-ray determined crystallinities are: (a) 58%; (b) 66%; (c) 70%; (d) 75%. For the region below  $80\text{cm}^{-1}$  the samples were increased in thickness (by layering) by the factors indicated

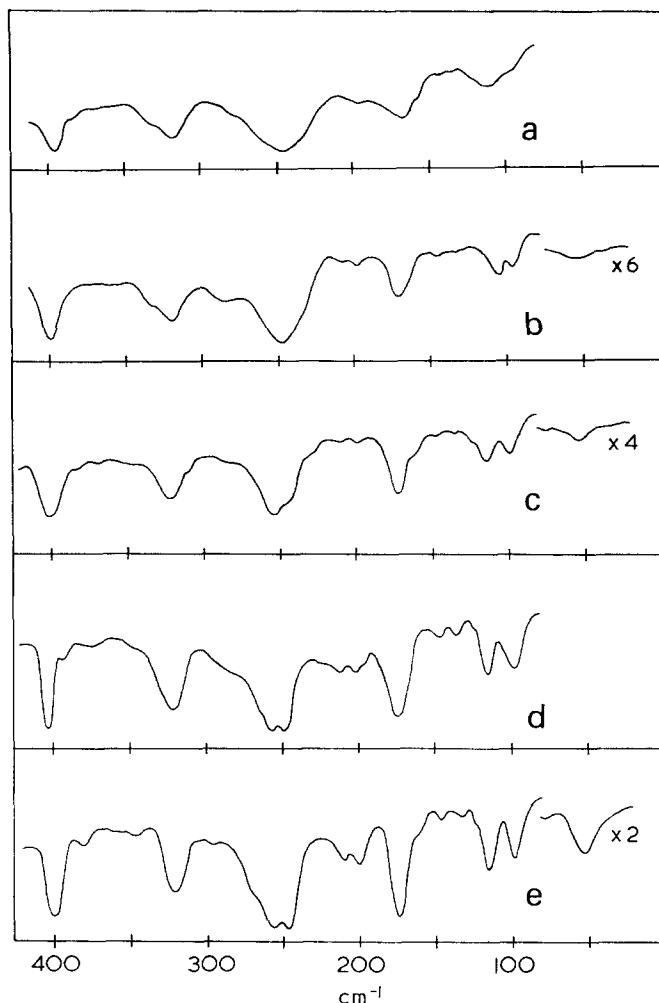


Figure 2 Far infra-red spectra of  $\alpha$ -IPP samples at  $\sim 100\text{K}$ . X-ray determined crystallinities are: (a) 52% (including 25% smectic form); (b) 58%; (c) 66%; (d) 70%; (e) 75%. For the region below  $80\text{cm}^{-1}$  the samples were increased in thickness (by layering) by the factors indicated

with liquid nitrogen; (ii) 3 or 4 pieces of drawn sample were sandwiched together with dry liquid paraffin to give a resultant thickness of 4–5 mm; (iii) ten spectra were obtained for each sample and then averaged to increase the signal:noise ratio. In this way, satisfactory spectra to  $\sim 80\text{cm}^{-1}$  were obtained.

## RESULTS

The spectra obtained in the region  $400\text{--}10\text{cm}^{-1}$  for samples of different crystallinity at ambient temperature and  $\sim 100\text{K}$  are shown in Figures 1 and 2. Bands observed are listed in Table 2. The intensity and sharpness of some of the bands is seen to increase markedly as the crystallinity of the specimen is increased. Two bands in particular, those at  $\sim 100\text{cm}^{-1}$  and  $\sim 50\text{cm}^{-1}$  show very interesting behaviour. The latter is not only seen to sharpen as one increases the crystallinity of the sample, but where the band maximum could be located with sufficient accuracy (crystallinities  $> 66\%$ ), it moves from 48 to  $55\text{cm}^{-1}$  as the temperature is lowered from ambient to  $\sim 100\text{K}$ . The band at  $\sim 100\text{cm}^{-1}$  is observed to split into two components as the temperature is decreased, the effect being most evident with the most highly crystalline samples at low temperature (e.g. for a

Table 2 Re-assignment of the infra-red spectrum of isotactic polypropylene in the region 400–10cm<sup>-1</sup>

$\nu(\text{obs.})$		Dichroism	Assignment†	$\nu(\text{calc.})^2$	Form of mode <sup>2‡</sup>
~300 K	~100 K				
400	400		$\nu_{22}(A)$	381	$\delta(\text{CH}_2\text{—CHMe—CH}_2)$ [45%, sym; 30%, asym]
321	321	⊥	$\nu_{23}(E)$	294	$\delta(\text{CH}_2\text{—CHMe—CH}_2)$ [65%, asym]
250	255		$\nu_{23}(A)$	266	$\delta(\text{CH}_2\text{—CHMe—CH}_2)$ [25%, sym; 30%, asym] and $\tau(\text{C—Me})$ [20%]
	245				
210	210	*	$\nu_{24}(E)$	222	$\tau(\text{C—Me})$ [95%]
198	198	*	$\nu_{24}(A)$	216	$\tau(\text{C—Me})$ [75%]
173	173	⊥	$\nu_{25}(E)$	145	$\delta(\text{CH}_2\text{—CHMe—CH}_2)$ [40%, asym] and $\delta(\text{CH—CH}_2\text{—CH})$ [35%]
145	145	*	$\nu_{25}(A)$	138	$\delta(\text{CH—CH}_2\text{—CH})$ [40%] and $\tau(\text{C—C}_{\text{eq}})$ [30%]
135	135				
100	113	⊥	$\nu_{26}(E)$	70	$\tau(\text{C—C}_{\text{ax}})$ [80%]
	98				
48	55	*	Lattice	—	—

\* Not possible to measure dichroism

† Symbols refer to C<sub>3</sub> line group modes

‡ Similar results given in refs 3–8, except torsional coordinates not always included

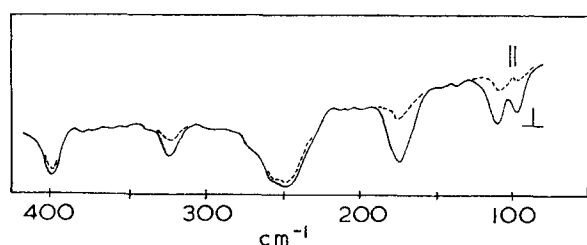


Figure 3 Polarized far infra-red spectra of oriented  $\alpha$ -IPP at ~100K. Symbols || and  $\perp$  correspond respectively to the electric vector of the radiation parallel and perpendicular to the direction in which the sample had been drawn

75% crystalline sample at ~100 K, the band resolves into components at 113 and 95 cm<sup>-1</sup>.

The dichroism of most of the bands in the region 400–80 cm<sup>-1</sup> was determined from polarization measurements carried out at ~100 K (Figure 3).

## DISCUSSION AND ASSIGNMENTS

Our assignments for IPP in the region 400–10 cm<sup>-1</sup> are listed in Table 2. From 400 to 160 cm<sup>-1</sup> our assignments of the main features are in agreement with those of previous workers<sup>2–5</sup>. Below 160 cm<sup>-1</sup> only two internal modes of the 3<sub>1</sub> helix are predicted to appear on the basis of a line group model (Table 1), viz.  $\nu_{26}(E)$  and the *A* component of  $\nu_{25}$ . However, we observe five bands in the region 160–10 cm<sup>-1</sup>. The most likely reasons for the appearance of the three extra bands are: (i) removal of the degeneracy of the *E* line group modes; (ii) correlation field splitting; and (iii) lattice modes.

The band at 48 cm<sup>-1</sup> has been previously assigned to an internal mode<sup>5</sup>. However, this can now quite clearly be seen to be wrong. There are two properties of this band which together provide compelling evidence for its assignment to an infra-red-active lattice mode: (a) the intensity of the band increases rapidly as the crystallinity of the sample is increased; (b) the band maximum shifts by 7 cm<sup>-1</sup> to higher frequency (55 cm<sup>-1</sup>) when the sample is cooled from room temperature to ~100 K.

The shift is considerably greater than is observed for any other band in the spectrum. The lattice modes which have been observed in other polymers (polyethylene<sup>11–16</sup>, polyoxymethylene<sup>17, 18</sup>, and polytetrafluoroethylene<sup>19</sup>), are generally characterized by shifts

to higher frequency of similar magnitude to that observed in the present work when the temperature of the sample is decreased. For example, the infra-red band at 72 cm<sup>-1</sup> in polyethylene at room temperature shifts by 7 cm<sup>-1</sup> to 79 cm<sup>-1</sup> on cooling to 100 K and has been assigned to one of the two predicted infra-red-active lattice modes ( $\nu_{11}$ ,  $B_{1u}$ )<sup>11</sup>. Hence the 48 cm<sup>-1</sup> band in IPP (room temperature value) is most likely an infra-red-active lattice mode, and not the internal mode  $\nu_{26}(E)$  as previously<sup>5</sup> thought.

In an attempt to define the nature of this lattice mode more precisely we have carried out a unit cell group analysis (commonly but erroneously<sup>20</sup> called factor group analysis), as described in the Appendix. It can be seen (Table 3) that five infra-red-active lattice-modes are predicted, two rotations ( $A_u + B_u$ ) and three translations ( $2A_u + B_u$ ), but it is not possible from our results to decide which gives rise to the 48 cm<sup>-1</sup> absorption band. We assume that the other four modes predicted to appear are either of inherently low intensity or are in too close proximity to the band observed to be resolved.

The second most noteworthy feature in the spectrum of IPP is the splitting of the band at ~100 cm<sup>-1</sup> into two components. This has been observed by previous workers who assigned the bands to the skeletal modes  $\nu_{25}(A)$  and  $\nu_{25}(E)$ <sup>5</sup>. This assignment is invalidated by our observation that both components have perpendicular dichroism\* (Table 2 and Figure 3). The separation of

\* We make the reasonable first-order approximation that the dichroism of the chain line group modes will be essentially unaffected by the influence of the crystal packing.

Table 3 Unit cell group analysis\* for isotactic  $\alpha$ -polypropylene in space group  $P2_1/c$  (isomorphous point group  $C_{2h}$ )

$C_{2h}$	$T'$	$T_A$	$T$	$R$	$n_L$	Activity
$A_g$	3	0	3	1	4	Raman
$B_g$	3	0	3	1	4	Raman
$A_u$	3	1	2	1	3	infra-red
$B_u$	3	2	1	1	2	infra-red

\*  $T'$ =total number of translational degrees of freedom;  $T_A$ =number of acoustic modes;  $T$ =number of optical translatory lattice modes ( $=T' - T_A$ );  $R$ =number of rotational lattice modes;  $n_L$ =total number of optical lattice modes ( $=T + R$ )

the two bands increases with increasing crystallinity of the sample, although the band positions are not observably dependent on temperature (providing the temperature is low enough for the splitting to be resolved). The similar behaviour of the two components of the doublet, especially their perpendicular dichroism, point to the origin of the component peaks being the same  $E$  line group internal chain mode. Since no lower frequency internal mode is found, this must be the lowest frequency chain mode calculated,  $\nu_{26}(E)$ .

The splitting could arise from either (a) a static field (site symmetry) effect [ $E(C_3$  line group) $\rightarrow 2A(C_1$  chain site)], or (b) a dynamic field (correlation splitting) effect. Possible effects are summarized in Table 4. The extent of splitting by either of these mechanisms is not easily predicted and in some cases it may be impossible to resolve the components. Thus observable splitting of some but not all  $E$  line group modes may occur. Correlation field splitting is expected to be more significant for vibrations of groups at the periphery of the chains. Examples of this are found in polyethylene ( $CH_2$  bending and rocking modes)<sup>13,21,22</sup>, and in  $\alpha$ -[CoCl<sub>2</sub>(pyridine)<sub>2</sub>]<sub>n</sub> (Co-N stretching modes)<sup>23</sup>. In IPP,  $\nu_{26}(E)$  is thought to be largely a mode of the polymer backbone ( $CH_2$ - $CHCH_3$  torsion)<sup>2,7,8</sup>, and will therefore involve appreciable motion of the  $CH_3$  groups. However, there does not appear to be any compelling evidence for distinguishing between static and dynamic field effects being the cause of the crystal field splitting of this mode.

The only other observed bands unaccounted for are those at 135 and 145  $cm^{-1}$ . We consider these too high in frequency to be lattice modes, and moreover they do not shift with decreasing temperature. The only internal chain mode remaining unassigned is the  $\nu_{25}(A)$  line group mode, calculated<sup>2</sup> to be at 138  $cm^{-1}$ . Since this  $A$  mode cannot split by a site symmetry effect, we attribute the 135, 145  $cm^{-1}$  pair of bands to the correlation-split  $\nu_{25}(A)$  line group mode. Unfortunately, these bands were too weak for their dichroism to be reliably determined, so that support for this assignment is at present lacking.

We note also that the band at 250  $cm^{-1}$ , assigned previously to the  $\nu_{23}(A)$  line group mode<sup>2,4,5</sup> (an assignment with which we concur), is also split in the spectra of highly crystalline samples at low tempera-

tures. Both components have parallel dichroism and the splitting, as in the case of that of  $\nu_{25}(A)$ , is therefore attributed to a correlation field effect.

#### ACKNOWLEDGEMENTS

We thank the SRC for a grant to purchase the FS-520 interferometer and for use of the PCMU (Harwell) service, Dr E. Gillam (City of London Polytechnic) for X-ray powder diffractometer facilities, and several colleagues for useful discussion.

#### REFERENCES

- Natta, G. and Corradini, P. *Nuovo Cim. Suppl.* 1960, **15**, 40
- Miyazawa, T., Fukushima, K. and Ideguchi, Y. *J. Polym. Sci. (B)* 1963, **1**, 385
- Miyazawa, T., Ideguchi, Y. and Fukushima, K. *J. Chem. Phys.* 1963, **38**, 2709
- Tadokoro, H., Kobayashi, M., Ukita, M., Yasufukum, K. and Murahashi, S. *J. Chem. Phys.* 1965, **42**, 1432
- Chantry, G. W., Fleming, J. W., Pardoe, G. W. F., Reddish, W. and Willis, H. A. *Infrared Phys.* 1971, **11**, 109
- Miyazawa, T. and Ideguchi, Y. *Bull. Chem. Soc. Japan* 1963, **36**, 1125
- Miyazawa, T. and Ideguchi, Y. *Bull. Chem. Soc. Japan* 1964, **37**, 1065
- Snyder, R. G. and Schachtschneider, J. H. *Spectrochim. Acta* 1964, **20**, 853
- Turner-Jones, A., Aizlewood, J. M. and Beckett, D. R. *Makromol. Chem.* 1964, **75**, 134
- Vincent, P. I. personal communication
- Bertie, J. E. and Whalley, E. *J. Chem. Phys.* 1964, **41**, 575
- Dean, G. D. and Martin, D. H. *Chem. Phys. Lett.* 1967, **1**, 415
- Tasumi, M. and Krimm, S. *J. Chem. Phys.* 1967, **46**, 755
- Bank, M. I. and Krimm, S. *J. Appl. Phys.* 1968, **39**, 4951
- Fleming, J. W., Chantry, G. W., Turner, P. A., Nicol, E. A., Willis, H. A. and Cudby, M. E. A. *Chem. Phys. Lett.* 1972, **17**, 84
- Krimm, S. and Bank, M. I. *J. Chem. Phys.* 1965, **42**, 4059
- Zerbi, G. and Masetti, G. *J. Mol. Spectros.* 1967, **22**, 284
- Boerio, F. J. and Cornell, D. D. *J. Chem. Phys.* 1972, **56**, 1516
- Chantry, G. W., Fleming, J. W., Nicol, E. A., Willis, H. A. and Cudby, M. E. A. *Chem. Phys. Lett.* 1972, **16**, 141
- Bertie, J. E. and Bell, J. W. *J. Chem. Phys.* 1971, **54**, 160
- Krimm, S., Liang, C. Y. and Sutherland, G. B. B. M. *J. Chem. Phys.* 1956, **25**, 549
- Tasumi, M. and Shimanouchi, T. *J. Chem. Phys.* 1965, **43**, 1245
- Goldstein, M. and Unsworth, W. D. *Inorg. Chim. Acta* 1970, **4**, 342
- Mencik, Z. *J. Macromol. Sci. (B)* 1972, **1**, 101
- Adams, D. M. and Newton, D. C. 'Tables for Factor Group and Point Group Analysis', Beckman-RIIC, London, 1970

#### APPENDIX

##### Unit cell group analysis

Two different space groups have been assigned to the  $\alpha$ -modification of IPP depending on the pre-treatment of the sample<sup>1,9,24</sup>. Unoriented but highly crystalline samples belong to space group  $C2/c$  ( $C_{2h}^6$ , No. 15)<sup>1,9</sup>, whereas for oriented fibres the space group symmetry is  $P2_1/c$  ( $C_{2h}^5$ , No. 14)<sup>24</sup>. The ideal  $P2_1/c$  unit cell contains four chains each with a particular combination of screw sense (left- or right-handed screws) and direction ('up' or 'down' with respect to the C- $CH_3$  direction). Randomization of these orientations among unit cells gives rise to the  $C2/c$  structure. This randomization is not expected to influence the number of lattice modes since each individual chain must be specifically oriented and randomization of orientation from one unit cell

Table 4 Correlation between chain line group, chain site group, and unit cell group for  $\alpha$ -IPP\*

Line group ( $C_3$ )	Site group ( $C_1$ )	Unit cell group ( $C_{2h}$ )
A	A	$A_g$
		$B_g$
		$A_u$
		$B_u$
E	2A	$2A_g$
		$2B_g$
		$2A_u$
		$2B_u$

\* Based on space group  $P2_1/c$  ( $z=4$ )



to the next will not affect the number of modes arising from individual cells. Consequently, it is appropriate to carry out the unit cell analysis in the idealized space group  $P2_1/c$ .

The analysis has been made using published tables<sup>25</sup>. The isomorphous point group is  $C_{2h}$  and each chain is in a general position in the crystal (Wyckoff 'e' sites) with a polymer chain site of  $C_1$ . The total number of translatory degrees of freedom is given by row 4E of Table 2 in ref. 25:

$$T' = 3A_g + 3B_g + 3A_u + 3B_u$$

This representation includes acoustic modes ( $A_u + 2B_u$ ) obtained from the  $C_{2h}$  character table. Hence the optical translations are given as:

$$T = 3A_g + 3B_g + 2A_u + B_u$$

The rotatory lattice modes are given directly from row 4E of Table 4 in ref. 25:

$$R = A_g + B_g + A_u + B_u.$$

The combined results are shown in Table 3.

# Synthesis and conformation studies of copolypeptides composed of $\gamma$ -methyl-L-glutamate and $\epsilon$ -N-carbobenzyloxy-L-lysine

Toshio Hayashi and Akio Nakajima

Department of Polymer Chemistry, Kyoto University, Sakyo-ku, Kyoto, Japan  
(Received 7 May 1973; revised 11 June 1973)

Copolypeptides (PMGCL) composed of  $\gamma$ -methyl-L-glutamate (MLG) and  $\epsilon$ -N-carbobenzyloxy-L-lysine (CBL) covering the whole range of copolymer composition were synthesized by the *N*-carboxyanhydride (NCA) method. The experimentally obtained monomer reactivity ratios were  $r_1(\text{MLG}) = 2.0 \pm 0.4$  and  $r_2(\text{CBL}) = 0.5 \pm 0.1$ , from which the fractions of monomer dyads and triads in copolymer were plotted against the initial comonomer composition. From experimental results on thermally induced coil-to-helix transition of the copolypeptides in dichloroacetic acid/1,2-dichloroethane (DCA-DCE) systems, it has been found that these copolypeptides can exist in the  $\alpha$ -helix conformation in the same manner as homopolypeptides PMLG and PCBL. The van't Hoff heat of transition  $\Delta H$  showed a minimum against the initial monomer composition. The enthalpy  $\Delta H_{\text{res}}$  of formation of intramolecular hydrogen bonds per peptide bond also showed a minimum against copolymer composition. Such behaviour on  $\Delta H$  and  $\Delta H_{\text{res}}$  was also found for copolypeptide (PBGCL) composed of  $\gamma$ -benzyl-L-glutamate (BLG) and  $\epsilon$ -N-carbobenzyloxy-L-lysine (CBL) in DCA-DCE systems reported in a previous paper. The presence of a minimum in these relationships may be attributed to specific interactions between the side chain of one comonomer and that of the other comonomer in a two component copolymer. It is also pointed out that these copolymer molecules can exist in the  $\alpha$ -helix conformation in the solid state.

## INTRODUCTION

In previous papers, we have reported the molecular conformation of copolypeptides<sup>1,2</sup> composed of  $\gamma$ -benzyl-L-glutamate (BLG) and  $\gamma$ -methyl-L-glutamate (MLG), homopolypeptides PMLG<sup>3</sup> and poly( $\epsilon$ -N-carbobenzyloxy-L-lysine) (PCBL)<sup>4</sup>, and copolypeptide<sup>5</sup> composed of BLG and CBL.

In this paper, we are concerned with copolypeptides composed of MLG and CBL. The transition temperature of homopolypeptide PMLG<sup>3</sup> is different from that of PCBL<sup>4</sup> in the same solvent composition system; hence, it is necessary to use various solvent mixtures in order to bring about the transition to a definite and available temperature range.

Copolypeptides (PMGCL) of MLG and CBL, covering monomer ratio in copolymer chain from 0 to 1 were synthesized by the *N*-carboxyanhydride (NCA) method initiated by triethylamine (TEA). TEA is known to yield polypeptides with high degrees of polymerization. Results obtained on the present systems for PMGCL will be compared with those<sup>5,6</sup> for copolypeptide PBGCL composed of BLG and CBL. Thermal transition of PMGCL will be discussed in comparison with that of PBGCL<sup>5</sup>.

## EXPERIMENTAL

### Materials

The monomers, *N*-carboxy- $\gamma$ -methyl-L-glutamate anhydride (MLG-NCA) and *N*-carboxy- $\epsilon$ -N-carbobenzyloxy-L-lysine anhydride (CBL-NCA) were prepared according to the method proposed by Blout and Karlson<sup>7</sup>, and purified by repeated recrystallizations from an ethyl acetate solution with the addition of petroleum ether. The MLG-NCA and CBL-NCA, in desired mole ratios, were dissolved in a 1:1 (v/v) mixture of dry dioxane and methylene dichloride. The total concentration of both anhydrides was kept at 2%. The polymerization was initiated with TEA at an anhydride: initiator ratio ( $[M]/[I]$ ) of 100. The polymerization was completed within about 48 h at 25°C.

Samples in Table 1 were obtained at a lower conversion rate so as to estimate the monomer reactivity ratios. The copolypeptides formed were precipitated in a large amount of cold methanol to eliminate the low

oxy-L-lysine anhydride (CBL-NCA) were prepared according to the method proposed by Blout and Karlson<sup>7</sup>, and purified by repeated recrystallizations from an ethyl acetate solution with the addition of petroleum ether. The MLG-NCA and CBL-NCA, in desired mole ratios, were dissolved in a 1:1 (v/v) mixture of dry dioxane and methylene dichloride. The total concentration of both anhydrides was kept at 2%. The polymerization was initiated with TEA at an anhydride: initiator ratio ( $[M]/[I]$ ) of 100. The polymerization was completed within about 48 h at 25°C.

Table 1 Copolymerization of  $\gamma$ -methyl-L-glutamate (MLG) with  $\epsilon$ -N-carbobenzyloxy-L-lysine (CBL) by the NCA method

Sample No.	Initial monomer ratio (CBL mol %)	Polymer composition (CBL mol %)	Conv. (%)	$[\eta]$ (DCA, 25°C) (dl/g)	$M_n$
1	100.0	100.0	58	1.70	143 000
2	85.5	76.5	44	0.98	
3	70.0	58.5	41	0.88	
4	45.5	34.5	20	0.65	51 000
5	44.5	34.0	44	0.90	80 000
6	45.0	35.5	55	1.55	157 000
7	36.0	27.5	38	1.15	
8	25.5	18.0	40	1.33	
9	0.0	0.0	57	1.69	123 000

molecular weight fraction and dried under reduced pressure at 50°C. The composition of these copoly-peptides was determined from elemental analyses for N, C and H atoms. These elemental analyses were carried out in the Organic Microanalyses Center in Kyoto University.

#### Measurements

The intrinsic viscosity  $[\eta]$  (dl/g) of PMGCL was determined in DCA at 25°C using Ubbelohde type capillary viscometers. The experimentally determined monomer ratio in the copolymer and the composition of the initial monomer mixture, together with the intrinsic viscosity  $[\eta]$ , are summarized in Table 1. The number-average molecular weights of some PMGCL samples were determined by osmotic pressure measurements in dimethylformamide (DMF) at 30°C and the results are also listed in Table 1.

Infra-red absorption spectra of solid films of the samples cast from chloroform solution were measured with a Perkin-Elmer Model 521 spectrophotometer in the region of 400–4000  $\text{cm}^{-1}$ .

Optical rotatory dispersion (o.r.d.) in a temperature range from 5 to 50°C was measured with a Yanagimoto OR-100 Type spectropolarimeter using a tungsten lamp as light source. The concentration of copolymer solution was 1.0 g/dl throughout these measurements. The solvent system used was a mixture of DCA–DCE.

## RESULTS AND DISCUSSION

#### Monomer reactivity ratios

Figure 1 illustrates the copolymer composition curve for the copolymerization of MLG with CBL at a conversion level of about 40%, taken from the data in Table 1. Figure 2 shows the MLG mol % in copolymer against the polymer conversion for the system initially containing 55 mol % MLG. To estimate the monomer reactivity ratios  $r_1$ (MLG) and  $r_2$ (CBL), the polymerization should be generally stopped at low conversions

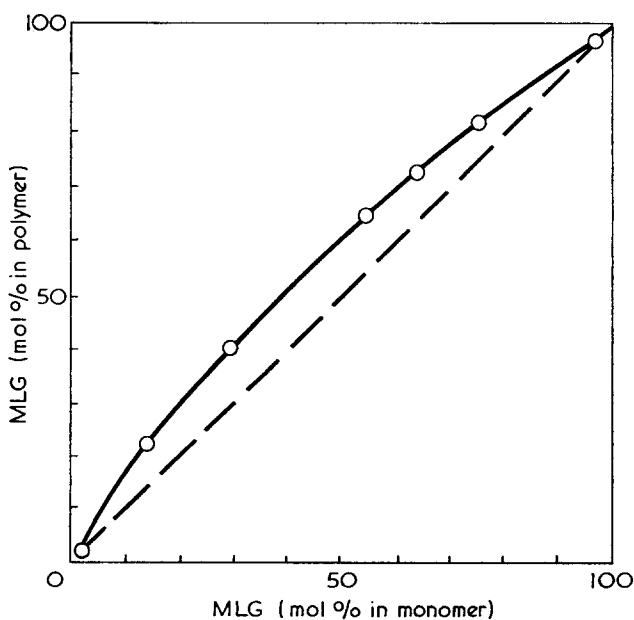


Figure 1 Copolymer composition curve for PMGCL copolymer at about 40% conversion. Data are taken from Table 1

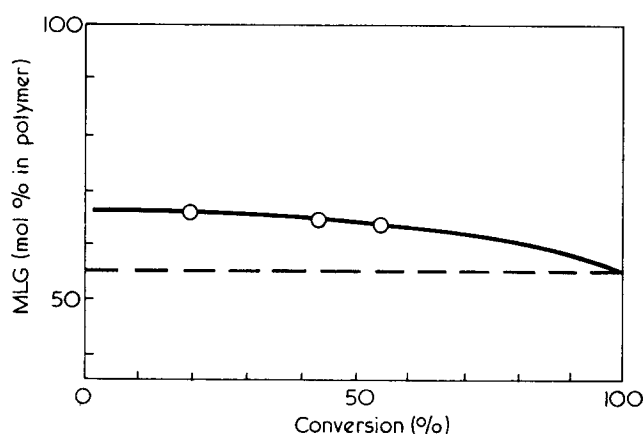


Figure 2 Copolymer composition vs. conversion curve for 55:45 mol % MLG/CBL system. The points represent the data of PMGCL-4, 5 and 6 in Table 1, from left to right

under 10–20%. On the other hand, by allowing polymerization to about 40% conversion, it was possible to prepare copolymers of sufficiently high molecular weight and yet with copolymer composition nearly the same as that at lower conversions. As is clear from Figure 1, MLG was more reactive than CBL. Now we denote the monomer reactivity ratios for the copolymerization of MLG with CBL by  $r_1$  and  $r_2$ , respectively. To obtain the monomer reactivity ratios, the method of Fineman and Ross<sup>8</sup> was employed. The numerical values of  $r_1$  and  $r_2$  obtained from the data shown in Table 1 were:  $r_1(\text{MLG}) = 2.0 \pm 0.4$ ; and  $r_2(\text{CBL}) = 0.5 \pm 0.1$ . It should be noticed here that the product  $r_1 \times r_2$  was equal to unity, which means that the monomers MLG and CBL are arranged at random along the chain in relative amounts specified by the composition of the initial monomer mixture. The same conclusion was also obtained for copolymerization of *N*-carboxyanhydrides of BLG and CBL. The numerical values obtained<sup>5</sup> were  $r_1(\text{BLG}) = 1.8 \pm 0.3$  and  $r_2(\text{CBL}) = 0.5 \pm 0.1$ .

Alfrey and Goldfinger<sup>9</sup> have related conditional probabilities,  $P_{11}$ ,  $P_{12}$ ,  $P_{21}$  and  $P_{22}$  to monomer reactivity ratios and feed composition data by assuming that only the last one monomer unit in the growing chain affects the probability of monomer addition in the course of copolymerization, and derived the following equations:

$$\begin{aligned} P_{11} &= \frac{r_1 F}{1 + r_1 F} \\ P_{12} &= \frac{1}{1 + r_1 F} \\ P_{21} &= \frac{1}{1 + r_2 / F} \\ P_{22} &= \frac{r_2 / F}{1 + r_2 / F} \end{aligned} \quad (1)$$

where  $F$  is the ratio of the initial mole fraction of monomer 1 to 2. Defining  $F_{11}$ ,  $F_{12}$ ,  $F_{21}$  and  $F_{22}$  as the fractions of bonds in the copolymer which connect specified monomer units (dyad), the following stoichiometric and steady-state relationships for the various dyad

distribution were introduced<sup>10, 11</sup>:

$$\begin{aligned} F_{11} &= \frac{r_1 F}{r_1 F + 2 + (r_2/F)} \\ F_{12} + F_{21} &= \frac{2}{r_1 F + 2 + (r_2/F)} \\ F_{22} &= \frac{r_2/F}{r_1 F + 2 + (r_2/F)} \\ F_{11} + F_{12} + F_{21} + F_{22} &= 1 \end{aligned} \quad (2)$$

The same relationships have been also introduced by Wall<sup>12</sup>.

Fractions of triad distributions in the copolymer can be calculated by multiplying the dyad distributions to the probabilities that the terminal units of these dyads are connected to other specified units. Thus the fractions of triads,  $F_{111}$ ,  $F_{112}$ ,  $F_{211}$ ,  $F_{121}$ ,  $F_{221}$ ,  $F_{112}$  and  $F_{222}$  are given by:

$$\begin{aligned} F_{111} &= \frac{r_1^2 F^3}{r_1^2 F^3 + 2r_1 F^2 + F^2 + F + 2r_2 F + r_2^2} \\ F_{112} + F_{211} &= \frac{2r_1 F^2}{r_1^2 F^3 + 2r_1 F^2 + F^2 + F + 2r_2 F + r_2^2} \\ F_{121} &= \frac{F^2}{r_1^2 F^3 + 2r_1 F^2 + F^2 + F + 2r_2 F + r_2^2} \\ F_{212} &= \frac{F}{r_1^2 F^3 + 2r_1 F^2 + F^2 + F + 2r_2 F + r_2^2} \\ F_{221} + F_{122} &= \frac{2r_2 F}{r_1^2 F^3 + 2r_1 F^2 + F^2 + F + 2r_2 F + r_2^2} \\ F_{222} &= \frac{r_2^2}{r_1^2 F^3 + 2r_1 F^2 + F^2 + F + 2r_2 F + r_2^2} \end{aligned} \quad (3)$$

$$F_{111} + F_{112} + F_{211} + F_{121} + F_{212} + F_{221} + F_{122} + F_{222} = 1$$

Now we calculate the normalized fractions of dyads and triads, respectively, from equations (2) and (3), by using experimental data of the monomer reactivity ratios for copolypeptide PMGCL. Figure 3 shows curves of the normalized fractions of monomer dyads,  $F_{11}$ ,  $F_{12} + F_{21}$  and  $F_{22}$ , as a function of the initial monomer

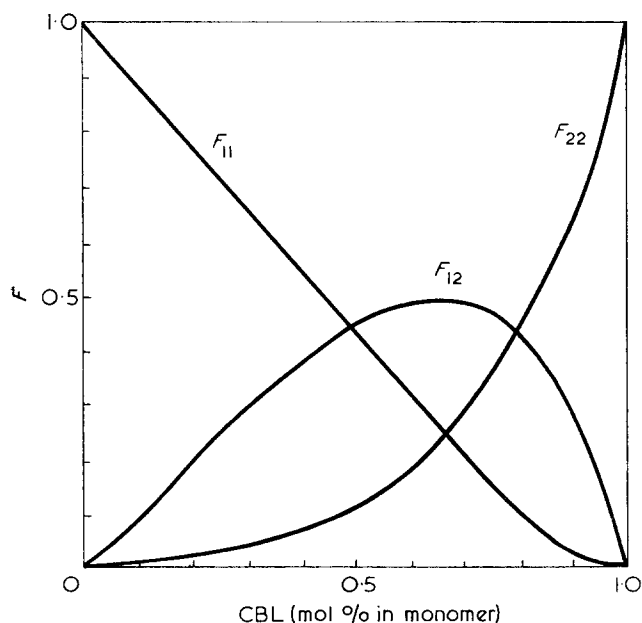


Figure 3 Normalized fractions of monomer dyads,  $F_{11}$ ,  $F_{12} + F_{21}$  and  $F_{22}$ , as a function of the initial monomer composition CBL mol % for PMGCL copolymer. 1 and 2 denote MLG and CBL, respectively.  $r_1 = 2.0$ ;  $r_2 = 0.5$

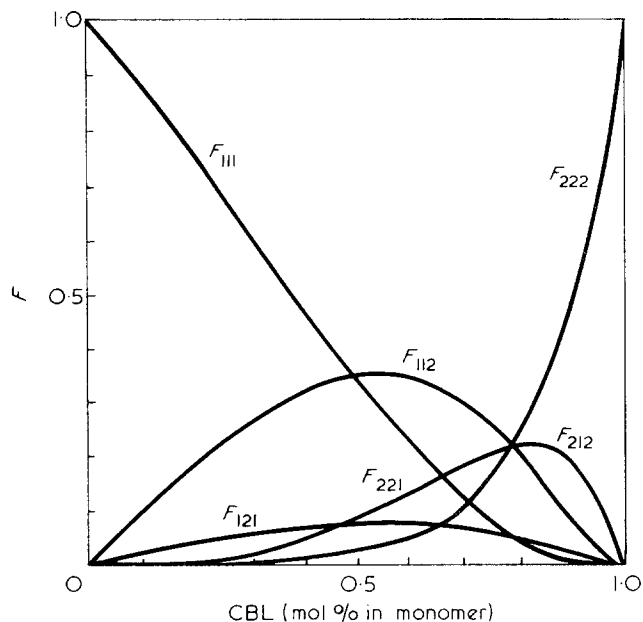


Figure 4 Normalized fractions of monomer triads,  $F_{111}$ ,  $F_{112}(=F_{112} + F_{211})$ ,  $F_{121}$ ,  $F_{212}$ ,  $F_{221}(=F_{221} + F_{122})$ , and  $F_{222}$ , as a function of the initial monomer composition CBL mol % for PMGCL copolymer. 1 and 2 denote MLG and CBL, respectively.  $r_1 = 2.0$ ;  $r_2 = 0.5$

composition CBL(mol %) for PMGCL. It is clear in Figure 3 that the curves obtained with fractions of alternate monomer dyad,  $F_{12} + F_{21}$ , have a maximum at about 70 mol % CBL of the initial monomer composition for PMGCL. It may be expected that the randomness of monomer dyad distribution is most remarkable at this initial monomer composition.

Figure 4 shows the normalized fractions of monomer triads,  $F_{111}$ ,  $F_{112}$ ,  $F_{121}$ ,  $F_{212}$ ,  $F_{221}$  and  $F_{222}$ , as a function of the initial monomer composition CBL (mol %) for copolypeptide PMGCL. In this case, the initial monomer composition exhibiting most remarkable randomness of monomer arrangement in the chain may be indicated more explicitly than that of Figure 3. It appeared at 72 mol % CBL for PMGCL.

#### Effect of solvent composition and temperature on transition

The results of o.r.d. measurements are examined in terms of the helix content  $X^H$  calculated by two different ways. One method is based on the coefficient  $b_0$  in the Moffitt equation<sup>13, 14</sup>:

$$[\alpha] = \left(\frac{100}{M_0}\right) \binom{n^2 + 2}{3} \left[ \frac{a_0 \lambda_0^2}{\lambda^2 - \lambda_0^2} + \frac{b_0 \lambda_0^4}{(\lambda^2 - \lambda_0^2)^2} \right] \quad (4)$$

where  $a_0$  is a constant which may vary with the nature of the side chain of polypeptide and depend on the kind of solvent, whereas the parameter  $b_0$  is a function of the helix content. Further,  $M_0$  is the molecular weight per peptide residue,  $n$  the refractive index of the solvent and  $\lambda$  (nm) the wavelength of the light source. In our previous analysis of the dispersion data on PMLG in some solvents in which the helix conformation is stable, we obtained  $b_0 = -630$  and  $\lambda_0 = 212$  nm. The helix content  $X^H$ , in this case, is estimated from:

$$X^H = \frac{b_0 - b_{0,c}}{b_{0,h} - b_{0,c}} \quad (5)$$

where,  $b_{0,h} (= -630)$  and  $b_{0,c} (= 0)$  denote the  $b_0$  values for perfect helix and random coil, respectively.

The other method is based on the coefficients in the

modified two-term Drude equation<sup>15</sup>:

$$[m'] = \frac{A_{(193)}\lambda_{193}^2}{\lambda^2 - \lambda_{193}^2} + \frac{A_{225}\lambda_{225}^2}{\lambda^2 - \lambda_{225}^2} \quad (6)$$

which gives the helix content  $X^H$  by the following equations

$$X^H = \frac{(A_{(193)} - A_{225}) + I}{K} \quad (7)$$

where  $A_{(193)}$  and  $A_{225}$  are the parameters relating to the helix content.  $I = 650$ , and  $K = 5580$  are used in this case.

We will turn to the conformational behaviour of these copolyptides resulting from change in temperature. Since the homopolypeptides, PMLG and PCBL, are rather different in helix stability in solvent, it was impossible to use the fixed composition of solvent

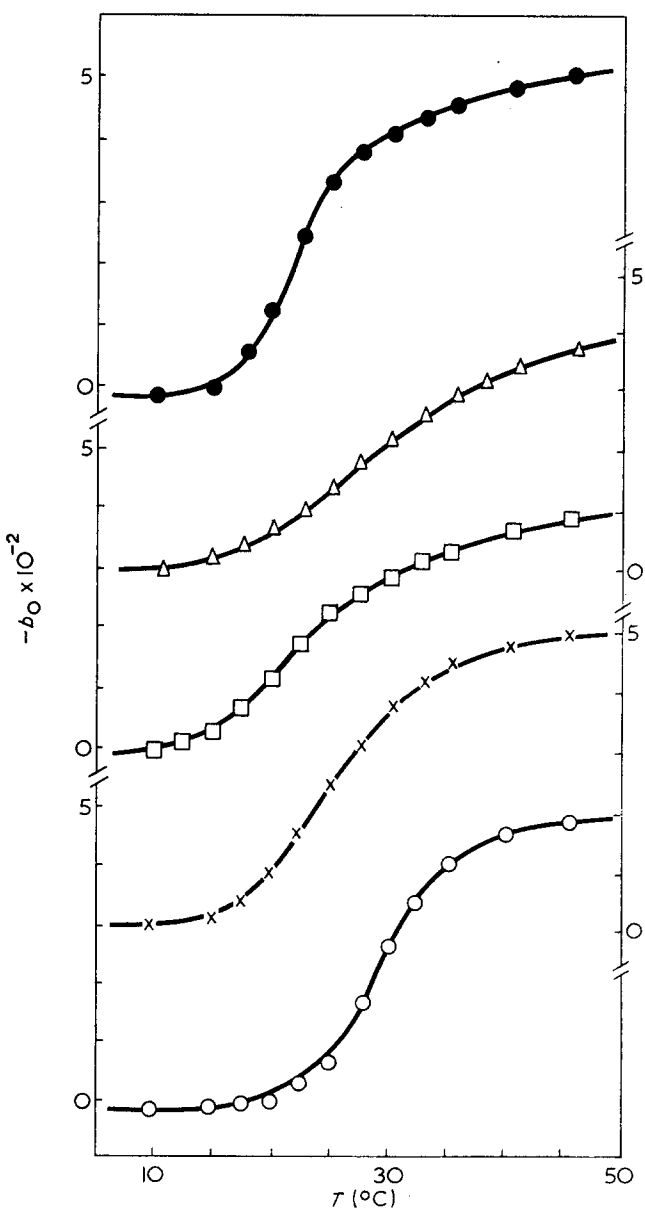


Figure 5 Temperature dependence of  $b_0$  for PMGCL copolyptides and component homopolypeptides PMLG and PCBL, in DCA-DCE mixture.  $\circ$ , PMLG-9 in DCA(69 mol %)-DCE(31 mol %);  $\times$ , PMGCL-7(27.5 mol % CBL) in DCA(65 mol %)-DCE(35 mol %);  $\square$ , PMGCL-6(35.5 mol % CBL) in DCA(61 mol %)-DCE(39 mol %);  $\triangle$ , PMGCL-2(76.5 mol % CBL) in DCA(50 mol %)-DCE(50 mol %); and  $\bullet$ , PCBL-1 in DCA(35 mol %)-DCE(65 mol %)

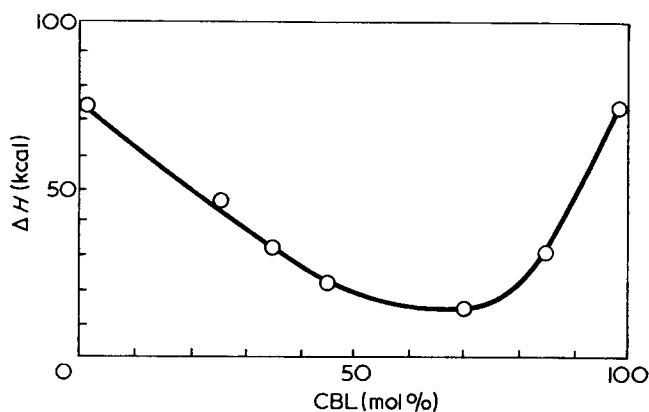


Figure 6 van't Hoff heat of transition,  $\Delta H$ , for thermal transition of PMGCL copolyptides in DCA-DCE mixture as a function of initial monomer composition CBL mol %

mixture to compare the thermal transition curves of these copolyptides. In order to keep the transitions within an available temperature range, different solvent compositions were used. The experimental results are shown in Figure 5. In Figure 5, experimentally observed thermal transition is illustrated for samples 1, 2, 6, 7 and 9. The sharpness of transition was quite different from case to case.

It is clear that the amount of DCA needed to bring the transitions within the same temperature range for the copolyptides PMGCLs are intermediate between those of the pure homopolypeptides PMLG and PCBL.

Experimental data relating to the thermally induced conformational transition have been analysed in terms of the Zimm-Bragg theory<sup>16-18</sup>. The helix content  $X^H$  was obtained as a function of temperature at a fixed solvent composition, hence the value of  $\Delta H$ , van't Hoff heat of transition, is readily determined experimentally from the slope of the  $b_0$  against temperature using the equation<sup>3</sup>:

$$\left(\frac{dX^H}{dT}\right)_{T_t} = \frac{1}{b_{0,h} - b_{0,c}} \left(\frac{db_0}{dT}\right)_{T_t} = \frac{\Delta H}{4RT_t^2} \quad (8)$$

The  $\Delta H$  calculated for these copolyptides PMGCLs, as well as their corresponding homopolypeptides, PMLG and PCBL, are illustrated in Figure 6 as a function of the initial monomer composition of CBL (mol %). It should be pointed out that the  $\Delta H$  showed a pronounced minimum against the initial monomer composition. Further, the initial monomer composition which gives the minimum value of  $\Delta H$  is in fair agreement with that obtained by theoretical calculation for monomer arrangement in PMGCL.

*Molecular conformations of PMGCL in DCA-DCE mixtures*

$A_{225}$  was plotted against  $A_{(193)}$  for copolyptide PMGCL in Figure 7, in which all points fall on the identical straight line. The same straight line relation was held for PMLG, PBLG, and PCBL. This fact suggests that structures other than  $\alpha$ -helix and random coil conformation are not present, and allows us to use the same equation as that for both homopolypeptides PMLG and PCBL to estimate the helix content.

Infra-red spectra were measured with an unoriented solid film of copolyptides PMGCLs with different copolymer compositions. Some typical illustrations of these spectra in the region of 400-900  $\text{cm}^{-1}$  and 2800-

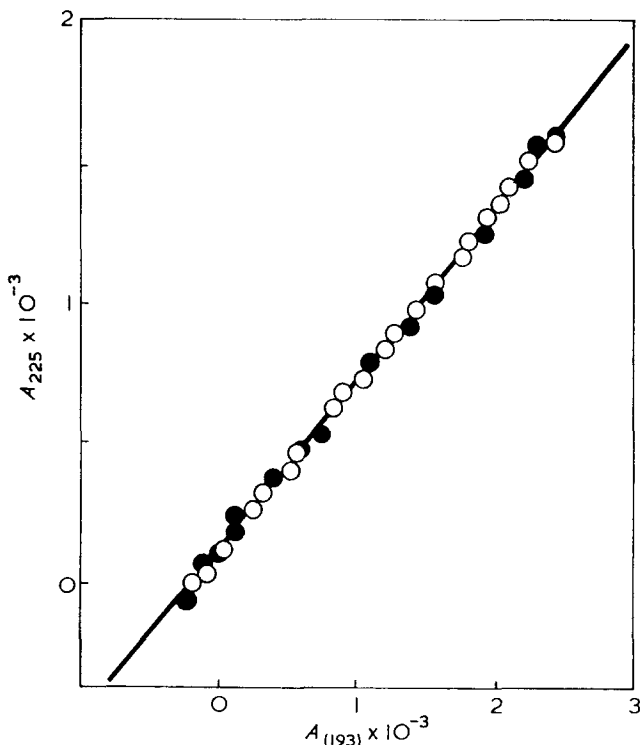


Figure 7 Plot of  $A_{(193)}$  against  $A_{225}$  for copolypeptides PMGCL (O) and PBGCL (●) in DCA-DCE mixtures, Polymer concentration is 1.0g/dl. Solid straight line denotes the relation obtained for PMLG, PBLG, and PCBL

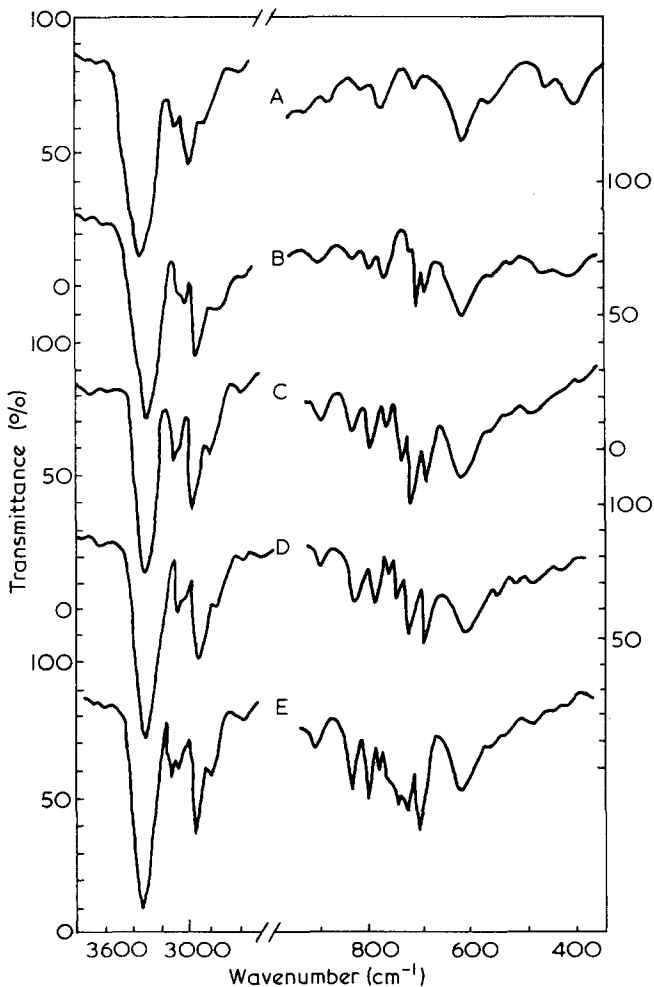


Figure 8 Infra-red spectra of unoriented solid films of samples cast from chloroform at 20°C. A, PMLG-9; B, PMGCL-8(18.0 mol % of CBL); C, PMGCL-6(35.5 mol % of CBL); D, PMGCL-3(58.5 mol % of CBL); E, PCBL-1

3600 $\text{cm}^{-1}$  are shown in Figure 8 together with those of homopolypeptides PMLG and PCBL. Of the low-frequency mode, the amide V vibration has been most useful in structural investigations. It involves N-H out-of-plane bending and depends considerably on the backbone conformations. The  $\alpha$ -helix and random coil conformations may now be distinguished even for unoriented films, and the fraction of the  $\alpha$ -helix conformation may be estimated in the presence of the disordered form. According to Miyazawa *et al.*<sup>19, 20</sup> and Masuda<sup>21</sup>, the amide V band of the  $\alpha$ -helix appears at 610–620 $\text{cm}^{-1}$  for PMLG and PCBL, while that of the disordered form at 650 $\text{cm}^{-1}$ . As is clear from Figure 8, the amide V band for copolypeptides PMGCLs appeared at 615 $\text{cm}^{-1}$ , just at the same wavenumber as that for PMLG and PCBL, with almost the same order of peak intensity as that of homopolypeptides PMLG and PCBL. Such a result means that these PMGCLs exist in helix conformation and, moreover, the helix content of these copolypeptides is nearly the same order as that of homopolypeptides.

Figure 9 shows the transition curves of PMGCL-3 (58.5 mol % of CBL) and of a 50:50 blend of PMLG and PCBL as a function of solvent composition at 25°C in DCA-DCE system. In the case of the blend, two transition regions were observed, while in the case of the copolypeptide, only one transition region was observed at about the middle point of the two transition regions observed for the blend. With respect to the polymer blend, the transition region at about 35 mol % DCA corresponds to that of PCBL, and that about 65 mol % DCA corresponding to that of PMLG. Comparison of these transition curves for the copolypeptide and the blend may suggest that, in the case of the blend, the transition takes place independently for PMLG and PCBL, while in the case of the copolypeptide the transition takes place cooperatively.

*Thermodynamic parameters for thermally induced coil-to-helix transition*

In the formulation of Zimm and Bragg<sup>16</sup> and of Applequist<sup>18</sup>,  $\Delta H$  of equation (8) is related to the enthalpy of formation  $\Delta H_{\text{res}}$  of intramolecular hydrogen bonds per residue in solvent, i.e., the transition enthalpy

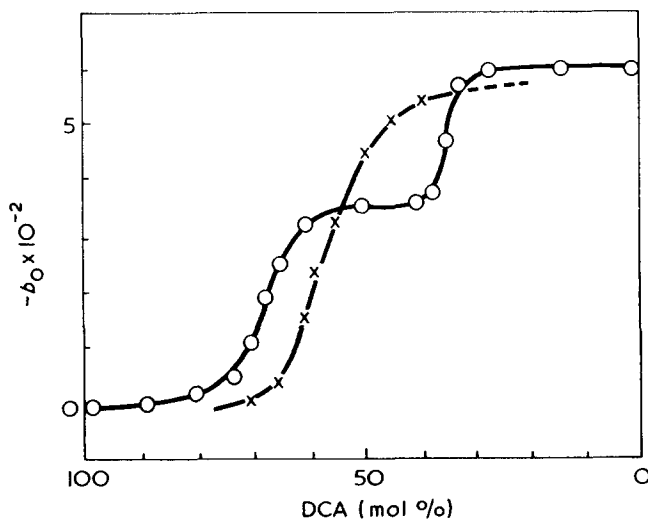


Figure 9  $b_0$  vs. solvent composition at 25°C for copolypeptide (x) containing 58.5 mol % of CBL (PMGCL-3), and for a polymer blend (O) containing 50:50 of PMLG and PCBL

per peptide residue associated with the transfer from coil to helix in solvent, by the equation  $\Delta H = \Delta H_{res}/\sigma^{1/2}$ . The parameter  $\sigma$  is designated as the cooperative parameter by Ackermann and Neumann<sup>22</sup>.

The value of  $\Delta H_{res}$  can be directly measured by a calorimetric technique<sup>23-25</sup>. The values of  $\Delta H_{res}$  obtained with PBLG by different authors<sup>22-25</sup> scattered from 525 to 950 cal/mol, because  $\Delta H_{res}$  of polypeptide was expected to depend on the molecular weight of polypeptide and also the concentration of polypeptide in the solution. With respect to PMLG and PCBL, however, reported results on  $\Delta H_{res}$  are very few. Recently, Giacometti *et al.*<sup>26</sup> have reported the results on the heat of solution of PCBL in DCA-DCE mixture, and obtained  $\Delta H_{res} = 620 \pm 40$  cal/mol for PCBL. They also estimated  $\Delta H_{res}$  with PMLG in DCA-DCE mixtures at 30°C by measuring the heat of solution<sup>24</sup>. Their experimental results have led to 650 cal/mol for the homopolypeptide, and they concluded that the difference of side chain in the polypeptides has no appreciable effect on the transition enthalpy, although it affects the helix stability as judged from solvent composition at the transition points.

Although the values of  $\Delta H_{res}$  should directly be measured by the calorimetric method described above, it also can be determined approximately by the method proposed by Karasz and O'Reilly<sup>27</sup>, which is based on the determination of heat of fusion from melting point depression (MPD). According to the MPD method, DCA molecules bound to the polypeptide have lost their translational freedom at temperatures below  $T_t$ , and are therefore in a 'solid' state. Above  $T_t$ , however, these DCA molecules are released and in normal liquid state. From the above relation and the ideal solution approximation for DCA, the following equation is obtained<sup>3, 27</sup>:

$$\frac{d(\ln X_{DCA})}{dT_t} = \frac{\Delta H_{DCA}}{RT_t^2} \quad (9)$$

where  $X_{DCA}$  is the mole fraction of DCA in the solvent mixture and  $\Delta H_{DCA}$  is the overall heat, per mole of DCA, associated with the transition of 'solid' DCA. Equation (9) was derived for the transition of DCA from 'solid' state to 'liquid' state. The total number of hydrogen bonds is not changed throughout the transition, and furthermore there is assumed a 1:1 molar equivalence between the bonded DCA molecules and the peptide residues on average. The 'melting point' of bonded DCA ('solid') is equated to the transition temperature  $T_t$  of the polypeptide. Hence  $\Delta H_{DCA}$  can be identified with the enthalpy of transition  $\Delta H_{res}$ .

Now we will refer to the thermal transition curves of the copolypeptide PMGCL-6 (35.5 mol % of CBL) in various DCA-DCE mixtures (see Figure 10). The sharpness of transition was different from case to case, and the value becomes lower as the DCA mol % in the DCA-DCE mixture increases.  $\Delta H_{res}$  was estimated from Figure 11, which showed the relation between the transition temperature  $T_t$  and the logarithm of the mole fraction of DCA in the mixture for PMGCL-6 (35.5 mol % of CBL) in DCA-DCE systems. The value of  $\Delta H_{res}$  thus obtained was about  $600 \pm 100$  cal/mol residue. Previously, we have reported that the values of  $\Delta H_{res}$  for PMLG and PCBL in DCA-DCE mixtures are  $920 \pm 100$  cal/mol<sup>3</sup> and  $740 \pm 100$  cal/mol<sup>5</sup>, respectively. Accordingly, the value of  $\Delta H_{res}$  for PMGCL

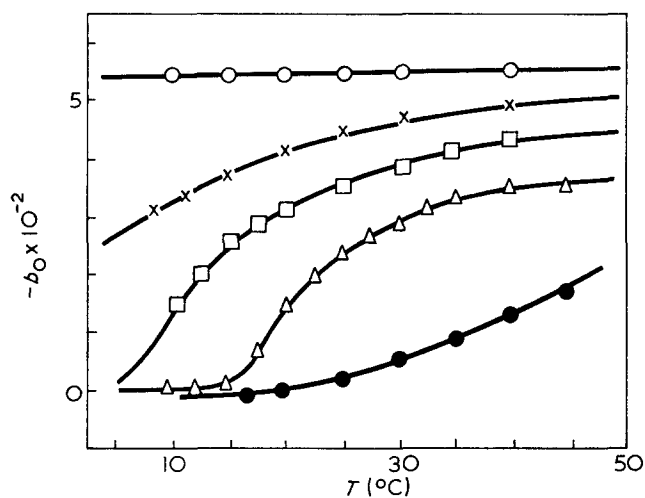


Figure 10 Temperature dependence of  $b_0$  in DCA-DCE mixture with various solvent compositions for copolypeptide PMGCL-6. O, 35; x, 50; □, 56; △, 60; ●, 64 mol % DCA

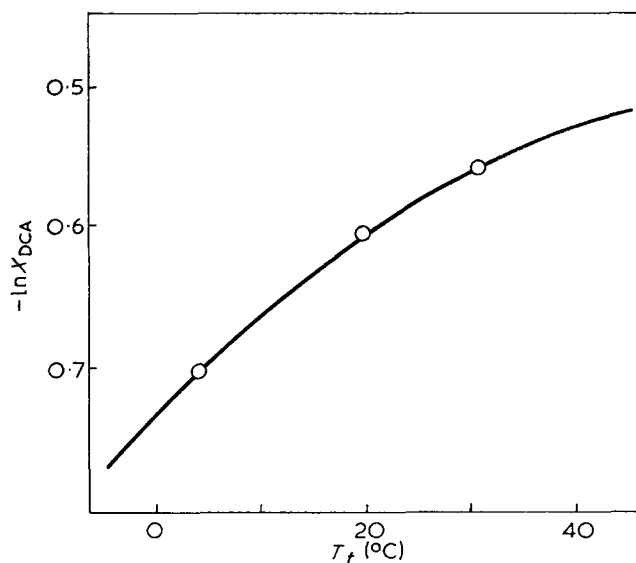


Figure 11  $\ln X_{DCA}$  plotted against the transition temperature  $T_t$  for copolypeptide PMGCL-6

copolypeptide (35.5 mol % of CBL) is smaller than those of both homopolypeptides PMLG and PCBL.

The MPD method is an approximation because equation (9) involves molar concentration rather than activity, and moreover it assumes stoichiometric relation between peptide residue and DCA. The number of DCA molecules bound to polypeptide coil may not equal exactly that of peptide residues if some polypeptide sites were incapable of binding a DCA molecule for steric reasons.

Recently, Ptitsyn and Birshtein<sup>29</sup> have derived a general equation to estimate the thermodynamic parameter of the conformational transition induced by the change in the external parameters such as temperature and solvent composition; i.e.,  $\Delta n = \Delta H_{res} d(1/RT_t)/d\mu$ , where  $\mu$  is the chemical potential of an active solvent component, DCA in this case, and  $\Delta n = n_2 - n_1$  is the difference in the number of molecules of DCA, which must be introduced into the systems containing polypeptide molecules in the two conformational states,  $\alpha$ -helix and random coil, for the creation of the chemical potential of the solvent system. In the simplest case when the interaction of DCA with the polypeptide is

reduced to a more or less firm binding of these molecules,  $\Delta n$  represents simply the difference in the numbers of molecules of DCA bound to the polypeptide residue in the two conformational states. By application of the ideal solution approximation to this relation, the following equation is derived:

$$\frac{d \ln X_{\text{DCA}}}{dT} = \frac{\Delta H_{\text{res}}}{\Delta n RT^2} \quad (10)$$

Equation (10) is reduced to equation (9) with  $\Delta n=1$ .

In the next stage, experimental data obtained with PMGCL in DCA-DCE mixture will be analysed by the method proposed by Fujita *et al.*<sup>30-32</sup>. They proposed a new procedure to estimate the parameters  $\Delta H_{\text{res}}$  and  $\sigma$  independently from o.r.d. measurements by using Nagai's theory for the helix-coil transition<sup>33</sup>. It has been shown that the helix content  $X^H$  of a polypeptide having degrees of polymerization  $P_n$  is represented to a good approximation by<sup>30, 31</sup>:

$$X_0^H = X^H - \frac{2X_0^H{}^{3/2}(1-X_0^H)^{1/2}}{P_n\sigma^{1/2}} \quad (11)$$

provided that  $\sigma^{1/2} \ll 1$ ,  $P_n \gg 1$  and  $P\sigma^{1/2} \gg 2$ . Here,  $X_0^H$  denotes the value of  $X^H$  for infinitely large  $P_n$  and is related to  $\sigma$ . Equation (11) predicts that a plot of  $X^H$  (at fixed solvent composition) versus  $1/P_n$  gives a straight line whose intercept  $A$  on the ordinate and slope  $B$  are equal to  $X_0^H$  and  $-2X_0^H{}^{3/2}(1-X_0^H)/\sigma^{1/2}$ , respectively. They have shown that experimental determination of  $A$  and  $B$  leads to the evaluation of  $\sigma^{1/2}$  by:

$$\sigma^{1/2} = -\left(\frac{2A}{B}\right)[A(1-A)]^{1/2} \quad (12)$$

We adopt equation (12) to samples PMGCL-4, -5 and -6 which have different molecular weights but constant (35 mol %) CBL content. Figure 12 illustrates the changes of  $b_0$  measured as a function of temperature at constant solvent composition in DCA-DCE mixture containing 59 mol % of DCA. Figure 13 shows plots of the helix content  $X^H$  against the reciprocal of number-average degrees of polymerization  $1/P_n$  from data in Figure 12.

Table 2 is a summary of thermodynamic parameters for copolyptides PMGCL and PBGCL<sup>4</sup> estimated by

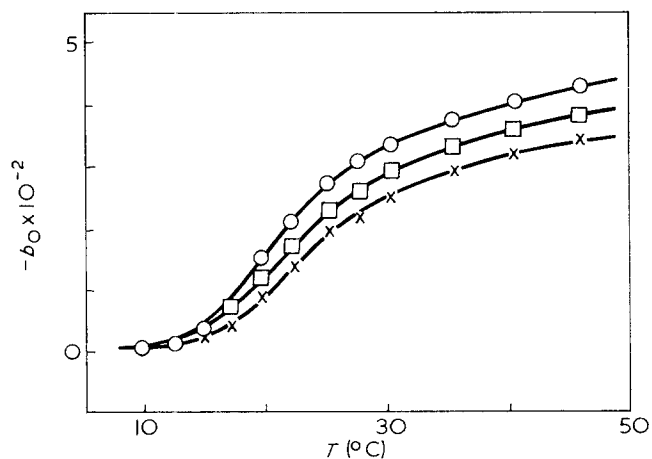


Figure 12 Temperature dependence of  $b_0$  in DCA(59 mol %)-DCE(41 mol %) mixture for PMGCL copolyptides with various molecular weights in:  $\circ$ , PMGCL-6 ( $M_n=157\ 000$ );  $\square$ , PMGCL-5 ( $M_n=80\ 000$ );  $\times$ , PMGCL-4 ( $M_n=51\ 000$ )

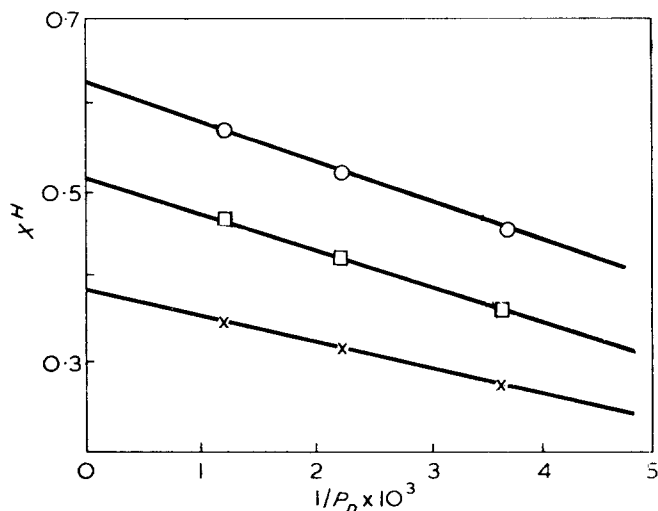


Figure 13 Plots of  $X^H$  against  $1/P_n$  for PMGCL-6 in DCA(59 mol %)-DCE(41 mol %) mixture at 30°C( $\circ$ ), 25°C( $\square$ ) and 22°C( $\times$ )

Table 2 Thermodynamic parameters of copolyptides PMGCL and PBGCL, and homopolypeptides PMLG, PBLG and PCBL, in DCA-DCE mixtures

Polymer	Polym. comp. (CBL mol %)	$X_{\text{DCA}}$	$\Delta H$ (kcal/mol)	$\Delta H_{\text{res}}$ (cal/mol)		$\sigma^{1/2}$
				From eqn (9)	From eqn (12)	
PMLG-9	0.0	0.69	$75 \pm 10$	$920 \pm 100$	$850 \pm 100$	0.011
PMGCL-6	35.5	0.59	$30 \pm 5$	$600 \pm 100$	$410 \pm 100$	0.014
PCBL-1	100.0	0.35	$75 \pm 10$	$740 \pm 100$	$640 \pm 100$	0.009
PBGCL-3 <sup>4</sup>	46.4	0.63	$35 \pm 10$	$680 \pm 100$	$430 \pm 100$	0.013
PBLG-8 <sup>4</sup>	0.0	0.69	$85 \pm 10$	$930 \pm 100$	$880 \pm 100$	0.010

the two different methods. In Table 2, values for homopolypeptides, PMLG, PBLG and PCBL, quoted from our previous papers are also cited. The values of  $\Delta H_{\text{res}}$  for PMGCL and PBGCL estimated by the two different methods are different from each other. The values obtained from equation (9) are much higher than those from equation (12). This fact suggests that the former method should overestimate  $\Delta H_{\text{res}}$  value though the cause is not clear at this stage. The difference  $\Delta n$  in the numbers of molecules of DCA bound to a copolyptide residue in the two conformational states are from 0.63 to 0.68 for both copolyptides, PMGCL containing 35 mol % of CBL and PBGCL containing 46 mol % of CBL, in DCA-DCE system. Finally the values of  $\sigma$  obtained from equation (12) for PMGCL (35 mol % of CBL) and PBGCL (46 mol % of CBL) are  $\sigma^{1/2} = 1.4 \pm 10^{-2}$  and  $1.3 \times 10^{-2}$ , respectively. These values are slightly higher than those of homopolypeptides PMLG, PBLG, and PCBL.

In summarizing our results,  $\Delta H$  for the copolyptides shows a minimum against copolymer composition and the values of  $\Delta H_{\text{res}}$  for the copolyptide are also lower than those for component homopolypeptides, differing from the result of Giacometti *et al.*<sup>26</sup>. They have reported results of heat of solution measurements on copolyptides of CBL with L-phenylalanine in mixtures of DCA-DCE. With their data, the values of  $\Delta H_{\text{res}}$  for PCBL and its copolymer with L-phenylalanine are all practically identical and equal to the value found for polyglutamate. Such result may



suggest a rather notable insensitivity of this quantity on the nature of the side chain. Roig *et al.*<sup>6</sup> independently studied the thermal behaviour of PBGCL copolyptides synthesized with sodium methoxide initiator in dioxane, and analysed the results in terms of Lifson and Roig's theory<sup>34</sup>. They concluded that the cooperativity parameter changed linearly with polymer and solvent compositions, whereas the heat of the transition  $\Delta H_{res}$  showed a very pronounced minimum as a function of polymer composition. One of the reasons for the appearance of the minimum is that each  $\Delta H_{res}$  was determined for a different solvent system, the effects of which might have a significant unknown effect on  $\Delta H_{res}$ .

#### REFERENCES

- 1 Kanamori, T. (Hayashi, T.), Itoh, K. and Nakajima, A. *Polymer J.* 1970, **1**, 524
- 2 Hayashi, T. and Nakajima, A. *Polymer J.* 1971, **2**, 1
- 3 Nakajima, A. and Hayashi, T. *Bull. Inst. Chem. Res., Kyoto Univ.* 1968, **46**, 62
- 4 Hayashi, T. and Nakajima, A. unpublished
- 5 Nakajima, A. and Hayashi, T. *Bull. Inst. Chem. Res., Kyoto Univ.* 1972, **50**, 303
- 6 Roig, A., Carcia, B. F. and Cortijo, M. *Biopolymers* 1971, **10**, 329
- 7 Blout, E. R. and Karlson, R. H. *J. Am. Chem. Soc.* 1956, **78**, 941
- 8 Fineman, M. and Ross, S. D. *J. Polym. Sci.* 1950, **5**, 269
- 9 Alfrey, T. and Goldfinger, G. *J. Chem. Phys.* 1944, **12**, 205
- 10 Harwood, H. J. and Ritchey, W. M. *J. Polym. Sci. (B)* 1964, **2**, 601
- 11 Harwood, H. J. *J. Polym. Sci. (C)* 1968, **25**, 37
- 12 Wall, F. T. *J. Am. Chem. Soc.* 1944, **66**, 2050
- 13 Moffitt, W. *J. Chem. Phys.* 1956, **25**, 467
- 14 Moffitt, W. and Yang, J. T. *Proc. Natl. Acad. Sci. U.S.* 1955, **42**, 595
- 15 Shechter, E. and Blout, E. R. *Proc. Natl. Acad. Sci. U.S.* 1964, **51**, 695
- 16 Zimm, B. H. and Bragg, J. K. *J. Chem. Phys.* 1958, **28**, 1246
- 17 Zimm, B. H. and Bragg, J. K. *J. Chem. Phys.* 1959, **31**, 526
- 18 Applequist, J. *J. Chem. Phys.* 1963, **38**, 934
- 19 Miyazawa, T. and Blout, E. R. *J. Am. Chem. Soc.* 1961, **83**, 712
- 20 Miyazawa, T., Masuda, Y. and Fukushima, K. *J. Polym. Sci.* 1962, **62**, S62
- 21 Masuda, Y. *Kobunshi Kagaku* 1963, **20**, 161, 166, 171, 206, 210
- 22 Ackermann, T. and Neumann, E. *Biopolymers* 1967, **5**, 649
- 23 Karasz, F. E. and O'Reilly, J. M. *Biopolymers* 1965, **3**, 241
- 24 Giacometti, G., Turolla, A. and Boni, R. *Biopolymers* 1968, **6**, 641
- 25 Kagemoto, A. and Fujishiro, R. *Biopolymers* 1968, **6**, 1753
- 26 Giacometti, G., Turolla, A. and Boni, R. *Biopolymers* 1970, **9**, 979
- 27 Karasz, F. E. and O'Reilly, J. M. *Biopolymers* 1967, **5**, 27
- 28 Nakajima, A., Hayashi, T. and Emi, S. unpublished
- 29 Ptitsyn, O. B. and Birshtein, T. M. *Biopolymers* 1969, **7**, 435
- 30 Okita, K., Teramoto, A. and Fujita, H. *Biopolymers* 1970, **9**, 717
- 31 Teramoto, A., Norisuye, T. and Fujita, H. *Polymer J.* 1970, **1**, 55
- 32 Norisuye, T., Matsuoka, M., Teramoto, A. and Fujita, H. *Polymer J.* 1970, **1**, 691
- 33 Nagai, K. *J. Chem. Phys.* 1961, **34**, 887
- 34 Lifson, S. and Roig, A. *J. Chem. Phys.* 1961, **34**, 1963

# Effect of polydispersity on the n.m.r. spectra of poly( $\gamma$ -benzyl-L-glutamate) through the helix $\rightarrow$ coil transition

E. M. Bradbury, C. Crane-Robinson and P. G. Hartman

*Biophysics Laboratories, Physics Department, Portsmouth Polytechnic, Portsmouth PO1 2QG, UK*  
(Received 23 May 1973)

High resolution n.m.r. and o.r.d. measurements on unfractionated poly( $\gamma$ -benzyl-L-glutamates) have been compared with results obtained on fractionated samples obtained therefrom by precipitation chromatography. It is concluded that the prime cause of the 'double-peak' main chain proton resonances observed in the helix-coil transition region is conformational heterogeneity resulting from molecular weight polydispersity.

## INTRODUCTION

Double peaks are frequently observed<sup>1</sup> in the  $\alpha$ -CH and NH regions of the proton spectra of many polypeptides. In the case of the  $\alpha$ -CH resonance, the upfield component is usually assigned to helix whilst the downfield is assigned to coil. Kinetic data<sup>2</sup> indicate, however, that a single averaged peak should be observed as a result of a fast helix-coil interconversion rate ( $10^7$  to  $10^8$  sec<sup>-1</sup>). Several suggestions have been put forward to account for this discrepancy. A slow nucleation step for the transition has been proposed by Ferretti and coworkers<sup>3</sup> whilst Joubert *et al.*<sup>4</sup> challenge the assignment of the two resonances to helix and coil states, proposing that they are due to solvated and unsolvated random coil residues. J. H. Bradbury *et al.*<sup>5</sup> have suggested that slow protonation of the coil peptide bond is the cause of the separate observation of the two conformations. These theories have been discussed elsewhere<sup>6</sup> and found unable to explain all the experimental observations. In a very recent study of poly(L-alanine), Goodman *et al.*<sup>7</sup> came to the conclusion that the strong upfield  $\alpha$ -CH resonance peak can be assigned to a time average of helix and coil, whilst the weaker peak to low field can be assigned to pure coil. [This accords closely with our own conclusions regarding poly(L-alanine).<sup>6</sup>] These authors then postulate that this might be the correct assignment for the two  $\alpha$ -CH components in all double peak spectra. Poly(L-alanine) is, however, not a typical polypeptide and we have explained elsewhere<sup>6</sup> the reasons for its exceptional behaviour. The most satisfactory explanation is that first developed by Ullman<sup>8</sup>, who concluded that the usual peak assignment is correct and that the double peak phenomenon can result from polydispersity and end-group effects, even though rapid interconversion of helix and coil states takes place. He pointed out that the free energy difference between helix initiation (in the middle of a polypeptide chain) and helix continuation

means that in the transition region a residue near the end of a polypeptide chain has a greater probability of being in the coil state than a residue in the middle of a chain, i.e. averaging of helix and coil states is not equivalent for all residues in the chain. This is sufficient to explain broadening of the peaks at intermediate molecular weights during the helix-coil transition and the observed disappearance of the effect at high molecular weight. However, to explain quite separate helix and coil peaks that remain fixed in position through the transition Ullman demonstrated that effects of molecular weight polydispersity must be considered. At low molecular weight the helicity of a given polypeptide chain under specified solvent conditions is very dependent on the chain length; in the middle of the helix coil transition therefore, a low molecular weight polydisperse sample will consist mainly of molecules that are either largely helical or largely random coil, and so contribute to the respective peaks. We have previously reported in this journal<sup>9</sup> the n.m.r. spectra of several unfractionated samples of poly( $\gamma$ -benzyl-L-glutamate) (PBLG) and concluded that polydispersity is indeed an important factor in the double peak phenomenon. In a recent note Nagayama and Wada<sup>10</sup> studied a sample of PBLG fractionated by gel permeation chromatography and having  $\overline{DP} = 45$ . In the middle of the helix-coil transition the  $\alpha$ -CH resonance of this fraction appeared as a broad single peak and this observation strongly supports the polydispersity explanation of the double peak phenomenon.

In this communication we give both nuclear magnetic resonance (n.m.r.) and optical rotatory dispersion (o.r.d.) results on fractionated PBLG samples, in particular fractions obtained by precipitation chromatography of the PBLG samples studied previously<sup>9</sup>. It is concluded that conformational heterogeneity in the helix-coil transition region which results from polydispersity is indeed the prime cause of the 'double peak' phenomenon in the n.m.r. spectrum of poly( $\gamma$ -benzyl-L-glutamate).

EXPERIMENTAL

PBLG samples R10 and S416 were synthesized by W. E. Hanby at the Courtaulds Research Laboratory, Maidenhead. Sample PH21 was prepared by initiation of  $\gamma$ -benzyl-L-glutamate *N*-carboxyanhydride (NCA) by *n*-hexylamine in dimethylformamide and P17 by initiation with diethylamine in dioxane.

Molecular weights were determined by measurement of viscosities in dichloroacetic acid (DCA), using the calibration of Doty *et al.*<sup>11</sup> and allowing for non-linearity at low molecular weight<sup>12</sup>. The n.m.r. spectra were recorded on a JEOL JNM-4H-100 MHz spectrometer and o.r.d. curves were obtained on a Bendix Polarmatic 62 spectropolarimeter.  $b_0$  values were calculated from the Moffitt equation using a  $\lambda_0$  value of 212 nm.

Precipitation chromatography

Baker and Williams<sup>13</sup> have developed the technique of precipitation chromatography for the fractionation of polystyrenes. This technique has been used to investigate the molecular weight distribution of poly( $\gamma$ -benzyl-L-glutamate)<sup>14</sup>, and appeared to lend itself to a more complete fractionation of polypeptides. The technique employs equilibration between a moving solution and a stationary precipitated phase along the length of a column, which is virtually a continuous series of filter beds covering a range of temperatures. The column (Figure 1) of 100 cm length was packed with glass beads of approximately 0.1 mm diameter, and was

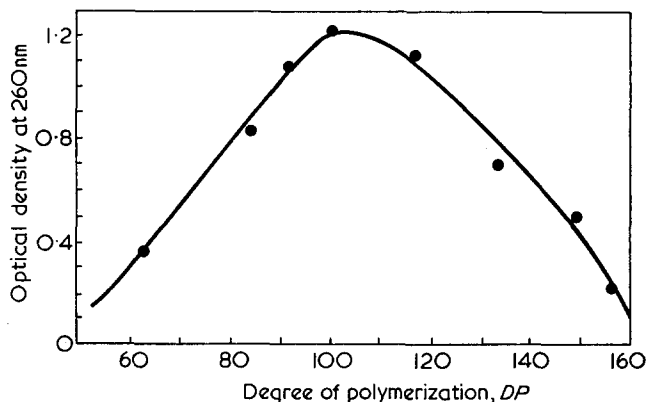


Figure 2 Molecular weight distribution curve for PBLG sample PH21 (degree of polymerization from viscosity measurements)

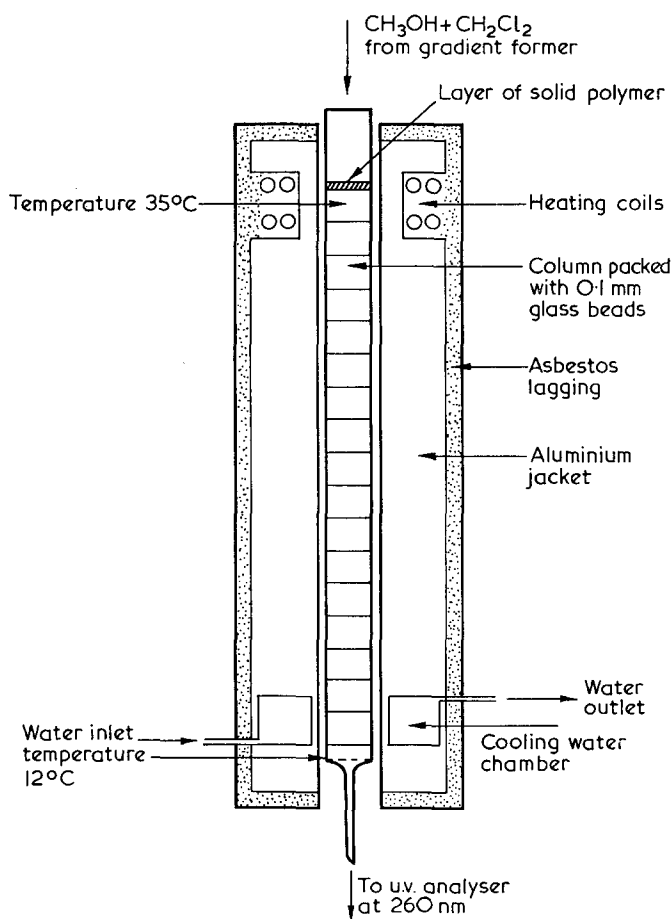


Figure 1 Precipitation chromatography column for polypeptide fractionation. Length, 100 cm; i.d., 2.4 cm

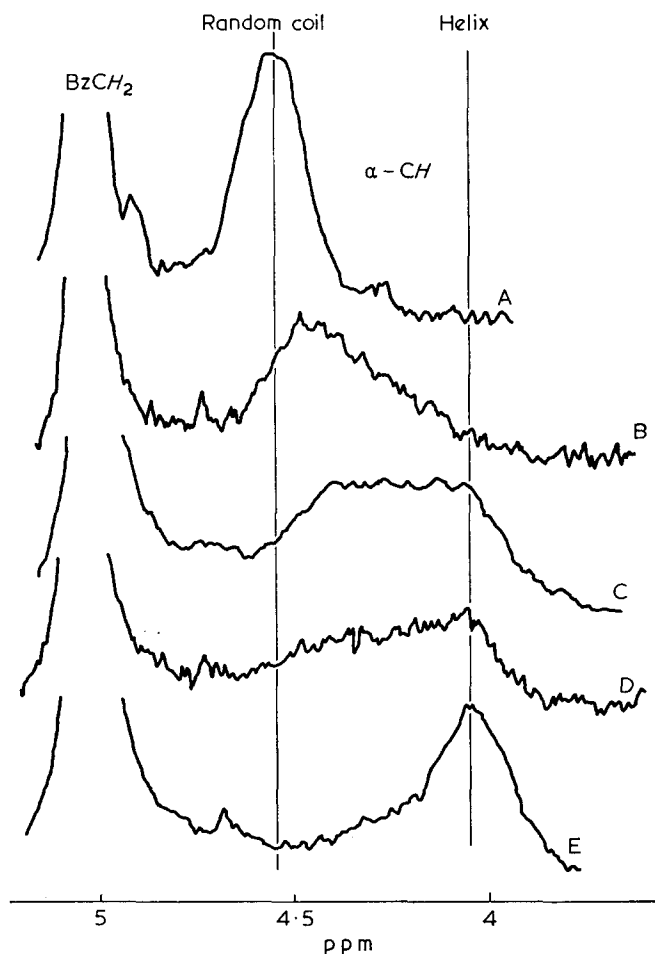


Figure 2a 100 MHz spectra of temperature induced helix-coil transition of PBLG sample PH21 ( $\overline{DP}=105$ ) in 10:90% TFA/ $CDCl_3$ . A, 4°C; B, 33°C; C, 37°C; D, 39°C; E, 50°C

enclosed in an aluminium jacket. The jacket was heated to 35°C at the top by means of an electrical winding and cooled to 12°C at the bottom by a water jacket. A solvent gradient (methanol, a non-solvent, slowly enriched with methylene chloride, a good solvent for PBLG) was run on to a layer of solid polymer situated at the top of the column. The temperature gradient down the column was found to be linear within 3% experimental error. The eluant from the column was passed through a spectrophotometer and the benzyl absorbance at 260 nm was measured. The technique is particularly applicable to PBLG owing to the ready

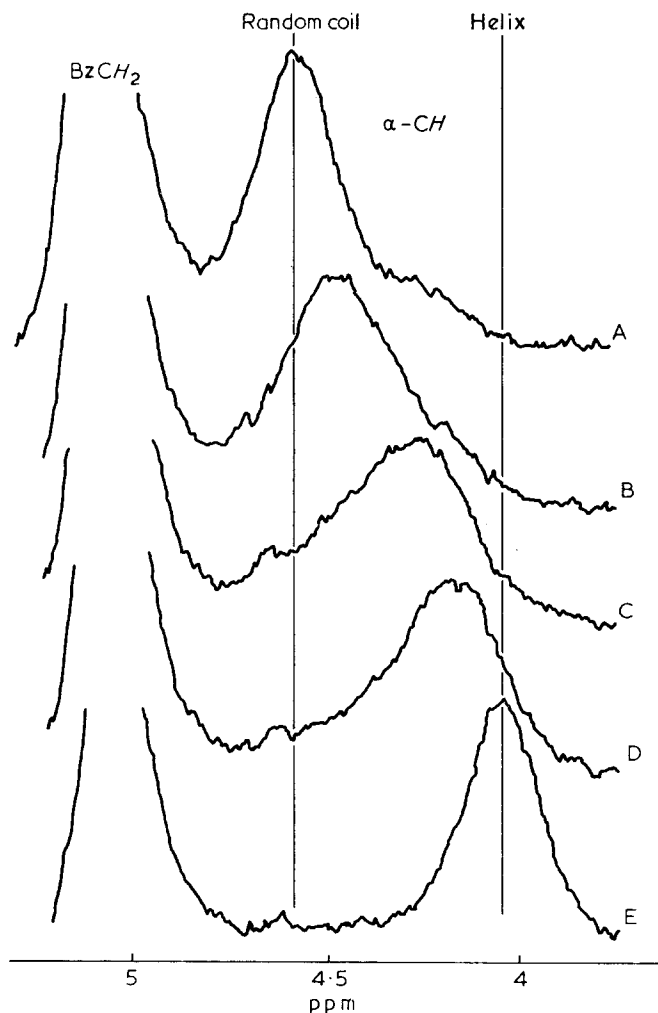


Figure 2b 100MHz spectra of temperature induced helix-coil transition of fraction X8 ( $\overline{DP}=80$ ) of PBLG sample PH21 in 10:90% TFA/ $CDCl_3$ . A, 9°C; B, 15°C; C, 19°C; D, 23°C; E, 33°C

availability of solvent (methylene chloride) and non-solvent (methanol) and the temperature dependence of the polymer solubility.

## RESULTS

Passage of sample PH21 through the column and viscosity measurements on the resulting fractions yielded the plot of degree of polymerization ( $DP$ ) against optical density shown in Figure 2. The curve is symmetrical ( $M_w/M_n \sim 1$ ) but shows a considerable spread of molecular weights. In addition, as with all PBLG samples, a certain amount of polymer of  $DP < 20$  was present, and this was removed before fractionation. Figures 2a and 2b show the n.m.r. spectra of the  $\alpha$ -CH region during a temperature-induced coil  $\rightarrow$  helix transition for unfractionated PH21 ( $\overline{DP} \sim 105$ ) and for fraction X8 which has a  $\overline{DP} \sim 80$ . Despite a lowering of the average chain length in fraction X8, the reduction of the range of molecular weight results in a sharpening of the resonance envelope (Figure 2b).

PBLG samples R10 and S416 both have  $\overline{DP} \sim 100$  yet the former shows a very clear 'double peak' spectrum whilst the latter exhibits a very broad single peak in the transition region. These polymers have already been discussed<sup>9</sup> and the polydispersity of R10 found to be greater than that of S416. This conclusion has now

been supported by molecular weight measurements on a complete range of fractions from both PBLG samples, and the data are given in Figure 3. The helix-coil transitions of R10 and S416 have been compared (Figure 4) to that of a high molecular weight sample (P17) by means of  $b_0$  measurements in DCA/chloroform. The molecular weight dependence of helix content at a specified solvent composition is very striking (compare for example R10 and S416 with P17 in the range 55 to 65% DCA), and it is also noted that the transition of

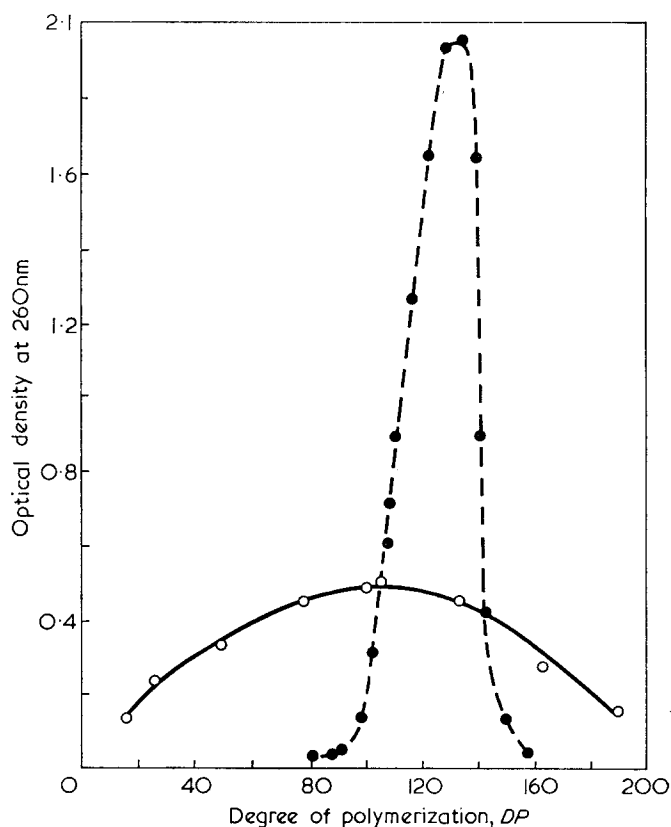


Figure 3 Molecular weight distribution curve for PBLG samples R10 (○) and S416 (●) (degree of polymerization from viscosity measurements)

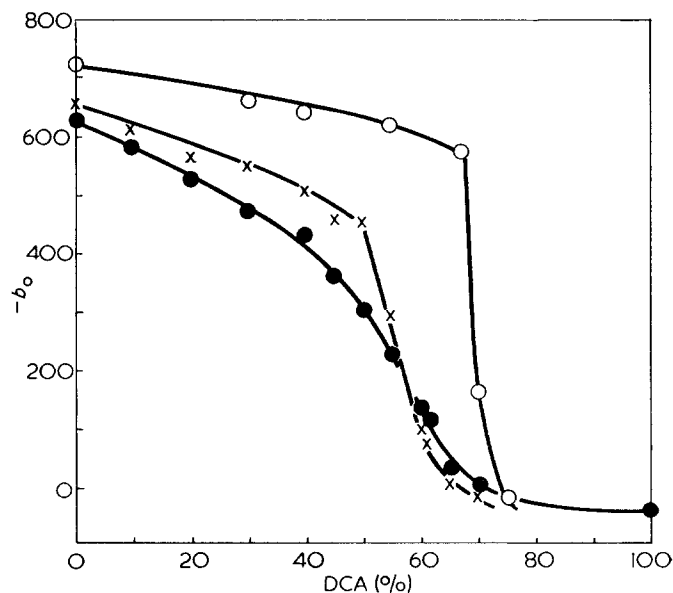


Figure 4  $b_0$  values in DCA/ $CHCl_3$  at 22°C for PBLG unfractionated samples P17 (○) ( $M_w=150 \times 10^3$ ), S416 (×) ( $M_w=20 \times 10^3$ ) and R10 (●) ( $M_w=22 \times 10^3$ )

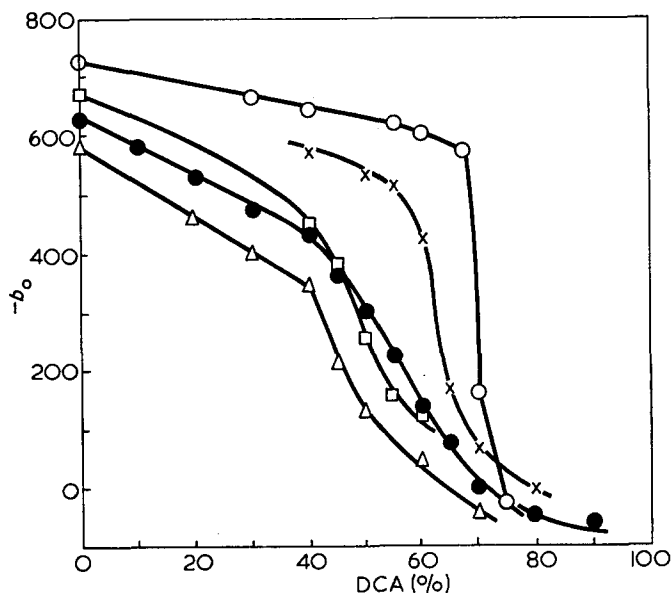


Figure 5  $b_0$  values in DCA/ $\text{CHCl}_3$  at 22°C for PBLG unfractionated samples P17 (○) (700 mer) and R10 (●) (92 mer). Fractionated samples of R10 are designated H58/59 (×) (130 mer), H50/51 (□) (80 mer) and H42/43 (△) (50 mer)

the transition for the  $DP \sim 130$  fraction does not differ greatly from that of the 700 mer, that of the  $DP \sim 50$  fraction shows virtually no sigmoidal character. Now the unfractionated polymer is half helical ( $b_0 = -315$ ) at 50% DCA. At this solvent composition fraction H42/43 (50 mer) has  $b_0 = -130^\circ$ , fraction H50/51 (80 mer) has  $b_0 = -260^\circ$ , and fraction H58/59 is almost fully helical with  $b_0 = -570^\circ$ . These fractions having different helicities at the midpoint of the transition for the unfractionated sample (50% DCA) will give rise to n.m.r. peaks at different chemical shift values and result in the observed multiple peak spectrum.

Figures 6 to 8 show  $\alpha\text{-CH}$  spectra of R10 and two

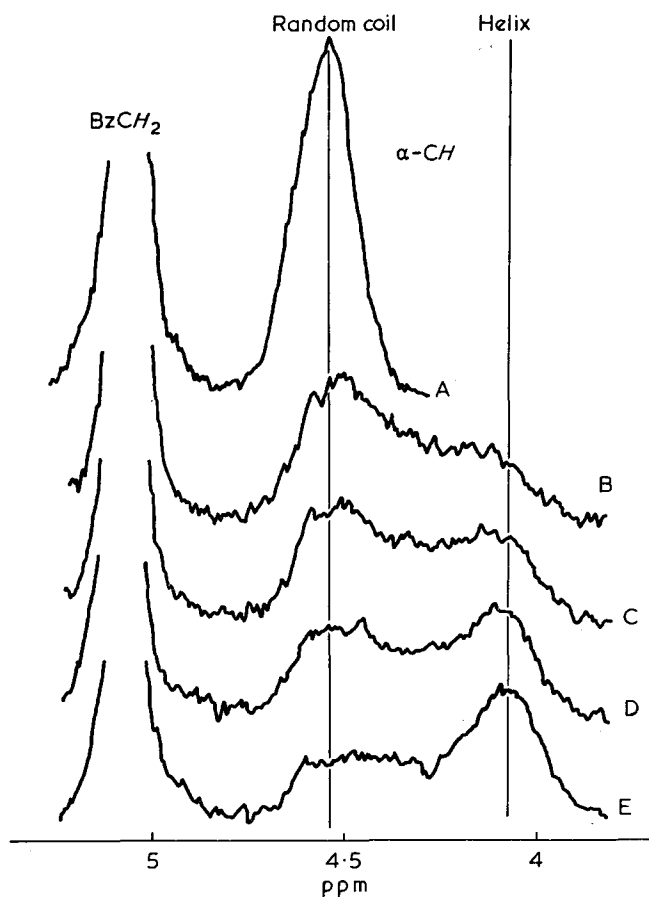


Figure 6 100MHz spectra of temperature induced helix-coil transition of PBLG sample R10 ( $DP=92$ ) in 20:80% TFA/ $\text{CDCl}_3$ . A, 36°C; B, 56°C; C, 62°C; D, 68°C; E, 78°C

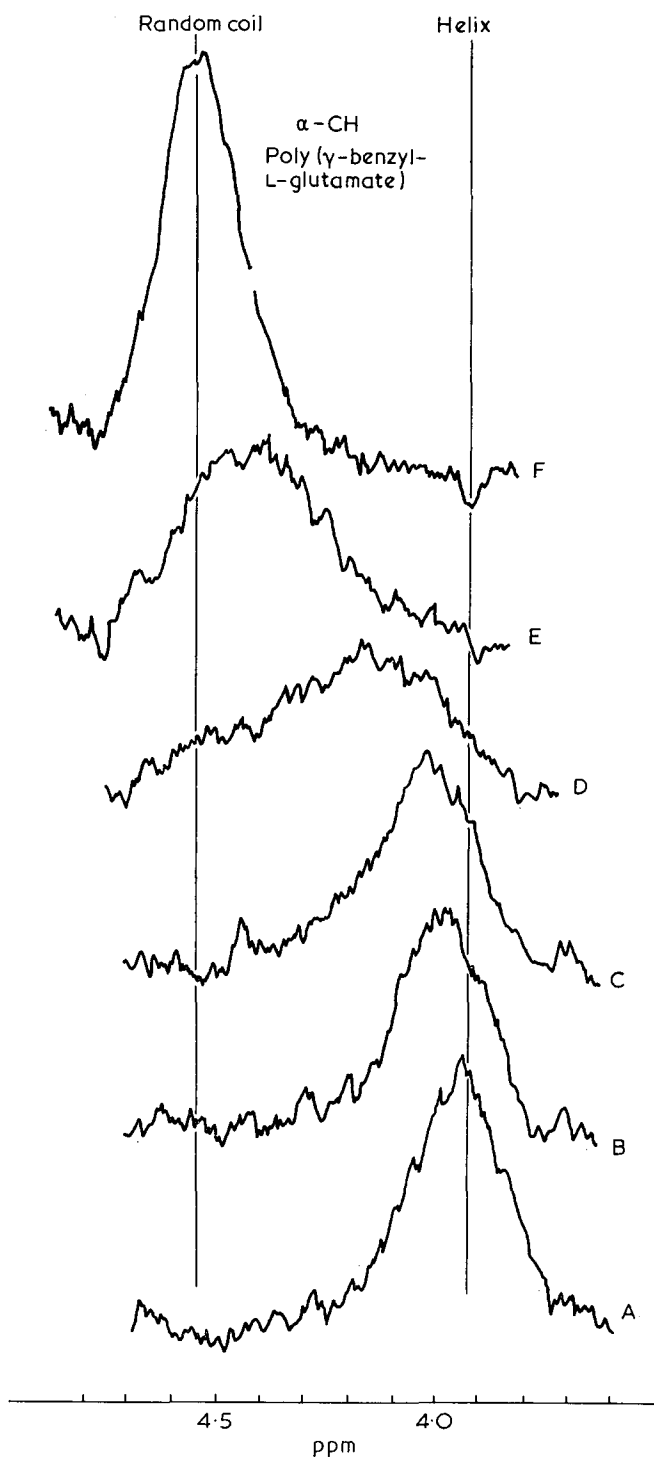


Figure 7 100MHz spectra in  $\text{CDCl}_3/\text{TFA}$  at 22°C of sample (130 mer) fractionated from R10. A, 1.3%; B, 8.4%; C, 9.6%; D, 10.7%; E, 11.8%; F, 14.0% TFA

the high molecular weight P17 is much sharper than that of R10 and S416. In addition that of R10 is even broader than that of S416. Figure 5 shows  $b_0$  curves (D), (E) and (F) for three fractions obtained from R10 (curve C). The data for the high molecular weight polymer P17 are included for comparison. It is striking that whilst

fractions obtained therefrom. In contrast to the unfractionated sample (Figure 6), showing the 'double peak' spectrum, the  $DP \sim 130$  fraction (Figure 7), shows only a moving resonance envelope. For the  $DP \sim 45$  fraction (Figure 8) the spectrum still shows a double peak character and this may be a consequence of polydispersity remaining at this low molecular weight. It might alternatively be due to very marked chain end effects that show up in a low molecular weight fraction. Residual polydispersity could be due to inefficient fractionation below  $DP \sim 50$  which results from the high sensitivity of the solubility at these chain lengths to slight inconsistencies in the temperature and solvent gradients on the column.

One fraction from R10 was subjected to refractionation by precipitation chromatography and of the resulting material a fraction A20, having  $DP \sim 110$ , i.e. close to that of the original R10, was investigated by n.m.r. Figure 9 shows the results which, on comparison with the corresponding spectra of R10 in Figure 6, demonstrate how a reduced polydispersity at the same molecular weight leads to disappearance of the 'double peak' spectrum.

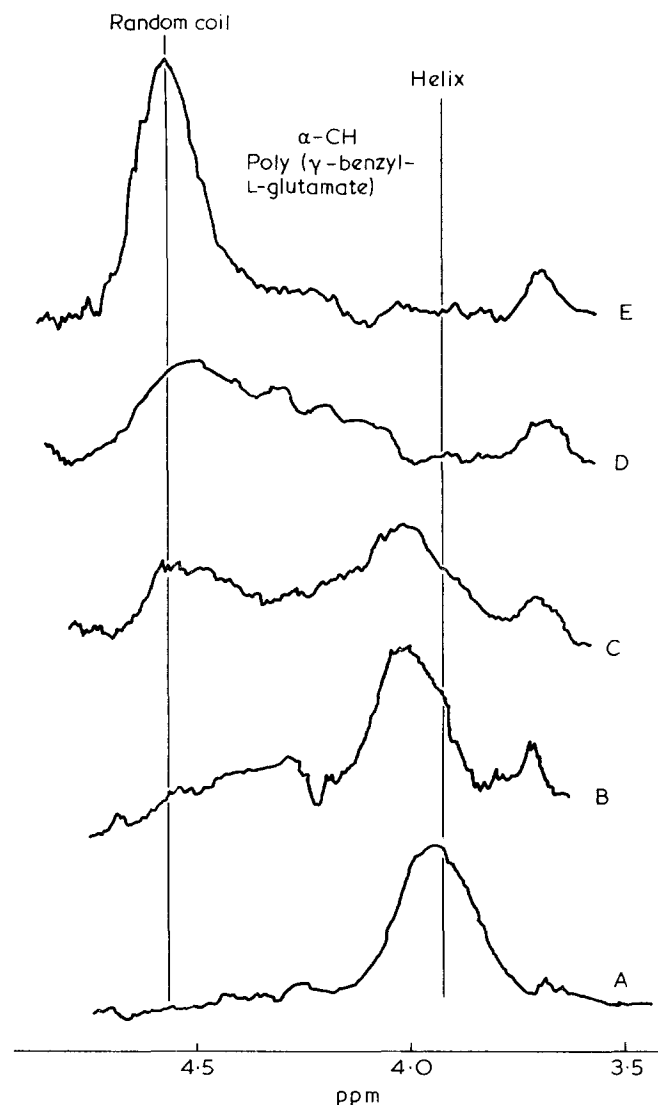


Figure 8 100MHz spectra in  $CDCl_3$ /TFA at 22°C of sample (45mer) fractionated from R10. A, 1.0%; B, 3.5%; C, 5.5%; D, 7.8%; E, 11.1% TFA

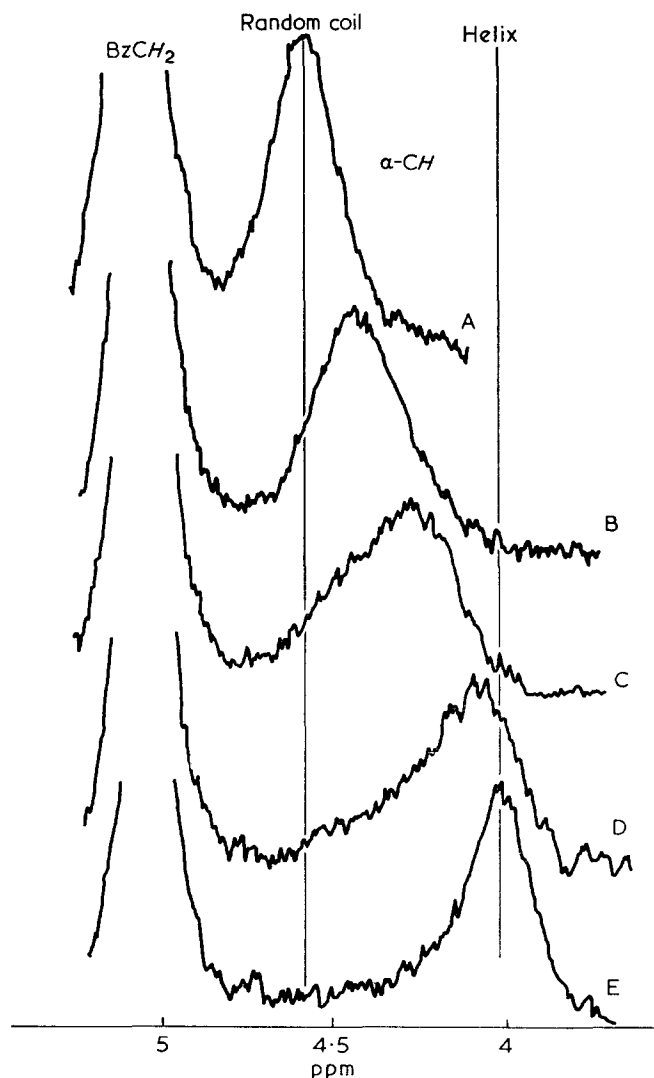


Figure 9 100MHz spectra of temperature induced helix-coil transition of PBLG sample R10 fraction A20 ( $DP=110$ ) in 12.88%  $CDCl_3$ . A, 5°C; B, 16°C; C, 19°C; D, 26°C; E, 38°C

## CONCLUSION

The above results demonstrate beyond doubt that polydispersity plays a major role in the appearance of 'double peak' main chain resonances for a sample having  $\overline{DP}$  of about 100. At  $\overline{DP} \sim 45$  our spectra still show some 'double peak' character. The recent results of Nagayama and Wada<sup>10</sup>, however, suggest that samples of  $\overline{DP} \sim 45$  of low polydispersity do show a single shifting peak. This implies that our  $\overline{DP} \sim 45$  sample may still be quite polydisperse. The present data compliment those of Nagayama and Wada and the sum total of both studies convincingly demonstrates that no contradiction exists between the observed n.m.r. spectra and the results of kinetic estimates of helix-coil exchange rates.

## ACKNOWLEDGEMENTS

We are grateful to Dr B. G. Carpenter of this laboratory for considerable assistance and advice during the course of the work. The continuing support of the SRC is also gratefully acknowledged.

REFERENCES

- 1 Ferretti, J. A. *Chem. Commun.* 1967, p 1030; Markley, J. L., Meadows, D. H. and Jardetzky, O. *J. Mol. Biol.* 1967, **27**, 25; Bradbury, E. M., Crane-Robinson, C., Goldman, H. and Rattle, H. W. E. *Nature* 1968, **217**, 812; Haylock, J. C. and Rydon, H. N. 'Peptides 1968' North Holland, Amsterdam, 1968
- 2 Schwarz, G. *J. Mol. Biol.* 1965, **11**, 64; Lumry, R., Legare, R. and Miller, W. G. *Biopolymers* 1964, **2**, 489; Barksdale, A. D. and Stuehr, J. E. *J. Am. Chem. Soc.* 1972, **94**, 3334
- 3 Ferretti, J. A., Ninham, B. W. and Parsegian, V. A. *Macromolecules* 1970, **3**, 34
- 4 Joubert, F. J., Lotan, N. and Scheraga, H. A. *Biochemistry* 1970, **9**, 2197
- 5 Bradbury, J. H. and Fenn, M. D. *Aust. J. Chem.* 1969, **22**, 357
- 6 Bradbury, E. M., Cary, P. D., Crane-Robinson, C. and Hartman, P. G. *Pure Appl. Chem.* 1973, **36**, in press
- 7 Goodman, M., Toda, F. and Ueyama, N. *Proc. Natl Acad. Sci. USA* 1973, **70**, 331
- 8 Ullman, R. *Biopolymers* 1970, **9**, 471
- 9 Bradbury, E. M., Crane-Robinson, C. and Rattle, H. W. E. *Polymer* 1970, **11**, 277
- 10 Nagayama, K. and Wada, A. *Chem. Phys. Lett.* 1972, **16**, 50
- 11 Doty, P., Bradbury, J. H. and Holtzer, A. M. *J. Am. Chem. Soc.* 1956, **78**, 947
- 12 Mitchell, J. C., Woodward, A. E. and Doty, P. *J. Am. Chem. Soc.* 1957, **79**, 3955
- 13 Baker, C. A. and Williams, R. J. P. *J. Chem. Soc.* 1956, p 2352
- 14 Peggion, A., Scoffone, E., Cosani, E. and Portolan, A. *Bio. polymers* 1966, **4**, 695

# Microtacticity of polymethacrylonitrile

T. Suzuki, S. Koshiro and Y. Takegami

Department of Hydrocarbon Chemistry, Faculty of Engineering, Kyoto University,  
Kyoto 606, Japan

(Received 5 March 1973; revised 14 May 1973)

220 MHz n.m.r. investigations of polymethacrylonitrile (PMAN) of different tacticities were carried out. A partly resolved pentad stereosequence distribution can be obtained from  $\alpha$ -methyl proton resonance. The pentad stereosequence distribution of PMAN prepared with free radical initiator can be explained by Bernoullian statistics, taking  $P_m=0.46$ . However, the stereosequence distribution of PMAN prepared with diethyl magnesium catalyst was neither explained by Bernoullian nor first-order Markov chain statistics. The stereosequence distribution of the dimethylformamide insoluble fraction of the above polymer agrees well with that calculated from Markov statistics, taking  $P_{m/m}=0.88$  and  $P_{r/m}=0.58$ .

## INTRODUCTION

In contrast to poly(methyl methacrylate) (PMMA), the microtacticity of polymethacrylonitrile (PMAN) has not been elucidated. Matsuzaki and Uryu<sup>1</sup> reported triad tacticity of PMAN prepared with free radical initiator. PMAN was converted to PMMA by alkaline hydrolysis followed by esterification and PMMA was subjected to nuclear magnetic resonance (n.m.r.) analysis. They concluded that radically initiated PMAN has almost a random configuration and slightly isotactic rich stereosequence distribution. Ishigure *et al.*<sup>2</sup> and Segre *et al.*<sup>3</sup> reported 100 MHz n.m.r. spectra of PMAN in trifluoroacetic acid. However, in this solvent methyl proton resonance did not show splitting according to triad stereosequences. Natta and Dallasta<sup>4</sup> and Joh *et al.*<sup>5</sup> reported several catalysts for the crystalline PMAN. Segre *et al.*<sup>3</sup> found that PMAN prepared with diethyl magnesium has a high concentration of isotactic dyad.

Recently Yamada and Yanagita<sup>6</sup> reinvestigated the microtacticity of PMAN. They concluded that PMAN prepared with radical initiator contains more syndiotactic substituents than isotactic ones. In addition they found splitting in the absorption of methyl proton of PMAN in nitromethane at 60 MHz, by different triad tacticities. These peaks are assigned to *rr*, *mr*, and *mm* triad sequences of PMAN in the order of increasing field strength. This assignment is just the opposite in the case of PMMA. There are still ambiguities in this assignment, as the crystalline PMAN prepared with an organometallic catalyst cannot be dissolved in nitromethane.

In this paper the present authors describe the 220 MHz n.m.r. spectra of PMAN prepared with radical and several organometallic catalysts.

## EXPERIMENTAL

The preparation of PMAN and extraction by acetone or dimethylformamide (DMF) were carried out as described by Joh *et al.*<sup>5</sup>. Polymer samples employed in this study are summarized in Table 1.

Table 1 Polymerization conditions and dyad fractions of PMAN

Run	Catalyst	Yield (%)	Dyad		Remarks
			<i>m</i>	<i>r</i>	
1	AIBN	36.0	0.46	0.54	Bulk at 60°C
2	Et <sub>2</sub> Mg	28.0	0.65	0.34	
2R		(49.0)	0.69	0.31	DMF-insoluble fraction
3	Et <sub>2</sub> Mg	41.8	0.53	0.47	at -78°C
4	n-BuLi	82.6	0.56	0.44	
4AR		(37.0)	0.58	0.42	Acetone-insoluble fraction
4AS		(63.0)	0.52	0.48	Acetone-soluble fraction
5	EtMg[AlEt <sub>2</sub> ]	48.0	0.64	0.36	
5R		(42.1)	0.70	0.30	DMF-insoluble fraction

Toluene, 27.0 ml; MAN, 3.0 ml; catalyst, 0.5 mmol; 70°C; 5 h

N.m.r. spectra were recorded at 220 MHz, with a Varian HR 220 spectrometer at 60~110°C, using tetramethylsilane as internal standard. Approximately 4-7% (wt/vol) solutions of PMAN in trifluoroacetic acid, acetonitrile-d<sub>3</sub>, benzonitrile, and nitromethane were employed.

Resolution of the n.m.r. spectrum into individual peaks was performed with a Fortran curve-resolution program, using a Facom 230-60 computer of Data Processing Center, Kyoto University. The parameters half-height width and peak height were optimized by fitting the computed curve to the experimental one, using Lorentzian line shape.

## RESULTS AND DISCUSSION

In Figure 1 220 MHz n.m.r. spectra of PMAN prepared with AIBN and the DMF insoluble fraction of PMAN prepared with Et<sub>2</sub>Mg are compared (in TFA solvent). Peaks at 1.95~2.05 $\delta$  in Figure 1a apparently are separated into three components, with two lower field peaks of relatively high intensity. On the other hand, the most characteristic feature in Figure 1b is the increase in the intensity of peak at 1.95 $\delta$ . According to the reported 100 MHz n.m.r. spectra these peaks cannot be separated in TFA. In addition at 100 MHz five peaks



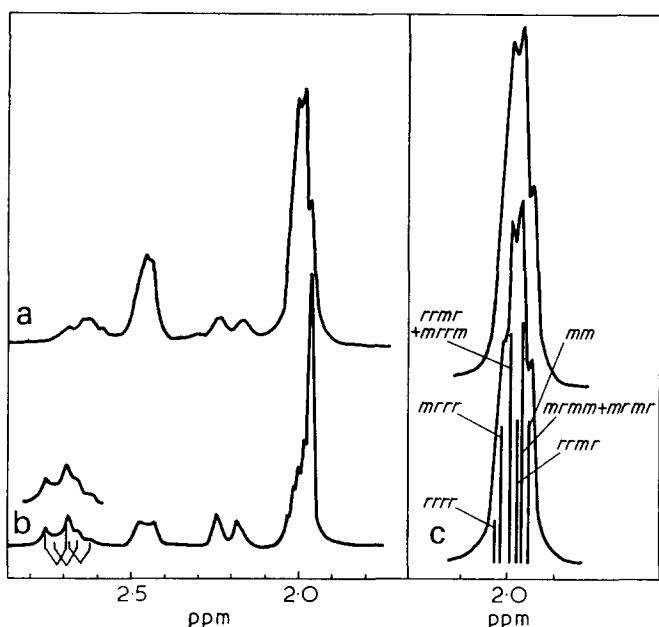


Figure 1 220 MHz n.m.r. spectra of polymethacrylonitrile. (a) Sample 1 (prepared with AIBN); (b) sample 2R (DMF-insoluble fraction prepared with  $\text{Et}_2\text{Mg}$ ); (c) calculated and observed (top) spectra of sample 1. Linewidth=4.0 Hz

are observed at 2.1~2.7 $\delta$ , which are assigned to AB quartet peaks of the meso dyad of PMAN methylene protons and a singlet peak (centre peak) of the racemic dyad of methylene protons. In 220 MHz spectrum (Figure 1a) higher field peaks exhibit part of an AB quartet but lower field peaks (2.57~2.70 $\delta$ ) present broad adsorption composed of an envelope of several lines. However, in the spectrum shown in Figure 1b part of the quartet at the higher field is sharper; in addition the lower field resonances can be resolved into three sets of AB quartets as shown in the block lines in Figure 1b. These resonances can be considered to be the tetrad stereosequences.\* The chemical shift differences of lower field resonances of methylene proton caused by configuration of remote units may be greater than those of higher field resonances of methylene proton. These features are also observed in PMMA<sup>7</sup>, and are quite different from those of poly(ethyl- $\alpha$ -chloroacrylate)<sup>8</sup>. However, chemical shift differences between the different tetrad sequences are very small compared with PMMA, in TFA solvent. Resonance of the racemic dyad cannot be observed as separate lines by the tetrad stereosequence. Therefore, further discussion about the tetrad sequences is not made.

As shown in Figure 1c  $\alpha$ -methyl proton resonances can be resolved into six components. The reason for this is interpreted as follows: (i) as shown in Figure 1b five relatively resolved peaks are observed in the isotactic rich polymer; (ii) well fitted calculated spectra cannot be obtained from resolution into three to five components, at any set parameter (half height width, peak height, and peak position).

As shown in Figure 1b the relative intensity of the *m* dyad increases as the relative intensity in the highest field  $\alpha$ -methyl peak increases. Therefore the highest field  $\alpha$ -methyl peak can be assigned to the *mm* triad stereosequence.

\* The measured tetrad sequences by curve resolution did not agree well with those calculated from first-order Markov chain model. This may be due to the influence of hexad sequences.

Although the accuracy of the estimated intensities of these resolved six lines were not good owing to poor resolution of the spectra, relative intensities of the resolved six lines do fit those calculated from Bernoullian statistics (see Table 2)<sup>6</sup>. Therefore, the assignment of the other five lines can be tentatively carried out as shown in the first column of Table 2 and Figure 1c. The estimated *mm* triad fraction of samples 1 and 2R are in considerably good agreement with the values obtained from PMMA converted from PMAN at 60 MHz by Yamada and Yanagita<sup>6</sup>. The fraction of the *m* dyad in sample 1 agrees well with that obtained by these authors, but that of sample 2R differs from the value obtained by them. Since resolution of the meso and racemic dyad peaks are complete at 220 MHz our results should be more reliable. In this polymer (sample 2R) the fraction of the *mm* triad is higher than that expected from the *m* dyad fraction calculated from Bernoullian statistics. Although due to partial overlapping of the pentad sequences, the fractions of the *mr* and *rr* triad cannot be determined, the *mr* and *rr* triad fractions were calculated from the stationary conditions of propagation ( $m = mm + \frac{1}{2}mr$ ;  $r = rr + \frac{1}{2}mr$ ). From these values, parameters of first-order Markov chain model were calculated, and in Table 3 the pentad fractions of the Markov trial are compared to those observed. Observed and calculated pentad sequences of sample 2R are in fairly good agreement, except *rrmr* + *mrrm* fractions.

Table 2 Calculated and observed pentad fractions of sample 1

$\delta$ in TFA	Sequence	Calcd <sup>a</sup>	In TFA	$\delta$ in $\text{CD}_3\text{CN}$	In $\text{CD}_3\text{CN}$
1.96	<i>mm</i>	0.21	0.19	1.75	0.19
1.98	<i>mrrm</i>	0.11	0.24	1.78	0.31
	<i>mrrmb</i>	0.12			
1.99	<i>rrmmb</i>	0.12			
2.00	<i>rrmr</i>	0.14	0.23	1.79	0.16
	<i>mrrm</i>	0.06		1.80	0.10
2.02	<i>rrrm</i>	0.14	0.15	1.81	0.15
2.03	<i>rrrr</i>	0.09	0.06	1.83	0.08

<sup>a</sup> Calculated from Bernoullian statistics  $P_m=0.46$

<sup>b</sup> These two sequences cannot be distinguished

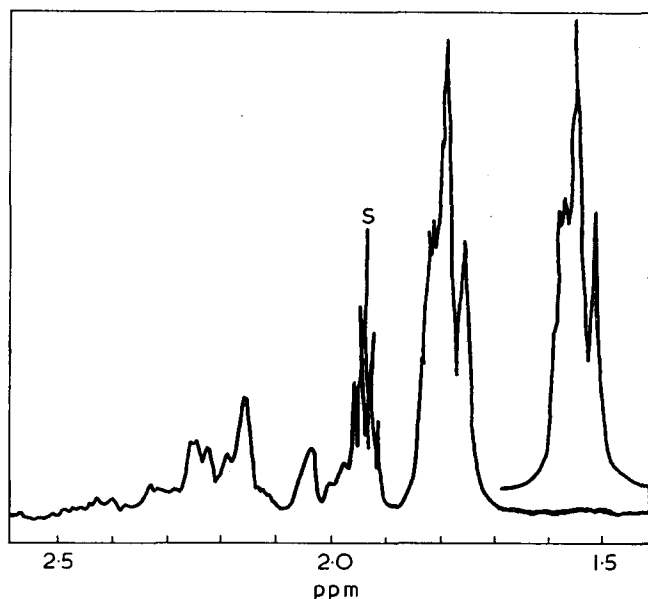


Figure 2 N.m.r. spectra of polymethacrylonitrile in  $\text{CD}_3\text{CN}$  (sample 1). S denotes solvent peak

Table 3 Calculated and observed pentad fractions of PMAN prepared with organometallic catalysts

Sequence	2	2R	Calcd <sup>a</sup>	3	Calcd <sup>b</sup>	5	5R	Calcd <sup>a</sup>	4	4AS	Calcd <sup>b</sup>	4AR
<i>mm</i>	0.47	0.62	0.61	0.25	0.28	0.46	0.58	0.58	0.28	0.25	0.28	0.31
<i>mrrm</i>	} 0.15	} 0.12	0.09	} 0.24	} 0.14	} 0.11	} 0.17	} 0.15	} 0.22	} 0.24	} 0.14	} 0.20
<i>mrmr</i>			0.03									
<i>rrmm</i>	0.11	0.07	0.09	0.09	0.12	0.17	0.06	0.10	0.13	0.09	0.12	0.15
<i>rrmr</i>	} 0.18	} 0.11	0.06	} 0.21	} 0.11	} 0.16	} 0.12	} 0.02	} 0.22	} 0.21	} 0.11	} 0.20
<i>mrrm</i>			0.02									
<i>rrrr</i>	0.07	0.05	0.06	0.14	0.11	0.09	0.05	0.03	0.09	0.11	0.11	0.13
<i>rrrr</i>	0.02	0.02	0.02	0.07	0.05	0.02	0.03	0.02	0.05	0.09	0.05	0.01

<sup>a</sup> Calculated from first-order Markov model

<sup>b</sup> Calculated from Bernoullian statistics

2R:  $P_{m/m}=0.88$ ;  $P_{r/m}=0.58$

5R:  $P_{m/m}=0.83$ ;  $P_{r/m}=0.73$

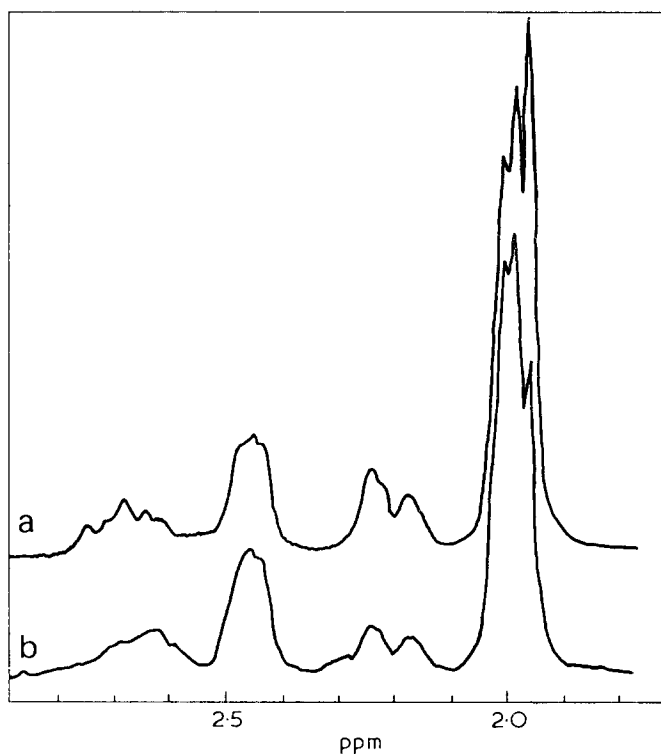


Figure 3 N.m.r. spectra of polymethacrylonitrile prepared with  $\text{Et}_2\text{Mg}$ . (a) Sample 2 (polymerized at  $70^\circ\text{C}$ ); (b) sample 3 (polymerized at  $-78^\circ\text{C}$ )

PMAN prepared with AIBN can be dissolved into acetonitrile, benzonitrile or nitromethane. In these solvents, as described by Yamada and Yanagita, more highly resolved spectra can be obtained as shown in Figure 2.

Resonances of methyl proton split into six lines with overlapping, and resonances of methylene protons show a completely different pattern in contrast to that obtained in TFA. This may be attributed to the absorptions of the tetrad and/or hexad stereosequences of the meso and racemic methylene protons. Unfortunately PMAN rich in the meso dyad such as sample 2R cannot be dissolved in these solvents, and in addition PMAN rich in the racemic dyad cannot be prepared. Therefore the assignment for these methylene proton absorptions is difficult. A tentative assignment of methyl peaks is shown in Table 2. Partly overlapped pentad sequences of different overlapping from those obtained in TFA are observed.

In Table 3 the relative intensity of the pentad stereosequence distribution of PMAN prepared with  $n\text{-BuLi}$  catalyst is compared. Relative intensity of the *mm* triad

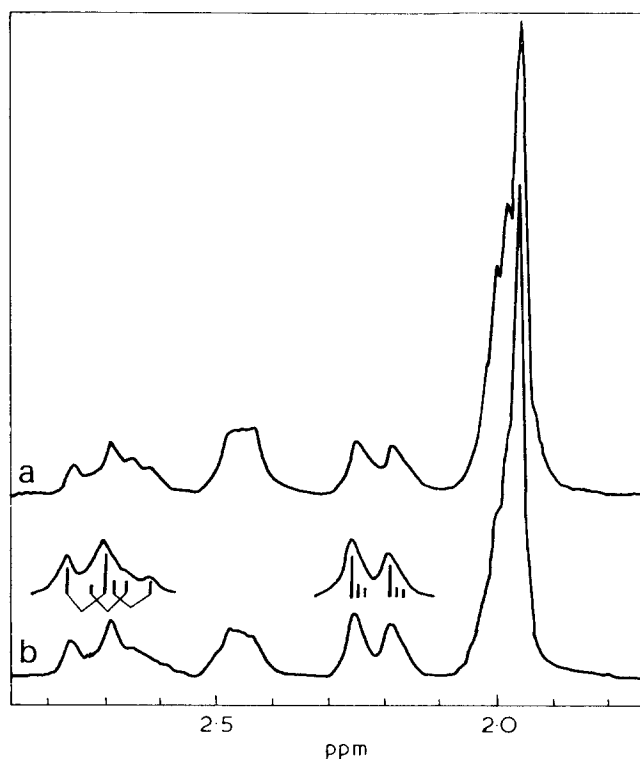


Figure 4 N.m.r. spectra of polymethacrylonitrile prepared with  $\text{EtMg}[\text{AlEt}_4]$ . (a) Sample 5 (whole polymer); (b) sample 5R (DMF-insoluble fraction)

fraction increases in the order  $\text{AS} < \text{W} < \text{AR}$ . This means that extraction by boiling acetone was possibly due to the difference in the stereosequence distribution. The pentad stereosequence distribution of the acetone-soluble fraction also fits that calculated from Bernoullian statistics. However, that of the acetone-insoluble fraction or the whole polymer was neither explained by Bernoulli or first-order Markov trial.

In Figure 3 n.m.r. spectra of PMAN prepared with  $\text{Et}_2\text{Mg}$  catalyst at  $-78^\circ\text{C}$  and  $70^\circ\text{C}$  are compared. Absorption of the *mm* triad in the polymer prepared at low temperature decreased markedly compared with that prepared at high temperature. The stereosequence distribution of PMAN prepared at  $-78^\circ\text{C}$  obeys Bernoullian statistics; on the other hand, PMAN prepared at  $70^\circ\text{C}$  neither obeyed Bernoullian nor first-order Markov statistics. We may conclude from these findings that diethyl magnesium presents the characteristics of multicentres of active species. At low temperature the catalyst produces predominantly atactic PMAN. At high temperature the catalyst has active centres

producing predominantly isotactic PMAN<sup>5</sup>. However, catalytic species producing atactic PMAN still exist, and produce atactic PMAN which was extracted by DMF, at high temperature. Therefore, DMF-insoluble polymer prepared with diethyl magnesium at high temperature (sample 2R) contains stereosequence obeying first order Markov statistics.

PMAN prepared with EtMg aluminium tetraethyl (ate) complex catalyst also has high concentrations of isotactic triad sequence as shown in *Figure 4* and *Table 3*. Stereosequence distribution of this polymer also deviates from Bernouillian and first-order Markov statistics. The DMF-insoluble fraction of this polymer has higher concentrations of the *mm* triad sequence as compared with whole polymer, and observed stereosequence distribution fits the calculated sequences obtained from first-order Markov trials.

The above results indicate that polymerization of methacrylonitrile by the organometallic catalyst proceeds according to at least two mechanisms; one is a coordinated anionic type of polymerization in which propagation proceeds by first-order Markov chain

model; the other may proceed via free anion-type propagation.

#### ACKNOWLEDGEMENT

We were grateful to Mr N. Nakayama for taking the n.m.r. spectra.

#### REFERENCES

- 1 Matsuzaki, K. and Uryu, T. *J. Polym. Sci. (B)* 1966, **4**, 255
- 2 Ishigure, K., Tabata, Y. and Oshima, K. *J. Polym. Sci. (B)* 1966, **4**, 669
- 3 Segre, A. L., Ciampelli, F. and Dall'asta, G. *J. Polym. Sci. (B)* 1966, **4**, 633
- 4 Natta, G. and Dall'asta, G. *Chim. Ind. (Milan)* 1964, **46**, 1429
- 5 Joh, Y., Yoshihara, T., Kotake, Y., Ide, F. and Nakatsuka, K. *J. Polym. Sci. (B)* 1966, **4**, 673; *J. Polym. Sci. (A-1)* 1967, **5**, 2503
- 6 Yamada, A. and Yanagita, M. *J. Polym. Sci. (B)* 1971, **9**, 103
- 7 Frisch, H. L., Mellows, C. L., Heatley, F. and Bovey, F. A. *Macromolecules* 1968, **1**, 533
- 8 Wesslén, B., Lenz, R. W. and Bovey, F. A. *Macromolecules* 1971, **4**, 709

# Configurational characteristics of ethylene–vinyl chloride copolymers

J. E. Mark

Department of Chemistry and the Macromolecular Research Center, University of Michigan, Ann Arbor, Michigan 48104, USA

(Received 7 May 1973)

Rotational isomeric state theory has been used to calculate mean-square unperturbed dimensions  $\langle r^2 \rangle_0$  and dipole moments  $\langle \mu^2 \rangle$  of ethylene–vinyl chloride copolymers as a function of chemical composition, chemical sequence distribution, and stereochemical composition of the vinyl chloride sequences. As was previously found for several other copolymeric chains,  $\langle \mu^2 \rangle$  is much more sensitive to chemical composition and chemical sequence distribution than is  $\langle r^2 \rangle_0$ . The present calculations also indicate that both  $\langle r^2 \rangle_0$  and  $\langle \mu^2 \rangle$  are most strongly dependent on chemical sequence distribution for ethylene–vinyl chloride chains having vinyl chloride sequences which are significantly syndiotactic in structure. In the case of ethylene–vinyl chloride copolymers in which the chemical sequences are relatively short and the vinyl chloride sequences are significantly isotactic, both  $\langle r^2 \rangle_0$  and  $\langle \mu^2 \rangle$  depend on chemical composition in an unexpectedly complex manner; under the cited conditions both of these statistical properties display a maximum and minimum in their variation with chemical composition.

## INTRODUCTION

The rotational isomeric state theory of chain molecules<sup>1</sup> has recently been used to give a very satisfactory interpretation of the mean-square dipole moments  $\langle \mu^2 \rangle$  of styrene/*p*-substituted styrene copolymers<sup>2</sup> and the temperature coefficient of the unperturbed dimensions  $\langle r^2 \rangle_0$  of ethylene–propylene copolymers<sup>3</sup>. Similar calculations have also been carried out on propylene–vinyl chloride chains<sup>4</sup>. Of particular interest in such studies is the sensitivity of these statistical properties to chemical sequence distribution since it should be feasible, at least under some conditions, to use experimental values of  $\langle r^2 \rangle_0$  and  $\langle \mu^2 \rangle$  to characterize such distributions in copolymeric chains. In addition, it is very important in general to understand the configurational characteristics of chemical copolymers (as opposed to stereochemical copolymers) since many commercial materials now fall into this category<sup>5,6</sup> and most polymers of biological interest are, of course, chemically copolymeric.

It is therefore the purpose of the present study to obtain a scheme for calculating statistical properties for copolymers of ethylene with any vinyl comonomer. The method may then be illustrated by application to ethylene–vinyl chloride copolymers, materials the preparation and study of which has become an area of very great current interest<sup>7–9</sup>. More specifically, we wish to obtain and interpret values of  $\langle r^2 \rangle_0$  and  $\langle \mu^2 \rangle$  for ethylene–vinyl chloride chains, calculated as a function of chemical composition, chemical sequence distribution, and stereochemical composition of the vinyl chloride sequences.

## THEORY

The chemical and stereochemical structure of an ethylene–vinyl comonomer chain may be adequately characterized

by the probability  $p_2$  of occurrence of units of type 2, the reactivity ratio product  $r_1 r_2$  (which controls the chemical sequence distribution at the specified value of  $p_2$ ), and the stereochemical replication probability  $p_r$  (probability of isotactic placement) characterizing the vinyl comonomer sequences. As has already been described<sup>1, 2, 10, 11</sup>, Monte Carlo methods may be used in conjunction with these variables in order to generate representative chains of any length which have the desired chemical composition, chemical sequence distribution, and stereochemical composition of the vinyl sequences.

The rotational isomeric state model for chain molecules has been extensively discussed elsewhere<sup>1</sup> as has been its specific application to the random-coil unperturbed dimensions of polyethylene<sup>1, 12–14</sup> and to both the unperturbed dimensions and dipole moments of a variety of vinyl chains, including poly(vinyl chloride)<sup>11</sup>. Following the analyses of such homopolymers, we adopt the rotational states *trans* (*t*), *gauche* positive (*g*<sup>+</sup>), and *gauche* negative (*g*<sup>−</sup>) for the skeletal bonds of the copolymer. Since intramolecular steric interactions may be relatively large within ethylene units, we allow for the displacement of these rotational states by an amount  $\Delta\phi$  from their symmetric locations at 0, 120, and  $-120^\circ$ <sup>1, 12</sup>. Specifically, these states are thus located at 0,  $120 - \Delta\phi$ , and  $-120 + \Delta\phi^\circ$ , respectively. Displacements of rotational states within vinyl comonomer units are also frequently significant<sup>1, 10</sup>. In the specific case of vinyl chloride units they are generally relatively minor, however, because of the small size of the pendant Cl atom<sup>11, 15, 16</sup>; in the case of this particular comonomer, the rotational states are therefore assumed to occur at 0,  $\pm 120^\circ$ .

The characterization of intramolecular interactions and the assignment of the corresponding statistical

weight factors is relatively simple in the case of copolymers of ethylene [CH<sub>2</sub>-CH<sub>2</sub>-] with a vinyl comonomeric unit [CH<sub>2</sub>-CHR-] where the pendant group R could be CH<sub>3</sub>, CH<sub>2</sub>-CH<sub>3</sub>, Cl, phenyl, etc. In the approximation that CH and CH<sub>2</sub> are sterically equivalent<sup>1,10</sup>, there are no intramolecular interactions occurring in such copolymeric chains not already characterized in analyses of the two homopolymers. Since, for example, such information is available for both polyethylene<sup>12-14</sup> and poly(vinyl chloride)<sup>11, 15, 16</sup>, both  $\langle r^2 \rangle_0$  and  $\langle \mu^2 \rangle$  can be directly calculated for ethylene-vinyl chloride chains without the need for additional approximations. The following analysis is therefore directly based on the schemes<sup>11-16</sup> developed for two such homopolymers. We consider first those interactions dependent on only one bond rotational angle. Conformations in which a CH or CH<sub>2</sub> group is *syn* to a CH<sub>2</sub> group are assigned a statistical weight factor of  $\sigma$ , whereas those in which a CH group is *syn* to an R group are given the factor  $\tau$ . Therefore, conformations in which CH is *syn* to both CH<sub>2</sub> and R are characterized by the product  $\sigma\tau$ . To facilitate comparison of the present analysis with that of the vinyl homopolymer itself, we normalize the factors  $\tau$ ,  $\sigma$ ,  $\sigma\tau$  to  $\eta$ , 1,  $\tau$  where  $\eta = \tau/\sigma$ <sup>11, 15, 17</sup>. If R is an articulated group such as CH<sub>2</sub>-CH<sub>3</sub>, then a pair of *trans* states about the bonds preceding and succeeding a substituted skeletal carbon atom give rise to interactions between the R group and the chain backbone which require the additional factor  $\tau^{*1, 10}$ . 'Pentane-type' interactions, dependent on rotational states of two consecutive skeletal bonds, are characterized by the factors  $\omega$ ,  $\omega'$ , and  $\omega''$ . The first of these,  $\omega$ , is introduced for conformations engendering interactions between a pair of CH or CH<sub>2</sub> groups. The second,  $\omega'$ , is associated with interactions between one of these groups and an R group, and the third,  $\omega''$ , with interactions between two R groups. Various combinations of these factors may be used to represent overall statistical weights for all possible conformations in ethylene-vinyl comonomer chains.

For the purpose of calculating configuration-dependent properties such as  $\langle r^2 \rangle_0$  and  $\langle \mu^2 \rangle$ , these statistical weights are used to construct statistical weight matrices  $U_i$ . In such matrices, rows are associated with rotational states about skeletal bond  $i-1$  and columns, with rotational states about skeletal bond  $i$ . Both rows and columns are indexed in the order  $t$ ,  $g^+$ ,  $g^-$ . For CH<sub>2</sub>-CH<sub>2</sub>-CH<sub>2</sub> (ethylene) bond pairs, the statistical weight matrix is designated  $U_e$  and has the form:

$$U_e = \begin{bmatrix} 1 & \tau/\eta & \tau/\eta \\ 1 & \tau/\eta & \tau\omega/\eta \\ 1 & \tau\omega/\eta & \tau/\eta \end{bmatrix} \quad (1)$$

For a pair of bonds meeting at a CHR group, the atomic configuration of the group must be specified. Adoption of the arbitrary  $d$ ,  $l$  convention previously employed<sup>1, 10, 11</sup> yields for the statistical weight matrix characterizing bonds meeting at a C atom of  $d$  configuration:

$$U_d = \begin{bmatrix} \eta\tau^* & 1 & \tau \\ \eta & 1 & \tau\omega \\ \eta & \omega & \tau \end{bmatrix} \quad (2)$$

By symmetry, the matrix  $U_l$  associated with a C atom

of  $l$  configuration is obtained by simple interchange of both the second and third rows and the second and third columns of  $U_d$ . In the case of pairs of bonds separating two CHR groups, the configuration of both groups must be specified. The statistical weight matrices for the dyads  $dd$  and  $dl$  are given by:

$$U_{dd} = \begin{bmatrix} \eta\omega'' & \tau\omega' & 1 \\ \eta & \tau\omega' & \omega \\ \eta\omega' & \tau\omega\omega'' & \omega' \end{bmatrix} \quad (3)$$

$$U_{dl} = \begin{bmatrix} \eta & \omega' & \tau\omega'' \\ \eta\omega' & 1 & \tau\omega \\ \eta\omega'' & \omega & \tau\omega'^2 \end{bmatrix} \quad (4)$$

The matrices  $U_{ll}$  and  $U_{ld}$  may be obtained from  $U_{dd}$  and  $U_{dl}$ , respectively, by the interchanges of rows and columns described above. Bond pairs CHR-CH<sub>2</sub>-CH<sub>2</sub> are characterized by the matrices  $U_{de}$  and  $U_{le}$  where:

$$U_{de} = \begin{bmatrix} \eta/\tau & \omega' & 1 \\ \eta/\tau & 1 & \omega \\ \eta/\tau & \omega & \omega' \end{bmatrix} \quad (5)$$

and  $U_{le}$  is related to  $U_{de}$  by the symmetry operations already described. Similarly, the matrices  $U_{ed}$  and  $U_{el}$  are associated with bond pairs CH<sub>2</sub>-CH<sub>2</sub>-CHR, with:

$$U_{ed} = \begin{bmatrix} \eta & \tau & 1 \\ \eta & \tau\omega' & \omega \\ \eta\omega' & \tau\omega & 1 \end{bmatrix} \quad (6)$$

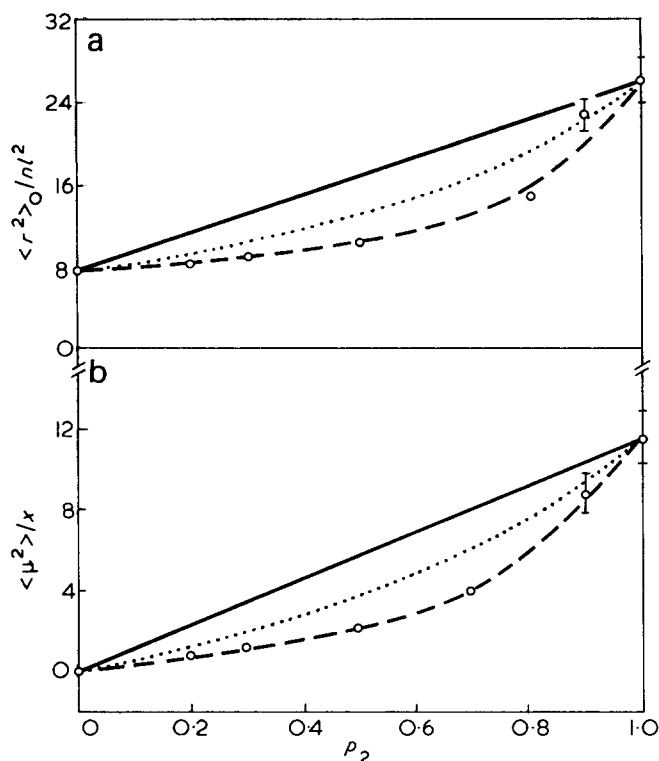
and  $U_{el}$  having the usual relationship to  $U_{ed}$ .

As described in detail elsewhere<sup>1, 10-12</sup>, these matrices may now be used in conjunction with bond lengths, bond angles, and group dipole moment vectors to calculate values of the mean-square unperturbed dimensions and dipole moments of the ethylene-vinyl comonomer chains generated by the Monte Carlo method. For convenience, these results will be expressed as the characteristic ratio  $\langle r^2 \rangle_0/nl^2$  (where  $n$  is the number of skeletal bonds, each of length  $l$ ) and the mean-square dipole moment per unit  $\langle \mu^2 \rangle/x$  (where  $x=n/2$  is the number of monomer units in the chain). The absence of a subscript zero on  $\langle \mu^2 \rangle$  is in recognition of the fact that long-range interactions should have no effect on the mean-square dipole moments of the copolymers chosen for the illustrative calculations, namely those of ethylene with vinyl chloride.<sup>11, 18, 19</sup>

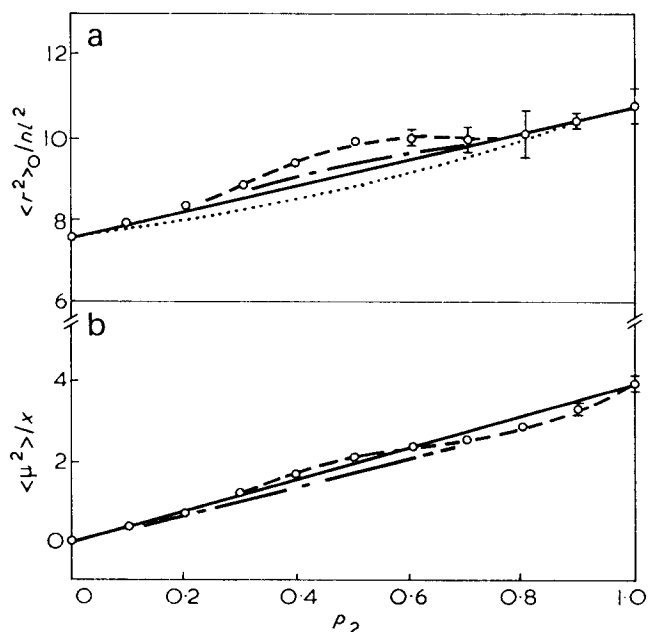
## RESULTS AND DISCUSSION

Calculations of  $\langle r^2 \rangle_0/nl^2$  and  $\langle \mu^2 \rangle/x$  for the ethylene-vinyl chloride copolymers were carried out using: (i) skeletal bond lengths of 1.53 Å and skeletal bond angles of 112°<sup>1, 10, 12</sup>; (ii) ethylene group dipole vectors of magnitude zero and vinyl chloride group dipole vectors of magnitude 2.00D, lying along C-Cl bonds tetrahedrally oriented with respect to the adjoining skeletal bonds<sup>11</sup>; (iii)  $\Delta\phi=0$  and 10°; (iv)  $p_r=0.05$ , 0.50, and 0.95 for the vinyl chloride sequences; (v)  $r_1r_2=0.01$ , 1.0, 100, 1000, and  $\infty$ ; (vi)  $x=n/2=100$ ; and (vii) values of the statistical weight factors appropriate for 25°C. These values are  $\eta=4.2$ ,  $\tau=0.45$ ,  $\tau^*=1.0$ ,  $\omega=\omega''=0.032$ , and  $\omega'=0.071$ <sup>1, 10-12, 15, 16</sup>.

Figures 1, 2 and 3 show some of the calculated results as a function of the chemical composition variable  $p_2$  (fraction of units which are vinyl chloride) and the



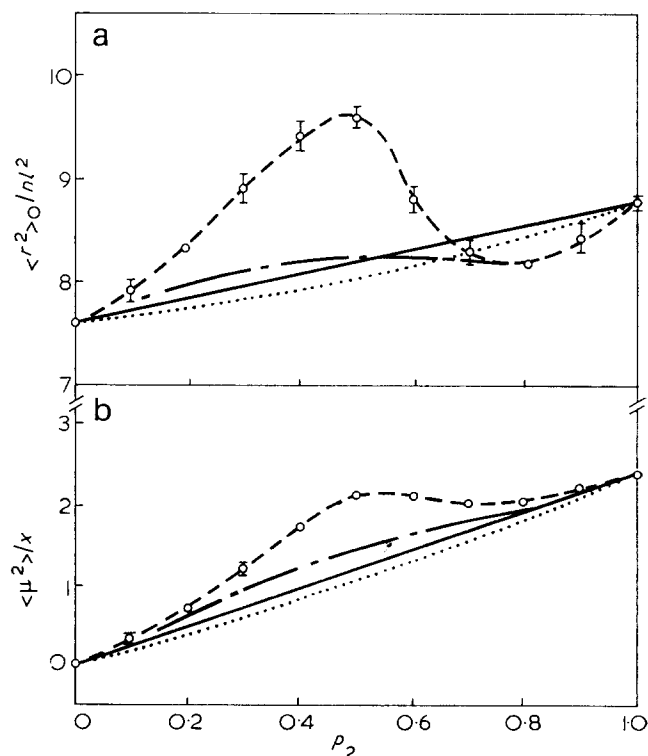
**Figure 1** Effect of chemical composition and chemical sequence distribution on (a) the characteristic ratio and (b) mean-square dipole moment per monomer unit of ethylene-vinyl chloride copolymers having vinyl chloride sequences of highly syndiotactic structure, at 25°C;  $p_r = 0.05$ . In this and the following Figures,  $p_r$  is the stereochemical replication probability and  $p_2$  is the probability that a given unit is of type 2 (vinyl chloride). In Figures 1-3, results are shown for rotational states located at  $\phi = 0, \pm 120^\circ$  (displacement  $\Delta\phi = 0^\circ$ ) and for selected values of the reactivity ratio product:  $r_1 r_2 = 0.01$  (---), 1.0 (— · —), 100 (·····), and  $\infty$  (—). Each circle (○) shown locates the average result calculated for five Monte Carlo chains, and the vertical lines through these points represent standard deviations. For purposes of clarity, calculated points and standard deviations are shown only for the case  $r_1 r_2 = 0.01$  in Figures 1-3, and for the case  $\Delta\phi = 0^\circ$  in Figures 4-6



**Figure 2** (a)  $\langle r^2 \rangle_0 / nl^2$  and (b)  $\langle \mu^2 \rangle / x$  shown as a function of  $p_2$  for selected values of  $r_1 r_2$  for ethylene-vinyl chloride copolymers having atactic vinyl chloride sequences;  $p_r = 0.50$ . See caption to Figure 1

reactivity ratio product  $r_1 r_2$ . Results are given for illustrative values of the replication probability  $p_r$  of 0.05, 0.50 and 0.95. More detailed results which show the dependence of  $\langle r^2 \rangle_0 / nl^2$  and  $\langle \mu^2 \rangle / x$  on  $\log r_1 r_2$  at equimolar composition ( $p_2 = 0.50$ ), are given in the remaining three Figures. As documented in detail elsewhere<sup>2, 3</sup>, increase in  $r_1 r_2$  at constant  $p_2$  corresponds to an increasing tendency to form long sequences ('blocks') of uniform chemical structure. For example, at  $p_2 = 0.50$ , values of  $r_1 r_2$  of 0.0 and 1000 give average sequence lengths  $n_1 = n_2$  of 1.0 and  $\sim 24$ , respectively, for a chain of  $x = 100$  units.

These results indicate that  $\langle \mu^2 \rangle / x$  is much more sensitive to chemical composition and chemical sequence distribution at constant composition than is  $\langle r^2 \rangle_0 / nl^2$ , a result of considerable importance with regard to possible characterization of such distributions by measurements of configuration-dependent properties. This conclusion is in agreement with results of previous studies on styrene/*p*-substituted styrene copolymers<sup>2</sup>, ethylene-propylene copolymers<sup>3</sup>, and propylene-vinyl chloride copolymers<sup>4</sup>. As has been previously pointed out<sup>4</sup>, this enhanced sensitivity in the case of  $\langle \mu^2 \rangle / x$  is obviously due to the fact that, in the calculation of  $\langle r^2 \rangle_0 / nl^2$  chemically different units differ in conformational energy, but have essentially identical values of the quantity being averaged, the skeletal bond vector, as expressed in the skeletal-bond coordinate system<sup>3, 4</sup>. On the other hand, in the calculation of  $\langle \mu^2 \rangle / x$ , both the conformational energy and the group dipole moment vector depend on the chemical nature of the comonomer unit<sup>2, 4</sup>. In the case of both  $\langle r^2 \rangle_0 / nl^2$  and  $\langle \mu^2 \rangle / x$  for ethylene-vinyl chloride chains, the strongest dependence on chemical sequence distribution is found in the stereochemical region of high syndiotacticity ( $p_r = 0.05$ ) of the vinyl chloride sequences.



**Figure 3** (a)  $\langle r^2 \rangle_0 / nl^2$  and (b)  $\langle \mu^2 \rangle / x$  shown as a function of  $p_2$  for selected values of  $r_1 r_2$  for ethylene-vinyl chloride copolymers having highly isotactic vinyl chloride sequences;  $p_r = 0.95$ . See caption to Figure 1

It is interesting to note that in the case of ethylene-vinyl chloride copolymers in which the chemical sequences are relatively short and the vinyl chloride sequences are significantly isotactic, both the characteristic ratio and the mean-square dipole moment per unit depend on chemical composition in an unexpectedly complex manner. For such copolymers, both of these statistical properties display a maximum and minimum in their variation with chemical composition. This behaviour can be readily understood by considering in detail the effect of chemical composition and chemical sequence distribution on, for example, the characteristic ratio  $\langle r^2 \rangle_0/nl^2$  of an ethylene-vinyl chloride copolymer having highly isotactic vinyl chloride sequences. As is shown in Figures 1-3,  $\langle r^2 \rangle_0/nl^2$  for a vinyl chloride homopolymer is larger than that of polyethylene homopolymer. Furthermore, addition of vinyl chloride units to a polyethylene chain increases its value of  $\langle r^2 \rangle_0/nl^2$ , while addition of ethylene units to a vinyl chloride chain decreases its value of  $\langle r^2 \rangle_0/nl^2$ . The characteristic ratio of a vinyl chloride homopolymer which is highly isotactic ( $p_r=0.95$ ) is, however, not very much larger than that of polyethylene and, consequently, the dependence of  $\langle r^2 \rangle_0/nl^2$  on composition exhibits the pronounced maximum and minimum shown in Figure 3. The effect is most pronounced at small values of the reactivity ratio product because of two circumstances. Increase in the characteristic ratio of a polyethylene chain due to addition of vinyl chloride units is greatest if these units are widely dispersed along the chain (small average sequence length due to small

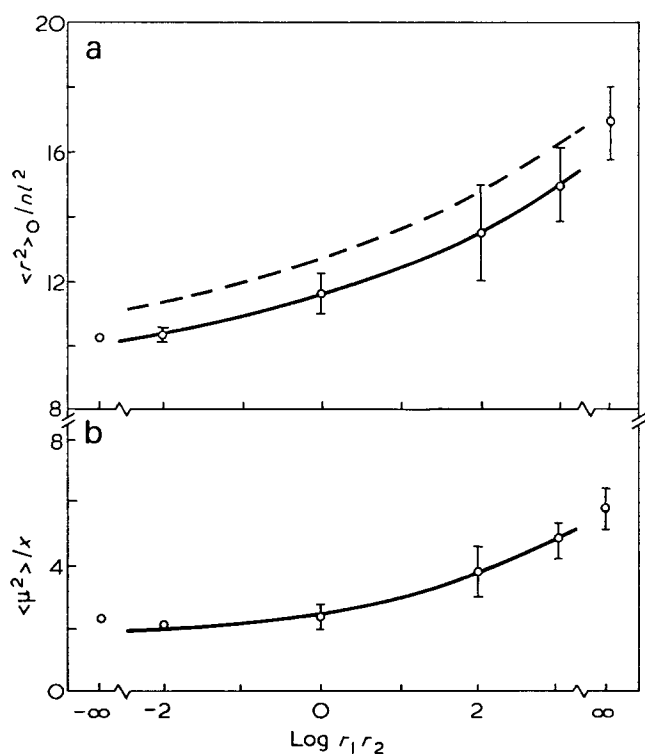


Figure 4 Dependence of (a) the characteristic ratio and (b) mean-square dipole moment per unit on the reactivity ratio product for ethylene-vinyl chloride chains of equimolar composition ( $p_2=0.50$ ) and highly syndiotactic vinyl chloride sequences, at 25°C;  $p_r=0.05$ . Circles (○) and solid lines (—) locate results calculated for  $\Delta\phi=0^\circ$ ; the broken lines (---) show results obtained upon alteration of  $\Delta\phi$  to  $10^\circ$  in the case of ethylene units, when these results differ significantly from those calculated for  $\Delta\phi=0^\circ$

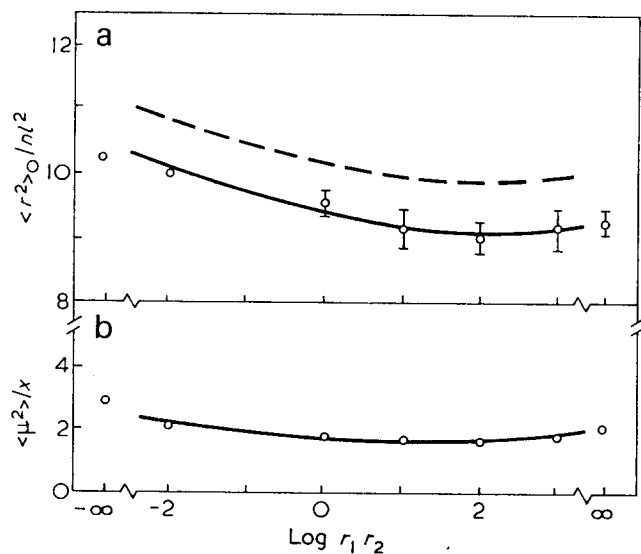


Figure 5 Dependence of (a)  $\langle r^2 \rangle_0/nl^2$  and (b)  $\langle \mu^2 \rangle/x$  on  $r_1 r_2$  for ethylene-vinyl chloride chains having  $p_2=0.50$  and atactic vinyl chloride sequences;  $p_r=0.50$ . See caption to Figure 4

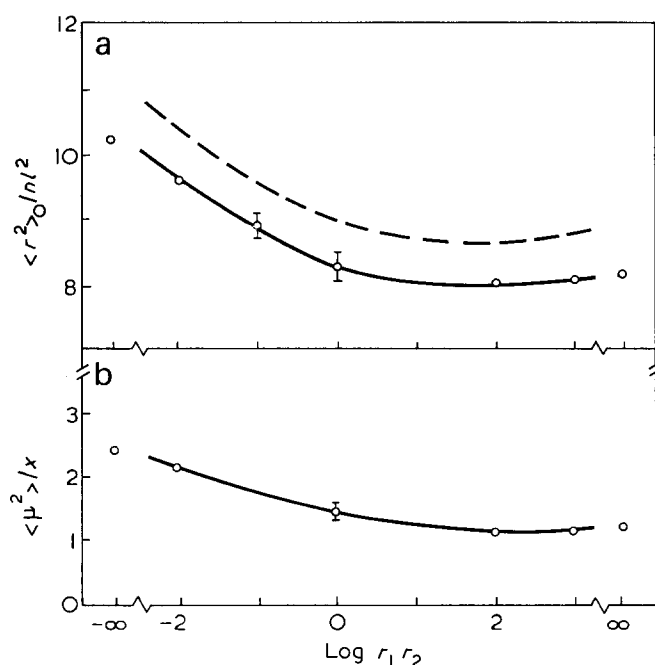


Figure 6 Dependence of (a)  $\langle r^2 \rangle_0/nl^2$  and (b)  $\langle \mu^2 \rangle/x$  on  $r_1 r_2$  for ethylene-vinyl chloride chains having  $p_2=0.50$  and highly isotactic vinyl chloride sequences;  $p_r=0.95$ . See caption to Figure 4

reactivity ratio product) since, in the case of highly isotactic vinyl chloride sequences, interactions between neighbouring vinyl chloride units decreases the preference for highly extended *trans* conformations in these units<sup>11, 15</sup>. Correspondingly, decrease in the characteristic ratio of an isotactic poly(vinyl chloride) chain upon incorporation of ethylene units is most pronounced when the ethylene units are widely dispersed, causing the largest number of disruptions of the extended helical conformations adopted by the isotactic vinyl chloride sequences<sup>11, 15</sup>. These maxima and minima would thus be expected to be less pronounced in the case of an ethylene-vinyl chloride copolymer having less highly isotactic vinyl chloride sequences and this is, in fact, shown by the results for the atactic case ( $p_r=0.50$ ) given in Figure 2. Similar arguments apply to  $\langle \mu^2 \rangle/x$  since, in vinyl chloride sequences, conforma-

tions of high chain extension are also of high dipole moment<sup>11</sup>.

It should be noted that the location of the rotational states is not of crucial importance in the present analysis. As can be seen from the broken lines in *Figures 4-6*, alteration of the displacement  $\Delta\phi$  from 0 to 10° in the case of ethylene units has only a relatively small effect on  $\langle r^2 \rangle_0/nl^2$  and no significant effect at all on  $\langle \mu^2 \rangle/x$ .

It is thus now apparent that although measurements of configuration-dependent properties of copolymers do show considerable promise, at least under some conditions, for use in characterizing chemical sequence distributions, the variation of such properties with chemical composition, chemical sequence distribution, and stereochemical composition can be exceedingly complex<sup>20</sup>.

#### ACKNOWLEDGEMENTS

Part of the work described here was carried out while the author was Visiting Professor at the University of Manchester during the Spring Term of 1972, and he would like to thank the members of the Department of Chemistry there for their hospitality. It is also a pleasure to acknowledge the financial support provided for this research by Grant GH-36205 from the National Science Foundation.

#### REFERENCES

- 1 Flory, P. J. 'Statistical Mechanics of Chain Molecules', Interscience, New York, 1969

- 2 Mark, J. E. *J. Am. Chem. Soc.* 1972, **94**, 6645
- 3 Mark, J. E. *J. Chem. Phys.* 1972, **57**, 2541
- 4 Mark, J. E. *J. Polym. Sci. (Polym. Phys.)* 1973, **11**, 1375
- 5 Aggarwal, S. L. (Ed.), 'Block Polymers', Plenum Press, New York, 1970
- 6 Molau, G. E. (Ed.) 'Colloidal and Morphological Behavior of Block and Graft Copolymers', Plenum Press, New York, 1971
- 7 See, for example, refs. 8 and 9 and relevant studies cited therein
- 8 Misono, A., Uchida, Y. and Yamada, K. *Bull. Chem. Soc. Japan* 1967, **40**, 2366
- 9 Misono, A., Uchida, Y., Yamada, K. and Saeki, T. *Bull. Chem. Soc. Japan* 1968, **41**, 2995
- 10 Flory, P. J., Mark, J. E. and Abe, A. *J. Am. Chem. Soc.* 1966, **88**, 639
- 11 Mark, J. E. *J. Chem. Phys.* 1972, **56**, 451
- 12 Abe, A., Jernigan, R. L. and Flory, P. J. *J. Am. Chem. Soc.* 1966, **88**, 631
- 13 Flory, P. J. and Jernigan, R. L. *J. Chem. Phys.* 1965, **42**, 3509
- 14 Jernigan, R. L. and Flory, P. J. *J. Chem. Phys.* 1969, **50**, 4178
- 15 Flory, P. J. and Williams, A. D. *J. Am. Chem. Soc.* 1969, **91**, 3118
- 16 Pickles, C. J. and Flory, P. J. *JCS Faraday Trans. II* 1973, **63**, 632
- 17 Williams, A. D. and Flory, P. J. *J. Am. Chem. Soc.* 1969, **91**, 3111
- 18 Nagai, K. and Ishikawa, T. *Polymer J.* 1971, **2**, 416
- 19 Doi, M. *Polymer J.* 1972, **3**, 252
- 20 The simple linear dependence of the statistical properties on chemical composition indicated for block copolymers in general was first pointed out by Stockmayer and coworkers [Stockmayer, W. H., Moore, L. D. Jr., Fixman, M. and Epstein, B. N. *J. Polym. Sci.* 1955, **16**, 517]. It has been experimentally verified for styrene-methyl methacrylate copolymers [Kotaka, T., Ohnuma, H. and Inagaki, H. *Polymer* 1969, **10**, 517; Kotaka, T., Tanaka, T., Ohnuma, H., Murakami, Y. and Inagaki, H. *Polymer J.* 1970, **1**, 245] and for styrene-isoprene copolymers [Urwin, J. R. and Girolamo, M. *Makromol. Chem.* 1972, **160**, 183]



# Molecular motion of polytetrafluoroethylene under high pressure

Chitoshi Nakafuku, Seiji Taki and Tetuo Takemura

Department of Applied Science, Faculty of Engineering, Kyushu University, Fukuoka, Japan  
(Received 21 May 1973; revised 18 June 1973)

The molecular motion of polytetrafluoroethylene under high pressure is seen directly by nuclear magnetic resonance (n.m.r.) study. The motional narrowing of the broad component at the high pressure phase shows that the interchain potential is fairly anharmonic and the vibration of the chain along the interchain direction becomes more incoherent on account of the active rotation of molecular chains, which are in a very compact phase.

## INTRODUCTION

Polytetrafluoroethylene (PTFE) has two first order transitions at atmospheric pressure, that is 20°C and 30°C transitions. Another transition under high pressure has been reported by some authors<sup>1</sup>. The phase diagram<sup>2</sup> obtained by the isobaric measurement of ultrasonic, linear thermal expansion and differential thermal analysis is shown in *Figure 1*. When the measuring temperature crosses over from phase II to phase III (high pressure phase), the attenuation increases, the sound velocity decreases, the volume decreases rapidly and the sharp endothermic peak appears at this transition point<sup>2</sup>. The Grüneisen parameter,  $\gamma$ , and the interchain specific heat,  $C_{inter}$ , by isothermal sound velocity and compressibility measurements become larger, and smaller, respectively at the high pressure phase<sup>3</sup>. The result and calculated values are shown in *Table 1*. The estimated value of the effective interchain force constant,  $g$  per effective intrachain force constant,  $f$  by Wada and Hayakawa's method<sup>4</sup> is about 0.1 at the high pressure phase, and the effective motional unit in the chain is about 6 CF<sub>2</sub> units in this region as shown in *Table 1*.

These results by indirect measurements show that the interchain potential is fairly anharmonic and the vibration of the chain along the interchain direction becomes more incoherent on account of an active rotation of molecular chains at the high pressure phase.

It is the purpose of this paper to obtain the direct proof of the molecular motion of this material under high pressure by n.m.r. measurements.

## APPARATUS

The measuring cell for n.m.r. measurement in a small magnet (diameter of pole piece 100 $\phi$ ) is shown in *Figure 2*.

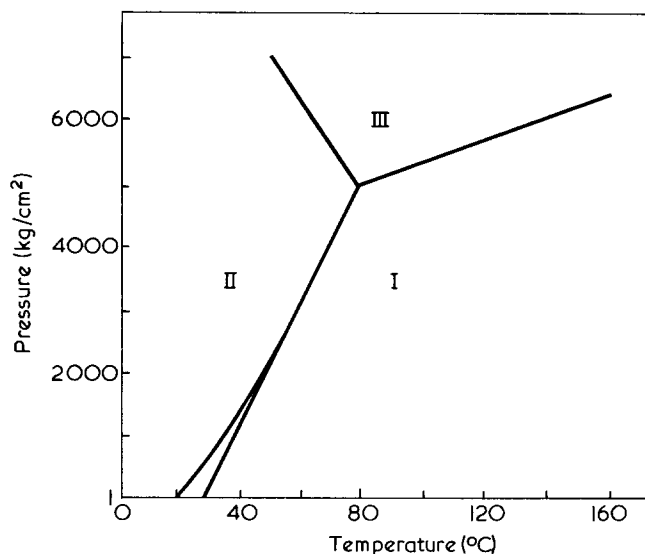


Figure 1 Phase diagram of PTFE<sup>2</sup>

Table 1 Thermodynamic quantities and motional unit of PTFE under high pressure

Pressure (kg/cm <sup>2</sup> )	15°C				48°C				65°C				81°C			
	$C_{inter}$ (J/K·g)	$g/f$	$N$	$\gamma$	$C_{inter}$ (J/K·g)	$g/f$	$N$	$\gamma$	$C_{inter}$ (J/K·g)	$g/f$	$N$	$\gamma$	$C_{inter}$ (J/K·g)	$g/f$	$N$	$\gamma$
1	0.125 <sup>II</sup>	0.25	4.0	4.8	0.100 <sup>I</sup>	0.16	5.0	5.3	0.116 <sup>I</sup>	0.22	4.3	5.2	0.124 <sup>I</sup>	0.25	4.0	5.2
1000	0.145 <sup>II</sup>	0.34	3.4	5.2	0.123 <sup>I</sup>	0.24	4.1	5.4	0.143 <sup>I</sup>	0.33	3.5	5.0	0.154 <sup>I</sup>	0.38	3.2	4.6
2000	0.160 <sup>II</sup>	0.41	3.1	5.4	0.142 <sup>I</sup>	0.32	3.5	5.0	0.171 <sup>I</sup>	0.47	2.9	4.6	0.182 <sup>I</sup>	0.53	2.7	4.4
3000	0.173 <sup>II</sup>	0.48	2.9	5.5	0.200 <sup>II</sup>	0.64	2.5	5.5	0.200 <sup>I</sup>	0.64	2.5	4.5	0.211 <sup>I</sup>	0.72	2.4	4.7
4000	0.183 <sup>II</sup>	0.54	2.7	5.8	0.228 <sup>II</sup>	0.84	2.2	5.2	0.240 <sup>I</sup>	0.93	2.1	4.4	0.236 <sup>I</sup>	0.90	2.1	4.8
5000	0.191 <sup>II</sup>	0.59	2.6	5.8	0.247 <sup>II</sup>	0.98	2.0	5.2	0.294 <sup>II</sup>	1.39	1.7	-3.0	0.276 <sup>I</sup>	1.22	1.8	2.8
6000	0.198 <sup>II</sup>	0.63	2.5	6.0	0.256 <sup>II</sup>	1.05	1.9	5.6	0.086 <sup>III</sup>	0.12	5.8	10.0	0.068 <sup>III</sup>	0.07	7.3	12.2

$C_{inter}$  is interchain specific heat,  $g/f$  is the effective interchain force constant per effective intrachain force constant,  $N$  is the number of the effective motional unit of CF<sub>2</sub>,  $\gamma$  is Grüneisen parameter  
I, II, III refer to phases I, II, III respectively

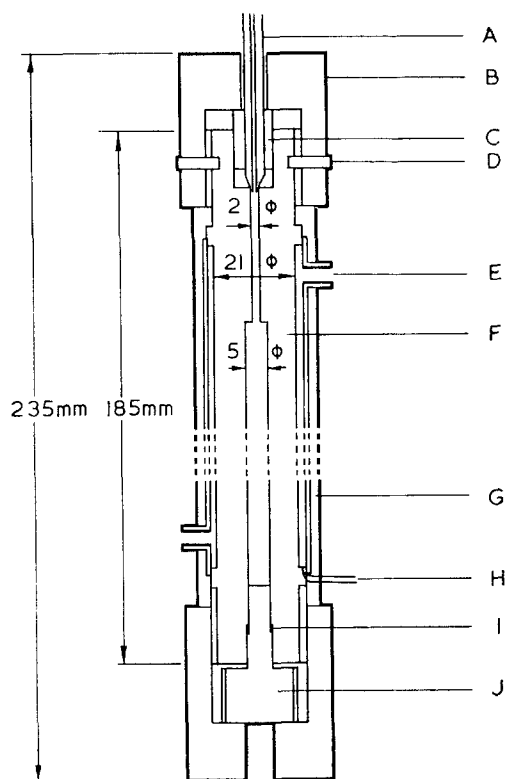


Figure 2a Beryllium-copper high pressure vessel. A, high pressure pipe; B, retaining screw of stainless steel; C, beryllium-copper collar; D, pin to avoid the rotation of the retaining screw; E, path for water or oil for temperature control; F, vessel; G, glass wool as thermal insulator; H, Pt/Pt-Rh 13% thermocouple attached to the surface of the vessel; I, copper seal; J, electrode plug

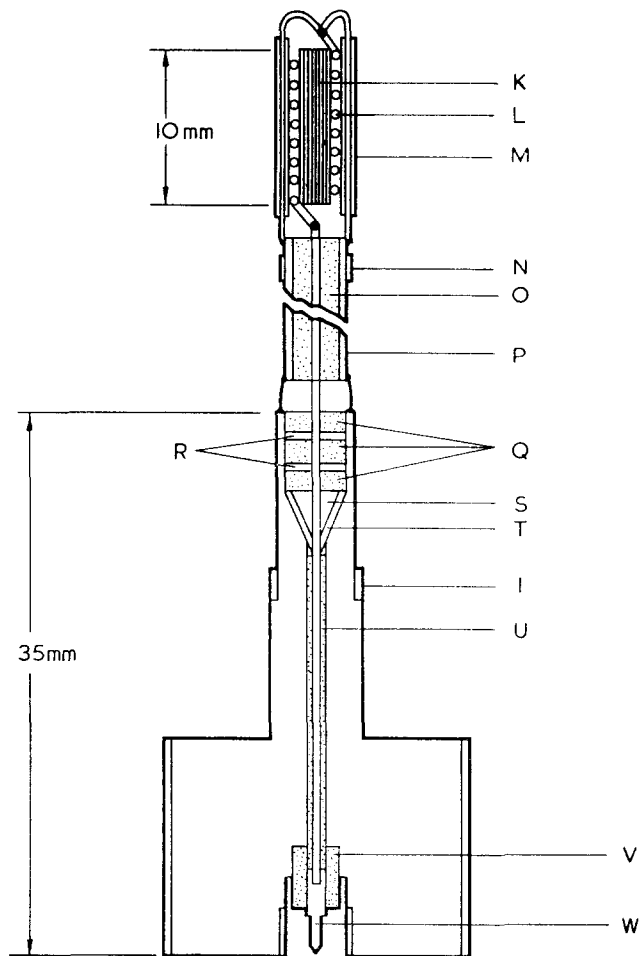


Figure 2b Beryllium-copper plug for vessel of Figure 2a. K, PTFE fibre sample; L, r.f. coil; M, PTFE tube for electric insulator; N, supporter; O, PTFE tube; P, brass tube; Q, epoxy resin; R, PTFE plate; S, beryllium-copper cone; T, sintered pyrophyllite and epoxy resin; I, copper seal; U, PTFE tube; V, PTFE tube; W, electrode

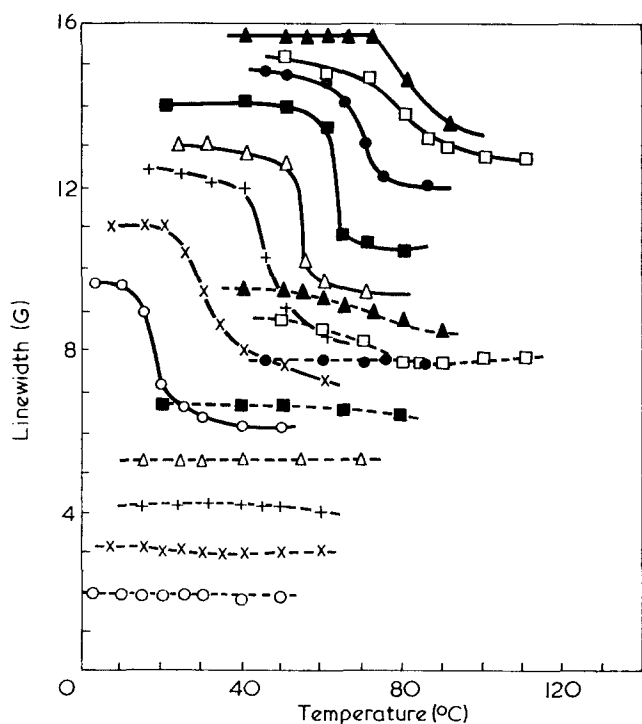


Figure 3 Linewidth versus temperature at elevated pressure for  $\theta=90^\circ$ . Motional narrowing occurs along II-I and II-III transition lines. In this Figure and Figure 4, the indications are shifted by the step of 1G/1000kg/cm<sup>2</sup> along vertical axis. ○, 1; ×, 1000; +, 2000; △, 3000; ■, 4000; ●, 5000; □, 5500; ▲, 6000kg/cm<sup>2</sup>. —, Broad component; ---, narrow component

The inner diameter and the outer diameter of this beryllium-copper cell ( $R_c=34$ ) were  $5\phi$  and  $21\phi$ , respectively, as shown in Figure 2a. The sample diameter was  $2\phi$ , and the sample weight was about 20 mg. Two kinds of coils wound on the bundle ( $2\phi$ ) of PTFE fibre (Toyoflon T 100) and the column ( $2\phi$ ) cut perpendicularly from the oriented fibre sheet bound by epoxy resin were used for the samples of  $\theta=90^\circ$  and  $0^\circ$ , where  $\theta$  is the angle between the fibre axis and the magnetic field. The coil and the electrode are shown in Figure 2b. The Amagat type seal was used for the electrode. The Pound and Knight type oscillating circuit<sup>5</sup> with a positive feed-back circuit was employed as a tool for the investigation of this small sample. The stable r.f. amplitude across the coil was 20 mV. In this experiment, a r.f. amplitude of 50 mV was used. The resonance radio frequency was set at 11.1919 MHz, for the poor  $Q$  value of the coil due to the Amagat electrode under high frequency.

The d.c. magnetic field produced was modulated at a rate of 37 or 150 Hz by the audio IC driver unit. The amplitude of modulation was set at 0.67 G, where the broadening of the linewidth of the broad and narrow component of this sample is not affected. A light oil was used as a pressure transmitting fluid. The proton resonance signal of this fluid on the oscilloscope is a good measure of the fluorine signal. The temperature

of the sample was controlled by the circulation of oil or water around the cell. The temperature was detected and controlled by the Pt/Pt-Rh 13% thermocouple.

RESULTS

The linewidth of the broad and narrow components for  $\theta=90^\circ$  and  $0^\circ$  under pressure are shown in Figures 3 and 4, respectively. In the case of  $\theta=90^\circ$ , the motional narrowing of the broad component occurs along the II-I transition line up to the triple point (about  $75^\circ\text{C}$ ,  $5000\text{ kg/cm}^2$ ) and this result is similar to the results at atmospheric pressure<sup>6</sup>. At the pressure range above this triple point the motional narrowing of the broad component occurs along the II-III transition line. On the other hand, in the case of  $\theta=0^\circ$ , the motional narrowing of the broad component does not occur along II-I

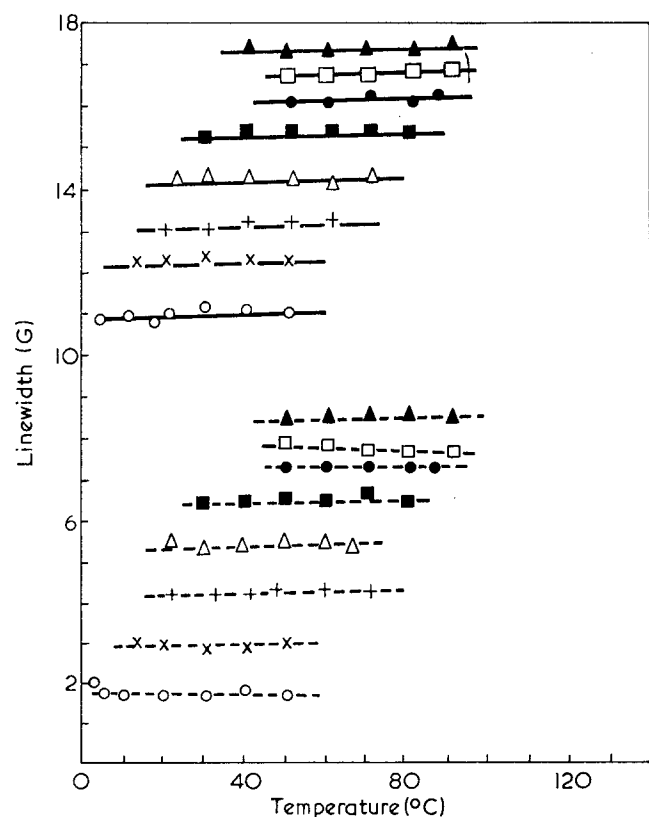


Figure 4 Linewidth versus temperature at elevated pressure for  $\theta=0^\circ$ . Motional narrowing cannot be seen in this Figure. —, Broad component; ----, narrow component. Symbols as in Figure 3

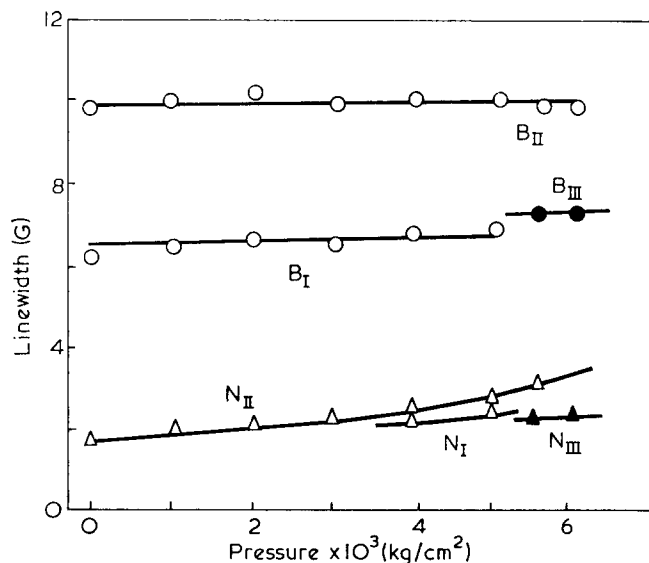


Figure 5 Linewidth versus pressure for each phase for  $\theta=90^\circ$ . B<sub>I</sub>, B<sub>II</sub>, and B<sub>III</sub> indicate linewidths of broad component for phases I, II, and III, respectively. N<sub>I</sub>, N<sub>II</sub>, and N<sub>III</sub> indicate linewidths of narrow component for phases I, II, and III

and II-III transition lines. The final behaviour of the linewidth of each component for  $\theta=90^\circ$  in each phase is shown in Figure 5.

These results show directly that the interchain potential is fairly anharmonic and the vibration of the chain along the interchain direction becomes more incoherent on account of the active rotation of molecular chain at the high pressure phase.

REFERENCES

- 1 Bridgman, P. W. *Proc. Am. Acad. Arts Sci.* 1948, **76**, 71; Weir, C. E. *J. Res. Natl. Bur. Stand.*, 1951, **46**, 207
- 2 Hirakawa, S. and Takemura, T. *Japan. J. Appl. Phys.* 1969, **8**, 635
- 3 Matsushige, K., Hirakawa, S. and Takemura, T. *Mem. Fac. Eng. Kyushu Univ.* 1972, **32**, 153
- 4 Wada, Y., Itani, A., Nishi, T. and Nagai, S. *J. Polym. Sci. (A-2)* 1966, **7**, 201; Wada, Y. and Hayakawa, R. *Progr. Polym. Sci. Japan* 1971, **3**, 215
- 5 Pound, R. V. and Knight, W. D. *Rev. Sci. Instrum.* 1950, **21**, 219
- 6 Slichter, W. P. *J. Polym. Sci.* 1957, **24**, 173; Hyndman, D. and Origlio, G. F. *J. Appl. Phys.* 1960, **31**, 1849; Yamagata, K. and Hirota, S. *Rep. Progr. Polym. Phys. Japan* 1962, **5**, 261; 1964, **7**, 279; McBrierty, V. J., McCall, D. W., Douglass, D. C. and Falcone, D. R. *Macromolecules* 1971, **4**, 584

# Triethylamine-sensitized photopolymerization of styrene

Kenji Yokota, Hideo Tomioka and Ken'ichiro Adachi

Materials Research Laboratory, Nagoya Institute of Technology, Gokiso-cho, Showa-ku, Nagoya, Japan

(Received 2 April 1973; revised 1 June 1973)

The photopolymerization of styrene in cyclohexane was accelerated by addition of triethylamine. The determination of the degree of polymerization of the polymer formed showed the acceleration was due to a concurrent sensitized initiation. Further kinetic studies revealed that the sensitization mechanism was analogous to that of the methyl methacrylate case reported earlier, in which an excited monomer and an amine formed an exciplex and gave an initiating radical species. The fluorescence of styrene was quenched effectively by addition of triethylamine in accordance with the kinetic argument.

## INTRODUCTION

In a previous paper<sup>1</sup>, the acceleration of the rate of photopolymerization of methyl methacrylate (MMA) by addition of several tertiary amines was described and the following initiation mechanism was proposed.

Excitation:



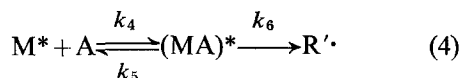
Self-quenching:



Direct photoinitiation:



Exciplex formation and sensitized initiation:



where M is the monomer, M\* is the excited monomer, A is the tertiary amine, (MA)\* is the exciplex, R· and R'· are initiating radical species and  $k_2$ – $k_6$  are reaction rate constants. This scheme is similar to the photo-reduction of aromatic ketones with tertiary amines<sup>2</sup> with respect to the mechanism which involves an exciplex formation between a donor (amine) and an excited acceptor (ester or ketone) and a hydrogen abstraction reaction on the  $\alpha$ -carbon adjacent to the nitrogen.

In the present paper, an analogous sensitization effect of triethylamine on the photopolymerization of styrene will be described. The sensitized photopolymerization of styrene has been extensively investigated using sensitizers such as dyes, polynuclear aromatic hydrocarbons, sulphur compounds and other miscellaneous compounds<sup>3</sup>. Tertiary amines, however, have been given little attention. The present sensitizer, tertiary amine, is not a real sensitizer in such a sense that the amine itself is not excited but interacts with the excited monomer to give an initiating radical species.

Mao and Eldred<sup>4</sup> showed that triphenylphosphine and MMA form a charge-transfer complex which is excited on irradiation and initiates the polymerization. They also showed that triphenylamine is not effective and that the polymerization of styrene is not sensitized with the phosphine.

## EXPERIMENTAL

### Materials

Styrene (extra pure) was successively washed with 10% sodium thiosulphate, 10% sodium hydroxide and distilled water, dried over anhydrous sodium sulphate, distilled under reduced nitrogen pressure and stored. Prior to the polymerization, this styrene was warmed to polymerize a part and distilled. Triethylamine (guaranteed) was stirred with crushed sodium thiosulphate and potassium hydroxide pellet and distilled under nitrogen. Cyclohexane (spectroscopic grade) was used as obtained.  $\alpha, \alpha'$ -Azobisisobutyronitrile (AIBN) was recrystallized twice from ethanol.

### Polymerization

The photopolymerization was carried out in a 10 ml Pyrex ampoule irradiating with a 300W Halos high-pressure mercury-vapour lamp from 260 mm distance. The dark polymerization with AIBN was carried out in a hard-glass ampoule wrapped with a thin black PVC film. Both polymerizations were conducted at 30.0°C in a thermostated bath and the rates of polymerization were determined by dilatometry. The contraction of styrene due to complete polymerization was estimated from the densities of monomer-polymer mixtures and calculated at 17.1% (lit.<sup>5</sup> 17.1%). A given mixture of styrene, triethylamine and cyclohexane in an ampoule was completely deoxygenated by repeated freeze-thaw cycles under vacuum before polymerization. The polymerization was continued after the determination of rate to 5–10% conversion, then the content of the ampoule was poured into methanol. The separated

polymer was twice reprecipitated with benzene-methanol and freeze-dried to a constant weight. The number-average degree of polymerization of the polymer was determined by osmometry on a Hewlett-Packard Model 501 Membrane Osmometer in toluene at 37°C.

### Spectroscopy

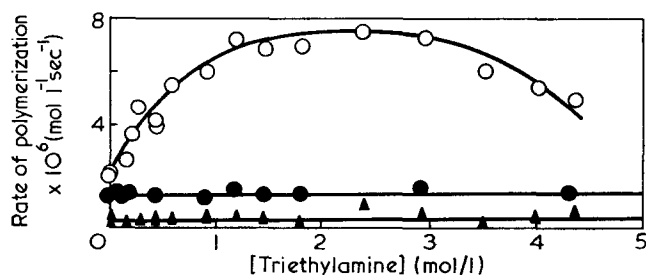
The ultra-violet spectra and the fluorescence spectra were recorded on a Shimadzu UV-200 Spectrometer and on a Hitachi MPF-2A Fluorescence Spectrometer. Cyclohexane was used as solvent throughout. Solutions for measurements were generally deoxygenated by repeated freeze-thaw cycles under vacuum.

## RESULTS AND DISCUSSION

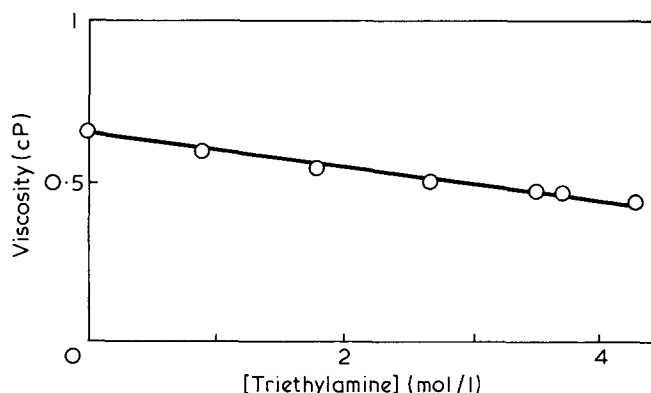
The effect of triethylamine concentration on the rate of polymerization of styrene (3.50 mol/l) in cyclohexane (a) under irradiation of mercury-vapour lamp, (b) with AIBN in the dark, and (c) without any initiator in the dark (thermal polymerization) are shown in *Figure 1*. The rate of thermal polymerization was determined interrupting the light beam for the polymerizing mixture for which the determination of the initial rate of photopolymerization had been just finished. As *Figure 1* shows, this remains constant and may be ignored in the following discussions. The rate of polymerization with AIBN in the dark also remains constant in the whole range of amine concentration and indicates the elementary reactions of AIBN-initiated polymerization are not influenced by the amine. On the other hand, the rate of photopolymerization is accelerated by addition of amine; with 0–1 mol/l of amine the rate increases steadily, with 1–3 mol/l of amine the rate reaches a plateau, and with still higher amine concentration the rate somewhat decreases. The maximum rate of sensitized photopolymerization is about four times that of the unsensitized rate. Thus it is clear that triethylamine has a sensitization effect on the rate of photopolymerization of styrene.

In the case of MMA of the previous work, it was necessary to correct the observed rate for the viscosity of the polymerizing mixture in order to estimate the net sensitization effect, because the termination reaction of the polymerization of MMA is diffusion-controlled<sup>6</sup>, and the addition of amine (substituting for solvent) changed the viscosity of the polymerizing mixture appreciably and thus caused the increase or decrease in rate irrespective of sensitization. The correction was made according to the following correlation:

$$R_p \propto \eta^{1/2} \quad (5)$$



*Figure 1* Effect of triethylamine concentration on the rate of polymerization of styrene in cyclohexane. [Styrene]=3.50 mol/l. O, Under irradiation of mercury-vapour lamp; ●, with AIBN in the dark; ▲, without any initiator in the dark (thermal polymerization)



*Figure 2* Effect of triethylamine concentration on the viscosity of the mixture of styrene, cyclohexane, and triethylamine. [Styrene]=3.50 mol/l

where  $R_p$  is the rate of polymerization, and  $\eta$  the viscosity of the polymerizing mixture. In the present case of styrene-triethylamine-cyclohexane, however, the correction of rate for viscosity was rather insignificant, because the addition of triethylamine substituting for cyclohexane, keeping the concentration of styrene constant, results in only a small change of viscosity (*Figure 2*), and because the effect of viscosity on the rate of polymerization of styrene is smaller<sup>7</sup>:

$$R_p \propto \eta^{1/4} \quad (6)$$

On assumptions that the addition of amine influences only the initiation reaction and not the propagation and termination reactions of photopolymerization and that the chain transfer reaction for triethylamine by polystyryl radical is not affected by the irradiation, the number-average degree of polymerization  $\bar{P}_n$  of the polymer formed is given by:

$$\bar{P}_n = \frac{k_t R_p}{2k_p^2 [\text{styrene}]^2} + C_s \frac{[\text{triethylamine}]}{[\text{styrene}]} + C_M \quad (7)$$

where  $k_p$  is the rate constant for propagation,  $k_t$  is the rate constant for termination,  $[\ ]$  is the concentration of the component,  $C_s$  is the chain transfer constant for triethylamine, and  $C_M$  is the chain transfer constant for styrene. The trivial chain transfer reaction for cyclohexane is neglected. The determination of  $C_s$  in the dark polymerization with AIBN at 30°C is shown in *Figure 3* and gives  $C_s = 1.1 \times 10^{-3}$ . By use of this  $C_s$  value and  $\bar{P}_n$  determined by osmometry for the polymer formed in the photopolymerization sensitized by triethylamine,  $1/\bar{P}_n - (C_s [\text{triethylamine}]/[\text{styrene}])$  is plotted against  $R_p$  and a straight line is obtained in *Figure 4*, the slope of which gives  $k_t/2k_p^2 [\text{styrene}]^2$ . Since  $[\text{styrene}] = 3.5 \text{ mol/l}$ ,  $k_t/k_p^2$  is given as  $1.05 \times 10^4$  that coincides with  $0.96 \times 10^4$  in the literature<sup>8</sup>. Therefore, it may be concluded that the increase of the rate of photopolymerization in the presence of triethylamine is attributable to the increase of the rate of initiation by a certain process involving this amine. Because the rate of polymerization is proportional to the square root of the rate of initiation, the maximum rate of initiation in the presence of the amine is about 16 times that of the unsensitized (direct) photoinitiation.

In order to reveal the mechanism of this sensitized initiation reaction, the monomer kinetic orders of styrene under various polymerization conditions were determined. *Figure 5* shows the plots of  $\log R_p$  against  $\log [\text{styrene}]$  in the polymerization under irradiation

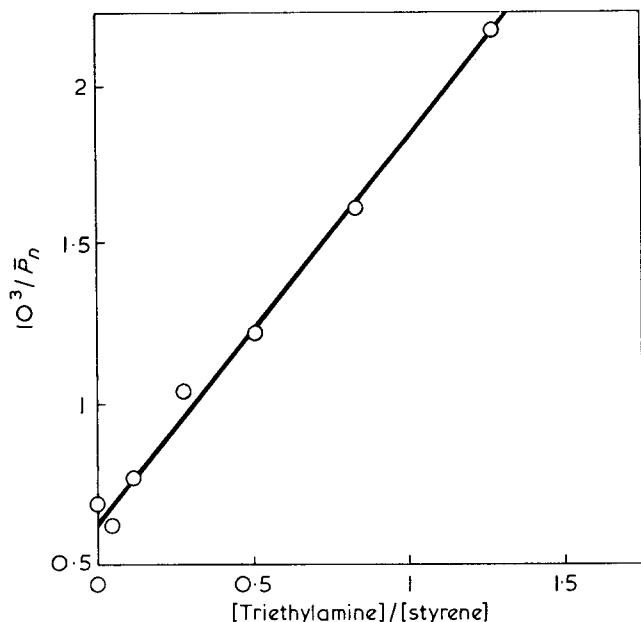


Figure 3 Determination of  $C_s$  for triethylamine in the dark, AIBN-initiated polymerization of styrene

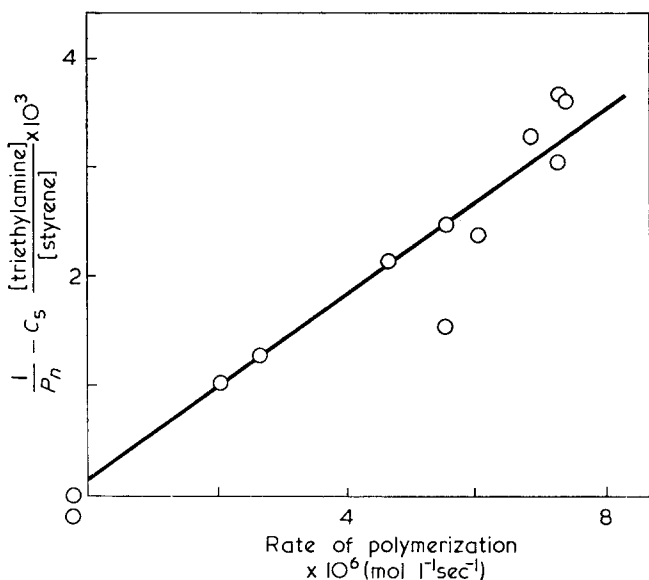


Figure 4 Determination of  $k_t/k_p^2$  in the photopolymerization of styrene in the presence of triethylamine

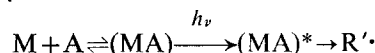
and with AIBN in the dark in cyclohexane solution without addition of triethylamine. The monomer kinetic orders given by the slopes of the plots are 1.24 for both methods of initiation. Olivé and Olivé<sup>9</sup> reported the identical value in this solvent for the AIBN-initiated polymerization at 50°C. One of the authors<sup>7</sup> has noticed that the monomer kinetic orders of styrene in various solvents are considerably affected by the viscosity of the solvent, although the quantitative explanation as for MMA<sup>10</sup> based on the diffusion-controlled termination theory<sup>6</sup> was unsuccessful. Because even in benzene solution an odd kinetic order (1.24<sup>7</sup> or 1.20<sup>9</sup>) is observed, the AIBN-initiated polymerization of styrene in cyclohexane may be considered to conform to the general scheme of radical polymerization. Then the direct photoinitiation reaction of the polymerization of styrene in cyclohexane should be of zeroth kinetic order with respect to styrene. This is most probable because the absorption of light (>310 nm) by styrene is very weak,

provided that a self-quenching reaction is predominant for the fate of excited styrene. Figure 5 also shows that the monomer kinetic orders in the presence of triethylamine (2.0 mol/l) under irradiation and with AIBN in the dark are consistently 1.24, and clearly demonstrates that the sensitized initiation should be of zeroth kinetic order with respect to styrene.

A definite kinetic order with respect to triethylamine in the sensitized photoinitiation cannot be evaluated, because in Figure 1 the effect of the amine concentration on rate is not uniform. The circumstances are similar to the MMA case where an initial increase in rate at low amine concentration tending to a plateau at higher amine concentration was observed. However, in the present styrene case a decrease in rate is observed at the highest amine concentration. The saturating sensitization effect was appropriately described by equation (8) on the basis of the reaction scheme, equations (1)–(4), in the previous work.

$$R'_i = \frac{2.30(k_6/k_2)I_0\epsilon d}{\left\{ \frac{(k_5+k_6)}{k_4} \right\} + 1} [A] \quad (8)$$

where  $I_0$  is the incident light intensity,  $\epsilon$  is the molar extinction coefficient of styrene at the wavelength employed,  $d$  is the optical length of the polymerizing ampoule. With increasing  $[A]$ , the numerator becomes smaller at first, then gradually approaches unity. Therefore  $R'_i$ , and ultimately  $R_p$ , increases at low amine concentration and tends to a plateau at higher amine concentration. An alternative possible interaction between monomer and amine as postulated for the phosphine-sensitization<sup>4</sup>:



did not fit the saturating profile. Equation (8) also explains the zeroth kinetic order with respect to monomer in the photoinitiation reaction. This rate expression may

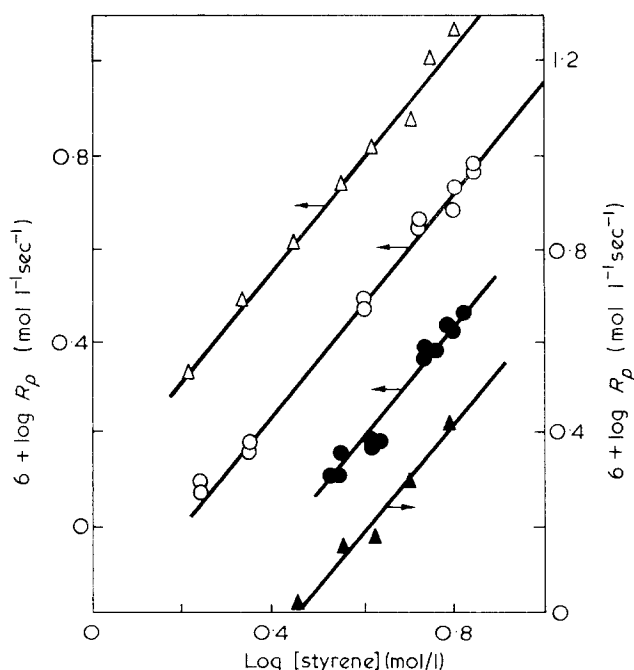


Figure 5 Determination of the monomer kinetic order in the polymerization of styrene under irradiation (○), with AIBN in the dark in cyclohexane (●), under irradiation (△), and with AIBN in the dark in triethylamine-cyclohexane (▲).  $[Triethylamine] = 2.0$  mol/l

also be applied to the present styrene case because the general kinetic aspects are analogous.

The decrease in rate at the highest amine concentration remains unexplained, however.

The ultra-violet spectra of the mixtures of styrene and triethylamine in cyclohexane were simple superpositions of spectra of the respective compounds either when they were very dilute ( $10^{-2} \sim 10^{-4}$  mol/l) or of polymerizing conditions (2 mol/l) and any charge transfer absorption band was not observed. The spectra of the concentrated solutions also showed that at the wavelength employed ( $> 310$  nm) only styrene absorbs light though very weakly ( $\epsilon < 0.1$ ). The fluorescence spectra of styrene with various concentrations of triethylamine are shown in Figure 6. Excitation was at 276 nm. Figure 6 shows that the intensity of the emission maximum at 306 nm decreases by the addition of triethylamine, a new emission at 400 nm appears instead, and an isosbestic point appear between them. The Stern-Volmer plot of this quenching process gives a straight line intercepting the ordinate at 1 as shown in Figure 7. The spectra of completely deoxygenated solutions decreased their intensities even during the scanning and gave a scattered plot. Probably the oxygen in the atmosphere disturbed the interaction between styrene and triethylamine. The quenching of the fluorescence of styrene by dissolved oxygen was recently reported<sup>11</sup> in connection with a sensitized photopolymerization. Such quenching processes by amines of the fluorescence of aromatic hydrocarbons have been studied and it is considered that the excited aromatic hydrocarbon behaves as an electron-

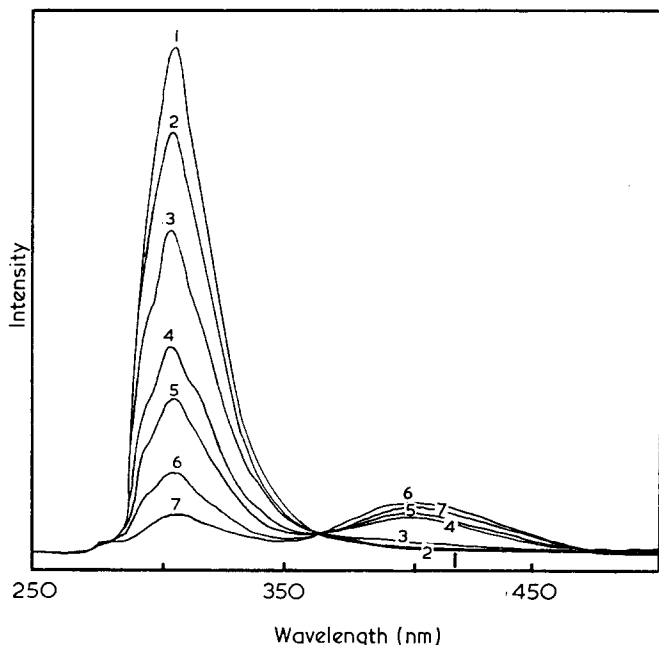


Figure 6 Fluorescence spectra of styrene with different concentrations of triethylamine. [Triethylamine]: 1, 0; 2, 1 mmol/l; 3, 4.4 mmol/l; 4, 14 mmol/l; 5, 23 mmol/l; 6, 59 mmol/l; 7, 150 mmol/l. The solutions were not deoxygenated

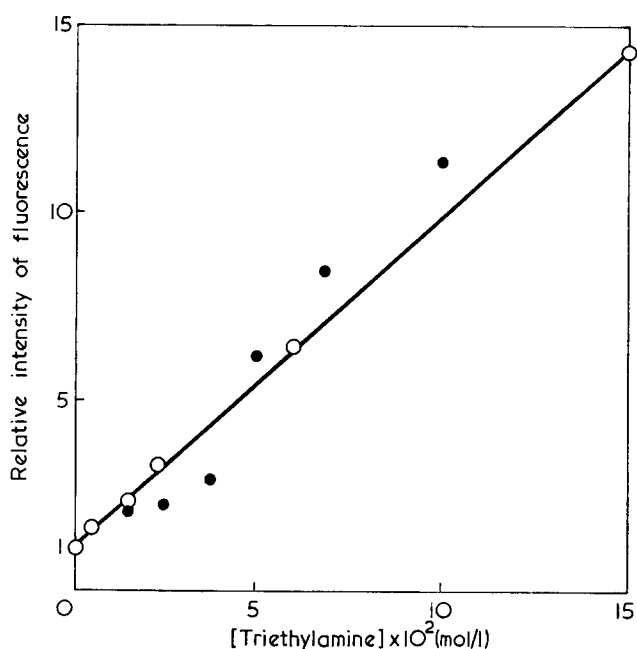


Figure 7 Stern-Volmer plot of the quenching process of the fluorescence of styrene at 306 nm by triethylamine. ○, Not deoxygenated; ●, deoxygenated

acceptor and interacts with electron-donating amine to give an exciplex which shows a new emission<sup>12</sup>. Izawa and Ogata<sup>13</sup> calculated the electron density of vinyl group in the lowest excited styrene by means of HMO method and proved its electron-accepting character. These observations and arguments lead to the conclusion that the excited styrene and triethylamine form an exciplex in agreement with the kinetic study.

#### ACKNOWLEDGEMENT

The authors are grateful to Professor Yasuji Izawa of Mie University for his helpful discussions.

#### REFERENCES

- 1 Yokota, K., Tomioka, H., Ono, T. and Kuno, F. *J. Polym. Sci. (A-1)* 1972, **10**, 1335
- 2 Cohen, S. G. and Chao, H. M. *J. Am. Chem. Soc.* 1968, **90**, 165
- 3 Nishijima, Y. and Yamamoto, M. *Kogyo Kagaku Zasshi* 1969, **72**, 31
- 4 Mao, T. J. and Eldred, R. J. *J. Polym. Sci. (A-1)* 1967, **5**, 1741
- 5 Kinoshita, M. and Imoto, M. *Kobunshi Kagaku* 1963, **20**, 631
- 6 North, A. M. and Reed, G. A. *J. Polym. Sci. (A)* 1963, **1**, 1311
- 7 Yokota, K., Kato, Y. and Tsuchikawa, S. *Abstr. SPSJ 18th Symp. Macromolecules, Tokyo* 1969, p 99
- 8 Imoto, M., Kinoshita, M. and Nishigaki, M. *Makromol. Chem.* 1965, **86**, 212
- 9 Olivé, G. H. and Olivé, S. *Makromol. Chem.* 1960, **42**, 251
- 10 Yokota, K. and Itoh, M. *J. Polym. Sci. (B)* 1968, **6**, 825
- 11 Kodaira, T., Hayashi, K. and Ohnishi, T. *Polymer J.* 1973, **4**, 1
- 12 Mataga, M. and Ezumi, K. *Bull. Chem. Soc. Japan* 1967, **40**, 1355
- 13 Izawa, Y. and Ogata, Y. *J. Org. Chem.* 1970, **35**, 3192

# Alternating copolymerization of methyl $\alpha$ -phenylacrylate and methyl methacrylate by *n*-BuLi

K. Hatada, J. Ohshima, T. Komatsu, S. Kokan and H. Yuki

*Department of Chemistry, Faculty of Engineering Science, Osaka University, Toyonaka, Osaka, Japan  
(Received 14 May 1973)*

The copolymerization of methyl  $\alpha$ -phenylacrylate (MPhA) and methyl methacrylate by *n*-BuLi was carried out in toluene at various temperatures with an initial monomer ratio of 1:1. At  $-78^{\circ}\text{C}$  the product was a homopolymer of MPhA. The copolymer obtained at  $-40^{\circ}\text{C}$  was a mixture of poly(methyl  $\alpha$ -phenylacrylate) and poly(methyl methacrylate) containing a small amount of alternating copolymer of both monomers. With further increase in the polymerization temperature the fraction of alternating copolymer increased and above  $30^{\circ}\text{C}$  all the copolymers obtained were alternate. With varying composition of feed monomers the copolymerization was carried out at  $30^{\circ}\text{C}$  and the alternating copolymer was obtained over a wide range of monomer feed ratios. In tetrahydrofuran the alternate sequence began to form at a lower temperature than in toluene, and all the copolymers obtained above  $0^{\circ}\text{C}$  were alternating ones. The mechanism of the copolymerization is discussed in some detail.

## INTRODUCTION

Stereoregulation in the anionic polymerization of methyl  $\alpha$ -phenylacrylate (MPhA) has been investigated<sup>1</sup>. It was found that this monomer could polymerize at low temperature giving a stereochemically random polymer under certain polymerization conditions, but gave no polymer above  $0^{\circ}\text{C}$  suggesting the ceiling temperature of this monomer lying around here.

We have briefly described also the copolymerization of MPhA and methyl methacrylate (MMA) by *n*-BuLi in toluene at various temperatures, where the alternating copolymer of these two monomers was produced above  $30^{\circ}\text{C}$ <sup>2</sup>.

In this work the copolymerization of MPhA and MMA was carried out by *n*-BuLi in toluene and in tetrahydrofuran at various temperatures. The investigation focused on the alternating tendency and the cotacticity of the copolymer. The mechanism of this alternating copolymerization is also discussed in some detail.

## EXPERIMENTAL

### *Materials*

MPhA was prepared and was purified as described in a previous paper<sup>1</sup>.

MMA obtained commercially was washed with a saturated aqueous solution of sodium hydrogensulphite and with 20% aqueous sodium chloride containing 5% sodium hydroxide. Then it was dried over molecular sieves type 4A and distilled under reduced nitrogen pressure. The MMA thus purified was redistilled over calcium hydride under high vacuum just before use.

Toluene was distilled over calcium hydride. Before use it was mixed with a small amount of *n*-BuLi in toluene and redistilled under high vacuum.

Tetrahydrofuran (THF) was refluxed over calcium hydride and was redistilled over lithium aluminium hydride under high vacuum.

Nitrobenzene-*d*<sub>5</sub> obtained commercially was used without further purification.

*n*-Butyllithium (*n*-BuLi) was prepared in *n*-heptane or toluene according to Ziegler's method from *n*-butyl chloride and metallic lithium under an argon atmosphere<sup>3</sup>.

Nitrogen and argon were purified by passing them through a column packed with molecular sieves type 4A cooled at  $-78^{\circ}\text{C}$ .

### *Polymerization*

A glass ampoule equipped with a three-way stopcock was evacuated by warming with the flame of a gas burner, and was filled with dry nitrogen. Then the solvent and the mixture of monomers were introduced into the ampoule with hypodermic syringes. The polymerization was initiated by adding the catalyst to the monomer solution at a given temperature. The ampoule was immediately sealed off.

After a desired reaction time the polymerization was stopped by adding a small amount of methanol, and the polymer produced was precipitated by pouring the reaction mixture into a large amount of methanol. After overnight standing, the polymer was collected by filtration, washed several times with methanol and dried *in vacuo*.



## Fractionation of copolymer

10 ml of nitromethane, 32 ml of methanol and 0.201 g of the copolymer obtained in toluene at  $-40^{\circ}\text{C}$  were placed in a 100 ml flask. The mixture was stirred magnetically for 8 h at room temperature and was allowed to stand overnight. Then the insoluble fraction was collected by filtration, washed several times with the mixture of nitromethane and methanol and dried *in vacuo*. The filtrate and the washings were combined and evaporated under reduced pressure. The soluble fraction thus obtained was redissolved in benzene and freeze-dried in order to remove the catalyst residue.

## Measurements

The p.m.r. spectrum of polymer was taken at  $150^{\circ}\text{C}$  on 10% w/v solution in nitrobenzene- $d_5$  at 100 MHz using a JEOL spectrometer (JNM-4H-100). Hexamethyldisilane was used as internal standard.

The solution viscosity of polymer was determined in toluene at  $30.0 \pm 0.02^{\circ}\text{C}$  using Ostwald viscometry. The concentration of the solution was 0.50 g/dl.

## RESULTS

## Copolymerization in toluene and p.m.r. spectra of copolymers

The copolymerization of MPhA and MMA was carried out in toluene by *n*-BuLi at various temperatures. The initial molar ratio of the two monomers was 1:1. The results are summarized in Table 1. The yield of the copolymer increased, reaching a maximum at  $0^{\circ}\text{C}$ , and then decreased with an increase in the temperature. The mole fraction of the MPhA unit in the copolymer was determined from the n.m.r. spectrum. The product obtained at  $-78^{\circ}\text{C}$  was found to be a homopolymer of MPhA, as has been reported by Tsuruta *et al.*<sup>4,5</sup>. The copolymer produced at  $-40^{\circ}\text{C}$  and above contained an equimolar ratio of the two monomers regardless of the polymerization temperature. The formation of the 1:1 copolymer of MMA and MPhA above  $0^{\circ}\text{C}$ , the ceiling temperature of MPhA<sup>1</sup>, strongly indicates the alternating incorporation of the two monomers in the copolymer.

The copolymerization was carried out at  $30^{\circ}\text{C}$  with varying composition of feed monomers. The results are shown in Figure 1. The 1:1 copolymer was obtained over a wide range of monomer feed ratios. This is additional evidence for the formation of alternating copolymer.

Table 1 Copolymerization of MPhA and MMA by *n*-BuLi in toluene<sup>a</sup>

No.	Temp. ( $^{\circ}\text{C}$ )	Time (h)	Yield (%)	MPhA unit in copolymer (mol %)	Alternate sequence (mol %)	$\eta_{sp}/C$ (dl/g)
1	-78	24	15	97	0	0.086
2	-40	72	68	44	31	0.142
9	-20	48	77	46	56	0.288
3	0	72	80	47	93	0.052
4	30	96	59	47	100	0.053
5	40	48	33	49	100	0.059
6	50	48	10	48	100	0.053

<sup>a</sup> MPhA, 6.8 mmol; MMA, 6.8 mmol; *n*-BuLi, 0.68 mmol; volume of reaction mixture, 10 ml

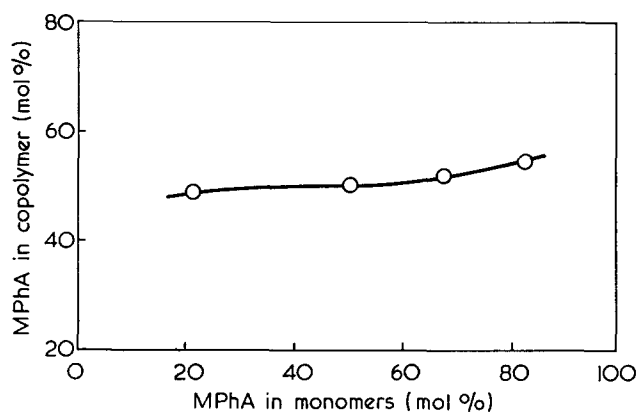


Figure 1 Copolymerization of MPhA and MMA by *n*-BuLi in toluene at  $30^{\circ}\text{C}$ . Total monomer, 13.6 mmol; *n*-BuLi, 0.68 mmol; volume of reaction mixture, 10 ml

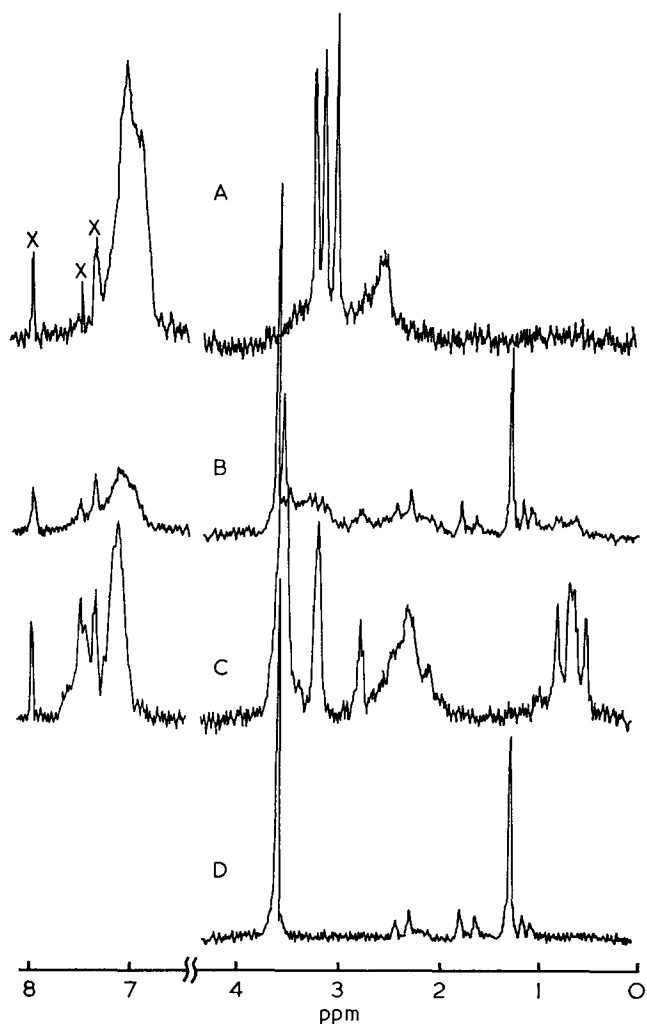


Figure 2 N.m.r. spectra of the copolymers of MPhA and MMA prepared at  $-78^{\circ}\text{C}$  (A),  $-40^{\circ}\text{C}$  (B) and  $30^{\circ}\text{C}$  (C) in toluene by *n*-BuLi, and of isotactic poly(methyl methacrylate) (D). The peaks labelled X are due to the phenyl protons of partially protonated nitrobenzene- $d_5$

The n.m.r. spectra of three samples of copolymers obtained at  $-78^{\circ}\text{C}$  (A),  $-40^{\circ}\text{C}$  (B) and  $30^{\circ}\text{C}$  (C) are shown in Figure 2, together with the spectrum of poly(methyl methacrylate) (PMMA) (D). The spectrum of polymer A was nearly the same as that of poly(methyl  $\alpha$ -phenylacrylate)<sup>1</sup> (PMPHA).

The spectrum of polymer B was close to the superposition of the spectra of PMPHA and isotactic PMMA.

The extraction of this polymer by nitromethane-methanol mixture gave a highly isotactic PMMA as an insoluble fraction as described in the next section. These facts suggest that most of the polymer was a mixture of PMPHA and PMMA. The weak absorption at 0.90~0.63 ppm may be due to the alternating copolymer as mentioned below.

The molar ratio of both monomer units in polymer C was nearly the same as that in polymer B. However, the spectrum of the former polymer was clearly distinguished from that of the latter by the following features: (a)  $\alpha$ -methyl proton resonance of MMA unit in polymer C appears at 0.90~0.63 ppm splitting into three peaks, but does not exist at 1.36~1.14 ppm, the region where the  $\alpha$ -methyl protons of PMMA resonate; (b) the resonance of methoxy methyl protons in polymer C is clearly different from those of PMMA and PMPHA. It splits into three peaks at 3.63, 3.28 and 2.85 ppm.

These results strongly indicate that the MMA and MPhA units in polymer C are arranged alternately. The high field shift observed in the  $\alpha$ -methyl proton resonance of the MMA unit may be due to the shielding effect of the benzene rings in MPhA units on both sides. Similar shift has been observed on the resonance of  $\alpha$ -methyl protons in alternating copolymer of MMA and styrene<sup>6</sup>.

The fractions of the alternate triad centred by the MMA unit were determined by the intensity measurement of the  $\alpha$ -methyl proton signal. The results are listed in Table 1. The fraction of alternating sequence increased with an increase in the polymerization temperature and the complete alternation was attained at 30°C and above.

The peak separations of  $\alpha$ -methyl and methoxy methyl resonances in the spectrum of the alternating copolymer should be due to the configurational differences among the sequences in the polymer chain. It is reasonably assumed that the diamagnetic shielding effect of the phenyl groups in MPhA units is the smallest on the methoxy methyl protons in MMA, if the configuration of the central MMA unit is the same as those of both the neighbouring MPhA units. Then the three peaks in the methoxy resonance region can be assigned to the methoxy methyl protons of centred MMA unit in co-isotactic (I), co-heterotactic (H) and co-syndiotactic (S) triads with increasing magnetic field. The first peak overlaps with the methoxy resonance of MPhA, which is not so sensitive to the stereochemical configuration of the chain as that in the spectrum of PMMA. The three peaks due to the  $\alpha$ -methyl protons, the situation of which is contrary to the methoxy methyl protons, can also be assigned to co-syndiotactic, co-heterotactic and co-isotactic triads with increasing magnetic field. Using these assignments triad cotacticities of the central

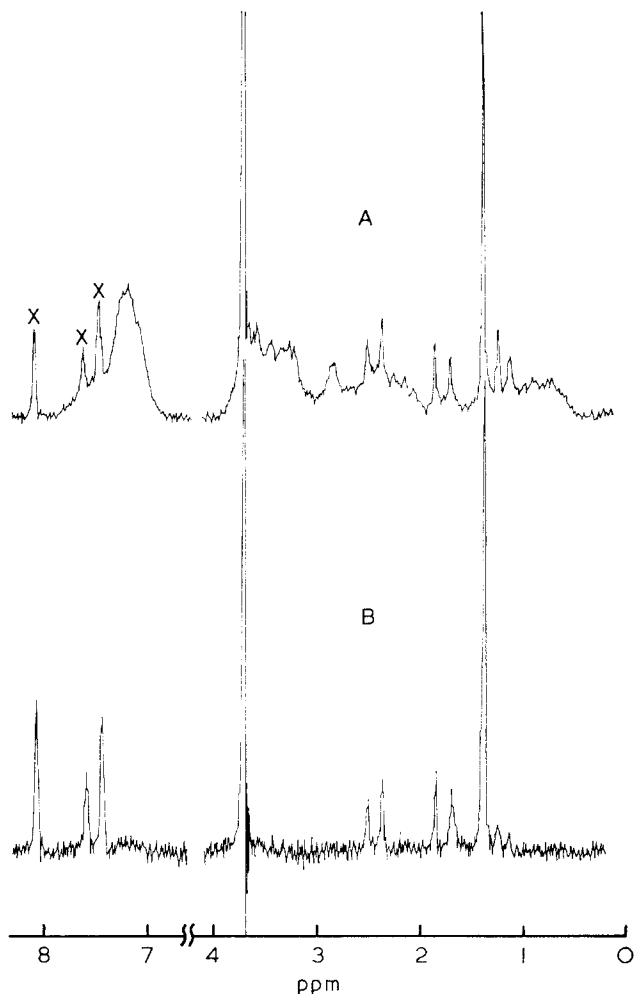


Figure 3 N.m.r. spectra of fractions of the copolymer obtained in toluene at  $-40^{\circ}\text{C}$ . A=soluble fraction; B=insoluble fraction. X, see Figure 2

MMA in the copolymers were determined as shown in Table 2. The values of tactic fractions calculated from the methoxy methyl proton resonance were in agreement with those from the  $\alpha$ -methyl proton resonance, which is considered to show the validity of the above assignments. The proportions of I:H:S in all the alternating copolymers were close to 1:2:1, indicating that the stereoregulation in this alternating copolymerization was almost random.

#### Fractionation of the copolymer obtained in toluene at $-40^{\circ}\text{C}$

Fractionation was carried out for the copolymer obtained by *n*-BuLi at  $-40^{\circ}\text{C}$  in toluene using a mixture of nitromethane and methanol. The insoluble fraction (13.9%) was found to be practically an isotactic PMMA, whose isotacticity (89.1% in triads) was extremely higher than that (62.9% in triads<sup>7</sup>) of the polymer obtained in the homopolymerization of MMA under the same condition (Figure 3). The soluble fraction appeared to be a mixture of PMPHA and isotactic PMMA from its n.m.r. spectrum.

#### Copolymerization in tetrahydrofuran

Copolymerization of MPhA and MMA was carried out by *n*-BuLi in THF at various temperatures. The results are summarized in Table 3 and Figure 4. The yield of the copolymer was highest at  $-20^{\circ}\text{C}$  and decreased with an increase in the polymerization temperature.

Table 2 Cotacticity of alternating copolymer of MPhA and MMA polymerized by *n*-BuLi in toluene

No.	Polymerization temp. ( $^{\circ}\text{C}$ )	From $\alpha$ -CH <sub>3</sub> of MMA			From -OCH <sub>3</sub> of MMA		
		I	H	S	I	H	S
3	0	20.6	48.0	31.4	14.2	53.4	32.4
4	30	24.8	50.4	24.8	25.6	52.1	22.3
5	40	24.2	50.7	25.1	18.7	55.6	25.7
6	50	22.7	49.8	27.5	18.3	58.0	23.7

I = co-isotactic; H = co-heterotactic; S = co-syndiotactic

Table 3 Copolymerization of MPhA and MMA by *n*-BuLi in THF for 48 h<sup>a</sup>

No.	Temp. (°C)	Yield (%)	MPhA unit in copolymer (mol %)	Alternate sequence (mol %)	$\eta_{sp}/C$ (dl/g)
15	-78	67	42	27	0.066
16	-40	79	47	71	0.066
19	-20	89	44	82	0.072
17	0	70	50	100	0.074
18	30	26	48	100	0.061
21	40	5	47	100	—
22	50	trace	—	—	—

<sup>a</sup> MPhA, 6.8 mmol; MMA, 6.8 mmol; *n*-BuLi, 0.68 mmol; volume of reaction mixture 10 ml

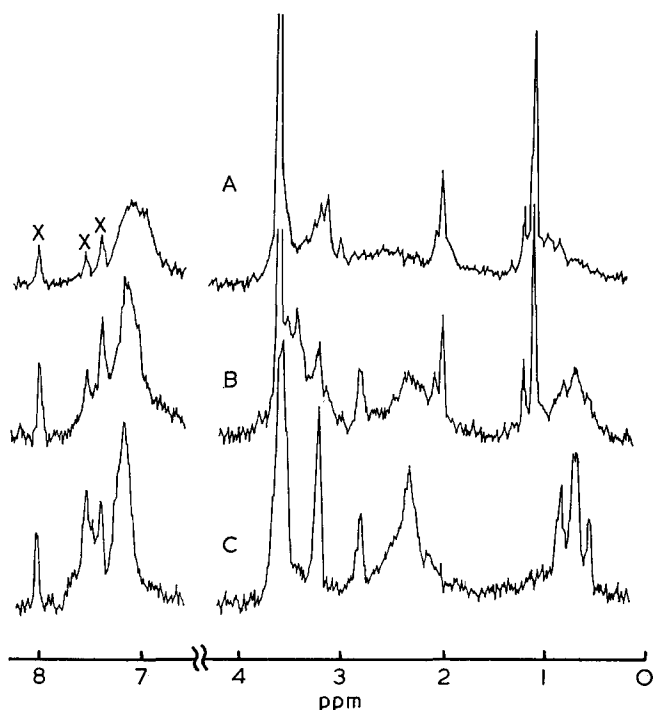


Figure 4 N.m.r. spectra of the copolymers of MPhA and MMA obtained at  $-78^{\circ}\text{C}$  (A),  $-40^{\circ}\text{C}$  (B) and  $30^{\circ}\text{C}$  (C) in THF by *n*-BuLi. X, see Figure 2

The spectrum of the copolymer obtained at  $-78^{\circ}\text{C}$  was nearly the superposition of those of PMPPhA and PMMA, as in the copolymerization in toluene at  $-40^{\circ}\text{C}$  (A in Figure 4). The configurational sequences of MMA units in this copolymer were found to be rich in syndiotactic configurations, while those the copolymer in toluene at  $-40^{\circ}\text{C}$  were rich in isotactic ones.

The spectrum of the copolymer obtained in THF at  $-40^{\circ}\text{C}$  (B in Figure 4) shows that a fairly large amount of alternate sequences were formed together with the long sequences of MMA units. In the copolymerization in THF the alternate sequences begin to form at lower temperature than in toluene. All the copolymers obtained at  $0^{\circ}\text{C}$  and above were alternating ones (Table 3). Their configurations were atactic, namely, the proportions of I:H:S being nearly equal to 1:2:1 (C in Figure 4).

#### DISCUSSION

In the anionic copolymerization of MMA and MPhA above the ceiling temperature of the latter (about  $0^{\circ}\text{C}$ ) the growing chain ending in MPhA unit cannot add this monomer. On the other hand, the MMA anion at the chain end may add predominantly MPhA owing to the higher reactivity of MPhA than MMA

towards the anion. The higher reactivity of MPhA is presumed by the lower charge density at the  $\beta$ -carbon of this monomer<sup>1</sup> and by the resonance stabilization of its anion due to the phenyl group. Thus the formation of alternating copolymer of MMA and MPhA in toluene at  $0^{\circ}\text{C}$  and above must be attributed to the crossover propagation occurring predominantly over homopolymerization of MMA.

The copolymerization in toluene at  $-78^{\circ}\text{C}$  produced only the homopolymer of MPhA. At  $-40^{\circ}\text{C}$  in toluene the highly isotactic PMMA was obtained together with PMPPhA in spite of the presence of highly reactive MPhA. In the polymerization of methacrylates by *n*-BuLi in a non-polar medium it is postulated<sup>8,9</sup> that the lithium atom can coordinate with the carbonyl oxygen of the penultimate monomer unit in the growing chain end and the resulting cyclic intermediate dominates the conformation of incoming monomer towards the lithium atom. The situation is nearly the same as in the case of MPhA. At low temperatures the Li-O interaction may be strong. This allows the growing anion to have a high selectivity towards the incoming monomer, and the anion can add only the same monomer as that at the chain end.

The result of the copolymerization in toluene at  $-78^{\circ}\text{C}$  indicates that the initiation reaction and, consequently, the propagation reaction occur predominantly on the MPhA side at this temperature. In the copolymerization at  $-40^{\circ}\text{C}$  the initiation reaction occurs on both monomer sides owing to the decrease in the reactivity of MPhA and the homopolymers of MPhA and MMA are obtained. It seems interesting that the PMMA obtained has a much higher isotacticity than that of the polymer obtained in the homopolymerization of MMA in toluene at  $-40^{\circ}\text{C}$ , although the reason for this is not clear at present.

Above  $0^{\circ}\text{C}$  the Li-O interaction will be loosened and the MMA anion at the chain end will lose its ability to the selectivity and the stereoregulation for incoming monomer, while the MPhA anion becomes incapable of adding MPhA. The situation may favour the formation of the alternate copolymer having an atactic configuration.

In the copolymerization in THF the Li-O interaction is not strong even at lower temperatures owing to the coordination of this polar solvent with the lithium atom, and the alternating copolymer begins to form at lower temperature than in toluene.

#### ACKNOWLEDGEMENTS

The authors are very grateful to Mr Y. Terawaki and Mr H. Okuda for the measurements of p.m.r. spectra. They also express their thanks to Mrs F. Yano for her clerical assistance in preparing the manuscript.

#### REFERENCES

- 1 Yuki, H., et al. *Polymer J.* 1971, **2**, 629
- 2 Yuki, H., et al. *Polymer J.* 1971, **2**, 812
- 3 Ziegler, K. and Gellert, H. G. *Justus Liebigs Annln Chem.* 1950, **567**, 179
- 4 Chikanishi, K. and Tsuruta, T. *Makromol. Chem.* 1965, **81**, 198
- 5 Chikanishi, K. and Tsuruta, T. *Makromol. Chem.* 1965, **81**, 211
- 6 Ikegami, T. and Hirai, H. *J. Polym. Sci. (A-1)* 1970, **8**, 195, 463
- 7 Yuki, H., Hatada, K. and Kokan, S. *Polymer J.* submitted
- 8 Cram, D. J. and Kopecky, K. R. *J. Am. Chem. Soc.* 1959, **81**, 2748
- 9 Bawn, C. E. H. and Ledwith, A. *Q. Rev. Chem. Soc.* 1962, **16**, 361

# Chemorheology of irradiation-cured natural rubbers: 1. Stress relaxation mechanisms for various curing systems in natural rubber at high temperature

Saburo Tamura and Kenkichi Murakami

*Chemical Research Institute of Non-Aqueous Solutions, Tohoku University, Sendai, Japan  
(Received 21 May 1973)*

Stress relaxation mechanisms were investigated for various curing systems in natural rubber, especially the 'complex' crosslinking irradiation cure systems containing sulphur or tetramethylthiuram disulphide (TMTD) in both air and nitrogen mainly at 100°C. With the systems, the chemical stress relaxation in air showed that in the main oxidative scission was the major cause of stress decay. However, the number of moles of main chain scission,  $q_m(t)$  seemed to be dependent on the chemical structure of the crosslink. In the TMTD curing system and irradiation-TMTD curing systems,  $q_m(t)$  is independent of the ratio,  $\rho$ , of the effective chain density  $N_c(0)$  based on the carbon-carbon crosslinkages to  $N_m(0)$  based on mono- and di-sulphide linkages. Stress decay in air of both accelerated-sulphur cures and irradiation-sulphur cures was shown to be due to both the interchange reaction of polysulphide linkages and random scission of the main chain. On the other hand, in nitrogen there are two simultaneous reactions at the crosslink: interchange and thermal scission.

## INTRODUCTION

The chemorheology of crosslinked rubbers has been extensively investigated by many workers<sup>1-3</sup>. We have also investigated the stress relaxation mechanisms on the crosslinked ethylene-propylene terpolymer (EPDM) differing only in the structure of crosslinks in both air and nitrogen<sup>4,5</sup>. The EPDM main chain is more stable to oxidative scission compared with the diene rubbers. Therefore the stress relaxation of these polymers can indicate the structural characteristics of the crosslinks. Further we have carried out stress relaxation measurement on dicumyl peroxide-cured EPDM under such experimental conditions that oxidative scission of the main chain occurs<sup>6</sup>. In this case, sulphur acts as an inhibitor against the oxidative scission of the main chain. On the other hand, the natural rubber chain is liable to undergo the oxidative scission. Tobolsky<sup>7</sup> suggested that for dicumyl peroxide-cured natural rubber stress decay occurred by oxygen-induced cleavage of the main chain. We<sup>8</sup> indicated that the number of moles of cleavages obtained directly from a stress relaxation measurement was approximately consistent with the one from the oxidation of non-crosslinked rubber in toluene solution under the same conditions.

Stress relaxation of crosslinked natural rubbers having different crosslink structures can be presumed to differ from that of EPDM. As regards the chemical stress relaxation mechanisms of crosslinked natural rubber, two contrary opinions were proposed by Tobolsky<sup>7</sup> and Berry and Watson<sup>9</sup>. Tobolsky reported that the

scission of those rubbers occurred at the network chain independent of the chemical structure of crosslinkage. Berry and Watson first concluded that the crosslinks were sites of cleavage for both dicumyl peroxide cures and for accelerated-sulphur cures. Watson *et al.*<sup>10</sup> later suggested that the crosslink was a site of reversible cleavage only in accelerated-sulphur cures, whereas the peroxide cures produced stable crosslinkages. In addition, Horix<sup>11</sup> by using sol-gel analysis suggested that the accelerated-sulphur cured natural rubber underwent both random scission in the network chains and scission directed by the crosslinkages. Thus the chemical stress relaxation mechanisms on the various crosslinking systems of natural rubber have still not been completely elucidated.

In this paper, the following problems are considered. First, the chemical relaxation mechanisms in air are investigated for various crosslinking systems of natural rubber, especially such complex crosslinking systems as irradiation cures containing sulphur or tetramethylthiuram disulphide. Secondly, from the results we are able to put forward suggestions relating to the contrary conclusions between Tobolsky and Watson *et al.* for accelerated-sulphur cured natural rubber.

## EXPERIMENTAL

Natural rubber (NR-RSS-1) was cold milled with curing ingredients under conditions described in *Table 1*. Sheets (about 0.5 mm) of milled polymer were pressed at

Table 1 Preparation of cured NR polymers

	Sample							
	1	2	3	4	5	6	7	8
Rubber	100	100	100	100	100	100	100	100
Sulphur	—	—	—	—	—	3	3	3
Zinc oxide	—	—	5	5	—	3	3	—
Stearic acid	—	—	2	2	—	0.5	0.5	—
TMTD	—	—	3	3	3	—	—	—
Mercaptobenzo-thiazole (MBT)	—	—	—	—	—	1	1	—
DCP	3	—	—	—	—	—	—	—
Hot-press curing*	10 min	—	10 min	10 min	—	30 min	30 min	—
Irradiation curing†	—	†	—	†	†	—	†	†

\* Curing temperature 145°C

† Total dose=12, 28.8 and 43.2Mrad

200 kg/cm<sup>2</sup> and 145°C. Samples 1, 3 and 6, respectively, were dicumyl peroxide (DCP)-cured NR, tetramethylthiuram disulphide (TMTD)-cured and accelerated-sulphurcured. It is evident that the crosslinking site, in these samples, consists of carbon-carbon bonds, mono- and di-sulphide linkages, and mono-, di- and poly-sulphide linkages for samples 1, 3 and 6, respectively. All other samples were prepared by  $\gamma$ -radiation from a <sup>60</sup>Co source at room temperature. The crosslink of sample 2 is due to carbon-carbon bonding. Samples 4 and 7 were prepared by exposing samples 3 and 6 to  $\gamma$ -rays. Samples 5 and 8 were prepared as follows: thin sheets (about 0.5mm) of non-crosslinked rubber containing TMTD for sample 5 and sulphur for sample 8 were made by milling and hot-pressing and the sheets were exposed to  $\gamma$ -rays. It can be assumed that the crosslinks of samples 4 and 5 are a mixture of carbon-carbon bonds and mono- and di-sulphide linkages, and those of samples 7 and 8 of carbon-carbon bonds, and mono-, di- and poly-sulphide linkages. All the samples were extracted with hot acetone for 48 h and dried *in vacuo*.

Continuous stress relaxation was mainly measured at 100°C in both air and nitrogen. In order to calculate the apparent activation energy of chemical stress relaxation based on the oxidative degradation for each curing system, measurements were also made at 109°C (or 110°C), 120°C and 140°C in air.

The stress relaxation apparatus used was constructed in our laboratory and included the usual strain-gauge system. All samples were held for 20 min at the experimental temperature before any stress was applied.

## RESULTS AND DISCUSSION

### Network chain density

The initial network chain density  $N(0)$  mol/ml was estimated by the stress-strain measurements based on the statistical theory of rubber-like elasticity:

$$f(0) = N(0)RT(\alpha - \alpha^{-2}) \quad (1)$$

where,  $f(0)$  is initial stress,  $R$  gas constant and  $T$  absolute temperature. The extension ratio  $\alpha$  was about 1.2. The initial chain density of the samples used here are given in Table 2 and shown in Figure 1. As can be seen from Figure 1,  $N(0)$  of all the samples increases linearly with radiation dose. However, we cannot define if this relation is held over the range of higher radiation doses. Sample 7 is able to form the effective network

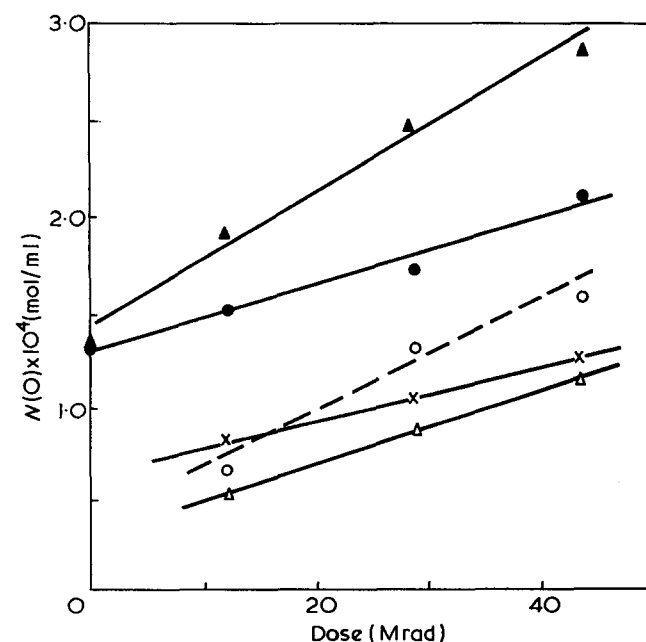
chain by  $\gamma$ -radiation compared with the other samples. This may be due to the polysulphide linkages, which exist in sample 6, undergoing the interchange reaction during irradiation to result in mono- and di-sulphide crosslinkages. In this paper, we do not intend to discuss the curing mechanisms.

### Chemorheology of crosslinked natural rubbers

*Chemical stress relaxation of DCP-cured NR (1) and irradiation-cured NR (2).* As described above, the crosslinkages of both samples 1 and 2 are known to consist of carbon-carbon bonds. If there should be no difference of chemical and physical structures between samples 1 and 2, the chemical and physical stress relaxation of both samples under the same condition, respectively, should be represented by a curve. Stress relaxation of samples 1 and 2 having the same density  $N(0) \approx 0.65 \times 10^{-4}$  mol/ml was measured in both air and nitrogen at 100°C. The relation of relative stress  $f(t)/f(0)$  versus logarithm of time ( $\log t$ ) is shown in Figure 2. It can be seen from this Figure that the relaxation of sample 1 in air and under nitrogen in each case is very closely consistent with that of sample 2. This suggests that both samples 1 and 2 have identical chemical and physical structures in spite of the difference in curing methods. However, the stress decay in air of sample 1 is slightly faster than that of sample 2 on the long-time side in Figure 2. Tobolsky *et al.*<sup>1,2</sup> also have recently found some difference of stress relaxation in the vacuum at

Table 2 Relation between radiation dose and initial chain density for samples 1-8

Radiation dose (Mrad)	Initial chain density at $n(0)=10$ (mol/ml)							
	1	2	3	4	5	6	7	8
0	1.27	—	1.32	—	—	1.31	—	—
12.0	—	0.64	—	1.48	0.79	—	1.89	0.52
28.4	—	1.30	—	1.72	1.03	—	2.45	0.85
43.2	—	1.53	—	2.10	1.21	—	2.84	1.13

Figure 1 Relation between initial chain density  $N(0)$  and irradiation dose. Samples: O, 2; ●, 3 and 4; x, 5; ▲, 6 and 7; △, 8

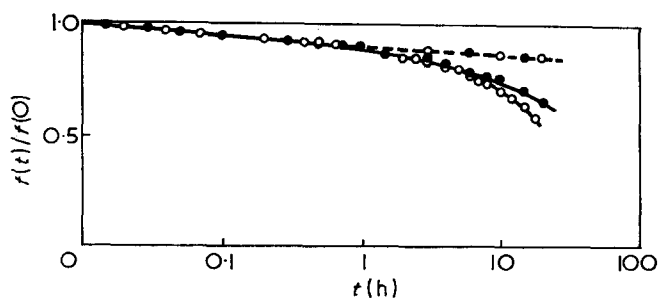


Figure 2 Stress relaxation of samples 1 (○) and 2 (●) in air and under nitrogen at 100°C. —, in air; ----, under nitrogen

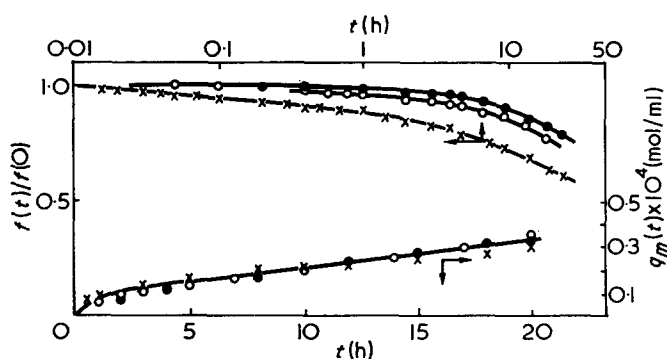


Figure 3 Stress relaxation of No. 1 samples having different initial chain density and relation between the number of moles of main chain scission  $q_m(t)$  and time  $t$ . ×, Irradiation dose=12 Mrad,  $N(0)=0.64 \times 10^{-4}$  mol/ml; ○, 28.8 Mrad,  $1.25 \times 10^{-4}$  mol/ml; ●, 43.2 Mrad,  $1.53 \times 10^{-4}$  mol/ml

higher temperature between peroxide cures and irradiation cures for both polyethylene and natural rubber, but this paper does not deal with these longer time differences. As we discuss now for the region where both curves agree among themselves, it can be assumed that there is no difference between samples 1 and 2.

The stress relaxation of three No. 1 samples having different initial chain densities  $N(0)$ , and prepared by the alteration of irradiation dose, was measured in air at 100°C. These stress relaxation curves given in Figure 3 show that the rate of stress relaxation decreases with increasing  $N(0)$ . The number of moles of main chain scission  $q_m(t)$  is represented by equation (2) which was proposed by Tobolsky<sup>13</sup>:

$$q_m(t) = -N(0) \ln f(t)/f(0) \quad (2)$$

Hence  $q_m(t)$  can be obtained directly from a stress-relaxation measurement. The relation between  $q_m(t)$  and  $t$  is also shown in Figure 3. The  $q_m(t)$  is independent of  $N(0)$ . This is a typical case of oxygen-induced cleavage of the main chain and consistent with the carbon-carbon crosslinking.

*Chemical stress relaxation of TMTD-cured NR (3) and TMTD-irradiation-cured NR (4 and 5).* First, we investigated the stress relaxation of both samples 4 and 5, respectively, in relation to the initial chain density  $N(0)$ . Figure 4 shows the chemical stress relaxation curves [ $\log f(t)/f(0)$  versus time] for samples 4 and 5 in air at 100°C. The stress decay of these samples is also dependent with  $N(0)$  as is the case of sample 2. Further linear relationships are seen for all samples over the longer time region. Therefore, it is assumed that only the main chain undergoes the oxidative scissions in these curing systems. The numbers of moles of the

main chain scission of these samples,  $q_m(t)$  were calculated from equation (2). The relation between  $q_m(t)$  versus time is shown in Figure 5. The value of  $q_m(t)$  is almost independent of  $N(0)$ . This suggests that the oxidative scission in both samples 4 and 5 also occurs on the main chain. What is further interesting in Figure 5 is independent of conditions of sample preparation. The crosslinkages of samples 4 and 5, as described above, are expected to consist of carbon-carbon bonds and mono- and di-sulphide linkages. Now, the effective chain density  $N_c(0)$  and  $N_m(0)$ , respectively, are considered based on the carbon-carbon crosslinkages and mono- and di-sulphide linkages. In this case,  $N(0)$  is equal to  $N_c(0) + N_m(0)$ . As the experimental method which estimates the values of  $N_c(0)$  and  $N_m(0)$  has not so far been made known, we cannot estimate them. The ratio,  $\rho$  of  $N_c(0)$  to  $N_m(0)$  may be different in samples 4 and 5. The  $\rho$  value, even in the same sample, can be expected to change with the irradiation dose. Nevertheless the relations of  $q_m(t)$  versus  $t$  are consistent with themselves.

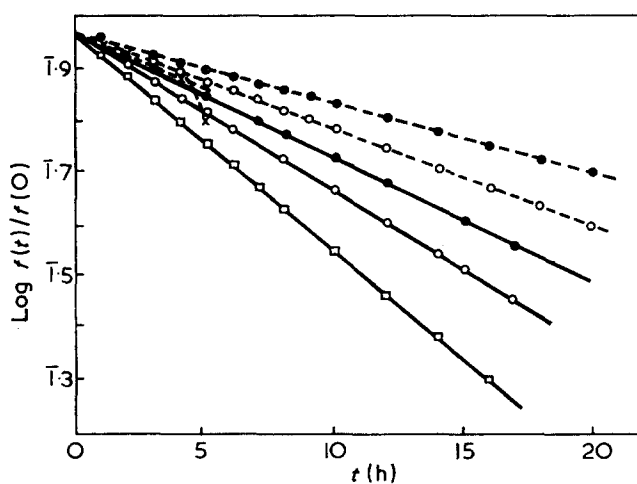


Figure 4 Stress relaxation of samples 3, 4 and 5 in air at 100°C. ×, Sample 3,  $N(0)=1.31 \times 10^{-4}$  mol/ml. ----, Sample 4: ○, irradiation dose=28.8 Mrad,  $N(0)=1.63 \times 10^{-4}$  mol/ml; ●, 43.2 Mrad,  $2.10 \times 10^{-4}$  mol/ml. —, Sample 5: □, 12 Mrad,  $0.79 \times 10^{-4}$  mol/ml; ○, 28.8 Mrad,  $1.03 \times 10^{-4}$  mol/ml; ●, 43.2 Mrad,  $1.21 \times 10^{-4}$  mol/ml

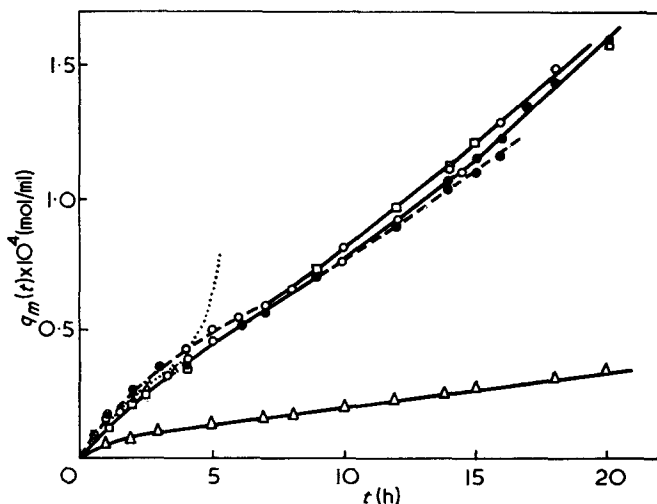


Figure 5 Relation between  $q_m(t)$  and  $t$  of samples 2, 3, 4 and 5: △, sample 2; ×, sample 3. ----, Sample 4: ○, irradiation dose=28.8 Mrad,  $N(0)=1.63 \times 10^{-4}$  mol/ml; ●, 43.2 Mrad,  $N(0)=2.10 \times 10^{-4}$  mol/ml. —, Sample 5: □, 12 Mrad,  $N(0)=0.79 \times 10^{-4}$  mol/ml; ○, 28.8 Mrad,  $N(0)=1.03 \times 10^{-4}$  mol/ml; ●, 43.2 Mrad,  $N(0)=1.21 \times 10^{-4}$  mol/ml

This suggests that both samples 4 and 5 undergo oxidative scission on the main chain independent of the  $\rho$  value, i.e. of the chemical structure of crosslinkages.

The result of the No. 3 sample having  $N(0) \approx 1.31 \times 10^{-4}$  mol/ml is also shown in both Figures 4 and 5. The crosslinkages of sample 3 consist of mono- and di-sulphide linkages. The stress relaxation mechanism for this sample is still not elucidated as shown in the different opinions between Tobolsky<sup>7</sup> and Watson *et al.*<sup>9</sup>. Recently, Takahashi and Tobolsky<sup>14</sup> reported that chemical stress relaxation in air showed that oxidative scissions along the main chains were major causes of stress decay for sample 3. They do not, however, provide sufficient experimental evidence for this suggestion. From Figure 5, it is apparent that the  $q_m(t)$  of sample 3 is consistent with that of samples 5 and/or 6 up to about 4 h. In the longer time region (after 4 h), it deviates from samples 5 and 6. This will be based on the rapid stress decay in this region, where the relaxation curve deviates from a linear relationship, i.e. Maxwellian curve. Such a phenomenon is also found in the No. 5 samples in Figure 5. The rapid stress decay is probably the physical relaxation based on micro- and/or macro-cracks formed in the samples. So, we are not able to give the chemorheological analysis in the longer time region. From the above, it can be concluded that the chemical stress relaxation up to 4 h of sample 3 is based on the oxidative scission along the main chain. Once again it is concluded that only the main chain scission occurs in these curing systems, and the  $q_m(t)$  is independent of  $\rho = N_c(0)/N_m(0)$ . However, this does not necessarily imply that  $q_m(t)$  is independent of  $\rho$  value from zero to infinity. The  $q_m(t)$  of sample 1 of  $\rho = \infty$  is appreciably smaller compared with that of samples 3, 4 and 5, as shown in Figure 5, i.e. the oxidative scission of the main chain is probably accelerated by having mono- or di-sulphide crosslinkages present, although the acceleration mechanism is still not understood.

Figure 6 shows the stress relaxation of samples 3, 4 and 5 in nitrogen at 100°C. From the Figure, it is evident that the relaxation of each sample is exhibited by a straight line independent of initial chain density  $N(0)$ . It was derived theoretically by Tobolsky that when scission occurs only at the crosslink in cross-linked polymer, the stress relaxation is expressed by a Maxwellian decay, i.e. equation (3) and is independent of  $n(0)$ .

$$f(t)/f(0) = \exp(-kt) \quad (3)$$

Therefore, it can be concluded that the stress relaxation of these curing systems in nitrogen is based on the scission of crosslinkage.

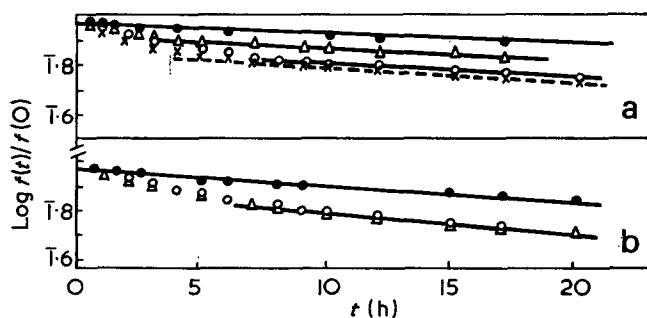


Figure 6 Stress relaxation of samples 3, 4, 5, 6, 7 and 8 under nitrogen at 100°C. (a) ●, 3 and 4; ×, 6; △ and ○, 7. (b) ●, 5; △ and ○, 8

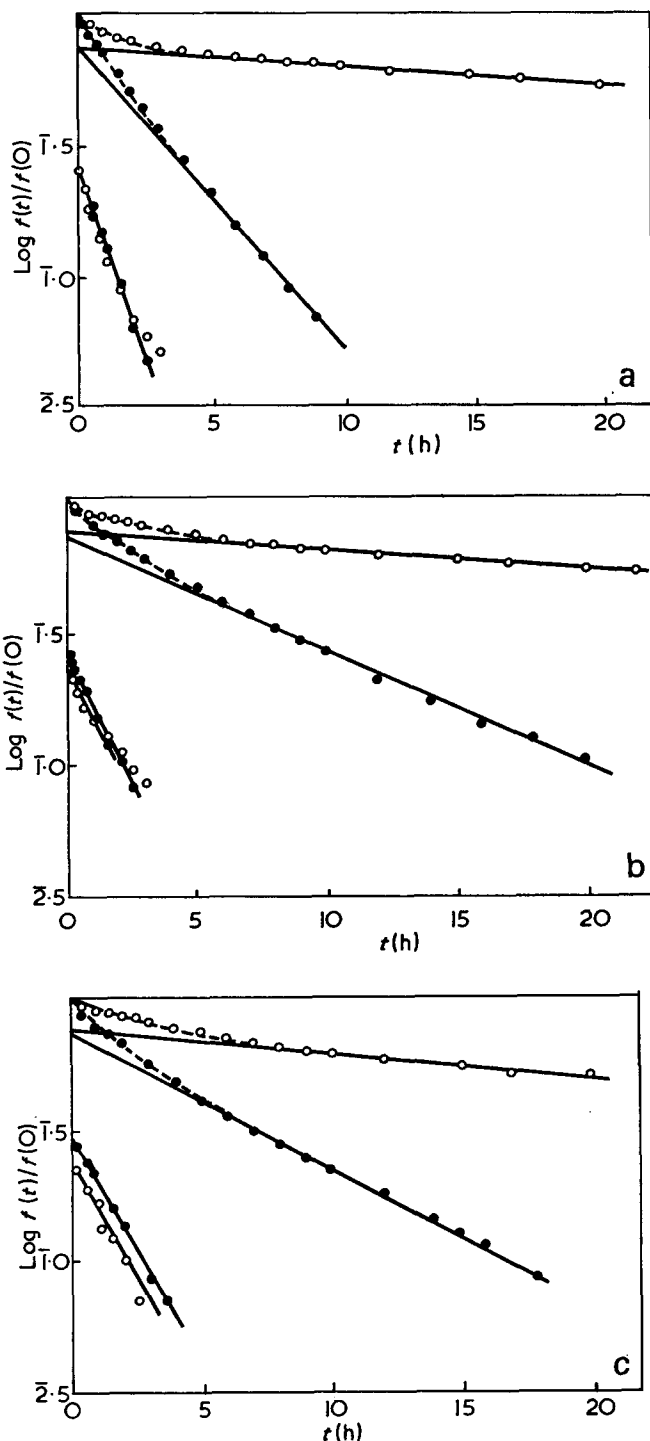


Figure 7 Stress relaxation in air and under nitrogen at 100°C. ●, In air; ○, under nitrogen. (a) sample 6; (b) sample 7 prepared by radiation of 28.8 Mrad; (c) sample 8 prepared by radiation of 28.8 Mrad

Chemical stress relaxation of accelerated sulphur-cured NR (sample 6) and irradiation-sulphur-cured NR (samples 7 and 8). Stress relaxation of samples 7 and 8 was measured in both and nitrogen at 100°C. The results are shown in Figure 7a for sample 6, 7b for sample 7 and 7c for sample 8. Samples 7 and 8 were prepared by the irradiation dose of 28.8 Mrad.

Crosslinkages of these samples consist of C-C bonds, and mono-, di- and poly-sulphide linkages as described previously. From Figure 7, it can be seen that all the stress relaxation curves decay rapidly in the short time region and then become linear with longer times. We

used the procedure suggested by Tobolsky and Murakami<sup>15</sup> and repeated it until we obtained a straight line in the whole time scale region. Either in air or under the nitrogen, all the stress relaxation curves for samples 6, 7 and 8, respectively, were divided into two definite straight lines as shown in Figures 7a, 7b and 7c. It is evident from the Figures that the stress relaxations in the short time region for each sample are in fair agreement with each other in both air and nitrogen, whereas the one in the long time region is apparently different between air and nitrogen. Thus, the above can be expressed by:

$$f(t)/f(0) = A \exp(-k_A t) + B \exp(-k_B t) \quad (\text{in air}) \quad (4)$$

$$f(t)/f(0) = A' \exp(-k_A t) + B' \exp(-k'_B t) \quad (\text{in nitrogen}) \quad (5)$$

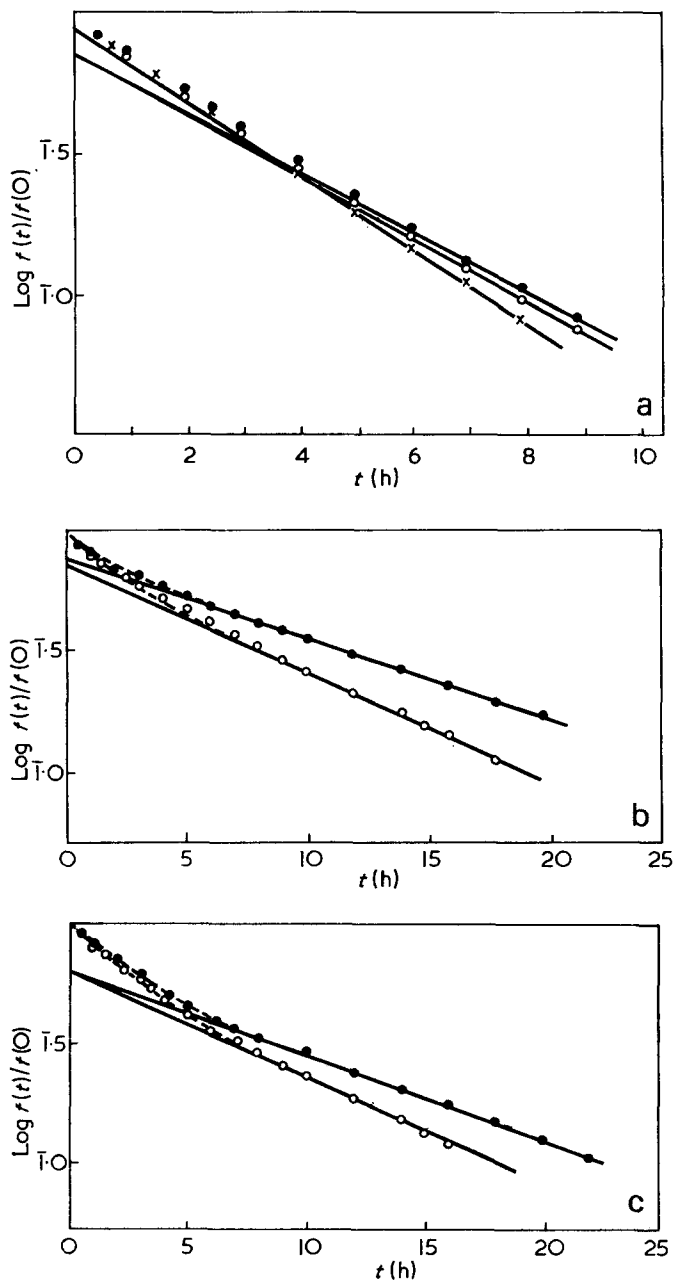


Figure 8 Dependence of initial chain density  $N(0)$  of the stress relaxation in air at 100°C for samples 6, 7 and 8. (a) 6:  $\times$ ,  $1.10 \times 10^{-4}$ ;  $\circ$ ,  $1.31 \times 10^{-4}$ ;  $\bullet$ ,  $1.46 \times 10^{-4}$  mol/ml; (b) 7:  $\circ$ ,  $2.45 \times 10^{-4}$ ;  $\bullet$ ,  $2.84 \times 10^{-4}$  mol/ml; (c) 8:  $\circ$ ,  $0.85 \times 10^{-4}$ ;  $\bullet$ ,  $1.13 \times 10^{-4}$  mol/ml

Figures 8a, 8b and 8c, respectively, show the dependence of initial chain density,  $n(0)$  of the stress relaxation in air for samples 6, 7 and 8. Those in nitrogen are shown in Figures 6a and 6b for the purpose of comparison with samples 3, 4 and 5. From the Figures, it can be seen that the  $k_B$  values in air depend on  $n(0)$ , while the  $k'_B$  value is independent of  $n(0)$ . From equations (4) and (5), it is expected that there are two different stress relaxation mechanisms in these curing systems either in air or in nitrogen; one is independent of the surroundings, the other will have completely different mechanisms between air and nitrogen. These stress relaxation behaviours can be explained as follows. The stress relaxation ( $k_A$ ) in the short time region will be based on the interchange reaction of polysulphide linkages which is independent of the surroundings. The interchange reaction of polysulphide linkages has been investigated in detail by Tobolsky<sup>16</sup>, Beevers<sup>17</sup>, and us<sup>4</sup>. In a previous paper<sup>18</sup>, we reported that the stress relaxation in nitrogen of accelerated-sulphur cured natural rubber (sample 6) was based on the interchange reaction of polysulphide linkages and the thermal scission of mono- and disulphide linkages. All the slopes ( $k'_B$ ) of straight lines for No. 7 samples in the long time region are not only independent of initial chain density  $n(0)$ , but are also equal to that of TMTD-cured natural rubber of which the crosslinkages consist of mono- and di-sulphides linkages. The slopes for sample 8 are also independent of  $n(0)$  and are in agreement with those for sample 5. It can thus be concluded that the stress relaxation in nitrogen of samples 7 and 8 in the long time region is also based on the thermal scission of crosslinkages. On the other hand, stress relaxation ( $k_B$ ) in air of samples 6, 7 and 8, respectively, apparently depend on the initial chain density  $n(0)$ . Therefore these vulcanizates also appear to undergo the oxidative scission of the main chain as the others. However, there is insufficient evidence, because in these curing systems we cannot calculate the number of moles of main chain scission,  $q_m(t)$ . In the curing systems, the presence of mono-, di- and poly-sulphide linkages also appears to accelerate the oxidative scission of the main chain.

*Temperature dependence of the chemical stress relaxation for each sample.* The temperature dependence of the rate of chemical stress relaxation in air for all the samples used here was investigated. The measurements were carried out at 100°, 110°, 120° and 140°C. For example, the result for samples 2, 5 and 8, which were prepared by a  $\gamma$ -irradiation dose of 28.8 Mrad, are shown in Figures 9a, 9b and 9c, respectively. The gradients of the lines in Figures 9 and 10 are the rate constants of the main chain scission reaction  $k$ , expressed by the Arrhenius equation as:

$$k = A \exp(-E_a/RT) \quad (6)$$

where  $E_a$  is the apparent activation energy (kcal/mol) for main scission reaction. Temperature dependence for all the samples is plotted as  $\log k$  ( $\text{h}^{-1}$ ) versus  $1/T$  (K) in Figure 10. In the Figure, the value of  $E_a$  for oxidative scission of main chains is also given. From Figure 10, we find that the value of  $k$  for samples 3, 4 and 5 containing mono- and di-sulphide crosslinkages, and for 6, 7 and 8 containing mono-, di- and poly-sulphide crosslinkages is very large compared with sample 2.

This suggests that although all the samples undergo



the main chain scission independent of the crosslinking structure, the number of moles of the scission is significantly dependent. Here, what is interesting and is not understandable is the agreement of the value of  $k$  between samples 7 and 8, in spite of the difference of initial chain density,  $n(0)$  (see Table 2). This is a large difference compared with the irradiation-TMTD cured NR (samples 5 and 6). As described above, the rate of stress relaxation of both samples 5 and 6 was independent of the method of preparation but was dependent of only the initial chain density  $N(0)$ . The value of  $E_a$  for samples 2, 6, 7 and 8 is about 21 kcal/mol. That for samples 3, 4 and 5 is about 27 kcal/mol.

CONCLUSIONS

(1) There was no difference of stress relaxation either in air or in nitrogen between DCP cures (sample 1) and irradiation cures (sample 2). This suggests that these vulcanizates have the same physical and chemical structures. In air samples 1 and 2 underwent the random scission of only the main chain.

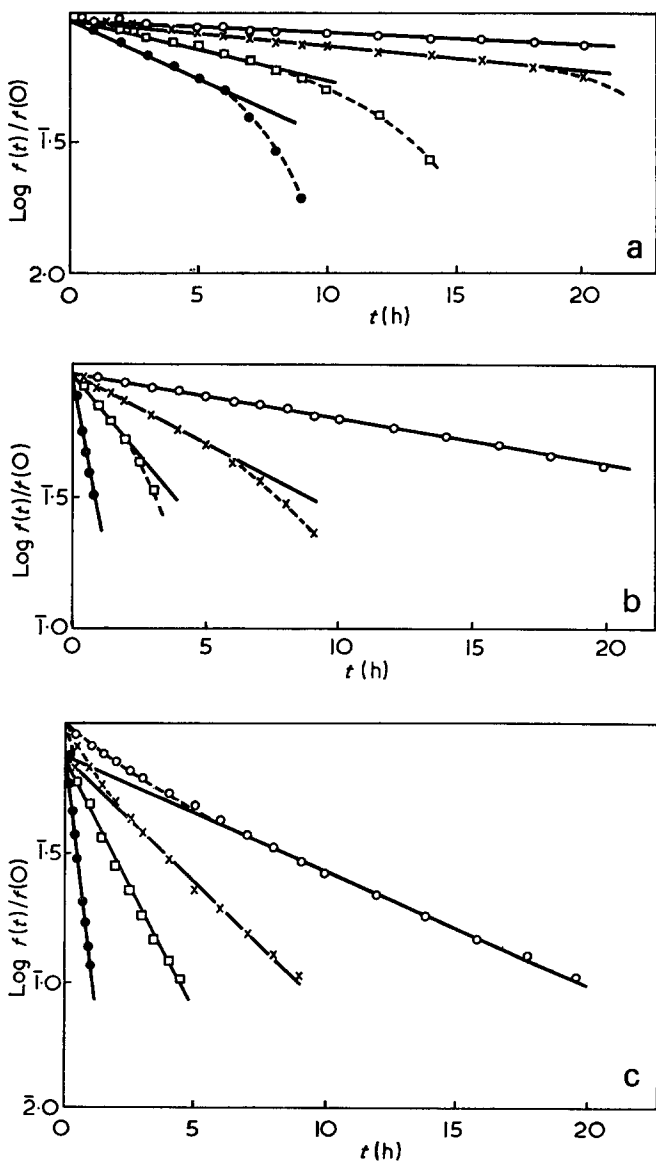


Figure 9 Temperature dependence of stress relaxation in air for samples 2, 5 and 8. ○, 100°C; ×, 110°C; □, 120°C; ●, 140°C. (a) Sample 2; (b) sample 5 prepared by radiation of 28.8Mrad; (c) sample 8 prepared by radiation of 28.8Mrad

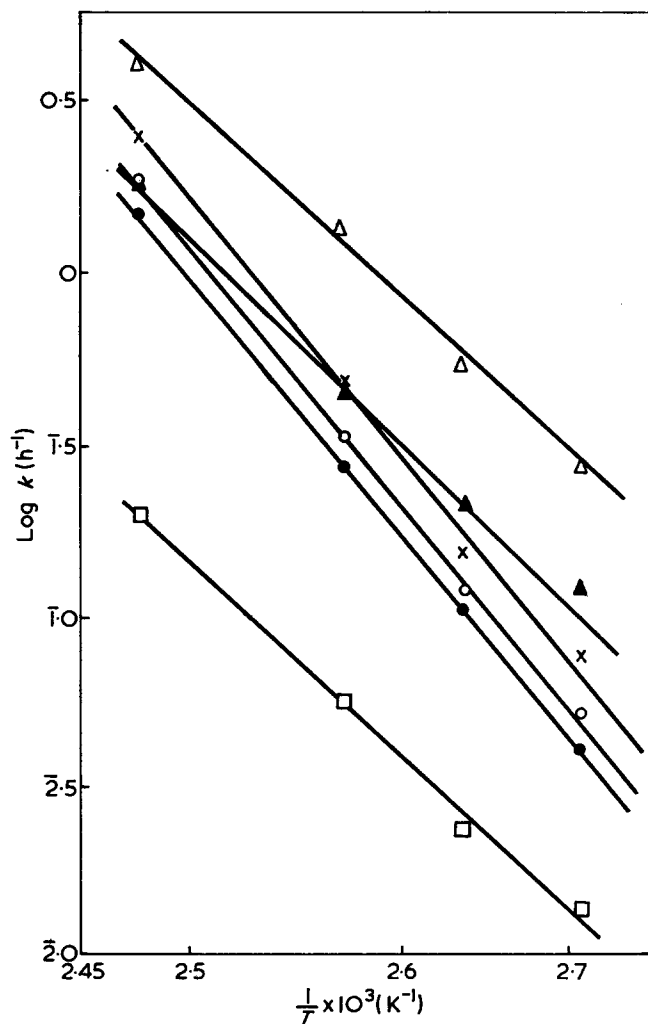


Figure 10 Plot of  $\log k$  versus  $1/T$  for each sample: □, 2; ○, 3; ×, 4; ●, 5; ▲, 6; △, 7 and 8

(2) In the case of irradiation-TMTD cures (samples 4 and 5), the stress decay was also based on the oxidative scission of the main chain. The number of moles of main chain scission,  $q_m(t)$  was independent of the ratio,  $\rho$  of  $N_c(0)$  based on the carbon-carbon bonds to  $N_m(0)$  based on the mono- and di-sulphide linkages. However, the  $q_m(t)$  was larger than that of sample 2. The oxidative scission of the main chain seemed to be accelerated by mono- and di-sulphide. It was found from comparison with samples 4 and 5 that TMTD cures (sample 3) underwent random scission on the main chain. The stress relaxation in nitrogen for samples 3, 4 and 5 was due to the thermal scission of the crosslink.

(3) The stress relaxation either in air or in nitrogen of both accelerated-sulphur cures (sample 6) and irradiation-sulphur cures (samples 7 and 8) was expressed by the sum of two exponential terms. The stress relaxation in air of samples 6, 7 and 8 could be explained by both the interchange reaction of polysulphide linkages and the random scission on the main chain. The stress decay in nitrogen of these vulcanizates was based on both the interchange reaction of polysulphide linkages and the thermal scission of the crosslinks. The rate of the interchange reaction in air was very closely consistent with the one in nitrogen.

(4) The apparent activation energy of the oxidative scission of the main chain was about 21 kcal/mol for samples 2, 6, 7 and 8 and some 27 kcal/mol for samples 3, 4 and 5.

REFERENCES

- 1 Tobolsky, A. V. 'Properties and Structure of Polymers', John Wiley, New York, 1962
- 2 Bueche, A. M. *J. Chem. Phys.* 1953, **21**, 614
- 3 Baxter, S. and Wilson, M. A. A. *Polymer* 1963, **4**, 163
- 4 Murakami, K. and Tamura, S. *J. Polym. Sci. (A-1)* 1971, **9**, 423
- 5 Murakami, K. and Tamura, S. *Polymer J.* 1971, **2**, 328
- 6 Tamura, S. and Murakami, K. *J. Appl. Polym. Sci.* 1972, **16**, 2803
- 7 Tobolsky, A. V., Prettyman, I. S. and Dillon, J. H. *J. Appl. Phys.* 1944, **15**, 380
- 8 Tamura, S. and Murakami, K. *J. Appl. Polym. Sci.* 1972, **16**, 1149
- 9 Berry, J. P. and Watson, W. F. *J. Polym. Sci.* 1955, **18**, 201
- 10 Dunn, J. R., Scanlan, J. and Watson, W. F. *Trans. Faraday Soc.* 1959, **55**, 667
- 11 Horix, M. M. *J. Polym. Sci.* 1956, **19**, 445
- 12 Shaw, T. and Tobolsky, A. V. *J. Polym. Sci. (A-1)* 1971, **9**, 1937
- 13 Tobolsky, A. V., Metz, D. J. and Mesrobian, R. B. *J. Am. Chem. Soc.* 1950, **72**, 1942
- 14 Takahashi, Y. and Tobolsky, A. V. *Polymer J.* 1971, **2**, 457
- 15 Tobolsky, A. V. and Murakami, K. *J. Polym. Sci.* 1959, **40**, 443
- 16 Tobolsky, A. V. *J. Polym. Sci. (B)* 1964, **2**, 823
- 17 Beevers, R. B. *J. Colloid Sci.* 1964, **19**, 40
- 18 Murakami, K. and Tamura, S. *J. Polym. Sci. (B)* in press

# A study of dilation coefficients of *cis*-polybutadiene in simple extension

C. Price and G. Allen

Department of Chemistry, University of Manchester, Manchester M13 9PL, UK  
(Received 8 May 1973)

Force–pressure measurements at constant length and temperature have been made on a sample of crosslinked *cis*-polybutadiene in the range  $1.11 < \alpha < 1.77$  in order to determine values of the dilation coefficient  $(\partial \ln V / \partial \alpha)_{P, T}$ . The results obtained, together with data reported earlier for natural rubber and butyl rubber, are compared with the predictions of (a) the Gaussian theory of rubber elasticity, and (b) a relationship based on the assumption that the linear compressibility is isotropic in extension.

## INTRODUCTION

The small volume changes which occur when a rubber is subjected to simple elongations may be readily determined from force–pressure measurements made at constant temperature and length<sup>1</sup>. The dilation coefficient  $(\partial \ln V / \partial \alpha)_{P, T}$  at a given elongation is obtained from the thermodynamic relation:

$$(\partial \ln V / \partial \alpha)_{P, T} = (L_i / V) (\partial f / \partial P)_{L, T} \quad (1)$$

where  $f$  is the total force,  $P$  the pressure,  $V$  the volume and  $\alpha = L / L_i$  where  $L_i$  and  $L$  are the lengths of the sample before and after deformation respectively. Values of  $(\partial \ln V / \partial \alpha)_{P, T}$  have been reported for crosslinked samples of natural rubber<sup>1</sup> ( $\alpha < 2.1$ ), butyl rubber<sup>2</sup> ( $\alpha < 1.48$ ) and a silicone rubber<sup>3</sup> ( $\alpha < 1.20$ ).

In the present study force–pressure measurements have been made on a sample of crosslinked *cis*-polybutadiene at five elongations below  $\alpha = 1.77$  so as to determine  $(\partial \ln V / \partial \alpha)_{P, T}$ . The results obtained are then compared with the data reported earlier for natural rubber and butyl rubber.

## EXPERIMENTAL

### Material

The *cis*-polybutadiene was crosslinked by heating for 1 h at 150°C with one part per hundred (by weight) of dicumyl peroxide.

### Measurements of $(\partial f / \partial P)_{L, T}$

The apparatus and experimental method are described in detail elsewhere<sup>1, 4</sup>. Briefly, changes in the retractive force exerted by the extended sample were determined from minute displacements of a calibrated steel strip; the displacements were measured by a Phillips displacement pick-up and direct-reading measuring bridge. During the force–pressure measurements the displacement of the spring never exceeded 1  $\mu\text{m}$  and could be detected to  $\pm 0.01 \mu\text{m}$ . The whole dynamometer assembly was housed inside a steel pressure vessel and a Budenberg

dead-weight gauge tester was used to supply the hydrostatic pressures. A thermostat surrounding the pressure vessel could be maintained to within  $\pm 0.002^\circ$  of the required temperature. The rubber test-piece was submerged in mercury in order to isolate it from the transformer oil, which surrounded the displacement pick-up and which transmitted pressure from the tester to the pressure vessel. Measurements of  $(\partial f / \partial P)_{L, T}$  were carried out at 30°C. A pressure of 1000 lbf/in<sup>2</sup> (1 lbf/in<sup>2</sup>  $\equiv$  6895 N/m<sup>2</sup>) was applied to the system at the start of each experiment. When the system had come to equilibrium the applied pressure was decreased in decrements of 100 lbf/in<sup>2</sup> to atmospheric pressure, and then increased in similar increments back to a pressure of 1000 lbf/in<sup>2</sup>. A period of between 10 and 15 min was found to be sufficient for the system to equilibrate at each new pressure.

### Force–extension measurements

The force–extension characteristics of the sample were studied using a Hounsfield Model E tensile tester fitted with an environmental chamber. Measurements were made for both increasing and decreasing loads. Between increments the sample was stretched at a rate of 0.5 cm/min. On reaching the required extension the sample was given a period of between 24 and 48 h to equilibrate. The extension was obtained by measuring the distance apart of two marks on the sample with a cathetometer to an accuracy of  $\pm 0.005 \text{ cm}$ . The equilibrium force was obtained using a calibrated load cell. Over the range studied ( $1.11 < \alpha < 1.77$ ) the force–extension results were found to fit quite closely the empirical Mooney equation,  $f / (\alpha - \alpha^{-2}) = C_1 + C_2 / \alpha$ , with  $C_1 = 2.65 \times 10^5 \text{ N/m}^2$  and  $C_2 = 1.58 \times 10^5 \text{ N/m}^2$ .

## RESULTS AND DISCUSSION

In Table 1, values of  $(\partial \ln V / \partial \alpha)_{P, T}$  determined from force–pressure measurements are listed for five extension ratios in the range  $1.11 < \alpha < 1.77$ . The results are com-

**Table 1** Values of  $(\partial \ln V / \partial \alpha)_{P,T}$  for a sample of crosslinked cis-polybutadiene

$\alpha$	$(\partial \ln V / \partial \alpha)_{P,T} \times 10^4$		
	From measurements of $(\partial f / \partial P)_{L,T}$	Calc. from eqn. (2) (Gaussian theory)	Calc. from eqn. (6)
1.113	1.90 ± 0.05	1.87	2.02
1.304	1.39 ± 0.05	1.29	1.65
1.498	1.26 ± 0.05	0.94	1.47
1.621	1.21 ± 0.05	0.78	1.41
1.765	1.13 ± 0.05	0.65	1.37

pared with the predictions of the Gaussian theory of rubber elasticity<sup>5, 6,\*</sup>

$$(\partial \ln V / \partial \alpha)_{P,T} = (L_i / V) f \kappa_{L,T} / (\alpha^3 - 1) \quad (2)$$

where  $\kappa_{L,T} = -(\partial \ln V / \partial P)_{L,T}$  is the bulk compressibility of the sample at constant length, and  $f$  is the total force. The reasonable assumption was made that the value of  $\kappa_{L,T}$  (which was taken as  $5.69 \times 10^{-10} \text{ N}^{-1} \text{ m}^2$ ) was independent of extension over the range of interest<sup>4, 7</sup>.

The experimental results are seen to fall above the values of  $(\partial \ln V / \partial \alpha)_{P,T}$  calculated from equation (2). This departure, however, is not surprising in view of the large magnitude of the ratio  $C_2/C_1$ ; the ratio  $C_2/C_1$  is often taken as an empirical measure of the deviation of stress-strain behaviour from the Gaussian equation of state. The departure of the theoretical and experimental values clearly becomes more pronounced as  $\alpha$  increases. Provided the measurements have been made under equilibrium conditions, the laws of classical thermodynamics require the two sets of values to converge at  $\alpha = 1$ .

#### Isotropy of linear compressibility

An alternative method of predicting  $(\partial \ln V / \partial \alpha)_{P,T}$ , proposed independently and in slightly different forms by Elliott and Lippmann<sup>8</sup>, and Gee<sup>9</sup>, involves making the assumption that the linear compressibility of a rubber in extension is isotropic, i.e.

$$A \equiv -3(\partial \ln L / \partial P)_{f,T} (\kappa_{f,T})^{-1} = 1 \quad (3)$$

where

$$\kappa_{f,T} = -(\partial \ln V / \partial P)_{f,T}$$

From thermodynamics:

$$\left(\frac{\partial \ln V}{\partial \alpha}\right)_{P,T} = -\frac{3}{\kappa_{f,T}} \left(\frac{\partial \ln L}{\partial P}\right)_{f,T} \cdot \frac{\kappa_{f,T} (L_i)}{3} \left(\frac{\partial f}{\partial \ln L}\right)_{P,T} \quad (4)$$

Hence from equations (3) and (4):

$$\left(\frac{\partial \ln V}{\partial \alpha}\right)_{P,T} = \frac{\kappa_{f,T} (L_i)}{3} \left(\frac{\partial f}{\partial \ln L}\right)_{P,T} \quad (5)$$

In a region in which the Mooney equation holds, equation (5) reduces to:

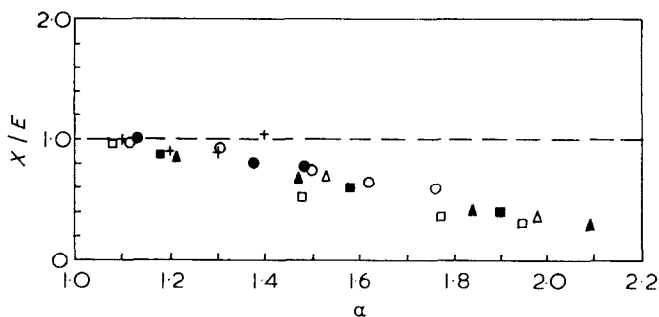
$$\left(\frac{\partial \ln V}{\partial \alpha}\right)_{P,T} = \frac{\kappa_{f,T} C_1 (\alpha^3 + 2)}{3} + \frac{\kappa_{f,T} C_2}{\alpha^3} \quad (6)$$

\* Our definition of the extension ratio, which is the same as that given in ref. 5, differs in a minor way from the definition used by Flory. Flory defines  $\alpha$  as the ratio of the length of the extended sample ( $L$ ) to the length of the sample in an isotropic state of volume  $V$ ;  $V$  is the volume of the extended sample under the conditions of the experiment. The difference between the two definitions, however, is trivial and has no detectable effect on the outcome of the results.

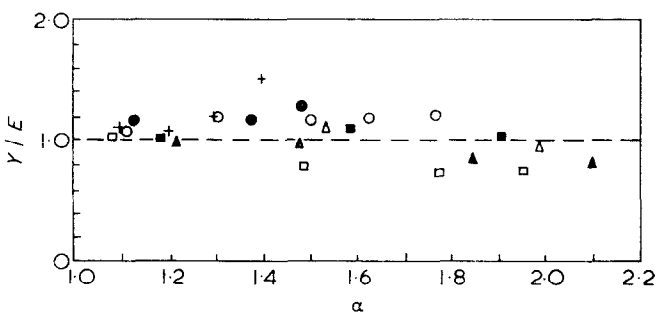
Values of  $(\partial \ln V / \partial \alpha)_{P,T}$  calculated from equation (6) for the crosslinked cis-polybutadiene are given in Table 1;  $\kappa_{f,T}$  was assumed to be independent of the applied stress and its value taken to be the same as that of  $\kappa_{L,T}$ . Equation (6) is seen to give a somewhat better representation of the observed experimental behaviour at the higher extension ratios than equation (2).

In Figures 1 and 2 the experimental values of  $(\partial \ln V / \partial \alpha)_{P,T}$  for cis-polybutadiene, natural rubber<sup>1</sup> and butyl rubber<sup>2</sup> are collected together and are compared with values predicted by equations (2) and (6) respectively. It is seen that the results for five different samples of crosslinked natural rubber in the dry state are also in closer agreement with the predictions of equation (6) than with those of equation (2). However, the limited data available for a single sample of butyl rubber in the dry state appears to favour equation (2). Four values of  $(\partial \ln V / \partial \alpha)_{P,T}$  from force-pressure measurements reported in an earlier study<sup>4</sup> for a single sample of natural rubber have not been included in the analysis because they are of lower precision than those given in ref. 1; the dynamometer assembly used in ref. 4 was set up specifically to measure  $(\partial f / \partial T)_{L,V}$  rather than  $(\partial f / \partial P)_{L,T}$ .

Direct studies of volume change on elongation reported for crosslinked natural rubber by Gee *et al.*<sup>10</sup> and by Christiansen and Hoeve<sup>11</sup> both gave results which were in accord with the integrated form of equation (4) rather than the integrated form of equation (2).



**Figure 1** Ratio,  $X/E$ , of values of  $(\partial \ln V / \partial \alpha)_{P,T}$  calculated from equation (2) ( $X$ ) to values determined by experiment ( $E$ ) at different extension ratios,  $\alpha$ . Samples:  $\circ$ , cis-polybutadiene; natural rubber:  $\square$ , sample A;  $\triangle$ , sample B;  $\blacksquare$ , sample C;  $\blacktriangle$ , sample D;  $\bullet$ , sample E; +, butyl rubber



**Figure 2** Ratio,  $Y/E$ , of values of  $(\partial \ln V / \partial \alpha)_{P,T}$  calculated from equation (6) ( $Y$ ) to values determined by experiment ( $E$ ) at different extension ratios,  $\alpha$ . Samples:  $\circ$ , cis-polybutadiene; natural rubber:  $\square$ , sample A;  $\triangle$ , sample B;  $\blacksquare$ , sample C;  $\blacktriangle$ , sample D;  $\bullet$ , sample E; +, butyl rubber

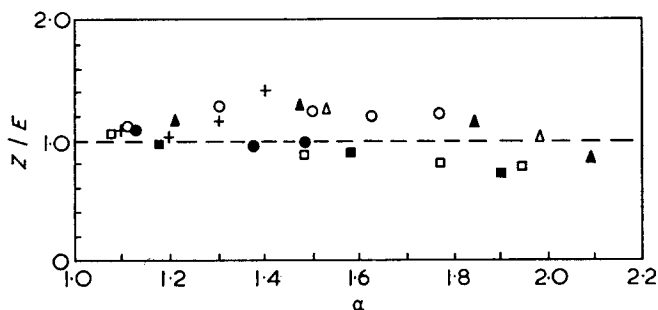


Figure 3 Ratio,  $Z/E$ , of values of  $(\partial \ln V / \partial \alpha)_{P, T}$  calculated from equation (7) ( $Z$ ) to values determined by experiment ( $E$ ) at different extension ratios,  $\alpha$ . Samples:  $\circ$ , *cis*-polybutadiene; natural rubber:  $\square$ , sample A;  $\triangle$ , sample B;  $\blacksquare$ , sample C;  $\blacktriangle$ , sample D;  $\bullet$ , sample E;  $+$ , butyl rubber

#### An empirical relationship

In Figure 3, experimental values of  $(\partial \ln V / \partial \alpha)_{P, T}$  are compared with those calculated from:

$$\left(\frac{\partial \ln V}{\partial \alpha}\right)_{P, T} = \frac{C_1 \kappa_{L, T}}{\alpha^2} + C_2 \kappa_{L, T} \quad (7)$$

where  $C_1$  and  $C_2$  are the Mooney constants. Equation (7) can be obtained from the Mooney equation if we assume  $C_1$  has the same volume dependence as the modulus predicted by the Gaussian theory, and assume  $C_2$  is inversely proportional to volume. This simple relationship is seen to provide a useful representation of the experimental data for natural rubber and *cis*-polybutadiene. It does not fit, however, the limited data available for butyl rubber.

The form of equation (7) leads one to expect that for highly swollen rubbers where  $C_2$  is small the dilation

coefficient  $(\partial \ln V / \partial \alpha)_{P, T}$  might be adequately predicted by equation (2). Some limited support for this viewpoint is offered by a number of results reported for highly swollen natural rubber networks<sup>1</sup>; unfortunately unequivocal conclusions cannot be drawn from the data since the maximum extension ratio covered was only 1.48.

#### ACKNOWLEDGEMENT

The authors wish to thank Dr F. P. Wolf for helpful discussions.

#### REFERENCES

- 1 Allen, G., Kirkham, M. J., Padget, J. C. and Price, C. *Trans. Faraday Soc.* 1971, **67**, 1278
- 2 Allen, G., Kirkham, M. C., Padget, J. C. and Price, C. 'Polymer Systems', (Eds R. E. Wetton and R. W. Whorlow), Macmillan, London, 1968, pp 51-58
- 3 Price, C., Padget, J. C., Kirkham, M. C. and Allen, G. *Polymer* 1969, **10**, 573
- 4 Allen, G., Bianchi, U. and Price, C. *Trans. Faraday Soc.* 1963, **59**, 2493
- 5 Khasanovich, T. N. *J. Appl. Phys.* 1959, **30**, 948
- 6 Flory, P. J. *Trans. Faraday Soc.* 1961, **57**, 829
- 7 Price, C., Padget, J. C., Kirkham, M. C. and Allen, G. *Polymer* 1969, **10**, 495
- 8 Elliott, D. R. and Lippmann, S. A. *J. Appl. Phys.* 1945, **16**, 50
- 9 Gee, G. *Trans. Faraday Soc.* 1946, **42**, 585
- 10 Gee, G., Stern, J. and Treloar, L. R. G. *Trans. Faraday Soc.* 1950, **46**, 1101
- 11 Christiansen, R. C. and Hoeve, C. A. J. *J. Polym. Sci. (A-1)* 1970, **8**, 1503

# Mechanical properties of polystyrene/low density polyethylene blends

W. M. Barentsen and D. Heikens

Laboratory of Polymer Technology, Eindhoven University of Technology,  
PO Box 513, Eindhoven, The Netherlands  
(Received 11 March 1973; revised 4 June 1973)

Some mechanical properties of blends of polystyrene and low density polyethylene have been derived from stress-strain and impact measurements. The strength and impact properties are improved by adding a graft copolymer of polystyrene and low density polyethylene to the blends. It is assumed that the copolymer acts as an adhesive at the interface of the homopolymers thus decreasing the stress concentrations around the dispersed polymer particles at yield. The impact strength and modulus of polystyrene-graft copolymer blends could be made comparable to those of commercial rubber-modified impact polystyrenes by adjusting the fraction of copolymer in the blend.

## INTRODUCTION

From literature data and our own preliminary experiments it was found that the modulus of elasticity of two phase blends of incompatible thermoplastic polymers follows an S-shaped curve if plotted against fractional weight composition. This is in agreement with Kerner's predicted modulus behaviour as was pointed out by Nielsen<sup>1</sup>. However, the tensile strength does not follow such a curve but shows a minimum around 50:50 compositions. Moreover, if one or both components shows a tough behaviour, their 50:50 blends have very low elongation at break<sup>2,3</sup>. These results suggest that the fracture path preferentially follows the weak interface between the polymer phases or that fracture is initiated at the interface. Polystyrene and low density polyethylene are recognized as incompatible polymers. Blends of these polymers can be considered as model compounds for blends with a glassy matrix and soft inclusions (e.g. impact polystyrene and ABS) if the fraction of low density polyethylene is low as well for blends with a soft matrix and hard inclusions if the fraction of polystyrene is low.

It was assumed that the adhesion between the homopolymers in the model blends could be improved by adding a graft copolymer to the polystyrene/low density polyethylene blends.

The influence of the concentration of a graft copolymer of low density polyethylene and polystyrene on some mechanical properties of polystyrene/low density polyethylene was investigated. It would be expected that by simple addition of the graft copolymer its influence on the mechanical properties of blends is more readily and firmly interpreted than is the effect of graft copolymers in composites such as high impact polystyrene and ABS. In the latter, copolymers are formed during the polymerization of styrene or styrene and acrylonitrile in the presence of rubber<sup>4-6</sup>. In these systems the amount of graft copolymer and its quantitative influence

on the properties of the composite are less easily determined. Furthermore, it is well known that matrix polymer can be incorporated in the rubber phase<sup>7</sup> and this phase can become crosslinked.

## EXPERIMENTAL

### Materials

Additive-free low density polyethylene (Stamylan 1510, DSM) and a general purpose polystyrene (Styron 666E, Dow) were used. Graft copolymers were prepared by a Friedel-Crafts alkylation of polystyrene (PS) with the low density polyethylene (LDPE) according to the method reported by Carrick<sup>8</sup>. During this reaction polyethylene is chemically coupled to polystyrene. In this way graft copolymers were prepared in high yield (50-70% of the starting amount of PS and LDPE) after very short reaction times (3-5 min). Free PS and LDPE were separated from the pure graft polymer by extraction of the reaction mixture with ethyl acetate and n-heptane. The copolymer used in this study contained 47% PS as determined by infra-red spectroscopy.

### Blends of PS and LDPE

Blends over the whole range of compositions were prepared on a Schwabenthan Laboratory Mill. The mixing conditions are listed in *Table 1*. The blends with a PS content of more than 30% by vol. were compression moulded to 160 × 160 × 3 mm sheets at 200°C. Tensile specimens with dimensions according to ASTM

Table 1 Mixing conditions for blend preparation

Batch	100 ml
Melt temperature	195°C
Circumferential speed of the rolls	6 and 18 cm/sec
Roll separation	0.8 mm
Mixing time	7 min

D 638 model 3 were machined from the sheets. From the blends with a PS content of less than 30% by vol. 1 mm thick sheets were compression moulded. Microtensile specimens according to ASTM D 1708 were stamped from these sheets. (It was found that the ASTM D 638 model 3 specimens of the latter blends had a deformation to break too large to be measured on the tensile tester.)

The structure of the blends was investigated by phase contrast microscopy. The method of cutting and immersion of thin polymer sections has been reported by Traylor<sup>9</sup>. A study on the micrographs of the blends led to the following conclusions: (1) discrete particles of the dispersed polymer are almost spherical; (2) particles in the core of the sheets from blends with more than 30% dispersed polymer are larger than those near the surface. It is believed to be caused by differences in the coalescence of the particles. During compression moulding the velocity gradient of the melt in the core of the sheet is small if compared with the gradient near the surface. Clearly, the higher gradient counteracts coalescence; (3) in blends with 40–60% LDPE by volume areas with two continuous phases could be observed.

*Blends of PS, LDPE and graft copolymer*

The graft copolymer was added to the PS/LDPE blends in which only one continuous and one dispersed phase was observed. PS was melt blended with 5 and 30% of graft copolymer if PS had to become the dispersed phase in the blends. Pre-blending of the copolymer and LDPE was carried out if LDPE was to form the dispersed phase. Additionally blends of only PS and graft copolymer (47% PS) were prepared. Tensile bars were machined or stamped from compression moulded sheets of blends and of pure graft copolymers of various compositions.

As the tensile properties of PS rich blends are notch sensitive, scratches on the tensile specimens were removed by wiping with benzene. Dynstat impact measurements according to DIN 53453 were carried out with unnotched compression moulded strips. Before conditioning at 21°C and 65% r.h. the test specimens were stored for 24 h at 60°C.

*Mechanical testing*

An Instron tensile tester was used for the stress-strain measurements. The cross-head speed was adjusted to give the samples an elongation rate of 50% of the original gauge length per minute. Young's modulus, yield strength, ultimate strength and elongation at yield and break were calculated from the stress-strain diagrams. From each blend 6–10 tests were run. The scatter in modulus and strength values for PS rich blends was 5% and for LDPE rich blends 10%. Thin sections of the blends were examined by phase contrast microscopy. Fracture surfaces of the blends were micrographed by a scanning electron microscope (Stereoscan Mark 2A, Cambridge Scientific Instruments Ltd). Impact measurements were carried out at -20°C and +20°C.

**RESULTS**

*Blends of PS and LDPE*

The Young's modulus of these blends can be described by the equation derived by Kerner<sup>10</sup>. As this equation

does not account for phase reversal, it can only be applied to blends with small fractions of dispersed polymer. Figure 1 shows that the graft copolymers have considerably higher moduli than blends with the same overall composition. These results indicate that the

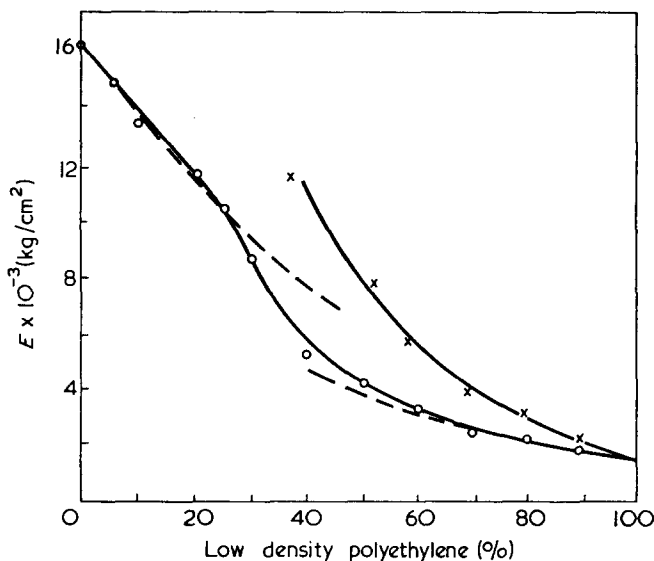


Figure 1 Young's modulus of blends and graft copolymers. ○, PS/LDPE blends; ×, graft copolymers; ----, Kerner

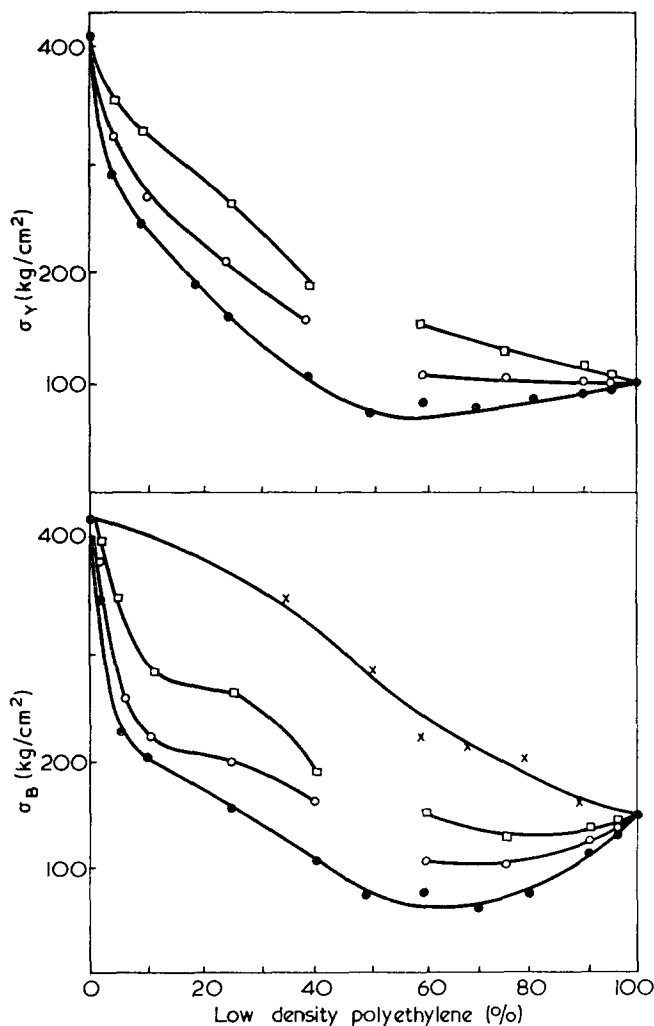


Figure 2 Yield strength and tensile strength of PS/LDPE blends. ●, Blends of PS and LDPE; ○, blends with 5% graft copolymer in the dispersed phase; □, blends with 30% graft copolymer in the dispersed phase; ×, graft copolymers

copolymers are partly crosslinked materials. The reaction scheme for the coupling of LDPE to PS suggested by Carrick and the observed resistance to flow at high temperatures are further evidence for the assumption.

The yielding of the blends is accompanied by whitening of the samples. Stress whitening is a well known phenomenon in impact polystyrene and ABS. The yield strength and the tensile strength pass through a minimum if plotted *versus* LDPE content (Figure 2).

Anderson *et al.*<sup>2</sup> observed this behaviour too but no explanation was put forward. As both PS and LDPE have higher yield strength and tensile strength than the 50:50 blends, it seems feasible to suppose that the phase boundary is the weakest spot in these blends. This was confirmed by scanning electron microscopy of fracture surfaces. No indication of adhesion between the two polymers could be found. The dispersed particles on the surfaces of the fracture are smooth as can be seen from Figures 3 and 4.

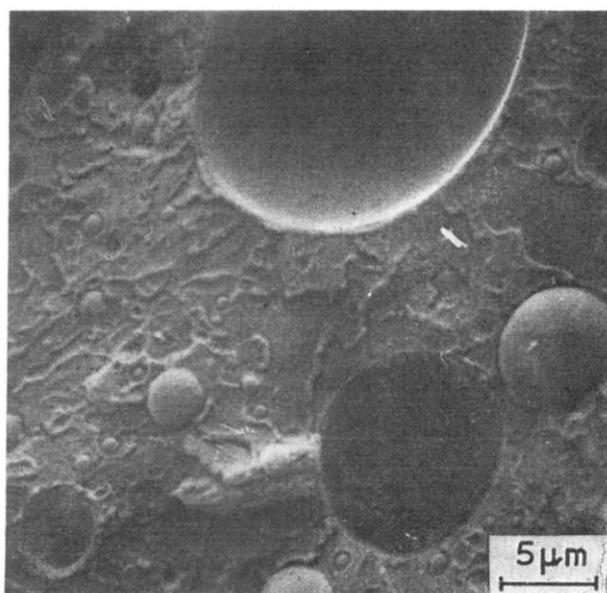


Figure 3 Fracture surface of the 75:25 PS/LDPE blend

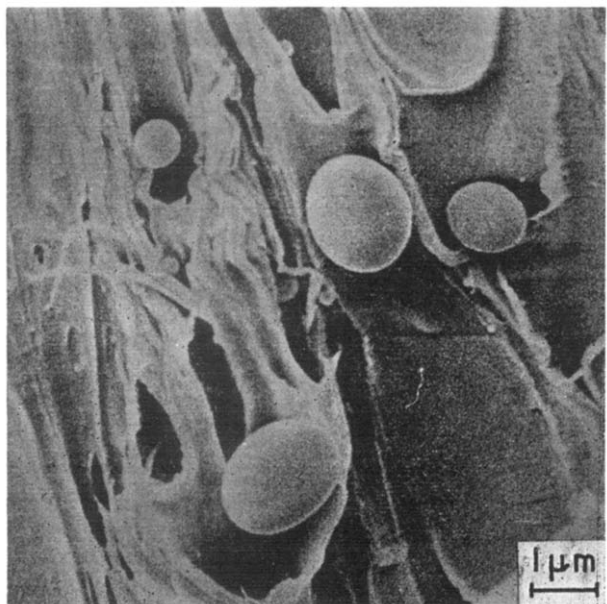


Figure 4 Fracture surface of the 25:75 PS/LDPE blend

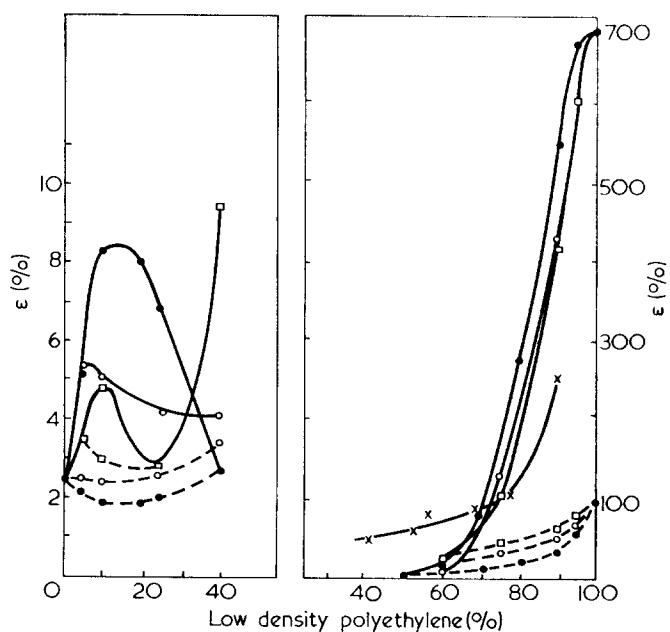


Figure 5 Elongation at yield and break of PS/LDPE blends and graft copolymers. ●, PS/LDPE blends; ○, blends with 5% graft copolymer (47% PS) in the dispersed phase; □, blends with 30% graft copolymer (47% PS) in the dispersed phase; ×, pure graft copolymers. —,  $\epsilon_B$ ; - - - ,  $\epsilon_Y$

The decrease in yield strength and tensile strength of PS and LDPE upon adding the second phase can be attributed to several causes: (1) the dispersed polymer does not adhere to the surrounding matrix. During the deformation of the blends holes are formed that contain the loose dispersed polymer particles. Accordingly, the stress bearing cross-section of the tensile bar is diminished by the presence of the dispersed polymer. The elongation at yield will decrease too as the total amount of yielding polymer decreases; (2) the presence of a second phase (polymer or hole) gives rise to stress concentrations around the inclusions<sup>11</sup>. Owing to the local concentrations of stress, yield will start at a lower average stress on the tensile bar and lower elongation than in a pure material.

#### Blends of PS, LDPE and graft copolymer (47% PS)

The Young's modulus of the blends to which the copolymer was added did not differ from the modulus of the blends without copolymer. The yield strength and the elongation at yield increase if the graft copolymer is added to the blends. However, the elongation at break diminishes as is shown in Figure 5.

These observations can be understood if the graft copolymer is present at the interface between PS and LDPE and thus improving the adhesion. Electron scanning micrographs of the fracture surfaces show that the phase boundary of the dispersed LDPE particles and the holes from which the particles are pulled out are covered with small globules (Figure 6). The total volume of these irregularities agrees well with the amount of added copolymer. This type of fracture surface was also found by Mann *et al.*<sup>6</sup> for an ABS polymer with grafted rubber particles. Dispersed PS particles are locally connected to the surrounding tough LDPE (Figure 7).

It may be concluded that the adhesion is still perfect at the yield point. So at yield the modulus ratio of matrix polymer and inclusion of these blends is lower



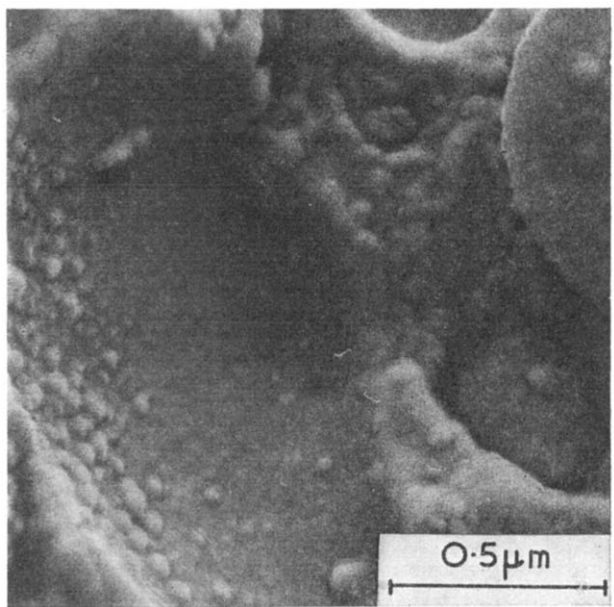


Figure 6 Fracture surface of the 75:25 PS/LDPE blend with 5% copolymer added to the amount of LDPE

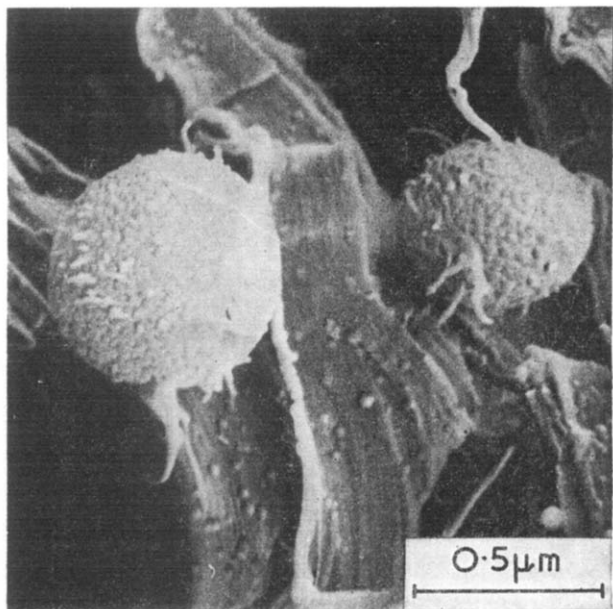


Figure 7 Fracture surface of the 25:75 PS/LDPE blend with 30% copolymer added to the amount of PS

than for blends without copolymer as in the latter cavitation due to lack of adhesion must be expected. As stress concentrations decrease upon decreasing modulus ratio, yield will occur at higher stress on the tensile specimen and at higher elongation.

The higher stress level in samples with added copolymer will influence the fracture process. Crazes in PS rich blends will spread faster under the increased load. The number of crazes that can be formed before the sample fractures will be less, which is in agreement with microscopic observations of thin sections of fractured blends<sup>12</sup>. This means that the elongation at break of blends with the graft copolymer will be less than of blends without the copolymer.

The blend with 40% LDPE to which 30% graft copolymer relative to the amount of LDPE was added, shows a rather large elongation at break. After microscopic examination it was concluded that the LDPE

was not dispersed as spherical particles as in other PS rich blends but as small interconnected discs. This may be caused by the compression moulding step in combination with the decrease in interfacial tension due to the presence of the copolymer at the interface in the highly filled blend.

Addition of the graft copolymer to the LDPE rich blends decreases the elongation at break also. It was concluded from observations by electron scanning microscopy, phase contrast microscopy and from the stress whitening phenomena that after yield but well before break most PS particles are torn loose from the surrounding highly oriented LDPE. Thus at break porous LDPE is stressed just like in blends without copolymer. No influence of the graft copolymer on the tensile strength would be expected then. As experiments showed that the graft copolymer is stronger than LDPE and has a higher modulus (Figures 2 and 5) the copolymer will enhance the strength of the porous LDPE. However, the elongation at break will be lower because before LDPE obtains its ultimate elongation, cracks in the copolymer skin of the holes are formed. These cracks will initiate fracture in LDPE thus lowering the elongation at break.

#### Impact strength

The impact strength measurements were carried out at +20°C and -20°C. No indication of a temperature dependence of the impact strength was found. In Figure 8 the impact data are related to the Young's modulus and the total LDPE content of the blends. The modulus-impact strength relationship follows the general pattern observed for many polymers. The impact strength increases as the modulus decreases<sup>13</sup>. In Figure 8 the data for three commercial impact polystyrenes are plotted. Blends of PS and LDPE can only obtain similar impact strength at the cost of rigidity. Such blends have a continuous LDPE phase and PS as dispersed phase. Impact strength and modulus comparable to the three impact polystyrenes were obtained for blends of PS and graft copolymer that contained 47% bound PS.

The impact behaviour of PS rich blends is in agreement with the general ideas about impact strength of rubber modified polystyrene<sup>14</sup> and ABS<sup>15</sup>. To ensure

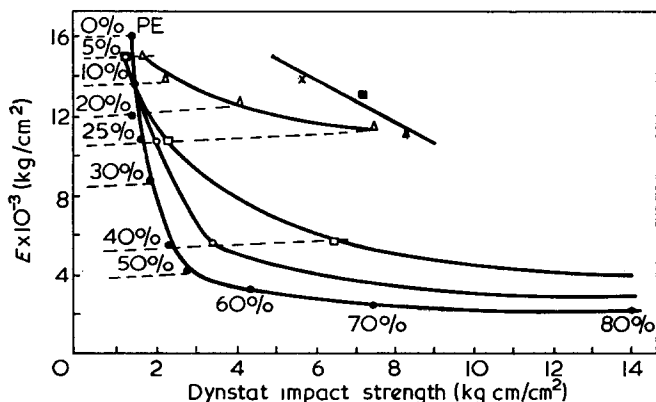


Figure 8 Dynstat impact strength of PS/LDPE blends. ●, PS/LDPE blends; ○, blends with 5% graft copolymer (47% PS) in the dispersed phase; □, blends with 30% graft copolymer (47% PS) in the dispersed phase; △, blends of PS and graft copolymer (47% PS). ▲, Styron 456 (Dow); ×, Polystyrol 457 (BASF); ■, Styron 453 (Dow)

tough behaviour, the dispersed phase must not only adhere to the surrounding glassy polymer but must also be crosslinked. With up to 50% LDPE only small reinforcement is noted. This behaviour of incompatible blends was also reported by Matsuo for poly(vinyl chloride)/polybutadiene blends<sup>16</sup>. The improved adhesion in blends with small amount of graft copolymer gives rise to an increase of impact strength. The best results are obtained for blends of PS and pure graft copolymer. The graft copolymer can be compared with the rubbery phase in impact PS which is also crosslinked and adheres to the polystyrene matrix. In general LDPE is not as effective as the rubbery phase in impact PS.

This may be caused by the sharp increase of modulus of LDPE as the result of the high speed of impact testing. Under such conditions, it must be expected that crazes are started at a higher average load on these blends than in impact polystyrene. Crazes and cracks will spread faster through the specimen. Less polystyrene will be converted to craze material. This plastic deformation of polystyrene is believed to be a major mechanism by which the impact strength of polystyrene is increased.

#### CONCLUSIONS

The Young's modulus of PS/LDPE blends can be predicted by the equation derived by Kerner. The close agreement does not hold for the blends containing 25–60% LDPE. In this composition range the phase inverts. The yield strength and the tensile strength pass through a minimum if plotted *versus* composition. For a particular composition yield strength and tensile strength can be improved if small amounts of graft copolymer of PS and LDPE are added to the blends.

It is found that the graft copolymer concentrates at the interface between the two homopolymers thus acting as an adhesive. It is most likely that the increase in strength at yield and break are caused by different mechanisms.

The impact strength of PS rich blends is best improved if the dispersed phase is crosslinked and adheres to the surrounding PS. The graft copolymer used in the blends fulfils these requirements like the rubbery phase in impact polystyrene. It is possible to adjust the ratio of the amounts of PS and graft copolymer to obtain impact strength and modulus close to the commercial grades of impact polystyrene.

#### REFERENCES

- 1 Nielsen, L. E. *J. Compos. Mater.* 1967, **1**, 100
- 2 Anderson, L. C., Rooper, D. A. and Rieke, J. K. *J. Polym. Sci.* 1960, **43**, 423
- 3 Heikens, D. and Barentsen, W. M. *Z. Werkstofftechn.* 1970, **1**, 49
- 4 Haward, R. N. and Mann, J. *Proc. R. Soc. (A)* 1964, **282**, 120
- 5 Mann, J., Bird, R. J. and Rooney, G. *Makromol. Chem.* 1966, **90**, 207
- 6 Bergen, R. L. *Appl. Polym. Symp.* 1968, **17**, 41
- 7 Kato, K. *Kolloid-Z. Z. Polym.* 1967, **220**, 24
- 8 Carrick, W. L. *J. Polym. Sci. (A-1)* 1970, **8**, 215
- 9 Traylor, A. *Analyt. Chem.* 1961, **33**, 1629
- 10 Kerner, E. H. *Proc. Phys. Soc. (B)* 1956, **69**, 808
- 11 Matsuo, M. *Polymer* 1966, **7**, 421
- 12 Barentsen, W. M. *Thesis* Eindhoven Technical University, 1972
- 13 van Krevelen, D. W. 'Properties of Polymers', Elsevier, Amsterdam, 1972
- 14 Bucknall, C. B. *J. Mater. Sci.* 1969, **4**, 214
- 15 Bohn, L. *Angew. Makromol. Chem.* 1971, **20**, 129
- 16 Matsuo, M., Ueda, A. and Kondo, Y. *Polym. Eng. Sci.* 1970, **10**, 253

# An approximate method of predicting the bending of thermoplastic beams

R. M. Ogorkiewicz

*Department of Mechanical Engineering, Imperial College of Science and Technology, Exhibition Road, London SW7 2BX, UK*

and A. A. M. Sayigh

*College of Engineering, University of Riyadh, Riyadh, Saudi Arabia  
(Received 31 May 1973)*

Availability of an increasing amount of data on the deformational characteristics of thermoplastics makes it possible to predict more accurately the deflection under load of plastics articles. This is shown by the close agreement between the calculated and observed deflections of PVC beams under bending loads of short and long duration.

## INTRODUCTION

The effort devoted in recent years to the study of the mechanical properties of thermoplastics has resulted in the publication of an increasing amount of data about their deformational characteristics<sup>1, 2</sup>. The generation of these data was inspired very largely by the hope that they would lead not only to a better understanding of the behaviour of plastics in general but also to the selection of thermoplastics more appropriate to particular applications and, ultimately, to a more rational design of thermoplastic articles. So far, however, relatively little has been published about the use of such data for the design of plastics components within limits of deflection prescribed by functional or aesthetic considerations.

Most of the data published so far about the deformational characteristics of thermoplastics has been based on their response under simple, uniaxial loading systems and in particular on tensile creep tests<sup>1-3</sup>. This type of data is generally considered to be best for characterizing deformational behaviour but it is not directly applicable to the design of plastics articles because in most cases they are subjected to more complex stress systems than uniaxial tension. There is a need, therefore, to devise or establish methods that would enable the basic data obtained under uniaxial loading systems to be used under other conditions which arise in engineering design with thermoplastics. In particular, this calls for methods of predicting the deflection of articles under loads of given magnitude and duration.

## METHODS OF PREDICTING DEFLECTIONS

### *General approach*

Since thermoplastics behave in general as non-linear viscoelastic materials rigorous solutions to the deformation of articles made of them are bound to be complicated and prohibitively so for general design purposes. It is

necessary, therefore, to resort to simpler, approximate methods<sup>4</sup>.

The approximate methods which have been put forward so far are based on adaptations of the theory of linear elastic materials established for many years with metals. One of the earliest adaptations of this is the procedure put forward by Baer *et al.*<sup>5</sup> which amounts to the substitution of a time-dependent modulus into the standard linear elastic solutions for deflections, the modulus being considered strain independent provided that the procedure is applied within prescribed strain limits<sup>5, 6</sup>. Similar procedures have been put forward, among others, by Alfrey and Gurnee<sup>7</sup>, as applicable to linear viscoelastic materials or, at least, the quasi-linear viscoelastic range of behaviour of polymeric materials.

This approach has already been applied with some success to beams by McCammond<sup>8</sup> who has found, however, that it predicted deflection less accurately than a method which took into account the variation of the modulus not only with time but also with strain. The second approach is obviously more realistic, particularly at other than small strains, and deserves further consideration, especially as it can be applied in an alternative and simpler form than McCammond's, which involves integration of areas under stress-strain curves. Moreover, the authors have had the opportunity of putting it to test in a bending apparatus more accurate and capable of taking more readings than those available to earlier workers.

### *Method used*

The method which has been followed is similar to that already applied to the deflection of plastics sandwich beams<sup>9</sup>. It is based on constant load isochronous stress-strain curves, which are now a common form of presenting basic data on thermoplastics<sup>2</sup> and from which corresponding values of stress and strain can be obtained

at different times from the commencement of the application of a constant load. Thus, selection of a particular strain  $\epsilon$  at a time  $t$  leads to the corresponding stress  $\sigma$  and the secant creep modulus  $E = \sigma/\epsilon$ .

Knowing the stress it is also possible to calculate the corresponding load  $W$  on a particular beam from the standard equation<sup>10</sup>:

$$\sigma = \frac{My}{I} \quad (1)$$

where  $M$  = bending moment,

$I$  = second moment of area of beam about its neutral axis,

$2y$  = thickness of the beam.

If  $\sigma$  is the skin stress at the mid-span of centrally loaded rectangular section beam equation (1) reduces to:

$$W = \frac{2bd^2}{3l} \sigma \quad (2)$$

where  $b$  = width of beam,

$d$  = thickness of beam,

$l$  = span of beam supports.

The theory of bending of beams also gives solutions to the deflection of beams in terms of  $W$ ,  $E$  and the geometry of the beam and loading system. For the particular case of the central deflection  $\delta$  of the centrally loaded rectangular section beam it is<sup>10</sup>:

$$\delta = \frac{Wl^3}{4Ebd^3} \quad (3)$$

Repeating the process for a series of values of  $\epsilon$  makes it possible to plot a curve of  $W$  vs.  $\delta$ , which can then be compared with the observed relationships between deflections and loads.

Although in the study of the bending of simply loaded plastics beams attention has tended to be focused on their central deflections, it is also of interest to consider deflection at other points along the beam. The authors have therefore done this at two additional points which are at a distance  $x = 7l/10$  and  $9l/10$ , measured from one of the supports. The equations to the deflection at these points obtained from classical beam theory<sup>10</sup> are:

at  $x = \frac{9}{10}l$

$$\delta = \frac{37}{5 \times 10^3} \frac{Wl^3}{Ebd^3} \quad (4)$$

and at  $x = \frac{7}{10}l$

$$\delta = \frac{99}{5 \times 10^3} \frac{Wl^3}{Ebd^3} \quad (5)$$

From some points of view the bending of beams simply supported at both ends and acted on by two identical, symmetrically disposed loads is of even greater interest, because of the constancy of the bending moment acting on the section of the beam between the loads. The authors have therefore considered the bending of beams under this condition also, with each load acting at a distance equal to  $l/4$  from the adjacent support. In this case the deflection at mid-span is:

$$\delta = \frac{11}{64} \frac{Wl^3}{Ebd^3} \quad (6)$$

and at the points of load application:

$$\delta = \frac{Wl^3}{8Ebd^3} \quad (7)$$

where  $W$  is the sum of the two equal loads acting on the beam.

## COMPARISON WITH EXPERIMENTAL RESULTS

To examine the validity of the theoretical approach, slender rectangular section beams of ICI Ltd Darvic 110 PVC were considered and their deflections were calculated from equations (3) to (7) for a series of values of load at 100 and 1000 sec from the applications of the loads using isochronous tensile stress-strain curves given for Darvic 110 in ref. 2, and additional tensile data obtained by the authors.

Corresponding Darvic 110 beams were then tested using an interrupted step-loading procedure, similar to that commonly used to obtain isochronous stress-strain curves in tension<sup>11</sup>, which gave 100 and 1000 sec isochronous load-deflection curves. The beams were nominally 6 mm thick and 24 mm wide and they were supported on small, fixed rollers, set 250 mm apart, which were adopted as a result of an earlier investigation into the effects of different supports on the results of bending tests<sup>12</sup>. The beams were loaded at their centre or at two symmetrically disposed points in a specially developed lever-loading machine and their deflections were recorded with capacitive transducers accurate to within  $\pm 0.005\%$ <sup>13</sup>.

A set of results for a beam in three-point bending 100 sec from the application of the load is shown in Figure 1. The correlation between the observed deflections and those calculated from equations (3), (4) and (5), respectively, at the centre of the beam and at 0.7 and 0.9 of the span is evidently close. Similarly, close agreement was obtained at 1000 sec from the application of the load.

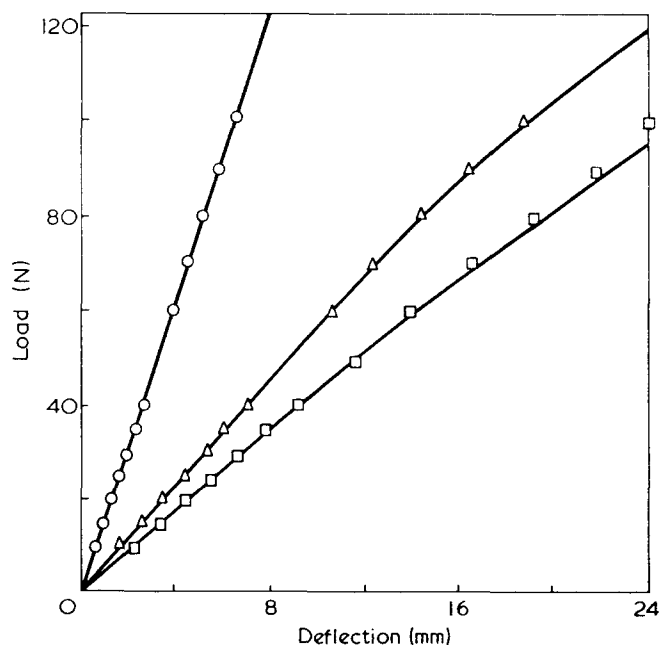


Figure 1 Comparison of calculated load-deflection curves and the observed deflections of a PVC beam in three-point bending at 100 sec after the application of loads at: □, mid-span; △, 0.7 of span; ○, 0.9 of span

Close agreement was also obtained in four-point bending. This is illustrated in Figure 2, which shows curves obtained from equations (6) and (7) for the deflection of the beam at mid-span and under the loads 100 sec after the application of the loads and the corresponding observed deflections. Similarly, close agreement was obtained at 1000 sec.

The agreement between the calculated and the observed results is brought out even more clearly by considering the deflected shape of the beams. This is shown in Figure 3 for a beam in three-point bending at 100 sec

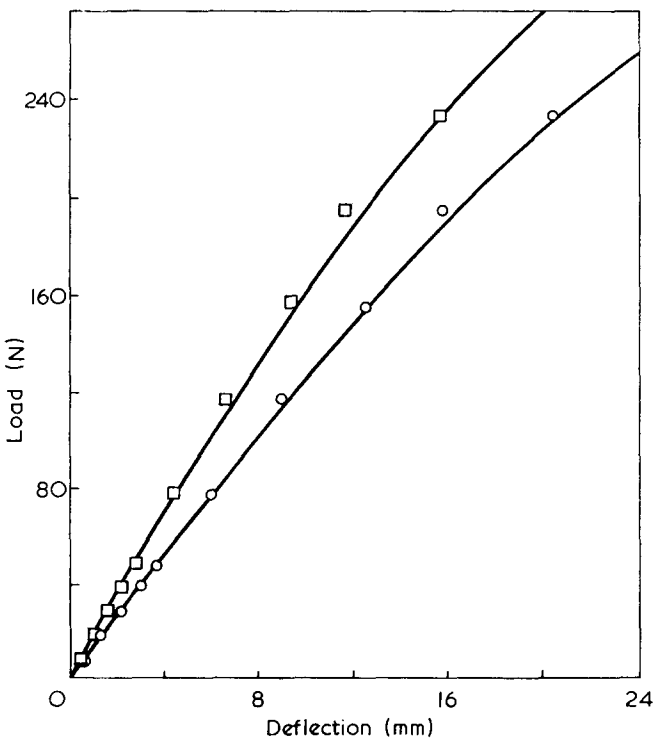


Figure 2 Comparison of calculated load-deflection curves and the observed deflection of a PVC beam in four-point bending at 100 sec after the application of the loads at: ○, mid-span; □, quarter span

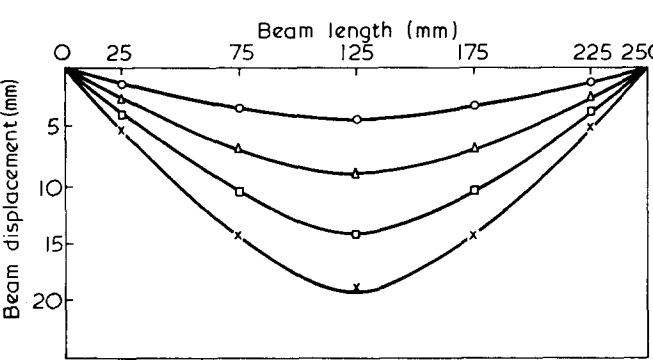


Figure 3 Comparison of calculated and observed deflected shapes of a PVC beam in three-point bending 100 sec after the application of different loads. ○, 19.6 N; △, 39.2 N; □, 58.8 N; ×, 78.4 N

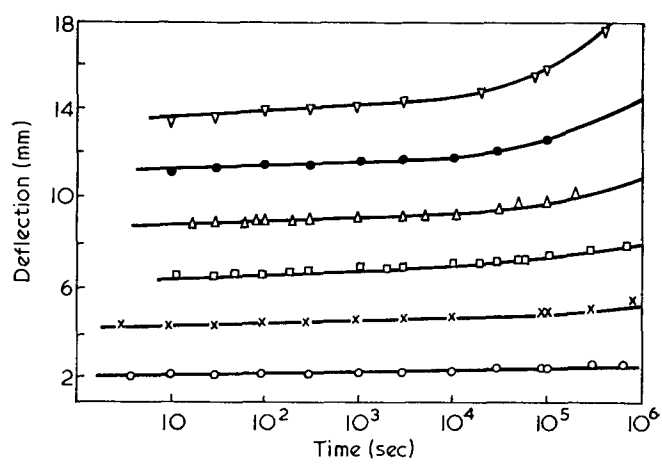


Figure 4 Calculated and observed creep deflections at the centre of a PVC beam in three-point bending. ○, 9.8 N; ×, 19.6 N; □, 29.4 N; △, 39.2 N; ●, 49.0 N; ▽, 58.8 N

after the application of each of a series of loads. The vertical scale in Figure 3 has been considerably magnified but, nevertheless, the deflections of different points of the beam come very close to its calculated shape.

PREDICTION OF CREEP

The agreement obtained at 100 and 1000 sec from the application of the load, led to an extension of the work to the prediction of creep deflections at times of up to 10<sup>6</sup> sec. This required the derivation of additional isochronous stress-strain curves from ref. 2 but otherwise followed the same procedure for working out series of values of load and deflection as before, except that each series was worked out for a constant load.

A typical set of results, for the central deflection of a beam in three-point bending, is shown in Figure 4. Evidently the agreement between the calculated and observed deflections is close. Similarly close agreement was obtained in four-point bending.

REFERENCES

- 1 'Shell Polyolefins—Engineering Design Data', Shell, London, 1966
- 2 'Engineering Properties of Thermoplastics', (Ed. Ogorkiewicz, R. M.), Wiley, London, 1970
- 3 Turner, S. *Br. Plast.* 1964, 37, 440
- 4 Turner, S. *Trans. J. Plast. Inst.* 1966, 34, 127
- 5 Baer, E., Knox, J. R., Linton, T. J. and Maier, R. E. *SPE JI.* 1960, 16, 396
- 6 'Designing with Du Pont Plastics', Du Pont, Wilmington, Delaware, 1961
- 7 Alfrey, T. and Gurnee, E. F. 'Organic polymers', Prentice-Hall, Englewood Cliffs, 1967
- 8 McCammond, D. *PhD Thesis* Queen's University, Belfast, 1968
- 9 Sayigh, A. A. M. *PhD Thesis* University of London, 1966
- 10 Timoshenko, S. 'Strength of Materials', Van Nostrand, New York, Vol 1, 1957
- 11 Thomas, D. A. and Turner, S. in 'Testing of Polymers', (Ed. W. E. Brown), Wiley, New York, Vol 4, 1969
- 12 Ogorkiewicz, R. M. and Mucci, P. E. R. *Composites* 1971, 2, 139
- 13 Mucci, P. E. R. and Ogorkiewicz, R. M. to be published

## Note to the Editor

### Preparation and characterization of some polymers terminated with primary amino groups

A. G. De Boos\*

Department of Chemistry, University of Manchester, Manchester M13 9PL, UK  
(Received 30 April 1973; revised 26 July 1973)

Techniques by which polymers with known terminal groups can be prepared have been known for some years, condensation polymers being the best examples. By suitable choice of reactant balance some control of the terminal groups in such polymers can be achieved. These products can then be used in the preparation of certain classes of block copolymers such as segmented polyurethanes<sup>1</sup>.

Preparation of addition polymers with known terminal groups requires different methods and can only be accomplished with certain monomers. Such polymers have been prepared using free radical initiators which incorporate the required functional groups<sup>2,3</sup> and by including a suitable chain transfer agent in the polymerizing mixture<sup>4,5</sup>. Free radical initiators incorporating the required functional groups are often difficult and tedious to prepare.

This communication describes a technique by which monofunctional primary amino-terminated polymers were prepared using a free radical polymerization technique. In the present work a chain transfer agent, 2-mercaptoethylammonium chloride, was included in the polymerizing mixture. This reagent was chosen as it could be readily obtained in the pure form and has a high radical chain transfer constant common to many aliphatic mercaptans<sup>6</sup>. The reagent was used as the quaternary ammonium salt to minimize any side reactions of the amino group. Alcohols were used as solvents because of their low radical transfer constants<sup>6</sup>. As radical transfer was the predominant mode of chain termination, the formation of  $\alpha$ - $\omega$  difunctional molecular chains, by combination of growing chains was expected to be low.

In a typical preparation, the initiator azobisisobutyronitrile (AIBN) (0.1% of the weight of monomer) and the transfer agent (1% of the weight of monomer) were dissolved in the appropriate solvent (200% of the weight of monomer) and the monomer was distilled into the reaction vessel which was then sealed under vacuum and held at 80°C for 24 h. The resultant polymer was purified by repeated solution and precipitation and was then dried under vacuum.

The polymers were characterized by the normal methods. Osmometric measurements were made with a Melabs recording osmometer (Model CSM-2) using tetrahydrofuran (THF) as solvent. Viscosity measurements were made in a Desreux-Bischoff viscometer at

25°C, the kinetic energy correction of which was negligible for the solvent (chloroform) used. Gel permeation chromatography (g.p.c.) was performed in THF in a Waters Associated Model 200 gel permeation chromatograph which had been calibrated with low dispersity linear polystyrene. End-group analysis was done by labelling the amino end groups with fluorodinitrobenzene (FDNB), followed by spectroscopic analysis

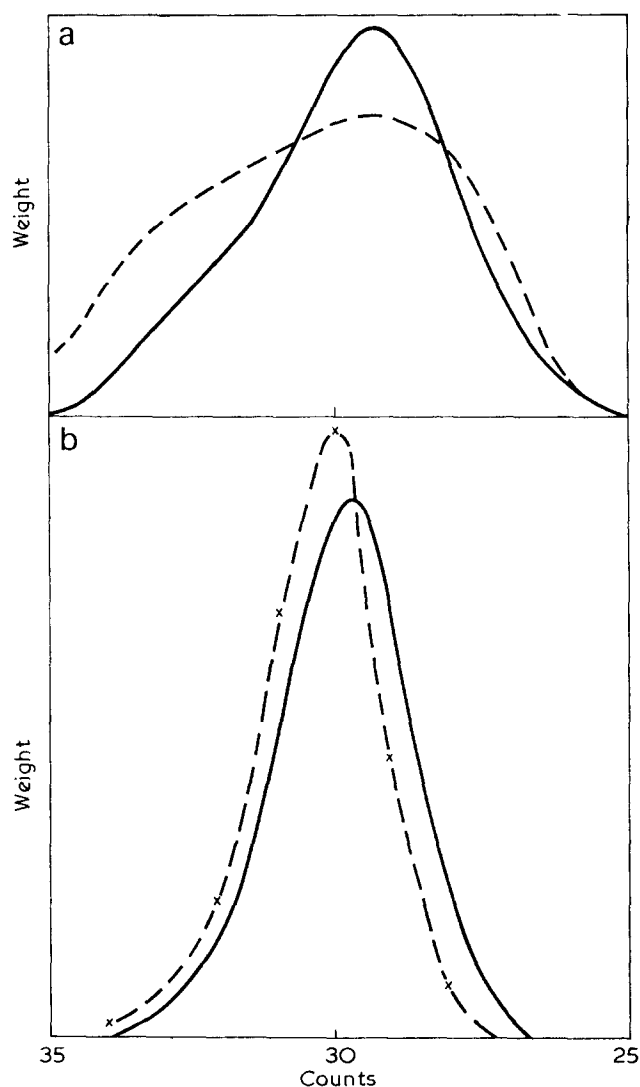


Figure 1 Gel permeation chromatographs of amine terminated (a) polystyrene (APS) and (b) poly(methyl methacrylate) (APMMA) prepared in the presence of two levels of mercapto-amine. —, 1%; ----, 2%

\* Present address: Division of Textile Industry, CSIRO, PO Box 21, Belmont, Victoria, Australia.

Table 1 Characterization of amine terminated polymers

Polymer <sup>a</sup>	Monomer	Solvent <sup>b</sup>	Initiator <sup>c</sup> (%)	Mercapto-amine <sup>c</sup> (%)	[ $\eta$ ]	$M_n \times 10^{-4}$	$M_w/M_n$	$\sigma$
APS0	S	THFA	0.1	0	0.62	5.8	2.4	0.00
APS1			0.1	1	0.29	1.9	2.7	0.63
APS2			0.2	2		1.2	3.1	0.52
APMMA0	MMA	THFA	0.1	0	1.02	8.7	3.7	0.00
APMMA1			0.1	1	0.29	2.3	1.9	0.56
APMMA2			0.1	2	0.23	1.9	1.4	0.63
APMMA3			0.2	2	0.18	1.4	1.5	0.50
APBMA0	BMA	THFA	0.1	0	0.65	7.5	2.4	0.00
APBMA1			0.1	1	0.21	2.0	1.5	0.55
APMA0	MA	THFA	0.1	0	0.17	0.67	2.1	
APMA1			0.1	1	0.13	0.66	1.9	
APEA0	EA	P	0.1	0		1.5	3.8	
APEA1			0.1	1		1.0	2.1	
APBA0	BA	P	0.1	0		1.6	3.2	
APBA1			0.1	1		0.81	2.0	

<sup>a</sup> APS= amine terminated polystyrene; APMMA= amine terminated poly(methyl methacrylate); APBMA= amine terminated poly(butyl methacrylate); APMA= amine terminated poly(methyl acrylate); APEA= amine terminated poly(ethyl acrylate); APBA= amine terminated poly(butyl acrylate)

<sup>b</sup> THFA= tetrahydrofurfuryl alcohol; P= propanol

<sup>c</sup> Of weight of monomer

Table 2 Characterization of APS1 fractions

Fraction	Weight fraction (%)	$M_n \times 10^{-4}$	$\sigma$
1	46.2	9.0	0.60
2	12.4	5.0	0.61
3	5.8	3.3	
4	9.3	2.5	
5	6.5	1.7	0.61
6	3.1	1.2	
7	16.7	0.68	0.84

of a solution of the purified polymer in chloroform ( $\lambda_{max}=350$  nm) and comparison with a suitable standard. The amino end-group frequency ( $\sigma$ ) was defined as the average number of functional end groups per molecule:

$$\sigma = A \cdot M_n$$

where  $A$  is the mol of end-group/g of polymer and  $M_n$  is the number-average molecular weight. The results obtained by these techniques are shown in Tables 1 and 2 and in Figure 1. Presence of the transfer agent in the polymerizing mixture lowered the molecular weight of the resultant polymer and, with the exception of polystyrene, narrowed the dispersity of the polymer. An increase in the concentration of the transfer agent enhanced this effect and simultaneously raised the functional end-group frequency. In the case of polystyrene and poly(methyl methacrylate), an increase in the initiator concentration lowered the molecular weight but broadened the molecular weight distribution and lowered the functional end-group frequency.

To determine the distribution of amino end groups in the polymer APS1 the material was fractionated and end-group analyses were performed on the fractions. The number-average molecular weights of the fractions were determined by g.p.c. as the molecular weights of the lower fractions were too low for reliable membrane osmometry. The low molecular weight fraction had an appreciably higher amino end-group frequency than the other fractions.

Difficulties in the purification of the polyacrylates prevented end group analysis of these polymers. The molecular weights were determined by g.p.c. because the materials were below the reliable limit for membrane osmometry. While this introduced some error the effect of the transfer agent could be qualitatively assessed.

The amino end-group frequency of the polymers was lower than expected from the reduction in molecular weight that resulted from the presence of the transfer agent. However, this may be explained by the existence of several competing chain-initiating and chain transfer reactions in the polymerizing medium, such as the direct initiation of chains by the radicals formed from AIBN or chain transfer to solvent or other molecules. The polymerizations were taken to high conversions so that it is probable that the concentrations of the various species and consequently the relative importance of competing reactions varied through the polymerization.

It is concluded that the inclusion of the chain transfer agent, mercaptoethylammonium chloride in the polymerizing mixture is a useful method of preparing polymers with primary amino terminal groups. Under the conditions used, the amino end-group frequencies achieved were not high, probably due to the existence of complicating reactions during the polymerization. However, higher frequencies could probably be achieved by suitable variation of these conditions. These polymers could be very useful starting materials for the preparation of block and graft copolymers or polymers of known geometry (comb or star shape).

#### REFERENCES

- 1 Bunn, C. W. *J. Polym. Sci.* 1955, **16**, 323
- 2 Bamford, C. H. and Jenkins, A. D. *Nature* 1955, **176**, 78
- 3 Roy, K., Pramanick, D. and Palit, S. *J. Polym. Sci. (B)* 1969, **7**, 765
- 4 Bamford, C. H. and White, E. F. T. *Trans. Faraday Soc.* 1956, **52**, 716
- 5 Bamford, C. H. and White, E. F. T. *Trans. Faraday Soc.* 1958, **54**, 268
- 6 Brandrup, J. and Immergut, E. H. 'Polymer Handbook', Interscience, New York, 1966

## Complexes of alkali metal ions with poly(ethylene oxide)

We wish to report the preparation of crystalline complexes of sodium and potassium salts with poly(ethylene oxide). The preparation of complexes of poly(ethylene oxide) with mercuric chloride has previously been reported<sup>1</sup> and their structures have been determined<sup>2, 3</sup>. The effect of certain alkali metal salts on the dilute solution viscosity of poly(ethylene oxide) has been studied by Lundberg *et al.*<sup>4</sup>. The latter workers also observed that the dissolution of potassium iodide in poly(ethylene oxide) disrupts the crystallinity of the polymer producing an elastomeric material at room temperature. Recently, Valenti *et al.*<sup>5</sup> have studied the depression of the melting point of nylon-6 by lithium salts.

When solvent is evaporated from a methanolic solution of sodium iodide and poly(ethylene oxide) in the proportions of 1 mol of sodium iodide to 4 mol of ethylene oxide repeating unit, a highly crystalline material is formed. As the material crystallizes the growth of spherulites may be observed in the usual manner through the polarizing microscope. The spherulites melt at a temperature of about 200°C (as compared to ~65°C for the pure polymer) and the X-ray and infrared spectra of the complex differ markedly from those of pure poly(ethylene oxide). Sodium and potassium thiocyanate similarly form highly crystalline complexes having high melting points (~170°C) from solutions having the same molar proportions (1 to 4) of salt to repeating unit. This stoichiometry was observed<sup>1, 2</sup> for the mercuric chloride complexes. However, a stoichiometry of 1 mol of salt to 1 mol of repeating unit as also observed<sup>3</sup> for the latter case has not been found for the alkali metal ion complexes. Alkali metal salt added in excess of 20 mol % of solids is recrystallized as the pure salt, the characteristic peaks of the salt appearing on X-ray spectra of the complex.

Potassium and sodium chlorides and bromides and potassium fluoride do not appear to form solid complexes although these salts take the polymer into solution in methanol at room temperature as observed by Lundberg *et al.*<sup>4</sup>. The chlorides and bromides are recrystallized from solution in well defined dendritic forms and the potassium fluoride in a finely divided form. Rubidium and caesium salts and lithium iodide and bromide similarly interact with the polymer in solution. Only with lithium iodide was spherulitic crystalline material observed and its nature is yet to be ascertained. The size of the cation may be a critical factor in the formation of complexes with poly(ethylene oxide).

The complexes can be drawn into highly oriented fibres and preliminary structural investigations show that the fibre repeats are reduced with respect to that of the pure polymer as found for the mercuric chloride

complexes. For example, for the KCNS complex  $c=8.1 \text{ \AA}$  as compared with the literature value<sup>1</sup> 19.25 Å for the pure polymer. The work of Iwamoto *et al.*<sup>2, 3</sup> and the extensive studies<sup>6-8</sup> of alkali metal ion-cyclic ether complexes, indicate that the ether oxygen atoms interact directly with the cations and not with the anions as suggested by Lundberg *et al.* in their solution study<sup>4</sup>. Similarities in the infra-red spectra of the poly(ethylene oxide) complexes and the cyclic ether complexes<sup>8</sup> suggest that the cations may be similarly disposed towards the oxygen atoms.

The electrical conductivity of the potassium thiocyanate complex is very sensitive to temperature and increases markedly as the degree of crystallinity is reduced. Work is continuing on the structure and properties of these complexes and their solutions.

D. E. Fenton

*Department of Chemistry,  
University of Sheffield,  
Sheffield S10 2TN, UK*

and J. M. Parker and P. V. Wright

*Department of Glass Technology,  
University of Sheffield,  
Sheffield S10 2TZ, UK*

(Received 21 August 1973)

### References

- 1 Blumberg, A. A., Pollack, S. S. and Hoeve, C. A. *J. Polym. Sci. (A)* 1964, **2**, 2499
- 2 Iwamoto, R., Saito, Y., Ishihara, H. and Tadokoro, H. *J. Polym. Sci. (A-2)* 1968, **6**, 1509
- 3 Yokoyama, M., Ishihara, H., Iwamoto, R. and Tadokoro, H. *Macromolecules* 1969, **2**, 184
- 4 Lundberg, R. F., Bailey, F. E. and Callard, R. W. *J. Polym. Sci. (A-1)* 1966, **4**, 1563
- 5 Valenti, B., Bianchi, E., Greppi, G., Jealdi, A. and Ciferri, A. *J. Phys. Chem.* 1973, **77**, 389
- 6 Pederson, C. J. *J. Am. Chem. Soc.* 1967, **89**, 7017
- 7 Fenton, D. E., Mercer, M., Poonia, N. S. and Truter, M. R. *JCS Chem. Commun.* 1972, p 66 and references therein
- 8 Dale, J. and Kristiansen, P. O. *Acta Chem. Scand.* 1972, **26**, 1471

## Pressure dependence of $\beta$ and $\gamma$ dispersion for polyethylene by n.m.r.

Polyethylene has three dispersion regions over the temperature range from  $-150^\circ\text{C}$  to the melting temperature and they are called  $\alpha$ ,  $\beta$  and  $\gamma$  dispersion in the order of descending temperature. Pressure dependences of these dispersions have been studied by some investigators<sup>1, 2</sup>. Wada *et al.*<sup>1</sup> measured the pressure dependence of the ultrasonic longitudinal wave velocity and found breaks in the curve. Kijima *et al.*<sup>2</sup> measured the pressure



dependence of  $\alpha$  dispersion by the measurement of ultrasonic wave velocity.

In this letter, the pressure dependence of  $\beta$  and  $\gamma$  dispersion in high density polyethylene by n.m.r. measurement is reported. Pressure dependence of n.m.r. linewidth of polyethylene at room temperature was investigated by Cleron *et al.*<sup>3</sup> They reported drastic broadening of n.m.r. linewidth at about 6000 kg/cm<sup>2</sup>. Heydemann and Houck<sup>4</sup> obtained the pressure dependence of bulk modulus  $B_T$  of polyethylene at 23°C and found a break at about 6000 kg/cm<sup>2</sup> in the  $B_T$  versus pressure curve. They discussed the pressure dependence of  $\beta$  and  $\gamma$  dispersion in relation with the data of Cleron. According to them, if the observed transition is identical with the  $\gamma$  relaxation then the pressure coefficient is  $dT_\gamma/dP = 0.022^\circ\text{C}/\text{kg}/\text{cm}^2$  and if it is identified with the  $\beta$  dispersion, the pressure coefficient of  $T_\beta$  is  $dT_\beta/dP = 0.007^\circ\text{C}/\text{kg}/\text{cm}^2$ .

The experimental technique employed here has been reported in detail already<sup>5</sup>. The resonance radio frequency of n.m.r. measurement was set at 11.1919 MHz, for the poor  $Q$  value of the coil due to Amagat electrode under high frequency. A fluorine oil was used as the pressure transmitting fluid because it did not contain protons. The rod sample of 2 mm diameter and 13 mm in length was shaped from the bulk of high density polyethylene (Hizex 2200J). The n.m.r. linewidth versus temperature curve at atmospheric pressure reported by some investigators shows narrowing of one step from about  $-100^\circ\text{C}$  to  $20^\circ\text{C}$ <sup>6-8</sup>. Until recently, it was difficult to determine whether this narrowing is caused by  $\beta$  or  $\gamma$  dispersion. However, by the application of pressure, it can be easily separated into two steps. Figure 1 shows the temperature dependence of the narrow component of n.m.r. linewidth of high density polyethylene at various pressures. By the application of pressure of only 800 kg/cm<sup>2</sup>, we can observe narrowing in two steps. Narrowing at higher temperature is caused by  $\beta$  dispersion and the lower one by  $\gamma$  dispersion. If we take breaks in the curve as the

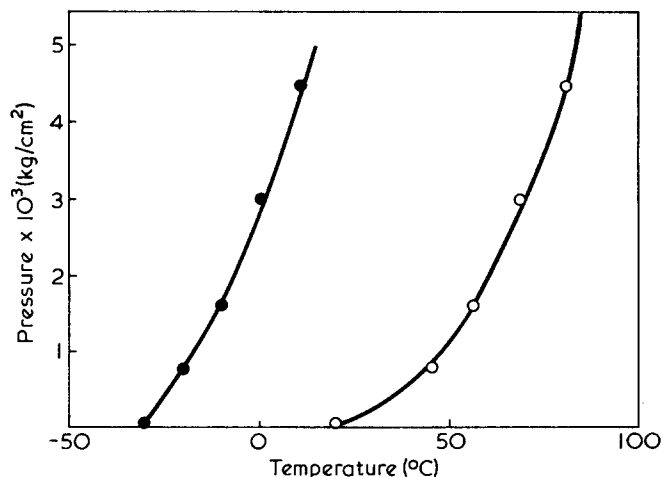


Figure 2 Pressure dependences of  $\beta$  (O) and  $\gamma$  (●) dispersion

transition point, the pressure dependence of each transition becomes as shown in Figure 2. From this Figure, the pressure coefficient of  $\gamma$  dispersion is about  $0.013^\circ\text{C}/\text{kg}/\text{cm}^2$  in the early stage. On the other hand,  $\beta$  dispersion increases more rapidly with pressure at  $0.032^\circ\text{C}/\text{kg}/\text{cm}^2$  in the early stage and then begins to saturate to about 5000 kg/cm<sup>2</sup>. This is slightly different from the data of Wada *et al.* who ascribed the breaks in the sound velocity versus pressure curve to the  $\beta$  dispersion but our data are self-consistent compared with the dispersion map of polyethylene. We believe that the data of Wada *et al.* refer to the  $\gamma$  dispersion and not to the  $\beta$  dispersion.

To know the effect of pressure on n.m.r. linewidth of polyethylene more precisely, it would be necessary to study the pressure dependence of n.m.r. linewidth for single crystal mat and low density polyethylene.

#### Acknowledgement

This work was supported in part by the Scientific Research Fund of the Ministry of Education.

Chitoshi Nakafuku, Seiji Taki and Tetuo Takemura

Department of Applied Science,  
Faculty of Engineering,  
Kyushu University,  
Fukuoka, Japan

(Received 10 August 1973)

#### References

- Wada, Y., Itani, A., Nishi, T. and Nagai, S. *J. Polym. Sci. (A-2)* 1969, 7, 201
- Kijima, T., Imada, K. and Takayanagi, M. *19th Symp. Polymers, Kyoto 1970*, p 901
- Cleron, V., Coston, C. J. and Drickamer, H. G. *Rev. Sci. Instrum.* 1966, 37, 68
- Heydemann, P. L. M. and Houck, J. C. *J. Polym. Sci. (A-2)* 1972, 10, 1631
- Nakafuku, C., Taki, S. and Takemura, T. *Polymer* 1973, 14, 558
- Nishioka, A., Komatsu, H. and Kakiuchi, Y. *J. Phys. Soc. Japan* 1957, 12, 283
- Rempel, R. C., Weaver, H. E. and Miller, R. L. *J. Appl. Phys.* 1957, 28, 1082
- Olf, H. G. and Peterlin, A. *J. Appl. Phys.* 1964, 35, 3108

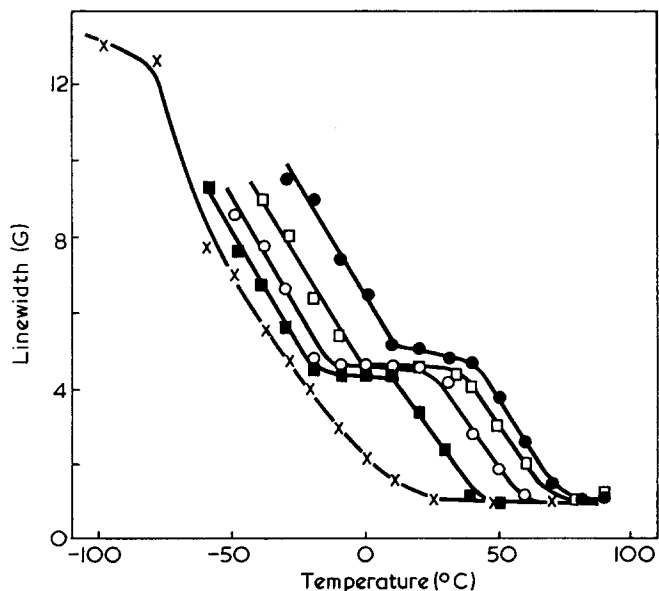


Figure 1 Variation with temperature of the linewidth of the narrow component of the proton resonance in polyethylene at various pressures:  $\times$ , 1;  $\blacksquare$ , 800;  $\circ$ , 1600;  $\square$ , 3000;  $\bullet$ , 4500 kg/cm<sup>2</sup>

# Letters

## Complexes of alkali metal ions with poly(ethylene oxide)

We wish to report the preparation of crystalline complexes of sodium and potassium salts with poly(ethylene oxide). The preparation of complexes of poly(ethylene oxide) with mercuric chloride has previously been reported<sup>1</sup> and their structures have been determined<sup>2, 3</sup>. The effect of certain alkali metal salts on the dilute solution viscosity of poly(ethylene oxide) has been studied by Lundberg *et al.*<sup>4</sup>. The latter workers also observed that the dissolution of potassium iodide in poly(ethylene oxide) disrupts the crystallinity of the polymer producing an elastomeric material at room temperature. Recently, Valenti *et al.*<sup>5</sup> have studied the depression of the melting point of nylon-6 by lithium salts.

When solvent is evaporated from a methanolic solution of sodium iodide and poly(ethylene oxide) in the proportions of 1 mol of sodium iodide to 4 mol of ethylene oxide repeating unit, a highly crystalline material is formed. As the material crystallizes the growth of spherulites may be observed in the usual manner through the polarizing microscope. The spherulites melt at a temperature of about 200°C (as compared to ~65°C for the pure polymer) and the X-ray and infrared spectra of the complex differ markedly from those of pure poly(ethylene oxide). Sodium and potassium thiocyanate similarly form highly crystalline complexes having high melting points (~170°C) from solutions having the same molar proportions (1 to 4) of salt to repeating unit. This stoichiometry was observed<sup>1, 2</sup> for the mercuric chloride complexes. However, a stoichiometry of 1 mol of salt to 1 mol of repeating unit as also observed<sup>3</sup> for the latter case has not been found for the alkali metal ion complexes. Alkali metal salt added in excess of 20 mol % of solids is recrystallized as the pure salt, the characteristic peaks of the salt appearing on X-ray spectra of the complex.

Potassium and sodium chlorides and bromides and potassium fluoride do not appear to form solid complexes although these salts take the polymer into solution in methanol at room temperature as observed by Lundberg *et al.*<sup>4</sup>. The chlorides and bromides are recrystallized from solution in well defined dendritic forms and the potassium fluoride in a finely divided form. Rubidium and caesium salts and lithium iodide and bromide similarly interact with the polymer in solution. Only with lithium iodide was spherulitic crystalline material observed and its nature is yet to be ascertained. The size of the cation may be a critical factor in the formation of complexes with poly(ethylene oxide).

The complexes can be drawn into highly oriented fibres and preliminary structural investigations show that the fibre repeats are reduced with respect to that of the pure polymer as found for the mercuric chloride

complexes. For example, for the KCNS complex  $c=8.1 \text{ \AA}$  as compared with the literature value<sup>1</sup> 19.25 Å for the pure polymer. The work of Iwamoto *et al.*<sup>2, 3</sup> and the extensive studies<sup>6-8</sup> of alkali metal ion-cyclic ether complexes, indicate that the ether oxygen atoms interact directly with the cations and not with the anions as suggested by Lundberg *et al.* in their solution study<sup>4</sup>. Similarities in the infra-red spectra of the poly(ethylene oxide) complexes and the cyclic ether complexes<sup>8</sup> suggest that the cations may be similarly disposed towards the oxygen atoms.

The electrical conductivity of the potassium thiocyanate complex is very sensitive to temperature and increases markedly as the degree of crystallinity is reduced. Work is continuing on the structure and properties of these complexes and their solutions.

D. E. Fenton

Department of Chemistry,  
University of Sheffield,  
Sheffield S10 2TN, UK

and J. M. Parker and P. V. Wright

Department of Glass Technology,  
University of Sheffield,  
Sheffield S10 2TZ, UK

(Received 21 August 1973)

### References

- 1 Blumberg, A. A., Pollack, S. S. and Hoeve, C. A. *J. Polym. Sci. (A)* 1964, **2**, 2499
- 2 Iwamoto, R., Saito, Y., Ishihara, H. and Tadokoro, H. *J. Polym. Sci. (A-2)* 1968, **6**, 1509
- 3 Yokoyama, M., Ishihara, H., Iwamoto, R. and Tadokoro, H. *Macromolecules* 1969, **2**, 184
- 4 Lundberg, R. F., Bailey, F. E. and Callard, R. W. *J. Polym. Sci. (A-1)* 1966, **4**, 1563
- 5 Valenti, B., Bianchi, E., Greppi, G., Jealdi, A. and Ciferri, A. *J. Phys. Chem.* 1973, **77**, 389
- 6 Pederson, C. J. *J. Am. Chem. Soc.* 1967, **89**, 7017
- 7 Fenton, D. E., Mercer, M., Poonia, N. S. and Truter, M. R. *JCS Chem. Commun.* 1972, p 66 and references therein
- 8 Dale, J. and Kristiansen, P. O. *Acta Chem. Scand.* 1972, **26**, 1471

## Pressure dependence of $\beta$ and $\gamma$ dispersion for polyethylene by n.m.r.

Polyethylene has three dispersion regions over the temperature range from  $-150^\circ\text{C}$  to the melting temperature and they are called  $\alpha$ ,  $\beta$  and  $\gamma$  dispersion in the order of descending temperature. Pressure dependences of these dispersions have been studied by some investigators<sup>1, 2</sup>. Wada *et al.*<sup>1</sup> measured the pressure dependence of the ultrasonic longitudinal wave velocity and found breaks in the curve. Kijima *et al.*<sup>2</sup> measured the pressure

# Book Reviews

## High resolution NMR of macromolecules

F. A. Bovey

Academic Press, New York, 1972, 466 pp. \$19.50

The author of this book is not only a leading exponent of the use of high resolution n.m.r. in the study of the solution spectra of synthetic polymers, but also a writer of already proven ability. This book is in accord with his previous standards of high clarity. The first chapter is a brief description of the fundamentals of n.m.r., similar to that in his general book on n.m.r. and 'intended to make the book more or less self contained'. Chapter 2 is a discussion of isomerism in polymer chains without special reference to n.m.r. Chapters 3 to 12 (180 pages) cover the interpretation of synthetic polymer spectra in terms of structure, stereochemical configuration, conformation and chain growth mechanisms. The division of this material into Chapters is by polymer class and the treatment is comprehensive in that mention is made of all the important polymers that have been studied by n.m.r. In these pages lies the book's main merit, and the exploitation of the unique ability of n.m.r. to provide details of sequence is fully described. Recent results from  $^{13}\text{C}$  spectroscopy are included although all spectra were obtained by accumulation in the CW mode, an approach already outdated. Although a great deal has been achieved to date on the study of synthetic polymers by n.m.r., a reading of these chapters makes it clear that the use of Fourier transform methods with both  $^1\text{H}$  and  $^{13}\text{C}$  together with data manipulation for resolution enhancement will yield more detailed spectral interpretations. Chapter 13, by way of a bridge to biopolymers (which take up the remainder of the book) deals with amino acids and synthetic polypeptides. These are subjects having considerable intrinsic interest but they do not bear greatly in fact on biopolymer studies. Synthetic polypeptides have recently been the subject of much study and the 'torrential' flow of papers described by the author continues unabated. One result is that since the writing of the book the apparent gross contradiction between n.m.r. and kinetic data on the rates of helix-coil conformational interconversion has been resolved in favour of an explanation rejected in the text. Nonetheless, the majority of the Chapter is useful, most particularly the introduction to the study of cyclic oligopeptides. The study of the solution conformations of cyclic antibiotics and hormones such as gramicidin, may prove to be one of the most significant contributions of high resolution n.m.r. to biology.

Chapter 14 is on globular proteins divided into (a) observations on the protein itself and (b) the binding of small molecules to proteins. In 46 pages only an introduction can be given to this large and rapidly expanding field, but those seeking an entré to the subject will find the chapter helpful. A great deal of significant work on proteins has appeared very recently and a contemporary view therefore requires the up to date literature. Similar considerations apply to the last chapter on nucleic acids, although the slower progress in this more difficult application makes the chapter more up to the minute. The four pages devoted to t-RNA make the most exciting reading in the book. In very rapidly expanding fields it is always difficult to review without seeming out of date, but when publication requires the inevitable delay to put it between hard covers it may not always be worth the effort. For example, at least one review of protein spectra appearing before the publication of this book consisted in considerable part of material not to be found in Chapter 4.

C. Crane-Robinson

## Instrumental analysis of cotton cellulose and modified cotton cellulose

Edited by Robert T. O'Connor

Marcel Dekker, New York, 1972, 490 pp. \$29.50

This book will be of assistance to many textile scientists attempting to keep pace with the dramatic changes which have taken place over the last decades in analytical methods. Since fabrics are

now constructed from fibres or fibre blends treated with one or more chemical finishing agents from a range of several hundred, quantitative analysis and quality control increasingly requires the use of modern instruments and computational refinement of data. This volume in the Fibre Science Series sets out to show the advances which have been made in the field of instrumental analysis of cotton cellulose and modified cotton cellulose, and is welcome evidence for increasing sophistication in a long established sector of the textile industry. The majority of contributors are from the Southern Regional Research Laboratory, New Orleans, Louisiana; others are from the Personal Products Company, Milltown, New Jersey, and the Department of Physics, San Fernando Valley College, Northridge, California. All have unequalled experience of celluloses both modified and unmodified, and the result of their collaboration is a complete bibliography of published work on cotton cellulose together with a wealth of operational and analytical detail.

The instrumental techniques surveyed in this book cover a wide range of the electromagnetic spectrum. The chapter on elemental analysis includes the relatively well known methods utilizing spectrochemical analysis of electron emission, atomic absorption and X-ray fluorescence, radiative methods including gamma-ray spectrometry with neutron activation, and non-radiative methods becoming known as electron spectroscopy for chemical analysis (ESCA), photoelectron spectroscopy (PES), and Auger electron spectroscopy (AES). Infra-red spectroscopy covers two chapters, one too many in my opinion, light microscopy and electron microscopy are discussed in separate chapters, as are X-ray diffraction and nuclear magnetic resonance spectroscopy (n.m.r.). The oxidation, degradation and pyrolysis of cellulose are described in terms of gas, paper, and thin-layer chromatography, mass spectroscopy, differential thermal analysis (d.t.a.) and thermogravimetric analysis (t.g.a.). The only omission from this exhaustive list appears to be that of electron resonance spectroscopy (e.s.r.).

The opening chapter, describing instrumental methods of elemental analysis, provides the reader with an exceptionally clear insight into the fundamental physical principles involved. Indeed this first chapter sets a very high standard, which, unfortunately, is not maintained throughout. In particular the rather dull and trivial introductions to both light and electron microscopy are a disappointment—we have enough specialist books of dubious quality in these fields already. I prefer the experimental section on Infra-red spectroscopy: 'we do not intend to discuss the general methods . . . since many books and review articles have covered this part in great detail'. Would that this directive had been issued to all contributors.

Although there is a storehouse of valuable information on instrumental technique in most chapters, the uncritical, bibliographic approach, and the unquestioning acceptance of data, will not win general acclaim. With a more complete mastery of his technique, the modern scientist can avoid many of the pitfalls encountered by his predecessors working with more primitive apparatus. For example, an appreciation of contrast-transfer theory in transmission electron microscopy enables the microscopist to understand that information concerning a complete range of object frequencies cannot be obtained in any one image plane without the use of a phase plate. Since many measurements must have been made on defocused low-resolution images enhancing a narrow frequency distribution, values for the size of elementary fibrils in cellulose should be treated with caution. The X-ray diffraction chapter also contains weaknesses: no serious worker would contemplate using a Geiger counter in diffractometry—scintillation and proportional counters have been proved to be more efficient especially when used with electronic discrimination. Again data reduction by electronic computer is hardly mentioned, yet a modern laboratory will make routine use of computational procedures. The section on light microscopy also has its limitations; despite a general discussion of modern phase, interference, and polarizing microscopes, no mention is made of compensator methods for measuring birefringence. It seems the antithesis of the purpose of this book to discuss only the Becke line method for refractive index evaluation.

Happily there are more forward looking sections; thus we are given details of a 'fingerprint' method for matching infra-red

## Book Reviews

spectra whereby a computer can compare a given spectrum with 100 000 spectra stored on magnetic tape. This must surely be the approach of the future to which the book is dedicated. Despite the disparities in style and outlook, the authors have provided a most valuable compendium for all fibre scientists working in the field of cotton cellulose which is probably worth the moderately high price of \$29.50.

*D. J. Johnson*

### **Europlastics Year Book 1973**

IPC Industrial Press, London. 670 pp. £12.00

This new annual guide to the plastics industry is the successor to *British Plastics Year Book*. It has been greatly expanded to provide information on products and services ranging from materials and plant equipment through to processors and manufactured products. The headings of all these entries, as well as the index to all products, are given in five languages (English, French, German, Italian and Spanish).

Each major section is usefully prefaced by an editorial chapter. These include: the latest developments in materials technology; comparative property data of different plastics materials and semi-finished plastics products; the latest design and performance of machines and process control; and the newest applications of plastics.

About half the book is devoted to company information on over 10 000 firms in 27 countries, which seems reasonable in a year book of this size. Overall impressions were good as far as presentation is concerned but the value of the data given in the comparative section on properties of plastics materials will be diminished by the mixed use of SI units with non-SI units. However, this probably reflects a basic deficiency in the trade literature emanating from the manufacturers. Hopefully, this will be remedied gradually over the next few years.

Certainly the book retains its reputation as the authoritative reference for the plastics industry in Britain and will be as equally considered in Europe as well. An added bonus is its reduced price of £8 if linked to a *europlastics monthly* subscription.

*C.J.R.*

#### *Conference Announcement*

### **IIIrd European Symposium on Polymer Spectroscopy**

Brunel University, London, 22-24 April 1974

This meeting is a Europhysics Conference organized on behalf of the Section of Macromolecular Physics of the Condensed Matter Division of the European Physical Society, the Polymer Physics Group of the Institute of Physics and the European Polymer Spectroscopy Group. Offers of contributed papers, of about 30 min duration, are invited on any aspect of the spectroscopy of polymers, including infrared and Raman spectroscopy, nuclear magnetic resonance, inelastic neutron scattering, polarized fluorescence and electron spin resonance but excluding structural studies by means of X-ray scattering. Provisional titles of papers should be sent as soon as possible to Dr D. I. Bower, Department of Physics, University of Leeds, Leeds LS2 9JT, UK. Abstracts of about 200 words (preferably in English) will be required by 1 February 1974.

#### *Conference Announcement*

### **Catalysis by Macromolecules**

University of Liverpool, 21 November 1973

The Chemical Society Macromolecular Group (in association with the North West Region of the Industrial Division, Chemical Society) is organizing the above one-day symposium. Fundamental and industrial aspects will be open to advanced discussion, with particular reference to developments in catalytically active synthetic macromolecules derived from advancing understandings of enzymic systems. The speakers will include: E. T. Kaiser (University of Chicago), A. J. Kirby (University of Cambridge), M. Lilley (University College, London), J. D. Littlehailes (ICI, Agricultural Division) and C. G. Overberger (University of Michigan). Further details and registration forms are available from H. L. Bennister, Industrial Division, The Chemical Society, Burlington House, London W1V 0BN, UK.

### **Otto Wichterle 60 years old**

Polymer scientists throughout the world would like to take this opportunity of congratulating Professor Otto Wichterle on his sixtieth birthday, 27 October 1973.

He has made unique advances in macromolecular chemistry which have had much scientific and industrial significance. We all remember the international conferences he organized in Prague in 1957 and 1965. The reputation of the Institute of Macromolecular Chemistry in Prague, which he founded, is considerable and world-wide.

The International Union of Pure and Applied Chemistry and all scientific workers in the field of macromolecules owe a great debt to him for his leadership in the creation of the Macromolecular Division of the Union, covering all aspects of the science of macromolecules. This occurred at the 1967 Conference of the Union in Prague. Under his leadership as first president, the Division worked with considerable success to bring about collaboration in macromolecular science between chemists and physicists, pure and applied workers, university and industry, all over the world.

For these and many other contributions to the world of science we thank Professor Wichterle and convey to him our respect and best wishes.

# Book Reviews

## High resolution NMR of macromolecules

F. A. Bovey

Academic Press, New York, 1972, 466 pp. \$19.50

The author of this book is not only a leading exponent of the use of high resolution n.m.r. in the study of the solution spectra of synthetic polymers, but also a writer of already proven ability. This book is in accord with his previous standards of high clarity. The first chapter is a brief description of the fundamentals of n.m.r., similar to that in his general book on n.m.r. and 'intended to make the book more or less self contained'. Chapter 2 is a discussion of isomerism in polymer chains without special reference to n.m.r. Chapters 3 to 12 (180 pages) cover the interpretation of synthetic polymer spectra in terms of structure, stereochemical configuration, conformation and chain growth mechanisms. The division of this material into Chapters is by polymer class and the treatment is comprehensive in that mention is made of all the important polymers that have been studied by n.m.r. In these pages lies the book's main merit, and the exploitation of the unique ability of n.m.r. to provide details of sequence is fully described. Recent results from  $^{13}\text{C}$  spectroscopy are included although all spectra were obtained by accumulation in the CW mode, an approach already outdated. Although a great deal has been achieved to date on the study of synthetic polymers by n.m.r., a reading of these chapters makes it clear that the use of Fourier transform methods with both  $^1\text{H}$  and  $^{13}\text{C}$  together with data manipulation for resolution enhancement will yield more detailed spectral interpretations. Chapter 13, by way of a bridge to biopolymers (which take up the remainder of the book) deals with amino acids and synthetic polypeptides. These are subjects having considerable intrinsic interest but they do not bear greatly in fact on biopolymer studies. Synthetic polypeptides have recently been the subject of much study and the 'torrential' flow of papers described by the author continues unabated. One result is that since the writing of the book the apparent gross contradiction between n.m.r. and kinetic data on the rates of helix-coil conformational interconversion has been resolved in favour of an explanation rejected in the text. Nonetheless, the majority of the Chapter is useful, most particularly the introduction to the study of cyclic oligopeptides. The study of the solution conformations of cyclic antibiotics and hormones such as gramicidin, may prove to be one of the most significant contributions of high resolution n.m.r. to biology.

Chapter 14 is on globular proteins divided into (a) observations on the protein itself and (b) the binding of small molecules to proteins. In 46 pages only an introduction can be given to this large and rapidly expanding field, but those seeking an entré to the subject will find the chapter helpful. A great deal of significant work on proteins has appeared very recently and a contemporary view therefore requires the up to date literature. Similar considerations apply to the last chapter on nucleic acids, although the slower progress in this more difficult application makes the chapter more up to the minute. The four pages devoted to t-RNA make the most exciting reading in the book. In very rapidly expanding fields it is always difficult to review without seeming out of date, but when publication requires the inevitable delay to put it between hard covers it may not always be worth the effort. For example, at least one review of protein spectra appearing before the publication of this book consisted in considerable part of material not to be found in Chapter 4.

C. Crane-Robinson

## Instrumental analysis of cotton cellulose and modified cotton cellulose

Edited by Robert T. O'Connor

Marcel Dekker, New York, 1972, 490 pp. \$29.50

This book will be of assistance to many textile scientists attempting to keep pace with the dramatic changes which have taken place over the last decades in analytical methods. Since fabrics are

now constructed from fibres or fibre blends treated with one or more chemical finishing agents from a range of several hundred, quantitative analysis and quality control increasingly requires the use of modern instruments and computational refinement of data. This volume in the Fibre Science Series sets out to show the advances which have been made in the field of instrumental analysis of cotton cellulose and modified cotton cellulose, and is welcome evidence for increasing sophistication in a long established sector of the textile industry. The majority of contributors are from the Southern Regional Research Laboratory, New Orleans, Louisiana; others are from the Personal Products Company, Milltown, New Jersey, and the Department of Physics, San Fernando Valley College, Northridge, California. All have unequalled experience of celluloses both modified and unmodified, and the result of their collaboration is a complete bibliography of published work on cotton cellulose together with a wealth of operational and analytical detail.

The instrumental techniques surveyed in this book cover a wide range of the electromagnetic spectrum. The chapter on elemental analysis includes the relatively well known methods utilizing spectrochemical analysis of electron emission, atomic absorption and X-ray fluorescence, radiative methods including gamma-ray spectrometry with neutron activation, and non-radiative methods becoming known as electron spectroscopy for chemical analysis (ESCA), photoelectron spectroscopy (PES), and Auger electron spectroscopy (AES). Infra-red spectroscopy covers two chapters, one too many in my opinion, light microscopy and electron microscopy are discussed in separate chapters, as are X-ray diffraction and nuclear magnetic resonance spectroscopy (n.m.r.). The oxidation, degradation and pyrolysis of cellulose are described in terms of gas, paper, and thin-layer chromatography, mass spectroscopy, differential thermal analysis (d.t.a.) and thermogravimetric analysis (t.g.a.). The only omission from this exhaustive list appears to be that of electron resonance spectroscopy (e.s.r.).

The opening chapter, describing instrumental methods of elemental analysis, provides the reader with an exceptionally clear insight into the fundamental physical principles involved. Indeed this first chapter sets a very high standard, which, unfortunately, is not maintained throughout. In particular the rather dull and trivial introductions to both light and electron microscopy are a disappointment—we have enough specialist books of dubious quality in these fields already. I prefer the experimental section on Infra-red spectroscopy: 'we do not intend to discuss the general methods . . . since many books and review articles have covered this part in great detail'. Would that this directive had been issued to all contributors.

Although there is a storehouse of valuable information on instrumental technique in most chapters, the uncritical, bibliographic approach, and the unquestioning acceptance of data, will not win general acclaim. With a more complete mastery of his technique, the modern scientist can avoid many of the pitfalls encountered by his predecessors working with more primitive apparatus. For example, an appreciation of contrast-transfer theory in transmission electron microscopy enables the microscopist to understand that information concerning a complete range of object frequencies cannot be obtained in any one image plane without the use of a phase plate. Since many measurements must have been made on defocused low-resolution images enhancing a narrow frequency distribution, values for the size of elementary fibrils in cellulose should be treated with caution. The X-ray diffraction chapter also contains weaknesses: no serious worker would contemplate using a Geiger counter in diffractometry—scintillation and proportional counters have been proved to be more efficient especially when used with electronic discrimination. Again data reduction by electronic computer is hardly mentioned, yet a modern laboratory will make routine use of computational procedures. The section on light microscopy also has its limitations; despite a general discussion of modern phase, interference, and polarizing microscopes, no mention is made of compensator methods for measuring birefringence. It seems the antithesis of the purpose of this book to discuss only the Becke line method for refractive index evaluation.

Happily there are more forward looking sections; thus we are given details of a 'fingerprint' method for matching infra-red

## Book Reviews

spectra whereby a computer can compare a given spectrum with 100 000 spectra stored on magnetic tape. This must surely be the approach of the future to which the book is dedicated. Despite the disparities in style and outlook, the authors have provided a most valuable compendium for all fibre scientists working in the field of cotton cellulose which is probably worth the moderately high price of \$29.50.

*D. J. Johnson*

### **Europlastics Year Book 1973**

IPC Industrial Press, London. 670 pp. £12.00

This new annual guide to the plastics industry is the successor to *British Plastics Year Book*. It has been greatly expanded to provide information on products and services ranging from materials and plant equipment through to processors and manufactured products. The headings of all these entries, as well as the index to all products, are given in five languages (English, French, German, Italian and Spanish).

Each major section is usefully prefaced by an editorial chapter. These include: the latest developments in materials technology; comparative property data of different plastics materials and semi-finished plastics products; the latest design and performance of machines and process control; and the newest applications of plastics.

About half the book is devoted to company information on over 10 000 firms in 27 countries, which seems reasonable in a year book of this size. Overall impressions were good as far as presentation is concerned but the value of the data given in the comparative section on properties of plastics materials will be diminished by the mixed use of SI units with non-SI units. However, this probably reflects a basic deficiency in the trade literature emanating from the manufacturers. Hopefully, this will be remedied gradually over the next few years.

Certainly the book retains its reputation as the authoritative reference for the plastics industry in Britain and will be as equally considered in Europe as well. An added bonus is its reduced price of £8 if linked to a *europlastics monthly* subscription.

*C.J.R.*

#### *Conference Announcement*

### **IIIrd European Symposium on Polymer Spectroscopy**

Brunel University, London, 22-24 April 1974

This meeting is a Europhysics Conference organized on behalf of the Section of Macromolecular Physics of the Condensed Matter Division of the European Physical Society, the Polymer Physics Group of the Institute of Physics and the European Polymer Spectroscopy Group. Offers of contributed papers, of about 30 min duration, are invited on any aspect of the spectroscopy of polymers, including infrared and Raman spectroscopy, nuclear magnetic resonance, inelastic neutron scattering, polarized fluorescence and electron spin resonance but excluding structural studies by means of X-ray scattering. Provisional titles of papers should be sent as soon as possible to Dr D. I. Bower, Department of Physics, University of Leeds, Leeds LS2 9JT, UK. Abstracts of about 200 words (preferably in English) will be required by 1 February 1974.

#### *Conference Announcement*

### **Catalysis by Macromolecules**

University of Liverpool, 21 November 1973

The Chemical Society Macromolecular Group (in association with the North West Region of the Industrial Division, Chemical Society) is organizing the above one-day symposium. Fundamental and industrial aspects will be open to advanced discussion, with particular reference to developments in catalytically active synthetic macromolecules derived from advancing understandings of enzymic systems. The speakers will include: E. T. Kaiser (University of Chicago), A. J. Kirby (University of Cambridge), M. Lilley (University College, London), J. D. Littlehailes (ICI, Agricultural Division) and C. G. Overberger (University of Michigan). Further details and registration forms are available from H. L. Bennister, Industrial Division, The Chemical Society, Burlington House, London W1V 0BN, UK.

### **Otto Wichterle 60 years old**

Polymer scientists throughout the world would like to take this opportunity of congratulating Professor Otto Wichterle on his sixtieth birthday, 27 October 1973.

He has made unique advances in macromolecular chemistry which have had much scientific and industrial significance. We all remember the international conferences he organized in Prague in 1957 and 1965. The reputation of the Institute of Macromolecular Chemistry in Prague, which he founded, is considerable and world-wide.

The International Union of Pure and Applied Chemistry and all scientific workers in the field of macromolecules owe a great debt to him for his leadership in the creation of the Macromolecular Division of the Union, covering all aspects of the science of macromolecules. This occurred at the 1967 Conference of the Union in Prague. Under his leadership as first president, the Division worked with considerable success to bring about collaboration in macromolecular science between chemists and physicists, pure and applied workers, university and industry, all over the world.

For these and many other contributions to the world of science we thank Professor Wichterle and convey to him our respect and best wishes.

# Electronic spectrum of polyisoprenyllithium in hydrocarbon solvents

J. E. L. Roovers and S. Bywater

Division of Chemistry, National Research Council of Canada, Ottawa K1A 0R9, Canada  
(Received 4 June 1973; revised 10 July 1973)

The study of the concentration, temperature and solvent dependence of polyisoprenyllithium spectra in hydrocarbons shows that the two maxima observed correspond to two forms of association of polyisoprenyllithium. The dissociation constants for a tetramer-dimer equilibrium are derived. The spectra of polybutadienyl- and polystyryl-lithium were found not to change on dilution.

## INTRODUCTION

In the course of the preparation of a series of styrene-isoprene block copolymers by *s*-butyl lithium initiated anionic polymerization in benzene, it was observed that the polyisoprenyllithium ultra-violet absorption spectrum was concentration dependent. The spectral changes could not be accounted for by fortuitous killing of living ends as the resulting block copolymers were homogeneous and had the expected molecular weight<sup>1</sup>. The high polymer concentrations employed in those experiments made analysis of the spectra difficult. The results of a more detailed study of the concentration, temperature and solvent dependence of the electronic spectrum of polyisoprenyllithium are now presented.

## EXPERIMENTAL

The vacuum techniques for the preparation of polyisoprenyllithium have been described<sup>1</sup>. *s*-Butyl lithium was used to ensure complete initiation. The initial 50 ml solution of polyisoprenyllithium was  $>3 \times 10^{-3}$  M in order to reduce the relative amount of fortuitous impurities. The lower concentrations of polyisoprenyllithium were obtained by internal dilution. To this end, about half the solution was poured into a sidearm equipped with a calibrated flask. The solvent was then distilled back to the main section by cooling the latter.

Quartz optical cells of 1 cm pathlength were equipped with removable quartz spacers that allowed 0.1, 0.05, 0.033 and 0.01 cm pathlengths. A 10 cm cylindrical cell was also available. All pathlengths were calibrated by means of  $K_2CrO_4$  solutions<sup>2</sup>. Spectra were recorded with a Cary 14 spectrophotometer and were reproducible to 1 nm. Temperatures were measured to 0.25°C with a copper-constantan thermocouple located in a Hg well above the optical cell. It was established that polyisoprene has no absorption in the wavelength region of interest. Extinction coefficients were assumed invariant with temperature.

## RESULTS

In a first series of experiments a solution of polyisoprenyllithium in *n*-hexane at 30.0°C was diluted successively

and the spectra of polyisoprenyllithium were recorded at each stage. When the spectra are compared, after correction by the experimental dilution factors, it is found that, on dilution, the absorption maximum shifts from 272 to 275 nm, the absorption at the maximum decreases, a shoulder develops with a new maximum between 315 and 320 nm, and that an isosbestic point occurs at about 290 nm. The observed changes in the spectrum are more pronounced at lower polyisoprenyllithium concentrations as can be seen from the examples shown in Figure 1.

In order to describe these observations quantitatively, the extinction coefficient of polyisoprenyllithium in *n*-hexane at 30.0°C was redetermined, at a high concentration of polyisoprenyllithium ( $1.7 \times 10^{-3}$  M), where the spectrum is only slightly dependent on the concentration. Three methods were used, the measurement of the polyisoprenyllithium spectrum before and after partial destruction with a known amount of *t*-butanol ( $\epsilon_{\max} = 7.95 \times 10^3$ ), lithium analysis after extraction with water

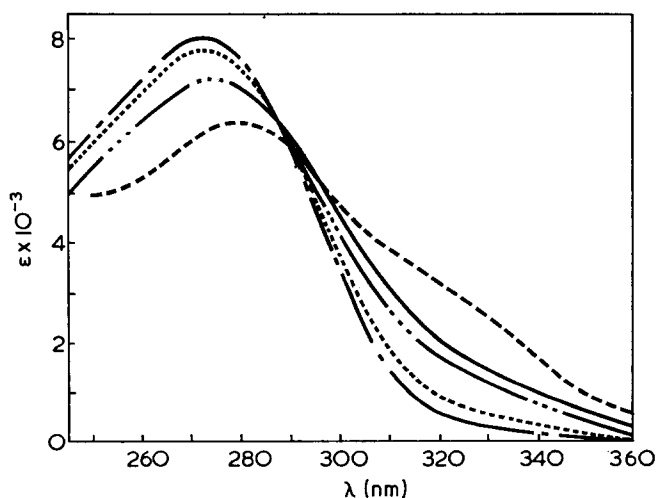


Figure 1 Ultra-violet absorption spectra of polyisoprenyllithium in *n*-hexane as a function of concentration. The broken curves show increasing absorption at 320 nm in the order:  $\cdots$ ,  $1.91 \times 10^{-3}$ ;  $-\cdot-\cdot-$ ,  $2.30 \times 10^{-4}$ ;  $-\cdot-\cdot-$ ,  $2.63 \times 10^{-5}$ ;  $-\cdot-\cdot-$ ,  $3.91 \times 10^{-6}$  M. —, Absorption in benzene for reference at a concentration of  $3.14 \times 10^{-4}$  M

( $\epsilon_{\max} = 8.4_3 \times 10^3$ ), and the determination of the number average molecular weight of the precipitated polyisoprene ( $\epsilon_{\max} = 8.2_0 \times 10^3$ ). Although objections can be made against each method, the agreement between them gives confidence that the mean  $\epsilon_{\max} = 8.05 \times 10^3$  is close to the true value\*. At the isosbestic point,  $\epsilon_{290} = 5.90 \times 10^3$  and this value was used to calculate the total polyisoprenyllithium concentration of all solutions. A number of spectra of polyisoprenyllithium in cyclohexane ( $2 \times 10^{-3}$  to  $3.75 \times 10^{-6}$  M) were investigated. The shoulder at 320 nm is somewhat more pronounced than in n-hexane at identical polyisoprenyllithium concentration.

The spectra of polyisoprenyllithium in benzene were examined in the range from  $1.11 \times 10^{-2}$  to  $5.06 \times 10^{-6}$  M. The polyisoprenyllithium absorption maximum (273 nm) is only accessible at the highest concentration because the benzene absorption becomes important below 285 nm. From the conversion of polystyryllithium to polyisoprenyllithium at different concentrations it was established that  $\epsilon_{290 \text{ nm}}^{\text{isosbestic}} = 6.05 \times 10^3$ , which is, within experimental error, the value obtained in n-hexane. The spectrum of polyisoprenyllithium in benzene above 290 nm is strongly dependent on the total polyisoprenyllithium concentration. The shoulder at 315–320 nm is significantly higher than in the aliphatic solvents at comparable concentration. An example is included in Figure 1.

In another series of experiments the spectra of a solution of polyisoprenyllithium in n-octane ( $\sim 6.5 \times 10^{-5}$  M) were recorded at different temperatures between 11.5° and 58°C. The spectra were standardized to a single concentration by correcting for the density change of n-octane. The examples in Figure 2 show that at this low concentration the spectrum of polyisoprenyllithium changes with higher temperature in a manner similar to the changes brought about by lowering the total polyisoprenyllithium concentration. The isosbestic point is clearly at 290 nm and the new maximum appears at 315–320 nm, this being more pronounced at the higher temperatures. The changes of the spectrum with temperature were completely reversible. However, keeping the

\* The results of the lithium analysis were not taken into account because the quantitative extraction of lithium salts from a polymer solution was difficult (units  $\text{cm l mol}^{-1}$ ).

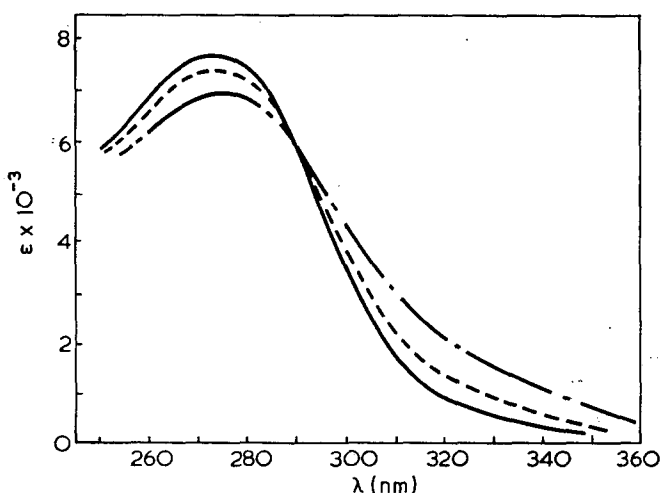


Figure 2 Temperature dependence of the absorption spectrum of polyisoprenyllithium in n-octane.  $[\text{PILi}] = 6.64 \times 10^{-5}$  M. —, 11.5°C; ----, 30.0°C; - · - · -, 54°C

polyisoprenyllithium solution at 80°C for 30 min produced some irreversible broadening of the spectrum.

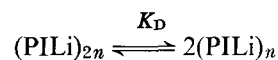
The spectrum of polybutadienyllithium in n-hexane at 30°C was found to be completely invariant with concentration in the range from  $6 \times 10^{-3}$  to  $2 \times 10^{-5}$  M. At no concentration was any increased absorption observed in the 300–400 nm region. Similarly, the spectrum of polystyryllithium in benzene at 30°C was found to be independent of concentration down to  $1 \times 10^{-6}$  M, in contrast with a claim by other workers<sup>3</sup>.

## DISCUSSION

The two discrete absorption maxima in the ultra-violet spectrum indicate the presence of two distinct species in solution. Because the relative peak heights depend on concentration, it is likely that we are observing partial dissociation of the aggregated species known to exist in hydrocarbon solvents. It has recently been shown<sup>4</sup> by measurements of the apparent molecular weight in cyclohexane that this phenomenon occurs. Kinetic results in benzene<sup>5</sup> may also indicate this effect. The spectral evidence presented here cannot distinguish between a tetramer–dimer or a dimer–monomer equilibrium. The evidence from association numbers and from kinetic analysis suggests that the major species present are tetramers, so the former case will be assumed. On this basis, the longer wavelength absorption corresponds to the dimer. This shift may indicate that increased delocalization occurs in this form.

The spectral shift is rather large but the structure of polyisoprenyllithium in the dimer may be quite different from that in the tetramer, which could resemble the local environment structure proposed for butyl lithium<sup>6</sup>. Also, the *cis*–*trans* ratio in the polyisoprenyllithium end may change on going from the tetramer to the dimer. Clearly, other unknown factors are also important in the determination of the energy levels in ground and excited states.

The assumption, that the observed spectral changes reflect the dissociation of the polyisoprenyllithium aggregates, can be tested by the constancy of the dissociation constant with total polyisoprenyllithium concentration:



where the discussion is pursued with  $n=2$ .

This dissociation constant can be calculated either from the decrease of the optical density at 272 nm or from the increase of the optical density at 320 nm. However, some assumptions have to be made concerning the extinction coefficient of the dimer, which cannot be obtained directly. A reasonable first approximation is to assume the extinction coefficient of the dimer at its maximum equal to that of the tetramer ( $8.05 \times 10^3$ ), and to assume the shape of the dimer absorption identical to that of the tetramer. The equilibrium constants calculated in this way show a satisfactory small scatter over the whole accessible concentration range, but the values of the dissociation constants calculated from the data at 320 nm are consistently 50% larger than the values obtained at 272 nm.

Increasing the extinction coefficient of the dimer at its maximum to  $1 \times 10^4$  results in a good agreement between the dissociation constants calculated from the 272 and 320 nm data. There is some justification for the higher



extinction coefficient as the spectrum of the dimer shows a markedly smaller half height width (plotted vs. wave number) than can be derived from the higher wavelength half of the tetramer spectrum. The results are collected in Table 1 and should be judged against the severe experimental difficulties and the assumptions underlying them.

For the three solvents no systematic trend of the dissociation constants is found over a 100-fold concentration range. In benzene, the dissociation constant decreases for polyisoprenyllithium concentrations below  $5 \times 10^{-5}$  M. The reasons for this are not clear but the spectrum may become complicated by the presence of monomeric species in this solvent. The order of the dissociation constants is n-hexane  $\approx$  n-octane < cyclohexane  $\ll$  benzene, parallel to the order of the dielectric constants of these solvents. The propagation rate constants of the alkyl lithium initiated isoprene polymerization are also in the order n-hexane < cyclohexane<sup>6</sup> < benzene<sup>5, 7</sup>. The present results suggest strongly that the complex propagation rate constants,  $k_p K_{Diss}^{1/4}$ , in which  $k_p$  is the rate constant for the addition of isoprene to the unassociated polyisoprenyllithium species and  $K_{Diss}$  is the overall equilibrium constant between tetrameric and monomeric polyisoprenyllithium, changes with solvent, in part, through the sensitivity of  $K_{Diss}$  to solvent. However, lack of knowledge about the dimer-monomer equilibrium constants precludes further speculation.

The greater ability of aromatic solvents to promote dissociation is in accordance with other data. *t*-Butyl lithium tetramers are more easily dissociated in toluene than in cyclopentane<sup>8</sup>. The differences observed in the kinetics of addition of lithium alkyls to double bonds between the two types of solvent can also be interpreted in this way. The small downward curvature in the logarithmic plot of propagation rate vs. concentration for polyisoprenyllithium in benzene has been noted earlier. It would be of interest to extend these data to concentrations lower than  $3 \times 10^{-4}$  M, to see if kinetic evidence for dissociation can be substantiated.

The dissociation constant obtained in cyclohexane at 30°C ( $1 \times 10^{-6}$ ) can be compared with the value obtained at 35°C by a completely different method ( $6 \times 10^{-6}$ )<sup>4</sup>. Considering the assumptions made and the difficulties involved in both types of measurement with such a low dissociation constant, the comparison must be regarded as satisfactory. Furthermore there is a gratifying parallelism between the fact that spectral changes only occur on dilution with polyisoprenyllithium and the observations<sup>4</sup> that the association number changes only with this compound and not with polybutadienyl- or polystyryl-lithium.

It is of some interest that the effect of addition of small amounts of tetrahydrofuran to polyisoprenyllithium in hydrocarbon solution produces gradually

Table 1 Dissociation constants for polyisoprenyllithium tetramers at 30.0°C

Solvent	$K_D \times 10^7$ at 272 nm (mol/l)	$K_D \times 10^7$ at 320 nm (mol/l)	No. of spectra	Conc. range (M)
n-Hexane	$4.2 \pm 1.2$	$5.4 \pm 1.2$	13	$2.3 \times 10^{-4} - 3.9 \times 10^{-6}$
n-Octane	$5.5 \pm 0.5$	$4.9 \pm 0.5$	2	$6.5 \times 10^{-6}$
Cyclohexane	$10 \pm 1$	$10 \pm 2$	7	$2.6 \times 10^{-4} - 3.7 \times 10^{-6}$
Benzene	—	$100 \pm 20$	13	$6 \times 10^{-8} - 5 \times 10^{-5}$

Table 2 Temperature dependence of the dissociation constant of polyisoprenyllithium in n-octane.  $[PILi] = 6.5 \times 10^{-5}$  at 30.0°C

Temp. (°C)	$K_D \times 10^7$ at 272 nm (mol/l)	$K_D \times 10^7$ at 320 nm (mol/l)
11.5	1.3	0.9
20.5	2.6	2.4
30	5.5	4.9
39.75	10.7	8.2
40.75	11.3	11.9
54	18	20
58	28	29

Table 3 Temperature dependence of the dissociation constant of polyisoprenyllithium in benzene.  $[PILi] = 2.11 \times 10^{-4}$  at 30.5°C

Temp. (°C)	$K_D \times 10^5$ at 320 nm (mol/l)
11.2	0.375
20.6	0.62
25.1	0.826
30.5	1.03
34.3	1.29
43.6	1.82

similar spectral changes with an isosbestic point at 290 nm. Polyisoprenyllithium ( $3 \times 10^{-3}$  M) is almost completely converted to a species absorbing at 315 nm when a 500-fold excess of tetrahydrofuran is present. This would suggest that, on addition of tetrahydrofuran, an initial dimer is formed. Addition of more tetrahydrofuran produces more complex changes and the calculation of equilibrium constants becomes impossible. It is curious, however, that in pure tetrahydrofuran, the absorption returns to a position close to that of the tetramer in hydrocarbon solvents. In this case, the spectrum corresponds to the monomeric (solvated) form in which charge delocalization would be expected to be even greater.

The results of the temperature variations are collected in Tables 2 and 3. In n-octane, these correspond to an enthalpy of dissociation of 12.3 kcal/mol and an entropy of dissociation of  $11.7 \text{ cal deg}^{-1} \text{ mol}^{-1}$ . The corresponding figures in benzene are 9.0 kcal/mol and  $7 \text{ cal deg}^{-1} \text{ mol}^{-1}$  respectively. The decreases in enthalpy and entropy in benzene are consistent with preferential solvation of the dissociation product in this solvent.

Finally, from a practical point of view, it should be noted that spectroscopic determinations of the total polyisoprenyllithium concentration should be made at 290 nm. The error caused by use of wavelengths closer to the maximum is, however, not large except at low concentrations.

## REFERENCES

- 1 Prud'homme, J., Roovers, J. E. L. and Bywater, S. *Eur. Polym. J.* 1972, 8, 901
- 2 Haupt, G. W. *J. Opt. Soc. Am.* 1952, 42, 441
- 3 Polyakov, D. K., Gantmakher, A. R. and Medvedev, S. S. *Polym. Sci. USSR* 1965, 7, 198
- 4 Worsfold, D. J. and Bywater, S. *Macromolecules* 1972, 6, 393
- 5 Alvario, J. M., Bello, A. and Guzman, G. M. *Eur. Polym. J.* 1972, 8, 53
- 6 Morton, M., Pett, R. A. and Fellers, J. F. *Prepr. IUPAC Macromol. Symp. Tokyo* 1966, 1, 69
- 7 Hsieh, H. L. *J. Polym. Sci. (A)* 1965, 3, 153, 173
- 8 Darenbourg, M. Y., Kimura, B. Y., Hartwell, G. E. and Brown, T. L. *J. Am. Chem. Soc.* 1970, 92, 1236

# Composites formed by interstitial polymerization of vinyl monomers in polyurethane elastomers:

## 1. Preparation and mechanical properties of methyl methacrylate based composites

G. Allen and M. J. Bowden\*

*Department of Chemistry, University of Manchester, Manchester M13 9PL, UK*

and D. J. Blundell, F. G. Hutchinson, G. M. Jeffs and J. Vyvoda

*Imperial Chemical Industries Ltd, Corporate Laboratory,  
The Heath, Runcorn, Cheshire WA7 4QE, UK  
(Received 22 May 1973)*

High-impact cast sheets of poly(methyl methacrylate) (PMMA) were prepared by the interstitial polymerization of the monomer in a polyurethane (PU) gel which had been prepared in a state of dilution in the monomer. The physical and mechanical properties of the composites depended on: (i) initiator concentration; (ii) molar ratio of isocyanate to hydroxyl groups; (iii) the time interval between gelation and subsequent polymerization of the MMA; (iv) the theoretical network crosslink density of the PU; and (v) the overall ratio of PMMA to PU. For a typical 80:20 PMMA/PU composite, with the above parameters at optimum values, measurements of  $12.5 \pm 1.0 \text{ kJ/m}^2$  and  $0.65 \pm 0.05 \text{ GN/m}^2$  were obtained for notched impact strength and shear modulus respectively compared to  $1.2 \pm 0.2 \text{ kJ/m}^2$  and  $1.47 \pm 0.03 \text{ GN/m}^2$  in PMMA homopolymer. Optical transmission was similar for both materials, i.e.  $\approx 90\%$ .

### INTRODUCTION

An established method of toughening plastics is the incorporation of rubber, either natural or synthetic, into the matrix. This approach has been the subject of several recent reviews<sup>1-4</sup>. Morphological studies on these materials (which include such commercially important products as high-impact polystyrene (HIPS) and the acrylonitrile-butadiene-styrene (ABS) terpolymers), show that they consist of a continuous glassy matrix throughout which is dispersed a large number of rubbery particles<sup>4-6</sup>. Factors which are important in determining the mechanical properties of such composite materials include the amount of rubber dispersed<sup>7</sup>, the size distribution and sub-structure of the rubber particles<sup>8</sup> and the degree of grafting of the glassy matrix to the rubber<sup>9</sup>. Other parameters such as the degree of crosslinking in the rubber and the molecular weight distribution of the continuous phase appear to be important<sup>8</sup>.

We wish to report a method for obtaining high-impact cast plastics by the interstitial polymerization of vinyl monomers within polyurethane elastomer gels. The process is shown schematically below:

Elastomer precursors + vinyl monomer

↓ urethane catalyst  
gel swollen with vinyl monomer  
↓ vinyl initiator  
composite

As the vinyl polymerization proceeds, a phase separation occurs between the polyvinyl and polyurethane to form a two-phase system. The extent of the phase separation is, however, controlled by the crosslinked polyurethane network. As will be shown later, although the final phase morphology is quite distinct from that of HIPS or ABS, the level of impact resistance obtained is very similar.

There are two important prerequisites in the choice of polymer for the success of the general scheme: (1) the elastomer precursors must be soluble in the vinyl monomer; and (2) there must exist a crosslinking mechanism chemically independent of vinyl initiation which can form the elastomer network prior to polymerization of the vinyl phase. These criteria are met by a polyurethane elastomeric system where the elastomer components (high molecular weight polyether or polyester polyols) are soluble in the vinyl monomer over the whole concen-

\* Present address: Bell Telephone Laboratories, Mountain Avenue, Murray Hill, NJ 07974, USA.

tration range and can be formed into a crosslinked network at room temperature by specific catalysts. One other desirable feature of such a scheme is that the solubility interaction parameter between the monomer and the gel should be such that the maximum swelling capacity of the gel is not exceeded (a phenomenon leading to macro-syneresis), and that the density of crosslinking is high enough to prevent macroscopic phase separation during subsequent polymerization of the vinyl component.

There is related work in the literature in which high-impact materials have been made by swelling pre-existing elastomers with a vinyl monomer and then polymerizing inside the swollen network. A feature which limits this approach is that the volume fraction of occluded monomer depends on the swelling characteristics of the rubber. Ceresa and Watson<sup>10,11</sup> swelled crosslinked natural rubber and then polymerized during the mastication of the swollen mass. They were able to combine up to 70% of the vinyl monomer, 'at which content the product behaved like a high-impact glassy plastic'. Corresponding work with synthetic elastomers has been carried out by Sperling *et al.*<sup>12,13</sup>, e.g. styrene monomer swelled into a preformed crosslinked network of poly(ethyl acrylate). However, their main aim was not to make high impact two-phase plastics but rather to study the characteristics of interpenetrating networks, their contention being that both phases are continuous and interpenetrating. Klemperer *et al.*<sup>14,15</sup> have also attempted to make interpenetrating networks by mixing emulsions of two polymers [e.g. poly(urethane urea) and poly(butadiene-acrylonitrile)] containing crosslinking agents followed by coagulation and simultaneous but chemically independent crosslinking. Recent dynamic mechanical and electron microscopic studies show that the interpenetrating networks of both Klemperer *et al.*<sup>16,17</sup> and Sperling *et al.*<sup>18</sup> exhibit a two-phase morphology very similar to the interstitial systems described in this present series of papers.

The present study deals with several aspects of the two-phase systems made by interstitial polymerization. This first paper discusses the parameters involved in the preparation of these composites with reference to the poly(methyl methacrylate) (PMMA)-polyurethane (PU) system<sup>19</sup>. Subsequent papers in this series deal with the relaxation properties and morphology of these composites and the extension to other monomeric systems. It is further hoped to extend this work using other elastomer systems.

## EXPERIMENTAL

### Purification of reagents

Diphenylmethane 4,4'-diisocyanate (Desmodur 44) was purified by vacuum distillation (b.p. 150°C at 0.1 mmHg). Poly(oxypropylene glycol) of molecular weight 2000 (PPG-2000) and oxypropylated glycerol derivatives of molecular weight 3000 (OPG-3000), 1500 (OPG-1500) and 1050 (OPG-1050) were vacuum dried with stirring (nitrogen bleed) at 120°C for 2-3 h. The polyester polyols, poly(ethylene adipate) and poly(propylene sebacate) both with a molecular weight of 2000 were similarly dried. Trimethylol propane, the chain extending agent used in the polyester studies was vacuum dried with stirring at about 60°C for several hours. All polyols were supplied by ICI Dyestuffs Division. Dibutyl-

tindilaurate (Alpha Inorganics Inc.) and azobisisobutyronitrile (Genitron) were used as supplied. Methyl methacrylate (BDH laboratory reagent) was freed from water and inhibitor by refluxing over CaH<sub>2</sub> followed by fractional distillation under reduced pressure (b.p. 51°C at 115 mmHg).

### Preparation of composites

The reaction was carried out in a one shot, two step procedure. All the reactants were mixed together at room temperature and dibutyltindilaurate (DBTL) added to promote urethane formation. The crosslinking points of the elastomer network were introduced via the trifunctional polyols. Prior to gelation, the solution was degassed and poured into a mould. The moulds consisted of either glass or metal glazing plates separated by a flexible gasket of Butyl 365 rubber (Esso Chemicals). The plates were spring loaded to minimize the problem of shrinkage during polymerization. The temperature was then raised to initiate polymerization of the vinyl phase. A variation of this procedure consisted of first preparing a prepolymer by reacting two parts of diisocyanate (MDI) to one part of polyol. The second stage of this so-called two shot technique involved the dissolution of the prepolymer together with a further one part of polyol in the monomer followed by the procedure outlined for the one shot process.

The gel time depended on the DBTL concentration while both gel time and the properties of the final gel depended on the ratio of vinyl (MMA) to polyurethane (PU) components and the theoretical molecular weight between crosslinks ( $\bar{M}_c$ ) of the network. At high vinyl concentrations (>85% w/w) the gelation of precursors designed to give a large value of  $\bar{M}_c$  was difficult, resulting in 'poor' gels in which macroscopic phase separation occurred during polymerizing of the MMA. This difficulty could be overcome by a slight adaptation of the normal procedure. In this case, a 50:50 MMA/PU composition was first prepared and just prior to gelation (<1 h) the mixture was diluted slightly with MMA progressively until the desired composition was reached. By means of this dilution technique, solutions containing 10% w/w PU with a theoretical  $\bar{M}_c$  of 4500 could be gelled in <3 h.

*Example.* 64 g methyl methacrylate (MMA), 0.16 g azobisisobutyronitrile (AIBN), 1.93 g MDI, 7.03 g PPG-2000, 7.03 g OPG-3000 and 0.26 g DBTL were mixed in a conical flask and allowed to stand at room temperature. For the above composition, [80:20 MMA/PU, molar ratio NCO/OH=1.1:1], gelation took about 4-5 h. Prior to gelation the sample was quickly degassed, poured into a mould and allowed to gel. After gelation, the casting was cured at 50°C for 15 h, 90°C for 1 h and 115-120°C for a further 2 h.

### Mechanical measurements

The number of different types of test has been kept to a minimum consistent with providing an indication of the mechanical properties of the composites. In general for each sample the notched impact strength (NIS) and shear modulus were measured. In the case of the variation of overall PU to PMMA composition, the tensile strength of the samples was also measured. All tests were carried out at room temperature (22-24°C).

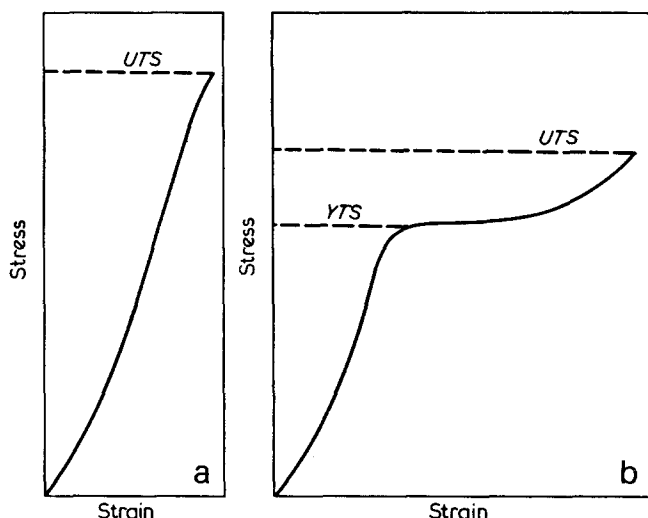


Figure 1 Typical stress-strain curves for (a) brittle and (b) ductile materials

**Notched impact strength.** As a measure of the toughness of the composites, the Charpy notched impact test<sup>20</sup> was used. The tests were performed with a Hounsfield Plastics Impact Tester. The samples were machined from the prepared sheets with dimensions approximately  $50 \times 5 \times 3$  mm and notched by a cutter of tip radius 0.25 mm. At least six samples were tested for each quoted value.

**Shear modulus.** The shear modulus ( $G'$ ) measured with a torsion pendulum operating at 1 Hz<sup>21</sup>, was chosen as a measure of the modulus of the composites. This test was preferred for its accuracy ( $\sim 2-3\%$ ) and small sample size ( $\sim 80 \times 7 \times 3$  mm) compared with other techniques of measuring moduli.

**Tensile strength.** The tensile properties of the composites were tested with a Hounsfield Tensometer (Type E) using a strain rate of 5 mm/min<sup>22</sup>. The tensile strength (TS) measured depended upon the type of stress-strain behaviour observed. In Figure 1a a typical stress-strain curve for a brittle material is shown where the ultimate tensile strength (UTS) is recorded. This type of behaviour was exhibited by PMMA homopolymer or by composites containing 10% by wt of PU. By comparison Figure 1b shows the typical stress-strain behaviour of a ductile material. For such a material the yield tensile strength (YTS) rather than the UTS is recorded since the former parameter is a more meaningful limit of application of the material. Ductile behaviour was shown by samples containing more than about 10% by wt of PU. In the results which follow tensile strength is quoted referring to UTS or YTS as appropriate.

## RESULTS

### Physical properties

The cast sheets have a transparent appearance. For samples made under optimized conditions the measured turbidity at 590 nm for a 3 mm sheet was less than  $\sim 0.02 \text{ mm}^{-1}$  over the whole composition range. This corresponds to a transmission of better than 87% in air. Electron microscopy studies which will be fully reported in the second paper of this series<sup>23</sup> show a morphology essentially consisting of PMMA domains in a PU matrix.

The dynamic mechanical results, also fully reported in Part 2<sup>23</sup> show that each component retained its separate glass transition, further supporting the conclusions drawn from electron microscopy. During tensile testing at high extensions and at the fracture surface of impact test samples, the highly strained regions of the samples were white and opaque in appearance. This phenomenon was not observed in PMMA homopolymer.

### Mechanical properties

Composites were prepared using mainly polyether polyols, but a few were prepared using polyester polyols. These had similar mechanical properties to the composites based on polyether polyols on which most of the studies of the effects of different parameters were made. Parameters varied in the composites included: (i) the initiator concentration for the polymerization of MMA; (ii) the molar ratio of isocyanate to hydroxyl groups; (iii) the time between gelation of the PU phase and the polymerization of the MMA at various polymerization temperatures; (iv) the theoretical PU crosslink density ( $\bar{M}_c$ ); and (v) the overall PMMA to PU composition. The effect of acid chloride was also studied.

**Effect of [AIBN].** The variation of impact strength and shear modulus for a set of 80:20 PMMA/PU composites prepared with varying amounts of vinyl initiator is shown in Table 1. The PU was formed from 50% w/w triol (OPG-3000) and 50% w/w diol (PPG-2000) giving a theoretical  $\bar{M}_c$  of 4500. The impact strength remained substantially constant over the range investigated although the modulus decreased at high initiator concentrations.

**Effect of molar ratio of isocyanate to hydroxyl groups.** The variation of impact strength and shear modulus for a series of composites prepared with various molar ratios of isocyanate to hydroxyl groups is shown in Figure 2. The overall composition of the composites and

Table 1 Effect of initiator (AIBN) concentrations on the mechanical properties of an 80:20 PMMA/PU composite

[AIBN] (%)	NIS (kJ/m <sup>2</sup> )	G' (GN/m <sup>2</sup> )
0.06	11.9 ± 0.8	0.71 ± 0.02
0.1	11.3 ± 0.6	0.69 ± 0.02
0.2	11.7 ± 0.6	0.68 ± 0.02
0.6	11.6 ± 0.7	0.59 ± 0.02

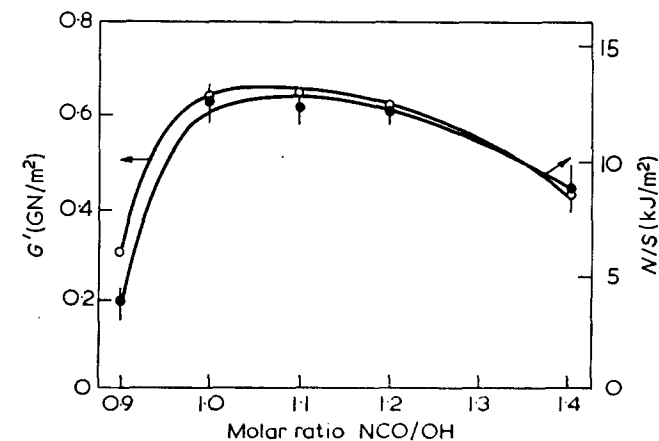


Figure 2 Effect of molar ratio of isocyanate to hydroxyl groups on the mechanical properties of 80:20 PMMA/PU composites. ○, Shear modulus; ●, notched impact strength

of the PU elastomer was the same as in the previous section. The initiator concentration was 0.2% based on total composite weight.

Both the impact strength and the modulus curves showed plateaux in the [NCO]/[OH] range of 1:1 to 1.2:1. At the low molar ratio limit of the series, both the impact strength and modulus decreased more rapidly than at high molar ratios.

*Effect of time difference between gelation and polymerization of MMA at various temperatures.* The effect of varying the time ( $t$ ) between the gelation of the PU components at room temperature and the initiation of vinyl polymerization at 50°C on impact strength and modulus is shown in Table 2. The gel point was taken as the time when the solution became too viscous to pour. A negative value of  $t$  indicates the time before normal gelation at room temperature when the sample was placed in the bath at elevated temperature. The overall composition of the composites and of the PU was the same as in the previous two sections. [AIBN] was 0.2% w/w and [NCO]/[OH] was 1.1:1.

The onset of polymerization could be detected by a faint cloudiness of the gel and usually occurred after an induction period of about 4–5 h. Samples placed in the bath at 50°C immediately after preparation ( $t = -5$  h) gelled within 2 h so that under all circumstances, gelation always took place prior to the commencement of polymerization. The data showed that variation of  $t$  from -5 h up to 7 days caused a slight decrease in impact strength. The modulus increased for intervals up to 4 days but then remained substantially constant.

Table 3 illustrates the effect of  $t$  upon the impact strength and shear modulus when polymerization was initiated at 70°C. In this case, the induction period was of the order of 20 min which was approximately the same time a sample placed in the bath immediately after preparation ( $t = -5$  h) took to gel. Thus it was possible to initiate polymerization as closely as possible to the real gel point. A strong dependence of shear modulus

Table 2 Dependence of mechanical properties on the time interval between gelation and polymerization at 50°C

$t$ (h)	NIS (kJ/m <sup>2</sup> )	$G'$ (GN/m <sup>2</sup> )
-5	12.5 ± 0.6	0.63 ± 0.02
1-2	12.8 ± 0.7	0.64 ± 0.02
22	12.1 ± 0.5	0.65 ± 0.02
96	11.8 ± 1.0	0.67 ± 0.02
120	11.3 ± 0.6	0.69 ± 0.02
168	11.7 ± 0.5	0.68 ± 0.02

Table 3 Dependence of mechanical properties on the time interval between gelation and polymerization at 70°C

$t$ (h)	NIS (kJ/m <sup>2</sup> )	$G'$ (GN/m <sup>2</sup> )
-5	11.7 ± 0.8	0.37 ± 0.02
-2	11.9 ± 0.6	0.39 ± 0.02
0	11.6 ± 0.6	0.50 ± 0.02
3	12.2 ± 0.3	0.53 ± 0.02
6	12.5 ± 0.3	0.60 ± 0.02
12	12.6 ± 0.5	0.64 ± 0.02
15	12.4 ± 0.6	0.67 ± 0.02
20	11.6 ± 0.5	0.79 ± 0.02
24	11.9 ± 0.7	0.68 ± 0.02
48	12.0 ± 0.4	0.69 ± 0.02
1 week	11.3 ± 0.6	0.70 ± 0.02

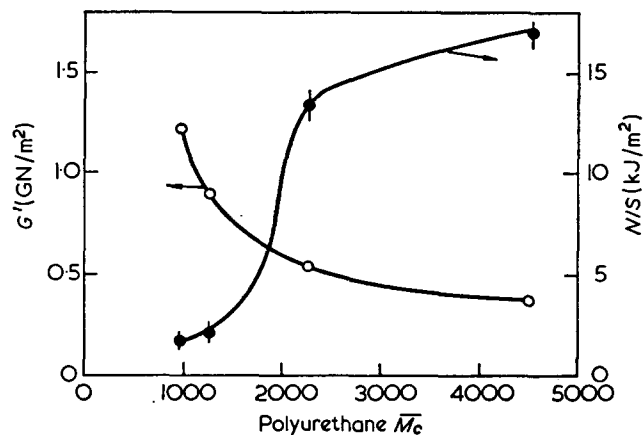


Figure 3 Effect of PU elastomer crosslinking density on the mechanical properties of 70:30 PMMA/PU composites. O, Shear modulus; ●, notched impact strength

on  $t$  was observed increasing with increasing  $t$ . A similar trend was observed in optical transmission at room temperature. In contrast, the impact strength remained constant to within experimental error.

*Effect of acid chloride.* The addition of a small amount of acid chloride, e.g. benzoyl chloride, is often recommended in urethane reaction chemistry where it is believed to react with any basic impurities in the polyol and small amounts of trace water<sup>24</sup>. The addition of small amounts of benzoyl chloride (<0.1% w/w) had a drastic effect on gelation time and on the final properties of the composites as can be seen in Table 4. Composition was 80:20 MMA/PU where the PU consisted of 50:50 OPG-3000/PPG-2000. The mechanical properties were unaffected up to about 0.02% w/w but the modulus decreased above this level of addition provided the stoichiometry of NCO to OH groups was maintained above 1:1. The impact strength was relatively unaffected. At a molar ratio of NCO/OH of 0.9:1, only a very weak gel formed and the addition of a trace of benzoyl chloride only resulted in a solution of increased viscosity for times up to one week, i.e. gelation did not occur.

*Effect of theoretical crosslink density ( $\bar{M}_c$ ).* The effect of the variation of the  $\bar{M}_c$  of the polyurethane upon impact strength and shear modulus is shown in Figure 3. The composites in this series were composed of 70:30 PMMA/PU. [AIBN] was 0.2% and molar ratio NCO/OH was 1.1:1. A time interval of 15 h was allowed between gelation and polymerization at 50°C.

Both modulus and impact strength were strongly dependent on  $\bar{M}_c$ . When the network was highly crosslinked (low  $\bar{M}_c$ ) the composites had a high modulus but were relatively brittle. Conversely for lightly crosslinked networks (high  $\bar{M}_c$ ) the composites had high impact strength but at the expense of modulus. At the higher  $\bar{M}_c$  values there was a tendency for both impact strength and modulus to level off.

*Effect of overall PMMA to PU composition.* The effect of overall composition upon the impact strength, shear modulus and tensile strength of the composites is shown in Figure 4. The various parameters discussed in the above five sections were set at or near their optimum values, viz. [AIBN]=0.2%, [NCO]/[OH]=1.1:1, time interval  $t=15$  h and polymerization temperature=50°C.

Table 4 Effect of benzoyl chloride on gelation and subsequent mechanical properties

Benzoyl chloride (% w/w)	0.9:1 [NCO]/[OH]			1:1 [NCO]/[OH]			1.1:1 [NCO]/[OH]		
	Approx. gel time (h)	NIS (kJ/m <sup>2</sup> )	G' (GN/m <sup>2</sup> )	Approx. gel time (h)	NIS (kJ/m <sup>2</sup> )	G' (GN/m <sup>2</sup> )	Approx. gel time (h)	NIS (kJ/m <sup>2</sup> )	G' (GN/m <sup>2</sup> )
0	> 48	7.47	5.03	4-5	13.92	6.78	4-5	11.16	6.98
0.025	∞	5.38	2.48	6-7	14.17	6.83	6-7	11.90	6.92
0.05	∞	5.6	2.20	10-12	13.51	6.42	10-12	12.39	6.56
0.1							~34	13.2	4.13

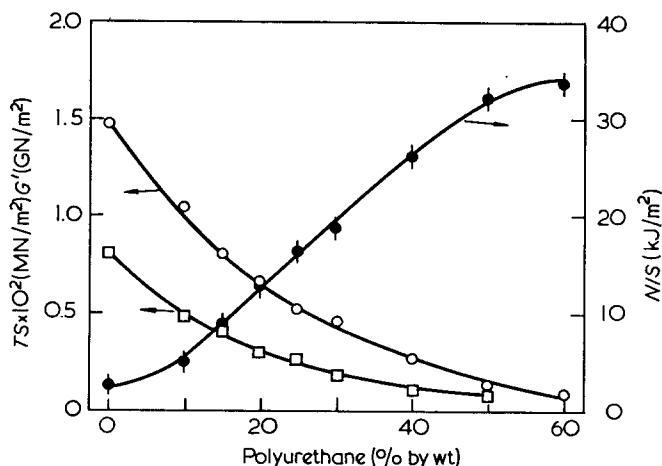


Figure 4 Effect of weight fraction of the PU elastomer on the mechanical properties of the composites. O, Shear modulus; □, tensile strength; ●, notched impact strength

The composition of the PU elastomer was chosen for high toughness, viz. equal proportions of PPG-2000 and OPG-3000 giving a theoretical  $\bar{M}_c$  of 4500.

Both the modulus and the tensile strength showed a fairly rapid fall from their values in PMMA homopolymer where  $G = 1.47 \pm 0.03$  GN/m<sup>2</sup> and  $TS = 79 \pm 3$  MN/m<sup>2</sup>. Above about 10% w/w PU, this fall was more gradual. The impact strength increased slowly from its value in PMMA homopolymer ( $1.2 \pm 0.2$  kJ/m<sup>2</sup>) but rose rapidly above 10% w/w PU. At 50% w/w PU the majority of the impact test samples did not break cleanly and tended to hinge.

**Other parameters.** The variation of DBTL concentration on the rate of reaction of the polyols with the diisocyanate did not produce any change in the mechanical properties of the composites. The procedure outlined earlier necessitated the formation of the PU network before polymerization of the MMA. Provided this was adhered to, the variation of DBTL concentration only affected the time to gel and not the mechanical properties of the composites.

The mechanical properties of composites prepared by either the one shot, two shot or dilution techniques were identical within experimental error.

The final curing procedure of heating the composites for 1 h at 90°C and 2 h at 115–120°C was sufficient to ensure complete conversion of the MMA to polymer. Provided the sample remained in the mould during the high temperature phase of the cure, there was no decrease in either modulus or impact strength for times ranging up to 24 h. When subjected to a similar heat treatment outside the mould, i.e. exposed to the air, the impact strength began to decrease after 2 h and by 24 h the sample was quite brittle. The causes of this effect are currently being investigated.

## DISCUSSION

The measured turbidity and associated transmittance of > 87% through a 3 mm sheet in air is almost as good as PMMA homopolymer. The turbidity depends on the size, nature of the dispersion and the difference in refractive index of the two phases. It has been possible to obtain a reasonable correlation between the turbidity and morphology as revealed by electron microscopy by using a modification of low-angle X-ray analysis<sup>25</sup>. The relation between structure and turbidity is currently being examined in greater detail. The low turbidity in the present case is due to the small size of the dispersion coupled with a small refractive index difference of about 0.015.

The results in Table 1 show that the shear modulus is sensitive to initiator concentration above about 0.2% indicating that the molecular weight of the PMMA is an important factor. Experiments on the bulk polymerization of MMA at different initiator concentrations showed a marked fall in molecular weight above a concentration of 0.1%. The polymerization of MMA is complicated by the autocatalytic or Trommsdorff effect<sup>26</sup> in which the increasing viscosity of the medium and associated decrease in termination rate constant with increasing conversion results in an increase in overall polymerization rate and molecular weight. This effect would be enhanced in the present system where polymerization is initiated in the gel phase thus leading to higher average molecular weights for higher initiator concentrations than in the corresponding case of pure MMA. On the other hand, the impact strength is not affected by the initiator concentration.

The curves in Figure 2 show very clearly a preferred range of molar ratios of isocyanate to hydroxyl groups extending from 1:1 to 1.2:1. It is interesting to note that the preferred range is not centred about the stoichiometric composition. This is obviously related to the problem of gelation in dilute solutions since molar ratios of 1.2:1 gel at times only slightly longer than 1:1 whereas it is only possible to produce gels of molar ratio 0.9:1 by the dilution technique and even then, a 'poor' gel is obtained. Flory<sup>27</sup> proposed a theory of gelation in non-linear polycondensation reactions assuming no intramolecular crosslinks and arrived at the condition for gelation as:

$$\alpha_c = \frac{1}{f-1} \quad (1)$$

where  $\alpha_c$  is the branching coefficient and is defined as the probability that a given functional group on a branch unit is connected to another branch unit. The term  $f$  is the functionality of reactant groups and has a value of 3 in the present system. Flory derived an expression relating  $\alpha_c$  to the extent of reaction for a mixture similar to the present system, e.g. a difunctional and

trifunctional polyol and a diisocyanate. This is given as

$$\alpha_c = \frac{p_{\text{NCO}}p_{\text{OH}}}{1 - p_{\text{NCO}}p_{\text{OH}}(1 - \rho)} \quad (2)$$

where  $p_{\text{NCO}}$  and  $p_{\text{OH}}$  are the extents of reaction of isocyanate and hydroxyl groups at the gel point and  $\rho$  is the ratio of hydroxyls on the branch unit to all hydroxyls in the system. By defining

$$\frac{[\text{NCH}]}{[\text{OH}]} = r = \frac{p_{\text{OH}}}{p_{\text{NCO}}} \quad (3)$$

and combining equations (2) with (3) we can deduce the limits within which gelation should take place. In the present case this is calculated to be  $0.67 < r < 1.5$ . These represent the widest limits since in practice  $\alpha_c$  is usually  $> 0.5$  due to the reaction of some of the functional groups to form intramolecular links or rings which do not contribute to the network. The ring size and the extent to which the rings are formed are determined by the probability of reaction between groups on the same molecule. This probability increases with dilution<sup>28</sup> and hence an increase in the value of  $\alpha_c$  would bring these limits closer together. Assuming that the limits remain reciprocally related in these circumstances the reason why solutions in which  $r=0.9$  do not gel, whereas those with  $r=1.2$  (reciprocal=0.83) do gel, is not immediately clear.

In their studies of the gelation of hexamethylene diisocyanate and a trifunctional polyol Peters and Stepto<sup>29</sup> found that gelations occurred at values of  $\alpha_c$  closer to the theoretical value of 0.5 when the hydroxyl component was in excess. Their system was not complicated by the presence of difunctional components and the initial concentration of isocyanate and hydroxyl groups was greater by a factor of about seven or eight. In our system it is possible that the gelation difficulties would be observed also on the high-isocyanate side of stoichiometry in the absence of trace amounts of water which probably react with the excess NCO groups resulting in functional groups (amines) and which then take part in further gelation reactions. The presence of trace water is suggested by the inhibition effect on gelation by acid chloride (Table 4) since these compounds are believed to act as inhibitors as a result of hydrolysis producing HCl, a known retarder<sup>24</sup>. Thus it is not altogether surprising that solutions on the high hydroxyl side of stoichiometry do not gel.

Soxhlet extractions of the composites prepared with low NCO/OH molar ratios and examination of the extracts by n.m.r. and i.r. spectroscopy, show quite large proportions of polyether and extended polyether fragments indicating that the network is incomplete. Hence the PU would not be expected to be fully efficient in promoting toughening and low impact strengths would result. The presence of these fragments would also be expected to have a plasticizing effect on the composition which would result in low moduli. Similarly at the higher [NCO]/[OH] ratios, the same phenomenon seems to be occurring, viz. incomplete build-up of the network but other secondary reactions are possible, e.g. allophanate formation, which lead to increased crosslinking and may be responsible for the slower fall off in mechanical properties.

It can be seen from Table 2 that the mechanical properties of the composites are almost independent of the time between gelation and vinyl polymerization provided

the latter is carried out at 50°C. This is true even when the sample is placed in the bath immediately after preparation. This time is critical, however, when polymerization is carried out at 70°C. It is known that gelation occurs well below complete reaction of functional groups but that these continue to react after gelation has occurred. This is evidenced by the improved viscoelastic properties of the gel with time and the absence of functional groups in the infra-red spectrum of the final composite. The accelerated rate of polymerization due to the decrease in the rate of termination can usually be detected by the temperature exotherm depending on initiator concentration and polymerization temperature. This exotherm will limit these variables to a range above which thermal runaway would occur<sup>30</sup>. Table 5 was obtained by measuring the temperature exotherm during polymerization at varying temperatures by embedding a thermocouple in the gel prior to polymerization. The initiator concentration was constant at 0.2%. Hence at 70°C the bulk of polymerization is completed within 1 h, at 60°C within 4 h and probably much longer at 50°C where it was not possible to observe a temperature exotherm. Above 70°C thermal runaway occurred.

It seems possible therefore that if polymerization takes place at 70°C immediately following gelation, the rubber network does not have time to form completely thereby resulting in inferior properties. At 50°C, however, the induction time appears long enough to allow reaction of nearly all functional groups, even if the sample is placed in the bath immediately after preparation. It is noteworthy though that it is the modulus, not the impact strength, which seems to depend on this parameter. When gelation is inhibited at 50°C using 0.1% acid chloride, a similar effect on the modulus is seen, as observed in Table 4.

Both the impact strength and modulus do depend upon the crosslink density of the PU network. As will be seen in Part 2 of this series<sup>23</sup> the glass transition temperature ( $T_g$ ) of the PU is strongly dependent upon this parameter. Composites with a PU phase of high  $\bar{M}_c$  have their glass transition temperatures near -50°C and as these elastomers show maximum improvement in impact strength, it suggests some correlation between these two parameters. The low  $T_g$  means the chains are highly mobile at room temperature and such lack of rigidity means that the PU would contribute little to the modulus of the composites. The low  $\bar{M}_c$  polymers have their glass transition temperatures near 0°C and consequently these chains are less mobile. Composites made from these polymers are less tough but have a higher modulus.

The composition of the composite, i.e. the relative proportions of PU and PMMA controls both modulus and impact strength of the composites in common with other rubber-toughened systems<sup>7</sup>. The question of how two materials of widely differing moduli combine to

Table 5 Effect of polymerization temperature on the sample temperature at constant [AIBN]

Polymerization temp. (°C)	Max. sample temp. (°C)	$\Delta T$ (°C)	Exotherm peak (h)
50	50	0	—
60	65	5	4
70	84.5	14.5	1
80	127	47	<1

give the composite modulus will be fully discussed in Part 5 of this series<sup>31</sup>. Toughness, as measured by the notched impact strength, increases approximately linearly over the range 10–50% w/w PU. Below 10%, brittle behaviour is reflected in the stress–strain measurements but above this value, ductile behaviour is shown.

## CONCLUSIONS

It has been shown that the interstitial method of combining PU elastomers with PMMA is successful in producing clear cast sheets whose toughness is much improved over that of unmodified PMMA. When the various preparation parameters are set at their optimum values then, typically, a ten-fold increase in toughness is achieved for a halving of modulus for a 80:20 PMMA/PU composite.

As the relative proportions of PMMA to PU decrease, the modulus of the composite falls and the toughness increases. Other parameters which affect the properties of the sheets are the molar ratio of isocyanate to hydroxyl groups, the time difference between gelation and polymerization of the MMA (at various temperatures) and the theoretical crosslink density of the PU. Other factors whose effects have been investigated but which do not have a profound effect upon the properties of the composites are the amount of vinyl initiator, the addition of acid chloride, the amount of urethane catalyst and variations in the final cure times and temperatures. No variation in modulus and toughness was detected in composites produced by one shot, two shot or dilution techniques.

The following papers in this series will report the results of investigations into the structure and loss properties of the composites and the preparations will be extended to include other vinyl systems.

## ACKNOWLEDGEMENTS

One of us (M.J.B.) is grateful to Imperial Chemical Industries Ltd and later to the University of Queensland for the award of successive Post-Doctoral Fellowships. All of the authors are indebted to Professor N. B. Graham for suggesting this field of work.

## REFERENCES

- 1 Rosen, S. L. *Polym. Eng. Sci.* 1967, **7**, 115
- 2 Bucknall, C. B. *Br. Plast.* 1967, **40** (11), 118; 1967, **40** (12), 84
- 3 Bowden, M. J. *Proc. R. Aust. Chem. Inst.* 1971, **39**, 190, 225
- 4 Williams, R. J. and Hudson, R. W. A. *Polymer* 1967, **8**, 643
- 5 Kato, K. *Polym. Eng. Sci.* 1967, **7**, 38
- 6 Matsuo, M., Nozaki, C. and Jyo, Y. *Polym. Eng. Sci.* 1969, **9**, 197
- 7 Fletcher, K., Haward, R. N. and Mann, J. *Chem. Ind.* 1965, p 1854
- 8 Wagner, E. R. and Robeson, L. M. *Rubber Chem. Technol.* 1970, **43**, 1129
- 9 Turley, S. G. *Appl. Polym. Symp.* 1968, **7**, 237
- 10 Ceresa, R. J. and Watson, W. F. *Trans. Inst. Rubber Ind.* 1959, **35**, 19
- 11 Ceresa, R. J. 'Block and Graft Copolymers', Butterworths, London, 1961
- 12 Sperling, L. H. and Friedman, D. W. *J. Polym. Sci. (A-2)* 1969, **7**, 425
- 13 Sperling, L. H., Taylor, D. W., Kirkpatrick, M. L. and George, H. F. *J. Appl. Polym. Sci.* 1970, **14**, 73
- 14 Frisch, H. L., Klempner, D. and Frisch, K. C. *J. Polym. Sci. (B)* 1969, **7**, 775
- 15 Klempner, D., Frisch, H. L. and Frisch, K. C. *J. Polym. Sci. (A-2)* 1970, **8**, 921
- 16 Matsuo, M., Kwei, T. K., Klempner, D. and Frisch, H. L. *Polym. Eng. Sci.* 1970, **10**, 327
- 17 Frisch, H. L. and Klempner, D. *Macromol. Rev.* 1970, **2**, 149
- 18 Sperling, L. M., Huelck, V. and Thames, D. A. in 'Polymer Networks', (Eds Champft and Newman), Plenum Press, New York, 1971
- 19 Br. Pat. 58947/70
- 20 ASTM D 256-56-method B, Am. Soc. Test. Mat., Philadelphia
- 21 ASTM D 2236-67T, Am. Soc. Test. Mat., Philadelphia
- 22 ASTM D 636-67T, Am. Soc. Test. Mat., Philadelphia
- 23 Allen, G., Bowden, M. J., Blundell, D. J., Jeffs, G. M., Vyvoda, J. and White, T. *Polymer* 1973, **14**, 604
- 24 Johnson, P. C. in 'Advances in Polyurethane Technology', (Eds J. M. Buist and H. Gudgeon), Maclaren, London, 1968
- 25 Blundell, D. J., Longman, G. W., Wignall, G. D. and Bowden, M. J. *Polymer* 1974, **15**, in press
- 26 North, A. M. and Reed, G. A. *Trans. Faraday Soc.* 1961, **57**, 859
- 27 Flory, P. J. in 'Principles of Polymer Chemistry', Cornell University Press, Ithaca, 1953, p 347
- 28 Dusek, K. and Prins, W. *Adv. Polym. Sci.* 1969, **6**, 1
- 29 Peters, R. H. and Stepto, R. F. T. *Soc. Chem. Ind. Monogr.* **20**, 1966, p 157
- 30 Schildknecht, C. E. in 'Polymer Processes' (Ed. C. E. Schildknecht), Interscience, New York, 1956
- 31 Allen, G., Bowden, M. J., Todd, S. M., Blundell, D. J., Jeffs, G. M. and Davies, W. E. A. *Polymer* 1974, **15**, in press
- 32 Bucknall, C. B. and Smith, R. R. *Polymer* 1965, **6**, 437
- 33 Kambour, R. P. *Appl. Polym. Symp.* 1968, **7**, 215
- 34 Boyer, R. F. *Polym. Eng. Sci.* 1968, **8**, 161



# Composites formed by interstitial polymerization of vinyl monomers in polyurethane elastomers: 2. Morphology and relaxation processes in methyl methacrylate based composites

G. Allen and M. J. Bowden\*

*Department of Chemistry, University of Manchester, Manchester M13 9PL, UK*

D. J. Blundell, G. M. Jeffs and J. Vyvoda

*Imperial Chemical Industries Ltd, Corporate Laboratory,  
The Heath, Runcorn, Cheshire WA7 4QE, UK*

and T. White

*Imperial Chemical Industries Ltd, Organics Division, Blackley, Manchester M9 3DA, UK  
(Received 22 May 1973)*

The morphology and loss properties of polymeric composites of poly(methyl methacrylate) (PMMA) and polyurethane (PU) prepared according to an interstitial method have been studied. To a first approximation the structure is shown to consist of PMMA domains embedded in a PU matrix. A second approximation shows that there is some molecular interaction between the polymeric species, probably at the domain boundaries. Variations in the domain size and molecular motions are studied as a function of composition and experimental variables. Attempts are made to correlate these results with the mechanical properties of the composites.

## INTRODUCTION

Part 1<sup>1</sup> of this series described the preparation and mechanical properties of two phase polymeric composites made by the interstitial polymerization of methyl methacrylate (MMA) in a polyurethane (PU) elastomer. This paper is concerned with the molecular motions within the composite and with the phase morphology at a supramolecular level. The aim is to correlate the observations amongst themselves and relate them to the observed mechanical properties<sup>1</sup>.

The interstitial polymerization process consists of two main stages—the formation *in situ* at room temperature of an elastomeric PU gel swollen by the MMA followed by polymerization at elevated temperature of the monomer to produce a toughened plastic. By incorporating 20% PU, the impact strength could be increased to ten times the value for PMMA homopolymer. The preparation conditions and how they affect the toughness and stiffness of the composites were fully described in Part 1<sup>1</sup>.

In this paper, the morphological structure of the phases is examined mainly by electron microscopy.

\* Present address: Bell Telephone Laboratories, Mountain Avenue, Murray Hill, NJ 07974, USA.

Results are also given for an associated study by small angle X-ray scattering; a full description of this work is to be published separately<sup>2</sup>. The motions of the polymer chains were studied by both low frequency dynamic mechanical and audio frequency dielectric relaxation techniques.

In the course of the morphological study it became apparent that the phase structure depended on the structure of the PU gel and the concentration of the gelling solution. Results are therefore also given of a brief study of changes in the elasticity of the pure PU system when gelled in different solution concentrations. Associated work is also reported on composites made by swelling these various preformed PU elastomers with MMA and then polymerizing. These composites show directly how variations in rubber structure can affect the morphology and physical properties.

## EXPERIMENTAL

### *Preparation of materials*

Composites were prepared as described in the previous paper by the formation, *in situ*, at room temperature of a PU gel swollen by MMA followed by polymerization

of the monomer. In some cases the polyether polyols of the PU networks were replaced by a hydroxy terminated polybutadiene<sup>3</sup> so that staining techniques for electron microscopy could be utilized.

The bulk PU elastomers were prepared by first dissolving freshly distilled diphenylmethane 4,4'-diisocyanate (MDI) in the required polyols. The mixture was then degassed and an amount of dibutyltin dilaurate (DBTL) catalyst was added such that the mixture gelled within about 30 min. On thickening, the material was cast between dried Melinex (ICI Ltd) sheets and after gelation was cured for about 15 h at 50°C.

The solution-gelled PU elastomers were prepared in moulds using the same formulation and general method as with the PMMA/PU composites, with the exception that 40 ppm quinol inhibitor was substituted for the azobisisobutyronitrile (AIBN) initiator. After gelling for 24 h at room temperature and curing for 15 h at 50°C, the mould was opened and the MMA monomer was carefully evaporated to obtain the PU elastomer.

PMMA/PU composites from existing PU elastomers were made by allowing the sheets to swell with the required quantity of MMA monomer containing 0.2% AIBN initiator. The swollen elastomer was then placed in a mould made from two glass sheets of the correct size and wrapped round with polyethylene sheet. After allowing up to 24 h for the monomer to disperse uniformly through the rubber, the monomer was polymerized for 15 h at 50°C followed by 1 h at 70°C and 1 h at 90°C.

#### Electron microscopy

Samples were prepared for electron microscopy by cutting sections about 100 nm thick with an LKB ultramicrotome at room temperature. Castings containing more than 50% w/w elastomer were too soft to cut. After mounting on grids, the sections were obliquely shadowed by vacuum evaporation with either chromium or gold/palladium alloy. It was found that the PMMA and PU phases had different cutting and deformation characteristics so that the resulting sections had surface topologies that were related to the bulk morphology. This structure is revealed in the electron microscope by the combined effect of the metal shadowing and the differences in electron absorption from variations in thickness. The resolution of the phase morphology obtained in this way depends on both the mechanical quality of the sections and on the size of the structural details relative to the thickness of the section. In some cases it was found that the phase structure could be further enhanced by subjecting the sections prior to shadowing to the preferential etching action of a low pressure gas discharge, using the method of Spit<sup>4</sup>. Another useful enhancing technique is to suspend the specimen grid on a wire mesh in the surface of carbon tetrachloride for several minutes. The solvent which mainly swells the PU phase, appears to loosen up the section so that on drying prior to shadowing, the PMMA phase is made to stand out more prominently. Neither of these enhancing techniques appears to change the basic morphological structure seen in the electron microscope.

In the case of the sample made with a polyurethane containing polybutadiene sequences, the staining technique reported by Kato<sup>5</sup> was used. A block of the casting about 5 mm across was preshaped for sectioning and then immersed in 1% osmium tetroxide solution for

2–3 days. The block was then washed and sectioned; only the top few sections were observed in the electron microscope.

#### Measurement of densities

The densities of PMMA/PU composites were determined by finding aqueous solutions of calcium nitrate that will just cause flotation. The density of the solutions and hence of the composites was then found using both hydrometers and a density balance method. The method gave results to an estimated accuracy of 0.0015 g/cm<sup>3</sup>.

#### Loss measurements

*Dynamic mechanical loss measurements.* The samples for dynamic mechanical measurements were cut from the prepared sheets to the approximate dimensions of 80 × 7 × 3 mm. The apparatus used was a torsion pendulum whose frequency could be maintained near 1 Hz by means of a variable-moment torsion bar. The apparatus was based upon a commercial compressed air bearing (Sangamo 03040) and the motion of the system was monitored by a displacement transducer. The period of the oscillation was determined by electronic means to within 1 ms and the damping was observed with the aid of a chart recorder (Brüel and Kjaer 2305) equipped with a logarithmic amplifier. The sample was enclosed in an environmental chamber which was thermostatically controlled to ±0.1°C over the temperature range from –140 to +150°C.

The dynamic shear modulus  $G'$  was calculated from the observed period ( $T$ ) of the pendulum, its moment of inertia ( $I$ ) and the sample dimensions according to the formula<sup>6</sup>:

$$G = \frac{64\pi^2 I l}{b t^3 \mu T^2}$$

where  $l$ ,  $b$  and  $t$  are the length, breadth and thickness respectively of the sample and  $\mu$  is a shape factor. The mechanical loss tangent,  $\tan \delta_M$ , was calculated from log decrement/ $\pi$ .

*Dielectric loss measurements.* The samples for dielectric loss measurements were cut into the form of discs, 50 mm diameter, whose thickness varied from 1.5 to 3 mm. The surfaces were machined so that variations in thickness in a single sample were less than 0.5%.

To ensure a good electrical contact, tinfoil electrodes were attached to the sample by a thin layer of silicon grease. The measurements were made in a conventional three-terminal dielectric cell by means of a General Radio transformer ratio-arm bridge (Model 1615-A) with its associated audio oscillator (1317A) and tuned amplifier/null detector (1232A). This equipment covers the frequency range from 60 Hz to 10 kHz. The temperature of the cell was thermostatically controlled to ±0.25°C in a liquid bath over the temperature range –196 to +180°C.

Measurements of dielectric permittivity,  $\epsilon'$  and loss tangent,  $\tan \delta_D$ , were made at the available frequencies and temperatures.

The loss measurements are illustrated in the results section by plots of either  $G'$  or  $\epsilon'$  and the respective loss tangents *versus* temperature. The imaginary part of the complex representation of the loss (either  $G'' = \tan \delta_M \times G'$  or  $\epsilon'' = \tan \delta_D \times \epsilon'$ ) was not chosen since, in many

instances, a peak in  $\tan \delta_M$  was not clearly shown in  $G''$  because of either a large change in  $G'$  accompanying the process or the occurrence of another process in the other phase of the composite.

#### Mechanical testing of elastomers

Simple elongation measurements were made on strips of about  $50 \times 10 \times 2$  mm using a Hounsfield Type E Tensometer extending at the rate of 0.25 mm/min. Similar results were obtained by loading incrementally and reading the extension after reaching equilibrium.

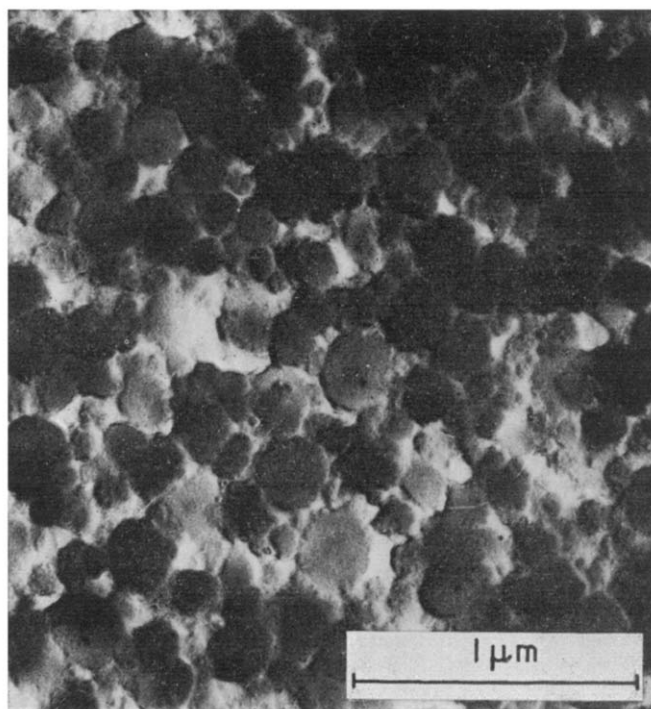
### MORPHOLOGY

#### General structure

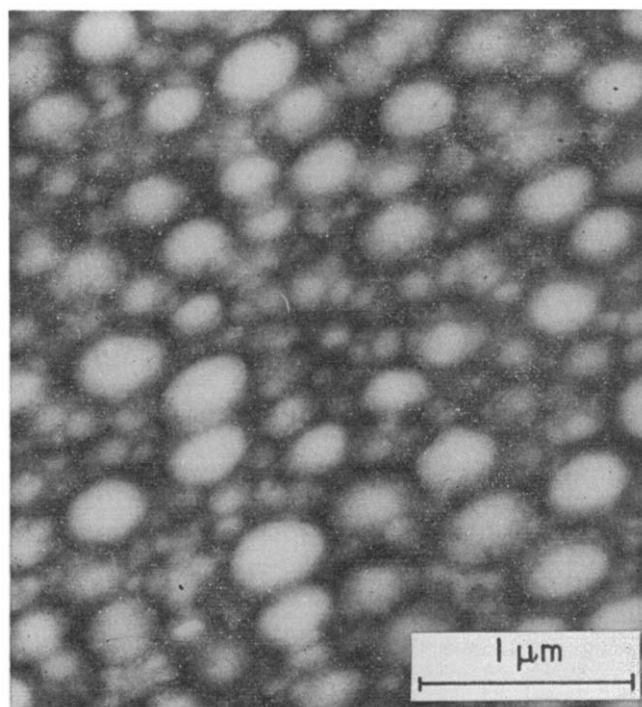
The basic morphology of the castings is best illustrated with compositions of 80% (w/w) PMMA and 20% PU. *Figure 1* is an electron micrograph of a shadowed section of one such sample in which the structure has been enhanced by preswelling in  $\text{CCl}_4$ . Most of the field is seen to be occupied by circular regions of varying sizes up to about 200 nm diameter, which are closely packed together. The simplest interpretation is that the composite has separated into submicroscopic phases where the circular regions represent PMMA, with the remaining region between them being occupied by PU rubber.

The picture of a simple two-phase structure is also consistent with the observed variation of the density with PMMA/PU composition. Within the accuracy of the measurements, it was found that the reciprocal of the observed density could be plotted against the weight fraction of PMMA to give a linear relation between a value of 0.947 for 0% PMMA to 0.838 for 100% PMMA.

The information obtained from an analysis of *Figure 1* is mainly representative of the structure on a random two-dimensional plane. It is important to decide whether this picture infers that in three dimensions the PMMA phases form closed cells or whether they join to form an open cell structure. The first possibility would involve the PMMA domains being completely separated by the PU phase, whereas in an open cell there would be a direct mechanical link between neighbouring domains. If the three-dimensional structure were an open cell, one would expect the random two-dimensional section to show a high proportion of neighbouring cells drawing out to join each other, whereas for closed cells all the domains would remain essentially circular. A scrutiny of micrographs such as *Figure 1* reveals that in the majority of cases, most of the domains, although not perfect circles, possess near-round smooth outlines, indicating a closed cell structure. Occasionally a pair of neighbouring cells appear to be well joined, but these are in the minority. However, the technique of preparing these electron microscope samples does not specifically show the location of the separate PMMA or PU phase, but only indicates the general nature of the texture. The apparent join of two domains could therefore be due to the inability to resolve intervening PU. In order to specifically resolve the rubber phase, use was made of the special composites containing a PU made from polybutadiene diols. The unsaturated polybutadiene sequences allow one to stain with osmium tetroxide and observe the location of the PU directly. *Figure 2* shows a stained section cut from a composite containing 80% w/w PMMA with the precursor polyol made from 60% Nisso 1000 polybutadiene and 40% OPG-3000. The



*Figure 1* Electron micrograph of a section from an 80:20 PMMA/PU composite shadowed with Cr



*Figure 2* Electron micrograph of a section from an 80:20 PMMA/PU composite made from a polybutadiene diol; PU phase stained with  $\text{OsO}_4$

dark regions represent the PU and clearly show that all the PMMA regions are smooth and circular in outline. Since some of the domains are smaller than the thickness of the section, an overlap of cells is seen in places. There is no strong evidence of a continuity of the PMMA between cells which would require a large proportion of cells to distort from circular outlines in order to join together.

From the point of view of the general morphology we therefore deduce that to a first approximation, the

composites consist of near spherical domains of PMMA closely packed and embedded in a continuous matrix of PU. The possibility of molecular interaction at phase boundaries and of molecular ties between domains is discussed with the results from the dynamic loss measurements later.

Compared with other systems made from spherical inclusions, the volume occupied by the PMMA spheres in the present composites is extremely high. Volume packing of the order of 80% of necessity requires a distribution of sphere sizes (cf. maximum of 74% for hexagonal close packing of identical spheres). The high efficiency of packing is achieved in the composites because the PMMA is formed *in situ* from pre-existing monomer, in which the sizes and positions of spheres are governed by the availability of unpolymerized monomer. Thus, for example, in the high PMMA compositions it is common to see the spaces between larger spheres occupied by smaller ones (Figure 4). Nevertheless, on the whole, the size distribution is still reasonably uniform for most of the composition range.

The size of the domain structure has been characterized by estimating the mean chord intercept length  $\bar{L}$  across the domains when a random line is drawn through the composite. Since the position of the domain boundaries is often difficult to resolve, this has been carried out by drawing lines on the micrographs and measuring  $N_L$  which is the average number of domains that are cut per unit length of line.  $\bar{L}$  is related to  $N_L$  according to<sup>7</sup>:  $\bar{L} = \chi/N_L$  where  $\chi$  is the volume fraction occupied by the domains. In practice  $\chi$  was calculated from the weight composition and density information by assuming a simple two phase model with sharp interfaces. The thickness of the PU network between domains can similarly be characterized by the quantity  $\lambda$  which is the mean free path between domains.  $\lambda$  is not independent of  $\bar{L}$  and is given by:  $\lambda = (1 - \chi)/N_L$ .

It is difficult to generalize on the accuracy of the measurements of  $\bar{L}$ , since it varies both with the quality of the micrographs and the domain sizes. For micrographs such as Figure 1, it has been estimated that  $\bar{L}$  can be determined to within about 15%; for smaller domains and poorer micrographs the accuracy is less. The actual value obtained for the sample shown in Figure 1 is  $\bar{L} = 115 \pm 15$  nm. The corresponding value of  $\lambda$  was found to be  $32.5 \pm 5$  nm. The same sample was also examined by small angle X-rays. A full report of this analysis is published separately<sup>2</sup>. It was found that the diffraction could be interpreted in terms of the theory described by Debye *et al.*<sup>8</sup> for a random two phase model. This gave an estimate of  $\bar{L} = 135$  nm which agrees well with the electron microscope result.

#### Variations in domain morphology

The variables of the system that could affect the domain morphology can be divided into three groups: (i) those associated with the technique and preparation conditions; (ii) variations in the PMMA/PU composition; and (iii) variations in the chemical reagents. Details of these variables were given in Part 1<sup>1</sup>. Except for variations in composition, all observations were made on castings containing 80% PMMA. In all cases examined, the general morphology did not depart from the domain structure of PMMA embedded in a PU matrix. The main variation observed was in the mean

domain size with occasional slight variations in the packing arrangement.

*Variations due to preparation method.* The difference in domain size when composites were prepared by the 'one shot' or 'two shot' techniques discussed previously<sup>1</sup> was found to be insignificant. The factor having the greatest effect was found to be the duration of the post-gelation period between the time of the gel point and the beginning of the vinyl cure. The effect is illustrated in Table 1 which shows the variations of  $\bar{L}$  for two series of samples where the temperature of the vinyl cure was 50°C and 70°C respectively.

In both series  $\bar{L}$  reduces as the post-gelation period is increased, although the effect is more pronounced for the 70°C cure. These results indicate that after the physical gel point an important proportion of the chemical linking of the PU continues to take place. The domain size appears to be determined by the state of gelation at the time when the vinyl polymerization occurs, further indicating the importance of the competing kinetics between the PU gelation and monomer polymerization<sup>1</sup>. The difference between the two series in Table 1 can be explained by the difference in induction times of the vinyl polymerization at the two temperatures. At 50°C the induction time is longer so that the gelation reaction is able to proceed relatively further than in the corresponding sample cured at 70°C. By the time polymerization actually begins, the network is tighter and more complete at 50°C so that the resulting domains are smaller. The results in Table 1 also show that when sufficient post gelation is allowed ( $\approx 20$  h),

Table 1 Variation of  $\bar{L}$  with post-gelation period

Post-gelation period (h)	$\bar{L}$ (nm)	
	1st series cured at 50°C	2nd series cured at 70°C
0	98	180
12	77	88
24	65	70
48	65	65

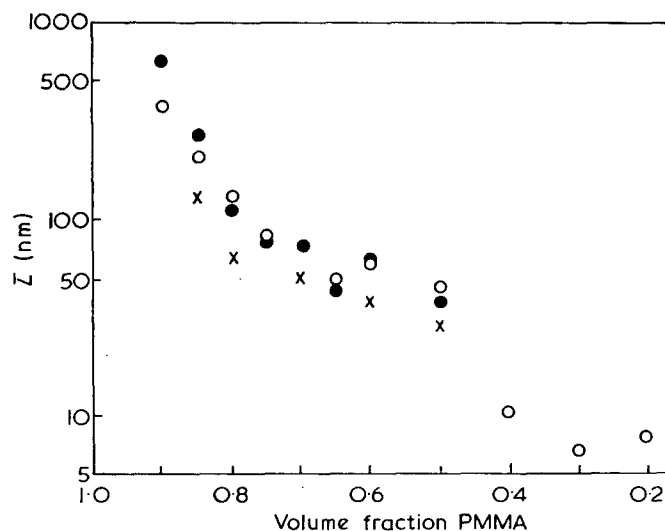


Figure 3  $\bar{L}$  as a function of weight fraction of PMMA. Electron microscope (●) results and low angle X-ray (○) results for a series of composites with zero post-gelation period. x, Electron microscope results for 5h post-gelation period

the effect of the vinyl polymerization temperature on the domain size becomes insignificant.

*Variations in composition.* The variations of  $\bar{L}$  with composition are shown in Figure 3. Results for two separate series of samples are plotted. For the first series, a zero post-gelation period was used. The second series, used a post-gelation period of 5 days. The results shown by solid circles were obtained from electron micrographs and the open circles from low angle X-ray analyses<sup>2</sup>. These pairs of results at identical compositions were determined from identical samples. The closeness of these two types of measurement is a measure of the success of the analytical methods and of the consistency of the morphological interpretation. Those for the second series were obtained from electron microscopy only.

Both series of results show a marked decrease in  $\bar{L}$  from greater than 500 nm with 90% PMMA to a few nanometres for 50% PMMA. In the region < 50% PMMA where samples were too soft to section, the two X-ray results indicate that the domain size continues to fall. The general shift in magnitude of  $\bar{L}$  between the two series of samples is a further demonstration of the effect of the post-gelation period. Examples of electron micrographs of the first series from which the  $\bar{L}$  measurements were obtained are shown in Figures 1, 4 and 5. Figure 1 for the 80% PMMA sample has already been discussed. Figure 4 shows the larger domains seen in the 90% PMMA sample. There is a marked increase in the breadth of the size distribution resulting from a tendency for a population of smaller domains to occupy the gaps between the larger ones. Some of the larger domains are also noticeably departing from the spherical shapes. Both these tendencies are observed whenever domains become very large (> 0.5  $\mu\text{m}$ ). Figure 5 shows the 50% PMMA sample where the domains are now only about 50 nm size and are seen as shadowed bumps embedded

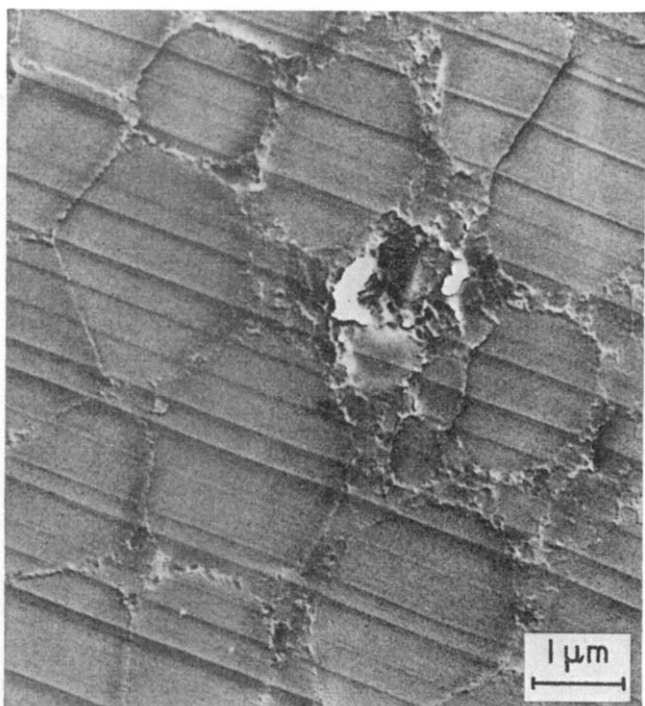


Figure 4 Electron micrograph of a section from a 90:10 PMMA/PU composite shadowed with Cr. Parallel lines are knife marks

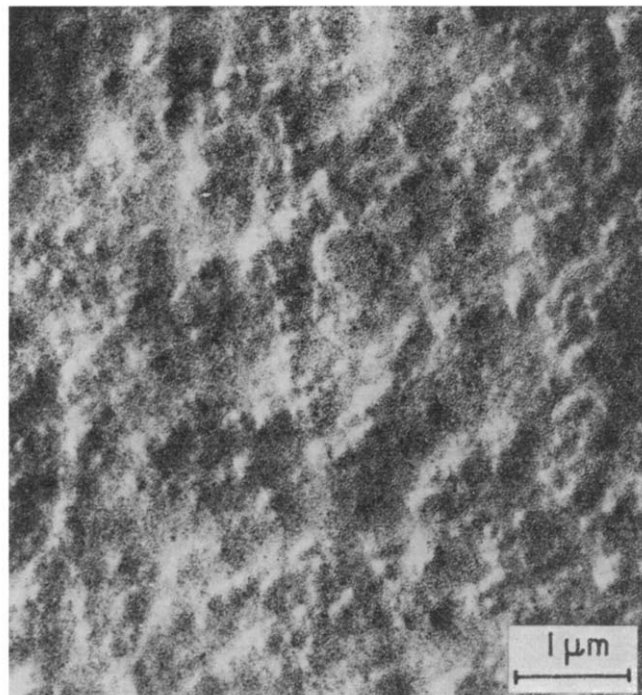


Figure 5 Electron micrograph of a section from a 50:50 PMMA/PU composite shadowed with Pd/Au

in the section. The interpretation becomes very difficult for domains of this size.

*Chemical variables.* In studying the effect of the chemical parameters, care was taken to use long enough post-gelation periods so that no complications were introduced from incomplete gelation before polymerization. The chemical variables can be subdivided into those which specifically affect the gelation and those affecting the vinyl polymerization. In the first category are the NCO/OH stoichiometry and the theoretical molecular weight between crosslink points ( $\bar{M}_c$ ). The effect of  $\bar{M}_c$  was examined by making the PU with OPG-3000 alone instead of the usual 50:50 mixture with PPG-2000 and OPG-3000. This gives a theoretical  $\bar{M}_c$  of 2250 instead of 4500 which is normally used. The morphology was more difficult to distinguish since the PU rubber is in this case more rigid. However, by slightly warming the sample during sectioning a domain structure with  $\bar{L}$  about 30 nm was revealed; this is about half of the normal value. The effect of varying [NCO]/[OH] is shown in Table 2. When the ratio of functional groups is close to the optimum value<sup>1</sup> of about 1:1,  $\bar{L}$  is fairly constant near the normal value. However, when the stoichiometry is well off balance in either direction so that the resulting PU networks are poorer, the resulting domains become very large. For effects relating to the vinyl polymerization, the concentration of AIBN initiator was varied from 0.05 to 0.5%. This, as with the temperature of the vinyl cure, should change the polymerization kinetics and molecular weight of the PMMA. However, as also observed with the polymerization temperature, if a post-gelation time greater than ~24 h is used, no significant change in  $\bar{L}$  is observed.

#### Discussion

The final domain size is thus independent of variations in the vinyl polymerization process, but very sensitive

Table 2 Variation of  $\bar{L}$  with stoichiometry of PU

[NCO]/[OH]	$\bar{L}$ (nm)
0.9:1	590
1.0:1	78
1.2:1	87
1.4:1	550

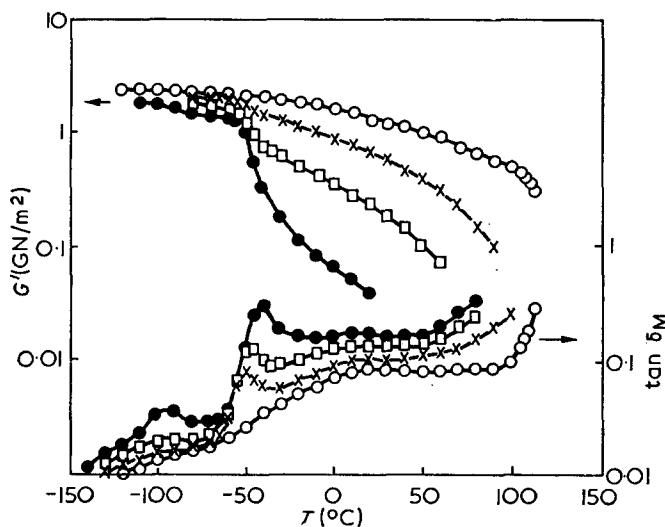


Figure 6 Shear modulus ( $G'$ ) and loss tangent ( $\tan \delta_M$ ) as functions of temperature ( $T$ ) for 100% PMMA (○) and for composites: ×, 80:20; □, 60:40; ●, 40:60 PMMA/PU

to the quality and molecular details of the swollen PU network and on the state of gelation at the time of polymerization. The mechanism by which the network structure determines the domain size is probably either by controlling the nucleation density of the domains, or by the elastic strain in the network acting as a restraint against growth (or by both). It is possible that the variation of  $\bar{L}$  with PMMA/PU composition is similarly connected with difference in the state and structure of the gel at different compositions. However, in this case, the relevant variations in PU structure are probably related to the fact that the gelations are taking place in different concentrations of MMA monomer, and are hence related to variations at a supramolecular level rather than a molecular level.

## LOSS PROPERTIES

### General loss properties and their variation with composition

The general loss properties of the composites are best illustrated by observing how they vary with overall composition and noting which elements of the loss properties of the homopolymers are observable in the spectra of the composites. Thus the order of presentation of this section differs from that of the previous section.

**Dynamic mechanical loss properties.** The dynamic mechanical loss properties of the PMMA/PU composites system are well represented in Figure 6 where both the shear modulus  $G'$  and the loss tangent,  $\tan \delta_M$  are plotted as functions of temperature for the pure vinyl polymer and for composites containing progressively increasing amounts of the PU phase.

Considering first the results for PMMA, the  $\tan \delta_M$  curve shows the presence of three loss regions. At low

temperature there is a broad, shallow region extending from  $-70^\circ\text{C}$  downwards in temperature. This effect is shown more clearly in the higher frequency dielectric results. The broadness of this process is reflected in the  $G'$  curve where no distinct 'step' is seen but rather a gradual decrease in modulus from the low temperature value of approximately  $2.5 \text{ GN/m}^2$ .

The next process observed, in order of increasing temperature, is the  $\beta$ -process of PMMA. This is another broad process which again produces a gradual decrease in  $G'$  with increasing temperature. The  $\tan \delta_M$  curve shows a broad peak near  $25^\circ\text{C}$  which, at high temperatures, begins to merge with the glass transition or  $\alpha$ -process of PMMA. This process is characterized by a sudden fall in modulus and a sharp increase in  $\tan \delta_M$  near  $110^\circ\text{C}$ .

The effect of the addition of PU is to introduce two loss processes into the spectrum. This is illustrated by the remaining curves on Figure 6 which show the results obtained for samples containing 20%, 40% and 60% w/w of PU. The theoretical  $\bar{M}_c$  of the PU in all cases was 4500. At low temperatures, near  $-90^\circ\text{C}$ , the  $\tan \delta_M$  curves show a peak (denoted PU- $\beta$ ) which gains in prominence as the relative proportion of PU increases. The modulus curves show a decrease from the PMMA curve and a distinct region where the fall is more marked is seen for the sample containing 60% w/w of PU. The effect of drying and wetting (in water) on a composite containing 30% w/w of PU is shown in Figure 11. The  $\tan \delta_M$  values for the sample dried under vacuum at  $120^\circ\text{C}$  for 2 h show the virtual absence of the PU- $\beta$  peak. Conversely, an enhanced peak is shown by the sample which had been immersed in water for 94 h. The uptake of water in this case was 1.45% w/w.

Near  $-50^\circ\text{C}$  a large loss process is seen. This gains in prominence with increasing proportion of PU and moves to slightly higher temperatures. This is the glass transition or  $\alpha$ -process in PU and marks the temperature at which the PU becomes rubbery in nature. Hence these peaks are accompanied by a distinct step in the  $G'$  curves. In the sample containing 60% PU the step merges into the general decrease caused by the  $\beta$ -process in PMMA. At high temperatures the  $\tan \delta_M$  curves for the composite show the characteristic increase on approaching the glass transition of PMMA.

**Dielectric loss properties.** The dielectric loss properties of the composites are illustrated in Figure 7, where the  $\tan \delta_D$  is plotted as a function of temperature at three representative frequencies, namely 200 Hz, 1 kHz and 10 kHz. Measurements were also taken at 60 Hz, 120 Hz, 500 Hz, 2 kHz and 5 kHz. The samples contained 60% w/w of PU whose  $\bar{M}_c$  was 4500. The results for a sample containing this high proportion of PU is chosen to emphasize the features of the polyurethane phase. Figure 7 also shows the values of  $\epsilon'$  measured at 1 kHz.

At low temperatures the PU- $\beta$  process is seen and the peak moves to higher temperatures as the frequency of measurement increases. This amplitude also increases with increasing frequency and at the highest frequency, 10 kHz, the peak shows a tendency to merge into the side of the  $\alpha$ -process. No significant change is observed in the  $\epsilon'$  values through this region.

The PU- $\alpha$  process is again well defined and is seen to move to higher temperatures with increasing frequency. The maximum  $\tan \delta_D$  values occur at  $-20^\circ$ ,  $-14^\circ$  and



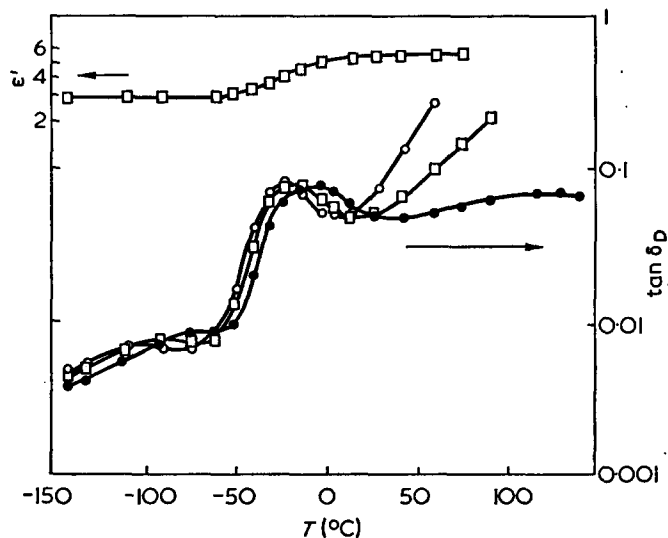


Figure 7 Dielectric permittivity ( $\epsilon'$ ) and loss tangent ( $\tan \delta_D$ ) as functions of temperature ( $T$ ) for a 40:60 PMMA/PU composite measured at:  $\circ$ , 200 Hz;  $\square$ , 1 kHz;  $\bullet$ , 10 kHz

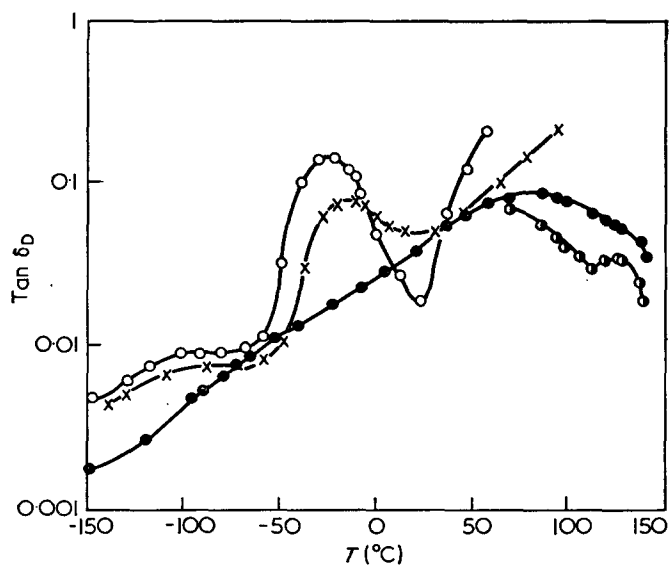


Figure 8 Dielectric loss tangent ( $\tan \delta_D$ ) measured at 1 kHz as a function of temperature ( $T$ ) for:  $\circ$ , 100% PU;  $\bullet$ , 100% PMMA;  $\times$ , 40:60 PMMA/PU composite. Additional points ( $\bullet$ ) for 100% PMMA measured at 120 Hz

$-8^\circ\text{C}$  for frequencies of 200 Hz, 1 kHz and 10 kHz respectively. This peak in  $\tan \delta_D$  is accompanied by an increase in  $\epsilon'$ . At higher temperatures the  $\tan \delta_D$  values measured at 200 and 1 kHz show increases to high values. The curve for measurements at 10 kHz shows evidence of the processes occurring in PMMA.

These processes in PMMA are more clearly shown in Figure 8 where  $\tan \delta_D$  measured at 1 kHz is shown as a function of temperature. In the temperature range from  $-100$  to  $-50^\circ\text{C}$  a shallow process is seen. This is the process shown less clearly by the dynamic mechanical results in Figure 6. The  $\beta$ -process in PMMA is shown in the dielectric results by a broad peak centred at  $80^\circ\text{C}$  (1 kHz) which tends to merge with and dominate the  $\alpha$ -process seen at about  $130^\circ\text{C}$ . The  $\beta$ -process is more clearly resolved at lower frequencies as shown by the curve representing measurements at 120 Hz.

$\tan \delta_D$ , measured at 1 kHz, for a wholly PU sample is also plotted in Figure 8. A broad PU- $\beta$  peak centred at  $-90^\circ\text{C}$  is seen together with the sharper PU- $\alpha$  peak

centred at  $-25^\circ\text{C}$ . At higher temperatures a rapid increase in  $\tan \delta_D$  is observed.

The final curve in Figure 8 is a plot of the results (1 kHz) for the composite containing 60% w/w of PU. A comparison of this curve with the corresponding curve for the PU homopolymer shows that the position of the PU- $\alpha$  peak in the composite is approximately  $14^\circ\text{C}$  higher in temperature than its position in the homopolymer.

**Correlation and discussion of loss properties.** Both the dynamic mechanical and the dielectric results are summarized in Figure 9, where the  $\log_{10}$  of the frequency of maximum loss is plotted against the increase of the absolute temperature. Starting at the higher temperatures the plots for the  $\alpha$ - and  $\beta$ -processes in PMMA are shown. Both plots are linear and good agreement is obtained between the higher frequency dielectric results and the single, low frequency, dynamic mechanical results. By means of the conventional Arrhenius approach, apparent activation energies for these processes have been obtained and the values are listed in Table 3.

The values of  $\Delta H$  for these processes in PMMA are in agreement with those obtained for atactic PMMA by other workers<sup>9-11</sup>. The high value of  $\Delta H$  of 445 kJ/mol is consistent with the larger scale motion occurring at the glass transition temperature. The value for  $\Delta H$  of 76 kJ/mol for the  $\beta$ -process is consistent with the rotation of the highly polar and bulky ester side group<sup>12</sup>. The

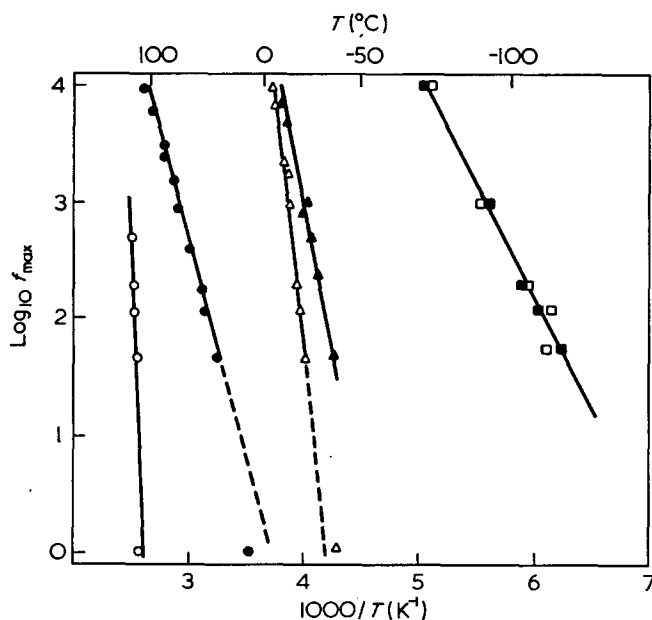


Figure 9  $\log_{10}$  of frequency of dielectric and dynamic mechanical maxima ( $\log_{10} f_{\max}$ ) versus reciprocal temperature ( $1000/T$ ).  $\circ$ , PMMA  $\alpha$ -process;  $\bullet$ , PMMA  $\beta$ -process;  $\triangle$ , PU- $\alpha$  process in composite;  $\blacktriangle$ , PU- $\alpha$  process in 100% PU. PU- $\beta$  process:  $\square$ , composite;  $\blacksquare$ , 100% PU

Table 3 Activation energies of different relaxation processes

Process	$\Delta H$ (kJ/mol)
PMMA- $\alpha$	$445 \pm 21$
PMMA- $\beta$	$76 \pm 2$
PU- $\alpha$ (composite)	$151 \pm 4$
PU- $\alpha$ (bulk)	$100 \pm 4$
PU- $\beta$	$37 \pm 4$

motion of this group relaxes the polar groups in this molecule at temperatures below that of the  $\alpha$ -process and, in the dielectric spectrum, the  $\alpha$ -peak is thus very much less prominent than the  $\beta$ -peak. The small process seen in PMMA at low temperature has been shown by other workers<sup>13</sup> to be due to the presence of moisture.

Linear relations are obtained in Figure 9 for the  $\alpha$ -process in the PU phase of 40:60 PMMA/PU. Fair agreement is obtained between the dielectric and the dynamic mechanical results for the composites ( $\tan \delta_M$  was not measured for bulk PU). The apparent activation energies are listed in Table 3. For the  $\alpha$ -process the values of  $\Delta H$  are rather low for a process which apparently involves large portions of the polymer molecule. This could be due to the movement being reduced to that of comparatively short lengths of polymer chain between the crosslink points. A significantly lower value for  $\Delta H$  is obtained for the PU homopolymer. The PU- $\alpha$  loss peak in the composition is seen to move to higher temperatures as the proportion of PU is increased. The shift in temperature compared with its position in bulk PU is especially noticeable in the loss curves, both dielectric and dynamic mechanical, for the 40:60 PMMA/PU sample.

The behaviour of the PU- $\alpha$  process, as exemplified by the activation energies and shifts in temperature, indicates a significant interaction between the phases in the form of a hindrance to the motion of the PU molecules. This hindrance can only arise from the more rigid PMMA molecules.

In terms of the domain morphology discussed earlier, any interaction between phases must occur at the interphase boundaries or be the result of direct molecular links of PMMA running through the rubber phase between domains. For a given fraction of PMMA the extent of interaction from both these effects will probably depend upon domain size. If the domains are made larger, then the thickness of PU separating the domains will be proportionately larger so that interdomain linking and associated interaction with PU molecules becomes less probable. At the same time, there will be a decrease in the specific interfacial area between phases so that there will also be a decrease in total molecular interaction at domain boundaries. By both these arguments, a composite with larger domains will provide less hindrance to motions in the PU and will, for a given composition, exhibit a more well-defined PU- $\alpha$  process. The shift to higher temperatures of the PU- $\alpha$  loss peak, as shown in Figure 6, with increasing amounts of PU, correlates well with the variation of domain size with compositional changes (Figure 5). The interaction between the phases increases as the domain size decreases and hence the interphase area increases. The effect is also well illustrated in the examples that follow and the question of interactions is further discussed in Part 4<sup>14</sup>, where further information is obtained by means of relaxation measurements on composites containing either polystyrene or polyacrylonitrile in place of PMMA.

The final plot in Figure 9 is for the  $\beta$ -process in PU. The results are insufficiently accurate to differentiate between the PU in the composite and in the bulk and consequently a single line has been drawn representing both cases. The drying and wetting experiments have shown that this process is enhanced by the presence of moisture and one can conclude that this  $\beta$ -process in PU is the relaxation of water molecules. The molecules

forming the PU network would be favourable to the hydrogen bonding of the water molecules and the apparent activation energy of this process of 37 kJ/mol is in good agreement to those obtained for similar processes in other polymeric systems<sup>15</sup>.

#### Variations in loss properties with preparation methods and chemical precursors

The effect of the variation of the post-gelation period between the gel point of the PU and the initiation of the polymerization of the vinyl (at 70°C) is shown in Figure 10 where  $G'$  and  $\tan \delta_M$  are plotted as functions of temperature for these composites. The  $\tan \delta_M$  curves show that the PU- $\alpha$  peak at about  $-50^\circ\text{C}$  decreases in magnitude as the post-gelation period is extended. The corresponding change in  $G'$  through the process also decreases as the period lengthens. These results imply that there is an increase in interaction between the PMMA and the PU as the post-gelation period is increased. This correlates well with the fall of domain size shown in Table 1 and the associated increase in interphase surface area.

The effect of the variation of crosslink density of the PU upon the loss properties of the composites is shown in Figure 11. Curves of both  $G'$  and  $\tan \delta_M$  are plotted for theoretical  $\bar{M}_c$  values of 4500, 2250, 1250 and 950 respectively for samples containing 30% w/w of PU.

The PU- $\beta$  process is little affected by this variable. However, a drastic change in the PU- $\beta$  process is seen. The sharp peak characteristic of the samples with  $\bar{M}_c$  of 4500 becomes progressively less distinct as the crosslink density increases. This is reflected in the  $G'$  curves where the drop in modulus becomes more diffuse and occurs at higher temperatures as the crosslink density increases. The curves for the composites of  $\bar{M}_c$  values of 1250 and 950 show a decrease in amplitude of the PMMA- $\beta$  process. The  $\tan \delta_M$  values for highly crosslinked samples,

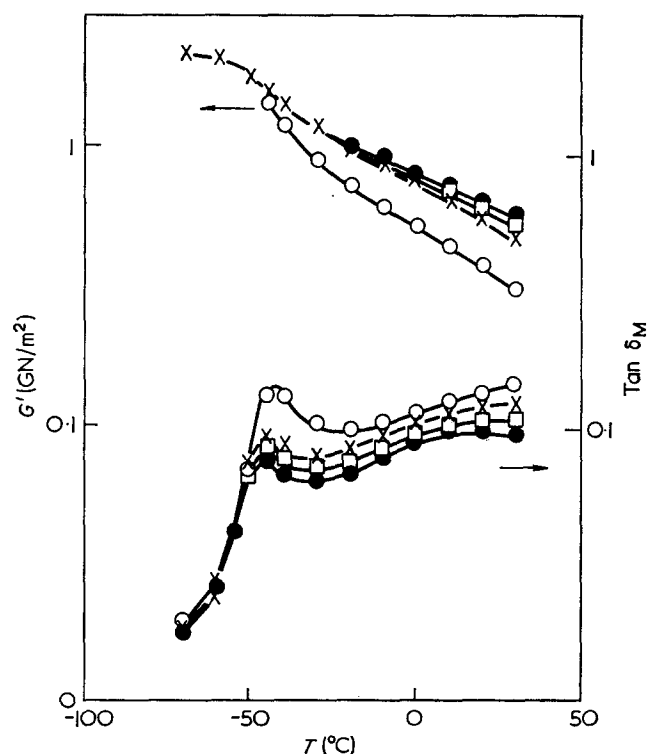


Figure 10 Shear modulus ( $G'$ ) and loss tangent ( $\tan \delta_M$ ) as functions of temperature ( $T$ ) for 80:20 PMMA/PU composites prepared with post-gelation periods of:  $\circ$ , 0h;  $\times$ , 12h;  $\square$ , 24h;  $\bullet$ , 48h



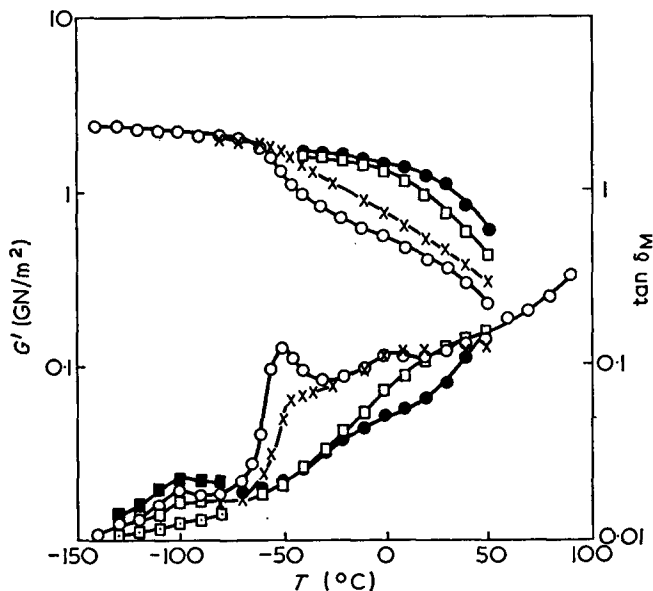


Figure 11 Shear modulus ( $G'$ ) and loss tangent ( $\tan \delta_M$ ) as functions of temperature ( $T$ ) for 80:20 PMMA/PU composites. PU theoretical  $\bar{M}_c$ :  $\circ$ , 4500;  $\times$ , 2250;  $\square$ , 1250;  $\bullet$ , 950. 4500  $\bar{M}_c$  sample vacuum dried ( $\square$ ) and wetted ( $\blacksquare$ )

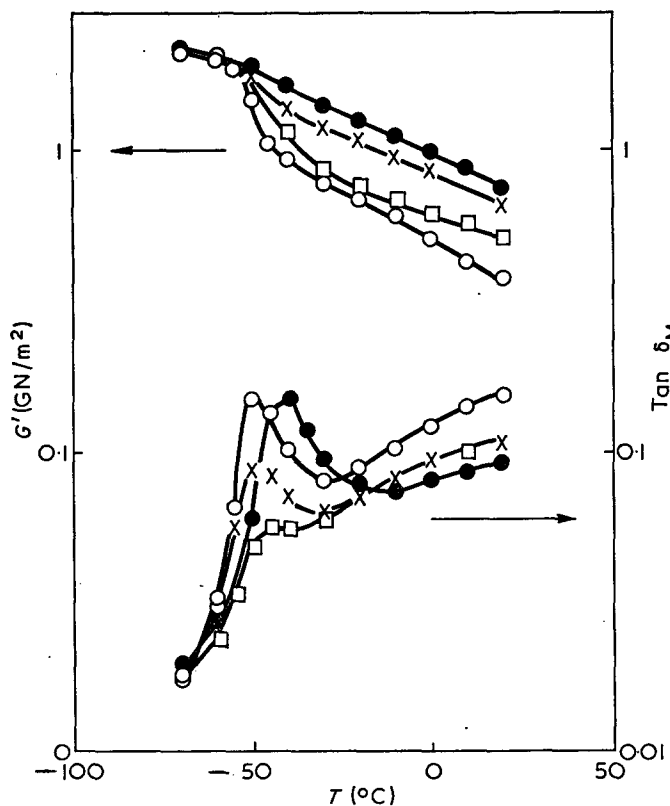


Figure 12 Shear modulus ( $G'$ ) and loss tangent ( $\tan \delta_M$ ) as function of temperature ( $T$ ) for 80:20 PMMA/PU composites. [NCO]/[OH] ratio:  $\circ$ , 0.9:1;  $\times$ , 1:1;  $\square$ , 1.2:1;  $\bullet$ , 1.4:1

show a reduction in the magnitude of the PMMA- $\beta$  loss peak. This is probably due to some of the ester groups being hindered by the highly polar PU molecules which will still be rigid at about 20°C when  $\bar{M}_c$  is of the order of 1000. In these composites the PMMA domains would be expected to be very small and hence the interaction between the polymer species will be large. The variation of impact strength with crosslink density of the PU, as reported in the first paper of this series, showed a distinct toughening as  $\bar{M}_c$  increases. This

correspondence suggests the importance of the size and definition of the PU- $\alpha$  process in the toughening of the composites.

The effect of the variation of the NCO/OH molar ratio upon the loss properties of the composites is shown in Figure 12 where  $G'$  and  $\tan \delta_M$  are plotted as functions of temperature for the samples of variable composition.

For the lowest and highest molar ratios, large well defined PU- $\alpha$  loss peaks and corresponding changes in  $G'$  are seen. For the samples prepared with the ratio nearer the stoichiometric amount the loss peaks and changes in  $G'$  are not so prominent. The results reported earlier<sup>1</sup> showed that the mechanical properties fell away at the extreme NCO/OH molar ratios. There is again a correlation with the domain sizes (Table 2), the large loss peaks at extreme NCO/OH molar ratios being associated with the larger domains and less interphase interaction. This is the only instance observed where an increase in molecular mobility, as detected by the sharpness and magnitude of the loss process, has been accompanied by a decrease in impact strength.

This effect can probably be attributed to the incomplete nature of the network. There will be a proportion of PU molecules which are not 'tied' to the network and will therefore be highly mobile and give rise to large loss peaks. The network will be more complete at the near stoichiometric ratios and the PU molecules will be less mobile and hence the loss peaks will be smaller. It would be expected that an incomplete network would not be very efficient at imparting toughness to the composite.

#### Variation of toughness with temperature

Figure 13 shows the variation of the toughness of the composites measured by the notched impact strength<sup>1</sup> as a function of temperature. Results are shown for PMMA, for a sample containing 30% w/w of PU of theoretical  $\bar{M}_c$  4500, and for a sample containing 30% w/w of PU of theoretical  $\bar{M}_c$  950. The notched impact strength ( $NIS$ ) of PMMA remains almost constant over the temperature range of the experiment and the PMMA- $\beta$  process imparts little toughness to the polymer.

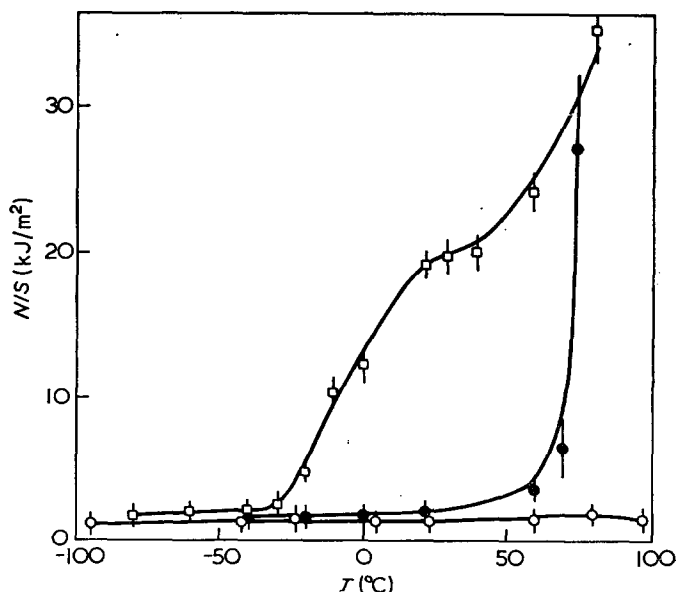


Figure 13 Charpy notched impact strength ( $NIS$ ) as a function of temperature ( $T$ ) for 100% PMMA ( $\circ$ ) and 70:30 PMMA/PU composites. PU theoretical  $\bar{M}_c$  4500 ( $\square$ ) and 950 ( $\bullet$ )

For the composite of the higher  $\bar{M}_c$  the onset of appreciable toughening occurs at about 0°C but does not coincide with the  $\tan \delta_M$  peak at -50°C, and agrees more closely with dielectric measurements of the PU- $\alpha$  peak at frequencies of about 1 kHz. This reinforces the view that there is a relation between toughening and main chain motions ( $\alpha$  processes).

The curve for the composite of low  $\bar{M}_c$  shows that when there is no distinct PU- $\alpha$  process at low temperatures, the material remains relatively brittle until well above room temperature. These results indicate that, for a polymeric material to be tough at room temperature, the presence of a low temperature loss process involving main chain motion is desirable.

## EXPERIMENTS WITH ELASTOMERS

### General elastic behaviour

The work on morphology emphasizes the importance of the gel structure of the PU in determining the size of the final PMMA domains. Experiments were therefore carried out to find how PU elastomers, gelled in MMA monomer, varied with amount of MMA present and in particular to find how they differed from a bulk cured PU made from the same constituents. PU elastomers were therefore gelled in various inhibited MMA solutions and then dried down to obtain the 100% elastomer. It was hoped that these dried down elastomers would be representative of the gel network in which the monomer is usually polymerized to make a composite. Corresponding elastomers were also cured in the bulk. All the elastomers were made from equal quantities of OPG-3000 and PPG-2000 crosslinked with MDI so that  $[\text{NCO}]/[\text{OH}] = 1.1:1$ .

The final rubbers were tested in simple elongation. Unfortunately, whereas gelled elastomers could be tested up to 100% strains, the bulk cured elastomers fractured at strains below 20%. For a complete comparison of all elastomers it was therefore decided to examine the initial elongation behaviour using the predictions of the simple statistical theory of elasticity<sup>16</sup>:

$$f = \frac{\langle r_i^2 \rangle}{\langle r_0^2 \rangle} \rho \frac{RT}{M_c} (\alpha - \alpha^{-2}) \quad (1)$$

where  $f$  is the equilibrium force per unit area of undeformed sample:  $\alpha$  is the extension ratio of extended length over original length:  $\rho$  is the density of chains actively contributing to the entropic force;  $M_c$  is the molecular weight of active chains between crosslinks and ideally should equal  $\bar{M}_c$ , which is calculated from the chemical formula:  $\langle r_i^2 \rangle / \langle r_0^2 \rangle$  is the so-called front factor<sup>17</sup> being the ratio of mean square lengths between chain ends in the undeformed sample and in the unperturbed reference state. For simplicity it was assumed that in the bulk elastomers  $r_i = r_0$ . For solution gelled elastomers it was assumed, following Price *et al.*<sup>18</sup> that  $\langle r_i^2 \rangle / \langle r_0^2 \rangle = \phi^{2/3}$ , where  $\phi$  is the volume fraction of the PU in the gel. In the limit for small extensions, equation (1) then simplifies to give Young's modulus:

$$Y = \frac{3\rho RT}{M_c} \phi^{2/3} \quad (2)$$

Table 4 summarizes the results of the experiments. The second column gives the mean initial moduli for each weight fraction of PU in the original gel. The third

Table 4 Results of simple elongation tests on PU elastomers

Weight fraction of PU in original gel	Initial modulus (MN/m <sup>2</sup> )	$M_c$ calculated from equation (2)
0.2	0.252	9800
0.3	0.373	8800
0.35	0.568	6400
0.4	0.450	8800
0.5	0.752	6200
1.0 (bulk rubber)	1.55	4900

column gives the values of  $M_c$  calculated from equation (2) taking  $\rho$  to be the bulk density of the elastomers (i.e. assuming that all chains actively contribute to the elasticity).

The modulus falls by a factor of about 6 when  $\phi$  is reduced from 1 to 0.2. Some of this will be due to the supercoiling of the chains resulting from drying off the MMA. In principle it should be possible to correct for this effect with the front factor in equation (2). The calculated  $M_c$  for the bulk elastomer agrees well with the theoretical  $\bar{M}_c$  of 4500, which is calculated from chemical formula. However, despite the use of the front factor, the calculated  $M_c$  still changes by a factor of about 2 when  $\phi$  is decreased to 0.2. Supercoiling cannot therefore account for all of the drop in modulus. A similar decrease in modulus with dilution was observed by Shen and Tobolsky<sup>19</sup> in their work on crosslinked acrylate elastomers. They attributed the effect to a decrease in physical entanglements at the higher dilutions. Whatever the true explanation it is clear from the initial modulus that there is an increase in the overall looseness of the network structures as the amount of MMA present at the gelation is increased.

In the region of larger strains ( $1.1 < \alpha < 2$ ) where our bulk PU could not be tested, the solution gelled elastomers were found to follow the Mooney-Rivlin type of relation:

$$f = C_1(\alpha - \alpha^{-2}) + C_2(1 - \alpha^{-3})$$

where  $C_1$  and  $C_2$  were constants for each elastomer. No obvious systematic trend was found in the relation between  $C_1$  and  $C_2$  for different elastomers. Typically  $C_2/C_1$  lay in the range 0.3 to 1.0. The value of  $C_1$  qualitatively followed the modulus observed for small strains. It is instructive to compare these observations for solution gelled PU with the findings of Blockland and Prins<sup>20</sup> for similar bulk cured PU. Chemically the polyurethanes of Blockland and Prins were essentially identical except that the MDI was replaced by toluene diisocyanate. All their bulk elastomers could be fitted to a Mooney-Rivlin relation in which  $C_2/C_1$  was typically in the range 0.3 to 0.5. The behaviour of solution gelled PU is therefore very similar to bulk cured PU except that their moduli are lower than the bulk PU. This is in marked contrast to recent observations of Price *et al.*<sup>18</sup> on natural rubbers. Whereas bulk vulcanized rubber usually gives  $C_2/C_1 \approx 3$ , Price *et al.* found that rubbers vulcanized in solution gave vanishingly small  $C_2$  terms. They associated the  $C_2$  term with physical entanglements and proposed that the diluent affected topology in such a way that the entanglements are reduced. Although similar topological effects could still be present, it is apparent that for the present solution gelled PU there are probably other factors contributing to the  $C_2$  term. In their paper on

bulk PU, Blockland and Prins associated their  $C_2$  term with a polar coupling of the urethane segments which gives rise to bundles within which the chains are not free to execute random walks. They give evidence for such structures from electron microscopy and light scattering and show that the observed elastic behaviour can be accounted for theoretically if 5% of the segments in each chain are involved in such bundle structures. It is presumed that similar polar couplings can be invoked to explain the  $C_2$  terms in the present solution gelled PU.

In addition to structure associated with specific polar interactions, other network imperfections can exist. These can range from defects at a molecular level such as unreacted free chains and closed loops, to large scale inhomogeneities in crosslink density. Such network defects are fully discussed by Dusek and Prins<sup>21</sup>. The presence of a diluent and the possibility of polar groupings could both encourage the formation of defects and inhomogeneities. It is the existence of these imperfections that most likely accounts for part of the increase in looseness of the network structure as  $\phi$  is decreased.

In the final swollen gel, bundle-like structures and inhomogeneities in crosslink density will be associated with corresponding fluctuations in the concentration of MMA monomer. It is tempting to speculate that in the preparation of normal PMMA/PU composites, it is those regions in the swollen gel that have low crosslink density and which are richer in monomer that will form the nucleation sites for the subsequent PMMA domains, and consequently control the final domain size.

#### Composites from swollen elastomers

This section describes the composites made from pre-existing PU elastomers by the method of swelling the elastomers with MMA monomer and then polymerizing in the swollen network. By varying the gelling conditions of the elastomers one can explore the connection between the structure of the precursor swollen gel and the domain morphology of the final composite. Use was made of both the bulk cured and the solution gelled elastomers that were discussed in the previous section.

The trends observed in the experiments are well illustrated by the results of the selected composites shown in Table 5. The first three composites were all made from the same dried down solution gelled elastomer. The fourth composite was made by swelling a bulk cured elastomer. The figures in parentheses in Table 5 are typical of those obtained from normal composites of corresponding composition.

All of the first three composites showed the normal domain morphology. For the 80:20 PMMA/PU composite, the domain size and mechanical properties are very

Table 5 Results for composites made from swollen elastomers

Sample	% of PMMA in final composite	% of MMA in original gel	$\bar{L}$ (nm)	$NIS$ (kJ/m <sup>2</sup> )	$G'$ (GN/m <sup>2</sup> )
1	90	80	55 ( $> 200$ )	2.0 (4.2)	0.97 (1.02)
2	80	80	60 (65)	9.4 (11.9)	0.65 (0.63)
3	70	80	65 (52)	Too soft (13.3)	0.036 (0.40)
4	70	bulk rubber	—	4.8 (13.3)	0.37 (0.40)

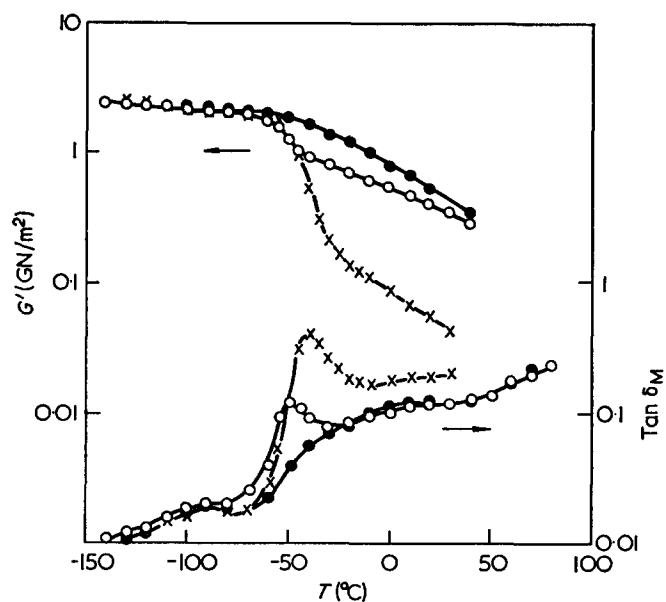


Figure 14 Shear modulus ( $G'$ ) and loss tangent ( $\tan \delta_M$ ) as functions of temperature ( $T$ ) for composites containing 70:30 PMMA/PU composites.  $\circ$ , Normal composite;  $\times$ , composite prepared from solution gelled PU;  $\bullet$ , composite prepared from bulk PU

close to those obtained from normal 80:20 PMMA/PU. This shows that the experimental processes of drying down the original swollen gel and of re-swelling with fresh monomer do not, in themselves, introduce any important artefacts.

The most striking feature of the morphological results is that for the same original rubber, the domain size becomes almost independent of the final PMMA content. This contrasts with the marked increase of  $\bar{L}$  with PMMA content in normal composites. In other similar experiments it has also been found that the value of  $\bar{L}$  obtained depends on the gelation conditions of the original elastomer and is usually very close to the value obtained from a normal composite made directly from the same gelation conditions. Thus if less MMA monomer is present during the gelation of the original elastomer so that a tighter network is formed, the domain sizes obtained after re-swelling the elastomer are smaller. These observations confirm the notion that the domain size in a composite depends on a structure in the swollen gel which is in turn determined by the conditions of gelation.

With composites made by swelling bulk cured elastomers, the morphology could not be determined with any certainty. However, there are strong indications from  $\tan \delta_M$  studies of swollen bulk elastomer composites that separate phases still exist. It is assumed therefore that the lack of structural detail in the electron microscope results from the inability of the PU to deform during sectioning due to hindrance of molecules from interacting PMMA chains.

Direct evidence of the molecular interactions in swollen elastomer composites is shown in the dynamic mechanical results in Figure 14. The results are for the third and fourth composites shown in Table 5. Curves for a typical normal composite containing 70% PMMA are also shown. The  $\tan \delta_M$  plot for the normal composite shows the usual PU- $\beta$  process at  $-90^\circ\text{C}$ , the PU- $\alpha$  process near  $-50^\circ\text{C}$  and the broad PMMA- $\beta$  process centred around  $20^\circ\text{C}$ . The  $G'$  plot is similar to that in Figure 6, the most distinct feature being the sharp drop in  $G'$

associated with the PU- $\alpha$  process. In the composite made from the swollen bulk elastomer, the important PU- $\alpha$  process is almost totally absent, whereas in the composite made from the 80% MMA solution gelled elastomer, the  $\tan \delta_M$  peak is much more pronounced than in the normal composite. This indicates that in comparison with the normal 70% PMMA composite, the interactions between PMMA and PU chains are more pronounced in the composite based on the bulk cured elastomer and less so in the composite from the 80% MMA solution gel. In view of the lack of electron microscope evidence, the absence of a  $\tan \delta_M$  peak in the bulk elastomer composite could be taken as evidence of a completely interpenetrating molecular network. However, when a 60% PMMA composite was made from the same bulk elastomer, a definite  $\tan \delta_M$  peak was observed indicating the presence of a distinct PU phase. It is presumed therefore that the large interaction in the 70% PMMA bulk elastomer composite should be associated with a very small domain structure with a correspondingly large specific interphase surface area. This interpretation would then be consistent with the general observed trend that when the pre-existing elastomer network is tighter, the resulting domains in the composite are smaller and the degree of molecular interaction between PMMA and PU is larger.

The variations in the PU motions are also reflected in the values of impact strength shown in *Table 5*. Although slightly lower, the *NIS* of sample 2 is similar to that of a typical normal 80:20 PMMA/PU composite. However, a normal 80:20 PMMA/PU composite has a far lower *NIS* than sample 3, which is made from the looser 80% MMA solution elastomer, but a higher *NIS* than sample 4, which is made from the tighter bulk elastomer. In these cases an increase in impact strength is seen to be accompanied in *Figure 14* by a sharpening of the PU- $\alpha$  process in the  $\tan \delta_M$  plot. In a similar way, a normally prepared 90:10 PMMA/PU composite is seen to have a higher *NIS* than sample 1 which is made from the relatively tighter 80% MMA solution elastomer. This agrees with the principle that a better impact strength is usually associated with a more well-defined PU- $\alpha$  process.

Except for sample 3, the room temperature shear moduli in *Table 5* do not differ significantly from the typical values of normal composites. It can be seen from *Figure 14* that the extremely low value of 37 MN/m<sup>2</sup> for sample 3 is related to the large drop in  $G'$  and the correspondingly sharp peak of  $\tan \delta_M$  associated with the PU- $\alpha$  process. This observation suggests that high values of modulus are usually attained in normal composites as a result of a certain amount of hindrance to the PU chains which will restrict the drop in  $G'$  in the region of the PU- $\alpha$  process. It also suggests an important principle that if samples are to be produced by the interstitial polymerization method, then a high modulus can only be attained if the structure of the gel is tight enough to limit the size of the domains so as to produce the required molecular interactions and hindrances.

## CONCLUSIONS

Electron microscopy shows that to a first approximation the morphology of the interstitial composites consists of spherical domains of PMMA closely packed and embedded in a continuous matrix of PU. The existence of the two distinct phases is confirmed by the observation

in the loss measurements of the two independent  $T_g$  processes of PMMA and PU respectively. However, the activation energy and shift in position of the PU- $\alpha$  process from that normally seen in bulk PU indicates an interaction between the PMMA and PU chains. This interaction probably occurs at the phase boundaries and suggests a region of transition between phases at the domain boundaries.

For a given PMMA/PU composition, the mean domain size is found to be independent of factors connected with the vinyl polymerization but very sensitive to the physical condition and molecular details of the PU gel at the time when the vinyl polymerization occurs. If the gel is 'loose', whether this is due to a molecular detail such as the choice of  $\bar{M}_c$  of the PU, or whether it is due to incompleteness of the gelation reaction, then the final domain size is larger than the domain size from a 'tight' network. If the parameters directly affecting the PU gel are kept constant, there is marked variation of domain size with composition, the domain size being large for the higher PMMA content. The observations on the PU elastomers gelled in solution under identical conditions to the gelation in the preparation of composites show that the network structure varies with the amount of MMA monomer present and is in fact looser when the amount of MMA is higher. This indicates that the variation of domain size with composition is probably due to variations in the tightness of the gel structure. This basic relation between the tightness of the swollen gel and the final domain size is confirmed directly with the composites made by swelling various pre-existing elastomers with monomer.

For a given composition there is always a good correlation between the domain size and the definition and size of the  $\tan \delta_M$  peak associated with the PU- $\alpha$  process, the peak being sharper whenever the domain size is larger. Since a broadening of the loss peak can be associated with an increase in molecular interaction between PMMA and PU, and also since the domain size is inversely proportional to the specific interphase surface, the observed correlation is consistent with a decrease in molecular interaction at the phase boundaries as the domain size increases.

It has already been noted<sup>1</sup> that in common with other rubber-modified plastics, the impact strength of the composites increases with the amount of rubber present. The comparison between impact strength and loss properties for varying values of the  $\bar{M}_c$  of the PU has shown that the rubber can only impart significant toughening against the standard impact test if the  $T_g$  of the PU is below about  $-30^\circ\text{C}$ . If the PMMA/PU composition and the theoretical  $\bar{M}_c$  are kept constant, the correlation between the mechanical strength properties discussed in Part 1 and the loss characteristics and morphology discussed in the present paper become more tenuous. However, two important trends emerge which are particularly well demonstrated by the swollen elastomer composites but which are also seen to a lesser extent in the normal composites. The first is that whenever there is an increase in the mobility of the rubber as judged by the sharpness of the PU- $\alpha$  process, there is also a tendency for a corresponding increase in impact strength. This does not necessarily mean that the energy absorption processes of the PU are in themselves responsible for the toughness, but rather that the toughening mechanism of the composites is more efficient when the

rubber is in a more mobile condition. The important exception to this correlation is the effect of varying the NCO/OH stoichiometry, where lower impact strengths were observed together with sharp loss peaks in either of the extreme stoichiometry cases. The poor impact properties in these instances are probably associated with the inefficient linking of the PU and shows that the toughening mechanism also requires completeness and good cohesion in the final rubber network.

The second important trend concerns the fall in the real part of the modulus which accompanies the PU- $\alpha$  loss process and which results in the room temperature modulus being lower whenever the loss peak is sharper. In terms of the structure of the interstitial system this means that an increase in modulus can be obtained by increasing the interaction between phases. Thus the balance in properties between stiffness and high impact strength can only be achieved with a certain compromise in how the structure is formed. For a better room temperature modulus, a tighter initial gel network is needed so that smaller domains will form and greater interaction will occur between phases. On the other hand, for improved impact properties a looser initial gel structure is needed so that larger domains will grow and there will be less interaction. In the normal composite system in which the gel is made *in situ* from polyols in solution, a reasonable compromise in gel structure seems to be made automatically by the solution gelling process. When, however, the swollen preformed elastomers are used, better control over the tightness of the elastomer is needed in order to produce balanced properties.

It will be noted that the morphology of these composites is essentially identical to the internal morphology of the embedded rubber modifying particles that are normally employed in high impact polystyrenes and acrylonitrile-butadiene-styrene resins<sup>22</sup>. In these other systems it is currently believed<sup>23</sup> that the main mechanism of toughening from the particles is one involving craze initiation in the surrounding glassy matrix polymer. The present work shows that the domain type morphology has a toughening mechanism of its own which could play an important additional role in the impact resistance of these other materials. However, the actual mechanisms

of toughening and stress whitening in the interstitial domain structure are not yet known and are presently under further investigation.

#### ACKNOWLEDGEMENTS

One of us (M.J.B.) is grateful to Imperial Chemical Industries Ltd, and later to the University of Queensland for the award of successive Post Doctoral Fellowships.

#### REFERENCES

- 1 Allen, G., Bowden, M. J., Blundell, D. J., Hutchinson, F. G., Jeffs, G. M. and Vyvoda, J. *Polymer* 1973, **14**, 597
- 2 Blundell, D. J., Longman, G. W., Wignall, G. D. and Bowden, M. J. *Polymer* 1974, **15**, in press
- 3 Allen, G., Bowden, M. J., Lewis, G., Blundell, D. J. and Jeffs, G. M. *Polymer* 1974, **15**, in press
- 4 Spit, B. J. *Polymer*, 1963, **4**, 109
- 5 Kato, K. *Polym. Eng. Sci.* 1967, **7**, 38
- 6 ASTM D2236-67T, Am. Soc. Test. Mat., Philadelphia
- 7 Underwood, E. E. 'Quantitative Stereology', Addison-Wesley, Reading, Massachusetts, 1970
- 8 Debye, P., Anderson, H. R. Jr. and Brumberger, H. *J. Appl. Phys.* 1957, **28**, 679
- 9 Saito, S. and Nakajima, T. *J. Appl. Polym. Sci.* 1959, **2**, 93
- 10 Mikhailov, G. P. and Borisova, T. I. *Sov. Phys. Tech. Phys.* 1958, **3**, 249
- 11 Deutsch, K., Hoff, E. A. W. and Reddish, W. J. *J. Polym. Sci.* 1954, **13**, 565
- 12 McCrum, N. G., Read, B. E. and Williams, G. 'Anelastic and Dielectric Effects in Polymeric Solids', Wiley, New York, 1967, p 247
- 13 Sall, W. G. and McCrum, N. G. *J. Polym. Sci.* 1961, **50**, 489
- 14 Allen, G., Bowden, M. J., Lewis, G., Blundell, D. J., Jeffs, G. M. and Vyvoda, J. *Polymer* 1974, **15**, in press
- 15 Allen, G., McAinsh, J. and Jeffs, G. M. *Polymer* 1971, **12**, 85
- 16 Flory, P. J. *Trans. Faraday Soc.* 1961, **57**, 829
- 17 Tobolsky, A. V., Carlsen, D. W. and Indictor, N. *J. Polym. Sci.* 1961, **54**, 175
- 18 Price, C., Allen, G., de Candia, F., Kirkham, M. C. and Subramanian, A. *Polymer* 1970, **11**, 486
- 19 Shen, M. C. and Tobolsky, A. V. *J. Polym. Sci. (A)* 1964, **2**, 2513
- 20 Blockland, R. and Prins, W. *J. Polym. Sci. (A-2)* 1969, **7**, 1595
- 21 Dusek, K. and Prins, W. *Adv. Polym. Sci.* 1969, **6**, 1
- 22 Matsuo, M., Nozaki, C. and Jyo, Y. *Polym. Eng. Sci.* 1969, **9**, 197
- 23 Kambour, R. P. *Appl. Polym. Symp.* 1968, **7**, 215

# Effect of hydrostatic pressure and temperature on the mechanical loss properties of polymers: 1. Polyethylene and polypropylene

E. Jones Parry and D. Tabor

*Physics and Chemistry of Solids, Cavendish Laboratory, University of Cambridge, Cambridge CB3 0HE, UK*

*(Received 16 April 1973; revised 1 August 1973)*

A torsion pendulum ( $\sim 1$ Hz) has been used to investigate the shear modulus and loss tangent of a number of hydrocarbon polymers as a function of temperature at pressures of up to 1200 atmospheres. Low density polyethylene (LDPE), high density polyethylene (HDPE), polypropylene (PP), a natural rubber and an ethylene-vinyl acetate copolymer have been studied. The results show that the relaxation temperatures are increased by the application of hydrostatic pressure, by amounts which range between about 5 and 20°C per 1000 atmospheres. However, it has only proved possible to correlate our results with theory in the case of PP because of the lack of other data, in particular the appropriate compressibility and thermal expansion coefficients. The results also show that if the crystallinity of LDPE and PP is reduced the  $\alpha$  relaxations are resolvable into two distinct processes.

## INTRODUCTION

Most previous studies on the viscoelastic properties of polymers have been concerned with the effect of temperature and rate (or frequency) of deformation. Since the dissipative process is known to involve the movement of chain segments or groups, the amount of free volume available must be an important factor. Consequently hydrostatic pressure should have a significant effect on viscoelastic behaviour. While some work has been carried out on dielectric loss as a function of hydrostatic pressure, only one previous paper has been published on the way in which mechanical loss varies with the application of hydrostatic pressure<sup>1</sup>. The present work is an extension of earlier investigations in this laboratory by Billingham and Tabor<sup>2</sup>. This paper deals with various hydrocarbon polymers, Part 2 with halogenated polymers and Part 3 with further polymers and copolymers.

We present first a brief account of theoretical relations which have been derived for the effect of pressure on the glass transition temperature. All these theories involve the compressibility and thermal expansion of the free volume itself. Unfortunately there are very little data available so that a direct comparison with experiment has only been possible for a few polymers. In some cases we have also attempted to discuss qualitatively the observed effect of pressure in terms of possible relaxation processes. These papers are essentially experimental in character and provide direct measurements of the effect of pressure on relaxation temperatures.

## EFFECT OF PRESSURE ON THE GLASS TRANSITION

A simple qualitative approach to the effect of pressure on the glass transition is to assume that the transition,

which involves widespread movement of the polymer chain, is associated with the availability of adequate free volume. If pressure is applied the free volume is reduced. Consequently to increase the free volume the temperature must be raised. Assuming that the glass transition occurs at a constant free volume it is evident that the shift in transition temperature with pressure will depend on the ratio of the compressibility  $\beta$  to the thermal expansion  $\alpha$ . More precisely these quantities should refer to the compressibility  $\Delta\beta$  and thermal expansion coefficient  $\Delta\alpha$  of the free volume itself, where  $\Delta\beta$  is defined as  $\beta_l - \beta_g$  and  $\Delta\alpha$  as  $\alpha_l - \alpha_g$ , the subscripts  $l$  and  $g$  referring to the liquid and glassy states respectively. We may therefore write<sup>1</sup>:

$$\frac{dT_g}{dP} = \frac{\Delta\beta}{\Delta\alpha} \quad (1)$$

A similar relation has been derived using thermodynamic arguments by Gee<sup>3</sup>. His basic assumption is that the glassy state is unchanged by pressure. This appears to be equivalent to the assumption that the free volume at the  $T_g$  is constant (see also Gee *et al.*<sup>3</sup>).

However, as Breuer and Rehage<sup>4</sup> have shown in the case of polystyrene the volume (and presumably the free volume) at the  $T_g$  is not constant but decreases somewhat at high pressures. There is indeed increasing evidence that a given volume change produced by temperature does not have the same effect on polymer properties as the same volume change produced by pressure<sup>5</sup>. Thus Bianchi<sup>6</sup> has shown that for PVC and poly(vinyl acetate) the glass is densified by the application of pressure above  $T_g$ . Assuming that  $\alpha_g$  contains a part that is due to an overall increase in molecular spacing that does not become available as free volume,  $\Delta\alpha$  is actually larger than that given by the definition

$\alpha_l - \alpha_g$ . Bianchi obtains a relation:

$$\frac{dT_g}{dP} = \frac{\Delta\beta}{\Delta\alpha + A}$$

where  $A$  is a term to allow for this inaccessible part of the volume. Again in their study of the shear strength of polymers, Baer *et al.*<sup>5</sup> observe that, for a given volume change, temperature has a larger effect than pressure. Baer uses a compensating factor to obtain 'true' iso-volume conditions and writes:

$$\frac{d(\text{strength})}{dP} = \gamma \cdot \frac{\Delta\beta}{\Delta\alpha}$$

where  $\gamma$  is a constant of the order of  $\frac{1}{2}$  to  $\frac{1}{3}$ .

Our own work suggests that the  $T_g$  is *not* determined simply by a constant free volume. If an applied pressure reduces the free volume a temperature rise sufficient to restore the free volume to its original value will in addition provide the polymer with more thermal energy. Thus we do not require to restore the free volume fully to its original value since the additional thermal energy will also contribute its part to the transition. A very simple model suggests a relation of the type:

$$\frac{dT_g}{dP} = \frac{\Delta\beta}{\Delta\alpha + Q/RT_g^2}$$

where  $Q$  is of the order of 1 kcal/mol. This is similar in form to Bianchi's equation but its physical basis is different.

We may therefore expect equation (1) to provide only a rough value of  $dT_g/dP$ : the observed result should be of the same order but smaller. In the few cases where such a comparison is possible we do, in fact, find that  $dT_g/dP$  is smaller than the theoretical value.

A different approach has been described by Goldstein<sup>7</sup>. He assumes that the glass transition occurs either under conditions of constant entropy change, or under conditions of constant enthalpy change: in both cases he obtains a relation:

$$\frac{dT_g}{dP} = TV \frac{\Delta\alpha}{\Delta C_p}$$

where  $\Delta C_p$  is the change in specific heat at constant pressure. In Parts 2 and 3 we are able to compare this with the observed results.

There appears to be no theory for the effect of pressure on other relaxations.

## EXPERIMENTAL

### Procedure

A torsion pendulum was constructed to function within a high pressure vessel as has been previously described<sup>8</sup>. The pendulum ( $\sim 1$  Hz) could be used to study the shear modulus,  $G'$ , and loss tangent,  $\tan \delta$ , of polymers as a function of temperature and hydrostatic pressure. The temperature range was  $-30^\circ\text{C}$  to  $+140^\circ\text{C}$  and the maximum gas pressure applied was 1400 atmospheres [ $1 \text{ atm} \equiv 101.33 \text{ kN/m}^2$ ]. The polymer samples used were shaped like tensile specimens and were 7 cm long, 0.5 cm wide, and about 0.1 cm thick. They were normally only subjected to a 0.5% strain and seldom more than 1% so that for cyclic deformation the behaviour may be considered to be within the linear viscoelastic regime. The error in  $G'$  was about 3% and that in  $\tan \delta$  about

5%. However, at temperatures below  $-10^\circ\text{C}$  the errors in  $\tan \delta$  increased rapidly and small changes below this temperature are generally unreliable.

Bianchi<sup>5</sup> has shown that the experimental path can critically affect the magnitude of the shift of the glass transition temperature with pressure. For this reason a standard procedure was used in all cases. The polymer was placed in position and the required pressure was applied to the containing vessel at room temperature. After leaving for about 1 h the temperature was varied at a rate of  $0.7^\circ\text{C}/\text{min}$  and the pressure only released when the polymer was again at room temperature. In most cases experiments at different pressures were carried out on different specimens which had been prepared from the same sheet, and all were carried out with temperature increasing. The experiments were reproducible to within 2%.

### Materials

The low density polyethylene (LDPE) used in our investigations was Alkathene WNC 71 of density  $0.917 \text{ g/cm}^3$ . The specimens were milled from a sheet which had been compression moulded at  $160^\circ\text{C}$  and  $60 \text{ kg/cm}^2$  and then cooled under pressure to room temperature over 8 h. Some prepared samples were placed in a glass tube which was then evacuated and subjected to 70 Mrad of radiation from a  $^{60}\text{Co}$  source of energy 6000 Ci. The density of these irradiated samples was measured as  $0.900 \text{ g/cm}^3$ . The high density poly-

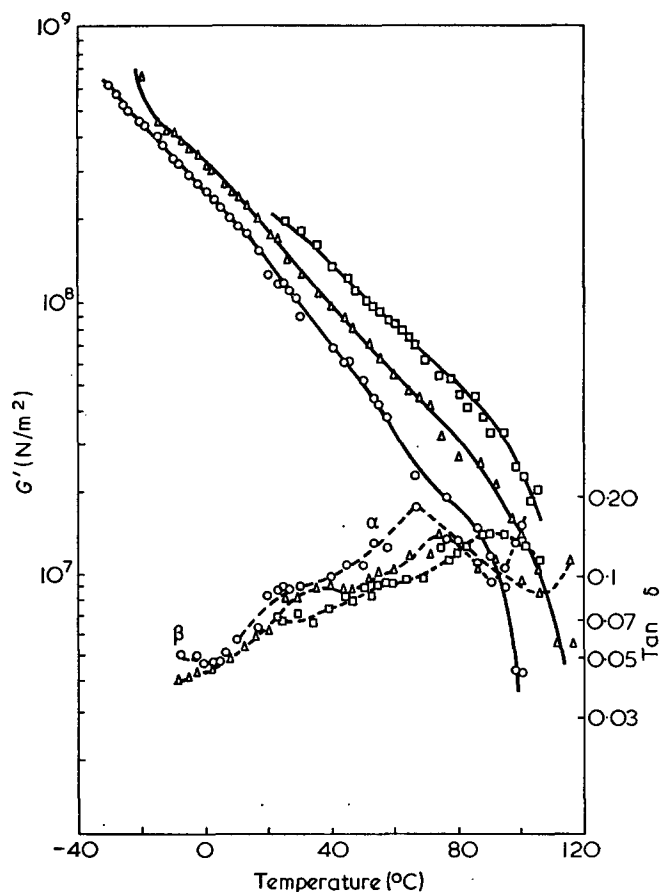


Figure 1 Temperature dependence of shear modulus (—) and loss tangent,  $\tan \delta$  (---) for low density polyethylene. The results are for pressures of 1 (O), 610 ( $\Delta$ ) and 1220 ( $\square$ ) atm. It is seen that the peaks corresponding to the  $\alpha$  relaxation are displaced to a higher temperature by the application of pressure. In general loss peaks show no systematic change in height with pressure

ethylene (HDPE) was Marlex 6001 of density  $0.960 \text{ g/cm}^3$ . Samples were prepared from a sheet which had been compression moulded at  $180^\circ\text{C}$  and  $60 \text{ kg/cm}^2$  and then slowly cooled under pressure. The polypropylene (PP) samples were milled from an extrusion moulded medium crystallinity sheet of density  $0.905 \text{ g/cm}^3$ . As in the case of LDPE some of the samples were exposed to 50 Mrad of radiation. The ethylene-vinyl acetate copolymer sample was prepared from a compression moulded sheet of 36% crystallinity and 18% acetate content. The natural rubber sample was cut from a sheet which had been cured for 20 min at  $151^\circ\text{C}$  and which was made up of 100 parts by weight of smoked sheet, 2 parts by weight of dicumyl peroxide and 1 part by weight of phenyl- $\beta$ -naphthylamine.

## RESULTS

Figure 1 shows plots of  $G'$  and  $\tan \delta$  against temperature at three pressures for LDPE. The  $\beta$  relaxation appears in the temperature range of low sensitivity. On the other hand, the  $\alpha$  relaxation is clearly non-linearly displaced to higher temperatures. Similar graphs are shown in Figure 2 for the irradiated low density sample.

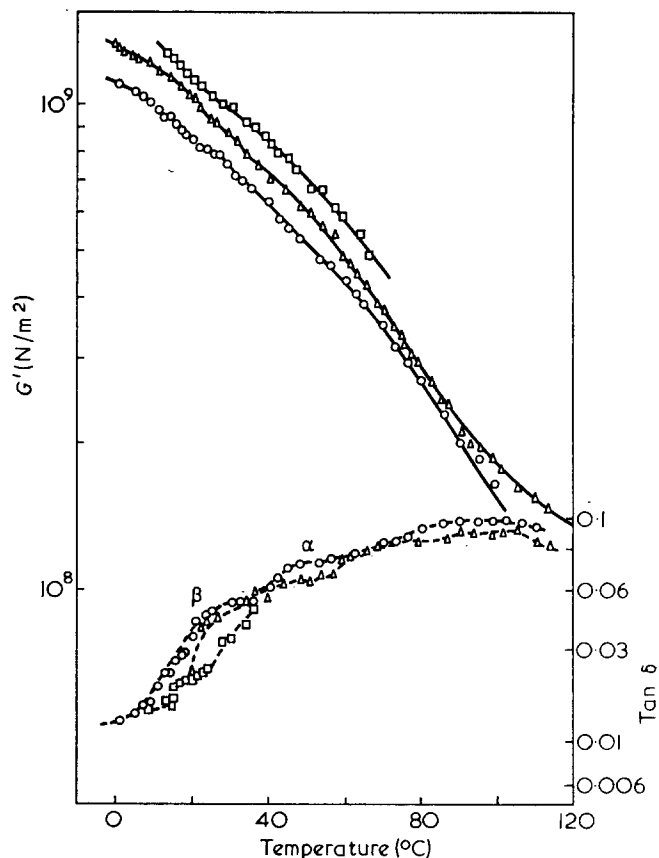


Figure 3 Temperature dependence of shear modulus (—) and loss tangent,  $\tan \delta$  (---) for high density polyethylene. The results are for pressures of 1 (○), 610 (△) and 1220 (□) atm. It is seen that the peaks corresponding to the  $\alpha$  and  $\beta$  relaxations are displaced to a higher temperature by the application of pressure

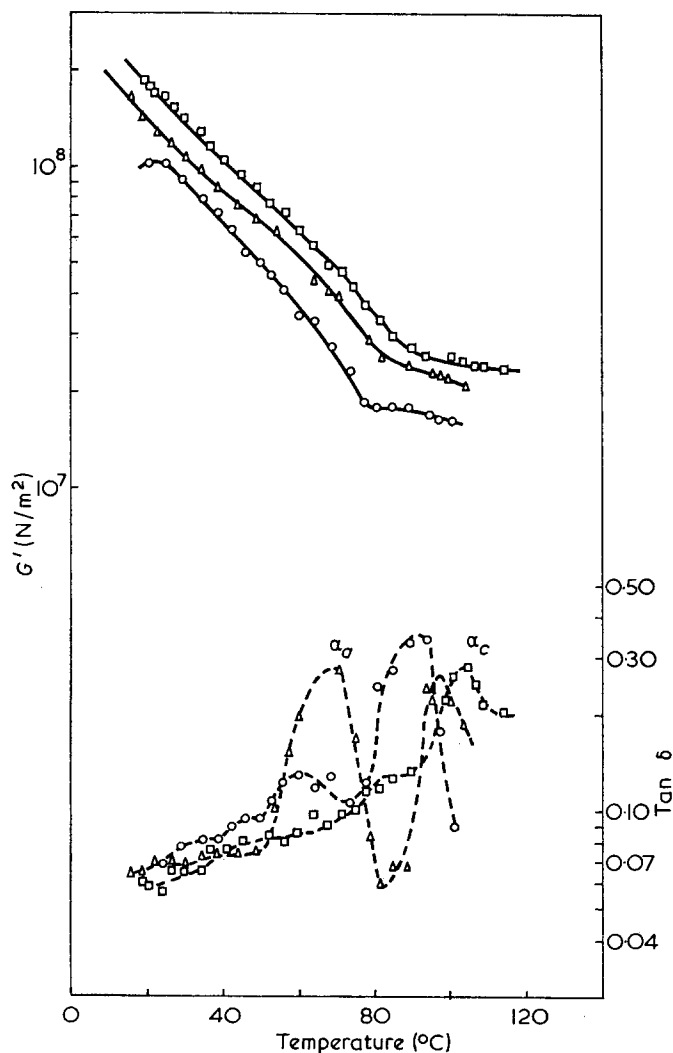


Figure 2 Temperature dependence of shear modulus (—) and loss tangent,  $\tan \delta$  (---) for irradiated low density polyethylene. The results are for pressures of 1 (○), 610 (△) and 1220 (□) atm. It is seen that the  $\alpha$  peak is split into two and that both the  $\alpha_a$  and  $\alpha_c$  peaks are displaced to a higher temperature by the application of pressure

It is seen that modulus is reduced by irradiation over the whole range of temperature and pressure, the reduction being least at atmospheric pressure but increasing with applied pressure for a given temperature. The density measurements confirm that this is due to the destruction of crystallites which lowers the modulus far more than any crosslinking increases it. In the irradiated sample the  $\alpha$  relaxation is split into two relaxations which are designated  $\alpha_a$  and  $\alpha_c$ : if merged these would correspond to the  $\alpha$  relaxation of the natural LDPE. The magnitudes of these relaxations are greater than that of the original  $\alpha$  relaxation. The  $\alpha_c$  relation is displaced linearly with pressure while the  $\alpha_a$  relaxation is displaced more at the higher pressure. These features are discussed later.

The results for HDPE are shown in Figure 3. Around  $15^\circ\text{C}$  small humps are observed in the  $\tan \delta$  curve. They are comparable with the experimental error and we tentatively identify them with the  $\beta$  relaxation which appears to be displaced by pressure. The  $\alpha$  relaxation is also poorly defined but again appears to be displaced from  $50^\circ$  to  $60^\circ\text{C}$  by the application of pressure of 610 atm.

The behaviour of PP is shown in Figure 4 and it is seen that there are two very clearly defined relaxations around  $0^\circ$  and  $80^\circ\text{C}$ . Earlier work by Flocke<sup>9</sup> on loss properties at atmospheric pressure has shown that the  $\beta$  relaxation increases in magnitude with decreasing crystallinity and he ascribes the relaxation to the glass-rubber transition. Our own measurements show that at atmospheric pressure and 1 Hz the  $\beta$  relaxation of PP occurs at  $2^\circ\text{C}$  and is displaced non-linearly upwards by



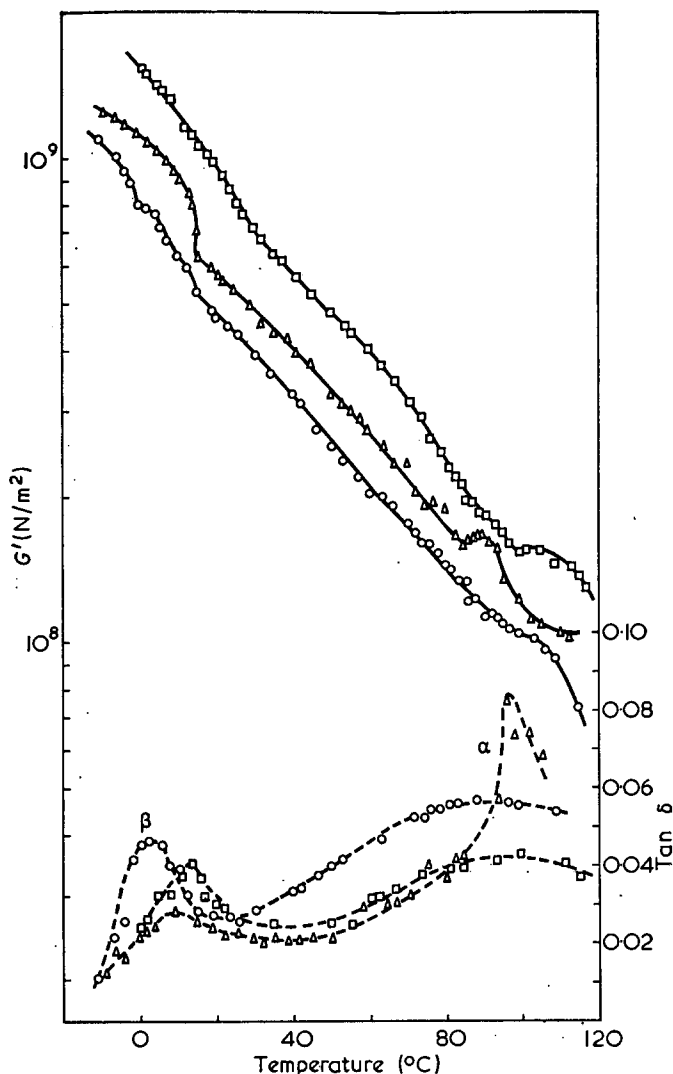


Figure 4 Temperature dependence of shear modulus (—) and loss tangent,  $\tan \delta$  (---) for polypropylene. The results are for pressures of 1 (O), 610 ( $\Delta$ ) and 1220 ( $\square$ ) atm. It is seen that the peaks corresponding to the  $\alpha$  and  $\beta$  relaxations are displaced to higher temperatures by the application of pressure

the application of pressure. The shift is greatest over the low pressure increment. The  $\alpha$  relaxation is linearly displaced by the applied pressure at a rate of  $5^\circ\text{C}/1000$  atm. However, the magnitude of the loss peaks does not increase monotonically with pressure. Figure 5 shows the temperature dependence of  $G'$  and  $\tan \delta$  for irradiated PP at three different pressures. Again the modulus of the irradiated polymer is always less than that of natural PP at any particular temperature and pressure. The  $\tan \delta$  curves are striking in that the broad  $\alpha$  relaxation of natural PP has been split up into two separate peaks,  $\alpha_a$  and  $\alpha_c$ , both of which are shifted upwards by the application of pressure. These peaks are also greater in magnitude than the relaxation in natural PP.

Split peaks are also seen in Figure 6 where the modulus and  $\tan \delta$  are plotted at two pressures for the ethylene-vinyl acetate copolymer. These peaks which are labelled  $\alpha_a$  and  $\alpha_c$  are displaced upwards by the application of pressure and are slightly greater in magnitude than the  $\alpha$  relaxation in the more crystalline natural LDPE.

Figure 7 shows the effect of temperature on the modulus  $G'$  of natural rubber at three pressures. The modulus is increased by the application of pressure but the modulus falls by about 10% for a temperature rise

from  $20^\circ$  to  $40^\circ\text{C}$ . With an 'ideal' rubber, of course, the modulus above the glass transition should increase linearly with absolute temperature, so that the increase between  $20$  and  $40^\circ\text{C}$  should be about 6%.

## DISCUSSION

Table 1 summarizes the effect of pressure on the various relaxations studied. It is not possible to make quantitative deductions from Figure 1 concerning the  $\beta$  relaxation in natural LDPE. On the other hand, the  $\beta$  relaxation in HDPE (see Figure 3) which is observed in a more favourable temperature range, suggests a shift of order  $5^\circ\text{C}/1000$  atm. The experiments of Schmieder and Wolf<sup>10</sup> at atmospheric pressure suggest that the  $\beta$  relaxation in polyethylene occurs in the amorphous regions. There are no other data on the effect of pressure<sup>11</sup> with which our results may be compared, and in view of the uncertainty as to the precise nature and location of the  $T_g$  in PE no attempt will be made to discuss the effect of pressure on the  $\beta$  relaxation in terms of glass transition behaviour under pressure.

The  $\alpha$  relaxations in LDPE are far more clearly defined. As is seen in Figure 1 for natural LDPE, this relaxation is displaced upwards by  $20^\circ\text{C}/1000$  atm. This is com-

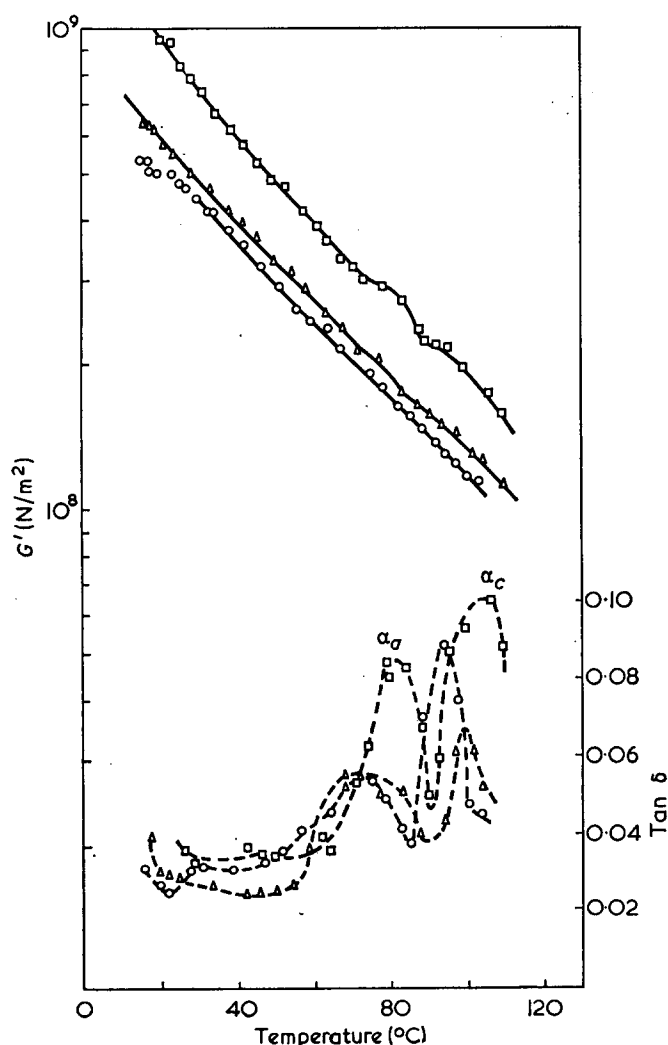


Figure 5 Temperature dependence of shear modulus (—) and loss tangent,  $\tan \delta$  (---) for irradiated polypropylene. The results are for pressures of 1 (O), 610 ( $\Delta$ ) and 1220 ( $\square$ ) atm. It is seen that the  $\alpha$  peak is split into two and that both the  $\alpha_a$  and  $\alpha_c$  peaks are displaced to a higher temperature by the application of pressure

Table 1 Pressure dependence of relaxation temperatures

Polymer	Relaxation	Relaxation temperature (°C) at			Mean value of shift (°C/1000atm)
		1 atm	610 atm	1220 atm	
Natural LDPE	$\alpha$	66	76	92	21±2
Irradiated LDPE	$\alpha_a$	61	68	80	17±2
	$\alpha_c$	91	97	103	10±1
HDPE	$\beta$	13	17	19	5±1
	$\alpha$	50	60	—	16±2
Natural PP	$\beta$	2	10	14	9±1
	$\alpha$	94	97	100	5±1
Irradiated PP	$\alpha_a$	70	75	82	10±1
	$\alpha_c$	95	99	103	7±1
Ethylene-vinyl acetate copolymer	$\alpha_a$	46	56	—	17±2
	$\alpha_c$	58	75	—	28±3

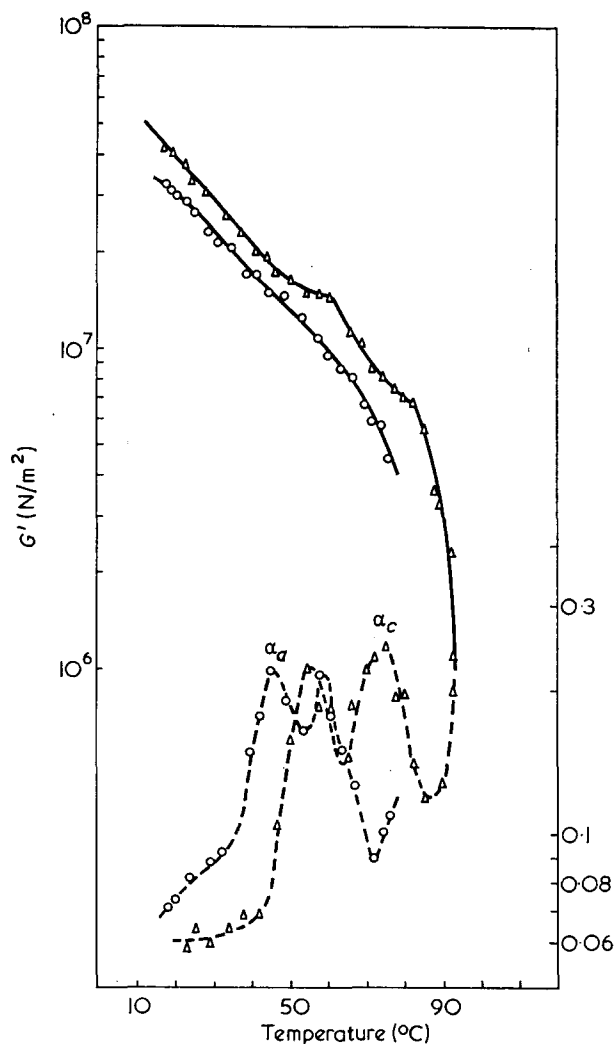


Figure 6 Temperature dependence of shear modulus (—) and loss tangent,  $\tan\delta$  (---) for 82:18% ethylene-vinyl acetate copolymer. The results are for pressures of 1 (○) and 610 (△) atm. It is seen that the peaks corresponding to the  $\alpha_a$  and  $\alpha_c$  relaxations are displaced to higher temperatures by the application of pressure

patible with the observed shift of 21°C/1000 atm in the melting temperature of polyethylene<sup>12</sup>. This supports Nielsen's view<sup>13</sup> that the  $\alpha$  relaxation is caused by crystal melting of a low molecular-weight constituent. On the other hand, in a more detailed study Nakayasu *et al.*<sup>14</sup> observed that the  $\alpha$  relaxation consisted of two distinct processes which they designated as  $\alpha_a$  and  $\alpha_c$ . Our experiments did not reveal a double  $\alpha$  relaxation with natural LDPE but as Figure 2 shows the double  $\alpha$

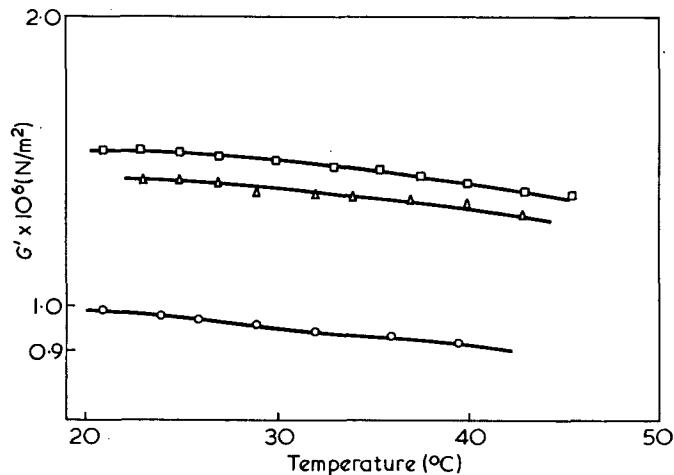


Figure 7 Temperature dependence of shear modulus for natural rubber at three pressures. ○, 1 atm; △, 610 atm, □, 1220 atm

relaxation is clearly seen for irradiated LDPE and for the natural copolymer. The splitting of the  $\alpha$  relaxation appears to become apparent when the crystalline content of the polyethylene is reduced and in the present investigation this occurs when the polymer is irradiated or when vinyl acetate is introduced. The lower temperature process is the  $\alpha_a$  relaxation and the other is the  $\alpha_c$  relaxation.

Iwayanagi<sup>15</sup> proposed that the  $\alpha_a$  relaxation was due to slip in the amorphous regions between the (crystalline) lamellae as they slip past each other to reorient their positions. This has been confirmed by Stein<sup>16</sup> who followed the time dependent changes in the average orientation of the crystal lattice planes as the polymer went through the relaxation. Our experiments which show that the  $\alpha_a$  relaxation is observed when the amorphous content of the polymer is increased is consistent with Iwayanagi's theory. The amount of shift is 17±1°C/1000 atm for both types of specimen. By contrast the  $\alpha_c$  shift has two rather different values, 10°C for the irradiated polyethylene, and 28°C/1000 atm for the copolymer. This difference may be associated with impurities in the copolymer but there is no direct evidence for this. There are two theories for the  $\alpha_c$  relaxation; the axial rotation theory and the incoherent lattice vibration theory but it is not possible to differentiate between them<sup>19</sup>.

The  $\alpha$  relaxation in natural PP consists of a single peak (see Figure 4) and its precise nature is uncertain. It has been postulated as being due to molecular relaxations within the crystal<sup>18</sup>, a lamellar slip mechanism<sup>15</sup> or to amorphous relaxations<sup>9</sup>. On the other hand, with irradiated PP (see Figure 5) the  $\alpha$  relaxation is resolved

into two distinct processes, the  $\alpha_a$  and  $\alpha_c$  relaxations, as is the case for the  $\alpha$  relaxation in polyethylene. The natural PP has a maximum value of  $\tan \delta = 0.06$  at the  $\alpha$  relaxation. In the irradiated sample where the amorphous content is greater the  $\alpha_a$  has a maximum value of  $\tan \delta = 0.09$  while the  $\alpha_c$  has a maximum value of 0.06. This is consistent with the  $\alpha_a$  relaxation being due to slip of the crystalline portions within the amorphous regions. The  $\alpha_c$  relaxation could be due to molecular relaxations within the crystal.

The glass transition temperature of PP is displaced non-linearly at an average rate of  $9 \pm 1^\circ\text{C}/1000\text{ atm}$ . Passaglia and Martin<sup>19</sup> have made a dilatometric study of the effect of pressure on the glass transition up to a maximum pressure of 700 atm. Their investigation showed that the effect was non-linear, the shift being greatest at the lowest pressures, and the mean shift was  $20^\circ\text{C}/1000\text{ atm}$ . Their measurements of compressibility  $\beta$  showed that it varies non-linearly with pressure, the change being greatest at low pressures. Thus the quantity  $\Delta\beta/\Delta\alpha$  agrees qualitatively with the observed trend of  $dT_g/dP$ . The difference between our values of  $dT_g/dP$  and those of Passaglia and Martin arise from two factors. First, as the earlier discussion indicates the ratio  $\Delta\beta/\Delta\alpha$  will always be greater than the observed values. Secondly, as will be shown in Parts 2 and 3, the magnitude of the shift is greater when more free volume is available. In our experiments the free volume is reduced by the presence of crystallites while in the dilatometric experiments of Passaglia and Martin the PP was almost entirely amorphous.

## CONCLUSION

The results show that the effect of hydrostatic pressure is to raise the relaxation temperatures of the polymers studied by amounts which range from about  $5^\circ$  to about  $25^\circ\text{C}$  per 1000 atm depending on the polymer and the transition in question. With polypropylene the glass transition and the  $\alpha$  relaxation are observed. With the polyethylenes the  $\alpha$  and  $\beta$  relaxations are observed.

It has not been possible to compare these shifts with

theoretical predictions except in the case of the  $\beta$  relaxation in polypropylene where the observed shift is appreciably less than that predicted. However, a broad general conclusion may be made concerning both LDPE and PP: when the crystallinity is reduced either by copolymerization or by  $\gamma$  radiation the  $\alpha$  relaxation is resolvable into two distinct processes. This is consistent with other experimental work which suggests that the  $\alpha$  relaxation consists of slip of crystalline lamellae within the amorphous region of the polymer together with internal motion within the crystal lamellae themselves.

## ACKNOWLEDGEMENTS

We wish to express our thanks to General Electric for a grant to the laboratory and also to Dr B. J. Briscoe for helpful discussions. One of us (E.J.P.) also wishes to thank the Thomas and Elizabeth Williams Scholarship Fund for a research grant. We are also grateful to the referee for helpful and constructive criticisms.

## REFERENCES

- 1 Zosel, A. *Kolloid Z.* 1961, **199**, 113
- 2 Billingham, P. R. and Tabor, D. *Polymer* 1971, **12**, 101
- 3 Gee, G. *Polymer* 1966, **7**, 177; Gee, G. *et al. Polymer* 1960, **1**, 365
- 4 Breuer, H. and Rehage, G. *Kolloid Z.* 1967, **216-217**, 159
- 5 Baer, E., Christiansen, A. W. and Radcliffe, S. V. *Phil. Mag.* 1971, **24**, 451
- 6 Bianchi, U. *J. Phys. Chem.* 1967, **71**, 3555
- 7 Goldstein, M. *J. Chem. Phys.* 1963, **39**, 3369
- 8 Jones Parry, E. and Tabor, D. *J. Phys. (D)* 1973, in press
- 9 Flocke, H. A. *Kolloid Z.* 1962, **180**, 118
- 10 Schmieder, K. and Wolf, K. *Kolloid Z.* 1953, **134**, 149
- 11 Heydemann, P. and Houck, J. *J. Polym. Sci. (A-2)* 1972, **10**, 1631
- 12 Matsuoka, S. *J. Polym. Sci.* 1962, **57**, 569
- 13 Nielsen, L. E. *J. Polym. Sci.* 1960, **42**, 357
- 14 Nakayasu, H., Markovitz, H. and Plazek, D. J. *Trans. Soc. Rheol.* 1961, **5**, 251
- 15 Iwayanagi, S. *Rep. Progr. Polym. Phys. Japan* 1962, **5**, 131
- 16 Stein, R. S. *Polym. Eng. Sci.* 1968, **8**, 259
- 17 Kambour, R. P. and Robertson, R. E. *GEC Rep. No. 70-C-104* 1970
- 18 McCrum, N. G. *J. Polym. Sci. (B)* 1964, **2**, 495
- 19 Passaglia, E. and Martin, G. M. *J. Res. Natl. Bur. Stand.* 1964, **68**, 519

# Effect of hydrostatic pressure and temperature on the mechanical loss properties of polymers:

## 2. Halogen polymers

E. Jones Parry and D. Tabor

*Physics and Chemistry of Solids, Cavendish Laboratory, University of Cambridge, Cambridge CB3 0HE, UK*

*(Received 16 April 1973; revised 1 August 1973)*

The shear modulus,  $G'$ , and loss tangent,  $\tan \delta$ , of a number of halogen polymers have been measured as a function of temperature at various pressures. The polymers studied were various poly(vinyl chloride) (PVC) samples, poly(vinylidene chloride) (PVDC), poly(vinyl fluoride) (PVF), poly(vinylidene fluoride) (PVDF) and a tetrafluoroethylene-hexafluoropropylene copolymer. The glass transition temperatures are shifted upwards by pressure by amounts varying between about 11°C and 25°C/1000 atm. In the case of PVC it has proved possible to compare the results with theory and the observed shift is found to be considerably smaller than the predicted value. In PVDC and PVDF the secondary relaxations are also shifted upwards by the application of pressure.

### INTRODUCTION

Since the loss processes in polymers involve some movement of chain segments or groups, the free volume available must play an important part. For that reason pressure would be expected to have a marked influence on viscoelastic behaviour and this has generally been found to be true<sup>1</sup>. A brief account of the background and theory in relation to the effect of pressure on the glass transition temperature has been given in Part 1<sup>1</sup>. This paper describes a direct experimental study of this effect in a series of halogen polymers. The experimental arrangement is the same as that described in the previous paper<sup>1</sup>.

### SAMPLES

A number of types of poly(vinyl chloride)(PVC) have been investigated. One was a rigid Breon PVC containing 150 parts by weight of polymer, 0.75 parts by weight of calcium stearate and 1.5 parts by weight of an organotin stabilizer. A plasticized sample of this polymer containing 33% dialkyl phthalate was also studied. The other two PVC samples were from the ICI Welvic range. In addition a prepared specimen of Welvic R7/622 was exposed in vacuum to 11 Mrad of radiation from a <sup>60</sup>Co source. On removal this sample was dark brown in colour whereas previously it had been white. The poly(vinylidene chloride) (PVDC), poly(vinyl fluoride) (PVF) and poly(vinylidene fluoride) (PVDF) used were commercial samples and the tetrafluoroethylene-hexafluoropropylene (TFE-HFP) copolymer contained 9% HFP. The apparatus used has been described previously<sup>2</sup>.

### RESULTS

*Figure 1* shows the temperature dependence of the shear modulus,  $G'$ , and  $\tan \delta$  for two samples of Breon PVC

at different pressures. The unplasticized PVC behaves like a typical amorphous polymer while the plasticized polymer is considerably less rigid and has a lower atmospheric pressure glass transition temperature. The glass transition temperatures are displaced upwards by the application of pressure. Similar results for a rigid and a plasticized Welvic PVC sample are shown in *Figure 2*. At atmospheric pressure the  $T_g$  of the irradiated Welvic R7/622 sample is higher than that of the natural R7/622 polymer as shown in *Figure 3*. The  $T_g$  of the irradiated polymer is displaced upwards by pressure but the magnitude of the shift is less than that for the natural polymer.

*Figure 4* shows modulus and loss as a function of temperature at three distinct pressures for the PVDC samples used in our experiments. Two loss peaks can be seen and the  $\beta$  relaxation is associated with a steep drop in modulus and has been assigned to the glass transition region. The  $\alpha$  relaxation like the  $\beta$  relaxation, is shifted non-linearly upwards in temperature with applied pressure and the magnitude of the loss peak is reduced.

The temperature dependence of shear modulus and loss tangent for PVF at three pressures is shown in *Figure 5*. The modulus behaviour with temperature is typical of a semi-crystalline polymer. The temperature of the  $\alpha$  relaxation is shifted non-linearly upwards by pressure and the magnitude of the relaxation changes but in a non-monotonic way.

In the experiments carried out on our samples of PVDF (Kynar 200) we attempted to locate the glass transition but the low temperature minimum of the apparatus prevented it. The results are plotted in *Figure 6*. The distinct  $\alpha$  relaxation is linearly displaced upwards by the pressure.

A preliminary study of the modulus of the TFE-HFP copolymer was made under 300 atm [1 atm  $\equiv$  101.33 kN/m<sup>2</sup>] of nitrogen pressure as a function of time exposed to

the gas. The gas was found to plasticize the polymer in such a way that the modulus of the polymer after 2 h exposure was less than its value at that temperature before the gas entered the system. For this reason the results shown in Figure 7 were carried out in helium which was found not to plasticize the material. The  $\alpha$  relaxation is clearly defined both by the fall in modulus

and by the loss peaks, and is shifted to a higher temperature by application of pressure.

Yasuda and Araki<sup>3</sup> observed volume changes in polytetrafluoroethylene (PTFE) as a function of temperature for various pressures. The temperature of the lower transition was shifted linearly upwards with pressure at a rate of 20°C/1000 atm. Billinghamurst and Tabor<sup>4</sup>

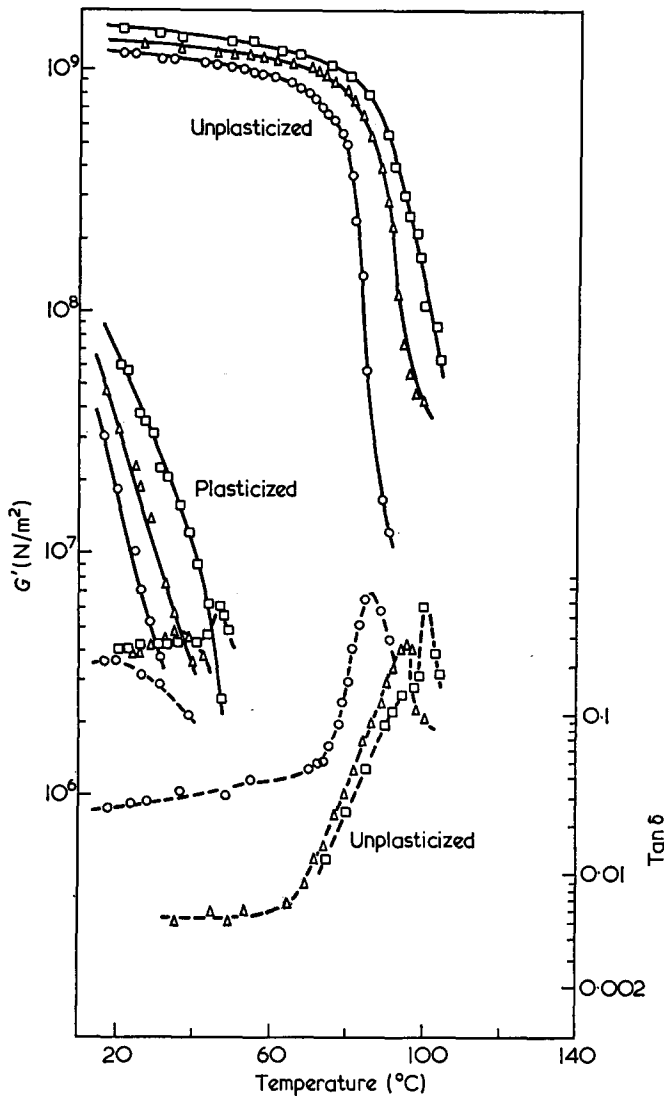


Figure 1 Temperature dependence of shear modulus (—) and loss tangent,  $\tan \delta$  (---) for plasticized and unplasticized PVC. The results are for pressures of 1 (○), 610 (△) and 1220 (□) atm. It is seen that the peaks corresponding to the  $\alpha$  relaxations are displaced to a higher temperature by the application of pressure

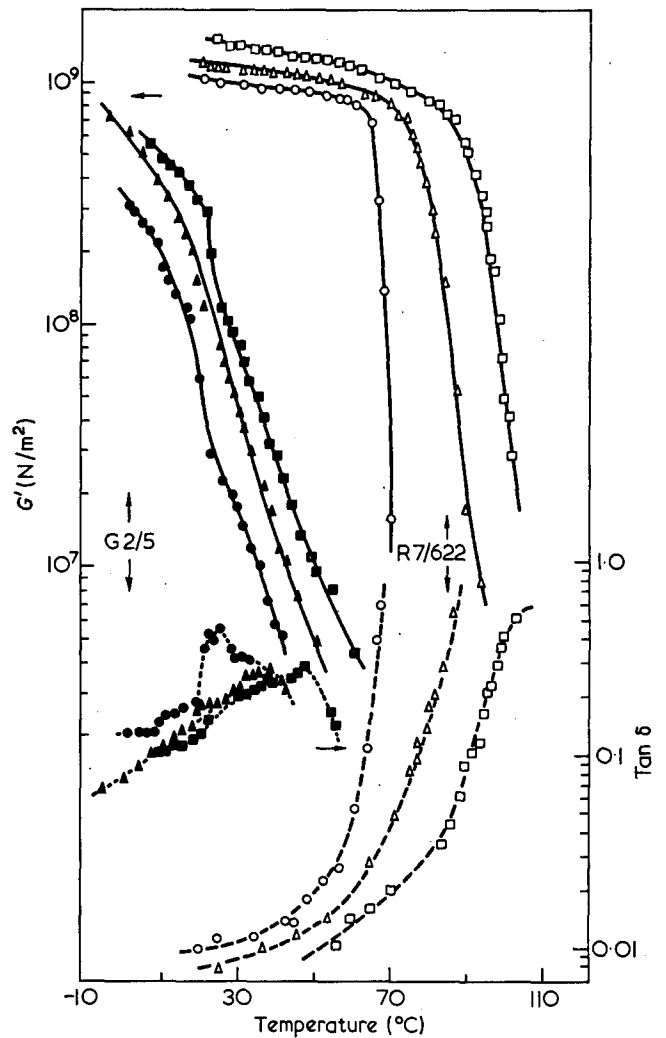


Figure 2 Temperature dependence of shear modulus (—) and loss tangent,  $\tan \delta$  (---) for R7/622 (open symbols) and G2/5 (solid symbols) poly(vinyl chlorides). The results are for pressures of 1 (○, ●), 610 (△, ▲) and 1220 (□, ■) atm. It is seen that the peaks corresponding to the  $\alpha$  relaxations are displaced to a higher temperature by the application of pressure

Table 1 Pressure dependence of relaxation temperatures

Polymer	Relaxation	Relaxation temperature (°C) at			Mean shift (°C/1000 atm)
		1 atm	610 atm	1220 atm	
Breon PVC	$\alpha$	85	92	98	11 ± 1
Breon + 33% dialkyl phthalate	$\alpha$	19	24	33	11 ± 1
Welvic G2/5	$\alpha$	19	27	33	11 ± 1
Welvic R7/622	$\alpha$	69	86	99	25 ± 2
Irradiated Welvic R7/622	$\alpha$	79	89	99	16 ± 2
PVDC	$\alpha$	81	85	100	16 ± 2
PVDC	$\beta$	13	19	32	16 ± 2
PVF	$\alpha$	53	62	67	12 ± 2
PVDF	$\alpha$	70	89	104	28 ± 2
TFE-HFP	$\alpha$	82	96	—	13 ± 2

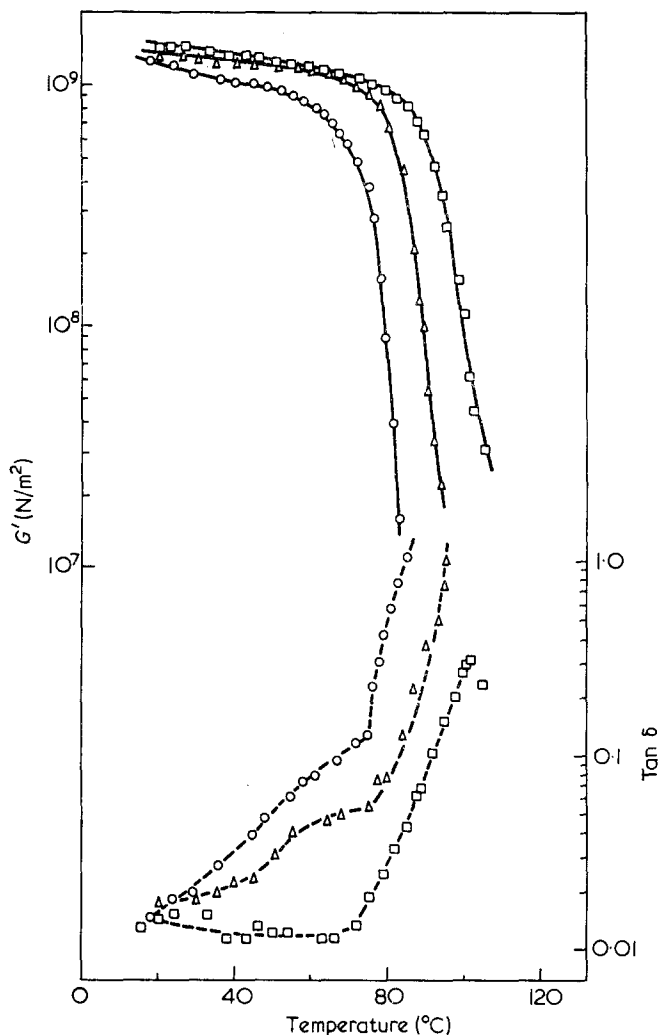


Figure 3 Temperature dependence of shear modulus (—) and loss tangent,  $\tan \delta$  (---) for irradiated R7/622 PVC. The results are for pressures of 1 (O), 610 ( $\Delta$ ) and 1220 ( $\square$ ) atm. It is seen that the peaks corresponding to the glass transition are displaced to a higher temperature by the application of pressure

measured the shear modulus against temperature at a number of pressures and found the  $\beta$  relaxation to be displaced by about  $18^\circ\text{C}/1000\text{ atm}$ . Unfortunately the upper temperature range of the present equipment is limited and consequently it has proved impossible to investigate the effect of pressure on the  $\alpha$  relaxation of PTFE. It is thus not possible to compare the behaviour of PTFE with its copolymer.

## DISCUSSION

We will first summarize the results for different polymers. Table 1 shows the pressure dependence of the relaxation temperatures.

For PVC most of the pressure shifts are non-linear and the plasticizer has had no effect on the magnitude of the shift of the  $T_g$  of the Breon samples. The Welvic G2/5 sample has the same overall shift but the R7/622 is displaced by a far greater amount. The shift in the glass transition of the irradiated R7/622 is less than that for the natural polymer. The atmospheric  $T_g$  of the irradiated sample is higher than that of the natural sample; this is consistent with the creation of crosslinks which pull the chains together and reduce the free volume. Because of this we would expect the shift with pressure to be less

for the crosslinked polymer as is in fact observed. A value of  $\Delta\beta/\Delta\alpha = 32^\circ\text{C}/1000\text{ atm}$  for natural PVC has been quoted by Hellwege *et al.*<sup>5</sup> while O'Reilly<sup>6</sup> quotes a value of  $TV(\Delta\alpha/\Delta C_p) = 30^\circ\text{C}/1000\text{ atm}$ . Both are very much higher than our experimental results. Of the polymers studied here PVC is the only one for which these data are available. From the discussion in Part 1<sup>1</sup> this discrepancy is to be expected.

On the other hand, other experimental studies of the shift of the  $T_g$  with pressure (dielectric, dilatometric, and mechanical) for PVC give values of order  $16^\circ\text{C}/1000\text{ atm}$  which is close to our own results.

The glass transition temperature of PVDC is significantly lower than that of PVC. PVDF also has a surprisingly low  $T_g$  and it appears to be a common feature in polymers where a symmetrical substitution of atoms occurs on alternate chain carbon atoms. Although the absolute values of the energy minima for PVDC are higher than for PVC because of steric hindrance, Gibbs and de Marzio<sup>7</sup> suggest that the potential energy barrier between the minima is less: consequently the  $T_g$  will be lower. This potential energy difference must be lower in PVDC than in PVC, despite the fact that the

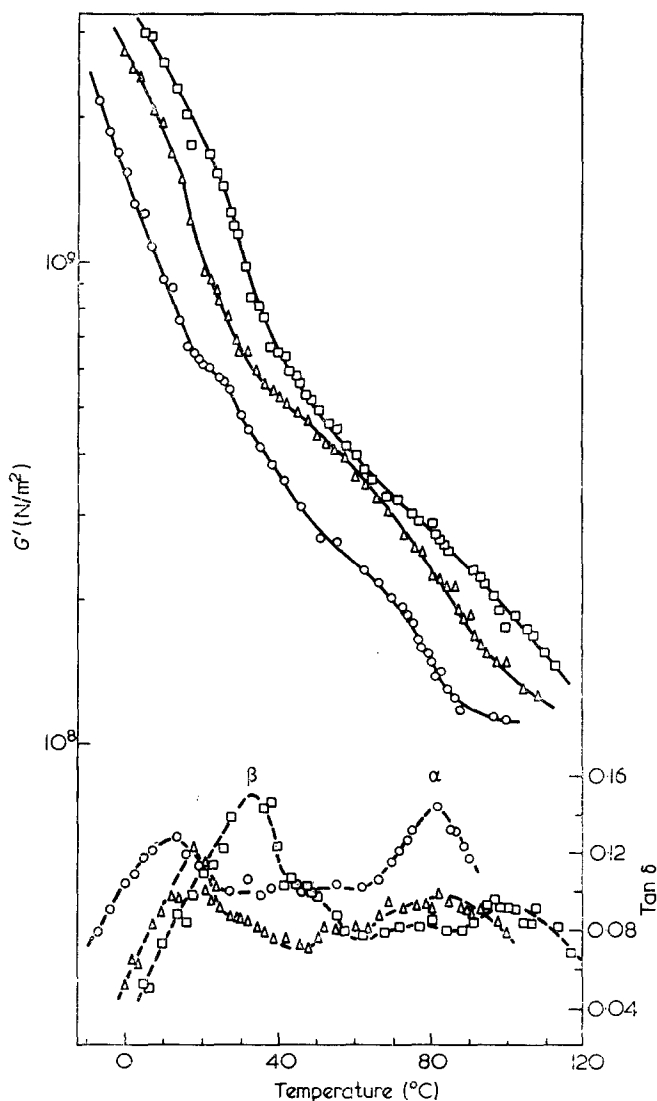


Figure 4 Temperature dependence of shear modulus (—) and loss tangent,  $\tan \delta$  (---) for PVDC. The results are for pressures of 1 (O), 610 ( $\Delta$ ) and 1220 ( $\square$ ) atm. It is seen that the peaks corresponding to the  $\alpha$  and  $\beta$  relaxations are displaced to a higher temperature by the application of pressure

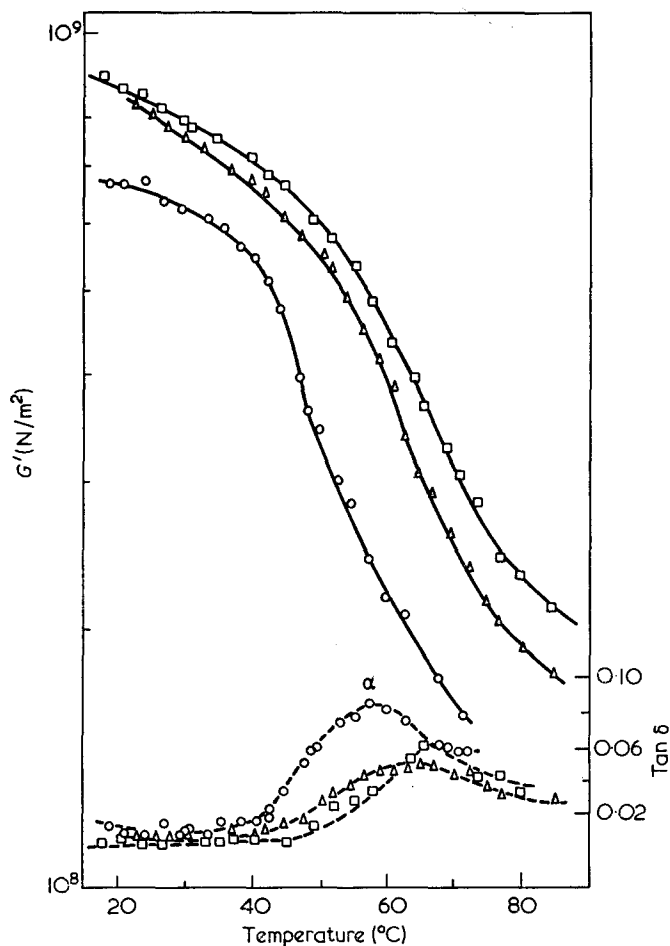


Figure 5 Temperature dependence of shear modulus (—) and loss tangent,  $\tan \delta$  (---) for PVF. The results are for pressures of 1 (○), 610 (△) and 1220 (□) atm. It is seen that the peaks corresponding to the  $\alpha$  relaxation are displaced to a higher temperature by the application of pressure

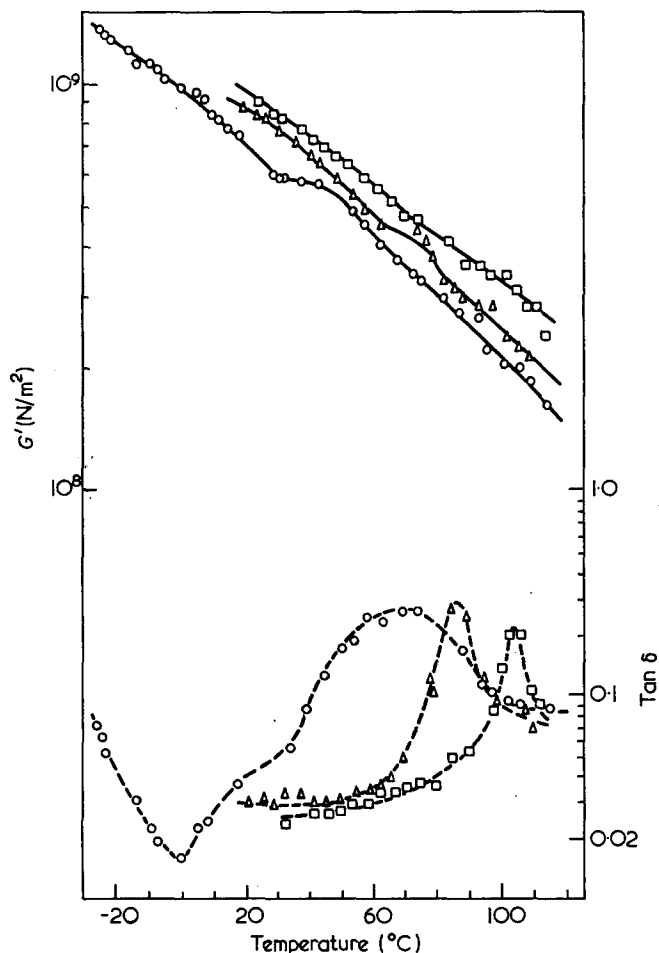


Figure 6 Temperature dependence of shear modulus (—) and loss tangent,  $\tan \delta$  (---) for PVDF. The results are for pressures of 1 (○), 610 (△) and 1220 (□) atm. It is seen that the peaks corresponding to the  $\alpha$  relaxation are displaced to a higher temperature by the application of pressure

absolute values will be larger because of steric factors. The magnitude of the  $\alpha$  peak in PVDC is reduced by pressure. If this relaxation entails the rotation of some main chain segments, some segments will be free to move while others are blocked by crystallites. The application of pressure blocks more segments and the relaxation is reduced in magnitude. Since the  $\alpha$  and  $\beta$  relaxations are shifted by an identical amount, then the movements involved in the  $\alpha$  relaxation are presumably on the same scale as the  $\beta$  relaxation. This is consistent with a 'crankshaft' type movement. For PVDF the  $\beta$  relaxation is displaced by a very large amount,  $28^\circ\text{C}/1000$  atm. This relaxation is believed to be crystalline in nature<sup>8</sup> and the shift is compatible with the process being due to some melting or reorientation process within the crystal regions of the polymer. Unfortunately we were unable to study the effect of crystallinity on this process.

The magnitude of the glass transition ( $\alpha$ ) in PVF is decreased by the application of pressure which 'blocks' certain segments. It is impossible to relate the magnitude of the shift in the  $\alpha$  relaxation for PVF to any theoretical quantities. Nor is this possible for the TFE-HFP copolymer.

#### CONCLUSIONS

The results show that the effect of pressure is to raise the glass transition temperature of PVC, PVDC, PVF and

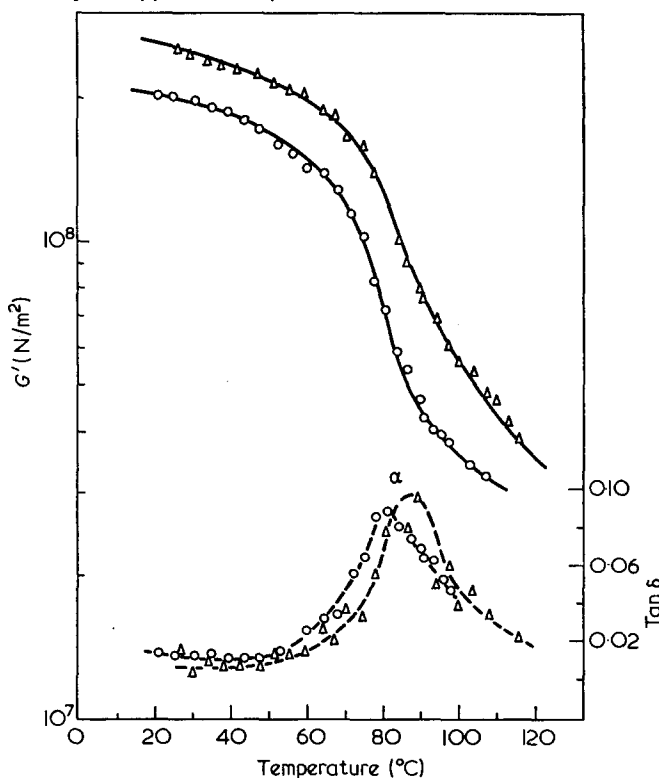


Figure 7 Temperature dependence of shear modulus (—) and loss tangent,  $\tan \delta$  (---) for TFE-HFP. The results are for pressures of 1 (○) and 610 (△) atm. It is seen that the peaks corresponding to the  $\alpha$  relaxation are displaced to a higher temperature by the application of pressure

the TFE-FEP copolymer by amounts varying between 11°C and 25°C/1000 atm. With PVC a comparison with theory is possible and shows that the experimental shift is appreciably less than the theoretical. With PVDC and PVDF the glass transition temperatures are lower than those for PVC and PVF respectively because of the symmetrical nature of the halogens in the main chains of the former polymers.

The secondary ( $\alpha$ ) relaxations in PVDC and PVDF are shifted upwards by 16 and 28°C/1000 atm respectively.

#### ACKNOWLEDGEMENTS

We wish to express our thanks to General Electric for a

grant to the laboratory and also to Dr B. J. Briscoe for helpful discussions. One of us (E.J.P.) also wishes to thank the Thomas and Elizabeth Williams Scholarship Fund for a research grant.

#### REFERENCES

- 1 Jones Parry, E. and Tabor, D. *Polymer* 1973, **14**, 617
- 2 Jones Parry, E. and Tabor D. *J. Phys. (D)* 1973, in press
- 3 Yasuda, T. and Araki, Y. *J. Appl. Polym. Sci.* 1961, **5**, 331
- 4 Billingham, P. R. and Tabor, D. *Polymer* 1971, **12**, 101
- 5 Hellwege, K. H., Knappe, W. and Lehman, P. *Kolloid Z.* 1963, **183**, 110
- 6 O'Reilly, J. M. *J. Polym. Sci.* 1962, **57**, 429
- 7 Gibbs, J. H. and Di Marzio, E. A. *J. Chem. Phys.* 1958, **28**, 373
- 8 Takamatsu, T. and Fukada, E. *Polymer J.* 1970, **1**, 101



# Effect of hydrostatic pressure and temperature on the mechanical loss properties of polymers: 3. PET, PVAC and vinyl chloride/vinyl acetate copolymers

E. Jones Parry and D. Tabor

*Physics and Chemistry of Solids, Cavendish Laboratory, University of Cambridge, Cambridge CB3 0HE, UK*

*(Received 16 April 1973; revised 1 August 1973)*

A torsion pendulum (1 Hz) has been used to determine the pressure dependence of the glass transition temperatures of poly(ethylene terephthalate) (PET), poly(vinyl acetate) (PVAC) and some vinyl chloride/vinyl acetate copolymers. Their glass transition temperatures are shifted upwards by amounts varying between 11 and 18°C/1000 atmospheres. In the case of PVAC it has proved possible to compare the results with theory and the observed shift is found to be much less than the predicted value. A study of poly(methyl methacrylate) (PMMA) shows the  $\beta$  relaxation to be displaced to a higher temperature at the rate of 4°C/1000 atm. Results are also presented for the temperature dependence of shear modulus,  $G'$ , and loss tangent,  $\tan \delta$  for a reinforced crosslinked polymer, Bakelite P17404, at different pressures.

## INTRODUCTION

The amount of available free volume present is known to influence the dissipative processes within a polymer. Hence we would expect the viscoelastic behaviour to be significantly affected by hydrostatic pressure, as discussed in Parts 1 and 2. This paper describes an experimental study on a further series of polymers.

## EXPERIMENTAL

### *Procedure*

A torsion pendulum was used within a high pressure vessel as has been previously described<sup>1</sup>. The shear modulus,  $G'$ , and loss tangent,  $\tan \delta$ , were calculated for a number of polymers as a function of temperature and pressure.

### *Materials*

Studies were made on amorphous and semi-crystalline samples of poly(ethylene terephthalate) (PET). The semi-crystalline samples were obtained by preparing two amorphous samples and annealing them between two thin steel plates in an oven for 24 h. The density was measured as 1.369 g/cm<sup>3</sup> at 20°C. They were then cooled uniformly to room temperature over a further period of 24 h. The data of Kilian *et al.*<sup>2</sup> suggest that these samples were then about 30% crystalline. Two different molecular weight samples of poly(vinyl acetate) (PVAC) were studied, Mowilith 50 (mol. wt. 260 000) and Mowilith 30 (mol. wt. 110 000). The samples were prepared by milling sheets which had been prepared by the compression moulding of granules at  $6 \times 10^6$  N/m<sup>2</sup>

and 100°C and 70°C respectively. This milling proved extremely difficult because of the brittle nature of the polymer on impact, and its low softening temperature.

The vinyl chloride/vinyl acetate copolymers were from the ICI Flovic range, while the laminate was Bakelite P17404. The poly(methyl methacrylate) (PMMA) was commercial Perspex. All the specimens were prepared by milling sheets of these materials.

## RESULTS

*Figure 1* shows the curves of  $G'$  against temperature for the PET samples at various pressures.  $\tan \delta$  is similarly plotted. It is seen that the modulus of the amorphous sample is always less than that of the semi-crystalline polymer over the whole range of temperature and pressure because of the strengthening provided by the crystallites. The modulus curves show the difference between the glass transition of amorphous and semi-crystalline polymers. In the former there is a sharp drop in modulus of about two decades, while for the latter the fall is more gradual because of the stiffness imparted by the crystallites. The loss maxima for the amorphous polymers were unattainable but the modulus behaviour shown by the various curves in *Figure 1* indicates that the atmospheric glass transition has been displaced to a higher temperature in the semi-crystalline polymer.  $\tan \delta$  has been reduced with the increase in crystallinity and its peak has broadened off on the high temperature side. The glass transition is clearly displaced to higher temperatures by the application of pressure.

The results for PVAC are shown in *Figures 2* and *3*. The atmospheric glass transition temperature of Mowilith

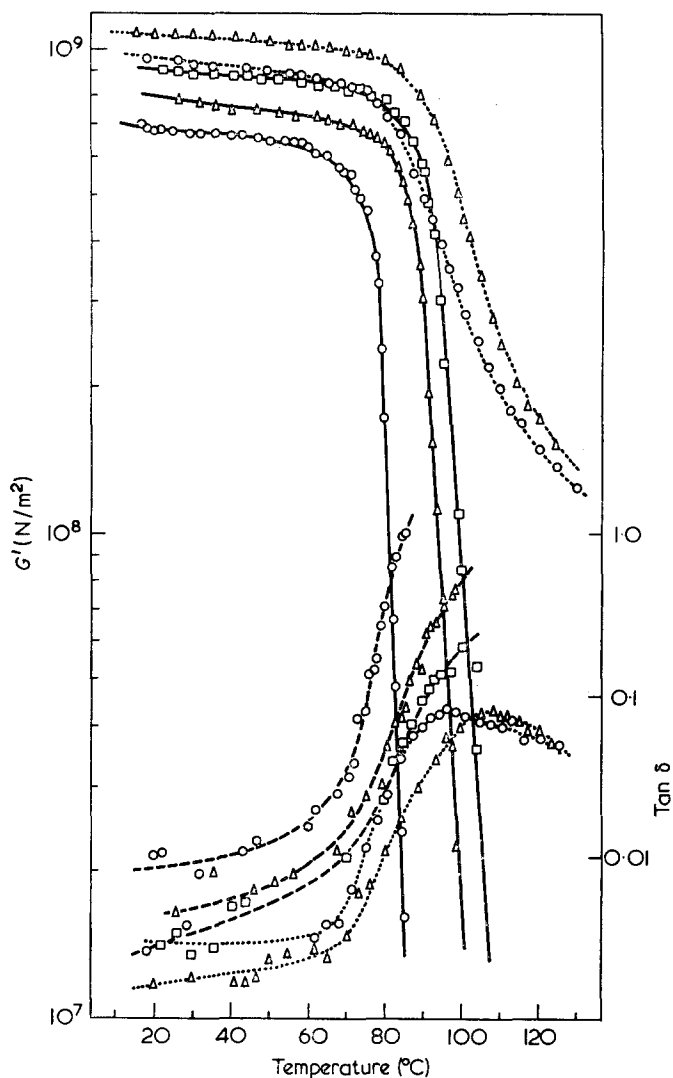


Figure 1 Temperature dependence of shear modulus (—, ····) and loss tangent,  $\tan \delta$  (---, ····) for amorphous (—, ---) and semi-crystalline (····) PET. The results are for pressures of 1 (○), 610 (△) and 1220 (□) atm. It is seen that the peaks corresponding to the glass transition are displaced to a higher temperature by the application of pressure

30 is less than that of Mowilith 50, but the shift of  $T_g$  with pressure is greater.

Studies have been made on three vinyl chloride/vinyl acetate copolymers containing respectively 2%, 11% and 17% of vinyl acetate. Results for the 2% acetate sample are shown in Figure 4. The results for the others will be quoted later. Each copolymer behaves like a typical amorphous polymer exhibiting one very marked glass transition which is a characteristic behaviour of random copolymers. The atmospheric glass transition is non-linearly shifted upwards in temperature by pressure.

The shear modulus,  $G'$ , and loss tangent,  $\tan \delta$ , of PMMA are plotted against temperature in Figure 5 for different pressures. Over the temperature range studied the modulus has dropped by about 35%. This is a greater fall than that of amorphous PET over a similar temperature range and is attributable to the  $\beta$  relaxation. The  $\tan \delta$  curves locate the position of this relaxation which is shifted to a slightly higher temperature by pressure.

Figure 6 shows the temperature dependence of shear modulus and loss tangent at three pressures for a Bakelite sample. As expected from crosslinked reinforced polymers with such complicated structures the loss curves do not

show the presence of any relaxations. The crosslinked nature of the resin and the presence of reinforcements cause the modulus to fall only gradually over the temperature range studied and to increase slightly with the application of pressure.

## DISCUSSION

Table 1 summarizes the effect of pressure on the relaxation temperatures of the polymers studied.

For PET the overall shift with pressure for the amorphous polymer appears to be less than for the semi-crystalline material. This is misleading since over the first 610 atm the shift for the amorphous polymer is actually greater. This emphasizes the non-linearity of the shift. Absence of any appropriate data makes it impossible to compare the magnitude of this shift with any theoretical expressions. In the case of PVAC this is possible, because O'Reilly<sup>3</sup> calculated  $TV(\Delta\alpha/C_p) = 25^\circ\text{C}/1000\text{ atm}$ , and McKinney and Belcher<sup>4</sup> found  $\Delta\beta/\Delta\alpha$  to

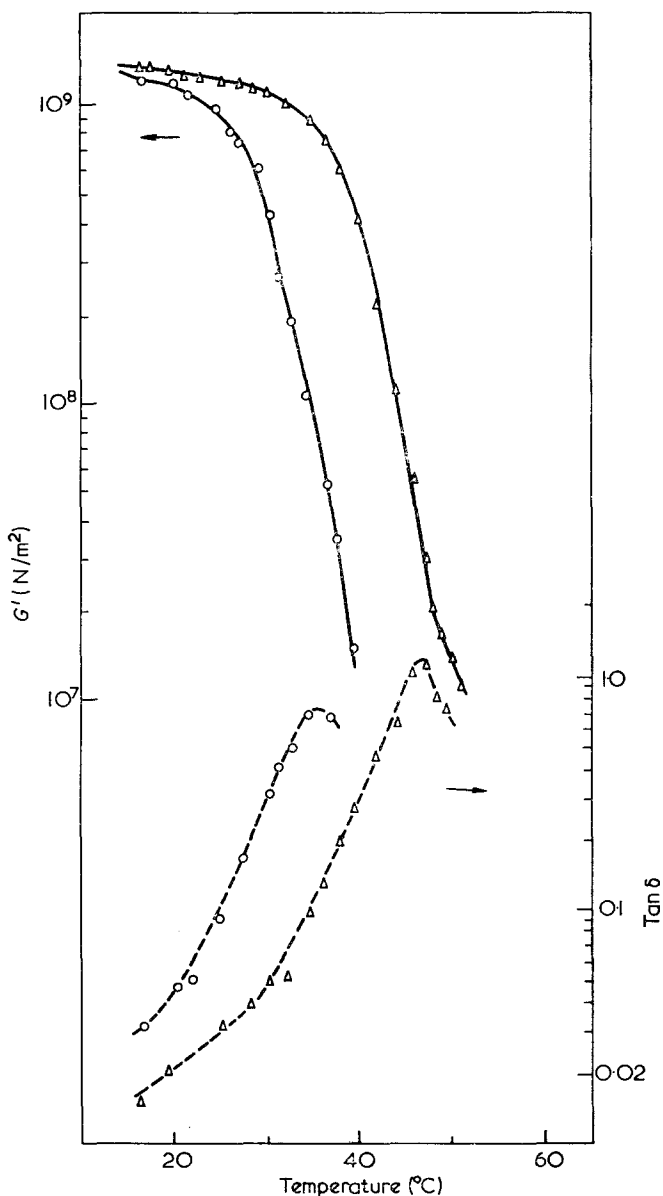


Figure 2 Temperature dependence of shear modulus (—) and loss tangent,  $\tan \delta$  (---) for PVAC (Mowilith 30). The results are for pressures of 1 (○) and 610 (△) atm. It is seen that the peaks corresponding to the glass transition are displaced to a higher temperature by the application of pressure

Table 1 Pressure dependence of relaxation temperatures

Polymer	Relaxation	Relaxation temperature (°C) at			Overall shift with pressure (°C/1000 atm)
		1 atm	610 atm	1220 atm	
Amorphous PET	$\alpha$	80	93	99	$16 \pm 2$
Semi-crystalline PET	$\alpha$	96	107	—	$18 \pm 2$
PVAC (Mowilith 30)	$\alpha$	33	44	—	$18 \pm 3$
PVAC (Mowilith 50)	$\alpha$	39	47	61	$18 \pm 3$
Vinyl chloride/vinyl acetate copolymer:	$\alpha$				
2% acetate/98% chloride		85	94	98	$11 \pm 1$
11% acetate/89% chloride		80	90	96	$13 \pm 1$
17% acetate/83% chloride		71	83	88	$14 \pm 1$
PMMA	$\beta$	29	31	34	$4 \pm 2$

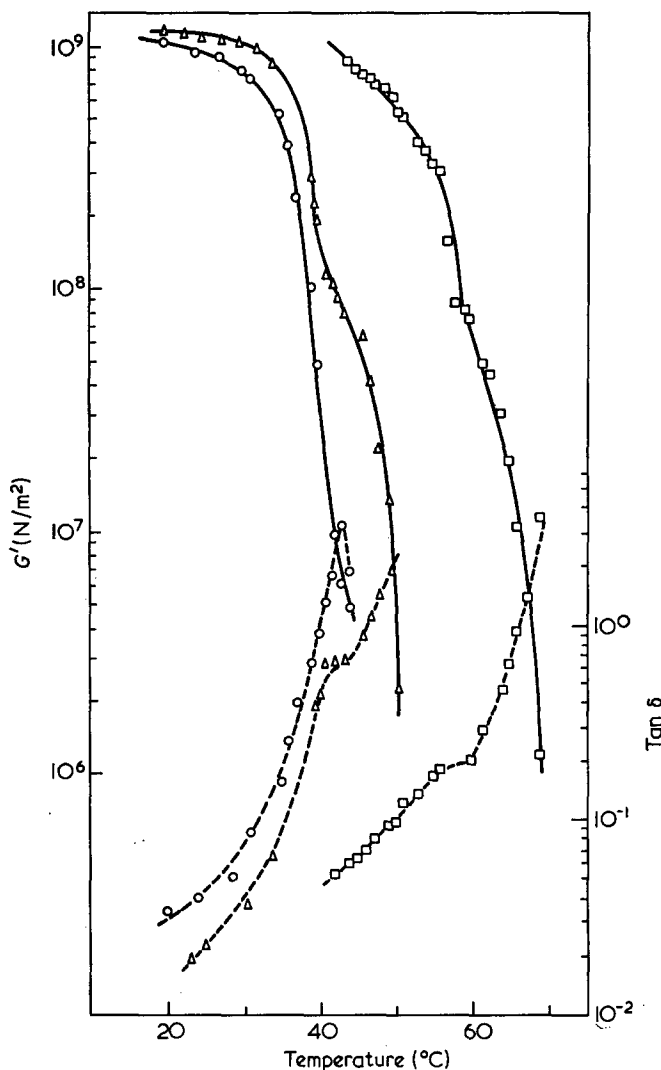


Figure 3 Temperature dependence of shear modulus (—) and loss tangent,  $\tan \delta$  (---) for PVAC (Mowilith 50). The results are for pressures of 1 (○), 610 (△) and 1220 (□) atm. It is seen that the peaks corresponding to the glass transition are displaced to a higher temperature by the application of pressure

be  $38^\circ\text{C}/1000\text{atm}$ . The former value is in approximate agreement with our observed shift of  $18^\circ\text{C}/1000\text{atm}$ , while the latter is over twice as great. The glass transition temperature of Mowilith 50 is non-linearly displaced with respect to pressure, the shift being greatest at higher pressures. This is in accord with the results of McKinney and Belcher who also found the quantity  $\Delta\beta/\Delta\alpha$  to increase slightly with increasing pressure. In general one would expect the opposite trend since polymers usually become less compressible at higher pressures but

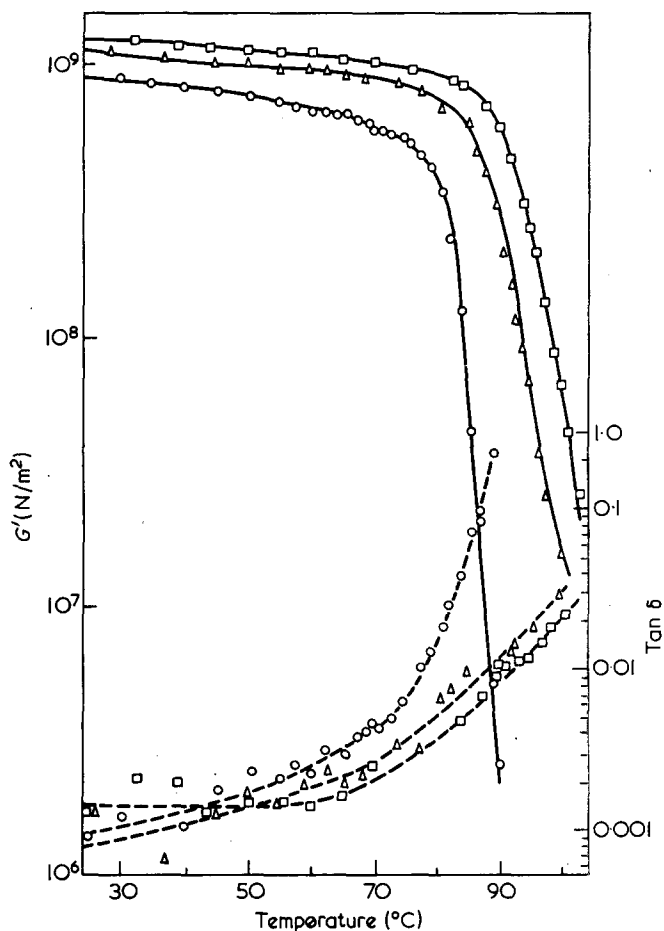


Figure 4 Temperature dependence of shear modulus (—) and loss tangent,  $\tan \delta$  (---) for 98% vinyl chloride/2% vinyl acetate copolymer. The results are for pressures of 1 (○), 610 (△) and 1220 (□) atm. It is seen that the peaks corresponding to the glass transition are displaced to a higher temperature by the application of pressure

we have observed a similar phenomenon with PVDC. Over the smaller pressure range the  $T_g$  of the lower molecular weight PVAC is shifted more than that of the other. The atmospheric pressure glass transition of the lower molecular weight sample is less than that of Mowilith 50. This is presumably because the larger number of chain ends in the lower molecular weight sample introduce extra free volume allowing the transition to occur at a lower temperature.

The atmospheric glass transition temperature of the vinyl chloride/vinyl acetate copolymers is reduced as the acetate content increases. The magnitude of this reduction indicates that the molecular motions involved at the glass transition must be long range, cooperative motions

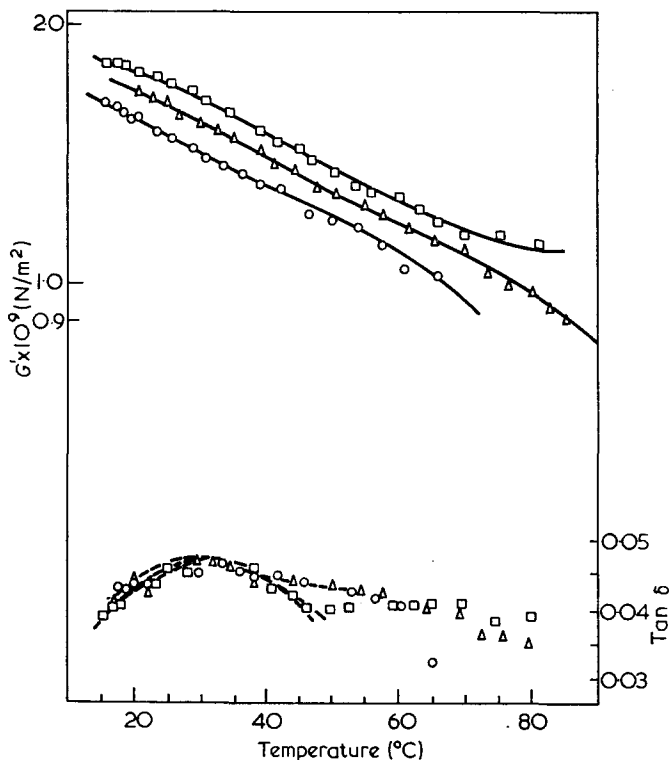


Figure 5 Temperature dependence of shear modulus (—) and loss tangent,  $\tan \delta$  (---) for PMMA. The results are for pressures of 1 (○), 610 (△) and 1220 (□) atm. It is seen that the peaks corresponding to the  $\beta$  relaxation are displaced to a higher temperature by the application of pressure

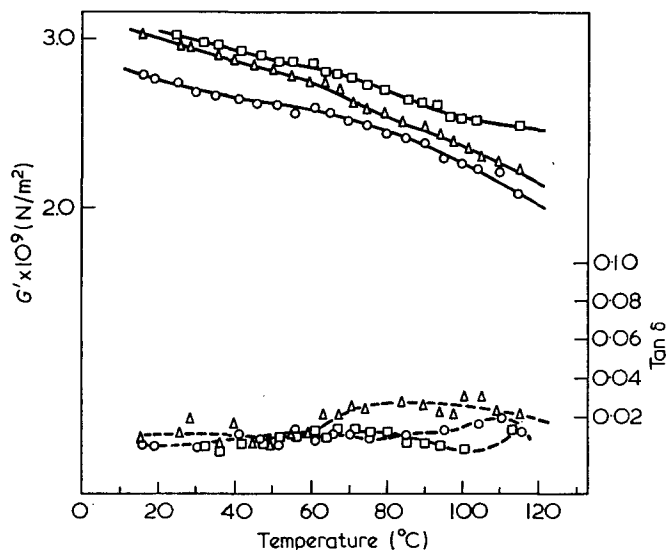


Figure 6 Temperature dependence of shear modulus (—) and loss tangent,  $\tan \delta$  (---) for Bakelite P17404<sup>2</sup>. The results are for pressures of 1 (○), 610 (△) and 1220 (□) atm.

because otherwise isolated vinyl acetate units would be unable to affect the motion of vinyl chloride units. The glass transition temperature is always non-linearly shifted with pressure, the shift being greatest over lower pressures. The mean shift increases as the acetate content increases. This is consistent with our earlier studies which have shown the  $T_g$  of poly(vinyl chloride) to be shifted by 11°C/1000 atm while the  $T_g$  of poly(vinyl acetate) is displaced by 18°C/1000 atm. It proved impossible to fit a Gordon-Taylor type expression to our results.

The  $\beta$  relaxation in PMMA has been generally assigned to the rotation of the  $-\text{COOCH}_3$  side group. It occurs at about room temperature because of the small amount of free volume necessary for this rotation. Thus the shift due to pressure is very low, about 4°C/1000 atm, and is in good agreement with Zosel's<sup>5</sup> observed shift of 2°C/1000 atm.

## CONCLUSIONS

The results show that the effect of hydrostatic pressure is to raise the glass transition temperatures of PET, PVAC and some vinyl chloride/vinyl acetate copolymers by amounts varying between 11 and 18°C/1000 atm. With PVAC the observed shift is less than that predicted by theory but as is indicated in Part 1 this is to be expected.

The  $\beta$  relaxation of PMMA is displaced upwards by 4°C/1000 atm. This small shift is attributed to the fact that this relaxation, involving the rotation of the  $-\text{COOCH}_3$  side groups, demands only a small free volume. Again, when the crystalline content of PET is increased, the molecular weight of PVAC increased and when PVC is irradiated to produce crosslinking the shifts in  $T_g$  with pressure are reduced. These results are consistent with the general conclusion, that a reduction in available free volume reduces the effect of pressure on relaxation temperatures.

## ACKNOWLEDGEMENTS

We wish to express our thanks to General Electric for a grant to the laboratory and also to Dr B. J. Briscoe for helpful discussions. One of us (E.J.P.) also wishes to thank the Thomas and Elizabeth Williams Scholarship Fund for a research grant.

## REFERENCES

- 1 Jones Parry, E. and Tabor, D. *J. Phys. (D)* 1973, in press
- 2 Kilian, H. G., Halboth, H. and Jenckel, E. *Kolloid Z.* 1960, **172**, 166
- 3 O'Reilly, J. M. *J. Polym. Sci.* 1961, **57**, 429
- 4 McKinney, J. and Belcher, H. *J. Res. Natl. Bur. Stand.* 1963, **67A**, 43
- 5 Zosel, A. *Kolloid Z.* 1964, **199**, 113

# The elastic modulus of nylons

T. R. Manley and C. G. Martin

Department of Materials Science, Newcastle upon Tyne Polytechnic,  
Newcastle upon Tyne NE1 8ST, UK  
(Received 17 April 1973; revised 19 July 1973)

The energy balance method previously described gives values for the elastic modulus of single crystals of nylons that are reasonably close to experimental data, where these are available, apart from nylon-6. Force constants were derived from Urey Bradley (*UBFF*) and valence (*VFF*) force fields. Modulus values, in GN/m<sup>2</sup>, are as follows:

Nylon-6	244.1 ( <i>UBFF</i> )	262.8 ( <i>VFF</i> )	164.8 (exp)
Nylon-11	243.5 ( <i>UBFF</i> )	241.4 ( <i>VFF</i> )	—
Nylon-6, 10	185.6 ( <i>UBFF</i> )	189.6 ( <i>VFF</i> )	196.2 (exp)
Nylon-6, 6	180.9 ( <i>UBFF</i> )	192.9 ( <i>VFF</i> )	172.6 (exp)
Nylon-7	180.2 ( <i>UBFF</i> )	188.6 ( <i>VFF</i> )	—

Consideration of the cross-sectional area and repeat distance of the polymer chain indicates that the modulus will decrease in the order given. The extensibility (*f* value) of each polymer was within the expected range (0.4 to 0.5 nN). The method is applicable to similar polymers, e.g. poly(tetramethylene hexamethylene sulphone) has a modulus of 176.7 GN/m<sup>2</sup> and an *f* value of 0.403 nN.

## INTRODUCTION

In a previous paper<sup>1</sup> we applied an energy balance method to the calculation of the elastic modulus of the helical polymer poly(phosphonitrilic chloride). No experimental values were available for the modulus of the crystal. Because of this the method was applied to a series of planar zig-zag polymers some of which had experimental results available for comparison with the calculated values. The polymers treated were polyethylene, s-PVC, s-PVF, s-PVA and s-PMMA<sup>2</sup>. These polymers are all of the simple  $-(A_1-A_2)-$  type with the exception of polyethylene which is of the  $-(A_1)-$  type. In this paper the method is applied to planar zig-zag polymers of a more complex basic structure. However, the principle of the method, does not change. The first polymer treated is nylon-6, 6 since the modulus of this polymer has been calculated previously<sup>3,4</sup> and experimental modulus results from X-ray techniques are available<sup>5</sup>. The method is then extended to other polyamides.

## DERIVATION OF MODULUS

### Nylon-6, 6

Nylon-6, 6 has a planar zig-zag structure similar to that of polyethylene; however, there are amide groups spaced at regular intervals along the chain (see *Figure 1a*). The repeat distance  $C_1C'_1$  contains 14 skeletal atoms, 12 carbon and 2 nitrogen which can be characterized by the following 'degrees of freedom'— $l_1, l_2, l_3, l_4, \alpha_1, \alpha_2, \alpha_3, \alpha_4$ , and  $\alpha_5$  where:

$$l_1 = C_1N_1 = N_2C_8$$

$$l_2 = N_1C_2 = C_7N_2$$

$$l_3 = C_2C_3 = C_3C_4 = C_4C_5 = C_5C_6 = C_6C_7 =$$

$$C_9C_{10} = C_{10}C_{11} = C_{11}C_{12}$$

$$l_4 = C_8C_9 = C_{12}C'_1$$

$$\alpha_1 = C_1N_1C_2 = C_7N_2C_8$$

$$\alpha_2 = N_1C_2C_3 = C_6C_7N_2$$

$$\alpha_3 = C_2C_3C_4 = C_3C_4C_5 = C_4C_5C_6 = C_5C_6C_7 =$$

$$C_9C_{10}C_{11} = C_{10}C_{11}C_{12}$$

$$\alpha_4 = N_2C_8C_9$$

$$\alpha_5 = C_{11}C_{12}C'_1$$

A two-dimensional Cartesian reference frame can be superimposed upon the repeat unit defining point  $C_1$  as the origin and direction  $C_1N_1$  as the *x* axis. The *y* axis is then through  $C_1$  and perpendicular to  $C_1N_1$  (see *Figure 1a*).

Vector components may now be assigned to each of the bonds making up the repeat unit as given below:

$$\begin{array}{c} \longrightarrow \\ C_1N_1 = (1, 0)l_1 \end{array}$$

$$\begin{array}{c} \longrightarrow \\ N_1C_2 = (\cos\theta_1, \sin\theta_1)l_2 \end{array}$$

$$\begin{array}{c} \longrightarrow \\ C_2C_3 = (\cos\eta_1, \sin\eta_1)l_3 \end{array}$$

$$\begin{array}{c} \longrightarrow \\ C_3C_4 = (\cos\theta_3, \sin\theta_3)l_3 \end{array}$$

$$\begin{array}{c} \longrightarrow \\ C_4C_5 = (\cos\eta_2, \sin\eta_2)l_3 \end{array}$$

$$\begin{array}{c} \longrightarrow \\ C_5C_6 = (\cos\theta_3, \sin\theta_3)l_3 \end{array}$$

$$\begin{array}{c} \longrightarrow \\ C_6C_7 = (\cos\eta_3, \sin\eta_3)l_3 \end{array}$$

$$\begin{array}{c} \longrightarrow \\ C_7N_2 = (\cos\theta_2, \sin\theta_2)l_2 \end{array}$$

$$\begin{array}{c} \longrightarrow \\ N_2C_8 = (\cos\eta_4, \sin\eta_4)l_1 \end{array}$$

$$\begin{array}{c} \longrightarrow \\ C_8C_9 = (\cos\theta_4, \sin\theta_4)l_4 \end{array}$$

$$\begin{aligned} \vec{C_9C_{10}} &= (\cos\eta_5, \sin\eta_5)l_3 \\ \vec{C_{10}C_{11}} &= (\cos\theta_3, \sin\theta_3)l_3 \\ \vec{C_{11}C_{12}} &= (\cos\eta_6, \sin\eta_6)l_3 \\ \vec{C_{12}C'_1} &= (\cos\theta_5, \sin\theta_5)l_4 \end{aligned}$$

where  $\theta_i$  and  $\eta_i$  are auxiliary angles (Figure 2), e.g.  $\theta_1$  is the angle between bond  $N_1C_2$  and the  $x$  axis,  $\eta_1$  is the angle between bond  $C_2C_3$  and the  $x$  axis and where initially  $\eta_i=0$  and

$$\theta_i = \pi - \alpha_i \tag{1}$$

The overall repeat vector  $\vec{C_1C'_1}$  is shown in Figure 3 and is designated

$$\vec{C_1C'_1} = (\cos\Omega, \sin\Omega)L = \vec{n} \cdot L \tag{2}$$

where  $L$  is the repeat distance.

The value of  $\Omega$  may be found by summing the  $y$  coordinates of the bonds in the repeat distance remembering that initially  $\eta=0$ ; therefore  $\sin\eta=0$  and  $\cos\eta=1$ .

$$\begin{aligned} \therefore L \sin\Omega &= \sum y_i = l_2 \sin\theta_1 + 3l_3 \sin\theta_3 + l_2 \sin\theta_2 + \\ & \quad l_4 \sin\theta_4 + l_4 \sin\theta_5 \end{aligned} \tag{3}$$

Hence from a knowledge of  $L$ ,  $l_i$  values and  $\theta_i$  values,  $\sin\Omega$  and hence  $\Omega$  can be calculated. As before if we consider the repeating unit  $L$  to undergo a change in

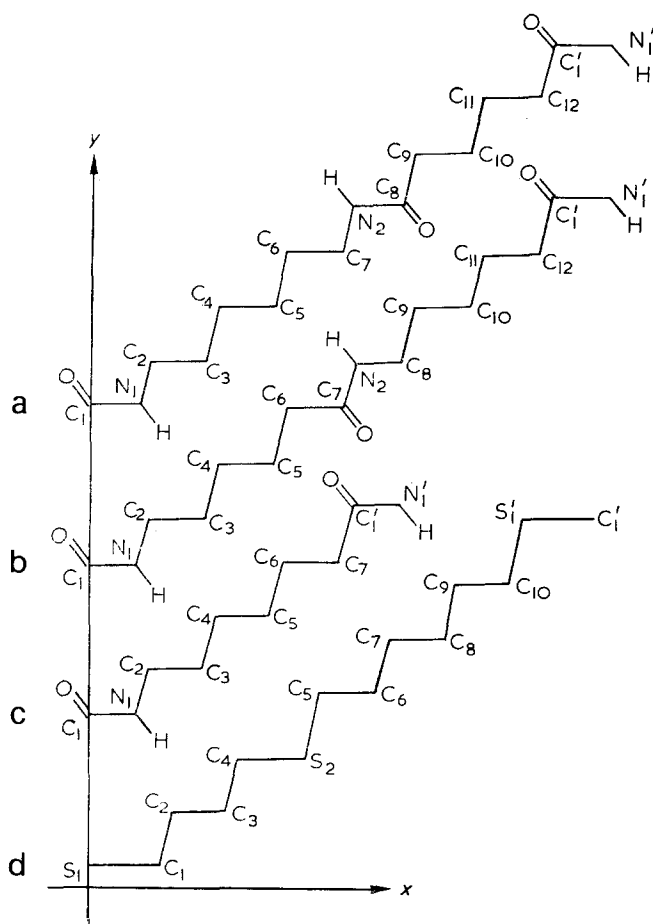


Figure 1 Conformation of nylons and PTHMS with superimposed Cartesian axes. (a) Nylon-6, 6; (b) nylon-6; (c) nylon-7; (d) PTHMS

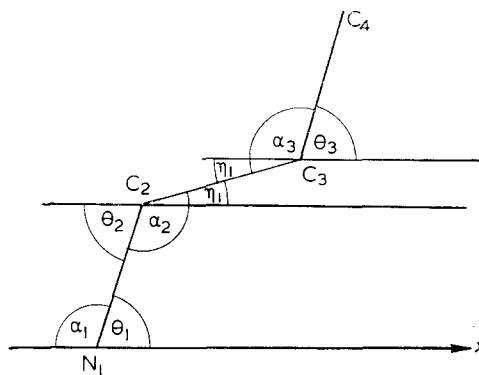


Figure 2 Designation of the auxiliary angles  $\theta$  and  $\eta$

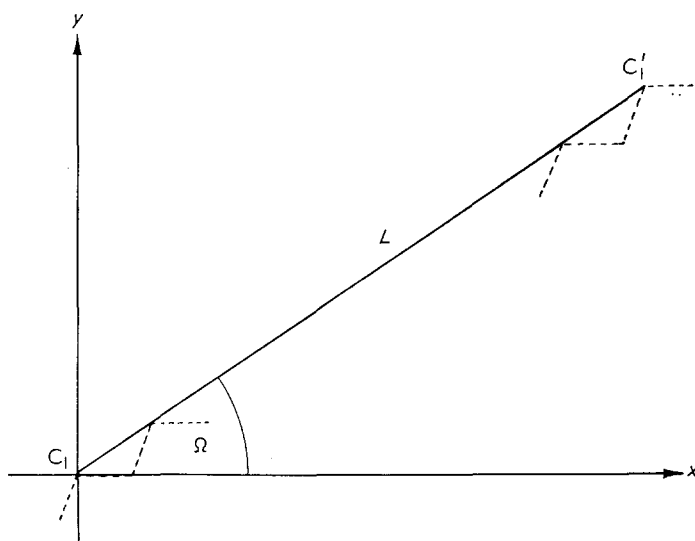


Figure 3 Relation of the repeat distance vector to the superimposed Cartesian axes

length  $dL$ , this change is made up as the sum of the small changes  $dL_i$  due to a small change  $dl_i$  in each degree of freedom, i.e.

$$dL = \sum_{i=1, \dots, n} dL_i$$

The small changes can be considered in two sections, first the bond length deformations:

$$dL_1 = 2\bar{n}(1, 0)dl_1 \tag{4}$$

$$dL_2 = 2\bar{n}(\cos\theta_1, \sin\theta_1)dl_2 \tag{5}$$

$$dL_3 = 5\bar{n}(1, 0)dl_3 + 3\bar{n}(\cos\theta_3, \sin\theta_3)dl_3 \tag{6}$$

$$dL_4 = 2\bar{n}(\cos\theta_4, \sin\theta_4)dl_4 \tag{7}$$

and secondly the bond angle deformations.

Considering only the portion of the chain  $N_1$  to  $N_2$  which is symmetric about the mid-point of  $C_4C_5$ :

$$\begin{aligned} dL_5 &= 2\{l_2\bar{n}[\partial/\partial\alpha_1(\cos\theta_1, \sin\theta_1)]d\alpha_1 + \\ & \quad l_3\bar{n}[\partial/\partial\alpha_1(\cos\eta_1, \sin\eta_1)]d\alpha_1 + \\ & \quad l_3\bar{n}[\partial/\partial\alpha_1(\cos\theta_3, \sin\theta_3)]d\alpha_1 + \\ & \quad \frac{1}{2}l_3\bar{n}[\partial/\partial\alpha_1(\cos\eta_2, \sin\eta_2)]d\alpha_1\} \end{aligned}$$

$$\begin{aligned} \therefore dL_5 &= 2\{l_2\bar{n}[\sin\theta_1, -\cos\theta_1] + l_3\bar{n}[\sin\eta_1, -\cos\eta_1] + \\ & \quad l_3\bar{n}[\sin\theta_3, -\cos\theta_3] + \frac{1}{2}l_3\bar{n}[\sin\eta_2, -\cos\eta_2]\}d\alpha_1 \end{aligned} \tag{8}$$

since  $\theta_1 = \pi - \alpha_1$ ,  $d\theta_1/d\alpha_1 = -1$  and also since  $\theta_2 = \theta_1 = \pi - \alpha_1 = \pi - \alpha_2 + \eta_1$  (see Figure 2)

$$\therefore d\eta_1/d\alpha_1 = -1$$

Similarly  $d\eta_2/d\alpha_1 = -1$ . Continuing as above:

$$dL_6 = 2\{l_3\bar{n}[-\sin\eta_1, \cos\eta_1] + l_3\bar{n}[-\sin\theta_3, \cos\theta_3] + \frac{1}{2}l_3\bar{n}[-\sin\eta_2, \cos\eta_2]\}d\alpha_2 \quad (9)$$

since  $d\eta_1/d\alpha_2 = +1$ ,  $d\theta_3/d\alpha_2 = +1$  and  $d\eta_2/d\alpha_2 = +1$ ,

$$dL_7 = 2\{l_3\bar{n}[\sin\theta_3, -\cos\theta_3] + \frac{1}{2}l_3\bar{n}[\sin\eta_2, -\cos\eta_2]\}d\alpha_3 \quad (10)$$

since  $d\theta_3/d\alpha_3 = -1$  and  $d\eta_2/d\alpha_3 = -1$ , and

$$dL_8 = l_3\bar{n}[-\sin\eta_2, \cos\eta_2]d\alpha_3 \quad (11)$$

since  $d\eta_2/d\alpha_3 = +1$ , [N.B.  $d\eta_2/d\alpha_3 \neq -1$  as in the previous differentiation since  $dL_7$  and  $dL_8$  refer to different positions of  $\alpha_3$ , i.e.  $C_2C_3C_4$  and  $C_4C_5C_6$  respectively.]

This completes section  $N_1$  to  $N_2$ . We must now consider section  $C_8$  to  $C'_1$  which is symmetric about the mid-point of  $C_{10}C_{11}$ .

$$dL_9 = 2\{l_4\bar{n}[\sin\theta_4, -\cos\theta_4] + l_3\bar{n}[\sin\eta_5, -\cos\eta_5] + \frac{1}{2}l_3\bar{n}[\sin\theta_3, -\cos\theta_3]\}d\alpha_4 \quad (12)$$

since  $d\theta_4/d\alpha_4 = -1$ ,  $d\eta_5/d\alpha_4 = -1$  and  $d\theta_3/d\alpha_4 = -1$ ,

$$dL_{10} = 2\{l_3\bar{n}[-\sin\eta_5, \cos\eta_5] + \frac{1}{2}l_3\bar{n}[-\sin\theta_3, \cos\theta_3]\}d\alpha_5 \quad (13)$$

since  $d\eta_5/d\alpha_5 = +1$  and  $d\theta_3/d\alpha_5 = +1$ , and finally

$$dL_{11} = l_3\bar{n}[\sin\theta_3, -\cos\theta_3]d\alpha_3 \quad (14)$$

since  $d\theta_3/d\alpha_3 = -1$ .

In all the previous expressions for  $dL_i$ ,  $\bar{n}$  is the repeat distance direction cosine:

$$\bar{n} = (\cos\Omega, \sin\Omega)$$

where  $\Omega$  is as defined earlier.

The delta values derived previously may then be utilized in the Jaswon formula<sup>1</sup> for the overall elastic constant,  $C$ :

$$C^{-1} = \frac{(dL_1)^2}{2K_1} + \frac{(dL_2)^2}{2K_2} + \frac{(dL_3)^2}{8K_3} + \frac{(dL_4)^2}{2K_4} + \frac{(dL_5)^2}{2H_{\alpha_1}} + \frac{(dL_6)^2}{2H_{\alpha_2}} + \frac{(dL_7)^2}{2H_{\alpha_3}} + \frac{(dL_8)^2}{2H_{\alpha_4}} + \frac{(dL_9)^2}{2H_{\alpha_4}} + \frac{(dL_{10})^2}{2H_{\alpha_5}} + \frac{(dL_{11})^2}{2H_{\alpha_3}} \quad (15)$$

where  $K_i$  and  $H_{\alpha}$  represent the appropriate stretching and bending force constants.

Finally, the Young's modulus  $c_{22}$  may be calculated from the relation:

$$c_{22} = \frac{CL^2}{V} = \frac{CL}{A}$$

where  $C$  is the overall elastic constant for the repeat unit as calculated above,  $L$  is the repeat distance and  $A$  is the effective cross-sectional area of the chain.

The force constants used by Treloar<sup>4</sup> in his treatment of nylon-6, 6 were obtained from an infra-red study of acetamide<sup>6</sup>. C-C(O)-N and C-C-N bending constants were assumed equal and that for C-N-C bending estimated from the stretching constants of the single bonds. The values used are given in Table 3. When Treloar's values and parameters are substituted in the above

equations, exactly the same result is obtained:  $c_{22} = 196.6$  GN/m<sup>2</sup>.

Owing to the uncertainty of those force constants a new set were calculated based on the Urey Bradley force field (UBFF)<sup>7</sup>.

#### DERIVATION OF FORCE CONSTANTS FROM A UREY BRADLEY TYPE FORCE FIELD

##### Nylon-6, 6

The parameters required and nomenclature for the Urey Bradley force field (UBFF) are shown in Figure 4.

The required force constants are then:

$$K_1 = K_{CONH} = K_{CN} + s_{32}^2 F_{CH_2NH} + s_{13}^2 F_{CH_2CO} + s_{21}' F_{N-CO} + s_{12}' F_{C-H} \quad (16)$$

$$K_2 = K_{NHCH_2} = K_{CN} + s_{23}^2 F_{CH_2NH} + s_{31}' F_{CH_2CO} + 2s_{23}' F_{N-H} + s_{32}' F_{C-H} \quad (17)$$

$$K_4 = K_{CH_2CO} = K_{CC} + s_{31}^2 F_{CH_2CO} + s_{32}^2 F_{CH_2NH} + 2s_{13}' F_{C-H} + s_{31}' F_{C-O} \quad (18)$$

where  $s_{32} = (r_{12} - r_{31} \cos\phi_1)/q_{32}$  and  $q_{32}^2 = r_{12}^2 + r_{31}^2 - 2r_{12}r_{31} \cos\phi_1$ .

It can be seen that  $s_{32} \equiv \cos x$  where  $x$  is the angle between  $q_{32}$  and  $r_{12}$  (see Figure 4). Similar relations for  $s_{13}$ ,  $s_{21}'$ ,  $s_{12}'$ ,  $s_{23}$ ,  $s_{31}$ ,  $s_{23}'$ ,  $s_{32}'$ ,  $s_{13}'$  and  $s_{31}'$  can be derived by considering similar angles. Also

$$H_{\alpha_1} = H^{\phi_1} = \rho_{32}^2 H_1 + t_{32}^2 \rho_{32}^2 F_{CH_2NH} + \rho_{23}^2 3\kappa/(8^{1/2} r_{31} r_{12}) \quad (19)$$

$$H_{\alpha_2} = H^{\phi_2} = \rho_{13}^2 H_2 + t_{13}^2 \rho_{13}^2 F_{CH_2CO} + \rho_{13}^2 3\kappa/(8^{1/2} r_{12} r_{23}) \quad (20)$$

$$H_{\alpha_3} = H^{\phi_3} = \rho_{23}^2 H_1 + t_{23}^2 \rho_{23}^2 F_{CH_2NH} + \rho_{23}^2 3\kappa/(8^{1/2} r_{23} r_{33}) \quad (21)$$

$$H_{\alpha_4} = H^{\phi_4} = \rho_{31}^2 H_3 + t_{31}^2 \rho_{31}^2 F_{CH_2CO} + \rho_{31}^2 3\kappa/(8^{1/2} r_{33} r_{31}) \quad (22)$$

where  $\rho_{32} = (r_{31} r_{12})^{1/2}$  and  $t_{32} = \rho_{32} \sin\phi_1/q_{32}$ .

It will be seen that  $t_{32} \equiv \sin x$  where  $x$  is as described above. Similarly, expressions for  $t_{13}$ ,  $t_{23}$  and  $t_{31}$  may be obtained by considering other angles.

Force constants  $K_3$  and  $H_{\alpha_5}$  for the polymethylene section of the chain are transferred directly from those obtained earlier for polyethylene<sup>2</sup>.

Molecular parameters and force constant data to be substituted into the previous equations are shown in Table 1. Unit cell data for nylon-6, 6 are in Table 3.

The resulting force constants are shown in Table 3 along with those used by Treloar and also a third set of force constants which are based on a valence force field (VFF).

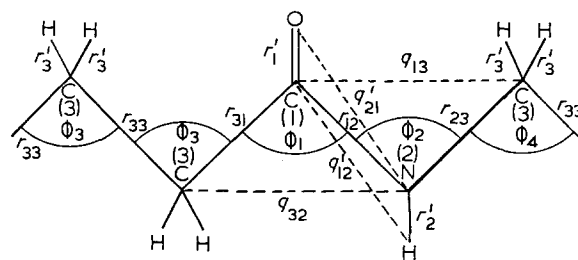


Figure 4 Parameters required for the derivation of the UBFF for nylon-6, 6

Table 1 Parameters used in modulus and force constant calculations

Molecular parameters <sup>a</sup>				Force constant datab			
Nylons <sup>9-11</sup>		PTHMS <sup>14</sup>		Nylons <sup>9-11</sup>		PTHMS <sup>14</sup>	
$l_1=r_{12}$	0.14	$l_1=r_{12}=r_{21}$	0.1778	KC-N	382	KC-S	187.8
$l_2=r_{23}$	0.147	$l_2=r_{23}=r_{32}$	0.154	KC-C	336	FCH <sub>2</sub> SO <sub>2</sub>	37.2
$l_3=r_{33}$	0.153	—	—	FCH <sub>2</sub> -CO	80	FCH <sub>2</sub> -CH <sub>2</sub>	20
$l_4=r_{31}$	0.153	—	—	FCH <sub>2</sub> -NH	-21	FC-O	35
$r'_1$	0.124	$r'_1$	0.1445	FNCO	132	FS-H	37.2
$r'_2$	0.1	$r'_2$	0.109	FCNH	32	H <sub>1</sub> =HcSC	23.2
$r'_3$	0.109	—	—	FN-H	35	H <sub>2</sub> =HcCS	20
$r'_4$	—	—	—	FC-O	54	$\kappa(\delta\text{CCS})$	-0.045
$\phi_1=\phi_3=\phi_4$	113° 32'	$\phi_1$	103°	FC-H	48.2	$\kappa(\delta\text{CSC})$	0.141
$\phi_2$	130° 48'	$\phi_2$	109° 28'	H <sub>1</sub>	100		
$\phi'_1$	120° 8'	$\phi'_1$	108° 48'	H <sub>2</sub>	28		
$\phi'_2$	114° 36'	$\phi'_2$	109° 28'	H <sub>3</sub>	11		
$\phi'_3$	109° 28'	—	—	$\kappa$	-0.049		
$\alpha_1=\alpha_2=\alpha_3=\alpha_4$	110°*	$\alpha_1=\alpha_2=\alpha_3$	109° 28'*				

<sup>a</sup> All bond lengths in nm

<sup>b</sup> All force constants in N/m except  $\kappa$  which is in aNm

\* For modulus calculation only

Table 2 Unit cell parameters for several polymer crystals

Polymer	Unit cell dimensions <sup>8</sup>						Number of chains in unit cell <sup>8</sup>	Effective cross-sectional area, A (nm <sup>2</sup> )	Crystal structure <sup>8</sup>
	a (nm)	b (nm)	c* (nm)	$\alpha$ (degrees)	$\beta$ (degrees)	$\gamma$ (degrees)			
Nylon-6, 6	0.49	0.54	1.72	48	77	63	1	0.2646	$\alpha$ -Form Triclinic
Nylon-6, 10	0.495	0.54	2.24	48	77	63	1	0.2646	Triclinic
Nylon-6	0.956	0.801	1.724	90	67.5	90	4	0.1914	$\alpha$ -Form Monoclinic
Nylon-7	0.49	0.54	0.985	49	77	63	1	0.2646	Triclinic
Nylon-11	0.96	0.42	1.50	72	90	64	2	0.2016	Triclinic
PTHMS	0.988	0.926	1.568	90	121.7	90	4	0.2287	Monoclinic

\* Fibre axis

Table 3 Force constants used in the calculations for nylon crystals

Parameter	Treloar <sup>4</sup>	UBFF	VFF <sup>13</sup>
$K_1(\text{KC}-\text{NH})$	780	561	611
$K_2(\text{KNH}-\text{CH}_2)$	574	510	527
$K_3(\text{KC}-\text{C})$	436	470*	453
$K_4(\text{KC}-\text{C})$	436	492	517
$H_{\alpha_1}(\text{HCO}-\text{N}-\text{CH}_2)$	140	81	232
$H_{\alpha_2}(\text{HN}-\text{C}-\text{C})$	82	191	156
$H_{\alpha_3}(\text{HC}-\text{C}-\text{C})$	82	222*	159
$H_{\alpha_4}(\text{HN}-\text{CO}-\text{C})$	82	195	253
$H_{\alpha_5}(\text{HC}-\text{C}-\text{CO})$	82	78	159

\* Transferred from polyethylene<sup>2</sup>

Stretching force constant units N/m

Bending force constant units aNm/rad

Some difficulty had been encountered in using a UBFF for amide force constant calculations<sup>12</sup> so Krimm and Jakes<sup>13</sup> have given a valence force field for the amide group and applied it to a study of the infra-red spectrum of nylon-6 and many other amides. The third set of force constants are transferred from their results. The results of the modulus calculation for nylon-6, 6 for each set of force constants are given in Table 4.

#### Nylon-6, 10

Nylon-6, 10 is very similar in structure to nylon-6, 6 but has 4 more CH<sub>2</sub> groups in its repeat distance and

can be analysed by an extension of the results obtained for nylon-6, 6, i.e. by including more terms in the expressions for the 'delta values'.

Molecular and force constant data were transferred directly from the values for nylon-6, 6 (Table 1) except for the dimensions of the triclinic unit cell<sup>8</sup> (see Table 2).

The effective cross-sectional area of the chain remained unchanged and the modulus of nylon-6, 10 was calculated using the three sets of force constants of Table 3. The calculated moduli are shown in Table 4.

#### Nylon-6

Nylon-6 departs further from the uniform planar zig-zag. Nylon-6 is less symmetrical than nylon-6, 6 and nylon-6, 10 due to the different way in which the chain is built up. In nylon-6, 6 the amide groups are in alternate directions along the chain as a result of the di-functional nature of its original reactants, e.g. a diamine and a diacid. Thus the sections of the nylon-6, 6/-6, 10 chain are symmetrical about a central point of a polymethylene section.

Nylon-6, however, being formed from one monomer has all the amide groups in the same direction. The structure of nylon-6 is shown in Figure 1b along with the superimposed axes as for nylon-6, 6 and nylon-6, 10. It can be seen there are two monomer units in the repeat distance since the carbonyl group falls on alternate sides of the chain.



Table 4 Calculated moduli and extensibilities of some polymer crystals

Polymer	Calculated modulus (GN/m <sup>2</sup> )			Calculated extensibility* (nN)			Experimental results <sup>5</sup> (GN/m <sup>2</sup> )
	UBFF	VFF	Force constants from ref. 4	UBFF	VFF	Force constants from ref. 4	
Nylon-6, 6	180.9	192.9	130.7	0.479	0.510	0.346	172.6
Nylon-6, 10	185.6	189.6	130.2	0.491	0.501	0.344	196.2
Nylon-6	244.1	262.8	179.7	0.468	0.501	0.343	164.8
Nylon-7	180.2	188.6	129.6	0.477	0.497	0.343	—
Nylon-11	243.5	241.4	165.2	0.488	0.486	0.333	—
PTHMS	176.7	—	—	0.403	—	—	—

\* For planar zig-zag polymers the extensibility should be in the range  $\approx 0.4$  to  $0.5 \text{ nN}^5$

Vector components for the bonds are then given as:

$$\begin{aligned} \vec{C}_1\vec{N}_1 &= (0, 1)l_1 \\ \vec{N}_1\vec{C}_2 &= (\cos\theta_1, \sin\theta_1)l_2 \\ \vec{C}_2\vec{C}_3 &= (\cos\eta_1, \sin\eta_1)l_3 \\ \vec{C}_3\vec{C}_4 &= (\cos\theta_3, \sin\theta_3)l_3 \\ \vec{C}_4\vec{C}_5 &= (\cos\eta_2, \sin\eta_2)l_3 \\ \vec{C}_5\vec{C}_6 &= (\cos\theta_3, \sin\theta_3)l_3 \\ \vec{C}_6\vec{C}_7 &= (\cos\eta_3, \sin\eta_3)l_4 \\ \vec{C}_7\vec{N}_2 &= (\cos\theta_5, \sin\theta_5)l_1 \\ \vec{N}_2\vec{C}_8 &= (\cos\eta_4, \sin\eta_4)l_2 \\ \vec{C}_8\vec{C}_9 &= (\cos\theta_2, \sin\theta_2)l_3 \\ \vec{C}_9\vec{C}_{10} &= (\cos\eta_5, \sin\eta_5)l_3 \\ \vec{C}_{10}\vec{C}_{11} &= (\cos\theta_3, \sin\theta_3)l_3 \\ \vec{C}_{11}\vec{C}_{12} &= (\cos\eta_6, \sin\eta_6)l_3 \\ \vec{C}_{12}\vec{C}'_1 &= (\cos\theta_4, \sin\theta_4)l_4 \end{aligned}$$

The angle  $\Omega$  made by the overall repeat distance  $\vec{C}_1\vec{C}'_1$  to the  $x$  axis is obtained by summing the  $y$  coordinates.

$$\therefore L \sin\Omega = l_2 \sin\theta_1 + 3l_3 \sin\theta_3 + l_1 \sin\theta_5 + l_3 \sin\theta_2 + l_4 \sin\theta_4 \quad (23)$$

and hence  $\bar{n}$  i.e.  $(\cos\Omega, \sin\Omega)$  may be calculated.

As for nylon-6, 6 and nylon-6, 10 the bond stretching deformations can be considered over the whole repeat distance.

$$\therefore dL_1 = \bar{n}(1, 0)dl_1 + \bar{n}(\cos\theta_5, \sin\theta_5)dl_1 \quad (24)$$

$$dL_2 = \bar{n}(\cos\theta_1, \sin\theta_1)dl_2 + \bar{n}(1, 0)dl_2 \quad (25)$$

$$dL_3 = 4\bar{n}(1, 0)dl_3 + 4\bar{n}(\cos\theta_3, \sin\theta_3)dl_3 \quad (26)$$

and

$$dL_4 = \bar{n}(1, 0)dl_4 + \bar{n}(\cos\theta_4, \sin\theta_4)dl_4 \quad (27)$$

The repeat distance  $\vec{C}_1\vec{C}'_1$  can be considered in two sections,  $\vec{N}_1$  to  $\vec{C}_6$  and  $\vec{C}_7$  to  $\vec{C}'_1$  with mid-points lying halfway along  $\vec{C}_3\vec{C}_4$  and  $\vec{C}_9\vec{C}_{10}$  respectively. Owing to

the lack of symmetry of the sections the method has to be modified slightly from that given for nylon-6, 6 and nylon-6, 10 when treating the bond angle deformation.

Consider first section  $\vec{N}_1\vec{C}_6$  and work from  $\vec{N}_1$  and  $\vec{C}_6$  alternately to the mid-point of  $\vec{C}_3\vec{C}_4$ :

$$\begin{aligned} dL_5 &= l_2\bar{n} \left[ \frac{\partial}{\partial\alpha_1} (\cos\theta_1, \sin\theta_1) \right] d\alpha_1 + \\ & l_3\bar{n} \left[ \frac{\partial}{\partial\alpha_1} (\cos\eta_1, \sin\eta_1) \right] d\alpha_1 + \\ & \frac{1}{2}l_3\bar{n} \left[ \frac{\partial}{\partial\alpha_1} (\cos\theta_3, \sin\theta_3) \right] d\alpha_1 \end{aligned}$$

$$\therefore dL_5 = \{l_2\bar{n}[\sin\theta_1, -\cos\theta_1] + l_3\bar{n}[\sin\eta_1, -\cos\eta_1] + \frac{1}{2}l_3\bar{n}[\sin\theta_3, -\cos\theta_3]\}d\alpha_1 \quad (28)$$

since  $d\theta_1/d\alpha_1 = -1$ ,  $d\theta_3/d\alpha_1 = -1$  and  $d\eta_1/d\alpha_1 = -1$ .

Also,

$$\begin{aligned} dL_6 &= l_3\bar{n} \left[ \frac{\partial}{\partial\alpha_4} (-\cos\theta_4, -\sin\theta_4) \right] d\alpha_4 + \\ & l_3\bar{n} \left[ \frac{\partial}{\partial\alpha_4} (-\cos\eta_2, -\sin\eta_2) \right] d\alpha_4 + \\ & \frac{1}{2}l_3\bar{n} \left[ \frac{\partial}{\partial\alpha_4} (-\cos\theta_3, -\sin\theta_3) \right] d\alpha_4 \end{aligned}$$

$$\therefore dL_6 = \{l_3\bar{n}[-\sin\theta_4, \cos\theta_4] + l_3\bar{n}[-\sin\eta_2, \cos\eta_2] + \frac{1}{2}l_3\bar{n}[-\sin\theta_3, \cos\theta_3]\}d\alpha_4 \quad (29)$$

since  $d\theta_4/d\alpha_4 = -1$ ,  $d\theta_3/d\alpha_4 = -1$  and  $d\eta_2/d\alpha_4 = -1$ . Similarly,

$$dL_7 = \{l_3\bar{n}[-\sin\eta_1, \cos\eta_1] + \frac{1}{2}l_3\bar{n}[-\sin\theta_3, \cos\theta_3]\}d\alpha_2 \quad (30)$$

since  $d\eta_1/d\alpha_2 = +1$  and  $d\theta_3/d\alpha_2 = +1$ ,

$$dL_8 = \{l_3\bar{n}[\sin\eta_2, -\cos\eta_2] + \frac{1}{2}l_3\bar{n}[\sin\theta_3, -\cos\theta_3]\}d\alpha_3 \quad (31)$$

since  $d\eta_2/d\alpha_3 = +1$  and  $d\theta_3/d\alpha_3 = +1$ , and

$$dL_9 = l_3\bar{n}[\sin\theta_3, -\cos\theta_3]d\alpha_3 \quad (32)$$

since  $d\theta_3/d\alpha_3 = -1$ .

We can revert to the shorter method as used for nylon-6, 6 at this point since for  $dL_9$  the remaining section of chain to be treated is symmetrical about the mid-point of  $\vec{C}_3\vec{C}_4$ .

Similarly, for section  $\vec{C}_7$  to  $\vec{C}'_1$  of the repeat unit we get:

$$dL_{10} = \{l_1\bar{n}[\sin\theta_5, -\cos\theta_5] + l_2\bar{n}[\sin\eta_4, -\cos\eta_4] + l_3\bar{n}[\sin\theta_2, -\cos\theta_2] + \frac{1}{2}l_3\bar{n}[\sin\eta_5, -\cos\eta_5]\}d\alpha_5 \quad (33)$$

since  $d\theta_5/d\alpha_5 = -1$ ,  $d\eta_4/d\alpha_5 = d\eta_5/d\alpha_5 = -1$  and  $d\theta_2/d\alpha_5 = -1$ ,

$$dL_{11} = \{l_4\bar{n}[-\sin\theta_5, \cos\theta_5] + l_3\bar{n}[-\sin\eta_6, \cos\eta_6] + l_3\bar{n}[-\sin\theta_3, \cos\theta_3] + \frac{1}{2}l_3\bar{n}[-\sin\eta_5, \cos\eta_5]\}d\alpha_5 \quad (34)$$

since  $d\theta_5/d\alpha_5 = -1$ ,  $d\eta_6/d\alpha_5 = d\eta_5/d\alpha_5 = -1$  and  $d\theta_3/d\alpha_5 = -1$ .

Continuing this procedure for the remainder of section  $C_7$  to  $C'_1$  we get:

$$dL_{12} = \{l_2\bar{n}[-\sin\eta_4, \cos\eta_4] + l_3\bar{n}[-\sin\theta_2, \cos\theta_2] + \frac{1}{2}l_3\bar{n}[-\sin\eta_5, \cos\eta_5]\}d\alpha_1 \quad (35)$$

since  $d\eta_4/d\alpha_1 = d\eta_5/d\alpha_1 = d\theta_2/d\alpha_1 = +1$ ,

$$dL_{13} = \{l_3\bar{n}[\sin\eta_6, -\cos\eta_6] + l_3\bar{n}[\sin\theta_3, \cos\theta_3] + \frac{1}{2}l_3\bar{n}[\sin\eta_5, -\cos\eta_5]\}d\alpha_4 \quad (36)$$

since  $d\eta_6/d\alpha_4 = d\eta_5/d\alpha_4 = d\theta_3/d\alpha_4 = +1$ ,

$$dL_{14} = \{l_3\bar{n}[\sin\theta_2, -\cos\theta_2] + \frac{1}{2}l_3\bar{n}[\sin\eta_5, -\cos\eta_5]\}d\alpha_2 \quad (37)$$

since  $d\theta_2/d\alpha_2 = d\eta_5/d\alpha_2 = -1$ ,

$$dL_{15} = \{l_3\bar{n}[-\sin\theta_3, \cos\theta_3] + \frac{1}{2}l_3\bar{n}[-\sin\eta_5, \cos\eta_5]\}d\alpha_3 \quad (38)$$

since  $d\theta_3/d\alpha_3 = d\eta_5/d\alpha_3 = -1$ . Finally,

$$dL_{16} = l_3\bar{n}[-\sin\eta_5, \cos\eta_5]d\alpha_3 \quad (39)$$

since  $d\eta_5/d\alpha_3 = +1$ .

It will be found that on calculation of the above delta values  $dL_6$ ,  $dL_8$ ,  $dL_{11}$ ,  $dL_{13}$  and  $dL_{15}$  give negative results. This is as expected since in their derivation the deformations are considered as acting in a  $-x$ ,  $-y$  sense.

No difficulty is encountered due to the sign of the  $dL_i$  since each  $dL_i$  is squared for inclusion in the expression for the overall elastic constant  $C$  which is given for nylon-6 as:

$$C^{-1} = \frac{(dL_1)^2}{2K_1} + \frac{(dL_2)^2}{2K_2} + \frac{(dL_3)^2}{8K_3} + \frac{(dL_4)^2}{2K_4} + \frac{(dL_5)^2}{H_{\alpha_1}} + \frac{(dL_6)^2}{H_{\alpha_2}} + \frac{(dL_7)^2}{H_{\alpha_3}} + \frac{(dL_8)^2}{H_{\alpha_4}} + \frac{(dL_9)^2}{2H_{\alpha_5}} + \frac{(dL_{10})^2}{H_{\alpha_6}} + \frac{(dL_{11})^2}{H_{\alpha_7}} + \frac{(dL_{12})^2}{H_{\alpha_8}} + \frac{(dL_{13})^2}{H_{\alpha_9}} + \frac{(dL_{14})^2}{H_{\alpha_{10}}} + \frac{(dL_{15})^2}{H_{\alpha_{11}}} + \frac{(dL_{16})^2}{2H_{\alpha_{12}}} \quad (40)$$

Using the value obtained for  $C^{-1}$  the elastic constant  $c_{22}$  may be calculated from:

$$c_{22} = \frac{CL}{A}$$

where  $L$  is the repeat distance and  $A$  the effective cross-sectional area of chain.

All molecular parameters and force constants for nylon-6 were transferred from nylon-6, 6, nylon-6, 10, etc. (Table 1). Unit cell data are in Table 2.

The calculated moduli of nylon-6, for three sets of force constants (Table 3) are shown in Table 4.

#### Nylon-7

Nylon-7 has a structure similar to that of nylon-6 but with one more  $-\text{CH}_2-$  group than nylon-6. The odd number of carbon atoms in the chemical unit results in a chain with all the carbonyl groups being on the same side. Hence, the repeat distance of nylon-7 is much

shorter than that of nylon-6 and contains only one monomer unit per chain repeat distance. The structure of nylon-7 and its superimposed set of axes are shown in Figure 1c.

Vector components are assigned and the bond stretching deformations derived, as before.

The shorter repeat distance of nylon-7, enables the bond angle deformations to be obtained by considering the complete repeat distance  $C_1C'_1$  at one time starting from  $C_1$  and  $C'_1$  and working towards the mid-point of the unit which is halfway between  $C_4$  and  $C_5$ .

The 'delta values'  $dL_i$  are used to obtain the overall elastic constant  $C$  for the repeat distance and the modulus  $c_{22}$  calculated from:

$$c_{22} = \frac{CL}{A}$$

Molecular parameters and force constant data were transferred from the calculation for nylon-6 (Tables 1 and 2).

The calculated elastic moduli of nylon-7 are shown in Table 4 for three sets of force constants (Table 3).

#### Nylon-11

Nylon-11 is similar to nylon-7 in that all the carbonyl groups lie on the same side of the chain. The only difference is that there are four more  $\text{CH}_2$  groups separating the amide groups than in nylon-7. Hence the modulus is calculated by a simple extension of the method given for nylon-6 and nylon-7, i.e. we include more terms in the expression for the  $dL_i$ 's.

Molecular parameters and initial force constant data are in Table 1, unit cell data in Table 2.

The moduli calculated using the force constants of Table 3 are given in Table 4.

#### Poly(tetramethylene hexamethylene sulphone) (PTHMS)

It was decided to calculate the modulus of a polymer with a similar type of long chemical unit in its repeat distance, viz. a polysulphone.

The structure of poly(tetramethylene hexamethylene sulphone)  $-(\text{CH}_2)_4.\text{SO}_2.(\text{CH}_2)_6.\text{SO}_2-$  is shown in Figure 1d with the Cartesian reference frame superimposed on the chain.

From this diagram the vector components of each bond can be obtained and the direction cosine ( $\bar{n}$ ) of the repeat distance vector obtained by summing the  $y$  coordinates making up the repeat distance.

The bond length deformations can then be written directly and the angular deformation obtained by considering the repeat distance in two sections  $S_1$  to  $S_2$  and  $S_2$  to  $S_1$ .

As both sections are symmetrical about the mid-points of  $C_2C_3$  and  $C_7C_8$  respectively the method used is exactly the same as for nylon-6, 6 and nylon-6, 10.

The overall elastic constant for the repeat unit is then obtained from:

$$C^{-1} = \frac{(dL_1)^2}{4K_1} + \frac{(dL_2)^2}{8K_2} + \frac{(dL_3)^2}{2H_{\alpha_1}} + \frac{(dL_4)^2}{2H_{\alpha_2}} + \frac{(dL_5)^2}{2H_{\alpha_3}} + \frac{(dL_6)^2}{2H_{\alpha_4}} + \frac{(dL_7)^2}{2H_{\alpha_5}} + \frac{(dL_8)^2}{2H_{\alpha_6}} \quad (41)$$

and finally the elastic modulus  $c_{22}$  from:

$$c_{22} = \frac{CL}{A}$$

where  $L$  is the repeat distance and  $A$  the effective cross-sectional area of the chain.

The force constants  $K_1$ ,  $K_2$ ,  $H_{\alpha_1}$ , and  $H_{\alpha_2}$  were derived from a Urey Bradley type of force field as shown below.

The required force constants are obtained from the following sets of equations:

$$K_1 = K_{\text{CH}_2\text{SO}_2} = K_{\text{C-S}} + s_{31}^2 F_{\text{CH}_2\text{SO}_2} + s_{22}^2 F_{\text{CH}_2\text{CH}_2} + 2s_{21}^2 F_{\text{C-O}} + 2s_{12}^2 F_{\text{S-H}} \quad (42)$$

$$H_{\alpha_1} = H^{\phi_1} = \rho_{22}^2 H_1 + \rho_{22}^2 t_{22}^2 F_{\text{CH}_2\text{CH}_2} + \rho_{22}^2 3\kappa / (8^{1/2} r_{21} r_{12}) \quad (43)$$

and

$$H_{\alpha_2} = H^{\phi_2} = \rho_{31}^2 H_2 + \rho_{31}^2 t_{31}^2 F_{\text{CH}_2\text{SO}_2} + \rho_{31}^2 3\kappa / (8^{1/2} r_{32} r_{21}) \quad (44)$$

where  $s_{31}$ ,  $s_{22}$ ,  $s_{21}$ ,  $s_{12}$ ,  $\rho_{22}$ ,  $\rho_{31}$ ,  $t_{22}$  and  $t_{31}$  may be derived as shown earlier for the nylons. The parameters and nomenclature are shown in Figure 5.

The values of  $K_2$  and  $H_{\alpha_2}$  for the polymethylene sections of the chain were transferred from the calculation for polyethylene carried out earlier<sup>2</sup>.

Molecular parameters, initial force constant data and unit cell dimensions are given in Tables 1 and 2. The calculated elastic modulus of PTHMS is given in Table 4.

## RESULTS

Table 3 gives the three sets of force constants used, those estimated by Treloar<sup>4</sup> and those from Urey Bradley or valence force fields. Table 4 shows the values calculated for the modulus, extensibility ( $f$  value) and experimental data where available.

Extensibility<sup>5</sup> is the force required to stretch the molecule by 1% in the direction of the molecular axis and is calculated as the product of the modulus and the cross-sectional area of a single molecule.

## DISCUSSION

The force constants used by Treloar were estimated from early work<sup>6</sup> on acetamide and are not further considered.

The *UBFF* constants are transferred from the normal coordinate analysis of *cis* and *trans* diacetamide, urea and substituted amides<sup>9-11</sup>. The *VFF* force constants were transferred directly from a valence force field set up specifically for the amide group and for the nylons<sup>13</sup> and thus could be expected to be the most accurate.

The close agreement between results for the modulus, based on *VFF* and *UBFF* force constants supports the use of the *UBFF* method for which more data are available.

As the modulus is proportional to the repeat distance  $L$  and inversely proportional to the cross-section area

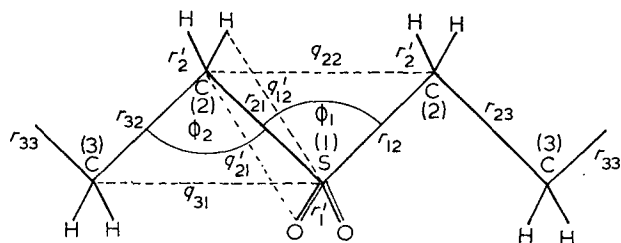


Figure 5 Parameters required for the derivation of the *UBFF* for poly(tetramethylene hexamethylene sulphone)

one would expect to find values of modulus decreasing in the series nylon-6 > nylon-11 > nylon-6, 10 > nylon-6, 6 > nylon-7, as nylon-6, 10; nylon 6, 6 and nylon-7 have a large cross-section area whilst nylon-6 and nylon-11 have low cross-section areas. It can be seen in Table 4 that the results fall in the expected sequence. The calculated and observed moduli for nylon-6, 6 and nylon-6, 10 are in fair agreement.

However, the observed result for nylon-6 is much lower than the calculated value and also is contrary to the prediction that nylon-6 should have the highest modulus.

Nylons have intermolecular hydrogen bonds when crystalline and therefore secondary bonding effects must play some part in the deformation of the crystal. The contribution depends on the crystal structure and since nylon-6 alone is monoclinic, the lower modulus for nylon-6 could be due to a lesser H-bonding effect in the monoclinic crystal structure. Since the present calculation only considers primary bonding effects, such changes in the modulus would not be apparent. Difficulties relating to the order of reflection used may also affect the experimental results<sup>5</sup>.

The extensibilities ( $f$  values) for the nylon series calculated from our results all lie within the range 0.4 to 0.5 nN as expected for a polymer with a planar zig-zag structure (see Table 4).

The method used in these calculations appears to be satisfactory for the nylons since the calculated moduli are in good agreement with the 'expected' moduli as described above.

Finally, the method was applied to a crystal of poly(tetramethylene hexamethylene sulphone) since the structure is quite similar to that of the nylons. No X-ray or previously calculated results were available. However, the extensibility of the polymer (0.404 nN) is within the range expected.

## ACKNOWLEDGEMENT

We thank the Science Research Council for a scholarship to C.G.M.

## REFERENCES

- 1 Manley, T. R. and Martin, C. G. *Polymer* 1971, **12**, 775
- 2 Manley, T. R. and Martin, C. G. *Polymer* 1973, **14**, 491
- 3 Lyons, W. J. *J. Appl. Phys.* 1958, **29**, 1429
- 4 Treloar, L. R. G. *Polymer* 1960, **1**, 95
- 5 Sakurada, I. and Kaji, K. *J. Polym. Sci. (C)* 1970, **31**, 57
- 6 Davies, M., Evans, J. C. and Jones, R. L. *Trans. Faraday Soc.* 1955, **51**, 761
- 7 Shimanouchi, T. *J. Chem. Phys.* 1949, **17**, 245, 734, 848
- 8 Alexander, L. E. 'X-Ray Diffraction Methods in Polymer Science', Wiley-Interscience, New York, 1969, Appendix 3, p 492
- 9 Kurado, Y., Saito, Y., Machida, K. and Uno, T. *Spectrochim. Acta* 1971, **27A**, 1481
- 10 Saito, Y., Machida, K. and Uno, T. *Spectrochim. Acta* 1971, **27A**, 991
- 11 Uno, T., Machida, K. and Saito, Y. *Spectrochim. Acta* 1971, **27A**, 833
- 12 Jakes, J. unpublished (1966)
- 13 Jakes, J. and Krimm, S. *Spectrochim. Acta* 1971, **27A**, 19
- 14 Uno, T., Machida, K. and Hanai, K. *Spectrochim. Acta* 1971, **27A**, 107

# Synthesis and homopolymerization studies of vinylimidazolium salts

J. C. Salamone\*, S. C. Israel, P. Taylor and B. Snider†

*Polymer Science Program, Department of Chemistry, Lowell Technological Institute, Lowell, Mass. 01854, USA and*

*Macromolecular Research Center, University of Michigan, Ann Arbor, Michigan 41805, USA (Received 27 April 1973; revised 24 July 1973)*

The preparations and characterizations of several monomeric vinylimidazolium salts are presented from the quaternizations of 1-vinylimidazole and 2-methyl-1-vinylimidazole with *n*-alkyl iodides and with dimethyl sulphate. Although vinylimidazolium salts have been reported in the patent literature, many of these salts were not isolated and characterized prior to their polymerization. From the reactions of 1-vinylimidazole with *n*-alkyl iodides, a homologous series of 3-*n*-alkyl-1-vinylimidazolium iodides were prepared in which the longer chain derivatives appeared to form micelles in aqueous solution. Dicationic cross-linking agents were also prepared through similar quaternization reactions. All the cationic vinyl monomers were homopolymerized in aqueous solution by free radical initiation. The solution behaviour of the resulting polyions indicated that the longer side-chain polyions had polysoap properties.

## INTRODUCTION

The free radical polymerization of cationic vinyl monomers has been an area of increased interest in recent years<sup>1,2</sup>. Although many such monomers have been synthesized, most of these have contained the positive charge far removed from the double bond. Very few studies have been concerned with monomers in which the positive charge was adjacent to the vinyl group, since these monomers can be difficult to polymerize. However, it has been found that when the cationic site is on an aromatic ring which is adjacent to a double bond, homo- and co-polymerization appears possible. This is illustrated by the free radical polymerizations of various vinylpyridinium<sup>3-7</sup> salts.

In this work are presented the preparation, characterization and polymerization of a variety of quaternary iodide and methylsulphate salts from 1-vinylimidazole and 2-methyl-1-vinylimidazole. Although mention has been made in the patent literature on the free radical polymerization of vinylimidazolium salts<sup>8</sup>, in many cases these quaternary monomers do not appear to have been isolated and characterized.

## EXPERIMENTAL

### *Monomer preparations*

**3-Methyl-1-vinylimidazolium iodide (Ia).** To 9.41 g (0.10 mol) of freshly distilled 1-vinylimidazole was added 85.20 g (0.60 mol) of reagent grade methyl iodide in 100 ml of dry ethyl acetate at  $-10^{\circ}\text{C}$ . The reaction mixture was stirred for 1 h and then brought to room

temperature overnight, during which time off-white crystals formed. The mixture was cooled and filtered, and the monomeric salt was washed three times with anhydrous diethyl ether, followed by three recrystallizations from *n*-propanol giving a 56% yield of off-white needles, m.p.  $77.5-78.0^{\circ}\text{C}$  (lit.  $85-86^{\circ}\text{C}$ )<sup>9</sup>.

Calculated for  $\text{C}_6\text{H}_9\text{N}_2\text{I}$ : C, 30.53%; H, 3.84%; N, 11.87%; I, 53.76%. Found: C, 30.44%; H, 3.79%; N, 11.82%; I, 53.77%.

**3-*n*-Propyl-1-vinylimidazolium iodide (Ib).** This monomer was prepared by a similar procedure to that for Ia except that stirring was conducted for 1 h at room temperature using 19.4 g (0.12 mol) of *n*-propyl iodide. After stirring, the solution was left overnight and an oily product separated. The oil was removed by decantation and triturated with diethyl ether. After a second trituration, solid formed. The quaternary salt was recrystallized from *n*-propanol giving a 58.9% yield with m.p.  $68.0-68.5^{\circ}\text{C}$ .

Calculated for  $\text{C}_8\text{H}_{13}\text{N}_2\text{I}$ : C, 36.38%; H, 4.97%; N, 10.60%; I, 48.05%. Found: C, 36.32%; H, 5.14%; N, 10.28%; I, 48.35%.

**3-*n*-Hexyl-1-vinylimidazolium iodide (Ic).** To 10.60 g (0.050 mol) of *n*-hexyl iodide in 25 ml of dry ethyl acetate at room temperature was added with stirring 2.35 g (0.025 mol) of 1-vinylimidazole. Stirring was continued for 8 h, during which time a light yellow oil separated. The product, which remained as an oil after several triturations with diethyl ether, was obtained in 10.5% yield.

Calculated for  $\text{C}_{11}\text{H}_{19}\text{N}_2\text{I}$ : C, 43.15%; H, 6.26%; N, 9.15%; I, 41.45%. Found: C, 42.44%; H, 6.48%; N, 9.44%; I, 41.74%.

\* To whom enquiries should be addressed.

† Present address: Dept. of Chemistry, Harvard University, Cambridge, Mass., USA.

**3-n-Heptyl-1-vinylimidazolium iodide (Id).** This monomer was prepared by a procedure similar to that for Ic except that the same molar amount of n-heptyl iodide was used. The reaction was stirred for 48 h, after which time the oily layer which formed was separated by decantation. After repeated triturations with diethyl ether, the product remained as an oil and was obtained in 17.5% yield.

Calculated for  $C_{12}H_{21}N_2I$ : C, 45.01%; H, 6.61%; N, 8.75%; I, 39.63%. Found: C, 44.82%; H, 6.80%; N, 8.77%; I, 39.77%.

**3-n-Dodecyl-1-vinylimidazolium iodide (Ie).** To 3.55 g (0.012 mol) of n-dodecyl iodide in 100 ml of dry ethyl acetate was added 1.00 g (0.0106 mol) of 1-vinylimidazole. After stirring the mixture for 48 h at room temperature, the solution was cooled to 0°C, and crystallization of the quaternary salt rapidly occurred. The crystals were filtered, washed with diethyl ether and recrystallized three times from ethyl acetate giving 2.02 g (51.0% yield) of off-white needles, m.p. 50.3–51.8°C.

Calculated for  $C_{17}H_{31}N_2I$ : C, 52.30%; H, 8.01%; N, 7.18%; I, 32.24%. Found: C, 52.04%; H, 8.46%; N, 7.08%; I, 32.15%.

**3-n-Hexadecyl-1-vinylimidazolium iodide (If).** This monomer was prepared by the same procedure as that for Ie except for the utilization of 4.23 g (0.012 mol) of n-hexadecyl iodide. After three recrystallizations from ethyl acetate, off-white needles formed in 30% yield, m.p. 68.0–68.5°C.

Calculated for  $C_{21}H_{39}N_2I$ : C, 56.50%; H, 8.81%; N, 6.27%; I, 28.42%. Found: C, 56.62%; H, 9.08%; N, 6.14%; I, 28.45%.

**2,3-Dimethyl-1-vinylimidazolium iodide (II).** Using the same conditions as that for Ia with the exception of conducting the entire reaction at room temperature, it was found that crystals formed rapidly. After washing the off-white crystals with diethyl ether followed by three recrystallizations from n-propanol, a 59.2% yield was obtained with m.p. 149.2–151.0°C.

Calculated for  $C_7H_{11}N_2I$ : C, 33.62%; H, 4.43%; N, 11.20%; I, 50.75%. Found: C, 33.80%; H, 4.43%; N, 11.18%; I, 50.64%.

**1,4-Butanediyl-3,3'-bis-1-vinylimidazolium diiodide (IIIa).** To a solution of 3.10 g (0.010 mol) of 1,4-diiodobutane in 20 ml of dry ethyl acetate was added 1.47 g (0.012 mol) of 1-vinylimidazole. After standing at room temperature for two weeks, the mixture was filtered and a crystalline product was obtained. The crystals were washed with ethyl acetate and then diethyl ether, followed by vacuum drying. The dicationic monomer was dissolved in 50 ml of water, 25 ml of acetone were added and the solution was concentrated *in vacuo* until crystals formed. The solution was stored in a refrigerator until crystallization was complete and the product was then filtered giving a 39.2% yield, m.p. 159.0–161.0°C.

Calculated for  $C_{14}H_{20}N_4I_2$ : C, 33.75%; H, 4.05%; N, 11.25%; I, 50.95%. Found: C, 33.70%; H, 4.01%; N, 11.31%; I, 50.75%.

**1,4-Butanediyl-3,3'-bis-2-methyl-1-vinylimidazolium diiodide (IIIb).** To a solution of 3.10 g (0.010 mol) of 1,4-diiodobutane in 100 ml of dry ethyl acetate at room

temperature was added 4.33 g (0.040 mol) of 2-methyl-1-vinylimidazole. A precipitate began to form within a few minutes. The solution was then stored overnight at 0°C and the product was then filtered and washed with ethyl acetate. After recrystallization in acetone–water by the procedure given for IIIa, a 53.3% yield of 2-methyl-3-(4-iodobutyl)-1-vinylimidazolium iodide, m.p. 141.0–144.0°C, was obtained. The incompletely quaternized product (1.72 g, 0.0042 mol) was dissolved in 20 ml of methanol and heated at 65°C for 3 h with 3.0 g (0.028 mol) of 2-methyl-1-vinylimidazole. The solution was cooled and poured into excess ethyl acetate to precipitate the dicationic salt. The final product was filtered, washed with diethyl ether and dried giving a 51% yield, m.p. 271.0–273.0°C.

Calculated for  $C_{16}H_{24}N_4I_2$ : C, 36.52%; H, 4.60%; N, 10.65%; I, 48.23%. Found: C, 35.70%; H, 4.54%; N, 10.56%; I, 48.18%.

**3-Methyl-1-vinylimidazolium methylsulphate (IVa).** To 15.14 g (0.12 mol) of freshly distilled dimethyl sulphate in 60 ml of dry ethyl acetate at –10°C was added 9.41 g (0.1 mol) of 1-vinylimidazole. A precipitate began to form within 10 min. After standing at 0°C for 4 h, the product was filtered, washed with ethyl acetate and then recrystallized from n-butanol. The white crystals were filtered, washed with diethyl ether and dried *in vacuo* at room temperature giving a 66.5% yield, m.p. 66.6–67.9°C. This product was found to be very hygroscopic.

Calculated for  $C_7H_{12}N_2SO_4$ : C, 38.17%; H, 5.49%; N, 12.72%; S, 14.56%. Found: C, 37.63%; H, 5.62%; N, 12.41%; S, 14.30%.

**2,3-Dimethyl-1-vinylimidazolium methylsulphate (IVb).** To 18.92 g (0.15 mol) of dimethyl sulphate in 60 ml of dry ethyl acetate at –10°C was added 10.81 g (0.10 mol) of freshly distilled 2-methyl-1-vinylimidazole. A precipitate was noted within 5 min. After standing at 0°C for 4 h, the monomeric salt was filtered, washed with ethyl acetate and recrystallized from n-propanol. After filtration, white hygroscopic crystals were obtained which were washed with diethyl ether and vacuum dried at room temperature giving a 42.2% yield with a m.p. of 65.0–66.2°C.

Calculated for  $C_8H_{14}N_2SO_4$ : C, 41.01%; H, 6.02%; N, 11.96%; S, 13.69%. Found: C, 40.89%; H, 5.91%; N, 11.96%; S, 13.57%.

#### Homopolymerization reactions

All homopolymerization reactions were conducted by the following procedure. To a heavy walled polymerization tube was added 10 ml of a 0.45 M aqueous solution of a monomeric salt (Ia–If, II, IVa, IVb) which contained 1 mol% of 4,4'-azobiscyanovaleic acid. The contents of the tube was flushed with nitrogen and sealed *in vacuo* after utilization of the freeze–thaw technique. The tubes were then placed in a constant temperature bath thermostated at 60°C for 20 h. In the cases of the completely water soluble, short chain length polymers (Va, Vb, VI, VIIa, VIIb), the polymeric salt solutions were exhaustively dialysed against de-ionized water and the products were obtained by lyophilization. The intermediate chain length polymers (Vc and Vd) were completely water insoluble and these products were dissolved in ethanol

and dialysed against ethanol-water and then water. Polymers Vc and Vd were then obtained in powder form by filtration. In the formation of the long side-chain polymers (Ve and Vf), the solutions turned opaque during the reaction and approximately 30% water insoluble polymer formed with the remainder existing in an emulsified solution. This solution was dialysed against de-ionized water and then isolated in aqueous solution. The percentage yields and elemental analyses of all polymers are given below.

*Poly(3-methyl-1-vinylimidazolium iodide) (Va)* obtained in 60.4% yield after lyophilization.

Calculated for  $C_6H_9N_2I$ : C, 30.53%; H, 3.84%; N, 11.87%; I, 53.76%. Found: C, 30.52%; H, 3.96%; N, 11.65%; I, 53.69%.

*Poly(3-n-propyl-1-vinylimidazolium iodide) (Vb)* obtained in 58.9% yield after lyophilization.

Calculated for  $C_8H_{13}N_2I$ : C, 36.38%; H, 4.97%; N, 10.60%. Found: C, 36.30%; H, 5.09%; N, 10.50%.

*Poly(3-n-hexyl-1-vinylimidazolium iodide) (Vc)* obtained in 65.0% yield after filtration.

Calculated for  $C_{11}H_{19}N_2I$ : C, 43.15%; H, 6.26%; N, 9.15%; I, 41.45%. Found: C, 43.21%; H, 6.27%; N, 9.54%; I, 40.74%.

*Poly(3-n-heptyl-1-vinylimidazolium iodide) (Vd)* obtained in 59.8% yield after filtration.

Calculated for  $C_{12}H_{21}N_2I$ : C, 45.01%; H, 6.61%; N, 8.75%; I, 39.63%. Found: C, 45.29%; H, 6.66%; N, 9.60%; I, 38.29%.

*Poly(3-n-dodecyl-1-vinylimidazolium iodide) (Ve)* obtained in a total yield of 63.1% (including water-soluble and water-insoluble polymer).

Calculated for  $C_{17}H_{31}N_2I$ : C, 52.30%; H, 8.01%; N, 7.18%; I, 32.24%. Found: C, 52.04%; H, 8.46%; N, 7.08%; I, 32.51%.

*Poly(3-n-hexadecyl-1-vinylimidazolium iodide) (Vf)* obtained in a total yield of 64.7% (including water-soluble and water-insoluble polymer).

Calculated for  $C_{21}H_{39}N_2I$ : C, 56.50%; H, 8.81%; N, 6.27%; I, 28.42%. Found: C, 56.32%; H, 8.62%; N, 6.37%; I, 28.58%.

*Poly(2,3-dimethyl-1-vinylimidazolium iodide) (VI)* obtained in 53.2% yield after lyophilization.

Calculated for  $C_7H_{11}N_2I$ : C, 33.62%; H, 4.43%; N, 11.20%; I, 50.75%. Found: C, 33.42%; H, 4.62%; N, 11.01%; I, 50.70%.

*Poly(3-methyl-1-vinylimidazolium methylsulphate) (VIIa)* obtained in 43.9% yield after lyophilization.

Calculated for  $C_7H_{12}N_2SO_4$ : C, 38.17%; H, 5.49%; N, 12.72%; S, 14.6%. Found: C, 38.12%; H, 5.41%; N, 12.67%; S, 14.54%.

*Poly(2,3-dimethyl-1-vinylimidazolium methylsulphate) (VIIb)* obtained in 67.6% yield after lyophilization.

Calculated for  $C_8H_{14}N_2SO_4$ : C, 41.01%; H, 6.02%; N, 11.96%. Found: C, 41.15%; H, 6.07%; N, 12.08%.

### Crosslinking reactions

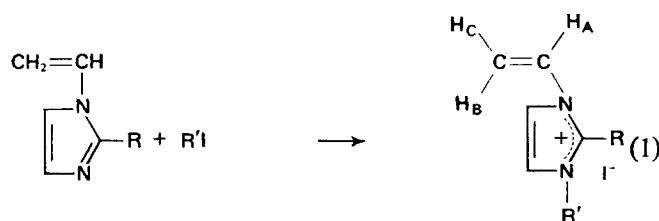
Copolymerization reactions of 1,4-butanediyl-3,3'-bis-1-vinylimidazolium diiodide (IIIa) with 3-methyl-1-vinylimidazolium iodide (Ia) and of 1,4-butanediyl-3,3'-bis-2-methyl-1-vinylimidazolium diiodide (IIIb) with 2,3-dimethylimidazolium iodide (II) were conducted in a similar manner to that of the homopolymerization reactions. Each solution contained a total monomer concentration of 0.45 M in 10 ml of water of which the crosslinking agent (IIIa or IIIb) amounted to 5 mol% of the monocationic salt (Ia or II). After copolymerization at 60°C for 24 h with 1 mol% 4,4'-azobiscyanovaleric acid, the products were obtained as soft gels which were exhaustively dialysed against water followed by lyophilization. The dried sample was then twice slurried in water and centrifuged to separate the soluble and insoluble portions. The reaction between Ia and IIIa gave a 68.5% yield of which 31.3% was water insoluble whereas the reaction between II and IIIb gave an 80.5% yield of which 53.5% was water insoluble.

## RESULTS AND DISCUSSION

### Monomer preparations

In this work, it was of interest to prepare a homologous series of quaternary vinylimidazolium salts in which the linear alkyl moiety could be increased in chain length. Such a series of monomeric salts could have varied hydrophilic-hydrophobic character such that they could function as 'normal' organic salts with the short alkyl moieties or as detergents with the long alkyl moieties. In a similar fashion, the progression in alkyl chain length would also be expected to effect markedly the solution behaviour of the resulting polycations.

The preparation of a homologous series of vinylimidazolium salts was readily achieved by the quaternization of 1-vinylimidazole (reaction 1, R=H) with a series of n-alkyl iodides in ethyl acetate as solvent according to the procedures given in the experimental section. This reaction results in quaternization of the 3-position of 1-vinylimidazole to give the corresponding 3-n-alkyl-1-vinylimidazolium iodide (Ia-If).



Ia: R = H, R' = CH<sub>3</sub>

Ib: R = H, R' = (CH<sub>2</sub>)<sub>2</sub>CH<sub>3</sub>

Ic: R = H, R' = (CH<sub>2</sub>)<sub>3</sub>CH<sub>3</sub>

Id: R = H, R' = (CH<sub>2</sub>)<sub>6</sub>CH<sub>3</sub>

Ie: R = H, R' = (CH<sub>2</sub>)<sub>11</sub>CH<sub>3</sub>

If: R = H, R' = (CH<sub>2</sub>)<sub>15</sub>CH<sub>3</sub>

II: R = R' = CH<sub>3</sub>

From the reactions of 1-vinylimidazole with methyl iodide, n-propyl iodide, n-dodecyl iodide and n-hexadecyl iodide, the cationic monomers of 3-methyl(Ia)-, 3-n-propyl(Ib)-, 3-n-dodecyl(Ie)- and 3-n-hexadecyl(If)-1-vinylimidazolium iodide were all obtained in the crystalline form as off-white needles. Upon standing,

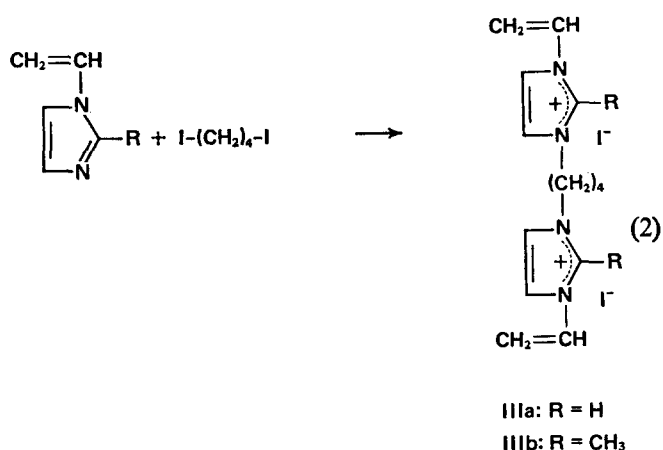
these needles had a tendency to yellow. Although it was possible to obtain crystals of the shortest and longest chain quaternary salts, this was not possible for the intermediate length salts 3-n-hexyl(Ic)- and 3-n-heptyl(Id)-1-vinylimidazolium iodide which remained as oils. In spite of the fact that the elemental analysis of the former compound was slightly in error, a verification of the purity of reagents used in the formation of both Ic and Id by gas chromatography indicated that impurities were not the cause of their non-crystallization behaviour. This characteristic is not unexpected, since intermediate chain length hydrocarbons can cause a phase change from a liquid to an oil or solid. For the shortest alkyl-substituted salt (Ia) it was found that this salt is very hygroscopic and difficult to handle. Furthermore, in the formation of this salt, it is possible to form an oil which can be difficult to crystallize. Recently, Shostakovskii *et al.*<sup>9</sup> prepared this salt and other vinylimidazolium and vinylbenzimidazolium salts for infra-red and ultra-violet spectral studies. Although these authors reported a melting point of 85–86°C in comparison to that which we obtained of 77.5–78.0°C, a detailed description of their preparation was not given.

The solubilities of the cationic monomers Ia–If in water were rather interesting. For the short chain length alkyl-substituted salts (Ia and Ib), it was found that they were readily soluble in water. For the intermediate chain length alkylated monomers (Ic and Id), these appeared to be less water soluble than compounds Ia and Ib, in accord with their greater hydrophobic character. For the long chain length alkyl substituents (Ie and If), it was found that these monomers behaved as detergents in aqueous solution with considerable frothing being noted. The monomer If appeared to be slightly less soluble than Ie. The solubility of the series of monomers in water thus illustrates a distinct change in solution behaviour depending on the length of the quaternary side-chain. The short chain monomers behave as typical water-soluble salts whereas the intermediate chain monomers are less water soluble because of their increased hydrophobic character, and the long chain monomers appear to form micelles in aqueous solution because of their highly hydrophobic character. Transitions in solution behaviour of this type often occur with ionic organic molecules where a hydrophobic moiety can be increased in chain length<sup>10</sup>.

For the monomer 2-methyl-1-vinylimidazole, the only quaternization reaction with an alkyl iodide that was studied was that with methyl iodide (reaction 1, R = R' = CH<sub>3</sub>). It was found that 2,3-dimethyl-1-vinylimidazolium iodide (II) formed very rapidly in comparison to the slower quaternization of 1-vinylimidazole with methyl iodide (reaction 1, Ia). On the basis of stereochemical considerations, this was surprising to note because the more hindered 2-methyl isomer would be expected to quaternize at a slower rate than the less hindered, unsubstituted isomer.

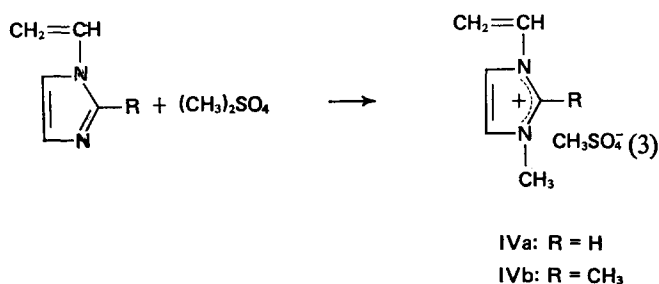
In conjunction with the quaternization of 1-vinylimidazole and 2-methyl-1-vinylimidazole by alkyl iodides, it was also of interest to prepare dicationic monomers that could be used as crosslinking agents. This was effected by the reaction of the nucleophilic vinyl monomers with the alkyl diiodide, 1,4-diiodobutane, in ethyl acetate (reaction 2). In this case it was found that the reaction with 1-vinylimidazole easily gave the dimeric product 1,4-butanediyl-3,3'-bis-1-vinylimidazolium diiodide

(IIIa). However, the reaction with 2-methyl-1-vinylimidazole initially gave the monoquaternized product 2-methyl-3-(4-iodobutyl)-1-vinylimidazolium iodide which underwent complete quaternization upon heating with excess 2-methyl-1-vinylimidazole to 1,4-butanediyl-3,3'-bis-2-methyl-1-vinylimidazolium diiodide (IIIb).



Previously, the only dicationic vinyl monomers that appear to have been reported and characterized have been those prepared from the diquaternization of amino acrylates and methacrylates<sup>2</sup>.

In further studies of the quaternization of 1-vinylimidazole and 2-methyl-1-vinylimidazole, it was also of interest to characterize the salts prepared from the reactions with dimethyl sulphate, since these monomers have been reported in the patent literature but apparently have not been isolated and structurally verified<sup>2, 9</sup>. Employing similar quaternization procedures as with the alkyl iodides, it was found that the quaternizations with dimethyl sulphate (reaction 3) occurred within minutes in cold ethyl acetate solution. As was expected, these quaternization reactions were considerably more rapid than the corresponding preparation of the iodide salts. Furthermore, it was again noted that 2-methyl-1-vinylimidazole appeared to quaternize more rapidly than its unsubstituted isomer.



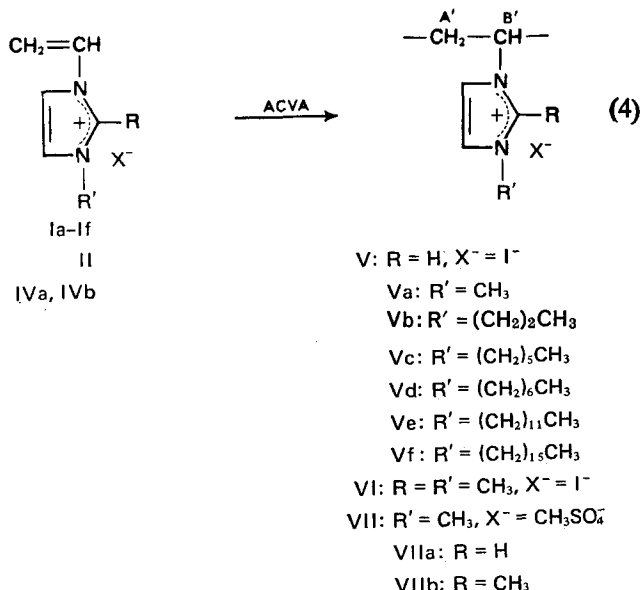
The monomers 3-methyl(IVa)- and 2,3-dimethyl(IVb)-1-vinylimidazolium methylsulphate were found to be extremely hygroscopic, and utilization of anhydrous conditions was needed in their characterization.

#### Polymerization reactions

It was previously indicated that several polyvinylimidazolium salts have been reported in the patent literature in which a variety of vinylimidazoles were quaternized and then free radically homo- or co-polymerized. Alternative preparations of polyvinylimidazolium salts have

also employed the initial formation of a neutral (nucleophilic) polyvinylimidazole, followed by treatment with an alkylating agent<sup>2</sup>. In the latter approach, it can be difficult to achieve complete quaternization.

In our experiments, we have found that the monomeric salts I, II and IV could be homopolymerized in water using the free radical initiator 4,4'-azobiscyanovaleric acid (ACVA, reaction 4) to their corresponding polyvinylimidazolium salts V-VII.



Each of the homopolymerization reactions were done under the same conditions. The solubilities of the resulting polymeric solutions were found to be related to the length of the alkyl chain. For the homologous alkyl iodide series Va-Vf, the short side-chain polyions of poly(3-methyl-1-vinylimidazolium iodide)(Va) and poly(3-n-propyl-1-vinylimidazolium iodide) (Vb) were found to be very soluble in water. The intermediate side-chain polyions of poly(3-n-hexyl-1-vinylimidazolium iodide) (Vc) and poly(3-n-heptyl-1-vinylimidazolium iodide) (Vd) were completely insoluble in water. On the other hand, the long side-chain polyions poly(3-n-dodecyl-1-vinylimidazolium iodide) (Ve) and poly(3-n-hexadecyl-1-vinylimidazolium iodide) (Vf) gave opaque solutions which frothed easily. From these solutions, it was indicated that the short side-chain polymers Va and Vb behaved as normal polyions whereas the long side-chain polyions Ve and Vf were sufficiently hydrophobic to cause micellarization of the macromolecules in aqueous solution such that polysoaps resulted. The intermediate side-chain length polyions Vc and Vd were apparently not sufficiently hydrophobic to cause the formation of polymeric micelles through the hydrophobic intramolecular or intermolecular interactions of the pendant groups. Transitions in solubility behaviour of this type have been reported by Strauss *et al.* on their studies of poly(4-vinylpyridine) which was first quaternized to a small degree with n-dodecyl bromide followed by greater quaternization with ethyl bromide<sup>11, 12</sup>.

In these polymerization reactions, it was noted that when the polysoap solutions were exhaustively dialysed and then lyophilized, the resulting dried solid was insoluble in water, even upon heating. Solubilization could then be effected only through the utilization of organic solutes. It is conceivable that this insolubility could be

caused by extensive intermolecular hydrophobic interactions between the long chain pendant groups such that the ionic charges would be buried in the interior and not near the surface as would occur in micellar solutions. A similar water insolubility of a dried anionic polysoap has been previously reported by Sinha and Medalia<sup>13</sup>.

The other short side-chain polyions, poly(2,3-dimethyl-1-vinylimidazolium iodide) (VI), poly(3-methyl-1-vinylimidazolium methylsulphate) (VIIa) and poly(2,3-dimethyl-1-vinylimidazolium methylsulphate) (VIIb) were also found to be very water soluble. Since the short side-chain monomers and their corresponding homopolymers were all highly water soluble, it was decided to test the crosslinking ability of the difunctional monomers IIIa and IIIb with the simplest monomeric salts, Ia and II, respectively. Using a 5 mol% solution of either crosslinking agent with Ia or II according to the conditions described for the homopolymerizations, followed by several washings with hot water to remove any uncrosslinked polymer, it was found that crosslinked hydrophilic gels resulted. A considerable amount of mechanical loss of crosslinked polymer was obtained by the rigorous purification technique because of the small size of the gel particles that were obtained.

#### N.m.r. measurements

N.m.r. spectra of imidazolium salts have been previously reported in the literature<sup>14-17</sup>. Although our preliminary investigation of the n.m.r. spectra of vinylimidazolium salts Ia and II was conducted in D<sub>2</sub>O<sup>1</sup>, as were most of the salts that have been reported in the literature, it was found that this solvent could not be used effectively for the various monomers and polymers because of their wide range in solubility behaviour. It was found, however, the DMSO-d<sub>6</sub> could be used for the greatest number of compounds, with only the 2,3-dimethyl-substituted iodide polymer (VI) being insoluble at ambient temperature.

The spectral data for the monomeric and polymeric salts prepared in this investigation are given in Tables 1 and 2, respectively. In both Tables, the substituent positions on the imidazolium ring are given by numbers 1-5 according to the numbering system shown in reaction (1). In the case of the monomeric salts, the vinyl hydrogens on the 1-position are denoted by A, B and C for positions *gem*, *cis* and *trans* to the imidazolium ring. In the case of the polyions, the chain-backbones are denoted by A' and B' (reaction 4) for the methylene and methine hydrogens of the 1-position.

In Table 1, it is seen that there is good agreement in chemical shift values for positions 1-5 of the monomers of the homologous series (Va-Vf). For each salt, the hydrogen of the 2-position is furthest downfield. In comparison to neutral (unquaternized) imidazole, the 2-hydrogen of each monomeric salt is shifted furthest downfield, apparently because of the cationic character of the 1- and 3-nitrogens. The chemical shifts and coupling constants for the vinyl hydrogens are in accord with those of other cationic, monomeric salts<sup>18, 19</sup>. Similar agreement in chemical shift data is also noted for the 2,3-dimethyl-substituted iodide (II), the dicationic crosslinking agents (IIa, IIb) and the methylsulphate salts (IVa, IVb). Relative to our previous spectral study of monomeric salts Ia and II in D<sub>2</sub>O<sup>1</sup>, it is found that DMSO-d<sub>6</sub> causes a significant shift downfield for all peak positions.



Table 1 N.m.r. spectra data of monomeric imidazolium salts in DMSO-d<sub>6</sub>

Mono- mer	Chemical shift, $\delta$ (ppm) from TMS													
	2a		4, 5b	Vinylc			Alkyl			Counter- ion	Coupling (Hz)			
	H	CH <sub>3</sub>		A	B	C	N-CH <sub>2</sub> -	-CH <sub>2</sub> -	-CH <sub>3</sub>		J <sub>45</sub>	J <sub>AB</sub>	J <sub>AC</sub>	J <sub>BC</sub>
Ia	9.92	—	8.34, 8.14	7.48	6.11	5.53	—	—	3.82s	—	1	16	9	2
Ib	9.93	—	8.46, 8.20	7.49	6.16	5.55	4.40t	2.35-0.95m	0.90t	—	1	16	9	1.5
Ic	9.95	—	8.34, 8.17	7.44	6.09	5.50	4.36t	2.20-1.15m	0.89t	—	1	16	9	2
Id	9.96	—	8.40, 8.14	7.51	6.15	5.52	4.44t	2.30-1.05m	0.86t	—	1	16	9	2.5
Ie	9.90	—	8.39, 8.15	7.46	6.10	5.48	4.37t	2.30-1.05m	0.89t	—	1	16	9	2
If	9.80	—	8.36, 8.10	7.42	6.05	5.47	4.32t	2.25-1.05m	0.86t	—	1	16	9	2
II	—	2.81	8.20, 7.89	7.58	5.96	5.45	—	—	3.92s	—	2	16	9	2.5
IIIa	9.82	—	8.37, 8.13	7.44	6.02	5.49	4.36t	1.91t	—	—	1	16	9	2
IIIb	—	2.89	8.29, 8.04	7.47	6.06	5.53	4.40t	1.91t	—	—	1	16	9	2
IVa	9.38	—	8.13, 7.88	7.26	5.93	5.45	—	—	3.92s	3.45s	2	16	9	2.5
IVb	—	2.71	8.08, 7.73	7.29	5.86	5.37	—	—	3.86s	3.44s	2	16	9	2.5

a All peaks in singlets

b All peaks in doublets

c All peaks in doublets of doublets

Table 2 N.m.r. spectral data of polymeric imidazolium salts in DMSO-d<sub>6</sub>

Polymer	Chemical shift, $\delta$ (ppm) from TMS								
	2		4, 5	Backbone		Alkyl			Counter-ion
	H	CH <sub>3</sub>		A'	B'	N-CH <sub>2</sub> -	-CH <sub>2</sub> -	-CH <sub>3</sub>	
Va	9.64	—	7.70	4.20	1.70	—	—	3.85	—
Vb	9.62	—	7.70	4.10	1.89	4.10	1.89	0.92	—
Vc	9.61	—	7.83	4.23	1.34	4.23	1.34	0.89	—
Vd	9.64	—	7.71	4.20	1.27	4.20	1.27	0.88	—
Ve	9.60	—	7.70	4.20	1.28	4.20	1.28	0.92	—
Vf	9.70	—	7.95	4.23	1.29	4.20	1.29	0.86	—
VIIa	9.06	—	7.70	3.02	1.77	—	—	3.45	3.45
VIIb	—	2.30	7.70	3.65	1.74	—	—	3.65	3.65

a All peaks are very broad

For the n.m.r. spectra of the polyions (Table 2), it was again found that good agreement occurred with all chemical shift data. Although the peak positions were rather broad, it can be seen that relative to the monomers in DMSO-d<sub>6</sub>, there are significant upfield shifts for positions 2, 4 and 5. This shift is most likely related to the conversion of the double bond of the monomer to the single bond of the chain-backbone. From these data, it is also apparent that the free radical polymerization of the cationic monomers proceeds through a normal vinyl addition in that there is no alteration of the imidazolium ring. In addition, in none of the spectra of the polymers was any monomer indicated. This is particularly important in the solubility properties of the polysoaps, since it indicates that their solubility in aqueous solution is most likely caused by the micellarization of the polymer chains and not by surrounding monomeric detergent molecules.

## CONCLUSION

This study has illustrated the preparations of a variety of homopolymers of vinylimidazolium salts. In the near future we hope to report further studies on the micellar character of the monomers and polymers as well as on the copolymerization behaviour of the monomeric salts.

## ACKNOWLEDGEMENT

The authors are grateful to Professor C. G. Overberger for his support and encouragement during the early stages of this work.

## REFERENCES

- Salamone, J. C., Snider, B., Israel, S. C., Taylor, P. and Raia, D. *Polymer Prepr.* 1972, **13**, 271
- For a review, see Hoover, M. F. *J. Macromol. Sci. (A)* 1970, **4**, 1327.
- Duling, I. R. and Price, C. C. *J. Am. Chem. Soc.* 1962, **84**, 578
- Shyluk, W. P. *J. Polym. Sci. (A)* 1964, **2**, 2191
- Monage, D. J. and Mosher, W. A. *Polymer Prepr.* 1969, **10**, 705
- Georgieva, V. R., Zubov, V. P., Kabanov, V. A. and Kargin, V. A. *Dokl. Acad. Nauk SSSR* 1970, **190**, 1128
- Gavurina, R. K., Karkozov, V. G. and Vybornov, O. Yu. *Vysokomol. Soedin. (B)* 1969, **11**, 589
- Ger. Pat. 847: 347 (1952) Ger. Pat. 932 699 (1955); Ger. Pat. 1 009 809 (1957); Ger. Pat. 1 108 436 (1959); Japan Pat. 12 510 (1965); Japan Pat. 10 411 (1966)
- Shostakovskii, M. V., Glaskova, N. P., Domnine, Ye. S., Belousova, L. V. and Shvortsova, G. C. *Khim. Geterst. Soedin.* 1971, **9**, 958
- Cordes, E. H. and Dunlap, R. B. *Acc. Chem. Res.* 1969, **2**, 329 and references cited therein
- Strauss, U. P. and Gershfeld, N. L. *J. Phys. Chem.* 1954, **58**, 747
- Strauss, U. P., Gershfeld, N. L. and Crook, E. H. *J. Phys. Chem.* 1956, **60**, 577
- Sinha, S. K. and Medalia, A. I. *J. Am. Chem. Soc.* 1957, **79**, 281
- Staab, H. A. and Mannschreck, A. *Tetrahedron Lett.* 1962, p 913; Mannschreck, A. and Staab, H. A. *Ber. Dtsch. Chem. Ges.* 1963, **67**, 470
- Overberger, C. G., Salamone, J. C. and Yaroslavsky, S. J. *Org. Chem.* 1965, **30**, 3580; Caesor, F. and Overberger, C. G. *J. Org. Chem.* 1958, **33**, 2971
- Olofson, R. A., Thompson, W. R. and Michelman, J. S. *J. Am. Chem. Soc.* 1965, **86**, 1865
- Haake, P., Bausher, L. P. and Miller, W. B. *J. Am. Chem. Soc.* 1969, **91**, 1113
- Ringsdorf, H. and Walter, G. *Makromol. Chem.* 1971, **149**, 295
- Salamone, J. C., Ellis, E. J. and Israel, S. C. *J. Polym. Sci. (B)* 1972, **10**, 605

# Vinylpyridine oxide copolymers: viscosity/pH relationship of aqueous solutions

P. F. Holt and B. Tamami

*Department of Chemistry, University of Reading, Reading RG6 2AD, UK  
(Received 18 May 1973; revised 20 June 1973)*

Complex variations with pH in the viscosity of poly(2-vinylpyridine 1-oxide) in aqueous solution have been observed and large changes in viscosity with small changes in pH at certain pH values have been related to conformational changes. A viscometer is described that allows the viscosity changes to be followed with greater accuracy. The new observations indicate that at some pH values the viscosity readings are not reproducible, probably because the change in viscosity is large over a pH range that is too small to measure accurately. This suggests that in passing from one extreme conformation to another the polymer passes through a highly unstable conformation. The variation of viscosity with pH has been studied for certain vinylpyridine oxide copolymers, namely poly(2-vinylpyridine 1-oxide-co-4-vinylpyridine 1-oxide), poly(2-vinylpyridine 1-oxide-co-2-methyl-5-vinylpyridine 1-oxide) and poly(4-vinylpyridine 1-oxide-co-2-methyl-5-vinylpyridine 1-oxide). The shapes of the viscosity/pH curves are interpreted in terms of the curves of the polymers formed from each comonomer.

## INTRODUCTION

Poly(2-vinylpyridine 1-oxide) (I) will inhibit the cytotoxicity of quartz dust. Poly(4-vinylpyridine 1-oxide) (II) is much less effective and a study<sup>1</sup> of the effectiveness of various poly(vinylpyridine 1-oxides) on the cytotoxicity of quartz in macrophage cultures has shown that the position of the *N*-oxide group and the presence of alkyl groups affect the activity of the polymer. By studying the viscosity of aqueous solutions of some of these polymers, Holt and Tamami<sup>2, 3</sup> attempted to deduce changes in the size and conformation at various pH values. Certain characteristic changes appeared to be associated with the several polymers.

There are practical difficulties in the determination of the viscosity/pH relationship of a dilute aqueous solution of a polymer; in particular, small pH changes are apt to occur while the solution is transferred from the pH meter to the viscometer. In previous studies<sup>2</sup>, when pH was adjusted outside the viscometer and the solution was filtered into the apparatus, the pH changed on transfer sometimes by as much as 0.2. A new viscometer has been designed that incorporates a glass electrode and that allows the addition of minute volumes of acid or alkali. The pH can then be adjusted and measured without transfer of the polymer solution. This has enabled more accurate and more numerous determinations of viscosity to be made at different pH values. Using the modified viscometer the pH can be determined to  $\pm 0.025$  inside the viscometer.

Certain of the viscosity/pH studies previously published were repeated using the new apparatus. The general shapes of the published curves were in each case confirmed but the impossibility of accurately replicating values in the region of certain peaks was emphasized.

It was previously argued that small peaks in the viscosity curves probably result from changes in conformation and if the intermediate between two extreme conformational forms is unstable, difficulty in reproducing viscosity values in this region must be anticipated. As an example, Holt and Tamami<sup>2</sup> suggested that the peak in the viscosity/pH curve of poly(2-vinylpyridine 1-oxide) at about pH 7–8 and 9–10 may be due to a changeover from an extreme conformation in which oxygens on adjacent rings are paired to another extreme conformation in which the oxygens alternate on either side of the ring. Models show that such a change is feasible but that the change is hindered by interference between oxygen and protons of the chain, i.e. this intermediate conformation must be unstable. A small change in pH would then be required to change the conformation from one extreme to the other. While the viscosity can be measured with considerable accuracy the pH cannot be determined to better than 0.05 and it is probable, therefore, that the inconsistencies at these points are due largely to slight errors in pH determination.

This paper records viscosity studies on copolymers each prepared from two of the following monomers: 2-vinylpyridine, 4-vinylpyridine, and 2-methyl-5-vinylpyridine (III) and subsequent oxidation. Since the vinylpyridine monomers were isomeric or differed only slightly in their empirical formulae, the composition of the copolymers could not be deduced from analytical figures. The composition was deduced from n.m.r. spectra, a method previously applied by Ritchey and Ball<sup>4</sup>, and Kulkarni *et al.*<sup>5</sup>.

Only block copolymers of 2-vinylpyridine and 4-vinylpyridine have previously been described<sup>6</sup> and these were not considered suitable for our viscosity studies.

Copolymers were therefore prepared by methods used in the homopolymerization of these monomers, free radical suspension polymerization being preferred because it favours highest molecular weight, although some anionic polymerizations were also effected. Copolymers of styrene and 2-vinylpyridine were also prepared but, on oxidation, the *N*-oxides proved insoluble in water and so were unsuitable for viscosity studies.

The following copolymers were prepared: poly(2-vinylpyridine 1-oxide-co-4-vinylpyridine 1-oxide) (IV) (free radical and anionic polymerization), poly(2-vinylpyridine 1-oxide-co-2-methyl-5-vinylpyridine 1-oxide) (V) and poly(4-vinylpyridine 1-oxide-co-2-methyl-5-vinylpyridine 1-oxide) (VI).

## EXPERIMENTAL

### Materials

The vinylpyridines were supplied by Midland Tar Distillers Ltd. The vinylpyridines and the styrene were purified by distillation under nitrogen at reduced pressure.

### Apparatus

Viscosities were determined with an Ubbelohde suspended level viscometer (Polymer Consultant Ltd) or in modified Ubbelohde viscometer. The modification consists of the removal of the bulb and its replacement by a larger bulb carrying a vertical tube wide enough to insert a glass electrode. The bulb carries a second tube through which passes a length of very fine (0.5 mm bore) polyethylene tubing, the upper end of which is connected to a micrometer syringe. Through this tubing very small quantities of acid or alkali can be added.

### Technique

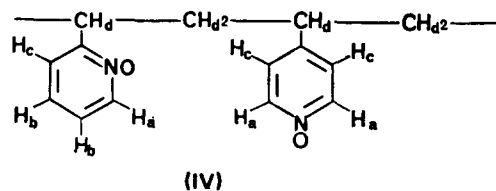
Viscometers were filled with chromic acid solution and kept at 70°C for 24 h. They were emptied, washed with conductivity water and then dried at 100–120°C.

Polymer solutions were prepared with conductivity water and stood for at least 24 h before measurement. Normally a concentration of 0.4 g/100 ml was used. Solutions were filtered into the viscometer through a grade 2 sinter. The thermostat temperature was held at 25° ± 0.05°C.

### Preparation of copolymers

*Poly(2-vinylpyridine 1-oxide-co-4-vinylpyridine 1-oxide)* (IV). (a) Free radical suspension. A suspension of calcium phosphate was prepared by addition of aqueous calcium chloride (22 ml, 1%) to a slowly stirred mixture of aqueous sodium phosphate (75 ml, 0.2%) and ammonia (1.6 ml, density 0.880). An equimolar mixture (40 g) of the two freshly distilled vinylpyridines with azobisisobutyronitrile (0.5 g) was dropped into the stirred calcium phosphate suspension, at 90°C, during 1 h. This temperature was maintained for a further 3 h. The copolymer, as small beads, was filtered off and washed several times with hot water to remove inorganic material. It was then dissolved in hydrochloric acid (2M) and precipitated with aqueous ammonia. The copolymer was twice precipitated as a white solid from methyl ethyl ketone solution by *n*-hexane (yield 17 g; softening point, ~150°C). Found: C, 78.43%; H, 6.64%; N, 13.12%. C<sub>7</sub>H<sub>7</sub>N, C<sub>7</sub>H<sub>7</sub>N requires C, 79.24%; H, 7.54%; N, 13.20%.

N.m.r. (structure IV): τ(CDCl<sub>3</sub>) centred at 1.55 br (s, H<sub>a</sub>); 2.75 b(s, M<sub>b</sub>); 3.50 br (s, H<sub>e</sub>); 8.35 br (s, H<sub>d</sub>).



Calculation based on the integral of the signal for (H<sub>a</sub>) gave the molar percentage of 2-vinylpyridine units as 67 ± 3.

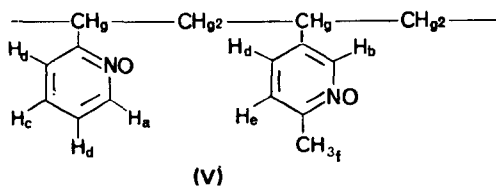
The copolymer was oxidized using hydrogen peroxide and acetic acid<sup>7</sup> to poly(2-vinylpyridine 1-oxide-co-4-vinylpyridine 1-oxide), a cream coloured, hygroscopic solid which decomposed at 275°C. I.r. showed a N–O stretching band at 1230 cm<sup>-1</sup>.

(b) Anionic. Dry toluene (90 ml) and phenyl magnesium bromide (570 mg) were introduced into a three-neck flask equipped with stirrer, nitrogen inlet, and dropping funnel. The well stirred mixture was heated to 45°C and during 30 min an equimolar mixture (10 g) of the two freshly distilled vinylpyridines was added dropwise. The solution was stirred for 4 h, when it became orange coloured. Hydrochloric acid (150 ml; 5%) was added and stirring was continued until the copolymer dissolved in the aqueous phase. The aqueous solution was then separated, diluted to 200 ml and dropped into ammonia (4%; 1 litre) containing ammonium chloride (20 g). The copolymer that was precipitated was filtered off, dissolved in dilute hydrochloric acid and then reprecipitated with ammonia. The dissolution and reprecipitation were repeated to give cream coloured flocks that were filtered off and dried at 60°C in vacuum (yield, 6 g). To obtain a polymer of better crystallinity, the dried copolymer was heated in decane<sup>8</sup> (50 ml) for 16 h. The solid was filtered off and vacuum dried. (softening point, ~280°C). Found: C, 79.60%; H, 6.53%; N, 13.21%. C<sub>7</sub>H<sub>7</sub>N, C<sub>7</sub>H<sub>7</sub>N requires C, 79.24%; N, 7.54%; N, 13.20%.

The n.m.r. is the same as that for the copolymer prepared by free radical suspension polymerization except that the broad signal centred at 8.35 due to chain hydrogen is a doublet centred at 8.15 and 8.40. Calculation based on the integral of the signal for (H<sub>a</sub>) gave the molar percentage of 2-vinylpyridine units as 50 ± 3. The copolymer was oxidized in the same manner as for copolymer (IV).

*Poly(2-vinylpyridine 1-oxide-co-2-methyl-5-vinylpyridine 1-oxide)*. Free radical suspension. The copolymer was prepared by the same procedure as for copolymer (IV) using an equimolar mixture of the two monomers. The copolymer was purified by repeated precipitation from methyl ethyl ketone solution with *n*-hexane (yield, 15 g; softening point, ~135°C). Found: C, 79.50%; H, 7.26%; N, 12.36%. C<sub>7</sub>H<sub>7</sub>N, C<sub>8</sub>H<sub>9</sub>N requires C, 80.35%; H, 7.14%; N, 12.51%.

N.m.r. (structure V): τ(CDCl<sub>3</sub>) centred at 1.75 br (s, H<sub>a</sub>); 2.45 br (s, H<sub>b</sub>); 2.90 br and 3.20 br (2s, H<sub>e</sub> and H<sub>d</sub>); 3.80 br (s, H<sub>e</sub>); 7.60 br (s, H<sub>f</sub>); 8.40 br (s, H<sub>g</sub>).

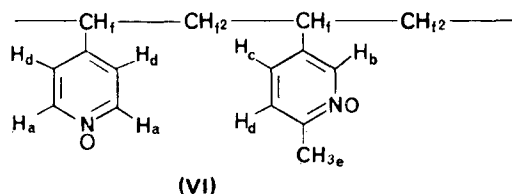


Calculation based on the integral of the signal for ( $H_a$ ) or protons of the ring, with respect to the chain and methyl protons, gave the molar percentage of 2-vinylpyridine units as  $49 \pm 3$ .

The copolymer was oxidized for 60 h by the method of Holt and Nasrallah<sup>7</sup>. Poly(2-vinylpyridine 1-oxide-co-2-methyl-5-vinylpyridine 1-oxide) was an extremely hygroscopic, cream coloured powder that decomposed at  $235^\circ\text{C}$ . I.r. showed a N-O stretching band at  $1230\text{ cm}^{-1}$ .

*Poly(2-methyl-5-vinylpyridine 1-oxide-co-4-vinylpyridine 1-oxide)*. Free radical suspension. The same procedure as for the last copolymer was used taking an equimolar mixture of 4-vinylpyridine and 2-methyl-5-vinylpyridine. The unoxidized copolymer was appreciably soluble in hot and slightly soluble in cold water. Unlike the other two copolymers it was insoluble in methyl ethyl ketone. It was purified by precipitation twice from a mixture of chloroform and methanol (3:1) with dry ether (yield, 15 g; softening point,  $\sim 215^\circ\text{C}$ ). Found: C, 79.59%; H, 7.16%; N, 12.31%.  $\text{C}_7\text{H}_7\text{N}$ ,  $\text{C}_8\text{H}_9\text{N}$  requires C, 80.35%; H, 7.14%; N, 12.51%.

N.m.r. (structure VI): ( $\text{CDCl}_3$ ) centred at 1.70 br (s,  $H_a$ ); 2.30 br (s,  $H_b$ ); 3.20 br (s,  $H_c$ ); 3.60 br (s,  $H_d$ ); 7.60 br (s,  $H_e$ ); 8.50 br (s,  $H_f$ ).

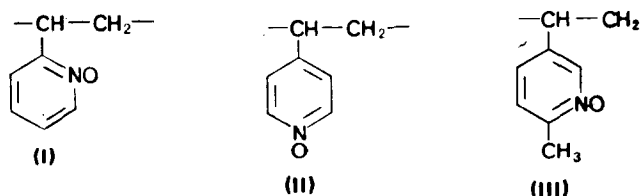


Calculation based on the sum of the integrals of the signals for ( $H_a$ ) and ( $H_b$ ), with respect to the chain and methyl protons gave the molar percentage of 4-vinylpyridine units as  $47 \pm 2$ . The copolymer was oxidized to the cream coloured, hygroscopic poly(2-methyl-5-vinylpyridine 1-oxide-co-4-vinylpyridine 1-oxide) that decomposed at  $250^\circ\text{C}$ . I.r. showed a N-O stretching band at  $1235\text{ cm}^{-1}$ .

## RESULTS

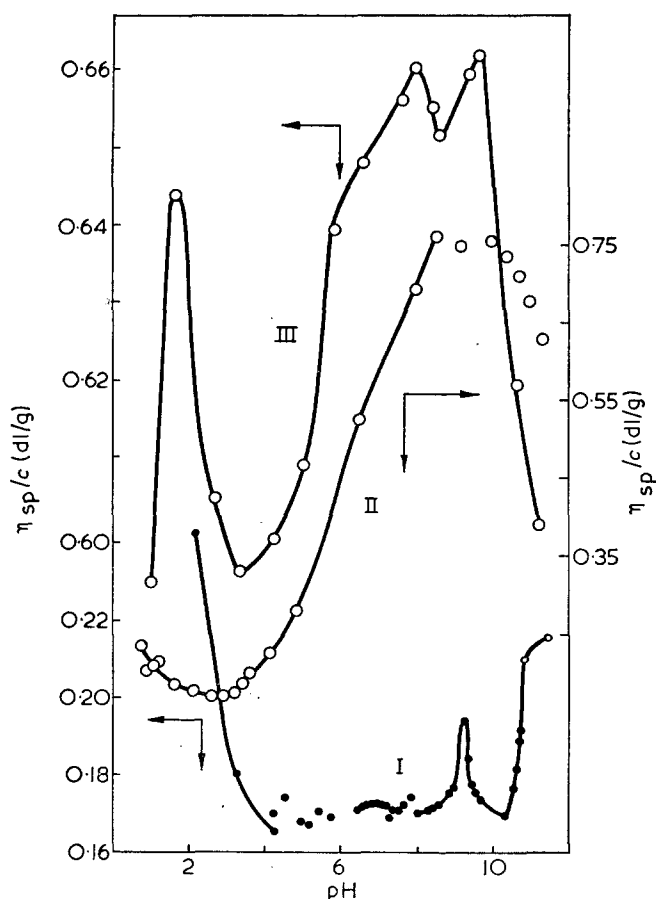
### *Poly(vinylpyridine 1-oxides)*

The curve of poly(2-vinylpyridine 1-oxide) (I) (*Figure 1*) obtained with the modified viscometer resembles that previously published, with minima at about pH 4, 8 and 10, and a sharp maximum at about pH 9. The viscosity increases steeply below pH and above pH 10. There appear to be breaks at about pH 4-5 and pH 7-8. The curves of poly(4-vinylpyridine 1-oxide) (II) and poly(2-methyl-5-vinylpyridine 1-oxide) (III) obtained with the modified viscometer were previously described<sup>3</sup>.



### *Poly(2-vinylpyridine 1-oxide-co-4-vinylpyridine 1-oxide)*

*Free radical polymerization.* The viscosity/pH curve has its lowest values at about pH 4.5 and 12.4. Below



*Figure 1* Viscosity/pH curve of poly(2-vinylpyridine 1-oxide) (I), poly(4-vinylpyridine 1-oxide) (II), poly(2-methyl-5-vinylpyridine 1-oxide) (III). 0.4% solutions;  $25^\circ\text{C}$

and above these values the viscosity increases and between them the curve has a broad maximum, centred at about pH 9, indicated by a number of irregular points (*Figure 2*).

*Anionic polymerization.* The rapid increase in viscosity either side of a minimum at pH 4 is also characteristic of this polymer (*Figure 2*). Above pH 9 the viscosity values are less certain but there is no evidence of the minimum at about pH 12 shown by the free radical copolymer.

### *Poly(2-vinylpyridine 1-oxide co-2-methyl-5-vinylpyridine 1-oxide) (V)*

The viscosity/pH curve rises steeply on either side of a minimum at pH 3-4. Points indicating a peak at pH 8-9 are indefinite (*Figure 2*).

### *Poly(2-methyl-5-vinylpyridine 1-oxide-co-4-vinylpyridine 1-oxide) (VI)*

The curve resembles that of polymer (V) in shape but has a definite maximum at about pH 3 (*Figure 2*). Between pH 8.4 and 10.5 the viscosity values are not reproducible.

## DISCUSSION

The exact structures of the copolymers are uncertain since it is not known to what extent the two units in the copolymers alternate. Since the comonomer molecules have different polarity, it is expected that alternation will be favoured especially in the case of copolymer (V) and (VI), where the difference in polarity of the comonomers

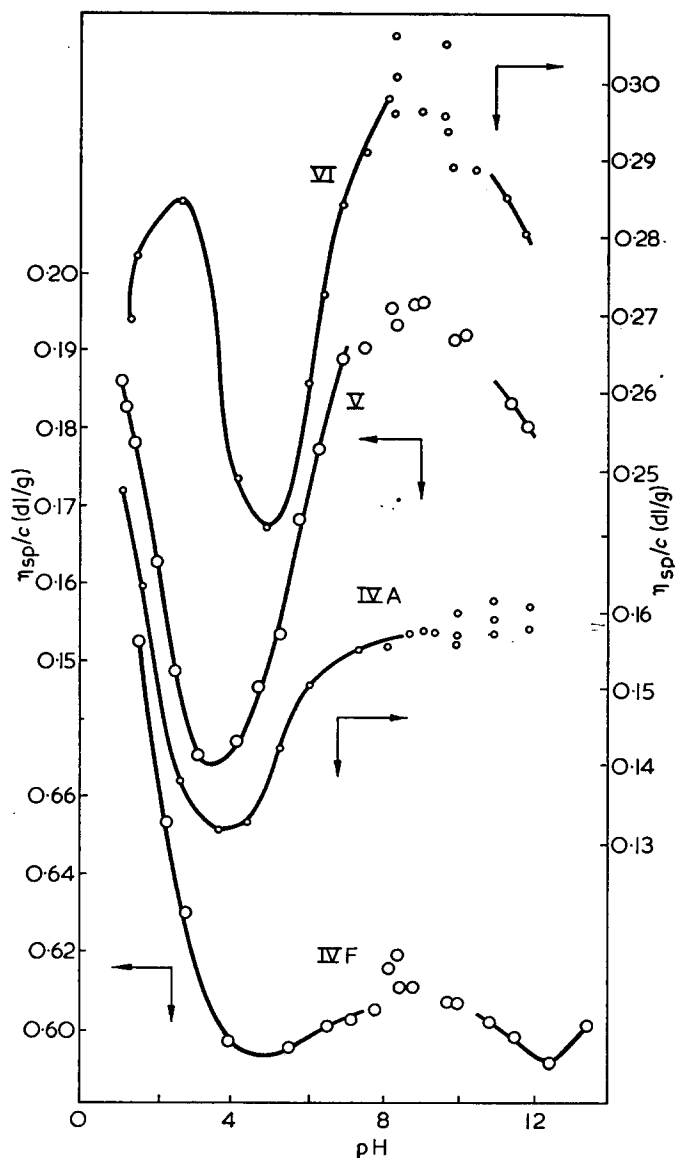


Figure 2 Viscosity/pH curve of poly(2-vinylpyridine 1-oxide-co-4-vinylpyridine 1-oxide) (IVF), free radical suspension, poly(2-vinylpyridine 1-oxide-co-4-vinylpyridine 1-oxide) (VIA), anionic, poly(2-vinylpyridine 1-oxide-co-2-methyl-5-vinylpyridine 1-oxide) (V), poly(4-vinylpyridine 1-oxide-co-2-methyl-5-vinylpyridine 1-oxide) (VI). 0.4% solutions; 25°C

is higher than in copolymer (IV). Supporting evidence for this is the observation that under the same experimental conditions the composition ratio of comonomers in copolymer (V) and (VI) are about 1:1, while that of copolymer (IV) is 2:1.

In copolymer (IV) the increase in viscosity below pH 4.5 is apparently a contribution from 2-vinylpyridine 1-oxide sequences of the copolymer, and the broad peak with the maximum at about pH 9 is a contribution from 4-vinylpyridine 1-oxide sequences. This peak is small compared to the height of the curve at low pH, possibly because there are far fewer 4-vinylpyridine oxide units than 2-vinylpyridine oxide units. In copolymer (V) the peak at about pH 9 is due to 2-methyl-5-vinylpyridine

oxide residues, and the increase at very low pH is due mainly to 2-vinylpyridine oxides. Copolymer (VI) has a high peak at about pH 9 which will have a contribution from both 2-methyl-5-vinylpyridine oxide and 4-vinylpyridine oxide residues. A smaller peak at about pH 3 is mainly due to 2-methyl-5-vinylpyridine oxide units. Any comparison of the viscosity values of the peaks at intermediate pH due to 4-vinylpyridine or 2-methyl-5-vinylpyridine units with those at low pH values, and any correlation of them with the molar percentage of the comonomers, should be made with reservation, since these two major viscosity changes are not of the same nature; one (at intermediate pH) is due to intermolecular interactions and the other (at low pH) is due to electrostatic repulsion<sup>2,3</sup>.

There are several off points in the viscosity/pH curves of these copolymers, especially in the case of copolymers (V) and (VI) around pH 9, where the points are not reproducible. These small viscosity changes are probably of the same nature as for the homopolymers<sup>2,3</sup>; they may be due to the conformational changes.

The viscosity/pH curve of poly(2-vinylpyridine 1-oxide-co-4-vinylpyridine 1-oxide) (IV) made by the anionic method is different from the curve for copolymer (IV) made by a free radical method. The viscosity increases above pH 5 and, unlike that for the copolymer made by the free radical method, it does not reach a maximum but flattens as the pH increases. Viscosity values are not exactly reproducible above about pH 8. These differences are most likely due to copolymers having different conformations. The anionic method is known to give isotactic homopolymers of vinylpyridines when the nitrogen is at the 2-position<sup>8</sup>.

It is interesting to see that the viscosity/pH curves of the above copolymers show similarities to those given by synthetic polyampholytes having different basic and acid groups. For example, Alfrey *et al.*<sup>9,10</sup> showed that viscosity/pH curves of poly(2-vinylpyridine-co-methacrylic acid) have peaks at high and low pH values due to the methacrylic acid units and vinylpyridine units respectively; and in the viscosity/pH curves of poly(methacrylic acid-co-diethylaminoethyl methacrylate), the position and height of the peaks can be changed simply by changing the molar percentage of the comonomers.

## REFERENCES

- 1 Beck, E. G., Holt, P. F. and Lindsay, H. *Br. J. Pharmacol.* 1970, **38**, 192
- 2 Holt, P. F. and Tamami, B. *Polymer* 1970, **11**, 553
- 3 Holt, P. F. and Tamami, B. *Makromol. Chem.* 1972, **155**, 55
- 4 Ritchey, W. M. and Ball, L. E. *J. Polym. Sci. (B)* 1966, **4**, 557
- 5 Kulkarni, N. G., Krishnamurti, N., Chatterjee, P. C. and Sivasamban, M. A. *Makromol. Chem.* 1970, **139**, 165
- 6 Grosius, P. P., Gallot, Y. and Skoulios, A. *Makromol. Chem.* 1970, **136**, 191
- 7 Holt, P. F. and Nasrallah, E. T. *J. Chem. Soc. (B)* 1968, p 400
- 8 Natta, G., Mozzant, G., Longi, P., Dall'Asta, G. and Bernadini, F. *J. Polym. Sci.* 1961, **51**, 487
- 9 Alfrey, T. and Morawetz, H. *J. Am. Chem. Soc.* 1952, **74**, 436
- 10 Alfrey, T., Raymond, M. F., Morawetz, H. and Pinner, H. *J. Am. Chem. Soc.* 1952, **74**, 438

## Kinetics of the reactions of polystyryl sodium with alkyl chlorides in dioxane

### Introduction

The propagation reaction in those anionic polymerizations which give rise to 'living' polymers is easily isolated and many studies of the effect of solvent and counter-ion on the kinetics of such reactions have been reported<sup>1</sup>. It is equally easy to isolate termination reactions by deliberately adding a terminating agent after polymerization is complete. We wish to report the preliminary results of a kinetic study of the reactions between alkyl chlorides and 'living' polystyrene in dioxane.

### Experimental

All reagents were rigorously purified and handled under high vacuum conditions using break-seals. 'Living' polymer solutions were prepared by contacting 1–2% solutions of styrene in dioxane with the appropriate alkali metal mirror. Concentrations of 'living ends' in the range  $8\text{--}20 \times 10^{-4}$  M were readily obtained. n-Butyl, s-butyl and t-butyl chlorides were dried over calcium hydride and then treated with freeze-dried 'living' polystyrene before use.

The reaction was followed spectrophotometrically using a reaction vessel consisting of a 1 cm silica cell containing the 'living' polymer solution and a break-seal ampoule containing the alkyl halide. After mixing the reagents, the cell was placed in a thermostated bath in the cell compartment of a Unicam SP500 spectrophotometer and the disappearance of the characteristic colour of the 'living ends' was monitored. Concordant results were obtained whether this was done at 340 nm ( $\lambda_{\text{max}}$ ) or at 530 nm, the latter being more convenient at high concentrations of 'living ends'.

### Results

Preliminary studies of the reaction between polystyryl sodium and t-butyl chloride in dioxane indicated that the reaction was relatively slow at room temperature. Using a large excess of t-butyl chloride, the disappearance of the 'living ends' was precisely first order over a period of at least 3 half-lives. The observed first order rate constants obtained at various initial

Table 1 Rates of reaction of polystyryl sodium with alkyl chlorides in dioxane at 20°C

Alkyl chloride	Run No.	[RCI] <sub>0</sub> (M)	$k_1 \times 10^3$ (sec <sup>-1</sup> )	$k_t \times 10^3$ (M <sup>-1</sup> sec <sup>-1</sup> )
t-butyl	138	0.134	0.81	6.04
	142	0.237	1.37	5.78
	140	0.391	2.27	5.80
	136	0.674	3.93	5.83
	133	0.06	3.53	59
s-butyl	128	0.027	6.07	225
n-butyl	129	0.071	14.67	207

Order of reactivity: n-butyl, 37; s-butyl, 10; t-butyl, 1

t-butyl chloride concentrations at 20°C are given in Table 1 and indicate a linear dependence of the first order rate constant on t-butyl chloride concentration. Thus the reaction appears to be a simple bimolecular process with a rate constant ( $k_t$ ) of  $5.9 \times 10^{-3}$  M<sup>-1</sup>sec<sup>-1</sup> at 20°C. The validity of the data is supported by the fact that different preparations of both polystyryl sodium and purified t-butyl chloride gave reproducible results. Similar results, not reported here, were obtained at other temperatures, although at higher temperatures a slow spontaneous decomposition of the 'living ends' (isomerization<sup>2</sup>) complicates the interpretation. It should be noted, however, that the rate of isomerization at 20°C was negligible in comparison with the rates of termination.

To estimate the variation in reactivity of the polystyryl sodium with other alkyl chlorides, one run was performed with a sample of s-butyl chloride and two with n-butyl chloride. Both reactions were first order with respect to 'living ends' and the values of  $k_t$  quoted in Table 1 assume a first order dependence on the alkyl chloride concentration and should therefore be regarded as estimates only at this stage.

Preliminary studies of the reaction of t-butyl chloride with polystyryl potassium and polystyryl caesium indicated little change in the overall rate of reaction. However, the disappearance of the 'living ends' showed deviations from first order behaviour beyond approximately 75% reaction so that firm conclusions must await a more detailed study.

### Discussion

The simple kinetic behaviour observed here with polystyryl sodium is consistent with what is known of 'living' polymers in dioxane. Studies of the propagation reaction with styrene indicate that the active centres are all present as ion-pairs, there being no evidence for significant concentrations of free ions or ion-pair aggregates. We would conclude, therefore, that the rate constants obtained refer to attack of the ion-pair on the alkyl chlorides. The products of the reactions have not yet been identified though by analogy with similar work in tetrahydrofuran<sup>3</sup> it seems probable that substitution predominates with n-butyl chloride while elimination is the major process with t-butyl chloride. The variation in reactivity n-butyl > s-butyl > t-butyl would support this view.

A. R. Baker and G. C. East

Department of Textile Industries,  
University of Leeds,  
Leeds LS2 9JT, UK  
(Received 10 October 1973)

### References

- 1 Szwarc, M. 'Carbanions, Living Polymers and Electron Transfer Processes', Interscience, New York, 1968, Ch VII
- 2 *Ibid.* p 407 and p 647 *et seq.*
- 3 Davis, A., Richards, D. H. and Scilly, N. F. *Makromol. Chem.* 1972, **152**, 133

# Classified Contents

- ABS/glass bead composites, mechanical behaviour and permeability, 21
- Acenaphthylene and methyl acenaphthylenes, cationic polymerization of, 352
- Active membrane, asymmetric catalytically, coupling of diffusion flux and chemical reaction in, 505
- Amino groups, primary, preparation and characterization of some polymers terminated with, 587
- Bending of thermoplastic beams, approximate method for predicting, 584
- Benzoin, benzoin methyl ether and benzil, mechanisms and relative efficiencies in radical polymerization photoinitiated by, 405
- Benzoyl peroxide, photo-dissociation 527
- Birefringence, flow, of polyelectrolytes: a poly(amide carboxylic acid) from pyromellitic anhydride and benzidine— influence of triethylamine on the molecular dimensions, 178
- Bis(2-hydroxyethyl)terephthalate, propagation and degradation reactions in polycondensation, 50
- Bisphenol-A epoxides/dicy systems, 91
- Butadiene-acrylonitrile copolymers, investigation of compatibility with poly(vinyl chloride), 347
- Carbonyls, metal, as photoinitiators for the polymerizations of tetrafluoroethylene and vinyl monomers containing tetrafluoroethylene, 38
- Catalysts, highly active, for ethylene polymerization by the reduction of  $TiCl_4$ , with organomagnesium compounds, 365
- Chain-extended growth and lamellar thickening of polyethylene, 387
- Chain extension by dianhydrides: new polymer systems, 466
- Characterization of stereoblock polymers of poly(methyl methacrylate) by thin-layer chromatography, 171
- Characterization of the crystalline, intermediate and amorphous phase in poly(ethylene terephthalate) fibres by X-ray diffraction, 9
- Chemorheology of irradiation-cured natural rubbers: 1. Stress relaxation mechanisms for various curing systems in natural rubber at high temperature, 569
- Cinnamic acid, copolymers of methyl methacrylate with, 409
- Composite elastomeric system, elastic properties and structure, 497
- Composites, ABS/glass bead, mechanical behaviour and permeability, 21
- Composites formed by interstitial polymerization of vinyl monomers in polyurethane elastomers: 1. Preparation and mechanical properties of methyl methacrylate based composites, 597. 2. Morphology and relaxation processes in methyl methacrylate based composites, 604
- Compression moulded TPX, morphology and fracture, 476
- Conformational transitions in heterogeneous oxidized-wool proteins, proton-magnetic resonance study, 523
- Cooling rate, influence of, on the heat capacity and thermal transitions of amorphous polyhexene-1, 167
- Copolymer, ethylene-vinyl acetate, study of thermoelastic properties, 290
- Copolymer of styrene and maleic anhydride, molecular motion, 68
- Copolymer, SIS three block, the cubic structure of, 145
- Copolymerization, alternating, of methyl  $\alpha$ -phenylacrylate and methyl methacrylate by  $n-BuLi$ , 565
- Copolymerization, radical, of *N*-(1,1-dimethyl-3-oxobutyl)-acrylamide in different solvents, 2
- Copolymers, butadiene-acrylonitrile, investigation of compatibility with poly(vinyl chloride), 347
- Copolymers, ethylene-vinyl chloride, configurational characteristics, 553
- Copolymers of methyl methacrylate with cinnamic acid, 409
- Copolymers, polystyrene-*g*-polyisoprene, synthesis and solution behaviour, 82
- Copolymers, vinylpyridine oxide: viscosity/pH relationship of aq. solutions, 645
- Copolyptides composed of  $\gamma$ -methyl-L-glutamate and  $\epsilon$ -*N*-carbobenzyloxy-L-lysine, synthesis and conformation studies, 535
- Craze shape and fracture in poly(methyl methacrylate), 469
- Crazing in a crystalline polymer (isotactic polypropylene) and the role of  $N_2$ ,  $O_2$ , and  $CO_2$  as crazing agents, 78
- Crystallization, chain-extended, of polyethylene: effect of sample thickness, 390
- Crystallization, flow induced, of polyethylene melts, 16
- Crystallization of polyamides under elevated pressure: nylon-6 (polycapramide), 463
- Degree of polymerization, effects of long branching on distribution of: 2, 524
- 2'-Deoxyadenosine, in DMSO-water mixtures, importance of 2:1 water-DMSO complex in the n.m.r. spectra, 332
- Dianhydrides, chain extension by: new polymer systems, 466
- Diels-Alder synthesis, cleavage of  $\beta$ -aryl ethers in dienylation of lignin, 395
- Diene polymer, asymmetric addition of thiol to, in the presence of optically active amines as catalyst, 427
- Diene polymer, reaction of thiol to, in the presence of various catalysts, 87
- Dienolysis of lignin: cleavage of  $\beta$ -aryl ethers by Diels-Alder synthesis, 395
- Die swell in a Newtonian liquid, a theoretical treatment, 262
- Die swell in elastic and viscous fluids, 297
- Diffusion flux, coupling of, and chemical reaction in an asymmetric catalytically active membrane, 505
- Diffusion, polymer translational: 1. Dilute theta solutions, polystyrene in cyclohexane, 151. 2. Non-theta solutions, polystyrene in butan-2-one, 293
- Dilation coefficients of *cis*-polybutadiene in simple extension, 576
- N*-(1,1-Dimethyl-3-oxobutyl)-acrylamide, radical copolymerization of, in different solvents, 2
- Dimethyl terephthalate, rate of transesterification with ethylene glycol, 55
- 1,3-Dioxolan, equilibrium bulk polymerization of, 355
- Elastic modulus of linear polymer crystals, 491
- Elastic modulus of nylons, 632
- Elastic properties and structure of a composite elastomeric system, 497
- Electrical conductivity in poly(vinyl chloride), 445
- Electron microscope studies of textile fibres and materials, 273
- Electron microscopic studies on the useful life of liquid permeated membranes, 411
- Electron microscopy studies of fracture processes in amorphous thermoplastics, 96
- Electron spin resonance studies of spin-labelled polymers: Part 5. Synthesis and characterization of *meta*-labelled polystyrene, 525
- Emulsion viscoses, rheological properties: 1. Influence of alkali concentration, reaction time and order of addition of reactants, 27. 2. Influence of cellulose origin, carbon disulphide ratio and temperature, 34
- Epoxy cure, kinetics of: 3. The systems bisphenol-A epoxides/dicy, 91
- Equilibrium ring concentrations and the statistical conformations of polymer chains: Part 11. Cyclics in poly(ethylene terephthalate), 185
- Etch technique for morphological studies of multiphase polymers containing polycarbonates, 509
- Ethylene-vinyl acetate copolymer, study of thermoelastic properties of, 290
- Ethylene-vinyl chloride copolymers, configurational characteristics, 549
- N*-Ethyl-2-vinylcarbazole, synthesis and polymerizability of, 124
- Fibre reinforced polymeric cage materials for rolling bearings, scanning electron microscopical study of, 130
- Flow, stability of wedge and channel, of highly viscous and elastic liquids, 209
- Fortisan, a variance analysis of the line broadening of X-ray profiles from, 402
- Fracture, and craze shape, in poly(methyl methacrylate), 469
- Fracture, and morphology, of compression moulded TPX, 476
- Fracture of poly(ethylene terephthalate) film, some observations on, 103
- Fracture of rubber-modified polystyrene, 451
- Fracture processes, electron microscopy studies of, in amorphous thermoplastics, 96
- Glass transition temperatures of oligosaccharides, 329
- Heat of dilution and density data for poly( $\beta$ -propiolactone) and poly( $\epsilon$ -caprolactone) in dioxane, 343
- Heat of dilution of polymer solution, estimation of: a trial on a correction of the heat of stirring ascribed to the viscosity difference before and after dilution, 237
- Hydroxymethyl groups, introduction of, into polystyrene and styrene, 330
- Infra-red spectrum ( $400-10\text{ cm}^{-1}$ ), far, of isotactic polypropylene, 530
- Initiation of free-radical polymerization by photoinduced electron transfer processes, 521

- Injection mouldings, thermoplastic, determination of frozen-in stresses, 193
- Interfacial and aqueous solution techniques, synthesis of titanium polyethers, 42
- Ionic end-groups in polymaleimide, 394
- Isobutylene, molecular-sieve catalysed polymerization, 333
- Isoxazoline and isoxazole heterocycles, electrical properties of polymers containing, 286
- $\alpha$ -Keratin, structure of, 61
- Kinetics of crosslinking of linear polyethylene with *t*-butyl peroxide, 156
- Kinetics of epoxy cure: 3. The systems bisphenol-A epoxides/dicy, 91
- Kinetics of the reactions of polystyryl sodium with alkyl chlorides in dioxane, 649
- Light scattering from terpolymer solutions, 460
- Light scattering Rayleigh linewidth measurements on some globular protein solutions, 359
- Lignin, dienolysis of: cleavage of  $\beta$ -aryl ethers by Diels-Alder synthesis, 395
- Long branching, effects of, on distribution of degree of polymerization: 2, 524
- Maleic anhydride, molecular motion in a copolymer of styrene and, 68
- Mechanical behaviour and permeability of ABS/glass bead composites, 21
- Mechanical loss properties of polymers, effect of hydrostatic pressure and temperature on: 1. Polyethylene and polypropylene, 617. 2. Halogen polymers, 623. 3. PET, PVAC and vinyl chloride/vinyl acetate copolymers, 628
- Mechanical properties of polystyrene/low density polyethylene blends, 579
- Melting of low molecular weight poly(ethylene oxide) with acetoxy- and trimethylsiloxy-end-groups, 300
- Membranes, liquid permeated, electron microscopic studies on the useful life of, 411
- Methyl acrylate, anionic polymerization of, 137
- Methyl methacrylate, copolymers of, with cinnamic acid, 409
- Methyl methacrylate, rôle of semi-pinacol radicals in the benzophenone-photo-initiated polymerization of, 250
- Microtacticity of polymethacrylonitrile, 549
- Molecular motion in a copolymer of styrene and maleic anhydride, 68
- Molecular motion of polytetrafluoroethylene under high pressure, 558
- Molecular motions in poly(dimethyl siloxane) oligomers and polymers, 423
- Molecular orientation in oriented poly(ethylene terephthalate) films, 111
- Molecular orientation in PET studied by polarized Raman scattering, 398
- Molecular-sieve catalysed polymerization of isobutylene, 333
- Molecular weight distribution in condensation polymerization, 462
- Molecular weight, variation of refractive index increment with, 133
- Morphology and fracture of compression moulded TPX, 476
- Natural rubbers, chemorheology of irradiation-cured: 1. Stress relaxation mechanisms for various curing systems in natural rubber at high temperature, 569
- Natural rubber vulcanized in the swollen state, thermoelastic and thermo-mechanical studies on, 338
- $\beta$ -Nitrostyrene, anionic polymerization, 172
- N.m.r., pressure dependence of  $\beta$  and  $\gamma$  dispersion for polyethylene by, 589
- N.m.r. spectra of 2'-deoxyadenosine in DMSO-water mixtures, importance of 2:1 water-DMSO complex, 332
- N.m.r. spectra of poly( $\gamma$ -benzyl-L-glutamate) through the helix-coil transition, effect of polydispersity on, 543
- N.m.r. studies of the helix-coil transition of polypeptides in non-protonating solvent mixtures, 303
- Nuclear magnetic relaxation on poly(*N*-amyl maleimide) and poly(*N*-dodecyl maleimide), 45
- Nylon-6 (polycapramide): crystallization of polyamides under elevated pressure, 463
- Nylons, elastic modulus of, 632
- 2,4,6-Octatriyne, solid-state polymerization of derivatives of: 9. Topochemical reactions of monomers with conjugated triple bonds, 433
- Oligosaccharides, glass transition temperatures of, 329
- Perfluorobutadiene, some steric regulation on radical polymerization of, 327
- PET, molecular orientation in, studied by polarized Raman scattering, 398
- Phosphonitrilic chloride: 21. Synthesis of chelating polymers with cyclophosphazene thiocarbamate and the properties of chelating polymers, 488
- Photo-dissociation of benzoyl peroxide, 527
- Photoinitiators, metal carbonyls, for the polymerization of tetrafluoroethylene and vinyl monomers containing tetrafluoroethylene, 38
- Photopolymerization of styrene, triethylamine-sensitized, 561
- Poly(amide carboxylic acid) from pyromellitic anhydride and benzidine—influence of triethylamine on the molecular dimensions, 178
- Polyamides, crystallization of, under elevated pressure: nylon-6 (polycapramide), 463
- Polyamides derived from squaric acid, 230
- Poly(amido acids) and polyimides, aliphatic, with cyclobutane ring in the main chain, 440
- Poly(*N*-amyl maleimide) and poly(*N*-dodecyl maleimide), nuclear magnetic relaxation, 45
- Poly( $\gamma$ -benzyl-L-glutamate), effect of polydispersity on n.m.r. spectra, through the helix-coil transition, 543
- cis*-Polybutadiene in simple extension, a study of dilation coefficients of, 576
- Poly( $\epsilon$ -caprolactone) in dioxane, heat of dilution and density data for poly( $\beta$ -propiolactone) and, 343
- Polycarbonates, multiphase polymers containing, an etch technique for morphological studies of, 509
- Polycondensation of bis(2-hydroxyethyl)terephthalate, propagation and degradation reactions, 50
- Poly(dimethyl siloxane) oligomers and polymers, molecular motions in, 423
- Poly(dinaphthyl alkylene ethers), preparation of, by oxidative polyarylation and their crystallization behaviour, 241
- Polyesters, structural studies of: 5. Molecular and crystal structures of optically active and racemic poly( $\beta$ -hydroxybutyrate), 267
- Polyethers, titanium, synthesis by the interfacial and aqueous solution techniques, 42
- Poly(ethyl acrylate) in dilute solution, 5
- Polyethylene, branched, steady flow and dynamic viscoelastic properties of, 384
- Polyethylene, chain-extended crystallization of: effect of sample thickness, 390
- Poly(ethylene-co-carbon monoxide) single crystals, morphology and structure of, 373
- Poly(ethylene glycol), spin-labelled, at high temperatures ( $T > T_g$ ), solid and liquid state relaxations in, 481
- Polyethylene, lamellar thickening and chain-extended growth of, 387
- Polyethylene, linear, kinetics of crosslinking with *t*-butyl peroxide, 156
- Polyethylene melts, flow induced crystallization, 16
- Poly(ethylene oxide), complexes of alkali metal ions with, 589
- Poly(ethylene oxide), melting of low molecular weight, with acetoxy- and trimethylsiloxy-end-groups, 300
- Polyethylene, pressure dependence of  $\beta$  and  $\gamma$  dispersion for, by n.m.r., 589
- Poly(ethylene terephthalate), cyclics in, 185
- Poly(ethylene terephthalate) fibres, characterization of the crystalline, intermediate and amorphous phase, by X-ray diffraction, 9
- Poly(ethylene terephthalate) film, some observations on the fracture of, 103
- Poly(ethylene terephthalate), molecular orientation in oriented films, 111
- Poly(ethylene terephthalate), studies on the formation: 1. Propagation and degradation reactions in the polycondensation of bis(2-hydroxyethyl)terephthalate, 50. 2. Rate of transesterification of dimethyl terephthalate with ethylene glycol, 55
- Polyhexene-1, amorphous, influence of cooling rate on the heat capacity and thermal transitions of, 167
- Poly( $\beta$ -hydroxybutyrate), optically active and racemic, molecular and crystal structures of, 267
- trans*-1,4-Polyisoprene spherulite, deformation of: small angle X-ray diffraction, thermal differential analysis and density studies, 71
- Polyisoprenyllithium, electronic spectrum in hydrocarbon solvents, 594
- Polymaleimide, ionic end-groups in, 394
- Polymerization, anionic, of methyl acrylate, 137
- Polymerization, anionic, of  $\beta$ -nitrostyrene, 172
- Polymerization, cationic, of acenaphthylene and methyl acenaphthylenes, 352
- Polymerization, condensation, molecular weight distribution in, 462
- Polymerization, effects of poor solvents on radical-radical termination of, 107
- Polymerization, equilibrium bulk, of 1,3-dioxolan, 355
- Polymerization, ethylene, highly active catalysts for, by reduction of  $TiCl_4$  with organomagnesium compounds, 365
- Polymerization, free-radical, initiation by photoinduced electron transfer processes, 521
- Polymerization of methyl methacrylate, rôle of semi-pinacol radicals in the benzophenone-photoinitiated, 250
- Polymerization, molecular-sieve catalysed, of isobutylene, 333



## Classified Contents

- Polymerization, radical, of perfluorobutadiene, some steric regulation on, 327
- Polymerization, radical, photoinitiated by benzoin, benzoin methyl ether and benzil, mechanisms and relative efficiencies in, 405
- Polymerization, solid-state, of derivatives of 2,4,6-octatriene: 9. Topochemical reactions of monomers with conjugated triple bonds, 433
- Polymerization, stereoregular, of vinyl chloride with the redox system ferrous sulphate/hydrogen peroxide/oxalic acid: 1. Influence of some synthesis conditions on the stereoregularity of PVC, 234
- Polymerization studies using modified Ziegler-Natta catalysts: 1. Polymerization of vinyl chloride, 215. 2. Polymerization of vinyl fluoride, 221. 3. The catalyst system, 224
- Polymerization of tetrafluoroethylene and vinyl monomers containing tetrafluoroethylene, metal carbonyls as photoinitiators, 38
- Polymer/particulate filler interaction—the bound rubber phenomena, 309
- Polymers from the hydrolysis of tetraethoxysilane, 420
- Polymethacrylonitrile, microtacticity of, 549
- Poly(methyl methacrylate), characterization of stereoblock polymers by t.l.c., 171
- Poly(methyl methacrylate), craze shape and fracture, 469
- Poly(methyl methacrylate-co-acrylonitrile), 324
- Polypeptides in non-protonating solvent mixtures, n.m.r. studies of the helix-coil transition of, 303
- Poly( $\beta$ -propiolactone) and poly( $\epsilon$ -caprolactone) in dioxane, heat of dilution and density data for, 338
- Polypropylene, isotactic, crazing in a crystalline polymer, and the role of  $N_2$ ,  $O_2$ , and  $CO_2$  as crazing agents, 78
- Polypropylene, isotactic, far infra-red spectrum (400–10  $cm^{-1}$ ), 530
- Polystyrene and styrene, introduction of hydroxymethyl groups into, 330
- Polystyrene-cyclohexane system, cloud-point curves of, near the critical point, 415
- Polystyrene, dilute theta solutions, in cyclohexane, 151
- Polystyrene, *meta*-labelled, synthesis and characterization of: electron spin resonance studies of spin-labelled polymers, Part 5, 525
- Polystyrene/low density polyethylene blends, mechanical properties of, 579
- Polystyrene, non-theta solutions, in butan-2-one, 293
- Polystyrene-*g*-polyisoprene copolymers, synthesis and solution behaviour, 82
- Polystyrene, rubber-modified, fracture of, 451
- Polystyryl sodium, kinetics of reactions with alkyl chlorides in dioxane, 649
- Polytetrafluoroethylene, molecular motion of, under high pressure, 558
- Polyurethane block polymers, effect of segment size and polydispersity on the properties of, 255
- Polyurethane elastomers, composites formed by interstitial polymerization of vinyl monomers in: 1. Preparation and mechanical properties of methyl methacrylate based composites, 597. 2. Morphology and relaxation processes in methyl methacrylate based composites, 604
- Poly(vinyl chloride), electrical conductivity in, 445
- Poly(vinyl chloride), investigation of the compatibility of butadiene-acrylonitrile copolymers with, 347
- Poly(vinyl chloride), reaction of, with ethylenediamine hydrotrisulphide and properties of the products, 515
- Protein, preferential interaction, with solvent components, sedimentation equilibrium study of, 502
- Proteins, heterogeneous oxidized-wool, proton magnetic resonance study of conformational transitions in, 523
- Protein solutions, globular, light scattering Rayleigh linewidth measurements on some, 359
- Proton magnetic resonance study of conformational transitions in heterogeneous oxidized-wool proteins, 523
- Radical-radical termination of polymerization, effects of poor solvents on, 107
- Radicals, semi-pinacol, rôle of, in the benzophenone-photoinitiated polymerization of methyl methacrylate, 250
- Raman scattering, polarized, molecular orientation in PET studies by, 398
- Redox system ferrous sulphate/hydrogen peroxide/oxalic acid, stereoregular polymerization of vinyl chloride with, 234
- Refractive index increment, variation with molecular weight, 133
- Relaxation, solid and liquid state, in spin-labelled poly(ethylene glycol) at high temperatures ( $T > T_g$ ), 481
- Rheological properties of emulsion viscoses: 1. Influence of alkali concentration, reaction time and order of addition of reactants, 27. 2. Influence of cellulose origin, carbon disulphide ratio and temperature, 34
- Rubber-modified plastics, transition magnitudes and impact improvement in, 161
- Rubber-modified polystyrene, fracture of, 451
- Scanning electron microscopical study of fibre reinforced polymeric cage materials for rolling bearings, 130
- Sedimentation equilibrium study on preferential interaction of protein with solvent components, 502
- Segment size and polydispersity, effect of, on the properties of polyurethane block polymers, 255
- Semi-crystalline polymers, application of small angle X-ray scattering to: 1. Experimental considerations and analysis of data, 379
- SIS three block copolymer, the cubic structure of, 145
- Solid and liquid state relaxations in spin-labelled poly(ethylene glycol) at high temperatures ( $T > T_g$ ), 481
- Squaric acid, polyamides derived from, 230
- Stereoregularity of PVC, influence of some synthesis conditions on, 234
- Stresses, frozen-in, determination in thermoplastic injection mouldings, 193
- Styrene, photopolymerization of, triethylamine-sensitized, 561
- Synthesis and polymerizability of *N*-ethyl-2-vinylcarbazole, 124
- Synthesis and solution behaviour of polystyrene-*g*-polyisoprene copolymers, 82
- Synthesis of titanium polyethers by the interfacial and aqueous solution techniques, 42
- Termination, radical-radical, of polymerization, effects of poor solvents on, 107
- Tetraethoxysilane, polymers from the hydrolysis of, 420
- Tetrafluoroethylene and vinyl monomers containing tetrafluoroethylene, metal carbonyls as photoinitiators, 38
- Textile fibres and materials, electron microscope studies of, 273
- Thermal differential analysis, small angle X-ray diffraction, and density studies: deformation of *trans*-1,4-polyisoprene spherulite, 71
- Thermoplastic injection mouldings, determination of frozen-in stresses, 193
- Thermoplastics, amorphous, electron microscopy studies of fracture processes, 96
- Thin-layer chromatography, characterization of stereoblock polymers of poly(methyl methacrylate), 171
- Thiol, asymmetric addition of, to diene polymer in the presence of optically active amines as catalyst, 427
- Thiol, reaction of, to diene polymer in the presence of various catalysts, 87
- Titanium polyethers, synthesis, by the interfacial and aqueous solution techniques, 42
- TPX, compression moulded, morphology and fracture of, 476
- Transesterification, rate, of dimethyl terephthalate with ethylene glycol, 55
- Vinyl chloride, polymerization studies using modified Ziegler-Natta catalysts, 215
- Vinyl chloride, stereoregular polymerization with the redox system ferrous sulphate/hydrogen peroxide/oxalic acid, 234
- Vinyl fluoride, polymerization studies using modified Ziegler-Natta catalysts of, 221
- Vinylimidazolium salts, synthesis and homopolymerization studies of, 639
- Vinylpyridine oxide copolymers: viscosity/pH relationship of aq. solutions, 645
- Wool proteins, heterogeneous oxidized, proton magnetic resonance study of conformational transitions in, 523
- X-ray diffraction, characterization of the crystalline, intermediate and amorphous phase in poly(ethylene terephthalate) fibres by, 9
- X-ray diffraction, small angle, thermal differential analysis and density studies: deformation of *trans*-1,4-polyisoprene spherulite, 71
- X-ray profiles, a variance analysis of the line broadening of, from Fortisan, 402
- X-ray scattering, small angle, application to semi-crystalline polymers: 1. Experimental considerations and analysis of data, 379
- Ziegler-Natta catalysts, modified, polymerization studies using: 1. Polymerization of vinyl chloride, 215. 2. Polymerization of vinyl fluoride, 221. 3. The catalyst system, 224

# Author Index

- Adachi, Ken'ichiro: *see* Yokota, Kenji; Tomioka, Hideo and Adachi, Ken'ichiro
- Alfonso, G. C., Fiorina, L., Martuscelli, E., Pedemonte, E. and Russo, S.: Morphology and structure of poly(ethylene-co-carbon monoxide) single crystals, 373
- Alfthan, Elisabeth; de Ruvo, Alf; and Brown, Wyn: Glass transition temperatures of oligosaccharides, 329
- Allegrezza, A. E.: *see* Ng, H. N., Allegrezza, A. E., Seymour, R. W. and Cooper, S. L.
- Allen, G.: *see* Price, C. and Allen, G.
- Allen, G., Bowden, M. J., Blundell, D. J., Hutchinson, F. G., Jeffs, G. M. and Vyvoda, J.: Composites formed by interstitial polymerization of vinyl monomers in polyurethane elastomers: 1. Preparation and mechanical properties of methyl methacrylate based composites, 597
- Allen, G., Bowden, M. J., Blundell, D. J., Jeffs, G. M., Vyvoda, J. and White, T.: Composites formed by interstitial polymerization of vinyl monomers in polyurethane elastomers: 2. Morphology and relaxation processes in methyl methacrylate based composites, 604
- Ashman, P. C. and Booth, C.: Melting of low molecular weight poly(ethylene oxide) with acetoxy- and trimethylsiloxy-end-groups, 300
- Bailey, J., Block, H., Cowden, D. R. and Walker, S. M.: Nuclear magnetic relaxation in poly(*N*-amyl maleimide) and poly(*N*-dodecyl maleimide), 45
- Bain, D. R.: *see* Margerison, D., Bain, D. R. and Kiely, B.
- Bajah, S. T.: *see* Carraher, C. E. Jr. and Bajah, S. T.
- Baker, A. R. and East, G. C.: Kinetics of the reactions of polystyryl sodium with alkyl chlorides in dioxane, 649
- Balakrishnan, M.: *see* Rao, G. Venkoba; Balakrishnan, M.; and Venkatasubramanian, N.
- Bamford, C. H. and Burley, J. W.: Ionic end-groups in polymaleimide, 394
- Bamford, C. H. and Lindsay, H.: Introduction of hydroxymethyl groups into polystyrene and styrene, 330
- Bamford, C. H. and Mullik, S. U.: Metal carbonyls as photoinitiators for the polymerizations of tetrafluoroethylene and vinyl monomers containing tetrafluoroethylene, 38
- Barentsen, W. M. and Heikens, D.: Mechanical properties of polystyrene/low density polyethylene blends, 579
- Bassett, D. C. and Carder, D. R.: Lamellar thickening and chain-extended growth of polyethylene, 387
- Bassett, D. C. and Khalifa, B. A.: Chain-extended crystallization of polyethylene: effect of sample thickness, 390
- Batchelor, J., Berry, J. P. and Horsfall, F.: Die swell in elastic and viscous fluids, 297
- Beahan, P., Bevis, M. and Hull, D.: Electron microscopy studies of fracture processes in amorphous thermoplastics, 96
- Bednarick, J.: *see* Labaig, J. J., Monge, Ph., and Bednarick, J.
- Belliard, P.: *see* Cohen, S., Belliard, P. and Marechal, E.
- Berry, J. P.: *see* Batchelor, J., Berry, J. P. and Horsfall, F.
- Berry, R. W. H. and Mazza, R. J.: Anionic polymerization of  $\beta$ -nitrostyrene, 172
- Berton, A.: *see* Bourdariat, J., Berton, A., Chaussy, J., Isnard, R. and Odin, J.
- Bevington, J. C.: *see* SenGupta, P. K. and Bevington, J. C.
- Bevington, J. C., Colley, F. R. and Ebdon, J. R.: Copolymers of methyl methacrylate with cinnamic acid, 409
- Bevis, M.: *see* Beahan, P., Bevis, M. and Hull, D.
- Bianchi, U.: *see* Pedemonte, E., Turturro, A., Bianchi, U. and Devetta, P.
- Binet, R. and Leonard, J.: Equilibrium bulk polymerization of 1,3-dioxolan, 355
- Block, H.: *see* Bailey, J., Block, H., Cowden, D. R. and Walker, S. M.
- Block, H., Collinson, M. E. and Walker, S. M.: Molecular motion in a copolymer of styrene and maleic anhydride, 68
- Blow, C. M.: Polymer/particulate filler interaction—the bound rubber phenomena, 309
- Blundell, D. J.: *see* Allen, G., Bowden, M. J., Blundell, D. J., Hutchinson, F. G., Jeffs, G. M. and Vyvoda, J.
- Blundell, D. J.: *see* Allen, G., Bowden, M. J., Blundell, D. J., Jeffs, G. M., Vyvoda, J. and White, T.
- Booth, C.: *see* Ashman, P. C. and Booth, C.
- Bourdariat, J., Berton, A., Chaussy, J., Isnard, R. and Odin, J.: Influence of cooling rate on the heat capacity and thermal transitions of amorphous polyhexene-1, 167
- Bowden, M. J.: *see* Allen, G., Bowden, M. J., Blundell, D. J., Hutchinson, F. G., Jeffs, G. M. and Vyvoda, J.
- Bowden, M. J.: *see* Allen, G., Bowden, M. J., Blundell, D. J., Jeffs, G. M., Vyvoda, J. and White, T.
- Bower, D. I.: *see* Purvis, J., Bower, D. I. and Ward, I. M.
- Bradbury, E. M., Crane-Robinson, C. and Hartman, P. G.: Effect of polydispersity on the n.m.r. spectra of poly( $\gamma$ -benzyl-L-glutamate) through the helix  $\rightarrow$  coil transition, 543
- Bradbury, E. M., Crane-Robinson, C., Paolillo, L. and Temussi, P.: N.m.r. studies of the helix-coil transition of polypeptides in non-protonating solvent mixtures, 303
- Brown, D. S., Fulcher, K. U. and Wetton, R. E.: Application of small angle X-ray scattering to semi-crystalline polymers: 1. Experimental considerations and analysis of data, 379
- Brown, H. R. and Ward, I. M.: Craze shape and fracture in poly(methyl methacrylate), 469
- Brown, Wyn: *see* Alfthan, Elisabeth; de Ruvo, Alf; and Brown, Wyn
- Bullock, A. T., Cameron, G. G. and Smith, P. M.: Electron spin resonance studies of spin-labelled polymers: Part 5. Synthesis and characterization of meta-labelled polystyrene, 525
- Burley, J. W.: *see* Bamford, C. H. and Burley, J. W.
- Busfield, W. K. and Methven, J. M.: Anionic polymerization of methyl acrylate, 137
- Buter, R., Tan, Y. Y. and Challa, G.: Characterization of stereoblock polymers of poly(methyl methacrylate) by thin-layer chromatography, 171
- Bywater, S.: *see* Roovers, J. E. L. and Bywater, S.
- Cameron, J.: *see* Cameron, G. G. and Cameron, J.
- Cameron, G. G.: *see* Bullock, A. T., Cameron, G. G. and Smith, P. M.
- Cameron, G. G. and Cameron, J.: Effects of poor solvents on radical-radical termination of polymerization, 107
- Carder, D. R.: *see* Bassett, D. C. and Carder, D. R.
- Carraher, C. E. Jr. and Bajah, S. T.: Synthesis of titanium polyethers by the interfacial and aqueous solution techniques, 42
- Challa, G.: *see* Buter, R., Tan, Y. Y. and Challa, G.
- Chatani, Y.: *see* Yokouchi, M., Chatani, Y., Tadokoro, H., Teranishi, K. and Tani, H.
- Chaussy, J.: *see* Bourdariat, J., Berton, A., Chaussy, J., Isnard, R. and Odin, J.
- Clarke, Jeanne S.: *see* Rhein, R. A. and Clarke, Jeanne S.
- Cohen, S., Belliard, P. and Marechal, E.: Cationic polymerization of acenaphthylene and methyl acenaphthylenes, 352
- Colley, F. R.: *see* Bevington, J. C., Colley, F. R. and Ebdon, J. R.
- Collinson, M. E.: *see* Block, H., Collinson, M. E. and Walker, S. M.
- Cooper, D. R. and Semlyen, J. A.: Equilibrium ring concentrations and the statistical conformations of polymer chains: Part 11. Cyclics in poly(ethylene terephthalate), 178
- Cooper, S. L.: *see* Ng, H. N., Allegrezza, A. E., Seymour, R. W. and Cooper, S. L.
- Cowden, D. R.: *see* Bailey, J., Block, H., Cowden, D. R. and Walker, S. M.
- Cowie, J. M. G. and McEwen, I. J.: Molecular motions in poly(dimethyl siloxane) oligomers and polymers, 423
- Crane-Robinson, C.: *see* Bradbury, E. M., Crane-Robinson, C. and Hartman, P. G.
- Crane-Robinson, C.: *see* Bradbury, E. M., Crane-Robinson, C., Paolillo, L. and Temussi, P.
- Crescenzi, Vittorio: *see* Manzini, Giorgio and Crescenzi, Vittorio
- Cunningham, A.: *see* Kashiwagi, M., Cunningham, A., Manuel, A. J. and Ward, I. M.
- Daffurn, P. C.: *see* Feasey, R. G., Turner-Jones, A., Daffurn, P. C. and Freeman, J. L.
- Dale, B. J. and Jones, D. W.: Proton magnetic resonance study of conformational transitions in heterogeneous oxidized-wool proteins, 523
- De Boos, A. G.: Preparation and characterization of some polymers terminated with primary amino groups, 587

## Author Index

- de Candia, F.: *see* Price, C., Evans, K. A. and de Candia, F.
- de Candia, F., Dontsov, A., Micera, G. and Pusino, A.: Elastic properties and structure of a composite elastomeric system, 497
- de Ruvo, Alf: *see* Alfthan, Elisabeth; de Ruvo, Alf and Brown, Wyn
- Devetta, P.: *see* Pedemonte, E., Turturro, A., Bianchi, U. and Devetta, P.
- DiBari, J. C.: *see* Toy, Madeline, S. and DiBari, J. C.
- Dimov, K. and Slavtcheva, L.: Stereoregular polymerization of vinyl chloride with the redox system ferrous sulphate/hydrogen peroxide/oxalic acid: 1. Influence of some synthesis conditions on the stereoregularity of PVC, 234
- Dontsov, A.: *see* de Candia, F., Dontsov, A., Micera, G. and Pusino, A.
- Drioli, E.: *see* Nicolais, L., Drioli, E. and Landel, R. F.
- Dwzelt, N. E.: *see* Kulshreshtha, A. K., Hunter, R. E. and Dwzelt, N. E.
- East, G. C.: *see* Baker, A. R. and East, G. C.
- Eastmond, G. C. and Smith, E. G.: An etch technique for morphological studies of multiphase polymers containing polycarbonates, 509
- Ebdon, F. R.: *see* Bevington, J. C., Colley, F. R. and Ebdon, J. R.
- Evans, K. A.: *see* Price, C., Evans, K. A. and de Candia, F.
- Feasey, R. G., Turner-Jones, A., Daffurn, P. C. and Freeman, J. L.: Preparation of poly(dinaphthyl alkylene ethers) by oxidative polyarylation and their crystallization behaviour, 241
- Fenton, D. E., Parker, J. M. and Wright, P. V.: Complexes of alkali metal ions with poly(ethylene oxide), 589
- Ferguson, R. J., Marshall, G. P. and Williams, J. G.: The fracture of rubber-modified polystyrene, 451
- Ferguson, R. J. and Williams, J. G.: Some observations on the fracture of poly(ethylene terephthalate) film, 103
- Fiorina, L.: *see* Alfonso, G. C., Fiorina, L., Martuscelli, E., Pedemonte, E. and Russo, S.
- Fletcher, K. L.: *see* Haward, R. N., Roper, A. N. and Fletcher, K. L.
- Franco, S. and Leoni, A.: Radical copolymerization of *N*-(1,1-dimethyl-3-oxobutyl)-acrylamide in different solvents, 2
- Fraser, R. D. B. and MacRae, T. P.: The structure of  $\alpha$ -keratin, 61
- Freeman, J. L.: *see* Feasey, R. G., Turner-Jones, A., Daffurn, P. C. and Freeman, J. L.
- Fujishiro, Ryoichi: *see* Tamura, Katsutoshi; Murakami, Sachio; and Fujishiro, Ryoichi
- Fulcher, K. U.: *see* Brown, D. S., Fulcher, K. U. and Wetton, R. E.
- Ghosh, S. K., Krishna, M. G. and Vankar, V. D.: Electron microscopic studies on the useful life of liquid permeated membranes, 411
- Glasser, Wolfgang G.: Dienolysis of lignin: cleavage of  $\beta$ -aryl ethers by Diels-Alder synthesis, 395
- Gogolewski, S. and Pennings, A. J.: Crystallization of polyamides under elevated pressure: nylon-6 (polycapramide), 463
- Goldstein, M., Seeley, M. E., Willis, H. A. and Zichy, V. J. I.: The far infra-red spectrum (400–10 cm<sup>-1</sup>) of isotactic polypropylene, 530
- Green, Brian R. and Neuse, Eberhard, W.: Polyamides derived from squaric acid, 230
- Hartman, P. G.: *see* Bradbury, E. M., Crane-Robinson, C. and Hartman, P. G.
- Hasegawa, Masaki: *see* Nakanishi, Fusae; Hasegawa, Masaki; and Takahashi, Hiroshi
- Hashimoto, M.: *see* Kajiwara, M., Hashimoto, M. and Saito, H.
- Haszeldine, R. N., Hyde, T. G. and Tait, P. J. T.: Polymerization studies using modified Ziegler-Natta catalysts: 1. Polymerization of vinyl chloride, 215. 2. Polymerization of vinyl fluoride, 221. 3. The catalyst system, 224
- Hatada, K., Ohshima, J., Komatsu, T., Kokan, S. and Yuki, H.: Alternating copolymerization of methyl  $\alpha$ -phenylacrylate and methyl methacrylate by *n*-BuLi, 565
- Haward, R. N., Roper, A. N. and Fletcher, K. L.: Highly active catalysts for ethylene polymerization by the reduction of TiCl<sub>4</sub> with organomagnesium compounds, 365
- Hayashi, Toshio and Nakajima, Akio: Synthesis and conformation studies of copolypeptides composed of  $\gamma$ -methyl-L-glutamate and  $\epsilon$ -*N*-carbobenzyloxy-L-lysine, 535
- Hearle, J. W. S. and Simmens, S. C.: Electron microscope studies of textile fibres and materials, 273
- Heikens, D.: *see* Barentsen, W. M. and Heikens, D.
- Holt, P. F. and Tamami, B.: Vinylpyridine oxide copolymers: viscosity/pH relationship of aqueous solutions, 645
- Honda, C.: *see* Kambe, Hirotaro; Kambe, Y.; and Honda, C.
- Hong, Suck-Ju: Electrical properties of polymers containing isoxazoline and isoxazole heterocycles, 286
- Horsfall, F.: A theoretical treatment of die swell in a Newtonian liquid, 262
- Horsfall, F.: *see* Batchelor, J., Berry, J. P. and Horsfall, F.
- Horvath, A.: *see* Noordermeer, J. W. M., Janeschitz-Kriegl, H. and Horvath, A.
- Hull, D.: *see* Beahan, P., Bevis, M. and Hull, D.
- Hull, D.: *see* Owen, T. W. and Hull, D.
- Hunter, A. K.: *see* Kulshreshtha, A. K., Hunter, R. E. and Dwzelt, N. E.
- Hutchinson, F. G.: *see* Allen, G., Bowden, M. J., Blundell, D. J., Hutchinson, F. G., Jeffs, G. M. and Vyvoda, J.
- Hutchinson, J., Lambert, M. C. and Ledwith, A.: Rôle of semi-pinacol radicals in the benzophenone-photoinitiated polymerization of methyl methacrylate, 250
- Hutchinson, J. and Ledwith, A.: Mechanisms and relative efficiencies in radical polymerization photoinitiated by benzoin, benzoin methyl ether and benzil, 405
- Hyde, P., Kricka, L. J. and Ledwith, A.: Synthesis and polymerizability of *N*-ethyl-2-vinylcarbazole, 124
- Hyde, T. G.: *see* Haszeldine, R. N., Hyde, T. G. and Tait, P. J. T.
- Ida, Hiroaki: *see* Tomita, Kosuke and Ida, Hiroaki
- Ingham, J. D.: *see* Rhein, R. A. and Ingham, J. D.
- Ingram, P.: *see* Wetton, R. E., Moore, J. D. and Ingram, P.
- Inoue, Hideo: Sedimentation equilibrium study on preferential interaction of protein with solvent components, 502
- Isnard, R.: *see* Bourdariat, J., Berton, A., Chaussy, J., Isnard, R. and Odin, J.
- Israel, S. C.: *see* Salamone, J. C., Israel, S. C., Taylor, P. and Snider, B.
- Janeschitz-Kriegl, H.: *see* Noordermeer, J. W. M., Janeschitz-Kriegl, H. and Horvath, A.
- Jeffs, G. M.: *see* Allen, G., Bowden, M. J., Blundell, D. J., Hutchinson, F. G., Jeffs, G. M. and Vyvoda, J.
- Jeffs, G. M.: *see* Allen, G., Bowden, M. J., Blundell, D. J., Jeffs, G. M., Vyvoda, J. and White, T.
- Jensen, M. and Whisson, R. R.: Determination of frozen-in stresses in thermoplastic injection mouldings, 193
- Jones, D. W.: *see* Dale, B. J. and Jones, D. W.
- Jones Parry, E. and Tabor, D.: Effect of hydrostatic pressure and temperature on the mechanical loss properties of polymers: 1. Polyethylene and polypropylene, 617. 2. Halogen polymers, 623. 3. PET, PVAC and vinyl chloride/vinyl acetate copolymers,
- Kaiser, J.: *see* Kiji, Jitsuo; Kaiser, J.; Wegner, G.; and Schultz, R. C.
- Kajiwara, M., Hashimoto, M. and Saito, H.: Phosphonitrilic chloride: 21. Synthesis of chelating polymers with cyclophosphazene thiocarbamate and the properties of chelating polymers, 488
- Kambe, Hirotaro; Kambe, Y.; and Honda, C.: Light scattering from terpolymer solutions, 460
- Kambe, Y.: *see* Kambe, Hirotaro; Kambe, Y.; and Honda, C.
- Kaneko, M.: *see* Kuwahara, N., Nakata, M. and Kaneko, M.
- Kashiwagi, M., Cunningham, A., Manuel, A. J. and Ward, I. M.: An investigation of molecular orientation in oriented poly(ethylene terephthalate) films, 111
- Keller, A.: *see* Mackley, M. R. and Keller, A.
- Khalifa, B. A.: *see* Bassett, D. C. and Khalifa, B. A.
- Kiely, B.: *see* Margerison, D., Bain, D. R. and Kiely, B.
- Kiji, Jitsuo; Kaiser, J.; Wegner, G.; and Schultz, R. C.: Solid-state polymerization of derivatives of 2,4,6-octatriene: 9. Topochemical reactions of monomers with conjugated triple bonds, 433
- King, T. A., Knox, A., Lee, W. I. and McAdam, J. D. G.: Polymer translational diffusion: 1. Dilute theta solutions, polystyrene in cyclohexane, 151
- King, T. A., Knox, A. and McAdam, J. D. G.: Polymer translational diffusion: 2. Non-theta solutions, polystyrene in butan-2-one, 293

- Knox, A.: *see* King, T. A., Knox, A., Lee, W. I. and McAdam, J. D. G.
- Knox, A.: *see* King, T. A., Knox, A. and McAdam, J. D. G.
- Kokan, S.: *see* Hatada, K., Ohshima, J., Komatsu, T., Kokan, S. and Yuki, H.
- Komatsu, T.: *see* Hatada, K., Ohshima, J., Komatsu, T., Kokan, S. and Yuki, H.
- Koshiro, S.: *see* Suzuki, T., Koshiro, S. and Takegami, Y.
- Kricka, L. J.: *see* Hyde, P., Kricka, L. J. and Ledwith, A.
- Krishna, M. G.: *see* Ghosh, S. K., Krishna, M. G. and Vankar, V. D.
- Kubín, M. and Špaček, P.: Coupling of diffusion flux and chemical reaction in an asymmetric catalytically active membrane, 505
- Kulshreshtha, A. K., Hunter, R. E. and Dweltz, N. E.: A variance analysis of the line broadening of X-ray profiles from Fortisan, 402
- Kuwahara, N., Nakata, M. and Kaneko, M.: Cloud-point curves of the polystyrene-cyclohexane system near the critical point, 415
- Labaig, J. J., Monge, Ph., and Bednarick, J.: Steady flow and dynamic viscoelastic properties of branched polyethylene, 384
- Lambert, M. C.: *see* Hutchison, J., Lambert, M. C. and Ledwith, A.
- Landel, R. F.: *see* Nicolais, L., Drioli, E. and Landel, R. F.
- Lättilä, H.: *see* Törmälä, P., Lättilä, H. and Lindberg, J. J.
- Ledwith, A.: *see* Hutchison, J., Lambert, M. C. and Ledwith, A.
- Ledwith, A.: *see* Hutchison, J. and Ledwith, A.
- Ledwith, A.: *see* Hyde, P., Kricka, L. J. and Ledwith, A.
- Ledwith, A. and Purbrick, M. D.: Initiation of free-radical polymerization by photo-induced electron transfer processes, 521
- Lee, W. I.: *see* King, T. A., Knox, A., Lee, W. I. and McAdam, J. D. G.
- Leonard, J.: *see* Binet, R. and Leonard, J.
- Leoni, A.: *see* Franco, S. and Leoni, A.
- Lindberg, J. J.: *see* Törmälä, P., Lättilä, H. and Lindberg, J. J.
- Lindner, W. L.: Characterization of the crystalline, intermediate and amorphous phase in poly(ethylene terephthalate) fibres by X-ray diffraction, 9
- Lindsay, H.: *see* Bamford, C. H. and Lindsay, H.
- McAdam, J. D. G.: *see* King, T. A., Knox, A., Lee, W. I. and McAdam, J. D. G.
- McAdam, J. D. G.: *see* King, T. A., Knox, A. and McAdam, J. D. G.
- McEwen, I. J.: *see* Cowie, J. M. G. and McEwen, I. J.
- Mackley, M. R. and Keller, A.: Flow induced crystallization of polyethylene melts, 16
- MacRae, T. P.: *see* Fraser, R. D. B. and MacRae, T. P.
- Mancarella, C.: *see* Martuscelli, E. and Mancarella, C.
- Manley, T. R. and Martin, C. G.: Elastic modulus of linear polymer crystals, 491. Elastic modulus of nylons, 632
- Manley, T. R. and Qayyum, M. M.: Kinetics of crosslinking of linear polyethylene with t-butyl peroxide, 156
- Mansour, O. Y., Nagaty, A. and Shukry, N.: Rheological properties of emulsion viscoses: 1. Influence of alkali concentration, reaction time and order of addition of reactants, 27. 2. Influence of cellulose origin, carbon disulphide ratio and temperature, 34
- Manuel, A. J.: *see* Kashiwagi, M., Cunningham, A., Manuel, A. J. and Ward, I. M.
- Manzini, Giorgio and Crescenzi, Vittorio: Heat of dilution and density data for poly( $\beta$ -propiolactone) and poly( $\epsilon$ -caprolactone) in dioxane, 343
- Marčinčin, K.: *see* Pollák, V., Romanov, A. and Marčinčin, K.
- Marechal, E.: *see* Cohen, S., Belliard, P. and Marechal, E.
- Margerison, D., Bain, D. R. and Kiely, B.: Variation of refractive index increment with molecular weight, 133
- Mark, J. E.: Configurational characteristics of ethylene-vinyl chloride copolymers, 553
- Marshall, G. P.: *see* Ferguson, R. J., Marshall, G. P. and Williams, J. G.
- Martin, C. G.: *see* Manley, T. R. and Martin, C. G.
- Martuscelli, E.: *see* Alfonso, G. C., Fiorina, L., Martuscelli, E., Pedemonte, E. and Russo, S.
- Martuscelli, E. and Mancarella, C.: Deformation of *trans*-1,4-polyisoprene spherulite: small angle X-ray diffraction, thermal differential analysis and density studies, 71
- Mayhan, K. G.: *see* Peace, B. W., Mayhan, K. G. and Montle, J. F.
- Mazza, R. J.: *see* Berry, R. W. H. and Mazza, R. J.
- Methven, J. M.: *see* Busfield, W. K. and Methven, J. M.
- Micera, G.: *see* de Candia, F., Dontsov, A., Micera, G. and Pusino, A.
- Mills, G. H.: *see* Scott, D. and Mills, G. H.
- Minoura, Yuji: *see* Yamaguchi, Koichi; Yamada, Nobuo; and Minoura, Yuji
- Monge, Ph.: *see* Labaig, J. J., Monge, Ph. and Bednarick, J.
- Montle, J. F.: *see* Peace, B. W., Mayhan, K. G. and Montle, J. F.
- Moore, J. D.: *see* Wetton, R. E., Moore, J. D. and Ingram, P.
- Mori, Kunio and Nakamura, Yoshiro: Reaction of poly(vinyl chloride) with ethylenediamine hydrotrisulphide and properties of the products, 515
- Mullik, S. U.: *see* Bamford, C. H. and Mullik, S. U.
- Murakami, Kenkichi: *see* Tamura, Saburo, and Murakami, Kenkichi
- Murakami, Sachio: *see* Tamura, Katsutoshi; Murakami, Sachio; and Fujishiro, Ryoichi
- Nagaty, A.: *see* Mansour, O. Y., Nagaty, A. and Shukry, N.
- Nakafuku, Chitoshi; Taki, Seiji; and Takemura, Tetuo: Molecular motion of polytetrafluoroethylene under high pressure, 558. Pressure dependence of  $\beta$  and  $\lambda$  dispersion for polyethylene by n.m.r., 589
- Nakajima, Akio: *see* Hayashi, Toshio and Nakajima, Akio
- Nakamura, Yoshiro: *see* Mori, Kunio
- Nakanishi, Fusae; Hasegawa, Masaki; and Takahashi, Hiroshi: Aliphatic poly(amido acids) and polyimides with cyclobutane ring in the main chain, 440
- Nakata, M.: *see* Kuwahara, N., Nakata, M. and Kaneko, M.
- Neuse, Eberhard, W.: *see* Green, Brian R. and Neuse, Eberhard, W.
- Ng, H. N., Allegrezza, A. E., Seymour, R. W. and Cooper, S. L.: Effect of segment size and polydispersity on the properties of polyurethane block polymers, 255
- Nicolais, L., Drioli, E. and Landel, R. F.: Mechanical behaviour and permeability of ABS/glass bead composites, 21
- Noordermeer, J. W. M., Janeschitz-Kriegl, H. and Horvath, A.: Flow birefringence of polyelectrolytes: a poly-(amide carboxylic acid) from pyromellitic anhydride and benzidine—influence of triethylamine on the molecular dimensions, 178
- Odin, J.: *see* Bourdariat, J., Berton, A., Chaussy, J., Isnard, R. and Odin, J.
- Ogorkiewicz, R. M. and Sayigh, A. A. M.: An approximate method of predicting the bending of thermoplastic beams, 584
- Ohshima, J.: *see* Hatada, K., Ohshima, J., Komatsu, T., Kokan, S. and Yuki, H.
- Olf, H. G. and Peterlin, A.: Crazing in a crystalline polymer (isotactic polypropylene) and the role of N<sub>2</sub>, O<sub>2</sub>, and CO<sub>2</sub> as crazing agents, 78
- Owen, Don R.: *see* Seymour, Raymond B., Owen, Don R. and Stahl, Glenn, A.
- Owen, T. W. and Hull, D.: Morphology and fracture of compression moulded TPX, 476
- Paolillo, L.: *see* Bradbury, E. M., Crane-Robinson, C., Paolillo, L. and Temussi, P.
- Parker, J. M.: *see* Fenton, D. E., Parker, J. M. and Wright, P. V.
- Parrini, Paolo: Electrical conductivity in poly(vinyl chloride), 445
- Peace, B. W., Mayhan, K. G. and Montle, J. F.: Polymers from the hydrolysis of tetraethoxysilane, 420
- Pearson, J. R. A. and Pickup, T. J. F.: Stability of wedge and channel flow of highly viscous and elastic liquids, 209
- Pedemonte, E.: *see* Alfonso, G. C., Fiorina, L., Martuscelli, E., Pedemonte, E. and Russo, S.
- Pedemonte, E., Turturro, A., Bianchi, U. and Devetta, P.: The cubic structure of a SIS three block copolymer, 145
- Pennings, A. J.: *see* Gogolewski, S. and Pennings, A. J.
- Peterlin, A.: *see* Olf, H. G. and Peterlin, A.
- Pickup, T. J. F.: *see* Pearson, J. R. A. and Pickup, T. J. F.
- Pollák, V., Romanov, A. and Marčinčin, K.: Study of thermoelastic properties of ethylene-vinyl acetate copolymer, 290
- Price, C. and Allen, G.: A study of dilation coefficients of *cis*-polybutadiene in simple extension, 576
- Price, C., Evans, K. A. and de Candia, F.: Thermoelastic and thermomechanical studies on natural rubber vulcanized in the swollen state, 338
- Price, C. and Woods, D.: Synthesis and solution behaviour of polystyrene-*g*-polyisoprene copolymers, 82
- Purbrick, M. D.: *see* Ledwith, A. and Purbrick, M. D.

## Author Index

- Purvis, J., Bower, D. I. and Ward, I. M.: Molecular orientation in PET studied by polarized Raman scattering, 398
- Pusino, A.: *see de Candia, F., Dontsov, A., Micera, G. and Pusino, A.*
- Qayyum, M. M.: *see Manley, T. R. and Qayyum, M. M.*
- Rao, G. Venkoba; Balakrishnan, M.; and Venkatasubramanian, N.: On the importance of 2 : 1 water-DMSO complex in the n.m.r. spectra of 2'-deoxyadenosine in DMSO-water mixtures, 332
- Rhein, R. A. and Clarke, Jeanne, S.: Molecular-sieve catalysed polymerization of isobutylene, 333
- Rhein, R. A. and Ingham, J. D.: New polymer systems: chain extension by dianhydrides, 466
- Romanov, A.: *see Pollák, V., Romanov, A. and Marcinčin, K.*
- Roovers, J. E. L. and Bywater, S.: Electronic spectrum of polyisoprenyllithium in hydrocarbon solvents, 594
- Roper, A. N.: *see Haward, R. N., Roper, A. N. and Fletcher, K. L.*
- Russo, S.: *see Alfonso, G. C., Fiorina, L., Martuscelli, E., Pedemonte, E. and Russo, S.*
- Sacher, E.: Kinetics of epoxy cure: 3. The systems bisphenol-A epoxides/dicy, 91
- Saito, H.: *see Kajiwara, M., Hashimoto, M. and Saito, H.*
- Salamone, J. C., Israel, S. C., Taylor, P. and Snider, B.: Synthesis and homopolymerization studies of vinylimidazolium salts, 639
- Santappa, M.: *see Srinivasan, K. S. V. and Santappa, M.*
- Sayigh, A. A. M.: *see Ogorkiewicz, R. M. and Sayigh, A. A. M.*
- Schultz, R. C.: *see Kiji, Jitsuo; Kaiser, J.; Wegner, G.; and Schultz, R. C.*
- Scott, D. and Mills, G. H.: Scanning electron microscopical study of fibre reinforced polymeric cage materials for rolling bearings, 130
- Seeley, M. E.: *see Goldstein, M., Seeley, M. E., Willis, H. A. and Zichy, V. J. I.*
- Sellen, D. B.: Light scattering Rayleigh linewidth measurements on some globular protein solutions, 359
- Semlyen, J. A.: *see Cooper, D. R. and Semlyen, J. A.*
- SenGupta, P. K. and Bevington, J. C.: Photo-dissociation of benzoyl peroxide, 527
- Seymour, Raymond B., Owen, Don R. and Stahl, Glenn A.: Poly(methyl methacrylate-co-acrylonitrile), 324
- Seymour, R. W.: *see Ng, H. N., Allegrezza, A. E., Seymour, R. W. and Cooper, S. L.*
- Shukry, N.: *see Mansour, O. Y., Nagaty, A. and Shukry, N.*
- Simmens, S. C.: *see Hearle, J. W. S. and Simmens, S. C.*
- Slavtcheva, L.: *see Dimov, K. and Slavtcheva, L.*
- Small, P. A.: Effects of long branching on distribution of degree of polymerization: 2, 524
- Smith, E. G.: *see Eastmond, G. C. and Smith, E. G.*
- Smith, P. M.: *see Bullock, A. T., Cameron, G. G. and Smith, P. M.*
- Snider, B.: *see Salamone, J. C., Israel, S. C., Taylor, P. and Snider, B.*
- Špaček, P.: *see Kubín, M. and Špaček, P.*
- Srinivasan, K. S. V. and Santappa, M.: Poly(ethyl acrylate) in dilute solution, 5
- Stahl, Glenn A.: *see Seymour, Raymond B., Owen, Don R. and Stahl, Glenn A.*
- Suzuki, T., Koshiro, S. and Takegami, Y.: Microtacticity of polymethacrylonitrile, 549
- Tabor, D.: *see Jones Parry, E. and Tabor, D.*
- Tadokoro, H.: *see Yokouchi, M., Chatani, Y., Tadokoro, H., Teranishi, K. and Tani, H.*
- Tait, P. J. T.: *see Haszeldine, R. N., Hyde, T. G. and Tait, P. J. T.*
- Takahashi, Hiroshi: *see Nakanishi, Fusae; Hasegawa, Masaki; and Takahashi, Hiroshi*
- Takegami, Y.: *see Suzuki, T., Koshiro, S. and Takegami, Y.*
- Takemura, Tetuo: *see Nakafuku, Chitoshi; Taki, Seiji; and Takemura, Tetuo*
- Taki, Seiji: *see Nakafuku, Chitoshi; Taki, Seiji; and Takemura, Tetuo*
- Tamami, B.: *see Holt, P. F. and Tamami, B.*
- Tamura, Katsutoshi; Murakami, Sachio; and Fujishiro, Ryoichi: Estimation of heat of dilution of polymer solution: a trial on a correction of the heat of stirring ascribed to the viscosity difference before and after dilution, 237
- Tamura, Saburo and Murakami, Kenkichi: Chemorheology of irradiation-cured natural rubbers: 1. Stress relaxation mechanisms for various curing systems in natural rubber at high temperature, 569
- Tan, Y. Y.: *see Buter, R., Tan, Y. Y. and Challa, G.*
- Tani, H.: *see Yokouchi, M., Chatani, Y., Tadokoro, H., Teranishi, K. and Tani, H.*
- Taylor, P.: *see Salamone, J. C., Israel, S. C., Taylor, P. and Snider, B.*
- Temussi, P.: *see Bradbury, E. M., Crane-Robinson, C., Paolillo, L. and Temussi, P.*
- Teranishi, K.: *see Yokouchi, M., Chatani, Y., Tadokoro, H., Teranishi, K. and Tani, H.*
- Tomioka, Hideo: *see Yokota, Kenji; Tomioka, Hideo; and Adachi, Ken'ichiro*
- Tomita, Kosuke: Studies on the formation of poly (ethylene terephthalate): 1. Propagation and degradation reactions in the polycondensation of bis(2-hydroxyethyl) terephthalate, 50
- Tomita, Kosuke and Ida, Hiroaki: Studies on the formation of poly(ethylene terephthalate): 2. Rate of transesterification of dimethyl terephthalate with ethylene glycol, 55
- Törmälä, P., Lättilä, H. and Lindberg, J. J.: Solid and liquid state relaxations in spin-labelled poly(ethylene glycol) at high temperatures ( $T > T_g$ ), 481
- Toy, Madeline S. and DiBari, J. C.: Some steric regulation on radical polymerization of perfluorobutadiene, 327
- Turner, J. C. R.: On the molecular weight distribution in condensation polymerization, 462
- Turner-Jones, A.: *see Feasey, R. G., Turner-Jones, A., Daffurn, P. C. and Freeman, J. L.*
- Turturro, A.: *see Pedemonte, E., Turturro, A., Bianchi, U. and Devetta, P.*
- Vankar, V. D.: *see Ghosh, S. K., Krishna, M. G. and Vankar, V. D.*
- Venkatasubramanian, N.: *see Rao, G. Venkoba; Balakrishnan, M.; and Venkatasubramanian, N.*
- Vyvoda, J.: *see Allen, G., Bowden, M. J., Blundell, D. J., Hutchinson, F. G., Jeffs, G. M. and Vyvoda, J.*
- Vyvoda, H.: *see Allen, G., Bowden, M. J., Blundell, D. J., Jeffs, G. M., Vyvoda, J. and White, T.*
- Walker, S. M.: *see Bailey, J., Block, H., Cowden, D. R. and Walker, S. M.*
- Walker, S. M.: *see Block, H., Collinson, M. E. and Walker, S. M.*
- Ward, I. M.: *see Brown, H. R. and Ward, I. M.*
- Ward, I. M.: *see Kashiwagi, M., Cunningham, A., Manuel, A. J. and Ward, I. M.*
- Ward, I. M.: *see Purvis, J., Bower, D. I. and Ward, I. M.*
- Wegner, G.: *see Kiji, Jitsuo; Kaiser, J.; Wegner, G.; and Schultz, R. C.*
- Wetton, R. E.: *see Brown, D. S., Fulcher, K. U. and Wetton, R. E.*
- Wetton, R. E., Moore, J. D. and Ingram, P.: Transition magnitudes and impact improvement in rubber-modified plastics, 161
- Whisson, R. R.: *see Jensen, M. and Whisson, R. R.*
- White, T.: *see Allen, G., Bowden, M. J., Blundell, D. J., Jeffs, G. M., Vyvoda, J. and White, T.*
- Williams, J. G.: *see Ferguson, R. J., Marshall, G. P. and Williams, J. G.*
- Williams, J. G.: *see Ferguson, R. J. and Williams, J. G.*
- Willis, H. A.: *see Goldstein, M., Seeley, M. E., Willis, H. A. and Zichy, V. J. I.*
- Woods, D.: *see Price, C. and Woods, D.*
- Wright, P. V.: *see Fenton, D. E., Parker, J. M. and Wright, P. V.*
- Yamada, Nobuo: *see Yamaguchi, Koichi; Yamada, Nobuo; and Minoura, Yuji*
- Yamaguchi, Koichi; Yamada, Nobuo; and Minoura, Yuji: Reaction of thiol to diene polymer in the presence of various catalysts, 87. Asymmetric addition of thiol to diene polymer in the presence of optically active amines as catalyst, 427
- Yokota, Kenji; Tomioka, Hideo; and Adachi, Ken'ichiro: Triethylamine-sensitized photopolymerization of styrene, 561
- Yokouchi, M., Chatani, Y., Tadokoro, H., Teranishi, K. and Tani, H.: Structural studies of polyesters: 5. Molecular and crystal structures of optically active and racemic poly( $\beta$ -hydroxybutyrate), 267
- Yuki, H.: *see Hatada, K., Ohshima, J., Komatsu, T., Kokan, S. and Yuki, H.*
- Zakrzewski, G. A.: Investigation of the compatibility of butadiene-acrylonitrile copolymers with poly(vinyl chloride), 347
- Zichy, V. J. I.: *see Goldstein, M., Seeley, M. E., Willis, H. A. and Zichy, V. J. I.*

## UK EDITORS

**C. H. Bamford** PhD, ScD, FRS  
Campbell Brown Professor of Industrial  
Chemistry, University of Liverpool,  
P.O. Box 147, Liverpool L69 3BX

**C. E. H. Bawn** CBE, FRS  
Grant Brunner Professor of Inorganic and  
Physical Chemistry, University of Liverpool,  
P.O. Box 147, Liverpool L69 3BX

**E. M. Bradbury** PhD  
Head of Biophysics Section,  
Portsmouth Polytechnic,  
Park Road, Portsmouth PO1 2DZ

**Geoffrey Gee** CBE, FRS  
Sir Samuel Hall Professor of Chemistry,  
University of Manchester,  
Manchester M13 9PL

**R. J. W. Reynolds** PhD, FPI  
Professor and Director,  
Institute of Polymer Technology,  
Loughborough University of Technology,  
Loughborough LE11 3TU

Annual subscription including postage  
UK £26; USA \$67.60 (surface mail)  
Airmail USA \$90; Japan £34  
Rates for other countries available on request

Published monthly by IPC Science and Technology  
Press Ltd, IPC House, 32 High Street,  
Guildford, Surrey, England  
Telephone: Guildford (0483) 71661  
Telegrams and Telex: Bisnespres 25137 London

Reprints (minimum quantity usually 100) of papers  
may be ordered from the publishers. Write to the  
Reprints Dept, IPC Science and Technology Press  
Ltd, at the above address

American Representatives: IPC (America) Ltd,  
205 East 42nd Street, New York, NY 10017, USA

© IPC Business Press Ltd, 1973

## OVERSEAS EDITORS

**H. C. Benoit** PhD  
Professor, Faculty of Science,  
University of Strasbourg  
Director, Centre de Recherches  
sur les Macromolécules,  
6, Rue Boussingault,  
67 Strasbourg, France

**S. Bywater** PhD  
Head, Polymer Section,  
National Research Council,  
Ottawa KIA OR9, Canada

**F. Danusso** PhD  
Professor of Macromolecular Chemistry,  
Istituto Chimica Industriale del Politecnico,  
Piazza Leonardo da Vinci 32,  
20133 Milano, Italy

**M. Szwarc** PhD, FRS  
Director, Polymer Research Center,  
State University of New York,  
College of Environmental Science and  
Forestry, Syracuse, NY 13210, USA

## MANAGING EDITOR

**J. A. G. Thomas** PhD

## ASSISTANT EDITOR

**C. J. Rawlins** BSc